Multiplex protein measurements in time course samples of traumatic brain injury patients using the antibody colocalization microarray

Author:
Véronique Laforte

Integrated Program in Neuroscience

McGill University, Montreal

December 2019

A thesis submitted to McGill University in partial fulfillment of the requirements for the degree of Doctor of Philosophy

Contents

List of Figures

List of Tables

Abstract

Traumatic brain injury (TBI) is a leading cause of death in young adults. Molecular mechanisms of damage and repair are very complex and have yet to be completely unraveled. However, the importance of anti- and pro-inflammatory mechanisms involved in injury progression and recovery has been shown. Moreover, there is a clinical need to identify potential biomarkers of injury severity, patient outcome, and to predict the development of harmful secondary injury. In order to better understand injury mechanisms, tools that can reliably and reproducibly sample and measure low-abundance proteins such as cytokines, chemokines, proteases and adhesion molecules are required. The goal of this thesis is to develop an assay that can efficiently and reliably measure proteins from human biofluids using the antibody colocalization microarray (ACM), a cross-reactivity free ELISA-based antibody microarray that is used to measure more than 100 proteins including cytokines and chemokines in hundreds of 20-30 µL samples. More specifically, the work in this thesis aims to 1) improve the reproducibility and reliability ACM, 2) improve the reliability of sampling of brain interstitial fluid by comparing different additives to a large molecular-weight cut-off cerebral microdialysis perfusion fluid and 3) measure several proteins involved in inflammation, injury and repair in TBI patients and explore their potential as biomarkers for injury severity, patient outcome or to predict secondary injury.

To improve reproducibility of ACM microarray spotting, new printing buffers with mixtures of hygroscopic additives were tested and evaluated based on spotting reliability and reproducibility, and for their capacity to prevent evaporation. To improve the assay reproducibility, the use of multiple fluorescent calibrants was tested and novel algorithms developed to help normalize and quantify microarray signals in large-scale experiments including several hundred samples. An improvement of 25 % in reproducibility was achieved using this novel calibration method. Next, to stabilize the

recovery of microdialysate fluid, three additives (albumin, low and high molecular dextrans) were added to cerebral microdialysis perfusion fluid. We performed *in vitro* tests comparing the relative recovery of proteins, leakage of additives through the microdialysis membrane, interference with protein quantification, and finally whether the additives modified protein secretion by glial cell in cultures, which could lead to erroneous protein measurements *in vivo*. Finally, we measured 103 proteins in 20-30 µL microdialysate, cerebrospinal fluid and blood time course samples of 8 patients with severe TBI, and blood time course samples of 5 patients with mild TBI and one patient with non-TBI trauma, as an exploratory study. We found evidence that some, but not all proteins detected in microdialysate of patients are produced by the brain, and found potential biomarkers of patient outcome, development of secondary injury, as well as injury severity.

The methods and solutions leading to improvements to the reproducibility and reliability of the ACM are directly transferable to other microarray platforms that make use of liquid handling and protein deposition on surfaces, and the comparison of additives for cerebral microdialysis is a step towards optimizing this valuable technique for indirect brain tissue sampling. The time course measurements of 103 proteins in cerebral microdialysis, cerebrospinal fluid and blood samples of TBI patients identified known and new potential biomarkers of injury severity, patient outcome and to predict the development of secondary injury. The time course data of 103 proteins can be used to further understand the mechanisms of brain injury and repair, and the potential biomarkers identified can be further studied and validated in bigger studies. Moreover, the improved ACM described in this thesis can be used to reliably measure proteins in different clinical populations in diseases which involve inflammation.

Résumé

Les traumatismes crâniens (TC) sont une des causes les plus fréquentes de décès chez les jeunes adultes. Les mécanismes moléculaires impliqués dans les lésions et réparations sont très complexes et ne sont aujourd'hui toujours pas entièrement compris. Cependant, l'importance des mécanismes inflammatoires et anti-inflammatoires impliqués dans la progression des lésions et le rétablissement des patients a été prouvé. De plus, il apparaît cliniquement essentiel de pouvoir identifier de potentiels biomarqueurs de la sévérité des lésions, du taux de rétablissement des patients et de prédiction à l'apparition de lésions secondaires dangereuses. Afin de mieux comprendre ces mécanismes de lésions, des outils capables d'échantillonner et de mesurer avec fiabilité et de façon reproductible des molécules telles que des cytokines, chémokines, protéases et molécules d'adhésion sont nécessaires. Cette thèse a pour but de développer un essai qui peut mesurer des protéines présentes dans les biofluides humains de façon fiable et efficace en utilisant l'"Antibody colocalization microarray" (ACM), une plateforme de microarray d'anticorps basée sur l'ELISA et capable de mesurer sans transréactivité plus de 100 protéines incluant des cytokines et chémokines dans des centaines d'échantillons de 20-30 µL. Plus spécifiquement, le travail décrit dans cette thèse a pour but de 1) améliorer la reproductibilité et la fiabilité de l'ACM, 2) améliorer la fiabilité de l'échantillonnage du fluide interstitiel du cerveau en comparant trois additifs ajoutés au liquide de perfusion de microdialyse (masse moléculaire à haute valeur de coupure) et 3) mesurer plusieurs protéines impliquées dans l'inflammation, les lésions et le rétablissement de patients souffrant de TC et en explorer le potentiel en tant que biomarqueurs de la sévérité des lésions, du taux de rétablissement des patients ou de prédiction à l'apparition de lésions secondaires.

Pour améliorer la reproductibilité d'impression des microarray de l'ACM, de nouveaux tampons d'impression contenant des mélanges d'additifs hygroscopiques ont été testés et évalués au regard

de la fiabilité et reproductibilité des dépôts imprimés et de leur capacité à prévenir l'évaporation. Pour améliorer la reproductibilité des essais, plusieurs calibrants fluorescents ont été testés et de nouveaux algorithmes développés pour aider à normaliser et quantifier les signaux des microarrays dans des expériences à grande échelle mesurant des centaines d'échantillons. Cette nouvelle méthode de calibration a permis d'améliorer de 25 % la reproductibilité des résultats. Par la suite, trois additifs (albumine et dextrans à faible et haute masse moléculaire) ont été ajoutés au fluide de perfusion de la microdialyse cérébrale afin de stabiliser sa récupération. Plusieurs tests *in vitro* ont été menés pour comparer la récupération des protéines, la fuite des additifs au travers de la membrane de microdialyse, l'interférence avec la quantification des protéines, et finalement pour déterminer si la présence des additifs modifiait la sécrétion de protéines par des cellules gliales en culture, ce qui pourrait générer des erreurs de mesure des protéines *in vivo*. Finalement, nous avons mesuré 103 protéines dans 20-30 µL d'échantillons successifs de microdialysat, de liquide céphalo-rachidien et de sang de 8 patients souffrant de TC sévère, ainsi que des échantillons successifs de sang de 6 patients souffrant de TC léger et un patient souffrant de trauma sans TC, en tant qu'étude exploratrice. Nous avons découvert des indices que certaines protéines - mais pas toutes - détectées dans les échantillons de microdialysat sont produites dans le cerveau, et avons pu identifier de potentiels biomarqueurs de la sévérité des lésions, du taux de rétablissement des patients, ainsi que du développement de lésions secondaires.

Les méthodes et solutions identifiées pour améliorer la reproductibilité et la fiabilité de l'ACM sont directement transférables aux autres plateformes de microarray qui manipulent les liquides et déposent des protéines à des surfaces, et la comparaison des additifs pour la microdialyse cérébrale est une étape vers l'optimisation de cette prometteuse technique d'échantillonnage indirect du tissu cérébral. La mesure de 103 protéines dans les échantillons successifs de microdialysat, de liquide céphalo-rachidien et de sang de patients souffrant de TC a permis de déterminer de potentiels biomarqueurs, connus et nouveaux, de la sévérité des lésions, du taux de rétablissement des patients et du développement des lésions secondaires. Les données successives des 103 protéines peuvent être également utilisées pour avancer la compréhension des mécanismes de lésion et réparation cérébrales, tandis que les biomarqueurs identifiés peuvent être étudiés et validés plus profondément dans de plus vastes études ultérieurement. De plus, l'ACM améliorée décrite dans cette thèse peut être utilisée pour mesurer des protéines dans des populations cliniques pour des maladies qui impliquent des processus inflammatoires.

Acknowledgements

My first thanks go to my supervisors, Dr. David Juncker and Dr. Judith Marcoux. David, I am very grateful for the amazing opportunity to work on this project, which was close to my heart, having lost a friend who was suffering the effects of a TBI for years. Thank you for your patience, for your feedback and questions, and for giving me the freedom to pursue the questions I felt were important in achieving the results that we did. Judith, I want to thank you for helping me along the way by encouraging me, showing me how things are done in the clinic, particularly in the operating theater, in the ICU and on the hospital floors, and for being open and eager to pursue research in spite of your very, very busy schedule as a neurosurgeon. Your support throughout the years has been invaluable.

I would like to thank Dr. Keith Murai and Dr. Clare Gallagher for serving as examiners for my thesis. It might look like a behemoth at the onset, but I hope you will reach the beginning of the appendices quickly. I am very grateful that you agreed to take valuable time out of your very busy schedules to read the fruit of many years of research and labor.

I want to thank Dr. Keith Murai and Dr. Amit Bar-Or, who counseled me from the start on my research and helped me focus on what was important. Your perspectives on my projects and your encouragement were very appreciated, and I looked forward to my yearly PhD committee meetings in order to hear your opinions. I always ended those meetings with the feeling that things were not so bad after all, that everything was moving along in the right direction, and having a better view of that direction. I want to thank Dr. Yasser Riazalhosseini for sitting on my comprehensive exam and providing valuable feedback afterwards.

I am especially grateful to Dr. Mathias Aebersold, Dr. Ayokunle Olanrewaju and Dr. Livie Dorwling-Carter for providing timely feedback on small and large parts of my thesis. Your feedback

was very much appreciated. I would like to thank Ms. Xuan Wang for providing me with information I needed for my thesis, which I could not obtain while being far away.

Three faculty members helped me and taught me valuable skills. I would like to thank Dr. Louis Collins for providing support more than once when work was difficult. I would like to thank Dr. Vanessa Dumeaux for introducing me to the wonderful and scary world of bioinformatics and answering my many questions. Programming is something I can do, but is not my favorite part of research. Discussing with Vanessa gave me the courage to tackle the challenge of doing all, and I mean *all*, my analyses in R when their complexity exploded with the development of calibration, making "button-pushing" with Excel and Prism virtually impossible from then on. I also would like to thank Dr. Simon Tinawi for allowing me to shadow him for one day in the clinic while he examined and helped patients who had suffered from mild TBI. It was an experience I greatly learned from, allowing me to witness first hand the effects of TBI on its victims. Spending time in the ICU, talking to ICU nurses, sometimes even interacting with families of comatose patients suffering from severe TBI, and perspectives of clinicians such as Dr. Tinawi and Dr. Marcoux have been extremely important to me throughout my PhD, providing the "why does it matter?" of my research goals, and a constant motivation.

While I really appreciate people I worked with and who supported me through my PhD years, I am very conscious that research cannot happen without proper funding. I would like to thank the following organizations who provided funding: the NSERC-CREATE training program in Integrated Sensors Systems, the McGill University Faculty of Medicine for awarding me an Alexander McFee studentship, the department of Systems Biology, Faculty of Medicine and CANSSI for providing travel awards that allowed me to attend conferences. I would like to give particular thanks to the family of the late Dr. Robert Ford, who provided the funds for the Award in Neurotrauma, an award I received which is part of the MUHC Research Institute Neurosurgery Research Awards.

When I started in David's lab in 2010 as a Master's student, I was surrounded by a great team that was in the final stages of the development of the Antibody Colocalization Microarray (ACM), a platform I later helped refine and used to measures clinical samples. I would like to thank Mateu Pla-Roca, Saule Tourekhanova, Emmanuel Moreau and Rym Leulmi for introducing me to the ACM platform.

I had the chance to work with three wonderful people on the ACM platform. I would like to thank Sébastien Bergeron for his constant encouragement, fresh perspective on research, and lively discussions in "Québecois" which allowed me not to completely lose my mother tongue. For part of my PhD the proteomics team was composed of Karen Gambaro, Pammy Lo and myself. While it lasted, I really enjoyed working "in a team" with two cheerful, hard-working, easy-going and extremely competent women. I felt like our work as a team was better and greater than the simple

addition of our individual work.

In the several years that I was working on my Master's project, which eventually turned into my PhD project, I had the chance to work alongside and supervise a few undergraduate students. I would like to thank Francesco Fiorini, David Zhang, Jack Mouhanna, Axelle Valet, Parth Vakyl, Madison Odabassian and Farah Musharbash for bring your passions, your cheerfulness, your questions, and your fresh perspectives on my research and your own, and contributing to my research projects while achieving your own goals. All of you are extremely brilliant individuals, and I truly enjoyed and benefited from the experience of supervising or helping your individual projects.

A lab is more than a supervisor and equipment, and one of the most valuable asset are its people. I would like to particularly thank my colleagues Philippe DeCorwin-Martin, Jeffrey Munzar, Andy Ng, Grant Ongo, Kate Turner, Milad Dagher, Anne Meunier, Gina Zhou, Sébastien Ricoult, Adiel Mallik, Mohsen Akbari, Ali Tamayol, Huiyan Li, Katie Clancy, Frédéric Normandeau, Greta Thompson-Steckel, Mohammad Qasaimeh, Mcolisi Dlamini, Florian Possel, Ahmet Turkdogan, Roozbeh Safavieh, Heidi Larkin, Myriam Kia, Arya Tavakoli and Donald McNearney for friendly and helpful discussions during my time in the lab. I would like to thank Hoai-Thu Vo, Geneviève Dancausse and Alexandre Belisle from the Genome Quebec Innovation Center for being friendly, professional and always helpful. Interacting with you was always a pleasure.

I would like to give special thanks for Ayokunle Olanrewaju, Jessica Lee and Alex Hernandez from the labs in Montreal for their support, discussions, encouragements and being good friends throughout the years. I spent the last three years of my PhD mostly in Zürich, Switzerland, which I now call my home. I spent many months squatting among the lab members of Prof. Janos Vörös's lab, where I've also made many friends. I would like to thank not only Prof. Vörös for generously letting me work in the student offices, but also Victoria, Raphael, Luca, Livie, Harald, Alex and Greta for welcoming me in Zürich and sharing with me your many different experiences of doing research as PhD students.

My family has always been there to encourage me, support me, help me, and have faith in me. I want to thank my mother France, Miville for their generosity and support, my grand-parents Yvette and Francis for their great hope and constant encouragements, Patricia, Nicolas, Guillaume, Wes, Christian, Misako, for being amazing siblings I could always count on and keeping me grounded as well as their constant support, Emily, Charles, Julien, Maël and Théo for letting me know that there are more important things in life than work and a PhD.

I have the chance to have a family not only in Montreal, but also in Zürich. I would like to thank Daniela, Beat, Isabelle and Moritz for welcoming me in their family with open arms, supporting and helping me while I finish my PhD. I always look forward to family gatherings and the many trips around Switzerland with you.

The last two people I would like to thank are my son Jan, and my husband Mathias. Jan, at two years old you have already taught me more things than I've learned in all my life before. Being your mom is more amazing than getting 1,000 PhDs and I do not regret for one second putting my PhD on hold in order to have you. Watching you grow up has been the best experience of my life. I also very much looking forward to meeting your little sister in just a couple of months. Mathias, I'm not sure if I can thank you enough with words on this page. I was more than lucky to have met you in the lab in Montreal when you came from ETH in Zürich to David's lab to do your final Master's thesis project. Since I met you, you have been my rock. I want to thank you for your faith in me, for always being there to talk, the countless times when you cooked, cleaned, took care of laundry while I was working, and most of all for allowing me to finish my PhD in spite of financial constraints. I will forever be grateful for everything you have given me, including our small but growing family. Thank you.

Contribution to Original Knowledge

Four chapters and one appendix contained in this thesis describe original research performed by the candidate. This section contains a list of this thesis' contributions to the body of scientific knowledge.

Chapter 3 describes a method for determining the combination of hygroscopic additives to microarray printing buffer that is best suited for any given brand or type of microarray slide in order to improve spot morphology, consistency and reproducibility. This method has not been described before and is simple to execute. Using this method, we have developed a new microarray printing buffer (2 M betaine, 25 % 2,3-butanediol in phosphate-buffered saline) which results in great spot morphology, enhanced signal intensity and reproducible microarray spots on reactive aldehyde microarray slides.

Chapter 4 presents a new method of calibrating microarray data to improve reproducibility of experiments by using multiple printed fluorescent molecules on each subarray of each microarray. The investigation of the mathematical relationship between calibrant and assay fluorescence signals has never been done before to our knowledge, and revealed a weighted logarithmic relationship between calibrant and assay fluorescence signals.

Chapter 5 presents the first quantitative measurement of leakage of albumin and dextrans through a commercially available cerebral microdialysis membrane. The study of the effect of additives on the measurements of small molecules and 96 proteins is also presented for the first time, as is the effect of additives, fresh whole blood and low-dose lipopolysaccharides on the levels of proteins secreted in the cell media of human U87 cells of CNS glial origin.

Finally, chapter 6 is the first to measure 103 low- to mid-abundance proteins using a cross-reactivity free immunoassay-based platform (the antibody colocalization microarray) in matched

microdialysate, cerebrospinal fluid, and blood time course samples of patients suffering from severe traumatic brain injury. Previous studies only measured up to 17 proteins in all three fluids. This chapter is the first to offer insight into the provenance of the proteins detected in microdialysate samples by comparing values in microdialysate, cerebrospinal fluid and blood, presenting a list of proteins that are likely to be produced in the brain, some that are likely to be produced elsewhere in the body, and others that are likely to produced in the brain as well as elsewhere in the body. This chapter is also the first to describe which blood collection tube is most appropriate for a given protein based on initial measurements and stability during a 2 h pre-centrifugation wait, instead of a picking a single blood collection tube. This data is used to analyze time course samples of severe and mild traumatic brain injury patients. Finally it offers time course data for 11 proteins never before measured in traumatic brain injury, and a list of new potential biomarkers of injury severity, development of secondary injury, and outcome.

Appendix A is a short conference proceeding that describes two new silicon quill pin designs which are robust, affordable and have high liquid capacity. This allows for printing thousands of spots from a single dipping in printing buffer. The new pin design was used in this thesis to print all microarray slides.

Preface and Contribution of Authors

This thesis is presented as a collection of manuscripts written by the candidate with the collaboration of co-authors. In his supervisory role, Prof. David Juncker appears as a co-author on all manuscripts to reflect his contribution to data interpretation and manuscripts preparation. As a secondary supervisor, Dr. Judith Marcoux appears as co-author on two of the four manuscripts for her contribution to data interpretation and manuscripts preparation. However, Dr. Judith Marcoux also participated in other parts of the projects as mentioned below.

The first manuscript (chapter 3) lists the candidate and Dr. Sébastien Bergeron as equal first authors. As such, Dr. Bergeron participated in the design and execution of experiments, as well as data analysis and writing of the manuscript. Pammy Lo participated in the carrying out of some of the experiments (with the pin printer) and analysis of them. Dr. Huiyan Li participated in the execution of a single experiment using the inkjet microarray printer. As equal first author, the candidate participated in the design, carrying out of some experiments involving the pin printer, analysis of experiments as well as the writing of the manuscript.

The second manuscript (chapter 4) lists Jack Mouhanna as co-author. As an undergraduate student under the supervision of the candidate, Jack helped execute about 20 % of the protocol optimization experiments. All the experimental design, carrying out of all experiments, data analysis, calibration code writing and validation, as well as manuscript writing was done by the candidate.

The third manuscript (chapter 5) lists Dr. Francesco Fiorini and David Kong Yu Zhang as co-authors. Both co-authors were undergraduate students working under the supervision of the candidate and helped perform some of the experiments. More specifically, Francesco performed the experiments involving microdialysis catheters, and analysed samples for small molecules.

David performed the experiments involving the U87 cell cultures. The candidate performed all the experiments involving the quantification of proteins in all samples using the antibody colocalization microarray. The candidate designed all experiments, and analysed all experiments except the small molecule measurements analysed by Francesco. The candidate wrote the manuscript. Dr. Judith Marcoux is also a co-author on the manuscript and provided materials and feedback during the project in a supervisory role.

The fourth manuscript (chapter 6) lists Dr. Rajeet Singh Saluja and Dr. Judith Marcoux as co-authors. As resident neurosurgeon at the time of sample collection from patients, Dr. Saluja was involved with identifying potential severe traumatic brain injury patients that could be recruited for the study, along with Dr. Marcoux. He helped place microdialysis catheters in the patients under Dr. Marcoux's supervision, and collected microdialysate samples. He also measured small molecules in microdialysate samples. Dr. Marcoux helped perform the sample collection and processing to study the effect of pre-analytical variables on protein quantities and stability with the candidate. Dr. Marcoux with various neurosurgery residents collected blood samples from mild traumatic brain injury patients. She and Dr. Juncker helped with the initial study design for the severe traumatic brain injury patients. Dr. Marcoux and the candidate designed the study for the mild traumatic brain injury patients. The candidate designed the study of pre-analytical variables and how to bring together the various studies in a single analysis. While nurses collected cerebrospinal fluid and blood samples of severe traumatic brain injury patients, the candidate processed them. The candidate performed the protein measurement experiments using the ACM, and performed all analyses, including biostatistical analyses. The candidate wrote the manuscript.

Appendix A is a refereed and published conference proceeding listing Dr. Ayokunle Olanrewaju as co-author. Dr. Olanrewaju helped design the serpentine silicon quill pin in a computer-assisted design (CAD) software. The candidate designed the double-channel silicon quill pin using the CAD software. Theoretical pin design and ideas were developed by the candidate, Dr. Olanrewaju and Dr. Juncker. Silicon quill pins were produced by trained staff in the "McGill Nanotools Microfab" microfabrication lab. The resulting pins were prepared for use and tested by the candidate. The conference proceeding was written by the candidate.

Appendix B is a book chapter written by the candidate, with comments from all co-authors (Pammy Lo, Dr. Huiyan Li and Dr. David Juncker). The candidate also produced all the graphics for the book chapter.

Appendix C to J refers to supplementary information for chapters 3 to 6 mentioned above, respectively. Therefore contributions to these chapters is as listed for their corresponding manuscripts.

All other sections of the thesis were written by the candidate.

List of Abbreviations

Ab	Antibody
ACM	Antibody colocalization microarray
aCSF	Artificial cerebrospinal fluid
Ag	Antigen
Alg	Algorithm
BSA	Bovine serum albumin
cAb	Capture antibody
CSF	Cerebrospinal fluid
CTAD	Citrate-theophylline, adenosine, dipyridamole
CV	Coefficient of variation (%)
dAb	Detection antibody
Dextran_{500}	500 kDa dextran
$\text{Dextran}_{\text{HMW}}$	High molecular weight (~250 kDa) dextran
$\text{Dextran}_{\text{LMW}}$	Low molecular weight (~75 kDa) dextran
Dx	Diagnosis
EDTA	Ethylenediamine tetraacetic acid
ELISA	Enzyme-linked immunosorbent assay
GCS	Glasgow coma scale
GOS-E	Extended Glasgow outcome scale
ICP	Intra-cranial pressure
IF	Interstitial fluid
IgG	Immunoglobulin G
LOD	Limit of detection
MD	Microdialysis
mTBI	Mild traumatic brain injury
mTBI_{C}	Mild complex traumatic brain injury
mTBI_{S}	Mild simple traumatic brain injury
MSA	Multiplexed sandwich assay
PBS	Phosphate-buffered saline

pnBlood	Pooled normal blood (serum or EDTA plasma)
pnCitrate	Pooled normal citrate plasma
pnCSF	Pooled normal cerebrospinal fluid
pnCTAD	Pooled normal CTAD plasma
pnEDTA	Pooled normal EDTA plasma
pnHeparin	Pooled normal heparin plasma
pnSerum	Pooled normal serum
sTBI	Severe traumatic brain injury

À ma grand-maman Yvette Morin, qui
s'est éteinte juste avant que j'obtienne
ce doctorat. Elle était si fière de sa
petite-fille, même avant la fin.
Tu me manques.

CHAPTER 1

Introduction

1.1 Background

A mechanical force that causes traumatic injury to the brain tissue inside the skull is called traumatic brain injury (TBI). It can be caused by sports accidents, falls, motor vehicle accidents, sound waves as experienced in explosions, and penetrating objects such as nails, knives, or bullets. TBI is a leading cause of death in young adults; it has an estimated incidence of 295 persons per 100,000 per year [1], therefore it can be estimated that in Canada in 2018, approximately 110,000 new cases of TBI were seen in emergency wards each year, of which roughly 15,000 were classified as moderate and severe TBI. Injury severity is commonly classified according to the Glasgow Coma Scale (GCS) [2] which quickly assesses the eye, verbal and motor responses of patients. The scale ranges from 15 (normal response) to 3 (no response) and depending on their GCS score, patients are classified into severe (score of 8 or less), moderate (score of 9 to 12) or mild (score of 13 or more) TBI categories. This categorization helps clinicians determine the best course of action for patient care. The incidence of TBI has increased in Quebec since the turn of the century [3] and overall, costs and mortality rates have also increased in the United States [4]. Public records of TBI incidence has been shown to underestimate the true incidence of TBI by 29 % [5], and up to 37 % of adult men will suffer from TBI at least once in their lifetime [6], therefore TBI is a widespread problem with considerable consequences for society.

In the case of severe TBI, the initial diagnosis is usually straightforward with patient examination and confirmation with a computed tomography (CT) scan. Diagnosing patients suffering from mild

TBI is more difficult. CT scans are negative in about 50 % of cases [7], and for patients whose GCS score is 15, a CT scan is only about 4 % sensitive, with no correlation of findings on CT scans with symptoms at 3 months post-injury [8]. Patient history of loss of consciousness or memory is not always accurate and remains the only method to diagnose mild TBI when CT scans are negative. Moreover, 10-15 % of patients who suffered a mild TBI develop direct long-term complications and never fully recover [9], therefore early outcome prediction would be useful to help prevent complications and identify patients in need of careful follow-up. In severe TBI, a number of patients develop general brain swelling (edema), which increases the intracranial pressure and can lead to further brain damage, called secondary injury, and death if left untreated. Outcome of patients is also difficult to predict - some patients recover fully while others die or are left disabled for life.

TBI has been linked to increased risks for a number of conditions such as neuropsychiatric disorders [10], multiple sclerosis [11], post-traumatic stress disorder [12], Parkinson's disease [13], Alzeihmer's disease [14] and chronic traumatic encephalopathy (CTE), a form of neurodegeneration [15]. Some of these findings could be explained by the fact that microglial activation can be seen for up to 17 years after TBI in specific regions of the whole brain [16].

Funding agencies have recognized the importance of finding new ways to diagnose and treat mild TBI, and clinical trials depend on accurate diagnosis and prognosis of patients. A quick, objective, non-invasive, sensitive and specific test does not currently exist to determine 1) signs of brain injury, 2) the prediction of secondary injuries, and 3) the prediction of outcome for patients. Such a tool would be of great help to clinicians in the diagnosis and management of TBI patients.

1.2 Rationale and objectives

In order to increase the chance of finding biomarkers for the diagnosis and management of TBI, a method that can measure numerous low-abundance proteins involved in inflammation, injury and repair, with good sensitivity and reproducibility, from samples with very small volume is required. The antibody colocalization microarray (ACM) is a platform that avoids false positive results due to antibody cross-reactivity, which is a challenge for all sandwich immunoassay-based multiplexed protein measurements platforms in which mixtures of detection antibodies are applied [17]. Indeed when detection antibodies are mixed, the identity of the detection antibody binding to antigens cannot be ascertained and the number of possible cross-reactivity events increases exponentially with the number of antigens being measured. The ACM physically separates detection antibodies, thereby avoiding all possible cross-reactivity, and allows the addition of proteins to be measured on the platform without extensive optimization as is required for other platforms.

However, optimization of the assay procedure and analysis is required to improve sensitivity and reproducibility that can allow reliable quantification of low-abundance proteins in hundreds of samples.

Proteins produced in the brain tissue are best measured through the use of cerebral microdialysis with a high molecular-weight cut-off, an indirect sampling method of the brain tissue interstitial fluid. Comparing the levels of proteins measured in microdialysate to that in cerebrospinal fluid (CSF) and blood in severe TBI patients can lead to the determination of the origin of production of the proteins, and whether they are measurable in blood, the only sample available from mild TBI patients. The levels of proteins can vary widely in the first three to five days post-injury [18], therefore it is best to sample microdialysate, CSF and blood samples at regular intervals over the course of a few days after the insertion of the cerebral microdialysis catheter. A study of the peaks and valleys in the evolution of levels of proteins can potentially give more information than a single level measurement, especially since proteins are known to peak at different times post-injury.

In order to properly compare levels of proteins measured in microdialysate to that of CSF and blood, a measure of the proportion of proteins which pass into the microdialysate compared to the quantity found in the sampled tissue needs to be calculated (called relative recovery), and is usually estimated using *in vitro* tests [19–28]. While the relative recovery of a few molecules have been calculated this way, it is affected by the composition of the perfusion fluid, the length and material of the catheters, and therefore should be measured for the proteins measured by the ACM, using the specific catheters used in collecting samples from severe TBI patients.

Finally, it is known that some proteins are best measured in plasma, while others are best measured in serum, since these two types of samples, although both originating from circulating blood, are considered to be distinct because of blood clotting which occurs when serum samples are collected. When measuring multiple proteins, it is therefore desirable to measure each of them in the sample type which best reflect the levels present in the blood circulation of patients.

1.3 Thesis outline

Chapter 2 present a review of the literature that describes how TBI is currently managed in clinical settings, known potential biomarkers of TBI, platforms for proteomic analyses, and factors that can affect protein quantification in different bodily fluids.

In chapter 3, a method for optimizing microarray printing buffers which prevent evaporation by adding mixtures of hygroscopic additives is presented, and is used to find a printing buffer for the reactive-aldehyde coated microarray slides used in the ACM. The printing buffer containing betaine and 2,3-butanediol increases sensitivity of assays, and improves the reproducibility of

spotting. These improvements allow the measurements of a few low-abundance proteins in small-scale experiments (less than 100 samples) with good sensitivity and reproducibility.

In chapter 4, a new method to improve reproducibility in large-scale experiments is presented, allowing the measurement of more than 100 proteins in hundreds of patient samples. It is based on the addition of multiple fluorescent calibrants to the capture antibody printing step, and the fluorescence signals obtained from the calibrants is used mathematically to compensate for local and systemic sources of noise and bias which normally leads to imprecision in protein measurements.

Chapter 5 presents a comparison of additives (albumin and dextrans) to the microdialysis perfusion fluid, normally used to stabilize the recovery of fluid which is a problem with high molecular-weight cutoff microdialysis. The calculation of relative recovery for 94 proteins is performed, required to properly infer the quantity of proteins measured in the brain tissue of severe TBI patients. Because there are concerns about the safety of the additives used in brain microdialysis, we also measure leakage through the microdialysis membrane *in vitro*, and the effect of the presence of additives on the measurement of small molecules and proteins. Finally, we study the effect of the presence of additives on the levels of proteins secreted by human U87 cells of glial origin.

In chapter 6, 103 proteins are measured in time course samples of microdialysate, cerebrospinal fluid and blood samples of severe TBI patients, as well as blood samples of mild TBI patients and a single non-TBI trauma patient as control. Both serum and plasma samples are collected, and the most appropriate blood sample type is determined for each protein using results from a small study of the effect of blood tube type and pre-processing waiting time and temperature using samples from healthy volunteers. Levels of proteins in the brain interstitial fluid of patients is estimated using the measurements of relative recovery obtained in the previous chapter, and levels in the brain, cerebrospinal fluid and blood are compared to determine the origin of production for each protein detected in microdialysate. Using this information, several known and new potential biomarkers of injury severity, development of secondary injuries and outcome are described.

Chapter 7 discusses the limitations and scope of the studies presented in this thesis and challenges encountered. It also compares the reproducibility and sensitivity of data obtained in each study, which improved with each chapter, and discusses how findings presented in the thesis can be used by the scientific community.

Finally, chapter 8 concludes the thesis by summarizing findings and providing an outlook and discussion on future work.

Appendix A describes the design and testing of improved silicon quill pins used to print microarrays for all chapters listed in this thesis.

Appendix B is a detailed description of the ACM platform and protocol used throughout the rest of the thesis.

References

1. Nguyen, R., Fiest, K. M., McChesney, J., Kwon, C. S., Jette, N., Frolkis, A. D., Atta, C., Mah, S., Dhaliwal, H., Reid, A., Pringsheim, T., Dykeman, J. & Gallagher, C. The international incidence of traumatic brain injury: A systematic review and meta-analysis. *Canadian Journal of Neurological Sciences* **43,** 774–785 (2016).
2. Teasdale, G. & Jennett, B. Assessment of coma and impaired consciousness. *The Lancet* **2,** 81–84 (1974).
3. De Guise, E., Marcoux, J., Maleki, M., Leblanc, J., Dagher, J., Tinawi, S., Feyz, M. & Lamoureux, J. Trends in hospitalization associated with TBI in an urban level 1 trauma centre. *Canadian Journal of Neurological Sciences* **41,** 466–475 (2014).
4. Farhad, K., Khan, H. M. R., Ji, A. B., Yacoub, H. A., Qureshi, A. I. & Souayah, N. Trends in outcomes and hospitalization costs for traumatic brain injury in adult patients in the United States. *Journal of Neurotrauma* **30,** 84–90 (2013).
5. Lasry, O., Dendukuri, N., Marcoux, J. & Buckeridge, D. L. Accuracy of Administrative Health Data for Surveillance of Traumatic Brain Injury. *Epidemiology* **29,** 876–884 (2018).
6. Zumstein, M. A., Moser, M., Mottini, M., Ott, S. R., Sadowski-Cron, C., Radanov, B. P., Zimmermann, H. & Exadaktylos, A. Long-term outcome in patients with mild traumatic brain injury: A prospective observational study. *Journal of Trauma - Injury, Infection and Critical Care* **71,** 120–127 (2011).
7. Smith, J. A., Das, A., Ray, S. K. & Banik, N. L. Role of pro-inflammatory cytokines released from microglia in neurodegenerative diseases. *Brain Research Bulletin* **87,** 10–20 (2012).
8. Lannsjö, M, Backheden, M, Johansson, U, Geijerstam, J. L. & Borg, J. Does head CT scan pathology predict outcome after mild traumatic brain injury ? *European Journal of Neurology,* 124–129 (2012).
9. Carroll, L., Cassidy, J. D., Peloso, P., Borg, J., von Holst, H., Holm, L., Paniak, C. & Pépin, M. Prognosis for mild traumatic brain injury: results of the WHO collaborating centre task force on mild traumatic brain injury. *Journal of Rehabilitation Medicine* **36,** 84–105 (2004).

10. Ciurli, P, Formisano, R, Bivona, U, Cantagallo, A & Angelelli, P. Neuropsychiatric disorders in persons with severe traumatic brain injury: prevalence, phenomenology, and relationship with demographic, clinical, and functional features. *The Journal of Head Trauma Rehabilitation* **26,** 116–126 (2011).

11. Kang, J.-H. & Lin, H.-C. Increased risk of multiple sclerosis after traumatic brain injury: a nationwide population-based study. *Journal of Neurotrauma* **29,** 90–5 (2012).

12. Kontos, A. P., Kotwal, R. S., Elbin, R., Lutz, R. H., Forsten, R. D., Benson, P. J. & Guskiewicz, K. M. Residual Effects of Combat-Related Mild Traumatic Brain Injury. *Journal of Neurotrauma* **30,** 680–686 (2013).

13. Gardner, R. C., Byers, A. L., Barnes, D. E., Li, Y., Boscardin, J. & Yaffe, K. Mild TBI and risk of Parkinson disease. *Neurology* **90,** e1771–e1779 (2018).

14. Mendez, M. F. What is the Relationship of Traumatic Brain Injury to Dementia? *Journal of Alzheimer's Disease* **57,** 667–681 (2017).

15. DeKosky, S. T. & Asken, B. M. Injury cascades in TBI-related neurodegeneration. *Brain Injury* **31,** 1177–1182 (2017).

16. Ramlackhansingh, A. F., Brooks, D. J., Greenwood, R. J., Bose, S. K., Turkheimer, F. E., Kinnunen, K. M., Gentleman, S., Heckemann, R. a., Gunanayagam, K., Gelosa, G. & Sharp, D. J. Inflammation after trauma: microglial activation and traumatic brain injury. *Annals of Neurology* **70,** 374–83 (2011).

17. Pla-Roca, M., Leulmi, R. F., Tourekhanova, S., Bergeron, S., Laforte, V., Moreau, E., Gosline, S. J. C., Bertos, N., Hallett, M., Park, M. & Juncker, D. Antibody colocalization microarray: a scalable technology for multiplex protein analysis in complex samples. *Molecular & Cellular Proteomics* **11,** M111.011460 (2012).

18. Helmy, A., Carpenter, K. L. H., Menon, D. K., Pickard, J. D. & Hutchinson, P. J. A. The cytokine response to human traumatic brain injury : temporal profiles and evidence for cerebral parenchymal production. *Journal of Cerebral Blood Flow & Metabolism* **31,** 658–670 (2010).

19. Rosenbloom, A. J., Sipe, D. M. & Weedn, V. W. Microdialysis of proteins: Performance of the CMA/20 probe. *Journal of Neuroscience Methods* **148,** 147–153 (2005).

20. Rosenbloom, A. J., Ferris, R., Sipe, D. M., Riddler, S. A., Connolly, N. C., Abe, K. & Whiteside, T. L. In vitro and in vivo protein sampling by combined microdialysis and ultrafiltration. *Journal of Immunological Methods* **309,** 55–68 (2006).

21. Trickler, W. J. & Miller, D. W. Use of osmotic agents in microdialysis studies to improve the recovery of macromolecules. *Journal of Pharmaceutical Sciences* **92,** 1419–1427 (2003).

22. Quist, S. R., Kirbs, C., Kloft, C. & Gollnick, H. P. Cytokine and chemokine recovery is increased by colloid perfusates during dermal microdialysis. *Materials* **11,** 682 (2018).

23. Dahlin, A. P., Purins, K., Clausen, F., Chu, J., Sedigh, A., Lorant, T., Enblad, P., Lewe, A. & Hillered, L. Refined Microdialysis Method for Protein Biomarker Sampling in Acute Brain Injury in the Neurointensive Care Setting. *Analytical Chemistry* **86,** 8671–8679 (2014).

24. Giorgi-Coll, S., Blunt-Foley, H., Hutchinson, P. J. & Carpenter, K. L. H. Heparin-gold nanoparticles for enhanced microdialysis sampling. *Analytical and Bioanalytical Chemistry* **409,** 5031–5042 (2017).

25. Helmy, A, Carpenter, K. L., Skepper, J. N., Kirkpatrick, P. J., Pickard, J. D. & Hutchinson, P. J. Microdialysis of cytokines: methodological considerations, scanning electron microscopy, and determination of relative recovery. *Journal of Neurotrauma* **26,** 549–561 (2009).

26. Hillman, J., Åneman, O., Anderson, C., Sjögren, F., Säberg, C. & Mellergård, P. A microdialysis technique for routine measurement of macromolecules in the injured human brain. *Neurosurgery* **56,** 1264–1270 (2005).

27. Hutchinson, P. J., O'Connell, M. T., Rothwell, N. J., Hopkins, S. J., Nortje, J., Carpenter, K. L. H., Timofeev, I., Al-Rawi, P. G., Menon, D. K. & Pickard, J. D. Inflammation in human brain injury: intracerebral concentrations of IL-1alpha, IL-1beta, and their endogenous inhibitor IL-1ra. *Journal of Neurotrauma* **24,** 1545–57 (2007).

28. Rosdahl, H., Hamrin, K., Ungerstedt, U. & Henriksson, J. A microdialysis method for the in situ investigation of the action of large peptide molecules in human skeletal muscle: Detection of local metabolic effects of insulin. *International Journal of Biological Macromolecules* **28,** 69–73 (2000).

CHAPTER 2

Literature Review

The brain is part of the central nervous system (CNS), which is highly protected by the skull. The spinal cord, also part of the CNS, is similarly protected by vertebrae. The brain and spinal cord both bathe in cerebrospinal fluid, produced in large part by choroid plexus cells lining the ventricules, which are hollow chambers within the brain. The CNS is made up of neuron cells, which collect signals from the body, process the information, and send signals to muscles, glands, etc. Neurons in the brain are surrounded by glia cells (figure 2.1) which provide nourishment, stability and protection to neurons as well as contribute to neurovascular interactions by modulating the blood brain barrier. Four cells types are considered to be glia: oligodendrocytes, astrocytes, ependymal cells, and microglia. Oligodendrocytes provide support and electrical insulation to neuron's axons (figure 2.1b), while astrocytes play roles in the nourishment of neurons, maintenance of the extracellullar milieu, and supporting the endothelial cells of blood capillaries that form the blood-brain barrier. Ependymal cells line the pial surface of the brain and like choroid plexus cells, are involved in the production of CSF. Finally microglia are the brain's resident macrophage cells, involved in the maintenance and repair of the brain. Because the CNS is protected from the rest of the body including pathogens, the role of microglia include recognizing and swallowing pathogens that might enter the brain.

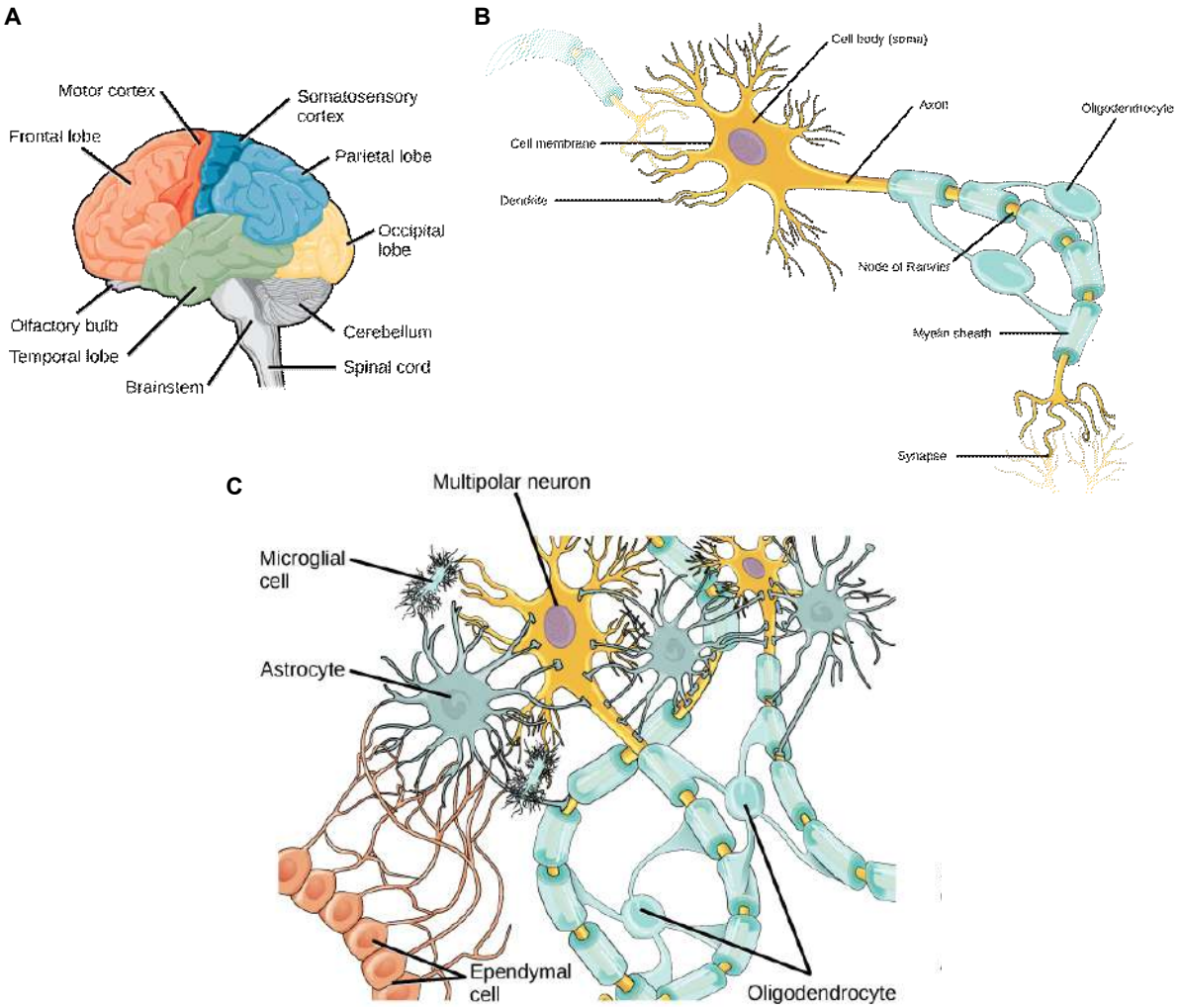

FIGURE 2.1: **Brain and brain cells. A** The human central nervous system (CNS) is composed of the brain including several lobes, a cerebellum, a brain stem and a spinal cord. **B** Neurons that inhabit the CNS are complex cells with dendrites to receive messages from other neurons, and an axon to transmit signals to other neurons. **C** The CNS is composed of neurons and glia, including astrocytes, oligodendrocytes, microglia and ependymal cells that serve to protect, nourish and sustain neurons. Images obtained from [29] under CC-BY 4.0.

2.1 Current methods in management of TBI

Traumatic brain injuries (TBI) happen when there is a physical blow to the head by an object or sound wave, which may or may not penetrate the skull to damage the brain tissue underneath. A hit to the head is often accompanied by a counter-hit which is the physical reaction of forcefully pushing the brain tissue towards one direction in the skull (figure 2.2a). Therefore hits to the head can produce multiple injuries across the brain, and not only at the exact site of injury. The section below describes current methods of diagnosing, prognosing and monitoring patients with TBI in the clinic.

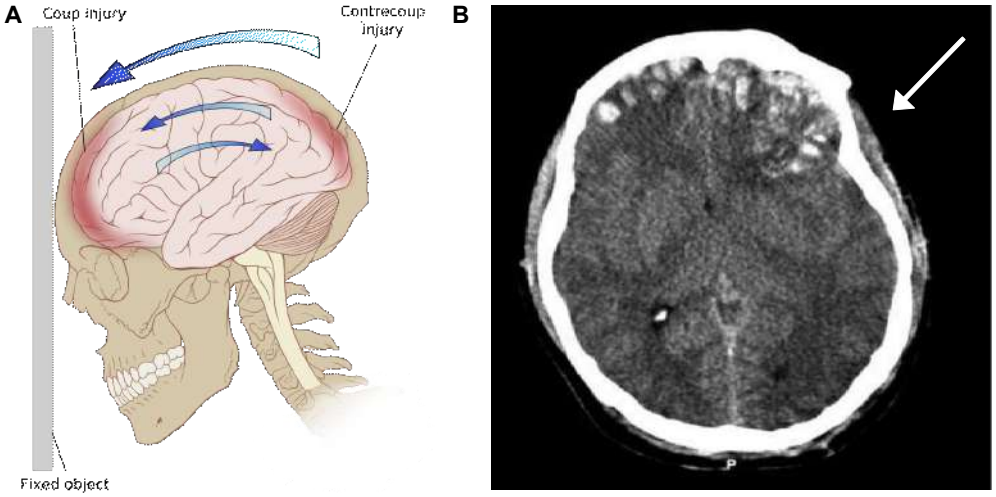

FIGURE 2.2: **Traumatic brain injury mechanism and CT scan. A** When the head is hit (coup), it is often accompanied by a contre-coup, which both cause lesions to opposite sides of the brain. Image obtained from [30] under CC-BY 2.5. **B** Preoperative CT scan of a patient while he had a GCS of 14. Image obtained from [31] under CC-BY 2.0.

2.1.1 Physiological description of TBI

TBIs are heterogeneous injuries that are caused by direct impact to the head, or acceleration and decelaration that can all cause injuries to the brain itself. In addition to skull fractures, penetrating injuries and brain lacerations, other pathologies can be present such as brain swelling, contusions, micro-bleeds, intracranial bleeding (hematomas and hemorrhages) and diffuse axonal injury (DAI). DAI causes cytoskeletal neuron damage, whereby normally intra-cellular cytoskeletal proteins can be found in the interstitial fluid of the brain tissue, flushed in the CSF and later into the blood circulation. Other injuries can induce blood-brain barrier disruptions, allowing proteins from the blood that are normally not present in the brain tissue to pass the blood-brain barrier and be detected in the brain tissue or cerebrospinal fluid (CSF). All types of injuries can be found in

both mild and severe TBIs because the severity is determined through the use of the GCS, which measures the response of the brain to the injuries. However, when injuries are visible on CT scans, patients suffering from mTBI most often have contusions and subarachnoid hemorrhages. DAI and subdural hematomas are most often seen in sTBI patients, in addition to contusions and subarachnoid hemorrhages.

Clinically, TBIs can lead to a plethora of symptoms such as loss of consciousness, convulsions, confusion, lightheadedness, difficulties speaking, sleepiness or lethargy, headache, vomiting, lack of muscular coordination, difficulty with balance, nausea, ringing in ears, strange taste in the mouth as well as mood changes and behavioural and cognitive changes such as difficulties with memory, attention, and concentration.

2.1.2 Diagnosis

The most commonly used diagnosis methods for TBI are the clinical history, CT scan (figure 2.2b) and neurological examination, and the GCS is used to monitor patients regularly. However, a study demonstrated that physicians are not always accurate in their evaluation of a patient's GCS score [32] due to the subjective nature of the evaluation, as well as potential patient alcohol intoxication at the time of injury [33]. The injury severity score (ISS) [34] is also determined, but it is not widely used in practice to monitor patients. In the case of polytrauma patients - patients who have injuries elsewhere such as abdominal, thoracic, or orthopedic injuries, a study has shown that GCS is inconsistent and the abbreviated ISS for the head is a more accurate measure of patients head injury [35]. Pupil reactivity [36] is a simple test used to determine if a patient requires urgent decompressive surgery. For mild TBI patients, age and clinical variables are stronger predictors of injury than CT scan [37] because of the lack of sensitivity of this technique.

2.1.3 Secondary injuries

Once diagnosed, patients are first treated for their acute injuries. Lesions that take up a substantial volume in the skull such as bleeds (hematomas) are evacuated by surgery [38, 39] as quickly as possible, because these lesions are life threatening and can lead to poor outcome if left untreated. However, secondary injuries can develop in the hours to days following the initial injury as an indirect effect of the primary injury, as a result of pathological biochemical pathways. The exact molecular processes involved in the development of secondary injuries are not well known, but can result in brain hypoxia (low oxygen), ischemia (low blood flow), hypotension (low blood pressure), breakdown of the blood-brain barrier and edema (swelling) which leads to raised intra-cranial pressure. Because raised intra-cranial pressure can lead to brain herniation, in which parts of

the brain are squeezed through openings in the cranium, interventions are necessary to prevent further damage to the brain. Patients suffering from sTBI are typically kept in a medically-induced coma in order to lower the requirements of the brain in oxygen, and help lower intra-cranial pressure by decreasing the amount of blood present in the brain. Other possible secondary injuries include hypercapnia (increased blood concentration of carbon dioxide), acidosis (decreased blood pH), meningitis, brain abscess, loss of cerebral autoregulation (of blood flow within the brain) and excitotoxicity (increased extracellular excitatory neurotransmitters such as glutamate). All secondary injuries can injure neurons that were not initially injured in the primary injury. Patients that suffered from TBI are monitored during their recovery period and in the case of severe TBI, medications or surgery is considered if secondary injuries develop. There exists no method for predicting the apparition of secondary injuries. Monitoring of patients vital signs, blood flow in the brain and intracranial pressure are currently the only ways to detect secondary injuries as they develop.

2.1.4 Prognosis/outcome prediction

Outcome of patients is categorized using the Glasgow Outcome Scale [40] or its extended version [41] which comprises 5 and 8 categories respectively between death and complete recovery. These scales are not foolproof and misclassifications are known to affect results of clinical trials [42]. Early outcome prediction, or prognosis, of patients is crucial in helping clinicians determine the best treatment for patients, and when accurate, can help families in decisions they may be required to make. A number of studies have looked at different factors that help predict outcome in patients: from age and injury severity [43, 44], post-traumatic amnesia, sitting balance and limb strength [45] to diffusion-weighted MRI findings [46]. The International Mission for Prognosis and Analysis of Clinical Trials in TBI (IMPACT) study has led to a more refined list of factors that appear to help predict patient outcome [47–50]. For example, it has shown that blood pressure at admission [47] and the cause of injury [48] do not improve reliability of prognosis, while pupil reactivity [49] and laboratory values at admission [50] (such as blood sodium, glucose, etc.) can help establishing a prognosis. Indeed, another study has shown that prognosis based on admission characteristics of patients has a specificity of 78-89% [51]. The IMPACT study shows that adding biomarkers can increase outcome prediction and differentiate between injury types [52], however no single potential biomarker has yet been found to be sensitive and specific enough to be used clinically.

2.2 Potential biomarkers of TBI

Many molecules measured in the blood or CSF have been studied as potential biomarkers to improve the clinical management of TBI patients. Figure 2.3 shows a list of biomarkers that have been studied and have shown good potential. Most of the molecules studied are proteins and they are normally released not only by neurons, but also astrocytes, microglia, liver and immune cells.

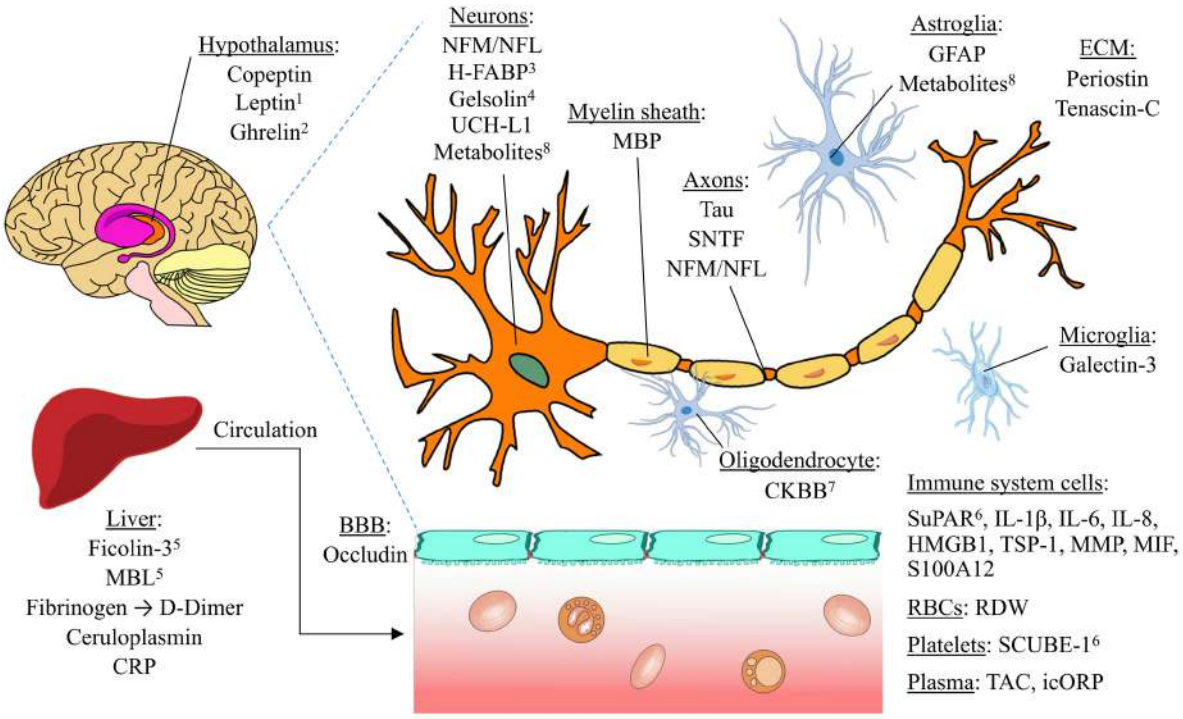

FIGURE 2.3: **Blood biomarkers of TBI.** Anatomical locations of potential TBI biomarkers. The biomarkers included in this schematic all rated as "good" (AUC=0.80→0.89) or better for any of the four clinical situations studied (detecting concussion, predicting intracranial damage after concussion, predicting delayed recovery after concussion, and predicting adverse outcome after severe TBI). Biomarkers with a pooled AUC <0.8 are not shown. [1]Also found in adipose tissue; [2]synthesized in cells of stomach and pancreas; [3]found mostly in pons; [4]also found extracellularly; [5]lectin pathway of the complement system; [6]also found in endothelial cells; [7]may regulate HPA axis; [8]panels of molecules. BBB: blood brain barrier. ECM: Extracellular matrix. AUC: Area under curve (predictive value). Image obtained from [53] under CC-BY 4.0.

2.2.1 Brain-specific proteins

The ideal TBI biomarkers has been described by Papa *et al.* in 2008 to be a protein or a panel of proteins or other molecules that 1) is highly specific for TBI and shows the degree of severity of injuries, 2) is sensitive, detecting all cases of TBI, 3) appears rapidly in the blood, urine or saliva

of patients after injury, 4) provides information about injury mechanisms, 5) has a well-defined time profile, 6) can be used to monitor progress, recovery and response to treatment, 7) can predict outcome and 8) is easily measured by a clinical analyzer or other FDA-approved devices [54].

A number of research groups have studied one or more proteins in patients who have suffered a TBI, by measuring them in blood, CSF or brain tissue through the use of cerebral microdialysis, in hope of finding a molecule whose level could predict injury severity or patient outcome. A number of brain-specific intracellular proteins have been studied as potential biomarker for injury severity, such as the cytoskeletal protein ubiquitin carboxy-hydroxylase L1 [55], however it is a poor predictor of injury for patients with negative CT scans [56]. Neuron-specific enolase [57], myelin basic protein [58], glial fibrillary acidic protein [59] and S100B [60] or secreted proteins involved in inflammation such as β-nerve growth factor [61], have been extensively studied and correlated with injury severity and outcome. However, they have not shown sufficient specificity and sensitivity [62].

Other molecules have been interrogated as potential biomarkers of TBI. Some proteins are intracellular (αII-spectrin degradation products due to calpain or caspase [63, 64], tau [65], hyper-phosphorylated neurofilament-heavy[66] and cytochrome c [67]) while others are extracellular and involved in inflammation, apoptosis or repair (adhesion molecules measured in CSF [68], intracellular adhesion molecule 1 [69], caspase-3 [70], α-microglobulin, soluble FAS receptor [71], brain gelatinases [72], matrix metalloproteinases [73, 74], interleukin-1β [75] and amyloid-$\beta_{1\text{-}42}$ [65]).

2.2.2 Proteins involved in inflammation

A gene expression microarray study has shown that over 1,200 genes are differentially expressed in the whole brain following severe TBI [76]. Because it is generally accepted that the whole brain exhibits a strong inflammatory response in TBI, which can help or hinder repair and recovery, the complex interactions between several anti- and pro-inflammatory proteins (cytokines and chemokines), which are small, low-abundance proteins with concentrations in the range of pg/mL have been studied [18, 20, 27, 77–89]. However, proteins involved in the inflammatory cascade are not specific to the brain, and TBI patients who also have injuries elsewhere most likely produce cytokines and chemokines in multiple places in the body, making it difficult to determine the origin of proteins detected in blood samples.

2.2.3 Genetics and other molecules

Additionally, a few gene polymorphisms have been associated with a poorer outcome, such as specific Apolipoprotein E [90], brain-derived neurotrophic factor [91], and interleukin-6 [92] gene

polymorphisms. High levels of estrogens and progesterone have also shown to have neuroprotective effects [93, 94]. Other molecules studied in relations with TBI are microRNAs [95] and small molecules that constitute the metabolome [96].

None of the proteins or other molecules studied have shown a specificity and sensitivity sufficient for use in the clinic. This can be due to the large patient variability in age, health condition and genetic traits which affect basal protein levels, as well as the type of head injury sustained. Patients also frequently have multiple injuries to the rest of their body, which can affect the levels of inflammatory proteins in the blood and CSF [97].

2.3 Effect of pre-analytical variables on sample measurements

Professor and physician Linda Papa expresses concerns over the number of studies of biomarkers in TBI [98]: *"The flurry of research in the area over the last decade is encouraging but is limited by small sample sizes, variable practices in sample collection, inconsistent biomarker-related data elements and disparate outcome measures. Future studies of biomarkers for pediatric TBI will require rigorous and more uniform research methodology, common data elements, and consistent performance measures."* Among the many factors listed, several pre-analytical variables pertaining to collection protocols of blood, CSF and cerebral microdialysis, are shown to have an impact on proteomic analyses.

2.3.1 Cerebral microdialysis

Cerebral microdialysis was invented and commercialized by Ungerstedt [102] and consists in a thin catheter that is 1-3 cm long, allowing contact with neurons and glia cells when inserted in the brain. It was originally inserted in the brain tissue of animals to study the effect of dopamine and for the delivery of different chemicals (figure 2.4a). Perfusion fluid, usually artificial CSF, is pumped through a very small, flexible tube to a tip made of a membrane 1-3 cm in length through which small molecules located in the brain tissue interstitial fluid can diffuse freely. The microdialysate is collected in small vials and the levels of different molecules can be measured. The relative recovery of molecules is based on their diffusion constant, which varies with molecular weight, temperature and flow rate of perfusion. Since it is an invasive technique, cerebral microdialysis was first used in humans suffering from strokes or severe TBI, and is not used on normal controls.

Small metabolites (glucose, glutamate, lactate and pyruvate) were first studied in the context of severe TBI [103] using a catheter with a 20 kDa cut-off (CMA 70). It was shown that high levels of cytotoxic glutamate can be seen as soon as three days after injury and can last up to nine days [104]. Relative level of recovery of small molecules is close to 100 %, and therefore is less

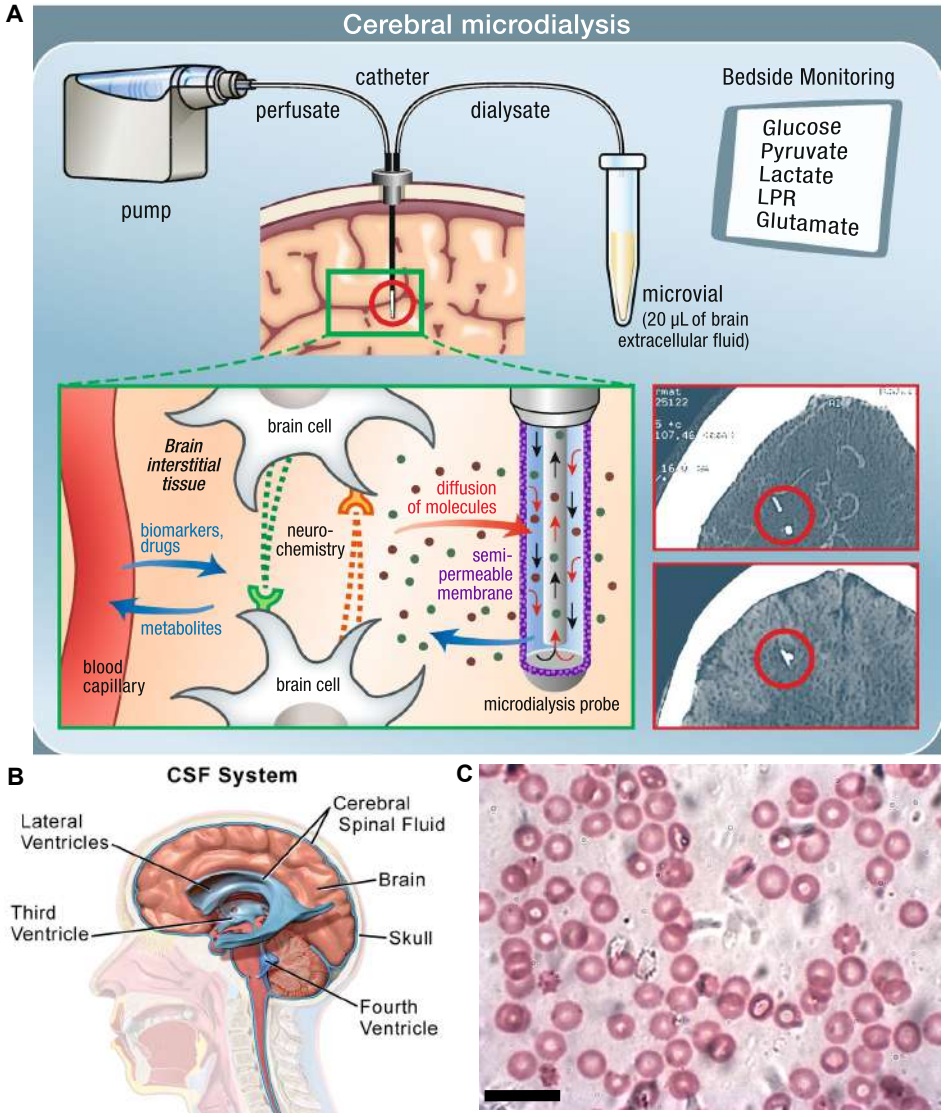

FIGURE 2.4: **Microdialysate, blood and cerebrospinal fluid.** **A** Cerebral microdialysis consists in indirectly sampling the brain tissue interstitial fluid (IF) at the point of insertion. Metabolites present in the IF diffuse freely inside the catheter, while drugs present in the perfusion fluid can diffuse freely into the brain. The collected microdialysate can be analyzed by the patient's bedside for small or large molecules. Location of the catheter gold-tip can be verified by CT scan. Image reproduced from [99] with permission. **B** The brain contains cerebrospinal fluid (CSF) which is produced in a large part in the ventricles by choroid plexus cells. It also surrounds the brain under the meninges, which are membranes under the skull that contain the brain and CSF. The CSF also envelops that spinal cord, where it can be obtained via a lumbar puncture. Image obtained from [100] under CC-BY 3.0. **C** Human red and white blood cells present in blood are in contact with all organs of the body. Blood also contains diluted CSF. Scale bar is 10 µm. Adapted from [101] under CC-BY 2.0.

affected by changes in perfusion flow rate. However, due to their higher molecular weight, the relative recovery rate of low-abundance IL-6 and IL-1β have been shown to be approximately 6 % at a flow rate of 0.5 µL/min [105]. In order to improve the relative recovery of proteins, a catheter with a membrane cut-off of 100 kDa was produced (CMA 71), which allows greater diffusion of proteins, and therefore recovery rate [106]. While the use of cerebral microdialysis to measure small molecules (glucose, lactate, pyruvate, glutamate, glycerol) using the 20 kDa catheter has been established in certain hospitals as part of routine care in North America [107] and Europe, the 100 kDa molecular weight cut-off catheter can only be used in research studies because it is not FDA-approved.

The use of heparin and heparin-covered microspheres [108] or 3.5 % human albumin [25] added to the perfusion fluid also increased the relative recovery of proteins when used with the 100 kDa molecular weight cut-off. Albumin also served to increase fluid recovery, defined as the ratio of the volume of microdialysate recovered to perfusate injected in the catheter. The manufacturer of cerebral microdialysis catheters recommends adding 3 % clinical grade dextran of molecular weight 60 kDa to improve fluid recovery, and they sell perfusion fluid containing 500 kDa dextran. Indeed, if there is a difference in osmolality between the perfusion fluid and the brain tissue, perfusion fluid can partially pass into the brain tissue by ultra-filtration, which additives such as albumin and dextrans prevent. On the other hand, albumin could leak through the membrane from the perfusion fluid and potentially affect the brain tissue locally. Neuron and glia are not normally exposed to albumin, and it has been shown that its presence activates astrocytes [109]. Leakage of 60 kDa dextran and albumin through the microdialysis membrane have not been measured quantitatively, but both have a size below 100 kDa, the molecular weight cut-off of the membrane.

Microdialysis vials are kept at 4 °C until small molecules can be measured or until frozen at −80 °C to prevent degradation of small molecules and proteins.

2.3.2 Cerebrospinal fluid

CSF is a clear liquid in which the brain tissue bathes (figure 2.4b). In patients suffering from severe TBI, it is collected through an extra-ventricular drain which helps regulate high intra-cranial pressure due to secondary injuries. It is however commonly collected through a lumbar puncture in normal controls, even though ventricular and lumbar quantities of proteins differs [110], and therefore the two should not be quantitatively considered equal. Studies have shown that CSF protein content appears to be free of degradation for at least two hours at room temperature [111], and that degradation can be seen when left at room temperature for four or more hours. This degradation was not improved by the addition of protease inhibitors [112].

2.3.3 Blood

Blood is composed of a liquid portion (plasma) which contains different types of cells, most importantly red blood cells, white blood cells of the immune response and platelets involved in blood coagulation cascades (figure 2.4c). Venous and arterial blood can be collected in several different tubes. Additive-free tubes for serum collection allows blood to clot at room temperature before centrifugation, which takes a few minutes to an hour, effectively trapping cells and ridding the serum from clotting factors. Studies have shown that the amount of time during which blood is allowed to clot alters the levels of some proteins, and this is in part due to the presence of platelets [113]. Platelets are known to produce gelatinases which can degrade certain proteins [114]. One study also shows that the presence of thrombin in serum causes broad-spectrum protein degradation [115]. Other blood collection tubes contain anticoagulant additives to prevent blood clotting, such as ethylenediaminetetraacetic acid (EDTA), heparin, or citrate. Cells contained in the blood are removed by centrifugation at 4 °C or room temperature.

In the past 20-30 years, certain groups started to study the stability of small metabolites and proteins in blood treated with different anti-coagulants [116], and the importance of studying the stability of analytes of interest during sample collection and processing was established [117]. Various groups looked at the effects of waiting time and temperature before and after centrifugation, storage temperature, addition of anti-coagulants [118], platelet-depletion by filtration [119] and also studied the addition of protease inhibitors to EDTA-containing blood collection tubes [120].

It has been widely shown that levels of proteins greatly vary between serum and plasma samples [113, 121] and the stability of proteins while waiting before and after centrifugation varies between serum and plasma collected in different blood collection tubes. Although the Human Proteome Organization (HUPO) recommends using EDTA-plasma to collect blood for proteomics studies [119], different proteins are best collected in different blood collection tubes and processed as quickly as possible in order to prevent degradation or release of proteins by blood cells while awaiting processing. While tedious, it is recommended that the most appropriate blood collection and processing protocol should be determined for each protein studied [122].

2.4 Multiplex protein measurements

Proteins are the products of gene expression in response to the body's internal and external environment. They are made of amino acid chains and are often glycosylated with complex sugar residues when they are normally secreted by cells to the extracellular fluid or the blood. With the advances of genomics, which is the study of all the genes that make up an organism, proteomics was developed to study the overall protein content of cells, organs or bodily fluids and gives information about

the function of genes in organisms [123]. Because proteomics can measure dozens to thousands of proteins in parallel instead of measuring a single protein in convential assays, the benefit can be enormous to virtually all scientists seeking to glean more information from precious samples. Proteomics has been used as a way to discover a large number of potential biomarkers of various diseases, but validation of potential biomarkers has not yet led to single biomarkers being used in the clinic due to their lack of sensitivity and specificity for diseases, and ultimately clinical utility. Most protein biomarkers in use today by clinicians have been discovered through the knowledge gained from studying a single protein at a time, which is a slow process [124].

Another potential utility of proteomics is the ability to quantify numerous proteins within single individuals, a concept called personalized or precision medicine [125]. Indeed, by measuring many proteins at once in blood or urine of patients, a complete picture of the health status could potentially be gleaned. However, the field of systems biology which deals with understanding the complexity of proteins networks seen in living organisms is still in its infancy. Proteomics is still a young discipline, and improvements in technologies and methodologies hold great promise in revolutionizing personalized medicine and clinicial diagnosis and prognosis of numerous diseases in the future. Two vastly different technologies used in proteomics are mass spectrometry, and immunoassay-based assays, which includes antibody microarrays and bead-based multiplex immunoassays. These two methods lead to very different information, which is explained in the following section.

2.4.1 Mass spectrometry

Mass spectrometry (MS)-based proteomics is a plethora of techniques that benefit from yearly technological advances. Proteins in samples are normally cut into smaller pieces of predictable sizes (peptides), and an MS instrument separates peptides by their molecular size and charge (figure 2.5a-b). MS allows the discovery of proteins in samples without prior hypothesis of presence or absence, and does not require specific reagents for individual proteins, such as antibodies, allowing the potential detection of any and all proteins found in a biofluid of interest. For example, a study on albumin and immunoglobulin-depleted serum in six TBI patients, found 95 proteins which were differentially expressed compared to normal controls [126]. However, MS-based techniques suffer from several limitations. The detection of proteins is limited to high- to mid-abundance proteins, and low-abundance proteins as seen in blood are often not detected by MS in spite of being quantified by more sensitive methods. Complex samples such as serum or plasma are pretreated to remove albumin and immunoglobulins which are high-abundance proteins, however these techniques are known to also deplete small and low-abundance proteins by as much as 27 % [127]. Quantification of proteins requires the use of isotope-labeled standards. Finally, the instrumentation

and bioinformatics databases required to use MS are often a deterrent in its adoption as a technique for the clinic.

In an effort to detect small, low-abundance proteins, a MS-based technique called Selected Reaction Monitoring (SRM-MS) has allowed the quantitative detection of 75 proteins with limits of detection in the high pg/mL range [131]. This is a significant improvement over previous MS techniques, however it requires an input list of proteins to monitor, and isotope-labeled standards to allow the quantification of those proteins. The sensitivity of this method is still not enough to detect a lot of cytokines and chemokines involved in the inflammatory response, which are found in the low- to -mid pg/mL range.

MS has been used to detect several proteins that were differentially expressed in TBI [126, 132–137] however most proteins detected were found in mid- to high-abundance and none of them were specific to TBI.

2.4.2 Immunoassay-based methods

The Enzyme-Linked Immunosorbent Assay [138] (ELISA) is the gold standard for the accurate, sensitive and specific detection of single proteins with limits of detection below pg/mL for some proteins. The antigen of interest is first bound to a capture antibody immobilized to the surface of a plate, and a matched detection antibody that recognizes a different epitope on the antigen of interest is incubated. The detection antibody is finally recognized by a reporter molecule (see figure 2.5c). Protein quantification by ELISA is very specific due to the need for the antigen to be be recognized at two different epitopes in order to generate quantitative signal. The method is also considered to be very sensitive thanks to the high affinity of matched antibodies used in the assay. It is also possible to detect proteins immobilized at a surface using a single antibody (reverse-phase detection), or by immobilizing antibodies to the surface and labeling all the proteins in a sample, however these methods suffer from cross-reactivity and lack of specificity due to the use of a single antibody for target recognition.

Current multiplexed technologies based on ELISA such as antibody microarrays or bead-based immunoassays (see figure 2.5d), do not give as accurate results as the gold standard used in the clinic and in hospitals [139, 140]. This can be explained by cross-reactivity interactions seen in multiplexed immunoassays and is a known problem that leads to loss of assay specificity and false positive results (figure 2.6) [17]. Extensive optimizations of commercially available antibody microarrays or multiplex bead arrays are required to keep the amount of cross-reactivity within an acceptable threshold, and limits the number of proteins that can be measured within the same assay to under 100.

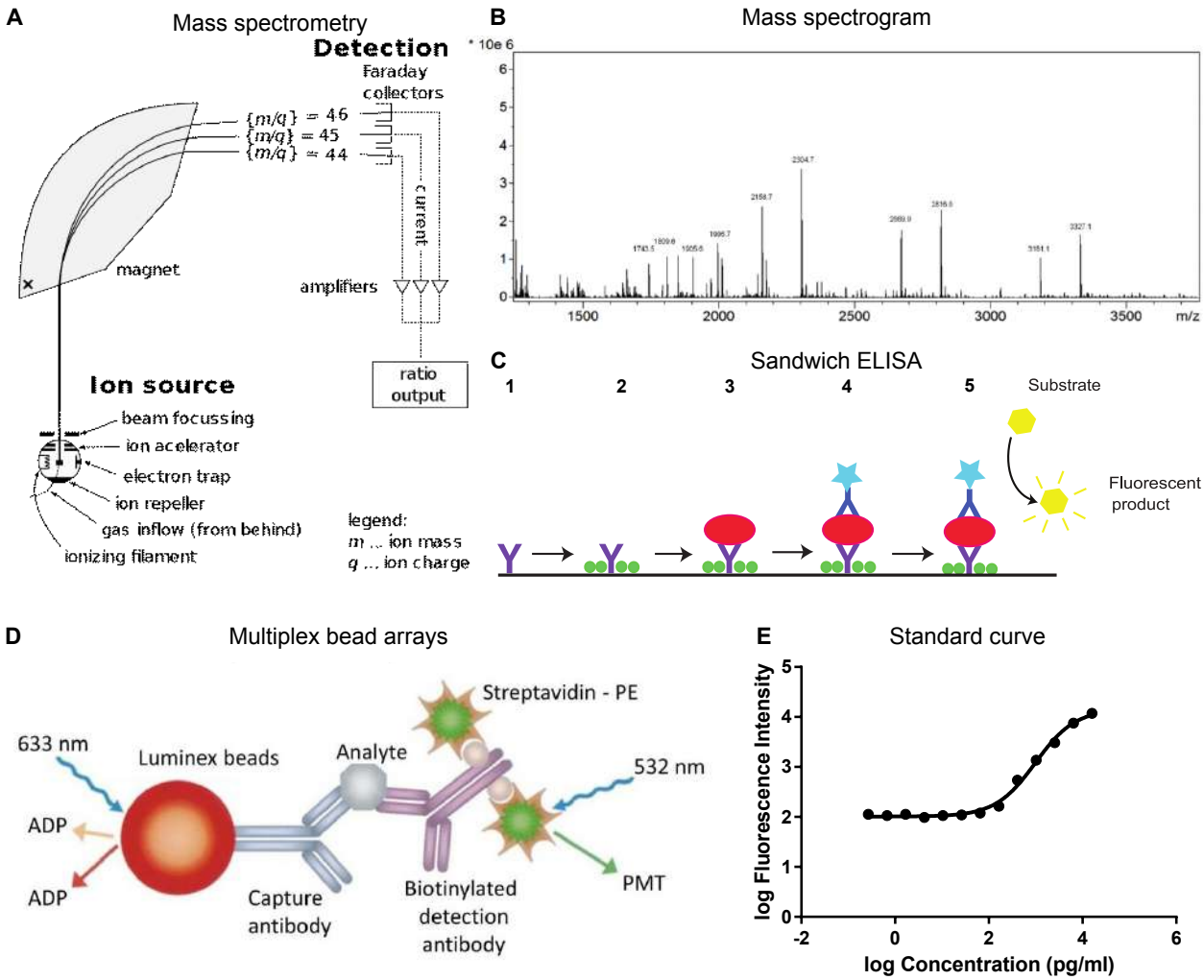

FIGURE 2.5: **Proteomics technologies. A** Mass spectrometry consists in ionizing small molecules and separating them by mass and charge (**B**), where complex databases and bioinformatics is used to infer protein identity. Image in **A** adapted from U.S. Geological Survey (public domain). Image in **B** obtained from [128] under a CC-BY 4.0. **C** The sandwich immunoassay protocol consists in (1) immobilizing capture antibodies on a surface, (2) blocking the surface to prevent non-specific adsorption of molecules in samples, (3) incubating samples, (4) incubating detection antibodies and (5) incubating a reporter molecule that produces a signal that can be quantified. Obtained from [129] under CC-BY 4.0. **D** Multiplex bead arrays use mixed beads with fluorescent codes to identify capture antibodies bound to the surface, and implement classical sandwich immunoassays as in **B**. Image obtained from [130] under CC-BY 4.0. **E** Quantification of proteins using immunoassays is performed by measuring multiple dilutions of a standard, and intrapolating the fluorescence intensity of unknown samples.

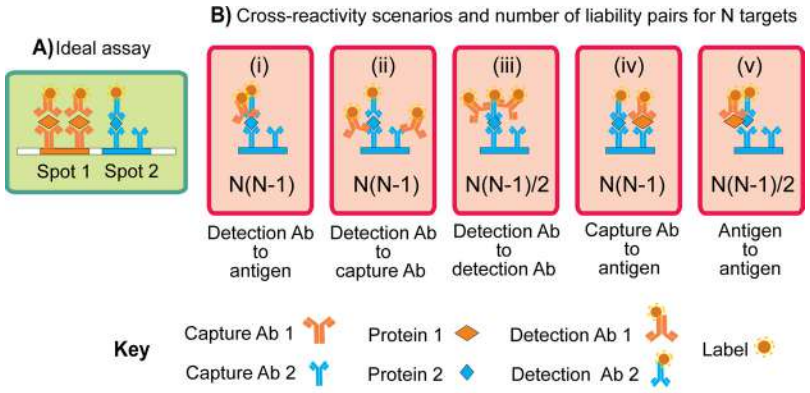

FIGURE 2.6: **Cross-reactivity in multiplex immunoassays.** **A**: The ideal assay result (in the absence of cross-reactivity) shows protein 1 (orange) sandwiched between cAb 1 and dAb 1 on spot 1, and protein 2 (blue) sandwiched between cAb 2 and dAb 2 on spot 2; protein 1 is abundant and saturates the spots, whereas protein 2 is scarce. **B**: Five scenarios of cross-reactivity (i-v) on spot 2 occurring as a result of the cross-reaction among a pair of non-matched Abs and analytes. A false positive signal is detected when the non-matched dAb 1 cross-reacts with protein 2 (i), cAb 2 (ii), and dAb 2 (iii). Cross-reactive binding of protein 1 to respectively cAb 2 (iv) or protein 2 (v) will result in the binding of dAb1 to spot 2 and a false positive signal. Modified from [17] under CC-BY 4.0.

The Antibody Colocalization Microarray (ACM) has been developed in Prof. David Juncker's lab to circumvent the cross-reactivity issues of multiplexed immunoassays, and thereby increase the accuracy of measurements for over 50 human proteins in a small volume of sample [17], with the possibility of easily adding matched antibody pairs to the platform to increase the number of proteins measured.

Similarly to ELISA assays, the ACM assay consists in printing pL-sized droplets of monoclonal antibodies in triplicate spots for over 50 proteins in each experiment subarray (figure 2.7a) on chemically-coated glass slides that allow binding of antibodies on the surface. Each microarray (glass slide) contains 16 subarrays which are physically separated by gaskets (figure 2.7c) during blocking, washing and incubation steps. Following slide blocking and antigen and samples incubation, the ACM avoids cross-reactivity by printing detection antibodies directly atop the corresponding capture antibodies, using silicon quill pins (figure 2.7b, see appendix A) that are precisely aligned at every spotting round (figure 2.7d) to ensure maximal alignment of spots during the different printing rounds. Detection antibodies, and therefore the bound target proteins, are quantified using fluorescently-labeled streptavidin, which is easily viewed using a fluorescent scanner (see figure 2.7 for an example of a fluorescent image of a single subarray). A complete description of the ACM protocol is located in appendix B.

Proteins measured using the ACM are typically found in low concentrations in samples, and most are involved in inflammatory processes. The current number of proteins measured with the

ACM is 50, but can be increased to 108, or more if the density of spots is increased in each subarray. The list of proteins measured includes cytokines and chemokines known to be involved in inflammation, as well as known or potential biomarkers of cancer and TBI to broaden the ACM's utility to several human diseases.

While the ACM has great potential, two limitations are mainly in the use of validated, commercially-available matched antibody-pairs normally used in ELISA, and the need for a microarrayer during the assay. To circumvent this last problem, the SnapChip™ was developed which pre-prints capture and detection antibodies spots on different microarray slides which are then stored [141–143]. During the assay, stored slides are brought in alignment using a small device. This method not only removes the requirement for a microarrayer by using stored microarray slides, it also shortens assay time. However, the density of spots printed is 75 % less than the density achieved with the ACM due to slight misalignments when slides are brought together, thereby decreasing the number of proteins that can be measured in the same volume of sample. The addition of new antibody pairs for the measurement of new proteins on the ACM and the SnapChip™ depends on the availability of antibody pairs and funding as they are expensive reagents with limited shelf life of 3-12 months.

Other platforms have been developed that circumvent cross-reactivity like the ACM, as reviewed elsewhere [144], such as the proximity extension assays (PEA) which has recently been used to measure 92 proteins in microdialysate samples of severe TBI patients [84]. While there is no need for extensive optimization of antibody pairs within a single assay, the number of proteins that can be measured is currently limited to 96 due to the detection method involving quantitative polymerase chain reaction (PCR) of resulting oligonucleotides that are produced when the capture and detection antibodies are brought together in close proximity due to the binding of an antigen on beads [145]. Because of this extra step of signal amplification, the sensitivity of PEA assays is better than that of ELISA or ACM by up to 100-fold, but is still limited by the binding affinity of antibodies to their target.

Therefore the ACM is a good choice of a platform for measuring 108 proteins or more in patient samples in discovery experiments to find potential biomarkers of TBI, which could potentially improve the way patients are diagnosed and monitor in the clinic.

References

17. Pla-Roca, M., Leulmi, R. F., Tourekhanova, S., Bergeron, S., Laforte, V., Moreau, E., Gosline, S. J. C., Bertos, N., Hallett, M., Park, M. & Juncker, D. Antibody colocalization microarray: a

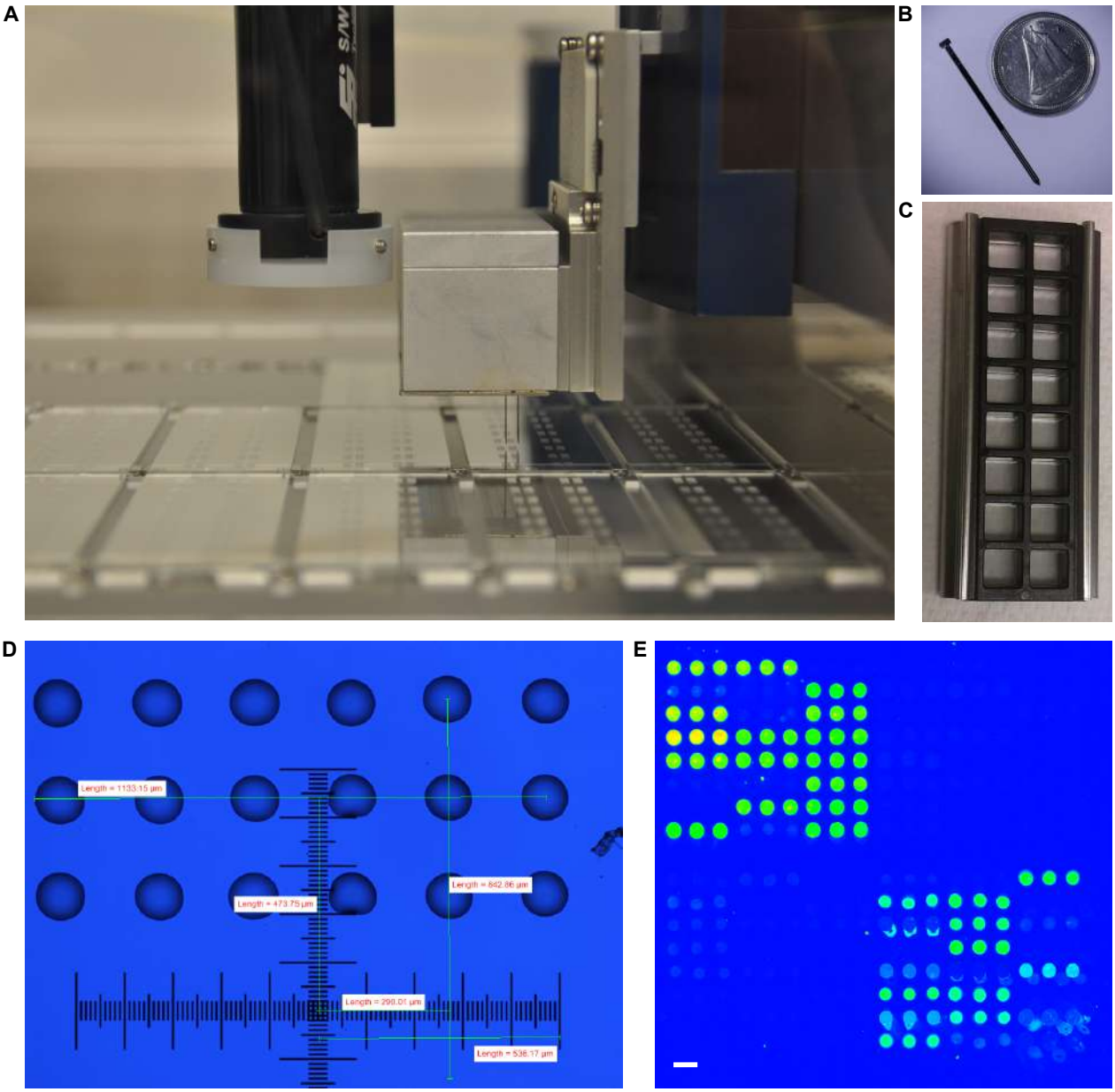

FIGURE 2.7: **Antibody colocalization microarray (ACM).** Multiple microarray slides are printed (**A**) using four custom-made silicon quill pins (**B**) in a pattern of 16 subarrays per slide. For washing, blocking, antigen and streptavidin incubation steps, a gasket (**C**) is fitted on every slide to physically separate the 16 subarrays. The ACM uses spring-clamping of slides (**A**) as well as a precise printing head positioning adjustment method (**D**) that uses a measurement slide on which test spots are printed before each spotting round. The resulting spots from microarray slides are imaged with a fluorescence scanner and fluorescence values are extracted using ArrayPro, as showed here for a single subarray (**E**). Distance between long bars in **D** is 100 µm. Scale bar in **E** is 250 µm.

scalable technology for multiplex protein analysis in complex samples. *Molecular & Cellular Proteomics* **11,** M111.011460 (2012).

18. Helmy, A., Carpenter, K. L. H., Menon, D. K., Pickard, J. D. & Hutchinson, P. J. A. The cytokine response to human traumatic brain injury : temporal profiles and evidence for cerebral parenchymal production. *Journal of Cerebral Blood Flow & Metabolism* **31,** 658–670 (2010).

20. Rosenbloom, A. J., Ferris, R., Sipe, D. M., Riddler, S. A., Connolly, N. C., Abe, K. & Whiteside, T. L. In vitro and in vivo protein sampling by combined microdialysis and ultrafiltration. *Journal of Immunological Methods* **309,** 55–68 (2006).

25. Helmy, A, Carpenter, K. L., Skepper, J. N., Kirkpatrick, P. J., Pickard, J. D. & Hutchinson, P. J. Microdialysis of cytokines: methodological considerations, scanning electron microscopy, and determination of relative recovery. *Journal of Neurotrauma* **26,** 549–561 (2009).

27. Hutchinson, P. J., O'Connell, M. T., Rothwell, N. J., Hopkins, S. J., Nortje, J., Carpenter, K. L. H., Timofeev, I., Al-Rawi, P. G., Menon, D. K. & Pickard, J. D. Inflammation in human brain injury: intracerebral concentrations of IL-1alpha, IL-1beta, and their endogenous inhibitor IL-1ra. *Journal of Neurotrauma* **24,** 1545–57 (2007).

29. Molnar, C. & Gair, J. *Concepts of Biology - 1st Canadian Edition* (ed University, R.) (BC Open Textbook, 2019).

30. Shaw, N. A. The neurophysiology of concussion. *Progress in Neurobiology* **67,** 281–344 (2002).

31. Rehman, T., Ali, R., Tawil, I. & Yonas, H. Rapid progression of traumatic bifrontal contusions to transtentorial herniation: A case report. *Cases Journal* **1,** 1–4 (2014).

32. Riechers, R. G., Ramage, A., Brown, W., Kalehua, A., Rhee, P., Ecklund, J. M. & Ling, G. S. Physician Knowledge of the Glasgow Coma Scale. *Journal of Neurotrauma* **22,** 1327–1334 (2005).

33. Golan, J. D., Marcoux, J., Golan, E., Schapiro, R., Johnston, K. M., Maleki, M., Khetarpal, S. & Jacques, L. Traumatic brain injury in intoxicated patients. *Journal of Trauma - Injury, Infection and Critical Care* **63,** 365–369 (2007).

34. Baker, S. P., O'Neill, B., Haddon, W. & Long, W. B. The injury severity score: a method for describing patients with multiple injuries and evaluating emergency care. *The Journal of Trauma* **14,** 187–196 (1974).

35. Grote, S, Bocker, W, Mutschler, W, Bouillon, B & Lefering, R. Diagnostic value of the Glasgow Coma Scale for traumatic brain injury in 18,002 patients with severe multiple injuries. *Journal of Neurotrauma* **28,** 527–534 (2011).

36. Chen, J. W., Gombart, Z. J., Rogers, S, Gardiner, S. K., Cecil, S & Bullock, R. M. Pupillary reactivity as an early indicator of increased intracranial pressure: The introduction of the Neurological Pupil index. *Surgical Neurology international* **2,** 82 (2011).

37. Jacobs, B., Beems, T., Stulemeijer, M., van Vugt, A. B., van der Vliet, T. M., Borm, G. F. & Vos, P. E. Outcome Prediction in Mild Traumatic Brain Injury: Age and Clinical Variables Are Stronger Predictors than CT Abnormalities. *Journal of Neurotrauma* **27,** 655–668 (2010).

38. Kramer, A. H., Deis, N., Ruddell, S., Couillard, P., Zygun, D. A., Doig, C. J. & Gallagher, C. Decompressive Craniectomy in Patients with Traumatic Brain Injury: Are the Usual Indications Congruent with Those Evaluated in Clinical Trials? *Neurocritical Care* **25,** 10–19 (2016).

39. Hutchinson, P. J., Kolias, A. G., Tajsic, T., Adeleye, A., Aklilu, A. T., Apriawan, T., Bajamal, A. H., Barthélemy, E. J., Devi, B. I., Bhat, D., Bulters, D., Chesnut, R., Citerio, G., Cooper, D. J., Czosnyka, M., Edem, I., El-Ghandour, N. M., Figaji, A., Fountas, K. N., Gallagher, C., Hawryluk, G. W., Iaccarino, C., Joseph, M., Khan, T., Laeke, T., Levchenko, O., Liu, B., Liu, W., Maas, A., Manley, G. T., Manson, P., Mazzeo, A. T., Menon, D. K., Michael, D. B., Muehlschlegel, S., Okonkwo, D. O., Park, K. B., Rosenfeld, J. V., Rosseau, G., Rubiano, A. M., Shabani, H. K., Stocchetti, N., Timmons, S. D., Timofeev, I., Uff, C., Ullman, J. S., Valadka, A., Waran, V., Wells, A., Wilson, M. H. & Servadei, F. Consensus statement from the International Consensus Meeting on the Role of Decompressive Craniectomy in the Management of Traumatic Brain Injury: Consensus statement. *Acta Neurochirurgica* **161,** 1261–1274 (2019).

40. Teasdale, G. & Jennett, B. Assessment and Prognosis of Coma After Head Injury. *Acta Neurochirurgica* **34,** 45–55 (1976).

41. Jennett, B., Snoek, J., Bond, M. R. & Brooks, N. Disability after severe head injury : observations on the use of the Glasgow Outcome Scale. *Journal of Neurology, Neurosurgery, and Psychiatry* **44,** 285–293 (1981).

42. Lu, J., Murray, G. D., Steyerberg, E. W., Butcher, I., McHugh, G. S., Lingsma, H., Mushkudiani, N., Choi, S., Maas, A. I. & Marmarou, A. Effects of Glasgow Outcome Scale misclassification on traumatic brain injury clinical trials. *Journal of Neurotrauma* **25,** 641–651 (2008).

43. De Guise, E., Leblanc, J., Dagher, J., Tinawi, S., Lamoureux, J., Marcoux, J., Maleki, M. & Feyz, M. Traumatic brain injury in the elderly: A level 1 trauma centre study. *Brain Injury* **29,** 558–564 (2015).

44. Julien, J., Alsideiri, G., Marcoux, J., Hasen, M., Correa, J. A., Feyz, M., Maleki, M. & de Guise, E. Antithrombotic agents intake prior to injury does not affect outcome after a traumatic brain injury in hospitalized elderly patients. *Journal of Clinical Neuroscience* **38,** 122–125 (2017).

45. Brown, A. W., Malec, J. F., McClelland, R. L., Diehl, N. N., Englander, J. & Cifu, D. X. Clinical Elements that Predict Outcome after Traumatic Brain Injury : A Prospective Multicenter Recursive Partitioning (Decision-Tree) Analysis. *Journal of Neurotrauma* **22,** 1040–1051 (2005).

46. Hou, D. J., Tong, K. A., Ashwal, S., Oyoyo, U., Joo, E., Shutter, L. & Obenaus, A. Diffusion-Weighted Magnetic Resonance Imaging Improves Outcome Prediction in Adult Traumatic Brain Injury. *Journal of Neurotrauma* **24,** 1558–1569 (2007).

47. Butcher, I., Maas, A. I., Lu, J., Marmarou, A., Murray, G. D., Mushkudiani, N. A., McHugh, G. S. & Steyerberg, E. W. Prognostic Value of Admission Blood Pressure in Traumatic Brain Injury: Results from The IMPACT Study. *Journal of Neurotrauma* **24,** 294–302 (2007).

48. Butcher, I, McHugh, G. S., Lu, J, Steyerberg, E. W., Hernandez, A. V., Mushkudiani, N, Maas, A. I., Marmarou, A & Murray, G. D. Prognostic value of cause of injury in traumatic brain injury: results from the IMPACT study. *Journal of Neurotrauma* **24,** 281–286 (2007).

49. Marmarou, A., Lu, J., Butcher, I., McHugh, G. S., Murray, G. D., Steyerberg, E. W., Mushkudiani, N. A., Choi, S. & Maas, A. I. Prognostic Value of The Glasgow Coma Scale And Pupil Reactivity in Traumatic Brain Injury Assessed Pre-Hospital And on Enrollment: An IMPACT Analysis. *Journal of Neurotrauma* **24,** 270–280 (2007).

50. Van Beek, J. G., Mushkudiani, N. A., Steyerberg, E. W., Butcher, I, McHugh, G. S., Lu, J, Marmarou, A, Murray, G. D. & Maas, A. I. Prognostic value of admission laboratory parameters in traumatic brain injury: results from the IMPACT study. *Journal of Neurotrauma* **24,** 315–328 (2007).

51. Hukkelhoven, C., Steyerberg, E., Habbema, J., Farace, E, Marmarou, A, Murray, G., Marshall, L. & Maas, A. Predicting Outcome after Traumatic Brain Injury: Admission Characteristics. *Journal of Neurotrauma* **22,** 1025–39 (2005).

52. Mondello, S., Jeromin, A., Buki, A., Bullock, R., Czeiter, E., Kovacs, N., Barzo, P., Schmid, K., Tortella, F., Wang, K. K. & Hayes, R. L. Glial Neuronal Ratio : A Novel Index for Differentiating Injury Type in Patients with Severe Traumatic Brain Injury. *Journal of Neurotrauma* **29,** 1096–1104 (2012).

53. Gan, Z. S., Stein, S. C., Swanson, R., Guan, S., Garcia, L., Mehta, D. & Smith, D. H. Blood biomarkers for traumatic brain injury: A quantitative assessment of diagnostic and prognostic accuracy. *Frontiers in Neurology* **10** (2019).

54. Papa, L., Robinson, G., Oli, M., Pineda, J., Demery, J., Brophy, G., Robicsek, S. A., Gabrielli, A., Robertson, C. S., Wang, K. K. & Hayes, R. L. Use of biomarkers for diagnosis and management of traumatic brain injury patients. *Expert Opinion on Medical Diagnostics* **2,** 937–945 (2008).

55. Papa, L., Akinyi, L., Liu, M. C., Pineda, J. a., Tepas, J. J., Oli, M. W., Zheng, W., Robinson, G., Robicsek, S. a., Gabrielli, A., Heaton, S. C., Hannay, H. J., Demery, J. a., Brophy, G. M., Layon, J., Robertson, C. S., Hayes, R. L. & Wang, K. K. W. Ubiquitin C-terminal hydrolase is a novel biomarker in humans for severe traumatic brain injury. *Critical Care Medicine* **38,** 138–44 (2010).

56. Papa, L., Lewis, L. M., Silvestri, S., Falk, J. L., Giordano, P., Brophy, G. M., Demery, J. A., Liu, M. C., Mo, J., Akinyi, L., Mondello, S., Schmid, K., Robertson, C. S., Tortella, F. C., Hayes, R. L. & Wang, K. K. Serum levels of ubiquitin C-terminal hydrolase distinguish mild traumatic brain injury from trauma controls and are elevated in mild and moderate traumatic brain injury patients with intracranial lesions and neurosurgical intervention. *Journal of Trauma and Acute Care Surgery* **72,** 1335–1344 (2012).

57. Herrmann, M., Curio, N., Jost, S., Wunderlich, M. T., Synowitz, H. & Wallesch, C. W. Protein S-100B and neuron specific enolase as early neurobiochemical markers of the severity of traumatic brain injury. *Restorative Neurology and Neuroscience* **14,** 109–114 (1999).

58. Thomas, D. G., Palfreyman, J. W. & Ratcliffe, J. G. Serum-Myelin-Basic-Protein Assay in Diagnosis and Prognosis of Patients With Head Injury. *The Lancet* **311,** 113–115 (1978).

59. Pelinka, L. E., Kroepfl, A., Schmidhammer, R., Krenn, M., Buchinger, W., Redl, H. & Raabe, A. Glial fibrillary acidic protein in serum after traumatic brain injury and multiple trauma. *Journal of Trauma - Injury, Infection and Critical Care* **57,** 1006–1012 (2004).

60. Berger, R. P., Pierce, M. C., Wisniewski, S. R., Adelson, P. D., Clark, R. S. B., Ruppel, R. A., Kochanek, P. M. & Background, A. Traumatic Brain Injury in Infants and Children. *Pediatrics* **109,** 2–7 (2002).

61. Chiaretti, A., Antonelli, A., Riccardi, R., Genovese, O., Pezzotti, P., Di Rocco, C., Tortorolo, L. & Piedimonte, G. Nerve growth factor expression correlates with severity and outcome of traumatic brain injury in children. *European Journal of Paediatric Neurology* **12,** 195–204 (2008).

62. Kleindienst, A. & Bullock, M. R. A critical analysis of the role of the neurotrophic protein S100B in acute brain injury. *Journal of Neurotrauma* **23,** 1185–1200 (2006).

63. Pike, B. R., Zhao, X., Newcomb, J. K., Posmantur, R. M., Wang, K. K. W. & Ca, R. L. H. Regional calpain and caspase-3 proteolysis of alpha-spectrin after traumatic brain injury. *Neuroreport* **9,** 2437–2442 (1998).

64. Ringger, N. C., O'Steen, B. E., Brabham, J. G., Silver, X, Pineda, J, Wang, K. K., Hayes, R. L. & Papa, L. A novel marker for traumatic brain injury: CSF alphaII-spectrin breakdown product levels. *Journal of Neurotrauma* **21,** 1443–1456 (2004).

65. Franz, G, Beer, R, Kampfl, A, Engelhardt, K, Schmutzhard, E, Ulmer, H & Deisenhammer, F. Amyloid beta 1-42 and tau in cerebrospinal fluid after severe traumatic brain injury. *Neurology* **60,** 1457–1461 (2003).

66. Shaw, G., Yang, C., Ellis, R., Anderson, K., Mickle, J. P., Scheff, S., Pike, B., Anderson, D. K. & Howland, D. R. Hyperphosphorylated neurofilament NF-H is a serum biomarker of axonal injury. *Biochemical and Biophysical Research Communications* **336,** 1268–1277 (2005).

67. Satchell, M. A., Lai, Y, Kochanek, P. M., Wisniewski, S. R., Fink, E. L., Siedberg, N. A., Berger, R. P., DeKosky, S. T., Adelson, P. D. & Clark, R. S. Cytochrome c, a biomarker of apoptosis, is increased in cerebrospinal fluid from infants with inflicted brain injury from child abuse. *Journal of Cerebral Blood Flow and Metabolism* **25,** 919–927 (2005).

68. Whalen, M. J., Carlos, T. M., Kochanek, P. M., Wisniewski, S. R., Bell, M. J., Carcillo, J. A., Clark, R. S., DeKosky, S. T. & Adelson, P. D. Soluble adhesion molecules in CSF are increased in children with severe head injury. *Journal of Neurotrauma* **15,** 777–787 (1998).

69. Pleines, U. E., Stover, J. F., Kossmann, T, Trentz, O & Morganti-Kossmann, M. C. Soluble ICAM-1 in CSF coincides with the extent of cerebral damage in patients with severe traumatic brain injury. *Journal of Neurotrauma* **15,** 399–409 (1998).

70. Beer, R, Franz, G, Srinivasan, A, Hayes, R. L., Pike, B. R., Newcomb, J. K., Zhao, X, Schmutzhard, E, Poewe, W & Kampfl, A. Temporal profile and cell subtype distribution of activated caspase-3 following experimental traumatic brain injury. *Journal of Neurochemistry* **75,** 1264–73 (2000).

71. Lenzlinger, P. M., Marx, A, Trentz, O, Kossmann, T & Morganti-Kossmann, M. C. Prolonged intrathecal release of soluble Fas following severe traumatic brain injury in humans. *Journal of Neuroimmunology* **122,** 167–174 (2002).

72. Vilalta, A, Sahuquillo, J, Rosell, A, Poca, M. A., Riveiro, M & Montaner, J. Moderate and severe traumatic brain injury induce early overexpression of systemic and brain gelatinases. *Intensive Care Medicine* **34,** 1384–1392 (2008).

73. Roberts, D. J., Jenne, C. N., Le, C., Kramer, A. H., Gallagher, C. N., Todd, S., Parney, I. F., Doig, C. J., Yong, V. W., Kubes, P. & Zygun, D. A. Association between the Cerebral Inflammatory and Matrix Metalloproteinase Responses after Severe Traumatic Brain Injury in Humans. *Journal of Neurotrauma* **30,** 1727–1736 (2013).

74. Roberts, D. J., Jenne, C. N., Léger, C., Kramer, A. H., Gallagher, C. N., Todd, S., Parney, I. F., Doig, C. J., Yong, V. W., Kubes, P. & Zygun, D. a. A prospective evaluation of the temporal matrix metalloproteinase response after severe traumatic brain injury in humans. *Journal of Neurotrauma* **30,** 1717–26 (2013).

75. Lu, K. T., Wang, Y. W., Yang, J. T., Yang, Y. L. & Chen, H. I. Effect of interleukin-1 on traumatic brain injury-induced damage to hippocampal neurons. *Journal of Neurotrauma* **22,** 885–895 (2005).

76. Michael, D. B., Byers, D. M. & Irwin, L. N. Gene expression following traumatic brain injury in humans: analysis by microarray. *Journal of Clinical Neuroscienceoscience* **12,** 284–290 (2005).

77. Buttram, S. D., Wisniewski, S. R., Jackson, E. K., Adelson, P. D., Feldman, K, Bayir, H, Berger, R. P., Clark, R. S. & Kochanek, P. M. Multiplex assessment of cytokine and chemokine levels in cerebrospinal fluid following severe pediatric traumatic brain injury: effects of moderate hypothermia. *Journal of Neurotrauma* **24,** 1707–1717 (2007).

78. Siman, R., Toraskar, N., Dang, A., McNeil, E., McGarvey, M., Plaum, J., Maloney, E. & Grady, M. S. A panel of neuron-enriched proteins as markers for traumatic brain injury in humans. *Journal of Neurotrauma* **26,** 1867–77 (2009).

79. Wilkinson, A. A., Simic, N., Frndova, H., Taylor, M. J., Choong, K., Fraser, D., Campbell, C., Dhanani, S., Kuehn, S., Beauchamp, M. H., Farrell, C., Anderson, V., Guerguerian, A. M., Dennis, M., Schachar, R. & Hutchison, J. S. Serum biomarkers help predict attention problems in critically ill children with traumatic brain injury. *Pediatric Critical Care Medicine* **17,** 638–648 (2016).

80. Di Battista, A. P., Rhind, S. G., Hutchison, M. G., Hassan, S., Shiu, M. Y., Inaba, K., Topolovec-Vranic, J., Neto, A. C., Rizoli, S. B. & Baker, A. J. Inflammatory cytokine and chemokine profiles are associated with patient outcome and the hyperadrenergic state following acute brain injury. *Journal of Neuroinflammation* **13,** 1–14 (2016).

81. Jastrow, K. M., Gonzalez, E. A., McGuire, M. F., Suliburk, J. W., Kozar, R. A., Iyengar, S., Motschall, D. A., McKinley, B. A., Moore, F. A. & Mercer, D. W. Early Cytokine Production Risk Stratifies Trauma Patients for Multiple Organ Failure. *Journal of the American College of Surgeons* **209,** 320–331 (2009).

82. Chiaretti, a, Barone, G, Riccardi, R, Antonelli, a, Pezzotti, P, Genovese, O, Tortorolo, L & Conti, G. Correlates With Severity and Outcome of Head Trauma in Children. *Neurology* (2009).

83. Mellergård, P., Sjögren, F. & Hillman, J. The Cerebral Extracellular Release of Glycerol, Glutamate, and FGF2 Is Increased in Older Patients following Severe Traumatic Brain Injury. *Journal of Neurotrauma* **29,** 112–118 (2011).

84. Dyhrfort, P., Shen, Q., Clausen, F., Thulin, M., Enblad, P., Kamali-Moghaddam, M., Lewén, A. & Hillered, L. Monitoring of Protein Biomarkers of Inflammation in Human Traumatic Brain Injury Using Microdialysis and Proximity Extension Assay Technology in Neurointensive Care. *Journal of Neurotrauma* **14,** 1–14 (2019).

85. Huie, J. R., Diaz-Arrastia, R., Yue, J. K., Sorani, M. D., Puccio, A. M., Okonkwo, D. O., Manley, G. T., Ferguson, A. R., Adeoye, O. M., Badjatia, N., Boase, K. D., Bodien-Guller, Y., Bullock, M. R., Chesnut, R. M., Corrigan, J. D., Crawford, K. L., Diaz-Arrastia, R., Dikmen, S. S., Duhaime, A.-C., Ellenbogen, R. G., Ezekiel, F., Feeser, V. R., Giacino, J. T., Goldman, D. P., Gonzales, L., Gopinath, S. P., Gullapalli, R. P., Hemphill, J. C., Hotz, G. A., Kramer, J. H., Levin, H., Lindsell, C. J., Machamer, J., Madden, C., Markowitz, A. J., Martin, A., Mathern, B. E., McAllister, T. W., McCrea, M. A., Merchant, R. E., Noel, F., Perl, D. P., Puccio, A. M., Rabinowitz, M., Robertson, C. S., Rosand, J., Sander, A. M., Satris, G., Schnyer, D. M., Seabury, S. A., Sergot, P., Sherer, M., Stein, D. M., Stein, M. B., Taylor, S. R., Temkin, N. R., Toga, A. W., Turtzo, L. C., Vespa, P. M., Wang, K. K., Zafonte, R. & Zhang, Z. Testing a Multivariate Proteomic Panel for Traumatic Brain Injury Biomarker Discovery: A TRACK-TBI Pilot Study. *Journal of Neurotrauma* **36,** 100–110 (2018).

86. Berger, R. P., Ta'asan, S., Rand, A., Lokshin, A. & Kochanek, P. Multiplex assessment of serum biomarker concentrations in well-appearing children with inflicted traumatic brain injury. *Pediatric Research* **65,** 97–102 (2009).

87. Robinson, S., Winer, J. L., Berkner, J., Chan, L. A. S., Denson, J. L., Maxwell, J. R., Yang, Y., Sillerud, L. O., Tasker, R. C., Meehan III, W. P., Mannix, R. & Jantzie, L. L. Imaging and serum biomarkers reflecting the functional efficacy of extended erythropoietin treatment in rats following infantile traumatic brain injury. *Journal of Neurosurgical Pediatry* **17,** 739–755 (2016).

88. Sankar, S. B., Pybus, A. F., Liew, A., Sanders, B., Shah, K. J., Wood, L. B. & Buckley, E. M. Low cerebral blood flow is a non-invasive biomarker of neuroinflammation after repetitive mild traumatic brain injury. *Neurobiology of Disease* **124,** 544–554 (2019).

89. Thelin, E. P., Just, D., Frostell, A., Häggmark-Månberg, A., Risling, M., Svensson, M., Nilsson, P. & Bellander, B. M. Protein profiling in serum after traumatic brain injury in rats reveals potential injury markers. *Behavioural Brain Research* **340,** 71–80 (2018).

90. Isoniemi, H, Tenovuo, O, Portin, R, Himanen, L & Kairisto, V. Outcome of traumatic brain injury after three decades–relationship to ApoE genotype. *Journal of Neurotrauma* **23,** 1600–1608 (2006).

91. McAllister, T. W., Tyler, A. L., Flashman, L. A., Rhodes, C. H., McDonald, B. C., Saykin, A. J., Tosteson, T. D., Tsongalis, G. J. & Moore, J. H. Polymorphisms in the Brain-Derived Neurotrophic Factor Gene Influence Memory and Processing Speed One Month after Brain Injury. *Journal of Neurotrauma* **29,** 1111–1118 (2011).

92. Dalla Libera, A. L., Regner, A., De Paoli, J., Centenaro, L., Martins, T. T. & Simon, D. IL-6 polymorphism associated with fatal outcome in patients with severe traumatic brain injury. *Brain Injury* **25,** 365–369 (2011).

93. Soustiel, J. F., Palzur, E., Nevo, O., Thaler, I. & Vlodavsky, E. Neuroprotective Anti-Apoptosis Effect of Estrogens in Traumatic Brain Injury. *Journal of Neurotrauma* **22,** 345–352 (2005).

94. Brotfain, E., E. Gruenbaum, S., Boyko, M., Kutz, R., Zlotnik, A. & Klein, M. Neuroprotection by Estrogen and Progesterone in Traumatic Brain Injury and Spinal Cord Injury. *Current Neuropharmacology* **14,** 641–653 (2016).

95. Bhomia, M., Balakathiresan, N. S., Wang, K. K., Papa, L. & Maheshwari, R. K. A Panel of Serum MiRNA Biomarkers for the Diagnosis of Severe to Mild Traumatic Brain Injury in Humans. *Scientific Reports* **6,** 1–12 (2016).

96. Parkin, G. M., Clarke, C., Takagi, M., Hearps, S., Babl, F. E., Davis, G. A., Anderson, V. & Ignjatovic, V. Plasma Tumor Necrosis Factor Alpha Is a Predictor of Persisting Symptoms Post-Concussion in Children. *Journal of Neurotrauma* **36,** 1768–1775 (2019).

97. Bromander, S., Anckarsäter, R., Kristiansson, M., Blennow, K., Zetterberg, H., Anckarsäter, H. & Wass, C. E. Changes in serum and cerebrospinal fluid cytokines in response to non-neurological surgery: an observational study. *Journal of Neuroinflammation* **9,** 242 (2012).

98. Papa, L., Ramia, M. M., Kelly, J. M., Burks, S. S., Pawlowicz, A. & Berger, R. P. Systematic Review of Clinical Research on Biomarkers for Pediatric Traumatic Brain Injury. *Journal of Neurotrauma* **30,** 324–338 (2013).

99. Oddo, M. & Hutchinson, P. J. Understanding and monitoring brain injury: the role of cerebral microdialysis. *Intensive Care Medicine* **44,** 1945–1948 (2018).

100. Blaus, B. Medical gallery of Blausen Medical. *WikiJournal of Medicine* **1** (2014).

101. Elson, J. A. *Red blood cell comparison* 2014.

102. Zetterström, T., Sharp, T., Marsden, C. A. & Ungerstedt, U. In Vivo Measurement of Dopamine and Its Metabolites by Intracerebral Dialysis: Changes After d-Amphetamine. *Journal of Neurochemistry* **41,** 1769–1773 (1983).

103. Meixensberger, J., Kunze, E., Barcsay, E., Vaeth, A. & Roosen, K. Clinical cerebral microdialysis: Brain metabolism and brain tissue oxygenation after acute brain injury. *Neurological Research* **23,** 801–806 (2001).

104. Vespa, P., Prins, M., Ronne-Engstrom, E., Caron, M., Shalmon, E., Hovda, D. A., Martin, N. A. & Becker, D. P. Increase in extracellular glutamate caused by reduced cerebral perfusion pressure and seizures after human traumatic brain injury: a microdialysis study. *Journal of Neurosurgery* **89,** 971–982 (1998).

105. Folkersma, H., Brevé, J. J. P., Tilders, F. J. H., Cherian, L., Robertson, C. S. & Vandertop, W. P. Cerebral microdialysis of interleukin (IL)-1ß and IL-6: extraction efficiency and production in the acute phase after severe traumatic brain injury in rats. *Acta Neurochirurgica* **150,** 1277–1284 (2008).

106. Afinowi, R, Tisdall, M, Keir, G, Smith, M, Kitchen, N & Petzold, A. Improving the recovery of S100B protein in cerebral microdialysis: implications for multimodal monitoring in neurocritical care. *Journal of Neuroscience Methods* **181,** 95–99 (2009).

107. Chen, J. W., Rogers, S. L., Gombart, Z. J., Adler, D. E. & Cecil, S. Implementation of cerebral microdialysis at a community-based hospital: A 5-year retrospective analysis. *Surgical Neurology international* **3,** 57 (2012).

108. Duo, J. & Stenken, J. A. Heparin-immobilized microspheres for the capture of cytokines. *Analytical and Bioanalytical Chemistry* **399,** 773–82 (2011).

109. Rossi, J. L., Ralay Ranaivo, H, Patel, F, Chrzaszcz, M, Venkatesan, C & Wainwright, M. S. Albumin causes increased myosin light chain kinase expression in astrocytes via p38 mitogen-activated protein kinase. *Journal of Neuroscience Research* **89,** 852–861 (2011).

110. Torres-Corzo, J. G., Tapia-Pérez, J. H., Sánchez-Aguilar, M., Della Vecchia, R. R., Chalita Williams, J. C. & Cerda-Gutiérrez, R. Comparison of cerebrospinal fluid obtained by ventricular endoscopy and by lumbar puncture in patients with hydrocephalus secondary to neurocysticercosis. *Surgical Neurology* **71,** 376–9 (2009).

111. Rosenling, T, Stoop, M. P., Smolinska, A, Muilwijk, B, Coulier, L, Shi, S, Dane, A, Christin, C, Suits, F, Horvatovich, P. L., Wijmenga, S. S., Buydens, L. M., Vreeken, R, Hankemeier, T, van Gool, A. J., Luider, T. M. & Bischoff, R. The Impact of Delayed Storage on the Measured Proteome and Metabolome of Human Cerebrospinal Fluid. *Clinical Chemistry* (2011).

112. Ranganathan, S, Polshyna, A, Nicholl, G, Lyons-Weiler, J & Bowser, R. Assessment of Protein Stability in Cerebrospinal Fluid Using Surface-Enhanced Laser Desorption/Ionization Time-of-Flight Mass Spectrometry Protein Profiling. *Clinical Proteomics* **2,** 91–101 (2006).

113. Banks, R. E., Stanley, A. J., Cairns, D. A., Barrett, J. H., Clarke, P, Thompson, D & Selby, P. J. Influences of blood sample processing on low-molecular-weight proteome identified by surface-enhanced laser desorption/ionization mass spectrometry. *Clinical Chemistry* **51,** 1637–1649 (2005).

114. Kälvegren, H., Jönsson, S. & Jonasson, L. Release of matrix metalloproteinases-1 and-2, but not-9, from activated platelets measured by enzyme-linked immunosorbent assay. *Platelets* **22,** 572–578 (2011).

115. O'Mullan, P., Craft, D., Yi, J. & Gelfand, C. A. Thrombin induces broad spectrum proteolysis in human serum samples. *Clinical Chemistry and Laboratory Medicine* **47,** 685–693 (2009).

116. Salazar, J.-F., Herbeth, B., Siest, G. & Leroy, P. Stability of blood homocysteine and other thiols: EDTA or acidic citrate? *Clinical Chemistry* **45,** 2016–2019 (1999).

117. Oddoze, C., Lombard, E. & Portugal, H. Stability study of 81 analytes in human whole blood, in serum and in plasma. *Clinical Biochemistry* **45,** 464–9 (2012).

118. Chan, B. Y. Y., Buckley, K. A., Durham, B. H., Gallagher, J. A. & Fraser, W. D. Effect of Anticoagulants and Storage Temperature on the Stability of Receptor Activator for Nuclear Factor-KB Ligand and Osteoprotegerin in Plasma and Serum. *Clinical Chemistry* **49,** 2083–2085 (2003).

119. Rai, A. J., Gelfand, C. A., Haywood, B. C., Warunek, D. J., Yi, J., Schuchard, M. D., Mehigh, R. J., Cockrill, S. L., Scott, G. B., Tammen, H., Schulz-Knappe, P., Speicher, D. W., Vitzthum, F., Haab, B. B., Siet, G. & Chan, D. W. HUPO Plasma Proteome Project specimen collection and handling: Towards the standardization of parameters for plasma proteome samples. *Proteomics* **5,** 3262–3277 (2005).

120. Hulmes, J. D., Bethea, D., Ho, K., Huang, S.-P., Ricci, D. L., Opiteck, G. J. & Hefta, S. A. An Investigation of Plasma Collection, Stabilization, and Storage Procedures for Proteomic Analysis of Clinical Samples. *Clinical Proteomics* **1,** 017–032 (2004).

121. Tammen, H, Schulte, I, Hess, R, Menzel, C, Kellmann, M, Mohring, T & Schulz-Knappe, P. Peptidomic analysis of human blood specimens: comparison between plasma specimens and serum by differential peptide display. *Proteomics* **5,** 3414–3422 (2005).

122. Jambunathan, K. & Galande, A. K. Sample collection in clinical proteomics - Proteolytic activity profile of serum and plasma. *Proteomics - Clinical Applications* **8,** 299–307 (2014).

123. Wilkins, M. R., Sanchez, J. C., Gooley, A. A., Appel, R. D., Humphery-Smith, I., Hochstrasser, D. F. & Williams, K. L. Progress with proteome projects: Why all proteins expressed by a genome should be identified and how to do it. *Biotechnology and Genetic Engineering Reviews* **13,** 19–50 (1996).

124. Garg, P., Morris, P., Fazlanie, A. L., Vijayan, S., Dancso, B., Dastidar, A. G., Plein, S., Mueller, C. & Haaf, P. Cardiac biomarkers of acute coronary syndrome: from history to high-sensitivity cardiac troponin. *Internal and Emergency Medicine* **12,** 147–155 (2017).

125. Whitcomb, D. C. What is personalized medicine and what should it replace? *Nature Reviews Gastroenterology and Hepatology* **9,** 418–424 (2012).

126. Haqqani, A. S., Hutchison, J. S., Ward, R & Stanimirovic, D. B. Biomarkers and diagnosis; protein biomarkers in serum of pediatric patients with severe traumatic brain injury identified by ICAT-LC-MS/MS. *Journal of Neurotrauma* **24,** 54–74 (2007).

127. Granger, J, Siddiqui, J, Copeland, S & Remick, D. Albumin depletion of human plasma also removes low abundance proteins including the cytokines. *Proteomics* **5,** 4713–4718 (2005).

128. Powers, T. W., Holst, S., Wuhrer, M., Mehta, A. S. & Drake, R. R. Two-dimensional N-glycan distribution mapping of hepatocellular carcinoma tissues by MALDI-imaging mass spectrometry. *Biomolecules* **5,** 2554–2572 (2015).

129. Thaitrong, N., Charlermroj, R., Himananto, O., Seepiban, C. & Karoonuthaisiri, N. Implementation of microfluidic sandwich ELISA for superior detection of plant pathogens. *PloS one* **8,** e83231 (2013).

130. Kuen, J. *Influence of 3D tumor cell/fibroblast co-culture on monocyte differentiation and tumor progression in pancreatic cancer* PhD thesis (Dec. 2017).

131. Shi, T., Fillmore, T. L., Sun, X., Zhao, R., Schepmoes, A. A., Hossain, M., Xie, F., Wu, S., Kim, J.-S., Jones, N., Moore, R. J., Pasa-Tolic, L., Kagan, J., Rodland, K. D., Liu, T., Tang, K., Camp, D. G., Smith, R. D. & Qian, W.-J. Antibody-free, targeted mass-spectrometric approach for quantification of proteins at low picogram per milliliter levels in human plasma/serum. *Proceedings of the National Academy of Sciences* **109,** 15395–15400 (2012).

132. Connor, D. E., Chaitanya, G. V., Chittiboina, P., McCarthy, P., Scott, L. K., Schrott, L., Minagar, A., Nanda, A. & Alexander, J. S. Variations in the cerebrospinal fluid proteome following traumatic brain injury and subarachnoid hemorrhage. *Pathophysiology* **24,** 169–183 (2017).

133. Crawford, F., Crynen, G., Reed, J., Mouzon, B., Bishop, A., Katz, B., Ferguson, S., Phillips, J., Ganapathi, V., Mathura, V., Roses, A. & Mullan, M. Identification of Plasma Biomarkers of TBI Outcome Using Proteomic Approaches in an APOE Mouse Model. *Journal of Neurotrauma* **29,** 246–260 (2012).

134. Hanrieder, J., Wetterhall, M., Enblad, P., Hillered, L. & Bergquist, J. Temporally resolved differential proteomic analysis of human ventricular CSF for monitoring traumatic brain injury biomarker candidates. *Journal of Neuroscience Methods* **177,** 469–478 (2009).

135. Kobeissy, F. H., Ottens, A. K., Zhang, Z, Liu, M. C., Denslow, N. D., Dave, J. R., Tortella, F. C., Hayes, R. L. & Wang, K. K. Novel differential neuroproteomics analysis of traumatic brain injury in rats. *Molecular & Cellular Proteomics* **5,** 1887–1898 (2006).

136. Lakshmanan, R, Angeles, L., Loo, J. A., Angeles, L., Drake, T, Angeles, L., Leblanc, J, Angeles, L., Ytterberg, A. J., Angeles, L., Mcarthur, D. L., Etchepare, M & Vespa, P. M. Metabolic Crisis After Traumatic Brain Injury is Associated with a Novel Microdialysis Proteome. *Neurocritical Care* **12,** 324–336 (2010).

137. Anada, R. P., Wong, K. T., Jayapalan, J. J., Hashim, O. H. & Ganesan, D. Panel of serum protein biomarkers to grade the severity of traumatic brain injury. *Electrophoresis* **39,** 2308–2315 (2018).

138. Engvall, E & Perlmann, P. Enzyme-linked immunosorbent assay (ELISA). Quantitative assay of immunoglobulin G. *Immunochemistry* **8,** 871–874 (1971).

139. De Koning, L., Liptak, C., Shkreta, A., Bradwin, G., Hu, F. B., Pradhan, A. D., Rifai, N. & Kellogg, M. D. A multiplex immunoassay gives different results than singleplex immunoassays which may bias epidemiologic associations. *Clinical Biochemistry* **45,** 848–851 (2012).

140. Phan, K., Sohn, K.-Y., Hill, S. a., Worster, A., You, J., Oremus, M., Devereaux, P. J., Jaffe, A. S. & Kavsak, P. a. Multiplex protein assay performance/evaluation and the requirement for precision and correlation to clinical assays. *Clinical Chemistry and Laboratory Medicine* **49,** 1915–8 (2011).

141. Li, H., Bergeron, S. & Juncker, D. Microarray-to-microarray transfer of reagents by snapping of two chips for cross-reactivity-free multiplex immunoassays. *Analytical Chemistry* **84,** 4776–4783 (2012).

142. Li, H., Munzar, J. D., Ng, A. & Juncker, D. A versatile snap chip for high-density sub-nanoliter chip-to-chip reagent transfer. *Scientific Reports* **5,** 11688 (2015).

143. Li, H., Bergeron, S., Larkin, H. & Juncker, D. Snap Chip for Cross-reactivity-free and Spotter-free Multiplexed Sandwich Immunoassays. *JoVE,* e56230 (2017).

144. Juncker, D., Bergeron, S., Laforte, V. & Li, H. Cross-reactivity in antibody microarrays and multiplexed sandwich assays: shedding light on the dark side of multiplexing. *Current Opinion in Chemical Biology* **18,** 29–37 (2014).

145. Assarsson, E., Lundberg, M., Holmquist, G., Björkesten, J., Thorsen, S. B., Ekman, D., Eriksson, A., Rennel Dickens, E., Ohlsson, S., Edfeldt, G., Andersson, A.-C., Lindstedt, P., Stenvang, J., Gullberg, M. & Fredriksson, S. Homogenous 96-Plex PEA Immunoassay Exhibiting High Sensitivity, Specificity, and Excellent Scalability. *PLoS ONE* **9,** e95192 (2014).

CHAPTER 3

Evaluating mixtures of 14 hygroscopic additives

Preface

Background and objectives

With the goal in mind of being able to measure over 100 proteins in hundreds of samples using the ACM, we first developed silicon quill pins that allowed us to print on 2D functionalized glass slides (see appendix A). The next step was to insure reproducible printing of spots on microarray slides. Printing buffers used in the first ACM manuscript evaporated quickly due to the double-channel nature of the silicon quill pins, in spite of the added glycerol. The relatively fast evaporation led to inconsistent quantities of capture antibodies bound at the surface and greatly affected the reproducibility of printing. Our next step was therefore to optimize additives in the printing buffer to prevent evaporation of the printing buffer, which would allow us to consistently spot hundreds or thousands of spots required to print multiple microarrays. Since the shape of microarray spots can greatly influence the quality of the quantitative data output, we also looked for additives that would optimize spot size, morphology and the consistency of signal intensity.

Challenges and encountered problems

When testing the different hygroscopic additives and their combinations, we were unable to survey all of the different hygroscopic additives available, nor the slides available, and we could not test the additives on more than three proteins in full assays. There exists hundreds, if not thousands

of hygroscopic compounds - no official list exists - therefore we picked ones that we considered to be compatible with protein assays in terms of preservation of antibody structure and function, that were easily available through vendors and fairly inexpensive. It is therefore quite conceivable that there exists better combinations of additives for the myriad of different slide types available commercially.

Reference

This chapter is based on an article in which I am co-first author: Sébastien Bergeron, Véronique Laforte, Pik Shan Lo, Huiyan Li and David Juncker, "Evaluating mixtures of 14 hygroscopic additives to improve antibody microarray performance" published in *Analytical and bioanalytical chemistry* in 2015 [146], reprinted here with permission. Minor changes were made to the version in this thesis from comments and questions from thesis reviewers.

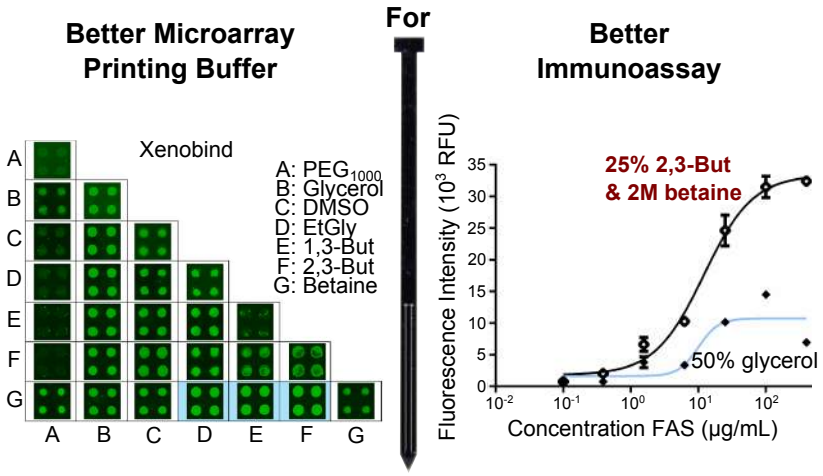

Evaluating mixtures of 14 hygroscopic additives to improve antibody microarray performance

Sébastien Bergeron[1,2,*], Véronique Laforte[1,2,3,*], Pik-Shan Lo[1,2], Huiyan Li[1,2], D. Juncker[1,2,3]

Affiliations

[1] McGill University and Genome Québec Innovation Center, McGill University,
740 Dr. Penfield Avenue, Montreal, Quebec, H3A 0G1
[2] Biomedical Engineering Department, McGill University, McGill University,
3775 University Street, Montreal, Quebec, Canada H3A 2B4
[3] Neurology and Neurosurgery Department, McGill University, McGill University,
3801 University Street, Montreal, Quebec, Canada H3A 2B4

[*] Sébastien Bergeron and Veronique Laforte contributed equally to this work.

Abstract

Microarrays allow the miniaturization and multiplexing of biological assays while only requiring minute amounts of samples. As a consequence of the small volumes used for spotting and the assays, evaporation often deteriorates the quality, reproducibility of spots, and the overall assay performance. Glycerol is commonly added to antibody microarray printing buffers to decrease evaporation; however, it often decreases the binding of antibodies to the surface, thereby negatively affecting assay sensitivity. Here, combinations of 14 hygroscopic chemicals were used as additives to printing buffers for contact-printed antibody microarrays on four different surface chemistries. The ability of the additives to suppress evaporation was quantified by measuring the residual buffer volume in open quill pins over time. The seven best additives were then printed either individually or as a 1:1 mixture of two additives, and the homogeneity, intensity, and reproducibility of both the spotted protein and of a fluorescently labeled analyte in an assay were quantified. Among the 28 combinations on the four slides, many were found to outperform glycerol, and the best additive mixtures were further evaluated by changing the ratio of the two additives. We observed that the

optimal additive mixture was dependent on the slide chemistry, and that it was possible to increase the binding of antibodies to the surface threefold compared to 50 % glycerol, while decreasing whole-slide coefficient of variation to 5.9 %. For the two best slides, improvements were made for both the limit of detection (1.6 × and 5.9 ×, respectively) and the quantification range (1.2 × and 2.1 ×, respectively). The additive mixtures identified here thus help improve assay reproducibility and performance, and might be beneficial to all types of microarrays that suffer from evaporation of the printing buffers.

Keywords: Antibody · Protein · Microarray · Low evaporation · Contact printing · Hygroscopic · Reproducibility

Abbreviations

1,3-But	1,3-Butanediol
2,3-But	2,3-Butanediol
Ab	Antibody
ACM	Antibody colocalization microarray
AF	Alexa Fluor
APTES	(3-Aminopropyl)triethoxysilane
cAb	Capture antibody
dAb	Detection antibody
DMSO	Dimethyl sulfoxide
DNA	Deoxyribonucleic acid
ELISA	Enzyme-linked immunosorbent assay
EtGly	Ethylene glycol
IgG	Immunoglobulin G
LOD	Limit of detection
OM	Orders of magnitude
PBS	Phosphate buffer saline
PBST	Phosphate buffer saline with 0.1 % Tween-20
PEG	Polyethylene glycol
PVA	Polyvinyl alcohol

3.1 Introduction

Over the past two decades, the miniaturization of biological assays such as DNA and antibody (Ab) microarrays has increased throughput while reducing consumption of reagents and samples. This

allows extracting more information from microliters of precious samples using smaller amounts of expensive reagents. Microarrays are fabricated by printing small droplets on a flat surface using direct pin printing or inkjet printing [147]. Solutions deposited on a microarray suffer from evaporation in the source well plate (5–20 µL) before and during dispensing, and after dispensing due to the minuscule (< 1 nL) size of spots [148, 149]. Because inkjet printing uses a closed nozzle, evaporation of solutions is minimized during printing, but in the case of pin-based printing of microarrays, there is significant evaporation of solutions in the pin during the printing process (100–400 nL depending on the printing technology used), leading to problems with the quality of pin printed microarrays [150].

Evaporation of solutions in the pin, prior to spot printing, leads to changes in concentration of reagents and can alter the viscosity of the solution, while evaporation following printing can lead to inhomogeneous spot morphology in the shape of a doughnut owing to the coffee ring effect [151], as well as many other irregularities such as egg-shape and cracking-like spots [152]. Quill pins have microscale slits that are filled by capillary effects, which offer long printing autonomy (i.e., the number of spots that can be printed before refilling) and can be made out of steel, silicon, or polymers [153, 154]. However, liquid in the open channel is in contact with air and, because of the high surface-to-volume ratio, evaporates quickly [155]. Evaporation can be mitigated by increasing the relative humidity in the chamber, but to prevent condensation on the slides and the instrument's electronics, it cannot be raised beyond 70–80 %. Cooling and sealing [156] of the source plates that contain reagents or the surface being printed on [157, 158], or printing solutions in a droplet of oil [159] is effective in avoiding evaporation for inkjet printing, but does not prevent evaporation from quill pins during printing.

The addition of hygroscopic chemicals such as glycerol to the printing buffer is therefore commonly used to reduce evaporation while improving inter- and intra-spot homogeneity [160], but it is often used at low concentrations ranging from 1 % [161] to 20 % [162], which is too low to completely prevent evaporation during printing. Moreover, it has been reported that glycerol interferes with the immobilization of proteins on surfaces [163–165], which results in a proportional reduction of the assay signal, thus affecting the performance and sensitivity of immunoassays [166].

Additives such as dimethyl sulfoxide (DMSO) [167] and betaine [168] have long been used in the printing buffers of DNA microarrays. Betaine is a naturally occurring osmoprotectant [169] that reduces evaporation (from both array and source plate), increases DNA binding to many surfaces, and improves spot morphology [168] The typical concentration of betaine in printing buffers is 0.75 to 1.5 M, but 6.8 M would be required to eliminate evaporation at 30 °C and 60 % relative humidity [168]. Betaine has also been tested in protein printing buffers because of its improvement to DNA spotting [170], but the potential benefits in terms of protein printing reproducibility have not been

documented to the best of our knowledge. Other hygroscopic additives such as sucrose, trehalose, and polyethylene glycol (PEG) that are known to preserve protein activity [171], or detergents such as Triton X-100 [172] and Tween-20 [173], which improve spot morphology, have also been tested but at low concentrations at which evaporation is still expected. The number of hygroscopic chemicals is large and not clearly defined. Many are organic solvents or polymers that are miscible in water, but only a few have been tested for microarrays and even fewer for antibody microarrays. Multiple so-called low evaporation printing buffers are available from many vendors (e.g., ArrayIt, Corning, BioTools, Grace Bio-Labs, Schott); however, vendors rarely provide evaporation data and printing buffers are generally optimized for only one slide surface, while the composition of buffers are kept proprietary.

The understanding of the impact of buffer additives on Ab microarrays spot quality and reproducibility remains limited. Yet there is a need for better printing buffer formulations that (i) minimize evaporation during Ab microarray printing, (ii) promote Ab binding to the surface, (iii) produce homogeneous spots, and (iv) do not decrease assay sensitivity. Here, we report the ability of 14 hygroscopic additives to effectively limit the evaporation of printing buffers and the effect of a number of mixtures of them on microarray printing quality and reproducibility, as well as immunoassay performance. First, the capacity of each additive to retain water was quantified by measuring the residual liquid in quill pins following evaporation. The seven additives that limited evaporation to 20 % or less were selected for further optimization. Twenty-eight pairwise combinations of these additives were used in antibody microarray assays. The signal intensity and homogeneity of the spots on four different slide surfaces with distinct surface chemistry were characterized. The two slides giving the highest signals and spot quality were selected, and the relative concentration of the two best additives was varied to identify the optimal ratio. The evaporation of the optimal buffers in the pin and in the source plate was quantified. Finally, slides were printed with either a standard buffer formulation containing 50 % glycerol or the optimal buffer solutions, and sandwich immunoassays against three distinct targets conducted. The optimized buffers lead to better printing reproducibility, as well as improved limits of detection (LOD) and larger quantification ranges for each of the targets.

3.2 Materials and Methods

3.2.1 Materials

Alexa Fluor-532 (AF-532) goat anti-mouse IgG and AF-647 chicken anti-goat IgG antibodies were purchased from Life Technologies (Carlsbad, CA, USA). Capture (cAb) and biotinylated detection

(dAb) antibodies against FAS, IL-1β, and TFN-RII, as well as the recombinants proteins, were obtained from R&D Systems (Minneapolis, MN, USA). The hydrogel-coated slide (Nexterion Slide H) and Nexterion Slide E and Slide AL were produced by Schott (Mainz, Germany), and Xenobind slides were obtained from Xenopore Corporation (Hawthorne, NJ, USA). Contact angle measurements of slides were performed with a VCA Optima 1 goniometer (AST Products, Billerica, MA, USA). Washing buffer (PBST) was composed of phosphate saline buffer (PBS, Fisher Scientific, Waltham, MA, USA) supplemented with 0.1 % Tween-20 (Sigma-Aldrich, St. Louis, MO, USA). Blocking buffer was made by dissolving 1 % IgG-free bovine serum albumin (BSA, Jackson ImmunoResearch Laboratories, West Grove, PA, USA) in PBST. The hygroscopic additives were purchased from Sigma-Aldrich: polyvinyl alcohol (PVA), Tween-20, sucrose, trehalose, PEG 1000 Da, PEG 8000 Da, DMSO, ethylene glycol, 1,3-butanediol, 2,3-butanediol, and betaine; Fisher Scientific: Triton X-100 and glycerol; and MP Biomedicals: magnesium sulfate. Protein Printing Buffer (PPB) was purchased from ArrayIt (Sunnyvale, CA, USA).

3.2.2 Quantification of evaporation in quill pins

Four silicon quill pins made in-house [154] were attached to a glass slide and used to simultaneously evaluate the evaporation of four different additives in 1 × PBS buffer. The tip of each pin was dipped in a solution containing an additive supplemented with 1 % food dye and placed in a closed chamber with 65 % relative humidity. Pictures were taken every minute for 10 to 15 min using a QX5 digital computer microscope (Digital Blue, Atlanta, GA, USA). The level of liquid in the pin was measured using Paint 6.1 software (Microsoft Corporation).

3.2.3 Microarray fabrication

cAbs were diluted in the different printing buffers at 100 µg/mL unless specified otherwise, and printed with a customized Nanoplotter 2.1 microarrayer (GeSiM GmbH, Grosserkmannsdorf, Germany) equipped with a silicon contact printing head and precision microfabricated collimator (Parallel Synthesis, Santa Clara, CA), and a customized slide tray with individual springloaded clamps for each slide (GeSIM). The relative humidity during printing was kept at 65 % and room temperature. Four silicon pins were used simultaneously and arrays with a pitch of 250 µm were produced with a contact time of 0.01 s. Sixteen identical arrays containing 6 or 16 replicate spots of each cAb were printed on each slide. Printed slides were incubated at room temperature with 65 % relative humidity overnight to allow antibodies to bind to the surfaces. To study the effect of evaporation in the source plate wells, microarrays were printed with an inkjet spotter (Nanoplotter 2.0, GeSIM GmbH) equipped with a single nozzle.

3.2.4 Immunoassay protocol

Gaskets (Proplate®, Grace Bio-Labs, Bend, OR, USA) were clamped onto printed slides so as to form 16 independent wells. Each well was filled with 80 µL of blocking buffer and the slides were washed three times at room temperature for 5 min on a rotary shaker at 450 rotations per minute (rpm) and subsequently blocked for 1 h with 80 µL of blocking buffer. Wells were manually emptied by knocking gaskets on absorbent paper. To incubate the analyte, wells were filled with 80 µL of blocking buffer containing 0.1 µg/mL AF-532 goat anti-mouse and incubated for 2 h on a rotary shaker at 450 rpm. Slides were washed three times with PBST, rinsed with double distilled water, blown-dry under a stream of compressed nitrogen, and immediately scanned.

For sandwich immunoassays, cAbs were printed at five different concentrations from 25 to 400 µg/mL as multiple sub-arrays. Slides were blocked and incubated with 80 µL of blocking buffer containing recombinant proteins in a four-fold dilution series and incubated for 2 h on a rotary shaker at 450 rpm. Slides were washed three times with PBST, and then incubated with a mixture of 0.1 µg/mL biotinylated dAbs for 1 h. Slides were washed three times and each well was loaded with 80 µL of 0.33 µg/mL Cy5-conjugated streptavidin (Rockland Immunochemicals, Gilbertsville, PA, USA) in PBS supplemented with 0.05 % Tween-20 and incubated for 30 min at 450 rpm and room temperature. After a final series of washing with PBST, slides were rinsed with double distilled water, blown-dry under a stream of nitrogen, and immediately scanned.

3.2.5 Fluorescence scanning, data extraction, and analysis

Slides were scanned using a SureScan Microarray Scanner from Agilent Technologies (Santa Clara, CA, USA). Spot morphology was analyzed using ImageJ. Mean Relative Fluorescence Unit (RFU) and standard deviations were calculated using ArrayPro 4.5 (MediaCybernetics, Rockville, MD, USA). The median local background of each spot was subtracted from the averaged intensity of each spot. Technical replicates were grouped for statistical analysis, and outlier removal was performed by removing points outside of each group's mean±3 standard deviations using Microsoft Excel (Microsoft Corporation, Redmond, WA, USA). Protein concentrations were calculated from a nonlinear four-parameter logistic curve fit using GraphPad Prism 5 (GraphPad Software Inc, La Jolla, CA, USA). The LOD for each protein was calculated by averaging the interpolated blank value plus 3 standard deviations from three independent standard curves. The quantification range was calculated by subtracting the log of the concentration which corresponds to 5 % above the lower LOD from the log of the concentration which corresponds to 5 % below the upper LOD (highest value). All experiments were performed in triplicate, and averages of the three experiments are reported.

3.3 Results

3.3.1 Minimizing evaporation

A major factor affecting printing consistency and autonomy is the evaporation of the printing buffers during printing of microarrays. To reproduce the evaporation occurring during microarray printing, in-house fabricated silicon pins were clamped on a microscope slide with tape and placed inside of the printing chamber at 65 % relative humidity. Pins were filled with buffer by contacting the tip with a solution, and the liquid level was recorded over time with a USB microscope (Fig. 3.1a). The evaporation was calculated based on the change in filling position of the residual liquid over time (Fig. 3.1b). In the first experiment, we tested the evaporation of solutions containing different concentrations of glycerol and thus observed in real time the evaporation of PBS, PBS with 10 and 20 % (v/v) glycerol, and of a commercial protein printing buffer (ArrayIt PPB). After 10 min, both the commercial buffer and PBS had almost completely evaporated. Glycerol slowed down the evaporation rate in a dose-dependent manner and a relatively stable level was reached after 10–12 min in both cases (Fig. fig:1-1b). Because 50 % of the volume evaporated from the 20 % glycerol solution, we calculated that glycerol stabilized at 40 %, slightly lower than the theoretical equilibrium (i.e., 55.5 %) [174] at 65 % relative humidity. This difference, and the initial plateau, can both be explained by the fact that initially the liquid is level with the pin, but as evaporation proceeds, a meniscus is slowly formed longitudinally along the pin before the liquid starts to retreat from the top [153]. Indeed, the difference was consistent and reproducible (variation ≤5 %), and thus does not affect the conclusions reached from these experiments.

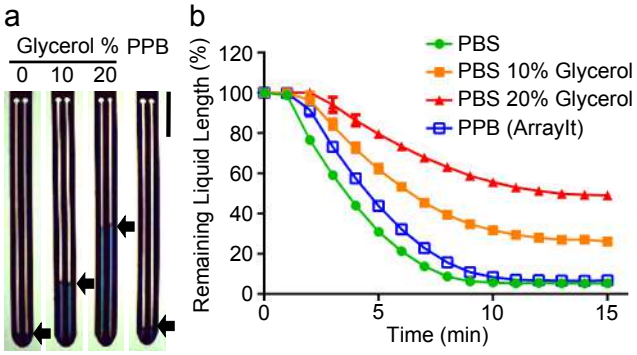

FIGURE 3.1: **Evaporation of glycerol containing printing buffers.** Pins were filled with four different printing buffers supplemented with 1 % food dye and incubated at 65 % relative humidity. **a** Representative image of the pins after 15 min of incubation. Scale bar is 2 mm. **b** Evaporation of water from the different printing buffers over 15 min shows that significant evaporation occurs in all four solutions.

Although high glycerol concentrations could entirely suppress evaporation, it was observed that 40 % glycerol diminishes the binding of antibodies to the surface of the widely used aldehyde-activated APTES silanized slides by 40 % [164]. To overcome the limitations of glycerol which negatively affect assay sensitivity, we selected 13 other hygroscopic chemicals based on potential compatibility with immunoassays: Triton X-100, PVA 9000 Da, Tween-20, sucrose, trehalose, PEG 1000 Da (PEG_{1000}), PEG 8000 Da (PEG_{8000}), DMSO, ethylene glycol (EtGly), 1,3-butanediol (1,3-But), 2, 3-butanediol (2,3-But), betaine, and magnesium sulfate (Table 3.1). Chemicals were selected not only for their potential hygroscopicity but also their known compatibility with protein assays, as well as cost and availability. Therefore, each of these chemicals was first evaluated for its ability to limit evaporation. The concentration of each additive was selected based on its solubility in PBS buffer as well as presumed compatibility with immunoassays. In this experiment, betaine was tested at a much higher concentration than previously used, and to our knowledge it is the first time that 1,3-But, 2,3-But, and magnesium sulfate were used in printing microarrays. We found seven additives that efficiently limited evaporation to 20 % or less, at 25 °C and 65 % relative humidity: PEG_{1000}, DMSO, EtGly, glycerol, 1,3-But, 2,3-But at concentrations of 50 % v/v and 4 M betaine (Fig. 3.2). The concentration of additives tested was not increased further once evaporation was efficiently limited, in order to minimize potential interference with protein immobilization and activity. On the other hand, we wanted to evaluate whether combinations of additives might be more beneficial than using a single one. To first test the effect of additive mixtures on evaporation, we mixed glycerol, DMSO, and EtGly in pairwise combinations of equal ratios, and found that mixtures of additives limited evaporation to the same degree as single additives (see Electronic Supplementary Material (ESM) Fig. C.S1).

3.3.2 Spot quality and immunoassay performance

After determining which additives effectively limit the evaporation of printing buffers, their effect on spot quality, antibody binding, and activity were studied for the individual additives, as well as their pairwise combinations (adding to a total of 28 conditions) on four slides with different surface chemistries. These slides include Schott Nexterion Slide E and Slide AL which are glass slides coated with silanes that have epoxy and aldehyde end groups and have contact angles of 52.5° and 46.8°, respectively. Xenopore's Xenobind slide is coated with a proprietary reactive aldehyde end group and has a contact angle of 61.2°. Schott Nexterion Slide H is coated with a thin polymer film with activated N-hydroxysuccinimide (NHS) groups and has a contact angle of 51.9°. Abs are covalently immobilized on all four slides by reaction of free amine groups on antibodies, either on the slide surface or inside of the hydrogel on Slide H.

TABLE 3.1: List of 14 hygroscopic additives tested for minimizing evaporation

Additive Name	Solubility (g/100 g H_2O) at 20 °C	Maximum concentration used	Chemical Structure and Formula	Vapor Pressure (mmHg)	First used in protein microarray
Triton X-100	Miscible	0.17 M (10 % v/v)	$(C_2H_4O)_nC_{14}H_{22}O$ n~9 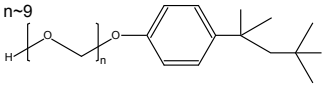	< 1.0	Tamaru *et al.* 2005 [175]
Poly(vinyl alcohol) 9-10 kDa, 80% hydrolyzed (PVA)	100	0.011 M (10 % w/v)	$(C_2H_4O)_n$ n~204-227 	Negl. [176]	Wu and Grainger 2006 [173]
Polysorbate 20 / Tween-20	Miscible	0.18 M (20 % v/v)	$C_{58}H_{114}O_{26}$ 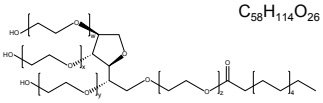	< 1.0	Xu *et al.* 2007 [177]
Sucrose	200 [178]	0.88 M (30 % w/v)	$C_{12}H_{22}O_{11}$ 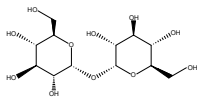	Negl.	Avseenko *et al.* 2001 [179]
Trehalose	68.9	0.88 M (30 % w/v)	$C_{12}H_{22}O_{11}$ 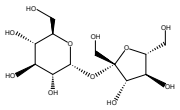	Negl.	Moerman *et al.* 2001 [180]
Polyethylene glycol 1000 Da (PEG_{1000})	80	0.5 M (50 % w/v)	$C_{2n}H_{4n+2}O_{n+1}$ n~22 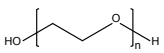	< 0.01	Lee and Kim 2002 [171][a] Wu and Grainger 2006 [173][b]
Polyethylene glycol 8000 Da (PEG_{8000})	63	0.04 M (30 % w/v)	$C_{2n}H_{4n+2}O_{n+1}$ n~181 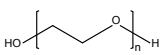	< 0.01	Wu and Grainger 2006 [173][c]
Dimethyl sulfoxide (DMSO)	Miscible	7.0 M (50 % v/v)	C_2H_6OS 	0.42	Xu *et al.* 2007 [177]
Ethylene glycol (EtGly)	Miscible	9.0 M (50 % v/v)	$C_2H_6O_2$ 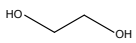	0.10	Moerman *et al.* 1999 [181]
1,3-butanediol (1,3-But)	Miscible	5.6 M (50 % v/v)	$C_4H_{10}O_2$ 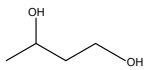	0.06	
2,3-butanediol (2,3-But)	Miscible	5.5 M (50 % v/v)	$C_4H_{10}O_2$ 	0.17	
Betaine	> 59	4.0 M (47 % w/v)	$C_5H_{11}NO_2$ 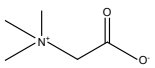	Negl.	Preininger *et al.* 2005 [170]
Magnesium sulfate	35.7 [182]	1.4 M (35.7 % w/v)	$MgSO_4$ 	Negl.	
Glycerol	Miscible	6.8 M (50 % v/v)	$C_3H_8O_3$ 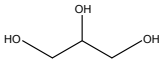	0.008	MacBeath and Schreiber 2000 [183]

Physical properties were obtained from the literature as cited, or from the manufacturer
Negl negligible
[a]PEG 200
[b]750 and 2000 were used
[c]PEG 6000 was used

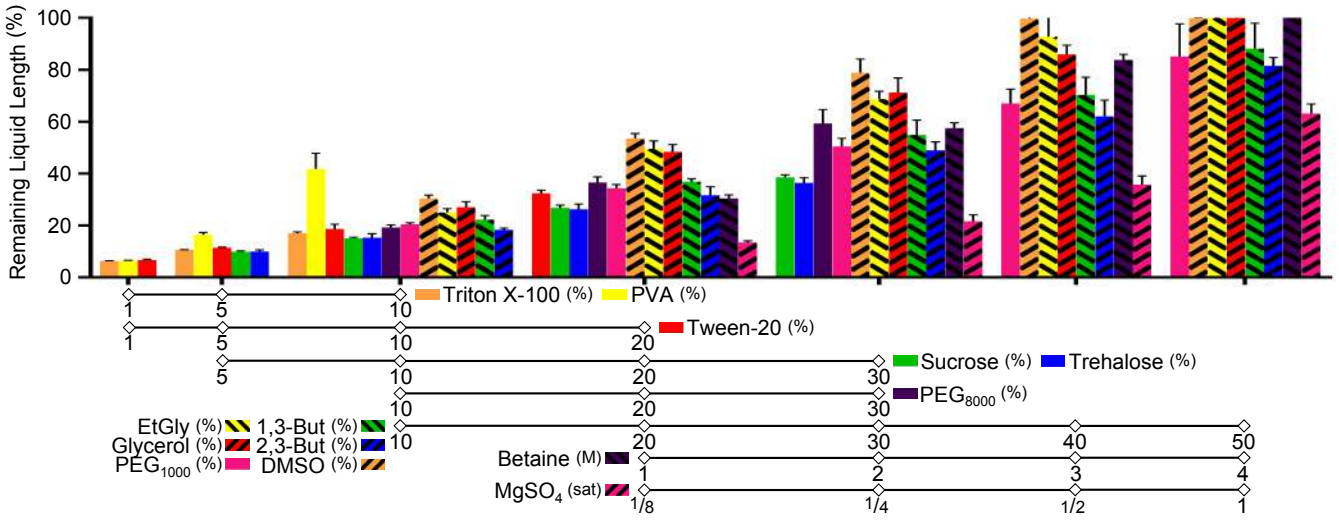

FIGURE 3.2: **Evaporation of buffers containing different additives.** Percentage length of liquid remaining in a pin after 10 min for different concentrations of various additives. The concentrations are expressed in percentage for all additives except betaine (molarity) and magnesium sulfate (level of saturation). Six additives limit evaporation to less than 20 %, namely PEG_{1000}, DMSO, EtGly, glycerol, 1,3-But, 2,3-But at a concentration of 50 % v/v, and betaine at 4 M.

Anti-goat IgG-AF647 was mixed at a concentration of 100 µg/mL in each of the 28 printing buffers. To evaluate the overall binding signal, arrays were incubated with goat IgG-AF532 as the analyte, and the fluorescence intensities quantified for the cAbs (immobilization signal) as well as the analyte (binding signal). The binding activity of the cAbs was calculated by dividing the binding signal by the immobilization signal. For comparison, we report the ratio of the signal intensities for the cAb immobilization (ESM Fig. C.S2), binding activity (ESM Fig. C.S3), and the binding signals (Fig. 3.3a–d) compared to that of 50 % glycerol on Xenobind because this additive is the most widely used in printing antibody microarrays. The most important performance metric is the capacity of each spot to bind its analyte, which constitutes the assay endpoint and only parameter being measured in practice.

The binding signal intensity was generally highest on Slide H, and was lower but homogeneous and consistent on Xenobind, while it was variable on Slide E and Slide AL (Fig. 3.3a–d). Immobilization signals on Xenobind and Slide H were again much higher than on Slide E and Slide AL. cAb binding activity was stable across all additives, suggesting that none of the additives denatured the cAbs significantly during the immobilization step. Hence, the density of immobilized antibodies on a surface was directly correlated to the binding signal, which was highest on Slide H and Xenobind.

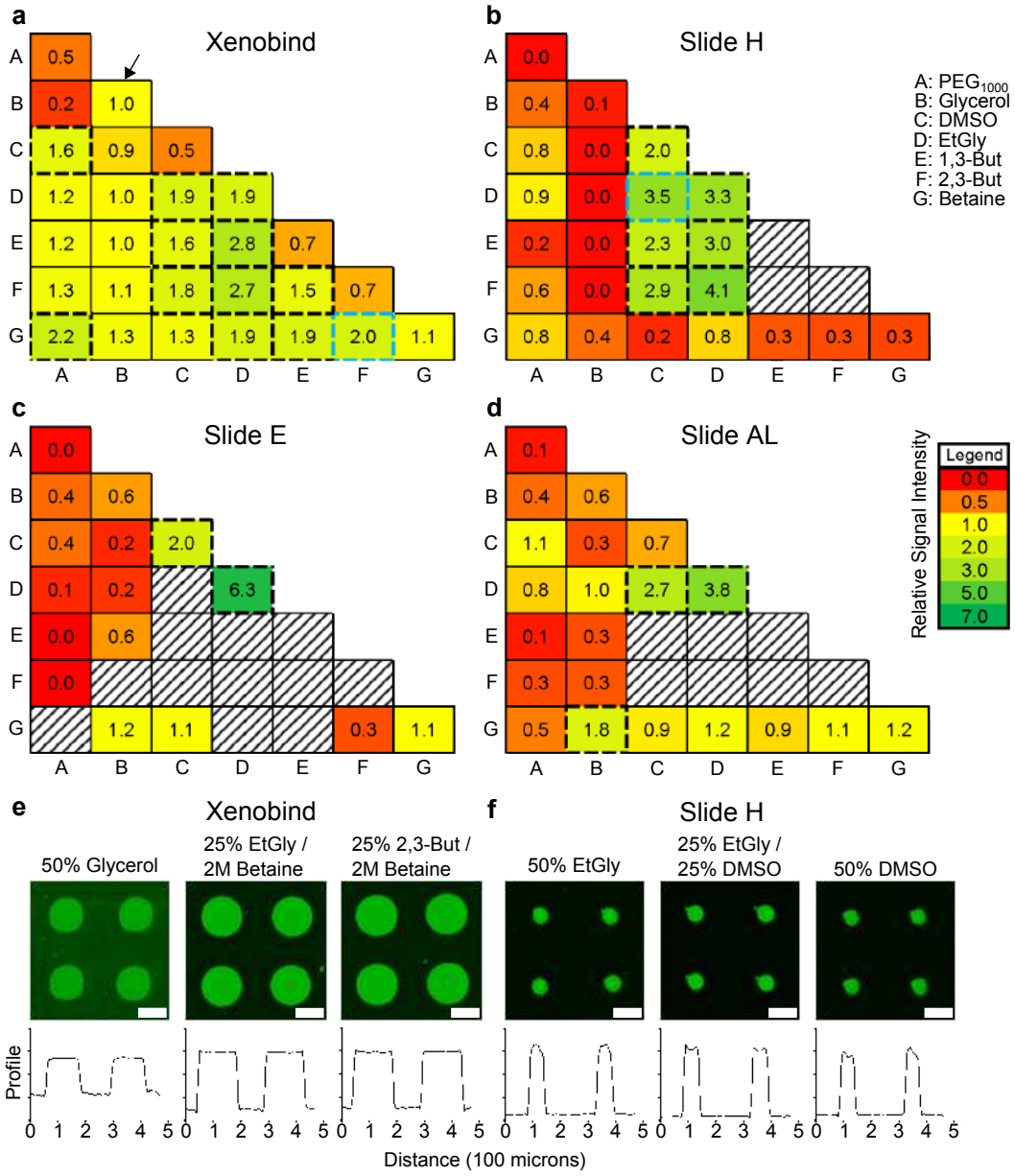

FIGURE 3.3: **Binding signal intensities of immunoassays on four different slides for 28 different printing buffer additive combinations.** Signal intensities of labeled analyte (0.1 µg/mL goat IgG-AF532) captured by anti-goat IgG on **a** Xenobind; **b** Slide H; **c** Slide E; and **d** Slide AL, and printed in different combinations of a total of 50 % v/v of additives in equal proportions (or 2 or 4 M betaine). Signals are reported relative to the signal obtained by printing with 50 % glycerol on Xenobind (arrow). Dashed outlines indicate signal values ≥ 1.5. Hatched boxes represent unquantifiable data owing to poor spot morphology or spots merging. Light blue dashed outlines on two boxes in **a** and **b** indicate the two mixtures of additives and slides that were found to be optimal on those surfaces in terms of spot morphology and binding signal intensity. Intensity profile across two spots, as shown for three different additives mixtures on **e** Xenobind and **f** Slide H. Scale bars are 100 µm.

Spot morphology (see ESM Fig. C.S4) can also affect the microarray performance and should be compatible with common automated data extraction algorithms. Poor spot morphology increases spot-to-spot and experiment-to-experiment variability [148, 172, 184]. We evaluated spot morphology by plotting the intensity profile of a cross-section of two spots (Fig. 3.3e, f and ESM Table C.S1) for all additive mixtures that yielded a binding signal greater than or equal to 1.5 times that of 50 % glycerol on Xenobind (thick dashed boxes on Fig. 3.3a–d). Spot morphology depended both on the additives and on the slide surface. All additives mixtures yielded spots with good morphology on Xenobind and Slide H, but not on Slide E and Slide AL. Whereas Slide E yielded spots with the highest fluorescence signals, the variability was greater, and the morphology was often egg-shaped resulting in inaccurate quantification data extraction software. Likewise, Slide AL produced high binding signals, but overall poor spot morphology. For these reasons, these two slide types were not considered further.

The morphology and intensity profile of the spots on Slide H and Xenobind shown in Fig. 3.3e, f were excellent with sharp edges and a constant intensity within spots (ESM Table C.S1). Three additives mixtures yielded excellent spot morphology and high binding signal on both Xenobind (betaine/EtGly, betaine/1,3-But and betaine/2,3-But) and Slide H (DMSO, EtGly, and DMSO/EtGly).

3.3.3 pH of additives mixtures

All the slides tested react with free amine groups that mediate antibody immobilization on the surface. Because amine groups are more likely to be deprotonated at high pH, and thus potentially more reactive, we tested the effect of printing buffer pH on immunoassay performance. The pI of antibodies varies from 6 to 9 [185], and we therefore prepared the six selected additives mixtures in PBS (pH 7.4) and carbonate buffers (pH 9.8). The pH of the resulting printing buffer solutions is listed in Table C.S2 in the ESM. An immunoassay was performed with the same antibodies as described earlier and printed in the three mixtures of additives found to have good performance as well as 50 % glycerol, and the immobilization and binding signals were measured. On Xenobind, there was no difference in either signals when antibodies were printed in PBS or carbonate buffers; however, on slide H, both the immobilization and binding signals were significantly decreased with carbonate buffer (ESM Fig. C.S5). Liu et al. have also reported weaker signals when using carbonate buffer on aldehyde-activated APTES slides [164]. For the slides and additives mixtures tested here, we conclude that binding of antibodies to the surface is not improved by increasing the printing buffer pH.

3.3.4 Optimization of the concentration of additives

In the experiments described above, the additives were mixed in equal ratio. The ratio of the best pair of additives identified (2,3-But/betaine for Xenobind and EtGly/DMSO for Slide H) was systematically varied to test whether the immobilization and binding signals might be further improved (Fig. 3.3). After confirming that the mixtures in different ratios still limit evaporation to below 20 % at 65 % relative humidity, we used them as printing buffers in an immunoassay as described previously, and we quantified both immobilization and binding signals. On Xenobind, the analyte binding signal increased slightly with higher concentration of 2,3-But (ESM Fig. C.S6a), and a number of combinations resulted in comparable immobilization and binding signal intensities (45 %/1 M, 45 %/1.5 M, and 35 %/1.5 M 2,3-But/betaine compared to 25 % 2,3-But/2 M betaine); however, spot morphology was deteriorated (ESM Fig. C.S6b). Therefore, 25 % 2,3-But/2 M betaine was retained as optimal additive mixture. On Slide H, a concomitant decrease of DMSO and increase in EtGly concentrations slightly increased the binding signal intensity (ESM Fig. C.S6c). Whereas 50 % EtGly yielded the highest binding signal along with good spot morphology on Slide H, spots dried out during long incubations, and therefore 15 % DMSO/35 % EtGly was selected.

3.3.5 Printing autonomy and consistency

Printing autonomy is the number of spots that can be printed following a single dip of the pin in a source well, and consistency refers to the variation in amount of antibodies delivered at each spot. Both can readily be assessed by measuring the fluorescence signal of spots printed consecutively. We expect that as a result of adding the additives that reduce evaporation a larger number of spots can be printed while maintaining a constant signal intensity. One thousand one hundred fifty-two spots were printed per single pin and a single pin loading of 20 µg/mL fluorescently labeled cAb using the two optimal buffers, and with three buffers with 10, 20, and 50 % v/v of glycerol, respectively, for comparison. A barcode at the bottom of Slide H gives a reduced printing area, and therefore only 1008 spots were printed. A lower concentration of cAb was used to avoid saturating the surface following evaporation and concentration of the reagents and antibodies in the buffer. To circumvent the possible evaporation in the source plate wells, printing was started immediately after depositing the solution in the source well plate. A full immunoassay was performed as in previous experiments.

The binding signal intensity of spots printed with 10, 20, and 50 % glycerol in PBS on Xenobind are shown in Fig. 3.4a. Evaporation of the printing buffers containing 10 and 20 % glycerol initially leads to significant increase in the amount of cAb immobilized on the surface and the analyte binding

signal as a result of concentration of the cAbs, followed by a slow decline in signal presumably due an increased concentration of glycerol resulting in a change in viscosity, a decrease in the delivered volume per spot, and decreased binding of cAbs on the surface. Spots printed with 50 % glycerol lead to good consistency, but overall low signal intensities compared to that of spots printed in 10 and 20 % glycerol.

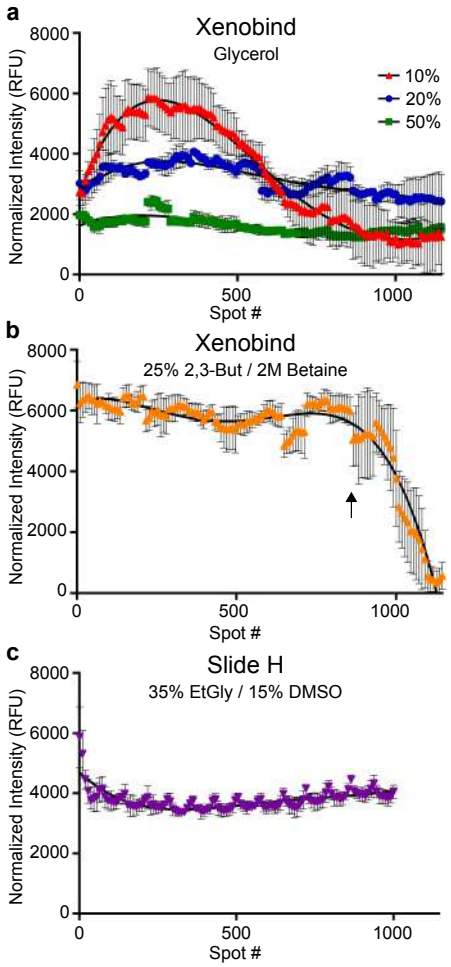

FIGURE 3.4: **Printing consistency of optimized buffers.** Binding signal intensities of 1152 spots where cAbs were consecutively printed in buffers containing **a** 10, 20, 50 % glycerol on Xenobind; **b** 25 % 2,3-But/2 M betaine on Xenobind; and **c** 35 % EtGly/15 % DMSO on Slide H. Each whole slide was printed in 45 min. Because of the bar code at the bottom of Slide H, only 1008 consecutive spots were printed. The arrow represents the spot number where two of the four pins were emptied of printing solution while printing with 25 % 2,3-But/2 M betaine on Xenobind, with the other two pins emptying shortly thereafter.

The binding signal intensity of spots printed with 25 % 2,3-But/2 M betaine on Xenobind slides is higher for the first spots than with all different concentrations of glycerol, and remains stable for about 864 spots, after which it falls off (Fig. 3.4b). These results indicate that this buffer

effectively prevents evaporation of the printing buffer, however owing to a different viscosity and surface tension, the volume deposited at each spot is higher, explaining why pins are drained more quickly. Spots printed with 35 % EtGly/15 % DMSO on Slide H also yield a high binding signal that is constant, while supporting in excess of the 1008 spots printed in this experiment (Fig. 3.4c). The higher printing autonomy is consistent with the smaller diameter, and volume, of solution deposited on this slide (see Fig. 3.3f).

The mean residual error is a measure of reproducibility and was calculated by taking the average of the difference between each spot binding signal and the mean binding signal of all spots. When printing with 10, 20, and 50 % glycerol on Xenobind, this mean residual error was 47.3, 13.7, and 13.3 %, respectively. On the other hand when printing with 25 % 2,3-But/2 M betaine on Xenobind or 35 % EtGly/15 % DMSO on Slide H, it was decreased to 5.9 % on both slides. These results demonstrate the benefit of using the optimized buffers on printing reproducibility while improving the signal intensity.

Printing buffers are stored in source well plates during printing, which can last for extended periods of time. Because of the low dead volume of quill pins, 6 µL of solution is largely sufficient for printing; however, such small volume may rapidly evaporate before it is used for printing. To evaluate the benefit of additives on the evaporation from the source well plate, printing of fluorescently labeled cAb was conducted at 2 h intervals over a period of 6 h while loading the pin from the same well, and proceeding with an immunoassay as previously performed. This experiment was not performed with a pin contact printer, but with an inkjet printer that uses a nozzle, which is closed and only open to the air at the tip, thus effectively eliminating evaporation while printing. Changes in signal intensities can therefore be ascribed to evaporation of printing buffers in the source well plate. Printing buffers with 10 and 20 % glycerol as well as 25 % 2,3-But/2 M betaine were used (ESM Fig. C.S7) on Xenobind. As expected, the printing buffers with low glycerol concentrations resulted in an increase in signal intensity over time that are consistent with evaporation, roughly tripling and doubling for 10 and 20 % glycerol, respectively. The binding signal obtained when using 25 % 2,3-But/2 M betaine was the highest as a result of increased immobilization of cAbs to the surface, and the mean of all spots within a slide varied only by 4.2 % between slides. This experiment also served to confirm the compatibility of the additives and buffers with inkjet printing. Indeed, the printing buffer containing 2,3-But and betaine has recently been used with inkjet printing in producing high-quality microarrays for SENSIA [186], a microarray platform for immunoassays that does not require the use of a fluorescent scanner.

3.3.6 Sandwich immunoassay binding curves

To further test the effect of the optimal additives, full sandwich immunoassays against FAS, IL-1β, and TFN-RII were carried out. The assays were performed in a multiplexed format, but unlike our recent work on the antibody colocalization microarray (ACM) [17], all dAbs were mixed in a solution prior to application to the microarray to avoid confounding effects from the evaporation of the dAb printing buffer used in ACM; we had established in previous experiments that these dAbs do not cross-react when applied in a mixed solution [17]. cAbs were printed at five different concentrations from 25 to 400 µg/mL on Xenobind and Slide H using the optimal buffer for each slide. We also printed cAbs in 50 % glycerol buffer on Xenobind only as a comparison because this buffer is not compatible with Slide H. After printing, each slide was incubated with a mixture of recombinant antigens in a series dilution, followed by the mixture of dAbs. Standard curves for each antigen and printing buffers were fitted (Fig. 3.5), and the LOD and quantification range were calculated for each curve.

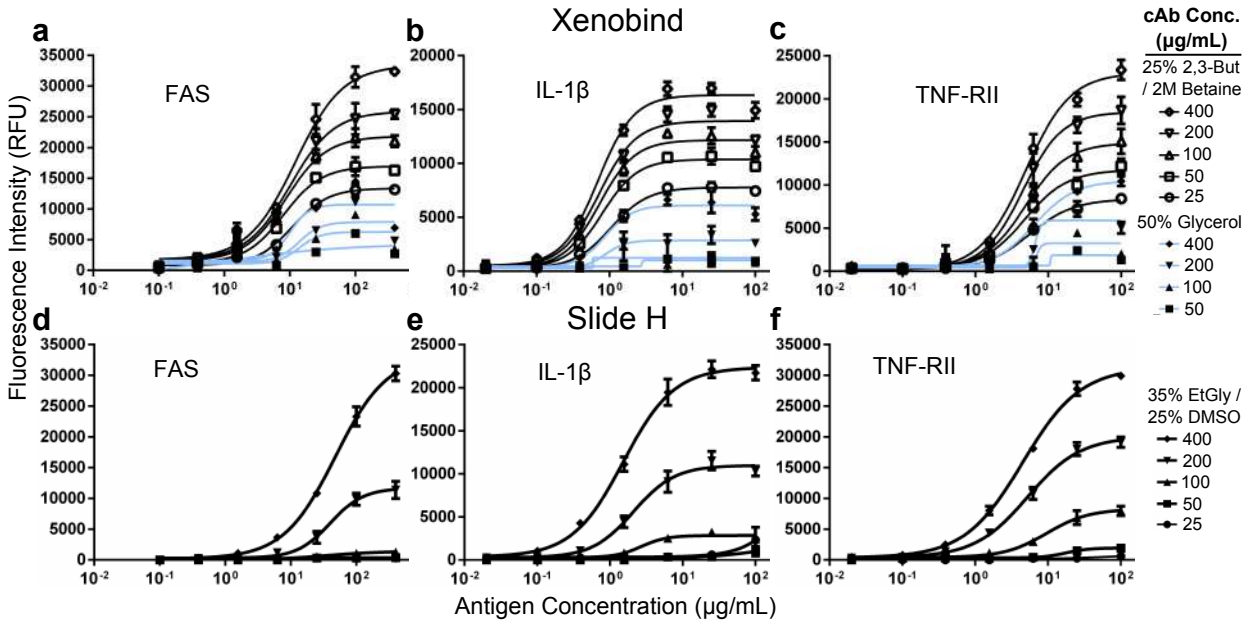

FIGURE 3.5: **Three-plex sandwich immunoassays with optimized buffers on Xenobind and Slide H.** Microarrays were prepared by printing cAbs against FAS, IL-1β, and TNF-RII at different concentrations on **a**–**c** Xenobind and **d**–**f** slide H using the optimized buffers, and compared to 50 % glycerol on Xenobind.

The quantification range of the binding curves was higher using the optimized buffers with the selected additives, and the signal increased markedly with increasing concentrations of the cAbs for both buffers, up to the highest concentration. Interestingly, cAbs printed on Xenobind at 25 µg/mL in 25 % 2,3-But/2 M betaine gave a similar signal than when printed at 400 µg/mL

with 50 % glycerol in PBS, suggesting that glycerol partially inhibits the binding of antibody on this surface. The LOD for all three analytes was improved from 1.6- to 5.9-fold (Table 3.2), while the LOD on Slide H was the lowest, possibly as a result of the 3D nature of the hydrogel surface, and consistent with prior studies [187, 188]. However, further studies using samples with complex matrices such as cell extracts or serum are needed to confirm the benefits of this surface in practice. These results demonstrate that the optimized printing buffers on Xenobind and Slide H improve the assay performance.

TABLE 3.2: Summary of printing buffer performance. Performance of the optimized printing buffers compared to that of various concentrations of glycerol in PBS in terms of mean residual error, lower limit of detection, and quantification range for three different protein standard curves.

Slide	Printing buffer	Mean residual error	Analyte	Lower LOD (ng/mL)	Quantification range (log)
Xenobind	10 % glycerol	47.3 %	N/A		
	20 % glycerol	13.7 %			
	50 % glycerol	13.3 %	FAS	7.0	1.39
			IL-1β	1.0	0.90
			TNF-RII	1.2	1.50
	25 % 2,3-But/2 M betaine	5.9 %[a]	FAS	2.7	1.73
			IL-1β	0.7	1.09
			TNF-RII	0.6	2.04
Slide H	35 % EtGly/15 % DMSO	5.9	FAS	1.4	2.04
			IL-1β	0.3	1.92
			TNF-RII	0.2	2.29

[a]Mean residual error calculated on the first 864 consecutive points after which the pins were empty of printing solution.

3.4 Discussion

We tested 14 hygroscopic chemicals as buffer additives for antibody spotting at 65 % relative humidity and tested 28 pairwise combinations of the seven most promising additives on four different slide surfaces. Using spot morphology and immunoassay binding signal as criteria, we identified 25 % 2,3-But/2 M betaine in PBS for use with Xenobind slides and 35 % EtGly/15 % DMSO in PBS for use with Nexterion Slide H. Nexterion Slide E and Slide AL were found to lead to inconsistent spot morphologies with many additives. The two optimized buffers led to a significant improvement in printing reproducibility, while also improving sandwich immunoassay sensitivity and quantification range. The increase in sensitivity of these two printing buffers compared to 50 %

glycerol might be due to their lower viscosity, thereby allowing more proteins to properly come in contact with the surface to bind during the limited incubation time. In addition, by using buffer additives, the spot morphology and printing consistency of pin contact-printed microarrays is as good, if not better, than that obtained by inkjet printing [147]. Whereas some prior studies found that overall binding activity tailed off for higher density of cAb immobilization due to crowding on the surface [189], even at the highest concentration of 400 µg/mL of cAb in the printing solution, no such effects were observed here. Overall, Slide H gave the best LOD and quantification range while yielding smaller spots; however, these advantages are counterbalanced by a high cost, need for storage at −20 °C with desiccant, and sensitivity to humidity which may reduce performance on long spotting runs. The choice of slide should be made in consideration of the particular application and circumstances.

There are additional hygroscopic chemicals that might be beneficial to antibody printing, as well as different slides with various surface chemistries. Considering that antibody binding was observed subsequent to spotting with all seven hygroscopic chemicals tested at a concentration of 50 % in buffer, expanding the range of chemicals, and increasing the concentration of additives, might improve assay performance further. Several of the chemicals that were tested initially but not studied in more depth because the lack of hygroscopic activity, as well as any other chemical with beneficial properties, could be tested in combination with the hygroscopic additives identified here. Such chemicals could include ones beneficial to microarray spot morphology such as sucrose [190] and PVA [173], or ones known to protect antibodies against freezing or dehydration such as trehalose [191] or sorbitol [185].

Here, only a small set of additives was tested, and only in pairwise combinations, which greatly improved printing reproducibility. We expect that assay sensitivity may be improved further by testing mixtures of three additives and by varying simultaneously other assay parameters. Provided that the working ranges for all additives are defined, large number of parameters could be evaluated simultaneously using design of experiment approaches such has the Taguchi method which we previously adopted for the optimization of antibody microarrays [192].

For assay platforms such as the ACM, it will also be necessary to optimize the buffer and additives for printing the dAbs atop of the cAb. Following dAb printing, binding of dAb to the captured antigen must be ensured, and hence additives may not interfere with antigen recognition and binding. At the same time, evaporation must be minimized as well. Thus, a new set of experiments is needed to identify the optimal buffer formulation for colocalized spotting of dAbs. Overall, this study shows that printing buffer formulations need to be optimized and tailored for a specific slide surface chemistry, although preliminary results show that 25 % 2,3-But/2 M betaine seems to perform very well on a number of other slide such as PolyAn 2D and 3D Epoxy, as

well as 2D Aldehyde slides. It was also found that many different chemicals, mixed at very high concentrations, are suitable as additives for printing antibodies without significant loss of antibody binding and activity during subsequent assays; the results suggest that a large number of other chemicals previously not tested for immunoassays may in fact be beneficial.

In this study, we used a pin printer to test mixtures of additives to the printing buffer because it is more sensitive to evaporation of solutions than an inkjet printer. We confirmed that the best mixtures of additives to the printing buffer are compatible with both pin and inkjet printers. In the future, we hope that additives will be used to improve assay performance and reproducibility of not only antibody microarrays but also DNA microarrays and microarrays used in MALDI, where evaporation of spots has recently been identified as a challenge when incubating enzymes for digestion of proteins on spots [193].

Supporting Information

Additional information as noted in the text. This material is available in appendix C.

Acknowledgements

We wish to thank Ayokunle Olanrewaju for his helpful comments on the manuscript, and the National Sciences and Engineering Research Council (NSERC) of Canada, the Canadian Institute of Health Research (CIHR), and the Canadian Cancer Society (CCS) for funding. DJ acknowledges a Canadian Research Chair (CRC), and VL the NSERC-Collaborative Research and Training Experience (NSERC-CREATE) Integrated Sensors Systems program for support.

Conflict of interest

The authors declare that they have no conflict of interest.

References

17. Pla-Roca, M., Leulmi, R. F., Tourekhanova, S., Bergeron, S., Laforte, V., Moreau, E., Gosline, S. J. C., Bertos, N., Hallett, M., Park, M. & Juncker, D. Antibody colocalization microarray: a scalable technology for multiplex protein analysis in complex samples. *Molecular & Cellular Proteomics* **11,** M111.011460 (2012).

146. Bergeron, S., Laforte, V., Lo, P. S., Li, H. & Juncker, D. Evaluating mixtures of 14 hygroscopic additives to improve antibody microarray performance. *Analytical and Bioanalytical Chemistry* **407,** 8451–8462 (2015).

147. Barbulovic-Nad, I., Lucente, M., Sun, Y., Zhang, M., Wheeler, A. R. & Bussmann, M. Bio-microarray fabrication techniques–a review. *Critical Reviews in Biotechnology* **26,** 237–59 (2006).

148. Ellington, A. A., Kullo, I. J., Bailey, K. R. & Klee, G. G. Antibody-based protein multiplex platforms: technical and operational challenges. *Clinical Chemistry* **56,** 186–93 (2010).

149. Dufva, M. & Christensen, C. B. V. Optimization of oligonucleotide sets for DNA microarrays. *Methods in Molecular Biology* **381** (ed Rampal, J. B.) 93–103 (2007).

150. Kricka, L. J. & Master, S. R. Quality control and protein microarrays. *Clinical Chemistry* **55,** 1053–1055 (2009).

151. Deegan, R. D., Bakajin, O., Dupont, T. F., Huber, G., Nagel, S. R. & Witten, T. A. Capillary flow as the cause of ring stains from dried liquid drops. *Nature* **389,** 827–829 (1997).

152. Angulo, J. Polar Modelling and Segmentation of Genomic Microarray Spots Using Mathematical Morphology. *Image Analytical Stereology* **27,** 107–124 (2008).

153. Safavieh, R., Pla-Roca, M., Qasaimeh, M. A., Mirzaei, M. & Juncker, D. Straight SU-8 pins. *Journal of Micromechanics and Microengineering* **20,** 055001–055009 (2010).

154. Laforte, V., Olanrewaju, A. & Juncker, D. *Low-cost , high liquid volume silicon quill pins for robust and reproducible printing of antibody microarrays* in *MicroTAS: miniaturized systems for chemistry and life sciences* (Chemical and Biological Microsystems Society (CBMS), Freiburg, Germany, 2013), 485–487.

155. McQuain, M. K., Seale, K., Peek, J., Levy, S. & Haselton, F. R. Effects of relative humidity and buffer additives on the contact printing of microarrays by quill pins. *Analytical Biochemistry* **320,** 281–291 (2003).

156. Gutmann, O., Kuehlewein, R., Reinbold, S., Niekrawietz, R., Steinert, C. P., de Heij, B., Zengerle, R. & Daub, M. Fast and reliable protein microarray production by a new drop-in-drop technique. *Lab on a Chip* **5,** 675–81 (2005).

157. Hartmann, M., Sjödahl, J., Stjernström, M., Redeby, J., Joos, T. & Roeraade, J. Non-contact protein microarray fabrication using a procedure based on liquid bridge formation. *Analytical and Bioanalytical Chemistry* **393,** 591–598 (2009).

158. Liberski, A., Zhang, R. & Bradley, M. Inkjet fabrication of polymer microarrays and grids - Solving the evaporation problem. *Chemical Communications* **3,** 334–336 (2009).

159. Sun, Y., Zhou, X. & Yu, Y. A novel picoliter droplet array for parallel real-time polymerase chain reaction based on double-inkjet printing. *Lab on a Chip* **14,** 3603–3610 (2014).

160. Olle, E. W., Messamore, J, Deogracias, M. P., McClintock, S. D., Anderson, T. D. & Johnson, K. J. Comparison of antibody array substrates and the use of glycerol to normalize spot morphology. *Experimental and Molecular Pathology* **79,** 206–209 (2005).

161. González-González, M., Bartolome, R., Jara-Acevedo, R., Casado-Vela, J., Dasilva, N., Matarraz, S., García, J., Alcazar, J. A., Sayagues, J. M., Orfao, A. & Fuentes, M. Evaluation of homo- and hetero-functionally activated glass surfaces for optimized antibody arrays. *Analytical Biochemistry* **450,** 37–45 (2014).

162. Zuo, P., Zhang, Y., Liu, J. & Ye, B. C. Determination of β-adrenergic agonists by hapten microarray. *Talanta* **82,** 61–66 (2010).

163. Rodríguez-Seguí, S. A., Pons Ximénez, J. I., Sevilla, L., Ruiz, A., Colpo, P., Rossi, F., Martínez, E. & Samitier, J. Quantification of protein immobilization on substrates for cellular microarray applications. *Journal of Biomedical Materials Research - Part A* **98,** 245–256 (2011).

164. Liu, Y. S., Li, C. M., Yu, L. & Chen, P. Optimization of printing buffer for protein microarrays based on aldehyde-modified glass slides. *Frontiers in Bioscience* **12,** 3768–3773 (2007).

165. Ruwona, T. B., McBride, R., Chappel, R., Head, S. R., Ordoukhanian, P., Burton, D. R. & Law, M. Optimization of peptide arrays for studying antibodies to hepatitis C virus continuous epitopes. *Journal of Immunological Methods* **402,** 35–42 (2014).

166. Monroe, M. R., Reddington, A. P., Collins, A. D., LaBoda, C., Cretich, M., Chiari, M., Little, F. F. & Ünlü, M. S. Multiplexed method to calibrate and quantitate fluorescence signal for allergen-specific IgE. *Analytical Chemistry* **83,** 9485–9491 (2011).

167. Hegde, P., Qi, R., Abernathy, K., Gay, C., Dharap, S., Gaspard, R., Hughes, J. E., Snesrud, E., Lee, N. & Quackenbush, J. A concise guide to cDNA microarray analysis. *BioTechniques* **29,** 548–62 (2000).

168. Diehl, F., Grahlmann, S., Beier, M. & Hoheisel, J. D. Manufacturing DNA microarrays of high spot homogeneity and reduced background signal. *Nucleic Acids Research* **29,** E38 (2001).

169. Csonka, L. N., Ikeda, T. P., Fletcher, S. A. & Kustu, S. The accumulation of glutamate is necessary for optimal growth of *Salmonella typhimurium* in media of high osmolality but not induction of the proU operon. *Journal of Bacteriology* **176,** 6324–6333 (1994).

170. Preininger, C., Sauer, U., Dayteg, J. & Pichler, R. Optimizing processing parameters for signal enhancement of oligonucleotide and protein arrays on ARChip Epoxy. *Bioelectrochemistry* **67,** 155–162 (2005).

171. Lee, C.-S. & Kim, B.-G. Improvement of protein stability in protein microarrays. *Biotechnology Letters* **24,** 839–844 (2002).

172. Rickman, D. S., Herbert, C. J. & Aggerbeck, L. P. Optimizing spotting solutions for increased reproducibility of cDNA microarrays. *Nucleic Acids Research* **31,** e109 (2003).

173. Wu, P. & Grainger, D. W. Comparison of hydroxylated print additives on antibody microarray performance. *Journal of Proteome Research* **5,** 2956–2965 (2006).

174. *Glycerine : an overview* tech. rep. (The Soap and Detergent Association, New York, NY, 1990), 1–27.

175. Tamaru, S.-I., Yamaguchi, S. & Hamachi, I. Simple and Practical Semi-wet Protein/Peptide Array Utilizing a Micelle-mixed Agarose Hydrogel. *Chemistry Letters* **34,** 294–295 (2005).

176. Finch, C. A. *Polyvinyl alcohol, properties and applications* (John Wiley & Sons, Ltd, New York, NY, 1973).

177. Xu, B.-J., Jin, Q.-H. & Zhao, J.-L. A Novel Method of Producing Protein Microarray for Immunoassay. *Chinese Journal of Analytical Chemistry* **35,** 153–158 (2007).

178. *The Merck Index: An Encyclopedia of Chemicals, Drugs, and Biologicals* 15th ed. (ed O'Neil, M.) (Merck Sharp & Dohme Corp., Whitehouse Station, NJ, 2014).

179. Avseenko, N. V., Morozova, T. Y., Ataullakhanov, F. I. & Morozov, V. N. Immobilization of proteins in immunochemical microarrays fabricated by electrospray deposition. *Analytical Chemistry* **73,** 6047–52 (2001).

180. Moerman, R., Frank, J., Marijnissen, J. C. M., Schalkhammer, T. G. M. & van Dedem, G. W. K. Miniaturized electrospraying as a technique for the production of microarrays of reproducible micrometer-sized protein spots. *Analytical Chemistry* **73,** 2183–2189 (2001).

181. Moerman, R., van den Doel, L. R., Picioreanu, S., Frank, J., Marijnissen, J. P. A., van Dedem, G. W. K., Hjelt, K. H., Vellekoop, M. J., Sarro, P. M. & Young, I. T. *Microinjection of sigma-D-glucose standards and Amplex Red reagent on microarrays* in *Micro- and Nanofabricated Structures and Devices for Biomedical Environmental Applications II* (ed Ferrari, M.) **3606** (International Society for Optics and Photonics, San Jose, CA, USA, 1999), 119–128.

182. Haynes, W. N. *CRC Handbook of Chemistry and Physics* 95th ed. (CRC Press, 2014).

183. MacBeath, G. & Schreiber, S. L. Printing proteins as microarrays for high-throughput function determination. *Science* **289,** 1760–1763 (2000).

184. Ressine, A., Marko-Varga, G. & Laurell, T. Porous silicon protein microarray technology and ultra-/superhydrophobic states for improved bioanalytical readout. *Biotechnology Annual Review* **13,** 149–200 (2007).

185. Mueller, M., Loh, M. Q., Tee, D. H., Yang, Y. & Jungbauer, A. Liquid formulations for long-term storage of monoclonal IgGs. *Applied Biochemistry and Biotechnology* **169,** 1431–1448 (2013).

186. Zhou, G., Bergeron, S. & Juncker, D. High-performance low-cost antibody microarrays using enzyme-mediated silver amplification. *Journal of Proteome Research* **14,** 1872–1879 (2015).

187. Wingren, C., Ingvarsson, J., Dexlin, L., Szul, D. & Borrebaeck, C. A. K. Design of recombinant antibody microarrays for complex proteome analysis: choice of sample labeling-tag and solid support. *Proteomics* **7,** 3055–3065 (2007).

188. Guilleaume, B., Buness, A., Schmidt, C., Klimek, F., Moldenhauer, G., Huber, W., Arlt, D., Korf, U., Wiemann, S. & Poustka, A. Systematic comparison of surface coatings for protein microarrays. *Proteomics* **5,** 4705–4712 (2005).

189. Zhao, X., Pan, F., Cowsill, B., Lu, J. R., Garcia-Gancedo, L., Flewitt, A. J., Ashley, G. M. & Luo, J. Interfacial immobilization of monoclonal antibody and detection of human prostate-specific antigen. *Langmuir* **27,** 7654–7662 (2011).

190. Wolter, A., Niessner, R. & Seidel, M. Preparation and characterization of functional poly(ethylene glycol) surfaces for the use of antibody microarrays. *Analytical Chemistry* **79,** 4529–4537 (2007).

191. Delehanty, J. B. & Ligler, F. S. A Microarray Immunoassay for Simultaneous Detection of Proteins and Bacteria. *Analytical Chemistry* **74,** 5681–5687 (2002).

192. Luo, W., Pla-Roca, M. & Juncker, D. Taguchi design-based optimization of sandwich immunoassay microarrays for detecting breast cancer biomarkers. *Analytical Chemistry* **83,** 5767–5774 (2011).

193. Küster, S. K., Pabst, M., Zenobi, R. & Dittrich, P. S. Screening for protein phosphorylation using nanoscale reactions on microdroplet arrays. *Angewandte Chemie - International Edition* **54,** 1671–1675 (2015).

CHAPTER 4

Improving ACM reproducibility with calibration

Preface

Background and objectives

Having optimized printing buffers to print spots with high reproducibility and sensitivity, the resulting performance for small-scale (4-8 slides) experiments was very good. We noticed that for mid-scale and large-scale experiments, reproducibility degraded, and therefore the next step was to address sources of variability which seemed to increase in importance with the number of slides and samples being measured in experiments.

Reproducibility issues of the ACM platform in large-scale experiments was preventing us from performing experiments with precious, low-volume clinical samples already collected. Without a way to reduce variability within large-scale experiments down to an acceptable level, we simply could not use the ACM to measure more than a hundred proteins in hundreds of samples as we did in this chapter and chapters 5 and 6. We had to 1) optimize assay steps which contributed to variability, 2) identify a proper calibrant using a well-defined set of criteria, 3) identify the mathematical relationship between the calibrant and assay signals, since we knew it was not a linear relationship, and 4) implement a way to calibrate data in large-scale experiments, which turned out to be a lot more complex than initially thought.

Challenges and encountered problems

We first attempted to implement normalization/calibration methods using a fluorescently-labeled spiked antibody added to capture antibodies, but quickly realized that there were several problems: 1) the presence of the calibrant led to significantly more protein being quantified due to cross-reactivity and 2) our method of calibrating by simply dividing fluorescence values did not reliably lead to a better reproducibility, suggesting that the relationship between calibrant and assay signal was not linear.

The timing of the optimizations experiments was critical. Our library of antibodies and antigens was getting less and less fresh by the day while awaiting to be used in large-scale experiments. Unfortunately we ran into quality problems with the PolyAn 2D Aldehyde slides, and we had no choice but to await new batches of slides from the manufacturer. This led to some of the standard curves having sub-optimal performance in this chapter and chapters 5 and 6, leading to some samples' proteins being left unquantified because their signal intensity was greater than the top plateau of their standard curves.

One major hurdle that I faced was the requirement for a completely new analysis of all the data. All previous analysis was performed using Microsoft Excel and GraphPad Prism, which requires the manual input of data and was sufficient for analyzing experiments measuring a few proteins and a few samples, without calibration. However the analysis of large-scale experiments measuring more than a hundred proteins and hundreds of samples combined with the data calibration which required to calculate 20-50 times more standard curves simply required a more automated, efficient way to analyze data. After much deliberation, I chose to convert the whole analysis pipeline to R, an open-source language for which many libraries used in bioinformatics are available. Many months were spent writing complex code, and debugging a large amount of code was no small feat. Final scripts of code took days to run.

The resulting calibration algorithm presented in this chapter was performant enough to improve reproducibility of results, however improvements could have been made as described in the chapter. These improvements were not implemented because it would have taken months of writing additional code and testing, with the ever present risk of introducing bugs in the code. There was simply no time for further improvements.

Reference

This chapter was written with the intention to submit to the journal *Analytical Chemistry* in the near future.

Multiple fluorescent calibrants improve antibody microarrays reproducibility

Veronique Laforte[1,2,3], Jack Mouhanna[1,3] and David Juncker[1,2,3,*]

Affiliations

[1] Department of Biomedical Engineering, McGill University, McGill University,
3775 University Street, Montreal, Quebec, Canada H3A 2B4
[2] Department of Neurology and Neurosurgery, McGill University, McGill University,
3801 University Street, Montreal, Quebec, Canada H3A 2B4
[3] McGill University and Genome Québec Innovation Center, McGill University,
740 Dr. Penfield Avenue, Montreal, Quebec, H3A 0G1

Abstract

The antibody colocalization microarray (ACM) is a cross-reactivity free antibody microarray that can measure over 100 proteins simultaneously in 16 samples probed in 16 subarrays per slide, while requiring two printing rounds. The reproducibility of antibody microarrays constitutes a weakness of microarrays relative to single protein assays, and is further exacerbated in the ACM which requires slow printing with silicon quill pins. Here, we investigate local and systemic sources of variability in the ACM and propose an improved experimental workflow and a new calibration method to improve reproducibility. First, trehalose is introduced as a protective agent which was found to minimize antibody degradation seen during long periods of time in the assay where spots are left to dry. Degradation was improved by $> 70\,\%$ but coating with trehalose led to greater local variability of technical replicates spots due to the presence of trehalose microcrystals. Therefore printing high-variability antibodies first is suggested to mitigate this variability due to the degradation of molecules in the dry state. Next, to compensate for local and systemic sources of variation such as slide surface variability, fluorescence degradation and time before spotting, we introduce the use of multiple calibrant molecules printed alongside or with capture antibodies (cAbs). We

compared goat anti-rabbit antibody conjugated to Alexa Fluor 555 (GAR-AF555) bovine-serum albumin conjugated to Alexa Fluor 555 (BSA-AF555), BSA-AF647 and AF555-hydrazide and found that BSA-AF555 most accurately reflected local variation in the quantity of cAbs on the surface when printed in low concentration with every cAb. We also chose to print biotinylated GAR antibody spiked with BSA-AF555 to compensate for systemic variations in streptavidin incubation and fluorophore degradation, as this molecule closely resembles the detection antibodies (dAbs) used in the assay. The mathematical relationship between BSA-AF555 and assay signals was found to be linear following log transformation of both fluorescence signals, with a slope that requires experimental estimation and an intercept that is related to antigen concentration. We compared methods for estimating calibration slopes within each experiment, and propose simple experimental layout rules that allow data calibration and verification of reproducibility improvement. Following ACM protocol optimization, the median reproducibility of two large-scale (36 and 48 slides) experiments measuring 103 proteins was improved by an average of 25 %. While the methods proposed here help improve the ACM reproducibility, they can be applied to other protein or antibody microarrays as calibrants are printed during the cAb printing step, and thereby improve the reproducibility of large-scale research and clinical studies.

Keywords: antibody colocalization microarray · trehalose · fluorophores · calibration · normalization · reproducibility

Abbreviations

Ab	Antibody
ACM	Antibody colocalization microarray
AF	Alexa Fluor
Ag	Antigen
Alg	Algorithm
Ang1	Angiopoietin 1
AR	Accuracy range
BSA	Bovine serum albumin
cAb	Capture antibody
CSE	Calibration slope estimation
CV	Coefficient of variation (%)
dAb	Detection antibody
ELISA	Enzyme-linked immunosorbent assay
Eq	Equation
GAM	Goat anti-mouse
GAR	Goat anti-rabbit
GAR-b	Goat anti-rabbit biotin-XX
h-AF555	Alexa Fluor 555 hydrazide
HGF-R	Hepatic growth factor receptor
IgG	Immunoglobulin G
LOD	Limit of detection
MCP4	Monocyte chemoattractant protein 4
MSA	Multiplexed sandwich assay
pnCSF	Pooled normal cerebrospinal fluid
pnPlasma	Pooled normal EDTA plasma
pnSerum	Pooled normal serum
PPD	Per-protein dilution
OM	Order of magnitude
PBS	Phosphate-buffered saline
PBST	Phosphate-buffered saline with 0.1 % Tween-20
QR	Quantification range
RH	Relative humidity
SC	Standard curve
SI	Supplementary information
Strept	Streptavidin
VEGFR2	Vascular endothelial growth factor receptor 2

4.1 Introduction

Antibody microarrays are used in research to measure dozens of proteins in small volumes of precious samples, thereby gaining more knowledge than the "gold standard" single-protein enzyme-linked immunosorbent assay (ELISA) [138] for the same amount of sample. They have the potential to get a broad view on the health status of patients by measuring hundreds to thousands of proteins, and to arrive at accurate clinical conclusions by analyzing hundreds to thousands of patients within single experiments. Reproducibility of their measurements is critical in arriving at accurate conclusions about clinical questions. Compared to ELISA, conventional antibody microarrays suffer from cross-reactivity of reagents due to mixing of detection antibodies (dAbs) which can lead to false positive measurements [17], and greater variability due to the complexity of assays. Reproducibility issues with antibody microarrays is well known as a factor that limits the adoption of the technology in academia, and the poor translation of findings into FDA-approved clinical biomarkers [150, 194–197].

Very few studies using antibody microarrays report reproducibility within their assays, since most of them do not use replicate samples from which reproducibility can be calculated. When reported, reproducibility values are often calculated using separate experiments with very small samples size (11 to 40 samples reported) [198–201], which may not reflect reproducibility seen in large-scale experiments with hundreds of samples. Many commercial antibody microarray platforms exist, such as the Quantibody® from RayBio Tech, for which the company claims assay coefficients of variation of <20 %. Abnova claims coefficients of variation of 5-10 % for their antibody microarrays, but no experimental details are provided for how this reproducibility was measured. In spite of the effort put forth in providing a "Minimum Information about a Microarray" (MIAME) [202] guideline which includes the use of replicate (reference) samples and where they are located within the experimental layout, users of commercial arrays often do not report measured reproducibility in their experiment. To the best of our knowledge, we know of a single study that quantified the variability of measurements across multiple sites in a protein microarray platform that measures IgE in samples. The authors found an average intra-site reproducibility of 17.3 %, however the experiments performed included only 11 samples [201]. Using the same microarray platform, a greater coefficient of variation of 22.9 % was measured with 29 human serum samples, indicating that variability increases with the number of samples measured [203]. We also found that reproducibility was deteriorated in large-scale experiments measuring several hundreds of samples compared to small-scale experiments measuring 60 to 70 samples, preventing us from publishing data from these large-scale experiments because of the unreliability of protein measurements obtained.

The antibody colocalization microarray (ACM) avoids cross-reactivity and therefore gives

more accurate data by physically separating dAbs with a second round of printing on top of the corresponding capture antibodies (cAbs), however the addition of a second round of printing introduces another source of variability to the assay [17]. This is exacerbated by the fact that the ACM prints spots using silicon quill pins, which allows for the great positional accuracy required to precisely print dAbs on top of cAbs, but is a slow process. The SnapChip™ was developed to circumvent the need for a microarrayer during the assay by pre-printing cAbs and dAbs on separate microarray slides and bringing them in contact during the assay in order to transfer dAbs on top of cAbs [141–143]. This method significantly reduces assay time and variability associated with slides waiting for dAb spots to be printed, however the density of spots is 75 % less than that achieved with the ACM due to slight misalignments when the cAb and dAb microarrays are brought together. Since all other steps (cAb printing, washing, reagent loadings, scanning) are the same as the ACM, variability that stems from these steps is similar as for the ACM. Printing time using silicon quill pins is proportional to the number of slides printed and can last up to 36 h in the case of a large-scale experiment using our setup (48 slides, 16 subarrays per slide, four quill pins). Accordingly, reproducibility of ACM assays worsens with increasing number of slides with the result that the precision of protein measurement is not usable in large-scale experiments.

Assay optimization is necessary to improve reproducibility [195], however in many cases it is not sufficient to lower variability to an acceptable level, and therefore calibration (also called normalization) has been used to further address local and systemic sources of variability. Traditionally, calibrants are samples containing a mixture of antigens (Ags) at known concentrations, diluted serially, and whose resulting fluorescence intensity is used as a standard curve to derive protein concentrations in samples by interpolation. These calibrants can also be called standards, and serve to translate spots fluorescence intensity into a protein concentration or quantity in any given sample. However, calibrants can also be molecules added to assays, whose fluorescence signal intensity varies in response to a given source of variability, and can be used to decrease the source of variability's effect on the assay signal fluorescence. In this manuscript, we use this definition of calibrant.

Four main methods of calibration or normalization have been used in the past. Spiking a calibrant with cAbs, or probing cAbs before or after the assay have been used to address local sources of variability which stems from the microarray slide surface coating. Other methods such as spiking a calibrant in samples, printing a positive control within microarray slides or subarrays and statistically normalizing data after the assay without the help of calibrants aim to address sytemic sources of variability due to biases introduced during assay protocols, where spatial bias or serialized steps introduce variability. Because of the well-known variability in the amount of molecules bound at the surface of microarray slides [204, 205], molecules such as antibodies

against GST [206], or molecular tags such as PolyHis [207] combined with GST or PolyHis-tagged proteins were spiked in samples. The calibrant signals were used in a simple division with the assay signal (GST) or qualitatively to confirm the presence of spots at the surface (PolyHis). As a pre- or post-assay step to determine the amount of cAb bound to the surface, groups have used universal antibodies [208] (post-assay) or IRIS, a label-free platform that calculates the quantity of cAbs within spots [166] (pre-assay). Several groups have spiked green fluorescent protein (GFP) in samples and standards [17, 209, 210], or cholera toxin subunit B [211]. To assess systemic variability and calibrate for variability in sample dilution, immunoglobulins were measured either on-chip or using ELISA [212], which requires an extra assay. Positive controls were added to arrays [213–215] and their signals were used to calculate a factor for every slide or subarray, by which all assay signals were multiplied. Finally to address systemic bias, a linear form of variability, purely statistical approaches to calibration were performed by measuring each slide's overall variability [216–218]. All these methods aim to address a single source of variability (local or systemic), whether it is the local amount of molecule bound to the surface, the variability in sample dilution, or systemic variability or bias due to serialized assay steps and spatial bias. Cross-reactivity between molecules used as calibrants and other molecules present in these assays were not investigated, nor was the effect of the sample matrix when spiking calibrants in samples.

Steps towards improving ACM assay reproducibility were taken by designing robust silicon quill pins that consistently deliver liquid at the slide surface [154], and by adding hygroscopic chemicals to the cAb printing buffer, avoiding its evaporation and thereby delivering a constant quantity of cAbs at the slide surface and improving spotting reproducibility [146]. However, the dAb printing buffer used up to now (20 % glycerol) has been shown to evaporate, and therefore a new dAb printing buffer is needed. Moreover, incubation times required for cAbs and dAbs to be maximally bound to the surface or their respective antigens still remains to be determined. Here, we further optimize the ACM assay to improve reproducibility, and investigate the degradation of cAbs and Ags left in the dry state during the long time before dAbs are printed in large-scale experiments, whose rate we decrease by coating slides with trehalose. We then propose the use of calibration to minimize multiple sources of experimental variability (local and systemic) that could not be mitigated by optimization of assay protocol steps. We compare Alexa Fluor (AF) 555 labeled goat anti-rabbit (GAR), bovine serum albumin (BSA) labeled with AF555 and AF647, and AF555-hydrazide in their ability to calibrate local variation in the amount of cAb bound on slides surfaces, and derive a mathematical model using calibrant and assay signals. We introduce biotinylated GAR (GAR-b) spiked with BSA-AF555 and spotted alongside cAbs on each of the 16 subarrays printed on every slide to address systemic biases, and use a standardized layout of samples and replicate samples in order to calibrate assay data using a small number of sample

subgroups in two large-scale experiments. We formulate five algorithms that encompass different combinations of sources of variability, and pick the best performing algorithm for calibrating 103 different proteins in two large-scale experiments measuring hundreds of samples each. We validate that the observed improvement in reproducibility can be translated to an increase in the precision of protein measurements for samples.

4.2 Materials and Methods

4.2.1 Materials

To collect blood for pooled normal serum and plasma replicate samples, we purchased serum (BD Vacutainer #367815), K_2EDTA (BD Vacutainer #367863), lithium heparin (BD Vacutainer #367886), citrate (BD Vacutainer #369714) and CTAD (BD Vacutainer #367599) blood collection tubes from Becton, Dickinson and Company (Franklin Lakes, NJ, USA). Pooled normal human lumber cerebrospinal fluid (pnCSF) was purchased from Gemini Bio-Products (West Sacramento, CA, USA). Phosphate-buffered saline (PBS) 10× solution, pure isopropanol and glycerol were obtained from Fisher Scientific (Hampton, NH, USA). Trehalose, sucrose, betaine, 2,3-butanediol, sodium borohydride and Tween-20® were obtained from Sigma-Aldrich (St. Louis, MO, USA). Pure ethanol was obtained from Commercial Alcohols (Greenfield Global, Brampton, ON, Canada). Protease-free, IgG-free bovine serum albumin (BSA) was obtained from Jackson ImmunoResearch Laboratories (West Grove, PA, USA). Unlabelled goat anti-rabbit (GAR) antibodies, GAR Alexa Fluor 555 (AF555), GAR-AF647, goat anti-mouse (GAM) AF647, GAR-biotinXX (GAR-b, where XX are two random amino acid spacers between GAR and biotin), BSA-AF555, BSA-AF647, AF555 hydrazide (h-AF555), streptavidin (Strept) AF555, Stretp-AF647 and 4 mm 0.45 µm PVDF syringe filters to filter detection antibody solutions were purchased from Thermo Fisher Scientific (Waltham, MA, USA). PolyAn 2D Aldehyde and 2D Epoxy microarray slides were obtained from PolyAn GmbH (Berlin, Germany). Xenobind microarray slides were purchased from Xenopore Corporation (Hawthorne, NJ, USA). ArrayIt SuperNHS, SuperAldehyde and SuperAldehyde2 microarray slides were obtained from ArrayIt Corporation ARYC (Sunnyvale, CA, USA). Capture antibodies, detection antibodies and recombinant antigens were purchased from R&D Systems (Minneapolis, MN, USA), Abnova (Taipei City, Taiwan), Abcam (Cambridge, UK), OriGene (Rockville, MD, USA), Fitzgerald Industries International (Acton, MA, USA), United States Biologicals (Salem, MA, USA), MBL International Corporation (Woburn, MA, USA) or Santa Cruz Biologicals (Santa Cruz, CA, USA) according to table D.S3 which also contains concentrations of all reagents used in experiments.

4.2.2 Samples Preparation

Pooled normal blood samples were prepared by collecting blood using a standard venipuncture procedure from a minimum of 10 healthy adult anonymous donors in one serum, one EDTA, two citrate, two CTAD and one heparin tubes. Serum tubes were left to coagulate for 30 min at room temperature while plasma tubes were processed immediately after inverting 8-10 ×. Tubes were centrifuged for 10 min at 1000 *g* and at room temperature. The supernatant was immediately collected, stored at 4 °C and pooled by blood tube type. The resulting mixture was aliquoted in cryotubes and stored at −80 °C. A second pooled normal serum sample (pnSerum2) was prepared from four healthy adult anonymous volunteers using a single serum blood collection tube per donor, which was processed as described above.

4.2.3 Quantification of evaporation of printing buffers

Measurement of evaporation of detection printing buffers was performed following a previously described protocol [146]. In short, various detection printing buffers containing 1 % blue food dye added were prepared. Silicon quill pins used for microarray printing but without proper tips were dipped in the detection printing buffer and incubated at 65 % relative humidity and room temperature. Pictures of the liquids in pin channels were taken every minute for 15 min after which no significant evaporation occurred.

4.2.4 Microarrays production

Printing of molecules on microarray slides, plasma-treatment of source well plates and the antibody colocalization microarray (ACM) protocol are explained in Laforte *et al.* [219]. In short, capture antibodies and other molecules were printed in 2 M betaine / 25 % 2,3-butanediol in PBS 1 × unless otherwise specified. A Nanoplotter 2.1 microarrayer (GeSiM GmbH, Radeberg, Germany) with an added microfabricated collimator (Parallel Synthesis, Santa Clara, CA, USA) fitted with four custom-made silicon quill pins [154] was used for printing. The Nanoplotter was equipped with a chamber where humidity could be controlled, and was set to 65 % relative humidity. Printing was performed in the dark and on cleaned Xenobind slides unless otherwise specified. Printing of 14 or 16 identical subarrays was generally performed on multiple slides. After printing, slides were incubated for 24 h or other specified amounts of time, before they were fitted onto gaskets (ProPlate®, Grace Bio-Labs, Bend, OR, USA) that separate subarrays into 16 independent liquid incubation chambers. Slides were then rinsed using washing buffer (PBS 1 × with 0.1 % Tween-20®) and the slide washing protocol consisting in rinsing slides three times rapidly with wash buffer, washing for 5 min with 450 rpm rotational shaking, and repeating this process twice. Blocking of

slides was performed by incubating for 3 h in 3 % BSA in PBST (PBS 1 × with 0.05 % Tween-20®) with 450 rpm rotational shaking. Samples diluted in PBST (high dilution: 1:30, low dilution: 1:3 if not specified) and serially diluted mixtures of antigens at known concentrations (diluted 1:2.5 13-15 × as indicated) as well as blanks (PBTS) were incubated on slides for a minimum of 18 h at 4 °C with 450 rpm rotational shaking unless specified otherwise. For ACM experiments, slides were washed using the above protocol and rinsed with pure water or 5 % trehalose diluted in pure water, then blown-dried with a stream of compressed nitrogen before being placed back in the nanoplotter chamber. Detection antibodies or other molecules in detection printing buffer (45 % glycerol, 1 % BSA, 0.001 % Tween-20®, filtered to avoid debris that could clog the silicon quill pins) were printed onto slides and left to incubate for 24 h unless specified otherwise. Slides were fitted back onto gaskets for further processing. For multiplex sandwich assays (MSA), following slide washing after samples and antigens incubation, slides were incubated with a mixture of detection antibodies at 0.2 µg/mL each in PBST for 1 h unless stated otherwise. For both ACM and MSA experiments, slides were washed using the previously mentioned protocol, and 0.5 µg/mL Strept-AF647 or other reporter molecules were incubated for 1 h in 3 % BSA in PBST, with 450 rpm rotational shaking. Deviations with the purpose of optimizing this protocol are stated directly in the results section.

4.2.5 Protocol optimization

Reductive amination of slides as specified was done using the following procedure: 20 mg of $NaBH_4$ was dissolved in 7.5 mL of PBS 1 × and 2.5 mL of pure ethanol. After the initial wash of capture antibodies using washing buffer, slides were rinsed with PBS 1 × and incubated in the freshly prepared solution of $NaBH_4$ described above with 450 rpm rotational shaking. Slides were washed 3 × 5 min in washing buffer with 450 rpm rotational shaking before proceeding with the slide blocking step. Because of its toxicity, liquids containing $NaBH_4$ were collected and quenched by adding ≈20 × the volume of isopropanol before disposing according to local environmental safety protocols.

4.2.6 Large-scale experiments

The large-scale experiment with trehalose coating was performed according to the above protocol, with 36 slides. Capture antibodies (for most: 100 µg/mL) and GAR-b (25 µg/mL) were spotted in triplicate in 50 % glycerol, 0.005 % Tween-20® with 20 µg/mL BSA-AF555 as spot calibrant. 14-point standard curves were located on slides 3, 12 and 35 and replicate samples pnSerum (dilutions 1:3 and 1:30), pnCSF (dilutions 1:3 and 1:15) and pnPlasma (dilutions 1:3 and 1:30) were located on each slide (one replicate type and dilution per slide). The large-scale experiment

without trehalose coating of slides was performed according to the above protocol, with 48 slides. Capture antibodies and GAR-b were spotted in 45 % glycerol, 0.005 % Tween-20® with 10 µg/mL BSA-AF555 as spot calibrant. 16-point standard curves were located on slides 2 and 16 and replicates samples of pnSerum at either dilution 1:3 or 1:30 were located on each slide. Each slide in both experiments also contained one or multiple blanks (subarrays incubated with PBST during the antigen/sample incubation step). Validation samples were produced by mixing pnSerum1 and pnSerum2 according to the schematic in figure D.S38 and applied to slides 1, 2, 7, 8, 13, 19, 25, 31 and 36 in the experiment with trehalose coating, and slides 1, 9, 23, 24, 33, 37, 38 and 39 in the experiment without trehalose coating. Capture and detection antibodies were spotted in order of decreasing %CV to minimize variability due to cAb and Ag degradation. This allowed proteins with large %CVs to benefit from the shortest duration of drying during dAb spotting. Because of missing spots in multiple validation samples, GRO-α, IGFBP-3 and SPARC were not analysed in the large-scale experiment with trehalose coating, while BDNF, Tie-2, PAI-1, IL-15, TGF-β2 and FAS were removed from the analysis of the large-scale experiment without trehalose coating.

4.2.7 Fluorescence scanning and data extraction

Microarray slides were scanned using the SureScan Microarray Scanner model 62505B/C (Agilent Technologies, Santa Clara, CA, USA) fitted with two lasers (red He/Ne 23 mW 632-638 nm and green solid-state 20 mW 532 nm) and corresponding emission filters (red 660-750 nm and green 550-615 nm). The scanner outputs 16-bit single-channel double images with a resolution of 5 µm/pixel. Files were viewed and analyzed with ArrayPro Analyzer 6.31 (Media Cybernetics Inc, Rockville, MD, USA). Grids of 18 × 18, 60 µm circles were manually overlaid on all subarrays of each microarray slides. The position of circles overlaid on top of groups of three technical replicates were moved together if the grid and the spots position did not correspond well. The mean fluorescence values of all pixels within each circle was outputted for further analysis.

4.2.8 Analysis and data calibration

Fluorescence data was imported and analysed in Excel (Microsoft Corporation, Redmond, WA, USA) and GraphPad Prism 5 (GraphPad Software Inc., La Jolla, CA, USA) for protocol optimization experiments and proof of concept experiments and R[220] for all calibration and performance measurements. Packages *onewaytests*[221], *outliers*[222], *drc*[223], *mblm*[224], *minpack.lm*[225], *limma*[226] and *MASS*[227] were used in the code. Standard curve fitting, quantification of samples and accuracy range (AR) calculations were modified from a website created by Murphy

and Dendukuri [228]. Exact details of calibration and measurement of performance are located in supplementary material appendix D.

4.3 Results

4.3.1 Assay Optimization

Previous optimizations were made to the ACM protocol in order to improve assay reproducibility and sensitivity, with the main goal of optimizing a slide and cAb printing buffer combination that minimizes evaporation [146]. Similarly, to minimize evaporation in the dAb printing buffer, we added 45 % glycerol, and to minimize non-specific binding, we added 1 % BSA and 0.001 % Tween-20 (figure D.S1). To further improve sensitivity, we increased blocking time and concentration of BSA in the blocking buffer and optimized Streptavidin incubation time and buffer composition. While previous studies using the ACM were done on Xenobind slides, they were no longer available. Therefore we investigated different slides in terms of signal intensity and reproducibility of the chemical coating and chose PolyAn 2D Aldehyde as it behaved similarly to Xenobind without modifications to the protocol. We changed the cAb printing buffer to 50 % glycerol with 0.005 % Tween-20 to improve assay reproducibility of one protein which was not reliably measured with the previously used 2 M betaine / 25 % 2,3-butanediol printing buffer, out of four protein tested. Supplementary figures D.S2 to D.S14 describe optimizations done to the assay protocol.

Figure 4.1 shows the ACM protocol steps with identified sources of variability that were mitigated with improvements to the assay protocol. Incubation of cAbs and dAbs need to be sufficiently long to allow them to be bound at equilibrium, thereby decreasing the variability between the first and last spot bound on the surface. We therefore measured the amount of time required to allow cAbs and dAbs to bind to the surface using logarithmic regression analysis (figure D.S15). We found that for cAbs and dAbs, an incubation time of 24 h following the last printed spot is required to achieve maximum binding and a difference less than 1 % (figures D.S16 and D.S17). We also selected an 18 h incubation for Ags and samples at 4 °C, allowing for low-abundance Ags to bind without degradation of samples, which is in agreement with a previous study [229].

4.3.2 Protecting spots from drying effects with trehalose

Some spots on the slides are left in a dry state for upwards of 36 h when measuring over 100 proteins in several hundred samples because the long spotting duration until every dAb is printed. We therefore investigated the stability of cAbs and Ags bound on the surface of slides while being exposed to the ambient environment. Figure 4.2a illustrates the effect of spot degradation using

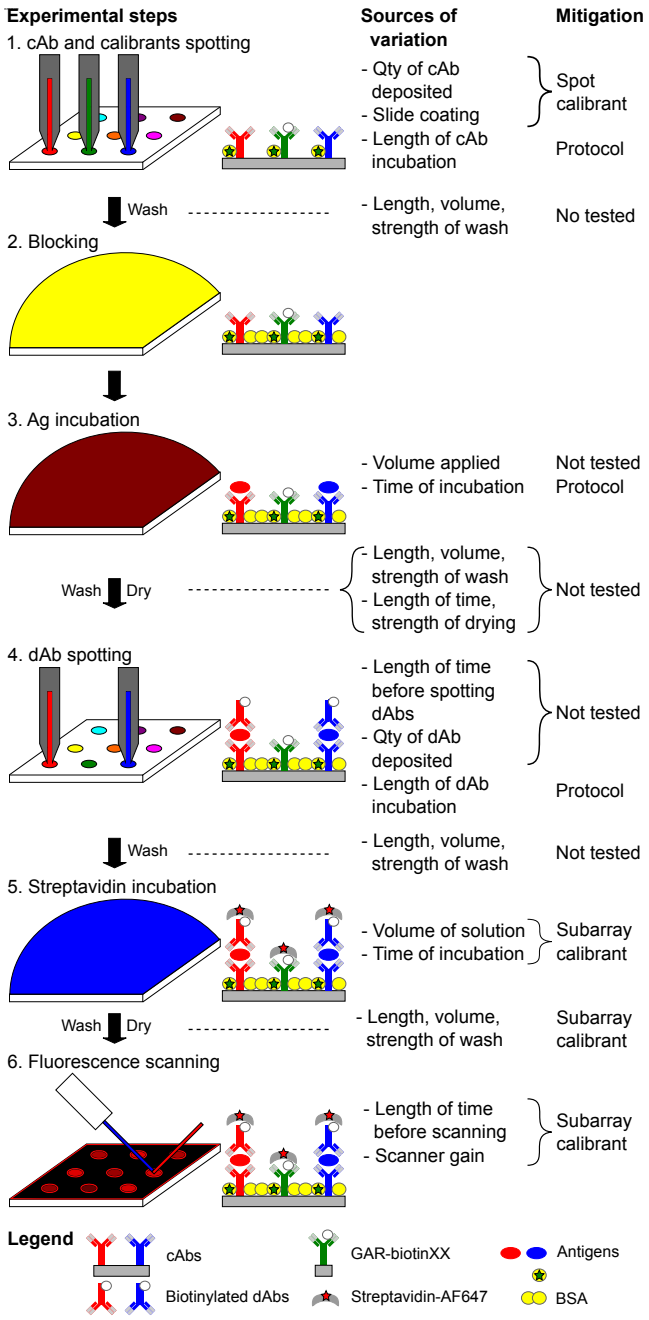

FIGURE 4.1: **Experimental sources of variability in ACM.** The ACM protocol consists of successive spotting (1, 4) and incubation (2, 3, 5) steps with slide processing such as washing and drying between steps. Some sources of variability are mitigated by modifications to the protocol while some are mitigated by the addition of a spot or subarray calibrants. Slides and spots layout is located on figure 4.5.

Ang1 as an example. cAb-Ag complexes were left in the dry state for different amount of times before spotting dAb printing buffer without dAb present, followed by incubation of dAbs in bulk and then incubation with goat anti-mouse (GAM) conjugated to AF647 at 1 µg/mL (figure D.S18)

and Strept-AF555. GAM-AF647 was used to quantify cAbs bound at the surface since Ang1 cAb is a mouse antibody, and Ang1 dAb is a goat antibody. We verified that GAM-AF647 did not cross-react with any of the dAbs used (figures D.S19 and D.S20). The quantity of Ag present on spots was quantified with Strept-AF555. A significant degradation in the GAM-AF647 signal was seen in as little as 12 h. We also determined that the degradation affected assay signals, notably degrading the LOD by a factor of up to 30 × (figure D.S22) due to the overall lower assay signal. While the degradation seen was prevented by immediately spotting dAb printing buffer on spots, dAb printing buffer printed on spots that had been left to dry and degrade did not reverse the degradation seen (figure D.S21). The amount of degradation varied on Xenobind, PolyAn 2D Aldehyde and PolyAn 2D Epoxy slides, indicating that the presence of various chemical coatings had an effect on the rate of degradation (figures D.S23 and D.S24).

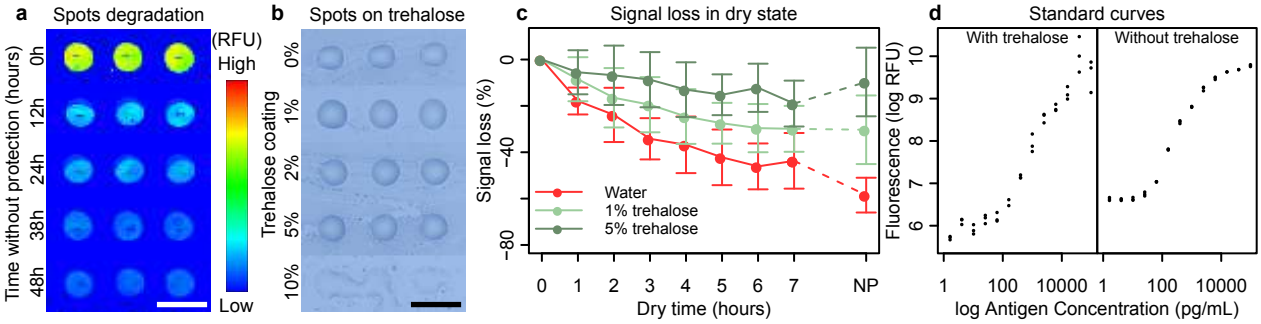

FIGURE 4.2: **Trehalose coating protects spots from degradation but increases local signal variability.** (**a**) Ang1 cAbs with bound Ag were washed with water, dried and left in the dry state for different amounts of time before dAb printing buffer was spotted. After incubation, slides were washed and incubated with GAM-AF647. (**b**) Microscope image of a blocked microarray slide that was coated with different concentrations of trehalose before drying and spotting dAb printing buffer. (**c**) Ang1 cAbs and bound Ag were coated with 1 or 5 % trehalose or rinsed with pure water and left to dry between one and up to seven hours before dAb printing buffer was spotted. (**d**) Ang1 immunoassay on slides protected with a trehalose coating leads to greater variability in the technical replicate signals than an Ang1 immunoassay without a trehalose coating. Size markers are 250 µm (**a** and **b**). Error bars are standard deviation (**c**). Dashed part of lines in **c** indicate a break in dry time. NP: Signal of spots onto which no dAb printing buffer was printed.

We coated slides with different concentrations of trehalose to attempt protecting spots from degradation, by incubating slides in the trehalose solution for a few seconds before drying using a stream of compressed nitrogen, effectively drying trehalose on top of the slides as a thin coating. We found that a maximum of 5 % trehalose could be spotted on slides and still allow dAb printing buffer to be printed on top (figure 4.2b). Compared to rinsing slides with water, coating slides with 5 % trehalose prevented up to 70 % of the observed degradation (figure 4.2c). Sucrose, BSA and glycerol were also tested, but they only provided minimal protection from degradation (figure D.S25) even though glycerol and BSA are already included at higher concentration in the dAb

printing buffer. Coating of slides with trehalose, sucrose and BSA led to the formation of small-scale crystals and introduced artifacts that affected assay signals and increased the local assay signal variability, as seen in the comparison of two standard curves of Ang1 in ACM assays of large-scale experiments (figure 4.2d). The standard curve from the slide coated with trehalose showed greater variability among triplicate spots at each antigen concentration compared to the slide without trehalose coating. In spite of the increased local variability due to coating slides with trehalose, this step was not dismissed because of the possibility that the spot calibrant tested next would address this extra source of variability, and therefore the slides of one large-scale experiment used to validate the proposed calibration method were coated in trehalose.

4.3.3 Choice of Spot Calibrant

We evaluated the use of spiked fluorescently-labeled molecules as calibrant to address local variability in the quantity of cAb bound to the surface at each spot. Because cAbs are monoclonal antibodies, and slides are blocked with BSA, we chose molecules which in theory should not interfere with the assay signal or cross-react with other molecules in the assay. We compared GAR-AF555, BSA-AF555 and AF555 hydrazide (h-AF555: a reactive version of AF555) that give signal in the green channel and BSA-AF647 that gives signals in the red channel. We compared these molecules using the following criteria: 1) absence of false positive signals, 2) sufficient signal intensity, 3) minimal interference with cAb binding to the surface, 4) stable binding to the surface within 24 h and 5) stability of the fluorescence signal in dry state before dAb printing (*i.e.* without trehalose coating).

When GAR-AF555 was added to cAbs to assay 10 different proteins, false positive signals were seen in at least four of them (figure D.S26), therefore GAR-AF555 was no longer considered for comparison. In order to determine the best concentration of spot calibrants, we printed 5, 10, 25 and 50 µg/mL BSA-AF555, BSA-AF647 and h-AF555 alone and mixed with GAR-b at 100 µg/mL. GAR-b was used as a replacement for cAb that can easily be probed with a fluorescently-labeled streptavidin in the opposite color channel as the spot calibrant tested. We incubated slides with Strept-AF555 and Strept-AF647 separately. All calibrants signal intensity increased proportionally with increasing concentrations (figure 4.3a), but only BSA-AF647 and BSA-AF555 showed decreasing GAR-b signal intensity with increasing spot calibrant concentration (figure 4.3b), indicating that they partially prevented GAR-b from binding to the slide surface. We also observed a small amount of fluorescence signal in the red channel used to measure AF647 when BSA-AF555 or h-AF555 were spotted, in the absence of AF647 (figure D.S27). From this experiment we picked concentrations of 8, 20, and 100 µg/mL for BSA-AF647, BSA-AF555 and h-AF555 respectively for further testing.

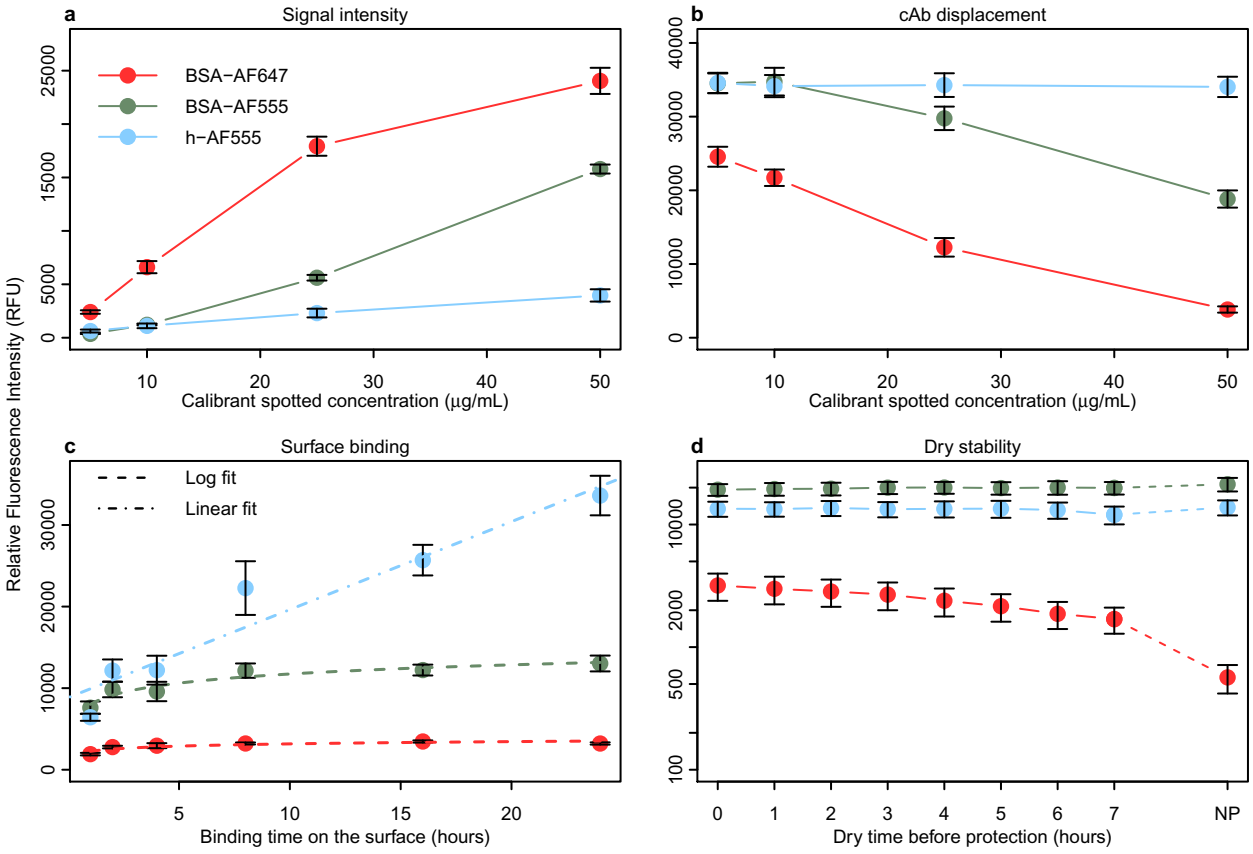

FIGURE 4.3: **BSA-AF555 performs best as spot calibrant.** BSA-AF647, BSA-AF555 and h-AF555 are compared in terms of (**a**) signal intensity and (**b**) displacement of cAb when spotted at different concentrations as a mixture with GAR-b at a constant concentration. (**c**) Calibrants at their ideal concentration mixed with GAR-b were allowed to bind on the slide for different amounts of time to determine their binding dynamics. h-AF555 shows a linear binding that does not accurately reflect the amount of GAR-b bound on the surface regardless of incubation time. (**d**) Calibrant spots mixed with GAR-b and bound for 24 h were left to dry for different amounts of time before being protected by dAb printing buffer spots. Fluorescence signals in (**a, c, d**) are from the spot calibrants, whereas in (**b**) they are from streptavidin conjugated to AF555 or AF647 to show GAR-b displacement. Error bars are standard deviation. Dashed part of lines in **d** indicate a break in dry time. NP: Signal of spots onto which no dAb printing buffer was printed.

The three spot calibrants were spotted at their optimal concentration and allowed to bind for different amounts of times to the slide to evaluate whether the signal intensities were stable after an incubation time of 24 h. We found that BSA-AF647 and BSA-AF555 both bound to the slide in a logarithmic fashion, while h-AF555 appeared to bind linearly (figure 4.3c). The signal intensity of h-AF555 was ~6 × greater without the presence of GAR-b, suggesting a complex mixture of binding rates between GAR-b, h-AF555 and the slide surface. Similarly to cAbs tested previously, the signal intensity of BSA-AF555 and BSA-AF647 varied by less than 1 % in large-scale experiments, while

binding of h-AF555 varied by much more than 1 % (figures D.S28 and D.S29).

We tested the stability of the three potential spot calibrants when left in the dry state for several hours before dAb printing, and found that h-AF555 and BSA-AF555 fluorescence signals were stable, while that of BSA-AF647 slowly degraded after 7 h (figure 4.3d). We tested the stability for a longer time duration (40 h) and found a slight degradation of BSA-AF555 fluorescence signal on Xenobind and PolyAn 2D Epoxy slides, but not PolyAn 2D Aldehyde (figures D.S30 to D.S32). BSA-AF647 fluorescence signal quickly degraded on all three slides, with up to 93 % decrease in signal intensity after 40 h. Similarly, we evaluated the stability of AF555 and AF647 in conditions simulating waiting time before scanning while being in the scanner at normal humidity and in the dark (figure D.S33) and found that both fluorophores were stable for up to 25 h. Finally, because calibrants can be left in the printing buffer in the source well plate for up to 36 h before being spotted onto microarray slides, we investigated their stability during storage in cAb printing buffer. Both BSA-AF647 and BSA-AF555 degraded slowly when stored for up to three days in the cAb printing buffer, although BSA-AF647 degraded ~3 × quicker than BSA-AF555 (figure D.S34).

h-AF555 did not bind with a similar rate as GAR-b, while BSA-AF555 and BSA-AF647 followed a logarithmic binding curve to the slide similar to that of cAbs. For this reason, h-AF555 was essentially useless as a predictor of the subtle differences in cAb quantity between spots. BSA-AF555 was selected over BSA-AF647 as spot calibrant because it interfered less with cAb binding and was more stable in the dry state. Therefore, BSA-AF555 was measured in the green channel, and the red channel was selected to measure the assay signal, which in our assay is also the most sensitive channel (figures D.S35 and D.S36).

4.3.4 Spot calibration

In order to model the mathematical relationship between the spot calibrant (BSA-AF555) and assay fluorescence signals, we serially diluted a mixture of spot calibrant and HGF-R cAb, while keeping the ratio of both molecules constant. Each subarray of a slide was spotted with the mixtures of spot calibrant and HGF-R cAb at different concentrations and subarrays were incubated with a 15-point standard curve of HGF-R. Figure 4.4a shows the different standard curves obtained with increasing concentrations of spot calibrant and cAb mixture. The relationship of spot calibrant and assay fluorescence signal intensities for the different antigen concentrations in the standard curve, corresponding to a relationship $A_{\mathrm{CAL}} = A/C_{\mathrm{S}}$ where $\mathrm{A_{CAL}}$ is the calibrated assay signal, $\mathrm{C_S}$ is the spot calibrant signal and A is the raw assay signal, are shown in Figure 4.4b. No simple mathematical relationship could be derived from this equation, and therefore it was not be possible to derive the antigen concentration from the simple ratio of assay to spot calibrant signals.

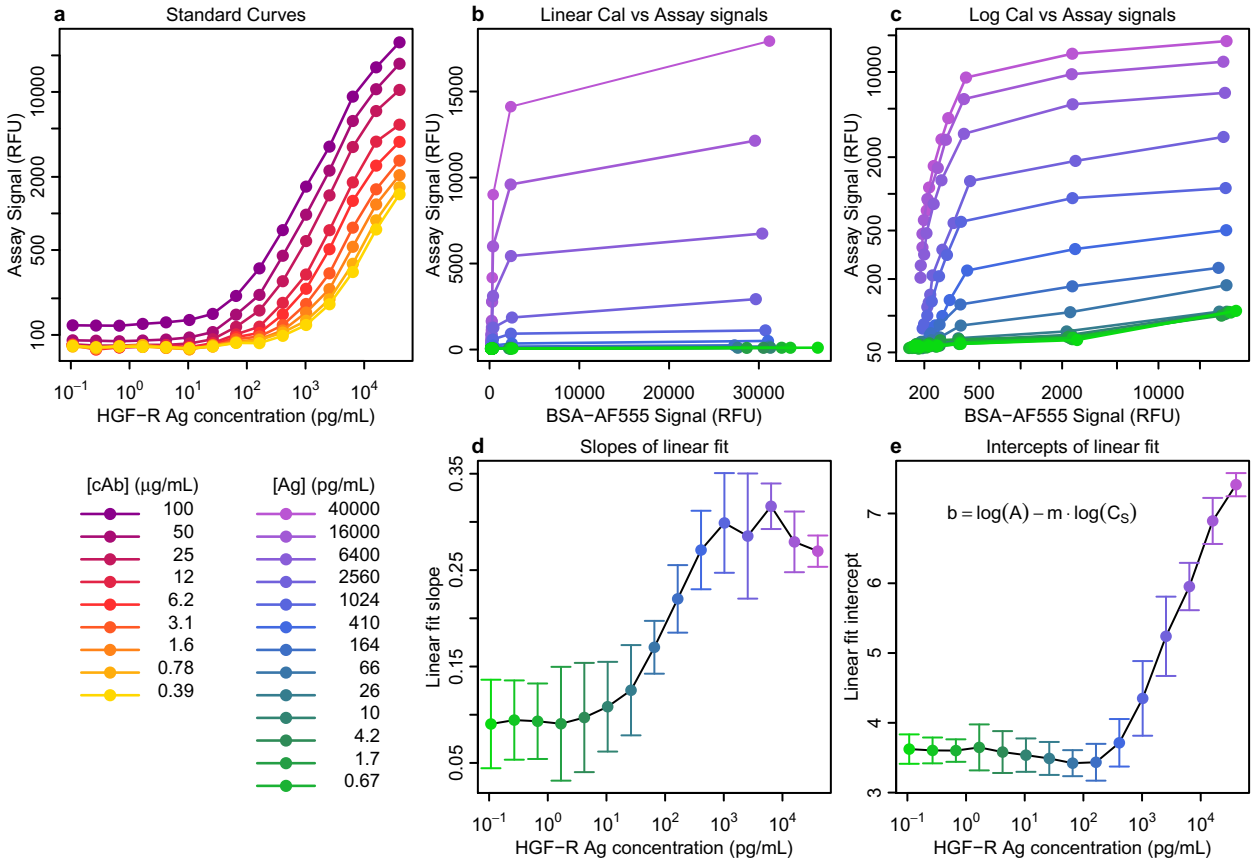

FIGURE 4.4: **Linear relationship between log assay and log spot calibrant signals.** A mixture of HGF-R cAb (Assay: A) and BSA-AF555 (spot calibrant Cal: C_S) at initial concentrations of 100 and 20 µg/mL respectively were diluted 1:2 nine times and spotted on a microarray slide. Following blocking, the microarray slide was incubated with a 15-point standard curve of HGF-R Ag serially diluted 1:2.5. (**a**) Nine standard curves of HGF-R of increasing concentrations of cAb/Cal. In (**b**) and (**c**), the spot calibrant signal is plotted against the assay signal in (**b**) linear-linear or (**c**) log-log scales, for each Ag concentration. Because the log-log graph (**c**) leads to parallel lines at high cAb/cal concentrations (25-100 µg/mL), they can be approximated by linear fits in this range for each cAb/cal concentration. The slope (**d**) and intercept (**e**) of these linear fits can be plotted against the Ag concentration. (**a-c**) are representative graphs while (**d**) and (**e**) are averages of three independent experiments. Error bars are standard deviation. Estimating the constant part of the calibration slopes (m) above the standard curves inflection points in (**d**) allows the calculation of Ag concentration by calculating the intercept (b) using the line equation $y = m \cdot x + b$.

Since the fluorescence intensity data obtained from microarrays is strongly heteroskedastic (figure D.S37) and that log transformations are used to make the data homoskedastic [230], both assay and spot calibrant signals were log transformed and plotted for each antigen concentration, corresponding to a relationship $A_{\mathrm{CAL}} = log(A)/log(C_S)$. Figure 4.4c shows that within the cAb concentration range of 25 to 100 µg/mL, the slopes (m) of log(C_S) vs log(A) were relatively constant. This slope was plotted against the antigen concentration in figure 4.4d. Similarly, the line intercepts

(b) were plotted against the corresponding antigen concentration in figure 4.4e. Approximately one order of magniture (OM) about the average point of inflection for the standard curves made by cAbs at concentrations 25 to 100 µg/mL, the slopes were relatively constant, while the intercepts appeared to be of a similar shape as an average of the first three standard curves shown in figure 4.4a. The intercepts were calculated using the equation $b = log(A) - m \cdot log(C_S)$ where A is the assay signal and C_C is the spot calibrant signal. By the law of logarithmic identities this corresponds to the following relationship between assay and spot calibration signals: $b = log(A/{C_S}^m)$.

4.3.5 Comparison of calibration algorithms

BSA-AF555 was selected as spot calibrant to address local variability due to differences in the surface coating of microarray slides. A subarray calibrant (GAR-b) was picked as subarray calibrant to compensate for systemic variability due to spatial bias and serialization of assay steps, specifically subtle differences in the duration of the Strept-AF647 incubation and following wash and variations during scanning. A subarray spot calibrant (BSA-AF555) was also mixed with the subarray calibrant GAR-b in order to compensate for local surface variability that could differentially affect binding rates of cAbs and spot calibrants. In total, three different calibrant signals were obtained in addition to the assay signal. Figure 4.5a shows the layout of cAbs and subarray calibrants for a single subarray that can measure 104 proteins from triplicate technical replicates. Figures 4.5b-c describe the molecules present at cAb and subarray calibrant spots, respectively.

We sought calibration equations that would allow the first calibrant to address the greatest source of variability (local or systemic), followed by the second calibrant addressing the second most important source of variability, and so on. We assumed that if a source of variability is very small, the calibrant signal which addresses this source of variability should not be used because in practical terms, it would simply add variability to the result. Therefore, we serially combined the three calibrant signals into five equations (figure 4.6) using different combinations of signals. Two of the resulting equations use a single calibrant (spot or subarray calibrant) and assume that the variability addressed by the other two calibrants is minimal. Two equations use the spot and subarray calibrants one after the other. The last equation uses the three calibrant signals, with the subarray spot calibrant first calibrating the spot calibrant signals.

Two large-scale experiments with 36 and 48 slides were performed to measure up to 103 proteins in clinical samples (analysed elsewhere). Table D.S3 lists the proteins measured along with the provenance and concentrations of reagents used. Because the use of trehalose coating of slides decreased the degradation of some molecules bound to the microarray slide surface, but introduced a local variability due to microcrystals being formed on the surface, one large-scale experiment (36 slides) received trehalose coating of its slides, while the other (48 slides) did not. Samples of the

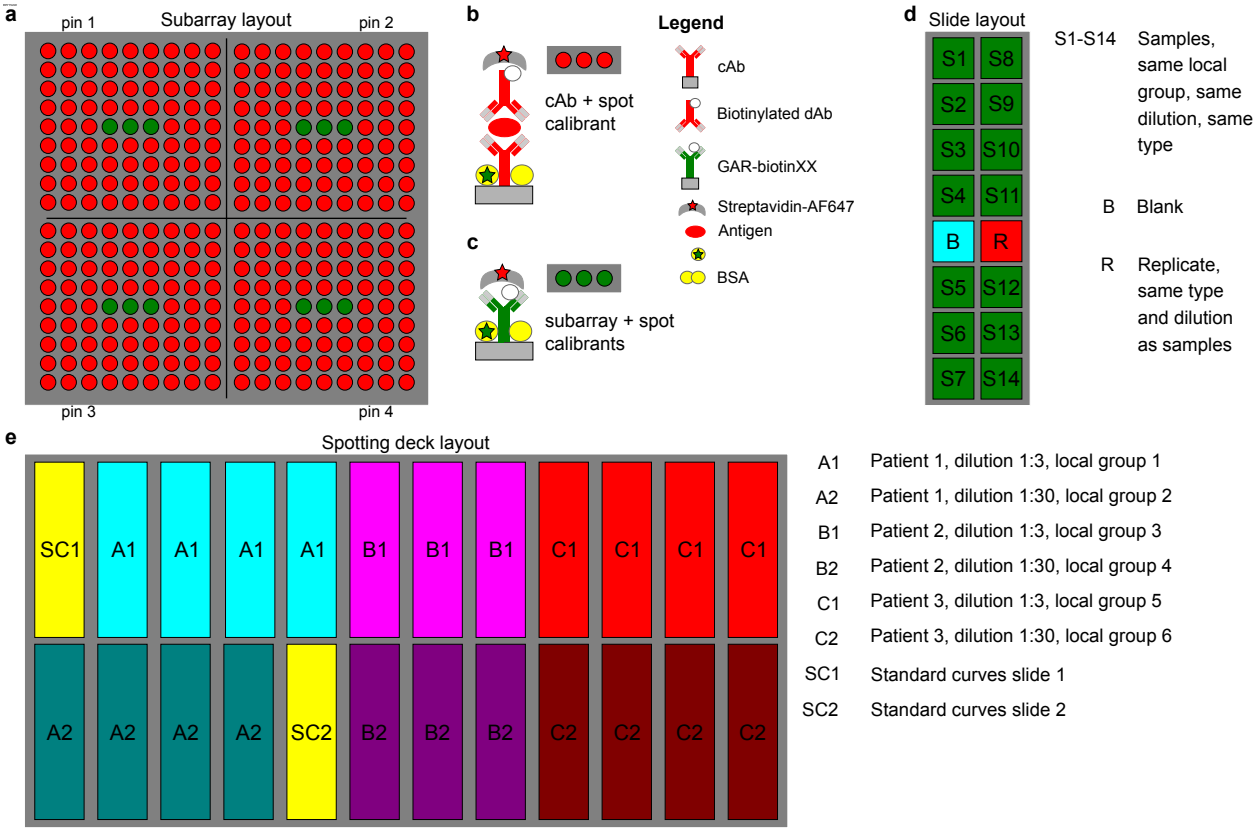

FIGURE 4.5: **Experimental design.** (**a**) The layout of cAbs, spot and subarray calibrants within a single subarray (used to measure a single Ag concentration or sample at a given dilution). The molecular composition of a spot containing (**b**) a cAb with spot calibrant and (**c**) a subarray calibrant with spot calibrant. (**d**) Slide layout containing 14 samples within a same local group, of the same type and dilution, and a single blank and replicate sample of the same type and dilution as that of the samples. (**e**) Example of a small deck layout containing 6 local groups, each of which composed of 3 or 4 slides with grouped samples to be compared (shown here as time course samples from a single patient), of the same sample type and dilution. The deck layout also contains two standard curves.

same type (serum, plasma, cerebrospinal fluid) and dilution (high or low) and in the case of patient time series, the same patient, were grouped together and the order of samples was randomized for each patient (as shown in figure 4.5e). This minimized variability within each small group, since variability is less in small-scale experiments compared to large-scale experiments. Each slide also contained a blank sample used for calculating the limit of detection (LOD), a measure of sensitivity. In order to calibrate assay signals, calibration slopes were estimated for each protein. We used pooled normal replicate samples on each slide, corresponding to the sample type and dilution of the slide (figure 4.5d) to estimate calibration slopes. To verify that reproducibility was also improved for clinical samples, a series of validation samples was added to both large-scale experiments, created from two different pooled normal serum samples (figure D.S38). Quantities

$$\text{Alg1: } b_1 = \log(\text{Assay}_R) - m_1 \cdot \log(\text{Cal}_{\text{spot-G}})$$

$$\text{Alg2: } b_2 = \log(\text{Assay}_R) - m_2 \cdot \log(\text{Cal}_{\text{subarray-R}})$$

$$\text{Alg3: } b_3 = b_2 - m_3 \cdot \log(\text{Cal}_{\text{spot-G}})$$

$$\text{Alg4: } b_4 = b_1 - m_4 \cdot \log(\text{Cal}_{\text{subarray-R}})$$

$$\text{Alg5: } b_5 = b_2 - m_5 \cdot (\log(\text{Cal}_{\text{spot-G}}) - m_6 \cdot \log(\text{Cal}_{\text{subarray-G}}))$$

FIGURE 4.6: **Equations for five calibration algorithms.** Alg1 and Alg2 are calibration algorithms that use a single calibrant (Cal variables, in red and green), Alg3 and Alg4 are extensions of Alg1 and Alg2 but use an additional calibrant, and finally Alg5 uses all three calibrants. For each protein, six calibration slopes (m, in blue) are estimated using the replicate samples located on each slide. A single calibration slope value is estimated for each local group, and the median of all the calculated calibration slopes is used to estimate the overall calibration slope.

of the four measured proteins did not vary significantly between the two different pooled samples (figure D.S39), however the measure of reproducibility calculated was the residual error, similar to coefficient of variation but with a non-zero regression line [146].

Replicate samples located throughout the slide layout of both large-scale experiments were used to both estimate calibration slopes and to calculate the resulting reproducibility. If care is not taken during the estimation of calibration slopes, it is possible for the improvement in reproducibility seen for replicate samples to not reflect a true improvement in reproducibility for the clinical samples being measured, a well-known statistical phenomenon called data overfitting [231]. We observed this phenomenon when performing an experiment where we used two different pooled normal samples (pnSerum1 and pnSerum2) to calculate calibration slopes and measured to resulting reproducibility on both replicate samples. Calibrating both replicates with a single calibration slope estimated from one of the replicates led to a much greater improvement in reproducibility in that replicate sample and small to little improvement in the other replicate sample (figure D.S40), proving that this method leads to overfitting. On the other hand, reproducibility was improved in both samples when the mean of the two calibration slopes obtained independantly from both replicates was used to calibrate both replicate samples (figure 4.7c). Moreover, the mean calibration slope estimated from low-dilution replicates improved low-dilution replicates reproducibility more than high-dilution replicates, and calibration slopes estimated using blanks did not improve reproducibility in most cases, indicating that using the proper dilution of replicate samples is important. Calibration slopes were therefore estimated by taking the mean or median of

several calibration slopes measured in individual local groups to avoid overfitting.

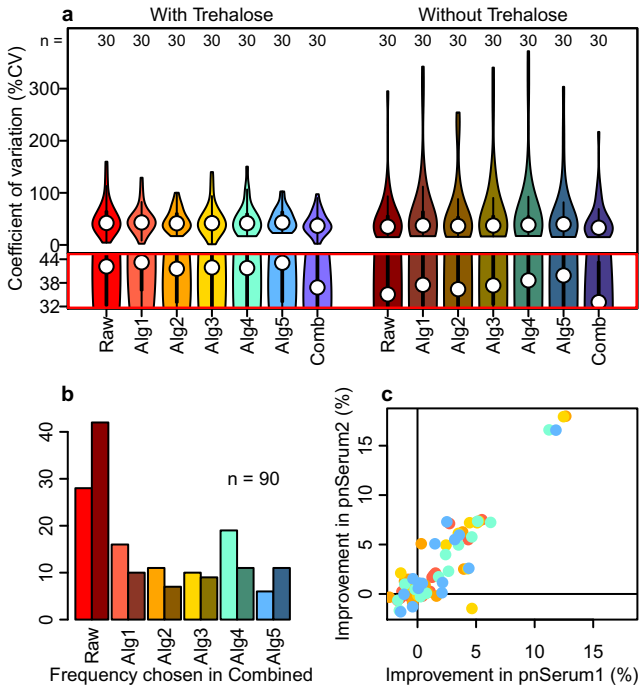

FIGURE 4.7: **Combination of five calibration algorithms improves assay reproducibility.** (**a**) Comparison with violin plots of reproducibility obtained with uncalibrated (Raw) data, five calibration algorithms and the best combination of these five algorithms per protein at dilution 1:3 in a large experiment where slides were coated or not coated with trehalose before drying. Only proteins (n = 30) where reproducibility could be calculated for all algorithms in both experiments are considered. Combined data is based on reproducibility of pnSerum at dilutions 1:3 and 1:30. (**b**) Frequency of use for each calibration algorithm in the final combined algorithm. Bright colors are for the experiment with trehalose, while dark colors are for the experiment without trehalose coating of slides. (**c**) In an experiment where two different replicates samples were applied several times (pnSerum1 and pnSerum2), the best improvement in reproducibility was obtained for both replicates when calibration slopes were calculated from the mean of calibration slopes obtained from both replicate samples.

We compared the improvement in reproducibility obtained using the five different equations. Median reproducibility of sample replicate quantities was used as a measure of the performance of calibration algorithms, as using the median is less skewed by outliers which are present in our reproducibility values distributions. Figure 4.7a shows that the reproducibility of 30 proteins, whose quantities were measured in both large-scale experiments, was equal or worse than reproducibility of uncalibrated data when using any of the five algorithms in both experiments. However when picking the best performing algorithm for each protein (or no calibration if none of the algorithms produced an improvement in reproducibility), median reproducibility was improved from 42.1 % to 36.8 % for the large-scale experiment with trehalose coating, and from 35.1 % to 33.1 % for the

other experiment. The frequency of selection of each algorithm for both large-scale experiments is shown in figure 4.7b and shows that data was left uncalibrated for about a third of the proteins for the large-scale experiment with trehalose coating, while for the other close to half the proteins were left uncalibrated. LOD was worse in the experiment with trehalose coating, and residual error of validation samples was improved with the combined algorithm in both experiments (figure D.S41).

We tested four different methods of estimating calibration slopes, described in the supplementary information. Calibration slopes were estimated by taking the mean or median of calibration slopes calculated within local groups, or estimated using the mean of calibration slopes estimated globally using different replicate samples types and dilutions (global) when more than one replicate type and dilution was present. In both cases, data for all protein dilutions were considered, or data only from a chosen dilution per protein. Most proteins were quantified at a lower dilution, except proteins found in larger quantities in samples (Ang1, CCL5, CD14, EGF-R, IGFBP-3, IGFBP-7, MMP-9, TGFβ RII, THBS-1, VCAM-1). We first compared different parameters (mean vs median, high vs low number of local groups, number of replicate types and dilutions) for each of the four method presented. We calculated reproducibility using replicate samples, residual error from validation samples, limit of detection (LOD), quantification range (QR: range between the minimum and maximum plateau of the standard curve fit) and accuracy range (AR: range of the standard curve with a precision $\leqslant$25 %) from uncalibrated raw data and data calibrated using the combined algorithm (figures D.S42 to D.S48). We found that in both experiments, calculating the median of local calibration slopes was better than the mean. The best performing number of local groups varied. Reproducibility and residual error improved further by picking the best method for estimating calibration slopes for each experiment, and in both cases taking the median of local calibration slopes performed best (figure D.S49 and D.S50).

4.3.6 Performance of combined calibration

In reporting final values of improvement in reproducibility, residual error and LOD, proteins for which values could be calculated using the calibrated and uncalibrated data in both large-scale experiments can be considered in order to compare the effect of trehalose coating of slides on assay performance. Figure 4.8 shows that reproducibility was better in the experiment without trehalose coating of slides, even though calibration improved reproducibility from 42.2 % to 30.0 % in the experiment with trehalose coating of slides and from 36.1 % to 27.2 % in the other experiment. Similarly, residual error was improved in both experiments, from 31.5 % to 24.1 % in the experiment with trehalose coating of slides and from 40.1 % to 30.6 % in the other experiment. Sensitivity was slightly better in the experiment without trehalose coating of slides (346 pg/mL vs 376 pg/mL)

even though calibration improved the LOD in the experiment with trehalose coating of slide, while sensitivity decreased slightly in the other experiment.

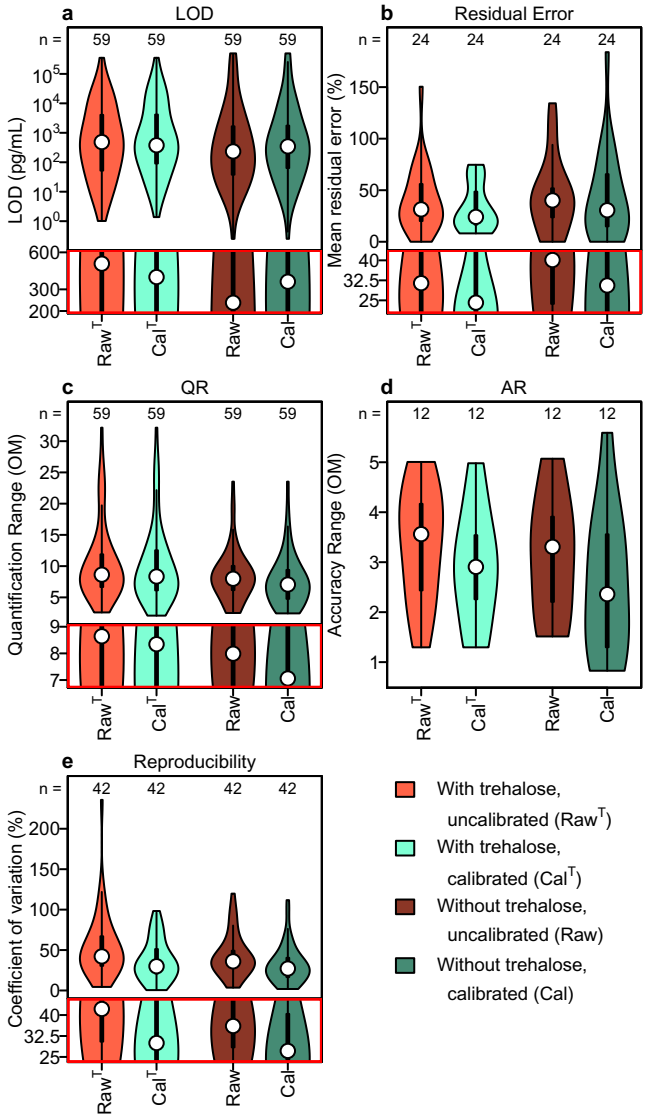

FIGURE 4.8: **Effect of calibration on assay performance.** Comparison of uncalibrated and calibrated data for experiment with and without trehalose coating in terms of (**a**) LOD, (**b**) mean residual error of validation samples, (**c**) QR, (**d**) AR of standard curves and (**e**) reproducibility of pnSerum sample replicates at dilution 1:3. Only proteins with standard curves and without unquantified replicate samples that have performance values in both experiments are considered.

On the other hand, the performance of calibration can be reported for each experiment individually. Because they measured a slightly different list of proteins, and because not all proteins had calculated values of reproducibility, residual error and LOD in both calibrated and uncalibrated data, the changes in performance due to calibration shown in figure D.S51 cannot be used to directly

compare the calibration performance for the two experiments. Reproducibility for the large-scale experiment with trehalose coating of slides improved from 42.9 % to 34.5 % and for the other experiment it improved from 36.8 % to 26.1 %. All performance values are reported in tables D.S1 and D.S2.

4.4 Discussion

As a first step to improving reproducibility of the ACM assay, steps of the protocol were examined for sources of variability that could be mitigated by modifications to the experimental protocol. We found a low-evaporation dAb printing buffer and lengthened both incubation times for cAb and dAb to 24 h to decrease the difference in the amount of antibodies bound to the surface between the first and last spot. These changes made to the protocol increased the overall time of the assay, making it last several days for large-scale experiments. However, the changes were very economical in their implementation. One step of the assay that happens several times and was performed entirely by hand was washing slides. Washing was performed with a squeeze bottle with high variability in the strength, volume and time of wash in each well of each slide. A similar problem was the loading of reagents, especially the standard curves, samples and replicate samples, as well as the Strept-AF647, which were done serially by hand and took over an hour for large-scale experiments. This step would also benefit from a higher consistency and quicker handling by automation. The automation of such steps has been shown to increase the reproducibility of assays [232–234], however the cost of additional equipment might be prohibitive.

While 2 M betaine / 25 % 2,3-butanediol cAb printing buffer performed with high sensitivity on all reactive aldehyde slide, it increased the variability of MCP4 on Xenobind slides, which was not seen with the Ang1, HGF-R and VEGFR2 assays. We determined that a cAb printing buffer composed of 50 % glycerol improved MCP4 assay reproducibility, and that the addition of 0.005 % Tween-20 helped increase the amount of liquid delivered on the surface by the silicon pins [165, 235], allowing the fluorescence intensity and therefore sensitivity to increase. MCP4's worse reproducibility on Xenobind slides was not observed on PolyAn 2D Aldehyde slides, suggesting that MCP4's variability in binding its Ag might arise from a susceptibility in surface coating variability that is specific to Xenobind. Despite the loss in sensitivity, we chose to print all antibodies in 50 % glycerol with 0.005 % Tween-20 on PolyAn 2D Aldehyde slides because of the yet unknown possibility that other cAbs among the 103 tested might be susceptible to variability in the surface coating of not only Xenobind slides, but also PolyAn 2D Aldehyde slides. Indeed, assay for two proteins (S100B and AFP) gave valid standard curves using the glycerol-based, but not the betaine/2,3-butanediol-based cAb printing buffers, even on PolyAn 2D aldehyde slides. Glycerol

is widely used to preserve the structure and function of proteins [236–240] whereas this is not the case for betaine or 2,3-butanediol. Many groups claim that glycerol in the cAb printing buffer prevents binding of molecules to the surface [163, 164]. Our results show that on reactive aldehyde based surfaces, binding of molecules to the surface in high glycerol content printing buffers was possible when a long enough incubation time was performed. This is consistent with McBeath *et al.* who spotted proteins in 40 % glycerol on reactive aldehyde slides [183]. Further research into a better combination of additives, for example by mixing betaine with glycerol and Tween-20, could also lead to a printing buffer that allows higher binding of molecules at the surface and still prevents the suspected denaturation of certain cAbs that are susceptible to denaturation due to the slides chemical coating.

After printing with a cAb printing buffer containing 50 % for the first large-scale experiment, we noticed that cAb spots printed in the first ~5 min swelled and merged, making 1-2 slides unusable each time pins were washed and dipped into the source well plate to load fresh reagents. This was most likely due the buffer absorbing up water from the high humidity, the other slides being usable because the cAb printing buffer in the pin had already absorbed water to an equilibrium state. We lowered the glycerol concentration to 45 % in the second large-scale experiment to resolve this issue. This difference between the two experiments might contribute in part to the worse LOD seen in the first large-scale experiment, although the trehalose coating of slides in this experiment probably contributed a larger proportion of the difference seen.

While we found Xenobind slides chemical coating to be stable during long waits at room temperature and high humidity before spotting, this was not the case for slides with printed cAbs and Ags in the dry state. We found no decrease in signal intensity of GAR-b that was left to dry for over 24 h and incubated with Strept-AF555. We therefore concluded that the degradation seen was not due to the breaking of bonds binding GAR-b to the surface, followed by washing away of cAb molecules, in spite of cAbs being bound by weak Schiff base bonds. Instead, we found significant degradation in mouse monoclonal cAbs ability to be bound by GAM-AF647. We presume that although GAM-AF647 is a polyclonal antibody, it was produced with structurally intact mouse IgGs and therefore a structural denaturation of cAbs on the surface would make them unable to be bound by GAM-AF647. When investigating the effect of degradation on Ags, we saw a less pronounced effect, which might be due to some Ags being less susceptible to denaturation than others, and/or some dAbs' ability to recognize the epitope on their respective Ag in a partially denatured form. Nonetheless, we saw an effect on assay signals, and therefore sensitivity of assays. The effect of degradation on assay signals differed between different types of slides, and therefore the degradation is likely partially due to the chemical coating on the slides surface. The time difference between the first and last printed spots for a single antibody in our protocol would be

80 min and therefore we assume that the difference in denaturation as a source of variability would not be very pronounced, although we did not measure the rate of denaturation of all cAbs and Ags in our assay. The greatest detrimental effect would be seen in sensitivity, where cAbs spotted last after 36 h of waiting in the dry state could have undergone significant degradation.

We observed that the degradation of cAbs and Ags when left in a dry state was partially mitigated by coating slide with a solution of 5 % trehalose, which we quickly blow-dried on slides using a stream of compressed nitrogen. While we used at 5 % trehalose solution, the solution dried on slides and therefore it is most likely the thickness of the coating along with how much water remained in that layer that protected cAbs and Ags. Drying slides manually was tricky and created variability not only because of the micro-crystals formed, visible under the microscope, but also in the thickness of the trehalose coating between slides and within single slides. This led to a worsening of the LOD and AR of assays, as there was more variability among technical replicate spots and blanks, making assays less precise. A better method of drying or depositing a uniform layer of trehalose with crystals of less than ~5 µm, the scanner resolution in our platform, would most likely lead to better reproducibility and sensitivity. Coating other chemicals or mixtures might also lead to a better protection of spots from degradation. A larger concentration of sucrose or trehalose dried on top of slides could be used for storing slides, combined with low temperatures, as is commonly used in lateral-flow assays using sucrose [241–243] or trehalose [244–246].

We found BSA-AF555 to be the best of four molecules at calibrating the amount of cAb bound to the microarray slide surface in every spot to address local variability. One of the other three molecules tested, GAR-AF555, showed significant false positive signals for half of the proteins tested. Assays which produced false positive measurements in the presence of GAR-AF555 were composed of goat polyclonal dAbs, which in theory should not lead to cross-reactivity because of the selection process by which antibodies are produced in mammals [247]. Therefore the reason why the presence of GAR-AF555 led to positive signal is unknown at this time. Since the blocking molecule in the ACM is BSA, and it is present in small proportion in every spot along with cAbs, it was not expected to lead to false positive signals in assays.

h-AF555 was a promising candidate as spot calibrant, as it does not contain a protein moiety and therefore cannot cross-react with other molecules in the assay. However the binding of h-AF555 on the surface was revealed to be more complex than for BSA-labeled molecules and could not be used as spot calibrant. A better use of h-AF555 would have been to pre-label all cAbs, however this labeling would have been cumbersome and lead to loss of costly antibodies during the purification step. Labeling of cAbs also could have modified their functionality and might have affected their stability.

Overall the performance of BSA-AF555 was better than that of BSA-AF647, whose affitiny for

the Xenobind surface appeared to be greater than that of BSA-AF555, thereby preventing some cAb from binding at the surface. The stability of the fluorophore, both in the dry state at high humidity and also at room temperature in the cAb printing buffer, made AF647 a bad candidate as spot calibrant. It was also necessary to consider the fluorophores with the background fluorescence of our slides and the performance of our scanner. Overall, the green channel had a higher fluorescence background and therefore it was a more sensible solution to use the spot calibrant in the green channel, with its fairly constant fluorescence intensity above the background. Therefore the red channel was left for assays which require more sensitivity and lower fluorescence backgrounds. A minimally working concentration of BSA-AF555 was however required to minimize cross-talk of the green signal into the red channel, most likely due to the emission tail of AF555 which slightly overlaps the emission tail of AF647. Picking two fluorophores which are further apart in their emission spectra and corresponding scanner laser and filters would most likely address this problem and improve sensitivity, although in this assay the crosstalk was fairly minimal.

We were surprised to see a rapid degradation of AF647 in the microarrayer chamber at high humidity, and a relative stability of fluorophores in the scanner, while both instruments were located in a room with controlled ozone below 5 ppm. It is known that AF647 is more sensitive to low levels of ozone than AF555 [248], but the difference between the two instruments was surprising and at this time it is unknown if AF647 was sensitive to high humidity or if there were differences in local concentrations of ozone between the two instruments. The degradation of AF647, and to a lesser degree AF555, occurred at different rates on the different slide types. This points to a type of degradation that might be facilitated by the chemical coating present at the slide surface, in high humidity or ozone.

To find out how to use calibrant signals when calibrating assay signals, we used BSA-AF555 spotted with cAbs at a constant ratio in different concentrations to elucidate the mathematical relationship between the spot calibrant and assay signals. We found that the relationship $b = log(A/{C_S}^m)$ is compatible with the fact that data is heteroskedastic and therefore log-transformed before data analysis. The exponent m accounts for differences in scanner gain and specific ratio of cAb to spot calibrant, and implies that the rate of difference relationship cannot be assumed to be 1:1. For example, a 100 % increase in assay signal may not translate to a 100 % increase in spot calibrant signal for the same antigen concentration, and m accounts for this difference in rate of change.

The fact that the constant slope relationship seen for the higher concentrations of Ag was only valid between 25 and 100 µg/mL of cAb concentration is not an issue in the ACM. Most antibodies are printed at concentrations of 100 µg/mL or more and we have seen less than 10 % difference in cAb quantities bound at the surface (as detected by GAM-AF647, data not shown). Therefore the

variability in quantity of cAb bound to the surface is well within the range where the slope between the log of spot calibrant and assay signals is linear.

Because of different affinities of cAbs and dAbs for their epitopes on the same antigen, and the degree of biotin labeling of dAbs varies from one protein assay to another, we observed that calibration slopes varied between different proteins. Moreover because of differences between experiments, we also observed that calibration slopes were different between experiments for the same protein. Therefore calibration slopes should be estimated for every protein, in every experiment, using replicate samples located throughout the experimental layout.

The strength of the mathematical relationship observed here is the fact that it can be serially combined when multiple calibrants signals are used. Since b_1 of the first equation is related to the antigen concentration just like the assay signal, it can replace the assay signal of a second equation using a second calibrant, obtaining a second intercept b_2 which can subsequently replace the assay signal in a third equation involving a third calibrant signal, and so on. Serially combining equations is a powerful technique but it must first calibrate the calibrant which corresponds to the greatest source of variability, followed by the calibrant addressing the second greatest source of variability. Since we could not possibly measure the amount of variability that each calibrant addressed in the assay for 103 proteins, we opted for devising five algorithms, each using specific combinations of one, two or three calibrants in different orders. There are a total of 15 ways to combine one, two or three calibrants serially and we used only five of them. It is possible that one of the untested equations might have led to a greater improvement of reproducibility for one or more proteins, but we picked the five listed in figure 4.6 because they made logical sense in the context of the assay.

We did not expect a single algorithm to prevail above all others and improve the reproducibility for all proteins tested, as we expected different cAbs, Ags and dAbs to be susceptible or sensitive to different sources of local and systemic variability. This was the case of MCP4 on Xenobind when it was printed in 2 M betaine / 25 % 2,3-butanediol compared to Ang1, HGF-R and VEGFR2 which were not sensitive to this printing buffer and slide combination. Therefore we decided to choose the best performing algorithm for each protein.

We were faced with a number of ways to estimate calibration slopes and found that taking the median of many calibration slopes calculated within 10-16 local groups performed best in two large-scale experiments, but the choice of which replicate types and dilutions to use, and how to best separate the experimental layout into local groups varied. For future experiment we recommend calculating the performance of each of the four ways of estimating calibration slopes and picking the method which leads to the best performance. This selection of the best method could also be done for each protein, which we did not do here and might improve calibration performance further. Using local groups in which samples are grouped by sample type, dilution and if possible, patient,

with randomization within local groups, also leads to increased reproducibility among samples located in the same local group, based on the fact that reproducibility is better in small-scale compared to large-scale experiments.

Because calibration slopes were calculated using replicate samples, and their performance was also verified using the same replicate samples, simply picking an m that would lead to the greatest improvement in reproducibility for the same replicate samples was not an option as it would have led to a form of overfitting. This would have led to improving reproducibility only in the replicates samples, and possibly worsening the true reproducibility and accuracy of clinical sample measurements. We therefore took care of estimating calibration slopes with many different local groups, or using different replicate types and dilutions. The use of validation samples allowed us to verify that our estimated calibration slopes did not lead to overfitting, and therefore the method we devised can be trusted to also improve clinical samples reproducibility and accuracy.

While the calibration slope m for each protein is constant above a certain antigen concentration, it is not constant across the whole range of antigen concentration used in our assays. Using replicate samples located throughout large-scale experiments allowed us to estimate calibration slopes if the quantity of antigen measured for a given protein was above the standard curve inflection point and located in the constant region of m. The fact that we estimated a single value for each protein's calibration slope (per calibrant) does not imply that the estimated calibration slope was in region of antigen concentration where calibration slopes are constant. This highly depended on the antigen concentration measured in the replicate samples. Calibration would be more accurate if the curve of m could be estimated throughout the whole range of Ag concentration, including below the standard curve inflection point. Because overfitting would have to be avoided at each estimation point of calibration slope curves for every protein, samples with various known concentrations of all antigens would be required in multiple replicates throughout the experimental layout, potentially requiring several slides with full standard curves, which would increase reagent costs and decrease space for clinical samples.

The two large-scale experiments had a number of differences during the execution of the experimetns and in their layouts. Other than the trehalose coating of slide *vs* washing slides with water before drying and dAb spotting, the number of slides were different, the cAb printing buffer had different concentrations of glycerol (with 45 % giving the least amount of change in the amount of cAb spotted throughout), they were spotted with different batches of PolyAn 2D Aldehyde slides, which showed different amounts of variability on their surfaces, and the validation samples were located at different places on the respective experimental slide layouts. Therefore the comparison of different performance measures in order to evaluate the role of trehalose coating is done with caution, as the effect of other experimental differences might not be insignificant. However, the

clear differences in AR and LOD is expected to be explained at least in part by the trehalose coating, as both these measures directly depend on noise among technical replicate spots.

Using the two large-scale experiments, we calculated the improvement in reproducibility and well as residual error for validation samples for both experiments. We found that in both cases, calibration improved reproducibility of replicate samples and also validation samples. Because of the differences in reproducibility, LOD and AR, trehalose coating as is currently described here is not recommended for large-scale experiments. To mitigate the potential degradation of some proteins, we suggest measuring this degradation for each protein, selecting proteins which are most sensitive to degradation and printing them first, thereby decreasing the amount of time they are left in the dry state before dAb printing.

Because in fact calibration slopes are not constant throughout the whole range of antigen concentration measured, AR, QR and LOD, which are affected by lack of reproducibility at the lower level of antigen concentration, were made worse by our calibration method. However since our calibration method can improve reproducibility at any level, in theory if one were to use blanks to calculate calibration slopes, sensitivity could be improved for experiments where it is deemed to be more important than reproducibility.

4.5 Conclusion

In this study we have addressed sources of variability on two fronts. First by optimizing certain protocol steps that are a source of variability, such as incubation times and cAb printing buffer. Second by introducing three new calibrants with an algorithm that combines five individual algorithms and allows the improvement in reproducibility of data after the experiment is performed. We obtained a 20 % and 30 % improvement in reproducibility in two large-scale experiments, which is better than the improvement obtained by using the robust linear model method of calibration [218], which led to a 19 % improvement in reproducibility. The calibration method proposed here does not assume that systemic sources of variability follow a linear model, since these sources of variability are in fact rarely linear [249]. From the large-scale experiment without trehalose coating where 103 proteins were measured in 768 wells located on 48 slides and printing times were 36 h, a median reproducibility of 26.1 % means that almost half of the 103 proteins measured have a reproducibility that is below the 25 % reproducibility required for FDA-approval of multiplexed assays used clinically to determine patient care [250].

In this study we have used replicate samples located on every slide in order to calculate reproducibility in two large-scale experiments, and similar control samples have only been used once previously [215]. Because of the importance of reproducibility in measuring and analyzing

clinical samples, we argue that multiplexed assays that contain replicate samples and from which reproducibility measures can be calculated for every analyte measured, is a more accurate way to assess the real reproducibility of assays, rather than performing a small-scale experiment prior to a large-scale experiment.

Several sources of variability in the ACM protocol were not optimized, nor addressed by calibrants, and contribute to the remaining variability measured in large-scale experiments. This includes washing and drying of slides, loading of reagents which were done entirely by hand, and dAb printing variability for which no calibrant was present. In fact, calibration of variability in dAb printing would be possible if a target molecule was spotted with the cAb and another fluorescently-labeled molecule was mixed with the dAb printing buffer to bind the target molecule in a way that is consistent with the amount of dAb delivered in each spot by printing. Possibly adding two more molecules to the ACM would however increase its complexity and increase chances of cross-reactivity, as well as require a scanner that can handle three or more colors. With further improvements to the assay by the addition of automation for washing, drying and loading of reagents unto slides, as well as calculating a non-linear calibration slope curve for each protein, even better reproducibility and sensitivity could be obtained. As seen also in previous studies, reproducibility is highly variable and depends on the protein measured or the matched antibody pair used [251], and therefore selection of more reliable antibodies might also help improve reproducibility further.

The methods explained here are not specific to pin printing with a contact microarrayer, and could be used with an inkjet microarray printer. cAb and dAb printing buffers might have to be re-optimized, but the use of the three calibrants and experimental layout recommendations are compatible with inkjet printers. It could also be used for regular MSA assays where dAbs are mixed rather than spotted, given that cross-reactivity from the mixing of dAbs has been minimized.

Supporting Information

Additional information as noted in the text. This material is available in appendix D.

Corresponding Author

*Email: david.juncker@mcgill.ca

Acknowledgements

This work was funded by the Natural Sciences and Engineering Research Council of Canada (NSERC), the Canadian Institutes of Health Research (CIHR) and the Canada Foundation for

Innovation (CFI). DJ acknowledges support from a Canada Research Chair in micro and nanobioengineering. VL acknowledges support from a Natural Sciences and Engineering Research Council of Canada - Collaborative Research and Training Experience Program (NSERC-CREATE) Award in Integrated Sensor Systems.

Conflict of interest

The authors declare no conflict of interest.

References

17. Pla-Roca, M., Leulmi, R. F., Tourekhanova, S., Bergeron, S., Laforte, V., Moreau, E., Gosline, S. J. C., Bertos, N., Hallett, M., Park, M. & Juncker, D. Antibody colocalization microarray: a scalable technology for multiplex protein analysis in complex samples. *Molecular & Cellular Proteomics* **11,** M111.011460 (2012).

138. Engvall, E & Perlmann, P. Enzyme-linked immunosorbent assay (ELISA). Quantitative assay of immunoglobulin G. *Immunochemistry* **8,** 871–874 (1971).

141. Li, H., Bergeron, S. & Juncker, D. Microarray-to-microarray transfer of reagents by snapping of two chips for cross-reactivity-free multiplex immunoassays. *Analytical Chemistry* **84,** 4776–4783 (2012).

142. Li, H., Munzar, J. D., Ng, A. & Juncker, D. A versatile snap chip for high-density sub-nanoliter chip-to-chip reagent transfer. *Scientific Reports* **5,** 11688 (2015).

143. Li, H., Bergeron, S., Larkin, H. & Juncker, D. Snap Chip for Cross-reactivity-free and Spotter-free Multiplexed Sandwich Immunoassays. *JoVE,* e56230 (2017).

146. Bergeron, S., Laforte, V., Lo, P. S., Li, H. & Juncker, D. Evaluating mixtures of 14 hygroscopic additives to improve antibody microarray performance. *Analytical and Bioanalytical Chemistry* **407,** 8451–8462 (2015).

150. Kricka, L. J. & Master, S. R. Quality control and protein microarrays. *Clinical Chemistry* **55,** 1053–1055 (2009).

154. Laforte, V., Olanrewaju, A. & Juncker, D. *Low-cost , high liquid volume silicon quill pins for robust and reproducible printing of antibody microarrays* in *MicroTAS: miniaturized systems for chemistry and life sciences* (Chemical and Biological Microsystems Society (CBMS), Freiburg, Germany, 2013), 485–487.

163. Rodríguez-Seguí, S. A., Pons Ximénez, J. I., Sevilla, L., Ruiz, A., Colpo, P., Rossi, F., Martínez, E. & Samitier, J. Quantification of protein immobilization on substrates for cellular microarray applications. *Journal of Biomedical Materials Research - Part A* **98,** 245–256 (2011).

164. Liu, Y. S., Li, C. M., Yu, L. & Chen, P. Optimization of printing buffer for protein microarrays based on aldehyde-modified glass slides. *Frontiers in Bioscience* **12,** 3768–3773 (2007).

165. Ruwona, T. B., McBride, R., Chappel, R., Head, S. R., Ordoukhanian, P., Burton, D. R. & Law, M. Optimization of peptide arrays for studying antibodies to hepatitis C virus continuous epitopes. *Journal of Immunological Methods* **402,** 35–42 (2014).

166. Monroe, M. R., Reddington, A. P., Collins, A. D., LaBoda, C., Cretich, M., Chiari, M., Little, F. F. & Ünlü, M. S. Multiplexed method to calibrate and quantitate fluorescence signal for allergen-specific IgE. *Analytical Chemistry* **83,** 9485–9491 (2011).

183. MacBeath, G. & Schreiber, S. L. Printing proteins as microarrays for high-throughput function determination. *Science* **289,** 1760–1763 (2000).

194. Chen, Z., Dodig-Crnković, T., Schwenk, J. M. & Tao, S. C. Current applications of antibody microarrays. *Clinical Proteomics* **15,** 1–15 (2018).

195. Sauer, U. Analytical protein microarrays: Advancements towards clinical applications. *Sensors (Switzerland)* **17,** 256 (2017).

196. Ko Ferrigno, P. Increasing experimental reproducibility, from antibodies to protein arrays. *Drug Discovery Today* **21,** 1197–1199 (2016).

197. Cretich, M., Damin, F. & Chiari, M. Protein microarray technology: How far off is routine diagnostics? *Analyst* **139,** 528–542 (2014).

198. Li, Z., Wen, F., Li, Z., Zheng, N., Jiang, J. & Xu, D. Simultaneous detection of α-Lactoalbumin, β-Lactoglobulin and Lactoferrin in milk by Visualized Microarray. *BMC Biotechnology* **17,** 72 (2017).

199. Gerdtsson, A., Dexlin-Mellby, L., Delfani, P., Berglund, E., Borrebaeck, C. & Wingren, C. Evaluation of Solid Supports for Slide- and Well-Based Recombinant Antibody Microarrays. *Microarrays* **5,** 16 (2016).

200. Ayling, K., Bowden, T., Tighe, P., Todd, I., Dilnot, E. M., Negm, O. H., Fairclough, L. & Vedhara, K. The application of protein microarray assays in psychoneuroimmunology. *Brain, Behavior, and Immunity* **59,** 62–66 (2017).

201. Van Hage, M., Schmid-Grendelmeier, P., Skevaki, C., Plebani, M., Canonica, W., Kleine-Tebbe, J., Nystrand, M., Jafari-Mamaghani, M. & Jakob, T. Performance evaluation of ImmunoCAP® ISAC 112: A multi-site study. *Clinical Chemistry and Laboratory Medicine* **55,** 571–577 (2017).

202. Brazma, A., Hingamp, P., Quackenbush, J., Sherlock, G., Spellman, P., Stoeckert, C., Aach, J., Ansorge, W., Ball, C. A., Causton, H. C., Gaasterland, T., Glenisson, P., Holstege, F. C., Kim, I. F., Markowitz, V., Matese, J. C., Parkinson, H., Robinson, A., Sarkans, U., Schulze-Kremer, S., Stewart, J., Taylor, R., Vilo, J. & Vingron, M. Minimum information about a microarray experiment (MIAME) - Toward standards for microarray data. *Nature Genetics* **29,** 365–371 (2001).

203. Martínez-Aranguren, R., Lizaso, M. T., Goikoetxea, M. J., García, B. E., Cabrera-Freitag, P., Trellez, O. & Sanz, M. L. Is the determination of specific IgE against components using ISAC 112 a reproducible technique? *PLoS ONE* **9,** 1–7 (2014).

204. Angenendt, P., Glökler, J., Murphy, D., Lehrach, H. & Cahill, D. J. Toward optimized antibody microarrays: a comparison of current microarray support materials. *Analytical Biochemistry* **309,** 253–260 (2002).

205. Harrison, A., Binder, H., Buhot, A., Burden, C. J., Carlon, E., Gibas, C., Gamble, L. J., Halperin, A., Hooyberghs, J., Kreil, D. P., Levicky, R., Noble, P. A., Ott, A., Pettitt, B. M., Tautz, D. & Pozhitkov, A. E. Physico-chemical foundations underpinning microarray and next-generation sequencing experiments. *Nucleic Acids Research* **41,** 2779–2796 (2013).

206. Löbke, C., Laible, M., Rappl, C., Ruschhaupt, M., Sahin, Ö., Arlt, D., Wiemann, S., Poustka, A., Sültmann, H. & Korf, U. Contact spotting of protein microarrays coupled with spike-in of normalizer protein permits time-resolved analysis of ERBB receptor signaling. *Proteomics* **8,** 1586–1594 (2008).

207. Ramani, S. R., Tom, I., Lewin-Koh, N., Wranik, B., Depalatis, L., Zhang, J., Eaton, D. & Gonzalez, L. C. A secreted protein microarray platform for extracellular protein interaction discovery. *Analytical Biochemistry* **420,** 127–138 (2012).

208. Olle, E. W., Sreekumar, A, Warner, R. L., McClintock, S. D., Chinnaiyan, A. M., Bleavins, M. R., Anderson, T. D. & Johnson, K. J. Development of an internally controlled antibody microarray. *Molecular & Cellular Proteomics* **4,** 1664–1672 (2005).

209. Zangar, R. C., Daly, D. S., White, A. M., Servoss, S. L., Tan, R. M. & Collett, J. R. ProMAT Calibrator : A Tool for Reducing Experimental Bias in Antibody Microarrays research articles. *Journal of Proteome Research* **8,** 3937–3943 (2009).

210. Jin, H. & Zangar, R. C. Antibody microarrays for high-throughput, multianalyte analysis. *Cancer Biomarkers* **6,** 281–290 (2009).

211. Ingvarsson, J., Larsson, A., Sjo, A. G., Truedsson, L., Jansson, B., Borrebaeck, C. A. K. & Wingren, C. Design of Recombinant Antibody Microarrays for Serum Protein Profiling : Targeting of Complement Proteins research articles. *Journal of Proteome Research* **6,** 3527–3536 (2007).

212. Hamelinck, D., Zhou, H., Li, L., Verweij, C., Dillon, D., Feng, Z., Costa, J. & Haab, B. B. Optimized Normalization for Antibody Microarrays and Application to Serum-Protein Profiling. *Molecular & Cellular Proteomics* **4,** 773–784 (2005).

213. Neuman de Vegvar, H. E., Amara, R. R., Steinman, L., Utz, P. J., Robinson, H. L. & Robinson, W. H. Microarray profiling of antibody responses against simian-human immunodeficiency virus: postchallenge convergence of reactivities independent of host histocompatibility type and vaccine regimen. *Journal of Virology* **77,** 11125–38 (2003).

214. Lv, L. L., Liu, B. C., Zhang, C. X., Tang, Z. M., Zhang, L. & Lu, Z. H. Construction of an antibody microarray based on agarose-coated slides. *Electrophoresis* **28,** 406–413 (2007).

215. Perlee, L., Christiansen, J, Dondero, R, Grimwade, B, Lejnine, S, Mullenix, M, Shao, W, Sorette, M, Tchernev, V., Patel, D. & Kingsmore, S. Development and standardization of multiplexed antibody microarrays for use in quantitative proteomics. *Proteome Science* **2,** 9 (2004).

216. List, M., Block, I., Pedersen, M. L., Christiansen, H., Schmidt, S., Thomassen, M., Tan, Q., Baumbach, J. & Mollenhauer, J. Microarray R-based analysis of complex lysate experiments with MIRACLE. *Bioinformatics* **30,** 631–638 (2014).

217. Rimini, R., Schwenk, J. M., Sundberg, M., Sjöberg, R., Klevebring, D., Gry, M., Uhlén, M. & Nilsson, P. Validation of serum protein profiles by a dual antibody array approach. *Journal of Proteomics* **73,** 252–66 (2009).

218. Sboner, A., Karpikov, A., Chen, G., Smith, M., Dawn, M., Freeman-cook, L., Schweitzer, B. & Gerstein, M. B. Robust-Linear-Model Normalization To Reduce Technical Variability in Functional Protein Microarrays. *Journal of Proteome Research* **8,** 5451–5464 (2009).

219. Laforte, V., Lo, P.-S., Li, H. & Juncker, D. Antibody Colocalization Microarray for Cross-Reactivity-Free Multiplexed Protein Analysis. *Methods in Molecular Biology* **1619** (eds Greening, D. W. & Simpson, R. J.) 239–261 (2017).

220. R Core Team. *R: A Language and Environment for Statistical Computing* R Foundation for Statistical Computing (Vienna, Austria, 2018).

221. Dag, O., Dolgun, A. & Konar, N. onewaytests: An R Package for One-Way Tests in Independent Groups Designs. *The R Journal* **10,** 175–199 (2018).

222. Komsta, L. *outliers: Tests for outliers* R package version 0.14 (2011).

223. Ritz, C., Baty, F., Streibig, J. C. & Gerhard, D. Dose-Response Analysis Using R. *PLOS ONE* **10** (12 2015).

224. Komsta, L. *mblm: Median-Based Linear Models* R package version 0.12 (2013).

225. Elzhov, T. V., Mullen, K. M., Spiess, A.-N. & Bolker, B. *minpack.lm: R Interface to the Levenberg-Marquardt Nonlinear Least-Squares Algorithm Found in MINPACK, Plus Support for Bounds* R package version 1.2-1 (2016).

226. Ritchie, M. E., Phipson, B., Wu, D., Hu, Y., Law, C. W., Shi, W. & Smyth, G. K. limma powers differential expression analyses for RNA-sequencing and microarray studies. *Nucleic Acids Research* **43,** e47 (2015).

227. Venables, W. N. & Ripley, B. D. *Modern Applied Statistics with S* Fourth. ISBN 0-387-95457-0 (Springer, New York, 2002).

228. Murphy, T. & Dendukuri, N. *R tutorial on fitting response curves for point-of-care diagnostic tests* http://weightinginbayesianmodels.github.io/poctcalibration/AMfunctions.html.

229. Saviranta, P., Okon, R., Brinker, A., Warashina, M., Eppinger, J. & Geierstanger, B. H. Evaluating sandwich immunoassays in microarray format in terms of the ambient analyte regime. *Clinical Chemistry* **50,** 1907–1920 (2004).

230. Yang, Y. H., Dudoit, S, Luu, P, Lin, D. M., Peng, V, Ngai, J & Speed, T. P. Normalization for cDNA microarray data: a robust composite method addressing single and multiple slide systematic variation. *Nucleic Acids Research* **30,** e15 (2002).

231. Babyak, M. What You See May Not Be What You Get: A Brief, Nontechnical Introduction to Overfitting in Regression-Type Models. *Psychosomatic Medicine,* 4–5 (2004).

232. Prüller, F., Wagner, J., Raggam, R. B., Hoenigl, M., Kessler, H. H., Truschnig-Wilders, M. & Krause, R. Automation of serum (1→3)-beta-D-glucan testing allows reliable and rapid discrimination of patients with and without candidemia. *Medical Mycology* **52,** 453–459 (2014).

233. Morschett, H., Wiechert, W. & Oldiges, M. Automation of a Nile red staining assay enables high throughput quantification of microalgal lipid production. *Microbial Cell Factories* **15,** 1–11 (2016).

234. Fu, Q., Kowalski, M. P., Mastali, M., Parker, S. J., Sobhani, K., Van Den Broek, I., Hunter, C. L. & Van Eyk, J. E. Highly Reproducible Automated Proteomics Sample Preparation Workflow for Quantitative Mass Spectrometry. *Journal of Proteome Research* **17,** 420–428 (2018).

235. Wang, S., Zhao, P. & Cao, B. Development and optimization of an antibody array method for potential cancer biomarker detection. *Journal of Biomedical Research* **25,** 63–70 (2011).

236. Wang, S., Oldenhof, H., Dai, X., Haverich, A., Hilfiker, A., Harder, M. & Wolkers, W. F. Protein stability in stored decellularized heart valve scaffolds and diffusion kinetics of protective molecules. *Biochimica et Biophysica Acta* **1844,** 430–438 (2014).

237. Vagenende, V., Yap, M. G. & Trout, B. L. Mechanisms of protein stabilization and prevention of protein aggregation by glycerol. *Biochemistry* **48,** 11084–11096 (2009).

238. Simpson, R. J. Stabilization of proteins for storage. *Cold Spring Harbor Protocols* **5** (2010).

239. Chen, X., Bhandari, B. & Zhou, P. Insight into the effect of glycerol on stability of globular proteins in high protein model system. *Food Chemistry* **278,** 780–785 (2019).

240. Pazhang, M., Mehrnejad, F., Pazhang, Y., Falahati, H. & Chaparzadeh, N. Effect of sorbitol and glycerol on the stability of trypsin and difference between their stabilization effects in the various solvents. *Biotechnology and Applied Biochemistry* **63,** 206–213 (2016).

241. Anfossi, L., Di Nardo, F., Profiti, M., Nogarol, C., Cavalera, S., Baggiani, C., Giovannoli, C., Spano, G., Ferroglio, E., Mignone, W. & Rosati, S. A versatile and sensitive lateral flow immunoassay for the rapid diagnosis of visceral leishmaniasis. *Analytical and Bioanalytical Chemistry* **410,** 4123–4134 (2018).

242. Bobosha, K., Tjon Kon Fat, E. M., van den Eeden, S. J. F., Bekele, Y., van der Ploeg-van Schip, J. J., de Dood, C. J., Dijkman, K., Franken, K. L. M. C., Wilson, L., Aseffa, A., Spencer, J. S., Ottenhoff, T. H. M., Corstjens, P. L. A. M. & Geluk, A. Field-Evaluation of a New Lateral Flow Assay for Detection of Cellular and Humoral Immunity against *Mycobacterium leprae*. *PLoS Neglected Tropical Diseases* **8** (2014).

243. Wang, Z., Zhi, D., Zhao, Y., Zhang, H., Wang, X., Ru, Y. & Li, H. Lateral flow test strip based on colloidal selenium immunoassay for rapid detection of melamine in milk, milk powder, and animal feed. *International Journal of Nanomedicine* **9,** 1699–1707 (2014).

244. Gussenhoven, G. C., Goris, M. G. A., Terpstra, W. J., Hartskeerl, R. A., Mol, B. E. N. W., W, C. O. R. & Smits, H. L. LEPTO Dipstick, a Dipstick Assay for Detection of Leptospira-Specific Immunoglobulin M Antibodies in Human Sera. *Microbiology* **35,** 92–97 (1997).

245. Ramachandran, S., Fu, E., Lutz, B. & Yager, P. Long-term dry storage of an enzyme-based reagent system for ELISA in point-of-care devices. *Analyst* **139,** 1456–1462 (2014).

246. Yu, C. Y., Ang, G. Y., Chua, A. L., Tan, E. H., Lee, S. Y., Falero-Diaz, G., Otero, O., Rodríguez, I., Reyes, F., Acosta, A., Sarmiento, M. E., Ghosh, S., Ramamurthy, T., Yean Yean, C., Lalitha, P. & Ravichandran, M. Dry-reagent gold nanoparticle-based lateral flow biosensor for the simultaneous detection of *Vibrio cholerae* serogroups O1 and O139. *Journal of Microbiological Methods* **86,** 277–282 (2011).

247. Nutt, S. L., Hodgkin, P. D., Tarlinton, D. M. & Corcoran, L. M. The generation of antibody-secreting plasma cells. *Nature Reviews Immunology* **15,** 160–171 (2015).

248. Berlier, J. E., Rothe, A., Buller, G., Bradford, J., Gray, D. R., Filanoski, B. J., Telford, W. G., Yue, S., Liu, J., Cheung, C. Y., Chang, W., Hirsch, J. D., Beechem, J. M., Haugland, R. P. & Haugland, R. P. Quantitative Comparison of Long-wavelength Alexa Fluor Dyes to Cy Dyes: Fluorescence of the Dyes and Their Bioconjugates. *Journal of Histochemistry and Cytochemistry* **51,** 1699–1712 (2003).

249. Tseng, G. C., Oh, M.-K., Rohlin, L., Liao, J. C. & Wong, W. H. Issues in cDNA microarray analysis: quality filtering, channel normalization, models of variations and assessment of gene effects. *Nucleic Acids Research* **29,** 2549–2557 (2001).

250. Sittampalam, G. S., Coussens, N. P., Nelson, H., Arkin, M., Auld, D., Austin, C., Bejcek, B., Glicksman, M., Inglese, J., Iversen, P. W., McGee, J., McManus, O., Minor, L., Napper, A., Peltier, J. M., Riss, T., Trask, O. J. & Weidner, J. *Assay Guidance Manual* tech. rep. (Eli Lilly & Company and the National Center for Advancing Translational Sciences, Bethesda, MD, 2016).

251. Paul, J., Sahaf, B., Perloff, S., Schoenrock, K., Wu, F., Nakasone, H., Coller, J. & Miklos, D. High-throughput allogeneic antibody detection using protein microarrays. *Journal of Immunological Methods* **432,** 57–64 (2016).

CHAPTER 5

Comparison of microdialysis additives

Preface

Background and objectives

While improving the ACM protocol, we had designed a clinical study which included collecting microdialysate samples from patients suffering from severe traumatic brain injury. Due to problems recovering microdialysate from one patient with particularly high intra-cranial pressure, we looked for additives to put in the perfusion fluid. When we searched the literature, we found that albumin and dextrans had been used for years to address this issue, but there was no quantitative measure of leakage into the brain and we were concerned about the safety of the leaked additives for patients, as well as the effect of the additives on the measurements of proteins.

Therefore the first step was to measure leakage of additives *in vitro*, and since I was planning to quantify several proteins in microdialysate samples of patients, we also had to measure the relative recovery of proteins through the microdialysis membrane. The second part of the study investigated the effect of the additives on human glial cells, as a first step that should be done *in vitro* before it is done *in vivo* in animals in the future. This would allow a more complete comparison of additives to the perfusion fluid of cerebral microdialysis, and in the future a standard procedure being agreed upon by clinicians around the world.

Challenges and encountered problems

Microdialysis catheters are expensive and while we attempted to optimize the amount of results we could obtain from a single catheter, we ran out of catheters before the end of our *in vitro* study. We had to reach out to scientists across the world to ask for catheters that were still usable, but whose sterility treatment had expired. We were very lucky to find two clinicians who sent us catheters, and allowed us to finish our study. Their donation of a catheter each is acknowledged in the chapter.

In order to study the effect of albumin on the U87 cell cultures, which are normally cultured with 10 % fetal bovine serum (FBS, which contains a fetal form of albumin), we attempted to culture the cells in a serum-free cell media. While there is increasing knowledge about the factors necessary for the sustenance of immortalized cells in culture, our attempts failed. The minimum amount of FBS we had to put in the cell media to keep cells alive (but not growing) was 1 %. After months of attempting to culture the U87 cells in a serum-free medium, we decided to grow cells in 10 % FBS, and then transfer them to multi-well plates in cell media containing only 1 % FBS, allowing the cells to survive but not to grow. This was used because we were adding 3.5 % albumin to the cell culture media, whose effect would have been hidden had we kept cells in media containing 10 % FBS.

Reference

This chapter was written with the intention to submit to the journal *Methods in Neuroscience* in the near future.

Comparison of albumin, low- and high-molecular weight dextrans as additives to brain microdialysis

Veronique Laforte[1,2,3], Francesco Fiorini[2,3], David KY Zhang[3,4], Judith Marcoux[2,5] and David Juncker[1,2,3,*]

Affiliations

[1] Department of Biomedical Engineering, McGill University,
3775 University Street, Montreal, Quebec, Canada H3A 2B4
[2] Department of Neurology and Neurosurgery, McGill University,
3801 University Street, Montreal, Quebec, Canada H3A 2B4
[3] McGill University and Genome Québec Innovation Center, McGill University,
740 Dr. Penfield Avenue, Montreal, Quebec, H3A 0G1
[4] Department of Microbiology and Immunology, McGill University,
3775 University Street, Montreal, Quebec, Canada H3A 2B4
[5] Department of Neurosurgery, McGill University Health Center,
1650 Cedar Avenue, Montreal, Quebec, H3G 1A4

Abstract

Cerebral microdialysis is used experimentally to monitor the progression of patients suffering from various severe brain injuries by indirectly measuring small molecules present in the brain tissue. A microdialysis catheter with a membrane cut-off of 100 kDa (CMA 71) was commercially produced to allow monitoring of large molecules such as proteins, however it leads to loss of perfusion fluid into the brain which can hinder or even prevent measurements. Several additives have been used to prevent fluid loss, but none were tested thoroughly for their leakage, effect on molecules measurements and brain cells. Here, we compare three different microdialysis additives (albumin, low-molecular weight and high-molecular weight dextrans) added to artificial cerebrospinal fluid as the base perfusion fluid in an *in vitro* testing environment. We found that all perfusates tested were stable after 20 minutes of flow, and that fluid recovery was above 100 % for all additives. Albumin leaked nine times more than high-molecular weight dextran through the membrane, and the leakage of low-molecular weight dextran resembled that of high-molecular weight dextran after four hours of perfusion. With respect to the effect of additives on the measurement of small (glucose, lactate, pyruvate and glutamate) and large (94 proteins measured with the antibody colocalization microarray) molecules, high-molecular weight dextran negatively affected the measurement of glutamate and a few proteins, whereas low-molecular weight dextran least affected measurements. Relative recovery of small and large molecules was also measured and again, high-molecular weight dextran was found to more strongly inhibit molecular diffusion across the membrane. Finally, additives were added to cell culture media of human glial U87 cells and proteins were measured at several time points afterwards. High-molecular weight dextran most strongly affected the profile of proteins secreted by glial cells, which is important because all additives tested leaked out of the catheter at various rates. Because all additives tested here leaked through the membrane and affected small molecules and proteins measurements directly and in glial cell cultures, no recommendation is made at this time. Instead, further testing is required to conclude about the safety of all additives *in vivo*.

Keywords: cerebral microdialysis · albumin · dextran · fluid recovery · relative recovery · leakage · matrix effect · U87 cells · antibody colocalization microarray

Abbreviations

ACM	Antibody colocalization microarray
aCSF	Artificial cerebrospinal fluid
BSA	Bovine serum albumin
BCA	Bicinchoninic acid
CSF	Cerebrospinal fluid
$Dextran_{500}$	500 kDa dextran
$Dextran_{HMW}$	High molecular weight (~250 kDa) dextran
$Dextran_{LMW}$	Low molecular weight (~75 kDa) dextran
FBS	Fetal bovine serum
ICP	Intracranial pressure
IF	Interstitial fluid
LPS	Lipopolysaccharide
pnCSF	Pooled normal cerebrospinal fluid
SI	Supplementary information
SM	Small molecules
sTBI	Severe traumatic brain injury

5.1 Introduction

Cerebral microdialysis is a technique by which molecules located in the interstitial fluid of the brain tissue are sampled by simple diffusion through a membrane inserted in the brain of patients who have suffered from traumatic brain injury or sub-arachnoid hemmorhage. A microdialysis catheter with a molecular weight cut-off of 20 kDa (CMA 70) has been used primarily to measure small molecules such as glucose, lactate, pyruvate, glutamate, urea and glycerol [252] using a commercial microdialysis analyzer which measures small molecules in parallel from approximately 2 µL per molecule measured. A microdialysis catheter with a higher molecular weight cut-off (CMA 71: 100 kDa) was developed for the measurement of macromolecules such as proteins, which can be measured with any platform in a research context.

Because of its larger pores, the high molecular weight cut-off microdialysis probe is subject to ultra-filtration [19, 21, 25] and regularly leaks liquid to the brain tissue being sampled. In order to circumvent this problem and restore diffusion-only based sampling, additives such as albumin and low and high-molecular weight dextrans have been used to increase the perfusion fluid osmolarity, thereby improving fluid recovery (the volume of microdialysate recovered compared to the volume of perfusate injected in the microdialysis catheter) and relative recovery of molecules (the concentration measured in the microdialysate compared to the concentration measured in the fluid or tissue being sampled). Albumin is a 66.5 kDa protein, generally monomeric, produced in the liver and accounts for half of the protein weight of plasma. It has been added to the microdialysis

perfusion fluid in order to improve fluid recovery and relative recovery of proteins [21, 25, 26, 253, 254], but leakage from the microdialysis probe has not been measured quantitatively, and the effect on small molecules and protein measurements as well as the effect on brain cells have not been investigated.

Dextrans are long neutral polymers of d-glucose monomers connected by α-1,6 links with occasional side chains, making up large, branched molecules between 3 and 2000 kDa. It is naturally produced by several bacteria, notably of the *lactobaccilus* family, and low-molecular weight dextrans (40 and 70 kDa) are used clinically to treat hypovolemia in patients due to their ability to increase plasma osmolarity [255]. Low-molecular weight dextran between 60 and 70 kDa ($\text{Dextran}_{\text{LMW}}$) was first used by Rosdahl et al. in 1997 in microdialysis [256], and subsequently used in several studies to increased fluid recovery in high molecular weight cut-off probes [19, 20, 26, 28, 257]. High ($\text{Dextran}_{\text{HMW}}$: 250 kDa) and very high (Dextran_{500}: 500 kDa) molecular weight dextrans were first used in microdialysis by Dahlin *et al.* in 2010 [258]. A qualitative study showed that dextrans of low (40 kDa) and high (250 kDa) molecular weights leaked through the 100 kDa molecular weight cut-off microdialysis membrane [259]. Therefore, Dextran_{500} was subsequently used in brain microdialysis of animals [23] and patients [260]. The effect of $\text{Dextran}_{\text{LMW}}$ on the relative recovery of proteins was measured for a small number (1-10) of proteins [19, 20, 258] and compared to perfusion fluid containing physiologically relevant concentrations of ions (CNS perfusion fluid, or artificial cerebrospinal fluid: aCSF). All studies found that while $\text{Dextran}_{\text{LMW}}$ improved fluid recovery, the relative recovery of most proteins was not improved with this additive. Quantitative leakage of dextrans, as well as the effect of $\text{Dextran}_{\text{HMW}}$ on the relative recovery of proteins, have not been measured.

The possible effect of albumin and dextrans on brain cells has not been explored. A single study qualitatively observed inflammation in rat skin where a high molecular weight cut-off microdialysis membrane was implanted and perfused with solutions containing different albumins and dextrans [261]. No study has compared albumin, $\text{Dextran}_{\text{LMW}}$ and $_{\text{HMW}}$ together quantitatively.

Here, we compare albumin and dextrans in a series of *in vitro* experiments in terms of flow stability, fluid recovery and relative recovery of small molecules and proteins. While leakage of additives has been mentioned twice previously [19, 258] as a theoretical notion and has been observed qualitatively [259], it has not yet been measured quantitatively. We measure the leakage of additives *in vitro*, and perform a thorough study of the effect of these additives on the measurement of small molecules and proteins. Finally, we test the effect of additives on brain cells, which is especially important if additives leak through the microdialysis membrane.

5.2 Materials and methods

5.2.1 Materials

Sodium chloride, potassium chloride, calcium chloride, magnesium chloride, Tris base, Tris hydrochloride, glycerol, sodium fluoride, sodium orthonitrate, phenylmethylsulfonyl fluoride (PMSF) and protease inhibitor cocktail (#P8340) were obtained from Sigma-Aldrich (St. Louis, MO, USA). Ethylenediaminetetraacetic acid (EDTA) and nonyl phenoxypolyethoxylethanol (NP-40) were purchased from Thermo Fisher Scientific (Waltham, MA, USA). Artificial CSF (aCSF: 147 mM NaCl, 2.7 mM KCl, 1.2 mM $CaCl_2$ and 0.85 mM $MgCL_2$ prepared in ultra-pure water) was used to dissolve immunoglobulin (IgG) and protease-free bovine serum albumin (BSA) (Jackson ImmunoResearch, West Grove, PA, USA), clinical grade low-molecular weight dextran ($Dextran_{LMW}$: 60-90 kDa) and clinical grade high-molecular weight dextran ($Dextran_{HMW}$: 200-300 kDa) (both dextrans were purchased from MP Biomedicals, Santa Ana, CA, USA). If not indicated, the additives were added at concentrations of 3.5 % (*w/v*) for BSA, and 3 % (*w/v*) for both dextrans. Liquid density was $\approx$ 1, 1.01, 1.03 and 1.02 g/mL for aCSF, BSA, $Dextran_{LMW}$ and $Dextran_{HMW}$, respectively. For the measurement of dextrans, pure phenol and sulfuric acid were obtained from Sigma-Aldrich. The cell culture medium Dulbecco's Modified Eagle Medium (DMEM), sterile phosphate-buffered saline (PBS), fetal bovine serum (FBS), lipopolysaccharides (LPS) from *Escherichia coli* O111:B4 were purchased from Sigma-Aldrich. Penicillin and streptomycin were obtained from Invitrogen (Carlsbad, CA, USA). The cell lysis buffer was composed of 20 mM Tris at pH 7.3, 140 mM NaCl, 10 % glycerol, 1 % NP-40, 2 mM EDTA with 10 mM NaF, 2 mM Na_3NO_4, 1 mM PMSF and 1:1000 protease inhibitor cocktail added just before use. PBS 10 × solution, goat anti-rabbit (GAR) AlexaFluor-647 (AF647), GAR-biotinXX, BSA-AF555, goat anti-mouse (GAM) AF647, streptavidin-AF647 and 4 mm 0.45 µm PVDF syringe filters used to remove debris from detection antibody solutions were obtained from Thermo Fisher Scientific. Tween-20® was purchased from Sigma-Aldrich. PBST solution consisted in PBS 1 ×, 0.05 % Tween-20® in pure water. Slides washing solution consisted in PBS 1 ×, 0.1 % Tween-20® in pure water. Capture antibodies, detection antibodies and recombinant proteins for 102 different assays (all proteins listed in appendix D except FGF-1 due to missing antibodies) were purchased from R&D Systems (Minneapolis, MN, USA), unless otherwise noted. BDNF, G-CSF, EpCAM, KLK14, FAS, TGF-β2, MCP4, and Cathepsin B were not measured due to missing spots in multiple samples. Concentrations used for each antibody and antigen are also listed in appendix D. Pooled normal human lumber cerebrospinal fluid (pnCSF) was purchased from Gemini Bio-Products (West Sacramento, CA, USA).

5.2.2 *In vitro* microdialysis measurements

Flow stability A microdialysis pump (CMA 107, μdialysis AB, Johanneshov, Sweden) containing a syringe filled with a perfusion fluid (aCSF, BSA, $\text{Dextran}_{\text{LMW}}$ or $\text{Dextran}_{\text{HMW}}$) and connected to a 100 kDa high-cut-off brain microdialysis catheter (CMA 71, 30 mm membrane, μdialysis AB) was used to pump the perfusion fluid into the catheter. The catheter tip was dipped in a microcentrifuge tube containing 500 µL of aCSF. The microdialysis microvial was located on a tared high-precision microbalance (XS204 DeltaRange Analytical Balance, Mettler Toledo, Colombus, OH, USA) and the weight was recorded every minute for 1 h. This experiment was done in triplicate each time with new catheters.

Fluid recovery and relative recovery of molecules Microdialysis catheters filled with aCSF and the different additives were dipped into sealed microcentrifuge tubes incubated at 37 °C and containing aCSF, normal pooled human lumbar cerebrospinal fluid (pnCSF, purchased from Gemini Bio-Products, West Sacramento, CA, USA) and a mixture of CMA 600 "Control Elevated" (μdialysis AB) containing a mixture of glucose, glycerol, glutamate, urea and pyruvate and lactate diluted 1:2 in aCSF. Catheters were perfused at 0.3 and 1 µL/min and pre-weighed vials were replaced every hour for three hours, followed by dialysis for three hours. Microcentrifuge tubes were also replaced at the same time to avoid depletion of molecules and to measure leakage of additives. Microvials from perfusion into the small molecule mixture, as well as the original mixture itself, were analysed for glucose, glutamate, pyruvate and lactate using the CMA 600 microdialysis analyzer (μdialysis AB). Microvials from perfusion into pnCSF were sealed and frozen at −80 °C for later measurement of proteins using the antibody colocalization microarray (ACM).

Leakage of additives The different additives were measured in the microcentrifuge tubes used to perfuse the additives solutions through aCSF. BSA was measured by spectrophotometry using a NanoDrop ND-1000 (Thermo Fisher Scientific) at 280 nm and quantified using a 31-point serial dilution series of BSA in aCSF with known concentrations (range of 0.01 ppm to 4 %). Samples from the microcentrifuge tubes containing leaked dextrans were measured by the phenol-sulphuric acid method [262] with optimized volumes of reagents to maximize sensitivity of the measurement. In short, 5 µL of the sample was mixed with 20 µL of 5 % phenol in water and 100 µL of pure sulfuric acid. The mixture was incubated at 55 °C for 5 min and promptly measured on the NanoDrop at 490 nm. The absorbance value was compared to a 31-point serial dilution series of both $\text{Dextran}_{\text{LMW}}$ and $\text{Dextran}_{\text{HMW}}$ diluted in aCSF with the same concentration as the BSA serial dilution series described earlier. The limits of detection of the spectrophotometric measurements of BSA, $\text{Dextran}_{\text{LMW}}$ and $\text{Dextran}_{\text{HMW}}$ were 0.06 %, 0.02 % and 0.03 %, respectively.

Matrix effect of additives A mixture of small molecules (CMA 600 "Control Normal", μdialysis AB) was mixed with BSA, $\text{Dextran}_{\text{LMW}}$ and $\text{Dextran}_{\text{HMW}}$ 1:2 diluted in aCSF to give a relatively

constant concentration of small molecules and increasing concentration of additives from 0.25 to 4 %. These dilutions were performed in triplicate with each additive and aCSF as measurement control, and the mixtures were frozen at −80 °C until they were measured with the microdialysis analyzer as described above. The experiment was repeated with pnCSF mixed with increasing concentrations of each additive, and the mixtures were measured with the ACM.

5.2.3 Cell culture

Human U87 cells that were tested to be mycoplasma-free were cultured in DMEM with the addition of 10 % sterile-filtered FBS and 100 µg/mL of penicillin and streptomycin. Cells were cultured in polystyrene flasks and kept at 37 °C and 5 % CO_2. To test the effect of additives in the cell medium, cells were trypsinized and 5000-10000 cells were seeded onto 24-well polystyrene plates in the growth medium described above. Cells were allowed to grow until they reached ~50 % confluency, after which medium containing DMEM, 1 % FBS and 100 µg/mL of penicillin and streptomycin was used. In each 24-well plate at 0, 24, 36, 42 and 46 h, three wells received this FBS-poor medium with either 3.5 % BSA, 3 % $\text{Dextran}_{\text{LMW}}$, 3 % $\text{Dextran}_{\text{HMW}}$, 5 % fresh anonymous whole blood obtained through finger-prick (BD Microtainer lancet #366593), or 100 ng/mL LPS. Two plates without cells received the same additives for whole blood and BSA and served as controls. After 48 h the cell culture medium of all wells (including controls which were not exposed to additives) were collected and frozen at −80 °C in microcentrifuge tubes. To lyse cells, cells were washed 3 × with sterile PBS, 50 µL of cell lysis buffer was added to each well and the 24-well plates were incubated for 30 min at 4 °C. The mixtures of cells and cell lysis buffer were removed with scraping to remove attached cells and placed in microcentrifuge tubes. Tubes were centrifuged for 10 min at 14 000 *g*. Supernatants were transferred to new tubes and analysed using the bicinchoninic acid (BCA) protein assay kit (Pierce, now Thermo Fisher Scientific).

5.2.4 Protein measurements

To measure proteins in samples, we fabricated ACM microarrays using protocols described in [219] and chapter 4, but no trehalose coating of slides was performed. In short, PolyAn 2D Aldehyde micorarray slides (PolyAn GmbH, Berlin, Germany) were placed in a Nanoplotter 2.1 microarrayer (GeSiM GmbH, Radeberg, Germany) with an added microfabricated collimator (Parallel Synthesis, Santa Clara, CA, USA) fitted with four custom-made silicon quill pins [154]. Capture antibodies or GAR-biotinXX (subarray calibrant, at 25 µg/mL) mixed with 20 µg/mL BSA-AF555 (spot calibrant) and diluted in 45 % glycerol, 0.005 % Tween-20® were printed onto slides as 14 identical subarrays at 65 % relative humidity and room temperature, in the dark. Following the end of

printing, slides were allowed to incubate in the chamber for 24 h in the same conditions. Slides were fitted in 16-well gaskets (ProPlate®, Grace Bio-Labs, Bend, OR, USA), washed for 3×5 min with washing solution and blocked with 3 % BSA in PBST for 3 h at room temperature with 450 rpm rotational shaking. The blocking solution was removed and samples diluted 1:3 or 1:15 as well as two standard curves (composed of recombinant antigens, except CA15-3 and CEA which were obtained from cancer patients, at known concentrations serially diluted 1:2.5 $13\times$) were incubated for 18 h at 4 °C with 450 rpm rotational shaking. Slides were washed with washing solution, rinsed with pure water, blown-dried with a stream of compressed nitrogen and carefully placed within the Nanoplotter chamber. Detection antibodies (biotinylated or mixed with a AF647-labeled reporter antibody) solutions mixed in 45 % glycerol with 1 % BSA and 0.001 % Tween-20® were filtered and spotted onto the slides at 65 % relative humidity, room temperature in the dark, followed by a 24 h incubation. Slides were once again fitted onto gaskets, washed as described before and incubated for 1 h with 0.5 µg/mL streptavidin-AF647 in PBST containing 3 % BSA, at room temperature with 450 rpm rotational shaking. Slides were washed one last time, dried with a compressed nitrogen stream and scanned with a SureScan Microarray Scanner (Agilent Technologies, Santa Clara, CA, USA) using two-colors and a resolution of 5 µm per pixel. We used ArrayPro Analyzer 6.31 (Media Cybernetics, Rockville, MD, USA) to extract raw fluorescence values from images produced by the scanner.

5.2.5 Statistical Analysis

All data were imported into and analyzed using R [220]. Calibration of the ACM data was based on chapter 4 with the goal of improving reproducibility or sensitivity as indicated. Reported values are mean ± standard deviation in graphs and tables. Trends of change in protein measurement with respect to time or additive concentration calculated with calibrated fluorescence values are reported as the difference between the mean value and the mean blank value divided by the measurement range for individual proteins.

5.3 Results

Immunoglobulin G (IgG) and protease-free bovine serum albumin (BSA) was used instead of human albumin solution because of its wide availability, and clinical-grade $\text{Dextran}_{\text{LMW}}$ and $\text{Dextran}_{\text{HMW}}$ dextrans in our study. Figure 5.1 shows a schematic of the *in vitro* setup used. Small molecules were measured with the CMA microdialysis analyzer while the remaining small volumes of microdialysate were analyzed using the antibody colocalization microarray (ACM)

[17], an immunoassay-based, cross-reactivity free antibody microarray that can measure over 100 proteins in a few microliters of samples with good reproducibility and sensitivity (chapter 4).

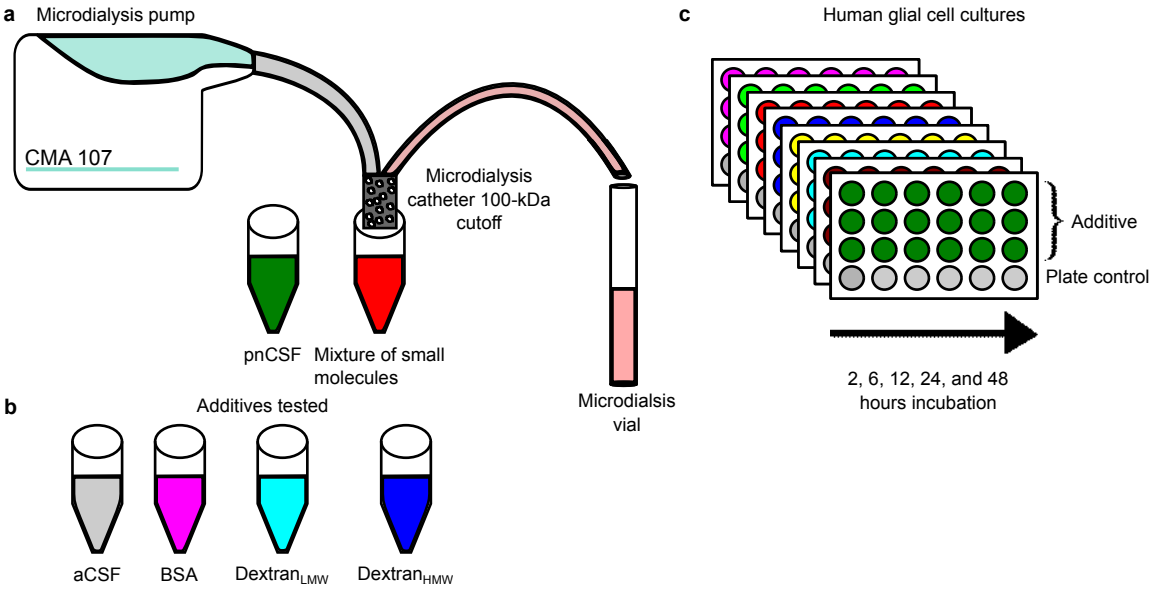

FIGURE 5.1: **Testing additives in the cerebral microdialysis perfusion fluid. a** A microdialysis pump connected to a 100-kDa molecular weight cut-off catheter was perfused in a mixture of small molecules or pooled normal lumbar CSF (pnCSF) and flow stability, fluid recovery, leakage and relative recovery were measured. Additives in (**b**) were perfused individually through the catheter bathing in a tube containing artificial CSF (aCSF), pnCSF or a mixture of small molecules, and the resulting microdialysate was collected in small microdialysis vials for measurement. **b** List of additives added to aCSF used in the microdialysis catheter (**a**) and used to calculate the possible interference with the measurement of small molecules and 94 different proteins. **c** Additives along with fresh blood and lipopolysaccharide (LPS) were added to 24-well plate containing human glial (U87) cell cultures at 0, 24, 36, 42 and 46 h to study their effect on the secretion of proteins by the cells, resulting in exposures to additives of 2, 6, 12, 24 and 48 h. Measurement of cell media with additives were done in triplicate at 48 h and each plate contained a row of controls.

5.3.1 Effects of additives on physical performance of perfusion

While starting the perfusion of fluids containing the various additives through the catheters, the time required for the flow to achieve the desired flow rate was measured in the first hour of perfusion. Within 20 min, all additives and artifical cerebrospinal fluid (aCSF) produced a stable output at a flow rate of 0.3 µL/min. Dextran$_{LMW}$ stabilized a few minutes later than the other additives (figure 5.2a).

Pooled normal lumbar CSF obtained from healthy controls was used to test the fluid recovery of perfusion fluids containing the different additives, which is defined as the ratio of the volume of output microdialysate to input perfusate. We chose to perfuse into pnCSF because it is the fluid

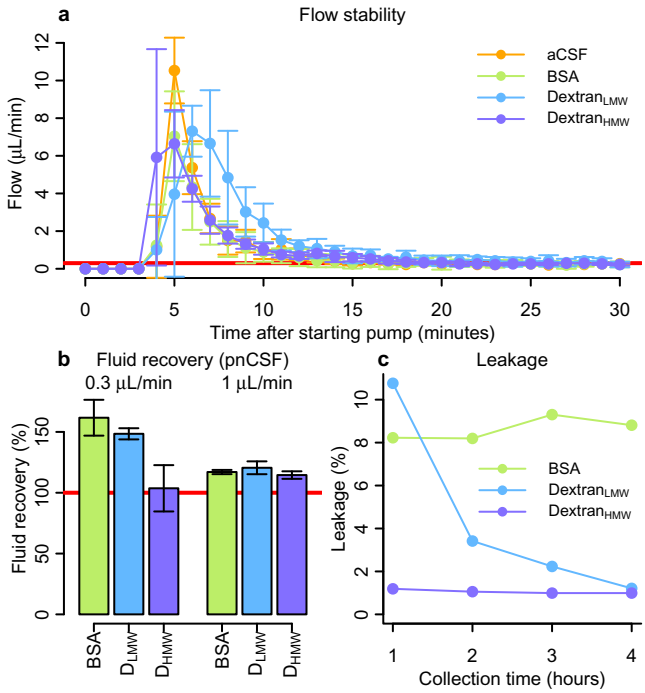

FIGURE 5.2: **Flow stability, additive leakage and fluid recovery of catheters containing additives.** **a** Flow rate at the microdialysis catheter tip after starting the pump at a flow rate of 0.3 µL/min when perfusing with aCSF, BSA, Dextran$_{LMW}$ or Dextran$_{HMW}$. The red line is a visual aid that indicates the set flow rate (0.3 µL/min). **b** Volume of microdialysate recovered from catheter tips submerged in pnCSF was used to measure fluid recovery and is expressed as a ratio to the volume of perfusate inputted in the catheter. The red line indicates a 100 % fluid recovery. **c** Leakage was measured by perfusing additives into tubes containing aCSF at a flow rate of 0.3 µL/min. BSA and dextrans reacted with a phenol-sulfuric acid method were detected with a spectrophotometer.

closest to brain interstitial fluid (IF) in terms of osmolality, as CSF is composed in part of IF in the normal brain. None of the additives tested lost liquid volume into the tube of pnCSF (figure 5.2b), and for BSA and Dextran$_{LMW}$, fluid recovery was greater at a flow rate of 0.3 µL/min than 1 µL/min, suggesting that fluid exchange at 1 µL/min was not at equilibrium for these two additives. When perfusing into aCSF, fluid recovery was greater than 100 % for all additives (figure E.S1) when compared to pnCSF, which contains proteins and other biomolecules in addition to the small ions present in aCSF.

Next, the presence of non-labeled additives was measured into tubes containing aCSF that were perfused for over an hour (figure 5.2c) in order to quantify leakage of additives through the microdialysis membrane. We used non-labeled additives instead of fluorescently-labeled additives because of the risk that the fluorescent labels modify the physical property of additives and affect leakage measurements. All leakage measurements reported here were above the limit of detected

determined spectrophotometrically using a 31-point standard curve made from the same additives. While BSA and $\text{Dextran}_{\text{HMW}}$ leaked steadily at rates of 8.6 % and 1.1 % respectively, the leakage of $\text{Dextran}_{\text{LMW}}$ started out high in the first hour (10.8 %) and progressively decreased until it reached 1.2 %, a level similar to that of $\text{Dextran}_{\text{HMW}}$.

5.3.2 Relative recovery of molecules

We found that glucose, lactate and pyruvate relative recoveries were not significantly affected by the presence of additives to the perfusion fluid, with the exception of $\text{Dextran}_{\text{HMW}}$ leading to slightly higher relative recovery values for all small molecules including glutamate (figure 5.3a-d). In spite of the high molecular weight cut-off of the membrane and the low flow rate (0.3 µL/min), the relative recovery of glutamate in the presence of additives were lower than in aCSF: 86.2 %, 67.3 %, 75.4 % and 77.3 % for aCSF, BSA, $\text{Dextran}_{\text{LMW}}$ and $\text{Dextran}_{\text{HMW}}$, respectively.

To evaluate the potential interference of additives with the quantification of 94 proteins, we used the ACM to measure microdialysate perfused in pnCSF. Because of the very low concentrations of most proteins in pnCSF, and the fact that no protein was detected in the microdialysate at a flow rate of 1 µL/min, we calibrated the ACM data with an improvement in sensitivity (figure E.S6) to obtain relative recovery measurements for a flow rate of 0.3 µL/min. This is possible because sensitivity is affected by variability of blank samples measured multiple times in the ACM experiment. This variability can be improved, and therefore sensitivity increased, by applying the calibration algorithm developed in chapter 4 using blank samples. This lead to an improvement in sensitivity from 69.0 to 40.5 pg/mL. All other protein measurements were done with calibration that improved median reproducibility from 30.9 % to 7.4 %. Details of calibration are found in the SI in figure E.S2 to table E.S2. Analysis of measurements were done with fluorescence values because a few samples with high values were not quantified using the standard curves.

The distribution of relative recovery for all proteins measured in microdialysate (figure 5.3e) shows that more proteins were detected in microdialysate with BSA than aCSF (13 compared to 7). BSA also allowed the detection of more proteins than Dextrans (10 each). When comparing the relative recovery for three proteins measured in high abundance in pnCSF: TGF-β1 (14 kDa), CD14 (56 kDa) and IGFBP-7 (29.1 kDa), we found that the median relative recovery in aCSF and BSA were comparable, $\text{Dextran}_{\text{LMW}}$ was a bit higher than aCSF and BSA, and the median relative recovery of $\text{Dextran}_{\text{LMW}}$ was the lowest. Since only three proteins had measured relative recovery values for aCSF and all additives, comparison between the additives is limited. Comparison of relative recovery values obtained between fluorescence values and quantified values shows a good correlation close to 1 (figure E.S7).

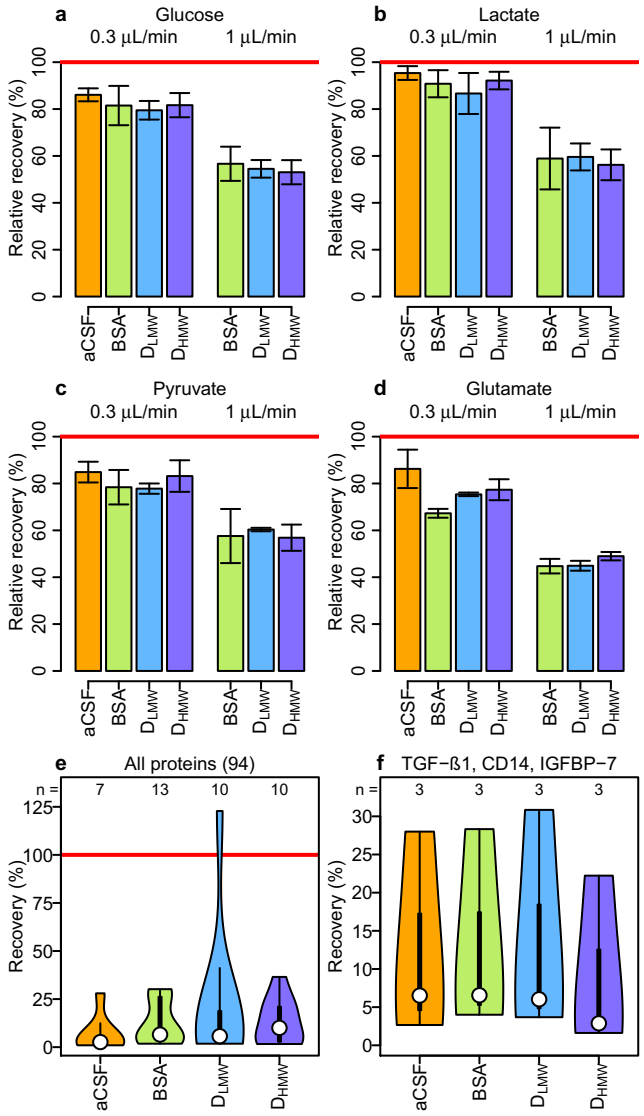

FIGURE 5.3: **Effect of additives on relative recovery of small molecules and proteins.** Catheters filled with aCSF or additives were perfused in (**a-d**) a mixture of small molecules or (**e-f**) pnCSF for 3×1 h. The quantity of **a** glucose, **b** lactate, **c** pyruvate, **d** glutamate or **e-f** proteins recovered in the microdialysate was compared to the measurement of the original solution (mixture of small molecules or pnCSF) to calculate relative recovery. **e** shows all values of relative recovery calculated, whereas **f** shows the relative recovery of only three proteins abundant in pnCSF for which a calculated value was calculated for all additives and aCSF (TGF-β1, CD14 and IGFBP-7). The list of relative recovery values for each protein is found in table E.S3. A red line in **a-e** is a visual aid that indicating a relative recovery of 100 %.

To better compare the additives in terms of proteins relative recovery, and using all the measured values of relative recovery (listed in table E.S3), we derived linear relationships with the estimated molecular size of proteins (table E.S4) for aCSF and all additives tested (figure 5.4), as done

previously with small molecules [263]. The recovery of proteins with higher molecular weight was better with $\text{Dextran}_{\text{LMW}}$, closely followed by aCSF. Relative recovery appeared to wane at ~90 kDa for BSA, while for $\text{Dextran}_{\text{HMW}}$, the cut-off was closer to 43 kDa. For all additives (but not aCSF), there appeared to be outliers to the linear relationships, especially proteins with a higher molecular weight which were recovered in unusually high proportion above the apparent cut-off.

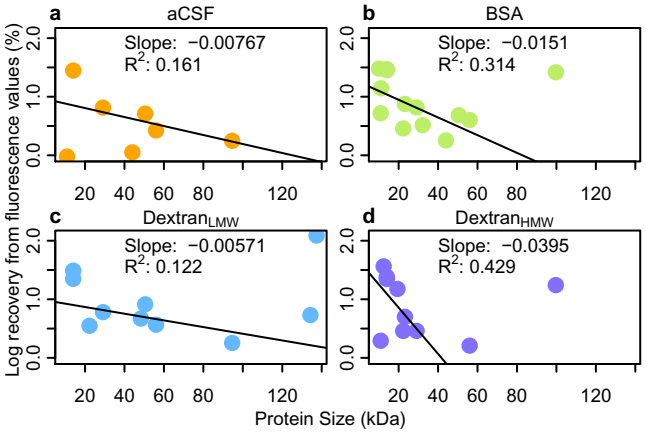

FIGURE 5.4: **Relationship between protein size and relative recovery.** Linear relationship between the log of relative recovery values and corresponding proteins effective molecular size which takes protein complexes into account. Linear fits were calculated using median-based linear regression. Relative recovery values were calculated only for proteins detected in microdialysate, which roughly corresponds to proteins found in sufficient abundance in pnCSF to allow detection in microdialysate.

5.3.3 Matrix effect of additives on molecules

Because the relative recovery of molecules can be influenced by the presence of additives in the sample at the time of measurement (also called matrix effect), we diluted small molecules and pnCSF in increasing concentrations of BSA, $\text{Dextran}_{\text{LMW}}$ and $\text{Dextran}_{\text{HMW}}$ and compared the obtained measurements with that of replicate samples of small molecules and pnCSF diluted in aCSF. The matrix effect of additives on small molecules is shown in figure 5.5a-d. While measurements of glucose, lactate and pyruvate (figure E.S8 to E.S10) did not suffer from matrix effect of any of the additives tested (less than 7 % loss), glutamate suffered considerably from the presence of 3 % BSA (45.4 %) and 3 % $\text{Dextran}_{\text{HMW}}$ (25.7 % loss), but not 3 % $\text{Dextran}_{\text{LMW}}$ (1.7 % loss). Measurement values for glutamate decreased proportionally with the increase in concentration of BSA and $\text{Dextran}_{\text{HMW}}$.

We also measured the matrix effect of additives on the measurement of proteins in pnCSF, using calibrated fluorescence values. The comparison of measurements obtained from fluorescence values

and intrapolated quantities shows that the correlation is good (R^2 of 0.655, 0.87 and 0.819) and that the percentage of the original protein measured obtained by fluorescence values should be multiplied by ~2.5-3 × to obtain the percentage of the original protein measured obtained from intrapolated quantities (figure E.S11). Figure 5.5e shows that while the presence of BSA generally does not affect measurement of proteins using the ACM, both $Dextran_{LMW}$ and $Dextran_{HMW}$ showed increased measurements of proteins, perhaps preventing protein from adsorbing into plastic pipette tips and tubes during processing. Table E.S5 gathers individual values of percent recovery calculated for the 29 proteins detected in this experiment. When fluorescence values are converted to quantities using the relationship from figure E.S11, we obtain ranges from 55 to 198 % for BSA, from 27 to 192 % for $Dextran_{LMW}$ and from 66 to 348 % for $Dextran_{HMW}$.

5.3.4 Effect of additives on human glial cell cultures

Because all additives tested showed detectable leakage through the high cut-off microdialysis membrane, we tested the possible effects of additives on U87 cells, originating from a human glioblastoma developed from CNS cells [264]. The ACM currently measures a number of cytokines and chemokines and glia has been shown to secrete a number of them during injury, therefore we chose these cells as an *in vitro* model of glia. U87 cells were grown in medium containing 10 % fetal bovine serum (FBS) and were seeded into 24-well plates in medium containing only 1 % FBS. Since FBS contains a lot of albumin, we used as little as possible in order not to overly skew the measurements of the effect of BSA on the cells. This lower concentration of FBS was found to be the minimal amount of FBS required to keep the U87 cells alive but not growing.

On each plate and at different times, we added 3.5 % BSA, 3 % $Dextran_{LMW}$, 3 % $Dextran_{HMW}$, 5 % fresh human blood obtained through finger-prick or 100 ng/mL lipopolysaccharides (LPS). One row of each plate did not receive additives and served as a negative control. Two plates that did not contain U87 cells received fresh blood and BSA and also served as control (figure 5.1). Since the effective concentration of additives leaked into the brain in an *in vivo* experiment consists in a decreasing gradient away from the microdialysis probe [259], we tested the full concentration of additives that could potentially be present locally and directly outside the microdialysis probe. We recorded the effect of the presence of additives for 2 to 48 h on the measurement of the 94 proteins in the cell media as an increase (or decrease) in the production of individual proteins by U87 measured over the 48 h period. As with measurements of relative recovery, changes in concentrations of proteins with time calculated with fluorescence values and quantified values led to a 1:1 correlation (figure E.S12). Linear regression parameters in each plate are listed for individual proteins in tables E.S6 to E.S13.

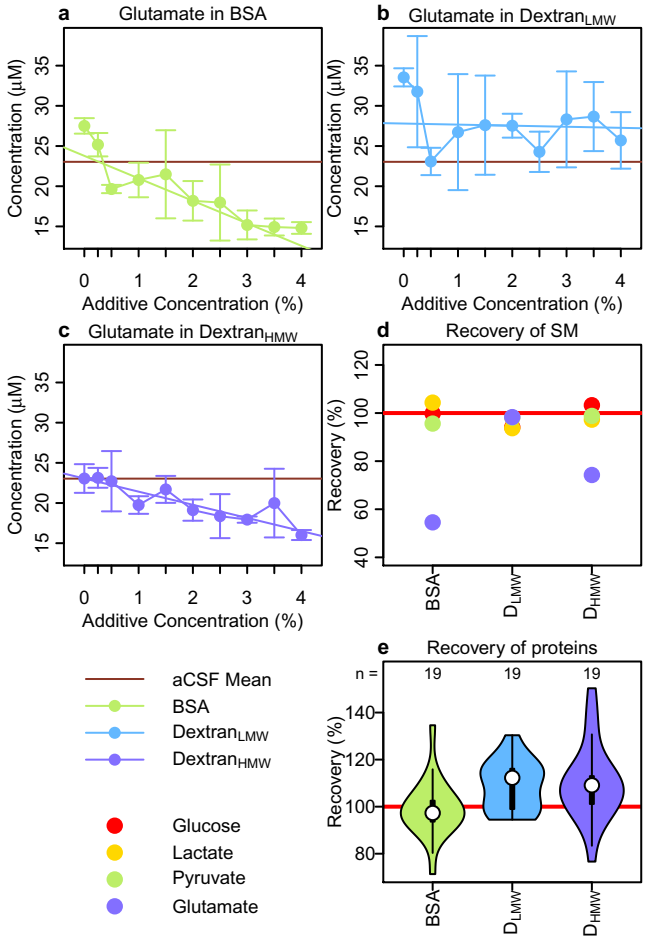

FIGURE 5.5: **Matrix effect of additives on glutamate and proteins.** A mixture of small molecules (glucose, lactate, pyruvate and glutamate at concentrations normally found in the brain) (**a-c**) or pnCSF (**e**) were mixed in aCSF containing increasing concentrations of additives. Recovery was calculated from the ratio of the predicted small molecule concentration at 0 % and 3.5 % (BSA) or 3 % (Dextran$_{LMW}$ and Dextran$_{HMW}$). Distribution of recovery for small molecules (**d**) and proteins (**e**) are shown for each additive. Only proteins for which a recovery was calculated with all three additives and aCSF are shown here. Graphs for glucose, lactate and pyruvate are found in figures E.S8-E.S10 and the matrix effect of additives on each protein are listed in table E.S5. Linear fits were calculated using a median-based linear model. The red lines in (**d-e**) are a visual aid where 100 % indicates no effect of additives on the measurement of a molecule. SM: small molecules.

A total of 51 proteins were detected in sufficient amounts to calculate values of production increase. A control plate that received no additives but was treated similarly to the other plates showed differences of up to 14.1 % (mean + 2 × standard deviation) when compared to its plate control, and therefore we identified differences for all additives and their respective controls (plate controls for Dextran$_{LMW}$, Dextran$_{HMW}$ and LPS, as well as plate controls and plate without cells for fresh blood and BSA) that were above 15 %. Table E.S14 shows a summary of all proteins that

TABLE 5.1: **List of proteins whose secretion were changed in the presence of additives.** Minimum amount of change recorded is 15 % of range when compared to plate control. Blood and BSA were also compared to their respective cell-free control. - : change less than 15 % or not detected.

	Protein name	None (%)	Blood (%)	BSA (%)	$\text{Dextran}_{\text{LMW}}$ (%)	$\text{Dextran}_{\text{HMW}}$ (%)	LPS (%)
11	CCL5	-	27.67	-	-	-	-
32	HGF	-	61.04	-	-	35.88	-
33	HGF-R	-	-	-	24.78	26.5	-
34	HMGB1	23.13	-	-	-	-	-
36	ICAM-1	-	-19.07	-	-	-	-
38	IGFBP-1	-	-26.44	-	19.51	51.35	-
44	IL-18	-	-	19.18	-	-	-
51	IL-6	-	-7.24*	-	-	-	-
53	IL-8	-	-	48.57	-	49.47	-
57	MCP1	-	25.29	-	-	-	-
59	MCP3	-	27.91	-	-	-	-
62	MIP-1α	-	-	-	-	29.96	-
63	MIP-1β	-	19.15	-	-	-	-
65	MMP-3	-	-	-	30.74	-	-
69	OPN	-	-	25.78	21.6	25.46	-
81	TGF-β1	-	29.27	-	-	-	-
82	THSB-1	-	22.28	-	-	-	-
88	uPA	-	-	-	-	18.42	-
91	VEGF-A	-	-	-17.96	-	-	-
	N^{o} Increase	1	8	3	4	7	0
	N^{o} Decrease	0	3	1	0	0	0

*: Strong peak at 12h followed by decrease.

were detected in the different controls, or were found to be produced or degraded in the presence of different cells. Eight proteins were detected in all samples of cell media (Ang1, HGF-R, IGFBP-7, IL-8, MIP-1α, THBS-1, uPA and VEGF-A) and the increase or decrease in levels is compared in figure E.S13, which shows that the greatest changes in production of proteins appeared in plates treated with fresh blood and $\text{Dextran}_{\text{HMW}}$, and to a lesser degree in $\text{Dextran}_{\text{LMW}}$. However, the changes in the plate containing $\text{Dextran}_{\text{LMW}}$ is not statistically significant, when compared to whole blood and $\text{Dextran}_{\text{HMW}}$ (table E.S15).

A total of 19 proteins were found to significantly change and are listed in table 5.1. The plate that received no additives shows a single protein whose production increase differed with its plate control (HMGB1) and can be considered an outlier. None of the other plates showed a significant change in the production increase of this protein. We measured the total cell protein using a bicinchoninic acid (BCA) protein assay kit and found that while there are differences between the total cell protein measured, the trends with time were relatively flat (figures E.S14 and E.S15) and

therefore the BCA data was not used to calibrate protein measurements. Cells treated with fresh blood show the greatest number of changes in protein production with time (11 proteins). It cannot be determined if the proteins were secreted by the U87 cells or cells found in the blood, however the origin of production of these proteins is not important in the context of microdialysis. BSA, $\text{Dextran}_{\text{LMW}}$ and $\text{Dextran}_{\text{HMW}}$ had an effect on the production of 4, 4 and 7 proteins, respectively. HGF-R, IGFBP-1 and OPN production by U87 cells were increased in the presence of both dextrans, but the effect was more pronounced with $\text{Dextran}_{\text{HMW}}$. Considering the increased matrix effect of $\text{Dextran}_{\text{HMW}}$ on the measurement of proteins with the ACM, it is likely that its effect on the cells is more considerable than shown here. LPS did not cause any protein to be increased or decreased in production, and indeed at the concentration used here (100 ng/mL) we did not expect any effect.

5.4 Discussion

All additives performed similarly in terms of flow stability. The period of time required for the liquid flow rate at the ouptut of the microdialysis catheter to stabilize is longer than the 5 min flush cycle of 15 µL/min indicated in the pump manufacturer's datasheet [265]. While it is a shorter amount of time than the first 1-5 h of microdialysate collection sometimes discarded [26, 253, 266] due to the micro-trauma of probe insertion that might alter protein measurements [20], many studies did not discard any of the collected microdialysate [18, 260, 267]. Since the first 20 min of catheter perfusion exhibits highly variable flow rate, and that proteins relative recoveries are affected by flow rate, we recommend discarding the microdialysate collected in the first 20 min immediately after powering the pump.

While albumin and dextrans have been shown to have fluid recoveries far above 100 % *in vitro*, they have been extensively shown to regulate fluid recovery closer to 100 % in patients or animals [20, 28, 256]. Moreover, fluid recovery of albumin has been shown not to vary within a clinically-significant range of intra-cranial pressure (ICP) of patients suffering from severe traumatic brain injury (sTBI) [18]. On the other hand, fluid recovery using dextran have been shown to be sensitive to patients ICP, but not in the presence of a polymer coating which also prevents membrane bio-fouling [23]. In our *in vitro* test here where no additional pressure with the use of gravity was present, all additives tested showed fluid volume recoveries above 100 %, and are expected to also prevent fluid loss *in vivo*.

The leakage of additives observed here are consistent with a previous study that used fluorescence microscopy to qualitatively observe leakage, which showed that dextrans of size 40 and 250 kDa both leaked, but not dextran of size 500 kDa [259]. We noted that the measurements in this study were performed for no longer than 6.5 min, and therefore a change in $\text{Dextran}_{\text{LMW}}$ leakage

was not observed. BSA along with $\text{Dextran}_{\text{LMW}}$ and Dextran_{500} were also tested as additives to microdialysis in rat skin tissue. In this study, $\text{Dextran}_{\text{LMW}}$ was found to leak and produced a strong local inflammatory response, while Dextran_{500} did not. When combined, these studies suggest that Dextran_{500} is too large to leak through the 100 kDa microdialysis membrane [261], but does not preclude a possible effect on rat skin. At this time it is unknown what caused the decrease in leakage observed for $\text{Dextran}_{\text{LMW}}$, however it might be due to a phenomenon similar to the membrane biofouling seen with proteins [268] which causes widespread occlusion and narrowing of pores of microdialysis catheters.

As expected, relative recovery of both small molecules and proteins were higher at the lower (0.3 µL/min) than the higher (1 µL/min) flow rates. The full relative recovery of small molecules was not achieved here at 0.3 µL/min, which is consistent with Rosdahl *et al.* who found that a flow rate of 0.15 µL/min is required for small molecules to be recovered at or close to 100 % [28]. All measures of relative recovery for proteins are low, most of them being lower than 25 %, which is consistent with other studies [269]. Contrary to studies which observed an increase in relative recovery of proteins using albumin [21, 25, 254], we found only a small increase compared to aCSF. Our results for $\text{Dextran}_{\text{LMW}}$ and $\text{Dextran}_{\text{HMW}}$ are surprising because the lower molecular weight dextran appears to improve the relative recovery of proteins, while the higher molecular weight dextran appears to impede it, which is not a graded effect compared to aCSF. However other studies have found that $\text{Dextran}_{\text{LMW}}$ both increases [26, 257] or slightly decreases [20] relative recoveries of different proteins, and therefore our results are consistent with the literature. We found no studies that found improvements in relative recovery with $\text{Dextran}_{\text{HMW}}$ when compared to aCSF or equivalent solution devoid of colloids. It is also important to note that the effect of additives on proteins measurements (matrix effect) can in part explain the difference in relative recovery measurement of individual proteins.

We measured the effect of additives on the measurement of small molecules, and found that glutamate concentration was significantly lower when BSA or $\text{Dextran}_{\text{HMW}}$ was added to the perfusion fluid. Strangely this was not the case when $\text{Dextran}_{\text{LMW}}$ was added to the perfusion fluid. This effect on the measurement of glutamate should be taken into consideration when comparing the cut-off or normal values of glutamate in clinical samples from sTBI patients. Values of recovery for proteins in the presence of additives that are above than 100 % are not of concern even if they are possibly overestimated as might be the case for SPARC, for which we measured a 348 % recovery in $\text{Dextran}_{\text{HMW}}$. Values of recovery that are significantly below 100 % are of concern especially if the measurement in aCSF would be close to the limit of detection of the assay. Assays in which the microdialysate is diluted in buffer are less likely to suffer from matrix effect due to the presence of additives, which are also diluted. Indeed, a previous study measured the matrix effect

of $\text{Dextran}_{\text{LMW}}$ on proteins using a bead-based multiplexed assay and measured on average no more than 5-10 % of difference between samples with and without $\text{Dextran}_{\text{LMW}}$ [20]. The samples used in this study were diluted in the bead assay, explaining the lack of effect of $\text{Dextran}_{\text{LMW}}$ on the measurement of proteins. On the other hand, samples were measured here without dilution to observe the true matrix effect of additives to the microdialysis perfusion fluid. This is also the case for small molecules measured by the CMA microdialysis analyzer, which uses a few microliters of pure microdialysate to measure small molecules in parallel. Apparent decrease in the amount of small molecules or protein measured when additives are present in the microdialysate can be acceptable if the assay used to measure them is sensitive enough, and the matrix effect is taken into consideration when comparing different sample types.

We observed the concentration change of 51 proteins in the cell culture media of U87 cells in which BSA, $\text{Dextran}_{\text{LMW}}$ and $\text{Dextran}_{\text{HMW}}$ were added, in addition to fresh blood and LPS as positive and negative controls, respectively. We detected 13 proteins that appeared to be produced by the U87 cells in the absence of any additives, all of which have been reported before (see table E.S14). LPS did not lead to any change in protein levels, which is consistent with another study which found no activation of U87 cells when stimulated with the concentration of LPS used here [270]. On the other hand, adding fresh blood to cell culture media was expected to induce a lot of changes in protein production, as was observed here. The results shown here for fresh blood have meaning in the context of the insertion of the microdialysis catheter in brain tissue, which can result in micro-bleeds [266], as well as in the context of brain injuries where bleeding can occur.

IL-1β is one of the first cytokine released in the inflammatory cascade response of the brain [27]. It was used in a previous study to stimulate U87 cells and investigate their specific response to inflammation [271]. Interestingly, five out of the eight proteins measured here in all cell media samples were found to be secreted by IL-1β-stimulated U87 cells in this study: IL-8, MIP-1α, IGFBP-7, THBS-1 and VEGF-A. These findings suggest that U87 cells kept in cell media containing only 1 % FBS are in a state of inflammation.

When looking at the effect of additives on the U87 cells, the amount of leakage needs to be considered. Since BSA leaked the most, the effect of BSA as additive is likely to be the most severe compared to both dextrans. A study found that serum albumin as additive to microdialysis did not trigger an inflammatory response in histological sections of rat skin, beyond the skin's reaction to the presence of the microdialysis probe itself [261]. The concentration of albumine in human subcutaneous tissue interstitial fluid was found to be 29.2 g/L [272] and therefore leakage of rat serum albumin in the skin tissue would not be expected to provoke an inflammatory reaction due to its already high concentration in the IF. On the other hand, the concentration of albumin in healthy brain tissue is approximately 50 mg/L, while in plasma, it is normally 35-50 g/L. Therefore

8.6 % leakage of a solution of 3.5 % albumin could lead to a concentration of 3.01 g/L in the brain immediately surrounding the microdialysis probe, which is ~60× higher than the normal concentration of albumin. While these calculations are a gross approximation, the combination with the increases in protein production seen in our *in vitro* model suggests that the presence of albumin as an additive to brain microdialysis might affect subsequent protein measurements as well as affect cells in the immediate vicinity of the microdialysis probe. The study by Keeler *et al.* reporting the effect of dextrans on the inflammatory response of rat skin also found that $\text{Dextran}_{\text{LMW}}$ provoked a strong inflammatory response, presumably from its leakage through the microdialysis membrane, while Dextran_{500} did not [261]. This is presumably due to the absence of leakage rather than an absence of effect on cells, as $\text{Dextran}_{\text{HMW}}$ caused more changes in protein production than $\text{Dextran}_{\text{LMW}}$ in our *in vitro* model of glia. Our results show that any leaked additives to the brain tissue during cerebral microdialysis has the potential to negatively affect cells in the vicinity of the microdialysis cathether.

Table 5.2 shows a summary of the comparison of BSA, $\text{Dextran}_{\text{LMW}}$ and $\text{Dextran}_{\text{HMW}}$. All additives performed similarly in terms of flow stability and fluid recovery. BSA was shown to leak significantly, while $\text{Dextran}_{\text{HMW}}$ leaked much less. $\text{Dextran}_{\text{LMW}}$ was shown to have an initial leakage greater than BSA, which quickly decreased to the level of $\text{Dextran}_{\text{HMW}}$ within four hours. In terms of small molecules relative recovery, $\text{Dextran}_{\text{HMW}}$ performed marginally better than BSA or $\text{Dextran}_{\text{LMW}}$, however the high-molecular weight cut-off microdialysis probe is used primarily for the measurement of proteins, where $\text{Dextran}_{\text{LMW}}$ performed better than the other additives. When studying the effect of additives on the measurement of small molecules and proteins, all additives showed a trend of improving measurements, although there was a lot of variability. Finally, all additives were shown to have an effect on the rate of production of proteins in U87 cells, with $\text{Dextran}_{\text{HMW}}$ showing the greatest effects on cells.

TABLE 5.2: **Summary of additives properties.** Performance is shown as very good (+++), good (++), acceptable (+) or not good (-). SM: small molecules.

	BSA	$\text{Dextran}_{\text{LMW}}$	$\text{Dextran}_{\text{HMW}}$
1. Flow stability	+++	+++	+++
2. Fluid recovery	+++	+++	+++
3. Leakage	-	+	++
4. Relative recovery (SM)	+	+	++
5. Relative recovery (proteins)	+	++	-
6. Matrix effect	+	+	+
7. Effect on cultured glial cells	+	+	-

In light of the possible allergic or anaphylactic reaction of some patients to dextran solutions [273], a dextran with higher molecular weight of 500 kDa has recently been used in cerebral microdialysis of patients using the CMA 71 [23, 260] because it was shown not to leak through the microdialysis membrane. At the time of performing experiments in the study presented here, a clinical grade version of Dextran_{500} was not available in Canada. If we extend results obtained here for $\text{Dextran}_{\text{HMW}}$ (200-300 kDa), we presume that the effect of Dextran_{500} on the measurement of glutamate might be even greater than that of $\text{Dextran}_{\text{HMW}}$, and that the relative recovery of proteins might also be worse, since for these two measures $\text{Dextran}_{\text{LMW}}$ performed better than $\text{Dextran}_{\text{HMW}}$. However, the coating of microdialysis probes perfused with Dextran_{500} with Pluronic F-127® has been shown to improve relative recovery of proteins by preventing biofouling, and the stability of fluid recovery in response to changes in patients brain ICP [23]. Adding heparin-coated gold nanoparticle to the microdialysis perfusion fluid could also enhance protein relative recovery [24].

5.5 Conclusion

The CMA 71, a high molecular weight cut-off cerebral microdialysis probe, has already proven to be a very powerful tool for monitoring the local inflammatory response of injured brains in animals models as well as human patients. We have shown that additives to the perfusion fluid, added to prevent ultra-filtration and loss of microdialysate, can leak through the membrane at different rates and affect measurements of small molecules and several proteins. We have also shown that a cell culture model of glial cells are affected by the presence of albumin and dextrans by measuring 94 proteins secreted by the cells in response to the presence of additives.

Therefore, while microdialysis for tissues other than the brain might safely benefit from the addition of human albumin, this might not be the case for brain microdialysis because of the very low endogenous concentration of albumin in the brain, and remains to be tested *in vivo*. Although it is used in the clinic, dextrans might also not be safe when leaked in the human brain tissue. Therefore improvements are still needed to optimize protein measurements with the CMA 71, more specifically to improve the relative recovery of proteins. More in-depth studies should be performed to measure the exact leakage of additives over longer periods of time, since in the clinic samples are collected from microdialysis catheters for up to 10 days. Finally, the safety of the different additives should be verified *in vivo* in brains of animal model organisms such as the pig.

Supporting Information

Additional information as noted in the text. This material is available in appendix E. Graphs of the matrix effect of additives on individual protein measurements are found in appendix G. Graphs of

the effect of additives and controls on the measurement of individual proteins in the cell culture media of U87 cells can be found in appendix H.

Corresponding Author

*Email: david.juncker@mcgill.ca

Acknowledgements

We want to thank Dr. Mathias Aebersold for his critical reading of the manuscript. This work was funded by the Natural Sciences and Engineering Research Council of Canada (NSERC), the Canadian Institutes of Health Research (CIHR) and the Canada Foundation for Innovation (CFI). DJ acknowledges support from a Canada Research Chair in micro and nanobioengineering. We are indebted to Rosanne Votapka from μdialysis, Inc. (N. Chelmsford, MA, USA) and Dr. Sandra Magnoni from the Neuroscience Intensive Care Unit, Department of Anesthesia and Intensive Care, Fondazione IRCCS Ca' Granda Ospedale Maggiore Policlinico (Milan, Italy) for donating a CMA 71 microdialysis catheter.

Conflict of interest

The authors declare no conflict of interest.

References

17. Pla-Roca, M., Leulmi, R. F., Tourekhanova, S., Bergeron, S., Laforte, V., Moreau, E., Gosline, S. J. C., Bertos, N., Hallett, M., Park, M. & Juncker, D. Antibody colocalization microarray: a scalable technology for multiplex protein analysis in complex samples. *Molecular & Cellular Proteomics* **11,** M111.011460 (2012).

18. Helmy, A., Carpenter, K. L. H., Menon, D. K., Pickard, J. D. & Hutchinson, P. J. A. The cytokine response to human traumatic brain injury : temporal profiles and evidence for cerebral parenchymal production. *Journal of Cerebral Blood Flow & Metabolism* **31,** 658–670 (2010).

19. Rosenbloom, A. J., Sipe, D. M. & Weedn, V. W. Microdialysis of proteins: Performance of the CMA/20 probe. *Journal of Neuroscience Methods* **148,** 147–153 (2005).

20. Rosenbloom, A. J., Ferris, R., Sipe, D. M., Riddler, S. A., Connolly, N. C., Abe, K. & Whiteside, T. L. In vitro and in vivo protein sampling by combined microdialysis and ultrafiltration. *Journal of Immunological Methods* **309,** 55–68 (2006).

21. Trickler, W. J. & Miller, D. W. Use of osmotic agents in microdialysis studies to improve the recovery of macromolecules. *Journal of Pharmaceutical Sciences* **92,** 1419–1427 (2003).

23. Dahlin, A. P., Purins, K., Clausen, F., Chu, J., Sedigh, A., Lorant, T., Enblad, P., Lewe, A. & Hillered, L. Refined Microdialysis Method for Protein Biomarker Sampling in Acute Brain Injury in the Neurointensive Care Setting. *Analytical Chemistry* **86,** 8671–8679 (2014).

24. Giorgi-Coll, S., Blunt-Foley, H., Hutchinson, P. J. & Carpenter, K. L. H. Heparin-gold nanoparticles for enhanced microdialysis sampling. *Analytical and Bioanalytical Chemistry* **409,** 5031–5042 (2017).

25. Helmy, A, Carpenter, K. L., Skepper, J. N., Kirkpatrick, P. J., Pickard, J. D. & Hutchinson, P. J. Microdialysis of cytokines: methodological considerations, scanning electron microscopy, and determination of relative recovery. *Journal of Neurotrauma* **26,** 549–561 (2009).

26. Hillman, J., Åneman, O., Anderson, C., Sjögren, F., Säberg, C. & Mellergård, P. A microdialysis technique for routine measurement of macromolecules in the injured human brain. *Neurosurgery* **56,** 1264–1270 (2005).

27. Hutchinson, P. J., O'Connell, M. T., Rothwell, N. J., Hopkins, S. J., Nortje, J., Carpenter, K. L. H., Timofeev, I., Al-Rawi, P. G., Menon, D. K. & Pickard, J. D. Inflammation in human brain injury: intracerebral concentrations of IL-1alpha, IL-1beta, and their endogenous inhibitor IL-1ra. *Journal of Neurotrauma* **24,** 1545–57 (2007).

28. Rosdahl, H., Hamrin, K., Ungerstedt, U. & Henriksson, J. A microdialysis method for the in situ investigation of the action of large peptide molecules in human skeletal muscle: Detection of local metabolic effects of insulin. *International Journal of Biological Macromolecules* **28,** 69–73 (2000).

154. Laforte, V., Olanrewaju, A. & Juncker, D. *Low-cost , high liquid volume silicon quill pins for robust and reproducible printing of antibody microarrays* in *MicroTAS: miniaturized systems for chemistry and life sciences* (Chemical and Biological Microsystems Society (CBMS), Freiburg, Germany, 2013), 485–487.

219. Laforte, V., Lo, P.-S., Li, H. & Juncker, D. Antibody Colocalization Microarray for Cross-Reactivity-Free Multiplexed Protein Analysis. *Methods in Molecular Biology* **1619** (eds Greening, D. W. & Simpson, R. J.) 239–261 (2017).

220. R Core Team. *R: A Language and Environment for Statistical Computing* R Foundation for Statistical Computing (Vienna, Austria, 2018).

252. Schulz, M. K., Wang, L. P., Tange, M. & Bjerre, P. Cerebral microdialysis monitoring: determination of normal and ischemic cerebral metabolisms in patients with aneurysmal subarachnoid hemorrhage. *Journal of Neurosurgery* **93,** 808–814 (2000).

253. Hillman, J, Aneman, O, Persson, M, Andersson, C, Dabrosin, C & Mellergard, P. Variations in the response of interleukins in neurosurgical intensive care patients monitored using intracerebral microdialysis. *Journal of Neurosurgery* **106,** 820–825 (2007).

254. Mertes, P. M., Beck, B., Jaboin, Y., Stricker, A., Carteaux, J. P., Pinelli, G., El Abassi, K., Villemot, J. P., Burlet, C. & Boulangé, M. Microdialysis in the estimation of interstitial myocardial neuropeptide Y release. *Regulatory Peptides* **49,** 81–90 (1993).

255. Varrier, M. & Ostermann, M. Fluid composition and clinical effects. *Critical Care Clinics* **31,** 823–837 (2015).

256. Rosdahl, H., Ungerstedt, U. & Henriksson, J. Microdialysis in human skeletal muscle and adipose tissue at low flow rates is possible if dextran-70 is added to prevent loss of perfusion fluid. *Acta Physiologica Scandinavica* **159,** 261–262 (1997).

257. Hillman, J., Milos, P., Yu, Z. Q., Sjögren, F., Anderson, C. & Mellergård, P. Intracerebral microdialysis in neurosurgical intensive care patients utilising catheters with different molecular cut-off (20 and 100 kD). *Acta Neurochirurgica (Wien)* **148,** 319–324 (2006).

258. Dahlin, A. P., Wetterhall, M, Caldwell, K. D., Larsson, A, Bergquist, J, Hillered, L & Hjort, K. Methodological aspects on microdialysis protein sampling and quantification in biological fluids: an in vitro study on human ventricular CSF. *Analytical Chemistry* **82,** 4376–4385 (2010).

259. Chu, J., Koudriavtsev, V., Hjort, K. & Dahlin, A. P. Fluorescence imaging of macromolecule transport in high molecular weight cut-off microdialysis. *Analytical and Bioanalytical Chemistry* **406,** 7601–7609 (2014).

260. Clausen, F., Marklund, N. & Hillered, L. Acute inflammatory biomarker responses to diffuse traumatic brain injury in the rat monitored by a novel microdialysis technique. *Journal of Neurotrauma* **36,** 201–211 (2019).

261. Keeler, G. D., Durdik, J. M. & Stenken, J. A. Comparison of microdialysis sampling perfusion fluid components on the foreign body reaction in rat subcutaneous tissue. *European Journal of Pharmaceutical Sciences* **57,** 60–67 (2014).

262. Masuko, T., Minami, A., Iwasaki, N., Majima, T., Nishimura, S.-I. & Lee, Y. C. Carbohydrate analysis by a phenol-sulfuric acid method in microplate format. *Analytical Biochemistry* **339,** 69–72 (2005).

263. Kendrick, K. M. Use of Microdialysis in Neuroendocrinology. *Methods in Enzymology* **168,** 182–205 (1989).

264. Allen, M., Bjerke, M., Edlund, H., Nelander, S. & Westermark, B. Origin of the U87MG glioma cell line: Good news and bad news. *Science Translational Medicine* **8,** 354re3 (2016).

265. *Product Note 107 Microdialysis Pump* 8001243h. CMA Microdialysis (Feb. 2016).

266. Bellander, B. M., Cantais, E., Enblad, P., Hutchinson, P., Nordström, C. H., Robertson, C., Sahuquillo, J., Smith, M., Stocchetti, N., Ungerstedt, U., Unterberg, A. & Olsen, N. V. Consensus meeting on microdialysis in neurointensive care. *Intensive Care Medicine* **30,** 2166–2169 (2004).

267. Hutchinson, P. J., O'Connell, M. T., Nortje, J., Smith, P., Al-Rawi, P. G., Gupta, A. K., Menon, D. K. & Pickard, J. D. Cerebral microdialysis methodology — evaluation of 20 kDa and 100 kDa catheters. *Physiological Measurement* **26,** 423–428 (2005).

268. Kjellström, S., Appels, N., Ohlrogge, M., Laurell, T. & Marko-Varga, G. Microdialysis - a membrane based sampling technique for quantitative determination of proteins. *Chromatographia* **50,** 539–546 (1999).

269. Schutte, R. J., Oshodi, S. A. & Reichert, W. M. In vitro characterization of microdialysis sampling of macromolecules. *Analytical Chemistry* **76,** 6058–6063 (2004).

270. Tarassishin, L. & Lee, S. C. Interferon regulatory factor 3 alters glioma inflammatory and invasive properties. *Journal of Neuro-Oncology* **113,** 185–194 (2013).

271. Tarassishin, L., Lim, J., Weatherly, D. B., Angeletti, R. H. & Lee, S. C. Interleukin-1-induced changes in the glioblastoma secretome suggest its role in tumor progression. *Journal of Proteomics* **99,** 152–168 (2014).

272. Lönsmann Poulsen, H. Interstitial fluid concentrations of albumin and immunoglobulin G in normal men. *Scandinavian Journal of Clinical and Laboratory Investigation* **34,** 119–122 (1974).

273. Shiratori, T., Sato, A., Fukuzawa, M., Kondo, N. & Tanno, S. Severe Dextran-Induced Anaphylactic Shock during Induction of Hypertension-Hypervolemia-Hemodilution Therapy following Subarachnoid Hemorrhage. *Case Reports in Critical Care* **2015,** 1–5 (2015).

CHAPTER 6

Potential biomarkers in TBI patients

Preface

Background and objectives

Once the ACM platform had improved reproducibility and sensitivity, and that the relative recovery of proteins in cerebral microdialysis was measured, analysis of the time course data from microdialysate, cerebrospinal fluid and blood samples of severe traumatic brain injury (TBI) patients, and blood samples of mild TBI patients could finally be performed.

Since we knew that some proteins are best measured in plasma or serum, but did not know which sample type to use for which protein, we measured all proteins in both sample types for all patients, and determined which to use for the analysis afterwards. To achieve this, we performed a mini-study of the effect of blood sample collection tubes and pre-processing waiting time and temperature on the initial value and stability of all proteins measured on the ACM.

The "holy grail" of TBI biomarkers are proteins which are produced exclusively in the brain and detected in very small quantities in the blood of patients, because it would offer a perfect specificity for TBI and the sensitivity would be related to the sensitivity of the technique used to detect this protein. Unfortunately while many potential biomarkers appear to be specific to the brain, most of them have been shown to be also produced elsewhere in the body. The reason why we measured proteins in microdialysate, cerebrospinal fluid and blood of severe TBI patients was to offer insights into the site of production of the proteins detected in microdialysate samples, even when proteins are

potentially also produced elsewhere in the body. Finally, with a complex data set of 103 proteins in 8 severe TBI, 6 mild TBI and one trauma patients, we sought to descriptively identify potential new biomarkers of injury severity, development of secondary injury and outcome. Another objective was to help increase the understanding of injury and repair mechanisms by presenting time course data for each protein and each patient, which can be freely examined by researchers in the scientific community.

Challenges and encountered problems

Recruiting severe TBI patients was the most difficult part of this study. In order to insert the cerebral microdialysis catheter, it was sometimes necessary for these severely injured patients to undergo surgery within the first few hours after their injury. This often did not leave a lot of time to identify unconscious patients, contact their families and obtain their consent. Therefore a lot of patients that fulfilled the inclusion criteria were not included in the study because consent could not be obtained. Patients also suffered from various different types and combinations of injuries, and it was not possible to group patients by injury type, which in a larger population would have led to a better and more precise analysis of protein patterns.

The time course data obtained in each bodily fluid and in each patient for 103 proteins was very interesting, and choosing the best way to analyze this data was challenging because of the amount of data and the many possible methods with which the data can be analyzed, each with advantages and disadvantages. When determining the origin of production of proteins, I chose to compare the mean of the 6 or 12 time points for each bodily fluid in each patient. However to determine potential biomarkers of injury severity, outcome and prediction of secondary injury, a descriptive method was chosen over a statistical method because of the low number of patients. This method allowed for a better overview of the trends obtained in patients, which might not have been selected using a statistical approach which unfortunately involves cut-offs and can sometimes miss interesting trends.

Reference

This chapter was written with the intention to submit to the journal *Journal of Neurotrauma* in the near future.

Time course proteomic analysis of matched microdialysis, cerebrospinal fluid and blood samples from severe and blood samples from mild traumatic brain injury patients

Veronique Laforte[1,2,3], Judith Marcoux[2,4], Rajeet Singh Saluja[2,4] and David Juncker[1,2,3,*]

Afilliations

[1] Department of Biomedical Engineering, McGill University, McGill University,
3775 University Street, Montreal, Quebec, Canada H3A 2B4
[2] Department of Neurology and Neurosurgery, McGill University, McGill University,
3801 University Street, Montreal, Quebec, Canada H3A 2B4
[3] McGill University and Genome Québec Innovation Center, McGill University,
740 Dr. Penfield Avenue, Montreal, Quebec, H3A 0G1
[4] Department of Neurosurgery, McGill University Health Center,
1650 Cedar Avenue, Montreal, Quebec, H3G 1A4

Abstract

Clinical diagnosis, management and prognosis of traumatic brain injury (TBI) has changed very little in the past 20-30 years, and is at times difficult and inaccurate. There is a clinical need to 1) correctly classify patients with possible TBI in order to best determine treatment and level of monitoring, 2) predict outcome and 3) predict the possible development of secondary injuries especially in patients with severe TBI. There is increasing interest in developing accurate and minimally invasive blood tests using protein biomarkers, but which proteins to measure, from which body fluid, and how soon after injury, is largely unknown. In this study we aim to find potential biomarkers of injury severity, outcome and secondary injury. To achieve this, we measured 103 proteins in microdialysate, cerebrospinal fluid and blood samples of eight patients with severe TBI, and blood samples of six patients with mild complex and simple TBI, every 12 hours (every hour for microdialysate) for the first three days following their injury. We propose a way to determine the

origin of production of proteins detected in the microdialysate of severe TBI patients by comparing the levels of proteins found in microdialysate, cerebrospinal fluid and blood samples. We found 14 proteins detected in the microdialysate samples that showed strong evidence of being produced by the brain, and 30 proteins that showed little evidence of being produced by the brain. We used this information to make a list of 16 different potential biomarkers of injury severity (of severe and mild TBI) using data from both severe and mild TBI patients. We found 16 potential protein biomarkers of secondary injury in severe TBI, 15 potential biomarkers of outcome in severe TBI and ten in mild TBI. Four of these proteins were different between severe and mild TBI patients with good and bad outcome (FGFb, HMGB1, IL-1β, S100B). When taken together, there is a potential for these biomarkers to better classify TBI severity, predict secondary injury and outcome in patients, which remains to be confirmed in larger-scale studies.

Keywords: traumatic brain injury · microdialysis · proteomics · brain-produced proteins · pre-analytical variables

Abbreviations

ACM	Antibody colocalization microarray
Alg	Algorithm
Amp.	Amplitude
CSF	Cerebrospinal fluid
CTAD	Citrate-theophylline, adenosine, dipyridamole
CV	Coefficient of variation (%)
Dx	Diagnosis
EDTA	Ethylenediamine tetraacetic acid
ELISA	Enzyme-linked immunosorbent assay
EVD	Extra-ventricular drain
GCS	Glasgow coma scale
GOS-E	Extended Glasgow outcome scale
ICP	Intra-cranial pressure
ISS	Injury severity scale
LOD	Limit of detection
LPR	Lactate to pyruvate ratio
MD	Microdialysis
mTBI	Mild traumatic brain injury
$mTBI_C$	Mild complex traumatic brain injury
$mTBI_S$	Mild simple traumatic brain injury
pnBlood	Pooled normal blood (serum or EDTA plasma)
pnCitrate	Pooled normal Citrate plasma
pnCSF	Pooled normal cerebrospinal fluid
pnCTAD	Pooled normal CTAD plasma
pnEDTA	Pooled normal EDTA plasma
pnHeparin	Pooled normal heparin plasma
pnSerum	Pooled normal serum
PRA	Peak and ratio analysis
SI	Supplementary Information
sTBI	Severe traumatic brain injury

6.1 Introduction

Traumatic brain injury (TBI) is one of the leading causes of death and disability in young adults, affecting as much as 10 million people per year worldwide and the incidence is predicted to increase in the future [3, 274]. TBIs can have long-lasting effects such as disability, but also links to early-onset dementia, Alzheimer's disease and Parkinson's disease are beginning to be discovered [13, 15, 275].

TBI is currently diagnosed with CT scans, clinical evaluation of the patient and self-reported symptoms. While diagnosing severe TBI (sTBI) is usually not a problem, mild TBI (mTBI) is

more difficult to diagnose and lesions are visible on computed tomography (CT) scans in only 10-15 % of cases [276]. Stratification of patients is based on the Glasgow Coma Scale (GCS) where patients with GCS of 12-15 are considered to have mild TBI, and patients with GCS of 8 or below are considered to have sTBI. Patients with GCS of 9-11 are classified as having moderate TBI. Penetrating injuries and intracranial bleeding that are sometimes present in sTBI require immediate neurosurgical intervention. However, treatment of other injury types such as contusions, micro-bleeds and diffuse axonal injury consists in assisting the recovery of patients and preventing complications, especially secondary injury which leads to brain edema, high intracranial pressure (ICP) and cerebral hypoperfusion in sTBI patients and leads to death in ~50 % of patients [277]. Despite this classification based on initial consciousness level, patients with sTBI can fully recovery even with the presence of secondary injuries and high ICP, while mTBI patients can suffer from permanent post-concussive syndrome and disability.

Therefore there is a clinical need for non-invasive biomarkers of TBI severity, outcome and to predict secondary injury [278, 279], such as is now the case for diagnosing myocardial infarction with a troponin blood test, which has greatly improved clinical management of patients with acute heart distress [280]. In spite of increased interest in finding biomarkers for TBI, none have yet been validated to the point of being used in clinical practice. S100B, GFAP, NSE, NF-L, UCHL1, tau and others have been well tested [281], but none were found to be specific or sensitive enough to be widely used in the clinic [282].

While most studies investigating potential biomarkers of TBI severity or diagnosis perform protein measurements in sTBI or mTBI patients separately, a few have performed measurements on both the patients suffering from the full spectrum of TBI severity [95, 137, 283–286]. This strategy allows the identification of molecules whose presence is specific to the more severe cases of TBI, while other molecules were identified that were specific to TBI regardless of severity, compared to normal controls.

Two strategies exist for finding potential biomarkers, using non-targeted and targeted approaches. The non-targeted approach is to use mass spectrometry to measure all proteins present in a given sample, thereby bypassing the need for less than perfect antibodies. This method has identified hundreds of potential biomarkers [126], however because of the bias towards mid- to high-abundance proteins, no biomarkers currently approved by the FDA have ever been identified using this technique [287]. Another non-targeted approach used phage display technology to identify GFAP in blood samples of mice subjected to TBI [288]. The targeted approach uses previous knowledge to identify potential targets and measure them using immunoassay-based techniques or targeted MS measurements (SRM-MS). Studies measuring one up to a few proteins in human TBI samples [26, 289–291] have increased the knowledge on molecular mechanisms of injury

and repair, but fail to grasp the bigger picture. Recently, the use of multiplex bead assays that measure from 21 to 143 proteins have helped gain a better understanding of the complex molecular mechanisms present in TBI [18, 77, 81, 85, 86, 88, 89, 260]. While the targeted approach uses platforms with very good sensitivity to measure low-abundance proteins, there is a potential to "miss" valuable information by not measuring enough proteins or proteins only known to be involved in TBI [292]. The antibody colocalization microarray (ACM) is a cross-reactivity free, immunoassay-based platform that can currently measure up to 104 proteins in hundreds of samples ([17] and chapter 4), 11 of which have never been measured before in TBI samples to the best of our knowledge. Any matched antibody pair can easily be added to the platform, making it more versatile than multiplex bead arrays. Recently, proximity elongation assays (PEA) have also been used to investigate 92 proteins in TBI samples, circumventing cross-reactivity by physically linking matched antibody pairs onto beads [84]. The targeted approach therefore benefits from using platforms that can accurately measure hundreds of proteins in single samples, with good sensitivity and reproducibility, effectively helping to better understand the complex molecular mechanisms of injury and repair by grasping a fuller picture of individual patients.

Three important points to consider in the design of studies are the choice of bodily fluid from which to measure proteins, the type of blood sample to use if measuring blood, and the time points at which samples should be collected. In all patients, blood samples are obtained quickly and non-invasively. For sTBI patients who are at risk of developing brain edema, ventricular cerebrospinal fluid (CSF) can be available when it is drained, as well as brain microdialysis, a method that allows indirect sampling of small and large molecules present in the interstitial fluid of the brain tissue. Proteins measured in microdialysate samples are thought to be produced by the brain, although in sTBI the presence of blood-brain barrier disruption can allow proteins to pass from the blood to the brain tissue, while other proteins produced elsewhere in the body can be found in smaller quantities in the brain tissue of normal individuals, such as albumin. A challenge posed by microdialysate sampling is the very low sample volume (~20 µL) and the very low concentration of proteins in samples. Proteins measured in CSF are thought to better reflect the status of the brain than blood, while proteins measured in blood can originate from anywhere in the body. Because of these differences, studies have compared proteins measured in microdialysate and blood [18, 72] or CSF and blood [293–305]. Studies investigated a small number of molecules such as IL-6 [306], 17 cytokines and matrix metalloproteinases [73, 74] or prostaglandins [307] in the three types of samples together and found that a majority of molecules were produced in the brain in TBI patients. Pharmacology studies on animals have measured small and large molecules in microdialysate, CSF and blood concurrently, and these studies have shown that molecules injected in the blood are generally detected in the brain tissue, albeit in varying proportion, proving that even large molecules

such as antibodies measured by microdialysis can have their origin elsewhere in the body [308].

The second point of consideration when measuring multiple proteins per sample is the question of which blood sample type to use. It is widely known that measuring proteins in serum and plasma can lead to different values. This can be due to a proportion of the protein measured being sequestered with the blood clot in serum samples [309–311], or this difference can be due to a different sources of the protein being measured [312–314]. An example is BDNF which is released by platelets upon blood clotting in serum, while levels measured in plasma is thought to more closely resemble levels present in the blood circulation [315]. On the other hand some proteins can degrade more quickly in plasma containing EDTA as anticoagulant, as is the case for BDNF [316]. Kaisar *et al.* reported significant degradation of 4 % of total proteins detected in EDTA plasma samples awaiting centrifugation and processing using mass spectrometry [317]. Therefore it is important that proteins are measured in conditions that best preserves proteins and accurately reflects levels in the blood circulation of patients, rather than levels measured from the release of blood cells during sample collection. Although the Human Proteome Organization (HUPO) recommends measuring proteins from EDTA plasma [119], there does not seem to be a single ideal blood collection tube that best preserves all proteins present and accurately reflect levels found in the blood circulation of patients.

Finally the question of when and how often to collect samples from patients is also crucial, as proteins levels have been shown to be dynamic, with GFAP and S100B having a delayed appearance in blood samples [276], whereas many proteins peak in the first 24 h after TBI injury in microdialysate samples [18, 299]. Time course measurements of proteins is the only way to capture the full dynamic of proteins levels in all bodily fluids.

Here, we measure 100 proteins in microdialysate, CSF, serum and EDTA plasma samples of sTBI patients over a course of 72 h starting within 24 h after their injury, in order to both increase the understanding of the molecular mechanisms of injury and repair and to identify the origin of proteins measured. We also measure 100 proteins in serum, EDTA and CTAD plasma samples of mTBI patients and a non-TBI trauma patient in a similar time course. We use stability measurements from two healthy volunteers to identify which blood sample type to analyze for each protein. We compare the levels of proteins in microdialysate, CSF and blood samples of sTBI patients to determine the origin of production of proteins detected in microdialysate samples, adding precious information about proteins identified as potential biomarkers of TBI severity, development of secondary injuries in sTBI patients, and outcome in both sTBI and mTBI patients.

6.2 Materials and Methods

6.2.1 Materials

Phosphate-buffered saline (PBS) 10 × solution and glycerol were purchased from Fisher Scientific (Hampton, NH, USA). Trehalose and Tween-20® were obtained from Sigma-Aldrich (St. Louis, MO, USA). Protease-free, IgG-free bovine serum albumin (BSA) was obtained from Jackson ImmunoResearch Laboratories (West Grove, PA, USA). BSA Alexa Fluor 555 (AF555), goat anti-rabbit (GAR)-AF647, goat anti-mouse (GAM) AF647, GAR-biotinXX (where XX are two random amino acid spacers between GAR and biotin), streptavidin-AF647 and 4 mm 0.45 µm PVDF syringe filters were purchased from Thermo Fisher Scientific (Waltham, MA, USA). PBST incubation solution consisted in PBS 1 ×, 0.05 % Tween-20® in pure water. Slides washing solution was prepared similarly but contained 0.1 % Tween-20®. Serum (BD Vacutainer #367815), K_2EDTA (BD Vacutainer #367863), lithium heparin (BD Vacutainer #367886), citrate (BD Vacutainer #369714) and CTAD (BD Vacutainer #367599) blood collection tubes were obtained from Becton, Dickinson and Company (Franklin Lakes, NJ, USA). Capture and detection antibodies as well as recombinant antigens to measure 103 different proteins (listed in appendix D) were purchased from R&D Systems (Minneapolis, MN, USA), unless otherwise noted. FAS-L, IL-2 and VEGFR2 were not measured in the sTBI experiment, and IL-6, SCGN and FGF-1 were not measured in the mTBI experiment due to missing antibodies or spots. Furthermore, β-NGF was not analysed in the study of effects of pre-analytical variables on the stability of proteins due to spots missing in multiple samples. Pooled normal human lumbar cerebrospinal fluid (pnCSF) was purchased from Gemini Bio-Products (West Sacramento, CA, USA). Pooled normal serum , plasma EDTA, CTAD, citrate and heparin plasma were made in-house with a minimum of 10 adult healthy anonymous volunteers as described in chapter 4.

6.2.2 Traumatic brain injury patients recruitment and sample collection

Severe TBI patients

Patients admitted at the Montreal General Hospital, a supraregional level 1 trauma center, with a diagnosis of severe TBI and requiring the insertion of an extra-ventricular drain (EVD) were considered for this study. Recruitment was prospective and occurred between July 2009 and October 2011. Consent for the insertion of a microdialysis probe was obtained prior to the insertion of clinically-required EVD, from patients' legal representatives, as all were in a comatose state and were unable to provide consent. A full informed consent was later sought for participants who regained their ability to consent. All participants were treated using standard care practices. Criteria

for selecting patients for an EVD insertion were in accordance with the guidelines [318] at the time of patient recruitment. A microdialysis (CMA 71, 30 mm high molecular weight cut-off membrane) catheter (μdialysis AB, Johanneshov, Sweden) was inserted in the right frontal lobe white matter via a twist-drill burr hole at the same time as the EVD as described in [319], secured with sutures to the patient's skin and attached to a microdialysis pump (CMA 107, μdialysis AB) filled with sterile perfusion fluid (Perfusion Fluid CNS, μdialysis AB). Catheter placement was verified by computed tomography. Perfusion fluid was injected at 0.3 µL/mL and the microdialysate collected every hour for 72 h in microdialysis vials (#P000001, μdialysis AB) situated at the level of the patient's head. Vials were immediately put on ice and frozen at −80 °C within 12 h of collection. CSF samples (1 mL, when available) were collected every 12 h from the EVD and processed within 1 h. At the same time, blood was collected into serum and K_2EDTA blood collection tubes through an arterial line in the radial artery. Serial bodily fluid collection started within 24 hours of injury. Serum tubes were allowed to clot untouched at room temperature, while EDTA tubes were inverted 8-10 × and stored on ice. Blood collection tubes were centrifuged less than one hour after collection for 10 min at 1000 *g* and the resulting serum and plasma along with the CSF were aliquoted into cryo-vials before storing at −80° for measurement with the ACM.

Mild TBI patients

Patients admitted to the Montreal General Hospital for at least 24 h and diagnosed with mild TBI (subjects) or trauma without a TBI (control), were eligible for the study. The recruitment was prospective and occured during the period of January to March 2016. Diagnosis of mild TBI was confirmed medically and included at least one of the following symptoms: period of loss or decreased level of consciousness, post-traumatic amnesia, alteration in mental state at the time of injury, neurological deficits (even transient) or the presence of a traumatic intracranial lesion on radiological scan [320]. Consent was obtained and serial blood collection started within 24 hours of injury. Blood was collected (in order) in serum, K_2EDTA and CTAD tubes using standard venipuncture procedures. Serum tubes were allowed to clot at room temperature while plasma tubes were inverted 8-10 × and stored on ice followed by centrifugation at 1000 *g* for 10 min in less than one hour. The resulting serum and plasma were transferred to cryo-vials and stored at −80 °C until measurement with the ACM.

Ethics and outcome measures

Both studies were approved by the McGill University Health Centers Institutional Review Board. For all patients, the following information were collected from medical records: age, gender, mechanism of trauma, medical history, Glasgow Coma Scale (GCS) [2] score upon initial presentation,

CT scan findings, type of surgical intervention, discharge destination, and functional dependency at discharge using the Extended Glasgow Outcome Scale (GOS-E) [321]. The GOS-E scale can be grossly divided as death (1) functionally dependent (≤ 4) and functionally independent (> 4).

6.2.3 Pre-analytical variables samples collection and processing

Blood samples were collected from two healthy anonymous adult males by standard venipuncture practice using a 23G size needle. Blood was collected (in order) into one partially-filled discard serum, one citrate, one serum, one lithium heparin, two K_2EDTA and two CTAD blood collection tubes per donor. All tubes were quickly inverted 8-10 $\times$ and aliquoted in six (12 for EDTA and CTAD) microcentrifuge tubes containing each 750 µL of whole blood for each blood collection type. Serum tubes were allowed to clot at room temperature for 15 min before being processed like the other tubes. Half of the microcentrifuge tubes were stored on ice, while the other half were left at room temperature. After 5, 30 and 120 min each, tubes were centrifuged for 10 min at 1000 *g*. Half of the EDTA and CTAD plasma from centrifuged tubes were filtered using a sterile 1 mL syringe fitted with a 0.22 µm sterile 13 mm PVDF membrane (MilliporeSigma™ GVWP01300, Burlington, MA, USA) to filter out remaining platelets from the plasma. The resulting serum/plasma were collected from the top of the red blood cells and were aliquoted by 50 µL. Samples were frozen immediately at −80 °C after processing, and were kept until measurement with the ACM.

6.2.4 Small molecules measurements

Microdialysis vials were thawed and kept at 4 °C until immediately before analysis to prevent proteins degradation in the samples. Glucose, lactate, pyruvate and glutamate were measured using a CMA 600 microdialysis analyzer (μdialysis AB). Remaining microdialysate fluid in vials was combined to make a pooled sample every 6 h, aliquoted by 20 µL and frozen at −80 °C until measurement with the ACM.

6.2.5 ACM experiments

ACM microarrays were produced using protocols in [219] and chapter 4. In short, GAR-biotinXX (subarray calibrant, at 25 µg/mL) and capture antibodies from matched ELISA antibody pairs were mixed with 50 % (sTBI experiment) or 45 % (mTBI experiment) glycerol and 0.005 % Tween-20® in PBS 1 $\times$ spiked with 20 µg/mL (sTBI experiment) or 10 µg/mL of BSA-AF555 spot calibrant before being printed on PolyAn 2D Aldehyde microarray slides (PolyAn GmbH, Berlin, Germany) as 16 identical subarrays. Printing was done with a customized Nanoplotter 2.1 microarrayer (GeSiM

GmbH, Radeberg, Germany) with an added microfabricated collimator (Parallel Synthesis, Santa Clara, CA, USA) fitted with four custom-made silicon quill pins [154]. Slides were incubated for 24 h following the end of printing, in the nanoplotter chamber with controlled humidity at 65 % RH and room temperature, in the dark. Slides were fitted onto gaskets (ProPlate®, Grace Bio-Labs, Bend, OR, USA) that separated subarrays into 16 independent liquid incubation chambers, washed with PBST and blocked for 3 h using 3 % BSA in PBST. Microdialysate, CSF, serum and plasma samples were thawed and diluted as indicated with slide washing buffer. Samples were loaded onto slides as well as three (sTBI experiment) or two (mTBI experiment) standard curves consisting of a mixture of recombinant antigens (except CA15-3 and CEA, which were antibody-purified from cancer patients) at known, high concentrations and diluted 15 times in a 1:2.5 serial dilution. Samples were incubated in the dark at 4 °C for a minimum of 18 h on a rotation shaker, before washing, rinsing in 5 % trehalose (sTBI experiment) or water (mTBI experiment), drying with a stream of compressed nitrogen and placing back with high precision in the nanoplotter chamber. Detection antibodies (either biotinylated or mixed with an AF647-labeled reporter antibody) mixed in 45 % glycerol with 1 % BSA and 0.001 % Tween-20® were printed on top of the capture antibodies and incubated for 24 h following the end of printing. Slides were fitted into the gaskets, washed, incubated for 1 h with a solution of Streptavidin-AF647 0.5 µg/mL in PBST with 3 % BSA at room temperature with rotational shaking, washed and then dried with a stream of compressed nitrogen and scanned using the SureScan Microarray Scanner (Agilent Technologies, Santa Clara, CA, USA) using two-colors and a resolution of 5 µm per pixel.

6.2.6 Statistical analysis

Fluorescence values were extracted from the images produced by the scanner and analyzed using ArrayPro Analyzer 6.31 (Media Cybernetics, Rockville, MD, USA). Fluorescence values were imported into R [220]. Calibration of data was based on chapter 4 with the goal of improving reproducibility or sensitivity as indicated. Linear regression of the relative recovery values of proteins versus their molecular weight was obtained from chapter 5. The R package *lme4* [322] was used for fitting linear mixed effect models to time course data, and package *limma* [323] was used for multivariate linear microarray models statistical analyses. Errors reported in graphs and tables are standard deviations. Groups of values were compared using Student's t-test or in the case of a single value compared to a group of values, Student's t-test with equal variance. Values for a single time course was considered to have a peak if the highest value was greater than 50 % above the mean of all values. The mean of values from each time course was considered to be above or below normal if it varied by more than 30 % from the mean value calculated for pnCSF or pnBlood.

6.3 Results

6.3.1 Patient characteristics

Serial microdialysate, CSF and blood samples were collected from eight patients suffering from sTBI for a total of 72 h starting within the first 24 h from injury. All were male between 19 and 83 (mean 45) years old and had an initial GCS between 3 and 14 (median GCS 7). Two patients were intubated at the time of admission. Five patients developed high intracranial pressure (ICP), for which two out of the five underwent decompressive surgery. The remaining three were given intravenous mannitol. Outcome at 6 months ranged from death to complete recovery (GOS-E 1 to 8). Similarly, serial blood samples were also collected from six patients suffering from mTBI (five with positive CT scan findings) and one non-TBI trauma patient. The six mTBI patients were male, and the trauma patient was female. The age of mTBI patients ranged from 57 to 91 (mean 70) years old, while the trauma patient was 66 at the time of injury. A single mTBI patient presented with an initial GCS of 14, the others had initial GCS of 15. Outcome of mTBI patients ranged from moderate disability to good recovery (GOS-E 6 to 8). None of the mTBI patients presented symptoms of high ICP.

TABLE 6.1: **Patient clinical information.** GCS: glasgow coma scale (level of consciousness), ISS: injury severity score, Dx: diagnosis (of TBI severity), sTBI: severe traumatic brain injury, $mTBI_C$ and $mTBI_S$: mild complex or simple traumatic brain injury, respectively, ICP: intracranial pressure, ICP Tx: treatment for high ICP, 6mo GOS-E: extended glasgow outcome scale at 6 months post-injury.

Patient ID	Initial GCS	ISS	Age	Gender	Dx	ICP	ICP Tx	6mo GOS-E
sTBI-001	3	26	25	Male	sTBI	High	Craniectomy day 1	5
sTBI-009	14	35	67	Male	sTBI	Low	-	1
sTBI-010	5T*	30	27	Male	sTBI	High	Medical	1
sTBI-011	8	38	57	Male	sTBI	Low	-	8
sTBI-013	3T*	43	27	Male	sTBI	High	Medical	2
sTBI-015	8	50	19	Male	sTBI	High	Craniectomy day 2	5
sTBI-016	13	43	57	Male	sTBI	High	Medical	8
sTBI-017	$14 \rightarrow 11 \rightarrow 7$	38	83	Male	sTBI	Low	-	3
mTBI-003	14	30	91	Male	$mTBI_C$	-	-	7
mTBI-004	15	9	61	Male	$mTBI_C$	-	-	6
mTBI-005	15	1	66	Female	Trauma	-	-	8
mTBI-006	15	10	86	Male	$mTBI_C$	-	-	8
mTBI-007	15	10	62	Male	$mTBI_C$	-	-	7
mTBI-008	15	20	57	Male	$mTBI_C$	-	-	8
mTBI-009	15	6	61	Male	$mTBI_S$	-	-	8

*:intubated

6.3.2 Brain metabolism in sTBI patients

Small molecules involved in brain metabolism (glucose, lactate, glutamate and pyruvate) were measured in the microdialysate of five sTBI patients for 72 h after catheter insertion. A single patient had bad dichotomized outcome (vegetative state) whereas other patients had good outcome (from moderate disability to complete recovery) and all but one patient had high ICP. Figures F.S1 to F.S5 show detailed time course measurements for all molecules measured, and figure 6.1 shows a statistical summary of the comparison in terms of outcome and secondary injury (high ICP). On average, mean lactate, lactate to pyruvate ratio were higher than normal values reported from microdialysate samples in healthy brain tissue [252], while glucose was lower than normal (figure 6.1c). Lactate to pyruvate ratio (LPR) was more elevated in patients suffering from high ICP (figure F.S5d), although the difference was not statistically significant (p-value 0.183). In the patient with low ICP, mean glucose was slightly elevated, whereas in all other patients mean glucose was found in very low concentration (below 2 mM) (figure F.S1a). In terms of outcome, the patient with bad outcome had a later glucose peak time (>36 h) whereas all others had earlier glucose peak times (<24 h) (figure F.S1c).

6.3.3 ACM experiments and choice of serum or plasma for each protein

We used the ACM to measure 103 proteins in two separate large-scale experiments, including low-abundance cytokines, chemokines, proteases, cell adhesion molecules, vascular signaling molecules, neurotrophin factors and two well-studied potential biomarkers of TBI, S100B and GFAP. The complete list of proteins is found in chapter 4 and more details can be found in chapter 5 appendices. The first experiment measured microdialysate, CSF, EDTA plasma and serum samples from sTBI patients, while the second experiment measured serum, EDTA and CTAD plasma from mTBI patients, as well as different blood samples from two healthy controls that was used to test the effect of pre-analytical variables on the measurement of proteins. Due to technical difficulties, each large-scale experiment had final measurements for 100 proteins, with six proteins being measured in a single large-scale experiment (FAS-L, IL-2 and VEGF-R2 in the mTBI experiment, and IL-6, SCGN and FGF-1 in the sTBI experiment). Details of the calibration can be found in the SI from figure F.S6 to table F.S2.

We performed an experiment to study the effect of blood collection tube types (serum, EDTA, citrate, heparin, CTAD), pre-processing waiting time and temperature and post-processing filtration to remove platelets on the initial protein measurements of 99 proteins as well as their stability during a 2 h waiting time before centrifugation. Using this data, we determined the most suitable sample type (serum or EDTA plasma) for each protein for the analysis of TBI patient samples time courses.

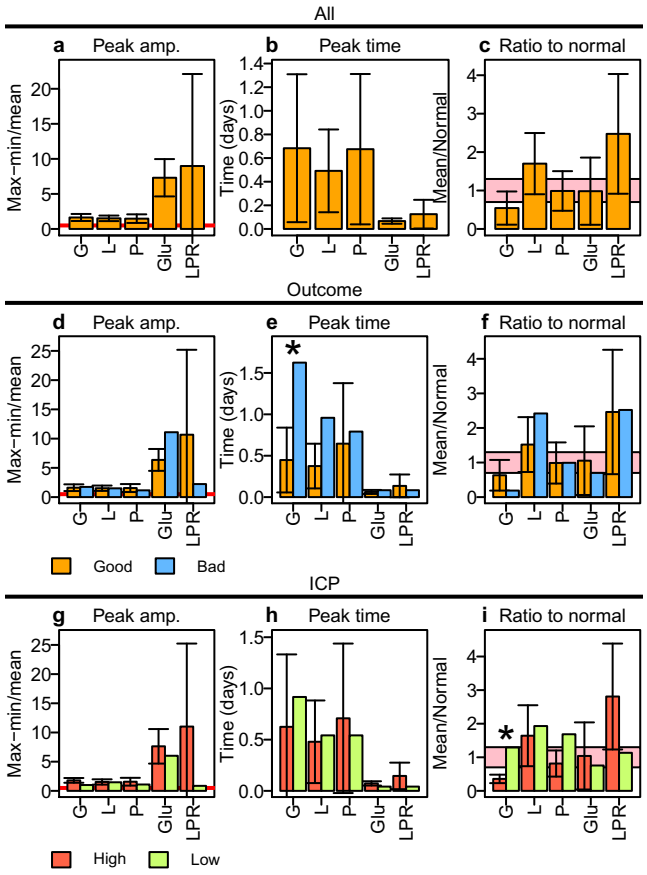

FIGURE 6.1: **Peak and ratio analysis for small molecules in brain microdialysate of sTBI patients.** Small molecules (G: glucose, L: lactate, P: pyruvate, Glu: glutamate, LPR: lactate to pyruvate ratio) were measured in the brain microdialysate of sTBI patients. The average (**a, d, g**) maximum value in the time course (peak), (**b, e, h**) time at which the peak occurred and (**c, f, i**) average value within time course compared to reported normal microdialysate values are shown. (**a-c**) Average of five sTBI patients. (**d-f**) Difference between patients with good (GOS-E 5-8) and bad (GOS-E 1-4) outcome. (**g-i**) Difference between patients with high and low ICP. Stars indicate a statistically significant difference (p-value < 0.01). The red lines in **a, d, g** show the threshold for a profile that is considered to have a peak, rather than being constant. The light red boxes in **c, f, i** show the threshold of comparison to the normal measured value.

Serum was chosen for 46 proteins, and EDTA plasma for 53 proteins based on the lower initial value that is assumed to reflect the true concentration of protein in the blood and stability during the 2 h waiting time before centrifugation. Initial value and stability measurements was not performed for IL-6, SCGN, FGF-1 and β-NGF, and EDTA plasma was picked based on the literature. Details of the effects of pre-analytical variables on the measurement of proteins can be found in the SI from figure F.S9 to table F.S6.

6.3.4 Evidence for brain production of proteins

All 100 proteins were detected in at least one blood sample of sTBI patients. Thirteen proteins were not detected in any microdialysate sample, and 26 proteins were not detected in any CSF sample. We estimated the original concentration of proteins in each sample type, taking into account sample dilution during measurement and for microdialysate samples, the relative recovery of each protein based on the regression line obtained for artificial CSF (aCSF) perfusion fluid in a previous study (chapter 5) (table F.S7). The ratio of estimated original concentration between microdialysate, CSF and blood samples is shown in figure 6.2. The majority of proteins detected in both microdialysate and CSF samples were found in higher concentration in microdialysate. Of the 87 proteins detected in microdialysate samples, 64 had higher concentrations in microdialysate than blood samples. Similarly, of the 74 proteins detected in CSF, only 11 were found in higher concentration in CSF than blood.

Comparing the estimated original concentration of each protein in the three different bodily fluids, 14 proteins were found in highest concentration in microdialysate samples and lowest in blood samples, which is evidence that these proteins were produced in the brain parenchyma (table 6.2) at the site of microdialysis sampling. A majority of proteins (55) were found in highest concentration in microdialysate samples, followed by blood and finally in lowest concentration in CSF, which suggests production in the brain as well as elsewhere in the body, *i.e.* a mixed production. A total of 30 proteins were found in highest concentration in the blood in spite of being detected in microdialysate samples, which suggests that these proteins were produced elsewhere in the body (systemic). A single protein (Ang1) was found in highest concentration in CSF.

6.3.5 Potential biomarkers of injury severity

We measured samples from multiple patients with sTBI, and mTBI with lesions found by CT scan ($mTBI_C$), as well as one mTBI patient without lesions found by CT scan ($mTBI_S$) and one patient who suffered a major trauma but no TBI. Considering that patients in these groups suffer from a decreasing scale of TBI severity, we compared the levels of each protein among the four groups to

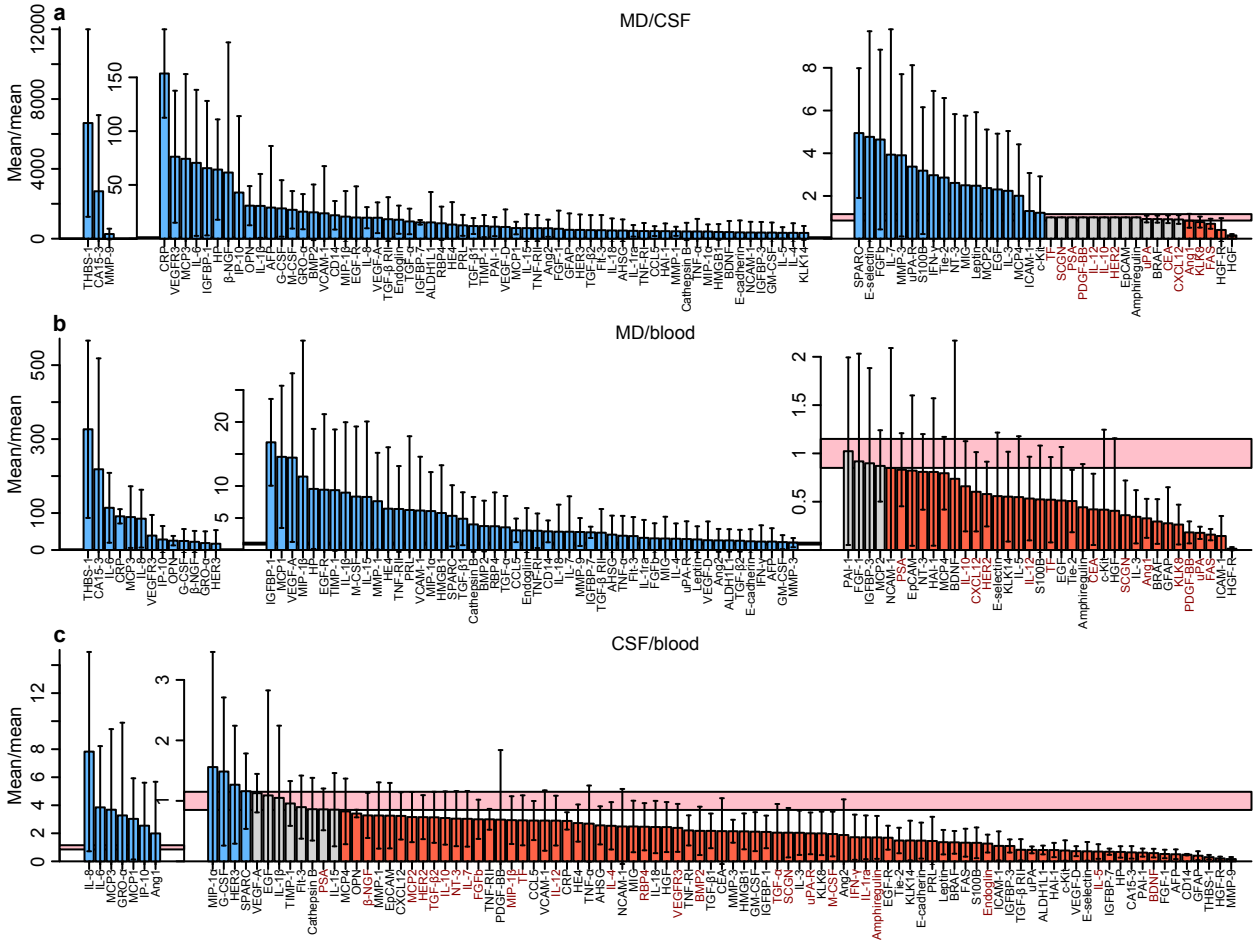

FIGURE 6.2: **Ratios of proteins between microdialysate, CSF and blood samples of sTBI patients.** Ratios of proteins between **a** microdialysate and CSF, **b** microdialysate and blood and **c** CSF and blood samples of sTBI patients. Values located in the light red box (gray) are considered to have similar concentrations, while those above (blue) and below (red) are considered to have different concentrations. Proteins with names in red were not detected and therefore their levels were assumed to be equal to that of LOD.

TABLE 6.2: **List of proteins detected in microdialysate samples produced in the brain and/or elsewhere in the body.** Examination of ratios between microdialysate, CSF and blood samples of sTBI patients shows evidence of brain production ($microdialysate > CSF \geq blood$) or evidence against brain production ($blood > CSF \geq microdialysate$ and $blood > microdialysate \geq CSF$). All other ratio combinations of proteins detected in microdialysate samples suggests a mixed production in the brain and also elsewhere in the body. MD: microdialysate.

MD > CSF ≥ Blood	MD ≥ Blood > CSF			Blood > MD ≥ CSF	
G-CSF	AFP	GM-CSF	MMP-3	Amphiregulin	PDGF-BB
GRO-α	AHSG	HE4	MMP-9	BRAF	PSA
HER3	ALDH1L1	HMGB1	OPN	CEA	S100B
IL-15	Ang2	HP	PAI-1	c-Kit	SCGN
IL-1β	BDNF	IFN-γ	PRL	CXCL12	TF
IL-6	BMP2	IGFBP-1	RBP4	EpCAM	Tie-2
IL-8	β-NGF	IGFBP-3	TGF-α	E-selectin	uPA
IP-10	CA15-3	IGFBP-7	TGF-β RII	GFAP	
MCP1	Cathepsin B	IL-18	TGF-β1	HAI-1	
MCP3	CCL5	IL-1ra	TGF-β2	HER2	
MIP-1α	CD14	IL-4	THSB-1	ICAM-1	
SPARC	CRP	IL-7	TNF-α	IL-10	
TIMP-1	E-cadherin	Leptin	TNF-RI	IL-12	
VEGF-A	EGF	MCP2	TNF-RII	IL-3	
	EGF-R	M-CSF	uPA-R	IL-5	
	Endoglin	MIG	VCAM-1	KLK14	
	FGF-1	MIP-1β	VEGF-D	MCP4	
	FGFb	MMP-1	VEGFR3	NCAM-1	
	Flt-3			NT-3	

CSF > MD > Blood	CSF > Blood > MD	Blood > CSF > MD
none	Ang1	FAS
		HGF
		HGF-R
		KLK8

protein levels measured in the pooled normal replicate serum or plasma samples (pnBlood) made from healthy controls (see figure 6.3 and tables F.S8 and F.S9). Because only blood samples were available for the mTBI and trauma patients, and ideally biomarkers of severity injury would be measured non-invasively as part of the diagnosis of patients presenting with possible TBIs, we only considered protein measurements in blood.

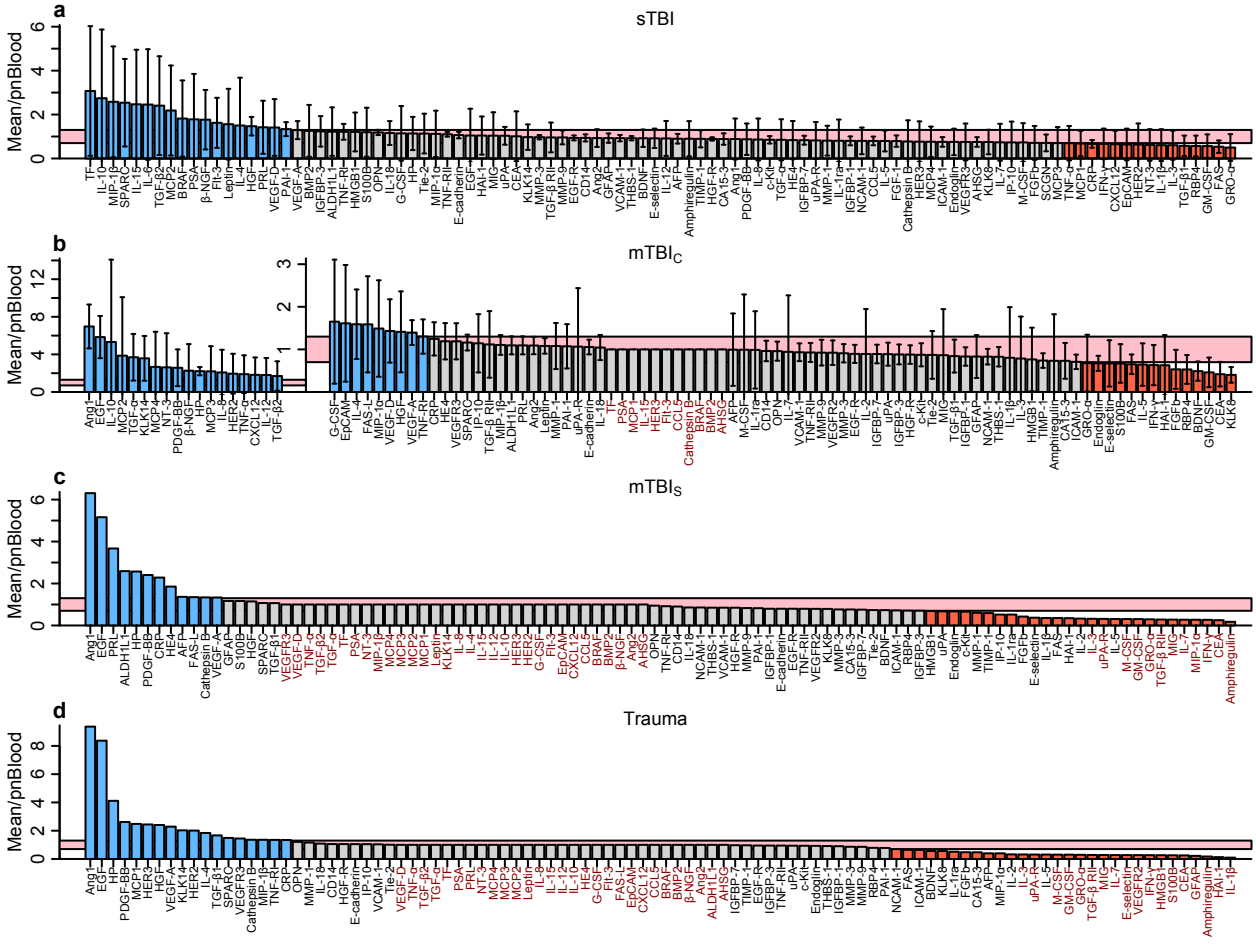

FIGURE 6.3: **Ratios of blood samples proteins to pnBlood in sTBI, mTBI$_C$, mTBI$_S$ and trauma patients.** Ratios of proteins to pnBlood in the blood samples of **a** sTBI, **b** mTBI$_C$, **c** mTBI$_S$ and **d** trauma patients compared to levels found in normal controls (pnBlood). Values located in the box (gray) are considered to have similar values to pnBlood, while those above (blue) and below (red) are considered to have values different from pnBlood. Proteins with names in red were not detected and therefore their levels were assumed to be equal to that of LOD.

A total of 18, 27, 12 and 18 proteins were found in higher concentration in blood samples of sTBI, mTBI$_C$, mTBI$_S$ and trauma patients, respectively, when compared to levels found in the normal control pnBlood. Similarly, 15, 14, 15 and 11 proteins were found in lower concentration in the same groups. As mentioned previously, all proteins were detected in at least one blood samples

of sTBI patients, while 11, 44 and 47 proteins were undetected in any of the $mTBI_C$, $mTBI_S$ or trauma patient blood samples, respectively.

Considering proteins that were elevated in at least 3/7 sTBI patient blood samples, or at least 2/5 $mTBI_C$ blood samples, several proteins were identified (table 6.3). Eight proteins were found to be elevated in sTBI patients blood samples only, one of which has been found to be produced by the brain in those patients (MCP1). Six proteins were found to be elevated in both sTBI and $mTBI_C$ patients blood samples, one of which was found to be produced in the brain of sTBI patients (MIP-1α). Two more proteins were unique to $mTBI_C$ patients, and five proteins were found to be elevated only in the $mTBI_S$ patient, including S100B and GFAP. Finally, two proteins were found to be elevated in most patients of all groups (MMP1 and OPN).

TABLE 6.3: **Summary of potential biomarkers of TBI severity from sTBI to mTBI.** Proteins listed were found to be elevated in one or more groups of different TBI severity (combined with +), and are separated by their presumed origin in sTBI patients. Parentheses note in how many patients the protein was found to be elevated. Total number of patients in each group is found in the title of each column.

Origin	sTBI (7)	sTBI (7) + $mTBI_C$ (5)	sTBI (7) + $mTBI_C$ (5) + $mTBI_S$ (1)	$mTBI_C$ (5)	$mTBI_C$ (5) + $mTBI_S$ (1)	$mTBI_S$ (1)	Trauma (1)	sTBI (7) + $mTBI_C$ (5) + $mTBI_S$ (1) + Trauma (1)
Brain	MCP1 (4)	MIP-1α (3, 3)	*none*	*none*	*none*	*none*	*none*	
Mixed	Ang2 (3) BMP2 (5) MIP-1β (3) BDNF (3)	HMGB1 (4, 2) PAI-1 (4, 2) TGF-a (3, 2) TGF-β RII (3, 2)	*none*	CA15-3 (2) FGFb (2)	*none*	AFP (1) ALDH1L1 (1)	*none*	MMP1 (3, 3, 1, 1) OPN (7, 2, 1, 1)
Other	IL-12 (3) NCAM-1 (3) TF (3)	E-selectin (3, 2)	*none*	*none*	*none*	GFAP (1) PDGF-BB (1) S100B (1)	*none*	*none*

6.3.6 Potential biomarkers of secondary injury in sTBI patients

Five out of eight sTBI patients developed high ICP in less than 48 h after their injury, therefore we compared proteins in microdialysate, CSF and blood samples whose levels were different between patients with low and high ICP in at least one bodily fluid (figure 6.4). The single patient with low ICP who had an microdialysis catheter inserted showed early peaks of MMP-9 and THBS-1 in the first day, while the level of CD14 was generally higher in microdialysate samples than the levels seen in patients with high ICP. In CSF, five proteins were found to be different between patients with high and low ICP. GRO-α and THBS-1 were elevated in patients with low ICP compared to pnCSF for the entire collection period, while IL-8 increased above the level of pnCSF also in patients with low ICP after 24 h. On the other hand, MMP-9 was normal compared to pnCSF in patients with low

ICP, and significantly decreased in patients with high ICP. A single protein (MMP-1) was found to be elevated in the CSF of patients with high ICP after 36 h. In blood samples, 11 proteins were found to be elevated in patients with high ICP compared to patients with low ICP. A single protein was found to be decreased in all sTBI patients (IL-3), however the level was far more decreased in patients with low ICP than high ICP. Similarly as in CSF, MMP-9 was found to be increased in patients with low ICP compared to pnBlood and patients with high ICP.

MMP-1 was found to be different in both CSF and blood samples, while MMP-9 was found to be different in microdialysate, CSF and blood samples. In both cases, the change seen in CSF was reflected in the blood, but in blood the difference was less pronounced for MMP-9 and more pronounced for MMP-1 compared to the difference seen in CSF. In contrast, the time course seen in microdialysate samples for MMP-9 is more complex, with a first increase (peak) in the patient with high ICP, followed by a decrease, whereas MMP-9 remained higher in patients with high ICP in CSF and blood.

6.3.7 Potential biomarkers of outcome

In sTBI patients as well as in $mTBI_C$ patients, some patients had a bad outcome and others had a good outcome. Therefore, we performed a similar comparison of protein levels in terms of dichotomized outcome. Because the outcome of sTBI patients varied from death to complete recovery, we separated patients in bad (GOS-E 1-4) or good (GOS-E 5-8) outcome categories, and compared microdialysate, CSF and blood samples. Figure 6.5 shows pronounced differences in microdialysate samples, with eight proteins being elevated in patients with bad outcome compared to good outcome. G-CSF, IL-1β, IL-8, MIP-1α and MIP-1β had an early peak during the first 24-30 h of sample collection, while IGFBP-1, IL-6 and TIMP-1 were increased until ~68 h in patients with bad outcome. In CSF samples, three proteins were decreased compared to levels measured in pnCSF in patients with bad outcome (EGF-R, TIMP-1, and VCAM-1). IL-18 was found to be above the level of pnCSF in patients with bad outcome, while the level seen in patient with good outcome was normal. VEGF-A was elevated in all sTBI patients, but it was more so in patients with bad than good outcome. In blood, only four proteins were found to be different between patients with good and bad outcome. FGFb was found to be normal in patients with bad outcome, and decreased in patients with good outcome. HMGB1 and S100B were found to be increased in patients with bad outcome, and normal in patients with good outcome. The opposite was seen with TIMP-1, whose levels were slightly decreased during day 2 in patients with bad outcome.

TIMP-1 was different between patients with good and bad outcome in microdialysate, CSF and blood samples. Surprisingly, the increase seen in microdialysate samples of patients with bad outcome was the opposite of the decrease seen in the CSF and blood samples of the same patients.

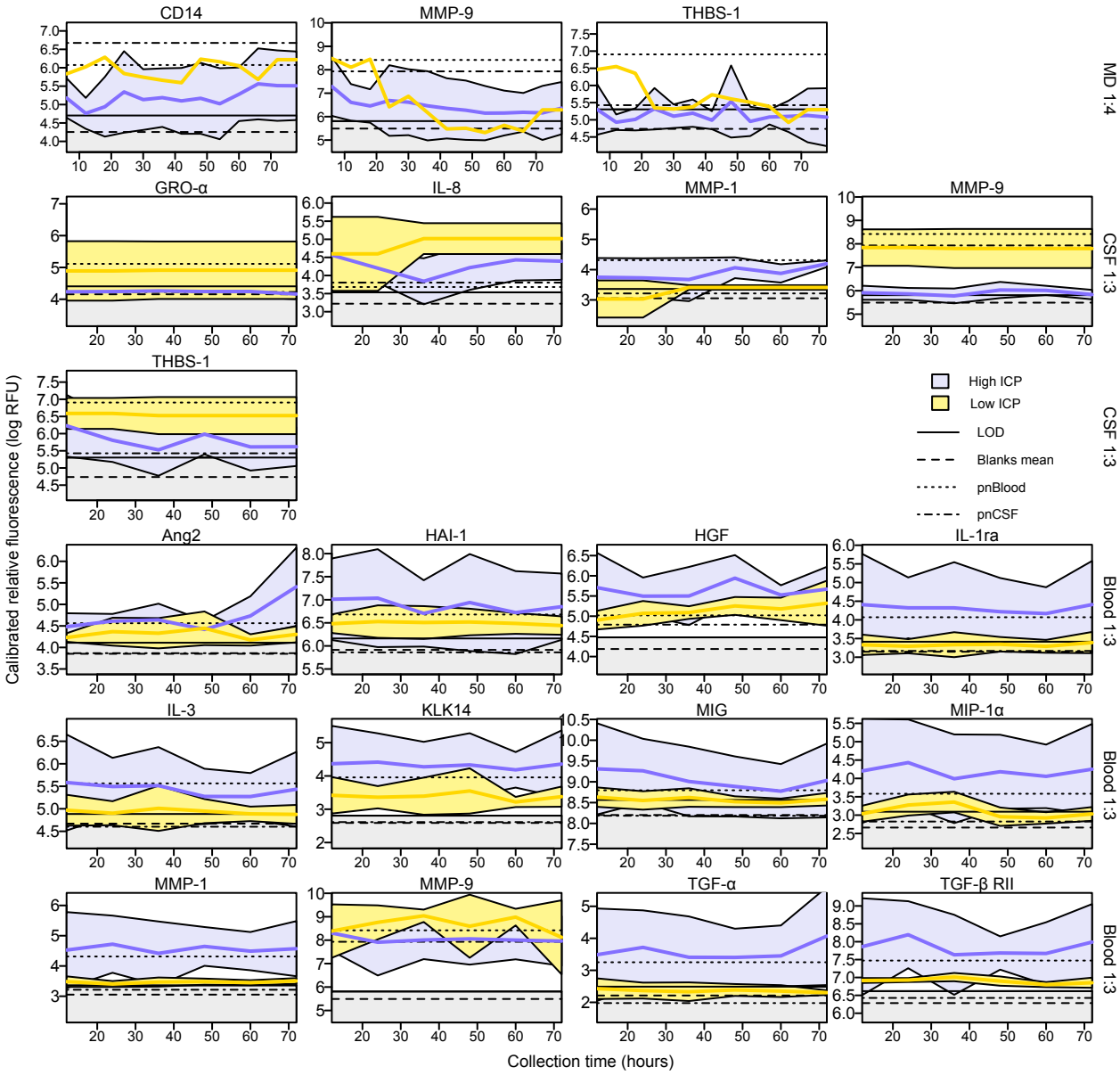

FIGURE 6.4: **Time courses of potential biomarkers of secondary injury in sTBI patients.** 16 potential biomarkers of secondary injury (high ICP) in sTBI patients are shown as average time profiles in microdialysate (row 1), CSF (rows 2-3) or blood (rows 4-6) samples, in a comparison of sTBI patients with low and high ICP. Thick yellow and purple lines are the mean value measured at a given time point for patients with low and high ICP, respectively. Lighter color polygons are ±1 SD. Levels are compared to pnCSF and pnBlood obtained from normal healthy controls. Grey area is below LOD. Time course and pnBlood values shown are for samples diluted as indicated on the right, except for MMP-9 in blood which was diluted 1:30. MD: microdialysate.

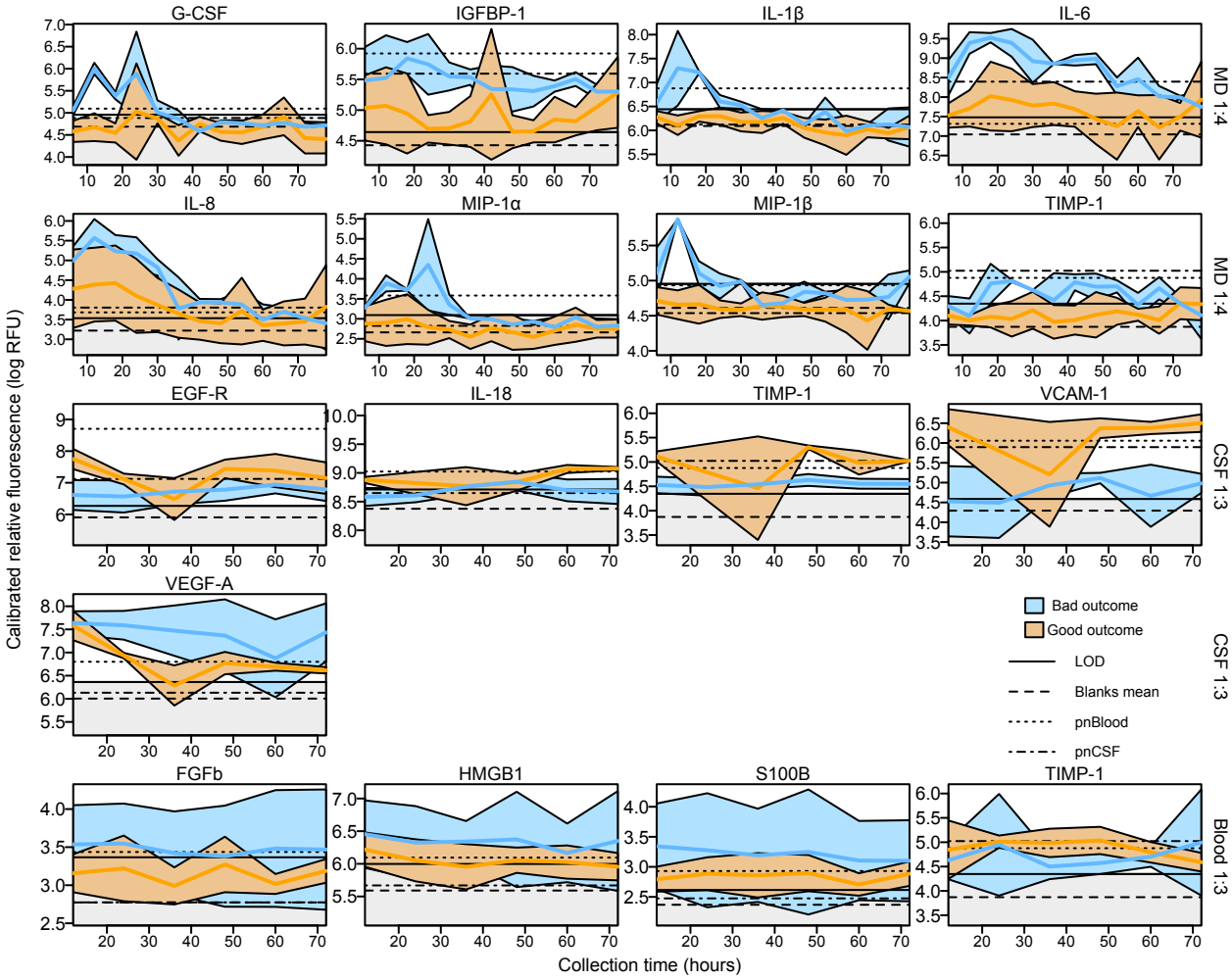

FIGURE 6.5: **Time courses of potential biomarkers of outcome in sTBI patients.** 15 potential biomarkers of outcome in sTBI patients are shown as average time profiles in microdialysate (rows 1-2), CSF (rows 3-4) or blood (row 5) samples, in a comparison of sTBI patients with good (GOS-E $\geq$ 5) and bad (GOS-E < 5) outcome. Thick orange and blue lines are the mean value measured at a given time point for patients with good and bad outcome, respectively. Lighter color polygons are $\pm$1 SD. Levels are compared to pnCSF and pnBlood obtained from normal healthy controls. Grey area is below LOD. Time course and pnBlood values shown are for samples diluted as indicated on the right. MD: microdialysate.

The differences seen in microdialysate and CSF samples were more pronounced than in blood samples.

We also compared the levels of proteins in blood samples of $mTBI_C$ patients patients with good and bad outcome. In this case the dichotomized outcome was separated in bad (GOS-E 6-7) and good (GOS-E 8) outcome, since patients with a single mTBI rarely suffer very bad outcome. In the patients studied here the worst outcome seen was GOS-E 6. We found 10 proteins that were different between patients with bad and good outcomes (figure 6.6). In all cases, the level of proteins measured in patients with bad outcome was similar to the level measured in pnBlood, while the levels measured in patients with good outcome was markedly lower. The difference seen in E-selectin, GFAP, IL-1ra, IL-5 and S100B was more pronounced after 24 h.

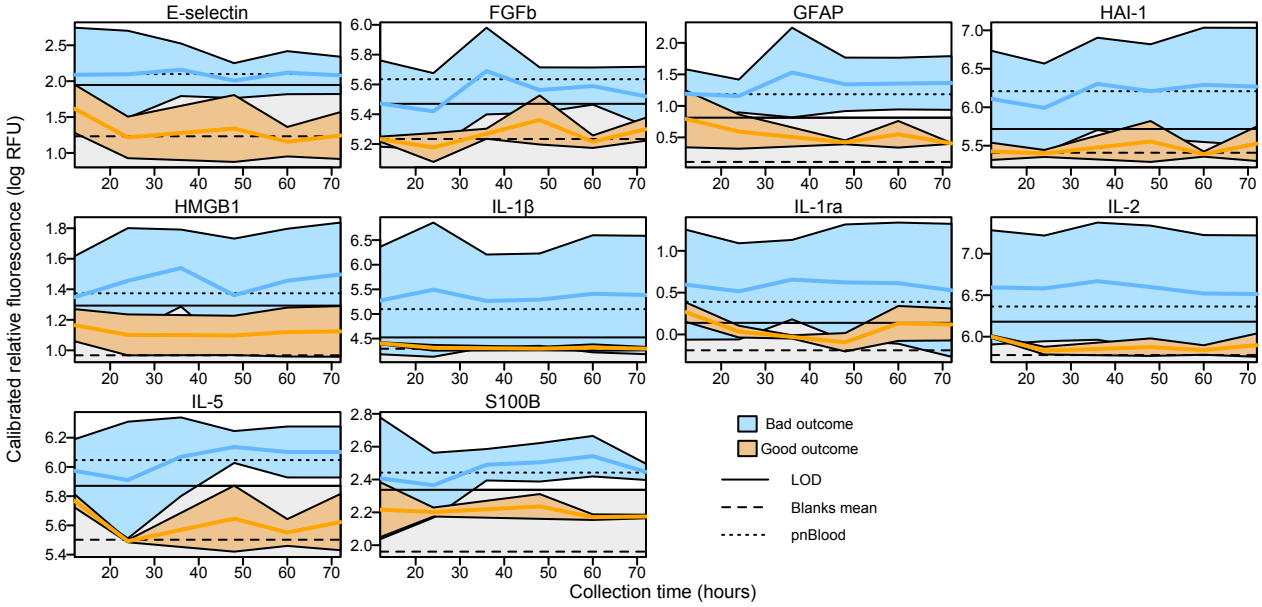

FIGURE 6.6: **Time courses of potential biomarkers of outcome in mTBI patients.** Ten potential biomarkers of outcome in mTBI patients are shown as average time profiles in blood samples, in a comparison of sTBI patients with good (GOS-E = 8) and bad (GOS-E < 8) outcome. Thick orange and blue lines are the mean value measured at a given time point for patients with good and bad outcome, respectively. Lighter color polygons are ±1 SD. Levels are compared to pnBlood obtained from normal healthy controls. Grey area is below LOD. Time course and pnBlood values shown are for blood samples diluted 1:3.

6.4 Discussion

This exploratory study measured 103 proteins in a total of 15 patients, which is a typical number in TBI studies where often 3 to 20 patients participate in multiplex TBI studies [18, 84, 126, 134,

136, 324]. As mentioned elsewhere [18], the combination of difficulties in rapidly recruiting sTBI patients shortly after their injury and the current maximum number of samples that can be measured in a single experiment limited the number of patients whose samples we could measure to under 20. Because of the low number of patients, stratification according to injury type was not possible.

While men are disproportionally affected by TBI compared to women (two-thirds of all reported mTBI and more than three-quarters of all sTBI patients are men [325–327]), our study included a single woman who suffered from trauma without a TBI. Because levels of some proteins such as IL-6 and IL-1β were reported to be elevated in microdialysate of women suffering from TBI compared to men [290], caution should be exercised when drawing conclusions from comparisons between sTBI and mTBI and the trauma patient in this study. Morever, validation of results in sex-representative populations of sTBI and mTBI patients is required in the future.

Increased lactate and lactate to pyruvate ratio has been previously observed in TBI [328], where surprisingly lactate has been shown to be an alternate source of energy for the injured brain [329]. The increase in lactate seen in figure 6.1 is due to glial cells producing lactate from glucose and damaged neuronal cells failing to uptake it as source of energy [330]. Along with the decreased glucose concentration in microdialysate samples of sTBI samples, these results indicate the presence of hypoxia and ischaemia in the brain tissue, resulting from an inadequate blood and oxygen supply [331]. We observed an inverse relationship between glucose concentration and ICP, which was previously observed in microdialysate samples of sTBI patients [332]. There was no evidence of prolonged excitotoxicity, as seen by a normal glutamate concentration.

We successfully measured 103 proteins in microdialysate, CSF and blood of sTBI and mTBI patients with the ACM. Each of these bodily fluids offers specific challenges. Microdialysate is a very low volume sample (~20 µL per aliquot) with very low concentration of proteins due to the limited recovery of proteins through the microdialysis membrane. CSF and blood are available in larger volumes, but CSF protein concentrations are typically very low. Proteins in blood (serum or plasma) can be found in very low to very high concentration, and the total protein concentration along with myriad of other molecules present can potentially interfere with the capture antibodies ability to bind their target, a phenomenon called matrix effect. All proteins were detected in at least one sample type, proving the versatility of the ACM in measuring 103 proteins in vastly differing samples. To our knowledge it's the first time that 11 of those proteins are studied in the context of TBI (AFP, AHSG, ALDH1L1, Amphiregulin, BRAF, EpCAM, Flt-3, HAI-1, HE4, HER2 and IGFBP-7). These proteins are measured on the ACM as part of its broad utility, not only in TBI but also in cancer and other diseases involving inflammation.

While determining from which blood sample, serum or plasma, to measure specific proteins, we observed a sharp increase in EGF in serum stored at room temperature before centrifugation.

Indeed, EGF is known to be secreted by platelets during clotting [312]. We also saw lower levels of OPN and HMGB1 in serum than in plasma, which is consistent with the literature [309, 311], suggesting that there is degradation of these proteins during clotting in serum. However, in spite of the difference in initial concentration, the levels of BDNF was more stable in serum than in EDTA after the initial clotting, as was reported previously [316]. Since levels of BDNF measured in serum are released by platelets, and in EDTA plasma the levels reflect that in the blood of patients, we picked EDTA plasma in spite of its worse stability even during as small as a two hour wait before centrifugation. Indeed, analyzing BDNF from EDTA plasma allowed us to see a difference between sTBI and mTBI patients, making it a potential biomarker of injury severity. This was not seen when analyzing BDNF data from serum. This highlights the importance of using the right type of blood specimen for each protein.

By comparing the levels of proteins found in microdialysate to that of CSF and blood in single patients, we were able to make a list of proteins that show evidence of brain tissue production at the site of sampling. To our knowledge, only one other study determined the origin of production of multiple proteins detected in microdialysate samples of 12 sTBI patients [18]. They detected all 42 proteins measured in microdialysate samples, of which only two (IL-10 and IL-12) were not detected here. They found that 19 out of the 42 proteins had higher levels in microdialysate than in plasma samples. 17 of those proteins were also measured in our study, and we found that only 3 of these had lower levels in microdialysate than blood samples. The remaining 13 proteins were also found to be produced in the brain (8) or produced in the brain and elsewhere in the body (4), proving a good agreement between our results and this study. Results from both studies indicate a strong inflammatory reaction throughout the brain tissue in sTBI patients. Out of the 14 proteins identified that have strong evidence of brain production, IL-1β, IL-6 and IL-8 have been well studied in TBI. Interestingly, SPARC has been shown to be involved in the development of the brain and normally not expressed in the adult brain, except in TBI where its expression is up-regulated [333], as is seen in patients here.

While measuring higher levels of proteins in microdialysate than in blood is a strong evidence for brain tissue production, measuring low levels of the same protein in CSF compared to microdialysate and blood is also a strong evidence for production elsewhere in the body. Indeed, 80-90 % of CSF is produced by cells of the choroid plexus that filters plasma of the majority of molecules that can be harmful for the brain tissue [334], and a small proportion of CSF has its origin in the fluid transport across the blood-brain barrier [335–337]. While there is exchange of small molecules between the brain interstitial fluid (IF) and CSF [338, 339] as it is a contiguous space, CSF has been recently considered to be a separate bodily fluid than IF [18]. Our results also show that concentrations vary widely between microdialysate and CSF and therefore these two sample types should be considered

as separate fluids.

Proteins that are detected in microdialysate in lower concentrations than blood could be explained by a much greater systemic production of the protein elsewhere in the body and 1) proteins from plasma crossing the brain through a compromised blood-brain barrier due to the TBI or 2) normal diffusion of proteins through an intact blood-brain barrier, as is the case for albumin or 3) normal lower concentration of proteins produced in the brain. Is it important to note that microdialysate only measures proteins present within a small tissue volume around the inserted probe and that proteins that were classified as being made elsewhere in the body could also be made locally at the site of injury, and therefore be undetected in microdialysate samples. Proteins such as GFAP and S100B could in fact have been produced locally at the site of injury in high concentration, broken down partially as is known for GFAP [285] in sTBI patients and therefore be measured in lower concentration in CSF, and finally also be produced elsewhere in the body. Indeed, both S100B and GFAP are known to be produced by cells outside of the brain [340, 341]. Moreover, both proteins were detected in small quantities in the pooled blood replicate samples (pnBlood) produced from healthy control individuals. Ang1 was measured at its highest level in CSF, suggesting that production of this protein also has its origin in the brain, however not at the site of microdialysis sampling. Ang1 is known to be produced in the brain after injury to initiate vascular repairs in patients with good outcome [342].

The comparison of elevated proteins in the blood of sTBI and $mTBI_C$ patients, including one $mTBI_S$ and one non-TBI trauma patients, led to the identification of eight proteins specific to sTBI, six proteins specific to sTBI and $mTBI_C$ patients, two proteins specific to $mTBI_C$ alone and five proteins specific to $mTBI_S$ (table 6.3). Because a single patient was compared to groups, AFP and ALDH1L1 that were found to be elevated specifically in the $mTBI_S$ patient are not likely to be biomarkers of very mild TBI injury. Rather, they are likely to be elevated in the context of individual baseline variation of proteins, or be involved in other diseases in this patient. However, it is interesting to note that GFAP and S100B were elevated in this patient but not consistently in any other groups. GFAP and S100B are astrocytic proteins that have been widely studied as biomarker of mTBI [285, 343–348]. Two proteins were found to be elevated in a majority of patients, MMP-1 and OPN, including the non-TBI trauma patient. The wide variety of biological functions of these two proteins involved in inflammation, prevention of apoptosis, tissue repair and remodeling can explain the elevation seen in blood samples of most patients.

TBIs have heterogeneous presentations; contusions and subarachnoid hemorrhages are the most common types of lesions observed in mTBI patients. Additionally, hematomas, diffuse axonal injuries, fractures and penetrating injuries may also all be present in sTBI patients [349]. The different types of lesions and the severity of the lesions may explain that different proteins

are elevated only in sTBI or $mTBI_C$ patients. Among the proteins that were elevated in sTBI patients only, MCP1 was elevated in four of the seven patients and its ability to distinguish sTBI patients from controls in blood has been reported before [350]. Likewise, BMP2 was elevated in five sTBI patients, and its elevation in sTBI patients has been observed in a previous study [351]. Therefore MCP1 and BMP2 are promising potential biomarkers of injury severity, having already been confirmed in previous studies.

Of the 17 proteins that were found to show different time course in microdialysate, CSF and blood samples of sTBI patients, MMP9 is the only protein that showed a difference in all three biofluids, with the same pattern of decrease in patients with high ICP (figure 6.4). The difference was greatest in CSF and varied little over the 72 h of samples collection. Because patients at risk of developing secondary injuries and high ICP are usually often equipped with an extra-ventricular drain (EVD: used to monitor and lower high ICP), CSF can easily be collected and analyzed in these patients. All other proteins identified in blood showed a constant level or late elevation (Ang2) in samples of sTBI patients with high ICP. Among these, MIP-1α appears to be the most promising potential biomarker of secondary injury, showing elevated levels throughout the collection period, although this elevation was not observed in all patients. It's likely that a combination of blood biomarkers would have to be considered to be able to predict secondary injuries in all patients with good specificity and sensitivity.

A number of proteins were found to correlate with the advent of high ICP in sTBI patients in previous studies, such as IL-8 [352, 353], IL-6 [354], IL-1ra, TNF-RI and IL-10 [355]. In our study all these proteins were found to be elevated in the blood of the same two out of four patients with high ICP, perhaps indicating common molecular events in these two patients.

As opposed to proteins that showed greater differences in blood samples of sTBI patients with high ICP, we observed greater differences in protein levels in microdialysate samples of sTBI patients with good and bad outcome compared to blood or CSF. MIP-1α, MIP-1β, IL-8, G-CSF and IL-1β all showed strong peaks in the first day of collection of patients with bad outcome. Peaks for IL-6, IGFBP-1 and TIMP-1 lasted longer for about 2.5 days. None of the proteins found to be different in microdialysate remained increased beyond this time period, suggesting that sampling of proteins through microdialysis would have to be done within the first 24-48 h to accurately predict bad outcome in patients. After this period of time, measurements of IL-18, TIMP-1 and VCAM-1 in CSF might provide information about outcome since the difference was sustained at 72 h after the beginning of sample collection. A previous study identified S100B as a predictor of bad outcome in CSF and serum samples of sTBI patients [356]. We also observed an elevation of S100B in blood samples of sTBI patients with bad outcome, however we did not observe any correlation in the CSF samples.

The differences in protein levels seen in mTBI patients blood samples was less pronounced than that seen in sTBI patients, with most proteins showing a stark decrease in levels in blood samples of mTBI patients with good outcome when compared to pnBlood. Proteins measured in patients with bad outcome were similar to that of pnBlood, except IL-1β, IL-1ra and IL-2 that showed slight increases compared to pnBlood. Both GFAP and S100B were identified as showing a difference between mTBI with good and bad outcome, which is consistent with other reports [357, 358].

It is interesting to note that several proteins were identified as potential biomarkers of outcome in both sTBI and mTBI patients (FGFb, IL-1β, HMGB1 and S100B) (figures 6.5 and 6.6). While IL-1β showed the greatest difference in microdialysate samples, the other three proteins all showed the difference in blood of both sTBI and mTBI patients. These are therefore potential biomarkers of outcome regardless of the severity of TBI incurred.

6.5 Conclusion

We successfully measured 103 proteins including cytokines and chemokines in microdialysate, CSF and blood samples of sTBI patients, as well as blood samples of mTBI patients, which showed that patients mounted a robust inflammatory response in the first 3-4 days following their injury. This response was observed in all three samples types, with the strongest peaks seen in microdialysate, followed by CSF and then blood. By measuring proteins simultaneously in microdialysate, CSF and blood samples of sTBI patients, we showed evidence of brain production for some proteins. Using this analysis on potential biomarkers in the future could help understand the provenance of proteins measured in any of the three samples types. It might be particularly beneficial to distinguish the origin of particular biomarkers or pattern of inflammatory response in polytrauma patients, suffering concurrently from TBI and other injuries. The method showed here requires the use of cerebral microdialysis, a precious tool that allows the sampling of proteins indirectly from the brain tissue.

We identified several proteins that were elevated specifically in sTBI and/or mTBI_C patients, and others that correlated with secondary injury in sTBI patients, or dichotomized outcome in sTBI and mTBI_C patients. While some proteins identified as potential biomarkers were known and indeed confirm previous results, others were, to our knowledge, never before identified as potential biomarkers in TBI. The complete description of time course data in microdialysate, CSF and blood samples of sTBI and blood samples of mTBI patients can also be used to further the understanding of TBI injury and repair within the three first days after injury. This study included a large number of proteins, and a small number of patients, and can therefore be described as exploratory or discovery

study. A future validation study measuring less proteins and a greater number of sTBI, mTBI, non-TBI patients and normal controls with representative gender distributions in a single experiment would provide material to properly analyze the predictive value of these proteins statistically.

Supporting Information

Additional information as noted in the text. This material is available in appendix F. Raw data of the effect of pre-analytical variables on protein initial measurements and stability is found in appendix I. Raw time course profiles for individual patients and proteins can be found in appendix J.

Corresponding Author

*Email: david.juncker@mcigll.ca

Acknowledgements

We thank Dr. Mathias Aebersold for his critical reading of the manuscript. This work was funded by the Natural Sciences and Engineering Research Council of Canada (NSERC), the Canadian Institutes of Health Research (CIHR) and the Canada Foundation for Innovation (CFI). DJ acknowledges support from a Canada Research Chair in micro and nanobioengineering. We thank Drs. Meshal Aljassar and Rakan Bokhari for collecting and processing blood samples from mTBI patients. We also want to thank patients and their families for participating to this study and allowing us to pursue our research goals.

Conflict of interest

The authors declare no conflict of interest.

References

2. Teasdale, G. & Jennett, B. Assessment of coma and impaired consciousness. *The Lancet* **2,** 81–84 (1974).

3. De Guise, E., Marcoux, J., Maleki, M., Leblanc, J., Dagher, J., Tinawi, S., Feyz, M. & Lamoureux, J. Trends in hospitalization associated with TBI in an urban level 1 trauma centre. *Canadian Journal of Neurological Sciences* **41,** 466–475 (2014).

13. Gardner, R. C., Byers, A. L., Barnes, D. E., Li, Y., Boscardin, J. & Yaffe, K. Mild TBI and risk of Parkinson disease. *Neurology* **90,** e1771–e1779 (2018).

15. DeKosky, S. T. & Asken, B. M. Injury cascades in TBI-related neurodegeneration. *Brain Injury* **31,** 1177–1182 (2017).

17. Pla-Roca, M., Leulmi, R. F., Tourekhanova, S., Bergeron, S., Laforte, V., Moreau, E., Gosline, S. J. C., Bertos, N., Hallett, M., Park, M. & Juncker, D. Antibody colocalization microarray: a scalable technology for multiplex protein analysis in complex samples. *Molecular & Cellular Proteomics* **11,** M111.011460 (2012).

18. Helmy, A., Carpenter, K. L. H., Menon, D. K., Pickard, J. D. & Hutchinson, P. J. A. The cytokine response to human traumatic brain injury : temporal profiles and evidence for cerebral parenchymal production. *Journal of Cerebral Blood Flow & Metabolism* **31,** 658–670 (2010).

26. Hillman, J., Åneman, O., Anderson, C., Sjögren, F., Säberg, C. & Mellergård, P. A microdialysis technique for routine measurement of macromolecules in the injured human brain. *Neurosurgery* **56,** 1264–1270 (2005).

72. Vilalta, A, Sahuquillo, J, Rosell, A, Poca, M. A., Riveiro, M & Montaner, J. Moderate and severe traumatic brain injury induce early overexpression of systemic and brain gelatinases. *Intensive Care Medicine* **34,** 1384–1392 (2008).

73. Roberts, D. J., Jenne, C. N., Le, C., Kramer, A. H., Gallagher, C. N., Todd, S., Parney, I. F., Doig, C. J., Yong, V. W., Kubes, P. & Zygun, D. A. Association between the Cerebral Inflammatory and Matrix Metalloproteinase Responses after Severe Traumatic Brain Injury in Humans. *Journal of Neurotrauma* **30,** 1727–1736 (2013).

74. Roberts, D. J., Jenne, C. N., Léger, C., Kramer, A. H., Gallagher, C. N., Todd, S., Parney, I. F., Doig, C. J., Yong, V. W., Kubes, P. & Zygun, D. a. A prospective evaluation of the temporal matrix metalloproteinase response after severe traumatic brain injury in humans. *Journal of Neurotrauma* **30,** 1717–26 (2013).

77. Buttram, S. D., Wisniewski, S. R., Jackson, E. K., Adelson, P. D., Feldman, K, Bayir, H, Berger, R. P., Clark, R. S. & Kochanek, P. M. Multiplex assessment of cytokine and chemokine levels in cerebrospinal fluid following severe pediatric traumatic brain injury: effects of moderate hypothermia. *Journal of Neurotrauma* **24,** 1707–1717 (2007).

81. Jastrow, K. M., Gonzalez, E. A., McGuire, M. F., Suliburk, J. W., Kozar, R. A., Iyengar, S., Motschall, D. A., McKinley, B. A., Moore, F. A. & Mercer, D. W. Early Cytokine Production Risk Stratifies Trauma Patients for Multiple Organ Failure. *Journal of the American College of Surgeons* **209,** 320–331 (2009).

84. Dyhrfort, P., Shen, Q., Clausen, F., Thulin, M., Enblad, P., Kamali-Moghaddam, M., Lewén, A. & Hillered, L. Monitoring of Protein Biomarkers of Inflammation in Human Traumatic Brain Injury Using Microdialysis and Proximity Extension Assay Technology in Neurointensive Care. *Journal of Neurotrauma* **14,** 1–14 (2019).

85. Huie, J. R., Diaz-Arrastia, R., Yue, J. K., Sorani, M. D., Puccio, A. M., Okonkwo, D. O., Manley, G. T., Ferguson, A. R., Adeoye, O. M., Badjatia, N., Boase, K. D., Bodien-Guller, Y., Bullock, M. R., Chesnut, R. M., Corrigan, J. D., Crawford, K. L., Diaz-Arrastia, R., Dikmen, S. S., Duhaime, A.-C., Ellenbogen, R. G., Ezekiel, F., Feeser, V. R., Giacino, J. T., Goldman, D. P., Gonzales, L., Gopinath, S. P., Gullapalli, R. P., Hemphill, J. C., Hotz, G. A., Kramer, J. H., Levin, H., Lindsell, C. J., Machamer, J., Madden, C., Markowitz, A. J., Martin, A., Mathern, B. E., McAllister, T. W., McCrea, M. A., Merchant, R. E., Noel, F., Perl, D. P., Puccio, A. M., Rabinowitz, M., Robertson, C. S., Rosand, J., Sander, A. M., Satris, G., Schnyer, D. M., Seabury, S. A., Sergot, P., Sherer, M., Stein, D. M., Stein, M. B., Taylor, S. R., Temkin, N. R., Toga, A. W., Turtzo, L. C., Vespa, P. M., Wang, K. K., Zafonte, R. & Zhang, Z. Testing a Multivariate Proteomic Panel for Traumatic Brain Injury Biomarker Discovery: A TRACK-TBI Pilot Study. *Journal of Neurotrauma* **36,** 100–110 (2018).

86. Berger, R. P., Ta'asan, S., Rand, A., Lokshin, A. & Kochanek, P. Multiplex assessment of serum biomarker concentrations in well-appearing children with inflicted traumatic brain injury. *Pediatric Research* **65,** 97–102 (2009).

88. Sankar, S. B., Pybus, A. F., Liew, A., Sanders, B., Shah, K. J., Wood, L. B. & Buckley, E. M. Low cerebral blood flow is a non-invasive biomarker of neuroinflammation after repetitive mild traumatic brain injury. *Neurobiology of Disease* **124,** 544–554 (2019).

89. Thelin, E. P., Just, D., Frostell, A., Häggmark-Månberg, A., Risling, M., Svensson, M., Nilsson, P. & Bellander, B. M. Protein profiling in serum after traumatic brain injury in rats reveals potential injury markers. *Behavioural Brain Research* **340,** 71–80 (2018).

95. Bhomia, M., Balakathiresan, N. S., Wang, K. K., Papa, L. & Maheshwari, R. K. A Panel of Serum MiRNA Biomarkers for the Diagnosis of Severe to Mild Traumatic Brain Injury in Humans. *Scientific Reports* **6,** 1–12 (2016).

119. Rai, A. J., Gelfand, C. A., Haywood, B. C., Warunek, D. J., Yi, J., Schuchard, M. D., Mehigh, R. J., Cockrill, S. L., Scott, G. B., Tammen, H., Schulz-Knappe, P., Speicher, D. W., Vitzthum, F., Haab, B. B., Siet, G. & Chan, D. W. HUPO Plasma Proteome Project specimen collection and handling: Towards the standardization of parameters for plasma proteome samples. *Proteomics* **5,** 3262–3277 (2005).

126. Haqqani, A. S., Hutchison, J. S., Ward, R & Stanimirovic, D. B. Biomarkers and diagnosis; protein biomarkers in serum of pediatric patients with severe traumatic brain injury identified by ICAT-LC-MS/MS. *Journal of Neurotrauma* **24,** 54–74 (2007).

134. Hanrieder, J., Wetterhall, M., Enblad, P., Hillered, L. & Bergquist, J. Temporally resolved differential proteomic analysis of human ventricular CSF for monitoring traumatic brain injury biomarker candidates. *Journal of Neuroscience Methods* **177,** 469–478 (2009).

136. Lakshmanan, R, Angeles, L., Loo, J. A., Angeles, L., Drake, T, Angeles, L., Leblanc, J, Angeles, L., Ytterberg, A. J., Angeles, L., Mcarthur, D. L., Etchepare, M & Vespa, P. M. Metabolic Crisis After Traumatic Brain Injury is Associated with a Novel Microdialysis Proteome. *Neurocritical Care* **12,** 324–336 (2010).

137. Anada, R. P., Wong, K. T., Jayapalan, J. J., Hashim, O. H. & Ganesan, D. Panel of serum protein biomarkers to grade the severity of traumatic brain injury. *Electrophoresis* **39,** 2308–2315 (2018).

154. Laforte, V., Olanrewaju, A. & Juncker, D. *Low-cost , high liquid volume silicon quill pins for robust and reproducible printing of antibody microarrays* in *MicroTAS: miniaturized systems for chemistry and life sciences* (Chemical and Biological Microsystems Society (CBMS), Freiburg, Germany, 2013), 485–487.

219. Laforte, V., Lo, P.-S., Li, H. & Juncker, D. Antibody Colocalization Microarray for Cross-Reactivity-Free Multiplexed Protein Analysis. *Methods in Molecular Biology* **1619** (eds Greening, D. W. & Simpson, R. J.) 239–261 (2017).

220. R Core Team. *R: A Language and Environment for Statistical Computing* R Foundation for Statistical Computing (Vienna, Austria, 2018).

252. Schulz, M. K., Wang, L. P., Tange, M. & Bjerre, P. Cerebral microdialysis monitoring: determination of normal and ischemic cerebral metabolisms in patients with aneurysmal subarachnoid hemorrhage. *Journal of Neurosurgery* **93,** 808–814 (2000).

260. Clausen, F., Marklund, N. & Hillered, L. Acute inflammatory biomarker responses to diffuse traumatic brain injury in the rat monitored by a novel microdialysis technique. *Journal of Neurotrauma* **36,** 201–211 (2019).

274. Hyder, A. A., Wunderlich, C. A., Puvanachandra, P., Gururaj, G. & Kobusingye, O. C. The impact of traumatic brain injuries: a global perspective. *NeuroRehabilitation* **22,** 341–353 (2007).

275. Gardner, R. C. & Yaffe, K. Epidemiology of mild traumatic brain injury and neurodegenerative disease. *Molecular and Cellular Neuroscience* **66,** 75–80 (2015).

276. Eierud, C., Craddock, R. C., Fletcher, S., Aulakh, M., King-Casas, B., Kuehl, D. & Laconte, S. M. Neuroimaging after mild traumatic brain injury: Review and meta-analysis. *NeuroImage: Clinical* **4,** 283–294 (2014).

277. Marmarou, A. Pathophysiology of traumatic brain edema: current concepts. *Acta Neurochirurgica. Supplement* **86,** 7–10 (2003).

278. Ichkova, A. & Badaut, J. New biomarker stars for traumatic brain injury. *Journal of Cerebral Blood Flow and Metabolism* **37,** 3276–3277 (2017).

279. Rodríguez-Rodríguez, A. & Egea-Guerrero, J. J. The utility of biomarkers in traumatic brain injury clinical management. *Critical Care* **20,** 5–6 (2016).

280. Goldstein, L. E. & McKee, A. C. Shining (laser) light on traumatic brain injury blood biomarkers. *JAMA Neurology* **74,** 1045 (2017).

281. Mondello, S., Schmid, K., Berger, R. P., Kobeissy, F., Italiano, D., Jeromin, A., Hayes, R. L., Tortella, F. C. & Buki, A. The Challenge of Mild Traumatic Brain Injury : Role of Biochemical Markers in Diagnosis of Brain Damage. *Medicinal Research Reviews* **34,** 503–531 (2014).

282. Tomar, G. S., Singh, G. P., Lahkar, D., Sengar, K., Nigam, R., Mohan, M. & Anindya, R. New biomarkers in brain trauma. *Clinica Chimica Acta* **487,** 325–329 (2018).

283. Rubenstein, R., Chang, B., Yue, J. K., Chiu, A., Winkler, E. A., Puccio, A. M., Diaz-Arrastia, R., Yuh, E. L., Mukherjee, P., Valadka, A. B., Gordon, W. A., Okonkwo, D. O., Davies, P., Agarwal, S., Lin, F., Sarkis, G., Yadikar, H., Yang, Z., Manley, G. T., Wang, K. K., Cooper, S. R., Dams-O'Connor, K., Borrasso, A. J., Inoue, T., Maas, A. I., Menon, D. K., Schnyer, D. M. & Vassar, M. J. Comparing plasma phospho tau, total tau, and phospho tau–total tau ratio as acute and chronic traumatic brain injury biomarkers. *JAMA Neurology* **74,** 1063–1072 (2017).

284. Orešič, M., Posti, J. P., Kamstrup-Nielsen, M. H., Takala, R. S., Lingsma, H. F., Mattila, I., Jäntti, S., Katila, A. J., Carpenter, K. L., Ala-Seppälä, H., Kyllönen, A., Maanpää, H. R., Tallus, J., Coles, J. P., Heino, I., Frantzén, J., Hutchinson, P. J., Menon, D. K., Tenovuo, O. & Hyötyläinen, T. Human Serum Metabolites Associate With Severity and Patient Outcomes in Traumatic Brain Injury. *EBioMedicine* **12,** 118–126 (2016).

285. Halford, J., Shen, S., Itamura, K., Levine, J., Chong, A. C., Czerwieniec, G., Glenn, T. C., Hovda, D. A., Vespa, P., Bullock, R., Dietrich, W. D., Mondello, S., Loo, J. A. & Wanner, I. B. New astroglial injury-defined biomarkers for neurotrauma assessment. *Journal of Cerebral Blood Flow and Metabolism* **37,** 3278–3299 (2017).

286. Diaz-arrastia, R., Wang, K. K. W., Papa, L., Sorani, M. D., Yue, J. K., Puccio, A. M., Mcmahon, P. J., Inoue, T., Yuh, E. L., Lingsma, H. F., Maas, A. I. R., Valadka, A. B., Okonkwo, D. O., Manley, G. T., Track-TBI Investigators, Casey, S. S., Cheong, M., Cooper, S. R., Connor, K. D.-o., Gordon, W. A., Hricik, A. J., Menon, D. K., Mukherjee, P., Schnyer, D. M., Sinha, T. K. & Vassar, M. J. Acute Biomarkers of Traumatic Brain Injury : Relationship between Plasma Levels of Ubiquitin C-terminal Hydrolase-L1 and Glial Fibrillary Acidic Protein. *Journal of Neurotrauma* **31,** 19–25 (2014).

287. Poste, G. Bring on the biomarkers. *Nature* **469,** 156–157 (2011).

288. Ghoshal, S., Bondada, V., Saatman, K. E., Guttmann, R. P. & Geddes, W. J. Phage Display for Identification of Serum Biomarkers of Traumatic Brain Injury. *Journal of Neuroscience Methods* **272,** 33–37 (2016).

289. Bogoslovsky, T., Wilson, D., Chen, Y., Hanlon, D., Gill, J., Jeromin, A., Song, L., Moore, C., Gong, Y., Kenney, K. & Diaz-Arrastia, R. Increases of Plasma Levels of Glial Fibrillary Acidic Protein, Tau, and Amyloid β up to 90 Days after Traumatic Brain Injury. *Journal of Neurotrauma* **34,** 66–73 (2017).

290. Mellergård, P., Åneman, O., Sjögren, F., Säberg, C. & Hillman, J. Differences in cerebral extracellular response of interleukin-1β, interleukin-6, and interleukin-10 after subarachnoid hemorrhage or severe head trauma in humans. *Neurosurgery* **68,** 12–9; discussion 19 (2011).

291. Mellergård, P., Åneman, O., Sjögren, F., Pettersson, P. & Hillman, J. Changes in extracellular concentrations of some cytokines, chemokines, and neurotrophic factors after insertion of intracerebral microdialysis catheters in neurosurgical patients. *Neurosurgery* **62,** 151–158 (2008).

292. Kulbe, J. R. & Geddes, J. W. Current status of fluid biomarkers in mild traumatic brain injury. *Experimental Neurology* **275,** 334–352 (2016).

293. Aisiku, I. P., Yamal, J. M., Doshi, P., Benoit, J. S., Gopinath, S., Goodman, J. C. & Robertson, C. S. Plasma cytokines IL-6, IL-8, and IL-10 are associated with the development of acute respiratory distress syndrome in patients with severe traumatic brain injury. *Critical Care* **20,** 1–10 (2016).

294. Bukovics, P., Czeiter, E., Amrein, K., Kovacs, N., Pal, J., Tamas, A., Bagoly, T., Helyes, Z., Buki, A. & Reglodi, D. Changes of PACAP level in cerebrospinal fluid and plasma of patients with severe traumatic brain injury. *Peptides* **60,** 18–22 (2014).

295. De Vos, A., Bjerke, M., Brouns, R., De Roeck, N., Jacobs, D., Van den Abbeele, L., Guldolf, K., Zetterberg, H., Blennow, K., Engelborghs, S. & Vanmechelen, E. Neurogranin and tau in cerebrospinal fluid and plasma of patients with acute ischemic stroke. *BMC Neurology* **17,** 1–8 (2017).

296. Feng, G., Feng, J., Zhang, S., Tong, Y., Zhang, Q., Yang, X. & Zhang, H. Altered levels of α-melanocyte stimulating hormone in cerebrospinal fluid and plasma of patients with traumatic brain injury. *Brain Research* **1696,** 22–30 (2018).

297. Gopcevic, A., Mazul-Sunko, B., Marout, J., Sekulic, A., Antoljak, N., Siranovic, M., Ivanec, Z., Margaritoni, M., Bekavac-Beslin, M. & Zarkovic, N. Plasma Interleukin-8 as a Potential Predictor of Mortality in Adult Patients with Severe Traumatic Brain Injury. *The Tohoku Journal of Experimental Medicine* **211,** 387–393 (2007).

298. Grossetete, M., Phelps, J., Arko, L., Yonas, H. & Rosenberg, G. A. Elevation of MMP-3 and MMP-9 in CSF and Blood in Patients with Severe Traumatic Brain Injury. *Neurosurgery* **65,** 702–708 (2009).

299. Maier, B., Lehnert, M., Laurer, H. L. & Marzi, I. Biphasic elevation in cerebrospinal fluid and plasma concentrations of endothelin 1 after traumatic brain injury in human patients. *Shock* **27,** 610–614 (2007).

300. Mondello, S., Buki, A., Barzo, P., Randall, J., Provuncher, G., Hanlon, D., Wilson, D., Kobeissy, F. & Jeromin, A. CSF and Plasma Amyloid-β Temporal Profiles and Relationships with Neurological Status and Mortality after Severe Traumatic Brain Injury. *Scientific Reports* **3,** 2–7 (2014).

301. Morel, N, Morel, O, Petit, L, Hugel, B, Cochard, J. F., Freyssinet, J. M., Sztark, F & Dabadie, P. Generation of procoagulant microparticles in cerebrospinal fluid and peripheral blood after traumatic brain injury. *The Journal of Trauma* **64,** 698–704 (2008).

302. Saw, M. M., Chamberlain, J., Barr, M., Morgan, M. P., Burnett, J. R. & Ho, K. M. Differential disruption of blood-brain barrier in severe traumatic brain injury. *Neurocritical Care* **20,** 209–216 (2014).

303. Seifman, M. A., Adamides, A. A., Nguyen, P. N., Vallance, S. A., Cooper, D. J., Kossmann, T, Rosenfeld, J. V. & Morganti-Kossmann, M. C. Endogenous melatonin increases in cerebrospinal fluid of patients after severe traumatic brain injury and correlates with oxidative stress and metabolic disarray. *Journal of Cerebral Blood Flow and Metabolism* **28,** 684–696 (2008).

304. Singhal, A., Baker, A., Hare, G., Reinders, F., Schlichter, L. & Moulton, R. Association between Cerebrospinal Fluid Interleukin-6 Concentrations and Outcome after Severe Human Traumatic Brain Injury. *Journal of Neurotrauma* **19,** 929–937 (2002).

305. Zheng, K., Li, C., Shan, X., Liu, H., Fan, W., Wang, Z. & Zheng, P. Matrix metalloproteinases and their tissue inhibitors in serum and cerebrospinal fluid of patients with moderate and severe traumatic brain injury. *Neurology India* **61,** 606–609 (2013).

306. Sarrafzadeh, A., Schlenk, F., Gericke, C. & Vajkoczy, P. Relevance of cerebral interleukin-6 after aneurysmal subarachnoid hemorrhage. *Neurocritical Care* **13,** 339–346 (2010).

307. Clausen, F., Marklund, N., Lewén, A., Enblad, P., Basu, S. & Hillered, L. Interstitial F 2 - Isoprostane 8-Iso-PGF 2α As a Biomarker of Oxidative Stress after Severe Human Traumatic Brain Injury. *Journal of Neurotrauma* **29,** 766–775 (2011).

308. Chang, H. Y., Morrow, K., Bonacquisti, E., Zhang, W. Y. & Shah, D. K. Antibody pharmacokinetics in rat brain determined using microdialysis. *mAbs* **10,** 843–853 (2018).

309. Basso, D., Padoan, A., Laufer, T., Aneloni, V., Moz, S., Schroers, H., Pelloso, M., Saiz, A., Krapp, M., Fogar, P., Cornoldi, P., Zambon, C. F., Rossi, E., La Malfa, M., Marotti, A., Brefort, T., Weis, T. M., Katus, H. A. & Plebani, M. Relevance of pre-analytical blood management on the emerging cardiovascular protein biomarkers TWEAK and HMGB1 and on miRNA serum and plasma profiling. *Clinical Biochemistry* **50,** 186–193 (2017).

310. Pérez de Ciriza, C., Lawrie, A. & Varo, N. Influence of pre-analytical and analytical factors on osteoprotegerin measurements. *Clinical Biochemistry* **47,** 1279–1285 (2014).

311. Lanteri, P., Lombardi, G., Colombini, A., Grasso, D. & Banfi, G. Stability of osteopontin in plasma and serum. *Clinical Chemistry and Laboratory Medicineedicine* **50,** 1979–84 (2012).

312. Lev-Ran, A., Hwang, D. L. & Snyder, D. S. Human serum and plasma have different sources of epidermal growth factor. *American Journal of Physiology* **259,** R545–R548 (1990).

313. Benoy, I., Salgado, R., Colpaert, C., Weytjens, R., Vermeulen, P. B. & Dirix, L. Y. Serum interleukin 6, plasma VEGF, serum VEGF, and VEGF platelet load in breast cancer patients. *Clinical Breast Cancer* **2,** 311–315 (2002).

314. Friebe, A. & Volk, H. D. Stability of tumor necrosis factor alpha, interleukin 6, and interleukin 8 in blood samples of patients with systemic immune activation. *Archives of Pathology and Laboratory Medicine* **132,** 1802–1806 (2008).

315. Amadio, P., Sandrini, L., Ieraci, A., Tremoli, E. & Barbieri, S. S. Effect of clotting duration and temperature on BDNF measurement in human serum. *International Journal of Molecular Sciences* **18** (2017).

316. Tsuchimine, S., Sugawara, N., Ishioka, M. & Yasui-Furukori, N. Preanalysis storage conditions influence the measurement of brain-derived neurotrophic factor levels in peripheral blood. *Neuropsychobiology* **69,** 83–88 (2014).

317. Kaisar, M., Van Dullemen, L. F., Thézénas, M. L., Zeeshan Akhtar, M., Huang, H., Rendel, S., Charles, P. D., Fischer, R., Ploeg, R. J. & Kessler, B. M. Plasma degradome affected by variable storage of human blood. *Clinical Proteomics* **13,** 1–11 (2016).

318. Brain Trauma Foundation, American Association of Neurological Surgeons, Congress of Neurological Surgeons, Joint Section on Neurotrauma and Critical Care, AANS/CNS, Bratton, S. L., Chestnut, R. M., Ghajar, J., Hammond, F. F. M., Harris, O. A., Hartl, R., Manley, G. T., Nemecek, A., Newell, D. W., Rosenthal, G., Schouten, J., Shutter, L., Timmons, S. D., Ullman, J. S., Videtta, W., Wildberger, J. E. & Wright, D. W. Guidelines for the management of severe traumatic brain injury. VI. Indications for intracranial pressure monitoring. *Journal of Neurotrauma* **24,** S37–S44 (2007).

319. Marcoux, J, McArthur, D. A., Miller, C, Glenn, T. C., Villablanca, P, Martin, N. A., Hovda, D. A., Alger, J. R. & Vespa, P. M. Persistent metabolic crisis as measured by elevated cerebral microdialysis lactate-pyruvate ratio predicts chronic frontal lobe brain atrophy after traumatic brain injury. *Critical Care Medicine* **36,** 2871–2877 (2008).

320. Menon, D. K., Schwab, K., Wright, D. W. & Maas, A. I. Position statement: Definition of traumatic brain injury. *Archives of Physical Medicine and Rehabilitation* **91,** 1637–1640 (2010).

321. Wilson, J. T. L., Pettigrew, L. E. L. & Teasdale, G. M. Structured Interviews for the Glasgow Outcome Scale and the Extended Glasgow Outcome Scale: Guidelines for Their Use. *Journal of Neurotrauma* **15,** 573–585 (1998).

322. Bates, D., Mächler, M., Bolker, B. & Walker, S. Fitting Linear Mixed-Effects Models Using lme4. *Journal of Statistical Software* **67,** 1–48 (2015).

323. Ritchie, M. E., Phipson, B., Wu, D., Hu, Y., Law, C. W., Shi, W. & Smyth, G. K. limma powers differential expression analyses for RNA-sequencing and microarray studies. *Nucleic Acids Research* **43,** e47 (2015).

324. Hill, L. J., Di Pietro, V., Hazeldine, J., Davies, D., Tomman, E., Logan, A. & Belli, A. Cystatin D (CST5): An ultra-early inflammatory biomarker of traumatic brain injury. *Scientific Reports* **7,** 1–10 (2017).

325. Gómez, P. A., Castaño-Leon, A. M., De-la Cruz, J., Lora, D. & Lagares, A. Trends in epidemiological and clinical characteristics in severe traumatic brain injury: Analysis of the past 25 years of a single centre data base. *Neurocirugia* **25,** 199–210 (2014).

326. Feigin, V. L., Theadom, A., Barker-Collo, S., Starkey, N. J., McPherson, K., Kahan, M., Dowell, A., Brown, P., Parag, V., Kydd, R., Jones, K., Jones, A. & Ameratunga, S. Incidence of traumatic brain injury in New Zealand: A population-based study. *The Lancet Neurology* **12,** 53–64 (2013).

327. De Guise, E., LeBlanc, J., Dagher, J., Tinawi, S., Lamoureux, J., Marcoux, J., Maleki, M. & Feyz, M. Outcome in Women with Traumatic Brain Injury Admitted to a Level 1 Trauma Center. *International Scholarly Research Notices* **2014,** 1–9 (2014).

328. Gallagher, C. N., Carpenter, K. L., Grice, P., Howe, D. J., Mason, A., Timofeev, I., Menon, D. K., Kirkpatrick, P. J., Pickard, J. D., Sutherland, G. R. & Hutchinson, P. J. The human brain utilizes lactate via the tricarboxylic acid cycle: A 13C-labelled microdialysis and high-resolution nuclear magnetic resonance study. *Brain* **132,** 2839–2849 (2009).

329. Jalloh, I., Helmy, A., Howe, D. J., Shannon, R. J., Grice, P., Mason, A., Gallagher, C. N., Murphy, M. P., Pickard, J. D., Menon, D. K., Carpenter, T. A., Hutchinson, P. J. & Carpenter, K. L. A Comparison of Oxidative Lactate Metabolism in Traumatically Injured Brain and Control Brain. *Journal of Neurotrauma* **35,** 2025–2035 (2018).

330. Lama, S., Auer, R. N., Tyson, R., Gallagher, C. N., Tomanek, B. & Sutherland, G. R. Lactate storm marks cerebral metabolism following brain trauma. *Journal of Biological Chemistry* **289,** 20200–20208 (2014).

331. Tisdall, M. M. & Smith, M. Cerebral microdialysis: Research technique or clinical tool? *British Journal of Anaesthesia* **97,** 18–25 (2006).

332. Ståhl, N., Mellergård, P., Hallström, A., Ungerstedt, U. & Nordström, C. H. Intracerebral microdialysis and bedside biochemical analysis in patients with fatal traumatic brain lesions. *Acta Anaesthesiologica Scandinavica* **45,** 977–985 (2001).

333. Jones, E. V., Bernardinelli, Y., Zarruk, J. G., Chierzi, S. & Murai, K. K. SPARC and GluA1-Containing AMPA Receptors Promote Neuronal Health Following CNS Injury. *Frontiers in Cellular Neuroscience* **12,** 1–13 (2018).

334. Dandy, W. E. Internal Hydrocephalus. An Experimental, Clinical and Pathological Study. *Annals of Surgery* **70,** 129–142 (1919).

335. Kimelberg, H. K. Water homeostasis in the brain: Basic concepts. *Neuroscience* **129,** 851–860 (2004).

336. Orešković, D. & Klarica, M. The formation of cerebrospinal fluid: Nearly a hundred years of interpretations and misinterpretations. *Brain Research Reviews* **64,** 241–262 (2010).

337. Redzic, Z. Molecular biology of the blood-brain and the blood-cerebrospinal fluid barriers: Similarities and differences. *Fluids and Barriers of the CNS* **8,** 3 (2011).

338. Abbott, N. J., Pizzo, M. E., Preston, J. E., Janigro, D. & Thorne, R. G. The role of brain barriers in fluid movement in the CNS: is there a 'glymphatic' system? *Acta Neuropathologica* **135,** 387–407 (2018).

339. Legros, C., Chesneau, D., Boutin, J. A., Barc, C. & Malpaux, B. Melatonin from cerebrospinal fluid but not from blood reaches sheep cerebral tissues under physiological conditions. *Journal of Neuroendocrinology* **26,** 151–163 (2014).

340. Dietrich, M. O., Tort, A. B., Schaf, D. V., Farina, M., Gonçalves, C. A., Souza, D. O. & Portela, L. V. Increase in Serum S100B Protein Level After a Swimming Race. *Canadian Journal of Applied Physiology* **28,** 710–716 (2003).

341. Middeldorp, J. & Hol, E. M. GFAP in health and disease. *Progress in Neurobiology* **93,** 421–443 (2011).

342. Zhou, S., Yin, D. P., Wang, Y., Tian, Y., Wang, Z. G. & Zhang, J. N. Dynamic changes in growth factor levels over a 7-day period predict the functional outcomes of traumatic brain injury. *Neural Regeneration Research* **13,** 2134–2140 (2018).

343. Babcock, L., Zhang, N., Leach, J. & Wade, S. L. Are UCH-L1 and GFAP promising biomarkers for children with mild traumatic brain injury? *Brain Injury* **30,** 1231–1238 (2016).

344. Lewis, L. M., Schloemann, D. T., Papa, L., Fucetola, R. P., Bazarian, J., Lindburg, M. & Welch, R. D. Utility of Serum Biomarkers in the Diagnosis and Stratification of Mild Traumatic Brain Injury. *Academic Emergency Medicine* **24,** 710–720 (2017).

345. Papa, L., Brophy, G. M., Welch, R. D., Lewis, L. M., Braga, C. F., Tan, C. N., Ameli, N. J., Lopez, M. A., Haeussler, C. A., Mendez Giordano, D. I., Silvestri, S., Giordano, P., Weber, K. D., Hill-Pryor, C. & Hack, D. C. Time course and diagnostic accuracy of glial and neuronal blood biomarkers GFAP and UCH-L1 in a large cohort of trauma patients with and without mild traumatic brain injury. *JAMA Neurology* **73,** 551–560 (2016).

346. Plog, B. A., Dashnaw, M. L., Hitomi, E., Peng, W., Liao, Y., Lou, N., Deane, R. & Nedergaard, M. Biomarkers of Traumatic Injury Are Transported from Brain to Blood via the Glymphatic System. *The Journal of Neuroscience* **35,** 518–526 (2015).

347. Raheja, A., Sinha, S., Samson, N., Bhoi, S., Subramanian, A., Sharma, P. & Sharma, B. S. Serum biomarkers as predictors of long-term outcome in severe traumatic brain injury: analysis from a randomized placebo-controlled Phase II clinical trial. *Journal of Neurosurgery* **125,** 631–641 (2016).

348. Ercole, A., Thelin, E. P., Holst, A., Bellander, B. M. & Nelson, D. W. Kinetic modelling of serum S100b after traumatic brain injury. *BMC Neurology* **16,** 1–8 (2016).

349. Dixon, K. J. Pathophysiology of Traumatic Brain Injury. *Physical Medicine and Rehabilitation Clinics of North America* **28,** 215–225 (2017).

350. Ho, L., Zhao, W., Dams-O'Connor, K., Tang, C. Y., Gordon, W., Peskind, E. R., Yemul, S., Haroutunian, V. & Pasinetti, G. M. Elevated plasma MCP-1 concentration following traumatic brain injury as a potential "predisposition" factor associated with an increased risk for subsequent development of Alzheimer's Disease. *Journal of Alzheimer's Disease* **31,** 301–313 (2012).

351. Wang, Y., Sun, W. F., Liu, X. G., Deng, J., Yan, B. E., Jiang, W. Y. & Lin, X. B. Comparative study of serum BMP-2 and heterotopic ossification in traumatic brain injury and fractures patients. *China Journal of Orthopedics and Traumatology* **24,** 399–403 (2011).

352. Stein, D. M., Lindell, A, Murdock, K. R., Kufera, J. A., Menaker, J, Keledjian, K, Bochicchio, G. V., Aarabi, B & Scalea, T. M. Relationship of serum and cerebrospinal fluid biomarkers with intracranial hypertension and cerebral hypoperfusion after severe traumatic brain injury. *The Journal of Trauma* **70,** 1096–1103 (2011).

353. Stein, D. M., Lindel, A. L., Murdock, K. R., Kufera, J. A., Menaker, J. & Scalea, T. M. Use of serum biomarkers to predict secondary insults following severe traumatic brain injury. *Shock* **37,** 563–568 (2012).

354. Hergenroeder, G. W., Ward III, N. H., Clifton, G. L., Moore, A. N., Dash, P. K., McCoy Jr, J. P. & Samsel, L. Serum IL-6: A candidate biomarker for intracranial pressure elevation following isolated traumatic brain injury. *Journal of Neuroinflammation* **7,** 1–13 (2010).

355. Shiozaki, T., Hayakata, T., Tasaki, O., Hosotubo, H., Fuijita, K., Mouri, T., Tajima, G., Kajino, K., Nakae, H., Tanaka, H., Shimazu, T. & Sugimoto, H. Cerebrospinal fluid concentrations of anti-inflammatory mediators in early-phase severe traumatic brain injury. *Shock* **23,** 406–410 (2005).

356. Goyal, A., Failla, M. D., Niyonkuru, C., Amin, K., Fabio, A., Berger, R. P. & Wagner, A. K. S100b as a Prognostic Biomarker in Outcome Prediction for Patients with Severe Traumatic Brain Injury. *Journal of Neurotrauma* **30,** 946–957 (2013).

357. Heidari, K., Asadollahi, S., Jamshidian, M., Abrishamchi, S. N. & Nouroozi, M. Prediction of neuropsychological outcome after mild traumatic brain injury using clinical parameters, serum S100B protein and findings on computed tomography. *Brain Injury* **29,** 33–40 (2015).

358. Mondello, S., Kobeissy, F., Vestri, A., Hayes, R. L., Kochanek, P. M. & Berger, R. P. Serum Concentrations of Ubiquitin C-Terminal Hydrolase-L1 and Glial Fibrillary Acidic Protein after Pediatric Traumatic Brain Injury. *Scientific Reports* **6,** 1–8 (2016).

CHAPTER 7

Comprehensive Discussion

The chapters included in this thesis truly built on top of each other. In order to compare the levels of proteins in microdialysate, cerebrospinal fluid (CSF) and blood samples of severe TBI patients in chapter 6, the relationship between the relative recovery of proteins and their molecular weight calculated in chapter 5 was required. The differences seen in several proteins when comparing levels of proteins between patients with different levels of TBI injury severity, or patients with good and bad outcome and patients with high and low intra-cranial pressure (ICP), reproducibility and sensitivity of the ACM was critical to obtaining good results. This was possible because of the improvements to the ACM developed in chapters 3 and 4. Moreover, the new calibration algorithms developed in chapter 4 would not have been possible without proper microarray printing buffers that prevent evaporation evaluated in chapter 3. Finally, no microarray would have been printed on 2D functionalized glass slides without the design and production of improve silicon quill pins presented in appendix A.

Therefore all improvements and calculations made in appendix A and chapters 3, 4 and 5 allowed the study of 103 proteins in multiple bodily fluids of severe and mild TBI patients in chapter 6, which identified several potential biomarkers of injury severity, outcome and development of secondary injury.

7.1 Performance

Chapters 3 and 4 had the specific purpose of improving ACM reproducibility, while preserving or improving sensitivity and the low sample volume requirement. As can be seen in table 7.1, where experiments are listed in the order that they were executed, sensitivity significantly improved until the last two experiments, where all experiment optimizations were defined. The two large-scale experiments whose performance is analyzed in chapter 4 (sTBI and MS), were performed with and without a trehalose coating, and the capture antibody printing buffer was decreased from 50 % to 45 % glycerol between the sTBI and MS experiment. Consequently, the reproducibility increased, and sensitivity improved. The further improvement in sensitivity and reproducibility seen in the last two experiments (MD and mTBI + PAV) can be attributed to higher quality batches of PolyAn 2D Aldehyde slides, as well as increased experience in executing the experiments, although which factor is most important remains unknown. The excellent reproducibility observed in the MD experiment can be attributed to the use of pnCSF as a replicate sample, which has very low concentration of most proteins, and therefore whose variability is closer to that of the slide surface coating itself. Good reproducibility values were also observed when blanks (buffer without proteins) were used as replicate samples throughout the experiments. Finally, the very good reproducibility seen in the experiments in chapter 3 (pnSerum) is simply due to the fact that reproducibility is calculated using a single slide, which indicates that reproducibility degrades as the number of slide processed is increased, which can be attributed to the long spotting and wait times in larger-scale experiments. Slide-to-slide variability was not measured in this chapter.

While the reproducibility achieved with improvements to the ACM reaches a median of 25 % or better, this value is sufficient for future statistical evaluation of clinical results obtained in large cohorts but not for actual protein measurements in individual patients in the clinic. The ACM is not aimed at rapid, low-cost measurements of a few proteins by the patient bedside, and it is expected that a better reproducibility of 5-10 % would be required by a point-of-care device measuring less than 10 potential biomarkers in patients.

While the median sensitivity reported in table 7.1 is sub-ng/mL, the numbers reported include sensitivity for low and mid-abudance proteins in blood samples. Most cytokines and chemokines' sensitivities were below that, with some even achieving sub-pg/mL performance. Therefore the sensitivity of the ACM is similar to that of classical ELISA, and is determined by the affinity of matched antibodies purchased, with antibodies against cytokines and chemokines having much stronger affinity for their target antigen because of their low-abundance in bodily fluids.

Results obtained in chapter 6, where time course samples of microdialysate, CSF and blood samples of sTBI and blood samples of mTBI patients were measured, were possible because of the reproducibility, sensitivity, low sample volume requirement and suppression of cross-reactivity

TABLE 7.1: **Comparison of performance obtained in different chapters** Comparison of the reproducibility and sensitivity obtained in the experiments presented in this thesis, from the first to the last experiment executed. All proteins were spotted in triplicates. MD: microdialysis additives, sTBI: severe traumatic brain injury, mTBI: mild traumatic brain injury, PAV: pre-analytical variables, MS: multiple sclerosis.

Experiment	Chapter	Trehalose	# of slides	# of spots per subarray	Replicate samples type	Reproducibility (%) (median)	Sensitivity pg/mL (median)
pnSerum	3	No	1	9	pnSerum	5.9	1333*
sTBI	4, 6	Yes	36	324	pnSerum pnEDTA pnCSF	34.5	548
MS	4	No	48	324	pnSerum	26.1	352
MD	5	No	39	324	pnCSF	7.4	187
mTBI + PAV	6	No	42	324	pnSerum pnEDTA pnCitrate pnCTAD pnHeparin	20.3	189

*: mean of three proteins

of the ACM. The time course of well-studied biomarkers of TBI such as S100B, IL-1β, GFAP and IL-6 we measured was in agreement with the literature, further supporting the accuracy and validity of the measurements made by the ACM.

The ACM was capable of measuring 103 low- to mid-abundance proteins in 20-30 µL of hundreds of samples with very low (microdialysate, CSF) and very high (blood) total protein concentrations without sample pre-treatment as is required for mass spectrometry. Although the number of proteins measured with the ACM could be increased while keeping the same number of subarrays per microarray, technical replicates and the same sample volume requirement simply by increasing the spot density, the maximum number of proteins that could be measured might be 150-200 with space optimization on microarray slides. While the performance and the characteristics of the ACM presented in this thesis was good and the number of proteins measured could be improved, a commercial platform or facility should be used with the capability of measuring more proteins in more samples along with proper quality assurance.

7.2 Limitations and scope

This thesis focused on measuring over 100 proteins in multiple bodily fluids of TBI patients with the goal of increasing the understanding of mechanisms involved in injury and repair in the first three days following injury, and identifying proteins whose levels correlated with injury severity,

outcome or the development of secondary injury. This thesis did not attempt to validate biomarkers related to TBI for use in the clinic, as the study using sTBI and mTBI samples included a limited number of patients.

The ACM platform was shown in this thesis to achieve performance in terms of reproducibility and sensitivity that was sufficient to allow the analysis of TBI patient samples in chapter 6. However, the ACM used custom-made parts and is not readily available commercially, thereby making it a bit of an artisanal platform with very clear limitations. The maximum number of slides that could be printed and processed together was 48, and this limited the number of samples that could be analyzed in a single experiment. The long spotting times due to the nature of the microarray (a contact-printer) unfortunately increased the variation in large-scale experiments, although this was mitigated partially by calibration in chapter 4. Spotting times can be greatly decreased in the future by the use of a high-quality injket microarray printer, as long as its spot positional accuracy is sufficient to allow two printing rounds on multiple slides in a single experiment.

Due to the great costs of antibodies and antigens (~600 $CAD per reagent), some of the reagents used in our library of 103 proteins were expired and some were missing after being unfortunately used up. It is virtually impossible for an academic lab to be expected to keep a fresh library of over 200 antibodies and 100 recombinant antigens commercially obtained that sometimes expired after only three months. However, for discovery experiments, the quality was sufficient to be able to draw conclusions from samples as obtained in chapters 5 and 6. In order to improve further the performance of the ACM, a high quality inkjet microarrayer was purchased that prints microarray slides faster than the contact-printer Nanoplotter used in this thesis. Another advancement was the development on the Snap-Chip, which currently uses the inkjet microarrayer to pre-spot capture and detection antibodies on separate slides, which are stored and brought together in alignment during the assay using a small mechanical device, thereby circumventing the need for a microarrayer in the middle of the assay [141–143].

For future experiments seeking to validate some of the proteins found in this thesis in a much greater number of sTBI, mTBI, and non-TBI trauma patients, as well as healthy controls, another platform should however be chosen. A company or laboratory facility that specializes in measuring low-volume samples using a multiplex immunoassay-based platform, that can measure hundreds of proteins with good sensitivity, reproducibility and little to no cross-reactivity in thousands of samples would be ideal. Additionally, the team that analyzes samples should have the expertise, fresh reagents, automated liquid handling, and quality control processes put in place, and measure performance (reproducibility and sensitivity) in every experiment. This would ensure that precious samples collected leads to the most meaningful clinical conclusions. While many commercial

platforms using multiplex bead arrays or microarrays do exist (R&D Systems, Luminex, Meso-scale Discovery and others), they suffer from cross-reactivity that cannot be completely eliminated and that can lead to a false overestimation of protein quantities. Because of the optimization required to minimize cross-reactivity, only a limited choice of proteins are available in a same assay, without the possibility of adding more proteins without performing a second assay entirely. Bead-based platforms have also been known to suffer from matrix effect particularly with plasma EDTA samples, which suffers from higher background values than serum samples [359]. As a better alternative, a service where samples are sent to a facility are now offered by Olink [360] that uses proximity extension assays (PEA) to measure from 92 to 1100 proteins in very low-volume samples without cross-reactivity, although the cost might be prohibitive for academia.

7.3 Challenges

Although the optimized capture antibody printing buffer developed in chapter 3 (containing 2 M betaine and 25 % 2,3-butanediol) decidedly increased the printing consistency of microarrays compared to traditional printing buffers which exhibited a lot of evaporation, we did not use this printing buffer in the large-scale experiments of chapters 4, 5 and 6. The optimized buffer performed similarly to 50 % glycerol in terms of reproducibility for many proteins, but was better in terms of sensitivity for all proteins. Because of the as yet unexplained increase of variation for one protein (MCP4) out of the four proteins tested in chapter 4, a glycerol-based printing buffer was used instead for all proteins, with the addition of Tween-20 to improve sensitivity of assays. Had time and resources been more generously available, it would have been best to test all proteins in the library of 103 assays to find out which proteins were consistently sensitive to the betaine/2,3-butanediol-based printing buffer, because the glycerol-based printing buffer did not match the betaine/2,3-butanediol-based printing buffer in terms of sensitivity, even with the addition of Tween-20. Therefore, experiments in chapters 5 and 6 significantly suffered because of this lack of sensitivity.

The interference of microdialysis additives with protein measurements seen in chapter 5 is a phenomenon that is well-known by developers of (singleplex or multiplex) immunoassays that measure one or more proteins in serum or plasma. Because serum samples have been clotted, a significant portion of proteins in the liquid part has been depleted, which often leads to lower assay background values than EDTA plasma, and therefore more difficulties achieving good sensitivity when measuring proteins in plasma [359, 361]. In order to avoid such performance discrepancies, we optimized the blocking step during the ACM with a high concentration of bovine serum albumin at 3 % for 3 h, which allowed us to have similar background fluorescence signal in microdialysate,

cerebrospinal fluid, serum and plasma samples. While we did not use specific assay diluents that mimic the sample matrix as suggested by Abcam and R&D Systems [362, 363], we diluted both recombinant antigens and samples in a phosphate-buffered saline in the presence of Tween-20® and diluted samples 1:3 or 1:30 in order to minimize matrix effects of complex blood samples. In spite of this, the matrix effect can never be fully mitigated in immunoassays, effectively making most immunoassay techniques, including the ACM, semi-quantitative.

Measurements of relative recovery of 94 proteins in cerebral microdialysate were performed in chapter 5 and was used in chapter 6 to calculate an approximate quantity of 100 proteins in microdialysis samples of sTBI patients. While other studies used the relative recovery values calculated *in vitro* to modify *in vivo* measurements [18], we used the linear fit produced by the relative recovery of proteins in relation to the proteins molecular weights. We used pooled normal lumbar CSF (pnCSF) to calculate relative recovery values of proteins *in vitro* because this sample contained real human proteins with glycosylation and isoforms normally found in the brain, as opposed to recombinantly-made, often partial-sized proteins lacking glycosylation. Owing to the very low concentration of proteins in this starting sample, measurement values obtained for those proteins recovered in microdialysate were very low, often undetected. Because the confidence in quantities recovered was not complete, we opted to use the linear regression which is an average of all the relative recovery values obtained and could be more highly trusted. While relative recovery values calculated *in vitro* are only estimates for the real relative recovery values *in vivo*, which cannot ethically be obtained using live human subjects, studies in animals have shown that values obtained *in vitro* are higher than *in vivo*, because sampling is done in tissue with a much greater resistance which impedes diffusion of molecules *in vivo* [364]. Therefore the quantities of proteins calculated in chapter 6 is most likely an underestimate of the true quantity of proteins that was present in the brain tissue of patients at the time of sampling.

Problems with fluid loss of microdialysate into the brain of one sTBI patient with very high intracranial pressure (not included in chapter 6) using the sterile, quality-controlled CNS Perfusion Fluid sold by MDialysis, led us to design the study described in chapter 5. At the time of sTBI patient recruitment, perfusion fluid containing additives, such as human albumin solution or dextrans, were not available in sterile, quality-controlled ampules. While clinical-grade low and high molecular weight dextrans were available commercially, we did not feel confident preparing solutions that would be perfused in the brains of human patients, for the lack of quality-control and no way to ensure the complete sterility of solutions. Also, we did not have access to clinical-grade, purified human serum albumin, which is costly and difficult to obtain [365]. Our main concern with all additives was leakage through the microdialysis membrane, and possible effects not only on the measurement of molecules, but the potentially detrimental effect on patients' brains if the additives

leaked. Therefore analysis of microdialysate samples obtained without additives was performed. While fluid recovery was not as high and stable as might have been obtained with the use of additives in the perfusion fluid, microdialysate samples were still recovered in sufficient amounts to measure proteins in microdialysate as reported in chapter 6, and also reported elsewhere [267].

7.4 Usability of findings

The findings presented in this thesis can be used by other researchers aiming to improve the performance of their platforms. For example the low-evaporation capture antibody printing buffer developed in chapter 3 performed very well on several brands of reactive-aldehyde microarray slides, and has even been used by different groups since the publication of the research [366, 367]. These buffers can be used with both contact (quill pins) and inkjet microarray printers. The method presented for quickly determining the performance of many mixtures of additives can also be used to optimize the printing buffer of any slide or surface.

The calibration method presented in chapter 4 can be applied to other antibody microarray platforms, and also be modified to be implemented fully or in part on other existing or future platforms. While the calibration method can still benefit from improvements by estimating calibration slopes for the entire antigen concentration range contained in the ACM assay, this would have required a substantial amount of time to build new code, and a different experimental layout in large-scale experiments. Nonetheless, we hope that this chapter convinces more researchers in academia and corporations to measure and report the performance of their experiments in terms of reproducibility and sensitivity.

The *in vitro* effect of additives on human glial cells, on the measurement of proteins, and their leakage through the microdialysis membrane observed in chapter 5 complements the current knowledge about additives to cerebral microdialysis. More work is required in animals to truly attest to the safety of additives on the brain tissue at the site of sampling. We hope that in the future a fully evaluated, safe technique using additives will be available to allow the precious sampling of proteins in the brain tissue of patients in neurocritical care.

Finally the time course measurements of 103 proteins in microdialysate, CSF and blood samples of sTBI patients and blood samples of mTBI patients presented in chapter 6 offers a method for determining the origin of proteins measured in microdialysate samples, and a list of new potential biomarkers of injury severity, secondary injury in sTBI patients, and outcome. We hope that future studies will attempt to validate those proteins as biomarkers in TBI. The list of proteins detected in each biofluid and their time profiles can contribute to a better understanding of underlying pathways of injury and repair in TBI patients, and present potential therapeutic targets in the future.

Future validation studies would benefit from measuring proteins listed in chapter 6 which were identified as potential biomarkers of secondary injury, injury severity or outcome in patients. Moreover, matched antibody pairs raised against proteins such as neuron specific enolase (NSE), hyper-phosphorylated neurofilament-heavy, αII-spectrin degradation products, tau and amyloid-$\beta_{1\text{-}42}$ should be added to the ACM if available commercially, or matched pairs found by testing combinations of available monoclonal and polyclonal antibodies (as was done here for SPARC). A more complete list of cytokines and chemokines, as well as matrix metalloproteinases, could also be measured by the ACM, and extensive literature search into known and inflammatory and anti-inflammatory processes could serve to extend the utility of the ACM list of protein measured in future studies.

References

18. Helmy, A., Carpenter, K. L. H., Menon, D. K., Pickard, J. D. & Hutchinson, P. J. A. The cytokine response to human traumatic brain injury : temporal profiles and evidence for cerebral parenchymal production. *Journal of Cerebral Blood Flow & Metabolism* **31,** 658–670 (2010).

141. Li, H., Bergeron, S. & Juncker, D. Microarray-to-microarray transfer of reagents by snapping of two chips for cross-reactivity-free multiplex immunoassays. *Analytical Chemistry* **84,** 4776–4783 (2012).

142. Li, H., Munzar, J. D., Ng, A. & Juncker, D. A versatile snap chip for high-density sub-nanoliter chip-to-chip reagent transfer. *Scientific Reports* **5,** 11688 (2015).

143. Li, H., Bergeron, S., Larkin, H. & Juncker, D. Snap Chip for Cross-reactivity-free and Spotter-free Multiplexed Sandwich Immunoassays. *JoVE,* e56230 (2017).

267. Hutchinson, P. J., O'Connell, M. T., Nortje, J., Smith, P., Al-Rawi, P. G., Gupta, A. K., Menon, D. K. & Pickard, J. D. Cerebral microdialysis methodology — evaluation of 20 kDa and 100 kDa catheters. *Physiological Measurement* **26,** 423–428 (2005).

359. Rosenberg-Hasson, Y., Hansmann, L., Liedtke, M., Herschmann, I. & Maecker, H. T. Effects of serum and plasma matrices on multiplex immunoassays. *Immunologic Research* **58,** 224–233 (2014).

360. *https://www.olink.com/* 2019.

361. Schwickart, M., Vainshtein, I., Lee, R., Schneider, A. & Liang, M. Interference in immunoassays to support therapeutic antibody development in preclinical and clinical studies. *Bioanalysis* **6,** 1939–1951 (2014).

362. Abcam. *Technical tips for ELISA and multiplex immunoassay development* 2019.

363. R&D Systems. *ELISA Development Guide*

364. Glick, S. D., Dong, N., Jr., R. W. K. & Carlson, J. N. Estimating Extracellular Concentrations of Dopamine and 3,4-Dihydroxyphenylacetic Acid in Nucleus Accumbens and Striatum Using Microdialysis: Relationships Between In Vitro and In Vivo Recoveries. *Journal of Neurochemistry* **62,** 2017–2021 (1994).

365. Giorgi-Coll, S., Thelin, E. P., Lindblad, C., Tajsic, T., Carpenter, K., Hutchinson, P. J. & Helmy, A. Dextran 500 improves recovery of inflammatory markers: an in vitro microdialysis study. *Journal of Neurotrauma,* Epub ahead of print (2019).

366. Clancy, K. F., Dery, S., Laforte, V., Shetty, P., Juncker, D. & Nicolau, D. V. Protein microarray spots are modulated by patterning method, surface chemistry and processing conditions. *Biosensors and Bioelectronics* **130,** 397–407 (2019).

367. Rivas, L., Reuterswärd, P., Rasti, R., Herrmann, B., Mårtensson, A., Alfvén, T., Gantelius, J. & Andersson-Svahn, H. A vertical flow paper-microarray assay with isothermal DNA amplification for detection of Neisseria meningitidis. *Talanta* **183,** 192–200 (2018).

CHAPTER 8

Summary and conclusion

8.1 Summary

This thesis presented a new and rapid method for determining the best combination of two hygroscopic additives to prevent evaporation of printing buffers on any surface, and a new betaine/2,3-butanediol-based printing buffer for printing on reactive-aldehyde functionalized microarray slides. Furthermore, a new method of calibrating microarray data to improve reproducibility of large-scale experiments was developed using multiple fluorescent molecules printed along with capture antibodies on microarrays. Next, albumin and low- and high-molecular weight dextrans as additives to the cerebral microdialysis perfusion fluid were compared in terms of leakage through a microdialysis membrane, possible interference on the measurement of small molecules and proteins, and activation of human U87 cells as measured by their protein secretion in culture. Finally, a time course analysis of over 100 proteins were measured using the improved ACM in microdialysate, cerebrospinal fluid and blood samples of severe TBI patients, as well as blood samples of mild TBI patients and relative recovery values of proteins from cerebrospinal fluid *in vitro* was established. The comparison of mean protein values in the three bodily fluids in severe TBI patients was used to infer the origin of production of proteins, and potential new biomarkers of injury severity, development of secondary injury, and outcome were described.

8.2 Conclusion

Improvements to the ACM from the design of new silicon quill pins, the development of an optimized printing buffer to the new calibration method presented in this thesis allowed us to measure up to 103 proteins in hundreds of samples from four separate large-scale experiments. The reproducibility and sensitivity of the ACM, with an improvement of 25 % in reproducibility and the low- to mid-pg/mL range sensitivity, were sufficient to measure precise time course measurements of low-abundance known low-abundance biomarkers of TBI in the last chapter, as well as finding new potential biomarkers. These results also demonstrated the importance of reproducibility when measuring proteins in multiplex immunoassays. Finally, the measurement of 100 proteins in the microdialysate, cerebrospinal fluid and blood of severe TBI patients has allowed us to confirm that only 13 proteins detected in the microdialysate samples were produced in majority in the brain, with the majority of proteins detected being produced both by the brain and elsewhere in the body.

8.3 Outlook and future work

The methods and strategies developed in this thesis for improving the ACM reproducibility and sensitivity could be used and adapted to improve the reproducibility of other multiplexed protein measurement platforms. More specifically, the improvement of spot morphology and printing consistency by quickly adding mixtures of hygroscopic additives to microarray printing buffers could allow researchers to find additives best suited to their platform in a matter of hours. The new calibration algorithm could be applied directly to other antibody microarrays and protein arrays. Improvements in reproducibility and/or sensitivity observed by using multiple fluorescent molecules for calibration could be also be adapted by researchers using various immunoassays platforms that suffer from local and systemic variation in the assay. In order to further improve the performance of calibration and the overall reproducibility of the ACM, the new calibration method could in the future include a non-linear calibration slope estimation to cover the whole range of antigen concentration.

Following the *in vitro* comparison of additives to cerebral microdialysis, *in vivo* comparisons and validation of the safety of additives in animals are the logical next step. To improve the predictive power of potential biomarkers of TBI and their specificity, proteins could be measured in multiple bodily fluids instead of a single one, and the ratio between fluids be analyzed. This method might be particularly useful for proteins which are released from the brain during TBI, but that are also produced elsewhere in the body. Finally, the proteins identified as potential biomarkers

of injury severity, development of secondary injury or outcome in this thesis would deserve to be validated in larger scale studies involving many more patients and controls.

APPENDIX A

Silicon Pins Design

Preface

Background and objectives

Early experiments using the ACM used triple-pronged silicon quill pins that broke easily and in stages - a single prong at a time, making it difficult to know when a pin was broken. Those quill pins also only printed on nitrocellulose pads due to the 3D nature of the surface, which the quill pins penetrated and left a mark, compressing the pad. Because of the high auto-fluorescence background of nitrocellulose pads, we wanted to test alternative microarray slides which have 2D functionalized glass surfaces, but the triple-pronged silicon quill pins could not print on these slides. A new silicon quill pin design was required to allow consistent contact between the pin tip and 2D functionalized glass slides. The goal was to design pins that were also physically robust, and would fail gracefully, *i.e.* letting us know right away when it fails. We wanted to retain the high liquid capacity of the previous pin design.

Challenges and encountered problems

The silicon quill pins were produced from a silicon wafer, and the critical step was the deep reactive ion etching (DRIE) which essentially shaped the pins on the wafer after protection of the non-etched parts. This critical step was highly sensitive on timing and other, unknown factors. A few batches of wafers ended up being over- or under-etched, making them useless. The single silicon wafer that

we used for printing all subsequent microarrays was slightly under-etched, which is what created the 3-walled channel at the very tip, making the pins very robust compared to pins that were properly etched. We were lucky to produce pins that were slightly under-etched, and I think it might be difficult to produce exactly the same under-etch without a proper study of the factors that influence the rate of etching in the exact conditions used.

Reference

This appendix is based on a peer-reviewed conference proceeding which I wrote: Véronique Laforte, Ayokunle Olanrewaju and David Juncker, "Low-cost, high liquid volume silicon quill pins for robust and reproducible printing of antibody microarrays" presented at MicroTAS in 2013 [154].

Low-cost, High Liquid Volume Silicon Quill Pins for Robust and Reproducible Printing of Antibody Microarrays

V. Laforte*, A. Olanrewaju and D. Juncker
McGill University, Montreal, Quebec, Canada

Abstract

Ideal silicon quill pins should be robust, low-cost, high volume and give good spot morphology that is reproducible over a printing run. Previously used silicon quill pins were brittle and did not print on all surfaces due to their pin tip design. We designed two new silicon quill pins with high volume (double-channel and serpentine-channel), a single 3-walled robust tip design, are not sensitive to microfabrication process variations, and lead to good spot morphology, printing on all surfaces tested, and good spot reproducibility. These pins help us achieve greater sensitivity and reproducibility in performing micro-ELISA assays using antibody microarrays.

Keywords: High-volume, silicon microfabrication, quill pins, microarray, contact printing

Introduction

Antibody microarrays are formed by spotting antibodies as micrometer sized spots on surfaces that are then used to measure the concentration of several proteins in a small volume of complex samples. The sensitivity of assays depends on good spots morphology, and low variation between spots. We have developed the antibody colocalization microarray [17] and use silicon pins in order to achieve the necessary alignment between multiple spotting on the same slides. In order to decrease the amount of reagents needed, as well as printing time, it is desirable to print multiple slides in a single run with a single loading event. Previous pins designed in our lab were flexible SU-8 pins [153], and high liquid volume capacity silicon pins with a double-channel tips (Figure A.1A). Due to variation in the lithographic process, tip shapes varied between pins, were brittle and led to high variation between and within spots (Figure A.1B). Here we present new silicon pins designed for high liquid volume capacity, robustness, good spot morphology and low variation between spots.

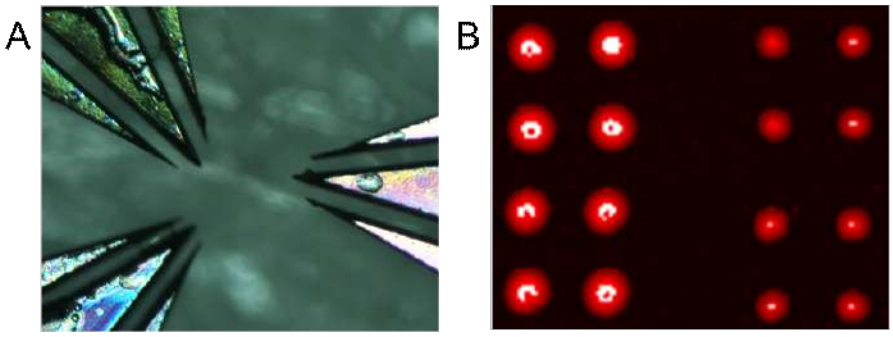

FIGURE A.1: Tips (A) of previously used silicon quill pins with double channel, and printed fluorescent spots (B) on nitrocellulose slide.

Theory

New pins have a single channel tip (Figure A.2A) with a flat tip to create a sufficiently large contact area between the pin and the slide and reliably transfer liquid. To increase liquid capacity, pins with a serpentine channel (Figure A.2D) and with a double-channel merging into a single channel 100 µm from the pin tip (Figure A.2C) were designed. Both designs include retention valves close to the top of channels to prevent drainage of the liquid and ensure the channels are repeatedly filled and drained [153]. Pins are fabricated by photolithography on a silicon-on-insulator wafer, etched by deep-reactive ion etching (DRIE), and detached from the carrier wafer in an HF bath. Pins are attached to a support on the side of the head (Figure A.2H) and are detached manually by breaking them off.

Because the channels are smallest at the tip, DRIE incompletely etches the tip, resulting in a 3-sided channel (Figure A.3A) which serves to improve the pins' mechanical robustness; new pins lasted over 1 year corresponding to over two million spots whereas prior designs failed after 500,000 spots. Moreover, pins that suffer considerable force (manual test) break at the retention valve and not at the tip, making it obvious when a pin has broken. A single wafer carries 232 pins, making each pin inexpensive to produce.

Experimental

Serpentine and y-junction pins were fabricated at the McGill Nanotool Microfabrication Facility (http://www.mcgill.ca/microfab). Chemicals were purchased from Sigma-Aldrich (St-Louis, MO, USA) unless otherwise noted. Both types of pins were used to print 20 mg/mL Alexa Fluor 647 conjugated chicken anti-goat IgG (H+L) (Life Technologies, Carlsbad, CA, USA) on Avid Oncyte slides (Grace Biolabs, Bend, OR, USA), which consists of a 10 micron thick nitrocellulose

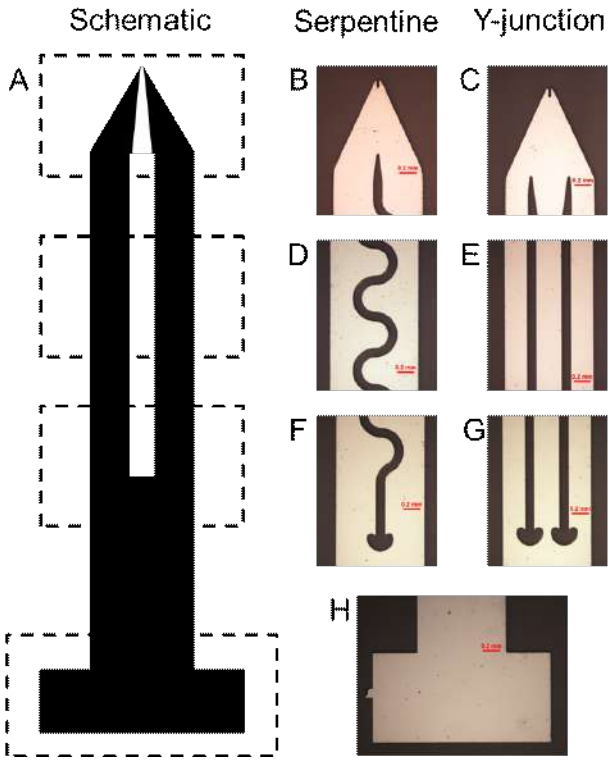

FIGURE A.2: Schematic (A) of pin design and pictures of backside of tip (B), channel (D), top of channel (F) of serpentine pin design, as well as backside of tip (C), double channels (E) and top (G) of y-junction pin design. Top of pin (H) is attached on the side to the remaining of the wafer.

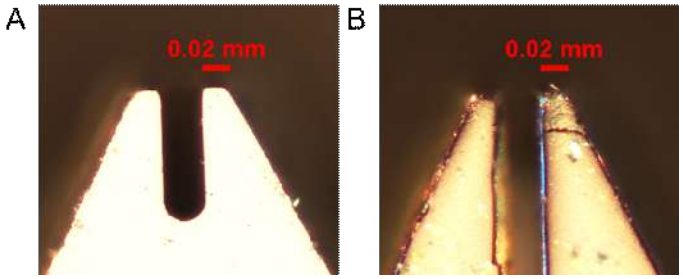

FIGURE A.3: Closed backside (A) and open front side (B) of y-junction pin show a 3-sided channel. The channel being the thinnest at this point, the DRIE process does not completely etch it.

and Xenobind slides (Xenopore Corp., Hawthorne, NJ, USA) which have a functionalized glass surface to test printing performance. Slides were printed using a customized nanoplotter (GeSim, Grosserkmannsdorf, Germany). Some slides were previously blocked for 1 hour with 1 % ultra-pure bovine serum albumin (Life Technologies) in 1 × phosphate buffer saline (PBS) with 0.1 % tween-20. All slides were washed in 1 × PBS with 0.1 % tween-20, three times five minutes on a rotary shaker before being rinsed with double-distilled water, dried with compressed nitrogen gas, and scanned with a 2-color DNA Microarray Scanner (Agilent Technologies, Santa Clara, CA,

USA).

Results and Discussion

Spot morphology from eight consecutively printed spots from a y-junction pin is excellent (Figure A.4), with sharp edges and consistent signal intensity throughout the spot. Figure A.5 shows that serpentine and y-junction pins print consistently on nitrocellulose and on glass slides, while the previous pins did not print on glass slides due to their non-flat tip design. The new flat pin tip design allows a good contact with the slide, and therefore consistent printing on both surfaces.

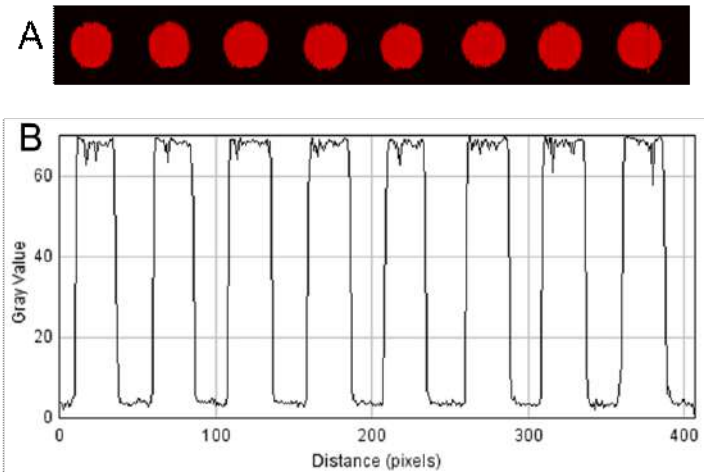

FIGURE A.4: Spot intensity profile printed with y-junction pin. Analyzed using ImageJ.

To test the new pins' liquid capacity and autonomy, we printed an entire slide (maximum 288 spots per pin) and observed how many spots were successfully printed before the pins were empty of liquid. Because we spotted slides before and after blocking it with BSA, we performed the experiment on the two different surfaces. We also spotted using different concentrations of glycerol, which is a hygroscopic additive that partially (10 %) or completely (50 %) prevents evaporation of the solution while spotting. Figure A.6 shows that liquid capacity for new pins is best on functionalized glass slides, and therefore we conclude that the volume of liquid delivered to the Xenobind slide is less than on the Avid Oncyte slide. The new pins hold 300 nL of liquid, and were not depleted after printing 288 spots, indicating that the dispensed volume is < 260 pL.

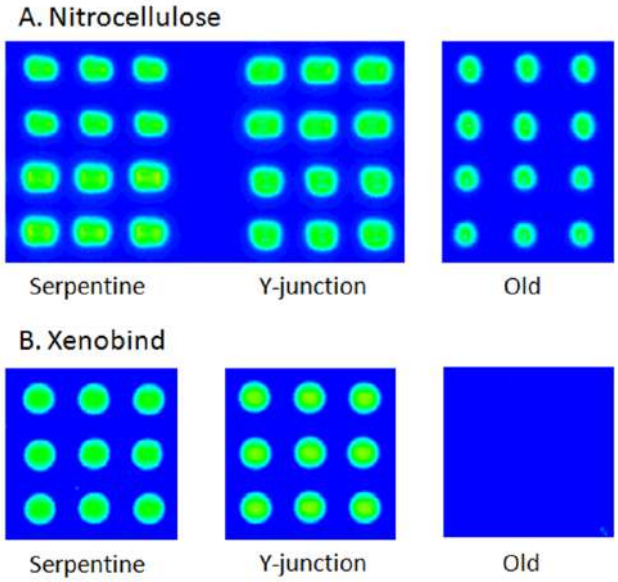

FIGURE A.5: Spot morphology printed on 3-D nitrocellulose (A) and 2-D Xenobind (B) surfaces shows that only serpentine and y-junction pins successfully print on 2-D surface.

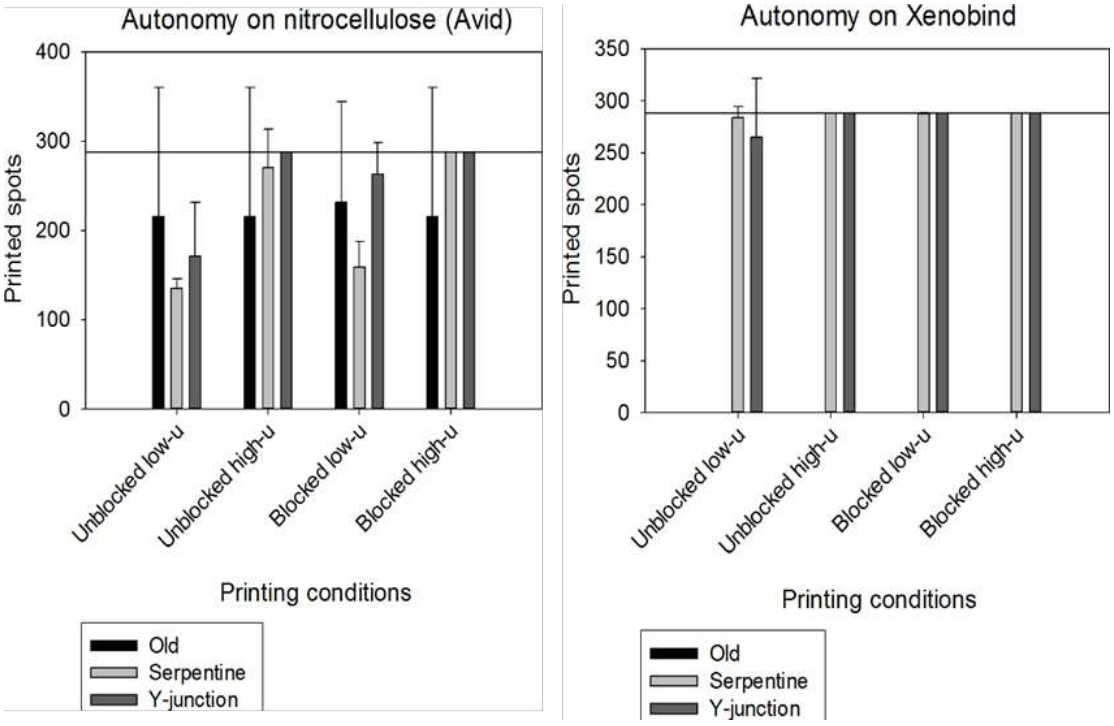

FIGURE A.6: Number of spots successfully printed on untreated and treated slides (blocked with 1 % bovine serum albumin (BSA) in 10 % and 50 % glycerol, on nitrocellulose and functionalized glass slide (Xenobind). Serpentine and y-junction pins print for the full run (reference line, 288 spots), while the previous pin design prints partially a single pin loading.

Conclusion

We presented two new silicon pins which performed equally well in terms of robustness, high liquid capacity, and lead to reproducible spots with excellent morphology. Using these pins to produce antibody microarrays helps maximize the sensitivity of assays by minimizing variation of the printing step, which helps improve the limit of detection. This allows us to detect low-abundance proteins in blood and other fluids.

Acknowledgments

The authors wish to acknowledge funding from the NSERC-CREATE training programs in integrated sensor systems and neuroengineering and grants from the Canadian Institute of Health Research. DJ holds a Canada Research chair.

References

17. Pla-Roca, M., Leulmi, R. F., Tourekhanova, S., Bergeron, S., Laforte, V., Moreau, E., Gosline, S. J. C., Bertos, N., Hallett, M., Park, M. & Juncker, D. Antibody colocalization microarray: a scalable technology for multiplex protein analysis in complex samples. *Molecular & Cellular Proteomics* **11,** M111.011460 (2012).

153. Safavieh, R., Pla-Roca, M., Qasaimeh, M. A., Mirzaei, M. & Juncker, D. Straight SU-8 pins. *Journal of Micromechanics and Microengineering* **20,** 055001–055009 (2010).

154. Laforte, V., Olanrewaju, A. & Juncker, D. *Low-cost , high liquid volume silicon quill pins for robust and reproducible printing of antibody microarrays* in *MicroTAS: miniaturized systems for chemistry and life sciences* (Chemical and Biological Microsystems Society (CBMS), Freiburg, Germany, 2013), 485–487.

Contact

*V. Laforte, tel: +1-514-3984400 ext. 09589; veronique.laforte@gmail.com

APPENDIX B

ACM: Cross-reactivity free multiplexed protein analysis

Preface

Background and objectives

The ACM protocol was improved until it was used to measure over one hundred proteins in hundreds of samples in chapters 4, 5 and 6. The protocol was complex, and it contained a lot of details and know-how that we felt was best to officially write up and share with the scientific community.

Challenges and encountered problems

While writing this book chapter, I was also working on optimizing the ACM platform and the calibration method reported in chapter 4. Some work in progress was not included in this book chapter, and part of the information gathered here became obsolete. However, this snap-shot of the ACM protocol still contains a lot of information which I hope to be useful to the scientific community.

Reference

This appendix is based on a book chapter which I wrote: Véronique Laforte, Pik Shan Lo, Huiyan Li and David Juncker, "Antibody Colocalization Microarray for cross-reactivity free multiplexed

protein analysis" published in the *Methods in Molecular Biology* book series in 2017 [219], reprinted here with permission.

Antibody Colocalization Microarray for cross-reactivity free multiplexed protein analysis

Veronique Laforte[1,2,3], Pik-Shan Lo[2,3], Huiyan Li[2,3], D. Juncker[1,2,3]

Affiliations

[1] Department of Neurology and Neurosurgery, McGill University, McGill University,
3801 University Street, Montreal, Quebec, Canada H3A 2B4
[2] Department of Biomedical Engineering, McGill University, McGill University,
3775 University Street, Montreal, Quebec, Canada H3A 2B4
[3] McGill University and Genome Québec Innovation Center, McGill University,
740 Dr. Penfield Avenue, Montreal, Quebec, H3A 0G1

Abstract

Measuring many proteins at once is of great importance to the idea of personalized medicine, in order to get a snapshot of a person's health status. We describe the antibody colocalization microarray (ACM), a variant of antibody microarrays which avoids reagent-induced cross-reactivity by printing individual detection antibodies atop their corresponding capture antibodies. We discuss experimental parameters that are critical for the success of ACM experiments, namely, the printing positional accuracy needed for the two printing rounds and the need for protecting dried spots during the second printing round. Using small sample volumes (less than 30 µL) and small quantities of reagents, up to 108 different targets can be measured in hundreds of samples with great specificity and sensitivity.

Keywords: Microarray, Antibody, Sandwich immunoassay, Multiplexed, Fluorescence

B.1 Introduction

Immunoassays are currently used in the clinic to quantify specific proteins in the blood and plasma of patients to give clues about their health status. Proteomics, the measurement of tens or hundreds of proteins in a single sample, has the potential to empower diagnostics and patient monitoring by providing a more complete snapshot picture of the health status of a person using very little sample. To achieve this multiplexed measurement goal in the future, technologies that measure multiple proteins simultaneously with high sensitivity, precision, and reproducibility are required.

Sandwich immunoassays consist in capturing a target in a sample to the surface using a surface-bound capture antibody, followed by the binding of a detection antibody which recognizes the same target (e.g., a protein) but at a different epitope as the capture antibody. Sandwich immunoassays offer high sensitivity due to the high affinity of antibodies to their target and high specificity, thanks to the double recognition of different epitopes on that target. Antibody microarrays can measure multiple targets at once using the same amount of sample as a classical ELISA and minimal amounts of costly antibodies. However, when multiple detection antibodies are mixed, specificity is often lost due to cross-reactivity between reagents [17] which can be mitigated by extensive selection, optimization of the reagents, and limiting the number of targets measured simultaneously. Cross-reactivity leads to significant false-positive signals, which can mask significant binding or conversely give the appearance of target binding when none occurred [144].

The antibody colocalization microarray (ACM) was developed to avoid cross-reactivity in multiplexed measurements by physically separating individual detection antibody solutions and printing them directly atop their corresponding capture antibodies. Because detection antibodies are not mixed, the same high level of specificity as ELISA is reached with the ACM. Microscope slides are printed with capture antibodies using a microarray printer with silicon quill pins that are fabricated in-house [154]. After blocking and incubating samples on the microarray slides, slides are dried and moved back to the microarray printer where detection antibodies are then spotted over their respective capture antibodies with great positional accuracy. Microarray slides are incubated with a reporter molecule (streptavidin conjugated to Alexa Fluor 647 (AF647)) and scanned with a fluorescence scanner (*see* Figure B.1). Capture and detection antibodies are printed in different low-evaporation buffers which are suited for each step. These low-evaporation printing buffers allow for long printings of several hours without changing the composition of the printed solutions, allowing for better printing reproducibility [146].

Many other methods have been devised to circumvent cross-reactivity in multiplexed measurements. Similar to the ACM, a system was developed with two spotting rounds and an aqueous two-phase system to separate individual detection antibodies. The caveat of this system is the size of spots which limits the density of targets that can be measured in one sample [368]. Proximity

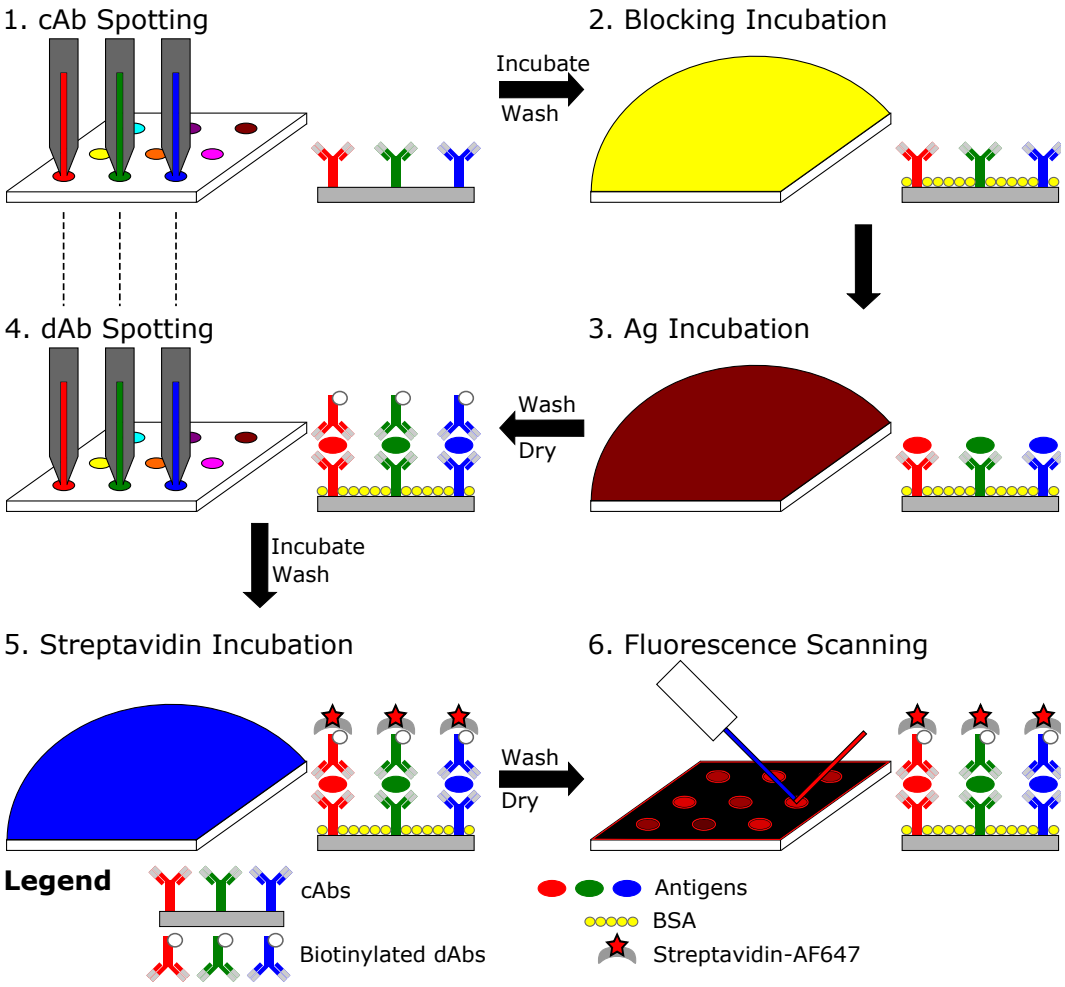

FIGURE B.1: Schematic of the antibody colocalization microarray. Capture antibodies are printed onto functionalized glass microarray slides (*1*) using silicon quill pins and incubated for 24 h. Microarray slides are washed and blocked (*2*), followed by an overnight incubation of diluted samples and antigen standard overnight at 4 °C (*3*). Microarray slides are then washed and dried before printing cognate biotinylated detection antibodies at the exact same location as previously printed capture antibodies (*4*). Microarray slides are incubated for 16–24 h before washing, followed by the incubation of fluorescent streptavidin (*5*). After washing and drying, microarray slides are scanned with a fluorescent scanner (*6*).

extension assays (PEA) [145] and proximity ligation assays (PLA) [369, 370] make use of matched antibody or aptamer pairs conjugated to corresponding short DNA fragments and real-time PCR to quantify the amount of antigen bound. These methods have been shown to accurately measure up to 96 targets in as little as 1 µL samples; however, it requires the labeling of each individual antibody and the use of a separate microfluidic platform. The Simple Plex [371] is a simple polymer chip that uses microfluidics to separate the flow of individual detection antibodies over separate capture

areas. The method can very quickly detect proteins in samples; however, the multiplexing capabilities are currently limited to detecting four targets in a same sample. Microarray chips that use force-based discrimination only leave tightly bound antibody on the surface, while cross-reacting antibodies that are expected to be weakly bound are removed [372]. This method was shown for eight targets. In short, while PEA and PLA have good performance and multiplexing capabilities, these assays are very complex. On the other hand, Simple Plex and the aqueous two-phase system platform are simpler but have limited multiplexing capabilities. In comparison, ACM is simple and allows for more than one hundred targets to be measured.

Several aspects of the procedure described in this chapter are critical to the success of ACM experiments. These are printing positional accuracy, spots protection with trehalose during detection antibody printing, duration of streptavidin incubation, features of the working environment, and experimental design. Each of these aspects contributes to the high accuracy, sensitivity, and reproducibility of the ACM platform, and they are described below.

Because detection antibodies are printed directly atop their corresponding capture antibodies, the microarray printer used, regardless of whether it is a contact printer or inkjet, should have excellent positional accuracy (10 µm) when a microarray slide is removed and handled between two spotting rounds on the same slide. In order to reach this level of performance, we found it important to avoid re-initializing the printer between printing rounds, as well as establishing a method for calibrating the printer head position. A microarray slide deck that is equipped with spring-loaded slots was used for accurate positioning of slides. Slides were pushed against a corner and the two adjoining sides. Precise and consistent alignment is also dependent on good manual dexterity, and slides were positioned at the same location on the deck.

Since spots containing the capture antibodies and targets are dried before printing the detection antibodies, it is important to coat the microarray slides with a protectant to prevent the degradation of antibodies and proteins at the surface [373]. Trehalose [374] was dried on the surface, forming a protective coating, without the presence of salts or buffer, which denature proteins because of the high salt concentration at the dry state. Detection antibodies are printed with a detection buffer containing glycerol and bovine serum albumin (BSA) that help protect the proteins at the surface during the following incubation. Printing many microarray slides (>10) takes several hours with our setup with four silicon pins used in parallel. In the absence of a trehalose coating just before detection antibody printing, we observed a slow degradation of capture antibodies and bound antigens at the surface that reduced assay reproducibility.

Following sample incubation which is done for ~18 h to allow the capture antibody to antigen binding to reach equilibrium, incubation times for the following steps are crucial. Because the detection antibody spots have very small volumes and high viscosity, which decreases the off-rate

of the antibody-antigen complex, the quantity of bound antigen to the capture antibodies is not significantly decreased in spite of the long incubation time. However, during the following washes and streptavidin-AF647 incubation, a trade-off must be found between minimizing incubation times to limit off-rate unbinding and providing sufficient time for the streptavidin to bind in order to give a strong signal. We found that 20–30 min of streptavidin incubation is sufficient in our experiments. After the final washing and drying, all microarray slides were scanned at once unless they are kept in the dark and in vacuum. Fluorophores used are sensitive to ozone below levels that can normally be detected, and keeping them in the presence of air or light for several hours leads to significant degradation to affect reproducibility and sensitivity.

A dedicated room was used for carrying out the procedures described below with lights turned off, ozone removal, and HEPA-filtered air. Ambient light and the presence of even small amounts (10 ppb) of ozone in the air during incubations, washes, and scanning can lead to fluorophore photobleaching and gradual degradation during scanning that can affect reproducibility of the assay. Alexa Fluor dyes are less sensitive to the effect of light than Cy dyes [375]; however, they are more sensitive to ozone [376]. Their use is still warranted by the fact that AF dyes have higher signals and decreased quenching compared to Cy5 and Cy3 [377, 378]. Their absorption and emission spectra also do not change when they are conjugated to antibodies [379]. Dust particles that are bigger than a spot size (100 µm) can lead to one or several missing spots and, hence, missing data points in an experiment. Moreover, many dust particles are autofluorescent. The use of cellulose-based cotton from lab coats or paper to blot liquids in the work environment should be avoided to prevent contamination by dust particles. Microfiber cloths were used, along with clean-room quality lab coats. Generally following guidelines for a dust-free room (such as a clean room) is helpful to obtain high-quality defect-free microarrays.

If a microarray printer is not readily available, pairs of microarray slides containing preprinted, mirrored capture antibodies and detection antibodies, respectively, can be purchased from Parallex Bioassays (http://www.parallexbio.com, Montreal, Canada) along with a snap-chip device. The ACM assay can then be conveniently performed by using the snap chip to precisely transfer the detection antibodies to the spots with the corresponding capture antibody spots following sample incubation [141, 142]. The snap-chip procedure (*see* Figure B.2) corresponds to the steps described below involving sample incubation, washing, streptavidin-AF647 incubation, and scanning. Steps that are specific to the ACM are the printing steps and the protection of microarray slides with trehalose. This is not necessary in the snap-chip procedure because all detection antibodies are applied at once in parallel. Overall, an experiment using the snap chip is shorter in time than with home-printed microarray slides.

Experimental design is important to the success of ACM experiments (*see* Figure B.3). Two

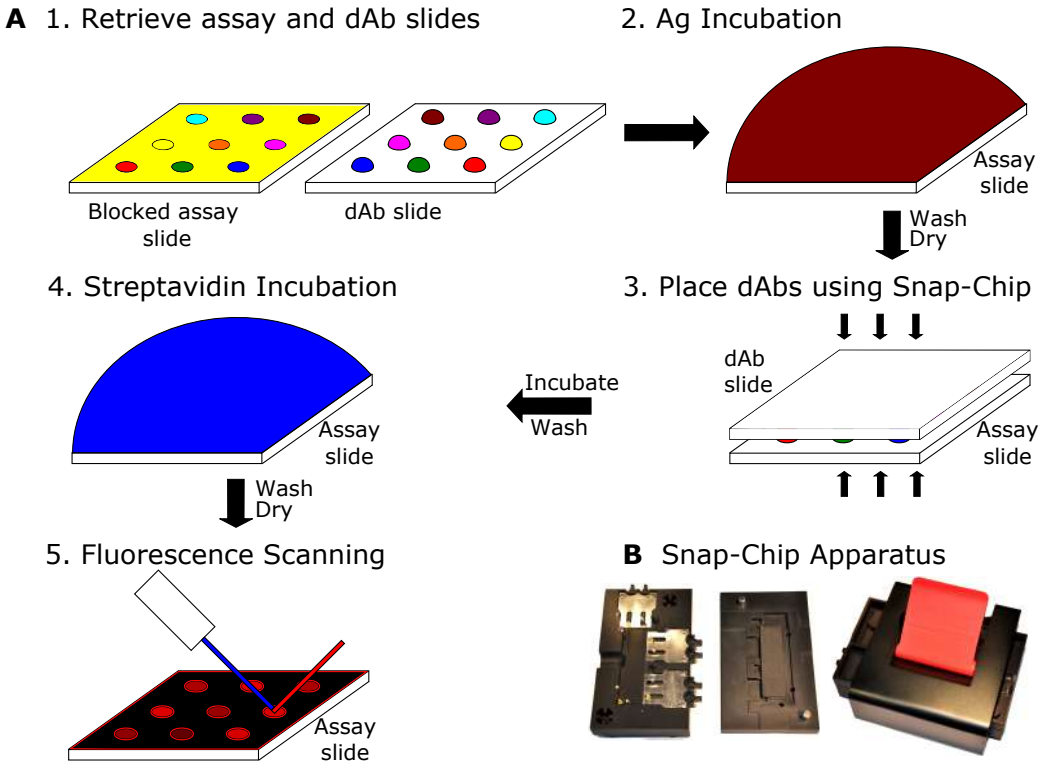

FIGURE B.2: Schematic of the ACM using a snap-chip apparatus. (**a**) The same number of assay (capture) and detection slides are pre-spotted with antibodies (*1*), and the assay slides are pre-rinsed, blocked, and dried prior to shipping. Assay slides are retrieved from storage by the user and incubated with diluted samples and antigen standards overnight at 4 °C (*2*). Assay slides are then washed and dried. After being retrieved from storage, detection slides are brought into contact with their respective assay slides using the snap-chip apparatus (*3*) which aligns the assay and detection slides and ensures incubation of each spot with a detection antibody solution for 1 h. Slides are then separated, and the assay slides are incubated with fluorescent streptavidin (*4*), washed, dried, and scanned (*5*) using a fluorescent scanner. (**b**) The snap-chip apparatus mechanically brings an assay slide and a detection slide in contact with precise force and alignment over the whole surface (pictures from Parallex Bioassays).

complete standard curves containing a mixture of known quantities of recombinant antigen that are serially diluted (1:2–1:4) with a minimum of seven points (but ideally 15 points to obtain an accurate curve fit) and a blank are included in the layout [250, 380]. Samples are measured at two different dilutions (e.g., 1:3 and 1:50) to allow the quantification of low- and high-abundance proteins. The well position of all samples is randomized to avoid measurement bias. Several blanks and normal replicate samples, for example, from a pooled normal serum or plasma sample, are measured at regular position intervals (e.g., once per microarray slide) in order to properly measure the limit of detection (LOD) and the reproducibility (coefficient of variation %CV for each target measured. All values of samples and replicates are quantified by interpolating the log-transformed

raw fluorescence value in a log-log curve fit using the standard curve values (without the blank).

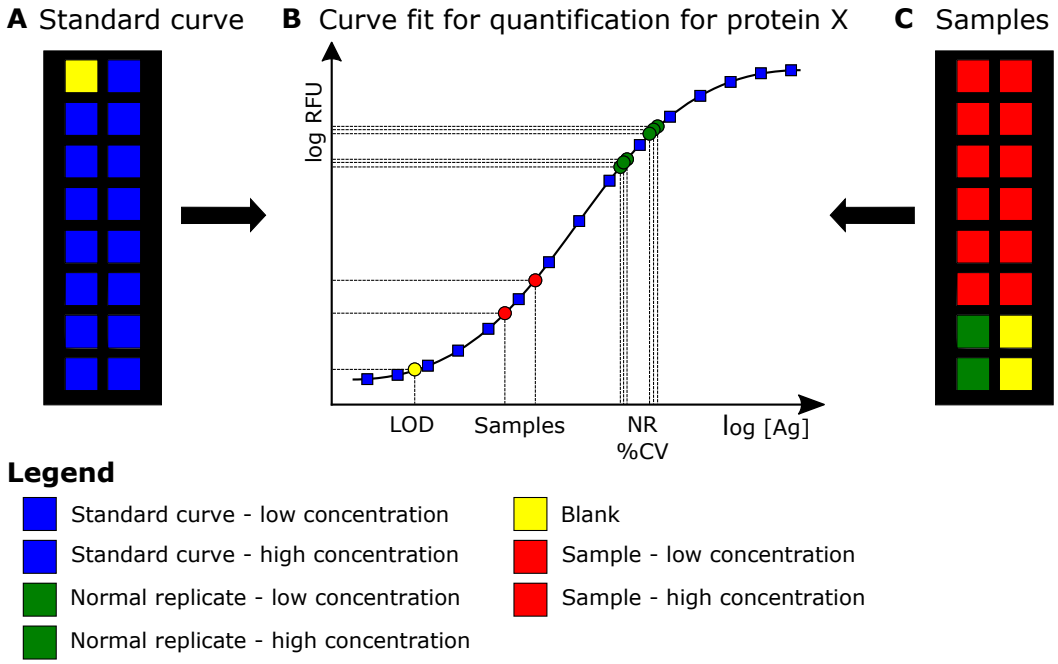

FIGURE B.3: Experimental design for ACM experiments. A slide containing 16 identical subarrays are incubated with (**a**) a serial dilution of recombinant antigen mixtures (varying shades of blue) and a blank (yellow). This standard curve is plotted on a log-log graph (**b**) and fitted with a four-parameter logistical curve. Other slides (**c**) are incubated with samples at different dilutions (red), blanks (yellow), and normal replicates (pooled samples from healthy individuals) at different dilutions (green). The concentration of each protein is derived by interpolating the values with the binding curves derived in (**a**). The limit of detection (LOD) is calculated as the mean + three times the standard deviation of blanks, whereas the assay coefficient of variation (%CV) is calculated from the interpolation of each normal replicate where the standard deviation is divided by the mean for each target.

The ACM has been used to measure up to 50 targets in 55 samples [17, 381]. Recently, the measurement of up to 108 targets with triplicate replicate spots per target and per sample and for upward of 300 samples with two dilutions per sample has been analyzed. The ACM has been used to measure human serum, plasma with different anticoagulants (EDTA, heparin, CTAD, and citrate), as well as other human fluids such as cerebrospinal fluid and urine. The sensitivity of assays using the ACM is comparable to that of ELISA, with LODs ranging from 0.1 pg/mL to 300 pg/mL depending on the antibody pair used. Reproducibility of assays also varies depending on the antibody pair and can be as good as 10 % variability over a large (>200 samples) experiment (unpublished results). Because of long duration of printing for large experiments, reproducibility is better when printing up to six to eight microarray slides with a 16-well gasket (*see* Figure B.2)

which leads to printing rounds that are less than 3 h. Reproducibility can be further improved by normalizing the data [382].

B.2 Materials

B.2.1 Buffers and Materials

All buffers are prepared using ultrapure water which has a resistance of at least 18 MΩ · cm at 25 °C. All reagents are analytical grade and stored at room temperature unless otherwise indicated. Follow local waste disposal regulations and MSDS recommendations for chemicals.

1. Wash buffer: 1 × phosphate-buffered saline (PBS) containing 0.1 % Tween 20. Mix 100 mL of 10 × PBS stock to 900 mL of ultrapure water. Add 1 mL of Tween 20 using a viscous liquid pipette (*see* **Note 1**). 1 × PBS can be prepared by other methods as long as it is free of small particles (*see* **Note 2**). This buffer can be stored in a squeeze bottle at 4 °C for 1 year.

2. Dilution buffer: 1 × PBS containing 0.05 % Tween 20. Mix 100 mL of 10 × PBS stock to 900 mL of ultrapure water. Add 0.5 mL of Tween 20 using a viscous liquid pipette (*see* **Note 1**). This buffer can be stored at 4 °C for 1 year.

3. Blocking buffer: 3 % protease-free bovine serum albumin (BSA) kept at 4 °C, 1 × PBS, and 0.05 % Tween 20. Mix 0.3 g BSA in 10 mL of dilution buffer. This solution is made fresh when needed.

4. Capture antibody printing buffer: make a 2.9 M betaine, 35.7 % 2,3-butanediol in 1 × PBS by mixing 1.6987 g of betaine to 1.785 mL 2,3-butanediol using the viscous liquid pipette (*see* **Note 1**), and 1.97 mL of 1 × PBS. Dilute this concentrated printing buffer to the required concentration by mixing with 1 × PBS before adding to individual capture antibodies. The final concentration for printing is 2 M betaine and 25 % 2,3-butanediol in 1 × PBS when antibodies have been added (*see* **Note 3**). This solution can be kept at room temperature for up to a week. Do not store this buffer at 4 °C (*see* **Note 4**).

5. Detection antibody printing buffer: make a concentrated BSA-T20 solution by mixing 0.15 g of protease-free BSA kept at 4 °C, 150 µL of wash buffer, and 4.85 mL of 1 × PBS. When preparing detection antibodies, mix the appropriate volume of this concentrated BSA-T20 (3 % BSA, 0.003 % Tween 20, 1 × PBS) to pure glycerol using the viscous liquid pipette (*see* **Note 1**) and 1 × PBS so that the final concentration of the additives is 1 % BSA, 0.001 % Tween 20, and 45 % glycerol solution in 1 × PBS after adding the detection antibody stock

solution (*see* **Note 3**). However, before adding the individual detection antibodies, filter the solution containing BSA, Tween 20, and glycerol with a 0.45 µm sterile filter, a syringe, and a hypodermic needle (*see* **Note 5**). Dispose of the hypodermic needle in a sharps container according to local waste management regulations. This solution is prepared fresh daily.

6. Slide rinsing solution: make 50 mL or more of 5 % trehalose solution in water by mixing 2.5 g of trehalose to 50 mL of ultrapure water. This solution is kept at 4 °C in a squeeze bottle.

7. Microarray slides: Xenobind slides (Xenopore Corp.) are standard size glass microarray slides with a proprietary reactive aldehyde surface. PolyAn's 2D aldehyde microarray slides also work well with this protocol, as it has the right surface-binding capacity and chemistry (*see* **Note 6**). Slides should be clean and free of dust or visible smudges. Their surface coating should be homogeneous and can be verified by scanning slides at a high gain before using. If slides are not clean, an in-house cleaning and quality control step can be performed (*see* **Note 7**) but should be validated for each slide type.

B.2.2 Equipment

The ACM protocol requires a number of specialized equipment. Below is the list of equipment and their characteristics or performance parameters that are critical to the success of ACM assays.

1. Microarray printing: printing is done using a contact microarray printer using custom-made silicon quill pins with high liquid capacity [3]. The printer has a spot positioning accuracy of 10 µm or less when microarray slides are taken out of the slide deck and replaced in the same position after further processing. The capture and detection printing buffers are compatible with silicon quill pins. Quill pins are treated once with the flame from an ordinary kitchen torch which forms a plasma that makes the pin channels hydrophilic. During normal operation, pins are washed with a soap solution, followed by distilled water, and then dried using a vacuum pump or absorbent paper. Neither the source plate nor the slide deck is cooled. An inkjet-type microarray printer can be used if it meets minimum performance requirements (*see* **Note 8**). The printing chamber is kept free from dust by filtering the incoming air to the humidifier and minimizing manipulations with hands inside the chamber. Gloves and dust-free (clean room) lab coats are worn at all times in the room where the printer is located, and hair is tied or covered. A HEPA filter and dust-minimizing practices are also recommended for this room. If using a 1536-well plate to dispense liquids, make sure that the plate fits tightly in its enclosure and is well aligned. To facilitate loading the plates, they

can be treated with a (gas) plasma. We found that 10 s at 100 W (PlasmaEtch PE-50) worked well for 1536-well plate for detection antibody solutions. The 1536-well plate for capture antibody solutions containing additives is not plasma-treated (*see* **Note 9**).

2. Rotary shaker: a type of flat rotary shaker that has a large surface area and small radius of rotation is used in order to maximize mixing within the 7 mm^2 wells. Moreover, it is compatible with temperatures down to 4 °C. In order to improve the adhesion between gaskets and the rotary shaker, a large, flat layer of polydimethylsiloxane (PDMS) is placed on top of the surface (*see* **Note 10**).

3. Fluorescent scanner: a microarray scanner which scans microarray slides in less than 15 min per slide at a resolution of 5 µm or less is recommended. At least one of the laser and filter combination should be compatible with the AF647 dye.

B.2.3 Antibody Pairs and Antigens

Assays should be performed with high-quality reagents that have undergone rigorous quality control. Only antibody pairs that have been validated for use as a pair in ELISA or on a microarray are used, and binding curves established using full-length proteins whenever available. All reagents are verified for binding against the species of the samples to be measured.

1. Capture antibodies: these antibodies are typically monoclonal antibodies, purified and unlabeled. If the stock concentration is not at least 0.25 mg/mL, a concentration and quantification step is required prior to aliquoting in working volumes and storing at the appropriate temperature as specified by the manufacturer. Capture antibodies should be free of carrier proteins (e.g., BSA) and contain less than 5 % glycerol (*see* **Note 11**).

2. Detection antibodies: these antibodies can be monoclonal or polyclonal antibodies and are purified and labeled with biotin. Other labels are possible (*see* **Note 12**) but should be compatible with the labels of all other assays within a microarray slide's subarray. Their concentration is at least 0.1 mg/mL and they are aliquoted in working volumes and stored according to the manufacturer's instructions. If the concentration is too low, a concentration step, for example, using spin columns, may be used before aliquoting and storing.

3. Antigens: antigens are typically recombinant and purified. Antigens that are obtained from animals or humans and purified can lead to significant cross-reactivity with other targets within the subarray (*see* **Note 13**). Antigen stock solutions should have as high concentration as possible for better storage stability and can be stored in the presence of carrier protein such as BSA in order to improve their shelf life.

B.2.4 Other Materials and Equipment

1. Microarray gaskets: the microarray gaskets used are Grace Bio-Labs ProPlate® Multi-Array Slide System, more specifically the gaskets with metal clips and 16 wells (2×8) that allow us to incubate 16 different samples per microarray slide. Printing of microarray slides is designed to print 16 identical subarrays that correspond to the 16 wells of the gasket. Different gasket layouts can be used in order to have more or less targets and samples on each slide as long as the microarray printing layout is adjusted.
2. Compressed nitrogen stream: many fluorescent dyes are sensitive to heat, oxygen, ozone, and light. When drying microarray slides, it is very important to use a stream of compressed gas that is free of oxygen in order to avoid degradation of the AF647 reporter dye.
3. Square 24.5 cm^2 petri dishes (optional, *see* **Note 10**).
4. Solvent- and water-resistant permanent marker (*see* **Note 14**).
5. Microfiber cloth.
6. 1536-well plate, not plasma-treated (*see* **Note 9**).
7. 1536-well plate, plasma-treated (*see* **Note 9**).
8. Pure ethanol, for washing.
9. 8-channel multichannel pipette.
10. Dust-free, ozone-free sealed room with HEPA filter.
11. 4 °C storage, ideally a cold room.

B.3 Methods

B.3.1 Sample Storage

Samples of serum, plasma (EDTA, heparin, citrate, or CTAD), or other biological fluids such as urine, cell culture supernatant, saliva, or cerebrospinal fluid can be collected using standard procedures. Serum samples are allowed to coagulate for 30–60 min before centrifugation. All samples are centrifuged for 10 min at $1500 \times g$ at room temperature to remove cells and other particles. The supernatant can be aliquoted in working volumes and kept at −80 °C for short periods of time (less than 1 year). For longer storage, samples are kept in the dry phase of a liquid nitrogen storage system.

B.3.2 Capture Antibody Printing

1. Mark clean slides with a small black line at the top right corner to identify the printed side, using a permanent marker that does not dissolve in water nor ethanol (*see* **Note 14**). In addition, identify each individual slide in the bottom corners using the same marker. Take care to always handle microarray slides by the sides, never touching the top or bottom with your hands or gloves.

2. Prepare the pin printer for printing by turning on the humidity to 65 % at room temperature and cleaning the pins according to the manufacturer's instructions. Make sure all wash buffer containers are full and waste recipients are empty. The humidity in the printing chamber should be stable before capture antibody solutions are placed in the printer. Verify printer alignment (*see* **Note 15**).

3. Prepare capture antibody solutions. Capture antibodies are printed at a concentration of 0.1 mg/mL in the capture antibody printing buffer, and the final concentration of additives is exactly 2 M betaine and 25 % 2,3-butanediol. For example, mix 2 µL of an antibody that has a stock concentration of 1.0 mg/mL to 8 µL of a capture antibody printing solution that contains 2.5 M betaine and 31.3 % of 2,3-butanediol. Any significant increase or decrease of the concentration of additives can prevent reproducible printing across all slides due to evaporation or swelling of solutions while printing. If loading a 1536-well plate, preparing 10 µL is sufficient for each individual antibody. If fluorescence signal is too low for all spots for a specific antibody solution, or if spots have streaks in their near vicinity, slightly increase or decrease the concentration accordingly until no streaking is seen and sufficient fluorescence is obtained for all spots (*see* **Note 16**).

4. Load 8 µL of each capture antibody solution into the 1536-well plate using pipette tips that are long and thin (e.g., as is used for loading polyacrylamide gels). Place the bottom of the tip at one of the bottom corner of a well before dispensing the solution slowly; this will ensure that no bubble is formed at the bottom of the well. The source well plate used for the capture antibody solutions is not plasma-treated (*see* **Note 9**).

5. Quickly remove dust from microarray slides using a stream of compressed nitrogen before loading them, as well as the 1536-well plate, into the printer when the relative humidity has reached 65 % in the printing chamber. Set up the printing program to print at least three technical replicate spots of each solution per subarray, and 16 identical subarrays on each microarray slide, in locations that fit exactly the 16-well gaskets used. The spacing between spots is at least 200 µm to prevent spots from merging during printing or the

subsequent incubation. Make sure that the microarray slides are secured in their position in a reproducible manner (*see* **Note 17**).

B.3.3 Slide Blocking

1. Clean and assemble gaskets to make them free of dust or chemical residues (*see* **Note 18**).

2. Apply incubated microarray slides onto the gaskets. Mark the top right corner of the slide on the gasket using a small tape, along with the microarray slide number.

3. Wash slides with wash buffer in a squeeze bottle (*see* **Note 19**) by filling the gasket wells halfway with wash buffer, dumping the wash buffer, repeating twice, followed by filling the gasket wells halfway with wash buffer, and leaving on the rotary shaker for 5 min at room temperature and 450 rotations per min (rpm). An entire wash cycle consists in repeating the above step 3 times in total.

4. After microarray slides are washed, load 80 µL of blocking buffer into each well using an 8-tip multichannel pipette, and incubate on the rotary shaker for 3 h at room temperature, 450 rpm.

B.3.4 Antigens and Sample Incubation

1. Prepare the antigen standard curve. Antigens are added to dilution buffer as a mixture of low volumes of stock for each antigen before diluting. If the antigen stock concentration is too high to measure at least 1 µL of antigen stock solution into the mixture, then pre-dilute with dilution buffer as necessary. The final mixture containing all antigens to be assayed is diluted 1:2.5 15 times by mixing 66.6 µL of the previous concentration to 100 µL of dilution buffer. Each antigen starting concentration (i.e., its individual concentration in the original mixture) is picked such that 15 serial dilutions cover the entire s-shape of the assay standard curve (*see* Figure B.2). Increase or decrease the starting concentration of an individual antigen in the mixture as needed to shift the resulting s-shaped curve.

2. Retrieve samples from storage and let them thaw for at least 10 min at room temperature or longer at 4 °C. Mix individual samples by pipetting up and down before diluting them. Prepare the samples by diluting them at 1:3 and 1:50 in dilution buffer. For example, mix 31.8 µL of pure serum or plasma to 63.6 µL of dilution buffer to make the 1:3 dilution. Mix 5.4 µL of the 1:3 dilution to 84.6 µL of dilution buffer to make the 1:50 dilution for a sample. Use multiples of these quantities for replicate samples.

3. Dump the blocking buffer from the microarray slides. Knock the remaining liquid from the gaskets by hitting a dust-free surface. Use a dry microfiber cloth (*see* **Note 20**) to wipe the top of the gasket to prevent well-to-well contamination (*see* **Note 21**). Do not leave the microarray slide to dry. Immediately load the samples for one microarray slide before dumping the blocking buffer for the next microarray slide.

4. Place all the microarray slides in a square 24.5 cm^2 petri dish with PDMS at the bottom (*see* **Note 10**). Close the petri dish with its lid, and seal it with two full layers of paraffin film.

5. Incubate overnight (minimum 16 h) at 4 °C on the rotary shaker, at 450 rpm.

B.3.5 Detection Antibody Printing

1. Prepare the pin printer for printing by turning on the humidity to 65 % at room temperature and cleaning the pins according to the manufacturer's instructions. Make sure all wash buffer containers are full and waste recipients are empty. The humidity in the printing chamber should be stable before both the detection antibody solutions and the microarray slides are placed in the printer. Verify alignment of the printer head (*see* **Notes 15** and **17**).

2. Prepare detection antibody solutions. Detection antibodies are printed at a concentration of 0.01 mg/mL in the detection antibody printing buffer, and the final concentration of additives should be exactly 45 % glycerol, 1 % BSA, and 0.001 % Tween 20. For example, mix 1 µL of an antibody that has a stock concentration of 0.2 mg mL^{-1} to 19 µL of a detection antibody solution that contains 47.4 % glycerol, 1.053 % BSA, and 0.001 053 % Tween 20. Because the detection antibody solutions are prone to making bubbles when mixing the components by pipetting up and down, make 20 µL even though only 8 µL is loaded onto a 1536-well plate.

3. Load 8 µL of each detection antibody solution into the 1536-well plate using the long and thin pipette tips. Place the bottom of the tip at one of the bottom corner of a well before dispensing the solution; this will ensure that no bubble is formed at the bottom of the well. The source well plate used for the detection antibody solutions is plasma-treated for proper loading without bubbles (*see* **Note 9**).

4. Incubate the slides at room temperature for 30 min before removing the paraffin film from the large square petri dish. This allows the slides to be at room temperature for further processing.

5. Wash microarray slides twice with washing buffer by performing two times Subheading B.3.3, **step 3**.

6. Rinse microarray slides rapidly in their gasket three times with PBS without Tween 20. Dump the PBS from the gaskets. Add 80 µL of slide rinsing solution to the gaskets and incubate 5 min at room temperature on the rotary shaker at 450 rpm.

7. Dump the slide rinsing solution from the gaskets. Remove the gasket from the microarray slide and rinse the top side of the slide with more slide rinsing solution with a squeeze bottle.

8. Immediately dry the slide under a forceful, perpendicular stream of compressed nitrogen. This step is done to ensure that a small consistent film of trehalose is left on the surface to protect the complexed capture antibodies and antigens spots during the detection printing step (*see* **Note 22**). Wash and dry a single microarray slide at a time.

9. Print all slides in the same order that capture antibody solutions were printed. Detection antibodies are printed directly atop their corresponding capture antibody solutions. Incubate the slides for 24 h after printing is finished to allow detection antibodies to fully bind to the targets. Printed spots should be visible on the microarray slides, immediately after printing and also after the incubation.

10. Clean and assemble gaskets (*see* **Note 18**).

B.3.6 Streptavidin Incubation

1. Apply incubated microarray slides onto clean gaskets. Mark the top right corner of the slide on the gasket using a small tape, along with the microarray slide number.

2. Wash microarray slides by performing Subheading B.3.3, **step 4**.

3. Prepare a solution of 0.5 µg/mL of streptavidin-AF647 in blocking buffer and apply 80 µL in each well using a multichannel pipette. To apply to several slides, apply in the same order that washes will be performed, waiting 15–20 s in between each slide (*see* **Note 23**).

4. Incubate for 30 min at room temperature on the rotary shaker at 450 rpm. The microarray slides are kept in the dark at this point because of the presence of a fluorescence marker.

5. Wash microarray slides again by performing Subheading B.3.3, **step 4**.

6. Remove the gasket and rinse both sides of the microarray slide with distilled water from a squeeze bottle or a gentle flow from a distilled water tap.

7. Immediately dry the microarray slide under a forceful stream of compressed nitrogen that is parallel to the small axis of the microarray slide, in order to remove all droplets of water. Rinse and dry a single microarray slide at a time.

B.3.7 Fluorescence Scanning

1. If using a fluorescence scanner that scans through the back of the slide, polish the back of all microarray slides using a dry microfiber cloth (*see* **Note 20**). Remove the microfiber dust particles using a stream of compressed nitrogen.

2. Turn on the scanner and allow enough time for the lasers to warm up. Refer to the manufacturer's instructions.

3. Set the photomultiplier gain to an appropriate number. This gain should be the highest that leads to no saturated pixel (*see* **Note 24**).

4. Scan all the microarray slides as quickly as possible after the experiment is done, and in as little time as possible (*see* **Note 25**).

5. Save all images as TIFF images. If compressing images, make sure that the compression algorithm is loss-less (*see* **Note 26**).

B.3.8 Data Extraction and Analysis

1. Verify that none of the microarray slide pictures have saturated pixels (*see* **Note 24**).

2. Align grids onto the TIFF images to extract all technical replicate spots on all subarrays and on all microarray slides. Grid spot size should be at least half of the size of the actual spots. For spots of approximately 100 µm in size, we use a grid spot size of 60 µm diameter.

3. Extract the data by outputting the raw fluorescent intensity. There should be no negative value in this data.

4. Log-transform the data by calculating the log10 of each individual outputted value.

5. Perform outlier removal using Peirce's criterion or Grubbs' test (*see* **Note 27**). Calculate the mean and standard deviation of technical replicates to obtain a log-transformed raw fluorescence intensity value for a specific assay in a given sample, sample replicate, blank, or standard curve dilution. Note that the value of the concentration of antigen should also be log10 transformed.

6. Perform a four-parameter logistical curve fit on each individual assay's standard curve using the values obtained in Subheading B.3.8, **step 5**. It is important to use the standard deviations obtained for the standard curve dilutions to obtain a more accurate curve fit.

7. In order to calculate the limit of detection for a curve fit, calculate the mean and standard deviation for all blank values (obtained in Subheading B.3.8 **step 5**) for a given assay within the experiment. Interpolate the value calculated by taking the mean + three times the standard deviation into the curve fit for the given assay. The concentration obtained is the log10 value of the lowest quantity of antigen that can be quantified using the assay.

8. In order to calculate the reproducibility for a given assay, interpolate all individual values from the replicate sample. Divide the standard deviation of all the quantities obtained by the mean of all those quantities. The value obtained is the coefficient of variation (%CV) for this assay.

9. Interpolate the values obtained in Subheading B.3.8 **step 5** for all samples in the curve fit for a given assay to obtain the quantities measured in that sample. If the values obtained at dilution 1:3 cannot be quantified because they are above the maximum value from the standard curve, quantify the samples in the 1:50 dilution. Multiply the quantities obtained by the dilution in order to infer the concentration in the original sample (*see* **Note 28**).

B.4 Notes

1. The volume and concentration of viscous liquids to be measured are critical for this application. Therefore, in order to measure viscous liquids such as glycerol, Tween 20, or 2,3-butanediol, we recommend using a viscous liquid pipette which uses a piston to displace the viscous liquid rather than air.

2. The $1\times$ PBS solution used throughout the protocol should be free of small particles that are often autofluorescent and can easily bind to the microarray surface or sometimes lead to missing spots if particles clog the silicon quill pins. For this reason we recommend buying a $10\times$ PBS stock solution that has been prefiltered by the manufacturer.

3. Antibodies are normally supplied as liquid in a PBS buffer base, or freeze-dried, in which case they are reconstituted in PBS. The presence of up to 5 % of glycerol or other cryopreservative chemicals did not affect our experiments. Antibodies supplied in a different buffer than PBS might also be used but should be individually tested. For calculations, we made the assumption that antibody stock solutions are the equivalent of $1\times$ PBS.

4. At a concentration of 2 M betaine and 25 % 2,3-butanediol, the capture printing buffer can safely be kept at 4 °C; however, at higher concentrations of betaine, this chemical can precipitate out of solution when kept at 4 °C. For this reason, it is best to keep the capture printing buffer at room temperature.

5. For the same reasons as listed (*see* **Note 2**) and because BSA has particles that can lead to missing spots, the detection printing buffers are filtered with a sterile 0.45 µm filter prior to mixing with individual stock detection antibody solutions. We do not recommend filtering the solutions once antibodies have been added, because the volumes are too small, in the range of 10–20 µL. However, 1 mL of the detection printing buffer containing glycerol, BSA, and Tween 20 can be filtered using a 3 mm luer-lock filter and a 1 mL sterile luer-lock syringe. A 1.5″ 18 G hypodermic luer-lock needle can be fitted to the 1 mL syringe to pick up the detection printing buffer before filtering. Dispose of the needle in a sharps container according to local waste management regulations.

6. The capture antibody printing buffer was optimized to work well on a 2D reactive aldehyde surface. While other surfaces with higher antibody-binding capacity were identified (e.g., high-capacity epoxy surfaces), antibody-target binding was strongest on the reactive aldehyde surface suggesting that antibodies were less denatured or less crowded.

7. Xenobind microarray slides can be cleaned by sonicating ten slides at a time in distilled water, followed by a quick rinse with distilled water and then pure ethanol using squeeze bottles, immediately followed by drying with a stream of compressed nitrogen. It's very important not to let the ethanol air-dry on the microarray slides, as it can leave visible chemical smudges.

8. The main requirements for the microarray printer are spot absolute positional accuracy in both the printing and in positioning slides on a deck, the compatibility with the high-viscosity printing buffers, and printing speed. Slower (several hours) printing leads to degradation of assay signal for spots that are printed earlier and therefore gives a worse reproducibility performance for the assay.

9. Excessive plasma treatment of microplates can lead to cross-contamination between wells as liquid films form on the surface, and the optimal plasma processing time should be carefully verified. We observed that when loading printing buffers containing betaine and 2,3-butanediol on a 1536-well plate, contamination between adjacent wells occurred readily. Therefore, the 1536-well plate used for capture antibody solutions is not plasma-treated. The additives present in the detection printing buffer (glycerol and BSA) do not however flow

easily onto the plastic surface and therefore require a short 10 s plasma treatment in order to easily be loaded into the 1536-well plate.

10. We prepared a flat PDMS surface that we laid on top of the rotary shaker surface by curing approximately 200 mL of PDMS in a 24.5 cm^2 square petri dish normally used for cell culture. Cured PDMS (Sylgard® 184, Corning) is prepared by mixing a ratio of 1:10 of curing agent to the polymer base, mixing thoroughly by hand before pouring into the petri dish. The dish is allowed to stand for 30 min to allow bubbles to escape and is then cured in a 60 °C oven for a minimum of 8 h. The PDMS can then be removed from the petri dish if needed. This step is optional if multiple microarray slide gaskets can be secured at once to the rotary shaker surface.

11. The presence of more than 5 % glycerol in the capture antibody printing solution can significantly hinder binding of the antibodies to the surface.

12. If all detection antibodies within an assay are biotinylated, then all can be detected using a fluorescently labeled streptavidin. Alternatively, detection antibodies can be directly labeled with a fluorescent molecule. If detection antibodies are not labeled, they should (1) have been made in an animal species different than that of the capture antibody and (2) be probed with a secondary antibody made in the same species as that of the capture antibody in order to avoid cross-reactivity to the capture antibody. For example, if the capture antibody of an antibody pair is a mouse IgG and the detection antibody is a goat IgG, then the labeled secondary antibody should be a mouse anti-goat IgG. However all matched antibody pairs should be compatible with the labeled secondary antibody within a subarray. Any other combination (such as a capture antibody that is a goat IgG) will lead to false-positive signals due to the labeling of the capture antibody rather than the detection antibody for this assay.

13. Proteins that are obtained by purification from animal or human samples (e.g., cancer related and other proteins that have particular glycosylation patterns that cannot readily be reproduced by recombinant protein synthesis methods) often contain impurities in the form of unrelated proteins, some of which may be targets in the same subarray. This can lead to significant assay signal and cross-reactivity in the standard curves of other targets even in the absence of those targets' specific recombinant antigens [383].

14. Marker pens that dissolve in either water or organic solvents readily leak onto the slide and may smear the surface with highly fluorescent chemicals. We suggest using the solvent-resistant permanent marker from Thermo Fisher Scientific (laboratory marking pen, ref. #2000) which doesn't leak or smear using this protocol.

15. Alignment of printing between the capture and the detection steps is critical for the success of this assay. For some printers, it is as simple as avoiding re-initialization of the printer between the two printing rounds. For others which suffer from printing position drift with time, a method for calibrating the printing head position is necessary. A microscope calibration slide can be used for this in the following way. First, wash the microscope calibration slide with pure ethanol using a squeeze bottle, and dry it with a stream of compressed nitrogen. Before the capture antibody printing step, quickly print a subarray on top of the calibration area, using a solution of 50 % glycerol in PBS. View the printed calibration spots under a microscope and make note of the position of a specific spot which lies within the calibration area, compared to the center of the slide. Before performing the detection antibody printing, redo this procedure. Adjust printing margins to compensate for any misalignment that occurred between the two printing rounds.

16. Individual capture antibodies will bind to the surface with different affinities and at different rates. To increase the amount of capture antibody bound on the surface, increase the concentration of that antibody in its printing solution while keeping the concentration of additives (betaine, 2,3-butanediol) the same. Conversely, if fluorescence signals are too strong or streaking is observed around a specific capture antibody, decrease its concentration in the printing solution while keeping the concentration of additives the same. The streaking is due to the surface being saturated by the capture antibody solution and the presence of unbound capture antibodies which quickly bind to the surface during the initial washing, prior to blocking the microarray slide surface.

17. The proper alignment of detection antibody spots onto their corresponding capture antibody spots requires a very precise positioning of the microarray slides within a slide deck and the accurate alignment of the printing head prior to both printing rounds (*see* **Note 15**). Therefore it is important that slides can be positioned accurately and reproducibly within the slide deck (with less than 10 µm variability). A spring-clamped slide deck and a proper manual technique for loading slides are essential and can achieve this reproducibility.

18. Gaskets that have dust or a very hydrophilic surface can lead to contamination between wells because of an incomplete seal. In order to thoroughly wash gaskets, our method is to first rinse all parts in a mild soap solution, then rinse many times with distilled water, and finally dip for 10–15 s with shaking in pure ethanol. The gasket parts are then dried with a stream of compressed nitrogen, before being assembled and ready for use. They are then stored in a closed petri dish that prevents dust from falling on them.

19. It is important to wash the microarray slides with wash buffer with enough force, which is why the wash buffer is placed in a squeeze bottle. This helps prevent fluorescent streaks on the microarray surface. If streaking of certain spots is still seen in spite of proper washing, slightly decrease the concentration of the capture antibody in the solution for the streaking spots (*see* **Note 16**).

20. Because paper generates a lot of fluorescent dust particles, even low-dust clean-room paper is avoided when wiping microarray slides or surfaces within the working environment. Instead, we use a microfiber cloth of the like that is used to clean lenses or eyeglasses. Particles generated by microfiber cloth are not fluorescent, and they can easily be removed with a stream of compressed nitrogen.

21. If a small film of liquid is present at the top of the gasket, it can lead to contamination between wells when samples and antigens are shaken. Do not cover the gasket unless this cover has a liquid-tight seal. Any seal that is not tight will also lead to contamination between wells and falsify results.

22. Most antibodies and antigens will degrade at varying speeds after they are dried on the surface. Therefore, spots should be protected with 5 % trehalose which was found to slow down degradation and in many cases even prevents it. The actual quantity of trehalose left on the surface after drying with the stream of compressed nitrogen is dependent on the drying method. A stream that is strong, and head-on, was found best to achieve an even surface. If the detection spots spread and lose their shape on the surface during detection antibody printing, then there is too much trehalose on the surface. It is then recommended to use a stronger stream of nitrogen and to hold the nozzle close to the microarray slide (2–3 cm), although using a slightly less concentrated solution of trehalose is also possible. However, a lower concentration of trehalose can lead to more degradation of antibodies and antigens.

23. Binding of streptavidin to the detection antibodies is not limited by the concentration of streptavidin used in these experiments. However, the streptavidin signal will increase with an increase in incubation time. In order to maximize reproducibility across slides, it is important to incubate the streptavidin solution for exactly the same amount of time per slide. Therefore, if it takes 15 s to wash a single slide, apply the streptavidin solution to each slide with a 15 s delay between each slide. This will ensure that all slides have exactly the same streptavidin incubation time.

24. Saturated pixels are pixels that have the maximum value (or very close to the maximum value of 65,535 in a 16-bit system) and are in fact too high to be recorded by the scanner at the gain

used. This leads to a loss of data and falsification of results. If a significant number of pixels are saturated for a given gain, all slides of the experiment should be re-scanned with a lower gain.

25. Fluorophores in a dry state slowly degrade in the presence of air (humidity, oxygen, heat), even in a sealed room where ozone is actively removed. For this reason it is important to scan all the slides in an experiment as quickly as possible to minimize the effect of this degradation on reproducibility. If it is necessary to scan slides multiples times at different gains, then first scan all slides at an initial gain, and then scan all of them at a second higher or lower gain depending on the results, rather than scanning each slide at multiple gains. This will maximize reproducibility between microarray slides.

26. When saving fluorescence images of microarray slides, it is very important to save the image data with high dynamic range (16 bit or 20 bit) while avoiding image compression. Formats such as GIF or JPEG may only accommodate 8 bit images and compress the data with information loss that will likely lead to false results. Image formats such as TIFF accommodate 16-bit and 20 bit images and also allow compression using loss-less LZW algorithms for example.

27. In instances where the number n of technical replicates is very low, the mean and standard deviation of the group of technical replicates is very sensitive to the presence of outliers. Therefore a test or method for removing outliers that is efficient at low n is required. A minimum of three technical replicates is required for proper statistics. Grubbs' test performs well with $n = 3$ or more, while Peirce's criterion only works with $n = 4$ or more.

28. Protein quantification is subject to matrix effects that limit the comparison of quantities of a target obtained in samples within a single dilution. Because of the matrix effects, the concentration values are not considered to be absolute, and a target concentration inferred from the 1:3 dilution may be lower than the one inferred from the 1:50 dilution. Different targets are subject to different matrix effects depending on the sample type and the dilution.

B.5 Acknowledgments

We wish to thank the National Science and Engineering Research Council (NSERC) of Canada, the Canadian Cancer Society (CCS), and the Canadian Institute of Health Research (CIHR) for funding. D.J. holds a Canada Research Chair (CRC) in Micro- and Nanobioengineering.

References

17. Pla-Roca, M., Leulmi, R. F., Tourekhanova, S., Bergeron, S., Laforte, V., Moreau, E., Gosline, S. J. C., Bertos, N., Hallett, M., Park, M. & Juncker, D. Antibody colocalization microarray: a scalable technology for multiplex protein analysis in complex samples. *Molecular & Cellular Proteomics* **11,** M111.011460 (2012).

141. Li, H., Bergeron, S. & Juncker, D. Microarray-to-microarray transfer of reagents by snapping of two chips for cross-reactivity-free multiplex immunoassays. *Analytical Chemistry* **84,** 4776–4783 (2012).

142. Li, H., Munzar, J. D., Ng, A. & Juncker, D. A versatile snap chip for high-density sub-nanoliter chip-to-chip reagent transfer. *Scientific Reports* **5,** 11688 (2015).

144. Juncker, D., Bergeron, S., Laforte, V. & Li, H. Cross-reactivity in antibody microarrays and multiplexed sandwich assays: shedding light on the dark side of multiplexing. *Current Opinion in Chemical Biology* **18,** 29–37 (2014).

145. Assarsson, E., Lundberg, M., Holmquist, G., Björkesten, J., Thorsen, S. B., Ekman, D., Eriksson, A., Rennel Dickens, E., Ohlsson, S., Edfeldt, G., Andersson, A.-C., Lindstedt, P., Stenvang, J., Gullberg, M. & Fredriksson, S. Homogenous 96-Plex PEA Immunoassay Exhibiting High Sensitivity, Specificity, and Excellent Scalability. *PLoS ONE* **9,** e95192 (2014).

146. Bergeron, S., Laforte, V., Lo, P. S., Li, H. & Juncker, D. Evaluating mixtures of 14 hygroscopic additives to improve antibody microarray performance. *Analytical and Bioanalytical Chemistry* **407,** 8451–8462 (2015).

154. Laforte, V., Olanrewaju, A. & Juncker, D. *Low-cost , high liquid volume silicon quill pins for robust and reproducible printing of antibody microarrays* in *MicroTAS: miniaturized systems for chemistry and life sciences* (Chemical and Biological Microsystems Society (CBMS), Freiburg, Germany, 2013), 485–487.

219. Laforte, V., Lo, P.-S., Li, H. & Juncker, D. Antibody Colocalization Microarray for Cross-Reactivity-Free Multiplexed Protein Analysis. *Methods in Molecular Biology* **1619** (eds Greening, D. W. & Simpson, R. J.) 239–261 (2017).

250. Sittampalam, G. S., Coussens, N. P., Nelson, H., Arkin, M., Auld, D., Austin, C., Bejcek, B., Glicksman, M., Inglese, J., Iversen, P. W., McGee, J., McManus, O., Minor, L., Napper, A., Peltier, J. M., Riss, T., Trask, O. J. & Weidner, J. *Assay Guidance Manual* tech. rep. (Eli Lilly & Company and the National Center for Advancing Translational Sciences, Bethesda, MD, 2016).

368. Frampton, J. P., White, J. B., Simon, A. B., Tsuei, M., Paczesny, S. & Takayama, S. Aqueous two-phase system patterning of detection antibody solutions for cross-reaction-free multiplex ELISA. *Scientific Reports* **4,** 4878 (2014).

369. Fredriksson, S., Dixon, W., Ji, H., Koong, A. C., Mindrinos, M. & Davis, R. W. Multiplexed protein detection by proximity ligation for cancer biomarker validation. *Nature Methods* **4,** 327–329 (2007).

370. Fredriksson, S., Gullberg, M., Jarvius, J., Olsson, C., Pietras, K., Gústafsdóttir, S. M., Östman, A. & Landegren, U. Protein detection using proximity-dependent DNA ligation assays. *Nature Biotechnology* **20,** 473–477 (2002).

371. Aldo, P., Marusov, G., Svancara, D., David, J. & Mor, G. Simple plex™: A novel multi-analyte, automated microfluidic immunoassay platform for the detection of human and mouse cytokines and chemokines. *American Journal of Reproductive Immunology* **75,** 678–693 (2016).

372. Blank, K., Lankenau, A., Mai, T., Schiffmann, S., Gilbert, I., Hirler, S., Albrecht, C., Benoit, M., Gaub, H. E. & Clausen-Schaumann, H. Double-chip protein arrays: force-based multiplex sandwich immunoassays with increased specificity. *Analytical and Bioanalytical Chemistry* **379,** 974–981 (2004).

373. Christendat, D., Yee, A., Dharamsi, A., Kluger, Y., Savchenko, A., Cort, J. R., Booth, V., Mackereth, C. D., Saridakis, V., Ekiel, I., Kozlov, G., Maxwell, K. L., Wu, N., McIntosh, L. P., Gehring, K., Kennedy, M. A., Davidson, A. R., Pai, E. F., Gerstein, M., Edwards, A. M. & Arrowsmith, C. H. Structural proteomics of an archaeon. *Nature Structural Biology* **7,** 903–909 (2000).

374. Kusnezow, W., Jacob, A., Walijew, A., Diehl, F. & Hoheisel, J. D. Antibody microarrays: An evaluation of production parameters. *Proteomics* **3,** 254–264 (2003).

375. Berlier, J. E., Rothe, A., Buller, G., Bradford, J., Gray, D. R., Filanoski, B. J., Telford, W. G., Yue, S., Liu, J., Cheung, C.-Y., Chang, W., Hirsch, J. D., Beechem, J. M., Haugland, R. P. & Haugland, R. P. Quantitative comparison of long-wavelength Alexa Fluor dyes to Cy dyes: fluorescence of the dyes and their bioconjugates. *The Journal of Histochemistry & Cytochemistry* **51,** 1699–1712 (2003).

376. Byerly, S., Sundin, K., Raja, R., Stanchfield, J., Bejjani, B. A. & Shaffer, L. G. Effects of ozone exposure during microarray posthybridization washes and scanning. *Journal of Molecular Diagnostics* **11,** 590–597 (2009).

377. Cox, W. G., Beaudet, M. P., Agnew, J. Y. & Ruth, J. L. Possible sources of dye-related signal correlation bias in two-color DNA microarray assays. *Analytical Biochemistry* **331,** 243–254 (2004).

378. Anderson, G. P. & Nerurkar, N. L. Improved fluoroimmunoassays using the dye Alexa Fluor 647 with the RAPTOR, a fiber optic biosensor. *Journal of Immunological Methods* **271,** 17–24 (2002).

379. Becker, W. Fluorescence lifetime imaging - techniques and applications. *Journal of Microscopy* **247,** 119–136 (2012).

380. Wilson, J. J., Burgess, R., Mao, Y. Q., Luo, S., Tang, H., Jones, V. S., Weisheng, B., Huang, R. Y., Chen, X. & Huang, R. P. Antibody Arrays in Biomarker Discovery. *Advances in Clinical Chemistry* **69,** 255–324 (2015).

381. Li, H., Bergeron, S., Annis, M. G., Siegel, P. M. & Juncker, D. Serial Analysis of 38 Proteins during the Progression of Human Breast Tumor in Mice Using an Antibody Colocalization Microarray. *Molecular & Cellular Proteomics* **14,** 1024–1037 (2015).

382. Wingren, C. & Borrebaeck, C. A. Antibody-based microarrays. *Methods in Molecular Biology* **509,** 57–84 (2009).

383. Gonzalez, R. M., Seurynck-Servoss, S. L., Crowley, S. A., Brown, M., Omenn, G. S., Hayes, D. F. & Zangar, R. C. Development and validation of sandwich ELISA microarrays with minimal assay interference. *Journal of Proteome Research* **7,** 2406–2414 (2008).

APPENDIX C

Evaluating mixtures of 14 hygroscopic additives: Supplementary Material

This appendix describes the Supplementary Material to chapter 3.

Analytical and Bioanalytical Chemistry

Electronic Supplementary Material

Evaluating mixtures of 14 hygroscopic additives to improve antibody microarray performance

Sébastien Bergeron, Véronique Laforte, Pik-Shan Lo, Huiyan Li, D. Juncker

List of SI figures

List of SI tables

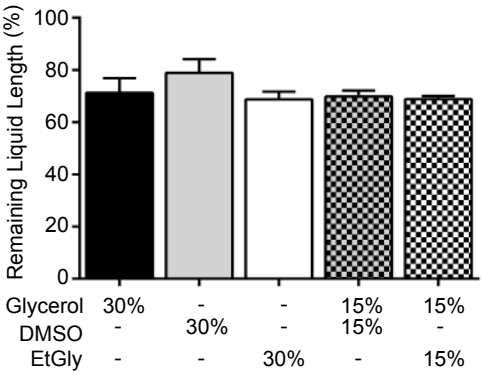

FIGURE C.S1: **Evaporation of mixtures of additives.** Percentage of liquid length remaining in a pin after 10 minutes for different single additives and pairwise mixtures with a total of 30 %v/v in PBS shows that the ability of a mixture of two additives to prevent evaporation is equal to that of a single additive in equal total concentration.

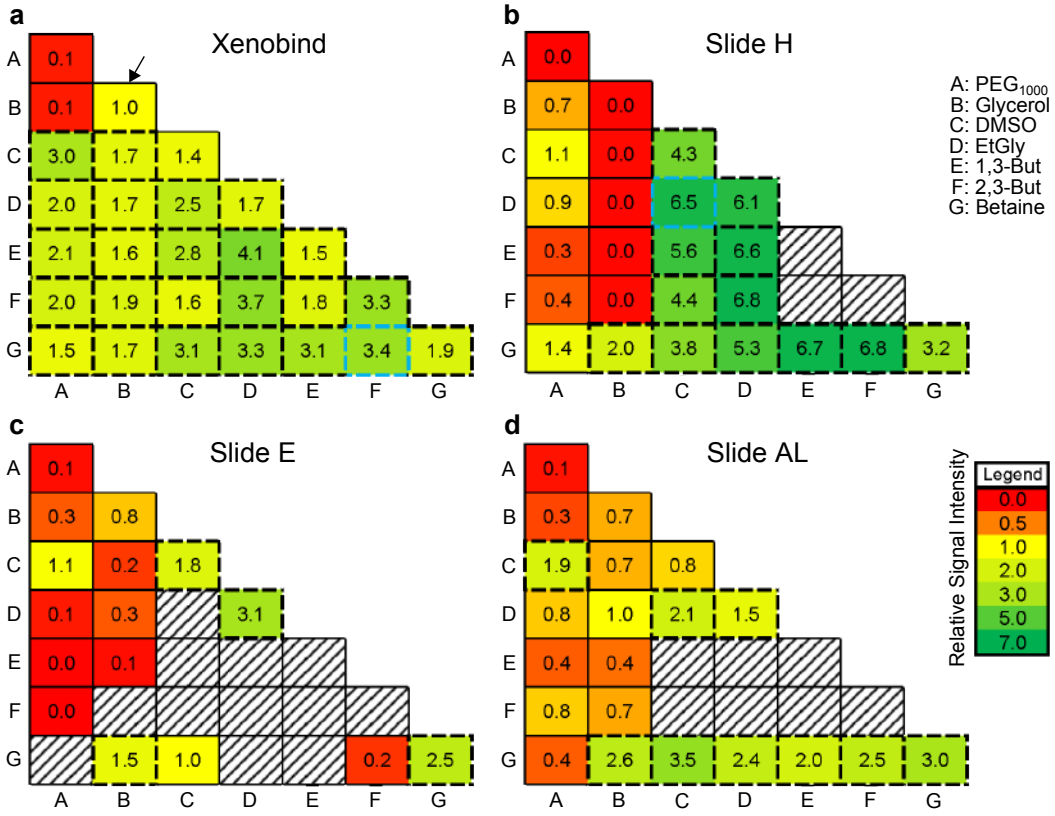

FIGURE C.S2: **Immobilization signal of cAb printed with different additives.** Fluorescently labeled anti-goat IgG was printed with different printing buffers on (a) Xenobind, (b) Slide H, (c) Slide E and (d) Slide AL. Printing buffers were composed of PBS containing 50 % of one additive listed above or 25 % of two additives each. We evaluated the immobilization of the cAb to the surface expressed as the ratio to the signal obtained by printing with glycerol 50 % on Xenobind (indicated by arrow). Dashed outlines indicate signal values ≥ 1.5 compared to 50 % glycerol on Xenobind. Hatched boxes represent unquantifiable data due to spot morphology or spots merging. Light blue dashed outlines on two boxes in (a) and (b) indicate the two mixtures of additives and slides that were found to be optimal because of their excellent spot morphology and binding signal intensities.

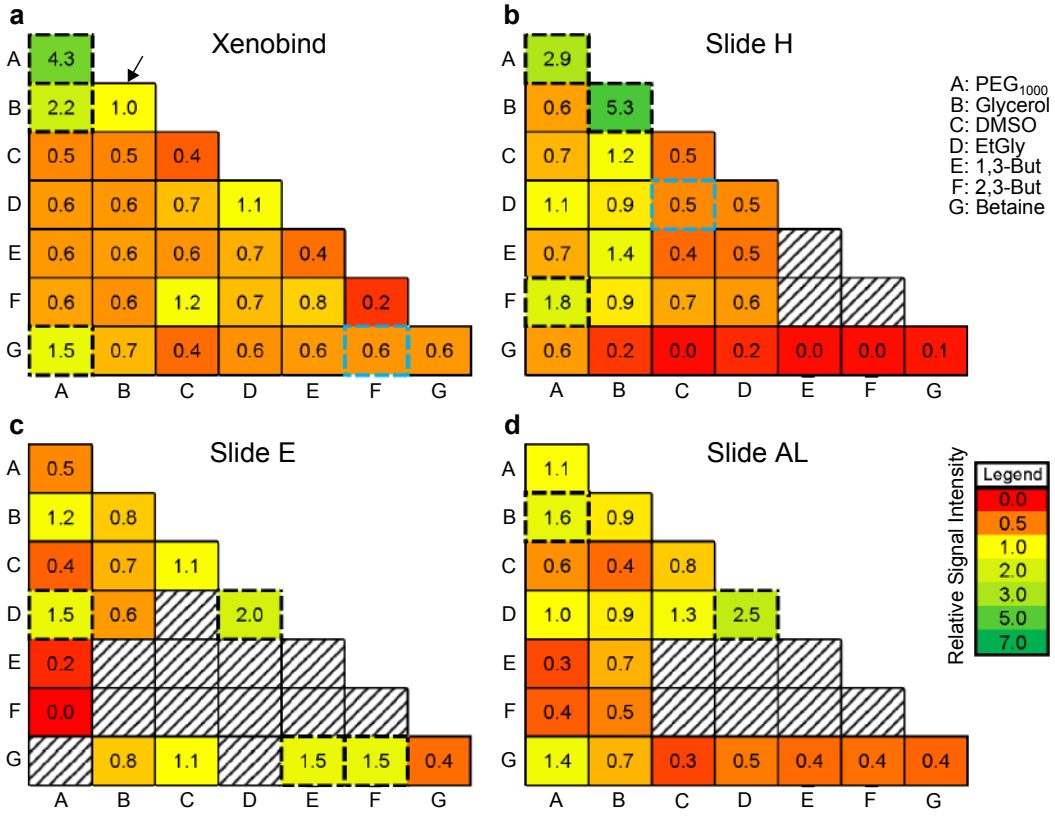

FIGURE C.S3: **Binding activity of cAb printed with different additives.** Fluorescently-labeled anti-goat IgG was printed with different printing buffers on (a) Xenobind, (b) Slide H, (c) Slide E and (d) Slide AL. Printing buffers were composed of PBS containing 50 % of one additive listed above or 25 % of two additives each. Slides were then incubated with fluorescently-labeled goat IgG analyte and the ratio of immobilization signal to binding signal is used to evaluate the cAb activity, shown here. The cAb activity is compared to that of 50 % glycerol on Xenobind (indicated by arrow). Dashed outlines indicate signal values ≥ 1.5 compared to 50 % glycerol on Xenobind. Hatched boxes represent unquantifiable data due to poor spot morphology or spots merging. Light blue dashed outlines on two boxes in (a) and (b) indicate the two mixtures of additives and slides that were further optimized because of their excellent spot morphology and binding signal intensities.

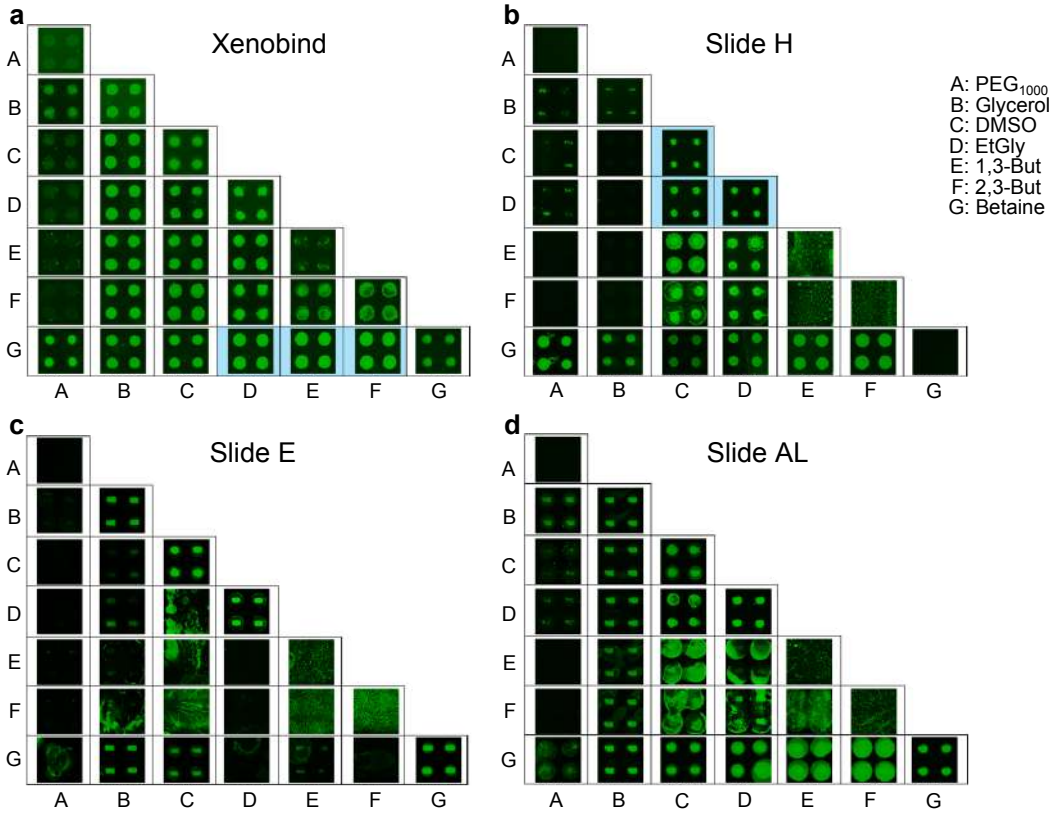

FIGURE C.S4: **Spot morphology of cAb printed with different additives.** Representative pictures of direct immunoassays with cAb printed in each printing buffers. The fluorescence signal is from the fluorescent analyte (binding signal).

TABLE C.S1: **Spot intensity profiles of cAb printed with different additives.** The uniformity and quality of spots was evaluated by plotting the fluorescence intensity profile of two adjacent spots using ImageJ software. The blue shading highlights buffers selected for further testing based on signal intensity and spot morphology (sharp edges and a uniform plateau).

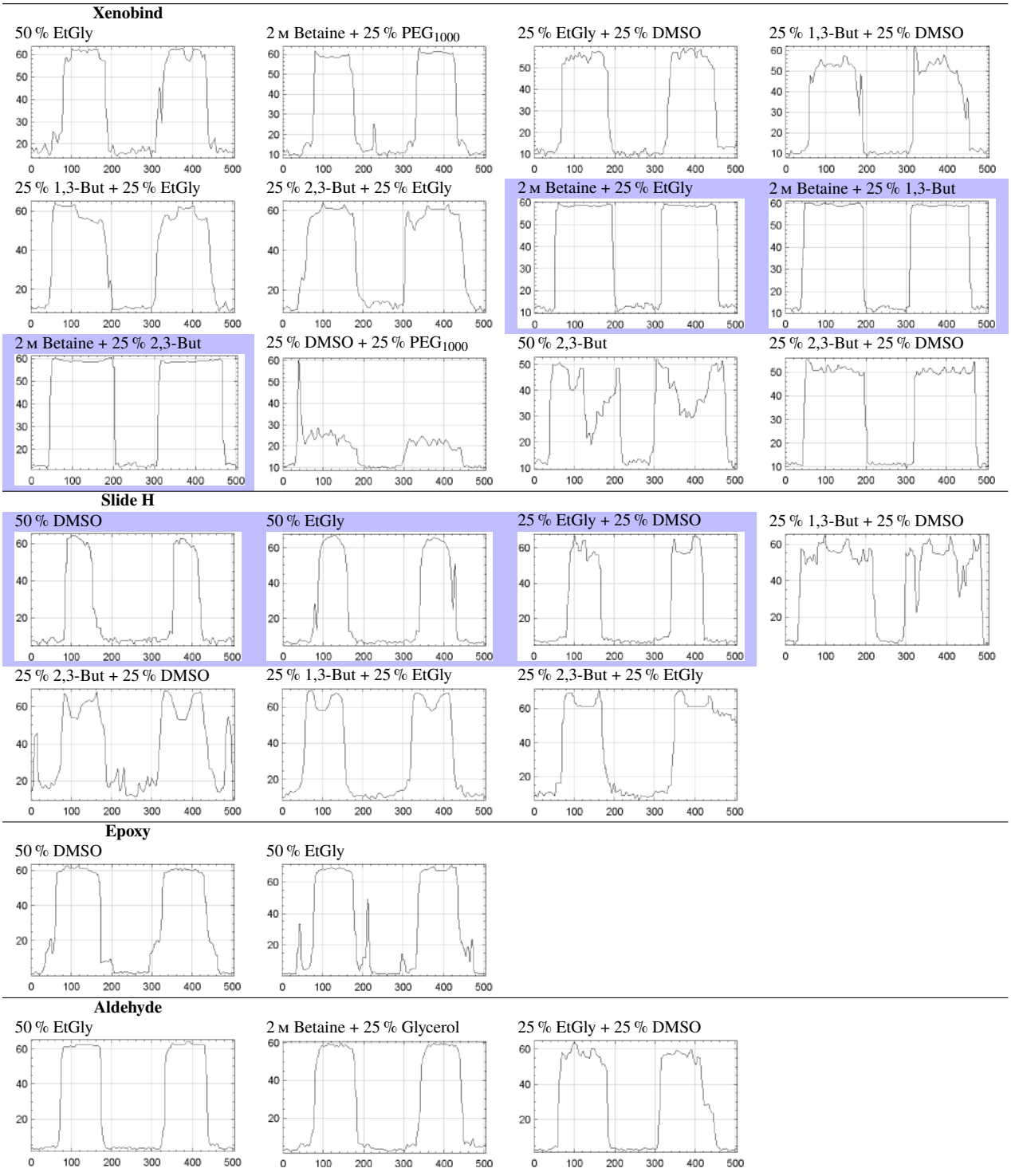

TABLE C.S2: **pH of select buffers in PBS and carbonate buffers.** Buffers with additives were prepared fresh. The pH was measured using a calibrated Fisher Scientific Accumet Basic AB15, after the reading was stable for at least 10 s.

		Prepared in	
	Printing Buffers (additives)	**PBS pH 7.4**	**Carbonate pH 9.8**
1	50 % Glycerol	6.75	9.44
2	2 M Betaine + 25 % EtGly	8.11	10.45
3	2 M Betaine + 25 % 1,3-But	8.39	10.83
4	2 M Betaine + 25 % 2,3-But	7.96	10.63
5	50 % DMSO	9.59	12.22
6	50 % EtGly	7.53	10.06
7	25 % EtGly + 25 % DMSO	8.35	10.93

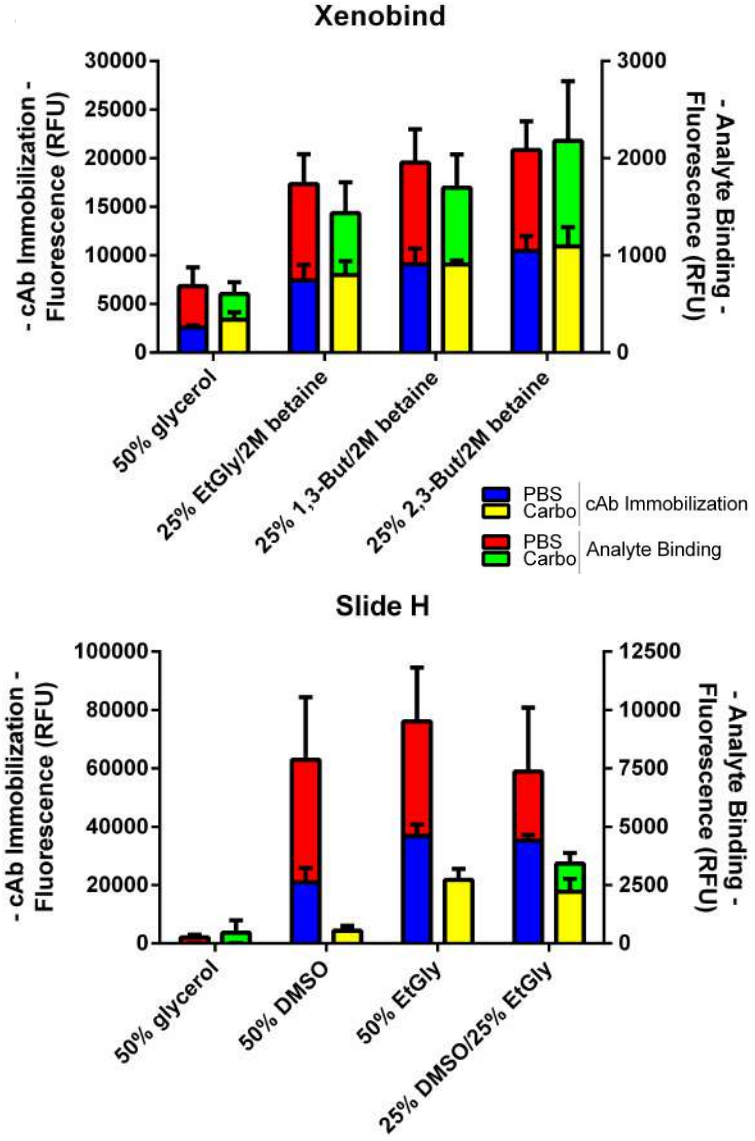

FIGURE C.S5: **Effect of pH and buffer composition on cAb immobilization and analyte binding.** The selected combinations of additives were prepared in both PBS pH 7.4 and carbonate buffer pH 9.8 and used to print fluorescently-labeled anti-goat IgG on (a) Xenobind and (b) Slide H. The slides were incubated with fluorescently-labeled goat IgG, rinsed and scanned for red and green fluorescence signals. The cAb immobilization signal (closed and gray bars) and analyte binding signals (hatched and open bars) are shown, respectively. These results show that printing with additives in PBS leads to greater signals on both surfaces.

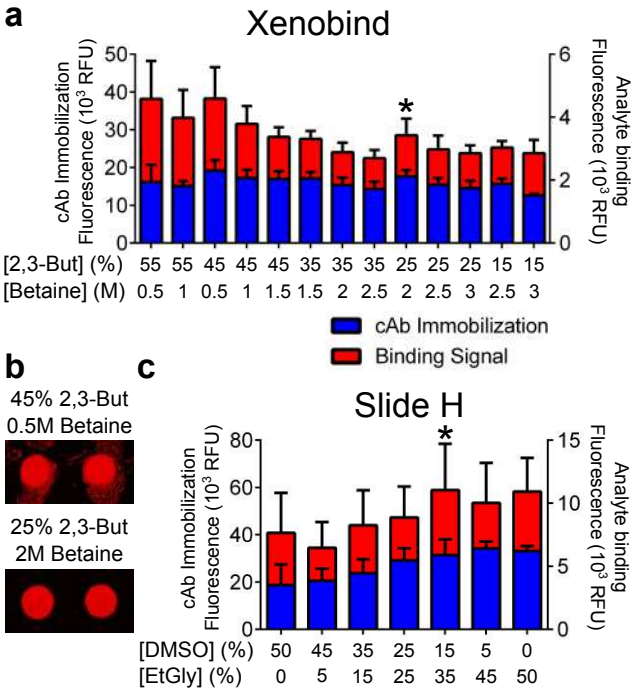

FIGURE C.S6: **Evaluation of varying additive ratios on cAb immobilization and binding signal.** (a) cAb immobilization and binding signals obtained from printing cAbs in buffers containing varying proportions of betaine and 2,3-But on Xenobind. (b) Spots printed in 45 % 2,3-But and 0.5 M betaine give the highest immobilization signal but poor spot morphology compared to spots printed in 25 % 2,3-butanediol and 2 M betaine. (c) cAb immobilization and binding signals obtained from printing cAbs in buffers containing varying proportions of DMSO and EtGly on Slide H. The optimal ratio for each buffer were selected based on binding signal and spot morphology and are indicated by (*).

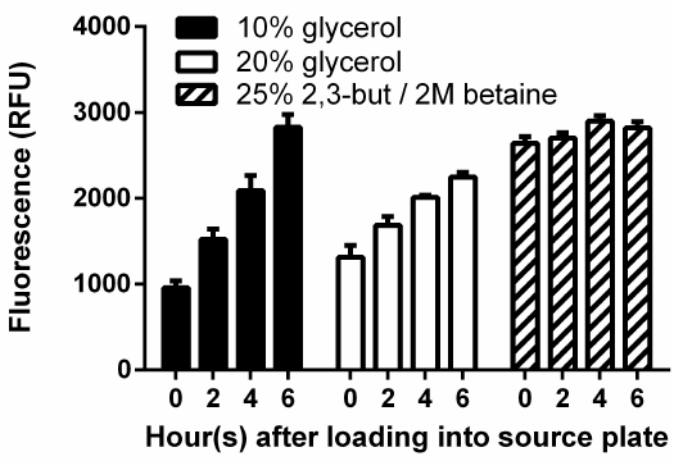

FIGURE C.S7: **Evaluation of the evaporation of printing buffers in the source well plate.** Anti-goat IgG diluted in printing buffer with different additives was loaded once in a source well plate of an inkjet (GeSim nanoplotter 2.0) printer. Every two hours, a whole Xenobind slide was printed with each buffer from the same source well. The slides were incubated with fluorescently-labeled goat IgG as analyte, whose signal intensity is shown here as binding signal. Evaporation of the buffer is expected to lead to higher concentration of cAb, leading to a greater density of antibody on the surface and higher binding signals. Results show increasing signals over time when printing with 10 % and 20 % glycerol, but no significant increase when printing the cAb in 25 % 2,3-butanediol and 2 M betaine on Xenobind. These results suggest that there is evaporation from the 10 % and 20 % glycerol, but not form the optimized buffer additive mixture.

APPENDIX D

Improving ACM reproducibility with calibration: Supplementary Material

This appendix describes the Supplementary Material to chapter 4.

Electronic Supplementary Material

Multiple fluorescent calibrants improve antibody microarrays reproducibility

Veronique Laforte, Jack Mouhanna and David Juncker

List of SI figures

List of SI tables

Supplementary Methods

SC parameters

The uncalibrated assay data was used to determine standard curve (SC) parameters that were subsequently used in the calibration computation. Two or three SCs were generated for each protein. An SC was considered valid if **a-** a well-fitted curve fit was generated from the data, **b-** the hill slope was between -3 and -0.18, and **c-** the fluorescence signal increased with an increase in Ag concentration. Additional constraints were placed on calibrated SCs, they consisted in less than 50 % variation on the hill slope and inflection parameters. The following SC parameters were determined. First the SC number was picked, and using that chosen SC, the rest of the parameters were chosen.

- *SC number:* large experiments contained two or three microarray slides with an SC rather than samples, blanks and sample replicates. To choose which SC to use for quantification on a per-protein basis, we considered whether the SC is valid and which SC had a better LOD.
- *Fluorescence threshold:* since the cAb printing buffer led to a slight fluorescence signal in the absence of any Ag or dAb, spots where no cAb were spotted could be removed by setting a fluorescence threshold that roughly corresponds to the value of the microarray background signal. In the distribution, this generally showed a bi-modal distribution where one or a very small number of values were significantly lower than the rest. By setting this fluorescence threshold, we are effectively ignoring values for which no cAb were spotted.
- *Hook number:* some SCs had a quickly saturating and then decreasing signal above a certain fluorescence value, that can be attributed to the hook effect [384]. The values that are decreasing below the maximum of the curve is of no use in standard curve fitting, therefore a hook number was used to remove one or more antigen concentrations from the standard curve for fitting after manual inspection of standard curves.
- *Dilution:* The distributions of samples and replicates compared to blanks were examined to choose a preferred dilution for sample quantification and analyzing certain SC performance parameters. Because a sample's matrix effect is greater at lower dilutions, a higher dilution was preferred but only if the lowest value of the replicates and samples were above the highest value of the blanks for the higher dilution. If that was not the case, the lower dilution was used, indicating that these proteins were found in very low quantity in the samples and more samples would be quantified by using the lower dilution.

SCs were used only when there were no unquantified replicates at the chosen dilution and for a given protein. Because most proteins had unquantified samples above the LOD, we decided to analyze the clinical data with fluorescence values. Therefore quantified sample replicates were only used to compute SC performance values.

Calibration slopes

Values for the subarray calibrant and its corresponding spot calibrant were calculated as the mean of the three replicates. If an outlier was found using Grubbs' test, the outlier was removed from the mean calculation. For the computation of calibration slopes, the data spots and their corresponding spot calibrants were considered individually. Calibration slopes were obtained using Theil-Sen estimators linear fits of four distinct groups of data:

- CSE_{local}: Calibration slopes were calculated for each local group of microarrays containing sample replicates of both low and high dilutions. The mean or median of all the local slopes was used to calculate global slopes. For algorithms involving more than one calibration slope, the global slope was used to calculate all but the last applied calibration slope to the algorithm.

- $CSE_{local\text{-}PPD}$: Calibration slopes were calculated for the local groups of microarrays containing sample replicates of the dilution determined to be optimal for each individual protein. The mean or median of all the local slopes was used to calculate global slopes. For algorithms involving more than one calibration slope, the global slope was used to calculate all but the last applied calibration slope to the algorithm.

- CSE_{global}: Calibration slopes were calculated for each sample replicate type and dilution combination across the whole experiment. Global calibration slopes were calculated from the mean of these slopes using different combinations of sample replicates type and dilution.

- $CSE_{global\text{-}PPD}$: Calibration slopes were calculated for each sample replicate type and dilution combination across the whole experiment. Global calibration slopes were calculated from the mean of the slopes using different combinations of sample replicates type at the dilution determined to be optimal for each individual protein.

The calculated global calibration slopes were then applied to uncalibrated data to obtain calibrated data using the five algorithms shown in Figure **??**.

Standard curve fitting

Standard curve fits were computed for uncalibrated data as well as each calibration algorithm. All assay values below the computed fluorescence threshold were ignored in further calculations. Standard curve values determined to show a hook effect were also ignored in the standard curve fit calculation. Standard curves were fitted using a 4-parameter logistic model and the nlsLM R function which implements the Levenberg-Marquardt fitting algorithm and requires estimating the bottom and top asymptotes of the standard curve. These were estimated using the lowest and highest values from the assay data used to calculate the standard curve. The model inflection and hill factor estimates were set to 3000 and -1, respectively. Outliers among technical replicates were ignored, and the remaining individual technical replicates was used to calculate the standard curve fit. A second round of fitting using the same function (recursively, with a maximum iteration of 500) but applying weights to the fitting algorithm was used to obtain a better-fitting curve fit with smaller residual weighted sum of squares. It essentially placed less emphasis on the points in the curve which had less accuracy. In the case that the resulting standard curve fit was invalid, the initial standard curve fit was subsequently used for assay data quantification. Likewise if the original standard curve fit from the uncalibrated data was deemed non-valid, the fit was ignored from further calculations and samples were left unquantified. The mean of technical replicates without outliers for blanks, sample replicates and samples values were interpolated in the final standard curve fit to obtain quantified data.

Standard curve fit performance

The global limit of detection (LOD) was calculated by interpolating the mean plus three standard deviations of all the blanks into the standard curve fit, while the local LODs were calculated using only blanks within a single local group of microarrays. Global reproducibility (coefficient of variation - %CV) was calculated by dividing the standard deviation by the mean of all the quantified values above LOD for a given replicate type and dilution, multiplied by 100. Local reproducibility was calculated using only the quantified values of sample replicates within a local group of microarray slides. Quantification range (QR) was calculated by interpolating the values corresponding to 5 % above the bottom and below the top of the standard curve fit and is a measure of the theoretical range of the standard curve fit in terms of antigen measurement. Similarly, the SC range with 25 % accuracy, called the accuracy range (AR) is a description of the range of antigen values for which the quantification is accurate at or below 25 % and was determined by a Taylor series approximation [228]. Residual errors from validation samples are a type of coefficient of variation and were calculated using quantified values which were above the LOD, by dividing the

mean difference between quantified values and the linear fit and the mean value of the linear fit, multiplied by 100.

Determination of combined algorithm data

For each protein, the reproducibility of quantified values for uncalibrated and calibrated data determines which data set was picked in the combined algorithm data. For proteins with a valid SC and no unquantified sample replicates at the chosen dilution, the algorithm with the best reproducibility of quantified sample replicates values was chosen. For proteins which did not have a valid SC or which had unquantified sample replicates, the standard deviation of the fluorescence values in the log domain were divided by the interquartile range of all values and these were ranked to find the best algorithm. Because some experiments contained many different types and dilutions of sample replicates, ranking was done to find the algorithm that led to the best reproducibility (of fluorescence or quantified values) across all sample replicates types and dilutions.

Supplementary Figures and Tables

The following figures and tables show additional results from the following sections:

1. Protocol modifications (Figures D.S1 to D.S13).
2. Trehalose protection of spots (Figures D.S18 to D.S25).
3. Choice of spot calibrant (Figures D.S26 to D.S36).
4. Spot calibration proof of concept (Figure D.S37).
5. Comparison of calibration algorithms (Figures D.S38to D.S50).
6. Performance of combined calibration (Figures D.S51 and D.S52 and tables D.S1 and D.S2).

Protocol Modifications

In this section, we present additional data that led to modifications to the ACM protocol in order to improve reproducibility of assays.

The use of open-channel silicon quill pins combined with long (up to 36 h) cAb and dAb printing times required to print ~48 slides can lead to variability if cAb and dAb printing buffers evaporate, changing the concentration of additives and molecules to be spotted. cAb printing buffers were already optimized to minimize evaporation and it was shown that low-evaporation

buffers prevent evaporation not only in the source well plate (where evaporation is slow) but also in the pins open-channels (where evaporation is fast) [146]. dAb printing buffers remained to be investigated and we opted for a similar strategy. We measured the evaporation of printing buffers containing 40, 45 and 50 % glycerol in PBS 1 × and found that 50 % glycerol did not evaporate (figure D.S1a). However, BSA and Tween-20 are required to avoid non-specific binding of dAb's to the slide surface, thereby increasing the signal to noise ratio of the assay. We found 1 % BSA and 0.001 % Tween-20 to be sufficient in preventing non-specific binding of dAbs, and a printing buffer containing only BSA and Tween-20 at these concentrations in PBS 1 × evaporated nearly as much as PBS 1 × by itself (figure D.S1b). When BSA and Tween-20 were added to 40, 45, and 50 % glycerol in PBS 1 ×, we found that the printing buffer with 50 % glycerol completely filled the pins double-channels, and swelled to the point of bursting the stop valve (figure D.S1c). On the other hand, the buffer containing 40 % glycerol failed to completely fill the double channels. The dAb printing buffer containing 45 % glycerol completely filled the pins double channels, and showed minimal evaporation that is less than the cAb printing buffer used on Xenobind (consisting of 2 M betaine and 25 % 2,3-butanediol, see figure D.S1a), and therefore was used for printing all dAbs in subsequent experiments.

The next step in assessing sources of variability in our assay was to verify the absence of contamination between source wells during cAb and dAb printing, as well as during pin washing and antigen incubation. Figure D.S2 shows no contamination during pin washing or antigen incubation, however we found that plasma-treated source well plates led to contamination of cAbs by allowing the printing buffer to leak into adjacent source plate wells. This was not a problem with the dAb printing buffer where plasma treatment is used to help manually load small volumes (10-15 µL) of viscous printing buffer in small, deep well. Therefore we used a non-plasma treated source well plate for cAb printing, and a plasma-treated source well plate for dAb printing. While we did not test if the contamination also occured with cAb printing buffers containing 50 % glycerol and 0.005 % Tween-20, we did not experience problems loading a non plasma-treated source plate with this cAb printing buffer.

Having confirmed that there is no contamination of reagents in the assay, we set out to quickly compare different slides surfaces, since variability in the chemical coating of slides can translate directly and even be amplified into variability in the assay. Slide surfaces variability in the amount of chemicals deposited at the surface can lead to different quantities of molecules bound to the surface, as well as different percentage of molecules whose function is preserved, in the case of antibodies their ability to bind their target molecule. It is therefore very important to choose a slide that has low surface variability. We first scanned Xenobind, ArrayIt SuperNHS, SuperAldehyde, SuperAldehyde2 and four different batches of PolyAn 2D Aldehyde slides immediately after unpacking

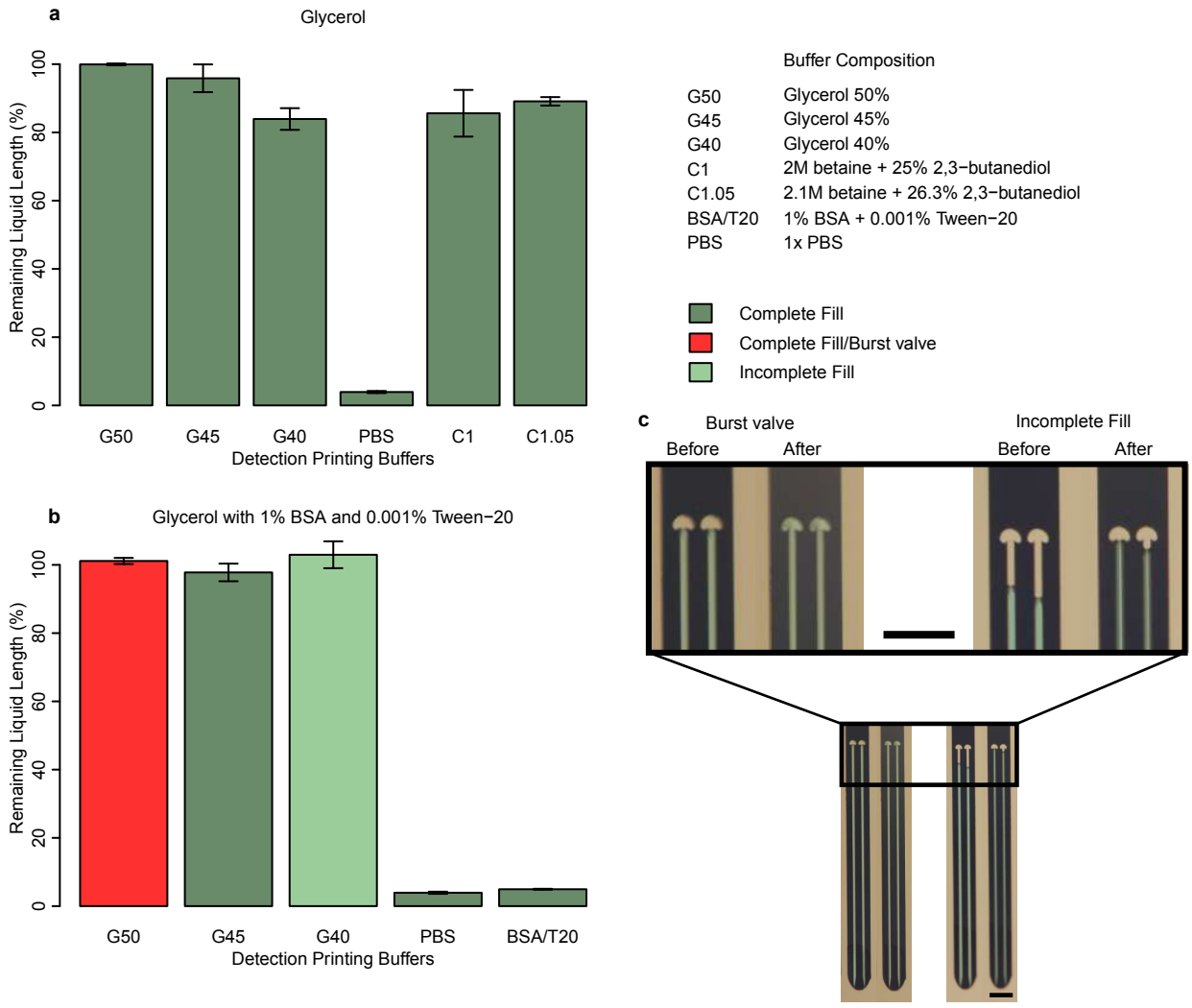

FIGURE D.S1: **Evaporation of detection printing buffers.** Silicon pins that were plasma-treated with an open flame were filled with buffers containing various additives **a** without and **b** with 1 % BSA and 0.001 % Tween-20 and blue food dye. The filled pins were incubated at 65 % relative humidity at room temperature, and pictures were taken every minute for 15 minutes. Remaining liquid length is the ratio of the length of liquid after and before evaporation. Buffer containing 50 % glycerol does not evaporate, but adding 1 % BSA and 0.001 % Tween-20 to 50 % glycerol leads to swelling of the buffer as it absorbs water from the air, thereby bursting the pin's retention valve (**b** and **c**, left). Instead, buffers containing 45 % or 40 % glycerol do not evaporate nor swell with the addition of 1 % BSA and 0.001 % Tween-20, however the buffer containing 40 % slowly and incompletely fills the pin (**b** and **c**, right). Black size markers are 1 mm.

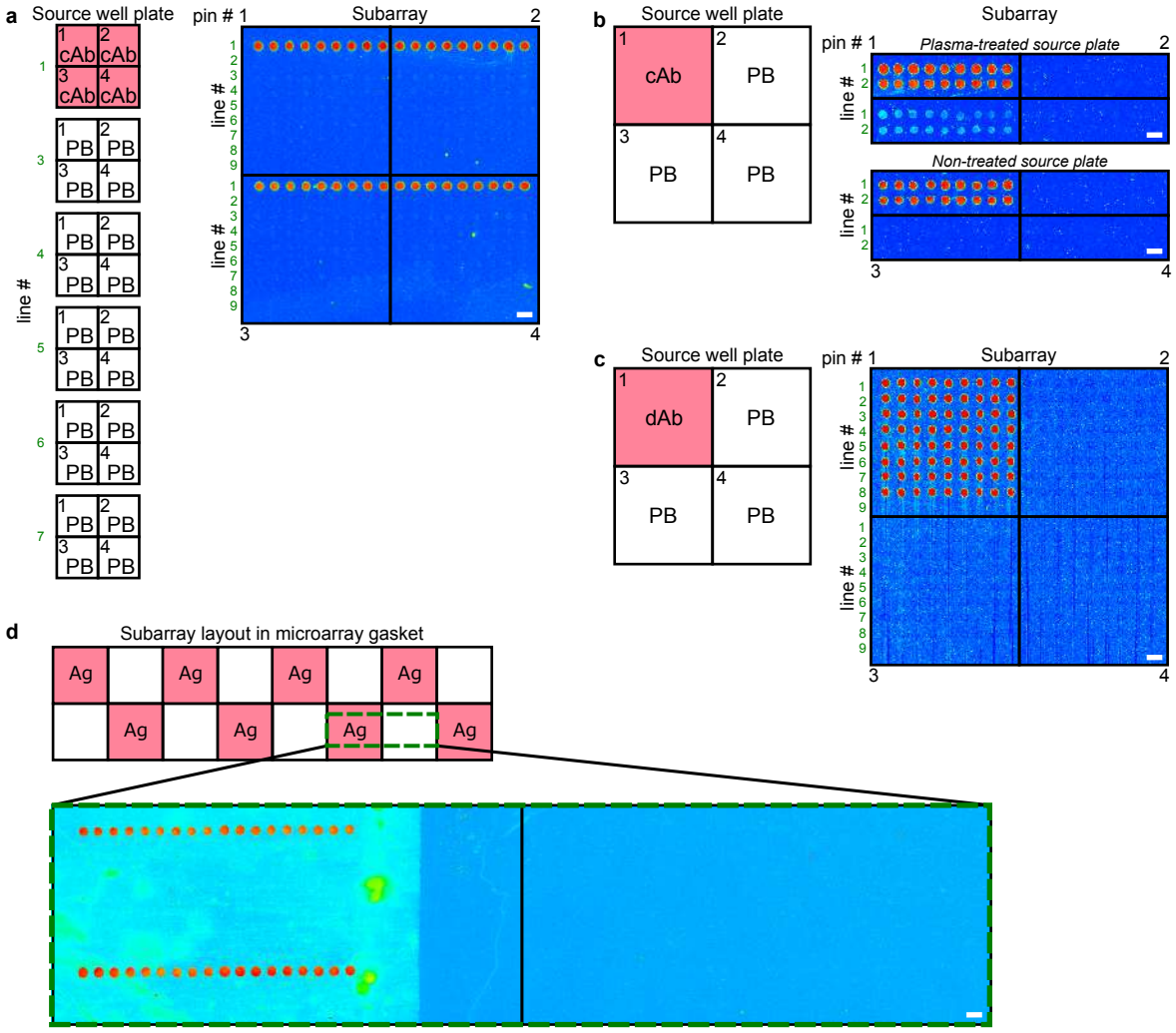

FIGURE D.S2: **Sources of contamination during spotting.** Investigation of **a** pin carry-over, contaminations in the **b** cAb and **c** dAb source well plates and **d** in the gasket. **a** Ang1 cAb (line 1) or printing buffer (PB: lines 3 to 7) were spotted. **b** Ang1 cAb (well/pin 1) and cAb printing buffer (wells/pins 2-4) were spotted on line 1, then pins were dipped again to spot on line 2. **c** Ang1 cAbs were spotted on lines 1-8 with all four pins. Ang1 Ag was incubated after blocking, and Ang1 dAb were spotted only with well/pin 1, with dAb printing buffer being printed in wells/pins 2-4. **d** Ang1 cAbs were spotted on line 1 in all four pins. Ag was incubated in a checkered pattern in the gasket, with incubation buffer in the remaining wells. Two adjacent subarrays with (left) and without Ag (right) are shown. White size markers are 250 µm. The only source of contamination found is in the cAb source well plate when it is plasma-treated. Omitting the plasma treatment resolved this source of contamination. Source well plates in **a** and **d** were not plasma-treated, while the source in **c** was plasma-treated.

to investigate both the variability and the amount of fluorescence backgrounds in both red and green channels. Figure D.S3a shows that ArrayIt slides have very low intra-slide variability and fluorescence backgrounds compared to Xenobind and PolyAn 2D Aldehyde slides. Xenobind showed similar fluorescence background and variability as PolyAn 2D Aldehyde, however it showed less inter-slide variability than PolyAn 2D Aldehyde when the fluorescence backgrounds was measured on four slides (figure D.S3b).

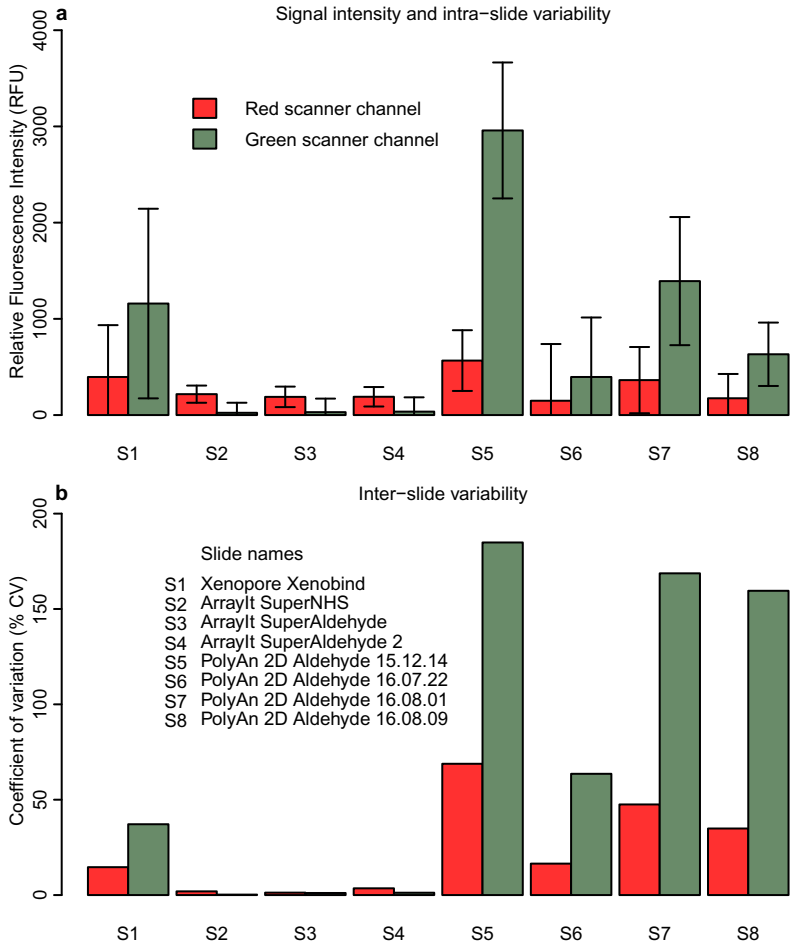

FIGURE D.S3: **Fluorescence background on eight slide types.** Four slides of eight different types were scanned dry without any treatment, except for Xenobind slides which were washed prior to scanning. **a** Signal intensity of the background and intra-slide variability (error bars) as well as **b** inter-slide variability are reported here.

While having low fluorescence backgrounds is important, the signal to noise ratio and assay signal variability of different slides is more important. We selected six matched antibody pairs (Ang1, HGF, HGF-R, MCP4, THBS-1 and VEGFR2) to test in multiplexed sandwich assays (MSA)

on the different slides. Because it does not contain a dAb printing step, instead incubating a mixture of dAbs, MSA assays have better overall reproducibility. We selected a concentration of 0.2 µg/mL for each dAb in the mixture and an incubation of 20 min to minimize the volume of costly antigen used, to avoid loss of weakly-bound antigens and obtain an acceptable signal to noise ratio (figure D.S4). In a first step we determined the amount of cross-reactivity between the six antibody pairs and found that there is significant cross-reactivity between HGF and HGF-R, as well as between the Ang1 dAb and THBS-1 and HGF (figure D.S5). For these reasons we decided to test the eight different slides with only four proteins (without HGF and THBS-1). We spotted the four cAbs and incubated slides with standard curves along replicates samples at dilutions 1:3 and 1:50 on four slides per slide type. Signal intensity for the four assay and their corresponding variability are shown for each protein in figures D.S7 to D.S10 with the average shown in figure D.S6. As can be seen in graphs D.S6a and D.S6b, after an MSA assay the background fluorescence of ArrayIt slides was actually greater than that of Xenobind and PolyAn 2D Aldehyde, but the background fluorescence variability of Xenobind, ArrayIt SuperAldehyde and SuperAldehyde2 was better than that of ArrayIt SuperNHS and all PolyAn 2D Aldehyde batches. We measured the variability in the four protein assays and found Xenobind and PolyAn 2D Aldehyde slides to perform best at around 20 %CV. Looking at the reproducibility of individual proteins, we noticed that assay reproducibility varied the most for MCP4 (40-100 % for the different replicates and blanks, see figure D.S9).

The low and reproducible fluorescent background of ArrayIt slides did not result in low and reproducible backgrounds after the assay, which suggests that variability in the chemical coating of ArrayIt slides was not visible by scanning slides with our scanner. On the other hand, higher variability in Xenobind and PolyAn 2D Aldehyde slides fluorescent background before the assay also resulted in higher variability in the fluorescent backgrounds and reproducibility of assays performed on those slides, suggesting that scanning these slides before the assay could serve as a quality assurance step.

The ACM protocol having been optimized for Xenobind slides, it was not surprising to see that the signal intensity of assays was very low for ArrayIt SuperNHS slides, notably because ArrayIt recommends printing antibodies on their proprietary Protein Printing Buffer. ArrayIt SuperAldehyde and SuperAldehyde2 gave similar signal intensities but slightly worse reproducibility as Xenobind and PolyAn 2D Aldehyde when printing with 2 M betaine / 25 % 2,3-butanediol, suggesting that this cAb printing buffer performs well on all slides based on a reactive aldehyde binding reaction.

To find out if the cAb printing buffer has an effect on the reproducibility of MCP4 assays, we printed the four proteins on eight Xenobind and PolyAn 2D Aldehyde slides using eight different cAb

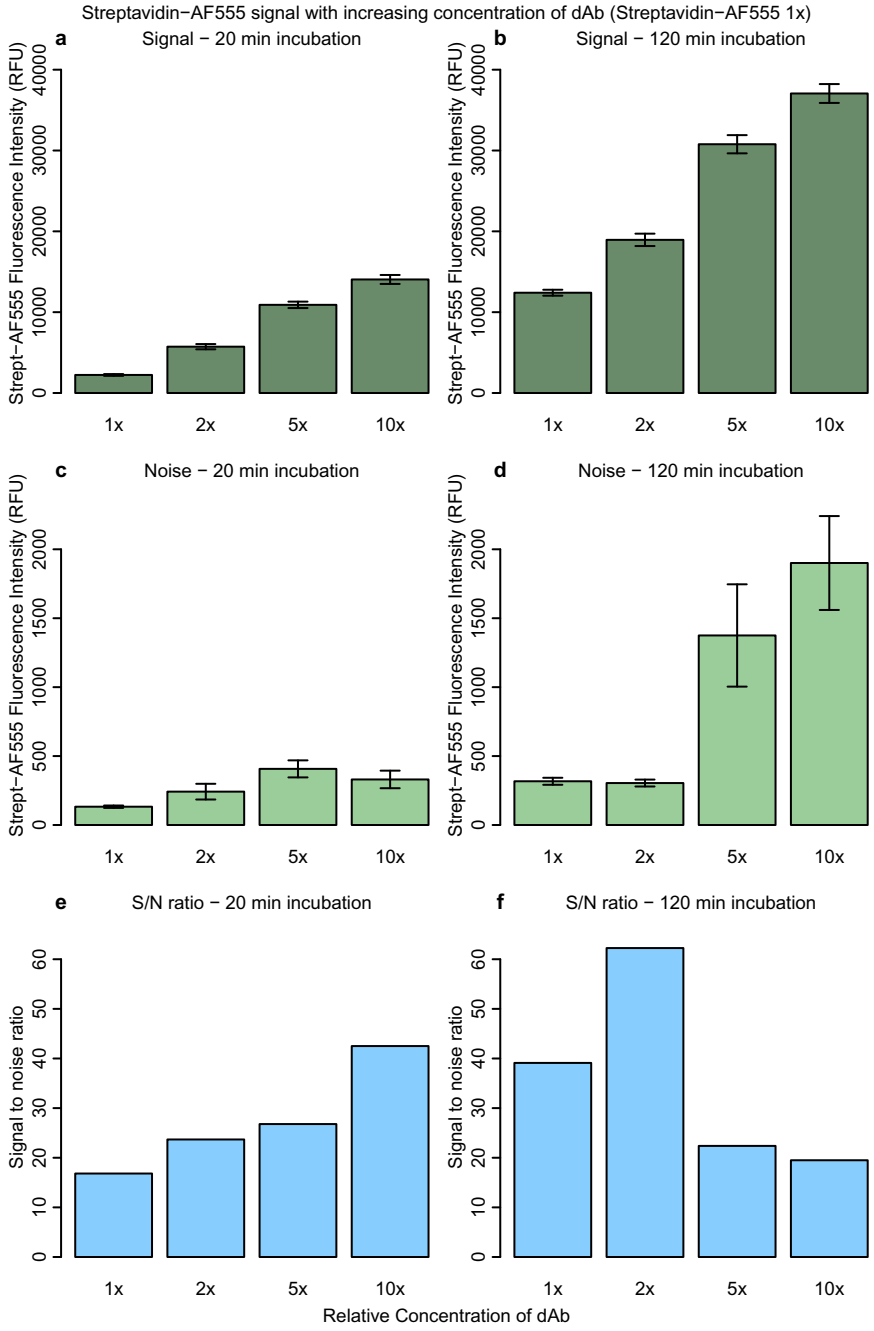

FIGURE D.S4: **Effect of dAb concentration on Strept-AF555 signal.** cAbs against 6 proteins (Ang1, HGF, HGF-R, MCP4, THBS-1, VEGFR2) were spotted onto two microarrays. An Ag mixture was incubated, followed by a dAb mixture at four different concentrations ($1\times = 0.1\,\mu g/mL$). As a second step, GAM-AF647 and Strept-AF555 were applied together at four different concentrations ($1\times = 0.1$ and $0.5\,\mu g/mL$, respectively) for either (**a, c, e**) 20 or (**b, d, f**) 120 min. Signal from GAM-AF647 (**a, b**) is shown as well as the green channel background (**c, d**) which are used to calculate a signal to noise ratio (**e, f**). All graphs are for Strept-AF555 at a concentration of $0.5\,\mu g/mL$. A dAb concentration of up to $1.0\,\mu g/mL$ is recommended with incubation time of 20 min to avoid antigen loss.

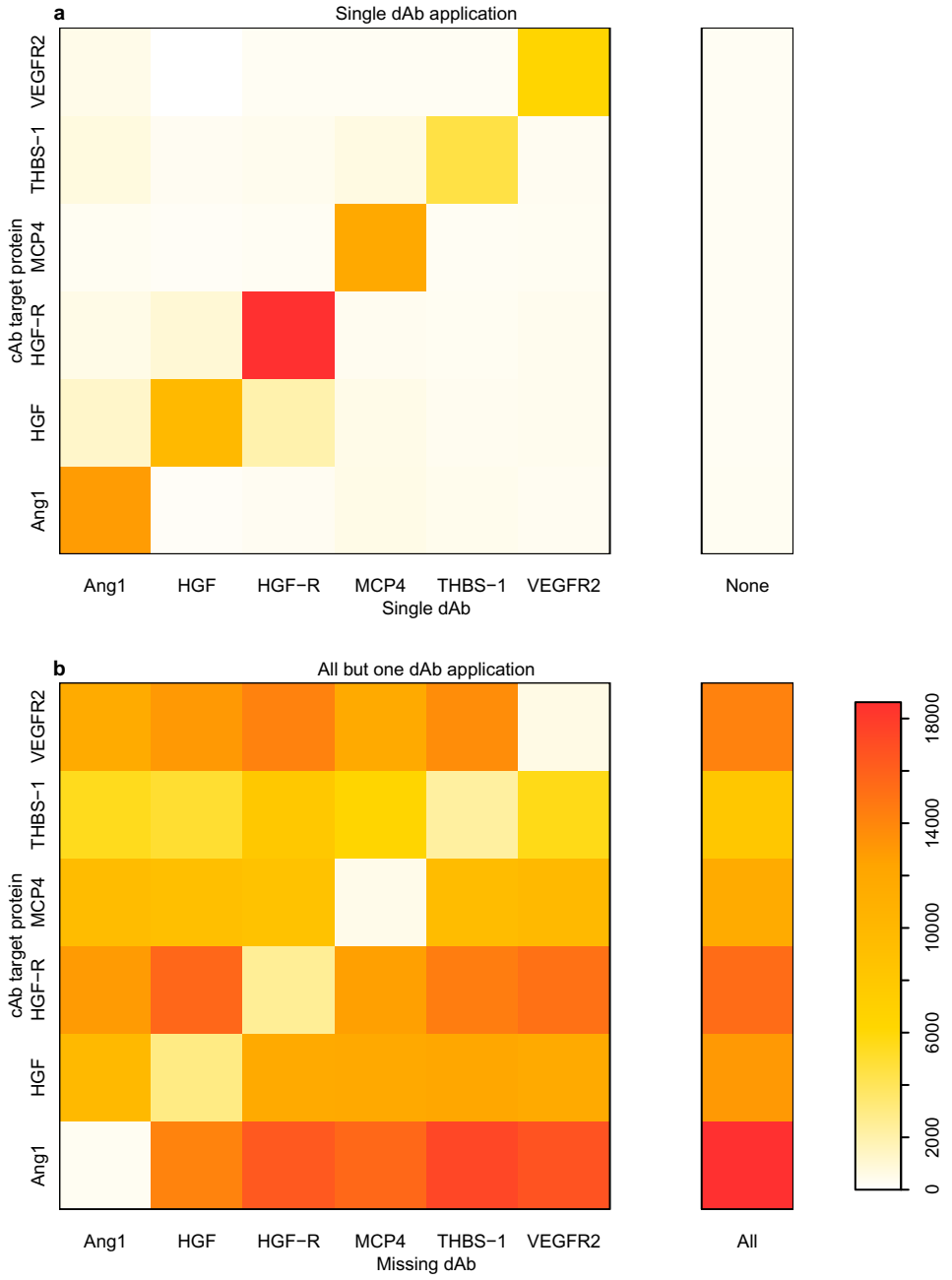

FIGURE D.S5: **Cross-reactivity in a 6-plex assay.** cAbs for 6 different proteins were spotted onto microarrays. All Ags were incubated, and then either a single dAb (**a**) or a mixture of all dAbs but one (**b**) were incubated on the microarray. A complete lack of cross-reactivity would show a single dark diagonal line on white background in **a** the reverse in **b**. Cross-reactivity is seen between HGF and HGF-R, as well as between the Ang1 dAb and THBS-1 and HGF.

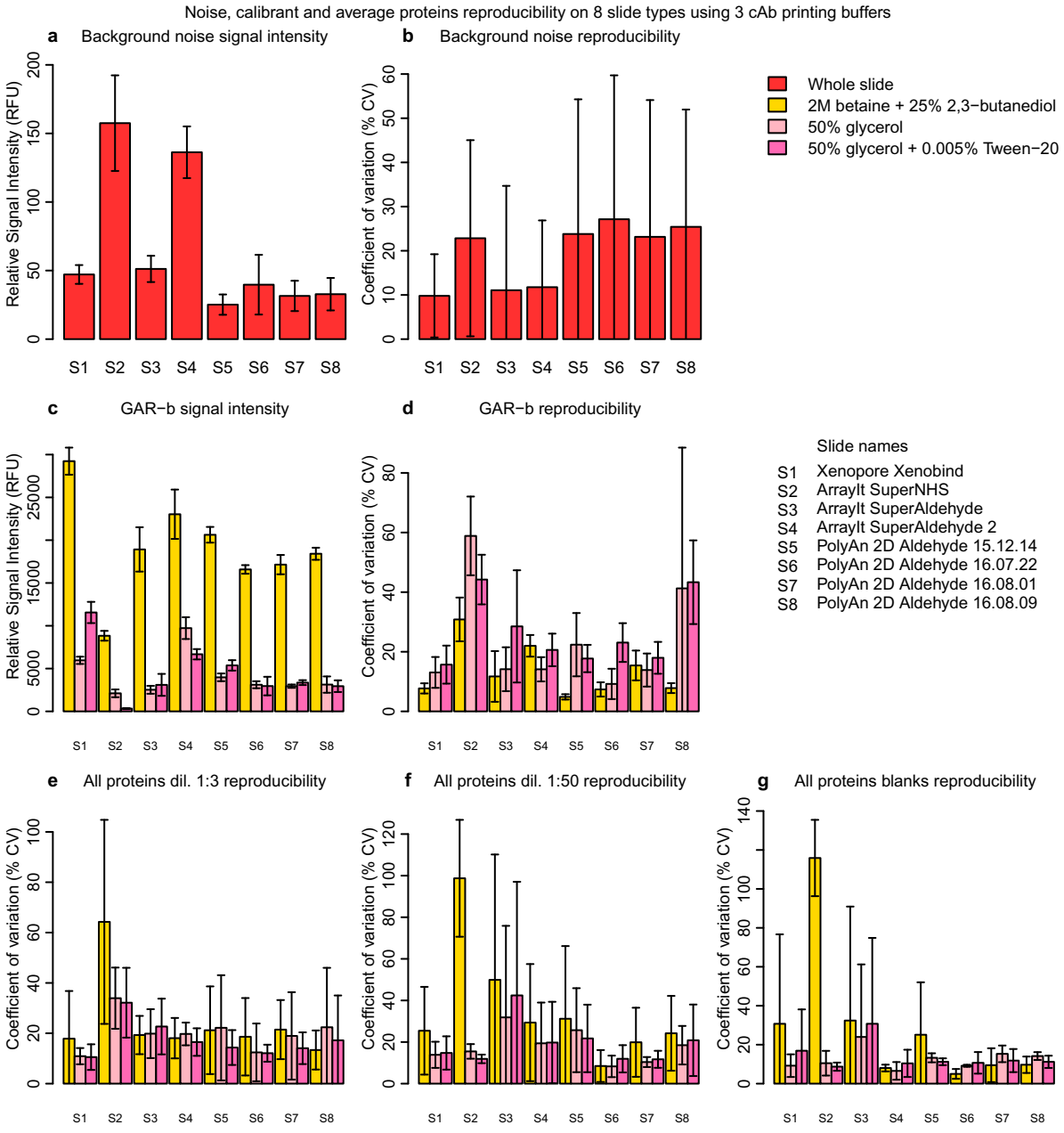

FIGURE D.S6: **Background, calibrant and average proteins on different slides and cAb printing buffer.** cAbs for four proteins and GAR-b were spotted with spot calibrant (BSA-AF555) on eight slide types using three different cAb printing buffers. Two different replicates (pnSerum1 and pnSerum2) were incubated at 1:3 and 1:50, as well as blanks. Here the signal intensity (**a, c**) and reproducibility values of background noise (**b**, after full assay) and the subarray calibrant GAR-b (**d**) are shown. The average reproducibility for the four proteins are shown in samples diluted 1:3 (**e**) and 1:50 (**f**) and blanks in (**g**).

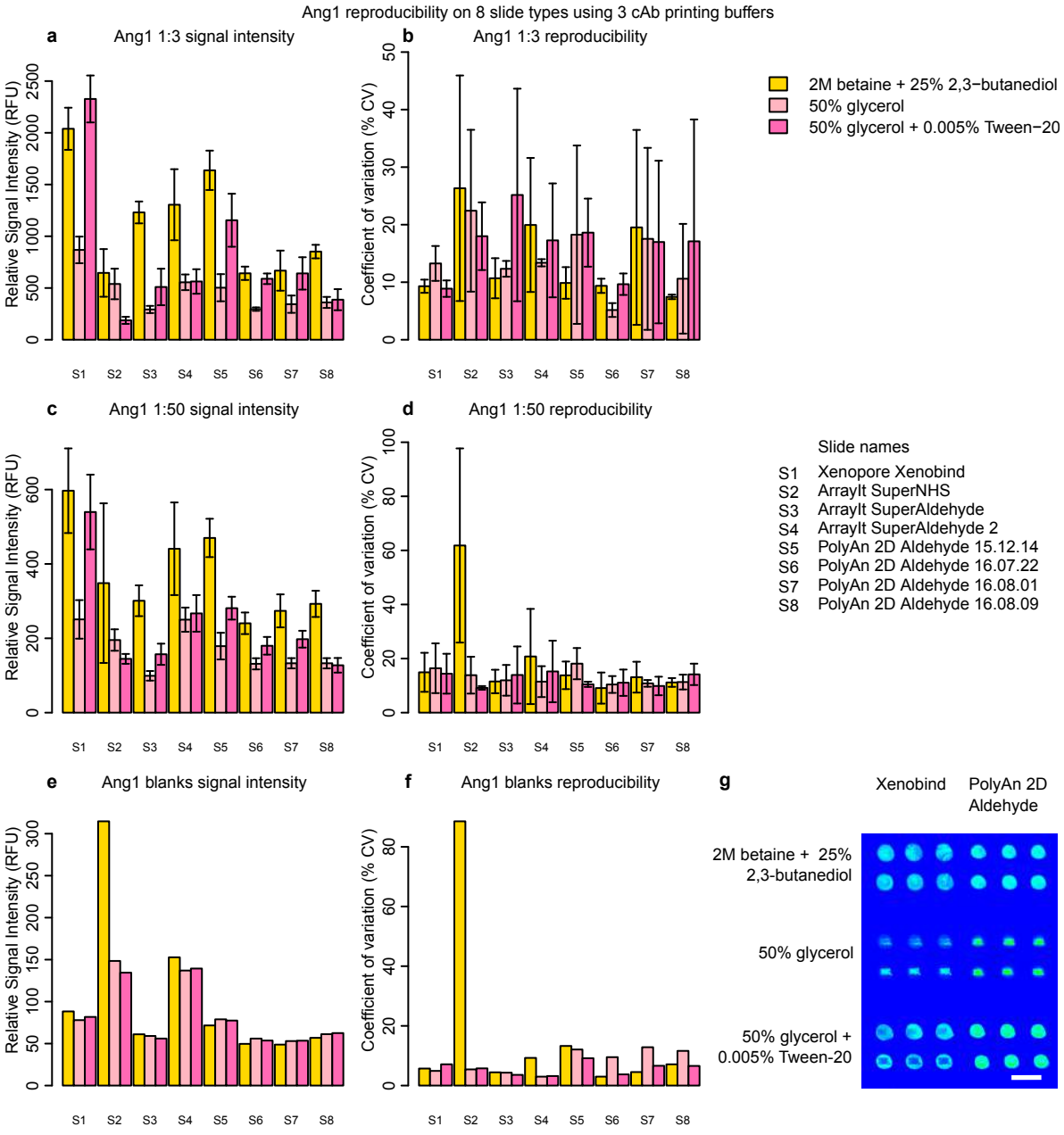

FIGURE D.S7: **Reproducibility and signal intensity of Ang1 on 8 different slides and 3 cAb printing buffer.** Ang1 cAbs were spotted with spot calibrant (BSA-AF555), on eight slide types using three different cAb printing buffers. Two different replicates (pnSerum1 and pnSerum2) were incubated at 1:3 and 1:50, as well as blanks. The signal intensity (**a, c, e**) and reproducibility (**b, d, f**) values of Ang1 blanks (**e, f**) and samples at dilution 1:3 (**a, b**) and 1:50 (**c, d**) are shown. In **g** pictures of spots using the three different printing buffers is shown for Xenobind and PolyAn 2D Aldehyde, with different image contrasts to best show spot morphology. White size marker is 250 µm.

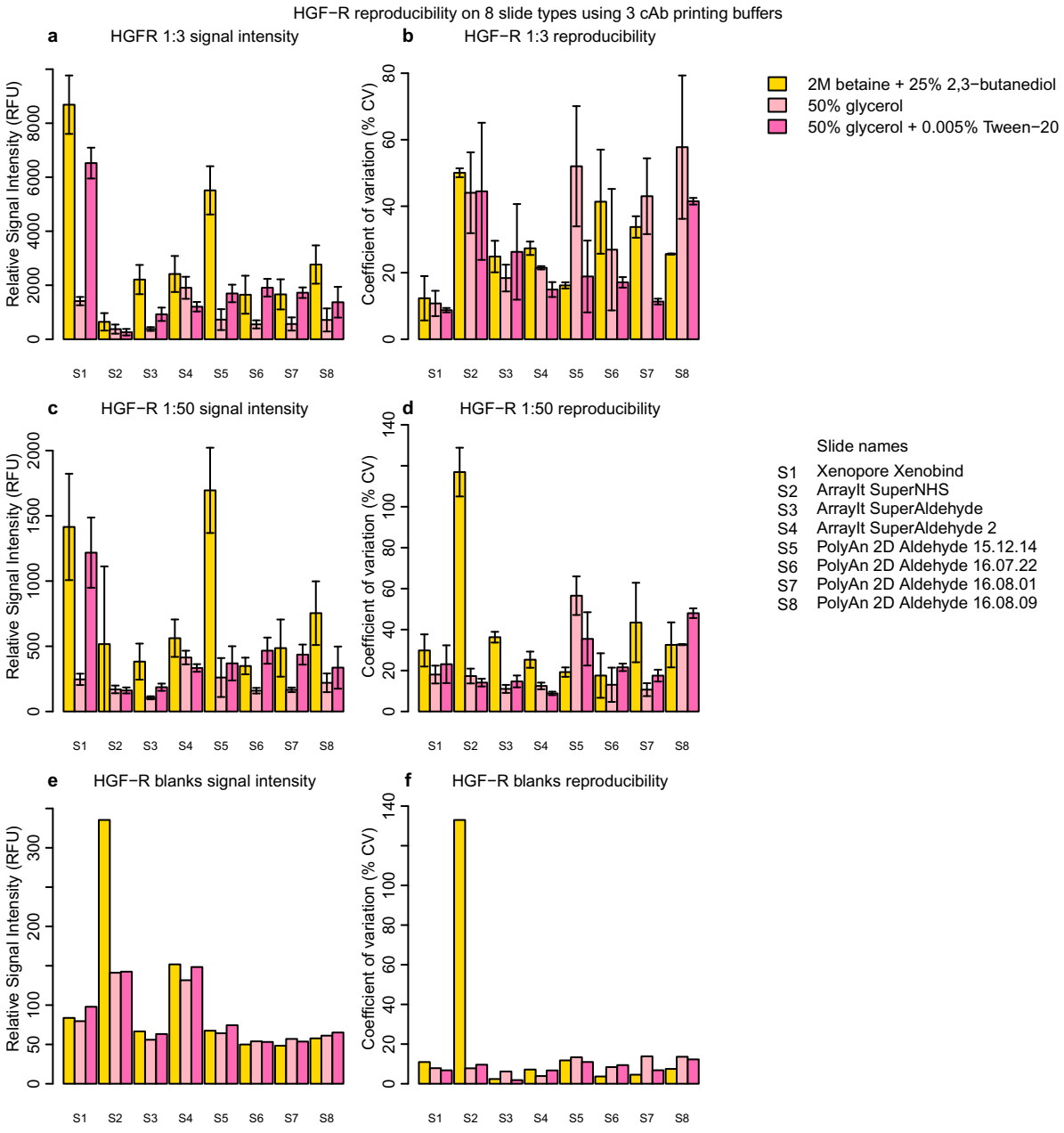

FIGURE D.S8: **Reproducibility and signal intensity of HGF-R on 8 different slides and 3 cAb printing buffer.** HGF-R cAbs were spotted with spot calibrant (BSA-AF555), on eight slide types using three different cAb printing buffers. Two different replicates (pnSerum1 and pnSerum2) were incubated at 1:3 and 1:50, as well as blanks. The signal intensity (**a, c, e**) and reproducibility (**b, d, f**) values of HGF-R blanks (**e, f**) and samples at dilution 1:3 (**a, b**) and 1:50 (**c, d**) are shown.

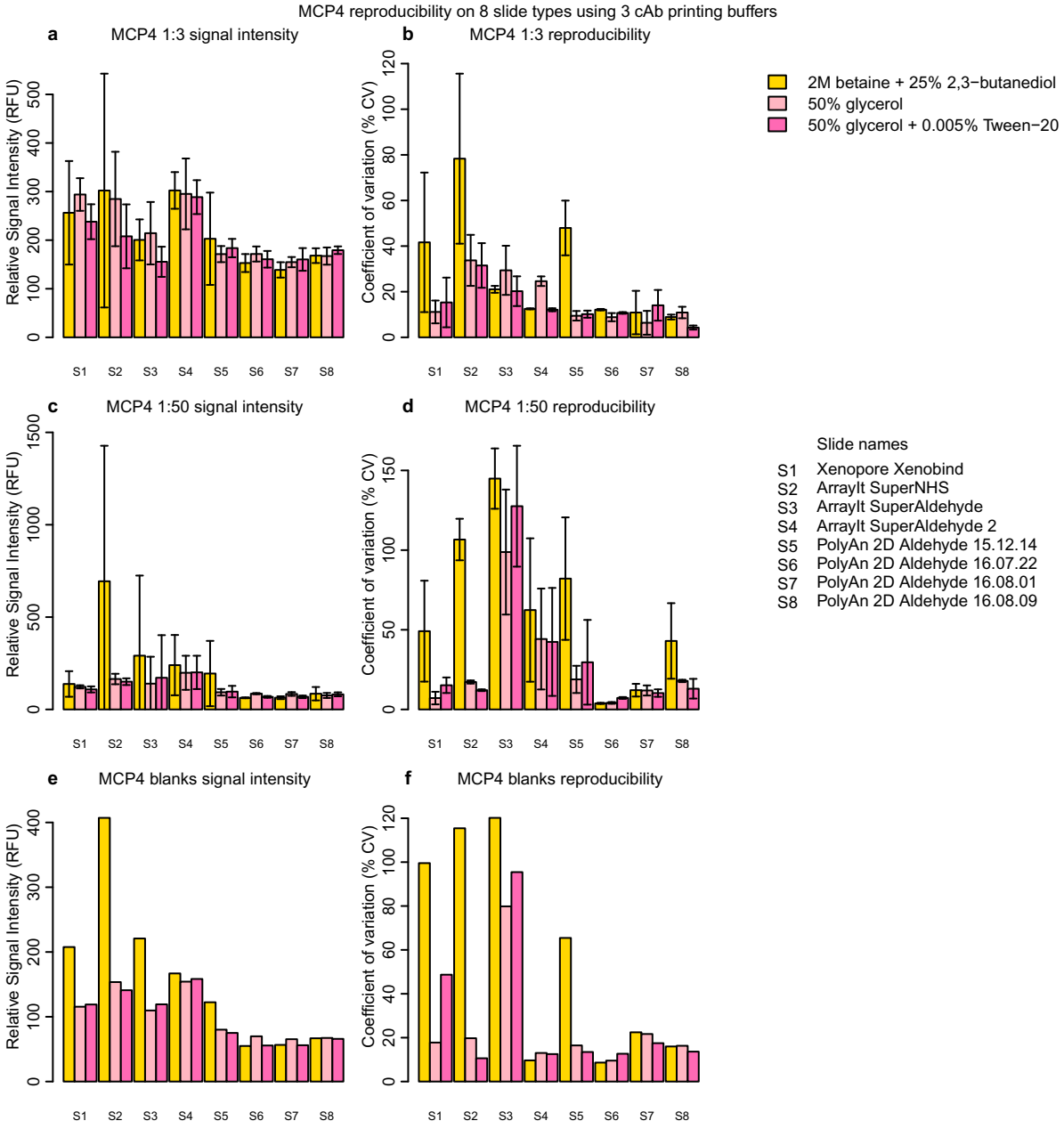

FIGURE D.S9: **Reproducibility and signal intensity of MCP4 on 8 different slides and 3 cAb printing buffer.** MCP4 cAbs were spotted with spot calibrant (BSA-AF555), on eight slide types using three different cAb printing buffers. Two different replicates (pnSerum1 and pnSerum2) were incubated at 1:3 and 1:50, as well as blanks. The signal intensity (**a, c, e**) and reproducibility (**b, d, f**) values of MCP4 blanks (**e, f**) and samples at dilution 1:3 (**a, b**) and 1:50 (**c, d**) are shown.

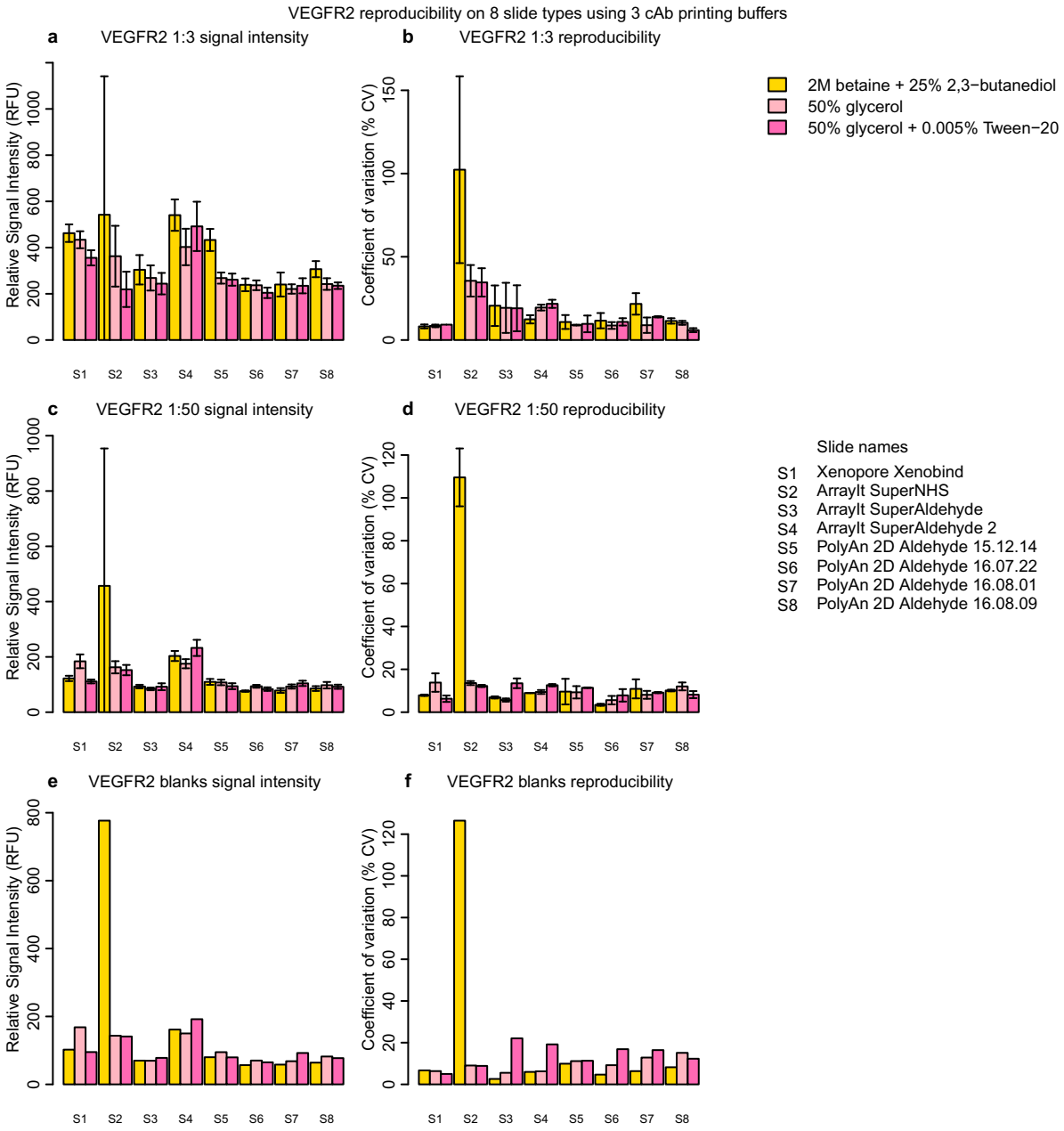

FIGURE D.S10: **Reproducibility and signal intensity of VEGFR2 on 8 different slides and 3 cAb printing buffer.** VEGFR2 cAbs were spotted with spot calibrant (BSA-AF555), on eight slide types using three different cAb printing buffers. Two different replicates (pnSerum1 and pnSerum2) were incubated at 1:3 and 1:50, as well as blanks. The signal intensity (**a, c, e**) and reproducibility (**b, d, f**) values of VEGFR2 blanks (**e, f**) and samples at dilution 1:3 (**a, b**) and 1:50 (**c, d**) are shown.

printing buffers on each slide (figures D.S11 and D.S12). The cAb printing buffers used contained various concentrations of betaine and 2,3-butanediol with the addition of various concentrations of glycerol and trehalose for which the total concentration would still prevent buffer evaporation during printing. We also tested 50 % glycerol as a control, and surprisingly found that the average reproducibility of proteins was better and more consistent with 50 % glycerol compared to any other printing buffer containing betaine and 2,3-butanediol (figure D.S11e). On PolyAn 2D Aldehyde, this improvement was not seen, as the reproducibility of assays printed in 50 % glycerol was similar to that of assays printed in 2 M betaine / 25 % 2,3-butanediol (figure D.S12e). In both cases, the signal intensity of HGF-R was decreased when printed in 50 % glycerol, but the three other proteins signal intensity did not change. Pictures of spots printed in 50 % glycerol (figure D.S7g) shows that much less liquid was delivered to the surface from the pins as shown by small, square footprints. Therefore we added 0.005 % Tween-20 to decrease the surface tension [165, 235]. As can be seen in this figure, spots from assays printed in 50 % glycerol with 0.005 % Tween-20 regained their round morphology, suggesting that more liquid (and quantity) of cAb were delivered to the surface at each spot. Figures D.S6 to D.S10 show that generally, assays printed in 50 % glycerol with 0.001 % Tween-20 led to better assay reproducibility on all slide types, but not always every protein. The largest improvement in reproducibility was seen in MCP-4 on both Xenobind and two of the four batches of PolyAn 2D Aldehyde slides.

Since printing for both cAbs in large-scale experiments takes upwards of 36 h, it was important to verify that the microarray slide surface is stable at room temperature and 65 % relative humidity (RH) during those two steps. We spotted GAR-AF647 and GAR-AF555 on Xenobind slides at various times and let them incubate for 24 h following the last spotting. As figure D.S13 demonstrates, we found no difference in binding of GAR-AF555 and GAR-AF647 to Xenobind slides that was just put in the Nanoplotter chamber and after staying for 24 h in the chamber at room temperature and 65 % RH.

To determine the concentration and incubation time for Strept-AF555, we varied its concentration (0.1, 0.2, 0.5 and 1 µg/mL) in a MSA with the four proteins used previously and found that while a concentration of 0.1 µg/mL incubated for 20 min or 2 h led to a greater signal to noise ratio (figure D.S14), in large experiments an incubation of 20 min was simply not feasible since the solution is applied by hand to over a thousand wells. Therefore a concentration of 0.5 µg/mL and an incubation time of 1 h was selected to minimize antigen loss and as a trade-off between making sure that the quantity of Strept-AF555 is not limiting and maximizing signal to noise ratio.

Having addressed variability at the surface, the next step was to determine the amount of time required to incubate cAbs and dAbs on the microarray slides before moving on to the next step in the ACM protocol. We printed the four cAbs as well as GAR-AF647 and GAR-AF555 on Xenobind

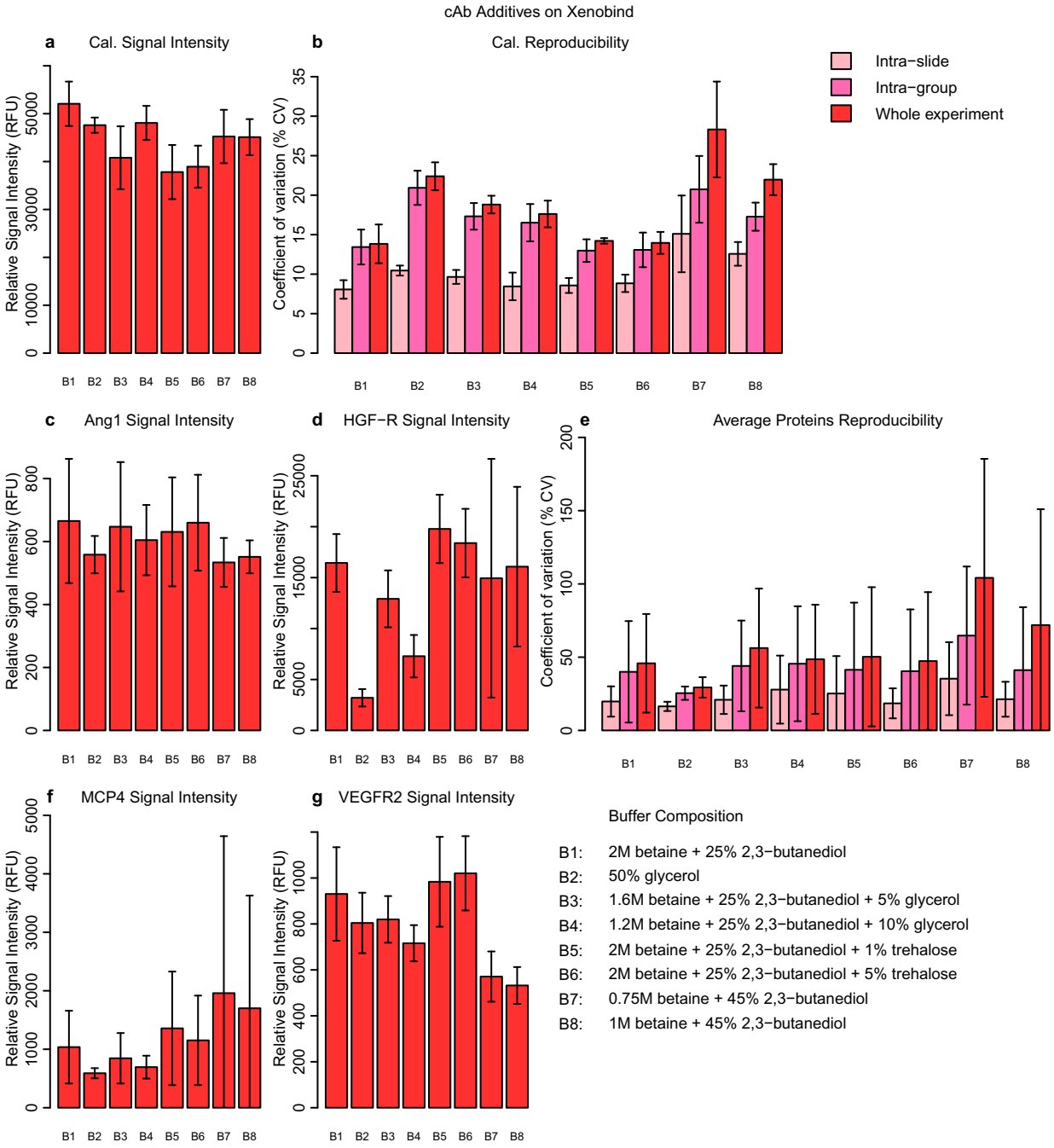

FIGURE D.S11: **cAb printing buffer additives on Xenobind.** cAbs for four proteins were spotted on a Xenobind slide with a spot calibrant (BSA-AF555) in eight different printing buffers. The signal intensity for the calibrant (**a**) and its reproducibility (**b**) within a slide, within a group (4 slides) and for the whole experiment (8 slides) were calculated. The signal intensity (**c, d, f, g**) for each protein and average reproducibility (**e**) also shown.

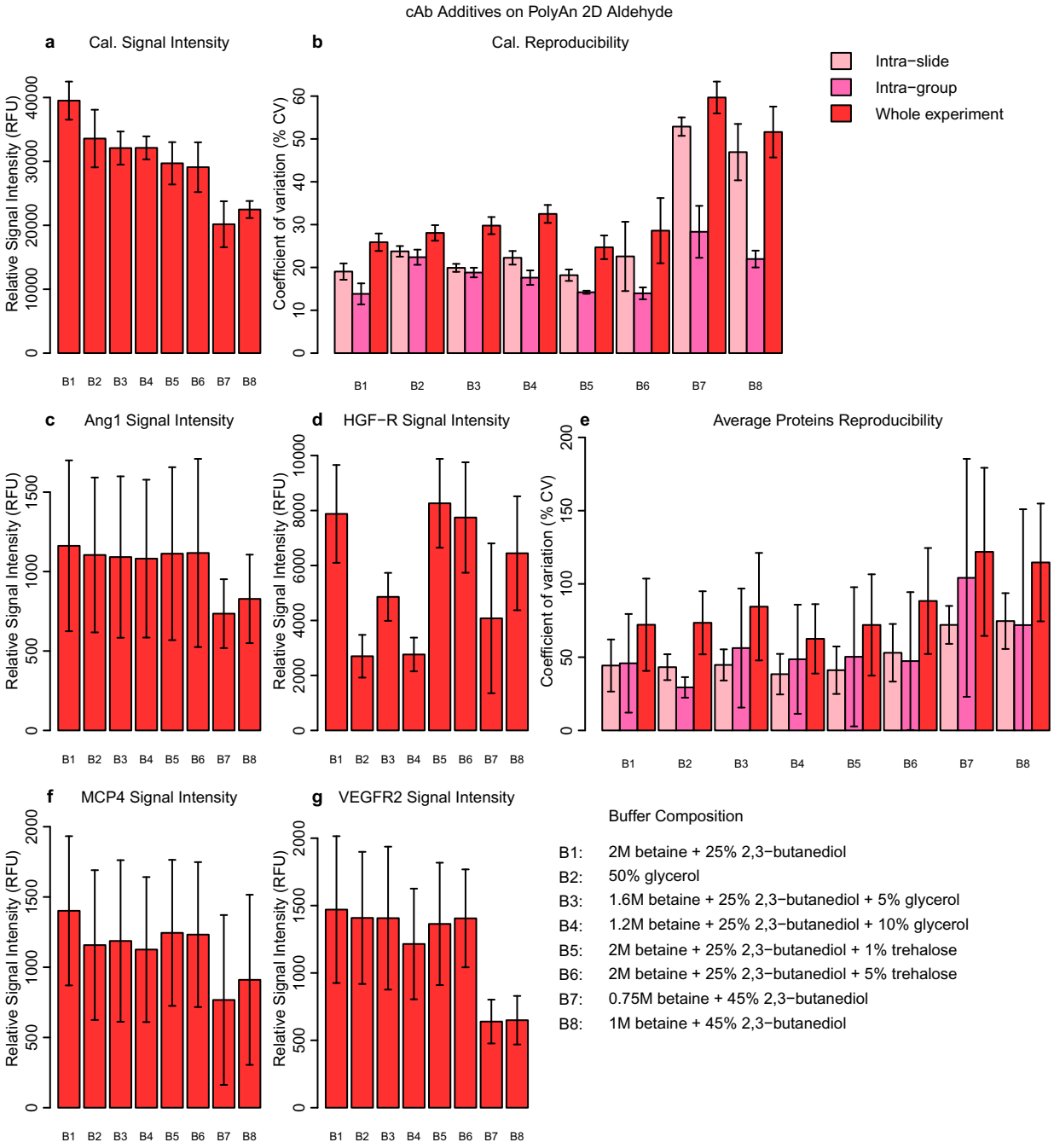

FIGURE D.S12: **cAb printing buffer additives on PolyAn 2D Aldehyde.** cAbs for four proteins were spotted on a PolyAn 2D Aldehyde slide with a spot calibrant (BSA-AF555) in eight different printing buffers. The signal intensity for the calibrant (**a**) and its reproducibility (**b**) within a slide, within a group (4 slides) and for the whole experiment (8 slides) were calculated. The signal intensity (**c, d, f, g**) for each protein and average reproducibility (**e**) also shown.

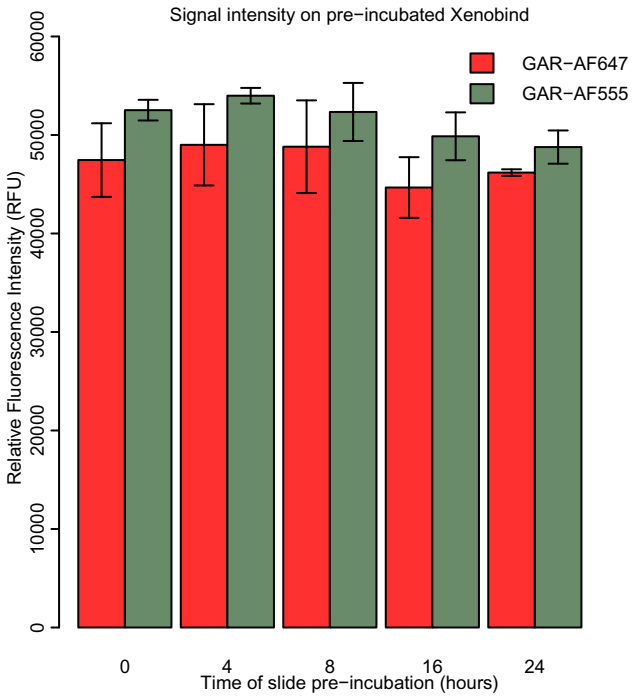

FIGURE D.S13: **Xenobind surface stability in high humidity.** Xenobind slides were pre-incubated in the nanoplotter chamber for different amounts of time before being spotted with GAR-AF555 and GAR-AF647. Slides were then incubated overnight. The Xenobind surface binding capacity is stable while it remains in the nanoplotter at room temperature and high humidity (65 %RH).

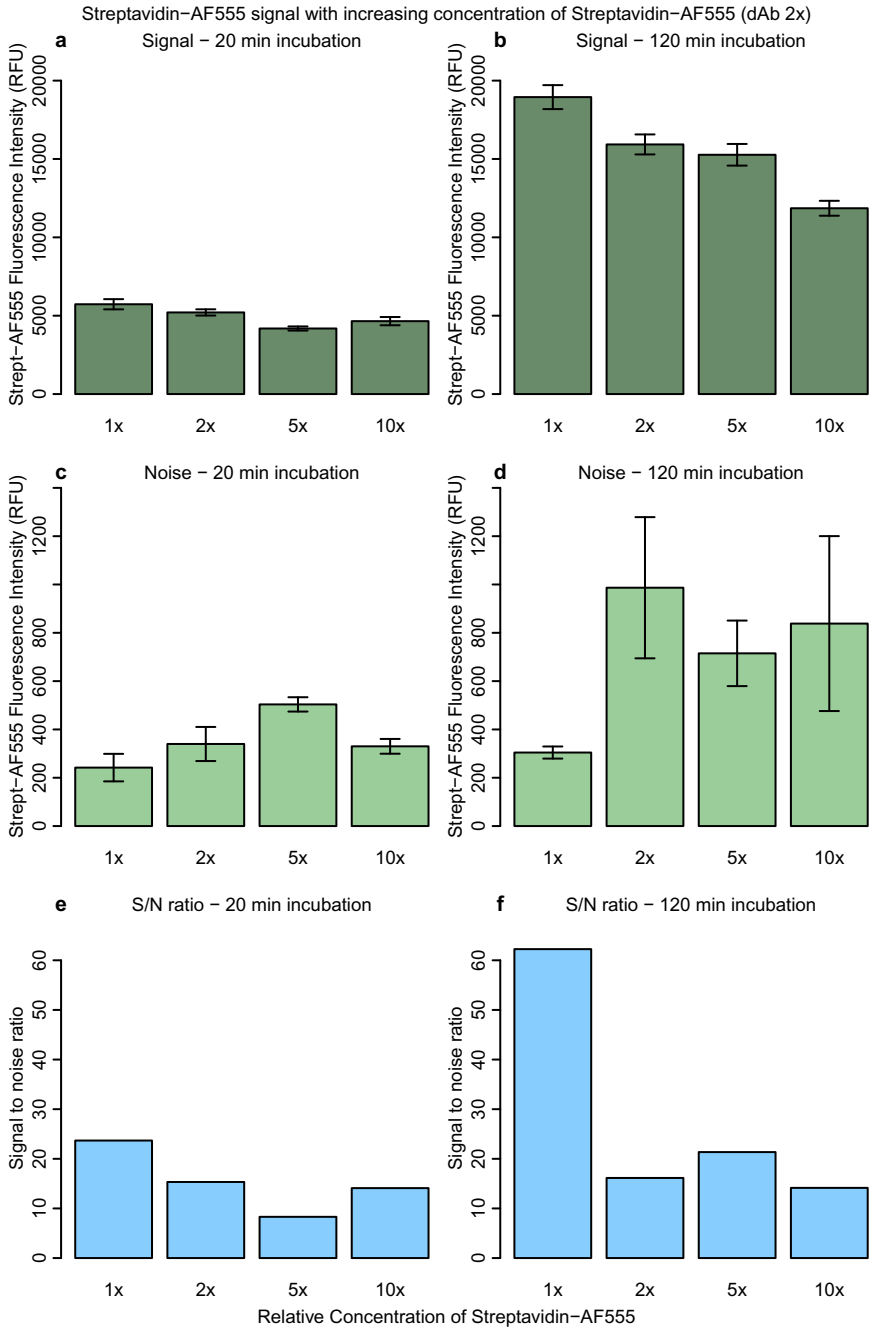

FIGURE D.S14: **Time and concentration of Strept-AF555 incubation.** cAbs against 6 proteins (Ang1, HGF, HGF-R, MCP4, THBS-1, VEGFR2) were spotted onto two microarrays. An Ag mixture was incubated, followed by a dAb mixture at four different concentrations ($1\times = 0.1\,\mu g/mL$). As a second step, GAM-AF647 and Strept-AF555 were applied together at four different concentrations ($1\times = 0.1$ and $0.5\,\mu g/mL$, respectively) for either (**a, c, e**) 20 or (**b, d, f**) 120 min. Signal from GAM-AF647 (**a, b**) is shown as well as the green channel background (**c, d**) which are used to calculate a signal to noise ratio (**e, f**). All graphs are for dAb concentration of $0.2\,\mu g/mL$. A Strept-AF555 concentration of $0.5\,\mu g/mL$ is recommended for 20 min to avoid antigen loss.

slides at different times in each subarray over a period of 24 h and found that all antibodies binding relationship with time followed roughly a logarithmic equation. The incubation time required to minimize the variability in binding to 1 %, 0.5 %, 0.2 % and 0.1 % for printing times of 15 min and 1 h were calculated and reflect the time required for printing four cAbs in parallel (using four pins) in a small-scale (~12 slides) and large-scale (~ 48 slides) experiment, respectively. Equations used in calculating those measures in a logarithmic and linear functions are shown in figure D.S15.

We found that 24 h incubation after printing of the last spot led to a difference in amount of cAb bound to the surface less than 0.2 % for five of the six molecules tested, and less than 0.1 % for the remainder in the case of short-scale experiments (figure D.S16). For large-scale experiments, a 24 h incubation time after the last spot printed led to differences in quantities of molecules bound to the surface of less than 1 % in the same five out of six molecules, and less than 0.2 % in the remainder.

Similarly, we tested the time required to incubate dAbs after spotting the last ones and found that for two dAbs (Ang1 and MCP4), binding was much faster than HGF-R and VEGFR2 dAbs (figure D.S17). For the slow-binding dAbs, an incubation period of 24 h led to a difference in quantity of dAbs bound of less than 0.2 % for small-scale experiments, and slightly greater but close to 0.5 % for large-scale experiments. For fast-binding dAbs, the difference in quantity of dAbs bound was less than 0.1 % for both small- and large-scale experiments.

While the measurement of cAb binding to Xenobind surface in 2 M betaine / 25 % 2,3-butanediol is most likely not the same as that of cAb binding on PolyAn 2D Aldehyde in 50 % glycerol / 0.005 % Tween-20, the fact that dAbs bind to their target in 45 % glycerol / 1 % BSA / 0.001 % Tween-20 within 24 h or less was sufficient to convince us that this length of time is also sufficient for cAbs to bind to the surface in glycerol-based printing buffers. Glycerol solutions have a very high viscosity (6 cP at 20 °C [174]) and compared to the viscosity of PBS 1 × (~1 cP at 20 °C), that of glycerol can significantly slow down molecular diffusion required for cAbs to bind to the surface, even in droplets of 100 pL or less. Since it was not tested, slides with cAbs printed in glycerol-based printing buffers might benefit from an even longer incubation time and therefore increase assay sensitivity and reproducibility.

While it is important for cAbs and dAbs binding to the surface to have reached an acceptable equilibrium to decrease variability, it is equally important to optimize the sample and antigen mixture incubation time, as well as the concentration and incubation time of Strept-AF555. The antigen incubation time was chosen to be a minimum of 18 h at 4 °C in order to allow greater amounts of low-abundance antigens to bind to cAbs, and also because it took ~1 h to load diluted samples and antigen mixtures into more than a thousand wells by hand during large-scale experiments. However, because the antigen concentration varies between samples, no amount of incubation time

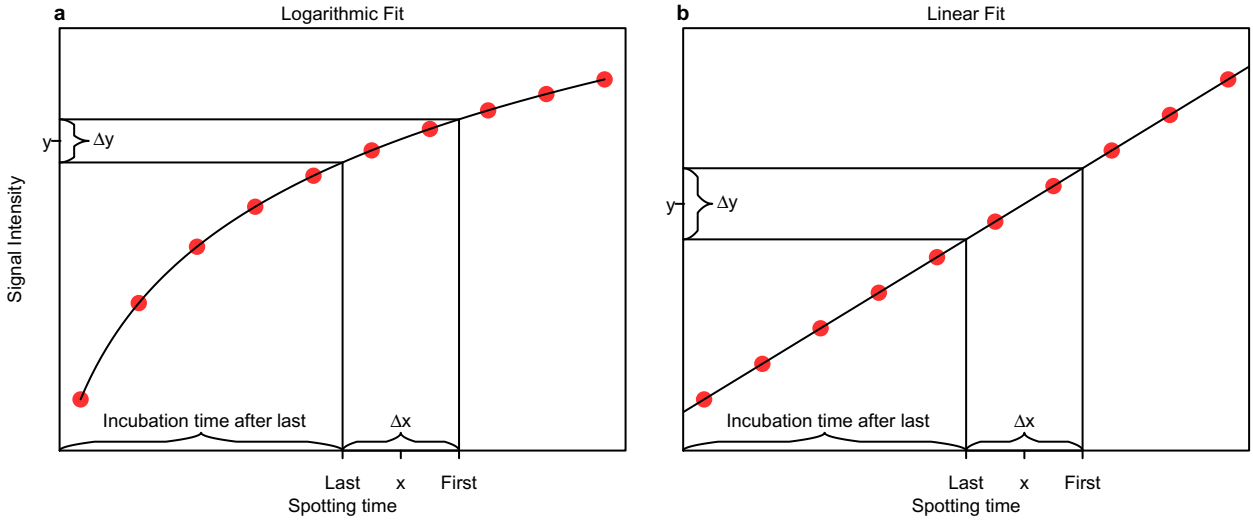

(1a) $y = c \cdot \ln(x) + b$

(1b) $y = m \cdot x + b$

(2a) $\frac{\Delta y}{\Delta x} = \frac{c}{x}$

(2b) $\frac{\Delta y}{\Delta x} = m$

(3a) $\frac{\Delta y}{y} = \frac{\Delta x}{x \cdot \ln(x) + \frac{x \cdot b}{c}}$ (A)

(3b) $\frac{\Delta y}{y} = \frac{\Delta x}{x + \frac{b}{m}}$ (A)

(4a) $x = \frac{\Delta x}{A \cdot W\left(\frac{\Delta x \cdot e^{b/c}}{A}\right)}$

(4b) $x = \frac{\Delta x}{A} - \frac{b}{m}$

FIGURE D.S15: **Schematics of calculations for binding to the surface.** Molecules binding to the surface of microarray slides can be modeled using **a** a logarithmic or **b** a linear equation. The first spot in a spotting round (for a given molecule) will have more time to incubate than the last spot. The first derivative of the function is found in the middle of the spotting round for a spotting range given by Δx. The corresponding range of signal intensity is Δy. For each function, the mathematical representation (eq. 1a and 1b) of the function is listed, as well as its first derivative (eq. 2a and 2b). The equation for the difference in binding to the surface as expressed by a percentage is calculated with eq. 3a and 3b and is equal to A, and those equations are re-arranged to solve for x in eq. 4a and 4b. The time reported by the calculation corresponds to the time of incubation after the last spot has been deposited for the spotting round ("Last" on the graph), for a given length of spotting (Δx) and difference of intensity between the first and last spot (A %). W in eq. 4a represents the Lambert W function.

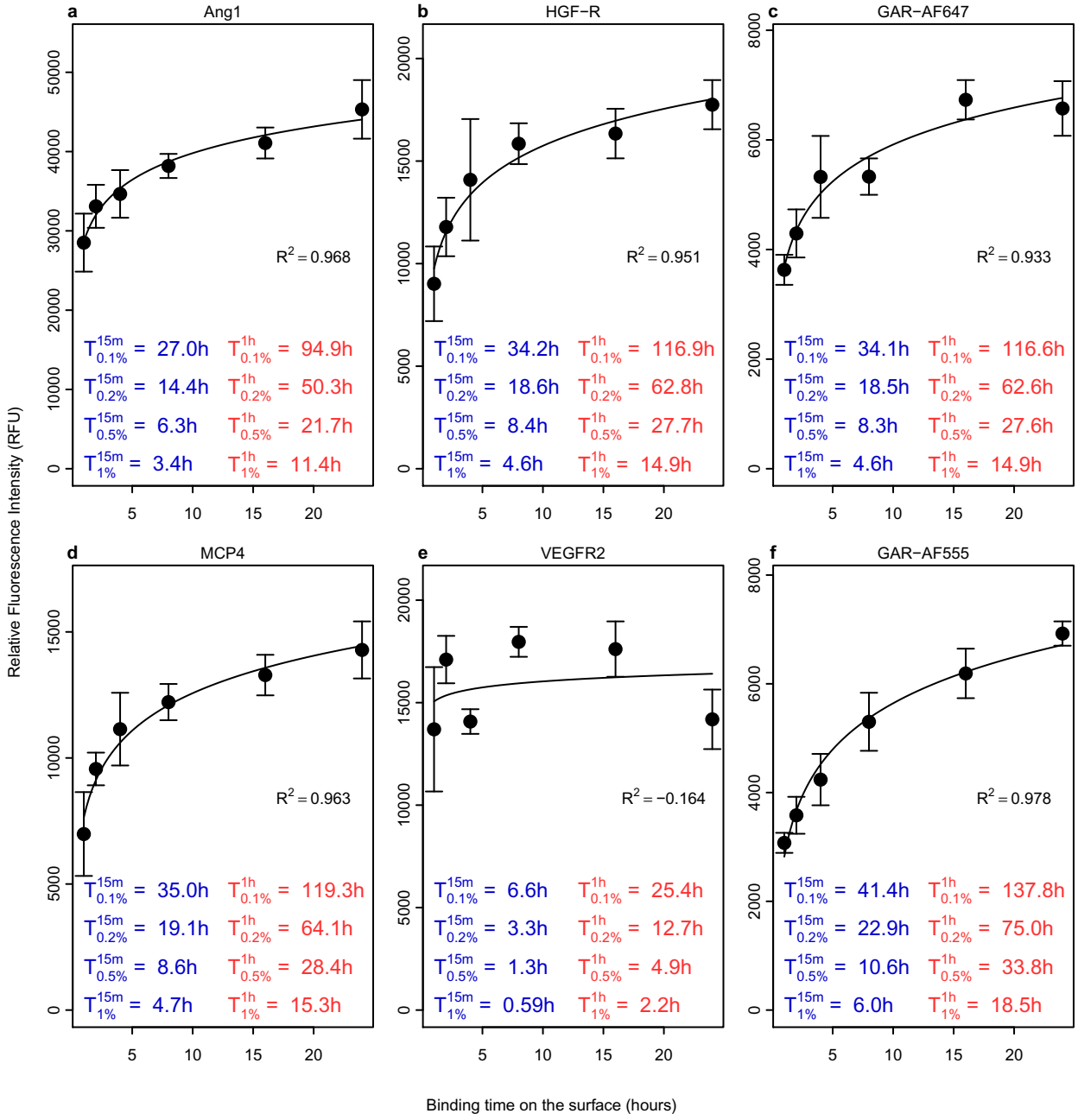

FIGURE D.S16: **Binding of cAbs to Xenobind.** cAbs for four different proteins were spotted on Xenobind slides and were incubated for different times before being washed and kept in washing buffer until incubated with (**a, b, d, e**) or without (**c, f**) GAM-AF647. All antibodies bind more or less in a logarithmic fashion, with similar times required to achieve different percentages of binding differences during short (15 min, blue) and long (1 h, red) spotting times. For long spotting times, a difference of roughly 0.5 % in binding of the cAb to the surface is achieved when leaving it for 24 h to incubate afterwards, whereas for short spotting times, a difference of surface binding of less than 0.2 % is achieved.

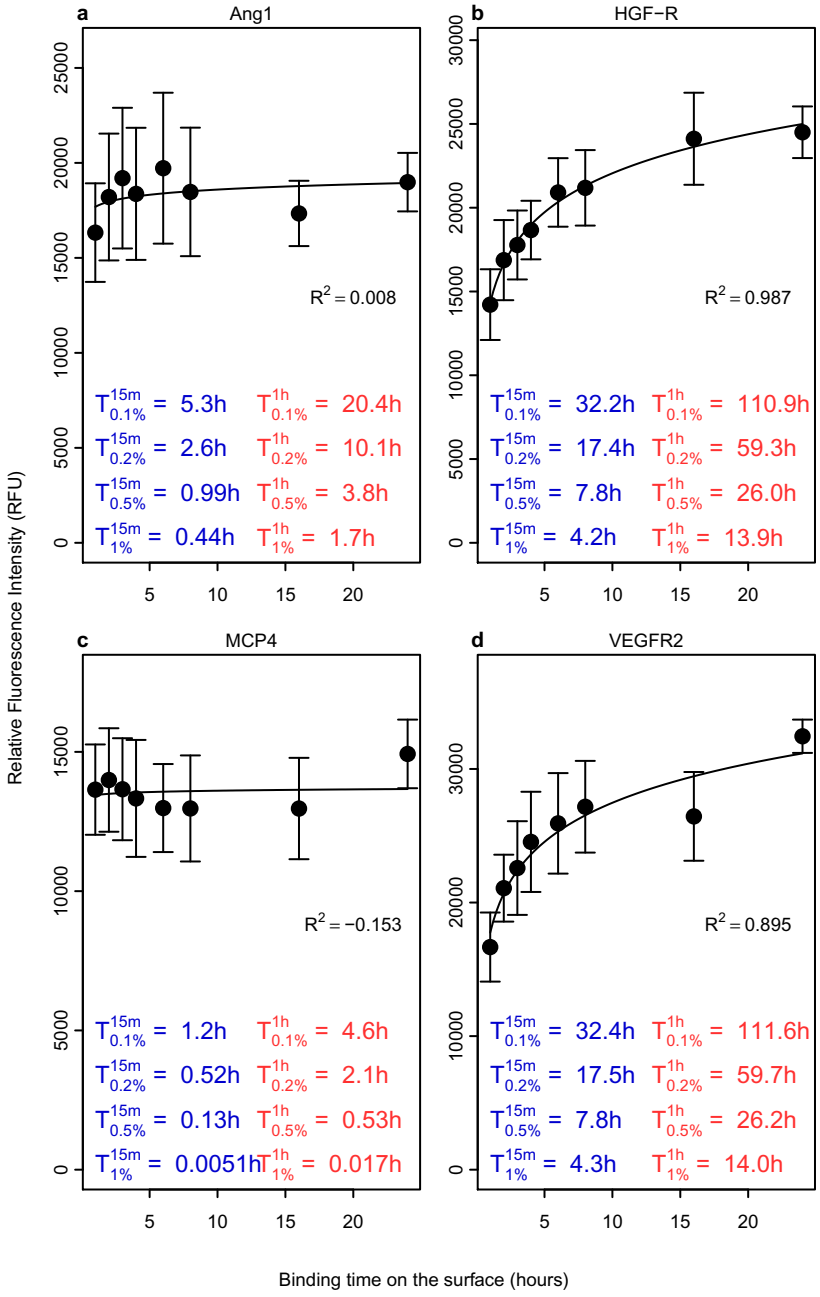

FIGURE D.S17: **Binding of dAbs.** cAbs for four proteins were spotted on Xenobind slides and allowed to bind for 24h. Slides were blocked and Ags were applied as a mixture overnight. Slides were rinsed with 5 % trehalose to avoid cAb and/or Ag degradation, and dAbs were then spotted at different times to achieve a range of dAb incubation times. Slides were washed, incubated with Strept-AF647, rinsed and scanned. Ang1 (**a**) and MCP4 (**c**) dAbs bind quickly to their respective Ag, while HGF-R (**b**) and VEGFR2 (**d**) bind more slowly. For long (1 h) spotting times, a difference of less than 0.1 % is achieved for Ang1 and MCP4, while for HGF-R and VEGFR2, a difference of slightly over 0.5 % is achieved.

would be sufficient to allow all antigens to reach a state of equilibrium in their binding to their corresponding cAbs. Therefore the incubation time has to be limited to what is practical.

Trehalose Protection of Spots

This sections presents additional details on experiments performed to study and attempt to mitigate the degradation of cAbs and Ags in the dry state while awaiting to be spotted on with dAb printing buffer.

To test the quantity of cAb bound at the surface of slides, we used a goat anti-mouse (GAM) conjugated to AF647 at 1 µg/mL (figure D.S18) that we incubated either by itself or with Strept-AF555. Since the four cAbs and dAbs used to assay Ang1, HGF-R, MCP4 and VEGFR2 are mouse and goat antibodies, respectively, the GAM-AF647 was not expected to cross-react with dAbs, and indeed it did not bind to dAbs (figures D.S19 and D.S20).

To investigate the nature of the cAb degradation in the dry state, we spotted half the spots with dAb printing buffer on slides where Ang1 cAbs had been printed, and Ang1 Ag had been incubated. The other half of spots were left to degrade in the dry state for 16, 24 and 40 h, before slides were washed and dAb printing buffer was printed on top of all spots. Slides were incubated for 24 h, washed and incubated with GAM-AF647. Figure D.S21 shows that spots which degraded in the dry state could not be rescued by the subsequent addition of dAb printing buffer. However, the degradation of spots on top of which dAb printing buffer was immediately printed, was minimized.

We attempted to determine whether Ags were also degraded and how it affected assay signals. Full standard curves assays as MSA were performed for Ang1 on four Xenobind slides, with the difference that each slide was washed with water and dried after washes following antigen incubation, placed in the Nanoplotter, and left in the dry state for 0, 16, 24 or 40 h before dAb printing buffer was printed on top of cAb spots. Figure D.S22a shows that assay signal increasingly diminished as the time left in the dry state was increased. This degradation affected sensitivity by up to 30 × when comparing slides that were left in the dry state for 0 and 40 h (figure D.S22b). Full Ang1 assays performed similarly on PolyAn 2D Aldehyde (figure D.S23) and 2D Epoxy (figure D.S24) slides shows that the degradation's effect on signal assay was greater at lower concentrations of Ang1 Ag on PolyAn 2D Aldehyde slides, and at higher concentrations of Ang1 Ag on PolyAn 2D Epoxy slides. As quantified by GAM-AF647, cAbs significantly degraded on both slides at a greater speed than on Xenobind slides (figure D.S22c).

When investigating the effect of this degradation on Ags, we saw a less pronounced effect, which might be due to some Ags because less susceptible to degradation than others, and/or some dAbs' ability to recognize their epitope in their partially denatured form. Nonetheless, we saw an effect on assay signals, and therefore sensitivity. The effect of degradation on assay signals

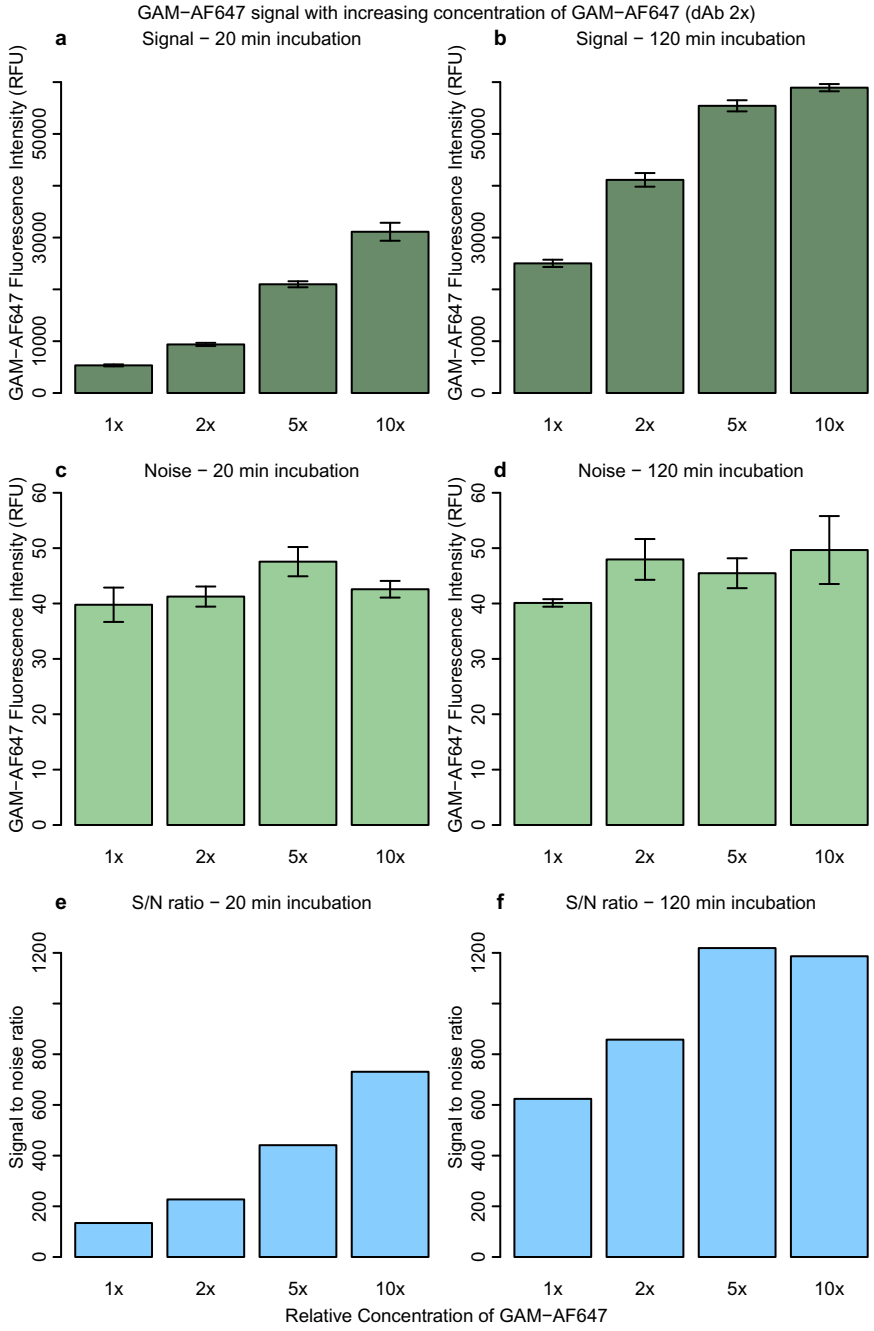

FIGURE D.S18: **Time and concentration of GAM-AF647 incubation.** cAbs against six proteins (Ang1, HGF, HGF-R, MCP4, THBS-1, VEGFR2) were spotted onto two microarrays. An Ag mixture was incubated overnight, followed by a dAb mixture at four different concentrations ($1\times$ = 0.1 µg/mL). As a second step, GAM-AF647 and Strept-AF555 were applied together at four different concentrations ($1\times$ = 0.1 and 0.5 µg/mL, respectively) for either (**a, c, e**) 20 or (**b, d, f**) 120 min. Signal from GAM-AF647 (**a, b**) is shown as well as the green channel background (**c, d**) which are used to calculate a signal to noise ratio (**e, f**). All graphs are for dAb concentration of 0.2 µg/mL. GAM-AF647 concentrations of 0.5 and 1.0 µg/mL are recommended for incubations of 120 and 20 min, respectively.

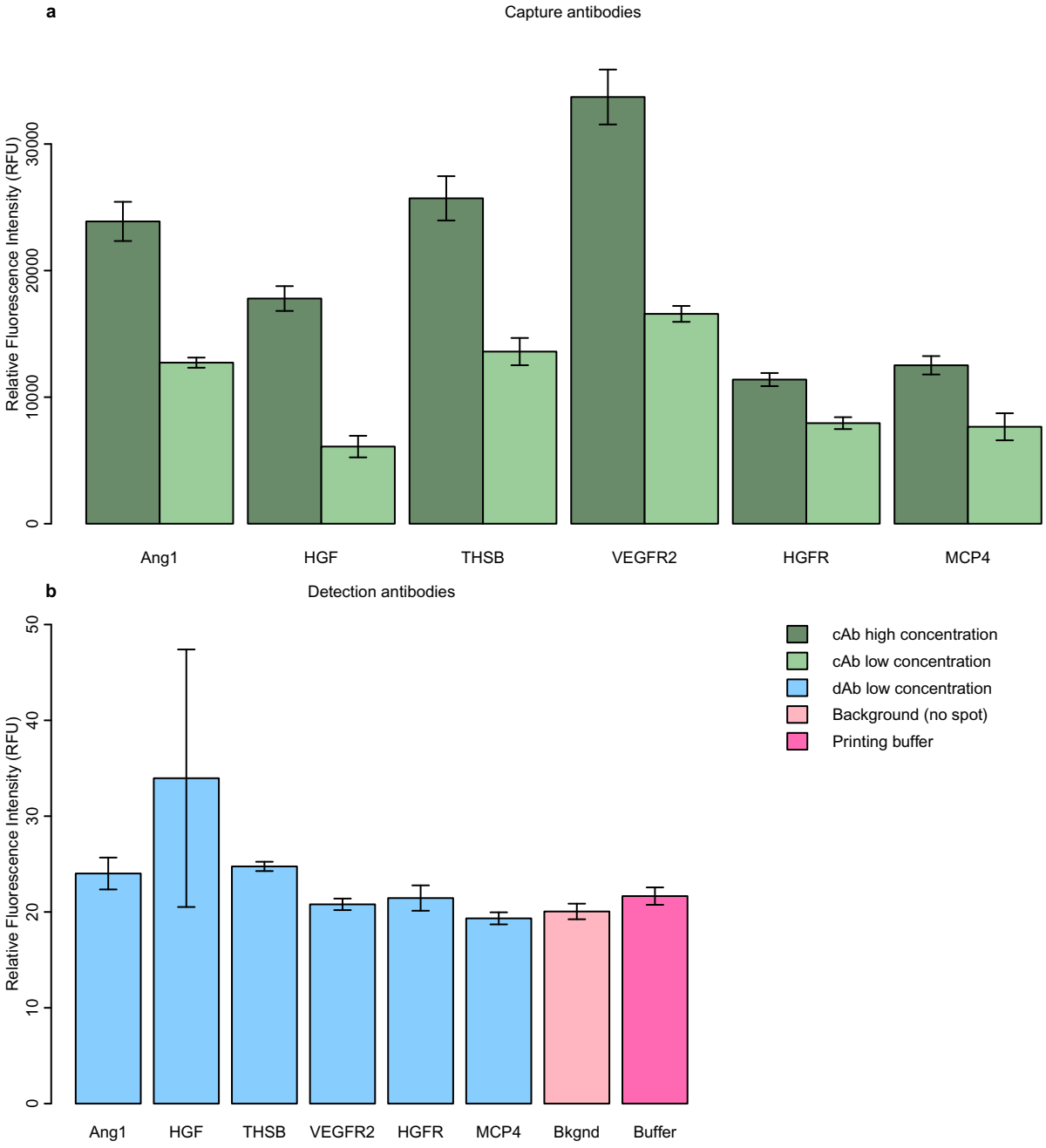

FIGURE D.S19: **GAM-AF647 binding to cAb and dAb.** cAbs (**a**) at two different concentrations and dAbs (**b**) for 6 pairs were bound on the surface of a microarray slide. The slide was washed, blocked, and incubated with GAM-AF647. Signal intensity from GAM-AF647 is strong and dose-dependent when binding to cAbs (monoclonal mouse Abs), and there appears to be minimal cross-reactivity to dAbs (polyclonal goat Abs).

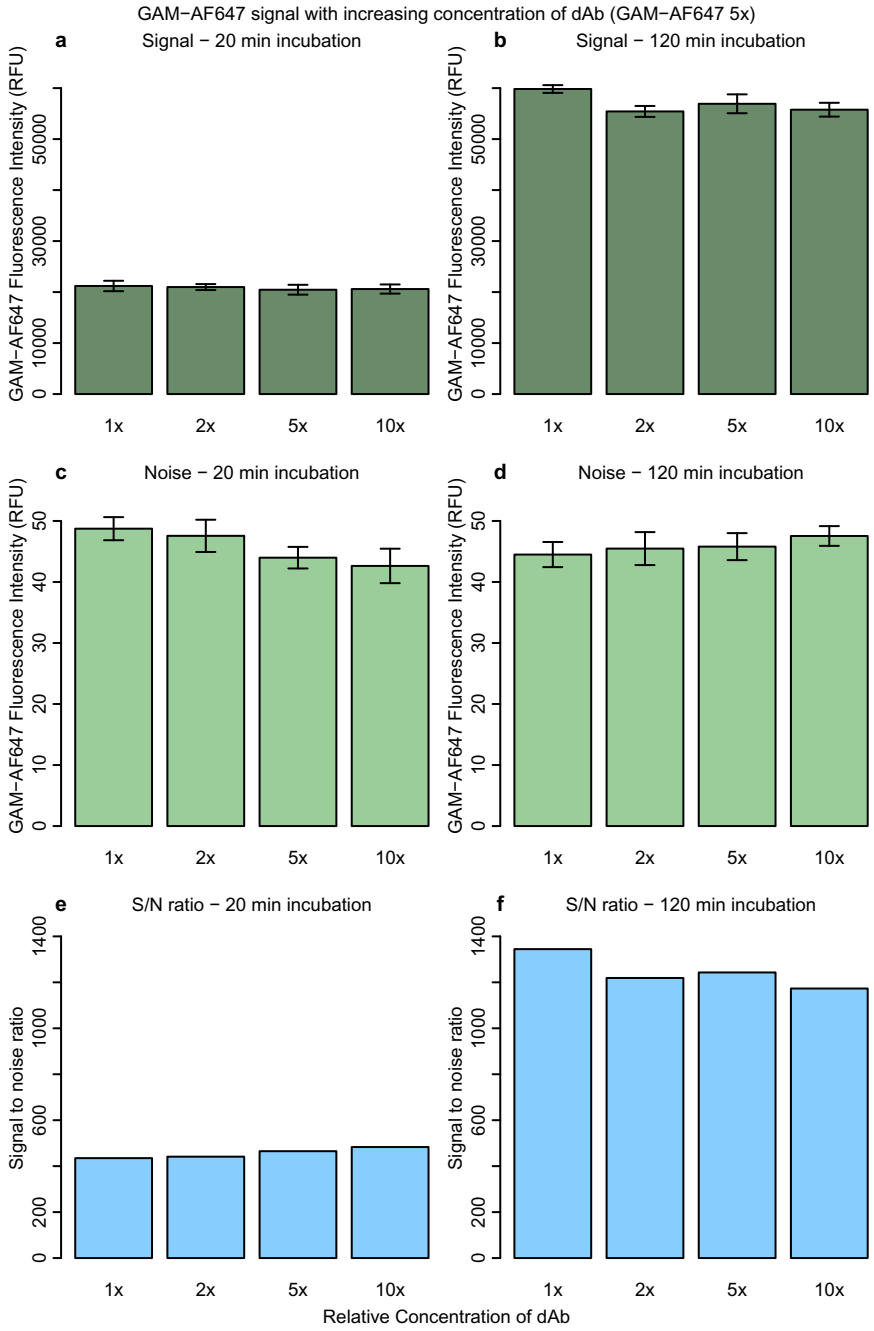

FIGURE D.S20: **Effect of dAb concentration on GAM-AF647 signal.** cAbs against 6 proteins (Ang1, HGF, HGF-R, MCP4, THBS-1, VEGFR2) were spotted onto two microarrays. An Ag mixture was incubated, followed by a dAb mixture at four different concentrations ($1\times = 0.1\,\mu g/mL$). As a second step, GAM-AF647 and Strept-AF555 were applied together at four different concentrations ($1\times = 0.1$ and $0.5\,\mu g/mL$, respectively) for either (**a, c, e**) 20 or (**b, d, f**) 120 min. Signal from GAM-AF647 (**a, b**) is shown as well as the green channel background (**c, d**) which are used to calculate a signal to noise ratio (**e, f**). All graphs are for GAM-AF647 at a concentration of $1\,\mu g/mL$. There is no effect on GAM-AF647 signal from increasing the concentration of dAbs.

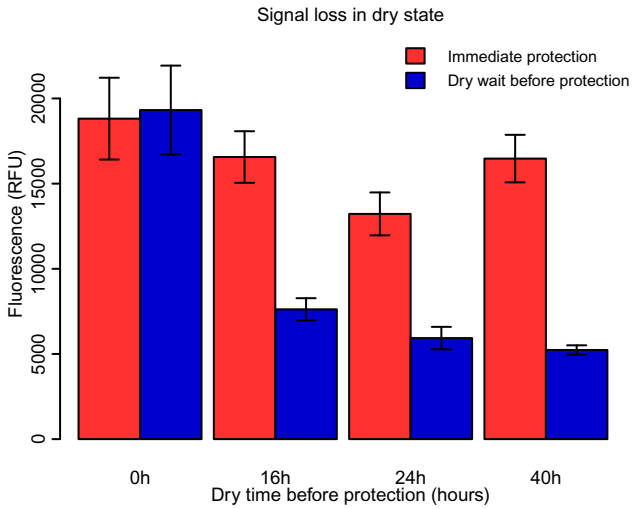

FIGURE D.S21: **Degradation of spots in dry state cannot be reversed.** Ang1 cAb spots with bound Ag were dried and either immediately protected with dAb printing buffer (red) or left in the dry state (blue) before the slide was washed and all cAbs with bound Ag were spotted with dAb printing buffer with Ang1 dAb. The slide was then incubated for 24 h before washing, GAM-AF647 incubation, and scanning.

differed between different types of slides, and therefore the degradation is likely partially due to the chemical coating on the slides surface. The time difference between the first and last printed spots for a single antibody in our protocol would be 80 min and therefore we assume that the difference in denaturation as a source of variability would not be very pronounced, although we did not measure the rate of denaturation of all cAbs and Ags in our assay. The greatest detrimental effect would be seen in sensitivity, where cAbs spotted last after 35 h of waiting in the dry state could have undergone significant degradation.

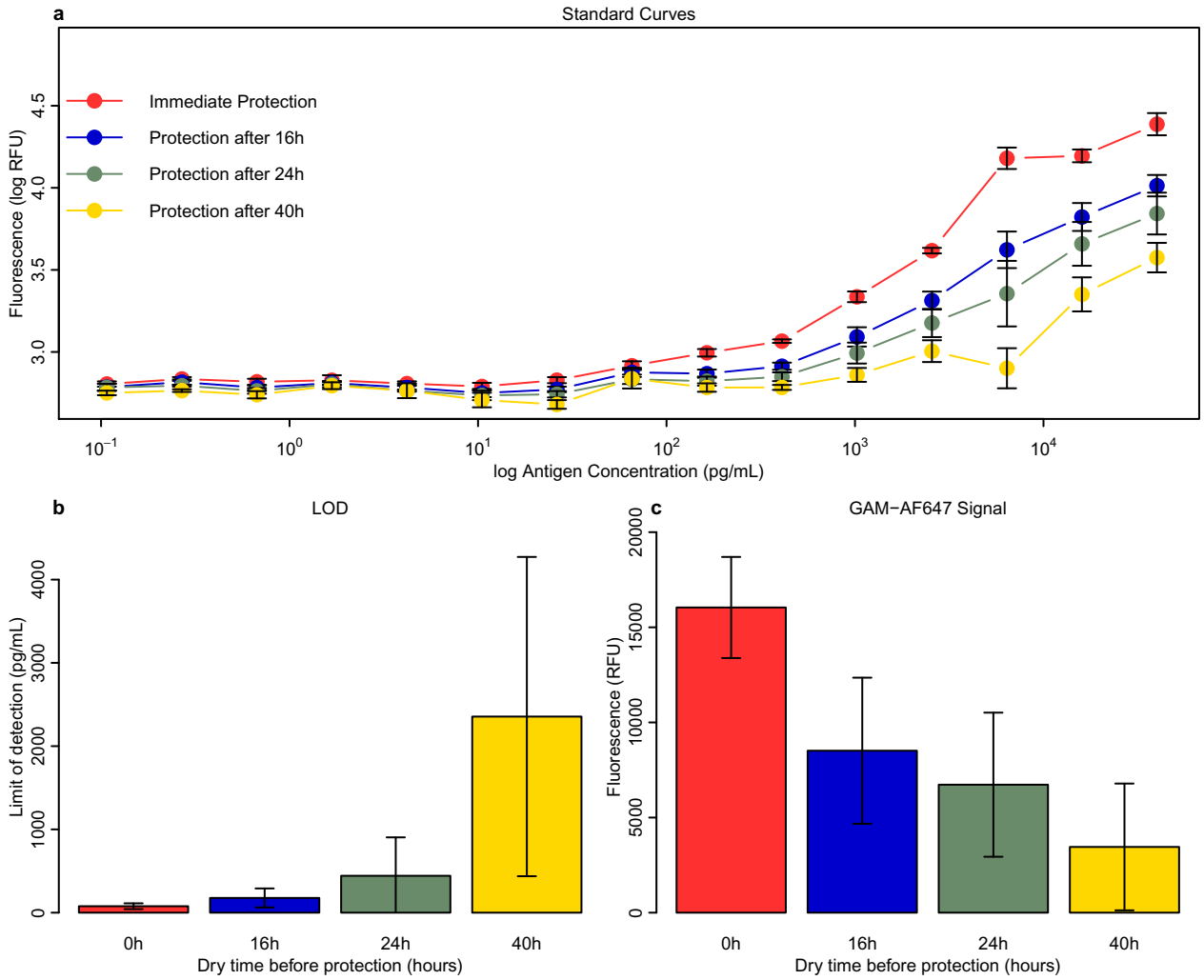

FIGURE D.S22: **Effect of spot degradation on assay performance.** Ang1 cAb were spotted on multiple lines of a Xenobind slide. Ag was applied in a SC and incubated overnight. The slide was dried and lines were protected with dAb printing buffer at different times. Ang1 dAb was incubated afterwards, as well as GAM-AF647 and Strept-AF555. **a** SCs from lines protected at different times show a decrease in sensitivity and signal intensity. **b** LOD is affected negatively by the decrease in signal intensity. **c** degradation is also seen from cAb as detected by GAM-AF647. Signal from **a** and **b** are from Strept-AF555.

To prevent the degradation of cAbs and Ags in the dry state, we also coated slides with different concentrations of glycerol, sucrose, and BSA on slides after the washing step following antigen incubation. The maximum concentration of sucrose, BSA and glycerol that could be dried on the surface of slides and still permit dAb printing was 5 %, 0.5 % and 0.5 % in water, respectively. Slides with printed cAb and complexed Ag and coated with the various chemicals at concentrations mentioned above were then blown-dried and left in the dry state for 0 up to 12 h before being printed with dAb printing buffer to assess cAb degradation. In spite of the fact that dAb printing buffer is largely composed of glycerol, figure D.S25 shows that at very low concentrations (0.2 % and 0.5 %), glycerol did not prevent cAb degradation in the dry state. BSA is also present in the dAb printing buffer and at concentrations of 0.2 % and 0.5 % it partially prevented the degradation of cAbs. Sucrose was better at preventing cAb degradation, but not as good as trehalose.

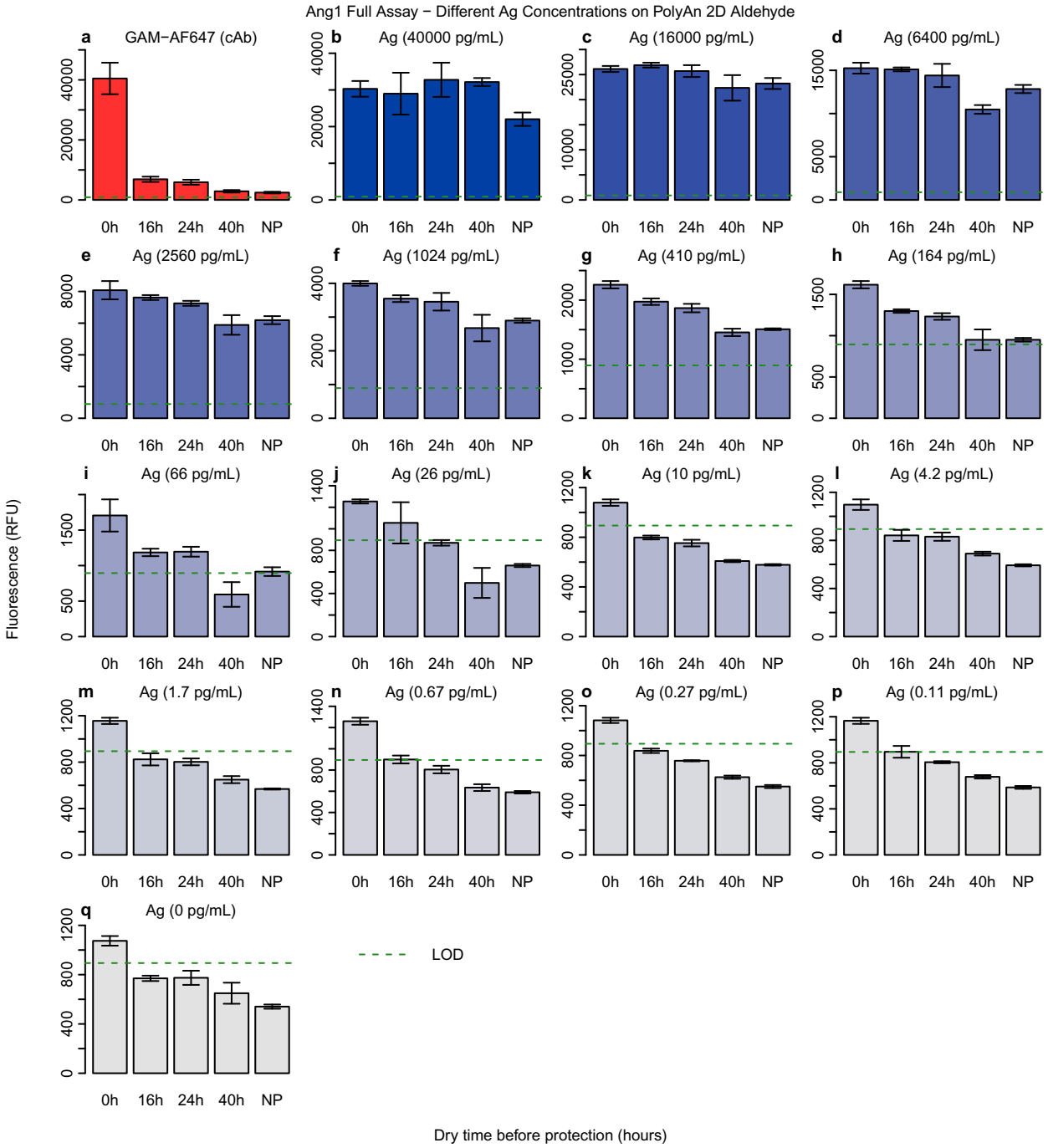

FIGURE D.S23: **Assay signal loss on PolyAn 2D Aldehyde.** Ang1 cAbs were spotted on multiple lines of a PolyAn 2D Aldehyde slide, Ag was applied as SC, and the slide was dried. Different lines were protected at different times with dAb printing buffer without dAb in it. dAb was incubated, followed by Strept-AF555 and GAM-AF647. Figure shows the effect of degradation on cAb as seen by GAM-AF647 (**a**) and assay (**b** to **q**) signal intensities. Signals from **b** to **q** are from Strept-AF555. Assay signal degradation is mainly seen in the lowest concentrations of Ang1 Ag (**e** to **p** including the blank **q**).

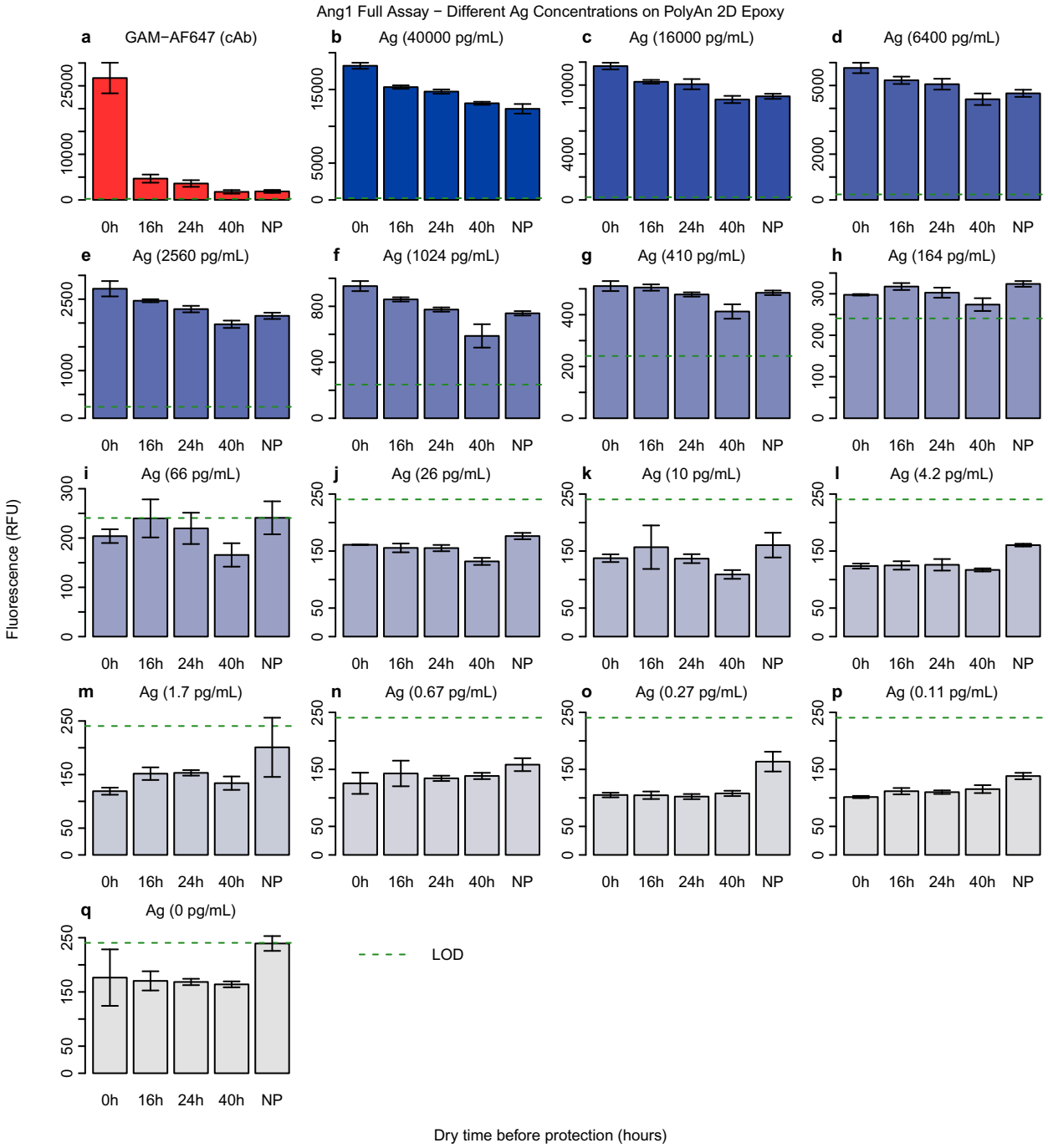

FIGURE D.S24: **Assay signal loss on PolyAn 2D Epoxy.** Ang1 cAbs were spotted on multiple lines of a PolyAn 2D Epoxy slide, Ag was applied as SC, and the slide was dried. Different lines were protected at different times with dAb printing buffer without dAb in it. dAb was incubated, followed by Strept-AF555 and GAM-AF647. Figure shows the effect of degradation on cAb as seen by GAM-AF647 (**a**) and assay (**b** to **q**) signal intensities. Signals from **b** to **q** are from Strept-AF555. Assay signal degradation is mainly seen in the highest concentrations of Ang1 Ag (**b** to **f**).

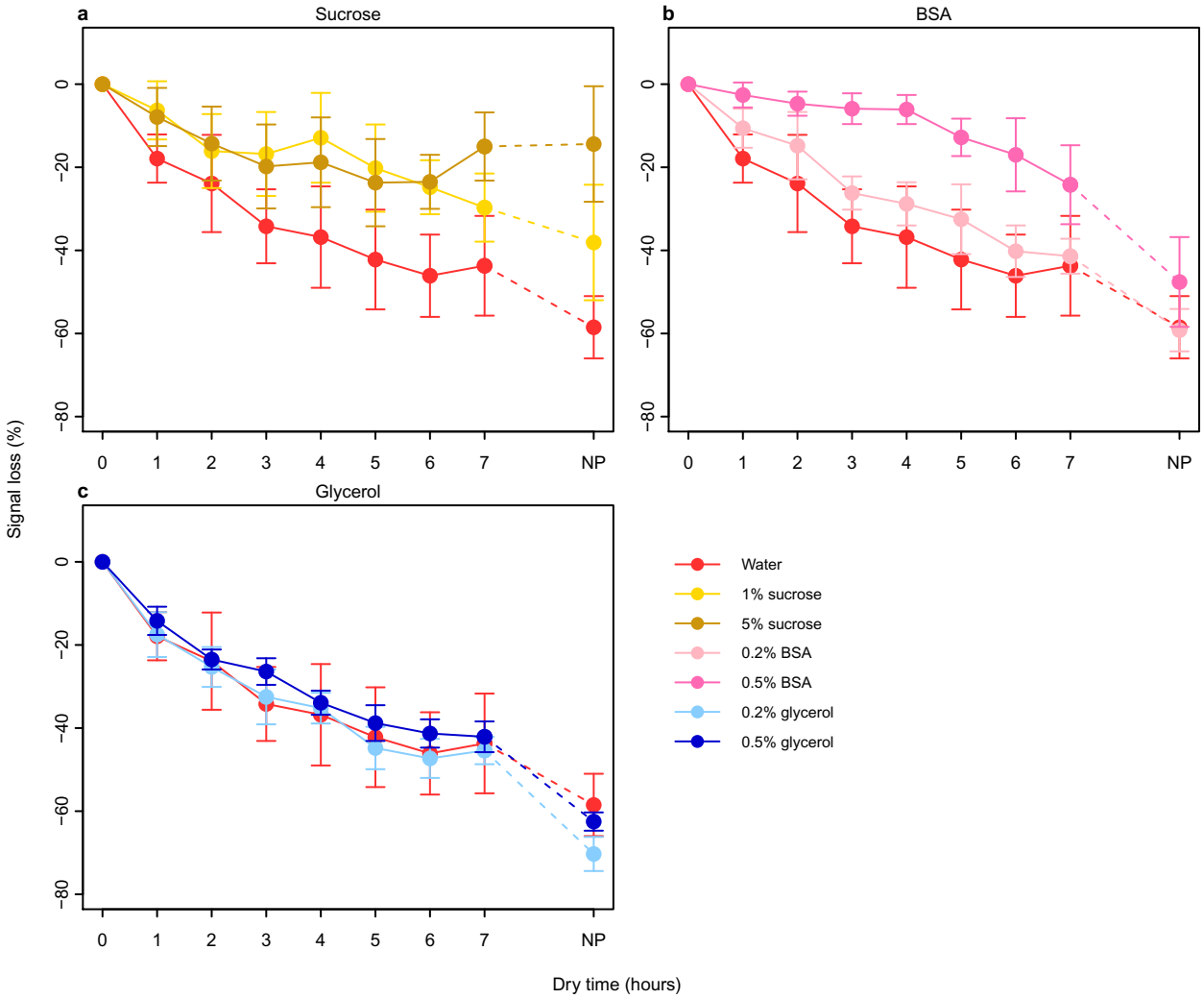

FIGURE D.S25: **Protection of spots by sucrose, BSA and glycerol.** Ang1 cAbs and bound Ag are protected with different concentrations of **a** sucrose, **b** BSA or **c** glycerol, or not protected (with water) and allowed to dry for up to seven hours before dAb printing buffer is spotted. Dashed part of lines to indicate a break in dry time. NP: Signal of spots onto which no dAb printing buffer was printed.

Choice of Spot Calibrant

This sections presents additional results from the comparison of GAR-AF555, BSA-AF555, BSA-AF647 and h-AF555 as potential spot calibrants.

Our primary concern in spiking molecules with cAb was to avoid the generation of false positive signal solely due to the presence of spot calibrants. Figure D.S26 shows a 10-protein ACM assay where cAbs were spiked with GAR-AF555, BSA-AF555 or h-AF555 were incubated with a standard curve and several replicate samples at dilutions 1:2 and 1:8. Calculations of average sample quantities show that six of the 10 proteins (Endoglin, IL-1β, IL-2, IL-6, MMP-9 and PSA) reported greater quantities of proteins in the replicate samples when cAbs were spiked with GAR-AF555 compared to cAbs spiked with BSA-AF555 or h-AF555. Only one protein (HGF-R) reported a greater quantity from cAbs spiked with BSA-AF555, and none with cAbs spiked with h-AF555. The false positive signals for Endoglin, MMP-9 and HGF-R all show a large error bar, indicating that an assay artefact might be responsible for the false positive signal rather than the presence of GAR-AF555 or BSA-AF555. However, four proteins still show clear false positive signals in the presence of GAR-AF555, and for this reason, it was not considered during subsequent comparisons.

In order to determine the best concentrations of spot calibrants, we mixed 5, 10, 25 and 50 µg/mL BSA-AF555, BSA-AF647 and h-AF555 alone or with GAR-b at 100 µg/mL and incubated slides with Strept-AF555 and Strept-AF647 separately. This experiment allowed us to not only determine an ideal concentration for each spot calibrant, but also to determine the amount of crosstalk (from green to red channel for h-AF555 and BSA-AF555 and red to green channel for BSA-AF647) (figure D.S27). We observed positive crosstalk (increasing) red signal in the presence of BSA-AF555 and h-AF555, without GAR-b or streptavidin, while we observed decreasing crosstalk in the presence of BSA-AF647 only. We also noticed that the signal intensity of h-AF555 was ~6 × greater without the presence of GAR-b.

At the chosen concentrations, we spotted the three spot calibrants and allowed them to bind for different amounts of times to the slide in order to find out if the signal intensity is relatively stable after an incubation time of 24 h. When mixed with HGF-R or MCP4, the difference in binding of BSA-AF555 was less than 0.2 % for a short-scale experiment and less than 1 % for a large-scale experiment, which was very similar to HGF-R (figure D.S28) and MCP4 (figure D.S29) binding. In contrast, the difference in binding of h-AF555 was greater than 0.5 % for a small-scale experiment and much larger than 1 % for a large-scale experiment. Therefore BSA-AF555 bound to the surface at similar rates as the cAb it was mixed in, while h-AF555 did not.

We investigated the stability of spot calibrants when bound on the microarray surface and waiting in the dry state before being spotted on with dAb printing buffer. We spotted the three

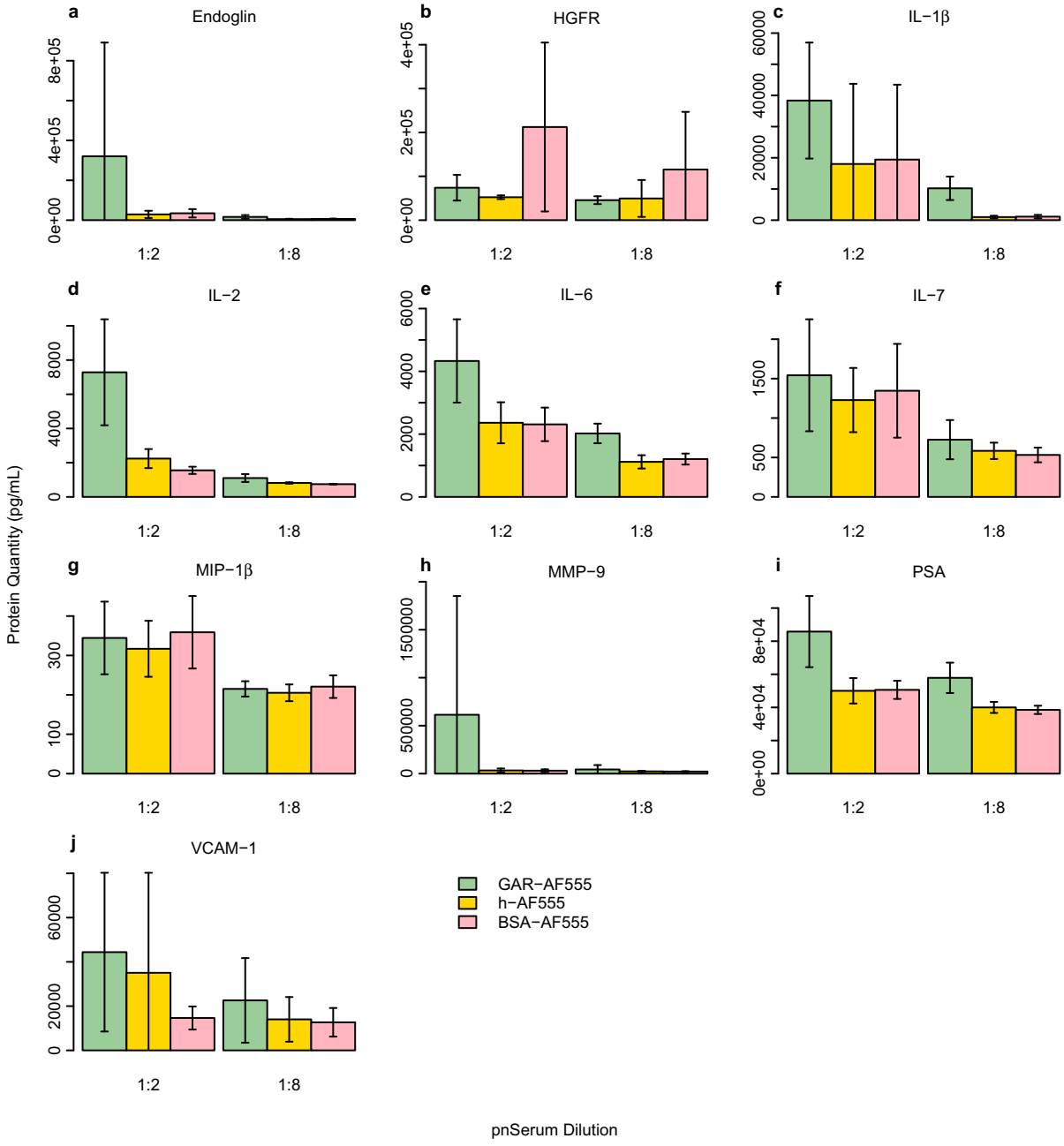

FIGURE D.S26: **Quantities of 10 proteins with 3 spot calibrants.** Ten cAbs against different proteins were spotted with spot calibrants (green: GAR-AF555, yellow: h-AF555, pink: BSA-AF555) on two microarray slides, one containing an SC and the other containing sample replicates at dilutions 1:2 and 1:8. False positive signal due to the presence of the spot calibrant is seen in graphs **a, c, d, e, h, i** for GAR-AF555 and **b** for BSA-AF555.

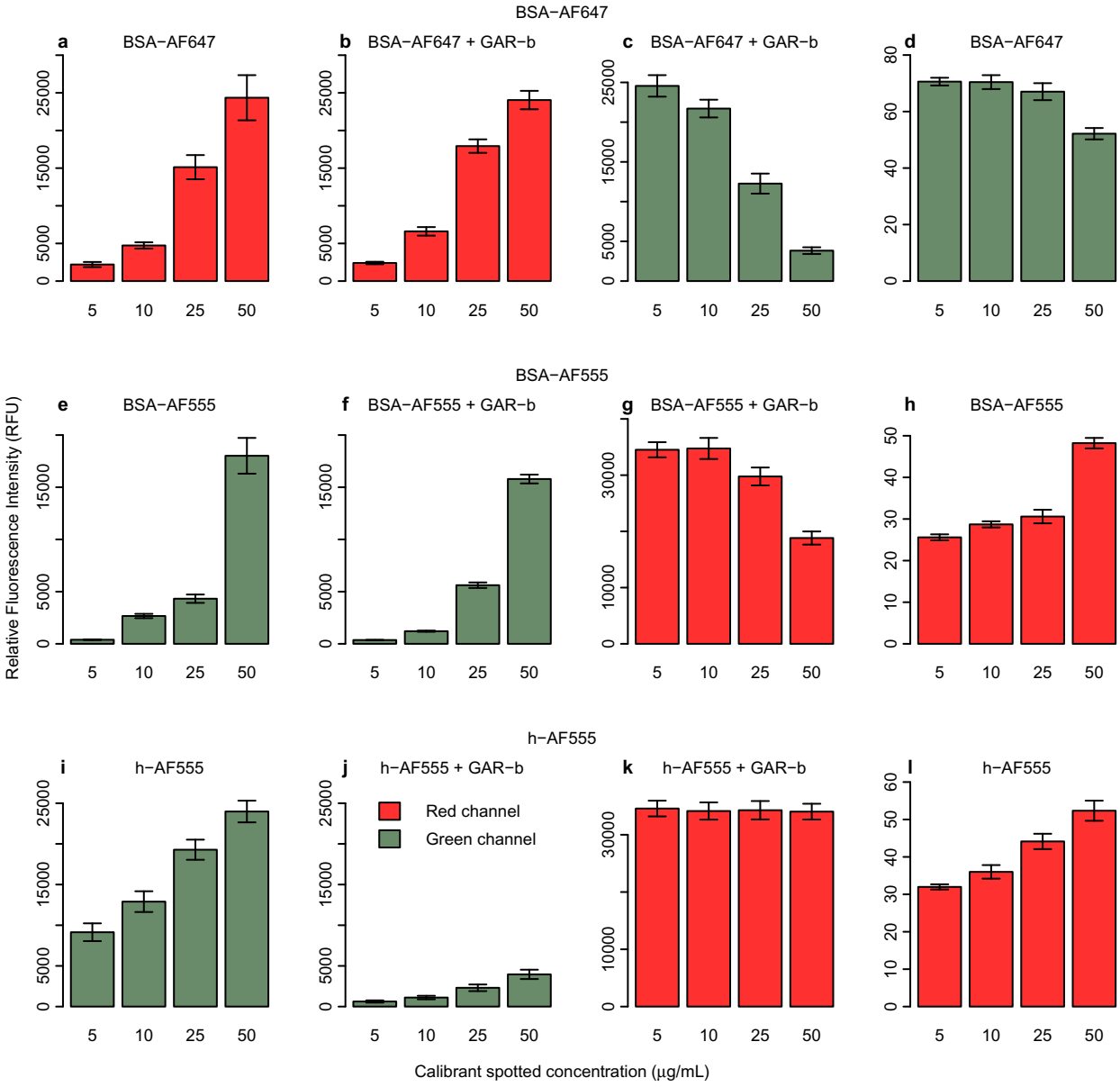

FIGURE D.S27: **Spot calibrants signal intensity, cAb displacement and crosstalk.** Spot calibrants were spotted at different concentrations with (columns 1 and 4) and without (columns 2 and 3) the presence of 100 µg/mL GAR-b. Slides were incubated overnight, washed, blocked and incubated with either Strept-AF555 or Strept-AF647. The first (**a, e, i**) and fourth(**e, h, l**) columns shows the signal intensity of each spot calibrant in the absence of GAR-b in the channel (first column) or the opposite channel (fourth column) as the spot calibrant's fluorophore. The second (**b, f, j**) and third (**c, g, k**) columns shows the signal intensity of (third columnn) each spot calibrant in the presence of GAR-b and (fourth column) Strept of the opposite fluorophore.

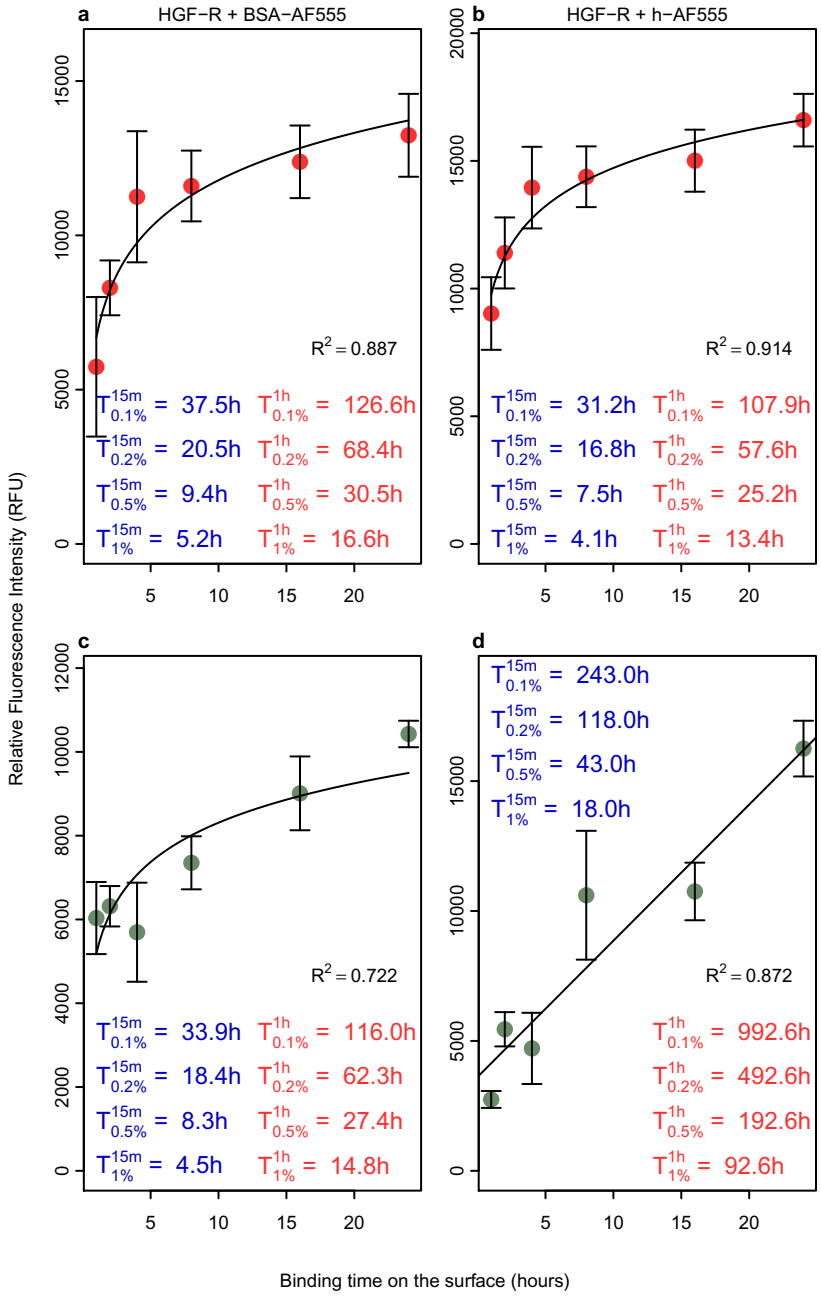

FIGURE D.S28: **Binding of HGF-R cAb and spot calibrants to Xenobind.** HGF-R cAb was mixed with BSA-AF555 (**a, c**) or h-AF555 (**b, d**) and spotted onto Xenobind slides. Slides were incubated for different times before being washed and kept in washing buffer until incubated with GAM-AF647. Red (**a, b**) graphs show the binding of cAb to the surface, while green (**c, d**) graphs show the binding of calibrants to the slide. BSA-AF555 (**c**) binds to the slide in a similar fashion as HGF-R (**a**), however h-AF555 (**d**) appears to bind linearly.

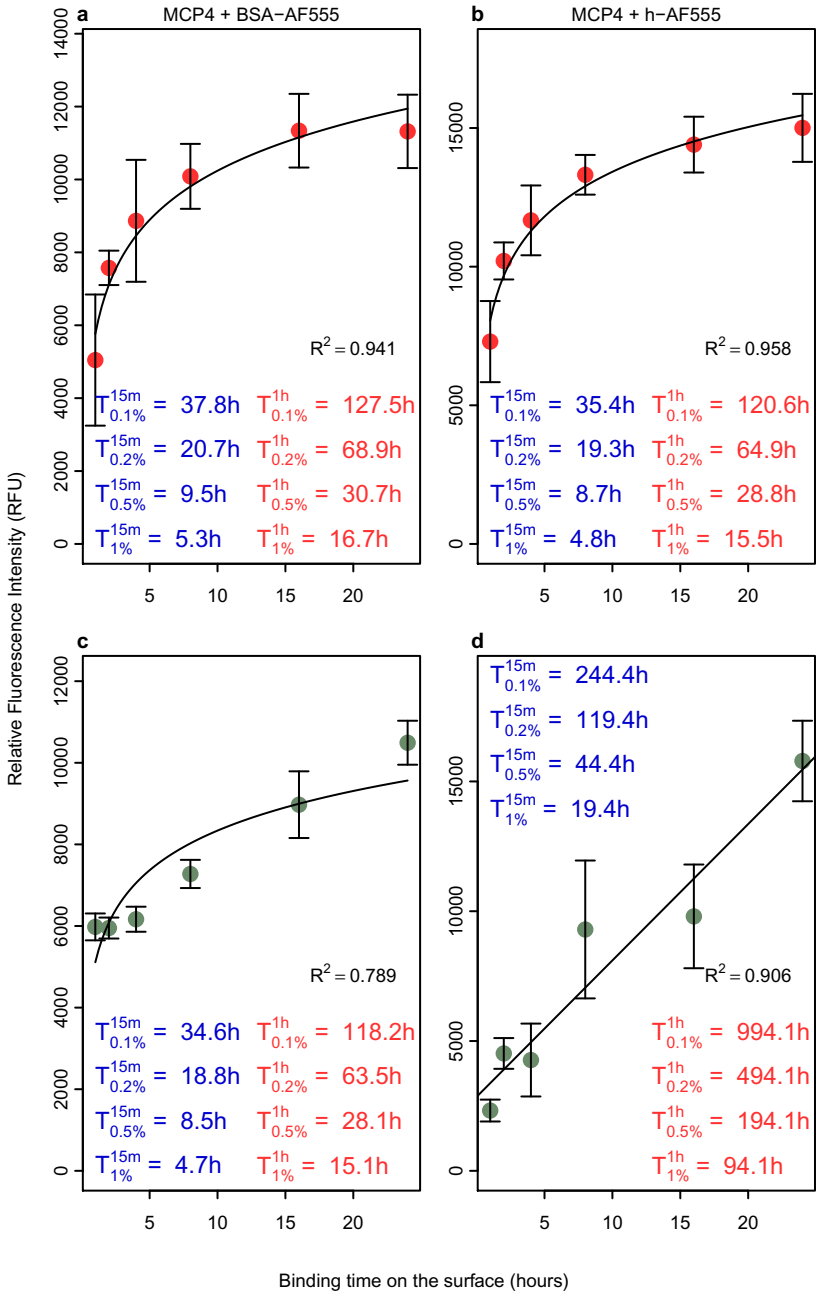

FIGURE D.S29: **Binding of MCP4 cAb and spot calibrants to Xenobind.** MCP4 cAb was mixed with BSA-AF555 (**a, c**) or h-AF555 (**b, d**) and spotted onto Xenobind slides. Slides were incubated for different times before being washed and kept in washing buffer until incubated with GAM-AF647. Red (**a, b**) graphs show the binding of cAb to the surface, while green (**c, d**) graphs show the binding of calibrants to the slide. BSA-AF555 (**c**) binds to the slide in a similar fashion as MCP4 (**a**), however h-AF555 (**d**) appears to bind linearly.

calibrants with GAR-b and incubated them for 24 h. We washed slides, dried them, and put them back in the Nanoplotter. Different lines of spots were protected by dAb printing buffer at 0, 16, 24 and 40 h, with one line not being protected before slides were washed and scanned. Figures D.S30, D.S31 and D.S32 show a slight degradation of BSA-AF555 (16 % and 19 %) on Xenobind and PolyAn 2D Epoxy slides respectively after 40 h, but no degradation on PolyAn 2D Aldehyde slides. BSA-AF647 degraded much faster on all three slides (86 %, 68 % and 93 %) on Xenobind, PolyAn 2D Aldehyde and 2D Epoxy slides, respectively. Reductive amination treatment significantly decreased the overall fluorescence signal of calibrants, but not GAR-b, suggesting that neither AF555 nor AF647 are compatible with $NaBH_4$ treatment. Of the fluorescence that remained after reductive amination of slides, the degradation of AF647 was only slowed down for 16 h on PolyAn 2D Aldehyde slides, but not Xenobind nor PolyAn 2D Epoxy slides.

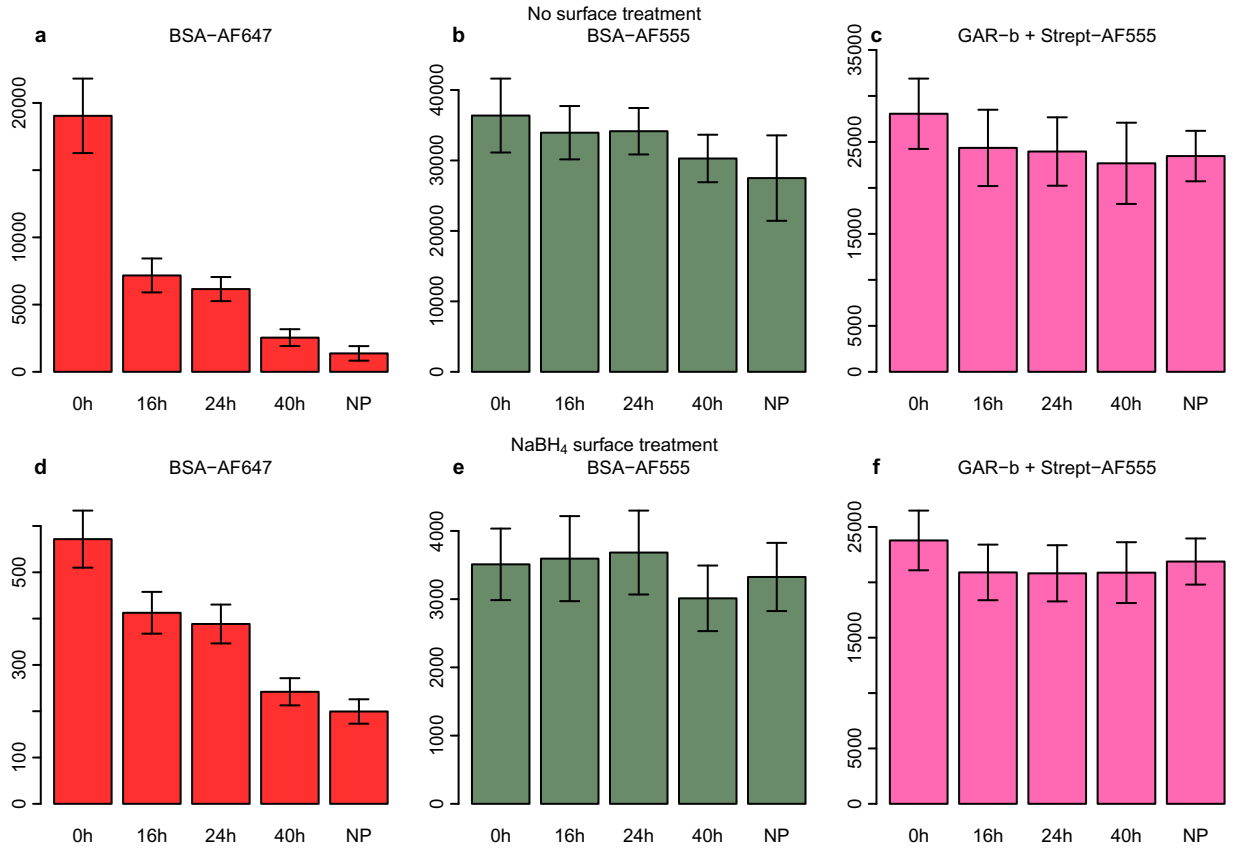

FIGURE D.S30: **Calibrants dry stability on Xenobind.** BSA-AF647, BSA-AF555 and GAR-b were spotted onto Xenobind slides and allowed to incubate for 24 h. Slides were then washed, received no treatment (**a, b, c**) or a $NaBH_4$ treatment (**d, e, f**), blocked and the spots were protected with dAb printing buffer at different times (or none before processing: NP), and finally incubated with Strept-AF555.

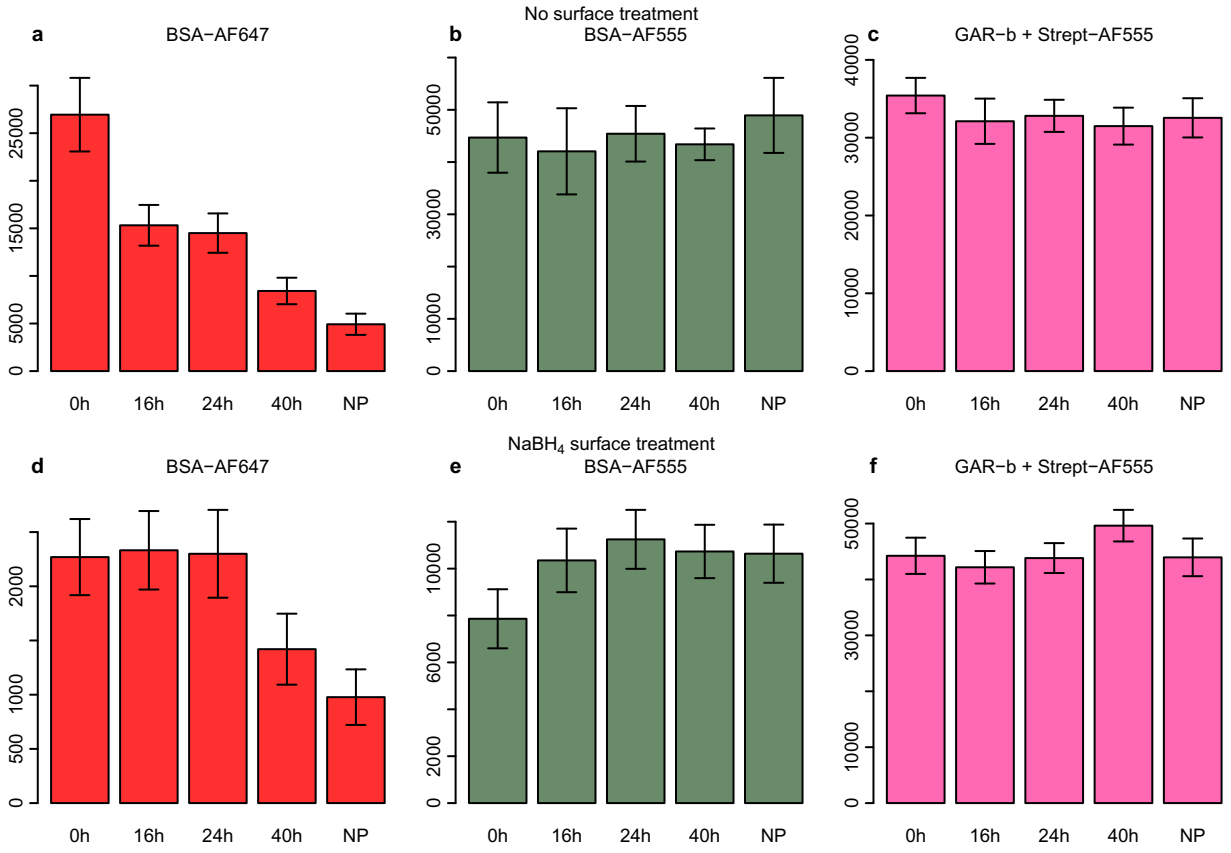

FIGURE D.S31: **Calibrants dry stability on PolyAn 2D Aldehyde.** BSA-AF647, BSA-AF555 and GAR-b were spotted onto PolyAn 2D Aldehyde slides and allowed to incubate for 24 h. Slides were then washed, received no treatment (**a, b, c**) or an $NaBH_4$ treatment (**d, e, f**), blocked and the spots were protected with dAb printing buffer at different times (or none before processing: NP), and finally incubated with Strept-AF555.

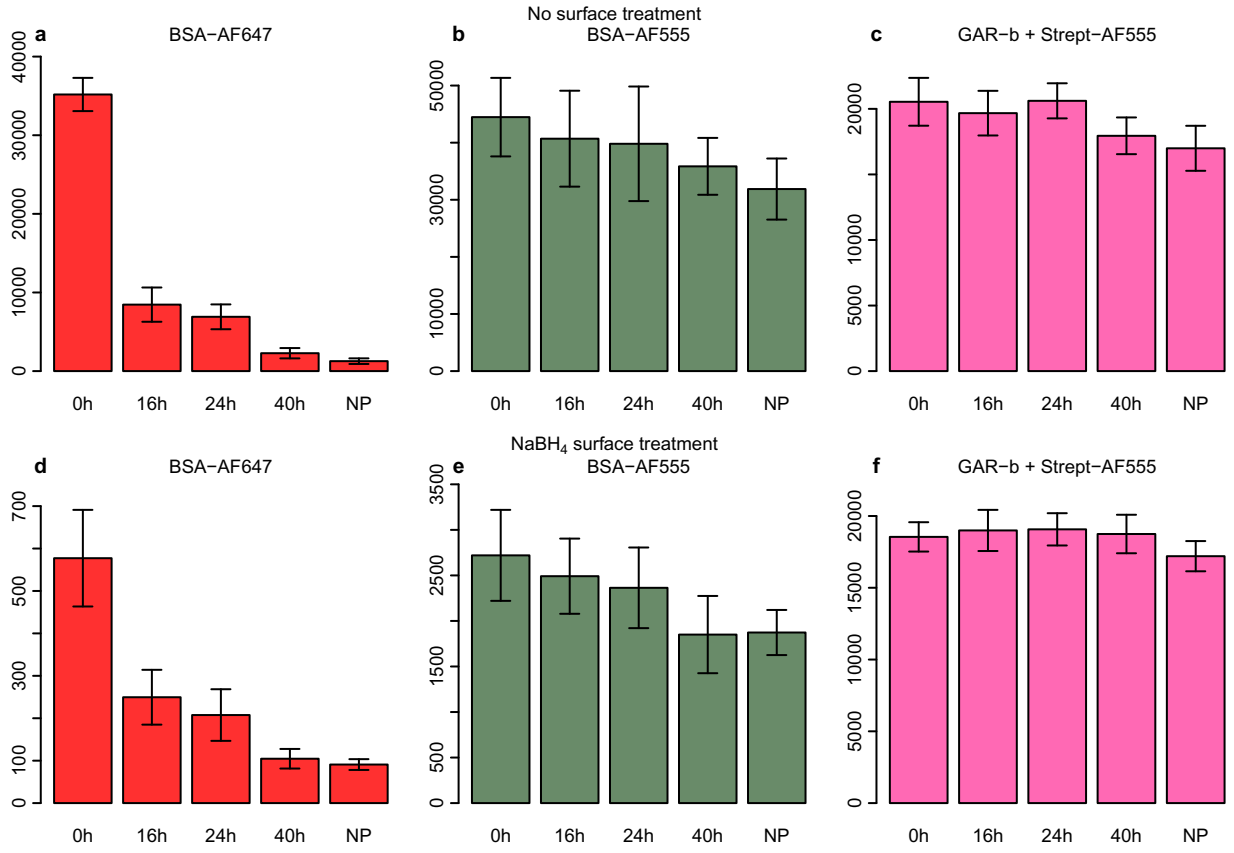

FIGURE D.S32: **Calibrants dry stability on PolyAn 2D Epoxy.** BSA-AF647, BSA-AF555 and GAR-b were spotted onto PolyAn 2D Epoxy slides and allowed to incubate for 24 h. Slides were then washed, received no treatment (**a, b, c**) or an $NaBH_4$ treatment (**d, e, f**), blocked and the spots were protected with dAb printing buffer at different times (or none before processing: NP), and finally incubated with Strept-AF555.

We also sought to determine whether AF647 and AF555 fluorophores are stable while awaiting scanning (at normal room temperature, normal humidity, in the dark) by spotting GAR-AF555 and GAR-AF647 on slides and waiting up to 25 h before scanning. Figure D.S33 shows that both AF555 and AF647 were stable during this time. As a last verification step of the fluorophores stability in cAb printing buffer, we prepared aliquots of BSA-AF555, BSA-AF647 and h-AF555 (with and without unlabeled GAR) and stored them for 24 and 72 h at 25, 4 and −20 °C. We found that while h-AF555 with and without GAR was stable for up to 72 h in cAb printing buffer at all temperatures, BSA-AF555 and BSA-AF647 suffered from degradation of the fluorescence signal, albeit at different rates. BSA-AF647 signal intensity degraded ∼3 × as fast as that of BSA-AF555 (figure D.S34).

To verify that the chosen spot calibrant (BSA-AF555) fits best with the rest of the assay, we verified which fluorescence channel had the best signal to noise ratio. We obtained more fluorescence from Strept-AF647 than Strept-AF555 (figure D.S35) using our scanner and the cAb printing buffer spotted by itself without any molecule leaves an increase in background fluorescence that is greater in the green channel than red channel (figure D.S36). Therefore the chosen spot calibrant was used in a channel with greater background and less sensitivity, which is acceptable because the spot calibrant was spiked at a concentration that led to signal intensities well above the LOD for this channel. On the other hand the more sensitive red channel was left for Strept-AF647 which measured signal intensities across several order of magnitudes of antigen concentrations.

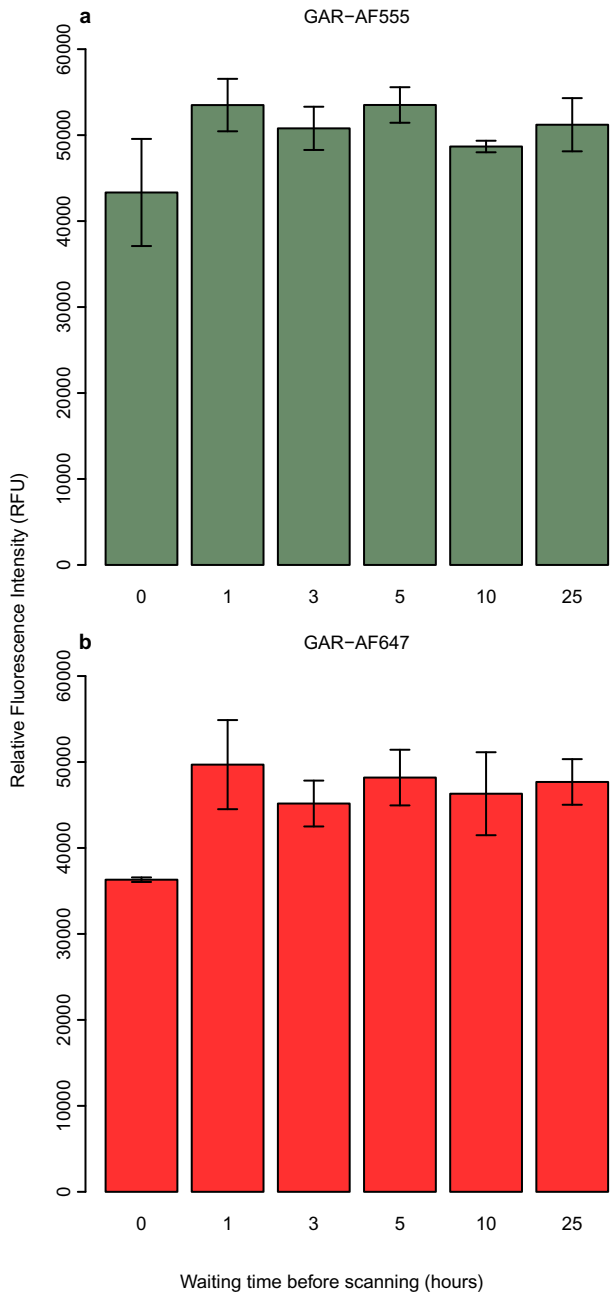

FIGURE D.S33: **Fluorophores stability before scanning.** Xenobind slides were spotted with **a** GAR-AF555 and **b** GAR-AF647 and incubated overnight for binding. Slides were then washed and incubated in the scanner for a number of hours before scanning.

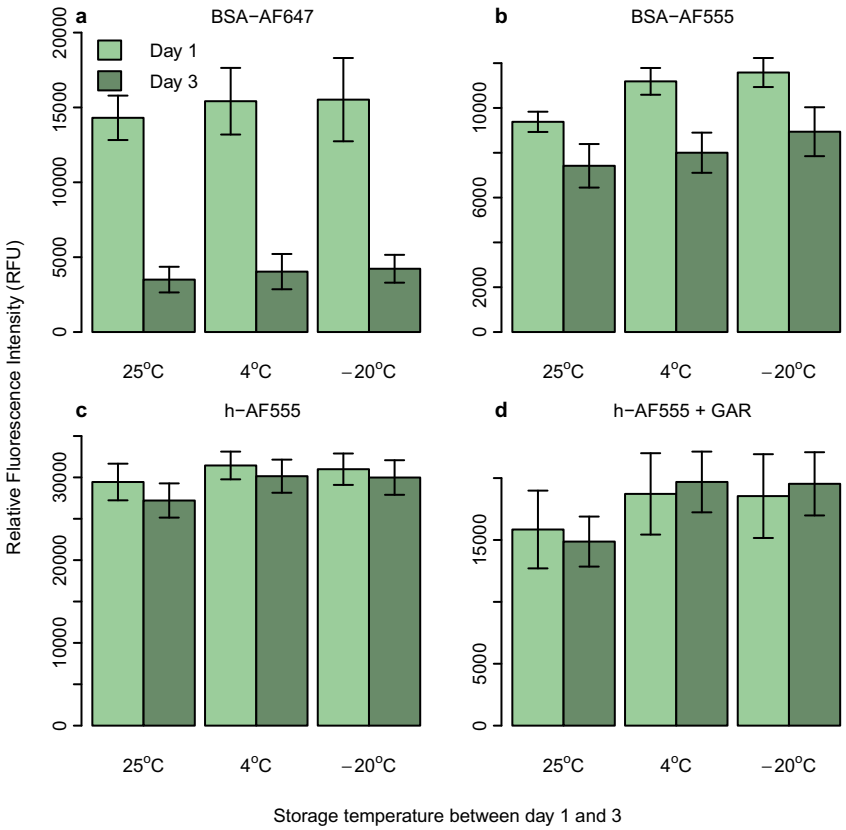

FIGURE D.S34: **Spot calibrants stability at different storage temperatures. a** BSA-AF647, **b** BSA-AF555, and h-AF555 without **c** or with **d** GAR were prepared in 2 M betaine + 25 % 2,3-butanediol. Aliquots were stored at three different temperatures for one (light green) or three (dark green) days. Aliquots that were retrieved after one day of storage were spotted onto a Xenobind slide, incubated and stored dry in vacuum while awaiting the same processing two days later with the remaining aliquots. Both slides were scanned together for quantitative comparison.

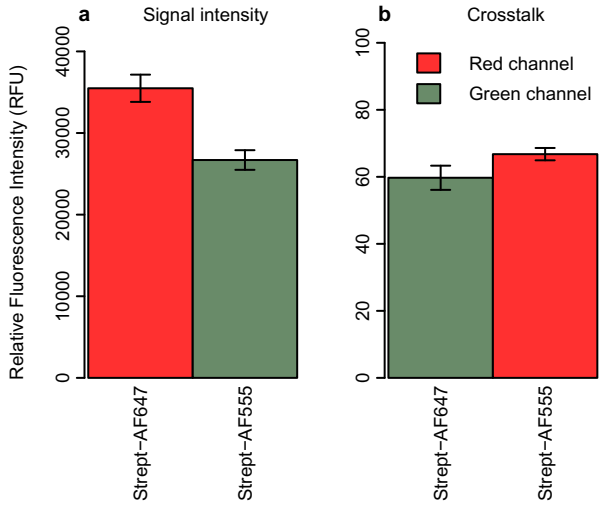

FIGURE D.S35: **Block calibrant signal intensity and crosstalk.** GAR-b was spotted onto slides and incubated overnight. Slide were then washed, blocked and incubated with either Strept-AF647 or -AF555. **a** Signal intensity from Strept-AF647 is greater than Strept-AF555. **b** Crosstalk from Strept-AF555's green channel into the red channel is more significant than the crosstalk from Strept-AF647's red channel into the green channel.

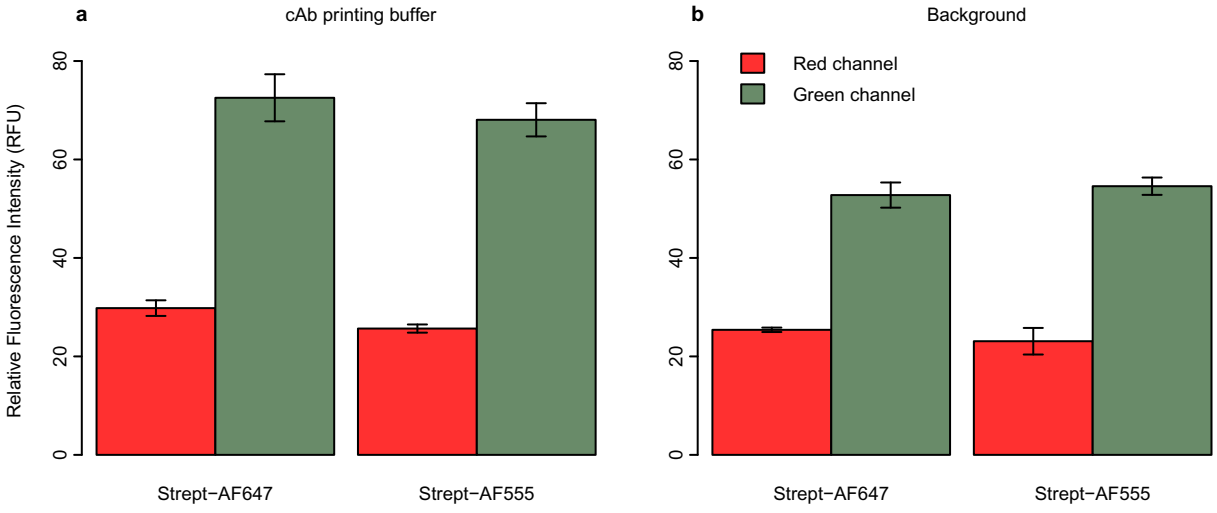

FIGURE D.S36: **cAb printing buffer and background signal intensity.** cAb printing buffer (**a**) was spotted onto slides and incubated overnight. Slides were then washed, blocked and incubated with either Strept-AF555 or -AF647. Background (**b**) refers to extracted data where nothing was spotted onto the slide. cAb printing buffer adds fluorescence intensity in the green channel, but not the red channel.

Spot calibration proof of concept

Fluorescence intensity data from ACM assays are heteroskedastic (figure D.S37). In order to normalize the amount of standard deviation accross the whole antigen range of individual assays, fluorescence intensity is log-transformed, which makes the data homoskedastic. In order for calibrant signals to be compared to assay signals, log-transformation allows both signals to be compared with similar standard deviations.

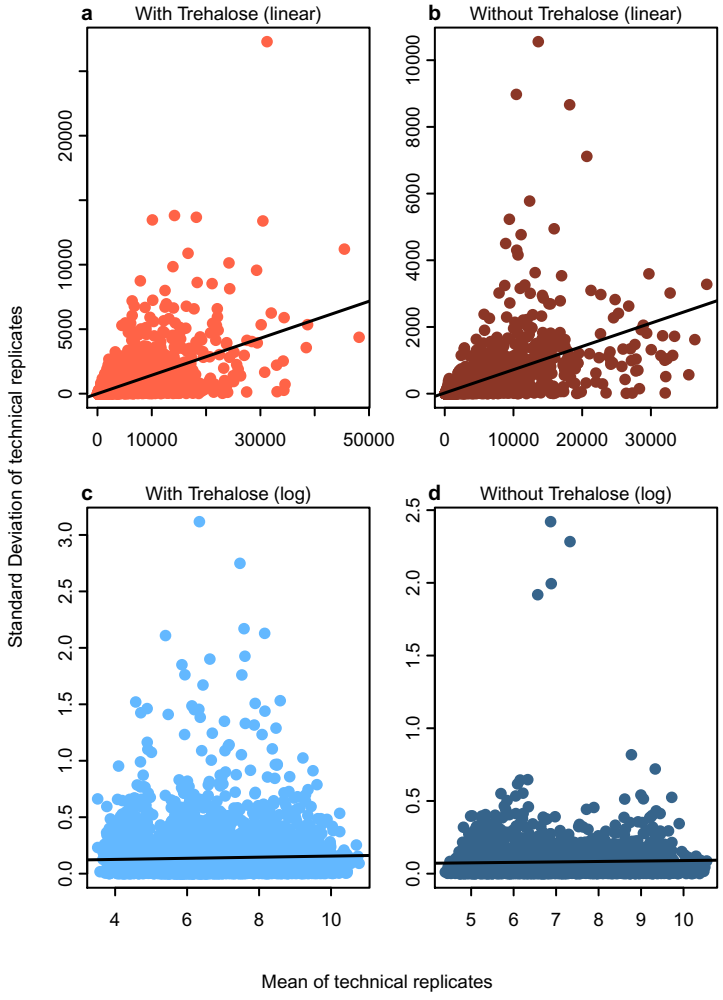

FIGURE D.S37: **Heteroskedasticity of fluorescence signal values.** The standard deviation (SD) is plotted against the mean of all technical replicates found on the three standard curves for the experiment with trehalose (**a, c**) and without trehalose (**b, d**). Data is either in the linear (**a, b**) or log (**c, d**) domain. Black lines are linear fits of all the points for each graph. Fluorescence values are heteroskedastic, and log-transforming the data makes it homoskedastic.

Comparison of calibration algorithms

In order to test the performance of calibration, validation samples were prepared from serial mixing of two different pooled normal serum samples (pnSerum1 and pnSerum2, figure D.S38). Figure D.S39 shows the measured quantities of Ang1, HGF-R, MCP4 and VEGFR2 in pnSerum1 and pnSerum2 at dilutions 1:3 and 1:50. None of the proteins showed significant differences in the quantities measured. Since they were different samples, a measure of residual error [146] was calculated rather than a coefficient of variation. Residual error measures how far away each data point is from the linear regression through all data points. The measure of coefficient of variation is the same if one assumes that the linear regression through all the points constitutes a completely horizontal line. Both experiments had validation samples located throughout their layout.

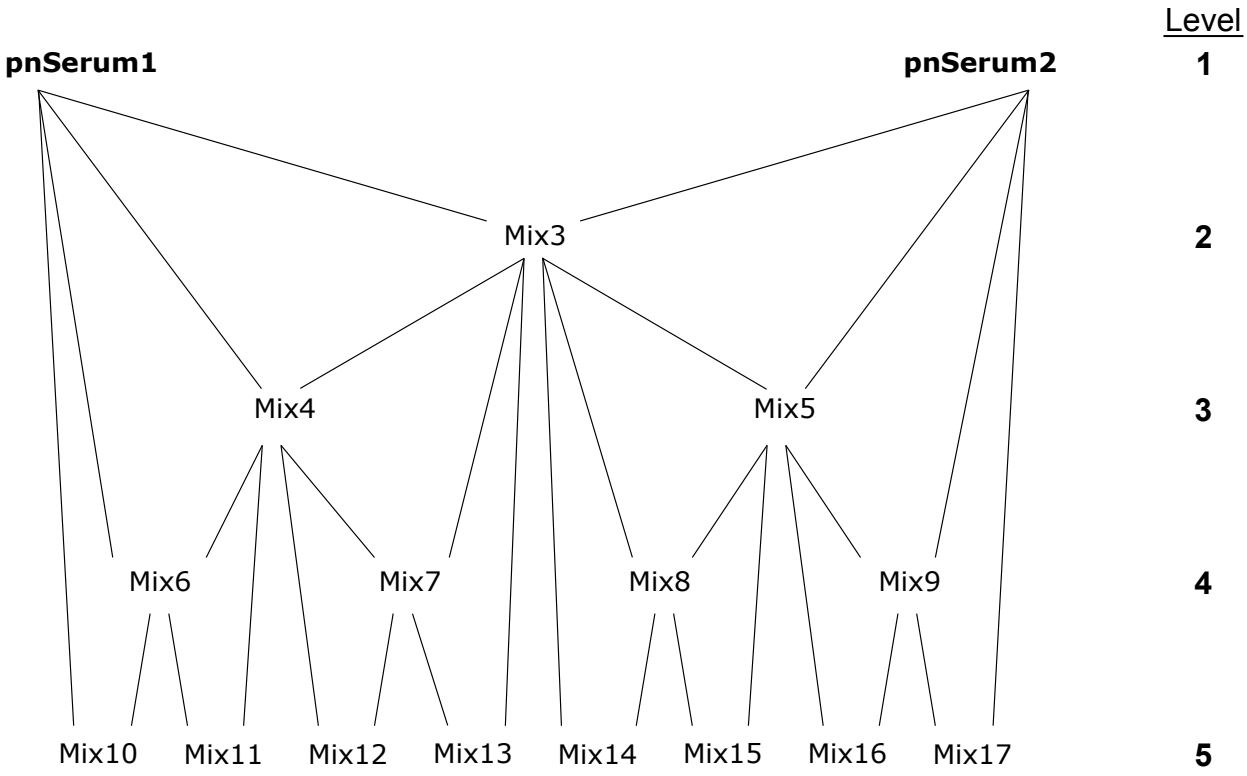

FIGURE D.S38: **Generation of validation samples from mixing pnSerum1 and pnSerum2.** Two different pooled normal serum samples (pnSerum1 and pnSerum2) were mixed to generate a group of 17 samples whose protein values theoretically form a linear gradient which may be differentiated when measured if the original values in pnSerum1 and pnSerum2 are significantly different.

Calibrating two different replicate samples with a single calibration slope estimated from one of the replicate samples led to a much greater improvement in reproducibility in that replicate sample and small to little improvement in the other replicate sample (figure D.S40). Also, the mean calibration slope estimated from low-dilution replicates improved low-dilution replicates

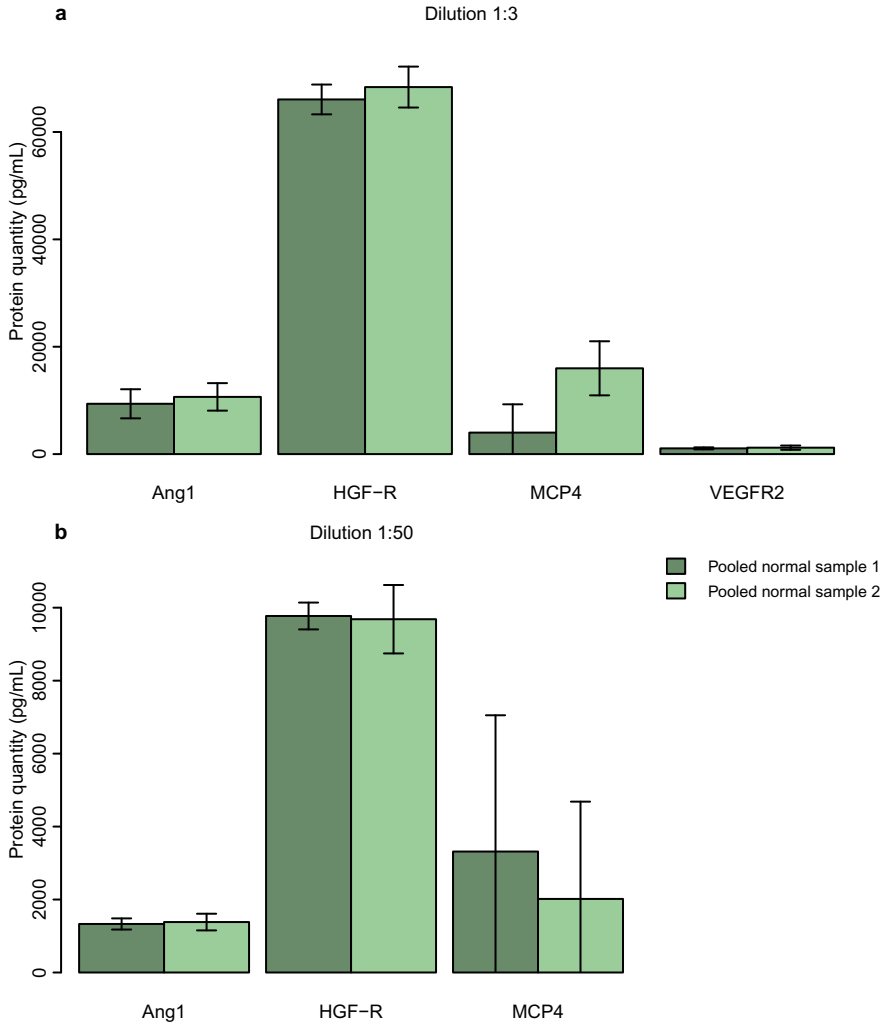

FIGURE D.S39: **Quantities of four proteins in two pnSerum sample replicates.** The quantities of four proteins in two different pnSerum samples at dilution 1:3 (**a**) and 1:50 (**b**) are shown in an MSA. The quantity of VEGFR2 is not detectable in either samples at dilution 1:50. cAbs were spotted with 2 M betaine + 25 % 2,3-butanediol printing buffer.

reproduciblity more than high-dilution replicates, and calibration slopes estimated using blanks did not improve reproducibility in most cases.

A comparison of uncalibrated data to data calibrated with the five algorithms or the combined algorithm in terms of residual errors of validation samples, LOD, quantification range (QR) and accuracy range (AR) shows that sensitivity was worse in the large-scale experiment with trehalose coating (figure D.S41). Because the estimated calibration slopes are not valid in the antigen concentration range containing the LOD, sensitivity is made worse by calibration in the large-scale experiment with trehalose coating, while it is left unchanged in the experiment without trehalose coating of slides. In both experiments, residuals errors improved in the combined algorithm compared to uncalibrated data, and QR was relatively unchanged. Too few proteins had a calculated AR (with curve precision <25 %) in the large-scale experiment with trehalose coating of slides to really be able to compare the effect of calibration.

In order to find the most suitable method for estimating calibration slopes, we first compared different parameters (mean vs median, high vs low number of local groups, number of replicate types and dilutions) for each of the four method presented in terms of changes in reproducibility, residual error, LOD, QR and AR from uncalibrated raw data to calibrated data using the combined algorithm (figures D.S42 to D.S48). We found that in both experiments, calculating the median of local calibration slopes was better than the mean (for CSE_{local} and $CSE_{local\text{-}PPD}$). For the large-scale experiment with trehalose coating of slides, a high number of local groups led to better reproducibility whereas the opposite was true for the large-scale experiment without trehalose coating of slides. For CSE_{global} in the case of the large-scale experiment with trehalose coating, using the low dilution of all three types of replicates (pnSerum, pnPlasma, and pnCSF) led to better reproducibility, and similarly for $CSE_{global\text{-}PPD}$, using the appropriate dilution for all three replicate types improved reproducibility the most, in spite of the fact that many proteins was found in much lower quantities in pnCSF. In the experiment without trehalose coating of slides where a single replicate type (pnSerum) was used at three different dilutions (1:3, 1:30 and 1:50), using the two lower dilution for CSE_{global} led to better reproducibility. No comparison could be made for this experiment for $CSE_{global\text{-}PPD}$ as a single dilution was picked for each protein.

A final comparison between methods was made with the parameters that gave the best improvement in reproducibility for each method. As seen in figure D.S49, reproducibility (from 39.4 % to 27.4 %) and residual error (from 31.7 % to 30.6 %) was best improved by CSE_{local} for the experiment with trehalose coating, even slightly improving the median LOD for this experiment (from 411 pg/mL to 400 pg/mL). On the other hand, the experiment without trehalose coating benefited most from calibration using the $CSE_{local\text{-}PPD}$ method (figure D.S50), with improvements in reproducibility (from 37.1 % to 25.4 %) and residual error (from 41.6 % to 36.3 %) although the median LOD became worse with this method (from 192 pg/mL to 346 pg/mL).

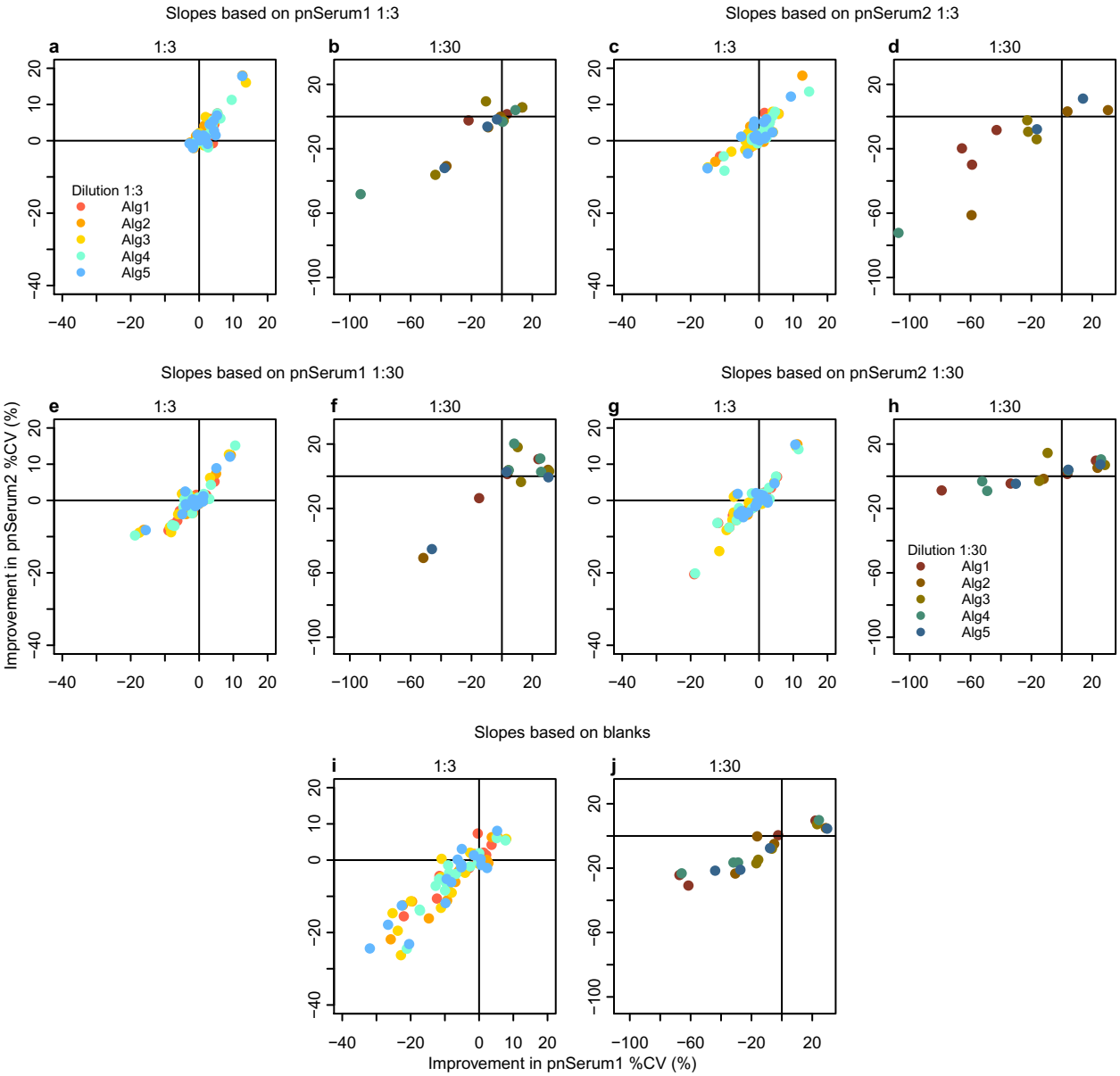

FIGURE D.S40: **Comparison of data sets used for calibration slope estimation.** Four proteins in two normal pooled sample replicates (pnSerum1 and pnSerum2) were quantified on PolyAn 2D Aldehyde slides. Calibration was done with slopes calculated from the mean of **a-b** pnSerum1 replicates at dilution 1:3, **c-d** pnSerum2 replicates at dilution 1:3, **e-f** pnSerum1 replicates at dilution 1:30, **g-h** pnSerum2 replicates at dilution 1:30 and **i-j** blanks. For each pair of graphs, the left graph corresponds to the correlation between improvements in reproducibility of pnSerum1 and pnSerum2 at dilution 1:3, and in the right graph, dilution 1:30.

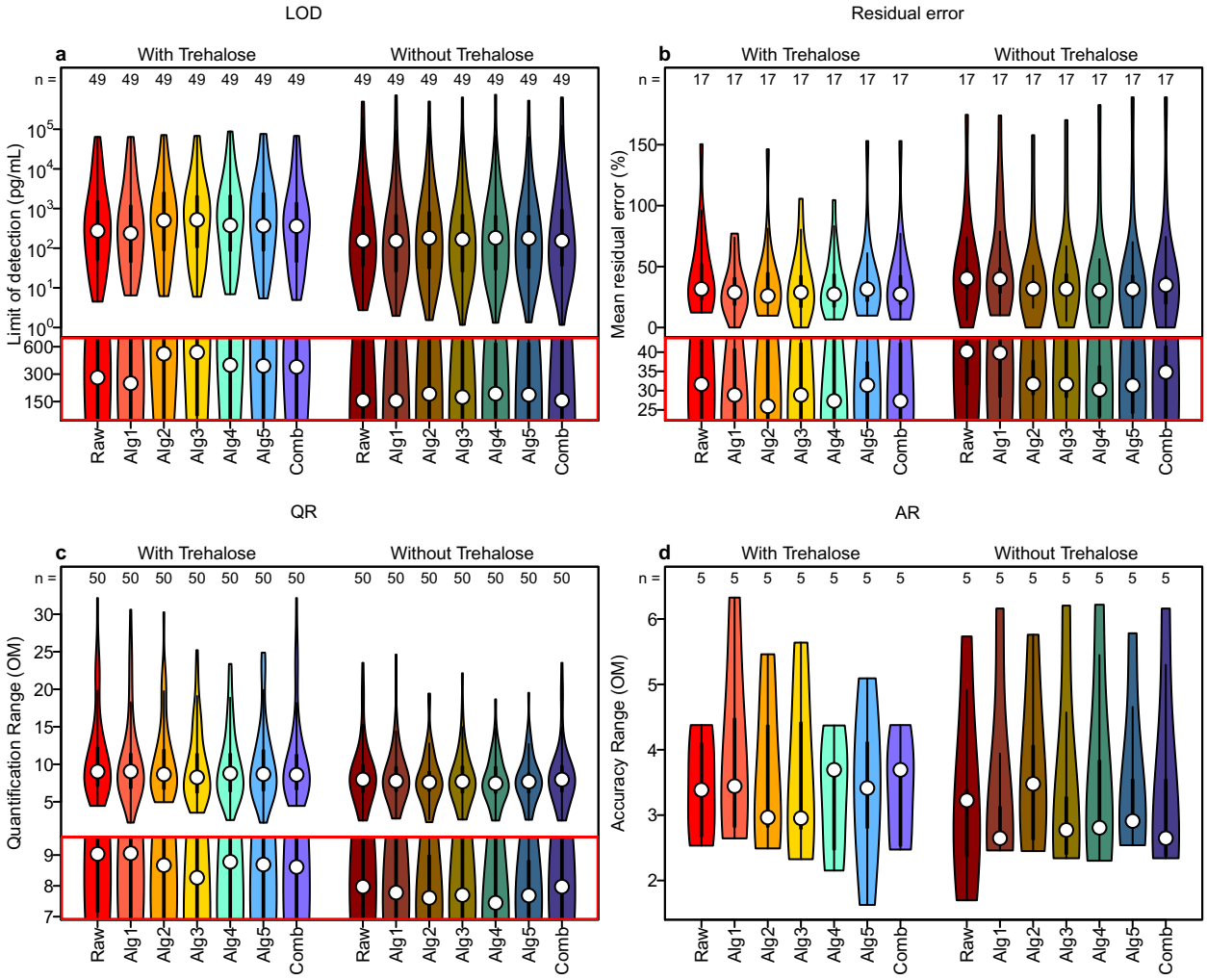

FIGURE D.S41: **Calibration algorithms comparison of LOD, residual error, QR and AR.** Calibration algorithms are compared in terms of (**a**) LOD, (**b**) validation samples mean residual error, (**c**) QR and (**d**) AR in two different large experiments, one with trehalose coating (left data set of each graph) and the other without (right data set of each graph). Only proteins for which a value was obtained for all calibration algorithms in both experiments are included in the comparison. Only proteins where the performance measures were calculated for all algorithms in both experiments are considered for each of the four performance measures. Combined data is based on reproducibility of pnSerum at dilutions 1:3 and 1:30.

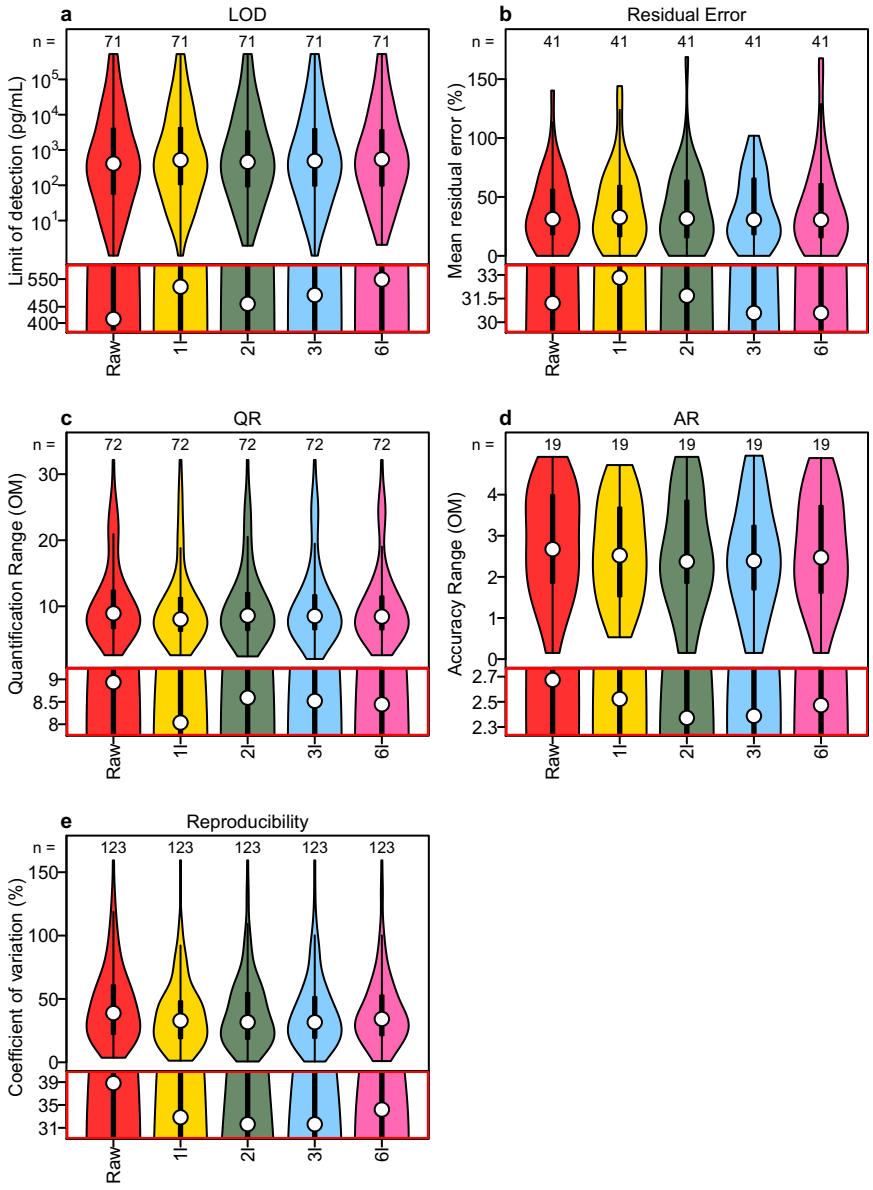

FIGURE D.S42: **Comparison of parameters for CSE_{global} with trehalose.** Comparison of (**a**) LOD, (**b**) validation samples mean residual error at the chosen dilution for each protein, (**c**) QR, (**d**) AR and (**e**) reproducibility at the chosen dilution for each protein from standard curves generated using a global method of calibration slope estimation in the experiment with trehalose coating. Calibration slopes and were estimated using calibration slopes from pnSerum 1:3 (1I), the mean of pnSerum 1:3 and pnPlasma 1:3 (2I), the mean of pnSerum 1:3, pnPlasma 1:3 and pnCSF 1:3 (3I) or the mean of pnSerum, pnPlasma at dilutions 1:3 and 1:30 and pnCSF at dilutions 1:3 and 1:15 (6I). Combined algorithm was chosen by ranking from the same replicates as for the calibration slope estimation. Proteins without a standard curve or whose standard curve did not allow for the quantification of all sample replicates in all parameter sets were not considered.

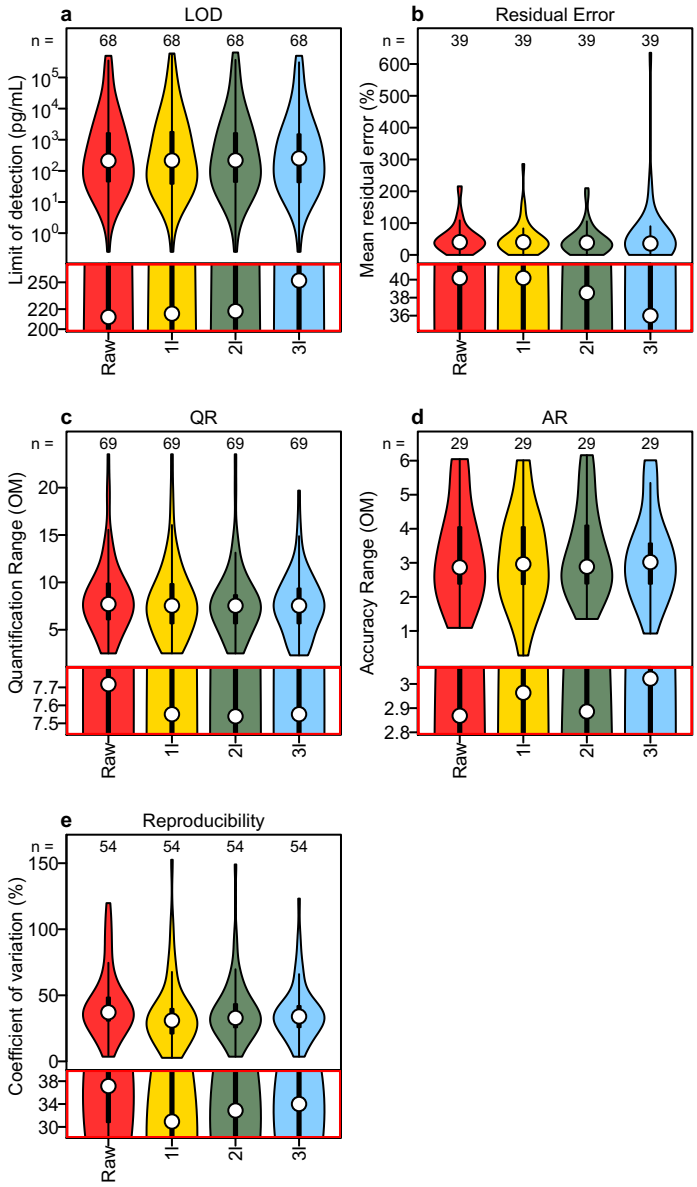

FIGURE D.S43: **Comparison of parameters for CSE_{global} without trehalose.** Comparison of (**a**) LOD, (**b**) validation samples mean residual error at the chosen dilution for each protein, (**c**) QR, (**d**) AR and (**e**) reproducibility at the chosen dilution for each protein from standard curves generated using a global method of calibration slope estimation in the experiment without trehalose coating. Calibration slopes were estimated using calibration slopes from pnSerum 1:3 (1I), the mean of pnSerum at dilutions 1:3 and 1:30 (2I) and the mean of pnSerum at dilutions 1:3, 1:30 and 1:50 (3I). Combined algorithm was chosen by ranking from the same replicates as for the calibration slope estimation. Proteins without a standard curve or whose standard curve did not allow for the quantification of all sample replicates in all parameter sets were not considered.

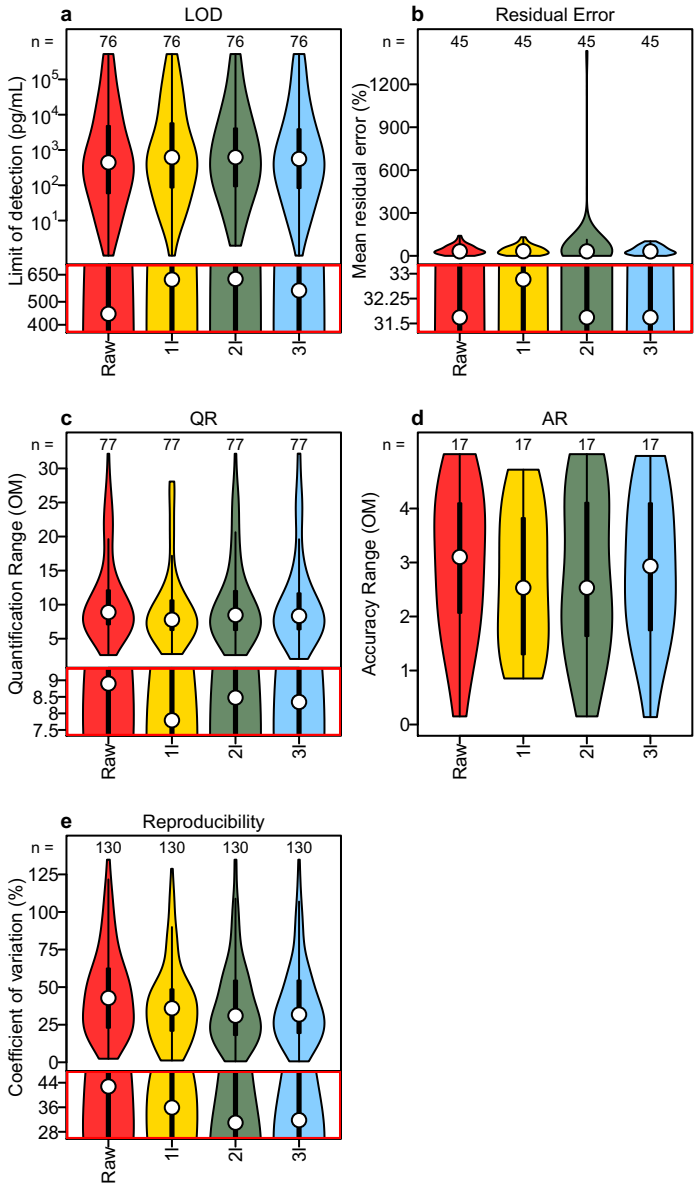

FIGURE D.S44: **Comparison of parameters for $CSE_{Global\text{-}PPD}$ with trehalose.** Comparison of (**a**) LOD, (**b**) validation samples mean residual error at the chosen dilution for each protein, (**c**) QR, (**d**) AR and (**e**) reproducibility at the chosen dilution for each protein from standard curves generated using a global method of calibration slope estimation in the experiment with trehalose coating. Calibration slopes were estimated using calibration slopes from pnSerum at the chosen dilution for each protein (1I), the mean of pnSerum and pnPlasma at the chosen dilution for each protein (2I) and the mean of pnSerum, pnPlasma and pnCSF at the chosen dilution for each protein (3I). Combined algorithm was chosen by ranking from the same replicates as for the calibration slope estimation. Proteins without a standard curve or whose standard curve did not allow for the quantification of all sample replicates in all parameter sets were not considered.

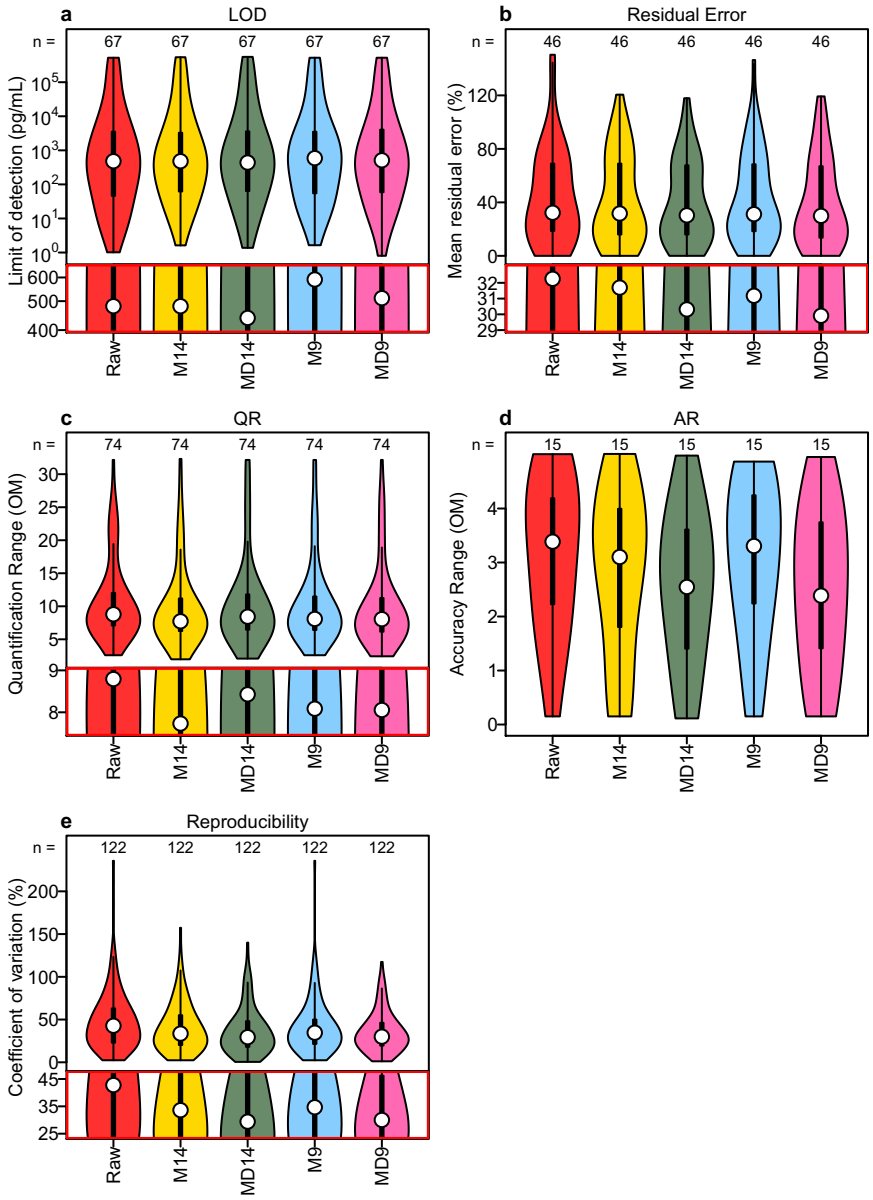

FIGURE D.S45: **Comparison of parameters for CSE_{Local} with trehalose.** Comparison of (**a**) LOD, (**b**) validation samples mean residual error at the chosen dilution for each protein, (**c**) QR, (**d**) AR and (**e**) reproducibility at the chosen dilution for each protein from standard curves generated using a local method of calibration slope estimation in the experiment with trehalose coating. Calibration slopes and were estimated using combinations of mean or median of calibration slopes calculated from local groups with a minimum of 2 (high number of local groups: 14) or 3 (low number of local groups: 9) sample replicates per local group. Combined algorithm was chosen by ranking from all sample replicates types and dilutions. Proteins without a standard curve or whose standard curve did not allow for the quantification of all sample replicates in all parameter sets were not considered.

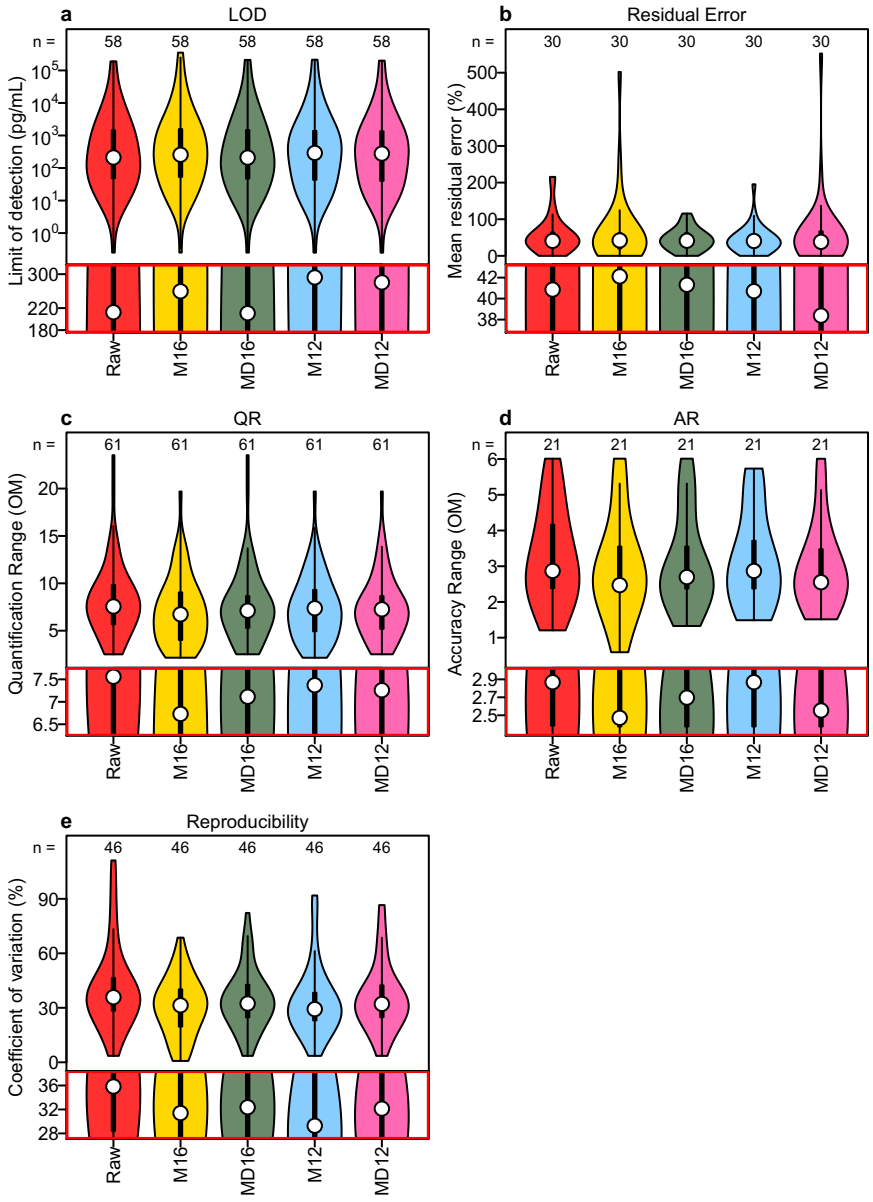

FIGURE D.S46: **Comparison of parameters for CSE_{Local} without trehalose.** Comparison of (**a**) LOD, (**b**) validation samples mean residual error at the chosen dilution for each protein, (**c**) QR, (**d**) AR and (**e**) reproducibility at the chosen dilution for each protein from standard curves generated using a local method of calibration slope estimation in the experiment without trehalose coating. Calibration slopes and were estimated using combinations of mean or median of calibration slopes calculated from local groups with a minimum of 2 (high number of local groups: 14) or 3 (low number of local groups: 9) sample replicates per local group. Combined algorithm was chosen by ranking from all sample replicates types and dilutions. Proteins without a standard curve or whose standard curve did not allow for the quantification of all sample replicates in all parameter sets were not considered.

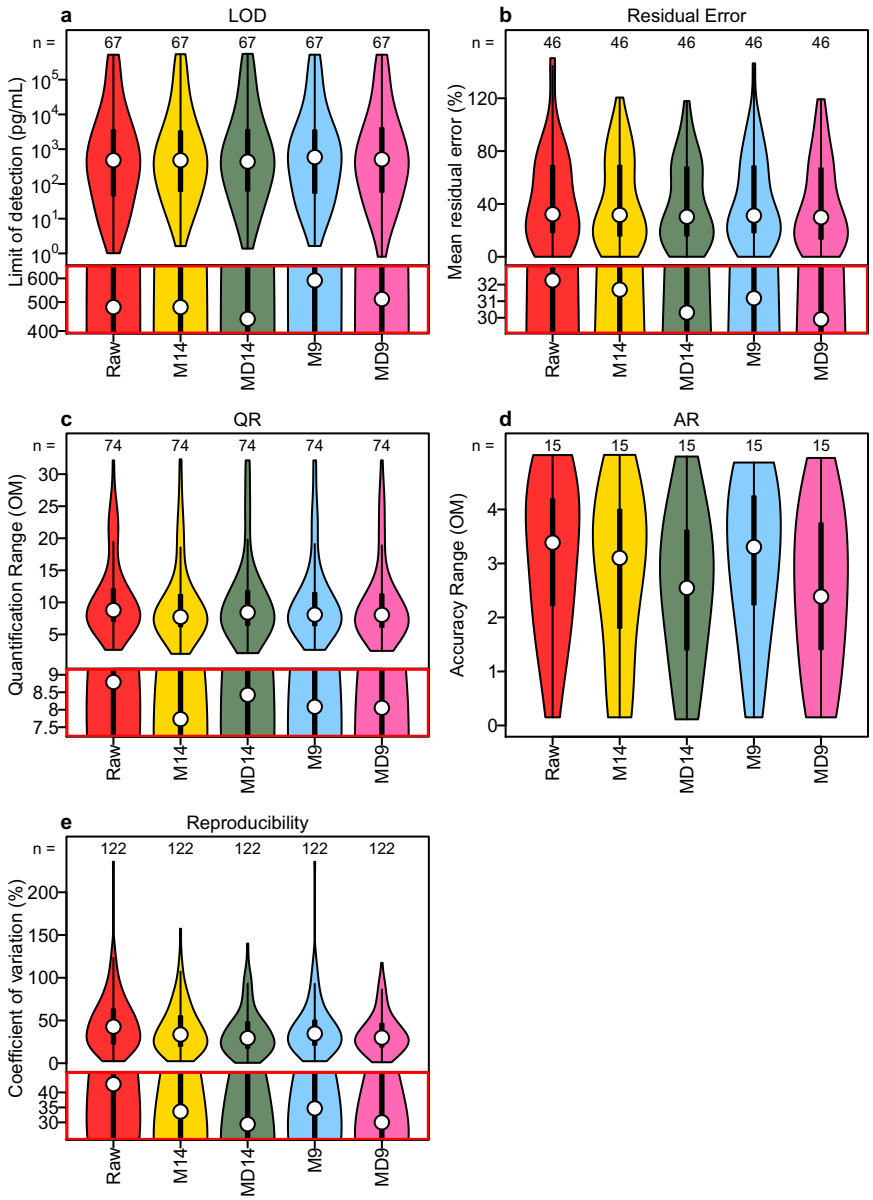

FIGURE D.S47: **Comparison of parameters for $CSE_{Local\text{-}PPD}$ with trehalose.** Comparison of (**a**) LOD, (**b**) validation samples mean residual error at the chosen dilution for each protein, (**c**) QR, (**d**) AR and (**e**) reproducibility at the chosen dilution for each protein from standard curves generated using a local method of calibration slope estimation in the experiment with trehalose coating. Calibration slopes and were estimated using combinations of mean or median of calibration slopes calculated from local groups with a minimum of 2 (high number of local groups: 14) or 3 (low number of local groups: 9) sample replicates per local group. Only local groups which contain the sample replicates at the chosen dilution for each protein were considered. Combined algorithm was chosen by ranking from all sample replicates types at the chosen dilution for each protein. Proteins without a standard curve or whose standard curve did not allow for the quantification of all sample replicates in all parameter sets were not considered.

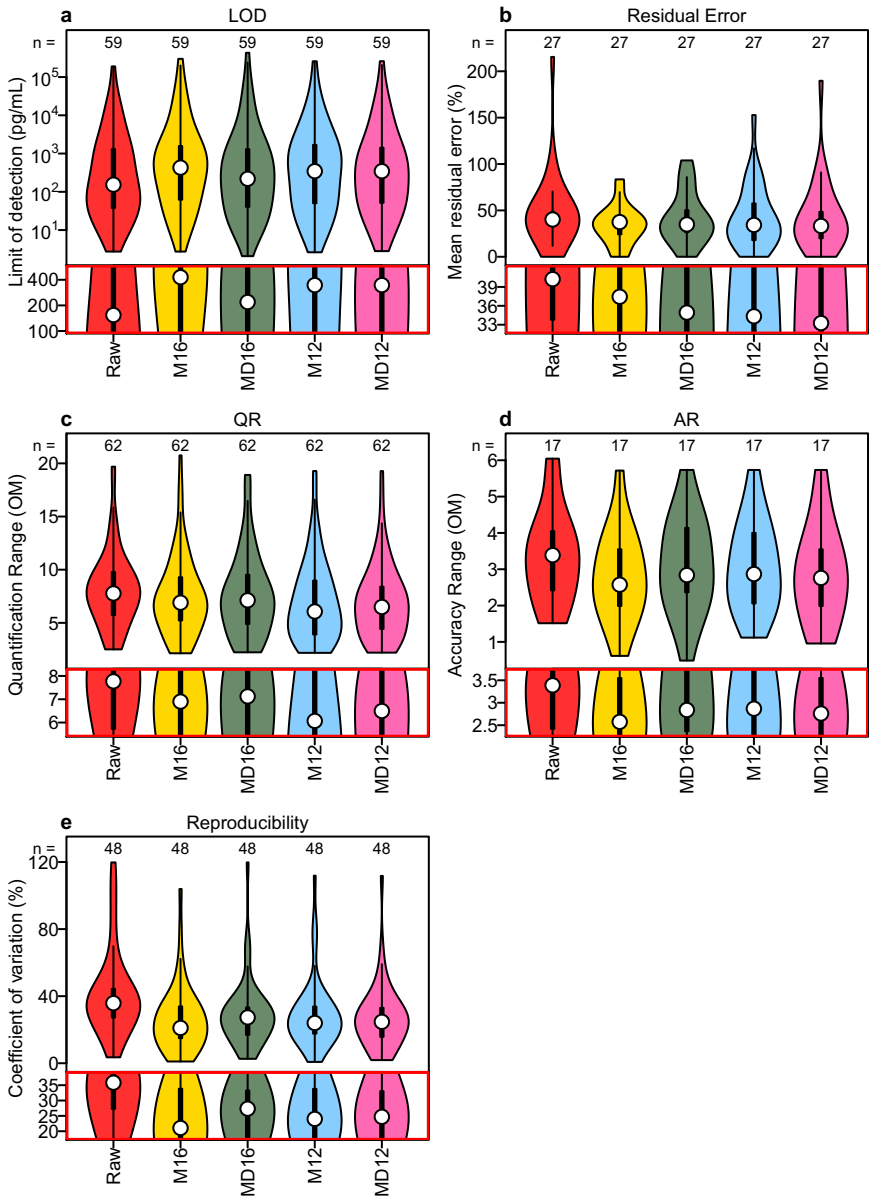

FIGURE D.S48: **Comparison of parameters for $CSE_{Local\text{-}PPD}$ without trehalose.** Comparison of (**a**) LOD, (**b**) validation samples mean residual error at the chosen dilution for each protein, (**c**) QR, (**d**) AR and (**e**) reproducibility at the chosen dilution for each protein from standard curves generated using a local method of calibration slope estimation in the experiment without trehalose coating. Calibration slopes and were estimated using combinations of mean or median of calibration slopes calculated from local groups with a minimum of 2 (high number of local groups: 16) or 3 (low number of local groups: 12) sample replicates per local group. Only local groups which contain the sample replicates at the chosen dilution for each protein were considered. Combined algorithm was chosen by ranking from the sample replicates at the chosen dilution for each protein. Proteins without a standard curve or whose standard curve did not allow for the quantification of all sample replicates in all parameter sets were not considered.

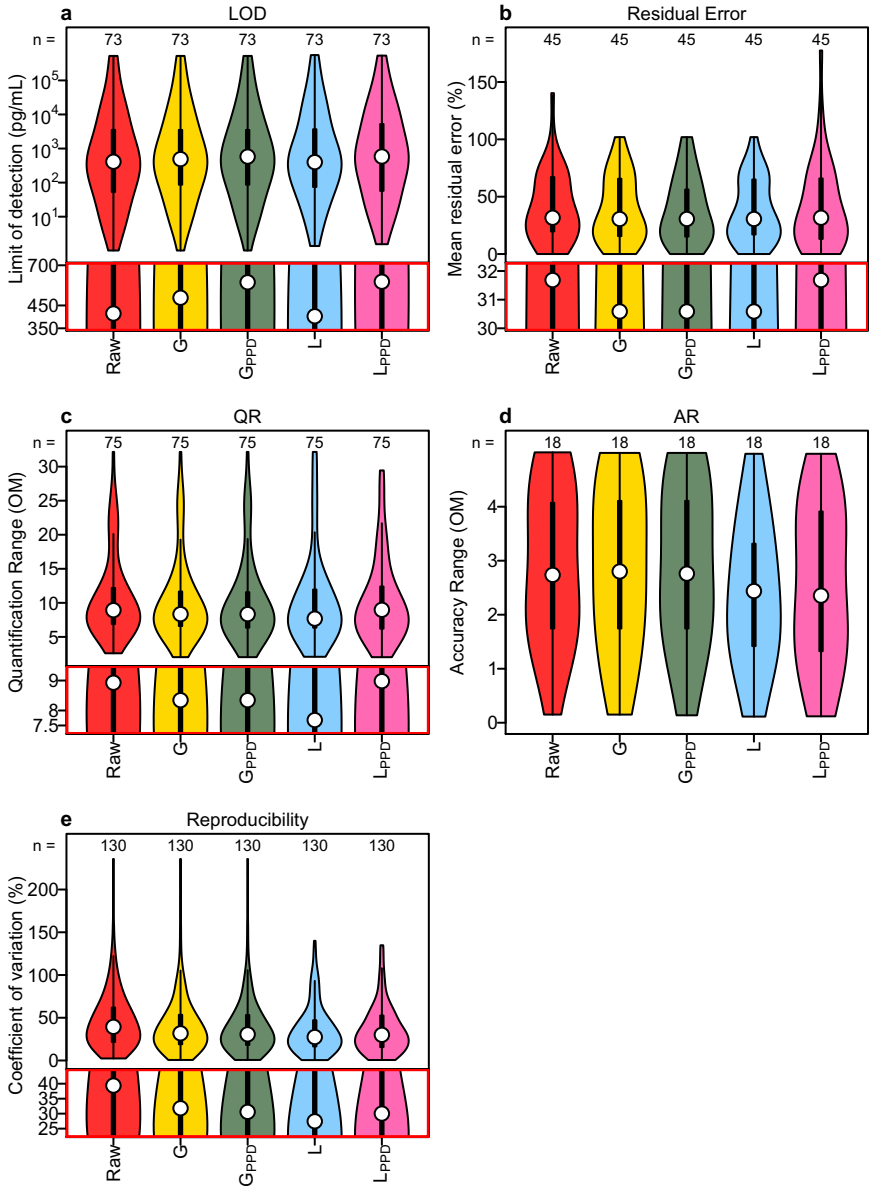

FIGURE D.S49: **Comparison of CSE methods with trehalose.** Comparison of (**a**) LOD, (**b**) validation samples mean residual error at the chosen dilution for each protein, (**c**) QR, (**d**) AR and (**e**) reproducibility at the chosen dilution for each protein from standard curves generated using a global (G), local (L) or global (G_{PPD}) or local (L_{PPD}) (with consideration for the chosen dilution for each protein) method of calibration slope estimation in the experiment with trehalose coating. Proteins without a standard curve or whose standard curve did not allow for the quantification of all sample replicates in all methods were not considered.

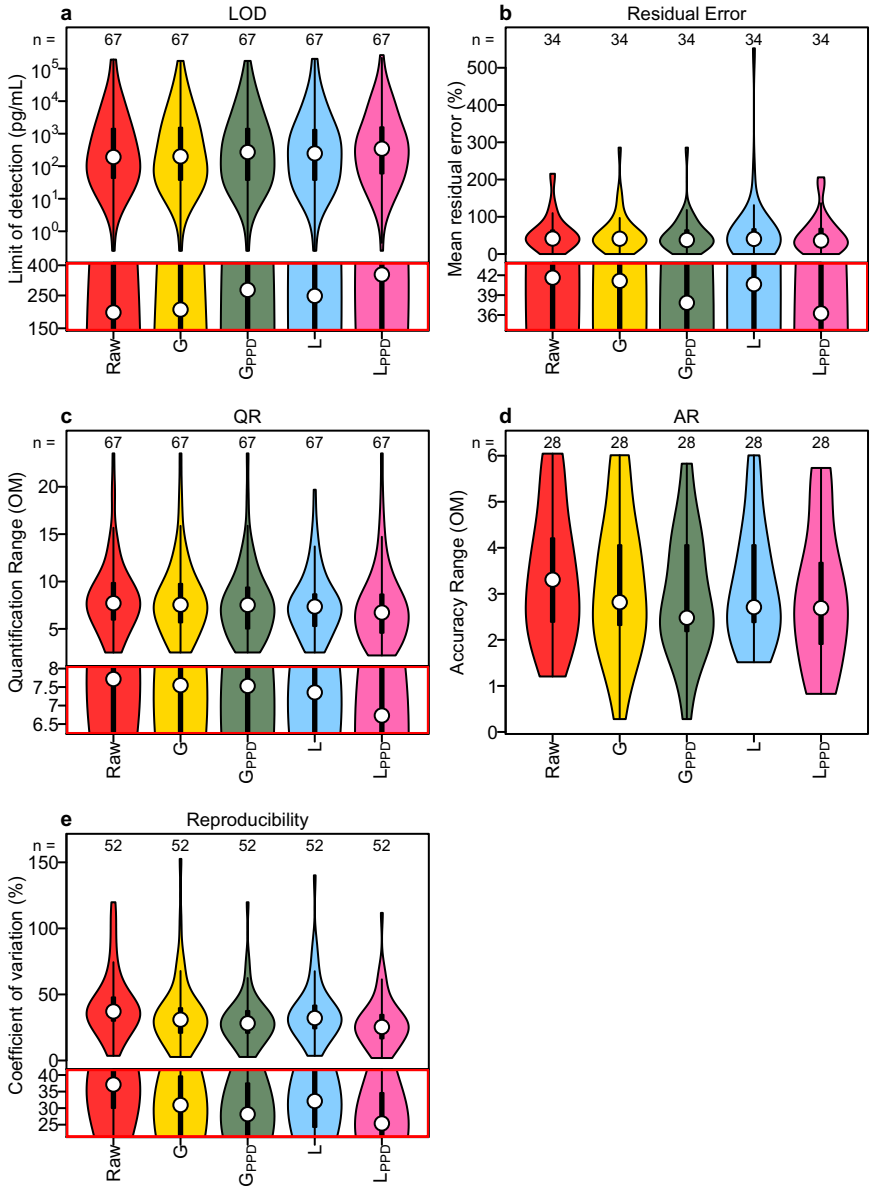

FIGURE D.S50: **Comparison of CSE methods without trehalose.** Comparison of (**a**) LOD, (**b**) validation samples mean residual error at the chosen dilution for each protein, (**c**) QR, (**d**) AR and (**e**) reproducibility at the chosen dilution for each protein from standard curves generated using a global (G), local (L) or global (G_{PPD}) or local (L_{PPD}) (with consideration for the chosen dilution for each protein) method of calibration slope estimation in the experiment without trehalose coating. Proteins without a standard curve or whose standard curve did not allow for the quantification of all sample replicates in all methods were not considered.

Performance of combined calibration

The performance of calibration can be reported for each experiment individually and are shown in figure D.S51. Performance values are reported in tables D.S1 and D.S2.

Reproducibility of all replicates types and dilutions are shown in figure D.S52 for both experiments. In spite of the fact that the same calibration slopes were used for all replicate samples types and dilutions in individual experiments, the reproducibility of all replicates samples types and dilutions improved, except for a single protein detected in pnCSF at high dilution, whose reproducibility worsened slightly.

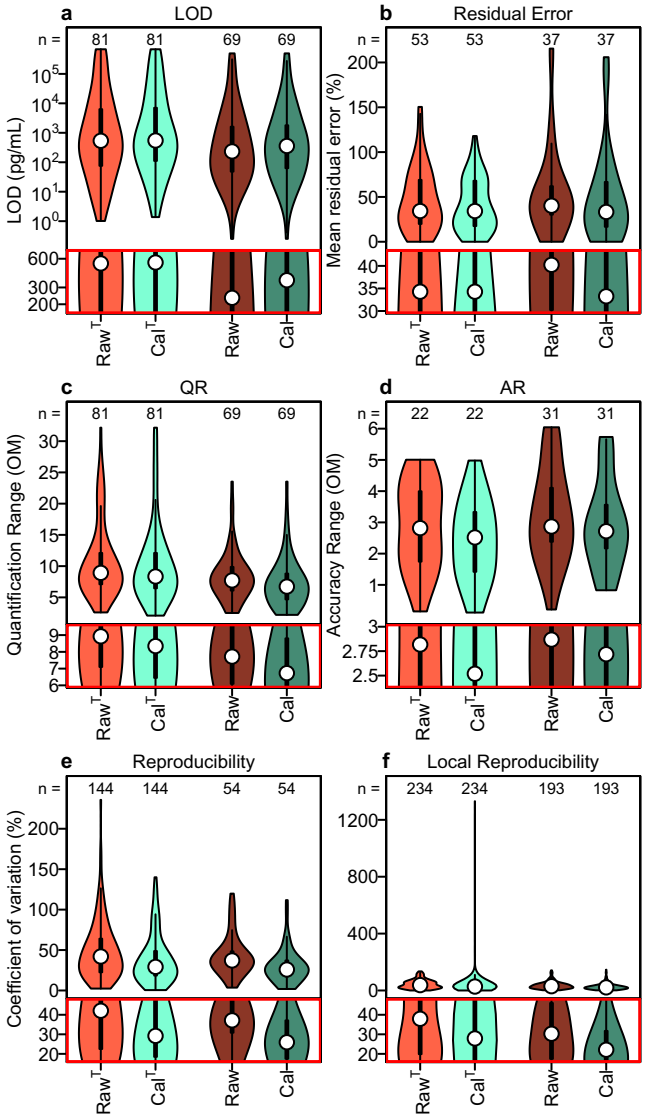

FIGURE D.S51: **Effect of calibration on quantification performance.** Comparison of uncalibrated data to calibrated (using combined algorithm) data with slopes calculated from the median of 14 local groups (with trehalose coating, left of graphs) and the median of 12 local groups with consideration to the chosen protein dilution (without trehalose coating, right of graphs) and their effect on the LOD (**a**), validation samples mean residual error (**b**) at the chosen dilution for each protein, QR (**c**), AR (**d**) and global (**e**) and local (**f**) reproducibility at the chosen dilution for each protein. Proteins with standard curves and unquantified sample replicates were not considered. The list of proteins for each experiment is different and independent.

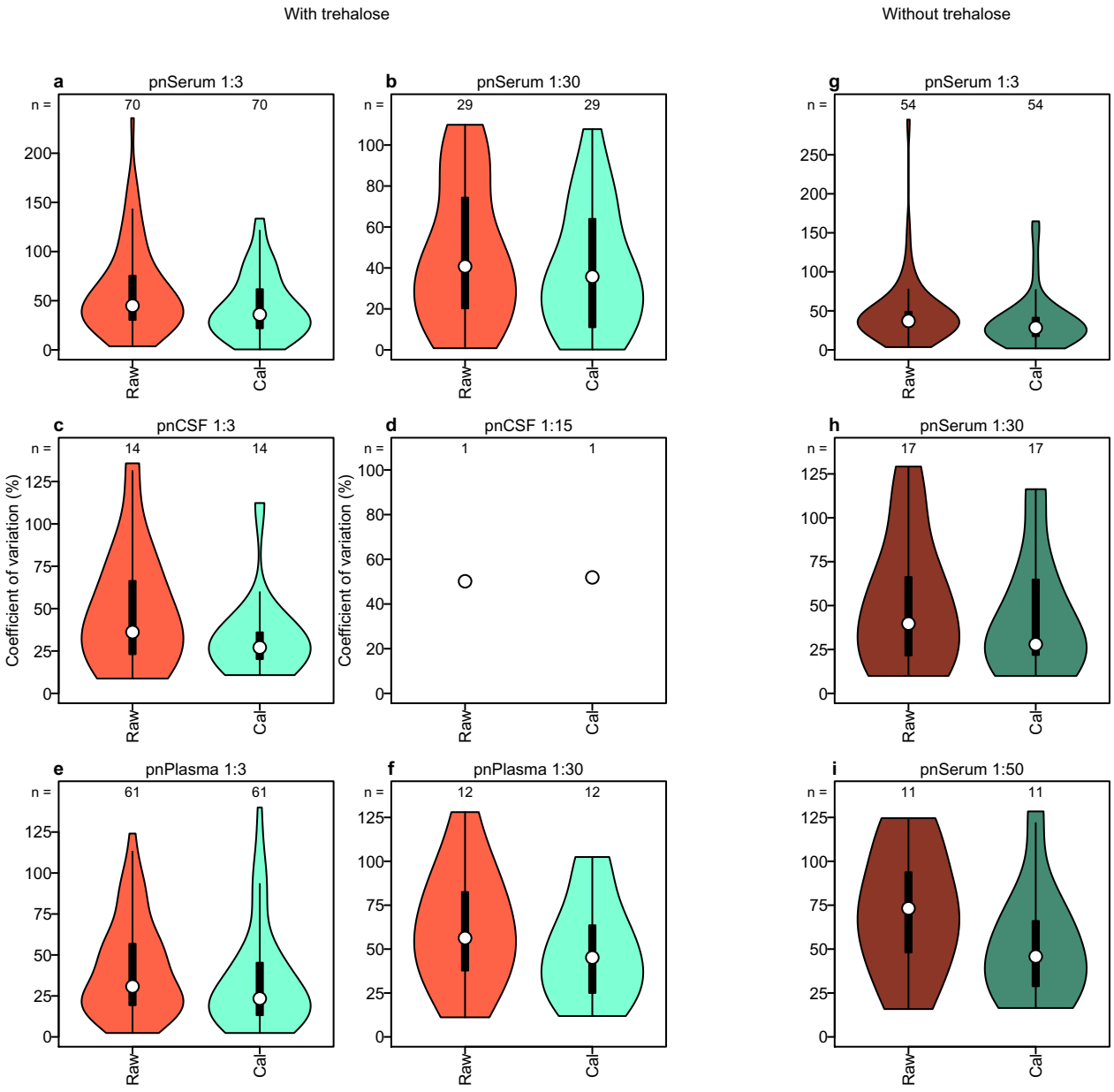

FIGURE D.S52: **Effect of calibration on sample replicates reproducibility.** Improved reproducibility of (**a-f**) six different replicate type and dilution combination in the experiment with trehalose coating and (**g-h**) three different replicate type and dilution combinations in the experiment without trehalose coating. Calibration parameters and methods is the best determined for each experiment. NCSF at dilution 1:15 (**d**) only had one quantifiable sample replicate protein, therefore the interquartile range of reproducibility could not be calculated. In both experiments, all replicates reproducibility are improved with calibration except the single protein quantified in pnCSF at dilution 1:15.

TABLE D.S1: **Calibration improvement of performance.** Only proteins whose performance values could be calculated in uncalibrated and calibrated data were considered, but the list of proteins differ between the two large-scale experiments. Standard deviation for LOD is listed as median ± 1 standard deviation. s.d.: standard deviation.

Performance measure	Slide coating	Uncalibrated Median	Uncalibrated s.d.	Calibrated Median	Calibrated s.d.	n
Reproducibility (%)	Trehalose	42.9	41.7	34.5	30.2	61
	Water	36.8	24.9	26.1	22.3	47
Residual error (%)	Trehalose	33.3	35.8	30.3	30	44
	Water	40.2	43.6	31.7	48.8	32
LOD* (pg/mL)	Trehalose	591	22 - 15785	548	22 - 13361	69
	Water	236	12 - 4581	352	20 - 6142	62
QR (OM)	Trehalose	8.7	6.2	8.3	6.9	69
	Water	7.9	4	7.0	4.1	62
AR (OM)	Trehalose	2.5	1.4	2.5	1.3	21
	Water	2.8	1.4	2.7	1.3	27

*: Median and standard deviation performed on log-transformed data.

TABLE D.S2: **Performance comparison of slide coating.** Only proteins whose performance values could be calculated in uncalibrated and calibrated data in both large-scale experiments were considered. Standard deviation for LOD is listed as median ± 1 standard deviation. s.d.: standard deviation.

Performance measure	Slide coating	Uncalibrated Median	Uncalibrated s.d.	Calibrated Median	Calibrated s.d.	n
Reproducibility (%)	Trehalose	42.2	40.3	30.0	25.5	42
	Water	36.1	26.1	27.2	23.3	42
Residual error (%)	Trehalose	31.5	31.8	24.1	22.3	24
	Water	40.1	36.2	30.6	42.9	24
LOD* (pg/mL)	Trehalose	486	28 - 8463	378	25 - 5743	59
	Water	234	12 - 4611	347	20 - 6155	59
QR (OM)	Trehalose	8.6	6.1	8.3	6.3	59
	Water	8.0	4.1	7.1	4.2	59
AR (OM)	Trehalose	3.6	1.2	2.9	1.2	12
	Water	3.3	1.2	2.4	1.5	12

*: Median and standard deviation performed on log-transformed data.

List of cAbs, Ags and dAb used in experiments

TABLE D.S3: **List of cAbs, Ags and dAbs used in large experiments.** All molecules listed were purchased from R&D Systems unless otherwise specified. cAb and dAb concentrations are µg/mL and Ag starting concentrations are ng/mL except for CA15-3 whose unit of concentration is the U/mL.

			Capture Ab			Antigen		Detection Ab			Reporter Molecule
	Name	Full name	Catalog Number	Species	[cAb]	Catalog Number	[Ag]	Catalog Number	Species	[dAb]	
1	AFP	Alpha feto-protein	H00000174-AP51[1]	mouse	150	ab114216[2]	800	H00000174-AP51[1]	rabbit	52.5	GAR-AF647
2	AHSG	Alpha-2-HS-glycoprotein	MAB11841	mouse	100	1184-PI-050	2000	BAF1184	goat	10	Strept-AF647
3	ALDH1L1	10-formyltetrahydrofolate dehydrogenase	TA600395[3]	mouse	100	TP313720[3]	200	TA700395[3]	mouse	25	Strept-AF647
4	Amphiregulin	Amphiregulin	MAB262	mouse	200	262-AR-100/CF	25	BAF262	goat	10	Strept-AF647
5	Ang1	Angiopoietin 1	MAB9231	mouse	100	923-AN	100	BAF923	goat	10	Strept-AF647
6	Ang2	Angiopoietin 2	MAB098	mouse	100	623-AN	20	BAM0981	mouse	12.5	Strept-AF647
7	BDNF	Brain-derived neurotrophic factor	MAB848	mouse	100	284-BD-005/CF	150	BAM648	mouse	25	Strept-AF647
8	BMP-2	Bone morphogenetic protein 2	MAB3551	mouse	200	35-BM-010/CF	25	BAM3552	mouse	25	Strept-AF647
9	β-NGF	Nerve growth factor	MAB256	mouse	100	256-GF	100	BAF256	goat	20	Strept-AF647
10	BRAF	B-Raf (kinase)	TA600012[3]	mouse	100	TF311013[3]	200	TA700012[3]	mouse	25	Strept-AF647
11	CA15-3	Cancer antigen 15-3 (derived from mucin 1)	10-CA15A[4]	mouse	100	10-C03F[4]	200	10-CA15B[4]	mouse	25	Strept-AF647
12	Cathepsin B	Cathepsin B	MAB2176	mouse	150	953-CY-010	4000	BAM21761	mouse	50	Strept-AF647
13	CCL5	Chemokine (C-Cmotif) ligand 5	MAB678	mouse	100	278-RN-010	200	BAF278	goat	10	Strept-AF647
14	CD14	Cluster of differentiation 14	MAB3833	mouse	100	383-CD-050/CF	2000	BAF383	sheep	10	Strept-AF647
15	CEA	Carcinoembryonic antigen	C1299-87H[5]	mouse	200	C1300-08E[5]	2000	C1299-87E[5]	mouse	50	Strept-AF647
16	c-kit	Mast/stem cell growth factor receptor	MAB332	mouse	200	332-SR-050/CF	1000	BAF332	goat	10	Strept-AF647
17	CRP	C-reactive protein	MAB17071	mouse	100	1707-CR	2000	BAM17072	mouse	10	Strept-AF647
18	CXCL12	Stromal cell-derived factor 1	MAB350	mouse	100	350-NS-010/CF	5000	BAF310	goat	40	Strept-AF647
19	E-Cadherin	Epithelial cadherin	MAB18382	mouse	100	648-EC-100	100	BAF648	goat	10	Strept-AF647
20	EGF	Epidermal growth factor	MAB636	mouse	200	236-EG	200	BAF236	goat	10	Strept-AF647
21	EGF-R	Epidermal growth factor receptor	AF231	goat	100	1095-ER	100	BAF231	goat	10	Strept-AF647
22	Endoglin	Endoglin	MAB10972	mouse	100	1097-EN	200	BAF1097	goat	10	Strept-AF647
23	EpCAM	Epithelial cell adhesion molecule	MAB9601	mouse	200	960-EP-050	50	BAF960	goat	10	Strept-AF647
24	E-selectin	Endothelial-leukocyte adhesion molecule 1	BBA16	mouse	200	ADP1	4000	BBA8	mouse	50	Strept-AF647
25	FAS	Fas cell surface death receptor	MAB144	mouse	200	326-FS	50	BAF326	goat	10	Strept-AF647
26	FAS-L	FAS ligand	MAB126	mouse	200	126-FL-010/CF	50	BAF126	goat	10	Strept-AF647
27	FGF-1	Acidic fibroblast growth factor	H00002246-AP21[1]	rabbit	75	H00002246-P01[1]	500	H00002246-AP21[1]	mouse	30	GAM-AF647
28	FGFb	Basic fibroblast growth factor	MAB233	mouse	100	233-FB	25	BAM233	mouse	25	Strept-AF647

Table D.S3 continued from previous page

			Capture Ab			Antigen		Detection Ab			Reporter Molecule
	Name	Full name	Catalog Number	Species	[cAb]	Catalog Number	[Ag]	Catalog Number	Species	[dAb]	
29	Flt-3	Fms-like tyrosine kinase 3	MAB608	mouse	100	308-FKN-005/CF	25	BAF308	goat	10	Strept-AF647
30	G-CSF	Granulocyte colony-stimulating factor	MAB214	mouse	200	214-CS	50	BAF214	goat	25	Strept-AF647
31	GFAP	Glial fibrillary acidic protein	H00002670-AP52[1]	mouse	150	ab114149[2]	1000	H00002670-AP52[1]	rabbit	20	GAR-AF647
32	GM-CSF	Granulocyte-macrophage colony-stimulating factor	MAB615	mouse	200	215-GM	100	BAM215	mouse	10	Strept-AF647
33	GRO-α	Chemokine (C-X-C motif) ligand 1	MAB275	mouse	100	275-GR	200	BAF275	goat	25	Strept-AF647
34	HAI-1	Hepatocyte growth factor activator inhibitor type 1	MAB10481	mouse	100	1048-PI-010	1000	BAM10482	mouse	25	Strept-AF647
35	HE4	Human epididymis protein 4	TA600333[3]	mouse	100	TP308491[3]	250	TA700330[3]	mouse	50	Strept-AF647
36	HER2	Human epidermal growth factor receptor 2	MAB1129	mouse	100	1129-ER	500	BAF1129	goat	10	Strept-AF647
37	HER3	Human epidermal growth factor receptor 3	MAB3481	mouse	100	348-RB-050	1000	BAM348	mouse	25	Strept-AF647
38	HGF	Hepatocyte growth factor	MAB694	mouse	200	294-HG-005/CF	100	BAF294	goat	10	Strept-AF647
39	HGF-R	Hepatocyte growth factor receptor	MAB3581	mouse	100	385-MT-100/CF	100	BAF358	goat	10	Strept-AF647
40	HMGB1	Amphoterin/High mobility group box 1	H00003146-AP42[1]	mouse	100	H00003146-P01[1]	250	H00003146-AP42[1]	mouse	20	Strept-AF647
41	HP	Haptoglobin	TA600399[3]	mouse	100	TP323612[3]	50	TA700399[3]	mouse	25	Strept-AF647
42	ICAM-1	Intercellular adhesion molecule 1	MAB720	mouse	100	ADP4-050	2000	BAF720	sheep	10	Strept-AF647
43	IFN-γ	Interferon gamma	MAB2852	mouse	100	285-IF-100/CF	100	BAF285	goat	10	Strept-AF647
44	IGFBP-1	Insulin-like growth factor-binding protein 1	MAB675	mouse	100	871-B1-025	200	BAF871	goat	10	Strept-AF647
45	IGFBP-3	Insulin-like growth factor-binding protein 3	MAB305	mouse	200	675-B3-025	1000	BAF675	goat	10	Strept-AF647
46	IGFBP-7	Insulin-like growth factor-binding protein 7	MAB1334	mouse	100	1334-B7-025	500	BAF1334	goat	10	Strept-AF647
47	IL-10	Interleukin 10	MAB2172	mouse	200	217-IL	25	BAF217	goat	10	Strept-AF647
48	IL-12	Interleukin 12 p70	MAB611	mouse	100	219-IL	25	BAF219	goat	10	Strept-AF647
49	IL-15	Interleukin 15	MAB647	mouse	100	247-ILB	25	BAF247	goat	25	Strept-AF647
50	IL-18	Interleukin 18	MAB1192	mouse	100	B001-5[6]	200	BAF119	goat	25	Strept-AF647
51	IL-1β	Interleukin 1 beta/Lymphocyte activating factor	MAB601	mouse	200	201-LB	25	BAF-201	goat	10	Strept-AF647
52	IL-1ra	Interleukin 1 receptor antagonist	MAB280	mouse	100	280-RA	200	BAF280	goat	20	Strept-AF647
53	IL-2	Interleukin 2	MAB602	mouse	100	202-IL	25	BAF202	goat	10	Strept-AF647
54	IL-3	Interleukin 3	MAB603	mouse	100	203-IL	25	BAF203	goat	10	Strept-AF647
55	IL-4	Interleukin 4	MAB604	mouse	100	204-IL	200	BAF204	goat	10	Strept-AF647
56	IL-5	Interleukin 5	MAB405	rat	100	205-IL	200	BAM6051	rat	100	Strept-AF647
57	IL-6	Interleukin 6	MAB206	mouse	100	206-IL	200	BAF206	goat	13.33	Strept-AF647
58	IL-7	Interleukin 7	MAB207	mouse	200	207-IL	25	BAF207	goat	10	Strept-AF647
59	IL-8	Interleukin 8	MAB208	mouse	200	208-IL	20	BAF208	goat	10	Strept-AF647
60	IP-10	Interferon gamma-induced protein 10	MAB266	mouse	200	266-IP	50	BAF266	goat	10	Strept-AF647

Table D.S3 continued from previous page

			Capture Ab			Antigen		Detection Ab			Reporter Molecule
	Name	Full name	Catalog Number	Species	[cAb]	Catalog Number	[Ag]	Catalog Number	Species	[dAb]	
61	KLK14	Kallikrein-14	AF2626	goat	100	AFG2626	2000	BAF2626	goat	10	Strept-AF647
62	KLK8	Kallikrein-8	TA600202[3]	mouse	150	2025-SE-010	500	TA700202[3]	mouse	50	Strept-AF647
63	Leptin	Leptin	MAB398	mouse	100	398-LP	500	BAM398	mouse	25	Strept-AF647
64	MCP1	Monocyte chemoattractant protein 1	MAB279	mouse	100	279-MC-010/CF	50	BAF279	goat	10	Strept-AF647
65	MCP2	Monocyte chemoattractant protein 2	MAB281	mouse	100	281-CP/CF	500	BAF281	goat	40	Strept-AF647
66	MCP3	Monocyte chemoattractant protein 3	MAB282	mouse	200	282-P3-010/CF	50	BAF282	goat	10	Strept-AF647
67	MCP4	Monocyte chemoattractant protein 4	MAB327	mouse	200	327-P4-025/CF	200	BAF327	goat	40	Strept-AF647
68	M-CSF	Macrophage colony-stimulating factor	MAB616	mouse	100	216-MC	100	BAF216	goat	10	Strept-AF647
69	MIG	Monokine induced by gamma interferon	MAB392	mouse	200	392-MG	200	BAF392	goat	10	Strept-AF647
70	MIP-1α	Macrophage inflammatory protein 1-alpha	AF-270-NA	goat	300	270-LD	50	BAF270	goat	10	Strept-AF647
71	MIP-1β	Macrophage inflammatory protein 1-beta	MAB271	mouse	200	271-BME	100	BAF271	goat	20	Strept-AF647
72	MMP-1	Matrix metalloproteinase-1	AF901	goat	100	901-MP-010	1000	BAF901	goat	25	Strept-AF647
73	MMP-3	Matrix metalloproteinase-3	AF513	goat	100	531-MP	500	BAF513	goat	25	Strept-AF647
74	MMP-9	Matrix metalloproteinase-9	MAB936	mouse	100	911-MP-010	500	BAF911	goat	10	Strept-AF647
75	NCAM-1	Neural cell adhesion molecule	MAB2408	mouse	100	2408-NC	2000	BAF2408	goat	10	Strept-AF647
76	NT-3	Neurotrophin-3	MAB267	mouse	200	267-N3-005/CF	500	BAF267	goat	10	Strept-AF647
77	OPN	Osteopontin	MAB14332	mouse	100	1433-OP	100	BAF1433	goat	20	Strept-AF647
78	PAI-1	Plasminogen activator inhibitor-1	MAB1786	mouse	100	1786-PI	2000	BAF1786	goat	10	Strept-AF647
79	PDGF-BB	Platelet-derived growth factor subunit BB	385-PR/CF	mouse	133	220-BB	200	BAF220	goat	10	Strept-AF647
80	PRL	Prolactin	H00005617-AP41[1]	mouse	100	H00005617-P01[1]	500	H00005617-AP41[1]	mouse	22	Strept-AF647
81	PSA	Prostate-specific antigen/Kallikrein-3	MAB13442	mouse	100	1344-SE	2000	BAF1344	goat	10	Strept-AF647
82	RBP4	Retinol binding protein 4	MAB33781	mouse	100	3378-LC	500	BAM33782	mouse	50	Strept-AF647
83	S100B	S100 calcium-binding protein B	H00006285-AP46[1]	mouse	100	H00006285-P01[1]	500	H00006285-AP46[1]	mouse	25	Strept-AF647
84	SCGN	Secretagogin	H00010590-AP21[1]	rabbit	200	H00010590-P01[1]	500	H00010590-AP21[1]	mouse	33	GAM-AF647
85	SPARC	Osteonectin	SC-73472[7]	mouse	30	941-SP	2000	BAF941	goat	40	Strept-AF647
86	TF	Tissue factor/Platelet tissue factor	MAB2339	mouse	100	2339-PA-010	100	BAF2339	goat	10	Strept-AF647
87	TGF-α	Transforming growth factor alpha	AF-239-NA	goat	100	239-A-100	500	BAF239	goat	10	Strept-AF647
88	TGF-β RII	Transforming growth factor beta receptor 2	AF-241-NA	goat	100	241-R2-025/CF	2000	BAF241	goat	10	Strept-AF647
89	TGF-β1	Transforming growth factor beta 1	MAB240	mouse	200	240-B-002/CF	200	BAF240	chicken	40	Strept-AF647
90	TGF-β2	Transforming growth factor beta 2	MAB612	mouse	200	302-B2-002/CF	180	BAF302	goat	40	Strept-AF647
91	THBS-1	Thrombospondin 1	MAB3074	mouse	200	3074-TH-050	250	BAF3074	goat	20	Strept-AF647
92	Tie-2	Angiopoietin-1 receptor	MAB3132	mouse	100	313-TI-100	1000	BAM3313	mouse	25	Strept-AF647

Table D.S3 continued from previous page

	Name	Full name	Capture Ab Catalog Number	Species	[cAb]	Antigen Catalog Number	[Ag]	Detection Ab Catalog Number	Species	[dAb]	Reporter Molecule
93	TIMP-1	TIMP metallopeptidase inhibitor 1	MAB970	mouse	100	970-TM-010	1000	BAF970	goat	10	Strept-AF647
94	TNF-α	Tumor necrosis factor	MAB610	mouse	200	210-TA	50	BAF210	goat	10	Strept-AF647
95	TNF-RI	Tumor necrosis factor receptor 1	MAB625	mouse	100	636-R1-025/CF	1000	BAF225	goat	25	Strept-AF647
96	TNF-RII	Tumor necrosis factor receptor 2	MAB726	mouse	200	1089-R2	200	BAF726	goat	10	Strept-AF647
97	uPA	Urokinase-type plasminogen activator	MAB1310	mouse	100	1310-SE	50	BAF1310	goat	10	Strept-AF647
98	uPA-R	Urokinase receptor	MAB807	mouse	100	807-UK-100/CF	500	BAF807	goat	10	Strept-AF647
99	VCAM-1	Vascular cell adhesion protein 1	MAB809	mouse	100	809-VR-050	200	BAF809	sheep	10	Strept-AF647
100	VEGF-A	Vascular endothelial growth factor A	MAB293	mouse	100	293-VE	25	BAF293	goat	10	Strept-AF647
101	VEGF-D	Vascular endothelial growth factor D	MAB2861	mouse	100	622-VD-005/CF	100	BAM286	mouse	25	Strept-AF647
102	VEGFR2	Vascular endothelial growth factor receptor 2	MAB3573	mouse	200	357-KD-050	500	BAF357	goat	10	Strept-AF647
103	VEGFR3	Vascular endothelial growth factor receptor 3	MAB349	mouse	100	349-F4-050	500	BAM3492	mouse	25	Strept-AF647

[1]: Abnova[2]: Abcam[3]: OriGene[4]: Fitzgerald Industries International[5]: US Biologicals[6]: MBL International Corporation[7]: Santa Cruz Biologicals

References

146. Bergeron, S., Laforte, V., Lo, P. S., Li, H. & Juncker, D. Evaluating mixtures of 14 hygroscopic additives to improve antibody microarray performance. *Analytical and Bioanalytical Chemistry* **407,** 8451–8462 (2015).

165. Ruwona, T. B., McBride, R., Chappel, R., Head, S. R., Ordoukhanian, P., Burton, D. R. & Law, M. Optimization of peptide arrays for studying antibodies to hepatitis C virus continuous epitopes. *Journal of Immunological Methods* **402,** 35–42 (2014).

174. *Glycerine : an overview* tech. rep. (The Soap and Detergent Association, New York, NY, 1990), 1–27.

228. Murphy, T. & Dendukuri, N. *R tutorial on fitting response curves for point-of-care diagnostic tests* http://weightinginbayesianmodels.github.io/poctcalibration/AMfunctions.html.

235. Wang, S., Zhao, P. & Cao, B. Development and optimization of an antibody array method for potential cancer biomarker detection. *Journal of Biomedical Research* **25,** 63–70 (2011).

384. Rodbard, D., Feldman, Y., Jaffe, M. & Miles, L. Studies on the nature of the 'high-dose hook effect'. *Immunochemistry* **15,** 77–82 (1978).

APPENDIX E

Comparison of microdialysis additives: Supplementary Material

This appendix describes the Supplementary Material to chapter 5.

Electronic Supplementary Material

Comparison of serum albumin, low- and high-molecular weight dextrans as additives to brain microdialysis

Veronique Laforte, Francesco Fiorini, David KY Zhang, Judith Marcoux and David Juncker

List of SI figures

List of SI tables

The following figures and tables show additional results from the following:

1. Physical performance of perfusion (figure E.S1).
2. Performance measures of ACM (figures E.S2 to E.S5 and tables E.S1 and E.S2).
3. Relative recovery of proteins in microdialysis (figures E.S6, E.S7 and tables E.S3 and E.S4).
4. Matrix effect of additives (figures E.S8 to E.S11 and table E.S5).
5. Effects of additives on U87 cell cultures (figures E.S12 to E.S15 and tables E.S6 to E.S14).

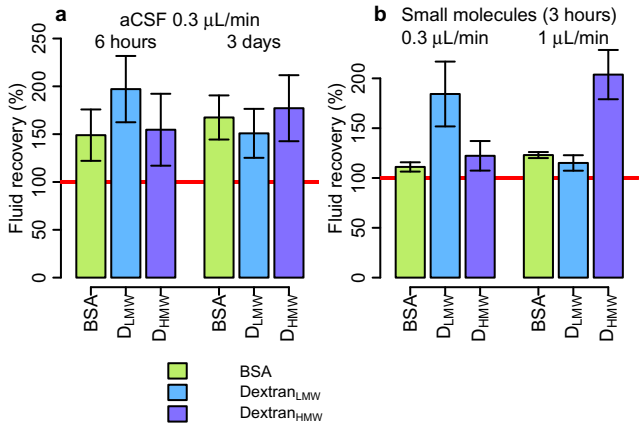

FIGURE E.S1: **Additives fluid recovery in aCSF and a mixture of small molecules.** Microdialysis catheters were loaded with BSA (3.5 %), $\text{Dextran}_{\text{LMW}}$ or $\text{Dextran}_{\text{HMW}}$ (both 3 %) diluted in aCSF. Catheters were perfused in (**a**) aCSF or (**b**) a mixture of small molecules for varying amounts of time and flow rate. Red lines are a visual aid that indicate the perfect value of fluid recovery (100 %).

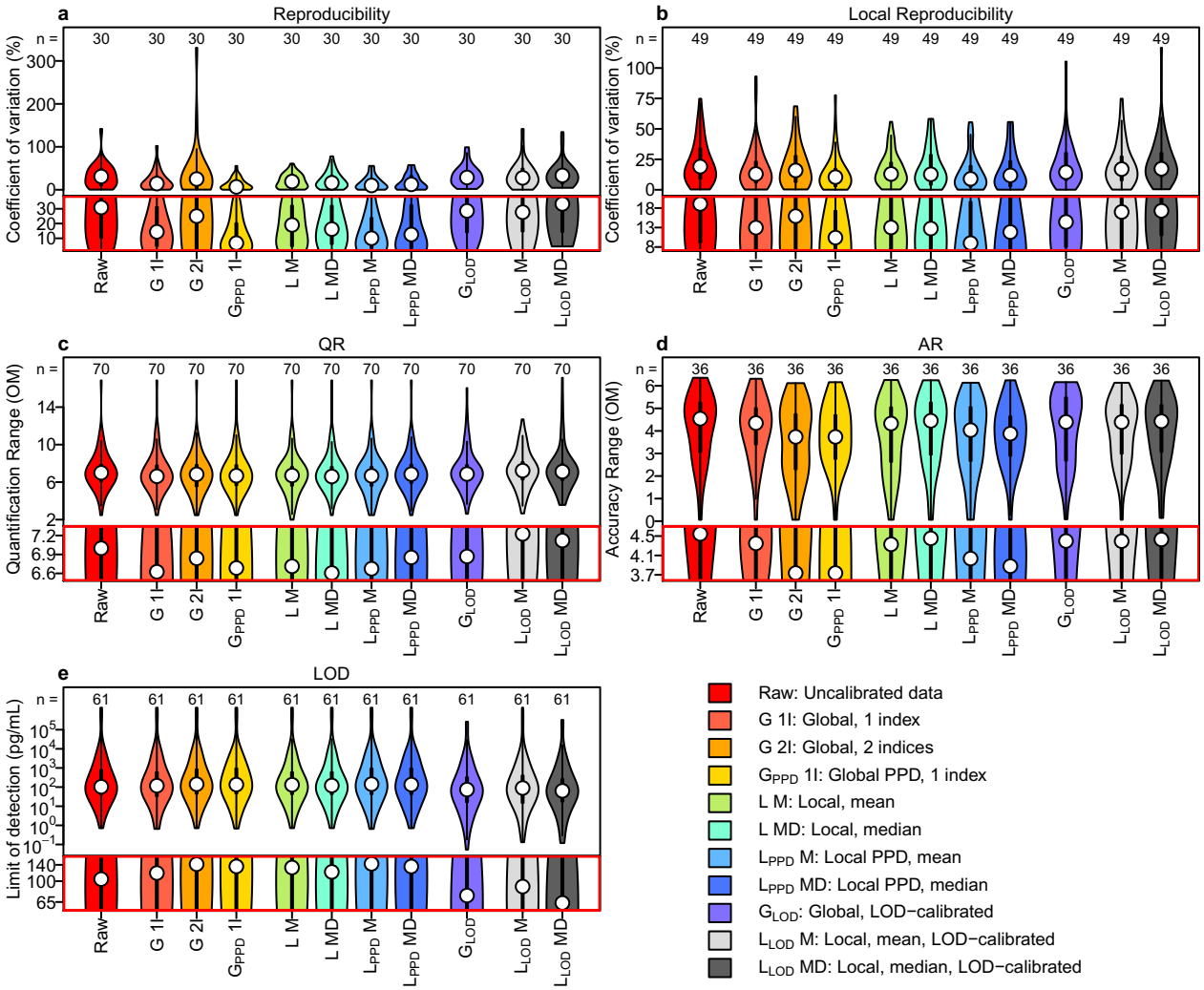

FIGURE E.S2: **Comparison of calibration parameters and methods with $LOD = Mean+3\times SD$.** Measurements of proteins using the ACM was calibrated using different calibration parameters and methods. These are compared in terms of (**a**) global and (**b**) local reproducibility, (**c**) quantification and (**d**) accuracy ranges and (**e**) sensitivity. The first seven data sets are calibrated with the intent to improve reproducibility, while the last three are calibrated with the intent to improve sensitivity.

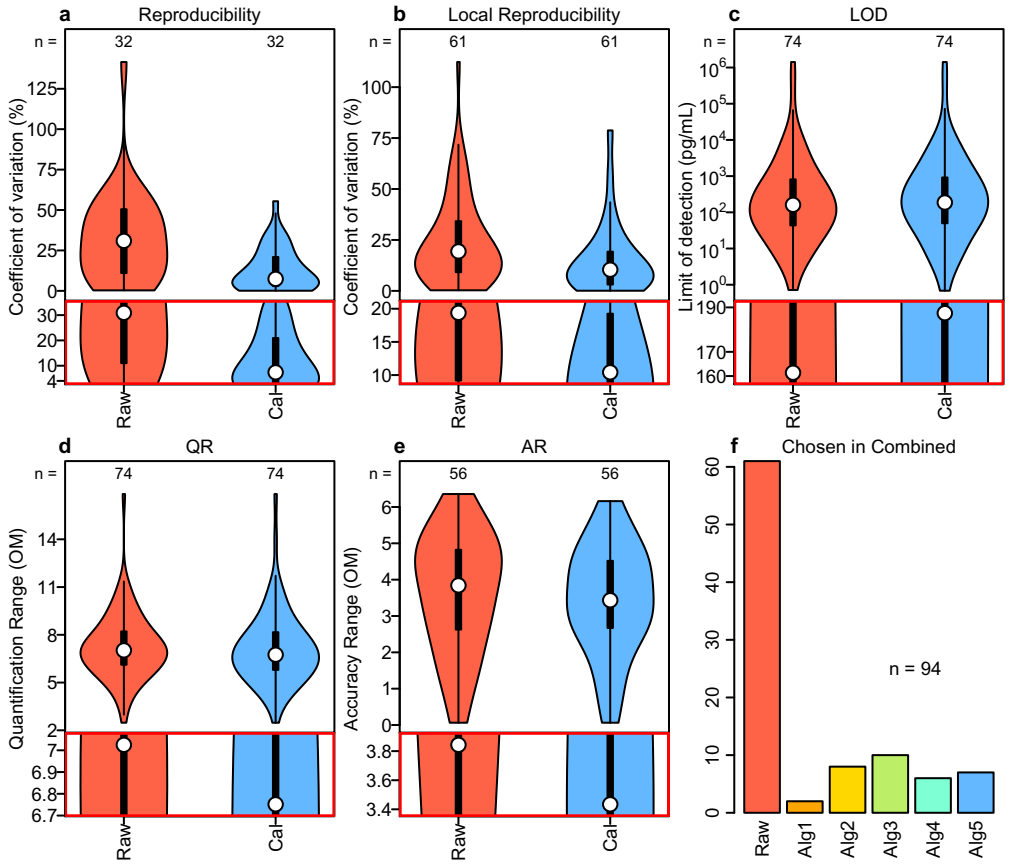

FIGURE E.S3: **ACM calibration performance based on reproducibility improvement with $LOD = Mean + 3 \times SD$. a-e** Comparison of uncalibrated with data calibrated using the global method of calibration using the chosen dilution for each protein (G_{PPD} 1 Index) in terms of (**a**) global and (**b**) local reproducibility, (**c**) quantification and (**d**) accuracy ranges and (**e**) sensitivity. **f** shows the frequency of each calibration algorithm chosen in the calibration.

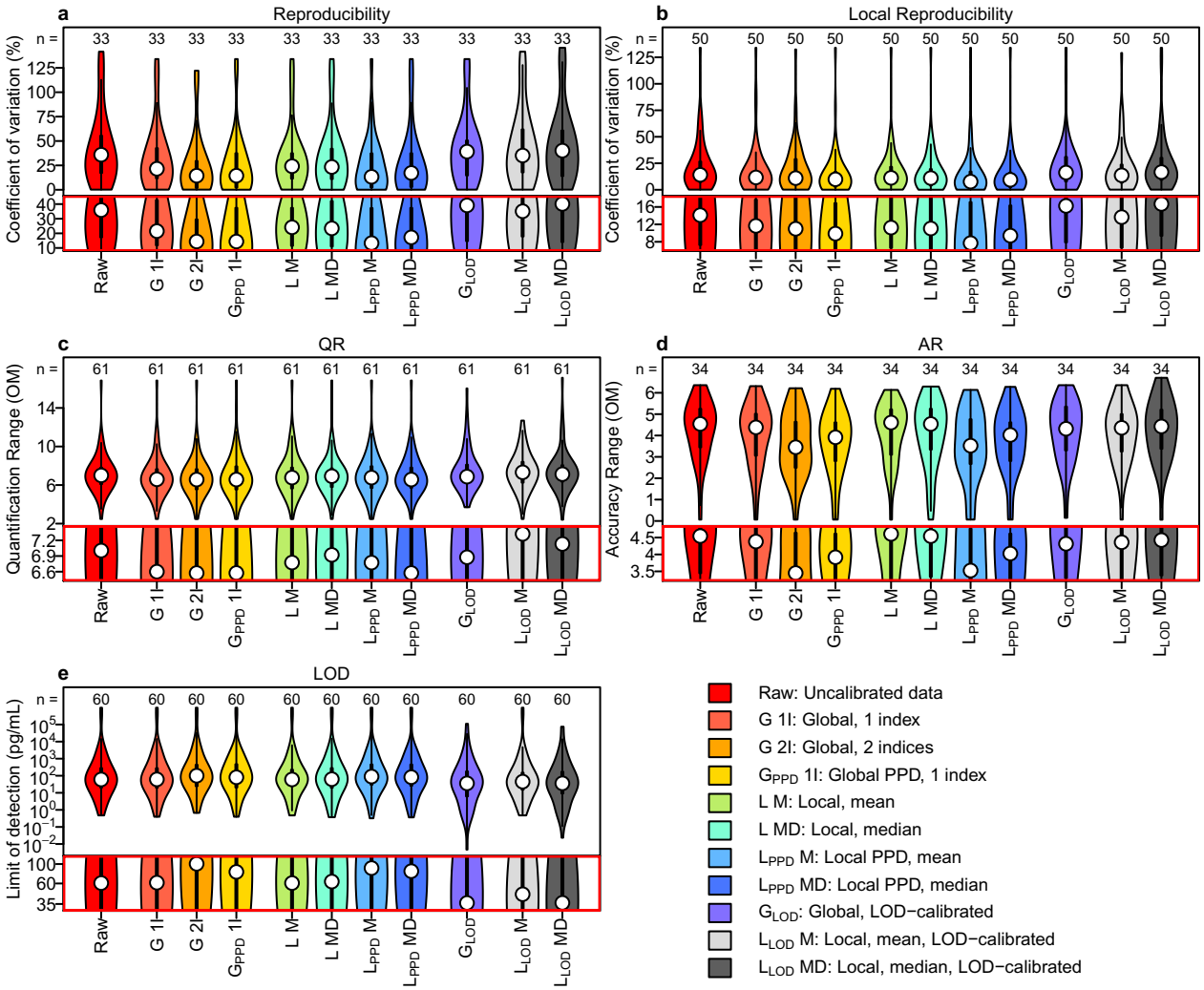

FIGURE E.S4: **Comparison of calibration parameters and methods with $LOD = Mean + 2 \times SD$.** Measurements of proteins using the ACM was calibrated using different calibration parameters and methods. These are compared in terms of (**a**) global and (**b**) local reproducibility, (**c**) quantification and (**d**) accuracy ranges and (**e**) sensitivity. The first seven data sets are calibrated with the intent to improve reproducibility, while the last three are calibrated with the intent to improve sensitivity.

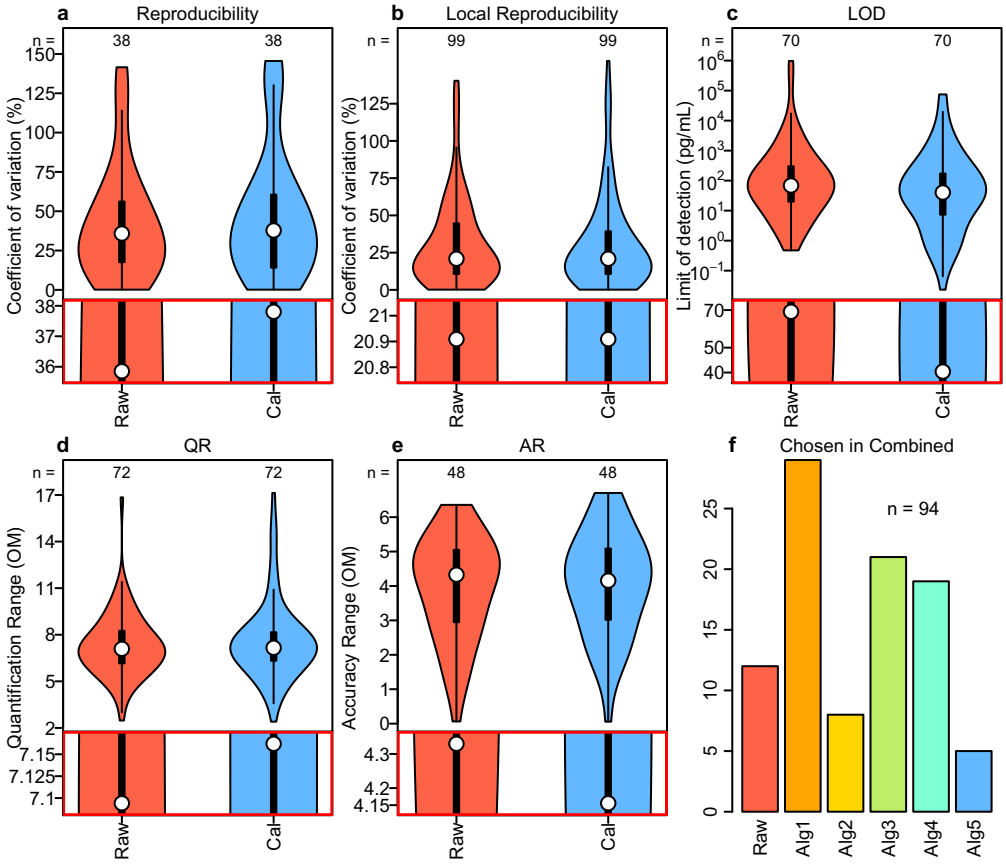

FIGURE E.S5: **ACM calibration performance based on sensitivity improvement with $LOD = Mean + 2 \times SD$. a-e** Comparison of uncalibrated with data calibrated using the local method of calibration using the median of all the local calibration slopes to calculate the global calibration slope (L_{LOD} median) in terms of (**a**) global and (**b**) local reproducibility, (**c**) quantification and (**d**) accuracy ranges and (**e**) sensitivity. **f** shows the frequency of each calibration algorithm chosen in the calibration.

TABLE E.S1: **Protein standard curve, calibration algorithm and performance measures with $LOD = Mean + 3 \times SD$.** This calibrated data was used for all protein measurements except relative recovery of proteins. SC: standard curve. Unquant. data? indicates whether samples or sample replicates above the LOD were not quantified by the standard curve. Cal. Alg: calibration algorithm. Repro pnCSF: reproducibility of pnCSF sample replicate measurements. LOD unit for CA15-3 is mU/mL.

	Protein name	SC Valid?	[Ag] (ng/mL)	Unquant. data?	SC#	Hook#	Threshold	Dilution	Cal. Alg	QR (OM)	AR (OM)	LOD (pg/mL)	Repro pnCSF
1	AFP	Yes	800	Yes	-	-	4.4	1 in 3	Alg1	-	-	-	-
2	AHSG	Yes	2000	Yes	-	-	-	1 in 15	None	-	-	-	-
3	ALDH1L1	Yes	200	No	1	-	-	1 in 3	Alg4	5.48	1.85	23.95	-
4	Amphiregulin	Yes	25	No	2	-	-	1 in 3	Alg1	6.36	5.52	45.3	-
5	Ang1	Yes	100	Yes	2	3	-	1 in 3	Alg1	3.88	0.67	30.25	-
6	Ang2	Yes	20	No	2	-	-	1 in 3	Alg1	5.28	3.12	717.08	-
7	BMP2	Yes	25	No	2	-	-	1 in 3	Alg1	4.42	4.23	157.01	-
8	β-NGF	Yes	100	Yes	2	-	-	1 in 3	Alg1	7.98	3.89	72.19	121.12%
9	BRAF	Yes	200	No	2	1	-	1 in 3	Alg4	6.05	3.88	656.84	-
10	CA15-3	Yes	200	Yes	1	-	-	1 in 3	Alg1	7.87	1.67	0.18	105.14%
11	CCL5	Yes	200	Yes	-	-	-	1 in 3	Alg1	-	-	-	-
12	CD14	No Ag	0	-	-	-	-	1 in 15	Alg1	-	-	-	-
13	CEA	Yes	2000	No	1	-	-	1 in 3	Alg3	6.53	1.99	71.98	-
14	c-Kit	Yes	1000	No	2	3	-	1 in 15	Alg4	8.86	3.38	188.43	12.17%
15	CRP	No	2000	-	-	-	-	1 in 3	Alg2	-	-	-	-
16	CXCL12	Yes	5000	Yes	2	-	-	1 in 3	Alg1	9.18	4.51	5668.28	33.36%
17	E-cadherin	Yes	100	No	2	-	-	1 in 3	Alg4	6.82	6.23	45.52	29.05%
18	EGF	Yes	200	No	2	8	5.2	1 in 3	Alg3	14.73	-	1.42	-
19	EGF-R	Yes	100	No	2	-	-	1 in 15	Alg5	8.14	0.28	63.77	7.98%
20	Endoglin	Yes	200	No	2	-	-	1 in 3	None	7.35	5.36	104.36	-
21	E-selectin	Yes	4000	No	1	-	-	1 in 3	Alg1	7.01	5.01	262.48	-
22	FAS-L	Yes	50	No	2	3	-	1 in 3	Alg4	7.22	3.84	2.85	56.07%
23	FGFb	Yes	25	No	2	-	-	1 in 3	Alg1	4.8	4.11	224.53	2.09%
24	Flt-3	Yes	25	No	2	-	5.75	1 in 3	Alg3	7.38	-	344.85	-
25	GFAP	No	1000	-	-	-	-	1 in 3	Alg3	-	-	-	-
26	GM-CSF	Yes	100	No	1	-	-	1 in 3	Alg1	7.32	5.66	6.83	-
27	GRO-α	Yes	200	Yes	1	-	-	1 in 3	Alg1	7.18	4.36	183.83	56.14%

Table E.S1 continued from previous page

	Protein name	SC Valid?	[Ag] (ng/mL)	Unquant. data?	SC#	Hook#	Threshold	Dilution	Cal. Alg	QR (OM)	AR (OM)	LOD (pg/mL)	Repro pnCSF
28	HAI-1	Yes	1000	No	2	-	-	1 in 3	Alg1	6.74	4.9	5259.28	-
29	HE4	Yes	250	Yes	2	-	-	1 in 3	Alg5	5.43	-	5029.16	-
30	HER2	Yes	500	No	1	-	-	1 in 3	Alg3	10.54	-	26.41	-
31	HER3	Yes	1000	No	2	-	-	1 in 3	Alg1	7.11	4.89	579.54	19.34%
32	HGF	Yes	100	Yes	2	-	-	1 in 3	Alg1	6.86	6.2	90.16	23.92%
33	HGF-R	Yes	100	No	2	1	-	1 in 3	Alg2	6.97	5.08	89.44	49.88%
34	HMGB1	No	250	-	-	-	4.8	1 in 3	Alg5	-	-	-	-
35	HP	Yes	50	No	2	-	-	1 in 3	Alg4	6.14	2.12	666.81	4.73%
36	ICAM-1	Yes	2000	No	2	4	-	1 in 3	Alg1	4.15	1.92	1477.55	27.42%
37	IFN-γ	Yes	100	No	2	-	-	1 in 3	Alg5	6.7	5.7	0.2	-
38	IGFBP-1	Yes	200	No	1	7	-	1 in 15	Alg5	5.91	2.9	0.97	20.56%
39	IGFBP-3	Yes	1000	No	2	-	-	1 in 15	Alg3	6.46	4.17	180.91	14.05%
40	IGFBP-7	Yes	500	Yes	-	-	5.3	1 in 15	Alg2	-	-	-	-
41	IL-10	No Ag	0	-	-	-	-	1 in 3	Alg4	-	-	-	-
42	IL-12	Yes	25	No	1	-	-	1 in 3	Alg4	11.51	-	1056.97	-
43	IL-15	Yes	25	No	1	-	-	1 in 3	Alg1	11.26	-	8.25	-
44	IL-18	No	200	-	-	-	-	1 in 15	Alg1	-	-	-	-
45	IL-1β	Yes	25	No	1	3	-	1 in 3	Alg1	5.39	3.07	0.12	-
46	IL-1ra	Yes	200	No	1	-	-	1 in 3	Alg3	8.01	5.24	127.4	-
47	IL-2	Yes	25	No	2	-	-	1 in 3	Alg3	12.04	-	3660.19	-
48	IL-3	Yes	25	No	2	1	-	1 in 3	Alg1	7.26	3.42	31.65	-
49	IL-4	Yes	200	No	2	-	-	1 in 3	Alg1	8.76	6.68	209.88	-
50	IL-5	No Ag	0	-	-	-	-	1 in 3	Alg4	-	-	-	-
51	IL-6	Yes	200	No	1	1	-	1 in 3	Alg4	7.71	-	15.06	29.01%
52	IL-7	Yes	25	No	1	-	-	1 in 3	Alg3	4.82	2.04	5.97	-
53	IL-8	Yes	20	Yes	1	2	6	1 in 3	Alg3	8.85	-	4.5	38.70%
54	IP-10	Yes	50	Yes	2	1	-	1 in 15	Alg3	6.21	5.12	16.5	8.62%
55	KLK8	No	500	-	-	-	-	1 in 3	Alg2	-	-	-	-
56	Leptin	No	500	-	-	-	-	1 in 3	None	-	-	-	-
57	MCP1	Yes	50	No	2	-	5.1	1 in 3	Alg4	7.19	-	258.09	33.30%
58	MCP2	Yes	500	No	2	-	-	1 in 3	Alg1	7.68	2.54	31.23	32.57%
59	MCP3	Yes	50	No	2	6	6	1 in 3	Alg4	8.39	2.84	4.37	53.42%
60	M-CSF	Yes	100	No	2	-	-	1 in 3	Alg3	14.93	-	108.41	-

Table E.S1 continued from previous page

	Protein name	SC Valid?	[Ag] (ng/mL)	Unquant. data?	SC#	Hook#	Threshold	Dilution	Cal. Alg	QR (OM)	AR (OM)	LOD (pg/mL)	Repro pnCSF
61	MIG	Yes	200	No	2	-	-	1 in 3	Alg1	7.96	4.77	201.43	-
62	MIP-1α	Yes	50	Yes	2	6	-	1 in 3	Alg1	7.71	2.83	2.89	47.61%
63	MIP-1β	Yes	100	Yes	2	3	-	1 in 3	Alg1	5.19	1.09	39.79	-
64	MMP-1	No Ag	0	-	-	-	-	1 in 3	Alg5	-	-	-	-
65	MMP-3	Yes	500	No	1	6	6	1 in 3	Alg3	6.85	-	99.18	35.87%
66	MMP-9	Yes	500	No	1	3	-	1 in 15	Alg4	6.72	5.43	33.76	5.57%
67	NCAM-1	Yes	2000	No	2	-	-	1 in 15	Alg2	7.56	5.22	1532.15	15.45%
68	NT-3	Yes	500	No	2	-	6	1 in 3	Alg5	4.99	3.89	4265.17	-
69	OPN	Yes	100	Yes	1	-	-	1 in 15	Alg1	7.61	4.52	42.33	41.80%
70	PAI-1	Yes	2000	No	1	-	5.2	1 in 3	Alg4	7.13	-	323523.79	-
71	PDGF-BB	Yes	200	No	2	-	-	1 in 3	None	8.23	4.73	75.03	-
72	PRL	No	500	-	-	-	-	1 in 3	Alg4	-	-	-	-
73	PSA	Yes	2000	No	2	-	-	1 in 3	Alg4	9.77	-	30052.89	-
74	RBP4	No	500	-	-	-	-	1 in 3	Alg1	-	-	-	-
75	S100B	Yes	500	No	1	-	-	1 in 3	Alg4	3.57	0.14	2.00E+05	-
76	SCGN	No	500	-	-	-	-	1 in 3	Alg5	-	-	-	-
77	SPARC	Yes	2000	No	1	-	-	1 in 15	Alg4	7.82	4.5	58.35	35.51%
78	TF	Yes	100	Yes	1	-	-	1 in 3	None	3.77	-	840.95	-
79	TGF-α	Yes	500	Yes	-	-	-	1 in 3	Alg4	-	-	-	-
80	TGF-β RII	Yes	2000	No	2	-	5.9	1 in 3	Alg5	7.19	2	296.45	-
81	TGF-β1	Yes	200	Yes	2	-	-	1 in 3	Alg3	7.11	5.54	51.87	61.88%
82	THBS-1	Yes	250	Yes	1	-	-	1 in 15	Alg1	6.73	1.93	19.56	6.40%
83	Tie-2	Yes	1000	No	1	-	-	1 in 3	Alg1	8.06	1.56	113.69	-
84	TIMP-1	No Ag	0	-	-	-	-	1 in 15	Alg4	-	-	-	-
85	TNF-α	Yes	50	No	2	6	-	1 in 3	Alg3	13.69	-	4.98	-
86	TNF-RI	Yes	1000	No	2	-	-	1 in 15	Alg4	6.67	3.92	17.35	38.30%
87	TNF-RII	Yes	200	Yes	1	6	-	1 in 15	Alg3	4.44	1.26	33.05	57.44%
88	uPA	Yes	50	Yes	1	2	-	1 in 3	Alg3	6.65	-	1.88	41.95%
89	uPA-R	Yes	500	No	2	-	6.2	1 in 3	None	5.45	3.38	154.12	4.47%
90	VCAM-1	Yes	200	Yes	1	-	-	1 in 15	Alg3	17.13	0.86	42.08	13.56%
91	VEGF-A	Yes	25	Yes	2	6	-	1 in 3	Alg1	7.67	2.63	0.73	134.33%
92	VEGF-D	Yes	100	No	2	-	-	1 in 3	Alg1	7.34	2.4	1110.57	-
93	VEGFR2	Yes	500	No	1	-	-	1 in 3	Alg1	6.22	3.08	397.8	-

Table E.S1 continued from previous page

	Protein name	SC Valid?	[Ag] (ng/mL)	Unquant. data?	SC#	Hook#	Threshold	Dilution	Cal. Alg	QR (OM)	AR (OM)	LOD (pg/mL)	Repro pnCSF
94	VEGFR3	No	500	-	-	-	-	1 in 3	Alg4	-	-	-	-

TABLE E.S2: **Protein standard curve, calibration algorithm and performance measures with $LOD = Mean + 2 \times SD$.** This calibrated data was used for measurements of relative recovery of proteins. SC: standard curve. Unquant. data? indicates whether samples or sample replicates above the LOD were not quantified by the standard curve. Cal. Alg: calibration algorithm. Repro pnCSF: reproducibility of pnCSF sample replicate measurements. LOD unit for CA15-3 is mU/mL.

	Protein name	SC Valid?	[Ag] (ng/mL)	Unquant. data?	SC#	Hook#	Threshold	Dilution	Cal. Alg	QR (OM)	AR (OM)	LOD (pg/mL)	Repro pnCSF
1	AFP	Yes	800000	Yes	-	-	4.4	1 in 3	Alg1	-	-	-	-
2	AHSG	Yes	2000000	Yes	-	-	-	1 in 15	None	-	-	-	-
3	ALDH1L1	Yes	200000	Yes	-	-	-	1 in 3	None	-	-	-	-
4	Amphiregulin	Yes	25000	No	2	-	-	1 in 3	Alg1	6.36	5.52	23.85	-
5	Ang1	Yes	100000	No	2	3	-	1 in 3	Alg3	6.73	6.7	18.38	36.91%
6	Ang2	Yes	20000	No	2	-	-	1 in 3	None	5.44	3.2	449.88	-
7	BMP2	Yes	25000	No	2	-	-	1 in 3	Alg3	4.52	4.35	109.13	-
8	b-NGF	Yes	100000	No	2	-	-	1 in 3	Alg1	7.98	3.89	34.87	145.55%
9	BRAF	Yes	200000	No	2	1	-	1 in 3	Alg4	6.05	3.88	481.27	-
10	CA15-3	Yes	200000	No	1	-	-	1 in 3	Alg2	8.73	-	0.79	121.84%
11	CCL5	Yes	200000	Yes	-	-	-	1 in 3	Alg1	-	-	-	-
12	CD14	No Ag	0	Yes	-	-	-	1 in 15	Alg1	-	-	-	-
13	CEA	Yes	2000000	No	1	-	-	1 in 3	Alg3	6.53	1.99	13.97	31.66%
14	c-Kit	Yes	1000000	No	2	3	-	1 in 15	Alg4	8.86	3.38	132.49	12.17%
15	CRP	No	2000000	Yes	-	-	-	1 in 3	Alg1	-	-	-	-
16	CXCL12	Yes	5000000	Yes	2	-	-	1 in 3	Alg1	9.18	4.51	2750.03	71.02%
17	E-cadherin	Yes	100000	No	2	-	-	1 in 3	Alg1	6.84	6.2	27.51	33.91%
18	EGF	Yes	200000	No	2	8	5.2	1 in 3	Alg3	14.73	-	0.15	-
19	EGF-R	Yes	100000	No	2	-	-	1 in 15	Alg5	8.14	0.28	34.05	7.98%
20	Endoglin	Yes	200000	No	2	-	-	1 in 3	Alg3	8.33	4.74	56.54	25.38%
21	E-selectin	Yes	4000000	No	1	-	-	1 in 3	Alg3	7.09	5.36	14.38	-
22	FAS-L	Yes	50000	No	2	3	-	1 in 3	Alg4	7.22	3.84	0.023	59.99%
23	FGFb	Yes	25000	No	2	-	-	1 in 3	Alg1	4.8	4.11	166.39	34.06%
24	Flt-3	Yes	25000	No	2	-	5.75	1 in 3	Alg3	7.38	-	170.09	-
25	GFAP	No	1000000	Yes	-	-	-	1 in 3	Alg3	-	-	-	-
26	GM-CSF	Yes	100000	No	1	-	-	1 in 3	Alg4	6.98	4.15	1.48	-
27	GRO-a	Yes	200000	No	1	-	-	1 in 3	None	5.49	3.86	57.32	44.72%

Table E.S2 continued from previous page

	Protein name	SC Valid?	[Ag] (ng/mL)	Unquant. data?	SC#	Hook#	Threshold	Dilution	Cal. Alg	QR (OM)	AR (OM)	LOD (pg/mL)	Repro pnCSF
28	HAI-1	Yes	1000000	No	2	-	-	1 in 3	Alg1	6.74	4.9	3587.8	-
29	HE4	Yes	250000	Yes	2	-	-	1 in 3	Alg5	5.43	-	2767.5	24.06%
30	HER2	Yes	500000	Yes	1	-	-	1 in 3	None	10.8	-	-	133.99%
31	HER3	Yes	1000000	No	2	-	-	1 in 3	Alg1	7.11	4.89	372.78	32.39%
32	HGF	Yes	100000	Yes	2	-	-	1 in 3	Alg1	6.86	6.2	58.38	30.67%
33	HGF-R	Yes	100000	Yes	2	1	-	1 in 3	Alg2	6.97	5.08	64.16	53.80%
34	HMGB1	No	250000	Yes	-	-	4.8	1 in 3	Alg5	-	-	-	-
35	HP	Yes	50000	No	2	-	-	1 in 3	Alg4	6.14	2.12	365.62	36.06%
36	ICAM-1	Yes	2000000	No	2	4	-	1 in 3	Alg1	4.15	1.92	964.15	27.42%
37	IFN-g	Yes	100000	Yes	-	-	-	1 in 3	Alg3	-	-	-	-
38	IGFBP-1	Yes	200000	No	1	7	-	1 in 15	Alg2	7.11	-	0.46	9.02%
39	IGFBP-3	Yes	1000000	No	2	-	-	1 in 15	Alg3	6.46	4.17	74.43	14.05%
40	IGFBP-7	Yes	500000	Yes	-	-	5.3	1 in 15	Alg2	-	-	-	-
41	IL-10	No Ag	0	Yes	-	-	-	1 in 3	Alg4	-	-	-	-
42	IL-12	Yes	25000	No	1	-	-	1 in 3	Alg4	11.51	-	279.6	-
43	IL-15	Yes	25000	No	1	-	-	1 in 3	Alg1	11.26	-	2.02	-
44	IL-18	No	200000	Yes	-	-	-	1 in 15	Alg1	-	-	-	-
45	IL-1b	Yes	25000	No	1	3	-	1 in 3	None	5.54	2.76	0.67	0.14%
46	IL-1ra	Yes	200000	No	1	-	-	1 in 3	Alg3	8.01	5.24	43.48	-
47	IL-2	Yes	25000	No	2	-	-	1 in 3	Alg1	12.16	-	1357.27	-
48	IL-3	Yes	25000	No	2	1	-	1 in 3	Alg1	7.26	3.42	19.19	-
49	IL-4	Yes	200000	Yes	2	-	-	1 in 3	Alg1	8.76	6.68	112.13	-
50	IL-5	No Ag	0	Yes	-	-	-	1 in 3	Alg4	-	-	-	-
51	IL-6	Yes	200000	No	1	1	-	1 in 3	Alg4	7.71	-	0.39	29.01%
52	IL-7	Yes	25000	No	1	-	-	1 in 3	Alg1	4.79	1.94	1.59	-
53	IL-8	Yes	20000	Yes	1	2	6	1 in 3	Alg3	8.85	-	2.14	38.70%
54	IP-10	Yes	50000	Yes	2	1	-	1 in 15	Alg3	6.21	5.12	10.2	8.62%
55	KLK8	No	500000	Yes	-	-	-	1 in 3	Alg2	-	-	-	-
56	Leptin	No	500000	Yes	-	-	-	1 in 3	None	-	-	-	-
57	MCP1	Yes	50000	No	2	-	5.1	1 in 3	Alg3	9.31	-	115.04	138.62%
58	MCP2	Yes	500000	No	2	-	-	1 in 3	Alg1	7.68	2.54	20.21	40.14%
59	MCP3	Yes	50000	No	2	6	6	1 in 3	Alg4	8.39	2.84	2.02	60.75%
60	M-CSF	Yes	100000	No	2	-	-	1 in 3	Alg3	14.93	-	50.59	-

Table E.S2 continued from previous page

	Protein name	SC Valid?	[Ag] (ng/mL)	Unquant. data?	SC#	Hook#	Threshold	Dilution	Cal. Alg	QR (OM)	AR (OM)	LOD (pg/mL)	Repro pnCSF
61	MIG	Yes	200000	No	2	-	-	1 in 3	Alg1	7.96	4.77	110.96	12.80%
62	MIP-1a	Yes	50000	Yes	2	6	-	1 in 3	Alg1	7.71	2.83	1.42	64.05%
63	MIP-1b	Yes	100000	Yes	2	3	-	1 in 3	Alg3	5.41	-	21.97	-
64	MMP-1	No Ag	0	Yes	-	-	-	1 in 3	Alg4	-	-	-	-
65	MMP-3	Yes	500000	No	1	6	6	1 in 3	Alg3	6.85	-	59.78	41.44%
66	MMP-9	Yes	500000	No	1	3	-	1 in 15	Alg2	6.4	6.1	12.35	8.59%
67	NCAM-1	Yes	2000000	No	2	-	-	1 in 15	Alg2	7.56	5.22	669.08	15.45%
68	NT-3	Yes	500000	No	2	-	6	1 in 3	None	6.24	4.17	2794.98	-
69	OPN	Yes	100000	Yes	1	-	-	1 in 15	Alg1	7.61	4.52	6.56	41.80%
70	PAI-1	Yes	2000000	No	1	-	5.2	1 in 3	Alg4	7.13	-	74731.78	-
71	PDGF-BB	Yes	200000	No	2	-	-	1 in 3	Alg2	8.22	5.01	37.46	-
72	PRL	No	500000	Yes	-	-	-	1 in 3	Alg4	-	-	-	-
73	PSA	Yes	2000000	No	2	-	-	1 in 3	Alg4	9.77	-	14659	-
74	RBP4	No	500000	Yes	-	-	-	1 in 3	Alg1	-	-	-	-
75	S100b	Yes	500000	No	1	-	-	1 in 3	Alg1	2.4	0.058	66469.9	-
76	SCGN	No	500000	Yes	-	-	-	1 in 3	Alg5	-	-	-	-
77	SPARC	Yes	2000000	No	1	-	-	1 in 15	Alg4	7.82	4.5	0.29	35.51%
78	TF	Yes	100000	Yes	1	-	-	1 in 3	None	3.77	-	429	-
79	TGF-a	Yes	500000	Yes	-	-	-	1 in 3	Alg4	-	-	-	-
80	TGF-b RII	Yes	2000000	No	2	-	5.9	1 in 3	Alg5	7.19	2	121.66	42.64%
81	TGF-b1	Yes	200000	Yes	2	-	-	1 in 3	Alg3	7.11	5.54	23.67	79.74%
82	THBS-1	Yes	250000	Yes	1	-	-	1 in 15	None	6.65	1.75	-	10.19%
83	Tie-2	Yes	1000000	No	1	-	-	1 in 3	Alg1	8.06	1.56	37.29	-
84	TIMP-1	No Ag	0	Yes	-	-	-	1 in 15	Alg4	-	-	-	-
85	TNF-a	Yes	50000	No	2	6	-	1 in 3	Alg3	13.69	-	2.66	-
86	TNF-RI	Yes	1000000	Yes	2	-	-	1 in 15	None	6.64	6.36	6.23	40.97%
87	TNF-RII	Yes	200000	Yes	1	6	-	1 in 15	Alg3	4.44	1.26	14.09	57.44%
88	uPA	Yes	50000	Yes	1	2	-	1 in 3	Alg4	7.81	4.09	0.75	66.89%
89	uPA-R	Yes	500000	No	2	-	6.2	1 in 3	None	5.45	3.38	108.62	14.43%
90	VCAM-1	Yes	200000	Yes	1	-	-	1 in 15	Alg3	17.13	0.86	13.99	13.56%
91	VEGF-A	Yes	25000	Yes	2	6	-	1 in 3	Alg1	7.67	2.63	0.36	134.33%
92	VEGF-D	Yes	100000	No	2	-	-	1 in 3	Alg1	7.34	2.4	425.89	-
93	VEGFR2	Yes	500000	No	1	-	-	1 in 3	Alg1	6.22	3.08	172.71	64.51%

Table E.S2 continued from previous page

	Protein name	SC Valid?	[Ag] (ng/mL)	Unquant. data?	SC#	Hook#	Threshold Dilution	Cal. Alg	QR (OM)	AR (OM)	LOD (pg/mL)	Repro pnCSF
94	VEGFR3	No	500000	Yes	-	-	-	1 in 3	Alg4	-	-	-	-

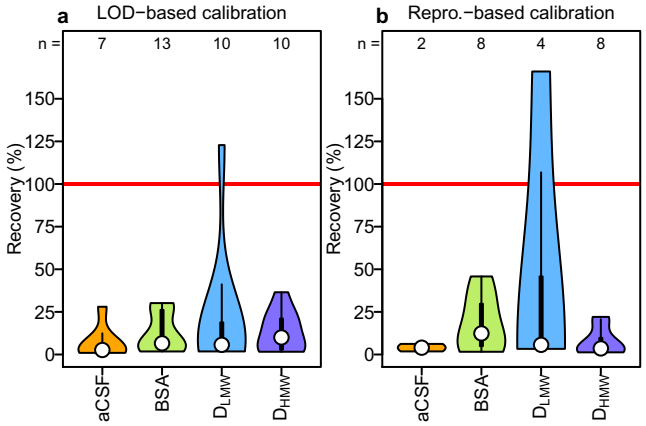

FIGURE E.S6: **Improvement of sensitivity using a modified calibration method.** Measurements of protein relative recovery using fluorescence values from data calibrated with (**a**) a method intended to improve the sensitivity and (**b**) a method intended to improve reproducibility. Graphs show that around twice as many low-abundance proteins were measured using the LOD-based calibration method, with $LOD = Mean + 2 \times SD$. Red lines are visual aids that indicate a perfect value of relative recovery at 100 %.

TABLE E.S3: **Relative recovery of proteins.** Quantities of proteins interpolated from standard curves are listed, as well as the relative recovery calculated using fluorescence values. Only proteins for which quantities were measured in pnCSF or the dialysate are listed here. No SC: no standard curve was generated for this protein.

			0.3 µL/mL				1.0 µL/mL		
	Protein name	pnCSF (pg/mL)	aCSF	BSA	LMW	HMW	BSA	LMW	HMW
1	AFP	No SC	-	-	122.8%	-	-	-	-
2	AHSG	No SC	-	-	-	-	2.8%	-	-
5	Ang1	64.4 ± 26.0	-	-	-	-	-	-	-
10	CA15-3	35.2 ± 42.0	-	-	-	-	-	-	-
12	CD14	No SC	2.7%	4.0% ± 2.3%	3.7% ± 2.4%	1.6%	5.1%	-	-
14	c-Kit	3346.9 ± 1129.5	-	-	-	-	-	-	-
17	E-cadherin	224.8 ± 152.4	-	26.2% ± 12.4%	-	17.5%	-	-	-
19	EGF-R	2749.4 ± 445.9	-	-	5.4%	-	-	-	-
22	FAS-L	26.6 ± 7.1	-	-	-	-	16.6%	-	-
27	GRO-α	1390.4 ± 633.9	-	-	-	-	-	-	-
30	HER2	7.8	-	-	-	-	-	-	-
31	HER3	2408 ± 1993.6	-	-	-	-	-	-	22.3%
32	HGF	1588.4 ± 615.5	-	-	-	-	-	-	-
33	HGF-R	794 ± 142.8	-	-	-	-	-	-	-
36	ICAM-1	7136.7 ± 387.2	-	-	-	15.0%	-	-	-
37	IFN-γ	No SC	-	-	-	-	-	-	-
38	IGFBP-1	675.2 ± 150.3	-	-	-	-	-	-	-
39	IGFBP-3	9743 ± 1980.4	-	3.3% ± 0.1%	-	-	-	-	-
40	IGFBP-7	No SC	6.5%	6.6% ± 0.7%	6.0% ± 0.7%	2.9% ± 3.1%	7.0%	-	-
44	IL-18	No SC	-	2.9%	3.5%	2.9%	-	-	-

Table E.S3 continued from previous page

			0.3 µL/mL				1.0 µL/mL		
	Protein name	pnCSF (pg/mL)	aCSF	BSA	LMW	HMW	BSA	LMW	HMW
51	IL-6	10.6 ± 2.2	-	-	-	-	-	-	-
53	IL-8	152.2 ± 24.7	-	13.9%	-	-	-	-	-
54	IP-10	6736.4 ± 2128.4	1.0%	5.2% ± 4.6%	-	2.0%	8.6%	-	-
59	MCP3	7.4 ± 5.6	-	-	-	36.5%	-	-	-
61	MIG	885 ± 208.9	-	29.6% ± 15.2%	22.4%	24.2%	29.1%	-	-
62	MIP-1α	13.6 ± 14.7	-	30.2%	-	-	-	-	-
65	MMP-3	223 ± 116.5	-	-	-	-	-	-	-
66	MMP-9	4591.4 ± 566.0	-	-	-	-	-	-	-
67	NCAM-1	162815.5 ± 88688	1.8%	-	1.8%	-	-	-	-
69	OPN	66588.5 ± 13201.9	1.1%	1.8%	-	-	-	-	-
77	SPARC	2686.2 ± 1199.9	-	-	-	-	-	-	-
81	TGF-β1	165.1 ± 76.2	28.0%	28.3%	30.8%	22.2%	27.4%	-	-
82	THBS-1	803.7 ± 561.0	-	-	-	-	-	-	6.7%
84	TIMP-1	No SC	-	7.5% ± 0.8%	-	5.0%	6.7%	-	10.2%
86	TNF-RI	3616.6 ± 700.0	5.1%	4.8%	8.2% ± 3.8%	-	3.2%	-	-
87	TNF-RII	1213.2 ± 219.1	-	-	4.7% ± 1.2%	-	-	-	-
88	uPA	7.5 ± 2.9	-	-	-	-	-	-	-
89	uPA-R	352.6 ± 58.3	-	-	-	-	-	-	46.9%
90	VCAM-1	204019.8 ± 73784.1	-	-	-	-	-	-	-
91	VEGF-A	2.6 ± 0.6	-	-	-	-	-	-	-

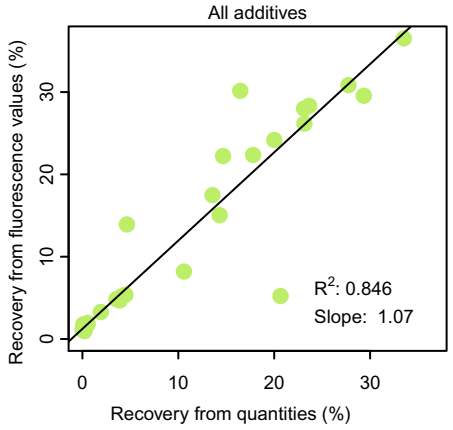

FIGURE E.S7: **Comparison of relative recovery of proteins calculated with fluorescence values and quantities.** The relative recovery of proteins measured when perfused with BSA, $\text{Dextran}_{\text{LMW}}$ or $\text{Dextran}_{\text{HMW}}$ was measured on calibrated fluorescence values (x-axis) and quantities interpolated from the standard curves (y-axis). The linear fit was calculated using median-based linear regression.

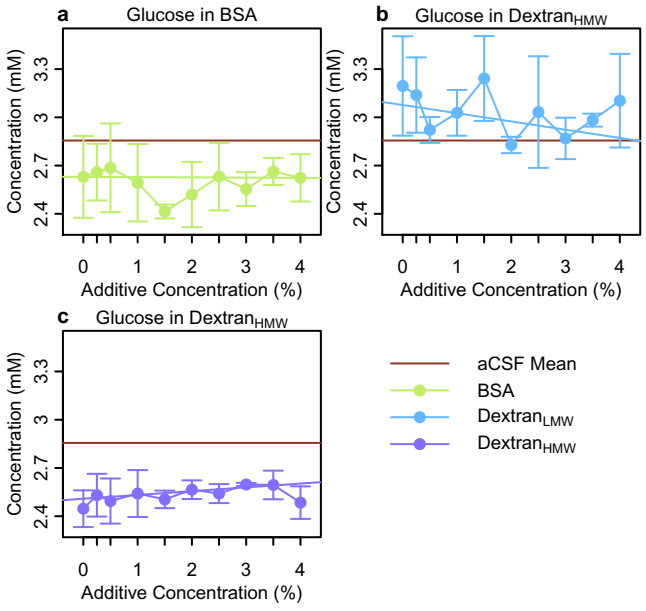

FIGURE E.S8: **Additives matrix effect on the measurement of glucose.** Measurement of glucose from a mixture of small molecules in aCSF buffer with increasing concentrations of (**a**) BSA, (**b**) $\text{Dextran}_{\text{LMW}}$ or (**c**) $\text{Dextran}_{\text{HMW}}$. Linear fits were calculated using median-based linear regression.

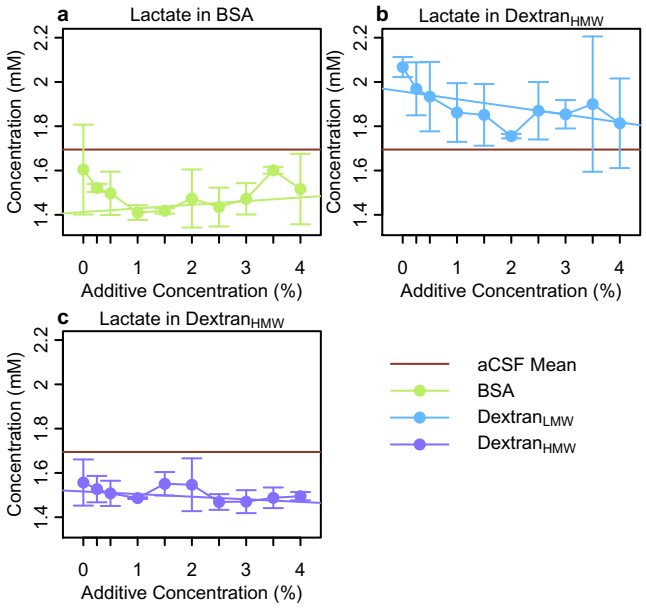

FIGURE E.S9: **Additives matrix effect on the measurement of lactate.** Measurement of lactate from a mixture of small molecules in aCSF buffer with increasing concentrations of (**a**) BSA, (**b**) Dextran$_{LMW}$ or (**c**) Dextran$_{HMW}$. Linear fits were calculated using median-based linear regression.

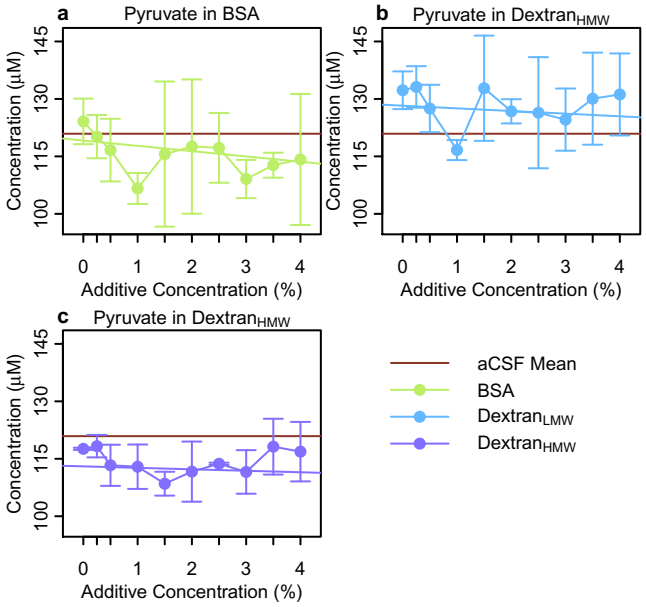

FIGURE E.S10: **Additives matrix effect on the measurement of pyruvate.** Measurement of pyruvate from a mixture of small molecules in aCSF buffer with increasing concentrations of (**a**) BSA, (**b**) Dextran$_{LMW}$ or (**c**) Dextran$_{HMW}$. Linear fits were calculated using median-based linear regression.

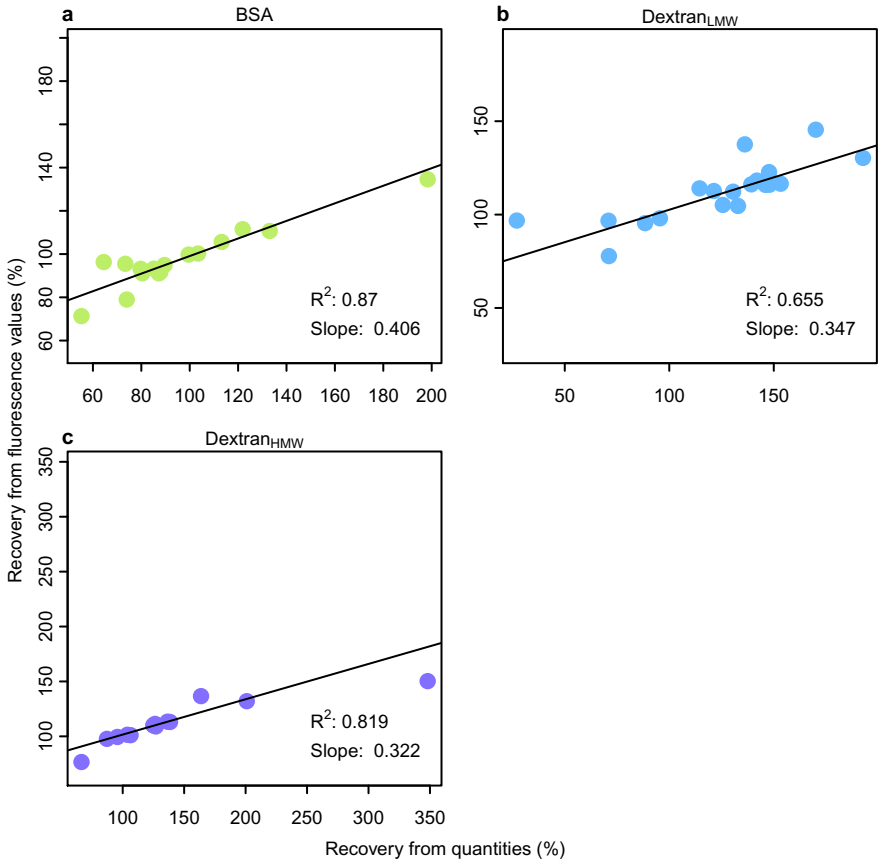

FIGURE E.S11: **Comparison of matrix effect of additives on proteins calculated with fluorescence values and quantities.** The recovery of proteins measured in increasing concentrations of (**a**) BSA, (**b**) Dextran$_{LMW}$ or (**c**) Dextran$_{HMW}$ was measured on calibrated fluorescence values (y-axes) and quantities interpolated from standard curves (x-axes). Linear fits were calculated using median-based linear regression.

TABLE E.S4: **Information on 94 proteins.** Information was obtained from the following sources: The Human Protein Atlas (www.proteinatlas.org) and the Human Protein Reference Database (www.hprd.org).

	Protein name	Full name	Unit size (kDa)	Size used (kDa)	Complexes	Glycosylation	Cell location	Detected in U87
1	AFP	Alpha feto-protein	68.7	137.4	1, 2, 3	Yes	Secreted	No
2	AHSG	Alpha-2-HS-glycoprotein	39.3	39.3		Yes	Secreted	No
3	ALDH1L1	10-formyltetrahydrofolate dehydrogenase	98.8	98.8		No	Cytoplasm	No
4	Amphiregulin	Amphiregulin	27.9	27.9		Probably	Membrane	No
5	Ang1	Angiopoietin 1	57.5	57.5		Yes	Secreted	Yes
6	Ang2	Angiopoietin 2	56.9	56.9		Probably	Secreted	No
7	BMP2	Bone morphogenetic protein 2	44.7	44.7		Yes	Secreted	Yes
8	b-NGF	Nerve growth factor	26.9	130	130-kDa complex	Probably	Secreted	Yes
9	BRAF	B-Raf (kinase)	84.4	84.4		Unknown	Cytoplasm	Yes
10	CA15-3	Cancer antigen 15-3 (derived from mucin 1)	122	375	250-500 kDa with glyco	Yes	Membrane	No
11	CCL5	Chemokine (C-Cmotif) ligand 5	99.9	8	Mature: 8 kDa	Yes	Secreted	No
12	CD14	Cluster of differentiation 14	48 or 56 (soluble)	56	Monomer	Probably	Secreted	Yes
13	CEA	Carcinoembryonic antigen (CEACAM 1)	57.5	60.7		Probably/Yes	Secreted	A bit
	CEA	Carcinoembryonic antigen (CEACAM 8)	38.1	60.7		Probably/Yes	Membrane	A bit
	CEA	Carcinoembryonic antigen (CEACAM 6)	37.2	60.7		Probably/Yes	Membrane	A bit
	CEA	Carcinoembryonic antigen (CEACAM 3)	27.1	60.7		Probably/Yes	Membrane	A bit
	CEA	Carcinoembryonic antigen (CEACAM 5)	76.8	60.7		Probably/Yes	Secreted	A bit
	CEA	Carcinoembryonic antigen (PSG1)	47.8	60.7		Probably/Yes	Secreted	A bit
14	c-Kit	Mast/stem cell growth factor receptor	109.9	109.9		Probably	Membrane	No
15	CRP	C-reactive protein	25	125	Pentameric: 125 kDa	Yes	Secreted	No
16	CXCL12	Stromal cell-derived factor 1	13.7	13.7		Probably	Secreted	No
17	E-cadherin	Epithelial cadherin-1	99.7	99.7		Probably	Membrane, secreted	No
18	EGF	Epidermal growth factor	6	6		Probably	Secreted	Yes
19	EGF-R	Epidermal growth factor receptor	134.3	134.3	Active homodimer membrane	Yes	Membrane, secreted	Yes
20	Endoglin	Endoglin	70.6	70.6	Homodimer	Yes	Membrane, secreted	Yes
21	E-selectin	Endothelial-leukocyte adhesion molecule 1	66.7	66.7		Probably	Membrane, secreted	No
22	FAS-L	FAS ligand	31.4	31.4	soluble FASL is smaller	Yes	Membrane, secreted	No
23	FGFb	Basic fibroblast growth factor	18	18		Unknown	Cytosol, nucleus, secreted	Yes
24	Flt-3	Fms-like tyrosine kinase 3	112.9	112.9		Probably	Membrane	No

Table E.S4 continued from previous page

	Protein name	Full name	Unit size (kDa)	Size used (kDa)	Complexes	Glycosylation	Cell location	Detected in U87
25	GFAP	Glial fibrillary acidic protein	49.9	49.9	Structural protein	No	Cytosol, secreted	Yes
26	GM-CSF	Granulocyte-macrophage colony-stimulating factor	16.3	32.6	Homodimer: 32.6	Yes	Secreted	Yes
27	GRO-a	Chemokine (C-X-Cmotif) ligand 1	11.3	11.3		Probably	Secreted	No
28	HAI-1	Hepatocyte growth factor activator inhibitor type 1	33.2 secreted	33.2		Probably	Membrane, secreted	No
29	HE4	Human epididymis protein 4	13	13		Probably	Cytosol, secreted	No
30	HER2	Human epidermal growth factor receptor 2	137.9	137.9			Membrane, cytosol, shed	No
31	HER3	Human epidermal growth factor receptor 3	148.1	148.1		Perhaps	Membrane, cytosol, secreted	No
32	HGF	Hepatocyte growth factor	83.1	83.1		Probably	Secreted	Yes
33	HGF-R	Hepatocyte growth factor receptor	157.8	21.3	Secreted: 21.3 kDa	Probably	Cytosol, membrane, secreted	Yes
34	HMGB1	Amphoterin/High mobility group box 1	24.9	24.9		Unknown	Cytosol, secreted	Yes
35	HP	Haptoglobin	45.2	167.4	Tetramer: ~167.4 kDa	Yes	Secreted	No
36	ICAM-1	Intercellular adhesion molecule 1	57.8	19.4	Secreted: 19.4 kDa	Yes	Membrane, secreted	Yes
37	IFN-g	Interferon gamma	19.3	38.6	Homodimer: 38.6	Yes	Secreted	No
38	IGFBP-1	Insulin-like growth factor-binding protein 1	27.9	27.9		Probably	Secreted	Yes
39	IGFBP-3	Insulin-like growth factor-binding protein 3	32.2	32.2	Heterotrimer: variable	Yes	Secreted	Yes
40	IGFBP-7	Insulin-like growth factor-binding protein 7	29.1	29.1		Probably	Secreted	Yes
41	IL-10	Interleukin 10	20.5	41	Homodimer: 41 kDa	Probably	Secreted	A bit
42	IL-12	Interleukin 12	~70 kDa active form	70	Heterodimer:	Yes	Secreted	
43	IL-15	Interleukin 15	18	18		Yes	Membrane, secreted	Yes
44	IL-18	Interleukin 18	22.3	22.3		Probably	Secreted	No
45	IL-1b	Interleukin 1 beta/Lymphocyte activating factor	17.5 kDa processed	17.5			Secreted	Yes
46	IL-1ra	Interleukin 1 receptor antagonist	19.9	19.9		Probably	Secreted	Yes
47	IL-2	Interleukin 2	17.6	17.6		Yes	Secreted	No
48	IL-3	Interleukin 3	17.2	17.2		Probably	Secreted	No
49	IL-4	Interleukin 4	17.4	17.4		Probably	Secreted	No
50	IL-5	Interleukin 5	15.2	15.2		Yes	Secreted	No
51	IL-6	Interleukin 6	23.7	23.7		Yes	Secreted	Yes
52	IL-7	Interleukin 7	20.2	20.2		Probably	Secreted	Yes
53	IL-8	Interleukin 8	11.1	11.1		Probably	Secreted	Yes
54	IP-10	Interferon gamma-induced protein 10	10.9	10.9		Probably	Secreted	No
55	KLK8	Kallikrein-8	33	33		Probably	Secreted	A bit
56	Leptin	Leptin	18.6	18.6		Probably	Secreted	A bit

Table E.S4 continued from previous page

	Protein name	Full name	Unit size (kDa)	Size used (kDa)	Complexes	Glycosylation	Cell location	Detected in U87
57	MCP1	Monocyte chemoattractant protein 1	11	11		Probably	Secreted	Yes
58	MCP2	Monocyte chemoattractant protein 2	11.2	11.2		Probably	Secreted	No
59	MCP3	Monocyte chemoattractant protein 3	12.4	12.4		Probably	Secreted	Yes
60	M-CSF	Macrophage colony-stimulating factor	60.1	120.2	Homodimer in blood	Yes	Secreted	Yes
61	MIG	Monokine induced by gamma interferon	14	14		Probably	Secreted	No
62	MIP-1a	Macrophage inflammatory protein 1-alpha	10	10		Probably	Secreted	Yes
63	MIP-1b	Macrophage inflammatory protein 1-beta	10.2	10.2		Probably	Secreted	No
64	MMP-1	Matrix metalloproteinase-1	54	54		Yes	Secreted	Yes
65	MMP-3	Matrix metalloproteinase-3	54	54		Probably	Secreted	Yes
66	MMP-9	Matrix metalloproteinase-9	78.5	78.5		Probably	Membrane, secreted	No
67	NCAM-1	Neural cell adhesion molecule	94.6	94.6		Yes	Membrane, secreted	Yes
68	NT-3	Neurotrophin-3	30.8	30.8		Probably	Secreted	No
69	OPN	Osteopontin	35.4	44	Apparent: 44 kDa	Yes	Secreted	Yes
70	PAI-1	Plasminogen activator inhibitor-1	45.1	45.1		Yes	Secreted	Yes
71	PDGF-BB	Platelet-derived growth factor subunit BB	27.3	54.6	Homodimer: 54.6	Probably	Secreted	A bit
72	PRL	Prolactin	22.6	22.6		Probably	Secreted	No
73	PSA	Prostate-specific antigen/Kallikrein-3	28.7	28.7		Yes	Secreted	No
74	RBP4	Retinol binding protein 4	23	23		Probably	Secreted	No
75	S100b	S100 calcium-binding protein B	10.7	10.7			Intracellular	A bit
76	SCGN	Secretagogin	32	32			Intracellular	No
77	SPARC	Osteonectin	34.6	34.6		Yes	Secreted	Yes
78	TF	Tissue factor/Platelet tissue factor	33.1	33.1		Yes	Membrane	Yes
79	TGF-a	Transforming growth factor alpha	17	17		Probably	Membrane, secreted	Yes
80	TGF-b RII	Transforming growth factor beta receptor II	67.5	67.5	Hetero or homodimeric	Probably	Secreted	Yes
81	TGF-b1	Transforming growth factor beta 1	14 or 44.3	14		Yes	Secreted	Yes
82	THSB-1	Thrombospondin 1	129.4	388.2	Homotrimeric: 388.2	Yes	Secreted	Yes
83	Tie-2	Angiopoietin-1 receptor	125.8	52	Secreted: 52 kDa	Probably	Membrane, secreted	Yes
84	TIMP-1	TIMP metallopeptidase inhibitor 1	23.2	23.2		Yes	Secreted	Yes
85	TNF-a	Tumor necrosis factor	25.6	51	Homotrimeric: 51 kDa	Probably	Membrane, secreted	No
86	TNF-RI	Tumor necrosis factor receptor 1	50.5	50.5		Probably	Membrane, secreted	Yes
87	TNF-RII	Tumor necrosis factor receptor 2	48.3	48.3		Probably	Membrane, secreted	Yes
88	uPA	Urokinase-type plasminogen activator	48.5	48.5		Probably	Membrane, secreted	Yes

Table E.S4 continued from previous page

	Protein name	Full name	Unit size (kDa)	Size used (kDa)	Complexes	Glycosylation	Cell location	Detected in U87
89	uPA-R	Urokinase receptor	37	50	With glyco: 50-60 kDa	Yes	Membrane, secreted	Yes
90	VCAM-1	Vascular cell adhesion protein 1	81.3	81.3		Yes	Membrane, secreted	A bit
91	VEGF-A	Vascular endothelial growth factor A	45.5	91	Homodimer: 91 kDa	Yes	Secreted	Yes
92	VEGF-D	Vascular endothelial growth factor D	40.4	40.4		Probably	Secreted	No
93	VEGFR2	Vascular endothelial growth factor receptor 2	151.5	151.5		Probably	Membrane	A bit
94	VEGFR3	Vascular endothelial growth factor receptor 3	152.8	152.8		Probably	Membrane, secreted	No

TABLE E.S5: **Additives matrix effect on proteins.** Comparison of linear regressions for each protein detected in pnCSF diluted in increasing concentrations of additives using fluorescence values. Linear regressions were obtained using a median-based linear model.

	Protein name	BSA				$Dextran_{LMW}$				$Dextran_{HMW}$			
		Slope	Intercept	R^2	Recovery (%)	Slope	Intercept	R^2	Recovery (%)	Slope	Intercept	R^2	Recovery (%)
2	AHSG	0.012	7.933	0.009	101.6	0.015	7.987	0.008	101.7	0.069	7.709	0.164	108.8
10	CA15-3	-	-	-	-	-0.003	1.403	0.001	96.8	-	-	-	-
12	CD14	-0.022	3.856	0.060	97.3	-0.038	4.095	0.035	96.3	0.011	3.813	0.015	101.2
14	c-Kit	-0.018	4.252	0.034	91.7	0.027	4.117	0.035	112.7	0.069	4.054	0.282	136.7
17	E-cadherin	-0.043	2.636	0.196	-	0.064	2.678	0.226	145.5	0.034	2.581	0.090	-
19	EGF-R	-0.030	1.480	0.031	93.3	0.082	1.414	0.217	116.5	0.047	1.484	0.076	109.1
22	FAS-L	0.032	1.250	0.130	-	-	-	-	-	-	-	-	-
31	HER3	0.050	3.376	0.203	-	-	-	-	-	-	-	-	-
32	HGF	-0.022	2.961	0.015	91.1	-0.060	2.889	0.174	77.8	-	-	-	-
33	HGF-R	-0.047	6.423	0.034	79.0	0.049	6.031	0.070	137.6	0.071	5.844	0.078	-
38	IGFBP-1	0.062	3.282	0.508	110.7	-0.032	3.330	0.094	95.4	0.010	3.347	0.013	101.5
39	IGFBP-3	-0.001	2.943	0.000	99.8	0.061	2.730	0.173	116.2	0.043	2.879	0.050	110.0
40	IGFBP-7	-0.006	5.444	0.000	99.3	-0.057	5.522	0.079	94.5	0.078	5.520	0.305	107.6
44	IL-18	0.018	3.100	0.052	103.4	0.000	3.081	0.000	100.0	0.062	2.755	0.167	112.8
53	IL-8	-0.089	1.841	0.458	71.3	0.049	1.566	0.078	118.2	0.031	1.564	0.062	111.4
54	IP-10	-0.026	4.839	0.031	96.3	0.035	4.422	0.022	105.2	-0.017	4.658	0.004	97.8
61	MIG	-0.064	4.089	0.253	-	0.022	3.985	0.024	114.1	0.064	3.867	0.041	-
66	MMP-9	0.048	-0.071	0.118	111.5	0.101	-0.189	0.262	122.8	-0.116	-0.028	0.423	76.6
67	NCAM-1	-0.034	4.108	0.073	93.2	0.068	3.632	0.081	115.9	0.054	3.584	0.048	113.1
69	OPN	0.002	5.241	0.001	100.3	-0.033	5.262	0.020	96.7	-0.005	5.044	0.002	99.5
77	SPARC	0.053	2.232	0.171	134.6	0.029	2.244	0.060	116.0	0.080	2.170	0.291	150.3
81	TGF-β1	-0.127	2.926	0.114	-	-	-	-	-	-	-	-	-
82	THBS-1	-0.029	6.356	0.077	91.1	0.087	6.086	0.212	130.4	0.083	6.007	0.242	132.1
84	TIMP-1	-0.017	4.469	0.014	94.0	0.033	4.261	0.029	112.8	-0.013	4.427	0.008	95.8
86	TNF-RI	0.029	1.673	0.112	105.6	-0.013	1.757	0.017	98.0	0.059	1.585	0.362	110.2
87	TNF-RII	-0.024	5.989	0.023	95.0	0.061	5.828	0.120	112.3	0.064	5.778	0.113	113.4
88	uPA	-	-	-	-	-	-	-	-	0.069	0.636	0.214	-
90	VCAM-1	-0.041	2.666	0.062	95.5	0.044	2.328	0.037	104.6	0.011	2.357	0.002	101.1
91	VEGF-A	-0.075	-1.772	0.478	-	-	-	-	-	-	-	-	-

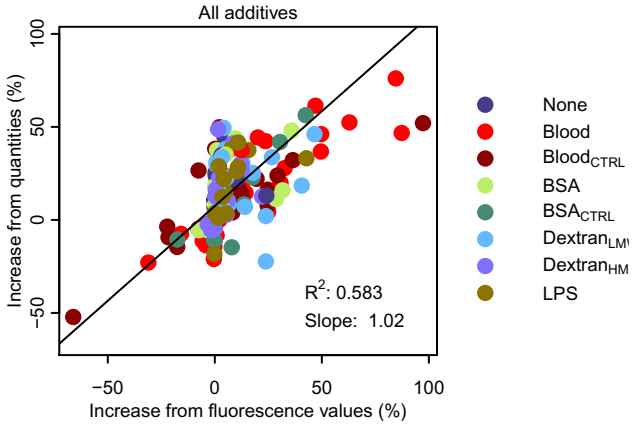

FIGURE E.S12: **Comparison of production increases of proteins in cell cultures calculated with fluorescence values and quantities.** The increase of proteins production in cell culture media as measured with calibrated fluorescence values (x-axes) and quantities interpolated from the standard curves (y-axes). **a** shows a number of outliers from fluorescence values. **b** shows the distribution of points that lead to the median-based linear regression. The linear fit were calculated using median-based linear regression.

TABLE E.S6: **Linear regressions of protein levels in the media of U87 cultures with no additives.** Stable human glial cells (U87) were cultured for two days in the absence of any additives in a 24-well culture plate. The last row of the plate is considered separately to study the normal variation seen in cell cultures.

		None							
		Additive				Plate control			
	Protein name	Slope	Intercept	R^2	Increase (%)	Slope	Intercept	R^2	Increase (%)
1	AFP	-	-	-	-	-	-	-	-
2	AHSG	-	-	-	-	-	-	-	-
5	Ang1	0.009	0.421	0.853	13.00	0.009	0.444	0.620	13.04
7	BMP2	-	-	-	-	-	-	-	-
8	b-NGF	-	-	-	-	0.013	3.112	0.523	21.80
9	BRAF	-	-	-	-	-	-	-	-
10	CA15-3	-	-	-	-	-	-	-	-
11	CCL5	-	-	-	-	-	-	-	-
12	CD14	-	-	-	-	-	-	-	-
14	c-Kit	-	-	-	-	-	-	-	-
17	E-cadherin	-	-	-	-	-	-	-	-
18	EGF	-	-	-	-	-	-	-	-
19	EGF-R	-	-	-	-	-	-	-	-
22	FAS-L	-	-	-	-	-	-	-	-
26	GM-CSF	-	-	-	-	-	-	-	-
27	GRO-a	-	-	-	-	-	-	-	-
32	HGF	0.008	2.199	0.534	7.51	0.005	2.319	0.340	7.32
33	HGF-R	0.011	5.723	0.968	10.33	0.011	5.701	0.885	9.15
34	HMGB1	-0.003	4.524	0.799	-12.08	-0.011	4.724	0.869	-35.21
36	ICAM-1	-	-	-	-	-	-	-	-
38	IGFBP-1	0.012	1.399	0.814	13.13	0.006	1.426	0.354	0.70

Table E.S6 continued from previous page

		None							
		Additive				Plate control			
	Protein name	Slope	Intercept	R^2	Increase (%)	Slope	Intercept	R^2	Increase (%)
39	IGFBP-3	-	-	-	-	-	-	-	-
40	IGFBP-7	0.026	2.960	0.762	41.53	0.023	3.019	0.850	35.76
44	IL-18	-	-	-	-	-	-	-	-
45	IL-1b	-	-	-	-	-	-	-	-
50	IL-5	-	-	-	-	-	-	-	-
51	IL-6	-	-	-	-	-	-	-	-
53	IL-8	0.017	1.777	0.253	25.53	0.007	2.171	0.039	10.75
54	IP-10	-	-	-	-	-	-	-	-
57	MCP1	-	-	-	-	-	-	-	-
59	MCP3	-	-	-	-	-	-	-	-
62	MIP-1a	0.006	4.646	0.128	9.90	0.004	4.552	0.071	6.76
63	MIP-1b	-	-	-	-	-	-	-	-
64	MMP-1	-	-	-	-	-	-	-	-
65	MMP-3	-	-	-	-	-	-	-	-
66	MMP-9	-	-	-	-	-	-	-	-
69	OPN	0.029	2.368	0.863	28.42	0.022	2.471	0.872	21.23
70	PAI-1	-	-	-	-	-	-	-	-
71	PDGF-BB	-	-	-	-	-	-	-	-
72	PRL	-	-	-	-	-	-	-	-
74	RBP4	-	-	-	-	-	-	-	-
77	SPARC	-	-	-	-	-	-	-	-
81	TGF-b1	-	-	-	-	-	-	-	-
82	THSB-1	0.003	6.341	0.167	3.77	-0.002	6.440	0.124	-2.94
84	TIMP-1	-	-	-	-	-	-	-	-
86	TNF-RI	-	-	-	-	-	-	-	-
87	TNF-RII	-	-	-	-	-	-	-	-
88	uPA	0.046	1.874	0.844	44.43	0.036	2.163	0.751	34.82
90	VCAM-1	-	-	-	-	-	-	-	-
91	VEGF-A	0.028	0.110	0.560	26.21	0.025	0.140	0.500	23.92
93	VEGFR2	-	-	-	-	-	-	-	-

TABLE E.S7: **Linear regressions of protein levels in the media of U87 cultures with whole blood.** Stable human glial cells (U87) were cultured for two days in media with whole blood in a 24-well culture plate. The last row of the plate is did not receive any additive.

		Blood							
		Additive				Plate control			
	Protein name	Slope	Intercept	R^2	Increase (%)	Slope	Intercept	R^2	Increase (%)
1	AFP	0.006	2.208	0.909	4.33	-	-	-	-
2	AHSG	-0.002	8.043	0.036	-2.33	-	-	-	-
5	Ang1	0.007	2.701	0.740	10.46	-0.002	0.787	0.084	-2.74
7	BMP2	-	-	-	-	-	-	-	-
8	b-NGF	-	-	-	-	-	-	-	-
9	BRAF	-	-	-	-	-	-	-	-
10	CA15-3	0.007	1.255	0.916	36.78	-	-	-	-
11	CCL5	0.018	1.475	0.913	30.13	-	-	-	-
12	CD14	0.009	3.526	0.736	12.75	-	-	-	-

Table E.S7 continued from previous page

		Blood Additive				Plate control			
	Protein name	Slope	Intercept	R^2	Increase (%)	Slope	Intercept	R^2	Increase (%)
14	c-Kit	0.006	3.971	0.755	27.88	-	-	-	-
17	E-cadherin	-0.001	3.159	0.015	-2.31	-	-	-	-
18	EGF	-0.003	1.637	0.407	-7.47	-	-	-	-
19	EGF-R	0.000	1.846	0.000	0.07	-	-	-	-
22	FAS-L	-	-	-	-	-	-	-	-
26	GM-CSF	-	-	-	-	-	-	-	-
27	GRO-a	0.015	-1.531	0.964	18.32	-	-	-	-
32	HGF	0.044	2.660	0.951	76.07	0.005	2.484	0.470	9.15
33	HGF-R	0.007	6.912	0.500	14.56	0.030	5.204	0.924	29.70
34	HMGB1	-	-	-	-	-	-	-	-
36	ICAM-1	-0.004	2.293	0.145	-8.32	-	-	-	-
38	IGFBP-1	0.009	1.575	0.570	15.30	0.030	1.027	0.967	41.74
39	IGFBP-3	0.002	3.628	0.301	4.37	-	-	-	-
40	IGFBP-7	0.007	4.423	0.751	11.39	0.022	2.738	0.913	34.44
44	IL-18	0.001	1.865	0.451	2.60	-	-	-	-
45	IL-1b	-	-	-	-	-	-	-	-
50	IL-5	-	-	-	-	-	-	-	-
51	IL-6	-0.002	2.199	0.011	-7.24	-	-	-	-
53	IL-8	0.041	1.982	0.670	61.41	-0.010	1.866	0.142	-14.41
54	IP-10	-	-	-	-	-	-	-	-
57	MCP1	0.015	3.773	0.889	42.34	-	-	-	-
59	MCP3	0.043	2.430	0.813	80.42	-	-	-	-
62	MIP-1a	0.015	4.744	0.316	25.96	0.008	4.415	0.401	14.36
63	MIP-1b	0.014	2.926	0.342	19.97	-	-	-	-
64	MMP-1	-	-	-	-	-	-	-	-
65	MMP-3	0.024	-2.780	0.868	52.43	0.026	-3.323	0.819	44.33
66	MMP-9	0.040	0.444	0.748	46.14	-	-	-	-
69	OPN	0.019	2.912	0.918	27.63	0.019	2.492	0.869	17.50
70	PAI-1	0.004	0.442	0.783	2.00	-	-	-	-
71	PDGF-BB	-0.008	6.137	0.381	-11.28	-	-	-	-
72	PRL	-	-	-	-	-	-	-	-
74	RBP4	-	-	-	-	-	-	-	-
77	SPARC	-0.006	2.232	0.373	-13.63	-	-	-	-
81	TGF-b1	-0.010	3.701	0.857	-22.90	-	-	-	-
82	THSB-1	0.014	7.831	0.923	18.67	-0.016	7.147	0.735	-21.01
84	TIMP-1	0.010	3.861	0.971	10.78	-	-	-	-
86	TNF-RI	0.002	0.369	0.548	5.08	-	-	-	-
87	TNF-RII	0.007	5.005	0.830	19.04	-	-	-	-
88	uPA	0.049	2.852	0.854	46.74	0.039	2.753	0.810	37.55
90	VCAM-1	0.001	1.309	0.021	1.96	-	-	-	-
91	VEGF-A	0.042	0.444	0.768	39.79	0.014	0.985	0.148	12.89
93	VEGFR2	-	-	-	-	-	-	-	-

TABLE E.S8: **Linear regressions of protein levels in cell culture media with whole blood and no U87 cells.** Whole blood was added to cell culture media in a 24-well culture plate and incubated over two days.

	Protein name	$Blood_{CTRL}$ Additive Slope	Intercept	R^2	Increase (%)
1	AFP	-	-	-	-
2	AHSG	-0.004	7.739	0.071	-5.95
5	Ang1	-0.001	2.703	0.017	-1.60
7	BMP2	-	-	-	-
8	b-NGF	-	-	-	-
9	BRAF	-	-	-	-
10	CA15-3	0.004	1.278	0.884	22.11
11	CCL5	0.002	1.898	0.131	2.46
12	CD14	0.006	3.300	0.486	7.88
14	c-Kit	0.007	3.879	0.499	32.16
17	E-cadherin	-0.004	3.360	0.493	-14.52
18	EGF	-0.004	1.792	0.377	-9.33
19	EGF-R	0.002	1.716	0.044	4.01
22	FAS-L	-	-	-	-
26	GM-CSF	-	-	-	-
27	GRO-a	0.012	-1.584	0.757	7.10
32	HGF	0.012	2.230	0.815	15.03
33	HGF-R	0.011	6.797	0.543	23.89
34	HMGB1	0.006	4.382	0.728	26.58
36	ICAM-1	0.005	1.838	0.193	10.75
38	IGFBP-1	-	-	-	-
39	IGFBP-3	-0.001	3.621	0.556	-2.73
40	IGFBP-7	0.001	4.025	0.024	2.26
44	IL-18	0.007	1.661	0.558	7.55
45	IL-1b	-	-	-	-
50	IL-5	-	-	-	-
51	IL-6	-	-	-	-
53	IL-8	0.034	1.636	0.603	49.84
54	IP-10	-	-	-	-
57	MCP1	0.011	3.714	0.947	17.05
59	MCP3	0.031	2.428	0.767	52.51
62	MIP-1a	0.014	3.942	0.914	15.92
63	MIP-1b	0.007	2.893	0.866	0.82
64	MMP-1	0.039	1.337	0.828	62.28
65	MMP-3	0.005	-2.781	0.194	10.11
66	MMP-9	0.045	0.556	0.878	52.06
69	OPN	-	-	-	-
70	PAI-1	-0.001	0.671	0.562	-4.73
71	PDGF-BB	-	-	-	-
72	PRL	-	-	-	-
74	RBP4	0.007	1.172	0.825	17.78
77	SPARC	0.000	2.213	0.001	0.68
81	TGF-b1	-0.022	3.975	0.958	-52.17
82	THSB-1	-0.003	8.003	0.942	-3.61
84	TIMP-1	0.010	3.865	0.651	12.43

Table E.S8 continued from previous page

		$Blood_{CTRL}$ Additive			
	Protein name	Slope	Intercept	R^2	Increase (%)
86	TNF-RI	0.005	0.394	0.488	13.97
87	TNF-RII	0.006	4.951	0.480	16.61
88	uPA	0.000	1.211	0.006	-0.18
90	VCAM-1	0.009	1.260	0.449	12.58
91	VEGF-A	0.041	-1.395	0.868	38.22
93	VEGFR2	0.003	-0.523	0.456	16.27

TABLE E.S9: **Linear regressions of protein levels in the media of U87 cultures with BSA.** Stable human glial cells (U87) were cultured for two days in media with BSA in a 24-well culture plate. The last row of the plate is did not receive any additive.

		BSA Additive				Plate control			
	Protein name	Slope	Intercept	R^2	Increase (%)	Slope	Intercept	R^2	Increase (%)
1	AFP	-	-	-	-	-	-	-	-
2	AHSG	-	-	-	-	-	-	-	-
5	Ang1	0.008	0.732	0.689	11.17	0.011	0.563	0.924	15.94
7	BMP2	-	-	-	-	-	-	-	-
8	b-NGF	-	-	-	-	-	-	-	-
9	BRAF	-	-	-	-	-	-	-	-
10	CA15-3	-	-	-	-	-	-	-	-
11	CCL5	-	-	-	-	-0.005	1.693	0.216	-7.85
12	CD14	-	-	-	-	-	-	-	-
14	c-Kit	-	-	-	-	-	-	-	-
17	E-cadherin	-	-	-	-	-0.004	2.694	0.060	-5.52
18	EGF	-	-	-	-	-	-	-	-
19	EGF-R	-	-	-	-	-	-	-	-
22	FAS-L	-	-	-	-	-	-	-	-
26	GM-CSF	-	-	-	-	-	-	-	-
27	GRO-a	-	-	-	-	-	-	-	-
32	HGF	0.011	2.178	0.794	11.89	0.006	2.363	0.213	10.05
33	HGF-R	0.009	5.730	0.835	7.04	0.010	5.587	0.869	2.97
34	HMGB1	-0.008	4.502	0.780	-15.17	-0.003	4.512	0.352	-14.80
36	ICAM-1	-	-	-	-	-	-	-	-
38	IGFBP-1	0.015	1.365	0.913	21.63	0.017	1.251	0.912	20.19
39	IGFBP-3	0.011	1.697	0.950	10.96	-	-	-	-
40	IGFBP-7	0.028	3.186	0.651	44.06	0.030	3.101	0.722	46.57
44	IL-18	-	-	-	-	-	-	-	-
45	IL-1b	-	-	-	-	-	-	-	-
50	IL-5	-	-	-	-	-	-	-	-
51	IL-6	-	-	-	-	-	-	-	-
53	IL-8	0.025	1.854	0.366	37.49	0.012	2.327	0.109	18.31
54	IP-10	-	-	-	-	-0.008	2.847	0.191	-5.42
57	MCP1	-	-	-	-	-	-	-	-
59	MCP3	-	-	-	-	-	-	-	-
62	MIP-1a	0.011	4.583	0.202	20.12	0.007	4.453	0.178	12.88
63	MIP-1b	-	-	-	-	-	-	-	-

Table E.S9 continued from previous page

		BSA							
		Additive				Plate control			
	Protein name	Slope	Intercept	R^2	Increase (%)	Slope	Intercept	R^2	Increase (%)
64	MMP-1	0.004	1.651	0.395	0.55	-	-	-	-
65	MMP-3	-	-	-	-	0.015	-3.602	0.760	5.95
66	MMP-9	0.022	-1.814	0.744	5.05	-	-	-	-
69	OPN	0.033	3.434	0.678	48.05	0.028	2.644	0.771	36.23
70	PAI-1	-	-	-	-	0.011	0.242	0.671	18.50
71	PDGF-BB	-	-	-	-	-	-	-	-
72	PRL	-	-	-	-	-	-	-	-
74	RBP4	-	-	-	-	-	-	-	-
77	SPARC	-	-	-	-	-	-	-	-
81	TGF-b1	-	-	-	-	-	-	-	-
82	THSB-1	0.005	6.364	0.706	6.97	0.006	6.367	0.407	8.28
84	TIMP-1	-	-	-	-	-	-	-	-
86	TNF-RI	-	-	-	-	-	-	-	-
87	TNF-RII	-	-	-	-	-	-	-	-
88	uPA	0.046	2.531	0.693	43.84	0.037	2.555	0.661	35.13
90	VCAM-1	-	-	-	-	-	-	-	-
91	VEGF-A	0.009	0.694	0.069	8.64	0.028	0.487	0.526	26.60
93	VEGFR2	-	-	-	-	-	-	-	-

TABLE E.S10: **Linear regressions of protein levels in cell culture media with BSA and no U87 cells.** BSA was added to cell culture media in a 24-well culture plate and incubated over two days.

		BSA_{CTRL}							
		Additive				Plate control			
	Protein name	Slope	Intercept	R^2	Increase (%)	Slope	Intercept	R^2	Increase (%)
1	AFP	-	-	-	-	-	-	-	-
2	AHSG	-	-	-	-	-	-	-	-
5	Ang1	0.006	0.450	0.894	8.38	-0.007	0.787	0.493	-10.55
7	BMP2	-	-	-	-	-	-	-	-
8	b-NGF	-	-	-	-	-	-	-	-
9	BRAF	-	-	-	-	-	-	-	-
10	CA15-3	-	-	-	-	-	-	-	-
11	CCL5	-	-	-	-	0.041	-0.392	0.722	5.09
12	CD14	-	-	-	-	-	-	-	-
14	c-Kit	-	-	-	-	-	-	-	-
17	E-cadherin	0.007	2.591	0.298	22.87	-	-	-	-
18	EGF	-	-	-	-	-	-	-	-
19	EGF-R	-	-	-	-	-	-	-	-
22	FAS-L	-	-	-	-	-	-	-	-
26	GM-CSF	-	-	-	-	-	-	-	-
27	GRO-a	-	-	-	-	-	-	-	-
32	HGF	0.007	2.265	0.846	8.78	-	-	-	-
33	HGF-R	0.013	5.615	0.964	10.51	-	-	-	-
34	HMGB1	-0.003	4.615	0.386	-14.69	-0.013	4.665	0.414	-29.31
36	ICAM-1	-	-	-	-	-	-	-	-
38	IGFBP-1	0.020	1.550	0.897	45.89	-	-	-	-
39	IGFBP-3	0.005	1.834	0.677	5.03	-	-	-	-

Table E.S10 continued from previous page

		BSA_{CTRL} Additive				Plate control			
	Protein name	Slope	Intercept	R^2	Increase (%)	Slope	Intercept	R^2	Increase (%)
40	IGFBP-7	0.028	2.510	0.950	37.78	-	-	-	-
44	IL-18	-	-	-	-	-	-	-	-
45	IL-1b	-	-	-	-	-	-	-	-
50	IL-5	-	-	-	-	-	-	-	-
51	IL-6	-	-	-	-	-	-	-	-
53	IL-8	-0.007	1.651	0.137	-11.08	-	-	-	-
54	IP-10	-	-	-	-	-	-	-	-
57	MCP1	-	-	-	-	-	-	-	-
59	MCP3	-	-	-	-	-	-	-	-
62	MIP-1a	0.013	4.200	0.865	23.07	-	-	-	-
63	MIP-1b	-	-	-	-	-	-	-	-
64	MMP-1	-	-	-	-	-	-	-	-
65	MMP-3	0.028	-3.179	0.909	56.32	-	-	-	-
66	MMP-9	-	-	-	-	-	-	-	-
69	OPN	0.023	2.430	0.782	22.27	-	-	-	-
70	PAI-1	-	-	-	-	-	-	-	-
71	PDGF-BB	-	-	-	-	-	-	-	-
72	PRL	-	-	-	-	-0.003	-1.087	0.019	-10.87
74	RBP4	-	-	-	-	-	-	-	-
77	SPARC	-	-	-	-	-	-	-	-
81	TGF-b1	-	-	-	-	-	-	-	-
82	THSB-1	0.002	6.490	0.300	2.10	-0.009	6.769	0.443	-11.34
84	TIMP-1	-	-	-	-	-	-	-	-
86	TNF-RI	-	-	-	-	-	-	-	-
87	TNF-RII	-	-	-	-	-	-	-	-
88	uPA	0.044	2.798	0.815	41.92	-	-	-	-
90	VCAM-1	-	-	-	-	-	-	-	-
91	VEGF-A	0.032	0.102	0.654	29.87	-	-	-	-
93	VEGFR2	-	-	-	-	-	-	-	-

TABLE E.S11: **Linear regressions of protein levels in the media of U87 cultures with $\mathbf{Dextran_{LMW}}$.** Stable human glial cells (U87) were cultured for two days in media with $Dextran_{LMW}$ in a 24-well culture plate. The last row of the plate is did not receive any additive.

		$Dextran_{LMW}$ Additive				Plate control			
	Protein name	Slope	Intercept	R^2	Increase (%)	Slope	Intercept	R^2	Increase (%)
1	AFP	-	-	-	-	-	-	-	-
2	AHSG	-	-	-	-	-	-	-	-
5	Ang1	0.005	0.700	0.885	7.05	0.013	0.557	0.947	18.46
7	BMP2	-	-	-	-	-	-	-	-
8	b-NGF	-	-	-	-	-	-	-	-
9	BRAF	-	-	-	-	0.011	1.678	0.579	46.09
10	CA15-3	-	-	-	-	-	-	-	-
11	CCL5	-	-	-	-	-	-	-	-
12	CD14	-	-	-	-	-	-	-	-
14	c-Kit	-	-	-	-	-	-	-	-

Table E.S11 continued from previous page

		$Dextran_{LMW}$ Additive				Plate control			
	Protein name	Slope	Intercept	R^2	Increase (%)	Slope	Intercept	R^2	Increase (%)
17	E-cadherin	-	-	-	-	-0.001	2.716	0.001	-2.45
18	EGF	-	-	-	-	-	-	-	-
19	EGF-R	-	-	-	-	-	-	-	-
22	FAS-L	-	-	-	-	0.006	1.079	0.554	14.53
26	GM-CSF	-	-	-	-	0.008	0.931	0.734	27.91
27	GRO-a	-	-	-	-	-	-	-	-
32	HGF	-	-	-	-	0.006	2.324	0.477	8.78
33	HGF-R	0.019	5.636	0.962	26.26	0.008	5.673	0.922	1.48
34	HMGB1	-0.005	4.590	0.477	-22.30	-0.010	4.641	0.562	-27.56
36	ICAM-1	-	-	-	-	-	-	-	-
38	IGFBP-1	0.018	1.472	0.906	33.78	0.013	1.365	0.712	14.27
39	IGFBP-3	0.010	1.650	0.922	8.47	-	-	-	-
40	IGFBP-7	0.031	3.162	0.822	49.30	0.028	3.087	0.731	43.99
44	IL-18	-	-	-	-	-	-	-	-
45	IL-1b	-	-	-	-	0.011	2.021	0.676	35.61
50	IL-5	-	-	-	-	0.010	-0.272	0.510	15.86
51	IL-6	-	-	-	-	-	-	-	-
53	IL-8	0.021	2.030	0.255	31.08	0.020	2.180	0.222	29.55
54	IP-10	-	-	-	-	-	-	-	-
57	MCP1	-	-	-	-	-	-	-	-
59	MCP3	-	-	-	-	-	-	-	-
62	MIP-1a	0.009	4.582	0.289	15.37	0.009	4.475	0.258	16.26
63	MIP-1b	-	-	-	-	-	-	-	-
64	MMP-1	-	-	-	-	-	-	-	-
65	MMP-3	0.026	-3.616	0.980	30.74	-	-	-	-
66	MMP-9	-	-	-	-	-	-	-	-
69	OPN	0.037	2.659	0.906	49.49	0.025	2.542	0.911	27.89
70	PAI-1	0.005	0.404	0.872	2.08	0.007	0.389	0.629	13.42
71	PDGF-BB	-	-	-	-	0.008	5.655	0.534	6.62
72	PRL	-	-	-	-	-	-	-	-
74	RBP4	-	-	-	-	-	-	-	-
77	SPARC	-	-	-	-	-	-	-	-
81	TGF-b1	0.005	2.808	0.774	8.25	-	-	-	-
82	THSB-1	0.001	6.512	0.149	1.34	0.002	6.487	0.080	3.06
84	TIMP-1	-	-	-	-	-	-	-	-
86	TNF-RI	-	-	-	-	-	-	-	-
87	TNF-RII	-	-	-	-	-	-	-	-
88	uPA	0.040	2.257	0.730	38.25	0.035	2.304	0.733	33.78
90	VCAM-1	-	-	-	-	-	-	-	-
91	VEGF-A	0.027	0.413	0.462	25.33	0.024	0.513	0.494	22.65
93	VEGFR2	-	-	-	-	-	-	-	-

TABLE E.S12: **Linear regressions of protein levels in the media of U87 cultures with Dextran$_{HMW}$.** Stable human glial cells (U87) were cultured for two days in media with Dextran$_{HMW}$ in a 24-well culture plate. The last row of the plate is did not receive any additive.

		Dextran$_{HMW}$ Additive				Plate control			
	Protein name	Slope	Intercept	R^2	Increase (%)	Slope	Intercept	R^2	Increase (%)
1	AFP	-	-	-	-	-	-	-	-
2	AHSG	-	-	-	-	-	-	-	-
5	Ang1	0.009	0.495	0.909	12.59	0.002	0.789	0.084	2.83
7	BMP2	-	-	-	-	-0.007	2.002	0.380	-8.50
8	b-NGF	-	-	-	-	-	-	-	-
9	BRAF	-	-	-	-	-	-	-	-
10	CA15-3	-	-	-	-	-	-	-	-
11	CCL5	-	-	-	-	-	-	-	-
12	CD14	-	-	-	-	-	-	-	-
14	c-Kit	-	-	-	-	-	-	-	-
17	E-cadherin	-	-	-	-	-	-	-	-
18	EGF	-	-	-	-	-	-	-	-
19	EGF-R	-	-	-	-	-	-	-	-
22	FAS-L	-	-	-	-	-	-	-	-
26	GM-CSF	-	-	-	-	-	-	-	-
27	GRO-a	-	-	-	-	-	-	-	-
32	HGF	0.022	2.145	0.938	30.48	-0.003	2.681	0.097	-5.40
33	HGF-R	0.017	5.742	0.965	26.50	-	-	-	-
34	HMGB1	-	-	-	-	-0.004	4.337	0.572	-0.63
36	ICAM-1	-	-	-	-	-	-	-	-
38	IGFBP-1	0.027	1.444	0.948	56.69	0.006	1.521	0.478	5.34
39	IGFBP-3	0.006	1.684	0.900	2.47	-	-	-	-
40	IGFBP-7	0.033	3.479	0.714	51.79	0.025	3.233	0.612	39.35
44	IL-18	-	-	-	-	-	-	-	-
45	IL-1b	-	-	-	-	-	-	-	-
50	IL-5	-	-	-	-	-	-	-	-
51	IL-6	-	-	-	-	0.006	1.694	0.212	6.04
53	IL-8	0.033	1.520	0.645	48.77	0.000	2.637	0.000	-0.70
54	IP-10	-	-	-	-	-	-	-	-
57	MCP1	-	-	-	-	-	-	-	-
59	MCP3	-	-	-	-	-	-	-	-
62	MIP-1a	0.006	4.642	0.232	10.49	-0.011	5.282	0.318	-19.47
63	MIP-1b	-	-	-	-	-	-	-	-
64	MMP-1	-	-	-	-	-	-	-	-
65	MMP-3	0.016	-3.564	0.981	10.72	-	-	-	-
66	MMP-9	-	-	-	-	-	-	-	-
69	OPN	0.030	2.600	0.875	38.08	0.010	2.765	0.395	12.62
70	PAI-1	-	-	-	-	-	-	-	-
71	PDGF-BB	-	-	-	-	-	-	-	-
72	PRL	-	-	-	-	-	-	-	-
74	RBP4	-	-	-	-	-	-	-	-
77	SPARC	0.002	2.001	0.190	3.27	-	-	-	-
81	TGF-b1	-	-	-	-	-0.012	2.942	0.472	-2.38
82	THSB-1	0.001	6.474	0.288	1.25	-0.004	6.560	0.453	-4.67
84	TIMP-1	-	-	-	-	-	-	-	-

Table E.S12 continued from previous page

		$Dextran_{HMW}$ Additive				Plate control			
	Protein name	Slope	Intercept	R^2	Increase (%)	Slope	Intercept	R^2	Increase (%)
86	TNF-RI	-	-	-	-	-	-	-	-
87	TNF-RII	-	-	-	-	-	-	-	-
88	uPA	0.043	2.503	0.659	41.15	0.024	2.580	0.714	22.73
90	VCAM-1	-	-	-	-	-	-	-	-
91	VEGF-A	0.025	0.517	0.561	23.31	0.017	0.575	0.305	16.36
93	VEGFR2	-	-	-	-	-	-	-	-

TABLE E.S13: **Linear regressions of protein levels in the media of U87 cultures with LPS.** Stable human glial cells (U87) were cultured for two days in media with LPS in a 24-well culture plate. The last row of the plate is did not receive any additive.

		LPS Additive				Plate control			
	Protein name	Slope	Intercept	R^2	Increase (%)	Slope	Intercept	R^2	Increase (%)
1	AFP	-	-	-	-	-	-	-	-
2	AHSG	-	-	-	-	-	-	-	-
5	Ang1	-0.001	0.498	0.076	-2.03	0.003	0.393	0.149	3.56
7	BMP2	-	-	-	-	-	-	-	-
8	b-NGF	-	-	-	-	-	-	-	-
9	BRAF	-	-	-	-	-	-	-	-
10	CA15-3	-	-	-	-	-	-	-	-
11	CCL5	-	-	-	-	0.003	1.637	0.048	4.96
12	CD14	-	-	-	-	-	-	-	-
14	c-Kit	-	-	-	-	-	-	-	-
17	E-cadherin	-	-	-	-	0.005	2.390	0.356	1.24
18	EGF	-	-	-	-	-	-	-	-
19	EGF-R	-	-	-	-	-	-	-	-
22	FAS-L	-	-	-	-	-	-	-	-
26	GM-CSF	-	-	-	-	-	-	-	-
27	GRO-a	-	-	-	-	-	-	-	-
32	HGF	0.003	2.322	0.210	2.59	0.007	2.366	0.569	12.31
33	HGF-R	0.012	5.747	0.803	15.17	0.012	6.015	0.604	26.12
34	HMGB1	-0.008	4.529	0.825	-17.75	-0.002	4.369	0.283	-3.92
36	ICAM-1	-	-	-	-	-	-	-	-
38	IGFBP-1	0.016	1.659	0.703	39.47	0.017	1.640	0.775	40.38
39	IGFBP-3	-	-	-	-	-	-	-	-
40	IGFBP-7	0.023	2.663	0.819	36.01	0.022	2.693	0.772	34.15
44	IL-18	-	-	-	-	-	-	-	-
45	IL-1b	-	-	-	-	-	-	-	-
50	IL-5	-	-	-	-	-	-	-	-
51	IL-6	-	-	-	-	-	-	-	-
53	IL-8	-0.003	1.843	0.006	-3.81	-0.017	1.833	0.275	-18.26
54	IP-10	-	-	-	-	-	-	-	-
57	MCP1	-	-	-	-	-	-	-	-
59	MCP3	-	-	-	-	-	-	-	-
62	MIP-1a	0.019	4.457	0.606	33.16	0.013	4.554	0.394	22.10
63	MIP-1b	-	-	-	-	-	-	-	-

Table E.S13 continued from previous page

		LPS Additive				Plate control			
	Protein name	Slope	Intercept	R^2	Increase (%)	Slope	Intercept	R^2	Increase (%)
64	MMP-1	-	-	-	-	-	-	-	-
65	MMP-3	0.024	-3.406	0.837	37.55	0.020	-3.378	0.921	28.39
66	MMP-9	-	-	-	-	-	-	-	-
69	OPN	0.024	2.497	0.713	25.27	0.026	2.469	0.840	27.94
70	PAI-1	-	-	-	-	-	-	-	-
71	PDGF-BB	-	-	-	-	-	-	-	-
72	PRL	-	-	-	-	-	-	-	-
74	RBP4	-	-	-	-	0.013	1.047	0.716	47.41
77	SPARC	-	-	-	-	-	-	-	-
81	TGF-b1	-	-	-	-	-	-	-	-
82	THSB-1	0.000	6.383	0.004	0.36	0.003	6.225	0.109	3.69
84	TIMP-1	-	-	-	-	-	-	-	-
86	TNF-RI	-	-	-	-	-	-	-	-
87	TNF-RII	-	-	-	-	-	-	-	-
88	uPA	0.040	2.664	0.659	38.05	0.043	2.598	0.687	41.61
90	VCAM-1	-	-	-	-	-	-	-	-
91	VEGF-A	0.031	0.194	0.520	28.86	0.031	0.224	0.513	28.84
93	VEGFR2	-	-	-	-	-	-	-	-

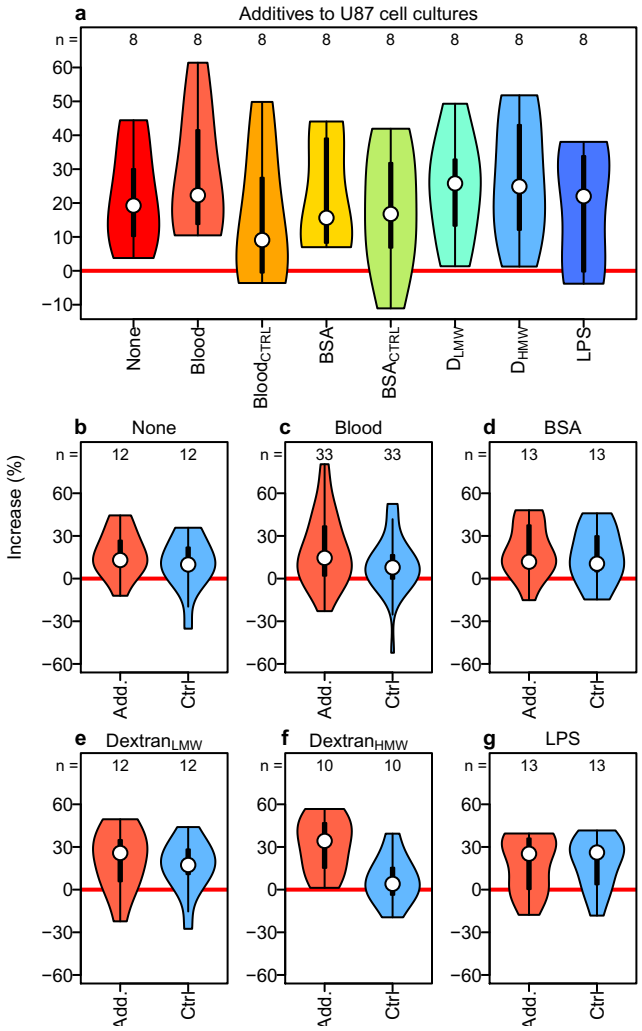

FIGURE E.S13: **Effect of additives on secretion of proteins in the medium of stable U87 cells.** Additives (**c** whole blood, **d** BSA, **e** $\text{Dextran}_{\text{LMW}}$, **f** $\text{Dextran}_{\text{HMW}}$ or **g** LPS) were added to three rows of a 24-well plate containing mycoplasma-free cultured human glial (U87) cells. The last row of each plate did not receive any additives and serves as a negative control. **a** is the comparison of the effect of additives on the secretion of proteins. Only proteins which were detected in all conditions is considered. **b-i** Each condition is shown compared to its plate control (**b, e-g**), to $\text{Blood}_{\text{CTRL}}$ (**c**) or BSA_{CTRL} (**d**). Only proteins detected in both the additive and the control are considered. Red lines are visual aids that show no increase nor decrease in protein levels measured in the cell culture media.

TABLE E.S14: **Summary of protein levels measured in cell cultures with additives and their possible provenance.**

		Detected in:			Produced by:		Degraded in:			
	Protein name	Media	BSA + media	Blood	U87 cells	Blood cells	BSA + media	Blood	Media	Media + U87 cells
2	AHSG	-	-	Yes	-	-	-	-	-	-
5	Ang1	Yes	Yes	Yes	Yes	-	Yes	-	Yes	-

Table E.S14 continued from previous page

		Detected in:			Produced by:			Degraded in:		
	Protein name	Media	BSA + media	Blood	U87 cells	Blood cells	BSA + media	Blood	Media	Media + U87 cells
10	CA15-3	-	-	-	-	Yes	-	-	-	-
11	CCL5	-	-	Yes	-	-	-	-	-	-
12	CD14	-	-	Yes	-	-	-	-	-	-
14	c-Kit	-	-	Yes	-	Yes	-	-	-	-
17	E-cadherin	-	Yes	Yes	-	-	Yes	-	-	-
18	EGF	-	-	Yes	-	-	-	-	-	-
19	EGF-R	-	-	Yes	-	-	-	-	-	-
27	GRO-α	-	-	Yes	-	-	-	-	-	-
32	HGF	-	Yes	Yes	Yes	Yes	Yes	-	-	-
33	HGF-R	-	Yes	Yes	Yes	Yes	Yes	-	-	-
34	HMGB1	Yes	Yes	Yes	-	Yes	-	-	Yes	Yes
36	ICAM-1	-	-	Yes	-	-	-	-	-	-
38	IGFBP-1	-	Yes	-	Yes	-	Yes	-	-	-
39	IGFBP-3	-	Yes	Yes	-	-	Yes	-	-	-
40	IGFBP-7	-	Yes	Yes	Yes	-	Yes	-	-	-
44	IL-18	-	-	Yes	-	-	-	-	-	-
51	IL-6	-	-	-	-	-	-	-	-	-
53	IL-8	-	Yes	-	Yes	Yes	Yes	-	-	Yes
57	MCP1	-	-	-	-	Yes	-	-	-	-
59	MCP3	-	-	-	-	Yes	-	-	-	-
62	MIP-1α	-	Yes	-	Yes	Yes	Yes	-	-	-
65	MMP-3	-	Yes	Yes	Yes	-	Yes	-	-	-
66	MMP-9	-	-	Yes	-	Yes	-	-	-	-
69	OPN	-	Yes	Yes	Yes	-	Yes	-	-	-
70	PAI-1	-	-	Yes	Yes	-	-	-	-	-
72	PRL	Yes	-	-	-	-	-	-	-	-
77	SPARC	-	-	Yes	-	-	-	-	-	-
81	TGF-β1	-	-	Yes	-	-	-	Yes	-	-
82	THBS-1	Yes	-	Yes	Yes	-	-	-	-	Yes
84	TIMP-1	-	-	-	-	Yes	-	-	-	-
86	TNF-RI	-	-	Yes	-	-	-	-	-	-
87	TNF-RII	-	-	Yes	-	-	-	-	-	-
88	uPA	-	Yes	Yes	Yes	-	Yes	-	-	-
90	VCAM-1	-	-	Yes	-	-	-	-	-	-
91	VEGF-A	-	Yes	Yes	Yes	Yes	Yes	-	-	-
93	VEGFR2	-	-	Yes	-	-	-	-	-	-
	Total	4	14	29	13	12	13	1	2	3

TABLE E.S15: **Statistical comparison of additives effects on U87 cell cultures.** The percent increase or decrease in the protein secretion in cell media was compared in the presence or absence of additive using each 24-well culture plate's last row as the negative control. Data normality was calculated using the Shapiro-Wilk normality test, as it is a requirement for the validity of paired t-tests. None, $\text{Dextran}_{\text{LMW}}$, $\text{Dextran}_{\text{HMW}}$ and LPS were compared to their plate controls, while Blood and BSA were compared to $\text{Blood}_{\text{CTRL}}$ and BSA_{CTRL} (plates containing blood and BSA without cells), respectively.

	None	Blood	BSA	$\text{Dextran}_{\text{LMW}}$	$\text{Dextran}_{\text{HMW}}$	LPS
Normality Additive	0.715	0.158	0.193	0.674	0.655	0.080
Normality Control	0.210	0.016	0.714	0.431	0.944	0.318
Normality Difference	0.160	0.092	0.049	0.227	0.242	0.434
Paired t-test p-value	0.004	0.003	0.492	0.167	0.001	0.657

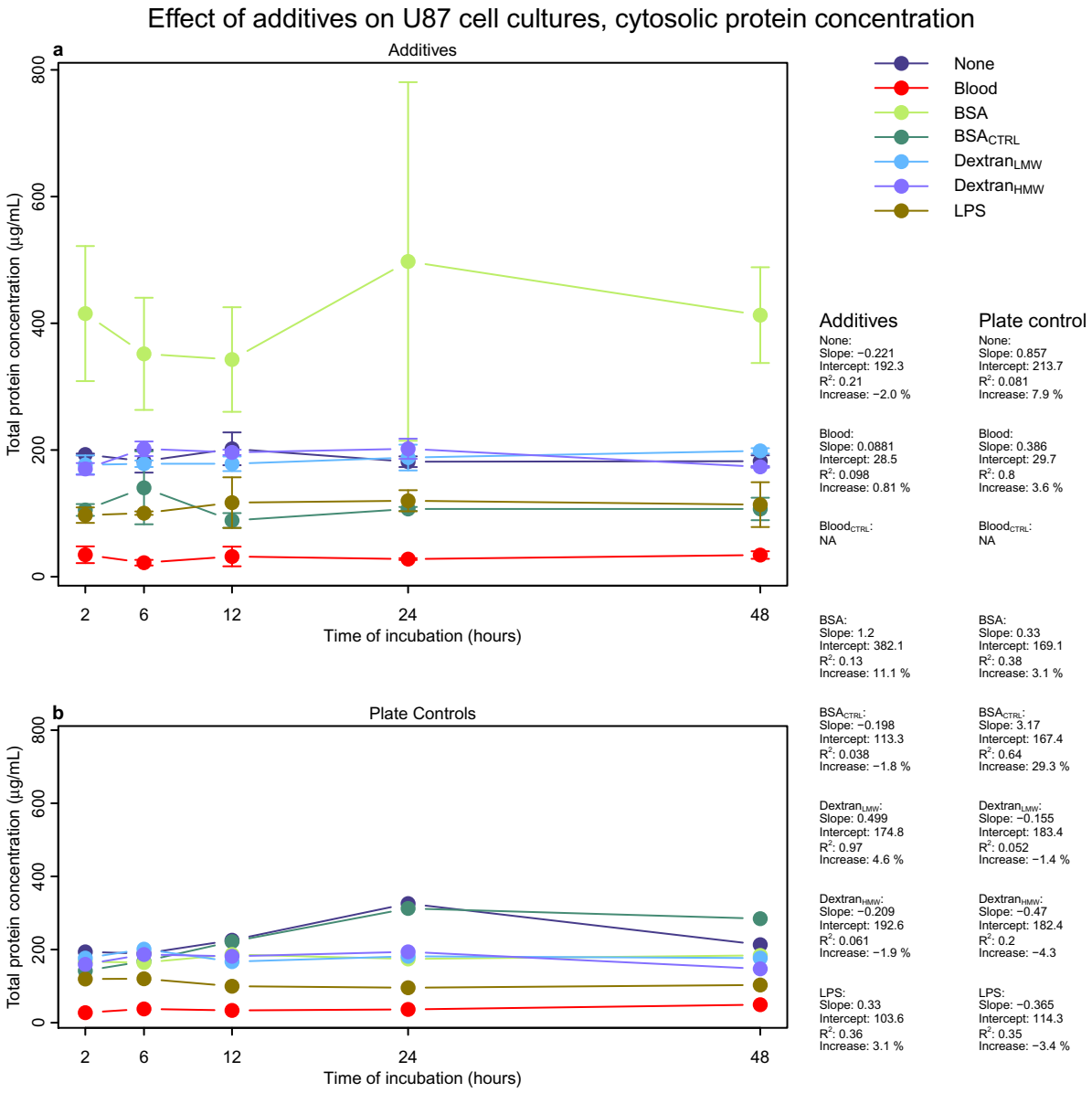

FIGURE E.S14: **Measure of quantity of cells in cell cultures subjected to additives.** Following media aspiration and freezing, remaining U87 cells from 24-well plates were washed and their number estimated by lysing and measuring the total protein concentration using a BCA assay.

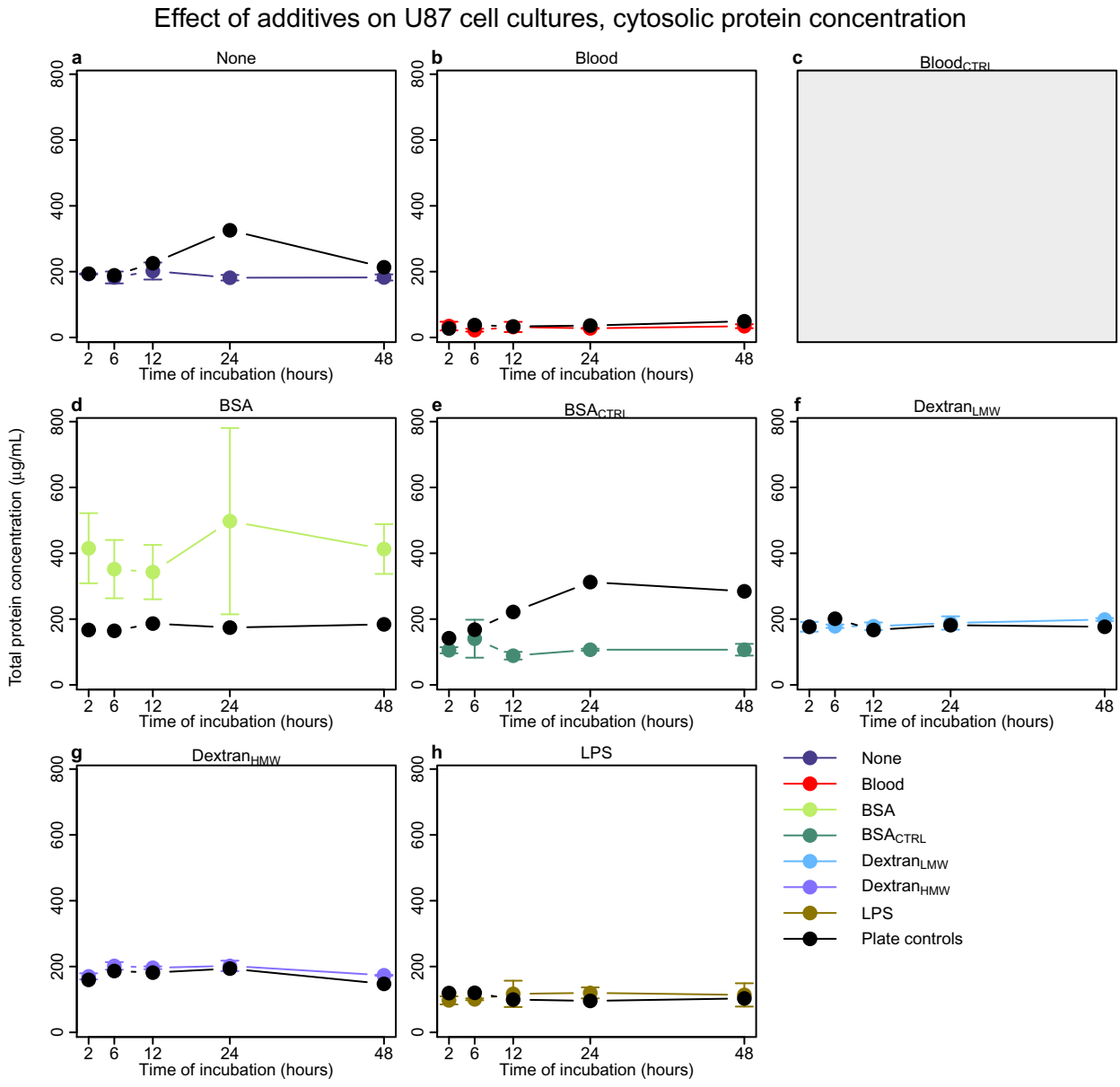

FIGURE E.S15: **Measure of quantity of cells in cell cultures subjected to additives.** Following media aspiration and freezing, remaining U87 cells from 24-well plates were washed and their number estimated by lysing and measuring the total protein concentration using a BCA assay. Total protein levels are shown here as separate graphs for each different 24-well plate. **c** Blood$_{CTRL}$ did not have any cells and therefore was not measured here.

APPENDIX F

Potential biomarkers in TBI patients: Supplementary Material

This appendix describes the Supplementary Material to chapter 6.

Electronic Supplementary Material

Time course proteomic analysis of matched microdialysis, cerebrospinal fluid and blood samples from severe and blood samples from mild traumatic brain injury patients

Veronique Laforte, Judith Marcoux, Rajeet Singh Saluja and David Juncker

List of SI figures

List of SI tables

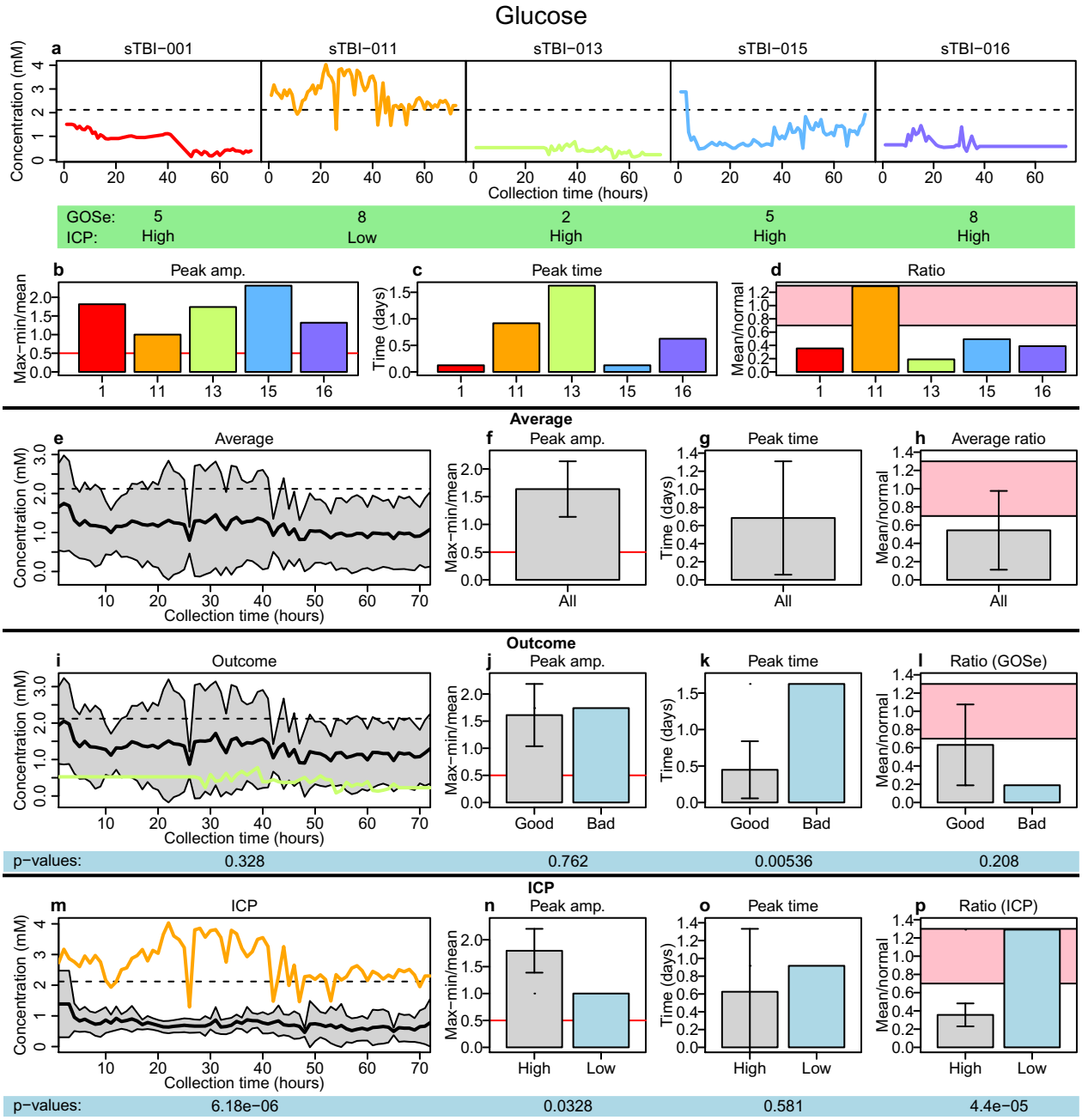

FIGURE F.S1: **Analysis of glucose levels in microdialysate samples of sTBI patients. a** Glucose concentration in the brain microdialysate samples of individual sTBI patients, whose clinical information is shown below, was measured and peaks amplitude, time and ratio of mean value to normal (PRA) (**b-d**) was calculated for each patient. The average glucose profile (**e**) and PRA (**f-h**) are shown. Glucose profiles (**i**, analyzed by mixed effect modeling) and PRA (**j-l**, t-tests) between patients with good (GOS-E 5-8) and bad (GOS-E 1-4) outcome were compared. Similarly, glucose profiles (**m**) and PRA (**n-p**) was compared between patients with high and low ICP. The dashed lines in **a, e, i, m** show the normal measured value while the red lines in **b, f, j, n** show a threshold for a profile that is considered to have a peak, rather than being constant. The light red boxes in **d, h, l, p** show the threshold of comparison to the normal measured value.

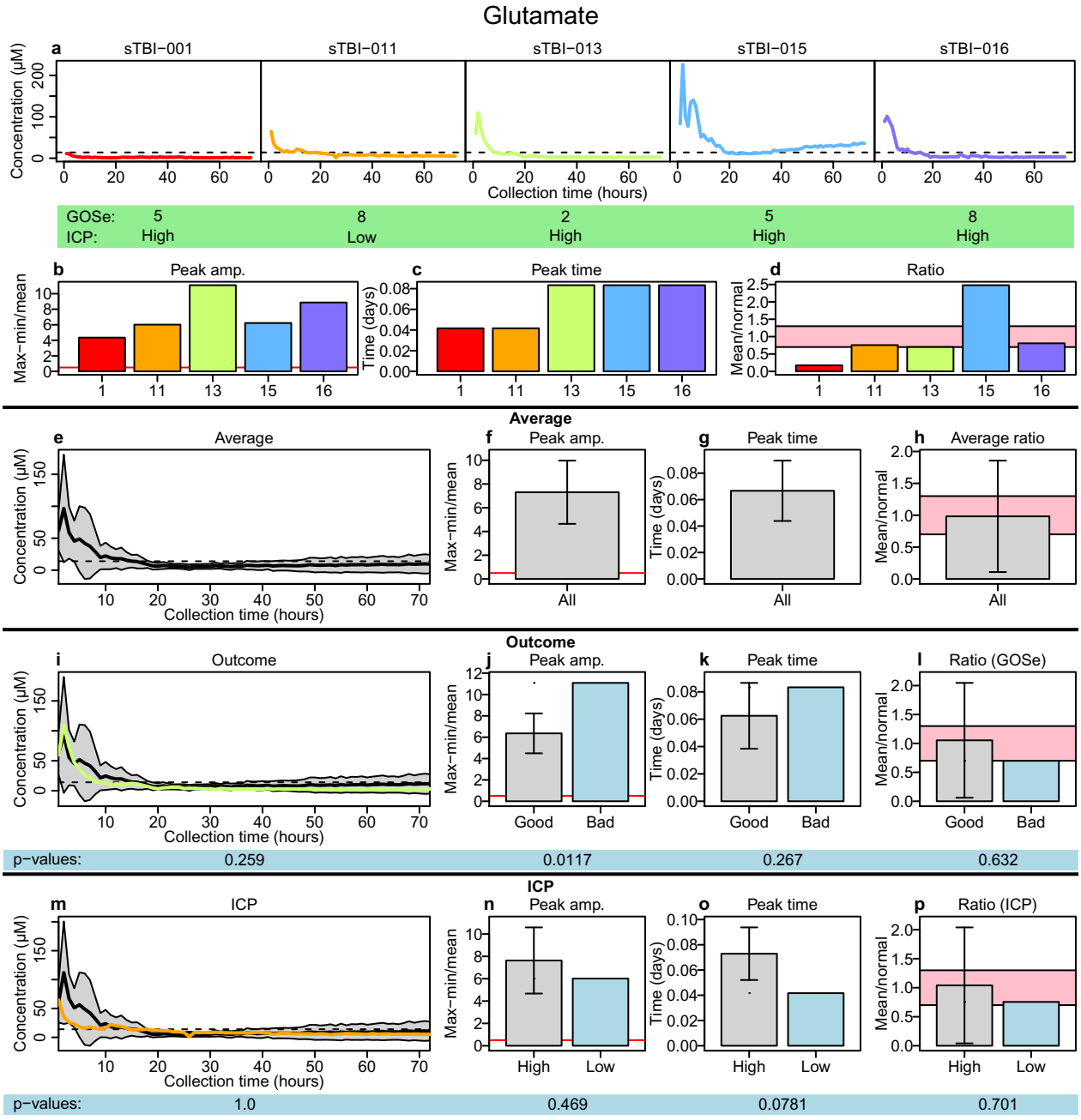

FIGURE F.S2: **Analysis of glutamate levels in microdialysate samples of sTBI patients. a** Glutamate concentration in the brain microdialysate samples of individual sTBI patients, whose clinical information is shown below, was measured and peaks amplitude, time and ratio of mean value to normal (PRA) (**b-d**) was calculated for each patient. The average glutamate profile (**e**) and PRA (**f-h**) are shown. Glutamate profiles (**i**, analyzed by mixed effect modeling) and PRA (**j-l**, t-tests) between patients with good (GOS-E 5-8) and bad (GOS-E 1-4) outcome were compared. Similarly, glutamate profiles (**m**) and PRA (**n-p**) was compared between patients with high and low ICP. The dashed lines in **a, e, i, m** show the normal measured value while the red lines in **b, f, j, n** show a threshold for a profile that is considered to have a peak, rather than being constant. The light red boxes in **d, h, l, p** show the threshold of comparison to the normal measured value.

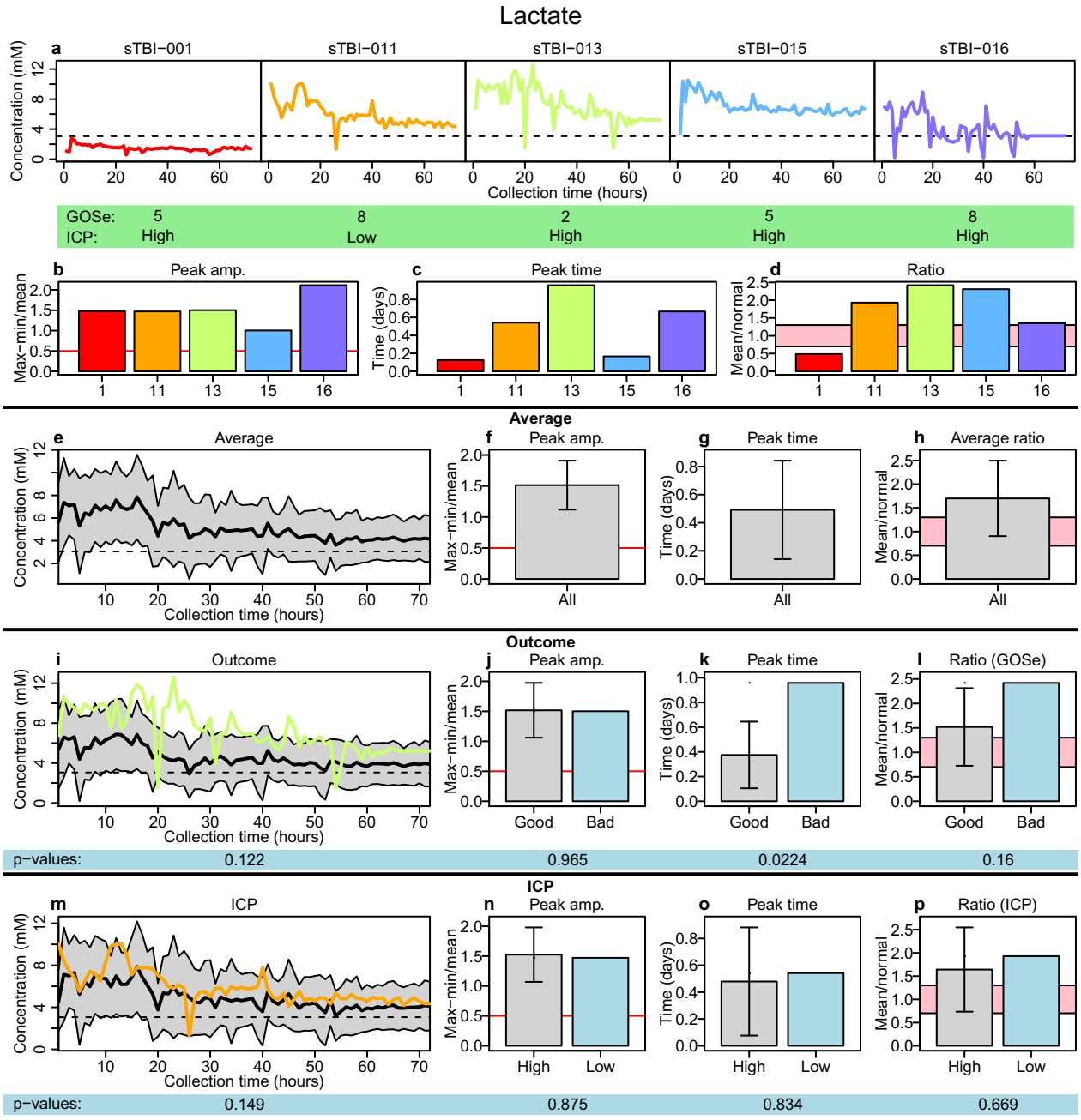

FIGURE F.S3: **Analysis of lactate levels in microdialysate samples of sTBI patients. a** Lactate concentration in the brain microdialysate samples of individual sTBI patients, whose clinical information is shown below, was measured and peaks amplitude, time and ratio of mean value to normal (PRA) (**b-d**) was calculated for each patient. The average lactate profile (**e**) and PRA (**f-h**) are shown. Lactate profiles (**i**, analyzed by mixed effect modeling) and PRA (**j-l**, t-tests) between patients with good (GOS-E 5-8) and bad (GOS-E 1-4) outcome were compared. Similarly, lactate profiles (**m**) and PRA (**n-p**) was compared between patients with high and low ICP. The dashed lines in **a, e, i, m** show the normal measured value while the red lines in **b, f, j, n** show a threshold for a profile that is considered to have a peak, rather than being constant. The light red boxes in **d, h, l, p** show the threshold of comparison to the normal measured value.

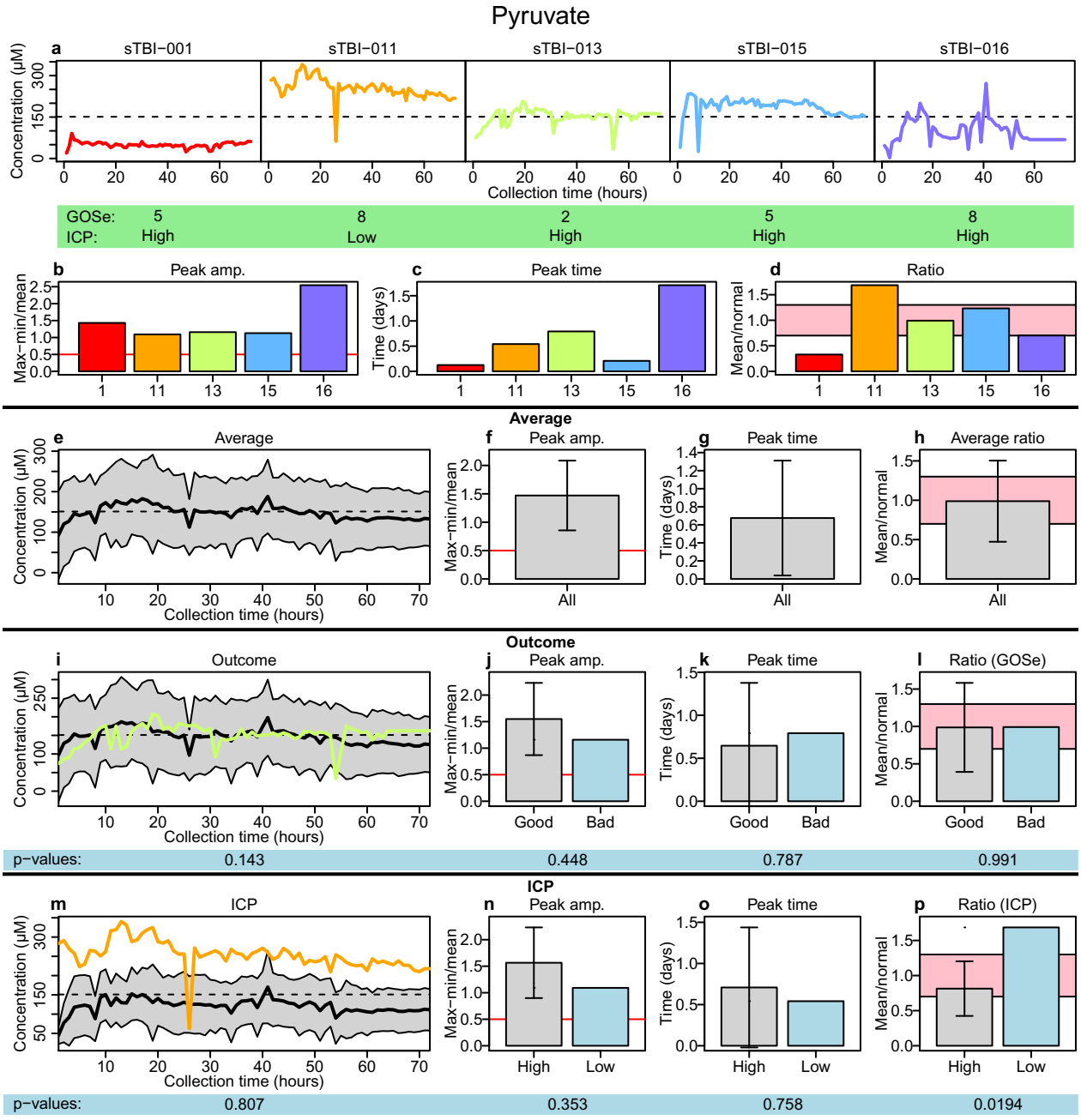

FIGURE F.S4: **Analysis of pyruvate levels in microdialysate samples of sTBI patients. a** Pyruvate concentration in the brain microdialysate samples of individual sTBI patients, whose clinical information is shown below, was measured and peaks amplitude, time and ratio of mean value to normal (PRA) (**b-d**) was calculated for each patient. The average pyruvate profile (**e**) and PRA (**f-h**) are shown. Pyruvate profiles (**i**, analyzed by mixed effect modeling) and PRA (**j-l**, t-tests) between patients with good (GOS-E 5-8) and bad (GOS-E 1-4) outcome were compared. Similarly, pyruvate profiles (**m**) and PRA (**n-p**) was compared between patients with high and low ICP. The dashed lines in **a, e, i, m** show the normal measured value while the red lines in **b, f, j, n** show a threshold for a profile that is considered to have a peak, rather than being constant. The light red boxes in **d, h, l, p** show the threshold of comparison to the normal measured value.

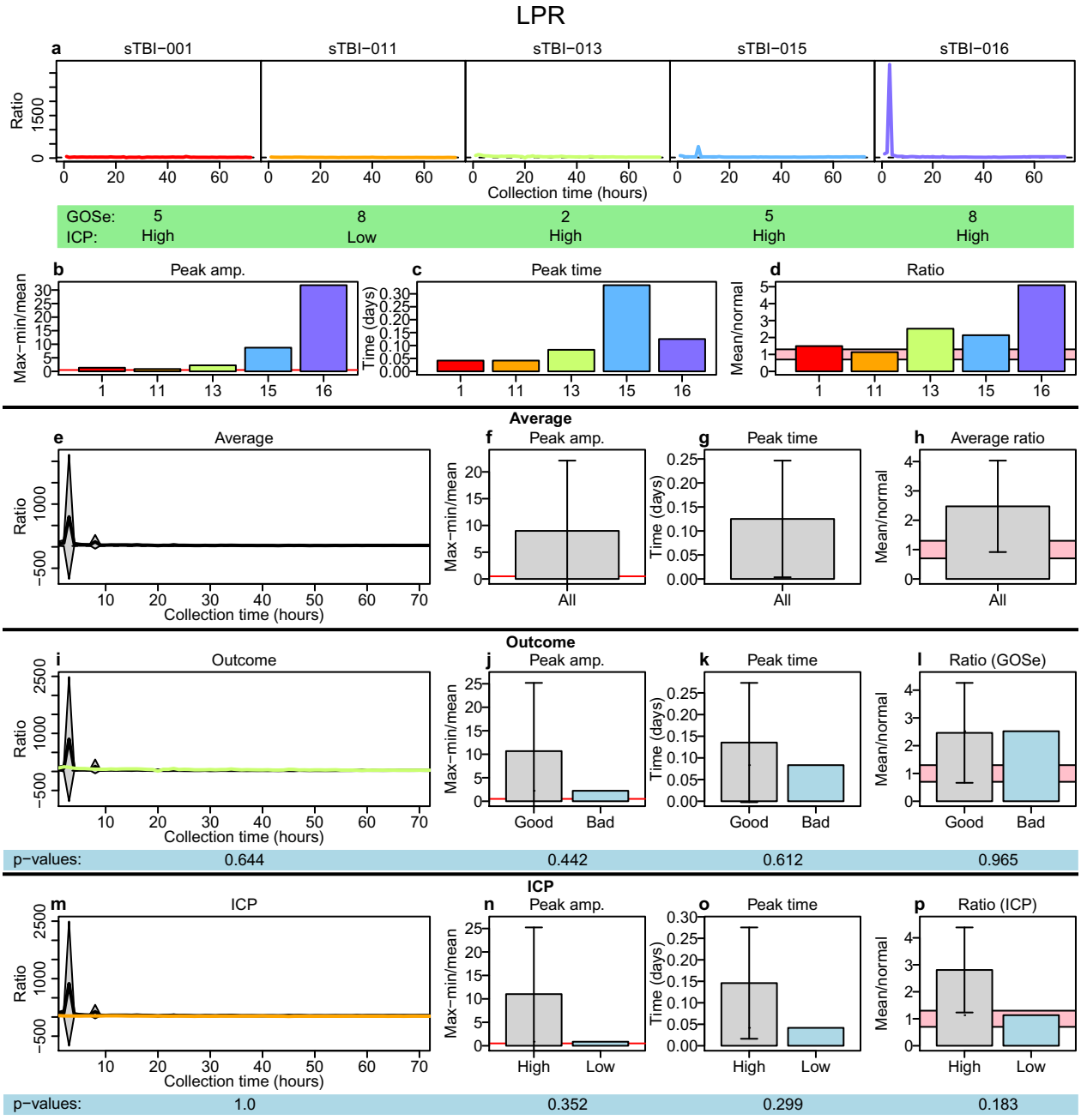

FIGURE F.S5: **Analysis of LPR levels in microdialysate samples of sTBI patients. a** Lactate to pyruvate ratio (LPR) in the brain microdialysate samples of individual sTBI patients, whose clinical information is shown below, was measured and peaks amplitude, time and ratio of mean value to normal (PRA) (**b-d**) was calculated for each patient. The average LPR profile (**e**) and PRA (**f-h**) are shown. LPR profiles (**i**, analyzed by mixed effect modeling) and PRA (**j-l**, t-tests) between patients with good (GOS-E 5-8) and bad (GOS-E 1-4) outcome were compared. Similarly, LPR profiles (**m**) and PRA (**n-p**) was compared between patients with high and low ICP. The dashed lines in **a, e, i, m** show the normal measured value while the red lines in **b, f, j, n** show a threshold for a profile that is considered to have a peak, rather than being constant. The light red boxes in **d, h, l, p** show the threshold of comparison to the normal measured value.

Because several samples were unquantified by standard curves, we used fluorescence values compared to a common sample replicate located throughout both experiments layouts to report protein measurements. The first large-scale experiment was calibrated for an improvement in sensitivity, while the second experiment was calibrated for an improvement in reproducibility, in order to roughly match the limit of detection of both experiments (205 and 189 pg/mL) to facilitate comparison of data (figure F.S6 and supplementary material on ACM calibration). Overall performance is shown in figures F.S7 and F.S8. Performance for individual proteins in both experiments are found in tables F.S1 and F.S2.

Proteins in sTBI patients samples were measured in a separate experiment as samples of mTBI patients because of the logistical limit to the number of samples that could be measured in a single experiment. While median LODs were adjusted to be roughly the same by selecting different methods of data calibration, mismatches in LOD of individual proteins sometimes led to the proteins being undetected in mTBI samples and detected in sTBI samples in spite of a real difference in ratio to pnBlood replicate samples, which were measured in both experiments. Therefore we compared fluorescence values measured to those of pnBlood, which is theoretically as reliable as quantifying proteins using standard curves, since subtle differences in curve fitting can lead to vast differences in quantified values. Conclusions drawn about potential biomarkers of injury severity, in which sTBI and mTBI samples are compared, should be taken with caution.

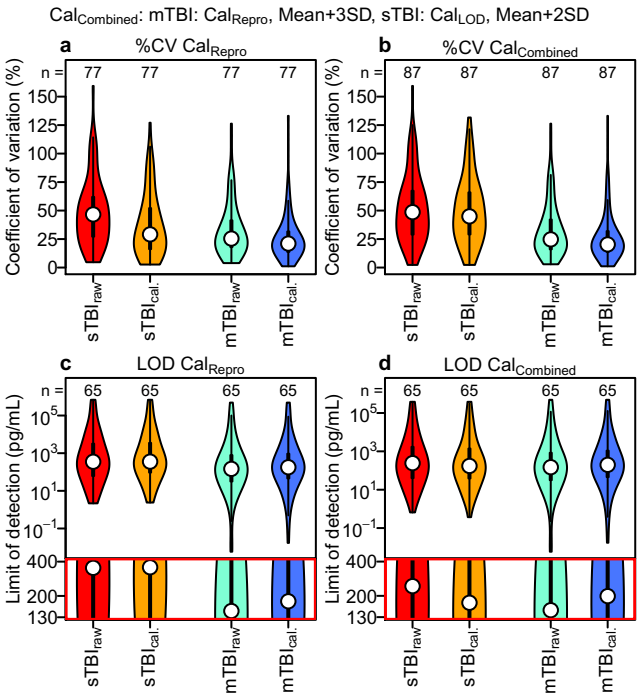

FIGURE F.S6: **Calibration performance adjustment of sTBI experiment using LOD-based calibration.** The mTBI experiment was calibrated using the recommended reproducibility-based parameters. **a** and **c** show the comparison between the sTBI and mTBI calibration performance when both experiments are calibrated using the reproducibility-based method. In contrast, **b** and **d** show the comparison when the sTBI experiment is calibrated using the LOD-based method. Only proteins for which a reproducibility and LOD were calculated in both experiments are considered.

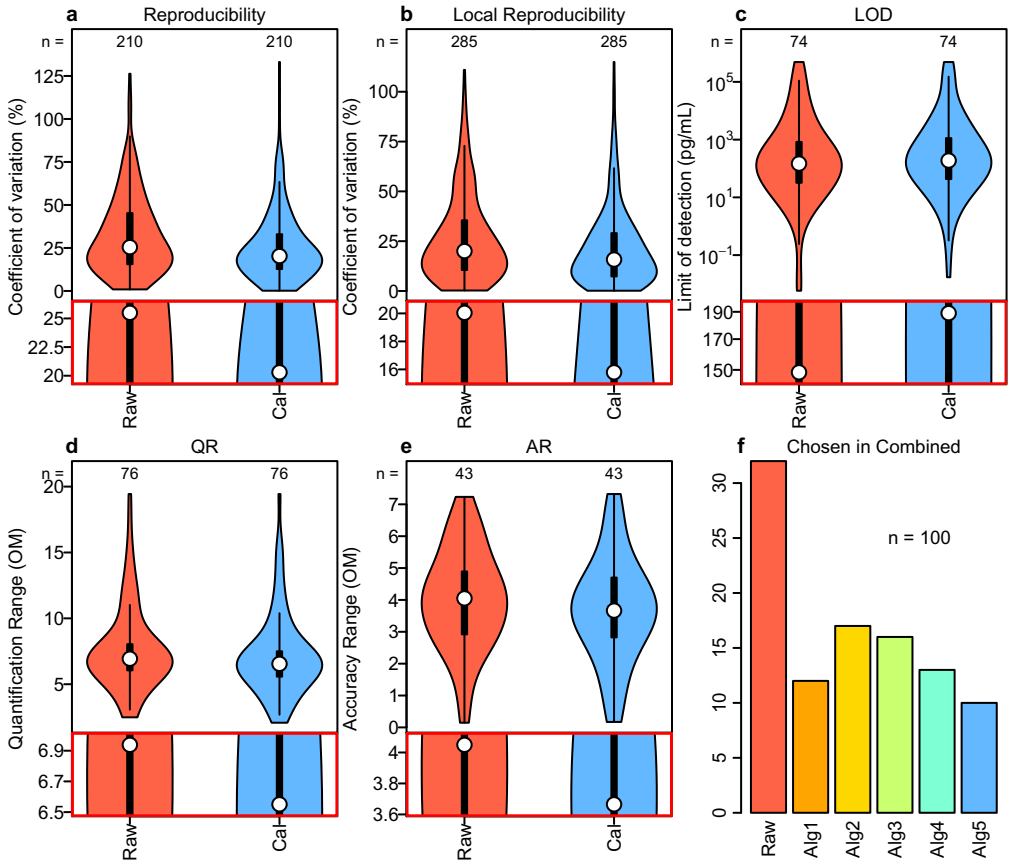

FIGURE F.S7: **ACM calibration performance based on reproducibility improvement for the mTBI analysis. a-e** Comparison of uncalibrated with data calibrated using the global method of calibration using the chosen dilution for each protein (G_{PPD} 1 Index) in terms of (**a**) global and (**b**) local reproducibility, (**c**) quantification and (**d**) accuracy ranges and (**e**) sensitivity. **f** shows the frequency of each calibration algorithm chosen in the calibration.

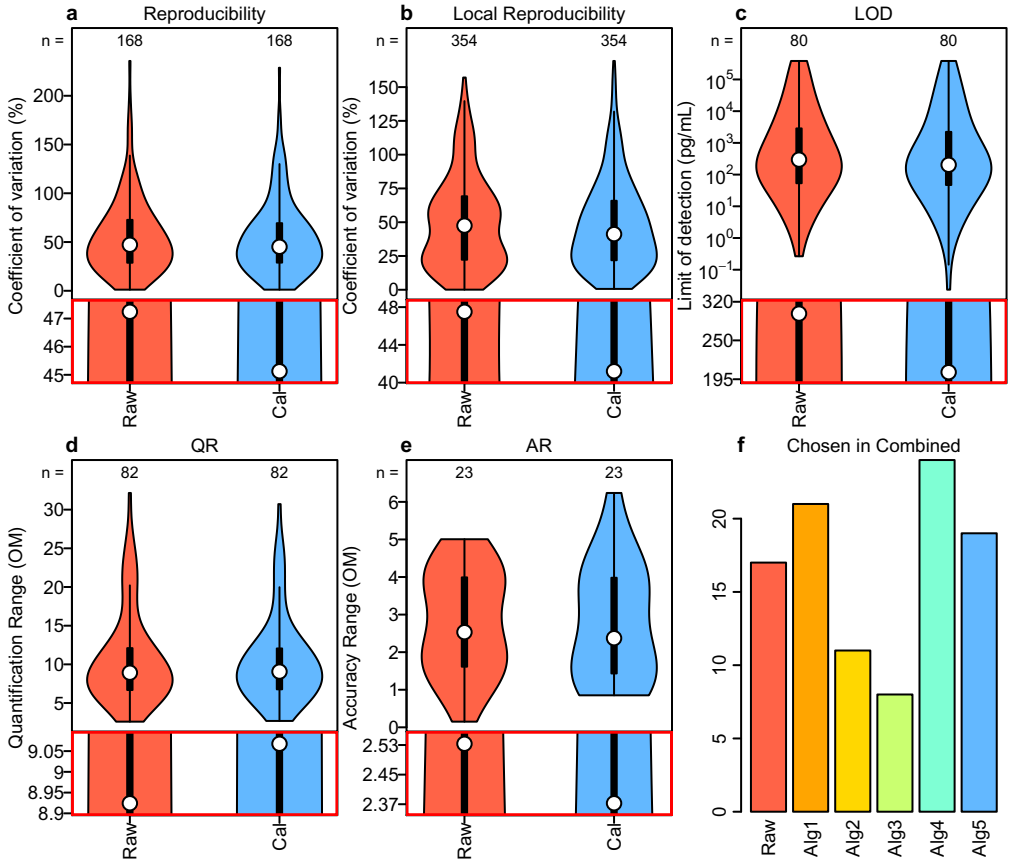

FIGURE F.S8: **ACM calibration performance based on sensitivity improvement for the sTBI analysis. a-e** Comparison of uncalibrated with data calibrated using the local method of calibration using the median of all the local calibration slopes to calculate the global calibration slope (L_{LOD} median) in terms of (**a**) global and (**b**) local reproducibility, (**c**) quantification and (**d**) accuracy ranges and (**e**) sensitivity. **f** shows the frequency of each calibration algorithm chosen in the calibration.

TABLE F.S1: **Proteins performance measures with reproducibility-based calibration for the mTBI/PAV experiment.** SC: standard curve. Unquant. data? indicates whether samples or sample replicates above the LOD were not quantified by the standard curve. Cal. Alg: calibration algorithm. Repro: reproducibility of pnCSF/pnSerum/pnEDTA sample replicate measurements. LOD unit for CA15-3 is mU/mL.

	Protein name	SC Valid?	[Ag] (ng/mL)	Unquant. data?	SC#	Hook#	Threshold	Dilution	Cal. Alg	QR (OM)	AR (OM)	LOD (pg/mL)	Repro pnSerum	Repro pnCitrate	Repro pnHeparin	Repro pnEDTA	Repro pnCTAD
1	AFP	Yes	800000	No	2	1	5	1 in 3	Alg4	10.63	-	179004.13	52.92%	40.32%	18.66%	26.88%	39.13%
2	AHSG	Yes	2000000	Yes	-	-	-	1 in 3	None	-	-	-	-	-	-	-	-
3	ALDH1L1	Yes	200000	No	1	-	-	1 in 3	Alg1	4.57	-	6215.19	-	-	-	23.97%	32.02%
4	Amphiregulin	Yes	25000	No	2	-	5.3	1 in 3	Alg2	5.14	4.15	45.8	40.12%	-	-	27.90%	48.68%
5	Ang1	Yes	100000	No	2	-	6	1 in 3	Alg3	5.11	3.06	73.47	6.66%	-	-	17.25%	-
6	Ang2	Yes	20000	No	2	-	-	1 in 3	None	5.62	1.51	713.24	-	-	-	-	-
7	BDNF	Yes	150000	No	2	1	-	1 in 3	Alg4	7.49	-	1404.36	28.58%	-	9.80%	35.66%	40.77%
8	BMP2	Yes	25000	No	2	-	-	1 in 3	Alg2	6.8	2.01	65.17	-	-	-	-	2.81%
9	β-NGF	Yes	100000	No	2	-	5	1 in 3	Alg1	9.36	3.86	33.47	-	-	-	-	6.68%
10	BRAF	Yes	200000	No	2	-	-	1 in 3	None	7.5	4.12	1087.65	-	-	-	-	-
11	CA15-3	Yes	200000	No	2	-	-	1 in 3	Alg5	5.28	3.15	65.86	21.08%	38.56%	32.56%	14.43%	7.57%
12	Cathepsin B	No Ag	0	-	-	-	-	1 in 3	None	-	-	-	-	-	-	-	-
13	CCL5	No	200000	-	-	-	-	1 in 3	None	-	-	-	-	-	-	-	-
14	CD14	No Ag	0	-	-	-	-	1 in 30	Alg3	-	-	-	-	-	-	-	-
15	CEA	Yes	2000000	No	2	6	-	1 in 3	None	6.67	-	149.6	10.98%	2.18%	5.33%	19.30%	8.73%
16	c-Kit	Yes	1000000	Yes	1	1	-	1 in 3	Alg5	5.62	5.07	171.24	30.17%	54.35%	2.33%	32.25%	49.32%
17	CRP	No	2000000	-	-	-	-	1 in 3	Alg1	-	-	-	-	-	-	-	-
18	CXCL12	Yes	5000000	No	1	-	-	1 in 3	None	7.16	3	7913.05	15.89%	-	-	15.63%	27.50%
19	E-cadherin	Yes	100000	No	1	1	-	1 in 3	None	7.3	6.73	207.63	7.08%	25.12%	3.35%	15.72%	20.18%
20	EGF	Yes	200000	No	2	7	-	1 in 3	None	19.44	3.66	0.017	56.33%	-	-	21.60%	72.35%
21	EGF-R	Yes	100000	No	1	-	-	1 in 30	Alg5	8.42	4.7	38.72	27.83%	5.17%	22.72%	32.49%	51.39%
22	Endoglin	Yes	200000	No	1	-	-	1 in 3	Alg4	7.18	3.9	422.13	19.84%	15.98%	1.18%	13.20%	24.54%
23	EpCAM	Yes	50000	No	2	-	-	1 in 3	None	6.47	2.68	25.21	-	-	-	-	-
24	E-selectin	No Ag	0	-	-	-	-	1 in 3	Alg2	-	-	-	-	-	-	-	-
25	FAS	Yes	50000	No	1	-	6	1 in 3	Alg2	6.76	6.87	12.73	26.32%	45.63%	21.24%	24.25%	43.53%
26	FAS-L	Yes	50000	No	1	-	-	1 in 3	Alg4	3.5	2.03	42.39	-	53.51%	-	18.83%	34.77%
27	FGFb	Yes	25000	No	1	-	-	1 in 3	None	6.12	-	2433.9	46.48%	-	24.68%	85.42%	47.44%
28	Flt-3	Yes	25000	No	1	-	5.5	1 in 3	None	6.87	-	419.25	-	-	-	-	-
29	G-CSF	Yes	50000	No	1	6	-	1 in 3	Alg3	9.48	6.6	3.75	-	-	-	-	15.18%
30	GFAP	No	1000000	-	-	-	-	1 in 3	Alg1	-	-	-	-	-	-	-	-

Table F.S1 continued from previous page

	Protein name	SC Valid?	[Ag] (ng/mL)	Unquant. data?	SC#	Hook#	Threshold	Dilution	Cal. Alg	QR (OM)	AR (OM)	LOD (pg/mL)	Repro pnSerum	Repro pnCitrate	Repro pnHeparin	Repro pnEDTA	Repro pnCTAD
31	GM-CSF	No Ag	0	-	-	-	-	1 in 3	None	-	-	-	-	-	-	-	-
32	GRO-α	Yes	200000	No	1	-	-	1 in 3	Alg4	5.03	2.69	6175.59	21.96%	-	-	22.72%	11.56%
33	HAI-1	Yes	1000000	No	1	-	-	1 in 3	Alg1	7.04	-	12262.75	60.06%	9.69%	31.05%	19.72%	36.44%
34	HE4	Yes	250000	No	1	-	-	1 in 3	Alg2	6.33	-	13900.06	-	-	27.04%	13.07%	21.69%
35	HER2	Yes	500000	No	2	-	-	1 in 3	None	6.37	4.46	39.03	-	-	-	-	-
36	HER3	Yes	1000000	No	1	-	-	1 in 3	None	6.92	5.77	137.42	66.46%	-	-	20.49%	24.90%
37	HGF	Yes	100000	No	1	-	6	1 in 3	Alg2	5.65	4.87	155.17	12.43%	15.79%	32.44%	31.66%	41.14%
38	HGF-R	Yes	100000	Yes	1	1	-	1 in 30	Alg4	5.45	3.87	352.4	22.16%	23.33%	10.32%	20.33%	37.30%
39	HMGB1	No	250000	-	-	-	-	1 in 3	Alg1	-	-	-	-	-	-	-	-
40	HP	Yes	50000	Yes	-	-	-	1 in 3	Alg1	-	-	-	-	-	-	-	-
41	ICAM-1	Yes	2000000	Yes	-	-	-	1 in 3	Alg3	-	-	-	-	-	-	-	-
42	IFN-γ	Yes	100000	Yes	-	-	-	1 in 3	Alg5	-	-	-	-	-	-	-	-
43	IGFBP-1	Yes	200000	No	2	6	5	1 in 30	Alg3	6.13	-	12.9	5.73%	17.06%	0.61%	15.94%	12.90%
44	IGFBP-3	Yes	1000000	No	2	1	-	1 in 30	None	7.46	4.78	415.86	3.90%	13.74%	1.02%	13.70%	16.54%
45	IGFBP-7	Yes	500000	Yes	2	-	5.4	1 in 30	None	5.09	3.89	245.73	9.14%	20.27%	15.38%	23.35%	12.51%
46	IL-10	No Ag	0	-	-	-	-	1 in 3	Alg2	-	-	-	-	-	-	-	-
47	IL-12	Yes	25000	No	2	-	-	1 in 3	Alg3	4.63	1.57	1143.57	26.36%	-	-	-	-
48	IL-15	Yes	25000	Yes	1	-	-	1 in 3	None	5.97	2.74	841.46	-	-	-	-	-
49	IL-18	No	200000	-	-	-	5.4	1 in 3	Alg3	-	-	-	-	-	-	-	-
50	IL-1β	Yes	25000	Yes	1	-	-	1 in 3	Alg1	6.49	4.8	0.45	77.00%	3.47%	74.95%	39.67%	37.64%
51	IL-1ra	Yes	200000	No	1	-	-	1 in 3	Alg3	2.08	-	3400.12	19.57%	32.27%	-	18.53%	18.91%
52	IL-2	Yes	25000	Yes	-	-	-	1 in 3	None	-	-	-	-	-	-	-	-
53	IL-3	Yes	25000	No	1	-	-	1 in 3	Alg3	6.44	4.7	75.23	52.31%	-	-	4.44%	31.41%
54	IL-4	Yes	200000	No	1	-	-	1 in 3	Alg1	7.26	3.36	555.63	2.64%	-	-	-	-
55	IL-5	No Ag	0	-	-	-	-	1 in 3	Alg2	-	-	-	-	-	-	-	-
56	IL-7	Yes	25000	No	1	5	5.65	1 in 3	Alg3	6.09	-	56.79	57.04%	32.60%	-	25.93%	17.84%
57	IL-8	Yes	20000	No	2	6	-	1 in 3	Alg2	2.69	0.77	12.62	-	-	-	-	4.96%
58	IP-10	Yes	50000	No	2	1	-	1 in 3	None	11.76	-	1.63	8.31%	64.11%	-	35.14%	76.04%
59	KLK14	Yes	2000000	Yes	2	6	6	1 in 3	Alg4	3.33	0.17	672.77	20.33%	-	-	1.53%	14.18%
60	KLK8	Yes	500000	No	2	-	-	1 in 3	None	15.14	-	487311.96	-	-	-	11.37%	-
61	Leptin	No	500000	-	-	-	-	1 in 3	None	-	-	-	-	-	-	-	-
62	MCP1	Yes	50000	No	2	-	-	1 in 3	None	6.18	-	317.53	-	-	-	2.89%	-
63	MCP2	Yes	500000	No	2	1	-	1 in 3	Alg1	12.89	-	6.59	46.91%	-	-	12.69%	45.95%
64	MCP3	Yes	50000	No	2	1	-	1 in 3	None	9.79	-	12.81	-	-	-	-	-
65	MCP4	Yes	200000	No	1	-	-	1 in 3	None	5.4	3.32	1330.39	-	-	-	-	-
66	M-CSF	Yes	100000	No	2	-	-	1 in 3	Alg4	8.86	-	174.19	30.34%	-	-	18.27%	36.09%

Table F.S1 continued from previous page

	Protein name	SC Valid?	[Ag] (ng/mL)	Unquant. data?	SC#	Hook#	Threshold	Dilution	Cal. Alg	QR (OM)	AR (OM)	LOD (pg/mL)	Repro pnSerum	Repro pnCitrate	Repro pnHeparin	Repro pnEDTA	Repro pnCTAD
67	MIG	Yes	200000	No	2	-	6.1	1 in 3	Alg4	3.77	3.67	459.89	17.81%	6.69%	-	19.39%	17.49%
68	MIP-1α	Yes	50000	No	2	6	6.1	1 in 3	Alg5	10.01	-	6.28	27.83%	-	-	30.27%	42.97%
69	MIP-1β	Yes	100000	No	2	6	-	1 in 3	None	3.02	-	79.53	-	-	-	-	-
70	MMP-1	No Ag	0	-	-	-	-	1 in 3	Alg3	-	-	-	-	-	-	-	-
71	MMP-3	Yes	500000	Yes	1	6	-	1 in 30	Alg4	6.55	3.44	120.59	13.29%	9.52%	12.27%	34.89%	31.10%
72	MMP-9	Yes	500000	No	1	-	-	1 in 30	None	6.49	6.25	76.23	17.46%	101.07%	45.54%	20.38%	22.15%
73	NCAM-1	Yes	2000000	No	2	-	-	1 in 3	Alg5	6.56	3.56	7655.16	68.25%	11.31%	29.18%	45.27%	61.26%
74	NT-3	Yes	500000	No	2	-	-	1 in 3	Alg3	3.42	3.52	198.89	29.77%	-	-	-	10.80%
75	OPN	Yes	100000	Yes	1	-	-	1 in 30	None	7.26	3.53	107.87	42.81%	34.14%	32.56%	33.13%	28.08%
76	PAI-1	Yes	1400000	No	2	-	5.3	1 in 3	Alg2	9.43	-	218096.92	26.82%	-	11.96%	19.98%	40.88%
77	PDGF-BB	Yes	200000	No	2	-	-	1 in 3	None	3.32	1.86	-	19.76%	-	55.38%	77.72%	-
78	PRL	No	500000	-	-	-	4.8	1 in 3	Alg3	-	-	-	-	-	-	-	-
79	PSA	Yes	2000000	No	1	-	5	1 in 3	Alg4	6.44	-	-	97.80%	8.67%	17.78%	62.62%	69.97%
80	RBP4	No	500000	-	-	-	5.2	1 in 3	Alg5	-	-	-	-	-	-	-	-
81	S100B	Yes	500000	No	1	-	-	1 in 3	Alg3	3.07	-	73069.94	24.03%	2.16%	-	6.62%	14.19%
82	SPARC	Yes	2000000	No	1	-	5.1	1 in 3	Alg2	7.5	4.21	938.6	22.67%	-	-	13.82%	2.76%
83	TF	Yes	100000	No	2	-	-	1 in 3	Alg5	5.81	-	-	72.15%	64.42%	10.36%	35.39%	42.76%
84	TGF-α	Yes	500000	No	1	9	5.5	1 in 3	Alg1	3.82	0.35	71.93	13.48%	-	-	8.66%	12.11%
85	TGF-β RII	Yes	2000000	Yes	1	6	6	1 in 3	Alg1	9.16	-	313.78	105.26%	-	-	38.14%	73.81%
86	TGF-β1	Yes	200000	No	2	5	-	1 in 3	Alg2	12.46	0.76	0.15	8.06%	-	-	133.10%	-
87	TGF-β2	Yes	180000	No	1	-	5.4	1 in 3	None	11.36	-	159529.35	-	-	-	-	-
88	THBS-1	Yes	250000	Yes	-	-	-	1 in 30	Alg3	-	-	-	-	-	-	-	-
89	Tie-2	Yes	1000000	No	2	-	-	1 in 3	Alg3	7.01	3.86	2753.83	1.74%	7.79%	2.85%	22.11%	29.36%
90	TIMP-1	No Ag	0	-	-	-	-	1 in 3	None	-	-	-	-	-	-	-	-
91	TNF-α	Yes	50000	No	1	5	-	1 in 3	Alg5	-	2.91	7.61	1.29%	-	-	1.09%	11.30%
92	TNF-RI	Yes	1000000	No	2	-	-	1 in 3	Alg2	7.06	5.6	290.89	10.34%	4.01%	11.65%	4.12%	19.48%
93	TNF-RII	Yes	200000	No	2	6	-	1 in 3	Alg4	15.29	0.64	34.38	13.52%	68.18%	1.36%	18.23%	24.36%
94	uPA	Yes	50000	No	1	-	-	1 in 3	Alg2	7.2	-	45.4	29.14%	2.87%	7.32%	19.94%	18.57%
95	uPA-R	Yes	500000	No	1	6	-	1 in 3	None	7.61	-	251.57	24.24%	-	-	9.22%	22.31%
96	VCAM-1	Yes	200000	No	2	1	5.5	1 in 30	Alg4	14.59	-	179.6	16.10%	5.95%	0.48%	19.37%	15.10%
97	VEGF-A	Yes	25000	No	1	-	5.5	1 in 3	Alg2	6.78	7.32	2.47	19.96%	15.71%	0.14%	19.28%	25.90%
98	VEGF-D	Yes	100000	No	1	-	-	1 in 3	Alg5	6.03	3.49	4015.13	15.84%	-	-	-	42.60%
99	VEGFR2	Yes	500000	No	2	-	-	1 in 3	Alg2	6.2	1.27	2921.6	18.46%	19.29%	-	23.95%	18.26%
100	VEGFR3	No	500000	-	-	-	-	1 in 3	Alg2	-	-	-	-	-	-	-	-

TABLE F.S2: **Proteins performance measures with LOD-based calibration for the sTBI experiment.** SC: standard curve. Unquant. data? indicates whether samples or sample replicates above the LOD were not quantified by the standard curve. Cal. Alg: calibration algorithm. Repro: reproducibility of pnCSF/pnSerum/pnEDTA sample replicate measurements. LOD unit for CA15-3 is mU/mL.

	Protein name	SC Valid?	[Ag] (ng/mL)	Unquant. data?	SC#	Hook#	Threshold	Dilution	Cal. Alg	QR (OM)	AR (OM)	LOD (pg/mL)	Repro pnCSF	Repro pnSerum	Repro pnEDTA
1	AFP	Yes	800000	Yes	2	3	-	1 in 3	Alg5	10.59	-	44344.37	-	-	-
2	AHSG	Yes	2000000	Yes	1	3	-	1 in 3	None	8.66	-	44258.69	51.27%	76.94%	82.08%
3	ALDH1L1	Yes	200000	No	2	1	-	1 in 3	Alg3	11.55	0.98	7928.15	18.92%	44.90%	29.22%
4	Amphiregulin	Yes	25000	No	2	-	-	1 in 3	Alg4	6.76	4.43	49.48	-	42.76%	27.18%
5	Ang1	Yes	100000	No	2	1	-	1 in 30	Alg4	13.26	1.81	28.47	-	43.83%	-
6	Ang2	Yes	20000	Yes	2	-	-	1 in 3	Alg5	5.61	2.04	115.69	-	100.27%	33.44%
7	BDNF	Yes	200000	No	1	-	-	1 in 3	Alg1	11.52	-	1487.6	-	61.27%	21.97%
8	BMP2	Yes	25000	No	2	-	-	1 in 3	Alg1	6.42	2.37	174.02	-	13.05%	51.23%
9	β-NGF	Yes	100000	No	2	-	-	1 in 3	Alg4	13.61	-	6.63	-	9.95%	-
10	BRAF	Yes	200000	No	2	-	-	1 in 3	Alg4	16.98	4.12	743.34	-	23.56%	8.03%
11	CA15-3	Yes	200000	No	3	-	-	1 in 3	Alg5	13.85	-	10.9	30.08%	31.87%	93.51%
12	Cathepsin B	No Ag	0	-	-	-	-	1 in 3	Alg5	-	-	-	-	-	-
13	CCL5	Yes	200000	Yes	-	-	-	1 in 3	Alg1	-	-	-	-	-	-
14	CD14	No Ag	0	-	-	-	-	1 in 30	Alg5	-	-	-	-	-	-
15	CEA	Yes	2000000	No	3	-	-	1 in 3	Alg5	9.48	-	227.52	-	37.31%	32.68%
16	c-Kit	Yes	1000000	No	1	4	-	1 in 3	Alg1	8.35	-	384.35	30.02%	38.18%	34.02%
17	CRP	Yes	2000000	No	2	-	-	1 in 3	Alg1	17.43	-	0.62	174.85%	228.73%	144.59%
18	CXCL12	Yes	5000000	No	2	-	-	1 in 3	None	12.78	-	2125.25	-	2.31%	42.59%
19	E-cadherin	Yes	100000	No	1	-	-	1 in 3	Alg4	10.95	-	93.7	30.48%	26.36%	16.36%
20	EGF	Yes	200000	No	2	8	-	1 in 3	Alg1	7.53	-	0.37	-	40.53%	81.86%
21	EGF-R	Yes	100000	Yes	1	-	-	1 in 3	None	8.9	-	53.03	44.88%	66.12%	84.52%
22	Endoglin	Yes	200000	No	1	-	-	1 in 3	Alg1	11.72	-	99.49	-	89.01%	58.49%
23	EpCAM	Yes	50000	No	1	1	-	1 in 3	Alg1	8.95	-	18.93	-	67.23%	28.87%
24	E-selectin	Yes	4000000	Yes	1	-	-	1 in 3	Alg2	7	-	72.48	-	41.79%	44.08%
25	FAS	Yes	50000	No	2	-	-	1 in 3	Alg1	8.13	1.01	38.59	-	75.53%	59.84%
26	FGF-1	Yes	500000	No	1	-	-	1 in 3	Alg2	11.44	-	270204.07	-	23.16%	27.92%
27	FGFb	Yes	25000	No	2	-	-	1 in 3	Alg4	5.33	4.05	429.44	-	126.38%	24.05%
28	Flt-3	Yes	25000	No	3	-	-	1 in 3	Alg4	11.85	-	332.23	-	-	-
29	G-CSF	Yes	50000	No	3	-	-	1 in 3	Alg4	5.23	-	6.16	11.42%	32.31%	29.60%
30	GFAP	No	1000000	-	-	-	-	1 in 3	Alg1	-	-	-	-	-	-

Table F.S2 continued from previous page

	Protein name	SC Valid?	[Ag] (ng/mL)	Unquant. data?	SC#	Hook#	Threshold	Dilution	Cal. Alg	QR (OM)	AR (OM)	LOD (pg/mL)	Repro pnCSF	Repro pnSerum	Repro pnEDTA
31	GM-CSF	Yes	100000	No	1	-	-	1 in 3	Alg4	7.93	-	0.54	-	60.96%	69.75%
32	GRO-α	Yes	200000	No	1	-	5.1	1 in 3	Alg4	12.05	-	1399.77	-	49.05%	46.88%
33	HAI-1	Yes	1000000	No	2	-	-	1 in 3	Alg2	-	-	29494.56	-	109.17%	47.94%
34	HE4	Yes	250000	Yes	3	-	-	1 in 3	Alg2	8.22	-	16332.44	-	72.73%	9.47%
35	HER2	Yes	500000	No	1	-	-	1 in 3	Alg1	30.72	-	523.04	-	53.32%	105.60%
36	HER3	Yes	1000000	No	1	2	-	1 in 3	None	7.44	-	828.77	-	114.18%	28.90%
37	HGF	Yes	100000	No	2	-	-	1 in 3	Alg1	6.48	3.56	108.82	30.91%	32.60%	35.62%
38	HGF-R	Yes	100000	No	1	2	-	1 in 30	Alg1	8.85	3.91	244.52	-	41.77%	52.77%
39	HMGB1	No	250000	-	-	-	-	1 in 3	None	-	-	-	-	-	-
40	HP	Yes	50000	No	2	1	-	1 in 3	Alg4	2.69	0.85	7760.68	-	7.78%	15.75%
41	ICAM-1	Yes	2000000	No	3	-	-	1 in 3	Alg2	9.18	-	640.36	80.28%	175.11%	75.00%
42	IFN-γ	Yes	100000	No	2	-	-	1 in 3	Alg3	6.21	3.83	0.024	-	53.40%	63.36%
43	IGFBP-1	Yes	200000	Yes	-	-	-	1 in 3	Alg3	-	-	-	-	-	-
44	IGFBP-3	Yes	1000000	Yes	3	4	5	1 in 3	Alg5	4.47	-	11516.57	-	26.04%	33.18%
45	IGFBP-7	Yes	500000	Yes	3	4	-	1 in 30	Alg5	6.46	3.12	66.27	53.90%	44.95%	8.62%
46	IL-10	No Ag	0	-	-	-	-	1 in 3	Alg4	-	-	-	-	-	-
47	IL-12	No	25000	-	-	-	-	1 in 3	Alg2	-	-	-	-	-	-
48	IL-15	Yes	25000	No	2	-	-	1 in 3	Alg4	10.3	-	100.04	-	-	-
49	IL-18	No	200000	-	-	-	-	1 in 3	Alg1	-	-	-	-	-	-
50	IL-1β	Yes	25000	No	1	-	-	1 in 3	None	7.11	-	2.07	-	74.64%	66.45%
51	IL-1ra	Yes	200000	No	1	-	-	1 in 3	Alg2	17.87	-	2524.13	-	80.80%	61.40%
52	IL-3	Yes	25000	No	1	-	-	1 in 3	Alg1	9.26	1.33	25.06	-	45.31%	64.73%
53	IL-4	Yes	200000	No	2	-	-	1 in 3	Alg4	20.03	-	276.27	-	122.55%	62.38%
54	IL-5	Yes	0	Yes	2	-	-	1 in 3	Alg5	-	-	-	-	-	-
55	IL-6	Yes	200000	No	1	-	-	1 in 3	None	8.95	-	148.94	36.03%	4.03%	-
56	IL-7	Yes	25000	No	2	3	-	1 in 3	None	8.2	3.1	10.03	-	69.18%	21.59%
57	IL-8	Yes	20000	Yes	1	1	-	1 in 3	Alg5	11.97	-	15.68	59.37%	53.00%	47.61%
58	IP-10	Yes	50000	No	2	-	5.8	1 in 3	Alg4	11.1	5.14	52.17	64.59%	104.65%	40.87%
59	KLK14	No Ag	0	-	-	-	-	1 in 3	Alg5	-	-	-	-	-	-
60	KLK8	Yes	500000	No	2	-	-	1 in 3	Alg2	5.04	1.17	266794.7	-	24.61%	8.24%
61	Leptin	No	500000	-	-	-	-	1 in 3	Alg4	-	-	-	-	-	-
62	MCP1	Yes	50000	Yes	2	-	-	1 in 3	Alg5	9.41	-	420.94	-	127.09%	59.83%
63	MCP2	Yes	500000	No	2	-	-	1 in 3	Alg3	24.78	-	570.47	-	34.53%	-
64	MCP3	Yes	50000	Yes	2	-	-	1 in 3	Alg5	5.69	0.97	5.42	-	42.19%	21.33%
65	MCP4	Yes	200000	No	2	-	-	1 in 3	Alg4	15.04	-	1400.07	-	-	-
66	M-CSF	Yes	100000	No	2	-	-	1 in 3	Alg3	24.46	-	182.98	-	95.19%	41.04%

Table F.S2 continued from previous page

	Protein name	SC Valid?	[Ag] (ng/mL)	Unquant. data?	SC#	Hook#	Threshold	Dilution	Cal. Alg	QR (OM)	AR (OM)	LOD (pg/mL)	Repro pnCSF	Repro pnSerum	Repro pnEDTA
67	MIG	Yes	200000	No	2	-	-	1 in 3	Alg1	9.81	6.24	322.24	-	78.86%	13.07%
68	MIP-1α	Yes	50000	No	1	1	-	1 in 3	Alg4	12.9	-	0.0038	-	132.66%	118.42%
69	MIP-1β	Yes	100000	No	1	1	-	1 in 3	Alg1	6.82	-	58.53	-	65.38%	-
70	MMP-1	Yes	1000000	No	1	-	-	1 in 3	Alg2	22.12	-	331.92	-	140.88%	70.21%
71	MMP-3	Yes	500000	Yes	3	-	-	1 in 3	None	12.05	-	40.17	43.18%	103.46%	58.20%
72	MMP-9	Yes	500000	Yes	-	-	-	1 in 30	None	-	-	-	-	-	-
73	NCAM-1	Yes	2000000	No	3	-	-	1 in 3	None	5.58	-	23483.02	-	61.98%	6.29%
74	NT-3	Yes	500000	No	2	-	-	1 in 3	Alg4	8.07	-	2052.36	-	40.83%	19.70%
75	OPN	Yes	100000	No	1	-	-	1 in 3	Alg5	12.53	-	85.08	33.56%	131.67%	105.06%
76	PAI-1	Yes	2000000	Yes	-	-	-	1 in 3	Alg5	-	-	-	-	-	-
77	PDGF-BB	Yes	200000	No	2	2	-	1 in 3	Alg3	6.21	4.41	66.9	-	21.65%	13.34%
78	PRL	Yes	500000	Yes	-	-	-	1 in 3	Alg5	-	-	-	-	-	-
79	PSA	Yes	2000000	No	2	-	-	1 in 3	Alg2	9.4	-	35198.54	-	-	-
80	RBP4	No	500000	-	-	-	-	1 in 3	Alg1	-	-	-	-	-	-
81	S100B	Yes	500000	No	1	-	-	1 in 3	Alg4	9.73	-	172289.09	-	21.26%	14.31%
82	SCGN	No	500000	-	-	-	-	1 in 3	None	-	-	-	-	-	-
83	SPARC	Yes	2000000	No	1	-	-	1 in 3	Alg4	8.95	-	3663.81	-	56.84%	3.66%
84	TF	Yes	100000	Yes	3	-	-	1 in 3	Alg5	5.64	-	2615.48	-	66.65%	-
85	TGF-α	Yes	500000	No	3	5	-	1 in 3	Alg5	14.02	-	0.73	-	145.68%	143.01%
86	TGF-β RII	Yes	2000000	Yes	2	-	-	1 in 3	None	22.35	-	8.56	-	129.95%	68.14%
87	TGF-β1	Yes	200000	No	2	1	-	1 in 3	Alg2	8.2	-	1.82	-	38.79%	74.82%
88	TGF-β2	Yes	180000	Yes	2	-	-	1 in 3	None	4.68	-	382984.37	10.29%	1.15%	-
89	THBS-1	Yes	250000	No	1	-	-	1 in 30	Alg1	25.46	-	2797.06	-	27.68%	53.40%
90	Tie-2	Yes	1000000	No	2	1	-	1 in 3	Alg1	10.74	-	983.3	-	36.48%	65.81%
91	TIMP-1	Yes	1000000	Yes	2	-	-	1 in 3	Alg3	4.62	0.86	110874.26	15.74%	80.26%	36.84%
92	TNF-α	Yes	50000	Yes	3	-	-	1 in 3	None	10.46	-	4.76	-	100.36%	59.06%
93	TNF-RI	Yes	1000000	No	1	-	-	1 in 3	Alg1	5.71	-	179.77	34.64%	24.49%	30.05%
94	TNF-RII	Yes	200000	Yes	1	5	-	1 in 3	Alg5	3.36	-	28.83	18.98%	53.23%	29.23%
95	uPA	Yes	50000	No	2	-	-	1 in 3	Alg4	6.21	1.6	144.95	-	56.74%	31.29%
96	uPA-R	Yes	500000	No	1	-	-	1 in 3	Alg3	12.49	-	155.21	5.32%	41.64%	57.88%
97	VCAM-1	Yes	200000	No	1	-	-	1 in 3	Alg4	20.92	-	171.98	74.54%	65.78%	97.61%
98	VEGF-A	Yes	25000	No	2	2	-	1 in 3	None	7.69	2.07	3.05	-	60.21%	13.76%
99	VEGF-D	Yes	100000	Yes	2	-	-	1 in 3	Alg4	2.94	1.54	13544.77	-	26.95%	18.84%
100	VEGFR3	Yes	500000	No	3	-	-	1 in 3	None	8.64	-	9755.78	-	46.84%	42.73%

In order to use the most reliable measurements for each protein in blood samples of TBI patients, we performed an experiment to study the effect of blood collection tube, wait time and temperature before centrifugation, and filtering of plasma prior to sample storage on the measurement of proteins. The different blood tubes were compared in terms of initial measurement value (with no wait before centrifugation) and stability during a 2 h wait before centrifugation at 4 °C or 25 °C. Starting values and stability measures were obtained for all conditions for 27 proteins and compared in figure F.S9, which gives an idea of overall trends in measurement reliability. Most proteins were reliably measured in all blood tubes, and the stability did not vary significantly with the temperature at which the blood tubes were held before processing. A single protein (EGF) showed a strong increase in serum when tubes were left for 0.5 to 2 h at 25 °C (table F.S3). The complete list of conditions that led to variation above or below 10 % of the measurement range is found in table F.S4.

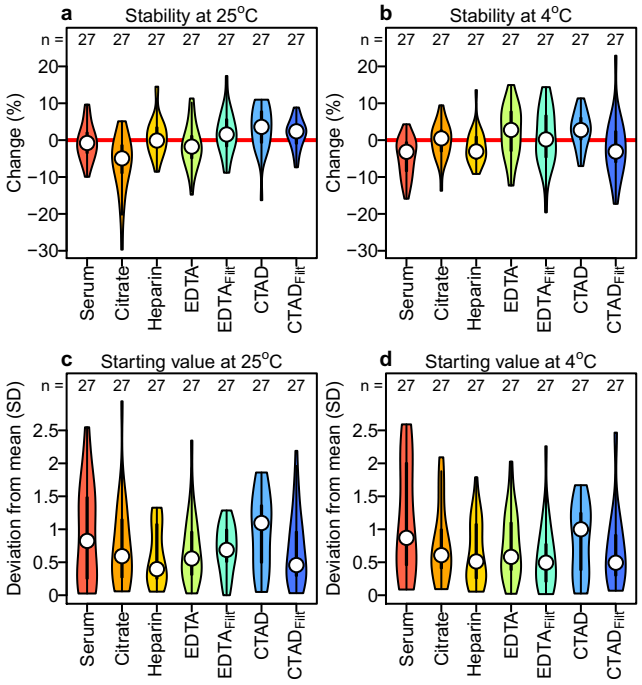

FIGURE F.S9: **Effect of tube collection type and filtering on proteins' initial measured value and stability before processing.** 103 proteins was measured in blood samples from two anonymous donors. Blood was collected in five different collection tubes and left at room temperature (**a, c**) or stored at 4 °C (**b, d**) for 5, 30 and 120 min. Serum tubes were left to coagulate for 15 min before storing and waiting. **a-b** show the aggregated stability of measured protein levels after 120 min and **c-d** the aggregated extrapolated value measured with no waiting time before processing. **c-d** are expressed as a number of standard deviations (SD) away from the mean of all collection tubes and post-centrifugal filtering for EDTA and CTAD plasma. A higher value indicates more deviation from the mean. Only proteins for which a starting value and stability values could be measured at both temperatures are considered.

Considering all proteins that were detected, the initial protein measurements varied between the different blood tube types, with eight proteins measuring higher in serum compared to plasma, and three measuring lower (table F.S3 and figure F.S10). Two proteins measured higher, and seven measured lower in plasma than in serum. Only EDTA plasma led to average initial protein measurements for all proteins. While filtering out platelets from CTAD appeared to give more reliable results in terms of initial protein measurement, filtering had no effect on the initial protein measurement of EDTA samples (figure F.S9c-d). Figures F.S11 and F.S12 show that values of initial measurement and stability calculated from fluorescence values are comparable to those calculated with quantities.

The lengths of time (5, 30 and 120 min) studied here as waiting time before centrifugation was very small compared to several studies where waiting time before centrifugation is often a maximum of 48 h. While a long wait time is common in clinical laboratories, samples taken for this study were usually processed within one hour and therefore the scale of waiting time chosen in this experiment corresponds to the scale of waiting time likely to be encountered by the sTBI and mTBI samples. In spite of the short waiting time, we found at least one protein (EGF) that was not stable even after 30 min in serum.

TABLE F.S3: **Proteins whose initial value are affected by different collection tubes.**

	Serum	Citrate	Heparin	EDTA/EDTA$_{\text{Filt}}$	CTAD/CTAD$_{\text{Filt}}$
Higher	Ang1 EGF[1] HGF MMP-1 PDGF-BB SPARC TGF-β1 VEGF-A	PRL	SPARC	*none*	PRL
Lower	E-cadherin HMGB1 OPN	IL-10 PAI-1 TGF-β RII TGF-β1	E-cadherin HMGB1	*none*	c-Kit IL-10 PAI-1 TGF-β RII TGF-β1

[1]: Accompanied by sharp increase in measured value with waiting time at room temperature before processing

The two blood collection tubes and storage temperature in common for sTBI and mTBI patients blood samples were serum kept at 25 °C and EDTA plasma kept at 4 °C. Comparing these two conditions, one of the two combinations of blood tube and pre-processing storage temperature was chosen for each protein, and the resulting list is found in tables F.S5 and F.S6.

TABLE F.S4: **Stability of proteins in different pre-analytical conditions**. Stability of a protein was deemed to be good (Y) if it was at least partially detected (above LOD) and its increase or decrease within 2 hours and its range (max-min) were below 10 % of the range. N represents a protein that was detected but where the range and/or the increase was above 10 % of the range. -: not detected. Acronyms: S-Serum, Ci-Citrate, H-Heparin, E-EDTA, E_F-$EDTA_{Filt}$, C-CTAD, C_F-C_{Filt}.

		4 °C, low dilution							4 °C, high dilution							25 °C, low dilution							25 °C, high dilution							Selected	
		S	Ci	H	E	EF	C	CF	S	Ci	H	E	EF	C	CF	S	Ci	H	E	EF	C	CF	S	Ci	H	E	EF	C	CF	Type	Dilution
1	AFP	N	Y	Y	Y	N	N	Y	Y	N	Y	Y	N	Y	Y	-	-	-	-	Y	Y	-	-	-	-	N	-	-	-	EDTA	3
2	AHSG	-	-	-	-	-	-	-	-	-	-	-	-	-	-	-	-	-	-	-	-	-	-	-	-	-	-	-	-	EDTA	3
3	ALDH1L1	-	-	-	N	-	-	-	-	-	-	-	-	-	-	-	-	-	-	-	-	-	-	-	-	-	-	-	-	Serum	3
4	Amphiregulin	Y	-	-	Y	-	-	-	-	-	-	-	Y	-	-	-	-	-	-	-	-	-	-	-	-	-	-	-	-	Serum	3
5	Ang1	Y	N	N	N	N	N	-	Y	Y	N	N	Y	-	-	Y	-	N	-	-	-	-	Y	-	N	-	-	-	-	EDTA	3
6	Ang2	-	-	-	-	-	-	-	-	-	-	-	-	-	-	-	-	-	-	-	-	-	-	-	-	-	-	-	-	Serum	3
7	BDNF	-	-	-	N	N	N	N	-	-	-	N	Y	-	Y	-	-	-	-	-	-	-	-	-	-	-	-	-	-	Serum	3
8	BMP2	-	-	-	-	-	-	-	-	-	-	-	-	-	-	-	-	-	-	-	-	-	-	-	-	-	-	-	-	EDTA	3
9	BRAF	-	-	-	-	-	-	-	-	-	-	-	-	-	-	-	-	-	-	-	-	-	-	-	-	-	-	-	-	EDTA	3
10	c-Kit	Y	Y	Y	Y	Y	Y	Y	Y	Y	Y	N	Y	Y	Y	N	Y	Y	Y	Y	N	N	N	Y	Y	Y	N	Y	Y	Serum	3
11	CA15-3	N	Y	Y	N	Y	N	Y	Y	Y	N	Y	N	Y	Y	-	N	Y	Y	Y	N	N	-	Y	N	Y	N	Y	N	Serum	3
12	Cathepsin B	-	-	-	-	-	-	-	-	-	-	-	-	-	-	-	-	-	-	-	-	-	-	-	-	-	-	-	-	EDTA	3
13	CCL5	-	-	-	-	-	-	-	-	-	-	-	-	-	-	-	-	-	-	-	-	-	-	-	-	-	-	-	-	EDTA	3
14	CD14	N	N	Y	N	N	Y	N	Y	Y	Y	Y	Y	Y	Y	Y	Y	N	Y	N	Y	Y	Y	Y	Y	Y	N	Y	Y	Serum	30
15	CEA	N	N	N	N	-	-	N	Y	-	Y	-	N	-	-	-	-	-	-	-	-	-	-	-	-	-	-	N	-	Serum	3
16	CRP	-	-	-	-	-	-	-	-	-	-	-	-	-	-	-	-	-	-	-	-	-	-	-	-	-	-	-	-	Serum	3
17	CXCL12	-	-	-	-	-	-	-	-	-	-	-	-	-	-	-	-	-	-	-	-	-	N	-	-	-	-	-	-	Serum	3
18	E-cadherin	Y	Y	Y	N	N	Y	Y	Y	Y	Y	N	N	Y	Y	Y	Y	Y	Y	Y	Y	Y	Y	Y	-	Y	Y	Y	Y	EDTA	3
19	E-selectin	N	-	N	Y	-	N	N	Y	N	N	-	Y	Y	Y	-	-	-	-	-	-	-	-	-	-	-	-	-	-	Serum	3

Table F.S4 continued from previous page

	4 °C, low dilution							4 °C, high dilution							25 °C, low dilution							25 °C, high dilution							Selected	
	S	Ci	H	E	E_F	C	C_F	S	Ci	H	E	E_F	C	C_F	S	Ci	H	E	E_F	C	C_F	S	Ci	H	E	E_F	C	C_F	Type	Dilution
20 EGF	Y	-	-	-	-	-	-	N	-	-	N	-	-	-	-	-	-	-	-	-	-	N	-	-	-	-	-	-	EDTA	3
21 EGF-R	Y	N	Y	Y	Y	Y	Y	Y	Y	Y	Y	Y	Y	Y	Y	Y	Y	Y	Y	Y	Y	N	N	Y	Y	N	N	Y	Serum	3
22 Endoglin	Y	Y	Y	Y	N	Y	Y	Y	N	Y	Y	Y	Y	N	-	-	-	-	-	-	-	-	-	-	-	-	-	-	EDTA	3
23 EpCAM	-	-	-	-	-	-	-	-	-	-	-	-	-	-	-	-	-	-	-	-	-	-	-	-	-	-	-	-	Serum	3
24 FAS	N	N	Y	Y	Y	Y	Y	Y	Y	Y	N	Y	Y	Y	-	-	-	-	-	-	-	-	-	-	-	-	-	-	Serum	3
25 FAS-L	N	N	-	N	N	-	N	-	N	-	N	N	-	N	-	-	-	-	-	-	-	-	-	-	-	-	-	-	Serum	3
26 FGFb	Y	Y	N	N	N	N	-	Y	N	Y	Y	N	Y	Y	Y	-	-	-	-	-	-	-	-	-	-	-	N	N	Serum	3
27 Flt-3	-	-	-	-	-	-	-	-	-	-	-	-	-	-	-	-	-	-	-	-	-	-	-	-	-	-	-	-	EDTA	3
28 G-CSF	-	-	-	-	-	-	-	-	-	-	-	-	-	-	-	-	-	-	-	-	-	-	-	-	-	-	-	-	Serum	3
29 GFAP	Y	N	Y	N	Y	Y	Y	Y	N	Y	Y	Y	N	Y	-	-	-	-	-	-	-	-	-	-	-	-	-	-	Serum	3
30 GM-CSF	-	-	-	-	-	-	-	-	-	-	N	-	-	-	-	-	-	-	-	-	-	-	-	-	-	-	-	-	Serum	3
31 GRO-α	-	-	-	-	-	-	-	-	-	-	-	-	-	-	-	-	-	-	-	-	-	-	-	-	-	-	-	-	Serum	3
32 HAI-1	Y	Y	Y	Y	Y	N	Y	-	N	-	Y	Y	Y	-	-	-	-	-	-	-	Y	-	-	-	-	-	-	-	Serum	3
33 HE4	-	-	-	N	Y	-	-	-	-	-	-	N	-	-	-	-	-	-	-	-	-	-	-	-	-	-	-	-	Serum	3
34 HER2	-	-	-	-	-	-	-	-	-	-	-	-	-	-	-	-	-	-	-	-	-	-	-	-	-	-	-	-	EDTA	3
35 HER3	-	-	-	-	-	-	-	-	-	-	-	N	-	-	-	-	Y	-	-	N	N	N	-	N	-	-	-	Y	EDTA	3
36 HGF	N	Y	Y	Y	Y	Y	Y	Y	Y	N	Y	Y	N	Y	-	-	-	-	-	-	-	-	-	-	-	Y	-	-	EDTA	3
37 HGF-R	Y	Y	Y	Y	Y	Y	N	Y	N	Y	Y	Y	Y	Y	Y	N	Y	Y	Y	N	N	Y	N	Y	Y	Y	Y	Y	EDTA	30
38 HMGB1	-	Y	-	N	Y	Y	N	-	N	-	N	N	Y	Y	-	-	-	-	-	-	-	-	-	-	-	-	-	-	EDTA	3
39 HP	Y	N	Y	Y	Y	Y	Y	N	N	Y	N	N	Y	Y	-	-	-	-	Y	Y	-	-	-	-	Y	Y	Y	Y	EDTA	3
40 ICAM-1	N	Y	Y	Y	Y	Y	Y	Y	Y	Y	N	Y	Y	Y	Y	Y	Y	Y	Y	N	Y	N	N	Y	Y	Y	N	Y	EDTA	3
41 IFN-γ	-	-	-	Y	N	N	-	-	-	-	-	-	-	-	-	-	-	-	-	-	-	-	-	-	-	-	-	-	Serum	3
42 IGFBP-1	Y	Y	N	Y	Y	N	Y	Y	Y	Y	N	Y	Y	N	Y	Y	Y	N	N	Y	N	Y	Y	Y	Y	Y	N	Y	Serum	3
43 IGFBP-3	Y	Y	Y	Y	Y	Y	Y	Y	Y	Y	Y	Y	Y	Y	Y	Y	Y	Y	Y	Y	Y	Y	Y	Y	Y	Y	Y	Y	EDTA	3

Table F.S4 continued from previous page

	4 °C, low dilution							4 °C, high dilution							25 °C, low dilution							25 °C, high dilution							Selected	
	S	Ci	H	E	E_F	C	C_F	S	Ci	H	E	E_F	C	C_F	S	Ci	H	E	E_F	C	C_F	S	Ci	H	E	E_F	C	C_F	Type	Dilution
44 IGFBP-7	Y	Y	Y	Y	N	Y	Y	Y	Y	Y	N	Y	Y	Y	Y	Y	Y	Y	Y	Y	Y	Y	Y	Y	Y	Y	N	Y	EDTA	30
45 IL-10	Y	-	Y	Y	N	-	-	-	-	Y	Y	Y	-	-	-	-	-	-	-	-	-	-	-	-	-	-	-	-	Serum	3
46 IL-12	-	-	-	-	-	-	-	-	-	-	-	-	-	-	-	-	-	-	-	-	-	-	-	-	-	-	-	-	EDTA	3
47 IL-15	-	-	-	-	-	-	-	-	-	-	-	-	-	-	-	-	-	-	-	-	-	-	-	-	-	-	-	-	Serum	3
48 IL-18	Y	N	Y	N	N	N	Y	Y	Y	Y	N	N	N	Y	-	-	-	-	Y	Y	-	-	-	-	N	-	N	-	Serum	3
49 IL-1β	N	Y	Y	Y	Y	Y	Y	Y	Y	Y	N	Y	Y	Y	-	-	-	-	-	-	-	-	-	-	-	-	-	-	Serum	3
50 IL-1ra	N	Y	-	Y	Y	Y	N	-	Y	-	N	Y	Y	Y	-	-	-	-	-	-	-	-	-	-	-	-	-	-	EDTA	3
51 IL-2	-	-	-	Y	-	-	-	-	-	-	N	-	-	-	-	-	-	-	-	-	-	-	-	-	-	-	-	-	Serum	3
52 IL-3	-	Y	-	-	-	N	-	-	N	-	-	-	-	-	-	-	-	-	-	-	-	-	-	-	-	-	-	-	Serum	3
53 IL-4	-	-	-	-	-	-	-	-	-	-	N	-	-	-	-	-	-	-	-	-	-	-	-	-	-	-	-	-	Serum	3
54 IL-5	-	-	N	N	-	-	-	-	-	-	N	Y	-	-	-	-	-	-	-	-	-	-	-	-	-	-	-	-	EDTA	3
55 IL-7	-	-	-	N	N	Y	Y	-	N	-	-	-	Y	-	-	-	-	-	-	-	-	-	-	-	-	-	-	-	Serum	3
56 IL-8	-	-	-	-	-	-	-	-	-	-	-	-	-	-	-	-	-	-	-	-	-	-	-	-	-	-	-	-	EDTA	3
57 IP-10	N	N	N	Y	Y	Y	Y	-	Y	N	N	N	-	Y	-	-	-	-	-	-	-	Y	-	-	-	N	-	-	EDTA	3
58 KLK14	-	-	-	N	-	-	-	-	-	-	N	-	-	-	N	-	-	-	-	-	-	Y	-	-	N	N	-	-	Serum	3
59 KLK8	-	-	-	Y	N	-	-	-	-	-	-	N	-	-	-	-	-	-	-	N	N	-	-	-	-	-	N	N	EDTA	3
60 Leptin	-	-	-	-	-	-	-	-	-	-	-	-	-	-	-	-	-	-	-	-	-	-	-	-	-	-	-	-	Serum	3
61 M-CSF	-	-	-	-	-	-	-	-	-	-	-	-	-	-	-	-	-	-	-	-	-	-	-	-	-	-	-	-	EDTA	3
62 MCP1	-	-	-	-	-	-	-	-	-	-	N	-	-	-	-	-	-	-	-	N	-	-	-	-	-	-	-	-	EDTA	3
63 MCP2	-	-	-	-	-	-	-	-	-	-	-	-	-	-	-	-	-	-	-	-	-	-	-	-	-	-	-	-	Serum	3
64 MCP3	-	-	-	-	-	-	-	-	-	-	-	-	-	-	-	-	-	-	-	-	-	-	-	-	-	-	-	-	EDTA	3
65 MCP4	-	-	-	-	-	-	-	-	-	-	-	-	-	-	-	-	-	-	-	-	-	-	-	-	-	-	-	-	EDTA	3
66 MIG	-	-	-	-	-	-	-	-	-	-	-	-	-	-	-	-	-	-	-	-	-	-	-	-	-	-	-	-	EDTA	3
67 MIP-1α	Y	N	N	Y	N	Y	N	Y	-	Y	Y	Y	Y	-	-	-	-	-	-	-	-	-	-	-	-	-	-	-	Serum	3

Table F.S4 continued from previous page

	4 °C, low dilution							4 °C, high dilution							25 °C, low dilution							25 °C, high dilution							Selected	
	S	Ci	H	E	E_F	C	C_F	S	Ci	H	E	E_F	C	C_F	S	Ci	H	E	E_F	C	C_F	S	Ci	H	E	E_F	C	C_F	Type	Dilution
68 MIP-1β	-	-	-	-	N	-	-	-	-	-	-	-	-	-	-	-	-	-	-	-	-	-	-	-	-	-	-	-	Serum	3
69 MMP-1	Y	-	-	Y	Y	-	-	N	-	-	N	-	-	-	-	-	-	-	-	-	-	-	-	-	-	-	-	-	EDTA	3
70 MMP-3	Y	Y	Y	Y	N	Y	Y	Y	Y	Y	Y	Y	Y	Y	Y	Y	N	Y	Y	Y	Y	Y	Y	Y	Y	N	Y	Y	EDTA	3
71 MMP-9	Y	Y	N	Y	Y	Y	N	Y	Y	Y	Y	Y	N	N	Y	Y	N	N	Y	Y	Y	Y	N	N	Y	Y	N	N	Serum	30
72 NCAM-1	Y	N	Y	Y	N	Y	Y	Y	N	Y	N	Y	Y	Y	Y	Y	Y	N	Y	Y	Y	Y	Y	Y	Y	N	Y	Y	Serum	3
73 NT-3	-	-	-	-	-	-	-	-	-	-	-	-	-	-	-	-	-	-	-	-	-	N	-	-	N	N	-	-	Serum	3
74 OPN	Y	Y	Y	Y	Y	Y	Y	N	Y	Y	Y	Y	Y	Y	Y	Y	Y	Y	Y	N	Y	Y	N	Y	Y	Y	N	Y	EDTA	3
75 PAI-1	Y	-	Y	Y	Y	-	-	Y	-	Y	Y	Y	-	-	-	-	-	-	-	-	-	-	-	-	-	-	-	-	Serum	3
76 PDGF-BB	Y	Y	-	N	N	N	-	N	-	-	Y	Y	-	-	N	-	-	-	N	-	-	Y	-	-	N	N	-	-	EDTA	3
77 PRL	-	N	-	-	-	-	N	-	N	-	-	-	-	Y	-	-	-	-	-	-	-	-	-	-	-	-	-	-	Serum	3
78 PSA	-	-	-	-	-	-	-	-	-	-	-	-	-	-	-	-	-	-	-	-	-	-	-	-	-	-	-	-	Serum	3
79 RBP4	-	-	-	-	-	-	-	-	-	-	-	-	-	-	-	-	-	-	-	-	-	-	-	-	-	-	-	-	EDTA	3
80 S100B	-	Y	-	-	-	-	-	-	N	-	-	-	-	-	-	-	-	-	-	-	-	-	-	-	-	-	-	-	Serum	3
81 SPARC	Y	-	N	N	Y	-	-	Y	-	Y	Y	-	-	-	-	-	-	-	-	-	-	-	-	-	-	-	-	-	EDTA	3
82 TF	-	-	-	-	-	-	-	-	-	-	-	-	-	-	-	-	-	-	-	-	-	-	-	-	-	-	-	-	Serum	3
83 TGF-α	-	-	-	-	-	-	-	-	-	-	N	-	-	-	-	-	-	-	-	-	-	-	-	-	-	-	-	-	EDTA	3
84 TGF-β RII	-	-	-	-	-	-	-	-	-	-	-	-	-	-	-	-	-	-	-	-	-	-	-	-	-	-	-	-	Serum	3
85 TGF-β1	Y	-	N	Y	N	-	-	N	-	N	N	N	-	-	N	-	-	-	-	-	-	-	-	-	-	-	-	-	EDTA	3
86 TGF-β2	-	-	-	-	-	-	-	-	-	-	-	-	-	-	-	-	-	-	-	-	-	-	-	-	-	-	-	-	Serum	3
87 THBS-1	Y	Y	Y	N	N	Y	N	Y	Y	Y	N	Y	Y	N	Y	N	N	Y	N	N	N	Y	N	Y	Y	N	N	N	Serum	30
88 Tie-2	-	N	-	N	-	Y	Y	-	N	-	-	Y	N	Y	-	-	-	-	-	-	-	-	-	-	-	-	-	-	EDTA	3
89 TIMP-1	Y	-	Y	N	Y	-	-	Y	-	Y	N	Y	-	-	-	-	-	-	-	N	-	-	-	-	-	-	Y	N	Serum	3
90 TNF-α	-	-	-	-	-	-	-	-	-	-	-	-	-	-	-	-	-	-	-	-	-	-	-	-	-	-	-	-	Serum	3
91 TNF-RI	N	Y	Y	Y	Y	Y	Y	Y	Y	Y	Y	Y	Y	Y	Y	-	-	-	Y	-	-	-	-	-	N	-	-	-	Serum	3

Table F.S4 continued from previous page

	4 °C, low dilution							4 °C, high dilution							25 °C, low dilution							25 °C, high dilution							Selected	
	S	Ci	H	E	E_F	C	C_F	S	Ci	H	E	E_F	C	C_F	S	Ci	H	E	E_F	C	C_F	S	Ci	H	E	E_F	C	C_F	Type	Dilution
92 TNF-RII	N	Y	Y	N	N	Y	N	Y	Y	N	Y	N	Y	Y	N	Y	Y	Y	Y	N	N	Y	Y	Y	Y	N	Y	Y	Serum	3
93 uPA	Y	Y	Y	Y	N	Y	Y	Y	Y	Y	Y	Y	Y	Y	-	-	-	-	-	-	-	Y	-	-	-	-	-	-	Serum	3
94 uPA-R	-	-	-	-	-	-	-	-	-	-	-	N	-	-	-	-	-	-	-	-	-	-	-	-	-	-	-	-	EDTA	3
95 VCAM-1	Y	Y	Y	Y	Y	Y	Y	Y	Y	Y	Y	Y	Y	Y	Y	Y	Y	Y	Y	Y	Y	Y	Y	Y	Y	Y	Y	Y	EDTA	3
96 VEGF-A	Y	Y	Y	N	N	-	Y	Y	Y	Y	Y	Y	-	-	Y	-	-	-	-	-	-	Y	-	-	-	-	-	-	EDTA	3
97 VEGF-D	-	-	-	-	-	-	-	-	-	-	-	-	-	-	-	-	-	-	-	-	-	-	-	-	-	-	-	-	EDTA	3
98 VEGFR2	Y	Y	Y	N	Y	N	N	Y	Y	-	-	Y	Y	Y	-	-	-	-	-	-	-	-	-	-	-	-	-	-	Serum	3
99 VEGFR3	-	-	-	-	-	-	-	-	-	-	-	-	-	-	-	-	-	-	-	-	-	-	-	-	-	-	-	-	Serum	3
# Y:	33	29	31	33	26	29	27	35	26	32	24	36	31	32	18	14	14	14	18	13	12	19	11	14	18	11	12	16		
# N:	14	14	11	24	24	13	14	6	16	7	28	16	5	5	5	3	5	3	4	11	8	7	6	4	6	12	11	6		
Total detected	47	43	42	57	50	42	41	41	42	39	52	52	36	37	23	17	19	17	22	24	20	26	17	18	24	23	23	22		

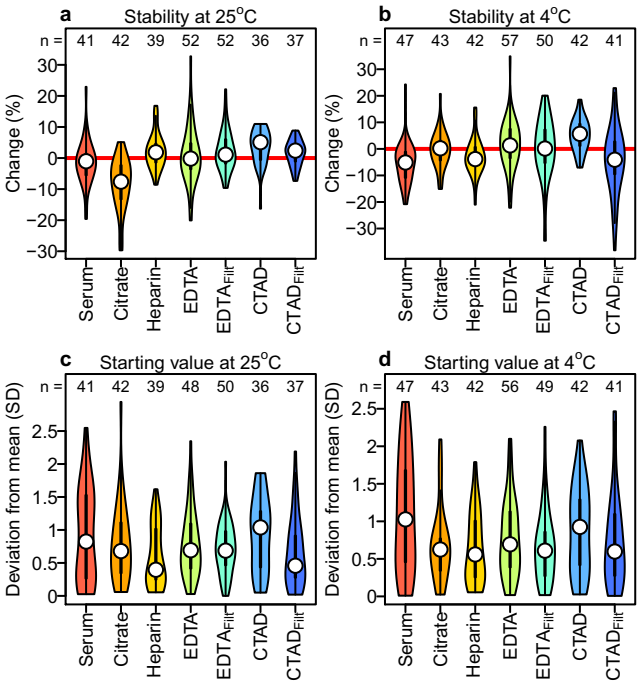

FIGURE F.S10: **Effect of tube collection type and filtering on proteins initial measured value and stability before processing, all proteins.** 103 proteins was measured in blood samples from two anonymous donors. Blood was collected in five different collection tubes and left at room temperature (**a, c**) or stored at 4 °C (**b, d**) for 5, 30 and 120 min. Serum tubes were left to coagulate for 15 min before storing and waiting. **a-b** show the aggregated stability of measured protein levels after 120 min and **c-d** the aggregated extrapolated value measured with no waiting time before processing. **c-d** are expressed as a number of standard deviations (SD) away from the mean of all collection tubes and post-centrifugal filtering for EDTA and CTAD plasma. A higher value indicates more deviation from the mean.

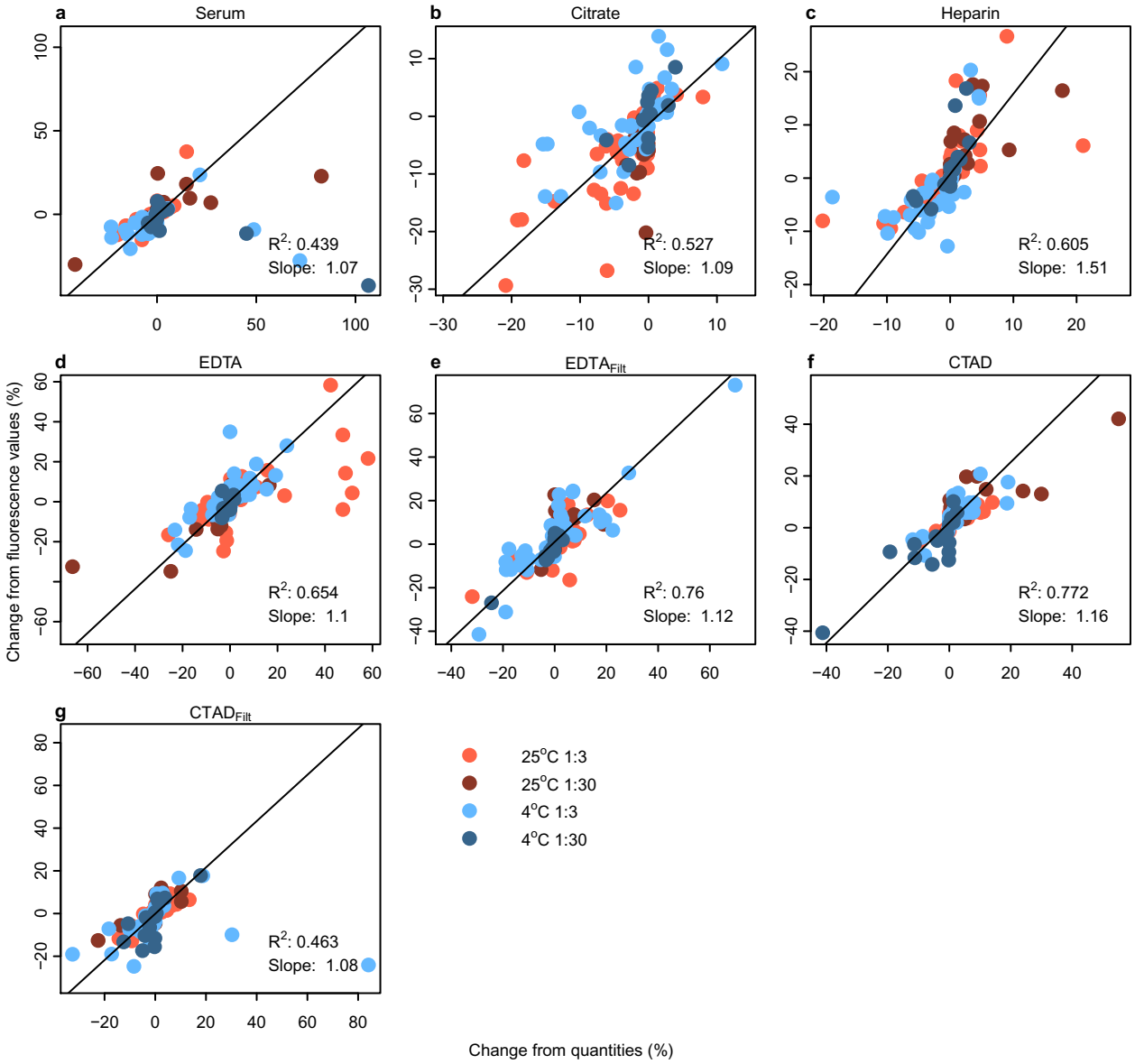

FIGURE F.S11: **Comparison of stability of proteins calculated with fluorescence values and quantities.** The effect of pre-analytical variables on protein stability of blood collected in **a** serum, **b** citrate, **c** heparin, **d-e** EDTA and **f-g** CTAD tubes while waiting for processing was measured with calibrated fluorescence values (y-axes) and quantities interpolated from the standard curves (x-axes). Graphs **e, g** shows stability values from plasma that were filtered before freezing. Linear fits were calculated using median-based linear regression.

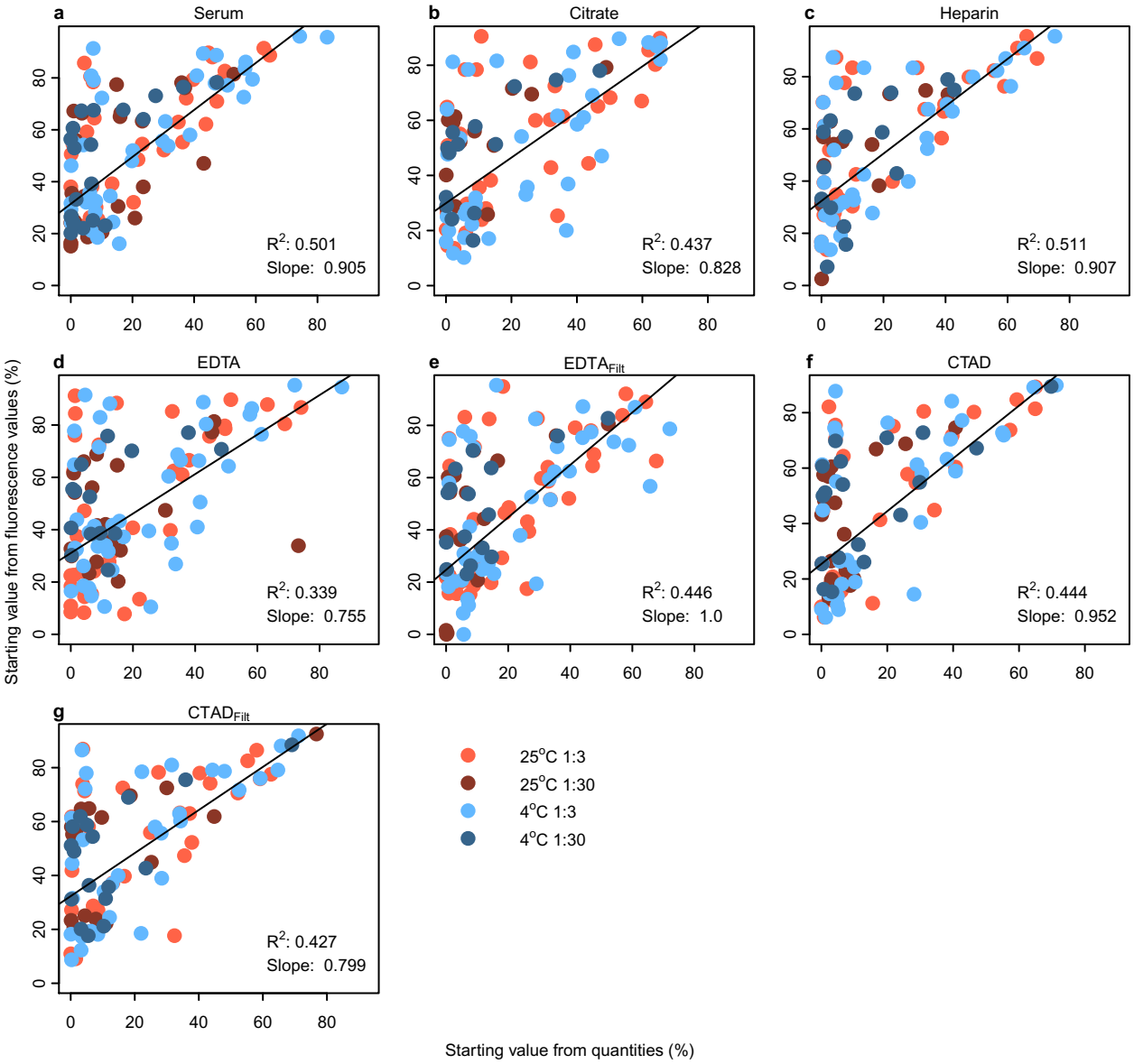

FIGURE F.S12: **Comparison of initial values of proteins calculated with fluorescence values and quantities.** The effect of pre-analytical variables on the initial values of proteins in blood collected in **a** serum, **b** citrate, **c** heparin, **d-e** EDTA and **f-g** CTAD tubes was measured with calibrated fluorescence values (y-axes) and quantities interpolated from the standard curves (x-axes). Graphs **e, g** shows stability values from plasma that were filtered before freezing. Linear fits were calculated using median-based linear regression.

TABLE F.S5: **Quantities of proteins found in pooled normal controls, low dilution.** All quantities are expressed in pg/mL, with standard deviations when available. -: not detected.

	Blood Type	Blood Dilution	Serum Normal Low	Citrate Normal Low	Heparin Normal Low	EDTA Normal Low	CTAD Normal Low
AFP	Serum	3	1387752.3 ± 734453.7	1234904.6	1583551.6 ± 3e+05	2e+06 ± 487500.4	1541678.6 ± 191052.0
AHSG	Serum	3	-	-	-	-	-
ALDH1L1	Serum	3	-	-	-	20567.0 ± 14237.8	24031.6
Amphiregulin	EDTA	3	296.9 ± 159.3	-	182.0 ± 97.3	301.7 ± 108.2	245.4 ± 93.5
Ang1	EDTA	3	3809.7 ± 253.8	398.1	-	-	-
Ang2	EDTA	3	-	-	-	-	-
β-NGF	EDTA	3	-	-	-	-	-
BDNF	Serum	3	5762.8 ± 1646.9	-	11131.5 ± 1091.0	15631.8 ± 5390.5	-
BMP2	Serum	3	-	-	-	-	-
BRAF	Serum	3	-	-	-	-	-
c-Kit	EDTA	3	5416.3 ± 1633.9	3604.8	8042.5 ± 187.6	8738.5 ± 2575.8	5657.6 ± 2120.1
CA15-3	Serum	3	615.6 ± 129.8	995.8	820.8 ± 267.2	818.5 ± 165.8	1019.9 ± 94.5
Cathepsin B	Serum	3	-	-	-	-	-
CCL5	Serum	3	-	-	-	-	-
CD14	Serum	30	-	-	-	-	-
CEA	Serum	3	662.7 ± 302.0	575.7	495.5 ± 26.4	677.1 ± 134.3	-
CRP	EDTA	3	-	-	-	-	-
CXCL12	EDTA	3	-	-	-	24190.0 ± 9843.7	25221.6 ± 11866.2
E-cadherin	Serum	3	2054.2 ± 145.5	3897.5	2933.0 ± 98.4	4169.7 ± 946.7	3262.6 ± 734.7
E-selectin	Serum	3	-	-	-	-	-
EGF	EDTA	3	4362.7 ± 2457.5	-	0.06 ± 0.081	0.22 ± 0.15	0.21
EGFR	Serum	3	11232.9 ± 3821.5	4233.0	12795.2 ± 8730.9	8658.8 ± 3115.0	5513.8 ± 3265.9
Endoglin	Serum	3	2131.3 ± 422.9	1887.2	2235.6 ± 26.4	2475.7 ± 299.6	2967.1 ± 688.2
EpCAM	EDTA	3	-	-	-	-	-
FAS	Serum	3	529.6 ± 139.4	546.8	429.5 ± 91.2	566.8 ± 195.1	336.8 ± 139.3
FAS-L	Serum	3	171.3 ± 112.2	130.5	-	189.1 ± 91.1	130.8 ± 76.8
FGF-1	EDTA	3	-	-	-	-	-
FGFb	Serum	3	20693.5 ± 15644.7	-	32100.2 ± 7920.9	48131.2 ± 43704.9	16774.1 ± 6061.9
Flt-3	EDTA	3	-	-	-	-	-
G-CSF	Serum	3	-	-	-	-	-
GFAP	Serum	3	-	-	-	-	-
GM-CSF	EDTA	3	-	-	-	-	-
GRO-α	Serum	3	22192.5 ± 7327.1	-	-	21236.0 ± 8193.1	-
HAI-1	Serum	3	153244.1 ± 92034.1	77111.3	98606.8 ± 30617.2	139449.4 ± 36344.1	141879.1 ± 45786.8
HE4	Serum	3	-	-	54501.7 ± 14736.9	67781.3 ± 25953.0	-
HER2	Serum	3	161.8 ± 269.4	-	-	-	-
HER3	Serum	3	565.0 ± 520.0	-	-	-	-
HGF	EDTA	3	2694.7 ± 335.1	1039.5	923.3 ± 299.5	1346.0 ± 481.8	1158.1 ± 530.6
HGF-R	Serum	30	15824.2 ± 3527.0	10123.3	20274.4 ± 7906.5	36804.2 ± 27650.9	29516.3 ± 7621.8
HMGB1	Serum	3	-	-	-	-	-
HP	Serum	3	-	-	-	-	-
ICAM-1	EDTA	3	-	-	-	-	-
IFN-γ	EDTA	3	-	-	-	-	-
IGFBP-1	Serum	3	539.5 ± 118.0	877.5	754.5 ± 19.5	774.1 ± 149.6	655.2 ± 85.1
IGFBP-3	Serum	3	1e+05 ± 26225.3	122322.9	145783.5 ± 8853.7	144382.2 ± 39814.9	89700.2 ± 6460.8
IGFBP-7	Serum	30	19160.0 ± 4303.3	15192.6	17644.0 ± 4319.9	17388.7 ± 7475.5	8456.4 ± 354.3
IL-10	EDTA	3	-	-	-	-	-
IL-12	EDTA	3	4312.4 ± 3245.6	-	-	-	-
IL-15	EDTA	3	-	-	-	-	-

Table F.S5 continued from previous page

	Blood Type	Blood Dilution	Serum Normal Low	Citrate Normal Low	Heparin Normal Low	EDTA Normal Low	CTAD Normal Low
IL-18	EDTA	3	-	-	-	-	-
IL-1β	EDTA	3	49.4 ± 38.1	24.0	18.0 ± 13.5	43.2 ± 18.8	45.5 ± 7.9
IL-1ra	EDTA	3	17083.7 ± 3343.7	10488.6	-	15843.2 ± 2631.3	13861.0 ± 2132.5
IL-2	EDTA	3	-	-	-	-	-
IL-3	EDTA	3	387.7 ± 241.5	-	-	254.6 ± 150.3	382.4 ± 106.8
IL-4	Serum	3	-	-	-	-	-
IL-5	EDTA	3	-	-	-	-	-
IL-6	EDTA	3	-	-	-	-	-
IL-7	EDTA	3	191.5 ± 166.9	172.3	-	231.7 ± 82.5	320.6 ± 13.9
IL-8	EDTA	3	-	-	-	-	-
IP-10	Serum	3	44.9 ± 49.1	20.2	10.8 ± 13.5	59.3 ± 33.5	53.0 ± 34.6
KLK14	EDTA	3	2215.4 ± 872.5	-	-	-	2048.1 ± 1051.7
KLK8	EDTA	3	-	-	2495248.6 ± 2305596.7	2197071.7 ± 810984.9	-
Leptin	Serum	3	-	-	-	-	-
M-CSF	EDTA	3	1518.8 ± 1081.7	-	-	827.5 ± 691.1	563.6 ± 589.2
MCP1	EDTA	3	-	-	1334.1	967.7 ± 358.7	-
MCP2	EDTA	3	36.8 ± 17.3	-	-	30.8 ± 21.5	60.0
MCP3	EDTA	3	-	-	-	-	-
MCP4	EDTA	3	-	-	-	-	-
MIG	EDTA	3	1694.8 ± 1322.4	1738.0	-	1787.0 ± 311.6	2177.1 ± 361.0
MIP-1α	EDTA	3	21.5 ± 10.4	-	20.2 ± 3.3	31.7 ± 12.1	27.5 ± 14.9
MIP-1β	EDTA	3	-	-	-	-	-
MMP-1	EDTA	3	-	-	-	-	-
MMP-3	Serum	3	9322.5 ± 2174.6	5592.5	15213.4 ± 262.1	12287.3 ± 6077.1	7254.5 ± 2279.8
MMP-9	EDTA	30	18715.6 ± 1314.0	5163.5	13894.7 ± 272.6	14154.2 ± 2675.9	16881.9 ± 369.7
NCAM-1	EDTA	3	168897.9 ± 115278.1	176312.3	324853.6 ± 94777.3	165748.3 ± 68800.6	254329.1 ± 127474.1
NT-3	EDTA	3	821.3 ± 244.5	-	-	-	-
OPN	EDTA	3	18900.2 ± 12796.6	19467.1	29662.7 ± 8235.4	175178.4 ± 282842.9	23199.8 ± 8574.3
PAI-1	EDTA	3	1267364.2 ± 569324.5	-	1857525.1 ± 222157.0	2222996.1 ± 756340.3	730451.7 ± 1e+05
PDGF-BB	EDTA	3	499.7 ± 98.7	-	73.7 ± 40.8	99.3 ± 77.2	-
PRL	Serum	3	-	-	-	-	-
PSA	Serum	3	27955.6 ± 27340.6	81621.5	16680.7 ± 2965.0	36532.1 ± 30789.2	68969.1 ± 39972.0
RBP4	EDTA	3	-	-	-	-	-
S100B	Serum	3	281297.7 ± 112244.3	288714.7	-	235768.8 ± 90783.3	265163.0 ± 42725.8
SCGN	EDTA	3	-	-	-	-	-
SPARC	EDTA	3	6924.6 ± 1570.0	-	-	3691.0 ± 458.5	-
TF	EDTA	3	1742.5 ± 1257.2	2399.5	4620.1 ± 478.8	4455.7 ± 1604.9	4079.9 ± 1407.8
TGF-α	EDTA	3	235.7 ± 94.3	-	-	-	252.0
TGF-β RII	EDTA	3	2199.6 ± 3537.7	-	-	2288.4 ± 1247.7	1735.0 ± 2810.3
TGF-β1	EDTA	3	753.3 ± 60.7	-	-	5.2 ± 7.4	-
TGF-β2	EDTA	3	-	-	-	-	-
THBS-1	Serum	30	-	-	-	-	-
Tie-2	Serum	3	8462.0 ± 1186.9	13211.0	9126.7 ± 259.8	12684.5 ± 2629.4	12875.9 ± 4178.8
TIMP-1	EDTA	3	-	-	-	-	-
TNF-α	EDTA	3	-	-	-	-	24.8 ± 10.6
TNF-RI	EDTA	3	3332.7 ± 344.6	3447.8	3541.9 ± 412.7	3284.4 ± 214.2	2569.3 ± 409.4
TNF-RII	Serum	3	2078.4 ± 281.1	4573.2	2038.5 ± 27.7	1724.9 ± 292.1	3372.7 ± 733.7
uPA	EDTA	3	1426.7 ± 415.8	931.8	729.7 ± 53.4	755.1 ± 146.6	757.3 ± 114.1
uPA-R	Serum	3	834.3 ± 227.5	-	-	795.6 ± 287.4	-
VCAM-1	Serum	3	87471.5 ± 10465.4	111902.6	84183.2 ± 24092.6	107549.6 ± 23820.1	124137.3 ± 32929.7
VEGF-A	EDTA	3	336.3 ± 67.1	13.5	22.2 ± 0.031	26.5 ± 6.8	9.4 ± 5.6

Table F.S5 continued from previous page

	Blood Type	Blood Dilution	Serum Normal Low	Citrate Normal Low	Heparin Normal Low	EDTA Normal Low	CTAD Normal Low
VEGF-D	Serum	3	-	-	-	-	-
VEGFR2	Serum	3	11751.9 ± 2169.0	13584.6	8996.6 ± 1071.9	9144.6 ± 1925.1	11893.1 ± 3653.3
VEGFR3	Serum	3	-	-	-	-	-

TABLE F.S6: **Quantities of proteins found in pooled normal controls, high dilution.** All quantities are expressed in pg/mL, with standard deviations when available. -: not detected.

	Blood Type	Blood Dilution	Serum Normal High	Citrate Normal High	Heparin Normal High	EDTA Normal High	CTAD Normal High
AFP	Serum	3	-	-	-	6483852.1 ± 6365814.2	-
AHSG	Serum	3	-	-	-	-	-
ALDH1L1	Serum	3	-	-	-	-	-
Amphiregulin	EDTA	3	-	-	-	-	-
Ang1	EDTA	3	21306.1 ± 10542.2	-	-	-	-
Ang2	EDTA	3	-	-	-	-	-
β-NGF	EDTA	3	-	-	-	-	-
BDNF	Serum	3	-	-	-	-	-
BMP2	Serum	3	-	-	-	-	-
BRAF	Serum	3	-	-	-	-	-
c-Kit	EDTA	3	21569.6 ± 4002.0	18542.8	16861.4	25432.7 ± 4427.0	24607.8 ± 8622.7
CA15-3	Serum	3	2623.8 ± 890.8	3810.5	2757.0	4761.8 ± 978.0	4699.7 ± 2043.6
Cathepsin B	Serum	3	-	-	-	-	-
CCL5	Serum	3	-	-	-	-	-
CD14	Serum	30	-	-	-	-	-
CEA	Serum	3	-	-	-	-	-
CRP	EDTA	3	-	-	-	-	-
CXCL12	EDTA	3	-	-	-	-	-
E-cadherin	Serum	3	6841.4 ± 697.6	6988.8	7974.4	9656.0 ± 2374.9	8328.6 ± 1472.7
E-selectin	Serum	3	-	-	-	-	-
EGF	EDTA	3	1697.2 ± 621.3	-	-	-	-
EGFR	Serum	3	20043.4 ± 4719.4	20541.7	17022.4	18898.9 ± 6139.4	20790.5 ± 10684.4
Endoglin	Serum	3	-	-	-	-	-
EpCAM	EDTA	3	-	-	-	-	-
FAS	Serum	3	689.7 ± 56.1	396.5	806.3	600.0 ± 101.5	459.7 ± 186.3
FAS-L	Serum	3	-	-	-	1449.4	-
FGF-1	EDTA	3	-	-	-	-	-
FGFb	Serum	3	-	-	105139.6	-	-
Flt-3	EDTA	3	-	-	-	-	-
G-CSF	Serum	3	-	-	-	-	-
GFAP	Serum	3	-	-	-	-	-
GM-CSF	EDTA	3	-	-	-	-	-
GRO-α	Serum	3	-	-	-	-	-
HAI-1	Serum	3	-	-	-	-	-
HE4	Serum	3	-	-	-	-	-
HER2	Serum	3	-	-	-	-	-
HER3	Serum	3	-	-	-	-	-
HGF	EDTA	3	-	-	-	-	-
HGF-R	Serum	30	72722.2 ± 15874.9	49919.7	48578.3	68154.3 ± 13853.6	79702.2 ± 29729.0
HMGB1	Serum	3	-	-	-	-	-
HP	Serum	3	-	-	-	-	-

Table F.S6 continued from previous page

	Blood Type	Blood Dilution	Serum Normal High	Citrate Normal High	Heparin Normal High	EDTA Normal High	CTAD Normal High
ICAM-1	EDTA	3	-	-	-	-	-
IFN-γ	EDTA	3	-	-	-	-	-
IGFBP-1	Serum	3	5144.7 ± 309.2	3846.5	4882.8	4688.1 ± 747.2	4697.2 ± 605.8
IGFBP-3	Serum	3	453243.7 ± 18607.4	518966.6	450723.4	511547.9 ± 70081.3	590374.8 ± 97652.3
IGFBP-7	Serum	30	48801.4 ± 10716.5	39046.3	51150.1	52985.4 ± 12372.4	55686.3 ± 6965.9
IL-10	EDTA	3	-	-	-	-	-
IL-12	EDTA	3	-	-	-	-	-
IL-15	EDTA	3	-	-	-	-	-
IL-18	EDTA	3	-	-	-	-	-
IL-1β	EDTA	3	-	-	-	110.5	-
IL-1ra	EDTA	3	-	-	-	-	-
IL-2	EDTA	3	-	-	-	-	-
IL-3	EDTA	3	-	-	-	-	-
IL-4	Serum	3	-	-	-	-	-
IL-5	EDTA	3	-	-	-	-	-
IL-6	EDTA	3	-	-	-	-	-
IL-7	EDTA	3	-	-	-	-	-
IL-8	EDTA	3	-	-	-	-	-
IP-10	Serum	3	-	-	-	-	-
KLK14	EDTA	3	-	-	-	-	-
KLK8	EDTA	3	-	-	-	-	-
Leptin	Serum	3	-	-	-	-	-
M-CSF	EDTA	3	-	-	-	-	-
MCP1	EDTA	3	-	-	-	-	10754.5 ± 7123.1
MCP2	EDTA	3	-	-	-	-	-
MCP3	EDTA	3	-	-	-	-	-
MCP4	EDTA	3	-	-	-	-	-
MIG	EDTA	3	-	-	-	15110.2	-
MIP-1α	EDTA	3	-	-	-	-	-
MIP-1β	EDTA	3	-	-	-	-	-
MMP-1	EDTA	3	-	-	-	-	-
MMP-3	Serum	3	18200.8 ± 2129.9	17283.5	20206.0	24992.1 ± 8718.8	20941.5 ± 6512.1
MMP-9	EDTA	30	343206.1 ± 77587.9	71413.0	116101.3	129837.4 ± 26454.6	190059.4 ± 42091.4
NCAM-1	EDTA	3	819893.0 ± 464646.2	1309647.5	1439684.1	884579.2 ± 277444.6	724756.1 ± 5e+05
NT-3	EDTA	3	-	-	-	-	-
OPN	EDTA	3	23812.1 ± 9690.5	29742.2	30752.4	41469.8 ± 13738.2	84403.2 ± 23703.2
PAI-1	EDTA	3	-	-	-	-	-
PDGF-BB	EDTA	3	-	-	-	-	-
PRL	Serum	3	-	-	-	-	-
PSA	Serum	3	237263.2 ± 141830.1	-	-	290661.3 ± 3e+05	335585.8 ± 330146.1
RBP4	EDTA	3	-	-	-	-	-
S100B	Serum	3	-	-	-	-	-
SCGN	EDTA	3	-	-	-	-	-
SPARC	EDTA	3	-	-	-	-	-
TF	EDTA	3	15224.3 ± 5094.3	31676.2	9391.0	28117.0 ± 13357.6	27896.1 ± 11900.7
TGF-α	EDTA	3	-	-	-	-	-
TGF-β RII	EDTA	3	-	-	-	-	-
TGF-β1	EDTA	3	-	-	-	21.3	-
TGF-β2	EDTA	3	-	-	-	-	-
THBS-1	Serum	30	-	-	-	-	-
Tie-2	Serum	3	-	-	-	-	-

Table F.S6 continued from previous page

	Blood Type	Blood Dilution	Serum Normal High	Citrate Normal High	Heparin Normal High	EDTA Normal High	CTAD Normal High
TIMP-1	EDTA	3	-	-	-	-	-
TNF-α	EDTA	3	-	-	-	-	-
TNF-RI	EDTA	3	-	-	-	-	-
TNF-RII	Serum	3	1828.8 ± 770.0	1709.5	-	3701.3 ± 3063.4	1444.3 ± 690.1
uPA	EDTA	3	-	-	-	-	-
uPA-R	Serum	3	-	-	-	-	-
VCAM-1	Serum	3	943985.6 ± 185368.9	736693.6	722453.8	851657.2 ± 164993.7	765215.7 ± 115565.3
VEGF-A	EDTA	3	381.5 ± 55.9	-	-	-	-
VEGF-D	Serum	3	-	-	-	-	-
VEGFR2	Serum	3	-	-	-	-	-
VEGFR3	Serum	3	-	-	-	-	-

TABLE F.S7: **TBI normals quantities and relative recovery values for microdialysis quantification.** LOD is expressed in pg/mL.

	Blood Type	Blood Dilution	mTBI LOD	mTBI pnBlood quantity (pg/mL)	sTBI LOD	sTBI pnBlood quantity (pg/mL)	CSF Dilution	sTBI pnCSF quantity (pg/mL)	Molecular size (kDa)	Relative recovery (%)
AFP	Serum	3	179004.1	1387752.3 ± 734453.7	44344.4	-	3	-	137.4	0.8
AHSG	Serum	3	-	-	44258.7	644780.4 ± 487173.9	3	186306.0 ± 2e+05	39.3	4.6
ALDH1L1	Serum	3	6215.2	-	7928.1	74970.1 ± 49275.1	3	22119.4 ± 25181.8	98.8	1.6
Amphiregulin	EDTA	3	45.8	301.7 ± 108.2	49.5	415.2 ± 120.4	3	-	27.9	5.6
Ang1	EDTA	3	73.5	219.5 ± 136.7	28.5	162.5 ± 23.9	3	-	57.5	3.3
Ang2	EDTA	3	713.2	1213.3 ± 256.1	115.7	1078.7 ± 282.2	3	-	56.9	3.3
β-NGF	EDTA	3	33.5	-	6.63	8.6 ± 5.8	3	-	130	0.92
BDNF	Serum	3	1404.4	5762.8 ± 1646.9	1487.6	45601.6 ± 37467.6	3	-	37.1	4.7
BMP2	Serum	3	65.2	87.3 ± 64.0	174	586.4 ± 228.4	3	191.8 ± 118.5	44.7	4.1
BRAF	Serum	3	1087.7	-	743.3	2556.4 ± 918.4	3	851.4 ± 1253.0	84.4	2.1
c-Kit	EDTA	3	171.2	8738.5 ± 2575.8	384.3	41181.5 ± 11633.7	3	1982.1 ± 545.9	109.9	1.3
CA15-3	Serum	3	65.9	615.6 ± 129.8	10.9	2329.0 ± 852.9	3	107.1 ± 74.3	375	0.012
Cathepsin B	Serum	3	-	-	-	-	3	-	30	5.4
CCL5	Serum	3	-	-	-	-	3	-	8	7.9
CD14	Serum	30	-	-	-	-	3	-	48	3.9
CEA	Serum	3	149.6	662.7 ± 302.0	227.5	1478.2 ± 806.2	3	-	60.7	3.1
CRP	EDTA	3	-	-	0.623	1e+07 ± 1.2e+07	3	770659.8 ± 1466364.8	125	1
CXCL12	EDTA	3	7913.1	24190.0 ± 9843.7	2125.2	12183.1 ± 9527.9	3	2145.8 ± 1135.8	13.7	7.2
E-cadherin	Serum	3	207.6	2054.2 ± 145.5	93.7	3357.9 ± 1185.7	3	346.1 ± 126.4	99.7	1.6
E-selectin	Serum	3	-	-	72.5	18129.4 ± 9425.5	3	256.3	66.7	2.8
EGF	EDTA	3	0.017	0.22 ± 0.15	0.37	17.0 ± 12.7	3	-	6	8.2
EGFR	Serum	3	38.7	11232.9 ± 3821.5	53	45268.9 ± 20620.9	3	1202.4 ± 338.4	134.3	0.85
Endoglin	Serum	3	422.1	2131.3 ± 422.9	99.5	1821.9 ± 1334.2	3	324.6 ± 534.9	70.6	2.6
EpCAM	EDTA	3	25.2	36.6 ± 16.5	18.9	252.7 ± 71.9	3	-	34.9	4.9
FAS	Serum	3	12.7	529.6 ± 139.4	38.6	2475.9 ± 1937.6	3	-	37.7	4.7
FAS-L	Serum	3	42.4	171.3 ± 112.2	-	-	3	-	31.4	5.2
FGF-1	EDTA	3	-	-	-	-	3	-	17.5	6.7
FGFb	Serum	3	2433.9	20693.5 ± 15644.7	429.4	1458.7 ± 506.5	3	-	18	6.6
Flt-3	EDTA	3	419.3	-	332.2	491.0 ± 487.6	3	364.4 ± 193.2	112.9	1.2
G-CSF	Serum	3	3.7	4.2	6.16	30.2 ± 19.7	3	12.6 ± 9.9	22.3	6.1
GFAP	Serum	3	-	-	-	-	3	-	49.9	3.8
GM-CSF	EDTA	3	-	-	0.542	270.4 ± 162.5	3	-	32.6	5.1

Table F.S7 continued from previous page

	Blood Type	Blood Dilution	mTBI LOD	mTBI pnBlood quantity (pg/mL)	sTBI LOD	sTBI pnBlood quantity (pg/mL)	CSF Dilution	sTBI pnCSF quantity (pg/mL)	Molecular size (kDa)	Relative recovery (%)
GRO-α	Serum	3	6175.6	22192.5 ± 7327.1	1399.8	44957.2 ± 23892.8	3	1696.1 ± 1644.2	11.3	7.5
HAI-1	Serum	3	12262.7	153244.1 ± 92034.1	29494.6	2709148.7 ± 1283650.5	3	-	33.2	5.1
HE4	Serum	3	13900.1	23870.2 ± 24232.9	16332.4	58717.2 ± 41090.4	3	21057.1 ± 11665.3	13	7.2
HER2	Serum	3	39	161.8 ± 269.4	523	4150.7 ± 2461.1	3	931.1 ± 633.4	137.9	0.8
HER3	Serum	3	137.4	565.0 ± 520.0	828.8	2760.8 ± 1509.9	3	1156.4 ± 378.1	148.1	0.67
HGF	EDTA	3	155.2	1346.0 ± 481.8	108.8	1081.8 ± 382.7	3	717.9 ± 123.6	83.1	2.1
HGF-R	Serum	30	352.4	72722.2 ± 15874.9	244.5	123655.9 ± 44026.1	3	2205.6 ± 902.4	21.3	6.3
HMGB1	Serum	3	-	-	-	-	3	-	24.9	5.9
HP	Serum	3	-	-	7760.7	38377.4 ± 3681.8	3	13642.3 ± 6158.1	167.4	0.47
ICAM-1	EDTA	3	-	-	640.4	1249055.2 ± 717166.3	3	7443.7 ± 5736.4	19.4	6.5
IFN-γ	EDTA	3	-	-	0.0235	12.4 ± 5.6	3	0.73	38.6	4.6
IGFBP-1	Serum	3	12.9	539.5 ± 118.0	-	-	3	-	27.9	5.6
IGFBP-3	Serum	3	415.9	1e+05 ± 26225.3	11516.6	54804.8 ± 12405.7	3	24645.9 ± 25016.1	32.2	5.2
IGFBP-7	Serum	30	245.7	48801.4 ± 10716.5	66.3	88609.5 ± 36023.1	3	51533.3 ± 29370.1	29.1	5.4
IL-10	EDTA	3	-	-	-	-	3	-	41	4.4
IL-12	EDTA	3	1143.6	-	-	-	3	-	70	2.6
IL-15	EDTA	3	841.5	-	100	188.4 ± 119.4	3	-	18	6.6
IL-18	EDTA	3	-	-	-	-	3	-	22.3	6.1
IL-1β	EDTA	3	0.45	43.2 ± 18.8	2.07	29.5 ± 14.2	3	4.8	17.5	6.7
IL-1ra	EDTA	3	3400.1	15843.2 ± 2631.3	2524.1	1e+05 ± 39026.7	3	3843.6 ± 3757.5	19.9	6.4
IL-2	EDTA	3	-	-	-	-	3	-	17.6	6.7
IL-3	EDTA	3	75.2	254.6 ± 150.3	25.1	791.9 ± 442.5	3	-	17.2	6.7
IL-4	Serum	3	555.6	926.7 ± 969.8	276.3	1447.0 ± 1315.3	3	-	17.4	6.7
IL-5	EDTA	3	-	-	-	-	3	-	15.2	7
IL-6	EDTA	3	-	-	-	-	3	-	23.7	6
IL-7	EDTA	3	56.8	231.7 ± 82.5	10	69.6 ± 9.4	3	-	20.2	6.4
IL-8	EDTA	3	12.6	31.6 ± 9.8	15.7	76.6 ± 36.5	3	103.7 ± 26.9	11.1	7.5
IP-10	Serum	3	1.6	44.9 ± 49.1	52.2	1707.5 ± 1013.0	3	1503.1 ± 1258.6	10.9	7.5
KLK14	EDTA	3	672.8	1732.4 ± 617.4	-	-	3	-	29.1	5.4
KLK8	EDTA	3	487312	2197071.7 ± 810984.9	266794.7	1415665.8 ± 116593.6	3	292165.8 ± 163933.9	33	5.1
Leptin	Serum	3	-	-	-	-	3	-	18.6	6.6
M-CSF	EDTA	3	174.2	827.5 ± 691.1	183	12370.6 ± 2658.2	3	-	120.2	1.1
MCP1	EDTA	3	317.5	967.7 ± 358.7	420.9	8727.0 ± 5221.6	3	-	11	7.5
MCP2	EDTA	3	6.6	30.8 ± 21.5	570.5	1363.6 ± 2235.9	3	-	11.2	7.5
MCP3	EDTA	3	12.8	-	5.42	20.0 ± 5.7	3	5.9 ± 0.84	12.4	7.3
MCP4	EDTA	3	1330.4	1454.1 ± 1452.0	1400.1	9583.1 ± 14830.0	3	-	11	7.5
MIG	EDTA	3	459.9	1787.0 ± 311.6	322.2	2345.7 ± 306.7	3	388.7 ± 497.9	14	7.1
MIP-1α	EDTA	3	6.3	31.7 ± 12.1	0.00375	179.8 ± 186.3	3	-	10	7.6
MIP-1β	EDTA	3	79.5	131.5 ± 54.9	58.5	170.0 ± 49.8	3	71.8 ± 55.3	10.2	7.6
MMP-1	EDTA	3	-	-	331.9	21575.1 ± 11840.8	3	648.5 ± 414.0	54	3.5
MMP-3	Serum	3	120.6	9322.5 ± 2174.6	40.2	56949.9 ± 19119.2	3	1045.4 ± 413.0	54	3.5
MMP-9	EDTA	30	76.2	129837.4 ± 26454.6	-	-	3	-	78.5	2.3
NCAM-1	EDTA	3	7655.2	165748.3 ± 68800.6	23483	192862.6 ± 8737.4	3	52871.9	94.6	1.7
NT-3	EDTA	3	198.9	378.0 ± 215.9	2052.4	11182.4 ± 2202.9	3	-	30.8	5.3
OPN	EDTA	3	107.9	175178.4 ± 282842.9	85.1	54201.8 ± 56265.8	3	1221.4 ± 595.1	44	4.2
PAI-1	EDTA	3	218096.9	2222996.1 ± 756340.3	-	-	3	-	45.1	4.1
PDGF-BB	EDTA	3	0	99.3 ± 77.2	66.9	471.5 ± 74.0	3	111.1 ± 67.8	54.6	3.5
PRL	Serum	3	-	-	-	-	3	-	22.6	6.1
PSA	Serum	3	0	27955.6 ± 27340.6	35198.5	-	3	-	28.7	5.5
RBP4	EDTA	3	-	-	-	-	3	-	23	6.1

Table F.S7 continued from previous page

	Blood Type	Blood Dilution	mTBI LOD	mTBI pnBlood quantity (pg/mL)	sTBI LOD	sTBI pnBlood quantity (pg/mL)	CSF Dilution	sTBI pnCSF quantity (pg/mL)	Molecular size (kDa)	Relative recovery (%)
S100B	Serum	3	73069.9	281297.7 ± 112244.3	172289.1	1779122.9 ± 460424.9	3	2e+05 ± 2e+05	10.7	7.5
SCGN	EDTA	3	-	-	-	-	3	-	32	5.2
SPARC	EDTA	3	938.6	3691.0 ± 458.5	3663.8	12037.5 ± 9812.9	3	6805.3 ± 3213.1	34.6	4.9
TF	EDTA	3	0	4455.7 ± 1604.9	2615.5	6063.2 ± 987.5	3	-	33.1	5.1
TGF-α	EDTA	3	71.9	165.9 ± 103.2	0.732	1183.7 ± 1398.0	3	-	17	6.7
TGF-β RII	EDTA	3	313.8	2288.4 ± 1247.7	8.56	22485.5 ± 8604.5	3	-	67.5	2.8
TGF-β1	EDTA	3	0.15	5.2 ± 7.4	1.82	205.1 ± 96.6	3	274.2	14	7.1
TGF-β2	EDTA	3	159529.3	-	382984.4	1202052.5 ± 654542.4	3	986142.1 ± 713958.3	50.6	3.7
THBS-1	Serum	30	-	-	2797.1	4673625.0 ± 1756480.2	3	16792.7 ± 11738.1	388.2	0.0096
Tie-2	Serum	3	2753.8	8462.0 ± 1186.9	983.3	5535.5 ± 1218.3	3	-	52	3.6
TIMP-1	EDTA	3	-	-	110874.3	877556.7 ± 219629.7	3	1109261.7 ± 219775.2	23.2	6
TNF-α	EDTA	3	7.6	17.6 ± 7.0	4.76	164.2 ± 54.8	3	-	51	3.7
TNF-RI	EDTA	3	290.9	3284.4 ± 214.2	179.8	5146.1 ± 1733.8	3	2865.6 ± 751.4	50.5	3.7
TNF-RII	Serum	3	34.4	2078.4 ± 281.1	28.8	745.3 ± 179.6	3	560.8 ± 108.7	48.3	3.9
uPA	EDTA	3	45.4	755.1 ± 146.6	144.9	965.1 ± 157.3	3	-	48.5	3.9
uPA-R	Serum	3	251.6	834.3 ± 227.5	155.2	1157.6 ± 600.0	3	280.2 ± 140.2	50	3.8
VCAM-1	Serum	3	179.6	87471.5 ± 10465.4	172	62006.5 ± 40157.4	3	72240.3 ± 81797.7	81.3	2.2
VEGF-A	EDTA	3	2.5	26.5 ± 6.8	3.05	25.8 ± 3.6	3	4.1 ± 3.5	91	1.8
VEGF-D	Serum	3	4015.1	8955.2 ± 6682.7	13544.8	72933.8 ± 22667.0	3	20965.1 ± 14332.2	40.4	4.5
VEGFR2	Serum	3	2921.6	11751.9 ± 2169.0	-	-	3	-	151.5	0.63
VEGFR3	Serum	3	-	-	9755.8	87696.2 ± 39177.9	3	10029.9 ± 13256.1	152.8	0.61

TABLE F.S8: **Ratio of proteins to pnBlood in sTBI, $mTBI_C$, $mTBI_S$ and trauma patients.** Numbers highlighted in blue and pink are more and less than 30 % above and below pnBlood, respectively.

	Protein name	sTBI	$mTBI_C$	$mTBI_S$	Trauma		Protein name	sTBI	$mTBI_C$	$mTBI_S$	Trauma
1	TF	3.07	1.00	1.00	1.00	53	TIMP-1	0.89	0.74	0.59	0.97
2	IL-10	2.74	5.32	1.00	1.00	54	HGF-R	0.89	0.88	0.85	1.05
3	MIP-1β	2.58	1.10	1.00	1.36	55	CA15-3	0.89	0.73	0.76	0.47
4	SPARC	2.54	1.16	1.07	1.49	56	Ang1	0.89	6.97	6.31	9.36
5	IL-15	2.47	1.00	1.00	1.00	57	PDGF-BB	0.88	2.58	2.40	2.62
6	IL-6	2.46	NA	NA	NA	58	IL-8	0.86	2.08	1.00	1.00
7	TGF-β2	2.41	1.70	1.00	1.00	59	c-Kit	0.85	0.87	0.66	0.93
8	MCP2	2.18	3.87	1.00	1.00	60	TGF-α	0.85	3.70	1.00	1.00
9	BRAF	1.82	1.00	1.00	1.00	61	HE4	0.84	1.19	1.85	1.00
10	PSA	1.78	1.00	1.00	1.00	62	IGFBP-7	0.83	0.89	0.75	0.97
11	β-NGF	1.77	2.27	1.00	1.00	63	uPA-R	0.82	1.06	0.31	0.31
12	Flt-3	1.62	1.00	1.00	1.00	64	MMP-1	0.81	1.08	0.61	1.16
13	Leptin	1.56	1.08	1.00	1.00	65	IL-1ra	0.81	0.99	0.52	0.51
14	IL-4	1.50	1.59	1.00	1.84	66	IGFBP-1	0.80	0.83	0.80	0.90
15	HGF	1.47	1.41	1.15	2.40	67	NCAM-1	0.80	0.83	0.86	0.70
16	PRL	1.42	1.09	3.67	1.00	68	CCL5	0.80	1.00	1.00	1.00
17	VEGF-D	1.41	1.43	1.00	1.00	69	IL-5	0.80	0.64	0.31	0.31
18	PAI-1	1.34	1.07	0.82	0.78	70	FGF-1	0.79	NA	NA	NA
19	VEGF-A	1.29	1.39	1.33	2.29	71	Cathepsin B	0.77	1.00	1.34	1.36
20	BMP2	1.26	1.00	1.00	1.00	72	HER3	0.77	1.00	1.00	2.44
21	IGFBP-3	1.24	0.88	0.70	0.95	73	MCP4	0.76	2.67	1.00	1.00
22	ALDH1L1	1.22	1.09	2.59	1.00	74	ICAM-1	0.75	0.71	0.72	0.64
23	TNF-RI	1.22	1.30	0.92	1.35	75	Endoglin	0.75	0.67	0.67	0.93
24	HMGB1	1.21	0.76	0.69	0.27	76	VEGFR3	0.75	1.19	1.00	1.45
25	S100B	1.20	0.67	1.17	0.26	77	AHSG	0.75	1.00	1.00	1.00
26	OPN	1.18	0.96	0.95	1.21	78	KLK8	0.75	0.40	0.79	0.56
27	IL-18	1.16	1.04	0.86	1.09	79	IL-7	0.74	0.94	0.28	0.28
28	G-CSF	1.14	1.65	1.00	1.00	80	IP-10	0.73	1.14	0.52	1.05
29	HP	1.14	2.21	2.57	4.11	81	M-CSF	0.73	0.99	0.31	0.31
30	Tie-2	1.13	0.87	0.73	1.01	82	BDNF	0.72	0.47	1.10	0.88
31	MIP-1α	1.12	1.49	0.27	0.40	83	FGFb	0.71	0.53	0.42	0.48
32	TNF-RII	1.10	0.93	0.80	0.95	84	SCGN	0.71	NA	NA	NA
33	E-cadherin	1.07	1.06	0.80	1.05	85	MCP3	0.70	2.20	1.00	1.00
34	EGF	1.04	5.84	5.16	8.37	86	TNF-α	0.70	1.90	1.00	1.00
35	HAI-1	1.04	0.63	0.35	0.13	87	MCP1	0.68	1.00	1.00	2.48
36	MIG	1.04	0.86	0.28	0.28	88	CRP	0.67	1.25	2.28	1.34
37	uPA	1.03	0.89	0.67	0.94	89	IFN-γ	0.66	0.63	0.27	0.27
38	CEA	1.01	0.42	0.25	0.25	90	CXCL12	0.65	1.83	1.00	1.00
39	KLK14	0.97	3.58	1.00	2.03	91	EpCAM	0.64	1.61	1.00	1.00
40	MMP-3	0.97	0.91	0.76	0.86	92	HER2	0.64	1.95	1.00	2.01
41	TGF-β RII	0.96	1.12	0.28	0.28	93	NT-3	0.61	2.62	1.00	1.00
42	MMP-9	0.96	0.92	0.83	0.86	94	IL-1β	0.61	0.80	0.36	0.10
43	EGF-R	0.94	0.89	0.80	0.95	95	IL-3	0.60	0.79	0.32	0.32
44	CD14	0.94	0.96	0.90	1.05	96	TGF-β1	0.58	0.84	1.07	1.67
45	Ang2	0.93	1.09	1.00	1.00	97	RBP4	0.57	0.53	0.71	0.79
46	GFAP	0.93	0.83	1.17	0.22	98	GM-CSF	0.57	0.46	0.30	0.30
47	VCAM-1	0.93	0.93	0.85	1.04	99	FAS	0.54	0.65	0.36	0.65
48	THBS-1	0.92	0.83	0.85	0.91	100	GRO-α	0.50	0.68	0.29	0.29
49	E-selectin	0.92	0.67	0.37	0.27	101	FAS-L	NA	1.59	1.35	1.00
50	IL-12	0.91	1.81	1.00	1.00	102	IL-2	NA	0.89	0.33	0.32
51	AFP	0.90	0.99	1.36	0.40	103	VEGFR2	NA	0.92	0.79	0.27
52	Amphiregulin	0.90	0.73	0.17	0.17						

TABLE F.S9: **Summary of proteins showing a peak and ratio analysis progression with respect to TBI severity.** Amp.: amplitude.

	Protein name	sTBI	$mTBI_C$	$mTBI_S$	Trauma	Peak amp.	Peak time	Ratio pnBlood		Protein name	sTBI	$mTBI_C$	$mTBI_S$	Trauma	Peak amp.	Peak time	Ratio pnBlood
1	FAS-L	-	Yes	Yes	No	↗	↘	↘	53	E-selectin	Yes	Yes	Yes	No	-	↘	↘
2	VEGFR2	-	Yes	Yes	No	↗	↗	↘	54	GFAP	Yes	Yes	Yes	No	↗	-	-
3	IL-2	-	Yes	Yes	Yes	-	-	↘	55	HAI-1	Yes	Yes	Yes	No	↗	-	↘
4	FGF-1	Yes	-	-	-	↘	↗	-	56	HE4	Yes	Yes	Yes	No	-	↘	-
5	IL-6	Yes	-	-	-	↘	↗	-	57	HMGB1	Yes	Yes	Yes	No	-	-	↘
6	SCGN	Yes	-	-	-	↘	↗	-	58	IL-1β	Yes	Yes	Yes	No	-	-	-
7	AHSG	Yes	No	No	No	↘	↗	-	59	PRL	Yes	Yes	Yes	No	-	↘	-
8	BMP2	Yes	No	No	No	↘	↗	-	60	S100B	Yes	Yes	Yes	No	↗	↘	-
9	BRAF	Yes	No	No	No	↘	↗	-	61	AFP	Yes	Yes	Yes	Yes	↗	-	-
10	CCL5	Yes	No	No	No	↘	↗	-	62	Ang1	Yes	Yes	Yes	Yes	-	-	-
11	Flt-3	Yes	No	No	No	↘	↗	-	63	BDNF	Yes	Yes	Yes	Yes	-	-	-
12	IL-15	Yes	No	No	No	↘	↗	-	64	CA15-3	Yes	Yes	Yes	Yes	↗	-	-
13	PSA	Yes	No	No	No	↘	↗	-	65	CD14	Yes	Yes	Yes	Yes	-	-	-
14	TF	Yes	No	No	No	↘	↗	-	66	c-Kit	Yes	Yes	Yes	Yes	-	-	-
15	HER3	Yes	No	No	Yes	-	-	-	67	CRP	Yes	Yes	Yes	Yes	-	-	-
16	MCP1	Yes	No	No	Yes	-	-	-	68	E-cadherin	Yes	Yes	Yes	Yes	-	-	-
17	Cathepsin B	Yes	No	Yes	Yes	-	-	↗	69	EGF	Yes	Yes	Yes	Yes	-	↗	-
18	Amphiregulin	Yes	Yes	No	No	↘	↗	-	70	EGF-R	Yes	Yes	Yes	Yes	-	-	-
19	Ang2	Yes	Yes	No	No	-	↘	-	71	Endoglin	Yes	Yes	Yes	Yes	-	-	-
20	β-NGF	Yes	Yes	No	No	↘	↗	-	72	FAS	Yes	Yes	Yes	Yes	-	-	-
21	CEA	Yes	Yes	No	No	-	↘	-	73	FGFb	Yes	Yes	Yes	Yes	-	-	-
22	CXCL12	Yes	Yes	No	No	↘	↘	-	74	HGF	Yes	Yes	Yes	Yes	-	-	-
23	EpCAM	Yes	Yes	No	No	↘	↗	-	75	HGF-R	Yes	Yes	Yes	Yes	-	-	-
24	G-CSF	Yes	Yes	No	No	↘	↗	-	76	HP	Yes	Yes	Yes	Yes	-	-	↗
25	GM-CSF	Yes	Yes	No	No	↘	-	-	77	ICAM-1	Yes	Yes	Yes	Yes	-	-	-
26	GRO-α	Yes	Yes	No	No	↘	↗	-	78	IGFBP-1	Yes	Yes	Yes	Yes	-	-	-
27	IFN-γ	Yes	Yes	No	No	↘	↘	-	79	IGFBP-3	Yes	Yes	Yes	Yes	-	-	-
28	IL-10	Yes	Yes	No	No	↘	↗	-	80	IGFBP-7	Yes	Yes	Yes	Yes	-	-	-
29	IL-12	Yes	Yes	No	No	↘	↗	-	81	IL-18	Yes	Yes	Yes	Yes	-	-	-
30	IL-3	Yes	Yes	No	No	↘	↗	-	82	IL-1ra	Yes	Yes	Yes	Yes	-	-	-
31	IL-7	Yes	Yes	No	No	↘	↗	-	83	IL-5	Yes	Yes	Yes	Yes	↗	-	-
32	IL-8	Yes	Yes	No	No	↘	↗	-	84	IP-10	Yes	Yes	Yes	Yes	-	-	-
33	Leptin	Yes	Yes	No	No	-	↗	-	85	KLK8	Yes	Yes	Yes	Yes	↗	-	-
34	MCP2	Yes	Yes	No	No	↘	↗	-	86	MMP-1	Yes	Yes	Yes	Yes	-	-	-
35	MCP3	Yes	Yes	No	No	↘	-	-	87	MMP-3	Yes	Yes	Yes	Yes	-	-	-
36	MCP4	Yes	Yes	No	No	↘	↗	-	88	MMP-9	Yes	Yes	Yes	Yes	-	-	-
37	M-CSF	Yes	Yes	No	No	↘	↗	-	89	NCAM-1	Yes	Yes	Yes	Yes	-	-	-
38	MIG	Yes	Yes	No	No	↘	↗	-	90	OPN	Yes	Yes	Yes	Yes	-	-	-
39	NT-3	Yes	Yes	No	No	↘	↗	-	91	PAI-1	Yes	Yes	Yes	Yes	-	-	↘
40	TGF-α	Yes	Yes	No	No	↘	↘	-	92	PDGF-BB	Yes	Yes	Yes	Yes	-	-	-
41	TGF-β RII	Yes	Yes	No	No	↘	↘	-	93	RBP4	Yes	Yes	Yes	Yes	-	-	-
42	TGF-β2	Yes	Yes	No	No	↘	↗	-	94	SPARC	Yes	Yes	Yes	Yes	-	-	-
43	TNF-α	Yes	Yes	No	No	↘	↘	-	95	TGF-β1	Yes	Yes	Yes	Yes	-	-	↗
44	uPA-R	Yes	Yes	No	No	↘	↘	-	96	THBS-1	Yes	Yes	Yes	Yes	-	-	-
45	VEGF-D	Yes	Yes	No	No	-	↗	-	97	Tie-2	Yes	Yes	Yes	Yes	-	-	-
46	HER2	Yes	Yes	No	Yes	-	-	-	98	TIMP-1	Yes	Yes	Yes	Yes	-	-	-
47	IL-4	Yes	Yes	No	Yes	-	-	-	99	TNF-RI	Yes	Yes	Yes	Yes	-	-	-
48	KLK14	Yes	Yes	No	Yes	-	-	-	100	TNF-RII	Yes	Yes	Yes	Yes	-	-	-
49	MIP-1α	Yes	Yes	No	Yes	-	-	-	101	uPA	Yes	Yes	Yes	Yes	-	-	-
50	MIP-1β	Yes	Yes	No	Yes	-	-	-	102	VCAM-1	Yes	Yes	Yes	Yes	-	↘	-
51	VEGFR3	Yes	Yes	No	Yes	-	-	-	103	VEGF-A	Yes	Yes	Yes	Yes	-	↗	-
52	ALDH1L1	Yes	Yes	Yes	No	-	-	-									

APPENDIX G

Comparison of microdialysis additives: Matrix effect of additives

This appendix is a supplementary material to chapter chapter 5 that describes the effect of additives on the measurement of 94 proteins.

Effect of additives on the measurement of protein measurements

Electronic Supplementary Material

Comparison of bovine serum albumin, low- and high-molecular weight dextrans as additives to brain microdialysis

Veronique Laforte, Francesco Fiorini, David KY Zhang, Judith Marcoux and David Juncker

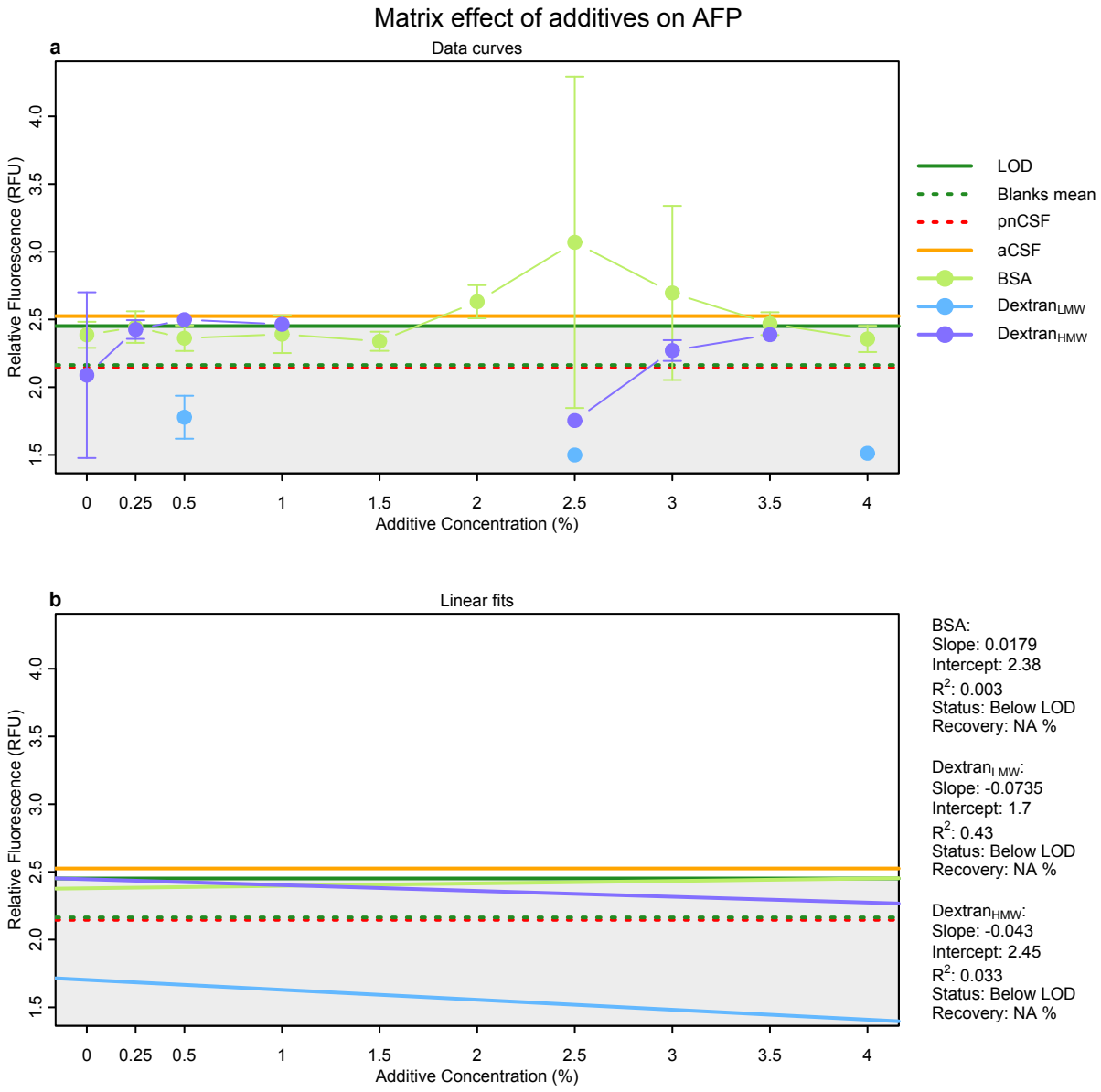

FIGURE G.S1: **Effect of additives on the measurement of AFP.** pnCSF mixed 0-4 % additives diluted in aCSF were measured using the ACM, in order to measure the possible interference of additives on the protein measurement (matrix effect). Linear regressions of measured calibrated fluorescence values of AFP were used to calculate the recovery at concentrations of additives used in cerebral microdialysis. **a** Data from the average of three independent replicates is shown. **b** Median-based linear regressions from the data in **a**.

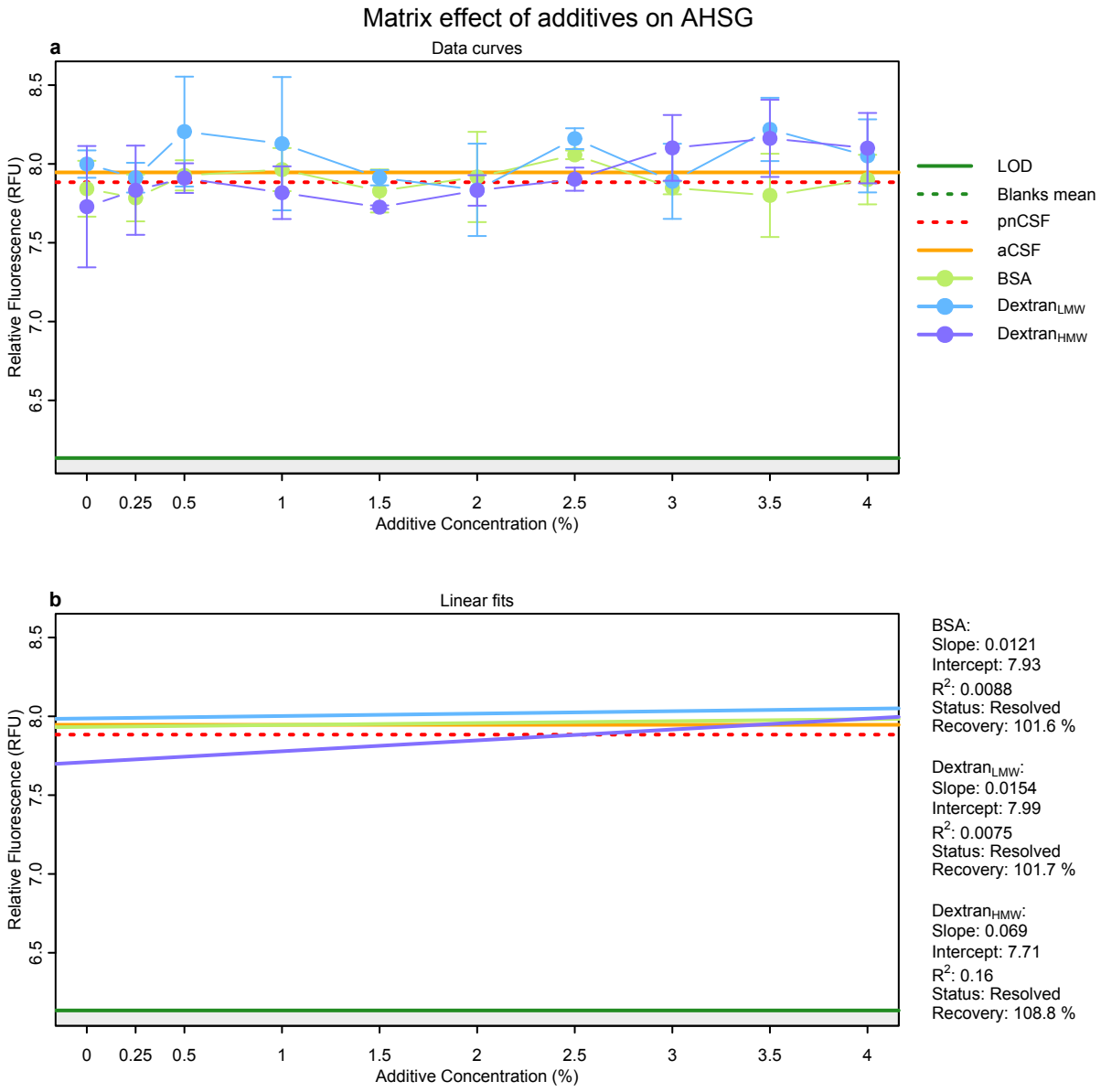

FIGURE G.S2: **Effect of additives on the measurement of AHSG.** pnCSF mixed 0-4 % additives diluted in aCSF were measured using the ACM, in order to measure the possible interference of additives on the protein measurement (matrix effect). Linear regressions of measured calibrated fluorescence values of AHSG were used to calculate the recovery at concentrations of additives used in cerebral microdialysis. **a** Data from the average of three independent replicates is shown. **b** Median-based linear regressions from the data in **a**.

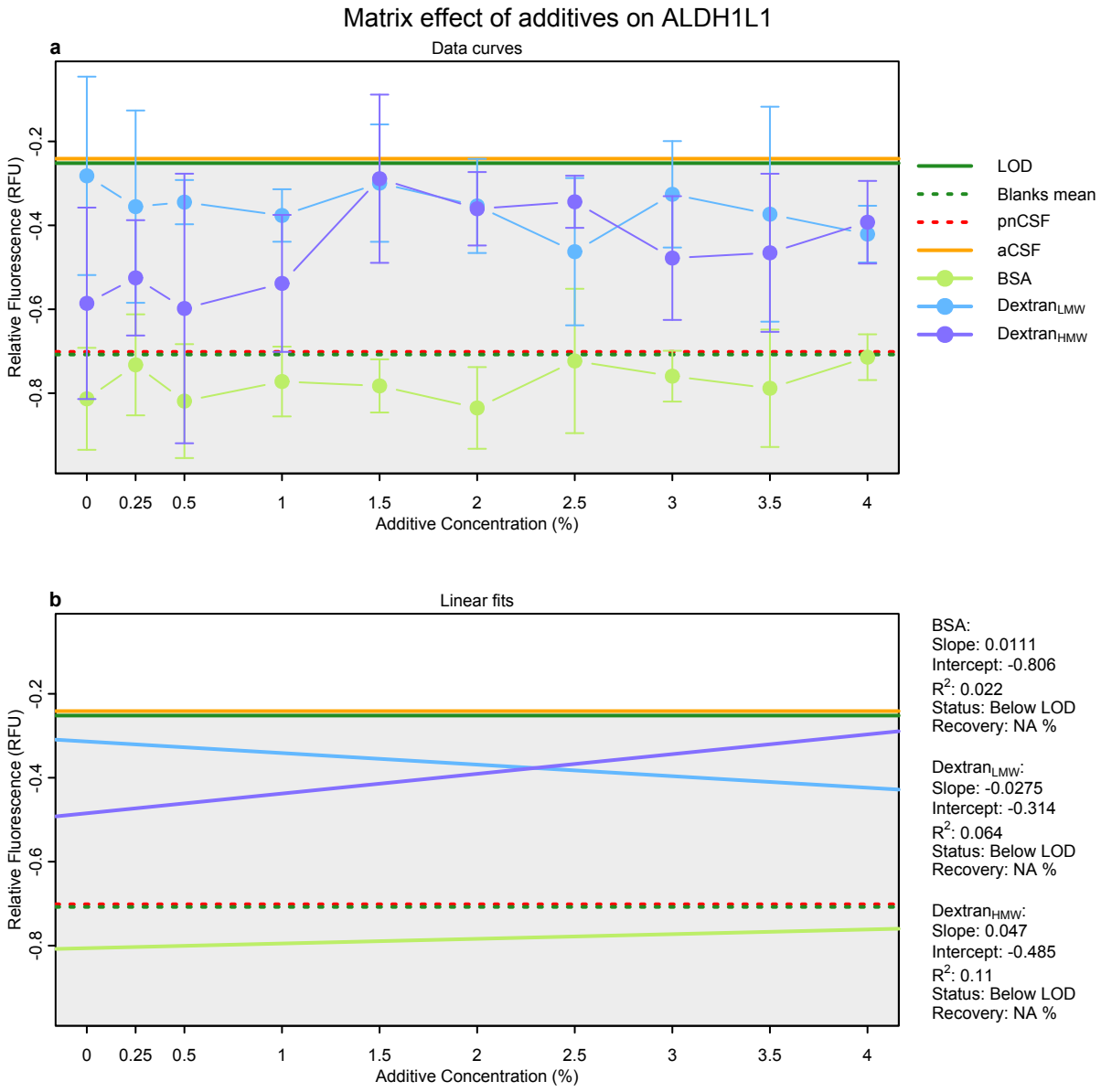

FIGURE G.S3: **Effect of additives on the measurement of ALDH1L1.** pnCSF mixed 0-4 % additives diluted in aCSF were measured using the ACM, in order to measure the possible interference of additives on the protein measurement (matrix effect). Linear regressions of measured calibrated fluorescence values of ALDH1L1 were used to calculate the recovery at concentrations of additives used in cerebral microdialysis. **a** Data from the average of three independent replicates is shown. **b** Median-based linear regressions from the data in **a**.

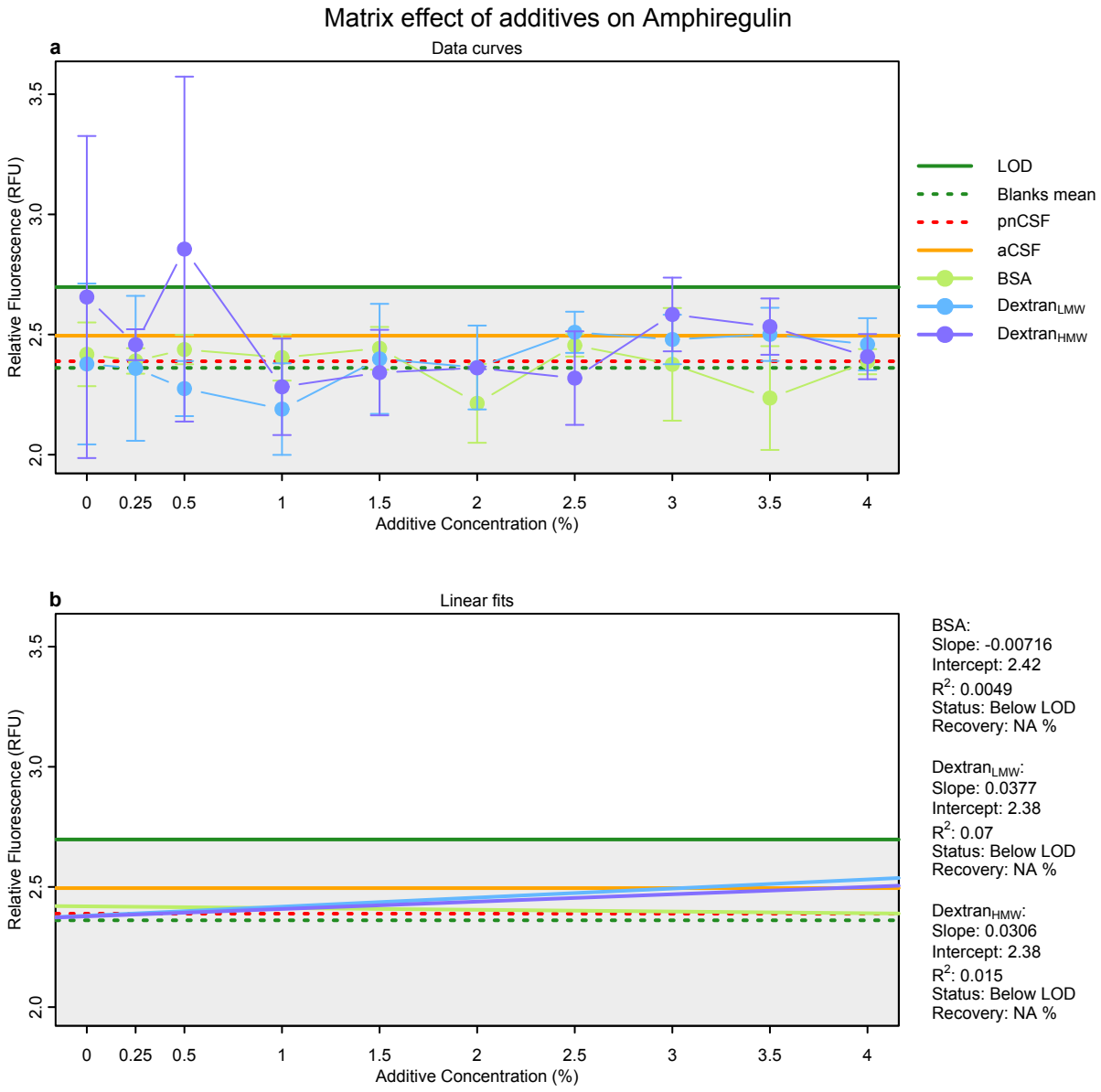

FIGURE G.S4: **Effect of additives on the measurement of Amphiregulin.** pnCSF mixed 0-4 % additives diluted in aCSF were measured using the ACM, in order to measure the possible interference of additives on the protein measurement (matrix effect). Linear regressions of measured calibrated fluorescence values of Amphiregulin were used to calculate the recovery at concentrations of additives used in cerebral microdialysis. **a** Data from the average of three independent replicates is shown. **b** Median-based linear regressions from the data in **a**.

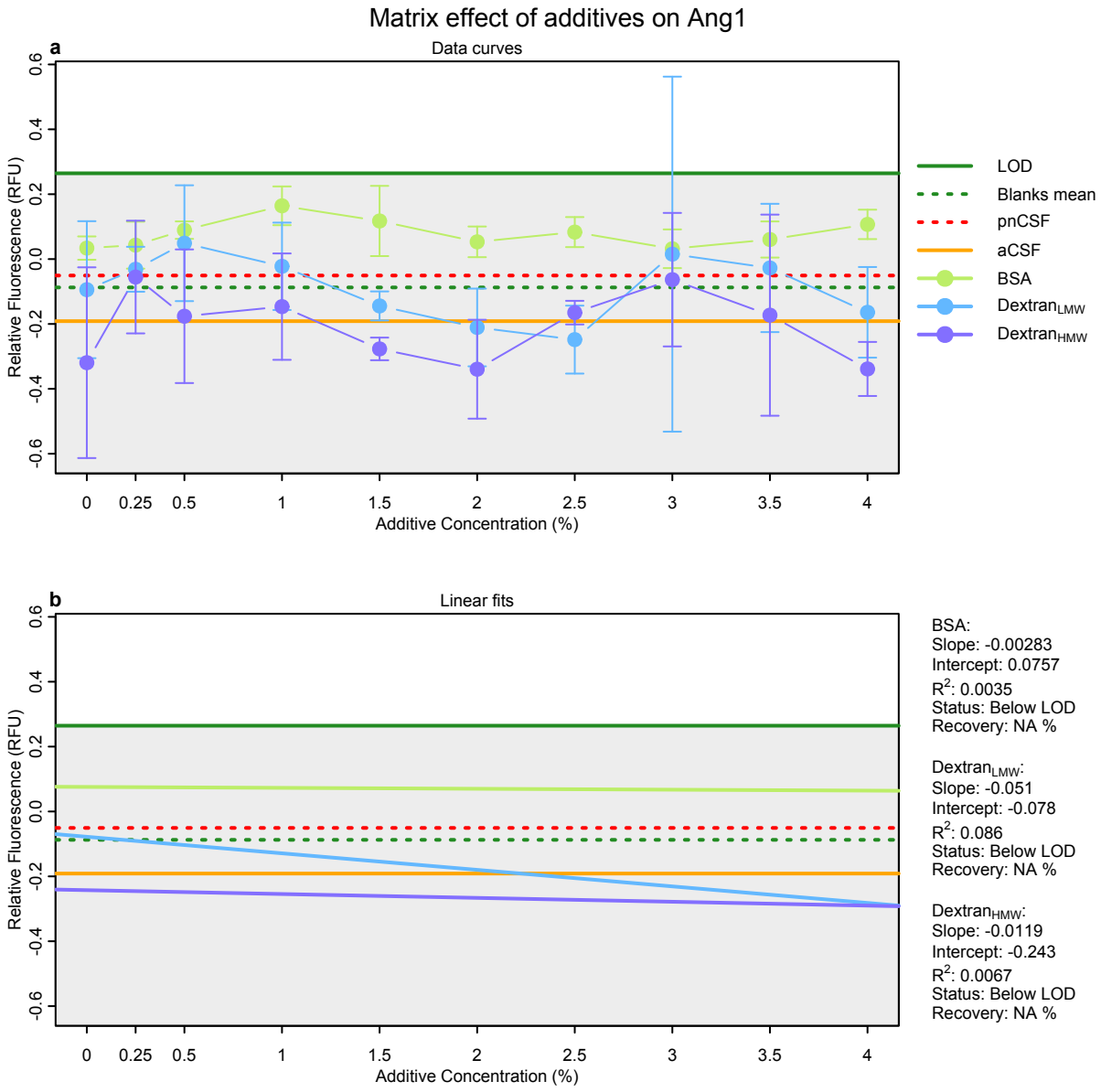

FIGURE G.S5: **Effect of additives on the measurement of Ang1.** pnCSF mixed 0-4 % additives diluted in aCSF were measured using the ACM, in order to measure the possible interference of additives on the protein measurement (matrix effect). Linear regressions of measured calibrated fluorescence values of Ang1 were used to calculate the recovery at concentrations of additives used in cerebral microdialysis. **a** Data from the average of three independent replicates is shown. **b** Median-based linear regressions from the data in **a**.

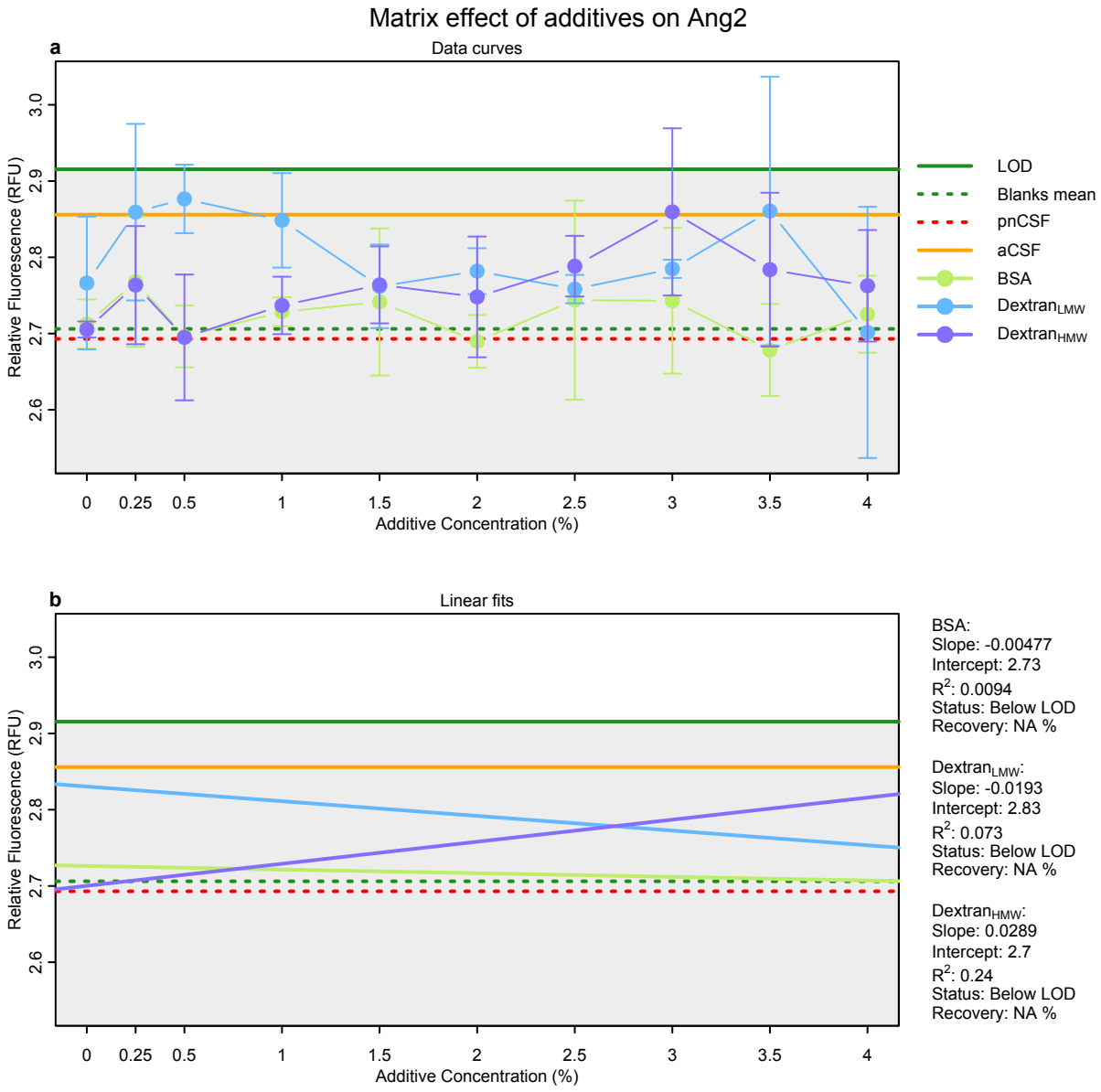

FIGURE G.S6: **Effect of additives on the measurement of Ang2.** pnCSF mixed 0-4 % additives diluted in aCSF were measured using the ACM, in order to measure the possible interference of additives on the protein measurement (matrix effect). Linear regressions of measured calibrated fluorescence values of Ang2 were used to calculate the recovery at concentrations of additives used in cerebral microdialysis. **a** Data from the average of three independent replicates is shown. **b** Median-based linear regressions from the data in **a**.

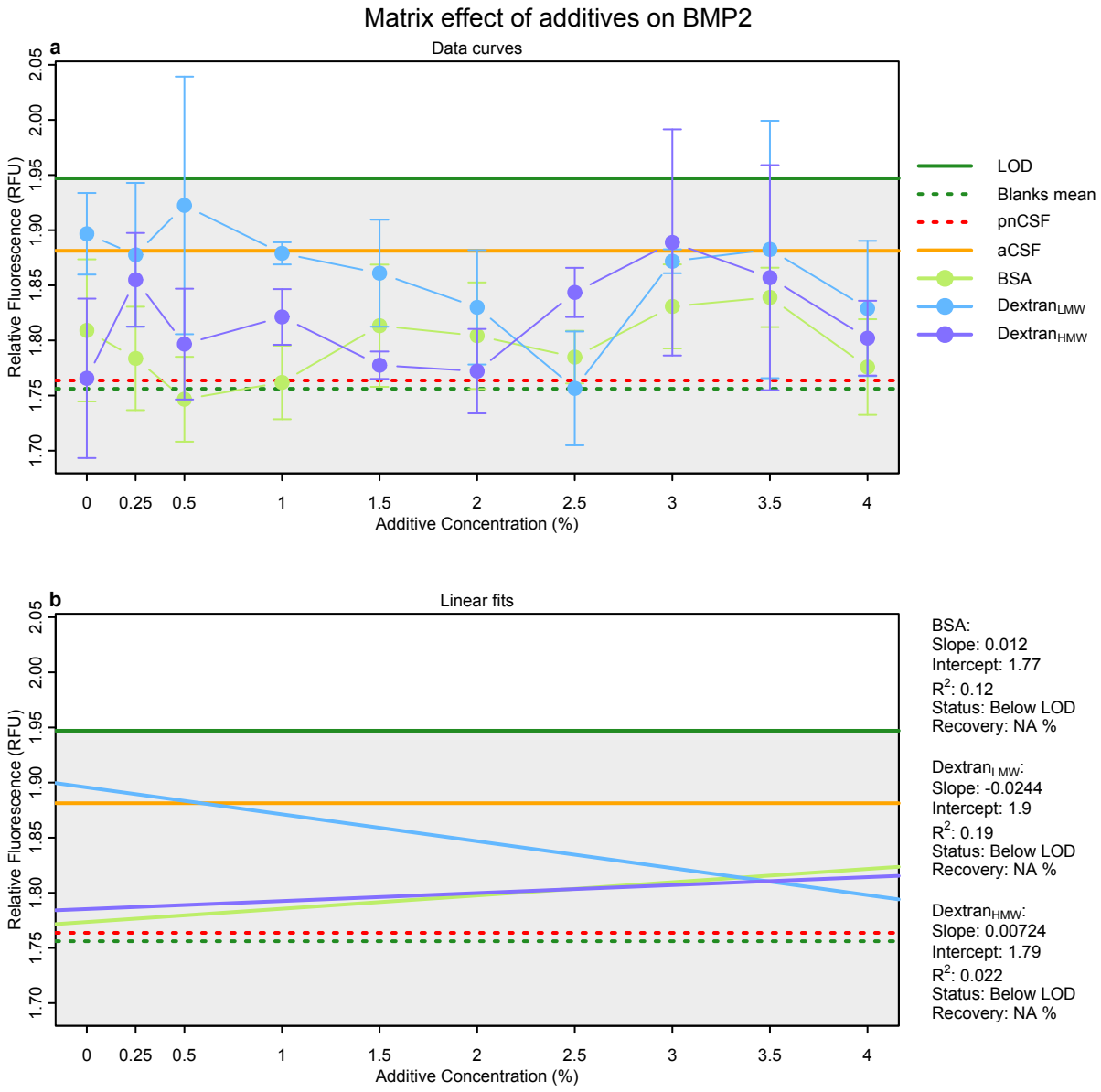

FIGURE G.S7: **Effect of additives on the measurement of BMP2.** pnCSF mixed 0-4 % additives diluted in aCSF were measured using the ACM, in order to measure the possible interference of additives on the protein measurement (matrix effect). Linear regressions of measured calibrated fluorescence values of BMP2 were used to calculate the recovery at concentrations of additives used in cerebral microdialysis. **a** Data from the average of three independent replicates is shown. **b** Median-based linear regressions from the data in **a**.

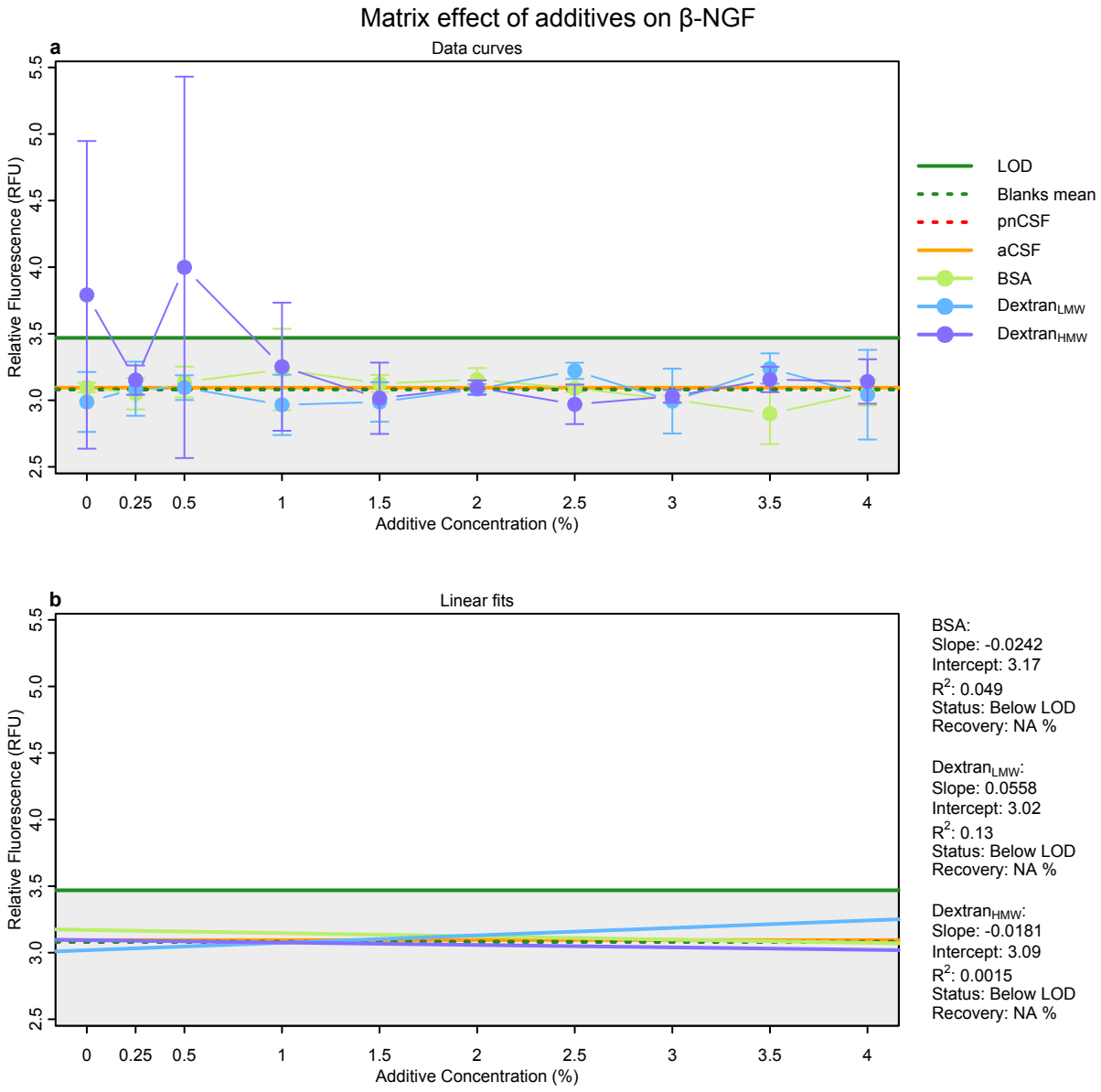

FIGURE G.S8: **Effect of additives on the measurement of β-NGF.** pnCSF mixed 0-4 % additives diluted in aCSF were measured using the ACM, in order to measure the possible interference of additives on the protein measurement (matrix effect). Linear regressions of measured calibrated fluorescence values of β-NGF were used to calculate the recovery at concentrations of additives used in cerebral microdialysis. **a** Data from the average of three independent replicates is shown. **b** Median-based linear regressions from the data in **a**.

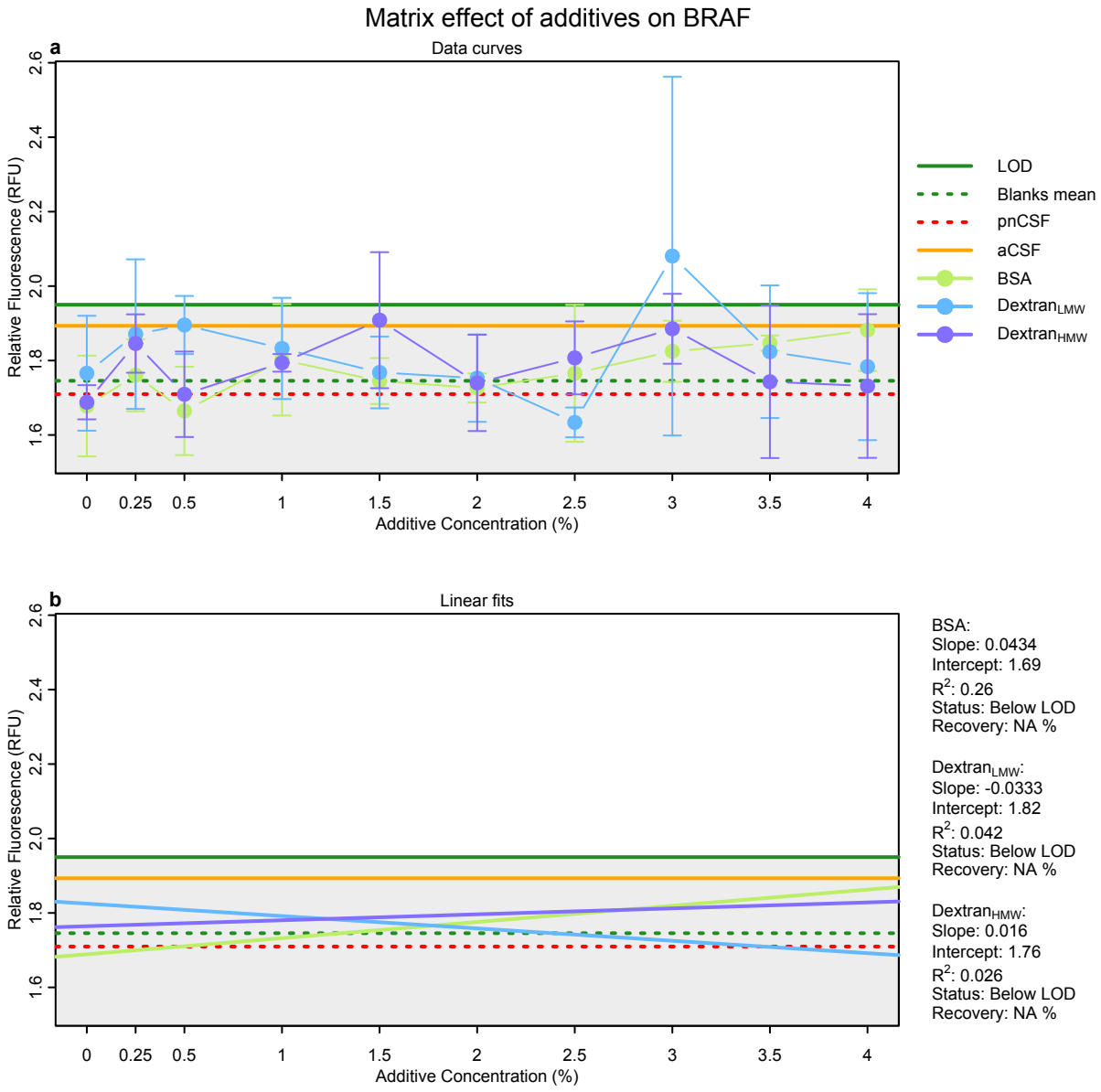

FIGURE G.S9: **Effect of additives on the measurement of BRAF.** pnCSF mixed 0-4 % additives diluted in aCSF were measured using the ACM, in order to measure the possible interference of additives on the protein measurement (matrix effect). Linear regressions of measured calibrated fluorescence values of BRAF were used to calculate the recovery at concentrations of additives used in cerebral microdialysis. **a** Data from the average of three independent replicates is shown. **b** Median-based linear regressions from the data in **a**.

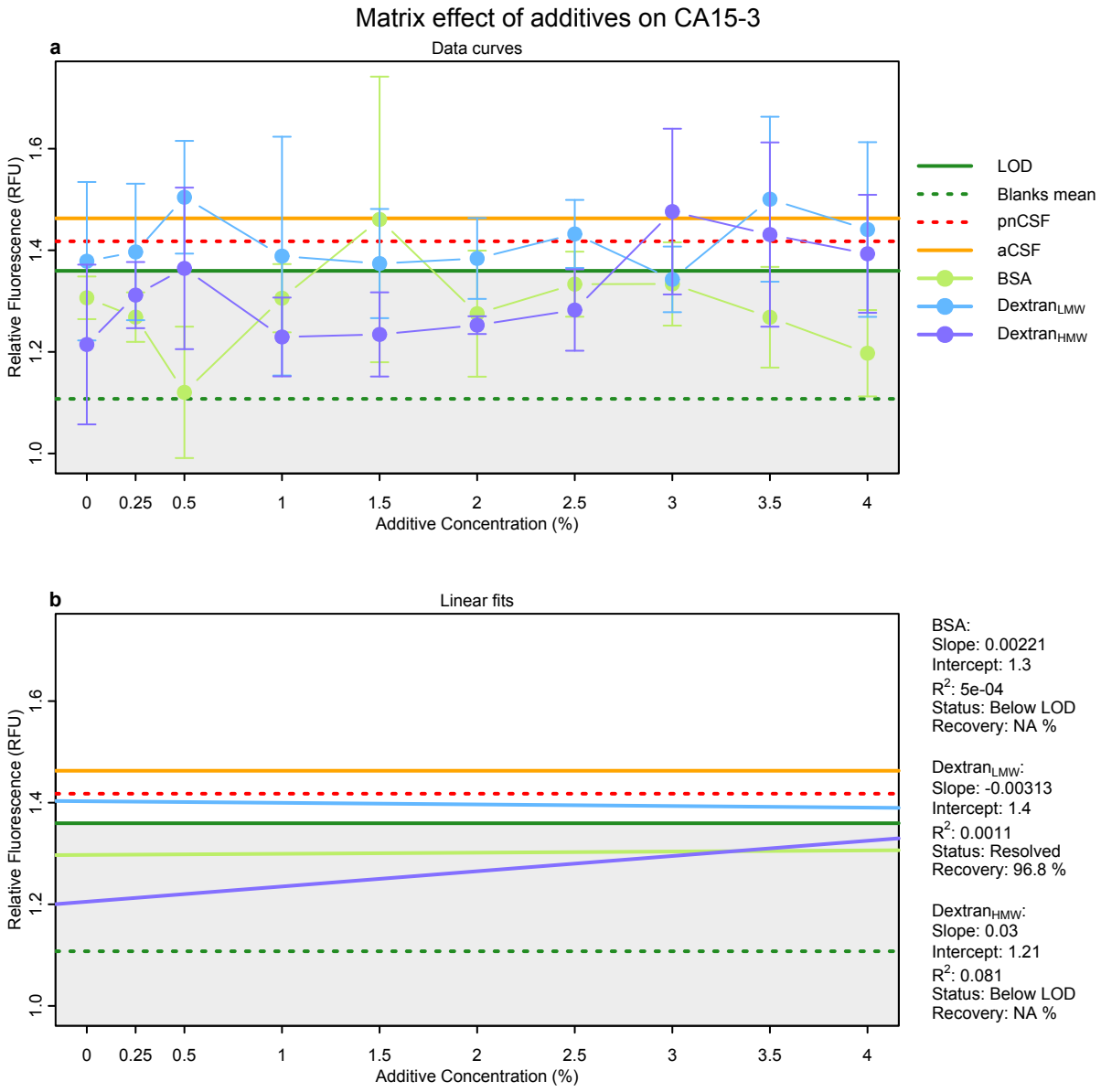

FIGURE G.S10: **Effect of additives on the measurement of CA15-3.** pnCSF mixed 0-4 % additives diluted in aCSF were measured using the ACM, in order to measure the possible interference of additives on the protein measurement (matrix effect). Linear regressions of measured calibrated fluorescence values of CA15-3 were used to calculate the recovery at concentrations of additives used in cerebral microdialysis. **a** Data from the average of three independent replicates is shown. **b** Median-based linear regressions from the data in **a**.

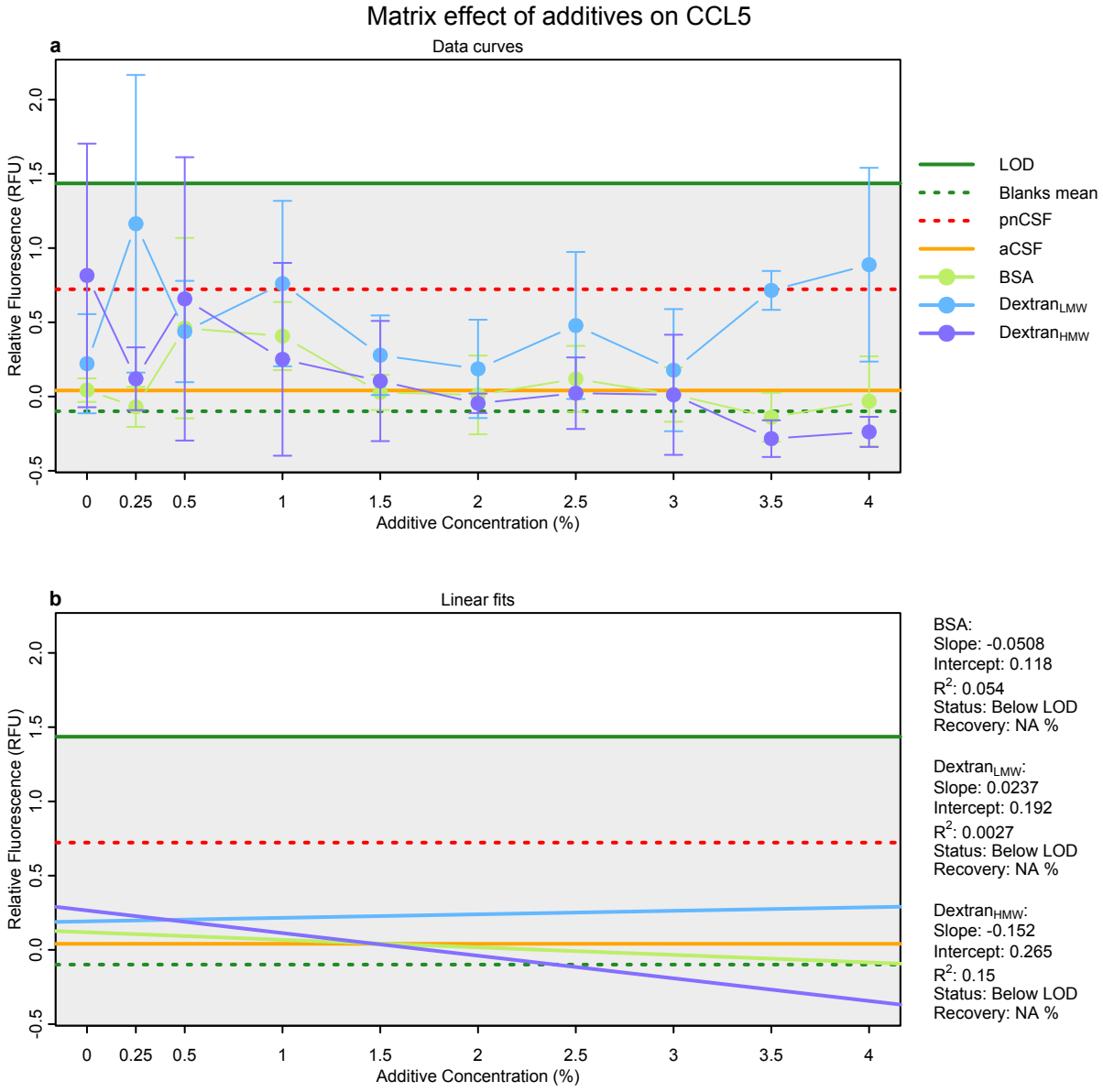

FIGURE G.S11: **Effect of additives on the measurement of CCL5.** pnCSF mixed 0-4 % additives diluted in aCSF were measured using the ACM, in order to measure the possible interference of additives on the protein measurement (matrix effect). Linear regressions of measured calibrated fluorescence values of CCL5 were used to calculate the recovery at concentrations of additives used in cerebral microdialysis. **a** Data from the average of three independent replicates is shown. **b** Median-based linear regressions from the data in **a**.

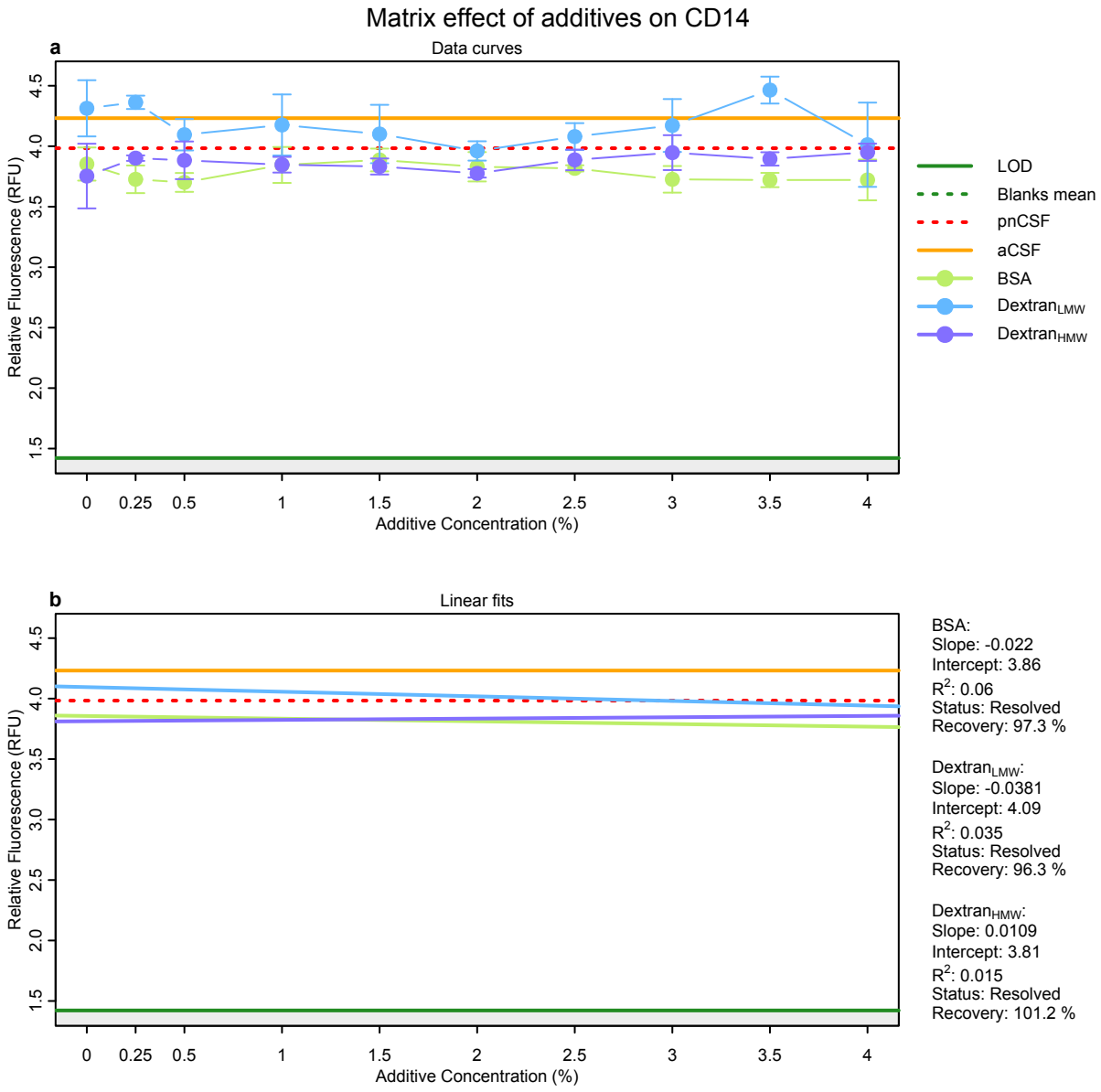

FIGURE G.S12: **Effect of additives on the measurement of CD14.** pnCSF mixed 0-4 % additives diluted in aCSF were measured using the ACM, in order to measure the possible interference of additives on the protein measurement (matrix effect). Linear regressions of measured calibrated fluorescence values of CD14 were used to calculate the recovery at concentrations of additives used in cerebral microdialysis. **a** Data from the average of three independent replicates is shown. **b** Median-based linear regressions from the data in **a**.

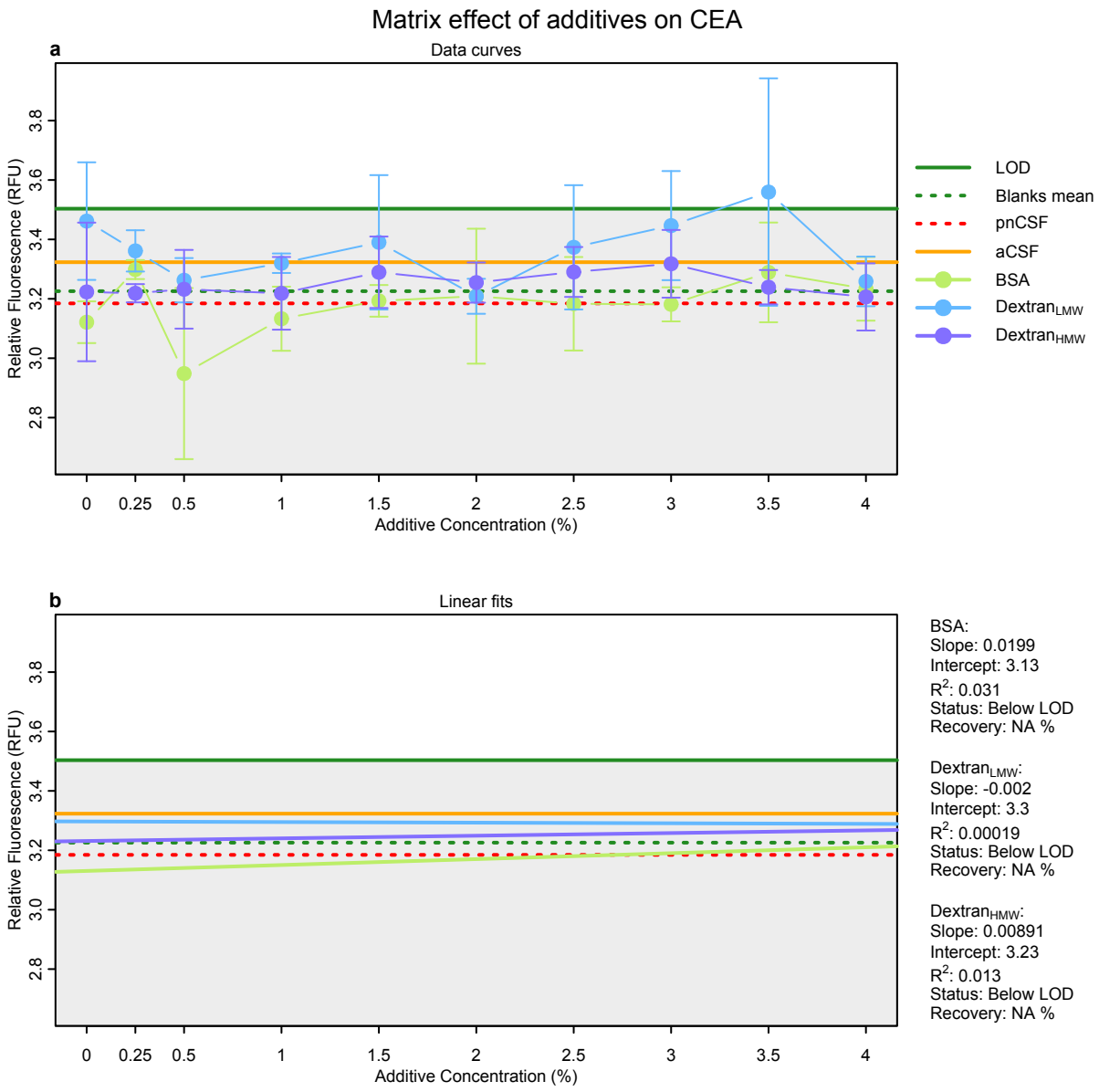

FIGURE G.S13: **Effect of additives on the measurement of CEA.** pnCSF mixed 0-4 % additives diluted in aCSF were measured using the ACM, in order to measure the possible interference of additives on the protein measurement (matrix effect). Linear regressions of measured calibrated fluorescence values of CEA were used to calculate the recovery at concentrations of additives used in cerebral microdialysis. **a** Data from the average of three independent replicates is shown. **b** Median-based linear regressions from the data in **a**.

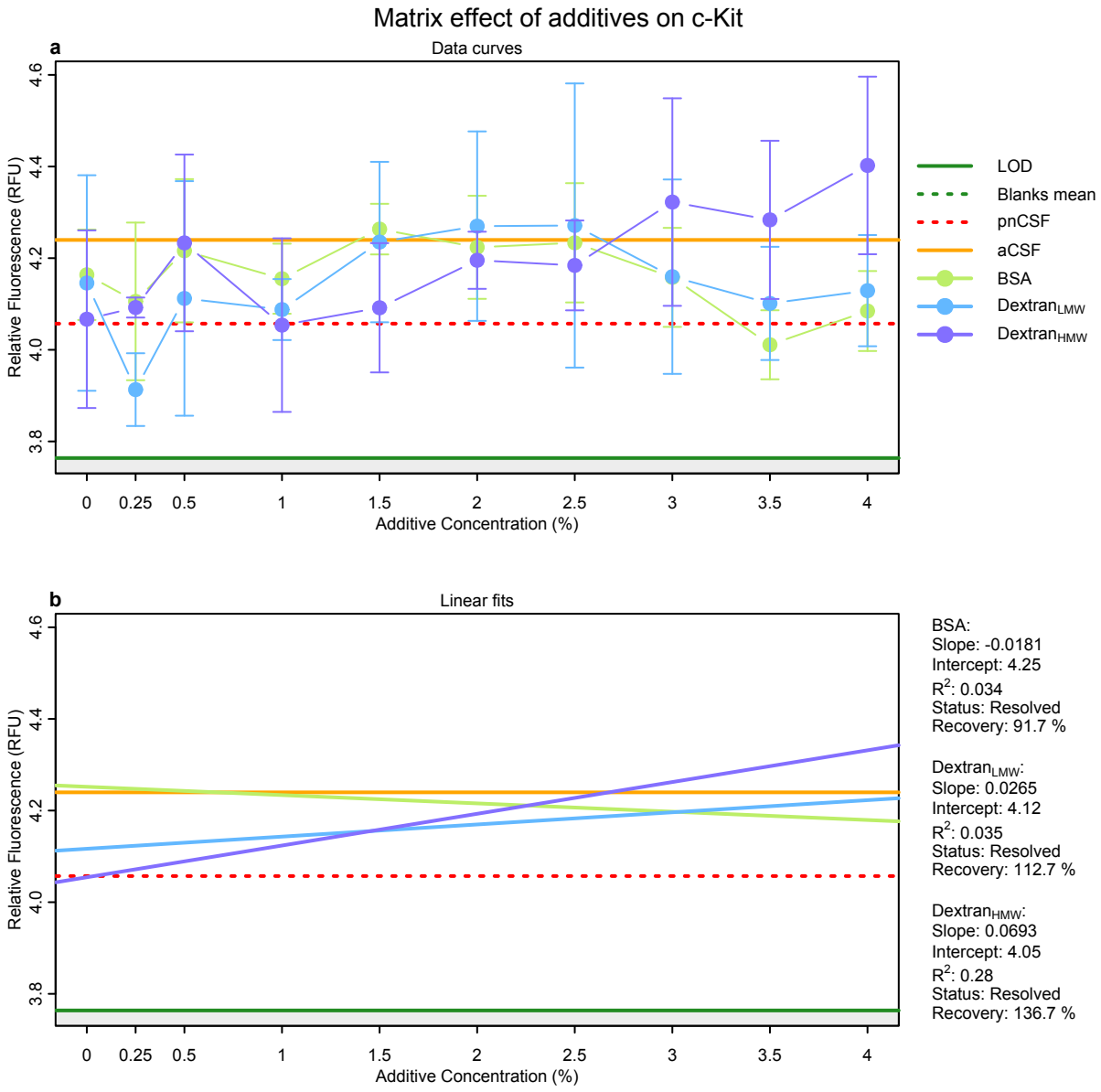

FIGURE G.S14: **Effect of additives on the measurement of c-Kit.** pnCSF mixed 0-4 % additives diluted in aCSF were measured using the ACM, in order to measure the possible interference of additives on the protein measurement (matrix effect). Linear regressions of measured calibrated fluorescence values of c-Kit were used to calculate the recovery at concentrations of additives used in cerebral microdialysis. **a** Data from the average of three independent replicates is shown. **b** Median-based linear regressions from the data in **a**.

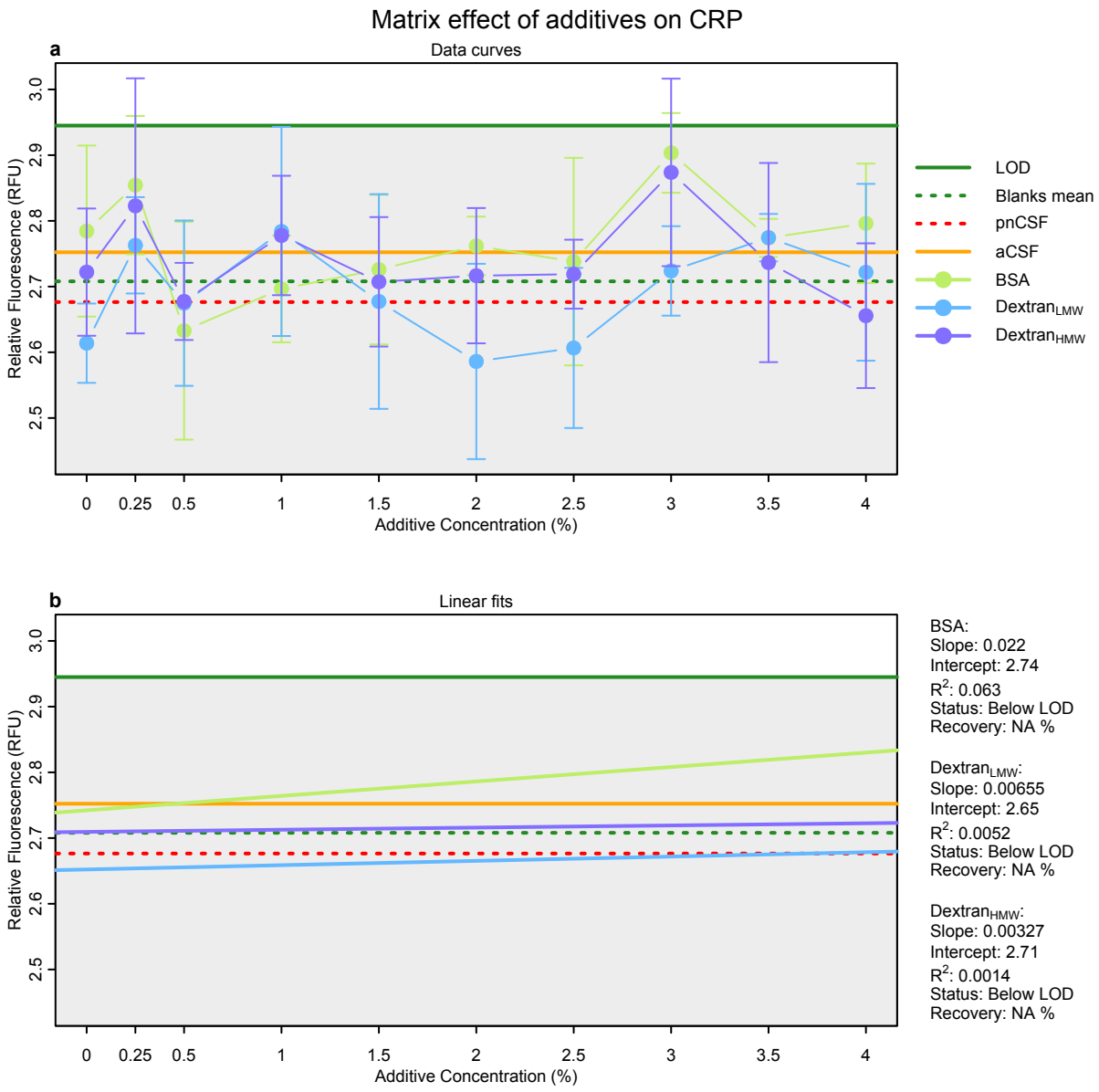

FIGURE G.S15: **Effect of additives on the measurement of CRP.** pnCSF mixed 0-4 % additives diluted in aCSF were measured using the ACM, in order to measure the possible interference of additives on the protein measurement (matrix effect). Linear regressions of measured calibrated fluorescence values of CRP were used to calculate the recovery at concentrations of additives used in cerebral microdialysis. **a** Data from the average of three independent replicates is shown. **b** Median-based linear regressions from the data in **a**.

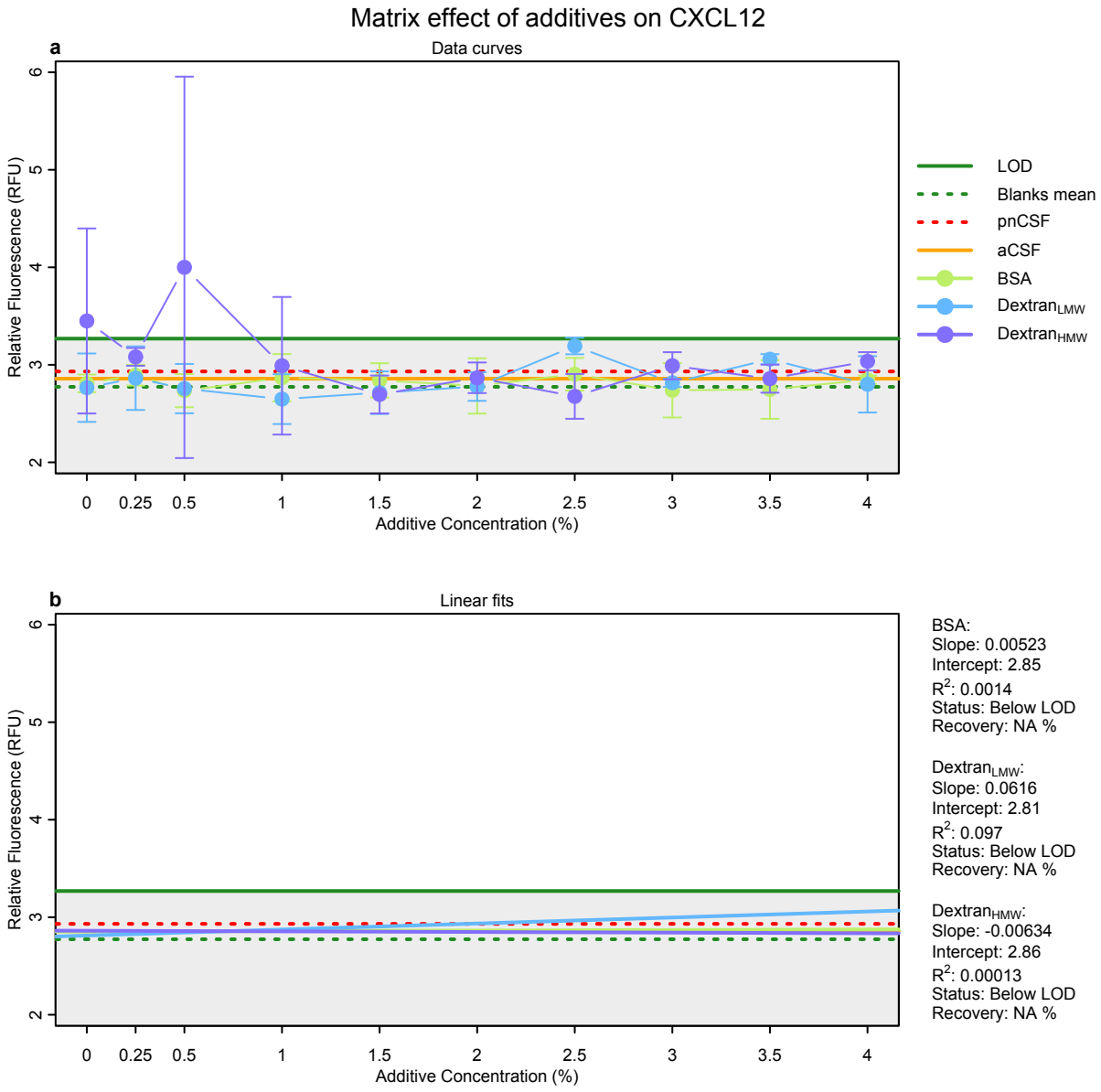

FIGURE G.S16: **Effect of additives on the measurement of CXCL12.** pnCSF mixed 0-4 % additives diluted in aCSF were measured using the ACM, in order to measure the possible interference of additives on the protein measurement (matrix effect). Linear regressions of measured calibrated fluorescence values of CXCL12 were used to calculate the recovery at concentrations of additives used in cerebral microdialysis. **a** Data from the average of three independent replicates is shown. **b** Median-based linear regressions from the data in **a**.

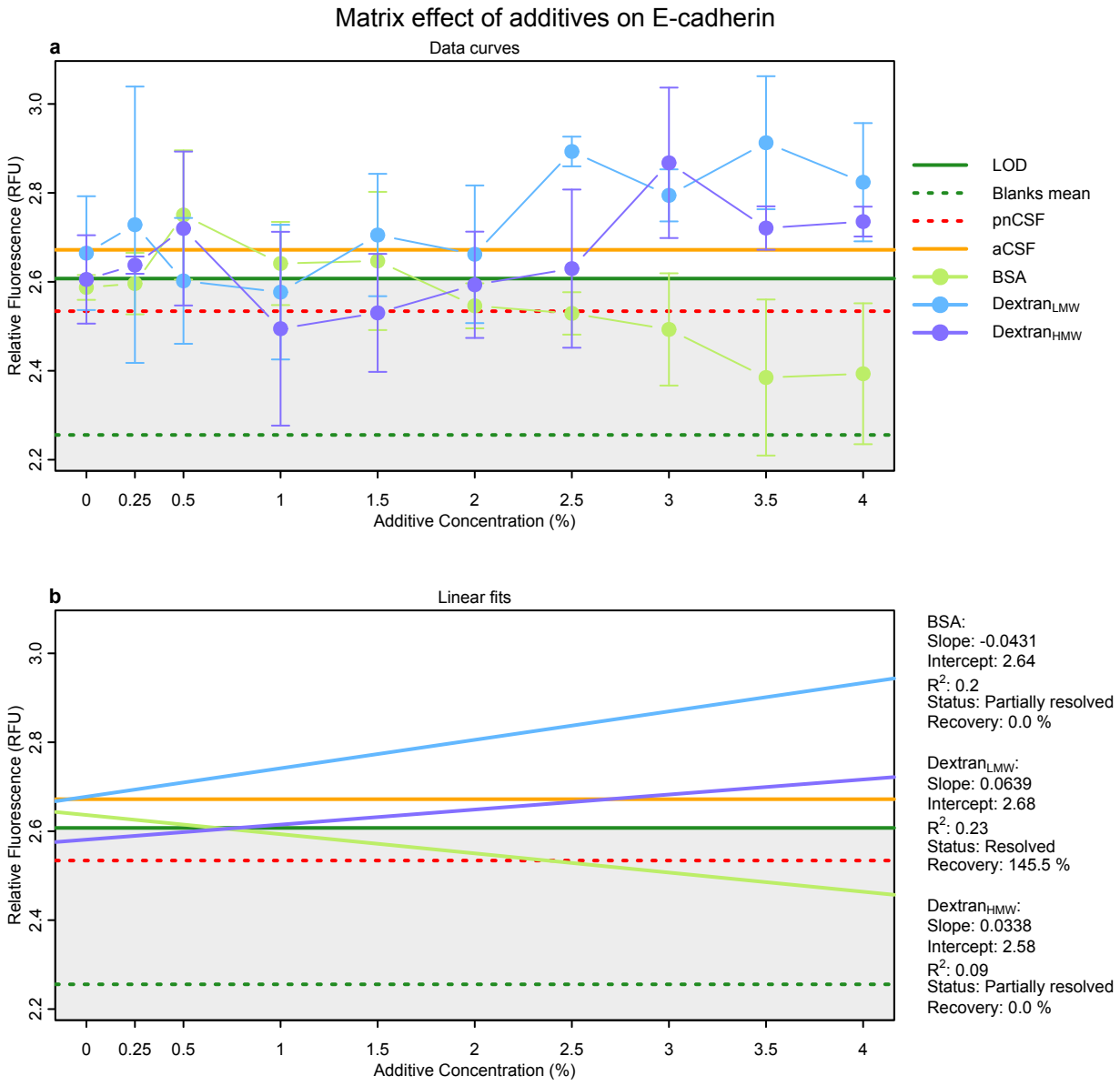

FIGURE G.S17: **Effect of additives on the measurement of E-cadherin.** pnCSF mixed 0-4 % additives diluted in aCSF were measured using the ACM, in order to measure the possible interference of additives on the protein measurement (matrix effect). Linear regressions of measured calibrated fluorescence values of E-cadherin were used to calculate the recovery at concentrations of additives used in cerebral microdialysis. **a** Data from the average of three independent replicates is shown. **b** Median-based linear regressions from the data in **a**.

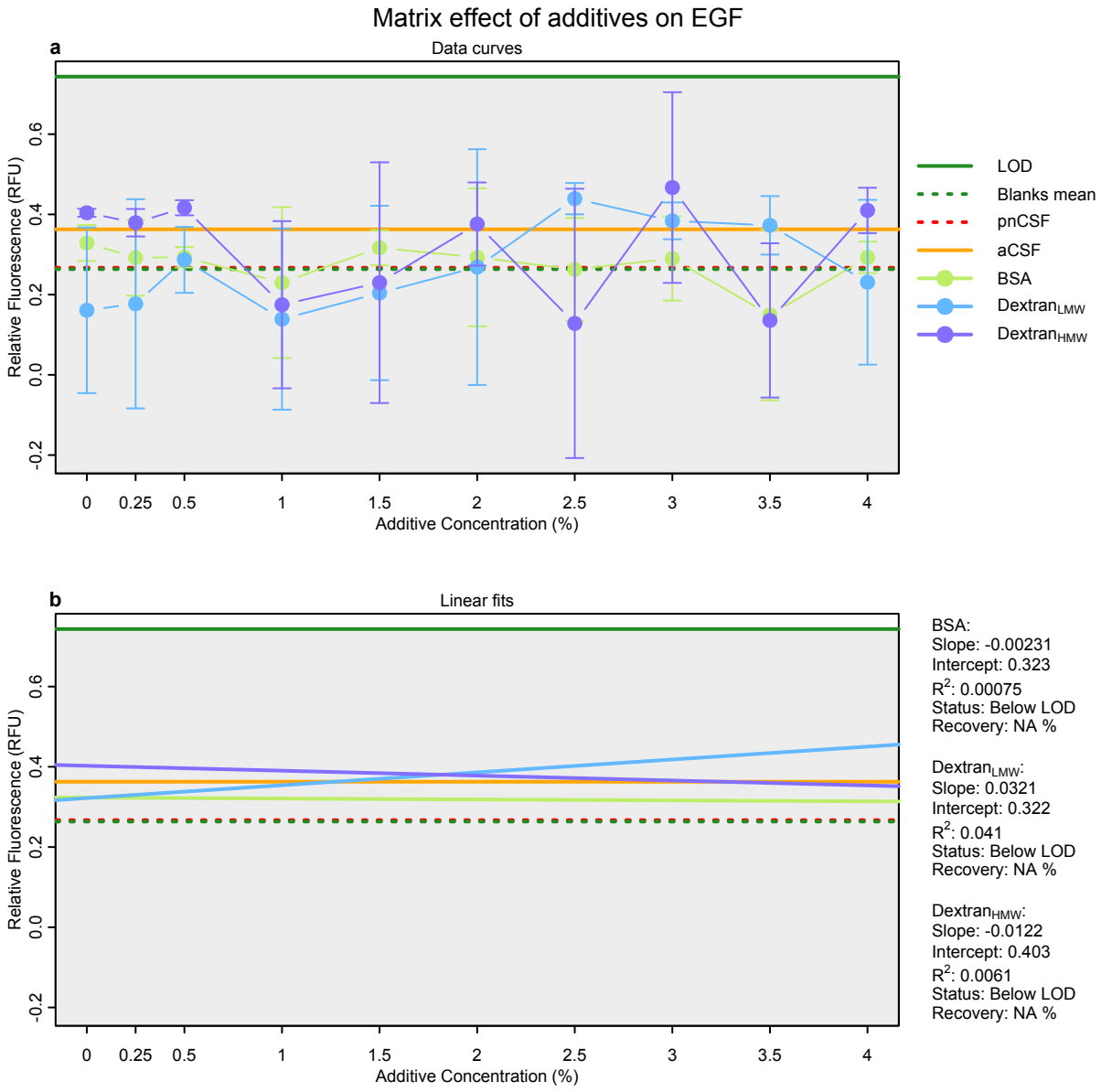

FIGURE G.S18: **Effect of additives on the measurement of EGF.** pnCSF mixed 0-4 % additives diluted in aCSF were measured using the ACM, in order to measure the possible interference of additives on the protein measurement (matrix effect). Linear regressions of measured calibrated fluorescence values of EGF were used to calculate the recovery at concentrations of additives used in cerebral microdialysis. **a** Data from the average of three independent replicates is shown. **b** Median-based linear regressions from the data in **a**.

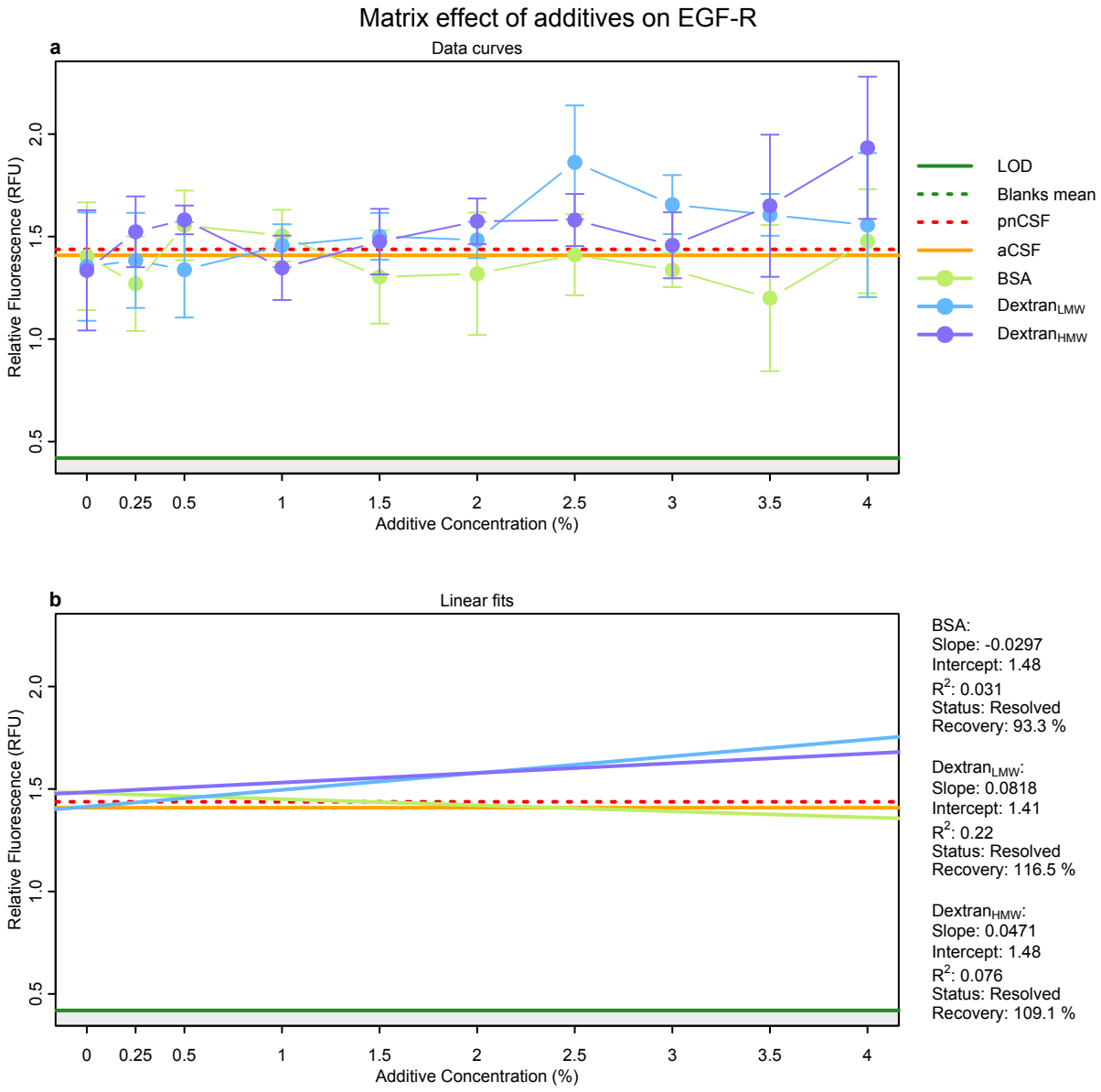

FIGURE G.S19: **Effect of additives on the measurement of EGF-R.** pnCSF mixed 0-4 % additives diluted in aCSF were measured using the ACM, in order to measure the possible interference of additives on the protein measurement (matrix effect). Linear regressions of measured calibrated fluorescence values of EGF-R were used to calculate the recovery at concentrations of additives used in cerebral microdialysis. **a** Data from the average of three independent replicates is shown. **b** Median-based linear regressions from the data in **a**.

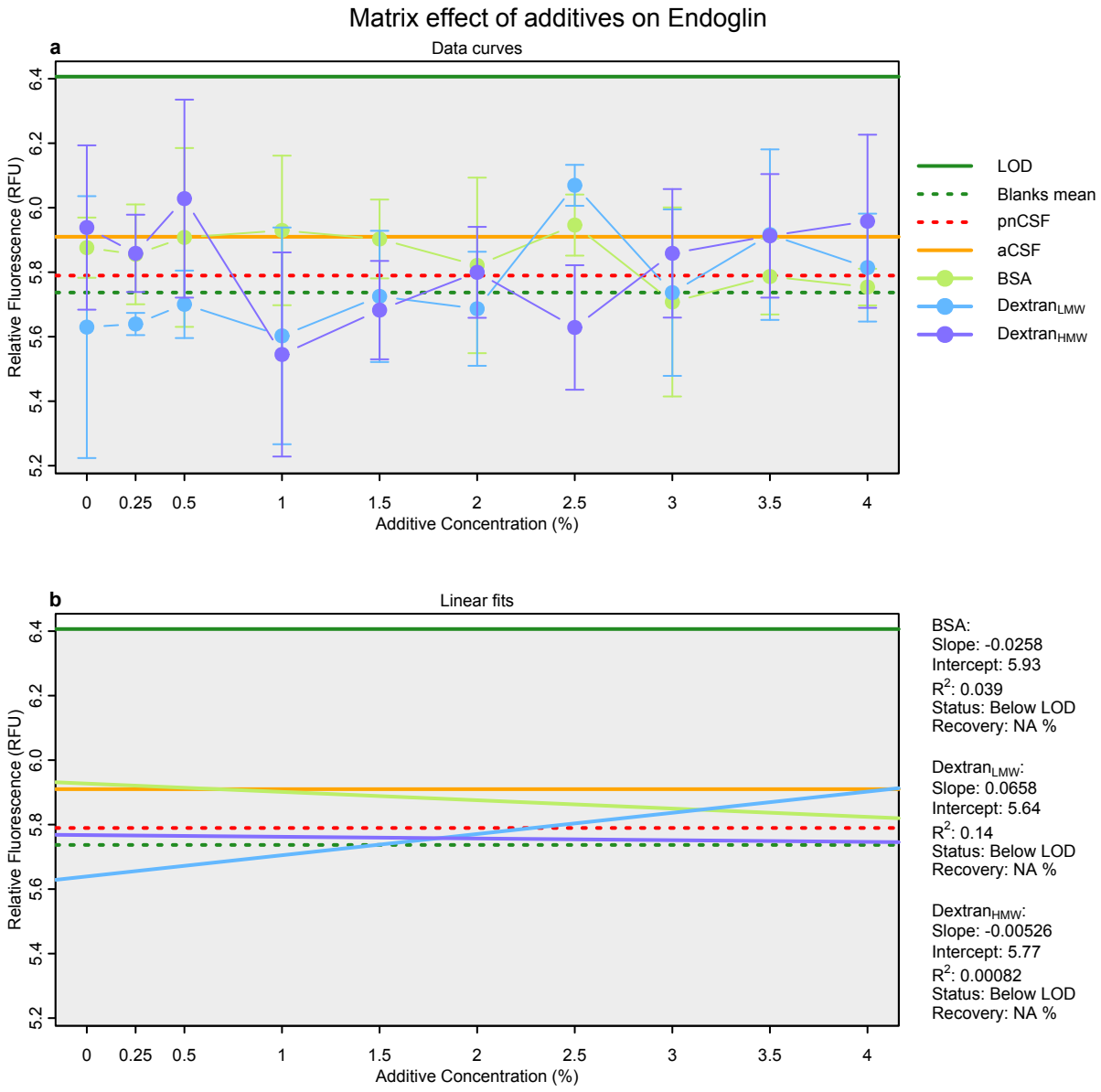

FIGURE G.S20: **Effect of additives on the measurement of Endoglin.** pnCSF mixed 0-4 % additives diluted in aCSF were measured using the ACM, in order to measure the possible interference of additives on the protein measurement (matrix effect). Linear regressions of measured calibrated fluorescence values of Endoglin were used to calculate the recovery at concentrations of additives used in cerebral microdialysis. **a** Data from the average of three independent replicates is shown. **b** Median-based linear regressions from the data in **a**.

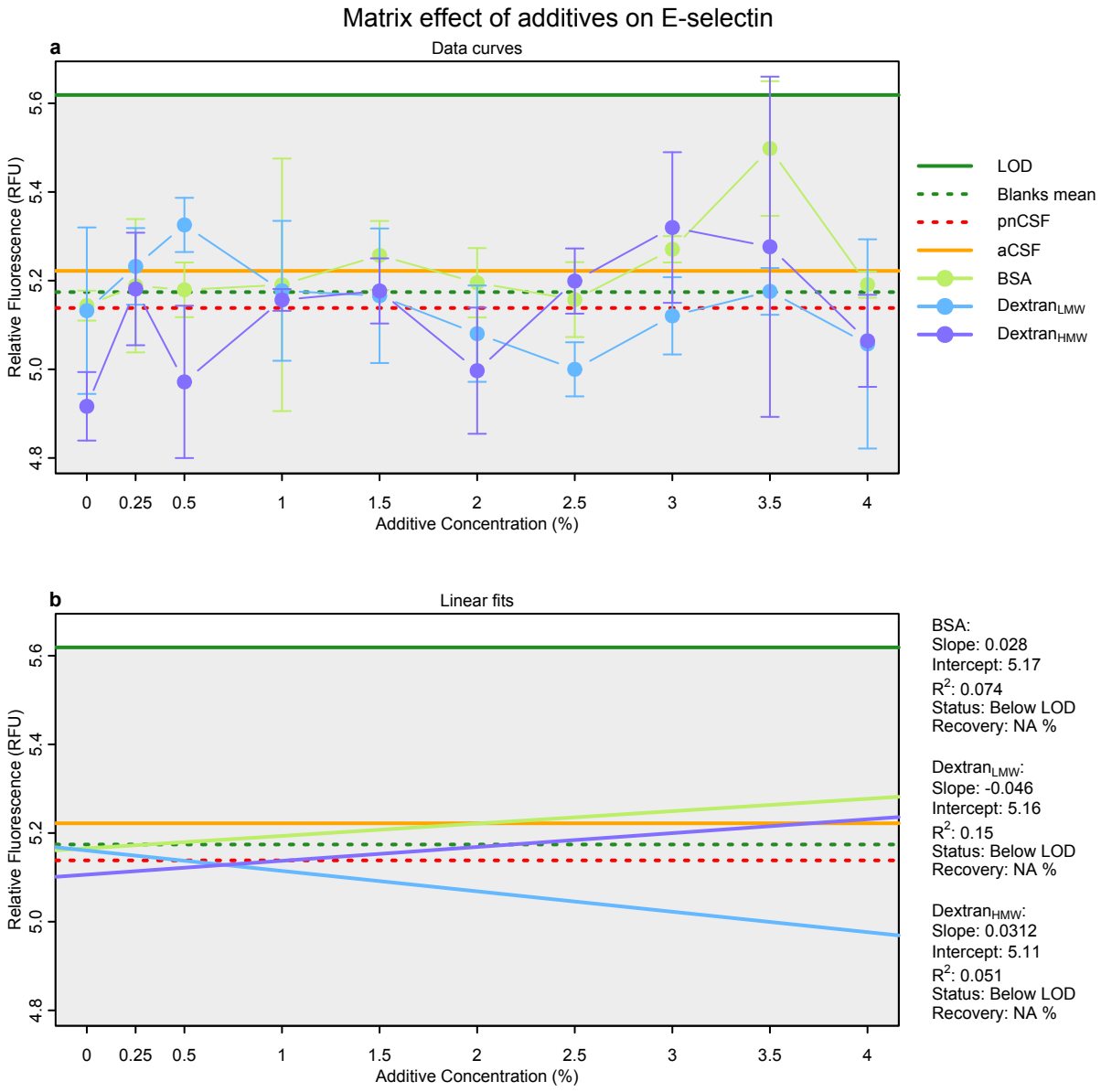

FIGURE G.S21: **Effect of additives on the measurement of E-selectin.** pnCSF mixed 0-4 % additives diluted in aCSF were measured using the ACM, in order to measure the possible interference of additives on the protein measurement (matrix effect). Linear regressions of measured calibrated fluorescence values of E-selectin were used to calculate the recovery at concentrations of additives used in cerebral microdialysis. **a** Data from the average of three independent replicates is shown. **b** Median-based linear regressions from the data in **a**.

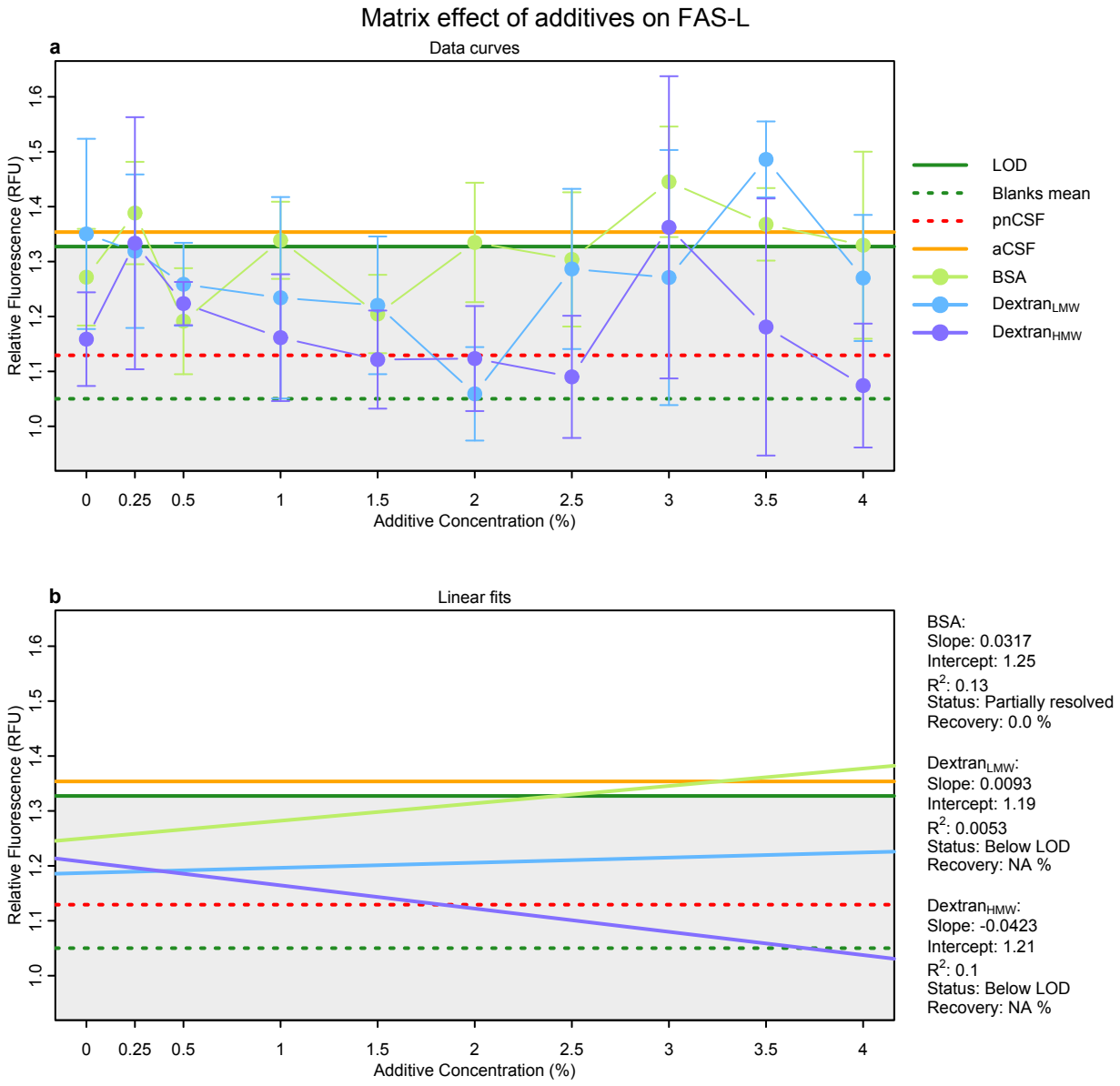

FIGURE G.S22: **Effect of additives on the measurement of FAS-L.** pnCSF mixed 0-4 % additives diluted in aCSF were measured using the ACM, in order to measure the possible interference of additives on the protein measurement (matrix effect). Linear regressions of measured calibrated fluorescence values of FAS-L were used to calculate the recovery at concentrations of additives used in cerebral microdialysis. **a** Data from the average of three independent replicates is shown. **b** Median-based linear regressions from the data in **a**.

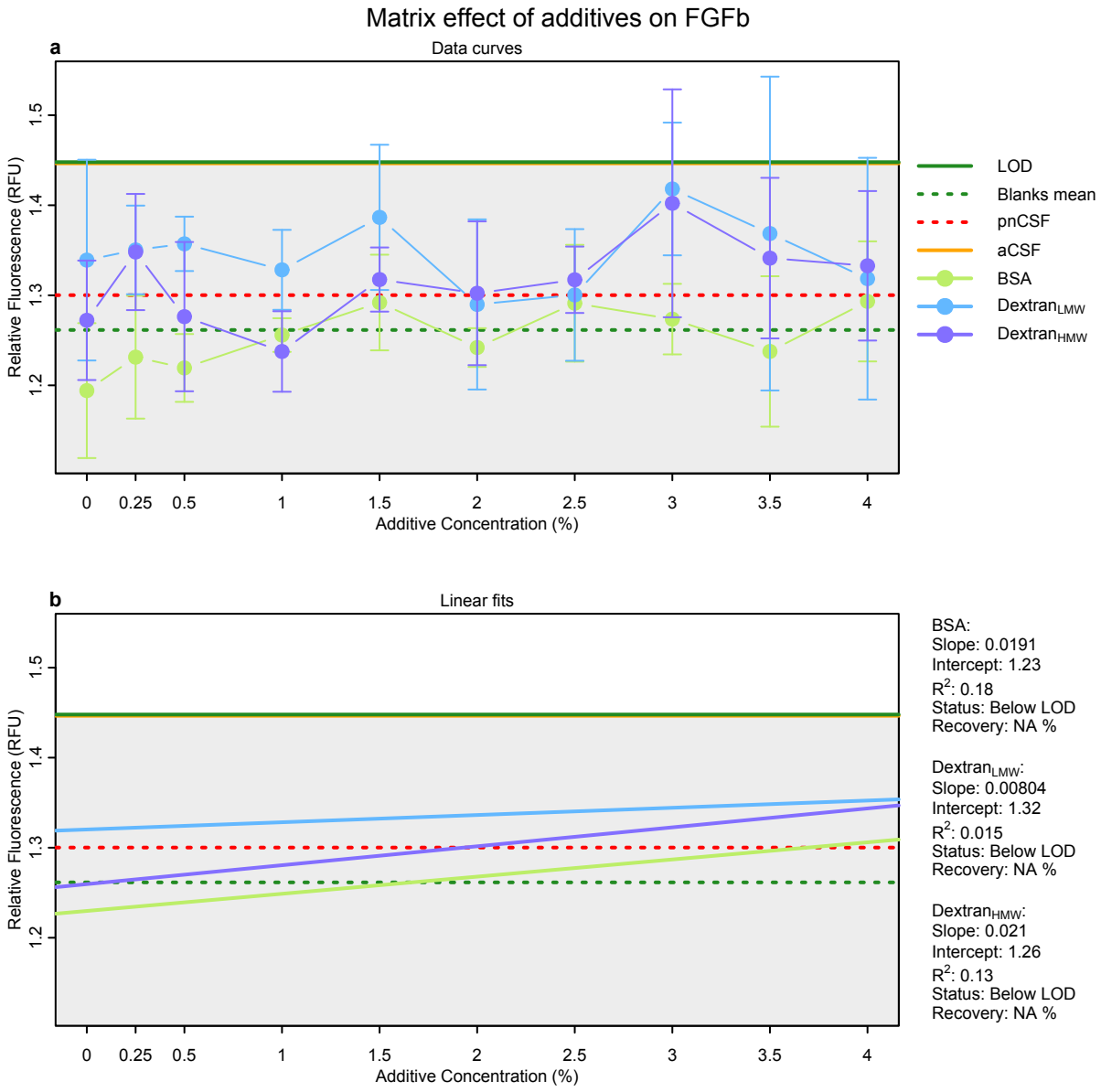

FIGURE G.S23: **Effect of additives on the measurement of FGFb.** pnCSF mixed 0-4 % additives diluted in aCSF were measured using the ACM, in order to measure the possible interference of additives on the protein measurement (matrix effect). Linear regressions of measured calibrated fluorescence values of FGFb were used to calculate the recovery at concentrations of additives used in cerebral microdialysis. **a** Data from the average of three independent replicates is shown. **b** Median-based linear regressions from the data in **a**.

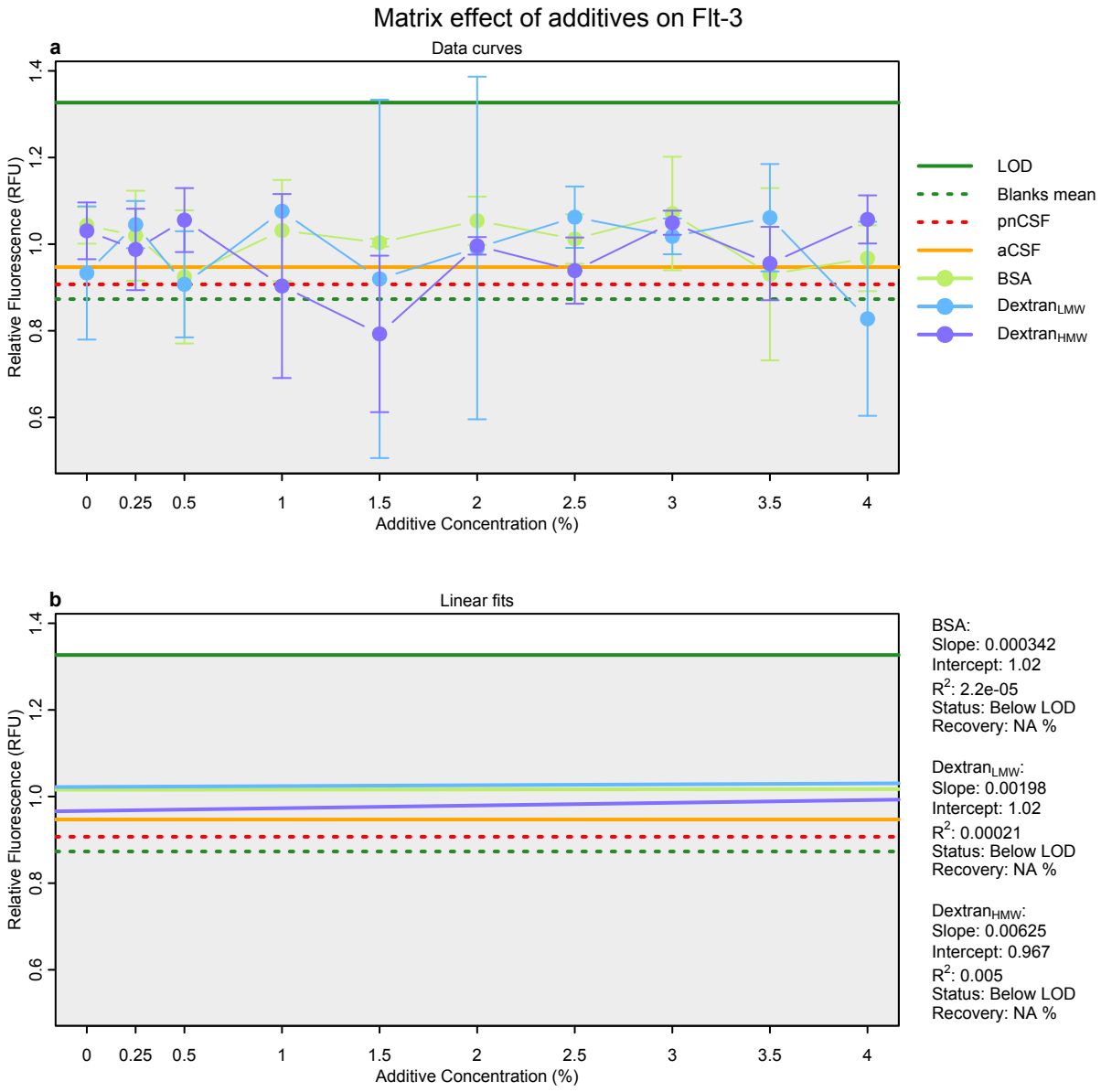

FIGURE G.S24: **Effect of additives on the measurement of Flt-3.** pnCSF mixed 0-4 % additives diluted in aCSF were measured using the ACM, in order to measure the possible interference of additives on the protein measurement (matrix effect). Linear regressions of measured calibrated fluorescence values of Flt-3 were used to calculate the recovery at concentrations of additives used in cerebral microdialysis. **a** Data from the average of three independent replicates is shown. **b** Median-based linear regressions from the data in **a**.

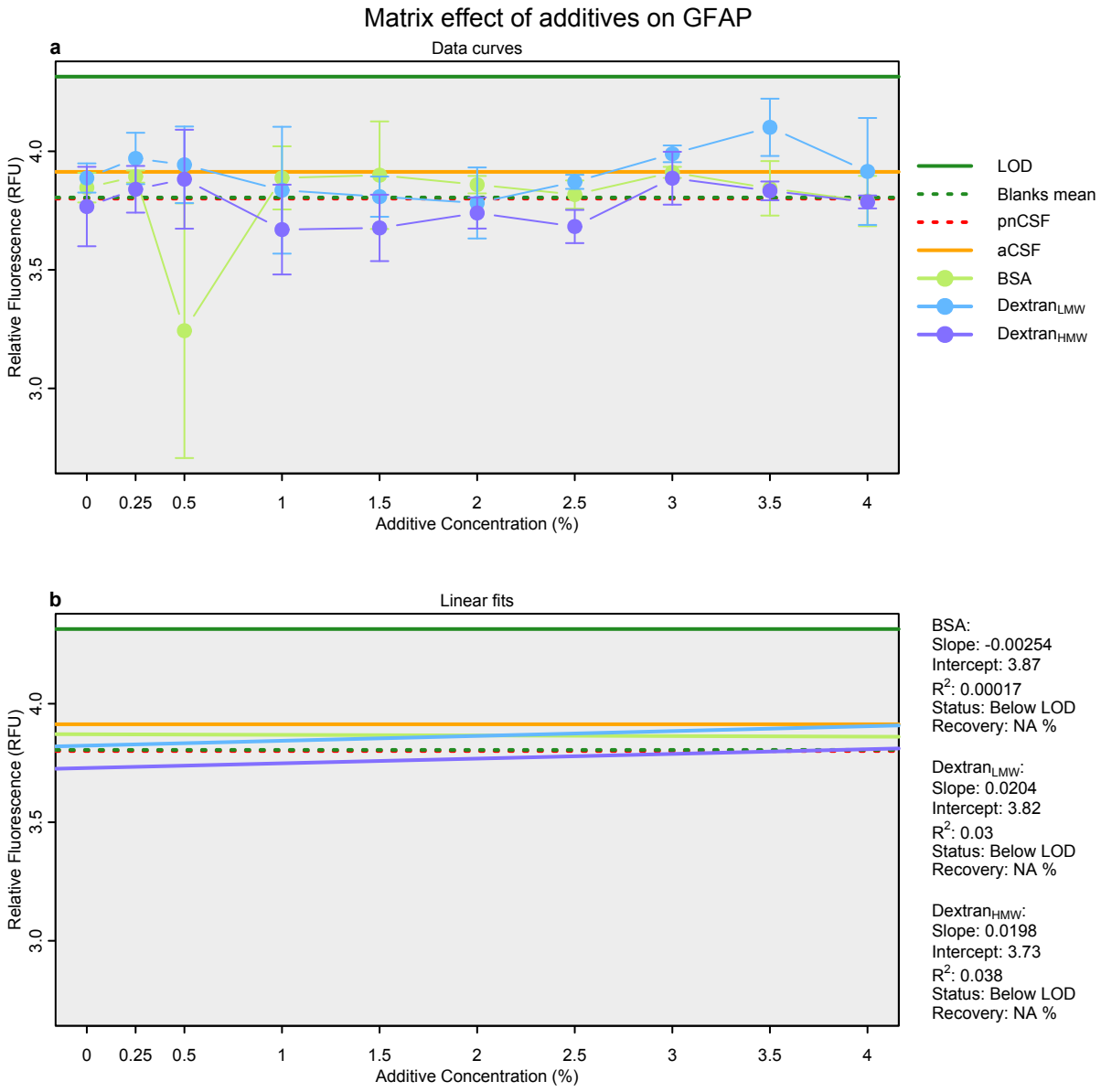

FIGURE G.S25: **Effect of additives on the measurement of GFAP.** pnCSF mixed 0-4 % additives diluted in aCSF were measured using the ACM, in order to measure the possible interference of additives on the protein measurement (matrix effect). Linear regressions of measured calibrated fluorescence values of GFAP were used to calculate the recovery at concentrations of additives used in cerebral microdialysis. **a** Data from the average of three independent replicates is shown. **b** Median-based linear regressions from the data in **a**.

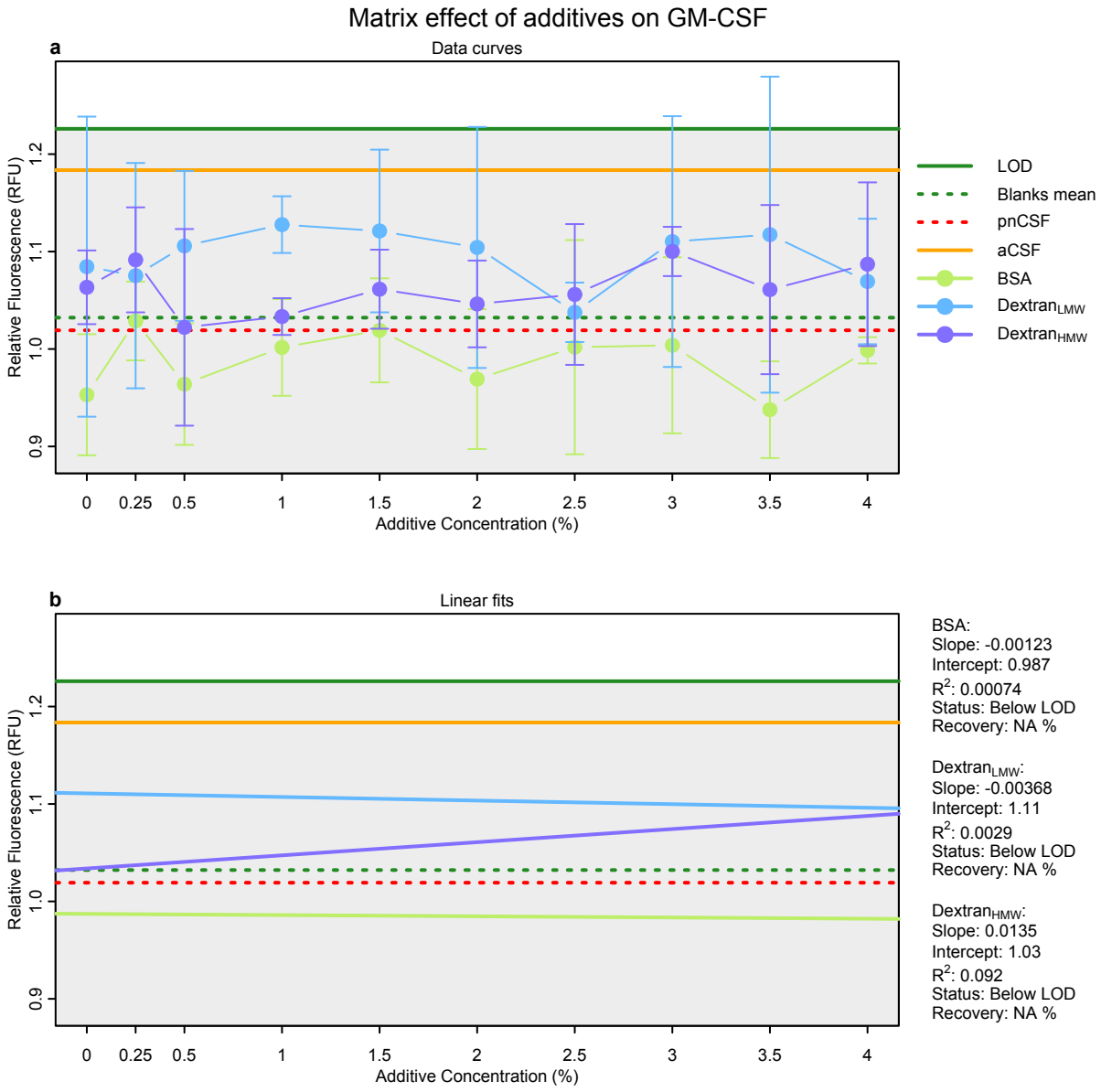

FIGURE G.S26: **Effect of additives on the measurement of GM-CSF.** pnCSF mixed 0-4 % additives diluted in aCSF were measured using the ACM, in order to measure the possible interference of additives on the protein measurement (matrix effect). Linear regressions of measured calibrated fluorescence values of GM-CSF were used to calculate the recovery at concentrations of additives used in cerebral microdialysis. **a** Data from the average of three independent replicates is shown. **b** Median-based linear regressions from the data in **a**.

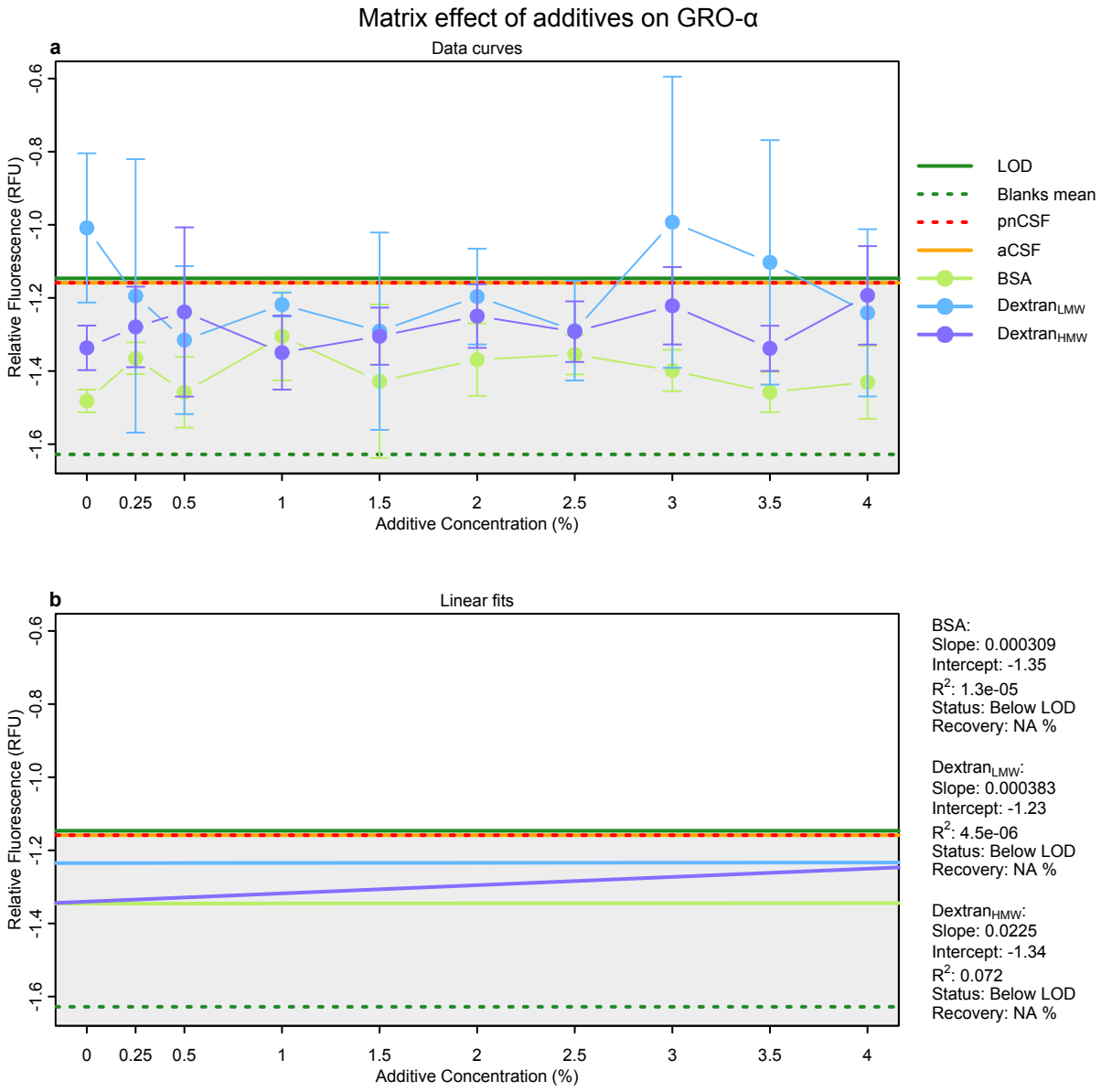

FIGURE G.S27: **Effect of additives on the measurement of GRO-α.** pnCSF mixed 0-4 % additives diluted in aCSF were measured using the ACM, in order to measure the possible interference of additives on the protein measurement (matrix effect). Linear regressions of measured calibrated fluorescence values of GRO-α were used to calculate the recovery at concentrations of additives used in cerebral microdialysis. **a** Data from the average of three independent replicates is shown. **b** Median-based linear regressions from the data in **a**.

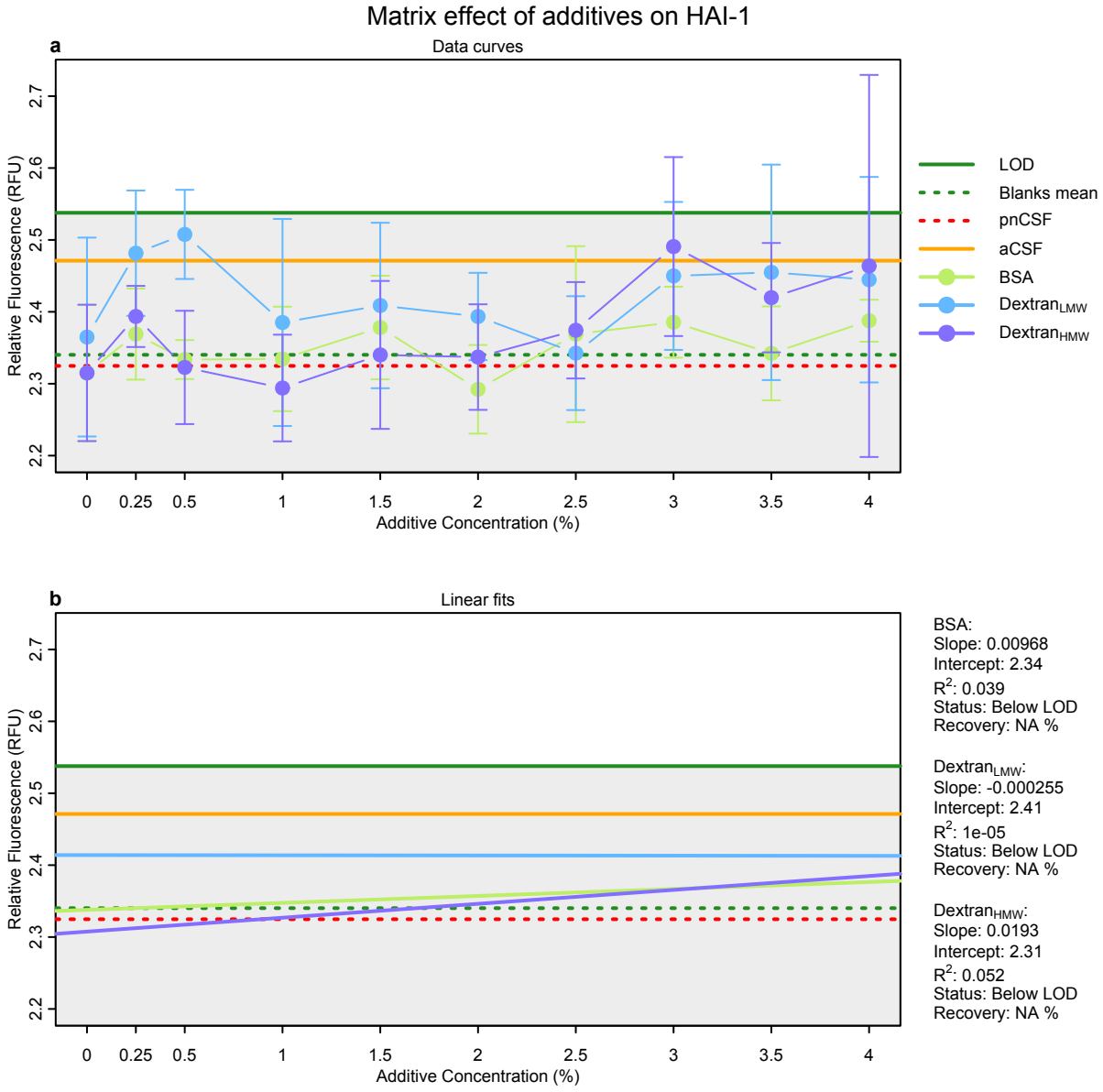

FIGURE G.S28: **Effect of additives on the measurement of HAI-1.** pnCSF mixed 0-4 % additives diluted in aCSF were measured using the ACM, in order to measure the possible interference of additives on the protein measurement (matrix effect). Linear regressions of measured calibrated fluorescence values of HAI-1 were used to calculate the recovery at concentrations of additives used in cerebral microdialysis. **a** Data from the average of three independent replicates is shown. **b** Median-based linear regressions from the data in **a**.

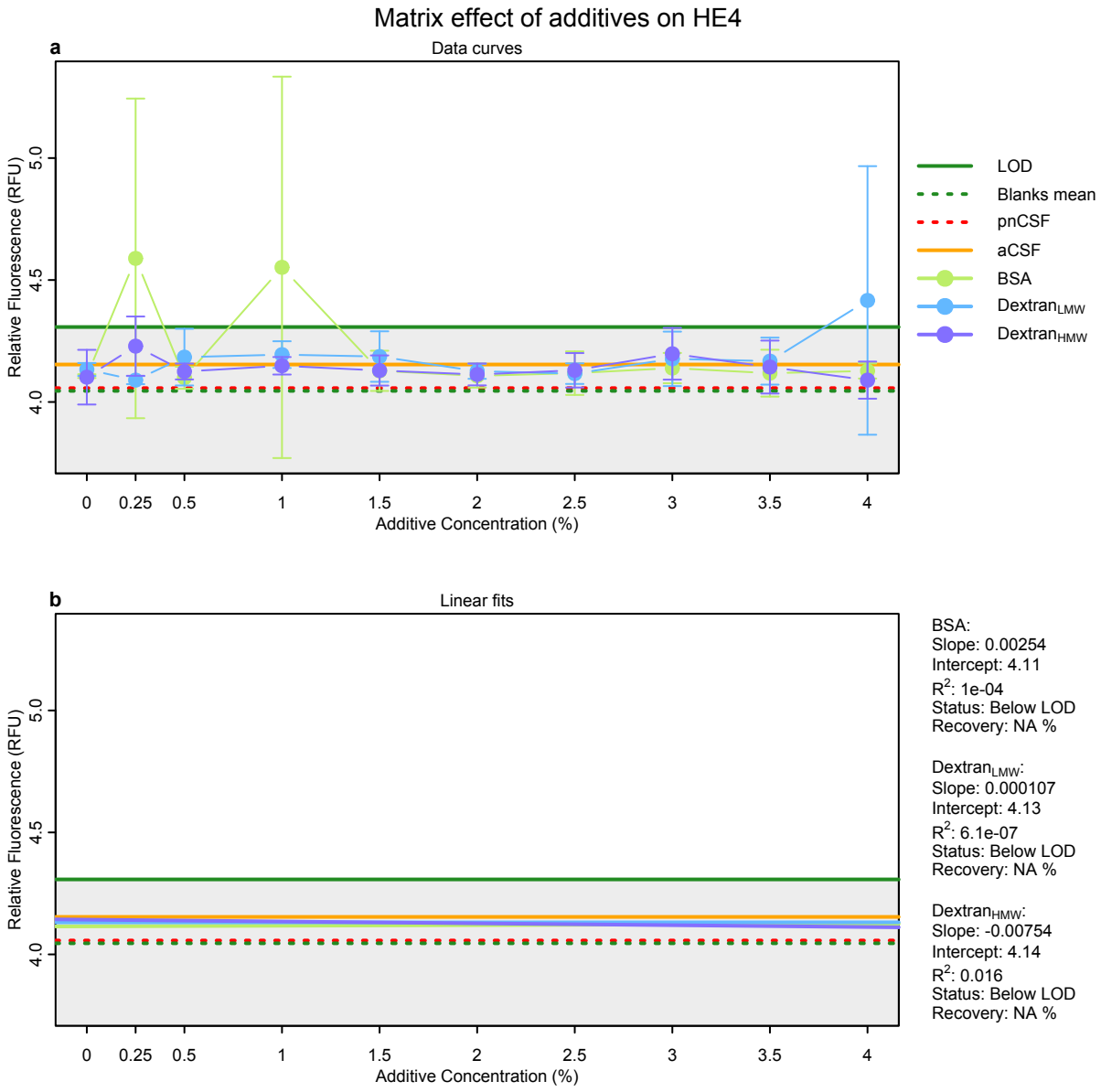

FIGURE G.S29: **Effect of additives on the measurement of HE4.** pnCSF mixed 0-4 % additives diluted in aCSF were measured using the ACM, in order to measure the possible interference of additives on the protein measurement (matrix effect). Linear regressions of measured calibrated fluorescence values of HE4 were used to calculate the recovery at concentrations of additives used in cerebral microdialysis. **a** Data from the average of three independent replicates is shown. **b** Median-based linear regressions from the data in **a**.

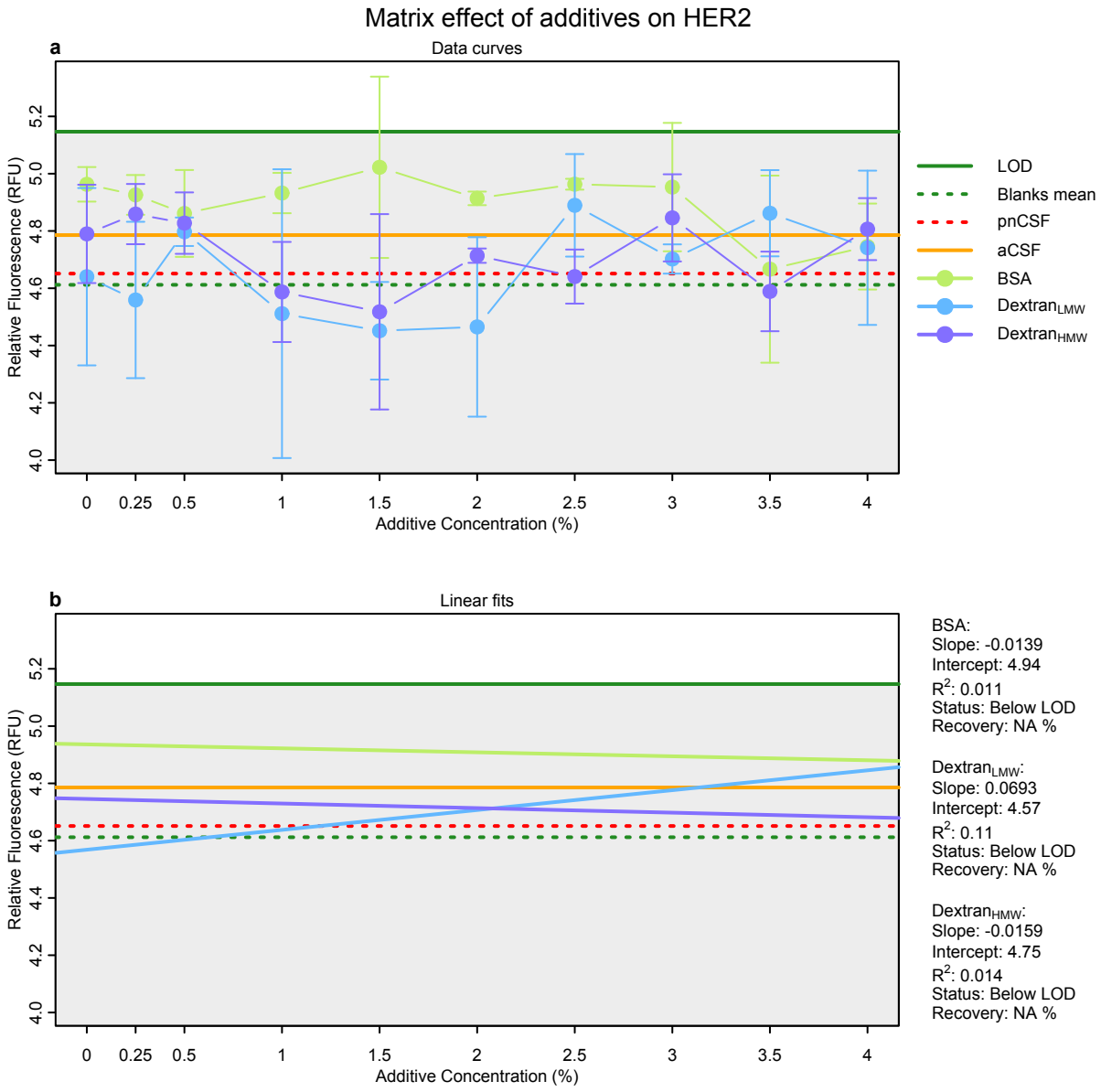

FIGURE G.S30: **Effect of additives on the measurement of HER2.** pnCSF mixed 0-4 % additives diluted in aCSF were measured using the ACM, in order to measure the possible interference of additives on the protein measurement (matrix effect). Linear regressions of measured calibrated fluorescence values of HER2 were used to calculate the recovery at concentrations of additives used in cerebral microdialysis. **a** Data from the average of three independent replicates is shown. **b** Median-based linear regressions from the data in **a**.

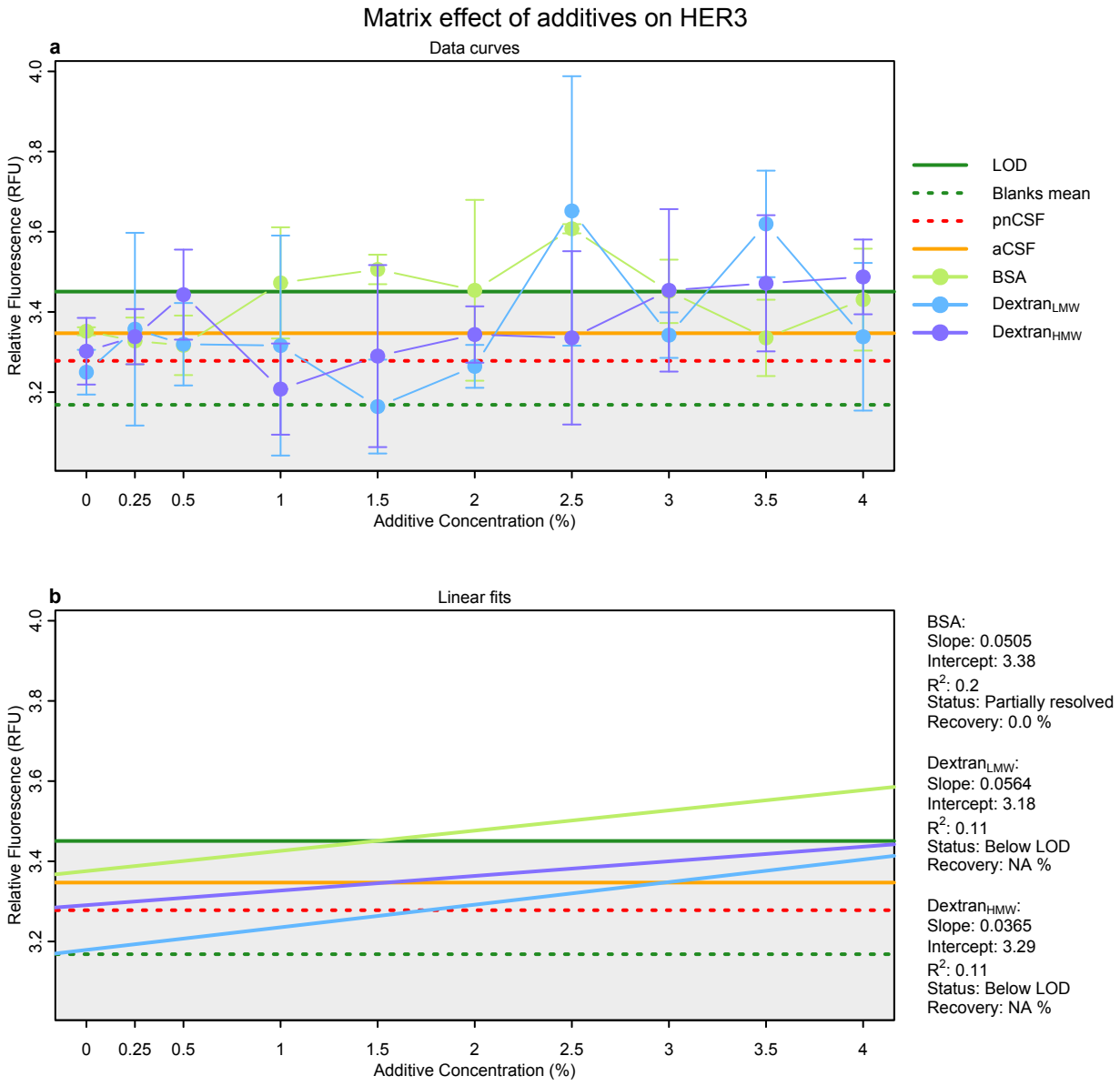

FIGURE G.S31: **Effect of additives on the measurement of HER3.** pnCSF mixed 0-4 % additives diluted in aCSF were measured using the ACM, in order to measure the possible interference of additives on the protein measurement (matrix effect). Linear regressions of measured calibrated fluorescence values of HER3 were used to calculate the recovery at concentrations of additives used in cerebral microdialysis. **a** Data from the average of three independent replicates is shown. **b** Median-based linear regressions from the data in **a**.

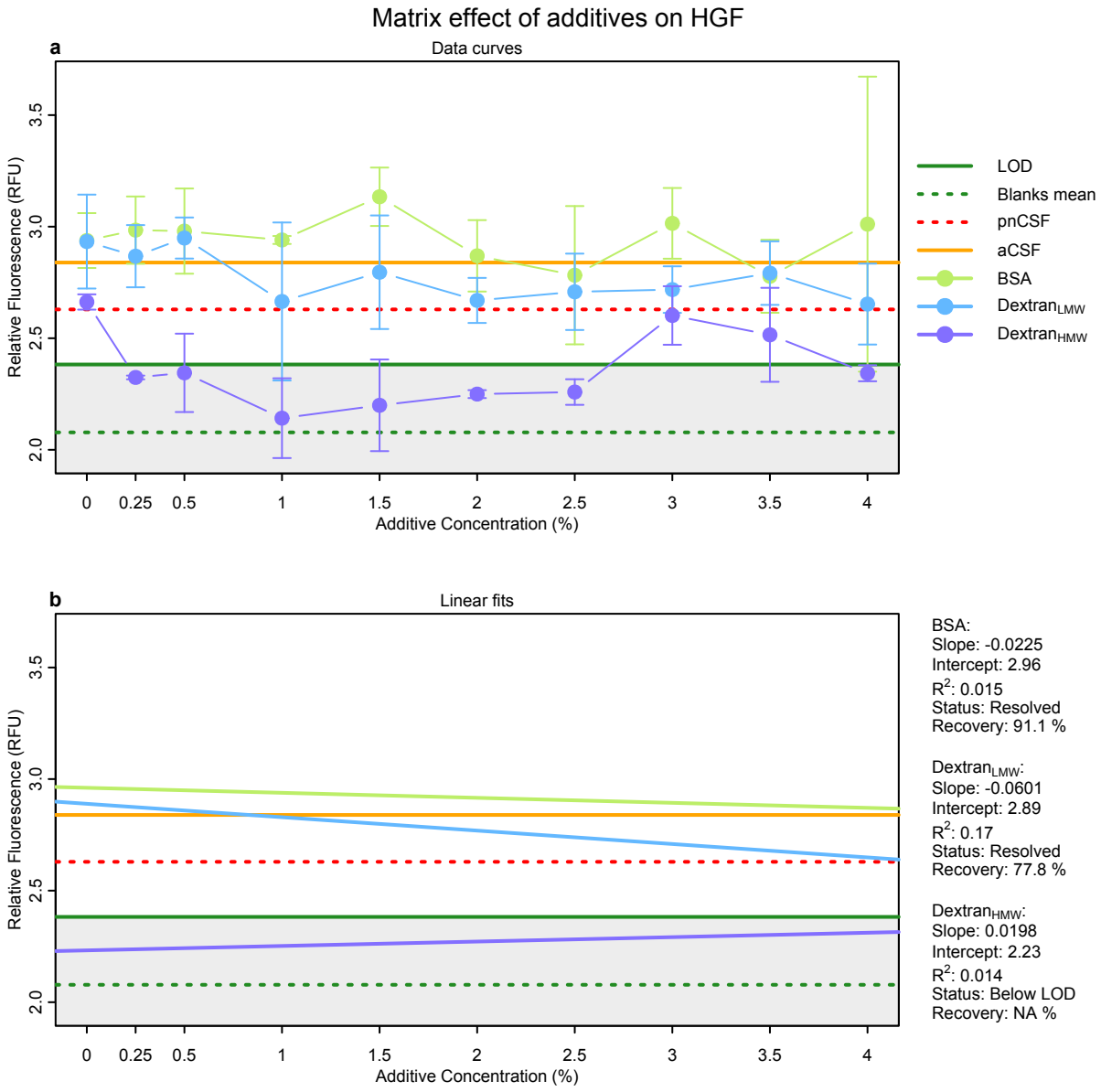

FIGURE G.S32: **Effect of additives on the measurement of HGF.** pnCSF mixed 0-4 % additives diluted in aCSF were measured using the ACM, in order to measure the possible interference of additives on the protein measurement (matrix effect). Linear regressions of measured calibrated fluorescence values of HGF were used to calculate the recovery at concentrations of additives used in cerebral microdialysis. **a** Data from the average of three independent replicates is shown. **b** Median-based linear regressions from the data in **a**.

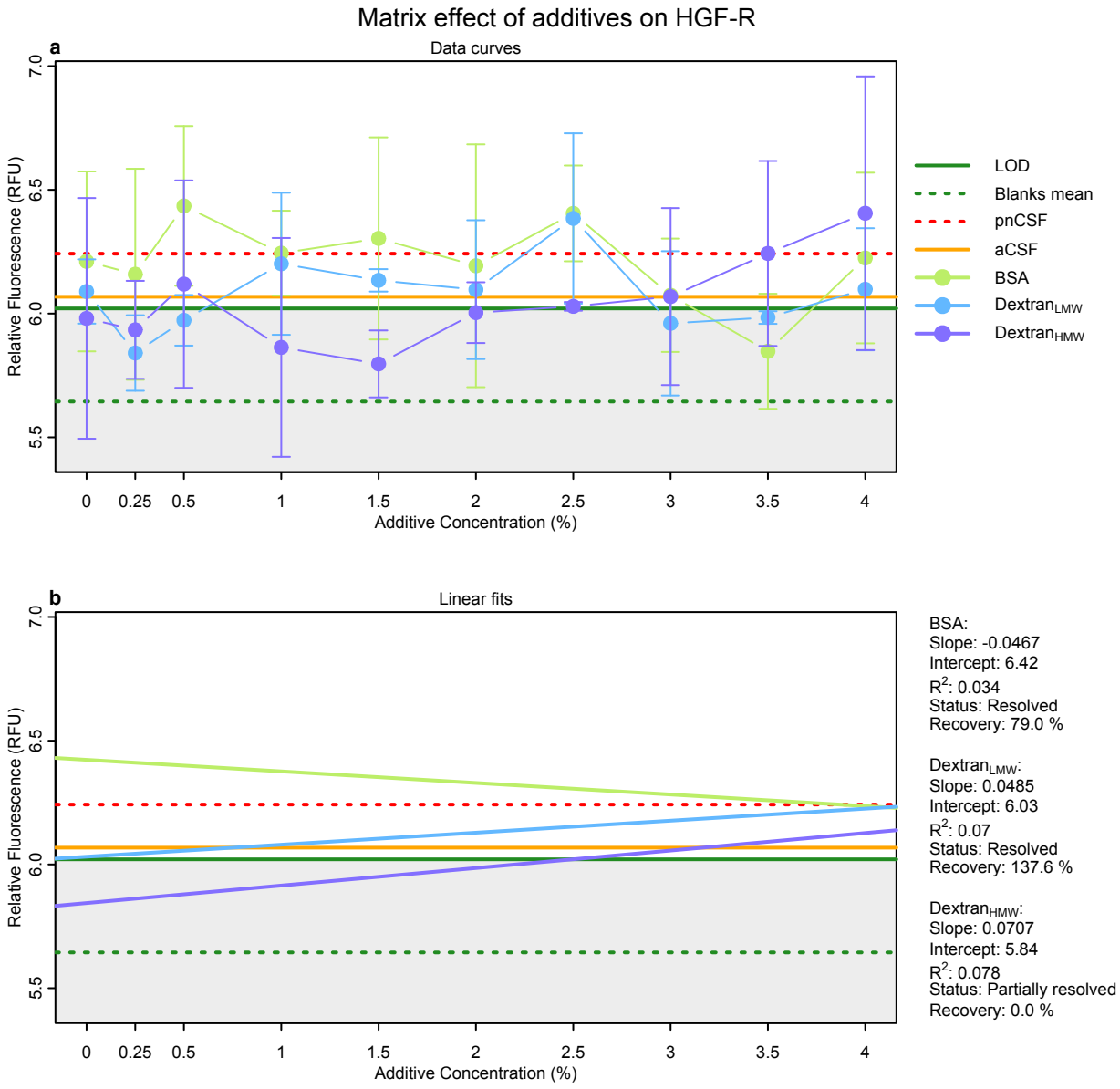

FIGURE G.S33: **Effect of additives on the measurement of HGF-R.** pnCSF mixed 0-4 % additives diluted in aCSF were measured using the ACM, in order to measure the possible interference of additives on the protein measurement (matrix effect). Linear regressions of measured calibrated fluorescence values of HGF-R were used to calculate the recovery at concentrations of additives used in cerebral microdialysis. **a** Data from the average of three independent replicates is shown. **b** Median-based linear regressions from the data in **a**.

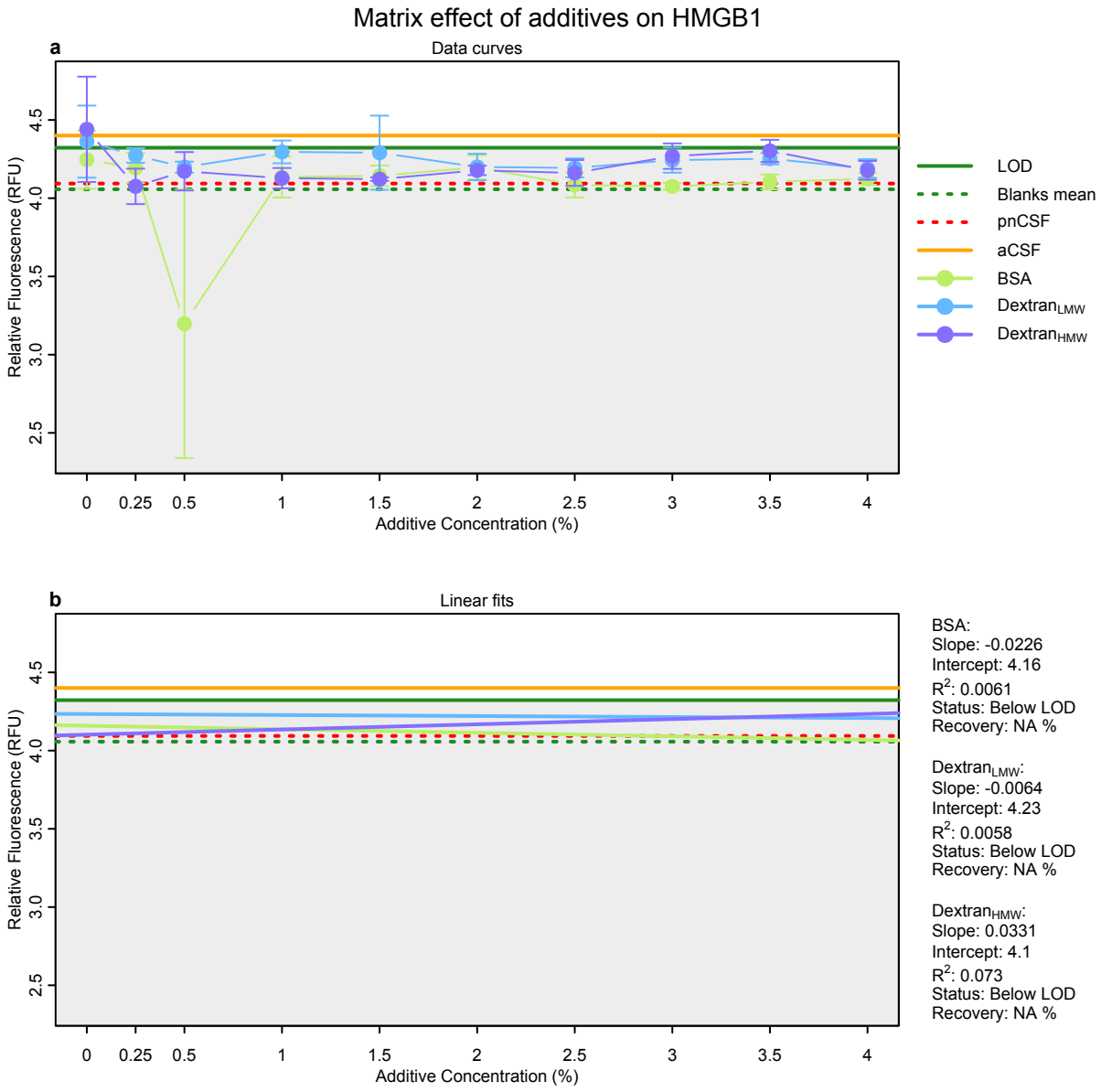

FIGURE G.S34: **Effect of additives on the measurement of HMGB1.** pnCSF mixed 0-4 % additives diluted in aCSF were measured using the ACM, in order to measure the possible interference of additives on the protein measurement (matrix effect). Linear regressions of measured calibrated fluorescence values of HMGB1 were used to calculate the recovery at concentrations of additives used in cerebral microdialysis. **a** Data from the average of three independent replicates is shown. **b** Median-based linear regressions from the data in **a**.

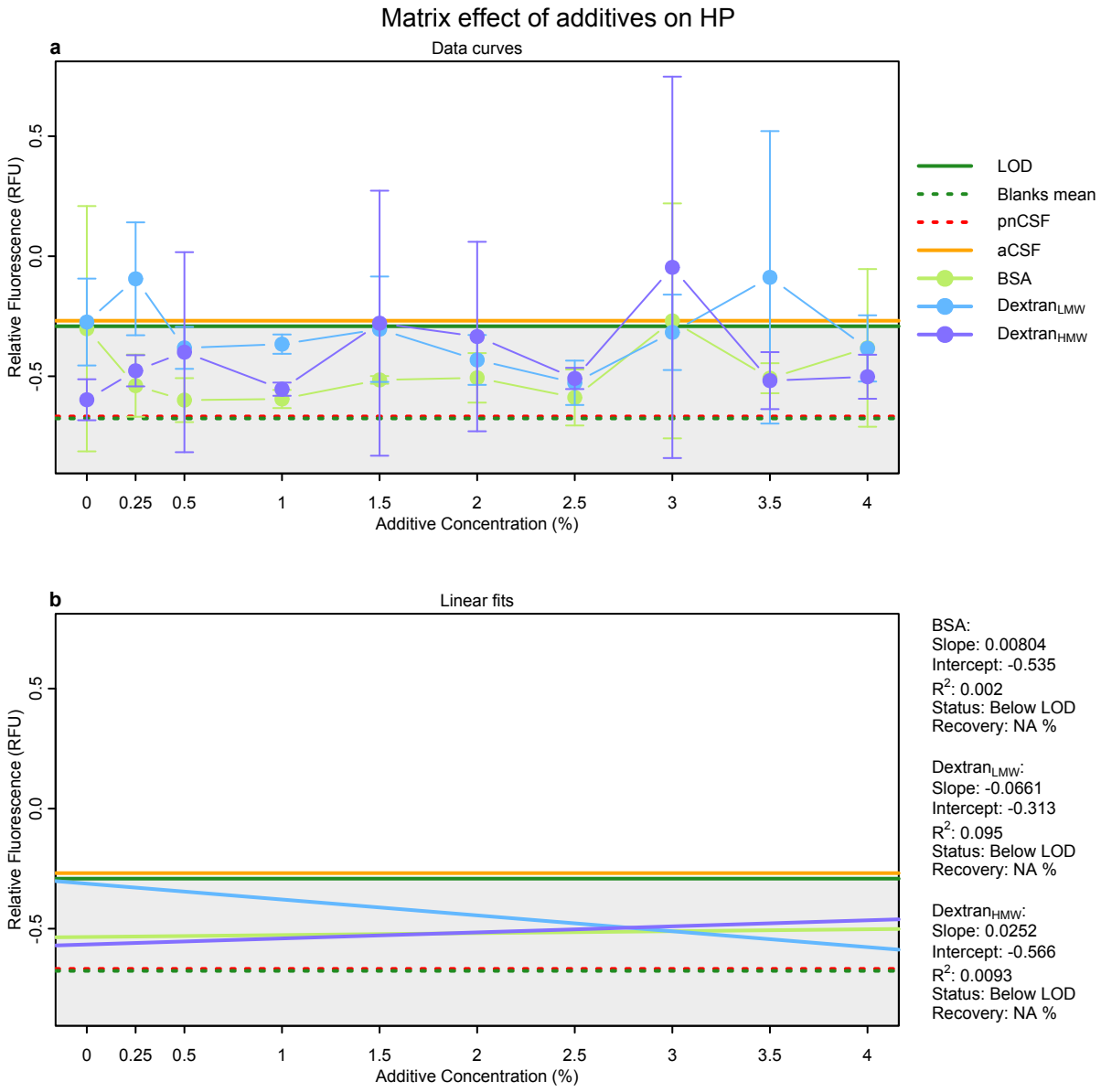

FIGURE G.S35: **Effect of additives on the measurement of HP.** pnCSF mixed 0-4 % additives diluted in aCSF were measured using the ACM, in order to measure the possible interference of additives on the protein measurement (matrix effect). Linear regressions of measured calibrated fluorescence values of HP were used to calculate the recovery at concentrations of additives used in cerebral microdialysis. **a** Data from the average of three independent replicates is shown. **b** Median-based linear regressions from the data in **a**.

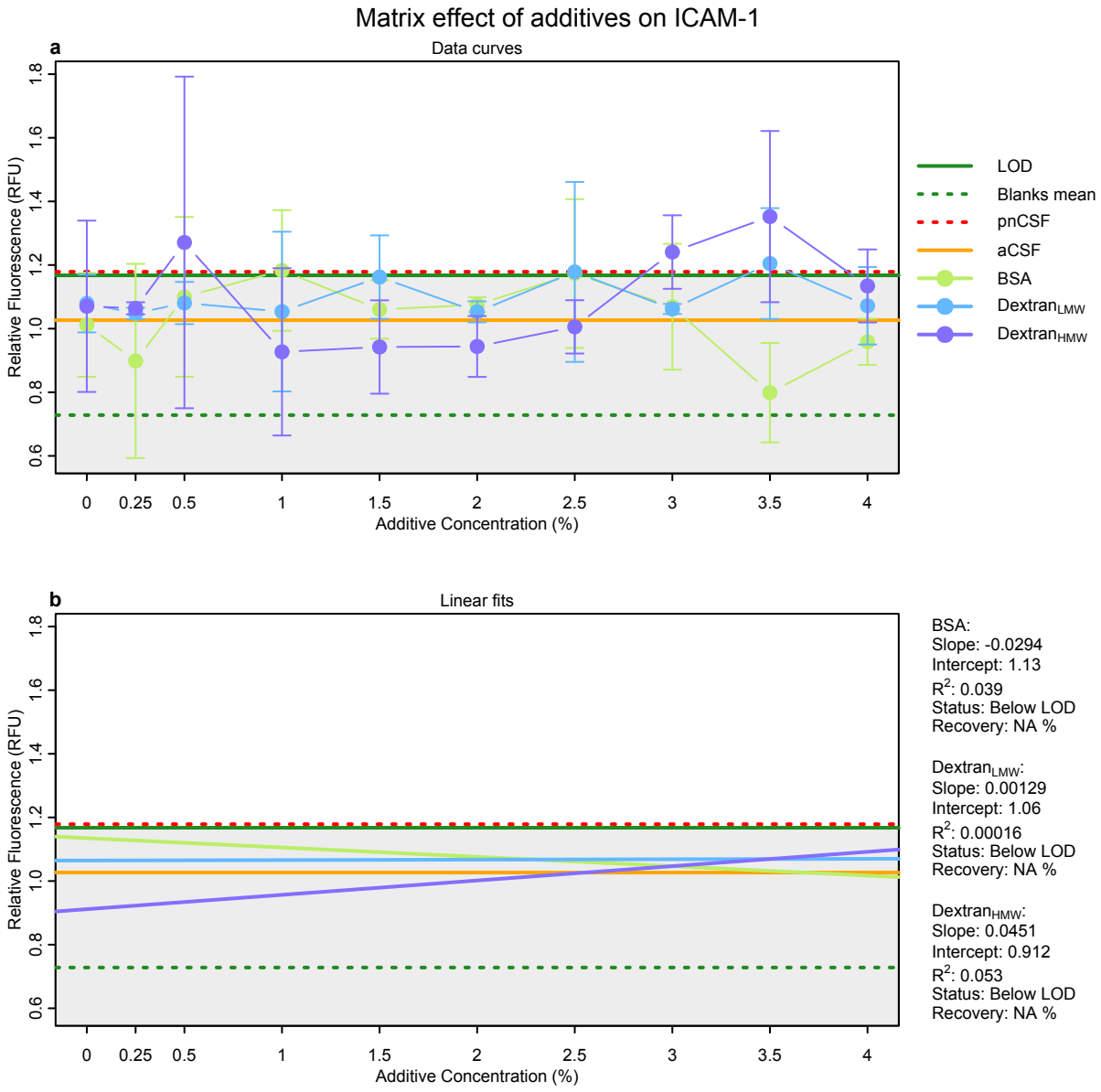

FIGURE G.S36: **Effect of additives on the measurement of ICAM-1.** pnCSF mixed 0-4 % additives diluted in aCSF were measured using the ACM, in order to measure the possible interference of additives on the protein measurement (matrix effect). Linear regressions of measured calibrated fluorescence values of ICAM-1 were used to calculate the recovery at concentrations of additives used in cerebral microdialysis. **a** Data from the average of three independent replicates is shown. **b** Median-based linear regressions from the data in **a**.

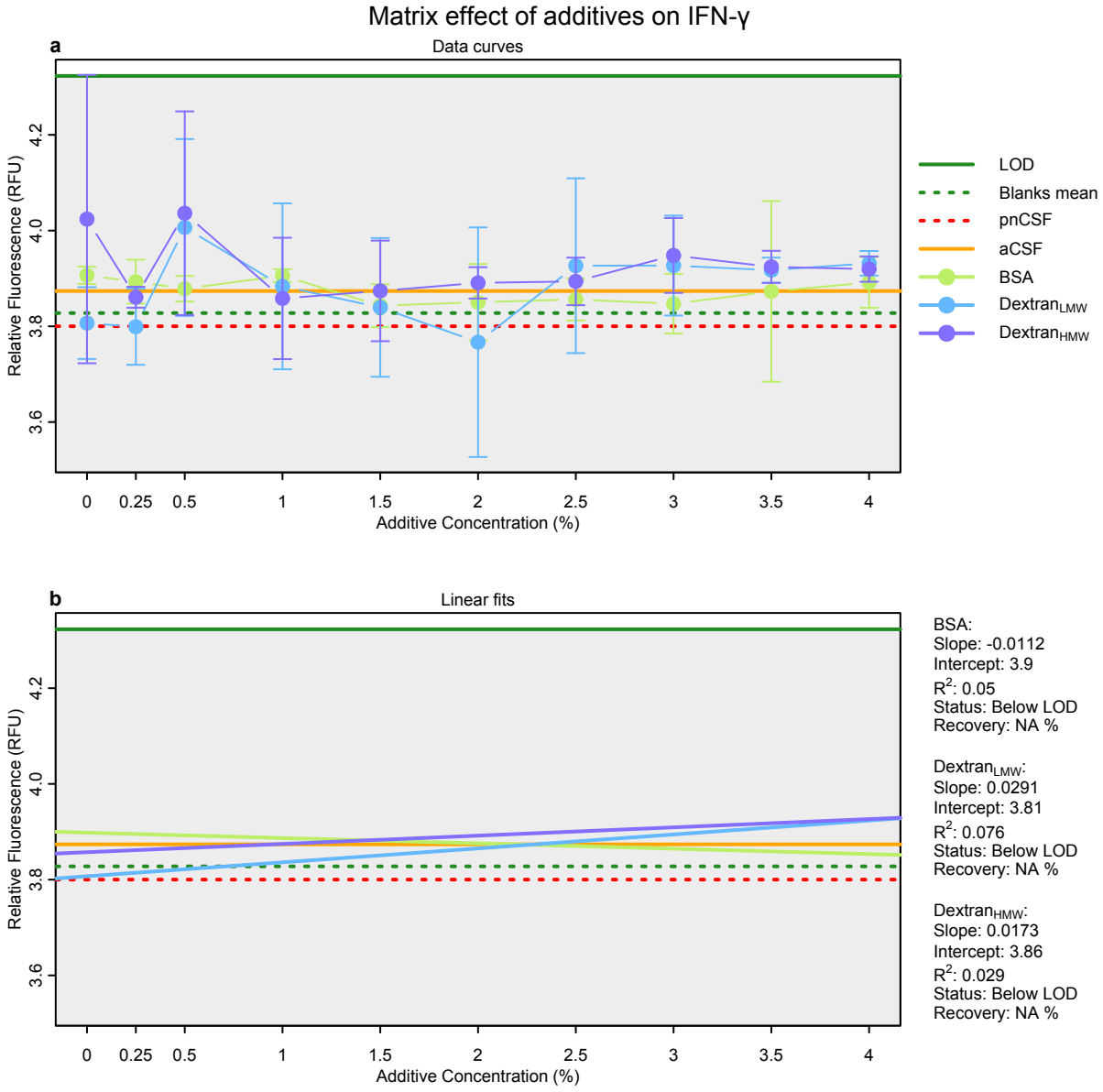

FIGURE G.S37: **Effect of additives on the measurement of IFN-γ.** pnCSF mixed 0-4 % additives diluted in aCSF were measured using the ACM, in order to measure the possible interference of additives on the protein measurement (matrix effect). Linear regressions of measured calibrated fluorescence values of IFN-γ were used to calculate the recovery at concentrations of additives used in cerebral microdialysis. **a** Data from the average of three independent replicates is shown. **b** Median-based linear regressions from the data in **a**.

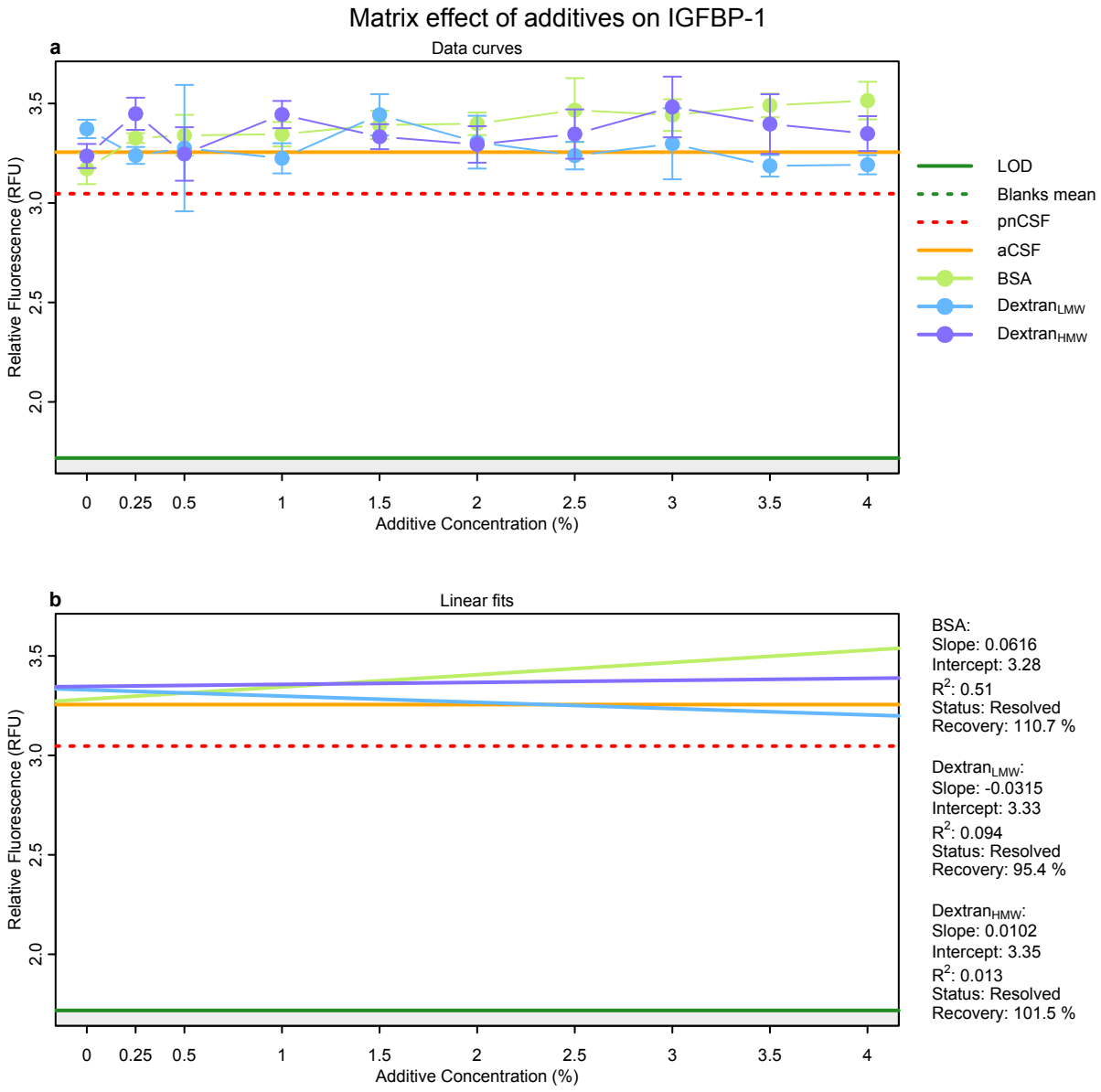

FIGURE G.S38: **Effect of additives on the measurement of IGFBP-1.** pnCSF mixed 0-4 % additives diluted in aCSF were measured using the ACM, in order to measure the possible interference of additives on the protein measurement (matrix effect). Linear regressions of measured calibrated fluorescence values of IGFBP-1 were used to calculate the recovery at concentrations of additives used in cerebral microdialysis. **a** Data from the average of three independent replicates is shown. **b** Median-based linear regressions from the data in **a**.

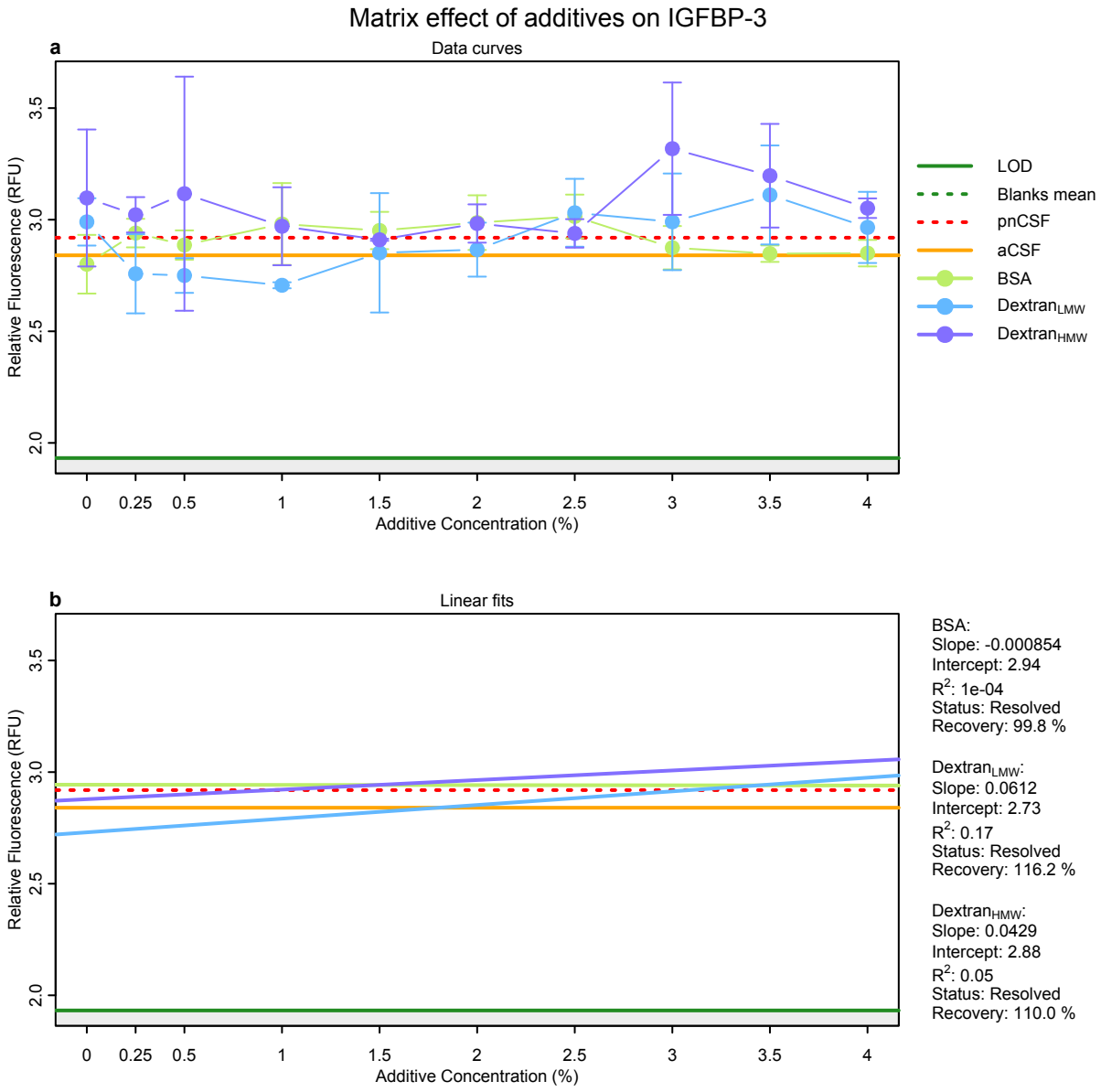

FIGURE G.S39: **Effect of additives on the measurement of IGFBP-3.** pnCSF mixed 0-4 % additives diluted in aCSF were measured using the ACM, in order to measure the possible interference of additives on the protein measurement (matrix effect). Linear regressions of measured calibrated fluorescence values of IGFBP-3 were used to calculate the recovery at concentrations of additives used in cerebral microdialysis. **a** Data from the average of three independent replicates is shown. **b** Median-based linear regressions from the data in **a**.

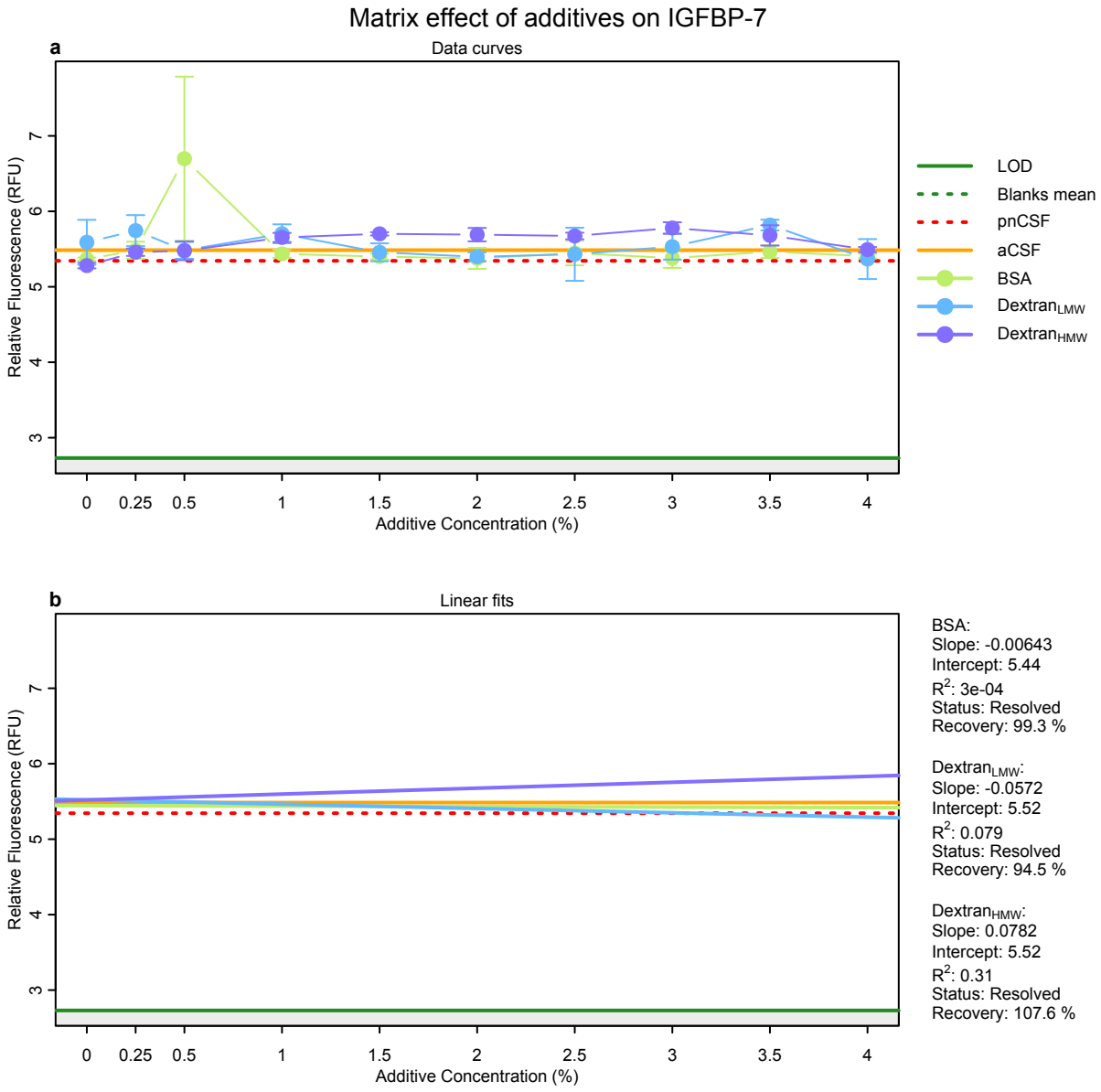

FIGURE G.S40: **Effect of additives on the measurement of IGFBP-7.** pnCSF mixed 0-4 % additives diluted in aCSF were measured using the ACM, in order to measure the possible interference of additives on the protein measurement (matrix effect). Linear regressions of measured calibrated fluorescence values of IGFBP-7 were used to calculate the recovery at concentrations of additives used in cerebral microdialysis. **a** Data from the average of three independent replicates is shown. **b** Median-based linear regressions from the data in **a**.

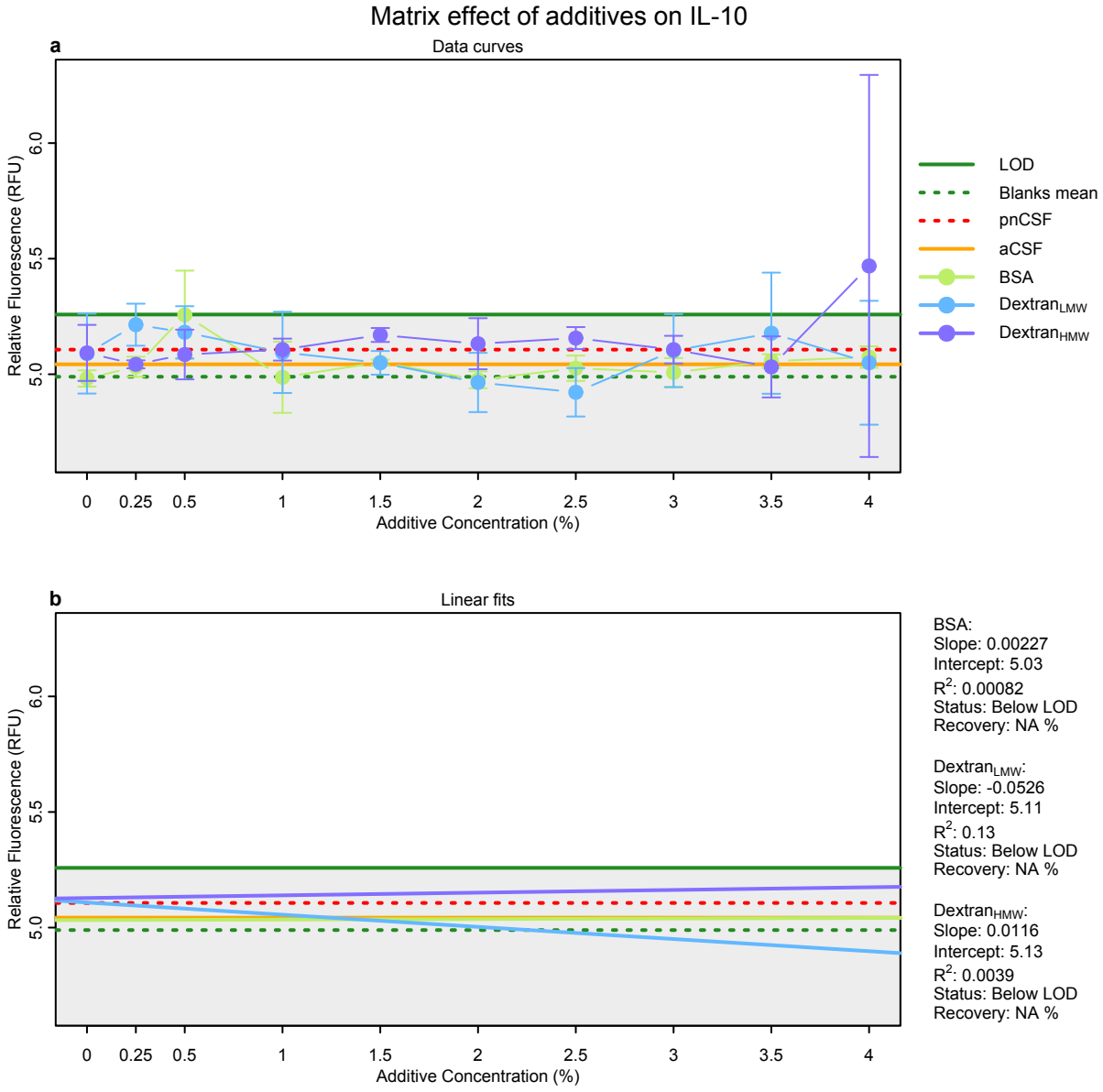

FIGURE G.S41: **Effect of additives on the measurement of IL-10.** pnCSF mixed 0-4 % additives diluted in aCSF were measured using the ACM, in order to measure the possible interference of additives on the protein measurement (matrix effect). Linear regressions of measured calibrated fluorescence values of IL-10 were used to calculate the recovery at concentrations of additives used in cerebral microdialysis. **a** Data from the average of three independent replicates is shown. **b** Median-based linear regressions from the data in **a**.

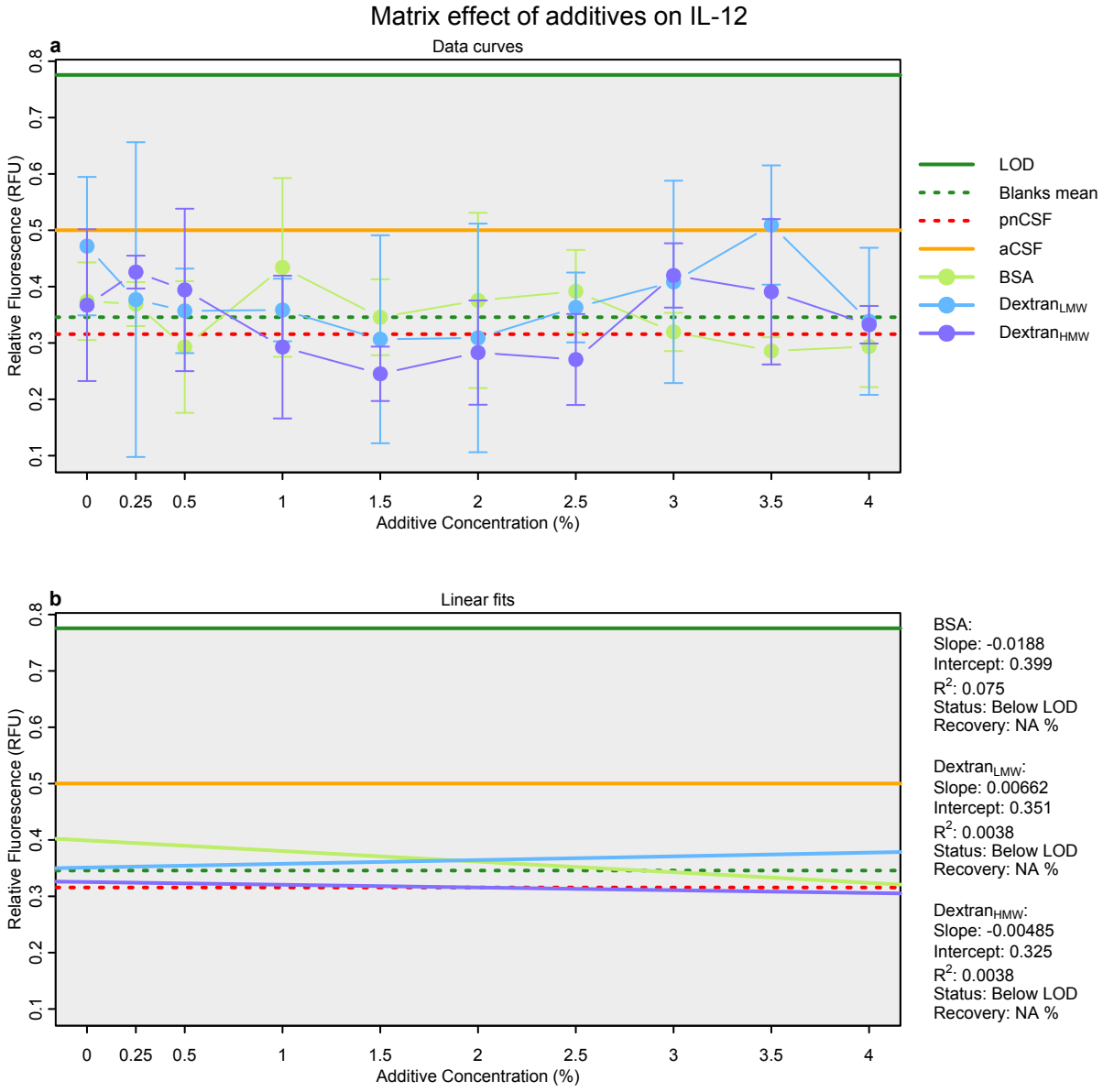

FIGURE G.S42: **Effect of additives on the measurement of IL-12.** pnCSF mixed 0-4 % additives diluted in aCSF were measured using the ACM, in order to measure the possible interference of additives on the protein measurement (matrix effect). Linear regressions of measured calibrated fluorescence values of IL-12 were used to calculate the recovery at concentrations of additives used in cerebral microdialysis. **a** Data from the average of three independent replicates is shown. **b** Median-based linear regressions from the data in **a**.

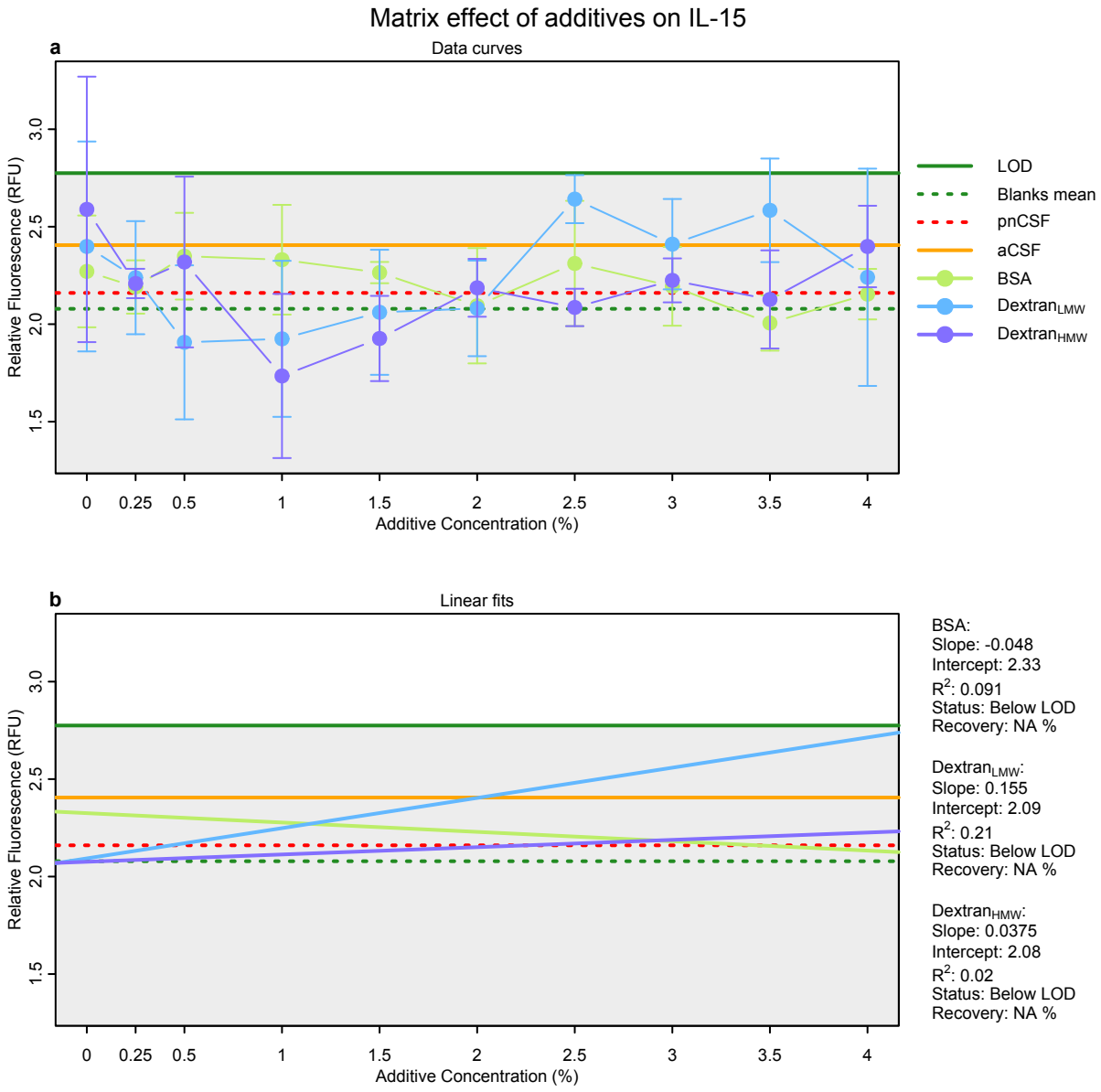

FIGURE G.S43: **Effect of additives on the measurement of IL-15.** pnCSF mixed 0-4 % additives diluted in aCSF were measured using the ACM, in order to measure the possible interference of additives on the protein measurement (matrix effect). Linear regressions of measured calibrated fluorescence values of IL-15 were used to calculate the recovery at concentrations of additives used in cerebral microdialysis. **a** Data from the average of three independent replicates is shown. **b** Median-based linear regressions from the data in **a**.

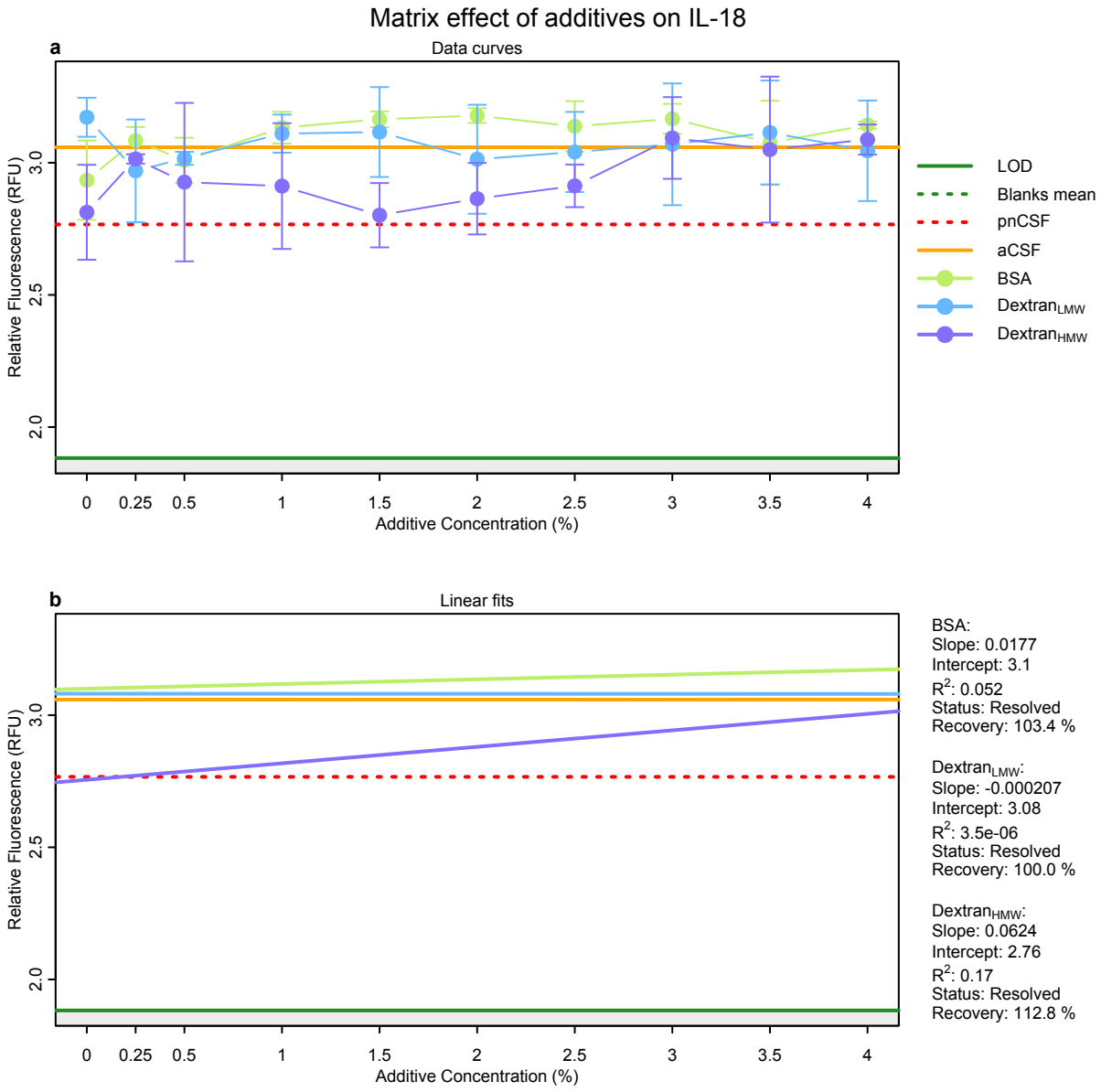

FIGURE G.S44: **Effect of additives on the measurement of IL-18.** pnCSF mixed 0-4 % additives diluted in aCSF were measured using the ACM, in order to measure the possible interference of additives on the protein measurement (matrix effect). Linear regressions of measured calibrated fluorescence values of IL-18 were used to calculate the recovery at concentrations of additives used in cerebral microdialysis. **a** Data from the average of three independent replicates is shown. **b** Median-based linear regressions from the data in **a**.

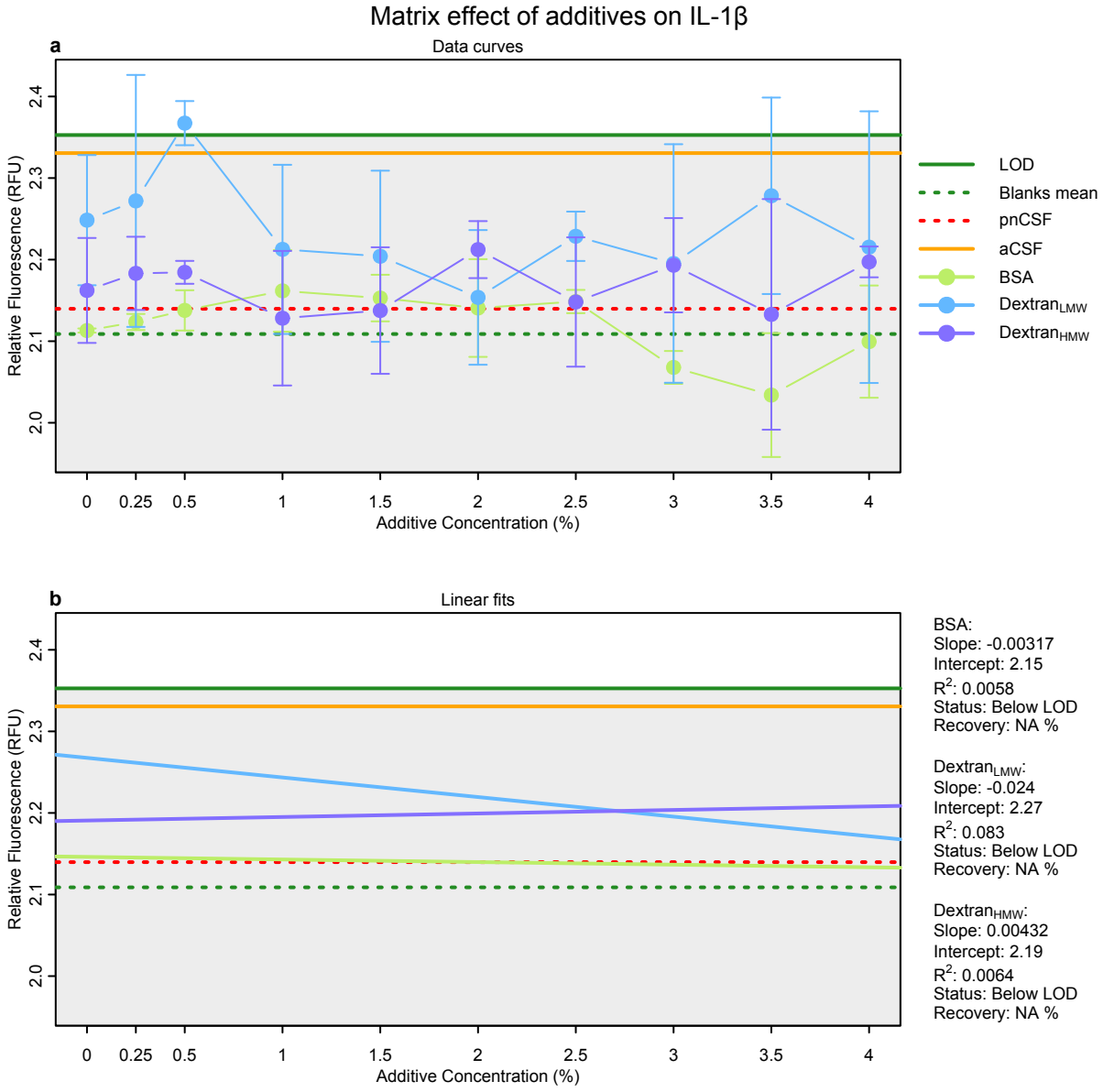

FIGURE G.S45: **Effect of additives on the measurement of IL-1β.** pnCSF mixed 0-4 % additives diluted in aCSF were measured using the ACM, in order to measure the possible interference of additives on the protein measurement (matrix effect). Linear regressions of measured calibrated fluorescence values of IL-1β were used to calculate the recovery at concentrations of additives used in cerebral microdialysis. **a** Data from the average of three independent replicates is shown. **b** Median-based linear regressions from the data in **a**.

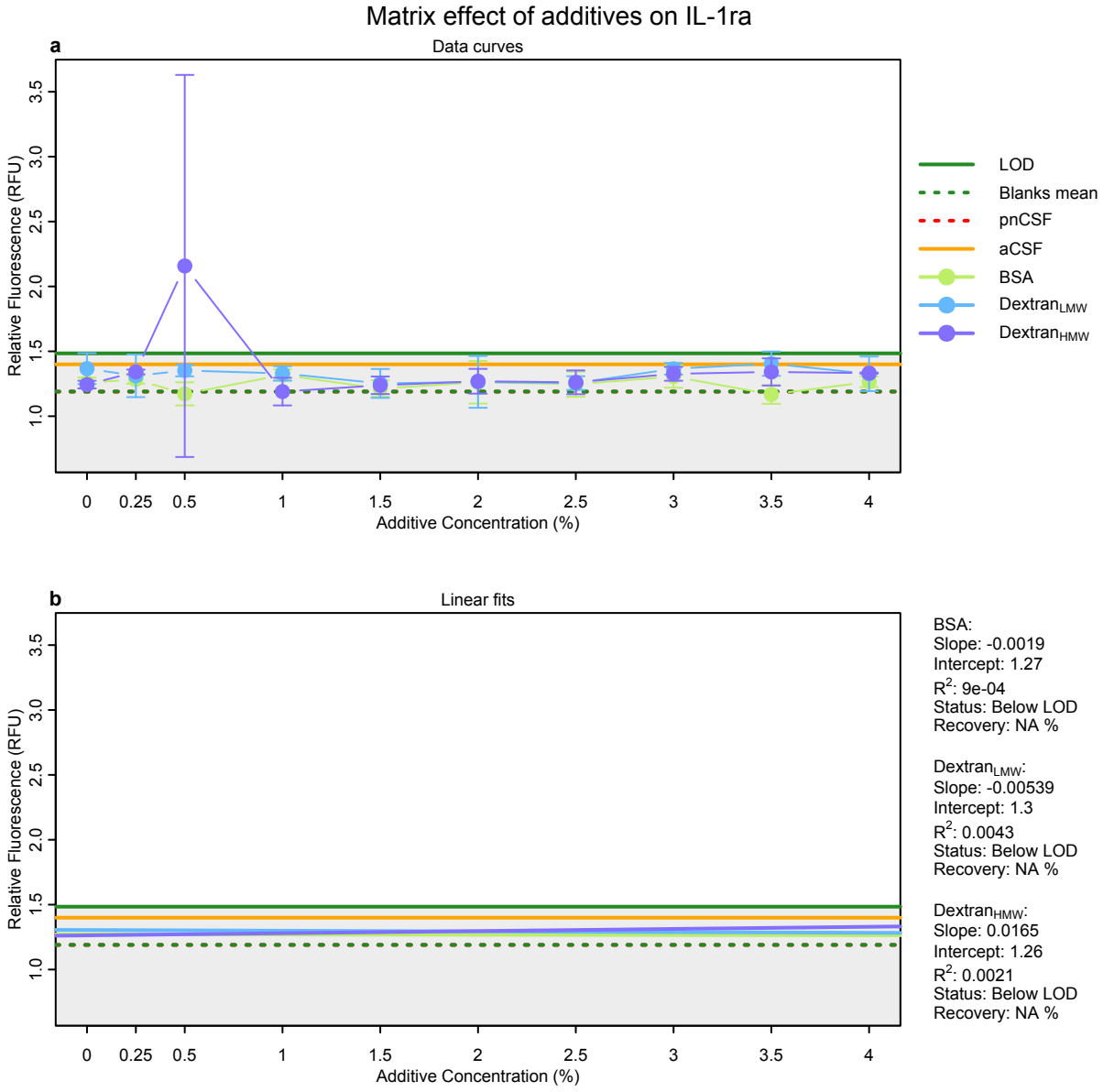

FIGURE G.S46: **Effect of additives on the measurement of IL-1ra.** pnCSF mixed 0-4 % additives diluted in aCSF were measured using the ACM, in order to measure the possible interference of additives on the protein measurement (matrix effect). Linear regressions of measured calibrated fluorescence values of IL-1ra were used to calculate the recovery at concentrations of additives used in cerebral microdialysis. **a** Data from the average of three independent replicates is shown. **b** Median-based linear regressions from the data in **a**.

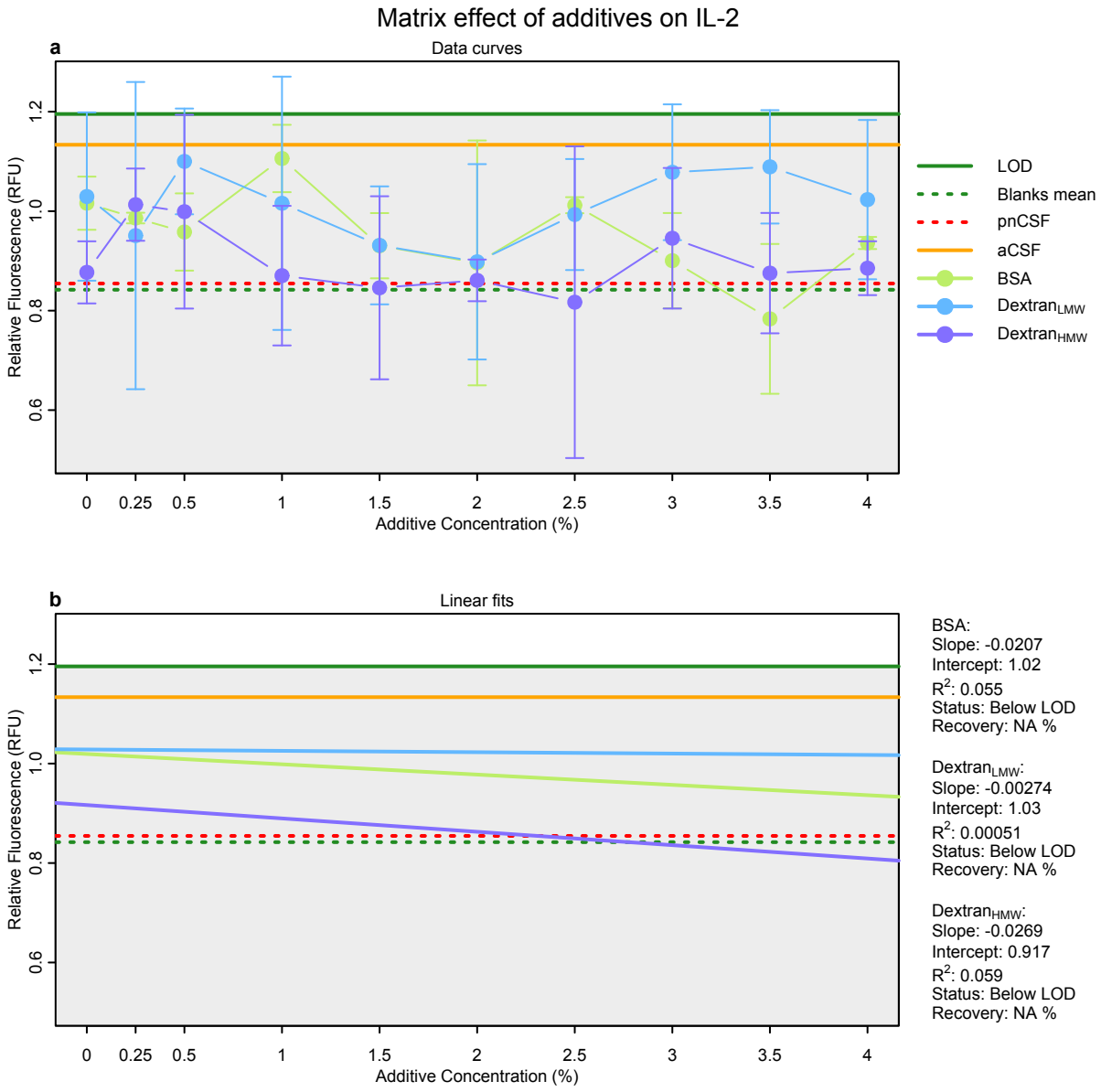

FIGURE G.S47: **Effect of additives on the measurement of IL-2.** pnCSF mixed 0-4 % additives diluted in aCSF were measured using the ACM, in order to measure the possible interference of additives on the protein measurement (matrix effect). Linear regressions of measured calibrated fluorescence values of IL-2 were used to calculate the recovery at concentrations of additives used in cerebral microdialysis. **a** Data from the average of three independent replicates is shown. **b** Median-based linear regressions from the data in **a**.

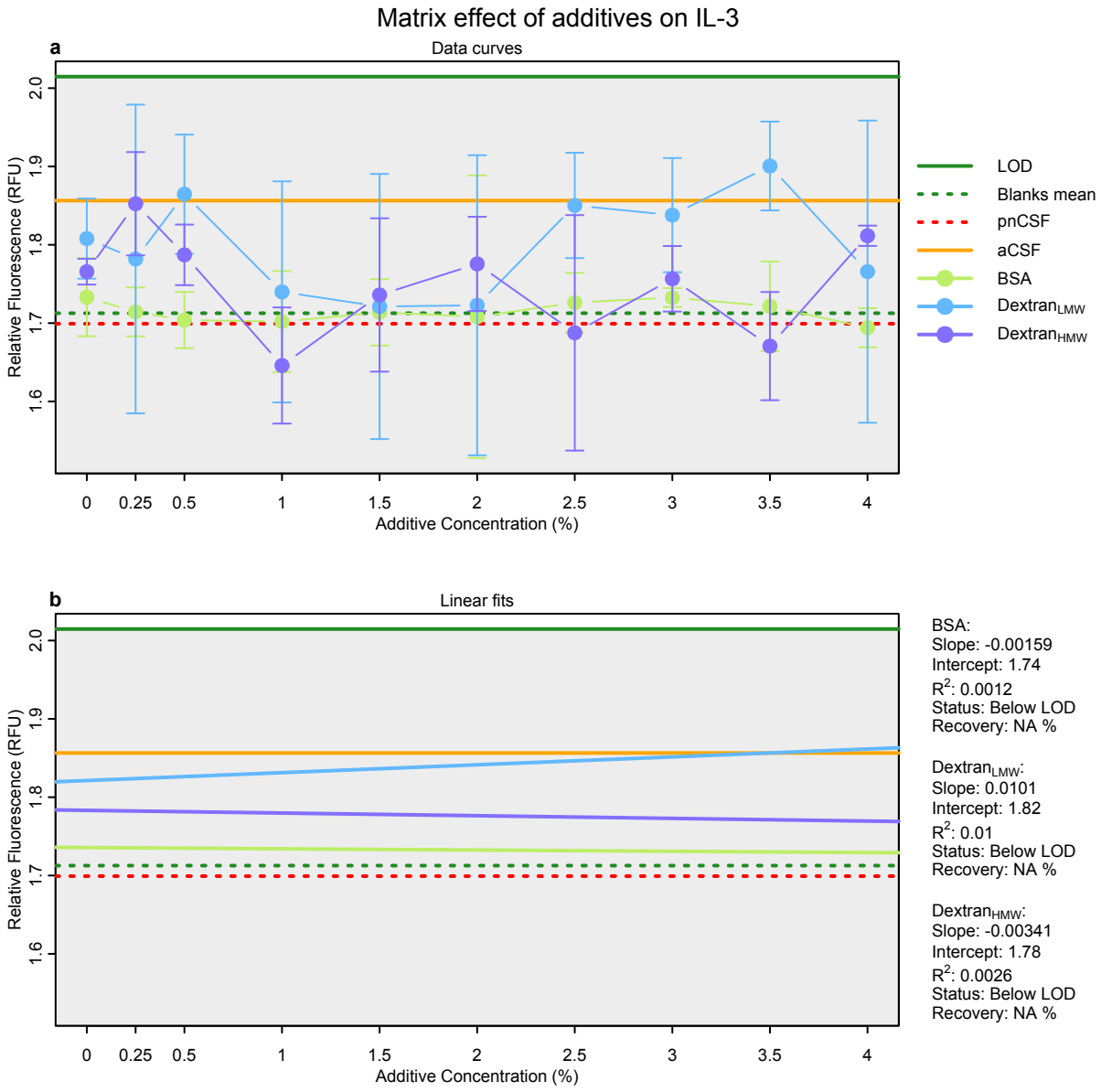

FIGURE G.S48: **Effect of additives on the measurement of IL-3.** pnCSF mixed 0-4 % additives diluted in aCSF were measured using the ACM, in order to measure the possible interference of additives on the protein measurement (matrix effect). Linear regressions of measured calibrated fluorescence values of IL-3 were used to calculate the recovery at concentrations of additives used in cerebral microdialysis. **a** Data from the average of three independent replicates is shown. **b** Median-based linear regressions from the data in **a**.

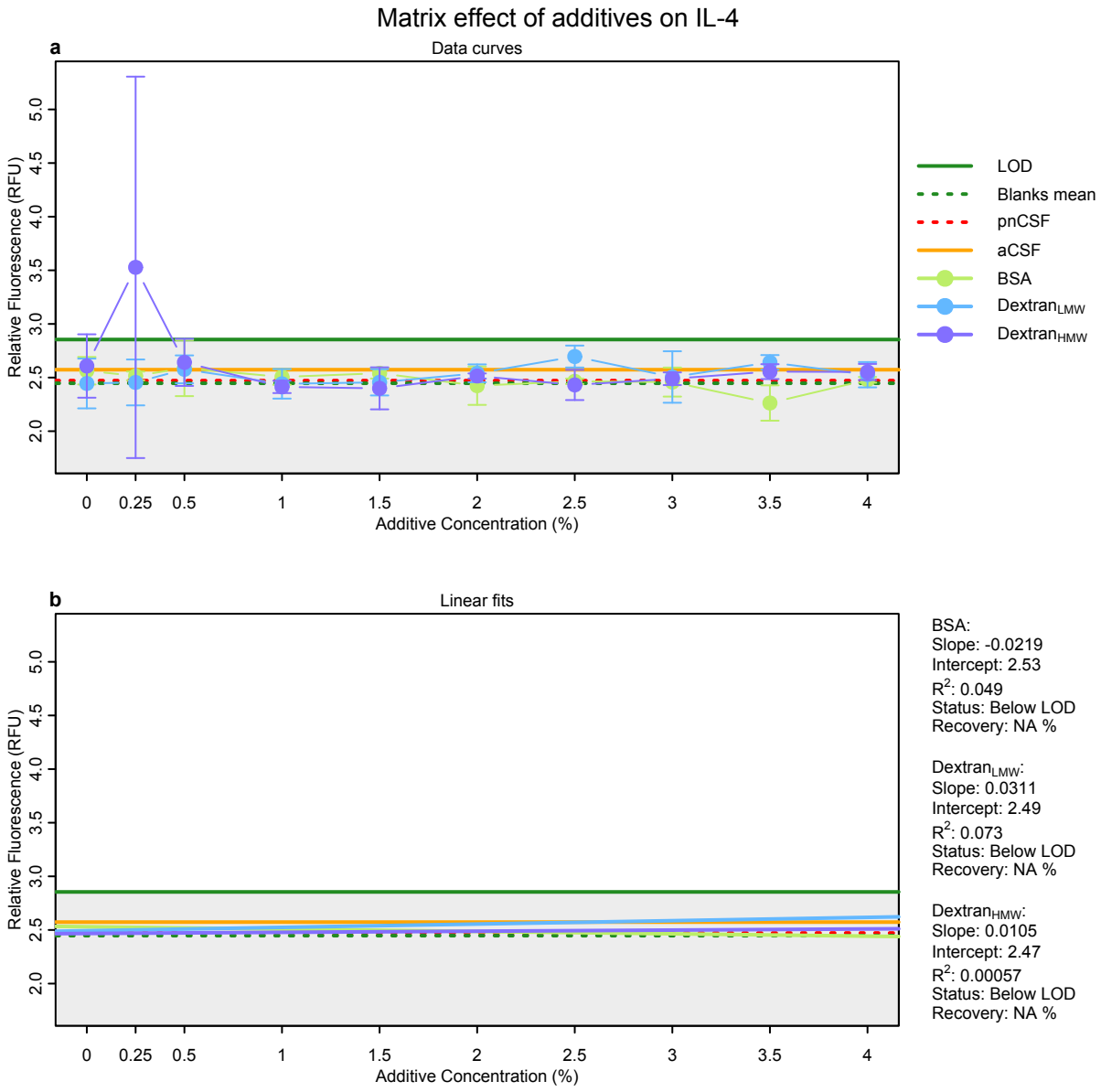

FIGURE G.S49: **Effect of additives on the measurement of IL-4.** pnCSF mixed 0-4 % additives diluted in aCSF were measured using the ACM, in order to measure the possible interference of additives on the protein measurement (matrix effect). Linear regressions of measured calibrated fluorescence values of IL-4 were used to calculate the recovery at concentrations of additives used in cerebral microdialysis. **a** Data from the average of three independent replicates is shown. **b** Median-based linear regressions from the data in **a**.

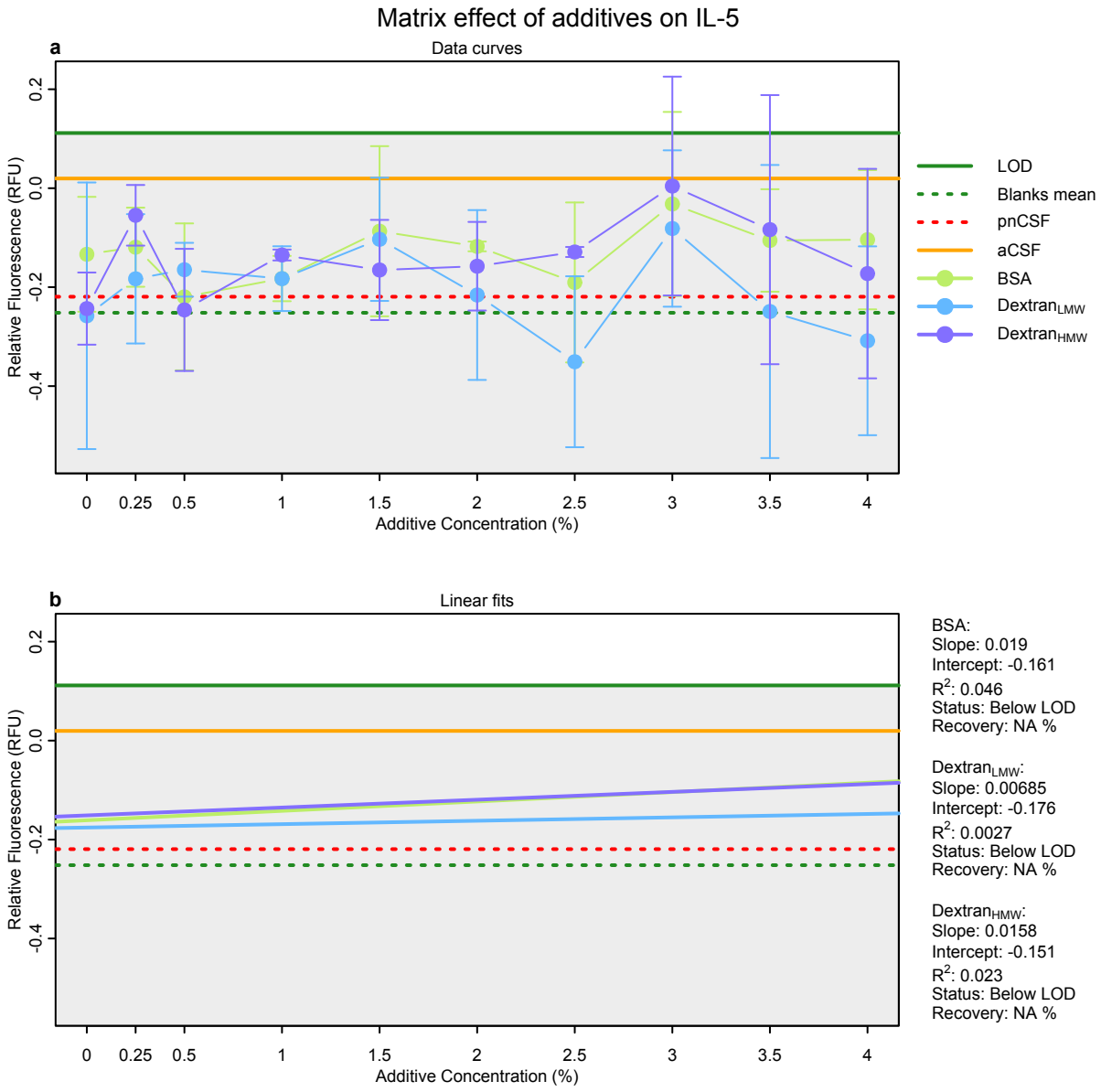

FIGURE G.S50: **Effect of additives on the measurement of IL-5.** pnCSF mixed 0-4 % additives diluted in aCSF were measured using the ACM, in order to measure the possible interference of additives on the protein measurement (matrix effect). Linear regressions of measured calibrated fluorescence values of IL-5 were used to calculate the recovery at concentrations of additives used in cerebral microdialysis. **a** Data from the average of three independent replicates is shown. **b** Median-based linear regressions from the data in **a**.

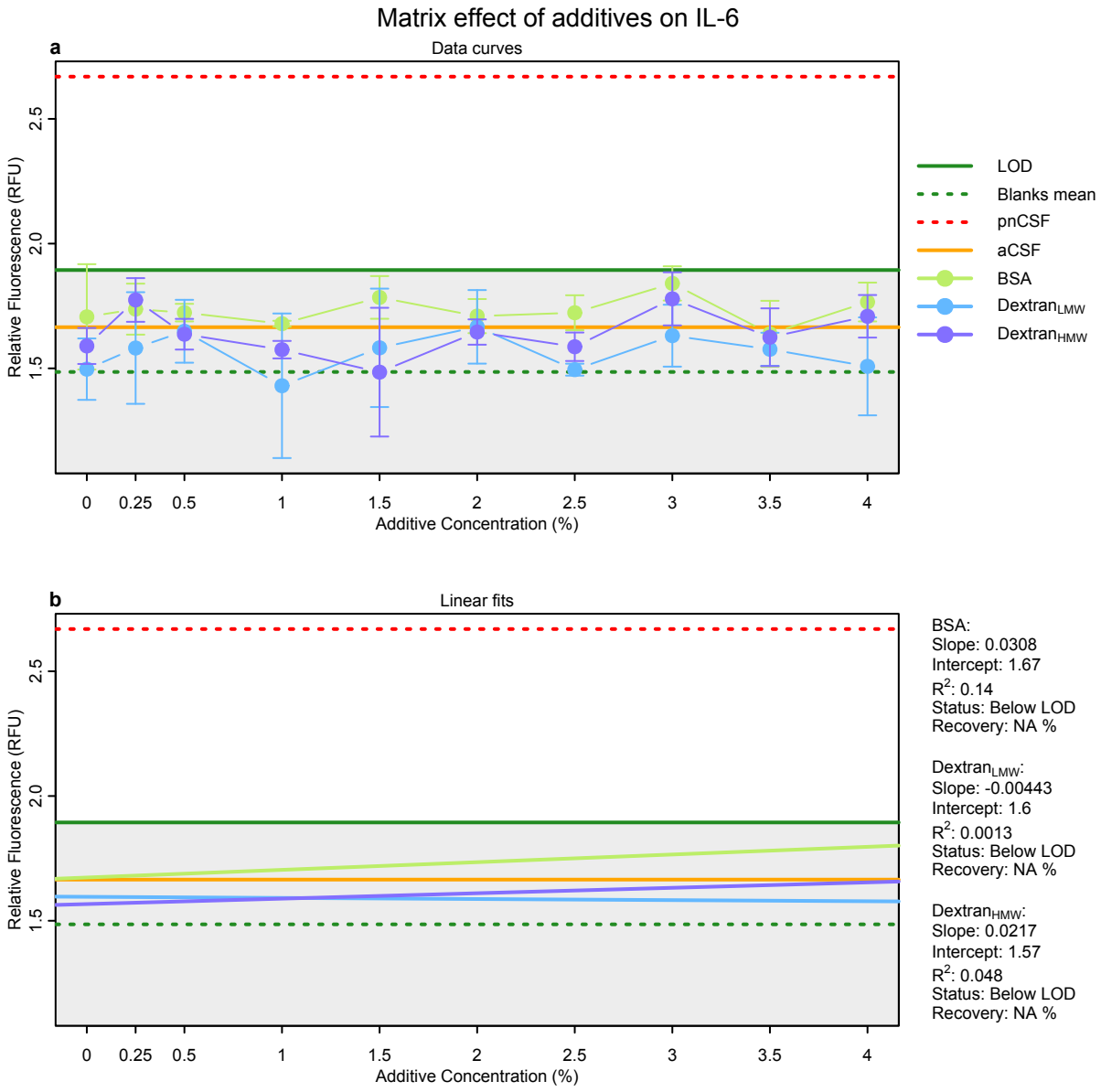

FIGURE G.S51: **Effect of additives on the measurement of IL-6.** pnCSF mixed 0-4 % additives diluted in aCSF were measured using the ACM, in order to measure the possible interference of additives on the protein measurement (matrix effect). Linear regressions of measured calibrated fluorescence values of IL-6 were used to calculate the recovery at concentrations of additives used in cerebral microdialysis. **a** Data from the average of three independent replicates is shown. **b** Median-based linear regressions from the data in **a**.

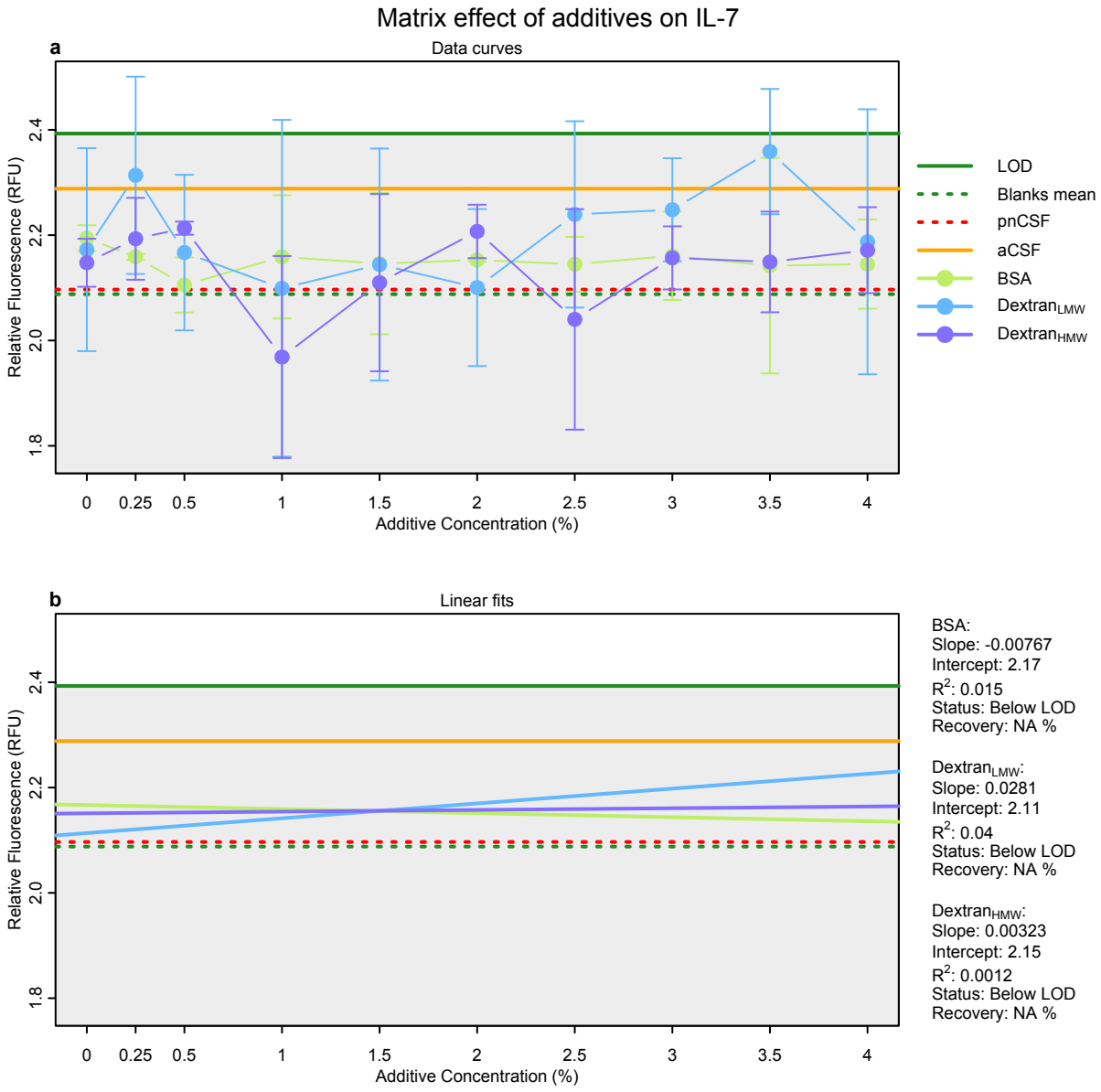

FIGURE G.S52: **Effect of additives on the measurement of IL-7.** pnCSF mixed 0-4 % additives diluted in aCSF were measured using the ACM, in order to measure the possible interference of additives on the protein measurement (matrix effect). Linear regressions of measured calibrated fluorescence values of IL-7 were used to calculate the recovery at concentrations of additives used in cerebral microdialysis. **a** Data from the average of three independent replicates is shown. **b** Median-based linear regressions from the data in **a**.

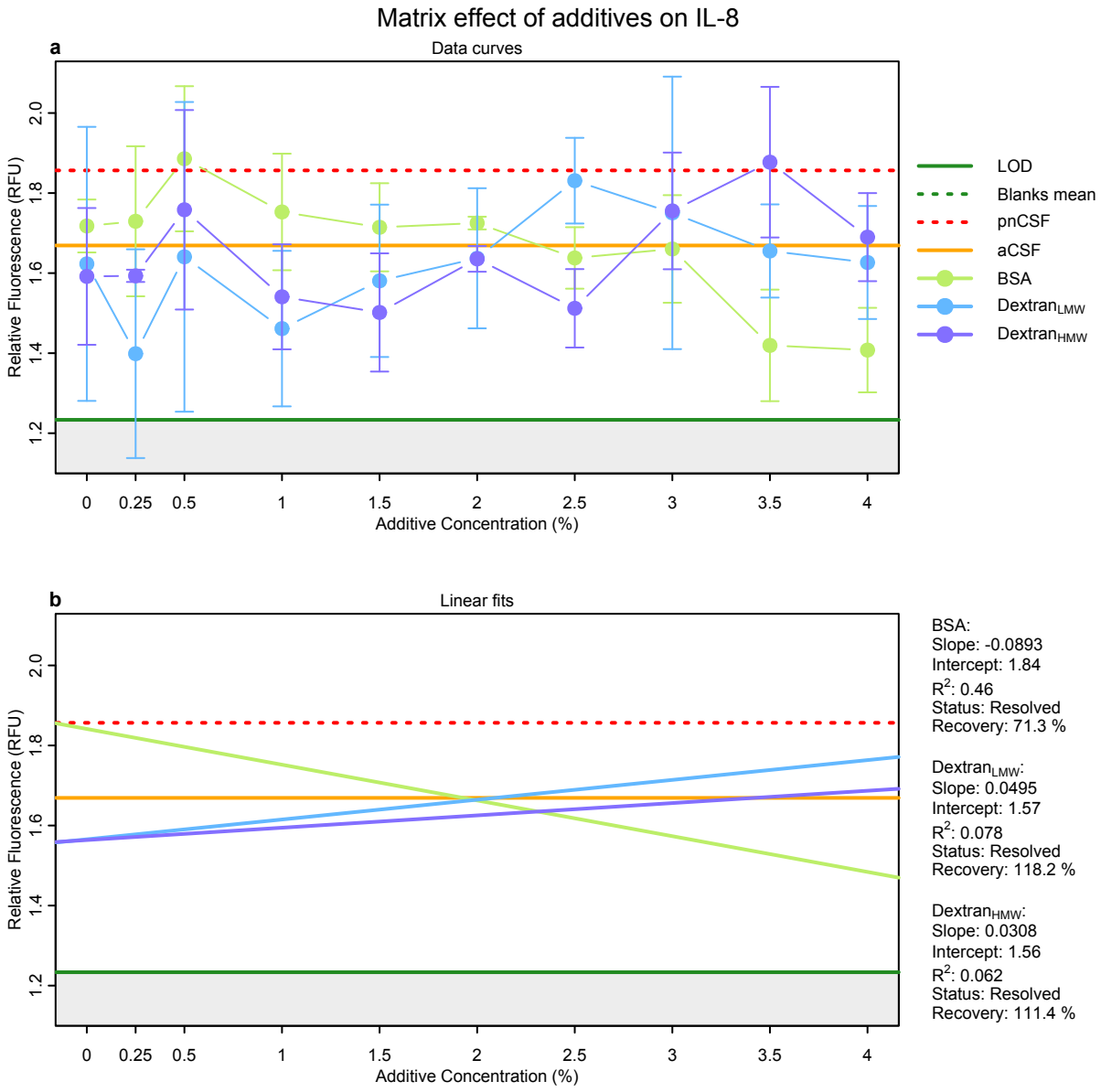

FIGURE G.S53: **Effect of additives on the measurement of IL-8.** pnCSF mixed 0-4 % additives diluted in aCSF were measured using the ACM, in order to measure the possible interference of additives on the protein measurement (matrix effect). Linear regressions of measured calibrated fluorescence values of IL-8 were used to calculate the recovery at concentrations of additives used in cerebral microdialysis. **a** Data from the average of three independent replicates is shown. **b** Median-based linear regressions from the data in **a**.

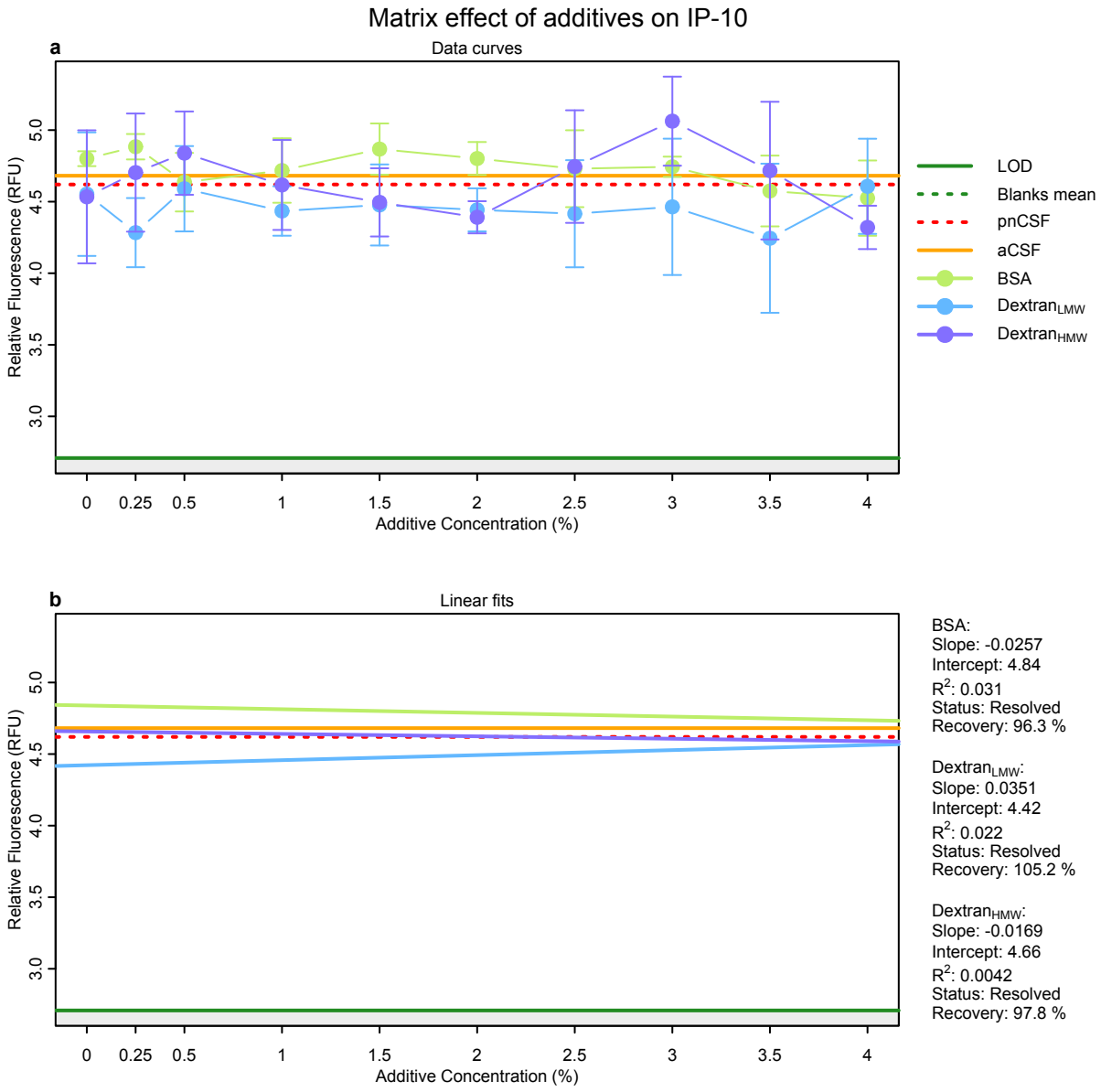

FIGURE G.S54: **Effect of additives on the measurement of IP-10.** pnCSF mixed 0-4 % additives diluted in aCSF were measured using the ACM, in order to measure the possible interference of additives on the protein measurement (matrix effect). Linear regressions of measured calibrated fluorescence values of IP-10 were used to calculate the recovery at concentrations of additives used in cerebral microdialysis. **a** Data from the average of three independent replicates is shown. **b** Median-based linear regressions from the data in **a**.

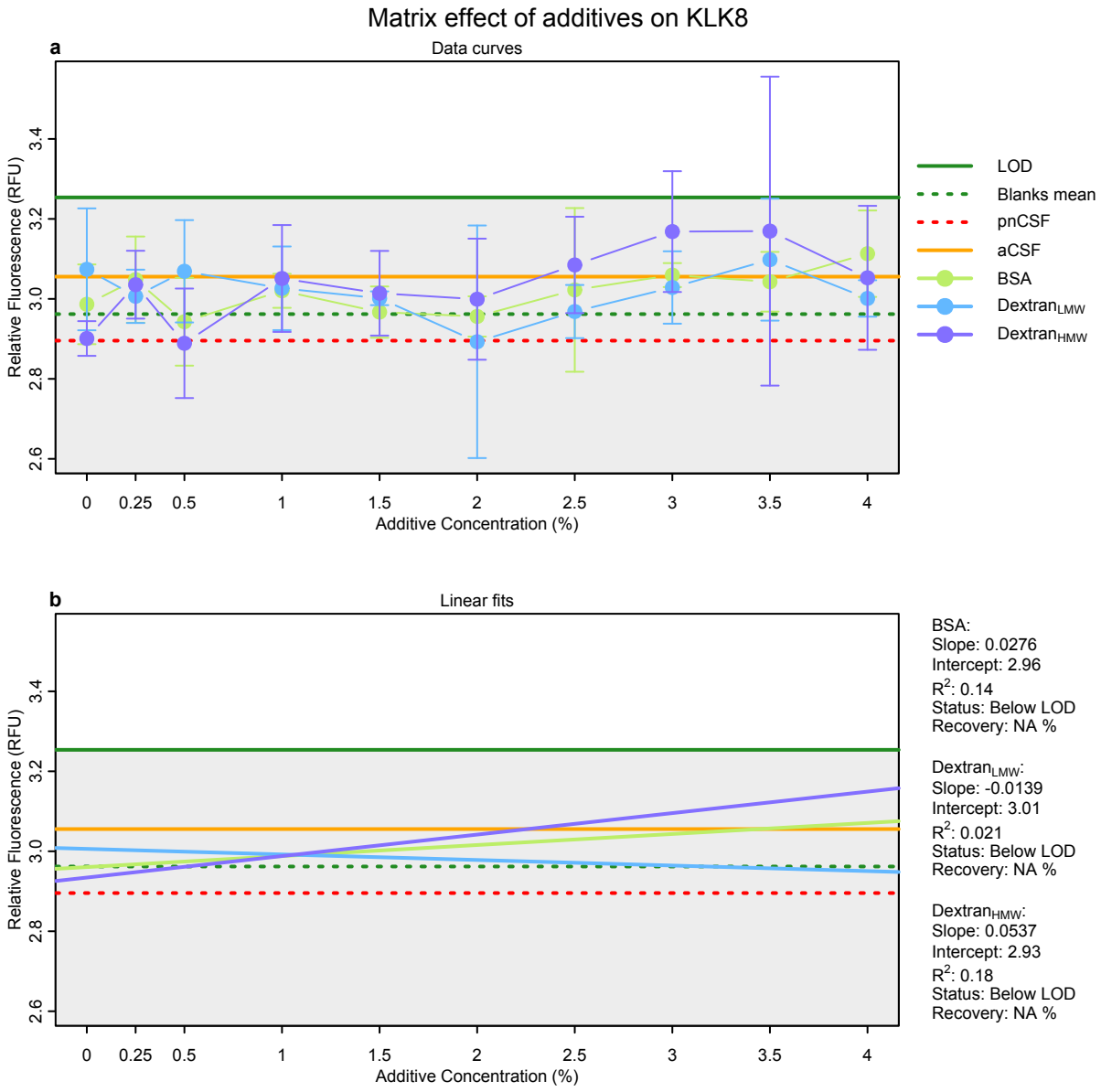

FIGURE G.S55: **Effect of additives on the measurement of KLK8.** pnCSF mixed 0-4 % additives diluted in aCSF were measured using the ACM, in order to measure the possible interference of additives on the protein measurement (matrix effect). Linear regressions of measured calibrated fluorescence values of KLK8 were used to calculate the recovery at concentrations of additives used in cerebral microdialysis. **a** Data from the average of three independent replicates is shown. **b** Median-based linear regressions from the data in **a**.

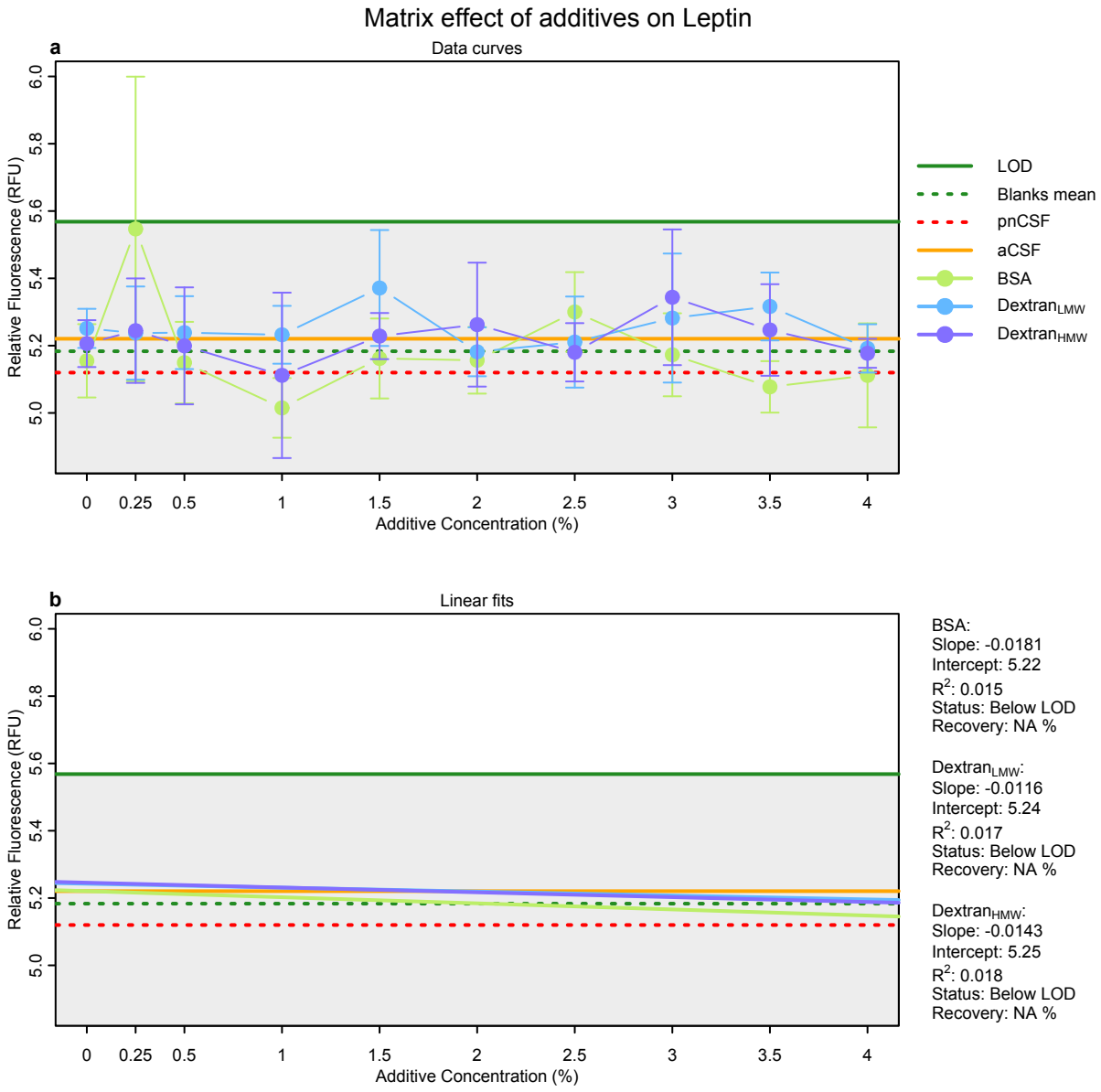

FIGURE G.S56: **Effect of additives on the measurement of Leptin.** pnCSF mixed 0-4 % additives diluted in aCSF were measured using the ACM, in order to measure the possible interference of additives on the protein measurement (matrix effect). Linear regressions of measured calibrated fluorescence values of Leptin were used to calculate the recovery at concentrations of additives used in cerebral microdialysis. **a** Data from the average of three independent replicates is shown. **b** Median-based linear regressions from the data in **a**.

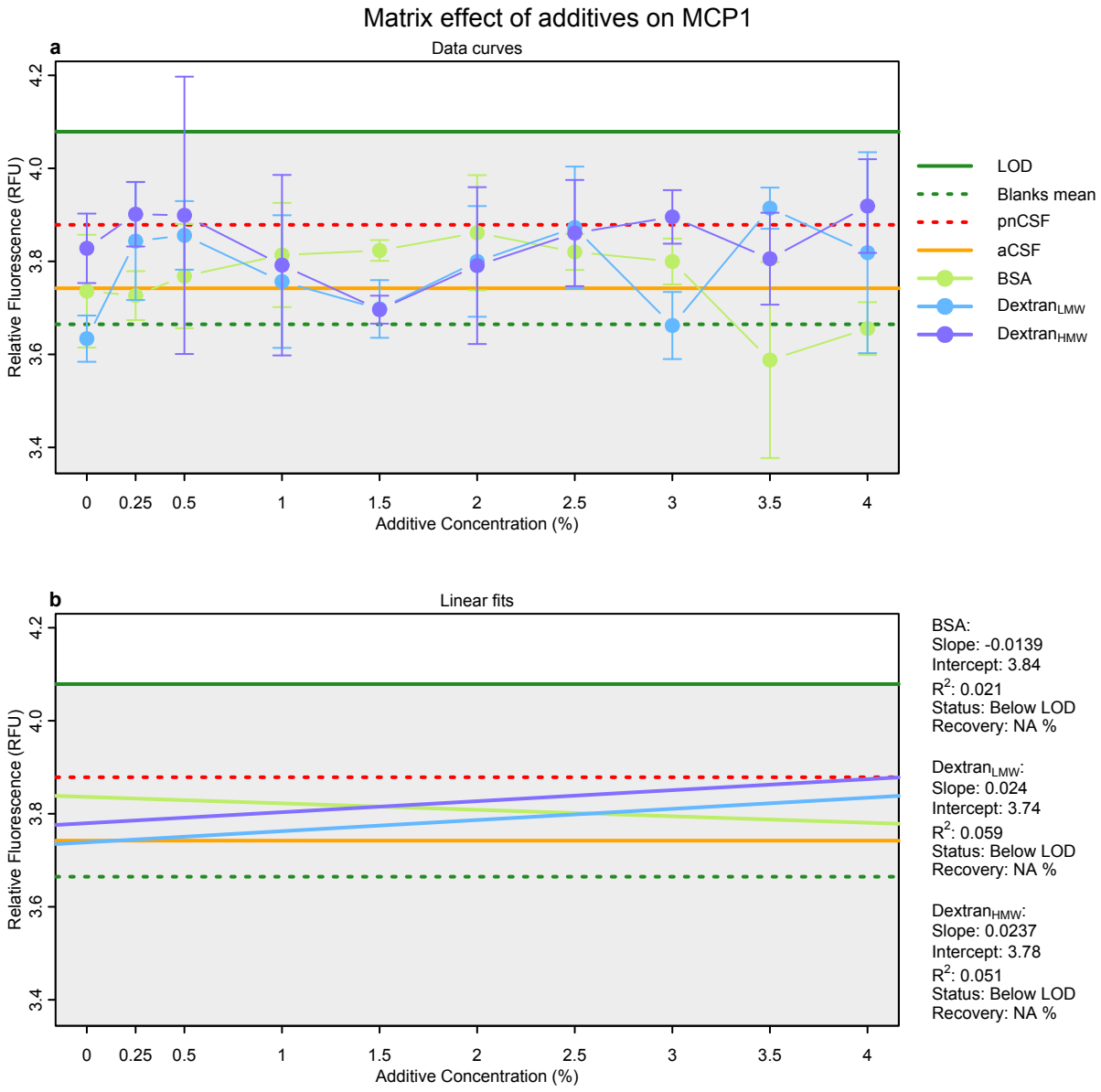

FIGURE G.S57: **Effect of additives on the measurement of MCP1.** pnCSF mixed 0-4 % additives diluted in aCSF were measured using the ACM, in order to measure the possible interference of additives on the protein measurement (matrix effect). Linear regressions of measured calibrated fluorescence values of MCP1 were used to calculate the recovery at concentrations of additives used in cerebral microdialysis. **a** Data from the average of three independent replicates is shown. **b** Median-based linear regressions from the data in **a**.

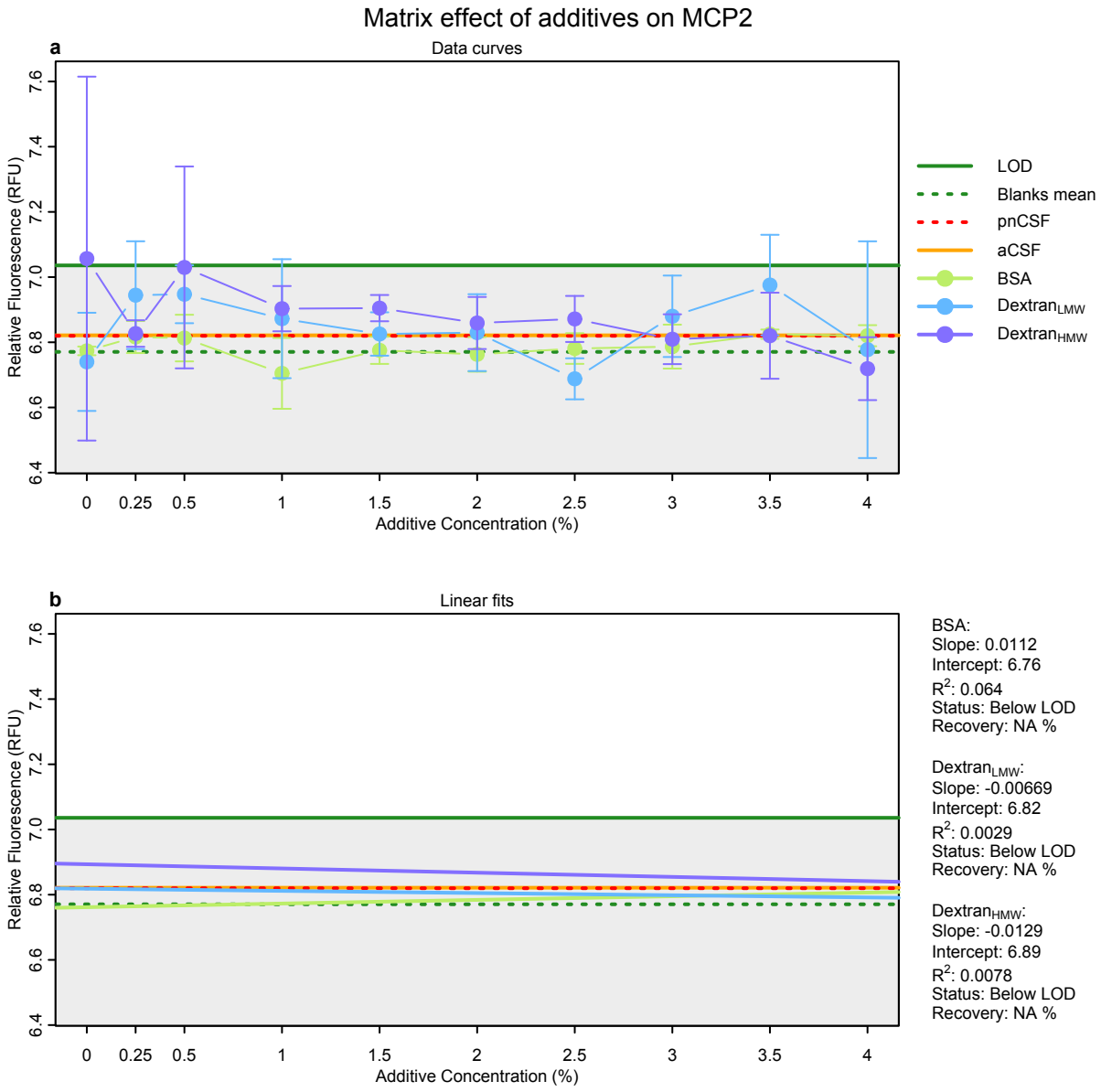

FIGURE G.S58: **Effect of additives on the measurement of MCP2.** pnCSF mixed 0-4 % additives diluted in aCSF were measured using the ACM, in order to measure the possible interference of additives on the protein measurement (matrix effect). Linear regressions of measured calibrated fluorescence values of MCP2 were used to calculate the recovery at concentrations of additives used in cerebral microdialysis. **a** Data from the average of three independent replicates is shown. **b** Median-based linear regressions from the data in **a**.

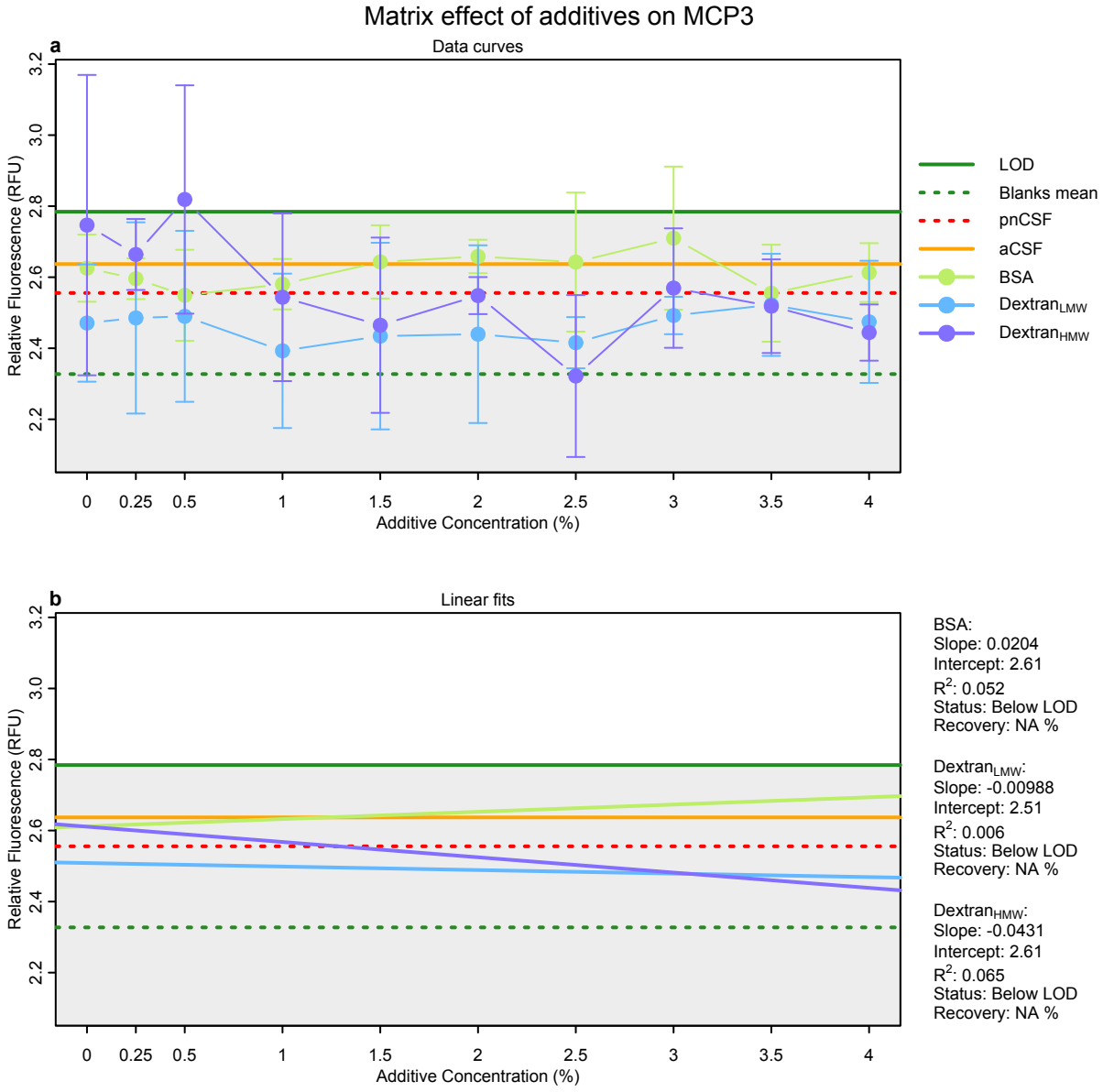

FIGURE G.S59: **Effect of additives on the measurement of MCP3.** pnCSF mixed 0-4 % additives diluted in aCSF were measured using the ACM, in order to measure the possible interference of additives on the protein measurement (matrix effect). Linear regressions of measured calibrated fluorescence values of MCP3 were used to calculate the recovery at concentrations of additives used in cerebral microdialysis. **a** Data from the average of three independent replicates is shown. **b** Median-based linear regressions from the data in **a**.

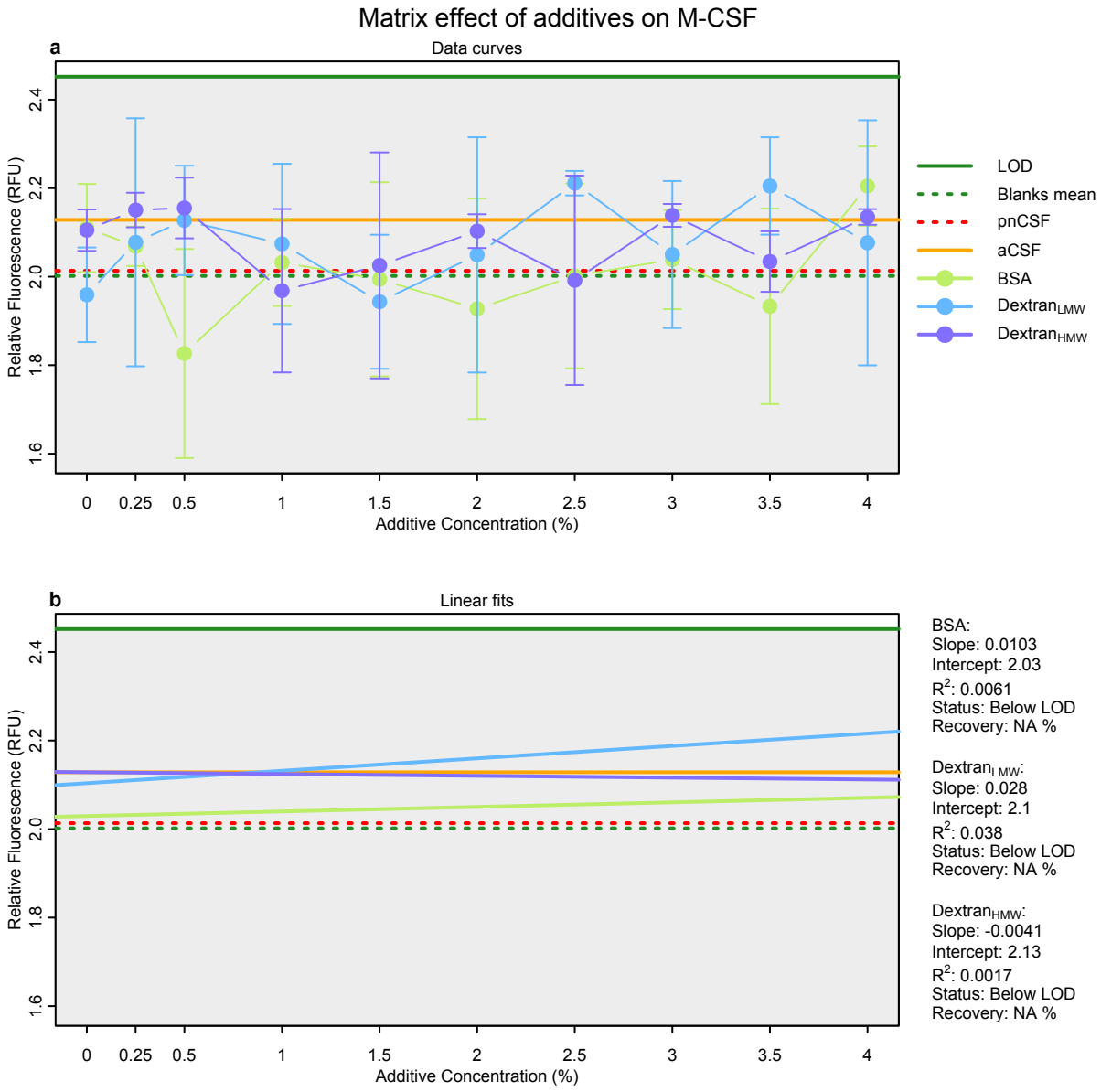

FIGURE G.S60: **Effect of additives on the measurement of M-CSF.** pnCSF mixed 0-4 % additives diluted in aCSF were measured using the ACM, in order to measure the possible interference of additives on the protein measurement (matrix effect). Linear regressions of measured calibrated fluorescence values of M-CSF were used to calculate the recovery at concentrations of additives used in cerebral microdialysis. **a** Data from the average of three independent replicates is shown. **b** Median-based linear regressions from the data in **a**.

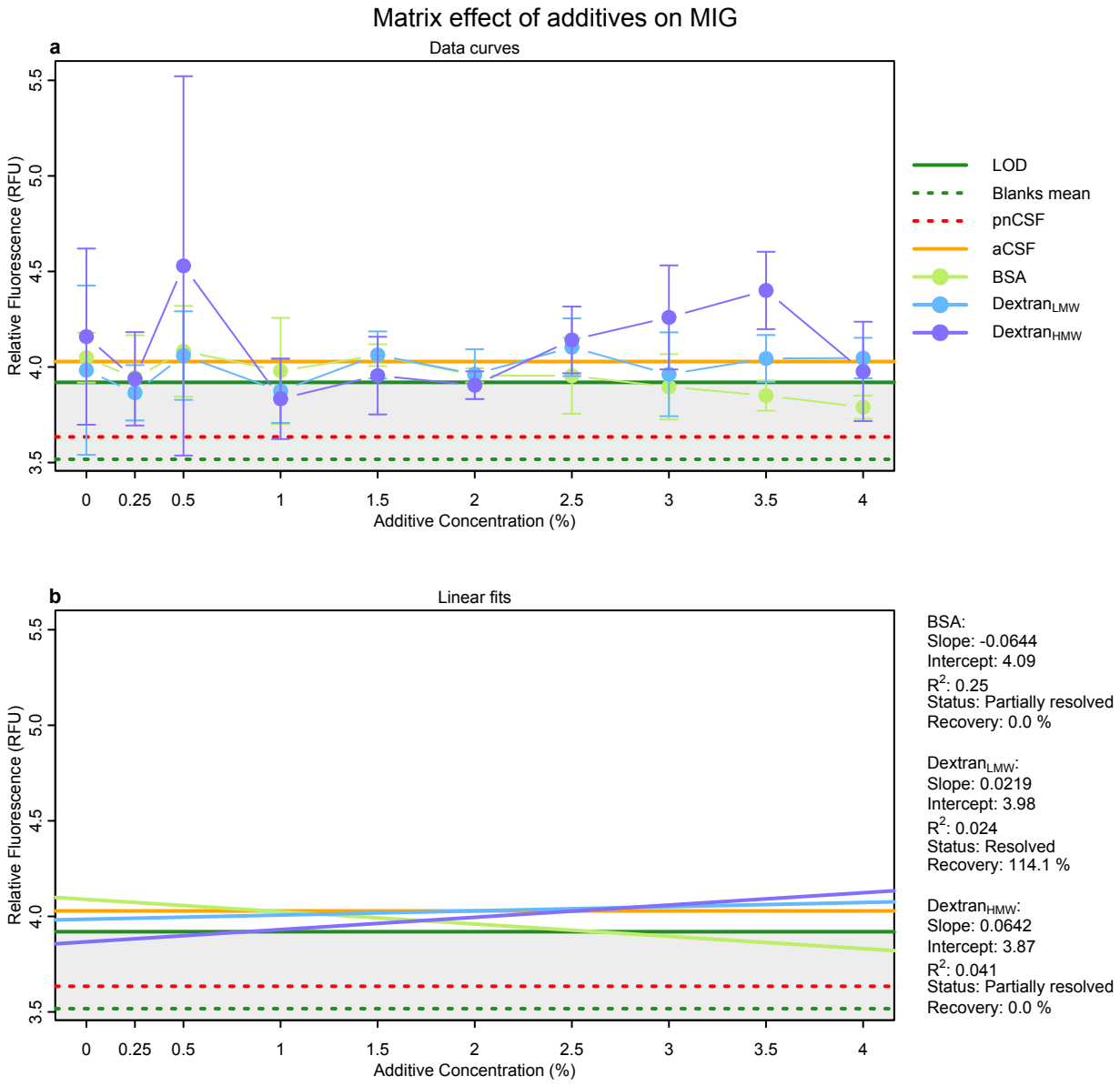

FIGURE G.S61: **Effect of additives on the measurement of MIG.** pnCSF mixed 0-4 % additives diluted in aCSF were measured using the ACM, in order to measure the possible interference of additives on the protein measurement (matrix effect). Linear regressions of measured calibrated fluorescence values of MIG were used to calculate the recovery at concentrations of additives used in cerebral microdialysis. **a** Data from the average of three independent replicates is shown. **b** Median-based linear regressions from the data in **a**.

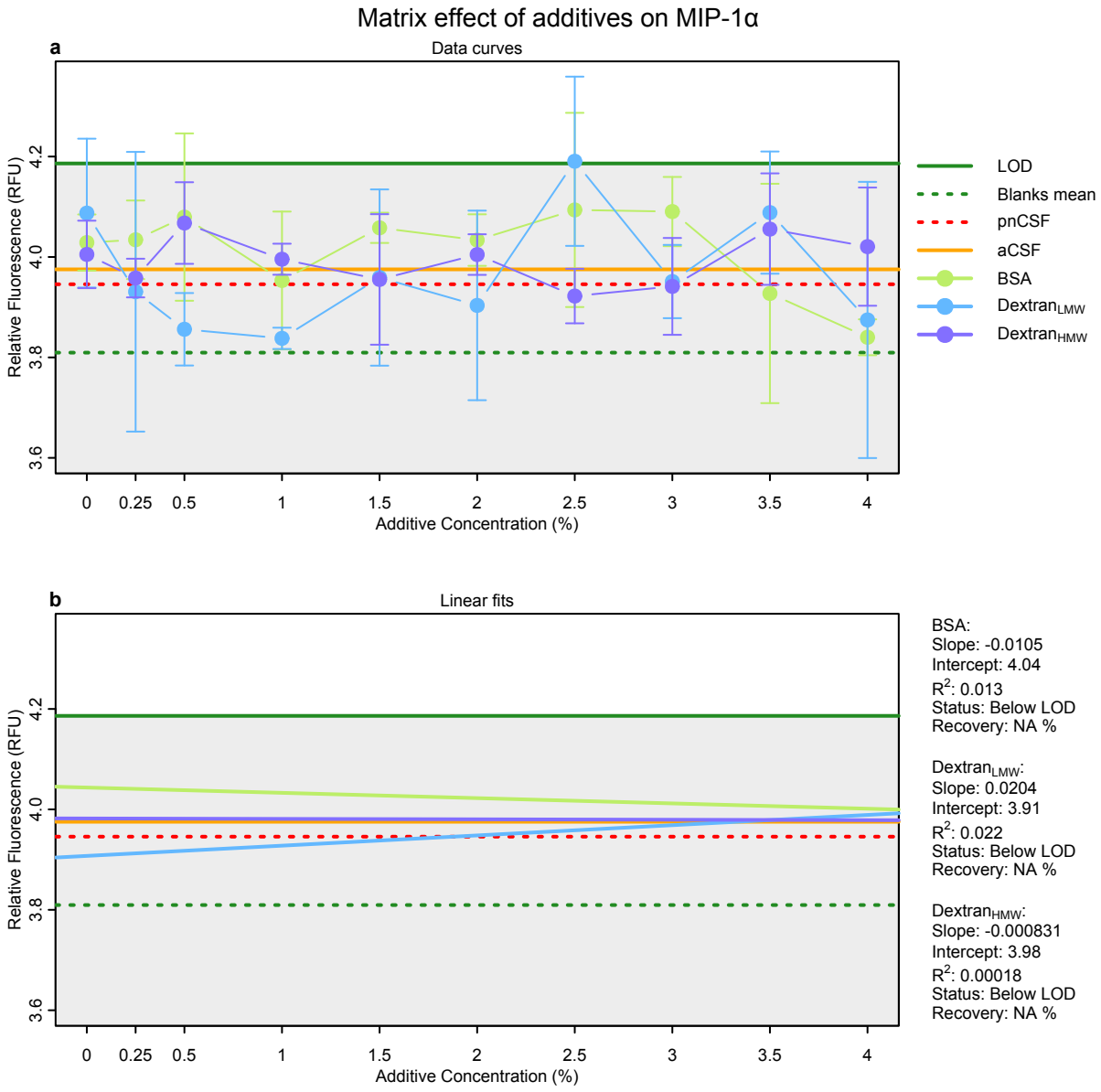

FIGURE G.S62: **Effect of additives on the measurement of MIP-1α.** pnCSF mixed 0-4 % additives diluted in aCSF were measured using the ACM, in order to measure the possible interference of additives on the protein measurement (matrix effect). Linear regressions of measured calibrated fluorescence values of MIP-1α were used to calculate the recovery at concentrations of additives used in cerebral microdialysis. **a** Data from the average of three independent replicates is shown. **b** Median-based linear regressions from the data in **a**.

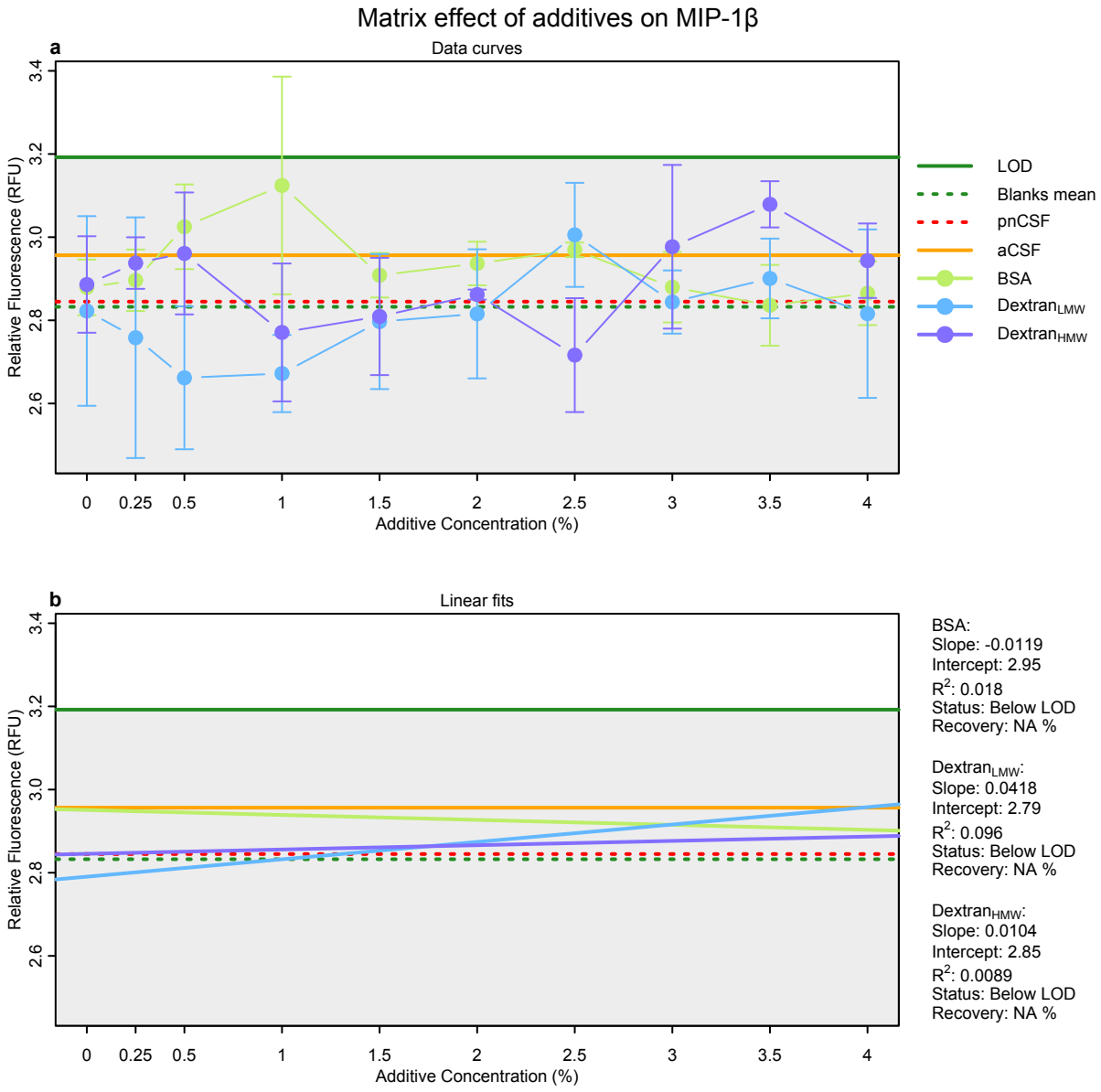

FIGURE G.S63: **Effect of additives on the measurement of MIP-1β.** pnCSF mixed 0-4 % additives diluted in aCSF were measured using the ACM, in order to measure the possible interference of additives on the protein measurement (matrix effect). Linear regressions of measured calibrated fluorescence values of MIP-1β were used to calculate the recovery at concentrations of additives used in cerebral microdialysis. **a** Data from the average of three independent replicates is shown. **b** Median-based linear regressions from the data in **a**.

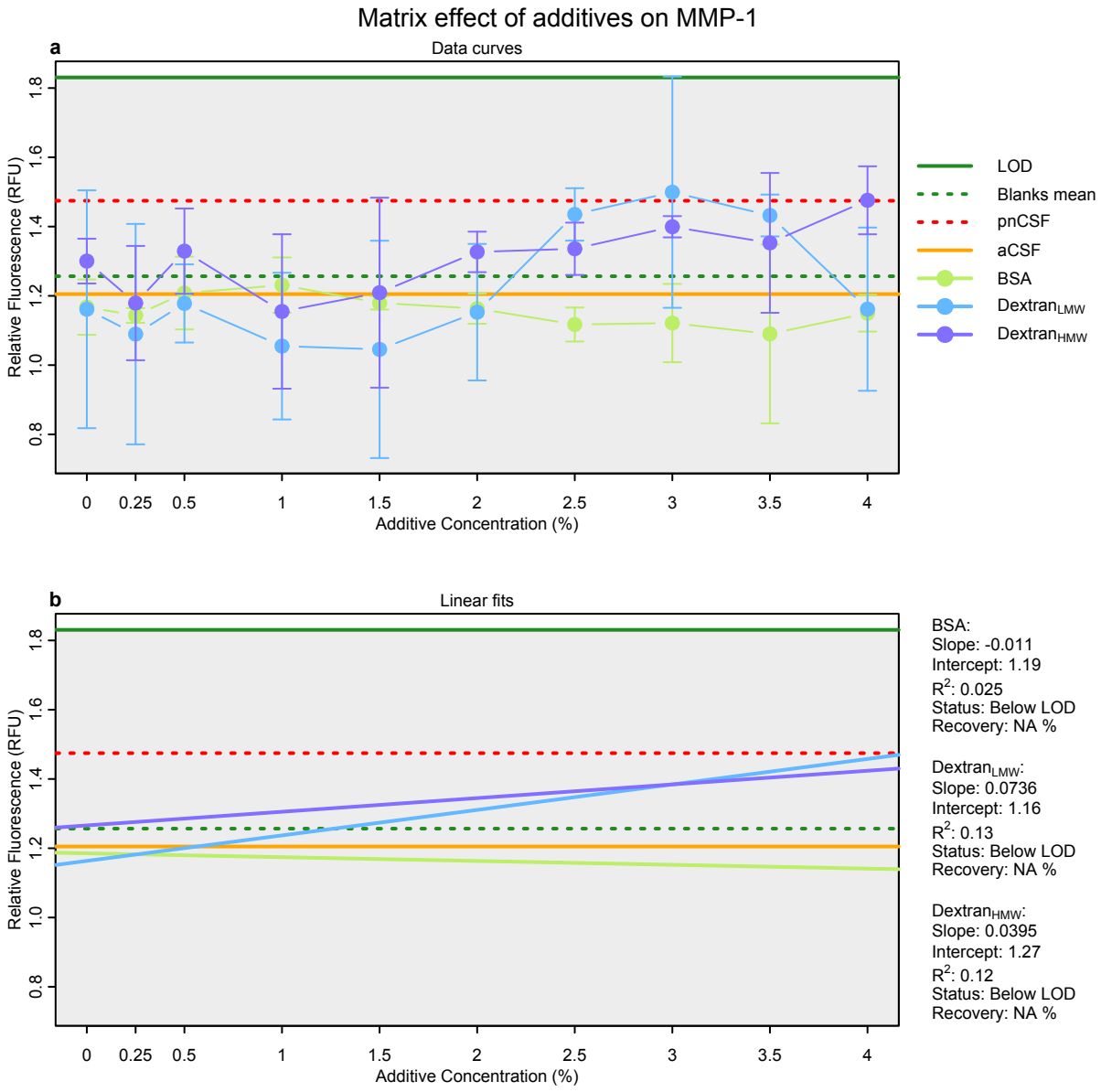

FIGURE G.S64: **Effect of additives on the measurement of MMP-1.** pnCSF mixed 0-4 % additives diluted in aCSF were measured using the ACM, in order to measure the possible interference of additives on the protein measurement (matrix effect). Linear regressions of measured calibrated fluorescence values of MMP-1 were used to calculate the recovery at concentrations of additives used in cerebral microdialysis. **a** Data from the average of three independent replicates is shown. **b** Median-based linear regressions from the data in **a**.

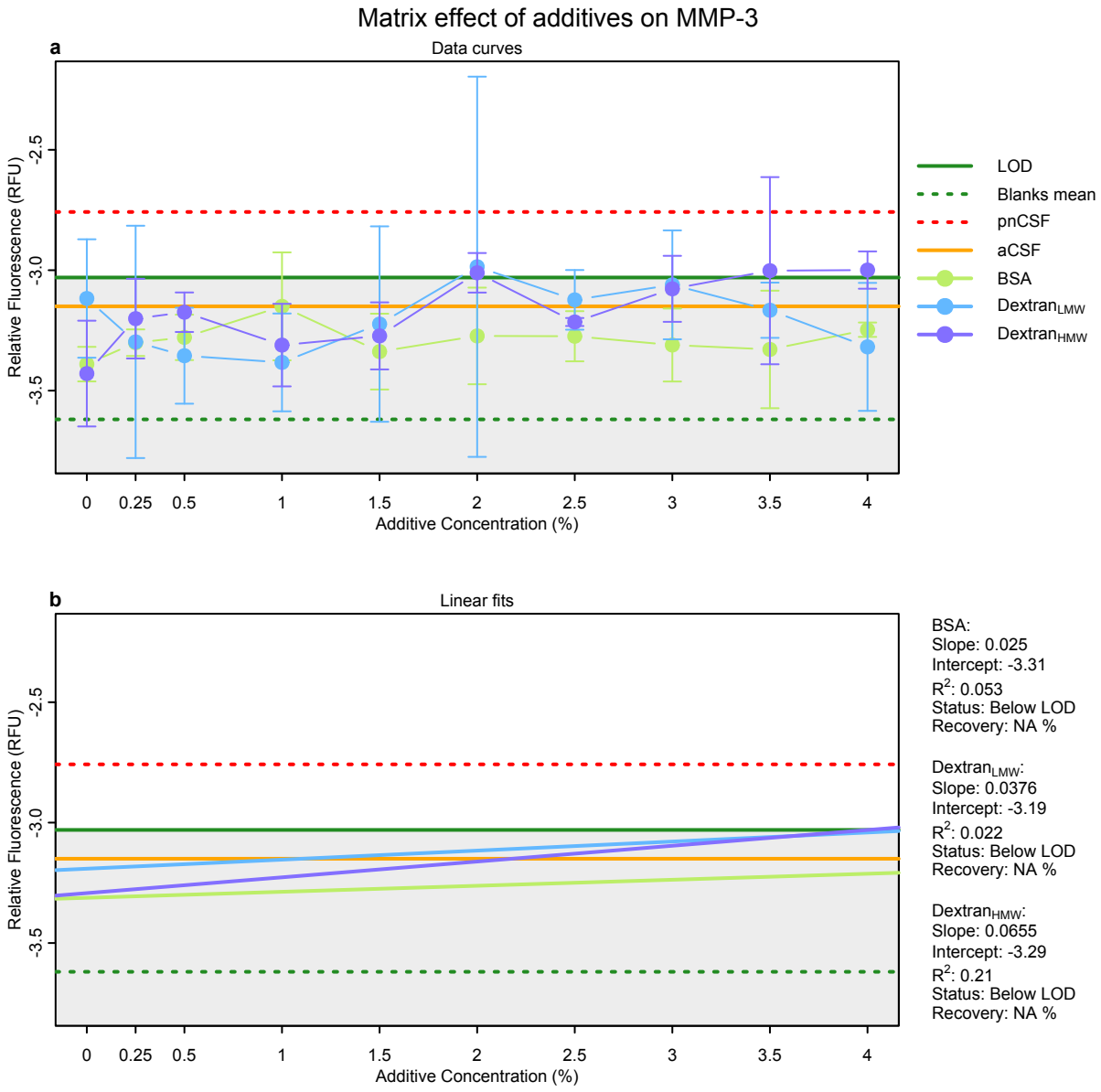

FIGURE G.S65: **Effect of additives on the measurement of MMP-3.** pnCSF mixed 0-4 % additives diluted in aCSF were measured using the ACM, in order to measure the possible interference of additives on the protein measurement (matrix effect). Linear regressions of measured calibrated fluorescence values of MMP-3 were used to calculate the recovery at concentrations of additives used in cerebral microdialysis. **a** Data from the average of three independent replicates is shown. **b** Median-based linear regressions from the data in **a**.

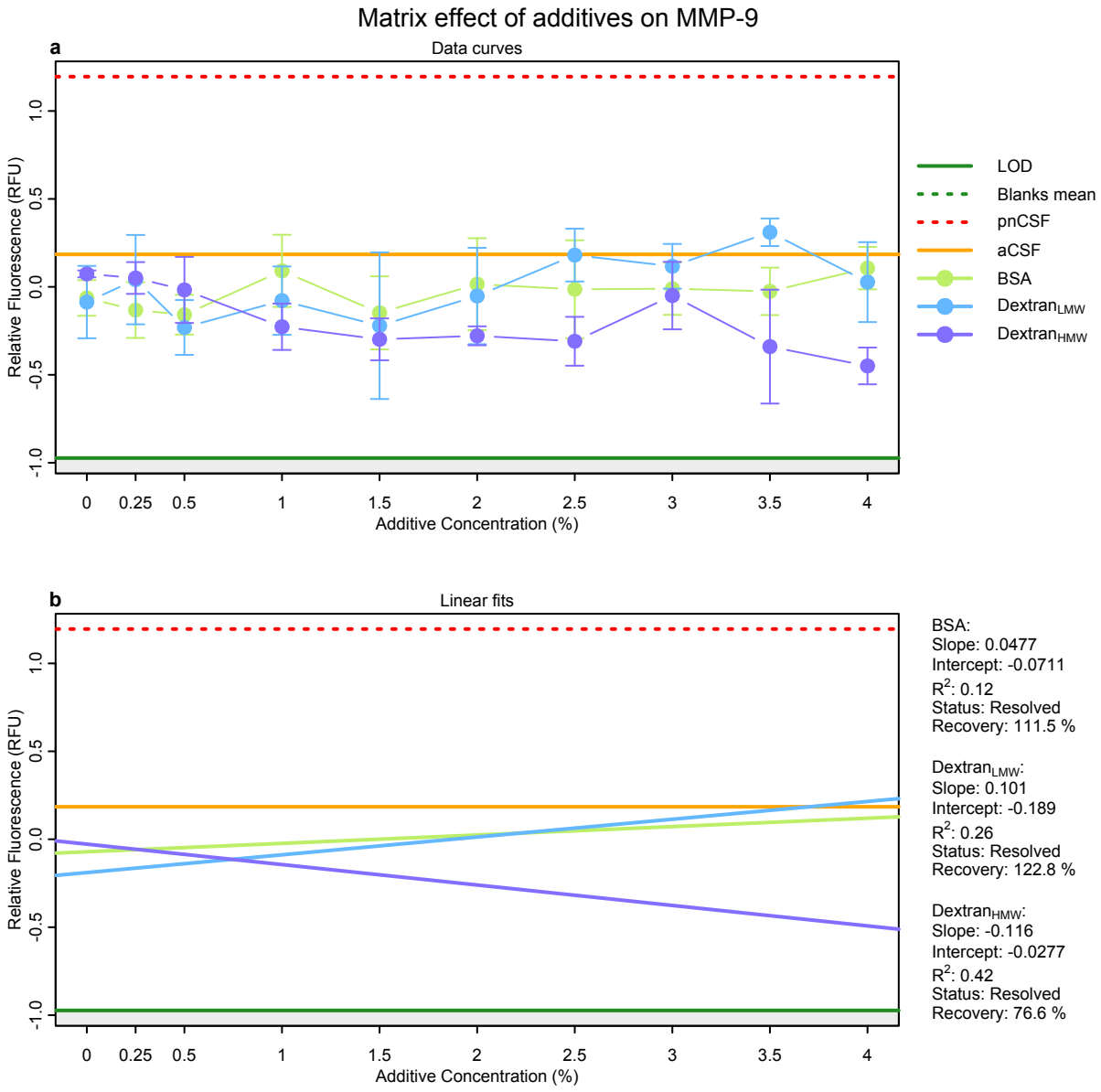

FIGURE G.S66: **Effect of additives on the measurement of MMP-9.** pnCSF mixed 0-4 % additives diluted in aCSF were measured using the ACM, in order to measure the possible interference of additives on the protein measurement (matrix effect). Linear regressions of measured calibrated fluorescence values of MMP-9 were used to calculate the recovery at concentrations of additives used in cerebral microdialysis. **a** Data from the average of three independent replicates is shown. **b** Median-based linear regressions from the data in **a**.

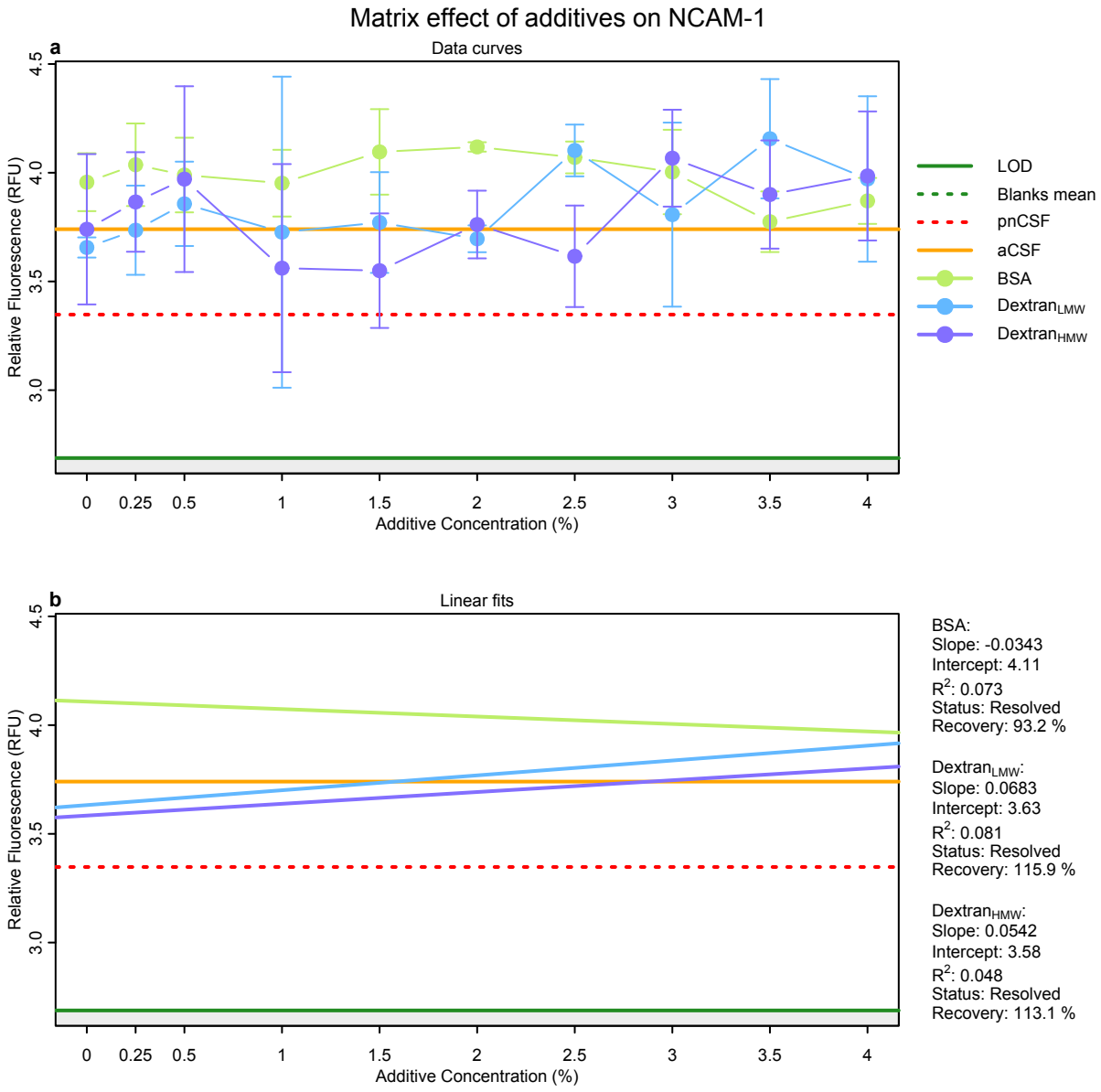

FIGURE G.S67: **Effect of additives on the measurement of NCAM-1.** pnCSF mixed 0-4 % additives diluted in aCSF were measured using the ACM, in order to measure the possible interference of additives on the protein measurement (matrix effect). Linear regressions of measured calibrated fluorescence values of NCAM-1 were used to calculate the recovery at concentrations of additives used in cerebral microdialysis. **a** Data from the average of three independent replicates is shown. **b** Median-based linear regressions from the data in **a**.

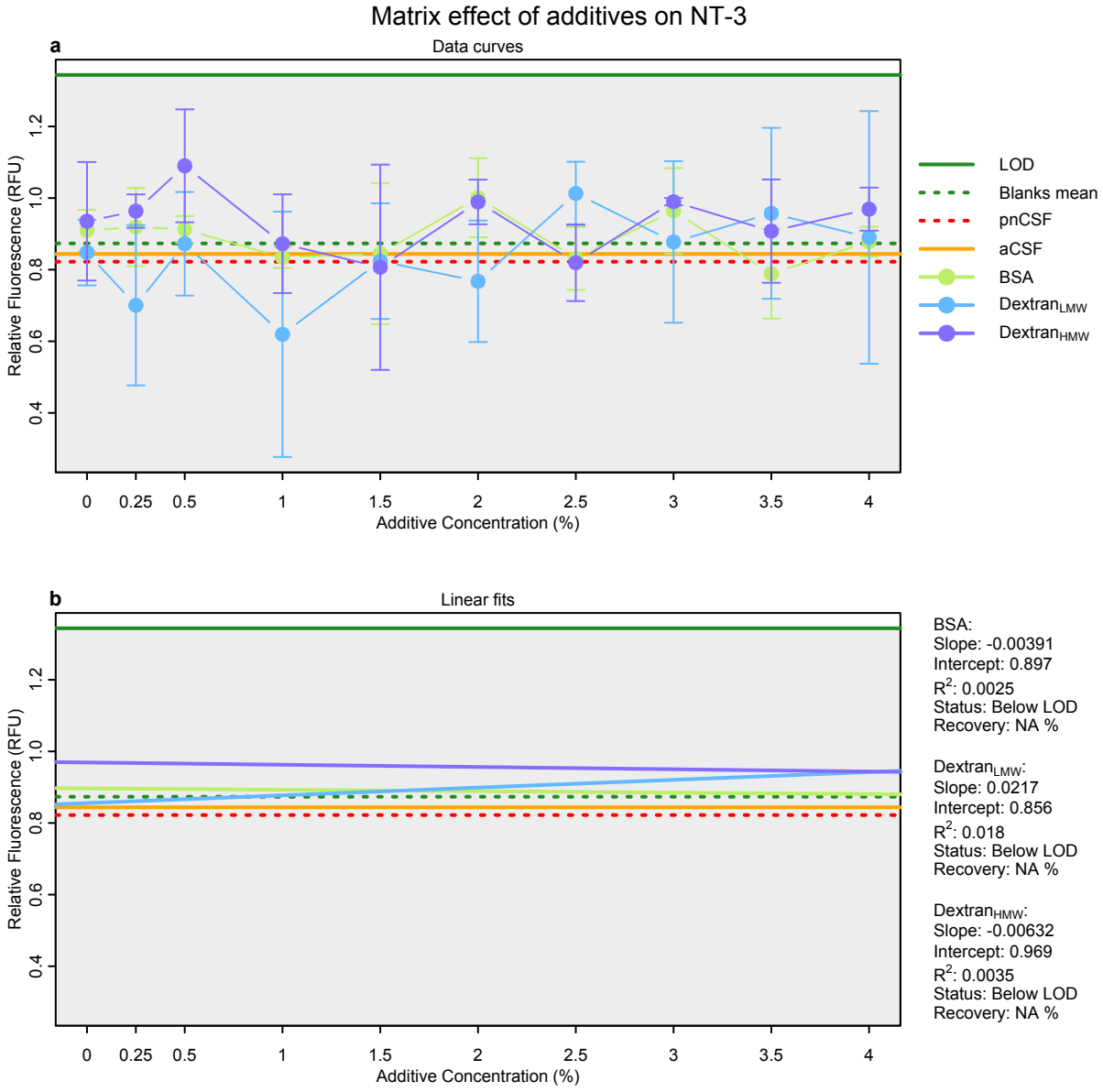

FIGURE G.S68: **Effect of additives on the measurement of NT-3.** pnCSF mixed 0-4 % additives diluted in aCSF were measured using the ACM, in order to measure the possible interference of additives on the protein measurement (matrix effect). Linear regressions of measured calibrated fluorescence values of NT-3 were used to calculate the recovery at concentrations of additives used in cerebral microdialysis. **a** Data from the average of three independent replicates is shown. **b** Median-based linear regressions from the data in **a**.

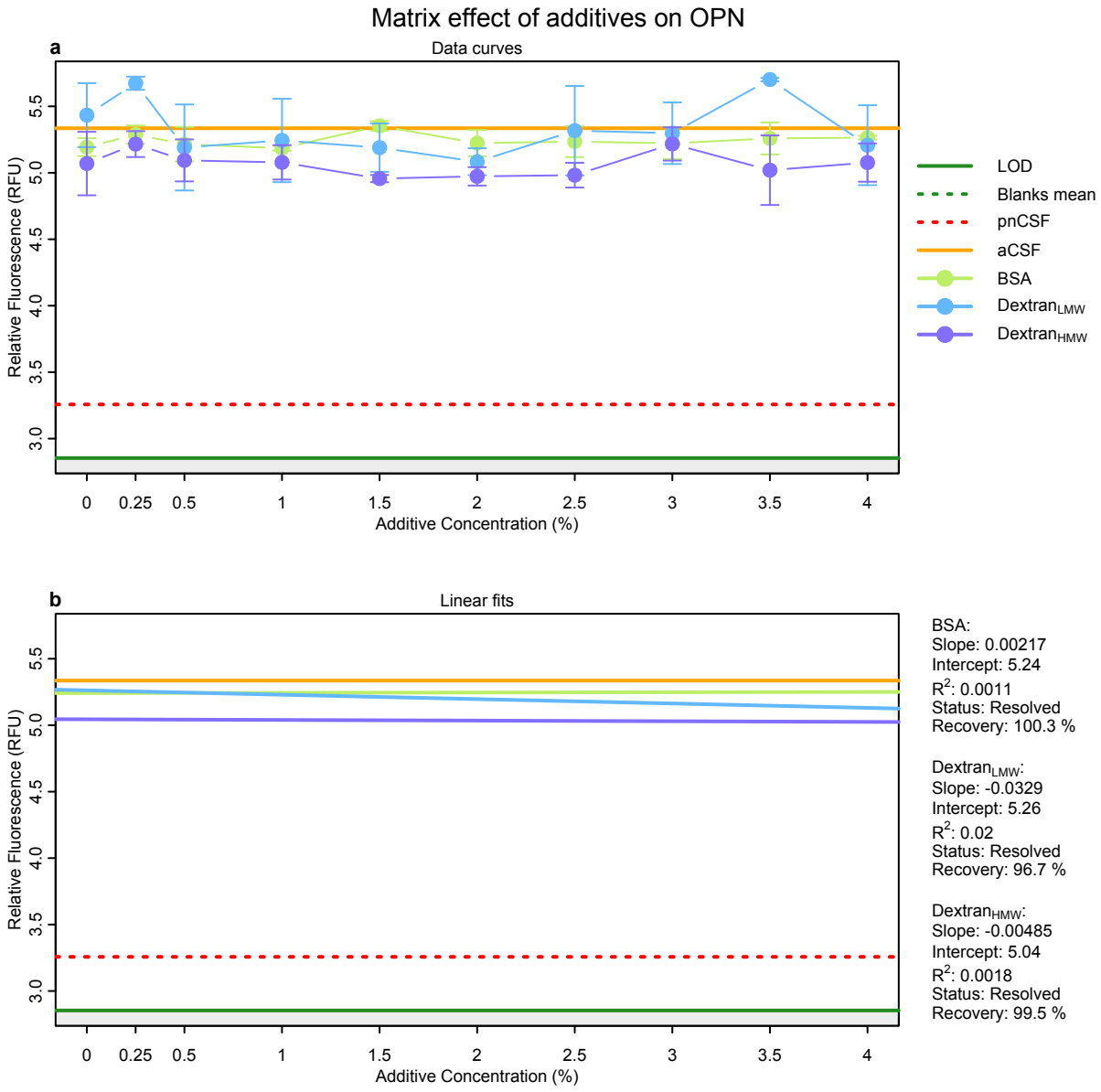

FIGURE G.S69: **Effect of additives on the measurement of OPN.** pnCSF mixed 0-4 % additives diluted in aCSF were measured using the ACM, in order to measure the possible interference of additives on the protein measurement (matrix effect). Linear regressions of measured calibrated fluorescence values of OPN were used to calculate the recovery at concentrations of additives used in cerebral microdialysis. **a** Data from the average of three independent replicates is shown. **b** Median-based linear regressions from the data in **a**.

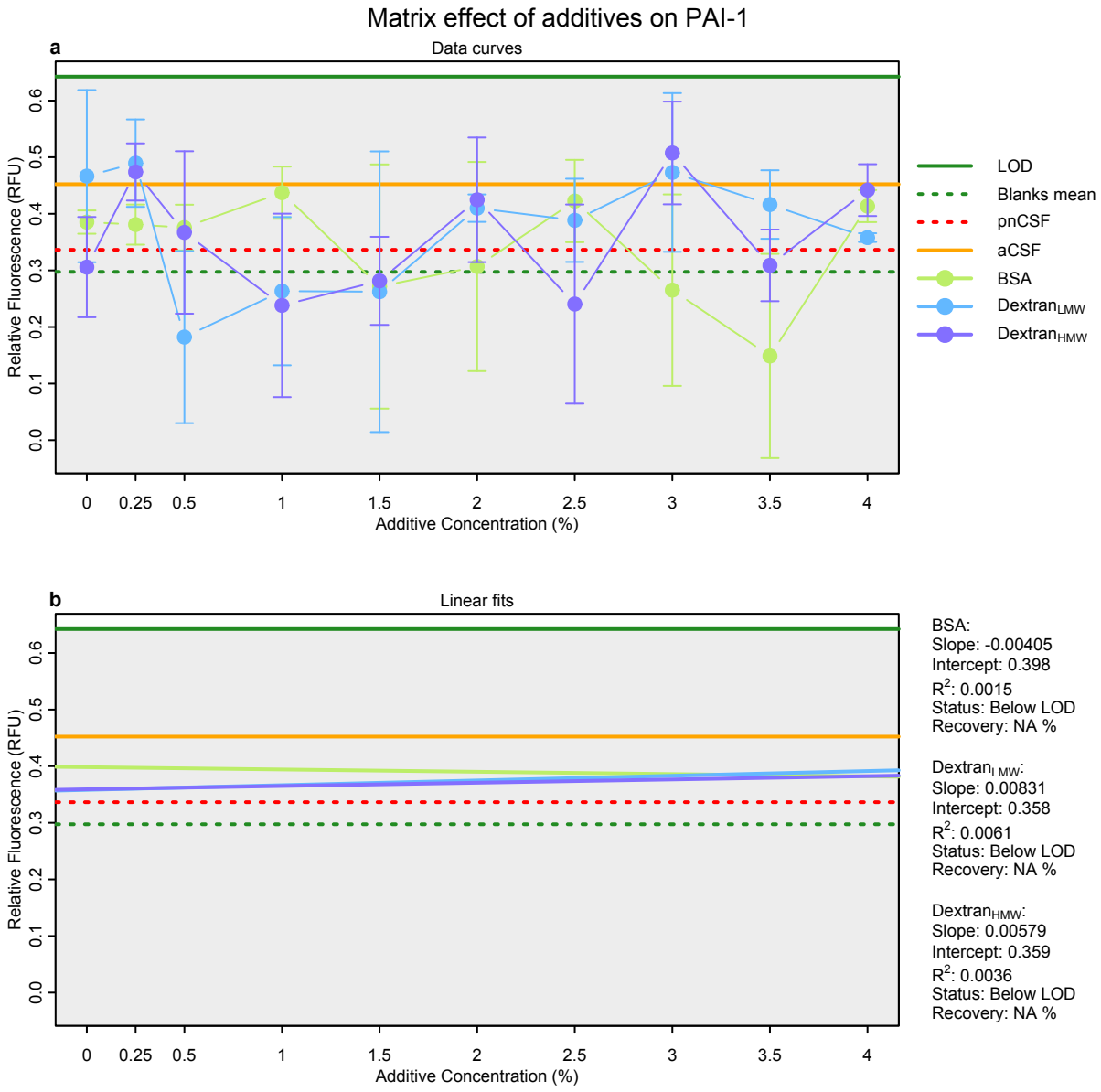

FIGURE G.S70: **Effect of additives on the measurement of PAI-1.** pnCSF mixed 0-4 % additives diluted in aCSF were measured using the ACM, in order to measure the possible interference of additives on the protein measurement (matrix effect). Linear regressions of measured calibrated fluorescence values of PAI-1 were used to calculate the recovery at concentrations of additives used in cerebral microdialysis. **a** Data from the average of three independent replicates is shown. **b** Median-based linear regressions from the data in **a**.

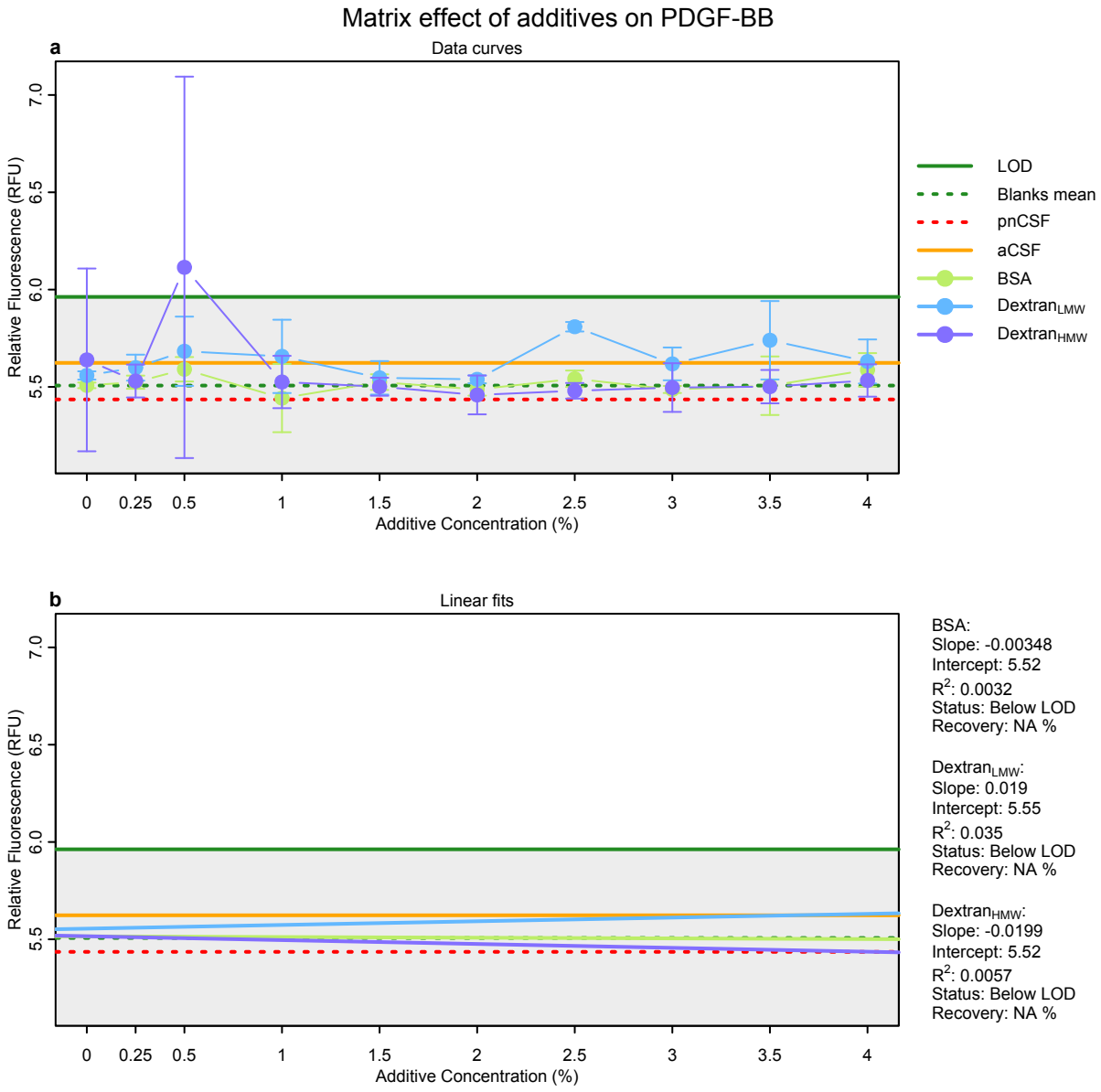

FIGURE G.S71: **Effect of additives on the measurement of PDGF-BB.** pnCSF mixed 0-4 % additives diluted in aCSF were measured using the ACM, in order to measure the possible interference of additives on the protein measurement (matrix effect). Linear regressions of measured calibrated fluorescence values of PDGF-BB were used to calculate the recovery at concentrations of additives used in cerebral microdialysis. **a** Data from the average of three independent replicates is shown. **b** Median-based linear regressions from the data in **a**.

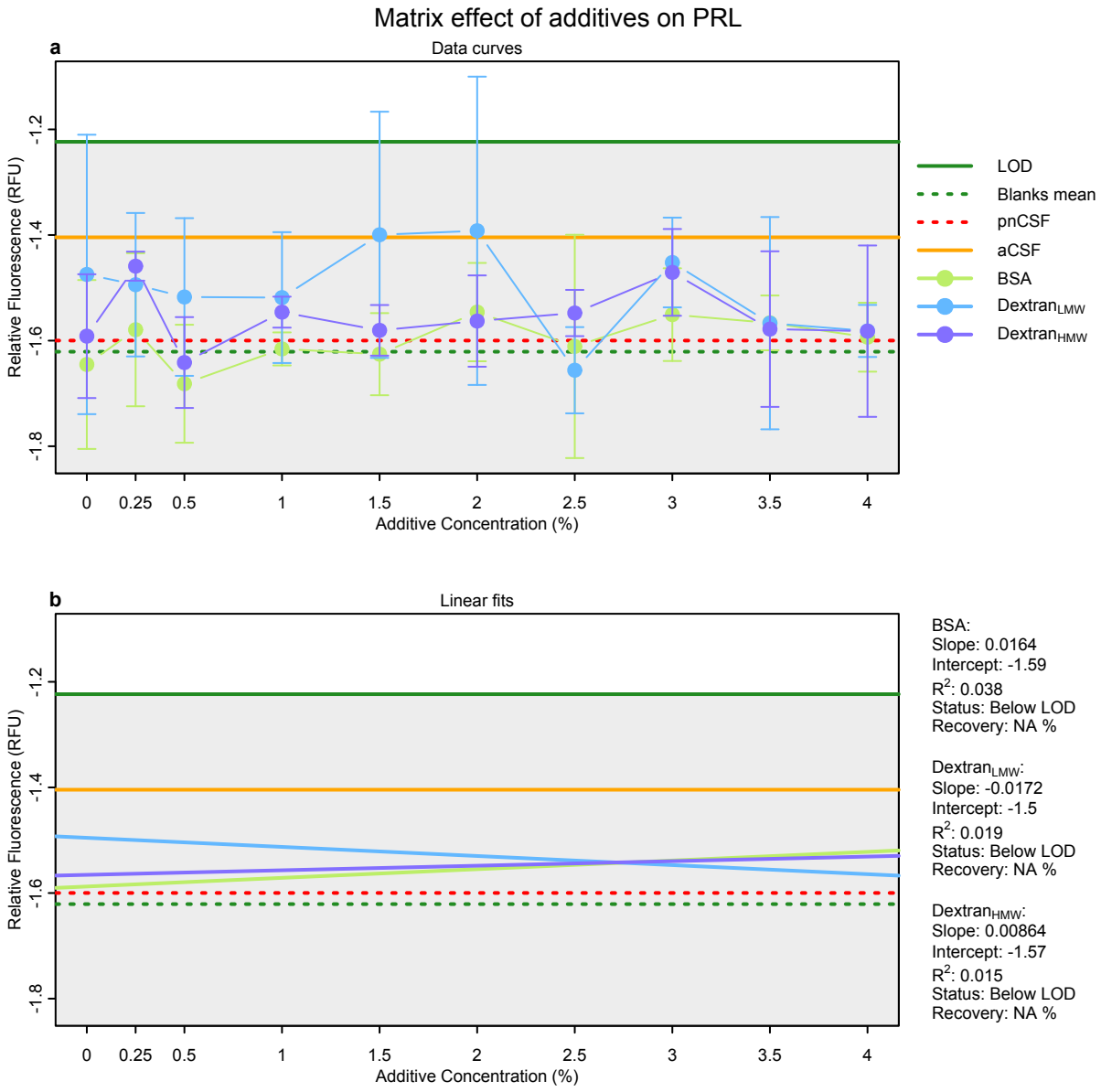

FIGURE G.S72: **Effect of additives on the measurement of PRL.** pnCSF mixed 0-4 % additives diluted in aCSF were measured using the ACM, in order to measure the possible interference of additives on the protein measurement (matrix effect). Linear regressions of measured calibrated fluorescence values of PRL were used to calculate the recovery at concentrations of additives used in cerebral microdialysis. **a** Data from the average of three independent replicates is shown. **b** Median-based linear regressions from the data in **a**.

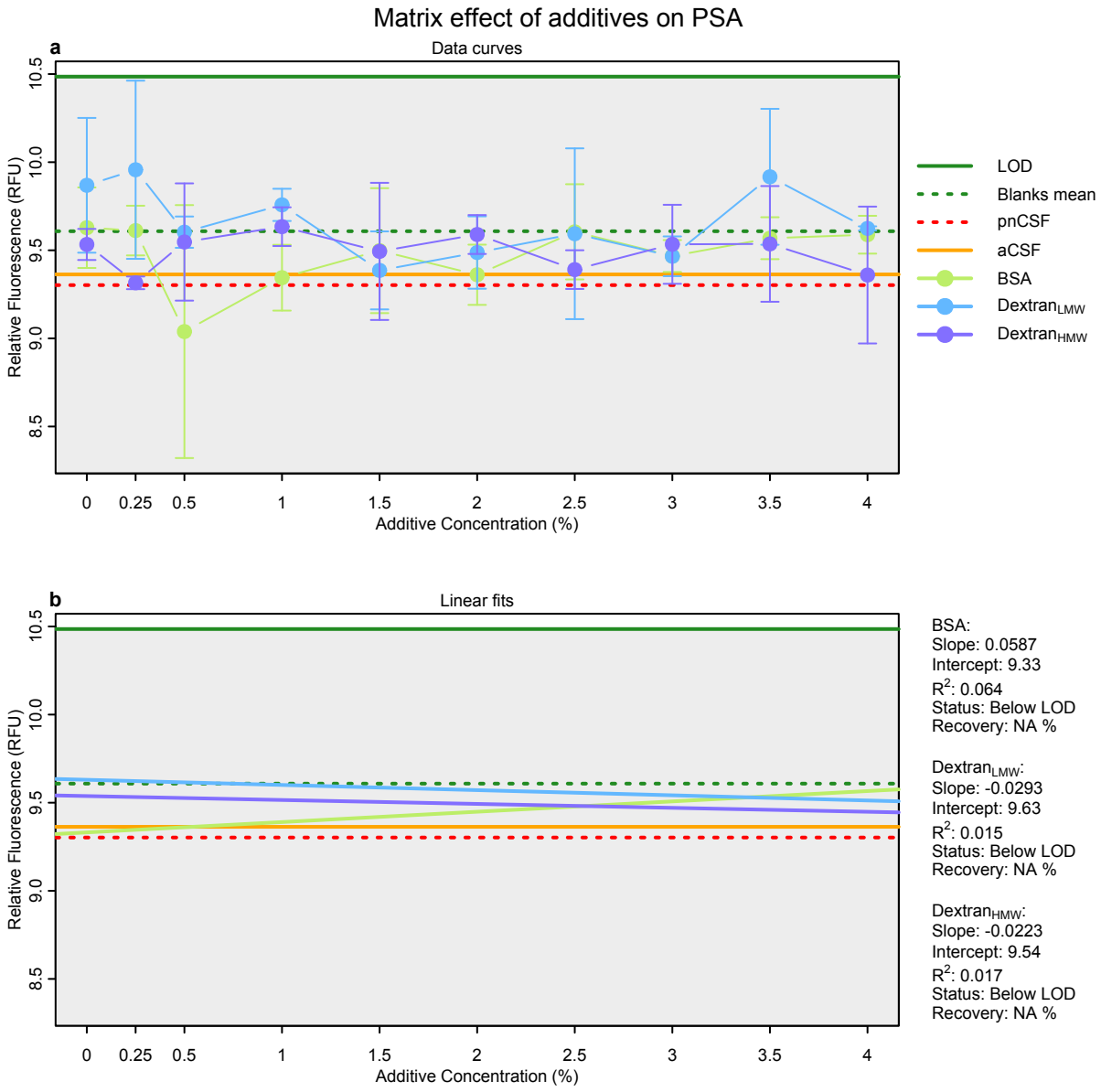

FIGURE G.S73: **Effect of additives on the measurement of PSA.** pnCSF mixed 0-4 % additives diluted in aCSF were measured using the ACM, in order to measure the possible interference of additives on the protein measurement (matrix effect). Linear regressions of measured calibrated fluorescence values of PSA were used to calculate the recovery at concentrations of additives used in cerebral microdialysis. **a** Data from the average of three independent replicates is shown. **b** Median-based linear regressions from the data in **a**.

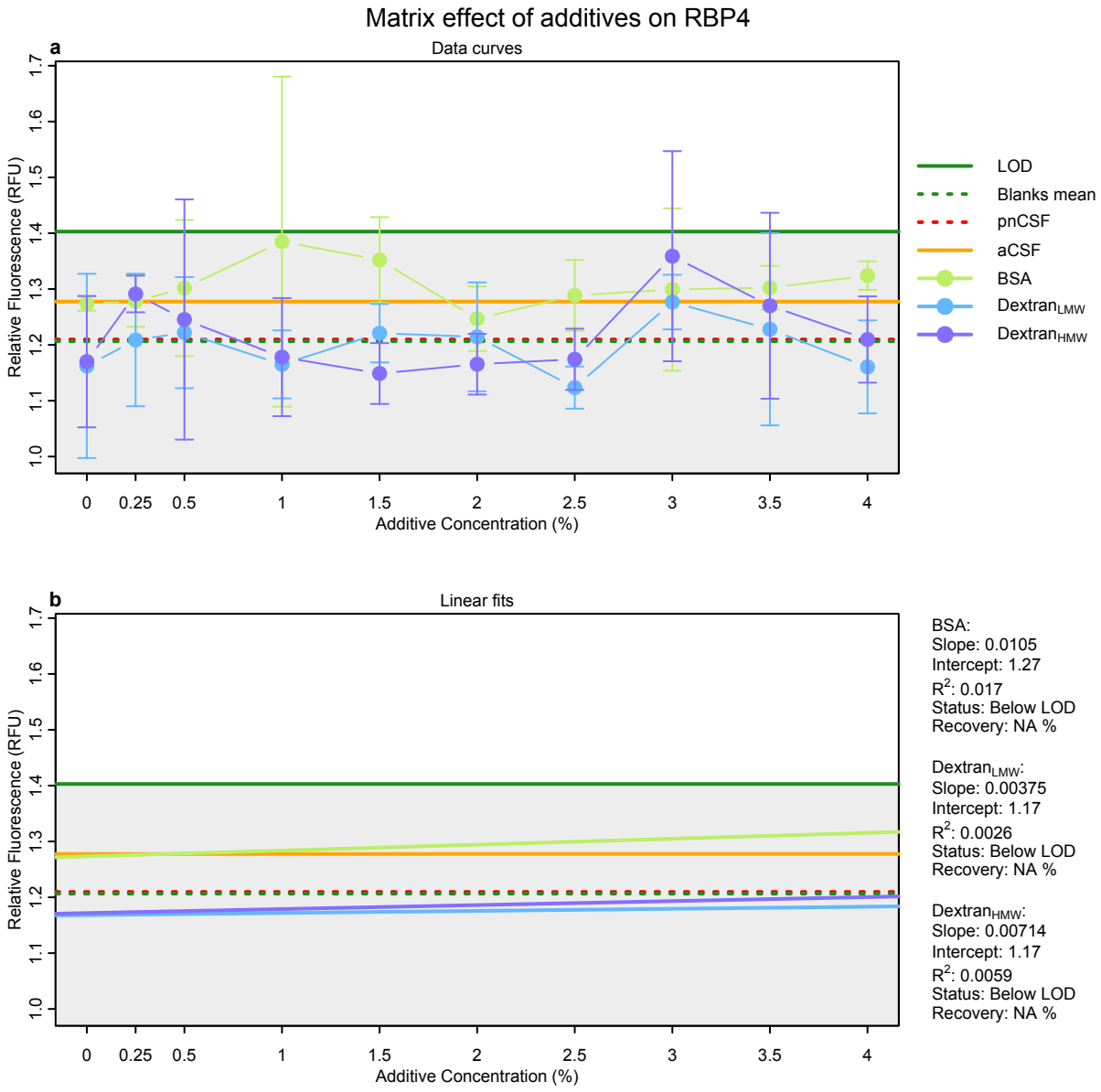

FIGURE G.S74: **Effect of additives on the measurement of RBP4.** pnCSF mixed 0-4 % additives diluted in aCSF were measured using the ACM, in order to measure the possible interference of additives on the protein measurement (matrix effect). Linear regressions of measured calibrated fluorescence values of RBP4 were used to calculate the recovery at concentrations of additives used in cerebral microdialysis. **a** Data from the average of three independent replicates is shown. **b** Median-based linear regressions from the data in **a**.

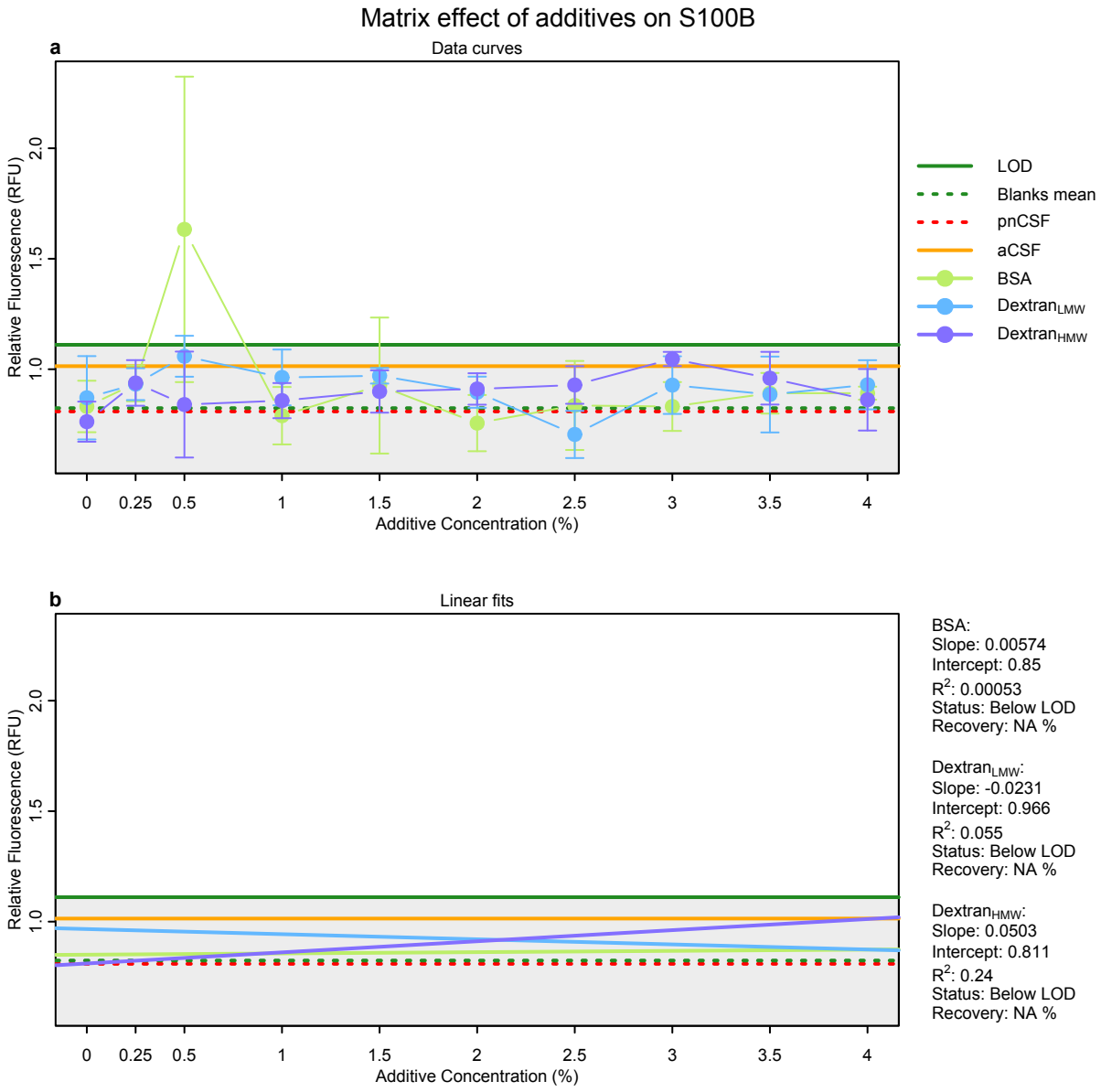

FIGURE G.S75: **Effect of additives on the measurement of S100B.** pnCSF mixed 0-4 % additives diluted in aCSF were measured using the ACM, in order to measure the possible interference of additives on the protein measurement (matrix effect). Linear regressions of measured calibrated fluorescence values of S100B were used to calculate the recovery at concentrations of additives used in cerebral microdialysis. **a** Data from the average of three independent replicates is shown. **b** Median-based linear regressions from the data in **a**.

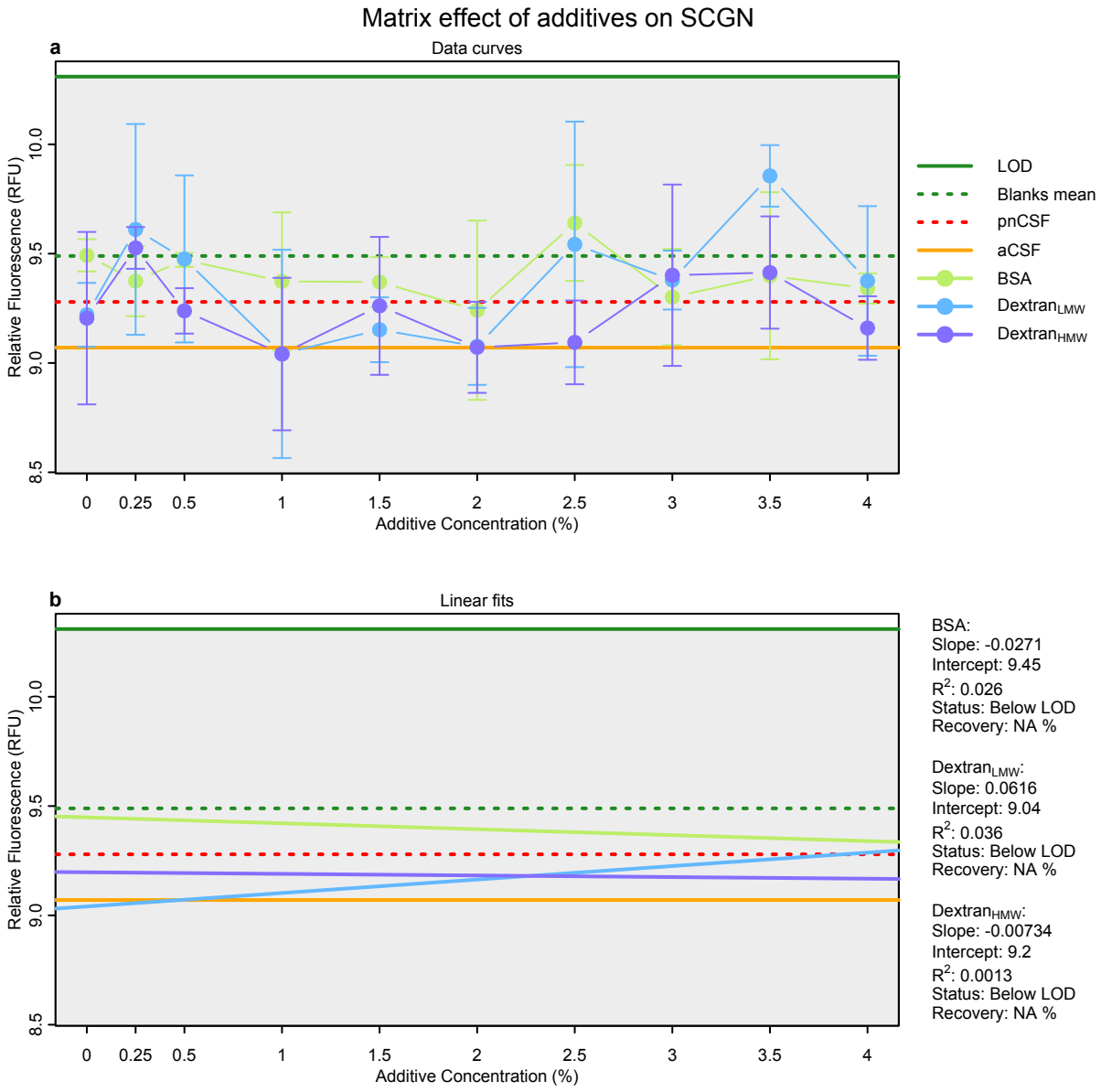

FIGURE G.S76: **Effect of additives on the measurement of SCGN.** pnCSF mixed 0-4 % additives diluted in aCSF were measured using the ACM, in order to measure the possible interference of additives on the protein measurement (matrix effect). Linear regressions of measured calibrated fluorescence values of SCGN were used to calculate the recovery at concentrations of additives used in cerebral microdialysis. **a** Data from the average of three independent replicates is shown. **b** Median-based linear regressions from the data in **a**.

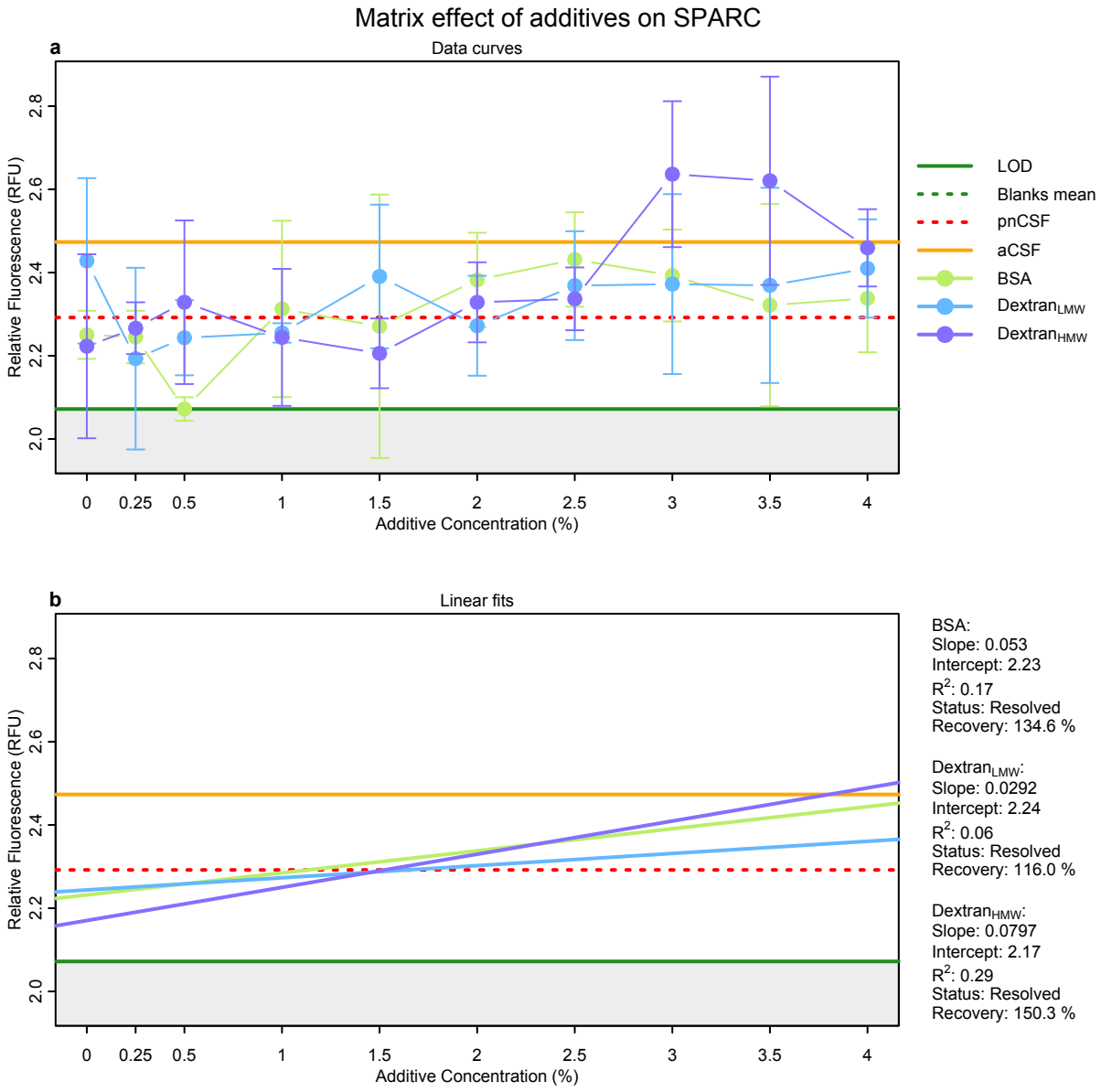

FIGURE G.S77: **Effect of additives on the measurement of SPARC.** pnCSF mixed 0-4 % additives diluted in aCSF were measured using the ACM, in order to measure the possible interference of additives on the protein measurement (matrix effect). Linear regressions of measured calibrated fluorescence values of SPARC were used to calculate the recovery at concentrations of additives used in cerebral microdialysis. **a** Data from the average of three independent replicates is shown. **b** Median-based linear regressions from the data in **a**.

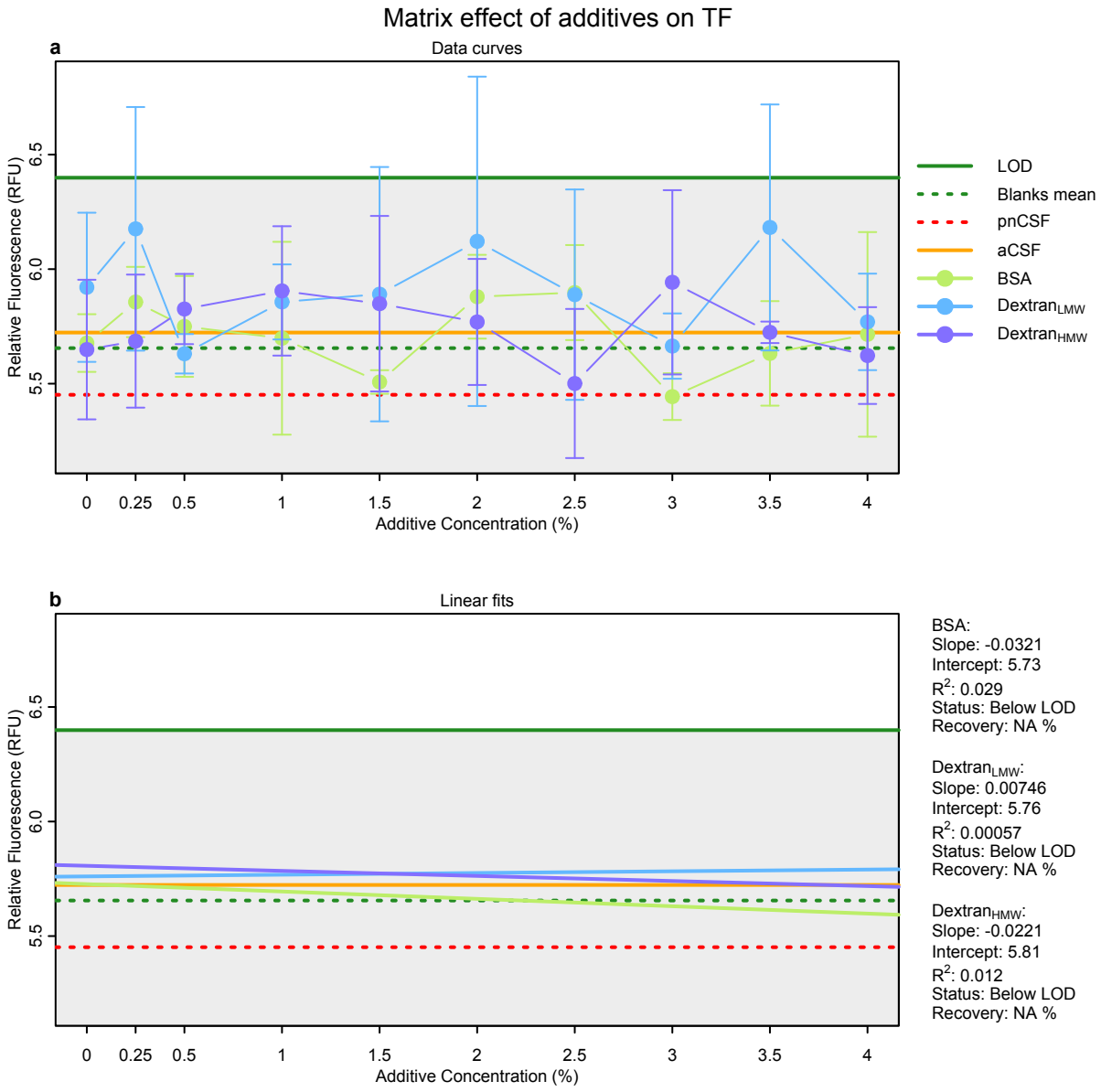

FIGURE G.S78: **Effect of additives on the measurement of TF.** pnCSF mixed 0-4 % additives diluted in aCSF were measured using the ACM, in order to measure the possible interference of additives on the protein measurement (matrix effect). Linear regressions of measured calibrated fluorescence values of TF were used to calculate the recovery at concentrations of additives used in cerebral microdialysis. **a** Data from the average of three independent replicates is shown. **b** Median-based linear regressions from the data in **a**.

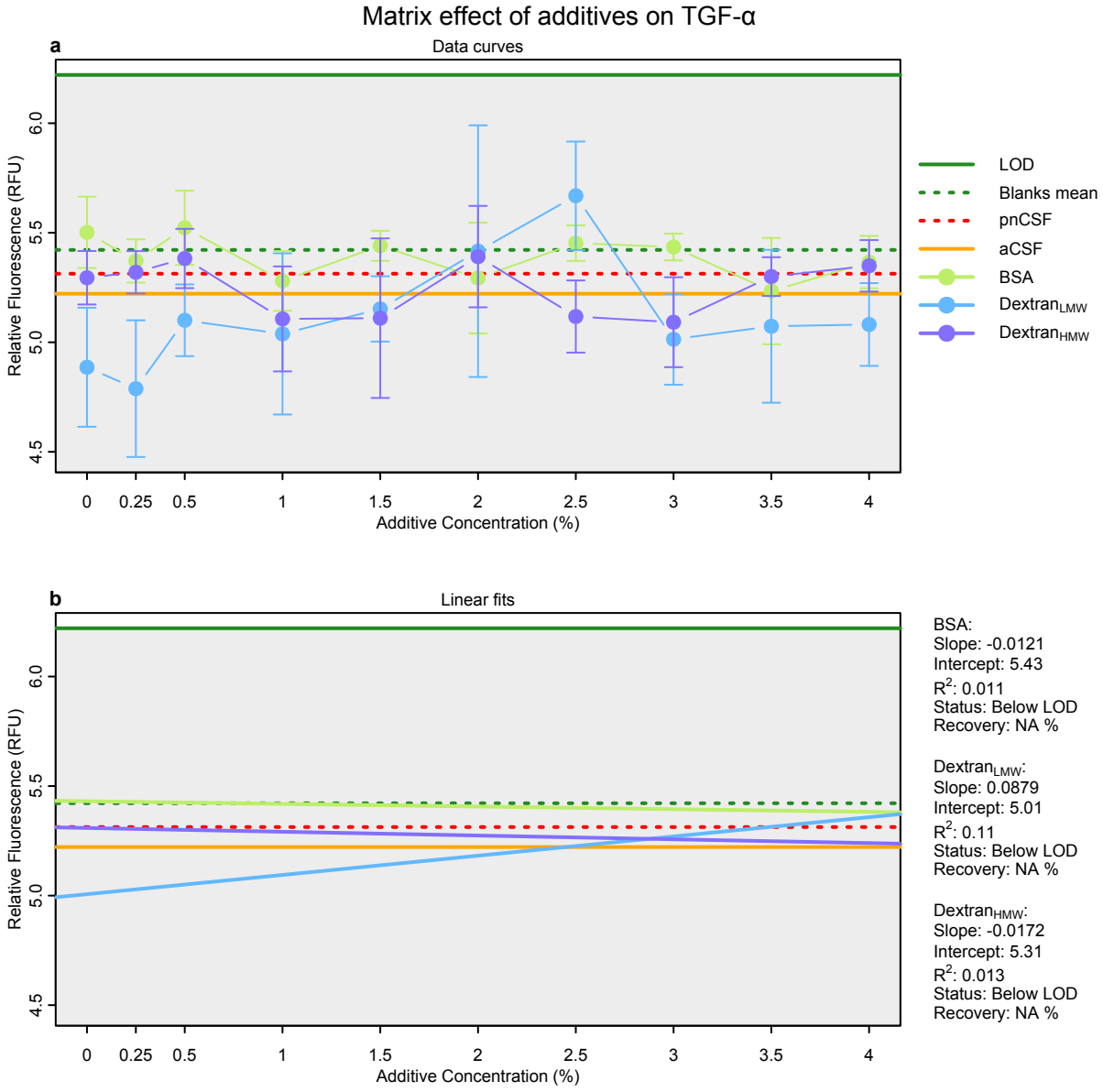

FIGURE G.S79: **Effect of additives on the measurement of TGF-α.** pnCSF mixed 0-4 % additives diluted in aCSF were measured using the ACM, in order to measure the possible interference of additives on the protein measurement (matrix effect). Linear regressions of measured calibrated fluorescence values of TGF-α were used to calculate the recovery at concentrations of additives used in cerebral microdialysis. **a** Data from the average of three independent replicates is shown. **b** Median-based linear regressions from the data in **a**.

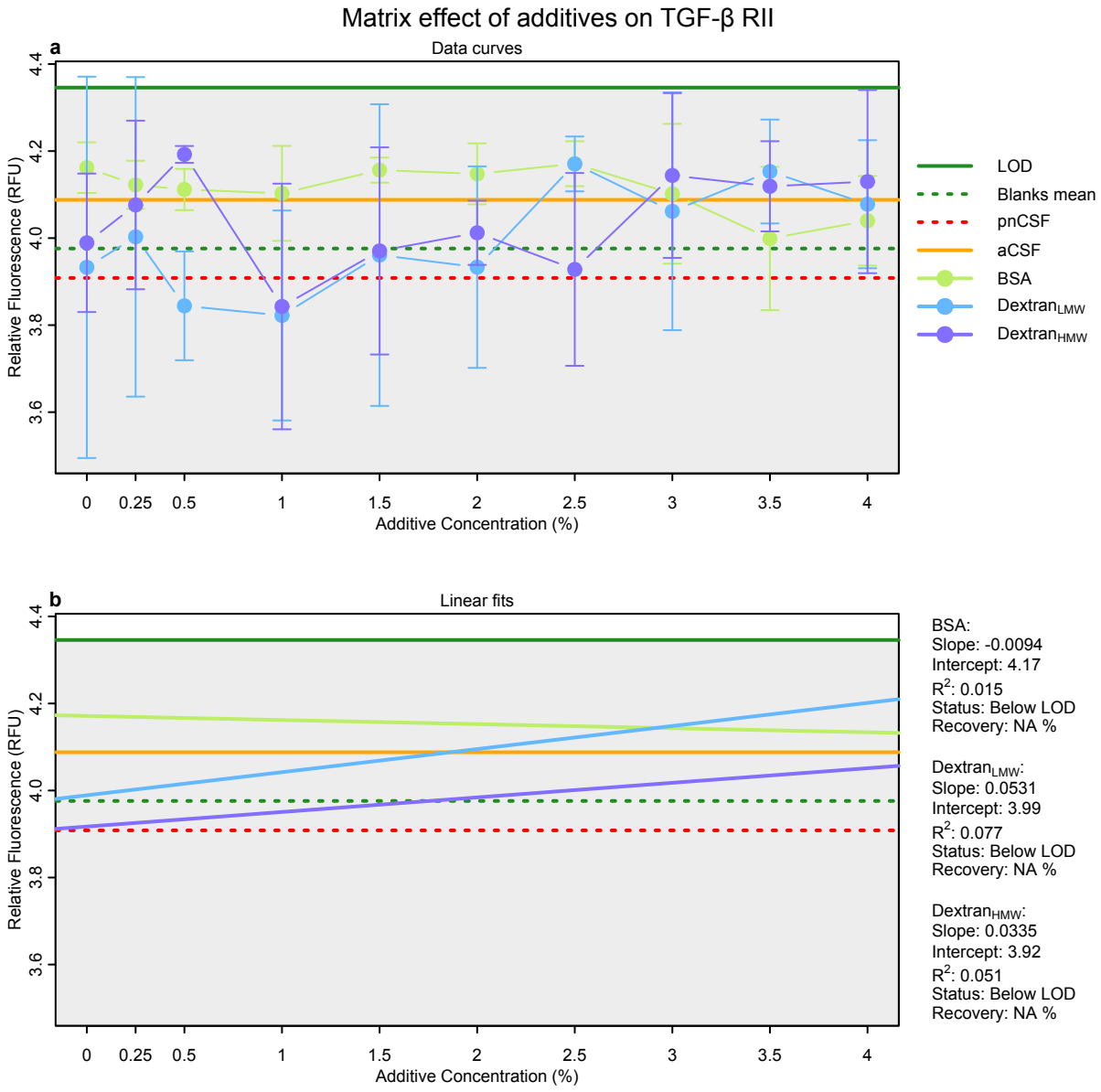

FIGURE G.S80: **Effect of additives on the measurement of TGF-β RII.** pnCSF mixed 0-4 % additives diluted in aCSF were measured using the ACM, in order to measure the possible interference of additives on the protein measurement (matrix effect). Linear regressions of measured calibrated fluorescence values of TGF-β RII were used to calculate the recovery at concentrations of additives used in cerebral microdialysis. **a** Data from the average of three independent replicates is shown. **b** Median-based linear regressions from the data in **a**.

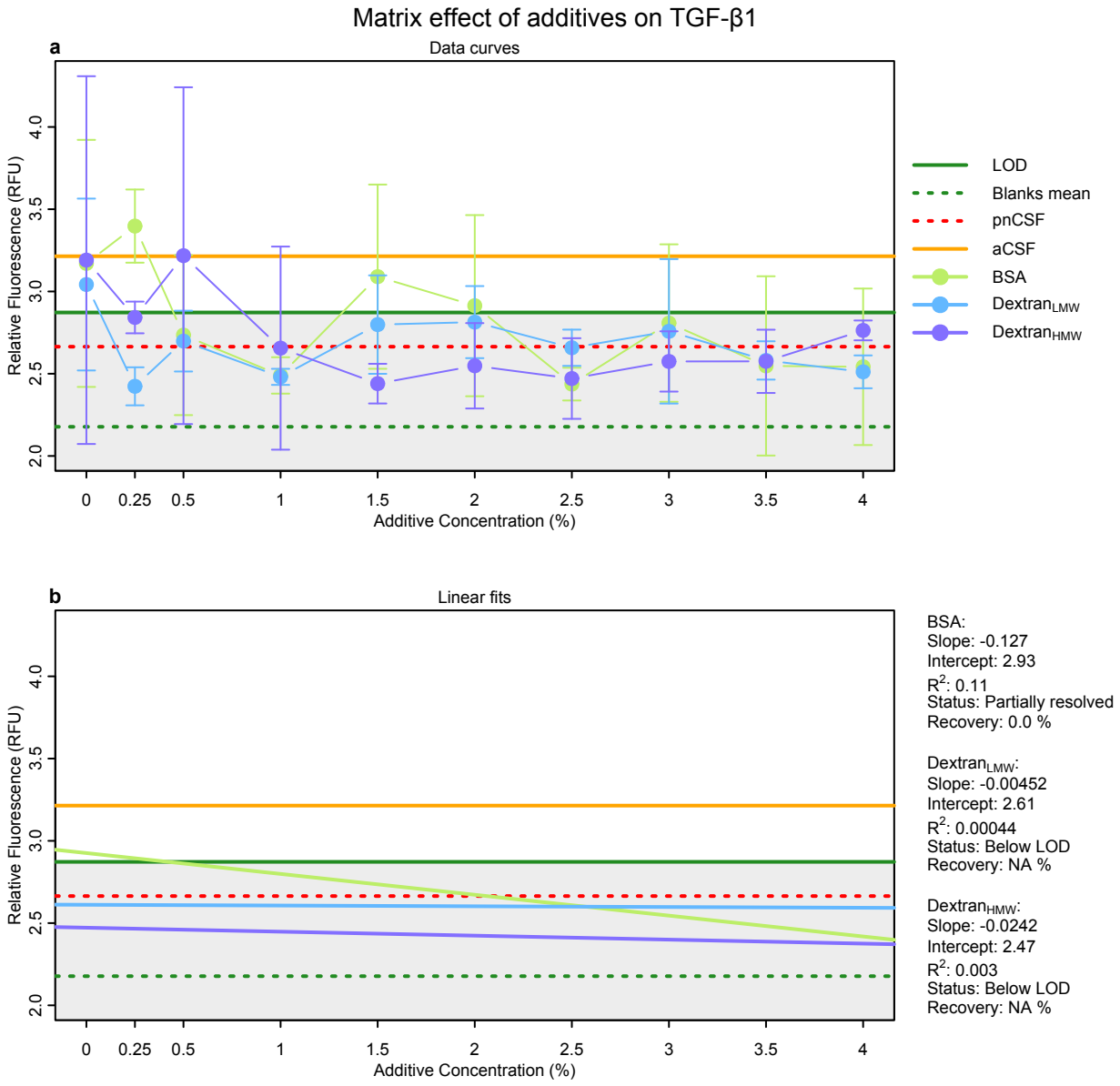

FIGURE G.S81: **Effect of additives on the measurement of TGF-β1.** pnCSF mixed 0-4 % additives diluted in aCSF were measured using the ACM, in order to measure the possible interference of additives on the protein measurement (matrix effect). Linear regressions of measured calibrated fluorescence values of TGF-β1 were used to calculate the recovery at concentrations of additives used in cerebral microdialysis. **a** Data from the average of three independent replicates is shown. **b** Median-based linear regressions from the data in **a**.

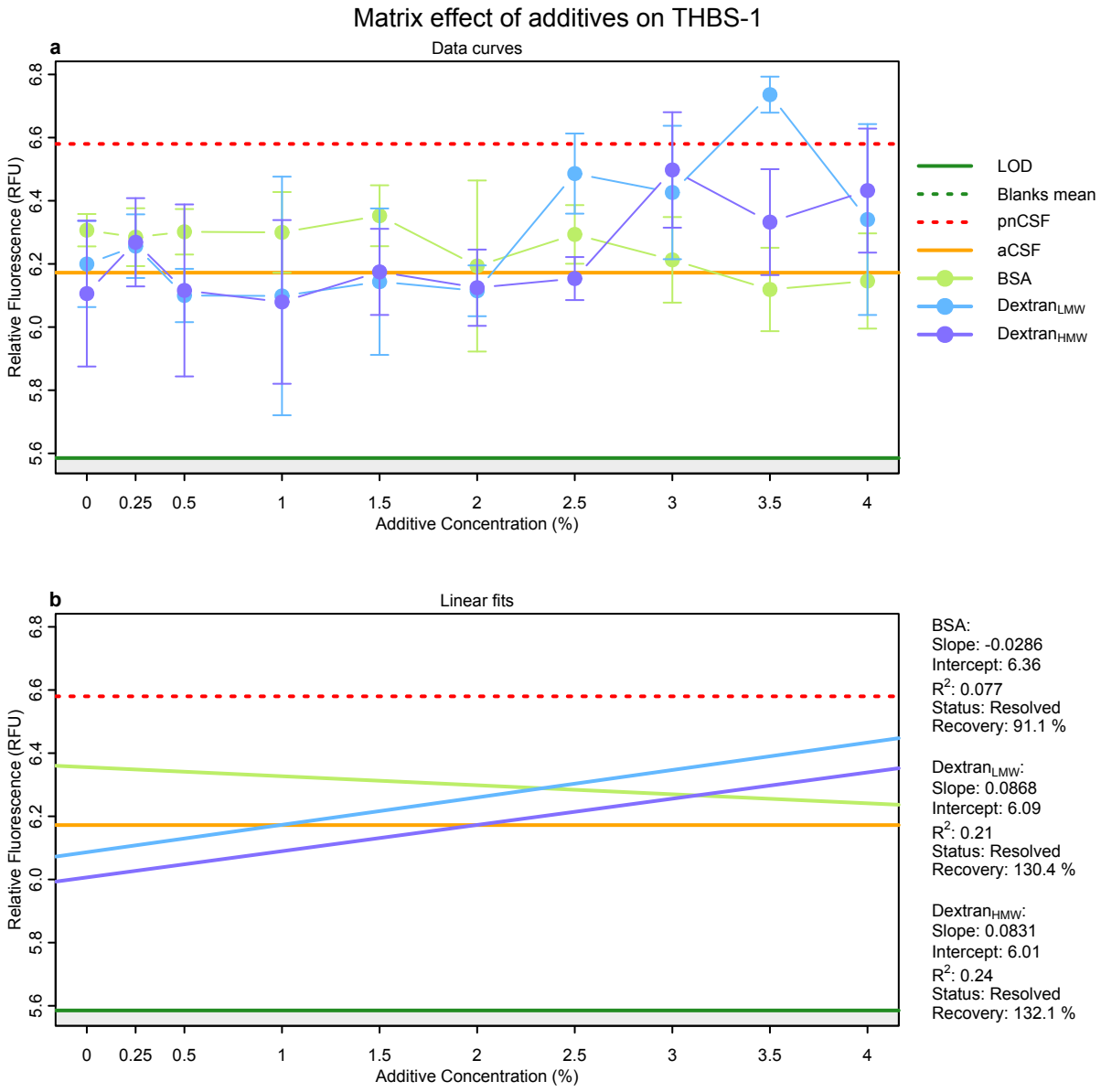

FIGURE G.S82: **Effect of additives on the measurement of THBS-1.** pnCSF mixed 0-4 % additives diluted in aCSF were measured using the ACM, in order to measure the possible interference of additives on the protein measurement (matrix effect). Linear regressions of measured calibrated fluorescence values of THBS-1 were used to calculate the recovery at concentrations of additives used in cerebral microdialysis. **a** Data from the average of three independent replicates is shown. **b** Median-based linear regressions from the data in **a**.

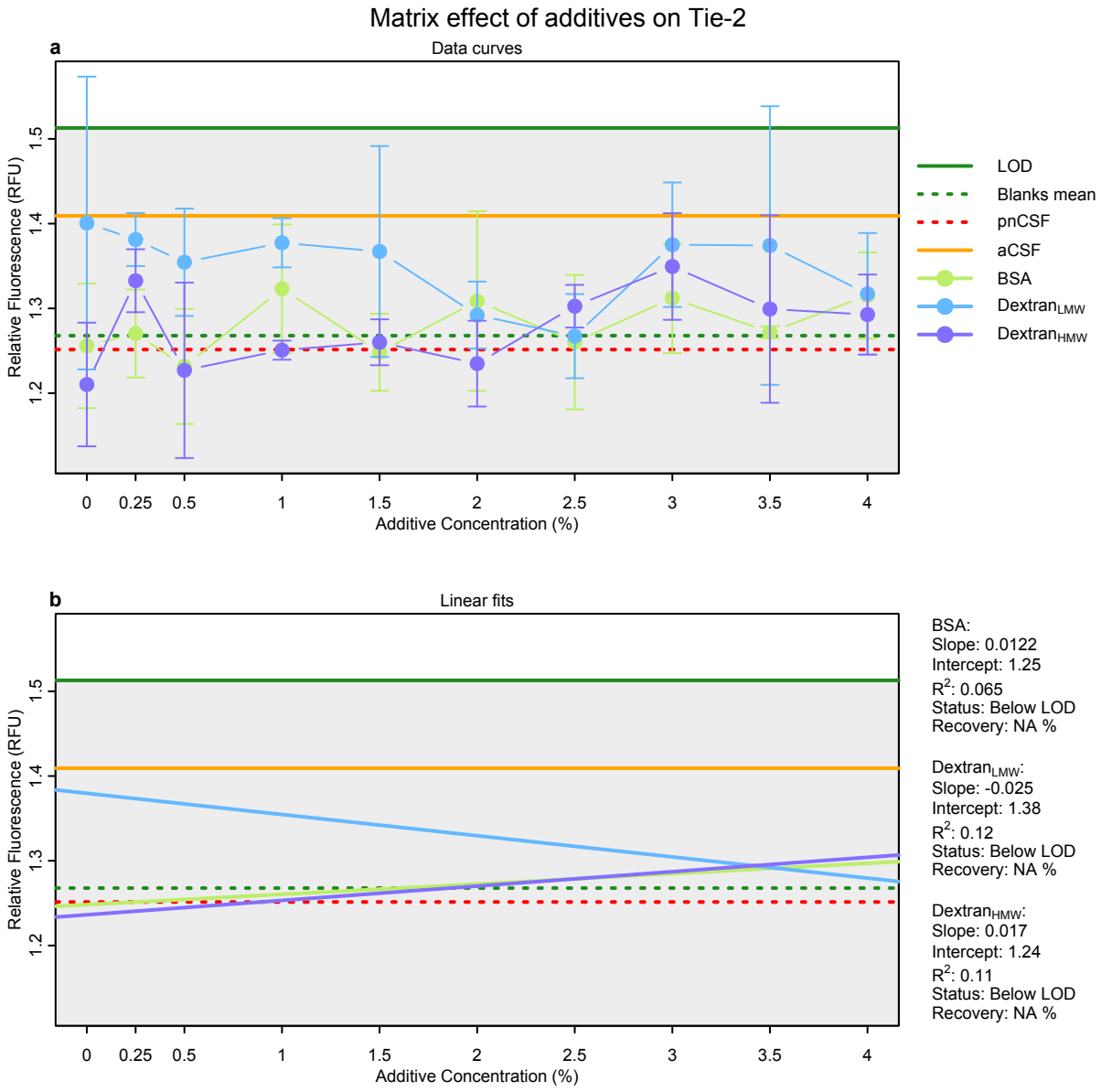

FIGURE G.S83: **Effect of additives on the measurement of Tie-2.** pnCSF mixed 0-4 % additives diluted in aCSF were measured using the ACM, in order to measure the possible interference of additives on the protein measurement (matrix effect). Linear regressions of measured calibrated fluorescence values of Tie-2 were used to calculate the recovery at concentrations of additives used in cerebral microdialysis. **a** Data from the average of three independent replicates is shown. **b** Median-based linear regressions from the data in **a**.

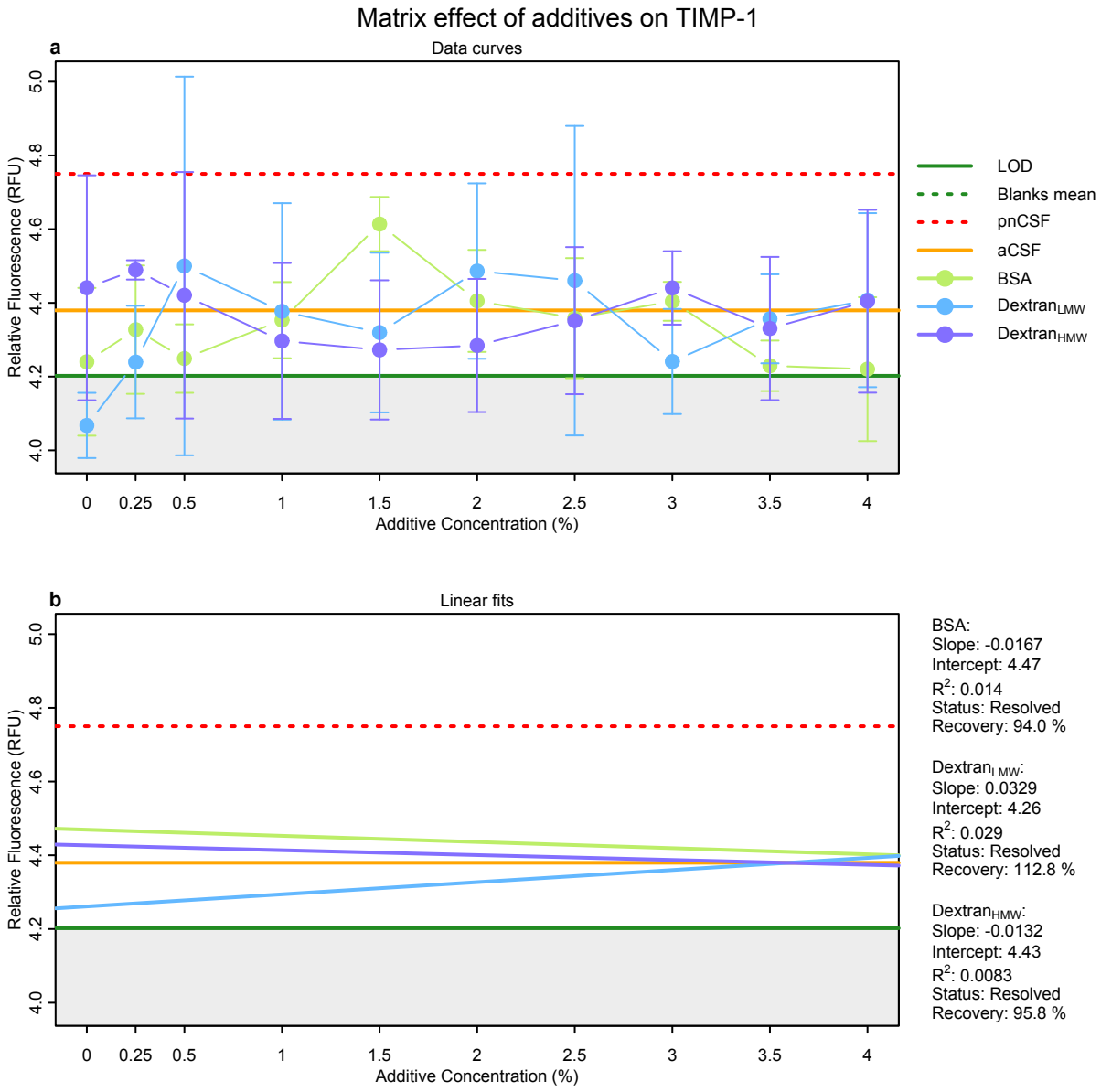

FIGURE G.S84: **Effect of additives on the measurement of TIMP-1.** pnCSF mixed 0-4 % additives diluted in aCSF were measured using the ACM, in order to measure the possible interference of additives on the protein measurement (matrix effect). Linear regressions of measured calibrated fluorescence values of TIMP-1 were used to calculate the recovery at concentrations of additives used in cerebral microdialysis. **a** Data from the average of three independent replicates is shown. **b** Median-based linear regressions from the data in **a**.

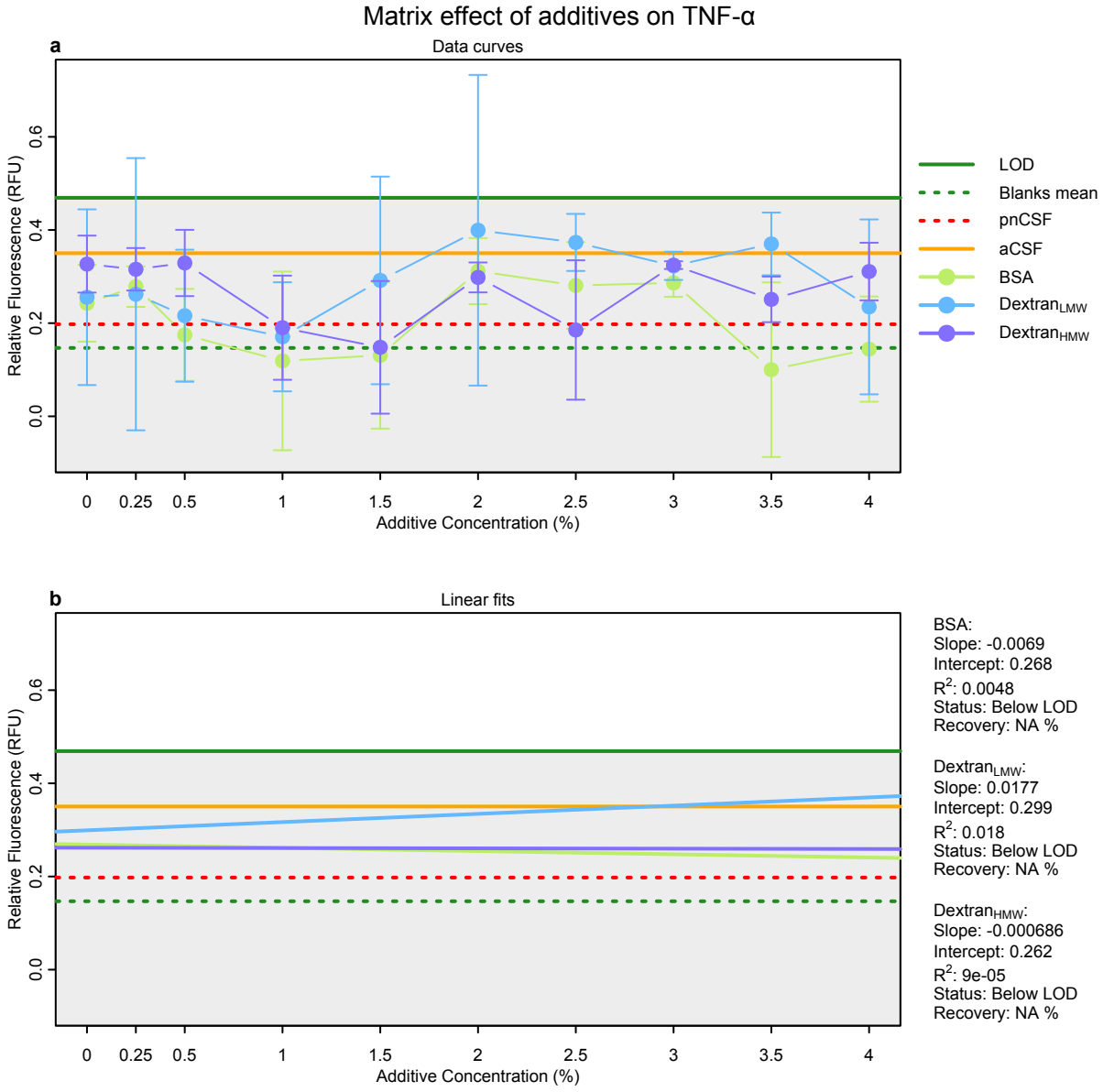

FIGURE G.S85: **Effect of additives on the measurement of TNF-α.** pnCSF mixed 0-4 % additives diluted in aCSF were measured using the ACM, in order to measure the possible interference of additives on the protein measurement (matrix effect). Linear regressions of measured calibrated fluorescence values of TNF-α were used to calculate the recovery at concentrations of additives used in cerebral microdialysis. **a** Data from the average of three independent replicates is shown. **b** Median-based linear regressions from the data in **a**.

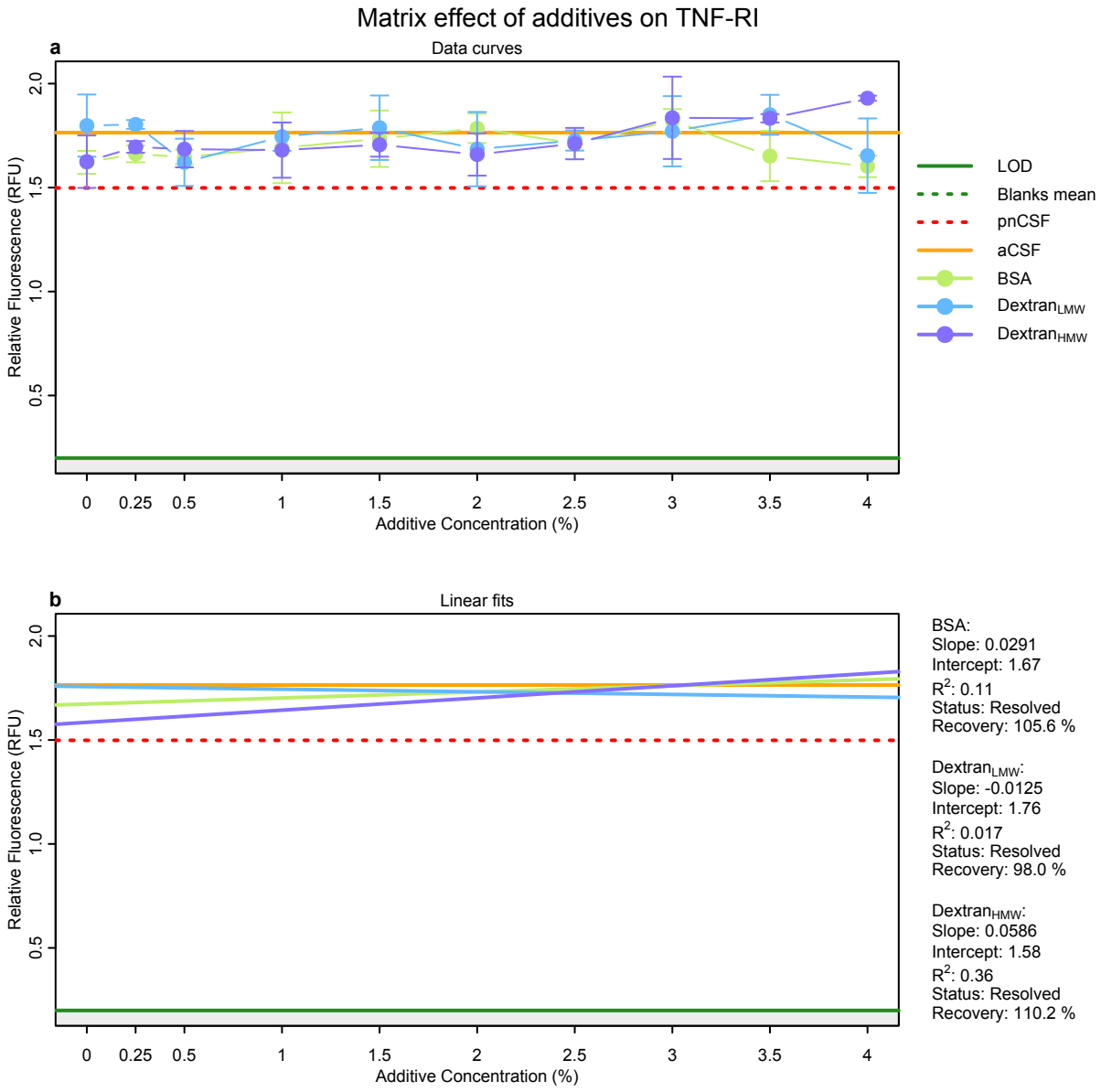

FIGURE G.S86: **Effect of additives on the measurement of TNF-RI.** pnCSF mixed 0-4 % additives diluted in aCSF were measured using the ACM, in order to measure the possible interference of additives on the protein measurement (matrix effect). Linear regressions of measured calibrated fluorescence values of TNF-RI were used to calculate the recovery at concentrations of additives used in cerebral microdialysis. **a** Data from the average of three independent replicates is shown. **b** Median-based linear regressions from the data in **a**.

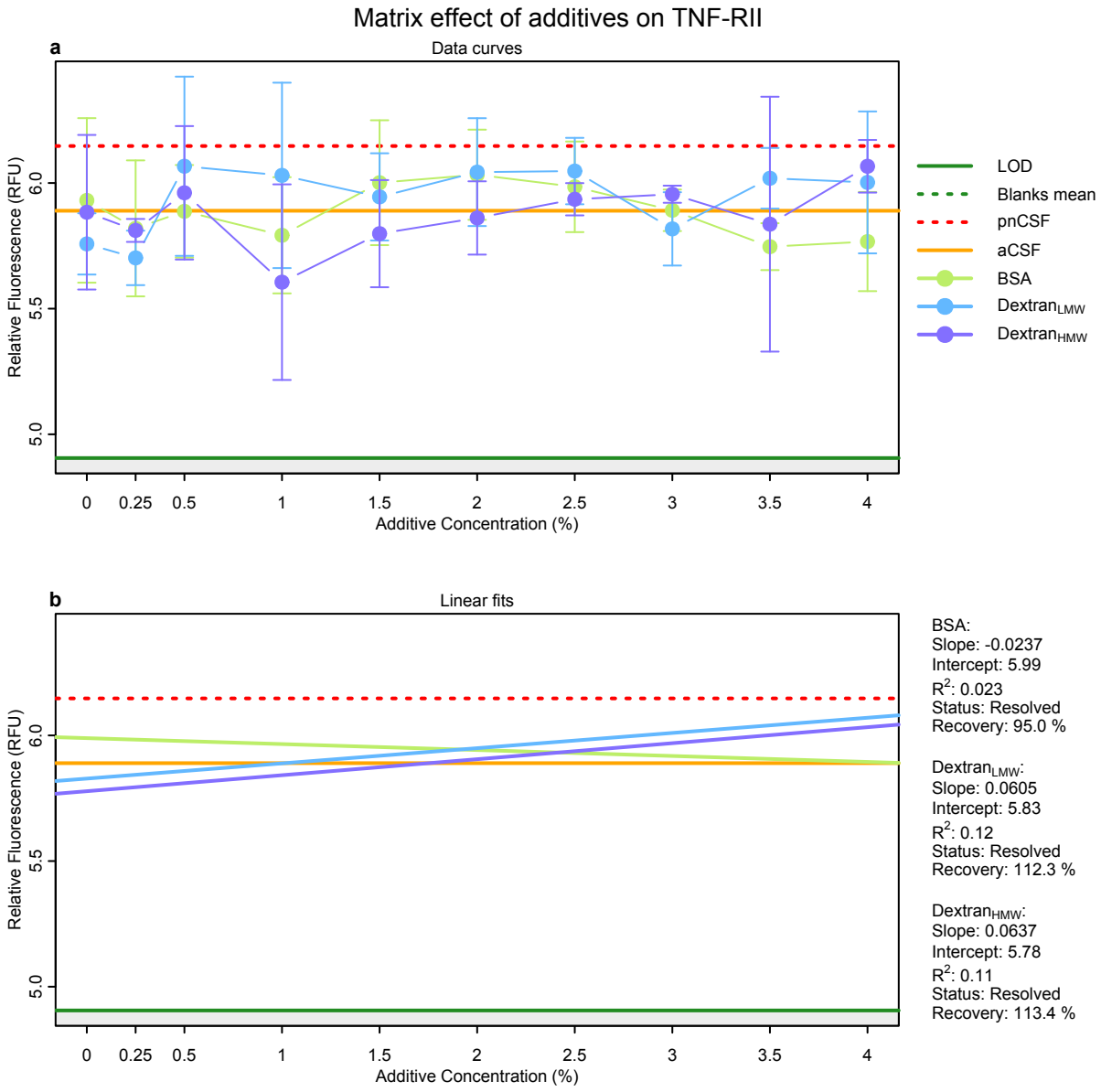

FIGURE G.S87: **Effect of additives on the measurement of TNF-RII.** pnCSF mixed 0-4 % additives diluted in aCSF were measured using the ACM, in order to measure the possible interference of additives on the protein measurement (matrix effect). Linear regressions of measured calibrated fluorescence values of TNF-RII were used to calculate the recovery at concentrations of additives used in cerebral microdialysis. **a** Data from the average of three independent replicates is shown. **b** Median-based linear regressions from the data in **a**.

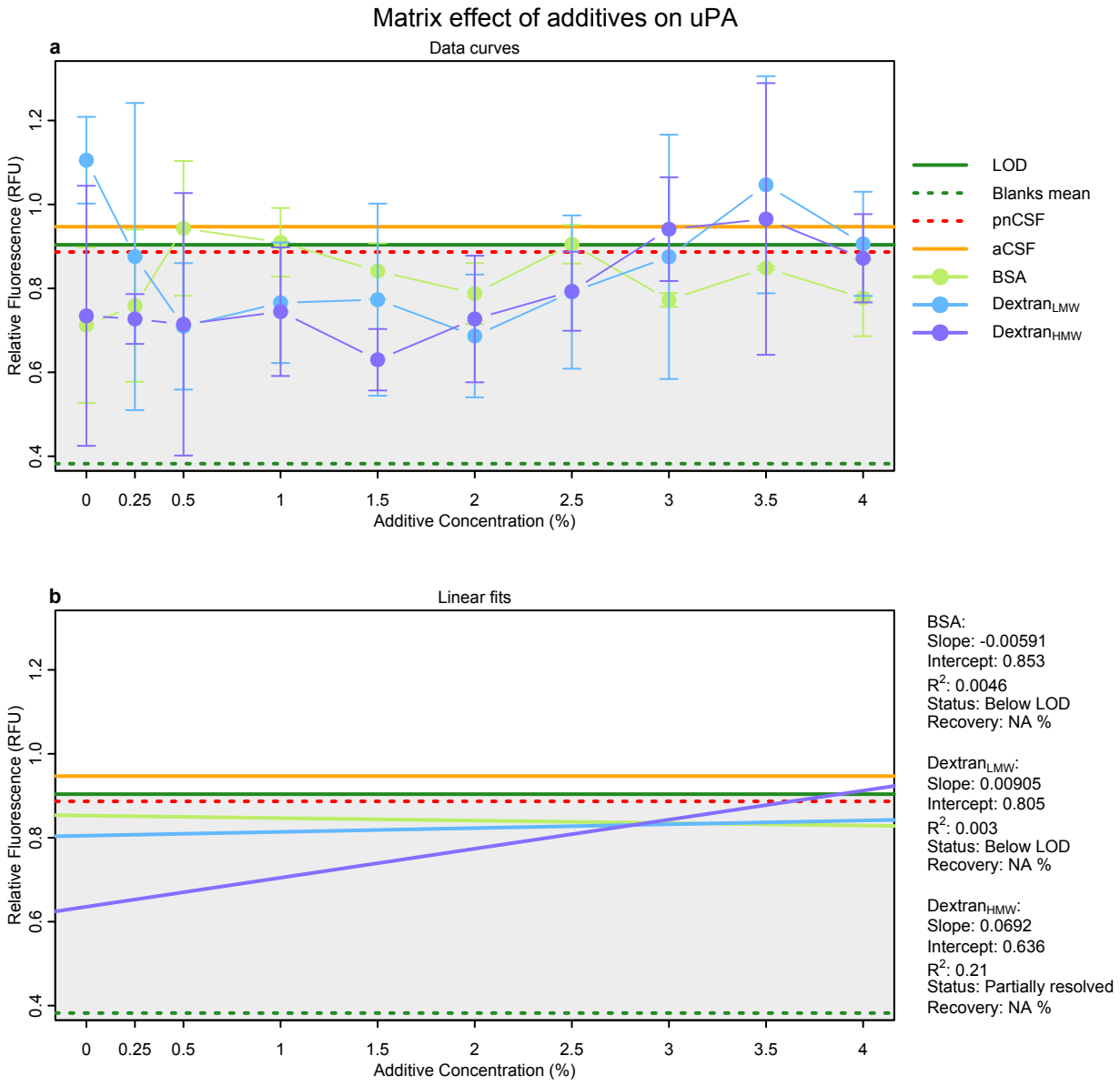

FIGURE G.S88: **Effect of additives on the measurement of uPA.** pnCSF mixed 0-4 % additives diluted in aCSF were measured using the ACM, in order to measure the possible interference of additives on the protein measurement (matrix effect). Linear regressions of measured calibrated fluorescence values of uPA were used to calculate the recovery at concentrations of additives used in cerebral microdialysis. **a** Data from the average of three independent replicates is shown. **b** Median-based linear regressions from the data in **a**.

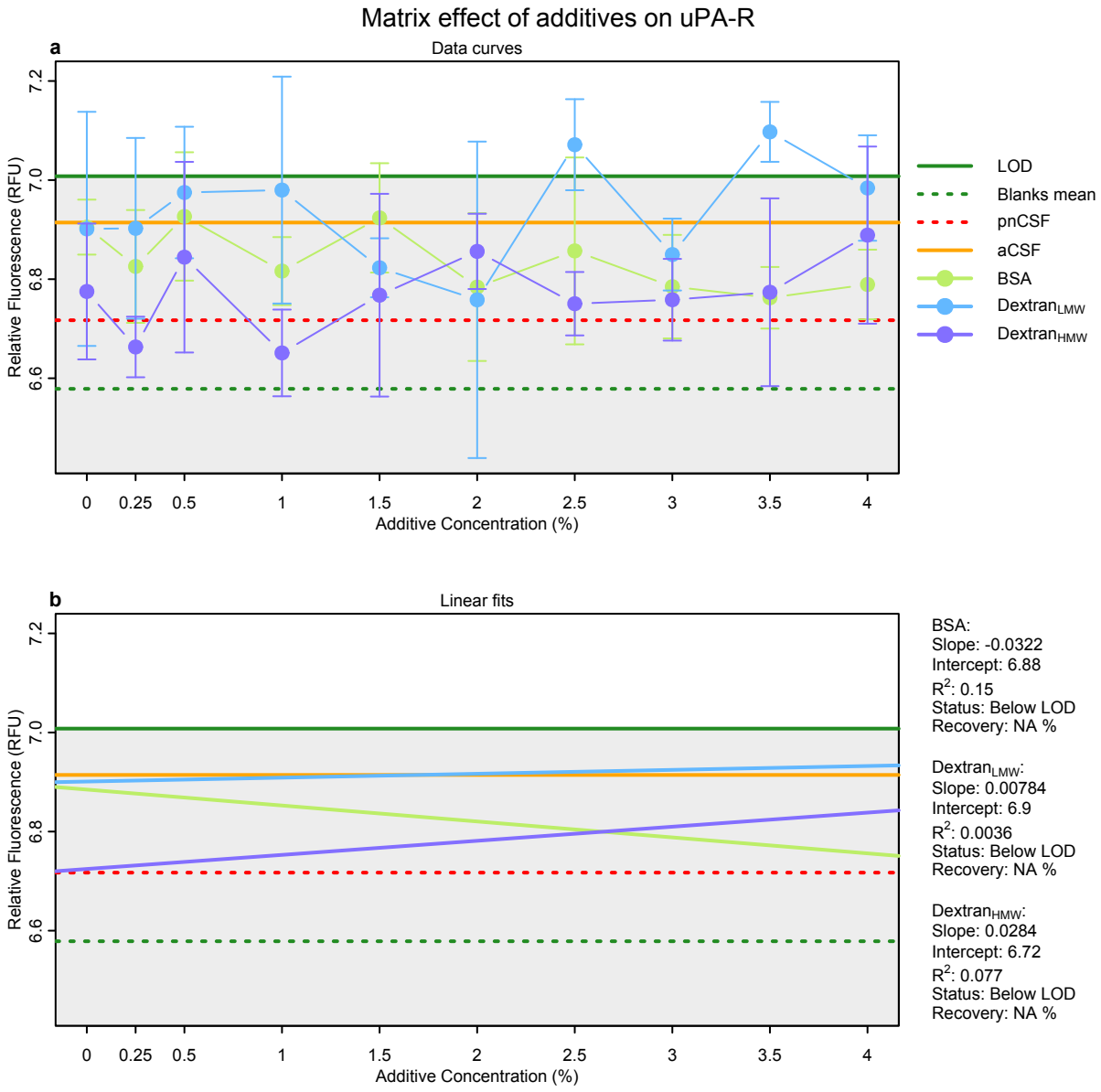

FIGURE G.S89: **Effect of additives on the measurement of uPA-R.** pnCSF mixed 0-4 % additives diluted in aCSF were measured using the ACM, in order to measure the possible interference of additives on the protein measurement (matrix effect). Linear regressions of measured calibrated fluorescence values of uPA-R were used to calculate the recovery at concentrations of additives used in cerebral microdialysis. **a** Data from the average of three independent replicates is shown. **b** Median-based linear regressions from the data in **a**.

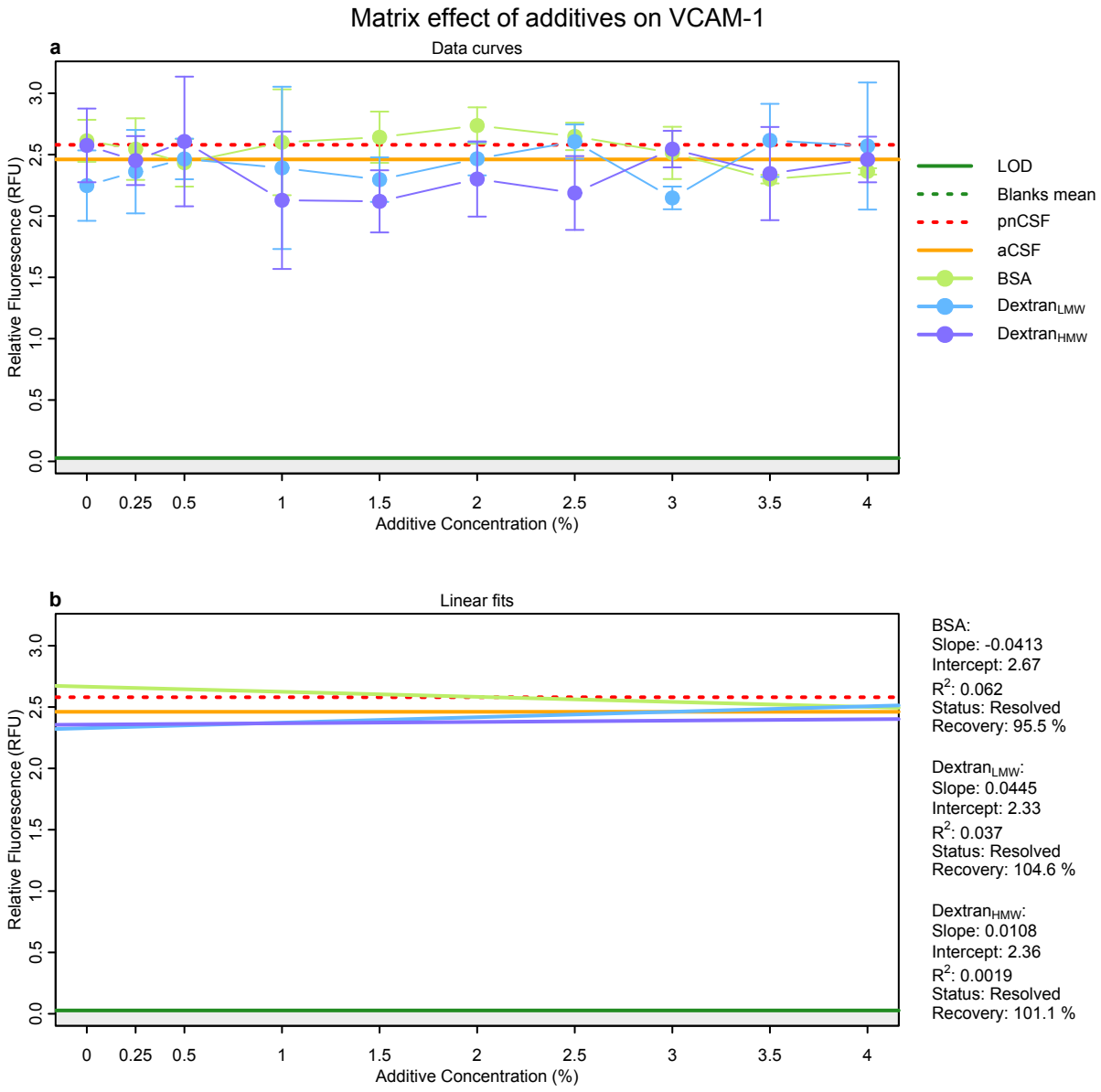

FIGURE G.S90: **Effect of additives on the measurement of VCAM-1.** pnCSF mixed 0-4 % additives diluted in aCSF were measured using the ACM, in order to measure the possible interference of additives on the protein measurement (matrix effect). Linear regressions of measured calibrated fluorescence values of VCAM-1 were used to calculate the recovery at concentrations of additives used in cerebral microdialysis. **a** Data from the average of three independent replicates is shown. **b** Median-based linear regressions from the data in **a**.

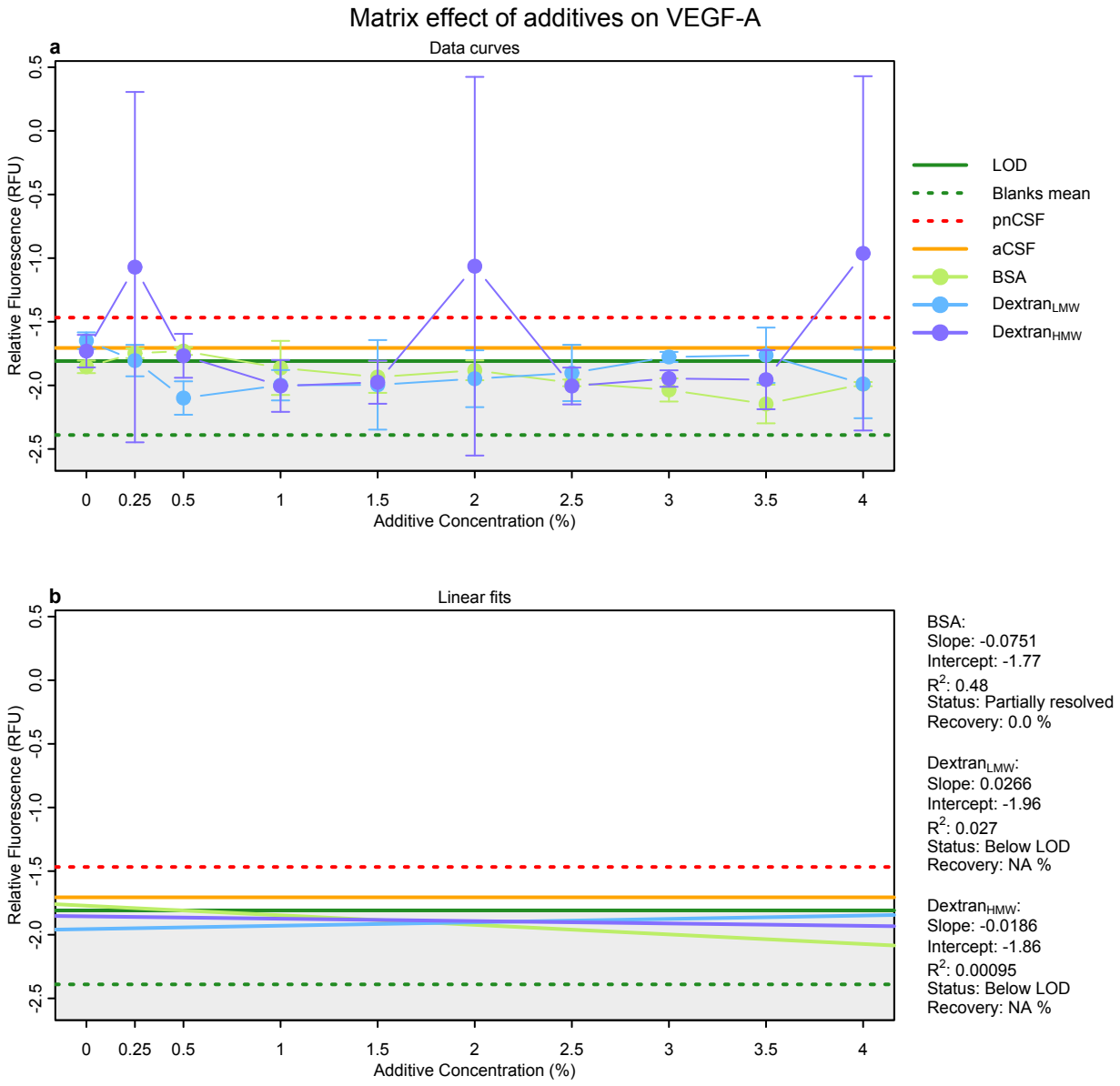

FIGURE G.S91: **Effect of additives on the measurement of VEGF-A.** pnCSF mixed 0-4 % additives diluted in aCSF were measured using the ACM, in order to measure the possible interference of additives on the protein measurement (matrix effect). Linear regressions of measured calibrated fluorescence values of VEGF-A were used to calculate the recovery at concentrations of additives used in cerebral microdialysis. **a** Data from the average of three independent replicates is shown. **b** Median-based linear regressions from the data in **a**.

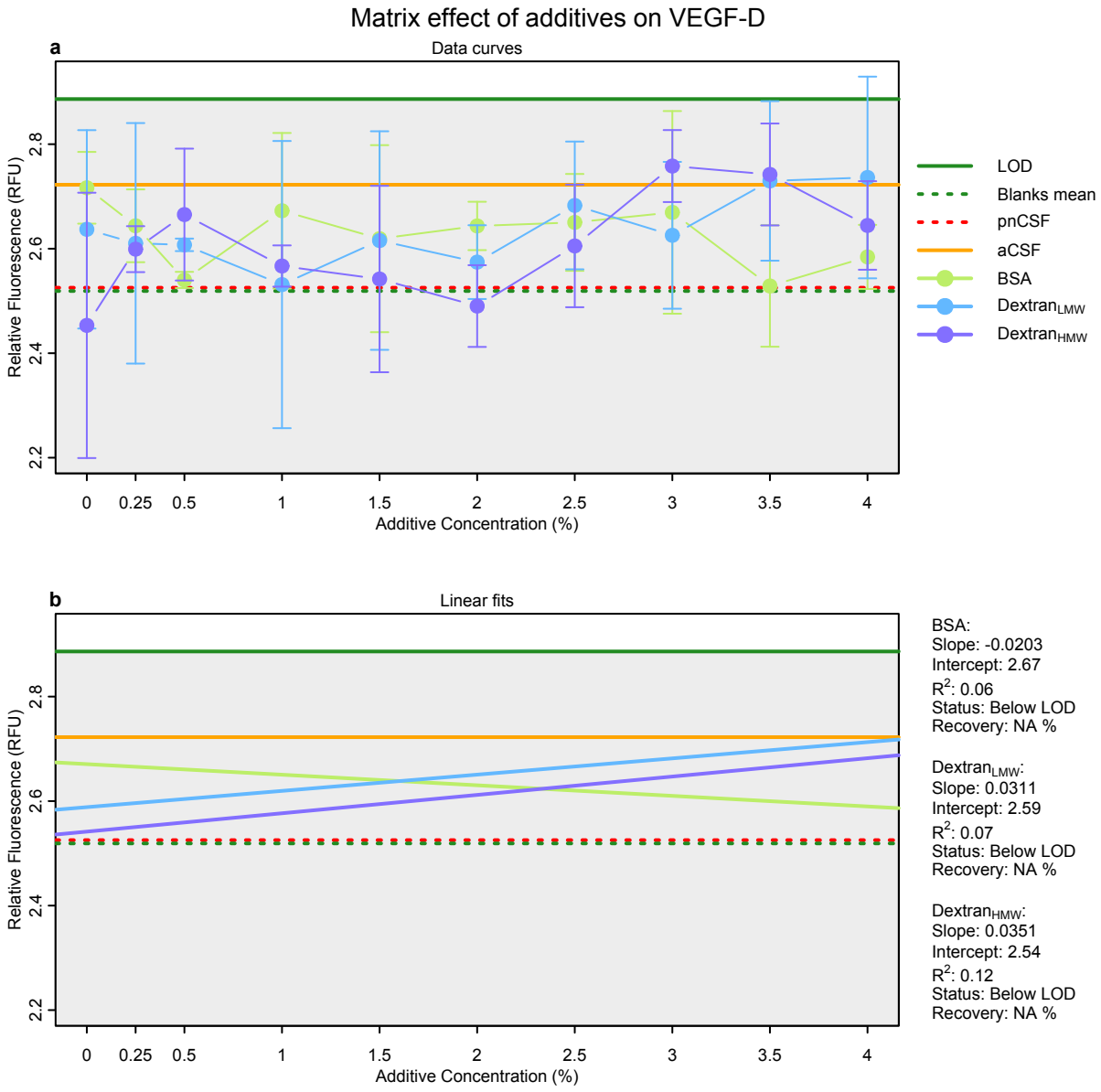

FIGURE G.S92: **Effect of additives on the measurement of VEGF-D.** pnCSF mixed 0-4 % additives diluted in aCSF were measured using the ACM, in order to measure the possible interference of additives on the protein measurement (matrix effect). Linear regressions of measured calibrated fluorescence values of VEGF-D were used to calculate the recovery at concentrations of additives used in cerebral microdialysis. **a** Data from the average of three independent replicates is shown. **b** Median-based linear regressions from the data in **a**.

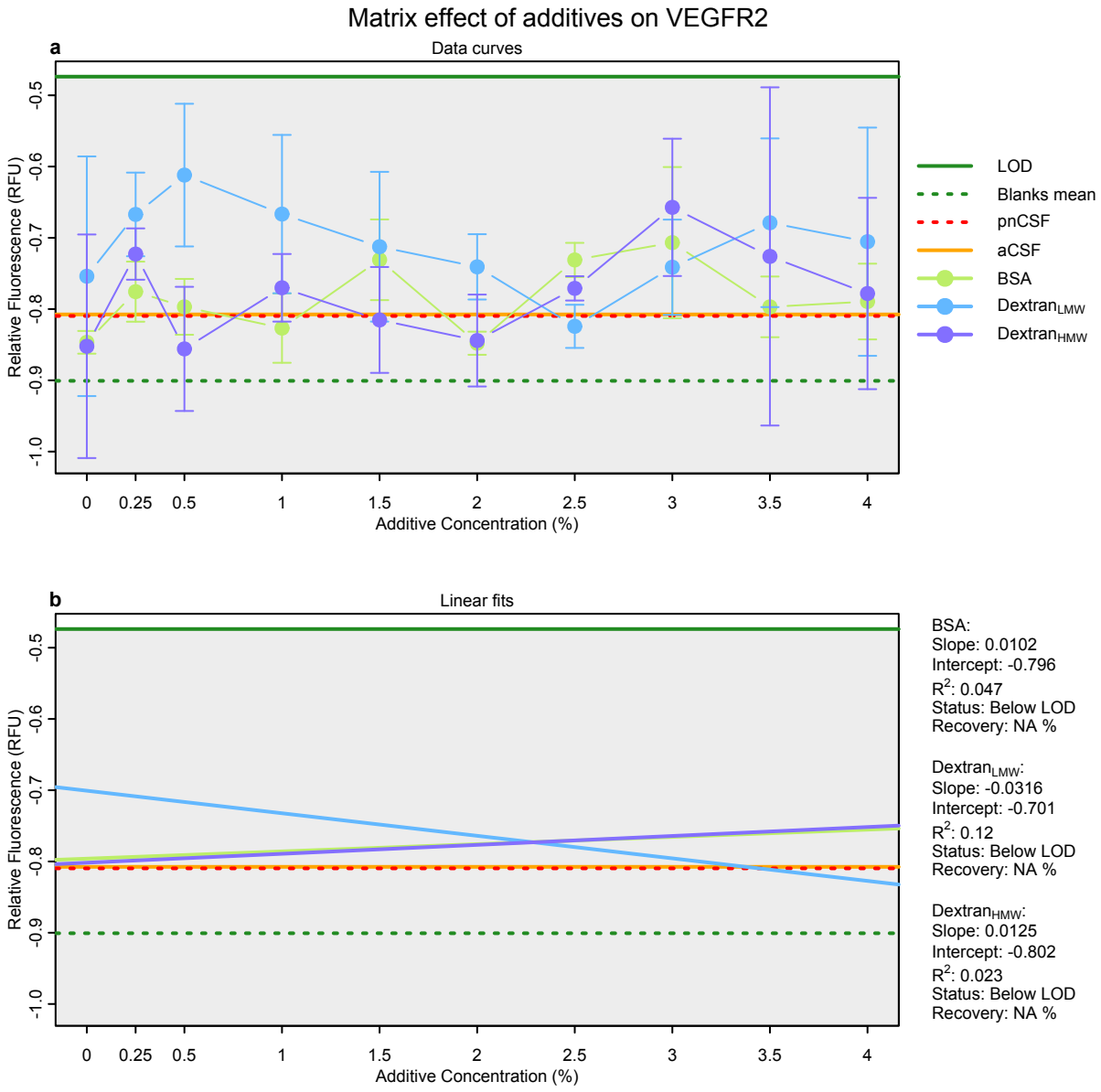

FIGURE G.S93: **Effect of additives on the measurement of VEGFR2.** pnCSF mixed 0-4 % additives diluted in aCSF were measured using the ACM, in order to measure the possible interference of additives on the protein measurement (matrix effect). Linear regressions of measured calibrated fluorescence values of VEGFR2 were used to calculate the recovery at concentrations of additives used in cerebral microdialysis. **a** Data from the average of three independent replicates is shown. **b** Median-based linear regressions from the data in **a**.

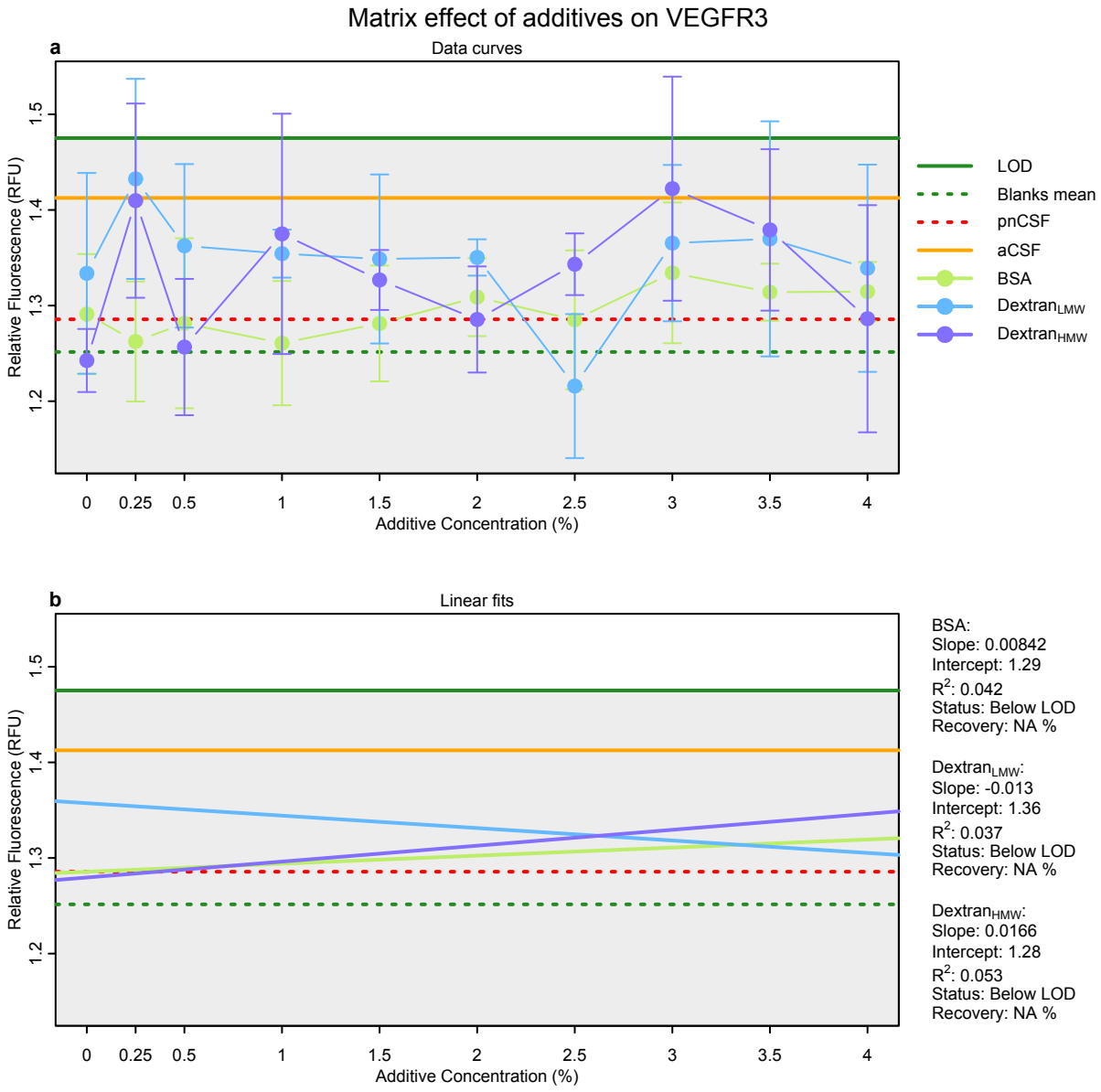

FIGURE G.S94: **Effect of additives on the measurement of VEGFR3.** pnCSF mixed 0-4 % additives diluted in aCSF were measured using the ACM, in order to measure the possible interference of additives on the protein measurement (matrix effect). Linear regressions of measured calibrated fluorescence values of VEGFR3 were used to calculate the recovery at concentrations of additives used in cerebral microdialysis. **a** Data from the average of three independent replicates is shown. **b** Median-based linear regressions from the data in **a**.

APPENDIX H

Comparison of microdialysis additives: Effect on U87 cells

This appendix is a supplementary material to chapter chapter 5 that describes the effect of additives on the measurement of 94 proteins in human microglial (U87) cell cultures.

Effect of additives on protein measurements in U87 cell cultures

Electronic Supplementary Material

Comparison of bovine serum albumin, low- and high-molecular weight dextrans as additives to brain microdialysis

Veronique Laforte, Francesco Fiorini, David KY Zhang, Judith Marcoux and David Juncker

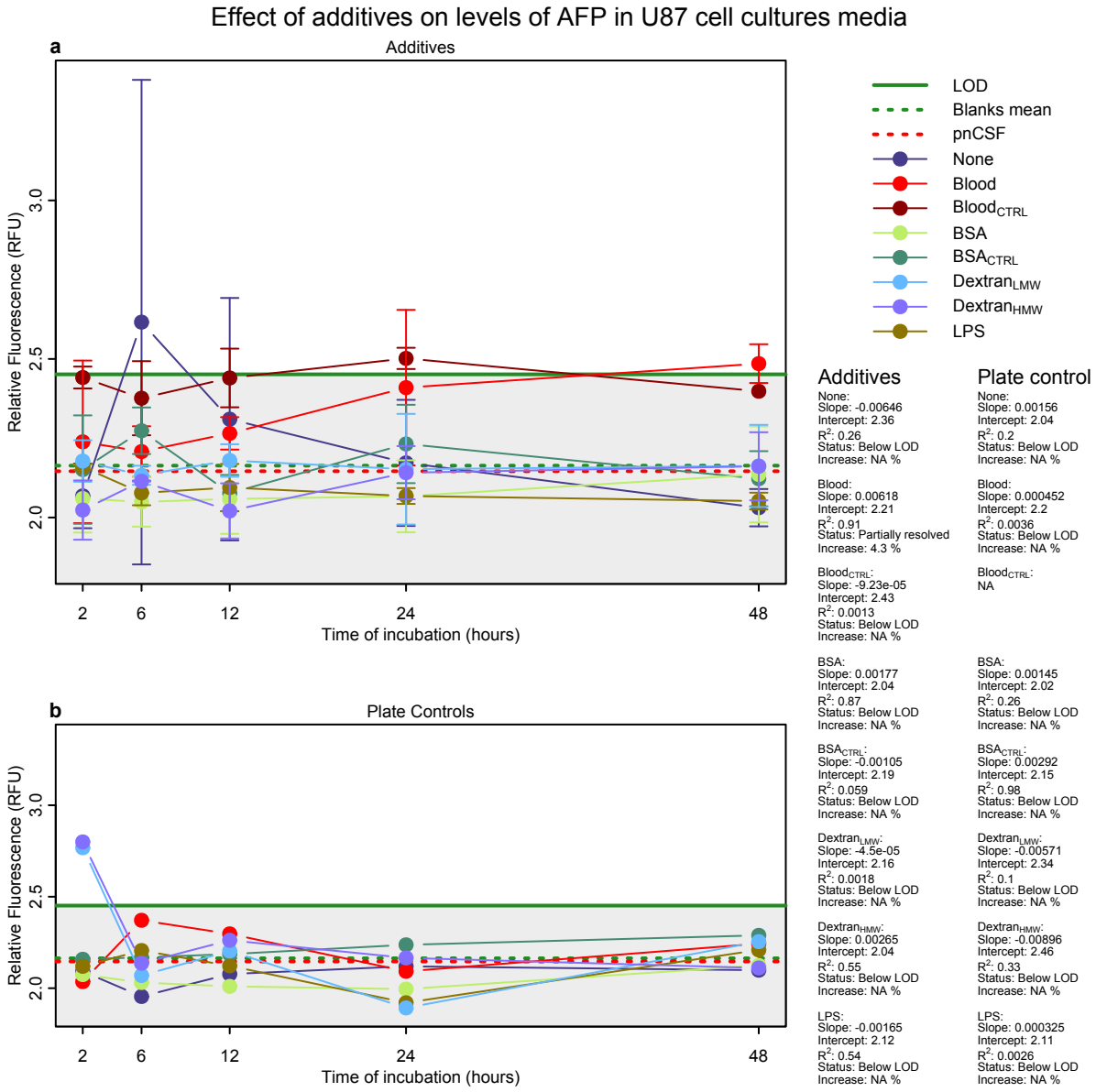

FIGURE H.S1: **Effect of additives on levels of AFP in U87 cell cultures media.** Additives along with fresh blood and LPS were added to mycoplasma-free human glial (U87) cells in triplicate wells of a 24-well plate and incubated for up to 48 h to measure the effect on levels of proteins measured in the cell media. Media was collected and frozen from successive triplicates at different intervals, then analyzed with the ACM. **a** Average values for AFP from three replicates for each point in every 24-well plate where a different additive was applied. **b** Data from the control cell media in each plate.

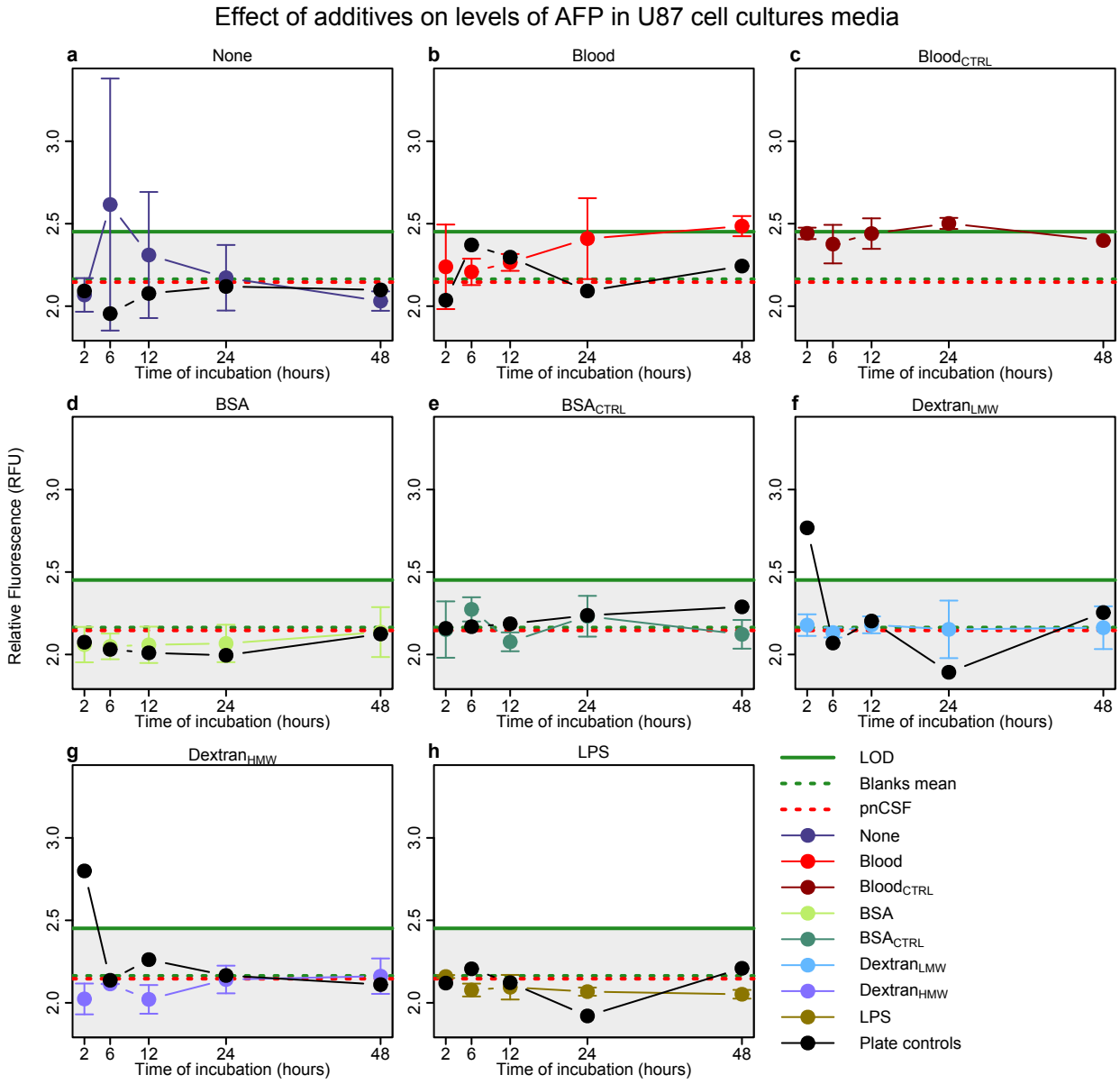

FIGURE H.S2: **Effect of additives on levels of AFP in U87 cell cultures media.** Additives along with fresh blood and LPS were added to mycoplasma-free human glial (U87) cells in triplicate wells of a 24-well plate and incubated for up to 48 h to measure the effect on levels of proteins measured in the cell media. Media was collected and frozen from successive triplicates at different intervals, then analyzed with the ACM. Each graph compares AFP values from cells incubated with a different additive to cells not incubated with additives located in the same 24-well plate. Plates in **c** and **e** did not contain any U87 cells, and **c** also did not have controls on the plate.

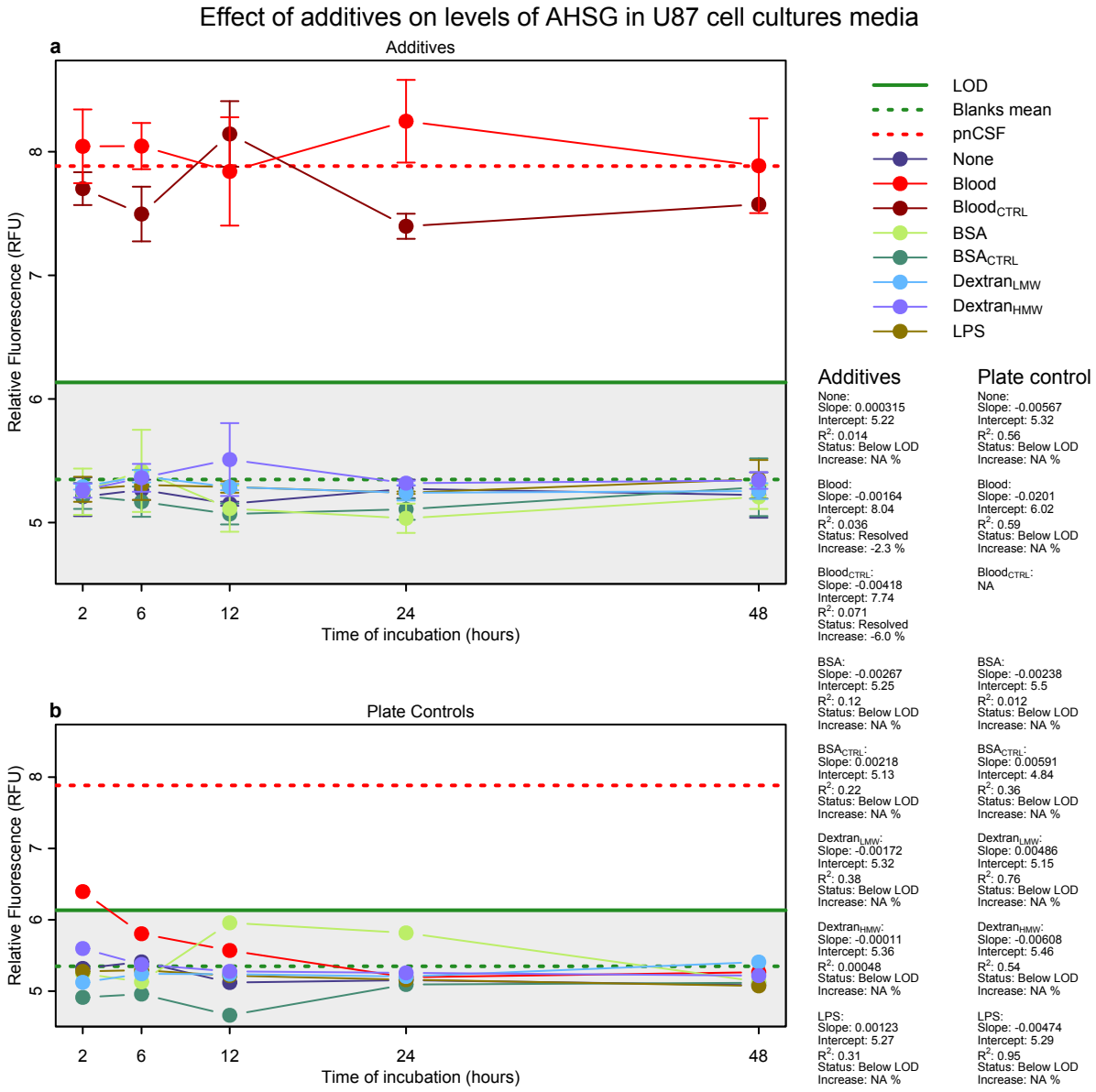

FIGURE H.S3: **Effect of additives on levels of AHSG in U87 cell cultures media.** Additives along with fresh blood and LPS were added to mycoplasma-free human glial (U87) cells in triplicate wells of a 24-well plate and incubated for up to 48 h to measure the effect on levels of proteins measured in the cell media. Media was collected and frozen from successive triplicates at different intervals, then analyzed with the ACM. **a** Average values for AHSG from three replicates for each point in every 24-well plate where a different additive was applied. **b** Data from the control cell media in each plate.

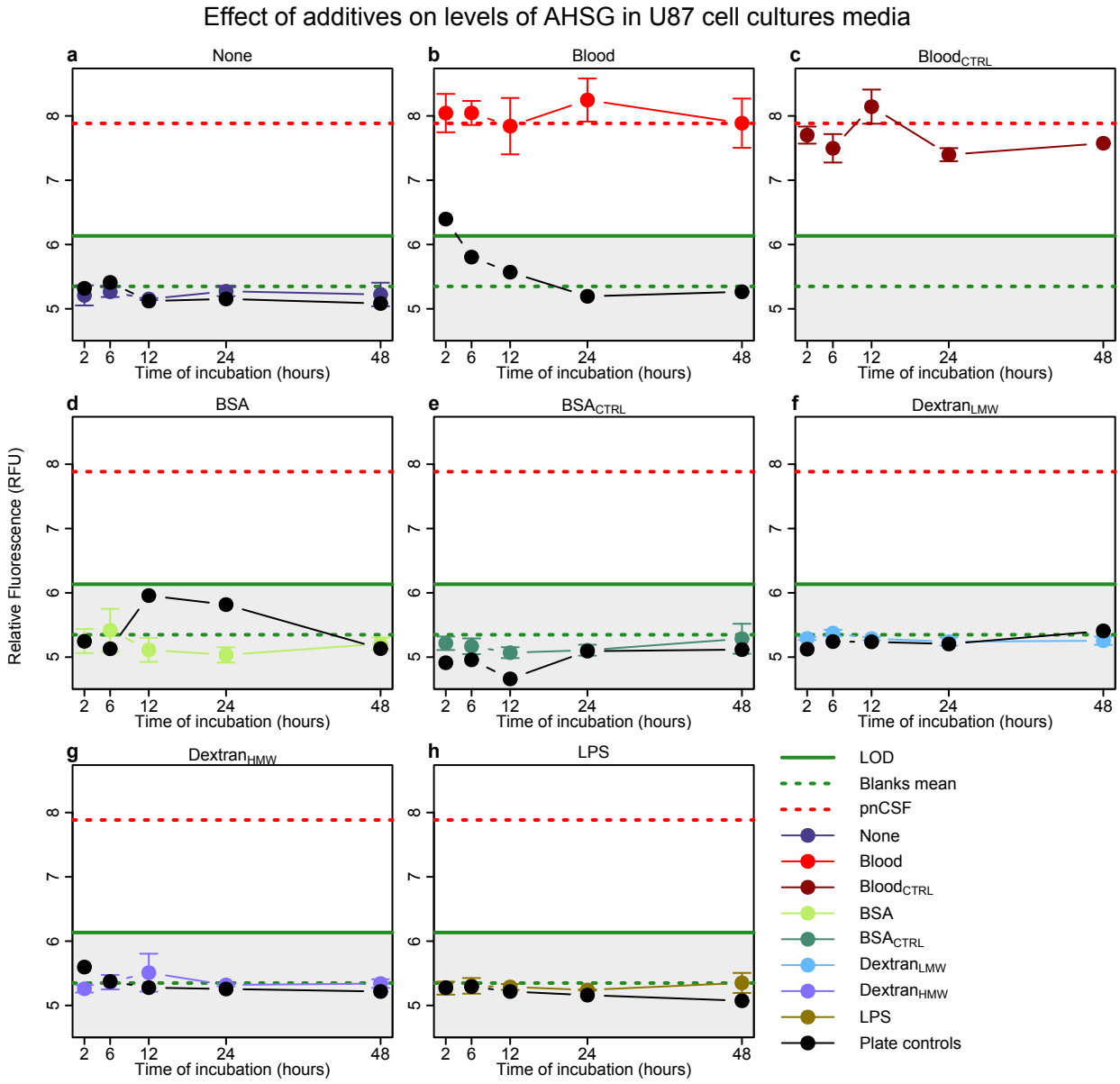

FIGURE H.S4: **Effect of additives on levels of AHSG in U87 cell cultures media.** Additives along with fresh blood and LPS were added to mycoplasma-free human glial (U87) cells in triplicate wells of a 24-well plate and incubated for up to 48 h to measure the effect on levels of proteins measured in the cell media. Media was collected and frozen from successive triplicates at different intervals, then analyzed with the ACM. Each graph compares AHSG values from cells incubated with a different additive to cells not incubated with additives located in the same 24-well plate. Plates in **c** and **e** did not contain any U87 cells, and **c** also did not have controls on the plate.

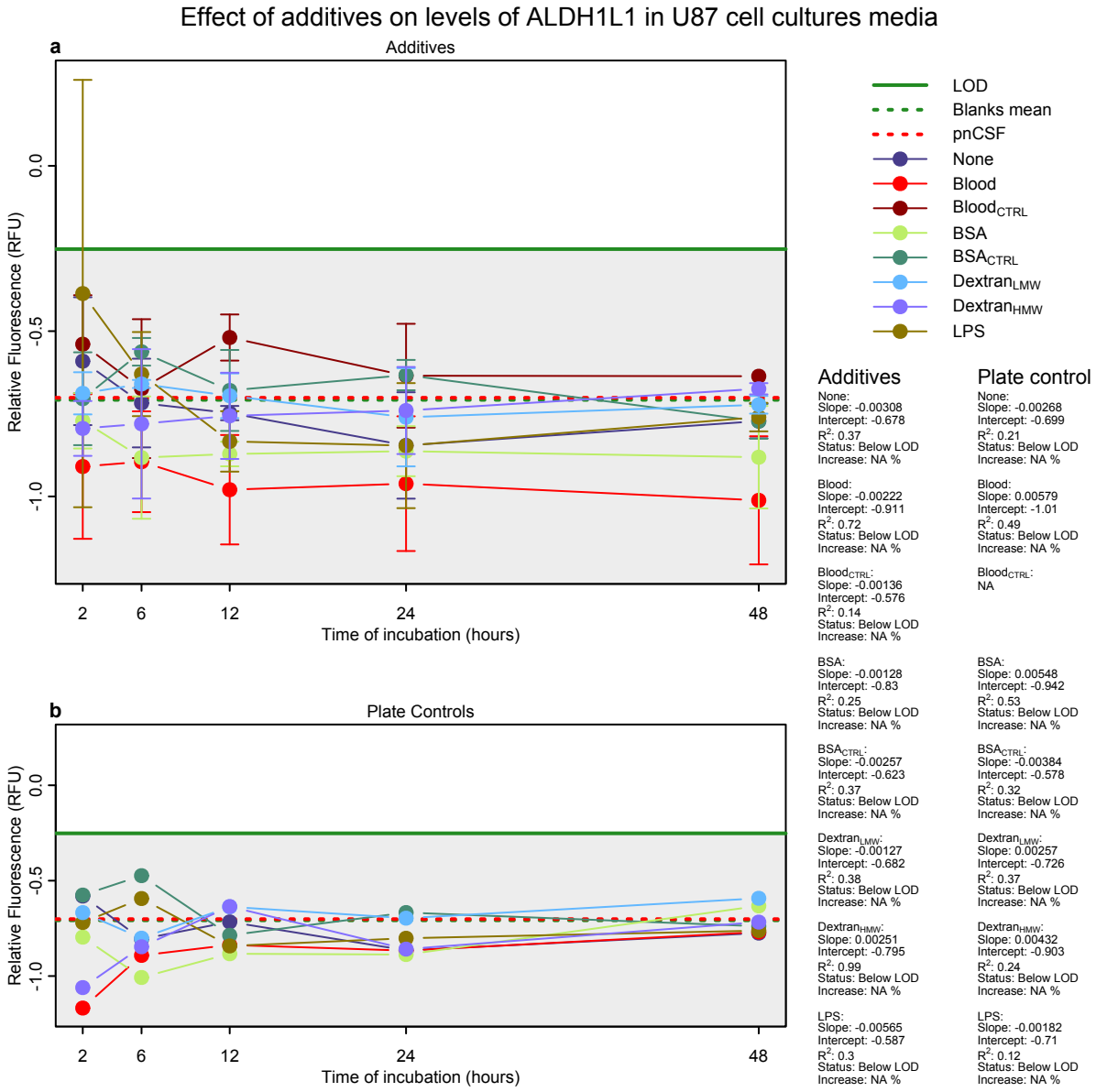

FIGURE H.S5: **Effect of additives on levels of ALDH1L1 in U87 cell cultures media.** Additives along with fresh blood and LPS were added to mycoplasma-free human glial (U87) cells in triplicate wells of a 24-well plate and incubated for up to 48 h to measure the effect on levels of proteins measured in the cell media. Media was collected and frozen from successive triplicates at different intervals, then analyzed with the ACM. **a** Average values for ALDH1L1 from three replicates for each point in every 24-well plate where a different additive was applied. **b** Data from the control cell media in each plate.

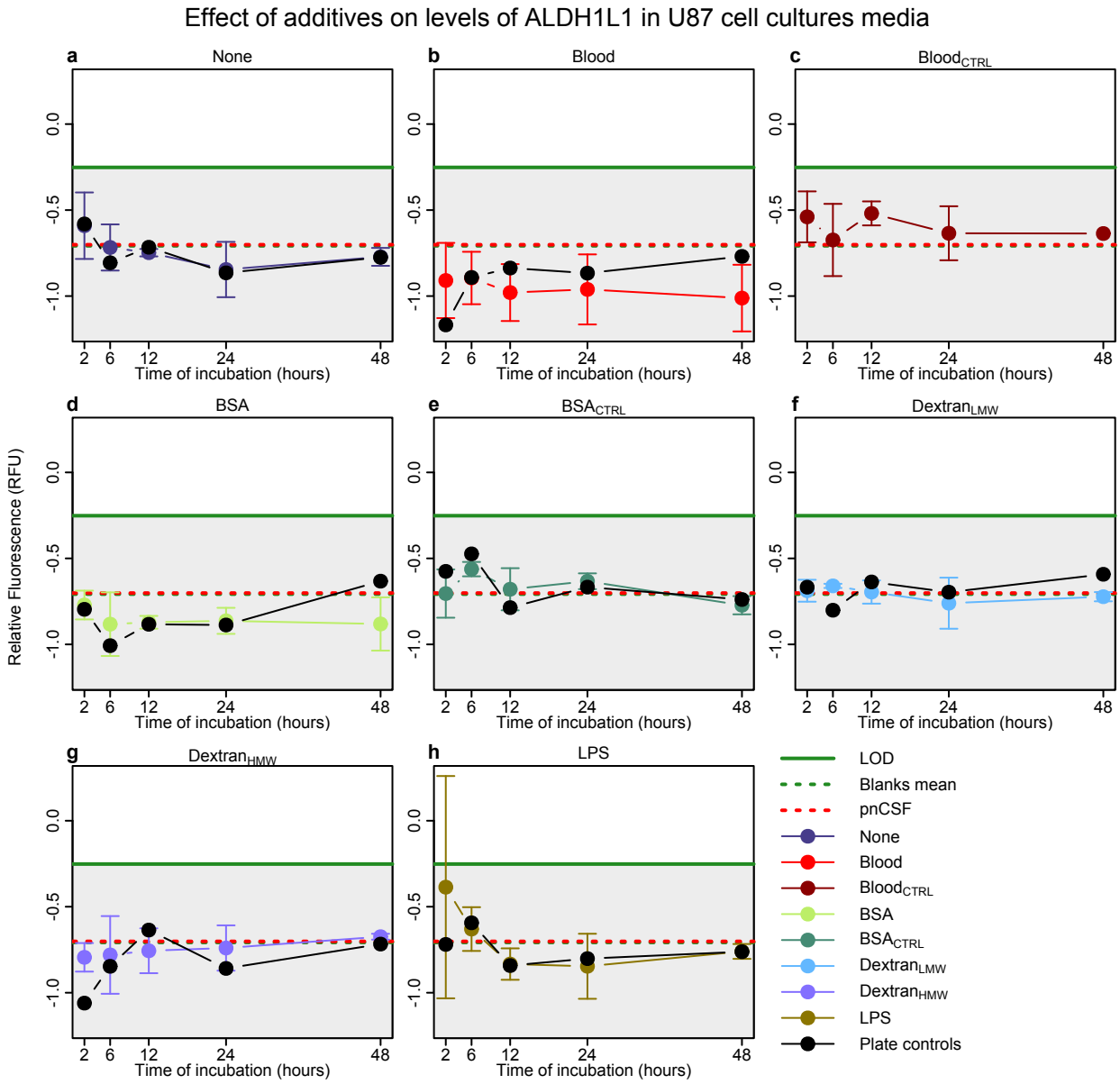

FIGURE H.S6: **Effect of additives on levels of ALDH1L1 in U87 cell cultures media.** Additives along with fresh blood and LPS were added to mycoplasma-free human glial (U87) cells in triplicate wells of a 24-well plate and incubated for up to 48 h to measure the effect on levels of proteins measured in the cell media. Media was collected and frozen from successive triplicates at different intervals, then analyzed with the ACM. Each graph compares ALDH1L1 values from cells incubated with a different additive to cells not incubated with additives located in the same 24-well plate. Plates in **c** and **e** did not contain any U87 cells, and **c** also did not have controls on the plate.

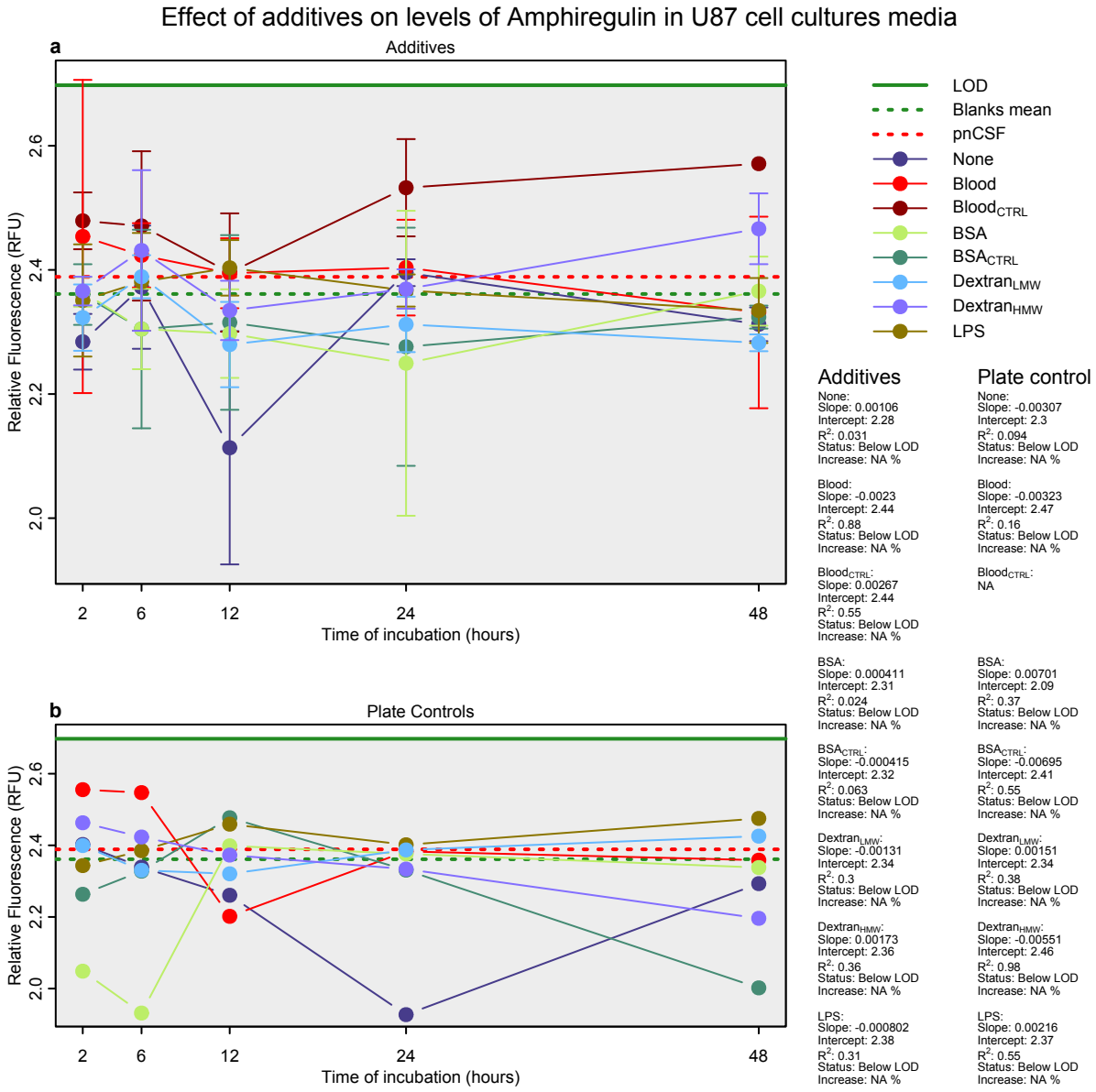

FIGURE H.S7: **Effect of additives on levels of Amphiregulin in U87 cell cultures media.** Additives along with fresh blood and LPS were added to mycoplasma-free human glial (U87) cells in triplicate wells of a 24-well plate and incubated for up to 48 h to measure the effect on levels of proteins measured in the cell media. Media was collected and frozen from successive triplicates at different intervals, then analyzed with the ACM. **a** Average values for Amphiregulin from three replicates for each point in every 24-well plate where a different additive was applied. **b** Data from the control cell media in each plate.

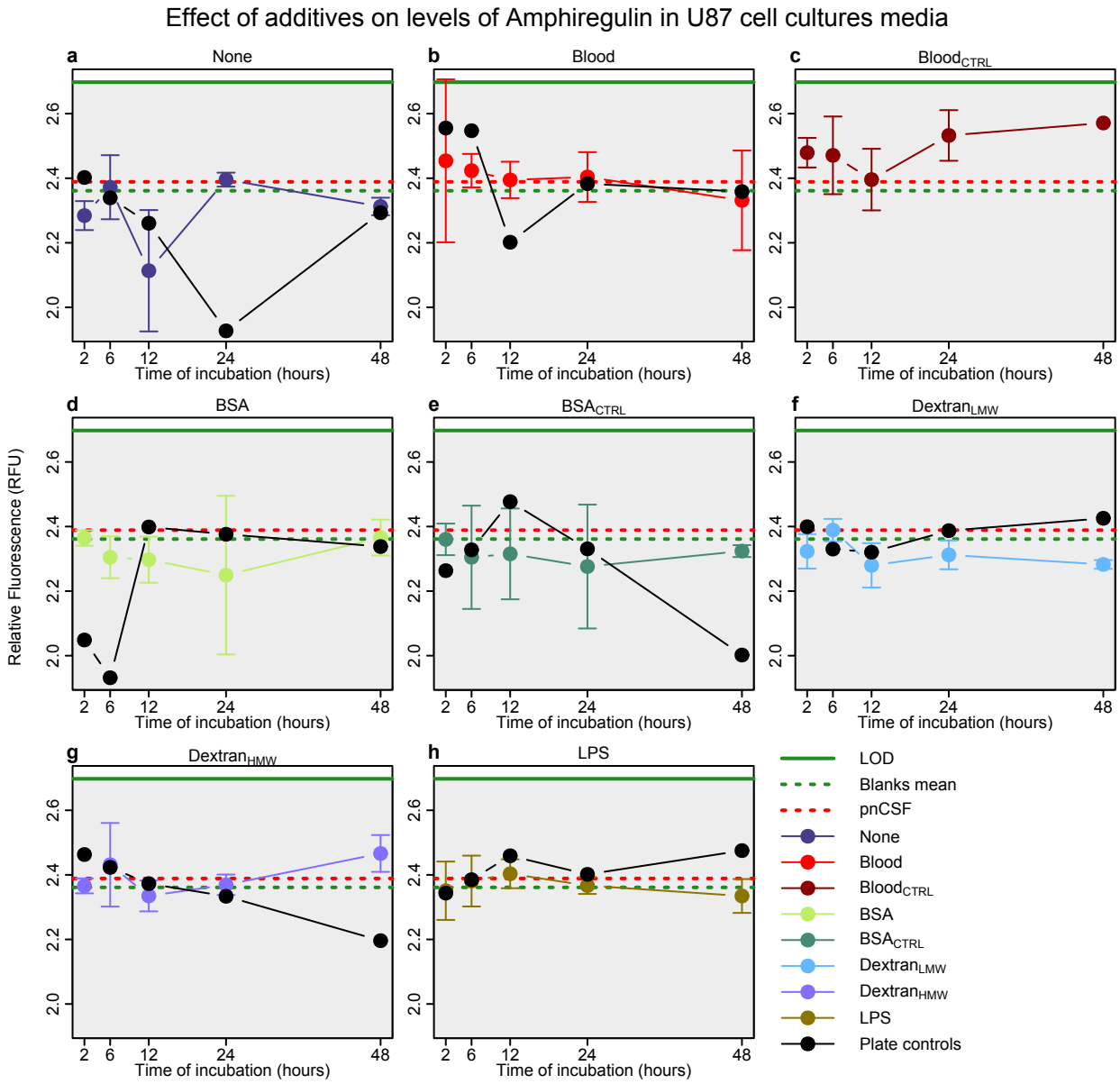

FIGURE H.S8: **Effect of additives on levels of Amphiregulin in U87 cell cultures media.** Additives along with fresh blood and LPS were added to mycoplasma-free human glial (U87) cells in triplicate wells of a 24-well plate and incubated for up to 48 h to measure the effect on levels of proteins measured in the cell media. Media was collected and frozen from successive triplicates at different intervals, then analyzed with the ACM. Each graph compares Amphiregulin values from cells incubated with a different additive to cells not incubated with additives located in the same 24-well plate. Plates in **c** and **e** did not contain any U87 cells, and **c** also did not have controls on the plate.

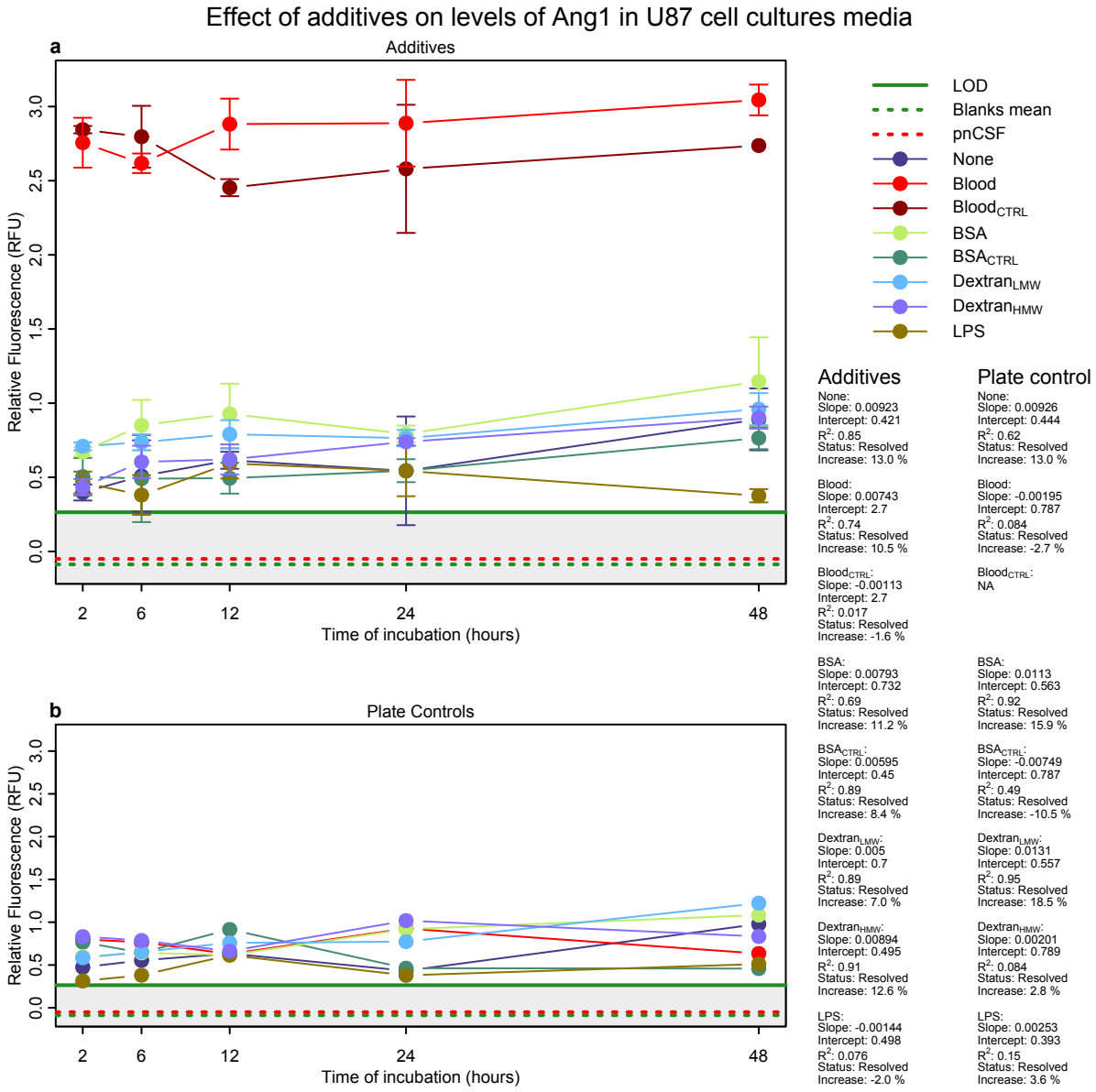

FIGURE H.S9: **Effect of additives on levels of Ang1 in U87 cell cultures media.** Additives along with fresh blood and LPS were added to mycoplasma-free human glial (U87) cells in triplicate wells of a 24-well plate and incubated for up to 48 h to measure the effect on levels of proteins measured in the cell media. Media was collected and frozen from successive triplicates at different intervals, then analyzed with the ACM. **a** Average values for Ang1 from three replicates for each point in every 24-well plate where a different additive was applied. **b** Data from the control cell media in each plate.

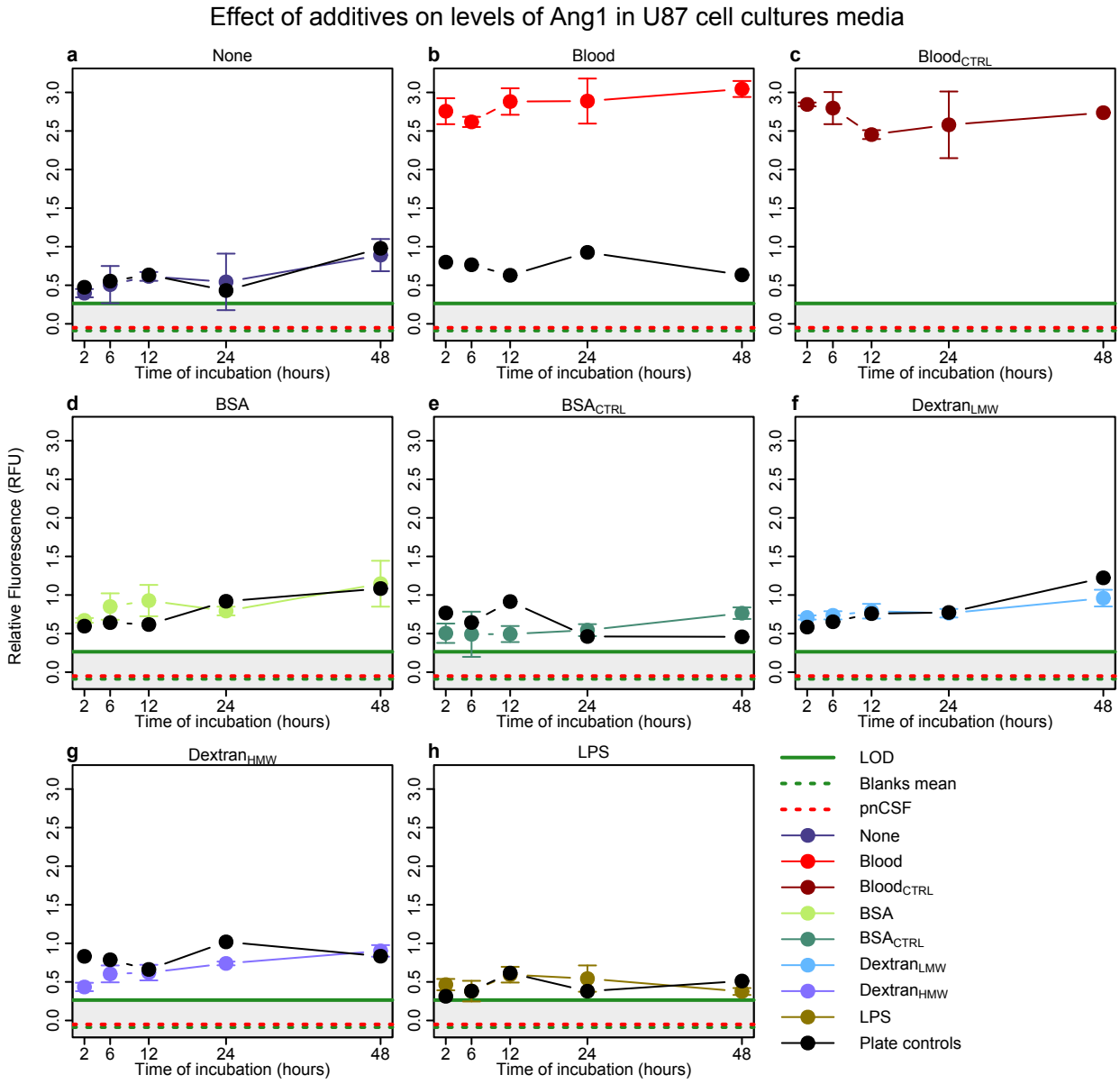

FIGURE H.S10: **Effect of additives on levels of Ang1 in U87 cell cultures media.** Additives along with fresh blood and LPS were added to mycoplasma-free human glial (U87) cells in triplicate wells of a 24-well plate and incubated for up to 48 h to measure the effect on levels of proteins measured in the cell media. Media was collected and frozen from successive triplicates at different intervals, then analyzed with the ACM. Each graph compares Ang1 values from cells incubated with a different additive to cells not incubated with additives located in the same 24-well plate. Plates in **c** and **e** did not contain any U87 cells, and **c** also did not have controls on the plate.

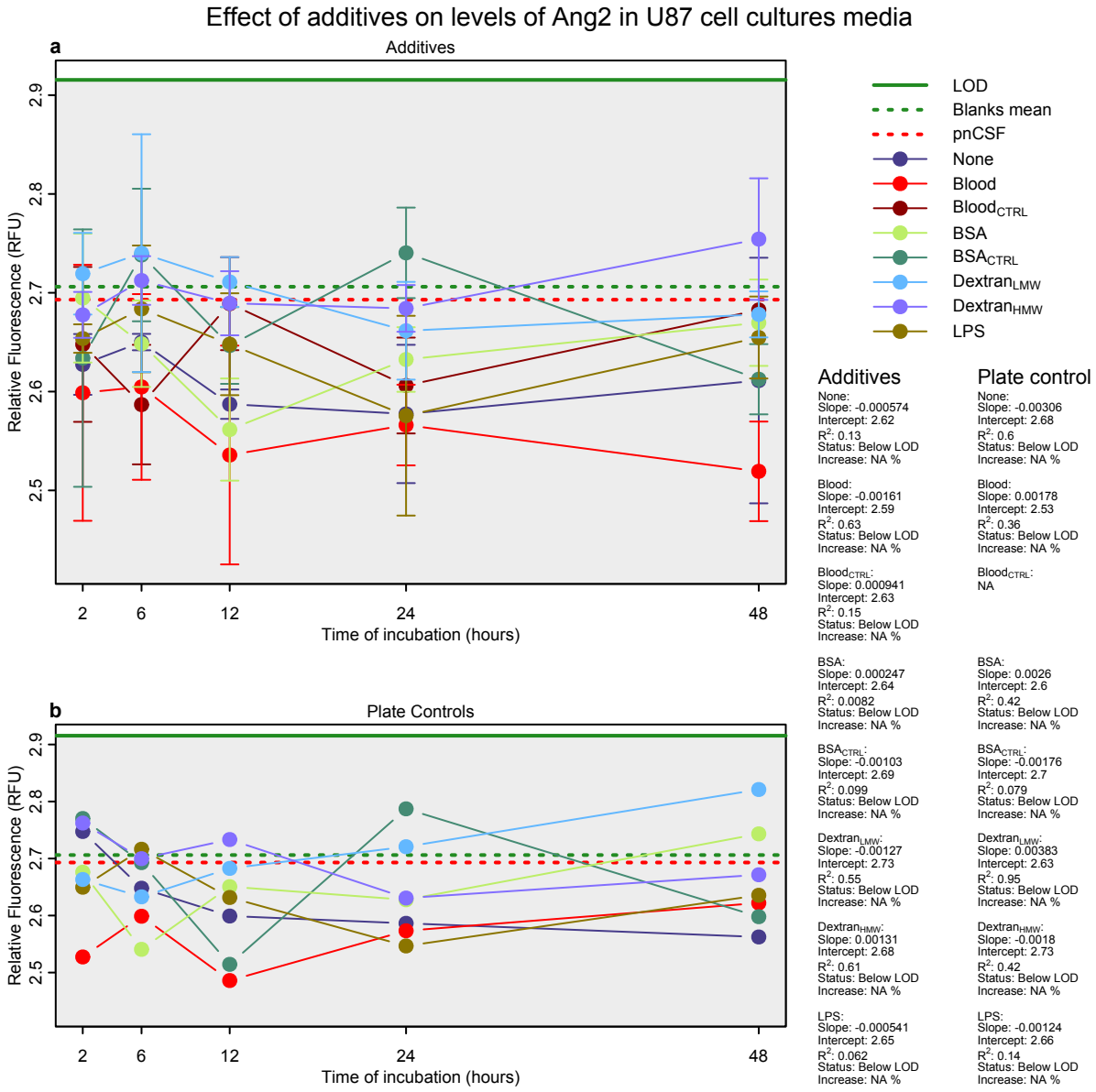

FIGURE H.S11: **Effect of additives on levels of Ang2 in U87 cell cultures media.** Additives along with fresh blood and LPS were added to mycoplasma-free human glial (U87) cells in triplicate wells of a 24-well plate and incubated for up to 48 h to measure the effect on levels of proteins measured in the cell media. Media was collected and frozen from successive triplicates at different intervals, then analyzed with the ACM. **a** Average values for Ang2 from three replicates for each point in every 24-well plate where a different additive was applied. **b** Data from the control cell media in each plate.

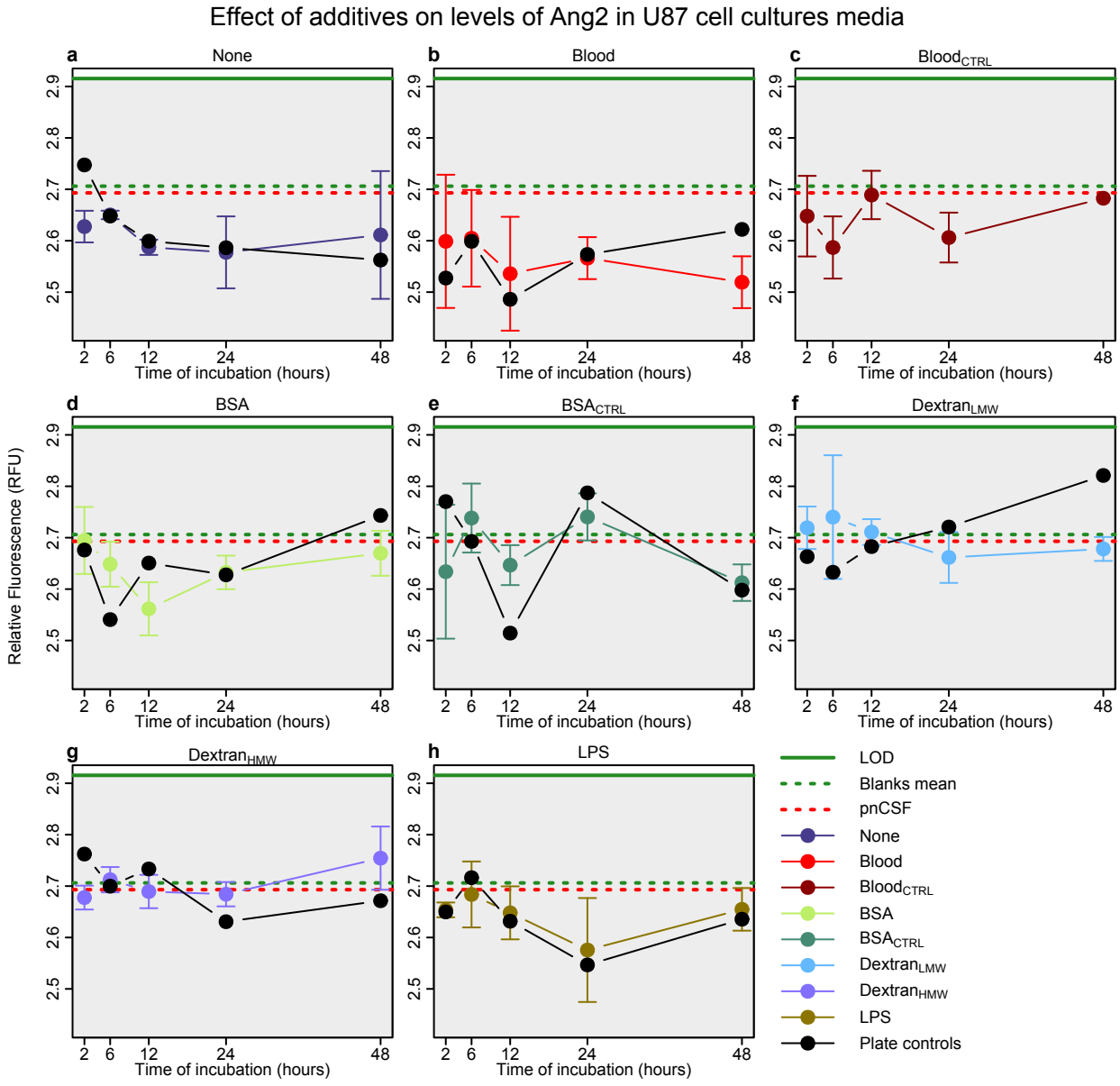

FIGURE H.S12: **Effect of additives on levels of Ang2 in U87 cell cultures media.** Additives along with fresh blood and LPS were added to mycoplasma-free human glial (U87) cells in triplicate wells of a 24-well plate and incubated for up to 48 h to measure the effect on levels of proteins measured in the cell media. Media was collected and frozen from successive triplicates at different intervals, then analyzed with the ACM. Each graph compares Ang2 values from cells incubated with a different additive to cells not incubated with additives located in the same 24-well plate. Plates in **c** and **e** did not contain any U87 cells, and **c** also did not have controls on the plate.

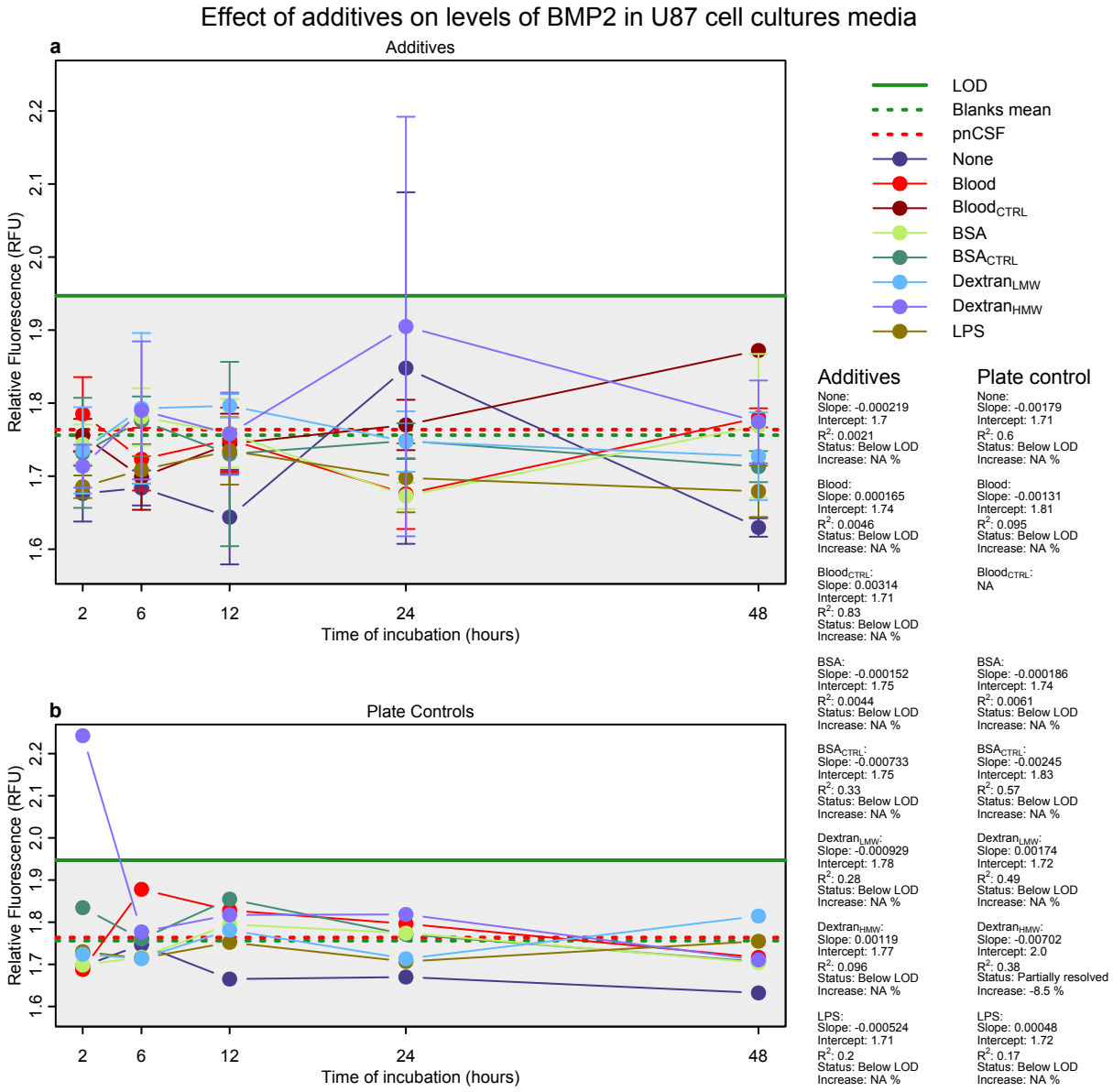

FIGURE H.S13: **Effect of additives on levels of BMP2 in U87 cell cultures media.** Additives along with fresh blood and LPS were added to mycoplasma-free human glial (U87) cells in triplicate wells of a 24-well plate and incubated for up to 48 h to measure the effect on levels of proteins measured in the cell media. Media was collected and frozen from successive triplicates at different intervals, then analyzed with the ACM. **a** Average values for BMP2 from three replicates for each point in every 24-well plate where a different additive was applied. **b** Data from the control cell media in each plate.

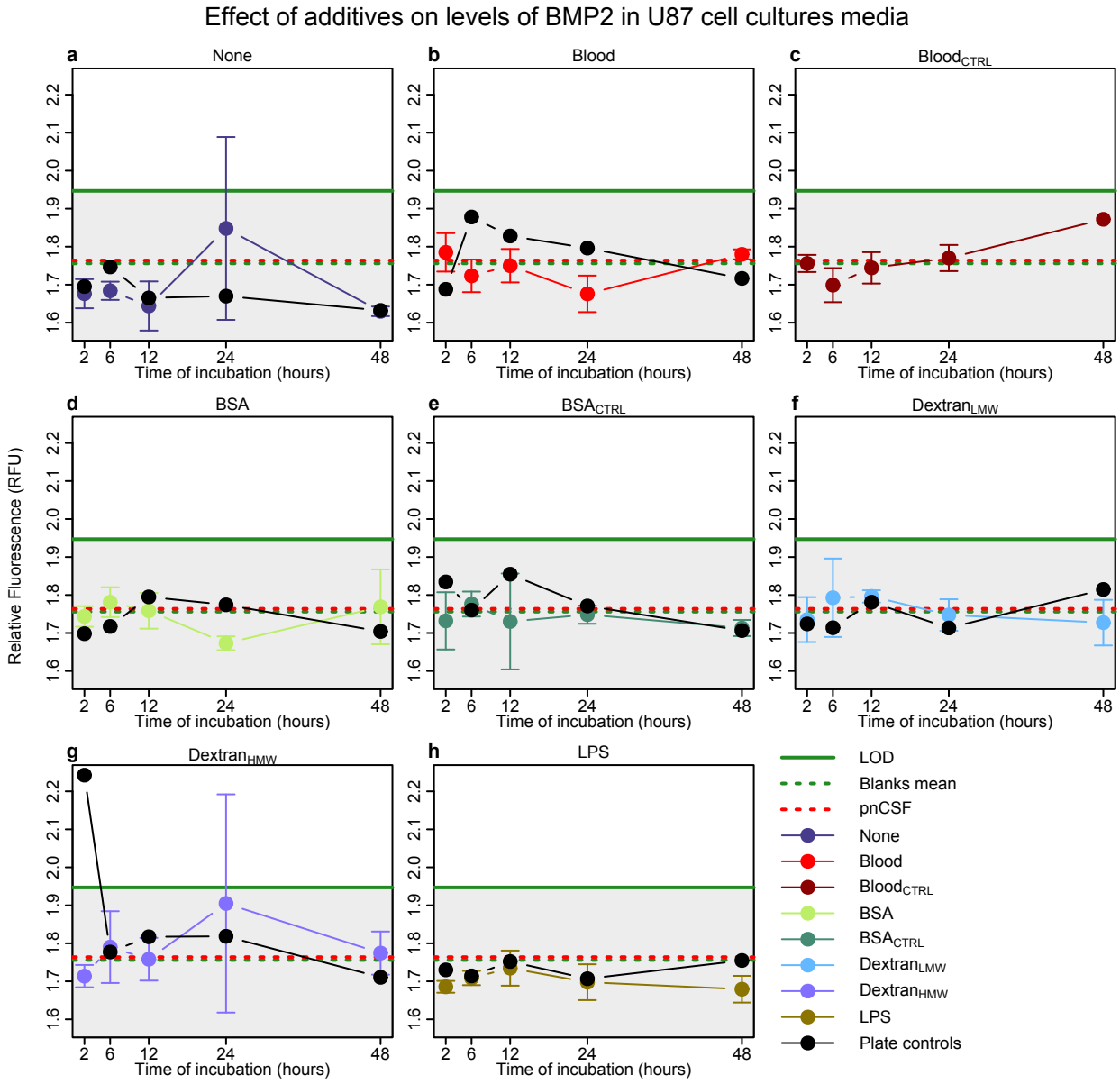

FIGURE H.S14: **Effect of additives on levels of BMP2 in U87 cell cultures media.** Additives along with fresh blood and LPS were added to mycoplasma-free human glial (U87) cells in triplicate wells of a 24-well plate and incubated for up to 48 h to measure the effect on levels of proteins measured in the cell media. Media was collected and frozen from successive triplicates at different intervals, then analyzed with the ACM. Each graph compares BMP2 values from cells incubated with a different additive to cells not incubated with additives located in the same 24-well plate. Plates in **c** and **e** did not contain any U87 cells, and **c** also did not have controls on the plate.

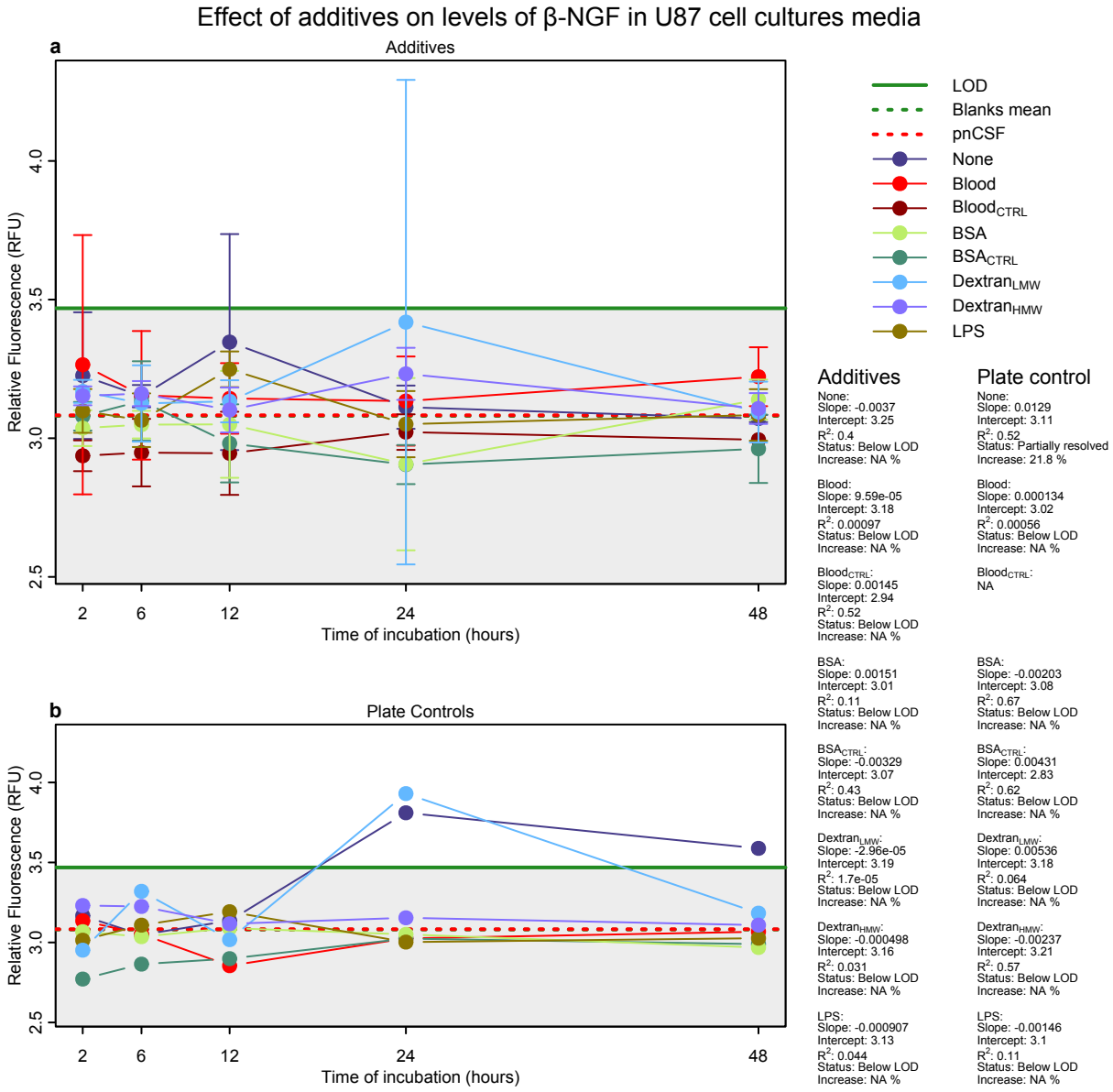

FIGURE H.S15: **Effect of additives on levels of β-NGF in U87 cell cultures media.** Additives along with fresh blood and LPS were added to mycoplasma-free human glial (U87) cells in triplicate wells of a 24-well plate and incubated for up to 48 h to measure the effect on levels of proteins measured in the cell media. Media was collected and frozen from successive triplicates at different intervals, then analyzed with the ACM. **a** Average values for β-NGF from three replicates for each point in every 24-well plate where a different additive was applied. **b** Data from the control cell media in each plate.

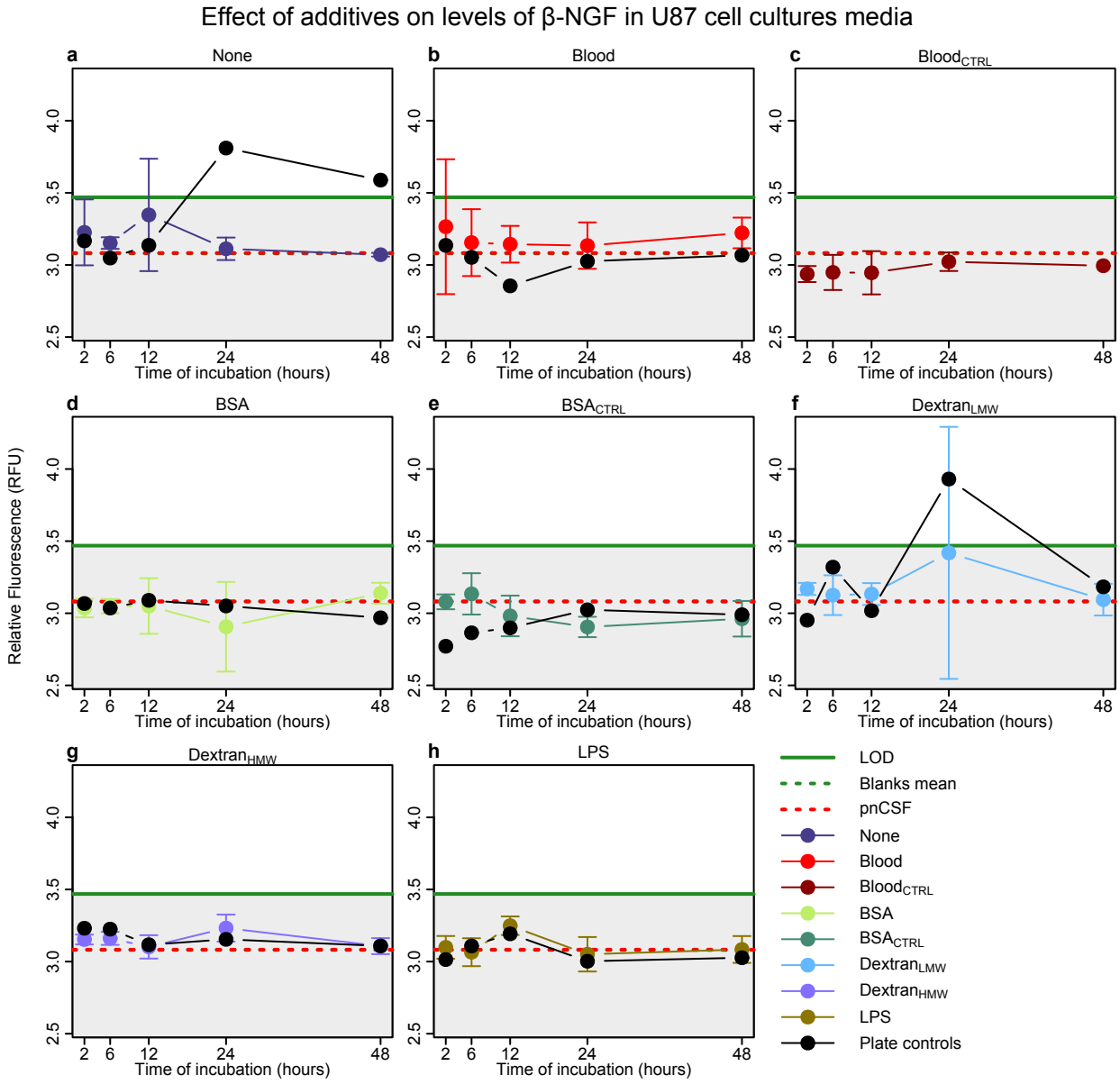

FIGURE H.S16: **Effect of additives on levels of β-NGF in U87 cell cultures media.** Additives along with fresh blood and LPS were added to mycoplasma-free human glial (U87) cells in triplicate wells of a 24-well plate and incubated for up to 48 h to measure the effect on levels of proteins measured in the cell media. Media was collected and frozen from successive triplicates at different intervals, then analyzed with the ACM. Each graph compares β-NGF values from cells incubated with a different additive to cells not incubated with additives located in the same 24-well plate. Plates in **c** and **e** did not contain any U87 cells, and **c** also did not have controls on the plate.

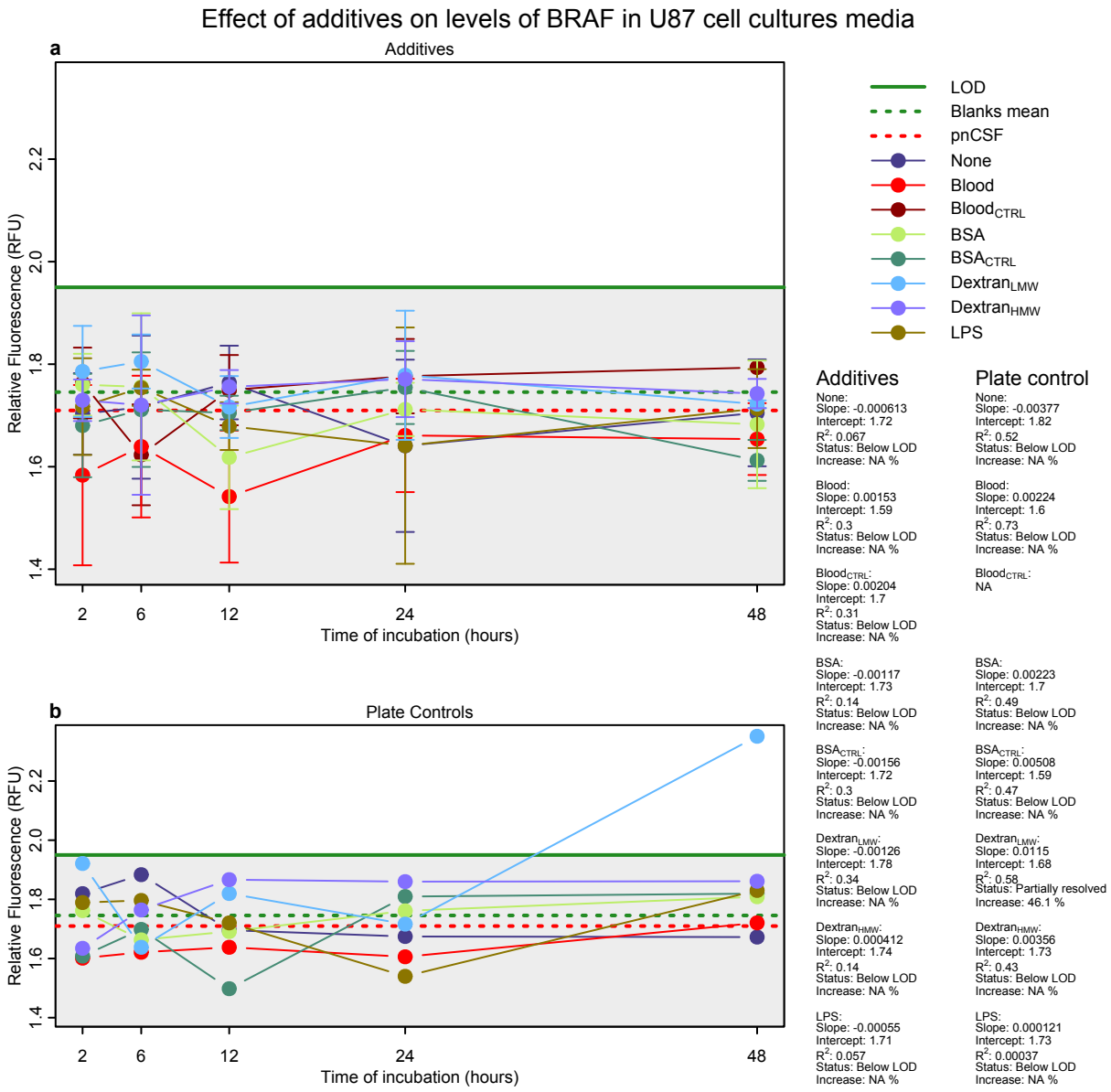

FIGURE H.S17: **Effect of additives on levels of BRAF in U87 cell cultures media.** Additives along with fresh blood and LPS were added to mycoplasma-free human glial (U87) cells in triplicate wells of a 24-well plate and incubated for up to 48 h to measure the effect on levels of proteins measured in the cell media. Media was collected and frozen from successive triplicates at different intervals, then analyzed with the ACM. **a** Average values for BRAF from three replicates for each point in every 24-well plate where a different additive was applied. **b** Data from the control cell media in each plate.

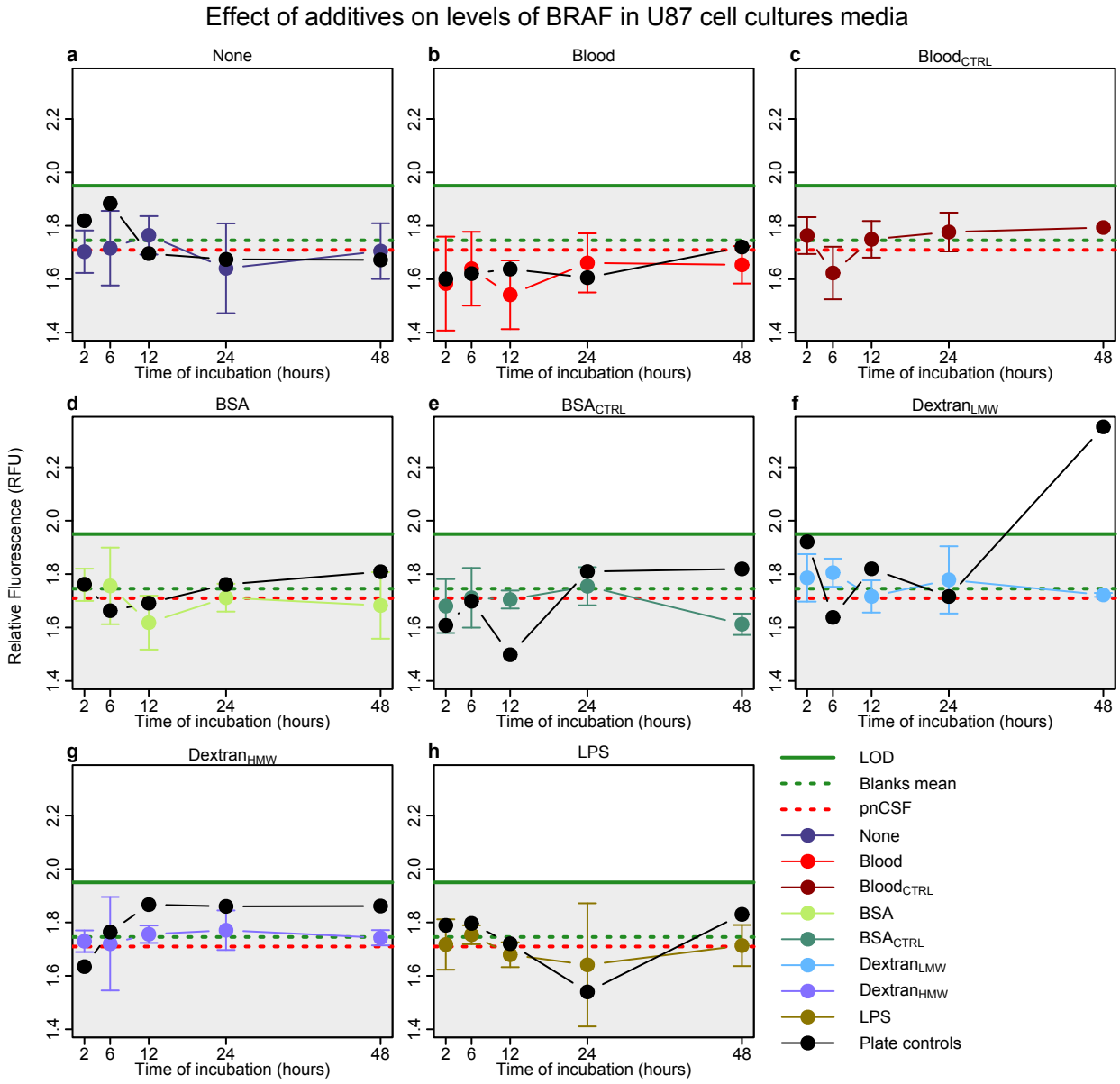

FIGURE H.S18: **Effect of additives on levels of BRAF in U87 cell cultures media.** Additives along with fresh blood and LPS were added to mycoplasma-free human glial (U87) cells in triplicate wells of a 24-well plate and incubated for up to 48 h to measure the effect on levels of proteins measured in the cell media. Media was collected and frozen from successive triplicates at different intervals, then analyzed with the ACM. Each graph compares BRAF values from cells incubated with a different additive to cells not incubated with additives located in the same 24-well plate. Plates in **c** and **e** did not contain any U87 cells, and **c** also did not have controls on the plate.

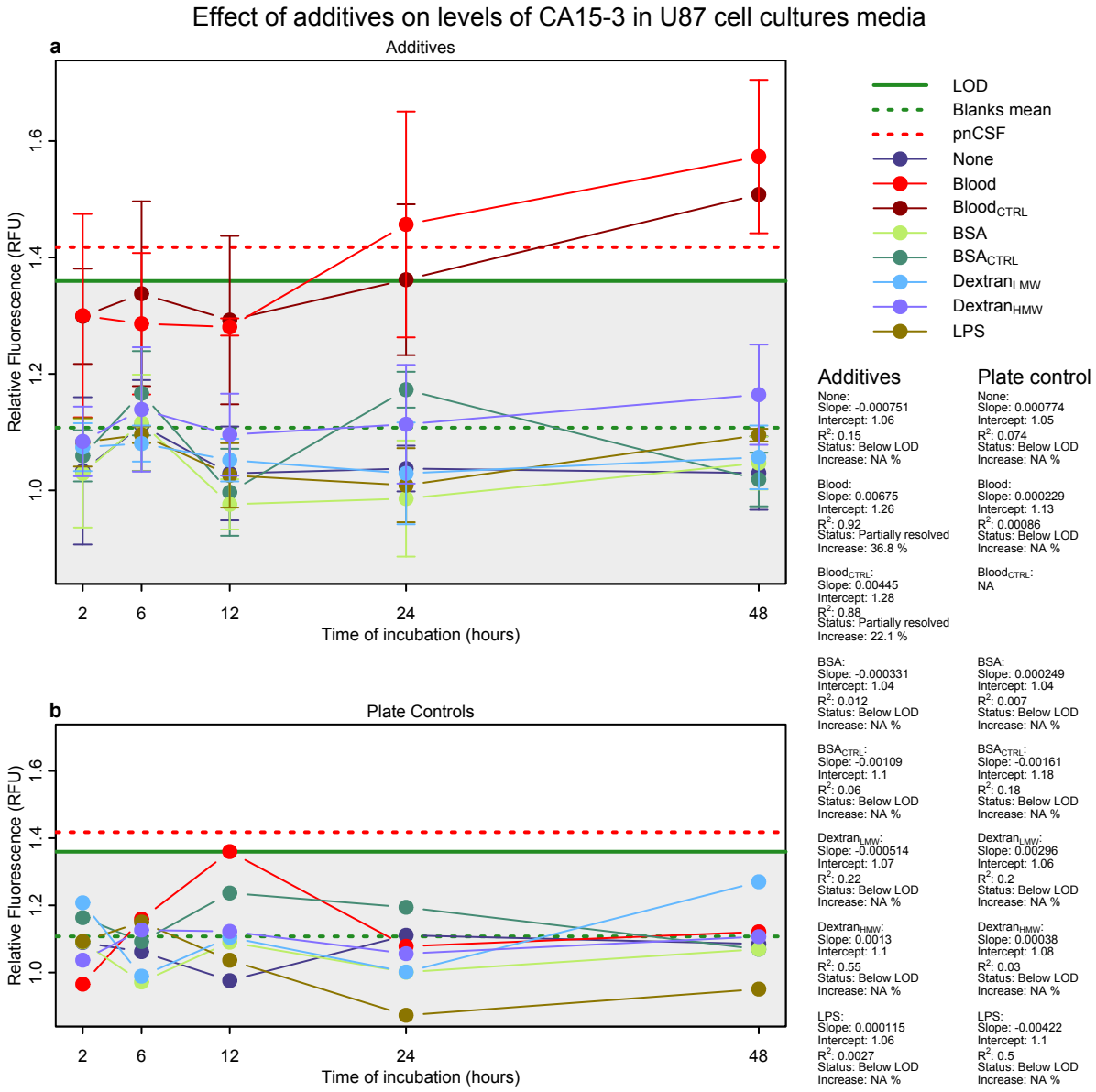

FIGURE H.S19: **Effect of additives on levels of CA15-3 in U87 cell cultures media.** Additives along with fresh blood and LPS were added to mycoplasma-free human glial (U87) cells in triplicate wells of a 24-well plate and incubated for up to 48 h to measure the effect on levels of proteins measured in the cell media. Media was collected and frozen from successive triplicates at different intervals, then analyzed with the ACM. **a** Average values for CA15-3 from three replicates for each point in every 24-well plate where a different additive was applied. **b** Data from the control cell media in each plate.

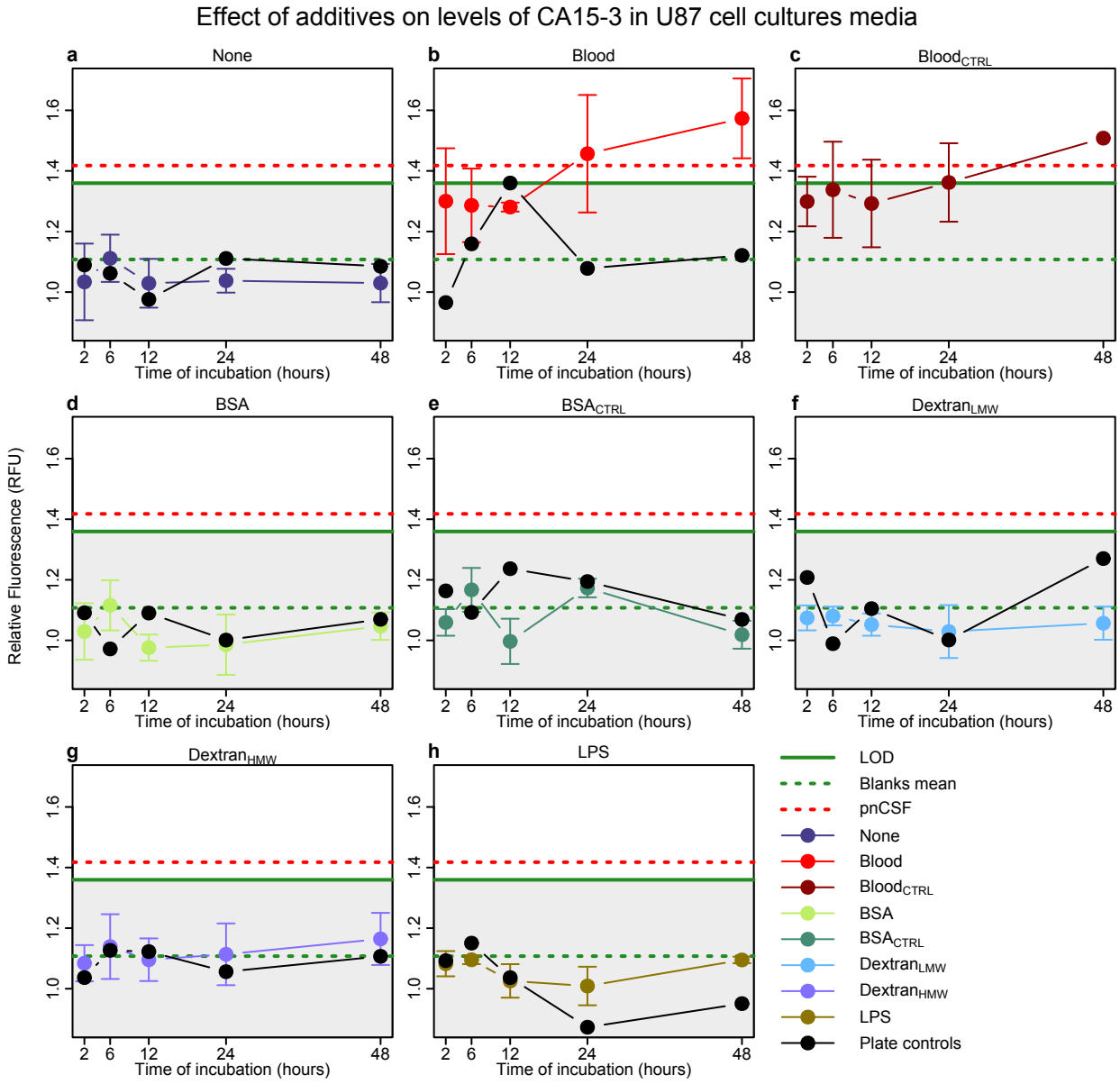

FIGURE H.S20: **Effect of additives on levels of CA15-3 in U87 cell cultures media.** Additives along with fresh blood and LPS were added to mycoplasma-free human glial (U87) cells in triplicate wells of a 24-well plate and incubated for up to 48 h to measure the effect on levels of proteins measured in the cell media. Media was collected and frozen from successive triplicates at different intervals, then analyzed with the ACM. Each graph compares CA15-3 values from cells incubated with a different additive to cells not incubated with additives located in the same 24-well plate. Plates in **c** and **e** did not contain any U87 cells, and **c** also did not have controls on the plate.

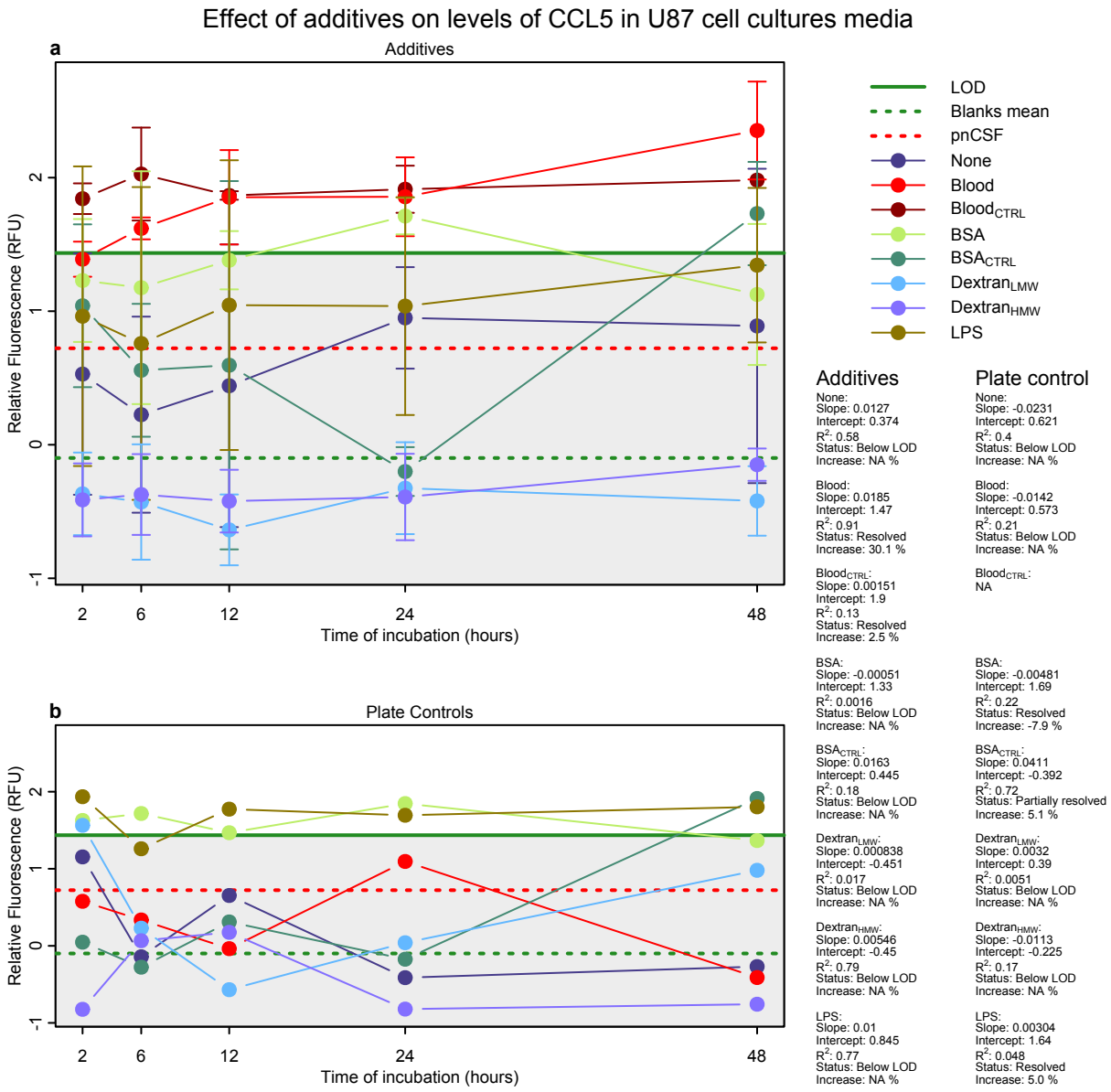

FIGURE H.S21: **Effect of additives on levels of CCL5 in U87 cell cultures media.** Additives along with fresh blood and LPS were added to mycoplasma-free human glial (U87) cells in triplicate wells of a 24-well plate and incubated for up to 48 h to measure the effect on levels of proteins measured in the cell media. Media was collected and frozen from successive triplicates at different intervals, then analyzed with the ACM. **a** Average values for CCL5 from three replicates for each point in every 24-well plate where a different additive was applied. **b** Data from the control cell media in each plate.

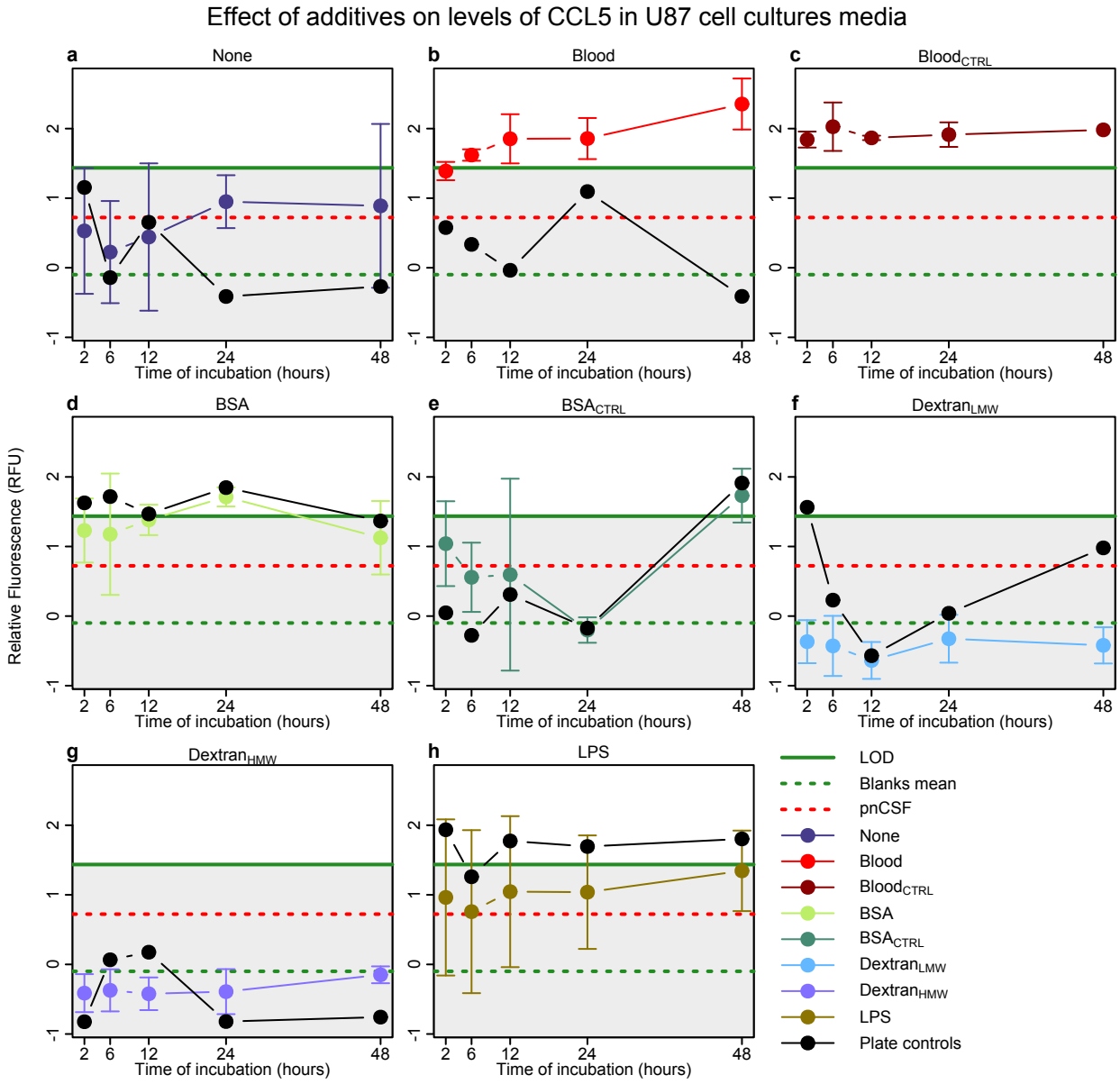

FIGURE H.S22: **Effect of additives on levels of CCL5 in U87 cell cultures media.** Additives along with fresh blood and LPS were added to mycoplasma-free human glial (U87) cells in triplicate wells of a 24-well plate and incubated for up to 48 h to measure the effect on levels of proteins measured in the cell media. Media was collected and frozen from successive triplicates at different intervals, then analyzed with the ACM. Each graph compares CCL5 values from cells incubated with a different additive to cells not incubated with additives located in the same 24-well plate. Plates in **c** and **e** did not contain any U87 cells, and **c** also did not have controls on the plate.

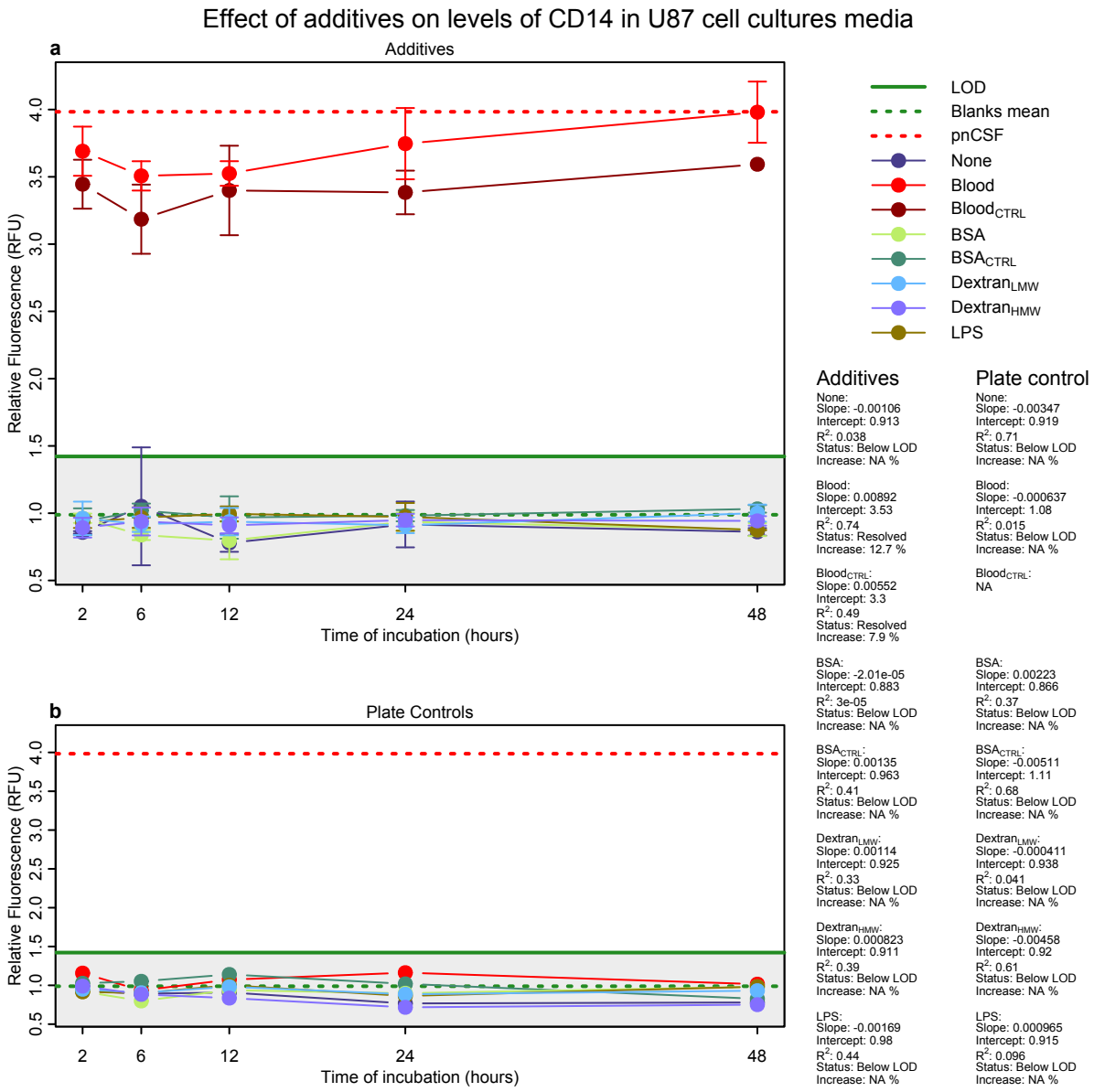

FIGURE H.S23: **Effect of additives on levels of CD14 in U87 cell cultures media.** Additives along with fresh blood and LPS were added to mycoplasma-free human glial (U87) cells in triplicate wells of a 24-well plate and incubated for up to 48 h to measure the effect on levels of proteins measured in the cell media. Media was collected and frozen from successive triplicates at different intervals, then analyzed with the ACM. **a** Average values for CD14 from three replicates for each point in every 24-well plate where a different additive was applied. **b** Data from the control cell media in each plate.

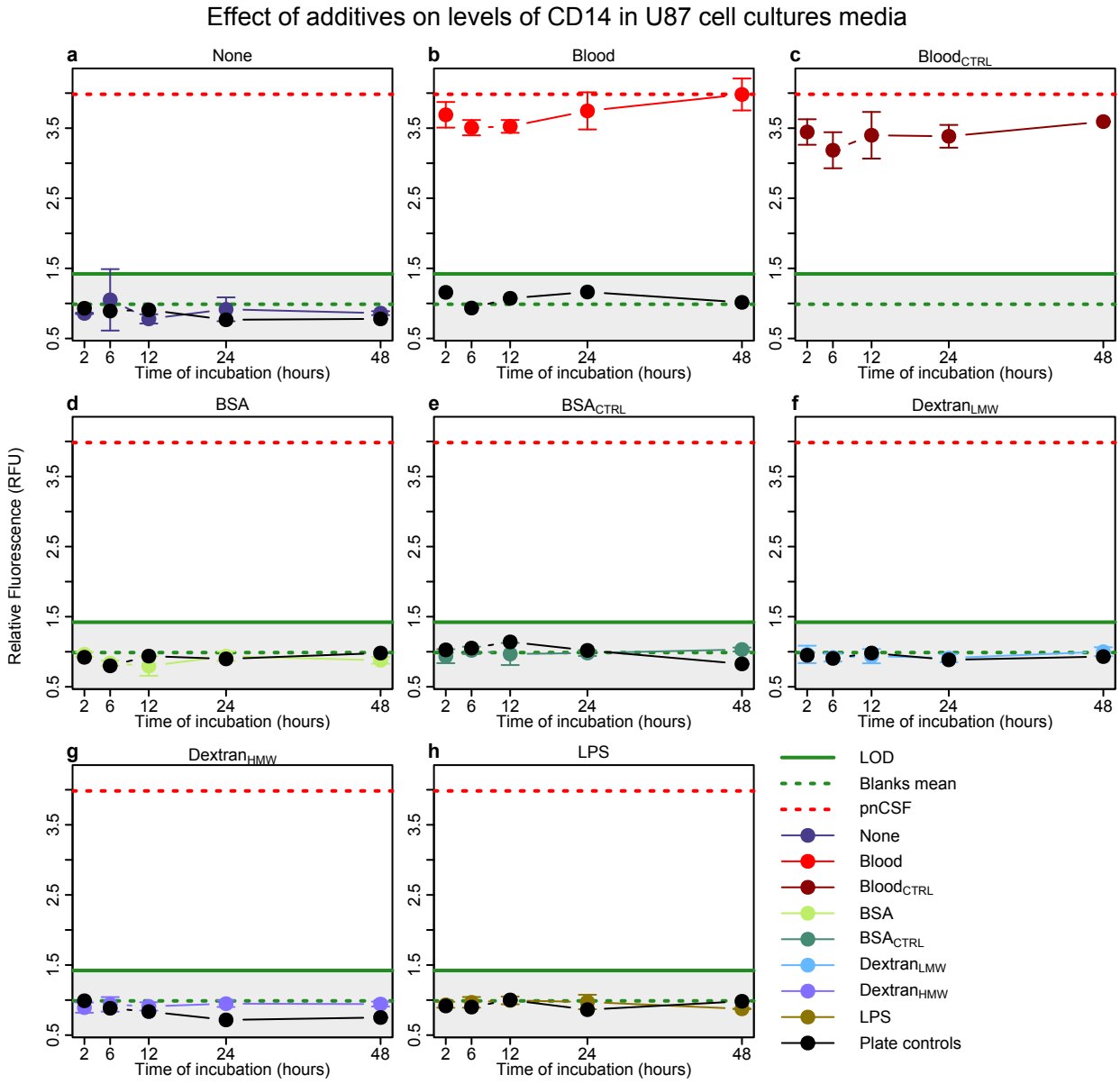

FIGURE H.S24: **Effect of additives on levels of CD14 in U87 cell cultures media.** Additives along with fresh blood and LPS were added to mycoplasma-free human glial (U87) cells in triplicate wells of a 24-well plate and incubated for up to 48 h to measure the effect on levels of proteins measured in the cell media. Media was collected and frozen from successive triplicates at different intervals, then analyzed with the ACM. Each graph compares CD14 values from cells incubated with a different additive to cells not incubated with additives located in the same 24-well plate. Plates in **c** and **e** did not contain any U87 cells, and **c** also did not have controls on the plate.

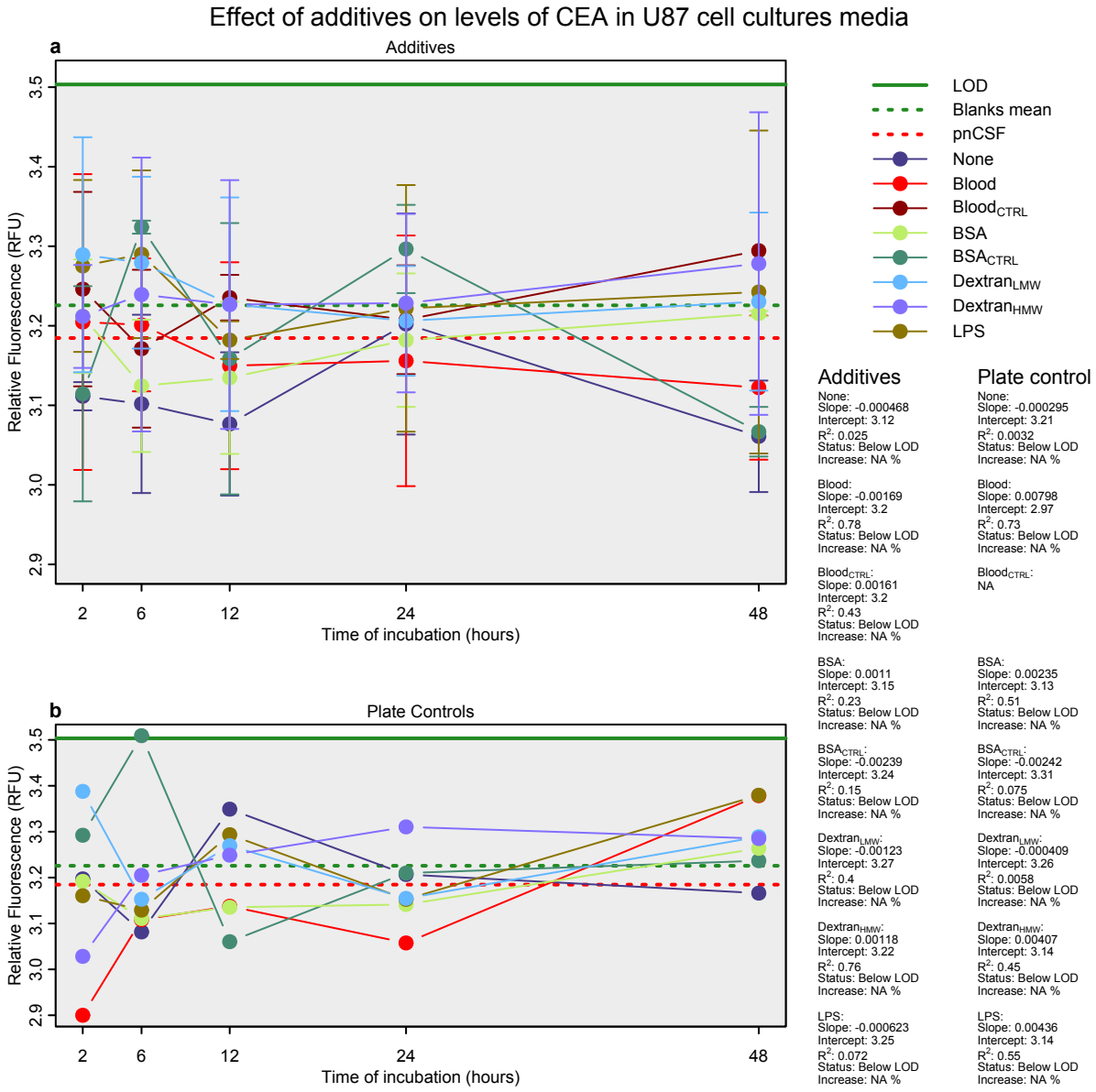

FIGURE H.S25: **Effect of additives on levels of CEA in U87 cell cultures media.** Additives along with fresh blood and LPS were added to mycoplasma-free human glial (U87) cells in triplicate wells of a 24-well plate and incubated for up to 48 h to measure the effect on levels of proteins measured in the cell media. Media was collected and frozen from successive triplicates at different intervals, then analyzed with the ACM. **a** Average values for CEA from three replicates for each point in every 24-well plate where a different additive was applied. **b** Data from the control cell media in each plate.

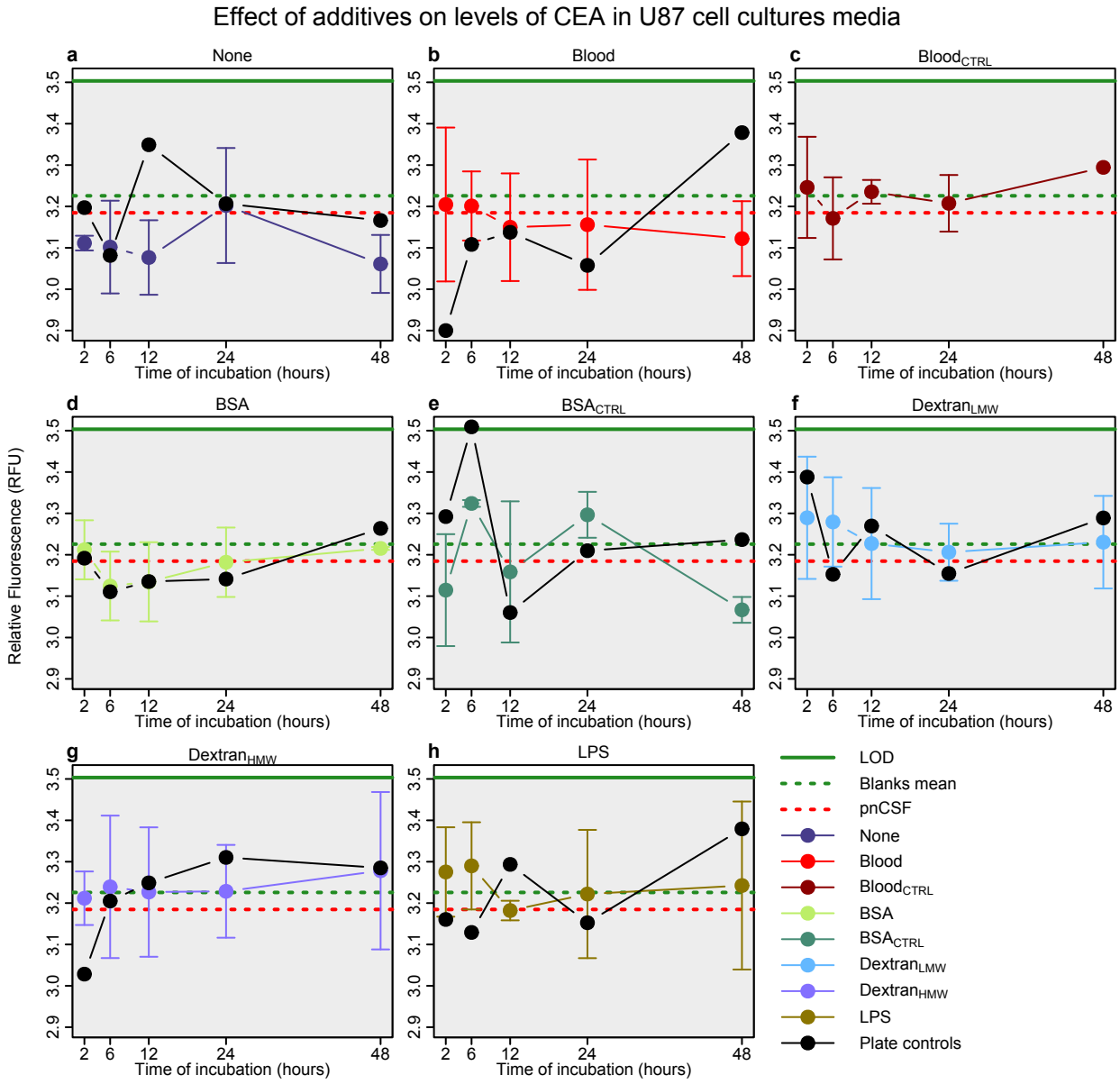

FIGURE H.S26: **Effect of additives on levels of CEA in U87 cell cultures media.** Additives along with fresh blood and LPS were added to mycoplasma-free human glial (U87) cells in triplicate wells of a 24-well plate and incubated for up to 48 h to measure the effect on levels of proteins measured in the cell media. Media was collected and frozen from successive triplicates at different intervals, then analyzed with the ACM. Each graph compares CEA values from cells incubated with a different additive to cells not incubated with additives located in the same 24-well plate. Plates in **c** and **e** did not contain any U87 cells, and **c** also did not have controls on the plate.

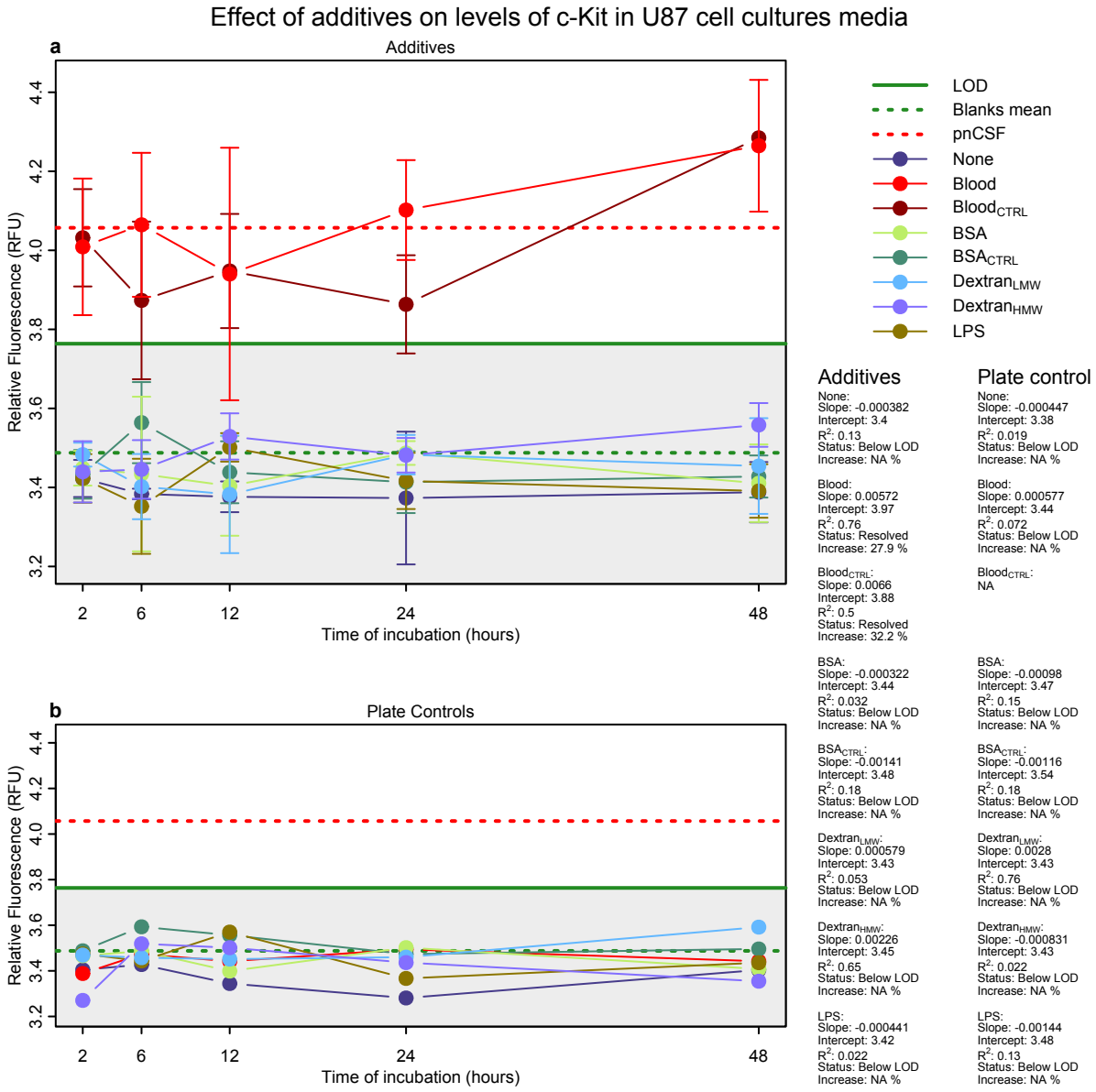

FIGURE H.S27: **Effect of additives on levels of c-Kit in U87 cell cultures media.** Additives along with fresh blood and LPS were added to mycoplasma-free human glial (U87) cells in triplicate wells of a 24-well plate and incubated for up to 48 h to measure the effect on levels of proteins measured in the cell media. Media was collected and frozen from successive triplicates at different intervals, then analyzed with the ACM. **a** Average values for c-Kit from three replicates for each point in every 24-well plate where a different additive was applied. **b** Data from the control cell media in each plate.

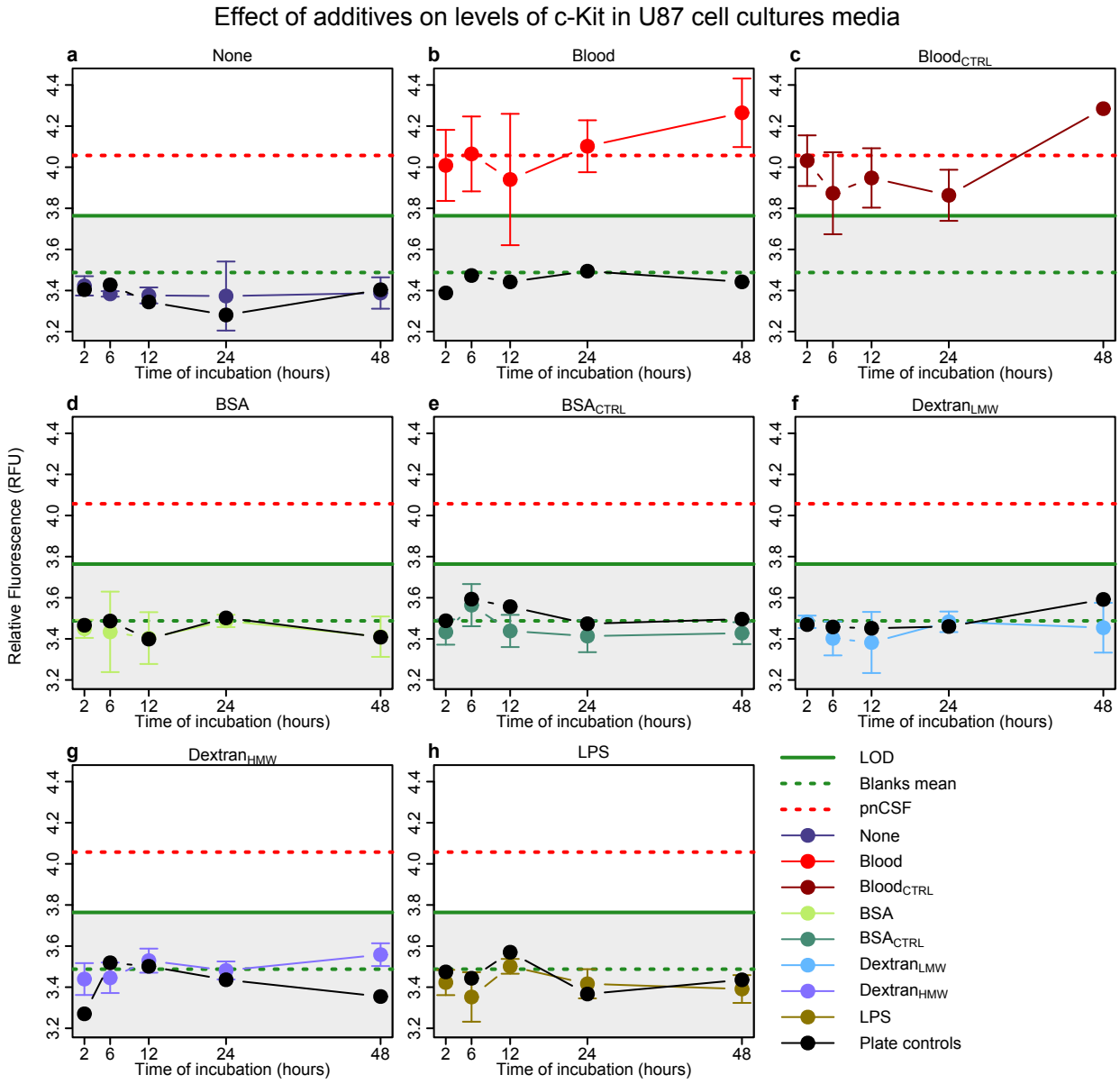

FIGURE H.S28: **Effect of additives on levels of c-Kit in U87 cell cultures media.** Additives along with fresh blood and LPS were added to mycoplasma-free human glial (U87) cells in triplicate wells of a 24-well plate and incubated for up to 48 h to measure the effect on levels of proteins measured in the cell media. Media was collected and frozen from successive triplicates at different intervals, then analyzed with the ACM. Each graph compares c-Kit values from cells incubated with a different additive to cells not incubated with additives located in the same 24-well plate. Plates in **c** and **e** did not contain any U87 cells, and **c** also did not have controls on the plate.

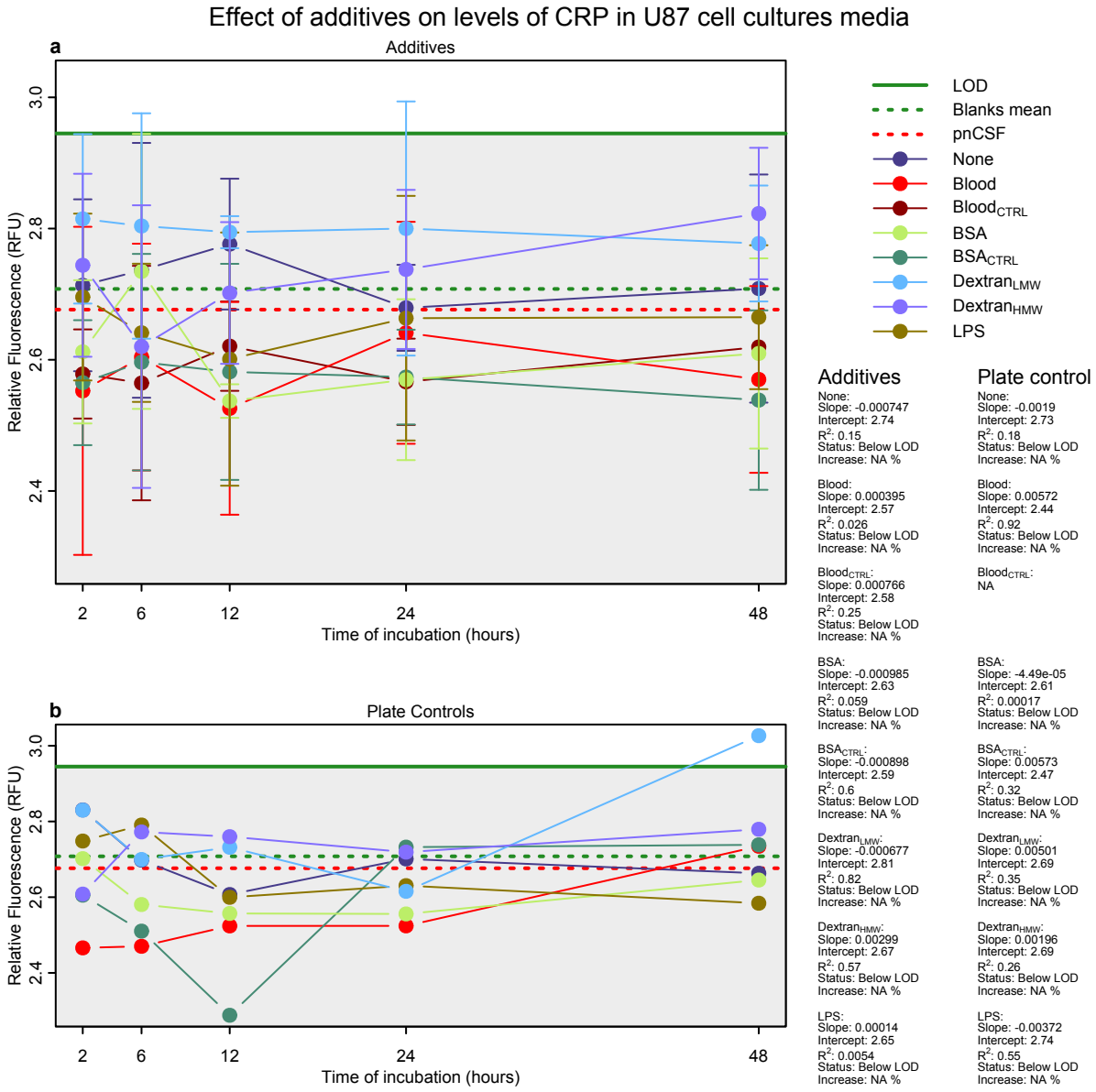

FIGURE H.S29: **Effect of additives on levels of CRP in U87 cell cultures media.** Additives along with fresh blood and LPS were added to mycoplasma-free human glial (U87) cells in triplicate wells of a 24-well plate and incubated for up to 48 h to measure the effect on levels of proteins measured in the cell media. Media was collected and frozen from successive triplicates at different intervals, then analyzed with the ACM. **a** Average values for CRP from three replicates for each point in every 24-well plate where a different additive was applied. **b** Data from the control cell media in each plate.

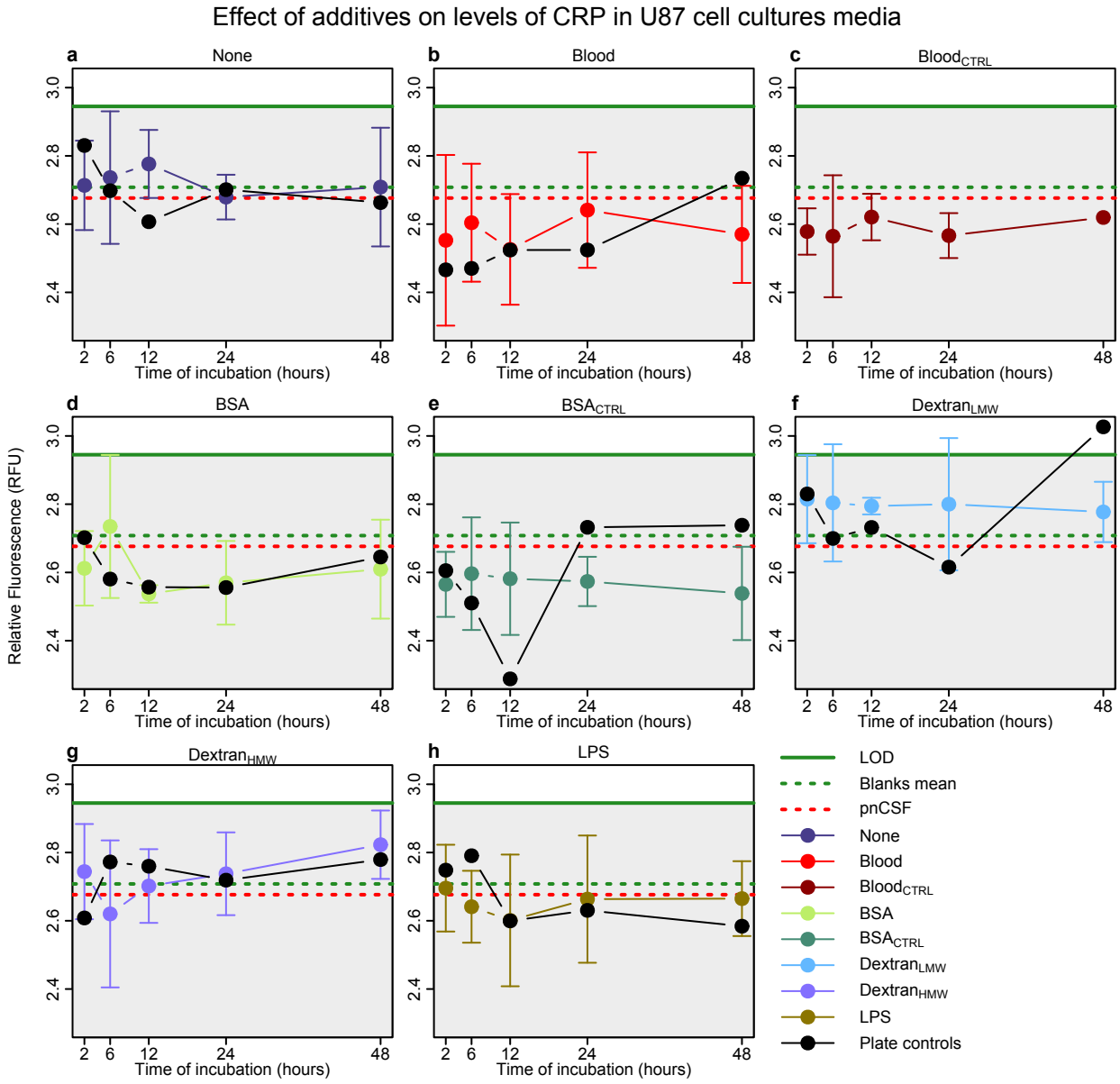

FIGURE H.S30: **Effect of additives on levels of CRP in U87 cell cultures media.** Additives along with fresh blood and LPS were added to mycoplasma-free human glial (U87) cells in triplicate wells of a 24-well plate and incubated for up to 48 h to measure the effect on levels of proteins measured in the cell media. Media was collected and frozen from successive triplicates at different intervals, then analyzed with the ACM. Each graph compares CRP values from cells incubated with a different additive to cells not incubated with additives located in the same 24-well plate. Plates in **c** and **e** did not contain any U87 cells, and **c** also did not have controls on the plate.

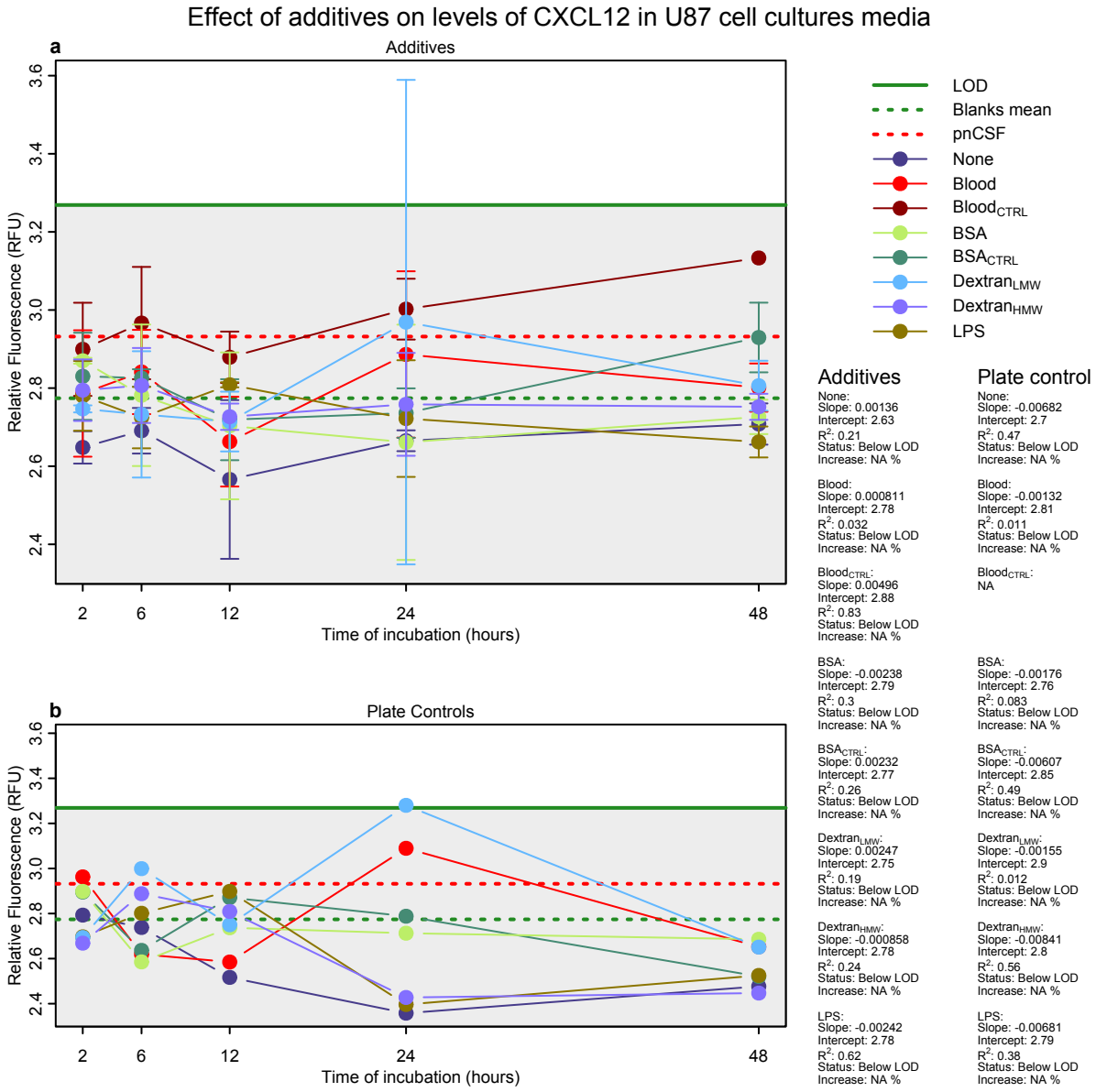

FIGURE H.S31: **Effect of additives on levels of CXCL12 in U87 cell cultures media.** Additives along with fresh blood and LPS were added to mycoplasma-free human glial (U87) cells in triplicate wells of a 24-well plate and incubated for up to 48 h to measure the effect on levels of proteins measured in the cell media. Media was collected and frozen from successive triplicates at different intervals, then analyzed with the ACM. **a** Average values for CXCL12 from three replicates for each point in every 24-well plate where a different additive was applied. **b** Data from the control cell media in each plate.

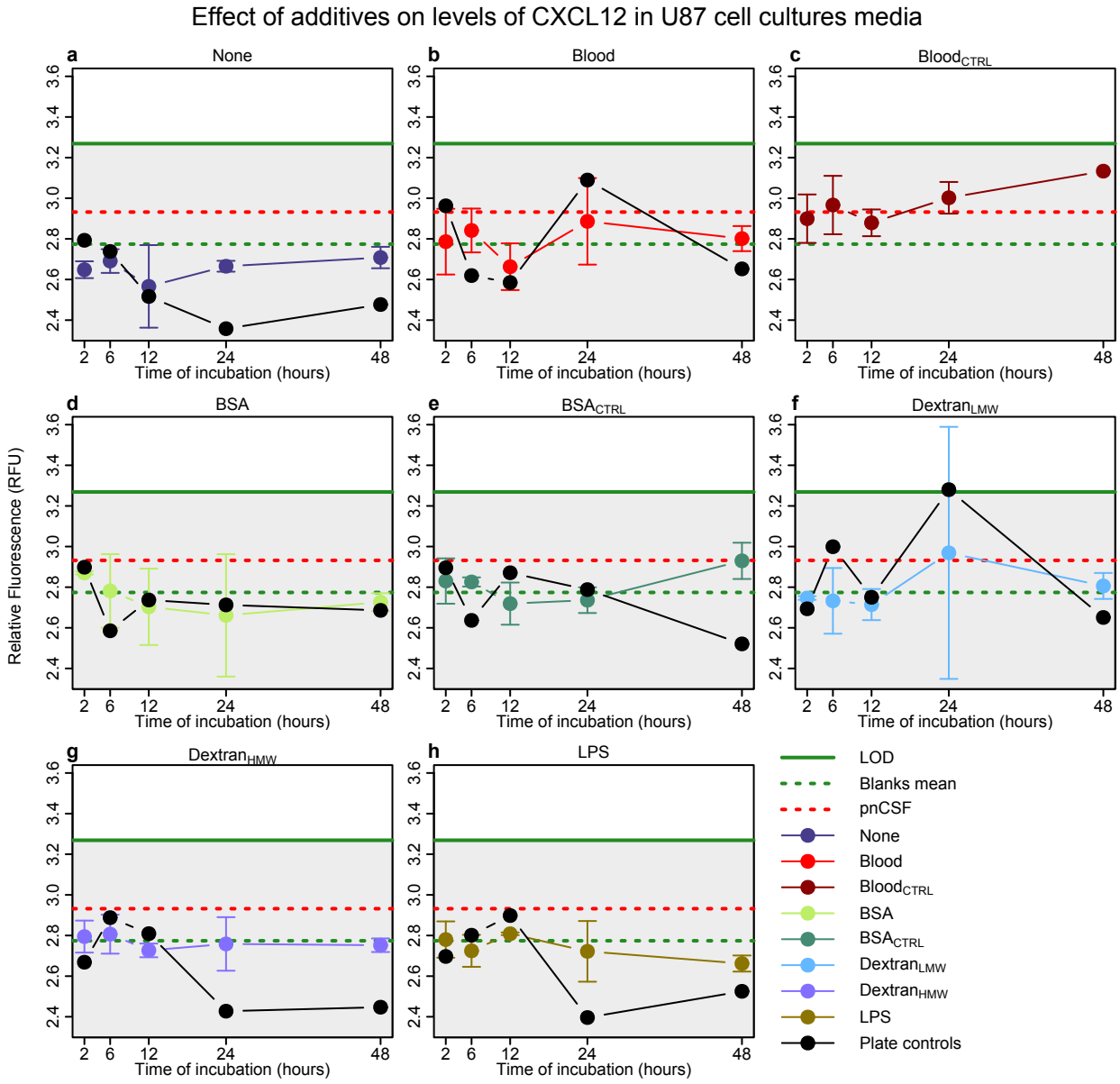

FIGURE H.S32: **Effect of additives on levels of CXCL12 in U87 cell cultures media.** Additives along with fresh blood and LPS were added to mycoplasma-free human glial (U87) cells in triplicate wells of a 24-well plate and incubated for up to 48 h to measure the effect on levels of proteins measured in the cell media. Media was collected and frozen from successive triplicates at different intervals, then analyzed with the ACM. Each graph compares CXCL12 values from cells incubated with a different additive to cells not incubated with additives located in the same 24-well plate. Plates in **c** and **e** did not contain any U87 cells, and **c** also did not have controls on the plate.

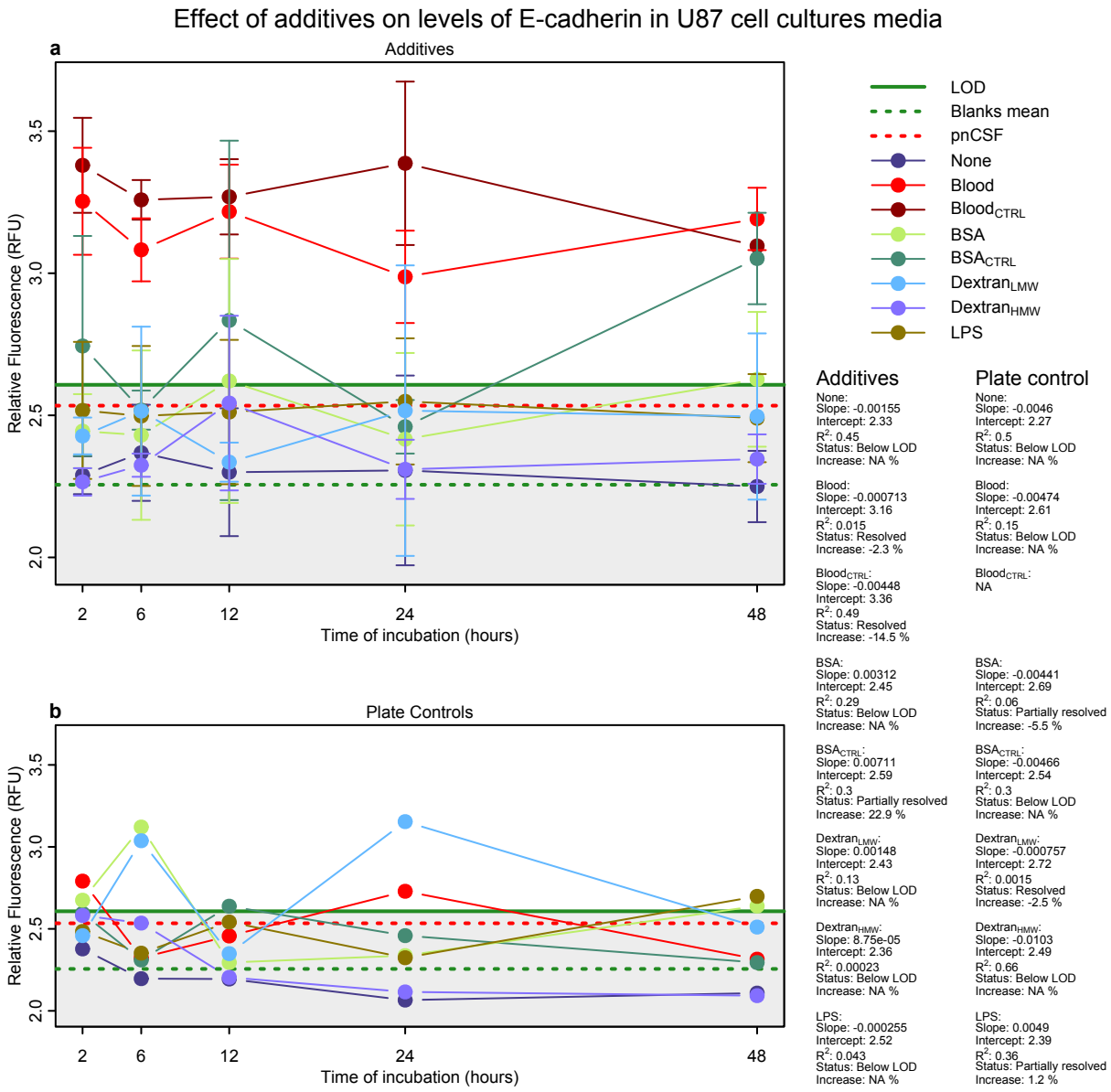

FIGURE H.S33: **Effect of additives on levels of E-cadherin in U87 cell cultures media.** Additives along with fresh blood and LPS were added to mycoplasma-free human glial (U87) cells in triplicate wells of a 24-well plate and incubated for up to 48 h to measure the effect on levels of proteins measured in the cell media. Media was collected and frozen from successive triplicates at different intervals, then analyzed with the ACM. **a** Average values for E-cadherin from three replicates for each point in every 24-well plate where a different additive was applied. **b** Data from the control cell media in each plate.

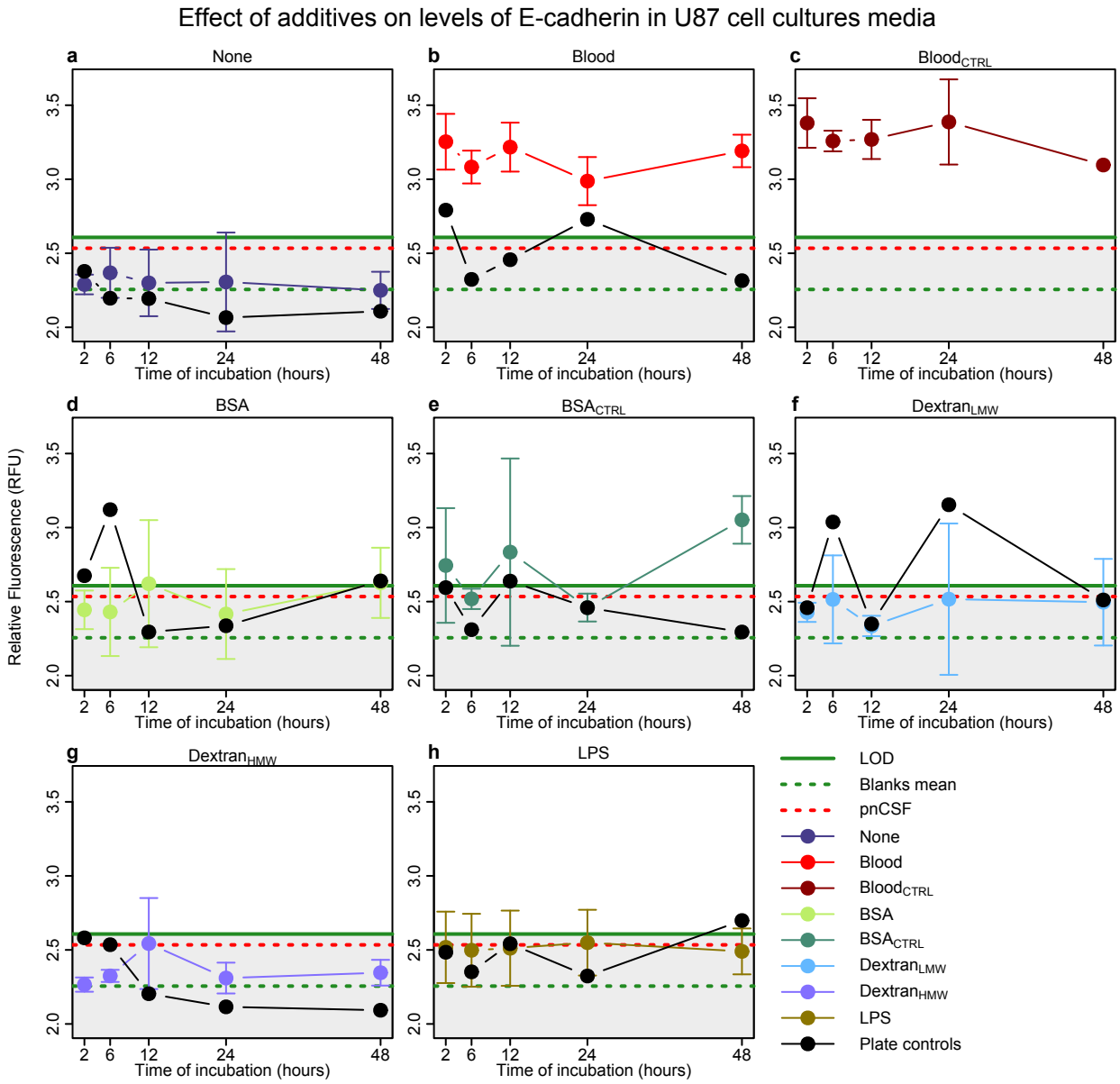

FIGURE H.S34: **Effect of additives on levels of E-cadherin in U87 cell cultures media.** Additives along with fresh blood and LPS were added to mycoplasma-free human glial (U87) cells in triplicate wells of a 24-well plate and incubated for up to 48 h to measure the effect on levels of proteins measured in the cell media. Media was collected and frozen from successive triplicates at different intervals, then analyzed with the ACM. Each graph compares E-cadherin values from cells incubated with a different additive to cells not incubated with additives located in the same 24-well plate. Plates in **c** and **e** did not contain any U87 cells, and **c** also did not have controls on the plate.

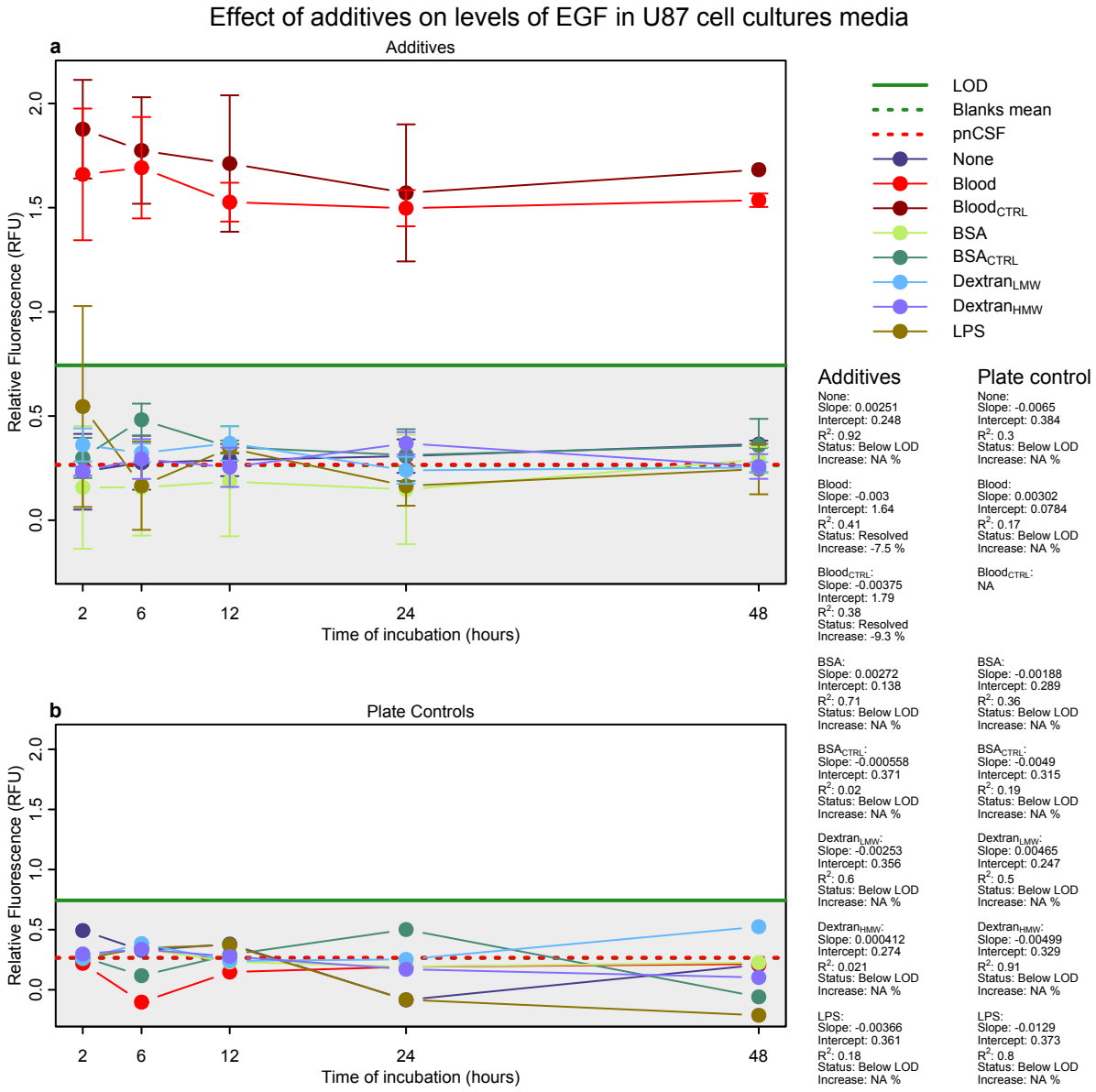

FIGURE H.S35: **Effect of additives on levels of EGF in U87 cell cultures media.** Additives along with fresh blood and LPS were added to mycoplasma-free human glial (U87) cells in triplicate wells of a 24-well plate and incubated for up to 48 h to measure the effect on levels of proteins measured in the cell media. Media was collected and frozen from successive triplicates at different intervals, then analyzed with the ACM. **a** Average values for EGF from three replicates for each point in every 24-well plate where a different additive was applied. **b** Data from the control cell media in each plate.

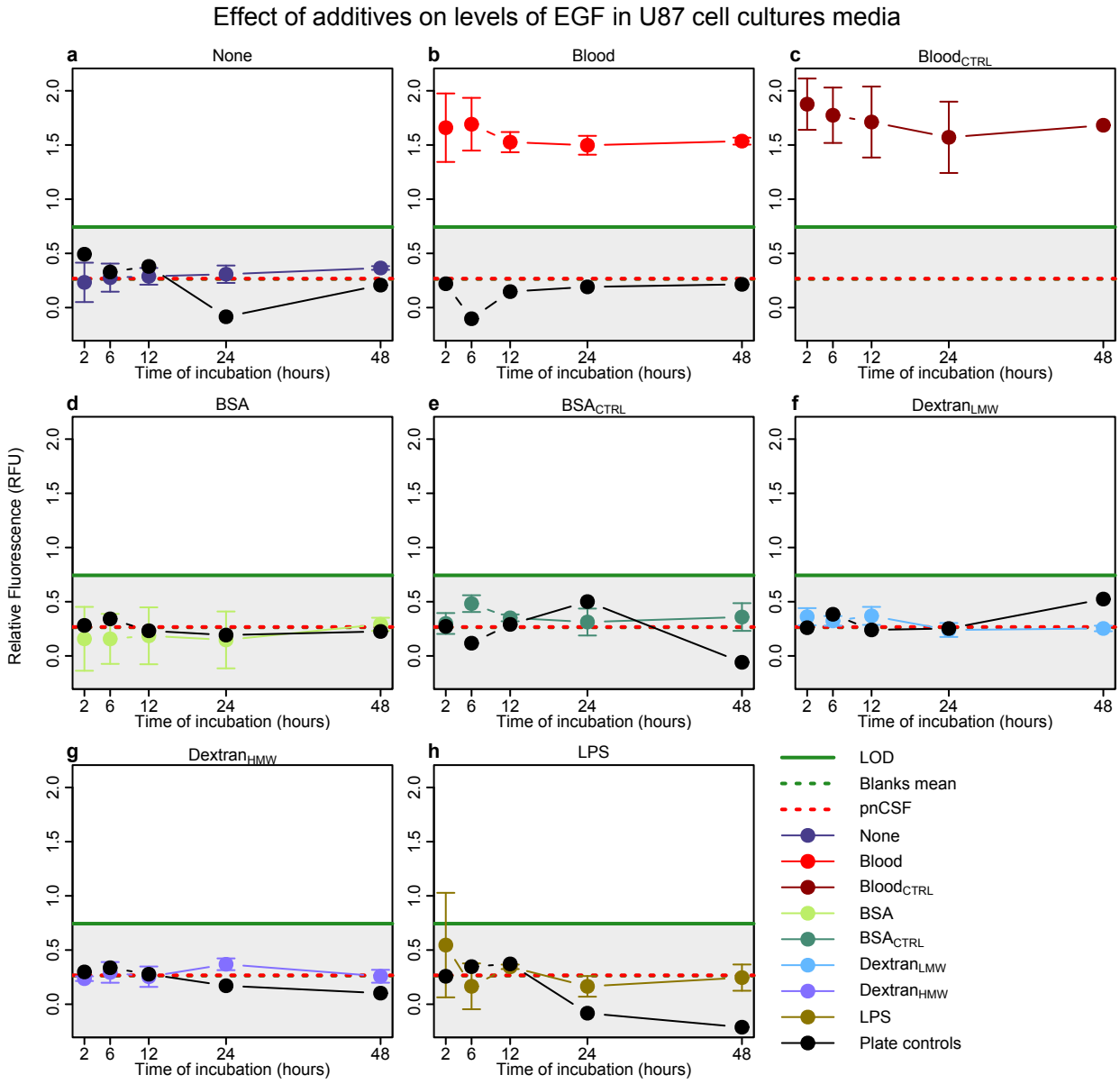

FIGURE H.S36: **Effect of additives on levels of EGF in U87 cell cultures media.** Additives along with fresh blood and LPS were added to mycoplasma-free human glial (U87) cells in triplicate wells of a 24-well plate and incubated for up to 48 h to measure the effect on levels of proteins measured in the cell media. Media was collected and frozen from successive triplicates at different intervals, then analyzed with the ACM. Each graph compares EGF values from cells incubated with a different additive to cells not incubated with additives located in the same 24-well plate. Plates in **c** and **e** did not contain any U87 cells, and **c** also did not have controls on the plate.

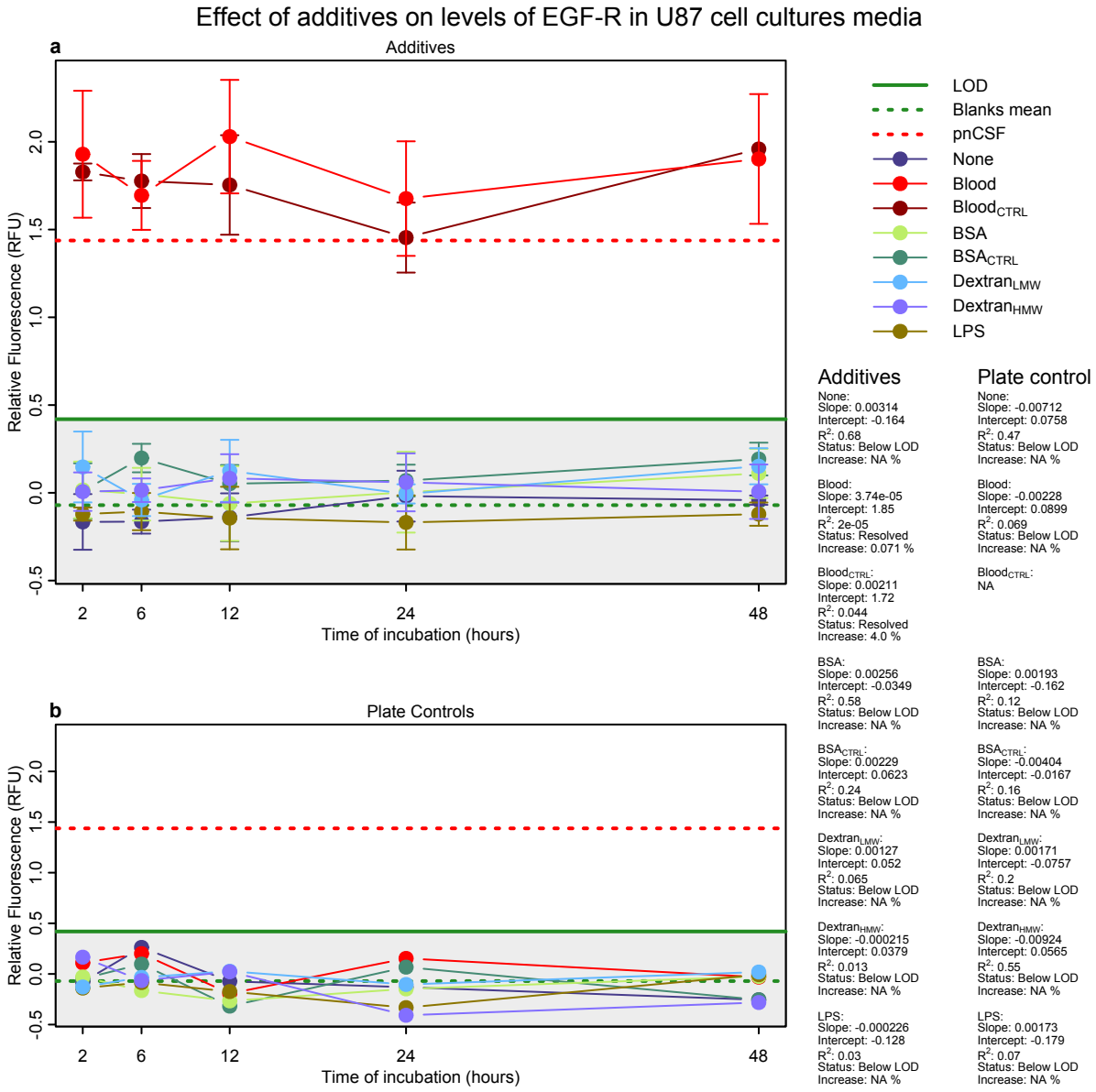

FIGURE H.S37: **Effect of additives on levels of EGF-R in U87 cell cultures media.** Additives along with fresh blood and LPS were added to mycoplasma-free human glial (U87) cells in triplicate wells of a 24-well plate and incubated for up to 48 h to measure the effect on levels of proteins measured in the cell media. Media was collected and frozen from successive triplicates at different intervals, then analyzed with the ACM. **a** Average values for EGF-R from three replicates for each point in every 24-well plate where a different additive was applied. **b** Data from the control cell media in each plate.

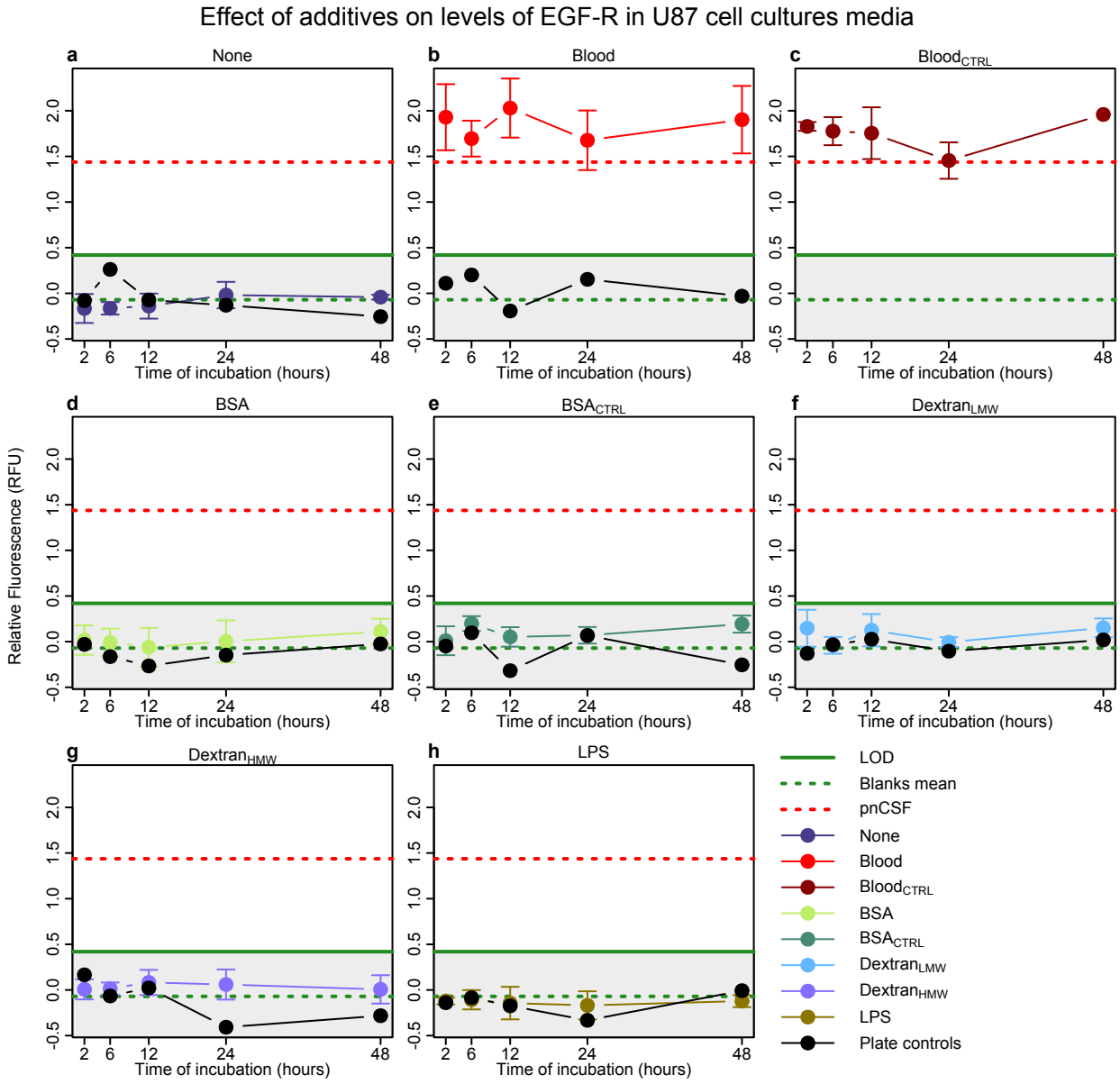

FIGURE H.S38: **Effect of additives on levels of EGF-R in U87 cell cultures media.** Additives along with fresh blood and LPS were added to mycoplasma-free human glial (U87) cells in triplicate wells of a 24-well plate and incubated for up to 48 h to measure the effect on levels of proteins measured in the cell media. Media was collected and frozen from successive triplicates at different intervals, then analyzed with the ACM. Each graph compares EGF-R values from cells incubated with a different additive to cells not incubated with additives located in the same 24-well plate. Plates in **c** and **e** did not contain any U87 cells, and **c** also did not have controls on the plate.

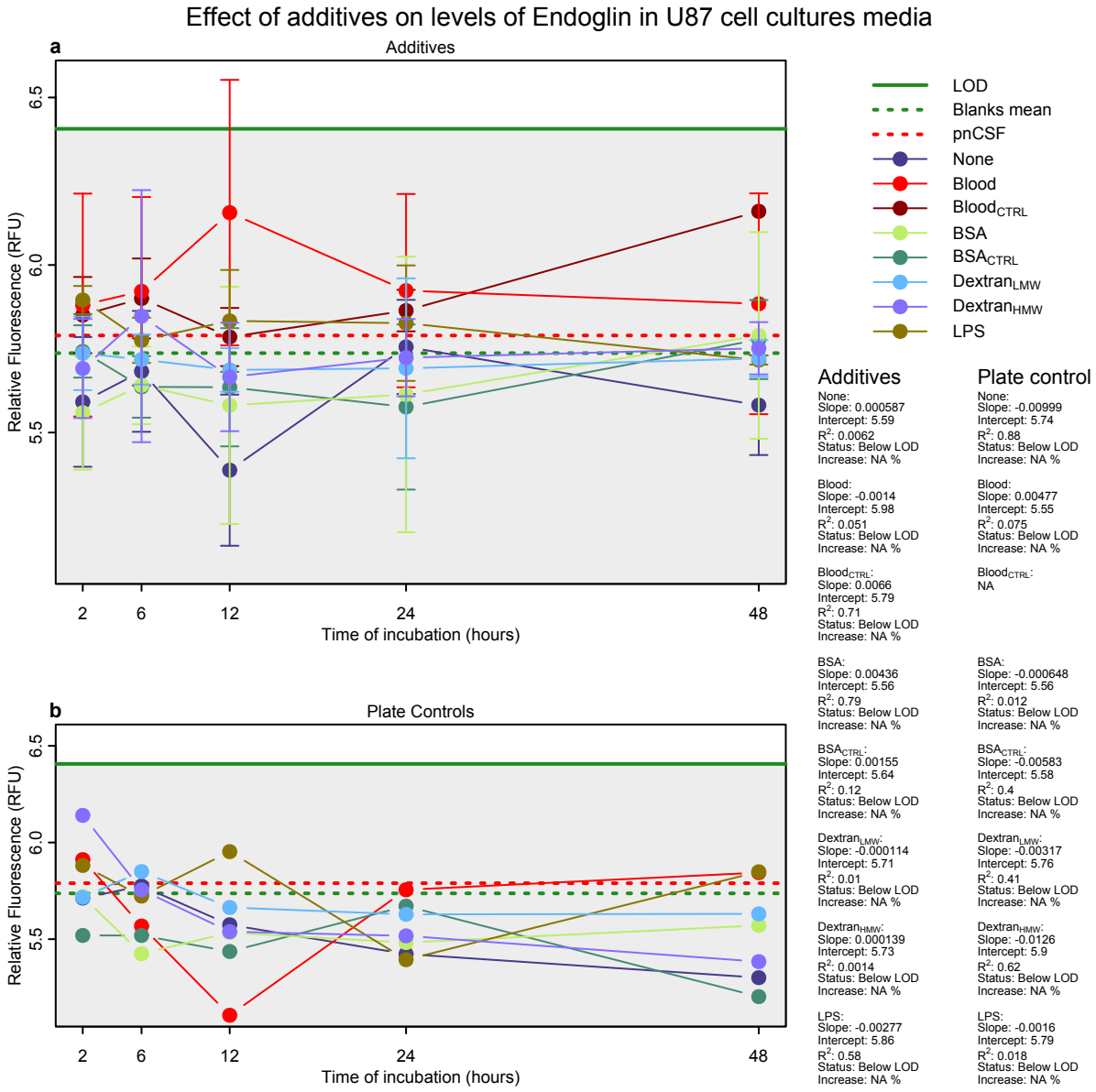

FIGURE H.S39: **Effect of additives on levels of Endoglin in U87 cell cultures media.** Additives along with fresh blood and LPS were added to mycoplasma-free human glial (U87) cells in triplicate wells of a 24-well plate and incubated for up to 48 h to measure the effect on levels of proteins measured in the cell media. Media was collected and frozen from successive triplicates at different intervals, then analyzed with the ACM. **a** Average values for Endoglin from three replicates for each point in every 24-well plate where a different additive was applied. **b** Data from the control cell media in each plate.

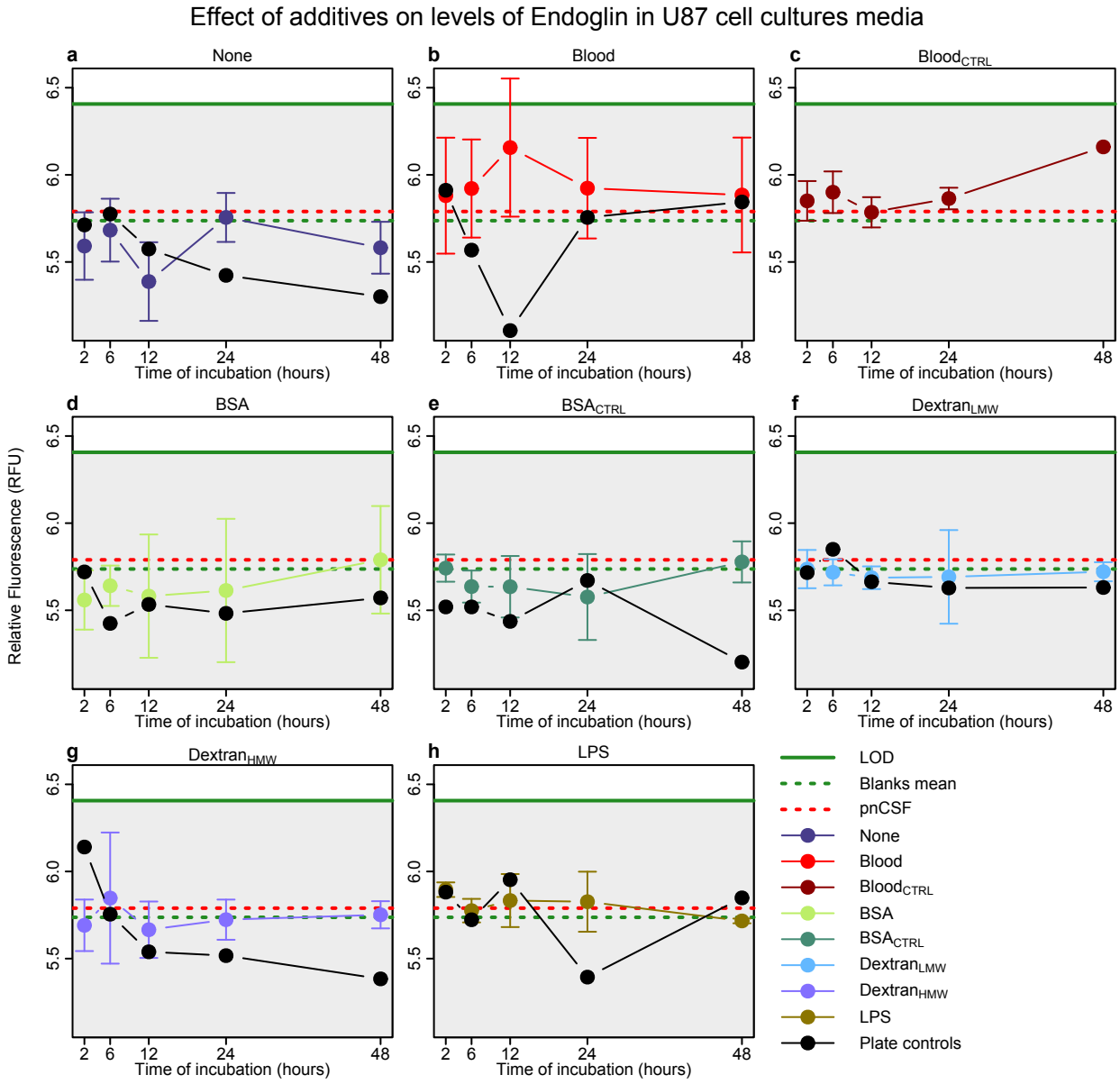

FIGURE H.S40: **Effect of additives on levels of Endoglin in U87 cell cultures media.** Additives along with fresh blood and LPS were added to mycoplasma-free human glial (U87) cells in triplicate wells of a 24-well plate and incubated for up to 48 h to measure the effect on levels of proteins measured in the cell media. Media was collected and frozen from successive triplicates at different intervals, then analyzed with the ACM. Each graph compares Endoglin values from cells incubated with a different additive to cells not incubated with additives located in the same 24-well plate. Plates in **c** and **e** did not contain any U87 cells, and **c** also did not have controls on the plate.

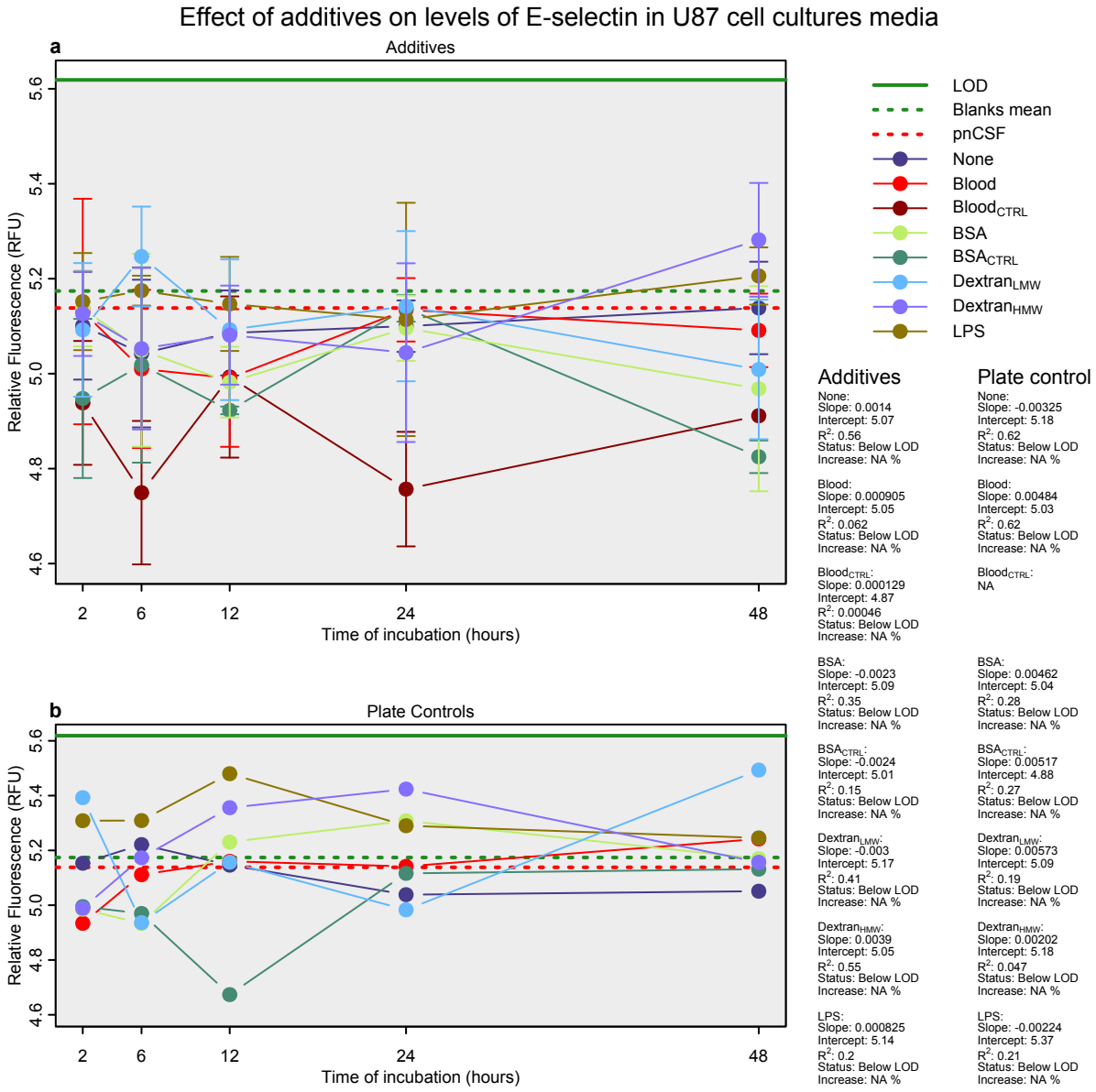

FIGURE H.S41: **Effect of additives on levels of E-selectin in U87 cell cultures media.** Additives along with fresh blood and LPS were added to mycoplasma-free human glial (U87) cells in triplicate wells of a 24-well plate and incubated for up to 48 h to measure the effect on levels of proteins measured in the cell media. Media was collected and frozen from successive triplicates at different intervals, then analyzed with the ACM. **a** Average values for E-selectin from three replicates for each point in every 24-well plate where a different additive was applied. **b** Data from the control cell media in each plate.

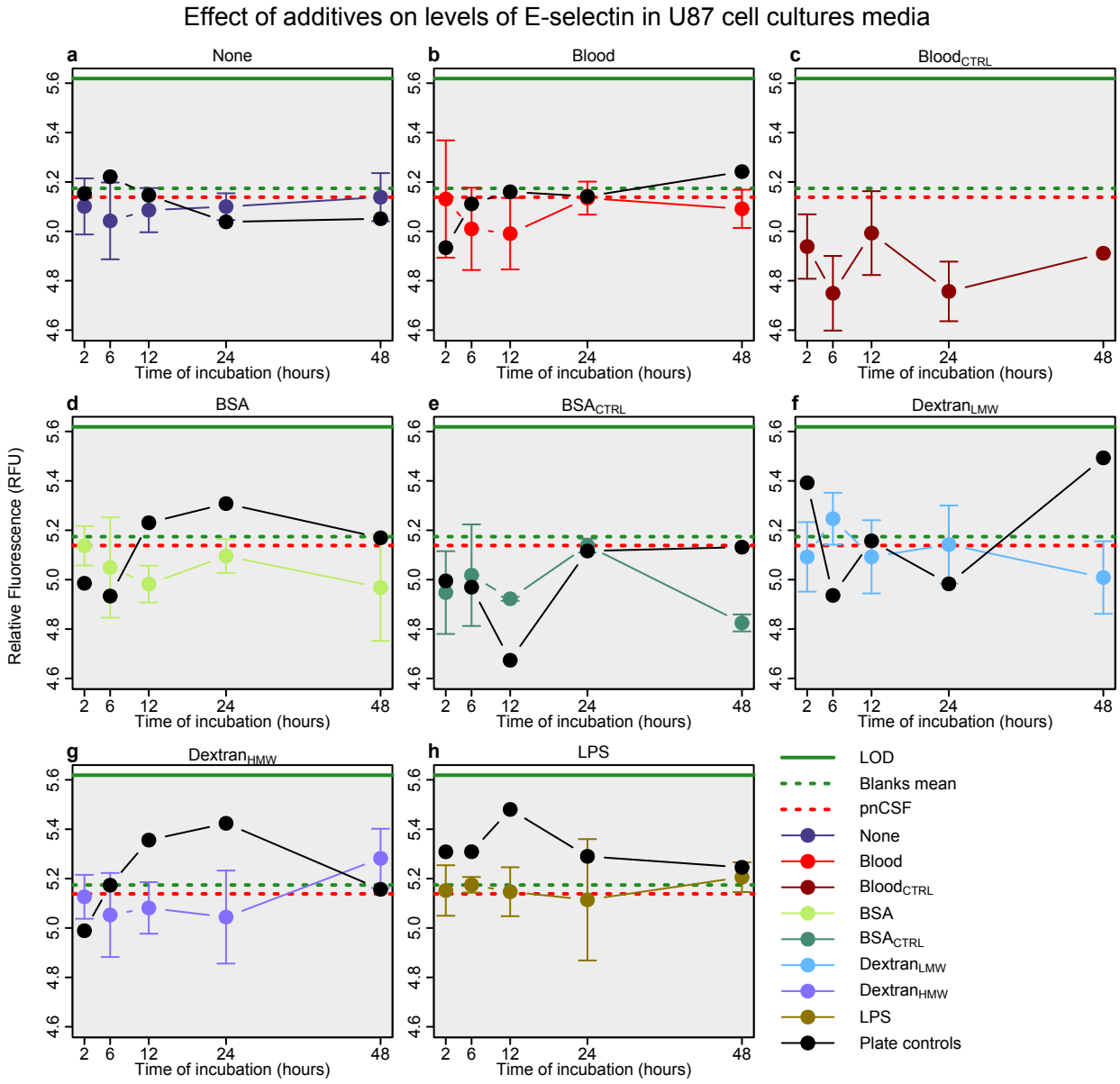

FIGURE H.S42: **Effect of additives on levels of E-selectin in U87 cell cultures media.** Additives along with fresh blood and LPS were added to mycoplasma-free human glial (U87) cells in triplicate wells of a 24-well plate and incubated for up to 48 h to measure the effect on levels of proteins measured in the cell media. Media was collected and frozen from successive triplicates at different intervals, then analyzed with the ACM. Each graph compares E-selectin values from cells incubated with a different additive to cells not incubated with additives located in the same 24-well plate. Plates in **c** and **e** did not contain any U87 cells, and **c** also did not have controls on the plate.

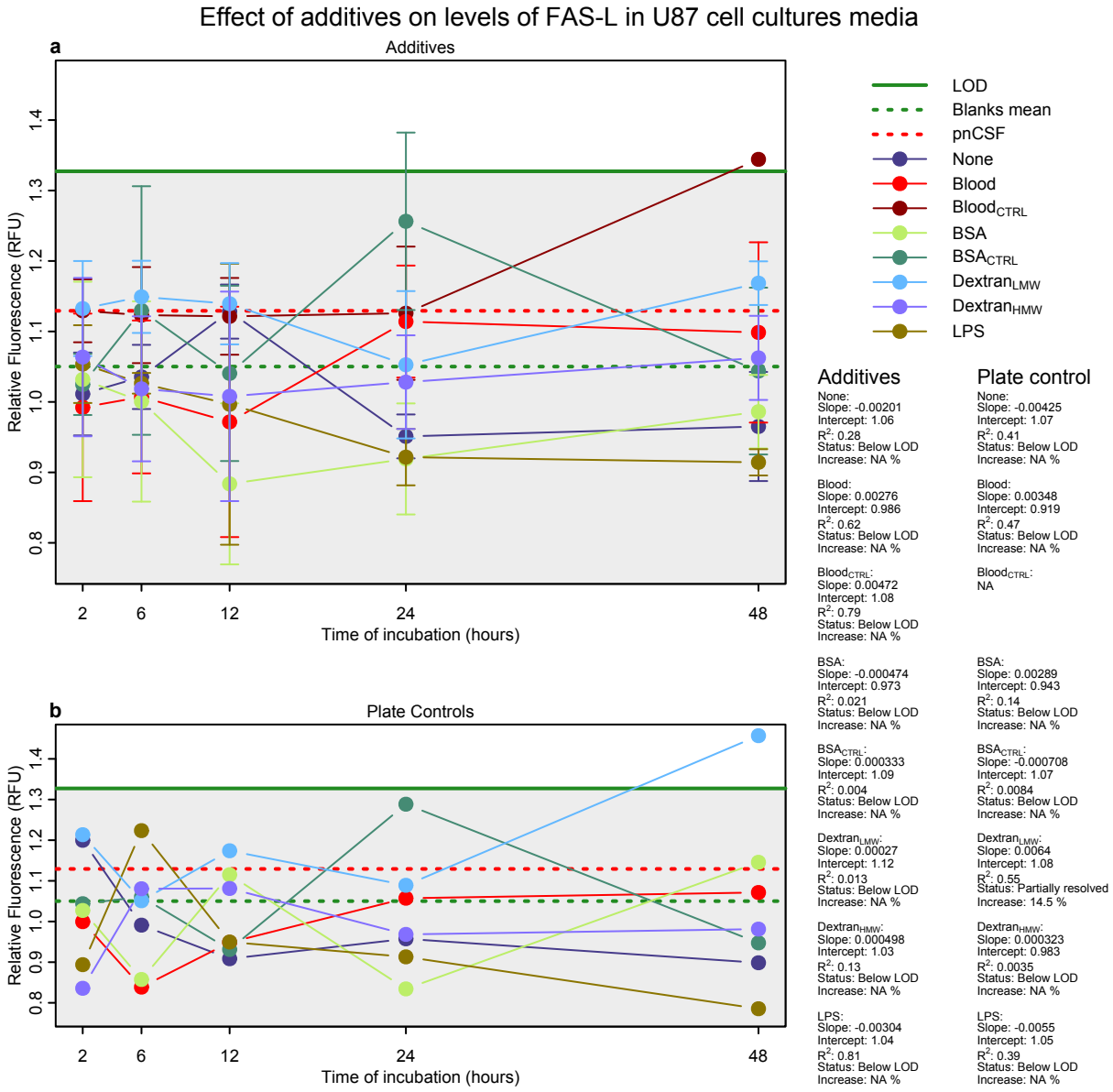

FIGURE H.S43: **Effect of additives on levels of FAS-L in U87 cell cultures media.** Additives along with fresh blood and LPS were added to mycoplasma-free human glial (U87) cells in triplicate wells of a 24-well plate and incubated for up to 48 h to measure the effect on levels of proteins measured in the cell media. Media was collected and frozen from successive triplicates at different intervals, then analyzed with the ACM. **a** Average values for FAS-L from three replicates for each point in every 24-well plate where a different additive was applied. **b** Data from the control cell media in each plate.

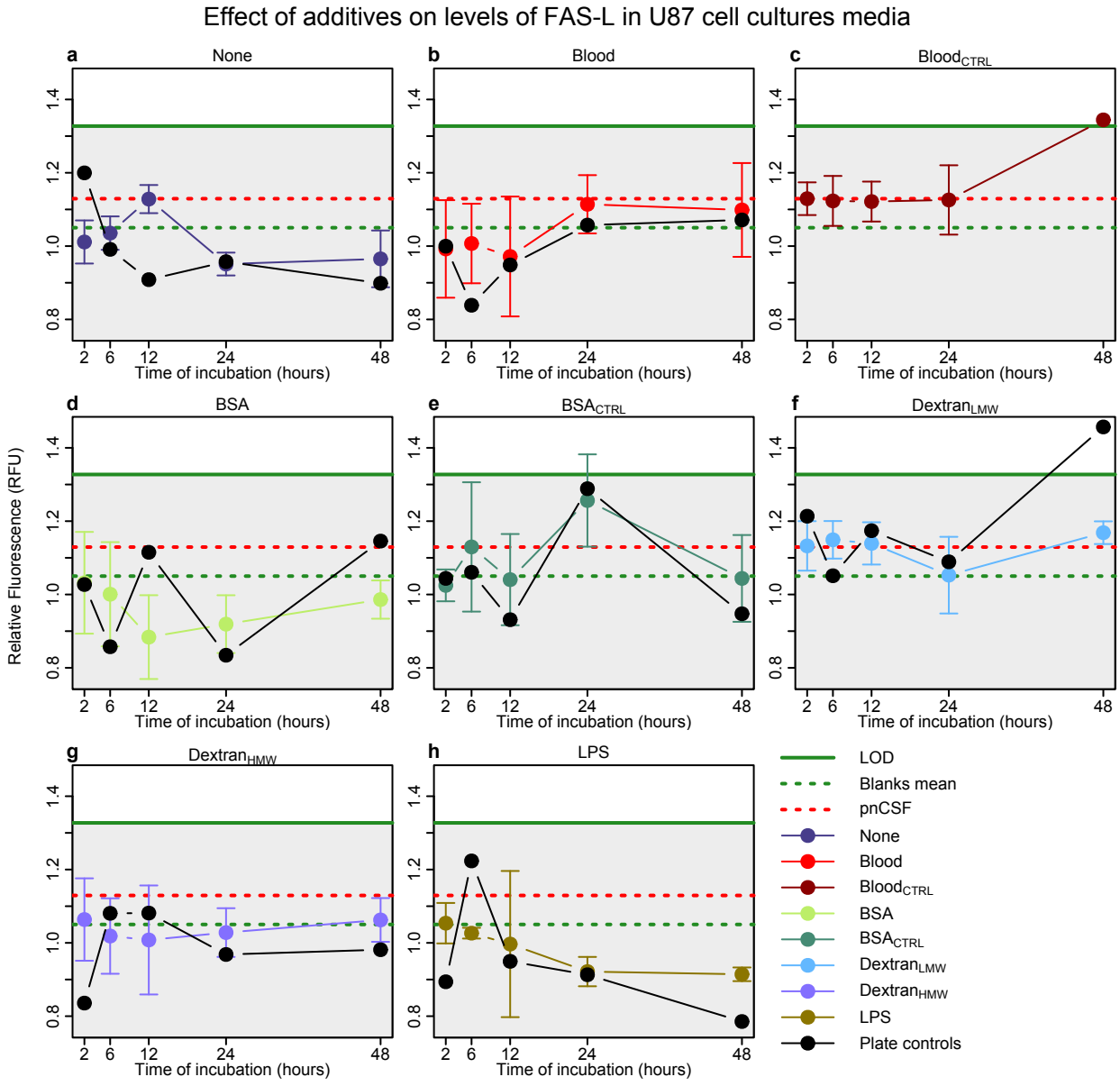

FIGURE H.S44: **Effect of additives on levels of FAS-L in U87 cell cultures media.** Additives along with fresh blood and LPS were added to mycoplasma-free human glial (U87) cells in triplicate wells of a 24-well plate and incubated for up to 48 h to measure the effect on levels of proteins measured in the cell media. Media was collected and frozen from successive triplicates at different intervals, then analyzed with the ACM. Each graph compares FAS-L values from cells incubated with a different additive to cells not incubated with additives located in the same 24-well plate. Plates in **c** and **e** did not contain any U87 cells, and **c** also did not have controls on the plate.

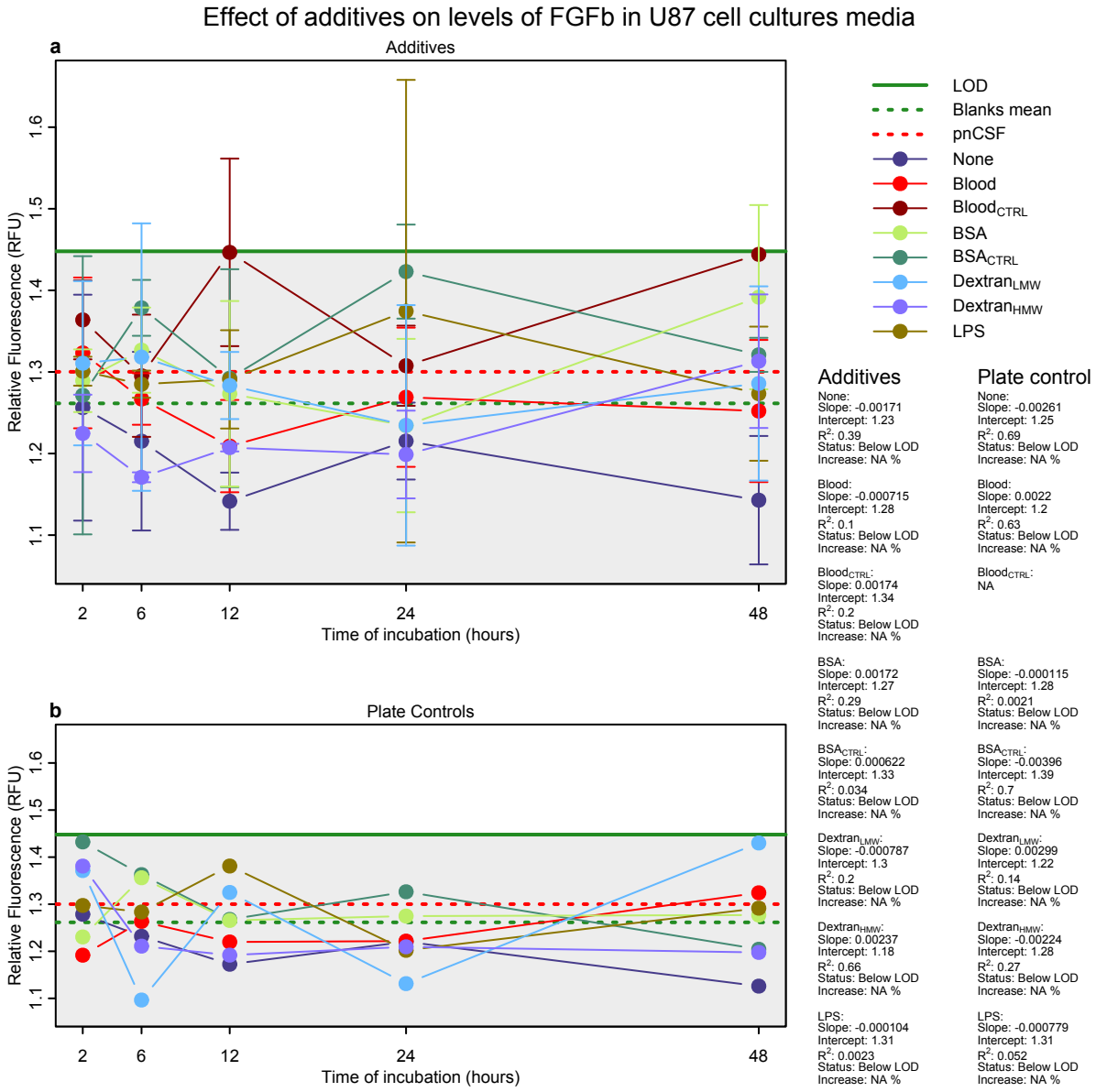

FIGURE H.S45: **Effect of additives on levels of FGFb in U87 cell cultures media.** Additives along with fresh blood and LPS were added to mycoplasma-free human glial (U87) cells in triplicate wells of a 24-well plate and incubated for up to 48 h to measure the effect on levels of proteins measured in the cell media. Media was collected and frozen from successive triplicates at different intervals, then analyzed with the ACM. **a** Average values for FGFb from three replicates for each point in every 24-well plate where a different additive was applied. **b** Data from the control cell media in each plate.

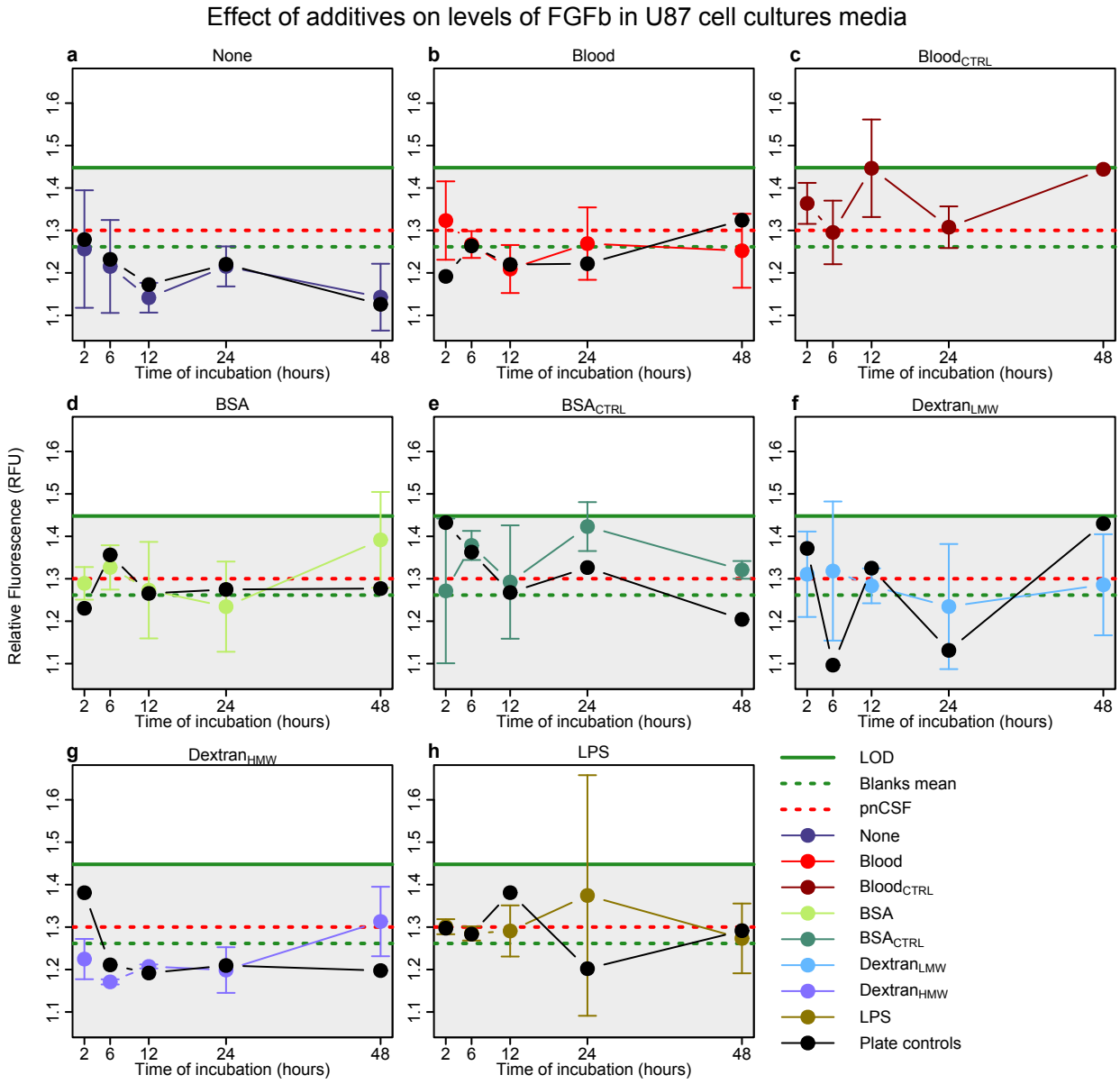

FIGURE H.S46: **Effect of additives on levels of FGFb in U87 cell cultures media.** Additives along with fresh blood and LPS were added to mycoplasma-free human glial (U87) cells in triplicate wells of a 24-well plate and incubated for up to 48 h to measure the effect on levels of proteins measured in the cell media. Media was collected and frozen from successive triplicates at different intervals, then analyzed with the ACM. Each graph compares FGFb values from cells incubated with a different additive to cells not incubated with additives located in the same 24-well plate. Plates in **c** and **e** did not contain any U87 cells, and **c** also did not have controls on the plate.

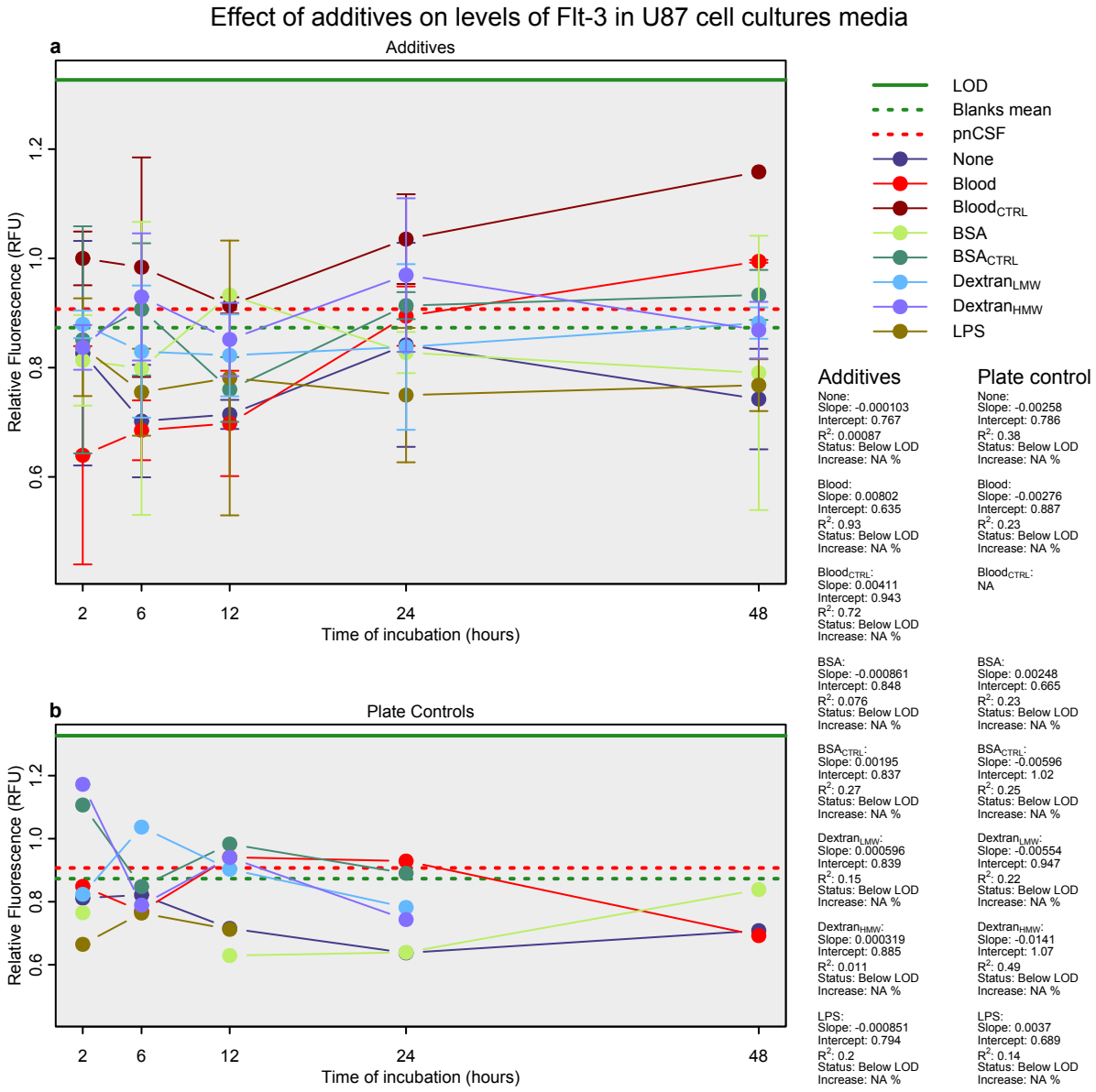

FIGURE H.S47: **Effect of additives on levels of Flt-3 in U87 cell cultures media.** Additives along with fresh blood and LPS were added to mycoplasma-free human glial (U87) cells in triplicate wells of a 24-well plate and incubated for up to 48 h to measure the effect on levels of proteins measured in the cell media. Media was collected and frozen from successive triplicates at different intervals, then analyzed with the ACM. **a** Average values for Flt-3 from three replicates for each point in every 24-well plate where a different additive was applied. **b** Data from the control cell media in each plate.

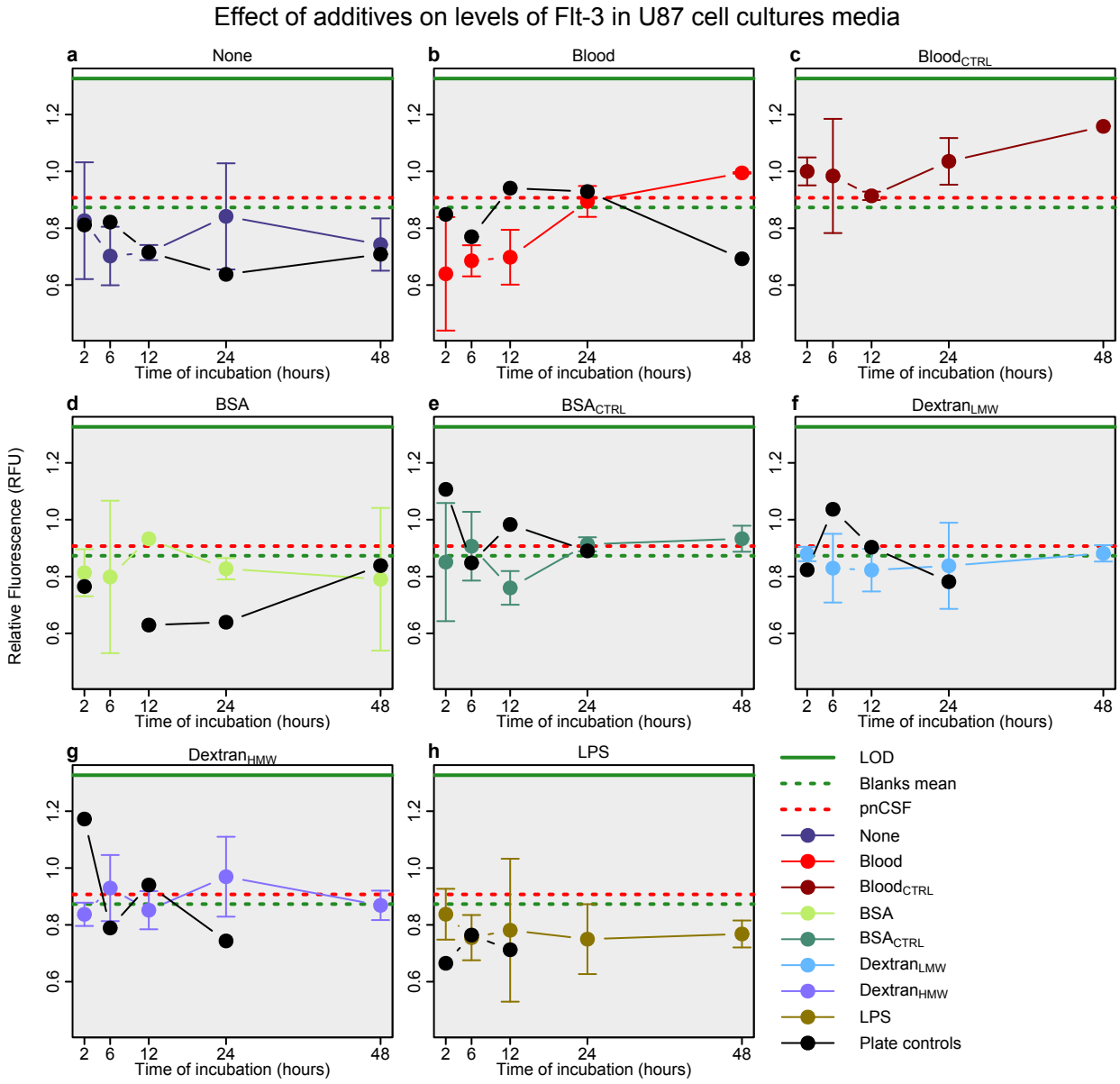

FIGURE H.S48: **Effect of additives on levels of Flt-3 in U87 cell cultures media.** Additives along with fresh blood and LPS were added to mycoplasma-free human glial (U87) cells in triplicate wells of a 24-well plate and incubated for up to 48 h to measure the effect on levels of proteins measured in the cell media. Media was collected and frozen from successive triplicates at different intervals, then analyzed with the ACM. Each graph compares Flt-3 values from cells incubated with a different additive to cells not incubated with additives located in the same 24-well plate. Plates in **c** and **e** did not contain any U87 cells, and **c** also did not have controls on the plate.

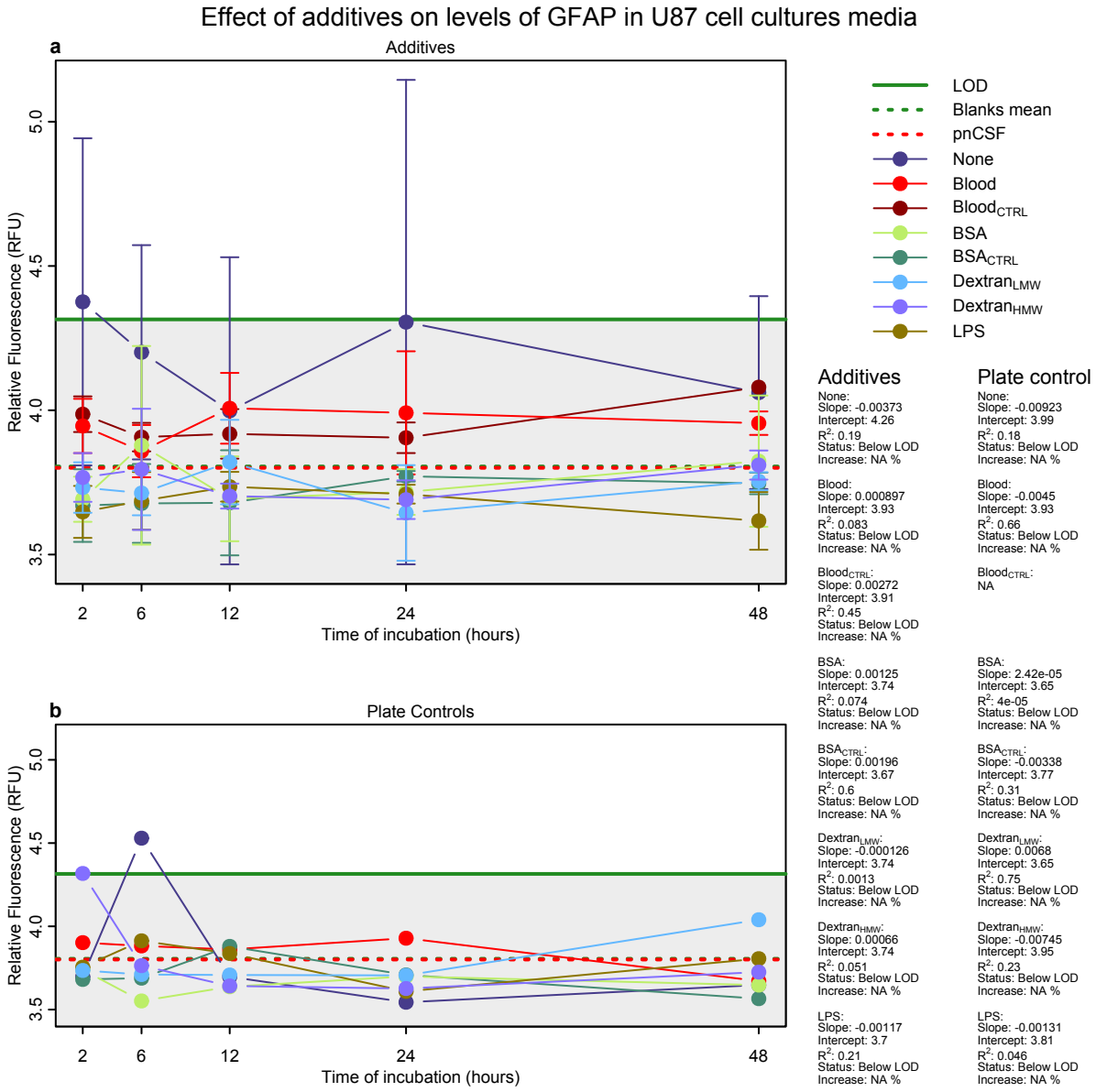

FIGURE H.S49: **Effect of additives on levels of GFAP in U87 cell cultures media.** Additives along with fresh blood and LPS were added to mycoplasma-free human glial (U87) cells in triplicate wells of a 24-well plate and incubated for up to 48 h to measure the effect on levels of proteins measured in the cell media. Media was collected and frozen from successive triplicates at different intervals, then analyzed with the ACM. **a** Average values for GFAP from three replicates for each point in every 24-well plate where a different additive was applied. **b** Data from the control cell media in each plate.

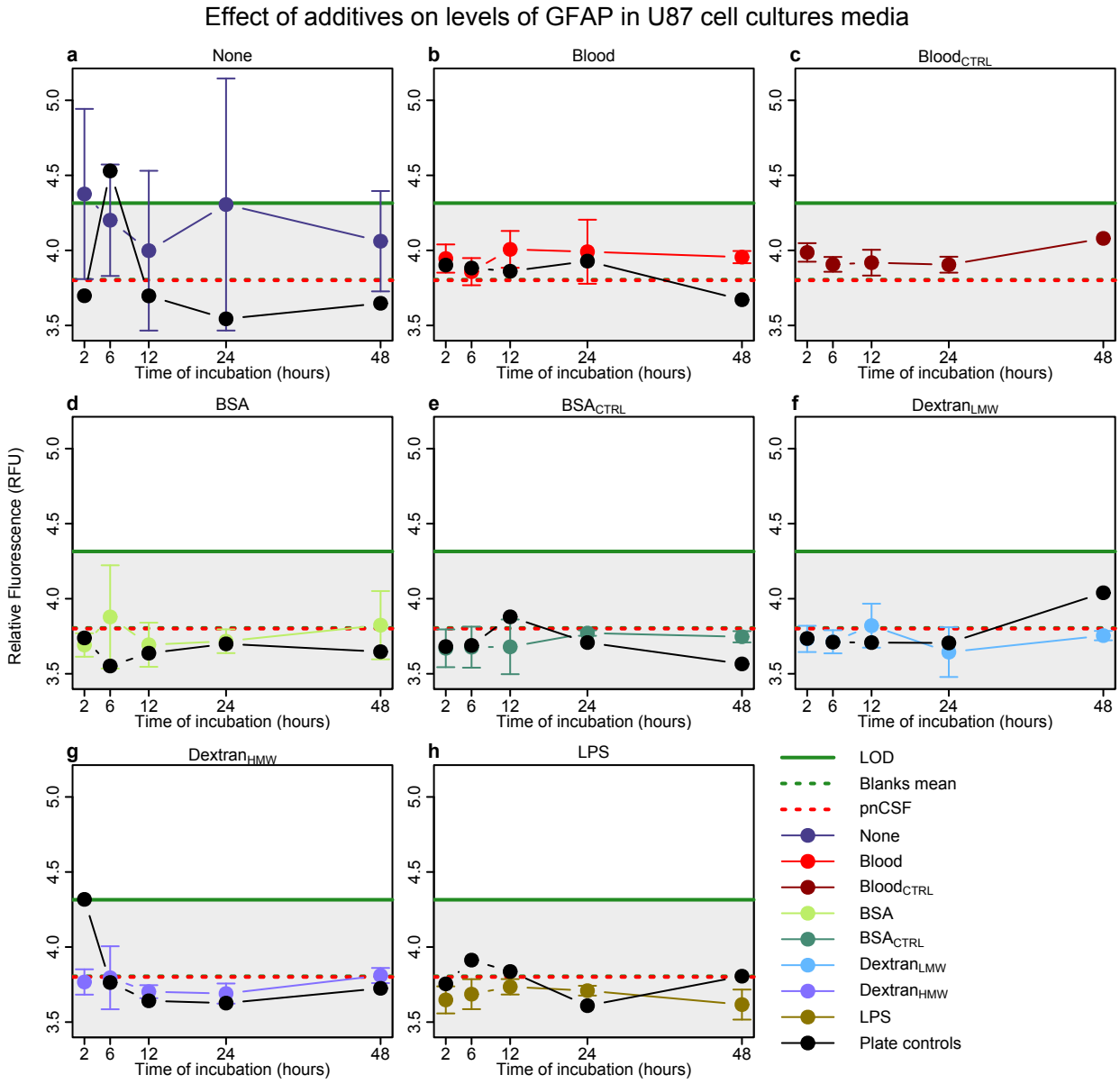

FIGURE H.S50: **Effect of additives on levels of GFAP in U87 cell cultures media.** Additives along with fresh blood and LPS were added to mycoplasma-free human glial (U87) cells in triplicate wells of a 24-well plate and incubated for up to 48 h to measure the effect on levels of proteins measured in the cell media. Media was collected and frozen from successive triplicates at different intervals, then analyzed with the ACM. Each graph compares GFAP values from cells incubated with a different additive to cells not incubated with additives located in the same 24-well plate. Plates in **c** and **e** did not contain any U87 cells, and **c** also did not have controls on the plate.

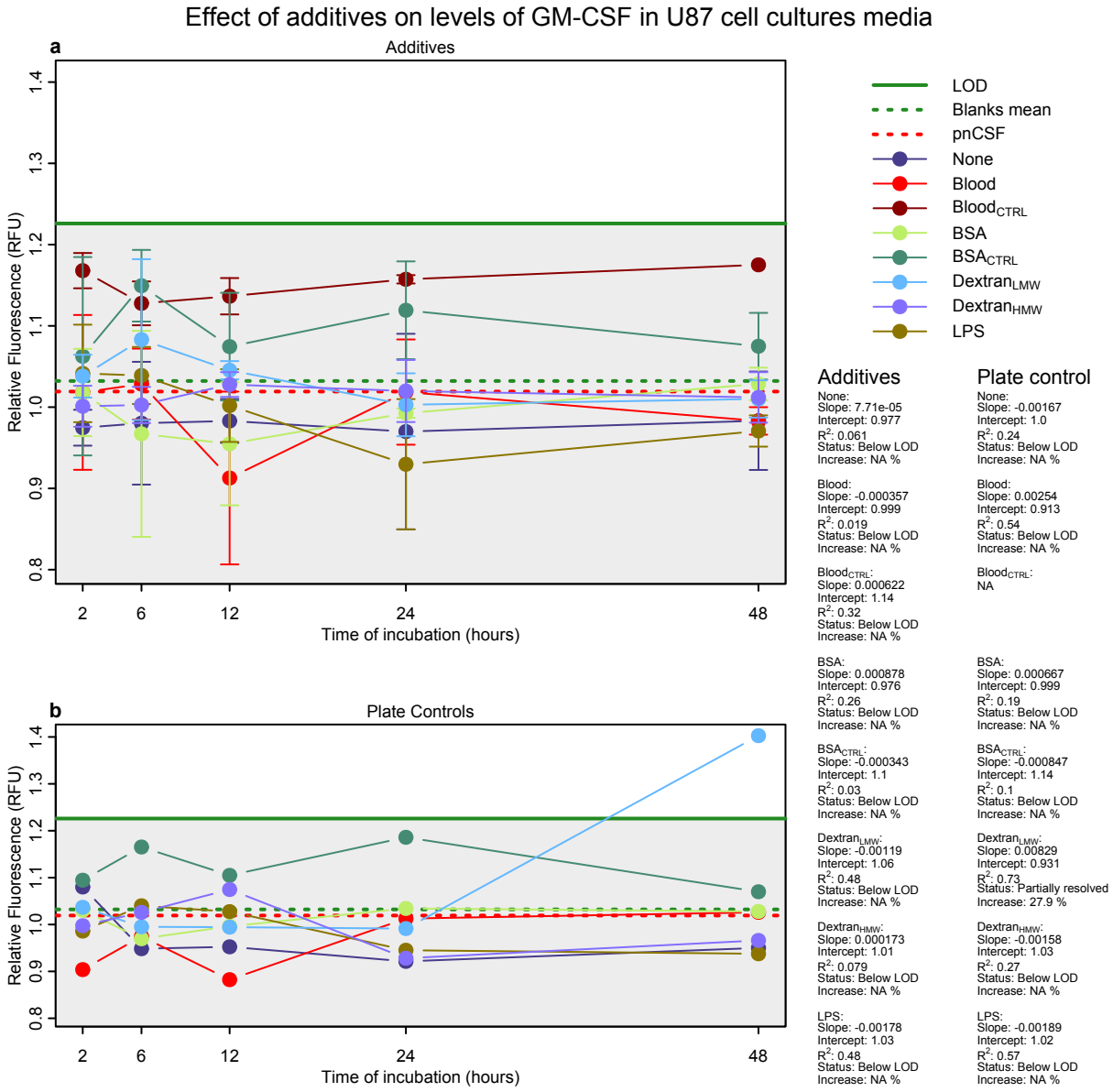

FIGURE H.S51: **Effect of additives on levels of GM-CSF in U87 cell cultures media.** Additives along with fresh blood and LPS were added to mycoplasma-free human glial (U87) cells in triplicate wells of a 24-well plate and incubated for up to 48 h to measure the effect on levels of proteins measured in the cell media. Media was collected and frozen from successive triplicates at different intervals, then analyzed with the ACM. **a** Average values for GM-CSF from three replicates for each point in every 24-well plate where a different additive was applied. **b** Data from the control cell media in each plate.

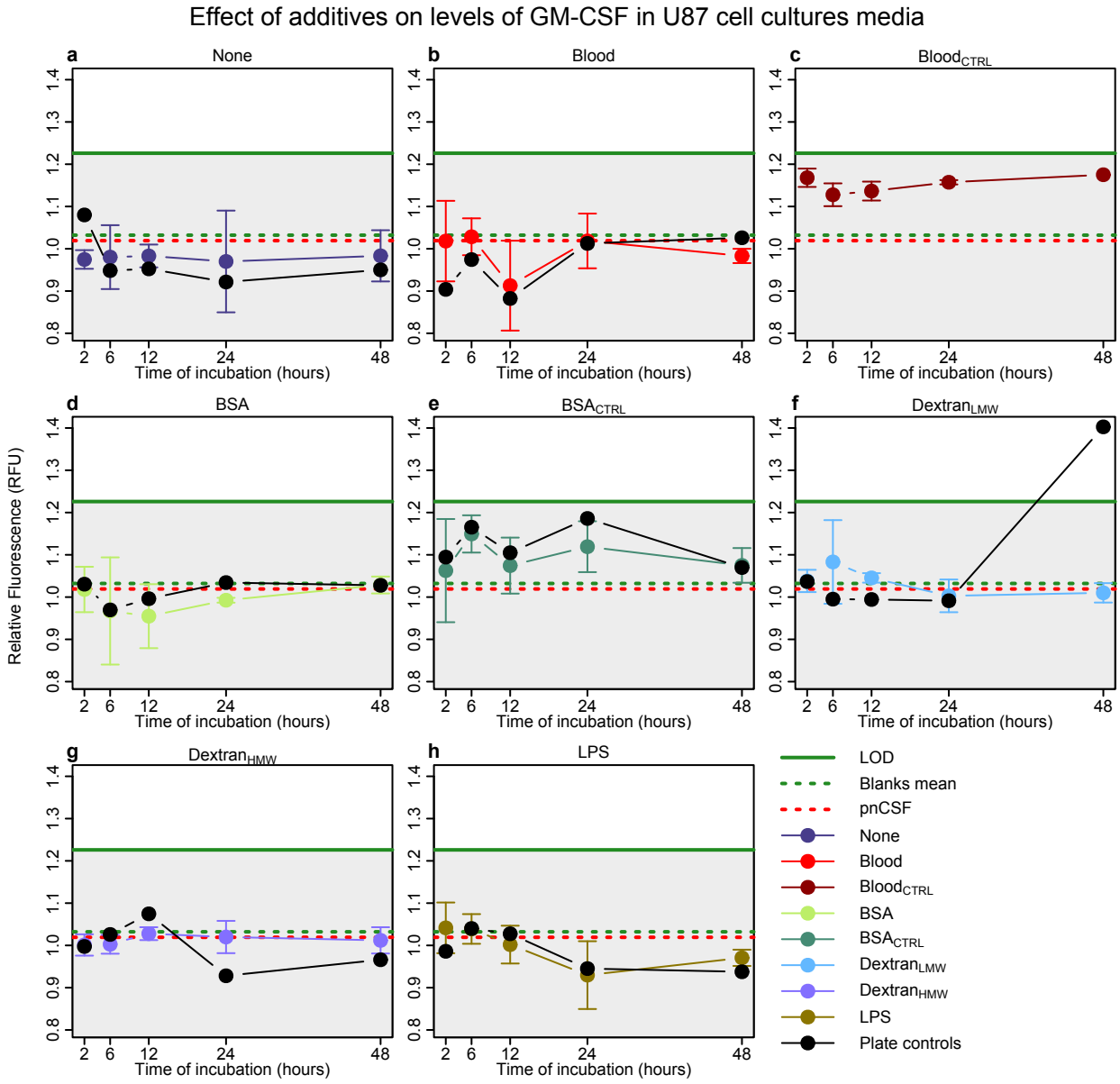

FIGURE H.S52: **Effect of additives on levels of GM-CSF in U87 cell cultures media.** Additives along with fresh blood and LPS were added to mycoplasma-free human glial (U87) cells in triplicate wells of a 24-well plate and incubated for up to 48 h to measure the effect on levels of proteins measured in the cell media. Media was collected and frozen from successive triplicates at different intervals, then analyzed with the ACM. Each graph compares GM-CSF values from cells incubated with a different additive to cells not incubated with additives located in the same 24-well plate. Plates in **c** and **e** did not contain any U87 cells, and **c** also did not have controls on the plate.

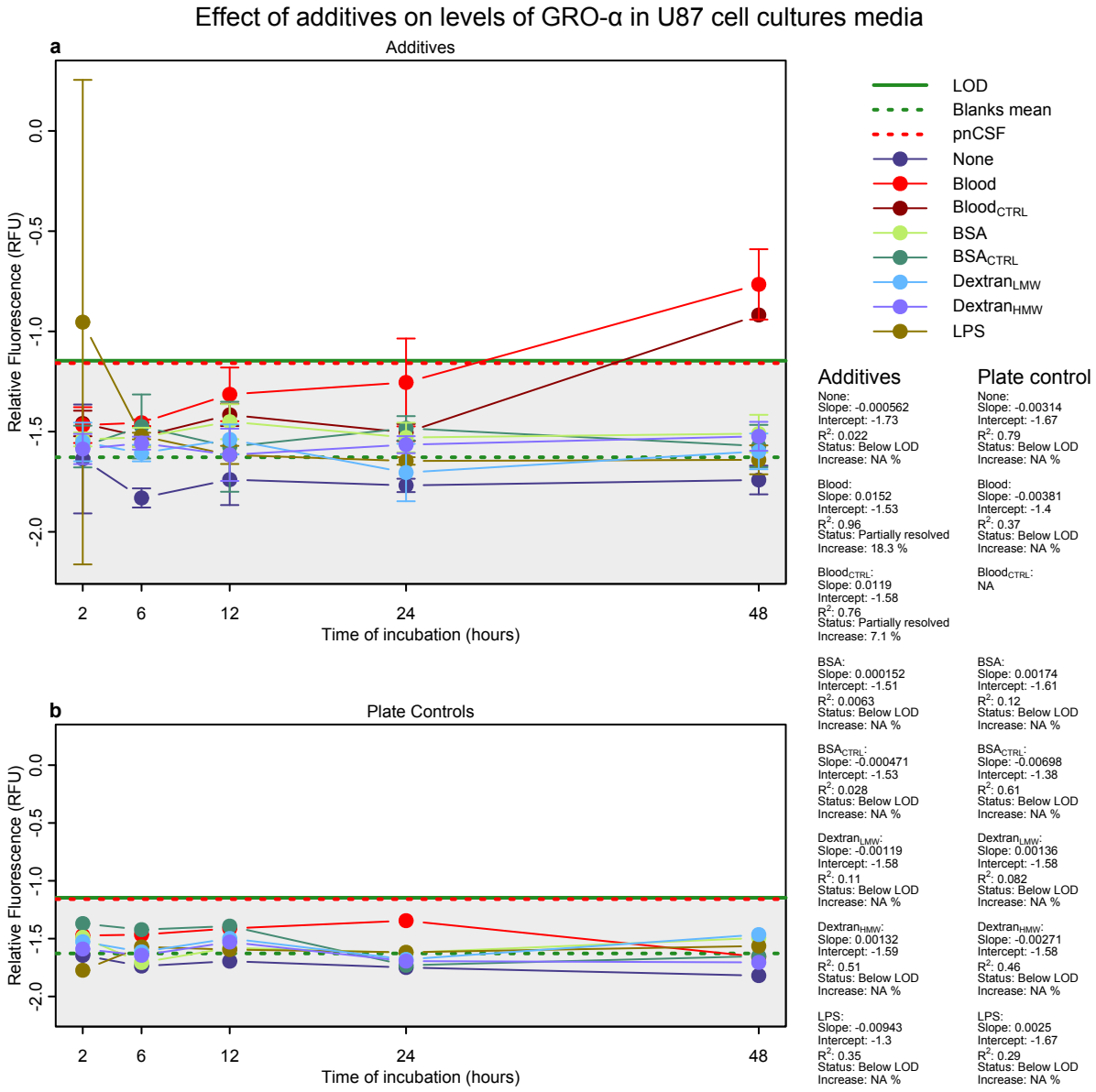

FIGURE H.S53: **Effect of additives on levels of GRO-α in U87 cell cultures media.** Additives along with fresh blood and LPS were added to mycoplasma-free human glial (U87) cells in triplicate wells of a 24-well plate and incubated for up to 48 h to measure the effect on levels of proteins measured in the cell media. Media was collected and frozen from successive triplicates at different intervals, then analyzed with the ACM. **a** Average values for GRO-α from three replicates for each point in every 24-well plate where a different additive was applied. **b** Data from the control cell media in each plate.

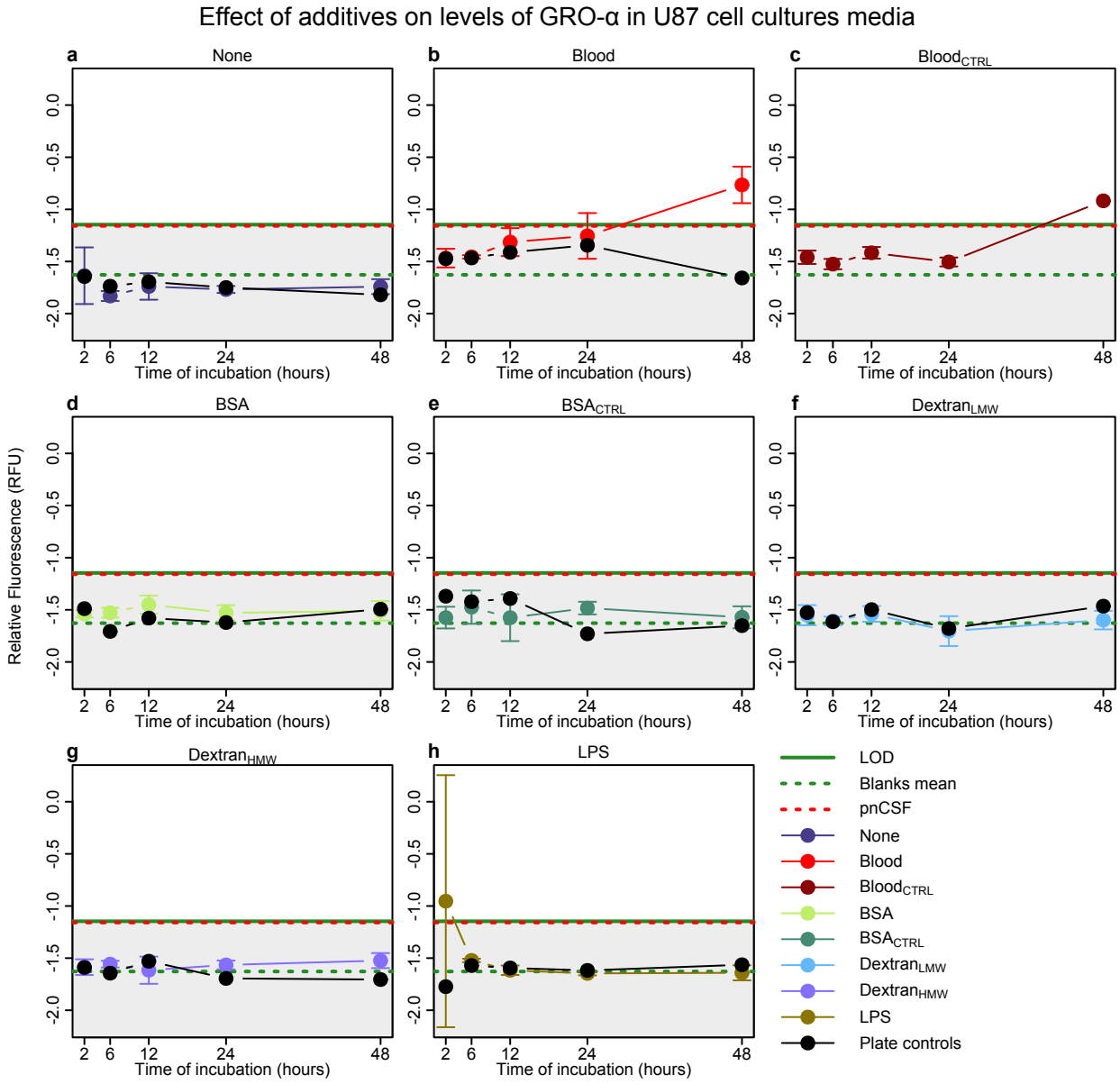

FIGURE H.S54: **Effect of additives on levels of GRO-α in U87 cell cultures media.** Additives along with fresh blood and LPS were added to mycoplasma-free human glial (U87) cells in triplicate wells of a 24-well plate and incubated for up to 48 h to measure the effect on levels of proteins measured in the cell media. Media was collected and frozen from successive triplicates at different intervals, then analyzed with the ACM. Each graph compares GRO-α values from cells incubated with a different additive to cells not incubated with additives located in the same 24-well plate. Plates in **c** and **e** did not contain any U87 cells, and **c** also did not have controls on the plate.

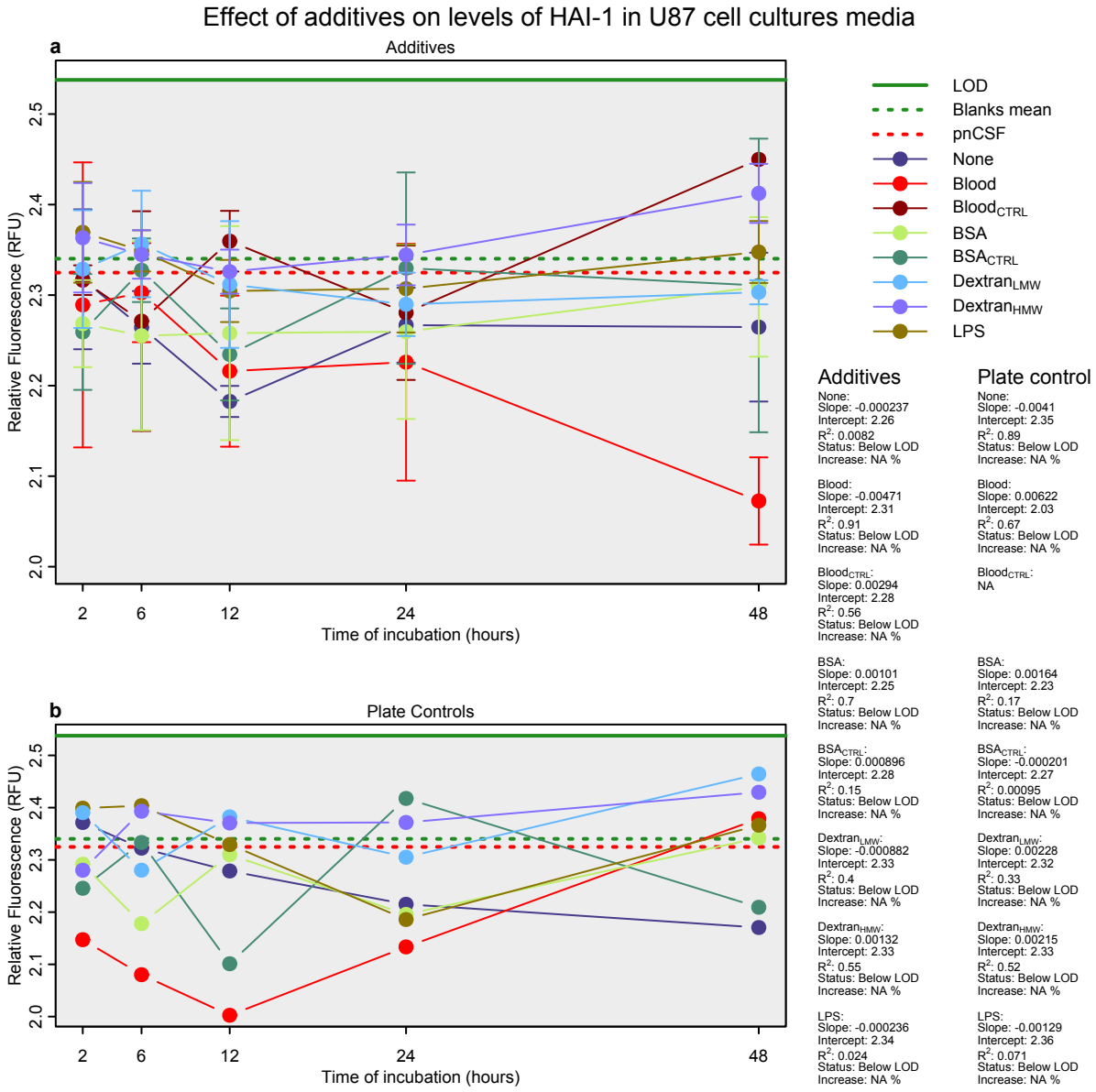

FIGURE H.S55: **Effect of additives on levels of HAI-1 in U87 cell cultures media.** Additives along with fresh blood and LPS were added to mycoplasma-free human glial (U87) cells in triplicate wells of a 24-well plate and incubated for up to 48 h to measure the effect on levels of proteins measured in the cell media. Media was collected and frozen from successive triplicates at different intervals, then analyzed with the ACM. **a** Average values for HAI-1 from three replicates for each point in every 24-well plate where a different additive was applied. **b** Data from the control cell media in each plate.

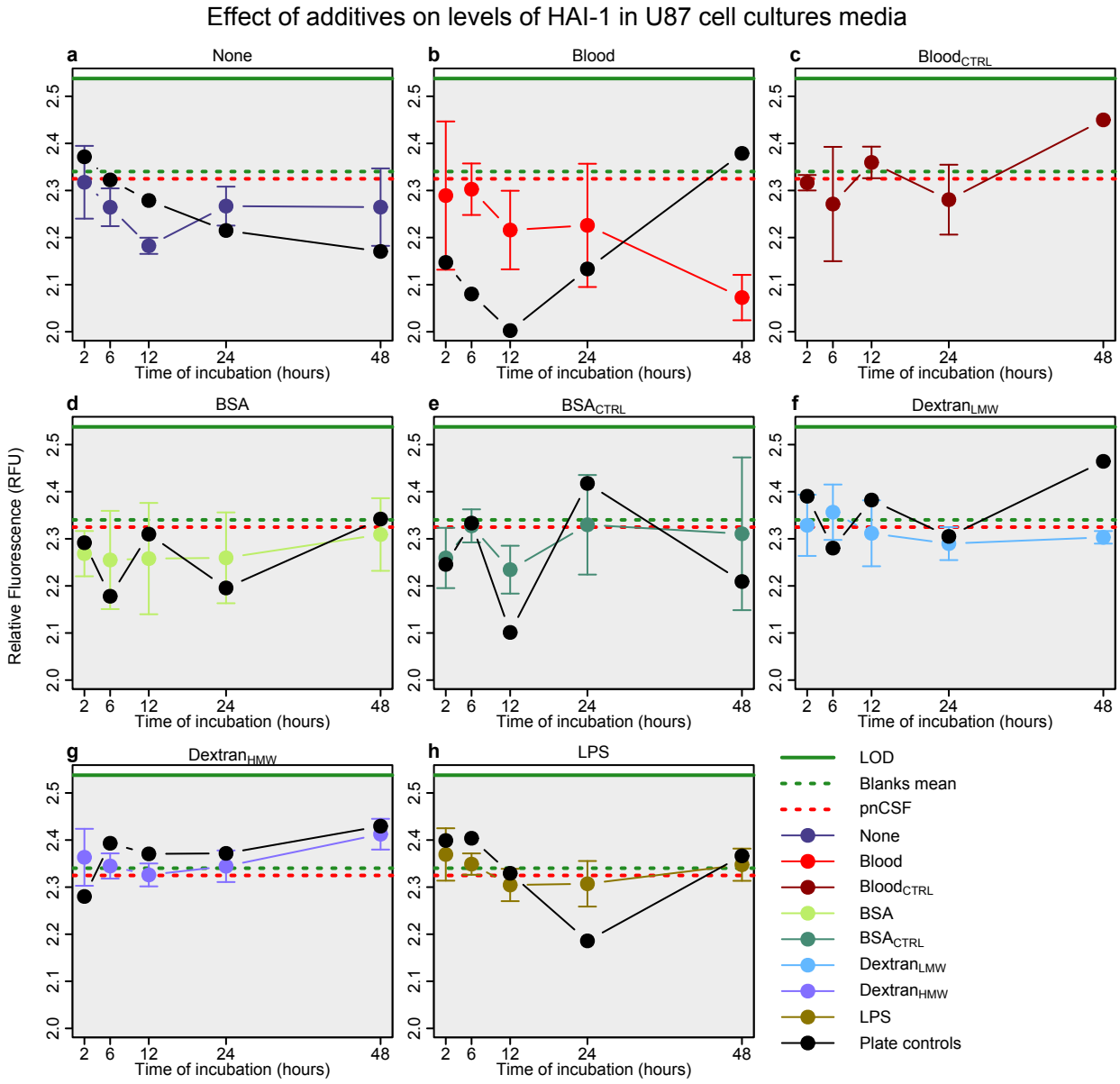

FIGURE H.S56: **Effect of additives on levels of HAI-1 in U87 cell cultures media.** Additives along with fresh blood and LPS were added to mycoplasma-free human glial (U87) cells in triplicate wells of a 24-well plate and incubated for up to 48 h to measure the effect on levels of proteins measured in the cell media. Media was collected and frozen from successive triplicates at different intervals, then analyzed with the ACM. Each graph compares HAI-1 values from cells incubated with a different additive to cells not incubated with additives located in the same 24-well plate. Plates in **c** and **e** did not contain any U87 cells, and **c** also did not have controls on the plate.

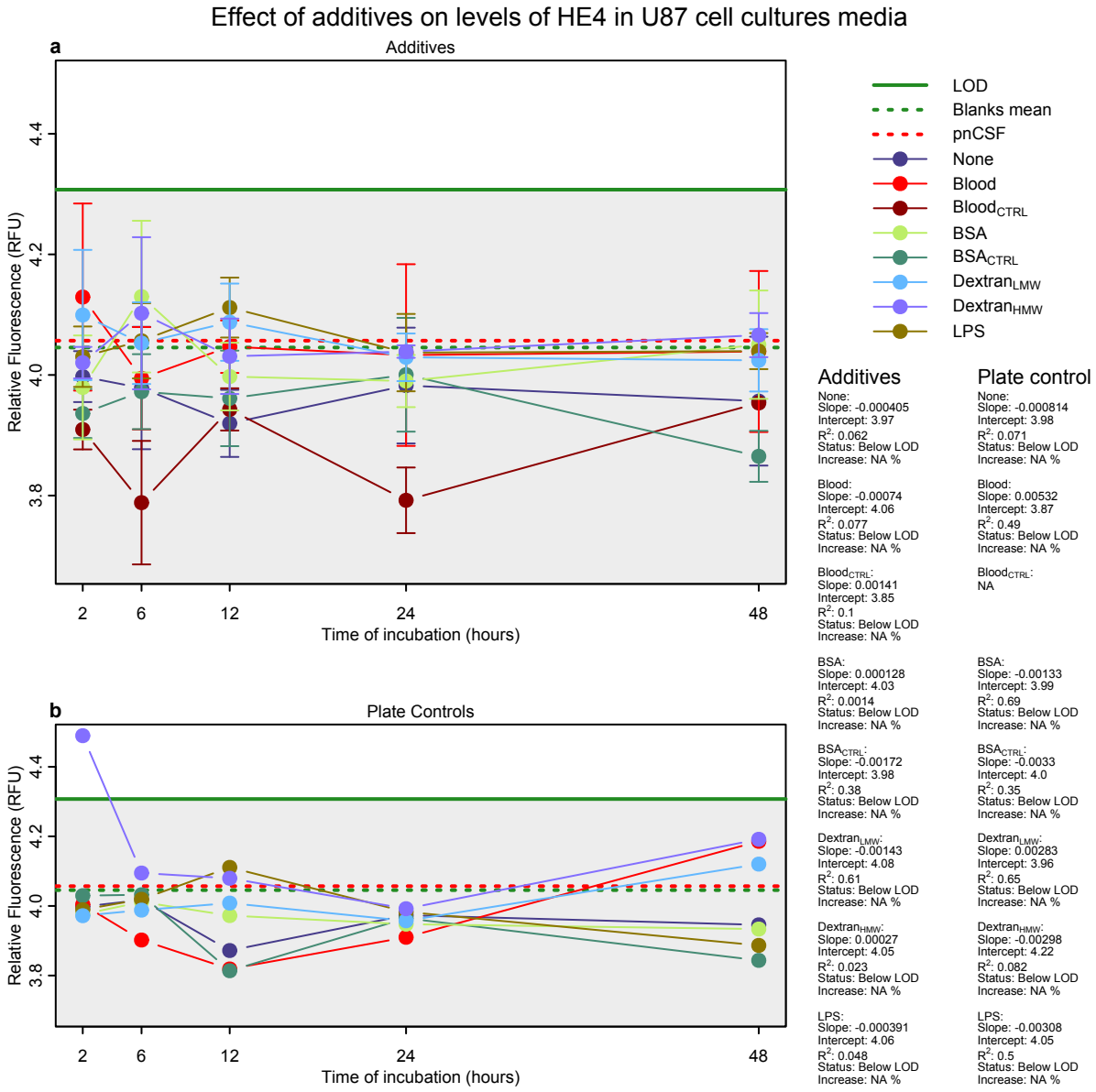

FIGURE H.S57: **Effect of additives on levels of HE4 in U87 cell cultures media.** Additives along with fresh blood and LPS were added to mycoplasma-free human glial (U87) cells in triplicate wells of a 24-well plate and incubated for up to 48 h to measure the effect on levels of proteins measured in the cell media. Media was collected and frozen from successive triplicates at different intervals, then analyzed with the ACM. **a** Average values for HE4 from three replicates for each point in every 24-well plate where a different additive was applied. **b** Data from the control cell media in each plate.

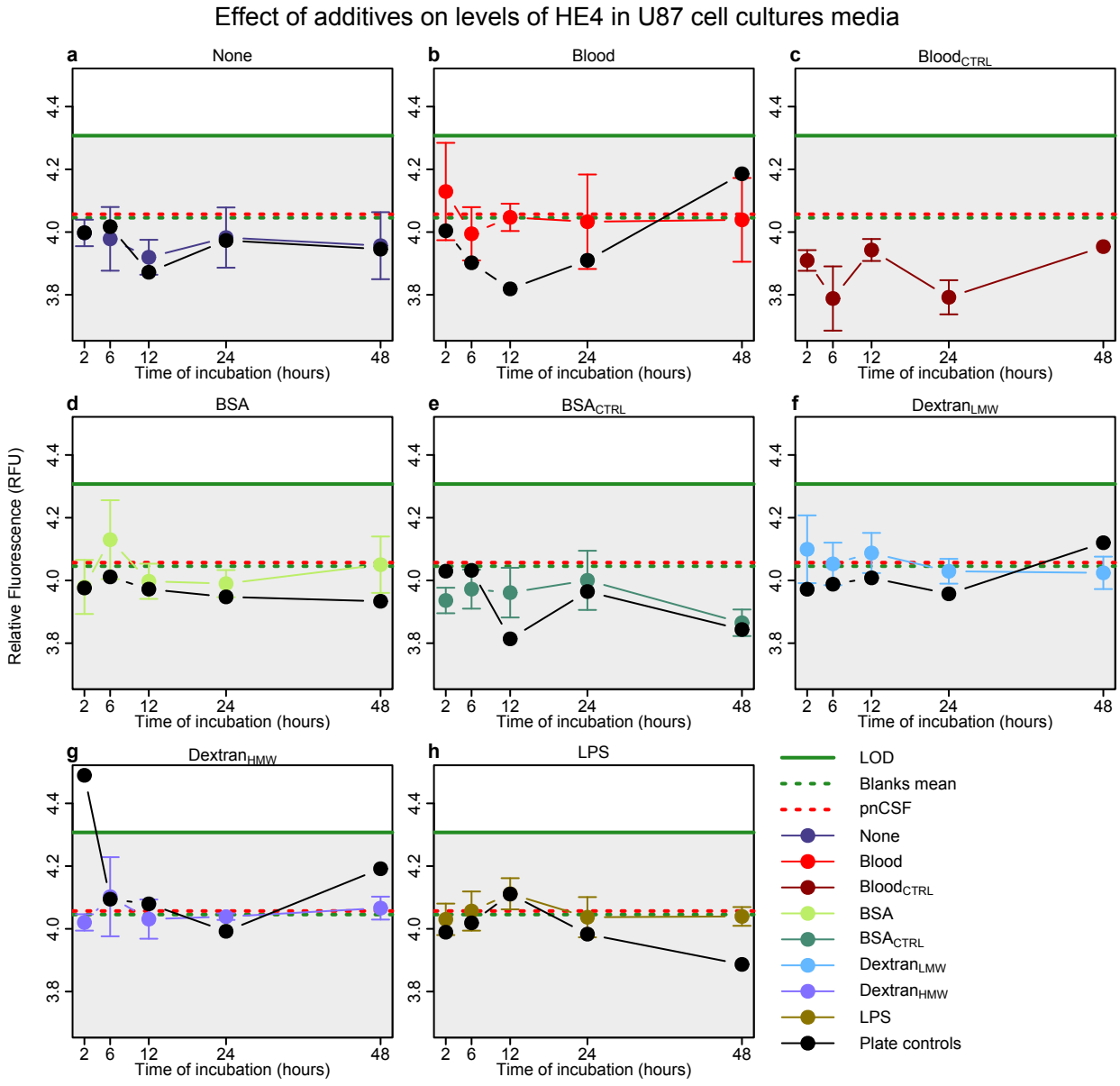

FIGURE H.S58: **Effect of additives on levels of HE4 in U87 cell cultures media.** Additives along with fresh blood and LPS were added to mycoplasma-free human glial (U87) cells in triplicate wells of a 24-well plate and incubated for up to 48 h to measure the effect on levels of proteins measured in the cell media. Media was collected and frozen from successive triplicates at different intervals, then analyzed with the ACM. Each graph compares HE4 values from cells incubated with a different additive to cells not incubated with additives located in the same 24-well plate. Plates in **c** and **e** did not contain any U87 cells, and **c** also did not have controls on the plate.

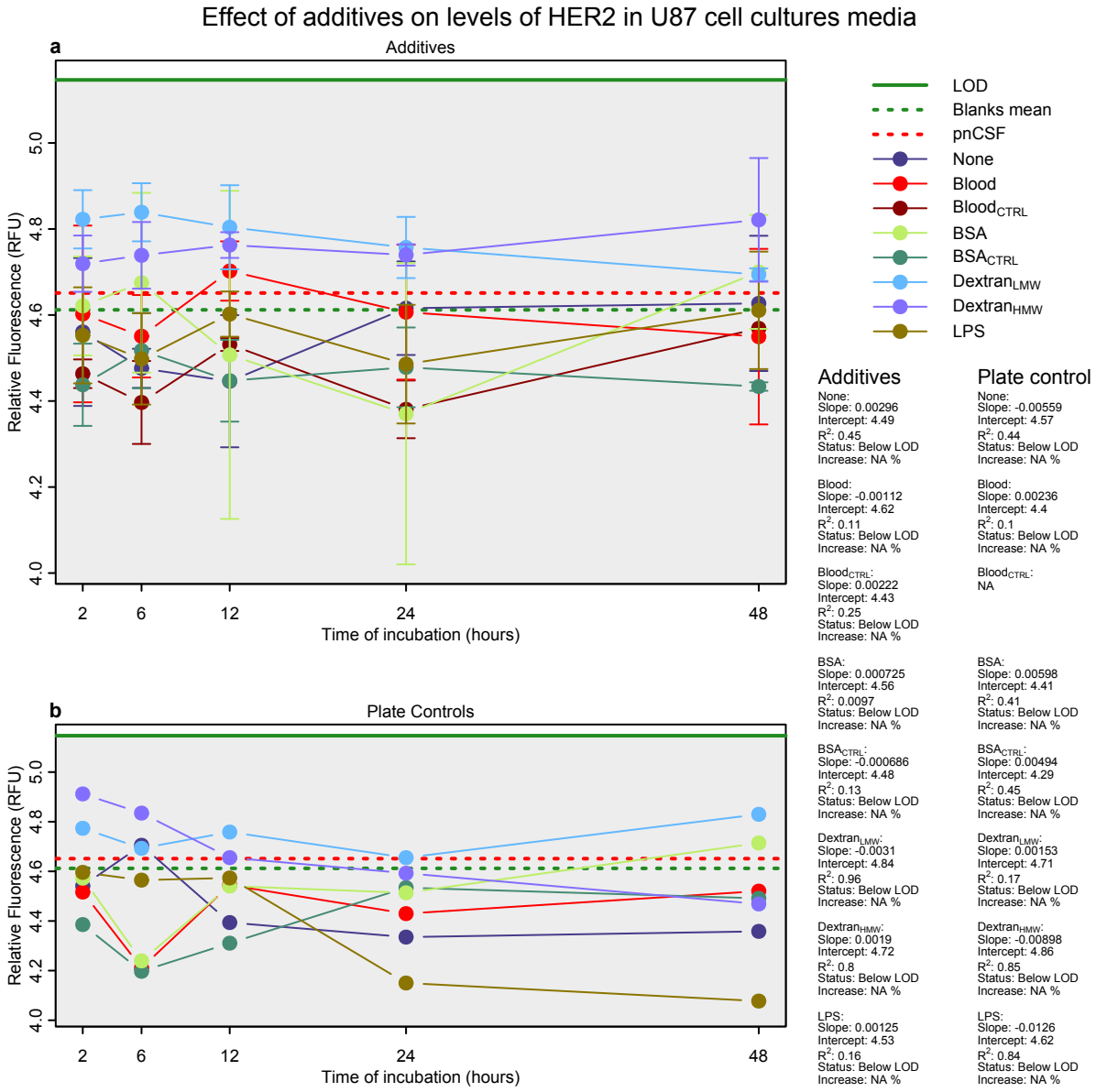

FIGURE H.S59: **Effect of additives on levels of HER2 in U87 cell cultures media.** Additives along with fresh blood and LPS were added to mycoplasma-free human glial (U87) cells in triplicate wells of a 24-well plate and incubated for up to 48 h to measure the effect on levels of proteins measured in the cell media. Media was collected and frozen from successive triplicates at different intervals, then analyzed with the ACM. **a** Average values for HER2 from three replicates for each point in every 24-well plate where a different additive was applied. **b** Data from the control cell media in each plate.

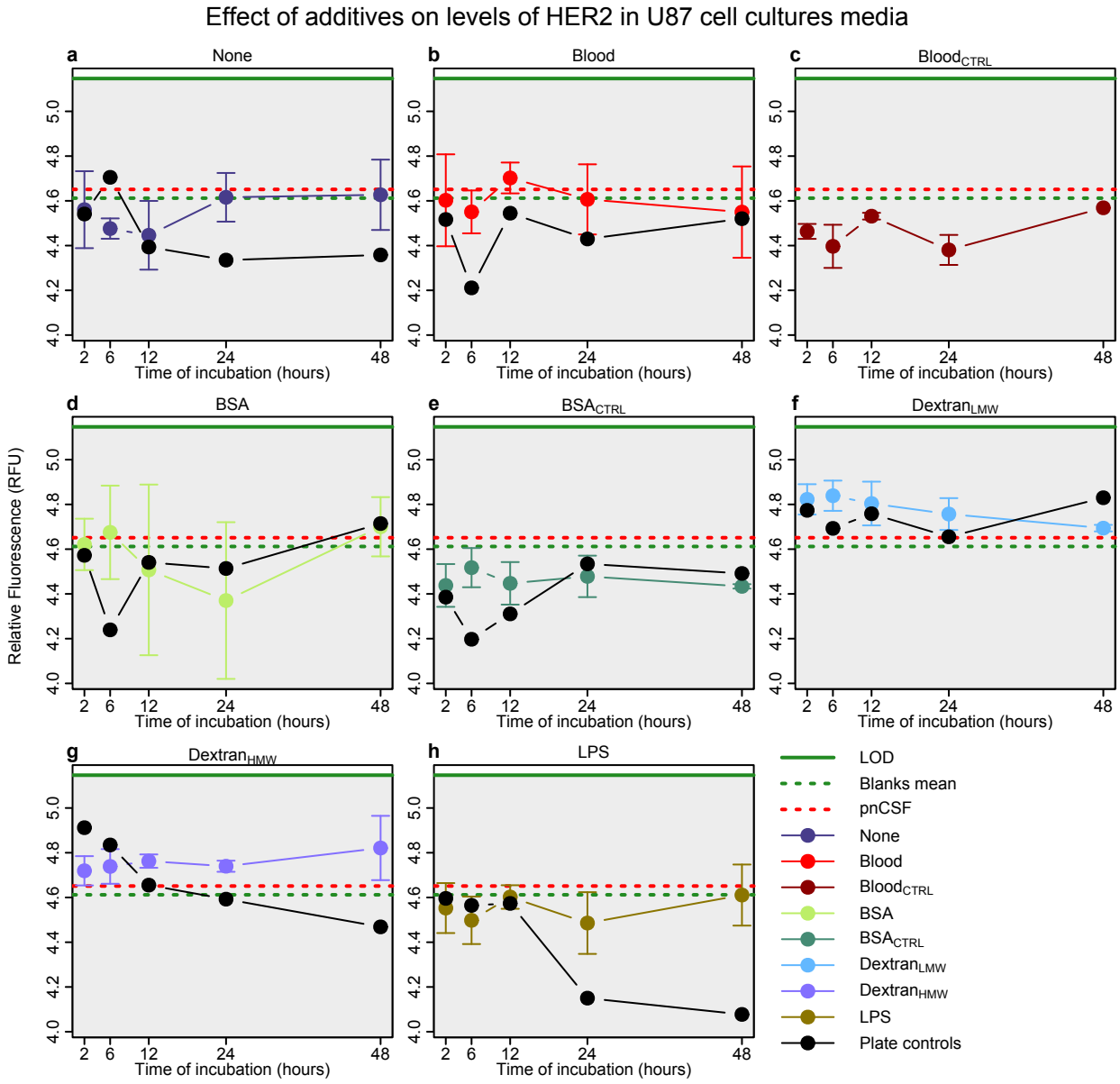

FIGURE H.S60: **Effect of additives on levels of HER2 in U87 cell cultures media.** Additives along with fresh blood and LPS were added to mycoplasma-free human glial (U87) cells in triplicate wells of a 24-well plate and incubated for up to 48 h to measure the effect on levels of proteins measured in the cell media. Media was collected and frozen from successive triplicates at different intervals, then analyzed with the ACM. Each graph compares HER2 values from cells incubated with a different additive to cells not incubated with additives located in the same 24-well plate. Plates in **c** and **e** did not contain any U87 cells, and **c** also did not have controls on the plate.

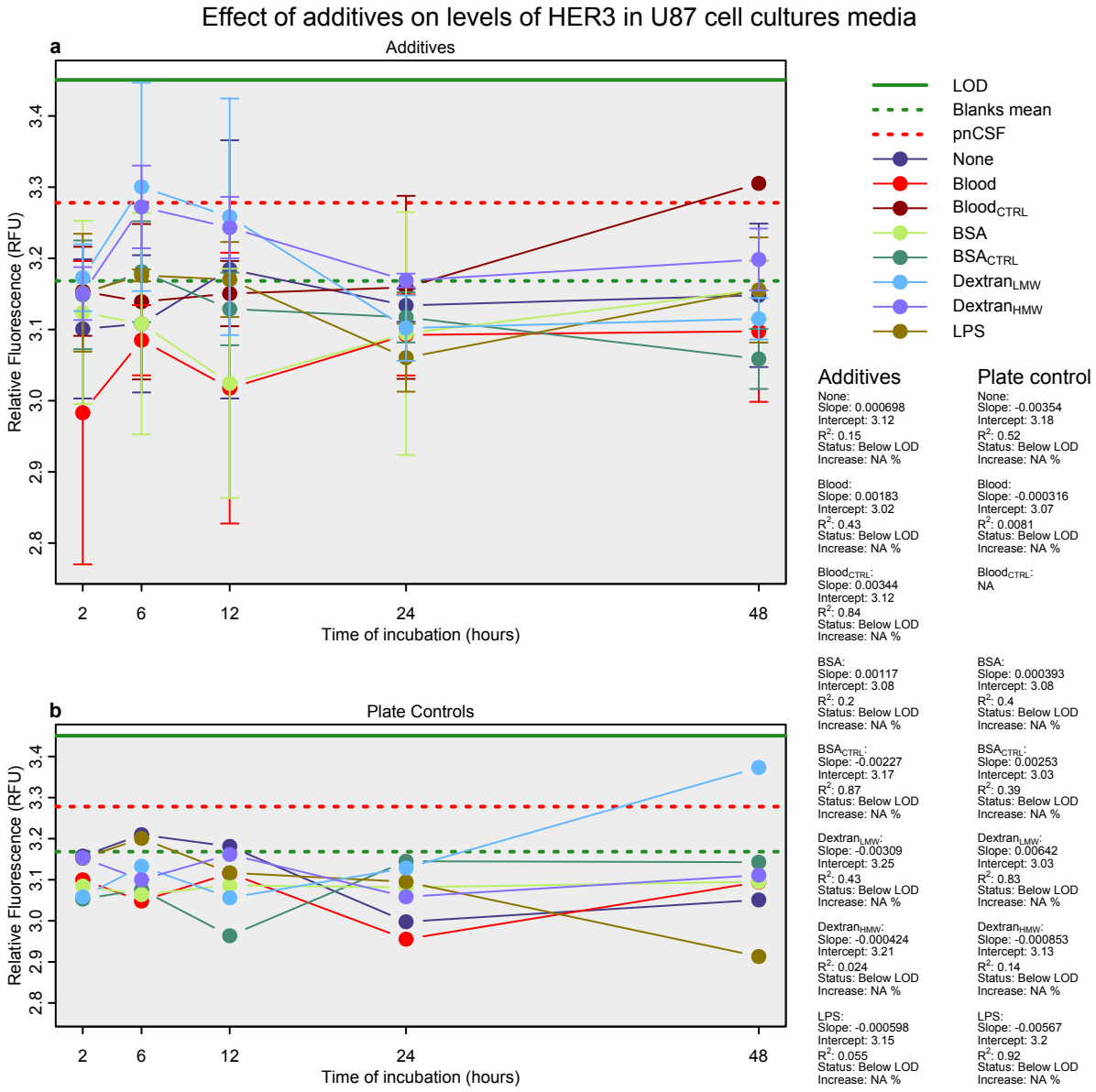

FIGURE H.S61: **Effect of additives on levels of HER3 in U87 cell cultures media.** Additives along with fresh blood and LPS were added to mycoplasma-free human glial (U87) cells in triplicate wells of a 24-well plate and incubated for up to 48 h to measure the effect on levels of proteins measured in the cell media. Media was collected and frozen from successive triplicates at different intervals, then analyzed with the ACM. **a** Average values for HER3 from three replicates for each point in every 24-well plate where a different additive was applied. **b** Data from the control cell media in each plate.

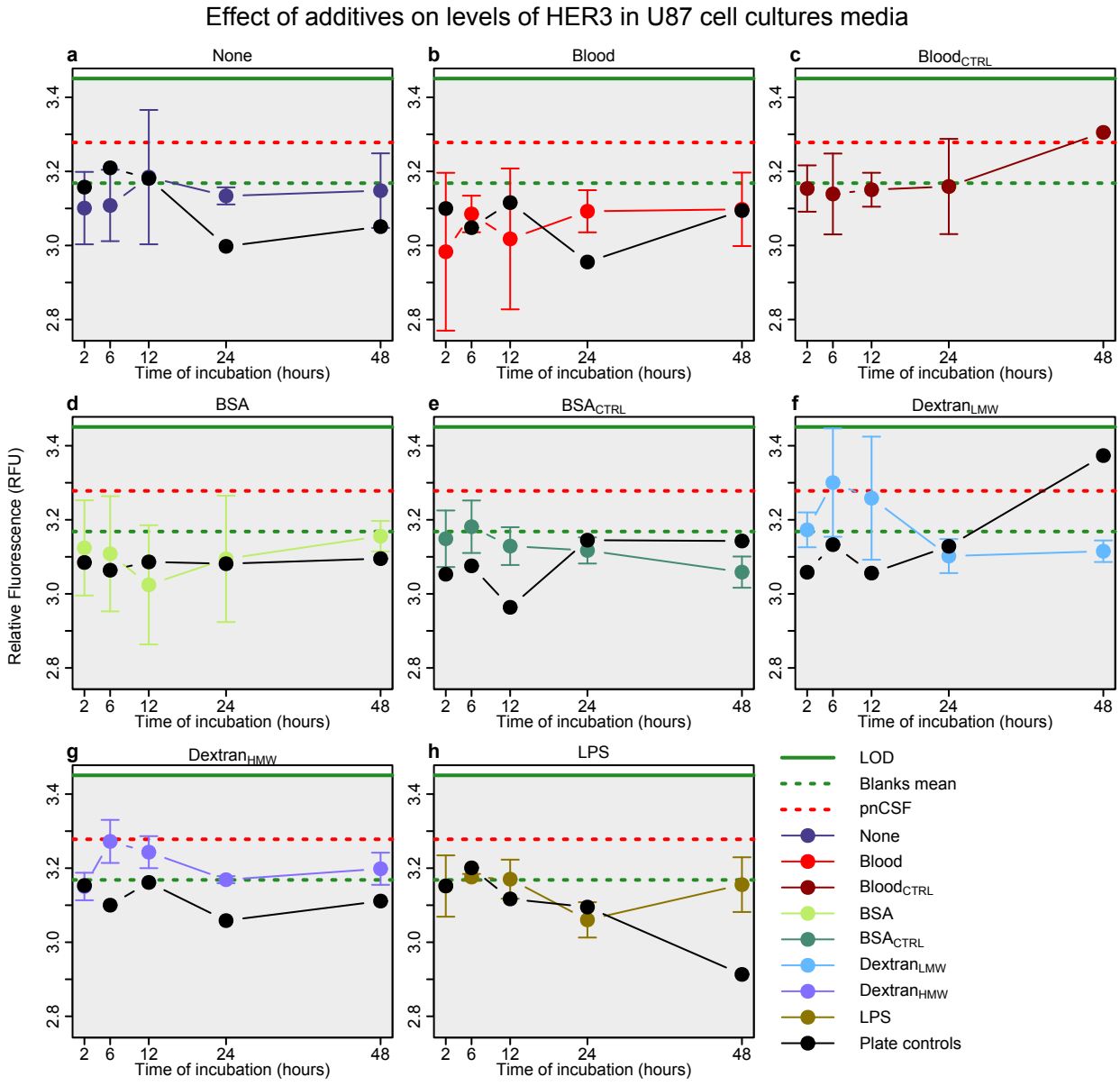

FIGURE H.S62: **Effect of additives on levels of HER3 in U87 cell cultures media.** Additives along with fresh blood and LPS were added to mycoplasma-free human glial (U87) cells in triplicate wells of a 24-well plate and incubated for up to 48 h to measure the effect on levels of proteins measured in the cell media. Media was collected and frozen from successive triplicates at different intervals, then analyzed with the ACM. Each graph compares HER3 values from cells incubated with a different additive to cells not incubated with additives located in the same 24-well plate. Plates in **c** and **e** did not contain any U87 cells, and **c** also did not have controls on the plate.

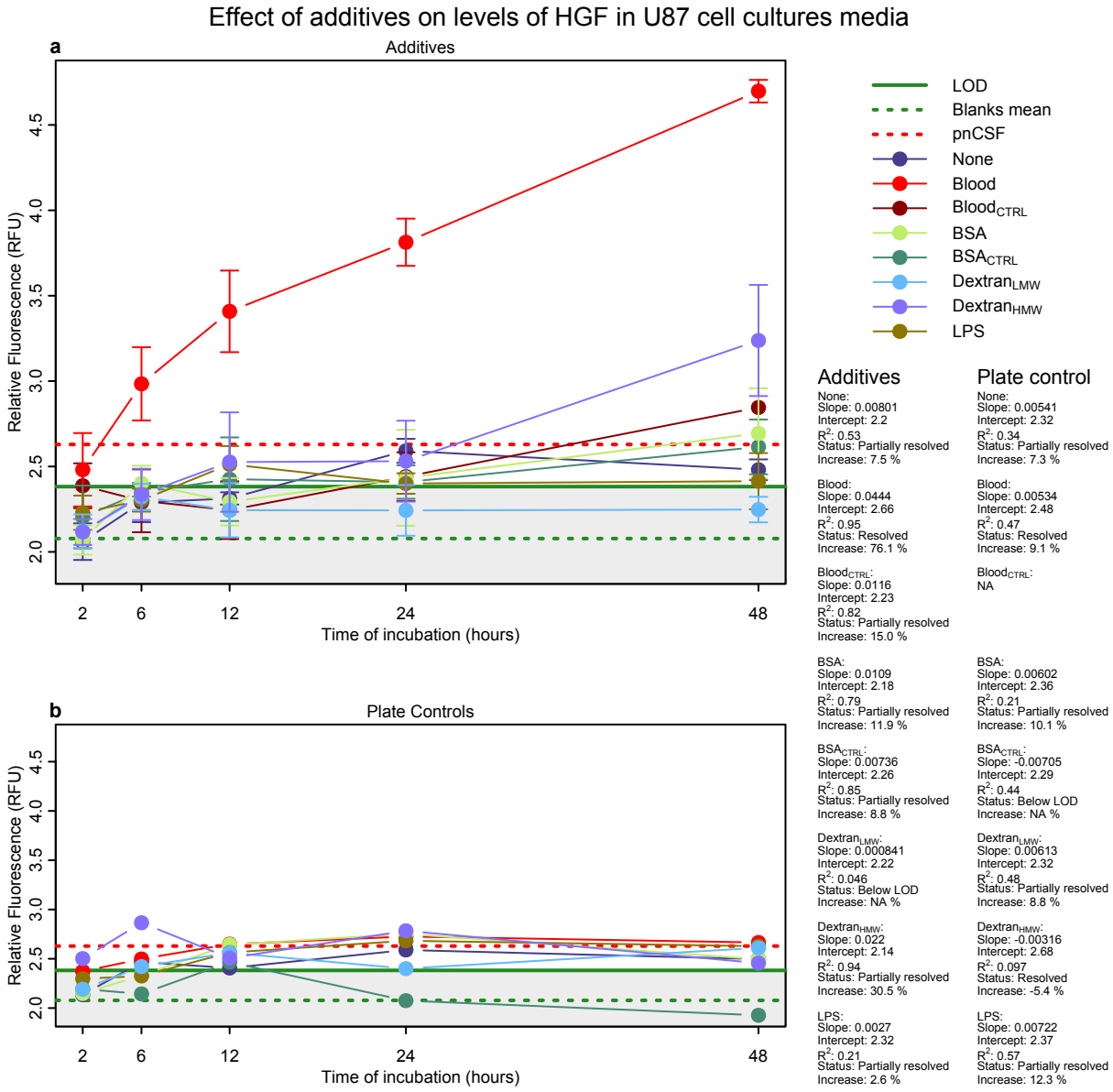

FIGURE H.S63: **Effect of additives on levels of HGF in U87 cell cultures media.** Additives along with fresh blood and LPS were added to mycoplasma-free human glial (U87) cells in triplicate wells of a 24-well plate and incubated for up to 48 h to measure the effect on levels of proteins measured in the cell media. Media was collected and frozen from successive triplicates at different intervals, then analyzed with the ACM. **a** Average values for HGF from three replicates for each point in every 24-well plate where a different additive was applied. **b** Data from the control cell media in each plate.

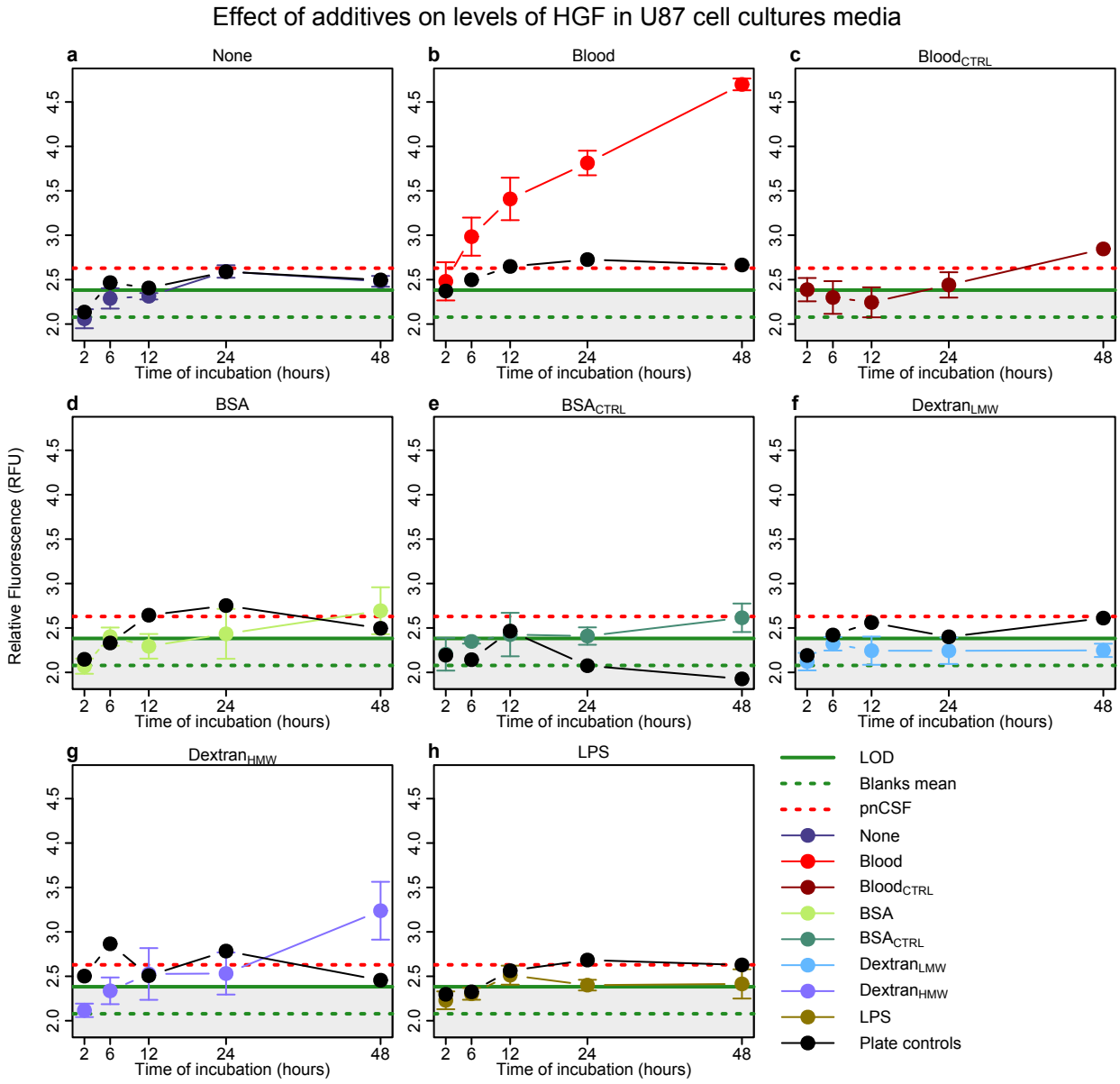

FIGURE H.S64: **Effect of additives on levels of HGF in U87 cell cultures media.** Additives along with fresh blood and LPS were added to mycoplasma-free human glial (U87) cells in triplicate wells of a 24-well plate and incubated for up to 48 h to measure the effect on levels of proteins measured in the cell media. Media was collected and frozen from successive triplicates at different intervals, then analyzed with the ACM. Each graph compares HGF values from cells incubated with a different additive to cells not incubated with additives located in the same 24-well plate. Plates in **c** and **e** did not contain any U87 cells, and **c** also did not have controls on the plate.

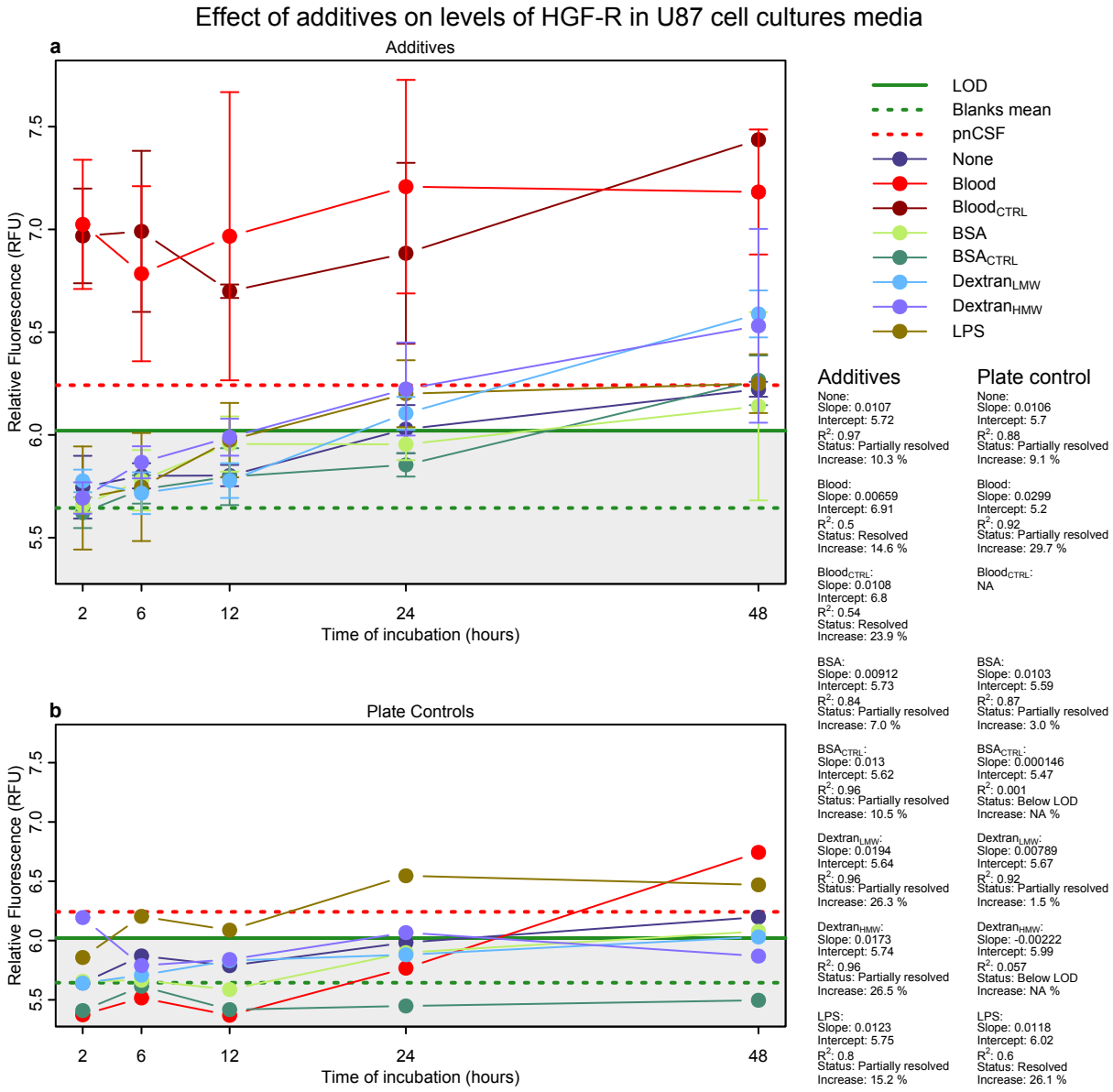

FIGURE H.S65: **Effect of additives on levels of HGF-R in U87 cell cultures media.** Additives along with fresh blood and LPS were added to mycoplasma-free human glial (U87) cells in triplicate wells of a 24-well plate and incubated for up to 48 h to measure the effect on levels of proteins measured in the cell media. Media was collected and frozen from successive triplicates at different intervals, then analyzed with the ACM. **a** Average values for HGF-R from three replicates for each point in every 24-well plate where a different additive was applied. **b** Data from the control cell media in each plate.

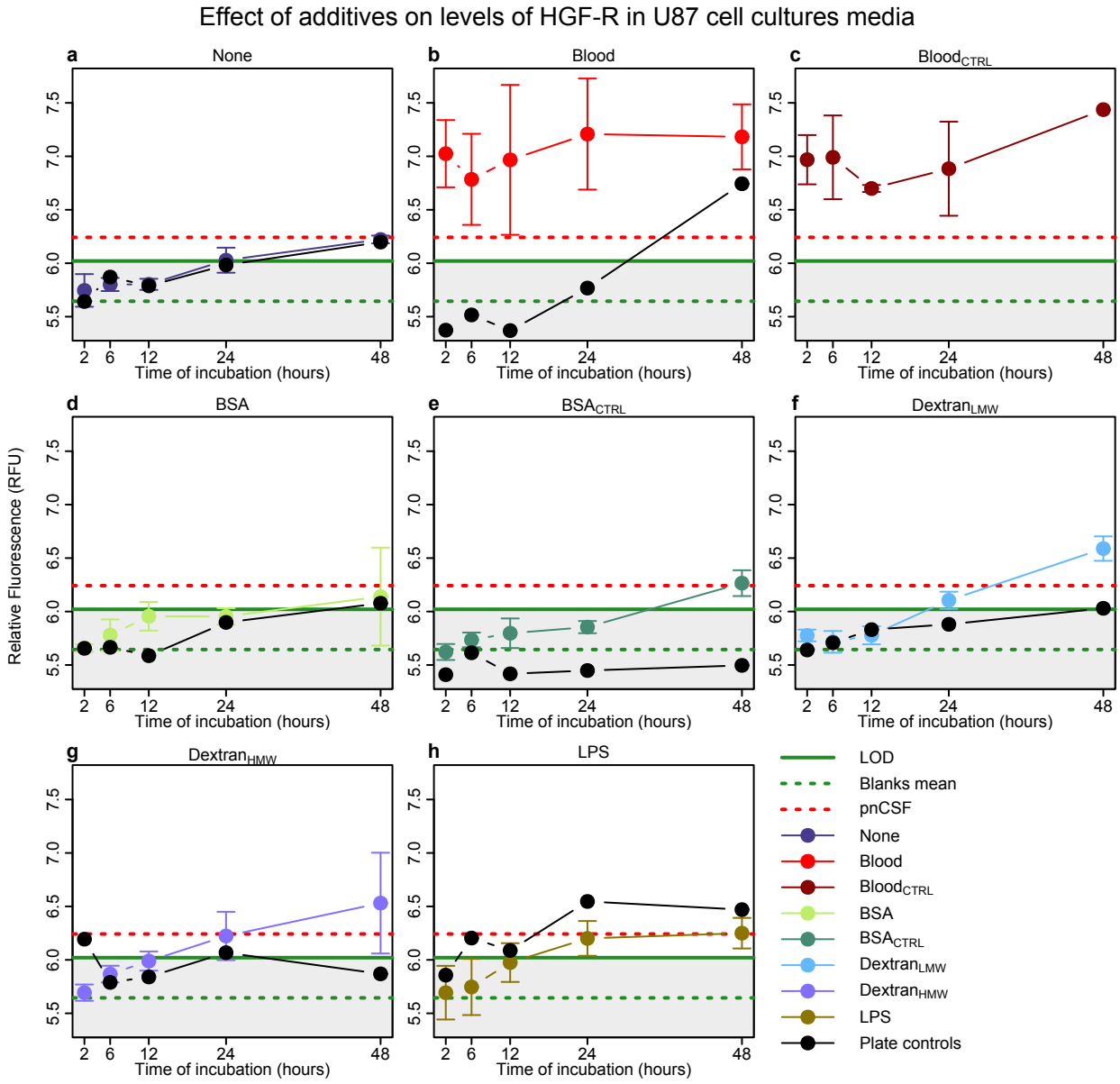

FIGURE H.S66: **Effect of additives on levels of HGF-R in U87 cell cultures media.** Additives along with fresh blood and LPS were added to mycoplasma-free human glial (U87) cells in triplicate wells of a 24-well plate and incubated for up to 48 h to measure the effect on levels of proteins measured in the cell media. Media was collected and frozen from successive triplicates at different intervals, then analyzed with the ACM. Each graph compares HGF-R values from cells incubated with a different additive to cells not incubated with additives located in the same 24-well plate. Plates in **c** and **e** did not contain any U87 cells, and **c** also did not have controls on the plate.

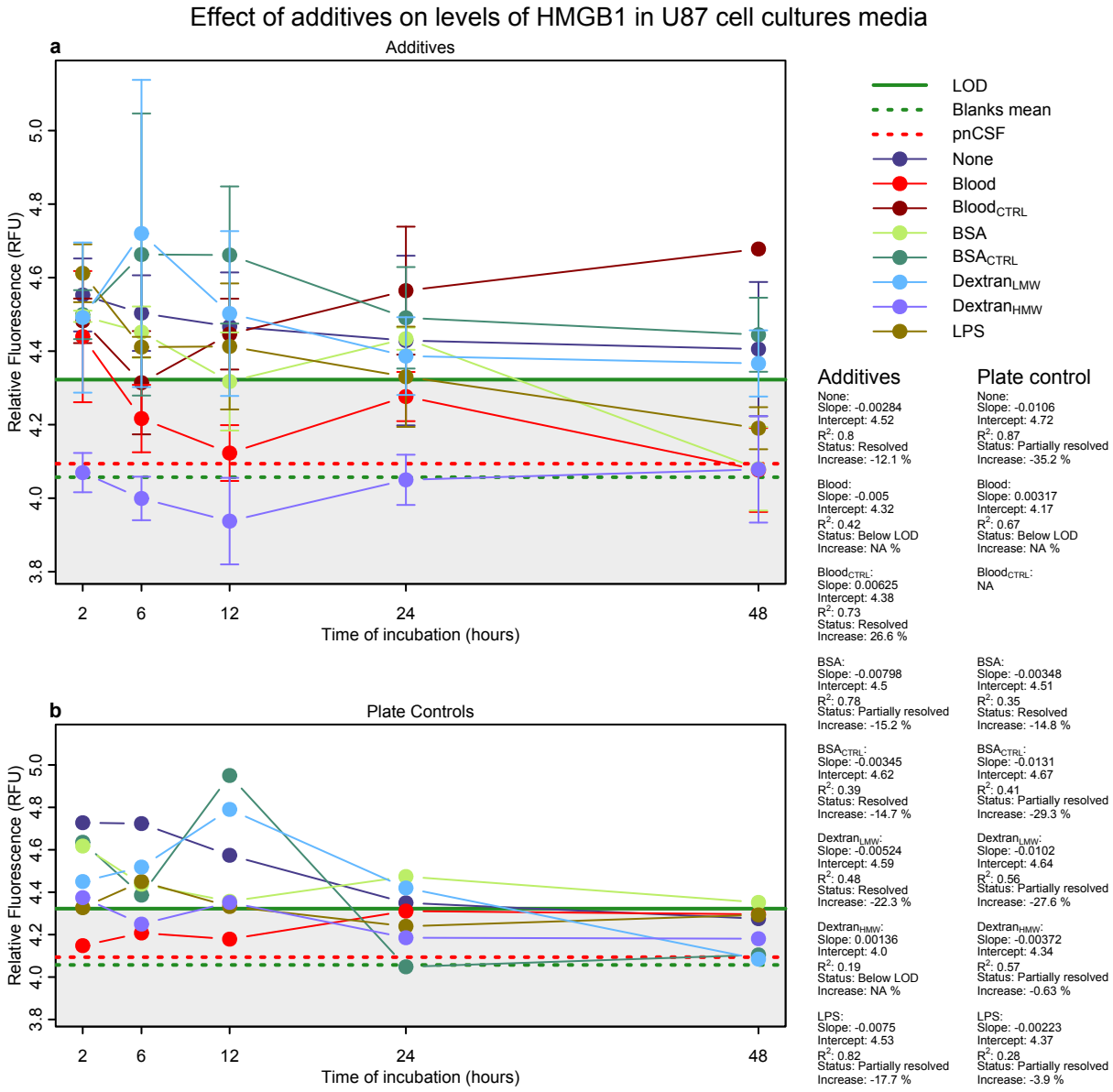

FIGURE H.S67: **Effect of additives on levels of HMGB1 in U87 cell cultures media.** Additives along with fresh blood and LPS were added to mycoplasma-free human glial (U87) cells in triplicate wells of a 24-well plate and incubated for up to 48 h to measure the effect on levels of proteins measured in the cell media. Media was collected and frozen from successive triplicates at different intervals, then analyzed with the ACM. **a** Average values for HMGB1 from three replicates for each point in every 24-well plate where a different additive was applied. **b** Data from the control cell media in each plate.

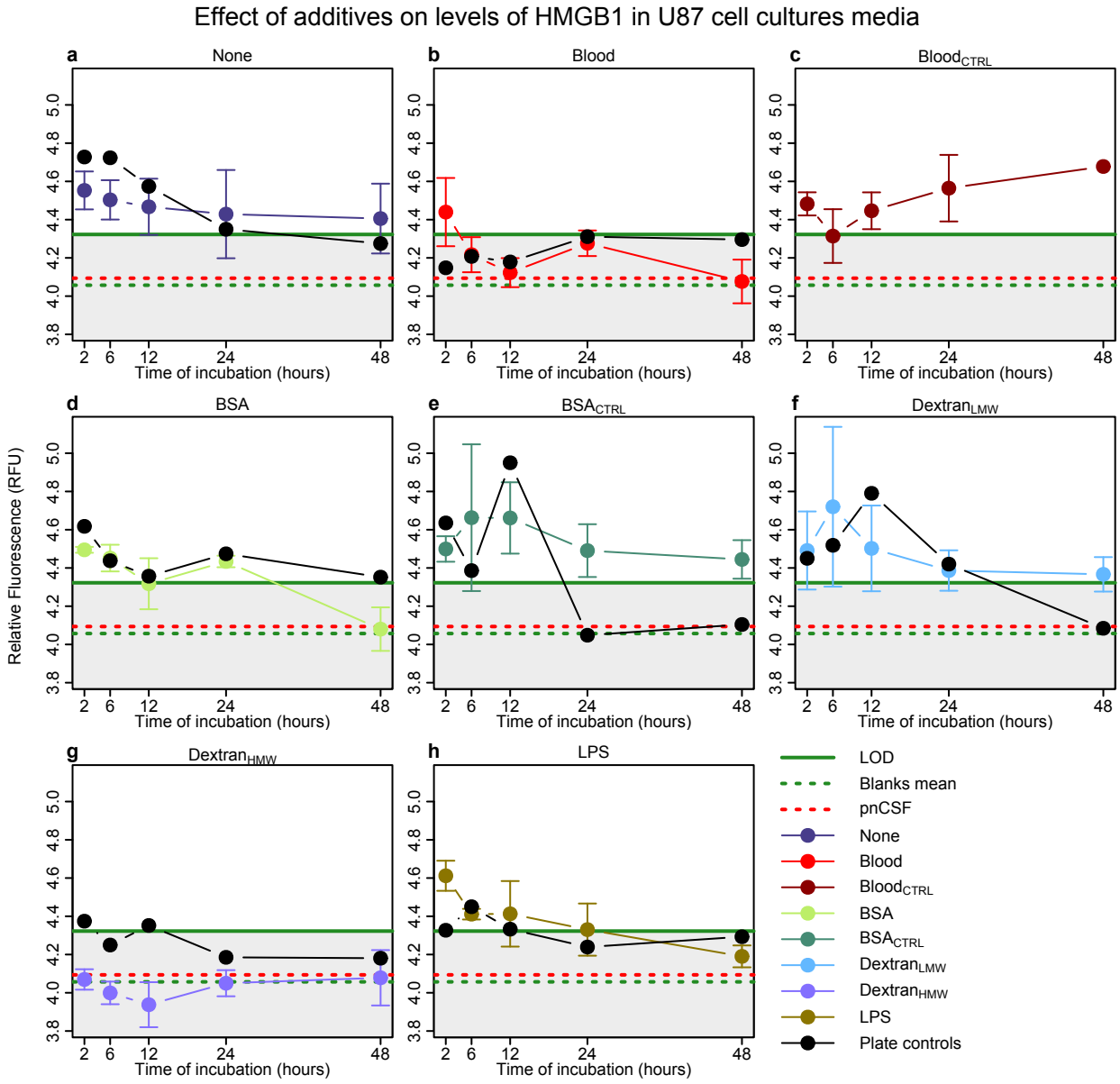

FIGURE H.S68: **Effect of additives on levels of HMGB1 in U87 cell cultures media.** Additives along with fresh blood and LPS were added to mycoplasma-free human glial (U87) cells in triplicate wells of a 24-well plate and incubated for up to 48 h to measure the effect on levels of proteins measured in the cell media. Media was collected and frozen from successive triplicates at different intervals, then analyzed with the ACM. Each graph compares HMGB1 values from cells incubated with a different additive to cells not incubated with additives located in the same 24-well plate. Plates in **c** and **e** did not contain any U87 cells, and **c** also did not have controls on the plate.

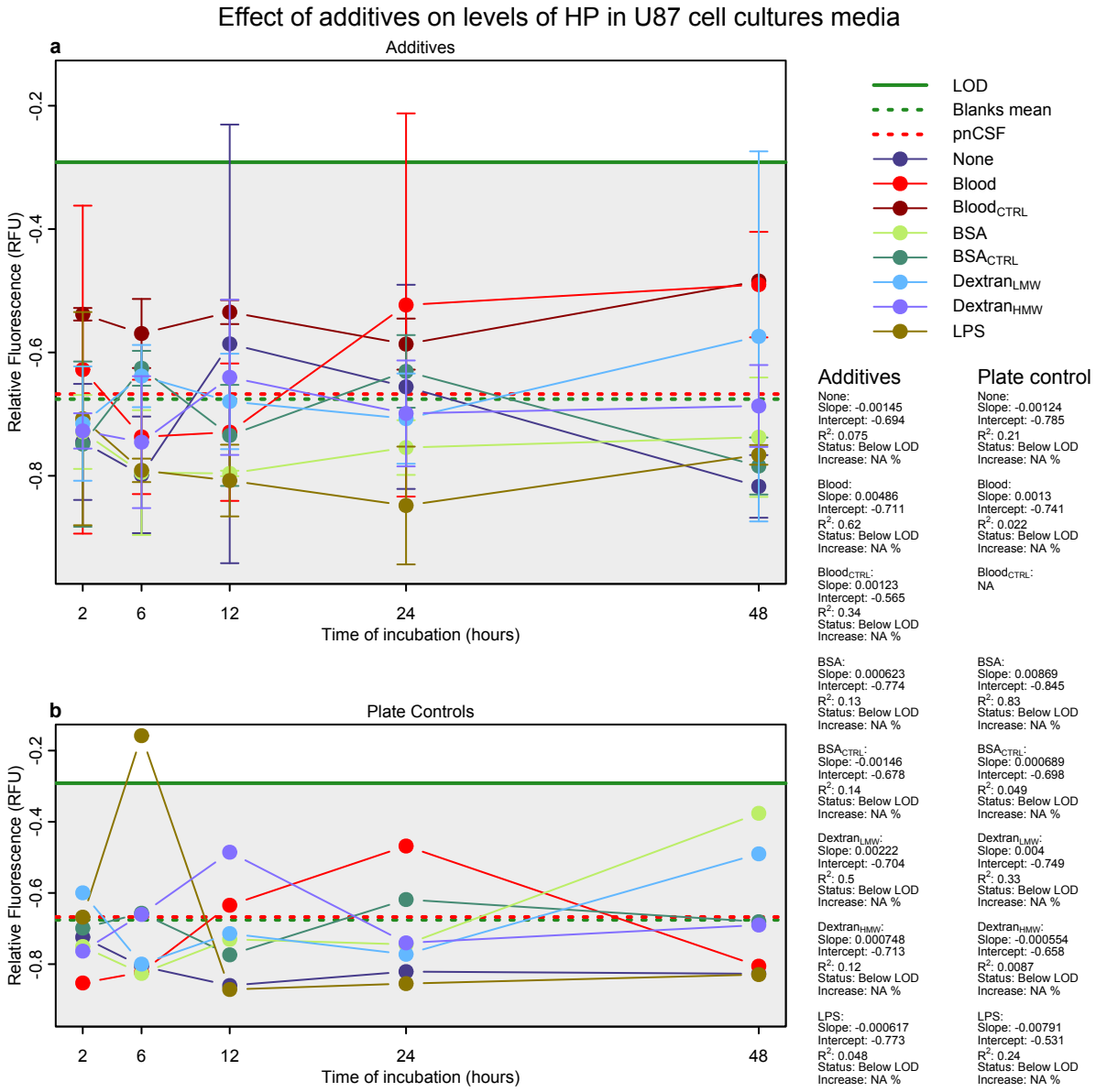

FIGURE H.S69: **Effect of additives on levels of HP in U87 cell cultures media.** Additives along with fresh blood and LPS were added to mycoplasma-free human glial (U87) cells in triplicate wells of a 24-well plate and incubated for up to 48 h to measure the effect on levels of proteins measured in the cell media. Media was collected and frozen from successive triplicates at different intervals, then analyzed with the ACM. **a** Average values for HP from three replicates for each point in every 24-well plate where a different additive was applied. **b** Data from the control cell media in each plate.

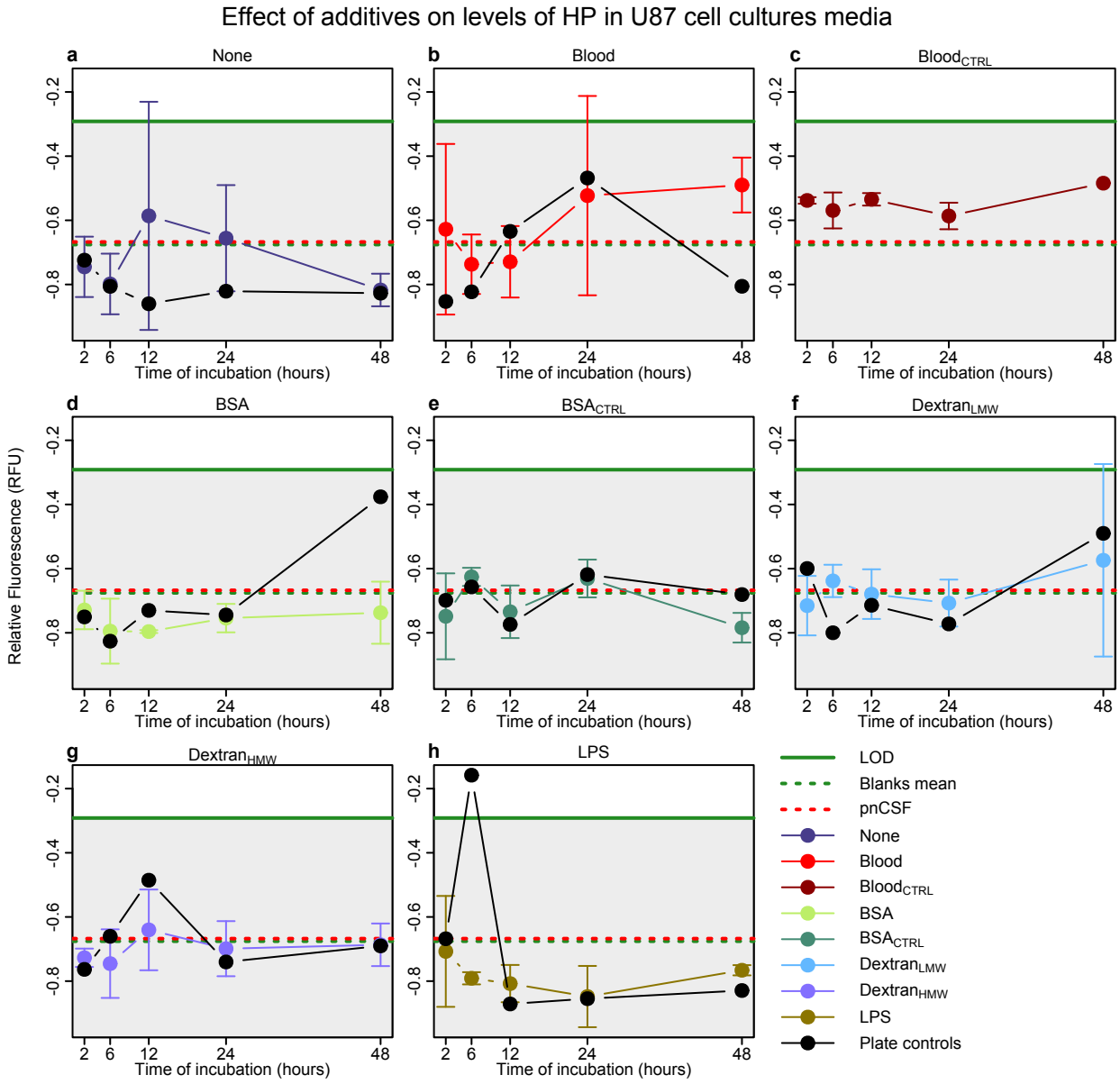

FIGURE H.S70: **Effect of additives on levels of HP in U87 cell cultures media.** Additives along with fresh blood and LPS were added to mycoplasma-free human glial (U87) cells in triplicate wells of a 24-well plate and incubated for up to 48 h to measure the effect on levels of proteins measured in the cell media. Media was collected and frozen from successive triplicates at different intervals, then analyzed with the ACM. Each graph compares HP values from cells incubated with a different additive to cells not incubated with additives located in the same 24-well plate. Plates in **c** and **e** did not contain any U87 cells, and **c** also did not have controls on the plate.

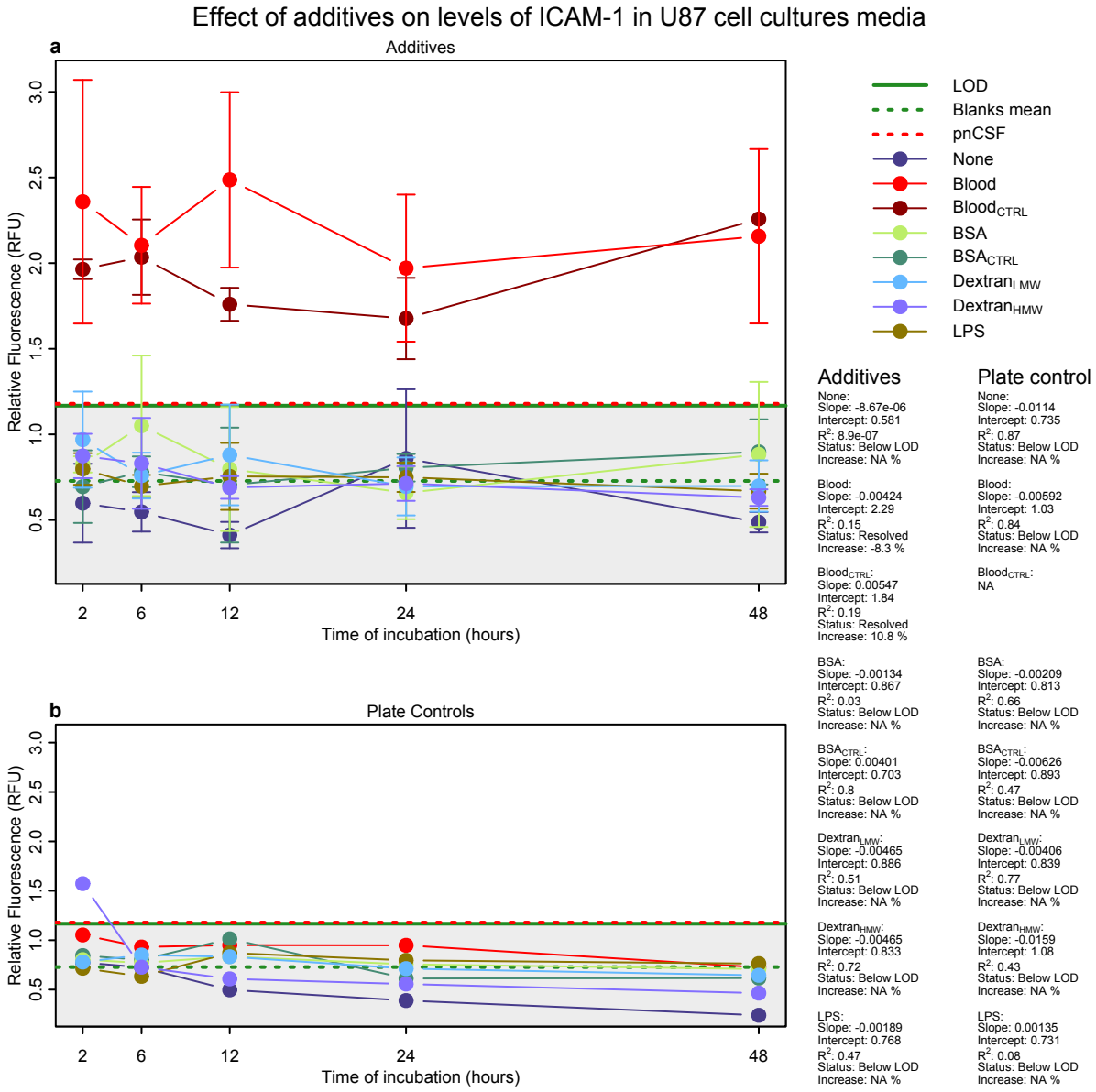

FIGURE H.S71: **Effect of additives on levels of ICAM-1 in U87 cell cultures media.** Additives along with fresh blood and LPS were added to mycoplasma-free human glial (U87) cells in triplicate wells of a 24-well plate and incubated for up to 48 h to measure the effect on levels of proteins measured in the cell media. Media was collected and frozen from successive triplicates at different intervals, then analyzed with the ACM. **a** Average values for ICAM-1 from three replicates for each point in every 24-well plate where a different additive was applied. **b** Data from the control cell media in each plate.

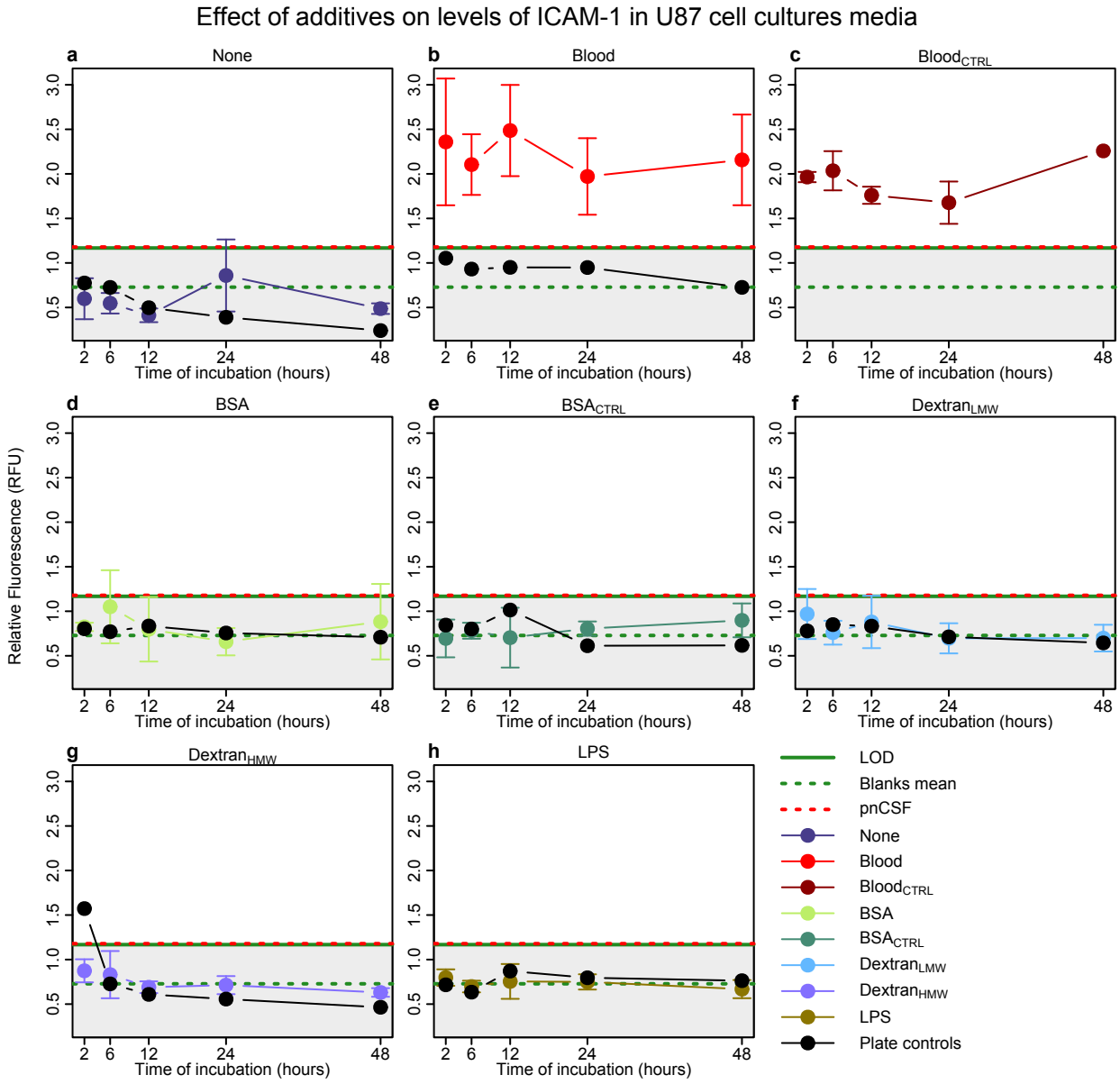

FIGURE H.S72: **Effect of additives on levels of ICAM-1 in U87 cell cultures media.** Additives along with fresh blood and LPS were added to mycoplasma-free human glial (U87) cells in triplicate wells of a 24-well plate and incubated for up to 48 h to measure the effect on levels of proteins measured in the cell media. Media was collected and frozen from successive triplicates at different intervals, then analyzed with the ACM. Each graph compares ICAM-1 values from cells incubated with a different additive to cells not incubated with additives located in the same 24-well plate. Plates in **c** and **e** did not contain any U87 cells, and **c** also did not have controls on the plate.

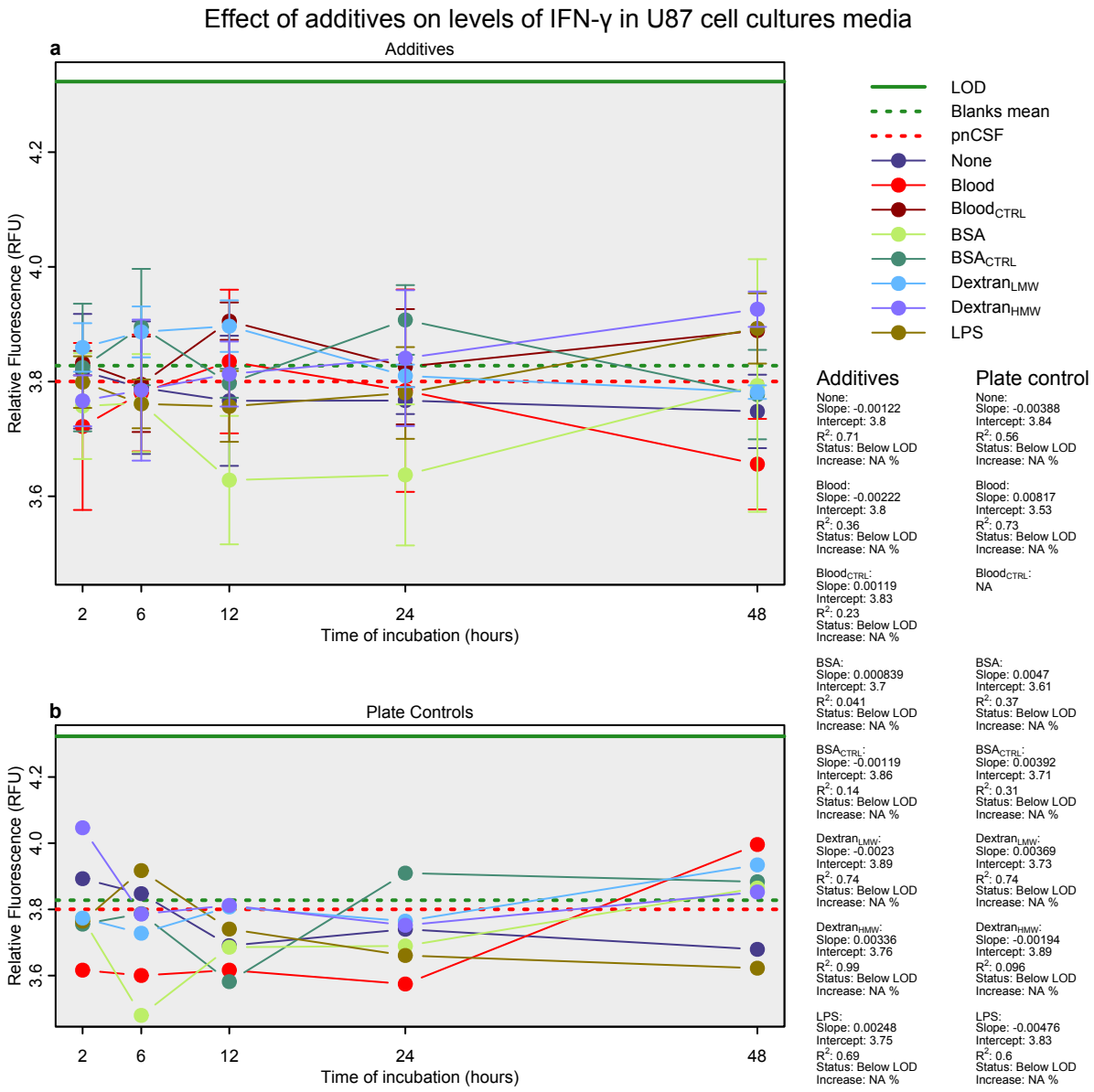

FIGURE H.S73: **Effect of additives on levels of IFN-γ in U87 cell cultures media.** Additives along with fresh blood and LPS were added to mycoplasma-free human glial (U87) cells in triplicate wells of a 24-well plate and incubated for up to 48 h to measure the effect on levels of proteins measured in the cell media. Media was collected and frozen from successive triplicates at different intervals, then analyzed with the ACM. **a** Average values for IFN-γ from three replicates for each point in every 24-well plate where a different additive was applied. **b** Data from the control cell media in each plate.

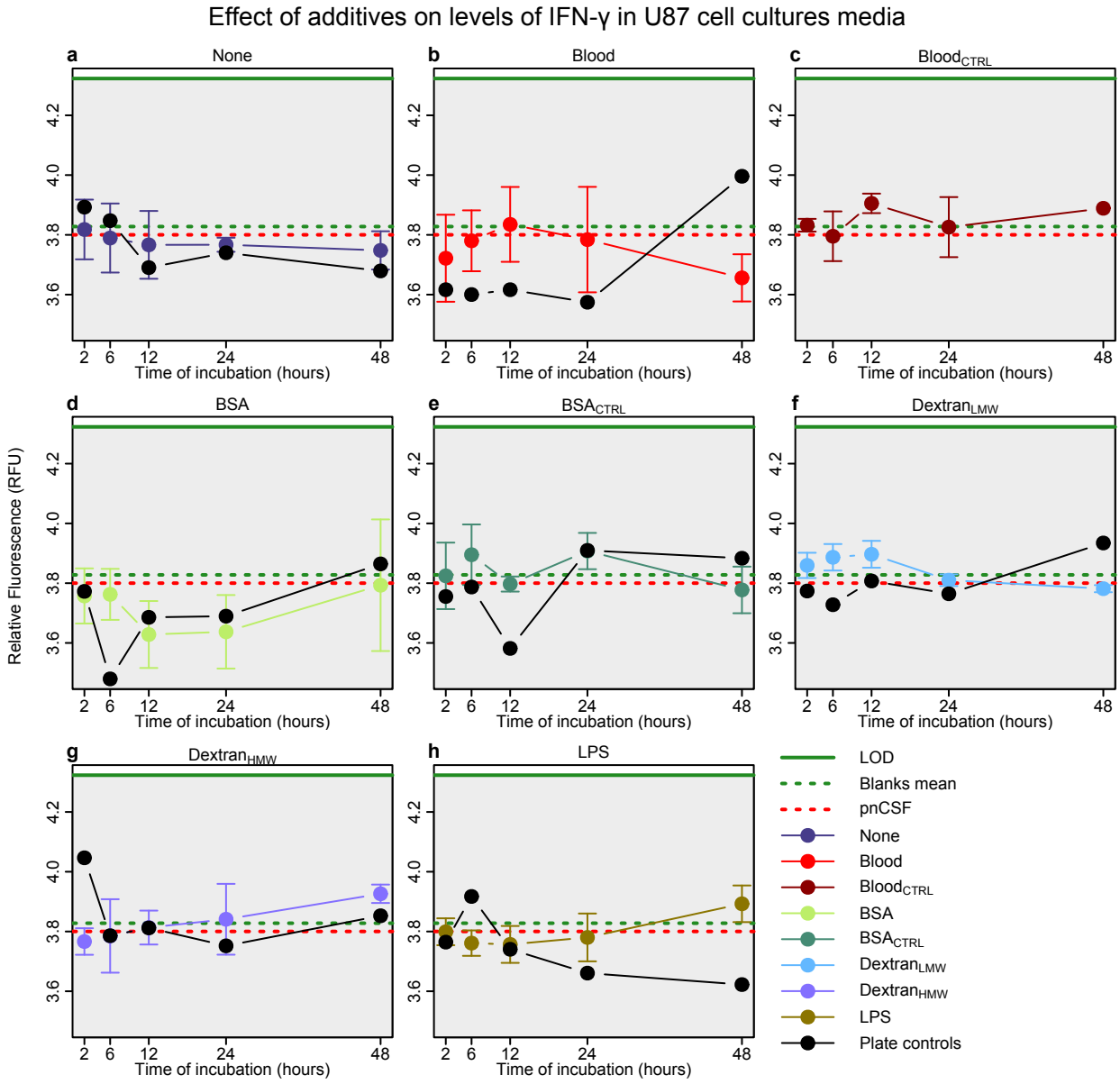

FIGURE H.S74: **Effect of additives on levels of IFN-γ in U87 cell cultures media.** Additives along with fresh blood and LPS were added to mycoplasma-free human glial (U87) cells in triplicate wells of a 24-well plate and incubated for up to 48 h to measure the effect on levels of proteins measured in the cell media. Media was collected and frozen from successive triplicates at different intervals, then analyzed with the ACM. Each graph compares IFN-γ values from cells incubated with a different additive to cells not incubated with additives located in the same 24-well plate. Plates in **c** and **e** did not contain any U87 cells, and **c** also did not have controls on the plate.

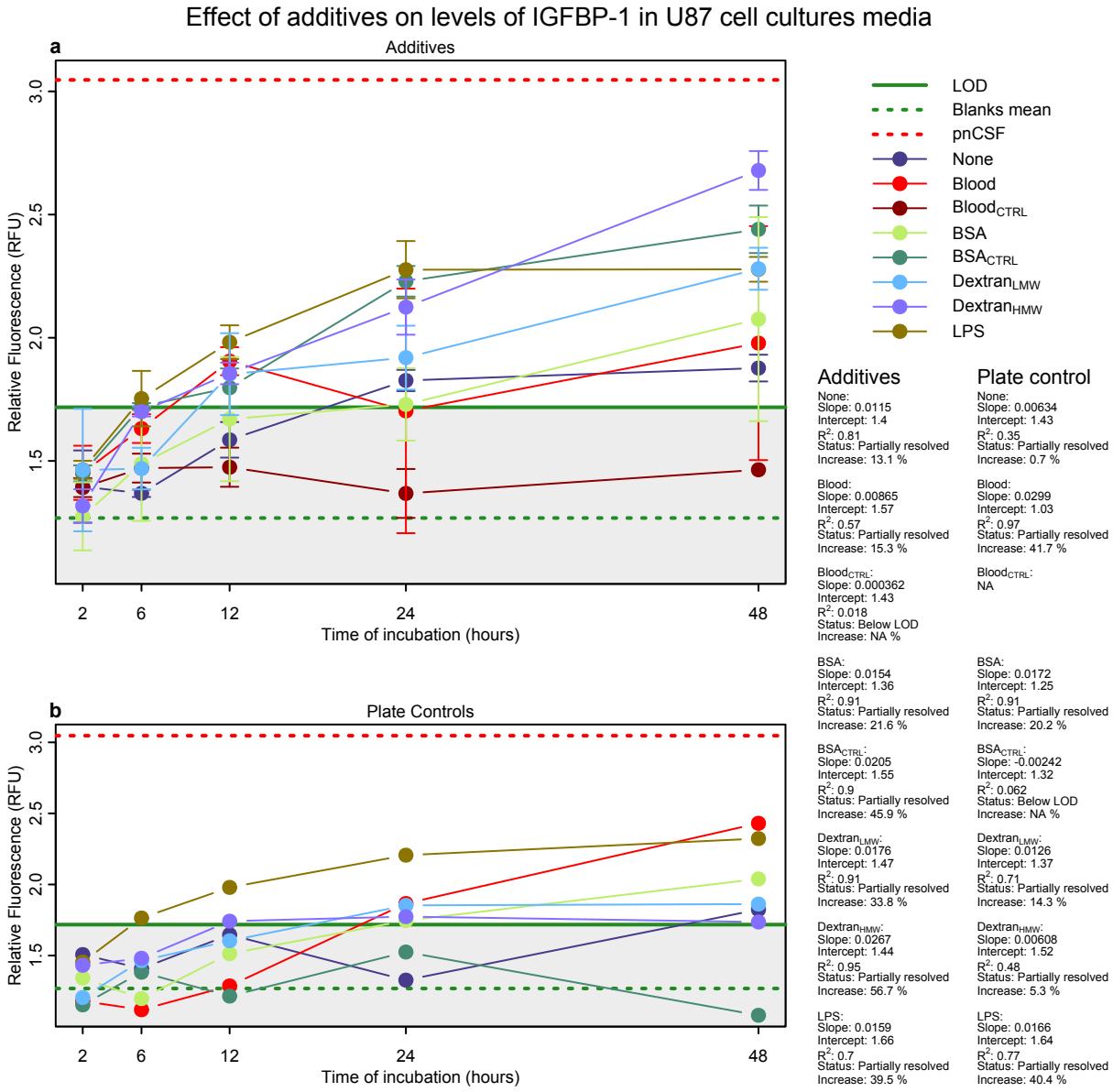

FIGURE H.S75: **Effect of additives on levels of IGFBP-1 in U87 cell cultures media.** Additives along with fresh blood and LPS were added to mycoplasma-free human glial (U87) cells in triplicate wells of a 24-well plate and incubated for up to 48 h to measure the effect on levels of proteins measured in the cell media. Media was collected and frozen from successive triplicates at different intervals, then analyzed with the ACM. **a** Average values for IGFBP-1 from three replicates for each point in every 24-well plate where a different additive was applied. **b** Data from the control cell media in each plate.

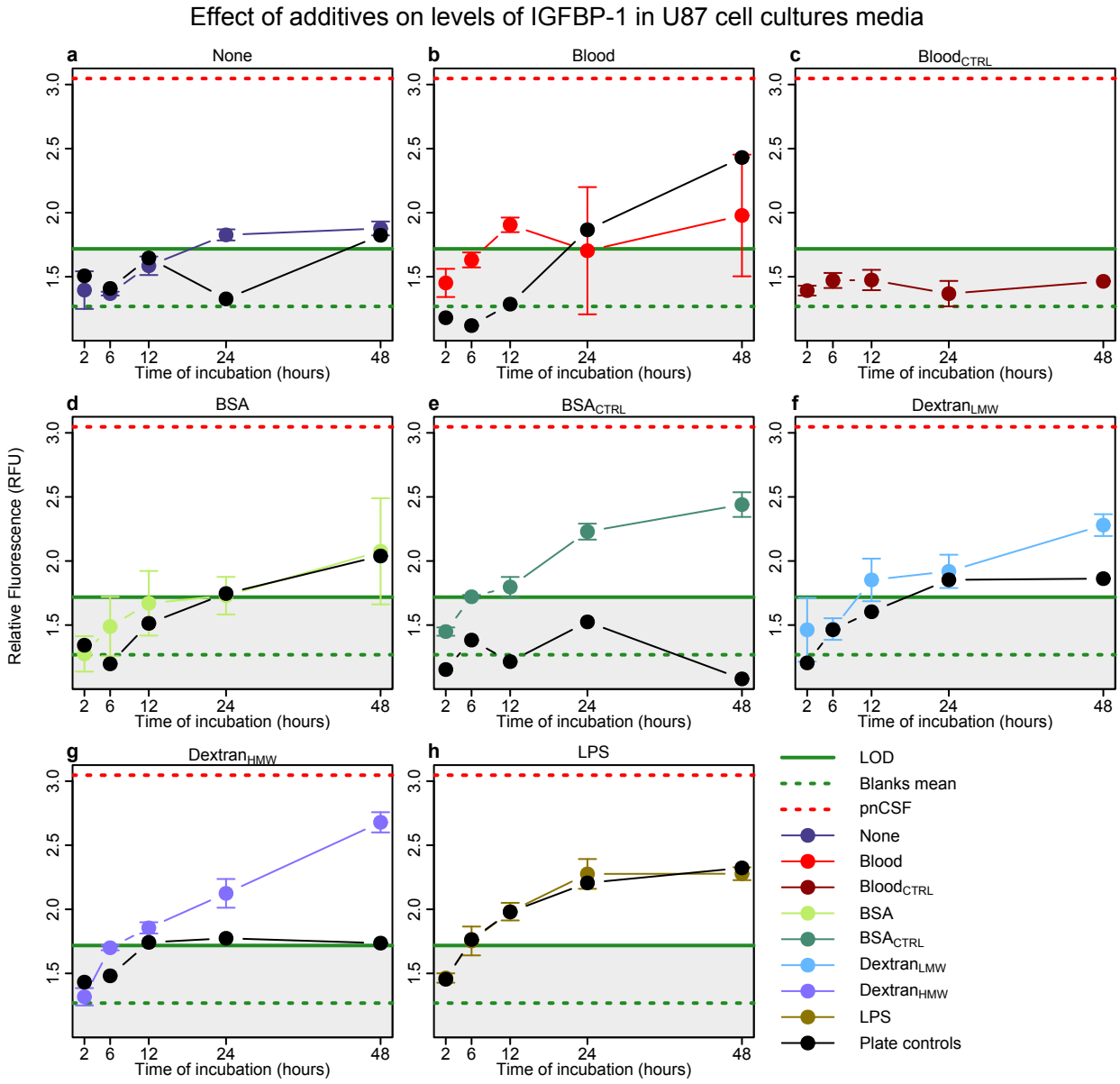

FIGURE H.S76: **Effect of additives on levels of IGFBP-1 in U87 cell cultures media.** Additives along with fresh blood and LPS were added to mycoplasma-free human glial (U87) cells in triplicate wells of a 24-well plate and incubated for up to 48 h to measure the effect on levels of proteins measured in the cell media. Media was collected and frozen from successive triplicates at different intervals, then analyzed with the ACM. Each graph compares IGFBP-1 values from cells incubated with a different additive to cells not incubated with additives located in the same 24-well plate. Plates in **c** and **e** did not contain any U87 cells, and **c** also did not have controls on the plate.

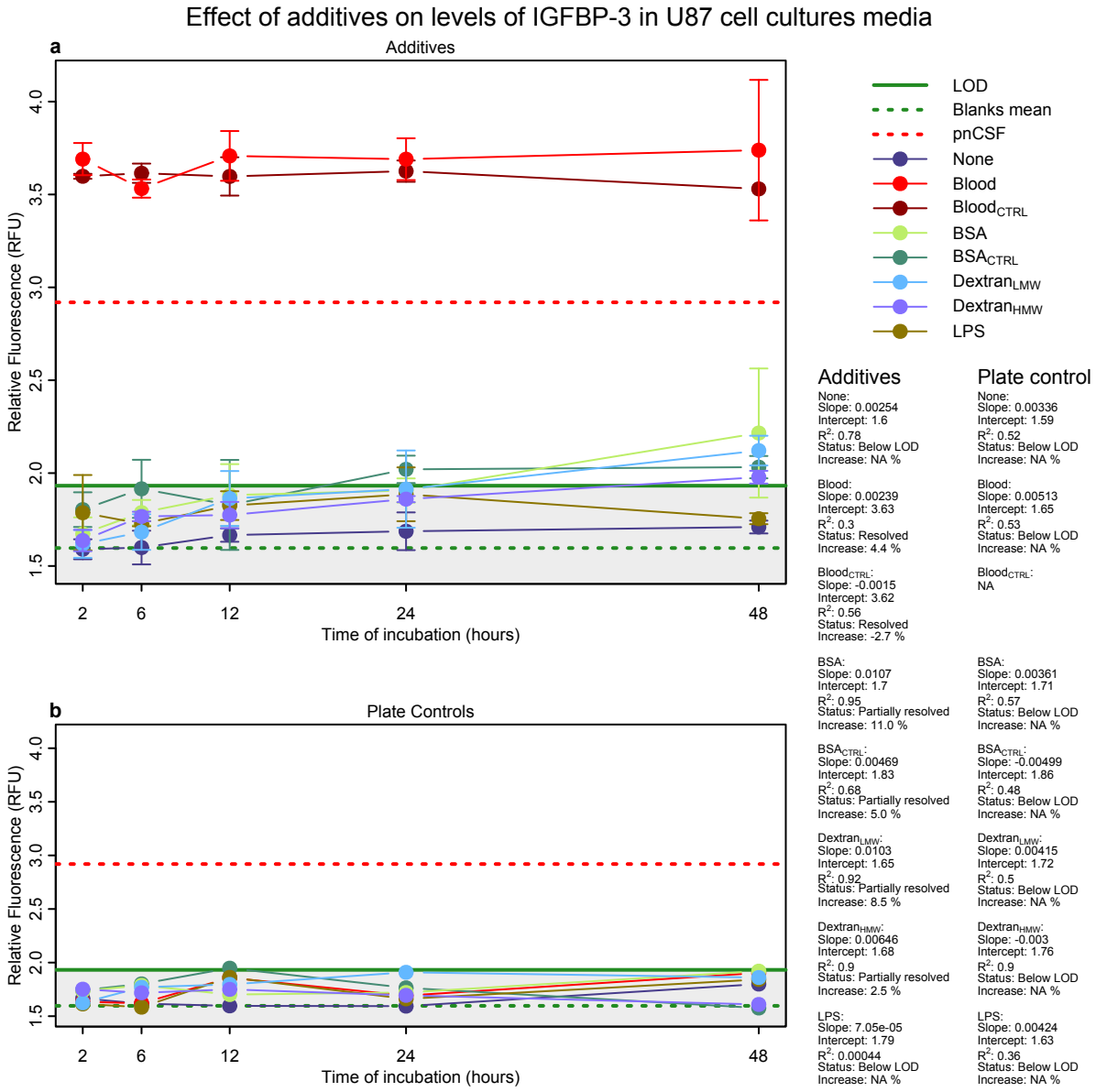

FIGURE H.S77: **Effect of additives on levels of IGFBP-3 in U87 cell cultures media.** Additives along with fresh blood and LPS were added to mycoplasma-free human glial (U87) cells in triplicate wells of a 24-well plate and incubated for up to 48 h to measure the effect on levels of proteins measured in the cell media. Media was collected and frozen from successive triplicates at different intervals, then analyzed with the ACM. **a** Average values for IGFBP-3 from three replicates for each point in every 24-well plate where a different additive was applied. **b** Data from the control cell media in each plate.

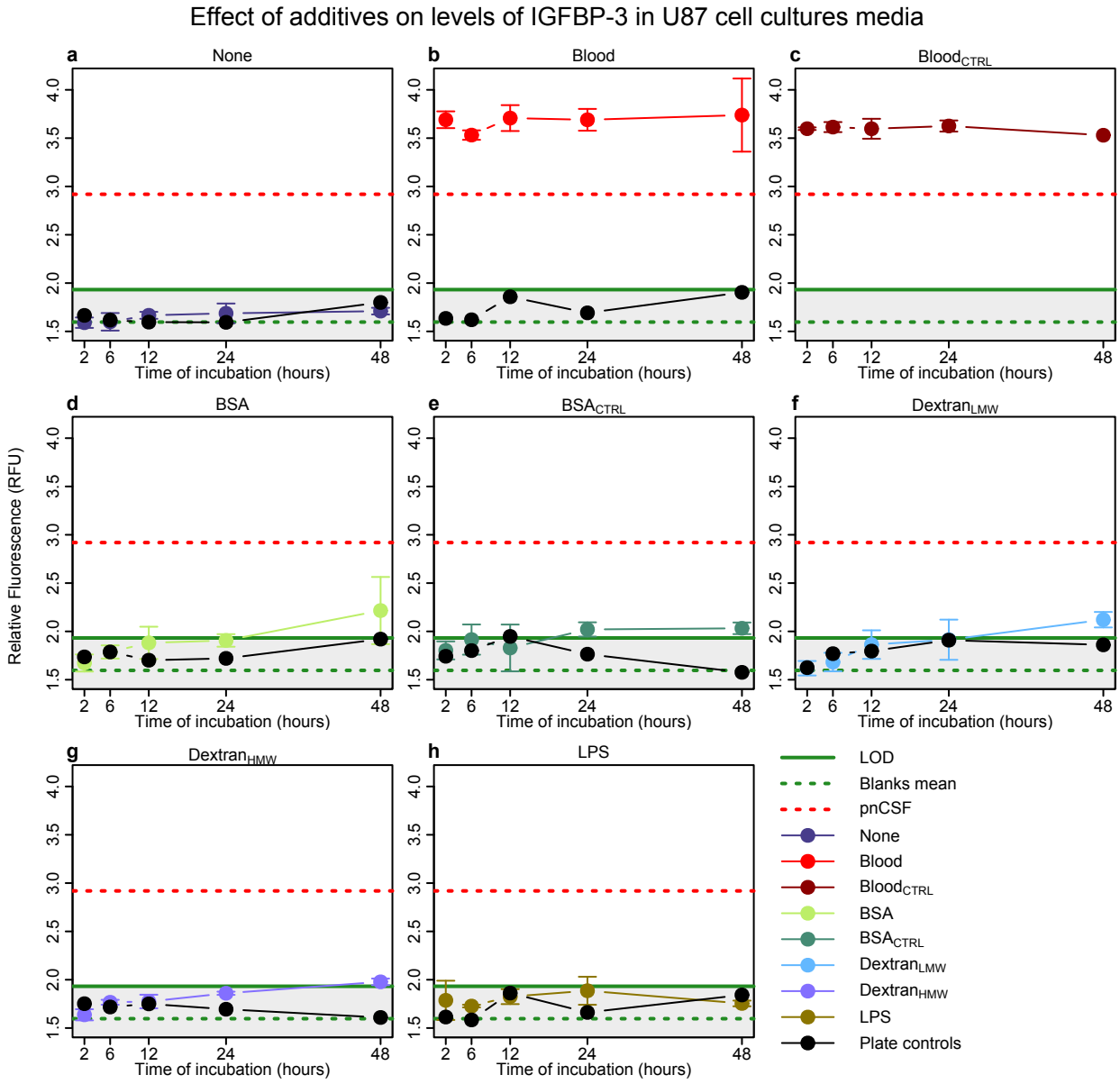

FIGURE H.S78: **Effect of additives on levels of IGFBP-3 in U87 cell cultures media.** Additives along with fresh blood and LPS were added to mycoplasma-free human glial (U87) cells in triplicate wells of a 24-well plate and incubated for up to 48 h to measure the effect on levels of proteins measured in the cell media. Media was collected and frozen from successive triplicates at different intervals, then analyzed with the ACM. Each graph compares IGFBP-3 values from cells incubated with a different additive to cells not incubated with additives located in the same 24-well plate. Plates in **c** and **e** did not contain any U87 cells, and **c** also did not have controls on the plate.

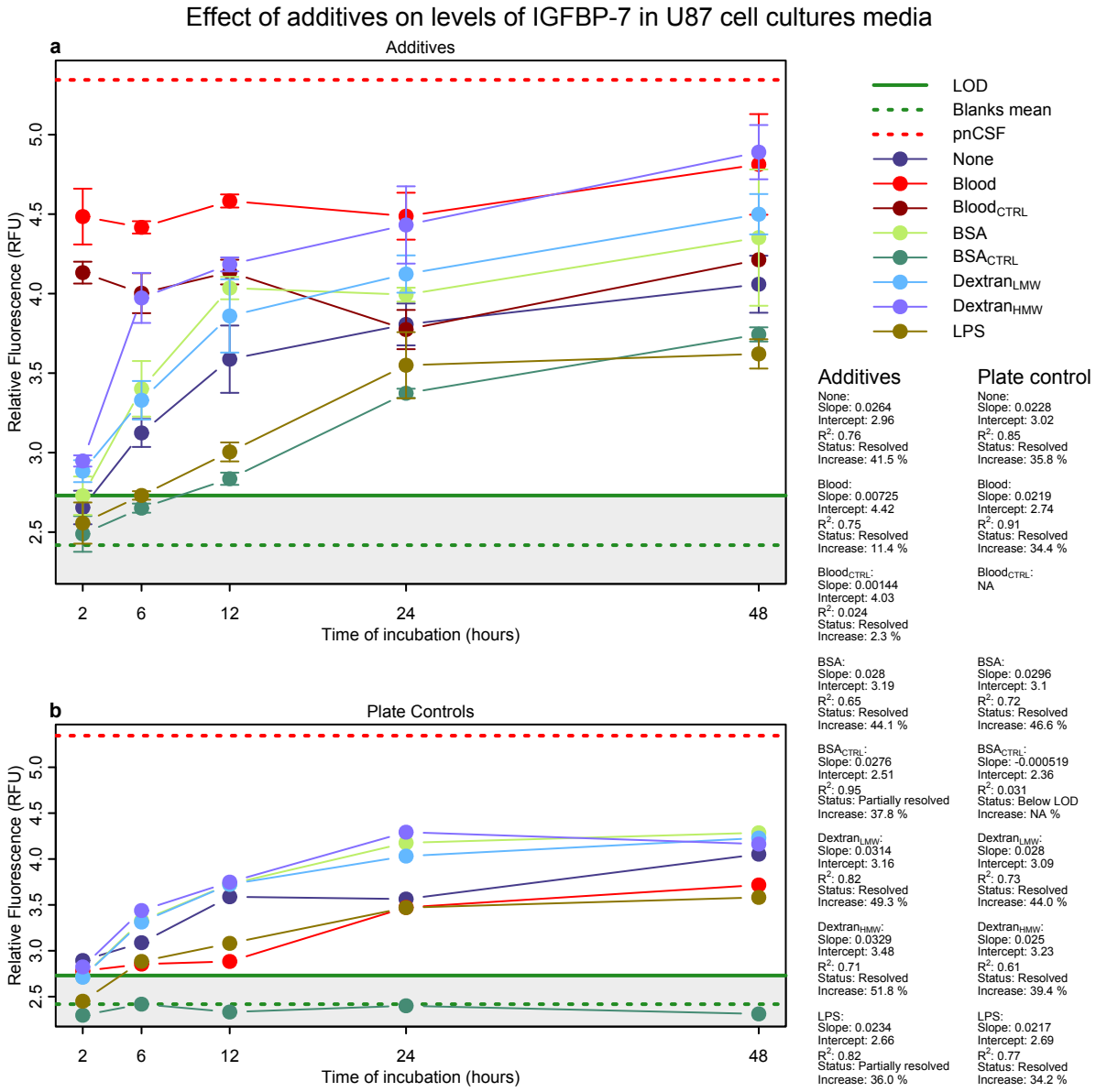

FIGURE H.S79: **Effect of additives on levels of IGFBP-7 in U87 cell cultures media.** Additives along with fresh blood and LPS were added to mycoplasma-free human glial (U87) cells in triplicate wells of a 24-well plate and incubated for up to 48 h to measure the effect on levels of proteins measured in the cell media. Media was collected and frozen from successive triplicates at different intervals, then analyzed with the ACM. **a** Average values for IGFBP-7 from three replicates for each point in every 24-well plate where a different additive was applied. **b** Data from the control cell media in each plate.

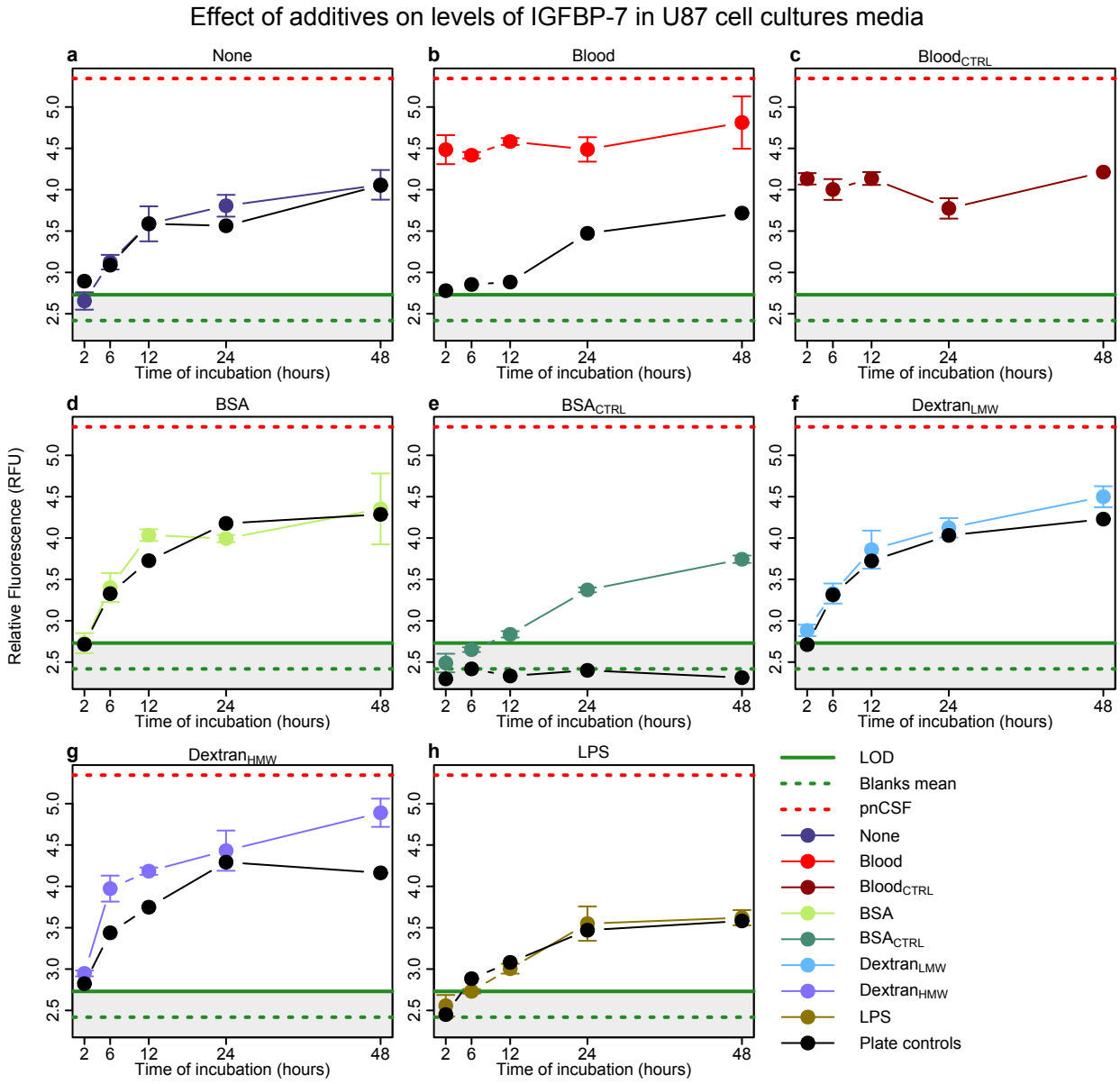

FIGURE H.S80: **Effect of additives on levels of IGFBP-7 in U87 cell cultures media.** Additives along with fresh blood and LPS were added to mycoplasma-free human glial (U87) cells in triplicate wells of a 24-well plate and incubated for up to 48 h to measure the effect on levels of proteins measured in the cell media. Media was collected and frozen from successive triplicates at different intervals, then analyzed with the ACM. Each graph compares IGFBP-7 values from cells incubated with a different additive to cells not incubated with additives located in the same 24-well plate. Plates in **c** and **e** did not contain any U87 cells, and **c** also did not have controls on the plate.

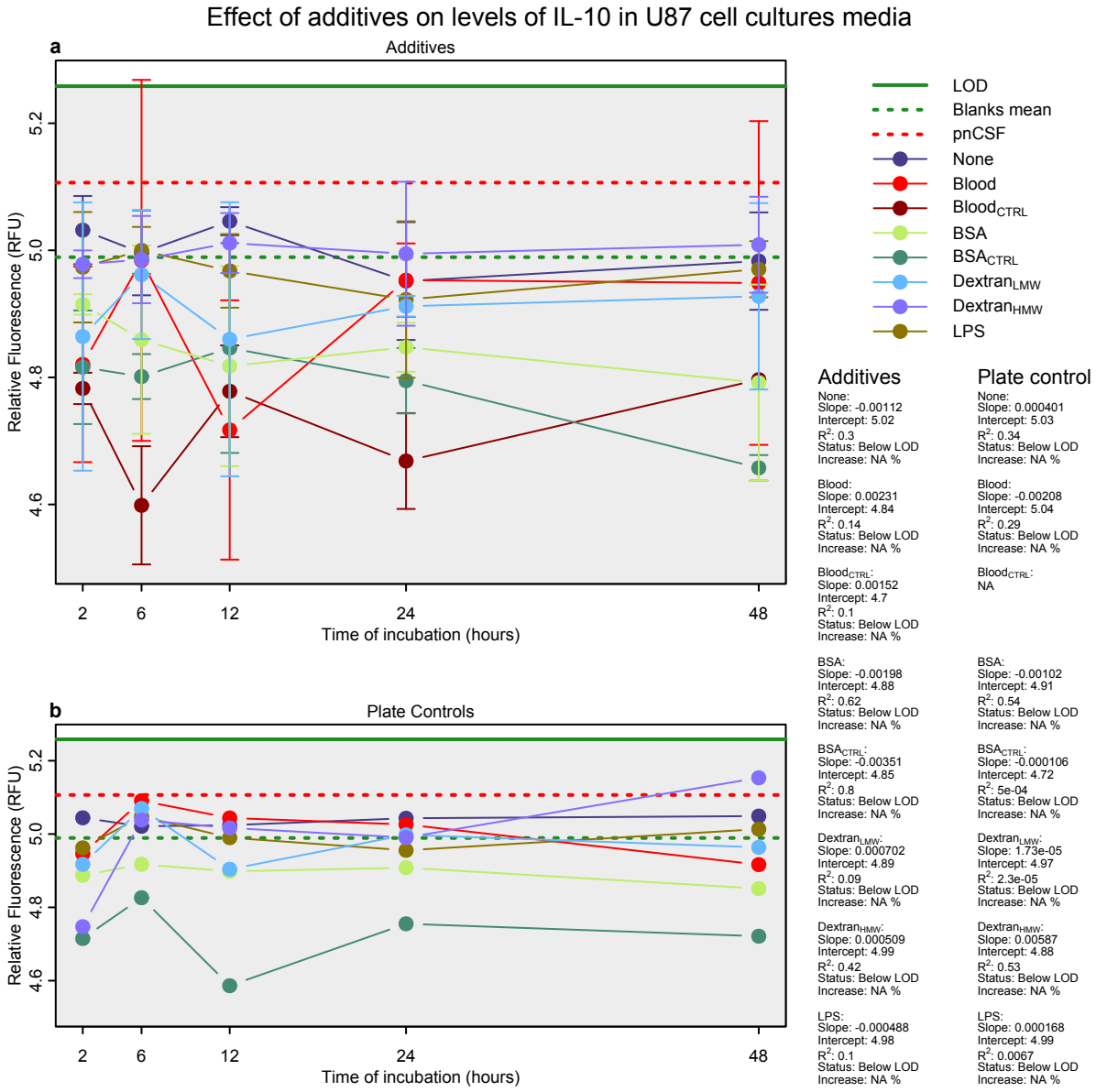

FIGURE H.S81: **Effect of additives on levels of IL-10 in U87 cell cultures media.** Additives along with fresh blood and LPS were added to mycoplasma-free human glial (U87) cells in triplicate wells of a 24-well plate and incubated for up to 48 h to measure the effect on levels of proteins measured in the cell media. Media was collected and frozen from successive triplicates at different intervals, then analyzed with the ACM. **a** Average values for IL-10 from three replicates for each point in every 24-well plate where a different additive was applied. **b** Data from the control cell media in each plate.

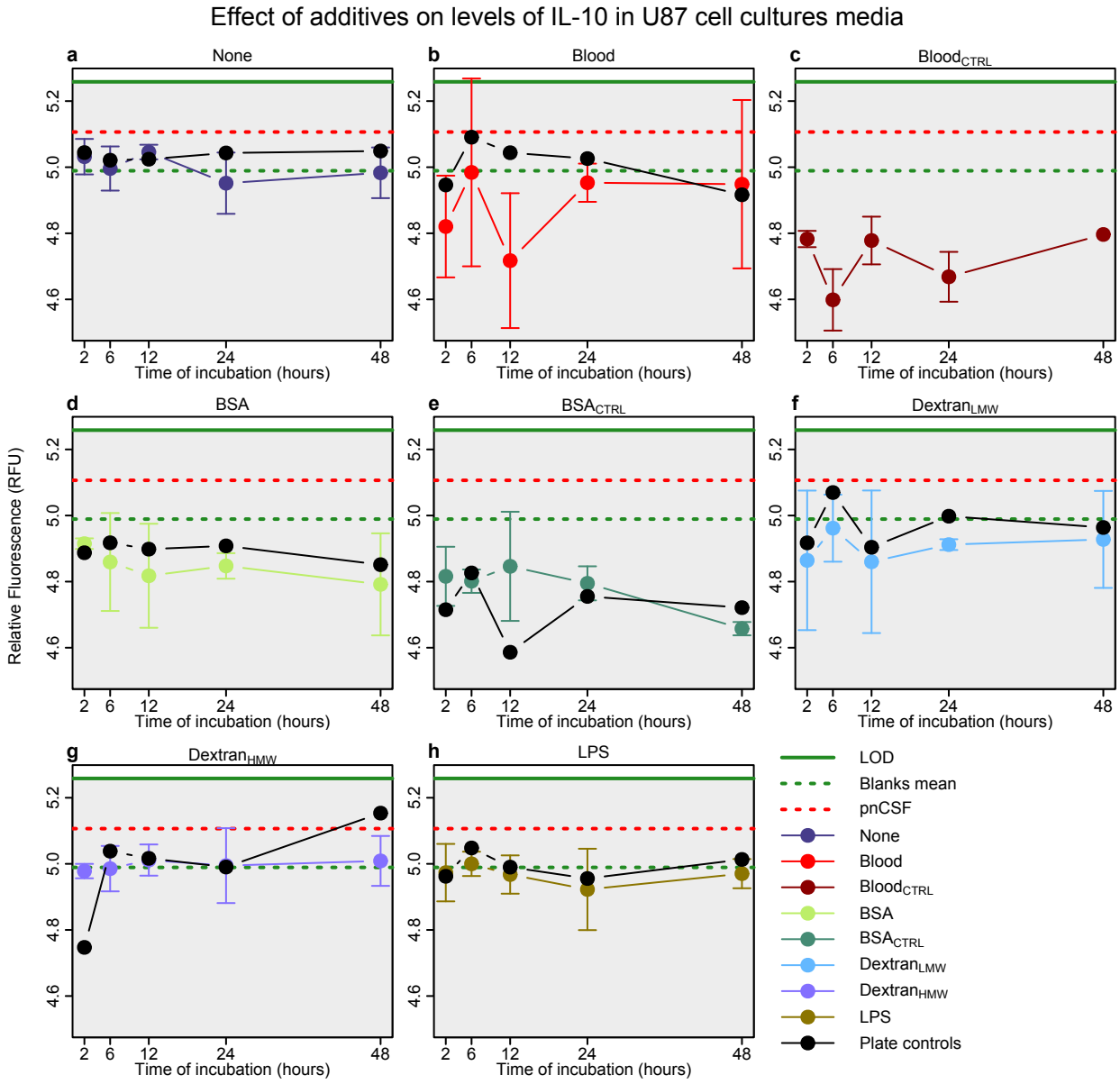

FIGURE H.S82: **Effect of additives on levels of IL-10 in U87 cell cultures media.** Additives along with fresh blood and LPS were added to mycoplasma-free human glial (U87) cells in triplicate wells of a 24-well plate and incubated for up to 48 h to measure the effect on levels of proteins measured in the cell media. Media was collected and frozen from successive triplicates at different intervals, then analyzed with the ACM. Each graph compares IL-10 values from cells incubated with a different additive to cells not incubated with additives located in the same 24-well plate. Plates in **c** and **e** did not contain any U87 cells, and **c** also did not have controls on the plate.

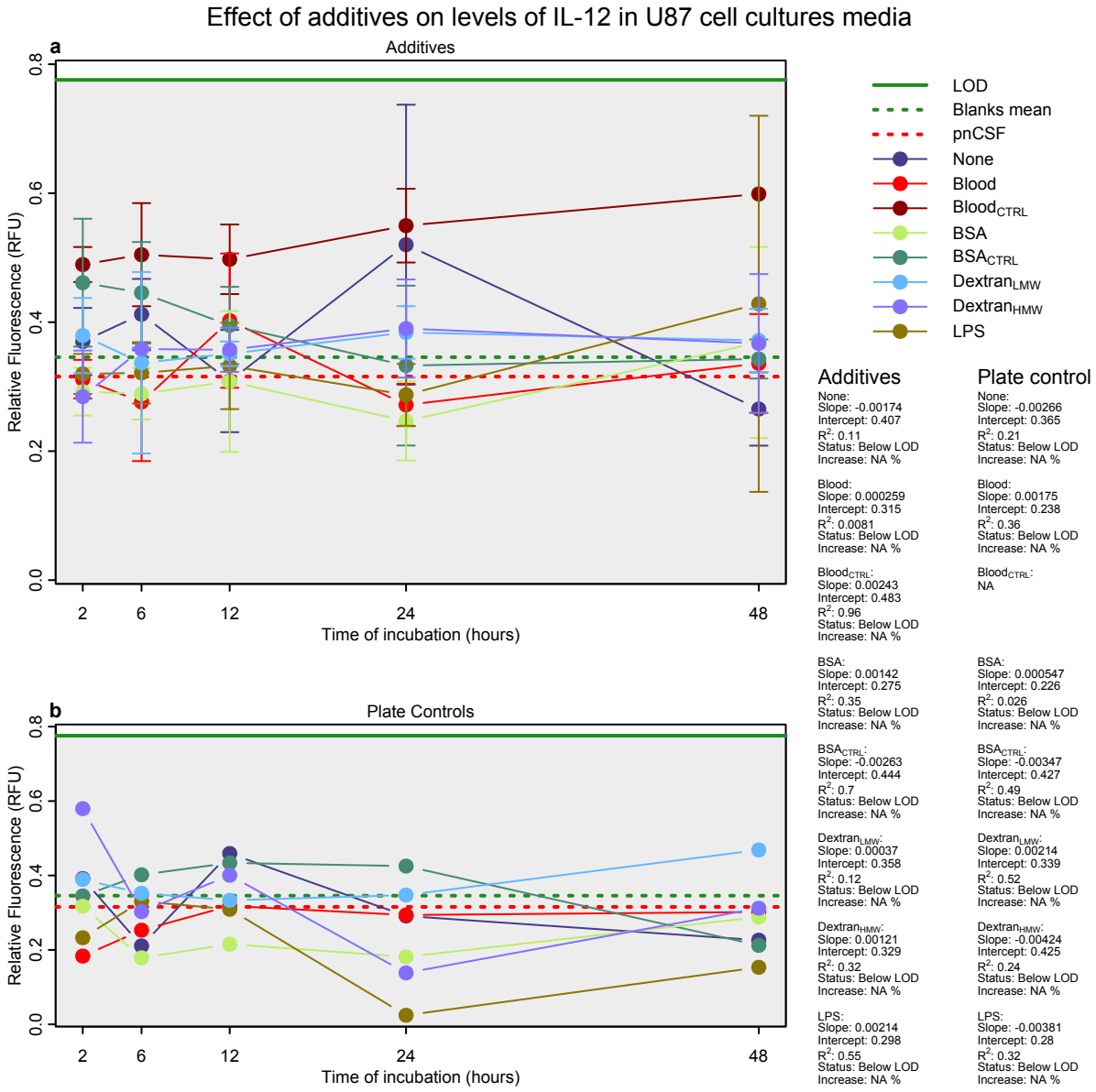

FIGURE H.S83: **Effect of additives on levels of IL-12 in U87 cell cultures media.** Additives along with fresh blood and LPS were added to mycoplasma-free human glial (U87) cells in triplicate wells of a 24-well plate and incubated for up to 48 h to measure the effect on levels of proteins measured in the cell media. Media was collected and frozen from successive triplicates at different intervals, then analyzed with the ACM. **a** Average values for IL-12 from three replicates for each point in every 24-well plate where a different additive was applied. **b** Data from the control cell media in each plate.

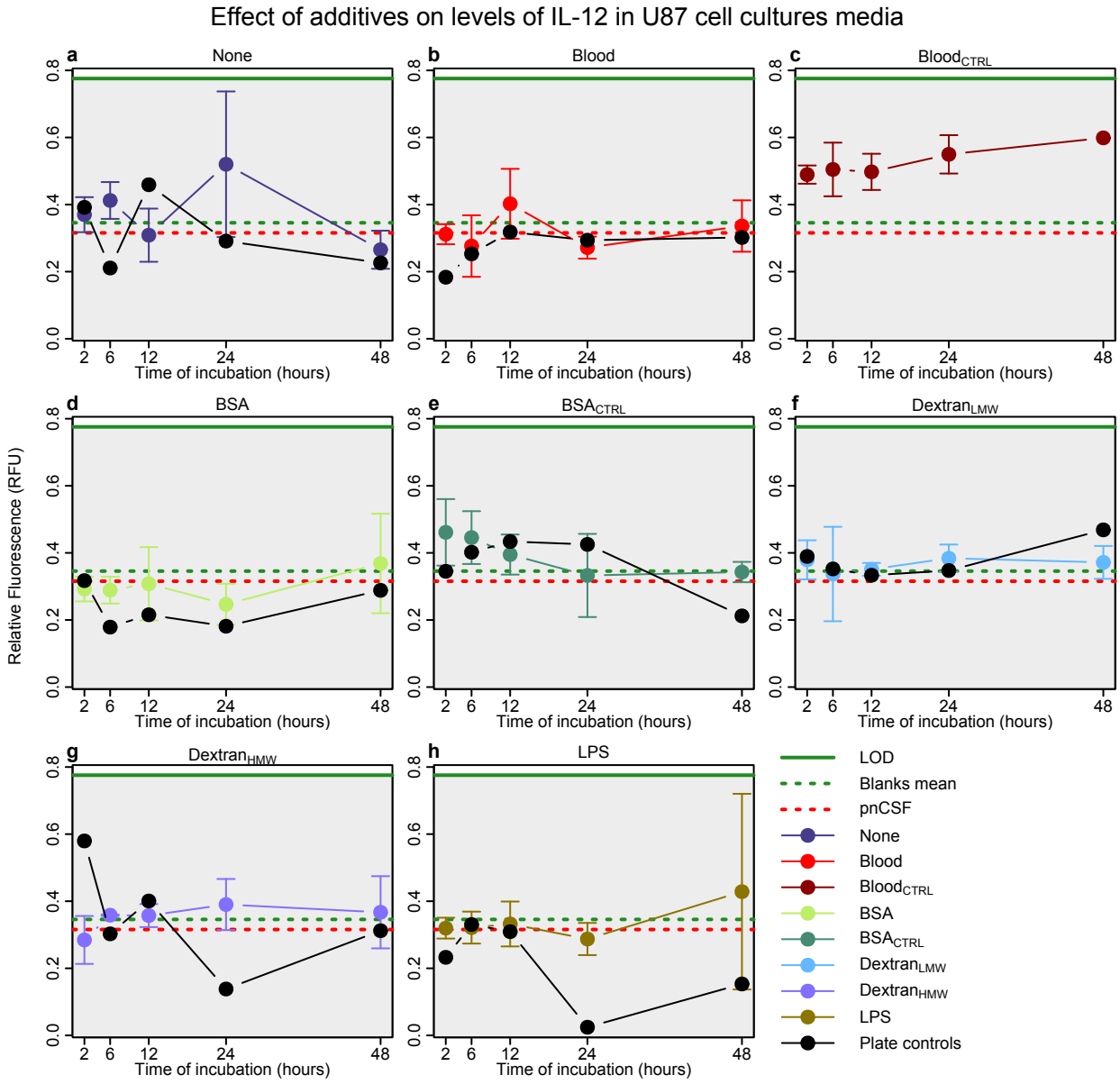

FIGURE H.S84: **Effect of additives on levels of IL-12 in U87 cell cultures media.** Additives along with fresh blood and LPS were added to mycoplasma-free human glial (U87) cells in triplicate wells of a 24-well plate and incubated for up to 48 h to measure the effect on levels of proteins measured in the cell media. Media was collected and frozen from successive triplicates at different intervals, then analyzed with the ACM. Each graph compares IL-12 values from cells incubated with a different additive to cells not incubated with additives located in the same 24-well plate. Plates in **c** and **e** did not contain any U87 cells, and **c** also did not have controls on the plate.

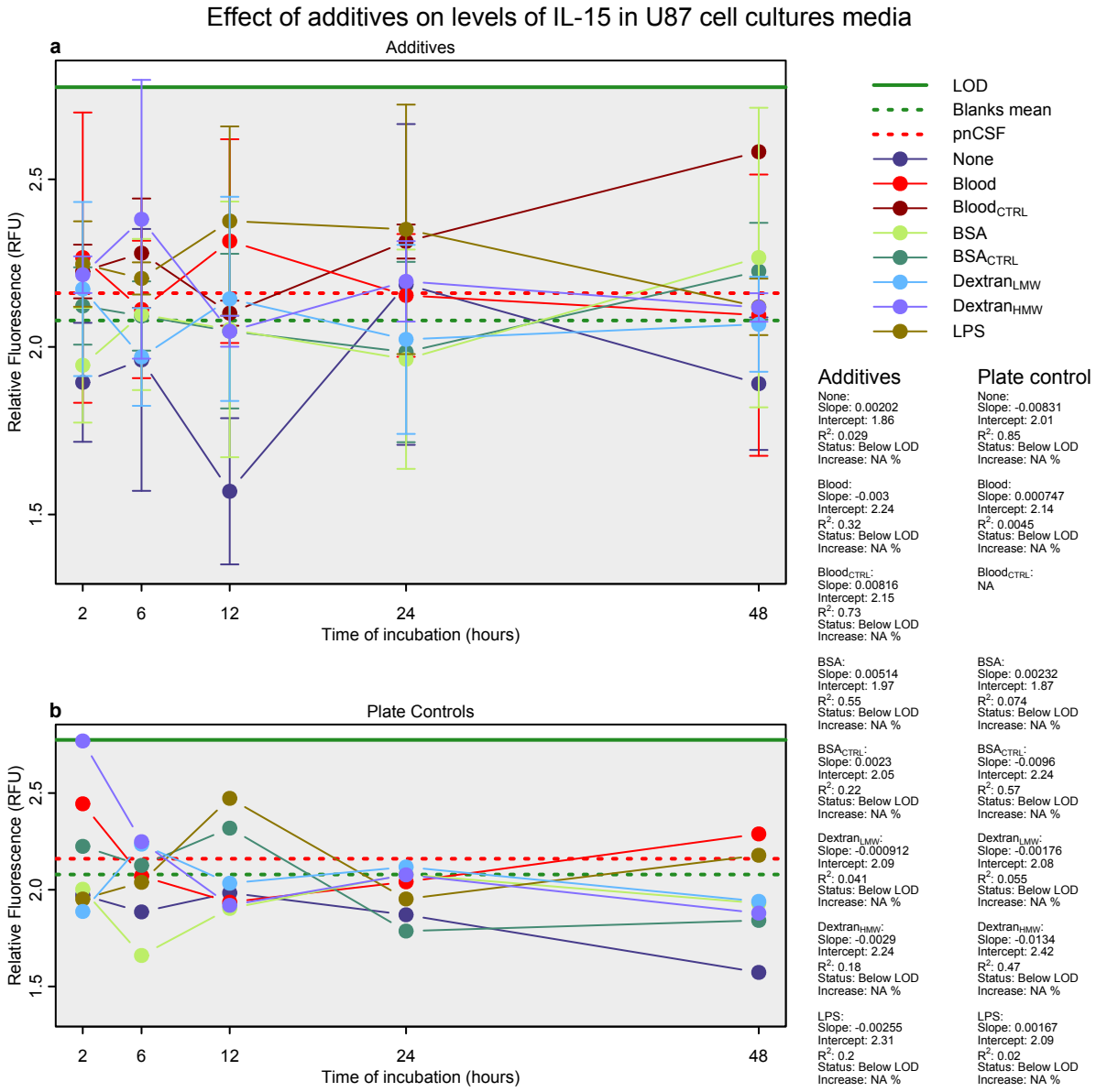

FIGURE H.S85: **Effect of additives on levels of IL-15 in U87 cell cultures media.** Additives along with fresh blood and LPS were added to mycoplasma-free human glial (U87) cells in triplicate wells of a 24-well plate and incubated for up to 48 h to measure the effect on levels of proteins measured in the cell media. Media was collected and frozen from successive triplicates at different intervals, then analyzed with the ACM. **a** Average values for IL-15 from three replicates for each point in every 24-well plate where a different additive was applied. **b** Data from the control cell media in each plate.

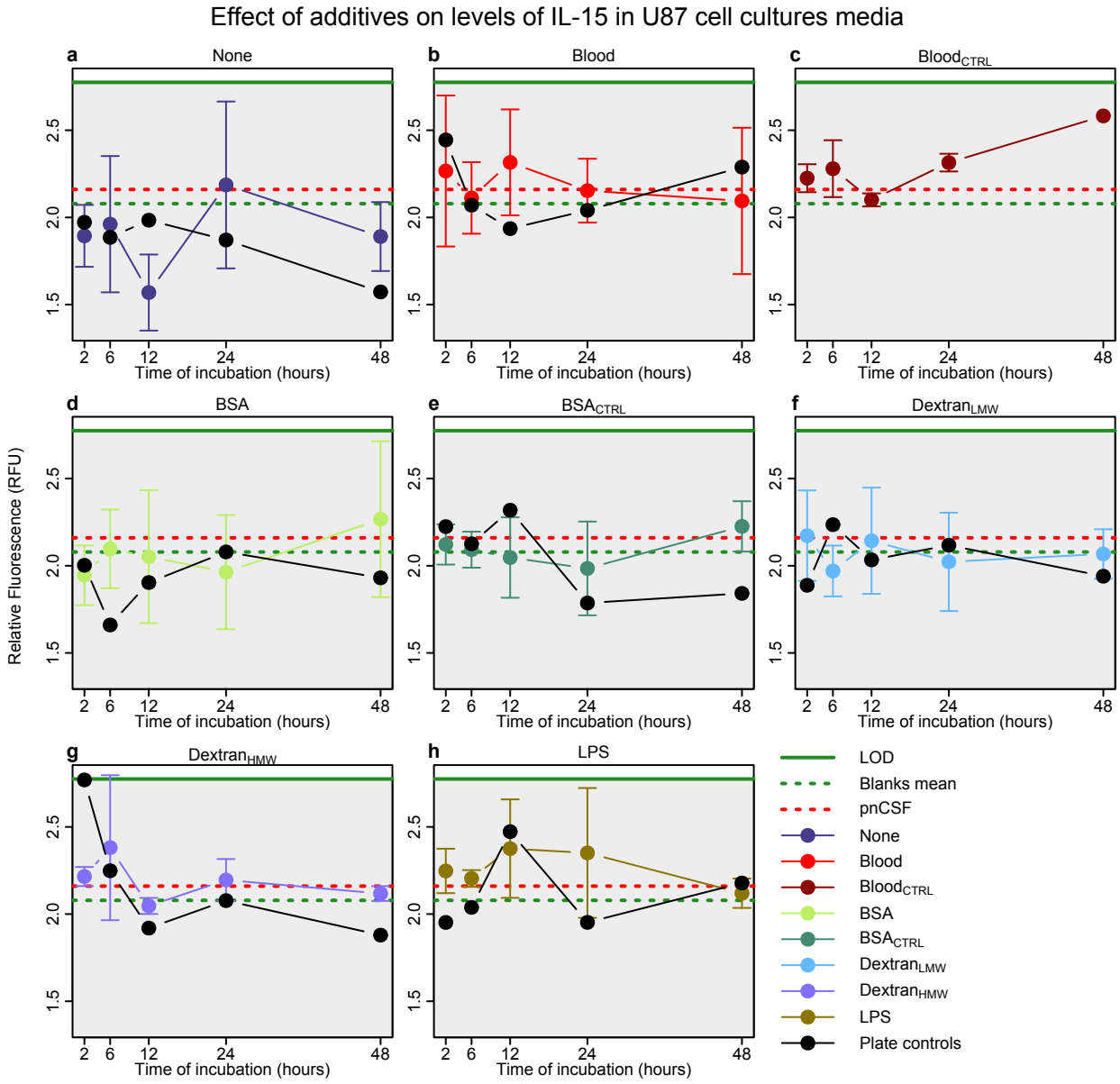

FIGURE H.S86: **Effect of additives on levels of IL-15 in U87 cell cultures media.** Additives along with fresh blood and LPS were added to mycoplasma-free human glial (U87) cells in triplicate wells of a 24-well plate and incubated for up to 48 h to measure the effect on levels of proteins measured in the cell media. Media was collected and frozen from successive triplicates at different intervals, then analyzed with the ACM. Each graph compares IL-15 values from cells incubated with a different additive to cells not incubated with additives located in the same 24-well plate. Plates in **c** and **e** did not contain any U87 cells, and **c** also did not have controls on the plate.

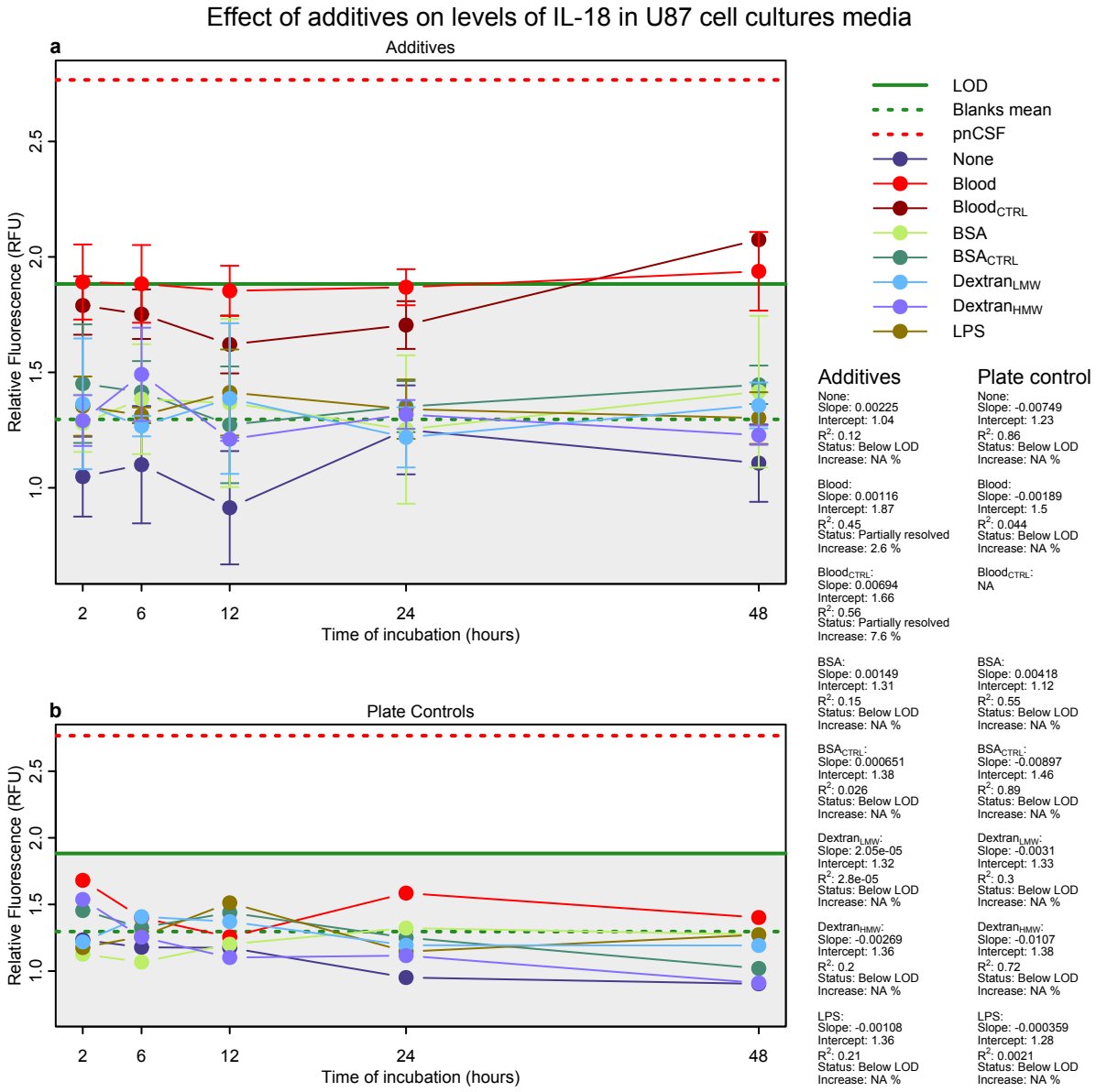

FIGURE H.S87: **Effect of additives on levels of IL-18 in U87 cell cultures media.** Additives along with fresh blood and LPS were added to mycoplasma-free human glial (U87) cells in triplicate wells of a 24-well plate and incubated for up to 48 h to measure the effect on levels of proteins measured in the cell media. Media was collected and frozen from successive triplicates at different intervals, then analyzed with the ACM. **a** Average values for IL-18 from three replicates for each point in every 24-well plate where a different additive was applied. **b** Data from the control cell media in each plate.

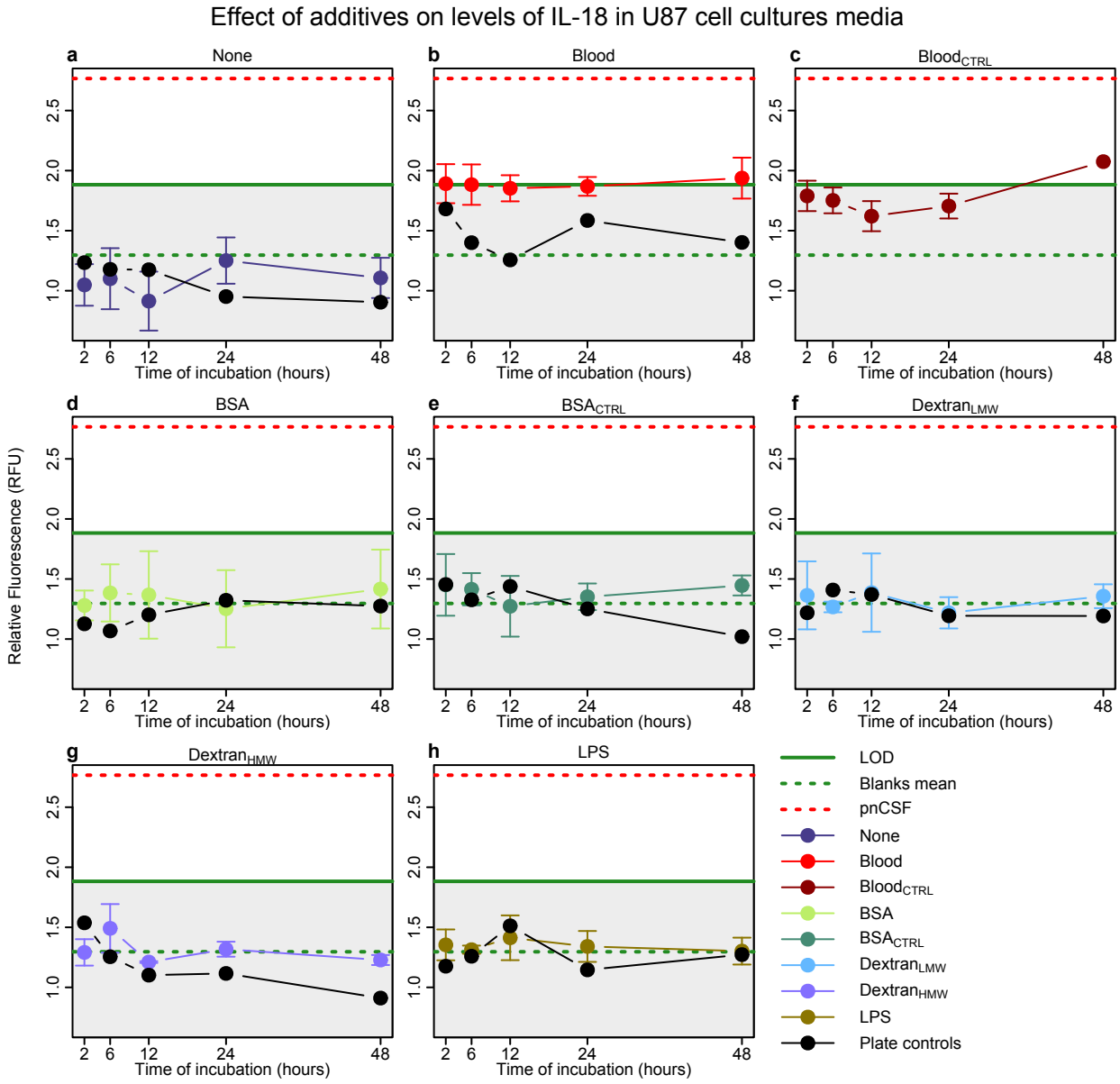

FIGURE H.S88: **Effect of additives on levels of IL-18 in U87 cell cultures media.** Additives along with fresh blood and LPS were added to mycoplasma-free human glial (U87) cells in triplicate wells of a 24-well plate and incubated for up to 48 h to measure the effect on levels of proteins measured in the cell media. Media was collected and frozen from successive triplicates at different intervals, then analyzed with the ACM. Each graph compares IL-18 values from cells incubated with a different additive to cells not incubated with additives located in the same 24-well plate. Plates in **c** and **e** did not contain any U87 cells, and **c** also did not have controls on the plate.

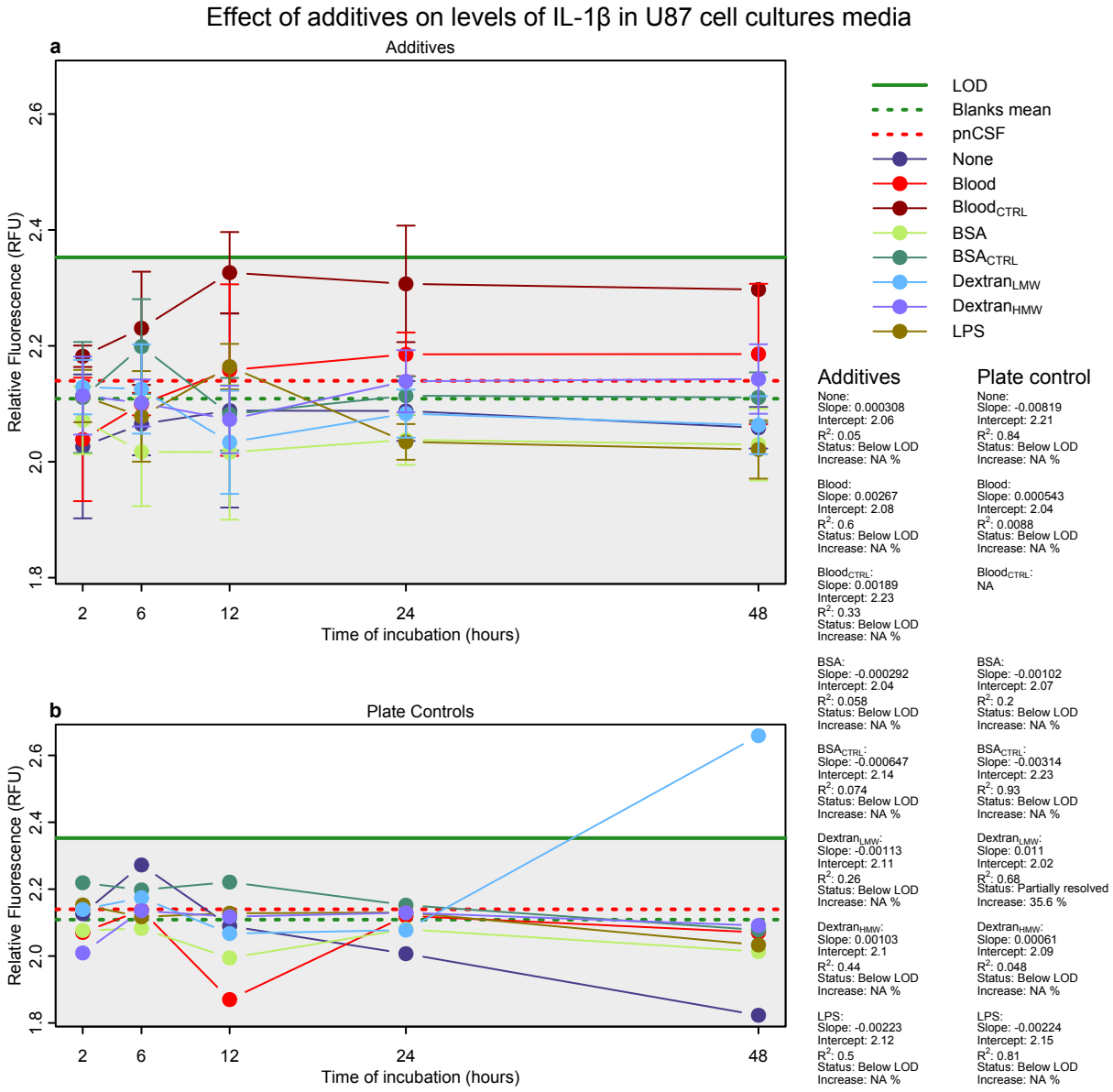

FIGURE H.S89: **Effect of additives on levels of IL-1β in U87 cell cultures media.** Additives along with fresh blood and LPS were added to mycoplasma-free human glial (U87) cells in triplicate wells of a 24-well plate and incubated for up to 48 h to measure the effect on levels of proteins measured in the cell media. Media was collected and frozen from successive triplicates at different intervals, then analyzed with the ACM. **a** Average values for IL-1β from three replicates for each point in every 24-well plate where a different additive was applied. **b** Data from the control cell media in each plate.

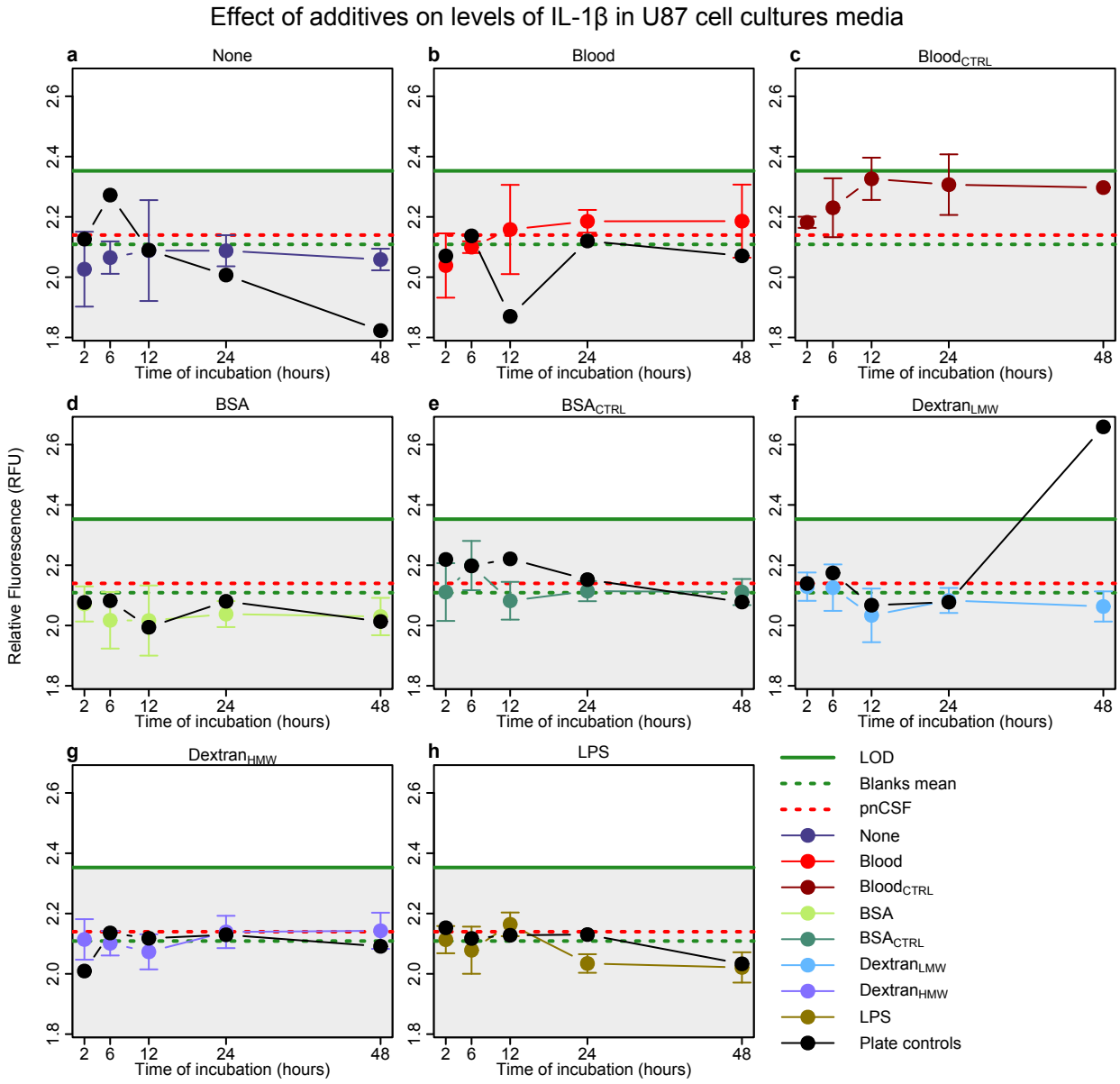

FIGURE H.S90: **Effect of additives on levels of IL-1β in U87 cell cultures media.** Additives along with fresh blood and LPS were added to mycoplasma-free human glial (U87) cells in triplicate wells of a 24-well plate and incubated for up to 48 h to measure the effect on levels of proteins measured in the cell media. Media was collected and frozen from successive triplicates at different intervals, then analyzed with the ACM. Each graph compares IL-1β values from cells incubated with a different additive to cells not incubated with additives located in the same 24-well plate. Plates in **c** and **e** did not contain any U87 cells, and **c** also did not have controls on the plate.

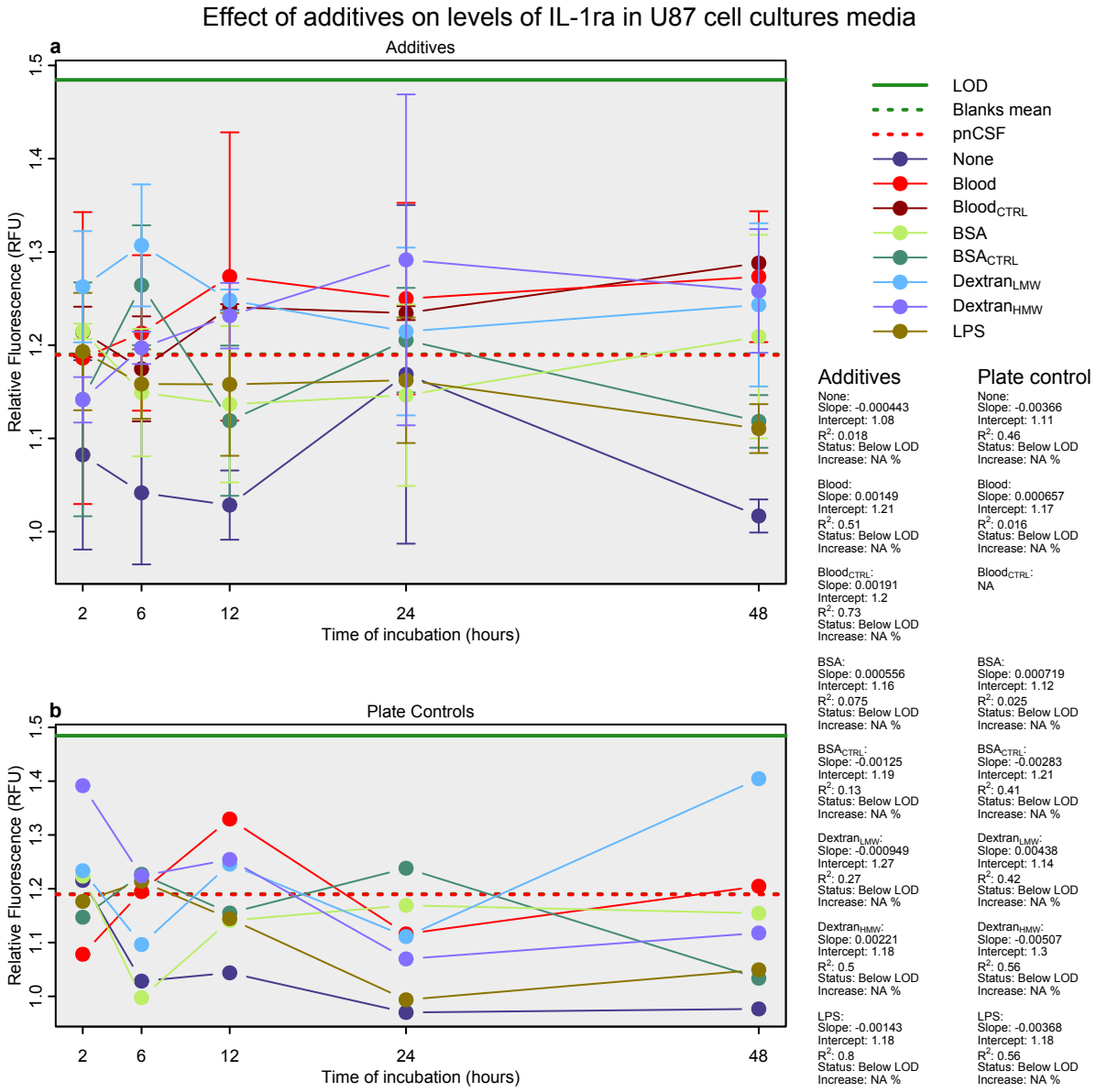

FIGURE H.S91: **Effect of additives on levels of IL-1ra in U87 cell cultures media.** Additives along with fresh blood and LPS were added to mycoplasma-free human glial (U87) cells in triplicate wells of a 24-well plate and incubated for up to 48 h to measure the effect on levels of proteins measured in the cell media. Media was collected and frozen from successive triplicates at different intervals, then analyzed with the ACM. **a** Average values for IL-1ra from three replicates for each point in every 24-well plate where a different additive was applied. **b** Data from the control cell media in each plate.

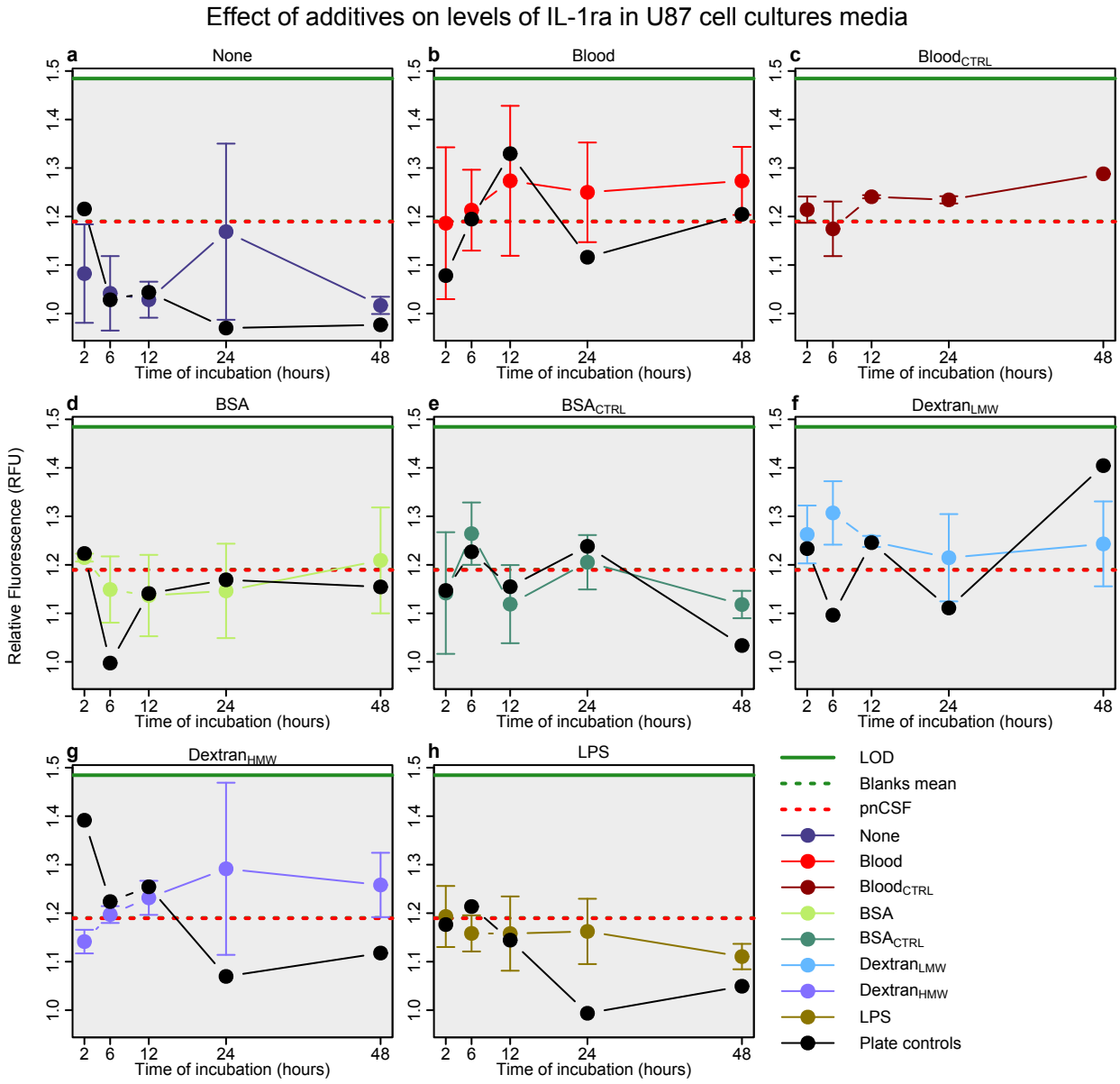

FIGURE H.S92: **Effect of additives on levels of IL-1ra in U87 cell cultures media.** Additives along with fresh blood and LPS were added to mycoplasma-free human glial (U87) cells in triplicate wells of a 24-well plate and incubated for up to 48 h to measure the effect on levels of proteins measured in the cell media. Media was collected and frozen from successive triplicates at different intervals, then analyzed with the ACM. Each graph compares IL-1ra values from cells incubated with a different additive to cells not incubated with additives located in the same 24-well plate. Plates in **c** and **e** did not contain any U87 cells, and **c** also did not have controls on the plate.

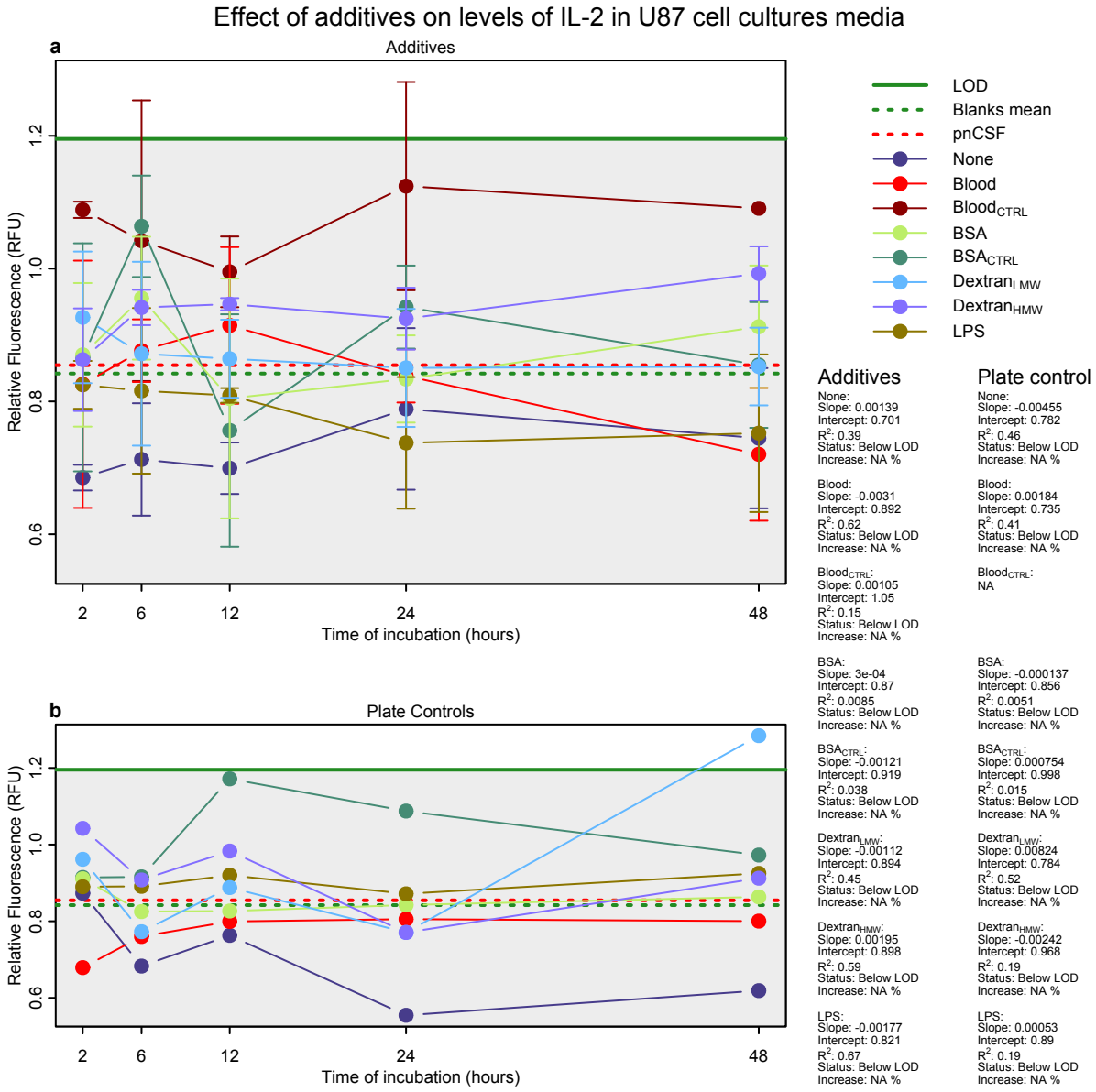

FIGURE H.S93: **Effect of additives on levels of IL-2 in U87 cell cultures media.** Additives along with fresh blood and LPS were added to mycoplasma-free human glial (U87) cells in triplicate wells of a 24-well plate and incubated for up to 48 h to measure the effect on levels of proteins measured in the cell media. Media was collected and frozen from successive triplicates at different intervals, then analyzed with the ACM. **a** Average values for IL-2 from three replicates for each point in every 24-well plate where a different additive was applied. **b** Data from the control cell media in each plate.

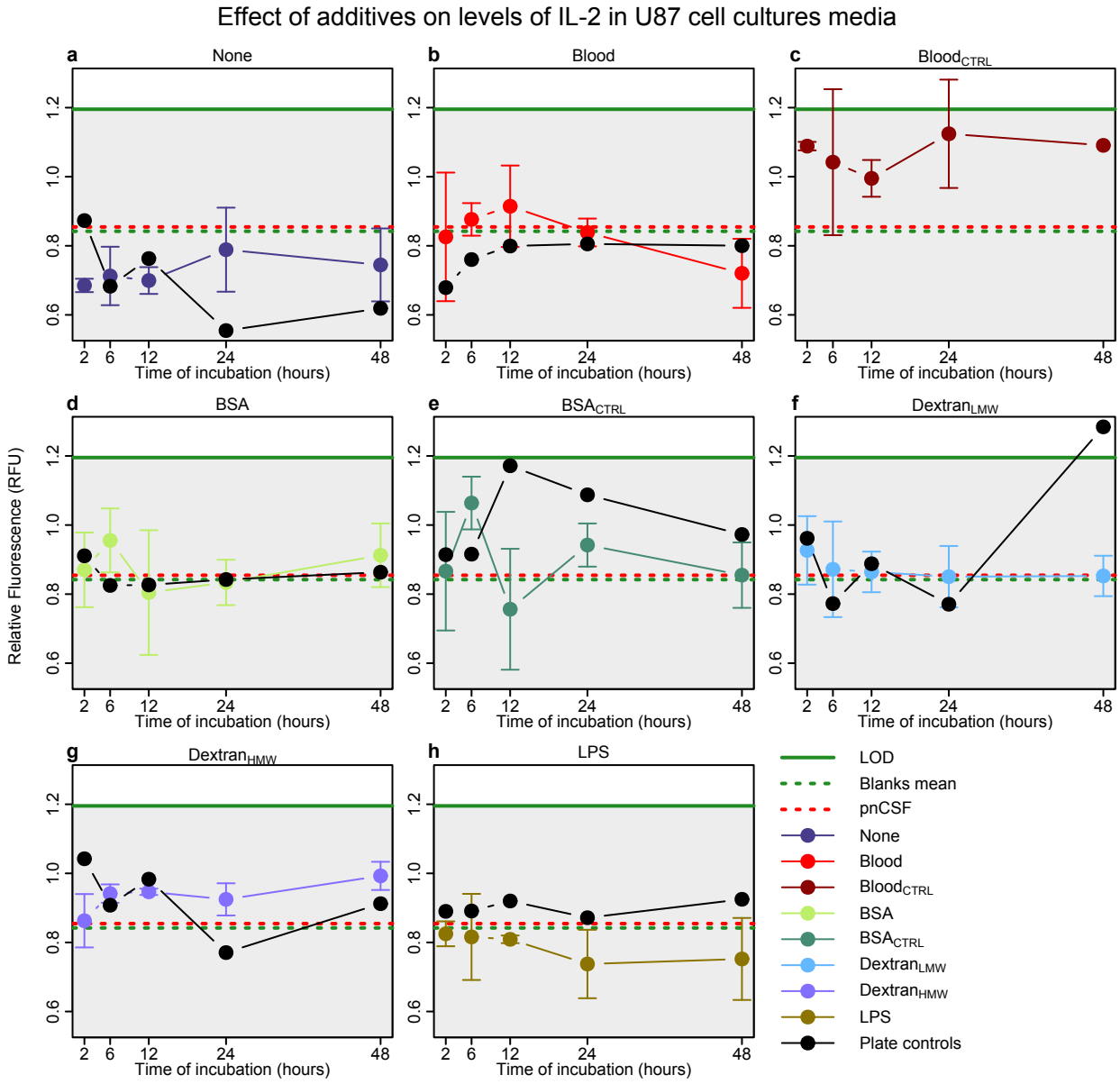

FIGURE H.S94: **Effect of additives on levels of IL-2 in U87 cell cultures media.** Additives along with fresh blood and LPS were added to mycoplasma-free human glial (U87) cells in triplicate wells of a 24-well plate and incubated for up to 48 h to measure the effect on levels of proteins measured in the cell media. Media was collected and frozen from successive triplicates at different intervals, then analyzed with the ACM. Each graph compares IL-2 values from cells incubated with a different additive to cells not incubated with additives located in the same 24-well plate. Plates in **c** and **e** did not contain any U87 cells, and **c** also did not have controls on the plate.

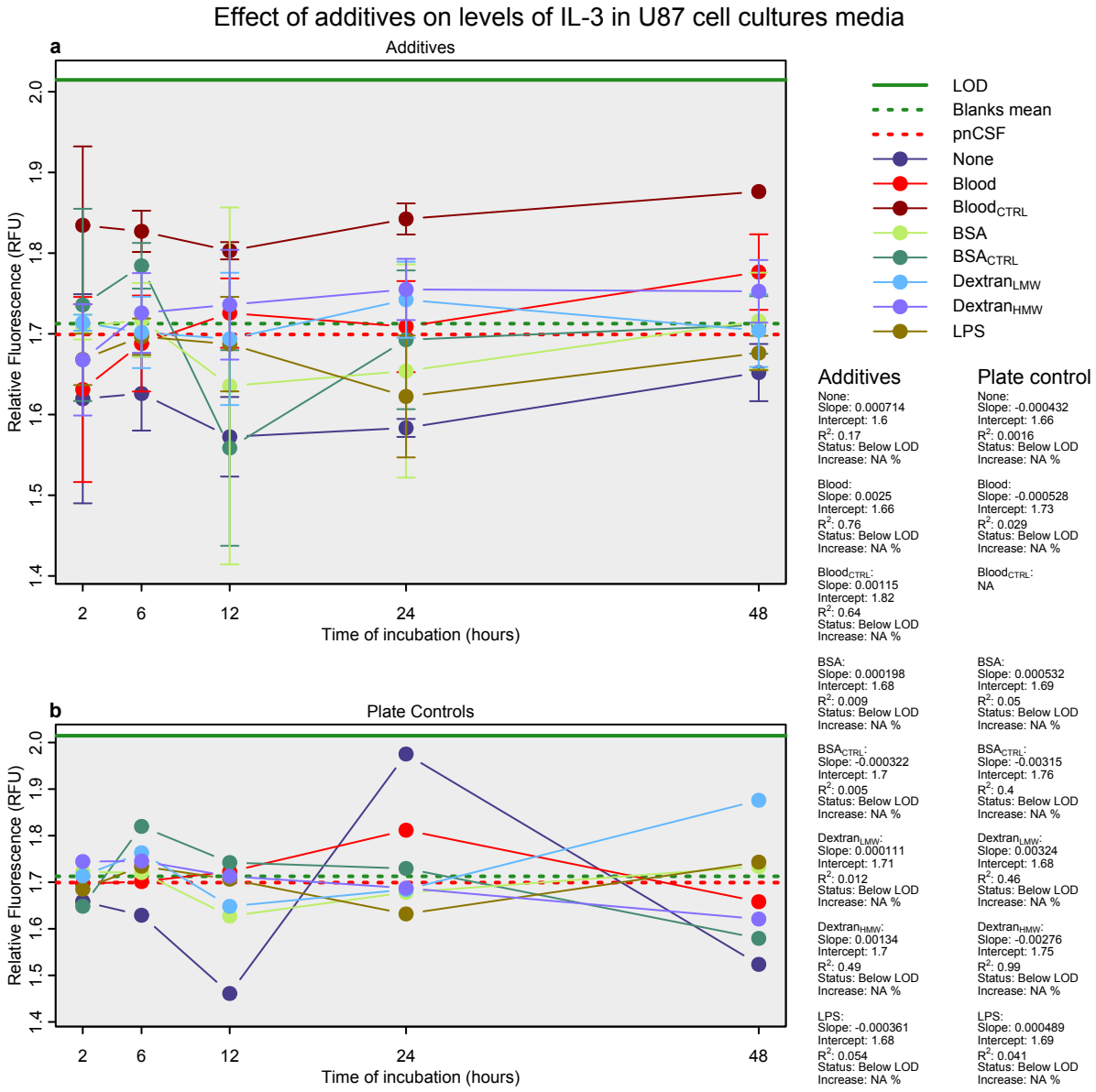

FIGURE H.S95: **Effect of additives on levels of IL-3 in U87 cell cultures media.** Additives along with fresh blood and LPS were added to mycoplasma-free human glial (U87) cells in triplicate wells of a 24-well plate and incubated for up to 48 h to measure the effect on levels of proteins measured in the cell media. Media was collected and frozen from successive triplicates at different intervals, then analyzed with the ACM. **a** Average values for IL-3 from three replicates for each point in every 24-well plate where a different additive was applied. **b** Data from the control cell media in each plate.

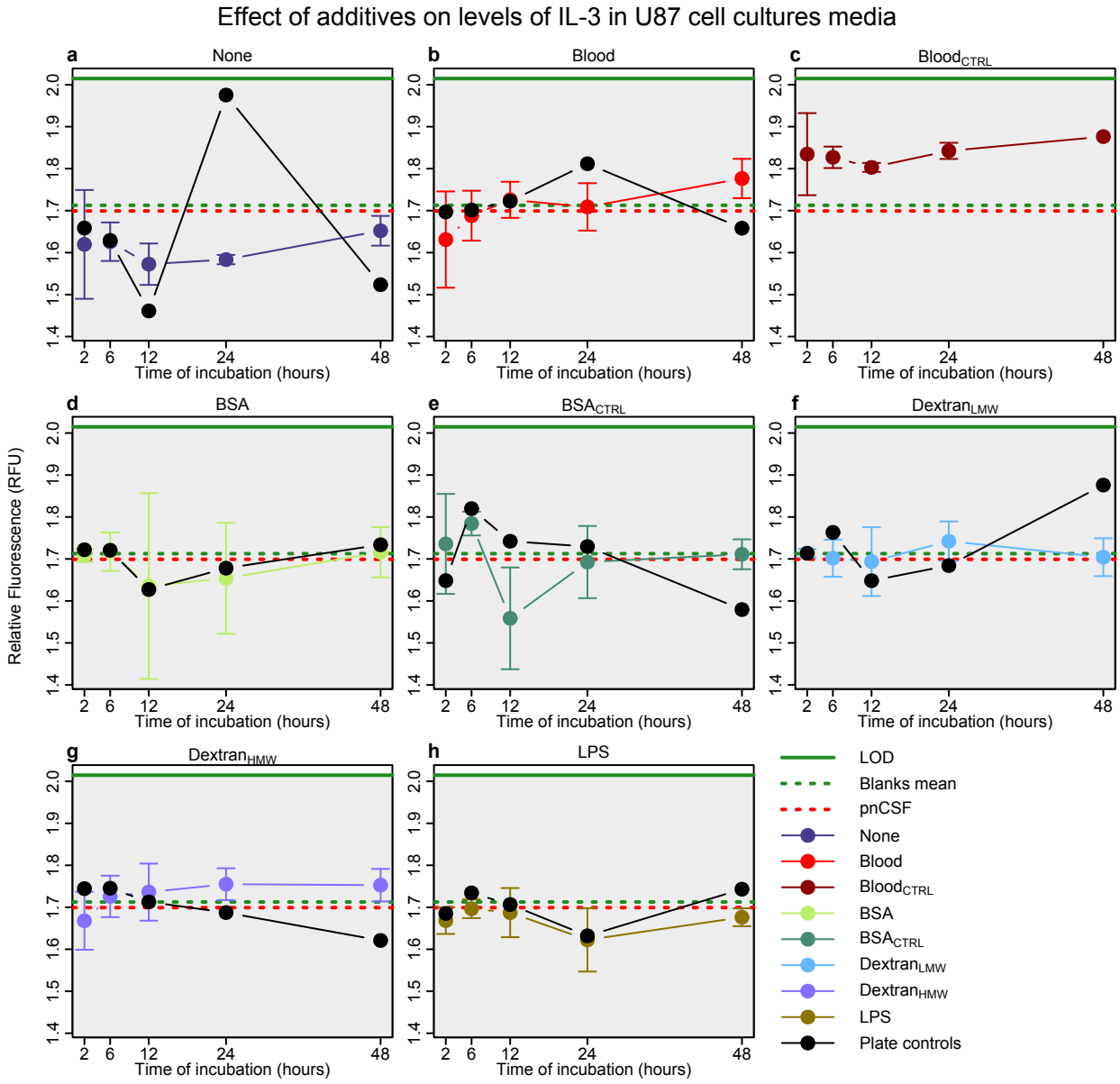

FIGURE H.S96: **Effect of additives on levels of IL-3 in U87 cell cultures media.** Additives along with fresh blood and LPS were added to mycoplasma-free human glial (U87) cells in triplicate wells of a 24-well plate and incubated for up to 48 h to measure the effect on levels of proteins measured in the cell media. Media was collected and frozen from successive triplicates at different intervals, then analyzed with the ACM. Each graph compares IL-3 values from cells incubated with a different additive to cells not incubated with additives located in the same 24-well plate. Plates in **c** and **e** did not contain any U87 cells, and **c** also did not have controls on the plate.

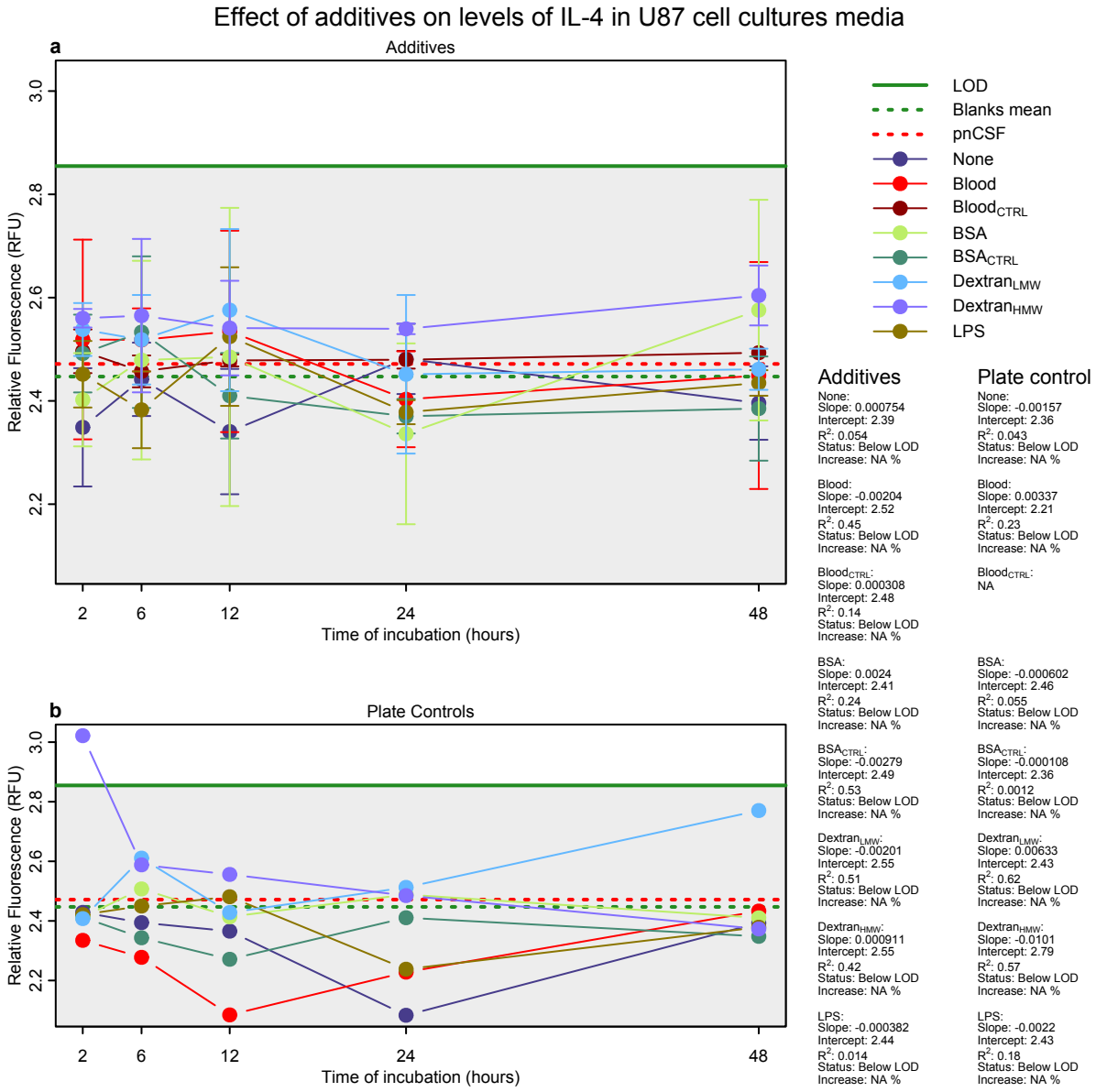

FIGURE H.S97: **Effect of additives on levels of IL-4 in U87 cell cultures media.** Additives along with fresh blood and LPS were added to mycoplasma-free human glial (U87) cells in triplicate wells of a 24-well plate and incubated for up to 48 h to measure the effect on levels of proteins measured in the cell media. Media was collected and frozen from successive triplicates at different intervals, then analyzed with the ACM. **a** Average values for IL-4 from three replicates for each point in every 24-well plate where a different additive was applied. **b** Data from the control cell media in each plate.

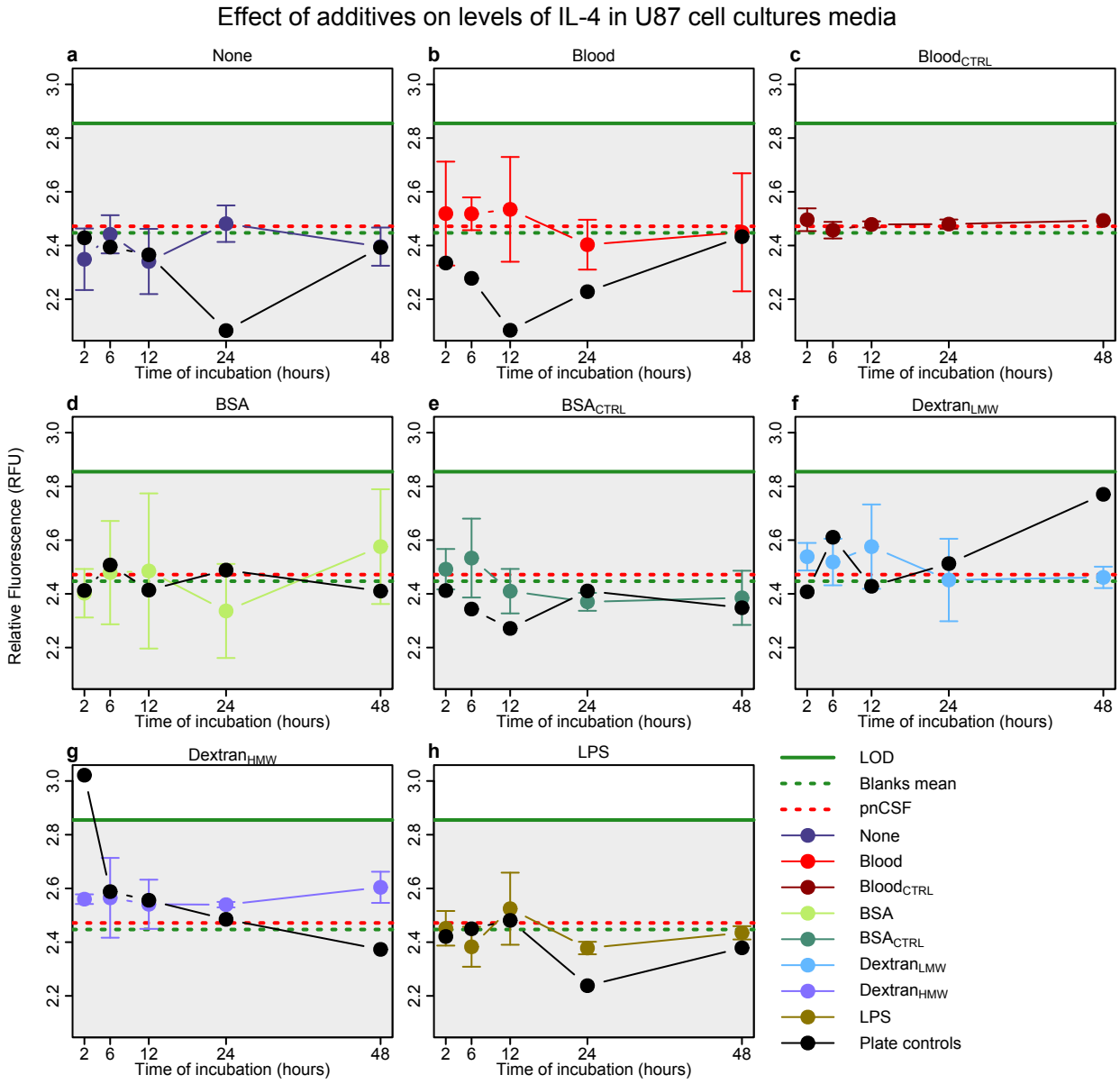

FIGURE H.S98: **Effect of additives on levels of IL-4 in U87 cell cultures media.** Additives along with fresh blood and LPS were added to mycoplasma-free human glial (U87) cells in triplicate wells of a 24-well plate and incubated for up to 48 h to measure the effect on levels of proteins measured in the cell media. Media was collected and frozen from successive triplicates at different intervals, then analyzed with the ACM. Each graph compares IL-4 values from cells incubated with a different additive to cells not incubated with additives located in the same 24-well plate. Plates in **c** and **e** did not contain any U87 cells, and **c** also did not have controls on the plate.

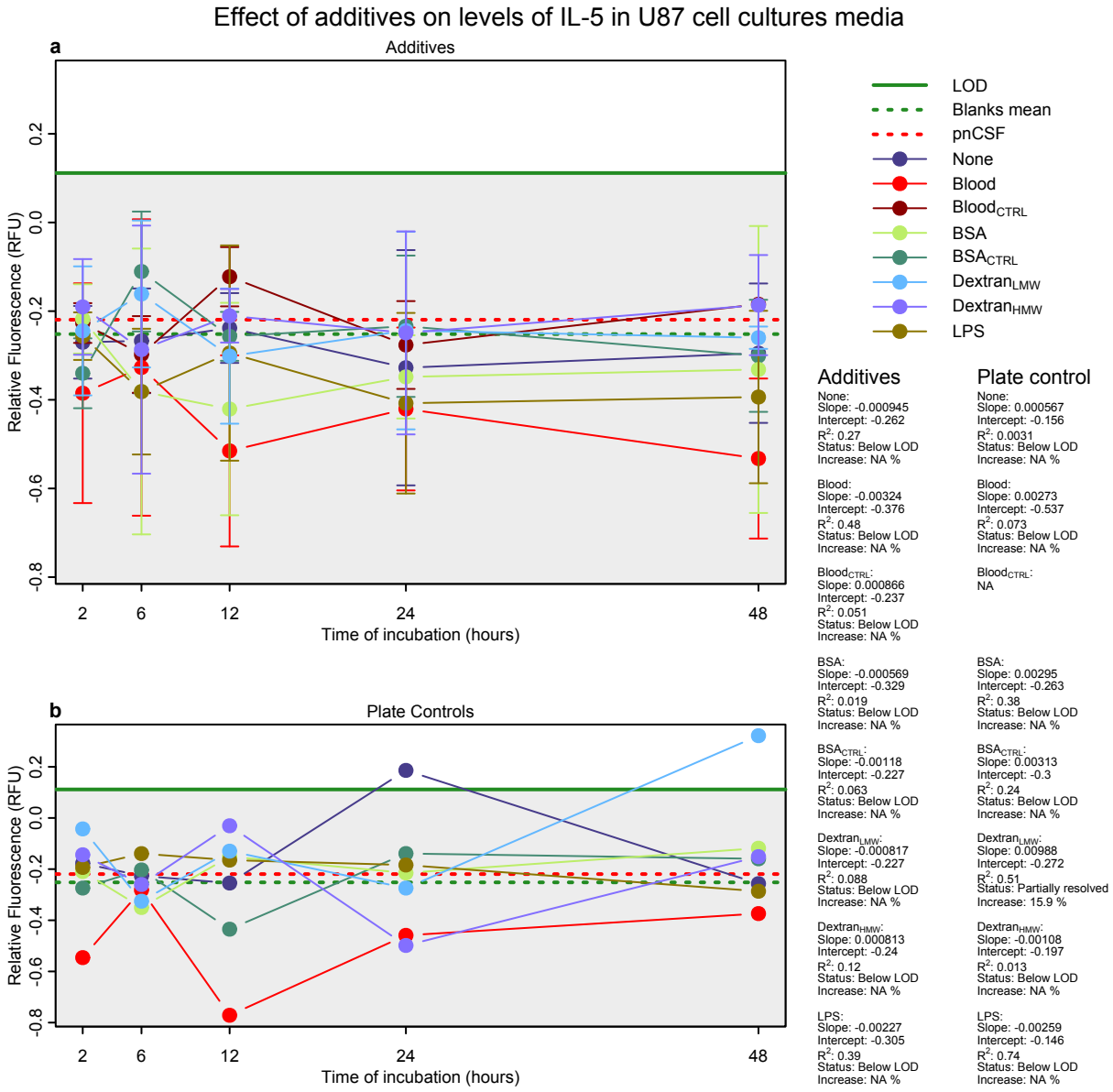

FIGURE H.S99: **Effect of additives on levels of IL-5 in U87 cell cultures media.** Additives along with fresh blood and LPS were added to mycoplasma-free human glial (U87) cells in triplicate wells of a 24-well plate and incubated for up to 48 h to measure the effect on levels of proteins measured in the cell media. Media was collected and frozen from successive triplicates at different intervals, then analyzed with the ACM. **a** Average values for IL-5 from three replicates for each point in every 24-well plate where a different additive was applied. **b** Data from the control cell media in each plate.

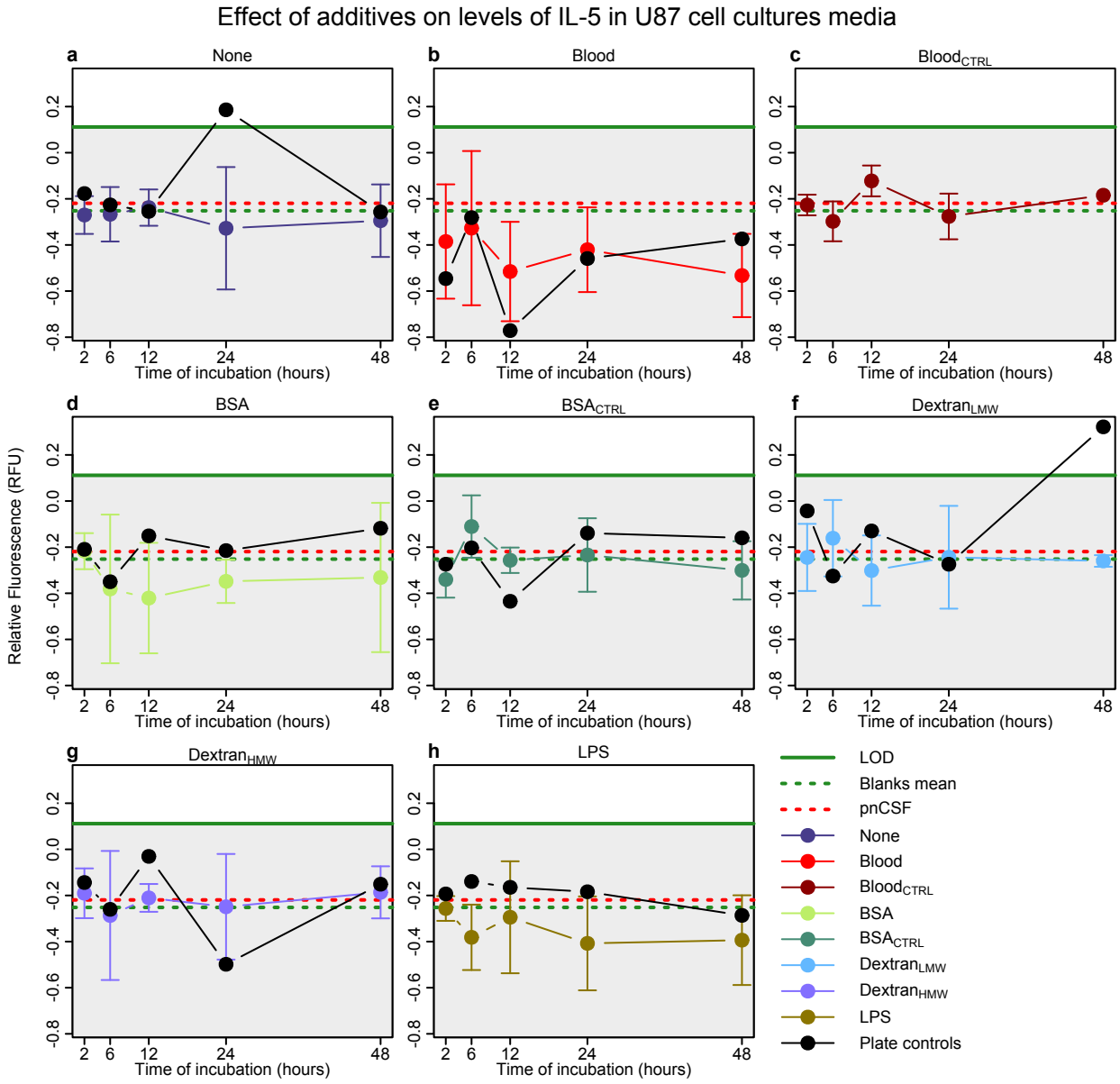

FIGURE H.S100: **Effect of additives on levels of IL-5 in U87 cell cultures media.** Additives along with fresh blood and LPS were added to mycoplasma-free human glial (U87) cells in triplicate wells of a 24-well plate and incubated for up to 48 h to measure the effect on levels of proteins measured in the cell media. Media was collected and frozen from successive triplicates at different intervals, then analyzed with the ACM. Each graph compares IL-5 values from cells incubated with a different additive to cells not incubated with additives located in the same 24-well plate. Plates in **c** and **e** did not contain any U87 cells, and **c** also did not have controls on the plate.

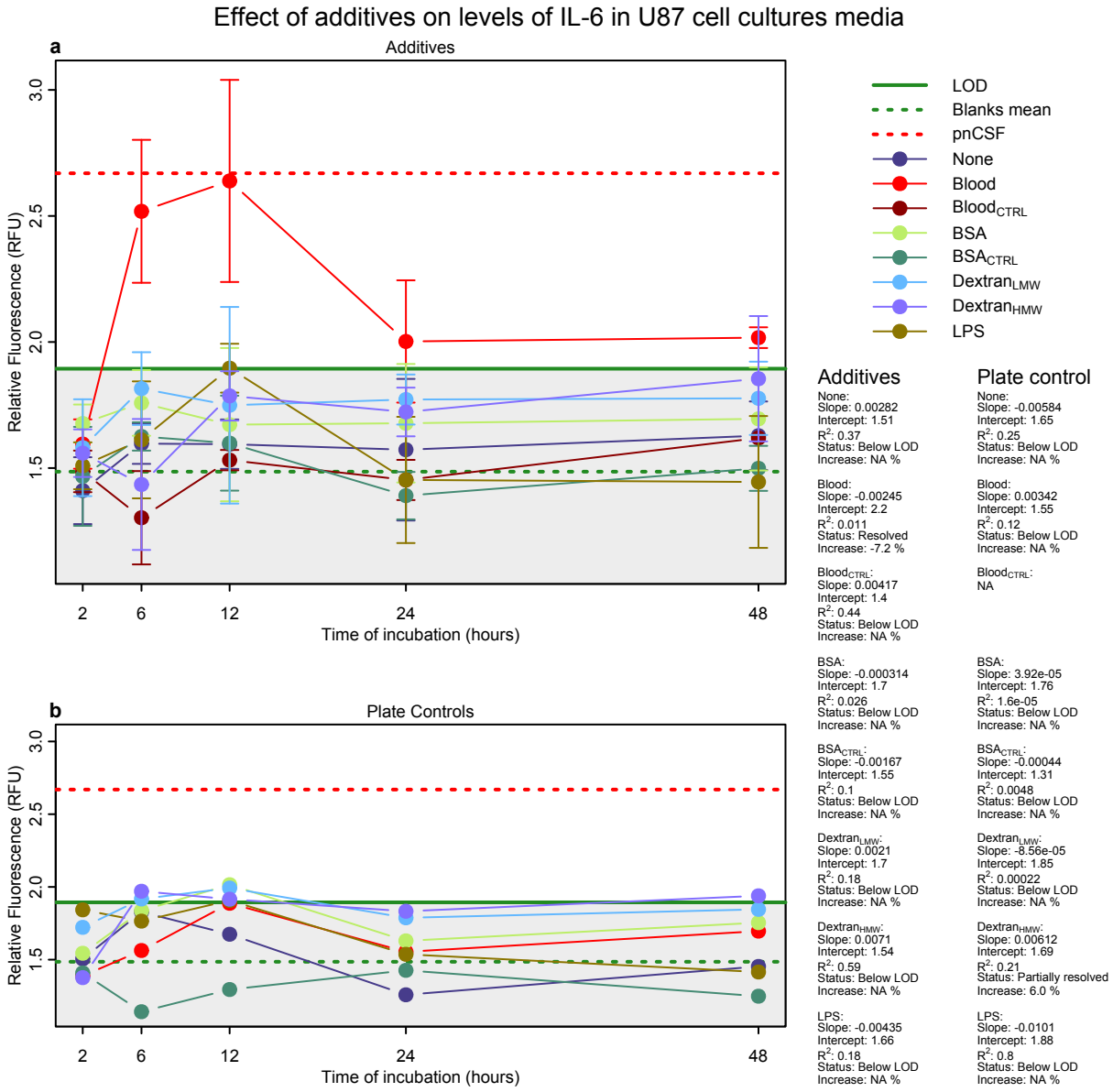

FIGURE H.S101: **Effect of additives on levels of IL-6 in U87 cell cultures media.** Additives along with fresh blood and LPS were added to mycoplasma-free human glial (U87) cells in triplicate wells of a 24-well plate and incubated for up to 48 h to measure the effect on levels of proteins measured in the cell media. Media was collected and frozen from successive triplicates at different intervals, then analyzed with the ACM. **a** Average values for IL-6 from three replicates for each point in every 24-well plate where a different additive was applied. **b** Data from the control cell media in each plate.

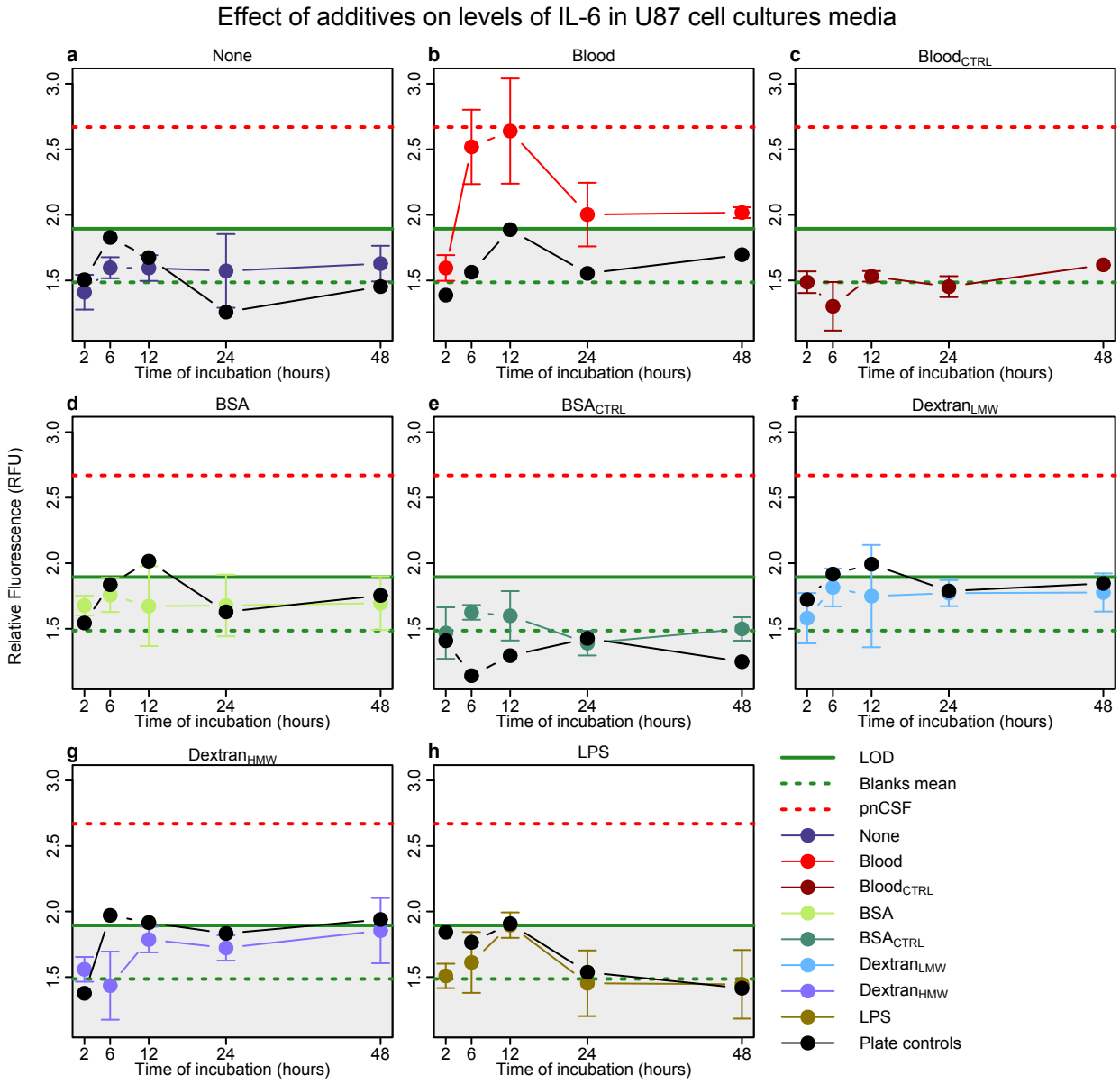

FIGURE H.S102: **Effect of additives on levels of IL-6 in U87 cell cultures media.** Additives along with fresh blood and LPS were added to mycoplasma-free human glial (U87) cells in triplicate wells of a 24-well plate and incubated for up to 48 h to measure the effect on levels of proteins measured in the cell media. Media was collected and frozen from successive triplicates at different intervals, then analyzed with the ACM. Each graph compares IL-6 values from cells incubated with a different additive to cells not incubated with additives located in the same 24-well plate. Plates in **c** and **e** did not contain any U87 cells, and **c** also did not have controls on the plate.

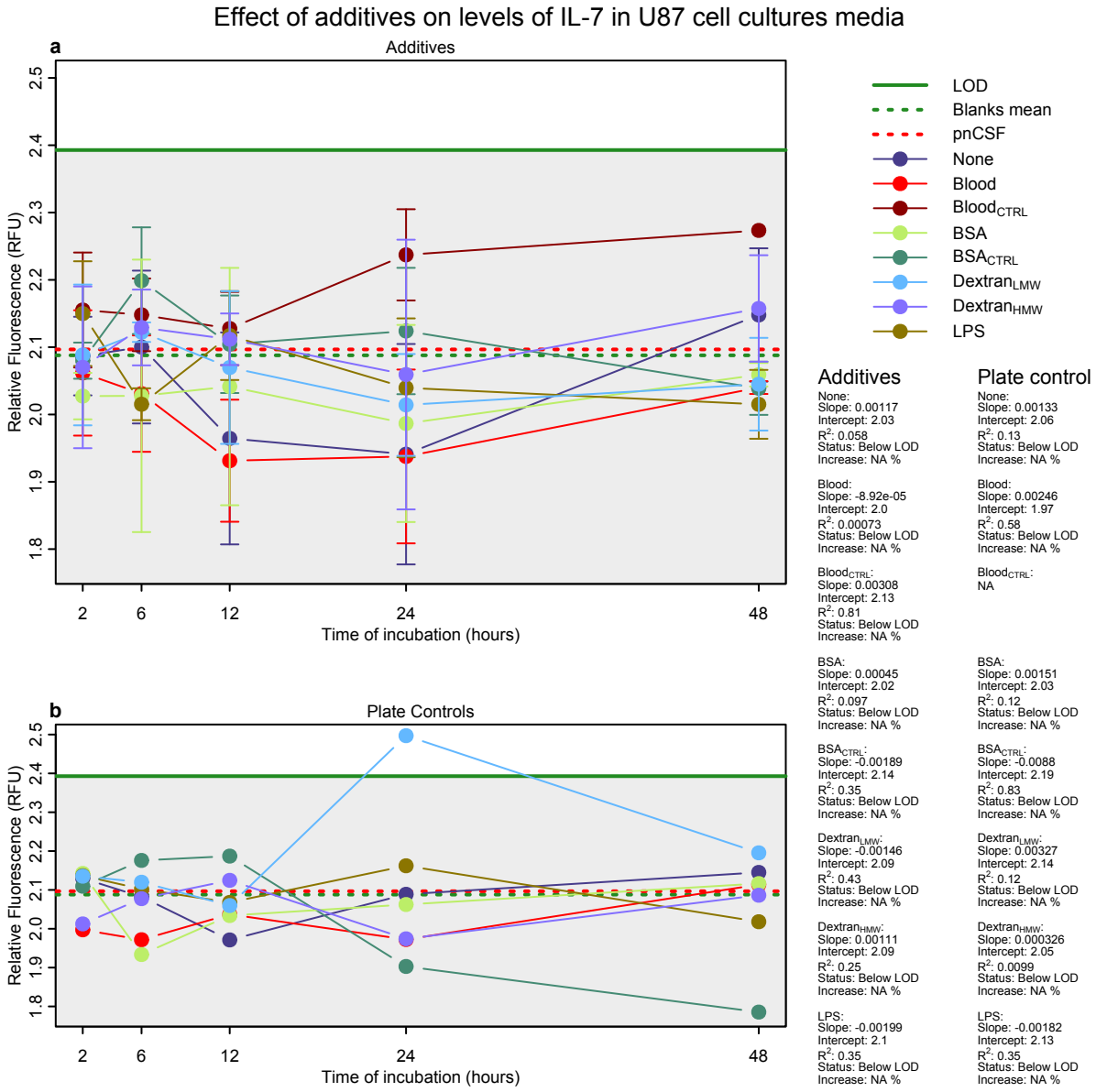

FIGURE H.S103: **Effect of additives on levels of IL-7 in U87 cell cultures media.** Additives along with fresh blood and LPS were added to mycoplasma-free human glial (U87) cells in triplicate wells of a 24-well plate and incubated for up to 48 h to measure the effect on levels of proteins measured in the cell media. Media was collected and frozen from successive triplicates at different intervals, then analyzed with the ACM. **a** Average values for IL-7 from three replicates for each point in every 24-well plate where a different additive was applied. **b** Data from the control cell media in each plate.

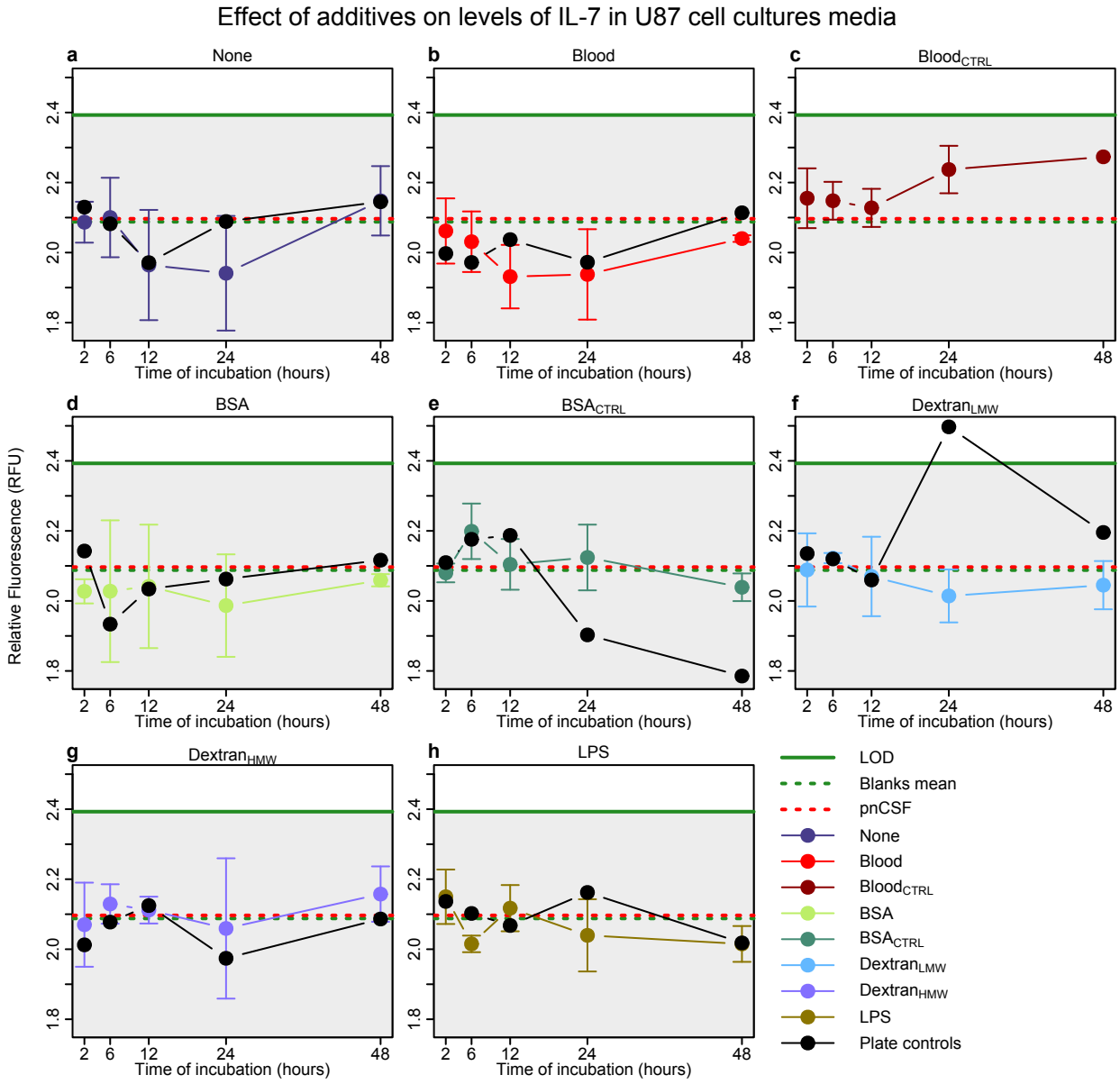

FIGURE H.S104: **Effect of additives on levels of IL-7 in U87 cell cultures media.** Additives along with fresh blood and LPS were added to mycoplasma-free human glial (U87) cells in triplicate wells of a 24-well plate and incubated for up to 48 h to measure the effect on levels of proteins measured in the cell media. Media was collected and frozen from successive triplicates at different intervals, then analyzed with the ACM. Each graph compares IL-7 values from cells incubated with a different additive to cells not incubated with additives located in the same 24-well plate. Plates in **c** and **e** did not contain any U87 cells, and **c** also did not have controls on the plate.

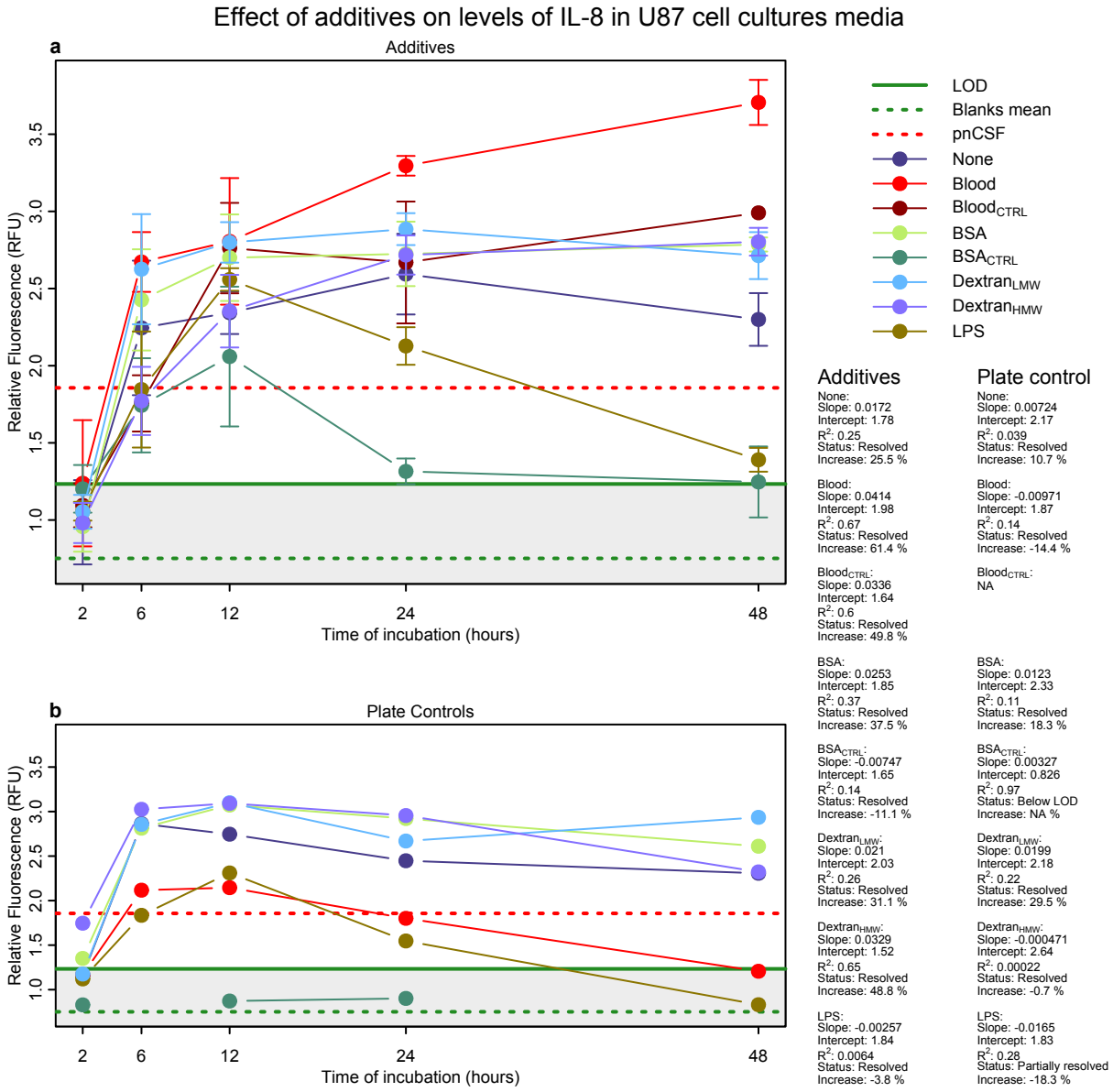

FIGURE H.S105: **Effect of additives on levels of IL-8 in U87 cell cultures media.** Additives along with fresh blood and LPS were added to mycoplasma-free human glial (U87) cells in triplicate wells of a 24-well plate and incubated for up to 48 h to measure the effect on levels of proteins measured in the cell media. Media was collected and frozen from successive triplicates at different intervals, then analyzed with the ACM. **a** Average values for IL-8 from three replicates for each point in every 24-well plate where a different additive was applied. **b** Data from the control cell media in each plate.

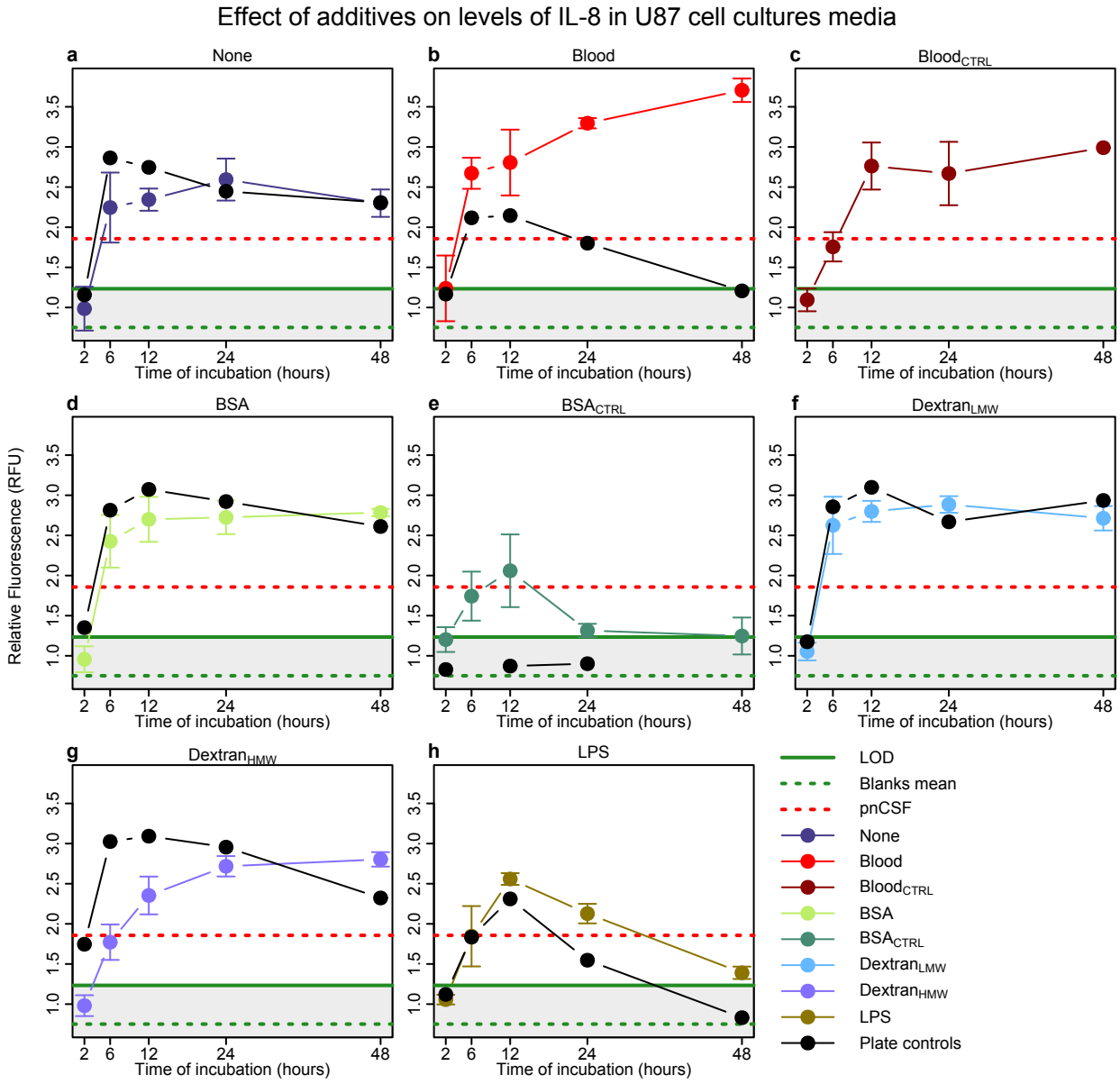

FIGURE H.S106: **Effect of additives on levels of IL-8 in U87 cell cultures media.** Additives along with fresh blood and LPS were added to mycoplasma-free human glial (U87) cells in triplicate wells of a 24-well plate and incubated for up to 48 h to measure the effect on levels of proteins measured in the cell media. Media was collected and frozen from successive triplicates at different intervals, then analyzed with the ACM. Each graph compares IL-8 values from cells incubated with a different additive to cells not incubated with additives located in the same 24-well plate. Plates in **c** and **e** did not contain any U87 cells, and **c** also did not have controls on the plate.

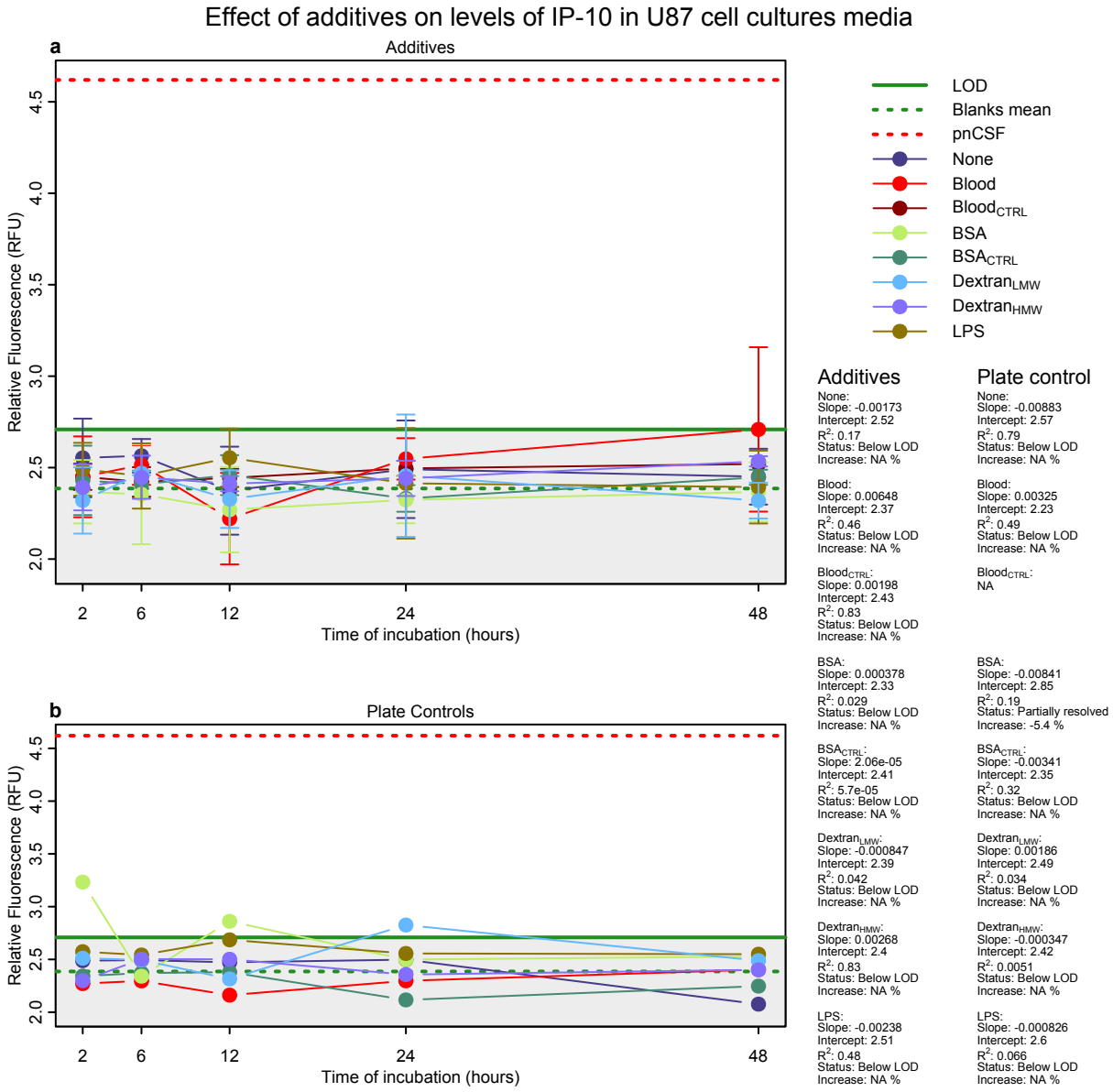

FIGURE H.S107: **Effect of additives on levels of IP-10 in U87 cell cultures media.** Additives along with fresh blood and LPS were added to mycoplasma-free human glial (U87) cells in triplicate wells of a 24-well plate and incubated for up to 48 h to measure the effect on levels of proteins measured in the cell media. Media was collected and frozen from successive triplicates at different intervals, then analyzed with the ACM. **a** Average values for IP-10 from three replicates for each point in every 24-well plate where a different additive was applied. **b** Data from the control cell media in each plate.

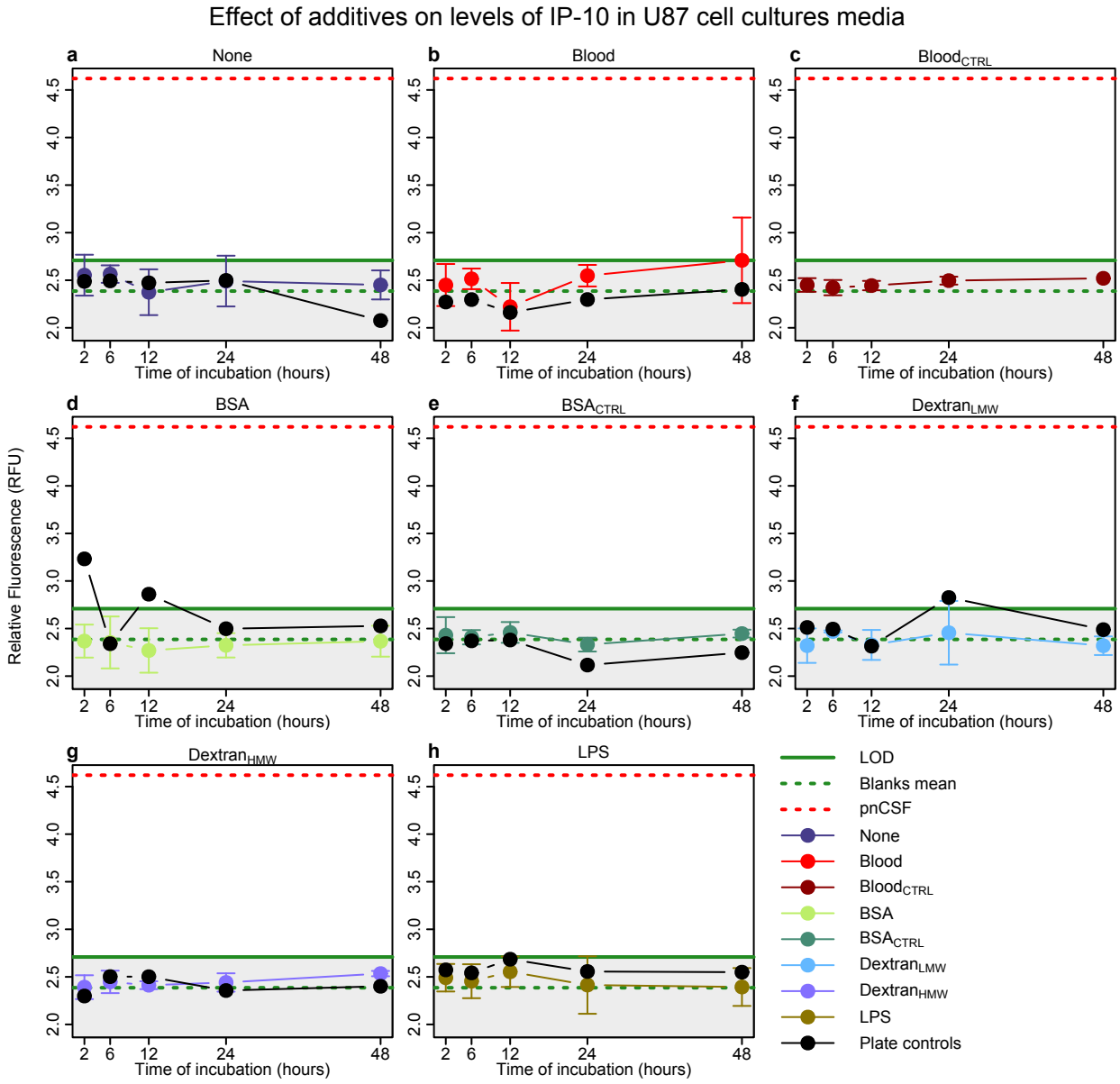

FIGURE H.S108: **Effect of additives on levels of IP-10 in U87 cell cultures media.** Additives along with fresh blood and LPS were added to mycoplasma-free human glial (U87) cells in triplicate wells of a 24-well plate and incubated for up to 48 h to measure the effect on levels of proteins measured in the cell media. Media was collected and frozen from successive triplicates at different intervals, then analyzed with the ACM. Each graph compares IP-10 values from cells incubated with a different additive to cells not incubated with additives located in the same 24-well plate. Plates in **c** and **e** did not contain any U87 cells, and **c** also did not have controls on the plate.

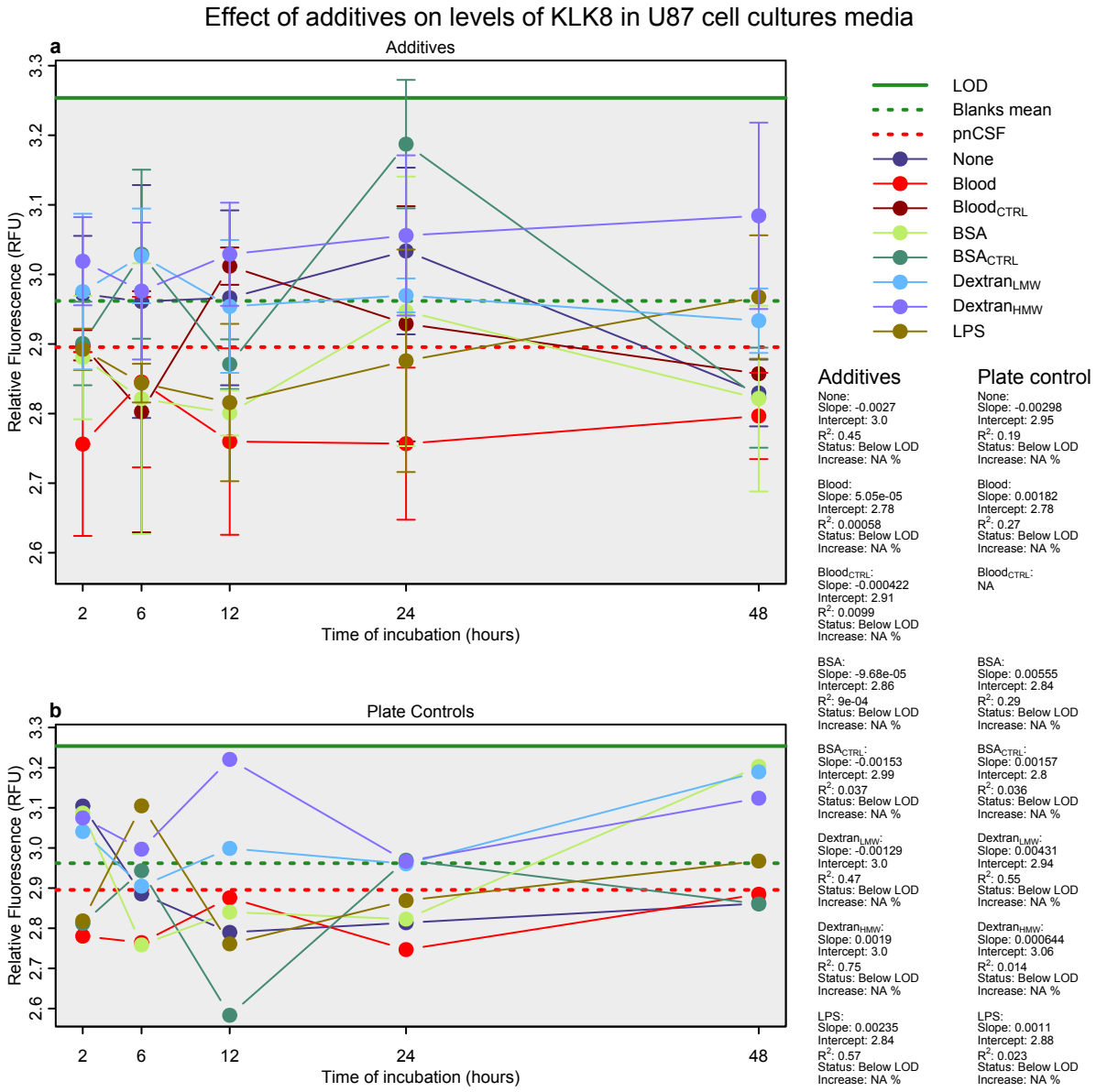

FIGURE H.S109: **Effect of additives on levels of KLK8 in U87 cell cultures media.** Additives along with fresh blood and LPS were added to mycoplasma-free human glial (U87) cells in triplicate wells of a 24-well plate and incubated for up to 48 h to measure the effect on levels of proteins measured in the cell media. Media was collected and frozen from successive triplicates at different intervals, then analyzed with the ACM. **a** Average values for KLK8 from three replicates for each point in every 24-well plate where a different additive was applied. **b** Data from the control cell media in each plate.

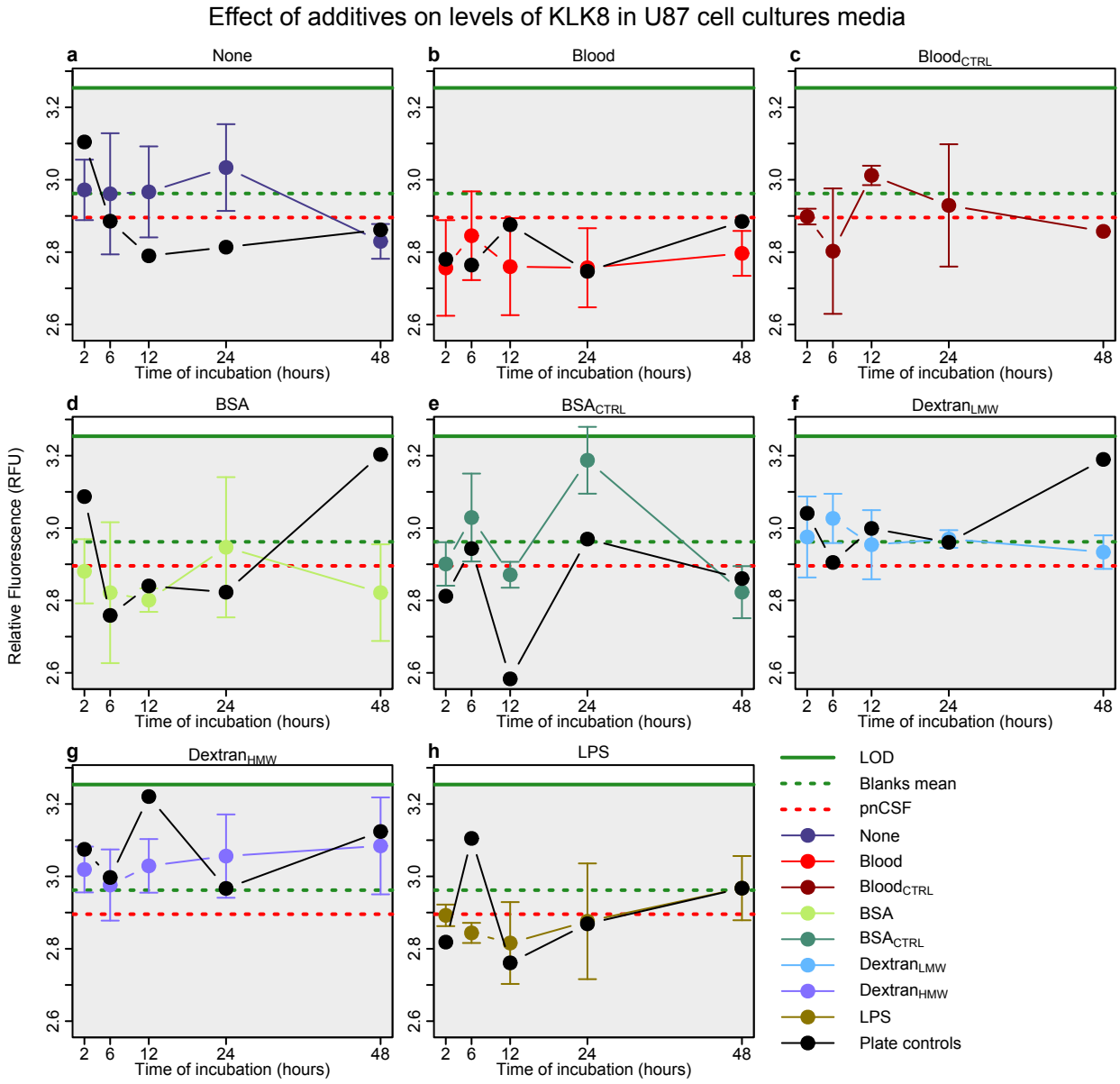

FIGURE H.S110: **Effect of additives on levels of KLK8 in U87 cell cultures media.** Additives along with fresh blood and LPS were added to mycoplasma-free human glial (U87) cells in triplicate wells of a 24-well plate and incubated for up to 48 h to measure the effect on levels of proteins measured in the cell media. Media was collected and frozen from successive triplicates at different intervals, then analyzed with the ACM. Each graph compares KLK8 values from cells incubated with a different additive to cells not incubated with additives located in the same 24-well plate. Plates in **c** and **e** did not contain any U87 cells, and **c** also did not have controls on the plate.

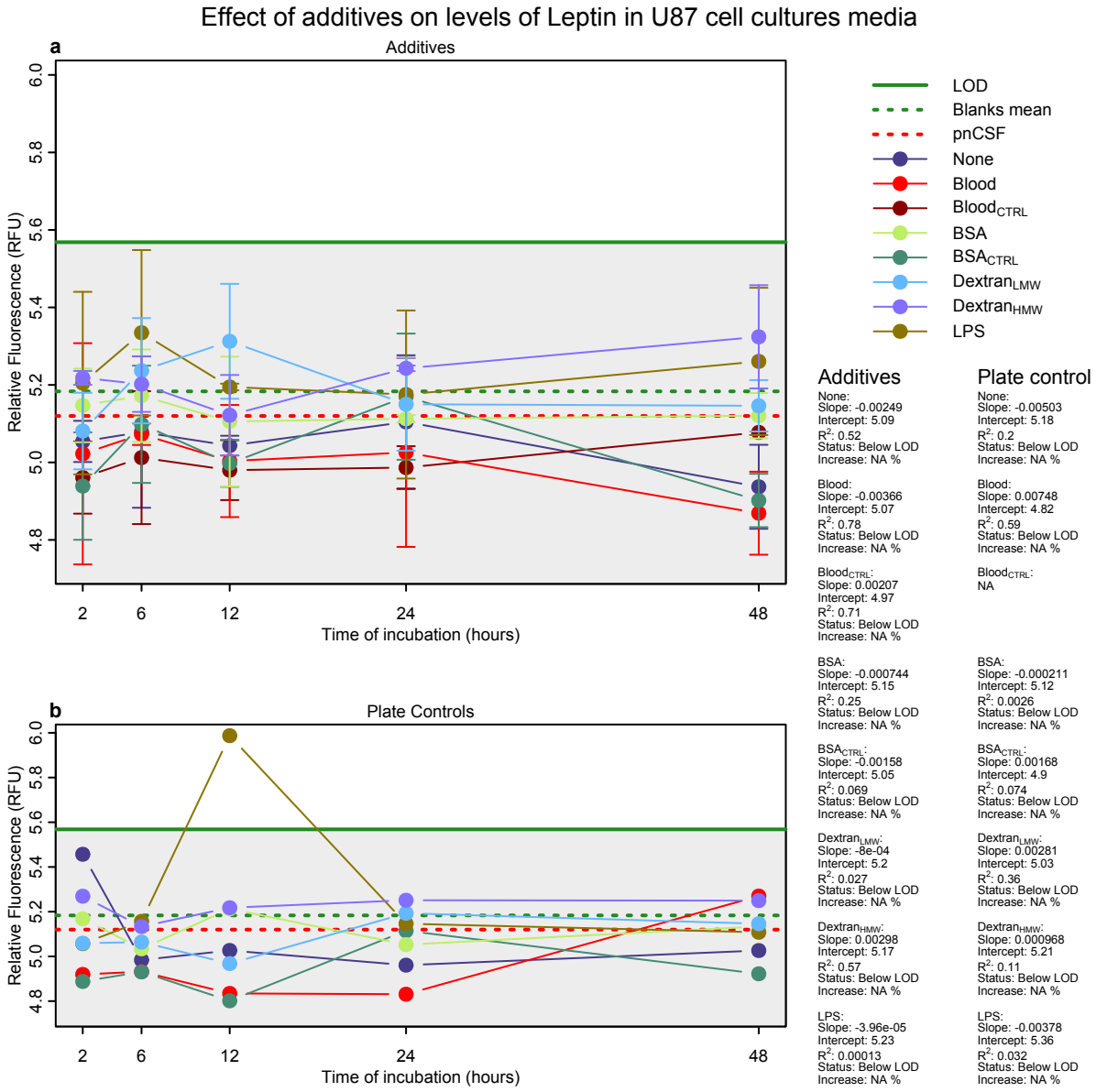

FIGURE H.S111: **Effect of additives on levels of Leptin in U87 cell cultures media.** Additives along with fresh blood and LPS were added to mycoplasma-free human glial (U87) cells in triplicate wells of a 24-well plate and incubated for up to 48 h to measure the effect on levels of proteins measured in the cell media. Media was collected and frozen from successive triplicates at different intervals, then analyzed with the ACM. **a** Average values for Leptin from three replicates for each point in every 24-well plate where a different additive was applied. **b** Data from the control cell media in each plate.

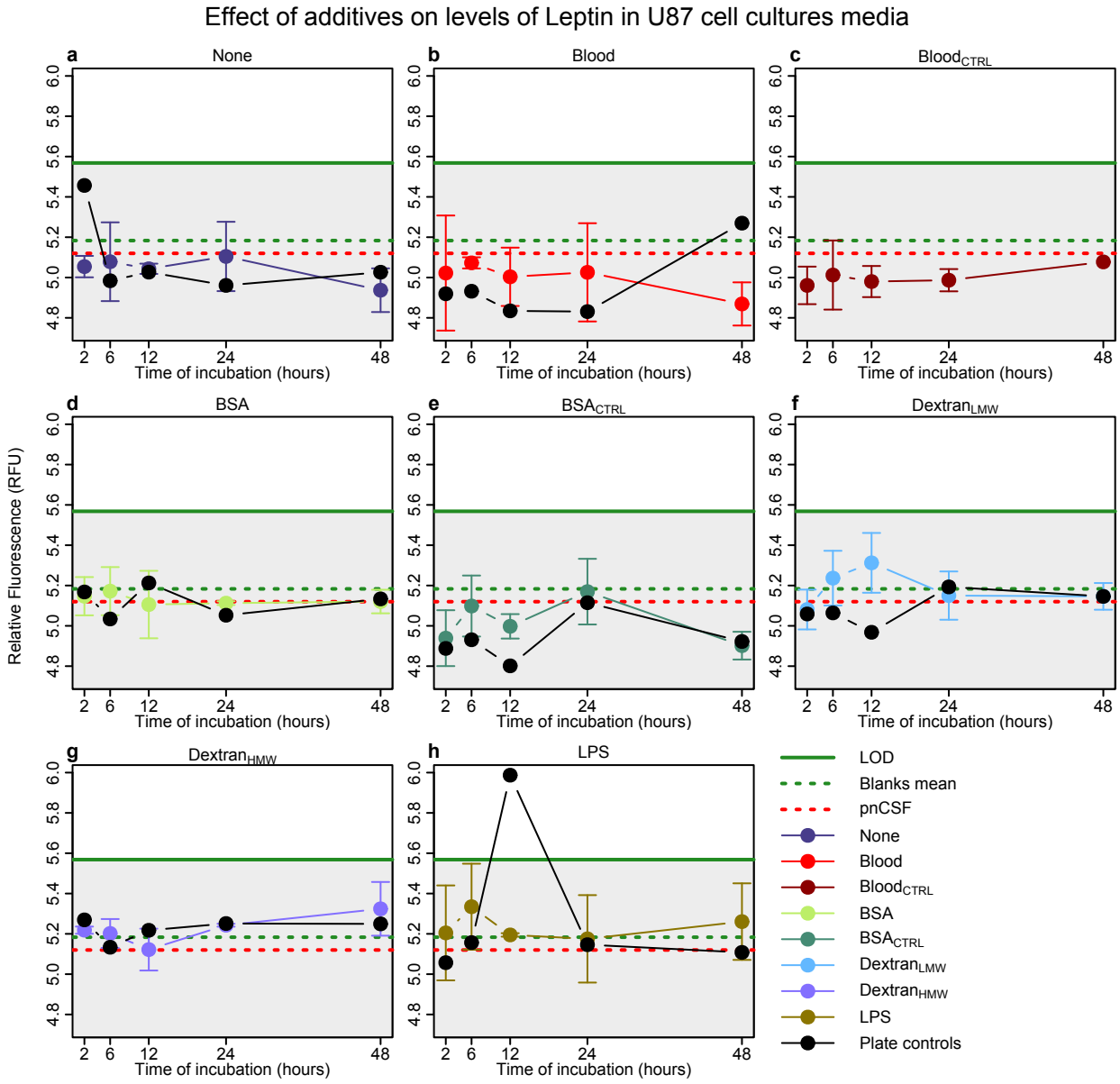

FIGURE H.S112: **Effect of additives on levels of Leptin in U87 cell cultures media.** Additives along with fresh blood and LPS were added to mycoplasma-free human glial (U87) cells in triplicate wells of a 24-well plate and incubated for up to 48 h to measure the effect on levels of proteins measured in the cell media. Media was collected and frozen from successive triplicates at different intervals, then analyzed with the ACM. Each graph compares Leptin values from cells incubated with a different additive to cells not incubated with additives located in the same 24-well plate. Plates in **c** and **e** did not contain any U87 cells, and **c** also did not have controls on the plate.

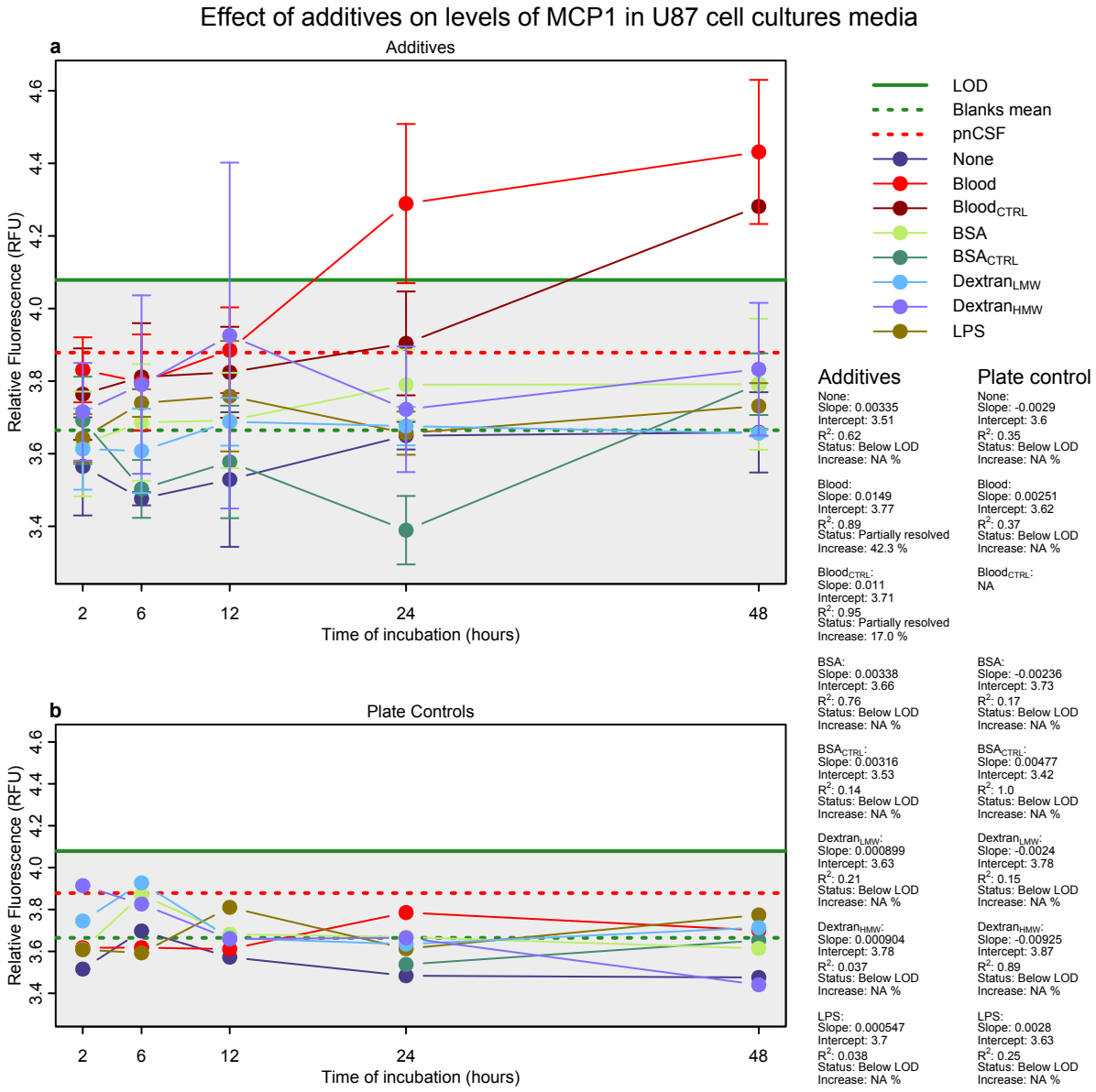

FIGURE H.S113: **Effect of additives on levels of MCP1 in U87 cell cultures media.** Additives along with fresh blood and LPS were added to mycoplasma-free human glial (U87) cells in triplicate wells of a 24-well plate and incubated for up to 48 h to measure the effect on levels of proteins measured in the cell media. Media was collected and frozen from successive triplicates at different intervals, then analyzed with the ACM. **a** Average values for MCP1 from three replicates for each point in every 24-well plate where a different additive was applied. **b** Data from the control cell media in each plate.

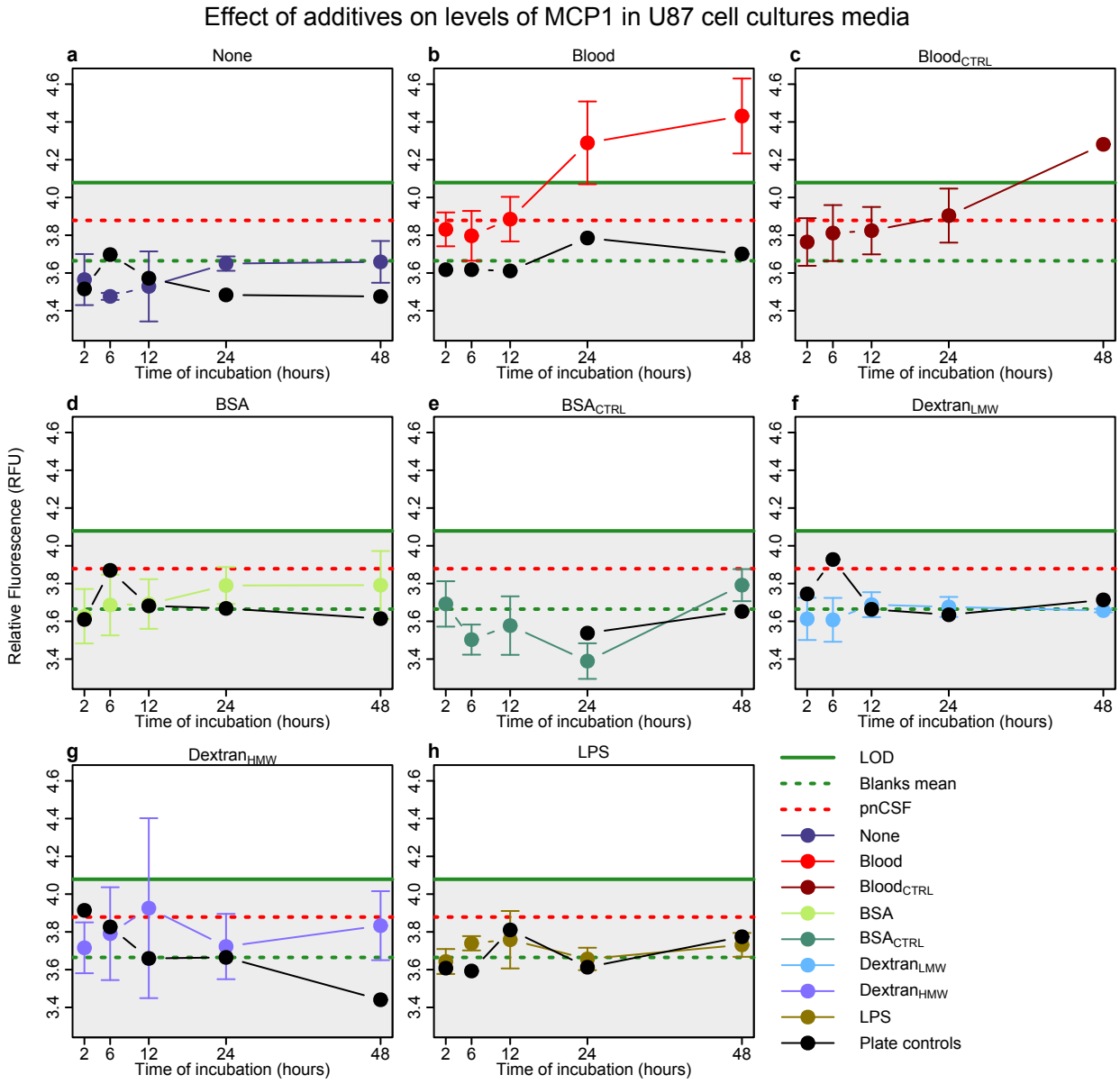

FIGURE H.S114: **Effect of additives on levels of MCP1 in U87 cell cultures media.** Additives along with fresh blood and LPS were added to mycoplasma-free human glial (U87) cells in triplicate wells of a 24-well plate and incubated for up to 48 h to measure the effect on levels of proteins measured in the cell media. Media was collected and frozen from successive triplicates at different intervals, then analyzed with the ACM. Each graph compares MCP1 values from cells incubated with a different additive to cells not incubated with additives located in the same 24-well plate. Plates in **c** and **e** did not contain any U87 cells, and **c** also did not have controls on the plate.

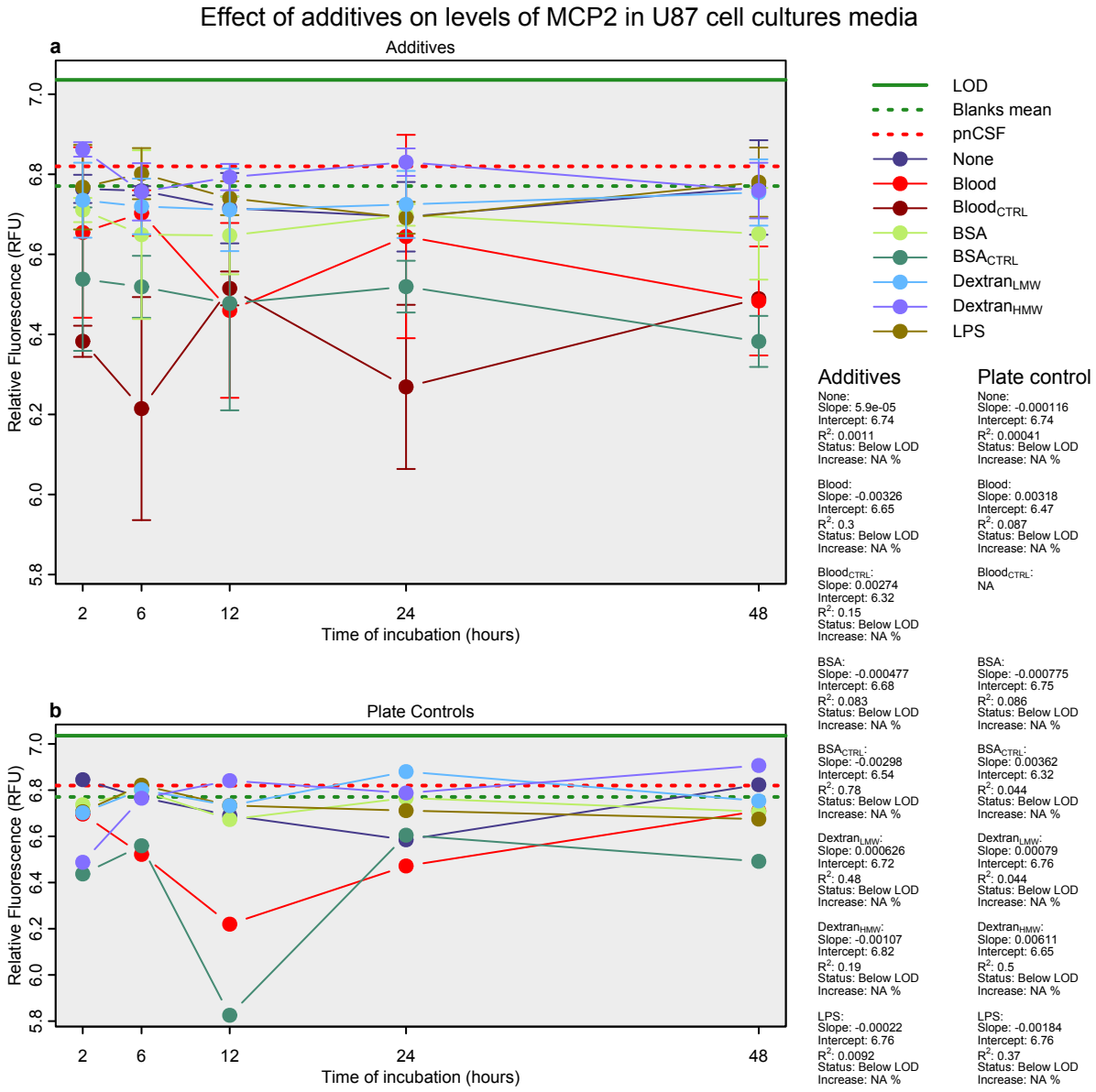

FIGURE H.S115: **Effect of additives on levels of MCP2 in U87 cell cultures media.** Additives along with fresh blood and LPS were added to mycoplasma-free human glial (U87) cells in triplicate wells of a 24-well plate and incubated for up to 48 h to measure the effect on levels of proteins measured in the cell media. Media was collected and frozen from successive triplicates at different intervals, then analyzed with the ACM. **a** Average values for MCP2 from three replicates for each point in every 24-well plate where a different additive was applied. **b** Data from the control cell media in each plate.

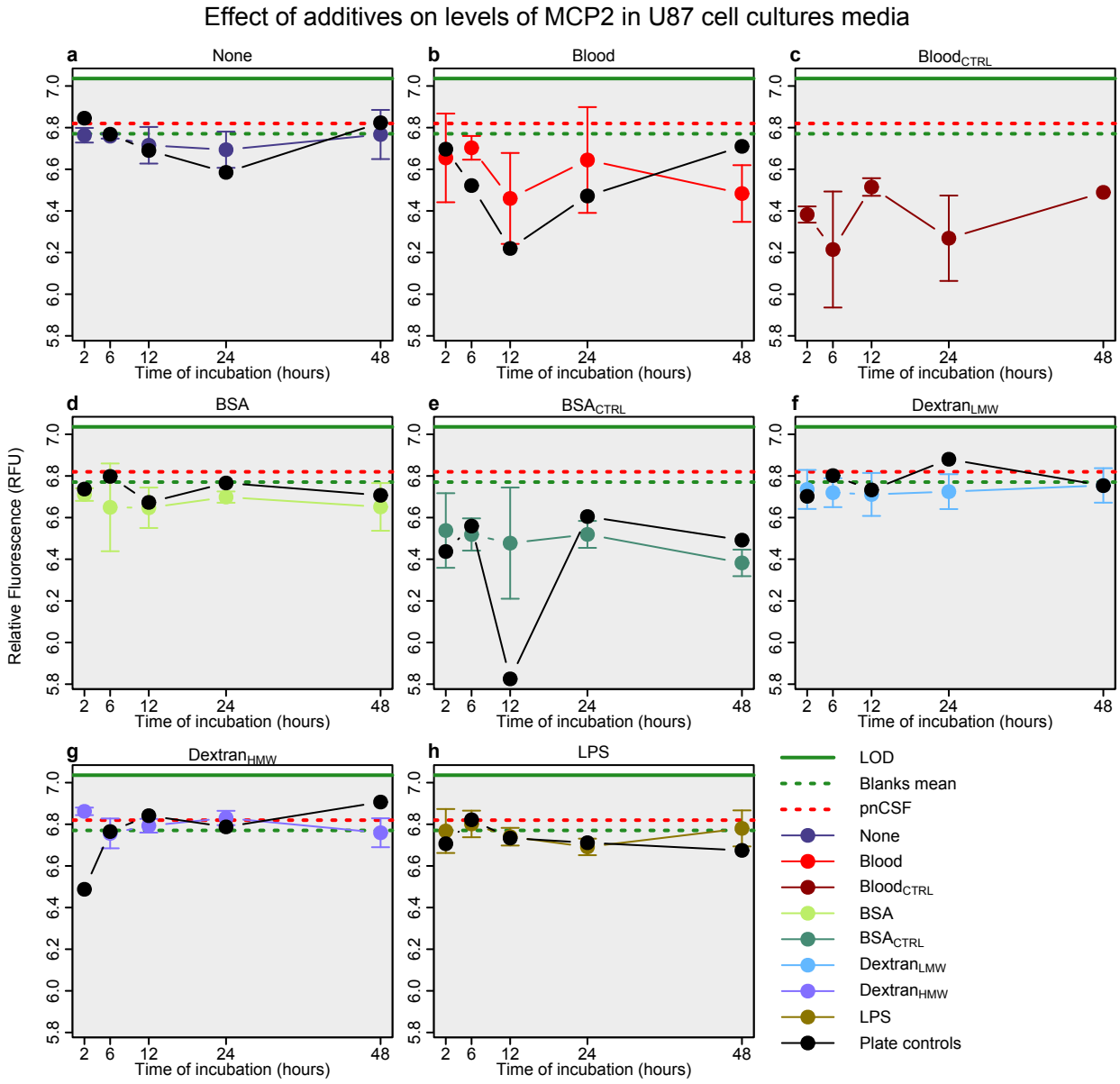

FIGURE H.S116: **Effect of additives on levels of MCP2 in U87 cell cultures media.** Additives along with fresh blood and LPS were added to mycoplasma-free human glial (U87) cells in triplicate wells of a 24-well plate and incubated for up to 48 h to measure the effect on levels of proteins measured in the cell media. Media was collected and frozen from successive triplicates at different intervals, then analyzed with the ACM. Each graph compares MCP2 values from cells incubated with a different additive to cells not incubated with additives located in the same 24-well plate. Plates in **c** and **e** did not contain any U87 cells, and **c** also did not have controls on the plate.

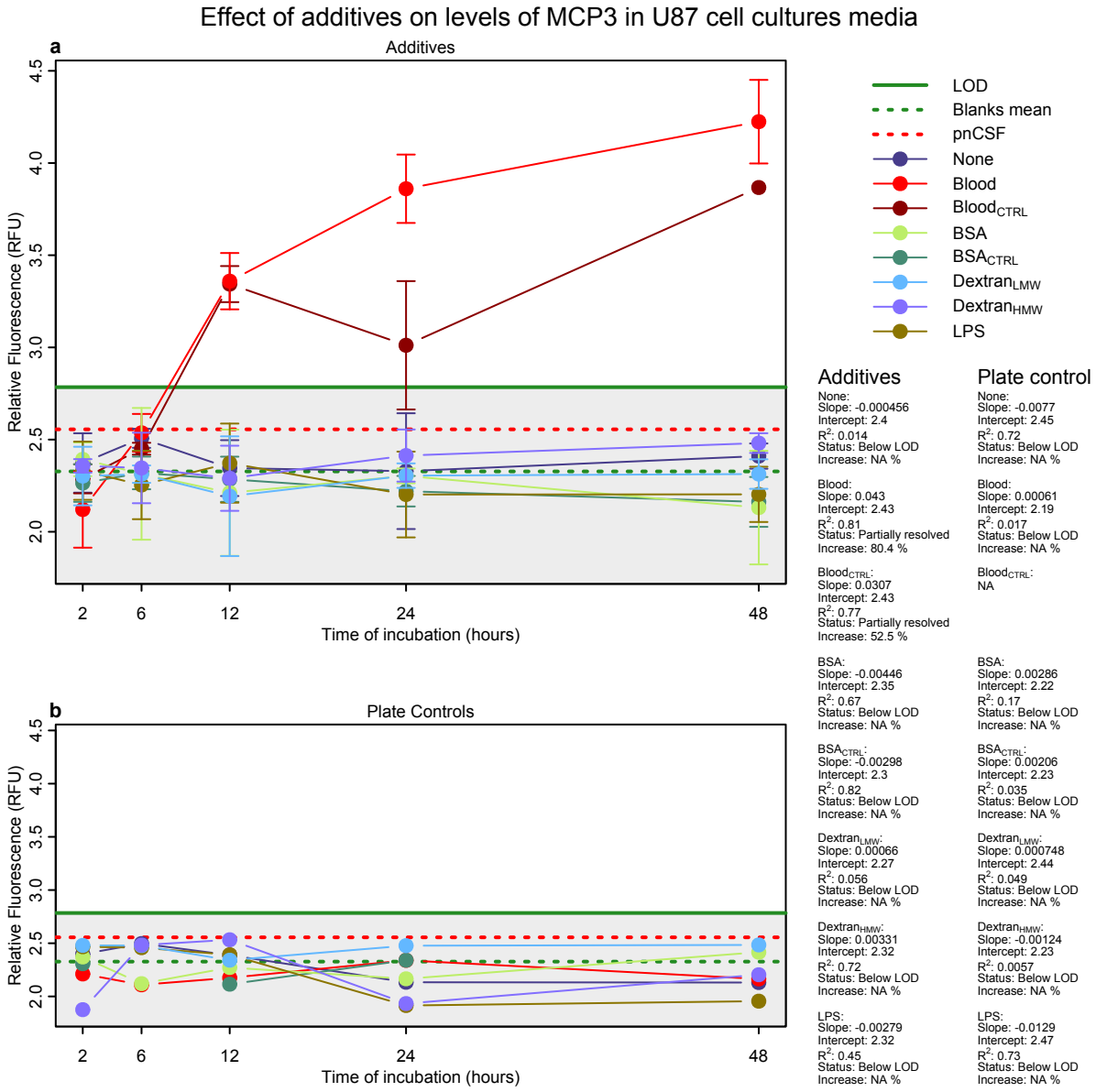

FIGURE H.S117: **Effect of additives on levels of MCP3 in U87 cell cultures media.** Additives along with fresh blood and LPS were added to mycoplasma-free human glial (U87) cells in triplicate wells of a 24-well plate and incubated for up to 48 h to measure the effect on levels of proteins measured in the cell media. Media was collected and frozen from successive triplicates at different intervals, then analyzed with the ACM. **a** Average values for MCP3 from three replicates for each point in every 24-well plate where a different additive was applied. **b** Data from the control cell media in each plate.

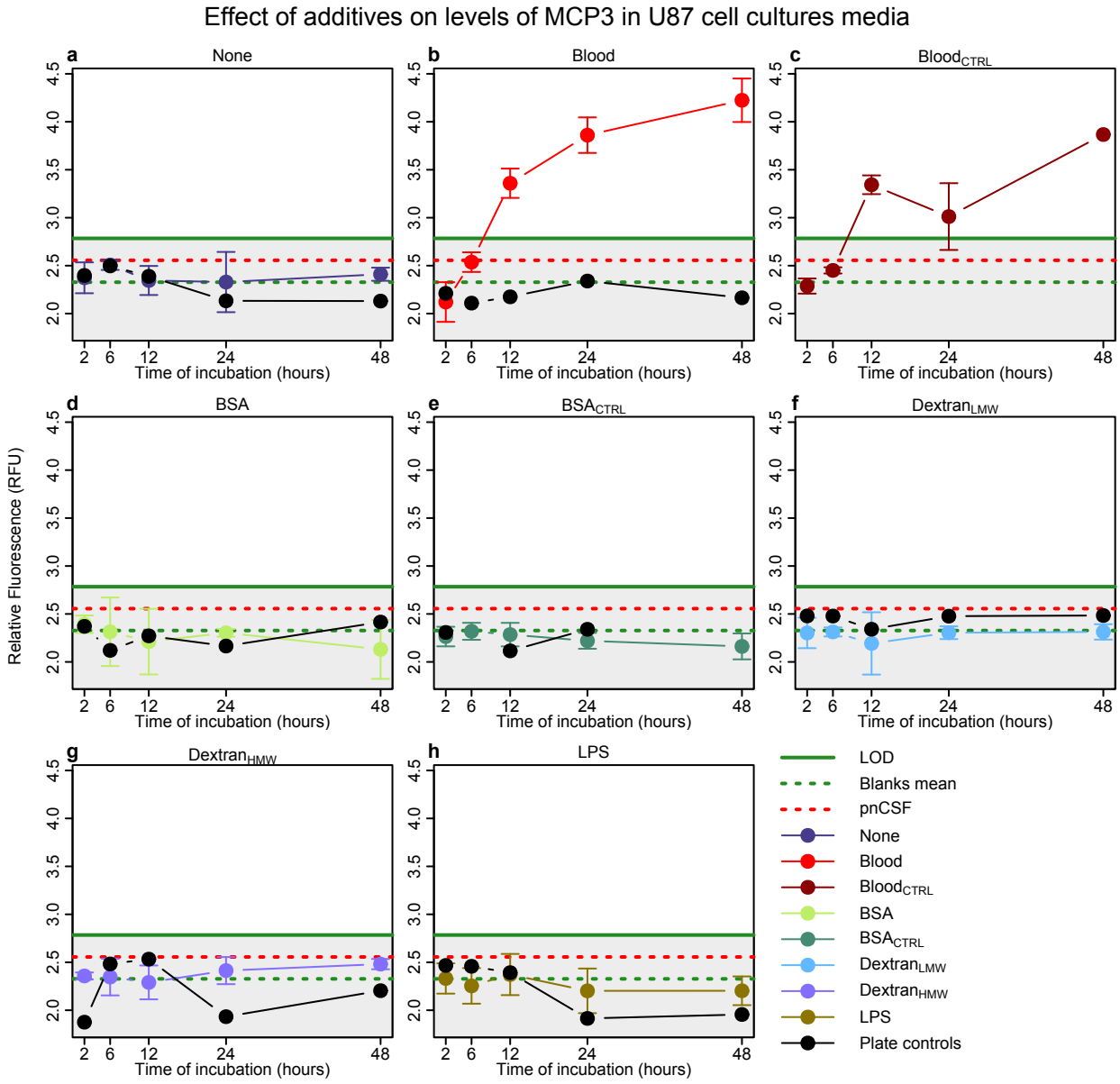

FIGURE H.S118: **Effect of additives on levels of MCP3 in U87 cell cultures media.** Additives along with fresh blood and LPS were added to mycoplasma-free human glial (U87) cells in triplicate wells of a 24-well plate and incubated for up to 48 h to measure the effect on levels of proteins measured in the cell media. Media was collected and frozen from successive triplicates at different intervals, then analyzed with the ACM. Each graph compares MCP3 values from cells incubated with a different additive to cells not incubated with additives located in the same 24-well plate. Plates in **c** and **e** did not contain any U87 cells, and **c** also did not have controls on the plate.

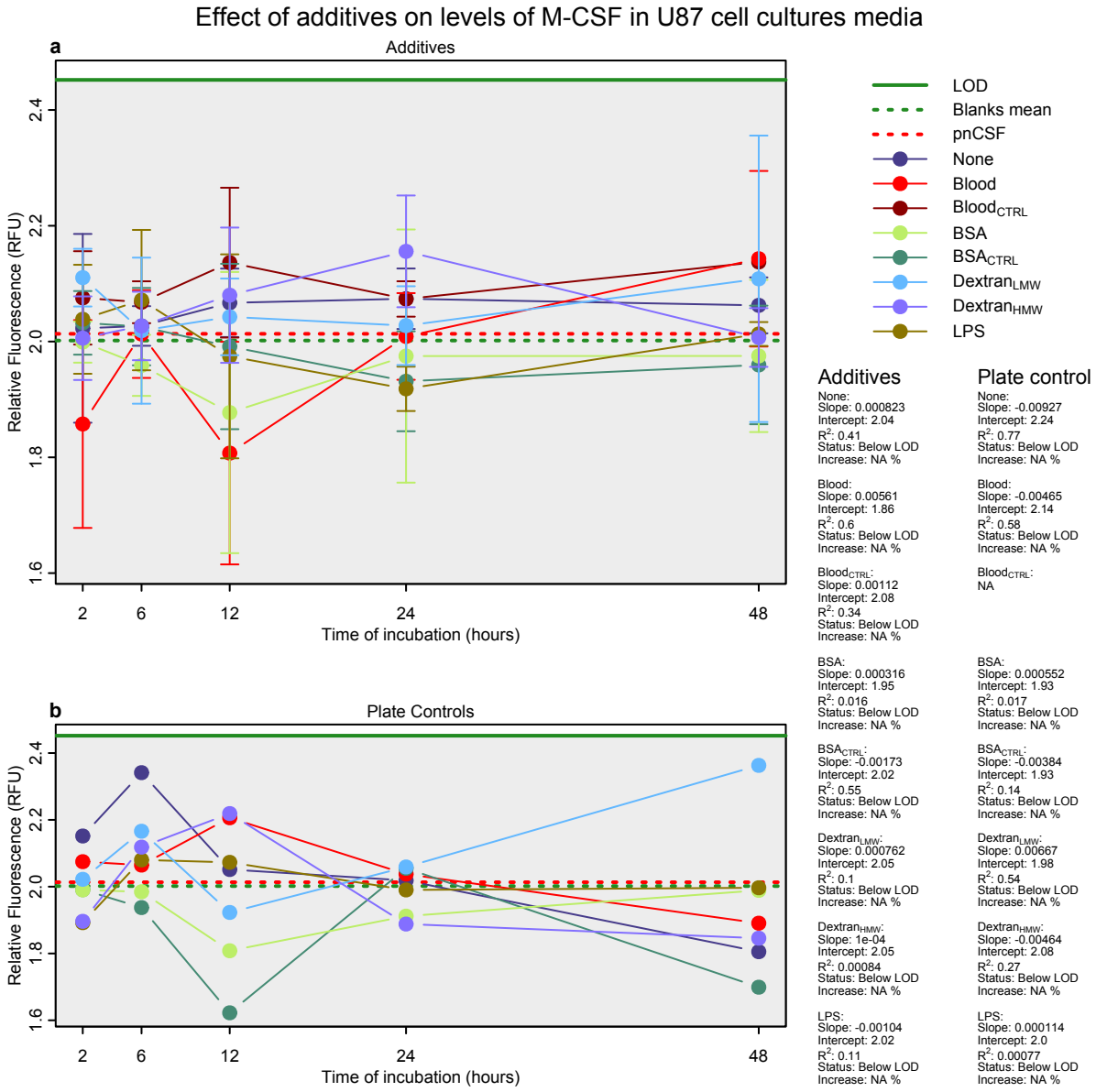

FIGURE H.S119: **Effect of additives on levels of M-CSF in U87 cell cultures media.** Additives along with fresh blood and LPS were added to mycoplasma-free human glial (U87) cells in triplicate wells of a 24-well plate and incubated for up to 48 h to measure the effect on levels of proteins measured in the cell media. Media was collected and frozen from successive triplicates at different intervals, then analyzed with the ACM. **a** Average values for M-CSF from three replicates for each point in every 24-well plate where a different additive was applied. **b** Data from the control cell media in each plate.

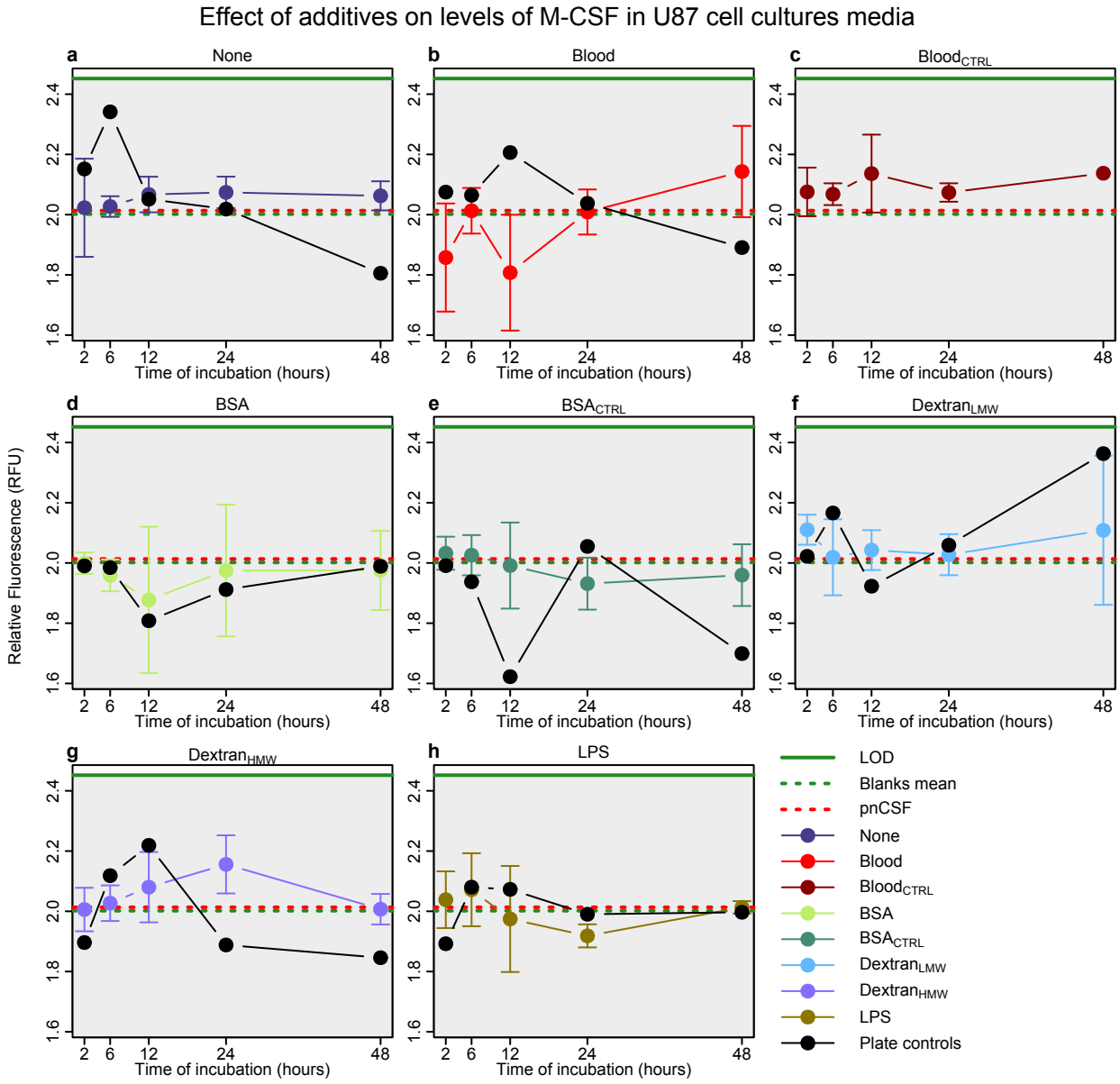

FIGURE H.S120: **Effect of additives on levels of M-CSF in U87 cell cultures media.** Additives along with fresh blood and LPS were added to mycoplasma-free human glial (U87) cells in triplicate wells of a 24-well plate and incubated for up to 48 h to measure the effect on levels of proteins measured in the cell media. Media was collected and frozen from successive triplicates at different intervals, then analyzed with the ACM. Each graph compares M-CSF values from cells incubated with a different additive to cells not incubated with additives located in the same 24-well plate. Plates in **c** and **e** did not contain any U87 cells, and **c** also did not have controls on the plate.

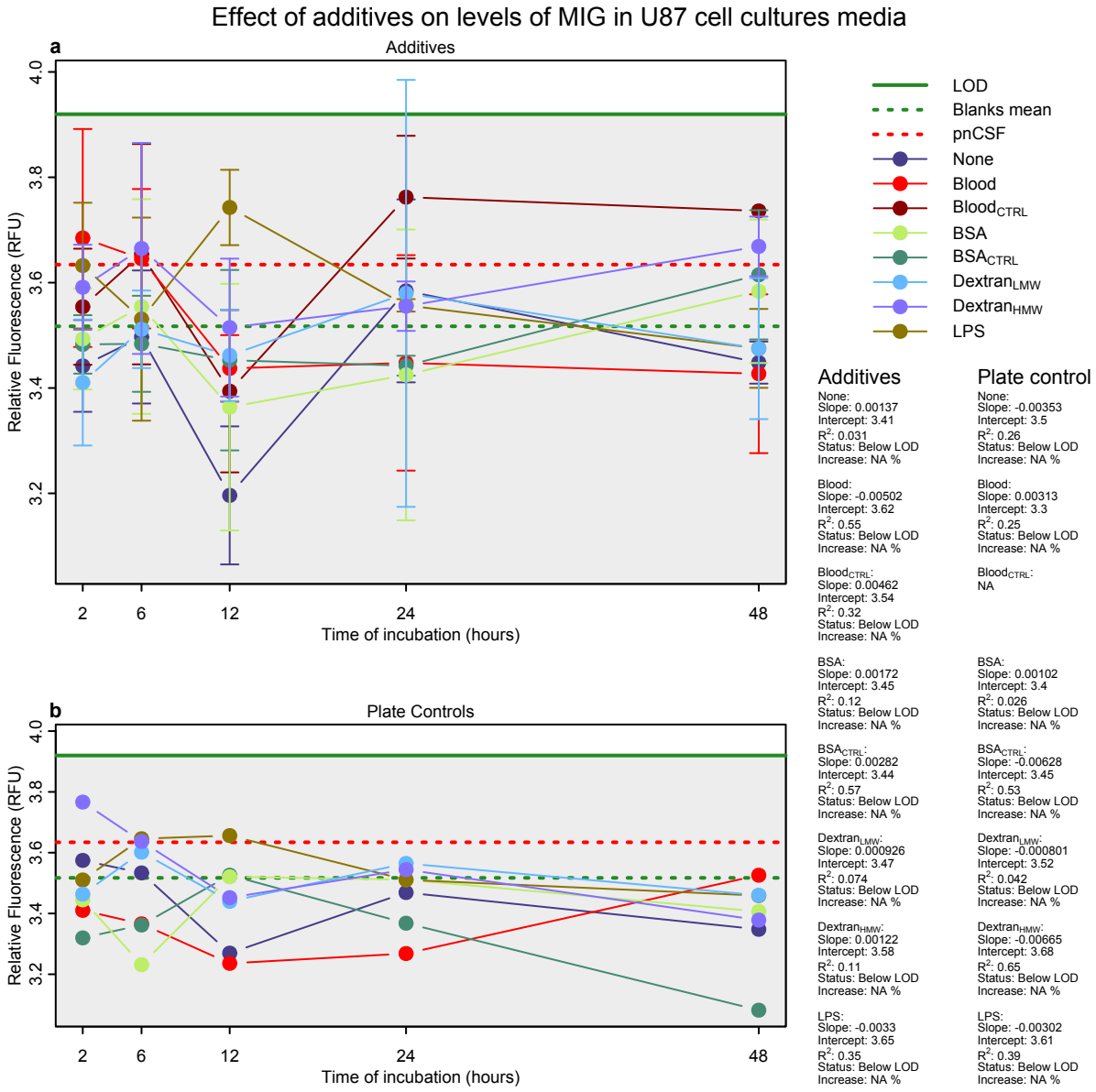

FIGURE H.S121: **Effect of additives on levels of MIG in U87 cell cultures media.** Additives along with fresh blood and LPS were added to mycoplasma-free human glial (U87) cells in triplicate wells of a 24-well plate and incubated for up to 48 h to measure the effect on levels of proteins measured in the cell media. Media was collected and frozen from successive triplicates at different intervals, then analyzed with the ACM. **a** Average values for MIG from three replicates for each point in every 24-well plate where a different additive was applied. **b** Data from the control cell media in each plate.

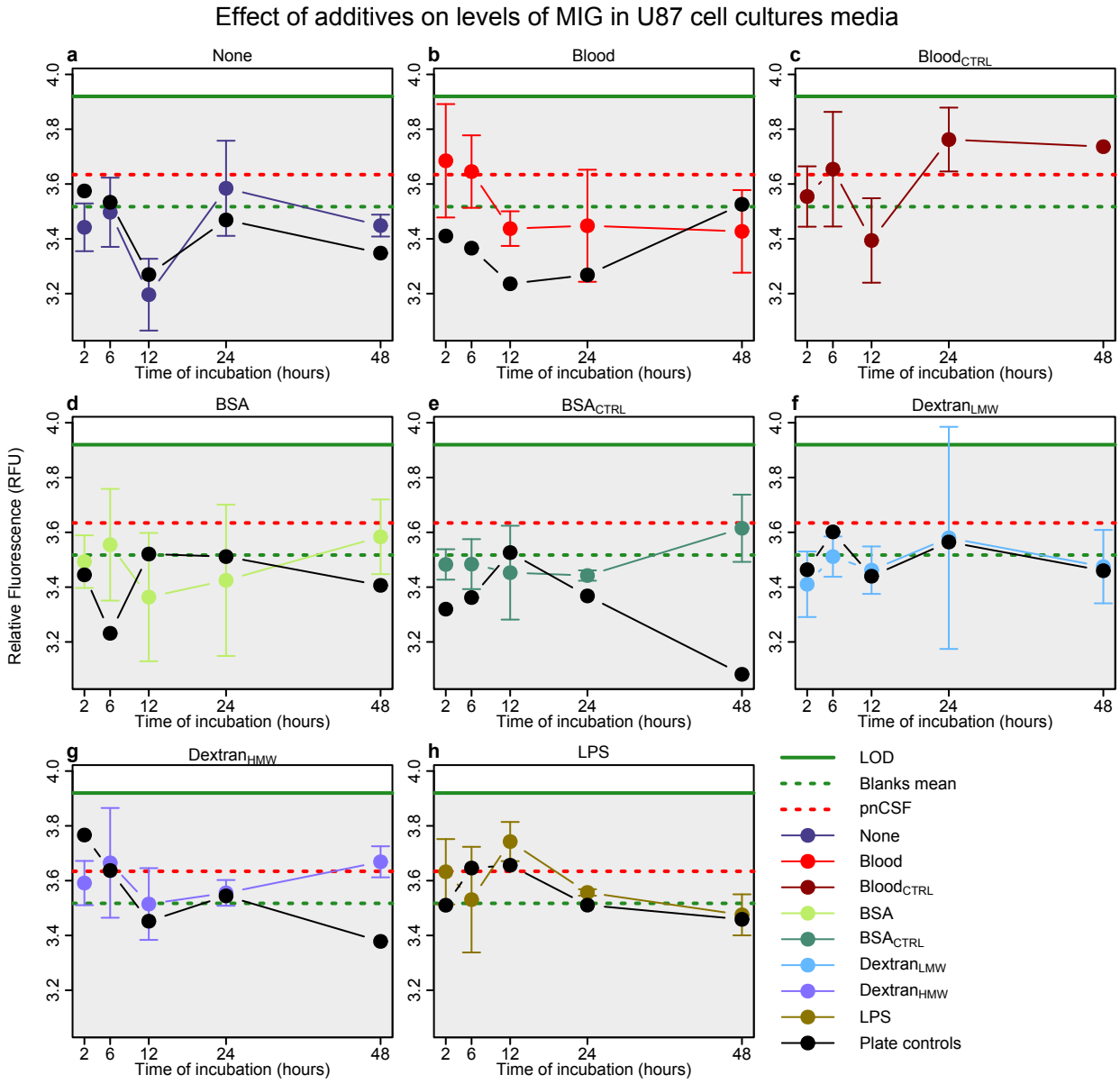

FIGURE H.S122: **Effect of additives on levels of MIG in U87 cell cultures media.** Additives along with fresh blood and LPS were added to mycoplasma-free human glial (U87) cells in triplicate wells of a 24-well plate and incubated for up to 48 h to measure the effect on levels of proteins measured in the cell media. Media was collected and frozen from successive triplicates at different intervals, then analyzed with the ACM. Each graph compares MIG values from cells incubated with a different additive to cells not incubated with additives located in the same 24-well plate. Plates in **c** and **e** did not contain any U87 cells, and **c** also did not have controls on the plate.

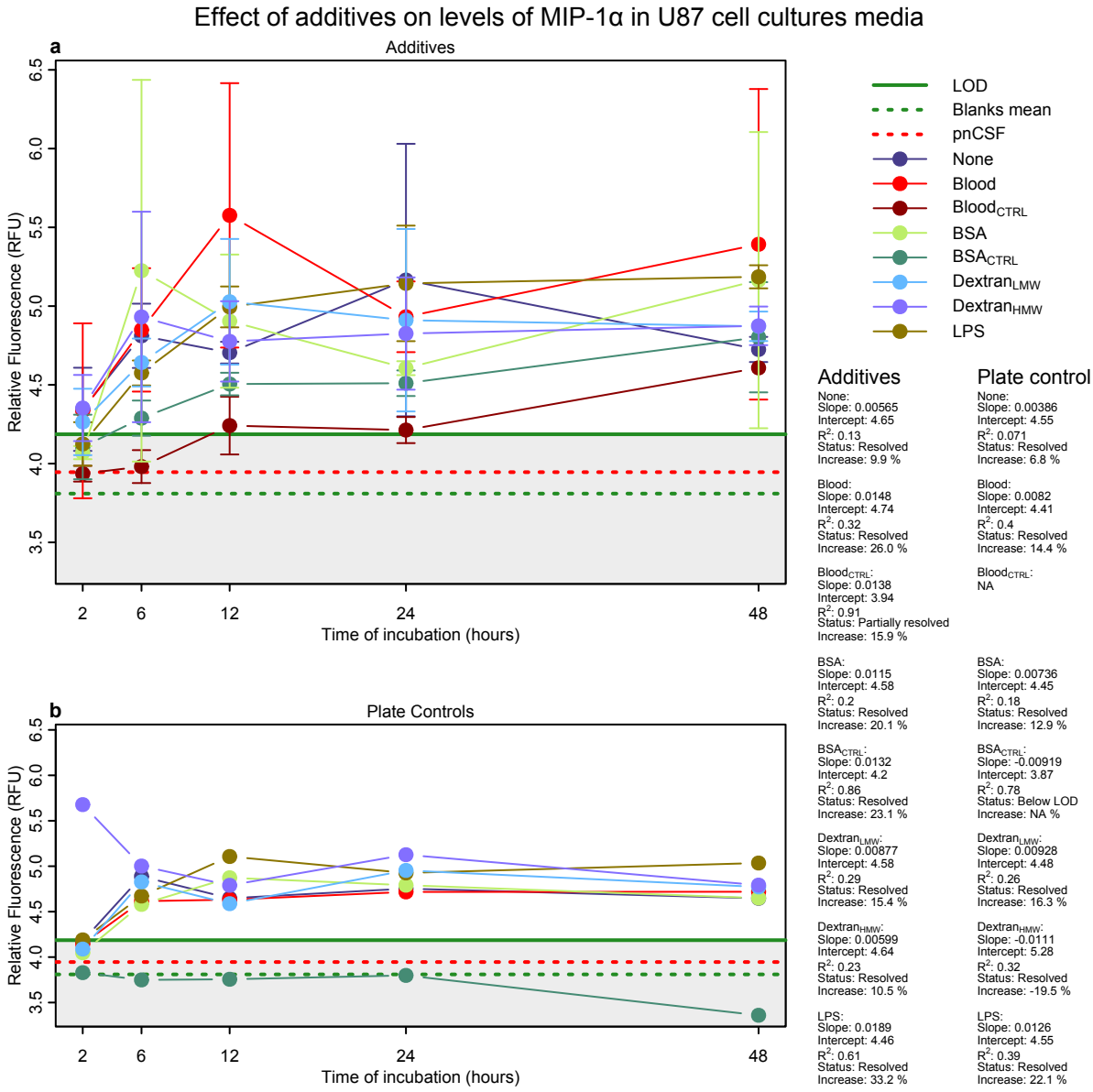

FIGURE H.S123: **Effect of additives on levels of MIP-1α in U87 cell cultures media.** Additives along with fresh blood and LPS were added to mycoplasma-free human glial (U87) cells in triplicate wells of a 24-well plate and incubated for up to 48 h to measure the effect on levels of proteins measured in the cell media. Media was collected and frozen from successive triplicates at different intervals, then analyzed with the ACM. **a** Average values for MIP-1α from three replicates for each point in every 24-well plate where a different additive was applied. **b** Data from the control cell media in each plate.

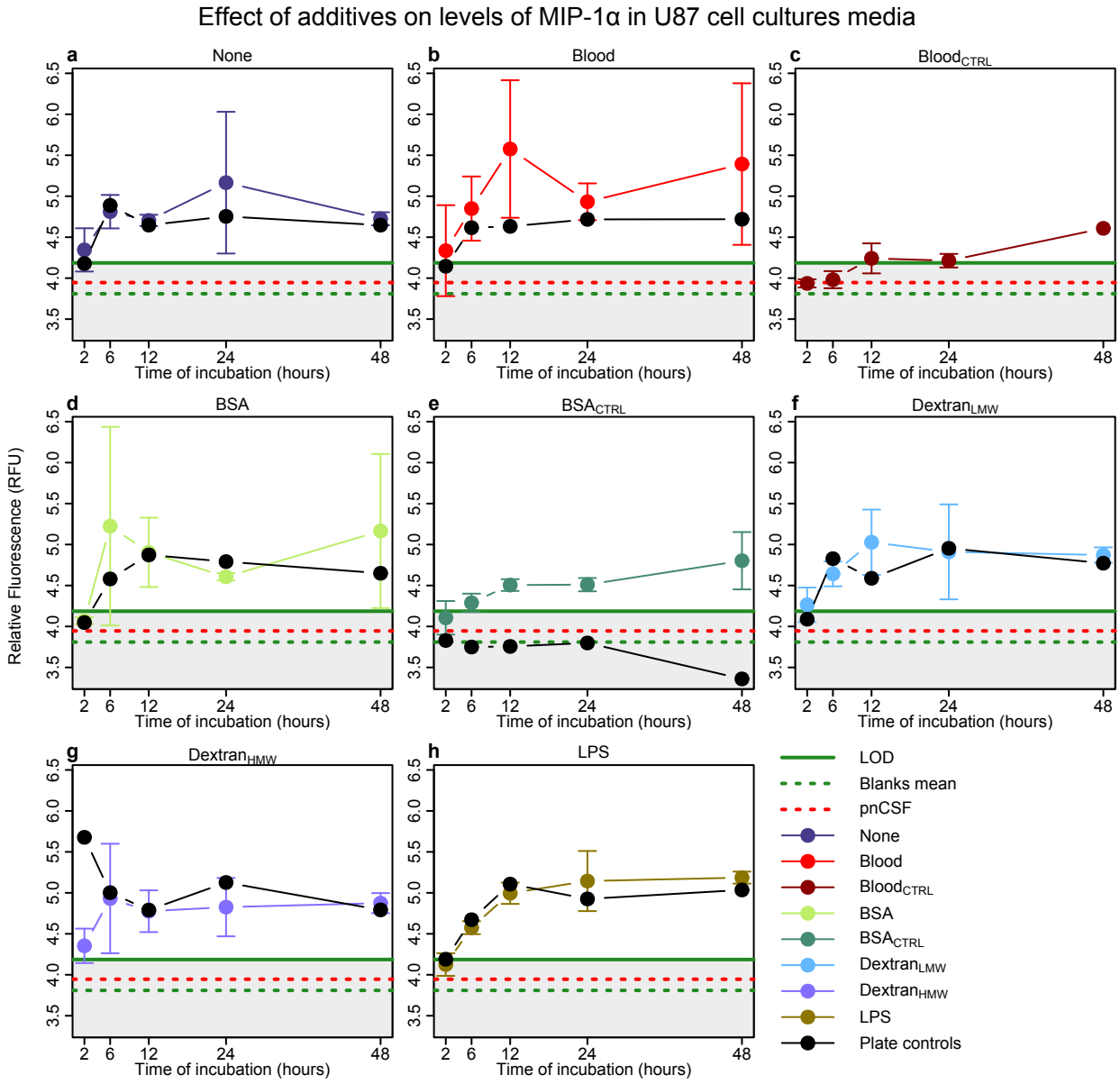

FIGURE H.S124: **Effect of additives on levels of MIP-1α in U87 cell cultures media.** Additives along with fresh blood and LPS were added to mycoplasma-free human glial (U87) cells in triplicate wells of a 24-well plate and incubated for up to 48 h to measure the effect on levels of proteins measured in the cell media. Media was collected and frozen from successive triplicates at different intervals, then analyzed with the ACM. Each graph compares MIP-1α values from cells incubated with a different additive to cells not incubated with additives located in the same 24-well plate. Plates in **c** and **e** did not contain any U87 cells, and **c** also did not have controls on the plate.

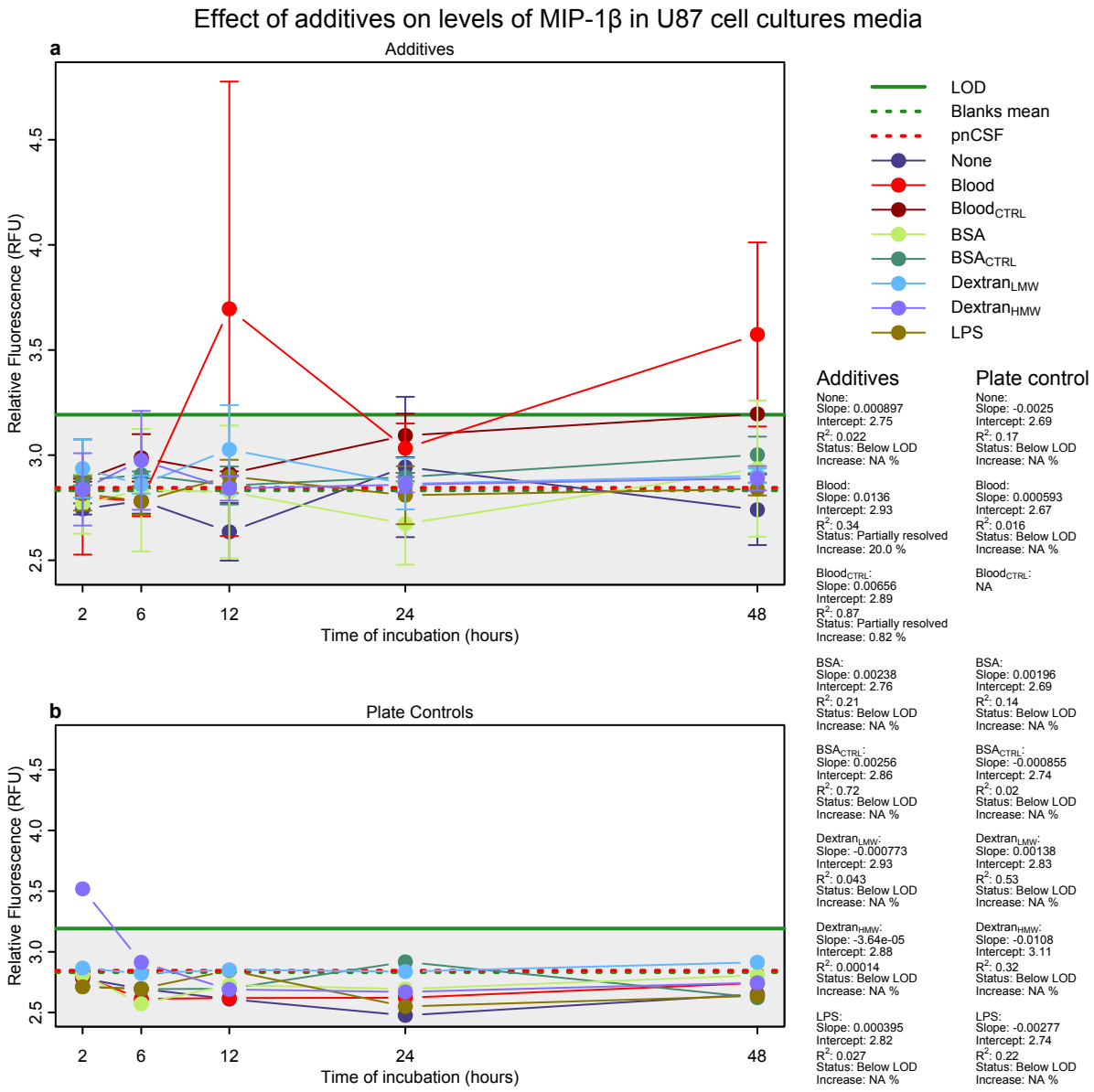

FIGURE H.S125: **Effect of additives on levels of MIP-1β in U87 cell cultures media.** Additives along with fresh blood and LPS were added to mycoplasma-free human glial (U87) cells in triplicate wells of a 24-well plate and incubated for up to 48 h to measure the effect on levels of proteins measured in the cell media. Media was collected and frozen from successive triplicates at different intervals, then analyzed with the ACM. **a** Average values for MIP-1β from three replicates for each point in every 24-well plate where a different additive was applied. **b** Data from the control cell media in each plate.

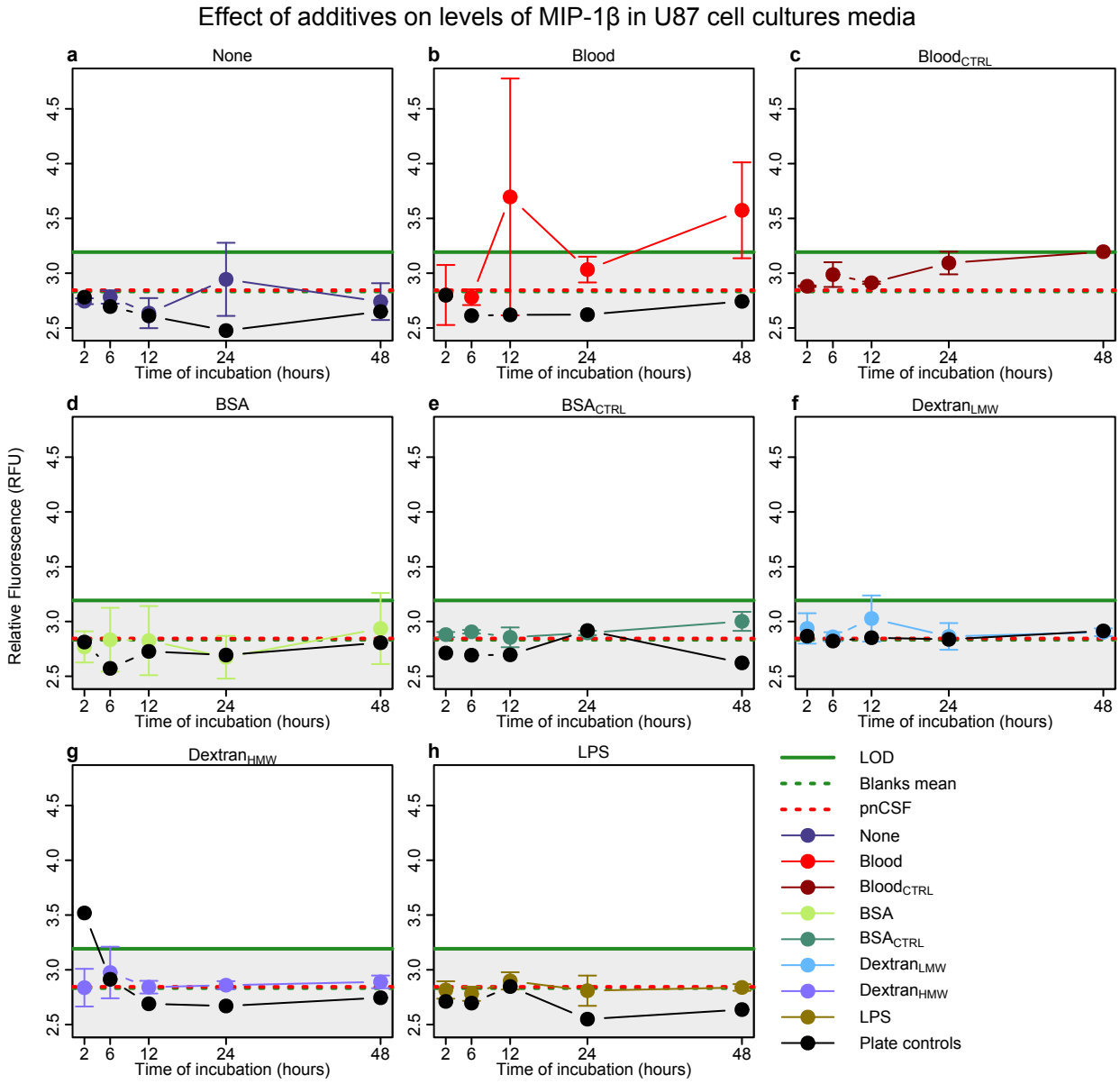

FIGURE H.S126: **Effect of additives on levels of MIP-1β in U87 cell cultures media.** Additives along with fresh blood and LPS were added to mycoplasma-free human glial (U87) cells in triplicate wells of a 24-well plate and incubated for up to 48 h to measure the effect on levels of proteins measured in the cell media. Media was collected and frozen from successive triplicates at different intervals, then analyzed with the ACM. Each graph compares MIP-1β values from cells incubated with a different additive to cells not incubated with additives located in the same 24-well plate. Plates in **c** and **e** did not contain any U87 cells, and **c** also did not have controls on the plate.

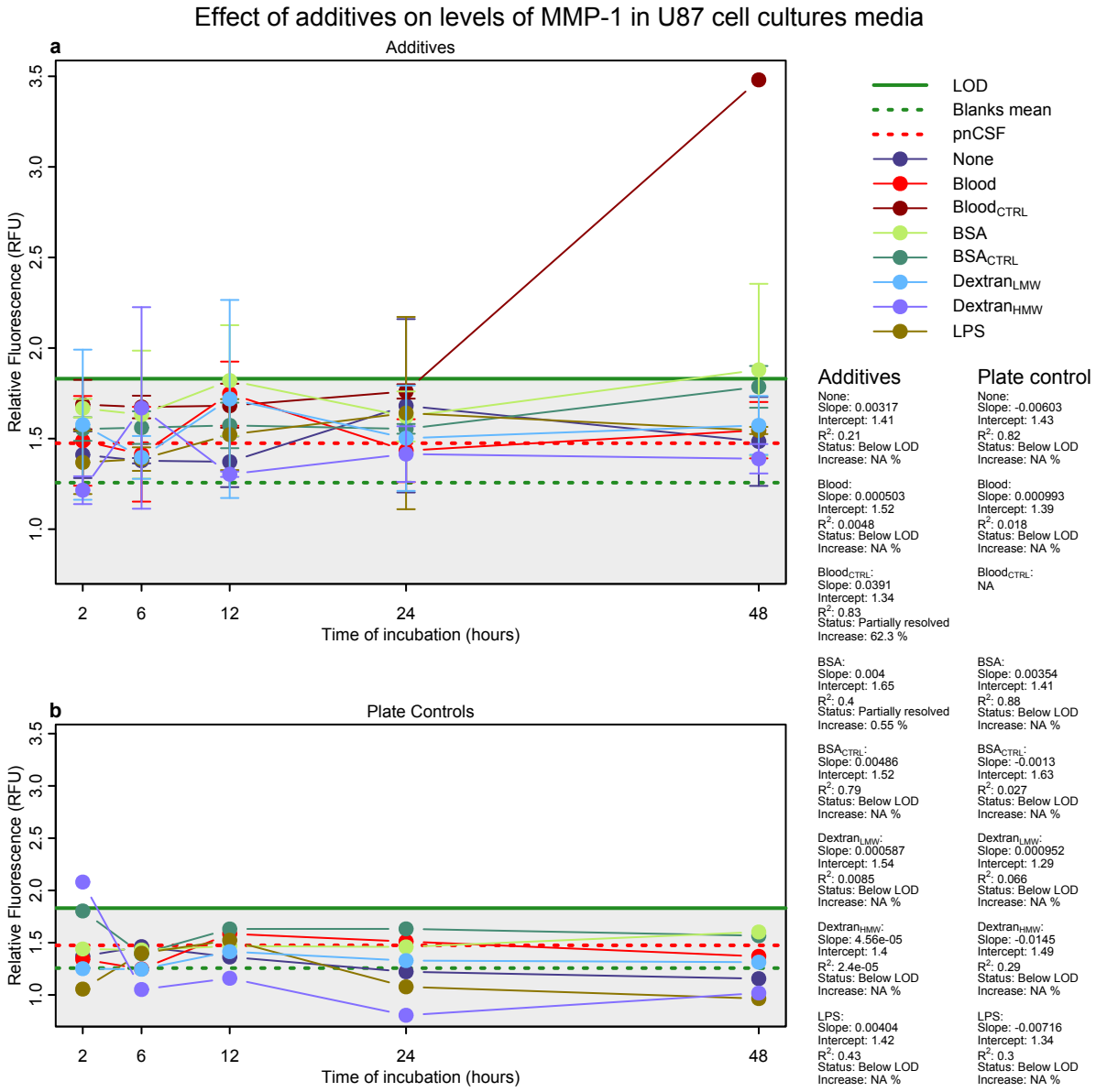

FIGURE H.S127: **Effect of additives on levels of MMP-1 in U87 cell cultures media.** Additives along with fresh blood and LPS were added to mycoplasma-free human glial (U87) cells in triplicate wells of a 24-well plate and incubated for up to 48 h to measure the effect on levels of proteins measured in the cell media. Media was collected and frozen from successive triplicates at different intervals, then analyzed with the ACM. **a** Average values for MMP-1 from three replicates for each point in every 24-well plate where a different additive was applied. **b** Data from the control cell media in each plate.

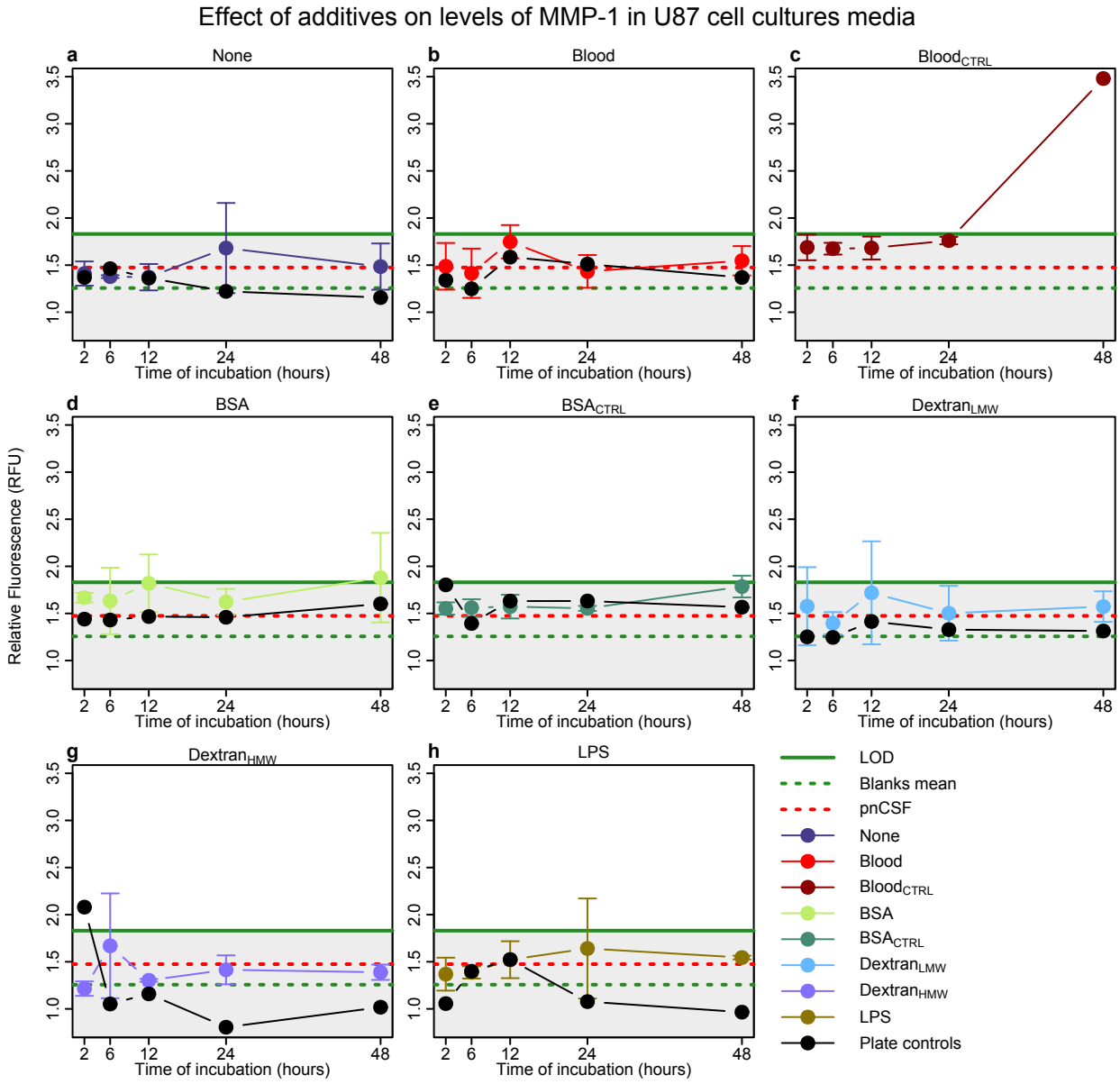

FIGURE H.S128: **Effect of additives on levels of MMP-1 in U87 cell cultures media.** Additives along with fresh blood and LPS were added to mycoplasma-free human glial (U87) cells in triplicate wells of a 24-well plate and incubated for up to 48 h to measure the effect on levels of proteins measured in the cell media. Media was collected and frozen from successive triplicates at different intervals, then analyzed with the ACM. Each graph compares MMP-1 values from cells incubated with a different additive to cells not incubated with additives located in the same 24-well plate. Plates in **c** and **e** did not contain any U87 cells, and **c** also did not have controls on the plate.

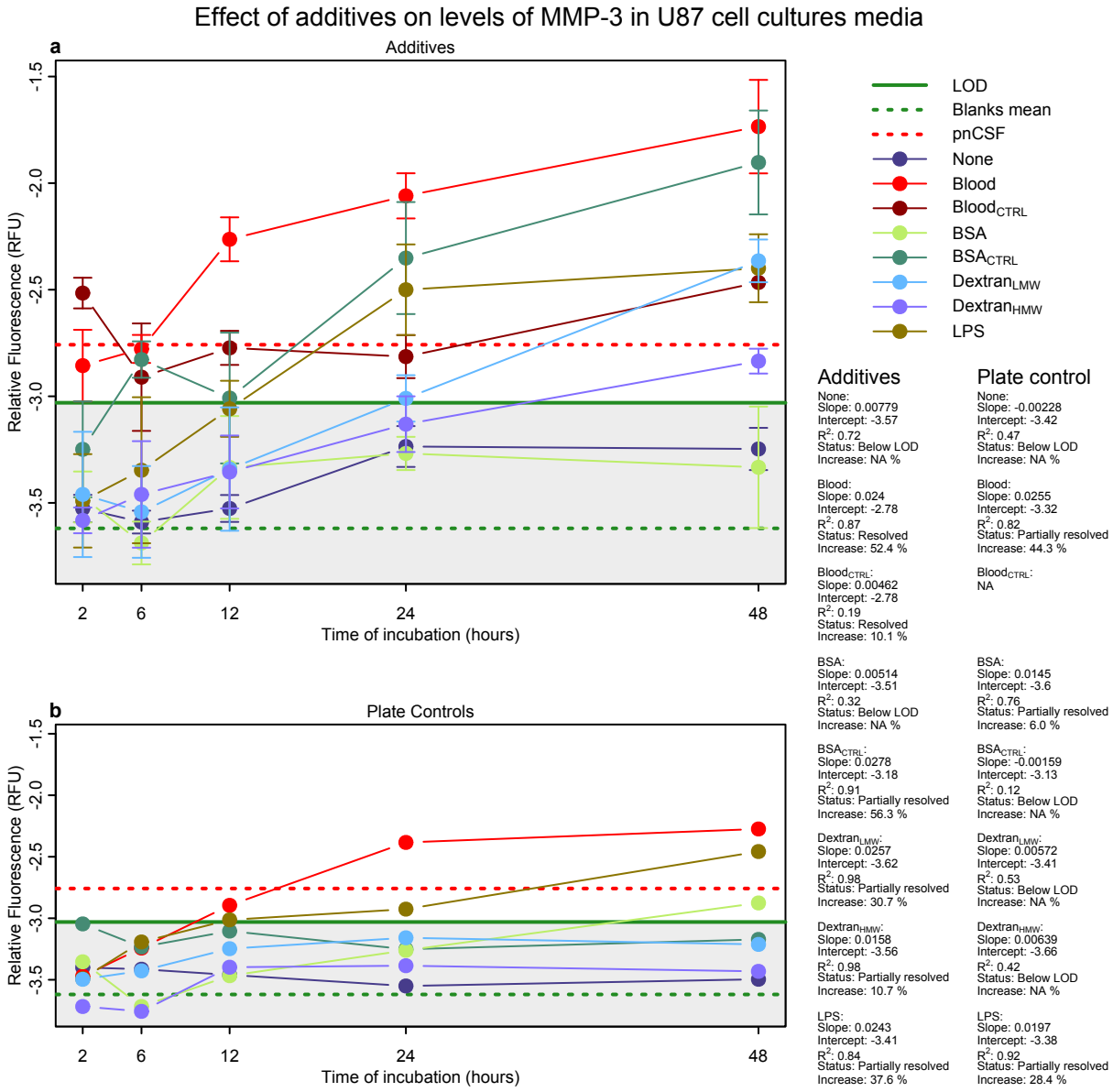

FIGURE H.S129: **Effect of additives on levels of MMP-3 in U87 cell cultures media.** Additives along with fresh blood and LPS were added to mycoplasma-free human glial (U87) cells in triplicate wells of a 24-well plate and incubated for up to 48 h to measure the effect on levels of proteins measured in the cell media. Media was collected and frozen from successive triplicates at different intervals, then analyzed with the ACM. **a** Average values for MMP-3 from three replicates for each point in every 24-well plate where a different additive was applied. **b** Data from the control cell media in each plate.

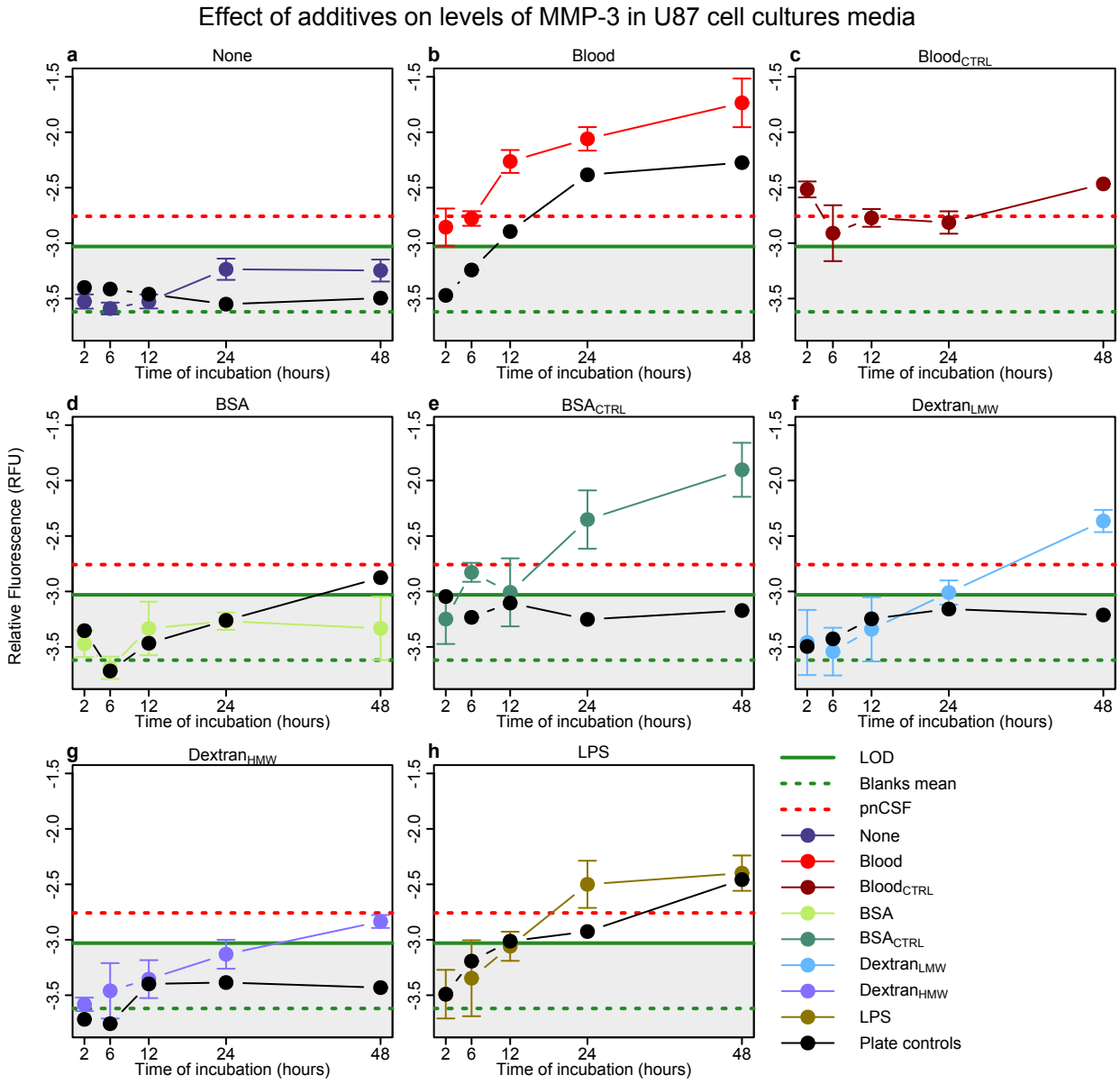

FIGURE H.S130: **Effect of additives on levels of MMP-3 in U87 cell cultures media.** Additives along with fresh blood and LPS were added to mycoplasma-free human glial (U87) cells in triplicate wells of a 24-well plate and incubated for up to 48 h to measure the effect on levels of proteins measured in the cell media. Media was collected and frozen from successive triplicates at different intervals, then analyzed with the ACM. Each graph compares MMP-3 values from cells incubated with a different additive to cells not incubated with additives located in the same 24-well plate. Plates in **c** and **e** did not contain any U87 cells, and **c** also did not have controls on the plate.

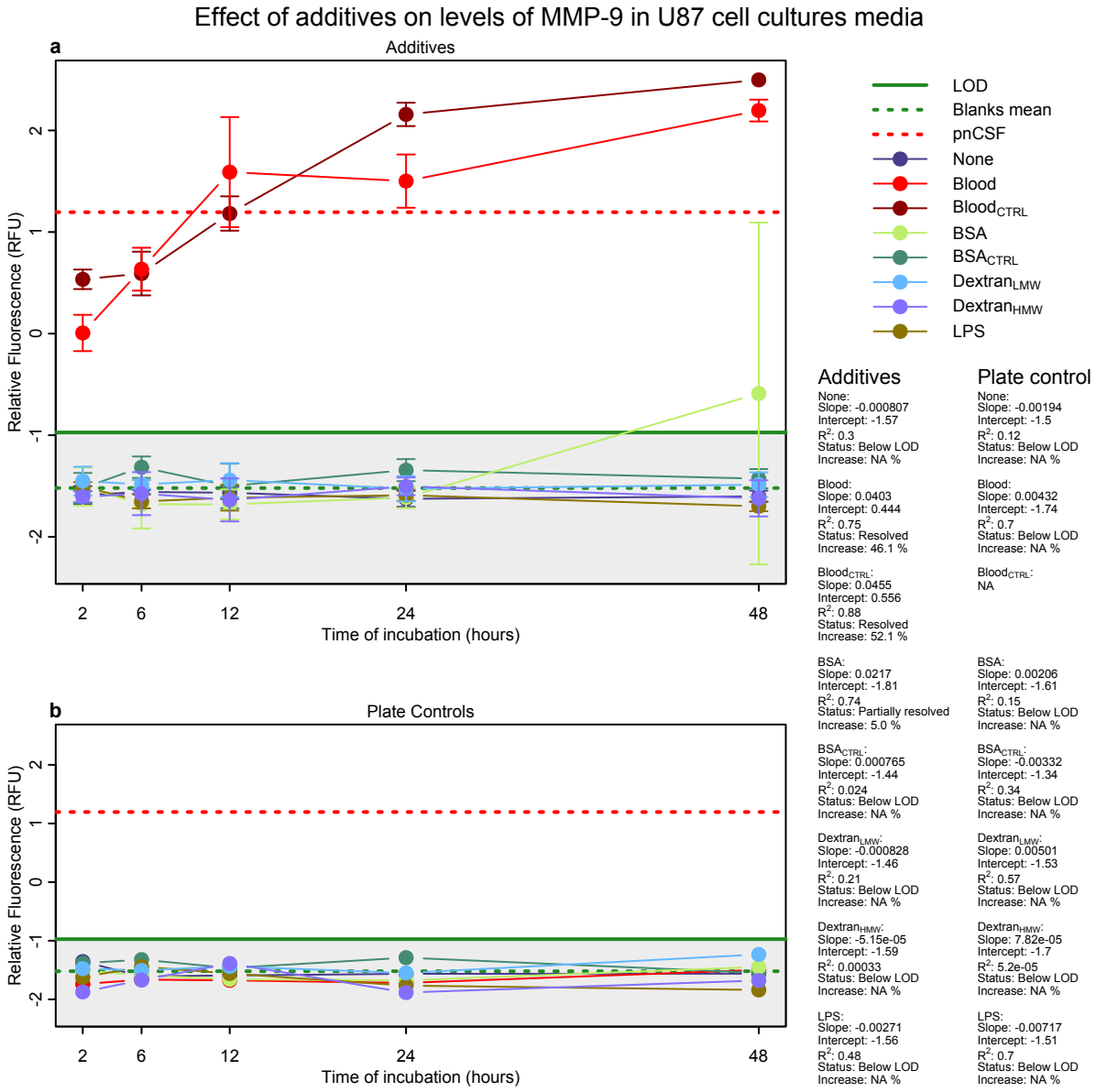

FIGURE H.S131: **Effect of additives on levels of MMP-9 in U87 cell cultures media.** Additives along with fresh blood and LPS were added to mycoplasma-free human glial (U87) cells in triplicate wells of a 24-well plate and incubated for up to 48 h to measure the effect on levels of proteins measured in the cell media. Media was collected and frozen from successive triplicates at different intervals, then analyzed with the ACM. **a** Average values for MMP-9 from three replicates for each point in every 24-well plate where a different additive was applied. **b** Data from the control cell media in each plate.

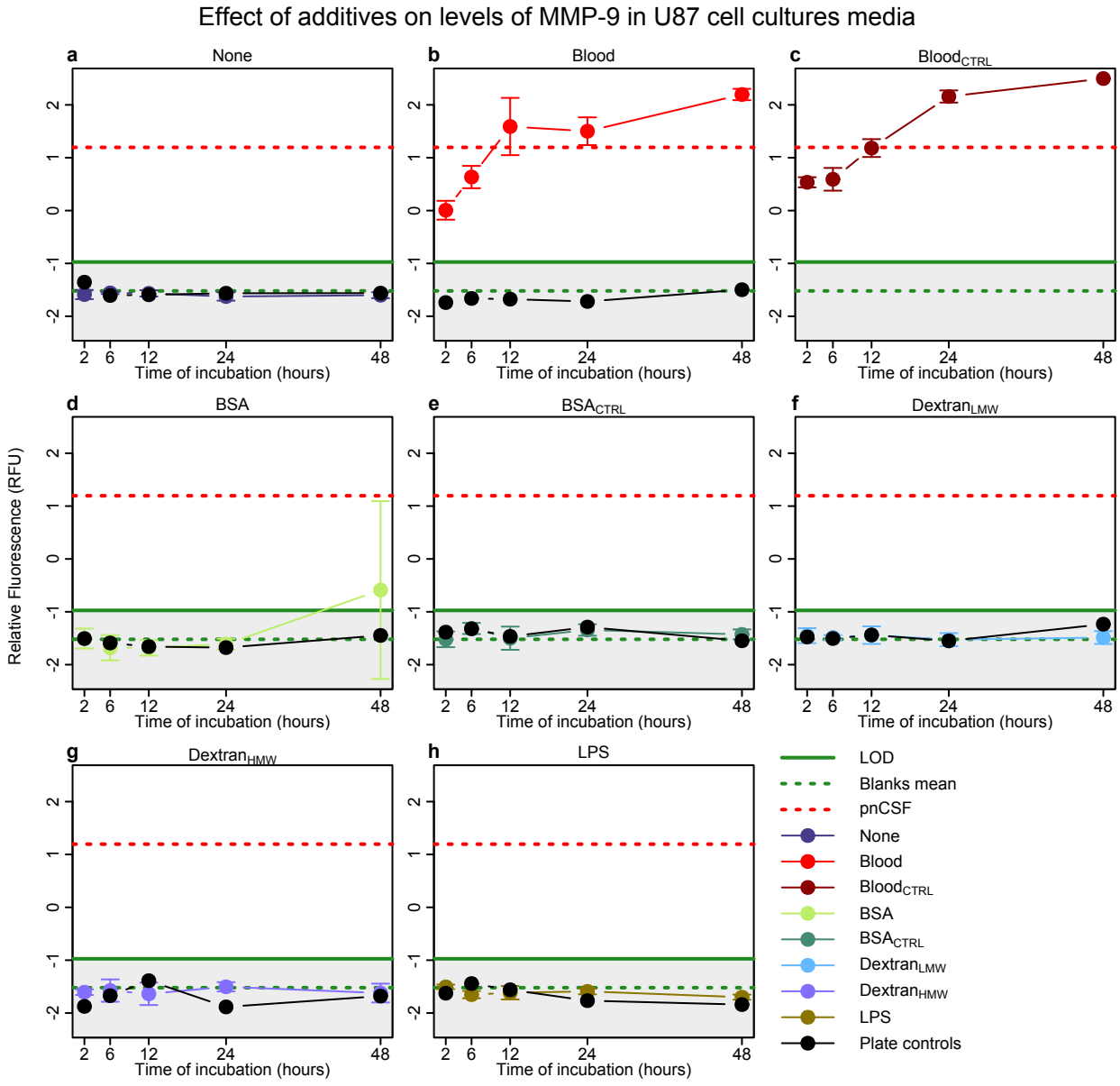

FIGURE H.S132: **Effect of additives on levels of MMP-9 in U87 cell cultures media.** Additives along with fresh blood and LPS were added to mycoplasma-free human glial (U87) cells in triplicate wells of a 24-well plate and incubated for up to 48 h to measure the effect on levels of proteins measured in the cell media. Media was collected and frozen from successive triplicates at different intervals, then analyzed with the ACM. Each graph compares MMP-9 values from cells incubated with a different additive to cells not incubated with additives located in the same 24-well plate. Plates in **c** and **e** did not contain any U87 cells, and **c** also did not have controls on the plate.

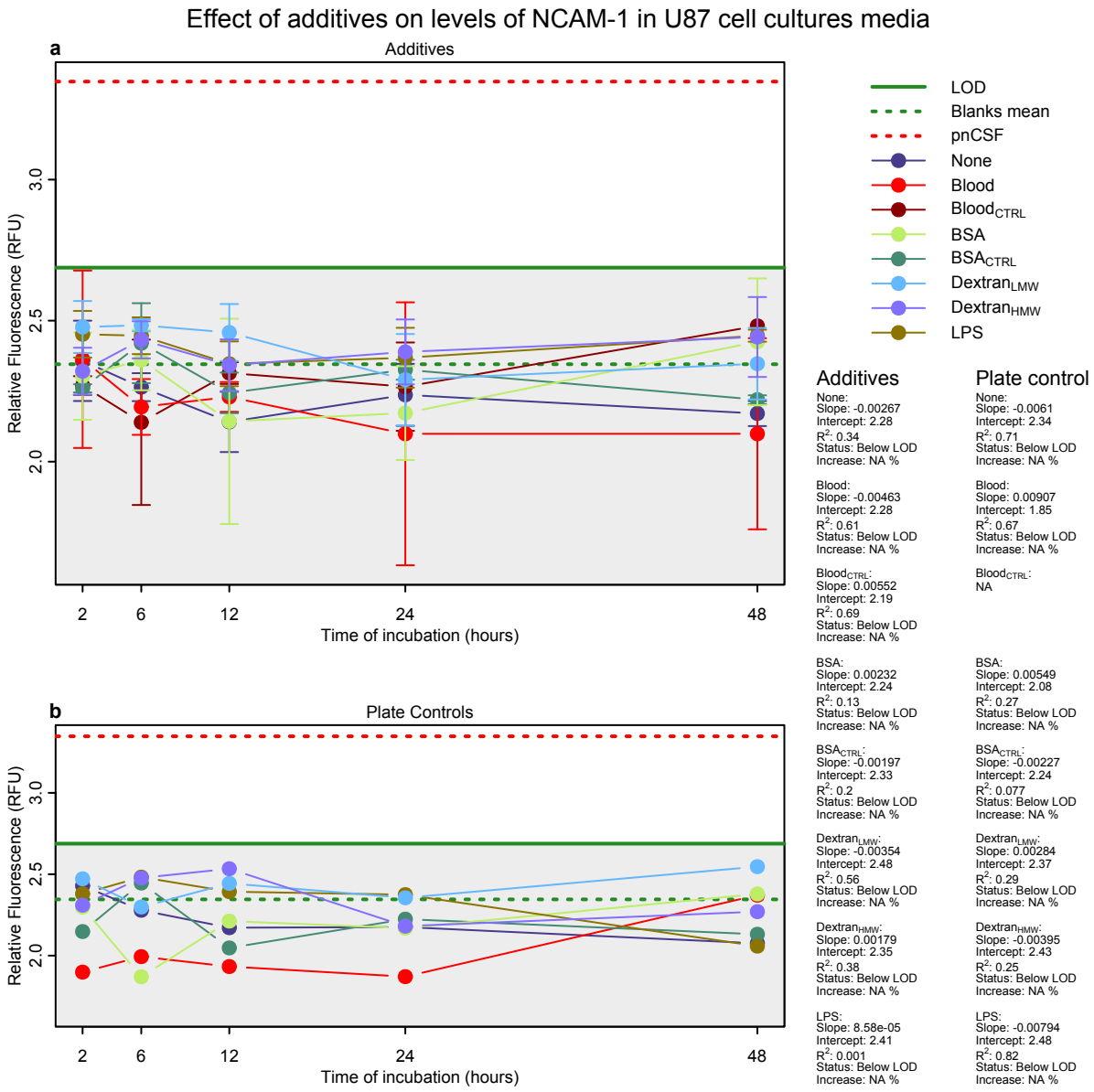

FIGURE H.S133: **Effect of additives on levels of NCAM-1 in U87 cell cultures media.** Additives along with fresh blood and LPS were added to mycoplasma-free human glial (U87) cells in triplicate wells of a 24-well plate and incubated for up to 48 h to measure the effect on levels of proteins measured in the cell media. Media was collected and frozen from successive triplicates at different intervals, then analyzed with the ACM. **a** Average values for NCAM-1 from three replicates for each point in every 24-well plate where a different additive was applied. **b** Data from the control cell media in each plate.

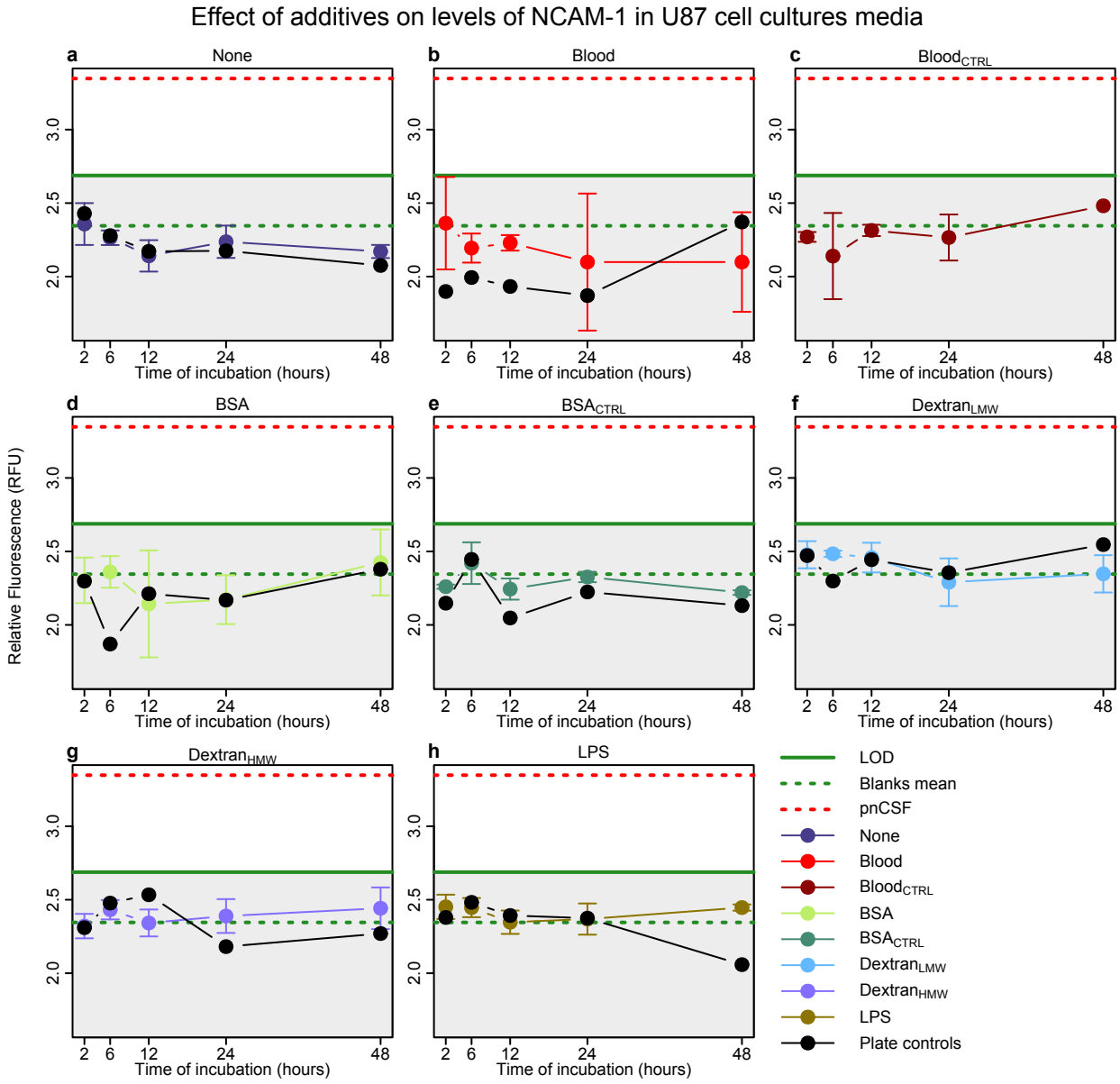

FIGURE H.S134: **Effect of additives on levels of NCAM-1 in U87 cell cultures media.** Additives along with fresh blood and LPS were added to mycoplasma-free human glial (U87) cells in triplicate wells of a 24-well plate and incubated for up to 48 h to measure the effect on levels of proteins measured in the cell media. Media was collected and frozen from successive triplicates at different intervals, then analyzed with the ACM. Each graph compares NCAM-1 values from cells incubated with a different additive to cells not incubated with additives located in the same 24-well plate. Plates in **c** and **e** did not contain any U87 cells, and **c** also did not have controls on the plate.

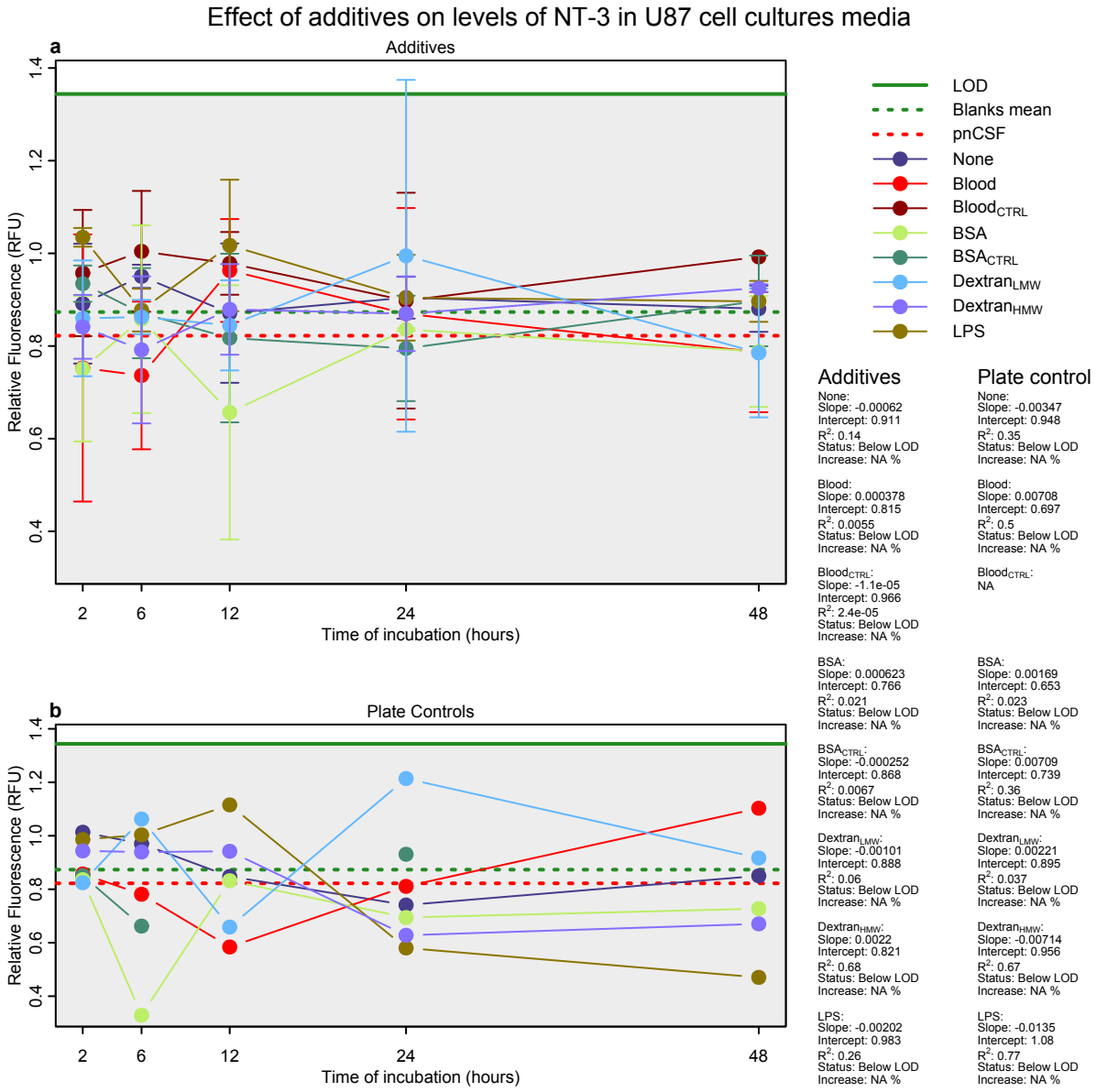

FIGURE H.S135: **Effect of additives on levels of NT-3 in U87 cell cultures media.** Additives along with fresh blood and LPS were added to mycoplasma-free human glial (U87) cells in triplicate wells of a 24-well plate and incubated for up to 48 h to measure the effect on levels of proteins measured in the cell media. Media was collected and frozen from successive triplicates at different intervals, then analyzed with the ACM. **a** Average values for NT-3 from three replicates for each point in every 24-well plate where a different additive was applied. **b** Data from the control cell media in each plate.

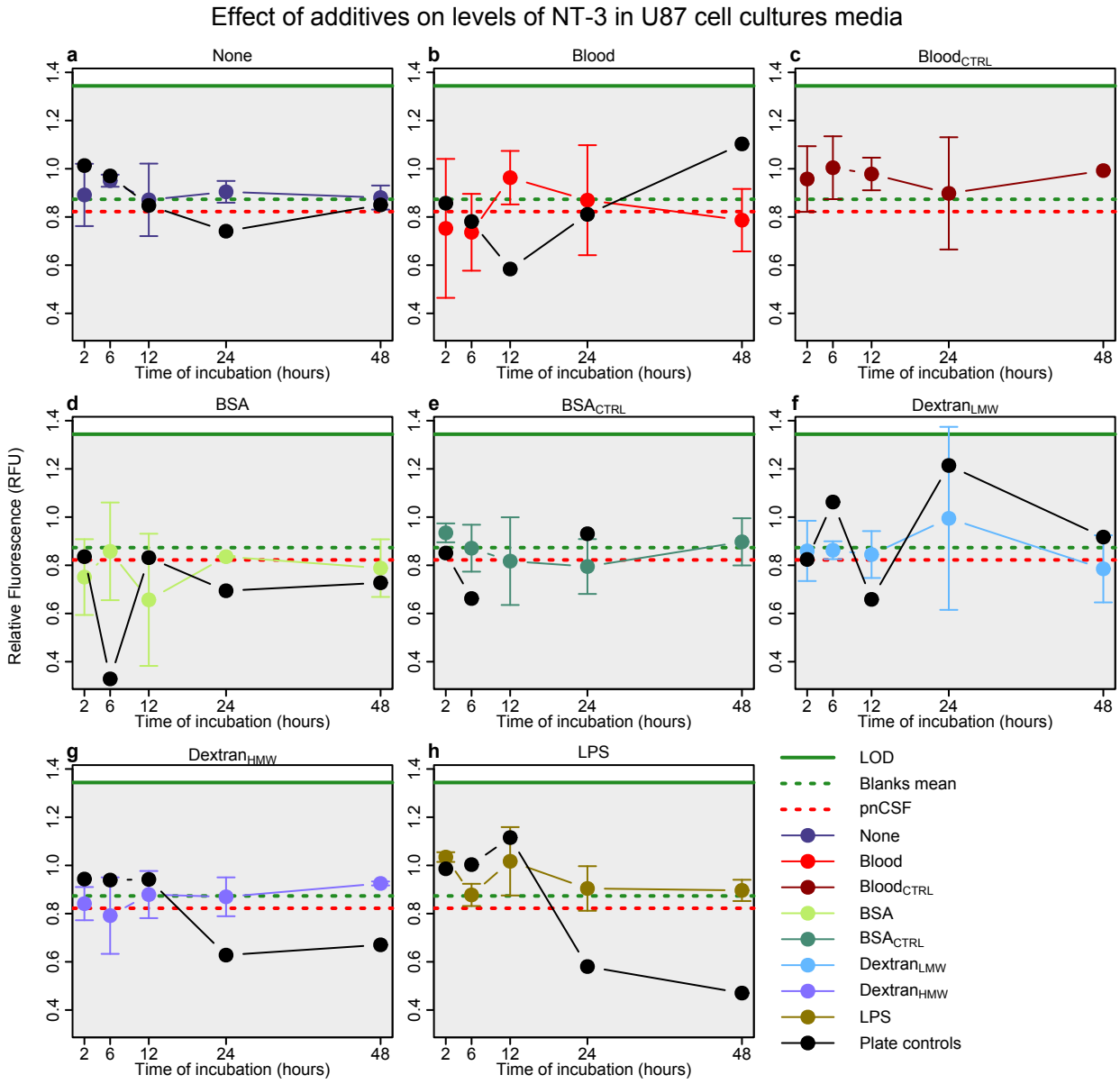

FIGURE H.S136: **Effect of additives on levels of NT-3 in U87 cell cultures media.** Additives along with fresh blood and LPS were added to mycoplasma-free human glial (U87) cells in triplicate wells of a 24-well plate and incubated for up to 48 h to measure the effect on levels of proteins measured in the cell media. Media was collected and frozen from successive triplicates at different intervals, then analyzed with the ACM. Each graph compares NT-3 values from cells incubated with a different additive to cells not incubated with additives located in the same 24-well plate. Plates in **c** and **e** did not contain any U87 cells, and **c** also did not have controls on the plate.

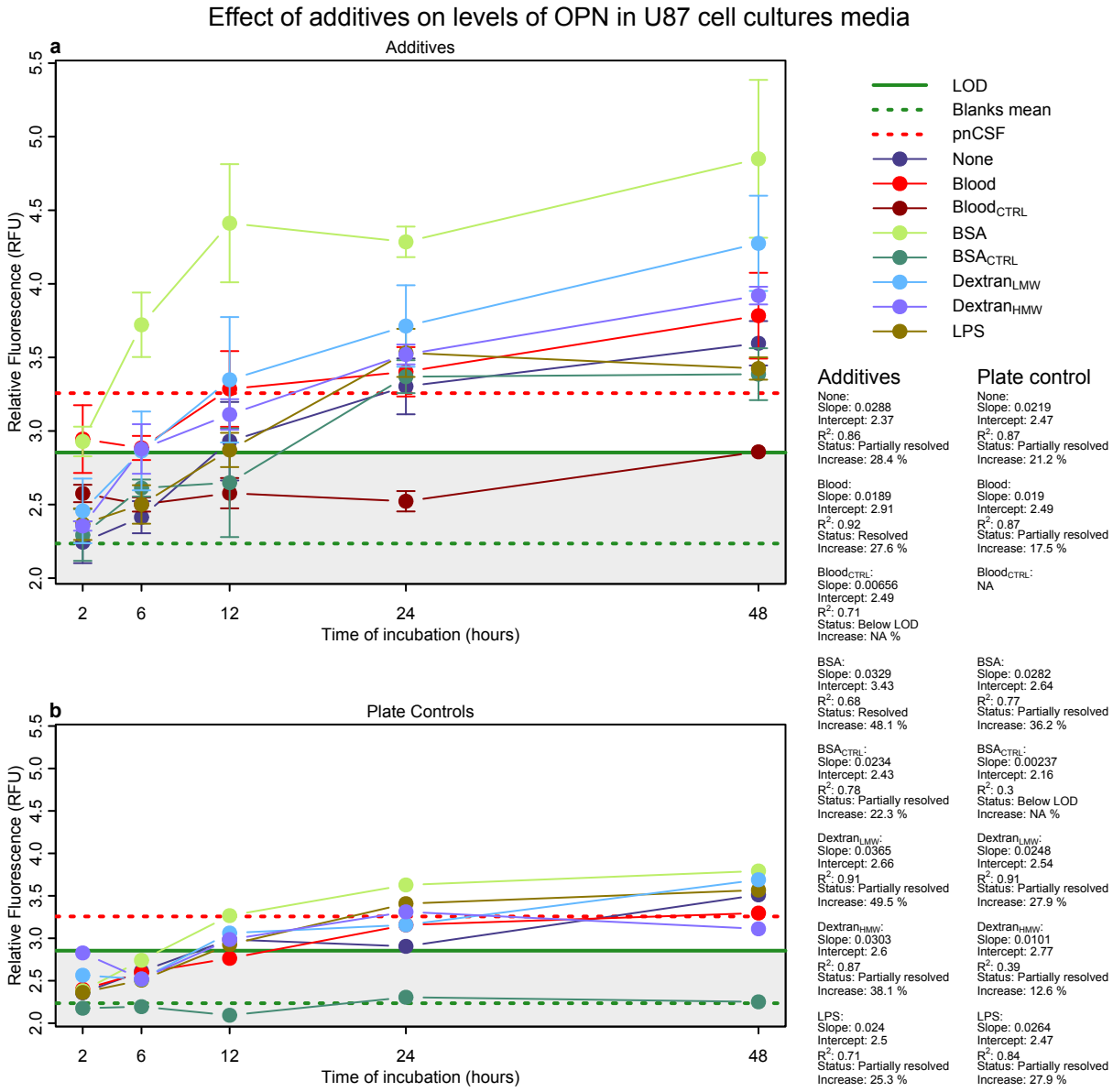

FIGURE H.S137: **Effect of additives on levels of OPN in U87 cell cultures media.** Additives along with fresh blood and LPS were added to mycoplasma-free human glial (U87) cells in triplicate wells of a 24-well plate and incubated for up to 48 h to measure the effect on levels of proteins measured in the cell media. Media was collected and frozen from successive triplicates at different intervals, then analyzed with the ACM. **a** Average values for OPN from three replicates for each point in every 24-well plate where a different additive was applied. **b** Data from the control cell media in each plate.

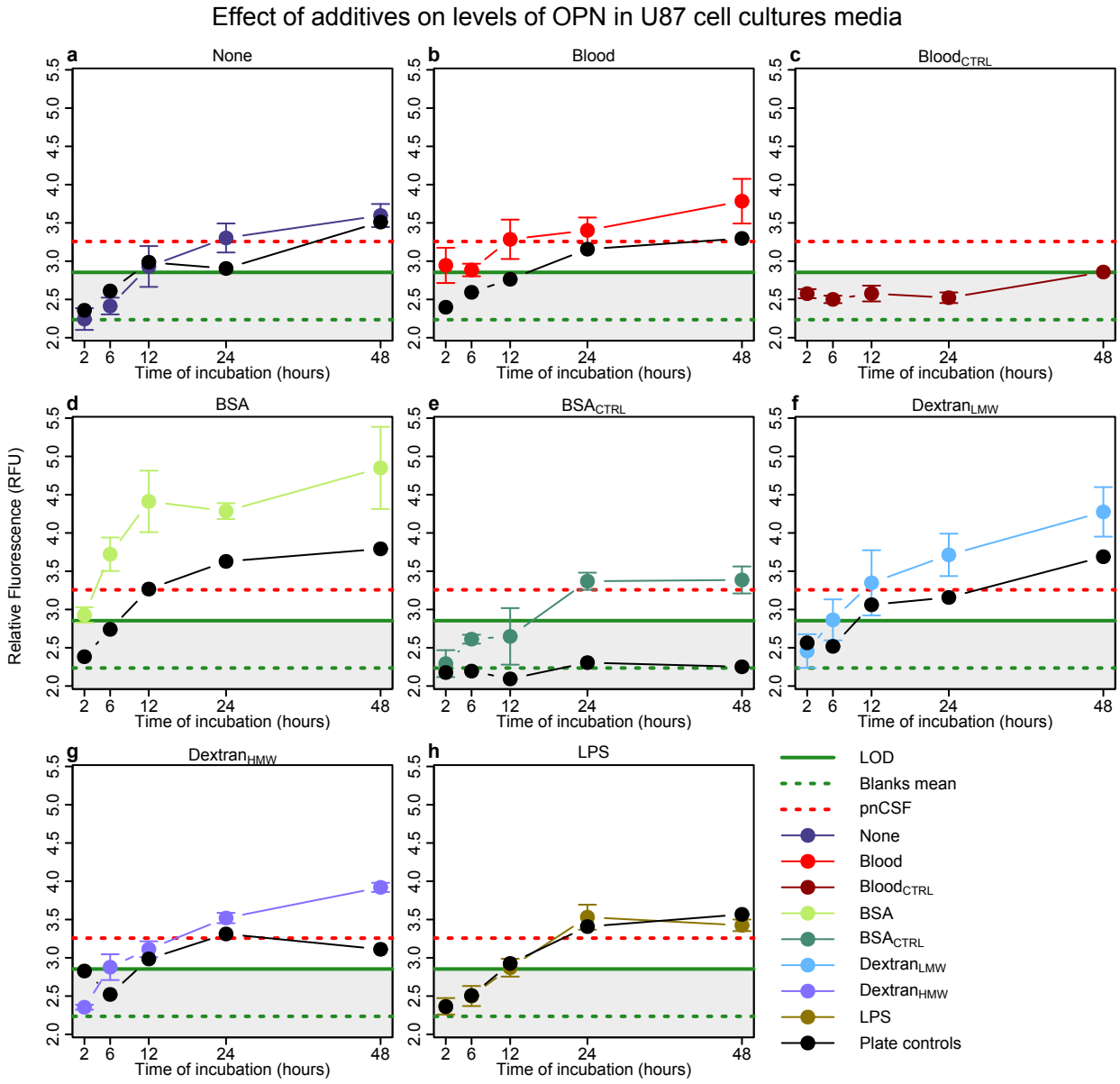

FIGURE H.S138: **Effect of additives on levels of OPN in U87 cell cultures media.** Additives along with fresh blood and LPS were added to mycoplasma-free human glial (U87) cells in triplicate wells of a 24-well plate and incubated for up to 48 h to measure the effect on levels of proteins measured in the cell media. Media was collected and frozen from successive triplicates at different intervals, then analyzed with the ACM. Each graph compares OPN values from cells incubated with a different additive to cells not incubated with additives located in the same 24-well plate. Plates in **c** and **e** did not contain any U87 cells, and **c** also did not have controls on the plate.

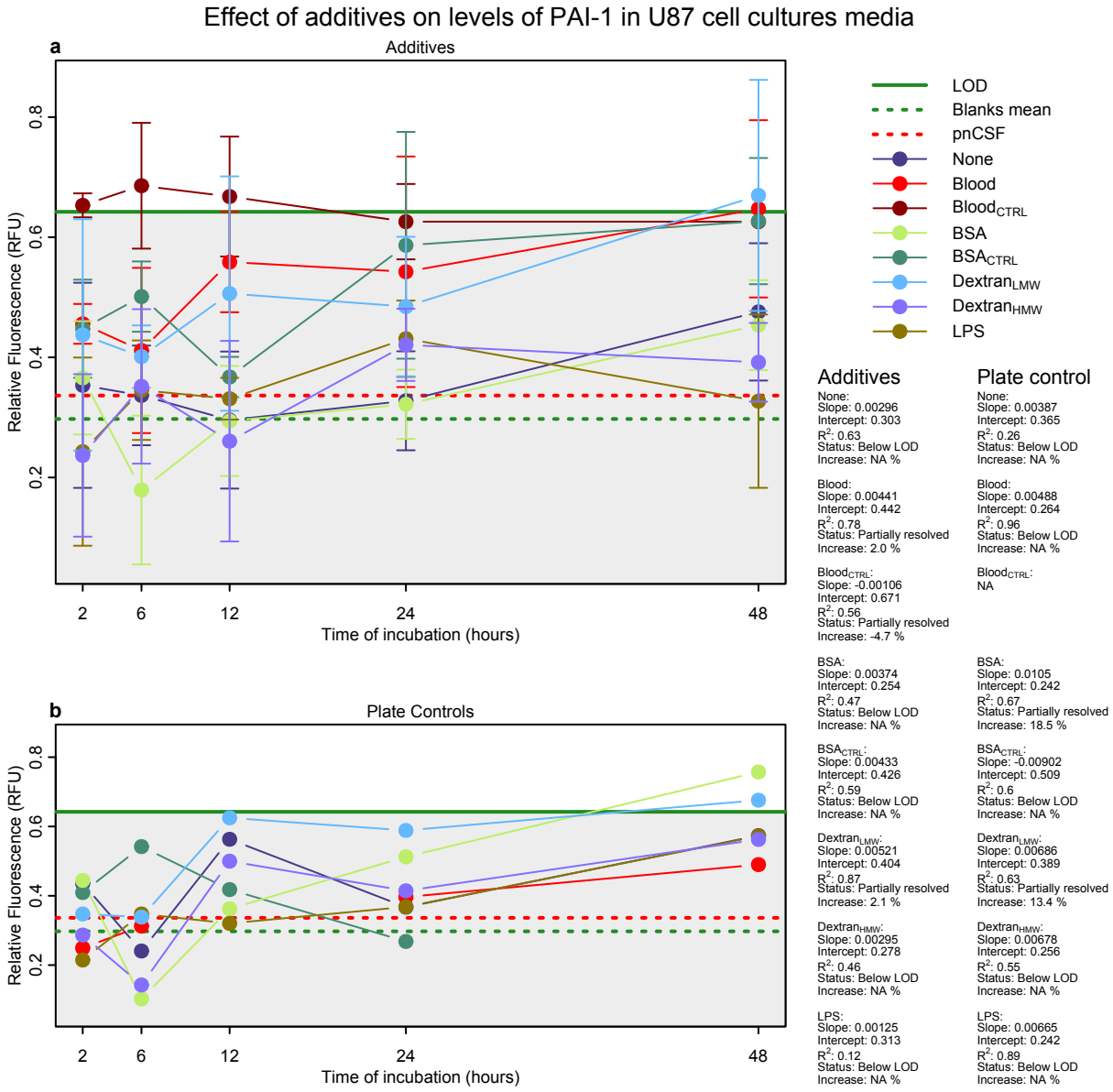

FIGURE H.S139: **Effect of additives on levels of PAI-1 in U87 cell cultures media.** Additives along with fresh blood and LPS were added to mycoplasma-free human glial (U87) cells in triplicate wells of a 24-well plate and incubated for up to 48 h to measure the effect on levels of proteins measured in the cell media. Media was collected and frozen from successive triplicates at different intervals, then analyzed with the ACM. **a** Average values for PAI-1 from three replicates for each point in every 24-well plate where a different additive was applied. **b** Data from the control cell media in each plate.

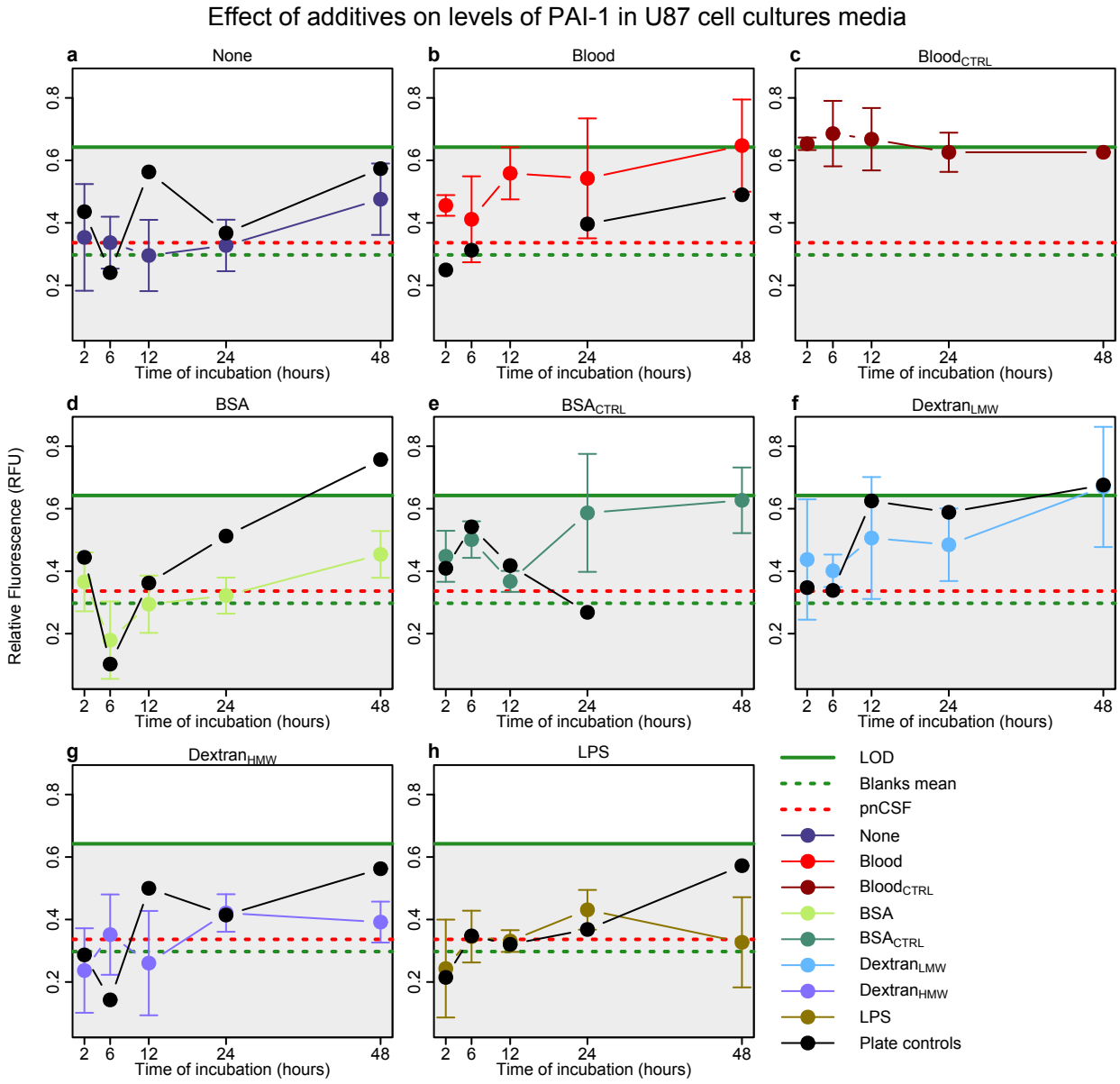

FIGURE H.S140: **Effect of additives on levels of PAI-1 in U87 cell cultures media.** Additives along with fresh blood and LPS were added to mycoplasma-free human glial (U87) cells in triplicate wells of a 24-well plate and incubated for up to 48 h to measure the effect on levels of proteins measured in the cell media. Media was collected and frozen from successive triplicates at different intervals, then analyzed with the ACM. Each graph compares PAI-1 values from cells incubated with a different additive to cells not incubated with additives located in the same 24-well plate. Plates in **c** and **e** did not contain any U87 cells, and **c** also did not have controls on the plate.

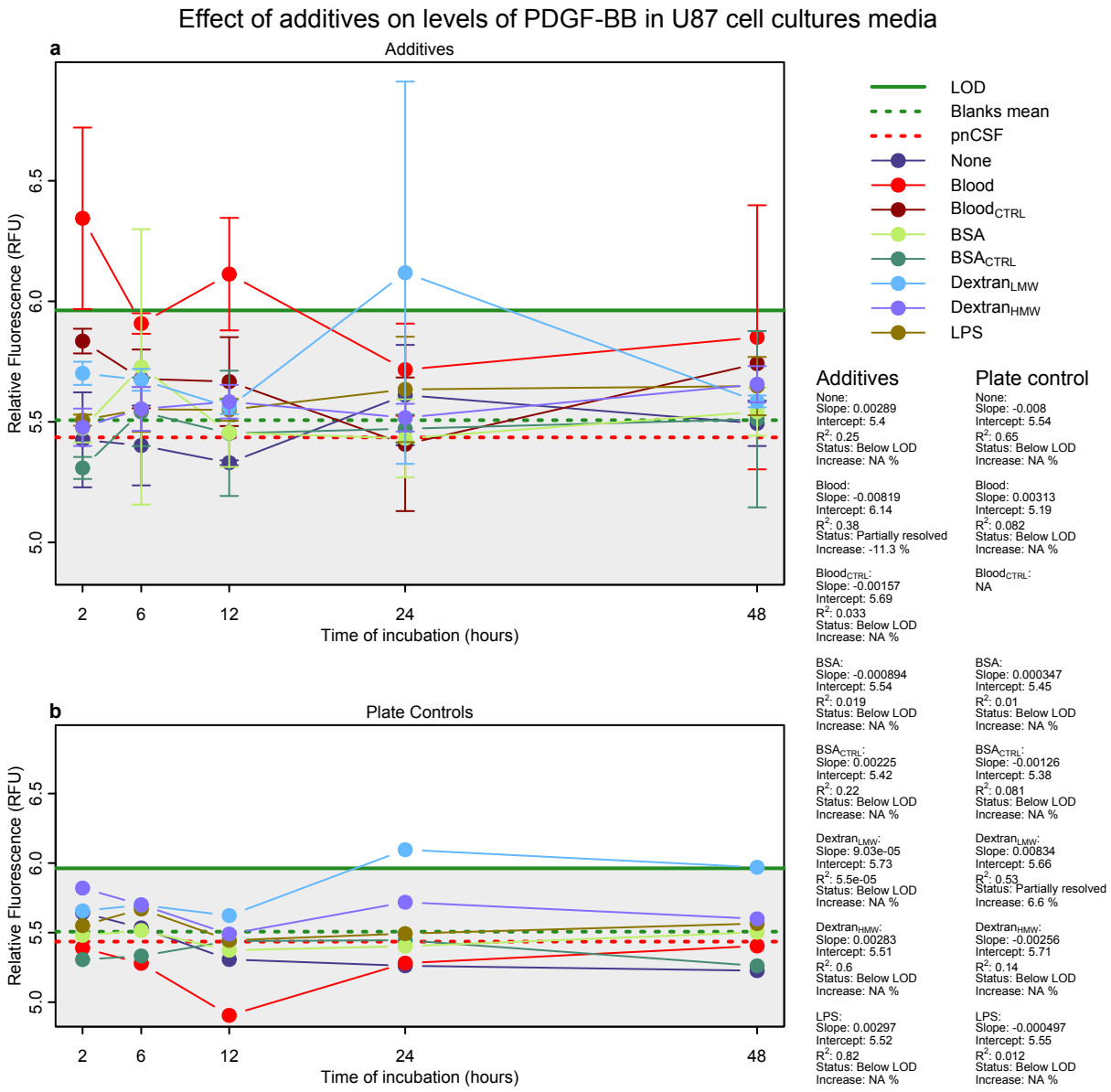

FIGURE H.S141: **Effect of additives on levels of PDGF-BB in U87 cell cultures media.** Additives along with fresh blood and LPS were added to mycoplasma-free human glial (U87) cells in triplicate wells of a 24-well plate and incubated for up to 48 h to measure the effect on levels of proteins measured in the cell media. Media was collected and frozen from successive triplicates at different intervals, then analyzed with the ACM. **a** Average values for PDGF-BB from three replicates for each point in every 24-well plate where a different additive was applied. **b** Data from the control cell media in each plate.

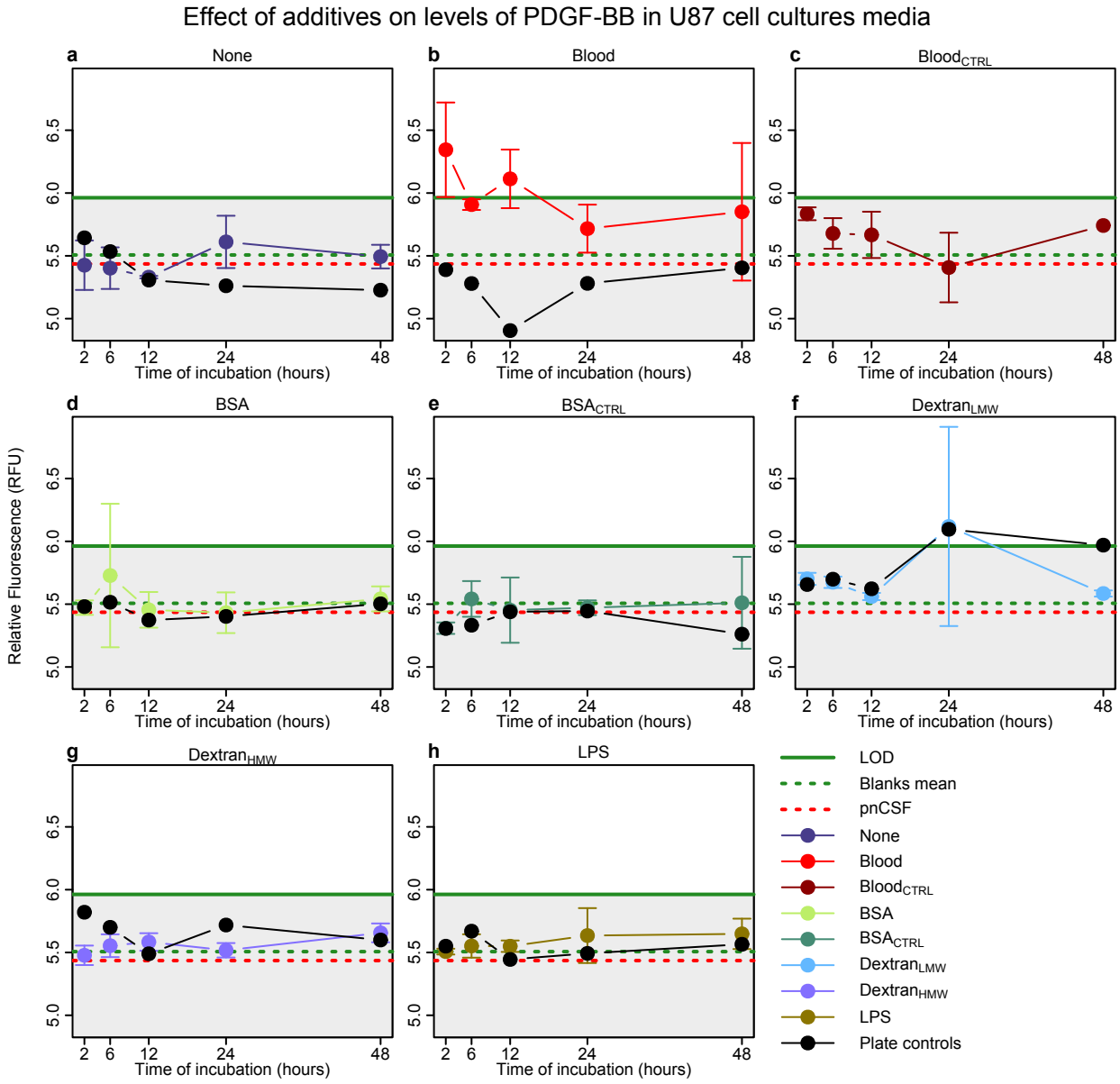

FIGURE H.S142: **Effect of additives on levels of PDGF-BB in U87 cell cultures media.** Additives along with fresh blood and LPS were added to mycoplasma-free human glial (U87) cells in triplicate wells of a 24-well plate and incubated for up to 48 h to measure the effect on levels of proteins measured in the cell media. Media was collected and frozen from successive triplicates at different intervals, then analyzed with the ACM. Each graph compares PDGF-BB values from cells incubated with a different additive to cells not incubated with additives located in the same 24-well plate. Plates in **c** and **e** did not contain any U87 cells, and **c** also did not have controls on the plate.

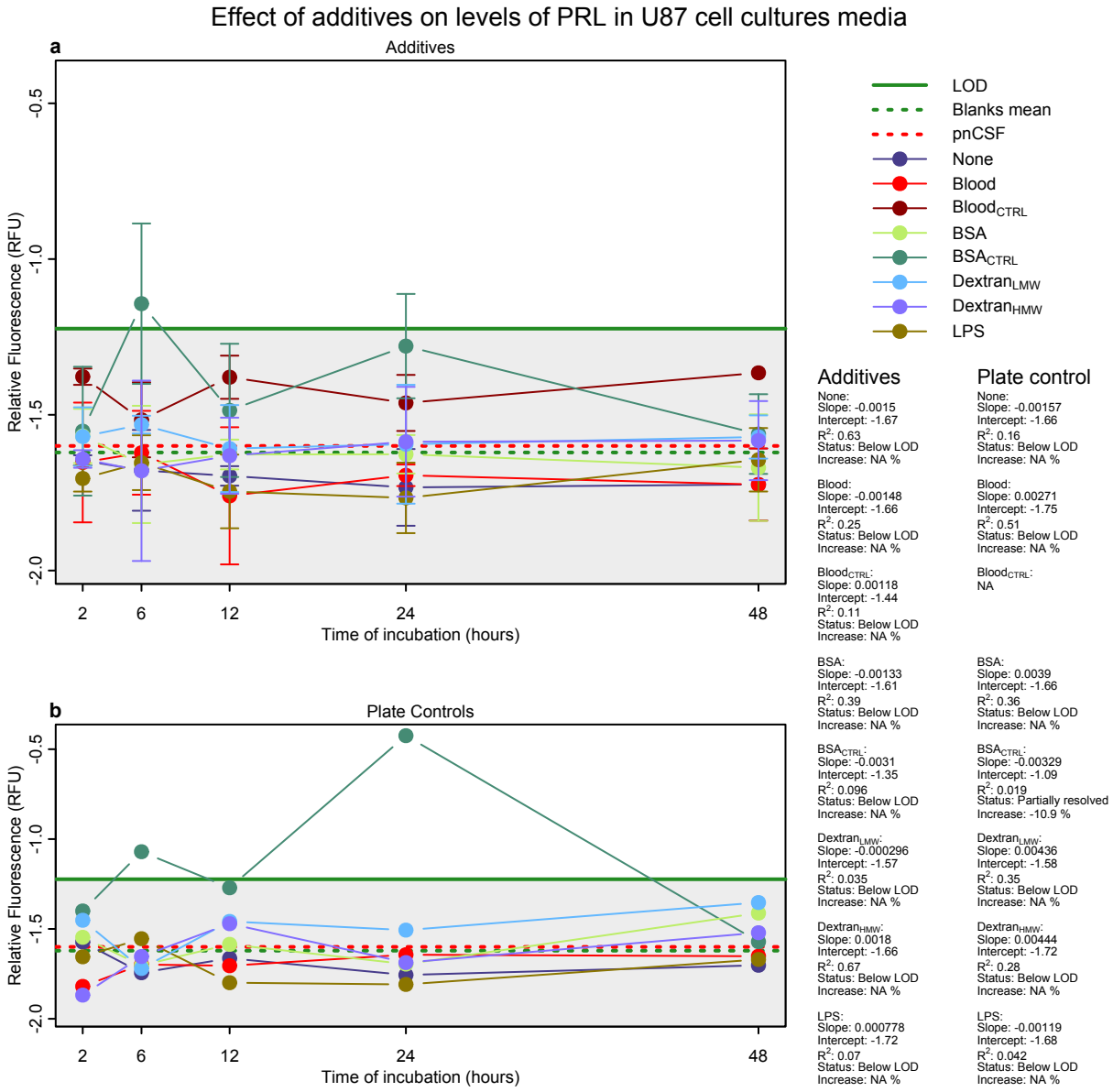

FIGURE H.S143: **Effect of additives on levels of PRL in U87 cell cultures media.** Additives along with fresh blood and LPS were added to mycoplasma-free human glial (U87) cells in triplicate wells of a 24-well plate and incubated for up to 48 h to measure the effect on levels of proteins measured in the cell media. Media was collected and frozen from successive triplicates at different intervals, then analyzed with the ACM. **a** Average values for PRL from three replicates for each point in every 24-well plate where a different additive was applied. **b** Data from the control cell media in each plate.

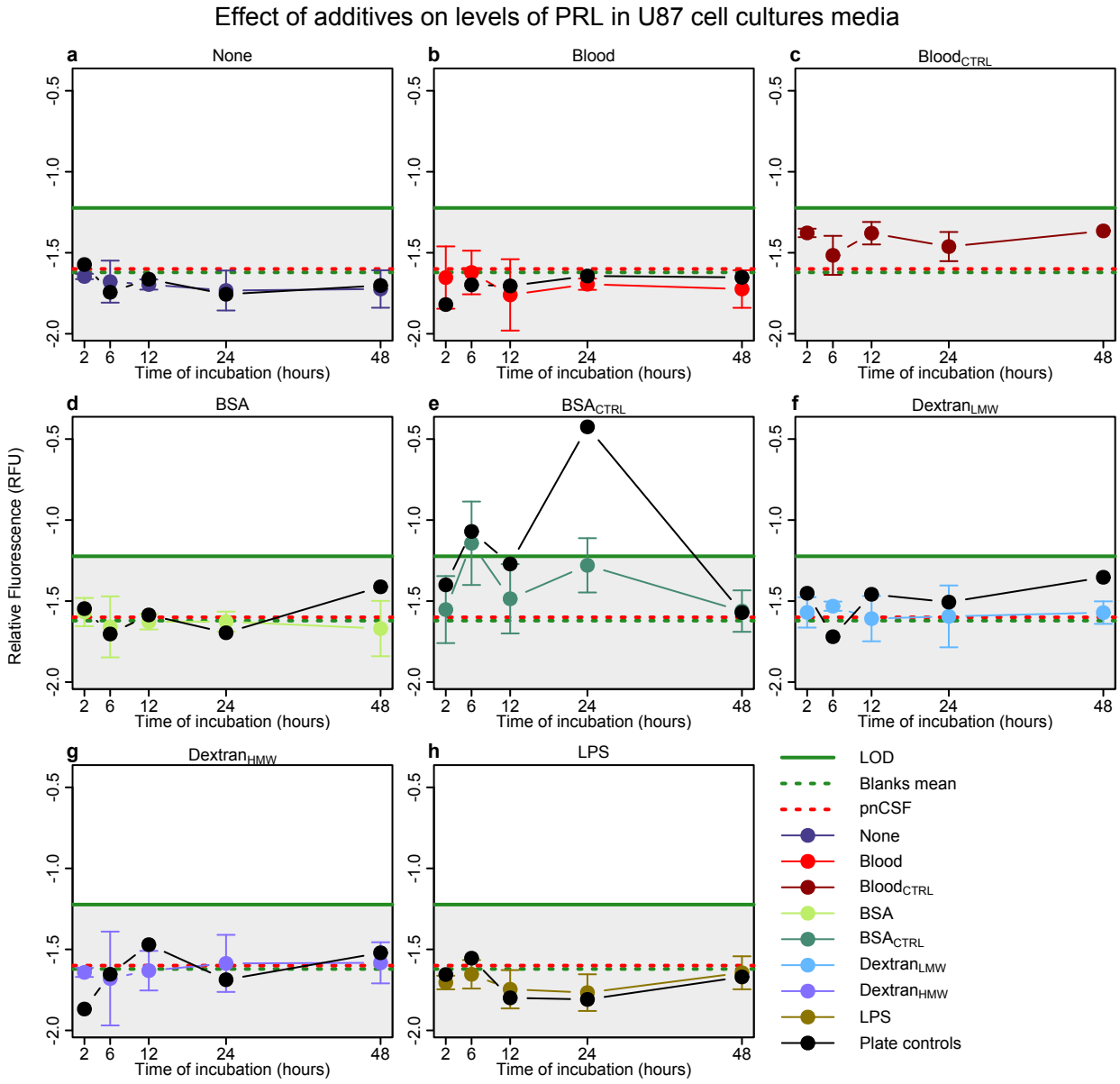

FIGURE H.S144: **Effect of additives on levels of PRL in U87 cell cultures media.** Additives along with fresh blood and LPS were added to mycoplasma-free human glial (U87) cells in triplicate wells of a 24-well plate and incubated for up to 48 h to measure the effect on levels of proteins measured in the cell media. Media was collected and frozen from successive triplicates at different intervals, then analyzed with the ACM. Each graph compares PRL values from cells incubated with a different additive to cells not incubated with additives located in the same 24-well plate. Plates in **c** and **e** did not contain any U87 cells, and **c** also did not have controls on the plate.

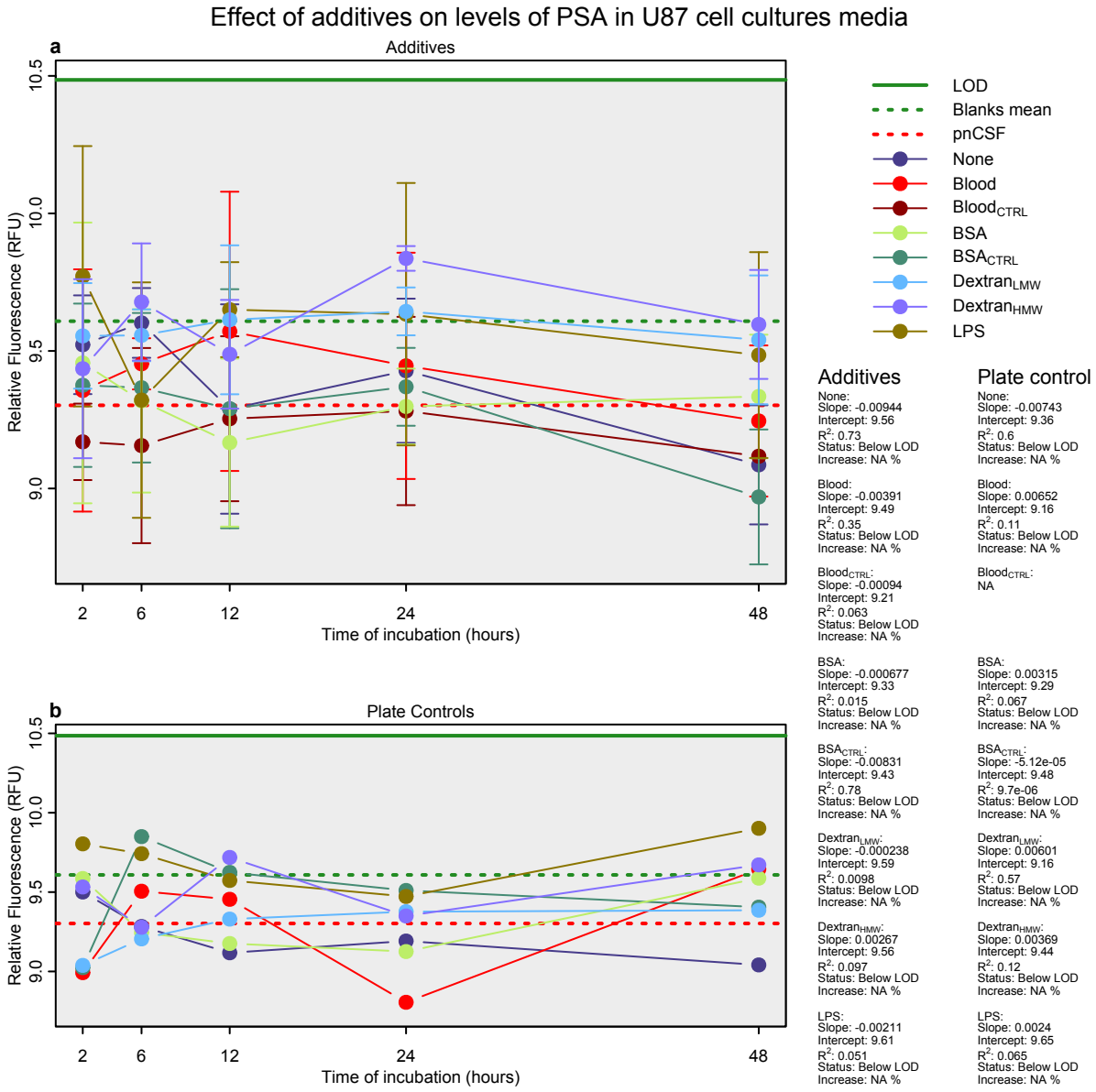

FIGURE H.S145: **Effect of additives on levels of PSA in U87 cell cultures media.** Additives along with fresh blood and LPS were added to mycoplasma-free human glial (U87) cells in triplicate wells of a 24-well plate and incubated for up to 48 h to measure the effect on levels of proteins measured in the cell media. Media was collected and frozen from successive triplicates at different intervals, then analyzed with the ACM. **a** Average values for PSA from three replicates for each point in every 24-well plate where a different additive was applied. **b** Data from the control cell media in each plate.

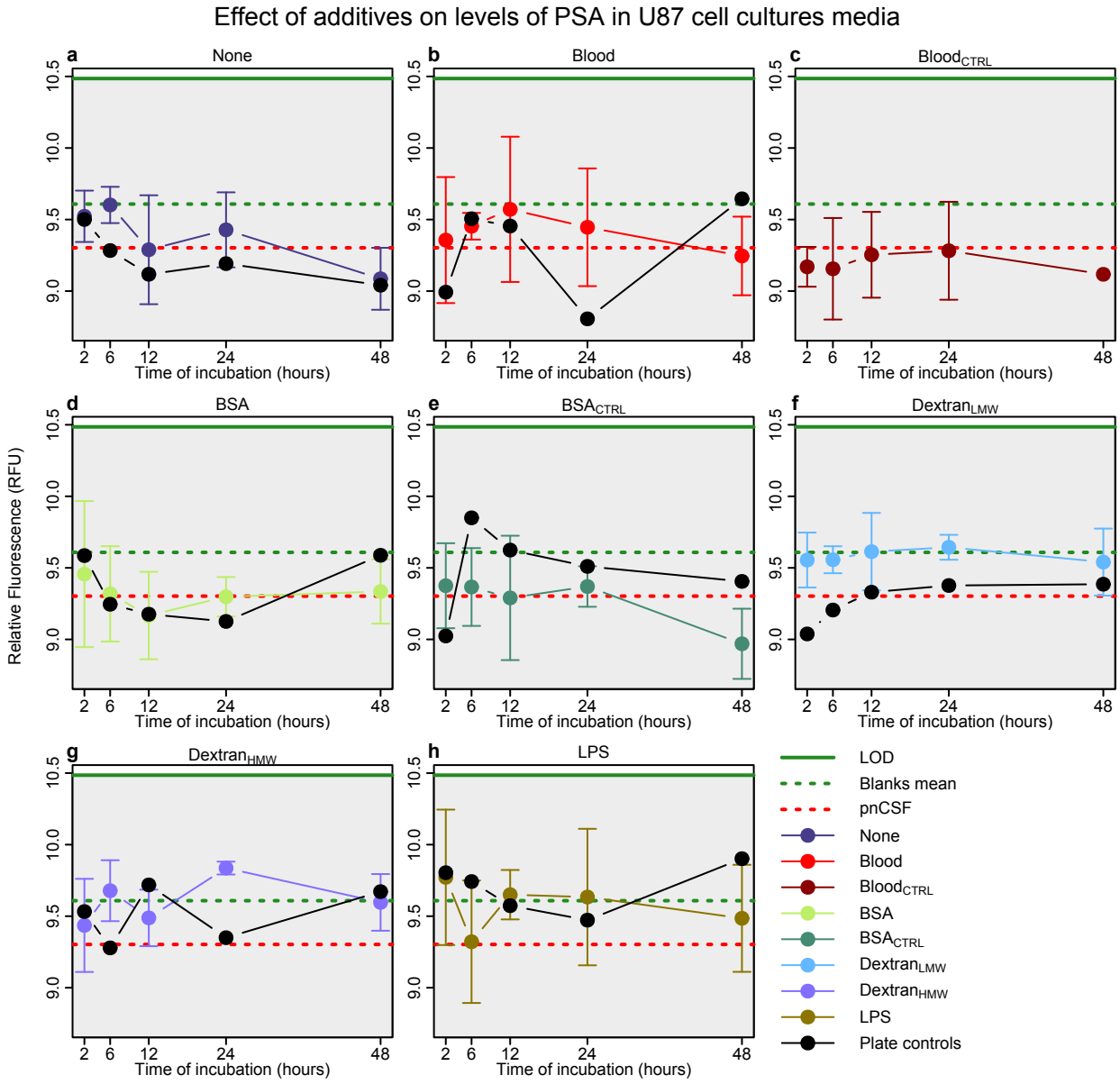

FIGURE H.S146: **Effect of additives on levels of PSA in U87 cell cultures media.** Additives along with fresh blood and LPS were added to mycoplasma-free human glial (U87) cells in triplicate wells of a 24-well plate and incubated for up to 48 h to measure the effect on levels of proteins measured in the cell media. Media was collected and frozen from successive triplicates at different intervals, then analyzed with the ACM. Each graph compares PSA values from cells incubated with a different additive to cells not incubated with additives located in the same 24-well plate. Plates in **c** and **e** did not contain any U87 cells, and **c** also did not have controls on the plate.

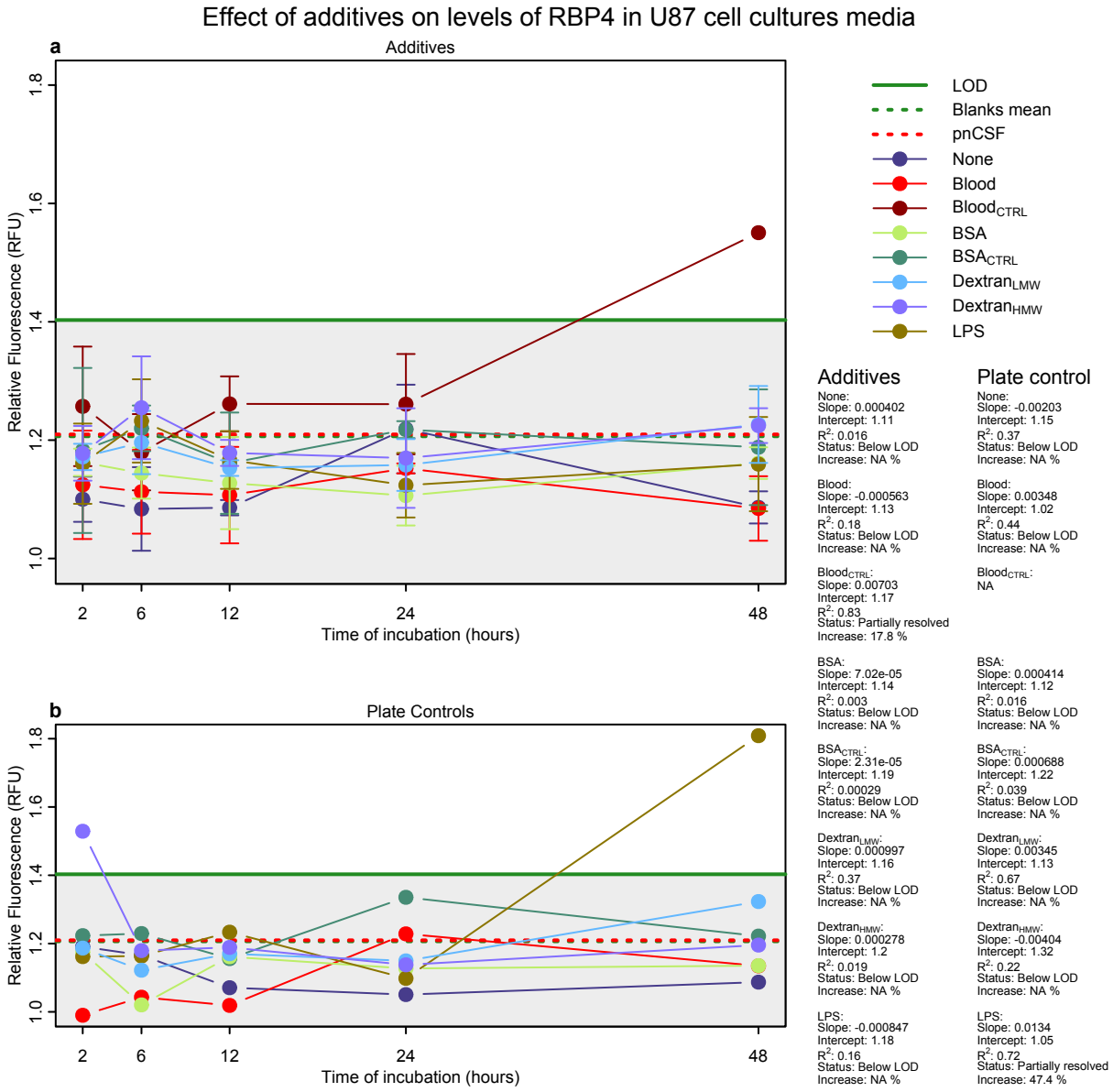

FIGURE H.S147: **Effect of additives on levels of RBP4 in U87 cell cultures media.** Additives along with fresh blood and LPS were added to mycoplasma-free human glial (U87) cells in triplicate wells of a 24-well plate and incubated for up to 48 h to measure the effect on levels of proteins measured in the cell media. Media was collected and frozen from successive triplicates at different intervals, then analyzed with the ACM. **a** Average values for RBP4 from three replicates for each point in every 24-well plate where a different additive was applied. **b** Data from the control cell media in each plate.

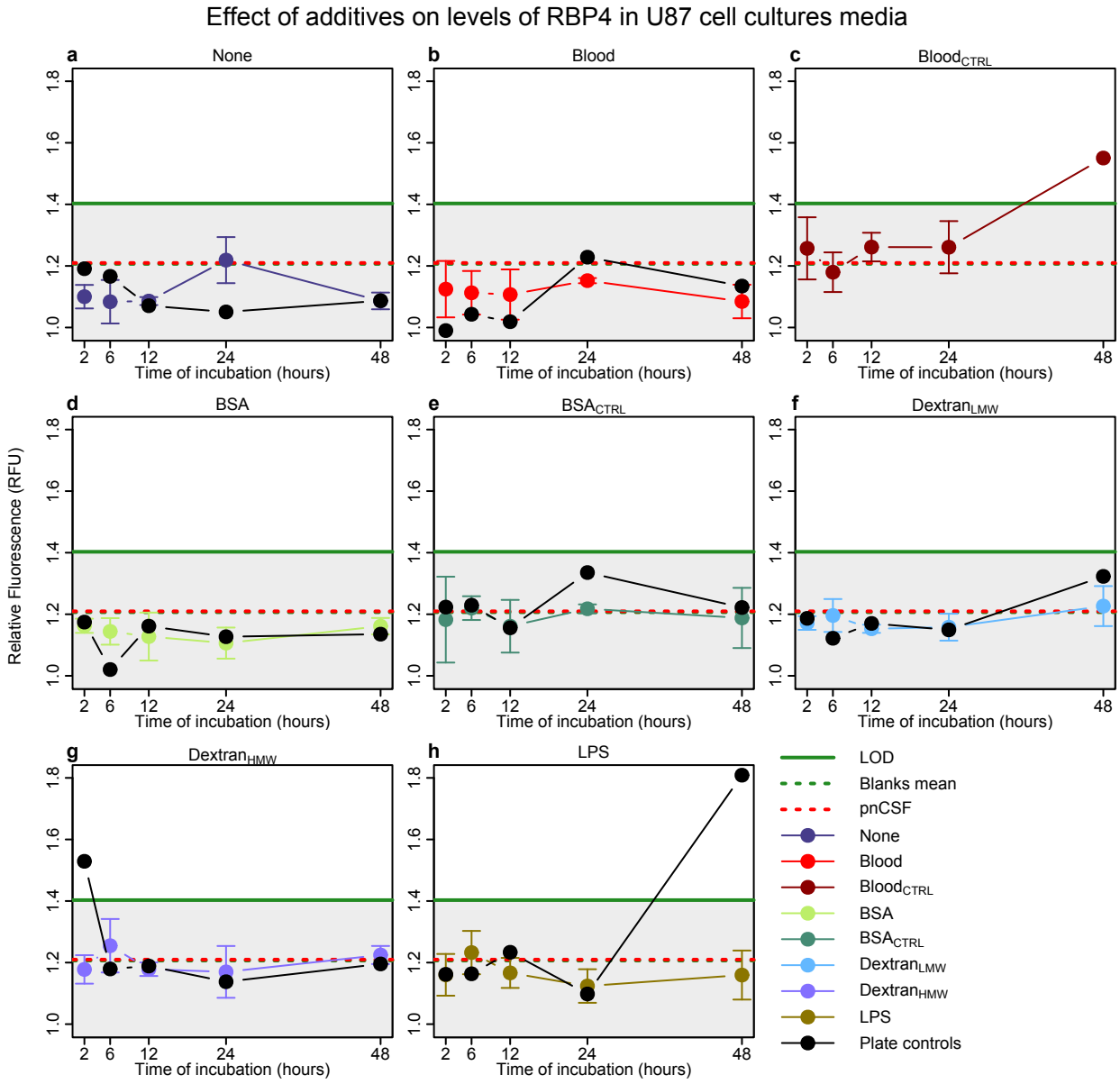

FIGURE H.S148: **Effect of additives on levels of RBP4 in U87 cell cultures media.** Additives along with fresh blood and LPS were added to mycoplasma-free human glial (U87) cells in triplicate wells of a 24-well plate and incubated for up to 48 h to measure the effect on levels of proteins measured in the cell media. Media was collected and frozen from successive triplicates at different intervals, then analyzed with the ACM. Each graph compares RBP4 values from cells incubated with a different additive to cells not incubated with additives located in the same 24-well plate. Plates in **c** and **e** did not contain any U87 cells, and **c** also did not have controls on the plate.

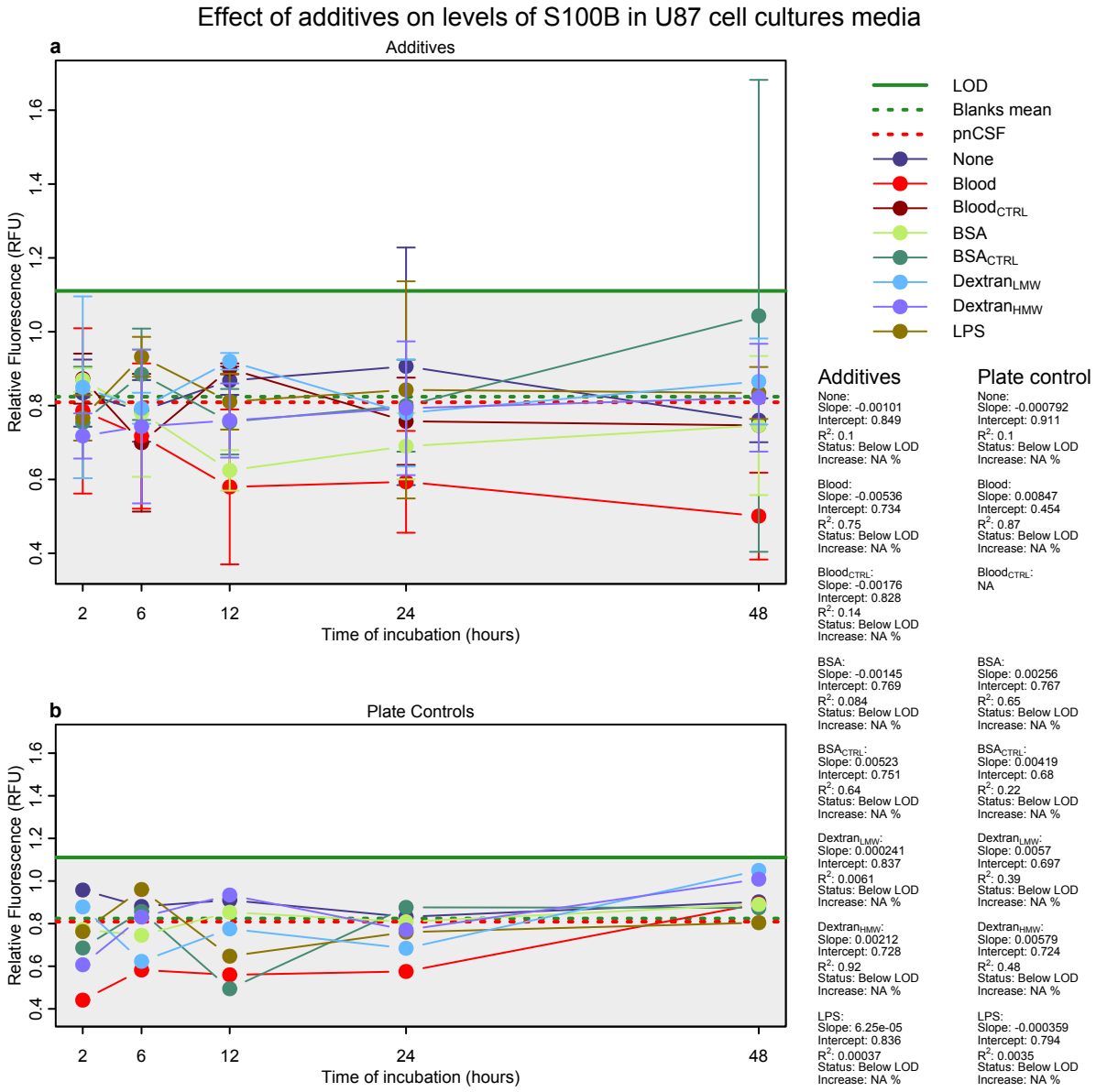

FIGURE H.S149: **Effect of additives on levels of S100B in U87 cell cultures media.** Additives along with fresh blood and LPS were added to mycoplasma-free human glial (U87) cells in triplicate wells of a 24-well plate and incubated for up to 48 h to measure the effect on levels of proteins measured in the cell media. Media was collected and frozen from successive triplicates at different intervals, then analyzed with the ACM. **a** Average values for S100B from three replicates for each point in every 24-well plate where a different additive was applied. **b** Data from the control cell media in each plate.

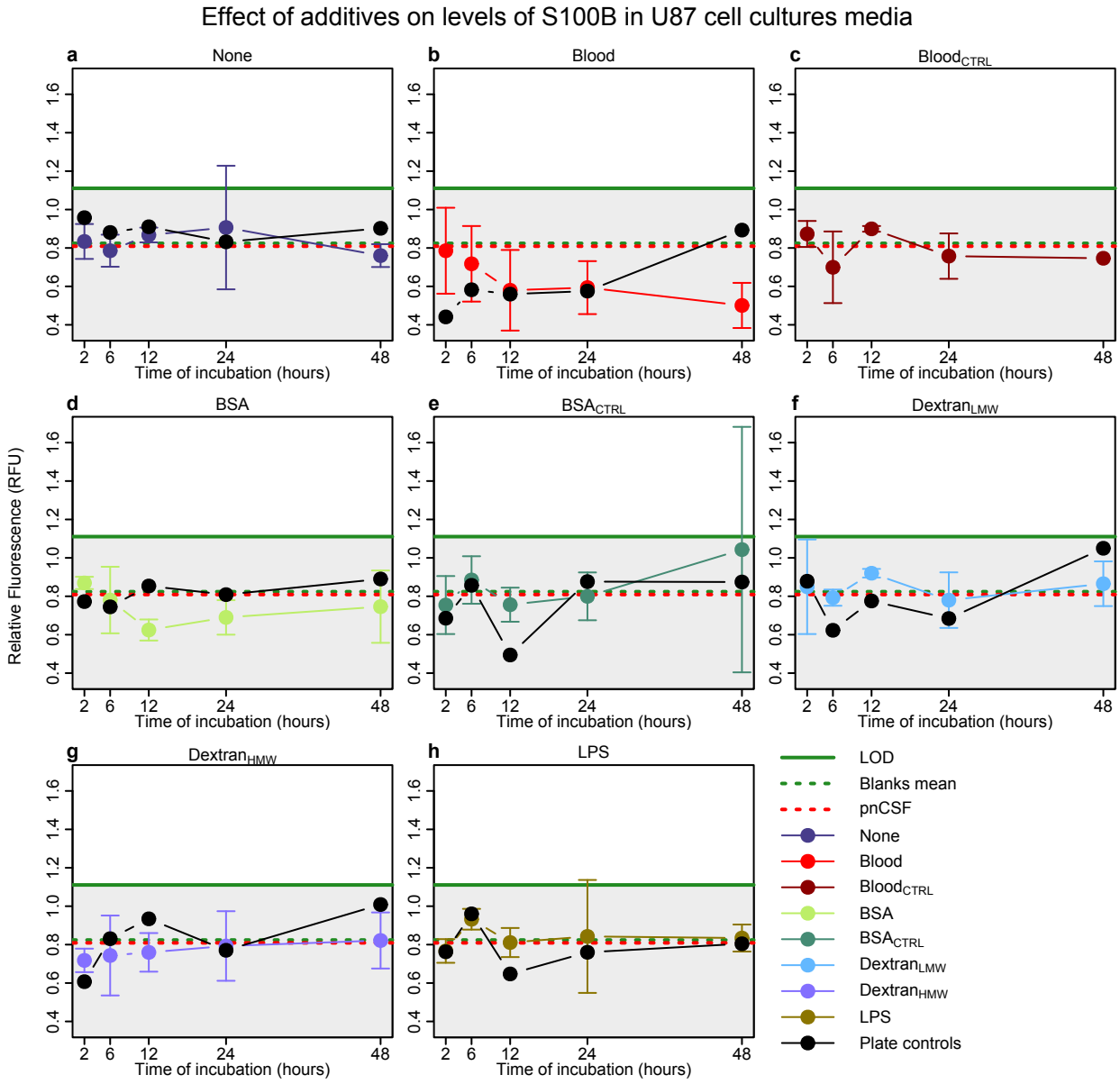

FIGURE H.S150: **Effect of additives on levels of S100B in U87 cell cultures media.** Additives along with fresh blood and LPS were added to mycoplasma-free human glial (U87) cells in triplicate wells of a 24-well plate and incubated for up to 48 h to measure the effect on levels of proteins measured in the cell media. Media was collected and frozen from successive triplicates at different intervals, then analyzed with the ACM. Each graph compares S100B values from cells incubated with a different additive to cells not incubated with additives located in the same 24-well plate. Plates in **c** and **e** did not contain any U87 cells, and **c** also did not have controls on the plate.

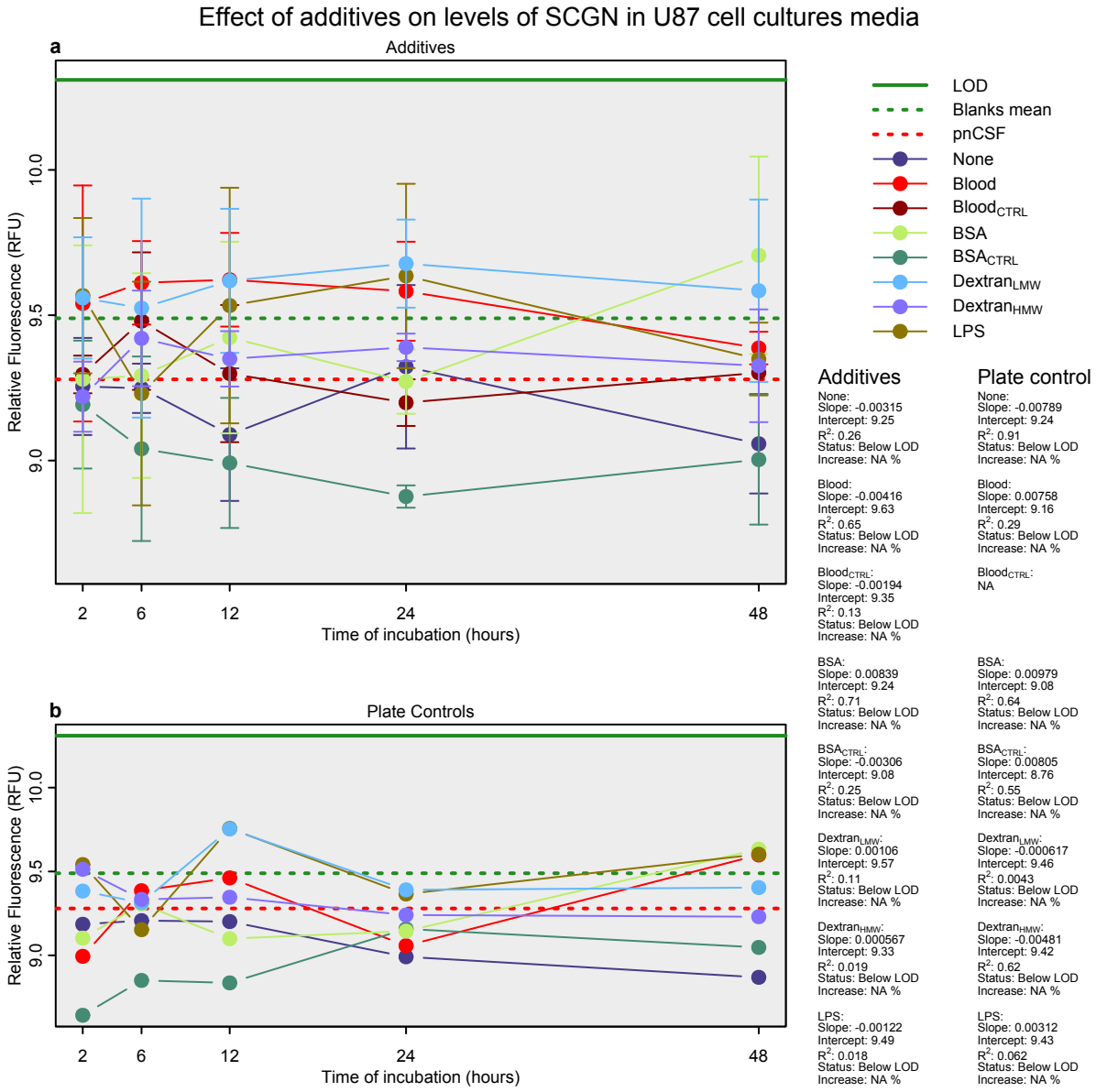

FIGURE H.S151: **Effect of additives on levels of SCGN in U87 cell cultures media.** Additives along with fresh blood and LPS were added to mycoplasma-free human glial (U87) cells in triplicate wells of a 24-well plate and incubated for up to 48 h to measure the effect on levels of proteins measured in the cell media. Media was collected and frozen from successive triplicates at different intervals, then analyzed with the ACM. **a** Average values for SCGN from three replicates for each point in every 24-well plate where a different additive was applied. **b** Data from the control cell media in each plate.

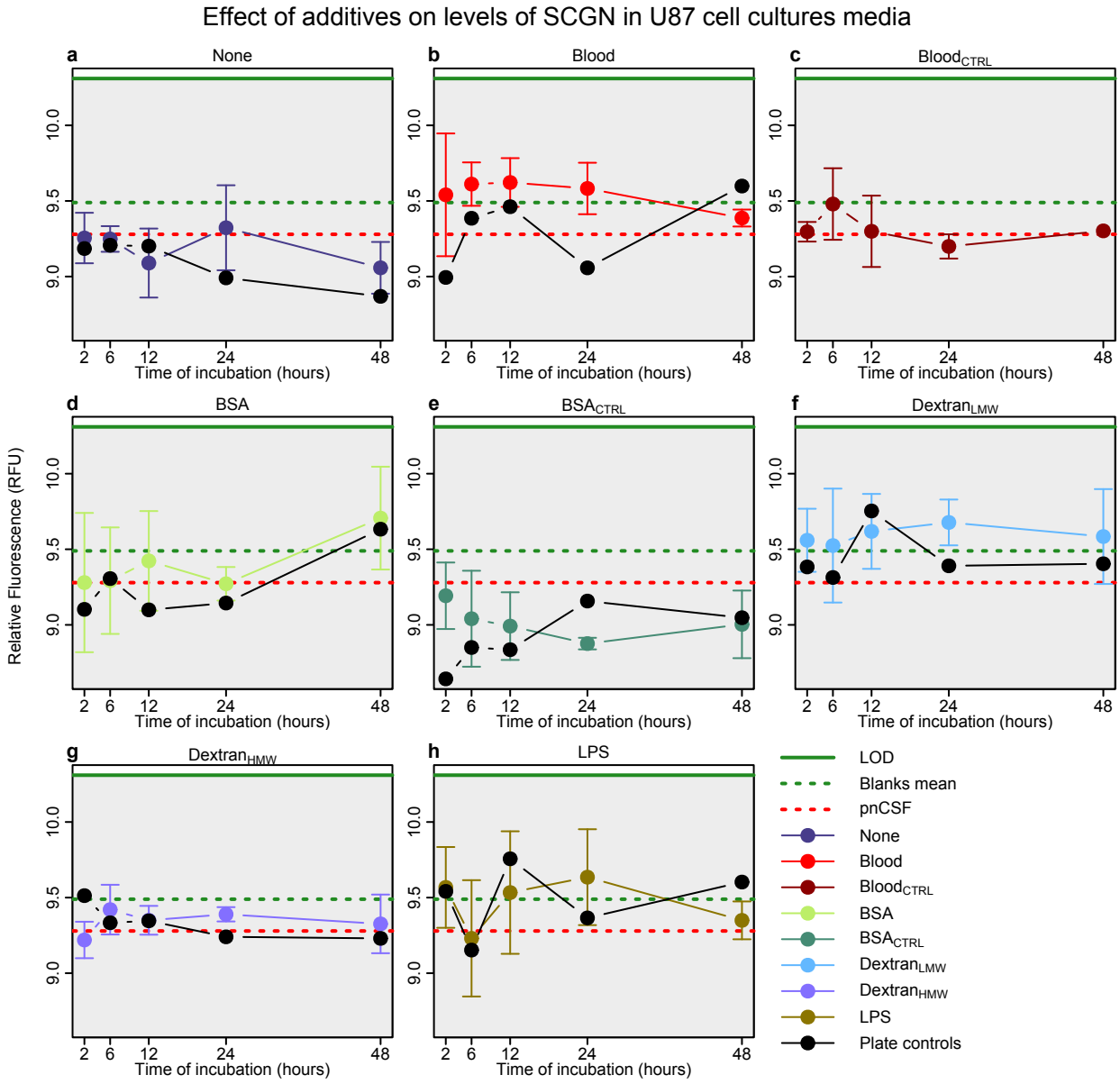

FIGURE H.S152: **Effect of additives on levels of SCGN in U87 cell cultures media.** Additives along with fresh blood and LPS were added to mycoplasma-free human glial (U87) cells in triplicate wells of a 24-well plate and incubated for up to 48 h to measure the effect on levels of proteins measured in the cell media. Media was collected and frozen from successive triplicates at different intervals, then analyzed with the ACM. Each graph compares SCGN values from cells incubated with a different additive to cells not incubated with additives located in the same 24-well plate. Plates in **c** and **e** did not contain any U87 cells, and **c** also did not have controls on the plate.

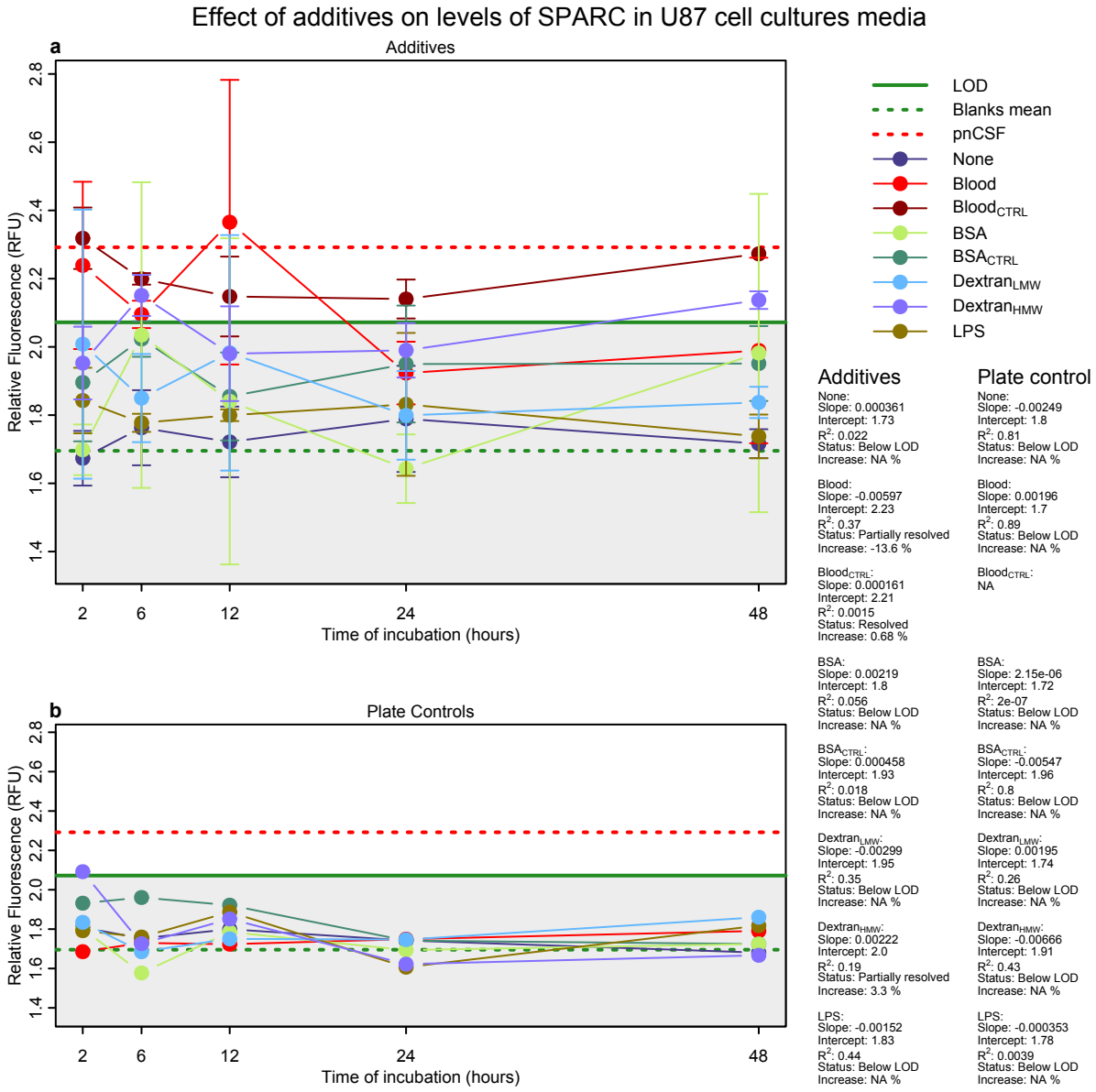

FIGURE H.S153: **Effect of additives on levels of SPARC in U87 cell cultures media.** Additives along with fresh blood and LPS were added to mycoplasma-free human glial (U87) cells in triplicate wells of a 24-well plate and incubated for up to 48 h to measure the effect on levels of proteins measured in the cell media. Media was collected and frozen from successive triplicates at different intervals, then analyzed with the ACM. **a** Average values for SPARC from three replicates for each point in every 24-well plate where a different additive was applied. **b** Data from the control cell media in each plate.

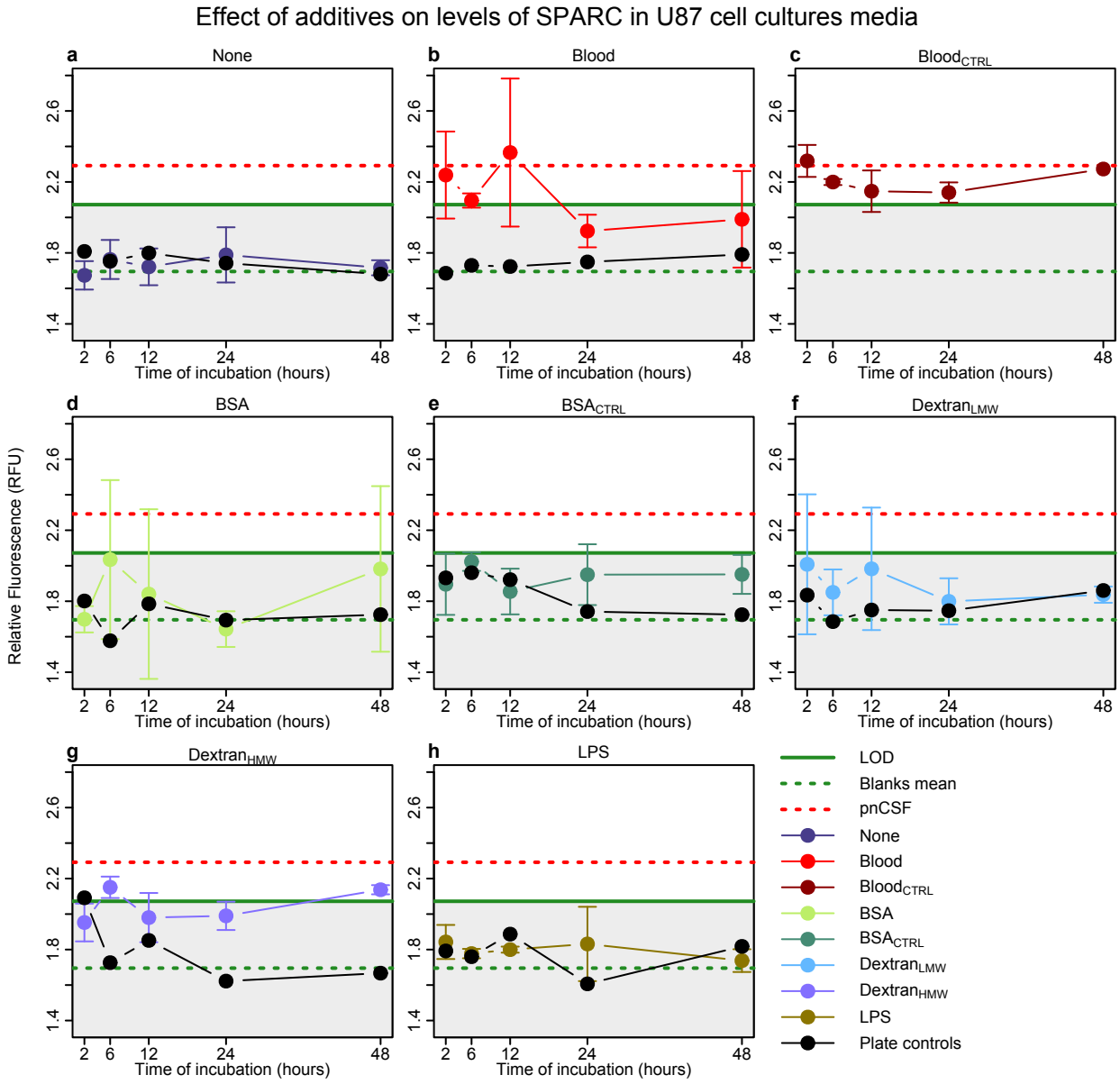

FIGURE H.S154: **Effect of additives on levels of SPARC in U87 cell cultures media.** Additives along with fresh blood and LPS were added to mycoplasma-free human glial (U87) cells in triplicate wells of a 24-well plate and incubated for up to 48 h to measure the effect on levels of proteins measured in the cell media. Media was collected and frozen from successive triplicates at different intervals, then analyzed with the ACM. Each graph compares SPARC values from cells incubated with a different additive to cells not incubated with additives located in the same 24-well plate. Plates in **c** and **e** did not contain any U87 cells, and **c** also did not have controls on the plate.

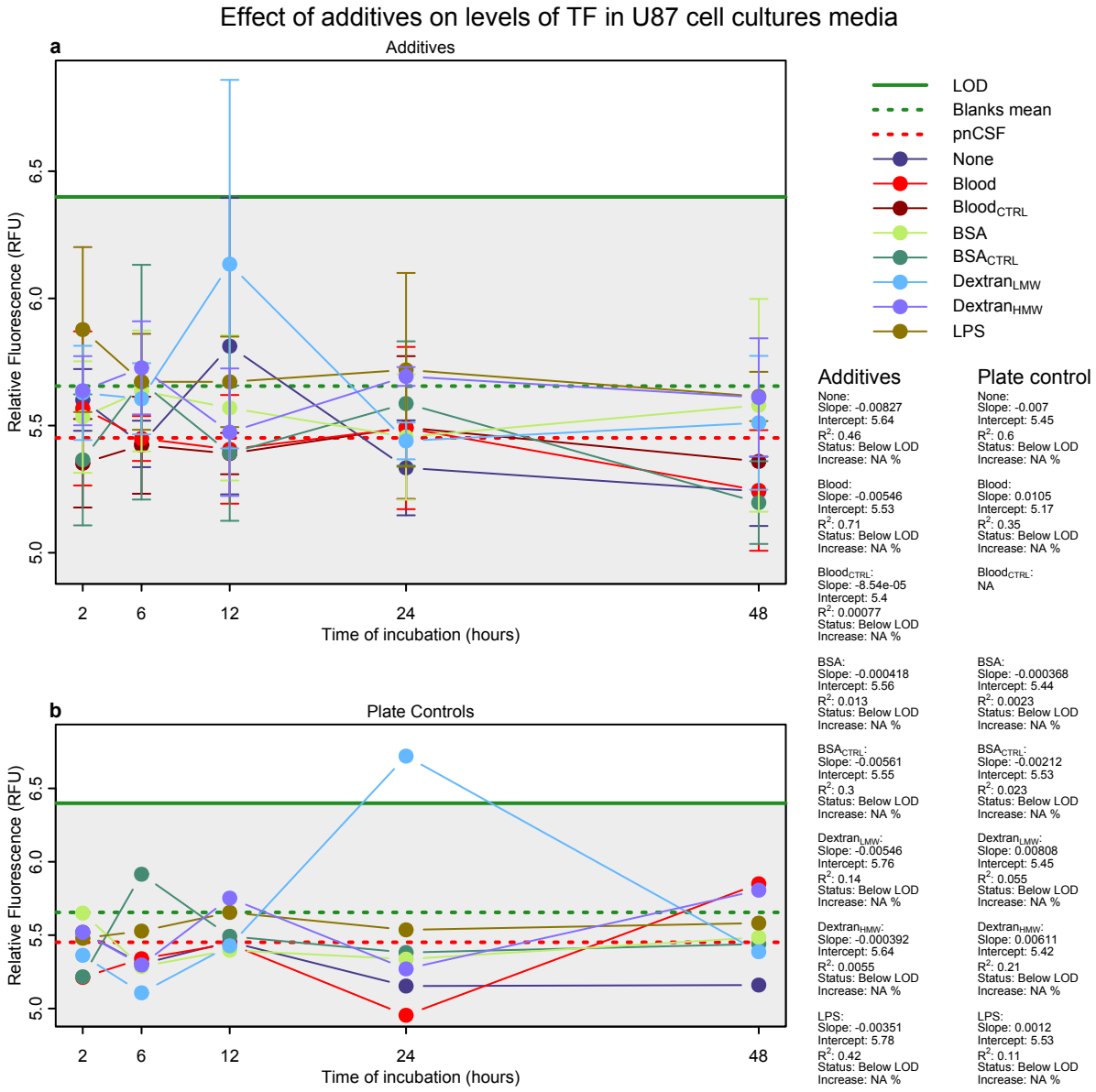

FIGURE H.S155: **Effect of additives on levels of TF in U87 cell cultures media.** Additives along with fresh blood and LPS were added to mycoplasma-free human glial (U87) cells in triplicate wells of a 24-well plate and incubated for up to 48 h to measure the effect on levels of proteins measured in the cell media. Media was collected and frozen from successive triplicates at different intervals, then analyzed with the ACM. **a** Average values for TF from three replicates for each point in every 24-well plate where a different additive was applied. **b** Data from the control cell media in each plate.

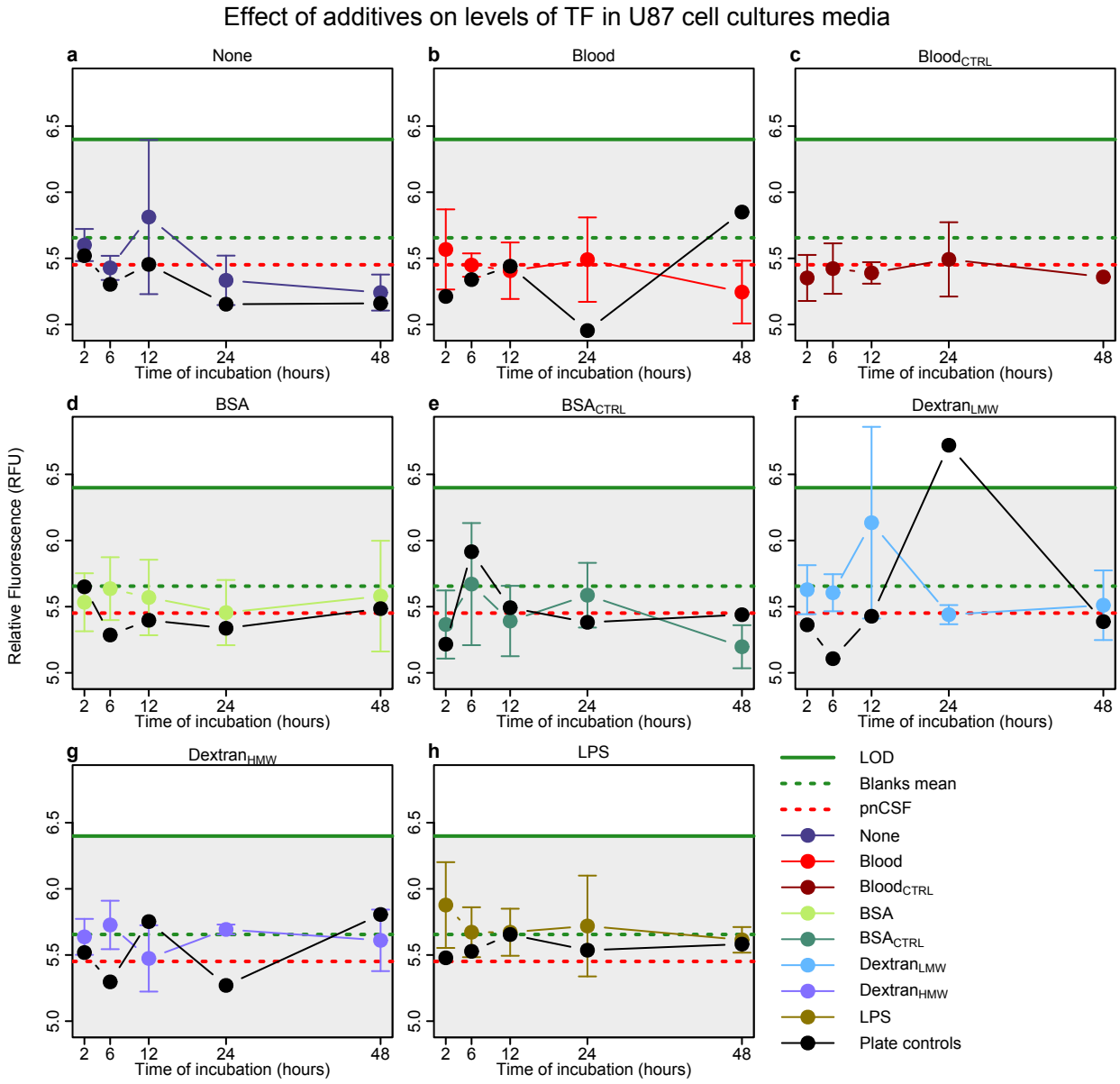

FIGURE H.S156: **Effect of additives on levels of TF in U87 cell cultures media.** Additives along with fresh blood and LPS were added to mycoplasma-free human glial (U87) cells in triplicate wells of a 24-well plate and incubated for up to 48 h to measure the effect on levels of proteins measured in the cell media. Media was collected and frozen from successive triplicates at different intervals, then analyzed with the ACM. Each graph compares TF values from cells incubated with a different additive to cells not incubated with additives located in the same 24-well plate. Plates in **c** and **e** did not contain any U87 cells, and **c** also did not have controls on the plate.

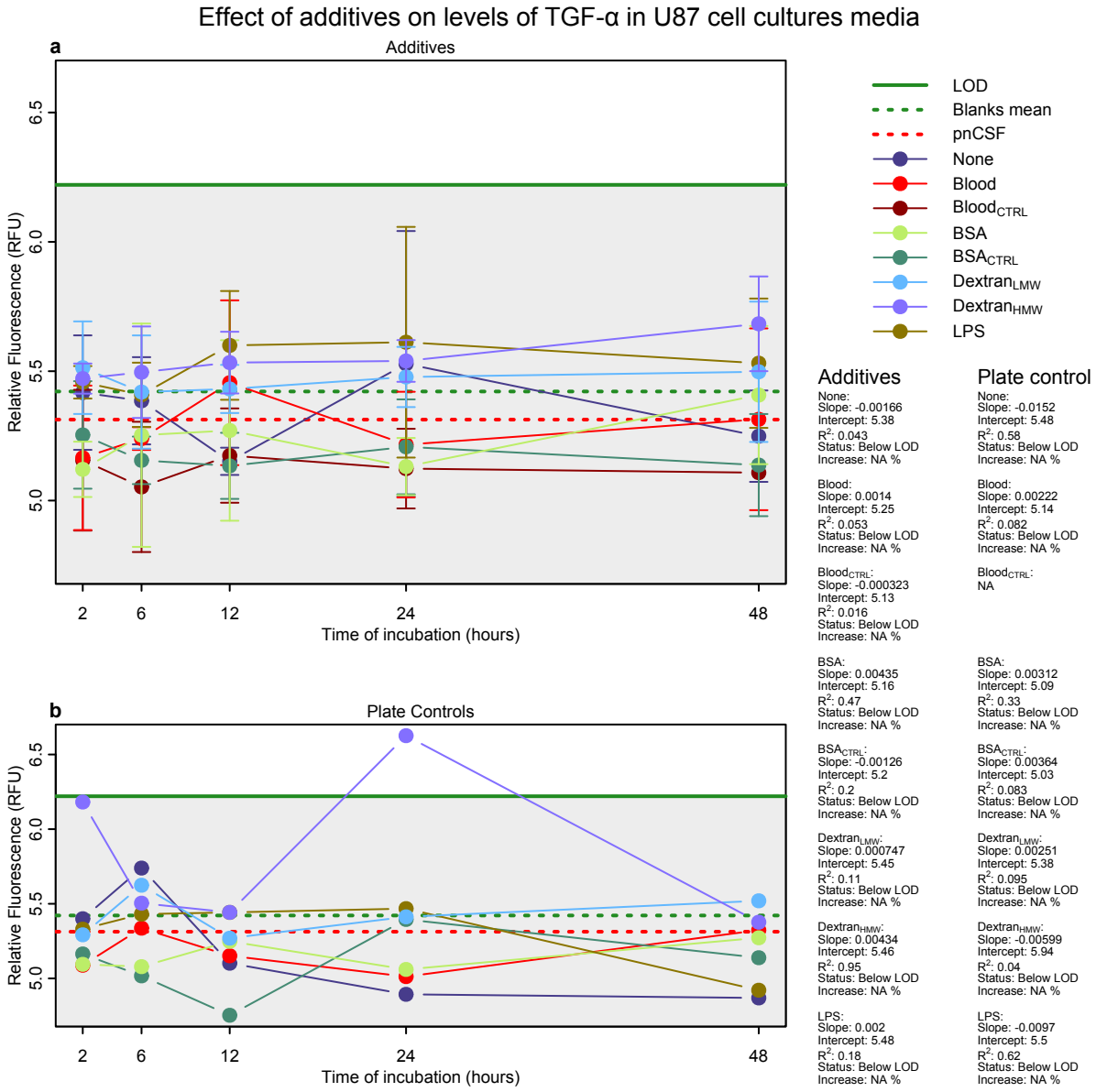

FIGURE H.S157: **Effect of additives on levels of TGF-α in U87 cell cultures media.** Additives along with fresh blood and LPS were added to mycoplasma-free human glial (U87) cells in triplicate wells of a 24-well plate and incubated for up to 48 h to measure the effect on levels of proteins measured in the cell media. Media was collected and frozen from successive triplicates at different intervals, then analyzed with the ACM. **a** Average values for TGF-α from three replicates for each point in every 24-well plate where a different additive was applied. **b** Data from the control cell media in each plate.

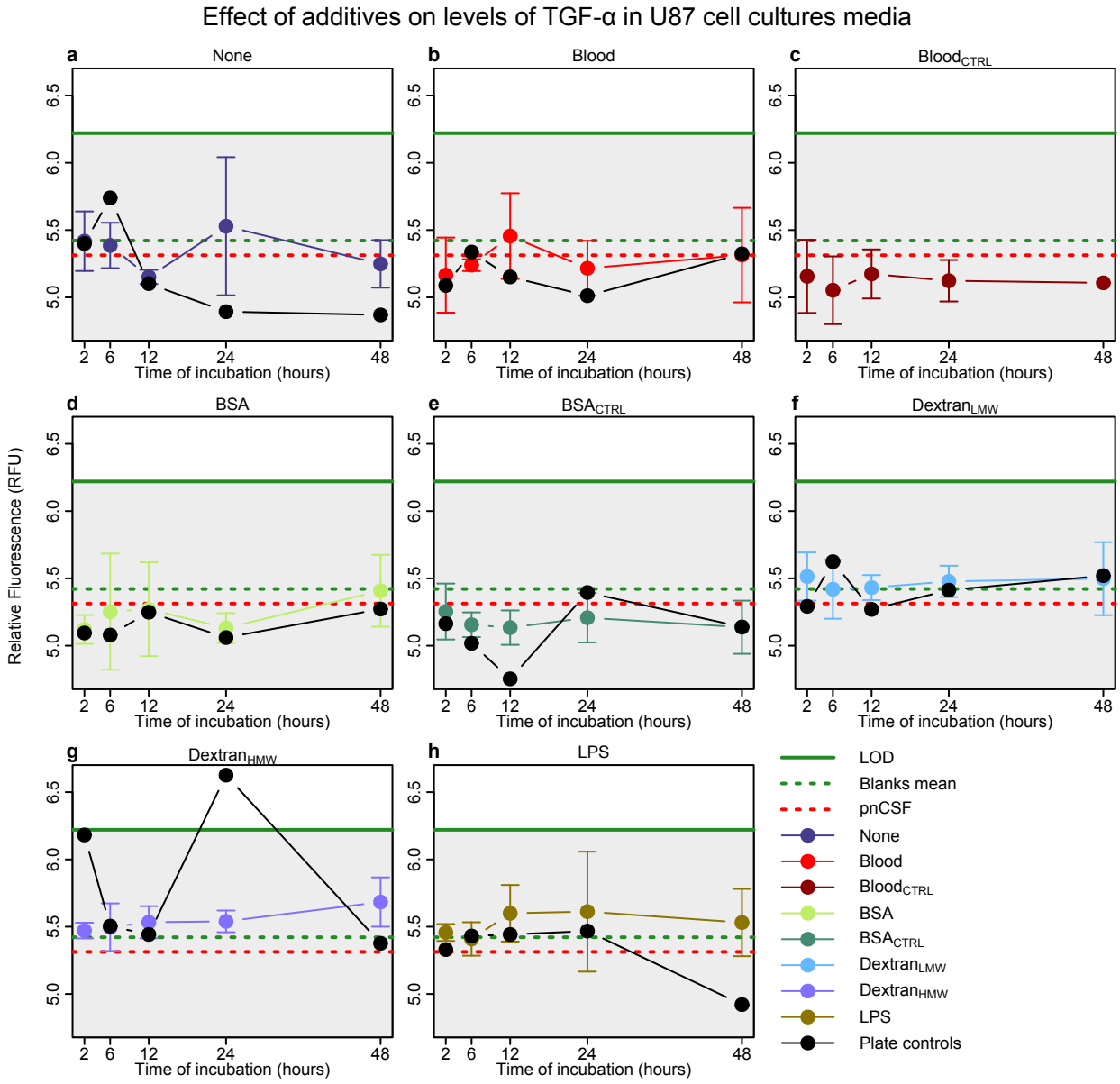

FIGURE H.S158: **Effect of additives on levels of TGF-α in U87 cell cultures media.** Additives along with fresh blood and LPS were added to mycoplasma-free human glial (U87) cells in triplicate wells of a 24-well plate and incubated for up to 48 h to measure the effect on levels of proteins measured in the cell media. Media was collected and frozen from successive triplicates at different intervals, then analyzed with the ACM. Each graph compares TGF-α values from cells incubated with a different additive to cells not incubated with additives located in the same 24-well plate. Plates in **c** and **e** did not contain any U87 cells, and **c** also did not have controls on the plate.

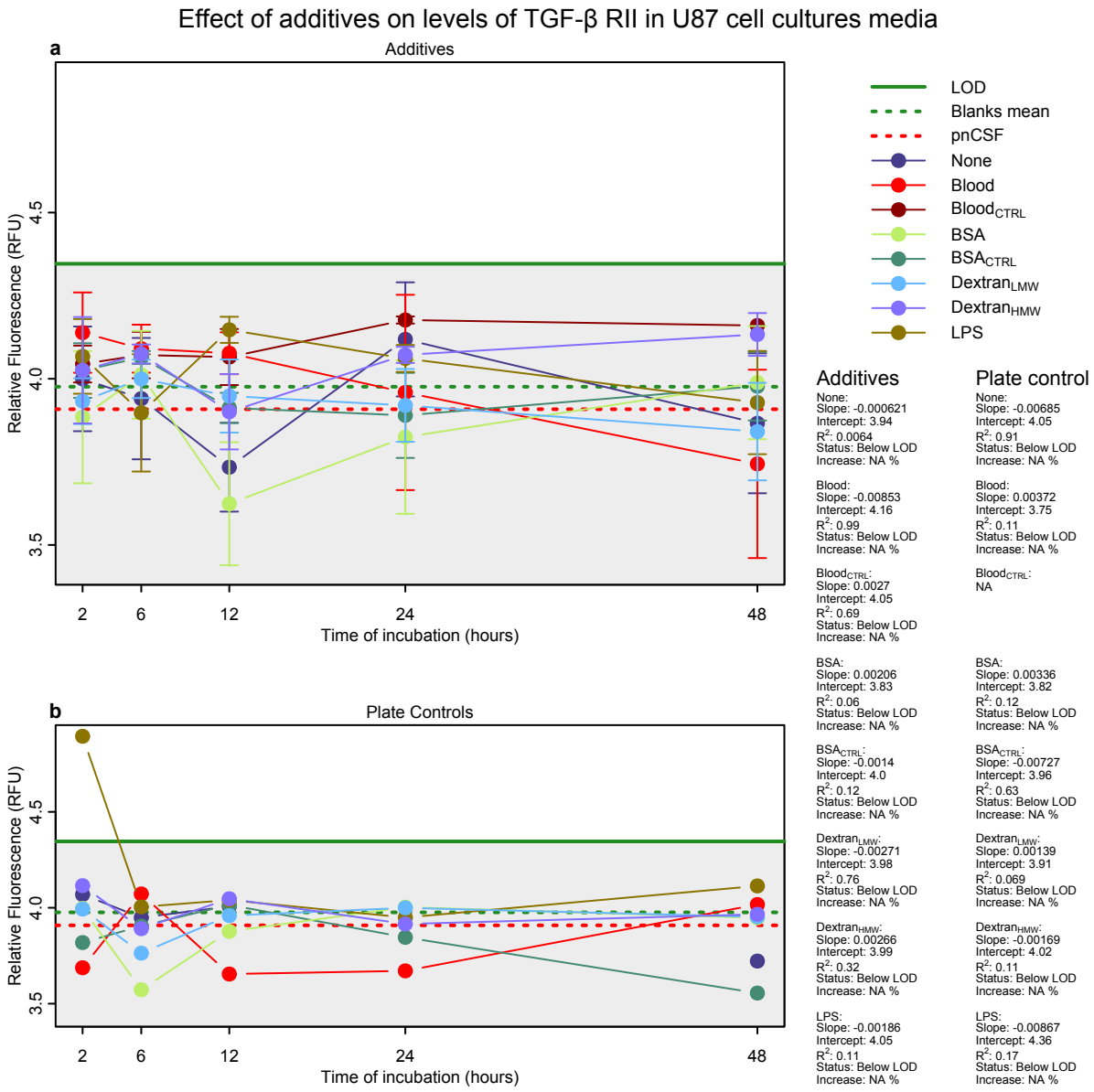

FIGURE H.S159: **Effect of additives on levels of TGF-β RII in U87 cell cultures media.** Additives along with fresh blood and LPS were added to mycoplasma-free human glial (U87) cells in triplicate wells of a 24-well plate and incubated for up to 48 h to measure the effect on levels of proteins measured in the cell media. Media was collected and frozen from successive triplicates at different intervals, then analyzed with the ACM. **a** Average values for TGF-β RII from three replicates for each point in every 24-well plate where a different additive was applied. **b** Data from the control cell media in each plate.

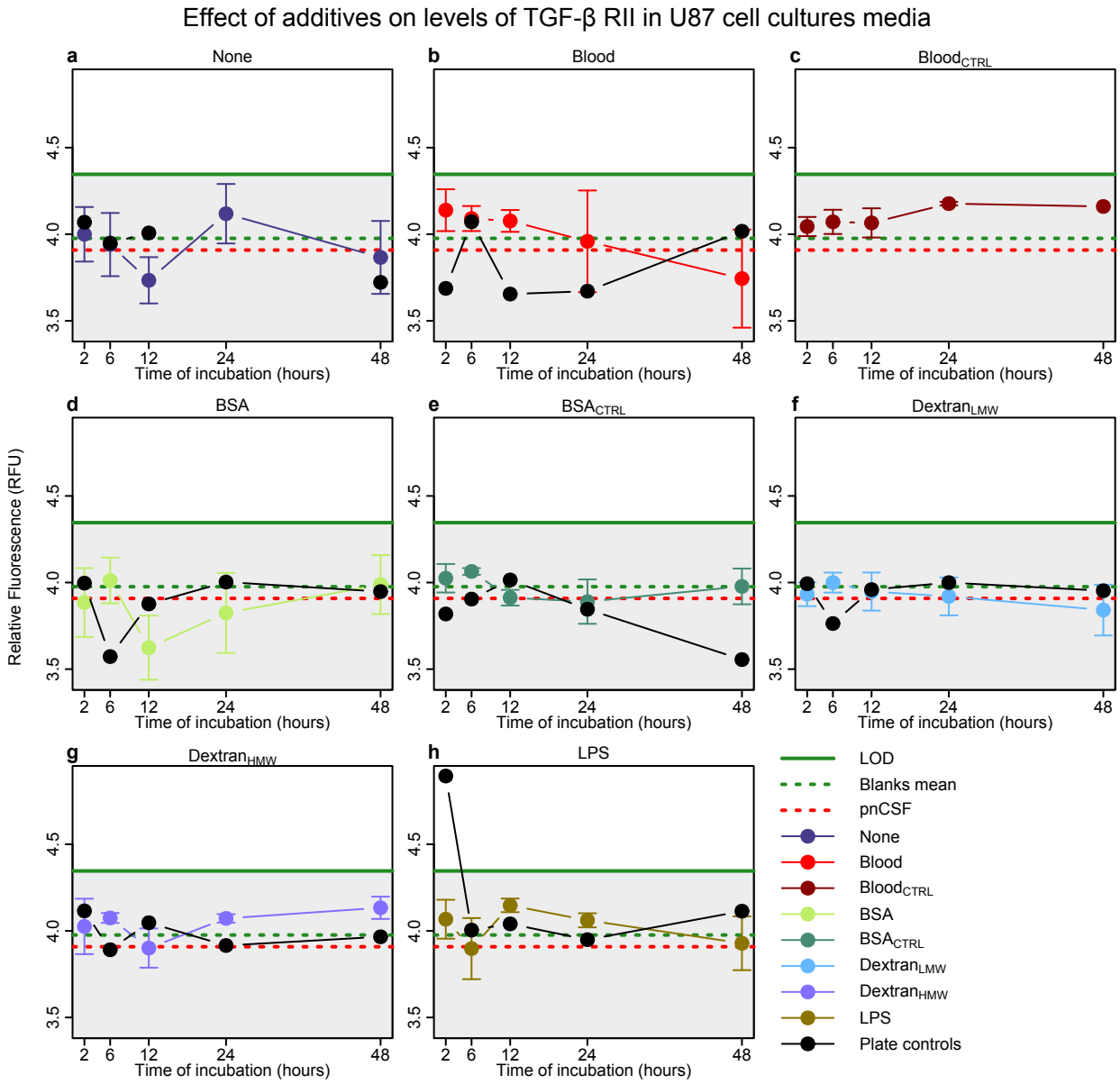

FIGURE H.S160: **Effect of additives on levels of TGF-β RII in U87 cell cultures media.** Additives along with fresh blood and LPS were added to mycoplasma-free human glial (U87) cells in triplicate wells of a 24-well plate and incubated for up to 48 h to measure the effect on levels of proteins measured in the cell media. Media was collected and frozen from successive triplicates at different intervals, then analyzed with the ACM. Each graph compares TGF-β RII values from cells incubated with a different additive to cells not incubated with additives located in the same 24-well plate. Plates in **c** and **e** did not contain any U87 cells, and **c** also did not have controls on the plate.

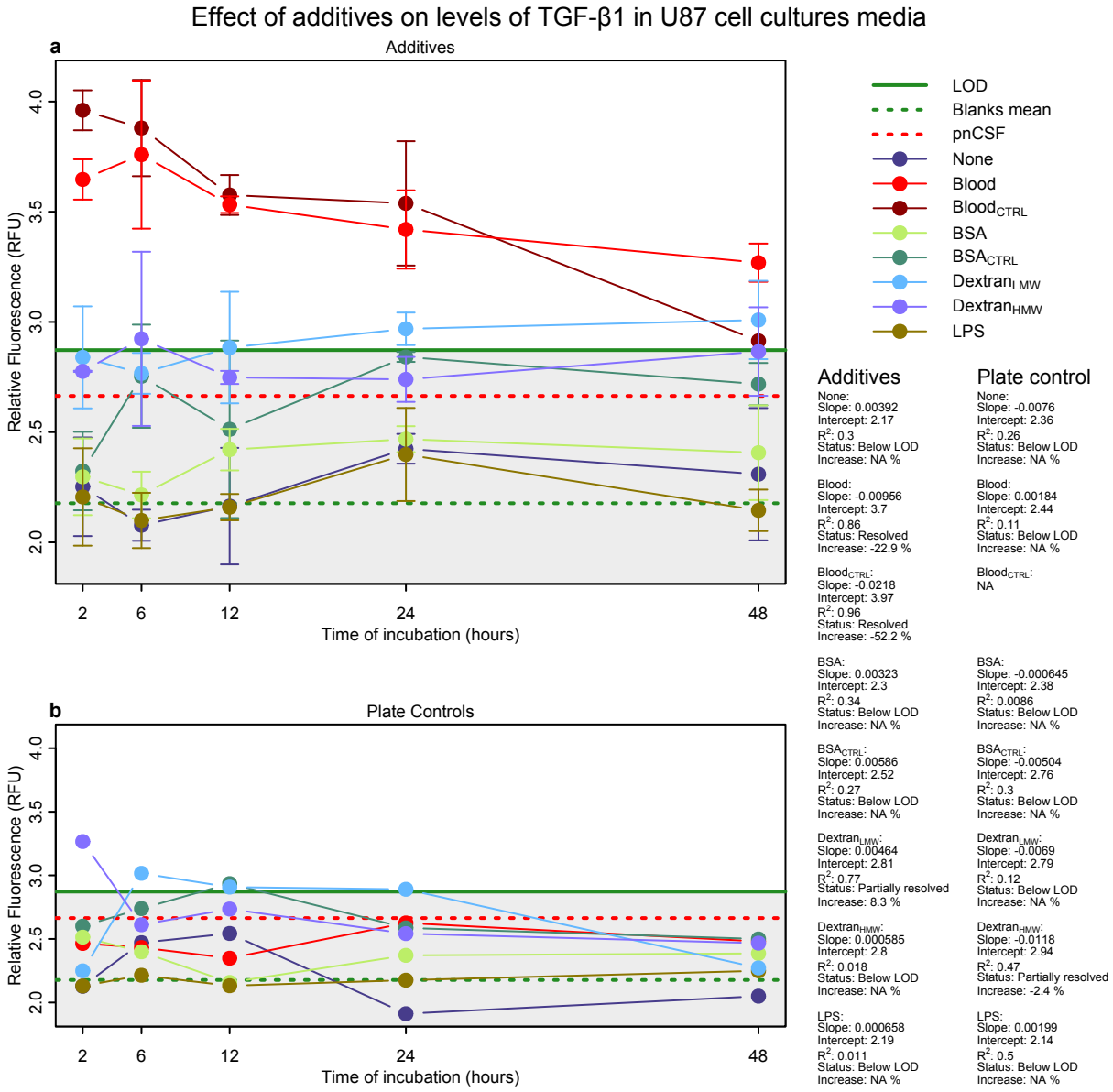

FIGURE H.S161: **Effect of additives on levels of TGF-β1 in U87 cell cultures media.** Additives along with fresh blood and LPS were added to mycoplasma-free human glial (U87) cells in triplicate wells of a 24-well plate and incubated for up to 48 h to measure the effect on levels of proteins measured in the cell media. Media was collected and frozen from successive triplicates at different intervals, then analyzed with the ACM. **a** Average values for TGF-β1 from three replicates for each point in every 24-well plate where a different additive was applied. **b** Data from the control cell media in each plate.

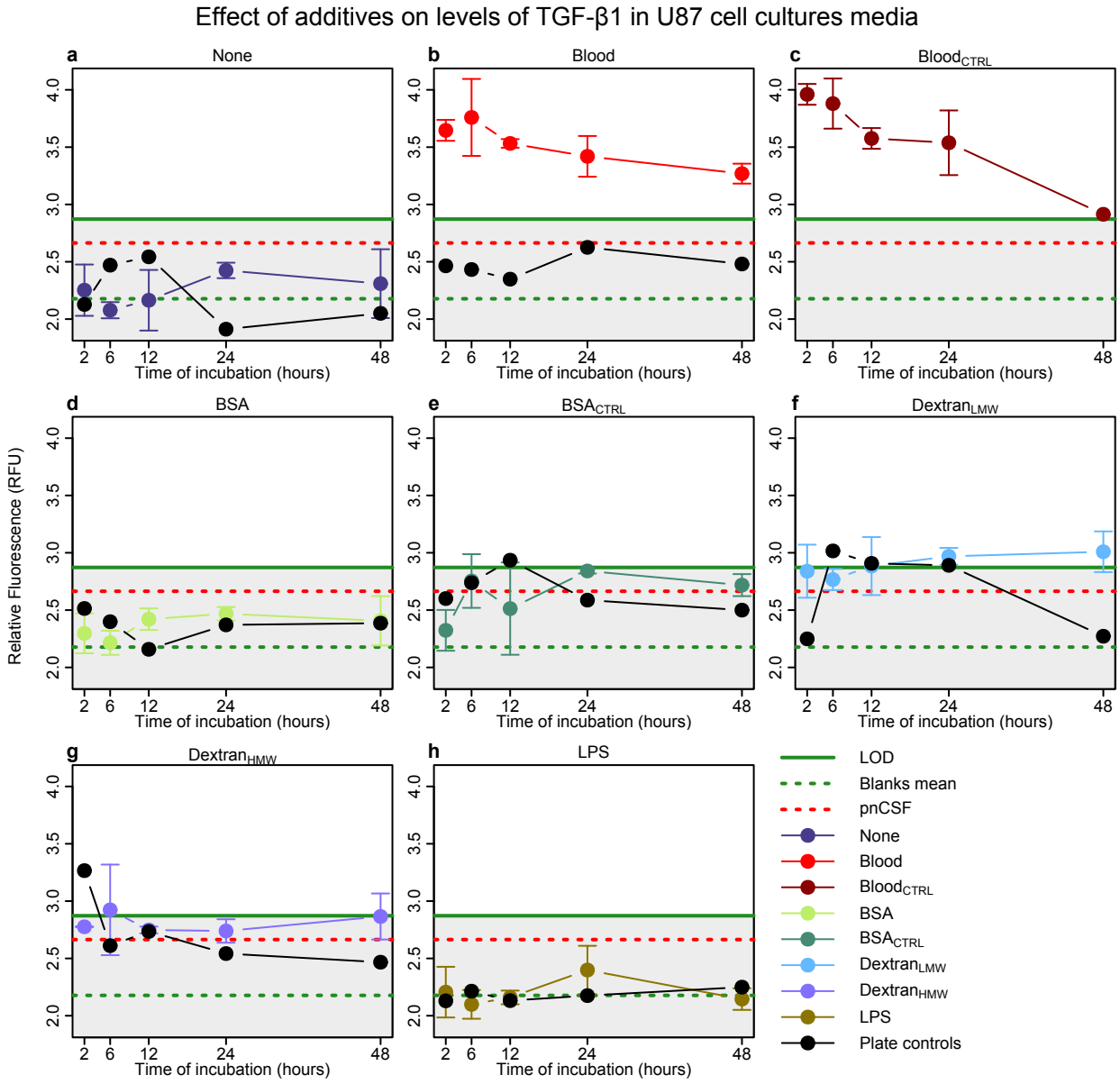

FIGURE H.S162: **Effect of additives on levels of TGF-β1 in U87 cell cultures media.** Additives along with fresh blood and LPS were added to mycoplasma-free human glial (U87) cells in triplicate wells of a 24-well plate and incubated for up to 48 h to measure the effect on levels of proteins measured in the cell media. Media was collected and frozen from successive triplicates at different intervals, then analyzed with the ACM. Each graph compares TGF-β1 values from cells incubated with a different additive to cells not incubated with additives located in the same 24-well plate. Plates in **c** and **e** did not contain any U87 cells, and **c** also did not have controls on the plate.

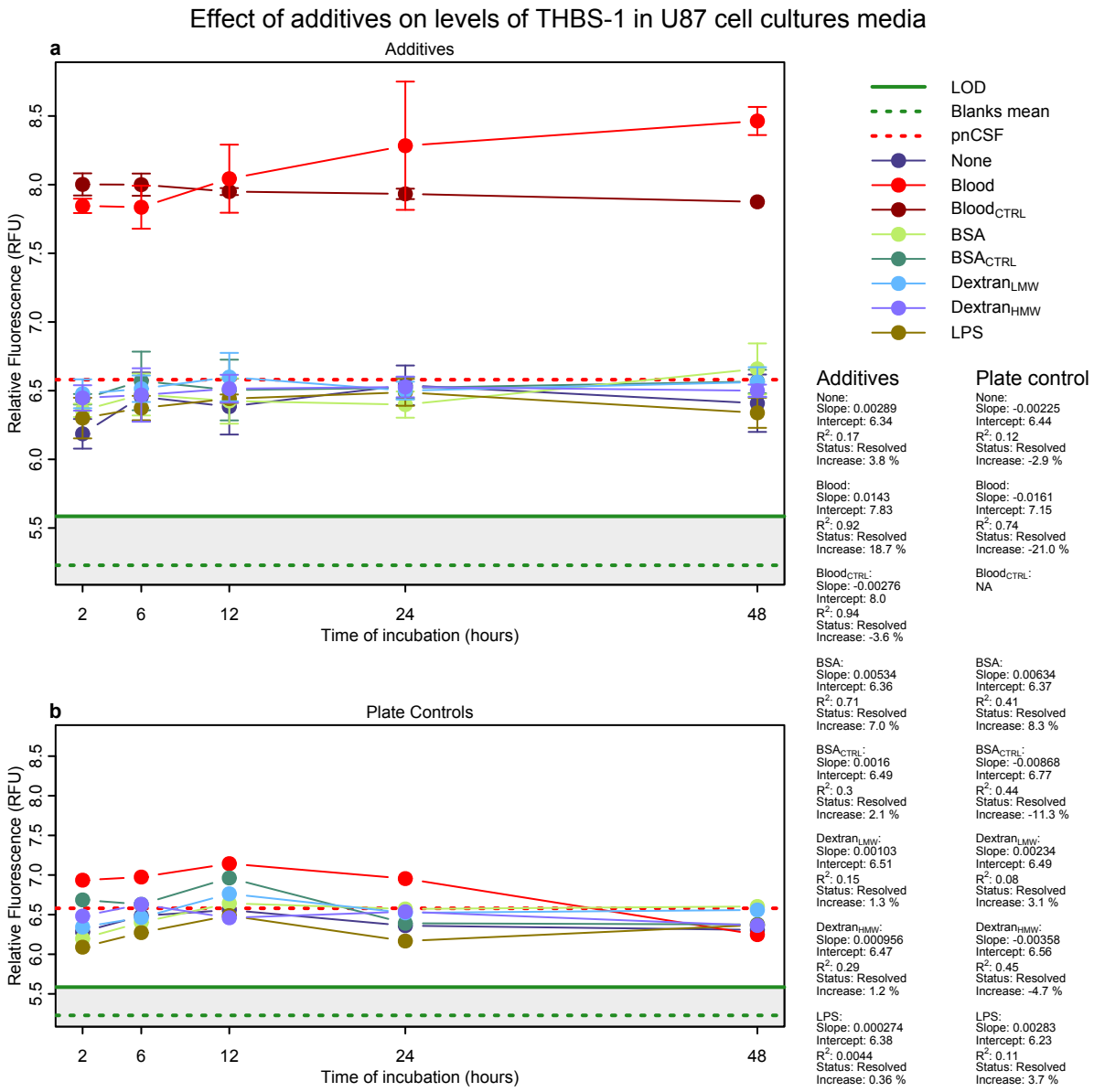

FIGURE H.S163: **Effect of additives on levels of THBS-1 in U87 cell cultures media.** Additives along with fresh blood and LPS were added to mycoplasma-free human glial (U87) cells in triplicate wells of a 24-well plate and incubated for up to 48 h to measure the effect on levels of proteins measured in the cell media. Media was collected and frozen from successive triplicates at different intervals, then analyzed with the ACM. **a** Average values for THBS-1 from three replicates for each point in every 24-well plate where a different additive was applied. **b** Data from the control cell media in each plate.

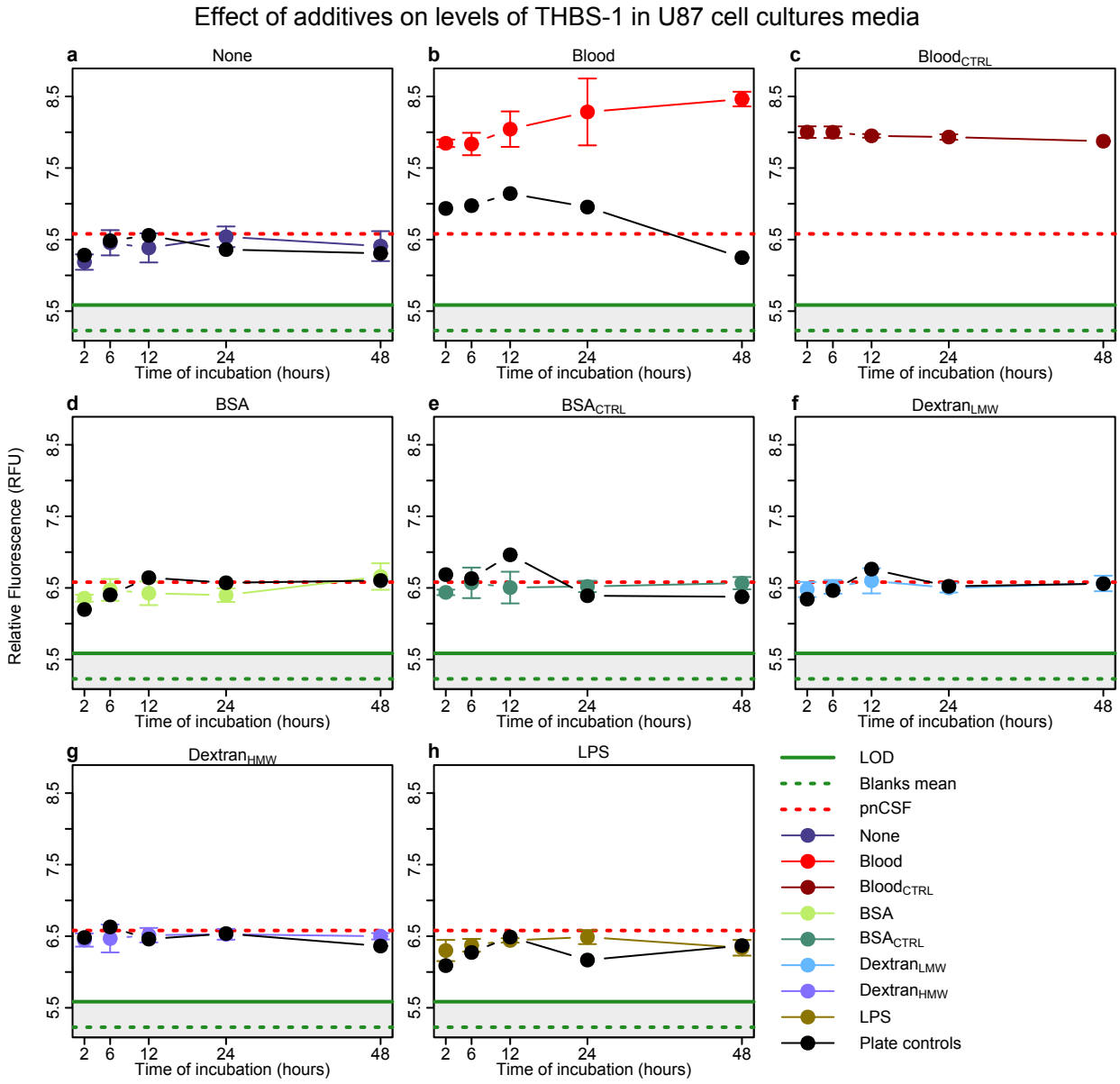

FIGURE H.S164: **Effect of additives on levels of THBS-1 in U87 cell cultures media.** Additives along with fresh blood and LPS were added to mycoplasma-free human glial (U87) cells in triplicate wells of a 24-well plate and incubated for up to 48 h to measure the effect on levels of proteins measured in the cell media. Media was collected and frozen from successive triplicates at different intervals, then analyzed with the ACM. Each graph compares THBS-1 values from cells incubated with a different additive to cells not incubated with additives located in the same 24-well plate. Plates in **c** and **e** did not contain any U87 cells, and **c** also did not have controls on the plate.

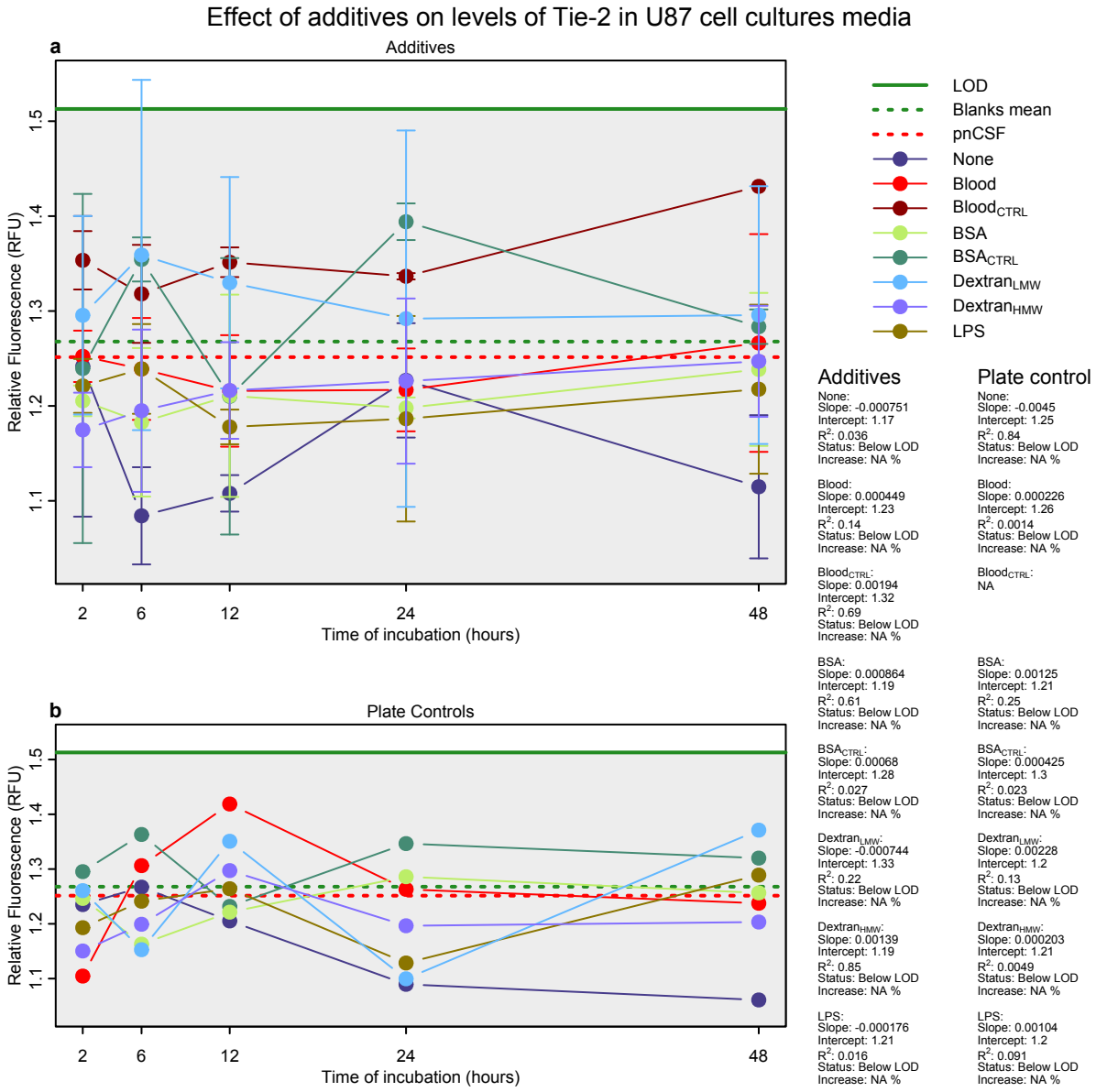

FIGURE H.S165: **Effect of additives on levels of Tie-2 in U87 cell cultures media.** Additives along with fresh blood and LPS were added to mycoplasma-free human glial (U87) cells in triplicate wells of a 24-well plate and incubated for up to 48 h to measure the effect on levels of proteins measured in the cell media. Media was collected and frozen from successive triplicates at different intervals, then analyzed with the ACM. **a** Average values for Tie-2 from three replicates for each point in every 24-well plate where a different additive was applied. **b** Data from the control cell media in each plate.

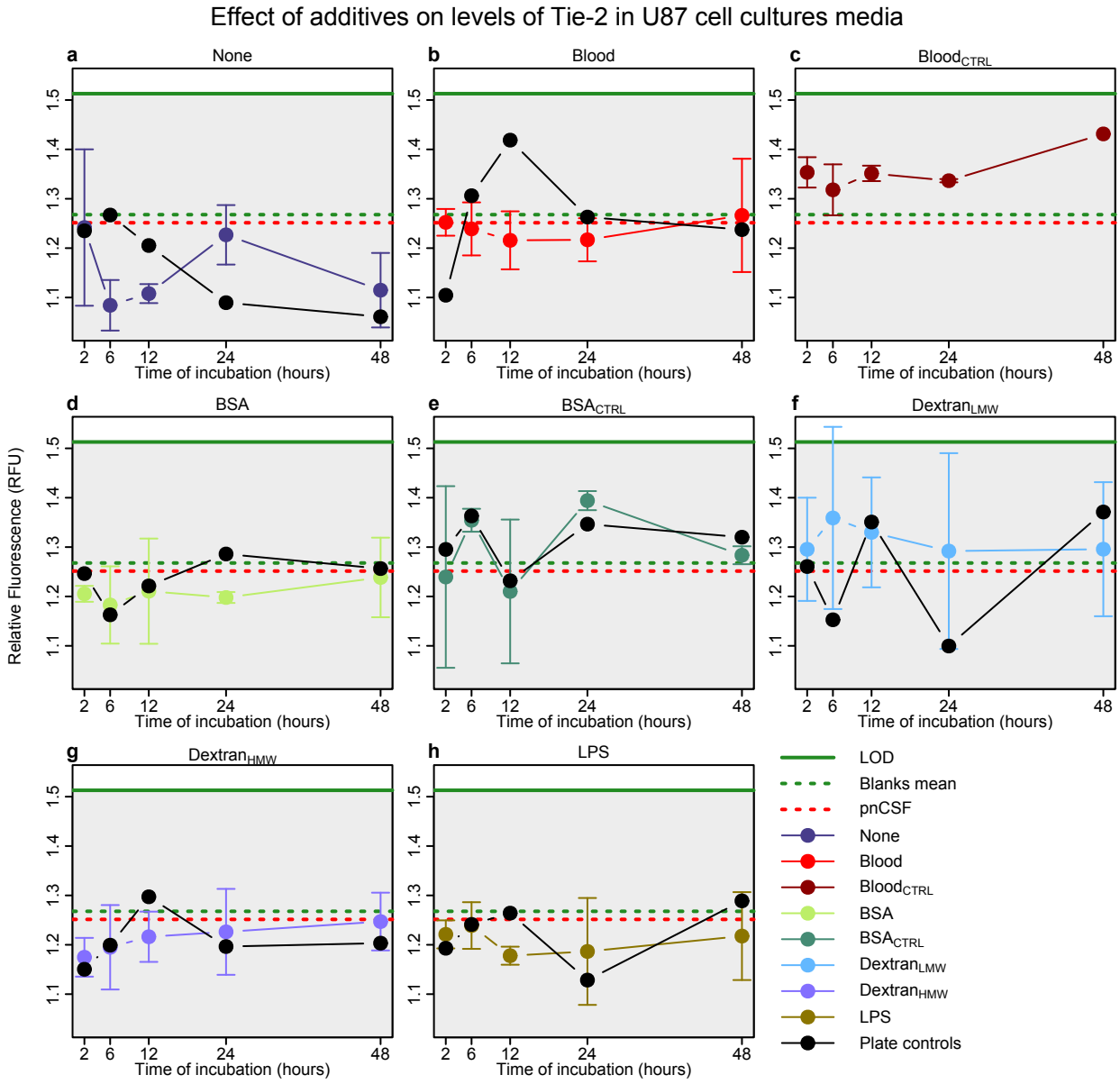

FIGURE H.S166: **Effect of additives on levels of Tie-2 in U87 cell cultures media.** Additives along with fresh blood and LPS were added to mycoplasma-free human glial (U87) cells in triplicate wells of a 24-well plate and incubated for up to 48 h to measure the effect on levels of proteins measured in the cell media. Media was collected and frozen from successive triplicates at different intervals, then analyzed with the ACM. Each graph compares Tie-2 values from cells incubated with a different additive to cells not incubated with additives located in the same 24-well plate. Plates in **c** and **e** did not contain any U87 cells, and **c** also did not have controls on the plate.

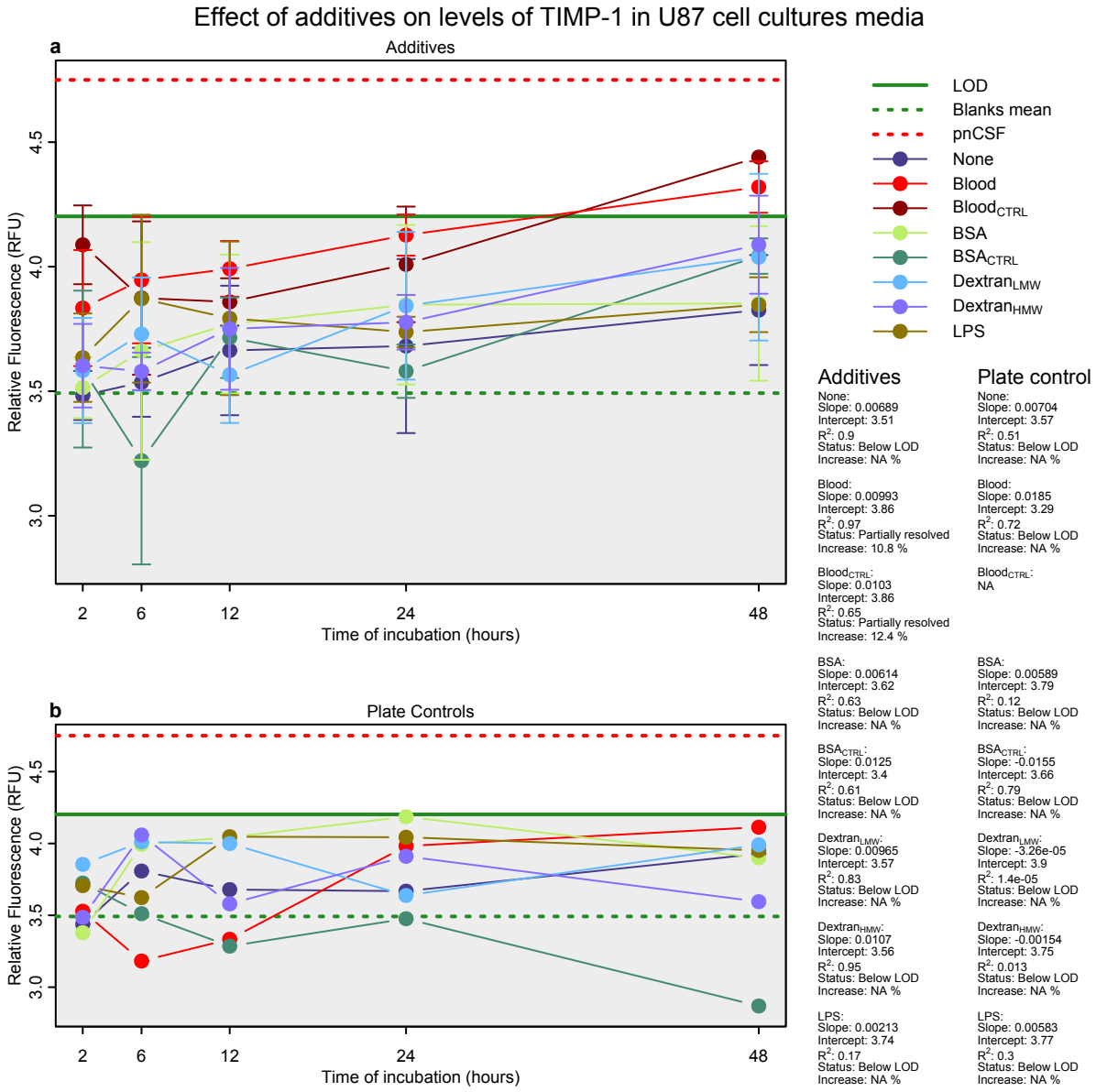

FIGURE H.S167: **Effect of additives on levels of TIMP-1 in U87 cell cultures media.** Additives along with fresh blood and LPS were added to mycoplasma-free human glial (U87) cells in triplicate wells of a 24-well plate and incubated for up to 48 h to measure the effect on levels of proteins measured in the cell media. Media was collected and frozen from successive triplicates at different intervals, then analyzed with the ACM. **a** Average values for TIMP-1 from three replicates for each point in every 24-well plate where a different additive was applied. **b** Data from the control cell media in each plate.

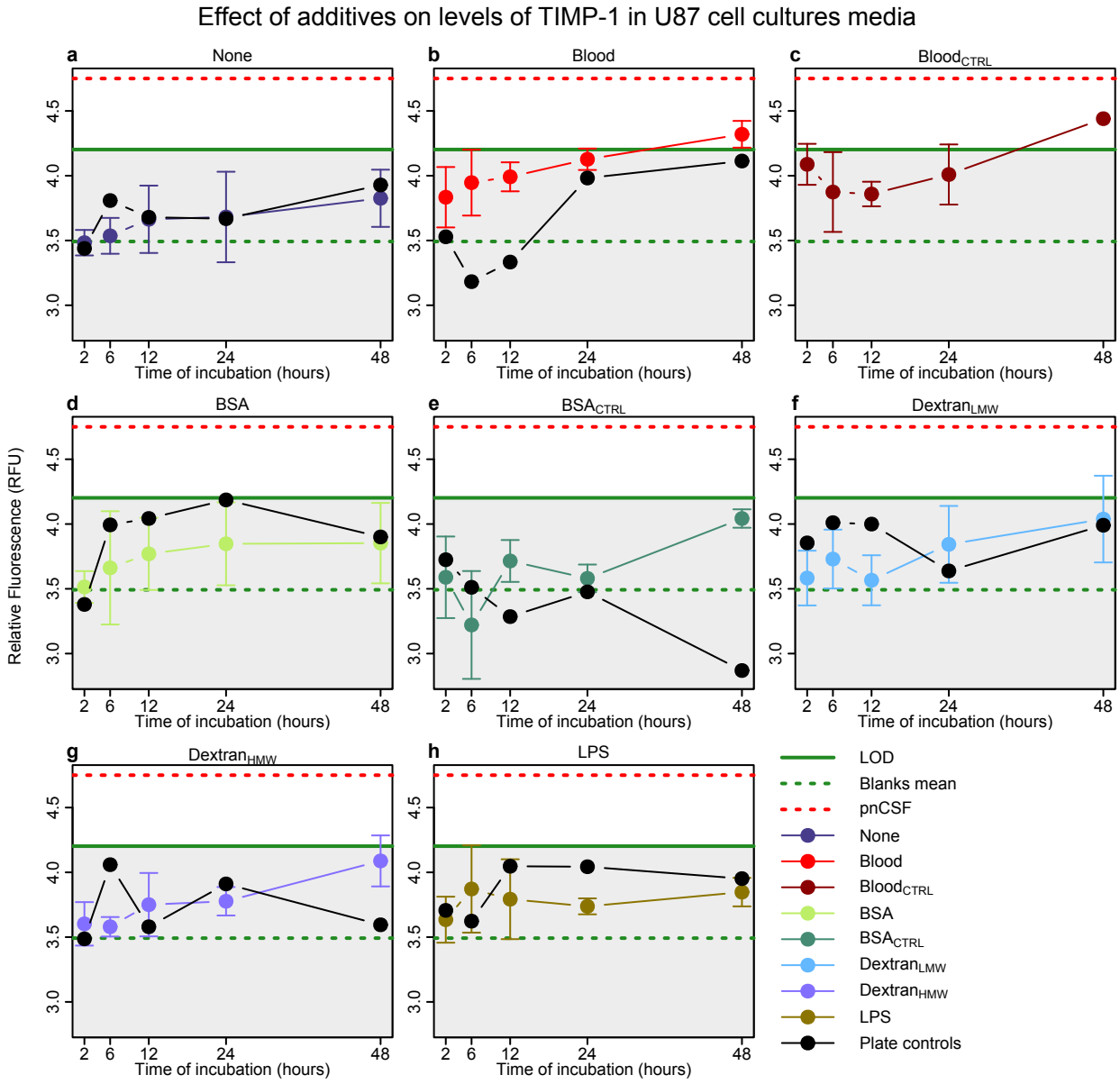

FIGURE H.S168: **Effect of additives on levels of TIMP-1 in U87 cell cultures media.** Additives along with fresh blood and LPS were added to mycoplasma-free human glial (U87) cells in triplicate wells of a 24-well plate and incubated for up to 48 h to measure the effect on levels of proteins measured in the cell media. Media was collected and frozen from successive triplicates at different intervals, then analyzed with the ACM. Each graph compares TIMP-1 values from cells incubated with a different additive to cells not incubated with additives located in the same 24-well plate. Plates in **c** and **e** did not contain any U87 cells, and **c** also did not have controls on the plate.

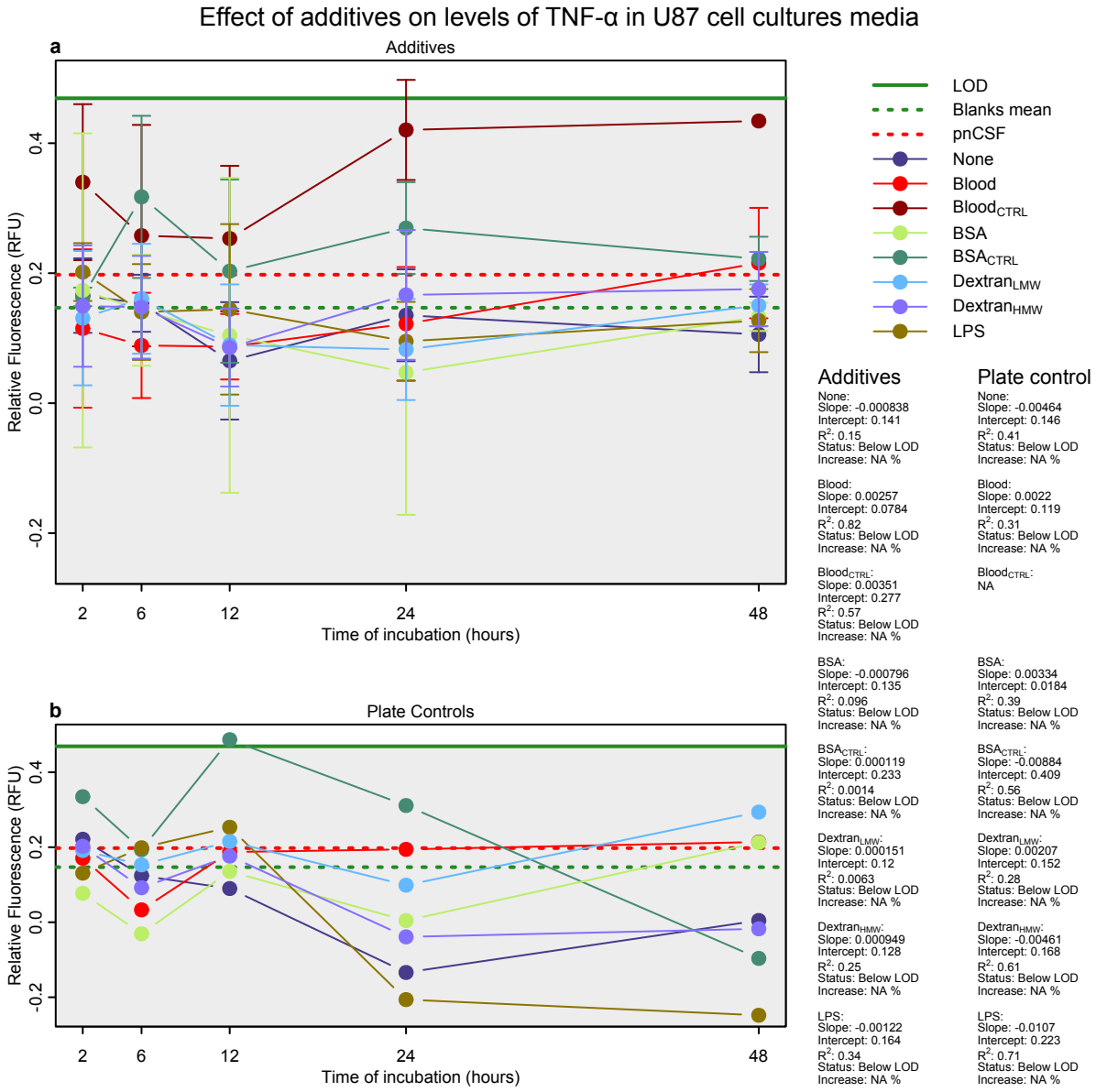

FIGURE H.S169: **Effect of additives on levels of TNF-α in U87 cell cultures media.** Additives along with fresh blood and LPS were added to mycoplasma-free human glial (U87) cells in triplicate wells of a 24-well plate and incubated for up to 48 h to measure the effect on levels of proteins measured in the cell media. Media was collected and frozen from successive triplicates at different intervals, then analyzed with the ACM. **a** Average values for TNF-α from three replicates for each point in every 24-well plate where a different additive was applied. **b** Data from the control cell media in each plate.

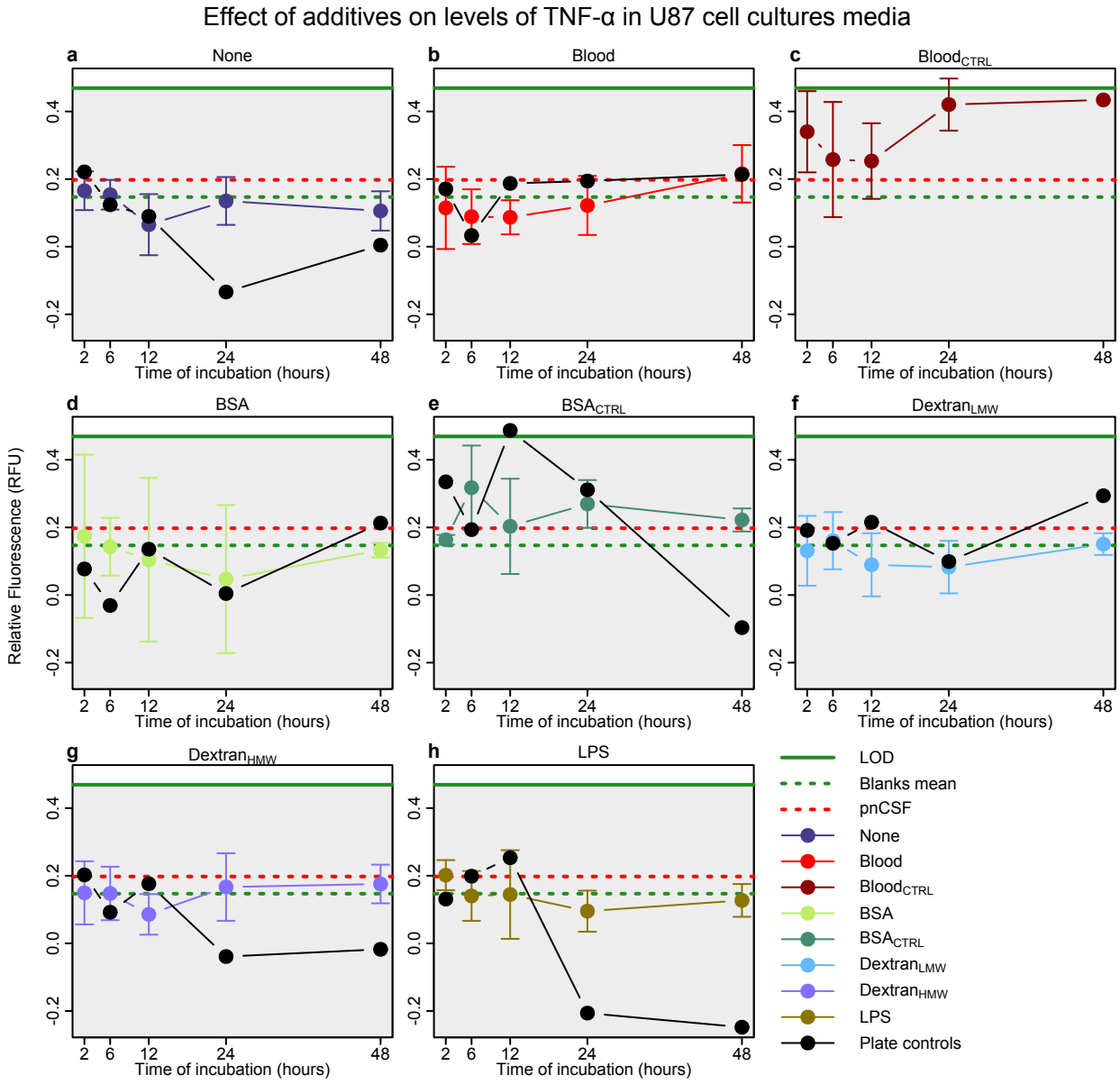

FIGURE H.S170: **Effect of additives on levels of TNF-α in U87 cell cultures media.** Additives along with fresh blood and LPS were added to mycoplasma-free human glial (U87) cells in triplicate wells of a 24-well plate and incubated for up to 48 h to measure the effect on levels of proteins measured in the cell media. Media was collected and frozen from successive triplicates at different intervals, then analyzed with the ACM. Each graph compares TNF-α values from cells incubated with a different additive to cells not incubated with additives located in the same 24-well plate. Plates in **c** and **e** did not contain any U87 cells, and **c** also did not have controls on the plate.

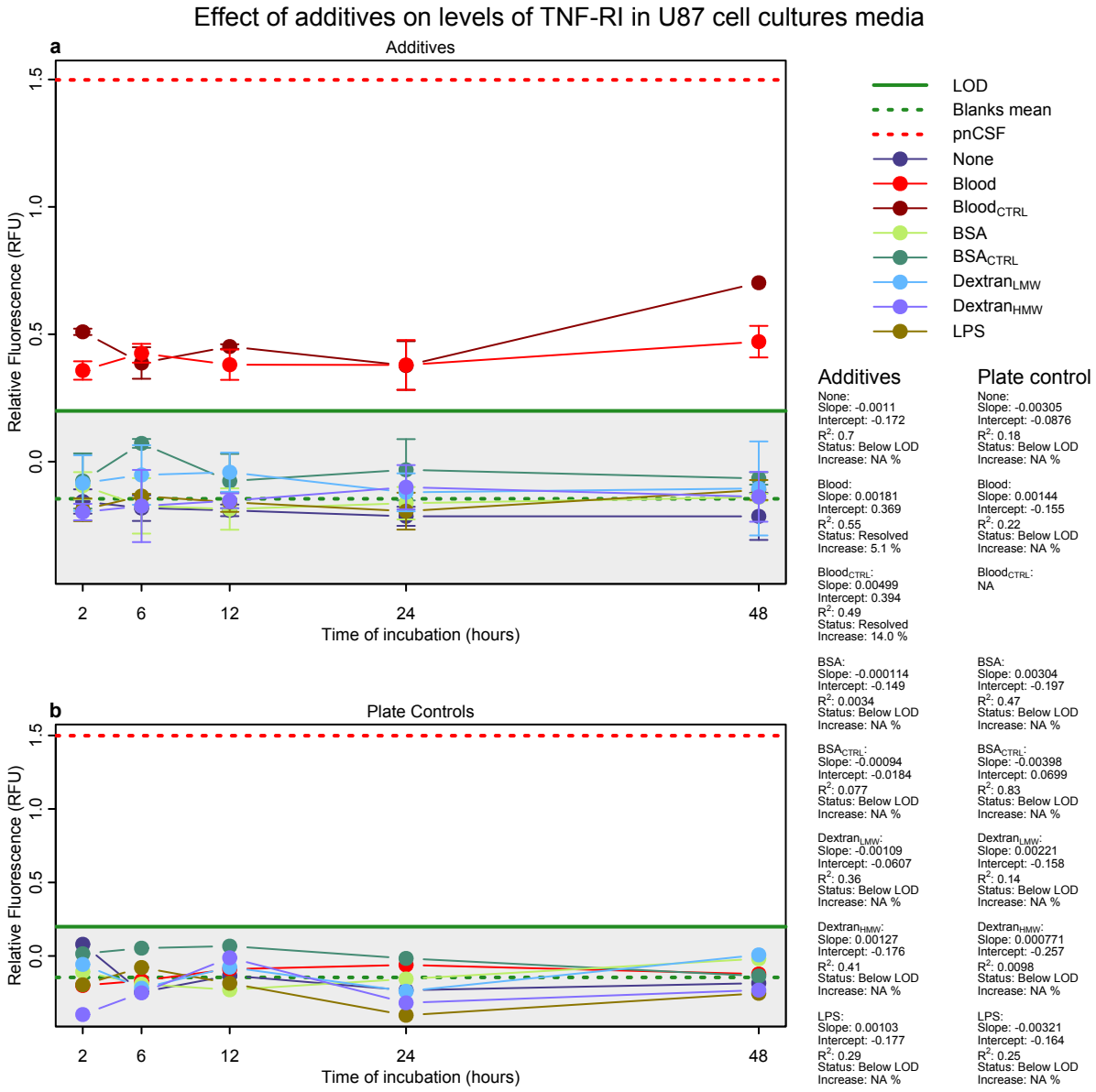

FIGURE H.S171: **Effect of additives on levels of TNF-RI in U87 cell cultures media.** Additives along with fresh blood and LPS were added to mycoplasma-free human glial (U87) cells in triplicate wells of a 24-well plate and incubated for up to 48 h to measure the effect on levels of proteins measured in the cell media. Media was collected and frozen from successive triplicates at different intervals, then analyzed with the ACM. **a** Average values for TNF-RI from three replicates for each point in every 24-well plate where a different additive was applied. **b** Data from the control cell media in each plate.

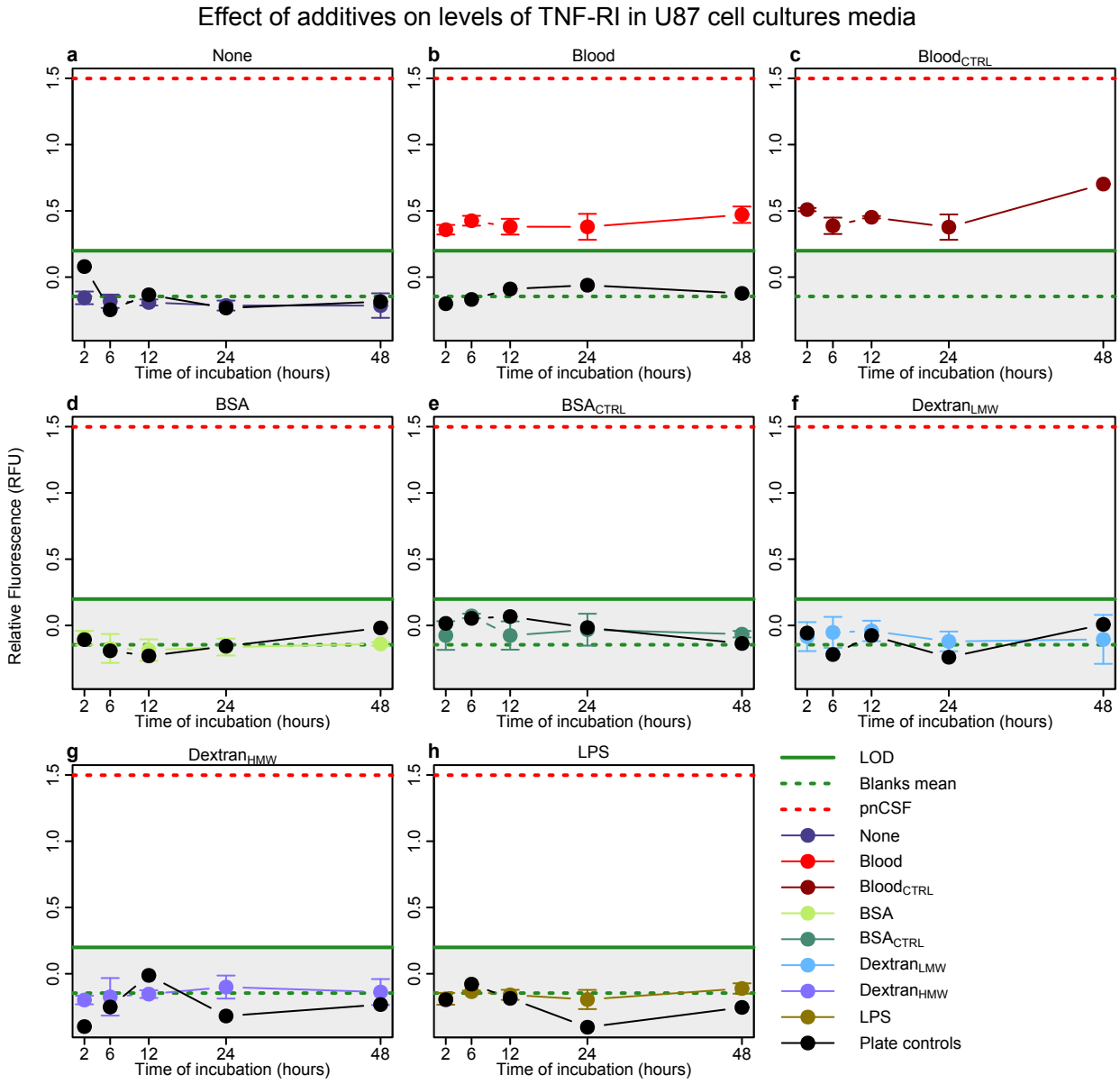

FIGURE H.S172: **Effect of additives on levels of TNF-RI in U87 cell cultures media.** Additives along with fresh blood and LPS were added to mycoplasma-free human glial (U87) cells in triplicate wells of a 24-well plate and incubated for up to 48 h to measure the effect on levels of proteins measured in the cell media. Media was collected and frozen from successive triplicates at different intervals, then analyzed with the ACM. Each graph compares TNF-RI values from cells incubated with a different additive to cells not incubated with additives located in the same 24-well plate. Plates in **c** and **e** did not contain any U87 cells, and **c** also did not have controls on the plate.

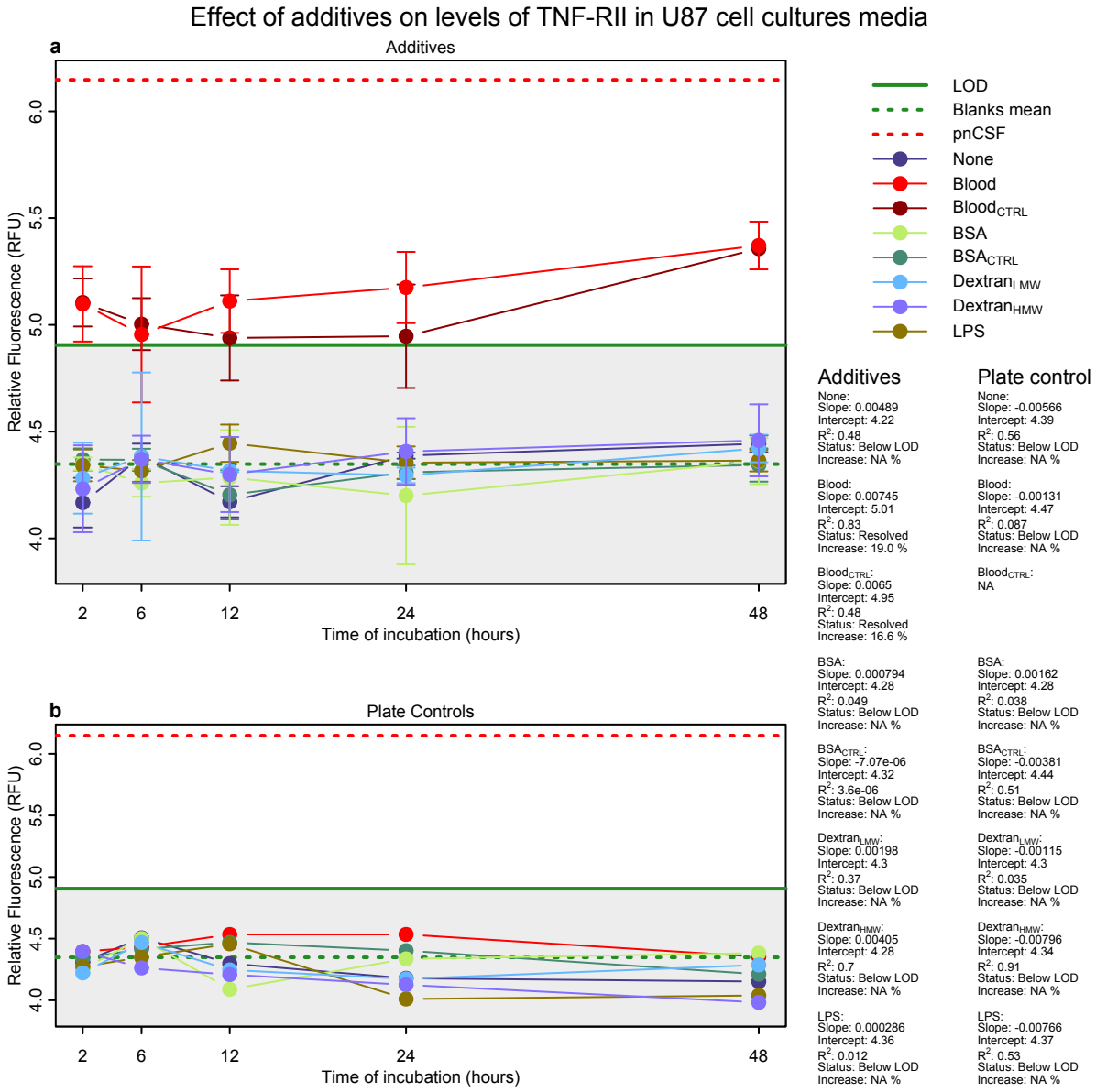

FIGURE H.S173: **Effect of additives on levels of TNF-RII in U87 cell cultures media.** Additives along with fresh blood and LPS were added to mycoplasma-free human glial (U87) cells in triplicate wells of a 24-well plate and incubated for up to 48 h to measure the effect on levels of proteins measured in the cell media. Media was collected and frozen from successive triplicates at different intervals, then analyzed with the ACM. **a** Average values for TNF-RII from three replicates for each point in every 24-well plate where a different additive was applied. **b** Data from the control cell media in each plate.

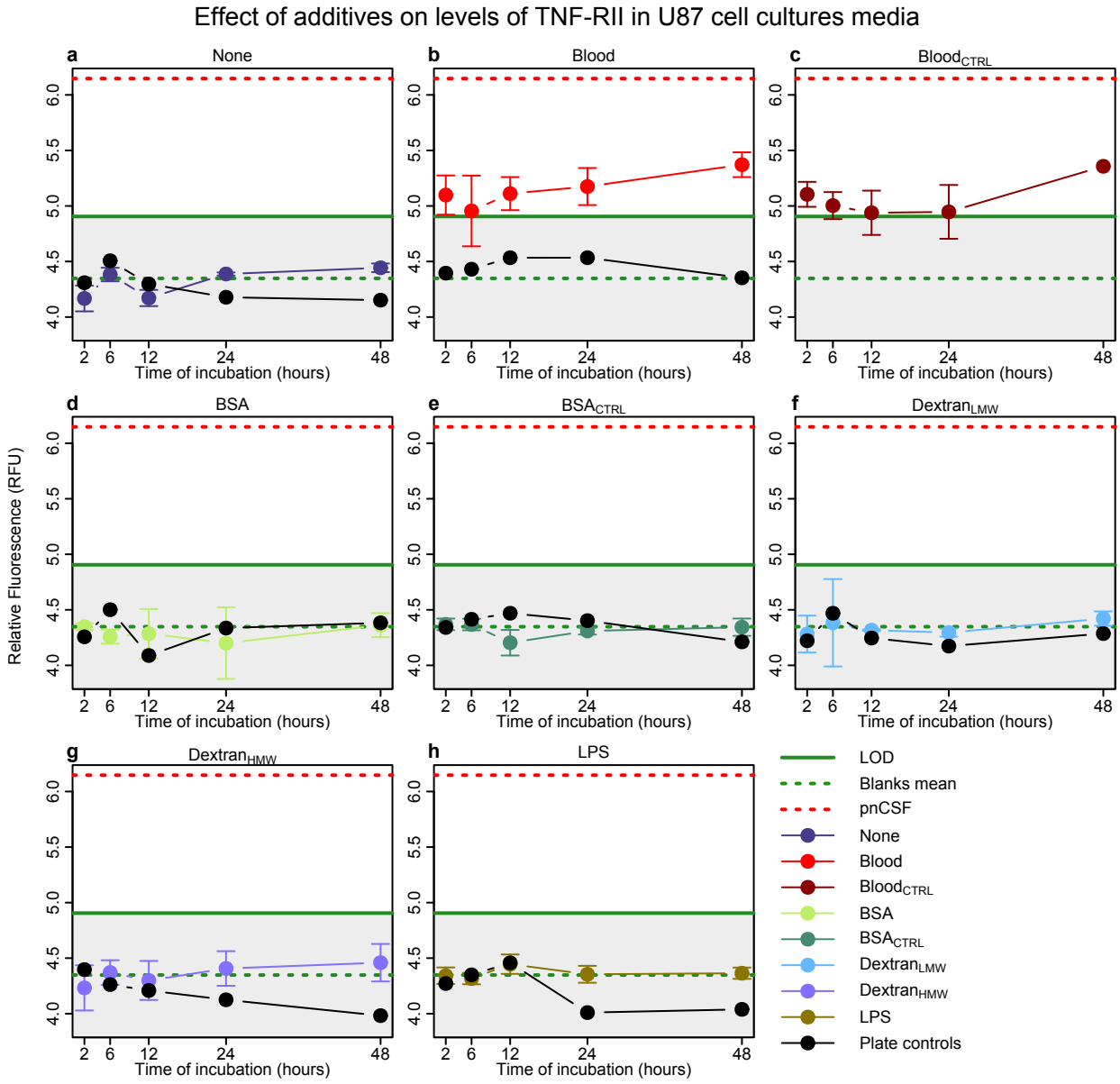

FIGURE H.S174: **Effect of additives on levels of TNF-RII in U87 cell cultures media.** Additives along with fresh blood and LPS were added to mycoplasma-free human glial (U87) cells in triplicate wells of a 24-well plate and incubated for up to 48 h to measure the effect on levels of proteins measured in the cell media. Media was collected and frozen from successive triplicates at different intervals, then analyzed with the ACM. Each graph compares TNF-RII values from cells incubated with a different additive to cells not incubated with additives located in the same 24-well plate. Plates in **c** and **e** did not contain any U87 cells, and **c** also did not have controls on the plate.

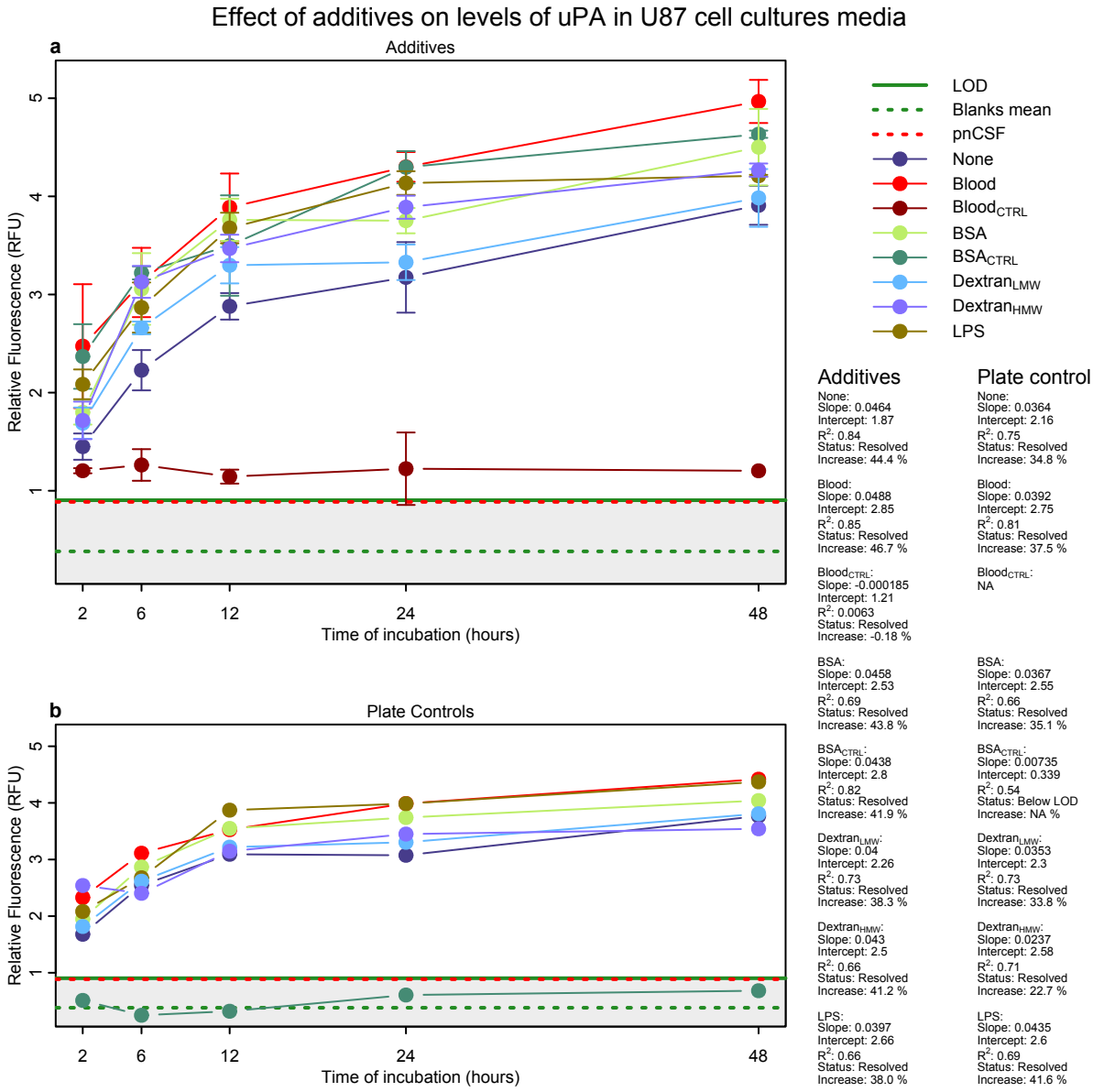

FIGURE H.S175: **Effect of additives on levels of uPA in U87 cell cultures media.** Additives along with fresh blood and LPS were added to mycoplasma-free human glial (U87) cells in triplicate wells of a 24-well plate and incubated for up to 48 h to measure the effect on levels of proteins measured in the cell media. Media was collected and frozen from successive triplicates at different intervals, then analyzed with the ACM. **a** Average values for uPA from three replicates for each point in every 24-well plate where a different additive was applied. **b** Data from the control cell media in each plate.

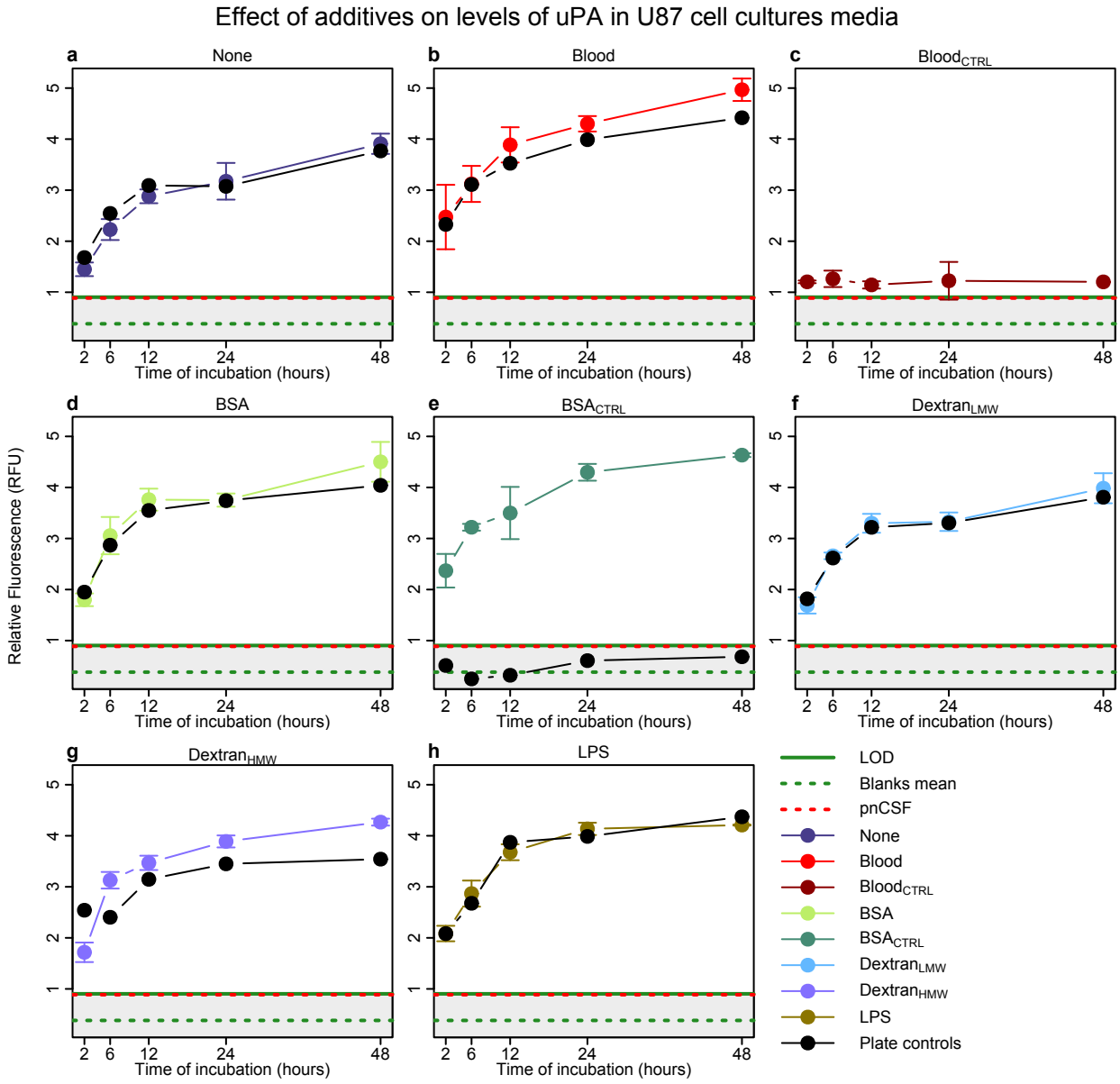

FIGURE H.S176: **Effect of additives on levels of uPA in U87 cell cultures media.** Additives along with fresh blood and LPS were added to mycoplasma-free human glial (U87) cells in triplicate wells of a 24-well plate and incubated for up to 48 h to measure the effect on levels of proteins measured in the cell media. Media was collected and frozen from successive triplicates at different intervals, then analyzed with the ACM. Each graph compares uPA values from cells incubated with a different additive to cells not incubated with additives located in the same 24-well plate. Plates in **c** and **e** did not contain any U87 cells, and **c** also did not have controls on the plate.

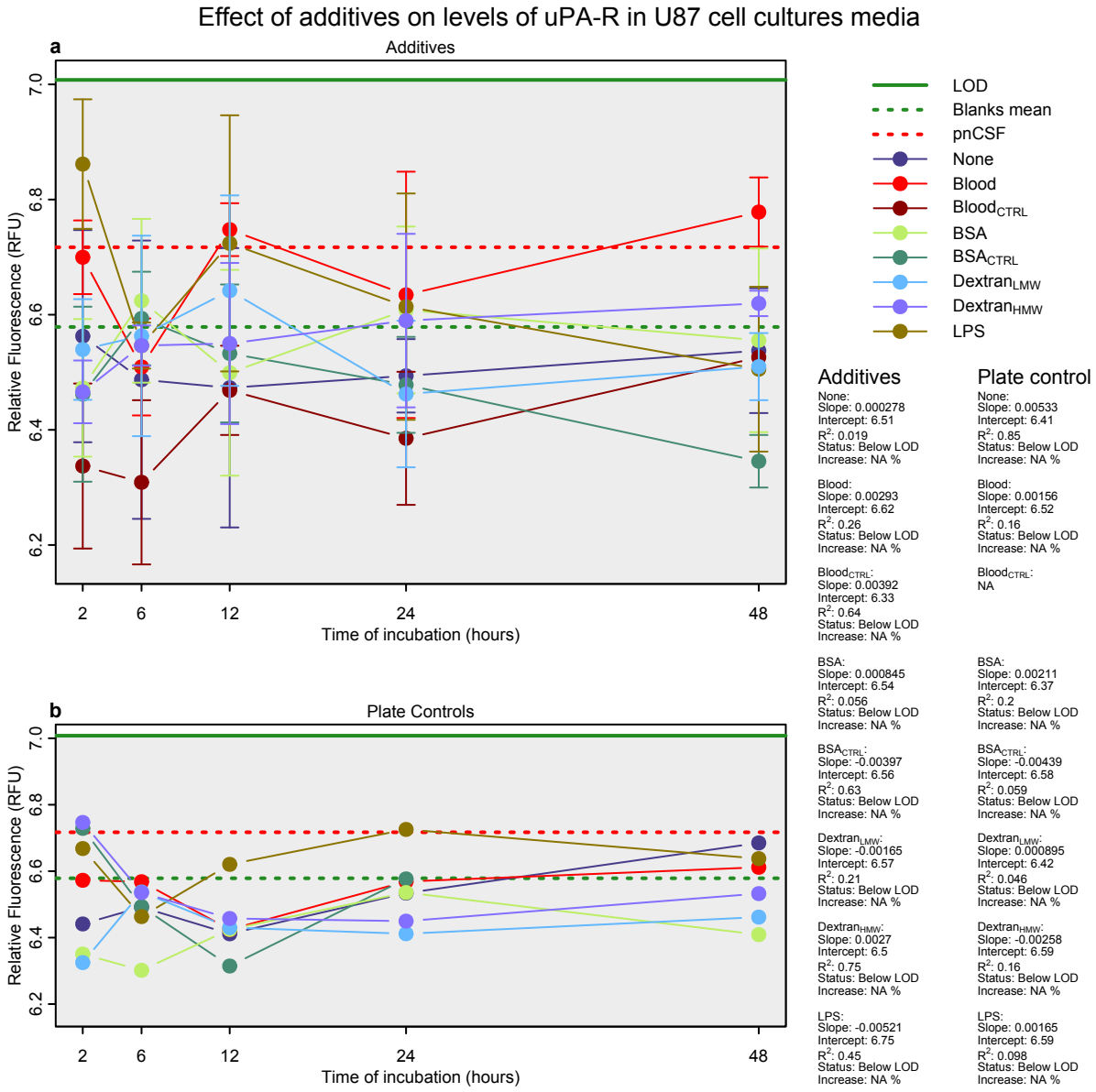

FIGURE H.S177: **Effect of additives on levels of uPA-R in U87 cell cultures media.** Additives along with fresh blood and LPS were added to mycoplasma-free human glial (U87) cells in triplicate wells of a 24-well plate and incubated for up to 48 h to measure the effect on levels of proteins measured in the cell media. Media was collected and frozen from successive triplicates at different intervals, then analyzed with the ACM. **a** Average values for uPA-R from three replicates for each point in every 24-well plate where a different additive was applied. **b** Data from the control cell media in each plate.

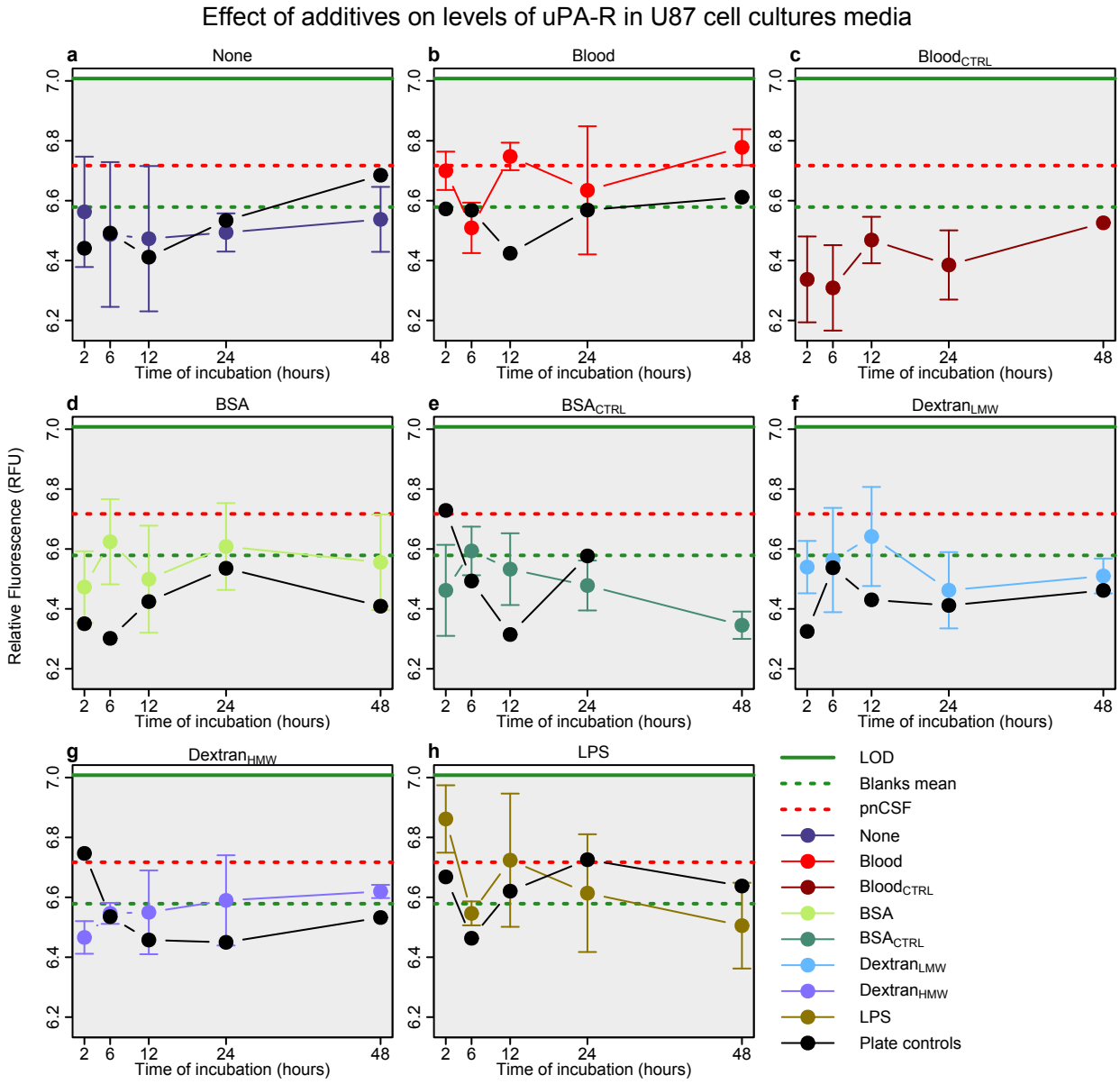

FIGURE H.S178: **Effect of additives on levels of uPA-R in U87 cell cultures media.** Additives along with fresh blood and LPS were added to mycoplasma-free human glial (U87) cells in triplicate wells of a 24-well plate and incubated for up to 48 h to measure the effect on levels of proteins measured in the cell media. Media was collected and frozen from successive triplicates at different intervals, then analyzed with the ACM. Each graph compares uPA-R values from cells incubated with a different additive to cells not incubated with additives located in the same 24-well plate. Plates in **c** and **e** did not contain any U87 cells, and **c** also did not have controls on the plate.

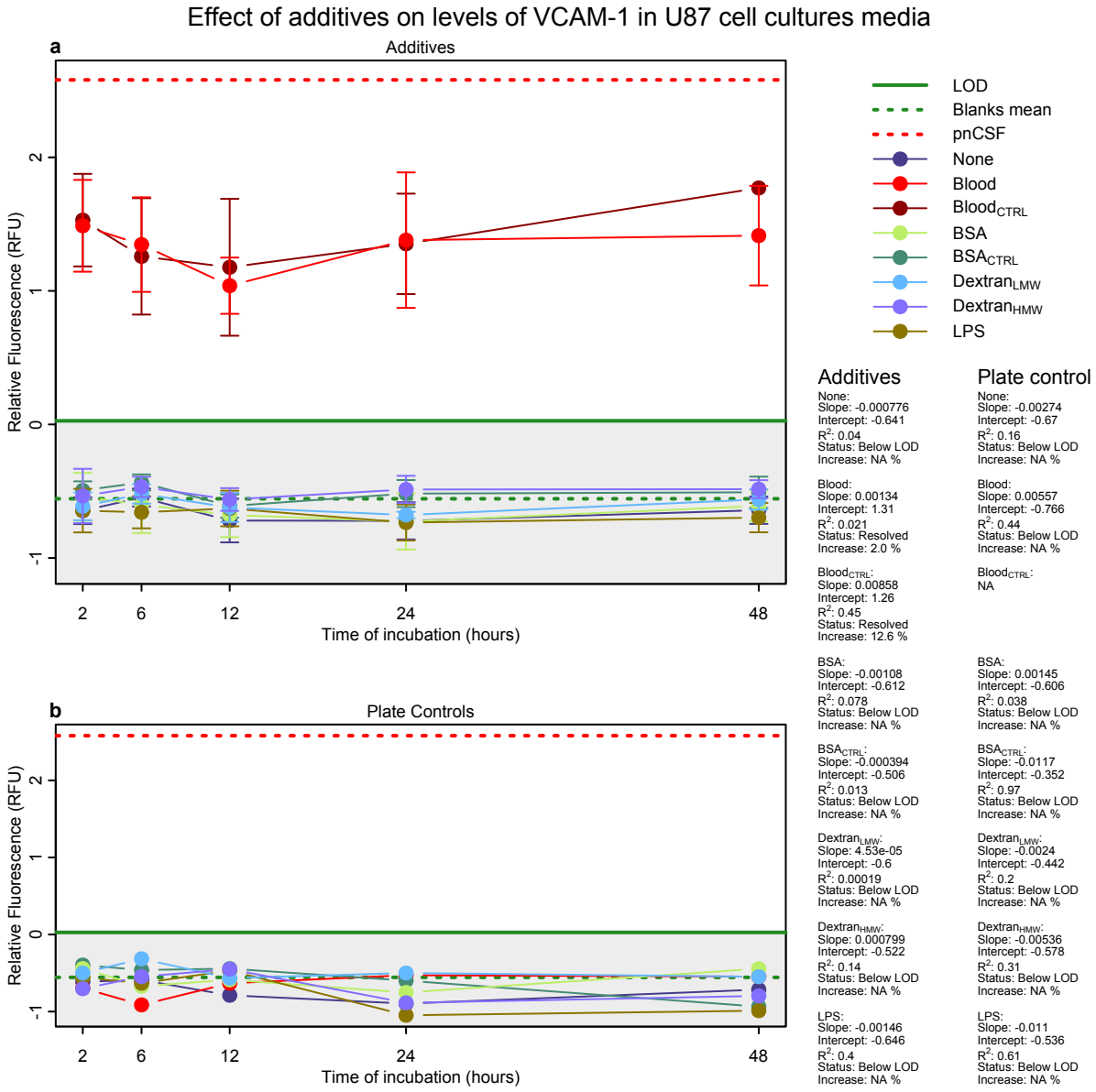

FIGURE H.S179: **Effect of additives on levels of VCAM-1 in U87 cell cultures media.** Additives along with fresh blood and LPS were added to mycoplasma-free human glial (U87) cells in triplicate wells of a 24-well plate and incubated for up to 48 h to measure the effect on levels of proteins measured in the cell media. Media was collected and frozen from successive triplicates at different intervals, then analyzed with the ACM. **a** Average values for VCAM-1 from three replicates for each point in every 24-well plate where a different additive was applied. **b** Data from the control cell media in each plate.

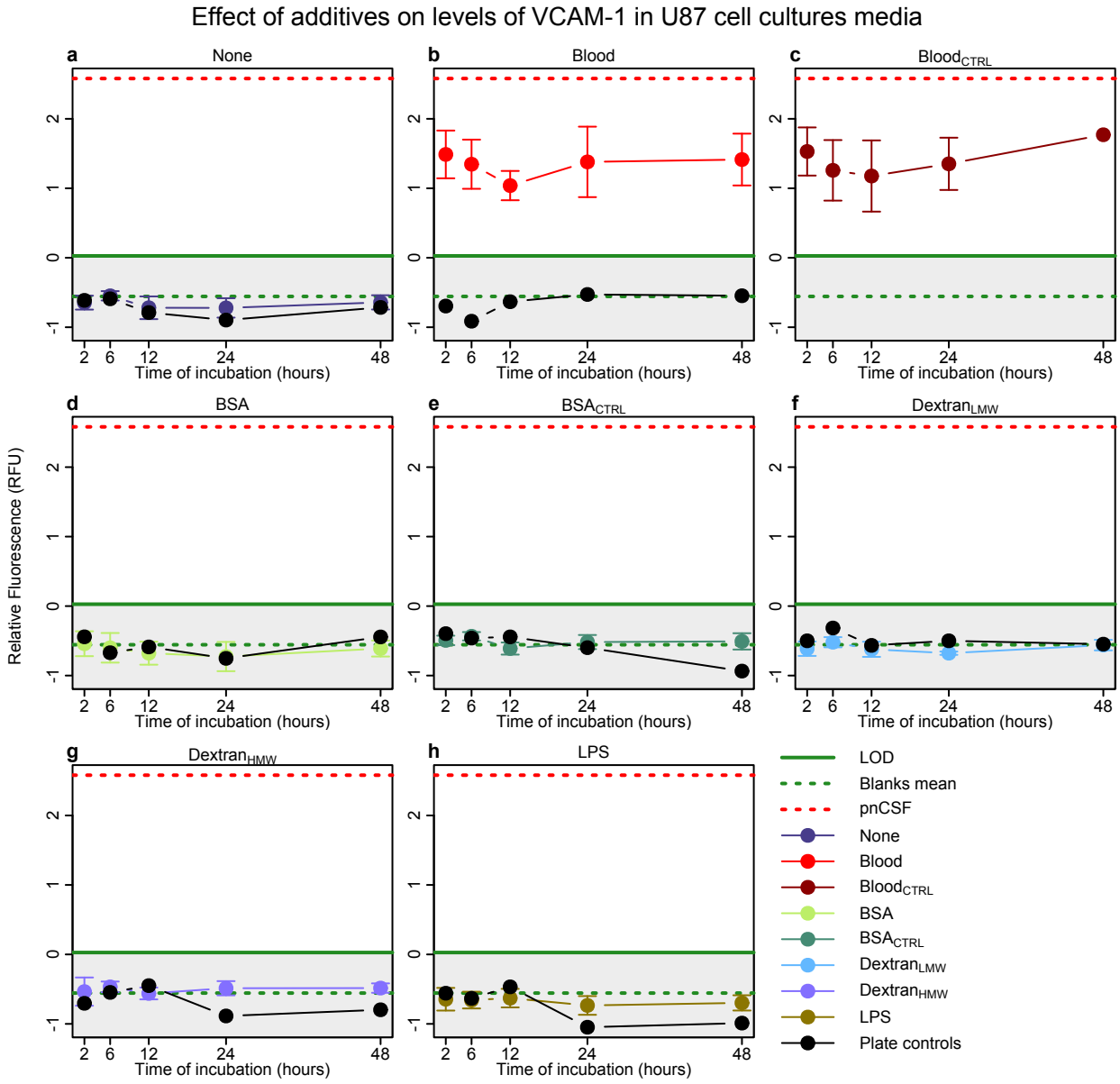

FIGURE H.S180: **Effect of additives on levels of VCAM-1 in U87 cell cultures media.** Additives along with fresh blood and LPS were added to mycoplasma-free human glial (U87) cells in triplicate wells of a 24-well plate and incubated for up to 48 h to measure the effect on levels of proteins measured in the cell media. Media was collected and frozen from successive triplicates at different intervals, then analyzed with the ACM. Each graph compares VCAM-1 values from cells incubated with a different additive to cells not incubated with additives located in the same 24-well plate. Plates in **c** and **e** did not contain any U87 cells, and **c** also did not have controls on the plate.

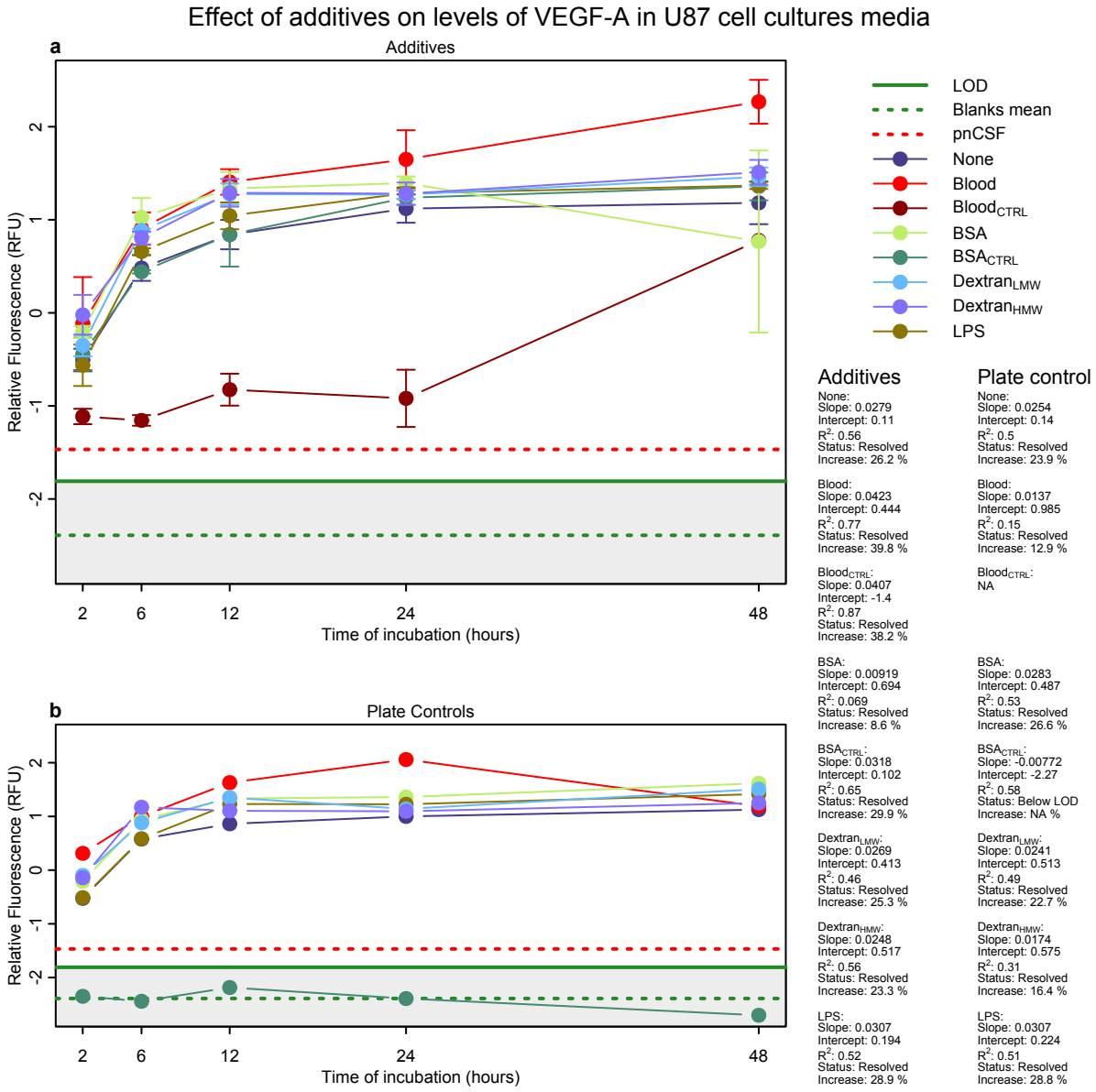

FIGURE H.S181: **Effect of additives on levels of VEGF-A in U87 cell cultures media.** Additives along with fresh blood and LPS were added to mycoplasma-free human glial (U87) cells in triplicate wells of a 24-well plate and incubated for up to 48 h to measure the effect on levels of proteins measured in the cell media. Media was collected and frozen from successive triplicates at different intervals, then analyzed with the ACM. **a** Average values for VEGF-A from three replicates for each point in every 24-well plate where a different additive was applied. **b** Data from the control cell media in each plate.

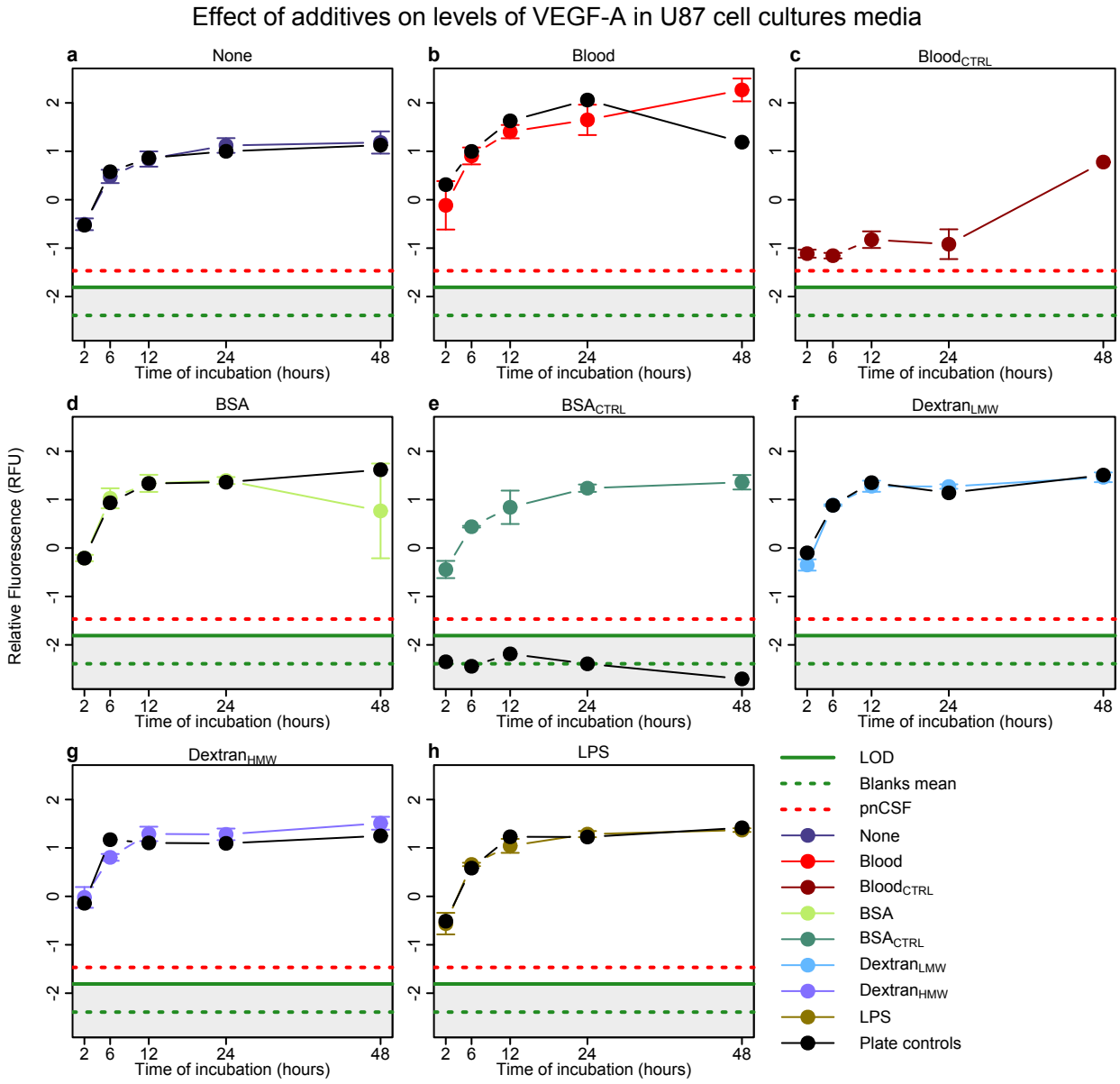

FIGURE H.S182: **Effect of additives on levels of VEGF-A in U87 cell cultures media.** Additives along with fresh blood and LPS were added to mycoplasma-free human glial (U87) cells in triplicate wells of a 24-well plate and incubated for up to 48 h to measure the effect on levels of proteins measured in the cell media. Media was collected and frozen from successive triplicates at different intervals, then analyzed with the ACM. Each graph compares VEGF-A values from cells incubated with a different additive to cells not incubated with additives located in the same 24-well plate. Plates in **c** and **e** did not contain any U87 cells, and **c** also did not have controls on the plate.

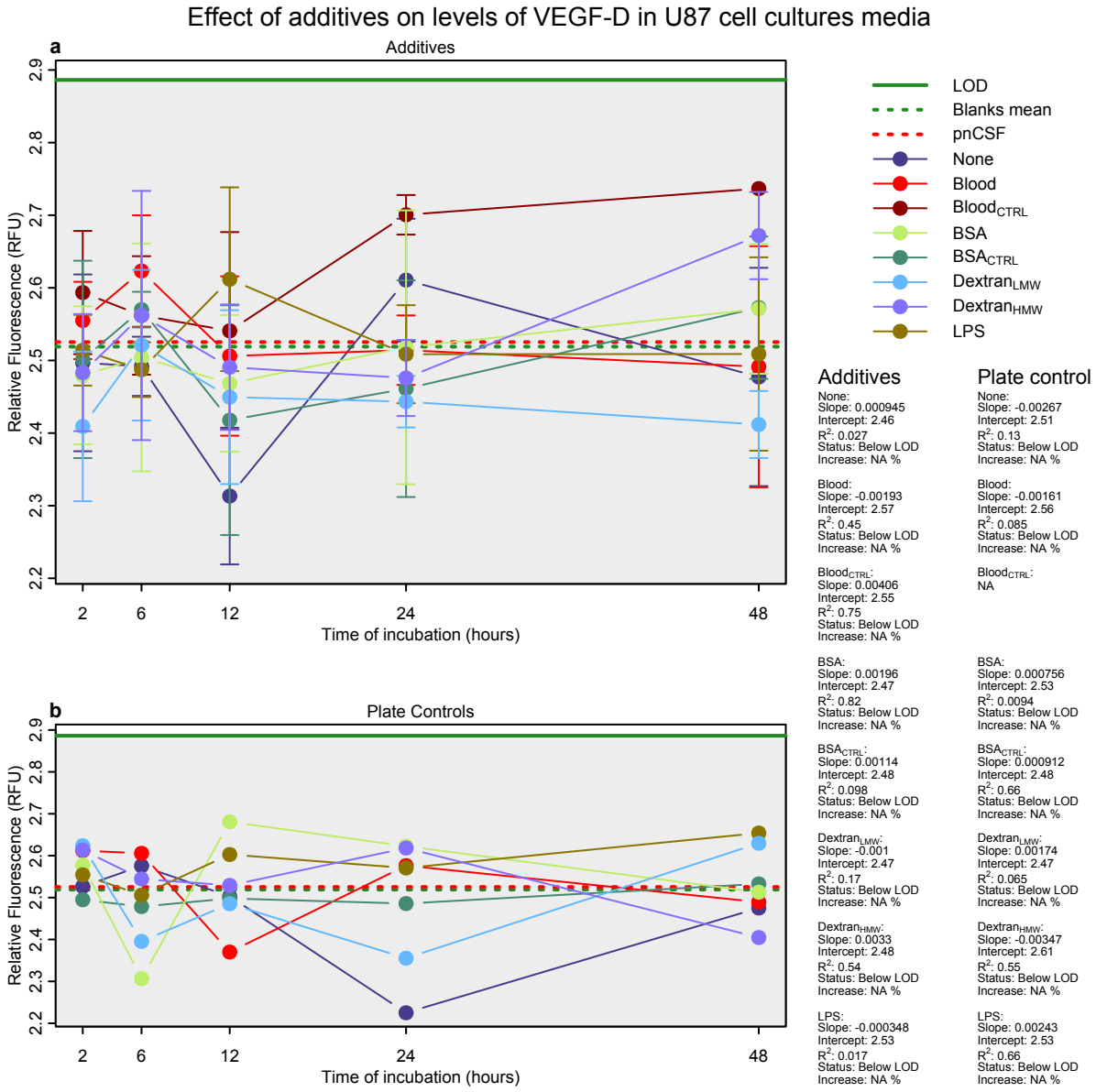

FIGURE H.S183: **Effect of additives on levels of VEGF-D in U87 cell cultures media.** Additives along with fresh blood and LPS were added to mycoplasma-free human glial (U87) cells in triplicate wells of a 24-well plate and incubated for up to 48 h to measure the effect on levels of proteins measured in the cell media. Media was collected and frozen from successive triplicates at different intervals, then analyzed with the ACM. **a** Average values for VEGF-D from three replicates for each point in every 24-well plate where a different additive was applied. **b** Data from the control cell media in each plate.

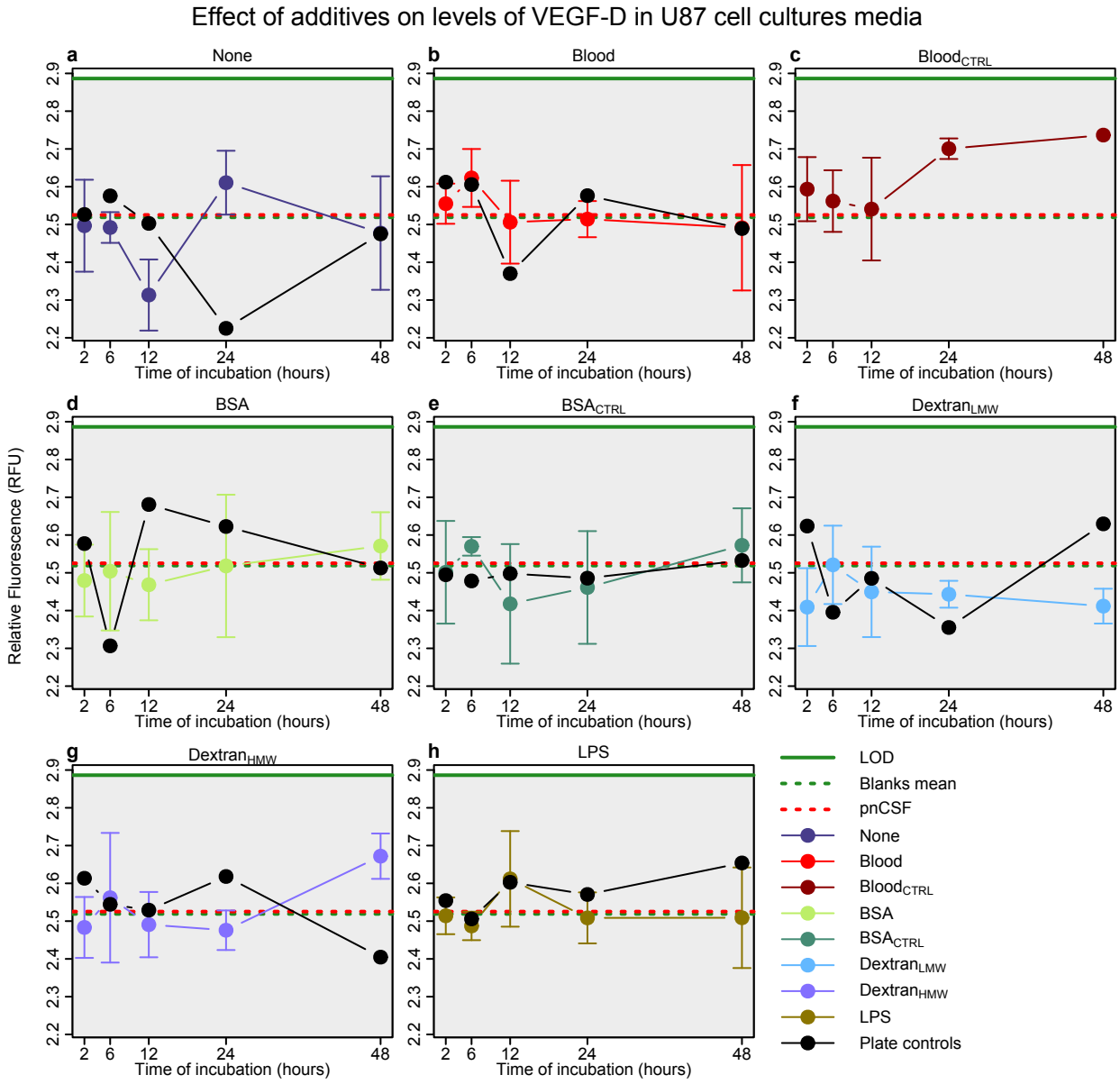

FIGURE H.S184: **Effect of additives on levels of VEGF-D in U87 cell cultures media.** Additives along with fresh blood and LPS were added to mycoplasma-free human glial (U87) cells in triplicate wells of a 24-well plate and incubated for up to 48 h to measure the effect on levels of proteins measured in the cell media. Media was collected and frozen from successive triplicates at different intervals, then analyzed with the ACM. Each graph compares VEGF-D values from cells incubated with a different additive to cells not incubated with additives located in the same 24-well plate. Plates in **c** and **e** did not contain any U87 cells, and **c** also did not have controls on the plate.

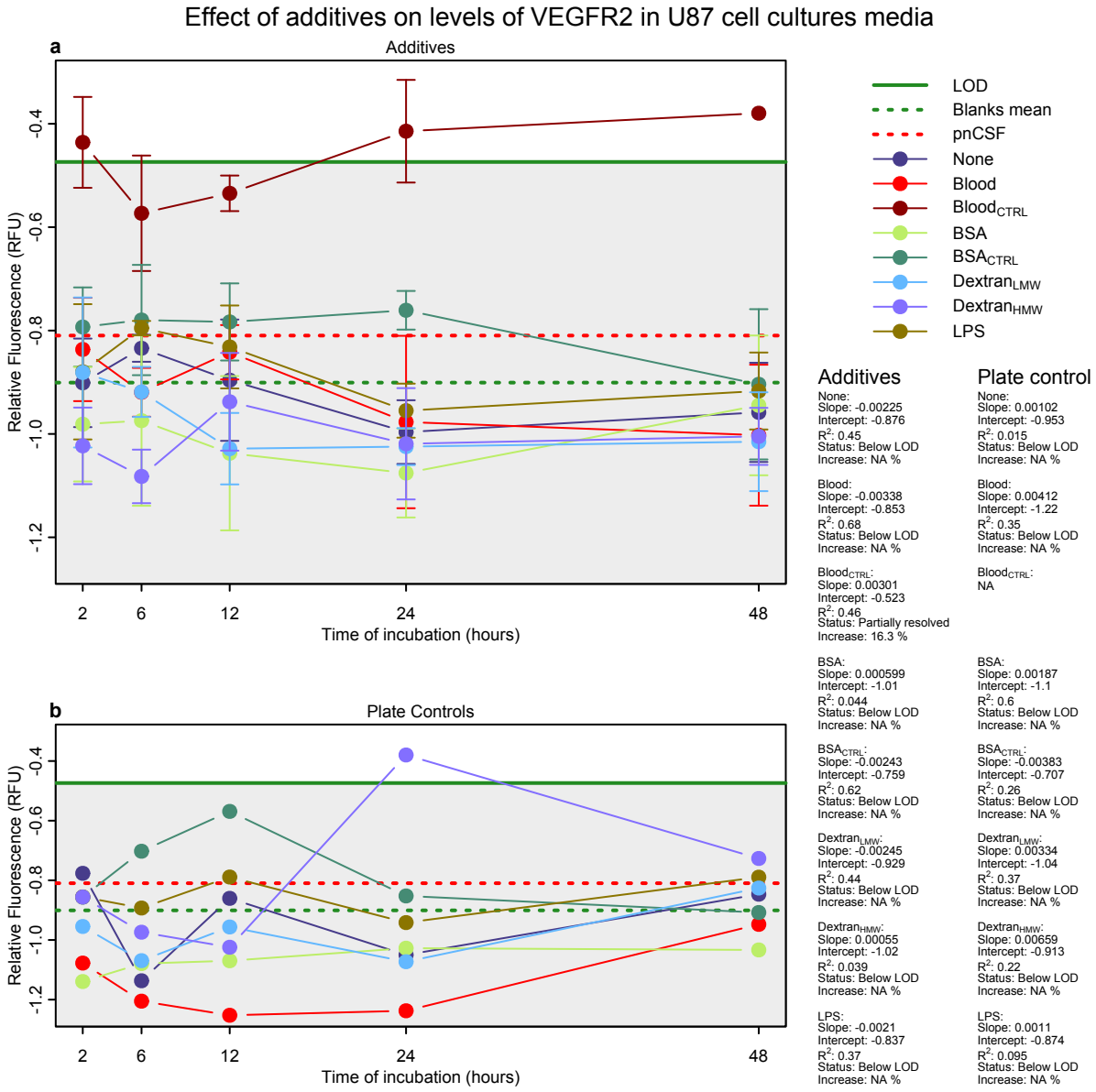

FIGURE H.S185: **Effect of additives on levels of VEGFR2 in U87 cell cultures media.** Additives along with fresh blood and LPS were added to mycoplasma-free human glial (U87) cells in triplicate wells of a 24-well plate and incubated for up to 48 h to measure the effect on levels of proteins measured in the cell media. Media was collected and frozen from successive triplicates at different intervals, then analyzed with the ACM. **a** Average values for VEGFR2 from three replicates for each point in every 24-well plate where a different additive was applied. **b** Data from the control cell media in each plate.

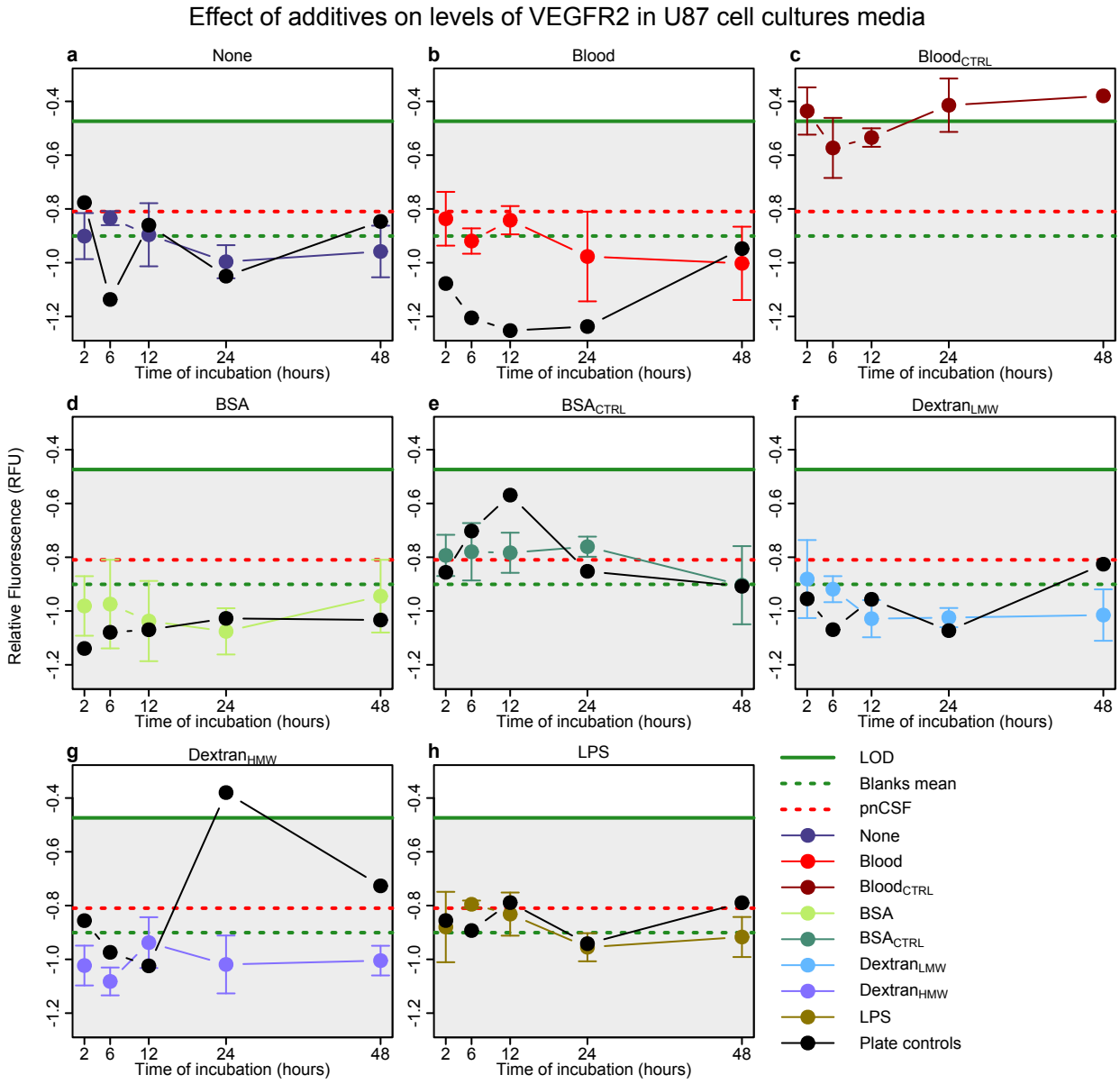

FIGURE H.S186: **Effect of additives on levels of VEGFR2 in U87 cell cultures media.** Additives along with fresh blood and LPS were added to mycoplasma-free human glial (U87) cells in triplicate wells of a 24-well plate and incubated for up to 48 h to measure the effect on levels of proteins measured in the cell media. Media was collected and frozen from successive triplicates at different intervals, then analyzed with the ACM. Each graph compares VEGFR2 values from cells incubated with a different additive to cells not incubated with additives located in the same 24-well plate. Plates in **c** and **e** did not contain any U87 cells, and **c** also did not have controls on the plate.

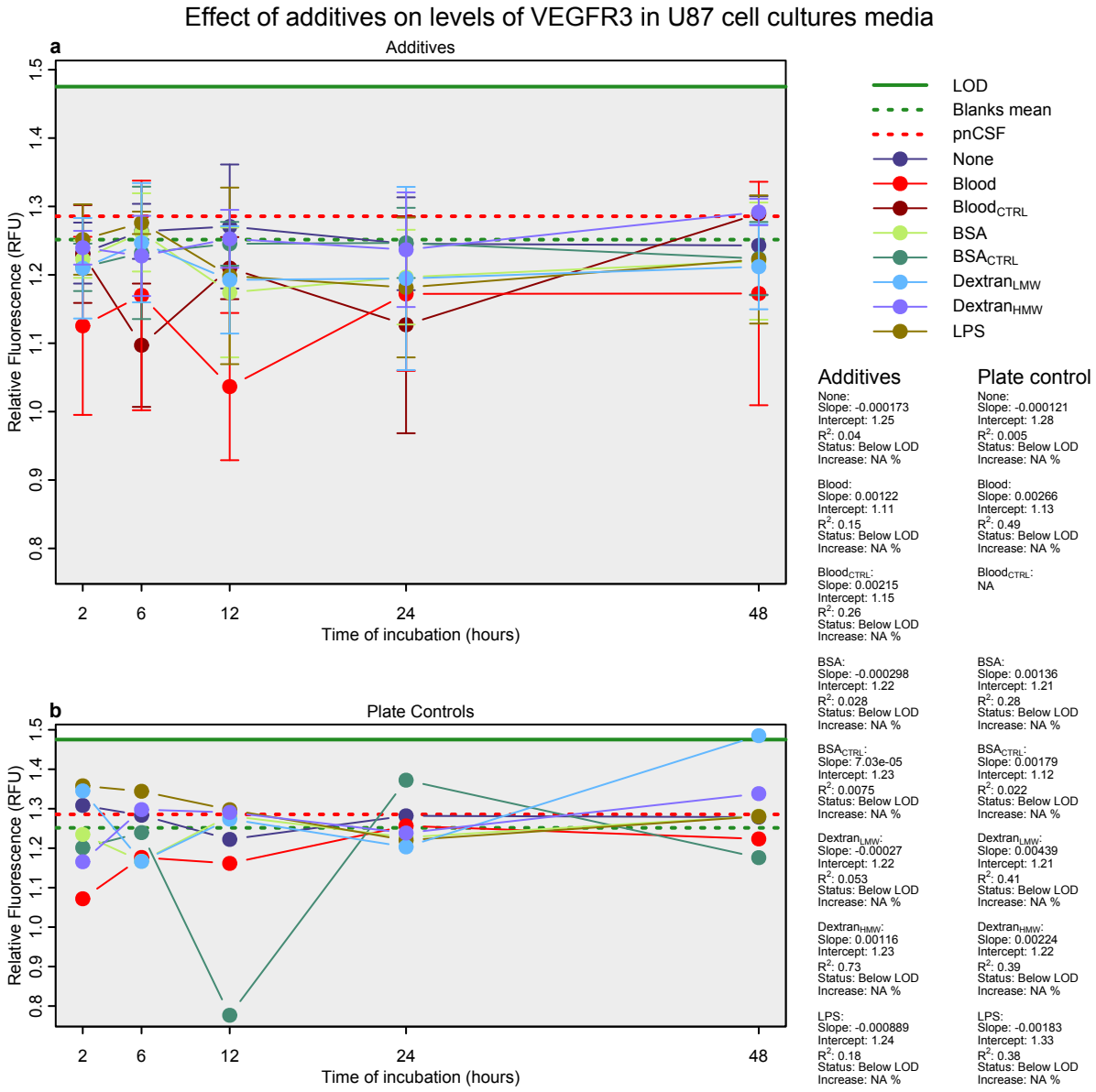

FIGURE H.S187: **Effect of additives on levels of VEGFR3 in U87 cell cultures media.** Additives along with fresh blood and LPS were added to mycoplasma-free human glial (U87) cells in triplicate wells of a 24-well plate and incubated for up to 48 h to measure the effect on levels of proteins measured in the cell media. Media was collected and frozen from successive triplicates at different intervals, then analyzed with the ACM. **a** Average values for VEGFR3 from three replicates for each point in every 24-well plate where a different additive was applied. **b** Data from the control cell media in each plate.

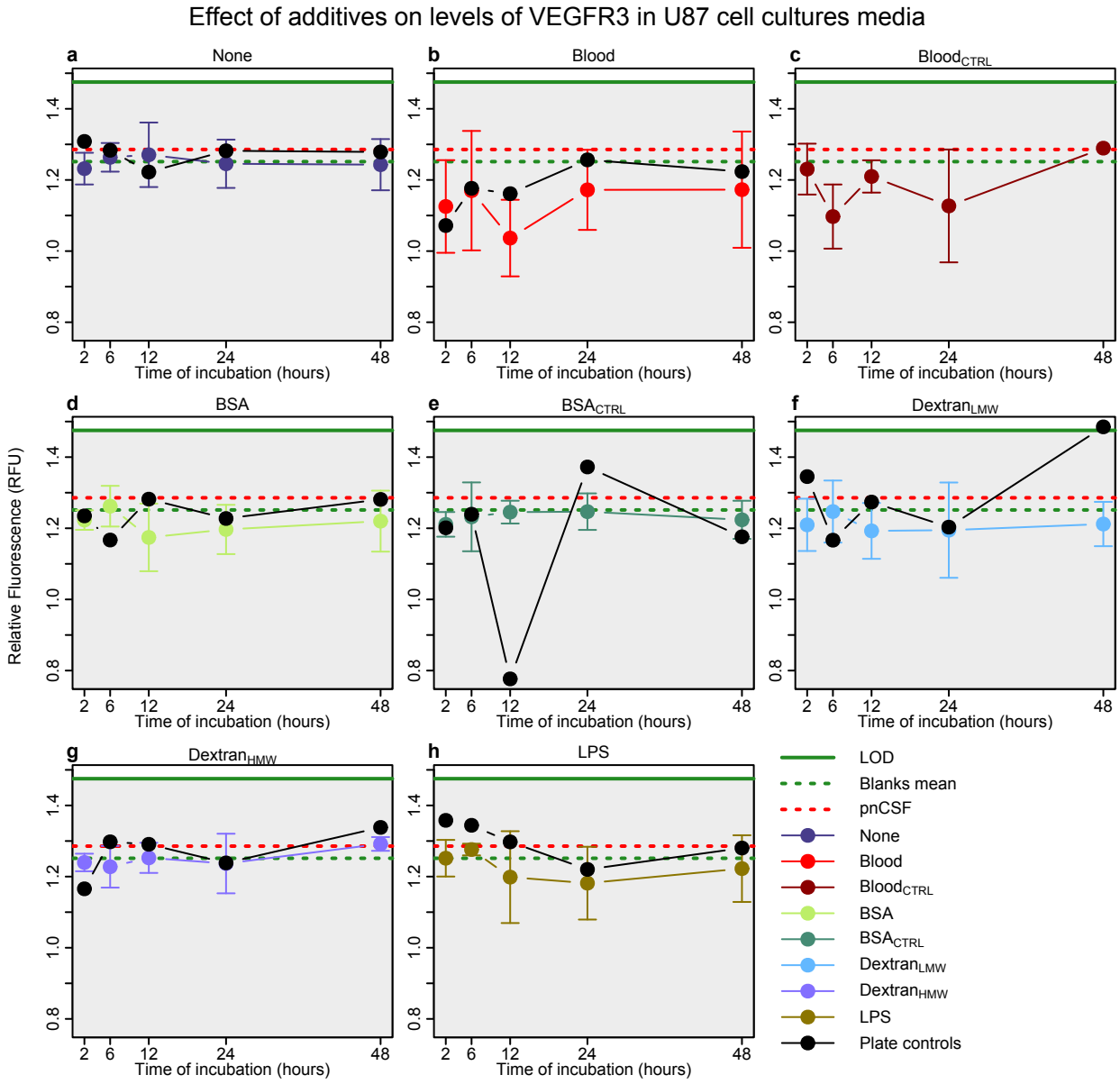

FIGURE H.S188: **Effect of additives on levels of VEGFR3 in U87 cell cultures media.** Additives along with fresh blood and LPS were added to mycoplasma-free human glial (U87) cells in triplicate wells of a 24-well plate and incubated for up to 48 h to measure the effect on levels of proteins measured in the cell media. Media was collected and frozen from successive triplicates at different intervals, then analyzed with the ACM. Each graph compares VEGFR3 values from cells incubated with a different additive to cells not incubated with additives located in the same 24-well plate. Plates in **c** and **e** did not contain any U87 cells, and **c** also did not have controls on the plate.

APPENDIX I

Potential biomarkers in TBI patients: Effect of pre-analytical variables

This appendix is a supplementary material to chapter chapter 6 that describes the pre-analytical effects on the initial measurement of proteins as well as their stability during a 2 h pre-centrifugation wait.

Effect of pre-processing storage temperature on protein measurements

Electronic Supplementary Material

Time course proteomic analysis of matched microdialysis, cerebrospinal fluid and blood samples from severe and blood samples from mild traumatic brain injury patients

Veronique Laforte, Judith Marcoux, Rajeet Singh Saluja and David Juncker

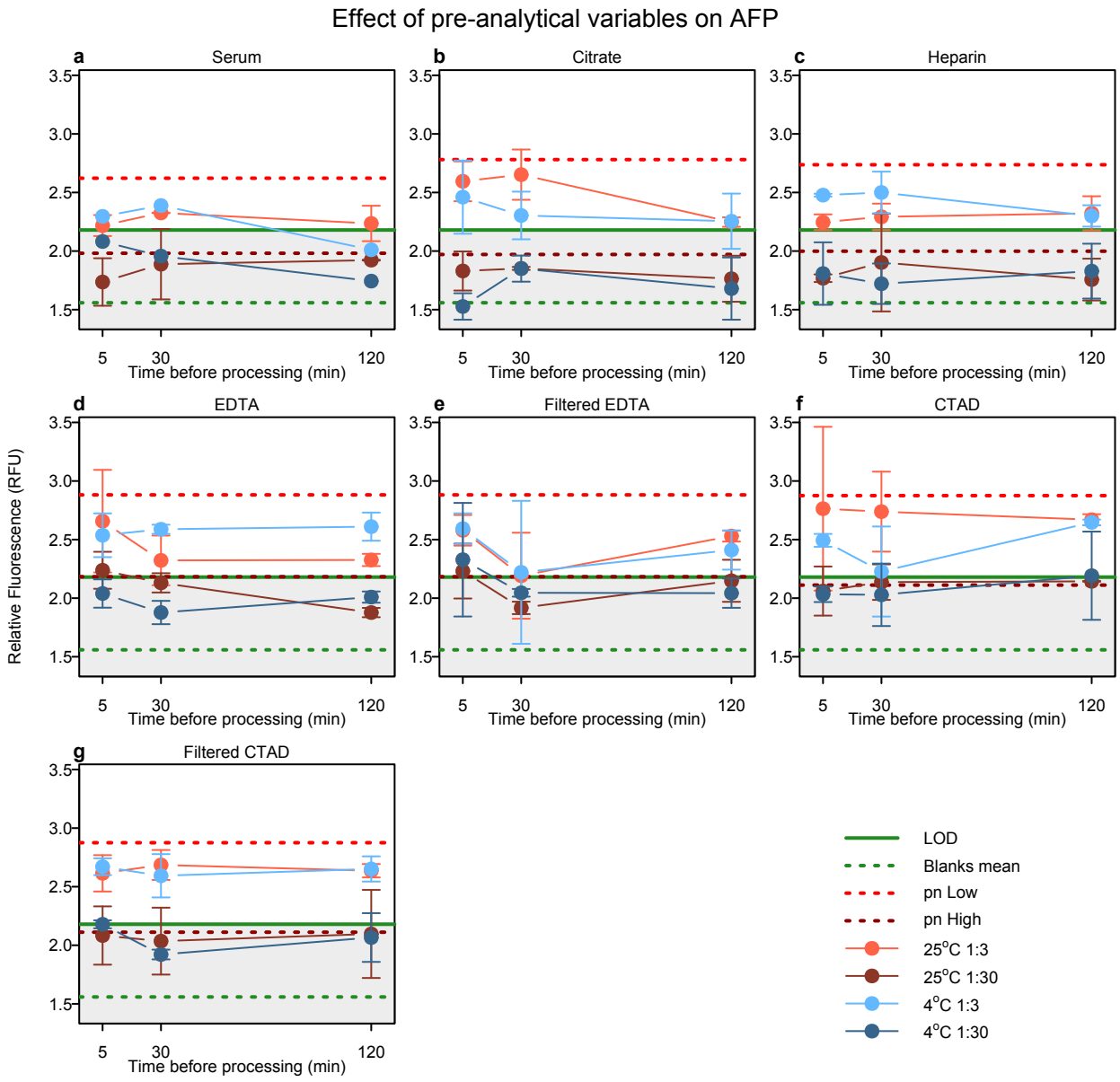

FIGURE I.S1: **Effect of blood collection tube on AFP stability and concentration.** Effects of blood collection tubes (**a**: serum, **b**: citrate, **c**: heparin, **d-e**: EDTA, **f-g**: CTAD), storage temperature and time before processing, and post-processing plasma filtering (**e, g**) on the initial value and pre-processing time stability of AFP measurements in blood. Information on the dilution of samples used for measuring, data range and the sample type selected are also shown.

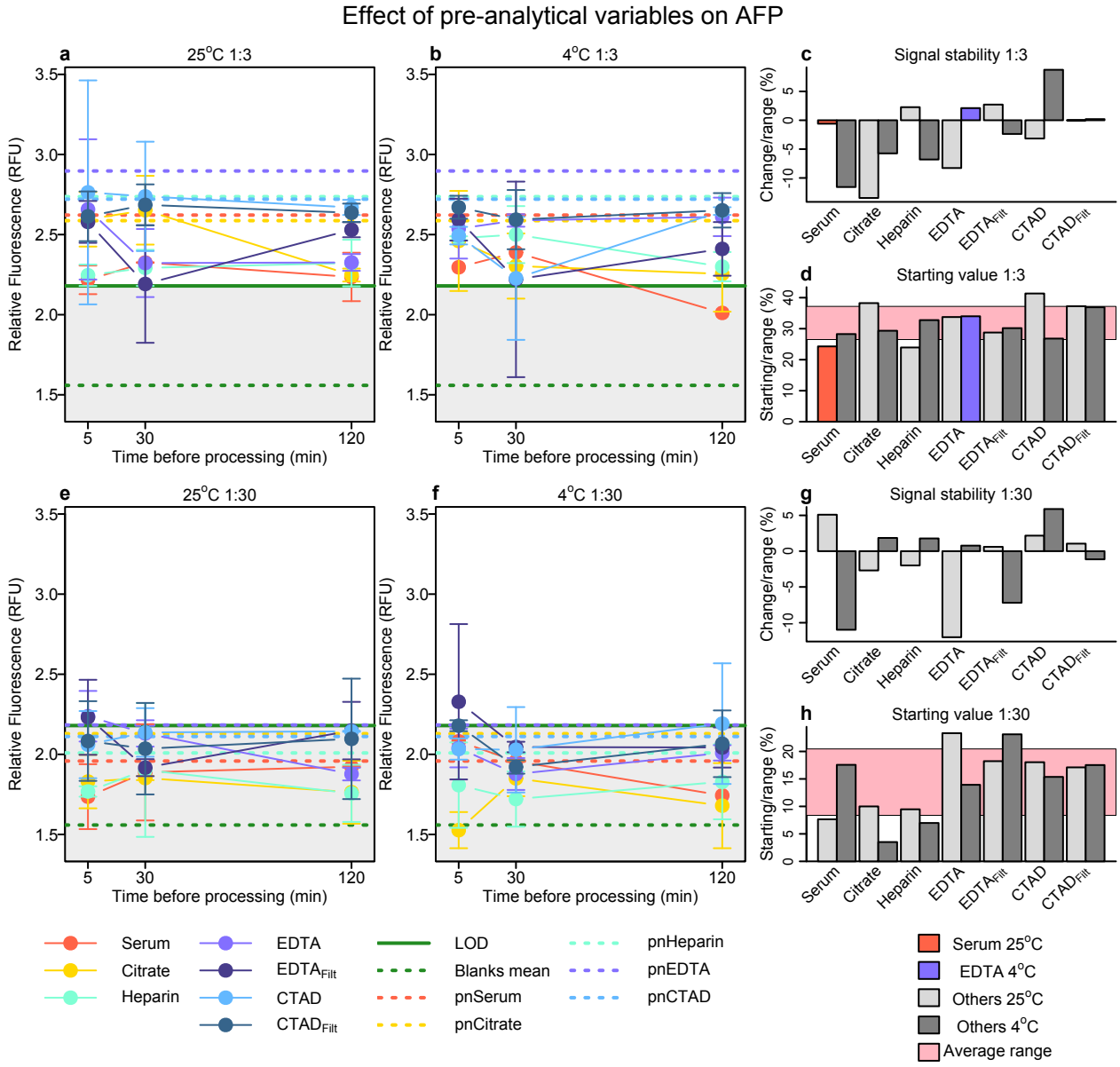

FIGURE I.S2: **Effect of pre-processing storage temperature on AFP stability and concentration.** Initial measured value and stability of AFP when stored at 25 °C (**a, e**) and 4 °C (**b, f**) before processing when collected in different tube types. The measured values are shown at low dilution of 1:3 (**a-b**) and high dilution of 1:30 (**e-f**). Stability before processing is expressed as an increase or decrease compared to the measurement range and is shown for low (**c**) and high (**g**) dilutions. Initial value is expressed as a portion of the measurement range when the linear regression is extrapolated to zero minutes and is shown for low (**d**) and high (**h**) dilutions. The pink box in graphs **d** and **h** indicate the region that is included by the *mean* ± *SD* of all the initial values and gives an indication of outliers when values lie outside this region. Red and purple bars in **c-d, g-h** are indicated at the measured dilution as the two choices for the TBI analysis.

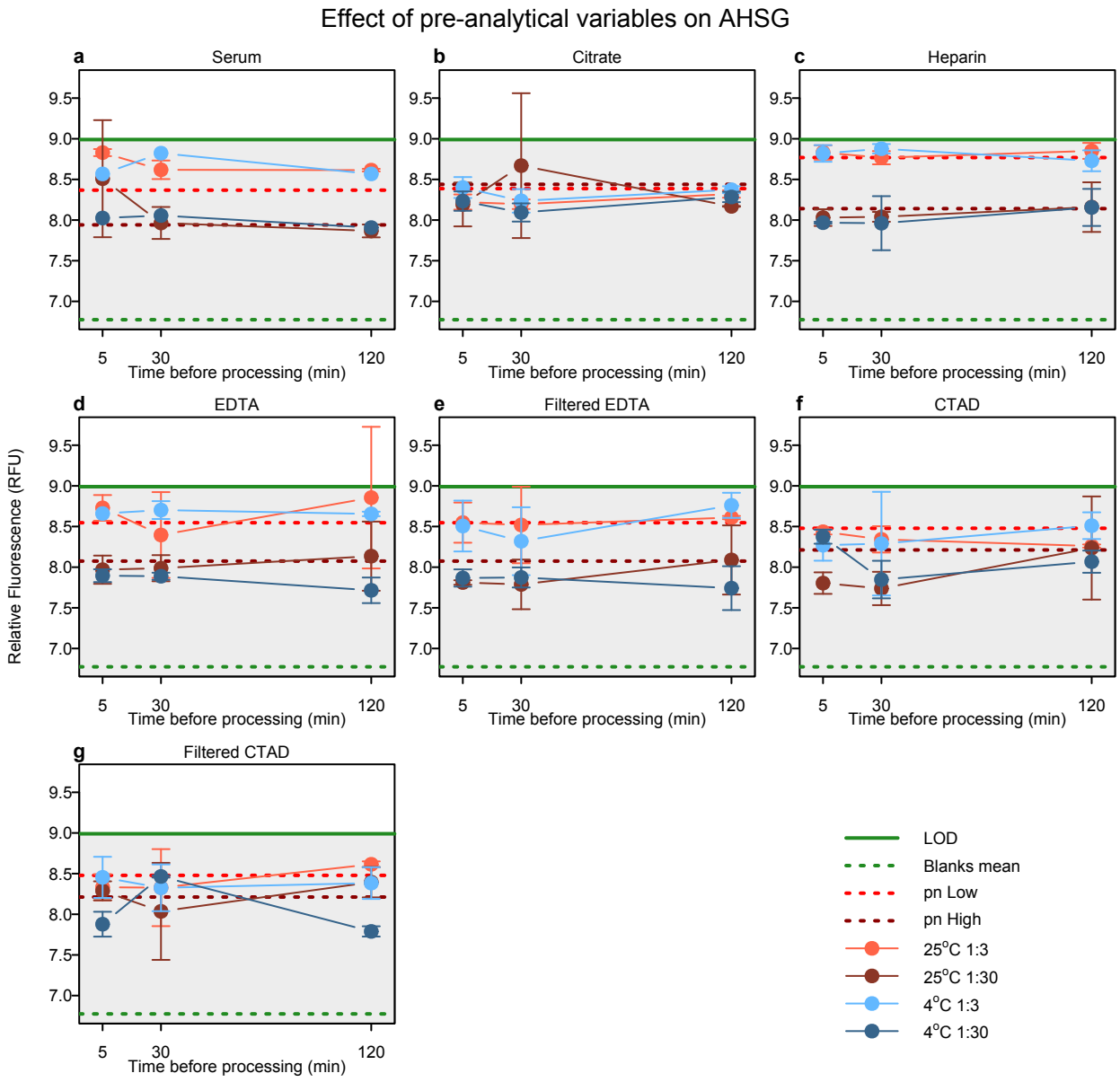

FIGURE I.S3: **Effect of blood collection tube on AHSG stability and concentration.** Effects of blood collection tubes (**a**: serum, **b**: citrate, **c**: heparin, **d-e**: EDTA, **f-g**: CTAD), storage temperature and time before processing, and post-processing plasma filtering (**e, g**) on the initial value and pre-processing time stability of AHSG measurements in blood. Information on the dilution of samples used for measuring, data range and the sample type selected are also shown.

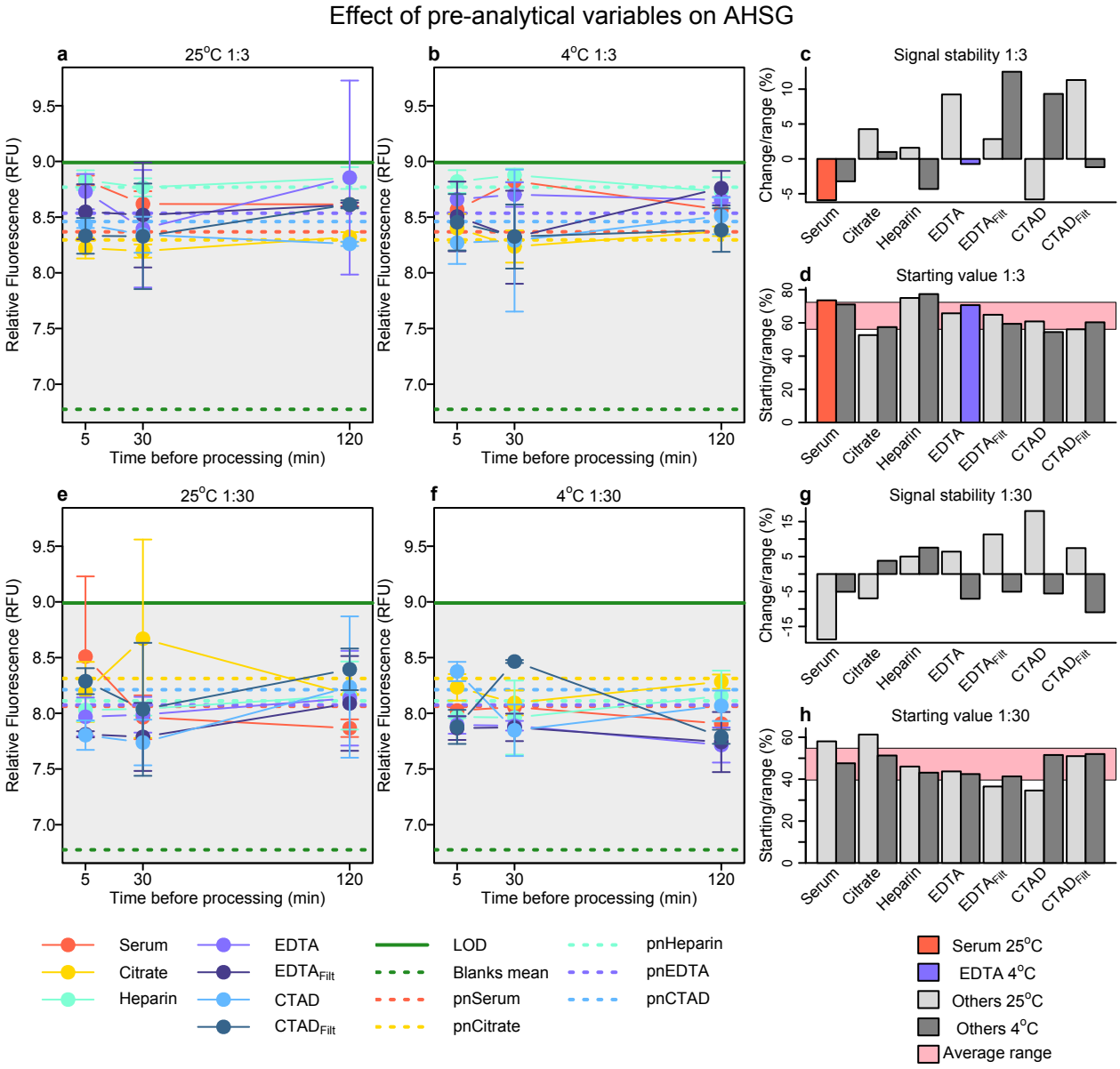

FIGURE I.S4: **Effect of pre-processing storage temperature on AHSG stability and concentration.** Initial measured value and stability of AHSG when stored at 25 °C (**a, e**) and 4 °C (**b, f**) before processing when collected in different tube types. The measured values are shown at low dilution of 1:3 (**a-b**) and high dilution of 1:30 (**e-f**). Stability before processing is expressed as an increase or decrease compared to the measurement range and is shown for low (**c**) and high (**g**) dilutions. Initial value is expressed as a portion of the measurement range when the linear regression is extrapolated to zero minutes and is shown for low (**d**) and high (**h**) dilutions. The pink box in graphs **d** and **h** indicate the region that is included by the *mean* ± *SD* of all the initial values and gives an indication of outliers when values lie outside this region. Red and purple bars in **c-d, g-h** are indicated at the measured dilution as the two choices for the TBI analysis.

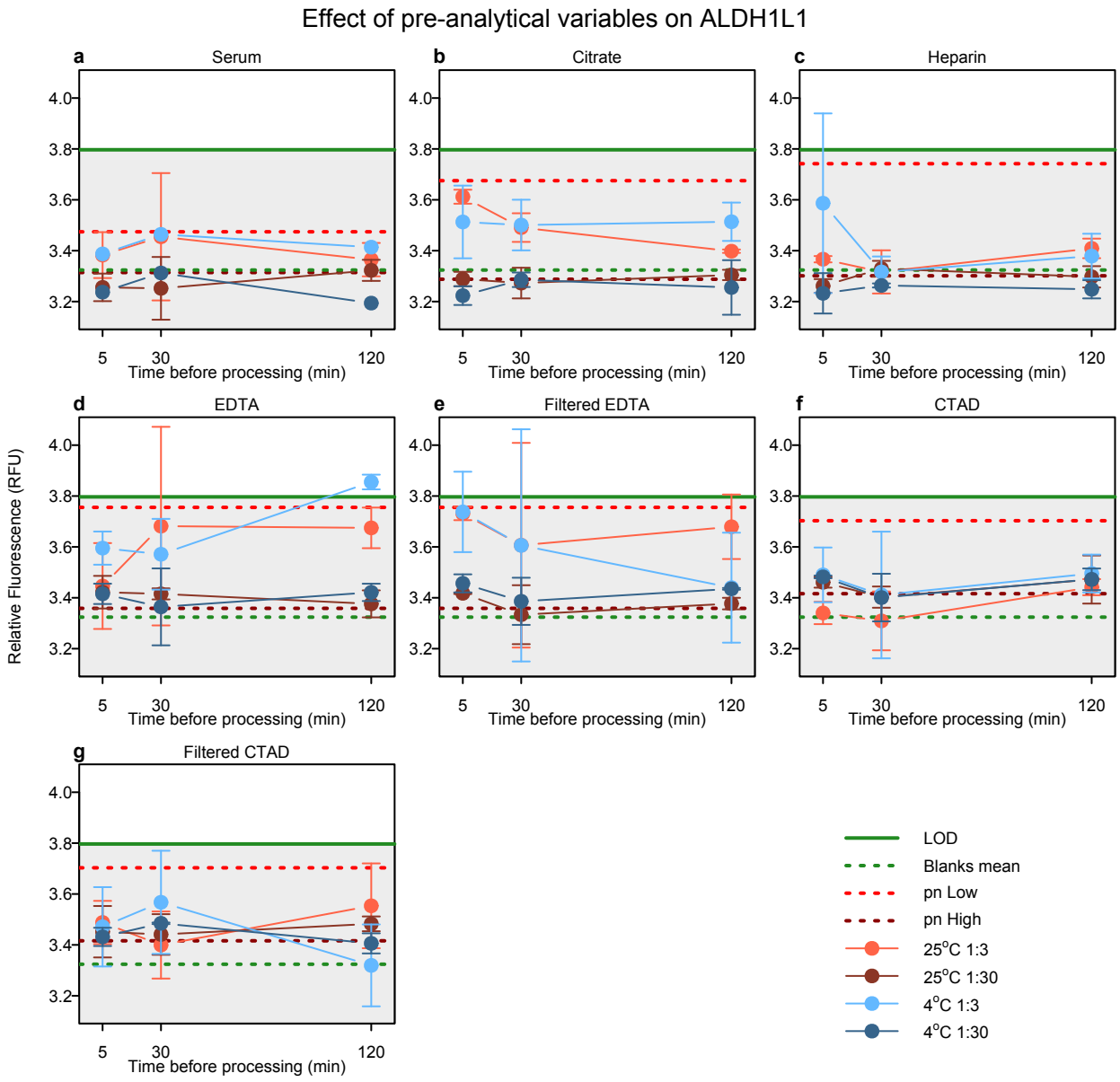

FIGURE I.S5: **Effect of blood collection tube on ALDH1L1 stability and concentration.** Effects of blood collection tubes (**a**: serum, **b**: citrate, **c**: heparin, **d-e**: EDTA, **f-g**: CTAD), storage temperature and time before processing, and post-processing plasma filtering (**e, g**) on the initial value and pre-processing time stability of ALDH1L1 measurements in blood. Information on the dilution of samples used for measuring, data range and the sample type selected are also shown.

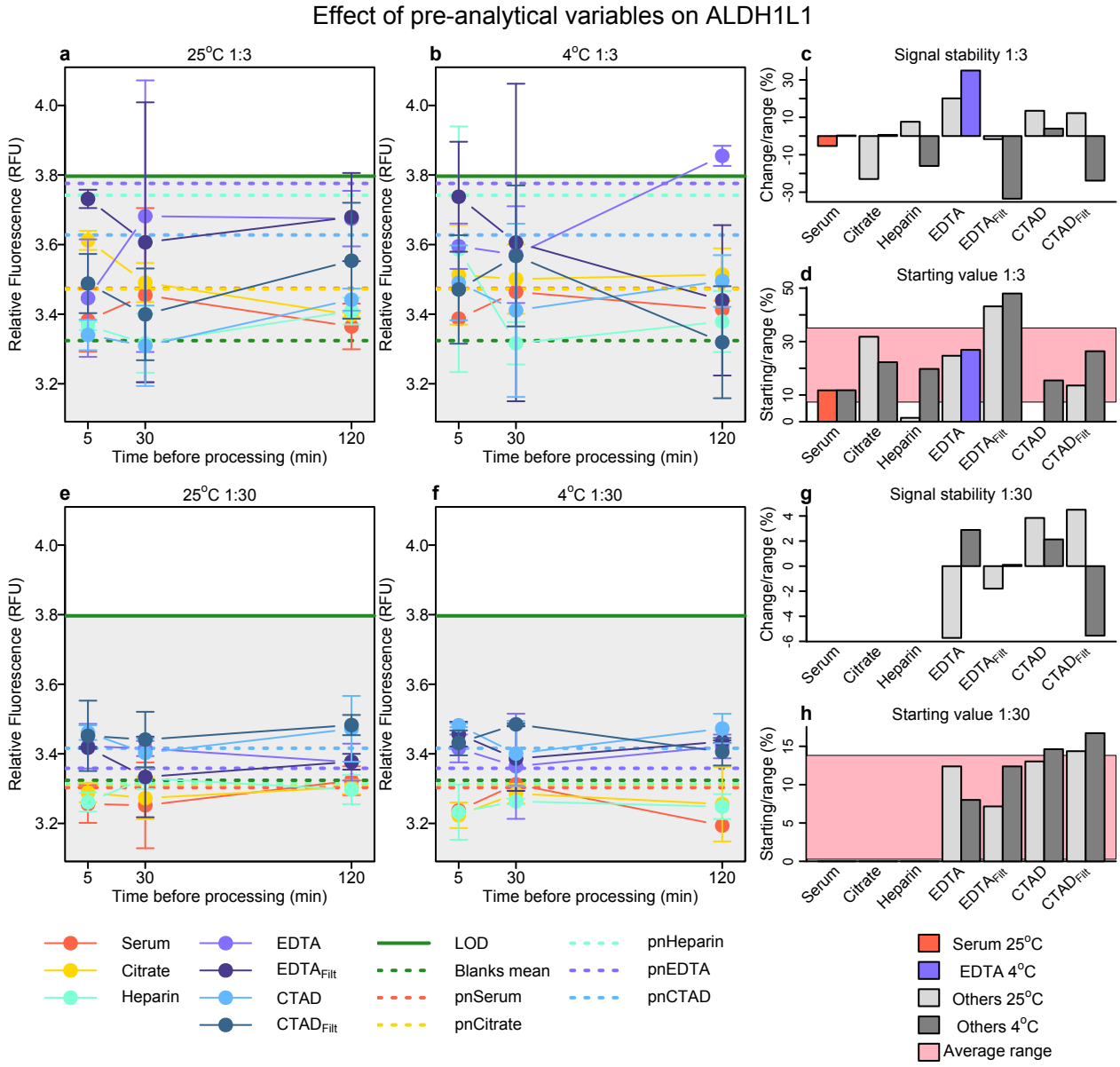

FIGURE I.S6: **Effect of pre-processing storage temperature on ALDH1L1 stability and concentration.** Initial measured value and stability of ALDH1L1 when stored at 25 °C (**a, e**) and 4 °C (**b, f**) before processing when collected in different tube types. The measured values are shown at low dilution of 1:3 (**a-b**) and high dilution of 1:30 (**e-f**). Stability before processing is expressed as an increase or decrease compared to the measurement range and is shown for low (**c**) and high (**g**) dilutions. Initial value is expressed as a portion of the measurement range when the linear regression is extrapolated to zero minutes and is shown for low (**d**) and high (**h**) dilutions. The pink box in graphs **d** and **h** indicate the region that is included by the *mean* ± *SD* of all the initial values and gives an indication of outliers when values lie outside this region. Red and purple bars in **c-d, g-h** are indicated at the measured dilution as the two choices for the TBI analysis.

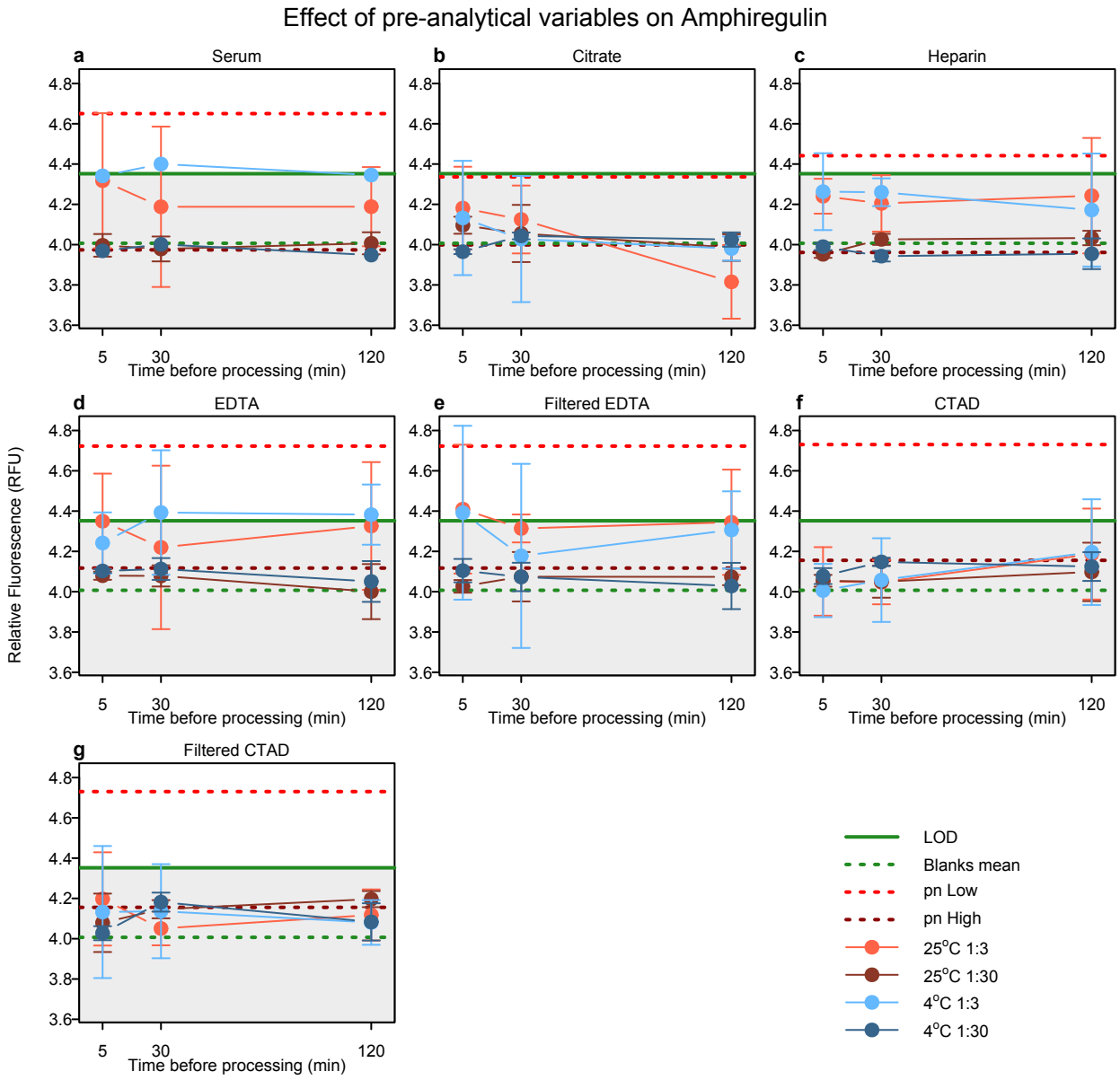

FIGURE I.S7: **Effect of blood collection tube on Amphiregulin stability and concentration.** Effects of blood collection tubes (**a**: serum, **b**: citrate, **c**: heparin, **d-e**: EDTA, **f-g**: CTAD), storage temperature and time before processing, and post-processing plasma filtering (**e, g**) on the initial value and pre-processing time stability of Amphiregulin measurements in blood. Information on the dilution of samples used for measuring, data range and the sample type selected are also shown.

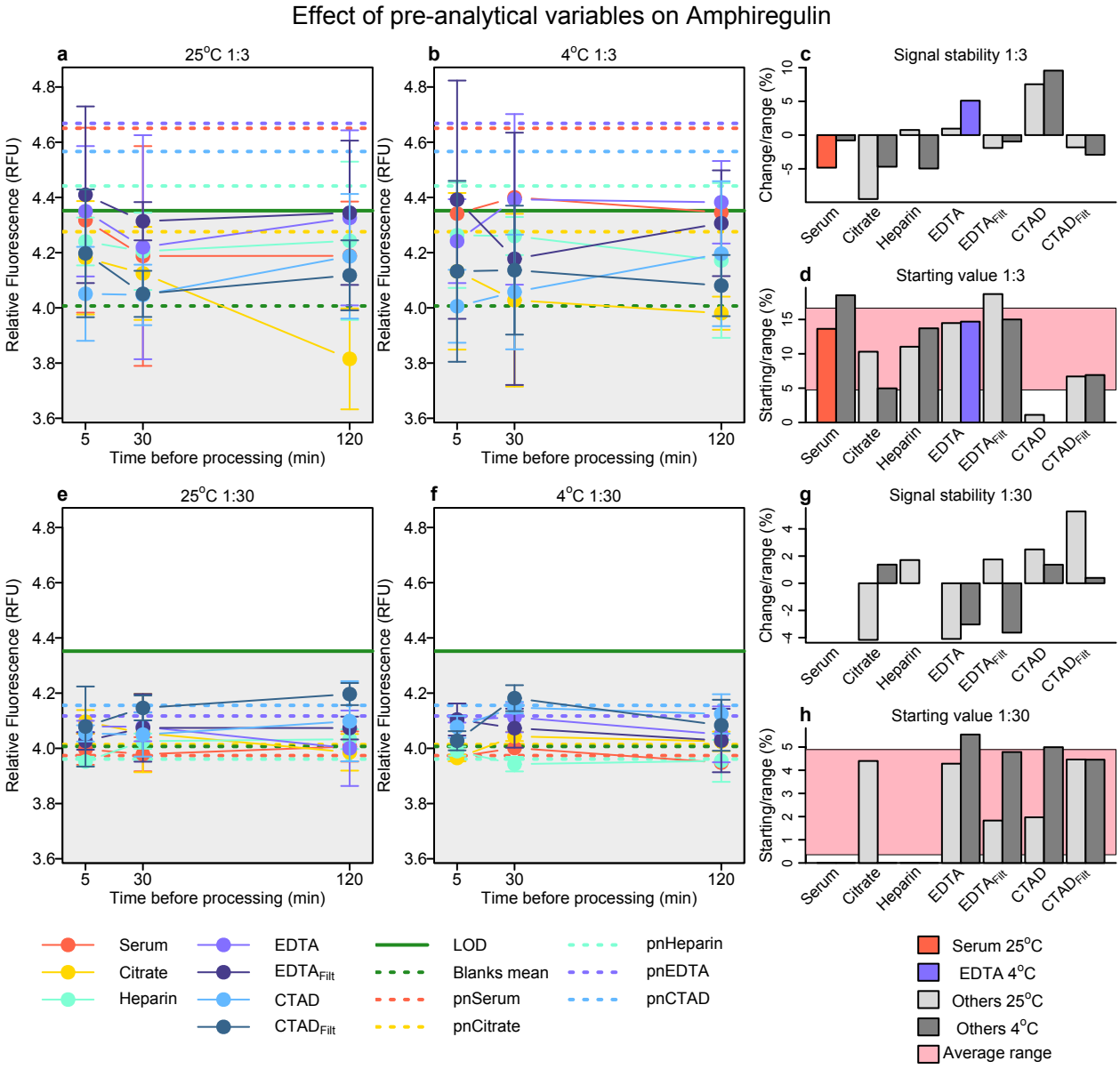

FIGURE I.S8: **Effect of pre-processing storage temperature on Amphiregulin stability and concentration.** Initial measured value and stability of Amphiregulin when stored at 25 °C (**a, e**) and 4 °C (**b, f**) before processing when collected in different tube types. The measured values are shown at low dilution of 1:3 (**a-b**) and high dilution of 1:30 (**e-f**). Stability before processing is expressed as an increase or decrease compared to the measurement range and is shown for low (**c**) and high (**g**) dilutions. Initial value is expressed as a portion of the measurement range when the linear regression is extrapolated to zero minutes and is shown for low (**d**) and high (**h**) dilutions. The pink box in graphs **d** and **h** indicate the region that is included by the *mean* ± *SD* of all the initial values and gives an indication of outliers when values lie outside this region. Red and purple bars in **c-d, g-h** are indicated at the measured dilution as the two choices for the TBI analysis.

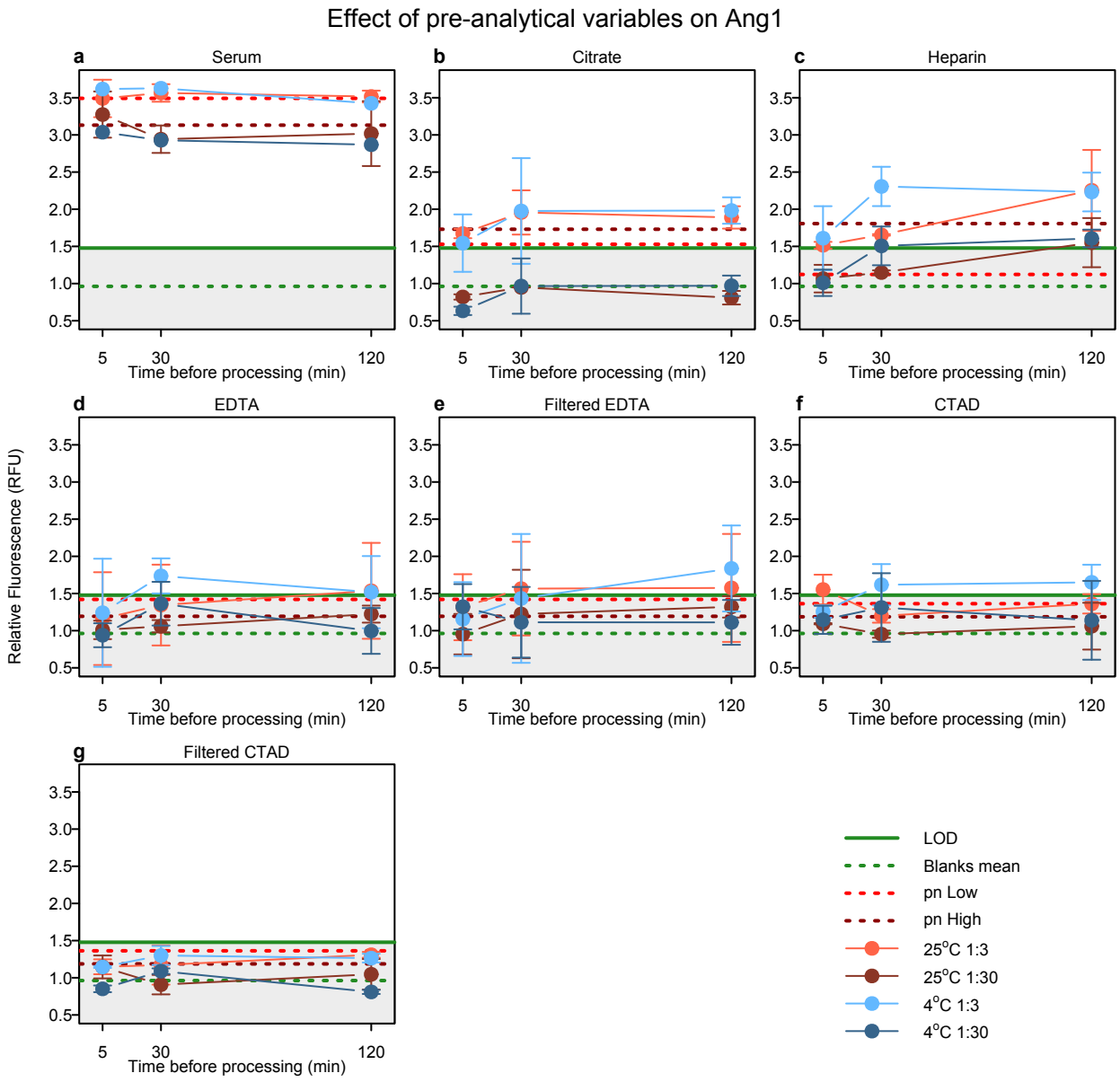

FIGURE I.S9: **Effect of blood collection tube on Ang1 stability and concentration.** Effects of blood collection tubes (**a**: serum, **b**: citrate, **c**: heparin, **d-e**: EDTA, **f-g**: CTAD), storage temperature and time before processing, and post-processing plasma filtering (**e, g**) on the initial value and pre-processing time stability of Ang1 measurements in blood. Information on the dilution of samples used for measuring, data range and the sample type selected are also shown.

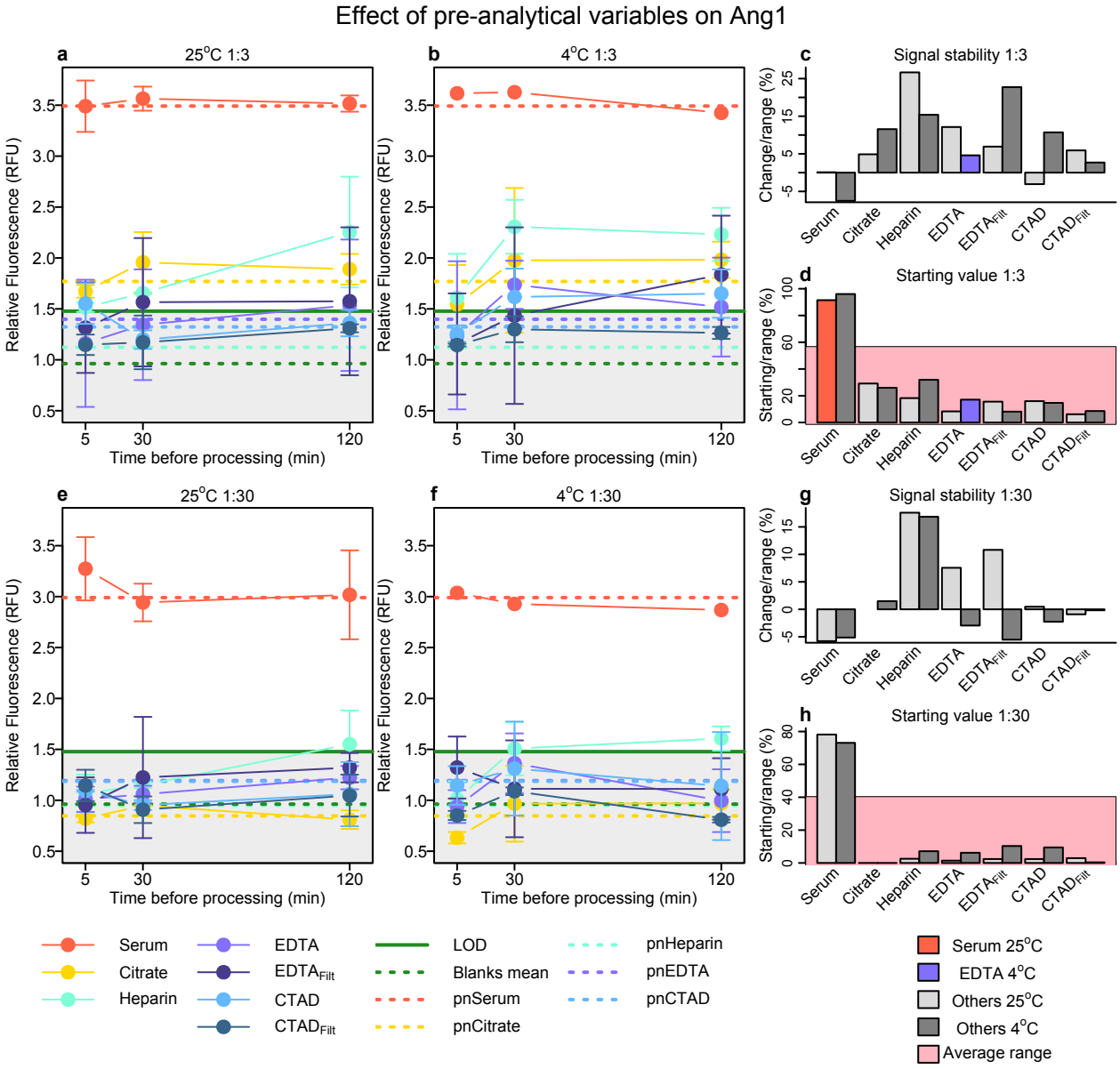

FIGURE I.S10: **Effect of pre-processing storage temperature on Ang1 stability and concentration.** Initial measured value and stability of Ang1 when stored at 25 °C (**a, e**) and 4 °C (**b, f**) before processing when collected in different tube types. The measured values are shown at low dilution of 1:3 (**a-b**) and high dilution of 1:30 (**e-f**). Stability before processing is expressed as an increase or decrease compared to the measurement range and is shown for low (**c**) and high (**g**) dilutions. Initial value is expressed as a portion of the measurement range when the linear regression is extrapolated to zero minutes and is shown for low (**d**) and high (**h**) dilutions. The pink box in graphs **d** and **h** indicate the region that is included by the *mean* ± *SD* of all the initial values and gives an indication of outliers when values lie outside this region. Red and purple bars in **c-d, g-h** are indicated at the measured dilution as the two choices for the TBI analysis.

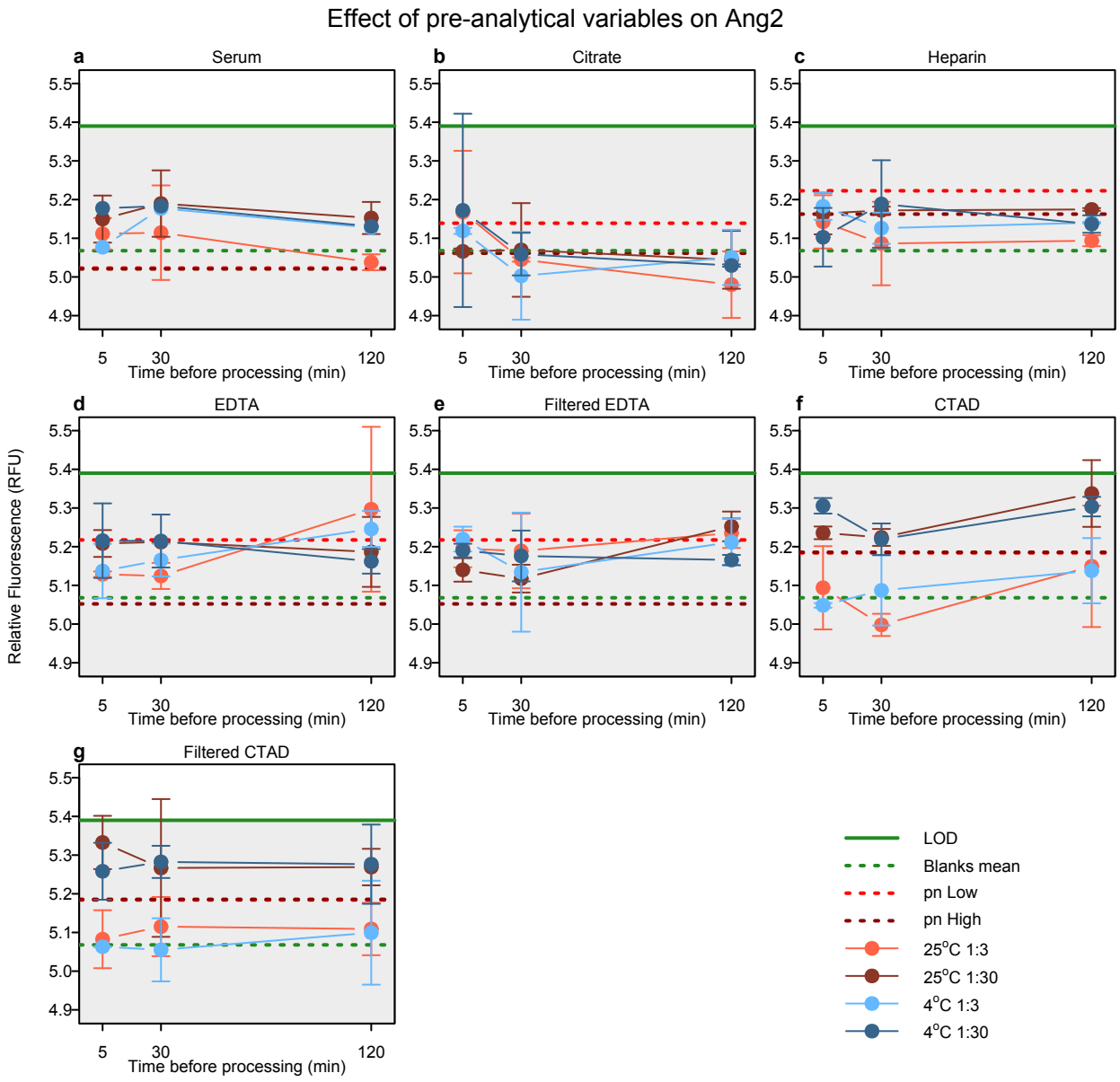

FIGURE I.S11: **Effect of blood collection tube on Ang2 stability and concentration.** Effects of blood collection tubes (**a**: serum, **b**: citrate, **c**: heparin, **d-e**: EDTA, **f-g**: CTAD), storage temperature and time before processing, and post-processing plasma filtering (**e, g**) on the initial value and pre-processing time stability of Ang2 measurements in blood. Information on the dilution of samples used for measuring, data range and the sample type selected are also shown.

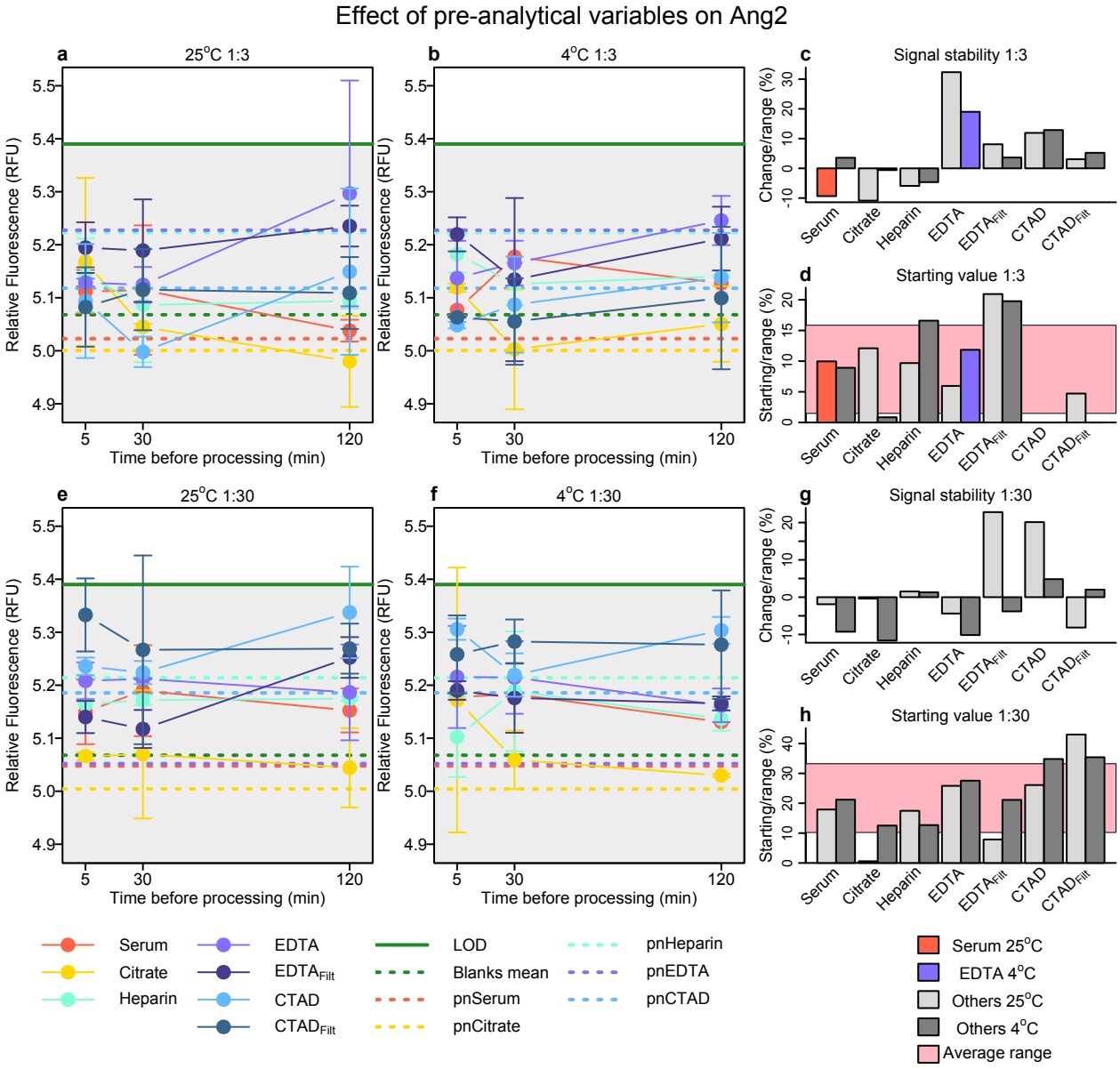

FIGURE I.S12: **Effect of pre-processing storage temperature on Ang2 stability and concentration.** Initial measured value and stability of Ang2 when stored at 25 °C (**a, e**) and 4 °C (**b, f**) before processing when collected in different tube types. The measured values are shown at low dilution of 1:3 (**a-b**) and high dilution of 1:30 (**e-f**). Stability before processing is expressed as an increase or decrease compared to the measurement range and is shown for low (**c**) and high (**g**) dilutions. Initial value is expressed as a portion of the measurement range when the linear regression is extrapolated to zero minutes and is shown for low (**d**) and high (**h**) dilutions. The pink box in graphs **d** and **h** indicate the region that is included by the *mean* ± *SD* of all the initial values and gives an indication of outliers when values lie outside this region. Red and purple bars in **c-d, g-h** are indicated at the measured dilution as the two choices for the TBI analysis.

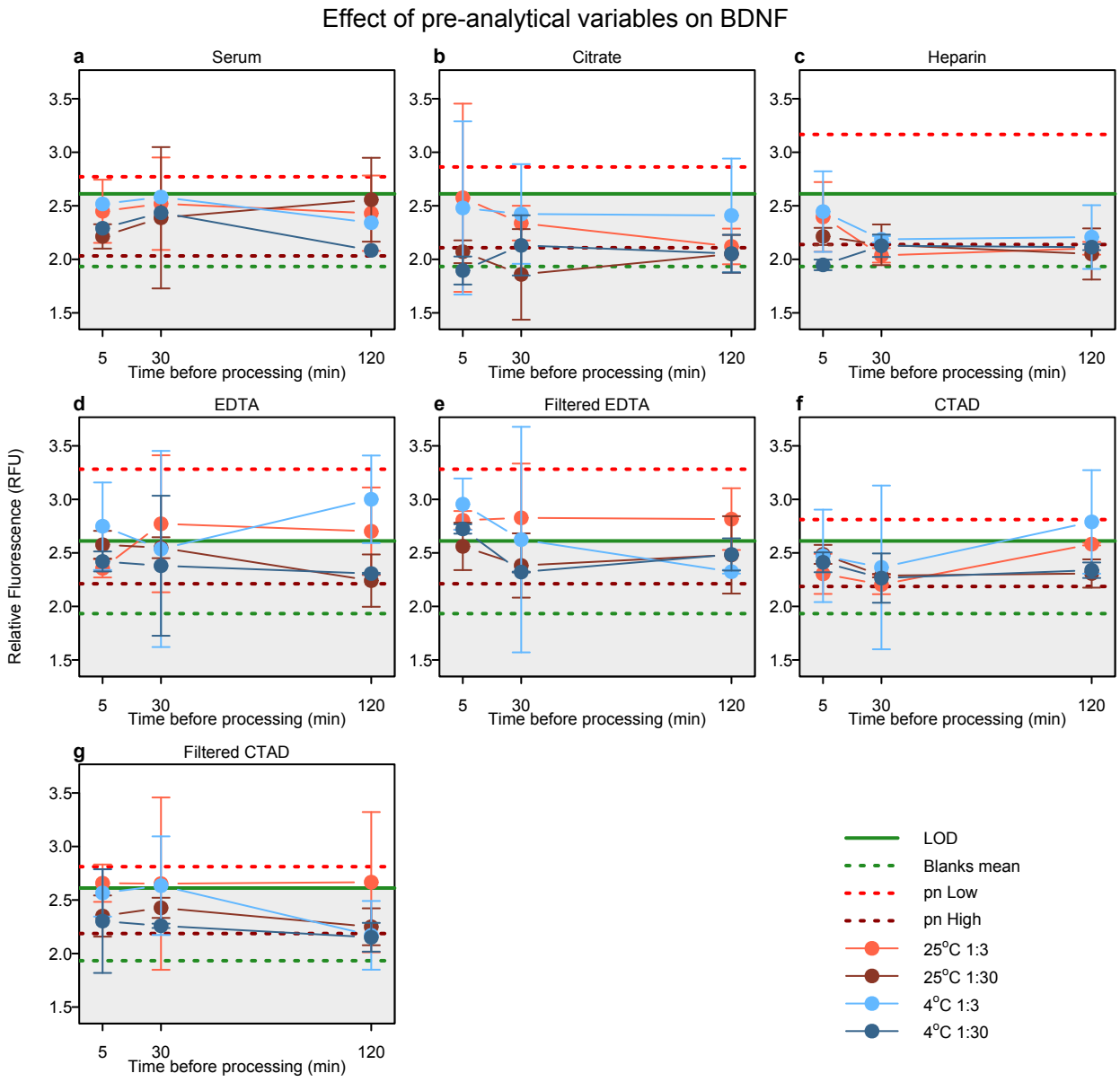

FIGURE I.S13: **Effect of blood collection tube on BDNF stability and concentration.** Effects of blood collection tubes (**a**: serum, **b**: citrate, **c**: heparin, **d-e**: EDTA, **f-g**: CTAD), storage temperature and time before processing, and post-processing plasma filtering (**e, g**) on the initial value and pre-processing time stability of BDNF measurements in blood. Information on the dilution of samples used for measuring, data range and the sample type selected are also shown.

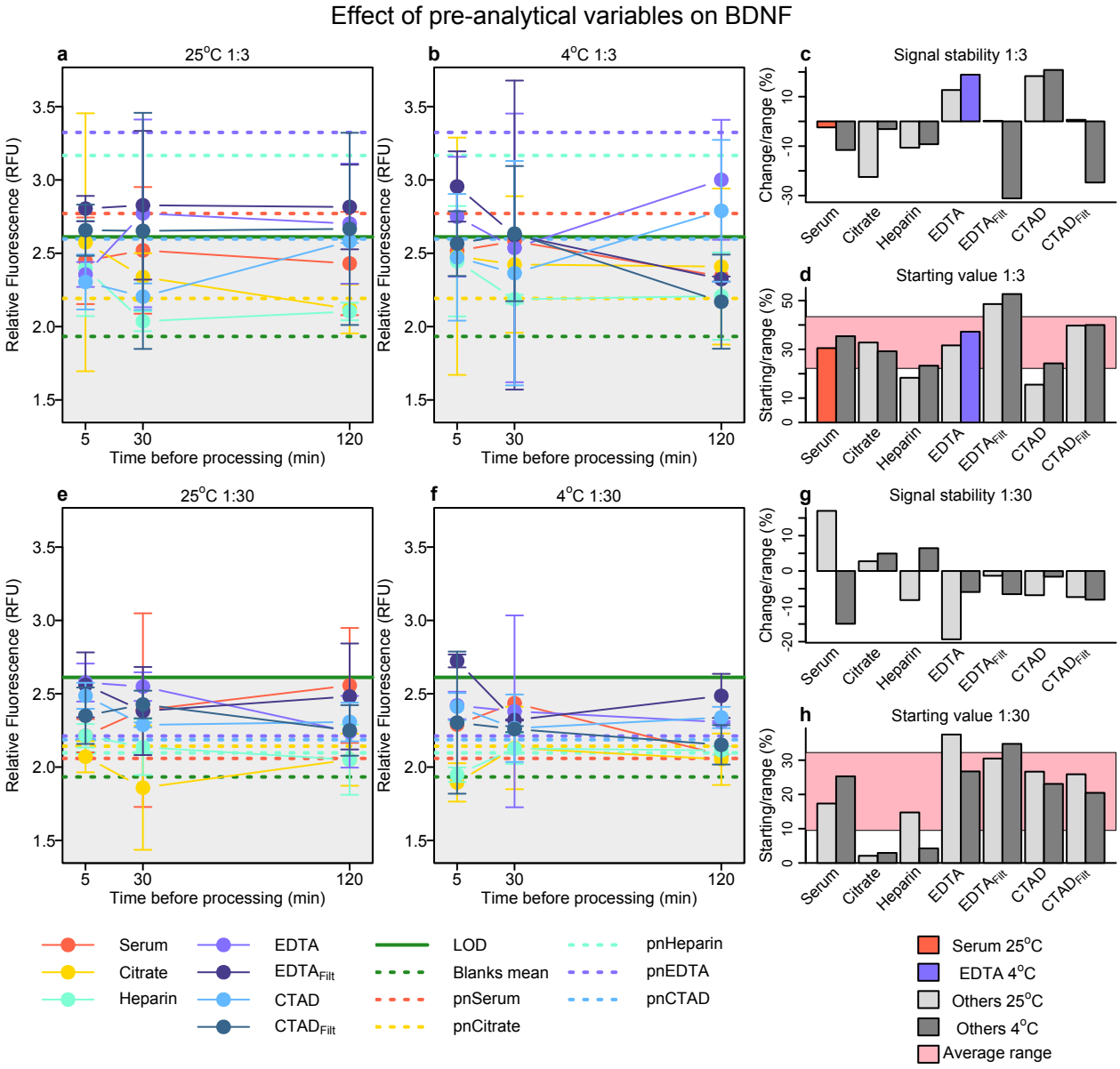

FIGURE I.S14: **Effect of pre-processing storage temperature on BDNF stability and concentration.** Initial measured value and stability of BDNF when stored at 25 °C (**a, e**) and 4 °C (**b, f**) before processing when collected in different tube types. The measured values are shown at low dilution of 1:3 (**a-b**) and high dilution of 1:30 (**e-f**). Stability before processing is expressed as an increase or decrease compared to the measurement range and is shown for low (**c**) and high (**g**) dilutions. Initial value is expressed as a portion of the measurement range when the linear regression is extrapolated to zero minutes and is shown for low (**d**) and high (**h**) dilutions. The pink box in graphs **d** and **h** indicate the region that is included by the *mean* ± *SD* of all the initial values and gives an indication of outliers when values lie outside this region. Red and purple bars in **c-d, g-h** are indicated at the measured dilution as the two choices for the TBI analysis.

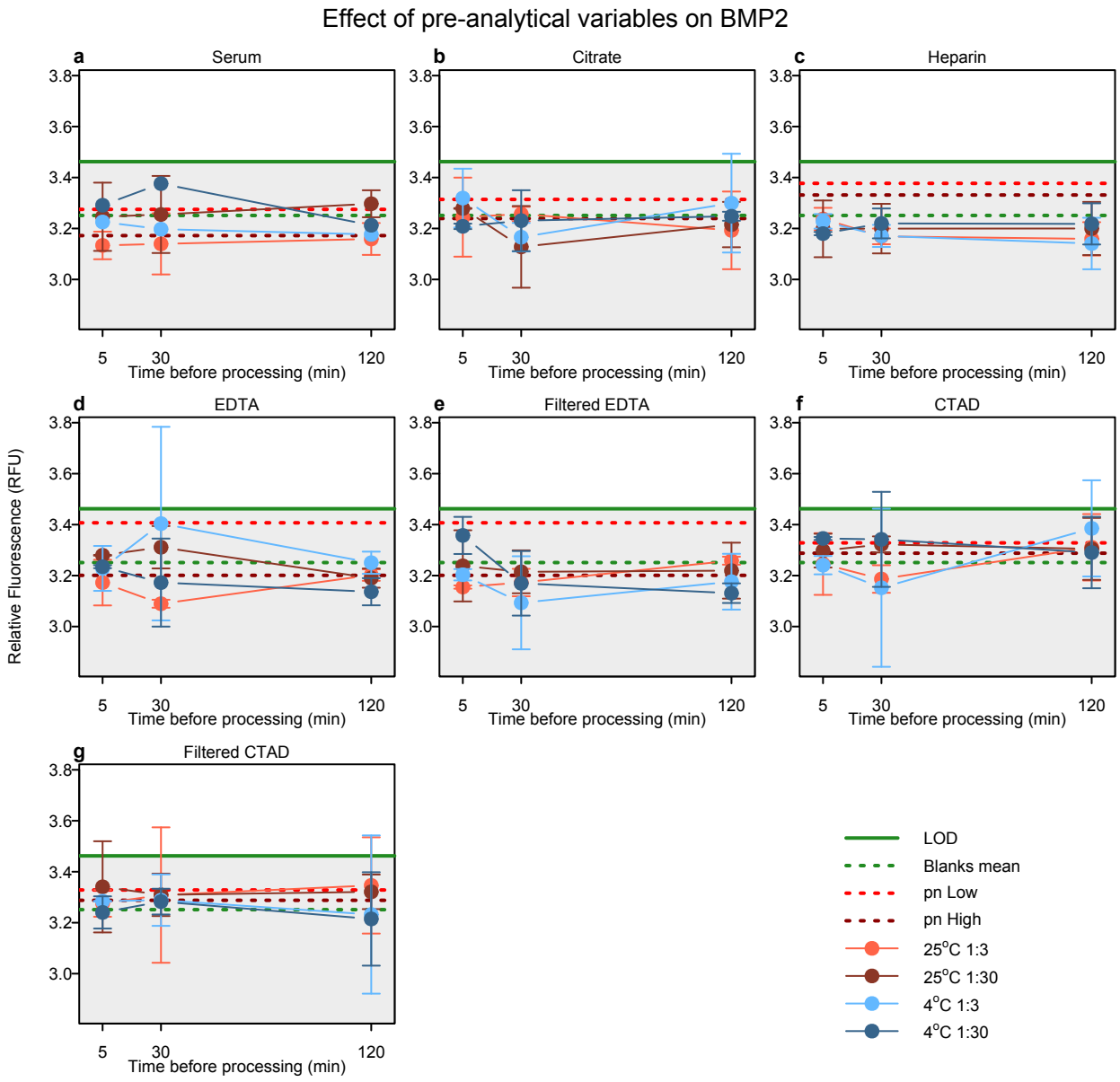

FIGURE I.S15: **Effect of blood collection tube on BMP2 stability and concentration.** Effects of blood collection tubes (**a**: serum, **b**: citrate, **c**: heparin, **d-e**: EDTA, **f-g**: CTAD), storage temperature and time before processing, and post-processing plasma filtering (**e, g**) on the initial value and pre-processing time stability of BMP2 measurements in blood. Information on the dilution of samples used for measuring, data range and the sample type selected are also shown.

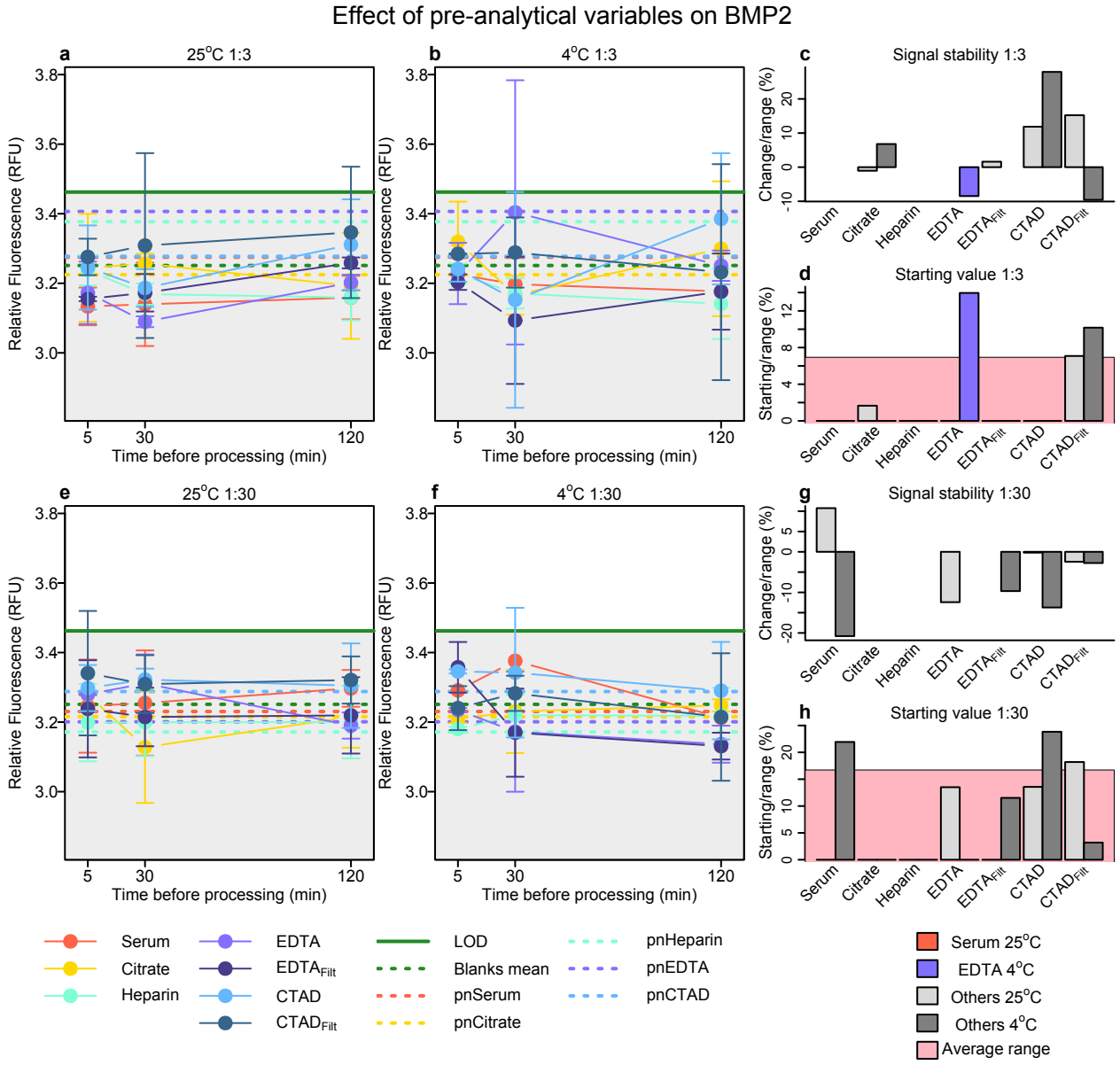

FIGURE I.S16: **Effect of pre-processing storage temperature on BMP2 stability and concentration.** Initial measured value and stability of BMP2 when stored at 25 °C (**a, e**) and 4 °C (**b, f**) before processing when collected in different tube types. The measured values are shown at low dilution of 1:3 (**a-b**) and high dilution of 1:30 (**e-f**). Stability before processing is expressed as an increase or decrease compared to the measurement range and is shown for low (**c**) and high (**g**) dilutions. Initial value is expressed as a portion of the measurement range when the linear regression is extrapolated to zero minutes and is shown for low (**d**) and high (**h**) dilutions. The pink box in graphs **d** and **h** indicate the region that is included by the *mean* ± *SD* of all the initial values and gives an indication of outliers when values lie outside this region. Red and purple bars in **c-d, g-h** are indicated at the measured dilution as the two choices for the TBI analysis.

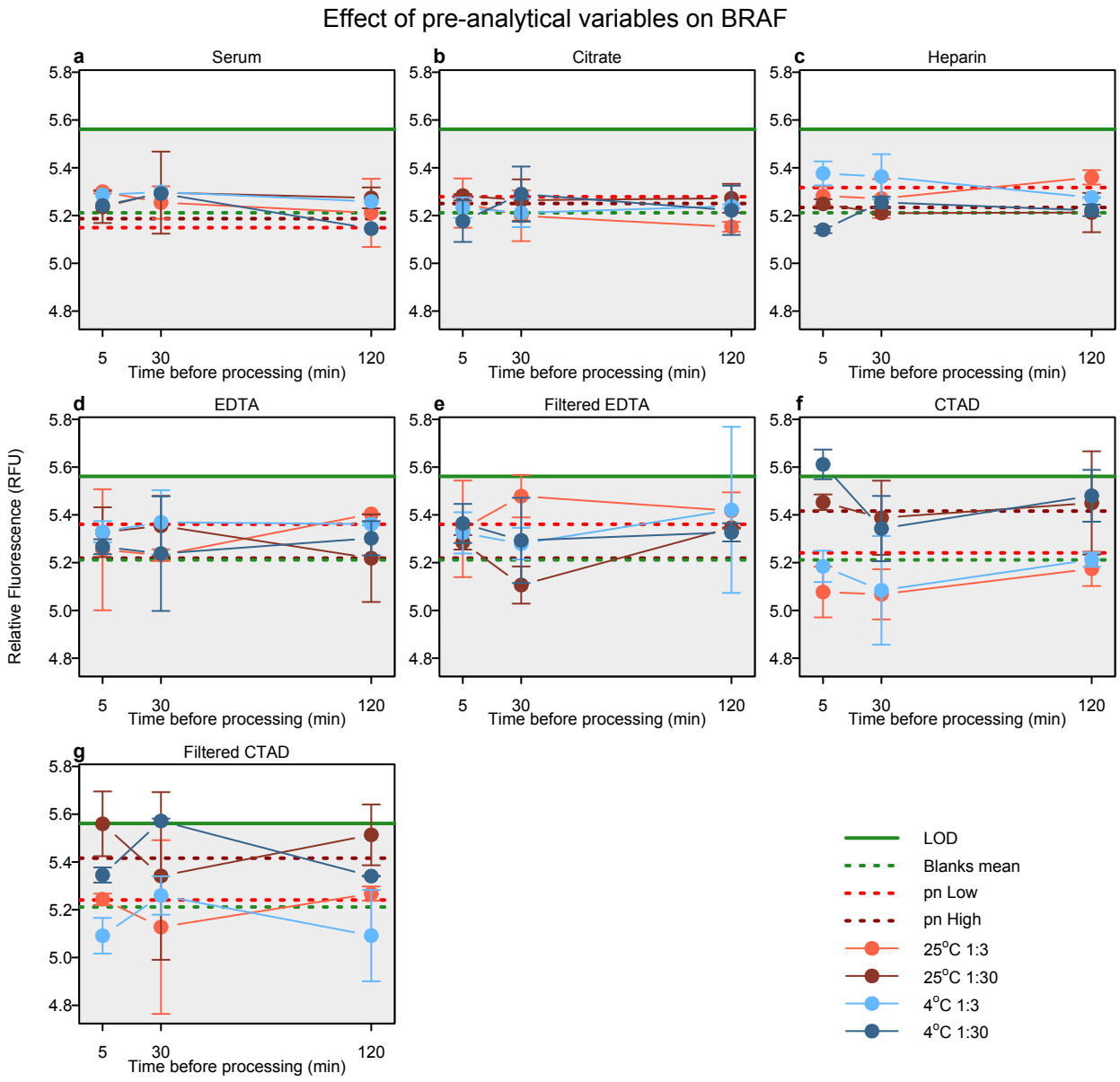

FIGURE I.S17: **Effect of blood collection tube on BRAF stability and concentration.** Effects of blood collection tubes (**a**: serum, **b**: citrate, **c**: heparin, **d-e**: EDTA, **f-g**: CTAD), storage temperature and time before processing, and post-processing plasma filtering (**e, g**) on the initial value and pre-processing time stability of BRAF measurements in blood. Information on the dilution of samples used for measuring, data range and the sample type selected are also shown.

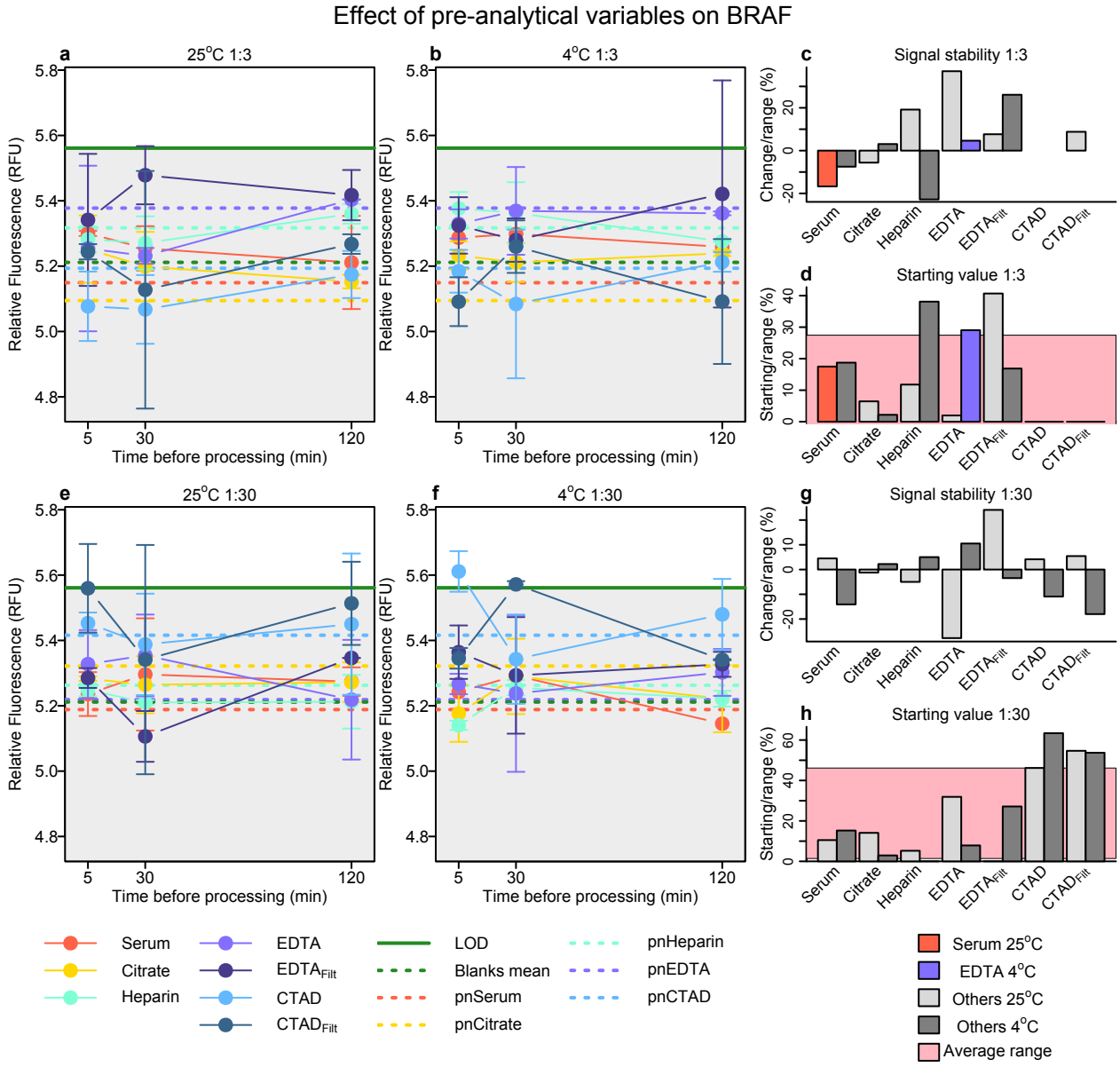

FIGURE I.S18: **Effect of pre-processing storage temperature on BRAF stability and concentration.** Initial measured value and stability of BRAF when stored at 25 °C (**a, e**) and 4 °C (**b, f**) before processing when collected in different tube types. The measured values are shown at low dilution of 1:3 (**a-b**) and high dilution of 1:30 (**e-f**). Stability before processing is expressed as an increase or decrease compared to the measurement range and is shown for low (**c**) and high (**g**) dilutions. Initial value is expressed as a portion of the measurement range when the linear regression is extrapolated to zero minutes and is shown for low (**d**) and high (**h**) dilutions. The pink box in graphs **d** and **h** indicate the region that is included by the *mean* ± *SD* of all the initial values and gives an indication of outliers when values lie outside this region. Red and purple bars in **c-d, g-h** are indicated at the measured dilution as the two choices for the TBI analysis.

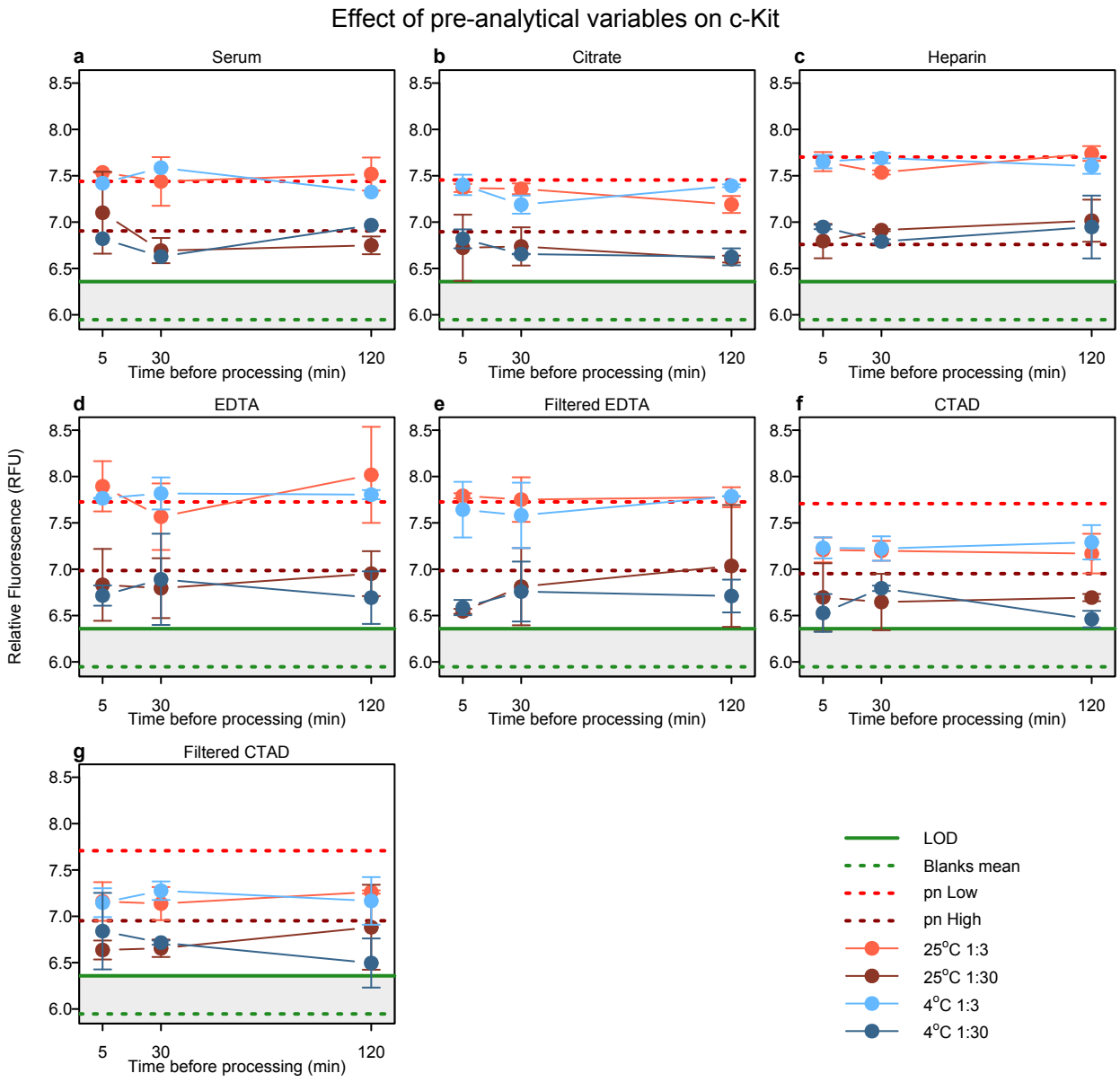

FIGURE I.S19: **Effect of blood collection tube on c-Kit stability and concentration.** Effects of blood collection tubes (**a**: serum, **b**: citrate, **c**: heparin, **d-e**: EDTA, **f-g**: CTAD), storage temperature and time before processing, and post-processing plasma filtering (**e, g**) on the initial value and pre-processing time stability of c-Kit measurements in blood. Information on the dilution of samples used for measuring, data range and the sample type selected are also shown.

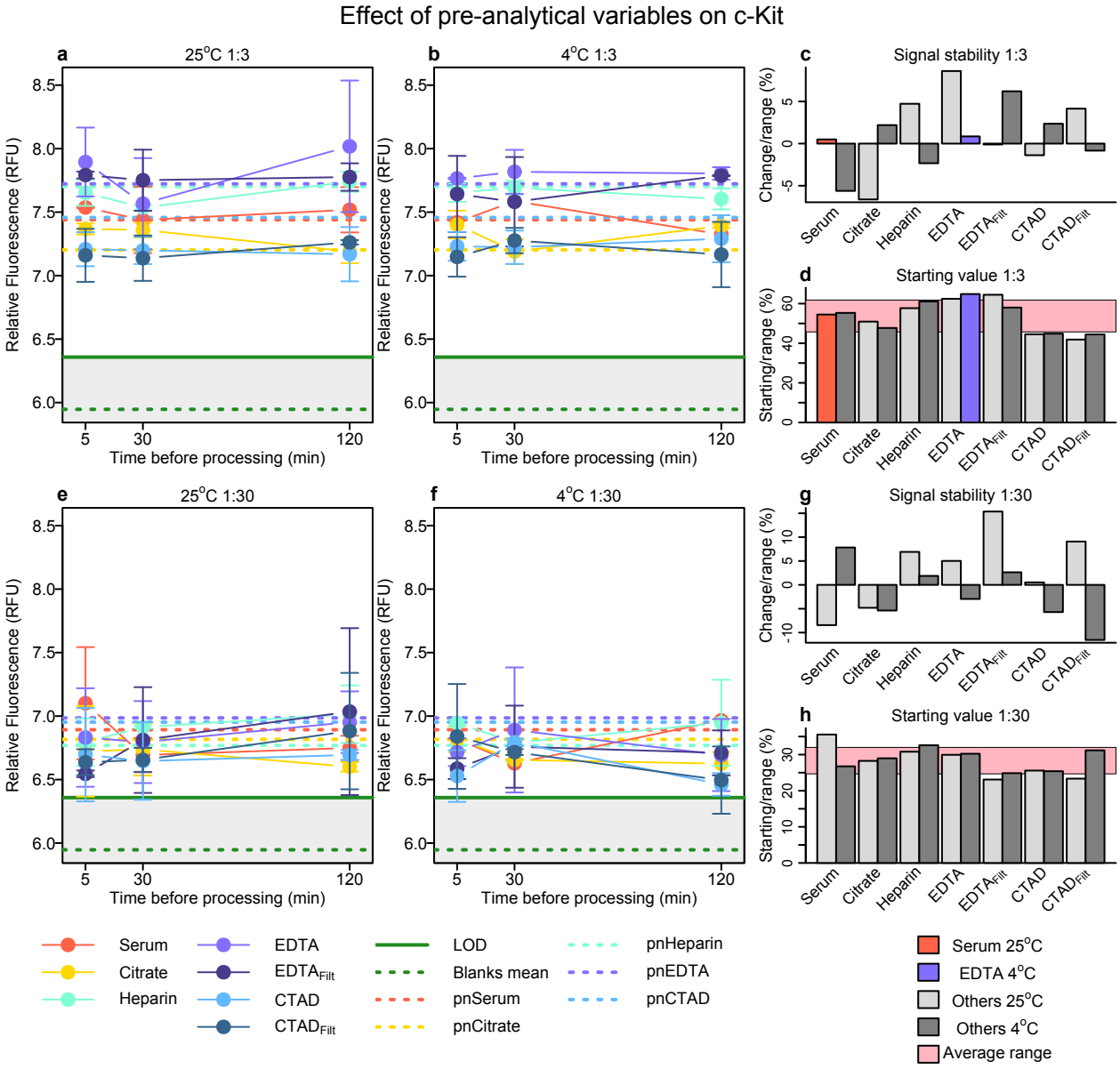

FIGURE I.S20: **Effect of pre-processing storage temperature on c-Kit stability and concentration.** Initial measured value and stability of c-Kit when stored at 25 °C (**a, e**) and 4 °C (**b, f**) before processing when collected in different tube types. The measured values are shown at low dilution of 1:3 (**a-b**) and high dilution of 1:30 (**e-f**). Stability before processing is expressed as an increase or decrease compared to the measurement range and is shown for low (**c**) and high (**g**) dilutions. Initial value is expressed as a portion of the measurement range when the linear regression is extrapolated to zero minutes and is shown for low (**d**) and high (**h**) dilutions. The pink box in graphs **d** and **h** indicate the region that is included by the *mean* ± *SD* of all the initial values and gives an indication of outliers when values lie outside this region. Red and purple bars in **c-d, g-h** are indicated at the measured dilution as the two choices for the TBI analysis.

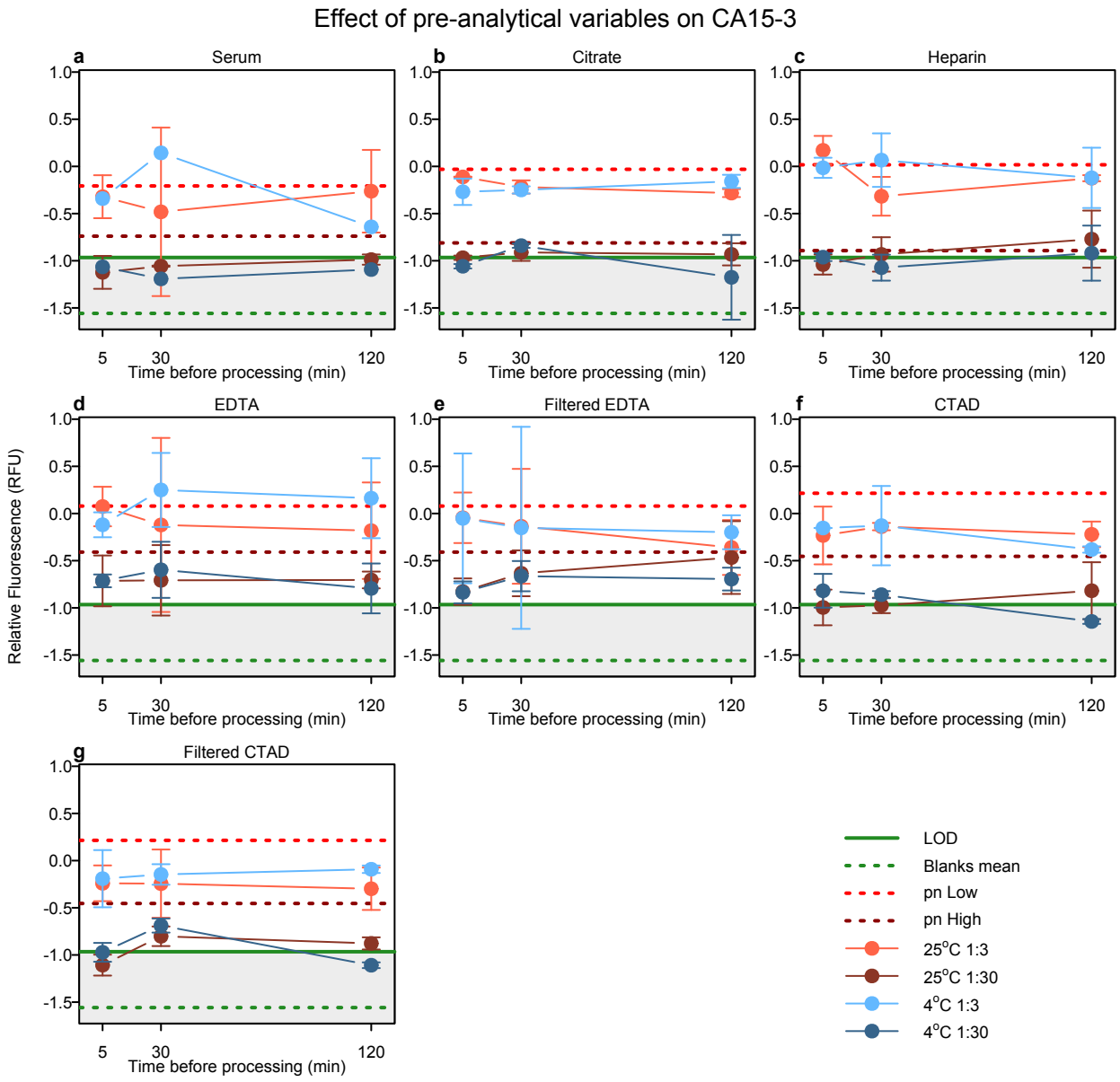

FIGURE I.S21: **Effect of blood collection tube on CA15-3 stability and concentration.** Effects of blood collection tubes (**a**: serum, **b**: citrate, **c**: heparin, **d-e**: EDTA, **f-g**: CTAD), storage temperature and time before processing, and post-processing plasma filtering (**e, g**) on the initial value and pre-processing time stability of CA15-3 measurements in blood. Information on the dilution of samples used for measuring, data range and the sample type selected are also shown.

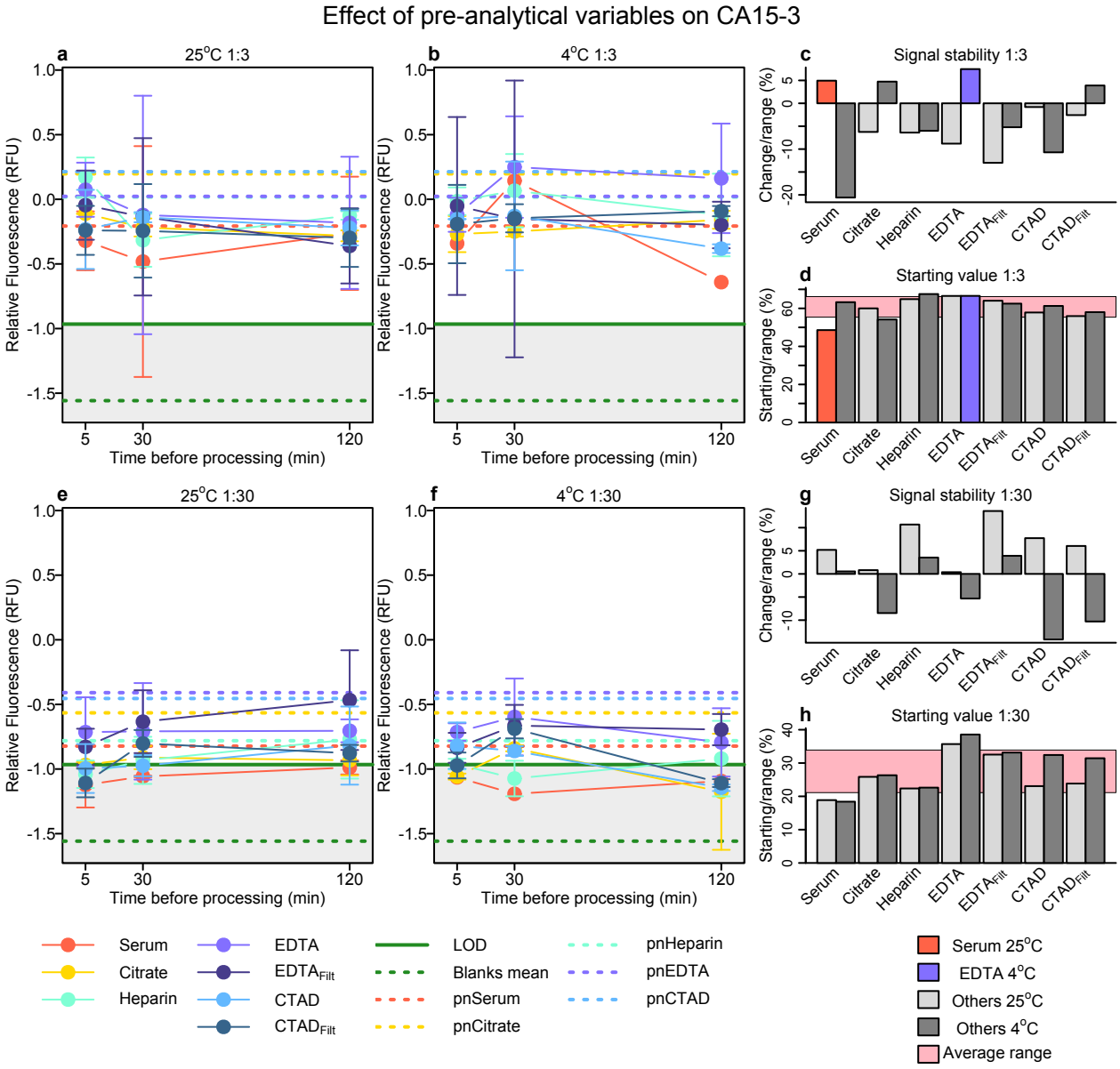

FIGURE I.S22: **Effect of pre-processing storage temperature on CA15-3 stability and concentration.** Initial measured value and stability of CA15-3 when stored at 25 °C (**a, e**) and 4 °C (**b, f**) before processing when collected in different tube types. The measured values are shown at low dilution of 1:3 (**a-b**) and high dilution of 1:30 (**e-f**). Stability before processing is expressed as an increase or decrease compared to the measurement range and is shown for low (**c**) and high (**g**) dilutions. Initial value is expressed as a portion of the measurement range when the linear regression is extrapolated to zero minutes and is shown for low (**d**) and high (**h**) dilutions. The pink box in graphs **d** and **h** indicate the region that is included by the *mean* ± *SD* of all the initial values and gives an indication of outliers when values lie outside this region. Red and purple bars in **c-d, g-h** are indicated at the measured dilution as the two choices for the TBI analysis.

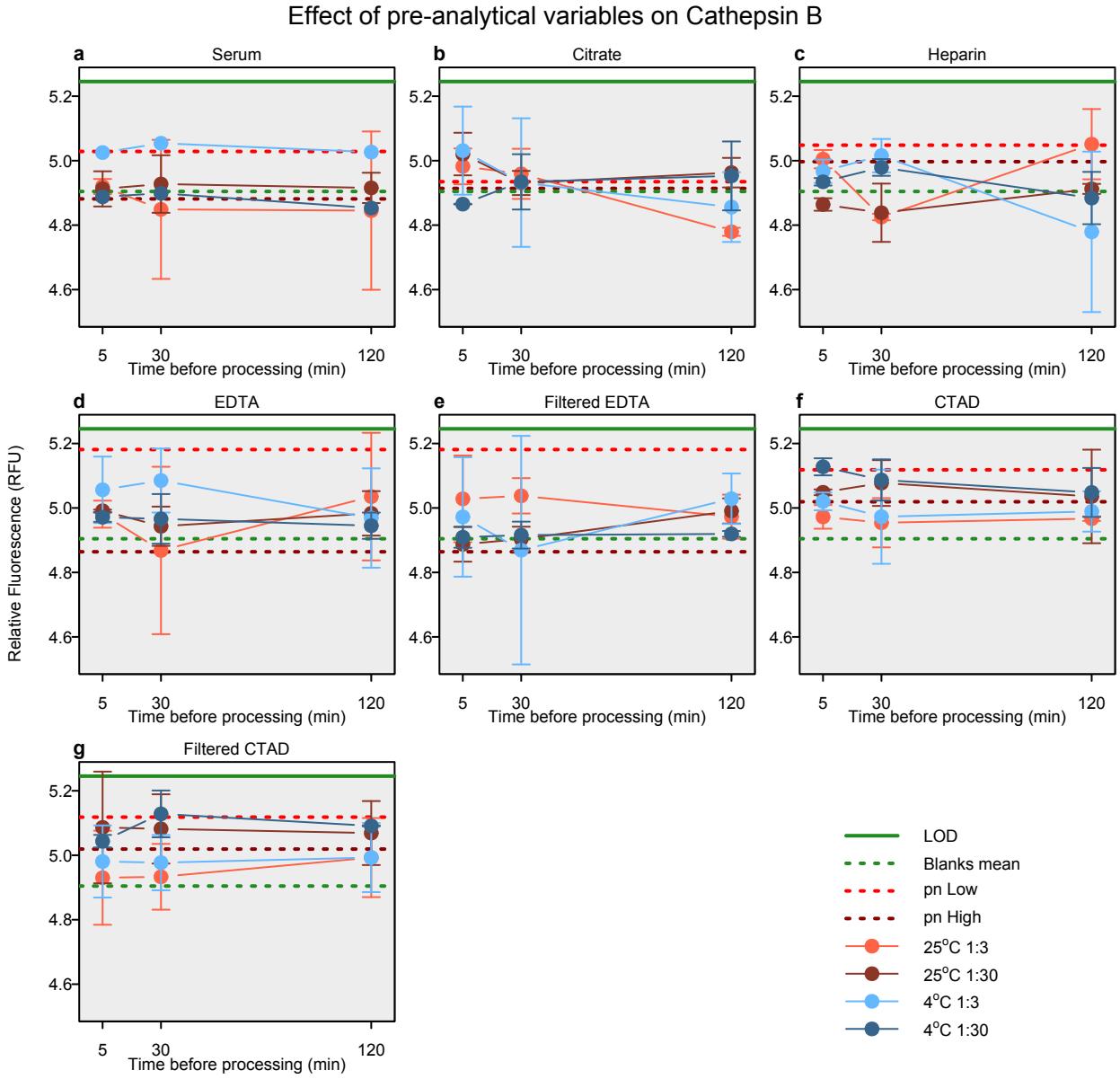

FIGURE I.S23: **Effect of blood collection tube on Cathepsin B stability and concentration.** Effects of blood collection tubes (**a**: serum, **b**: citrate, **c**: heparin, **d-e**: EDTA, **f-g**: CTAD), storage temperature and time before processing, and post-processing plasma filtering (**e, g**) on the initial value and pre-processing time stability of Cathepsin B measurements in blood. Information on the dilution of samples used for measuring, data range and the sample type selected are also shown.

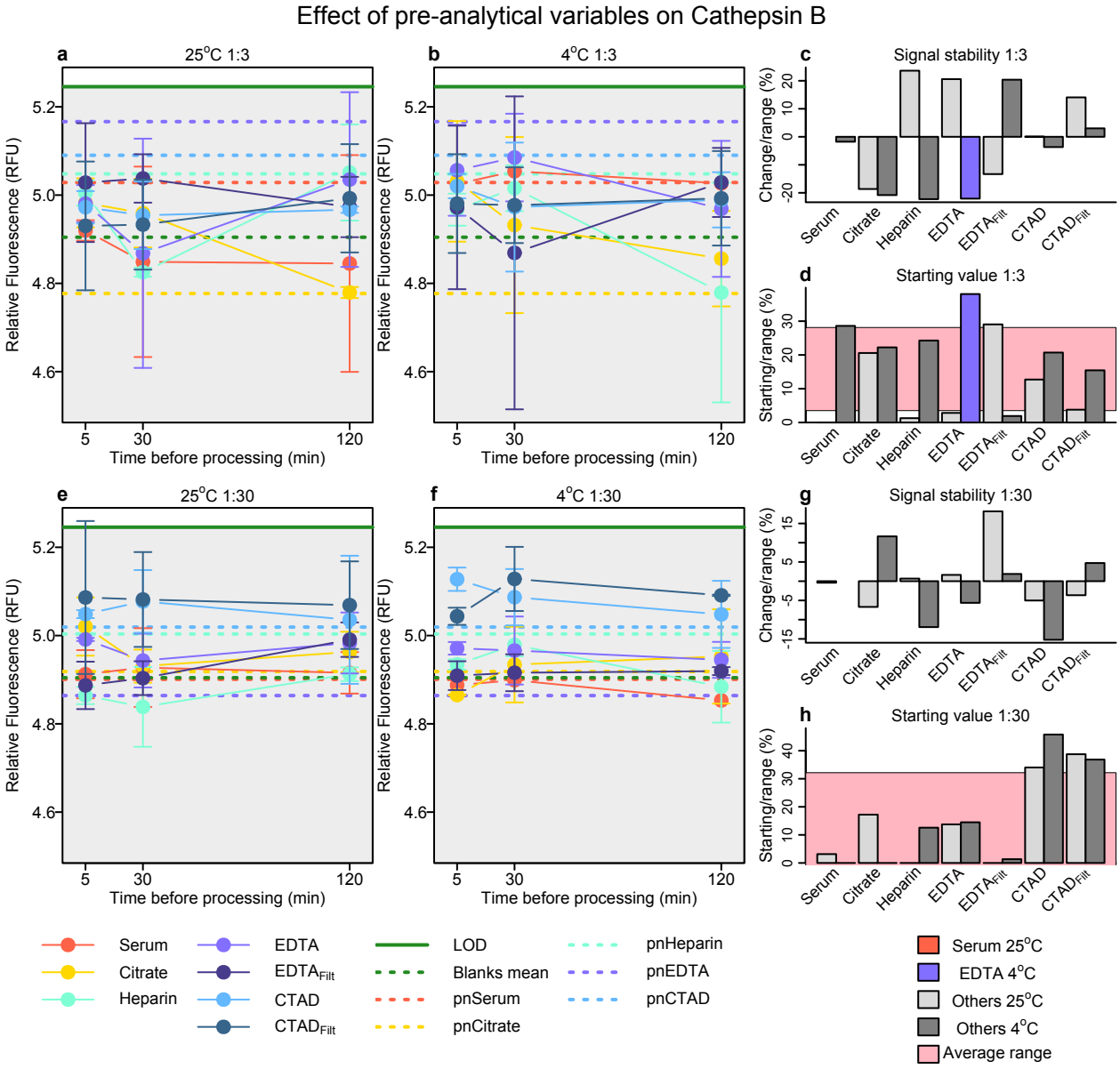

FIGURE I.S24: **Effect of pre-processing storage temperature on Cathepsin B stability and concentration.** Initial measured value and stability of Cathepsin B when stored at 25 °C (**a, e**) and 4 °C (**b, f**) before processing when collected in different tube types. The measured values are shown at low dilution of 1:3 (**a-b**) and high dilution of 1:30 (**e-f**). Stability before processing is expressed as an increase or decrease compared to the measurement range and is shown for low (**c**) and high (**g**) dilutions. Initial value is expressed as a portion of the measurement range when the linear regression is extrapolated to zero minutes and is shown for low (**d**) and high (**h**) dilutions. The pink box in graphs **d** and **h** indicate the region that is included by the *mean* ± *SD* of all the initial values and gives an indication of outliers when values lie outside this region. Red and purple bars in **c-d, g-h** are indicated at the measured dilution as the two choices for the TBI analysis.

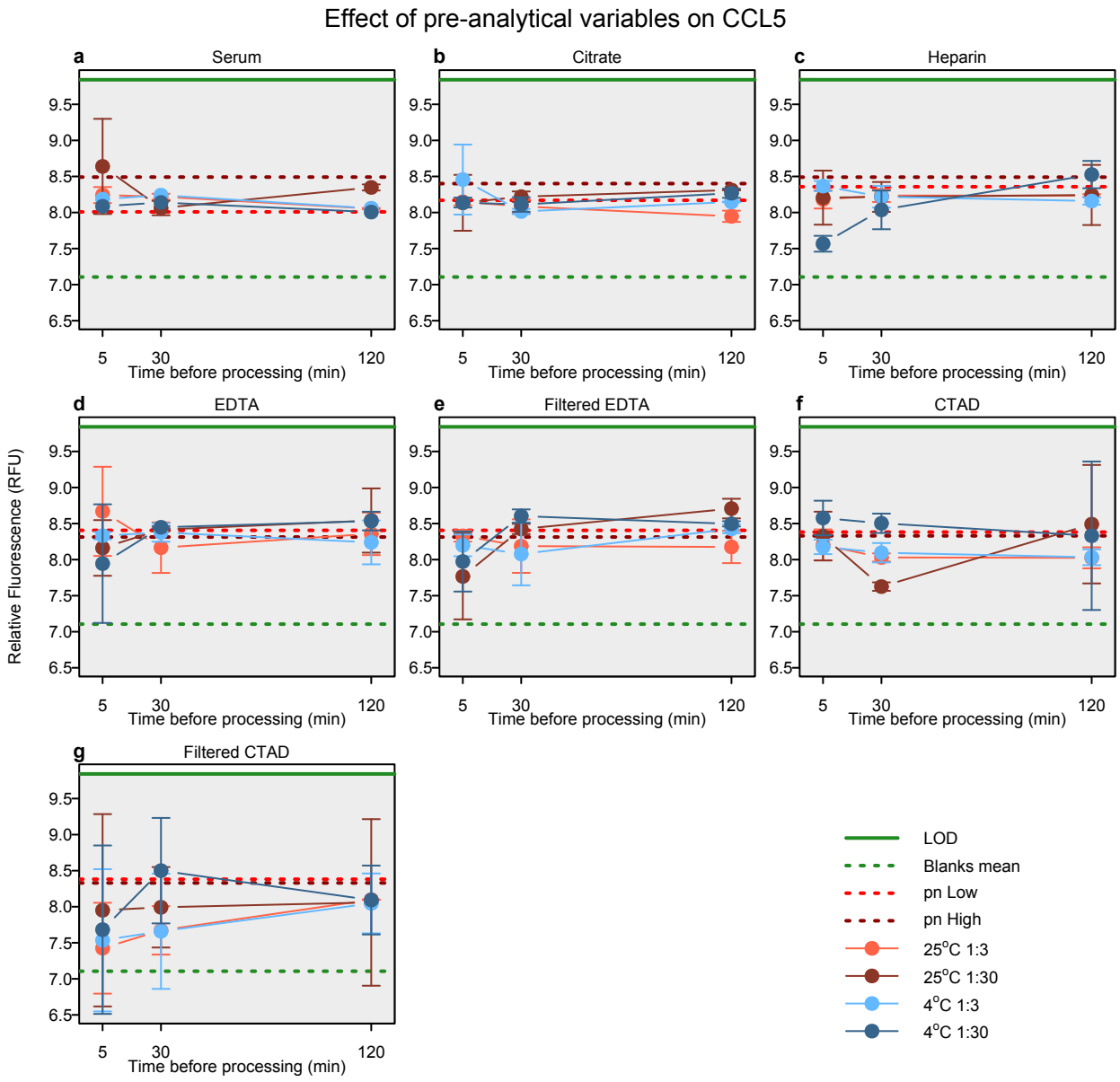

FIGURE I.S25: **Effect of blood collection tube on CCL5 stability and concentration.** Effects of blood collection tubes (**a**: serum, **b**: citrate, **c**: heparin, **d-e**: EDTA, **f-g**: CTAD), storage temperature and time before processing, and post-processing plasma filtering (**e, g**) on the initial value and pre-processing time stability of CCL5 measurements in blood. Information on the dilution of samples used for measuring, data range and the sample type selected are also shown.

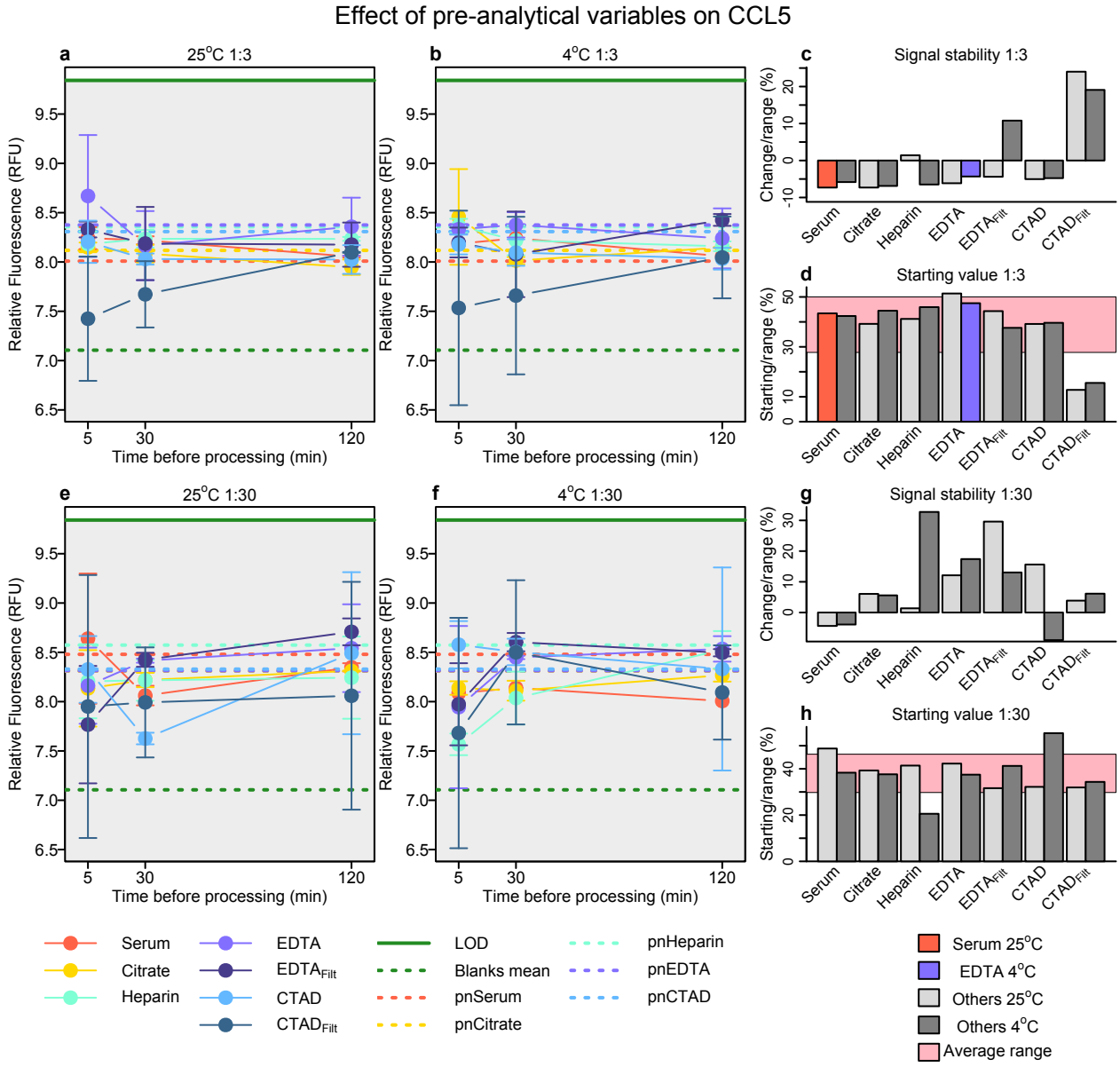

FIGURE I.S26: **Effect of pre-processing storage temperature on CCL5 stability and concentration.** Initial measured value and stability of CCL5 when stored at 25 °C (**a, e**) and 4 °C (**b, f**) before processing when collected in different tube types. The measured values are shown at low dilution of 1:3 (**a-b**) and high dilution of 1:30 (**e-f**). Stability before processing is expressed as an increase or decrease compared to the measurement range and is shown for low (**c**) and high (**g**) dilutions. Initial value is expressed as a portion of the measurement range when the linear regression is extrapolated to zero minutes and is shown for low (**d**) and high (**h**) dilutions. The pink box in graphs **d** and **h** indicate the region that is included by the *mean* ± *SD* of all the initial values and gives an indication of outliers when values lie outside this region. Red and purple bars in **c-d, g-h** are indicated at the measured dilution as the two choices for the TBI analysis.

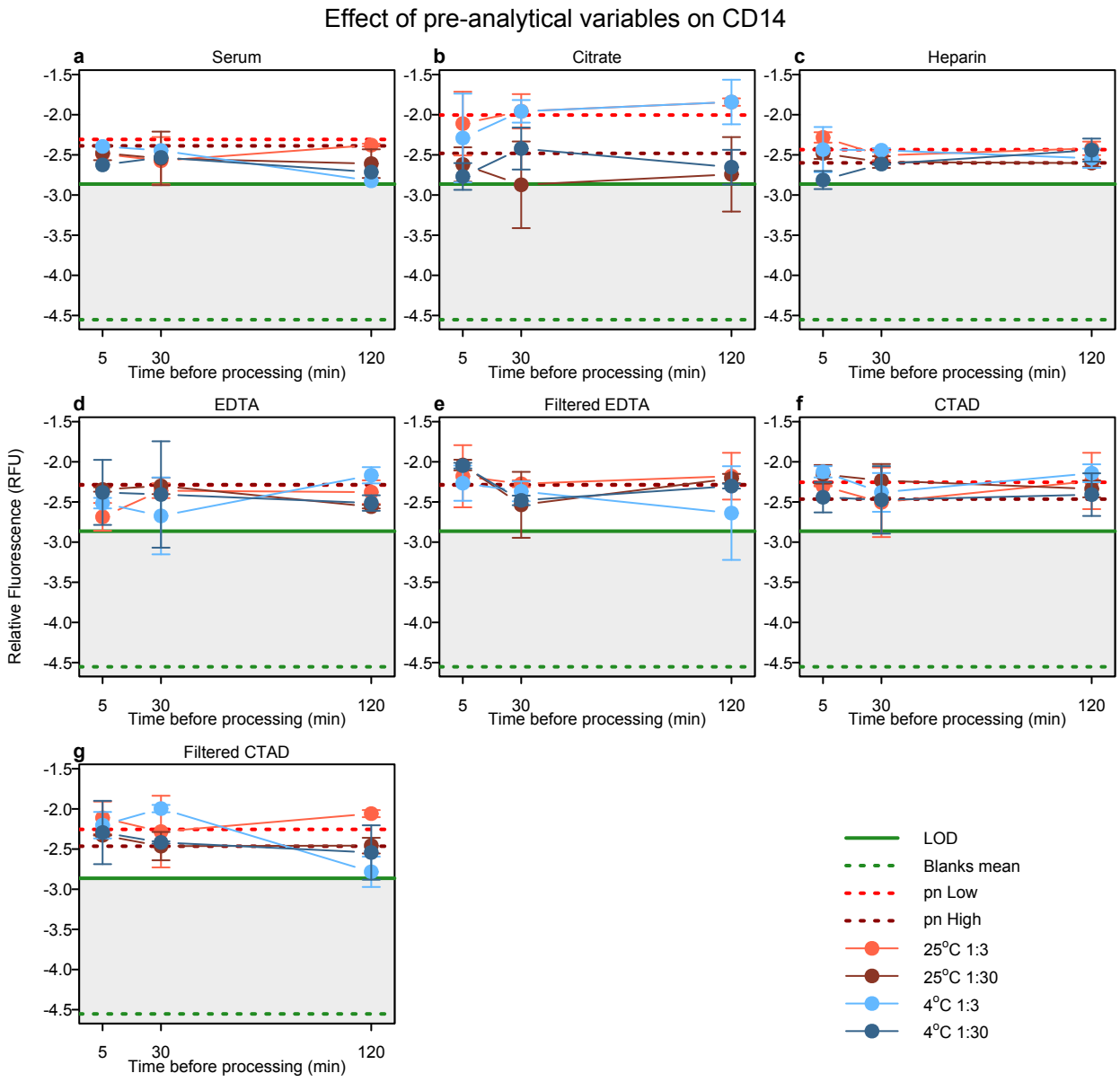

FIGURE I.S27: **Effect of blood collection tube on CD14 stability and concentration.** Effects of blood collection tubes (**a**: serum, **b**: citrate, **c**: heparin, **d-e**: EDTA, **f-g**: CTAD), storage temperature and time before processing, and post-processing plasma filtering (**e, g**) on the initial value and pre-processing time stability of CD14 measurements in blood. Information on the dilution of samples used for measuring, data range and the sample type selected are also shown.

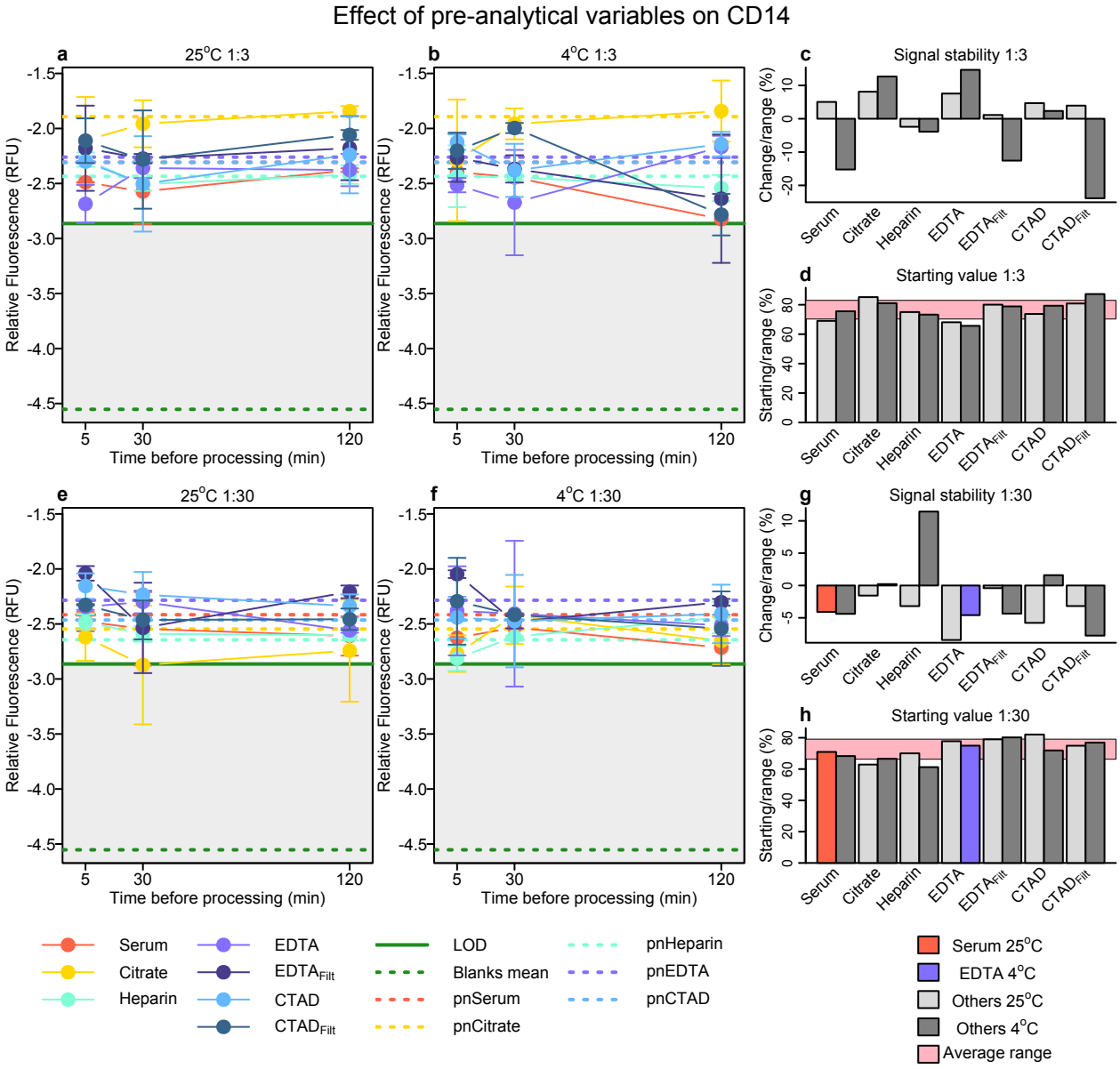

FIGURE I.S28: **Effect of pre-processing storage temperature on CD14 stability and concentration.** Initial measured value and stability of CD14 when stored at 25 °C (**a, e**) and 4 °C (**b, f**) before processing when collected in different tube types. The measured values are shown at low dilution of 1:3 (**a-b**) and high dilution of 1:30 (**e-f**). Stability before processing is expressed as an increase or decrease compared to the measurement range and is shown for low (**c**) and high (**g**) dilutions. Initial value is expressed as a portion of the measurement range when the linear regression is extrapolated to zero minutes and is shown for low (**d**) and high (**h**) dilutions. The pink box in graphs **d** and **h** indicate the region that is included by the *mean* ± *SD* of all the initial values and gives an indication of outliers when values lie outside this region. Red and purple bars in **c-d, g-h** are indicated at the measured dilution as the two choices for the TBI analysis.

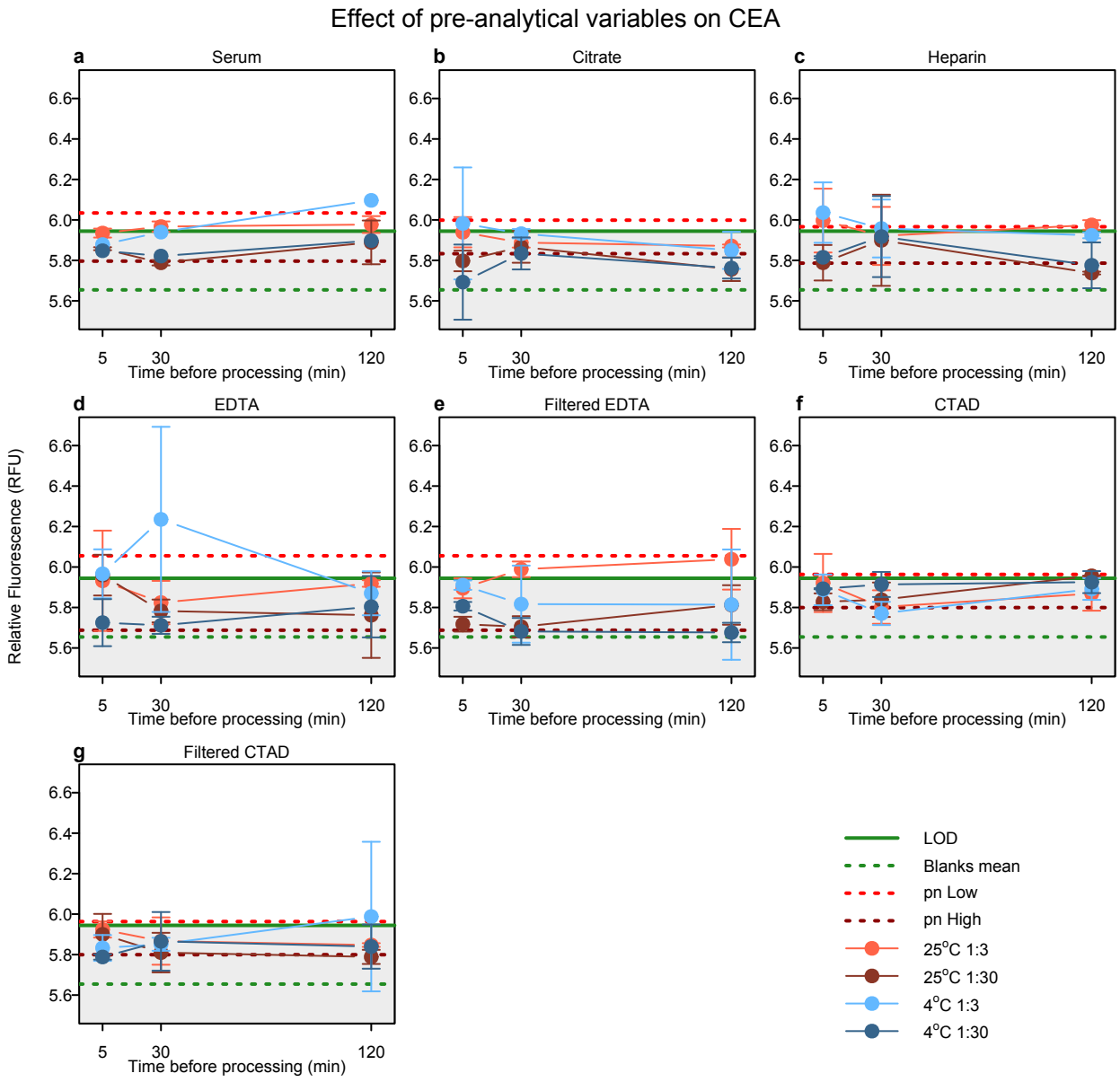

FIGURE I.S29: **Effect of blood collection tube on CEA stability and concentration.** Effects of blood collection tubes (**a**: serum, **b**: citrate, **c**: heparin, **d-e**: EDTA, **f-g**: CTAD), storage temperature and time before processing, and post-processing plasma filtering (**e, g**) on the initial value and pre-processing time stability of CEA measurements in blood. Information on the dilution of samples used for measuring, data range and the sample type selected are also shown.

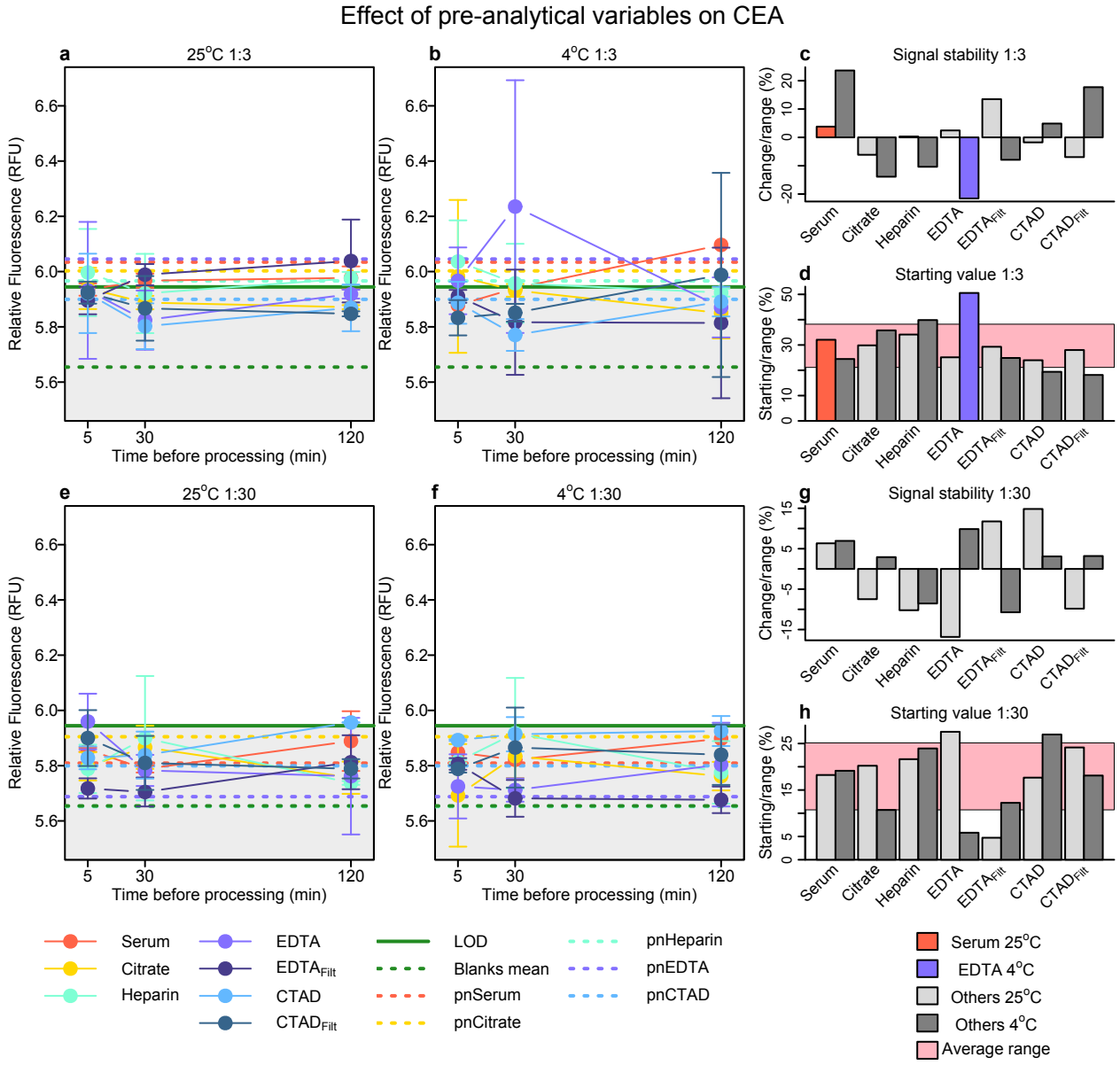

FIGURE I.S30: **Effect of pre-processing storage temperature on CEA stability and concentration.** Initial measured value and stability of CEA when stored at 25 °C (**a, e**) and 4 °C (**b, f**) before processing when collected in different tube types. The measured values are shown at low dilution of 1:3 (**a-b**) and high dilution of 1:30 (**e-f**). Stability before processing is expressed as an increase or decrease compared to the measurement range and is shown for low (**c**) and high (**g**) dilutions. Initial value is expressed as a portion of the measurement range when the linear regression is extrapolated to zero minutes and is shown for low (**d**) and high (**h**) dilutions. The pink box in graphs **d** and **h** indicate the region that is included by the *mean* ± *SD* of all the initial values and gives an indication of outliers when values lie outside this region. Red and purple bars in **c-d, g-h** are indicated at the measured dilution as the two choices for the TBI analysis.

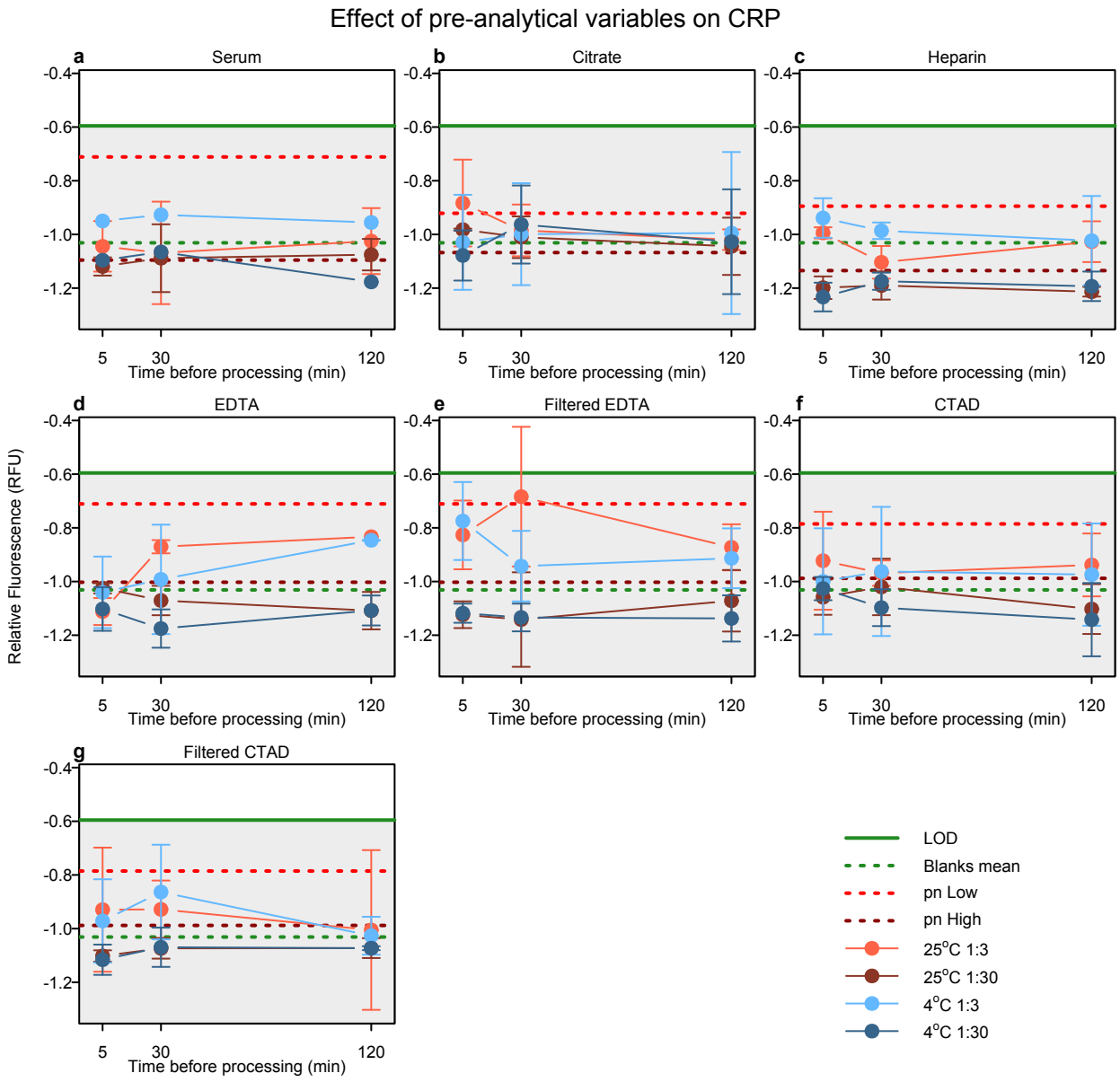

FIGURE I.S31: **Effect of blood collection tube on CRP stability and concentration.** Effects of blood collection tubes (**a**: serum, **b**: citrate, **c**: heparin, **d-e**: EDTA, **f-g**: CTAD), storage temperature and time before processing, and post-processing plasma filtering (**e, g**) on the initial value and pre-processing time stability of CRP measurements in blood. Information on the dilution of samples used for measuring, data range and the sample type selected are also shown.

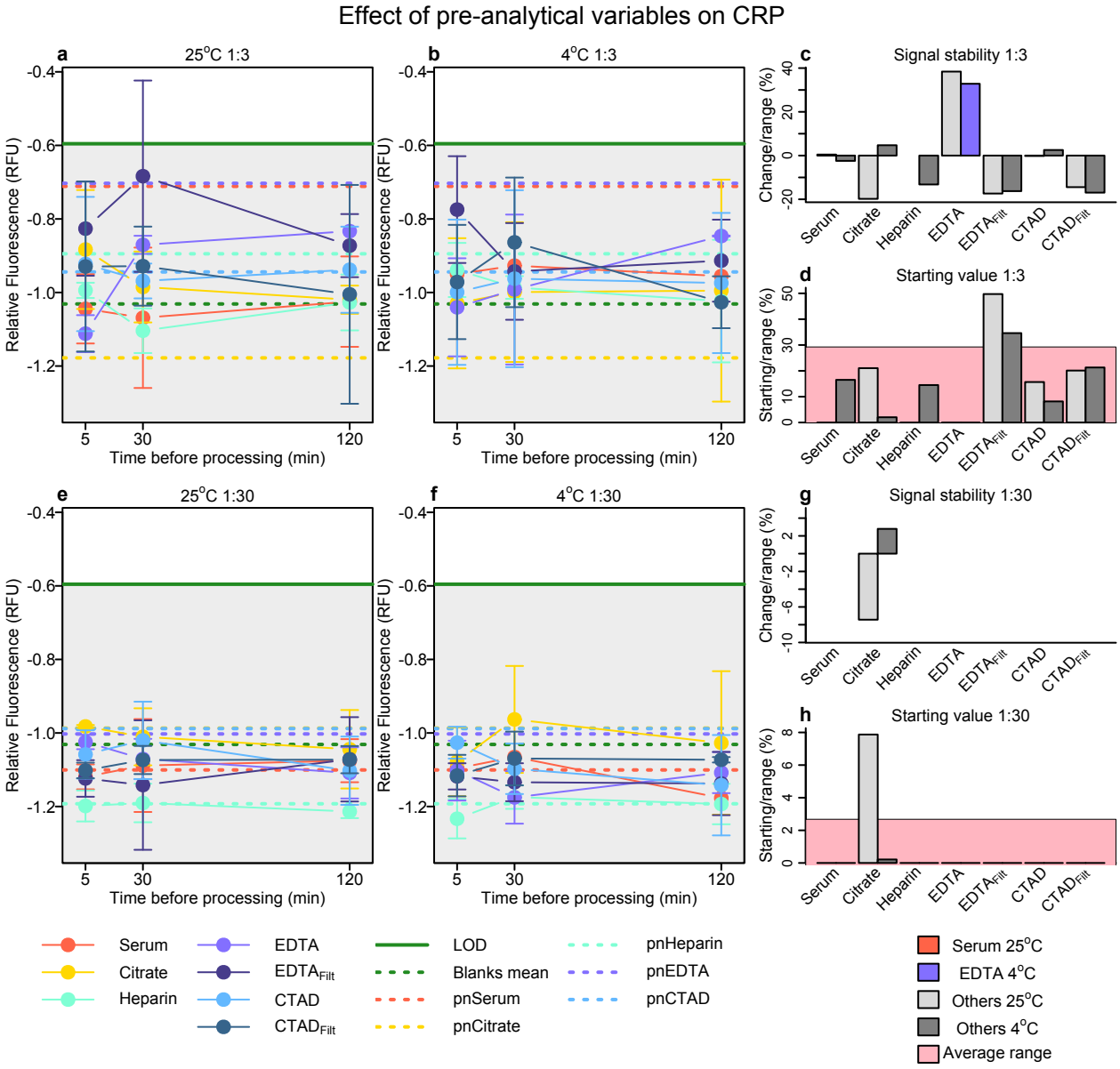

FIGURE I.S32: **Effect of pre-processing storage temperature on CRP stability and concentration.** Initial measured value and stability of CRP when stored at 25 °C (**a, e**) and 4 °C (**b, f**) before processing when collected in different tube types. The measured values are shown at low dilution of 1:3 (**a-b**) and high dilution of 1:30 (**e-f**). Stability before processing is expressed as an increase or decrease compared to the measurement range and is shown for low (**c**) and high (**g**) dilutions. Initial value is expressed as a portion of the measurement range when the linear regression is extrapolated to zero minutes and is shown for low (**d**) and high (**h**) dilutions. The pink box in graphs **d** and **h** indicate the region that is included by the *mean* ± *SD* of all the initial values and gives an indication of outliers when values lie outside this region. Red and purple bars in **c-d, g-h** are indicated at the measured dilution as the two choices for the TBI analysis.

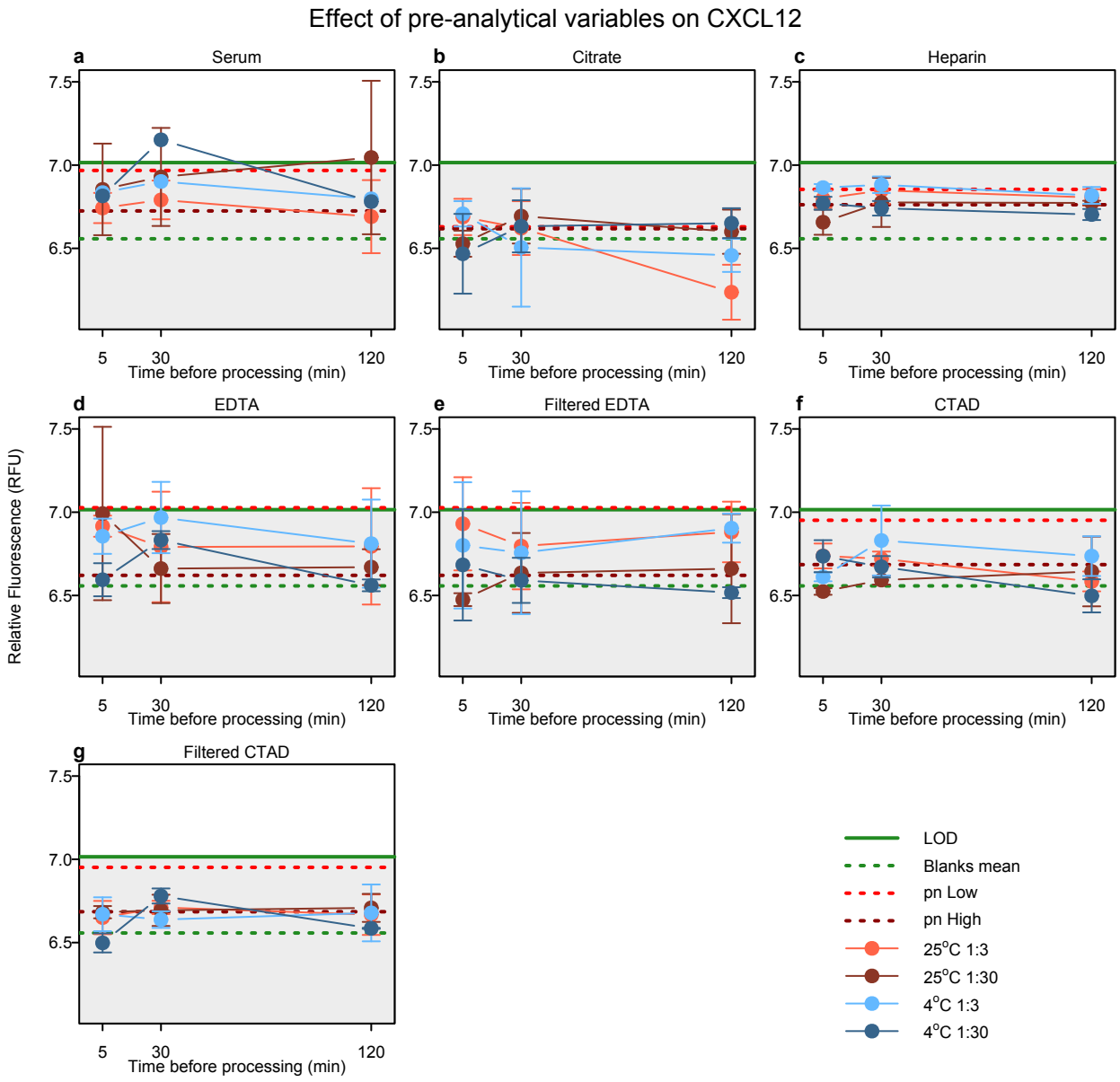

FIGURE I.S33: **Effect of blood collection tube on CXCL12 stability and concentration.** Effects of blood collection tubes (**a**: serum, **b**: citrate, **c**: heparin, **d-e**: EDTA, **f-g**: CTAD), storage temperature and time before processing, and post-processing plasma filtering (**e, g**) on the initial value and pre-processing time stability of CXCL12 measurements in blood. Information on the dilution of samples used for measuring, data range and the sample type selected are also shown.

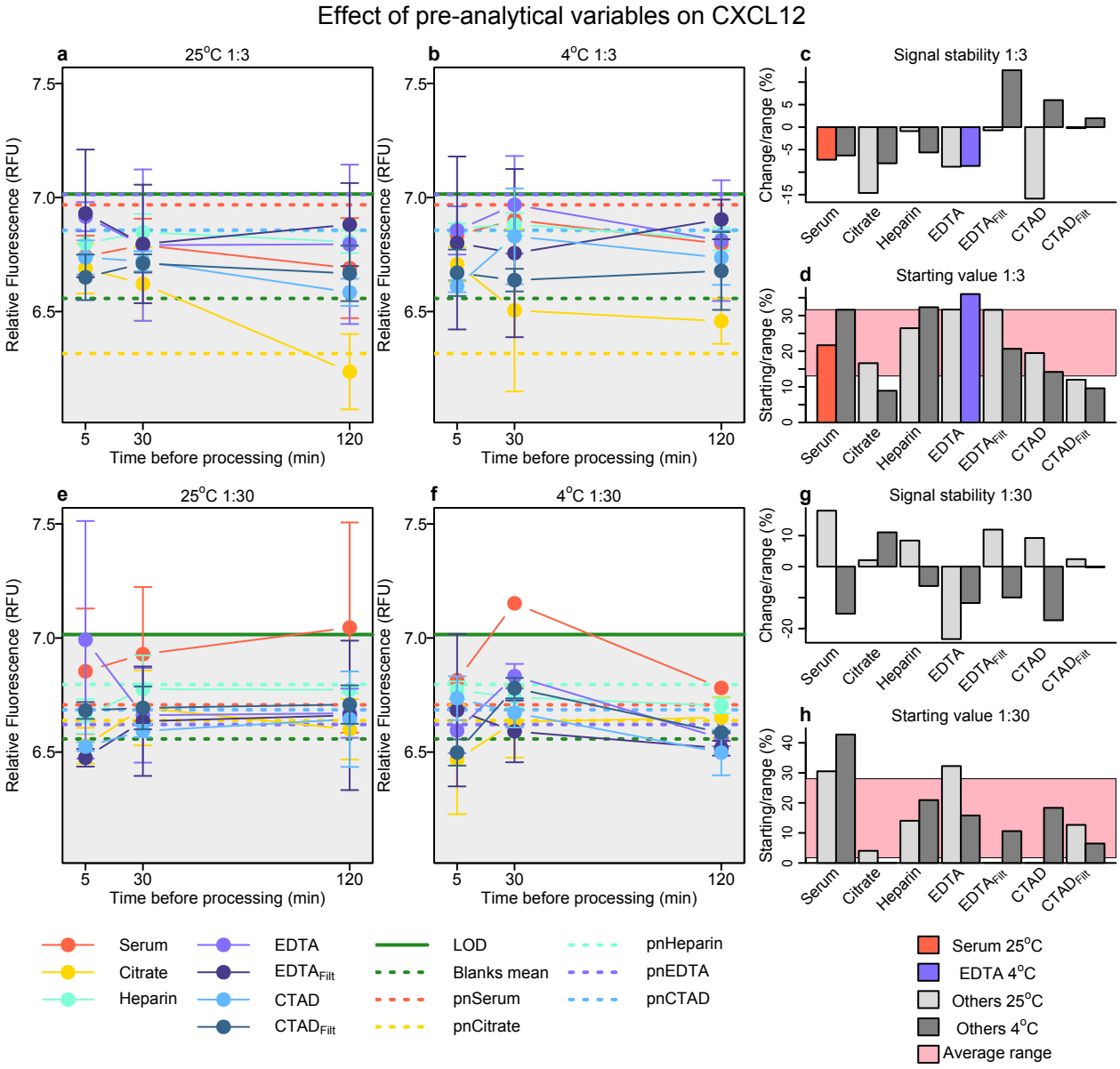

FIGURE I.S34: **Effect of pre-processing storage temperature on CXCL12 stability and concentration.** Initial measured value and stability of CXCL12 when stored at 25 °C (**a, e**) and 4 °C (**b, f**) before processing when collected in different tube types. The measured values are shown at low dilution of 1:3 (**a-b**) and high dilution of 1:30 (**e-f**). Stability before processing is expressed as an increase or decrease compared to the measurement range and is shown for low (**c**) and high (**g**) dilutions. Initial value is expressed as a portion of the measurement range when the linear regression is extrapolated to zero minutes and is shown for low (**d**) and high (**h**) dilutions. The pink box in graphs **d** and **h** indicate the region that is included by the *mean* ± *SD* of all the initial values and gives an indication of outliers when values lie outside this region. Red and purple bars in **c-d, g-h** are indicated at the measured dilution as the two choices for the TBI analysis.

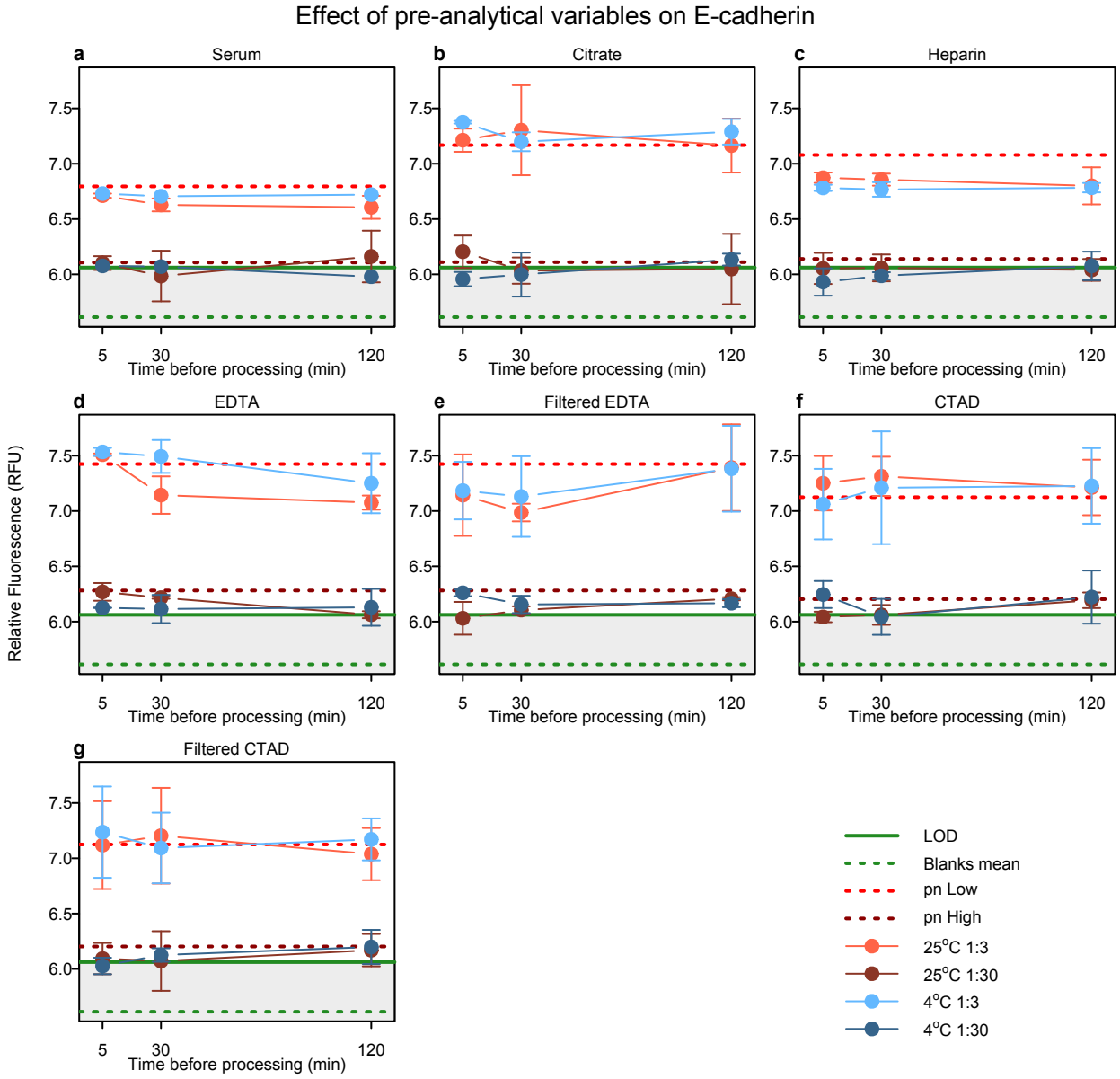

FIGURE I.S35: **Effect of blood collection tube on E-cadherin stability and concentration.** Effects of blood collection tubes (**a**: serum, **b**: citrate, **c**: heparin, **d-e**: EDTA, **f-g**: CTAD), storage temperature and time before processing, and post-processing plasma filtering (**e, g**) on the initial value and pre-processing time stability of E-cadherin measurements in blood. Information on the dilution of samples used for measuring, data range and the sample type selected are also shown.

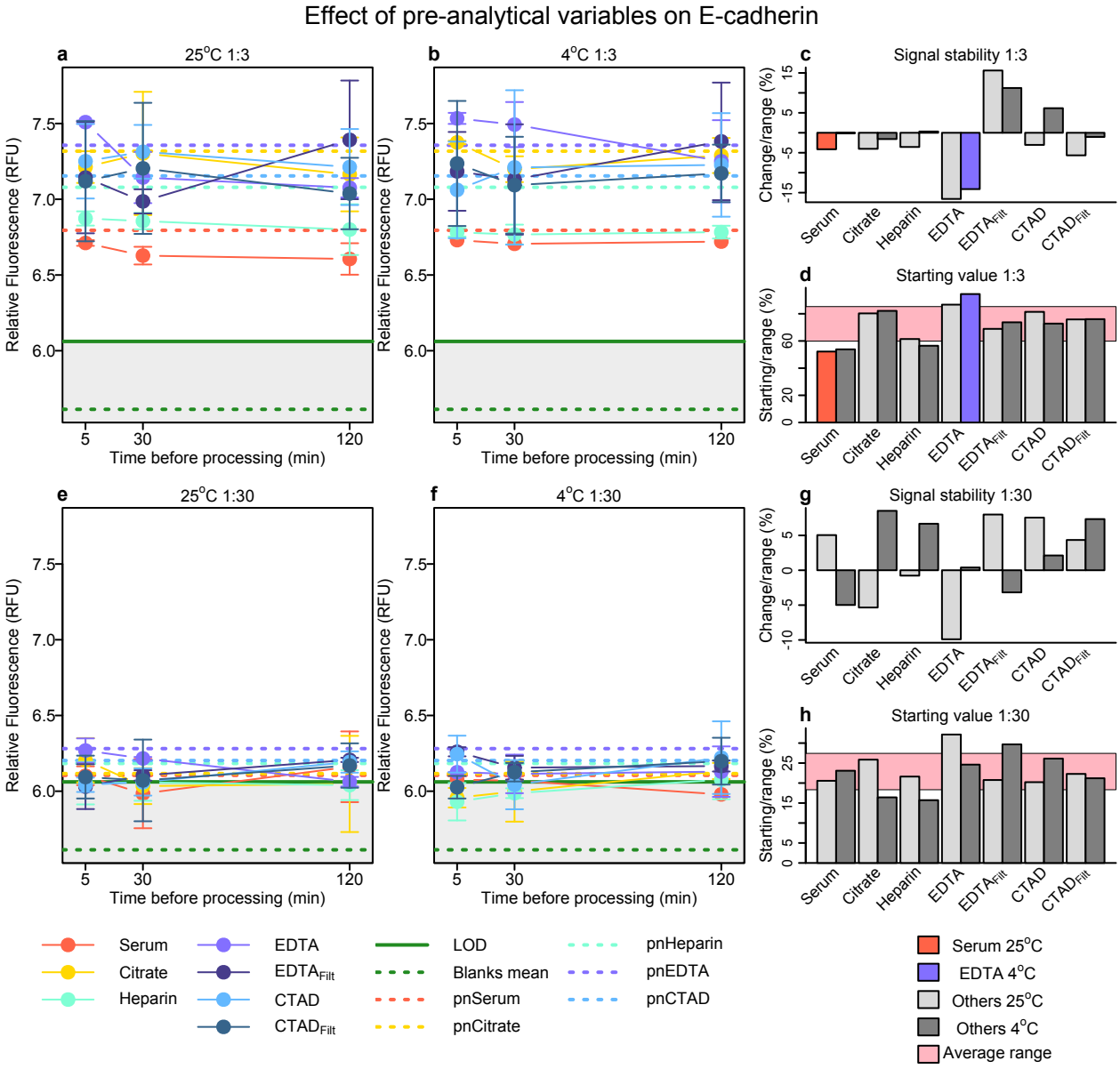

FIGURE I.S36: **Effect of pre-processing storage temperature on E-cadherin stability and concentration.** Initial measured value and stability of E-cadherin when stored at 25 °C (**a, e**) and 4 °C (**b, f**) before processing when collected in different tube types. The measured values are shown at low dilution of 1:3 (**a-b**) and high dilution of 1:30 (**e-f**). Stability before processing is expressed as an increase or decrease compared to the measurement range and is shown for low (**c**) and high (**g**) dilutions. Initial value is expressed as a portion of the measurement range when the linear regression is extrapolated to zero minutes and is shown for low (**d**) and high (**h**) dilutions. The pink box in graphs **d** and **h** indicate the region that is included by the *mean* ± *SD* of all the initial values and gives an indication of outliers when values lie outside this region. Red and purple bars in **c-d, g-h** are indicated at the measured dilution as the two choices for the TBI analysis.

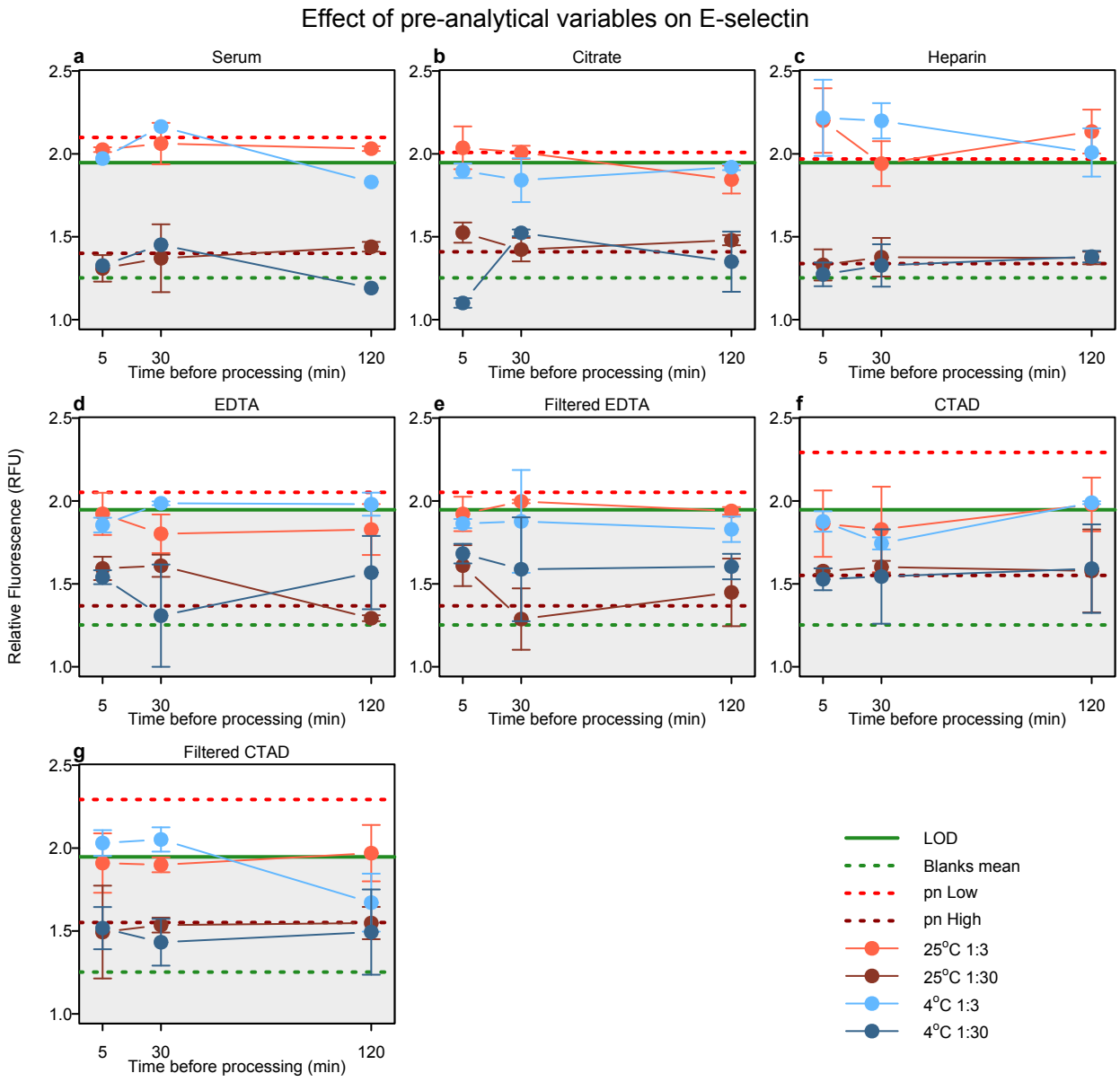

FIGURE I.S37: **Effect of blood collection tube on E-selectin stability and concentration.** Effects of blood collection tubes (**a**: serum, **b**: citrate, **c**: heparin, **d-e**: EDTA, **f-g**: CTAD), storage temperature and time before processing, and post-processing plasma filtering (**e, g**) on the initial value and pre-processing time stability of E-selectin measurements in blood. Information on the dilution of samples used for measuring, data range and the sample type selected are also shown.

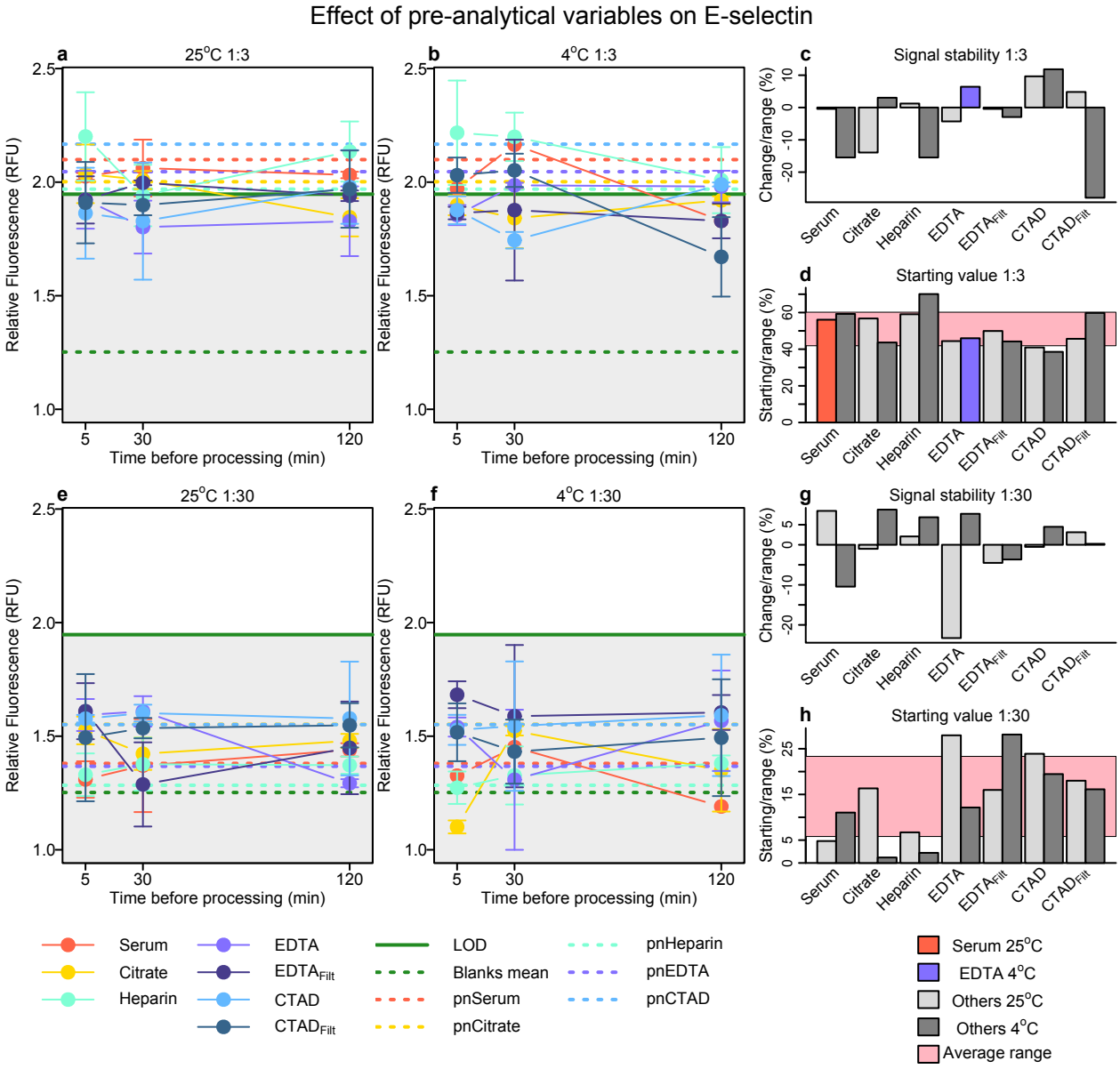

FIGURE I.S38: **Effect of pre-processing storage temperature on E-selectin stability and concentration.** Initial measured value and stability of E-selectin when stored at 25 °C (**a, e**) and 4 °C (**b, f**) before processing when collected in different tube types. The measured values are shown at low dilution of 1:3 (**a-b**) and high dilution of 1:30 (**e-f**). Stability before processing is expressed as an increase or decrease compared to the measurement range and is shown for low (**c**) and high (**g**) dilutions. Initial value is expressed as a portion of the measurement range when the linear regression is extrapolated to zero minutes and is shown for low (**d**) and high (**h**) dilutions. The pink box in graphs **d** and **h** indicate the region that is included by the *mean* ± *SD* of all the initial values and gives an indication of outliers when values lie outside this region. Red and purple bars in **c-d, g-h** are indicated at the measured dilution as the two choices for the TBI analysis.

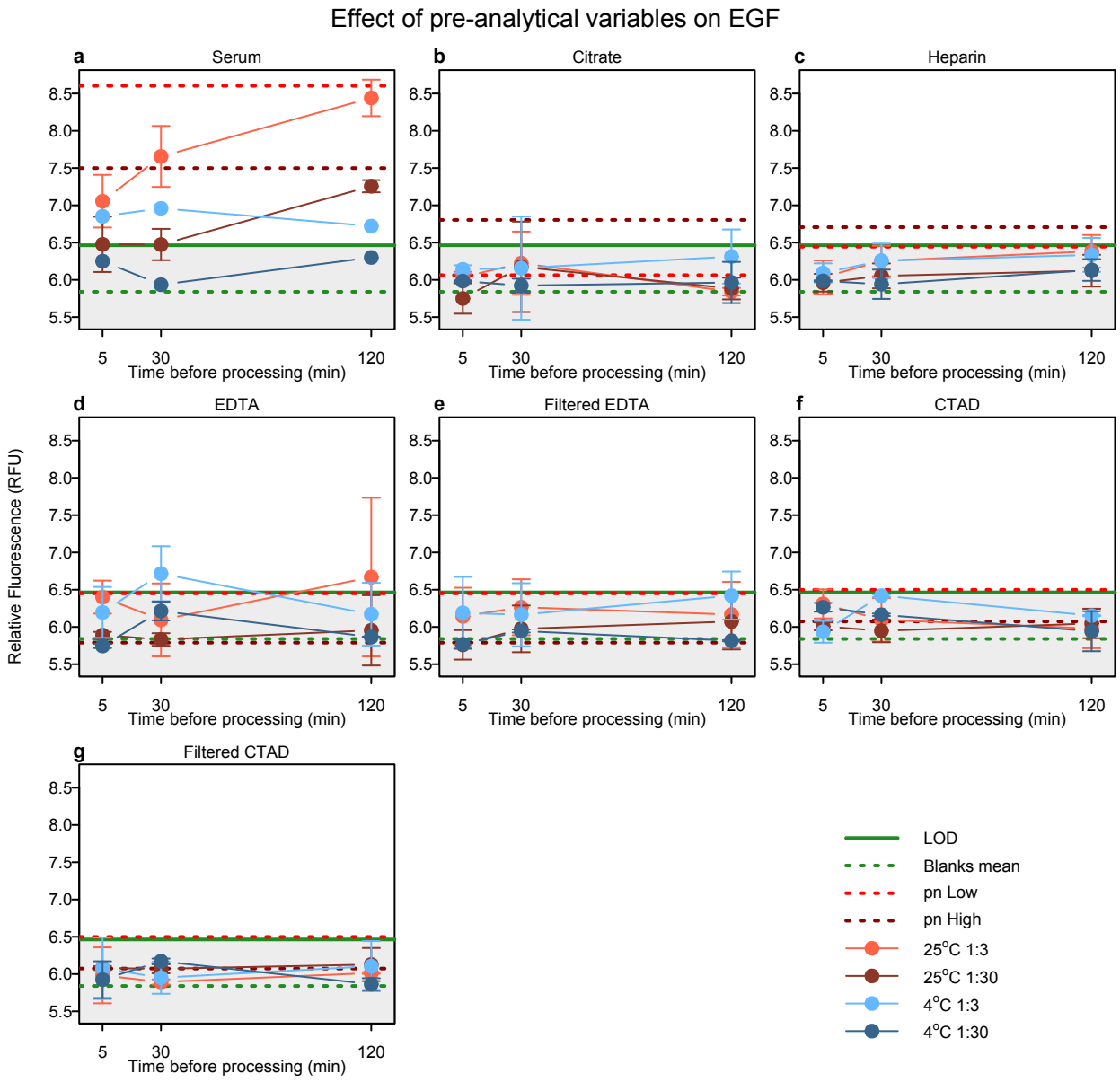

FIGURE I.S39: **Effect of blood collection tube on EGF stability and concentration.** Effects of blood collection tubes (**a**: serum, **b**: citrate, **c**: heparin, **d-e**: EDTA, **f-g**: CTAD), storage temperature and time before processing, and post-processing plasma filtering (**e, g**) on the initial value and pre-processing time stability of EGF measurements in blood. Information on the dilution of samples used for measuring, data range and the sample type selected are also shown.

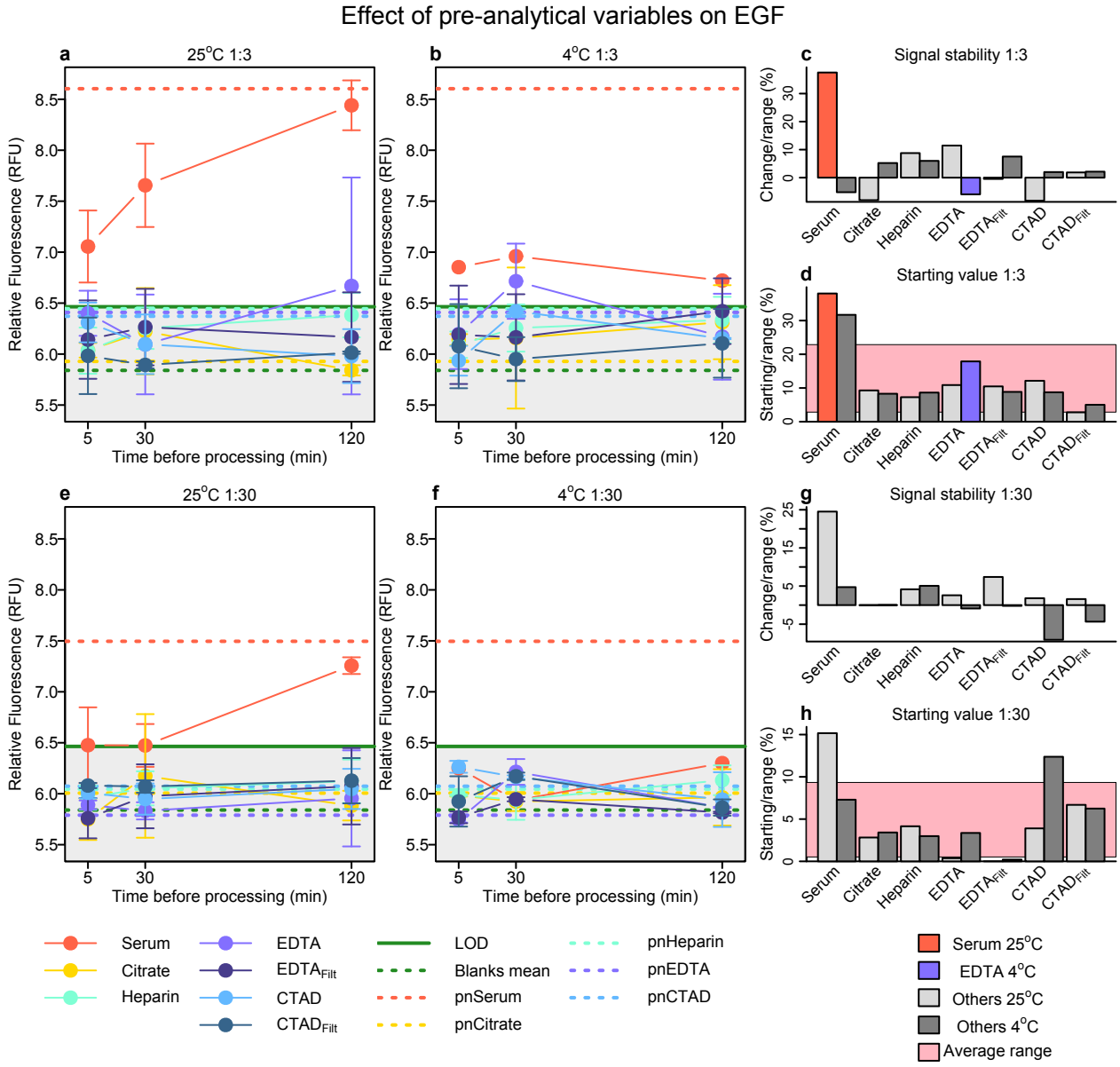

FIGURE I.S40: **Effect of pre-processing storage temperature on EGF stability and concentration.** Initial measured value and stability of EGF when stored at 25 °C (**a, e**) and 4 °C (**b, f**) before processing when collected in different tube types. The measured values are shown at low dilution of 1:3 (**a-b**) and high dilution of 1:30 (**e-f**). Stability before processing is expressed as an increase or decrease compared to the measurement range and is shown for low (**c**) and high (**g**) dilutions. Initial value is expressed as a portion of the measurement range when the linear regression is extrapolated to zero minutes and is shown for low (**d**) and high (**h**) dilutions. The pink box in graphs **d** and **h** indicate the region that is included by the *mean* ± *SD* of all the initial values and gives an indication of outliers when values lie outside this region. Red and purple bars in **c-d, g-h** are indicated at the measured dilution as the two choices for the TBI analysis.

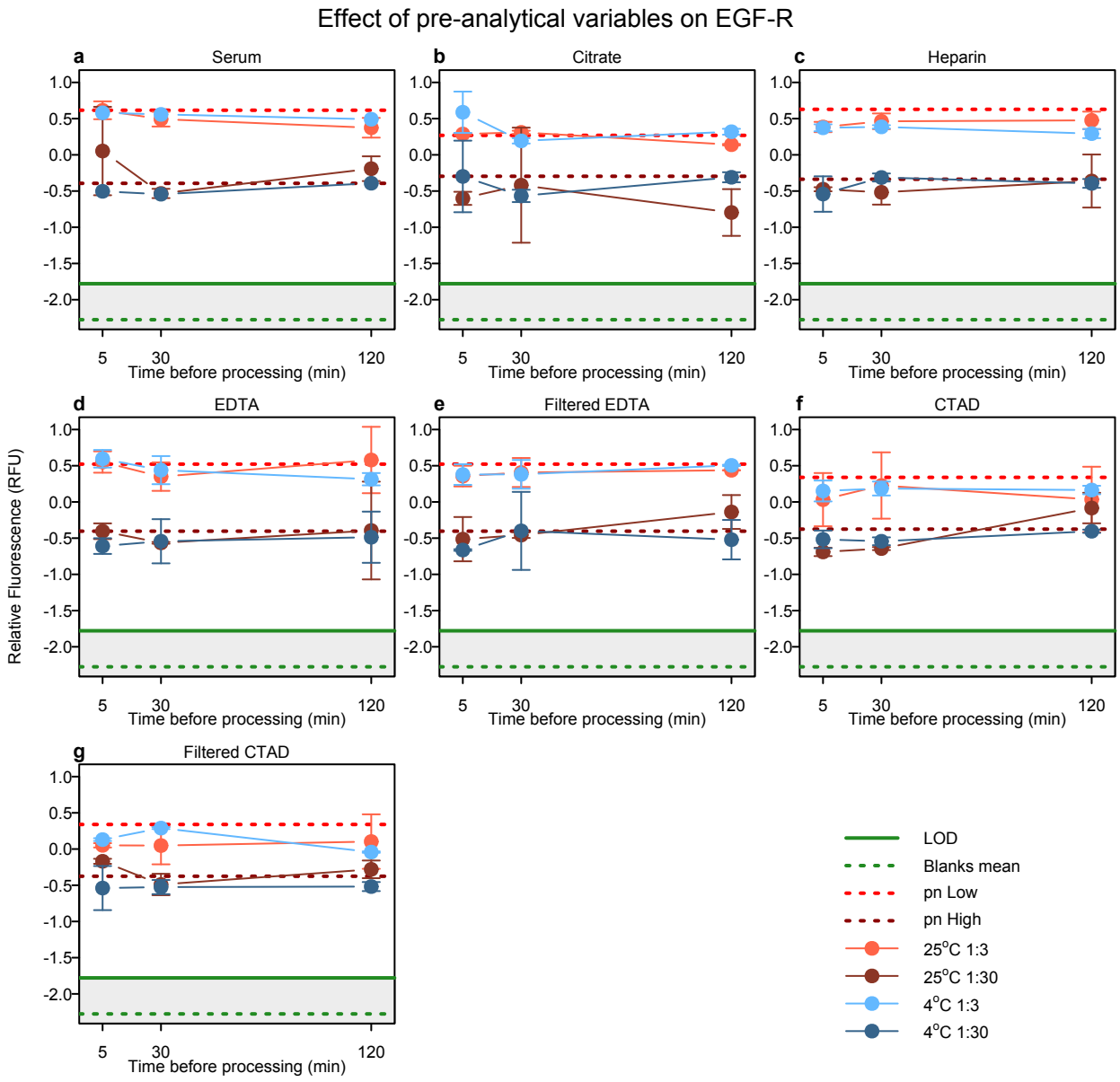

FIGURE I.S41: **Effect of blood collection tube on EGF-R stability and concentration.** Effects of blood collection tubes (**a**: serum, **b**: citrate, **c**: heparin, **d-e**: EDTA, **f-g**: CTAD), storage temperature and time before processing, and post-processing plasma filtering (**e, g**) on the initial value and pre-processing time stability of EGF-R measurements in blood. Information on the dilution of samples used for measuring, data range and the sample type selected are also shown.

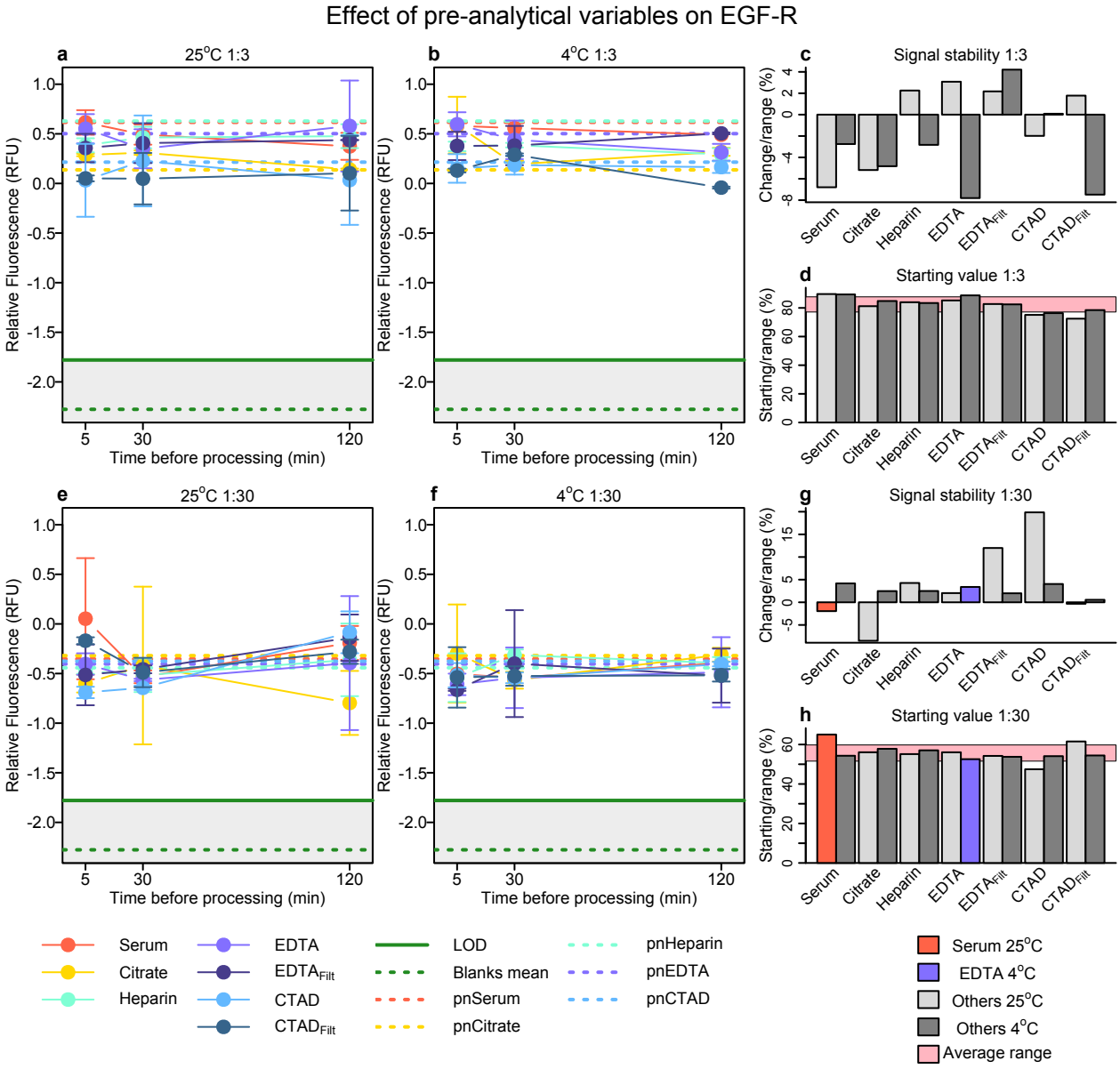

FIGURE I.S42: **Effect of pre-processing storage temperature on EGF-R stability and concentration.** Initial measured value and stability of EGF-R when stored at 25 °C (**a, e**) and 4 °C (**b, f**) before processing when collected in different tube types. The measured values are shown at low dilution of 1:3 (**a-b**) and high dilution of 1:30 (**e-f**). Stability before processing is expressed as an increase or decrease compared to the measurement range and is shown for low (**c**) and high (**g**) dilutions. Initial value is expressed as a portion of the measurement range when the linear regression is extrapolated to zero minutes and is shown for low (**d**) and high (**h**) dilutions. The pink box in graphs **d** and **h** indicate the region that is included by the *mean* ± *SD* of all the initial values and gives an indication of outliers when values lie outside this region. Red and purple bars in **c-d, g-h** are indicated at the measured dilution as the two choices for the TBI analysis.

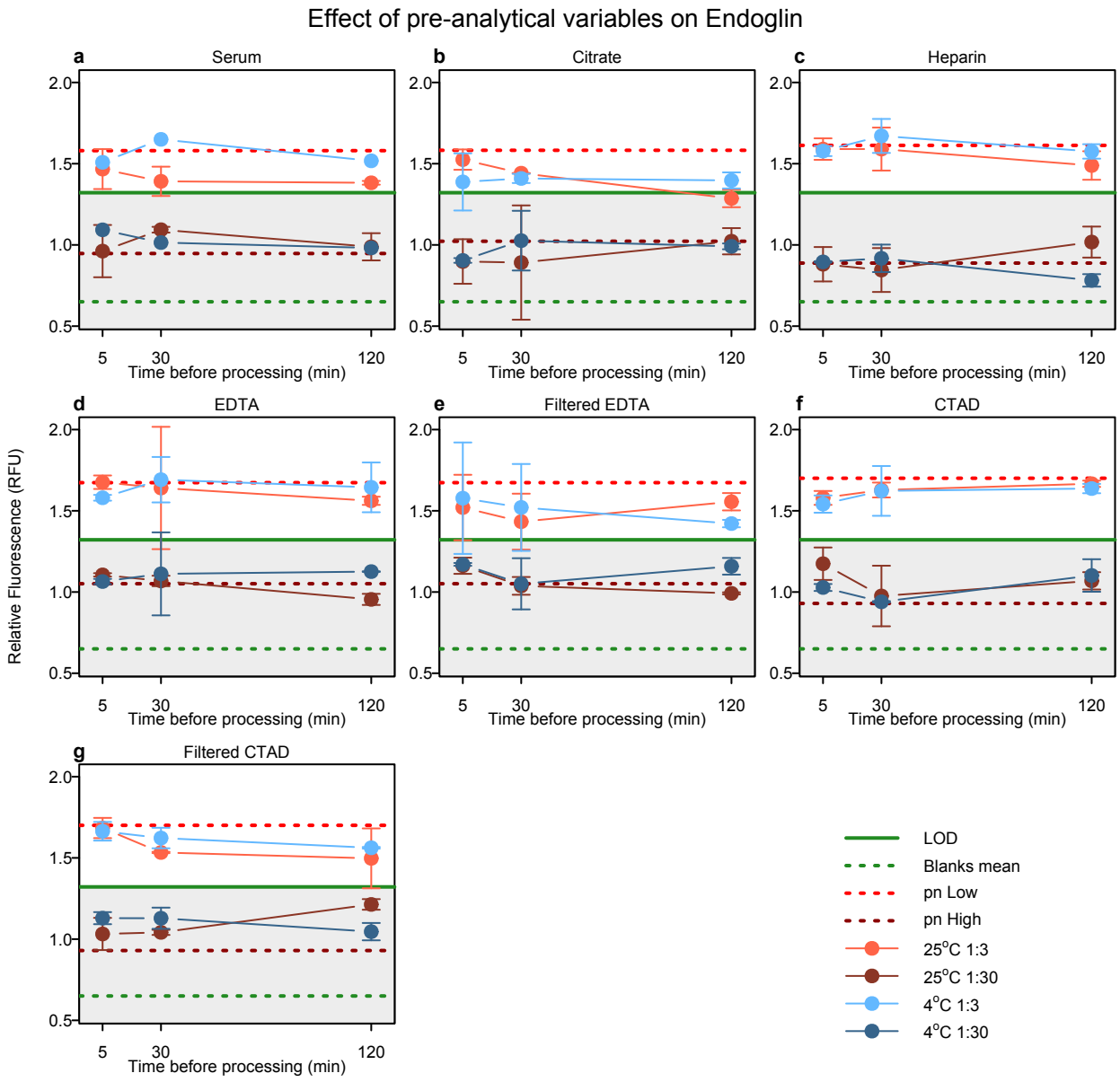

FIGURE I.S43: **Effect of blood collection tube on Endoglin stability and concentration.** Effects of blood collection tubes (**a**: serum, **b**: citrate, **c**: heparin, **d-e**: EDTA, **f-g**: CTAD), storage temperature and time before processing, and post-processing plasma filtering (**e, g**) on the initial value and pre-processing time stability of Endoglin measurements in blood. Information on the dilution of samples used for measuring, data range and the sample type selected are also shown.

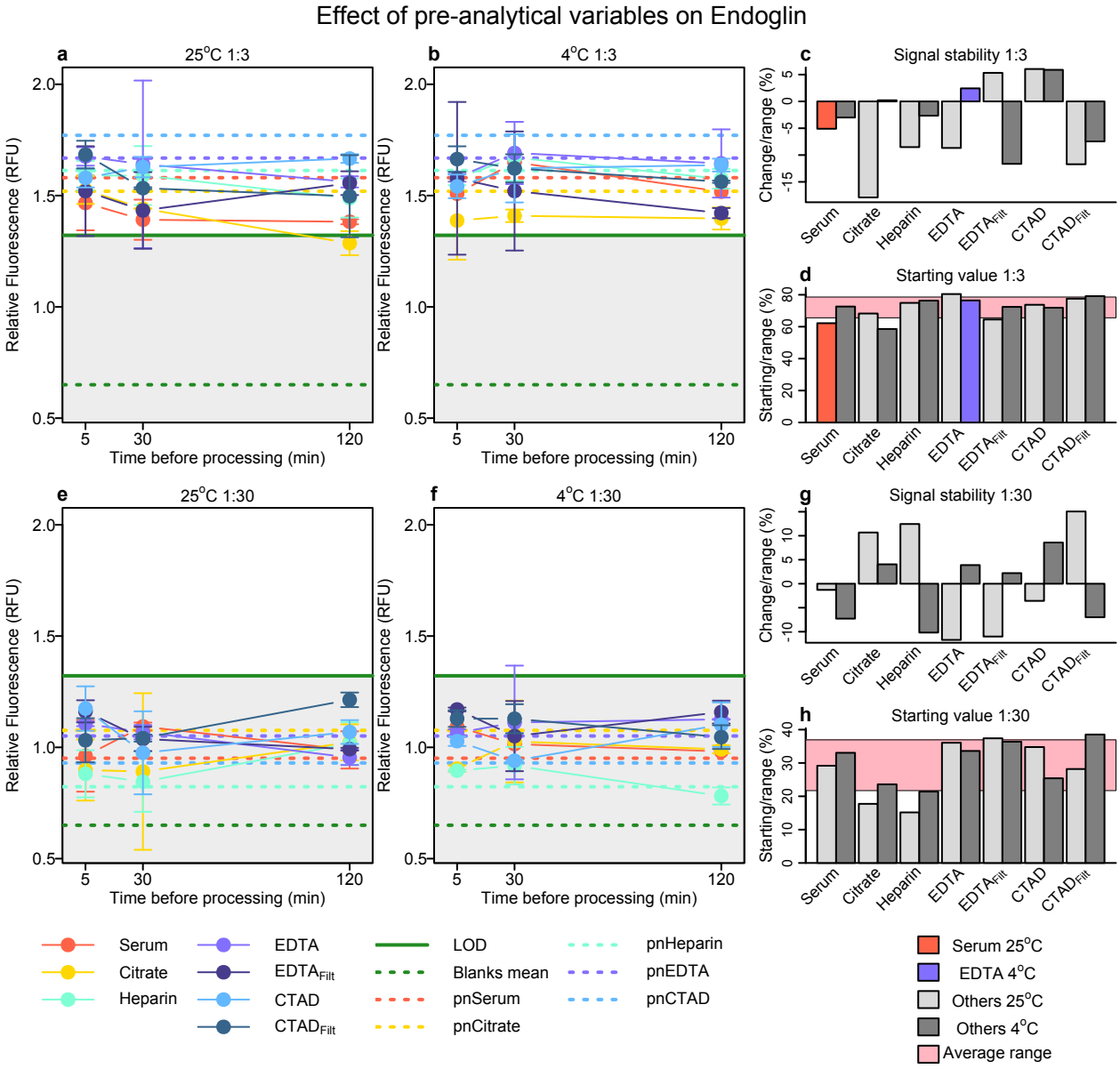

FIGURE I.S44: **Effect of pre-processing storage temperature on Endoglin stability and concentration.** Initial measured value and stability of Endoglin when stored at 25 °C (**a, e**) and 4 °C (**b, f**) before processing when collected in different tube types. The measured values are shown at low dilution of 1:3 (**a-b**) and high dilution of 1:30 (**e-f**). Stability before processing is expressed as an increase or decrease compared to the measurement range and is shown for low (**c**) and high (**g**) dilutions. Initial value is expressed as a portion of the measurement range when the linear regression is extrapolated to zero minutes and is shown for low (**d**) and high (**h**) dilutions. The pink box in graphs **d** and **h** indicate the region that is included by the *mean* ± *SD* of all the initial values and gives an indication of outliers when values lie outside this region. Red and purple bars in **c-d, g-h** are indicated at the measured dilution as the two choices for the TBI analysis.

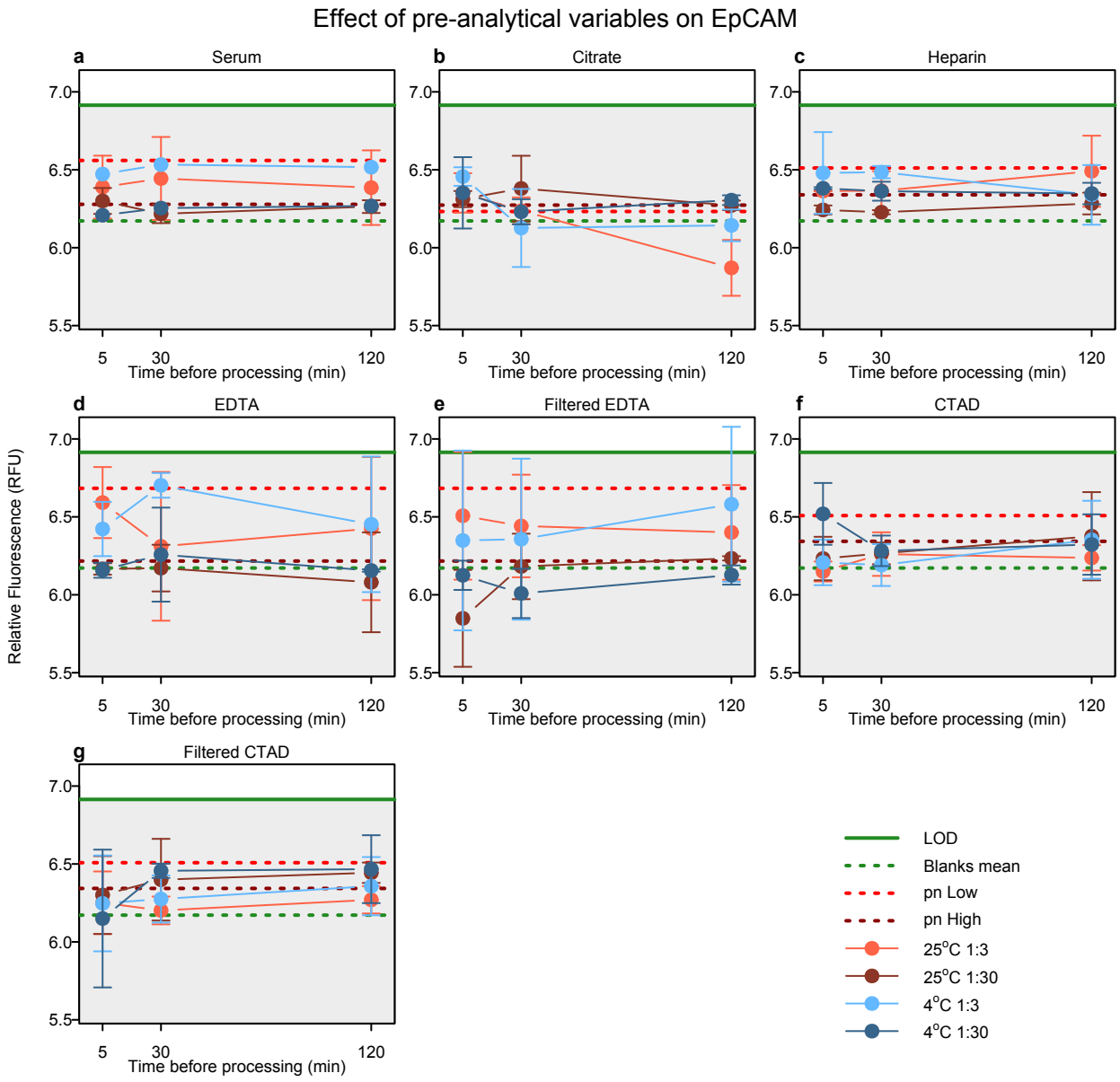

FIGURE I.S45: **Effect of blood collection tube on EpCAM stability and concentration.** Effects of blood collection tubes (**a**: serum, **b**: citrate, **c**: heparin, **d-e**: EDTA, **f-g**: CTAD), storage temperature and time before processing, and post-processing plasma filtering (**e, g**) on the initial value and pre-processing time stability of EpCAM measurements in blood. Information on the dilution of samples used for measuring, data range and the sample type selected are also shown.

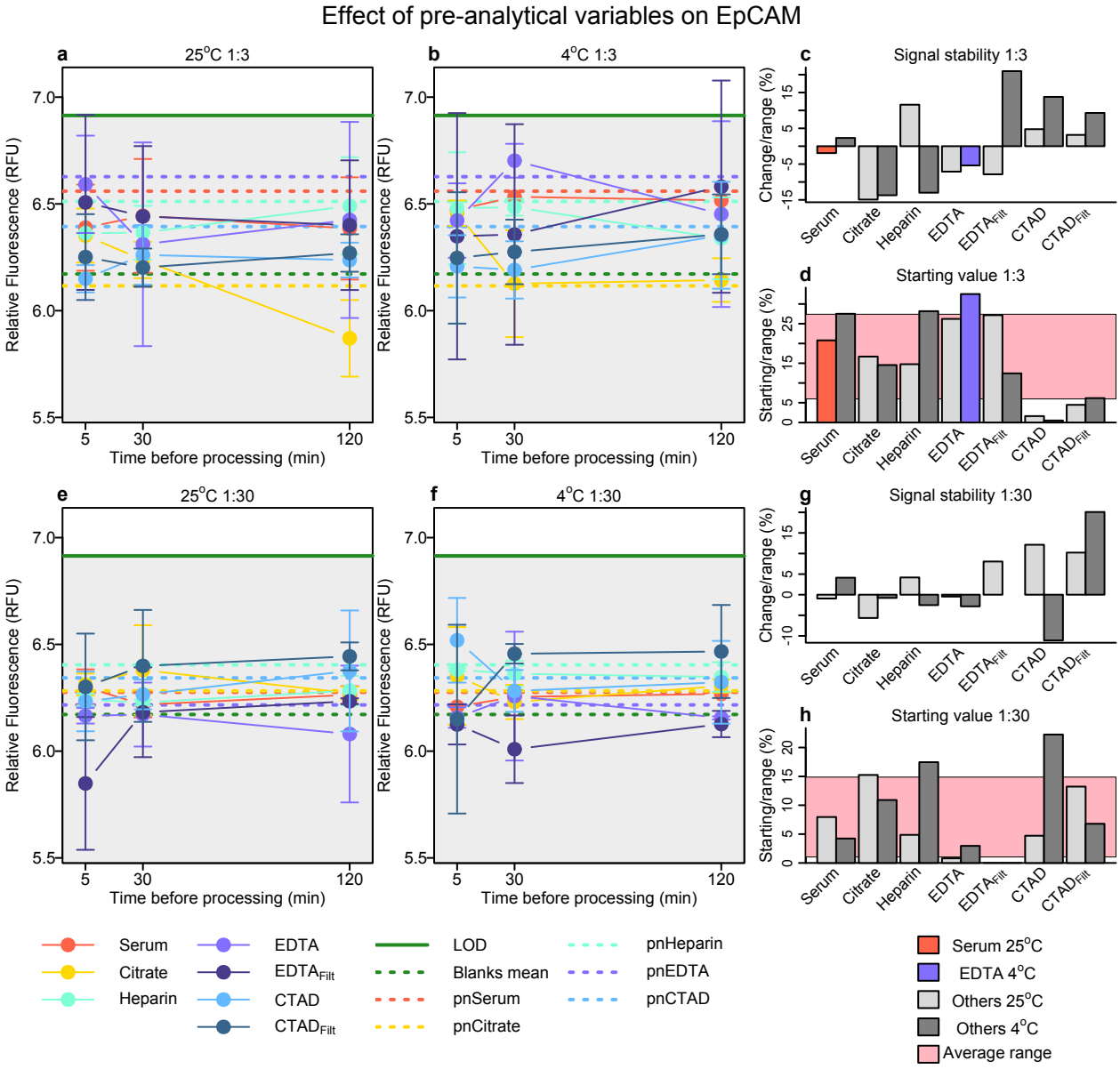

FIGURE I.S46: **Effect of pre-processing storage temperature on EpCAM stability and concentration.** Initial measured value and stability of EpCAM when stored at 25 °C (**a, e**) and 4 °C (**b, f**) before processing when collected in different tube types. The measured values are shown at low dilution of 1:3 (**a-b**) and high dilution of 1:30 (**e-f**). Stability before processing is expressed as an increase or decrease compared to the measurement range and is shown for low (**c**) and high (**g**) dilutions. Initial value is expressed as a portion of the measurement range when the linear regression is extrapolated to zero minutes and is shown for low (**d**) and high (**h**) dilutions. The pink box in graphs **d** and **h** indicate the region that is included by the *mean* ± *SD* of all the initial values and gives an indication of outliers when values lie outside this region. Red and purple bars in **c-d, g-h** are indicated at the measured dilution as the two choices for the TBI analysis.

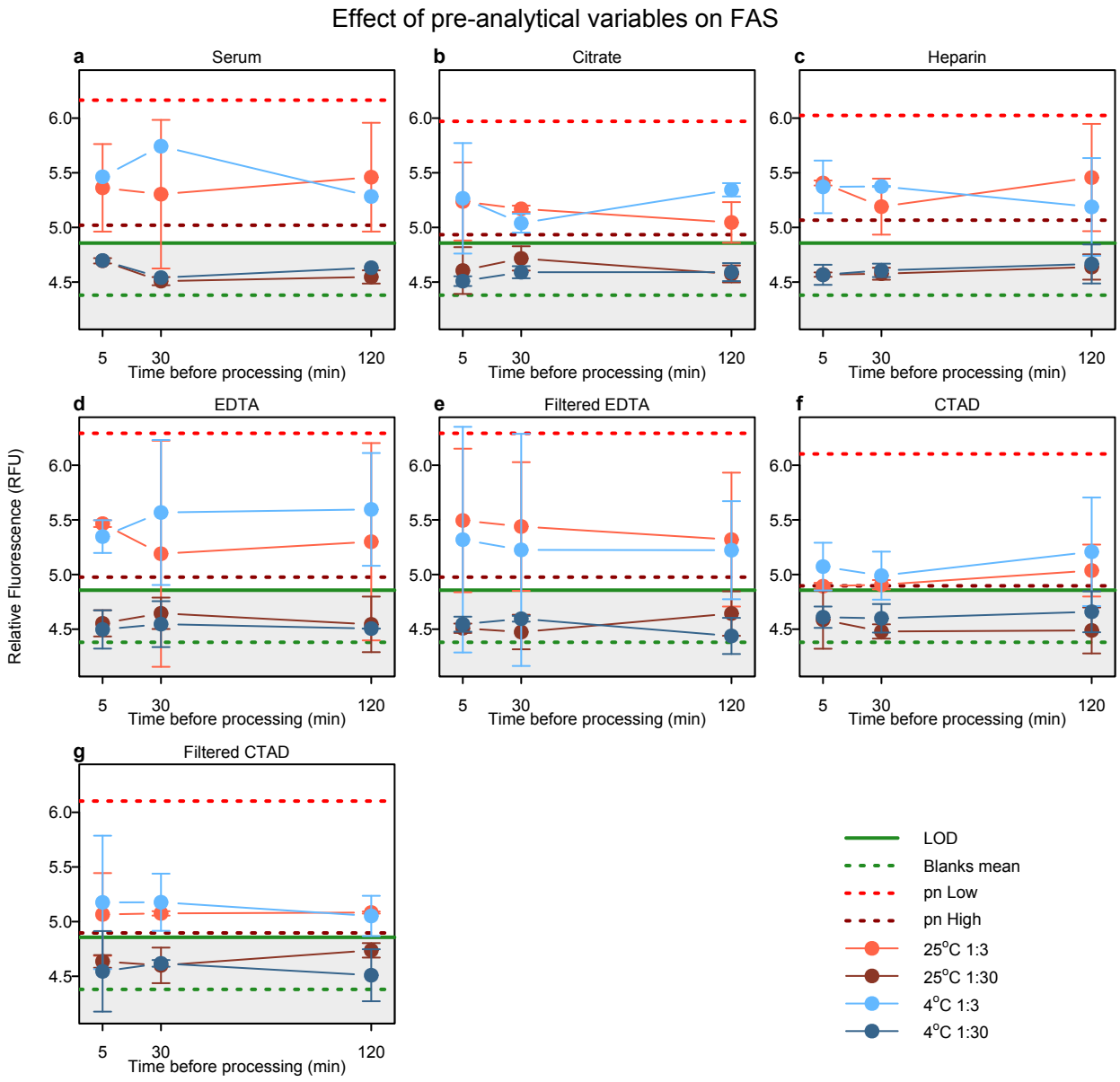

FIGURE I.S47: **Effect of blood collection tube on FAS stability and concentration.** Effects of blood collection tubes (**a**: serum, **b**: citrate, **c**: heparin, **d-e**: EDTA, **f-g**: CTAD), storage temperature and time before processing, and post-processing plasma filtering (**e, g**) on the initial value and pre-processing time stability of FAS measurements in blood. Information on the dilution of samples used for measuring, data range and the sample type selected are also shown.

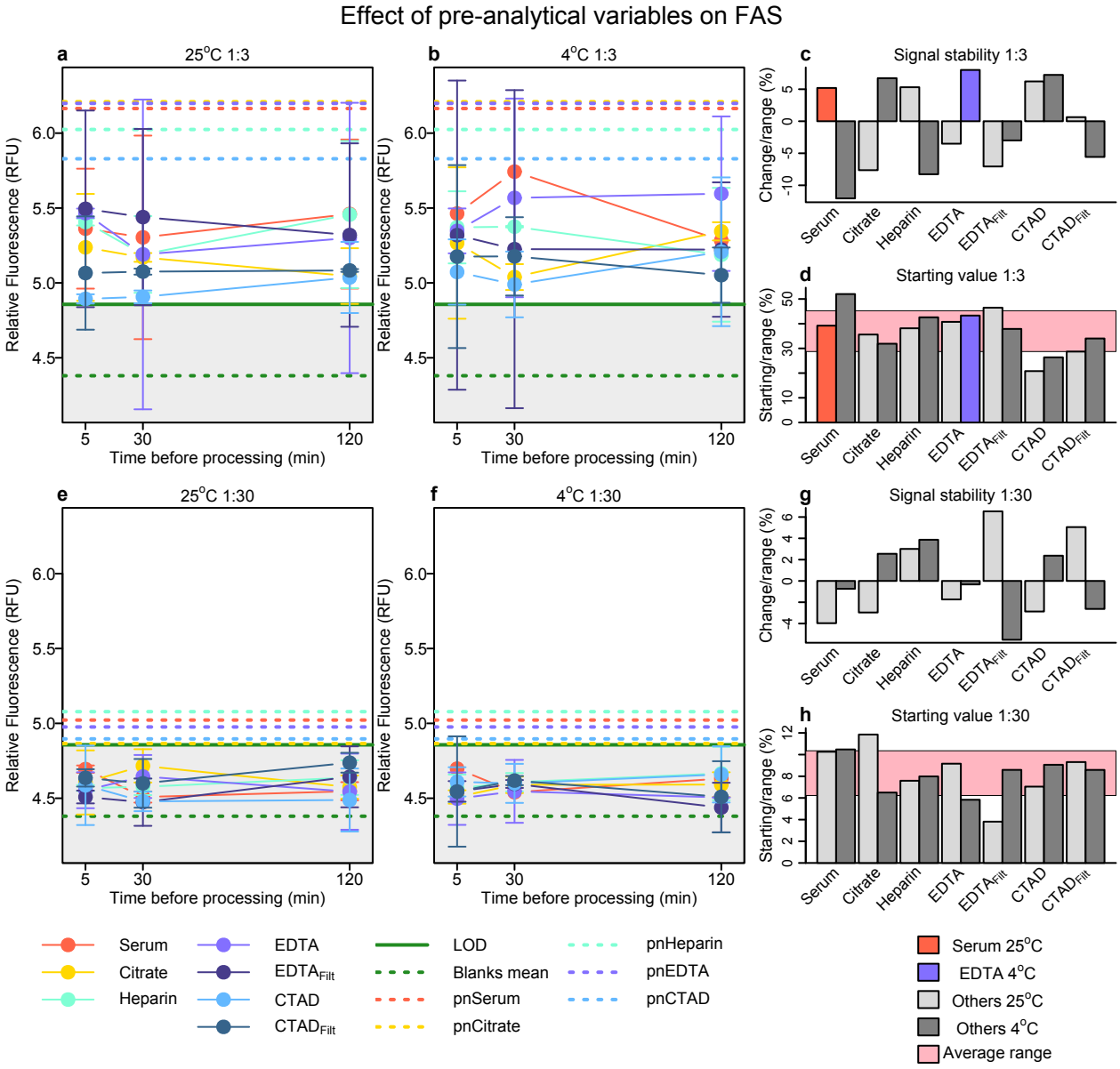

FIGURE I.S48: **Effect of pre-processing storage temperature on FAS stability and concentration.** Initial measured value and stability of FAS when stored at 25 °C (**a, e**) and 4 °C (**b, f**) before processing when collected in different tube types. The measured values are shown at low dilution of 1:3 (**a-b**) and high dilution of 1:30 (**e-f**). Stability before processing is expressed as an increase or decrease compared to the measurement range and is shown for low (**c**) and high (**g**) dilutions. Initial value is expressed as a portion of the measurement range when the linear regression is extrapolated to zero minutes and is shown for low (**d**) and high (**h**) dilutions. The pink box in graphs **d** and **h** indicate the region that is included by the *mean* ± *SD* of all the initial values and gives an indication of outliers when values lie outside this region. Red and purple bars in **c-d, g-h** are indicated at the measured dilution as the two choices for the TBI analysis.

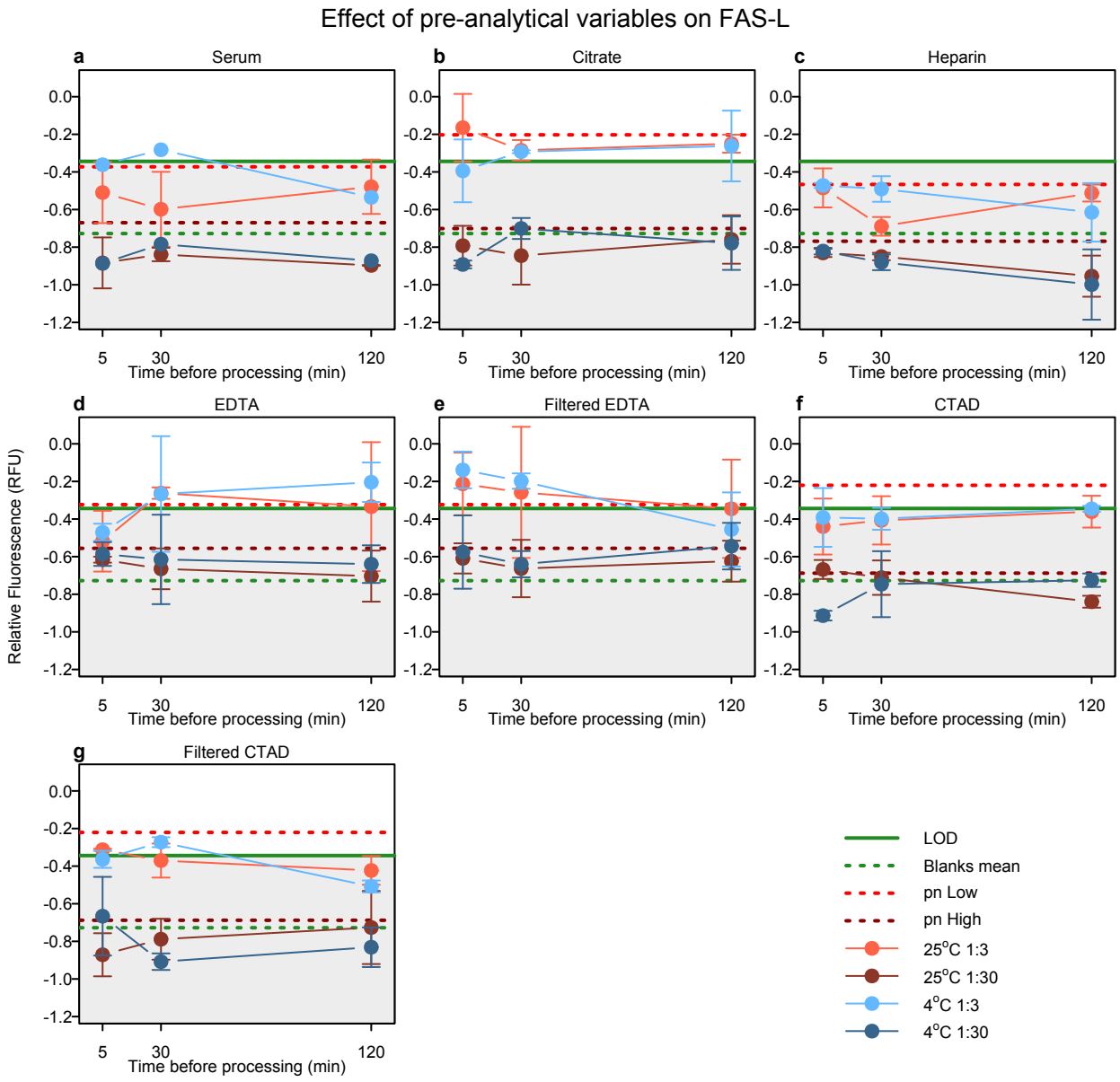

FIGURE I.S49: **Effect of blood collection tube on FAS-L stability and concentration.** Effects of blood collection tubes (**a**: serum, **b**: citrate, **c**: heparin, **d-e**: EDTA, **f-g**: CTAD), storage temperature and time before processing, and post-processing plasma filtering (**e, g**) on the initial value and pre-processing time stability of FAS-L measurements in blood. Information on the dilution of samples used for measuring, data range and the sample type selected are also shown.

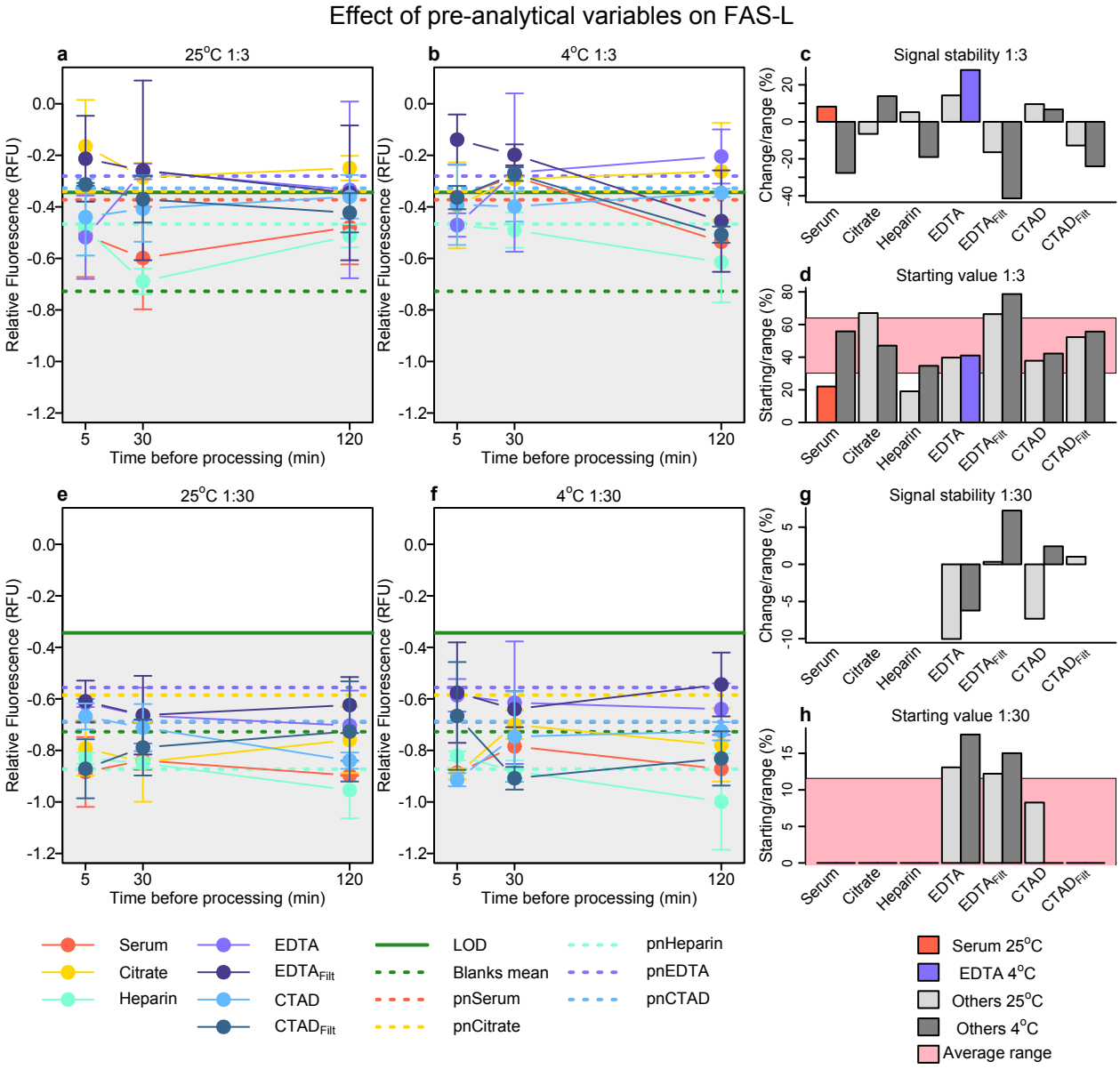

FIGURE I.S50: **Effect of pre-processing storage temperature on FAS-L stability and concentration.** Initial measured value and stability of FAS-L when stored at 25 °C (**a, e**) and 4 °C (**b, f**) before processing when collected in different tube types. The measured values are shown at low dilution of 1:3 (**a-b**) and high dilution of 1:30 (**e-f**). Stability before processing is expressed as an increase or decrease compared to the measurement range and is shown for low (**c**) and high (**g**) dilutions. Initial value is expressed as a portion of the measurement range when the linear regression is extrapolated to zero minutes and is shown for low (**d**) and high (**h**) dilutions. The pink box in graphs **d** and **h** indicate the region that is included by the *mean* ± *SD* of all the initial values and gives an indication of outliers when values lie outside this region. Red and purple bars in **c-d, g-h** are indicated at the measured dilution as the two choices for the TBI analysis.

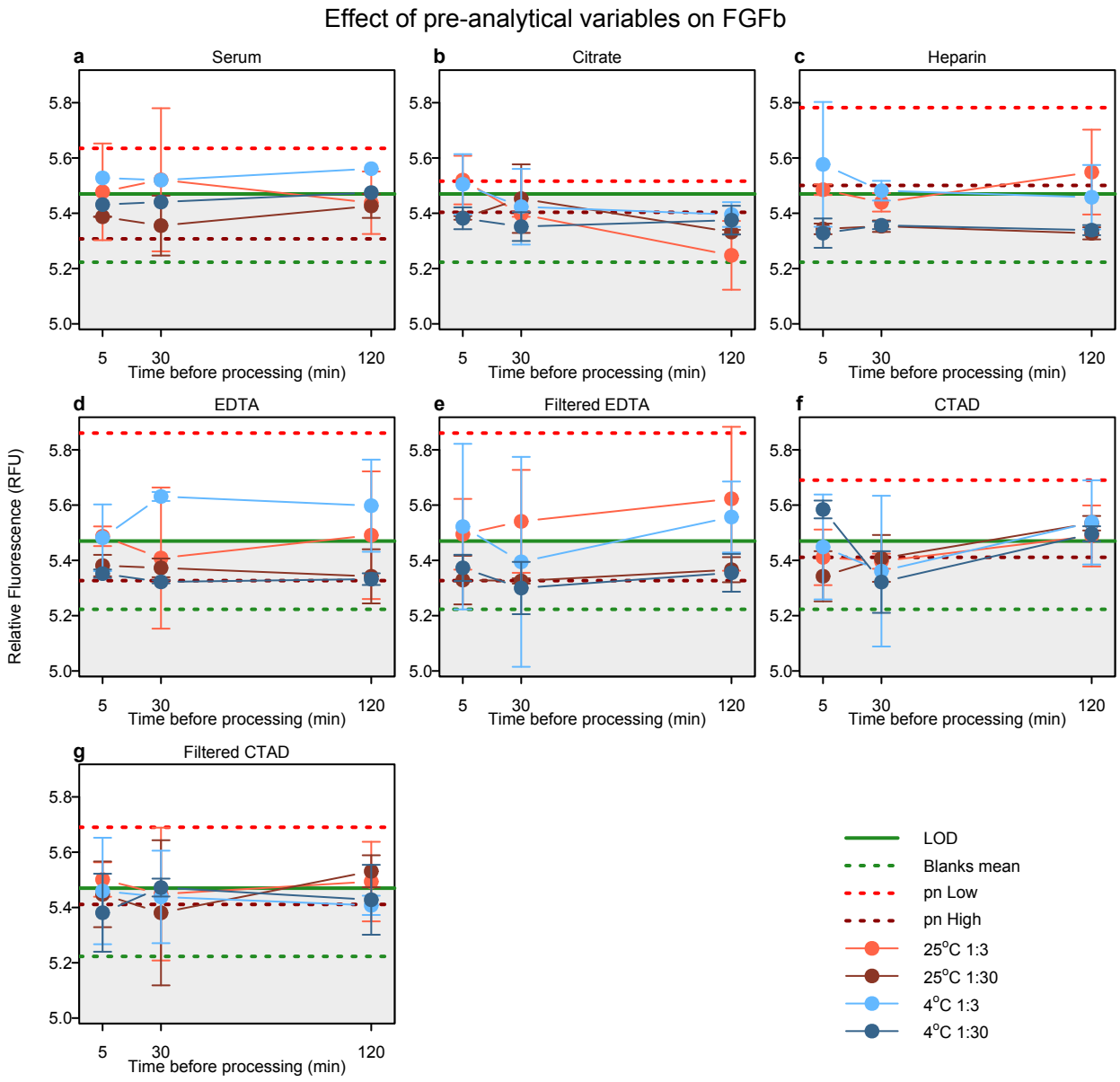

FIGURE I.S51: **Effect of blood collection tube on FGFb stability and concentration.** Effects of blood collection tubes (**a**: serum, **b**: citrate, **c**: heparin, **d-e**: EDTA, **f-g**: CTAD), storage temperature and time before processing, and post-processing plasma filtering (**e, g**) on the initial value and pre-processing time stability of FGFb measurements in blood. Information on the dilution of samples used for measuring, data range and the sample type selected are also shown.

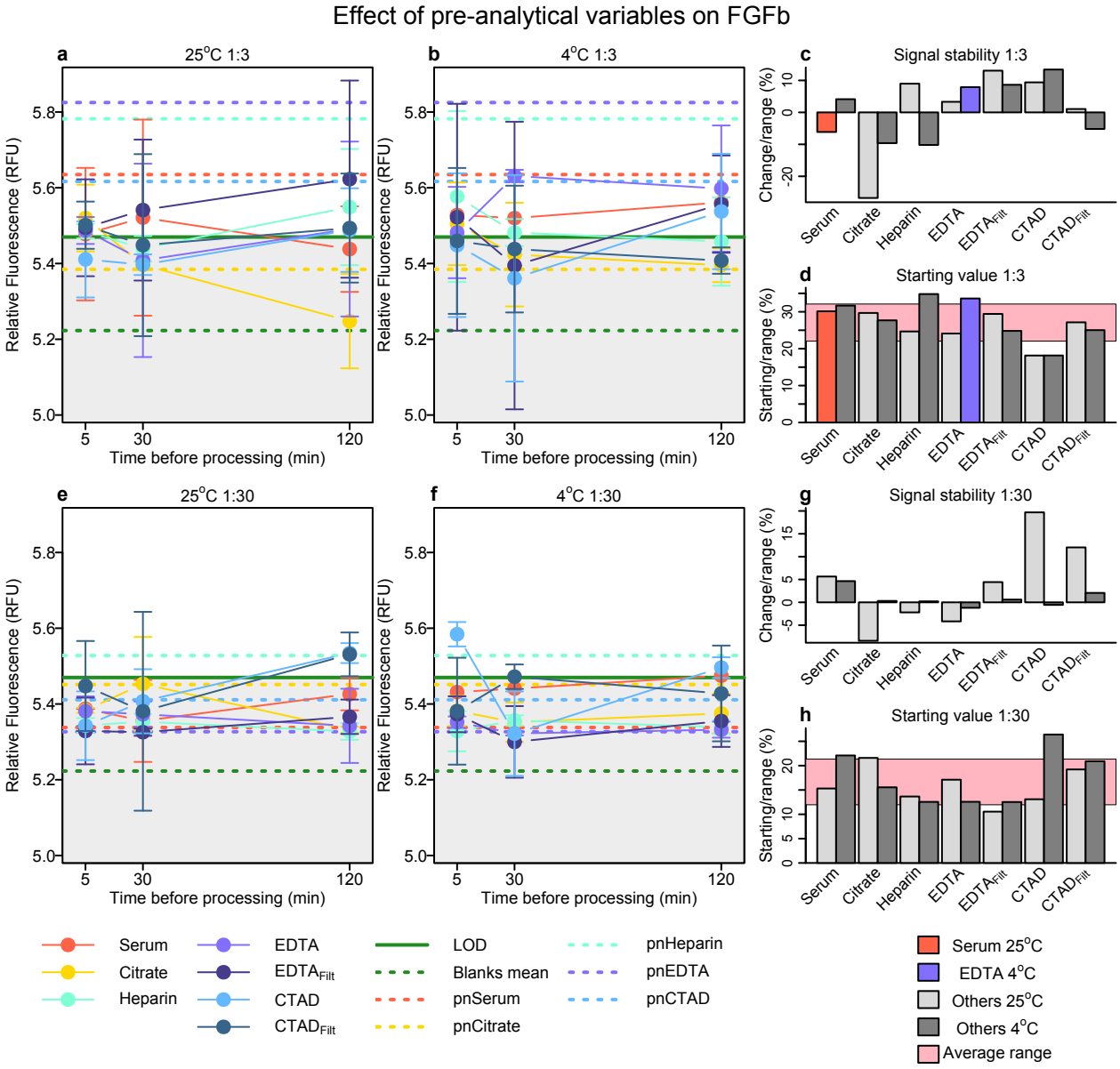

FIGURE I.S52: **Effect of pre-processing storage temperature on FGFb stability and concentration.** Initial measured value and stability of FGFb when stored at 25 °C (**a, e**) and 4 °C (**b, f**) before processing when collected in different tube types. The measured values are shown at low dilution of 1:3 (**a-b**) and high dilution of 1:30 (**e-f**). Stability before processing is expressed as an increase or decrease compared to the measurement range and is shown for low (**c**) and high (**g**) dilutions. Initial value is expressed as a portion of the measurement range when the linear regression is extrapolated to zero minutes and is shown for low (**d**) and high (**h**) dilutions. The pink box in graphs **d** and **h** indicate the region that is included by the *mean* ± *SD* of all the initial values and gives an indication of outliers when values lie outside this region. Red and purple bars in **c-d, g-h** are indicated at the measured dilution as the two choices for the TBI analysis.

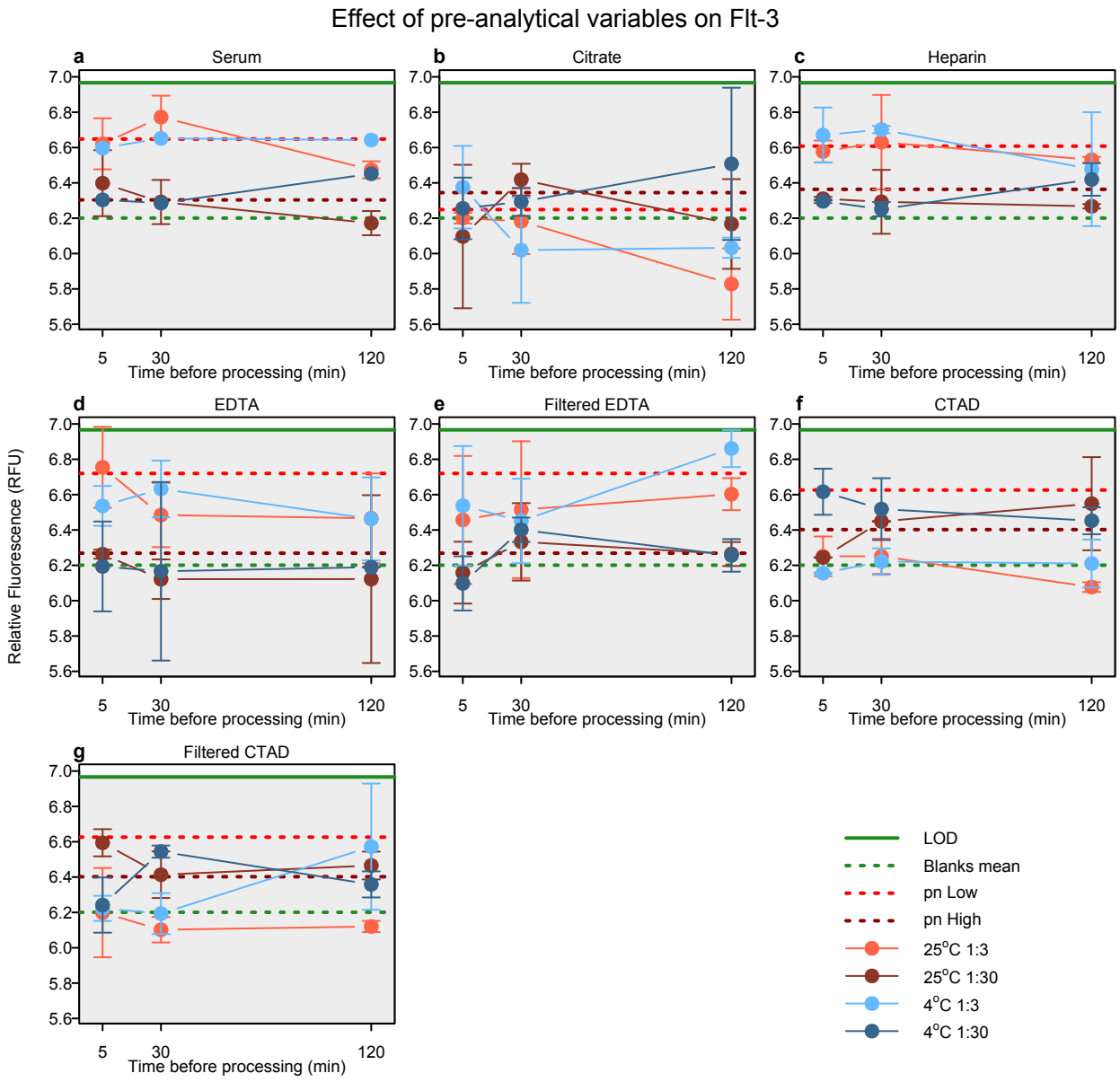

FIGURE I.S53: **Effect of blood collection tube on Flt-3 stability and concentration.** Effects of blood collection tubes (**a**: serum, **b**: citrate, **c**: heparin, **d-e**: EDTA, **f-g**: CTAD), storage temperature and time before processing, and post-processing plasma filtering (**e, g**) on the initial value and pre-processing time stability of Flt-3 measurements in blood. Information on the dilution of samples used for measuring, data range and the sample type selected are also shown.

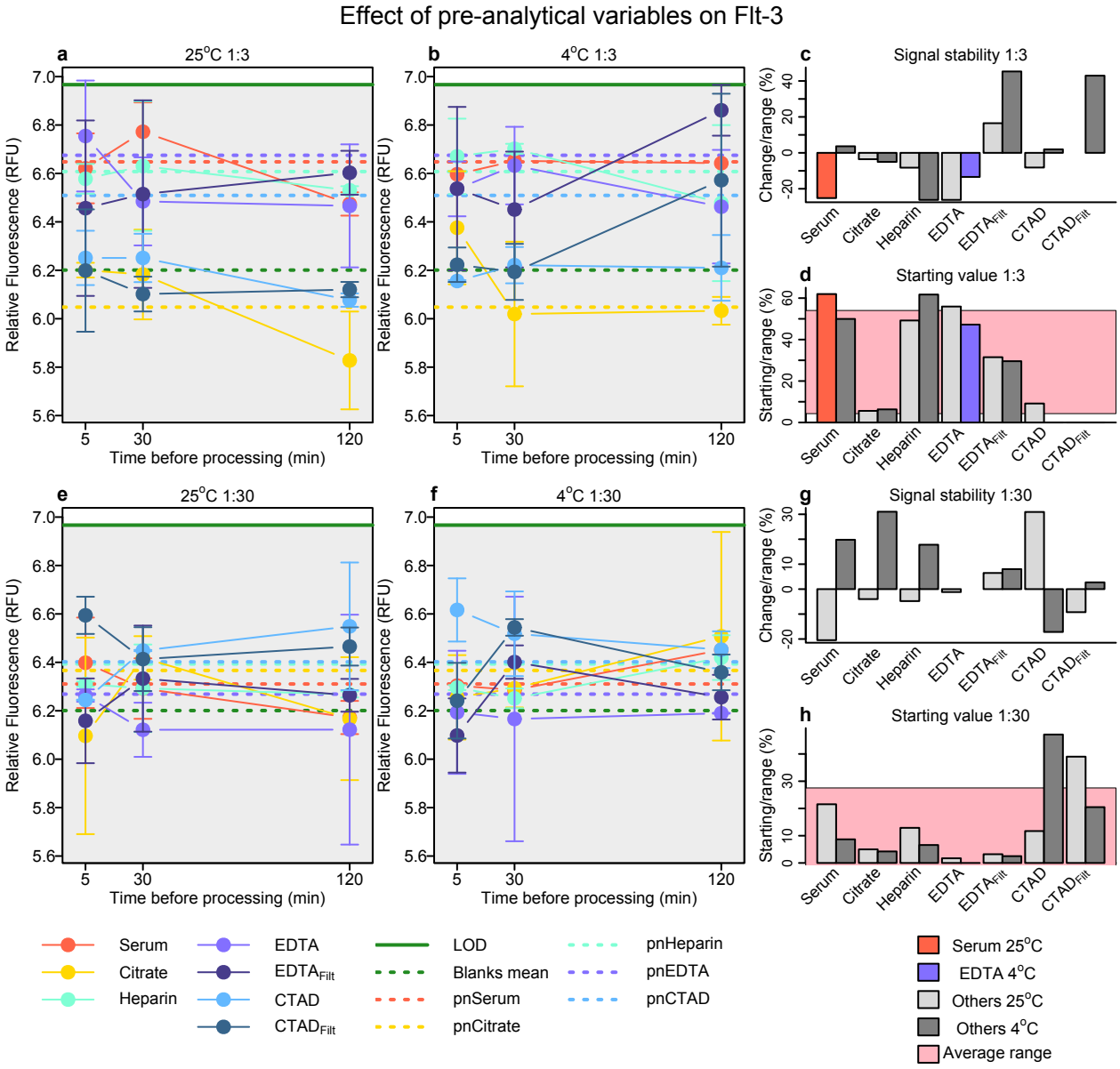

FIGURE I.S54: **Effect of pre-processing storage temperature on Flt-3 stability and concentration.** Initial measured value and stability of Flt-3 when stored at 25 °C (**a, e**) and 4 °C (**b, f**) before processing when collected in different tube types. The measured values are shown at low dilution of 1:3 (**a-b**) and high dilution of 1:30 (**e-f**). Stability before processing is expressed as an increase or decrease compared to the measurement range and is shown for low (**c**) and high (**g**) dilutions. Initial value is expressed as a portion of the measurement range when the linear regression is extrapolated to zero minutes and is shown for low (**d**) and high (**h**) dilutions. The pink box in graphs **d** and **h** indicate the region that is included by the *mean* ± *SD* of all the initial values and gives an indication of outliers when values lie outside this region. Red and purple bars in **c-d, g-h** are indicated at the measured dilution as the two choices for the TBI analysis.

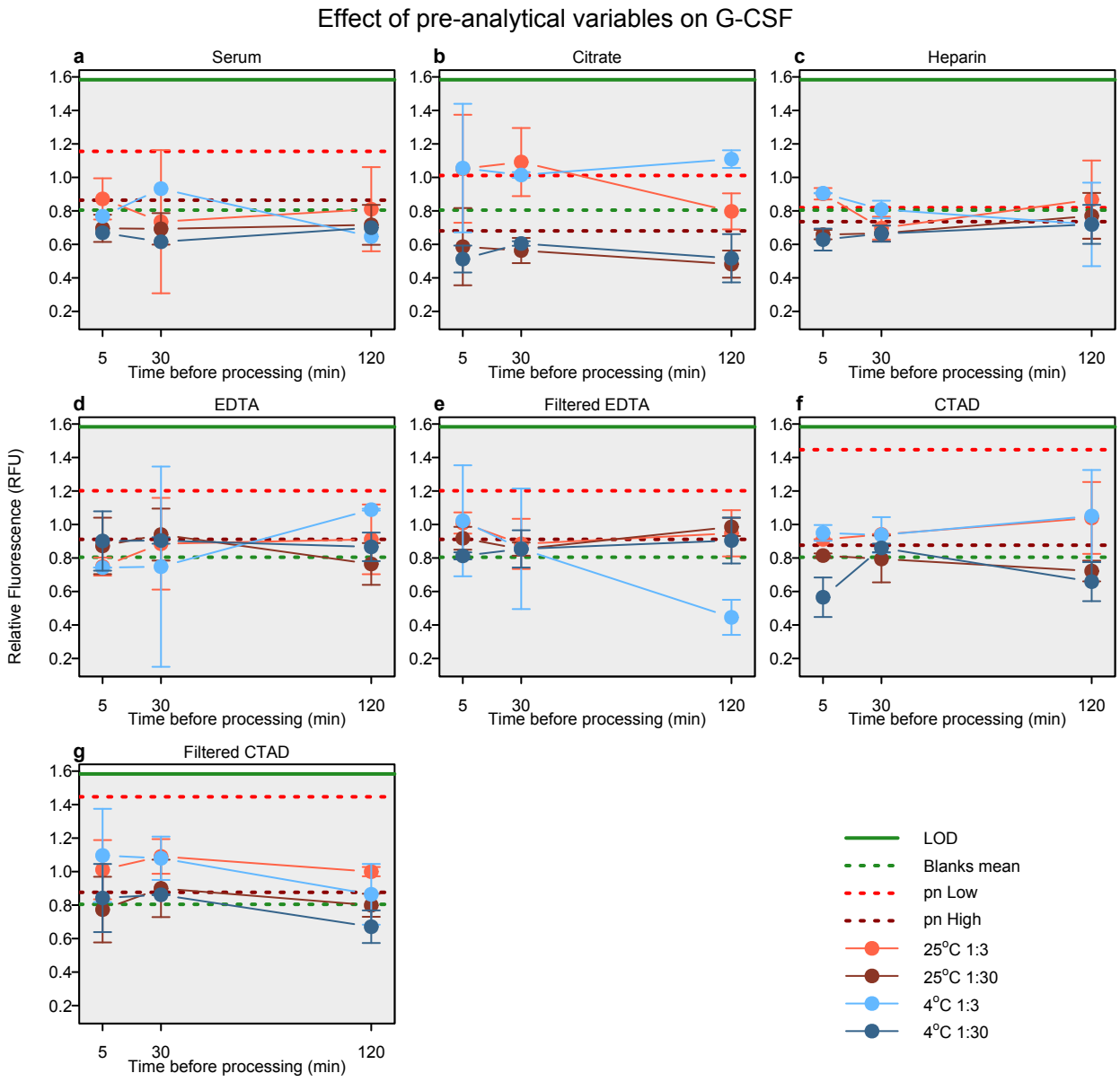

FIGURE I.S55: **Effect of blood collection tube on G-CSF stability and concentration.** Effects of blood collection tubes (**a**: serum, **b**: citrate, **c**: heparin, **d-e**: EDTA, **f-g**: CTAD), storage temperature and time before processing, and post-processing plasma filtering (**e, g**) on the initial value and pre-processing time stability of G-CSF measurements in blood. Information on the dilution of samples used for measuring, data range and the sample type selected are also shown.

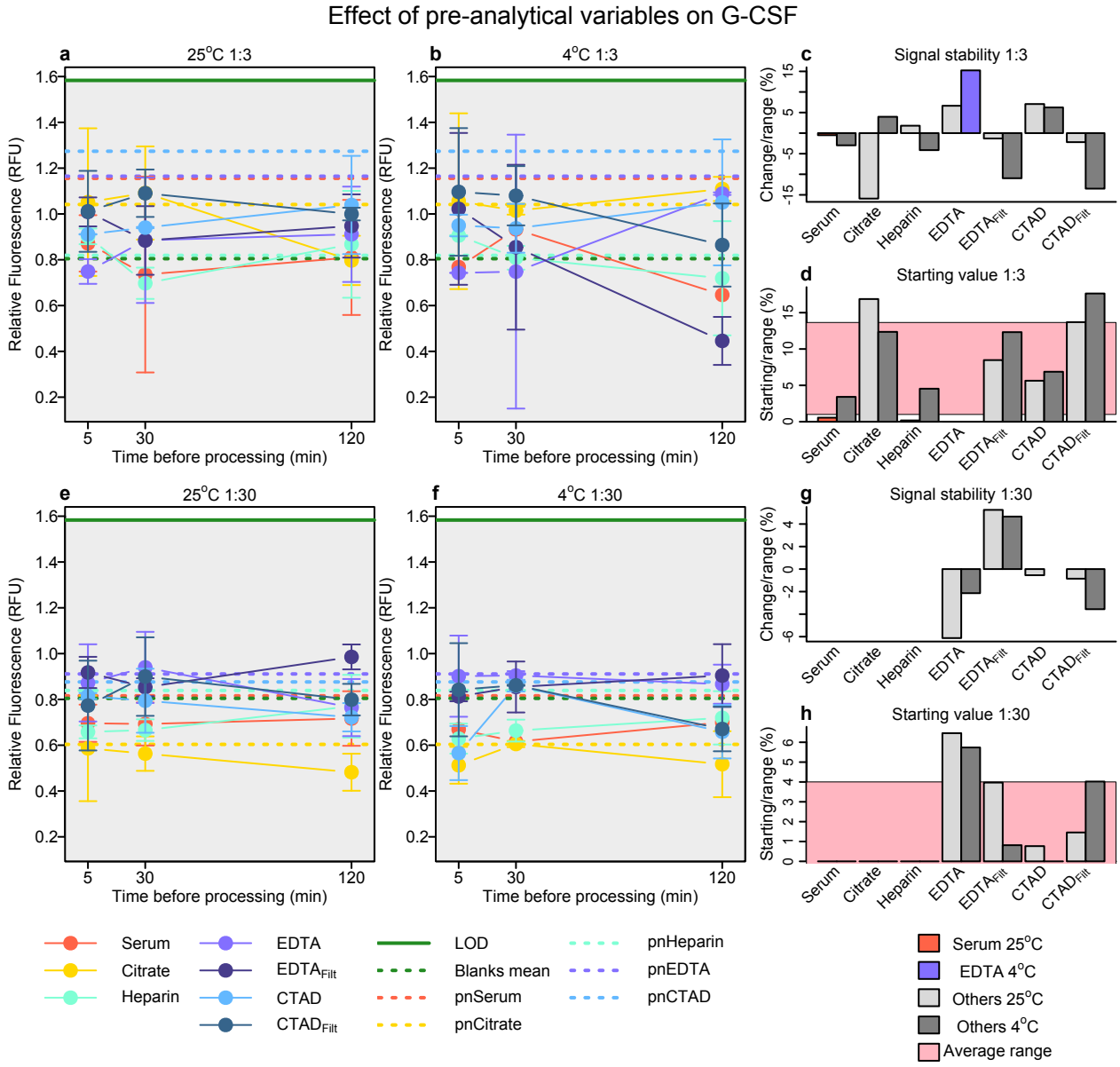

FIGURE I.S56: **Effect of pre-processing storage temperature on G-CSF stability and concentration.** Initial measured value and stability of G-CSF when stored at 25 °C (**a, e**) and 4 °C (**b, f**) before processing when collected in different tube types. The measured values are shown at low dilution of 1:3 (**a-b**) and high dilution of 1:30 (**e-f**). Stability before processing is expressed as an increase or decrease compared to the measurement range and is shown for low (**c**) and high (**g**) dilutions. Initial value is expressed as a portion of the measurement range when the linear regression is extrapolated to zero minutes and is shown for low (**d**) and high (**h**) dilutions. The pink box in graphs **d** and **h** indicate the region that is included by the *mean* ± *SD* of all the initial values and gives an indication of outliers when values lie outside this region. Red and purple bars in **c-d, g-h** are indicated at the measured dilution as the two choices for the TBI analysis.

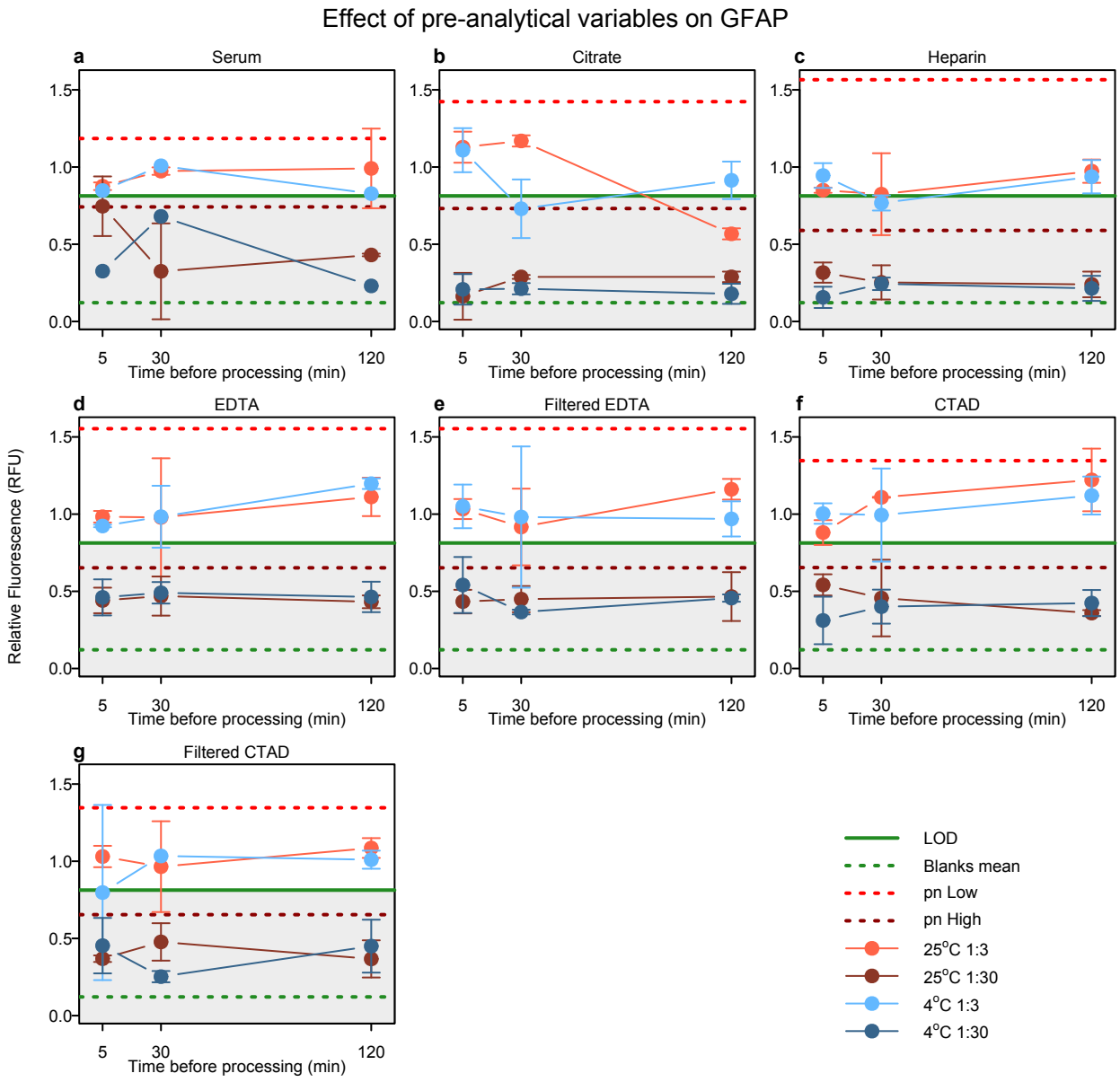

FIGURE I.S57: **Effect of blood collection tube on GFAP stability and concentration.** Effects of blood collection tubes (**a**: serum, **b**: citrate, **c**: heparin, **d-e**: EDTA, **f-g**: CTAD), storage temperature and time before processing, and post-processing plasma filtering (**e, g**) on the initial value and pre-processing time stability of GFAP measurements in blood. Information on the dilution of samples used for measuring, data range and the sample type selected are also shown.

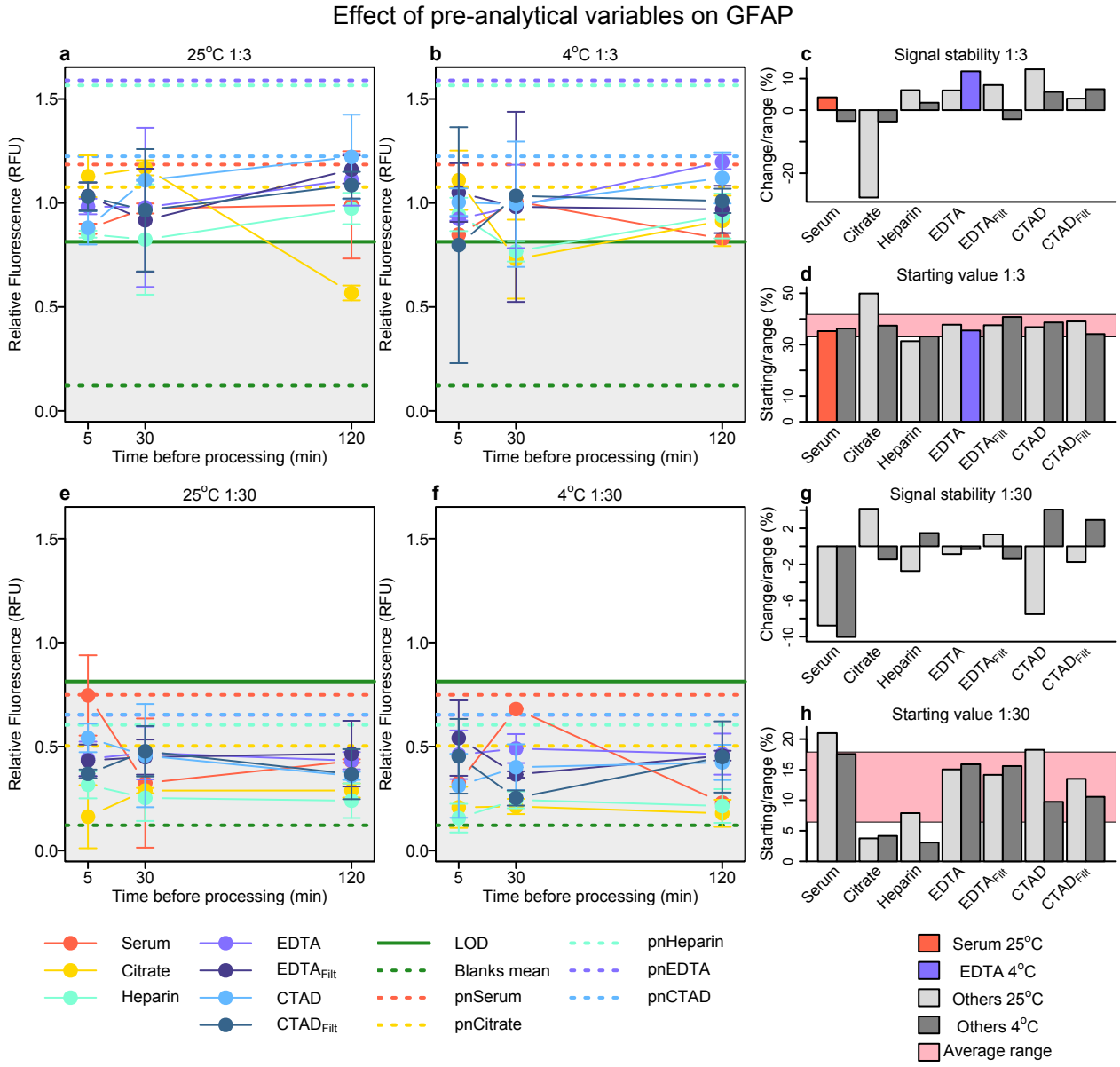

FIGURE I.S58: **Effect of pre-processing storage temperature on GFAP stability and concentration.** Initial measured value and stability of GFAP when stored at 25 °C (**a, e**) and 4 °C (**b, f**) before processing when collected in different tube types. The measured values are shown at low dilution of 1:3 (**a-b**) and high dilution of 1:30 (**e-f**). Stability before processing is expressed as an increase or decrease compared to the measurement range and is shown for low (**c**) and high (**g**) dilutions. Initial value is expressed as a portion of the measurement range when the linear regression is extrapolated to zero minutes and is shown for low (**d**) and high (**h**) dilutions. The pink box in graphs **d** and **h** indicate the region that is included by the *mean* ± *SD* of all the initial values and gives an indication of outliers when values lie outside this region. Red and purple bars in **c-d, g-h** are indicated at the measured dilution as the two choices for the TBI analysis.

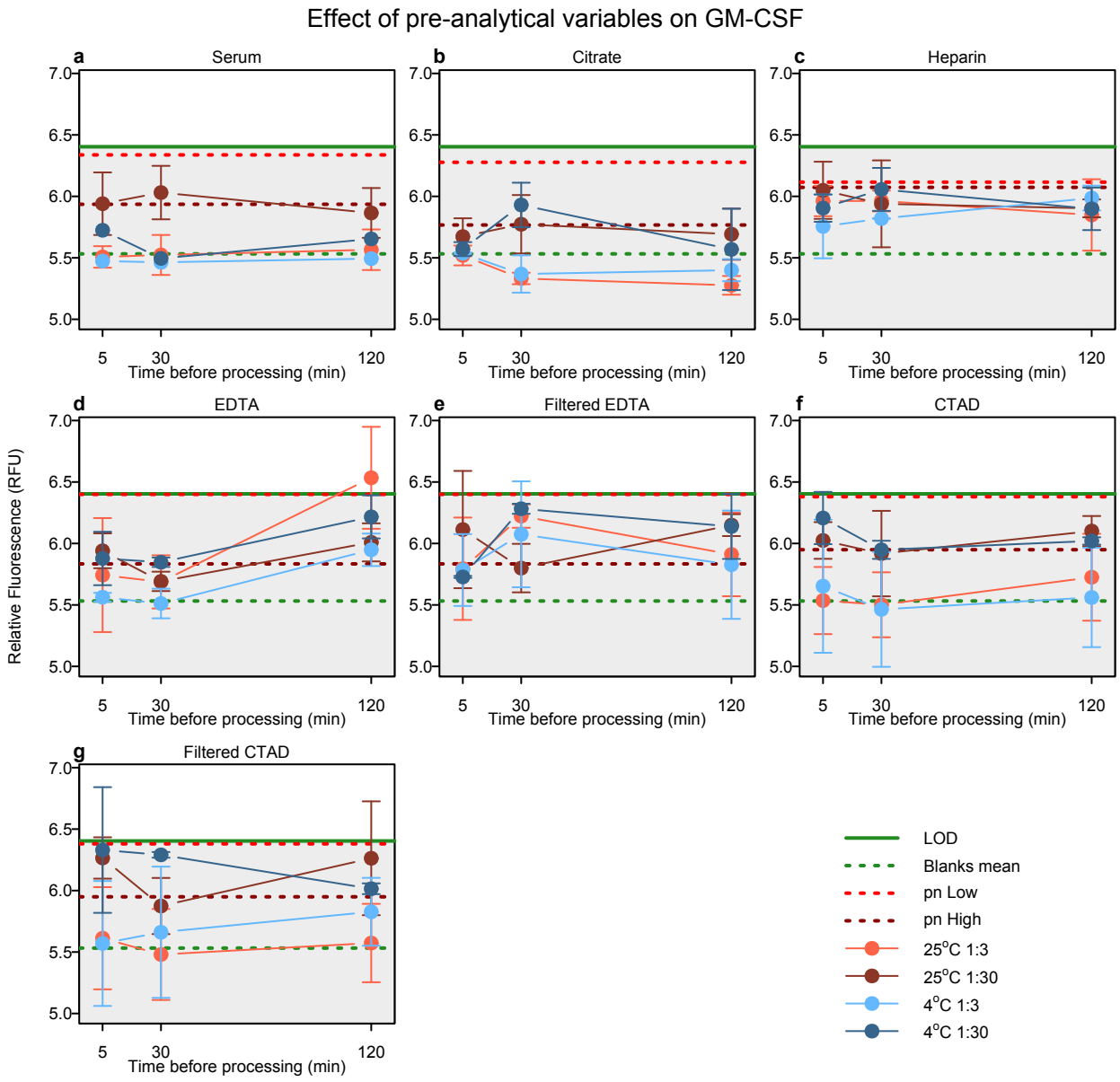

FIGURE I.S59: **Effect of blood collection tube on GM-CSF stability and concentration.** Effects of blood collection tubes (**a**: serum, **b**: citrate, **c**: heparin, **d-e**: EDTA, **f-g**: CTAD), storage temperature and time before processing, and post-processing plasma filtering (**e, g**) on the initial value and pre-processing time stability of GM-CSF measurements in blood. Information on the dilution of samples used for measuring, data range and the sample type selected are also shown.

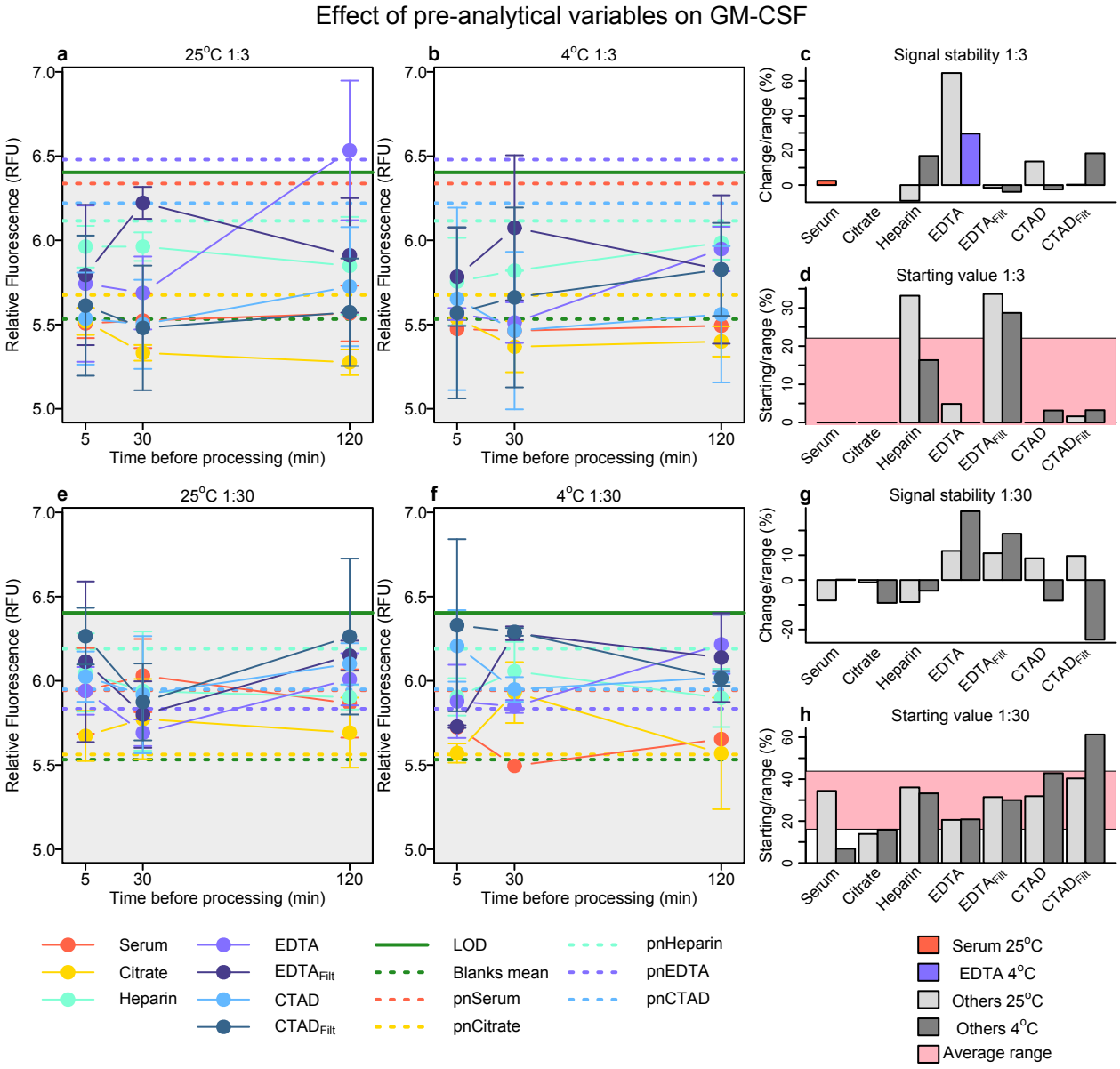

FIGURE I.S60: **Effect of pre-processing storage temperature on GM-CSF stability and concentration.** Initial measured value and stability of GM-CSF when stored at 25 °C (**a, e**) and 4 °C (**b, f**) before processing when collected in different tube types. The measured values are shown at low dilution of 1:3 (**a-b**) and high dilution of 1:30 (**e-f**). Stability before processing is expressed as an increase or decrease compared to the measurement range and is shown for low (**c**) and high (**g**) dilutions. Initial value is expressed as a portion of the measurement range when the linear regression is extrapolated to zero minutes and is shown for low (**d**) and high (**h**) dilutions. The pink box in graphs **d** and **h** indicate the region that is included by the *mean* ± *SD* of all the initial values and gives an indication of outliers when values lie outside this region. Red and purple bars in **c-d, g-h** are indicated at the measured dilution as the two choices for the TBI analysis.

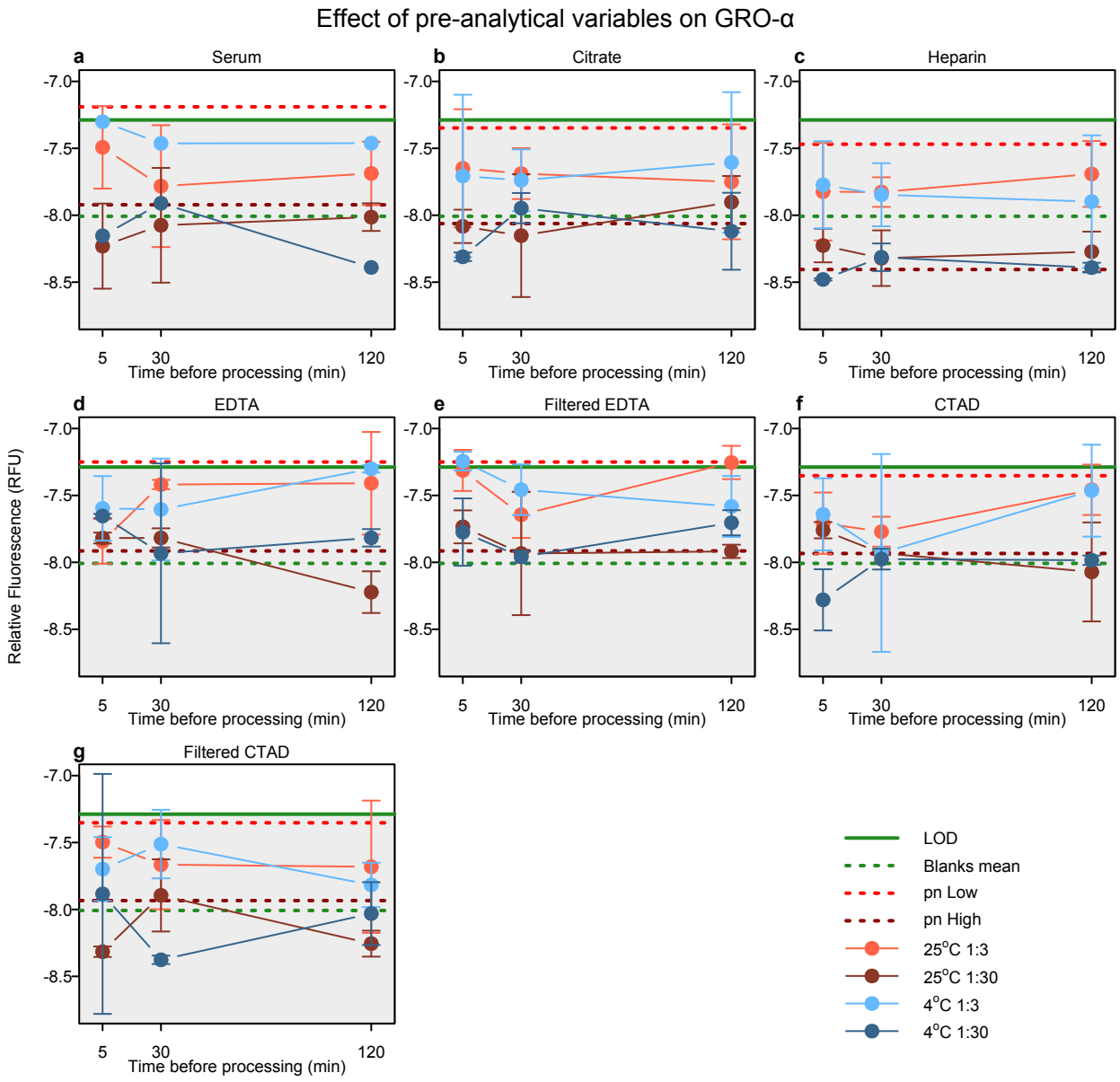

FIGURE I.S61: **Effect of blood collection tube on GRO-α stability and concentration.** Effects of blood collection tubes (**a**: serum, **b**: citrate, **c**: heparin, **d-e**: EDTA, **f-g**: CTAD), storage temperature and time before processing, and post-processing plasma filtering (**e, g**) on the initial value and pre-processing time stability of GRO-α measurements in blood. Information on the dilution of samples used for measuring, data range and the sample type selected are also shown.

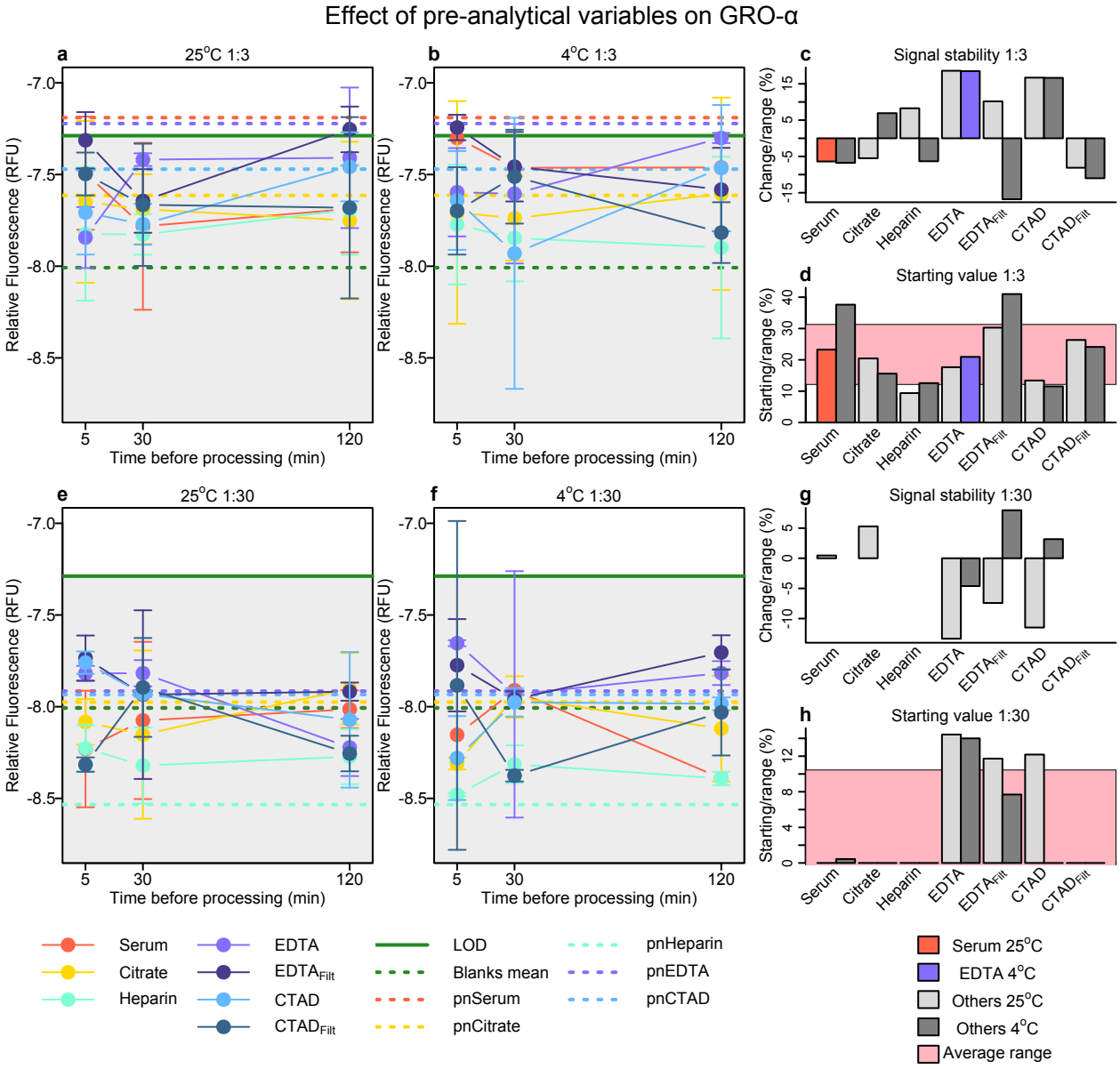

FIGURE I.S62: **Effect of pre-processing storage temperature on GRO-α stability and concentration.** Initial measured value and stability of GRO-α when stored at 25 °C (**a, e**) and 4 °C (**b, f**) before processing when collected in different tube types. The measured values are shown at low dilution of 1:3 (**a-b**) and high dilution of 1:30 (**e-f**). Stability before processing is expressed as an increase or decrease compared to the measurement range and is shown for low (**c**) and high (**g**) dilutions. Initial value is expressed as a portion of the measurement range when the linear regression is extrapolated to zero minutes and is shown for low (**d**) and high (**h**) dilutions. The pink box in graphs **d** and **h** indicate the region that is included by the *mean* ± *SD* of all the initial values and gives an indication of outliers when values lie outside this region. Red and purple bars in **c-d, g-h** are indicated at the measured dilution as the two choices for the TBI analysis.

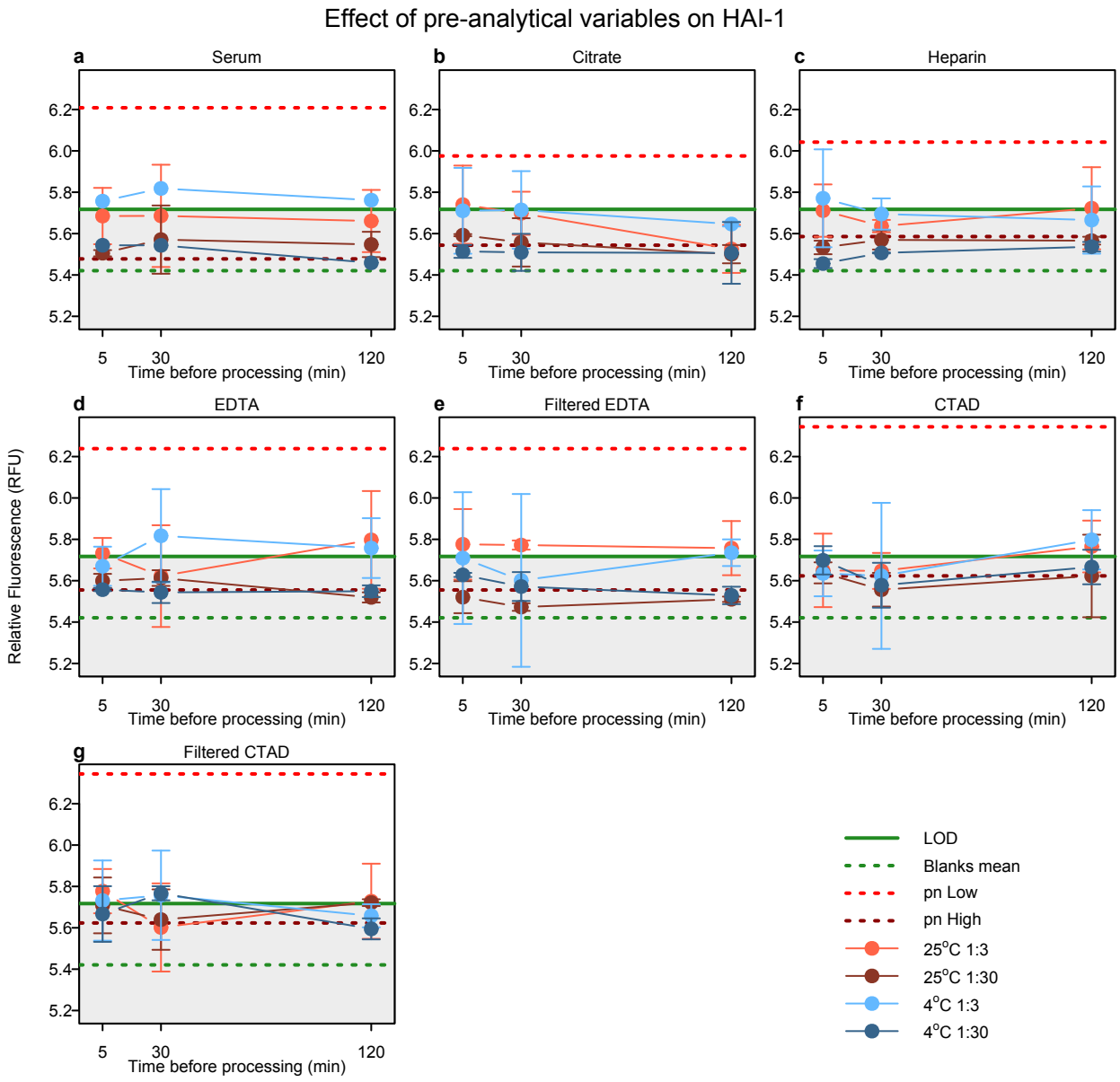

FIGURE I.S63: **Effect of blood collection tube on HAI-1 stability and concentration.** Effects of blood collection tubes (**a**: serum, **b**: citrate, **c**: heparin, **d-e**: EDTA, **f-g**: CTAD), storage temperature and time before processing, and post-processing plasma filtering (**e, g**) on the initial value and pre-processing time stability of HAI-1 measurements in blood. Information on the dilution of samples used for measuring, data range and the sample type selected are also shown.

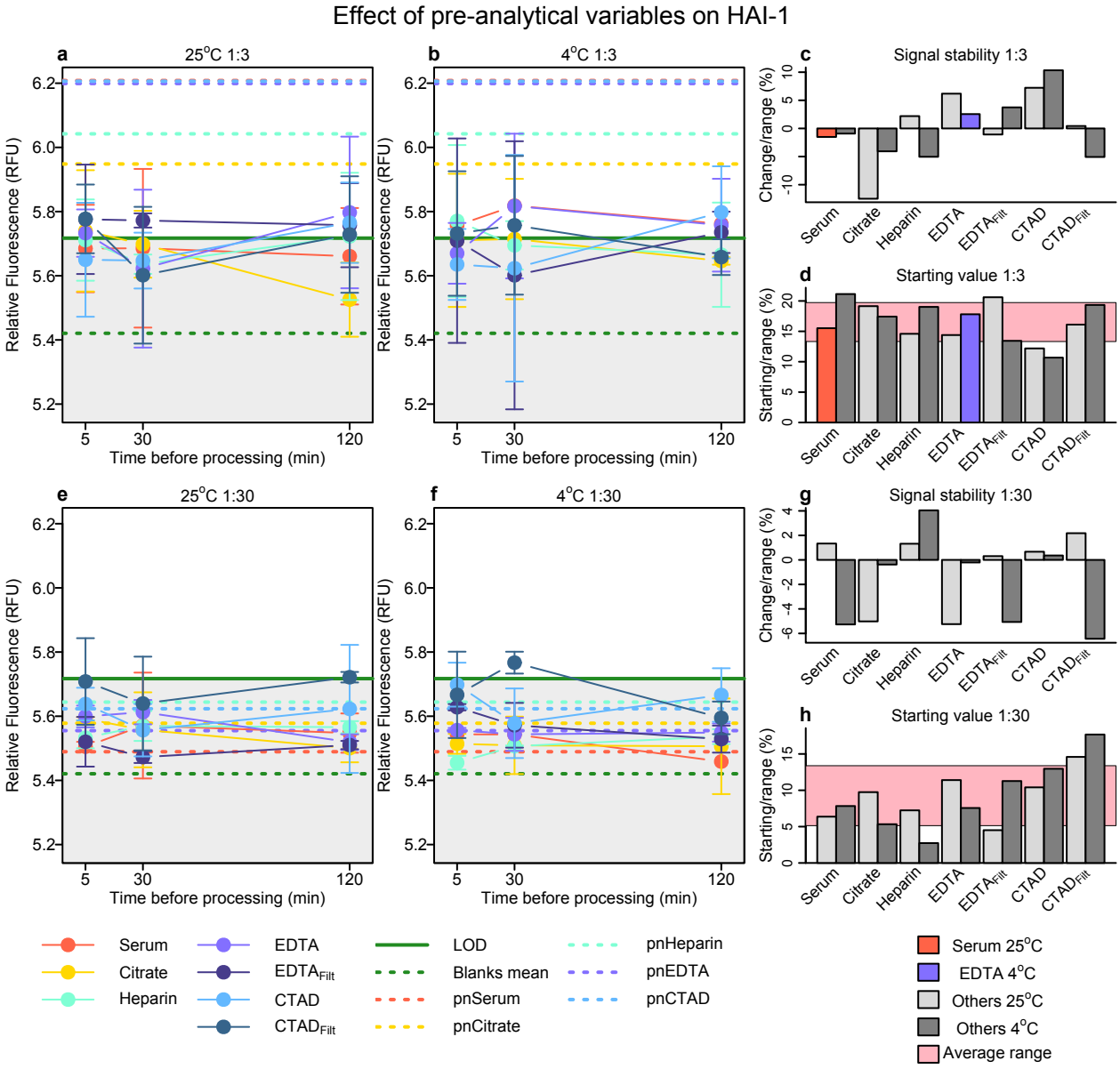

FIGURE I.S64: **Effect of pre-processing storage temperature on HAI-1 stability and concentration.** Initial measured value and stability of HAI-1 when stored at 25 °C (**a, e**) and 4 °C (**b, f**) before processing when collected in different tube types. The measured values are shown at low dilution of 1:3 (**a-b**) and high dilution of 1:30 (**e-f**). Stability before processing is expressed as an increase or decrease compared to the measurement range and is shown for low (**c**) and high (**g**) dilutions. Initial value is expressed as a portion of the measurement range when the linear regression is extrapolated to zero minutes and is shown for low (**d**) and high (**h**) dilutions. The pink box in graphs **d** and **h** indicate the region that is included by the *mean* ± *SD* of all the initial values and gives an indication of outliers when values lie outside this region. Red and purple bars in **c-d, g-h** are indicated at the measured dilution as the two choices for the TBI analysis.

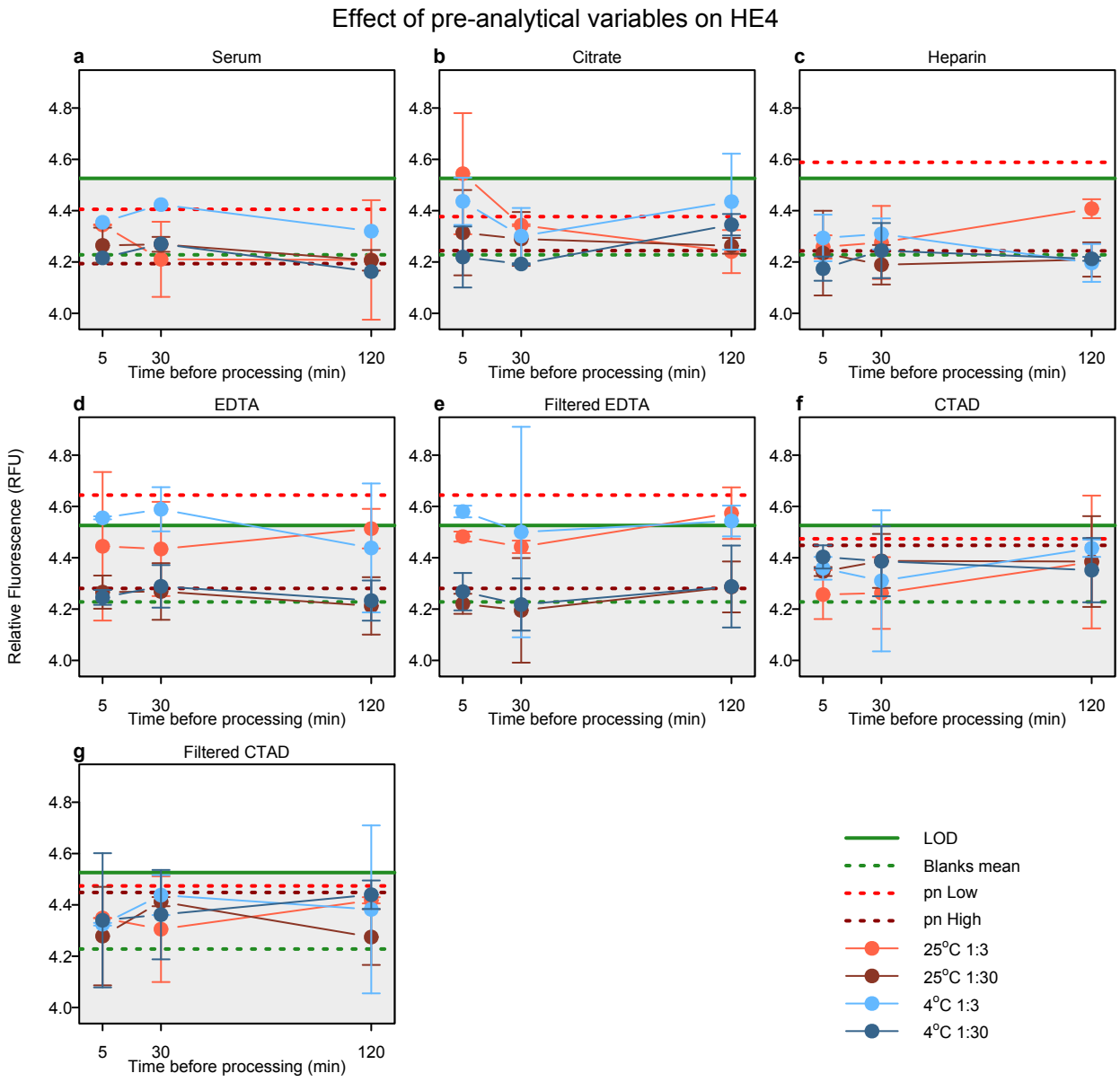

FIGURE I.S65: **Effect of blood collection tube on HE4 stability and concentration.** Effects of blood collection tubes (**a**: serum, **b**: citrate, **c**: heparin, **d-e**: EDTA, **f-g**: CTAD), storage temperature and time before processing, and post-processing plasma filtering (**e, g**) on the initial value and pre-processing time stability of HE4 measurements in blood. Information on the dilution of samples used for measuring, data range and the sample type selected are also shown.

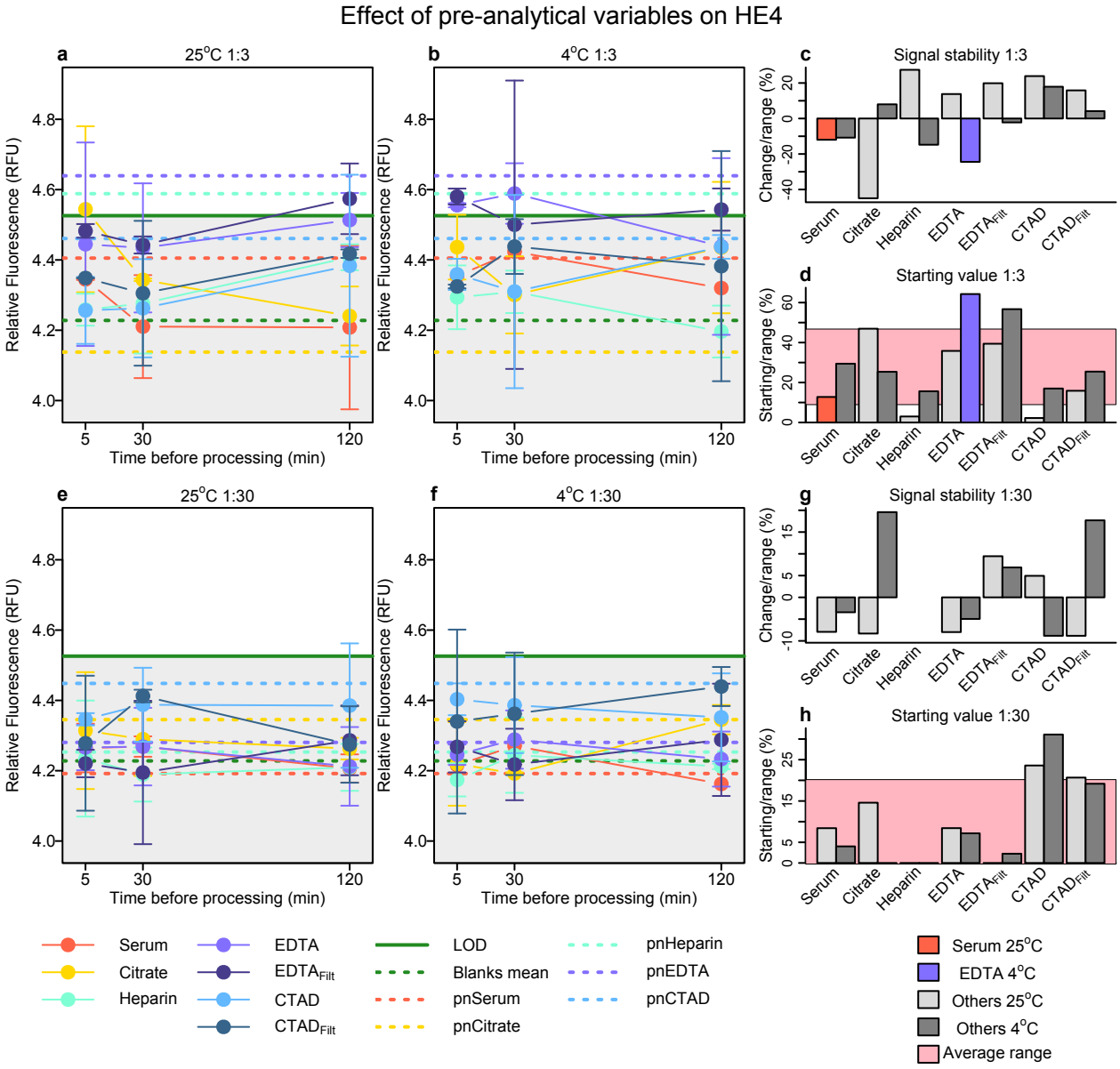

FIGURE I.S66: **Effect of pre-processing storage temperature on HE4 stability and concentration.** Initial measured value and stability of HE4 when stored at 25 °C (**a, e**) and 4 °C (**b, f**) before processing when collected in different tube types. The measured values are shown at low dilution of 1:3 (**a-b**) and high dilution of 1:30 (**e-f**). Stability before processing is expressed as an increase or decrease compared to the measurement range and is shown for low (**c**) and high (**g**) dilutions. Initial value is expressed as a portion of the measurement range when the linear regression is extrapolated to zero minutes and is shown for low (**d**) and high (**h**) dilutions. The pink box in graphs **d** and **h** indicate the region that is included by the *mean* ± *SD* of all the initial values and gives an indication of outliers when values lie outside this region. Red and purple bars in **c-d, g-h** are indicated at the measured dilution as the two choices for the TBI analysis.

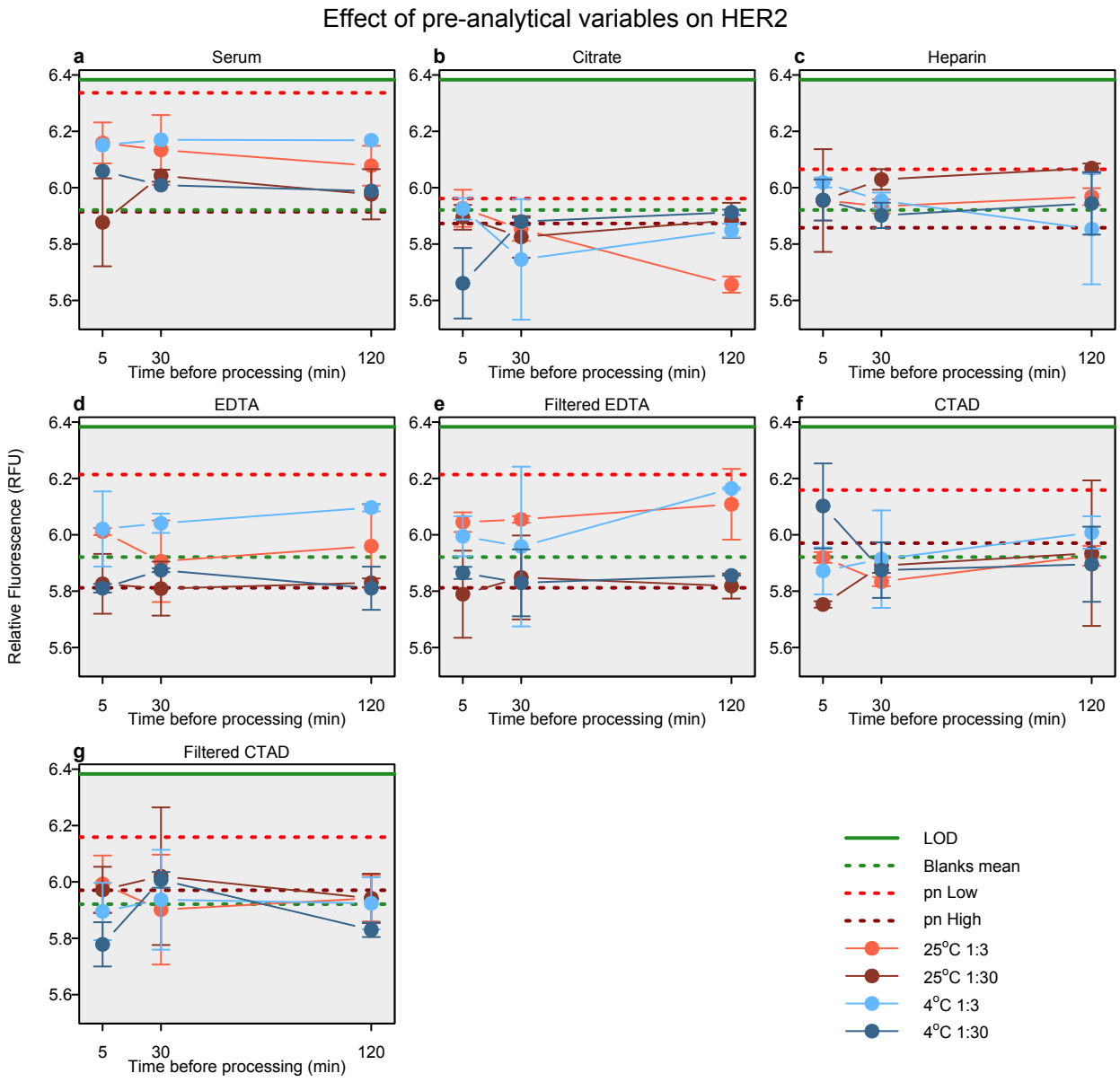

FIGURE I.S67: **Effect of blood collection tube on HER2 stability and concentration.** Effects of blood collection tubes (**a**: serum, **b**: citrate, **c**: heparin, **d-e**: EDTA, **f-g**: CTAD), storage temperature and time before processing, and post-processing plasma filtering (**e, g**) on the initial value and pre-processing time stability of HER2 measurements in blood. Information on the dilution of samples used for measuring, data range and the sample type selected are also shown.

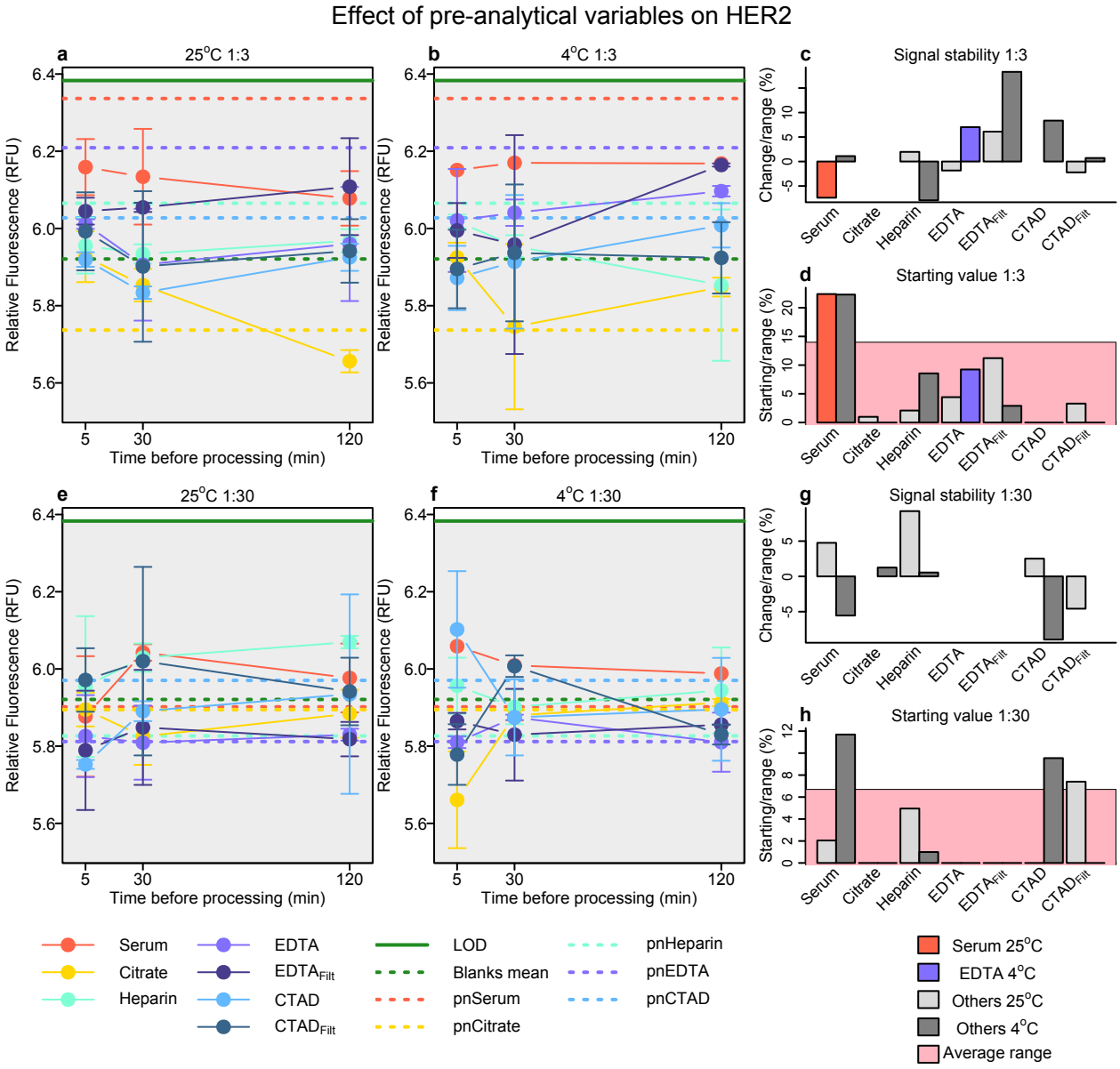

FIGURE I.S68: **Effect of pre-processing storage temperature on HER2 stability and concentration.** Initial measured value and stability of HER2 when stored at 25 °C (**a, e**) and 4 °C (**b, f**) before processing when collected in different tube types. The measured values are shown at low dilution of 1:3 (**a-b**) and high dilution of 1:30 (**e-f**). Stability before processing is expressed as an increase or decrease compared to the measurement range and is shown for low (**c**) and high (**g**) dilutions. Initial value is expressed as a portion of the measurement range when the linear regression is extrapolated to zero minutes and is shown for low (**d**) and high (**h**) dilutions. The pink box in graphs **d** and **h** indicate the region that is included by the *mean* ± *SD* of all the initial values and gives an indication of outliers when values lie outside this region. Red and purple bars in **c-d, g-h** are indicated at the measured dilution as the two choices for the TBI analysis.

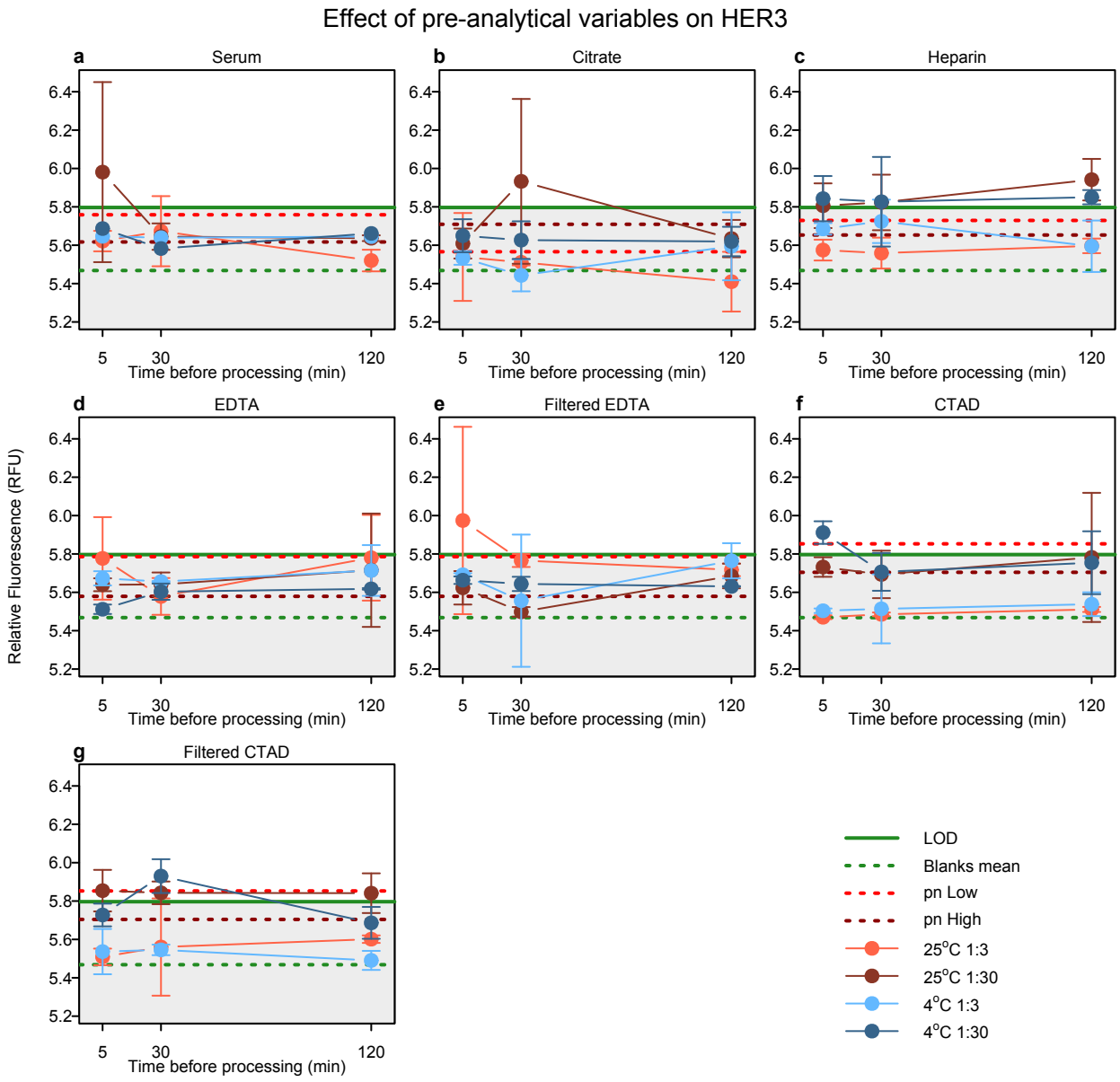

FIGURE I.S69: **Effect of blood collection tube on HER3 stability and concentration.** Effects of blood collection tubes (**a**: serum, **b**: citrate, **c**: heparin, **d-e**: EDTA, **f-g**: CTAD), storage temperature and time before processing, and post-processing plasma filtering (**e, g**) on the initial value and pre-processing time stability of HER3 measurements in blood. Information on the dilution of samples used for measuring, data range and the sample type selected are also shown.

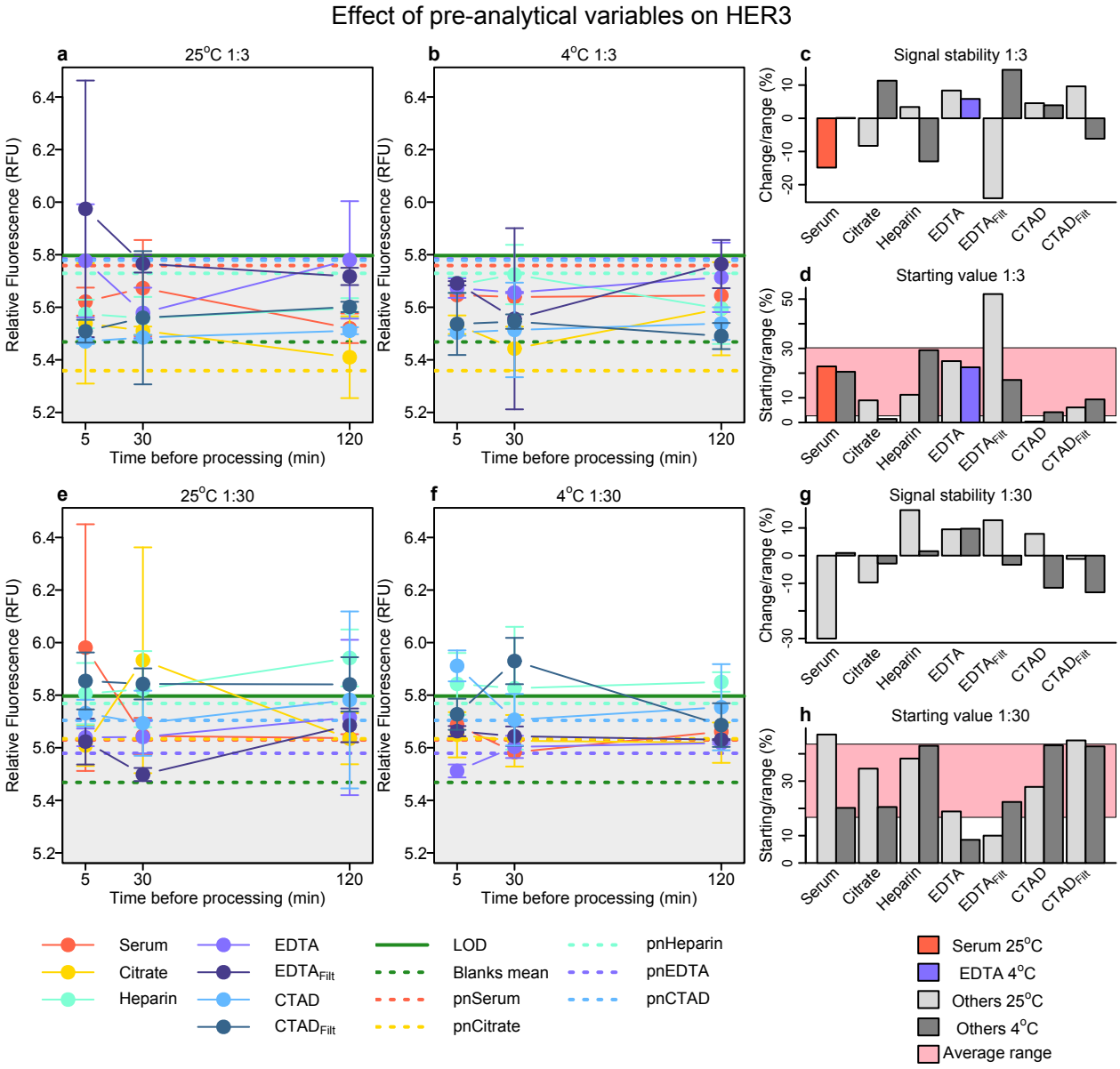

FIGURE I.S70: **Effect of pre-processing storage temperature on HER3 stability and concentration.** Initial measured value and stability of HER3 when stored at 25 °C (**a, e**) and 4 °C (**b, f**) before processing when collected in different tube types. The measured values are shown at low dilution of 1:3 (**a-b**) and high dilution of 1:30 (**e-f**). Stability before processing is expressed as an increase or decrease compared to the measurement range and is shown for low (**c**) and high (**g**) dilutions. Initial value is expressed as a portion of the measurement range when the linear regression is extrapolated to zero minutes and is shown for low (**d**) and high (**h**) dilutions. The pink box in graphs **d** and **h** indicate the region that is included by the *mean* ± *SD* of all the initial values and gives an indication of outliers when values lie outside this region. Red and purple bars in **c-d, g-h** are indicated at the measured dilution as the two choices for the TBI analysis.

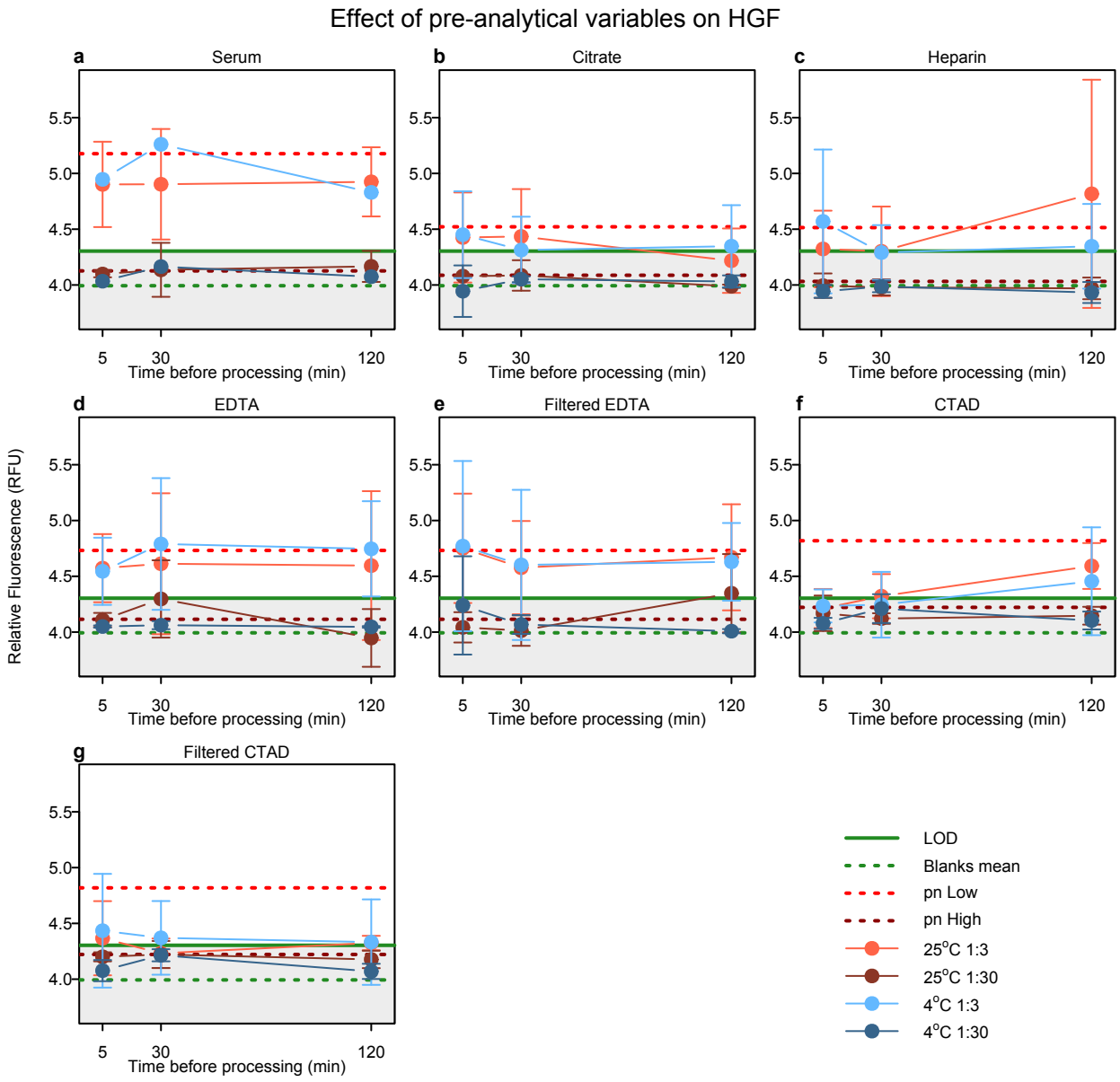

FIGURE I.S71: **Effect of blood collection tube on HGF stability and concentration.** Effects of blood collection tubes (**a**: serum, **b**: citrate, **c**: heparin, **d-e**: EDTA, **f-g**: CTAD), storage temperature and time before processing, and post-processing plasma filtering (**e, g**) on the initial value and pre-processing time stability of HGF measurements in blood. Information on the dilution of samples used for measuring, data range and the sample type selected are also shown.

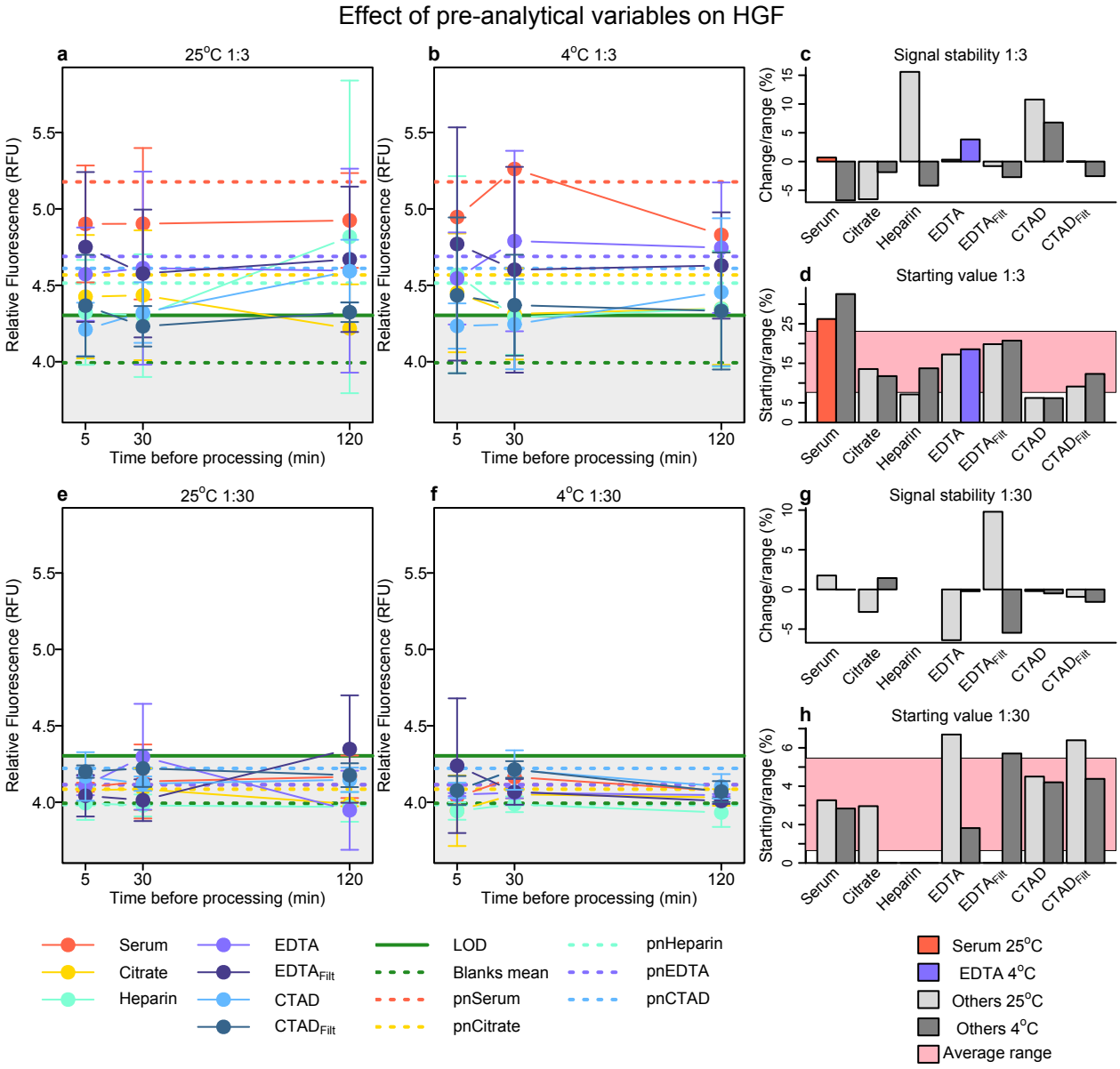

FIGURE I.S72: **Effect of pre-processing storage temperature on HGF stability and concentration.** Initial measured value and stability of HGF when stored at 25 °C (**a, e**) and 4 °C (**b, f**) before processing when collected in different tube types. The measured values are shown at low dilution of 1:3 (**a-b**) and high dilution of 1:30 (**e-f**). Stability before processing is expressed as an increase or decrease compared to the measurement range and is shown for low (**c**) and high (**g**) dilutions. Initial value is expressed as a portion of the measurement range when the linear regression is extrapolated to zero minutes and is shown for low (**d**) and high (**h**) dilutions. The pink box in graphs **d** and **h** indicate the region that is included by the *mean* ± *SD* of all the initial values and gives an indication of outliers when values lie outside this region. Red and purple bars in **c-d, g-h** are indicated at the measured dilution as the two choices for the TBI analysis.

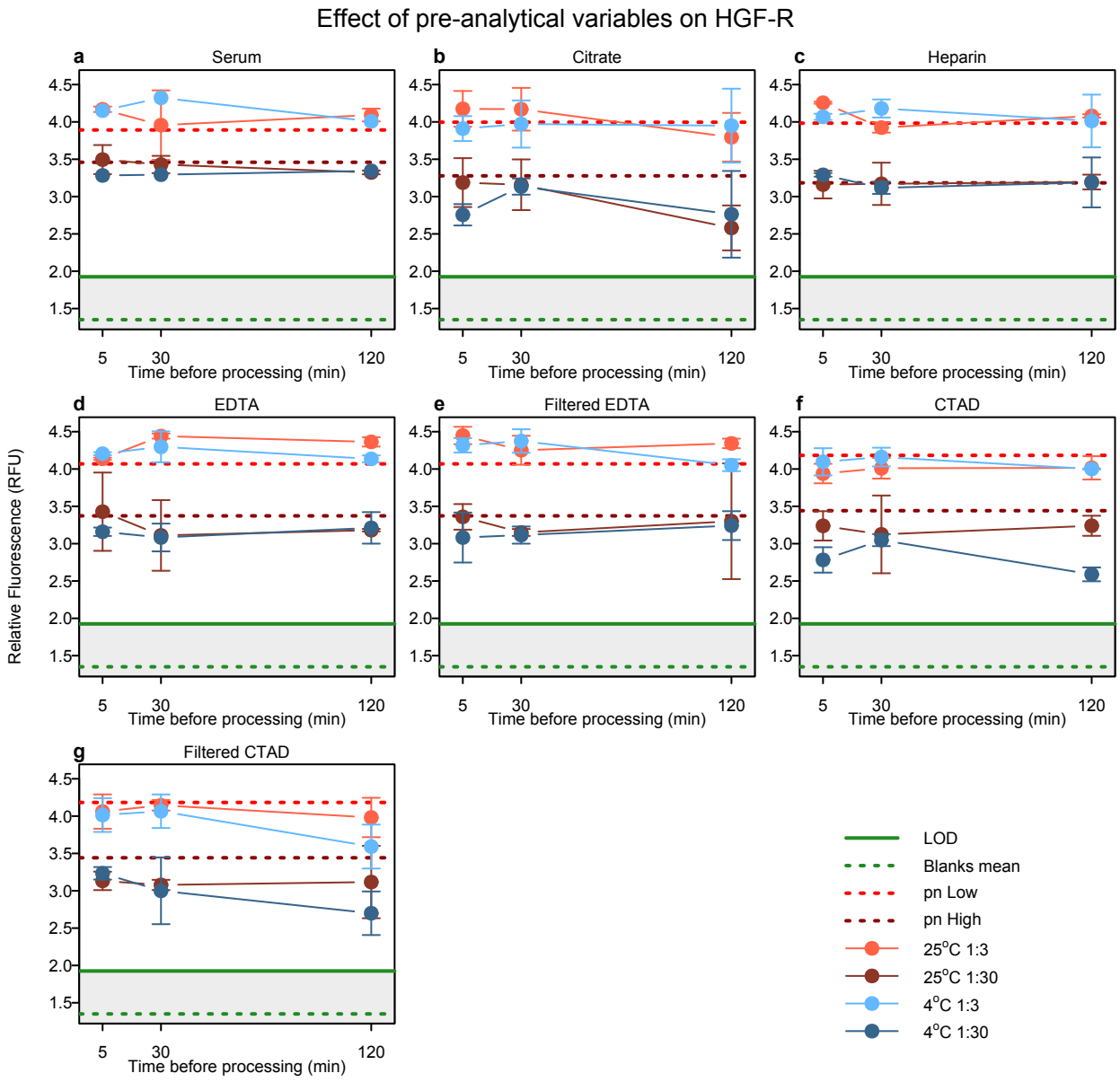

FIGURE I.S73: **Effect of blood collection tube on HGF-R stability and concentration.** Effects of blood collection tubes (**a**: serum, **b**: citrate, **c**: heparin, **d-e**: EDTA, **f-g**: CTAD), storage temperature and time before processing, and post-processing plasma filtering (**e, g**) on the initial value and pre-processing time stability of HGF-R measurements in blood. Information on the dilution of samples used for measuring, data range and the sample type selected are also shown.

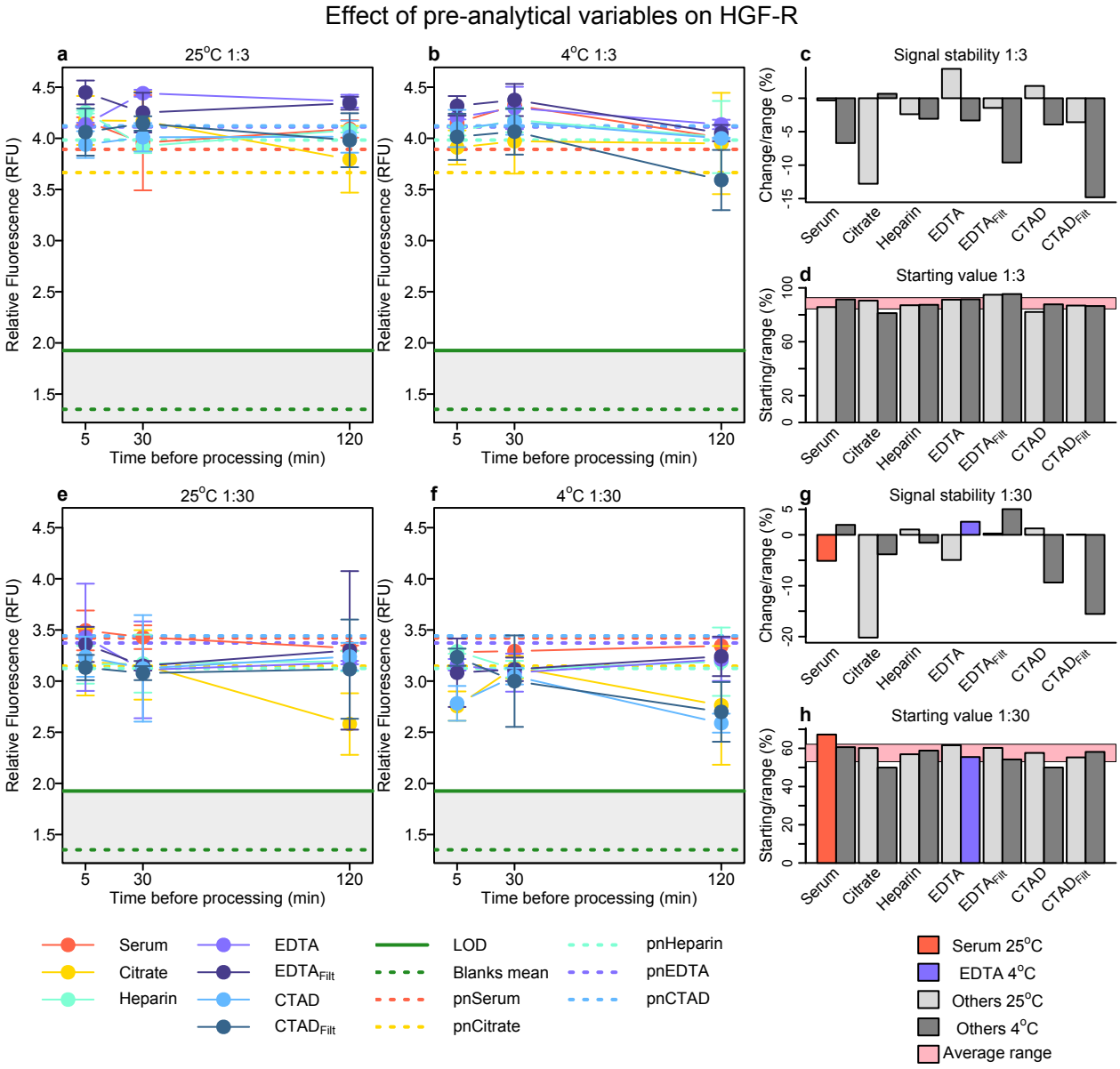

FIGURE I.S74: **Effect of pre-processing storage temperature on HGF-R stability and concentration.** Initial measured value and stability of HGF-R when stored at 25 °C (**a, e**) and 4 °C (**b, f**) before processing when collected in different tube types. The measured values are shown at low dilution of 1:3 (**a-b**) and high dilution of 1:30 (**e-f**). Stability before processing is expressed as an increase or decrease compared to the measurement range and is shown for low (**c**) and high (**g**) dilutions. Initial value is expressed as a portion of the measurement range when the linear regression is extrapolated to zero minutes and is shown for low (**d**) and high (**h**) dilutions. The pink box in graphs **d** and **h** indicate the region that is included by the *mean* ± *SD* of all the initial values and gives an indication of outliers when values lie outside this region. Red and purple bars in **c-d, g-h** are indicated at the measured dilution as the two choices for the TBI analysis.

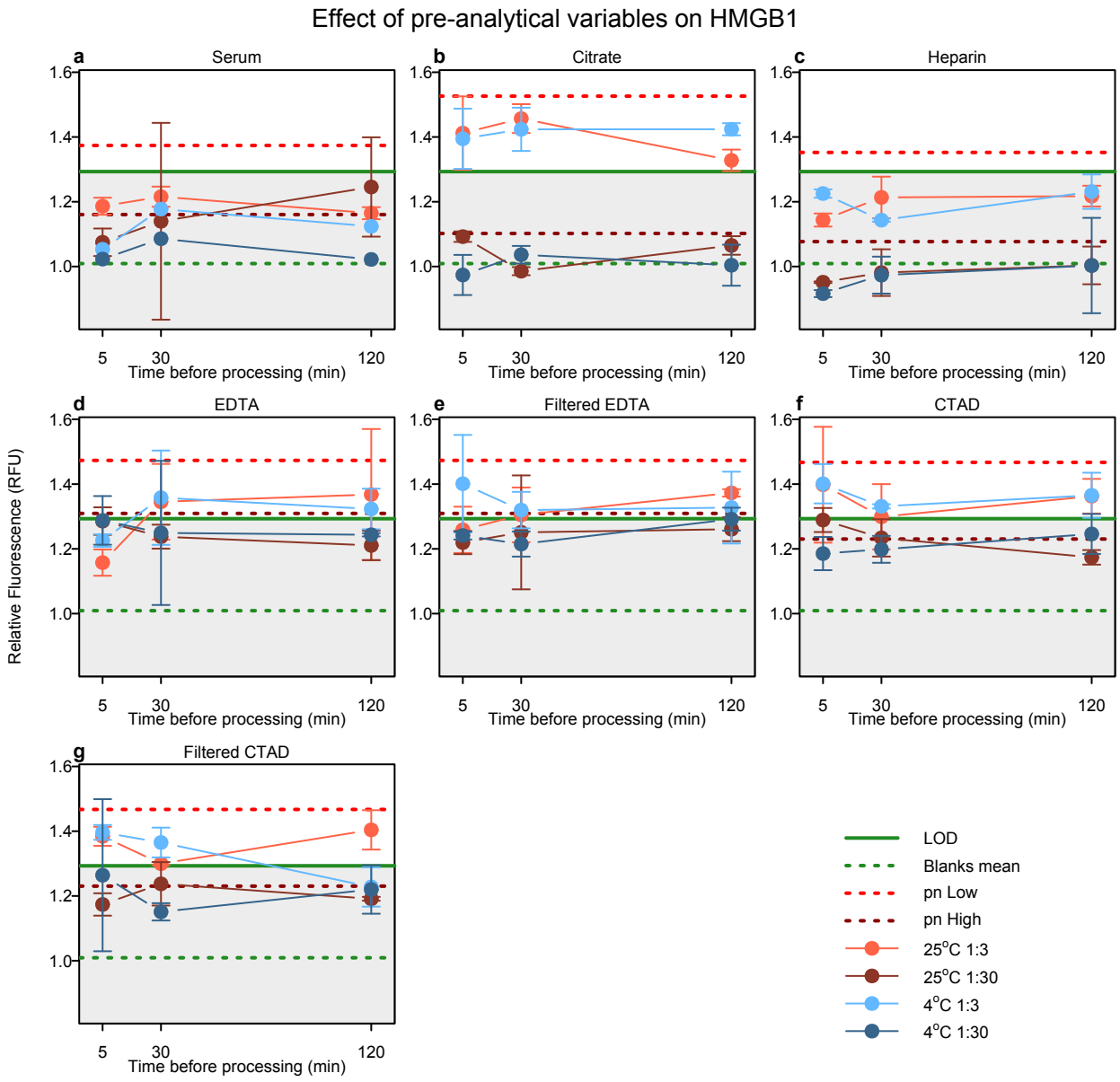

FIGURE I.S75: **Effect of blood collection tube on HMGB1 stability and concentration.** Effects of blood collection tubes (**a**: serum, **b**: citrate, **c**: heparin, **d-e**: EDTA, **f-g**: CTAD), storage temperature and time before processing, and post-processing plasma filtering (**e, g**) on the initial value and pre-processing time stability of HMGB1 measurements in blood. Information on the dilution of samples used for measuring, data range and the sample type selected are also shown.

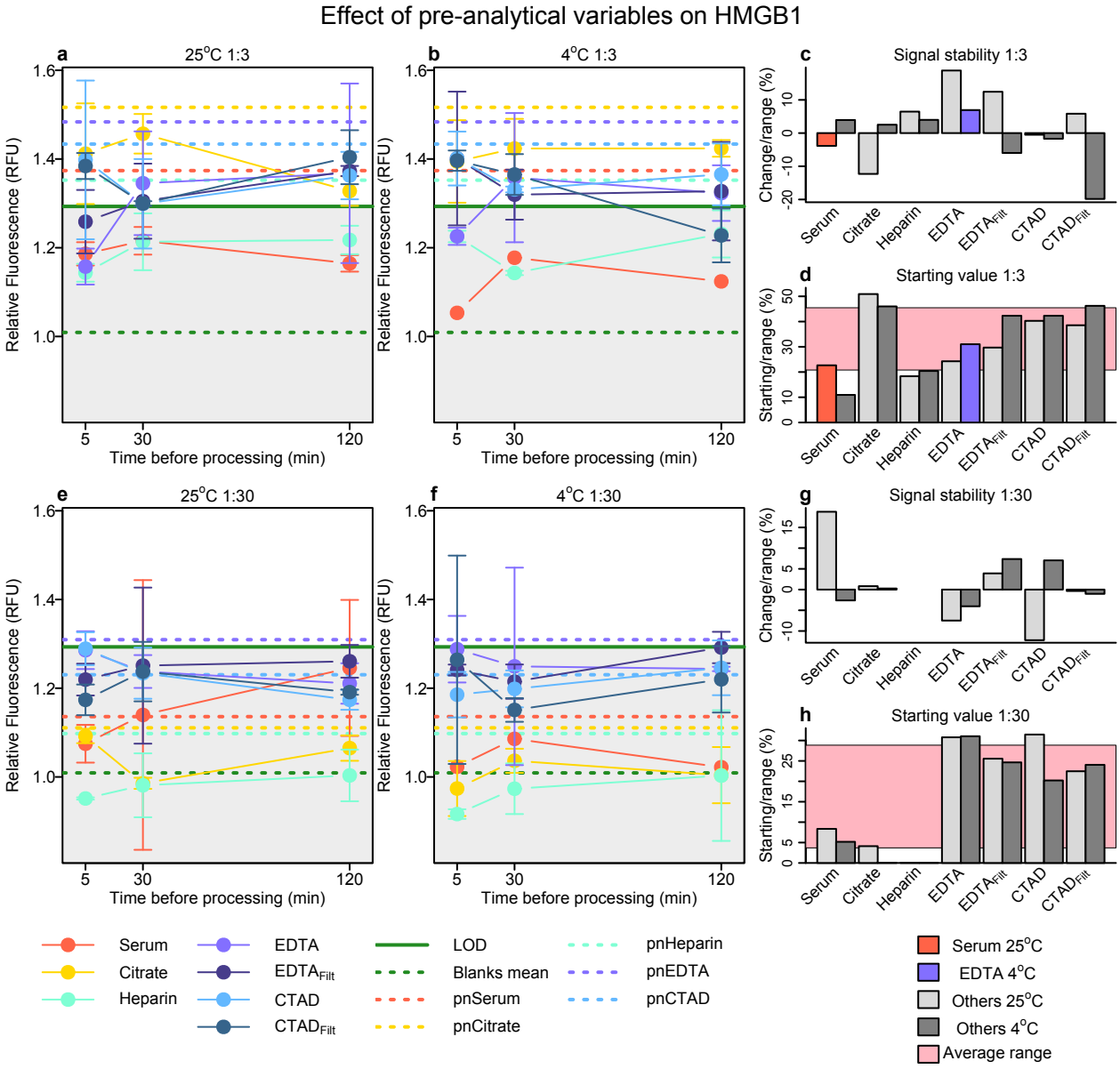

FIGURE I.S76: **Effect of pre-processing storage temperature on HMGB1 stability and concentration.** Initial measured value and stability of HMGB1 when stored at 25 °C (**a, e**) and 4 °C (**b, f**) before processing when collected in different tube types. The measured values are shown at low dilution of 1:3 (**a-b**) and high dilution of 1:30 (**e-f**). Stability before processing is expressed as an increase or decrease compared to the measurement range and is shown for low (**c**) and high (**g**) dilutions. Initial value is expressed as a portion of the measurement range when the linear regression is extrapolated to zero minutes and is shown for low (**d**) and high (**h**) dilutions. The pink box in graphs **d** and **h** indicate the region that is included by the *mean* ± *SD* of all the initial values and gives an indication of outliers when values lie outside this region. Red and purple bars in **c-d, g-h** are indicated at the measured dilution as the two choices for the TBI analysis.

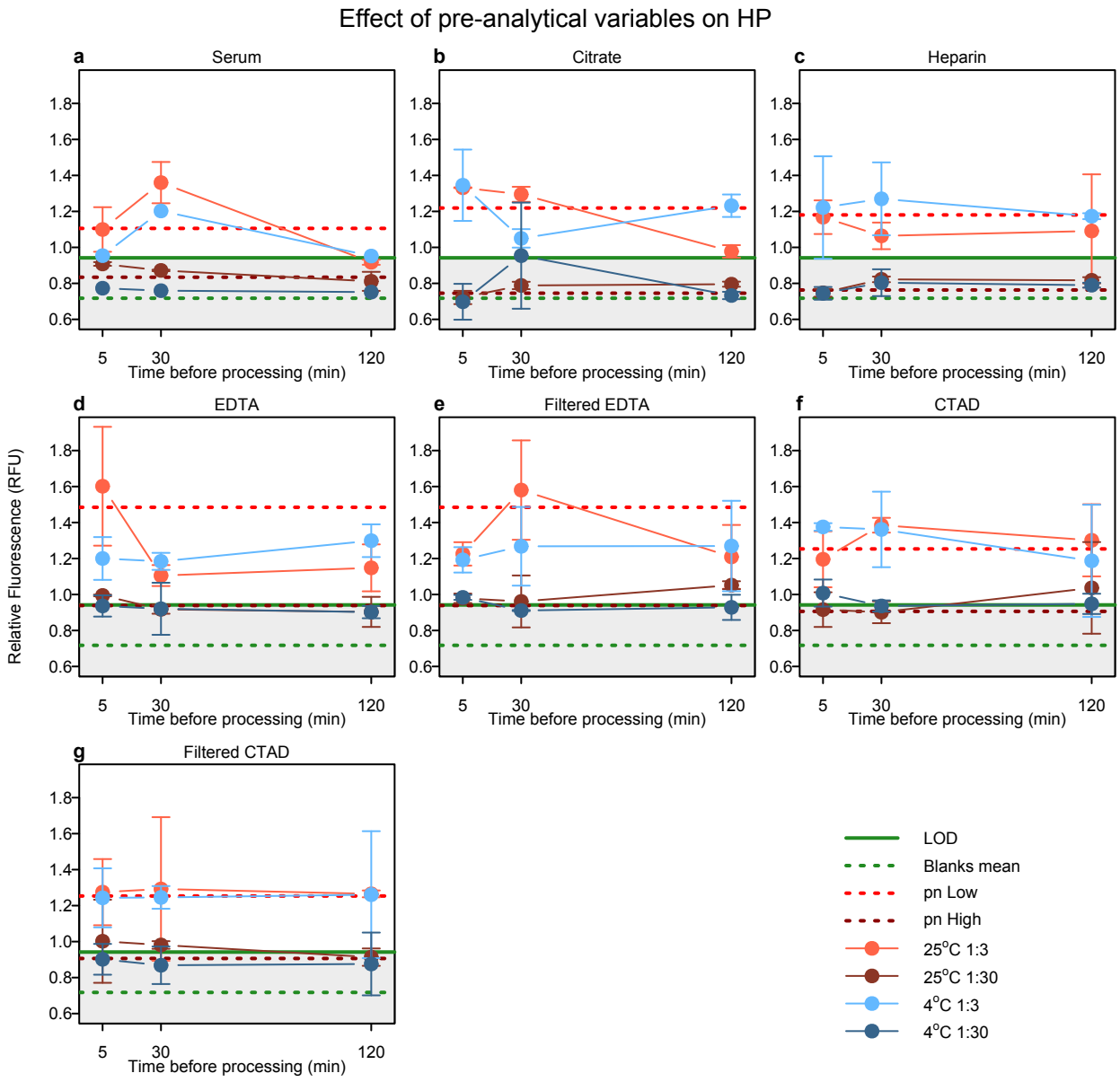

FIGURE I.S77: **Effect of blood collection tube on HP stability and concentration.** Effects of blood collection tubes (**a**: serum, **b**: citrate, **c**: heparin, **d-e**: EDTA, **f-g**: CTAD), storage temperature and time before processing, and post-processing plasma filtering (**e, g**) on the initial value and pre-processing time stability of HP measurements in blood. Information on the dilution of samples used for measuring, data range and the sample type selected are also shown.

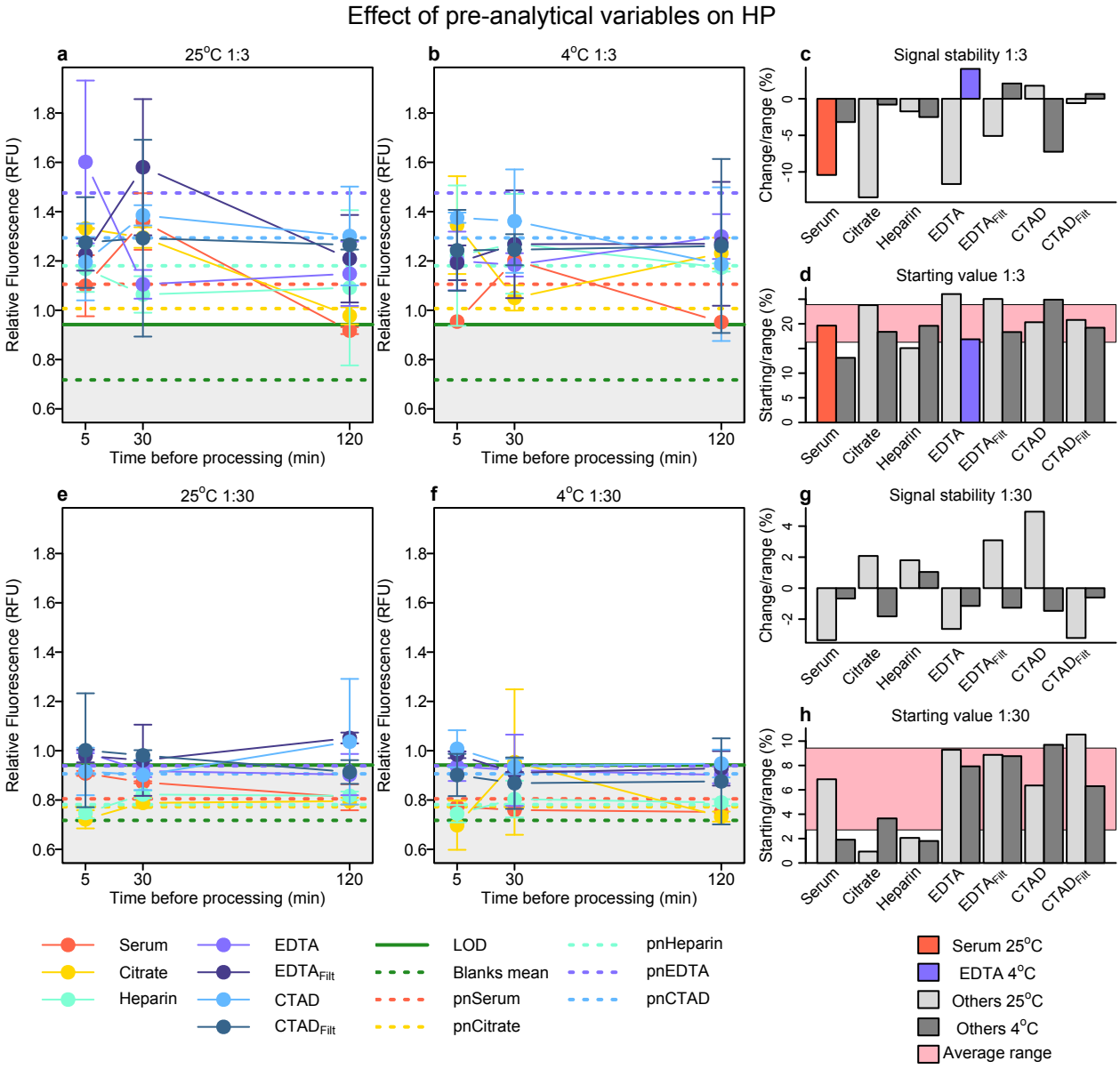

FIGURE I.S78: **Effect of pre-processing storage temperature on HP stability and concentration.** Initial measured value and stability of HP when stored at 25 °C (**a, e**) and 4 °C (**b, f**) before processing when collected in different tube types. The measured values are shown at low dilution of 1:3 (**a-b**) and high dilution of 1:30 (**e-f**). Stability before processing is expressed as an increase or decrease compared to the measurement range and is shown for low (**c**) and high (**g**) dilutions. Initial value is expressed as a portion of the measurement range when the linear regression is extrapolated to zero minutes and is shown for low (**d**) and high (**h**) dilutions. The pink box in graphs **d** and **h** indicate the region that is included by the *mean* ± *SD* of all the initial values and gives an indication of outliers when values lie outside this region. Red and purple bars in **c-d, g-h** are indicated at the measured dilution as the two choices for the TBI analysis.

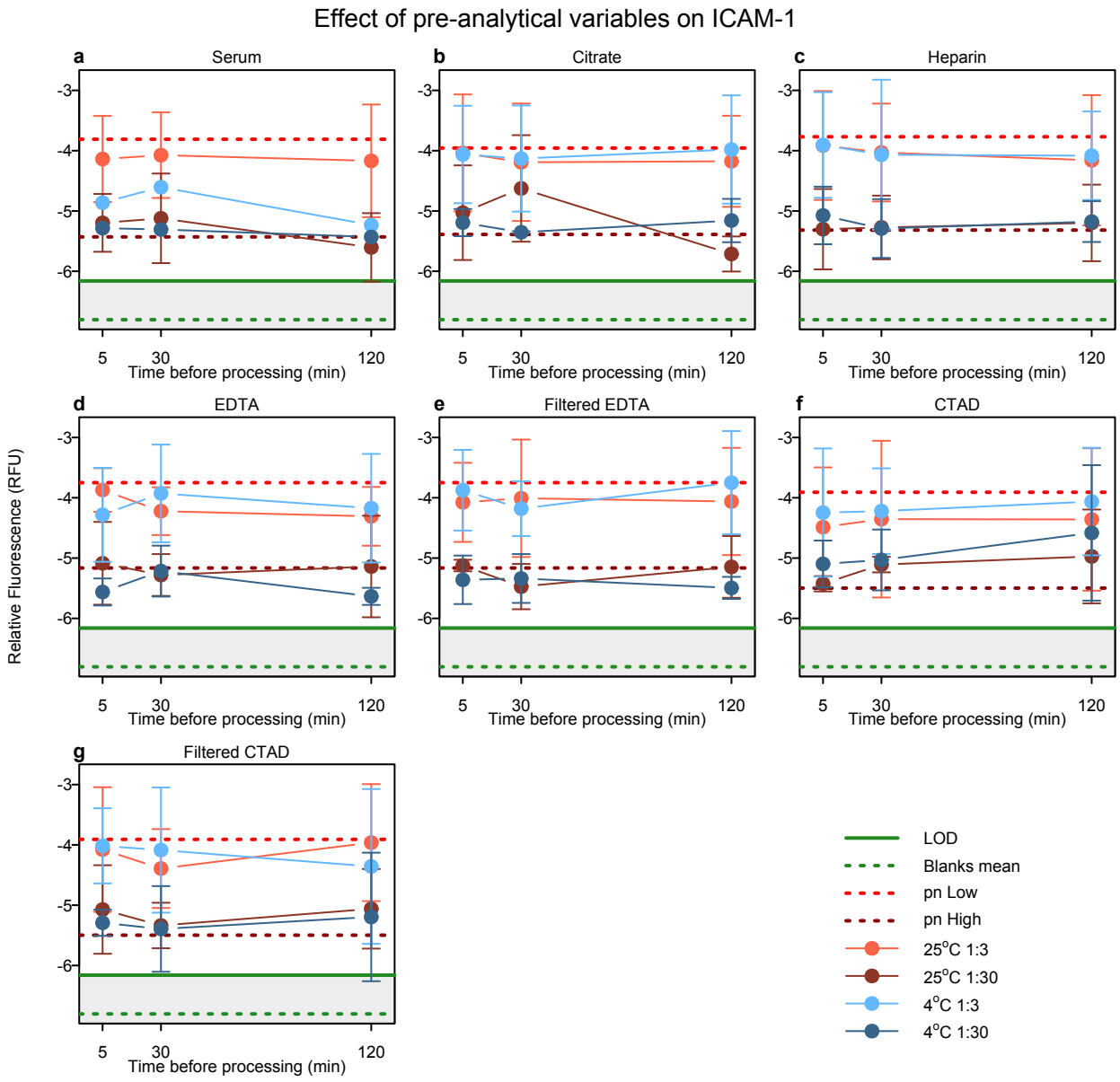

FIGURE I.S79: **Effect of blood collection tube on ICAM-1 stability and concentration.** Effects of blood collection tubes (**a**: serum, **b**: citrate, **c**: heparin, **d-e**: EDTA, **f-g**: CTAD), storage temperature and time before processing, and post-processing plasma filtering (**e, g**) on the initial value and pre-processing time stability of ICAM-1 measurements in blood. Information on the dilution of samples used for measuring, data range and the sample type selected are also shown.

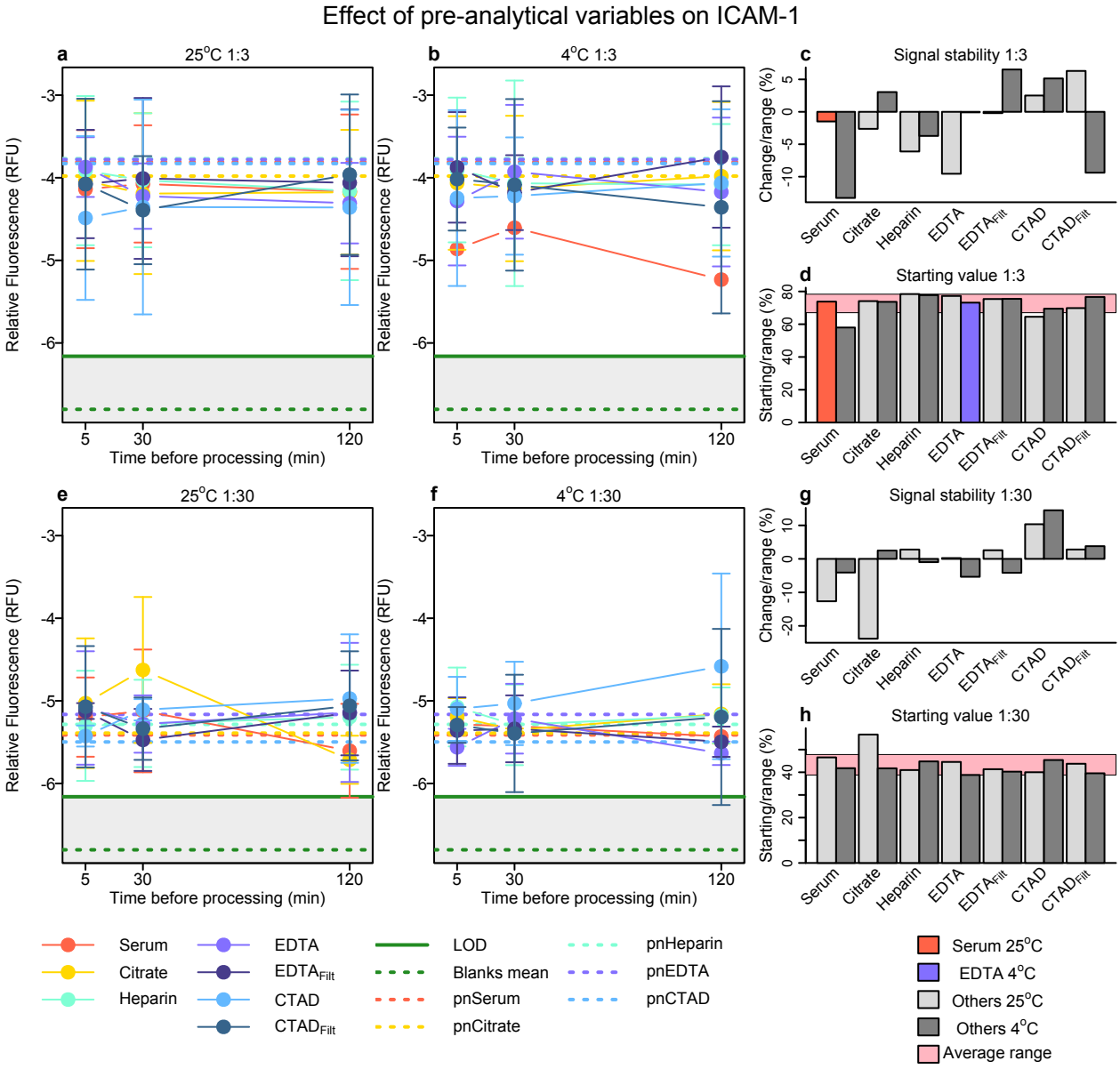

FIGURE I.S80: **Effect of pre-processing storage temperature on ICAM-1 stability and concentration.** Initial measured value and stability of ICAM-1 when stored at 25 °C (**a, e**) and 4 °C (**b, f**) before processing when collected in different tube types. The measured values are shown at low dilution of 1:3 (**a-b**) and high dilution of 1:30 (**e-f**). Stability before processing is expressed as an increase or decrease compared to the measurement range and is shown for low (**c**) and high (**g**) dilutions. Initial value is expressed as a portion of the measurement range when the linear regression is extrapolated to zero minutes and is shown for low (**d**) and high (**h**) dilutions. The pink box in graphs **d** and **h** indicate the region that is included by the *mean* ± *SD* of all the initial values and gives an indication of outliers when values lie outside this region. Red and purple bars in **c-d, g-h** are indicated at the measured dilution as the two choices for the TBI analysis.

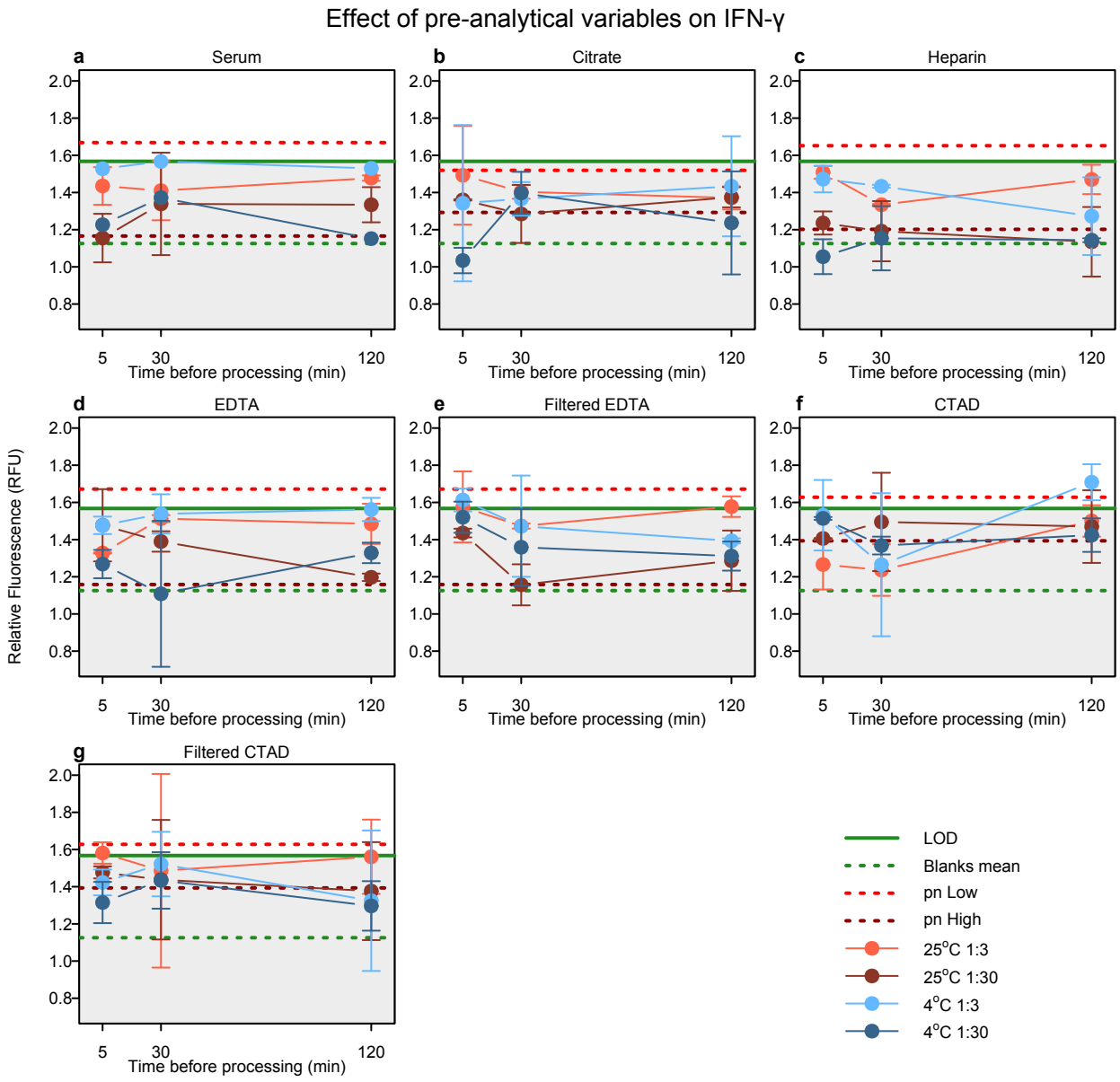

FIGURE I.S81: **Effect of blood collection tube on IFN-γ stability and concentration.** Effects of blood collection tubes (**a**: serum, **b**: citrate, **c**: heparin, **d-e**: EDTA, **f-g**: CTAD), storage temperature and time before processing, and post-processing plasma filtering (**e, g**) on the initial value and pre-processing time stability of IFN-γ measurements in blood. Information on the dilution of samples used for measuring, data range and the sample type selected are also shown.

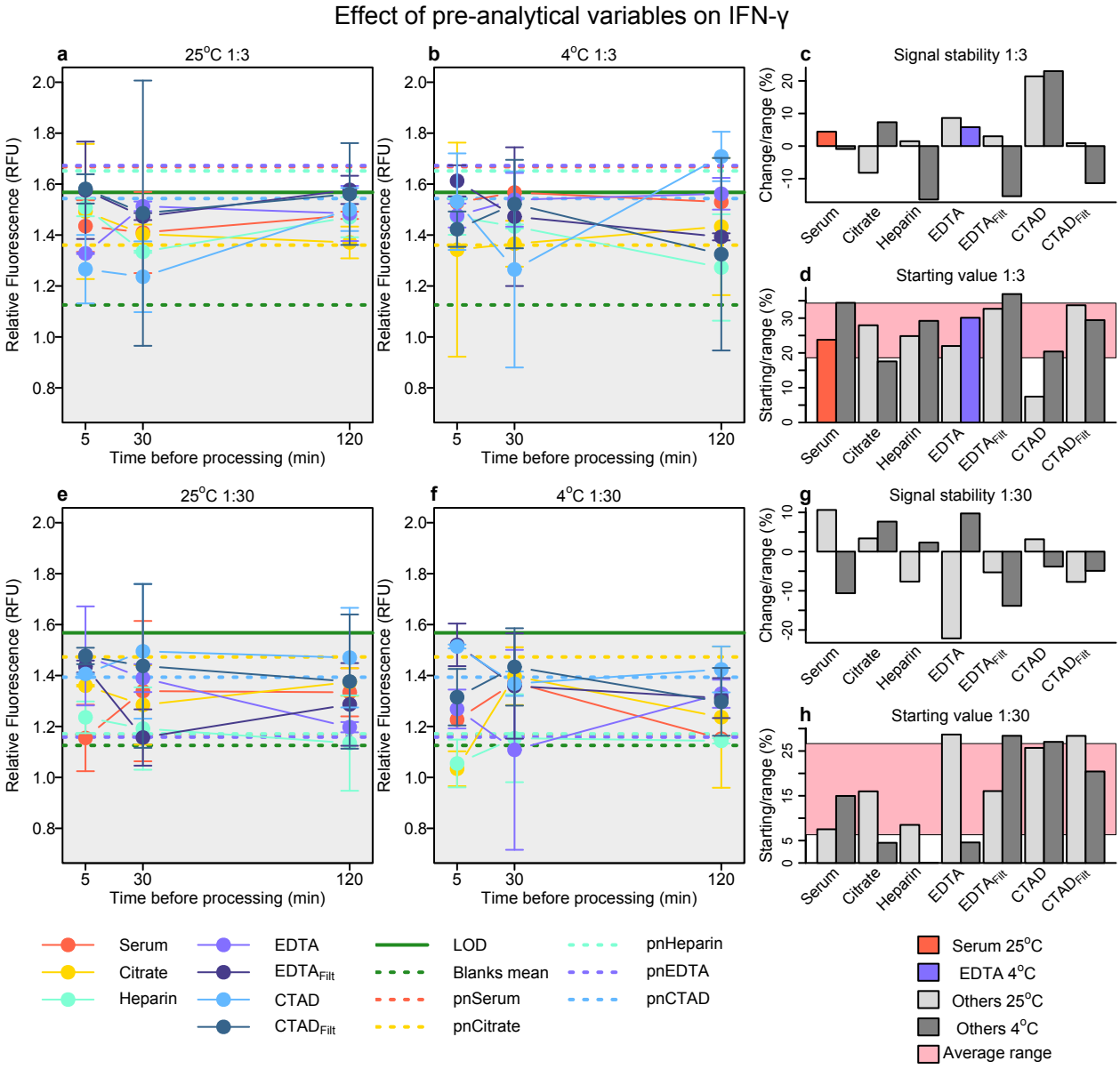

FIGURE I.S82: **Effect of pre-processing storage temperature on IFN-γ stability and concentration.** Initial measured value and stability of IFN-γ when stored at 25 °C (**a, e**) and 4 °C (**b, f**) before processing when collected in different tube types. The measured values are shown at low dilution of 1:3 (**a-b**) and high dilution of 1:30 (**e-f**). Stability before processing is expressed as an increase or decrease compared to the measurement range and is shown for low (**c**) and high (**g**) dilutions. Initial value is expressed as a portion of the measurement range when the linear regression is extrapolated to zero minutes and is shown for low (**d**) and high (**h**) dilutions. The pink box in graphs **d** and **h** indicate the region that is included by the *mean* ± *SD* of all the initial values and gives an indication of outliers when values lie outside this region. Red and purple bars in **c-d, g-h** are indicated at the measured dilution as the two choices for the TBI analysis.

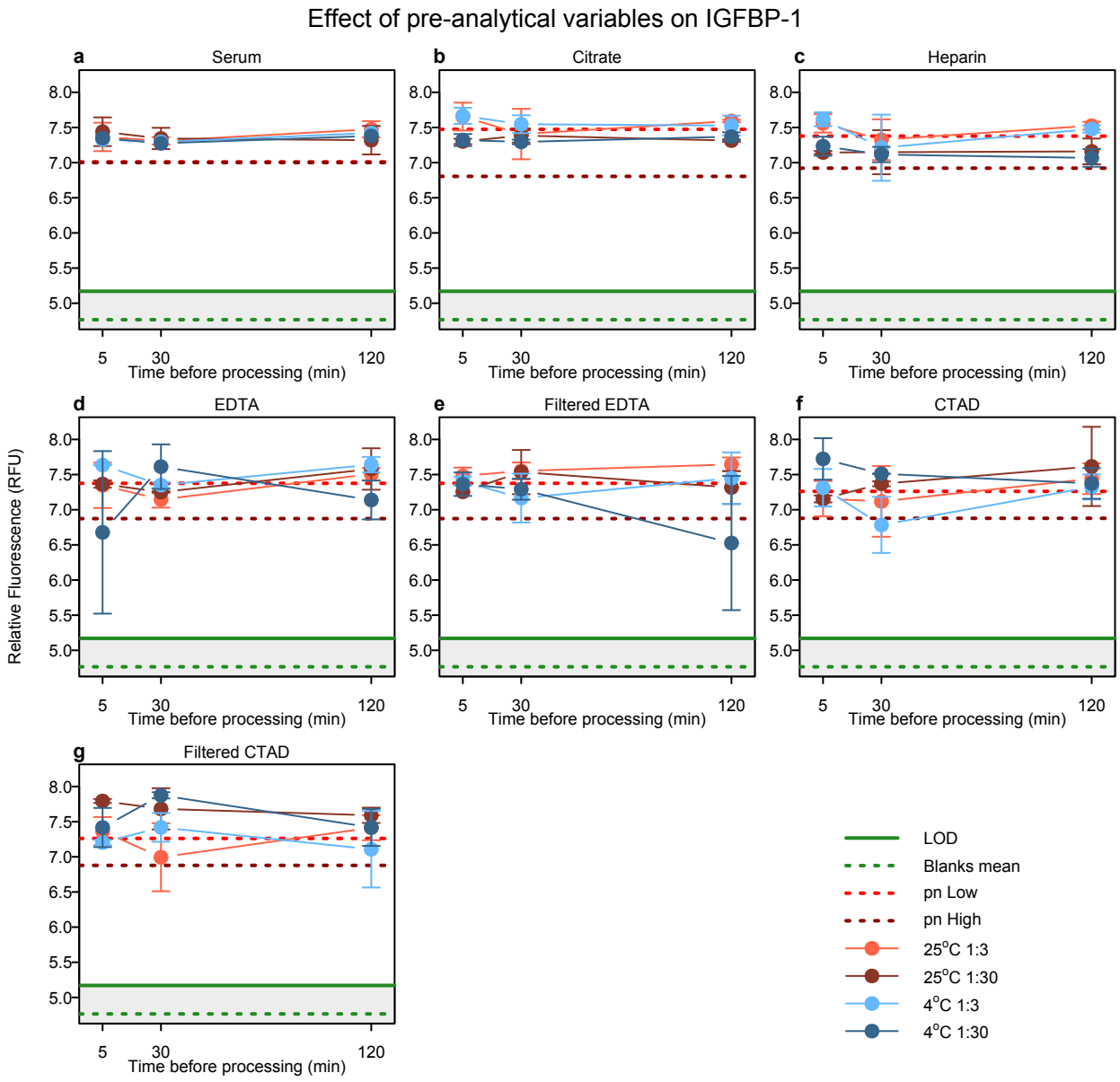

FIGURE I.S83: **Effect of blood collection tube on IGFBP-1 stability and concentration.** Effects of blood collection tubes (**a**: serum, **b**: citrate, **c**: heparin, **d-e**: EDTA, **f-g**: CTAD), storage temperature and time before processing, and post-processing plasma filtering (**e, g**) on the initial value and pre-processing time stability of IGFBP-1 measurements in blood. Information on the dilution of samples used for measuring, data range and the sample type selected are also shown.

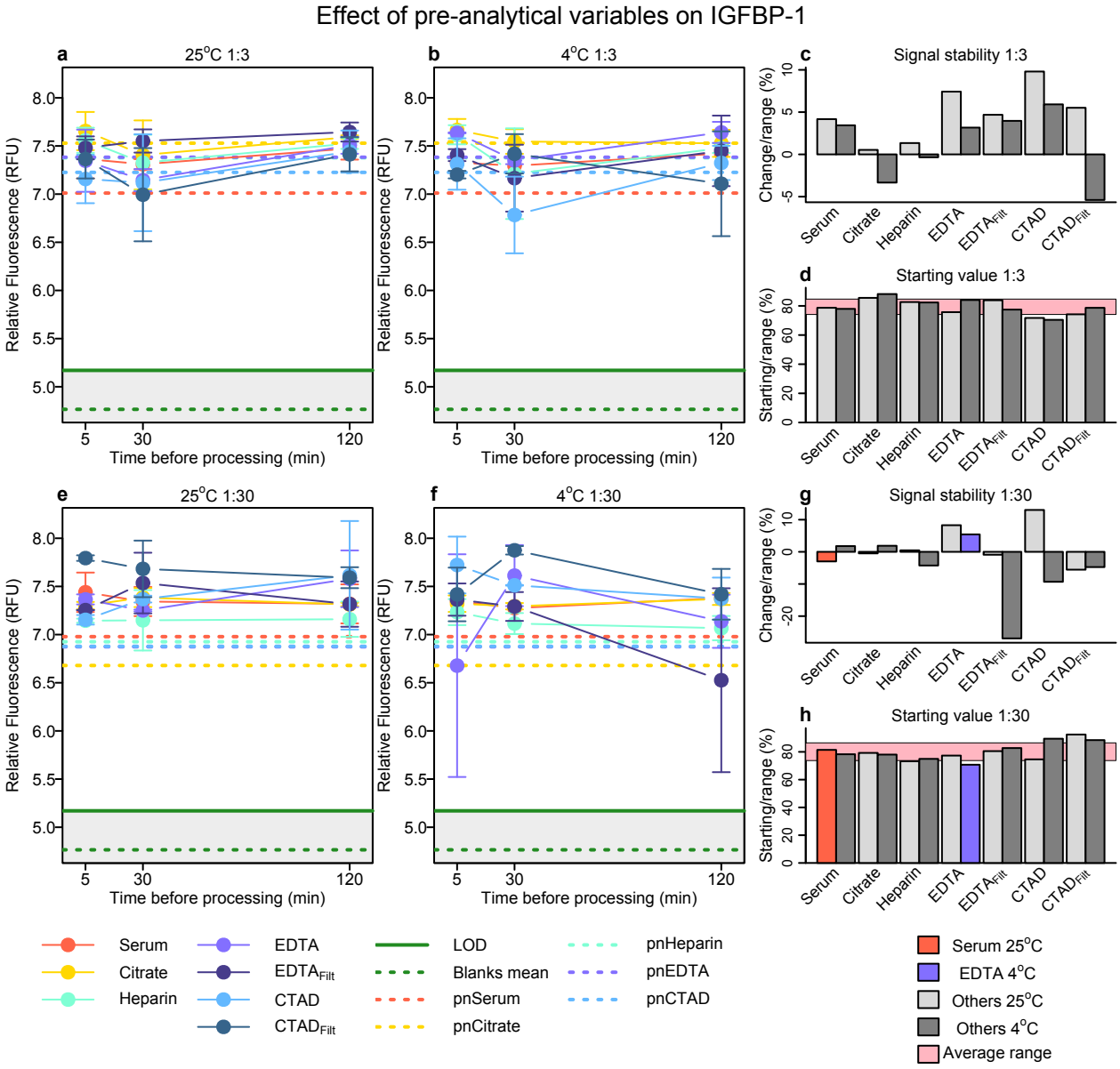

FIGURE I.S84: **Effect of pre-processing storage temperature on IGFBP-1 stability and concentration.** Initial measured value and stability of IGFBP-1 when stored at 25 °C (**a, e**) and 4 °C (**b, f**) before processing when collected in different tube types. The measured values are shown at low dilution of 1:3 (**a-b**) and high dilution of 1:30 (**e-f**). Stability before processing is expressed as an increase or decrease compared to the measurement range and is shown for low (**c**) and high (**g**) dilutions. Initial value is expressed as a portion of the measurement range when the linear regression is extrapolated to zero minutes and is shown for low (**d**) and high (**h**) dilutions. The pink box in graphs **d** and **h** indicate the region that is included by the *mean* ± *SD* of all the initial values and gives an indication of outliers when values lie outside this region. Red and purple bars in **c-d, g-h** are indicated at the measured dilution as the two choices for the TBI analysis.

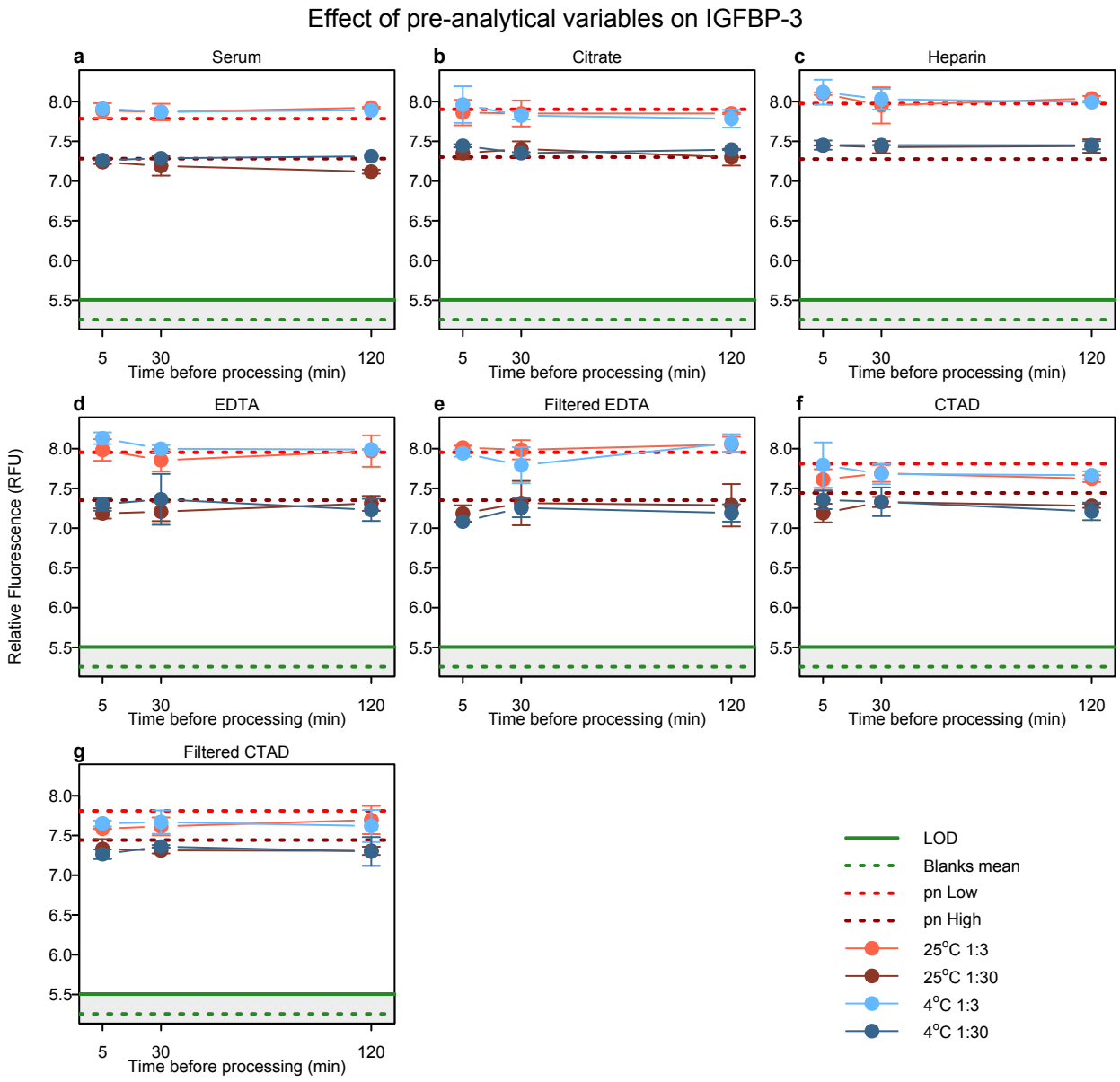

FIGURE I.S85: **Effect of blood collection tube on IGFBP-3 stability and concentration.** Effects of blood collection tubes (**a**: serum, **b**: citrate, **c**: heparin, **d-e**: EDTA, **f-g**: CTAD), storage temperature and time before processing, and post-processing plasma filtering (**e, g**) on the initial value and pre-processing time stability of IGFBP-3 measurements in blood. Information on the dilution of samples used for measuring, data range and the sample type selected are also shown.

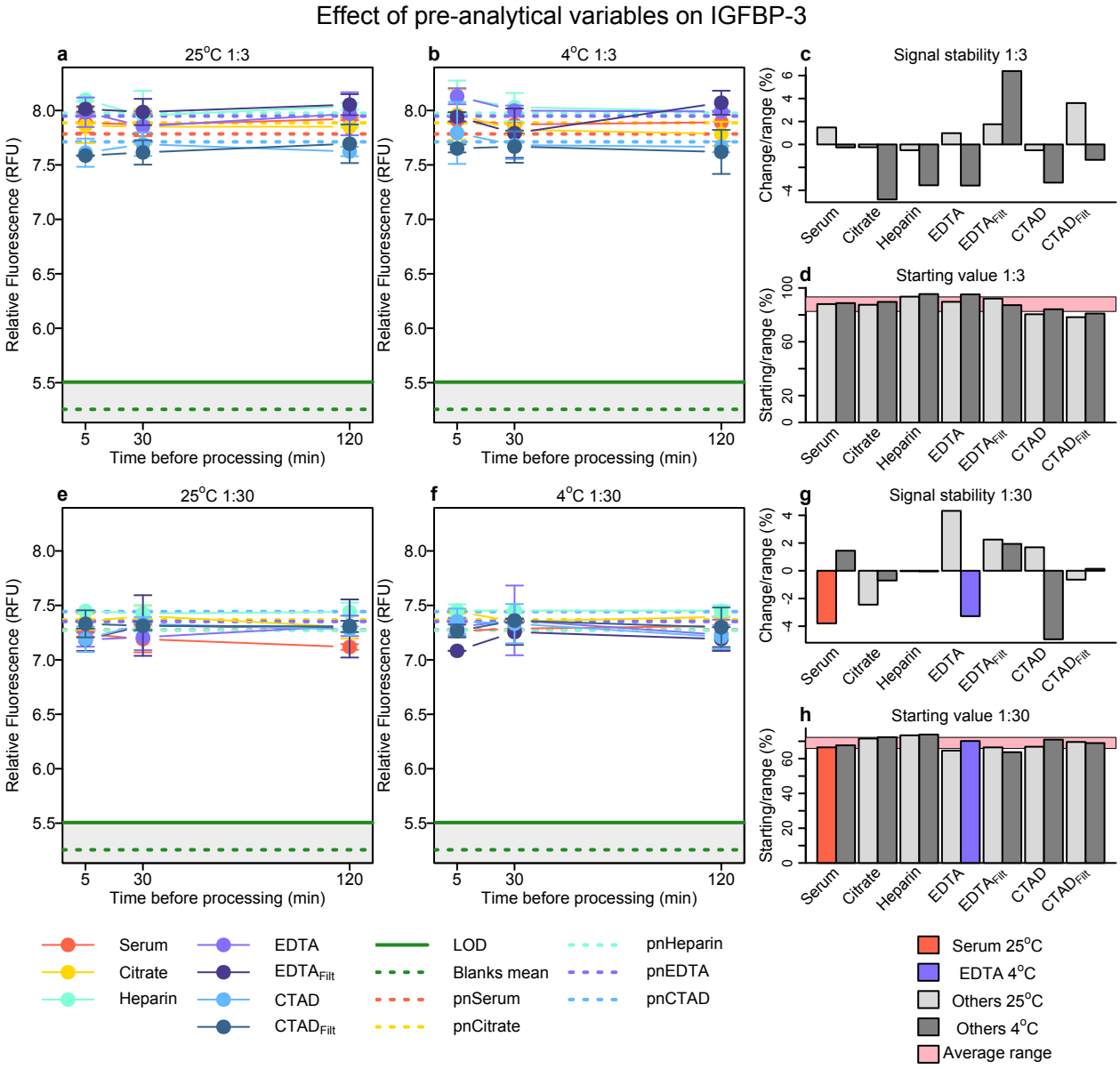

FIGURE I.S86: **Effect of pre-processing storage temperature on IGFBP-3 stability and concentration.** Initial measured value and stability of IGFBP-3 when stored at 25 °C (**a, e**) and 4 °C (**b, f**) before processing when collected in different tube types. The measured values are shown at low dilution of 1:3 (**a-b**) and high dilution of 1:30 (**e-f**). Stability before processing is expressed as an increase or decrease compared to the measurement range and is shown for low (**c**) and high (**g**) dilutions. Initial value is expressed as a portion of the measurement range when the linear regression is extrapolated to zero minutes and is shown for low (**d**) and high (**h**) dilutions. The pink box in graphs **d** and **h** indicate the region that is included by the *mean* ± *SD* of all the initial values and gives an indication of outliers when values lie outside this region. Red and purple bars in **c-d, g-h** are indicated at the measured dilution as the two choices for the TBI analysis.

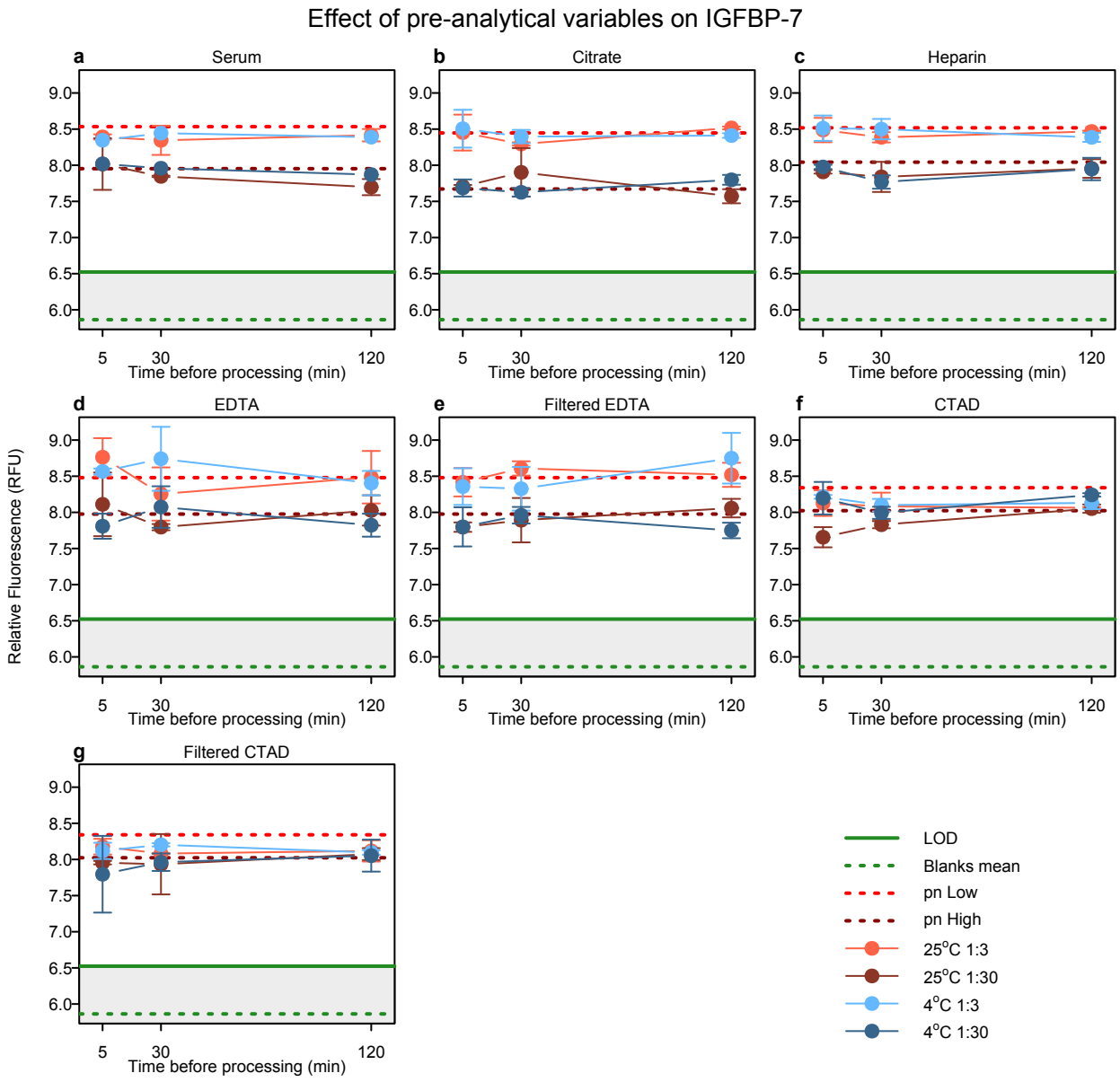

FIGURE I.S87: **Effect of blood collection tube on IGFBP-7 stability and concentration.** Effects of blood collection tubes (**a**: serum, **b**: citrate, **c**: heparin, **d-e**: EDTA, **f-g**: CTAD), storage temperature and time before processing, and post-processing plasma filtering (**e, g**) on the initial value and pre-processing time stability of IGFBP-7 measurements in blood. Information on the dilution of samples used for measuring, data range and the sample type selected are also shown.

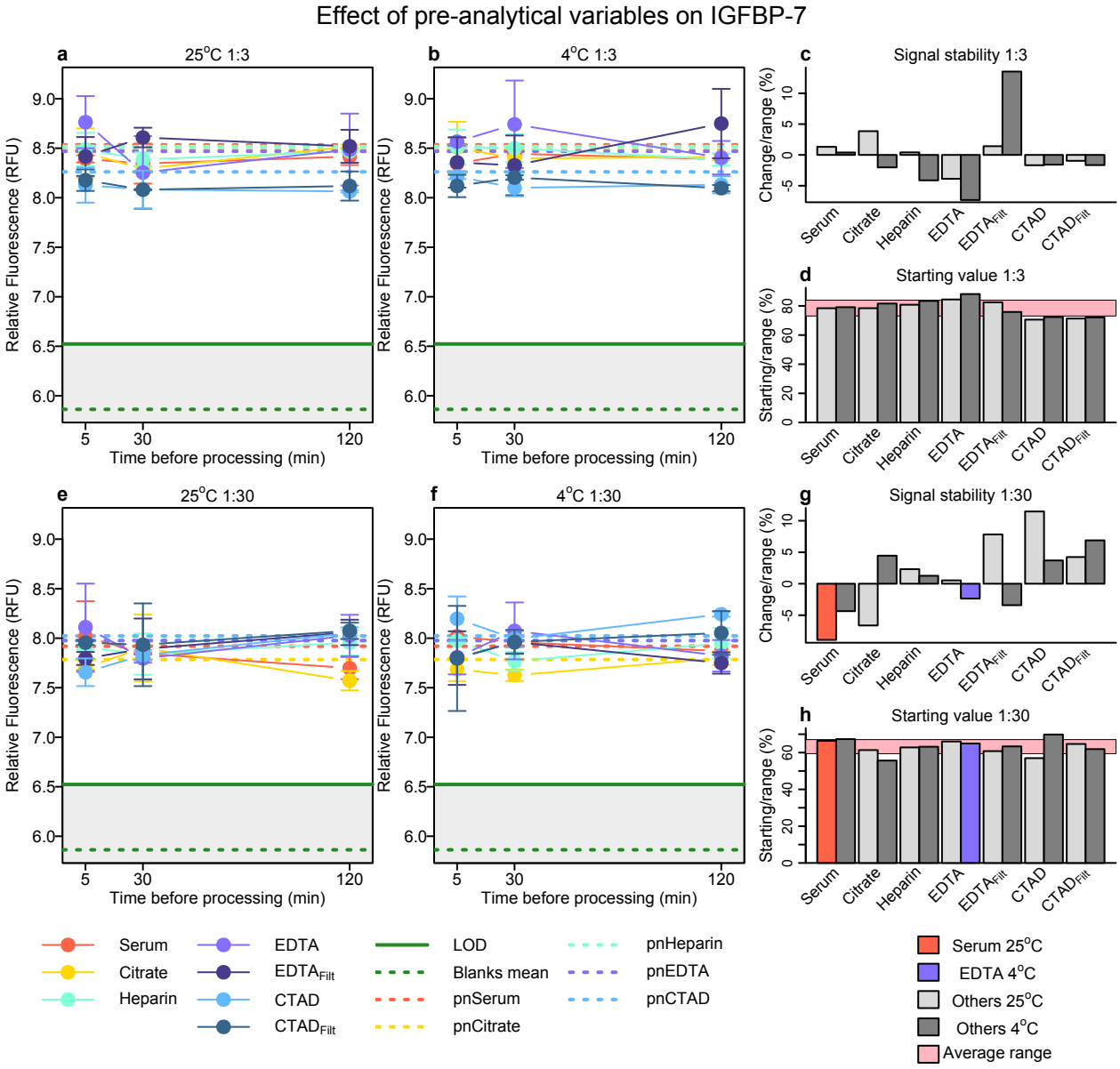

FIGURE I.S88: **Effect of pre-processing storage temperature on IGFBP-7 stability and concentration.** Initial measured value and stability of IGFBP-7 when stored at 25 °C (**a, e**) and 4 °C (**b, f**) before processing when collected in different tube types. The measured values are shown at low dilution of 1:3 (**a-b**) and high dilution of 1:30 (**e-f**). Stability before processing is expressed as an increase or decrease compared to the measurement range and is shown for low (**c**) and high (**g**) dilutions. Initial value is expressed as a portion of the measurement range when the linear regression is extrapolated to zero minutes and is shown for low (**d**) and high (**h**) dilutions. The pink box in graphs **d** and **h** indicate the region that is included by the *mean* ± *SD* of all the initial values and gives an indication of outliers when values lie outside this region. Red and purple bars in **c-d, g-h** are indicated at the measured dilution as the two choices for the TBI analysis.

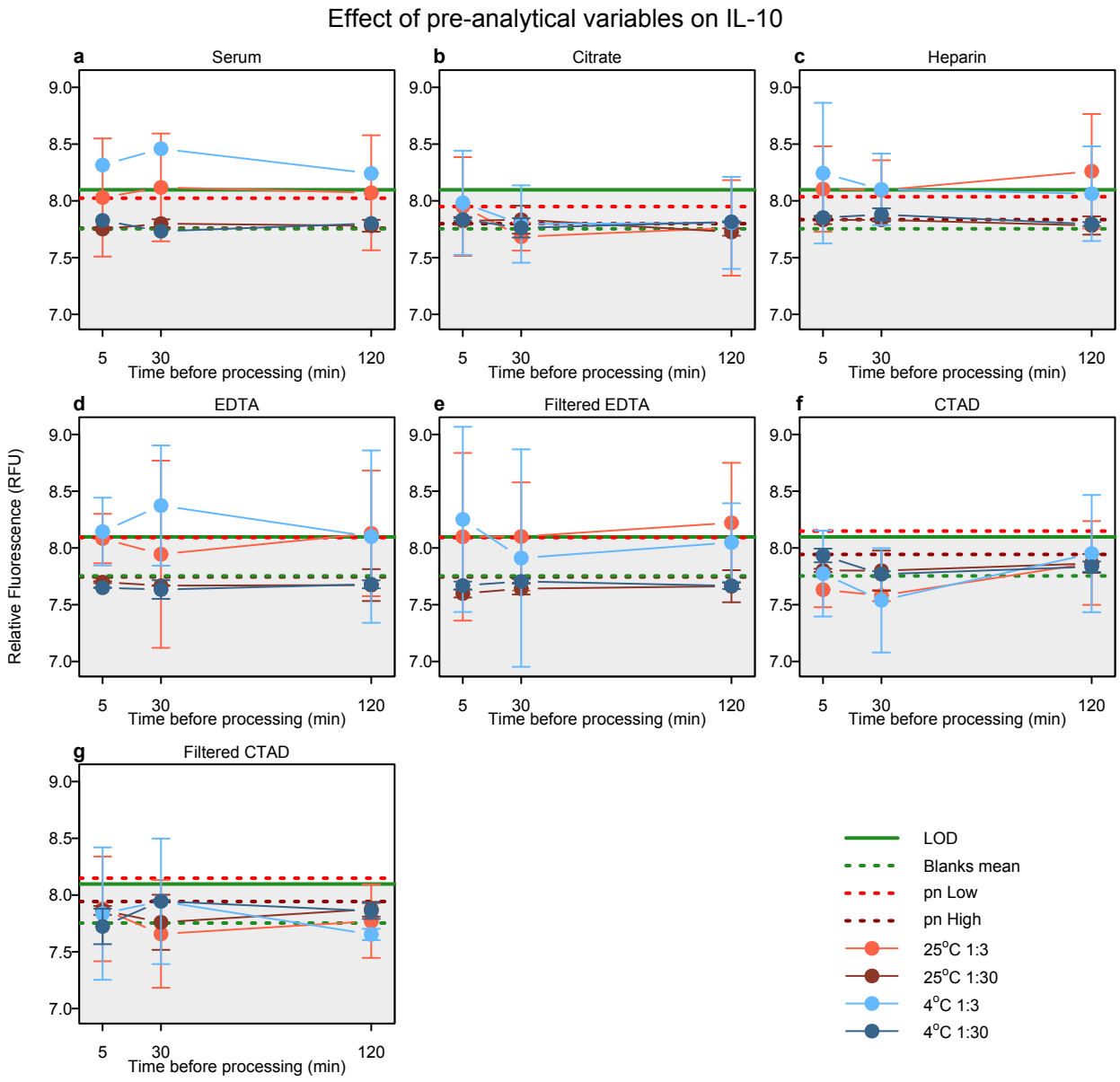

FIGURE I.S89: **Effect of blood collection tube on IL-10 stability and concentration.** Effects of blood collection tubes (**a**: serum, **b**: citrate, **c**: heparin, **d-e**: EDTA, **f-g**: CTAD), storage temperature and time before processing, and post-processing plasma filtering (**e, g**) on the initial value and pre-processing time stability of IL-10 measurements in blood. Information on the dilution of samples used for measuring, data range and the sample type selected are also shown.

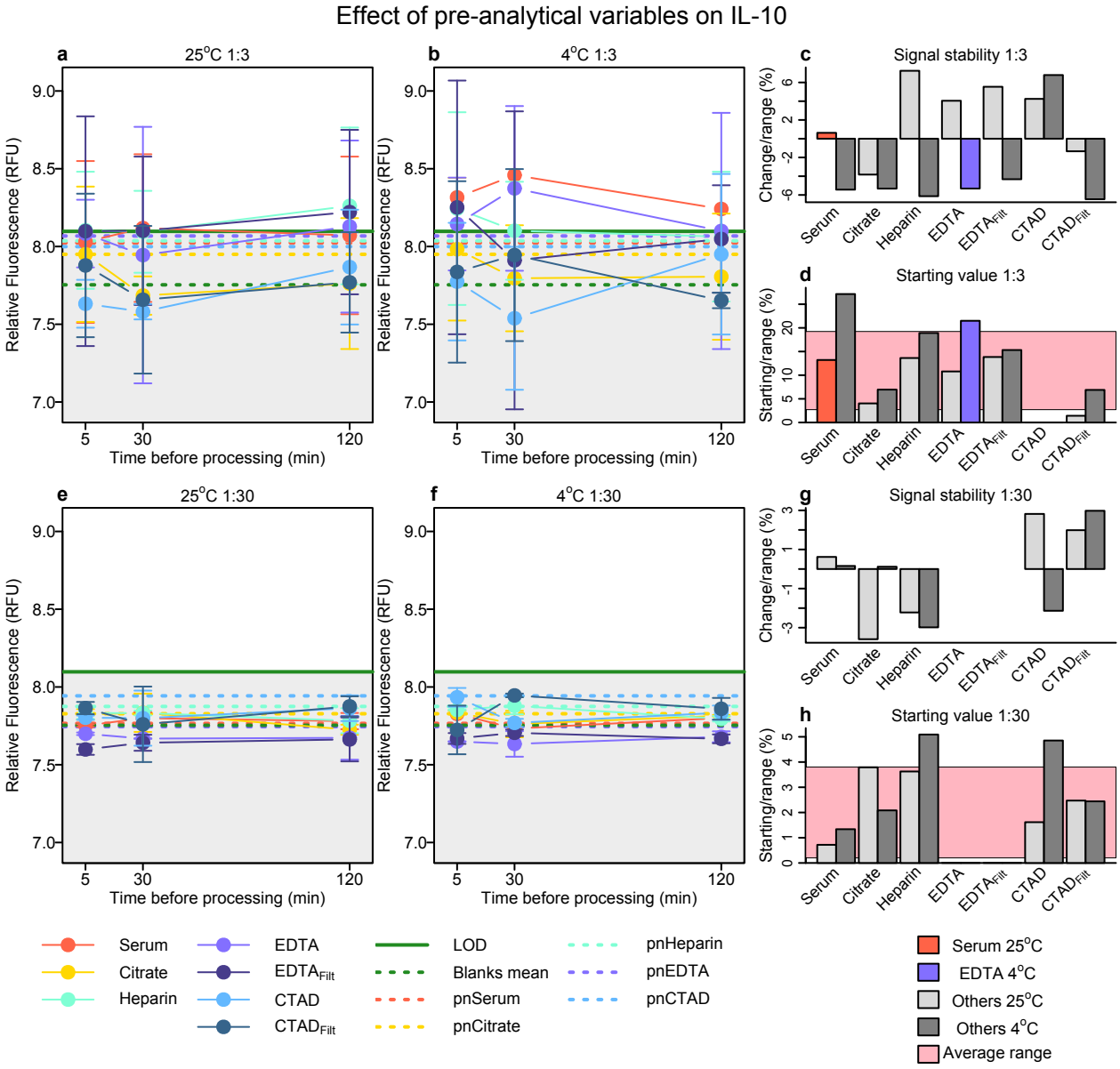

FIGURE I.S90: **Effect of pre-processing storage temperature on IL-10 stability and concentration.** Initial measured value and stability of IL-10 when stored at 25 °C (**a, e**) and 4 °C (**b, f**) before processing when collected in different tube types. The measured values are shown at low dilution of 1:3 (**a-b**) and high dilution of 1:30 (**e-f**). Stability before processing is expressed as an increase or decrease compared to the measurement range and is shown for low (**c**) and high (**g**) dilutions. Initial value is expressed as a portion of the measurement range when the linear regression is extrapolated to zero minutes and is shown for low (**d**) and high (**h**) dilutions. The pink box in graphs **d** and **h** indicate the region that is included by the *mean* ± *SD* of all the initial values and gives an indication of outliers when values lie outside this region. Red and purple bars in **c-d, g-h** are indicated at the measured dilution as the two choices for the TBI analysis.

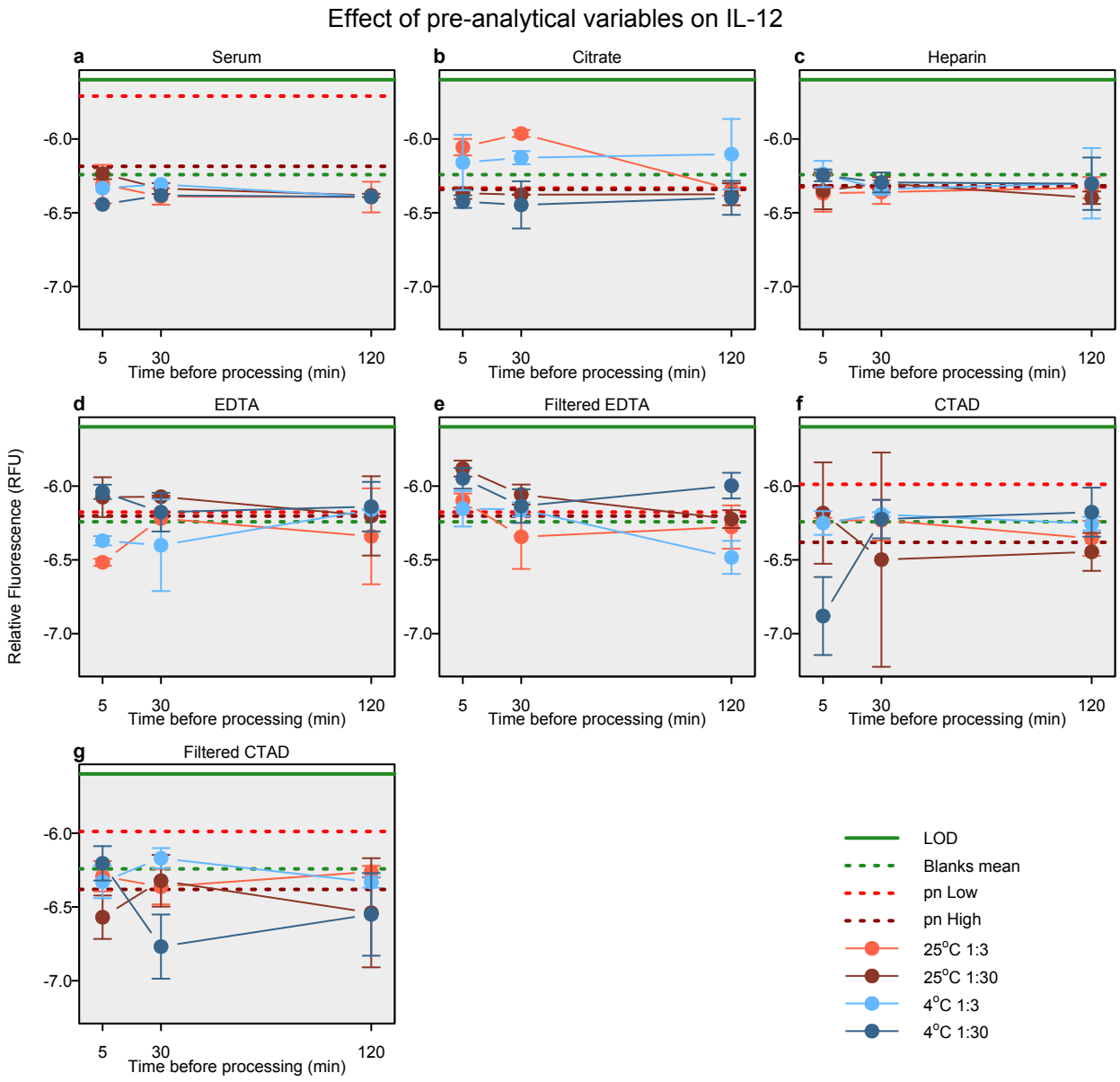

FIGURE I.S91: **Effect of blood collection tube on IL-12 stability and concentration.** Effects of blood collection tubes (**a**: serum, **b**: citrate, **c**: heparin, **d-e**: EDTA, **f-g**: CTAD), storage temperature and time before processing, and post-processing plasma filtering (**e, g**) on the initial value and pre-processing time stability of IL-12 measurements in blood. Information on the dilution of samples used for measuring, data range and the sample type selected are also shown.

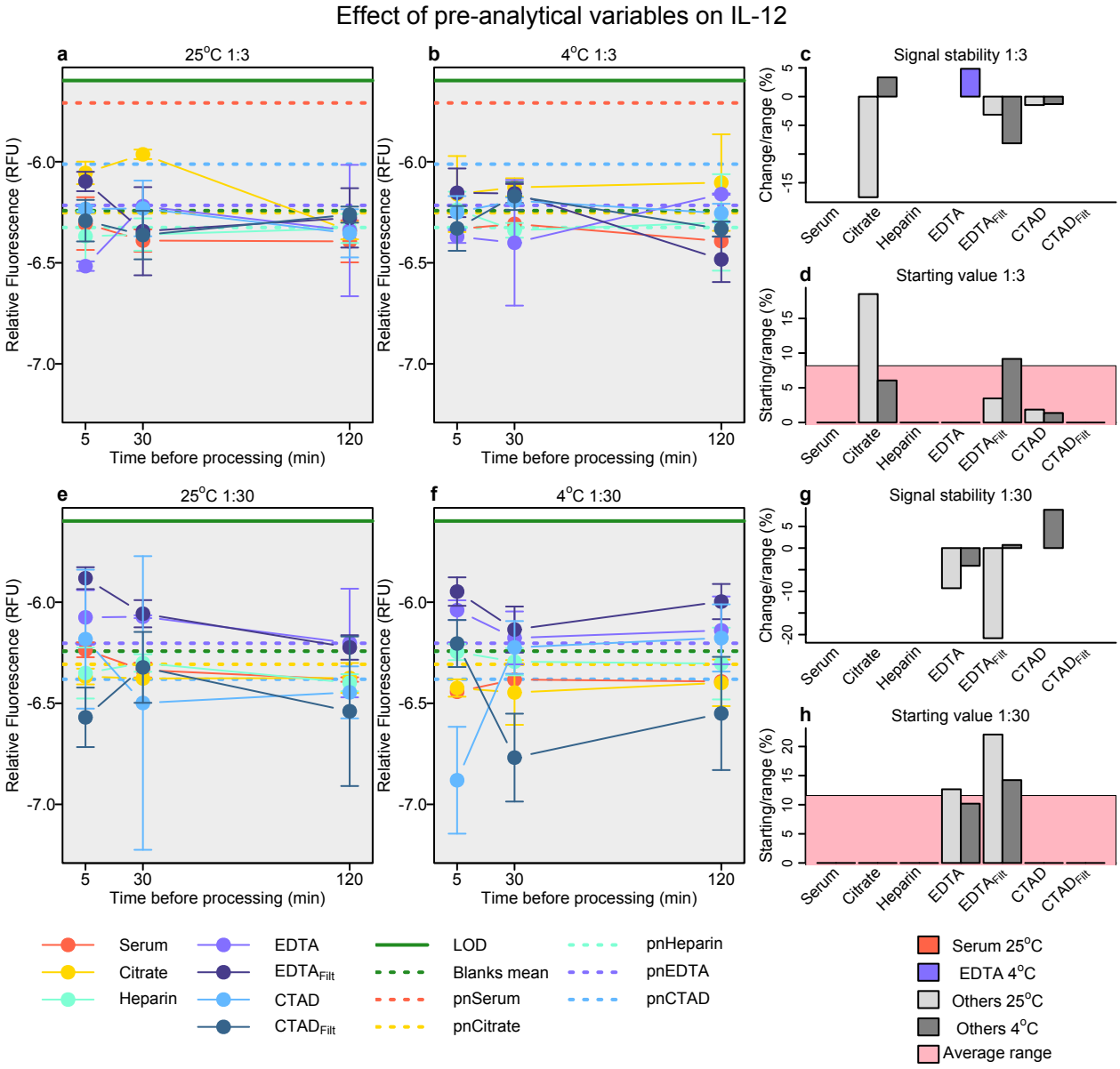

FIGURE I.S92: **Effect of pre-processing storage temperature on IL-12 stability and concentration.** Initial measured value and stability of IL-12 when stored at 25 °C (**a, e**) and 4 °C (**b, f**) before processing when collected in different tube types. The measured values are shown at low dilution of 1:3 (**a-b**) and high dilution of 1:30 (**e-f**). Stability before processing is expressed as an increase or decrease compared to the measurement range and is shown for low (**c**) and high (**g**) dilutions. Initial value is expressed as a portion of the measurement range when the linear regression is extrapolated to zero minutes and is shown for low (**d**) and high (**h**) dilutions. The pink box in graphs **d** and **h** indicate the region that is included by the *mean* ± *SD* of all the initial values and gives an indication of outliers when values lie outside this region. Red and purple bars in **c-d, g-h** are indicated at the measured dilution as the two choices for the TBI analysis.

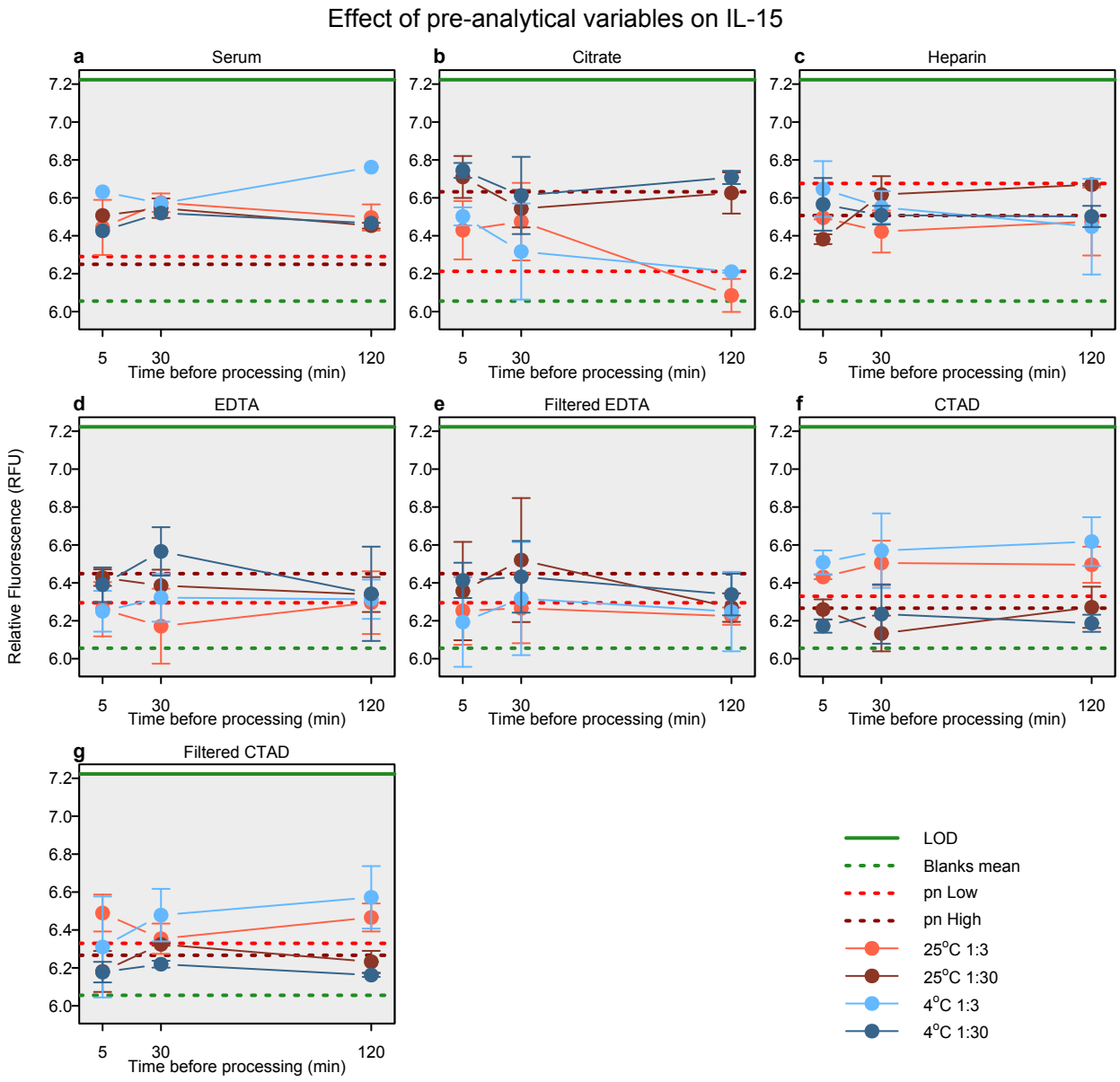

FIGURE I.S93: **Effect of blood collection tube on IL-15 stability and concentration.** Effects of blood collection tubes (**a**: serum, **b**: citrate, **c**: heparin, **d-e**: EDTA, **f-g**: CTAD), storage temperature and time before processing, and post-processing plasma filtering (**e, g**) on the initial value and pre-processing time stability of IL-15 measurements in blood. Information on the dilution of samples used for measuring, data range and the sample type selected are also shown.

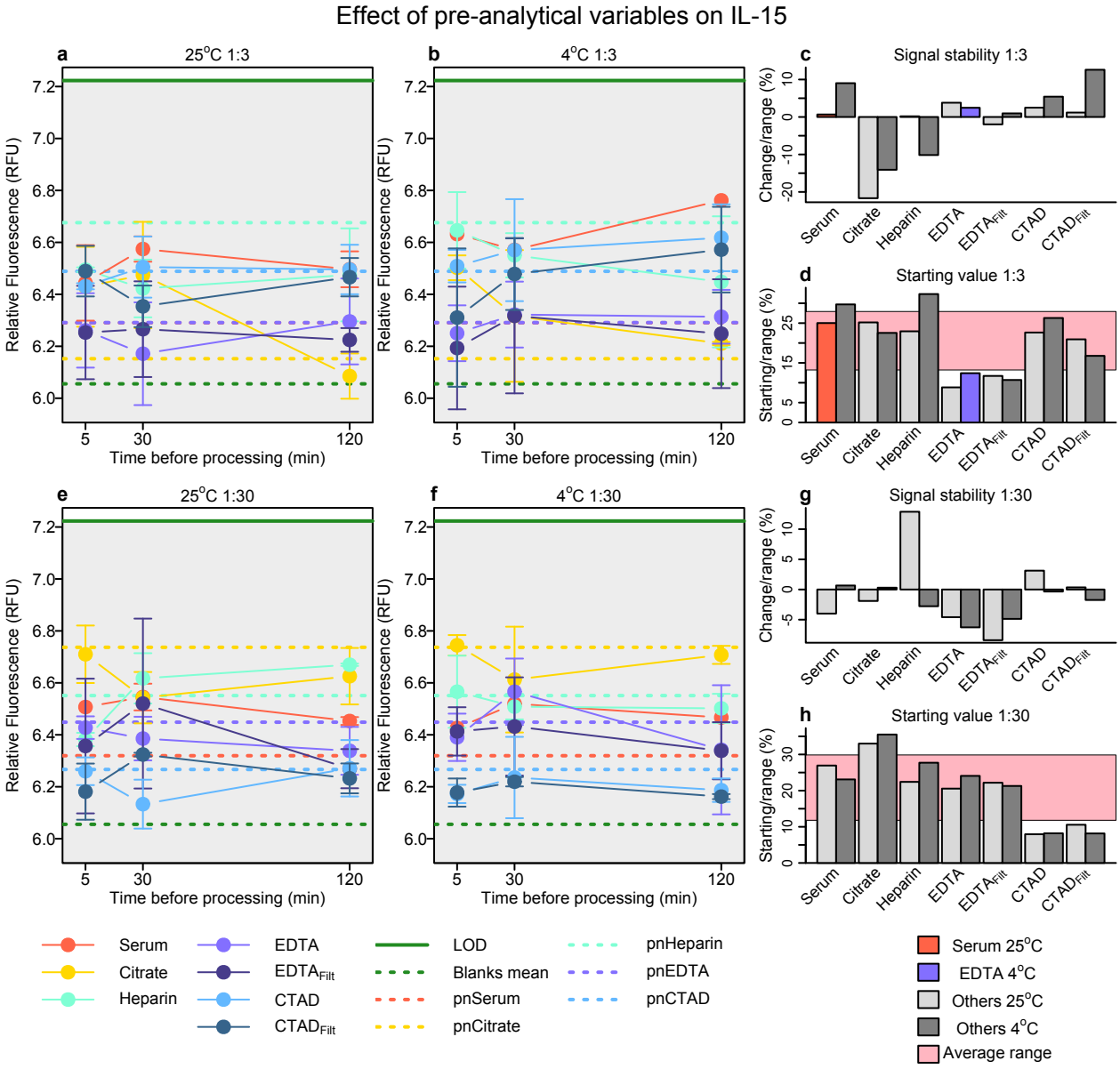

FIGURE I.S94: **Effect of pre-processing storage temperature on IL-15 stability and concentration.** Initial measured value and stability of IL-15 when stored at 25 °C (**a, e**) and 4 °C (**b, f**) before processing when collected in different tube types. The measured values are shown at low dilution of 1:3 (**a-b**) and high dilution of 1:30 (**e-f**). Stability before processing is expressed as an increase or decrease compared to the measurement range and is shown for low (**c**) and high (**g**) dilutions. Initial value is expressed as a portion of the measurement range when the linear regression is extrapolated to zero minutes and is shown for low (**d**) and high (**h**) dilutions. The pink box in graphs **d** and **h** indicate the region that is included by the *mean* ± *SD* of all the initial values and gives an indication of outliers when values lie outside this region. Red and purple bars in **c-d, g-h** are indicated at the measured dilution as the two choices for the TBI analysis.

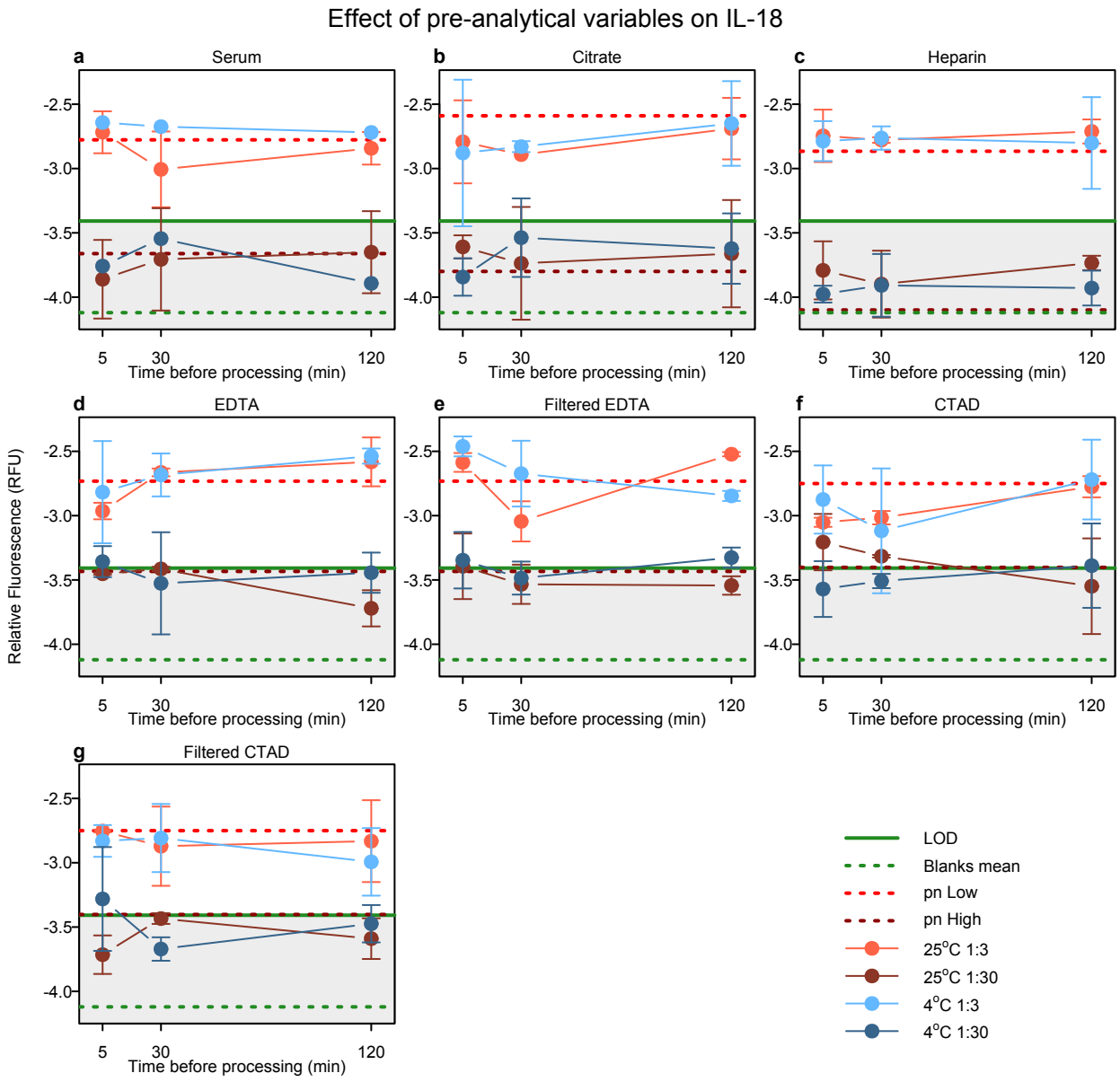

FIGURE I.S95: **Effect of blood collection tube on IL-18 stability and concentration.** Effects of blood collection tubes (**a**: serum, **b**: citrate, **c**: heparin, **d-e**: EDTA, **f-g**: CTAD), storage temperature and time before processing, and post-processing plasma filtering (**e, g**) on the initial value and pre-processing time stability of IL-18 measurements in blood. Information on the dilution of samples used for measuring, data range and the sample type selected are also shown.

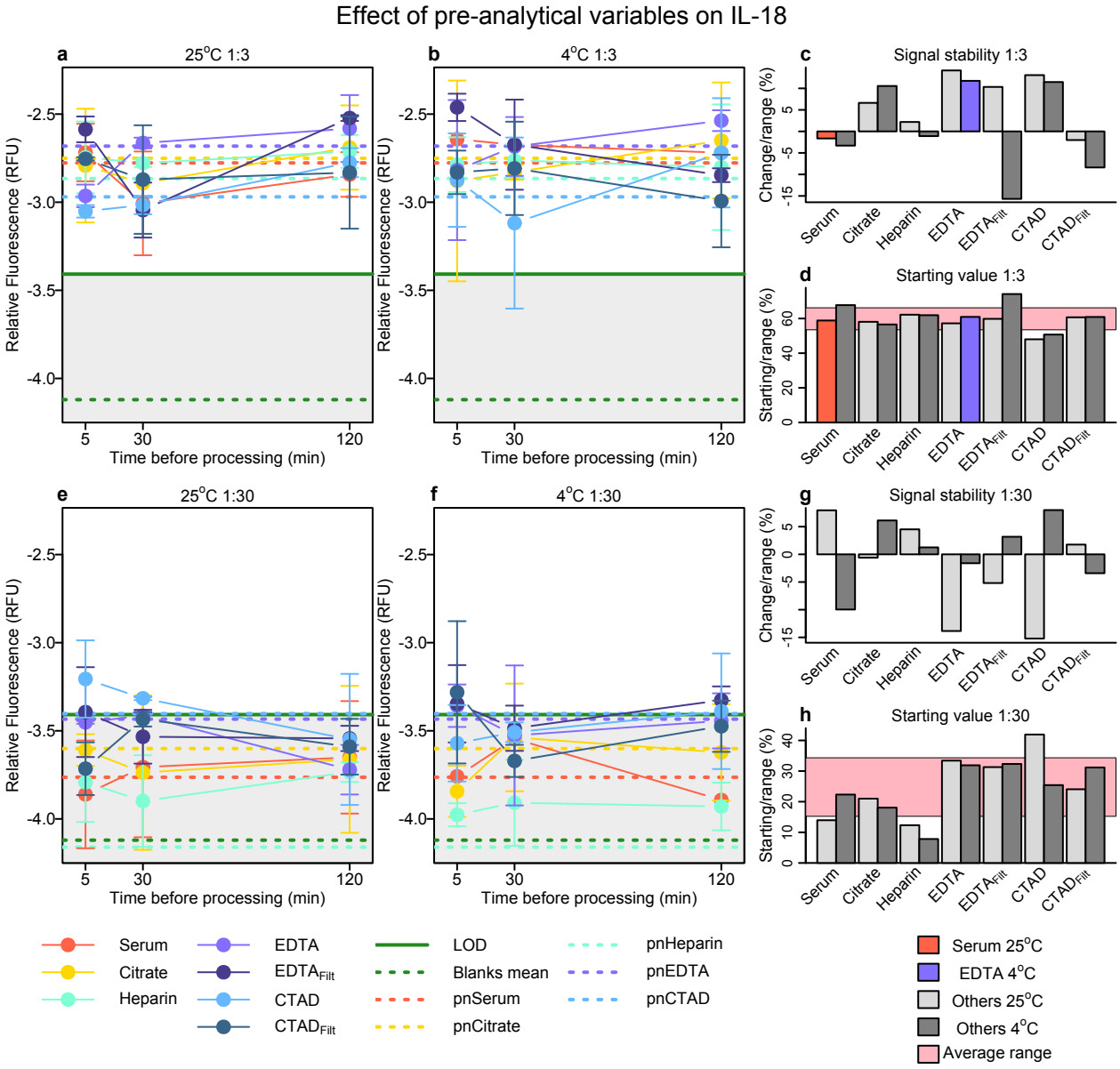

FIGURE I.S96: **Effect of pre-processing storage temperature on IL-18 stability and concentration.** Initial measured value and stability of IL-18 when stored at 25 °C (**a, e**) and 4 °C (**b, f**) before processing when collected in different tube types. The measured values are shown at low dilution of 1:3 (**a-b**) and high dilution of 1:30 (**e-f**). Stability before processing is expressed as an increase or decrease compared to the measurement range and is shown for low (**c**) and high (**g**) dilutions. Initial value is expressed as a portion of the measurement range when the linear regression is extrapolated to zero minutes and is shown for low (**d**) and high (**h**) dilutions. The pink box in graphs **d** and **h** indicate the region that is included by the *mean* ± *SD* of all the initial values and gives an indication of outliers when values lie outside this region. Red and purple bars in **c-d, g-h** are indicated at the measured dilution as the two choices for the TBI analysis.

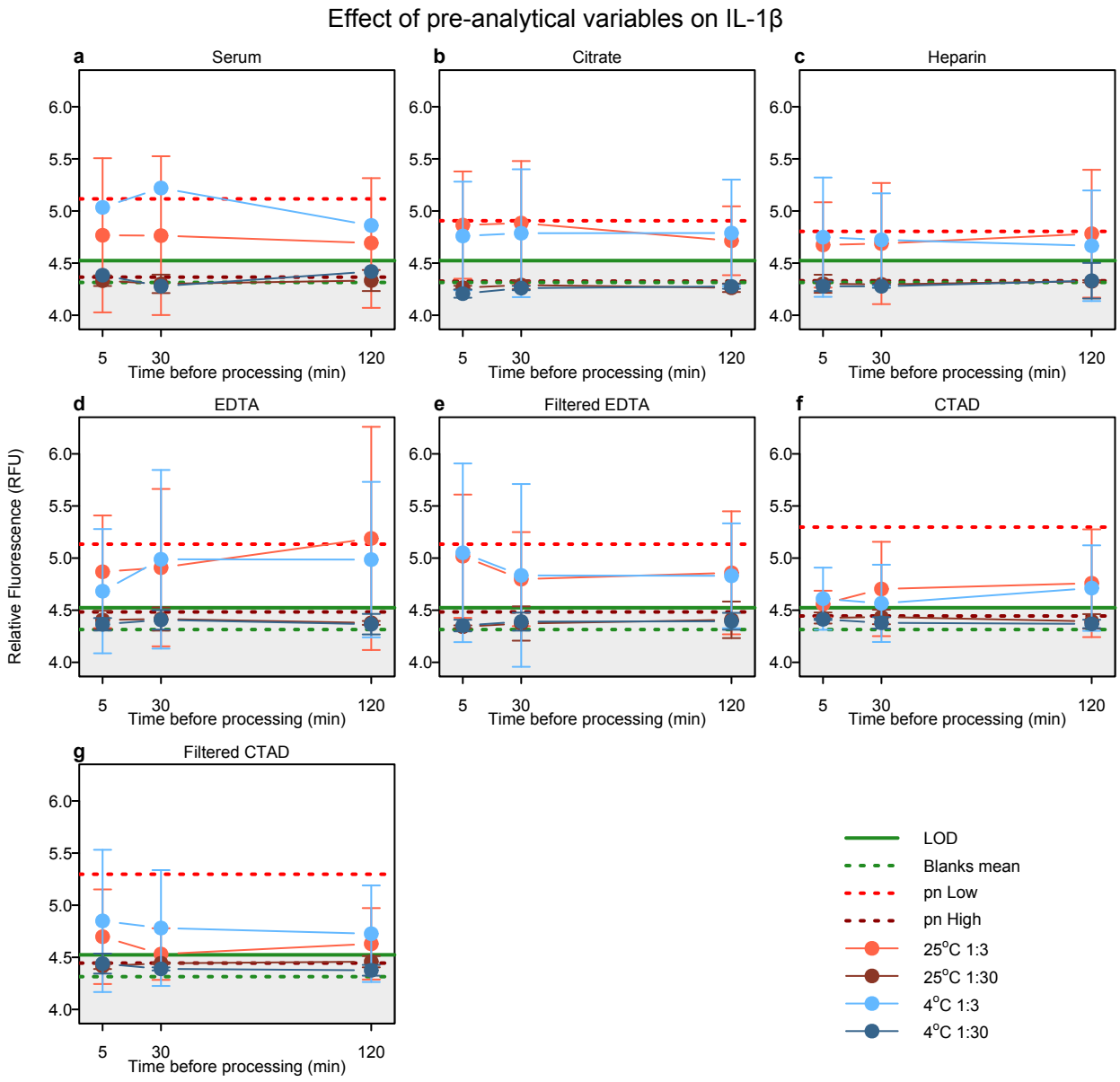

FIGURE I.S97: **Effect of blood collection tube on IL-1β stability and concentration.** Effects of blood collection tubes (**a**: serum, **b**: citrate, **c**: heparin, **d-e**: EDTA, **f-g**: CTAD), storage temperature and time before processing, and post-processing plasma filtering (**e, g**) on the initial value and pre-processing time stability of IL-1β measurements in blood. Information on the dilution of samples used for measuring, data range and the sample type selected are also shown.

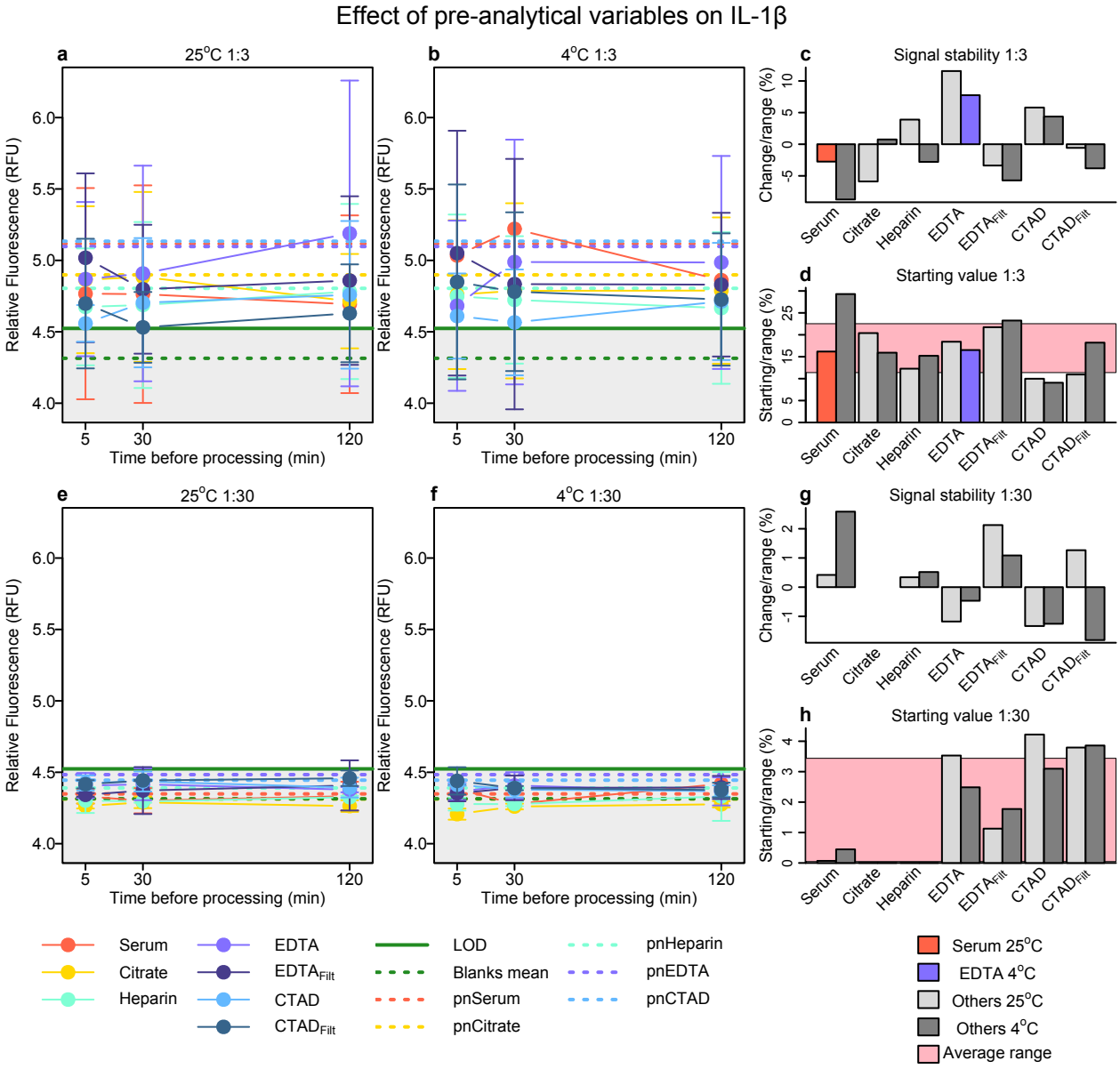

FIGURE I.S98: **Effect of pre-processing storage temperature on IL-1β stability and concentration.** Initial measured value and stability of IL-1β when stored at 25 °C (**a, e**) and 4 °C (**b, f**) before processing when collected in different tube types. The measured values are shown at low dilution of 1:3 (**a-b**) and high dilution of 1:30 (**e-f**). Stability before processing is expressed as an increase or decrease compared to the measurement range and is shown for low (**c**) and high (**g**) dilutions. Initial value is expressed as a portion of the measurement range when the linear regression is extrapolated to zero minutes and is shown for low (**d**) and high (**h**) dilutions. The pink box in graphs **d** and **h** indicate the region that is included by the *mean* ± *SD* of all the initial values and gives an indication of outliers when values lie outside this region. Red and purple bars in **c-d, g-h** are indicated at the measured dilution as the two choices for the TBI analysis.

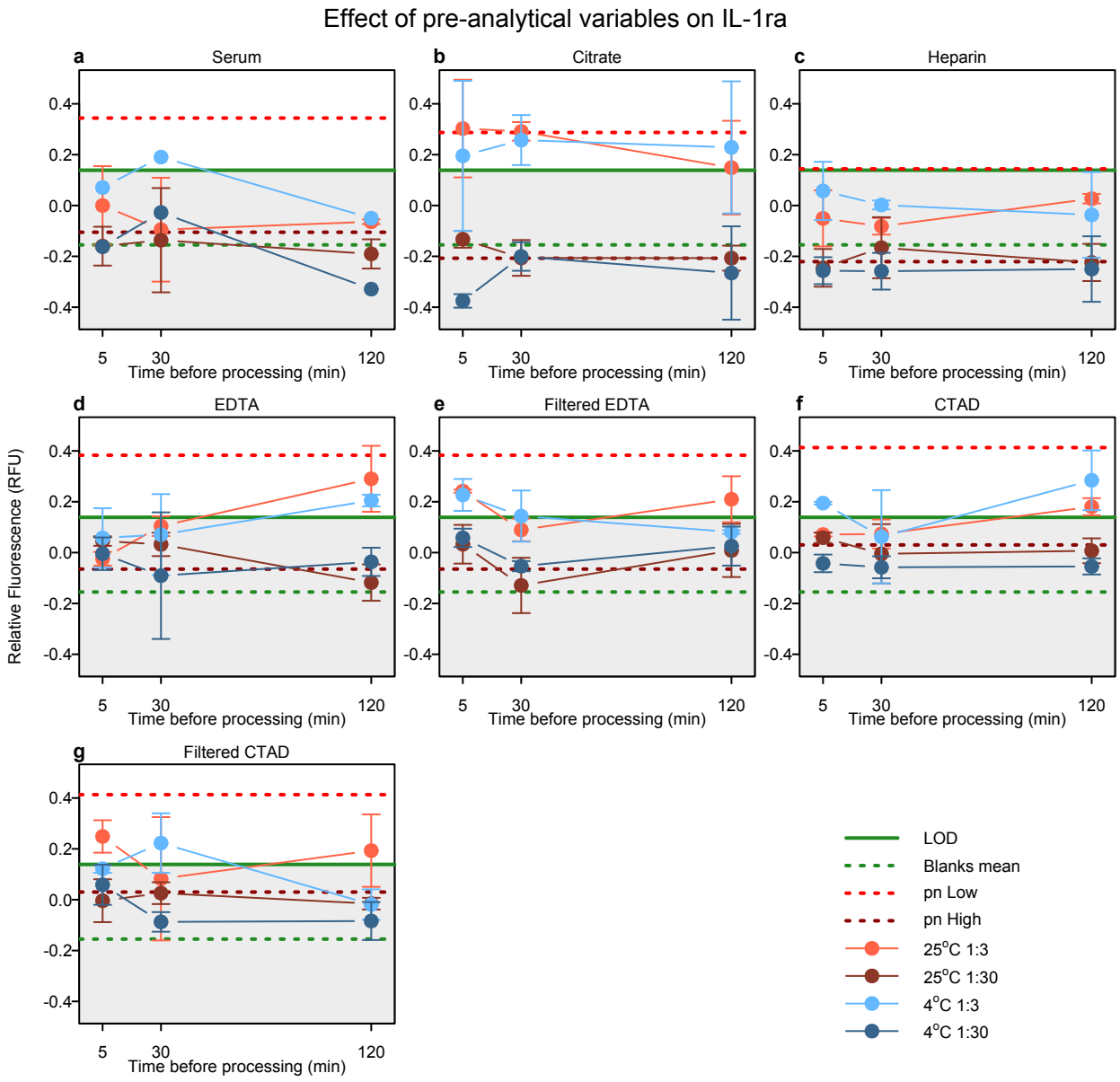

FIGURE I.S99: **Effect of blood collection tube on IL-1ra stability and concentration.** Effects of blood collection tubes (**a**: serum, **b**: citrate, **c**: heparin, **d-e**: EDTA, **f-g**: CTAD), storage temperature and time before processing, and post-processing plasma filtering (**e, g**) on the initial value and pre-processing time stability of IL-1ra measurements in blood. Information on the dilution of samples used for measuring, data range and the sample type selected are also shown.

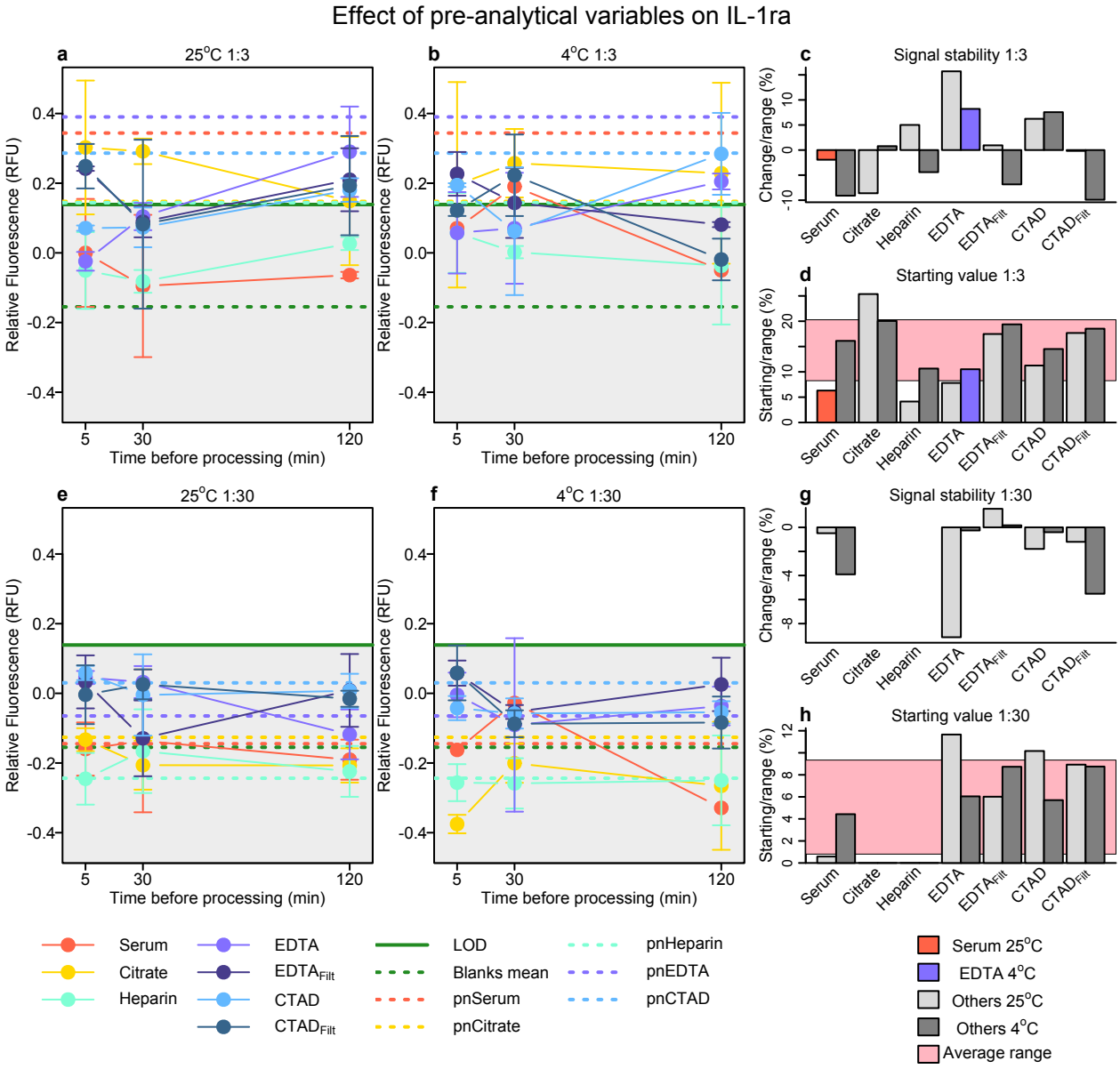

FIGURE I.S100: **Effect of pre-processing storage temperature on IL-1ra stability and concentration.** Initial measured value and stability of IL-1ra when stored at 25 °C (**a, e**) and 4 °C (**b, f**) before processing when collected in different tube types. The measured values are shown at low dilution of 1:3 (**a-b**) and high dilution of 1:30 (**e-f**). Stability before processing is expressed as an increase or decrease compared to the measurement range and is shown for low (**c**) and high (**g**) dilutions. Initial value is expressed as a portion of the measurement range when the linear regression is extrapolated to zero minutes and is shown for low (**d**) and high (**h**) dilutions. The pink box in graphs **d** and **h** indicate the region that is included by the *mean* ± *SD* of all the initial values and gives an indication of outliers when values lie outside this region. Red and purple bars in **c-d, g-h** are indicated at the measured dilution as the two choices for the TBI analysis.

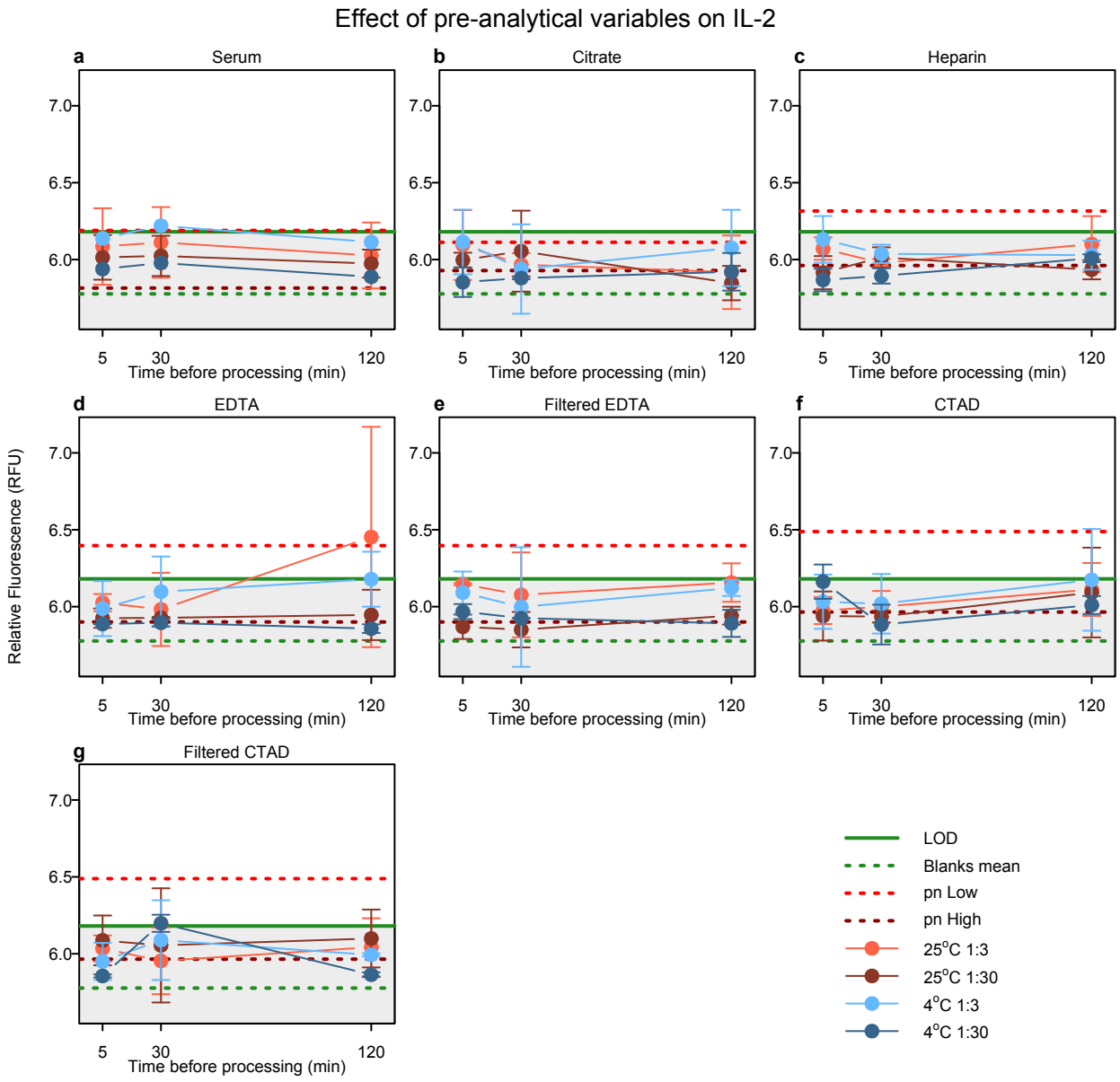

FIGURE I.S101: **Effect of blood collection tube on IL-2 stability and concentration.** Effects of blood collection tubes (**a**: serum, **b**: citrate, **c**: heparin, **d-e**: EDTA, **f-g**: CTAD), storage temperature and time before processing, and post-processing plasma filtering (**e, g**) on the initial value and pre-processing time stability of IL-2 measurements in blood. Information on the dilution of samples used for measuring, data range and the sample type selected are also shown.

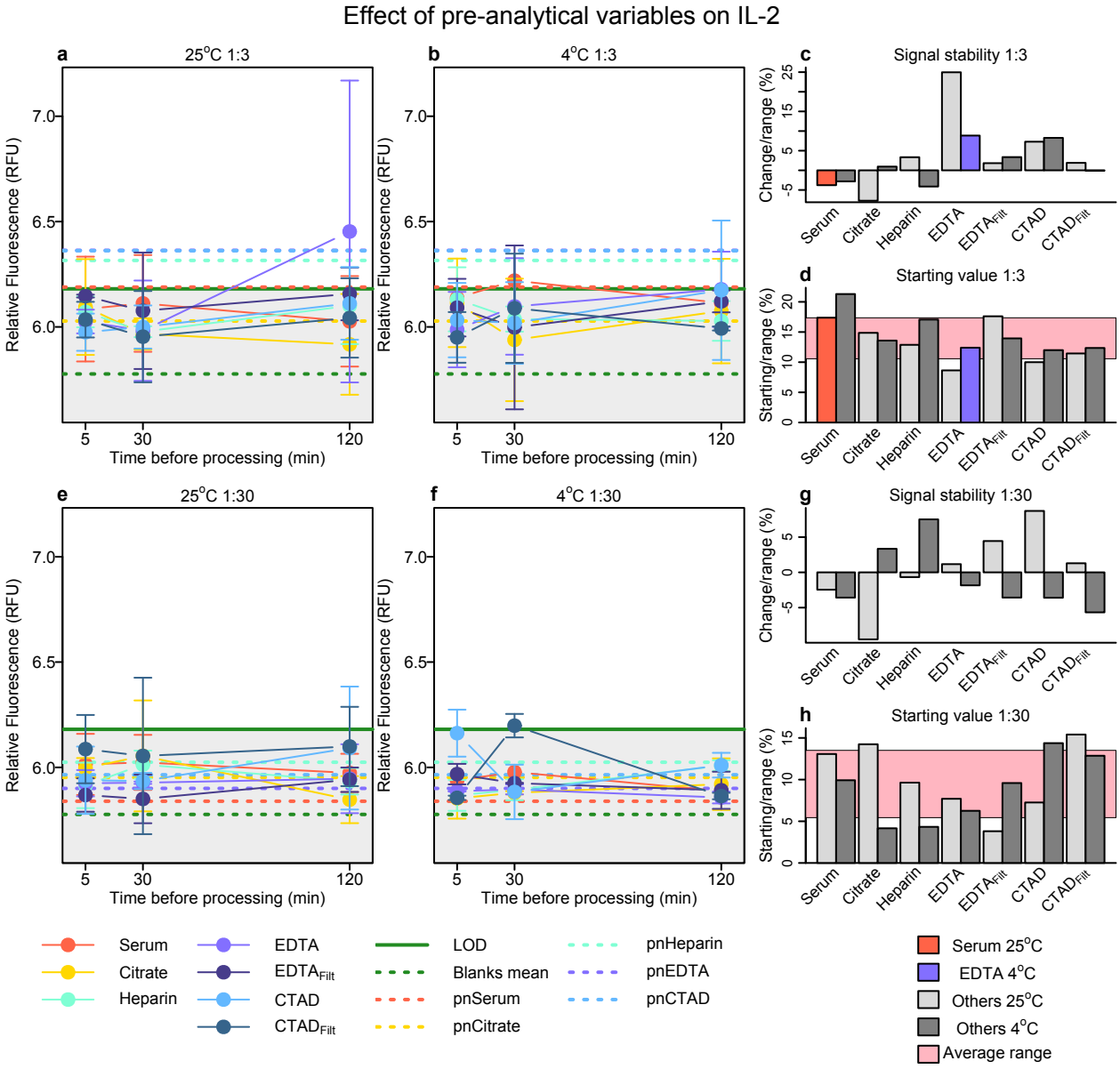

FIGURE I.S102: **Effect of pre-processing storage temperature on IL-2 stability and concentration.** Initial measured value and stability of IL-2 when stored at 25 °C (**a, e**) and 4 °C (**b, f**) before processing when collected in different tube types. The measured values are shown at low dilution of 1:3 (**a-b**) and high dilution of 1:30 (**e-f**). Stability before processing is expressed as an increase or decrease compared to the measurement range and is shown for low (**c**) and high (**g**) dilutions. Initial value is expressed as a portion of the measurement range when the linear regression is extrapolated to zero minutes and is shown for low (**d**) and high (**h**) dilutions. The pink box in graphs **d** and **h** indicate the region that is included by the *mean* ± *SD* of all the initial values and gives an indication of outliers when values lie outside this region. Red and purple bars in **c-d, g-h** are indicated at the measured dilution as the two choices for the TBI analysis.

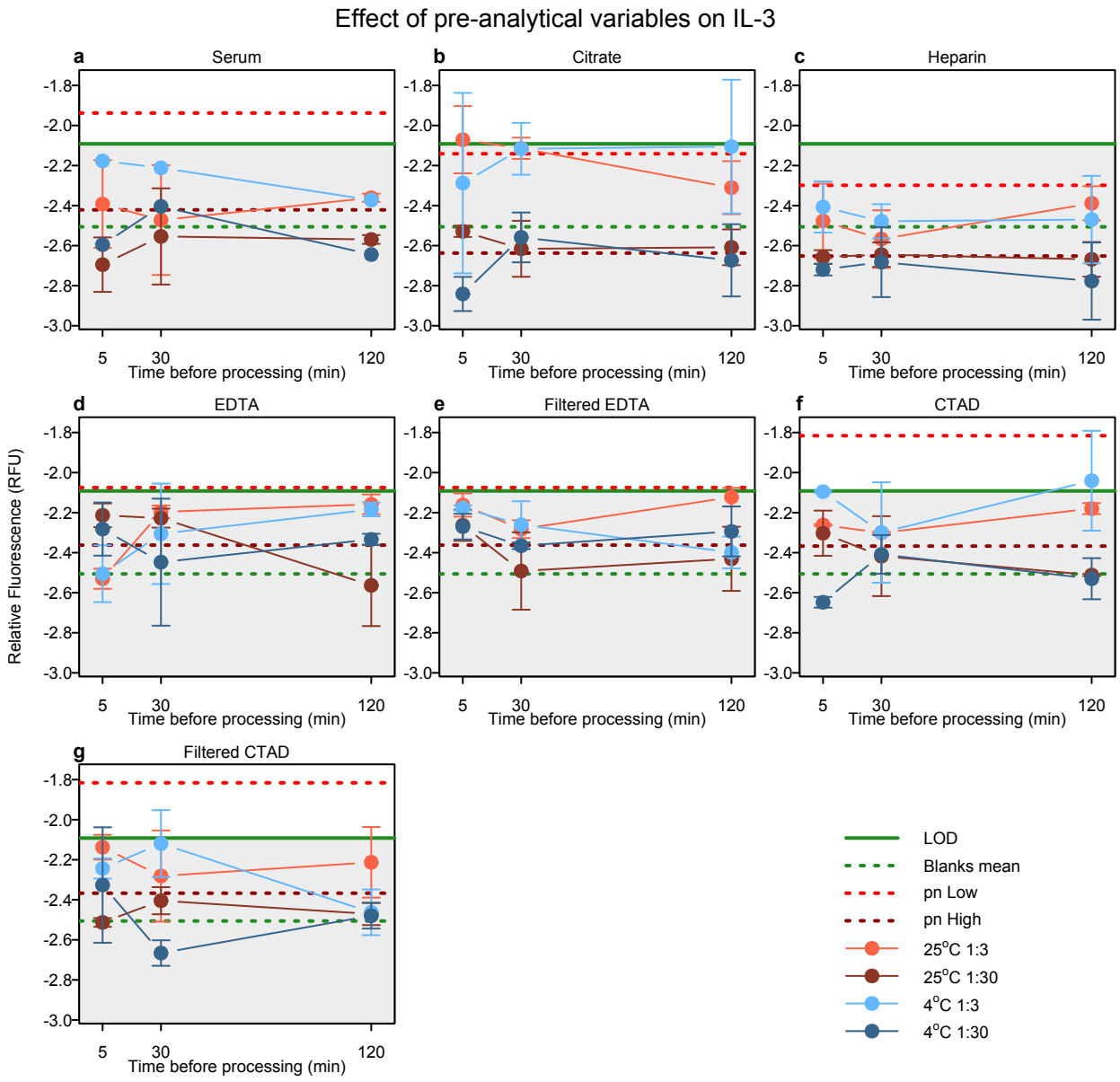

FIGURE I.S103: **Effect of blood collection tube on IL-3 stability and concentration.** Effects of blood collection tubes (**a**: serum, **b**: citrate, **c**: heparin, **d-e**: EDTA, **f-g**: CTAD), storage temperature and time before processing, and post-processing plasma filtering (**e, g**) on the initial value and pre-processing time stability of IL-3 measurements in blood. Information on the dilution of samples used for measuring, data range and the sample type selected are also shown.

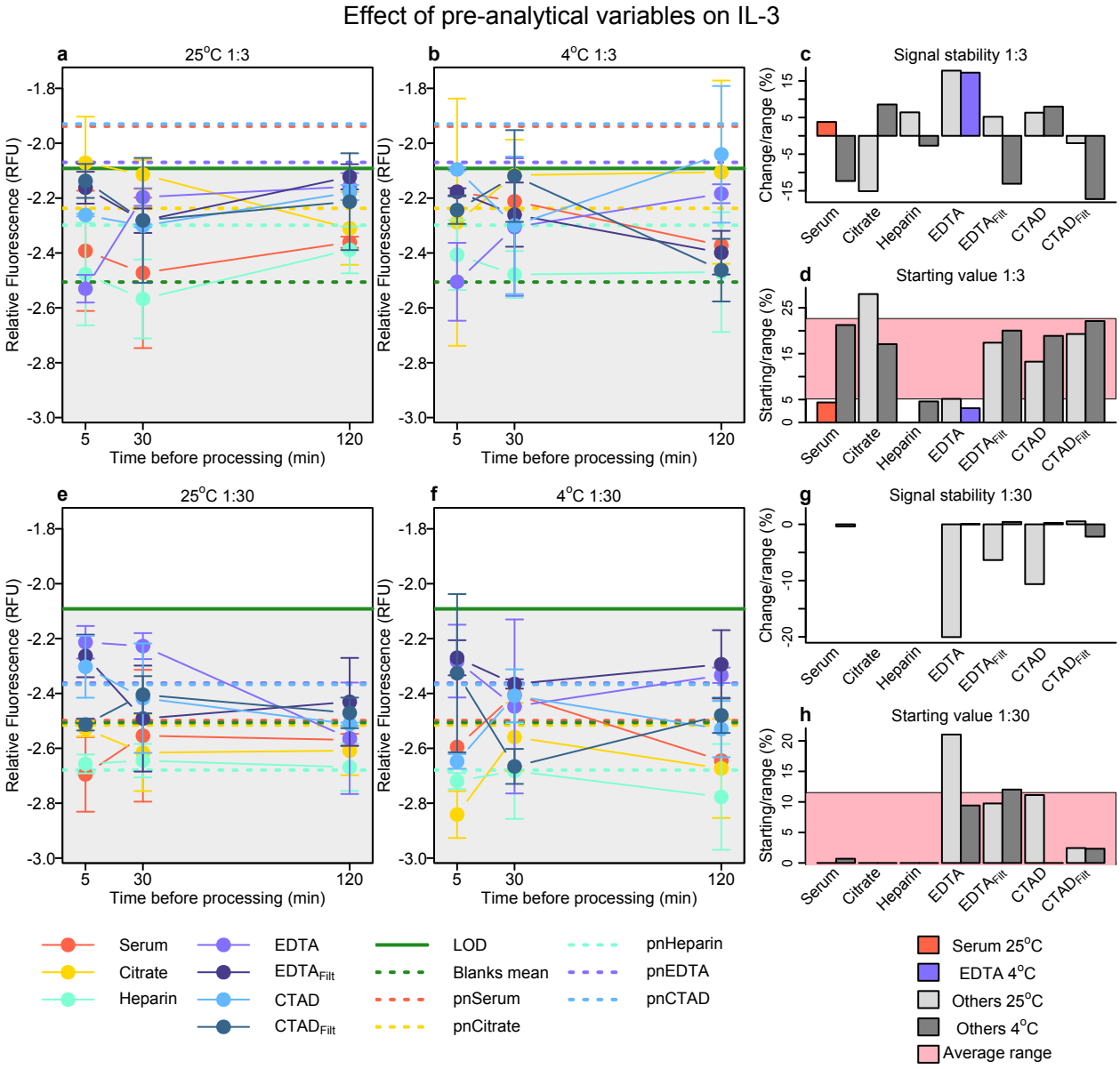

FIGURE I.S104: **Effect of pre-processing storage temperature on IL-3 stability and concentration.** Initial measured value and stability of IL-3 when stored at 25 °C (**a, e**) and 4 °C (**b, f**) before processing when collected in different tube types. The measured values are shown at low dilution of 1:3 (**a-b**) and high dilution of 1:30 (**e-f**). Stability before processing is expressed as an increase or decrease compared to the measurement range and is shown for low (**c**) and high (**g**) dilutions. Initial value is expressed as a portion of the measurement range when the linear regression is extrapolated to zero minutes and is shown for low (**d**) and high (**h**) dilutions. The pink box in graphs **d** and **h** indicate the region that is included by the *mean* ± *SD* of all the initial values and gives an indication of outliers when values lie outside this region. Red and purple bars in **c-d, g-h** are indicated at the measured dilution as the two choices for the TBI analysis.

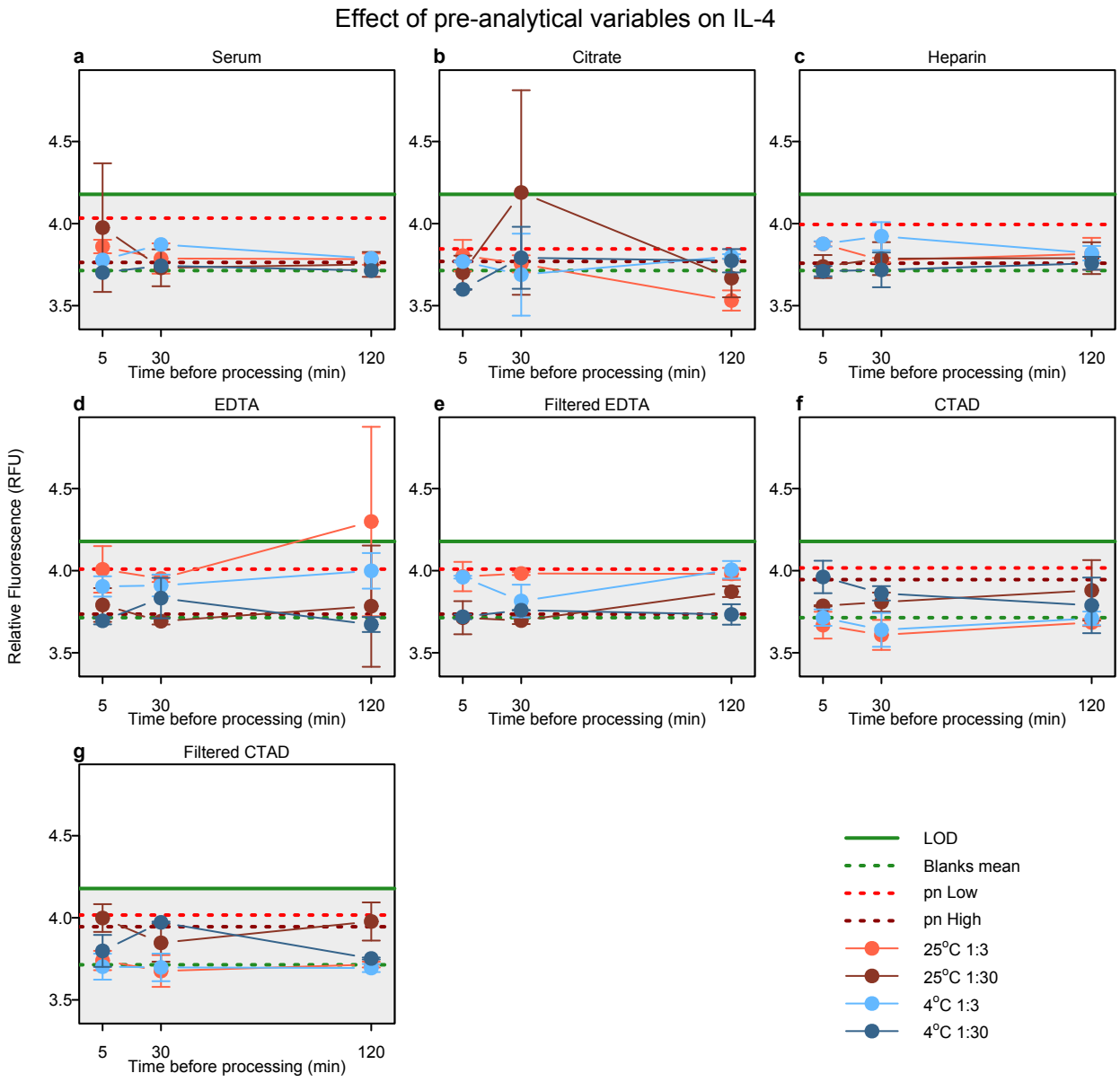

FIGURE I.S105: **Effect of blood collection tube on IL-4 stability and concentration.** Effects of blood collection tubes (**a**: serum, **b**: citrate, **c**: heparin, **d-e**: EDTA, **f-g**: CTAD), storage temperature and time before processing, and post-processing plasma filtering (**e, g**) on the initial value and pre-processing time stability of IL-4 measurements in blood. Information on the dilution of samples used for measuring, data range and the sample type selected are also shown.

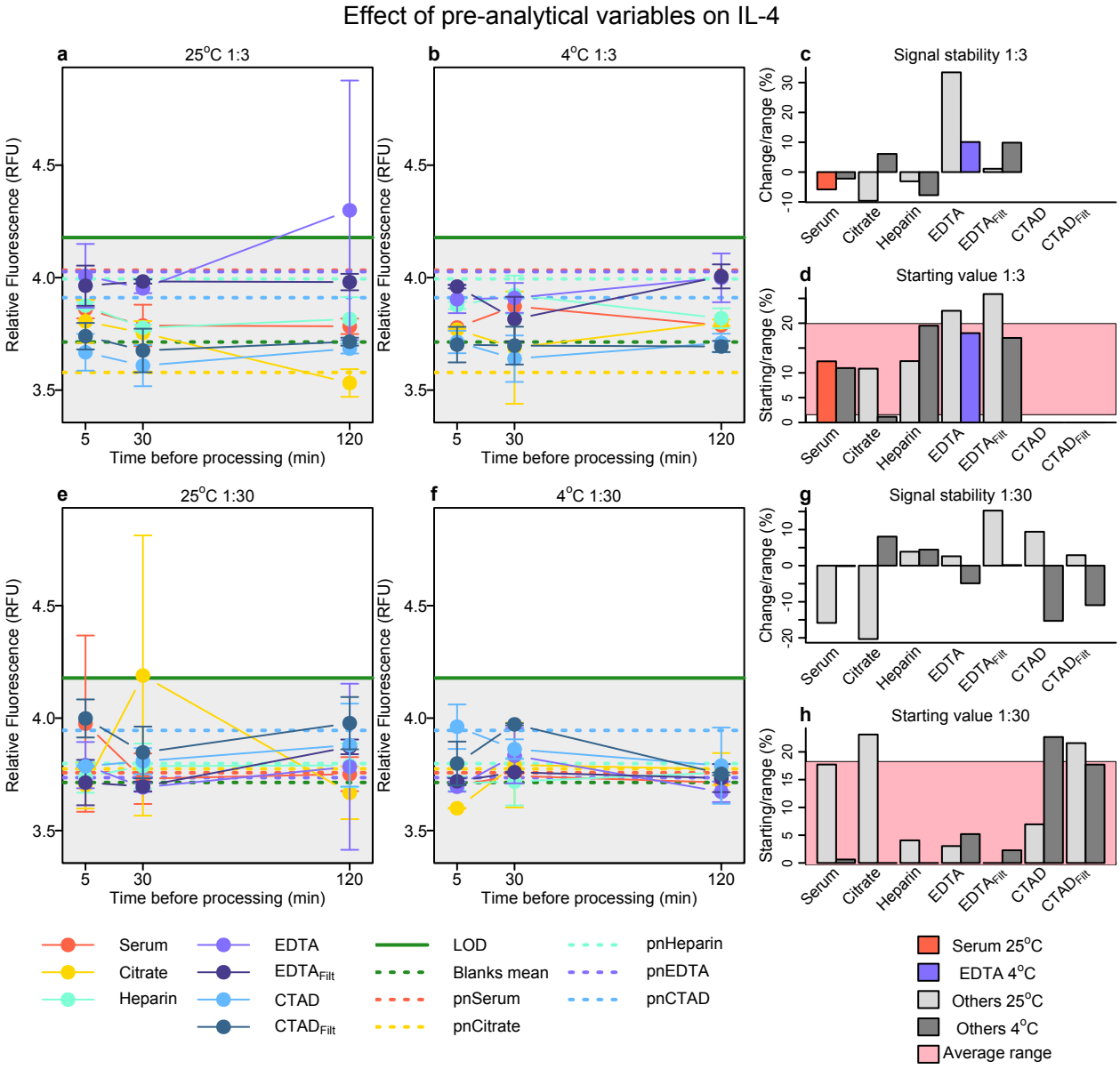

FIGURE I.S106: **Effect of pre-processing storage temperature on IL-4 stability and concentration.** Initial measured value and stability of IL-4 when stored at 25 °C (**a, e**) and 4 °C (**b, f**) before processing when collected in different tube types. The measured values are shown at low dilution of 1:3 (**a-b**) and high dilution of 1:30 (**e-f**). Stability before processing is expressed as an increase or decrease compared to the measurement range and is shown for low (**c**) and high (**g**) dilutions. Initial value is expressed as a portion of the measurement range when the linear regression is extrapolated to zero minutes and is shown for low (**d**) and high (**h**) dilutions. The pink box in graphs **d** and **h** indicate the region that is included by the *mean* ± *SD* of all the initial values and gives an indication of outliers when values lie outside this region. Red and purple bars in **c-d, g-h** are indicated at the measured dilution as the two choices for the TBI analysis.

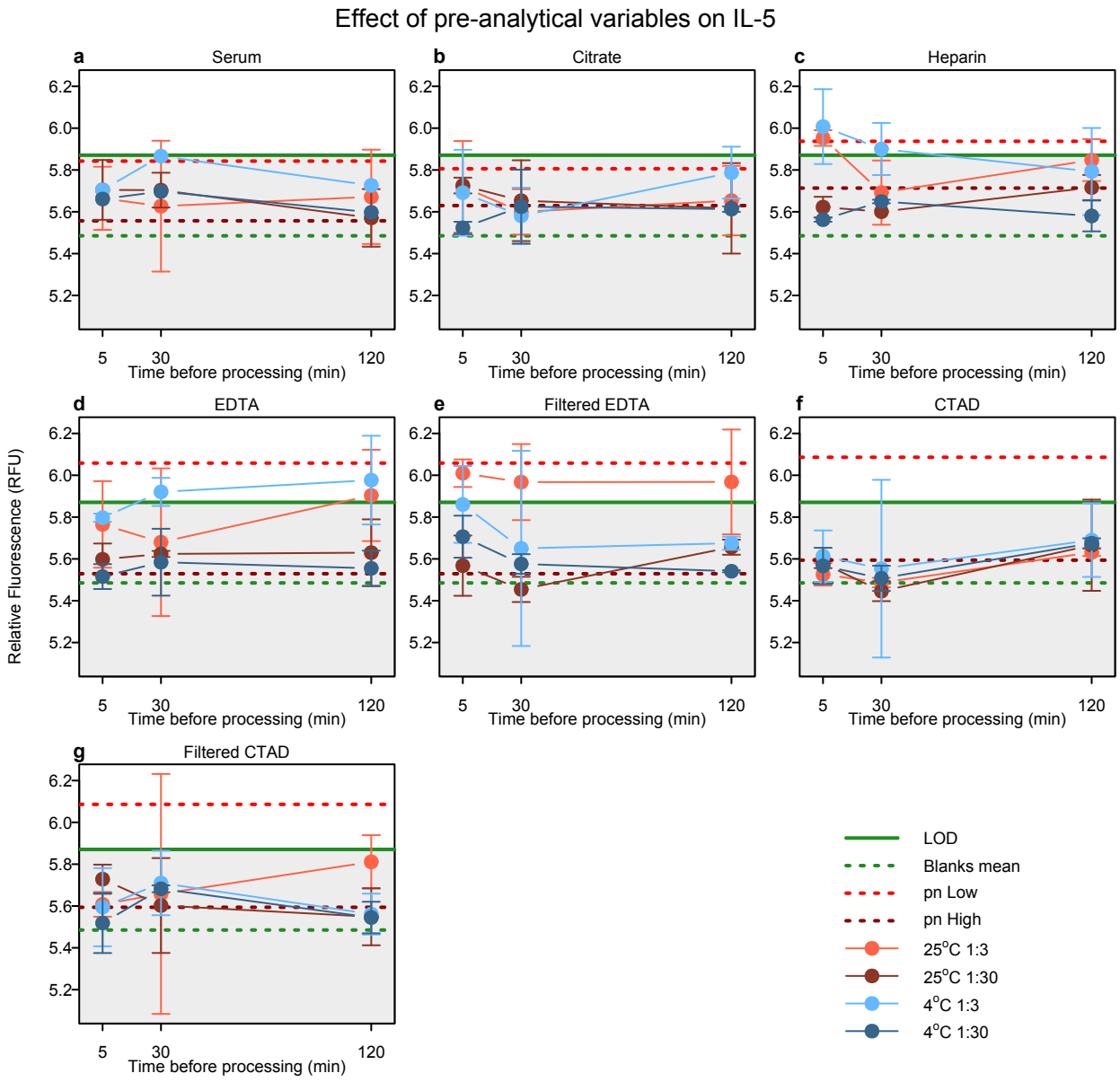

FIGURE I.S107: **Effect of blood collection tube on IL-5 stability and concentration.** Effects of blood collection tubes (**a**: serum, **b**: citrate, **c**: heparin, **d-e**: EDTA, **f-g**: CTAD), storage temperature and time before processing, and post-processing plasma filtering (**e, g**) on the initial value and pre-processing time stability of IL-5 measurements in blood. Information on the dilution of samples used for measuring, data range and the sample type selected are also shown.

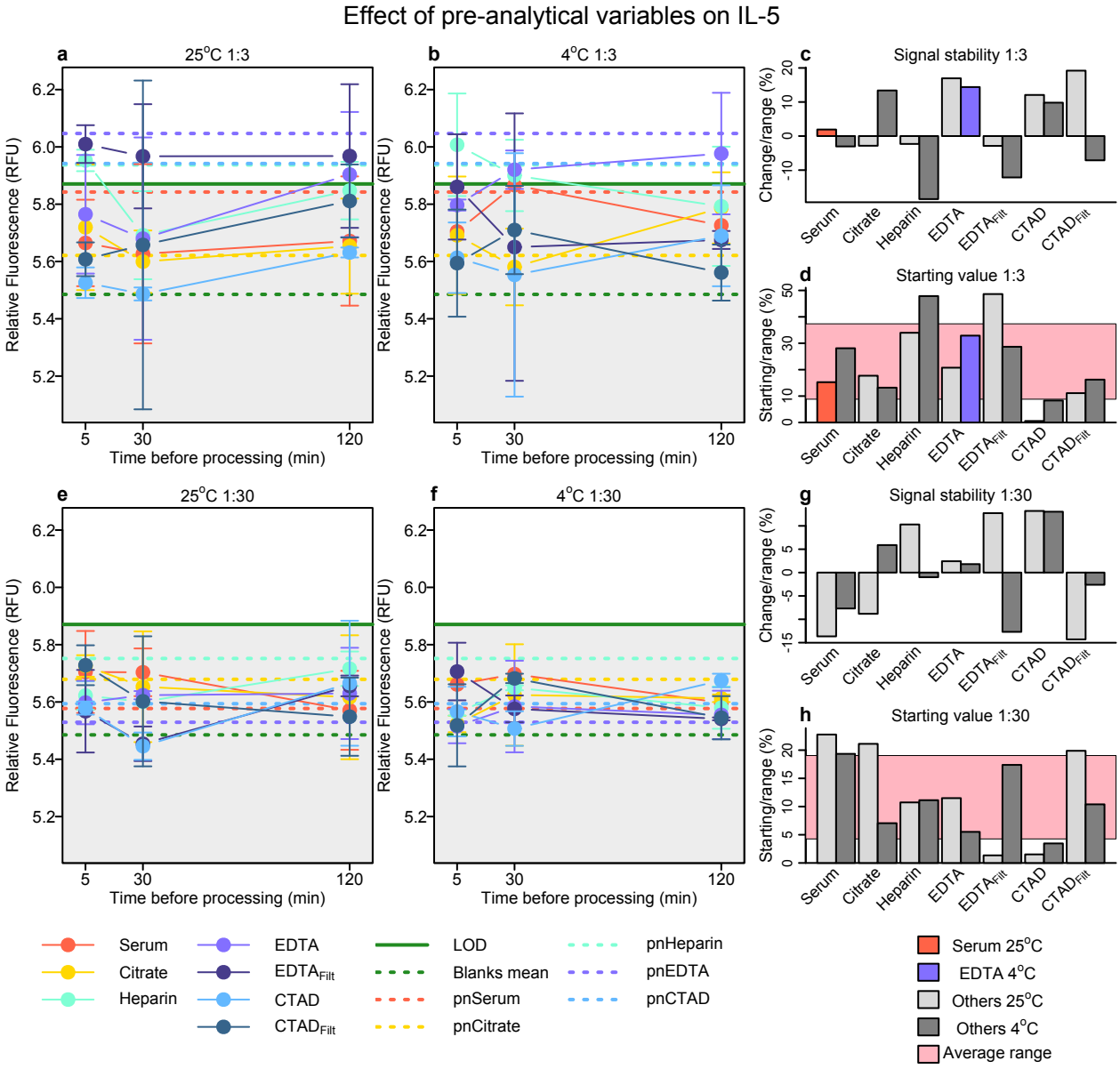

FIGURE I.S108: **Effect of pre-processing storage temperature on IL-5 stability and concentration.** Initial measured value and stability of IL-5 when stored at 25 °C (**a, e**) and 4 °C (**b, f**) before processing when collected in different tube types. The measured values are shown at low dilution of 1:3 (**a-b**) and high dilution of 1:30 (**e-f**). Stability before processing is expressed as an increase or decrease compared to the measurement range and is shown for low (**c**) and high (**g**) dilutions. Initial value is expressed as a portion of the measurement range when the linear regression is extrapolated to zero minutes and is shown for low (**d**) and high (**h**) dilutions. The pink box in graphs **d** and **h** indicate the region that is included by the *mean* ± *SD* of all the initial values and gives an indication of outliers when values lie outside this region. Red and purple bars in **c-d, g-h** are indicated at the measured dilution as the two choices for the TBI analysis.

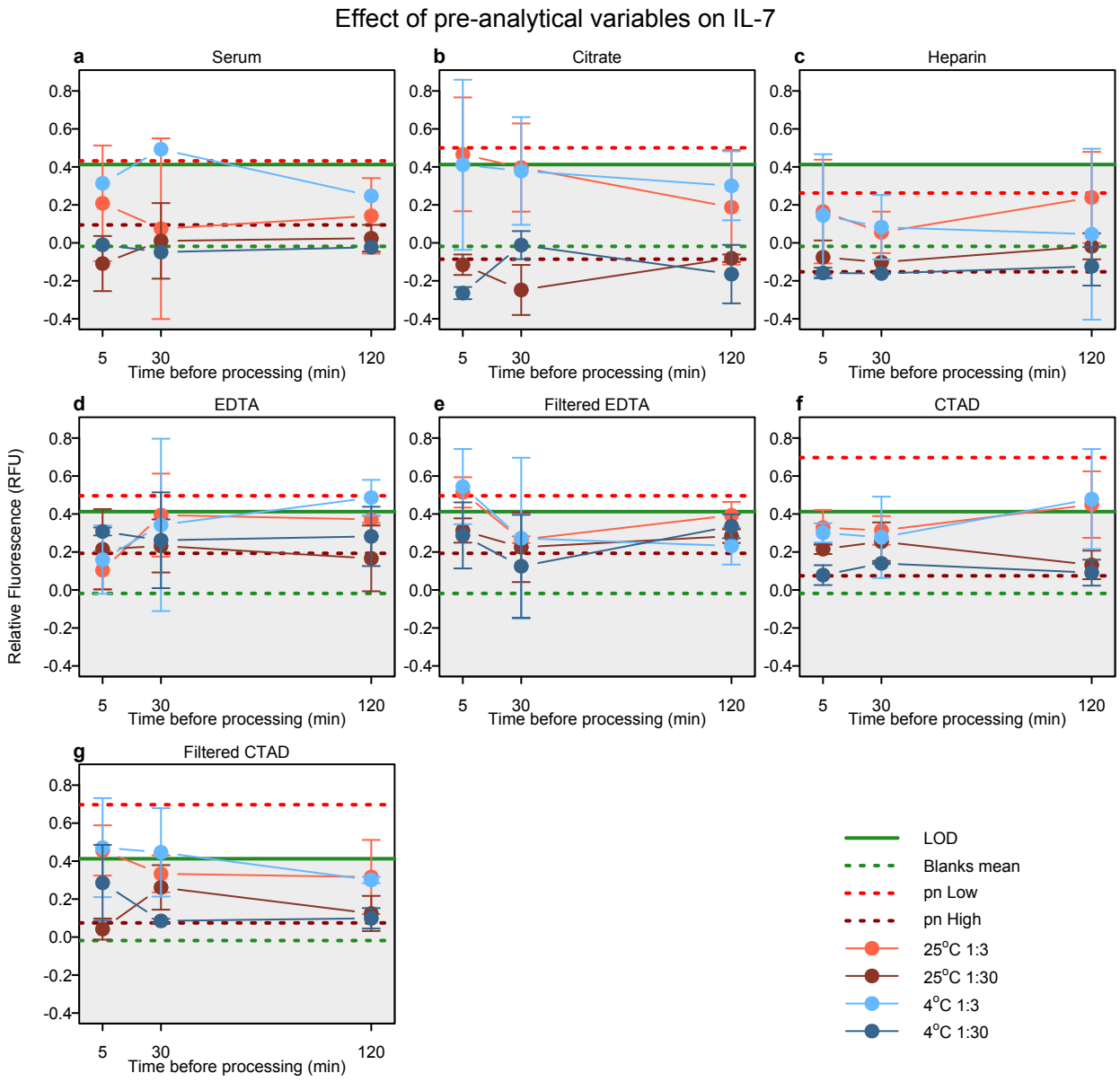

FIGURE I.S109: **Effect of blood collection tube on IL-7 stability and concentration.** Effects of blood collection tubes (**a**: serum, **b**: citrate, **c**: heparin, **d-e**: EDTA, **f-g**: CTAD), storage temperature and time before processing, and post-processing plasma filtering (**e, g**) on the initial value and pre-processing time stability of IL-7 measurements in blood. Information on the dilution of samples used for measuring, data range and the sample type selected are also shown.

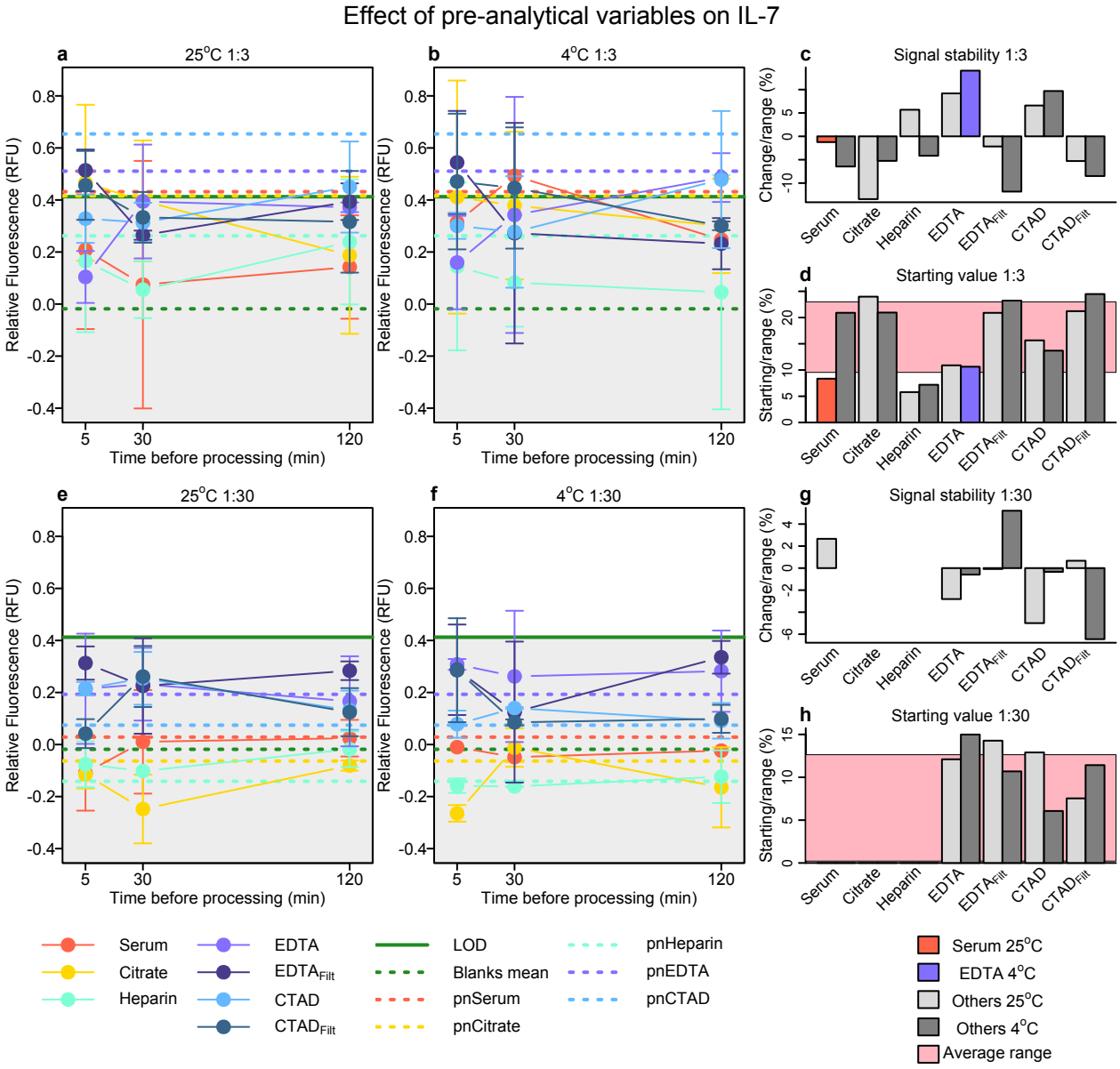

FIGURE I.S110: **Effect of pre-processing storage temperature on IL-7 stability and concentration.** Initial measured value and stability of IL-7 when stored at 25 °C (**a, e**) and 4 °C (**b, f**) before processing when collected in different tube types. The measured values are shown at low dilution of 1:3 (**a-b**) and high dilution of 1:30 (**e-f**). Stability before processing is expressed as an increase or decrease compared to the measurement range and is shown for low (**c**) and high (**g**) dilutions. Initial value is expressed as a portion of the measurement range when the linear regression is extrapolated to zero minutes and is shown for low (**d**) and high (**h**) dilutions. The pink box in graphs **d** and **h** indicate the region that is included by the *mean* ± *SD* of all the initial values and gives an indication of outliers when values lie outside this region. Red and purple bars in **c-d, g-h** are indicated at the measured dilution as the two choices for the TBI analysis.

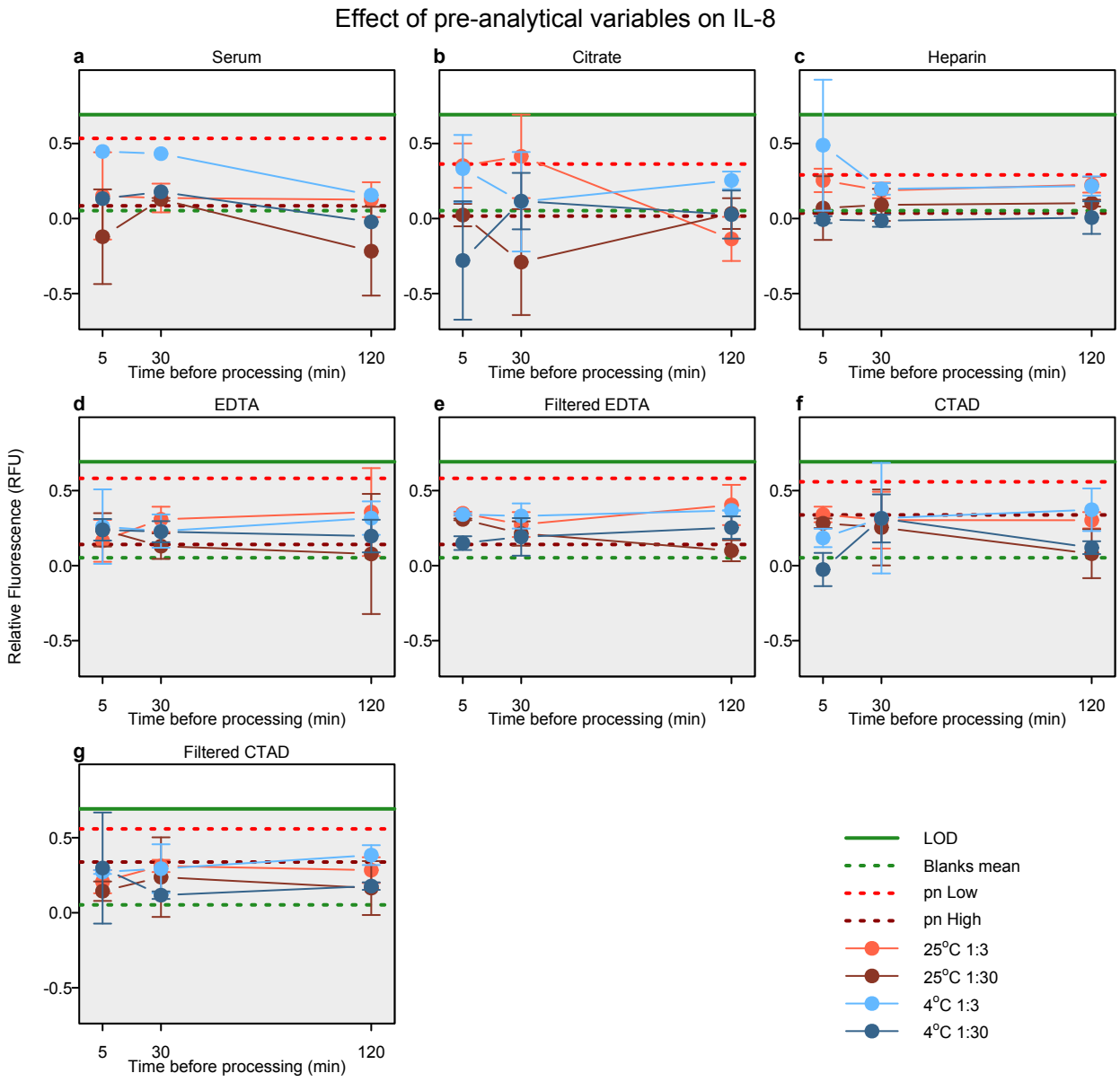

FIGURE I.S111: **Effect of blood collection tube on IL-8 stability and concentration.** Effects of blood collection tubes (**a**: serum, **b**: citrate, **c**: heparin, **d-e**: EDTA, **f-g**: CTAD), storage temperature and time before processing, and post-processing plasma filtering (**e, g**) on the initial value and pre-processing time stability of IL-8 measurements in blood. Information on the dilution of samples used for measuring, data range and the sample type selected are also shown.

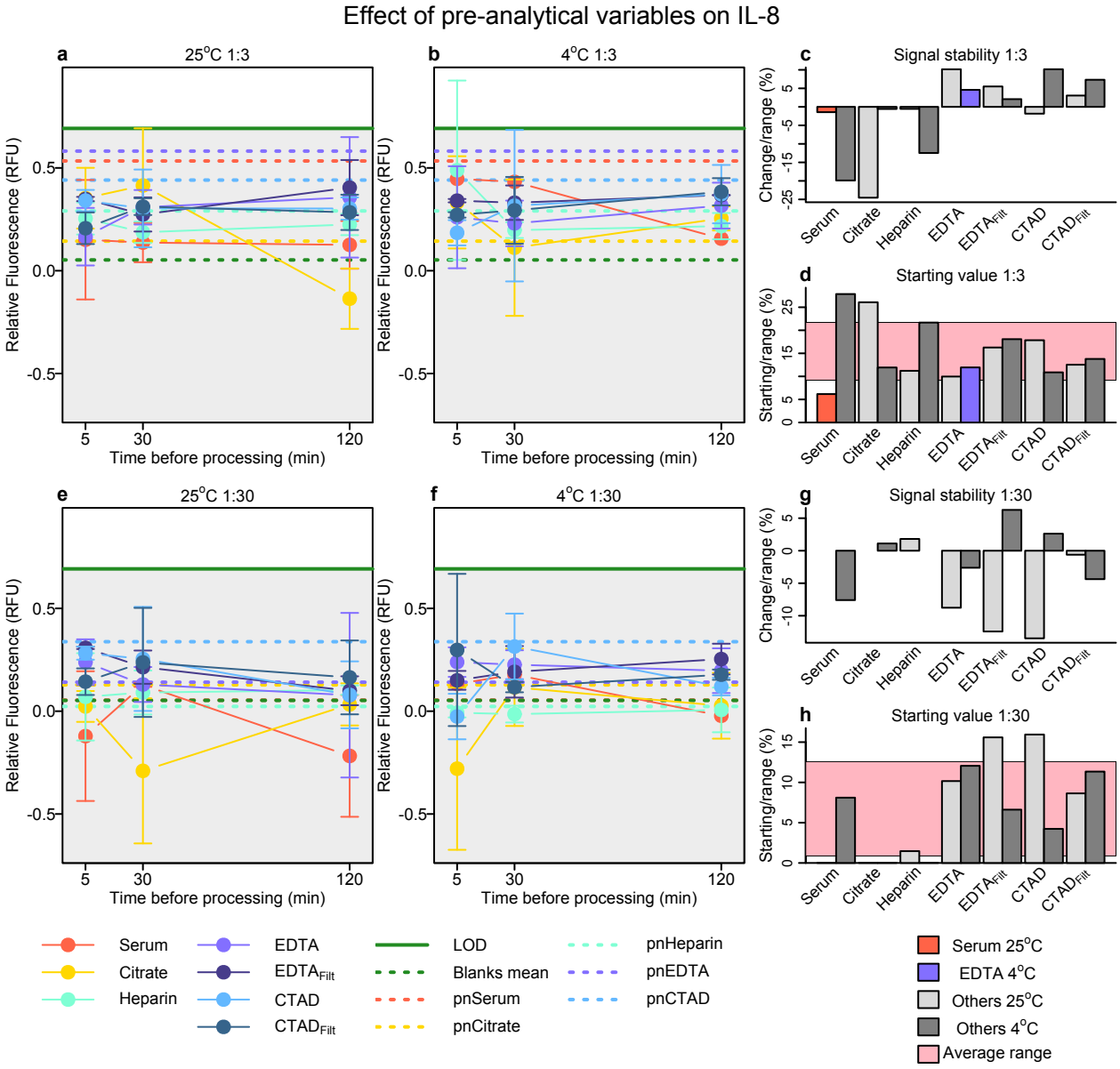

FIGURE I.S112: **Effect of pre-processing storage temperature on IL-8 stability and concentration.** Initial measured value and stability of IL-8 when stored at 25 °C (**a, e**) and 4 °C (**b, f**) before processing when collected in different tube types. The measured values are shown at low dilution of 1:3 (**a-b**) and high dilution of 1:30 (**e-f**). Stability before processing is expressed as an increase or decrease compared to the measurement range and is shown for low (**c**) and high (**g**) dilutions. Initial value is expressed as a portion of the measurement range when the linear regression is extrapolated to zero minutes and is shown for low (**d**) and high (**h**) dilutions. The pink box in graphs **d** and **h** indicate the region that is included by the *mean* ± *SD* of all the initial values and gives an indication of outliers when values lie outside this region. Red and purple bars in **c-d, g-h** are indicated at the measured dilution as the two choices for the TBI analysis.

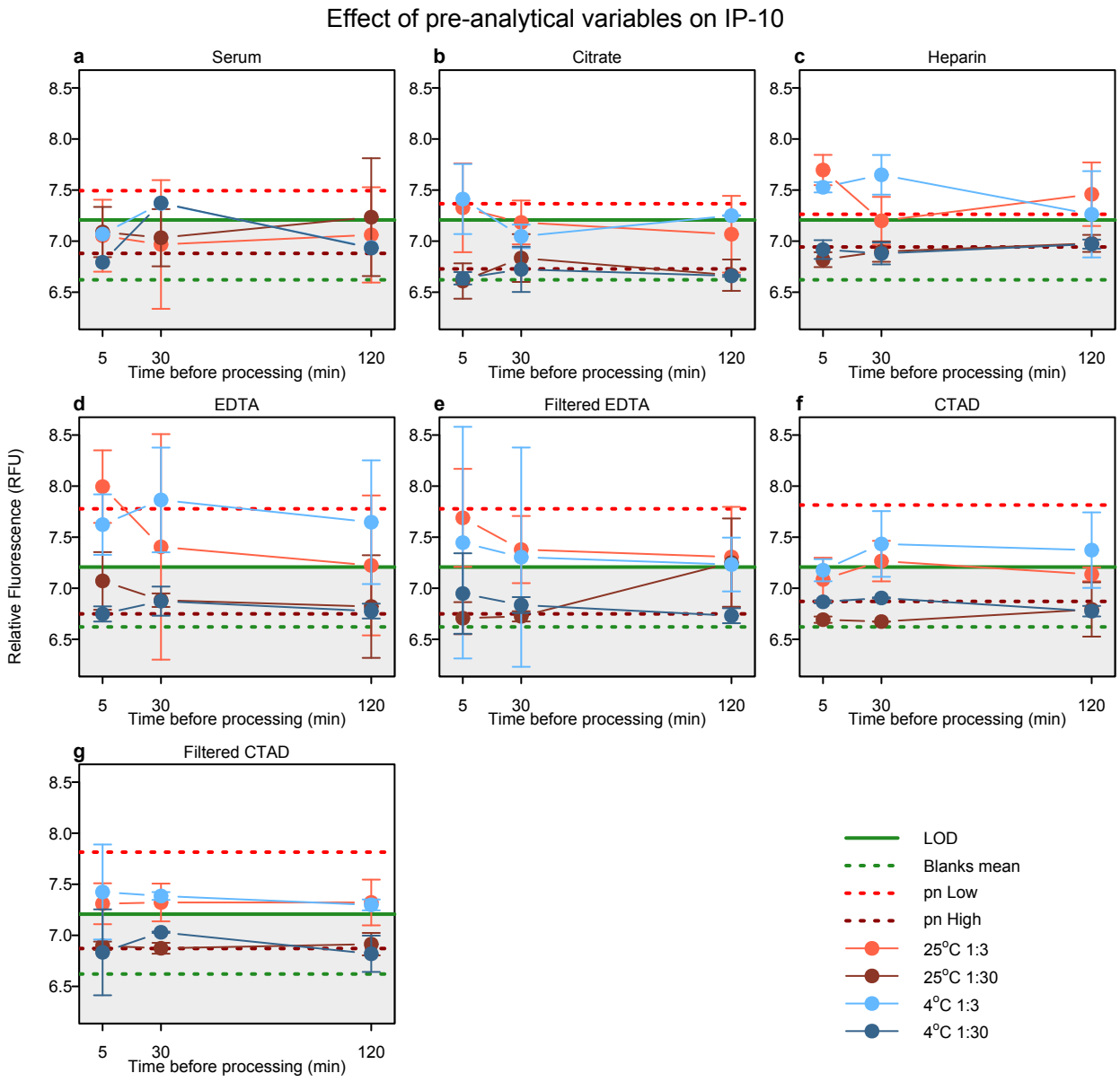

FIGURE I.S113: **Effect of blood collection tube on IP-10 stability and concentration.** Effects of blood collection tubes (**a**: serum, **b**: citrate, **c**: heparin, **d-e**: EDTA, **f-g**: CTAD), storage temperature and time before processing, and post-processing plasma filtering (**e, g**) on the initial value and pre-processing time stability of IP-10 measurements in blood. Information on the dilution of samples used for measuring, data range and the sample type selected are also shown.

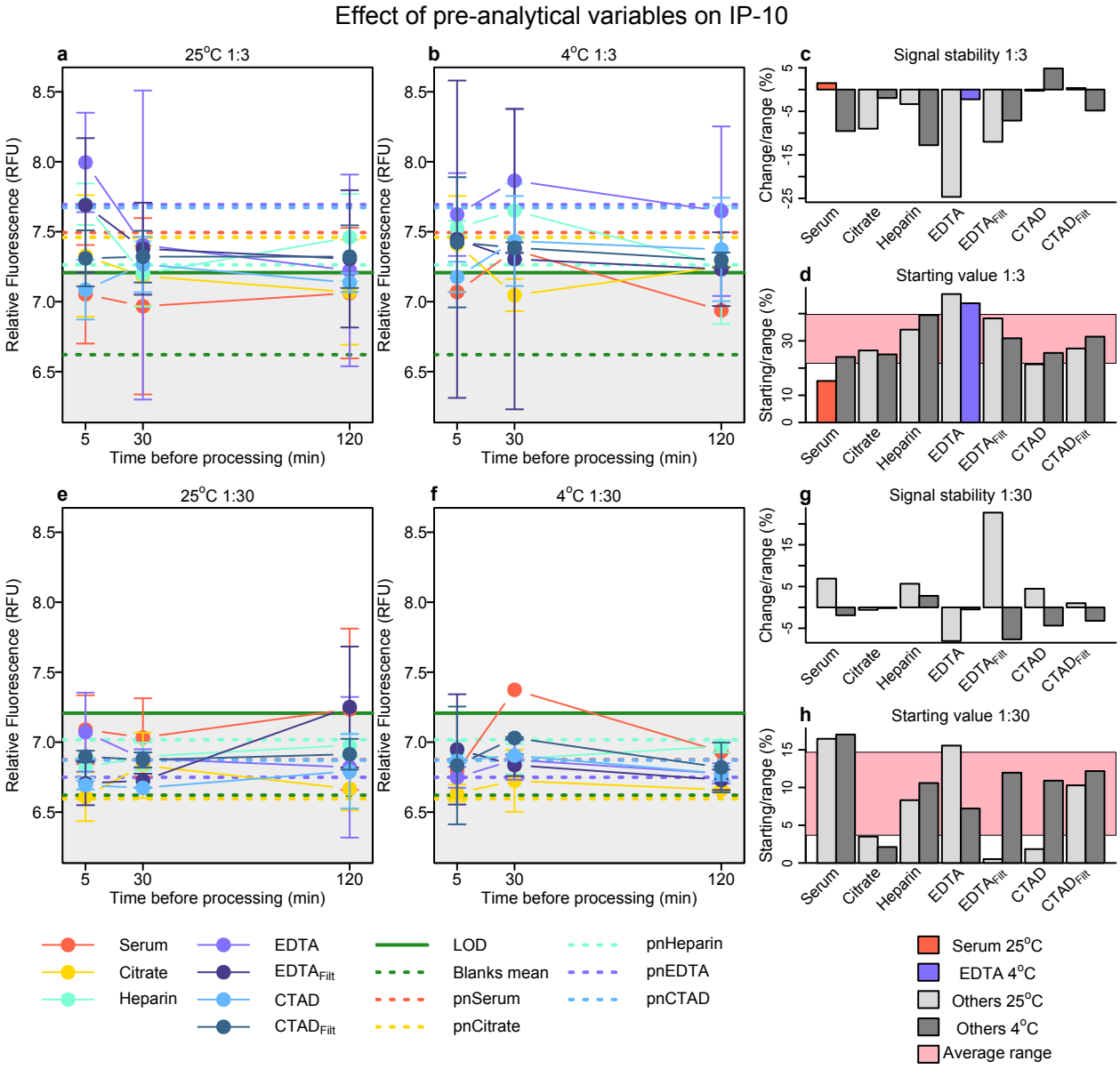

FIGURE I.S114: **Effect of pre-processing storage temperature on IP-10 stability and concentration.** Initial measured value and stability of IP-10 when stored at 25 °C (**a, e**) and 4 °C (**b, f**) before processing when collected in different tube types. The measured values are shown at low dilution of 1:3 (**a-b**) and high dilution of 1:30 (**e-f**). Stability before processing is expressed as an increase or decrease compared to the measurement range and is shown for low (**c**) and high (**g**) dilutions. Initial value is expressed as a portion of the measurement range when the linear regression is extrapolated to zero minutes and is shown for low (**d**) and high (**h**) dilutions. The pink box in graphs **d** and **h** indicate the region that is included by the *mean* ± *SD* of all the initial values and gives an indication of outliers when values lie outside this region. Red and purple bars in **c-d, g-h** are indicated at the measured dilution as the two choices for the TBI analysis.

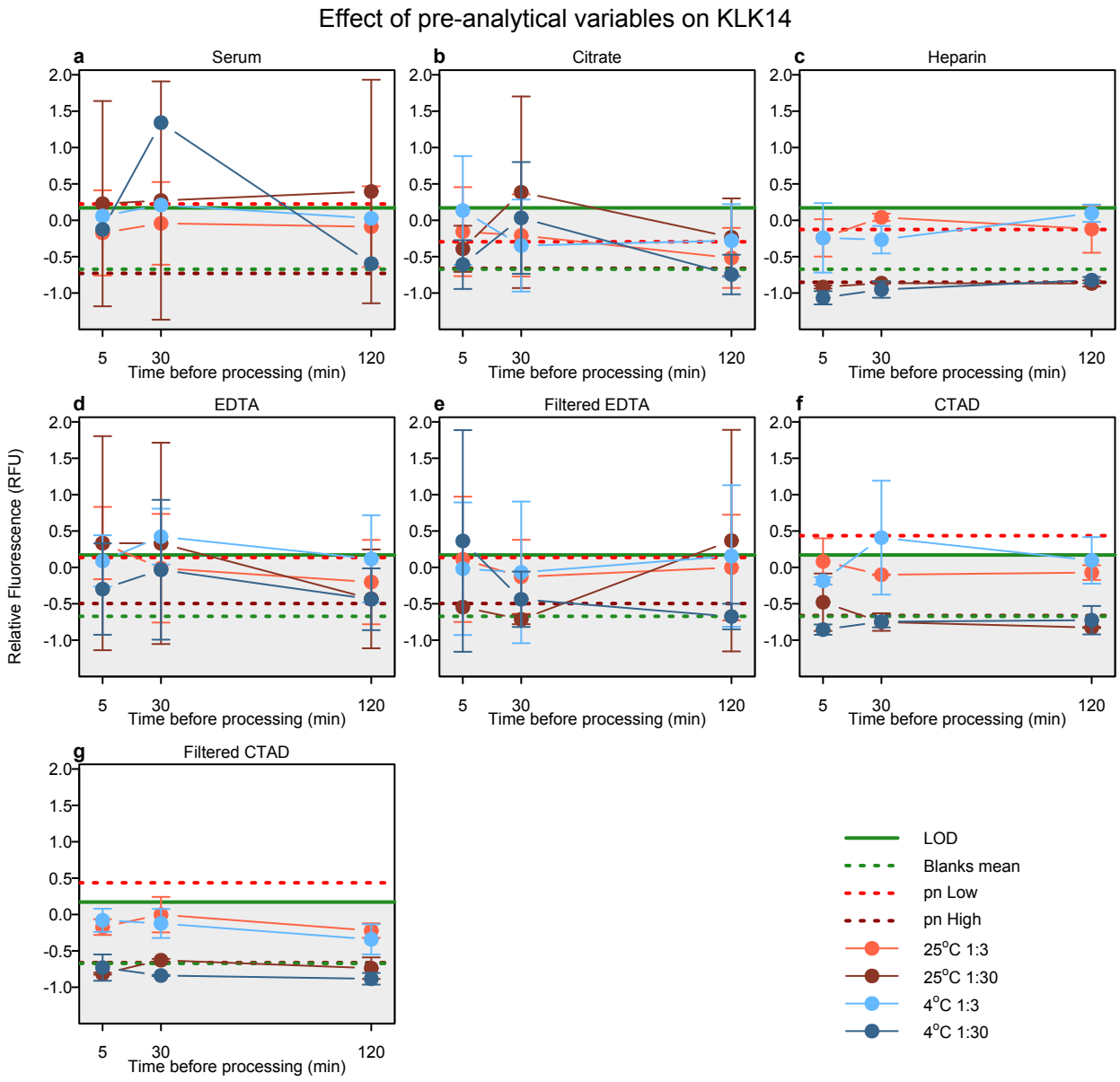

FIGURE I.S115: **Effect of blood collection tube on KLK14 stability and concentration.** Effects of blood collection tubes (**a**: serum, **b**: citrate, **c**: heparin, **d-e**: EDTA, **f-g**: CTAD), storage temperature and time before processing, and post-processing plasma filtering (**e, g**) on the initial value and pre-processing time stability of KLK14 measurements in blood. Information on the dilution of samples used for measuring, data range and the sample type selected are also shown.

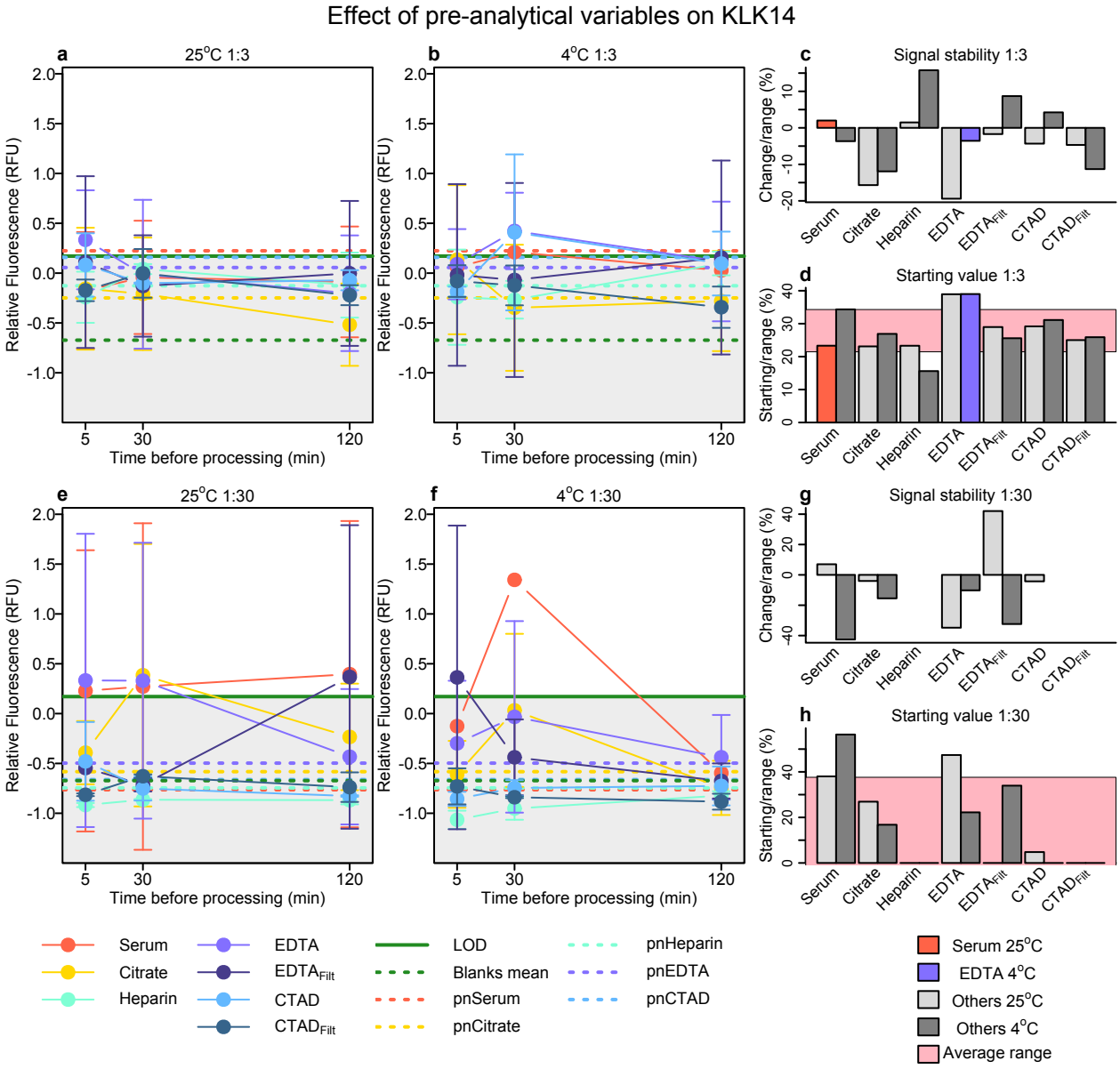

FIGURE I.S116: **Effect of pre-processing storage temperature on KLK14 stability and concentration.** Initial measured value and stability of KLK14 when stored at 25 °C (**a, e**) and 4 °C (**b, f**) before processing when collected in different tube types. The measured values are shown at low dilution of 1:3 (**a-b**) and high dilution of 1:30 (**e-f**). Stability before processing is expressed as an increase or decrease compared to the measurement range and is shown for low (**c**) and high (**g**) dilutions. Initial value is expressed as a portion of the measurement range when the linear regression is extrapolated to zero minutes and is shown for low (**d**) and high (**h**) dilutions. The pink box in graphs **d** and **h** indicate the region that is included by the *mean* ± *SD* of all the initial values and gives an indication of outliers when values lie outside this region. Red and purple bars in **c-d, g-h** are indicated at the measured dilution as the two choices for the TBI analysis.

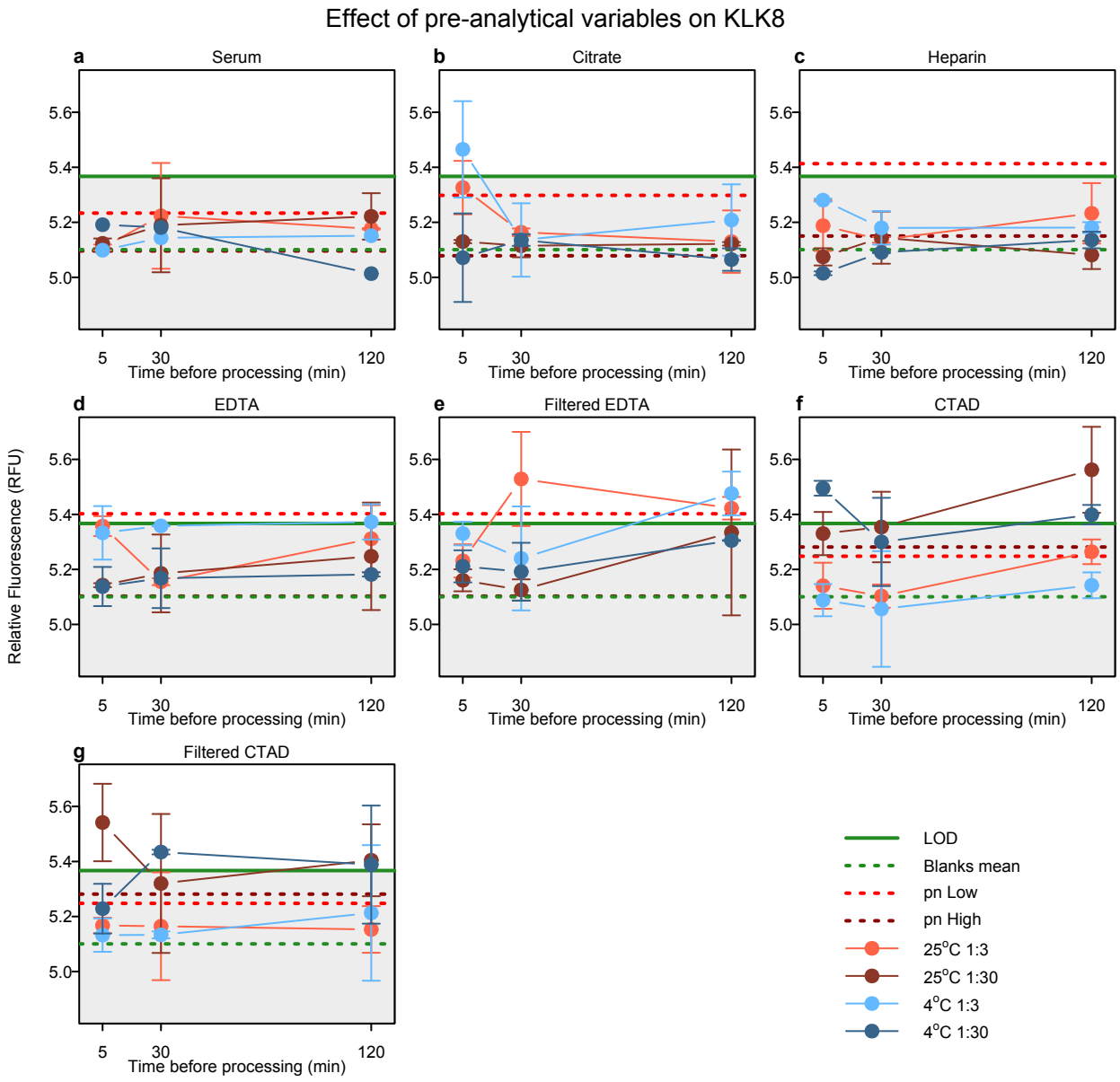

FIGURE I.S117: **Effect of blood collection tube on KLK8 stability and concentration.** Effects of blood collection tubes (**a**: serum, **b**: citrate, **c**: heparin, **d-e**: EDTA, **f-g**: CTAD), storage temperature and time before processing, and post-processing plasma filtering (**e, g**) on the initial value and pre-processing time stability of KLK8 measurements in blood. Information on the dilution of samples used for measuring, data range and the sample type selected are also shown.

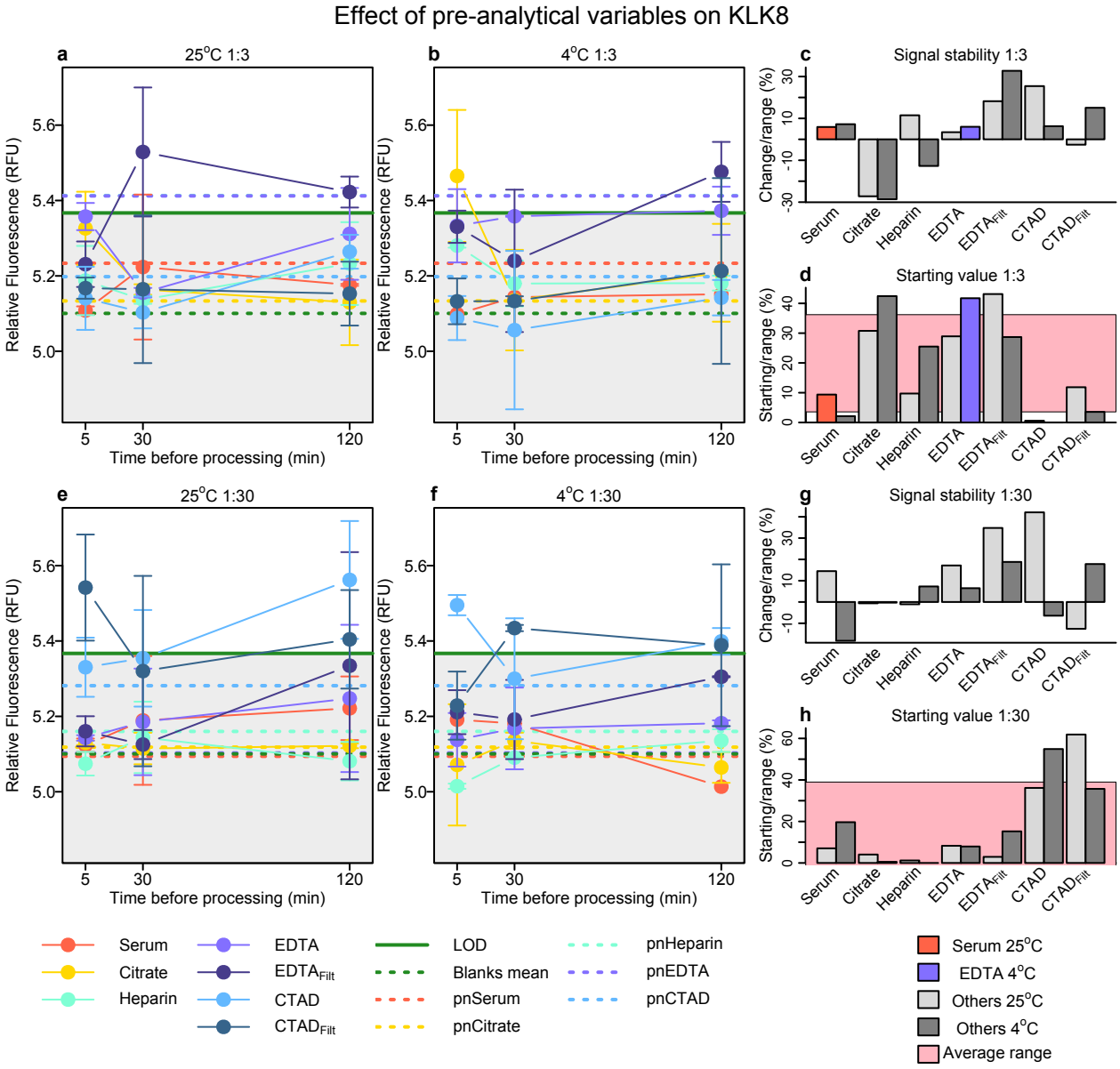

FIGURE I.S118: **Effect of pre-processing storage temperature on KLK8 stability and concentration.** Initial measured value and stability of KLK8 when stored at 25 °C (**a, e**) and 4 °C (**b, f**) before processing when collected in different tube types. The measured values are shown at low dilution of 1:3 (**a-b**) and high dilution of 1:30 (**e-f**). Stability before processing is expressed as an increase or decrease compared to the measurement range and is shown for low (**c**) and high (**g**) dilutions. Initial value is expressed as a portion of the measurement range when the linear regression is extrapolated to zero minutes and is shown for low (**d**) and high (**h**) dilutions. The pink box in graphs **d** and **h** indicate the region that is included by the *mean* ± *SD* of all the initial values and gives an indication of outliers when values lie outside this region. Red and purple bars in **c-d, g-h** are indicated at the measured dilution as the two choices for the TBI analysis.

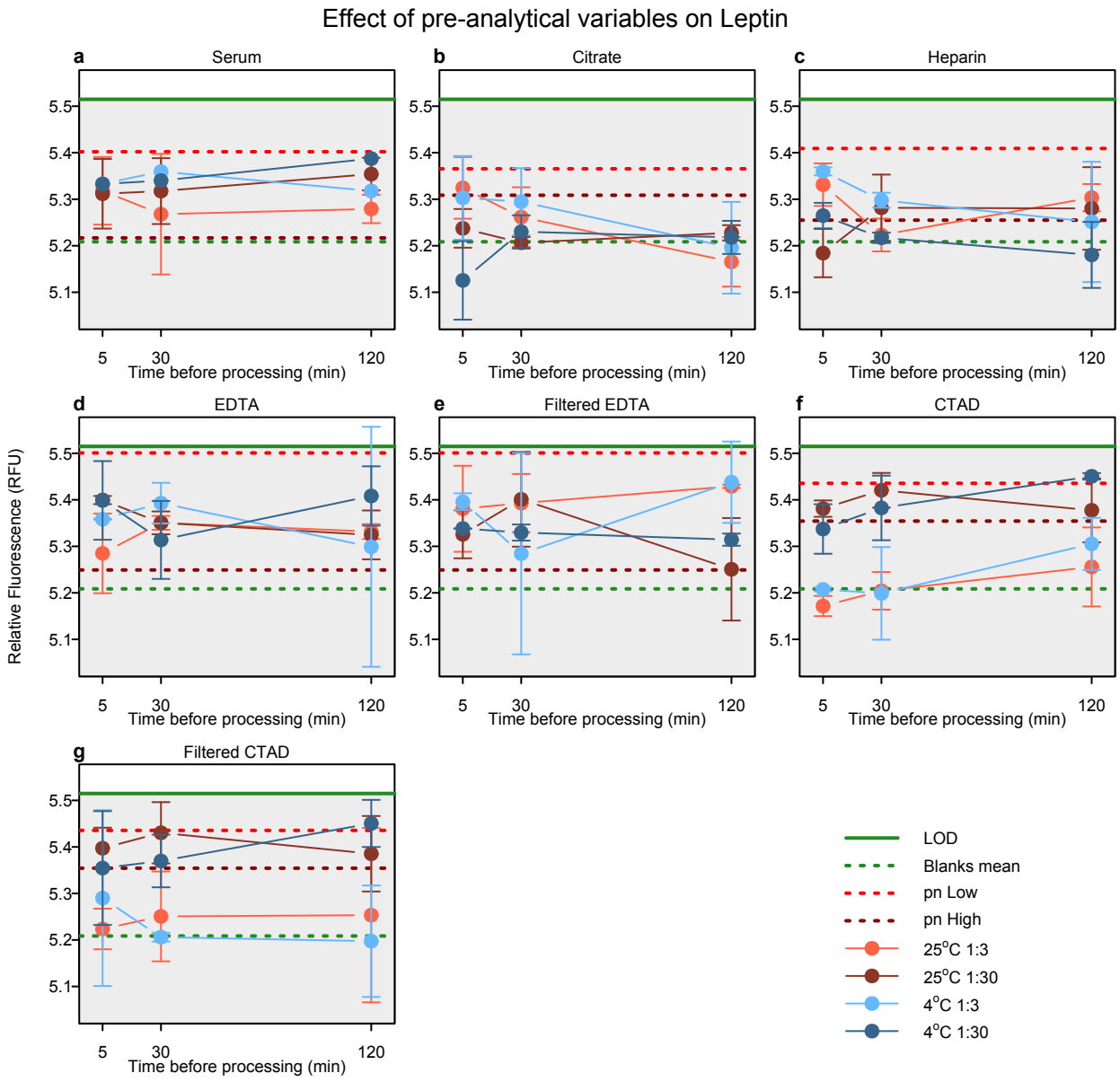

FIGURE I.S119: **Effect of blood collection tube on Leptin stability and concentration.** Effects of blood collection tubes (**a**: serum, **b**: citrate, **c**: heparin, **d-e**: EDTA, **f-g**: CTAD), storage temperature and time before processing, and post-processing plasma filtering (**e, g**) on the initial value and pre-processing time stability of Leptin measurements in blood. Information on the dilution of samples used for measuring, data range and the sample type selected are also shown.

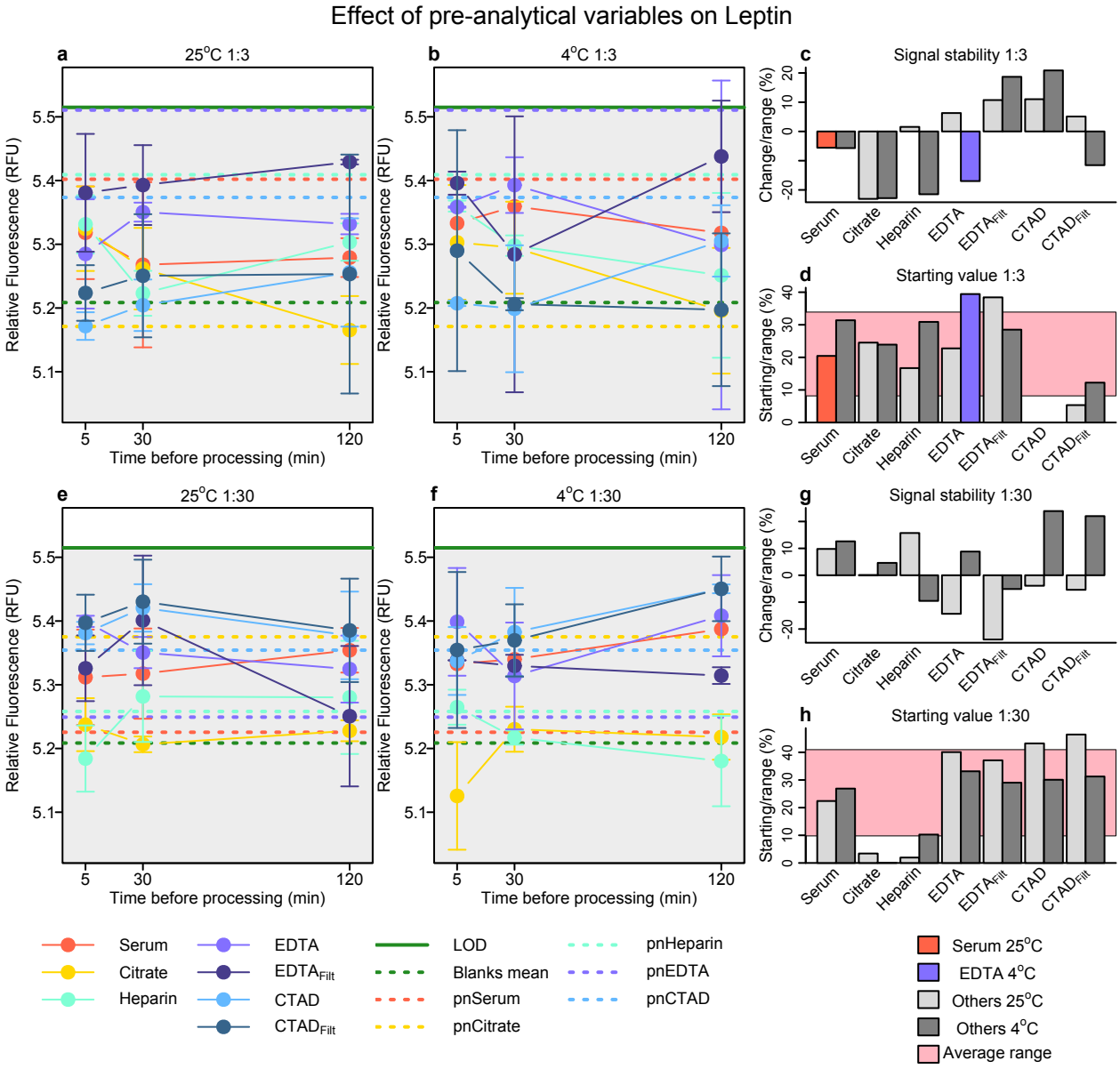

FIGURE I.S120: **Effect of pre-processing storage temperature on Leptin stability and concentration.** Initial measured value and stability of Leptin when stored at 25 °C (**a, e**) and 4 °C (**b, f**) before processing when collected in different tube types. The measured values are shown at low dilution of 1:3 (**a-b**) and high dilution of 1:30 (**e-f**). Stability before processing is expressed as an increase or decrease compared to the measurement range and is shown for low (**c**) and high (**g**) dilutions. Initial value is expressed as a portion of the measurement range when the linear regression is extrapolated to zero minutes and is shown for low (**d**) and high (**h**) dilutions. The pink box in graphs **d** and **h** indicate the region that is included by the *mean* ± *SD* of all the initial values and gives an indication of outliers when values lie outside this region. Red and purple bars in **c-d, g-h** are indicated at the measured dilution as the two choices for the TBI analysis.

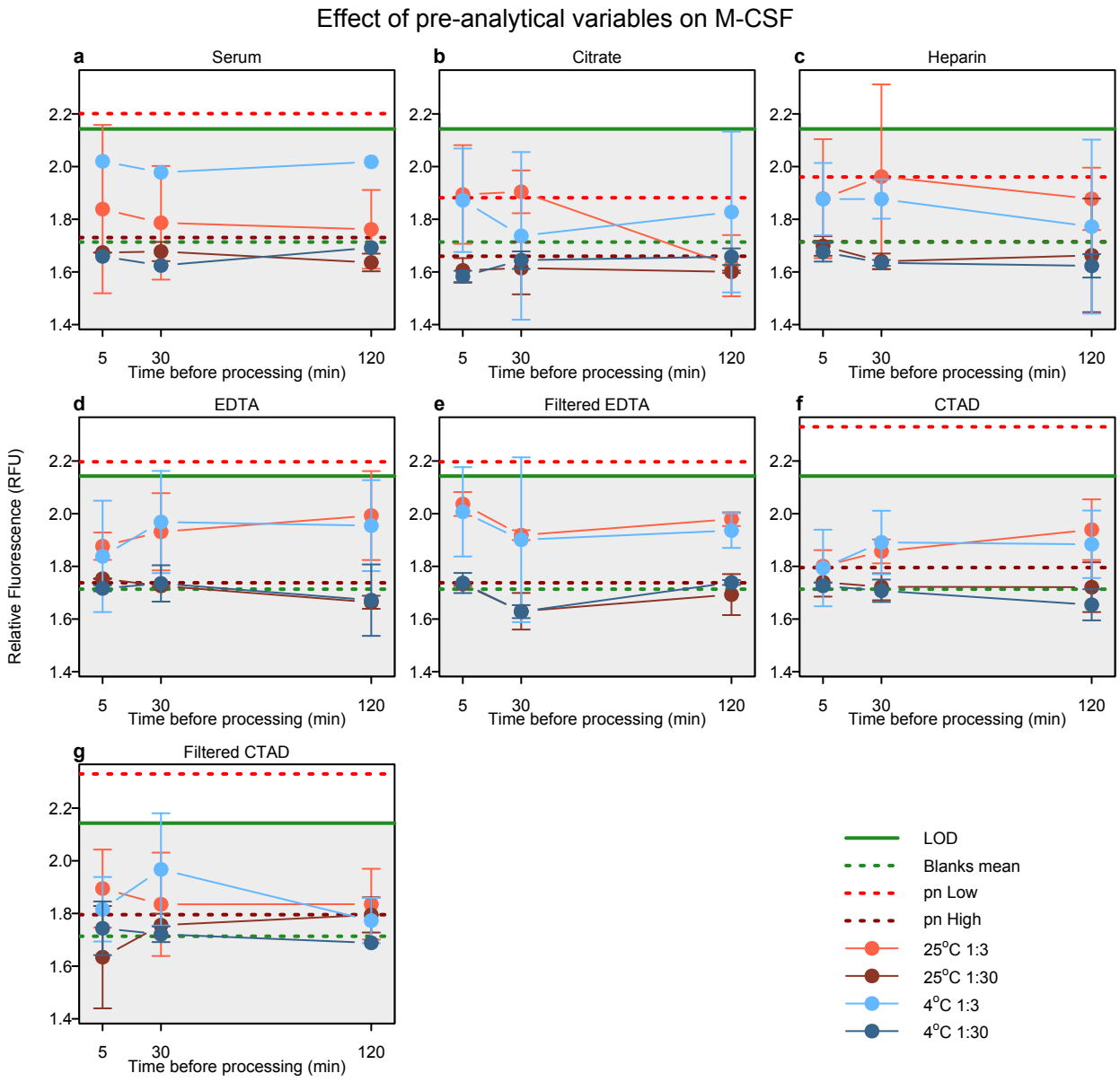

FIGURE I.S121: **Effect of blood collection tube on M-CSF stability and concentration.** Effects of blood collection tubes (**a**: serum, **b**: citrate, **c**: heparin, **d-e**: EDTA, **f-g**: CTAD), storage temperature and time before processing, and post-processing plasma filtering (**e, g**) on the initial value and pre-processing time stability of M-CSF measurements in blood. Information on the dilution of samples used for measuring, data range and the sample type selected are also shown.

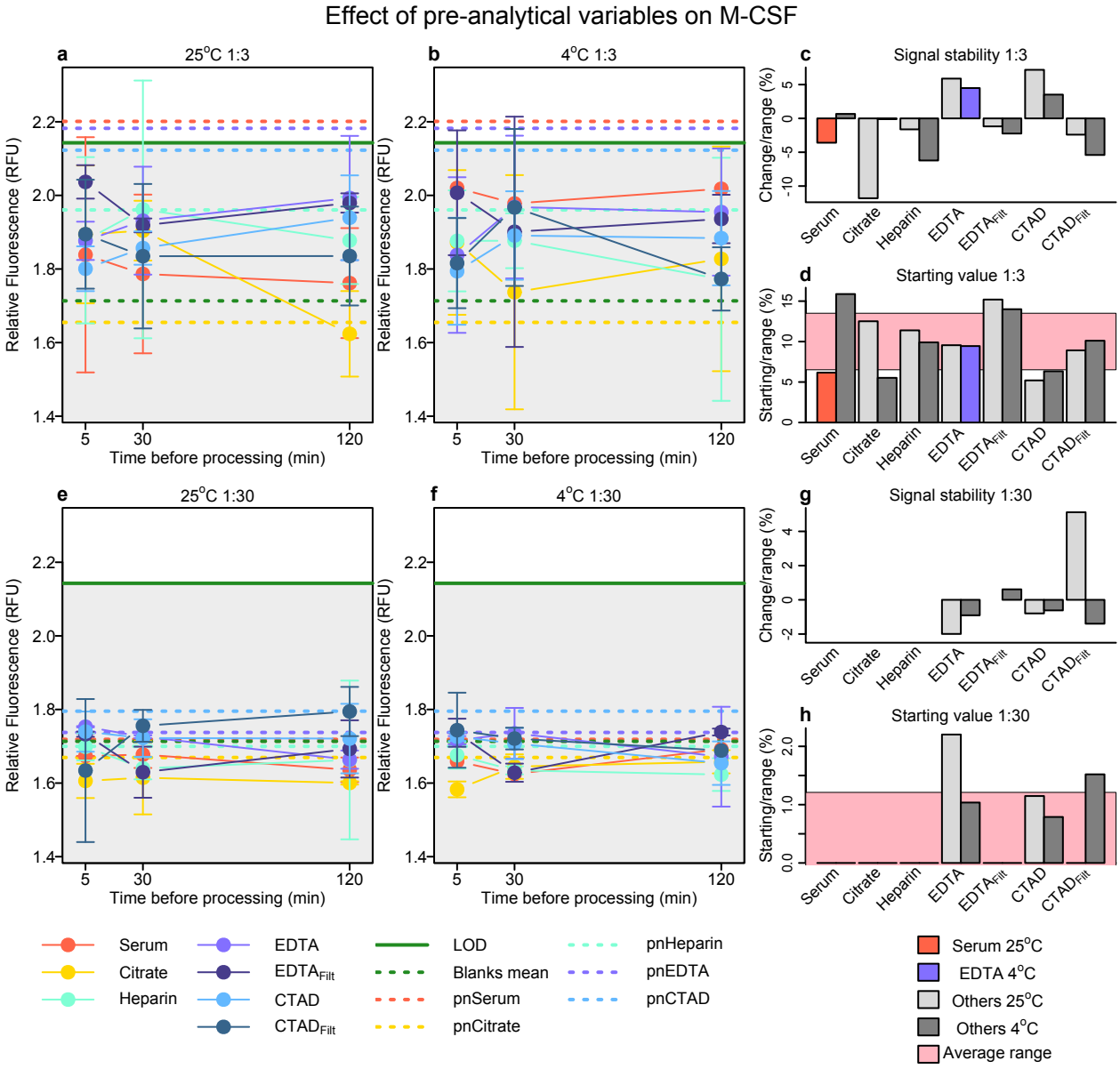

FIGURE I.S122: **Effect of pre-processing storage temperature on M-CSF stability and concentration.** Initial measured value and stability of M-CSF when stored at 25 °C (**a, e**) and 4 °C (**b, f**) before processing when collected in different tube types. The measured values are shown at low dilution of 1:3 (**a-b**) and high dilution of 1:30 (**e-f**). Stability before processing is expressed as an increase or decrease compared to the measurement range and is shown for low (**c**) and high (**g**) dilutions. Initial value is expressed as a portion of the measurement range when the linear regression is extrapolated to zero minutes and is shown for low (**d**) and high (**h**) dilutions. The pink box in graphs **d** and **h** indicate the region that is included by the *mean* ± *SD* of all the initial values and gives an indication of outliers when values lie outside this region. Red and purple bars in **c-d, g-h** are indicated at the measured dilution as the two choices for the TBI analysis.

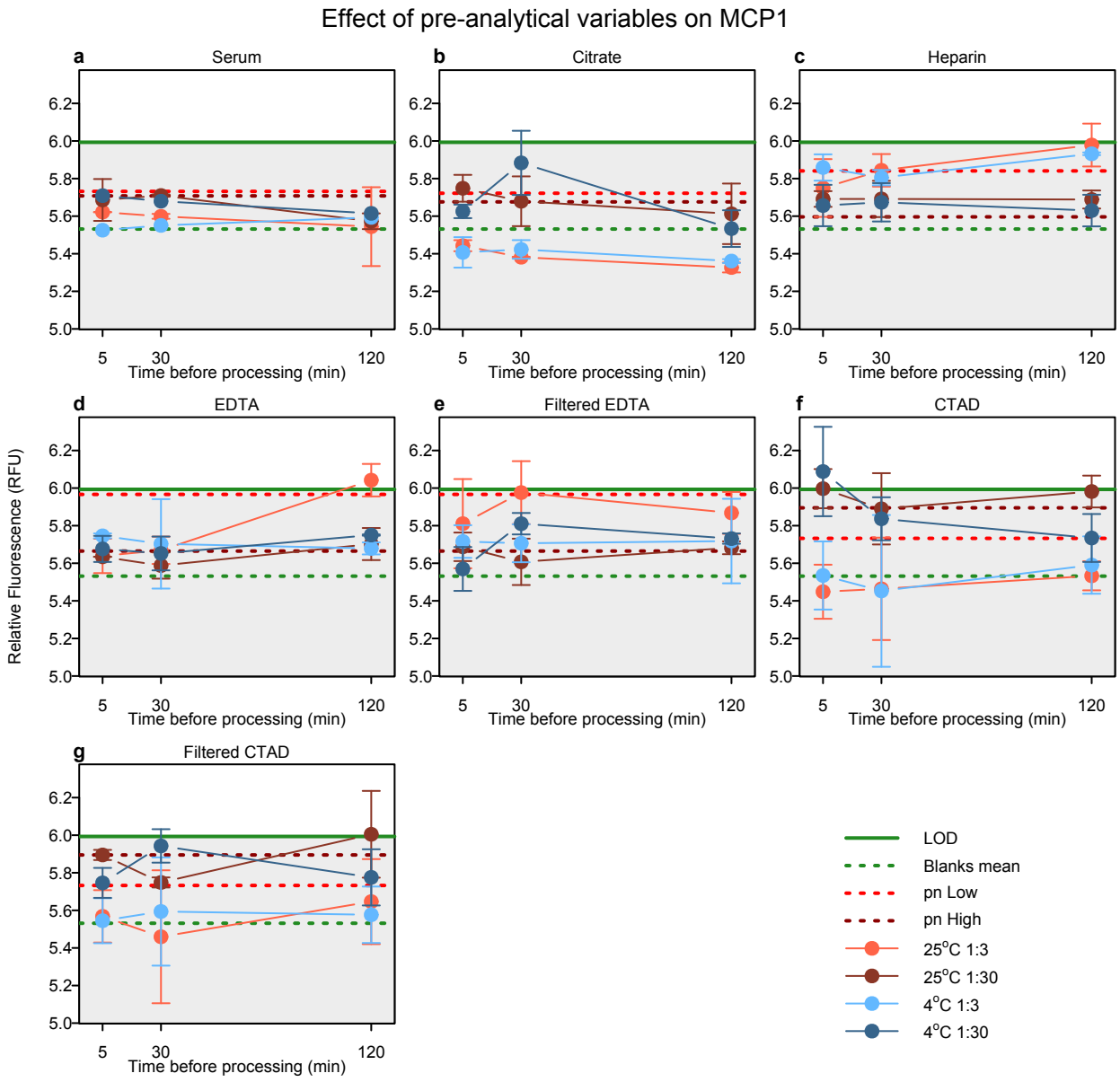

FIGURE I.S123: **Effect of blood collection tube on MCP1 stability and concentration.** Effects of blood collection tubes (**a**: serum, **b**: citrate, **c**: heparin, **d-e**: EDTA, **f-g**: CTAD), storage temperature and time before processing, and post-processing plasma filtering (**e, g**) on the initial value and pre-processing time stability of MCP1 measurements in blood. Information on the dilution of samples used for measuring, data range and the sample type selected are also shown.

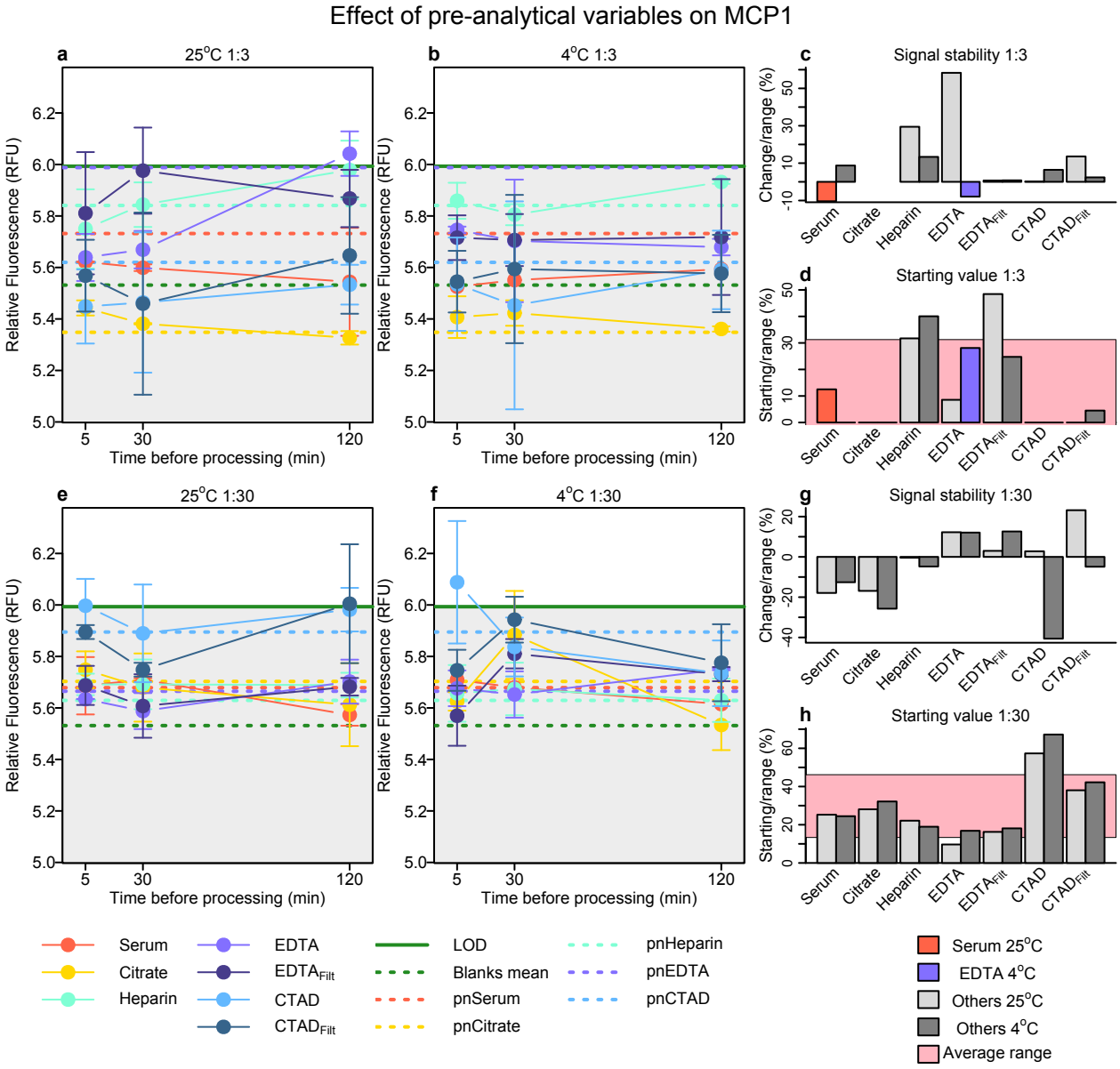

FIGURE I.S124: **Effect of pre-processing storage temperature on MCP1 stability and concentration.** Initial measured value and stability of MCP1 when stored at 25 °C (**a, e**) and 4 °C (**b, f**) before processing when collected in different tube types. The measured values are shown at low dilution of 1:3 (**a-b**) and high dilution of 1:30 (**e-f**). Stability before processing is expressed as an increase or decrease compared to the measurement range and is shown for low (**c**) and high (**g**) dilutions. Initial value is expressed as a portion of the measurement range when the linear regression is extrapolated to zero minutes and is shown for low (**d**) and high (**h**) dilutions. The pink box in graphs **d** and **h** indicate the region that is included by the *mean* ± *SD* of all the initial values and gives an indication of outliers when values lie outside this region. Red and purple bars in **c-d, g-h** are indicated at the measured dilution as the two choices for the TBI analysis.

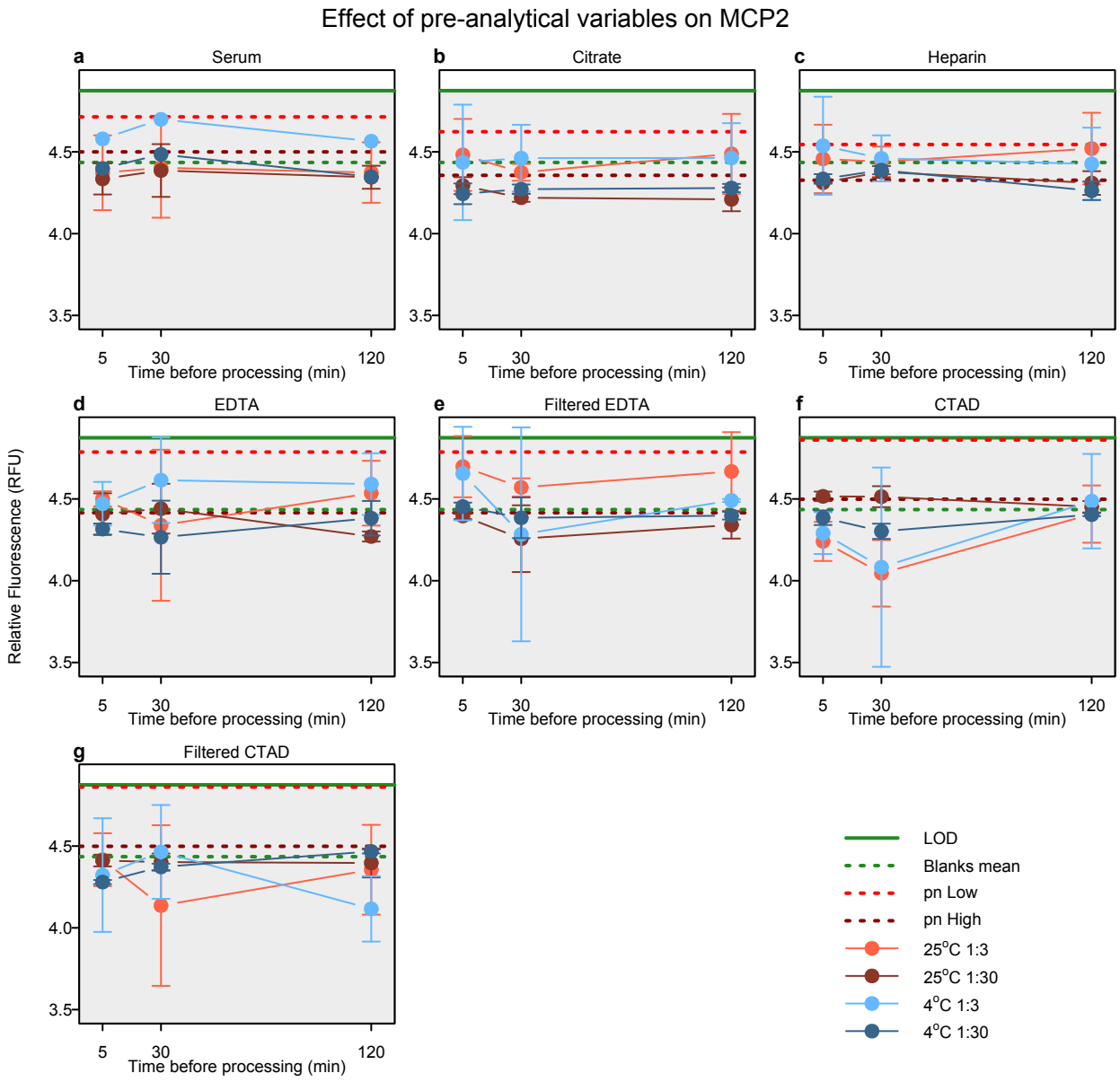

FIGURE I.S125: **Effect of blood collection tube on MCP2 stability and concentration.** Effects of blood collection tubes (**a**: serum, **b**: citrate, **c**: heparin, **d-e**: EDTA, **f-g**: CTAD), storage temperature and time before processing, and post-processing plasma filtering (**e, g**) on the initial value and pre-processing time stability of MCP2 measurements in blood. Information on the dilution of samples used for measuring, data range and the sample type selected are also shown.

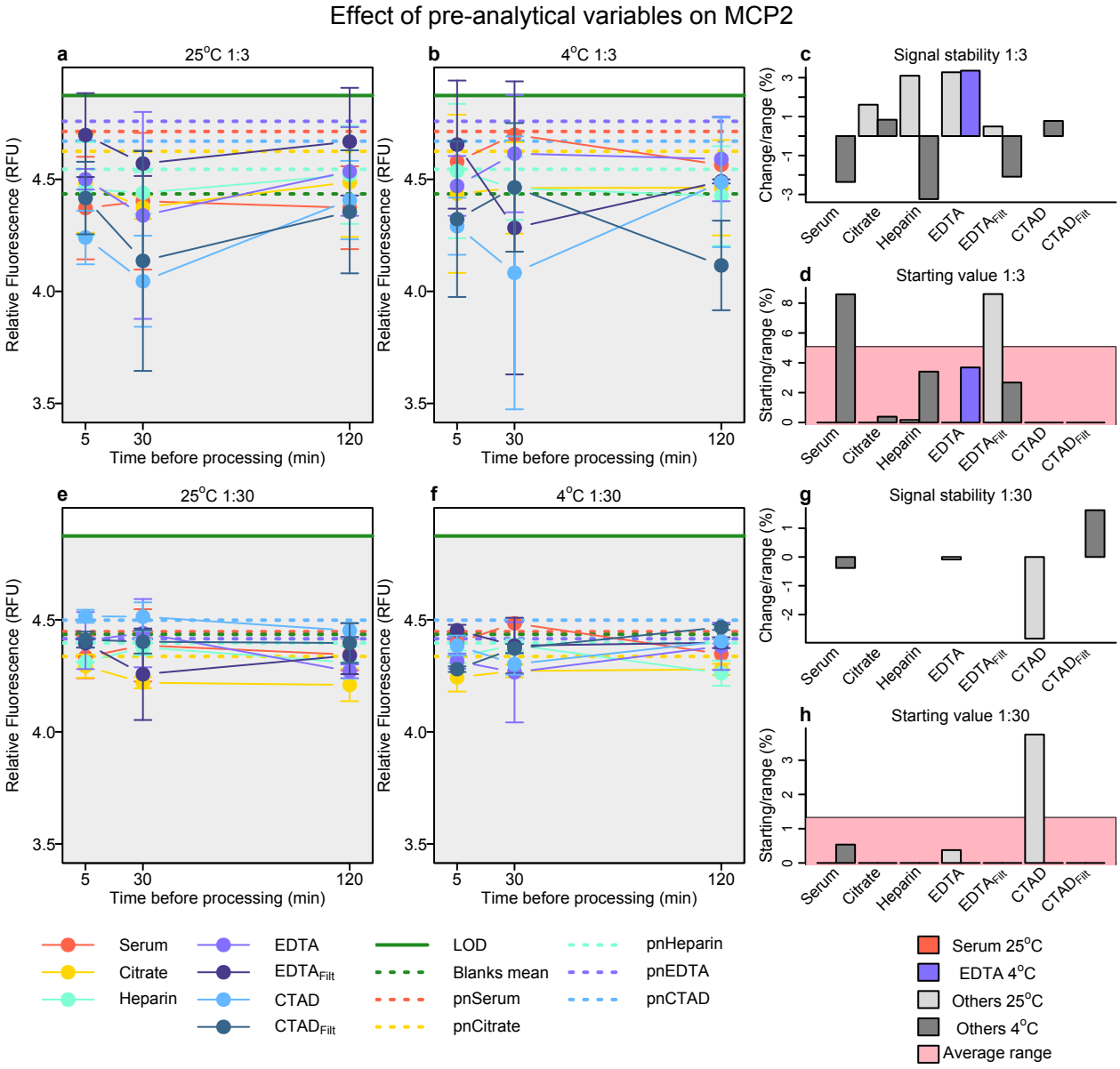

FIGURE I.S126: **Effect of pre-processing storage temperature on MCP2 stability and concentration.** Initial measured value and stability of MCP2 when stored at 25 °C (**a, e**) and 4 °C (**b, f**) before processing when collected in different tube types. The measured values are shown at low dilution of 1:3 (**a-b**) and high dilution of 1:30 (**e-f**). Stability before processing is expressed as an increase or decrease compared to the measurement range and is shown for low (**c**) and high (**g**) dilutions. Initial value is expressed as a portion of the measurement range when the linear regression is extrapolated to zero minutes and is shown for low (**d**) and high (**h**) dilutions. The pink box in graphs **d** and **h** indicate the region that is included by the *mean* ± *SD* of all the initial values and gives an indication of outliers when values lie outside this region. Red and purple bars in **c-d, g-h** are indicated at the measured dilution as the two choices for the TBI analysis.

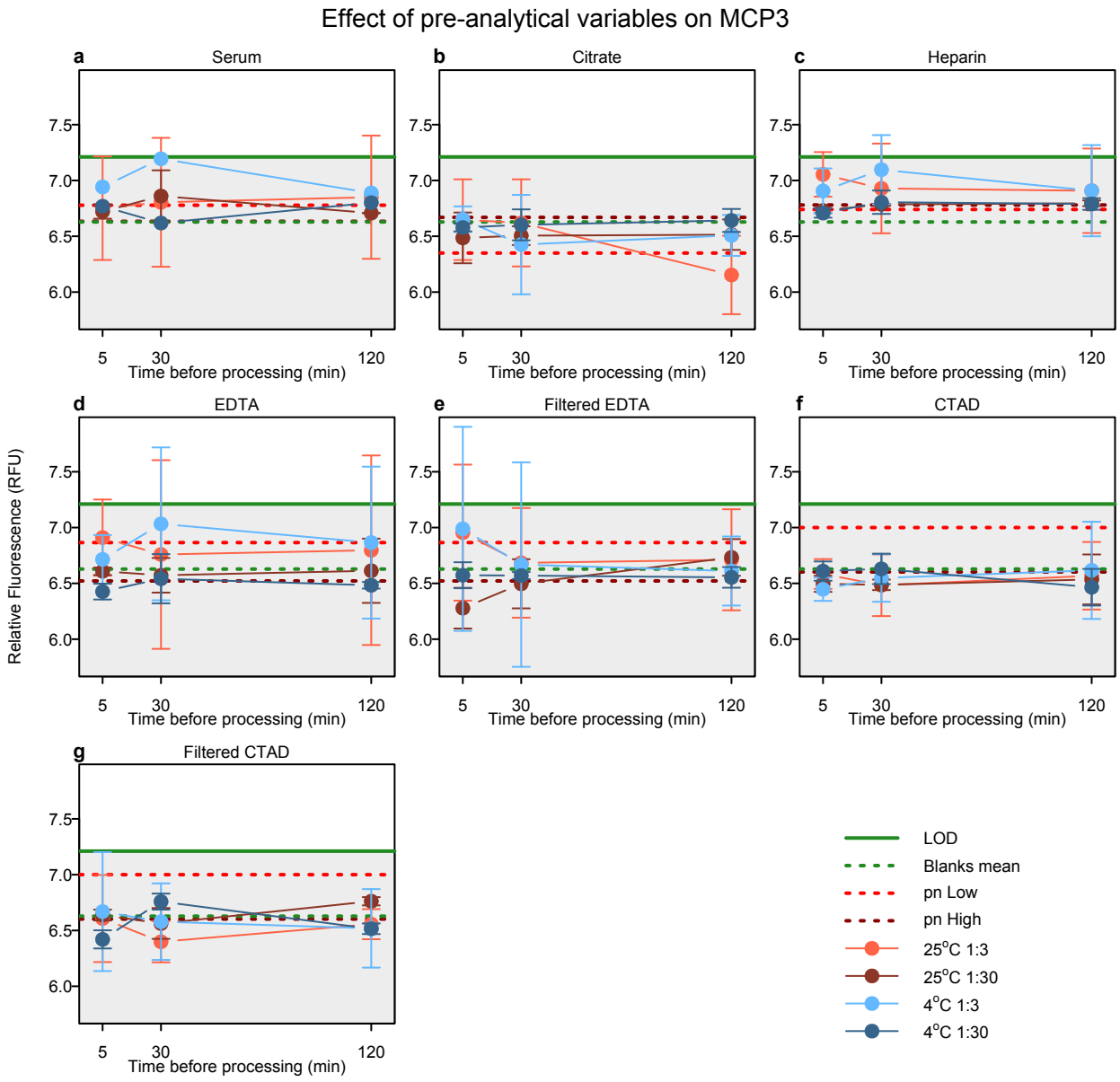

FIGURE I.S127: **Effect of blood collection tube on MCP3 stability and concentration.** Effects of blood collection tubes (**a**: serum, **b**: citrate, **c**: heparin, **d-e**: EDTA, **f-g**: CTAD), storage temperature and time before processing, and post-processing plasma filtering (**e, g**) on the initial value and pre-processing time stability of MCP3 measurements in blood. Information on the dilution of samples used for measuring, data range and the sample type selected are also shown.

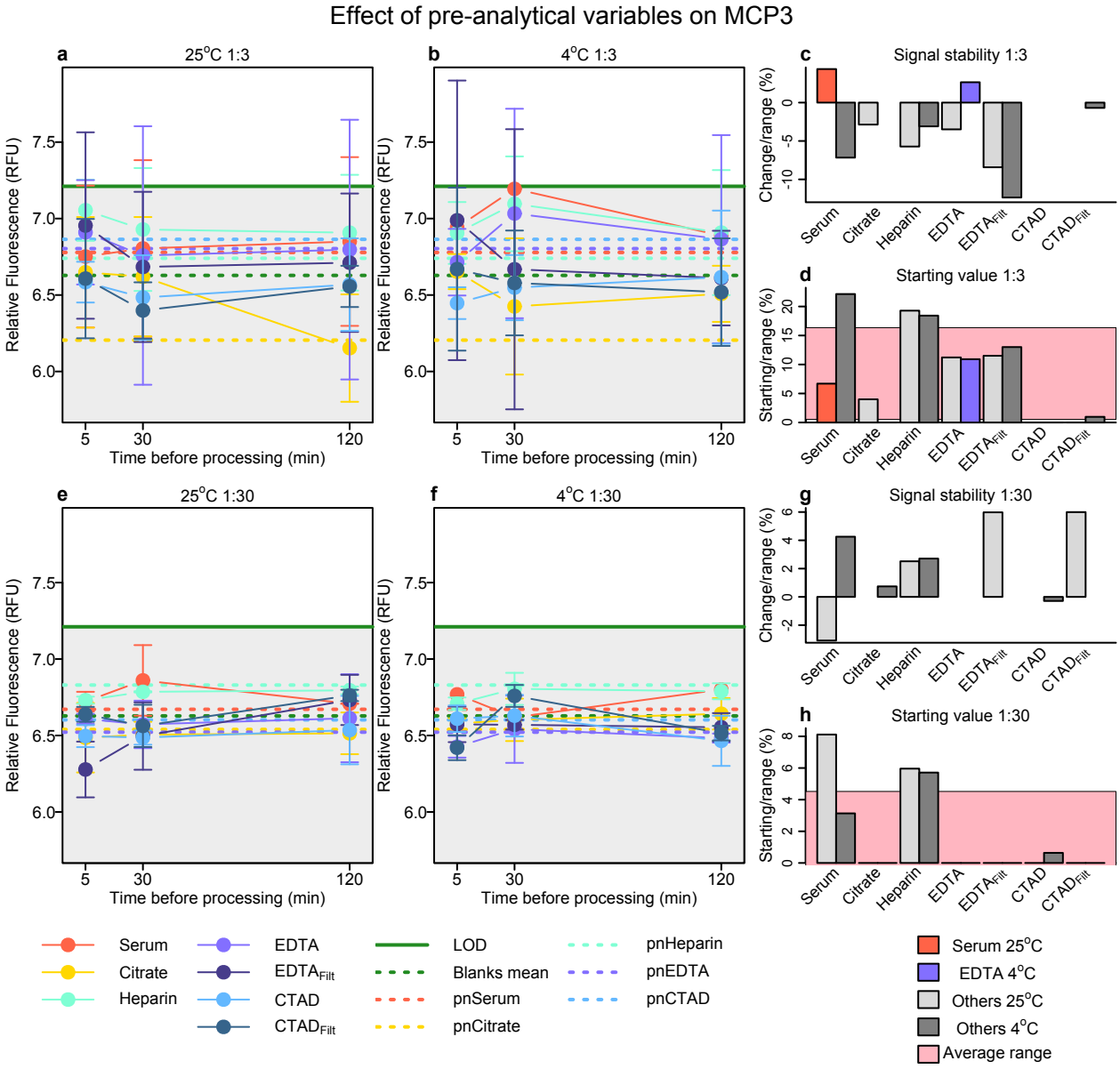

FIGURE I.S128: **Effect of pre-processing storage temperature on MCP3 stability and concentration.** Initial measured value and stability of MCP3 when stored at 25 °C (**a, e**) and 4 °C (**b, f**) before processing when collected in different tube types. The measured values are shown at low dilution of 1:3 (**a-b**) and high dilution of 1:30 (**e-f**). Stability before processing is expressed as an increase or decrease compared to the measurement range and is shown for low (**c**) and high (**g**) dilutions. Initial value is expressed as a portion of the measurement range when the linear regression is extrapolated to zero minutes and is shown for low (**d**) and high (**h**) dilutions. The pink box in graphs **d** and **h** indicate the region that is included by the *mean* ± *SD* of all the initial values and gives an indication of outliers when values lie outside this region. Red and purple bars in **c-d, g-h** are indicated at the measured dilution as the two choices for the TBI analysis.

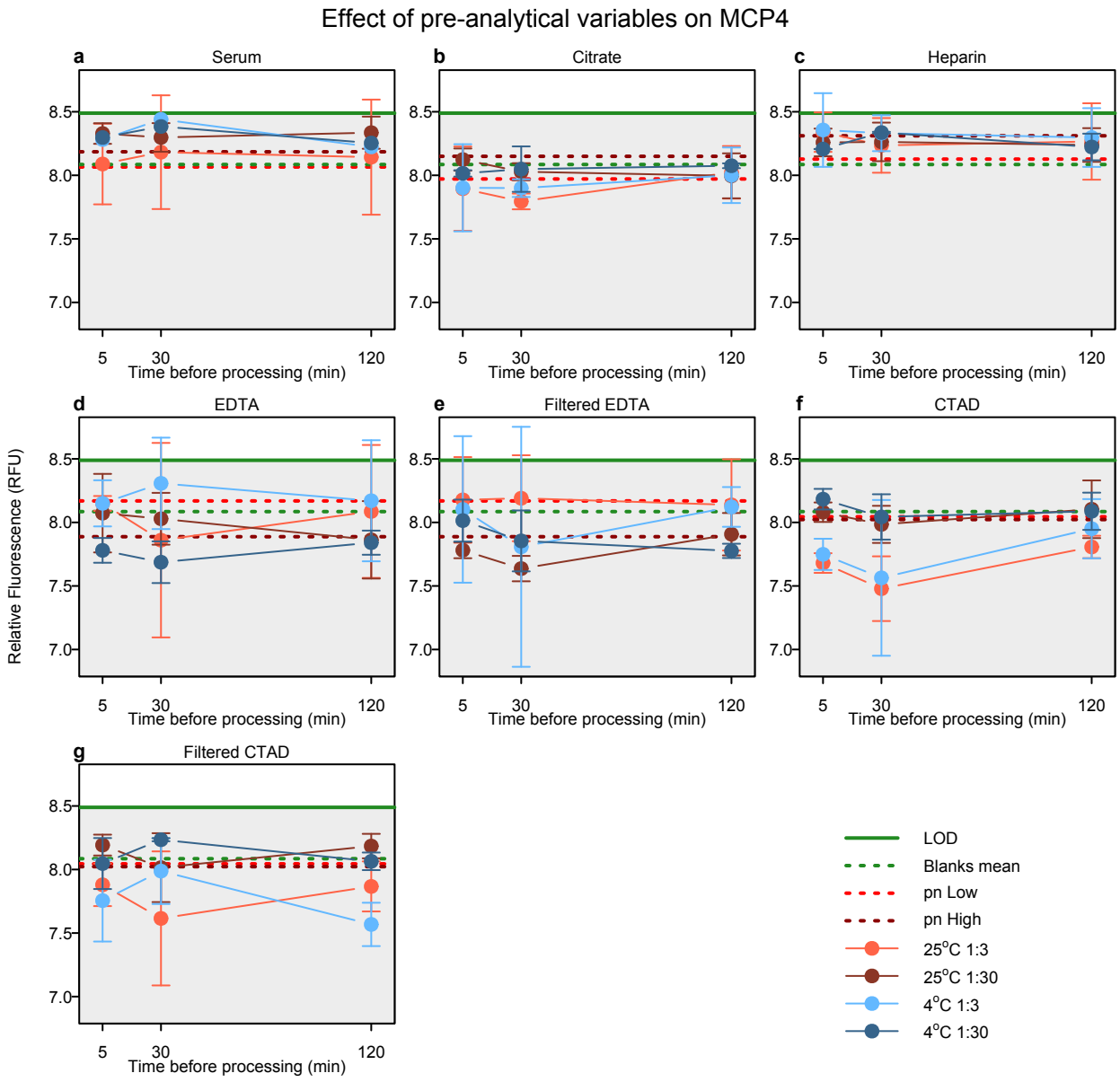

FIGURE I.S129: **Effect of blood collection tube on MCP4 stability and concentration.** Effects of blood collection tubes (**a**: serum, **b**: citrate, **c**: heparin, **d-e**: EDTA, **f-g**: CTAD), storage temperature and time before processing, and post-processing plasma filtering (**e, g**) on the initial value and pre-processing time stability of MCP4 measurements in blood. Information on the dilution of samples used for measuring, data range and the sample type selected are also shown.

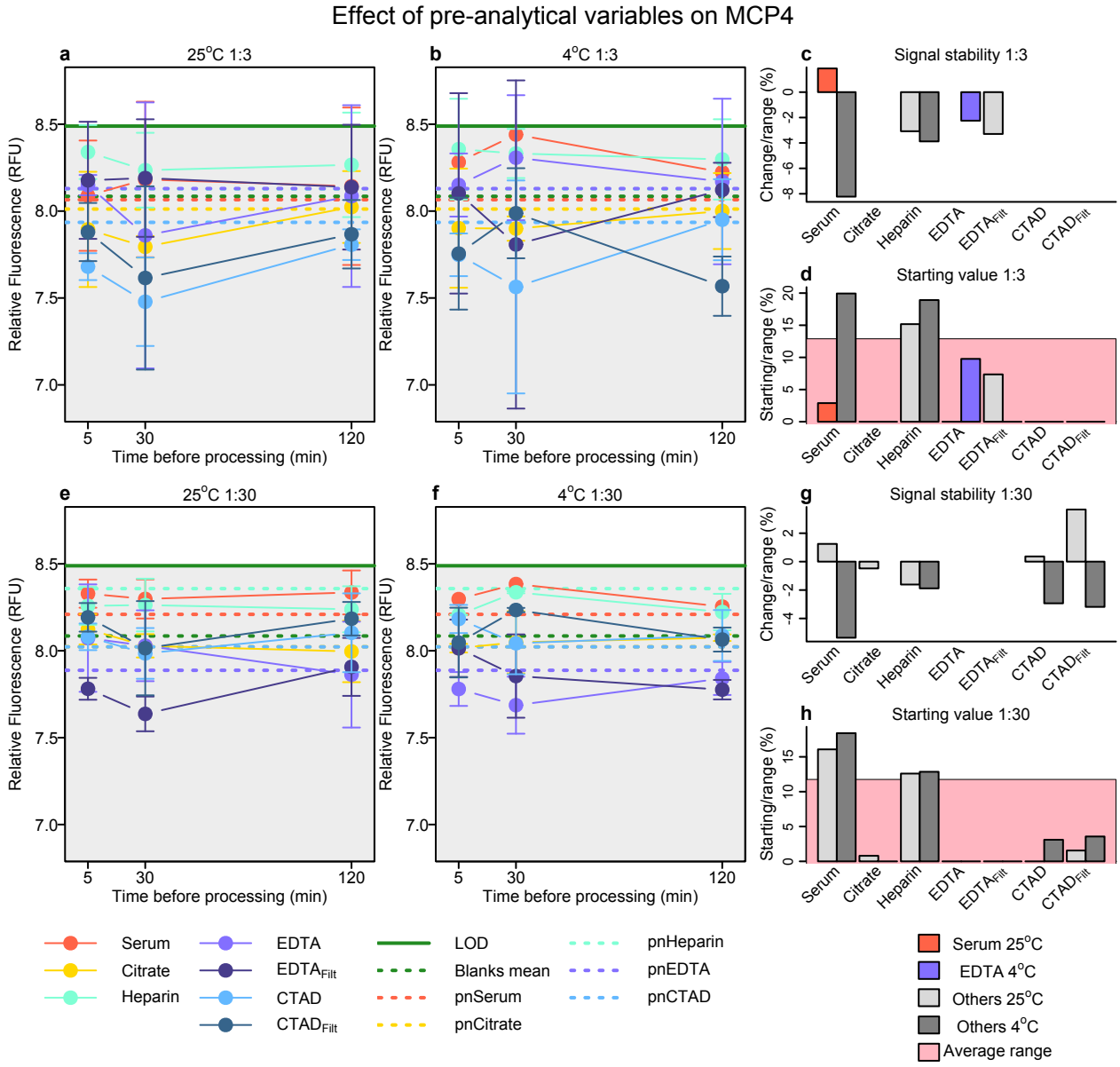

FIGURE I.S130: **Effect of pre-processing storage temperature on MCP4 stability and concentration.** Initial measured value and stability of MCP4 when stored at 25 °C (**a, e**) and 4 °C (**b, f**) before processing when collected in different tube types. The measured values are shown at low dilution of 1:3 (**a-b**) and high dilution of 1:30 (**e-f**). Stability before processing is expressed as an increase or decrease compared to the measurement range and is shown for low (**c**) and high (**g**) dilutions. Initial value is expressed as a portion of the measurement range when the linear regression is extrapolated to zero minutes and is shown for low (**d**) and high (**h**) dilutions. The pink box in graphs **d** and **h** indicate the region that is included by the *mean* ± *SD* of all the initial values and gives an indication of outliers when values lie outside this region. Red and purple bars in **c-d, g-h** are indicated at the measured dilution as the two choices for the TBI analysis.

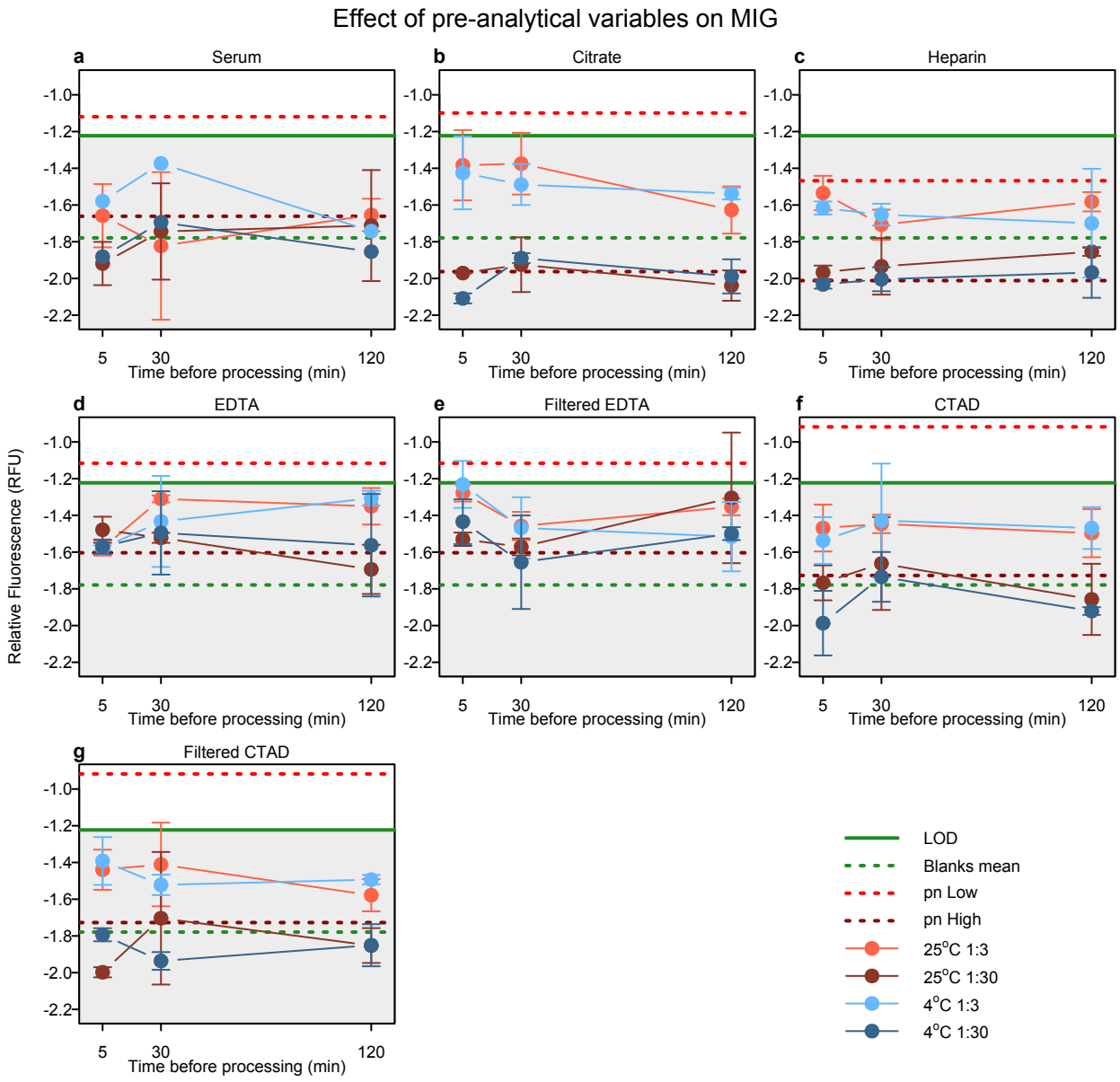

FIGURE I.S131: **Effect of blood collection tube on MIG stability and concentration.** Effects of blood collection tubes (**a**: serum, **b**: citrate, **c**: heparin, **d-e**: EDTA, **f-g**: CTAD), storage temperature and time before processing, and post-processing plasma filtering (**e, g**) on the initial value and pre-processing time stability of MIG measurements in blood. Information on the dilution of samples used for measuring, data range and the sample type selected are also shown.

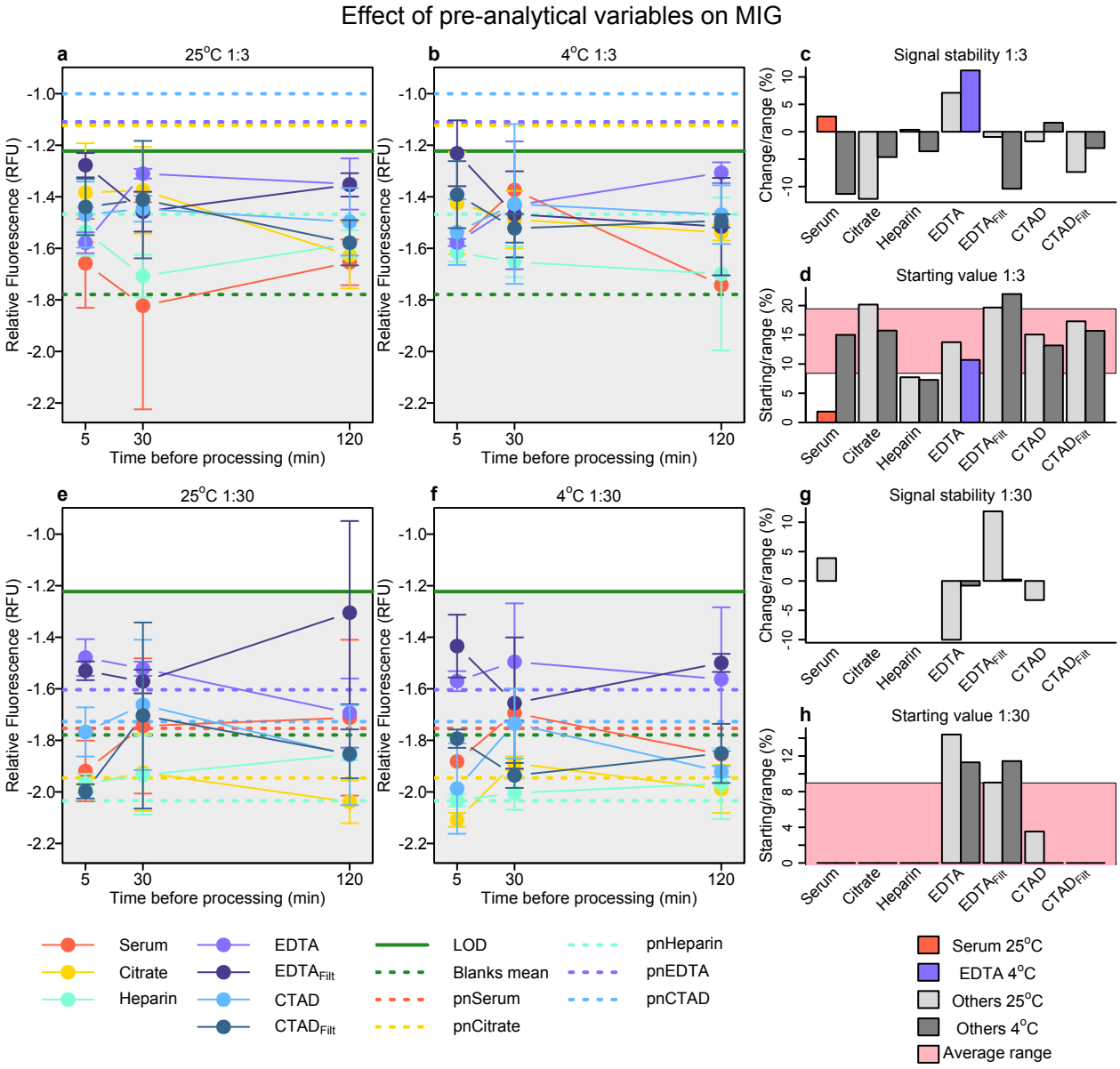

FIGURE I.S132: **Effect of pre-processing storage temperature on MIG stability and concentration.** Initial measured value and stability of MIG when stored at 25 °C (**a, e**) and 4 °C (**b, f**) before processing when collected in different tube types. The measured values are shown at low dilution of 1:3 (**a-b**) and high dilution of 1:30 (**e-f**). Stability before processing is expressed as an increase or decrease compared to the measurement range and is shown for low (**c**) and high (**g**) dilutions. Initial value is expressed as a portion of the measurement range when the linear regression is extrapolated to zero minutes and is shown for low (**d**) and high (**h**) dilutions. The pink box in graphs **d** and **h** indicate the region that is included by the *mean* ± *SD* of all the initial values and gives an indication of outliers when values lie outside this region. Red and purple bars in **c-d, g-h** are indicated at the measured dilution as the two choices for the TBI analysis.

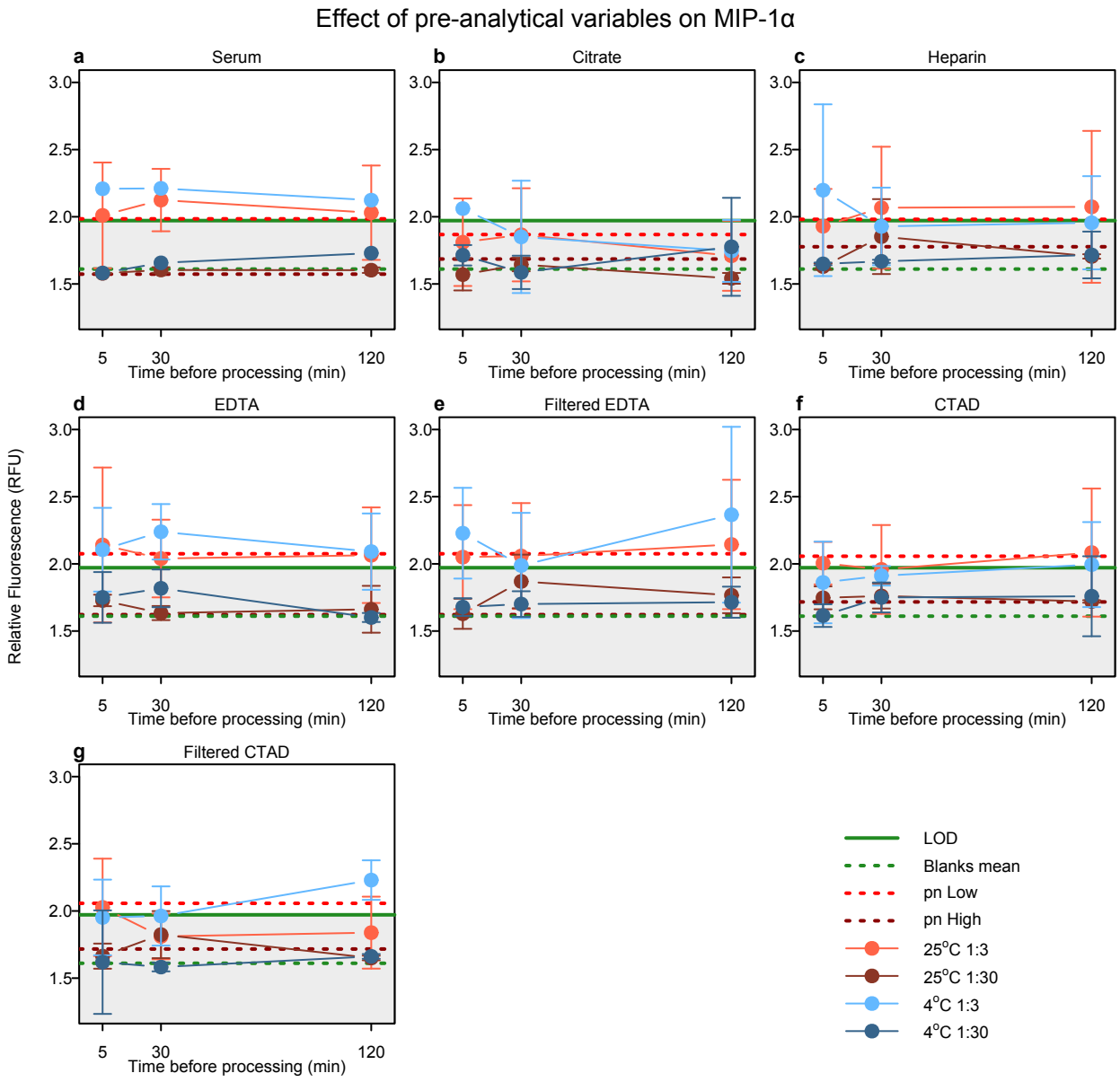

FIGURE I.S133: **Effect of blood collection tube on MIP-1α stability and concentration.** Effects of blood collection tubes (**a**: serum, **b**: citrate, **c**: heparin, **d-e**: EDTA, **f-g**: CTAD), storage temperature and time before processing, and post-processing plasma filtering (**e, g**) on the initial value and pre-processing time stability of MIP-1α measurements in blood. Information on the dilution of samples used for measuring, data range and the sample type selected are also shown.

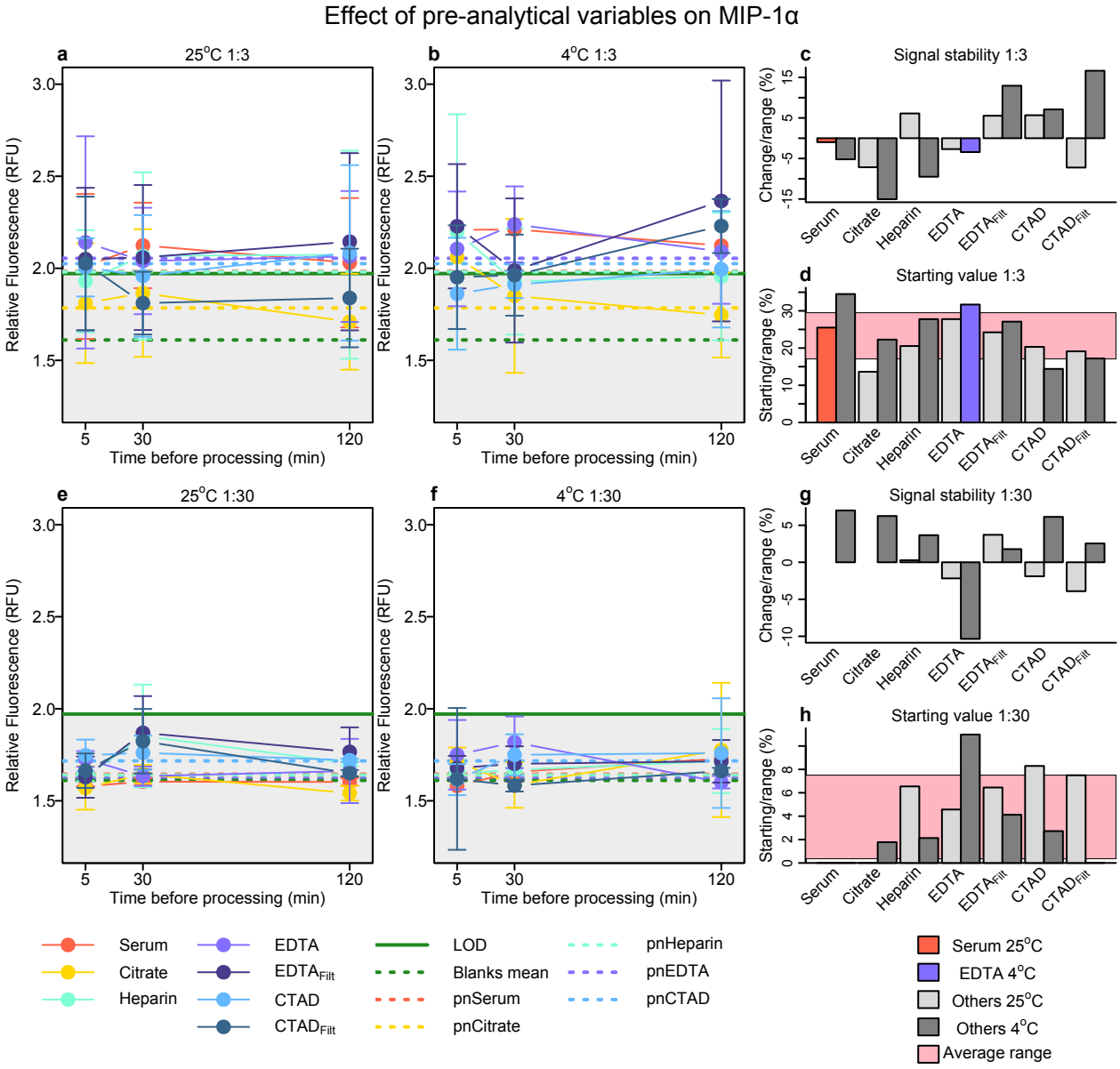

FIGURE I.S134: **Effect of pre-processing storage temperature on MIP-1α stability and concentration.** Initial measured value and stability of MIP-1α when stored at 25 °C (**a, e**) and 4 °C (**b, f**) before processing when collected in different tube types. The measured values are shown at low dilution of 1:3 (**a-b**) and high dilution of 1:30 (**e-f**). Stability before processing is expressed as an increase or decrease compared to the measurement range and is shown for low (**c**) and high (**g**) dilutions. Initial value is expressed as a portion of the measurement range when the linear regression is extrapolated to zero minutes and is shown for low (**d**) and high (**h**) dilutions. The pink box in graphs **d** and **h** indicate the region that is included by the *mean* ± *SD* of all the initial values and gives an indication of outliers when values lie outside this region. Red and purple bars in **c-d, g-h** are indicated at the measured dilution as the two choices for the TBI analysis.

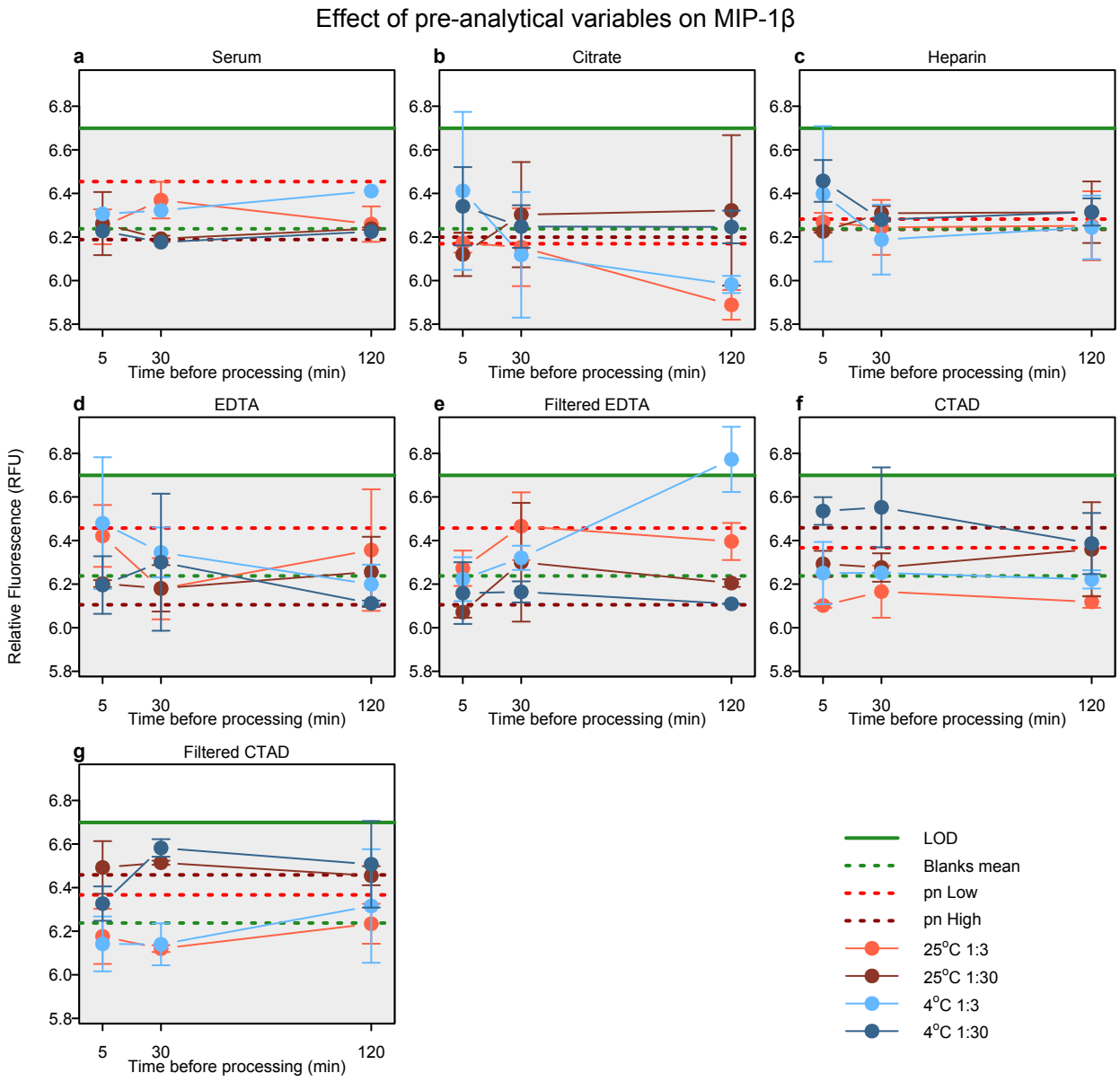

FIGURE I.S135: **Effect of blood collection tube on MIP-1β stability and concentration.** Effects of blood collection tubes (**a**: serum, **b**: citrate, **c**: heparin, **d-e**: EDTA, **f-g**: CTAD), storage temperature and time before processing, and post-processing plasma filtering (**e, g**) on the initial value and pre-processing time stability of MIP-1β measurements in blood. Information on the dilution of samples used for measuring, data range and the sample type selected are also shown.

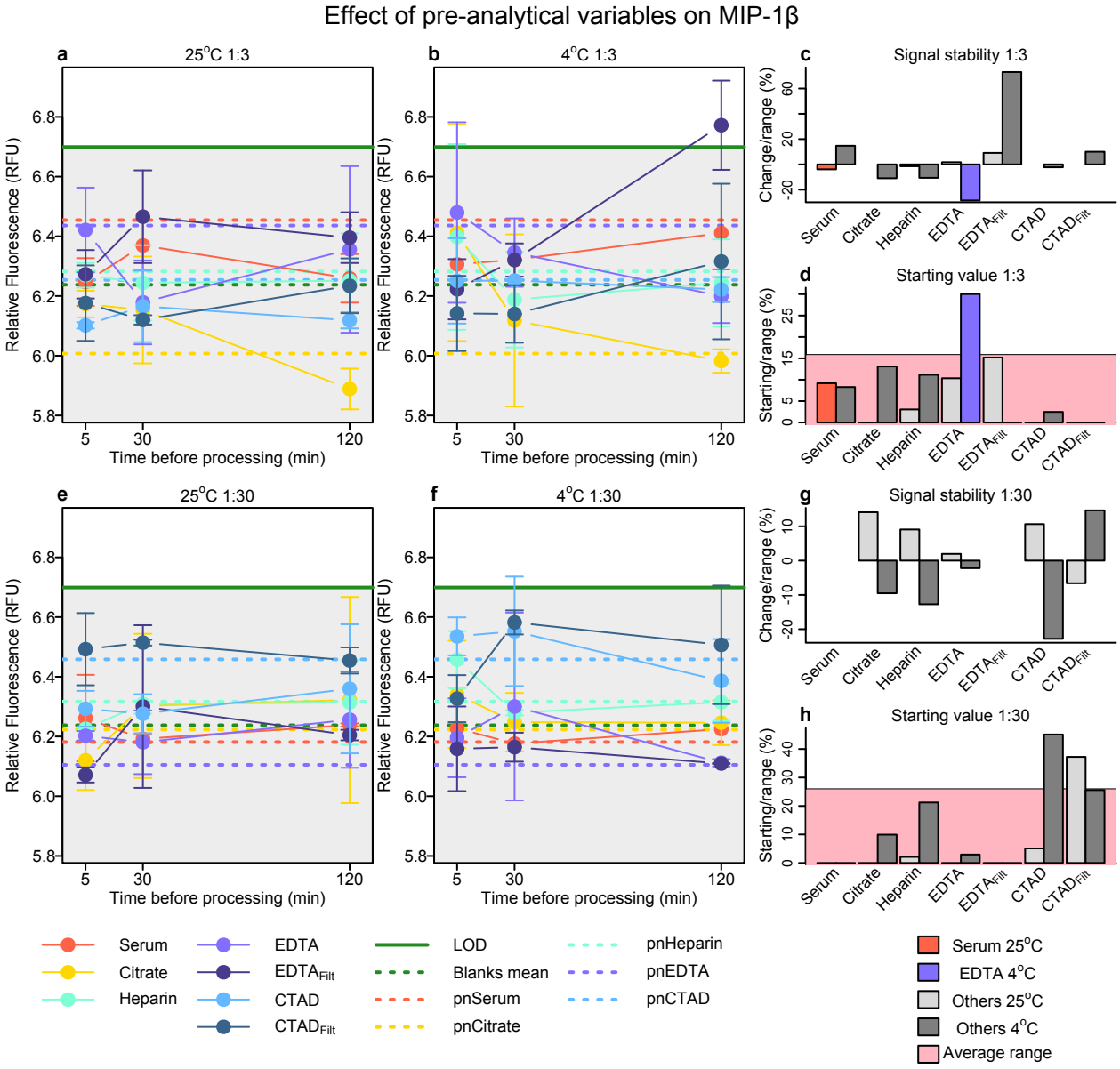

FIGURE I.S136: **Effect of pre-processing storage temperature on MIP-1β stability and concentration.** Initial measured value and stability of MIP-1β when stored at 25 °C (**a, e**) and 4 °C (**b, f**) before processing when collected in different tube types. The measured values are shown at low dilution of 1:3 (**a-b**) and high dilution of 1:30 (**e-f**). Stability before processing is expressed as an increase or decrease compared to the measurement range and is shown for low (**c**) and high (**g**) dilutions. Initial value is expressed as a portion of the measurement range when the linear regression is extrapolated to zero minutes and is shown for low (**d**) and high (**h**) dilutions. The pink box in graphs **d** and **h** indicate the region that is included by the *mean* ± *SD* of all the initial values and gives an indication of outliers when values lie outside this region. Red and purple bars in **c-d, g-h** are indicated at the measured dilution as the two choices for the TBI analysis.

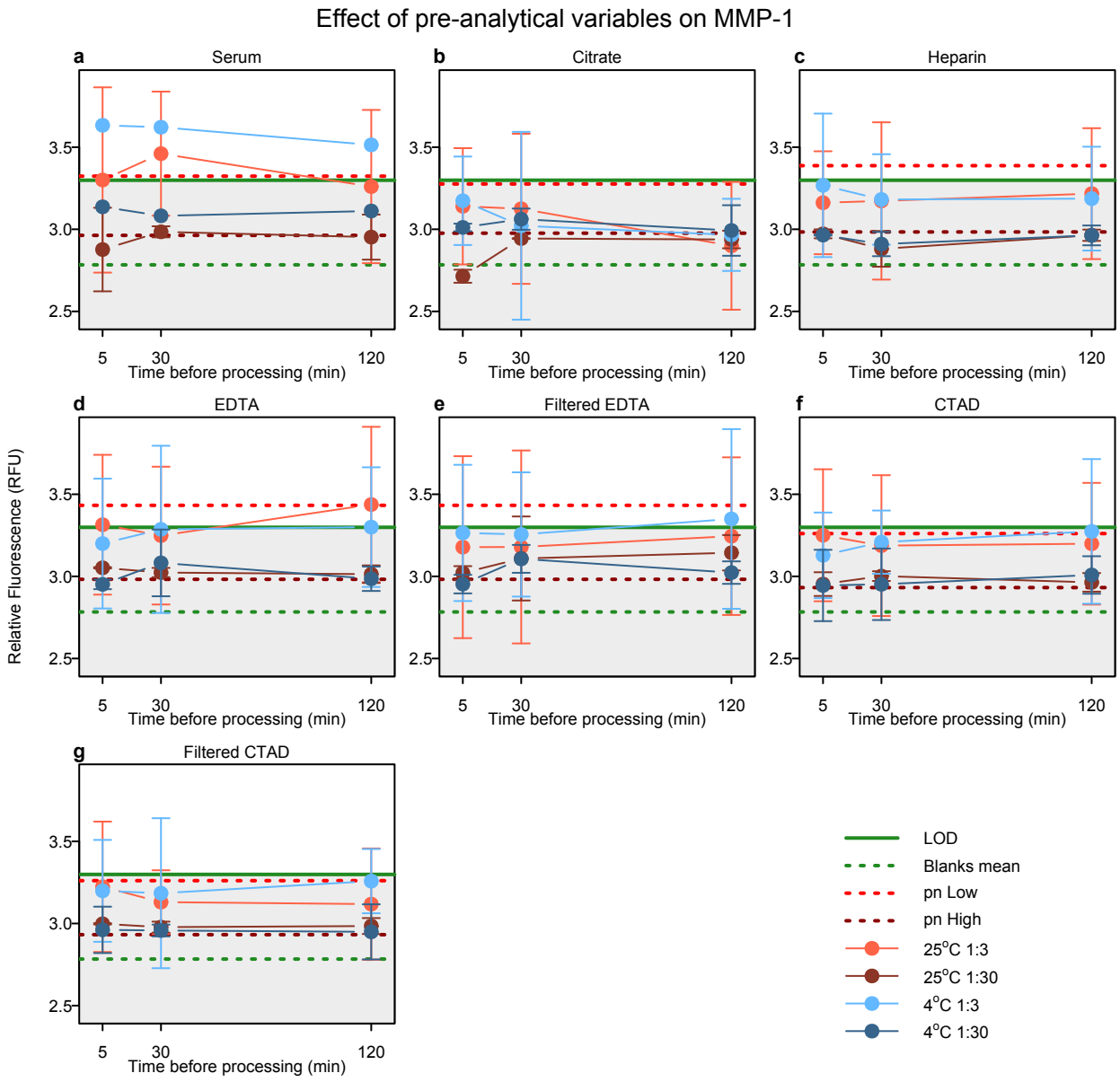

FIGURE I.S137: **Effect of blood collection tube on MMP-1 stability and concentration.** Effects of blood collection tubes (**a**: serum, **b**: citrate, **c**: heparin, **d-e**: EDTA, **f-g**: CTAD), storage temperature and time before processing, and post-processing plasma filtering (**e, g**) on the initial value and pre-processing time stability of MMP-1 measurements in blood. Information on the dilution of samples used for measuring, data range and the sample type selected are also shown.

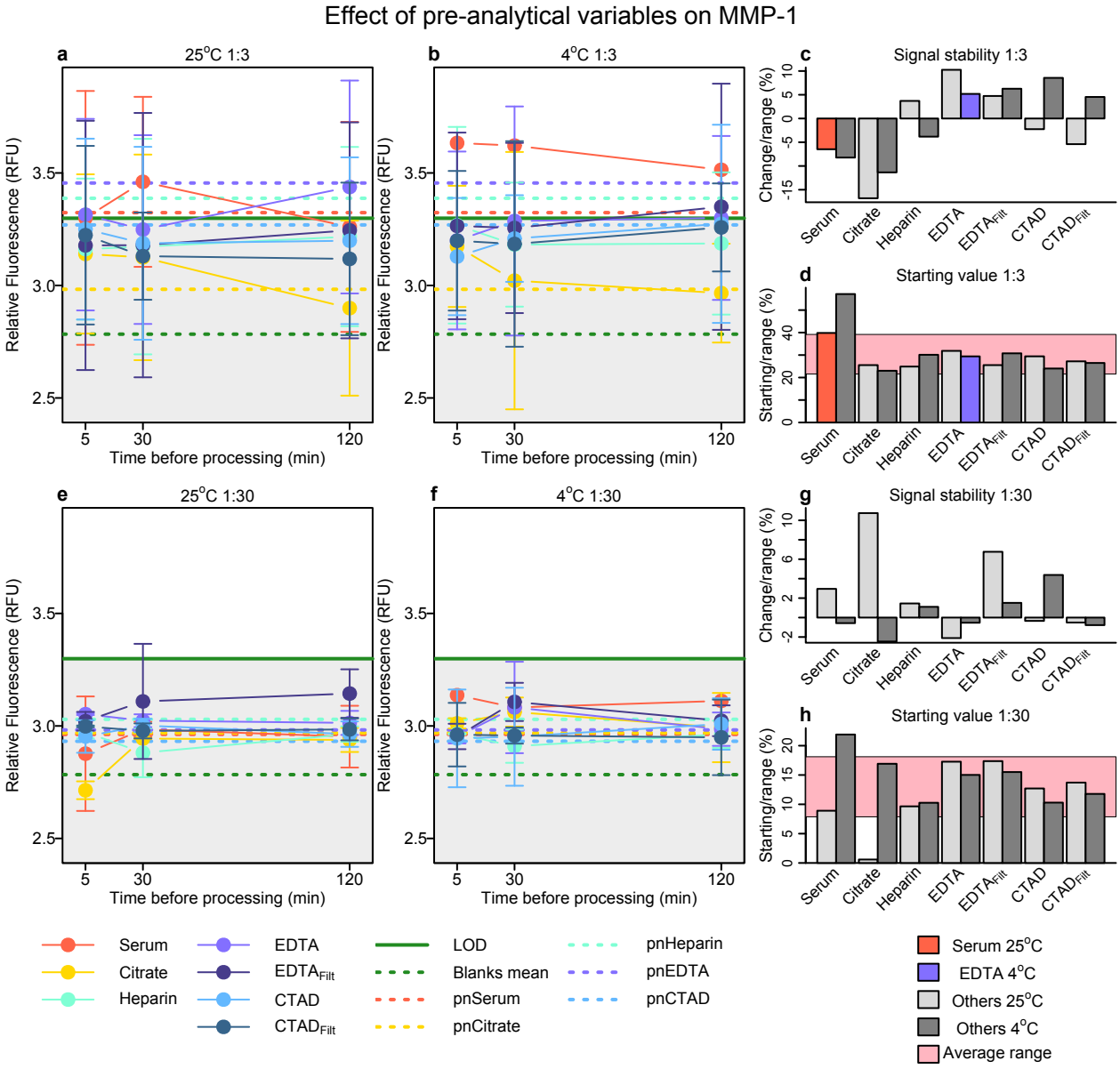

FIGURE I.S138: **Effect of pre-processing storage temperature on MMP-1 stability and concentration.** Initial measured value and stability of MMP-1 when stored at 25 °C (**a, e**) and 4 °C (**b, f**) before processing when collected in different tube types. The measured values are shown at low dilution of 1:3 (**a-b**) and high dilution of 1:30 (**e-f**). Stability before processing is expressed as an increase or decrease compared to the measurement range and is shown for low (**c**) and high (**g**) dilutions. Initial value is expressed as a portion of the measurement range when the linear regression is extrapolated to zero minutes and is shown for low (**d**) and high (**h**) dilutions. The pink box in graphs **d** and **h** indicate the region that is included by the *mean* ± *SD* of all the initial values and gives an indication of outliers when values lie outside this region. Red and purple bars in **c-d, g-h** are indicated at the measured dilution as the two choices for the TBI analysis.

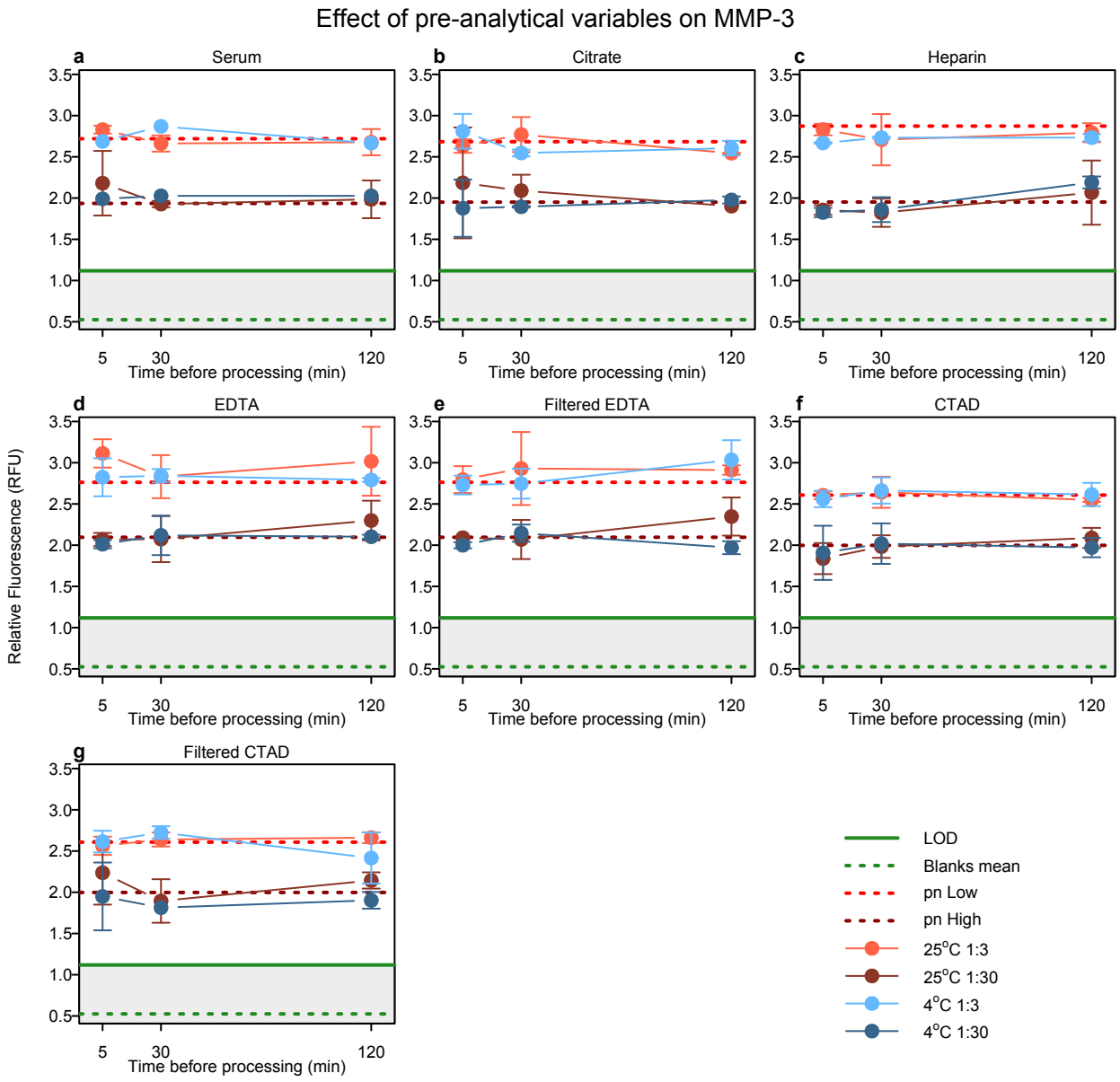

FIGURE I.S139: **Effect of blood collection tube on MMP-3 stability and concentration.** Effects of blood collection tubes (**a**: serum, **b**: citrate, **c**: heparin, **d-e**: EDTA, **f-g**: CTAD), storage temperature and time before processing, and post-processing plasma filtering (**e, g**) on the initial value and pre-processing time stability of MMP-3 measurements in blood. Information on the dilution of samples used for measuring, data range and the sample type selected are also shown.

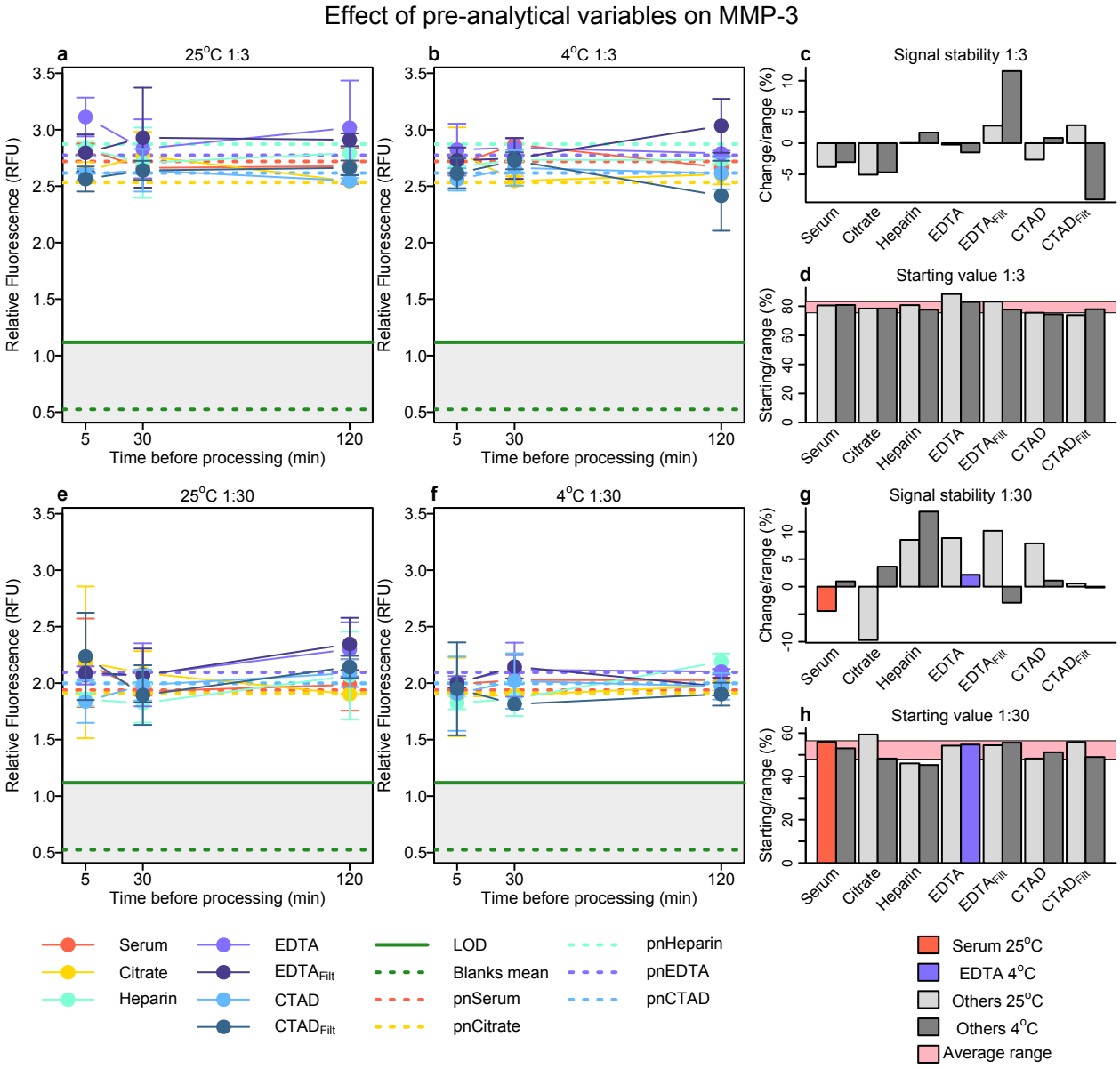

FIGURE I.S140: **Effect of pre-processing storage temperature on MMP-3 stability and concentration.** Initial measured value and stability of MMP-3 when stored at 25 °C (**a, e**) and 4 °C (**b, f**) before processing when collected in different tube types. The measured values are shown at low dilution of 1:3 (**a-b**) and high dilution of 1:30 (**e-f**). Stability before processing is expressed as an increase or decrease compared to the measurement range and is shown for low (**c**) and high (**g**) dilutions. Initial value is expressed as a portion of the measurement range when the linear regression is extrapolated to zero minutes and is shown for low (**d**) and high (**h**) dilutions. The pink box in graphs **d** and **h** indicate the region that is included by the *mean* ± *SD* of all the initial values and gives an indication of outliers when values lie outside this region. Red and purple bars in **c-d, g-h** are indicated at the measured dilution as the two choices for the TBI analysis.

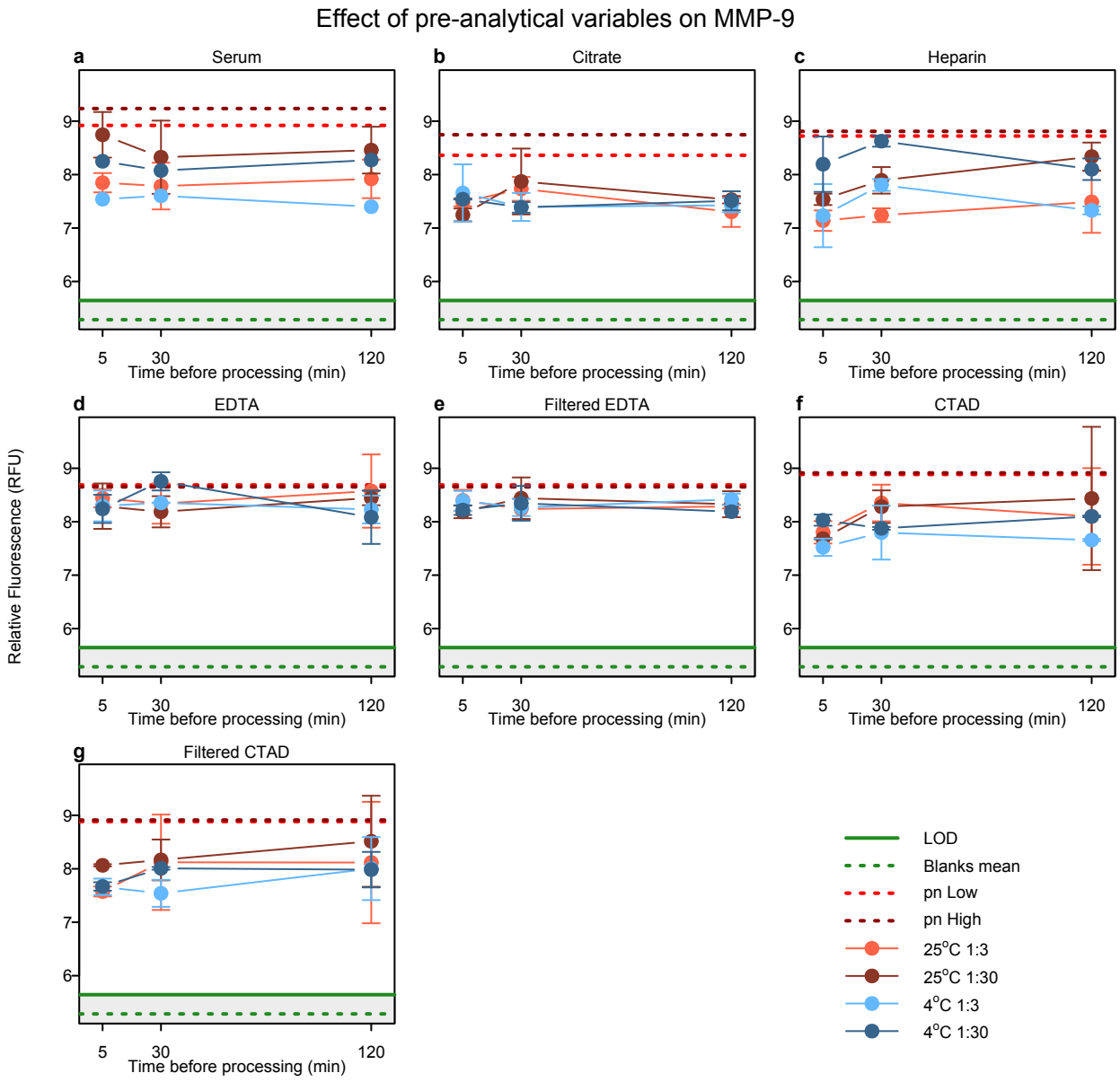

FIGURE I.S141: **Effect of blood collection tube on MMP-9 stability and concentration.** Effects of blood collection tubes (**a**: serum, **b**: citrate, **c**: heparin, **d-e**: EDTA, **f-g**: CTAD), storage temperature and time before processing, and post-processing plasma filtering (**e, g**) on the initial value and pre-processing time stability of MMP-9 measurements in blood. Information on the dilution of samples used for measuring, data range and the sample type selected are also shown.

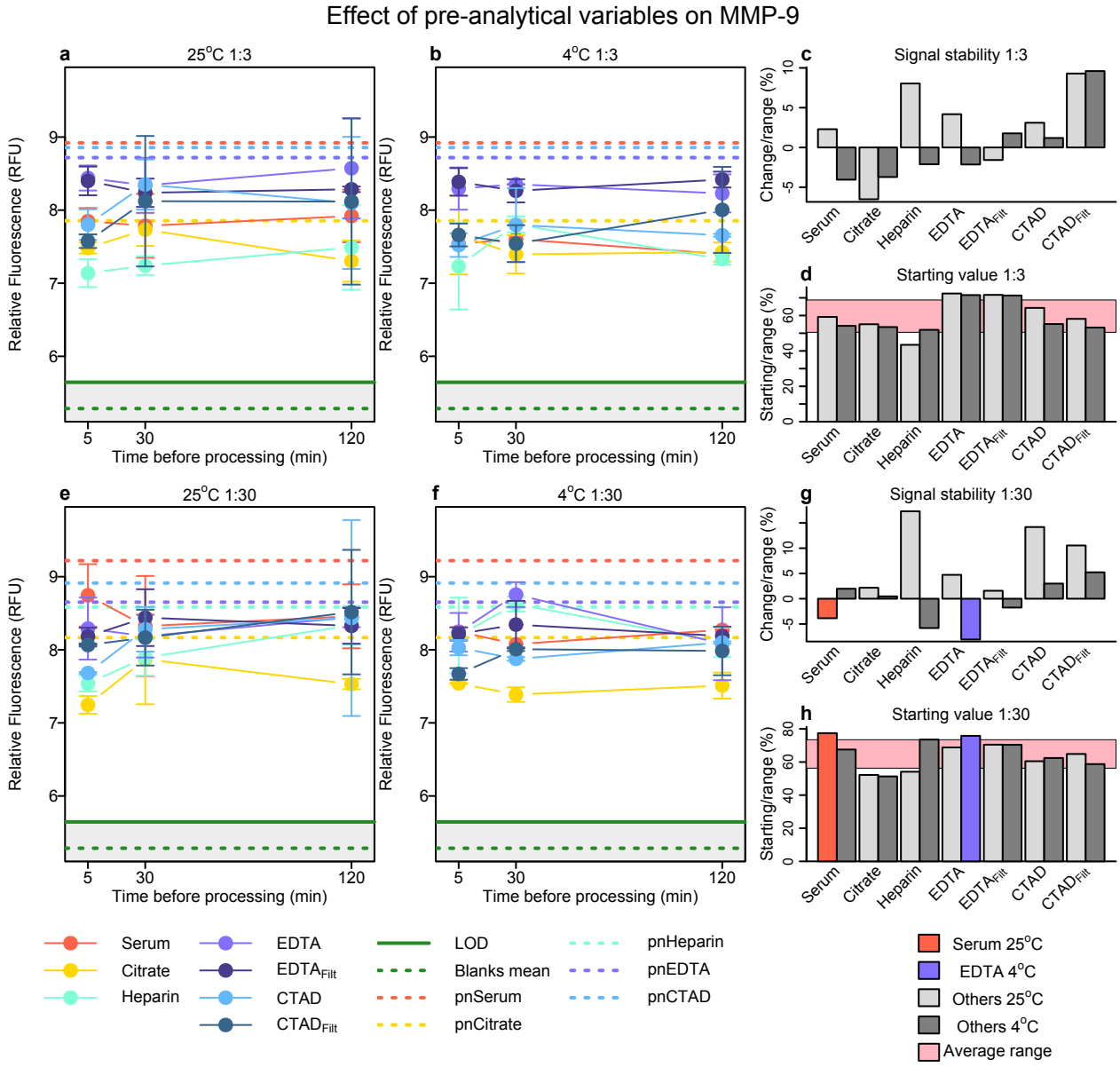

FIGURE I.S142: **Effect of pre-processing storage temperature on MMP-9 stability and concentration.** Initial measured value and stability of MMP-9 when stored at 25 °C (**a, e**) and 4 °C (**b, f**) before processing when collected in different tube types. The measured values are shown at low dilution of 1:3 (**a-b**) and high dilution of 1:30 (**e-f**). Stability before processing is expressed as an increase or decrease compared to the measurement range and is shown for low (**c**) and high (**g**) dilutions. Initial value is expressed as a portion of the measurement range when the linear regression is extrapolated to zero minutes and is shown for low (**d**) and high (**h**) dilutions. The pink box in graphs **d** and **h** indicate the region that is included by the *mean* ± *SD* of all the initial values and gives an indication of outliers when values lie outside this region. Red and purple bars in **c-d, g-h** are indicated at the measured dilution as the two choices for the TBI analysis.

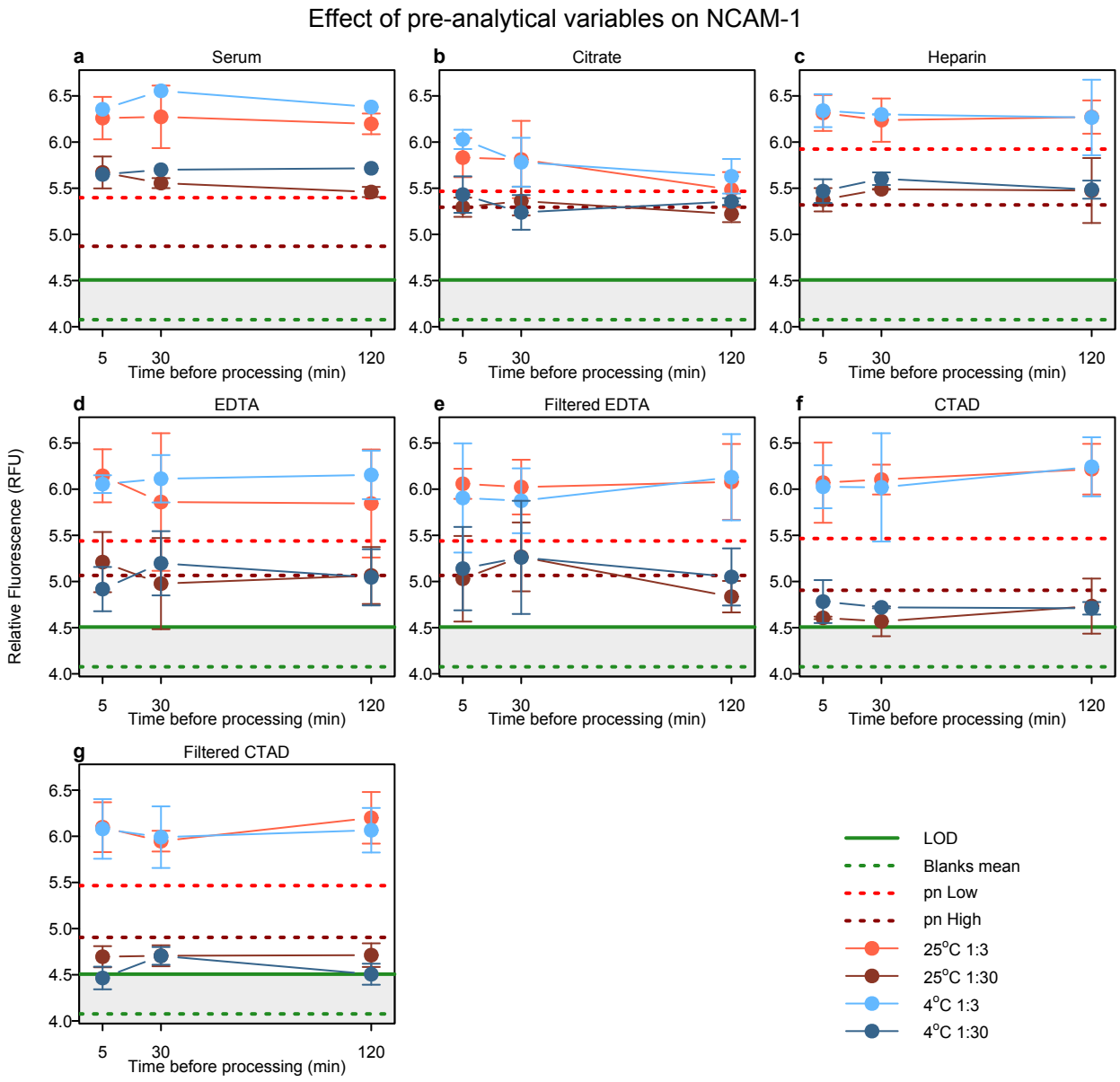

FIGURE I.S143: **Effect of blood collection tube on NCAM-1 stability and concentration.** Effects of blood collection tubes (**a**: serum, **b**: citrate, **c**: heparin, **d-e**: EDTA, **f-g**: CTAD), storage temperature and time before processing, and post-processing plasma filtering (**e, g**) on the initial value and pre-processing time stability of NCAM-1 measurements in blood. Information on the dilution of samples used for measuring, data range and the sample type selected are also shown.

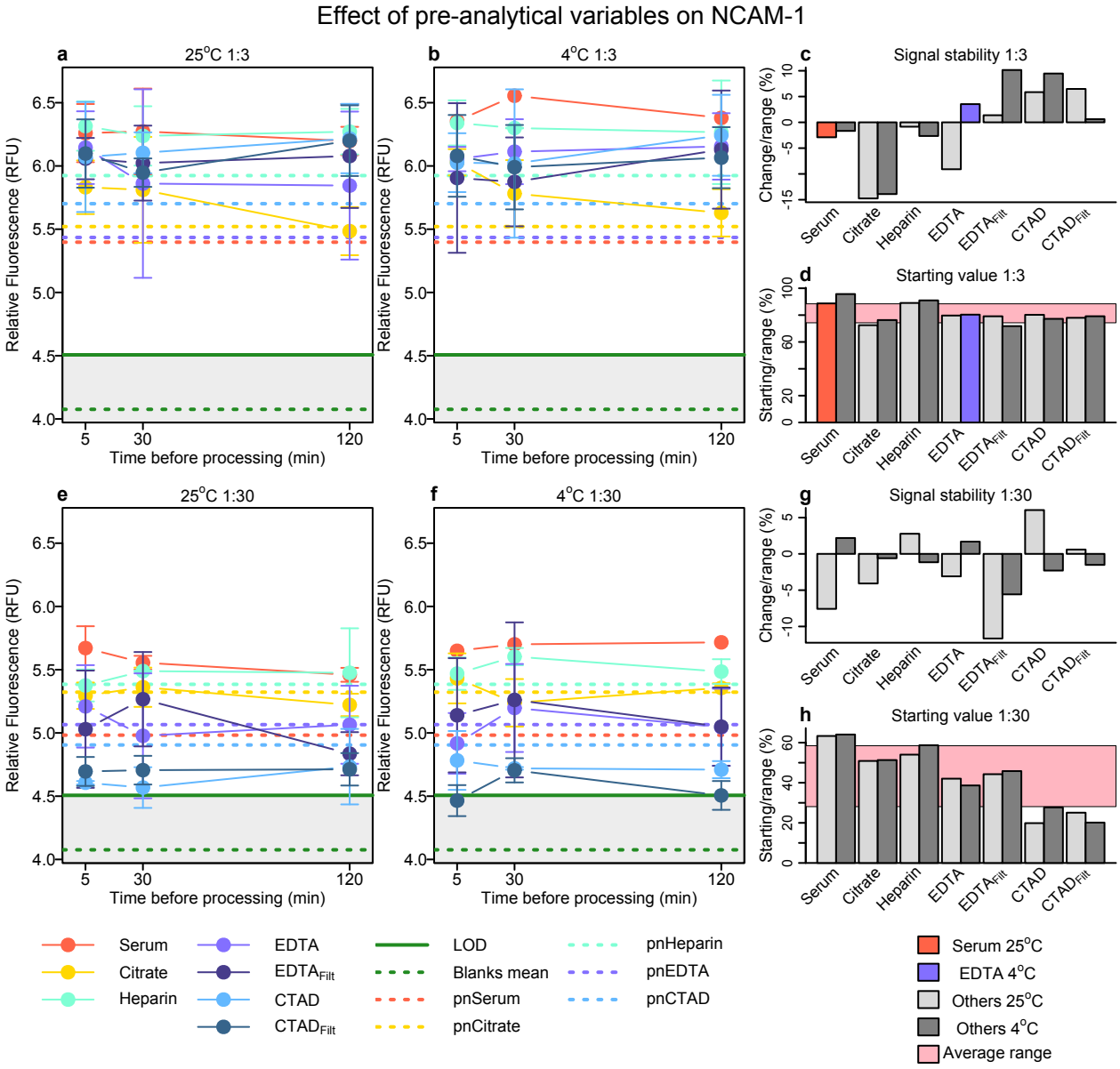

FIGURE I.S144: **Effect of pre-processing storage temperature on NCAM-1 stability and concentration.** Initial measured value and stability of NCAM-1 when stored at 25 °C (**a, e**) and 4 °C (**b, f**) before processing when collected in different tube types. The measured values are shown at low dilution of 1:3 (**a-b**) and high dilution of 1:30 (**e-f**). Stability before processing is expressed as an increase or decrease compared to the measurement range and is shown for low (**c**) and high (**g**) dilutions. Initial value is expressed as a portion of the measurement range when the linear regression is extrapolated to zero minutes and is shown for low (**d**) and high (**h**) dilutions. The pink box in graphs **d** and **h** indicate the region that is included by the *mean* ± *SD* of all the initial values and gives an indication of outliers when values lie outside this region. Red and purple bars in **c-d, g-h** are indicated at the measured dilution as the two choices for the TBI analysis.

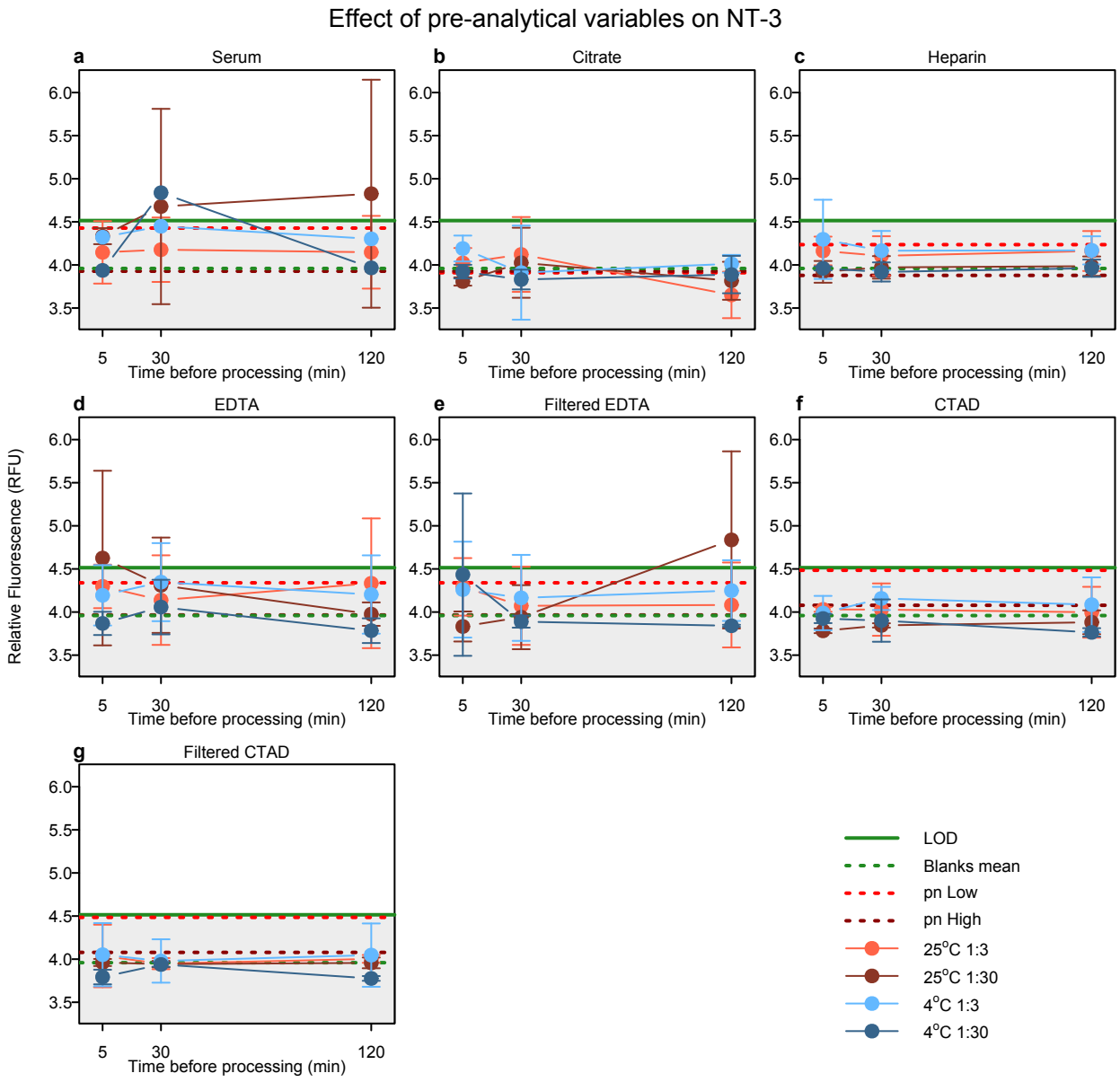

FIGURE I.S145: **Effect of blood collection tube on NT-3 stability and concentration.** Effects of blood collection tubes (**a**: serum, **b**: citrate, **c**: heparin, **d-e**: EDTA, **f-g**: CTAD), storage temperature and time before processing, and post-processing plasma filtering (**e, g**) on the initial value and pre-processing time stability of NT-3 measurements in blood. Information on the dilution of samples used for measuring, data range and the sample type selected are also shown.

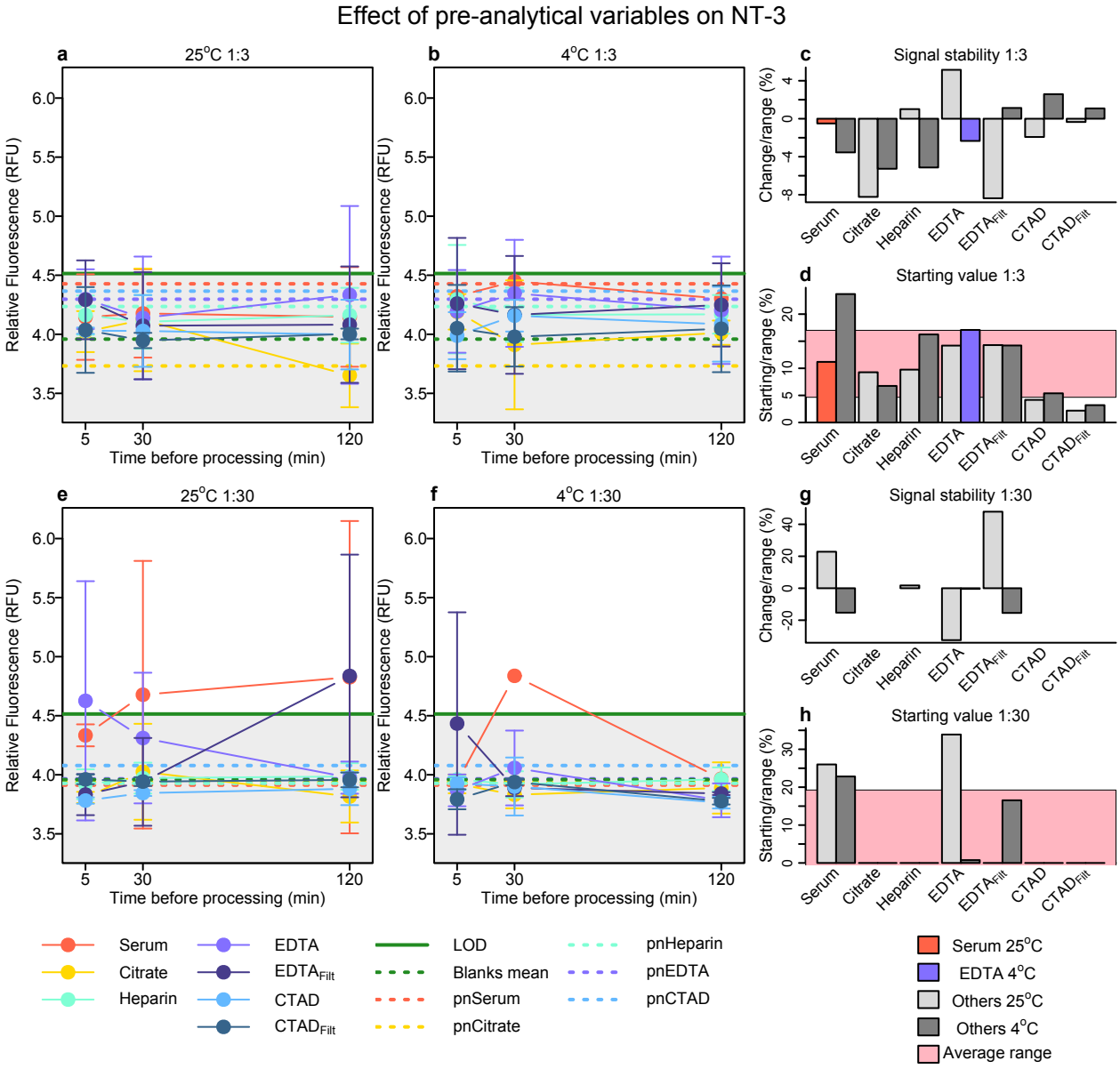

FIGURE I.S146: **Effect of pre-processing storage temperature on NT-3 stability and concentration.** Initial measured value and stability of NT-3 when stored at 25 °C (**a, e**) and 4 °C (**b, f**) before processing when collected in different tube types. The measured values are shown at low dilution of 1:3 (**a-b**) and high dilution of 1:30 (**e-f**). Stability before processing is expressed as an increase or decrease compared to the measurement range and is shown for low (**c**) and high (**g**) dilutions. Initial value is expressed as a portion of the measurement range when the linear regression is extrapolated to zero minutes and is shown for low (**d**) and high (**h**) dilutions. The pink box in graphs **d** and **h** indicate the region that is included by the *mean* ± *SD* of all the initial values and gives an indication of outliers when values lie outside this region. Red and purple bars in **c-d, g-h** are indicated at the measured dilution as the two choices for the TBI analysis.

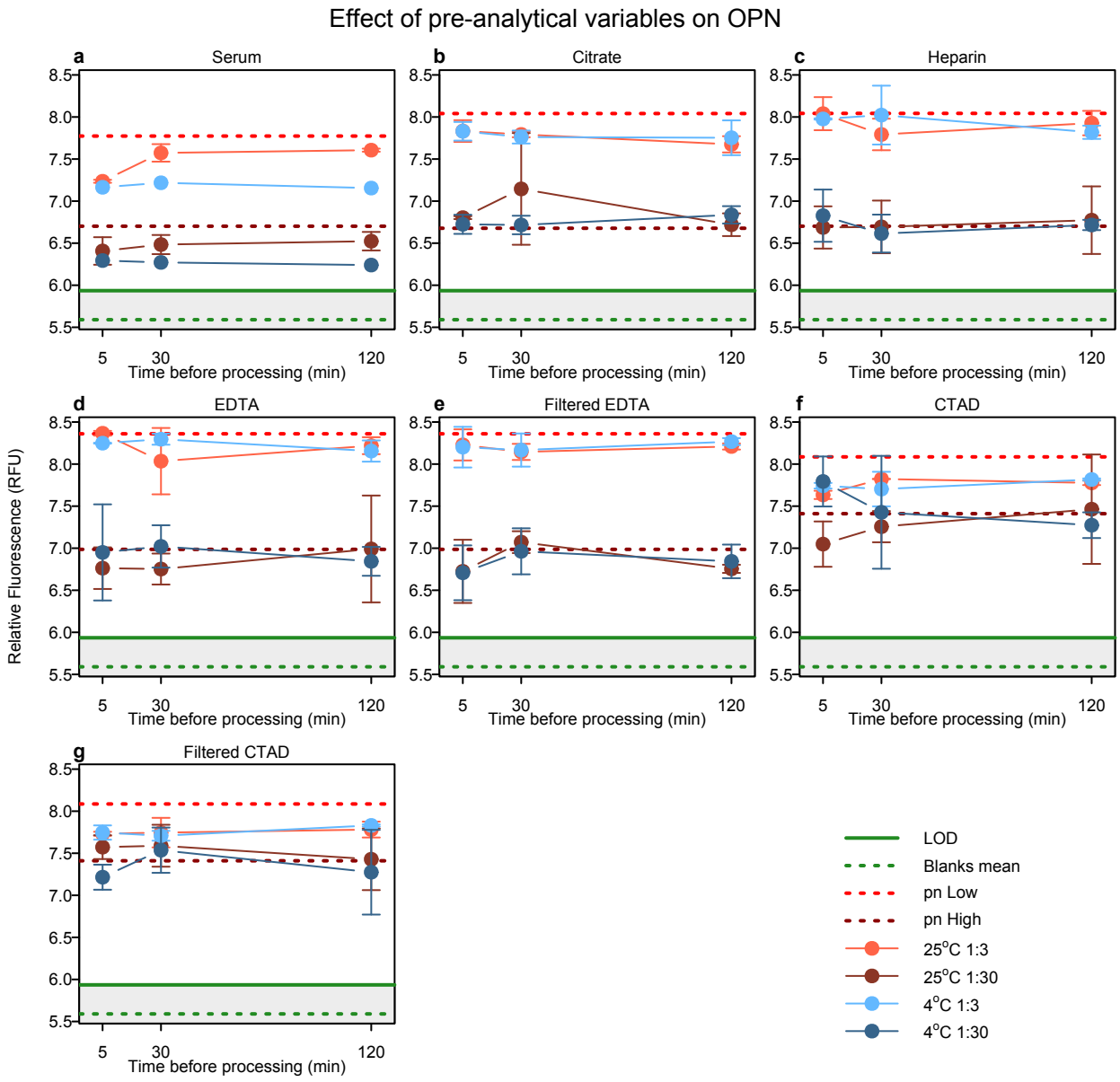

FIGURE I.S147: **Effect of blood collection tube on OPN stability and concentration.** Effects of blood collection tubes (**a**: serum, **b**: citrate, **c**: heparin, **d-e**: EDTA, **f-g**: CTAD), storage temperature and time before processing, and post-processing plasma filtering (**e, g**) on the initial value and pre-processing time stability of OPN measurements in blood. Information on the dilution of samples used for measuring, data range and the sample type selected are also shown.

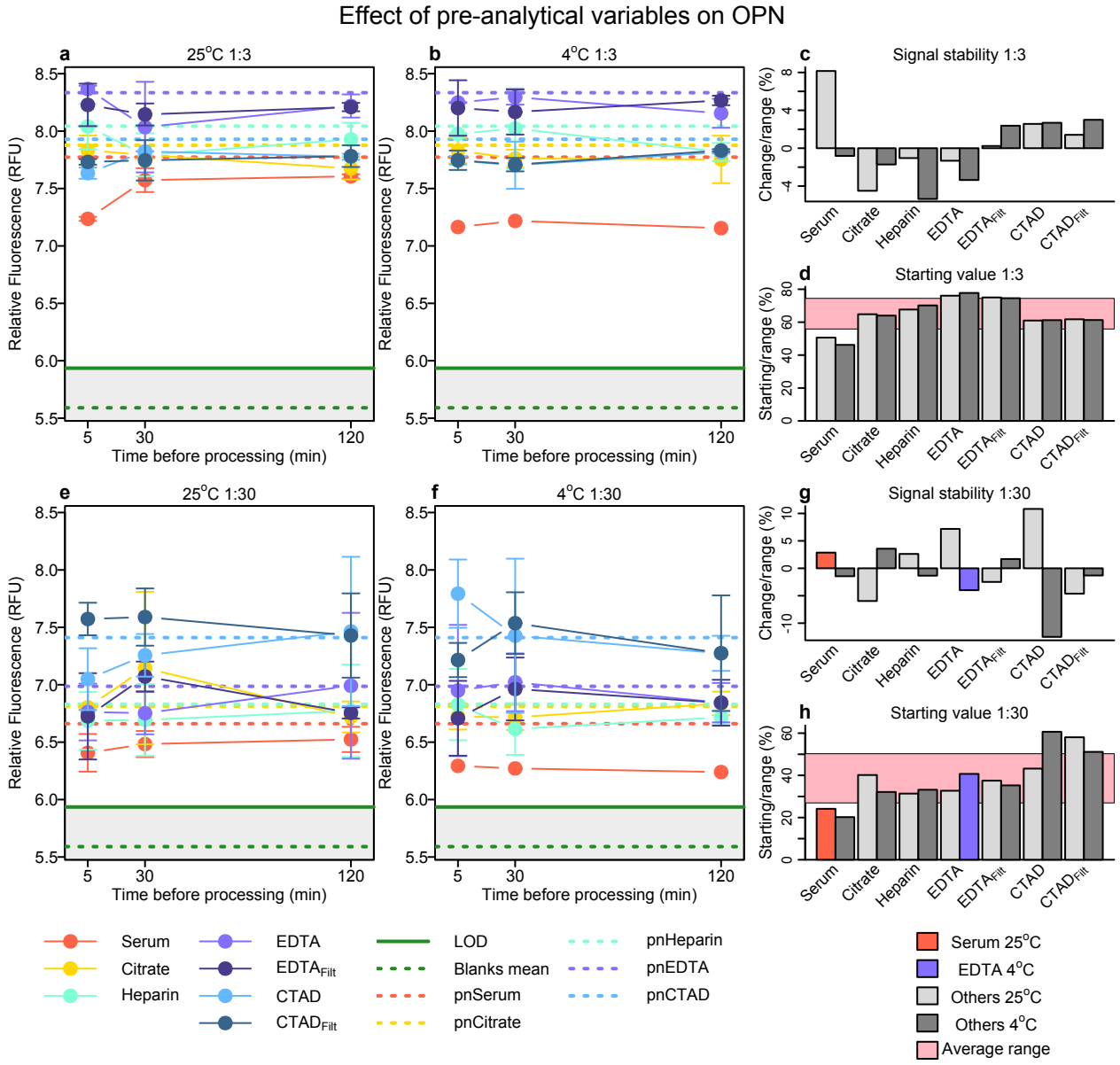

FIGURE I.S148: **Effect of pre-processing storage temperature on OPN stability and concentration.** Initial measured value and stability of OPN when stored at 25 °C (**a, e**) and 4 °C (**b, f**) before processing when collected in different tube types. The measured values are shown at low dilution of 1:3 (**a-b**) and high dilution of 1:30 (**e-f**). Stability before processing is expressed as an increase or decrease compared to the measurement range and is shown for low (**c**) and high (**g**) dilutions. Initial value is expressed as a portion of the measurement range when the linear regression is extrapolated to zero minutes and is shown for low (**d**) and high (**h**) dilutions. The pink box in graphs **d** and **h** indicate the region that is included by the *mean* ± *SD* of all the initial values and gives an indication of outliers when values lie outside this region. Red and purple bars in **c-d, g-h** are indicated at the measured dilution as the two choices for the TBI analysis.

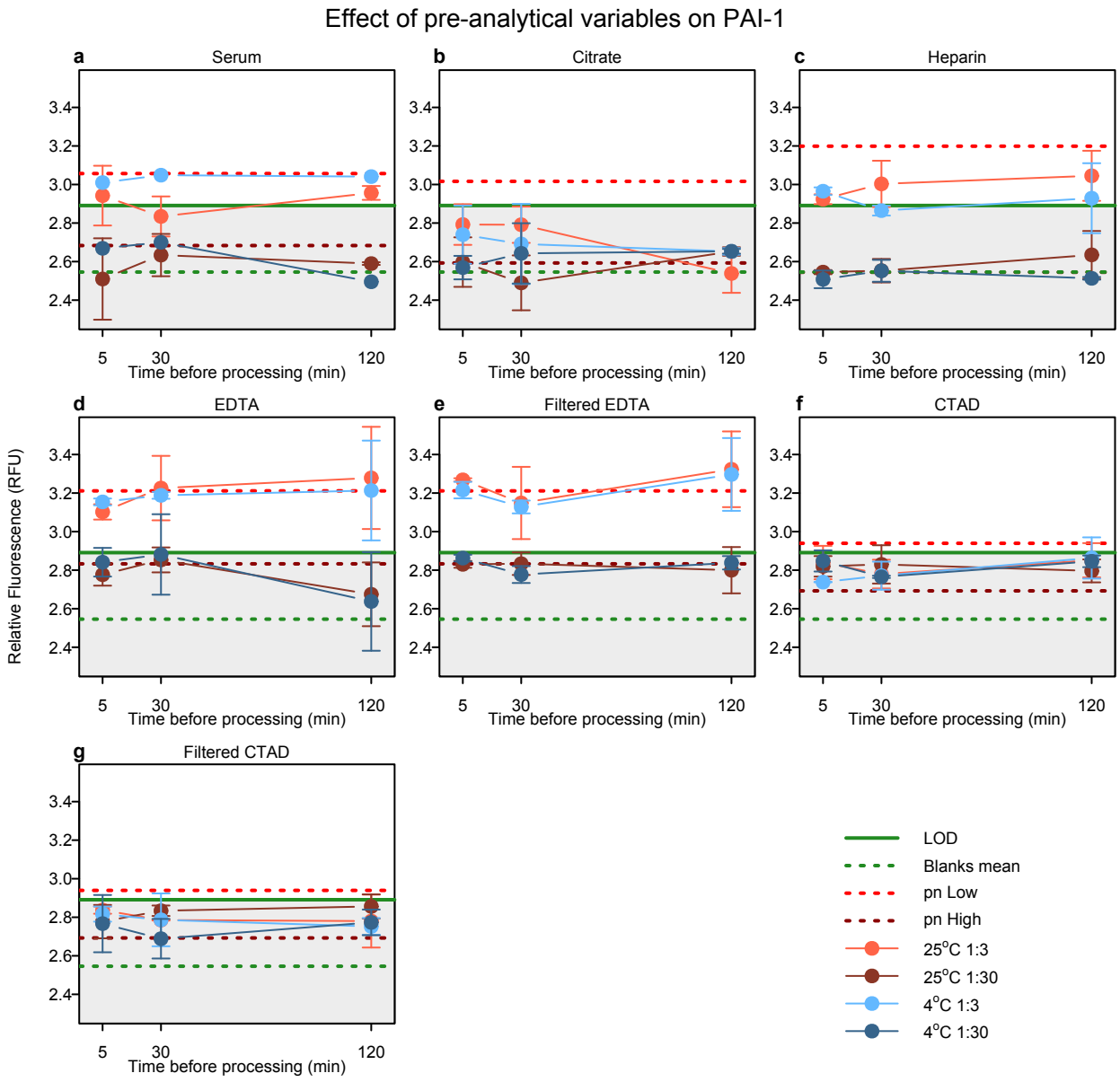

FIGURE I.S149: **Effect of blood collection tube on PAI-1 stability and concentration.** Effects of blood collection tubes (**a**: serum, **b**: citrate, **c**: heparin, **d-e**: EDTA, **f-g**: CTAD), storage temperature and time before processing, and post-processing plasma filtering (**e, g**) on the initial value and pre-processing time stability of PAI-1 measurements in blood. Information on the dilution of samples used for measuring, data range and the sample type selected are also shown.

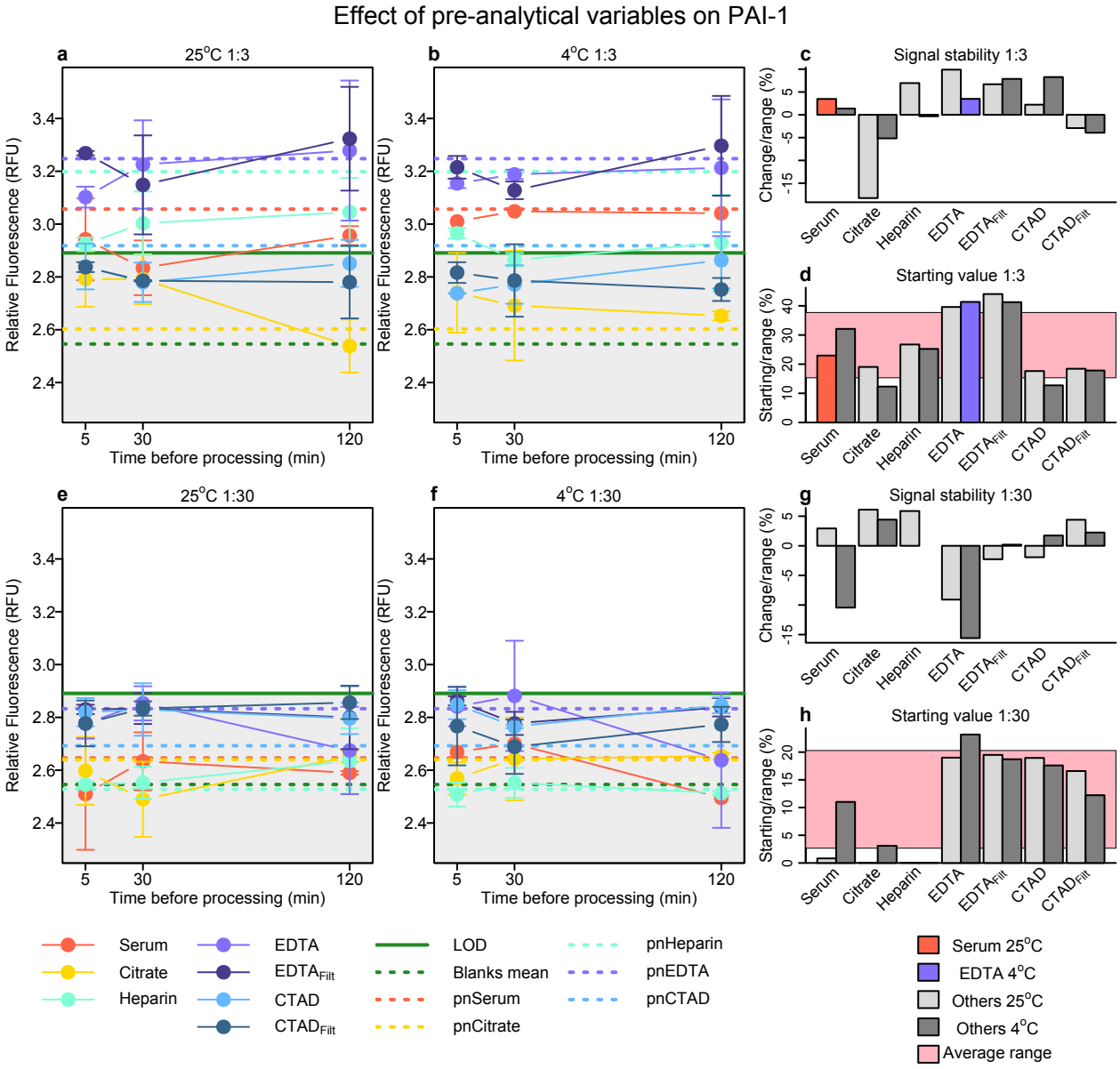

FIGURE I.S150: **Effect of pre-processing storage temperature on PAI-1 stability and concentration.** Initial measured value and stability of PAI-1 when stored at 25 °C (**a, e**) and 4 °C (**b, f**) before processing when collected in different tube types. The measured values are shown at low dilution of 1:3 (**a-b**) and high dilution of 1:30 (**e-f**). Stability before processing is expressed as an increase or decrease compared to the measurement range and is shown for low (**c**) and high (**g**) dilutions. Initial value is expressed as a portion of the measurement range when the linear regression is extrapolated to zero minutes and is shown for low (**d**) and high (**h**) dilutions. The pink box in graphs **d** and **h** indicate the region that is included by the *mean* ± *SD* of all the initial values and gives an indication of outliers when values lie outside this region. Red and purple bars in **c-d, g-h** are indicated at the measured dilution as the two choices for the TBI analysis.

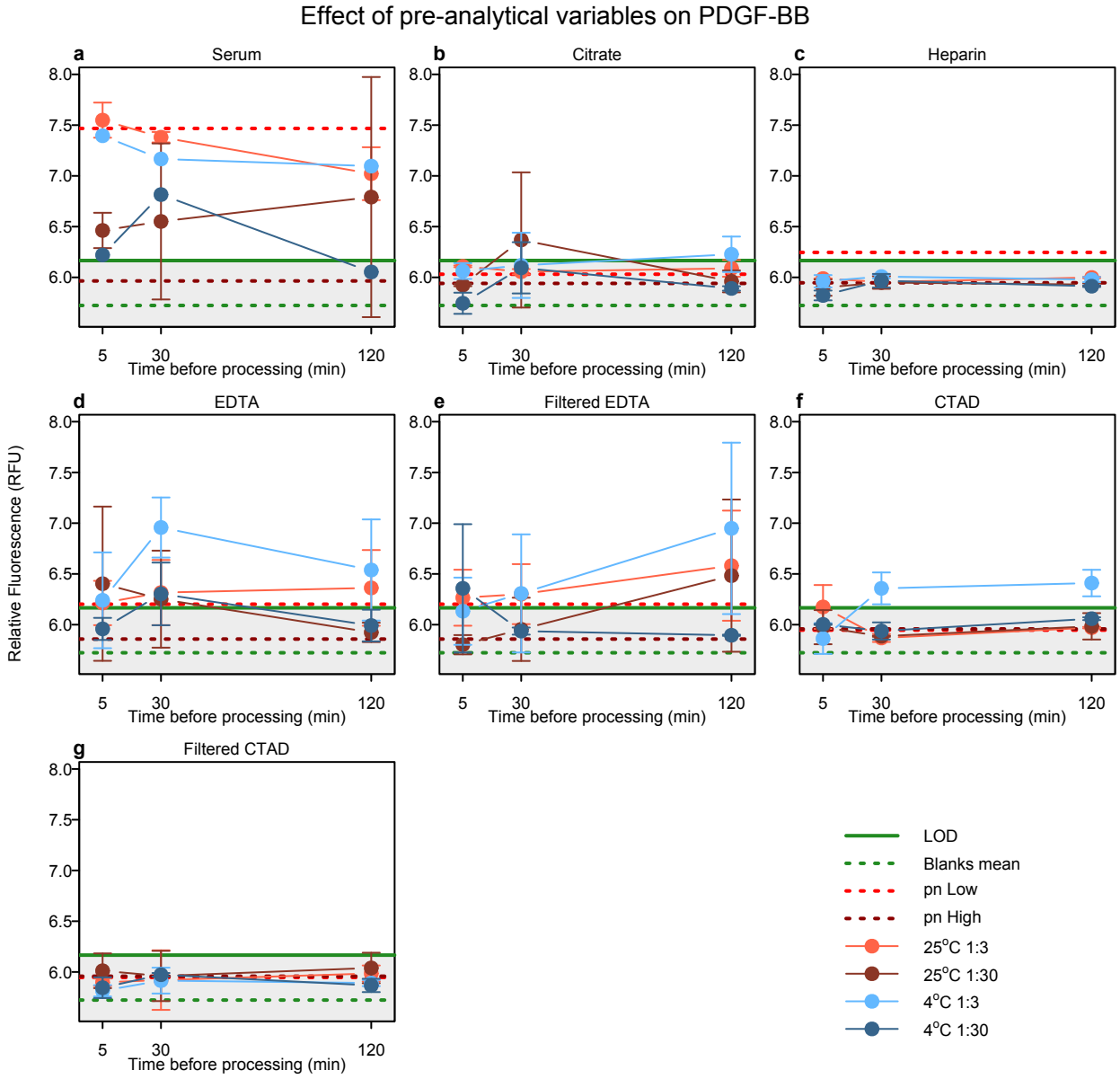

FIGURE I.S151: **Effect of blood collection tube on PDGF-BB stability and concentration.** Effects of blood collection tubes (**a**: serum, **b**: citrate, **c**: heparin, **d-e**: EDTA, **f-g**: CTAD), storage temperature and time before processing, and post-processing plasma filtering (**e, g**) on the initial value and pre-processing time stability of PDGF-BB measurements in blood. Information on the dilution of samples used for measuring, data range and the sample type selected are also shown.

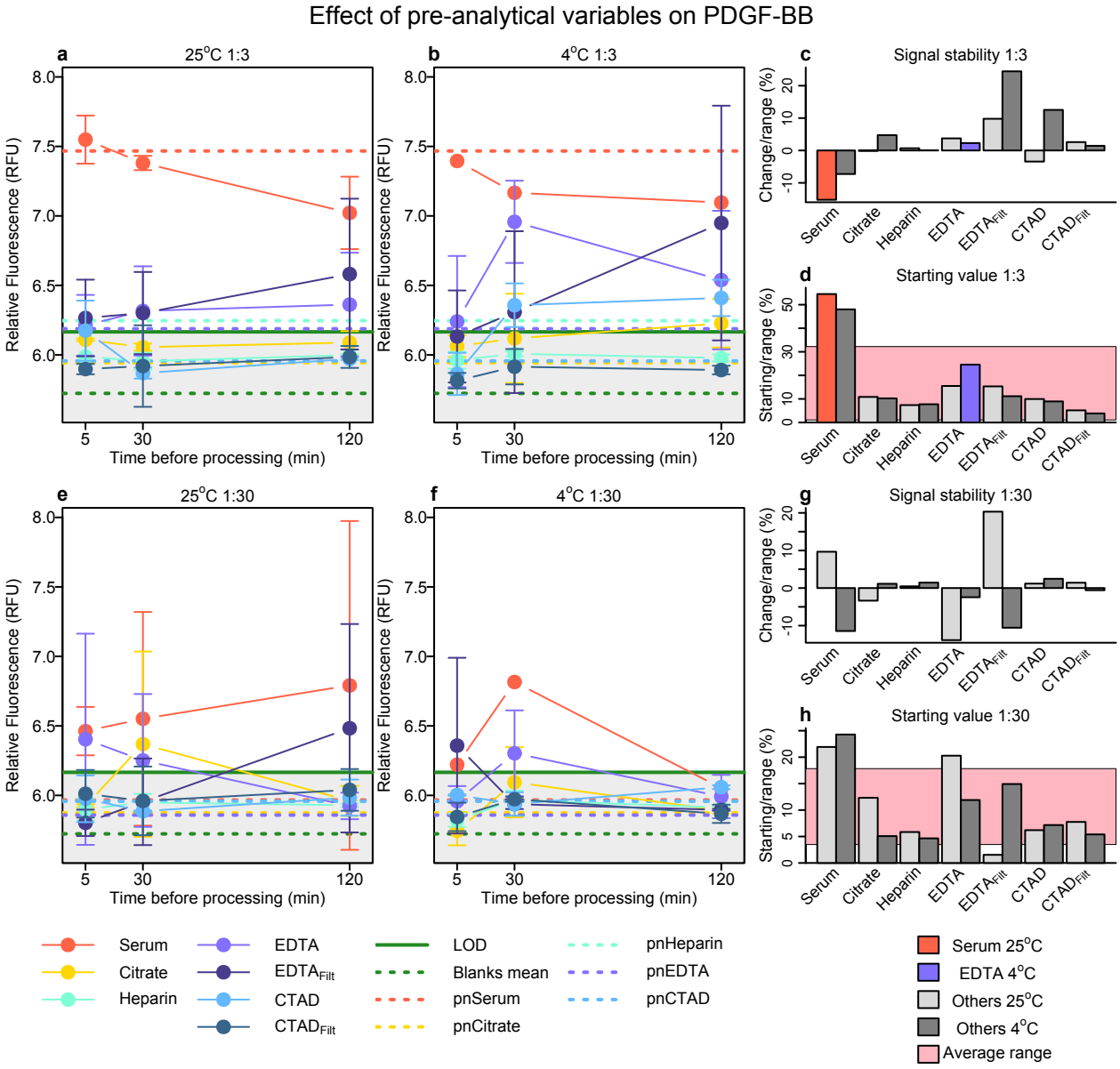

FIGURE I.S152: **Effect of pre-processing storage temperature on PDGF-BB stability and concentration.** Initial measured value and stability of PDGF-BB when stored at 25 °C (**a, e**) and 4 °C (**b, f**) before processing when collected in different tube types. The measured values are shown at low dilution of 1:3 (**a-b**) and high dilution of 1:30 (**e-f**). Stability before processing is expressed as an increase or decrease compared to the measurement range and is shown for low (**c**) and high (**g**) dilutions. Initial value is expressed as a portion of the measurement range when the linear regression is extrapolated to zero minutes and is shown for low (**d**) and high (**h**) dilutions. The pink box in graphs **d** and **h** indicate the region that is included by the *mean* ± *SD* of all the initial values and gives an indication of outliers when values lie outside this region. Red and purple bars in **c-d, g-h** are indicated at the measured dilution as the two choices for the TBI analysis.

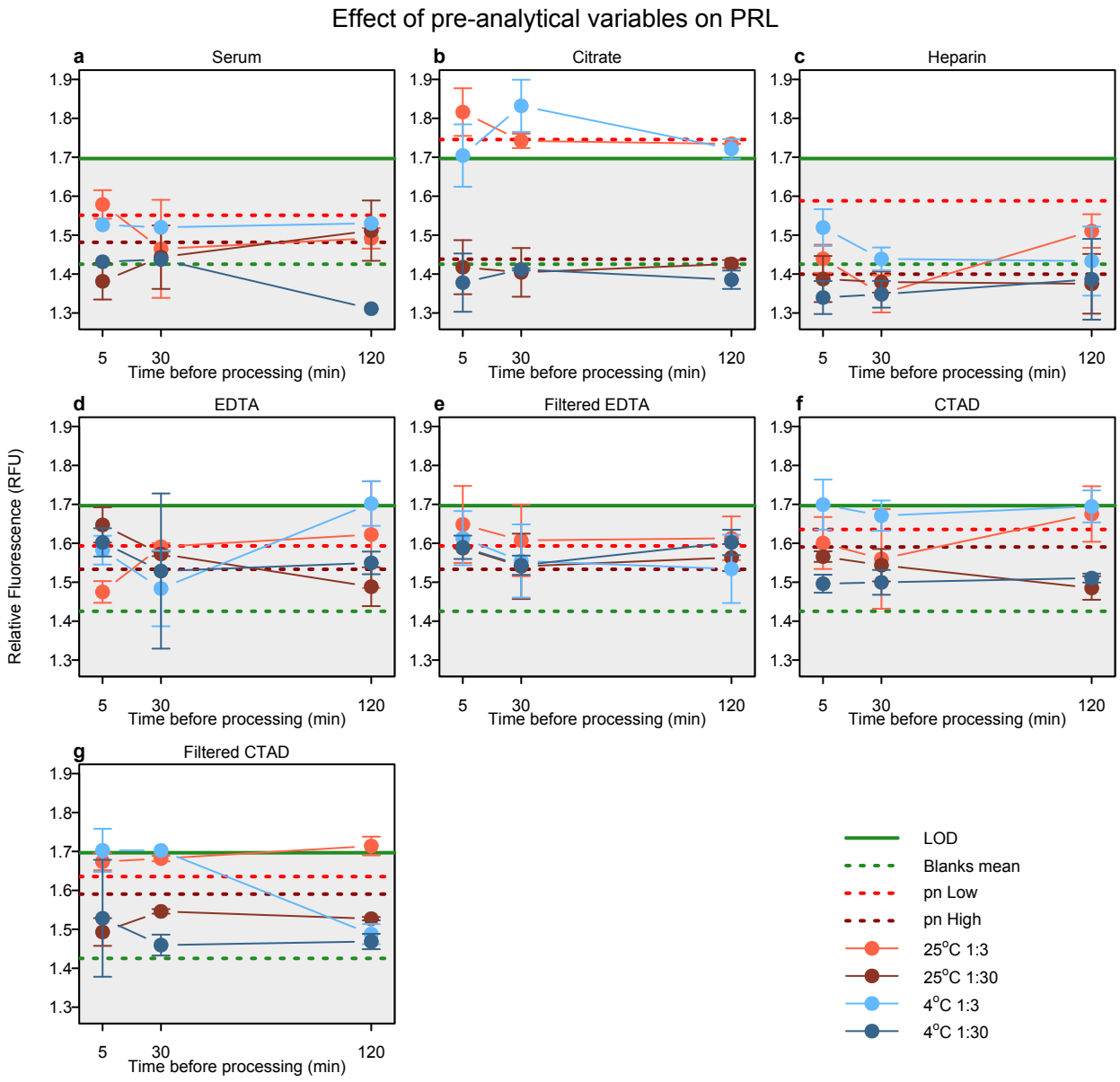

FIGURE I.S153: **Effect of blood collection tube on PRL stability and concentration.** Effects of blood collection tubes (**a**: serum, **b**: citrate, **c**: heparin, **d-e**: EDTA, **f-g**: CTAD), storage temperature and time before processing, and post-processing plasma filtering (**e, g**) on the initial value and pre-processing time stability of PRL measurements in blood. Information on the dilution of samples used for measuring, data range and the sample type selected are also shown.

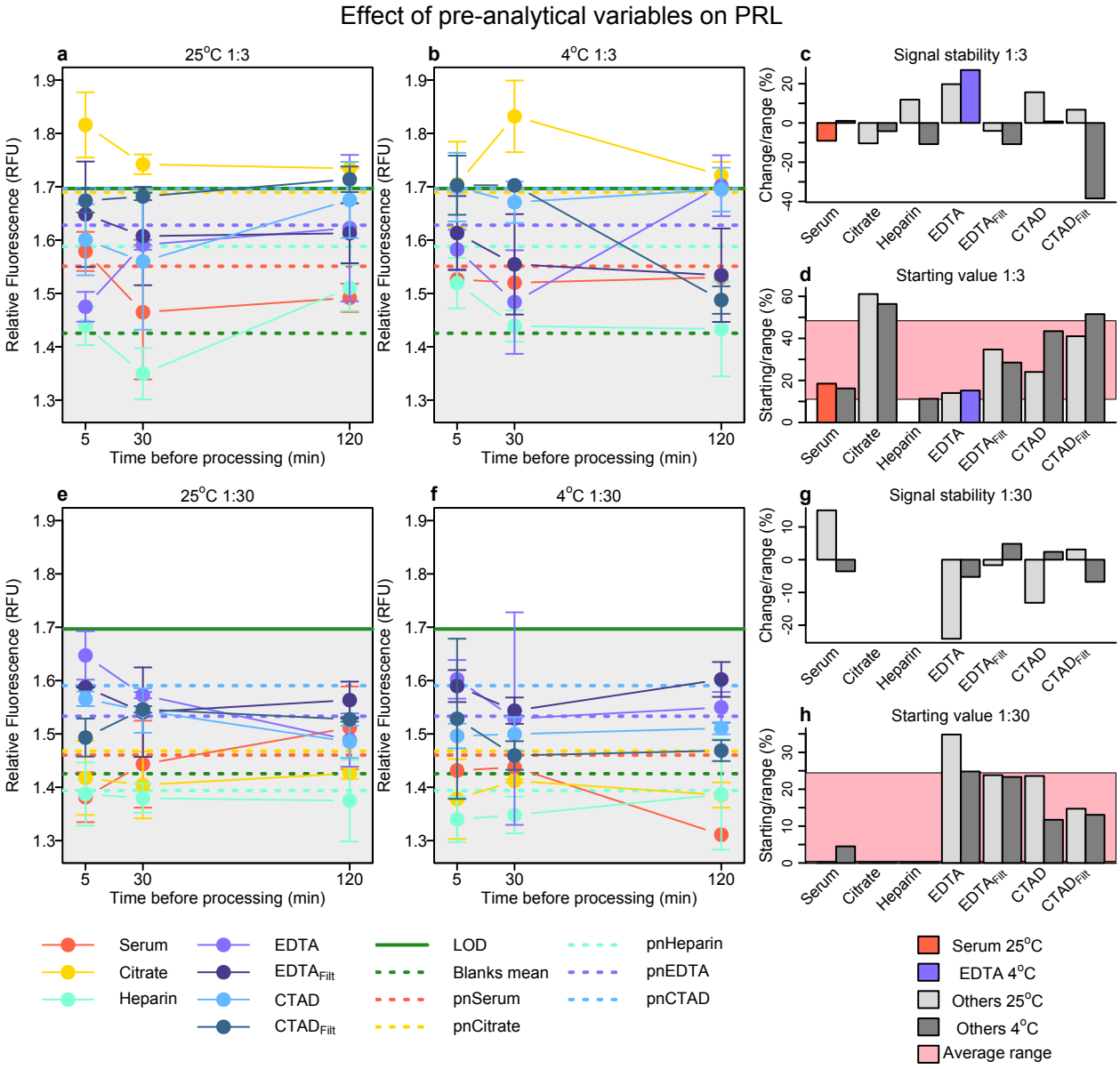

FIGURE I.S154: **Effect of pre-processing storage temperature on PRL stability and concentration.** Initial measured value and stability of PRL when stored at 25 °C (**a, e**) and 4 °C (**b, f**) before processing when collected in different tube types. The measured values are shown at low dilution of 1:3 (**a-b**) and high dilution of 1:30 (**e-f**). Stability before processing is expressed as an increase or decrease compared to the measurement range and is shown for low (**c**) and high (**g**) dilutions. Initial value is expressed as a portion of the measurement range when the linear regression is extrapolated to zero minutes and is shown for low (**d**) and high (**h**) dilutions. The pink box in graphs **d** and **h** indicate the region that is included by the *mean* ± *SD* of all the initial values and gives an indication of outliers when values lie outside this region. Red and purple bars in **c-d, g-h** are indicated at the measured dilution as the two choices for the TBI analysis.

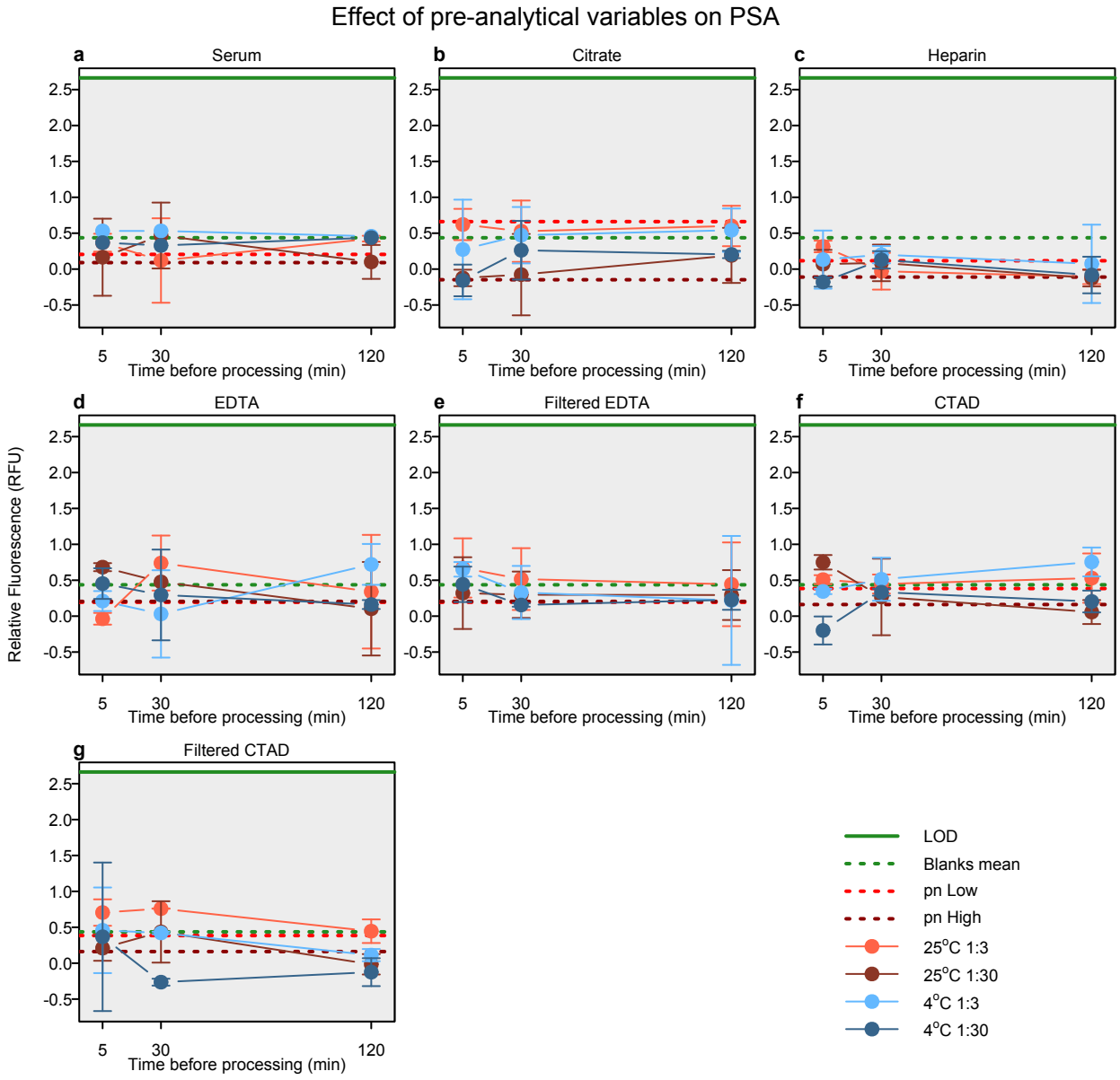

FIGURE I.S155: **Effect of blood collection tube on PSA stability and concentration.** Effects of blood collection tubes (**a**: serum, **b**: citrate, **c**: heparin, **d-e**: EDTA, **f-g**: CTAD), storage temperature and time before processing, and post-processing plasma filtering (**e, g**) on the initial value and pre-processing time stability of PSA measurements in blood. Information on the dilution of samples used for measuring, data range and the sample type selected are also shown.

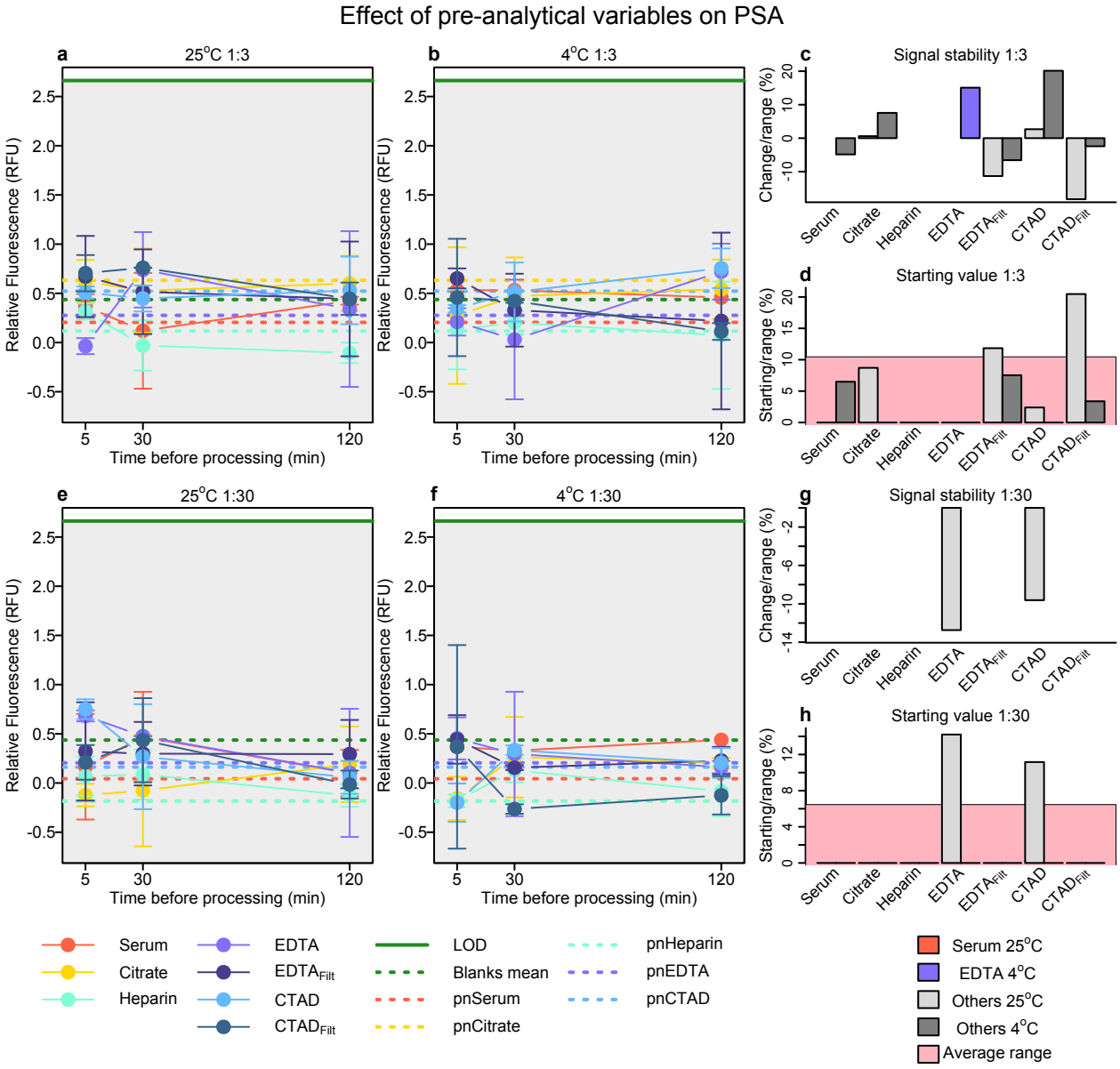

FIGURE I.S156: **Effect of pre-processing storage temperature on PSA stability and concentration.** Initial measured value and stability of PSA when stored at 25 °C (**a, e**) and 4 °C (**b, f**) before processing when collected in different tube types. The measured values are shown at low dilution of 1:3 (**a-b**) and high dilution of 1:30 (**e-f**). Stability before processing is expressed as an increase or decrease compared to the measurement range and is shown for low (**c**) and high (**g**) dilutions. Initial value is expressed as a portion of the measurement range when the linear regression is extrapolated to zero minutes and is shown for low (**d**) and high (**h**) dilutions. The pink box in graphs **d** and **h** indicate the region that is included by the *mean* ± *SD* of all the initial values and gives an indication of outliers when values lie outside this region. Red and purple bars in **c-d, g-h** are indicated at the measured dilution as the two choices for the TBI analysis.

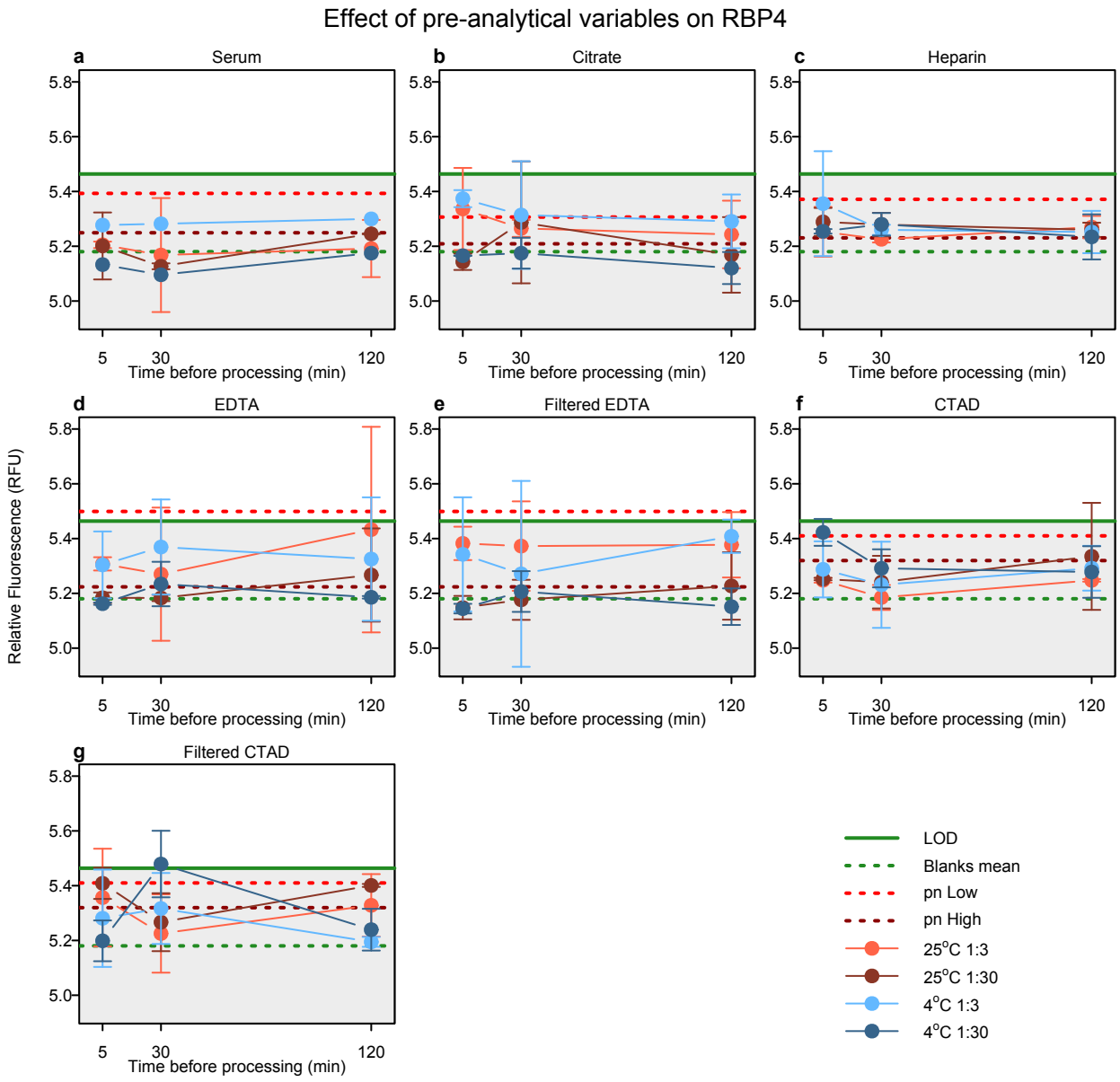

FIGURE I.S157: **Effect of blood collection tube on RBP4 stability and concentration.** Effects of blood collection tubes (**a**: serum, **b**: citrate, **c**: heparin, **d-e**: EDTA, **f-g**: CTAD), storage temperature and time before processing, and post-processing plasma filtering (**e, g**) on the initial value and pre-processing time stability of RBP4 measurements in blood. Information on the dilution of samples used for measuring, data range and the sample type selected are also shown.

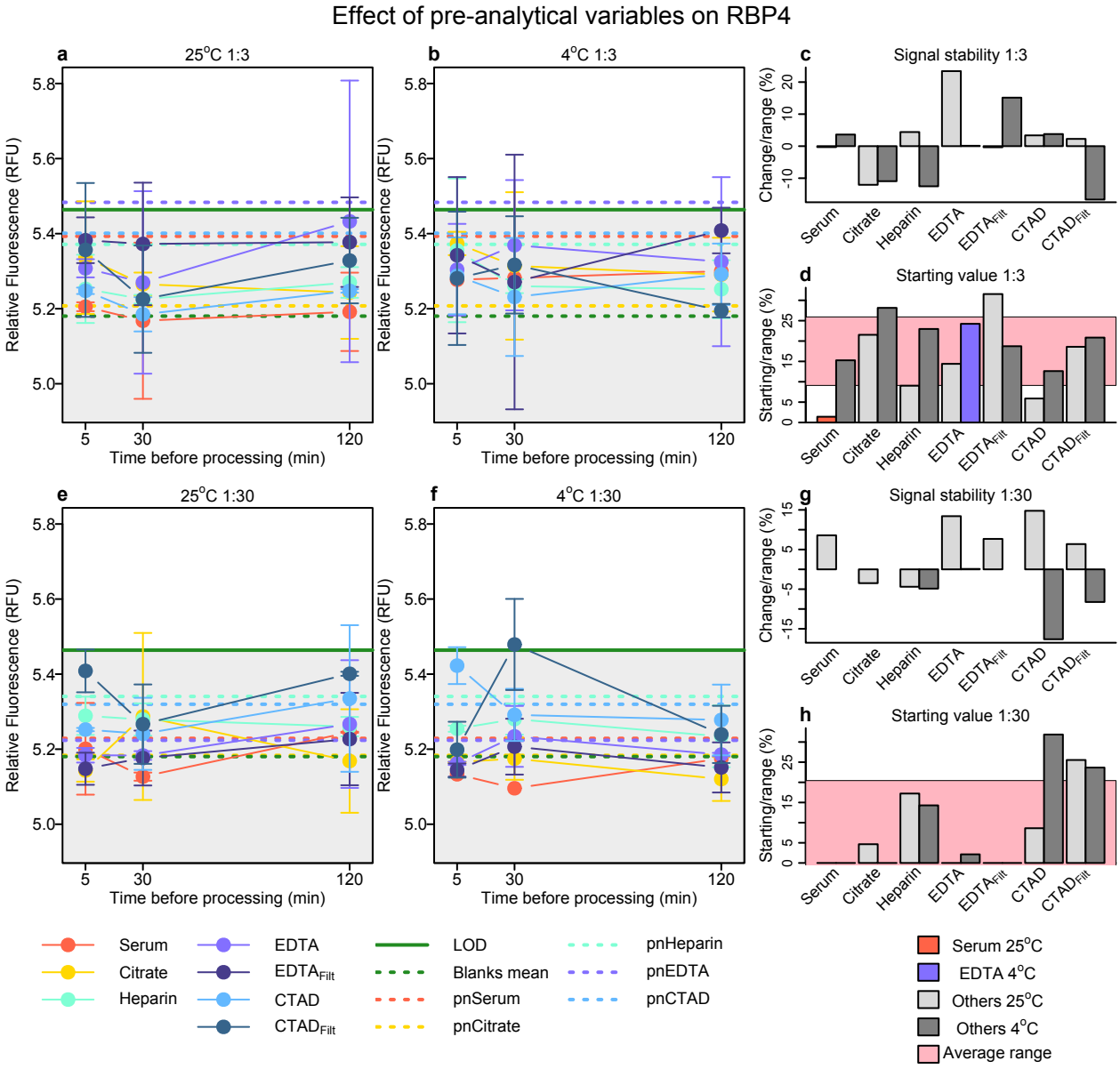

FIGURE I.S158: **Effect of pre-processing storage temperature on RBP4 stability and concentration.** Initial measured value and stability of RBP4 when stored at 25 °C (**a, e**) and 4 °C (**b, f**) before processing when collected in different tube types. The measured values are shown at low dilution of 1:3 (**a-b**) and high dilution of 1:30 (**e-f**). Stability before processing is expressed as an increase or decrease compared to the measurement range and is shown for low (**c**) and high (**g**) dilutions. Initial value is expressed as a portion of the measurement range when the linear regression is extrapolated to zero minutes and is shown for low (**d**) and high (**h**) dilutions. The pink box in graphs **d** and **h** indicate the region that is included by the *mean* ± *SD* of all the initial values and gives an indication of outliers when values lie outside this region. Red and purple bars in **c-d, g-h** are indicated at the measured dilution as the two choices for the TBI analysis.

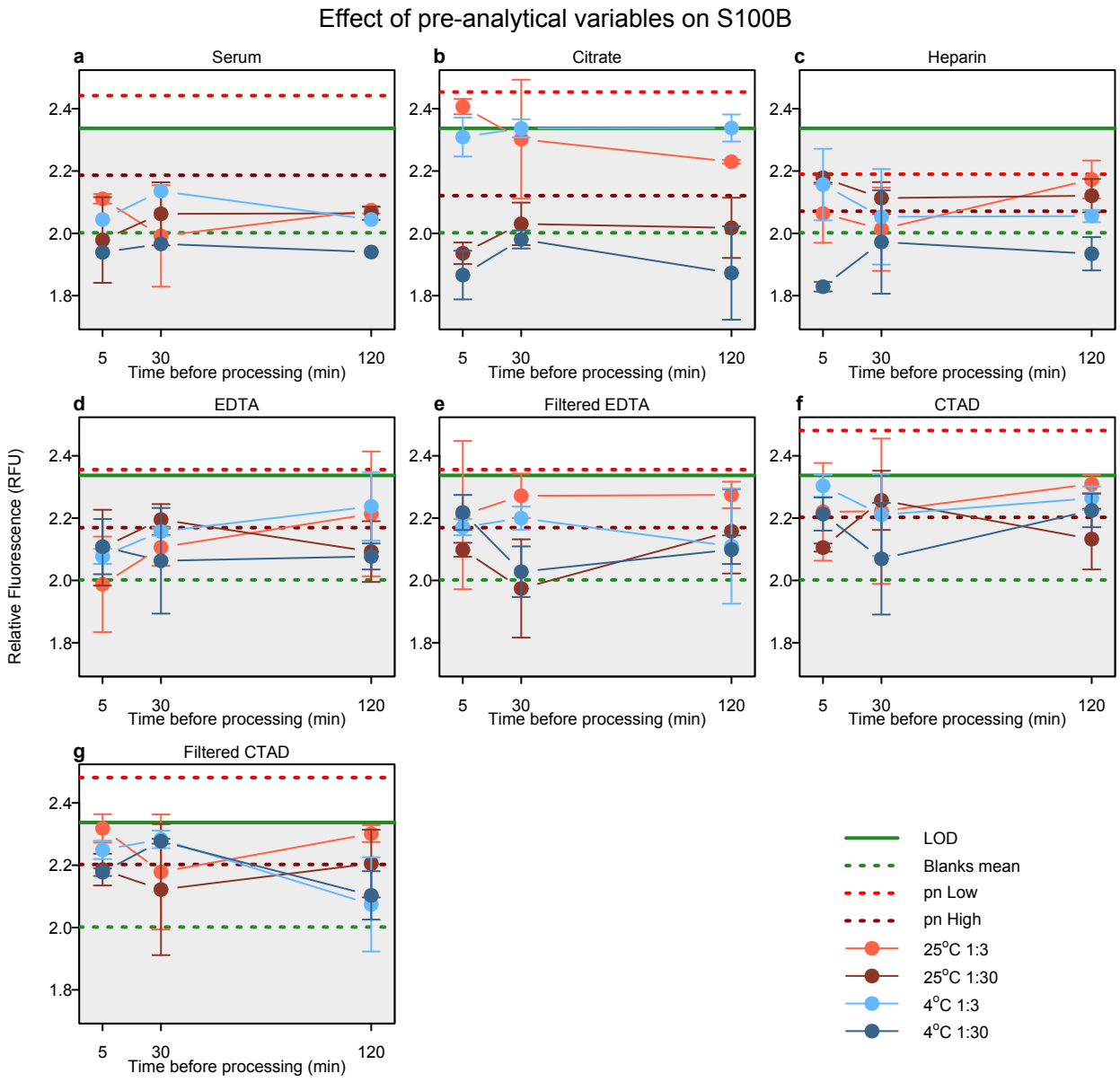

FIGURE I.S159: **Effect of blood collection tube on S100B stability and concentration.** Effects of blood collection tubes (**a**: serum, **b**: citrate, **c**: heparin, **d-e**: EDTA, **f-g**: CTAD), storage temperature and time before processing, and post-processing plasma filtering (**e, g**) on the initial value and pre-processing time stability of S100B measurements in blood. Information on the dilution of samples used for measuring, data range and the sample type selected are also shown.

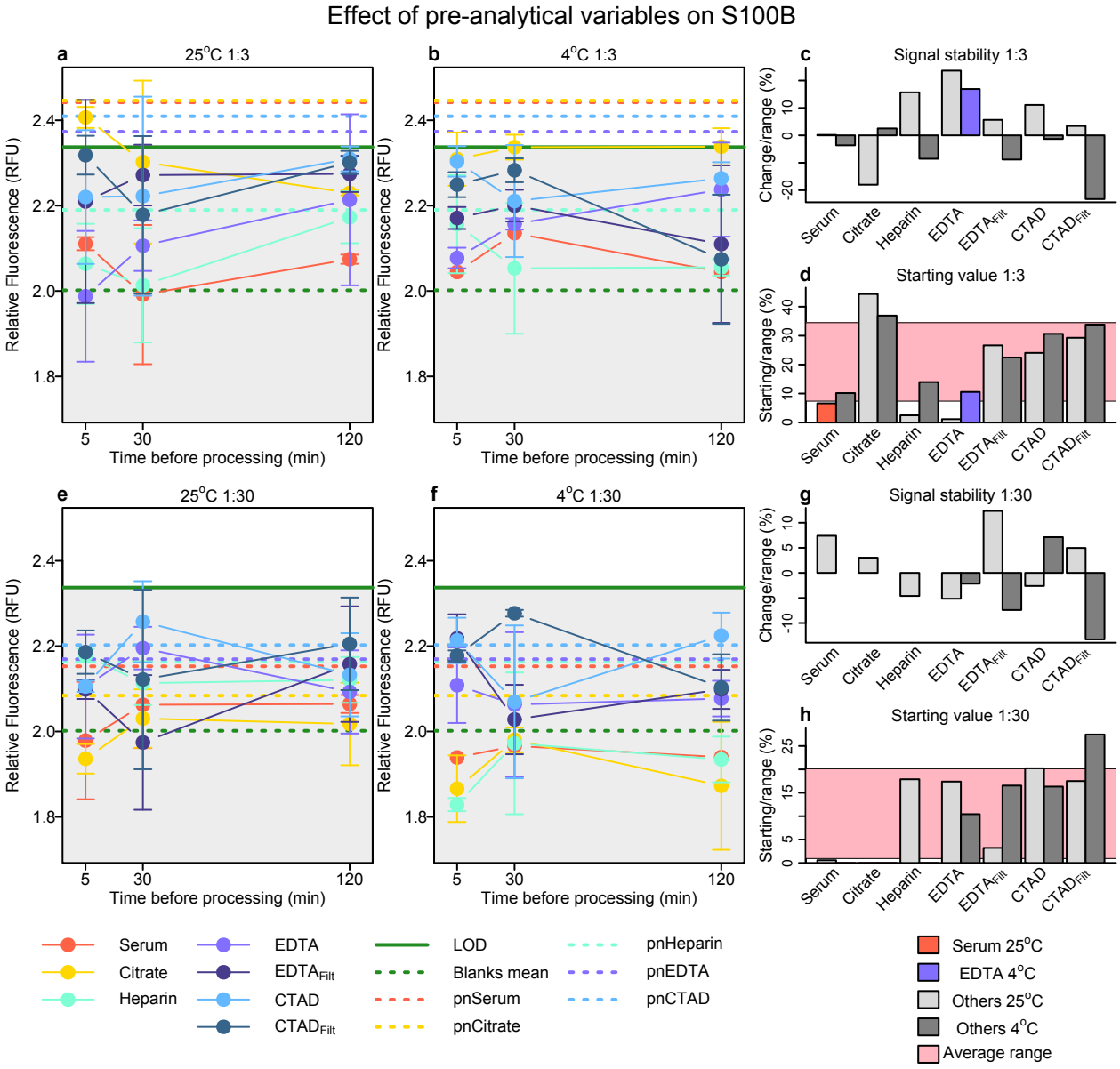

FIGURE I.S160: **Effect of pre-processing storage temperature on S100B stability and concentration.** Initial measured value and stability of S100B when stored at 25 °C (**a, e**) and 4 °C (**b, f**) before processing when collected in different tube types. The measured values are shown at low dilution of 1:3 (**a-b**) and high dilution of 1:30 (**e-f**). Stability before processing is expressed as an increase or decrease compared to the measurement range and is shown for low (**c**) and high (**g**) dilutions. Initial value is expressed as a portion of the measurement range when the linear regression is extrapolated to zero minutes and is shown for low (**d**) and high (**h**) dilutions. The pink box in graphs **d** and **h** indicate the region that is included by the *mean* ± *SD* of all the initial values and gives an indication of outliers when values lie outside this region. Red and purple bars in **c-d, g-h** are indicated at the measured dilution as the two choices for the TBI analysis.

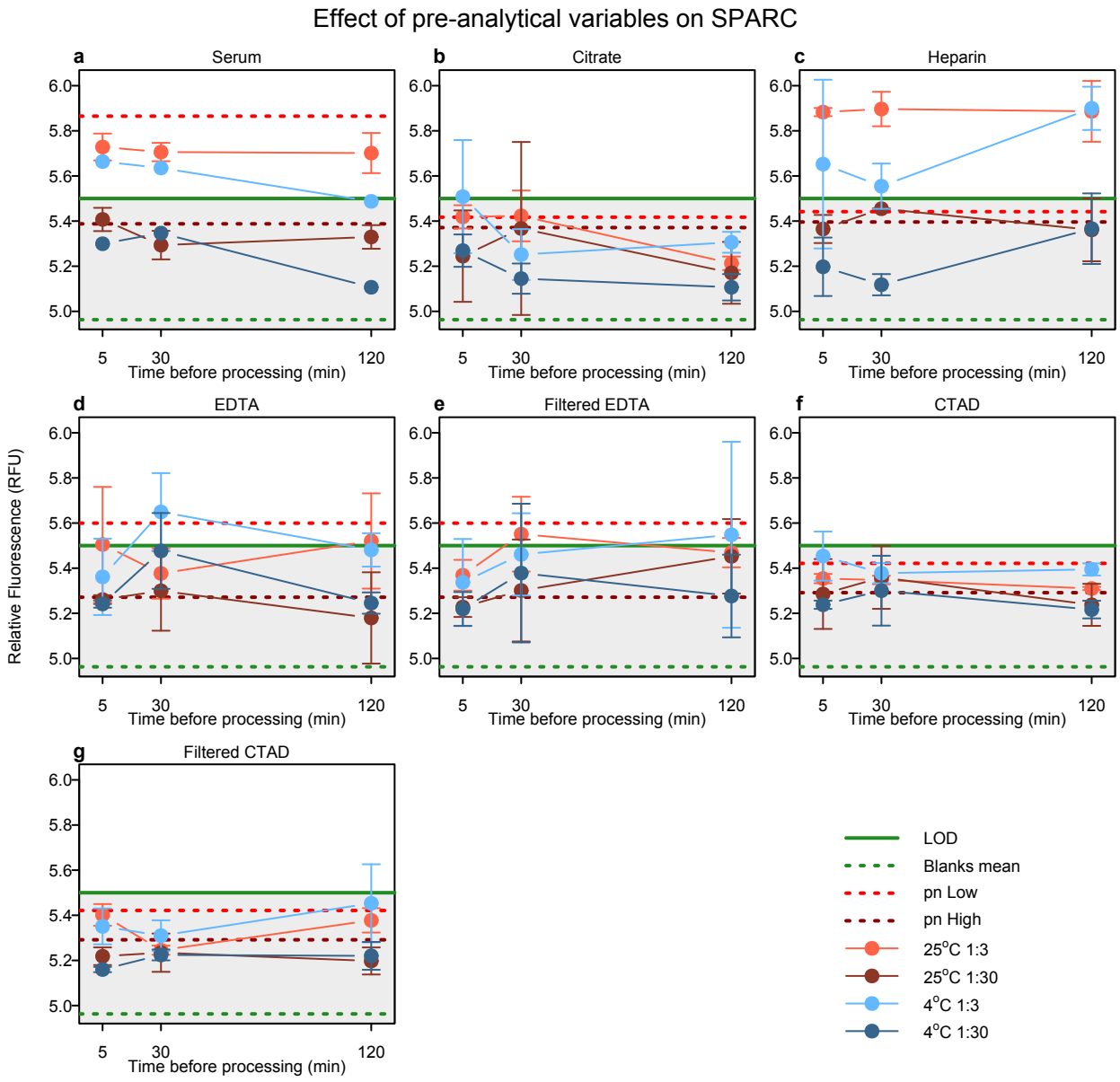

FIGURE I.S161: **Effect of blood collection tube on SPARC stability and concentration.** Effects of blood collection tubes (**a**: serum, **b**: citrate, **c**: heparin, **d-e**: EDTA, **f-g**: CTAD), storage temperature and time before processing, and post-processing plasma filtering (**e, g**) on the initial value and pre-processing time stability of SPARC measurements in blood. Information on the dilution of samples used for measuring, data range and the sample type selected are also shown.

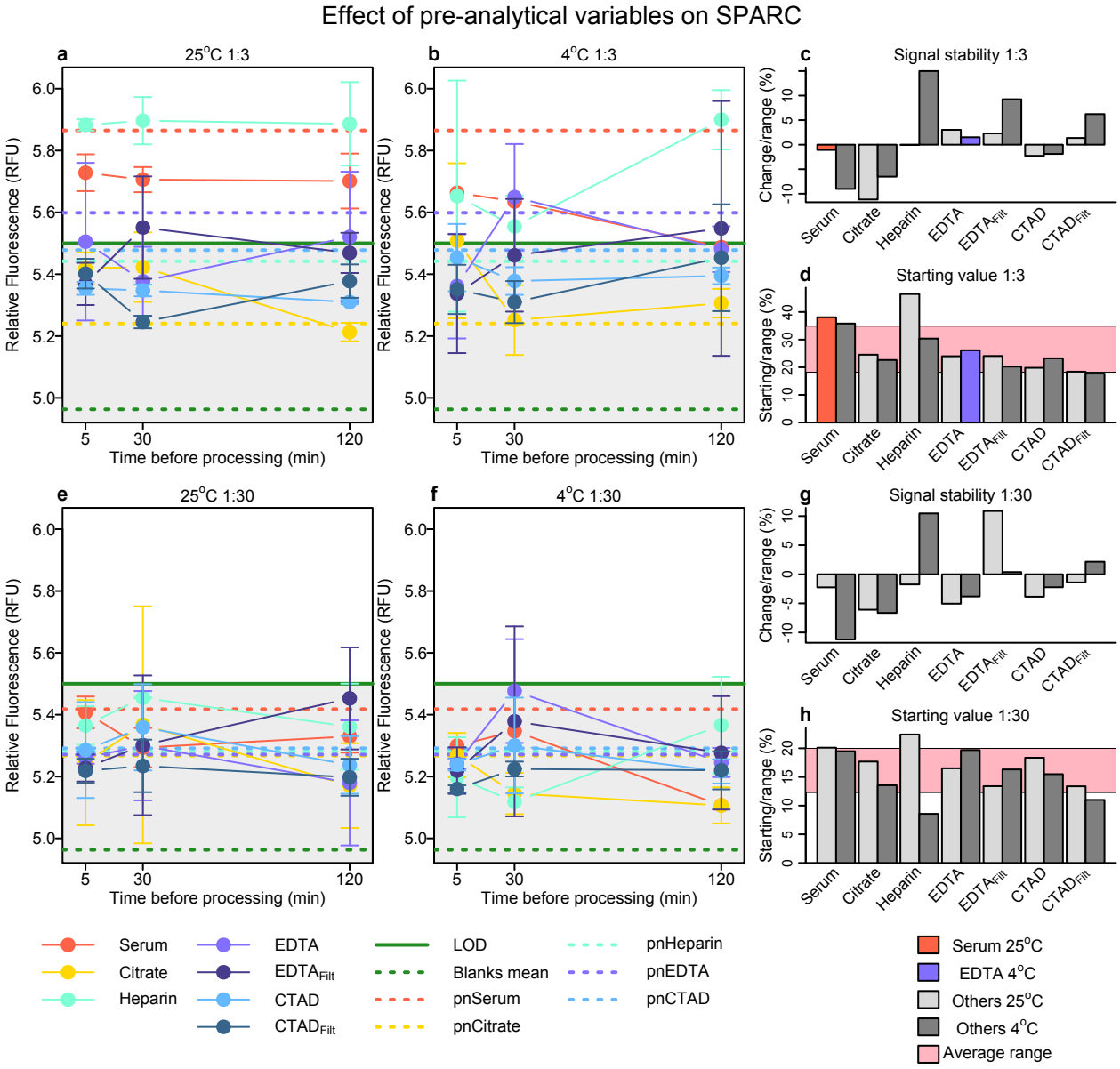

FIGURE I.S162: **Effect of pre-processing storage temperature on SPARC stability and concentration.** Initial measured value and stability of SPARC when stored at 25 °C (**a, e**) and 4 °C (**b, f**) before processing when collected in different tube types. The measured values are shown at low dilution of 1:3 (**a-b**) and high dilution of 1:30 (**e-f**). Stability before processing is expressed as an increase or decrease compared to the measurement range and is shown for low (**c**) and high (**g**) dilutions. Initial value is expressed as a portion of the measurement range when the linear regression is extrapolated to zero minutes and is shown for low (**d**) and high (**h**) dilutions. The pink box in graphs **d** and **h** indicate the region that is included by the *mean* ± *SD* of all the initial values and gives an indication of outliers when values lie outside this region. Red and purple bars in **c-d, g-h** are indicated at the measured dilution as the two choices for the TBI analysis.

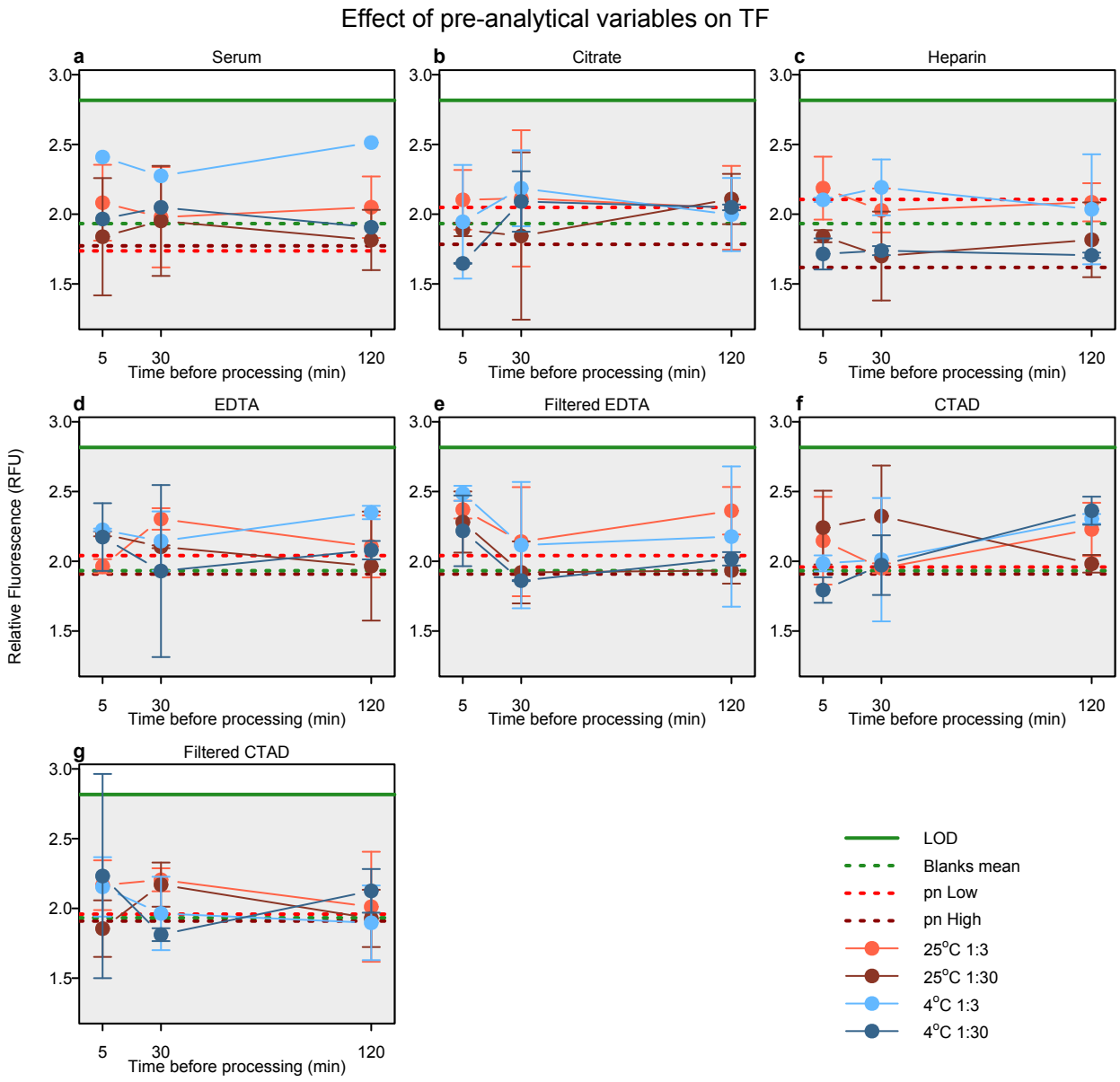

FIGURE I.S163: **Effect of blood collection tube on TF stability and concentration.** Effects of blood collection tubes (**a**: serum, **b**: citrate, **c**: heparin, **d-e**: EDTA, **f-g**: CTAD), storage temperature and time before processing, and post-processing plasma filtering (**e, g**) on the initial value and pre-processing time stability of TF measurements in blood. Information on the dilution of samples used for measuring, data range and the sample type selected are also shown.

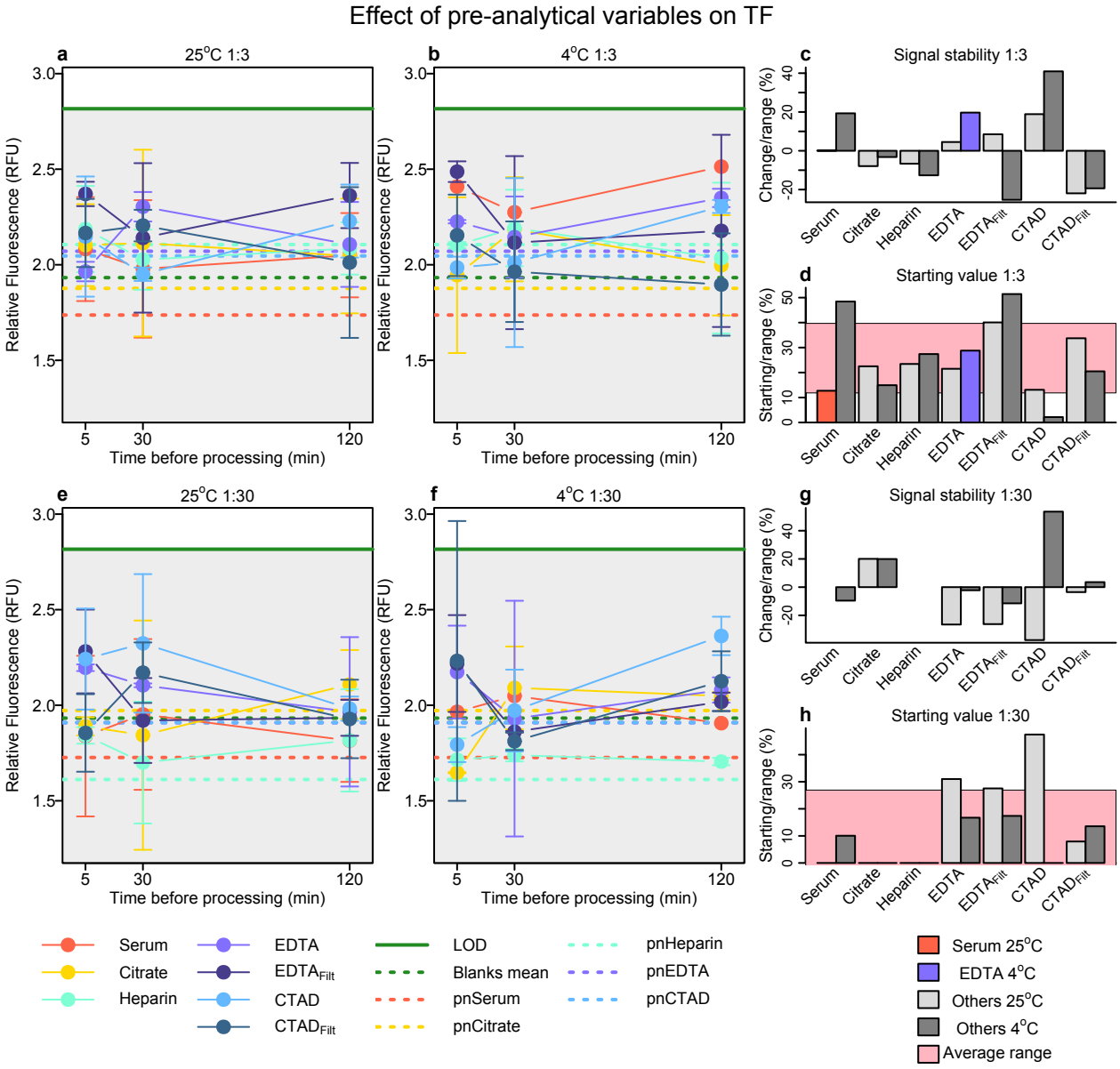

FIGURE I.S164: **Effect of pre-processing storage temperature on TF stability and concentration.** Initial measured value and stability of TF when stored at 25 °C (**a, e**) and 4 °C (**b, f**) before processing when collected in different tube types. The measured values are shown at low dilution of 1:3 (**a-b**) and high dilution of 1:30 (**e-f**). Stability before processing is expressed as an increase or decrease compared to the measurement range and is shown for low (**c**) and high (**g**) dilutions. Initial value is expressed as a portion of the measurement range when the linear regression is extrapolated to zero minutes and is shown for low (**d**) and high (**h**) dilutions. The pink box in graphs **d** and **h** indicate the region that is included by the *mean* ± *SD* of all the initial values and gives an indication of outliers when values lie outside this region. Red and purple bars in **c-d, g-h** are indicated at the measured dilution as the two choices for the TBI analysis.

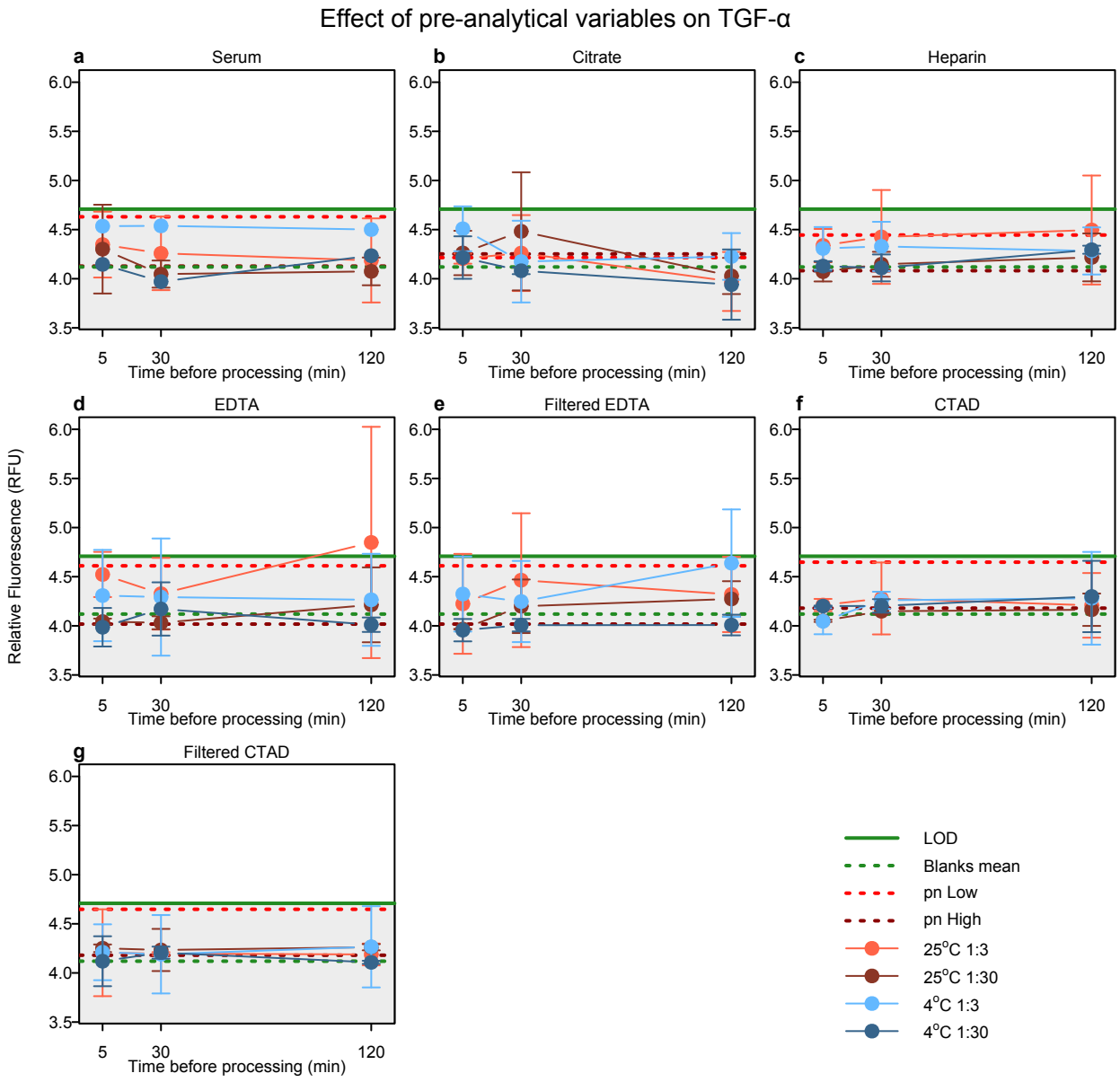

FIGURE I.S165: **Effect of blood collection tube on TGF-α stability and concentration.** Effects of blood collection tubes (**a**: serum, **b**: citrate, **c**: heparin, **d-e**: EDTA, **f-g**: CTAD), storage temperature and time before processing, and post-processing plasma filtering (**e, g**) on the initial value and pre-processing time stability of TGF-α measurements in blood. Information on the dilution of samples used for measuring, data range and the sample type selected are also shown.

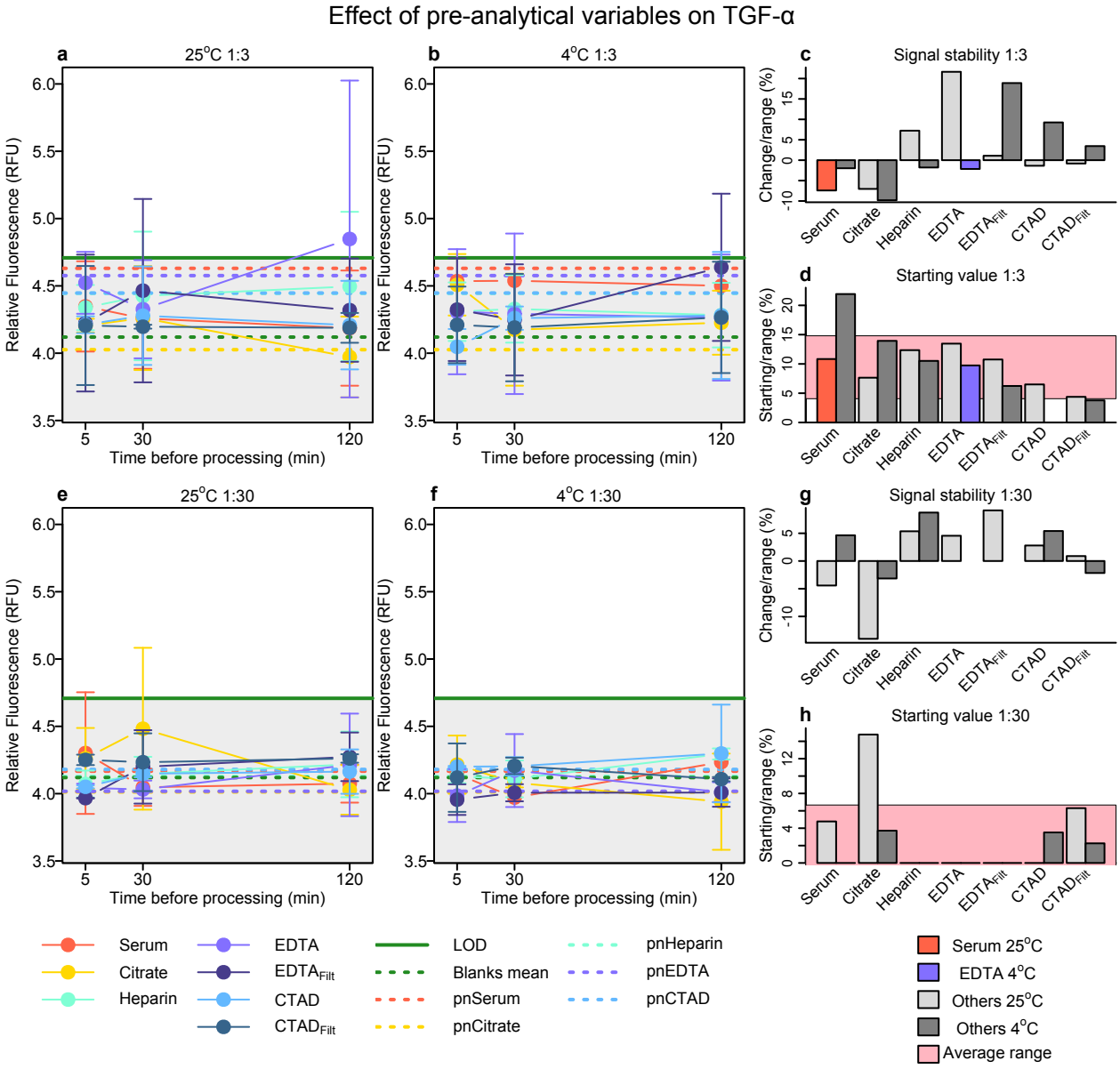

FIGURE I.S166: **Effect of pre-processing storage temperature on TGF-α stability and concentration.** Initial measured value and stability of TGF-α when stored at 25 °C (**a, e**) and 4 °C (**b, f**) before processing when collected in different tube types. The measured values are shown at low dilution of 1:3 (**a-b**) and high dilution of 1:30 (**e-f**). Stability before processing is expressed as an increase or decrease compared to the measurement range and is shown for low (**c**) and high (**g**) dilutions. Initial value is expressed as a portion of the measurement range when the linear regression is extrapolated to zero minutes and is shown for low (**d**) and high (**h**) dilutions. The pink box in graphs **d** and **h** indicate the region that is included by the *mean* ± *SD* of all the initial values and gives an indication of outliers when values lie outside this region. Red and purple bars in **c-d, g-h** are indicated at the measured dilution as the two choices for the TBI analysis.

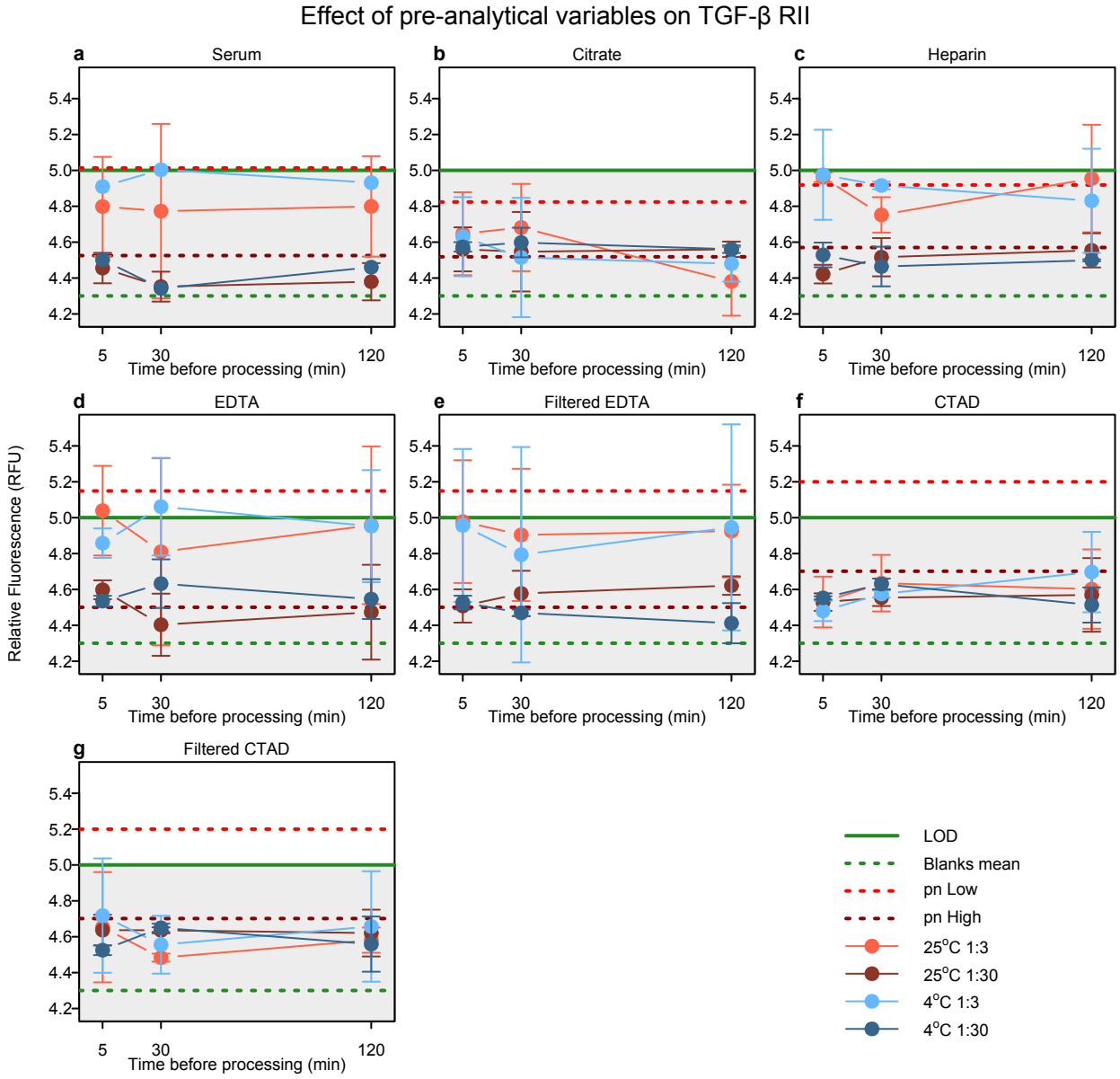

FIGURE I.S167: **Effect of blood collection tube on TGF-β RII stability and concentration.** Effects of blood collection tubes (**a**: serum, **b**: citrate, **c**: heparin, **d-e**: EDTA, **f-g**: CTAD), storage temperature and time before processing, and post-processing plasma filtering (**e, g**) on the initial value and pre-processing time stability of TGF-β RII measurements in blood. Information on the dilution of samples used for measuring, data range and the sample type selected are also shown.

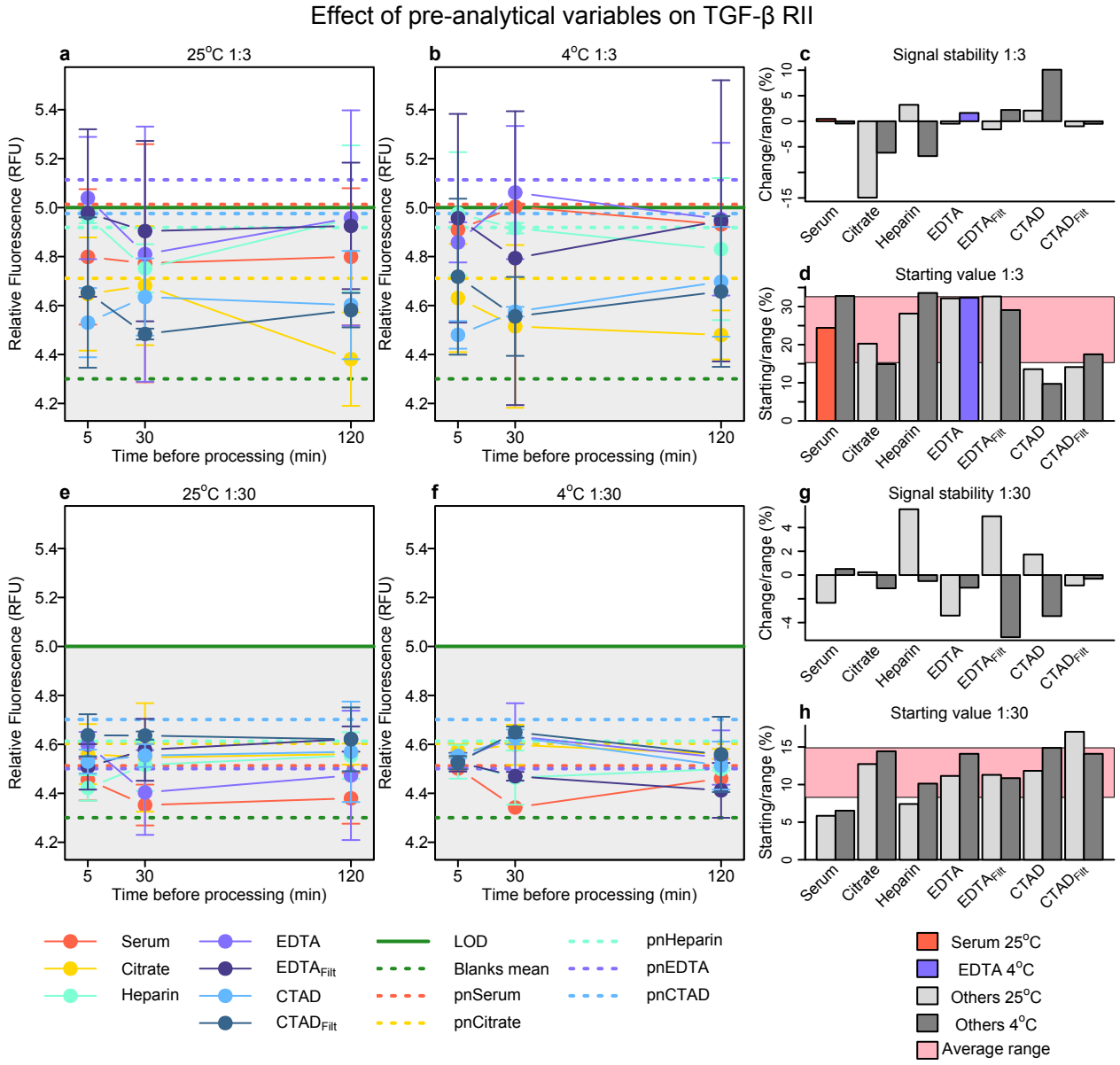

FIGURE I.S168: **Effect of pre-processing storage temperature on TGF-β RII stability and concentration.** Initial measured value and stability of TGF-β RII when stored at 25 °C (**a, e**) and 4 °C (**b, f**) before processing when collected in different tube types. The measured values are shown at low dilution of 1:3 (**a-b**) and high dilution of 1:30 (**e-f**). Stability before processing is expressed as an increase or decrease compared to the measurement range and is shown for low (**c**) and high (**g**) dilutions. Initial value is expressed as a portion of the measurement range when the linear regression is extrapolated to zero minutes and is shown for low (**d**) and high (**h**) dilutions. The pink box in graphs **d** and **h** indicate the region that is included by the *mean* ± *SD* of all the initial values and gives an indication of outliers when values lie outside this region. Red and purple bars in **c-d, g-h** are indicated at the measured dilution as the two choices for the TBI analysis.

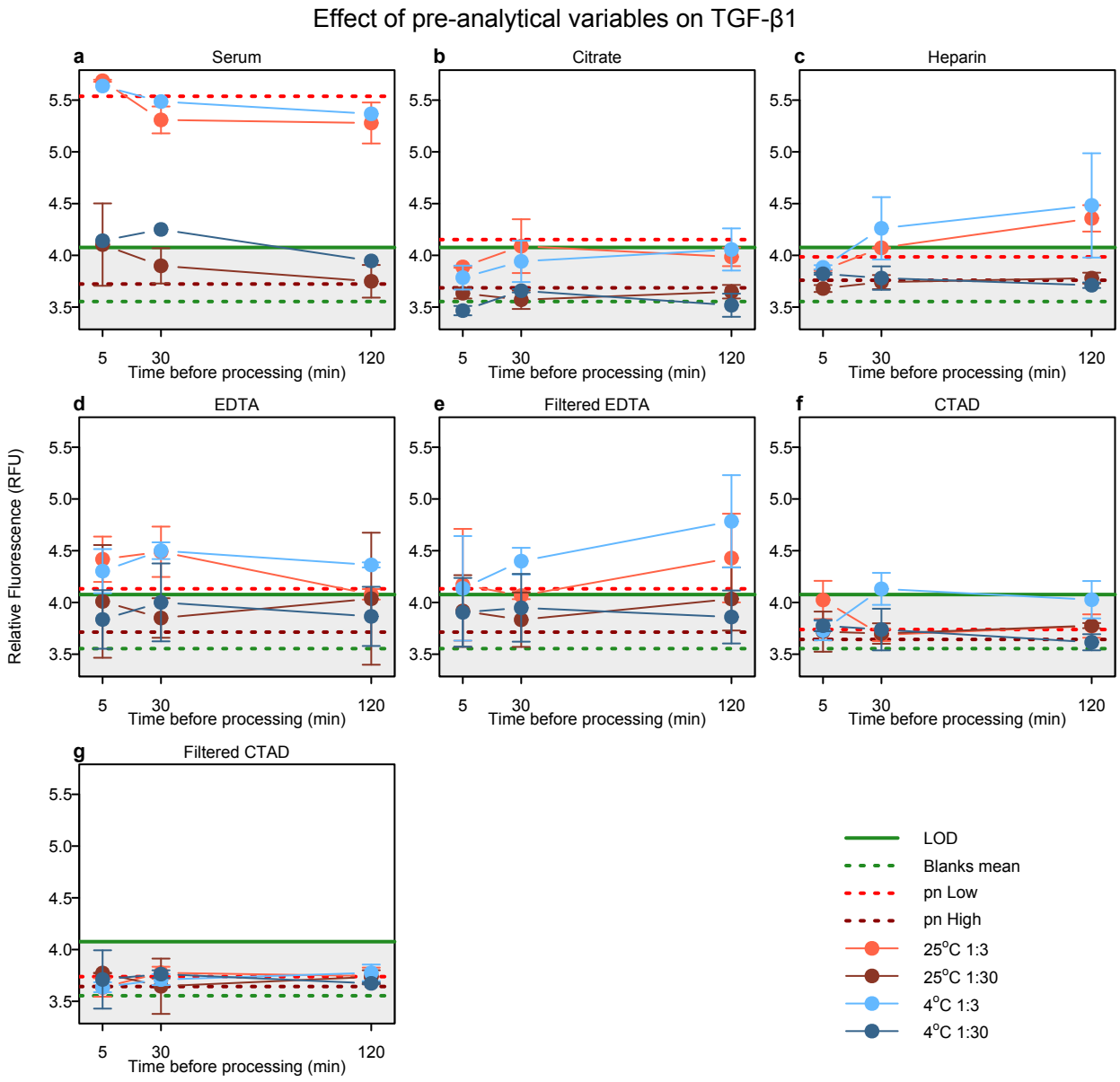

FIGURE I.S169: **Effect of blood collection tube on TGF-β1 stability and concentration.** Effects of blood collection tubes (**a**: serum, **b**: citrate, **c**: heparin, **d-e**: EDTA, **f-g**: CTAD), storage temperature and time before processing, and post-processing plasma filtering (**e, g**) on the initial value and pre-processing time stability of TGF-β1 measurements in blood. Information on the dilution of samples used for measuring, data range and the sample type selected are also shown.

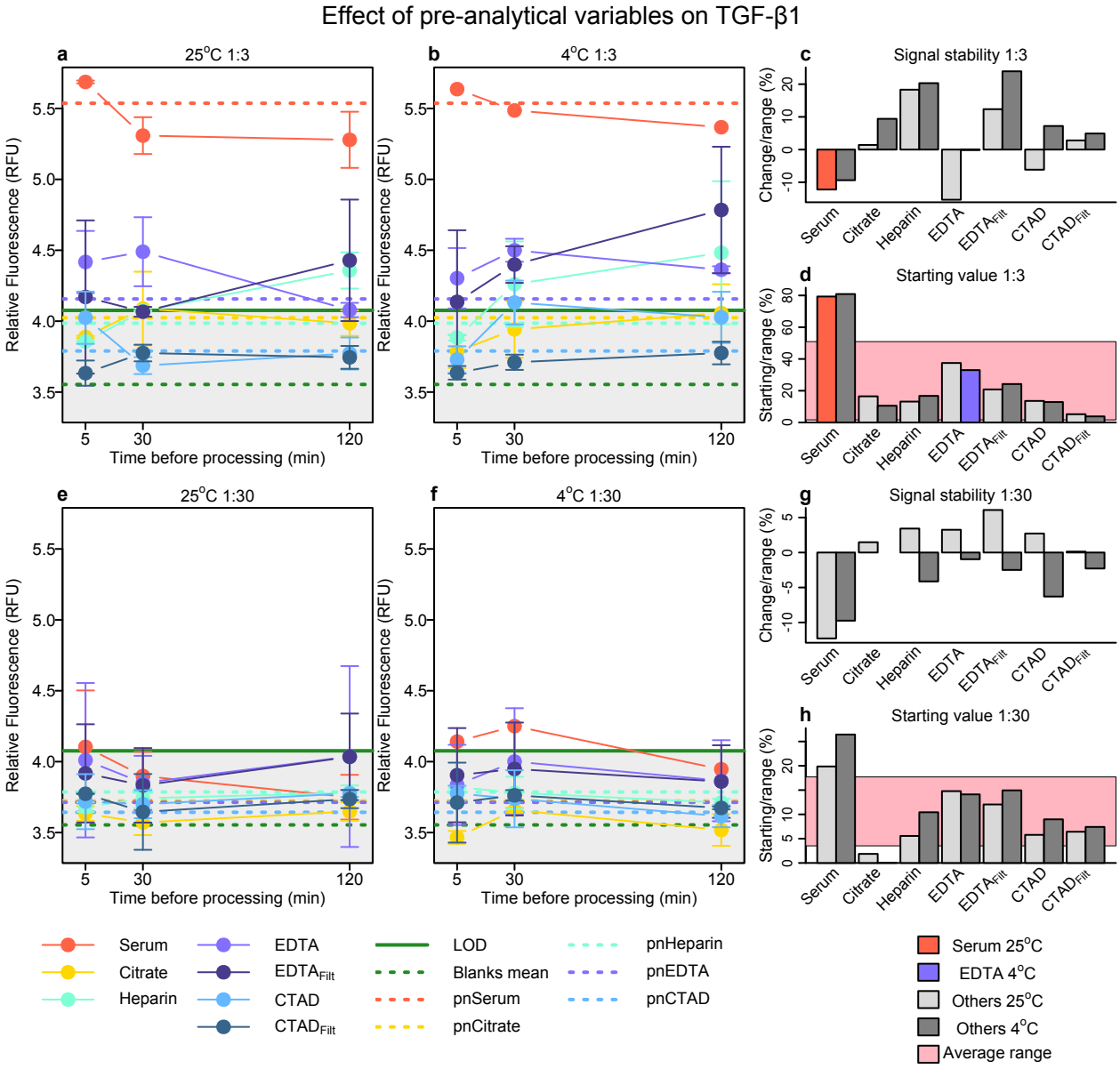

FIGURE I.S170: **Effect of pre-processing storage temperature on TGF-β1 stability and concentration.** Initial measured value and stability of TGF-β1 when stored at 25 °C (**a, e**) and 4 °C (**b, f**) before processing when collected in different tube types. The measured values are shown at low dilution of 1:3 (**a-b**) and high dilution of 1:30 (**e-f**). Stability before processing is expressed as an increase or decrease compared to the measurement range and is shown for low (**c**) and high (**g**) dilutions. Initial value is expressed as a portion of the measurement range when the linear regression is extrapolated to zero minutes and is shown for low (**d**) and high (**h**) dilutions. The pink box in graphs **d** and **h** indicate the region that is included by the *mean* ± *SD* of all the initial values and gives an indication of outliers when values lie outside this region. Red and purple bars in **c-d, g-h** are indicated at the measured dilution as the two choices for the TBI analysis.

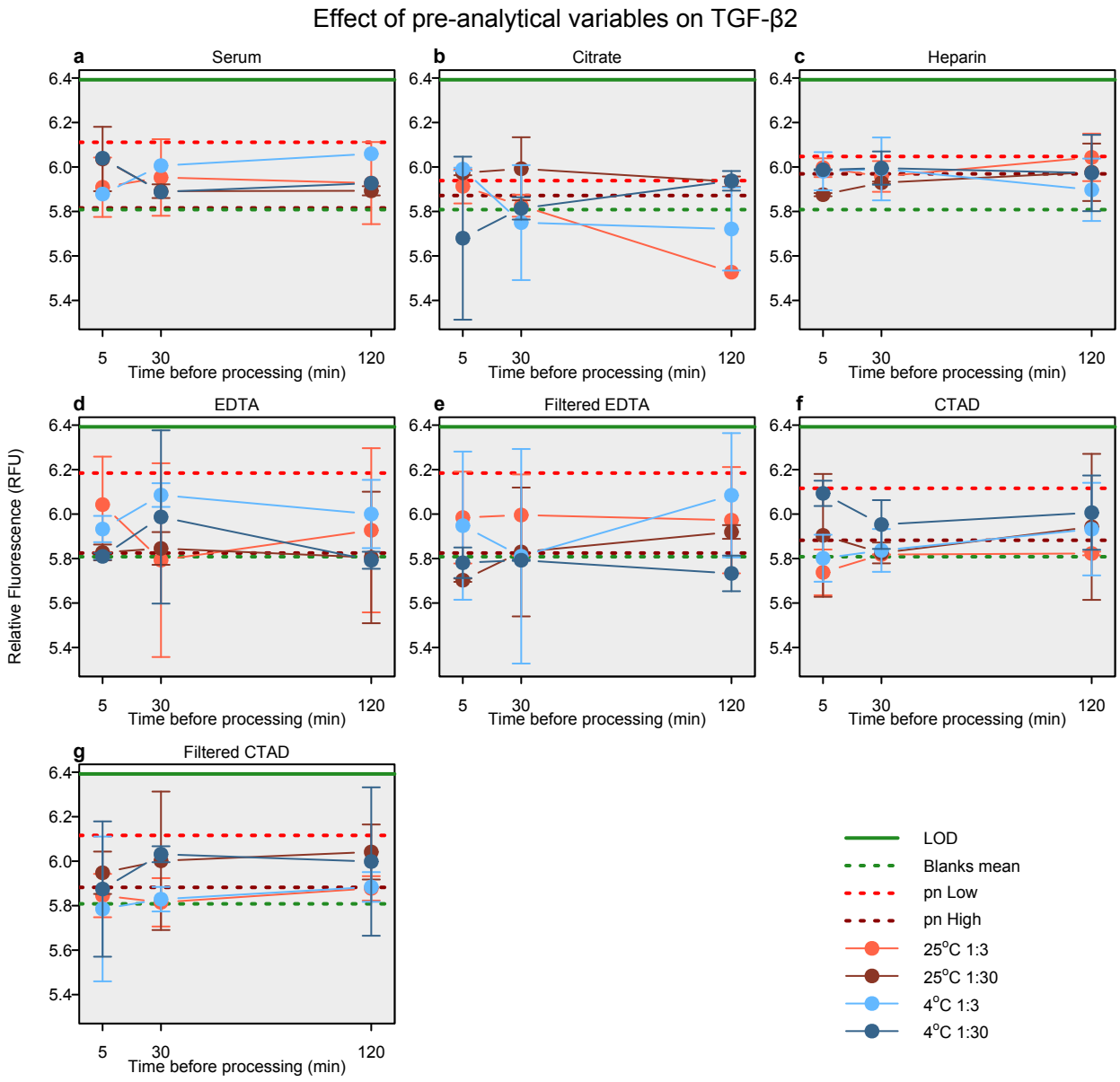

FIGURE I.S171: **Effect of blood collection tube on TGF-β2 stability and concentration.** Effects of blood collection tubes (**a**: serum, **b**: citrate, **c**: heparin, **d-e**: EDTA, **f-g**: CTAD), storage temperature and time before processing, and post-processing plasma filtering (**e, g**) on the initial value and pre-processing time stability of TGF-β2 measurements in blood. Information on the dilution of samples used for measuring, data range and the sample type selected are also shown.

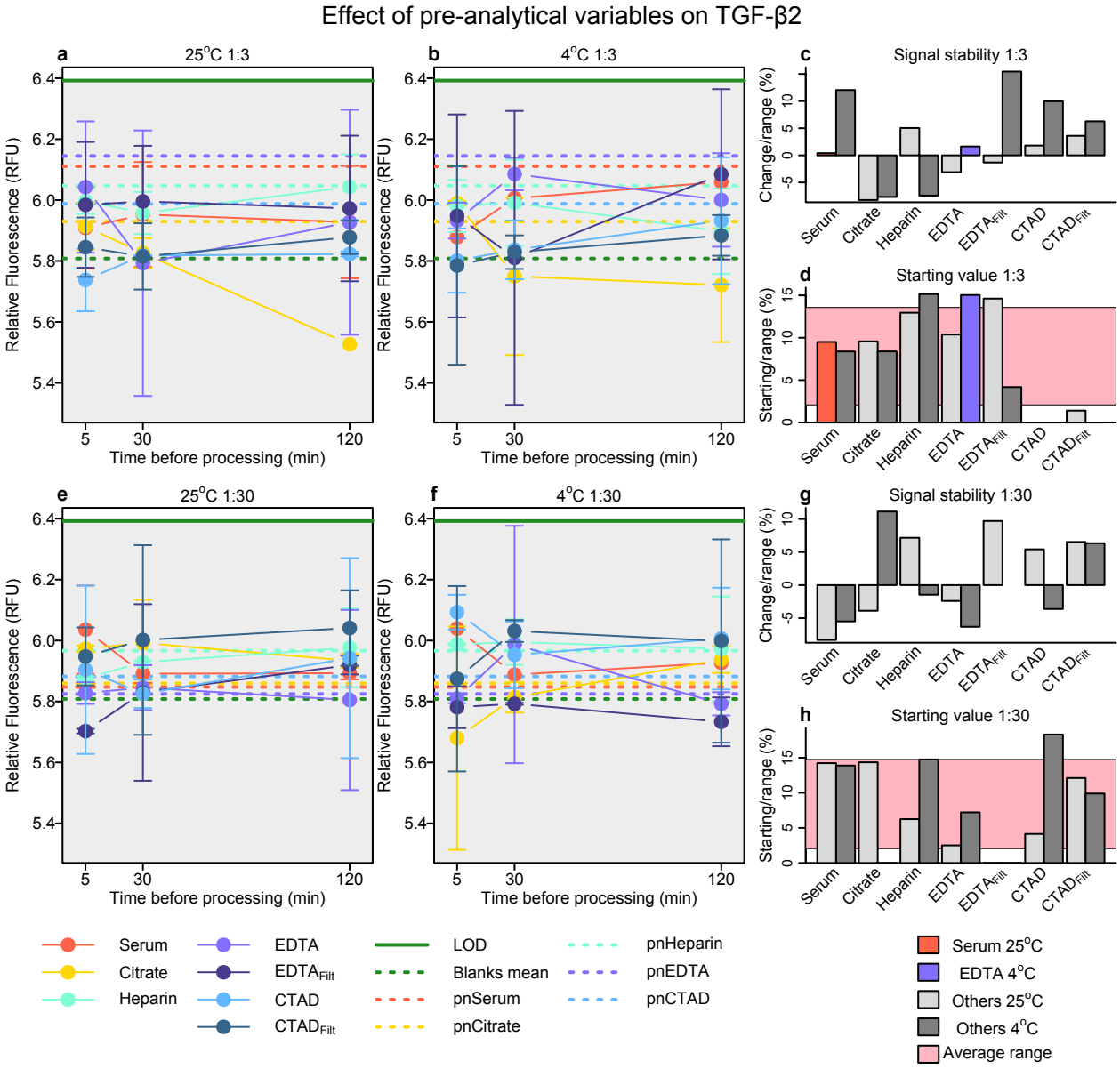

FIGURE I.S172: **Effect of pre-processing storage temperature on TGF-β2 stability and concentration.** Initial measured value and stability of TGF-β2 when stored at 25 °C (**a, e**) and 4 °C (**b, f**) before processing when collected in different tube types. The measured values are shown at low dilution of 1:3 (**a-b**) and high dilution of 1:30 (**e-f**). Stability before processing is expressed as an increase or decrease compared to the measurement range and is shown for low (**c**) and high (**g**) dilutions. Initial value is expressed as a portion of the measurement range when the linear regression is extrapolated to zero minutes and is shown for low (**d**) and high (**h**) dilutions. The pink box in graphs **d** and **h** indicate the region that is included by the *mean* ± *SD* of all the initial values and gives an indication of outliers when values lie outside this region. Red and purple bars in **c-d, g-h** are indicated at the measured dilution as the two choices for the TBI analysis.

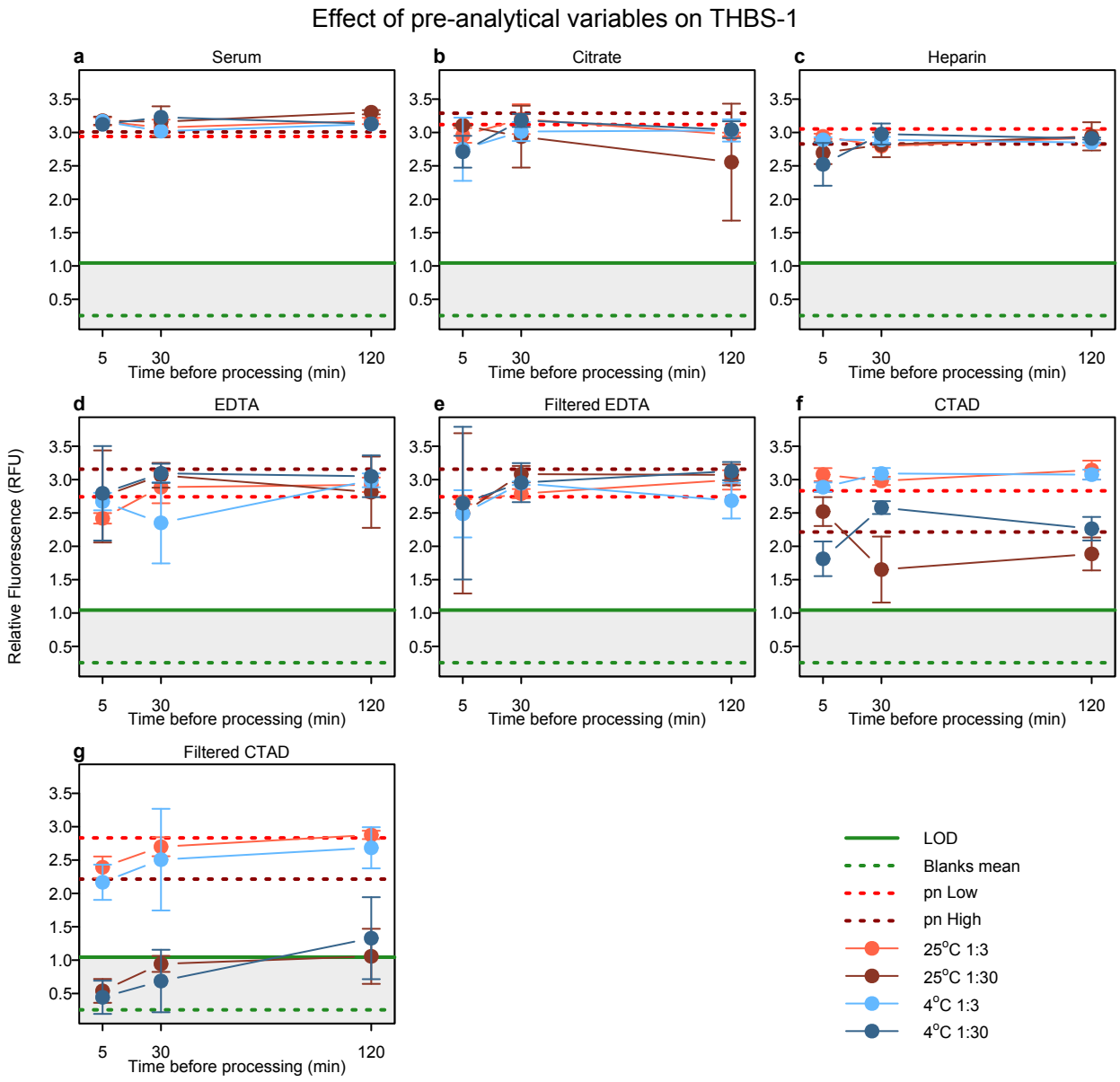

FIGURE I.S173: **Effect of blood collection tube on THBS-1 stability and concentration.** Effects of blood collection tubes (**a**: serum, **b**: citrate, **c**: heparin, **d-e**: EDTA, **f-g**: CTAD), storage temperature and time before processing, and post-processing plasma filtering (**e, g**) on the initial value and pre-processing time stability of THBS-1 measurements in blood. Information on the dilution of samples used for measuring, data range and the sample type selected are also shown.

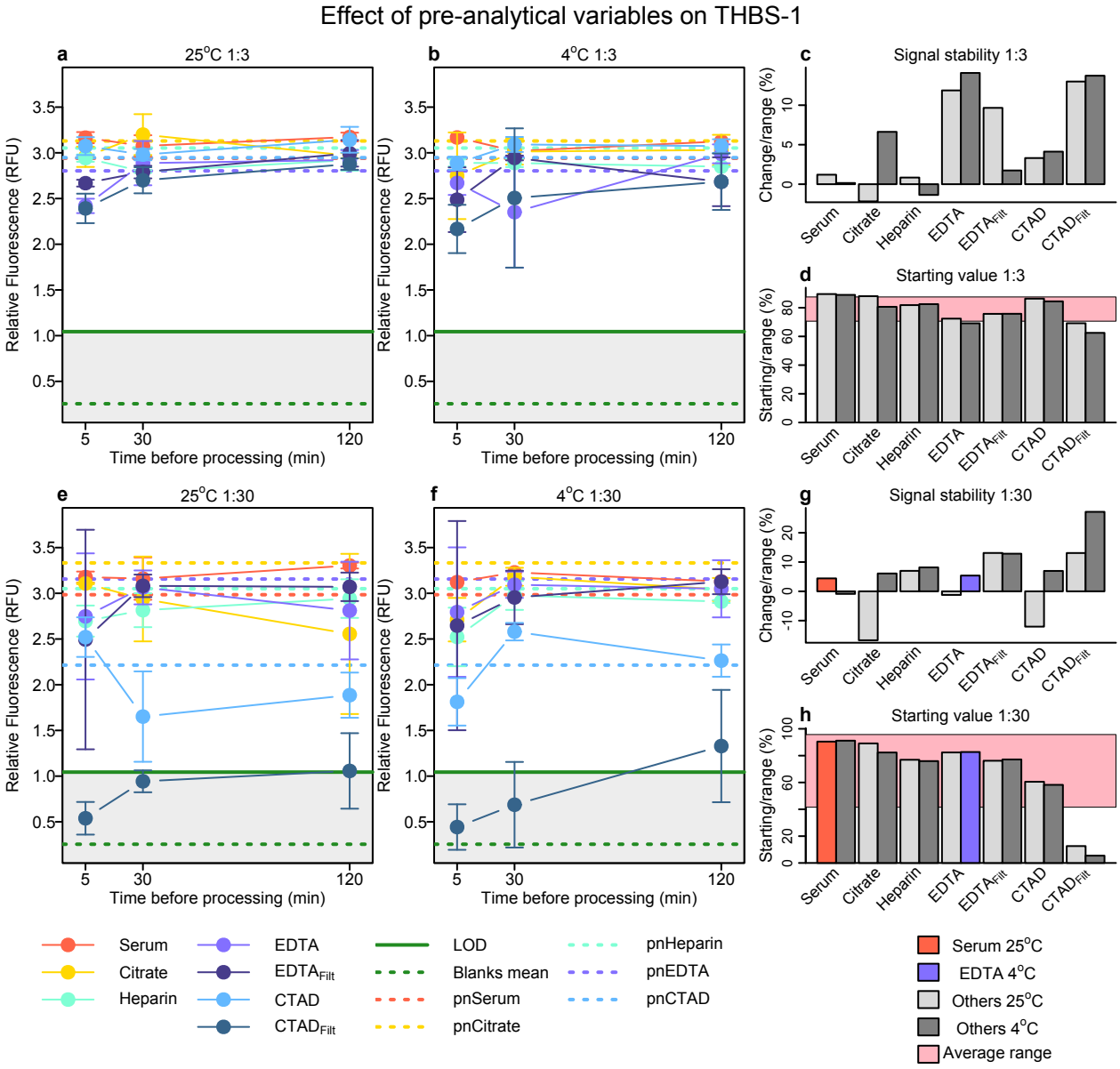

FIGURE I.S174: **Effect of pre-processing storage temperature on THBS-1 stability and concentration.** Initial measured value and stability of THBS-1 when stored at 25 °C (**a, e**) and 4 °C (**b, f**) before processing when collected in different tube types. The measured values are shown at low dilution of 1:3 (**a-b**) and high dilution of 1:30 (**e-f**). Stability before processing is expressed as an increase or decrease compared to the measurement range and is shown for low (**c**) and high (**g**) dilutions. Initial value is expressed as a portion of the measurement range when the linear regression is extrapolated to zero minutes and is shown for low (**d**) and high (**h**) dilutions. The pink box in graphs **d** and **h** indicate the region that is included by the *mean* ± *SD* of all the initial values and gives an indication of outliers when values lie outside this region. Red and purple bars in **c-d, g-h** are indicated at the measured dilution as the two choices for the TBI analysis.

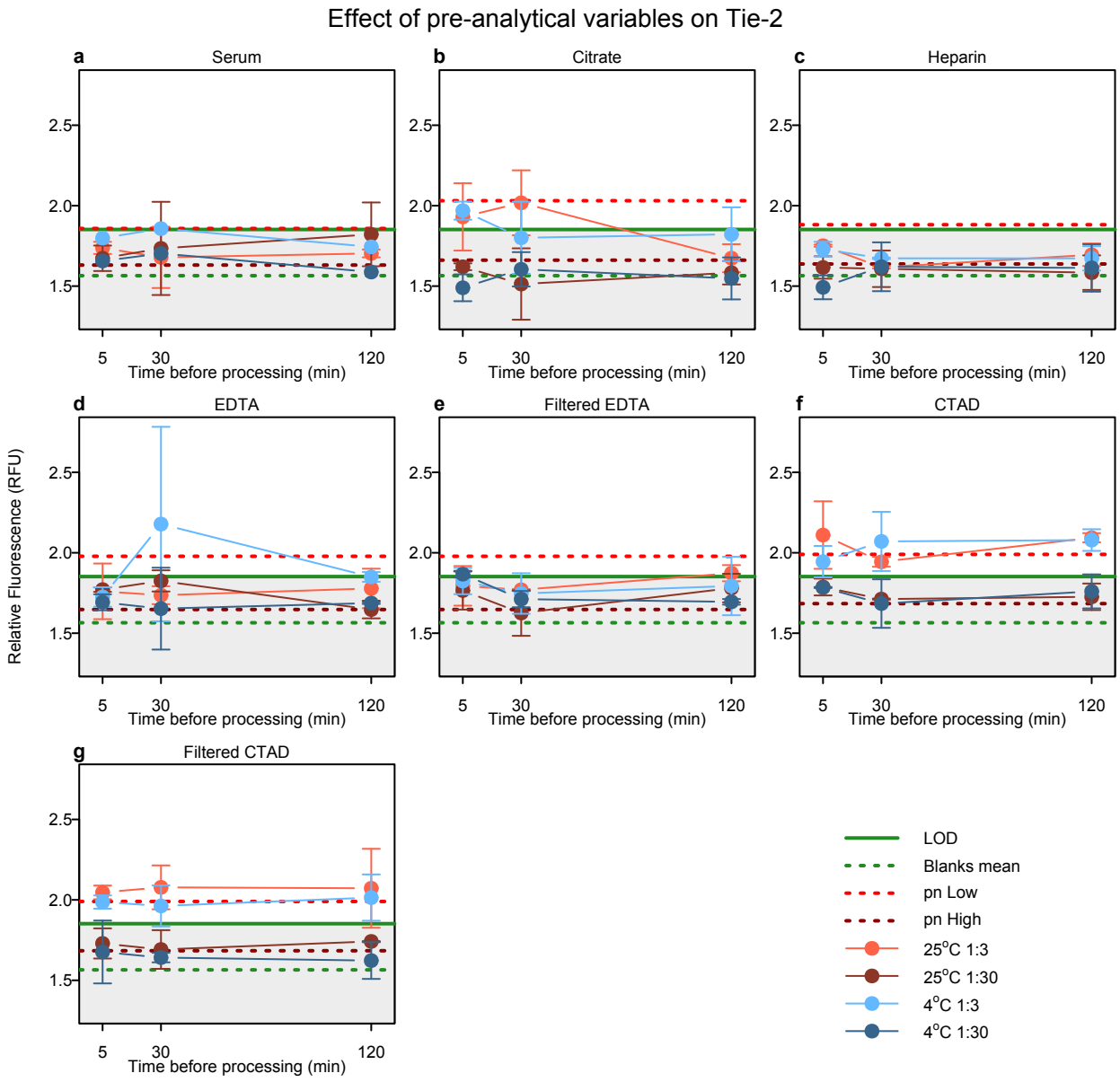

FIGURE I.S175: **Effect of blood collection tube on Tie-2 stability and concentration.** Effects of blood collection tubes (**a**: serum, **b**: citrate, **c**: heparin, **d-e**: EDTA, **f-g**: CTAD), storage temperature and time before processing, and post-processing plasma filtering (**e, g**) on the initial value and pre-processing time stability of Tie-2 measurements in blood. Information on the dilution of samples used for measuring, data range and the sample type selected are also shown.

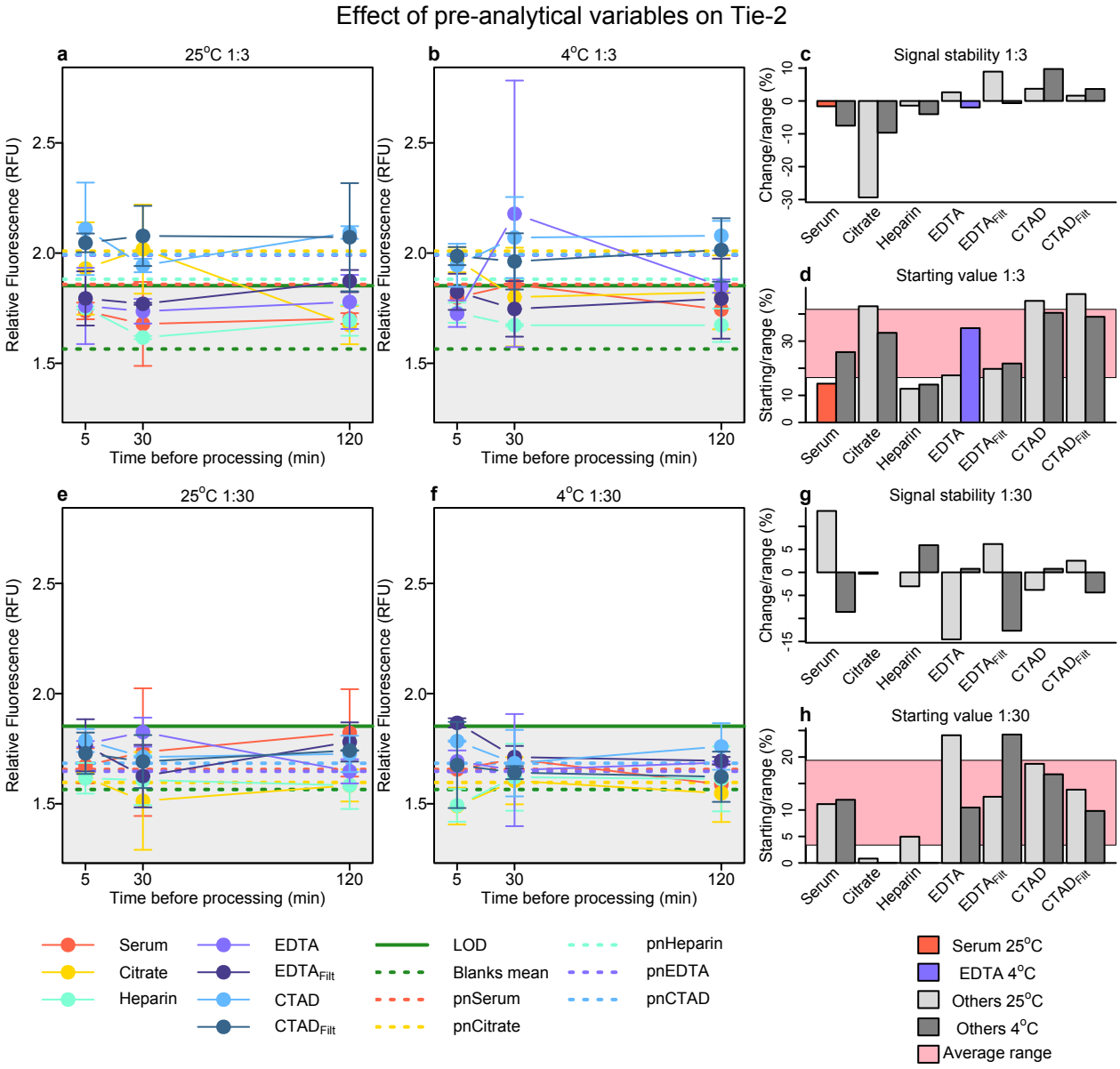

FIGURE I.S176: **Effect of pre-processing storage temperature on Tie-2 stability and concentration.** Initial measured value and stability of Tie-2 when stored at 25 °C (**a, e**) and 4 °C (**b, f**) before processing when collected in different tube types. The measured values are shown at low dilution of 1:3 (**a-b**) and high dilution of 1:30 (**e-f**). Stability before processing is expressed as an increase or decrease compared to the measurement range and is shown for low (**c**) and high (**g**) dilutions. Initial value is expressed as a portion of the measurement range when the linear regression is extrapolated to zero minutes and is shown for low (**d**) and high (**h**) dilutions. The pink box in graphs **d** and **h** indicate the region that is included by the *mean* ± *SD* of all the initial values and gives an indication of outliers when values lie outside this region. Red and purple bars in **c-d, g-h** are indicated at the measured dilution as the two choices for the TBI analysis.

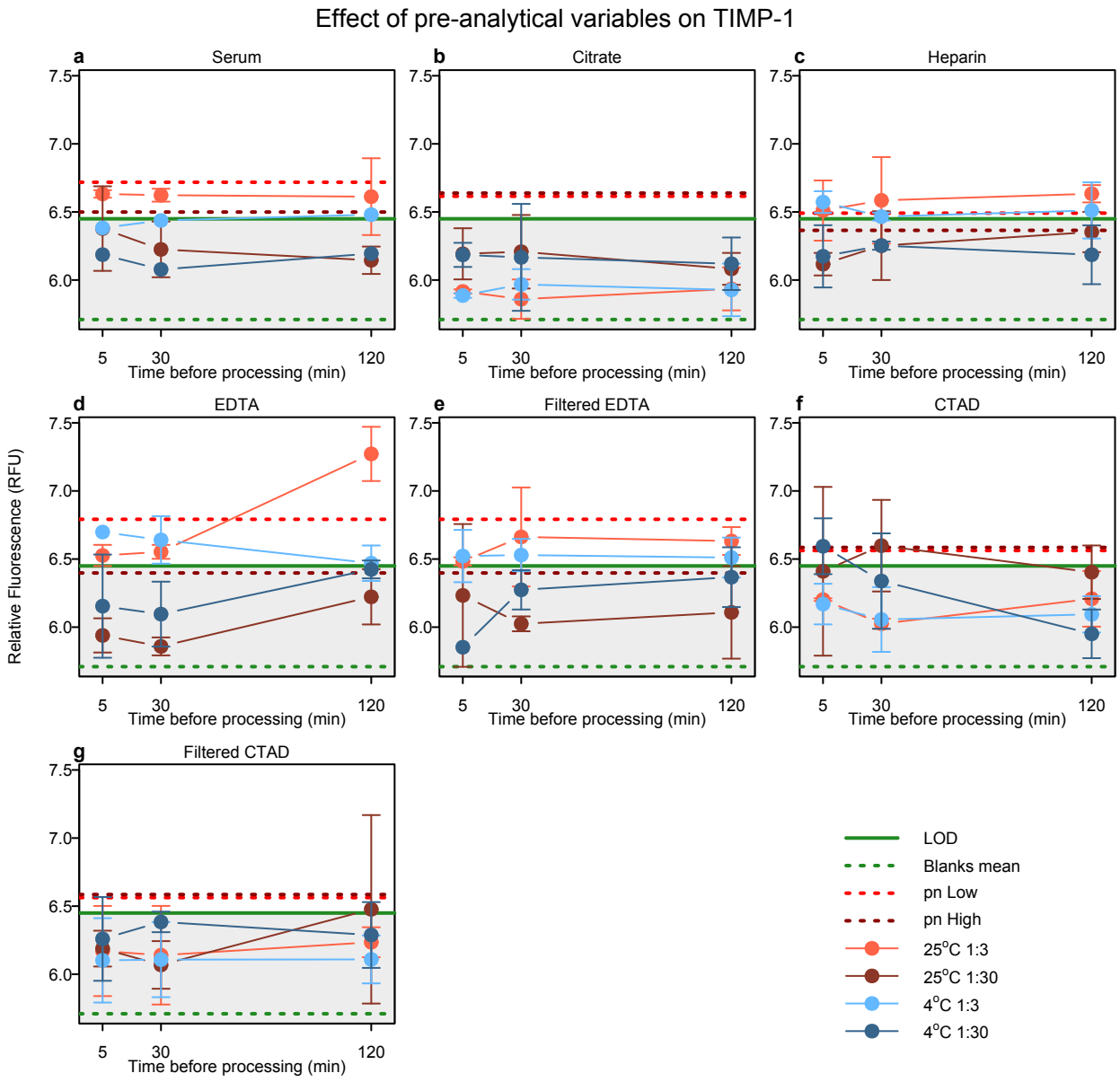

FIGURE I.S177: **Effect of blood collection tube on TIMP-1 stability and concentration.** Effects of blood collection tubes (**a**: serum, **b**: citrate, **c**: heparin, **d-e**: EDTA, **f-g**: CTAD), storage temperature and time before processing, and post-processing plasma filtering (**e, g**) on the initial value and pre-processing time stability of TIMP-1 measurements in blood. Information on the dilution of samples used for measuring, data range and the sample type selected are also shown.

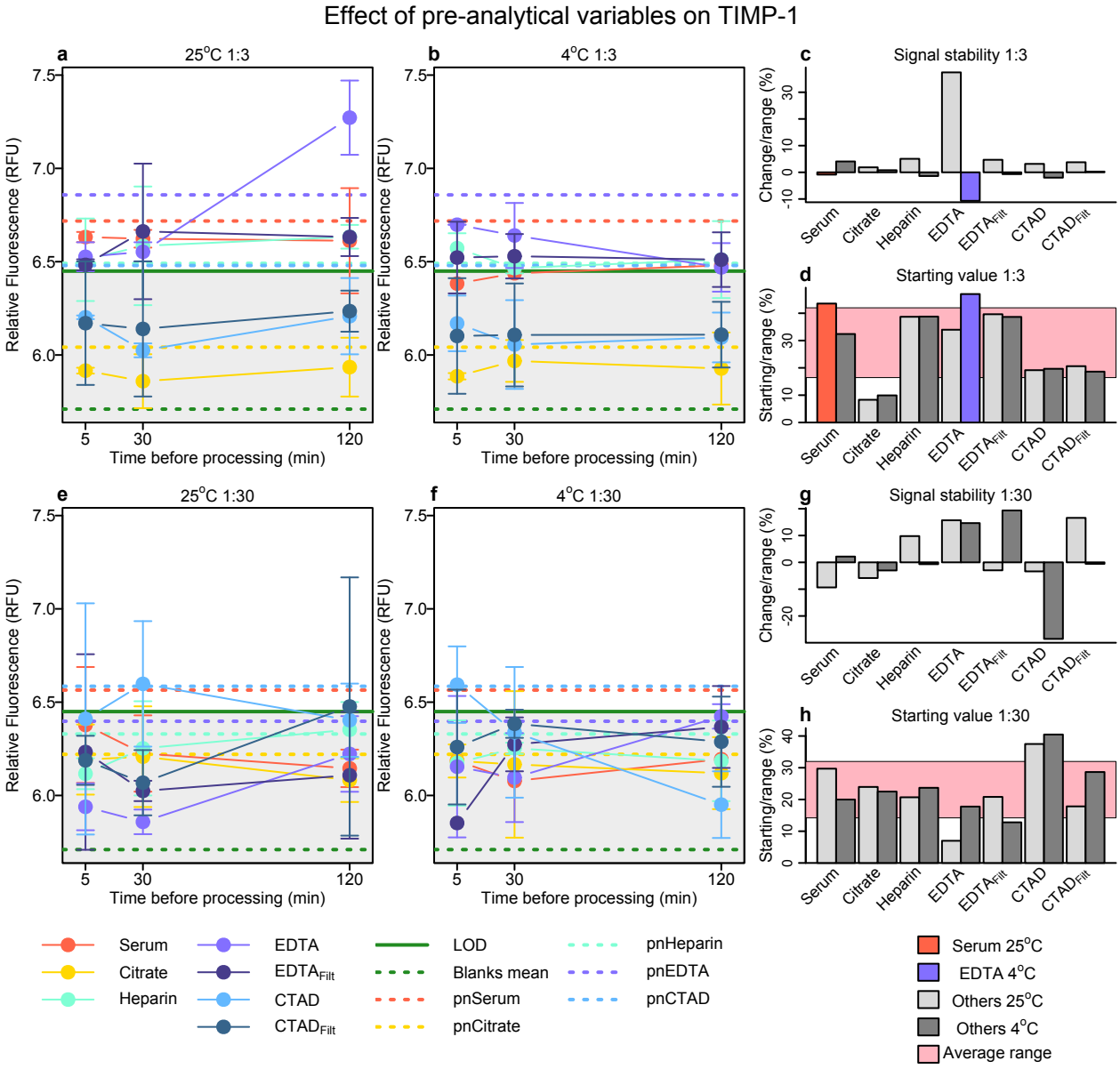

FIGURE I.S178: **Effect of pre-processing storage temperature on TIMP-1 stability and concentration.** Initial measured value and stability of TIMP-1 when stored at 25 °C (**a, e**) and 4 °C (**b, f**) before processing when collected in different tube types. The measured values are shown at low dilution of 1:3 (**a-b**) and high dilution of 1:30 (**e-f**). Stability before processing is expressed as an increase or decrease compared to the measurement range and is shown for low (**c**) and high (**g**) dilutions. Initial value is expressed as a portion of the measurement range when the linear regression is extrapolated to zero minutes and is shown for low (**d**) and high (**h**) dilutions. The pink box in graphs **d** and **h** indicate the region that is included by the *mean* ± *SD* of all the initial values and gives an indication of outliers when values lie outside this region. Red and purple bars in **c-d, g-h** are indicated at the measured dilution as the two choices for the TBI analysis.

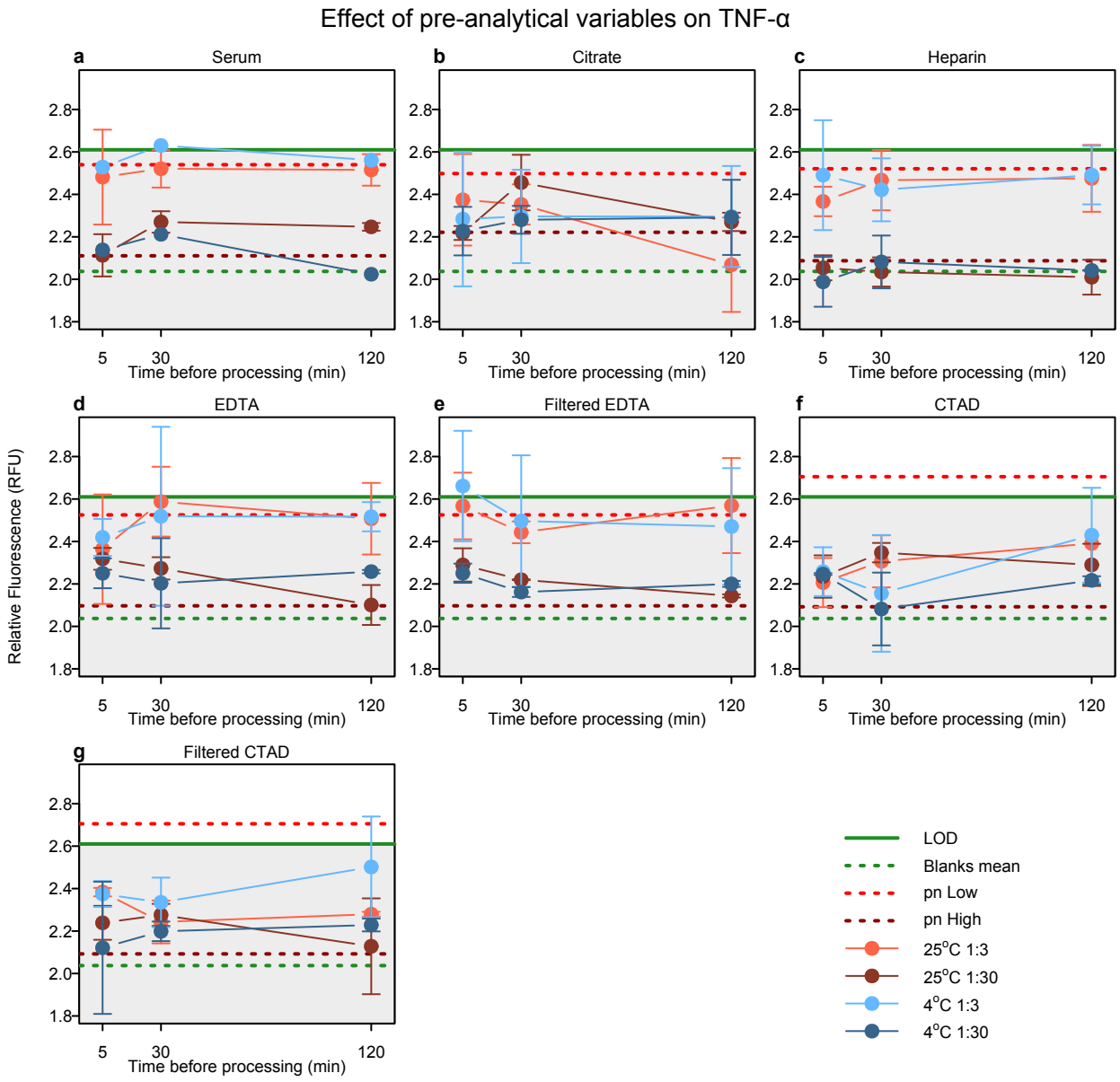

FIGURE I.S179: **Effect of blood collection tube on TNF-α stability and concentration.** Effects of blood collection tubes (**a**: serum, **b**: citrate, **c**: heparin, **d-e**: EDTA, **f-g**: CTAD), storage temperature and time before processing, and post-processing plasma filtering (**e, g**) on the initial value and pre-processing time stability of TNF-α measurements in blood. Information on the dilution of samples used for measuring, data range and the sample type selected are also shown.

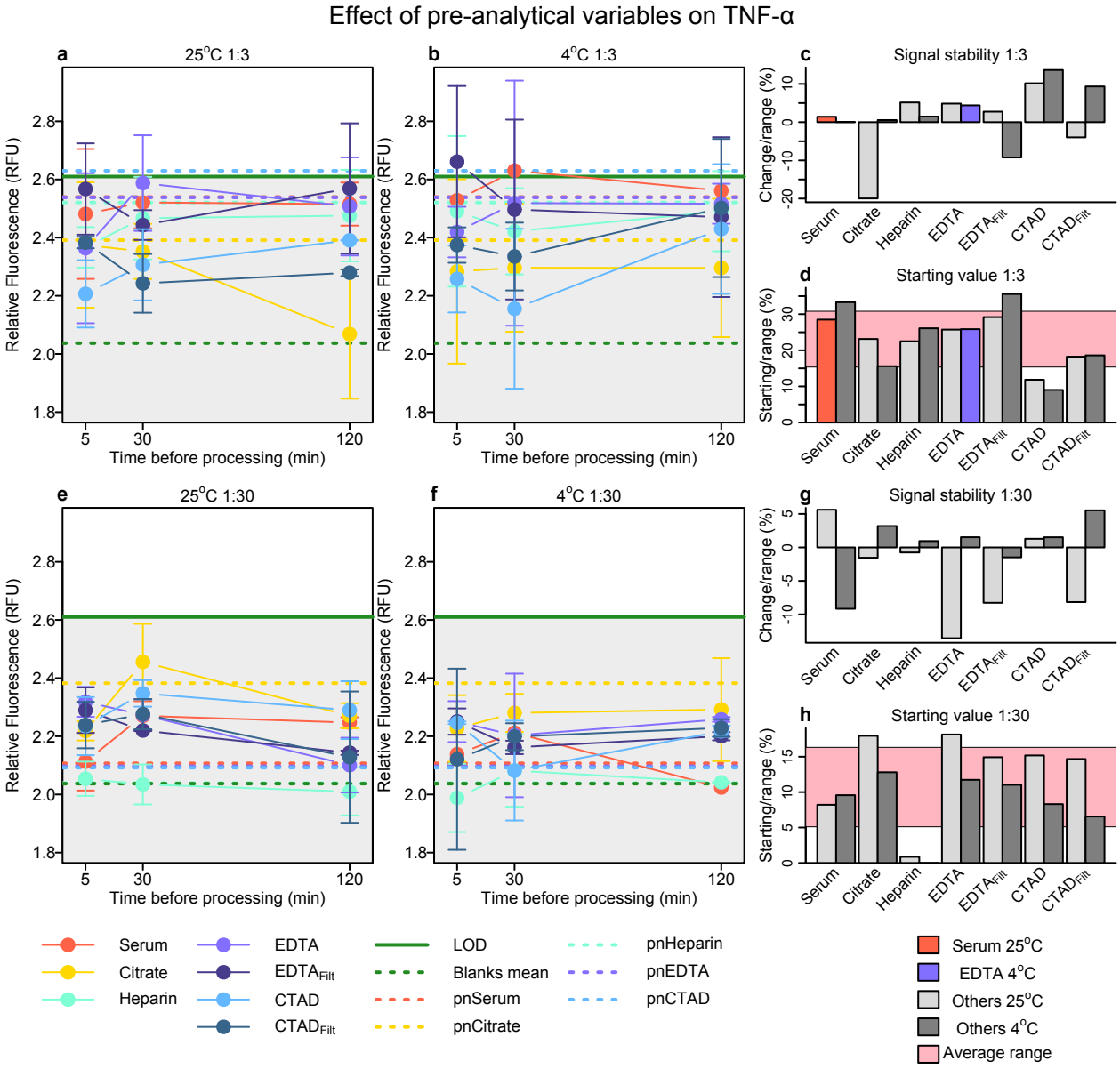

FIGURE I.S180: **Effect of pre-processing storage temperature on TNF-α stability and concentration.** Initial measured value and stability of TNF-α when stored at 25 °C (**a, e**) and 4 °C (**b, f**) before processing when collected in different tube types. The measured values are shown at low dilution of 1:3 (**a-b**) and high dilution of 1:30 (**e-f**). Stability before processing is expressed as an increase or decrease compared to the measurement range and is shown for low (**c**) and high (**g**) dilutions. Initial value is expressed as a portion of the measurement range when the linear regression is extrapolated to zero minutes and is shown for low (**d**) and high (**h**) dilutions. The pink box in graphs **d** and **h** indicate the region that is included by the *mean* ± *SD* of all the initial values and gives an indication of outliers when values lie outside this region. Red and purple bars in **c-d, g-h** are indicated at the measured dilution as the two choices for the TBI analysis.

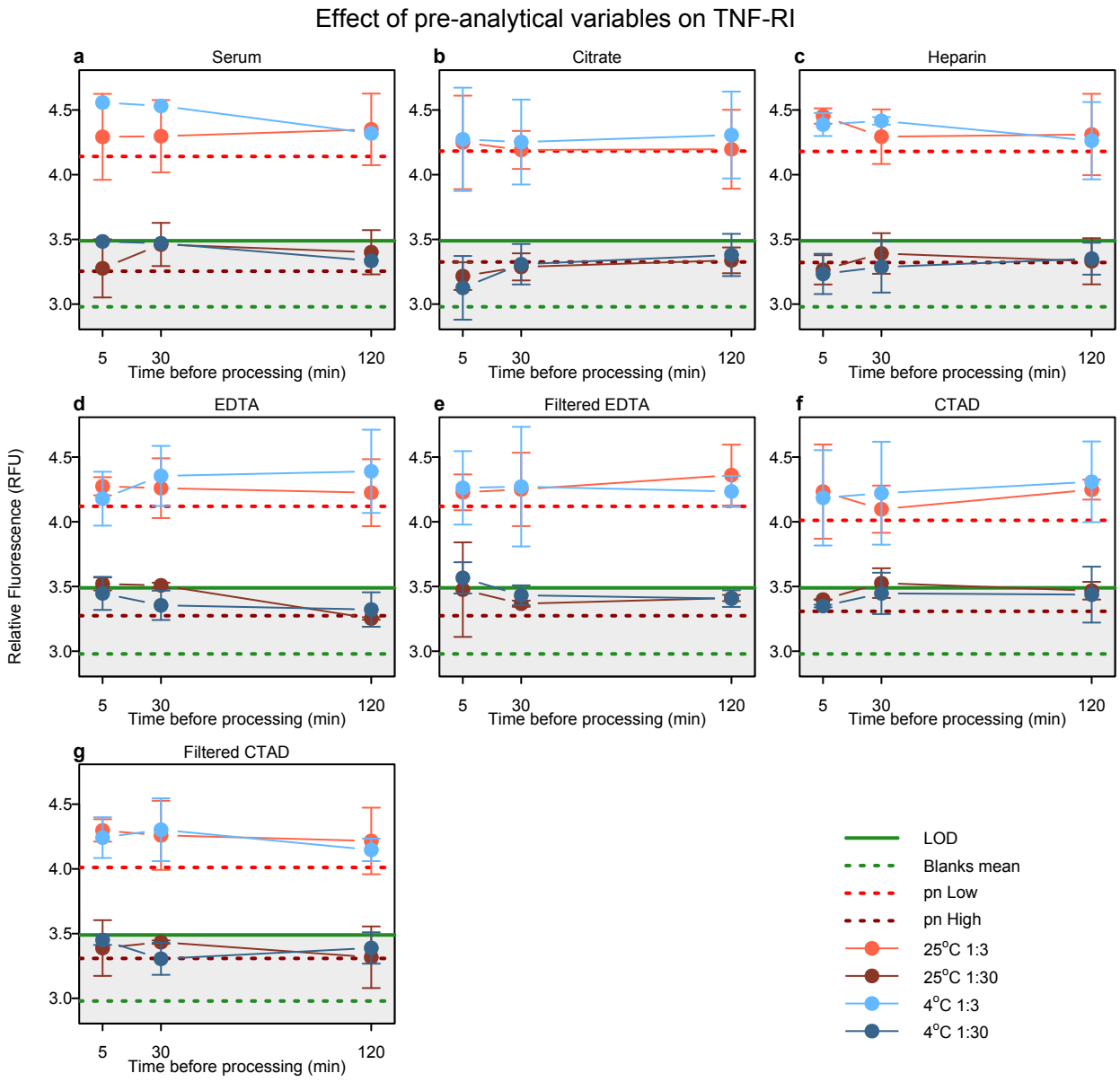

FIGURE I.S181: **Effect of blood collection tube on TNF-RI stability and concentration.** Effects of blood collection tubes (**a**: serum, **b**: citrate, **c**: heparin, **d-e**: EDTA, **f-g**: CTAD), storage temperature and time before processing, and post-processing plasma filtering (**e, g**) on the initial value and pre-processing time stability of TNF-RI measurements in blood. Information on the dilution of samples used for measuring, data range and the sample type selected are also shown.

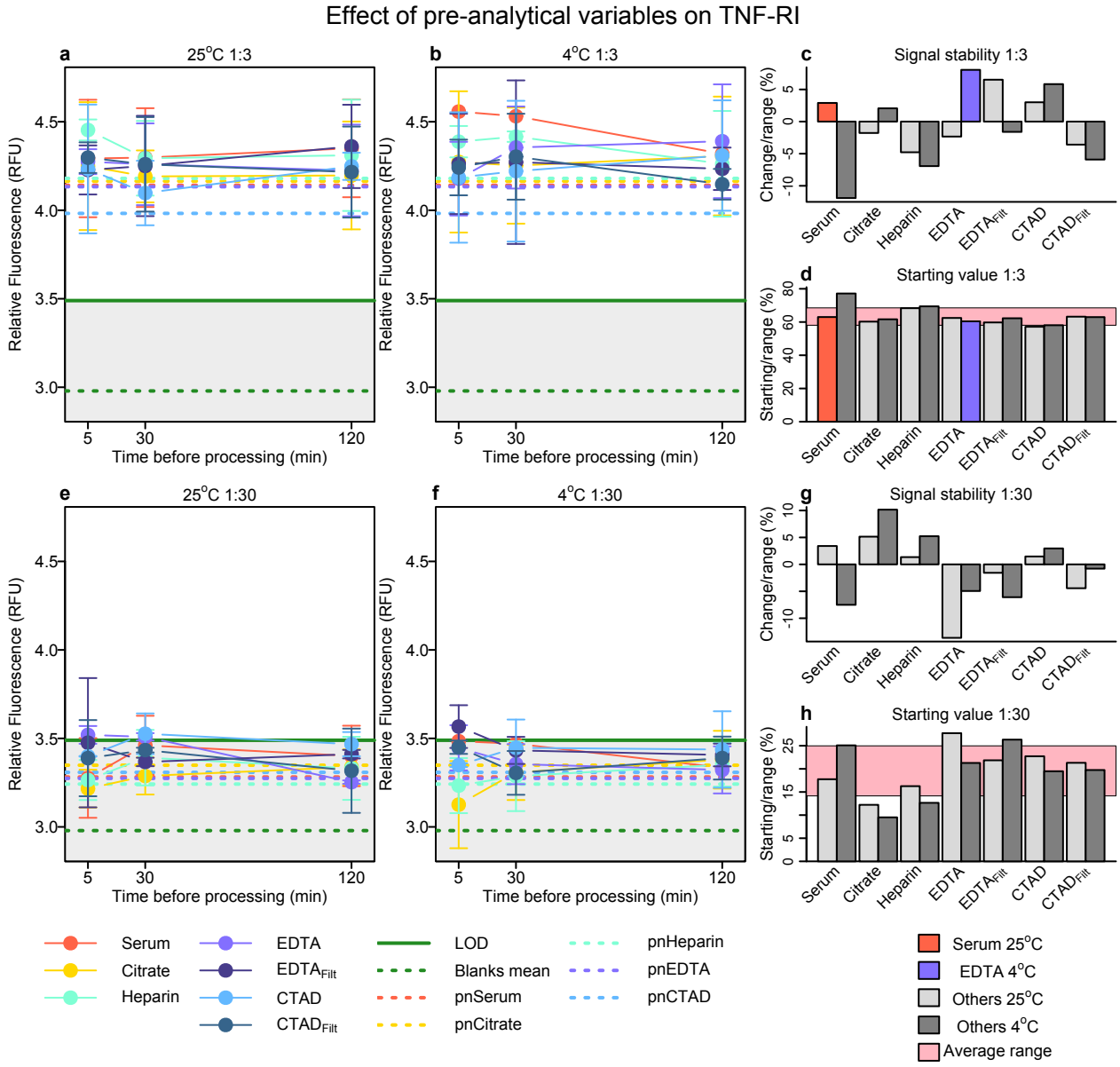

FIGURE I.S182: **Effect of pre-processing storage temperature on TNF-RI stability and concentration.** Initial measured value and stability of TNF-RI when stored at 25 °C (**a, e**) and 4 °C (**b, f**) before processing when collected in different tube types. The measured values are shown at low dilution of 1:3 (**a-b**) and high dilution of 1:30 (**e-f**). Stability before processing is expressed as an increase or decrease compared to the measurement range and is shown for low (**c**) and high (**g**) dilutions. Initial value is expressed as a portion of the measurement range when the linear regression is extrapolated to zero minutes and is shown for low (**d**) and high (**h**) dilutions. The pink box in graphs **d** and **h** indicate the region that is included by the *mean* ± *SD* of all the initial values and gives an indication of outliers when values lie outside this region. Red and purple bars in **c-d, g-h** are indicated at the measured dilution as the two choices for the TBI analysis.

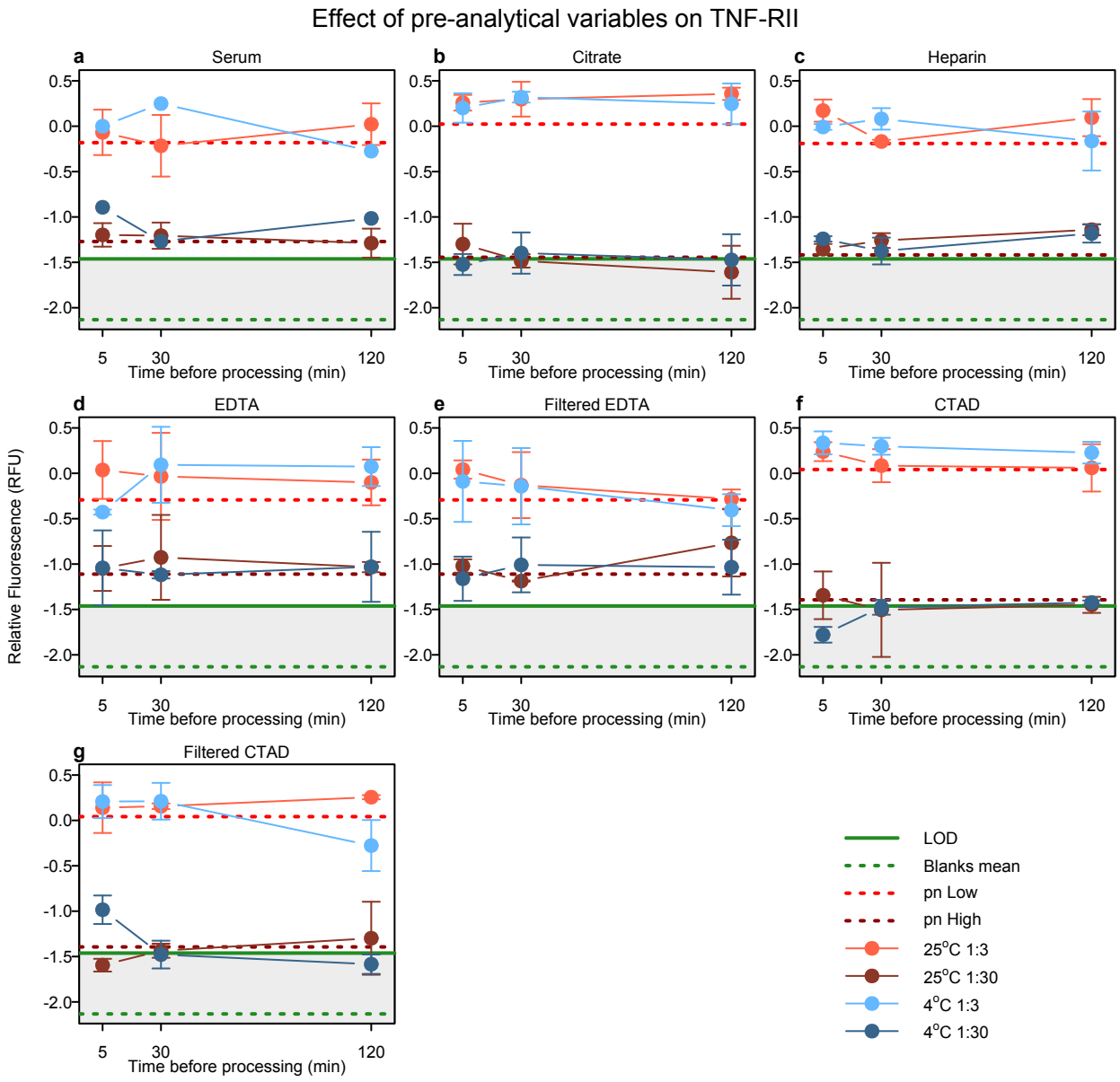

FIGURE I.S183: **Effect of blood collection tube on TNF-RII stability and concentration.** Effects of blood collection tubes (**a**: serum, **b**: citrate, **c**: heparin, **d-e**: EDTA, **f-g**: CTAD), storage temperature and time before processing, and post-processing plasma filtering (**e, g**) on the initial value and pre-processing time stability of TNF-RII measurements in blood. Information on the dilution of samples used for measuring, data range and the sample type selected are also shown.

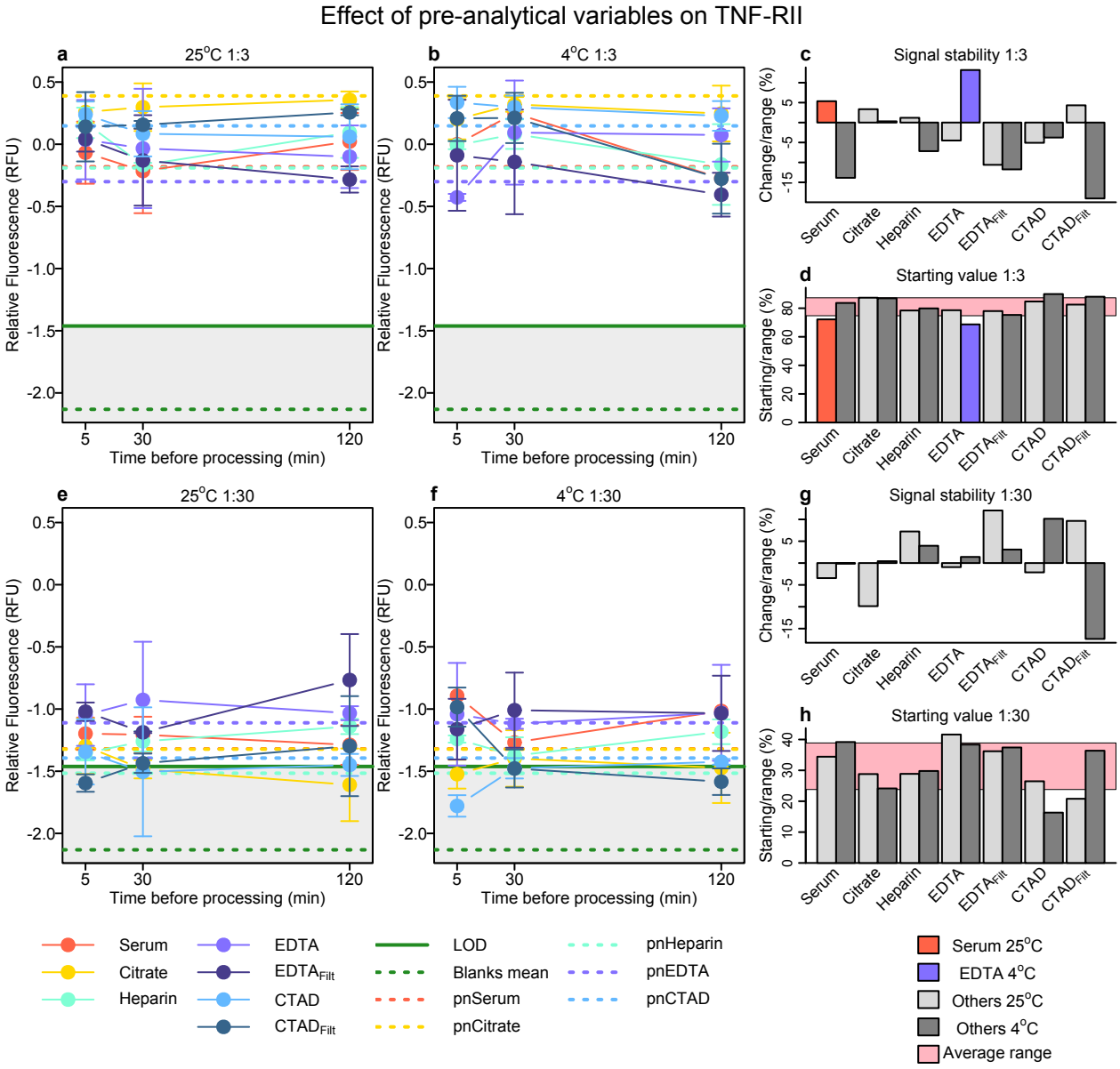

FIGURE I.S184: **Effect of pre-processing storage temperature on TNF-RII stability and concentration.** Initial measured value and stability of TNF-RII when stored at 25 °C (**a, e**) and 4 °C (**b, f**) before processing when collected in different tube types. The measured values are shown at low dilution of 1:3 (**a-b**) and high dilution of 1:30 (**e-f**). Stability before processing is expressed as an increase or decrease compared to the measurement range and is shown for low (**c**) and high (**g**) dilutions. Initial value is expressed as a portion of the measurement range when the linear regression is extrapolated to zero minutes and is shown for low (**d**) and high (**h**) dilutions. The pink box in graphs **d** and **h** indicate the region that is included by the *mean* ± *SD* of all the initial values and gives an indication of outliers when values lie outside this region. Red and purple bars in **c-d, g-h** are indicated at the measured dilution as the two choices for the TBI analysis.

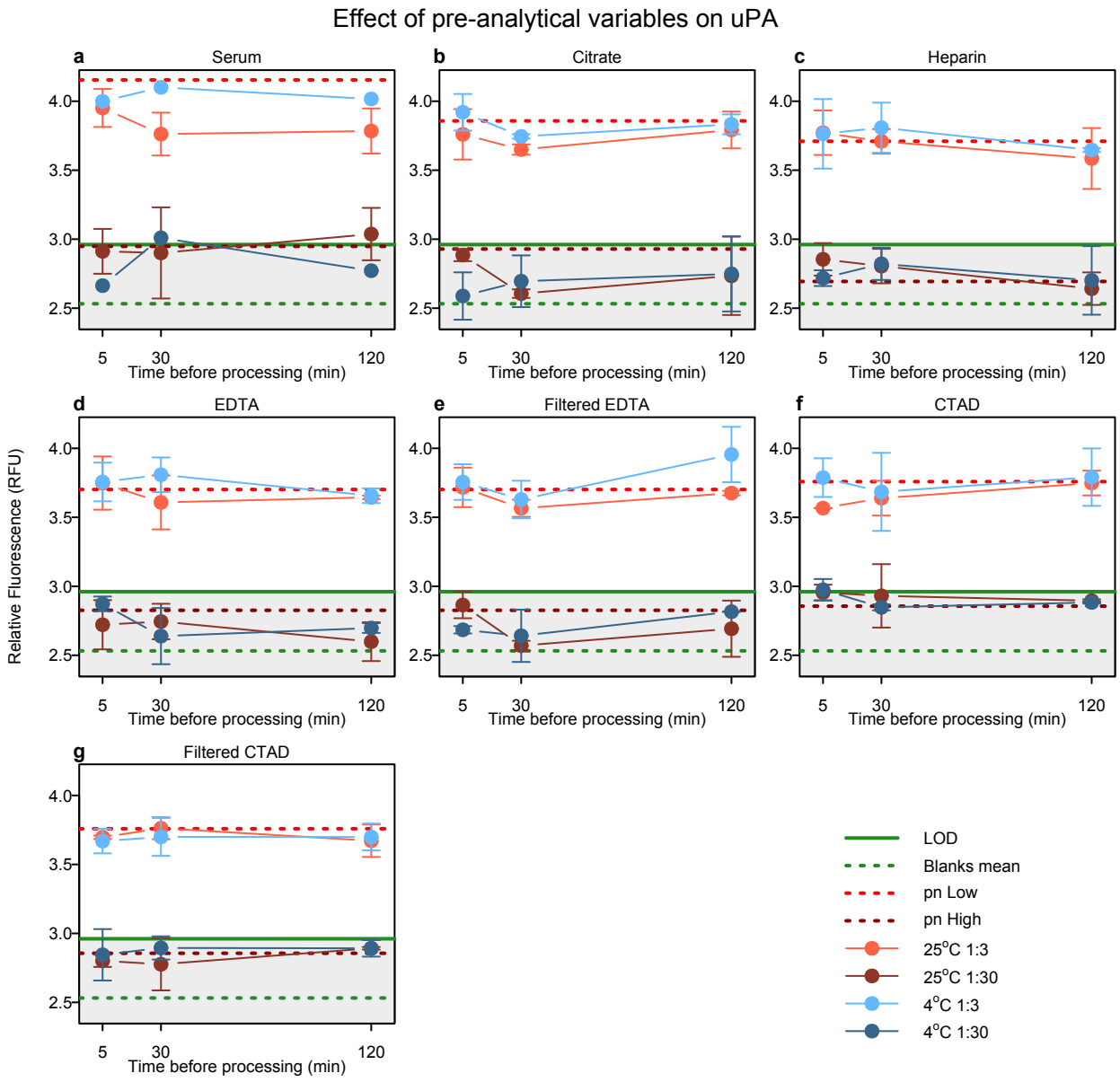

FIGURE I.S185: **Effect of blood collection tube on uPA stability and concentration.** Effects of blood collection tubes (**a**: serum, **b**: citrate, **c**: heparin, **d-e**: EDTA, **f-g**: CTAD), storage temperature and time before processing, and post-processing plasma filtering (**e, g**) on the initial value and pre-processing time stability of uPA measurements in blood. Information on the dilution of samples used for measuring, data range and the sample type selected are also shown.

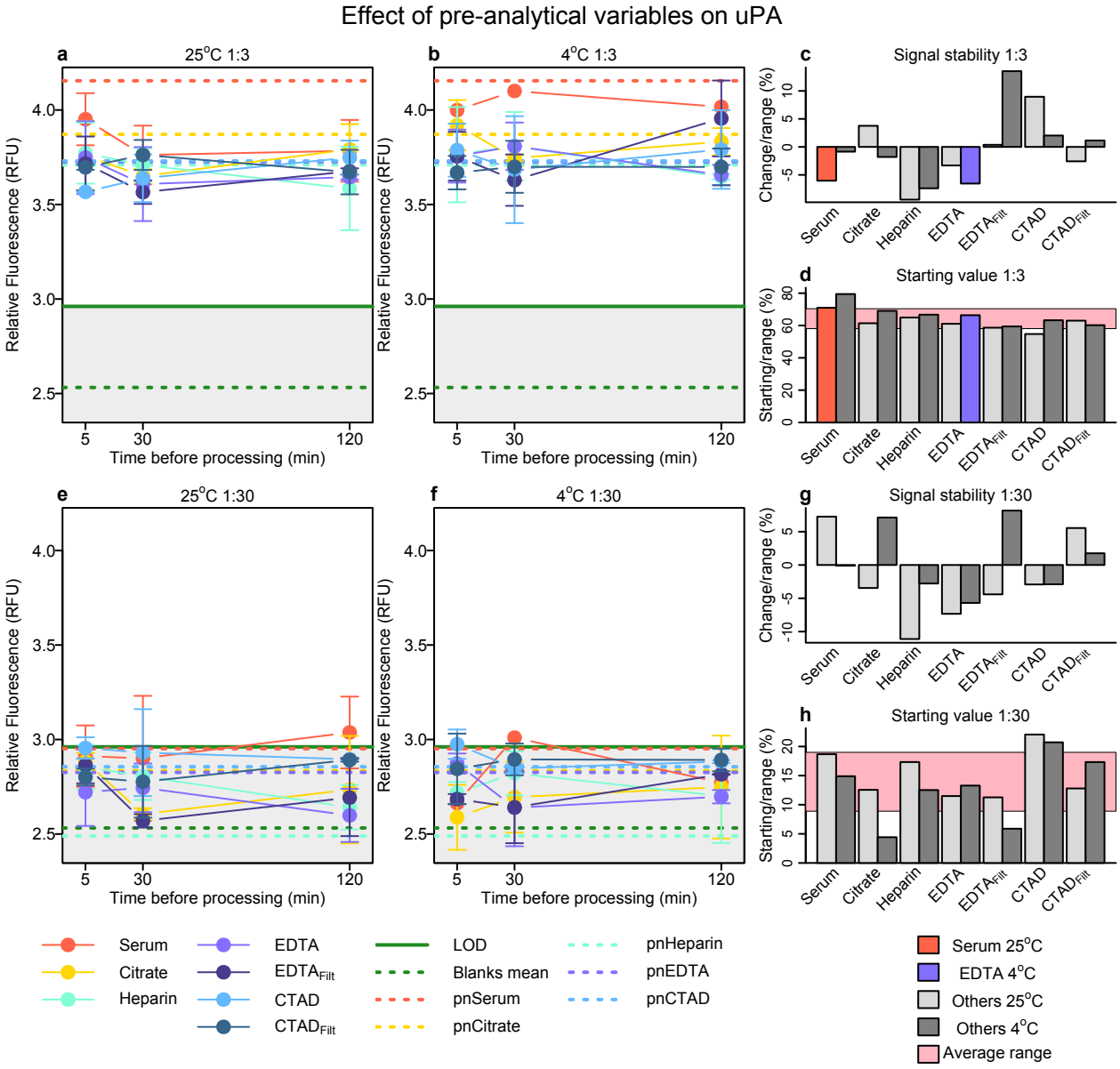

FIGURE I.S186: **Effect of pre-processing storage temperature on uPA stability and concentration.** Initial measured value and stability of uPA when stored at 25 °C (**a, e**) and 4 °C (**b, f**) before processing when collected in different tube types. The measured values are shown at low dilution of 1:3 (**a-b**) and high dilution of 1:30 (**e-f**). Stability before processing is expressed as an increase or decrease compared to the measurement range and is shown for low (**c**) and high (**g**) dilutions. Initial value is expressed as a portion of the measurement range when the linear regression is extrapolated to zero minutes and is shown for low (**d**) and high (**h**) dilutions. The pink box in graphs **d** and **h** indicate the region that is included by the *mean* ± *SD* of all the initial values and gives an indication of outliers when values lie outside this region. Red and purple bars in **c-d, g-h** are indicated at the measured dilution as the two choices for the TBI analysis.

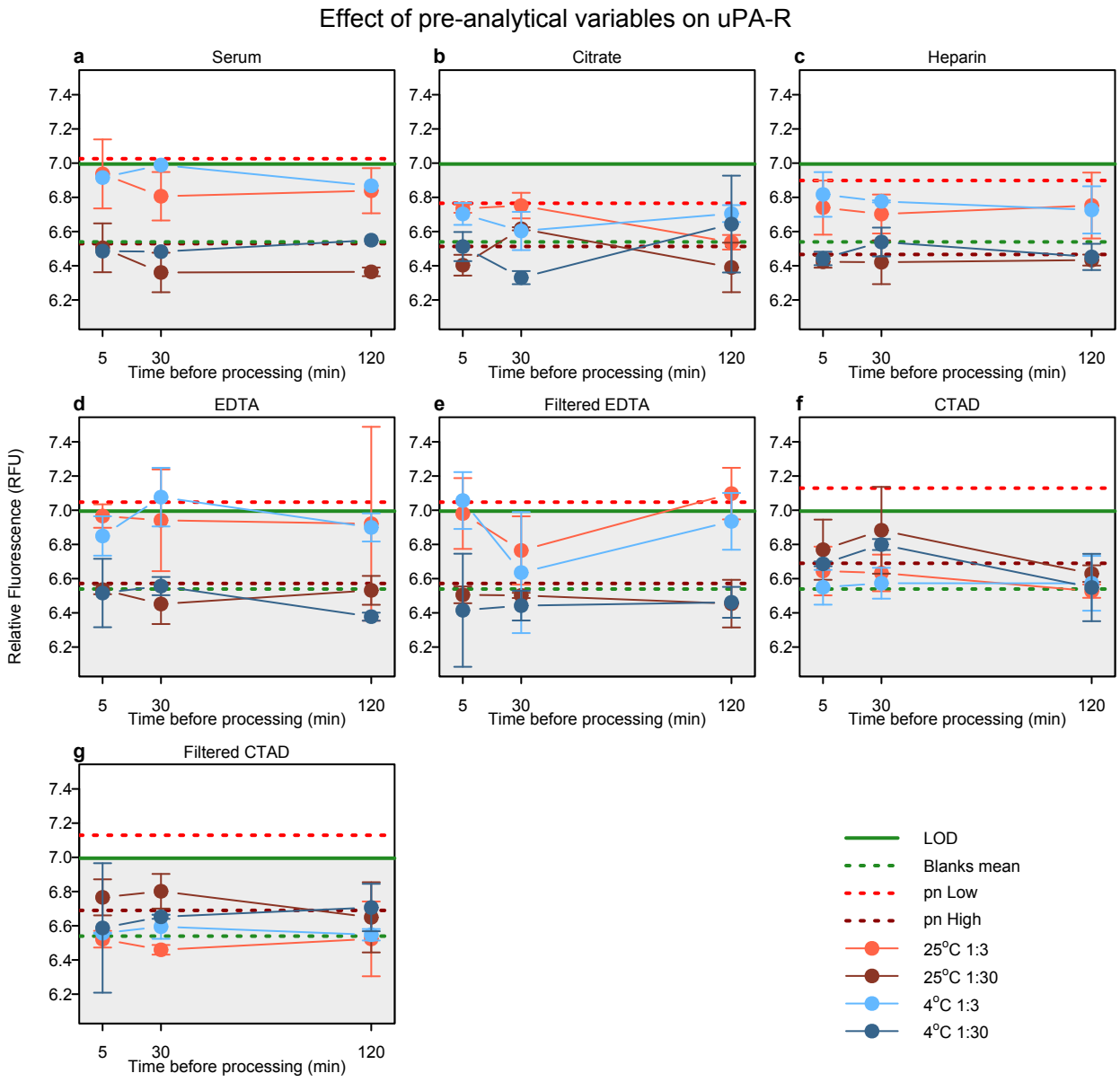

FIGURE I.S187: **Effect of blood collection tube on uPA-R stability and concentration.** Effects of blood collection tubes (**a**: serum, **b**: citrate, **c**: heparin, **d-e**: EDTA, **f-g**: CTAD), storage temperature and time before processing, and post-processing plasma filtering (**e, g**) on the initial value and pre-processing time stability of uPA-R measurements in blood. Information on the dilution of samples used for measuring, data range and the sample type selected are also shown.

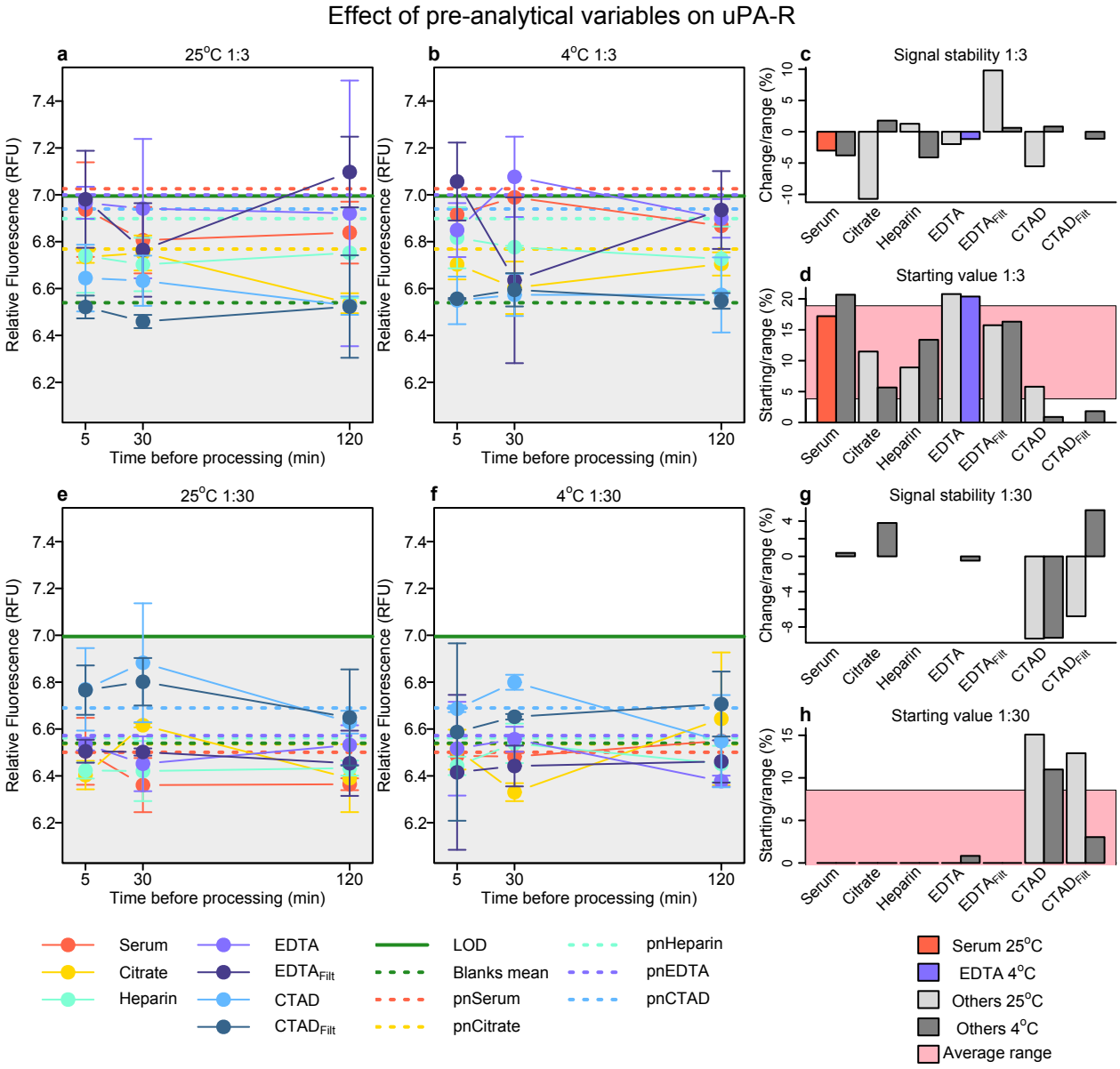

FIGURE I.S188: **Effect of pre-processing storage temperature on uPA-R stability and concentration.** Initial measured value and stability of uPA-R when stored at 25 °C (**a, e**) and 4 °C (**b, f**) before processing when collected in different tube types. The measured values are shown at low dilution of 1:3 (**a-b**) and high dilution of 1:30 (**e-f**). Stability before processing is expressed as an increase or decrease compared to the measurement range and is shown for low (**c**) and high (**g**) dilutions. Initial value is expressed as a portion of the measurement range when the linear regression is extrapolated to zero minutes and is shown for low (**d**) and high (**h**) dilutions. The pink box in graphs **d** and **h** indicate the region that is included by the *mean* ± *SD* of all the initial values and gives an indication of outliers when values lie outside this region. Red and purple bars in **c-d, g-h** are indicated at the measured dilution as the two choices for the TBI analysis.

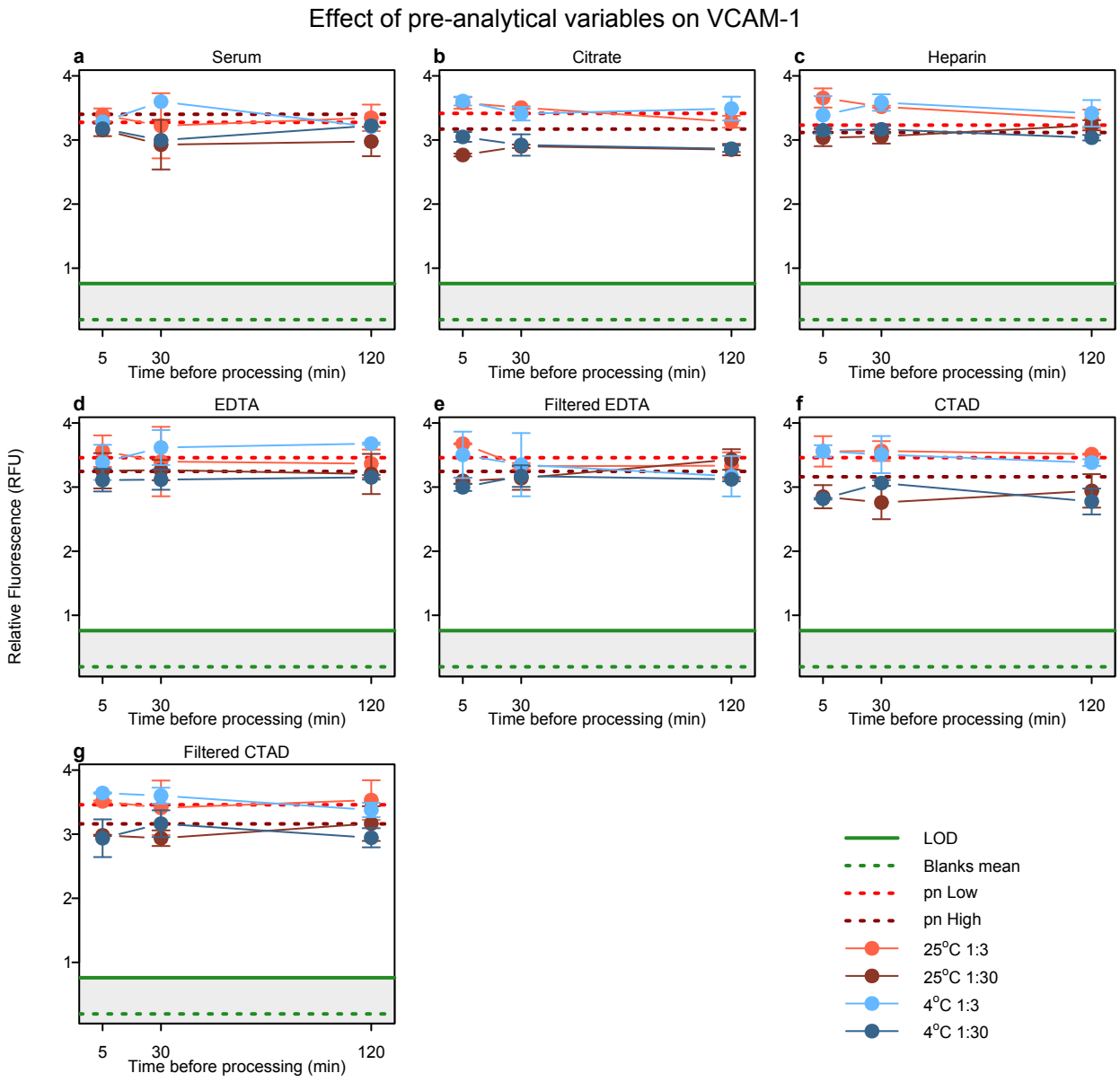

FIGURE I.S189: **Effect of blood collection tube on VCAM-1 stability and concentration.** Effects of blood collection tubes (**a**: serum, **b**: citrate, **c**: heparin, **d-e**: EDTA, **f-g**: CTAD), storage temperature and time before processing, and post-processing plasma filtering (**e, g**) on the initial value and pre-processing time stability of VCAM-1 measurements in blood. Information on the dilution of samples used for measuring, data range and the sample type selected are also shown.

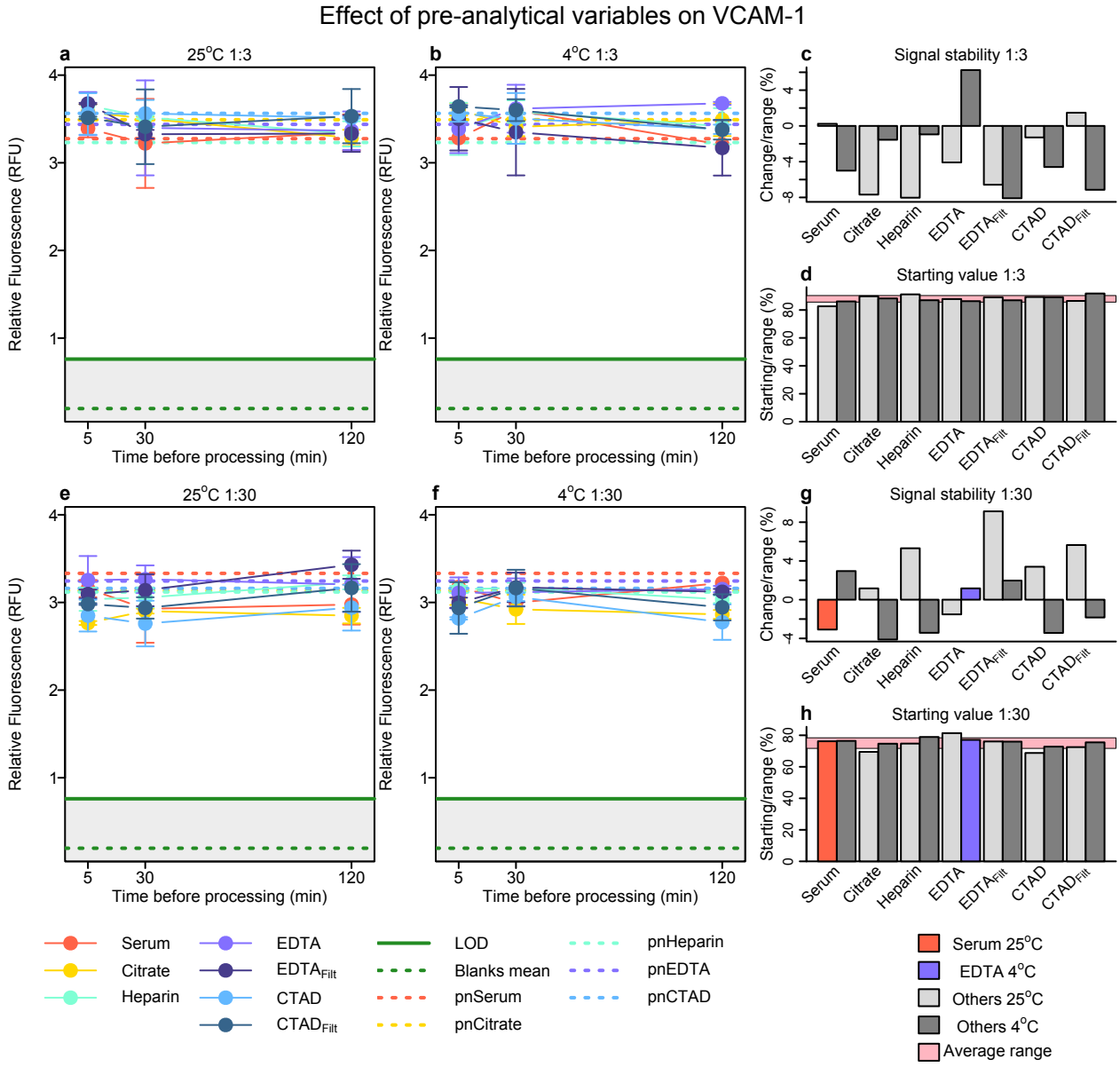

FIGURE I.S190: **Effect of pre-processing storage temperature on VCAM-1 stability and concentration.** Initial measured value and stability of VCAM-1 when stored at 25 °C (**a, e**) and 4 °C (**b, f**) before processing when collected in different tube types. The measured values are shown at low dilution of 1:3 (**a-b**) and high dilution of 1:30 (**e-f**). Stability before processing is expressed as an increase or decrease compared to the measurement range and is shown for low (**c**) and high (**g**) dilutions. Initial value is expressed as a portion of the measurement range when the linear regression is extrapolated to zero minutes and is shown for low (**d**) and high (**h**) dilutions. The pink box in graphs **d** and **h** indicate the region that is included by the *mean* ± *SD* of all the initial values and gives an indication of outliers when values lie outside this region. Red and purple bars in **c-d, g-h** are indicated at the measured dilution as the two choices for the TBI analysis.

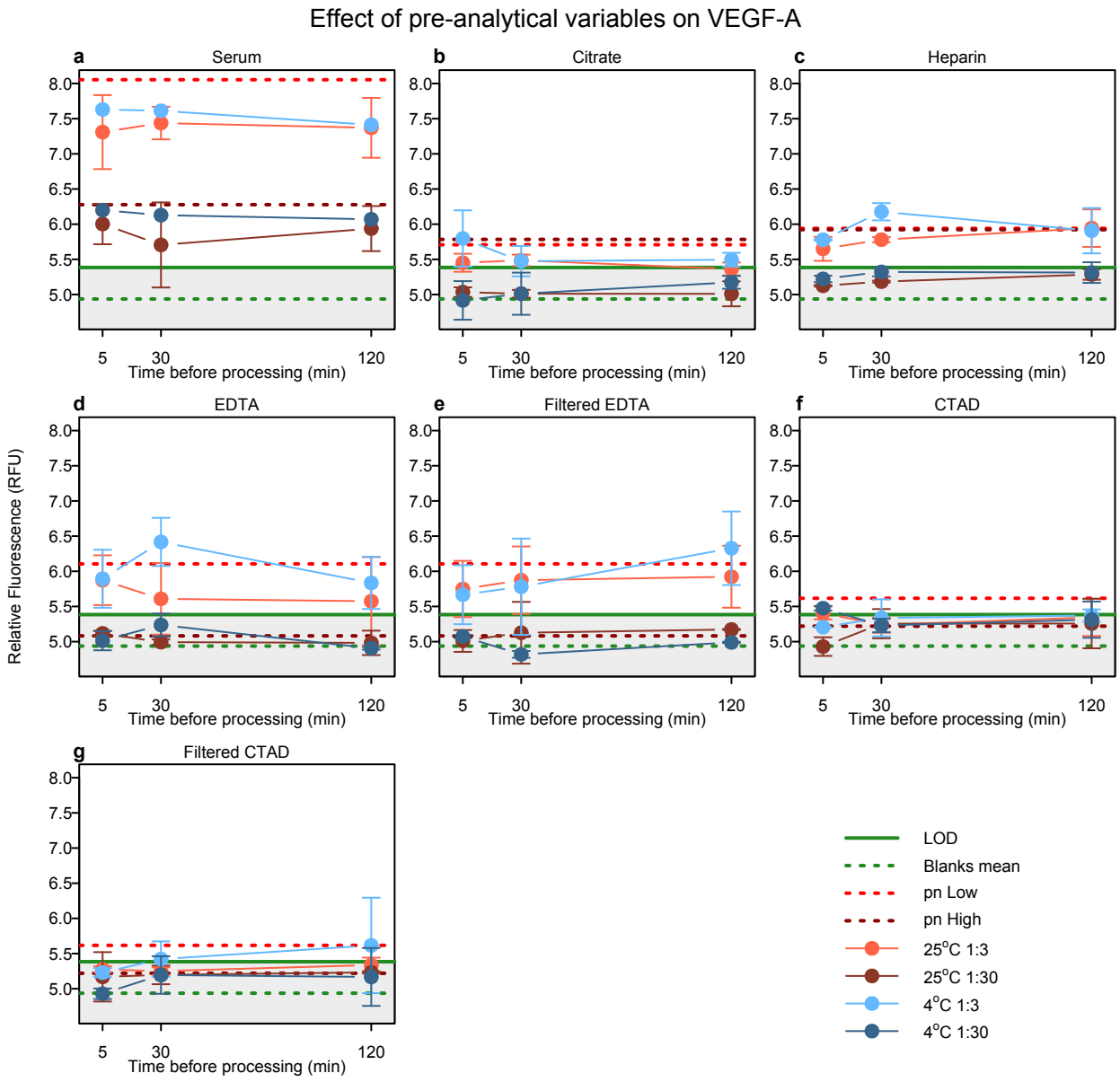

FIGURE I.S191: **Effect of blood collection tube on VEGF-A stability and concentration.** Effects of blood collection tubes (**a**: serum, **b**: citrate, **c**: heparin, **d-e**: EDTA, **f-g**: CTAD), storage temperature and time before processing, and post-processing plasma filtering (**e, g**) on the initial value and pre-processing time stability of VEGF-A measurements in blood. Information on the dilution of samples used for measuring, data range and the sample type selected are also shown.

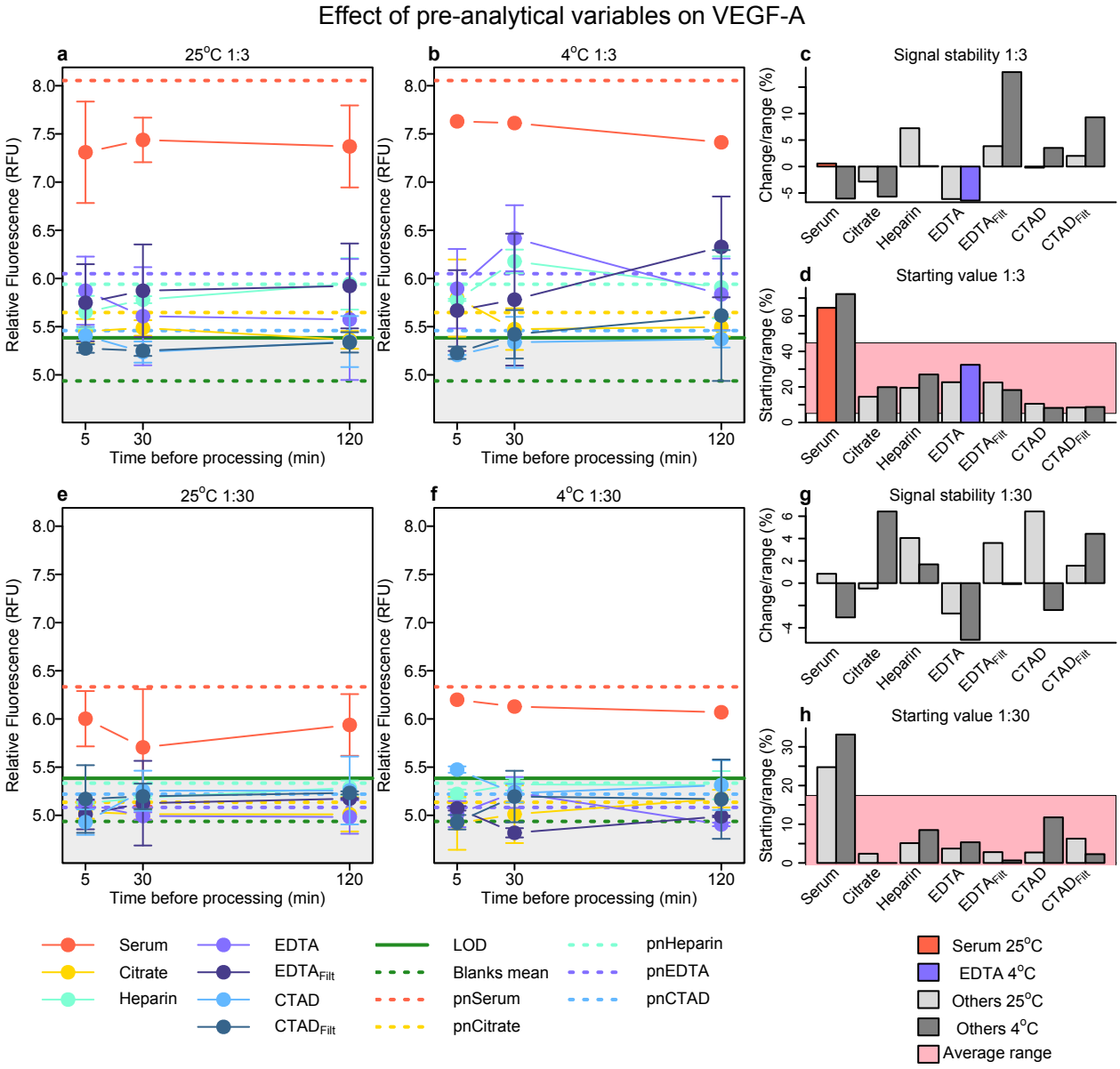

FIGURE I.S192: **Effect of pre-processing storage temperature on VEGF-A stability and concentration.** Initial measured value and stability of VEGF-A when stored at 25 °C (**a, e**) and 4 °C (**b, f**) before processing when collected in different tube types. The measured values are shown at low dilution of 1:3 (**a-b**) and high dilution of 1:30 (**e-f**). Stability before processing is expressed as an increase or decrease compared to the measurement range and is shown for low (**c**) and high (**g**) dilutions. Initial value is expressed as a portion of the measurement range when the linear regression is extrapolated to zero minutes and is shown for low (**d**) and high (**h**) dilutions. The pink box in graphs **d** and **h** indicate the region that is included by the *mean* ± *SD* of all the initial values and gives an indication of outliers when values lie outside this region. Red and purple bars in **c-d, g-h** are indicated at the measured dilution as the two choices for the TBI analysis.

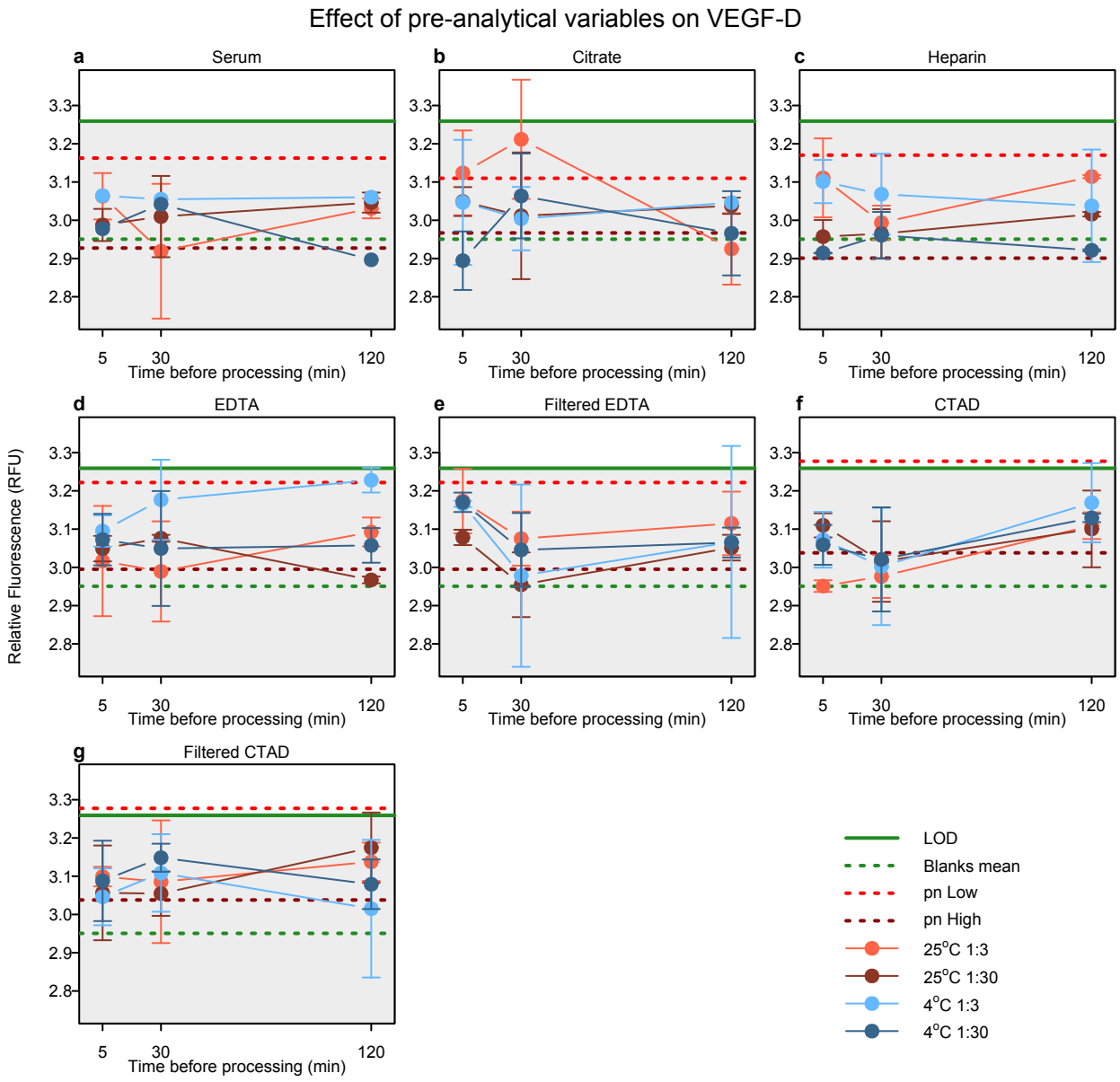

FIGURE I.S193: **Effect of blood collection tube on VEGF-D stability and concentration.** Effects of blood collection tubes (**a**: serum, **b**: citrate, **c**: heparin, **d-e**: EDTA, **f-g**: CTAD), storage temperature and time before processing, and post-processing plasma filtering (**e, g**) on the initial value and pre-processing time stability of VEGF-D measurements in blood. Information on the dilution of samples used for measuring, data range and the sample type selected are also shown.

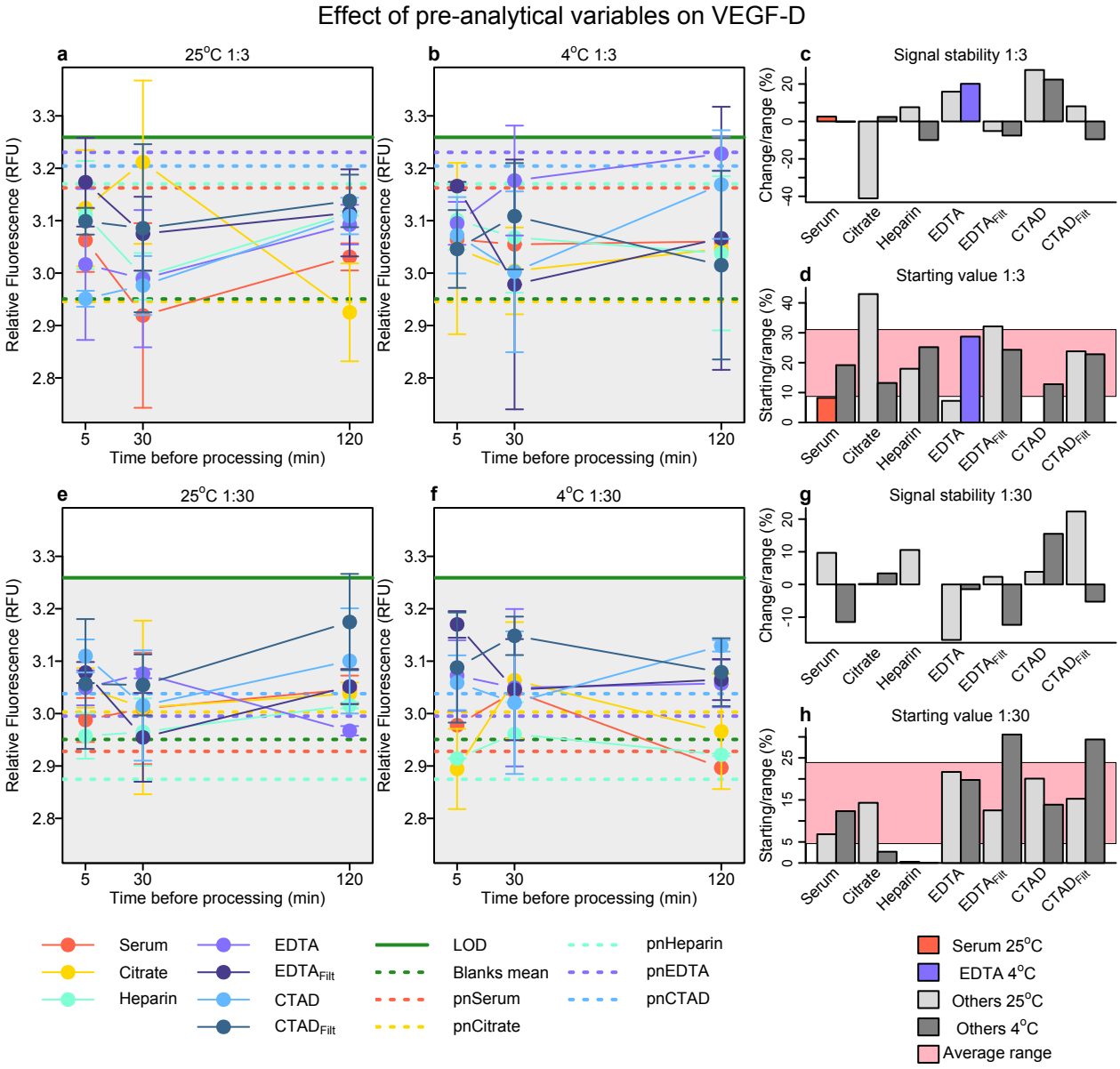

FIGURE I.S194: **Effect of pre-processing storage temperature on VEGF-D stability and concentration.** Initial measured value and stability of VEGF-D when stored at 25 °C (**a, e**) and 4 °C (**b, f**) before processing when collected in different tube types. The measured values are shown at low dilution of 1:3 (**a-b**) and high dilution of 1:30 (**e-f**). Stability before processing is expressed as an increase or decrease compared to the measurement range and is shown for low (**c**) and high (**g**) dilutions. Initial value is expressed as a portion of the measurement range when the linear regression is extrapolated to zero minutes and is shown for low (**d**) and high (**h**) dilutions. The pink box in graphs **d** and **h** indicate the region that is included by the *mean* ± *SD* of all the initial values and gives an indication of outliers when values lie outside this region. Red and purple bars in **c-d, g-h** are indicated at the measured dilution as the two choices for the TBI analysis.

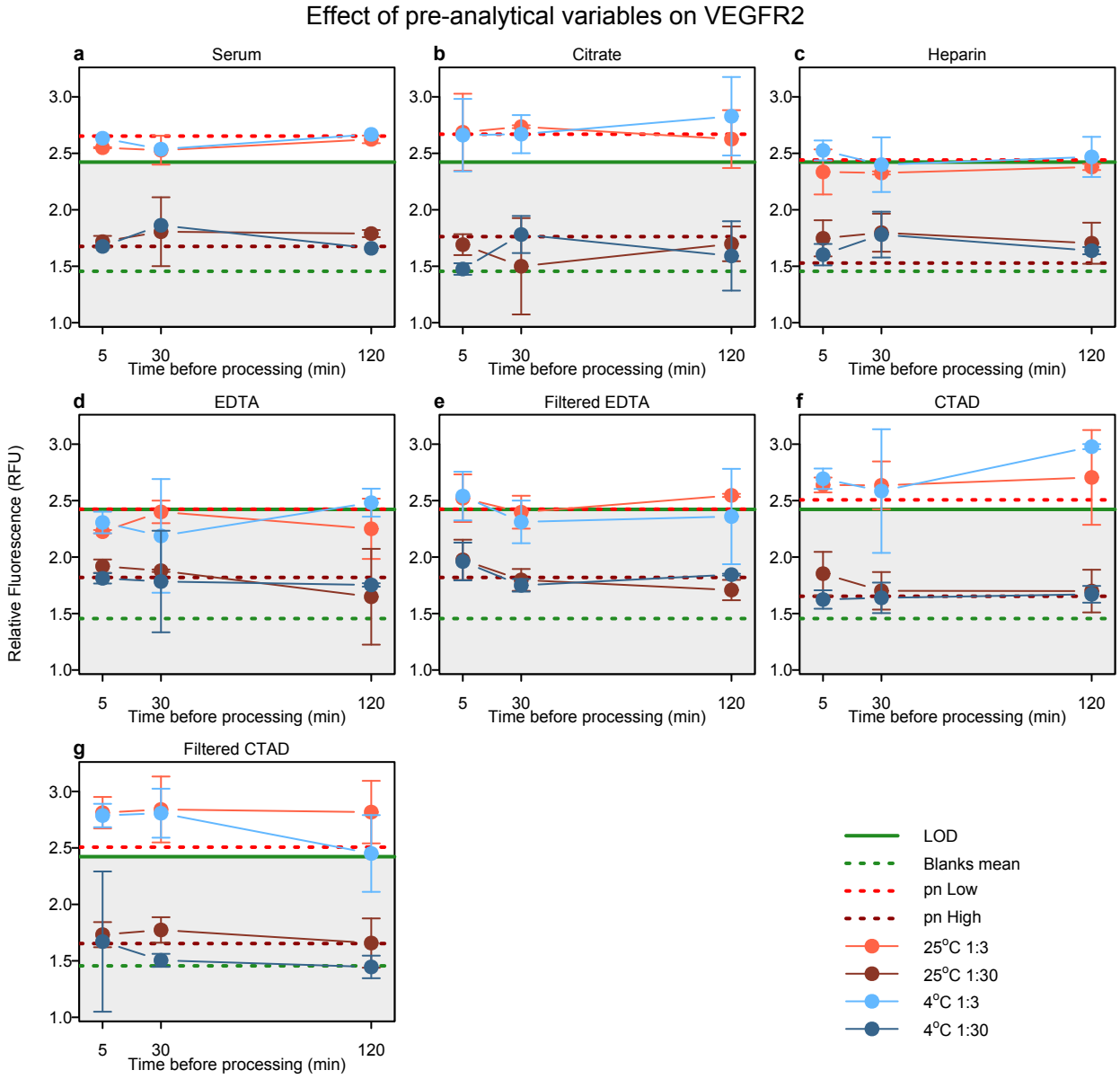

FIGURE I.S195: **Effect of blood collection tube on VEGFR2 stability and concentration.** Effects of blood collection tubes (**a**: serum, **b**: citrate, **c**: heparin, **d-e**: EDTA, **f-g**: CTAD), storage temperature and time before processing, and post-processing plasma filtering (**e, g**) on the initial value and pre-processing time stability of VEGFR2 measurements in blood. Information on the dilution of samples used for measuring, data range and the sample type selected are also shown.

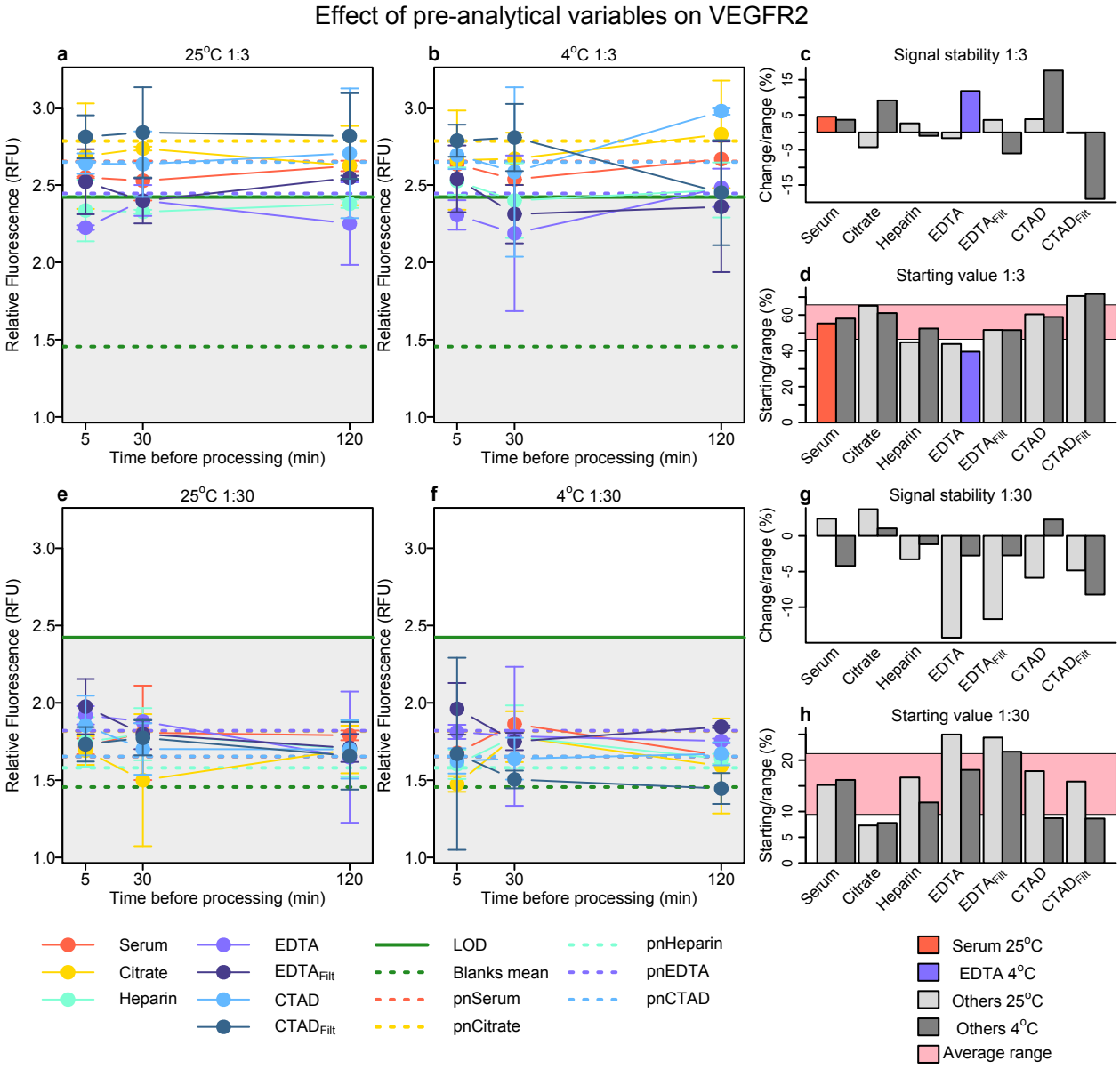

FIGURE I.S196: **Effect of pre-processing storage temperature on VEGFR2 stability and concentration.** Initial measured value and stability of VEGFR2 when stored at 25 °C (**a, e**) and 4 °C (**b, f**) before processing when collected in different tube types. The measured values are shown at low dilution of 1:3 (**a-b**) and high dilution of 1:30 (**e-f**). Stability before processing is expressed as an increase or decrease compared to the measurement range and is shown for low (**c**) and high (**g**) dilutions. Initial value is expressed as a portion of the measurement range when the linear regression is extrapolated to zero minutes and is shown for low (**d**) and high (**h**) dilutions. The pink box in graphs **d** and **h** indicate the region that is included by the *mean* ± *SD* of all the initial values and gives an indication of outliers when values lie outside this region. Red and purple bars in **c-d, g-h** are indicated at the measured dilution as the two choices for the TBI analysis.

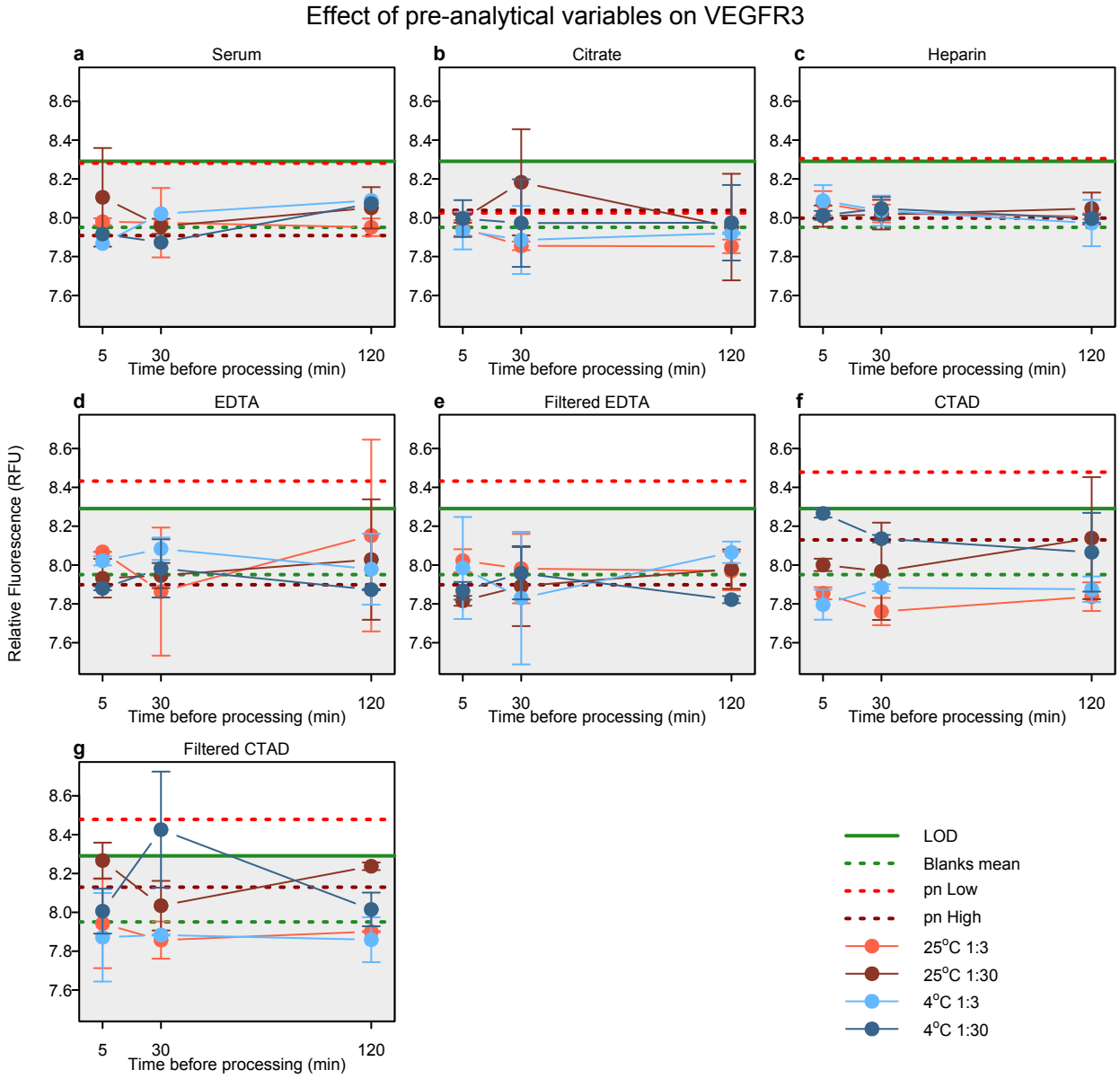

FIGURE I.S197: **Effect of blood collection tube on VEGFR3 stability and concentration.** Effects of blood collection tubes (**a**: serum, **b**: citrate, **c**: heparin, **d-e**: EDTA, **f-g**: CTAD), storage temperature and time before processing, and post-processing plasma filtering (**e, g**) on the initial value and pre-processing time stability of VEGFR3 measurements in blood. Information on the dilution of samples used for measuring, data range and the sample type selected are also shown.

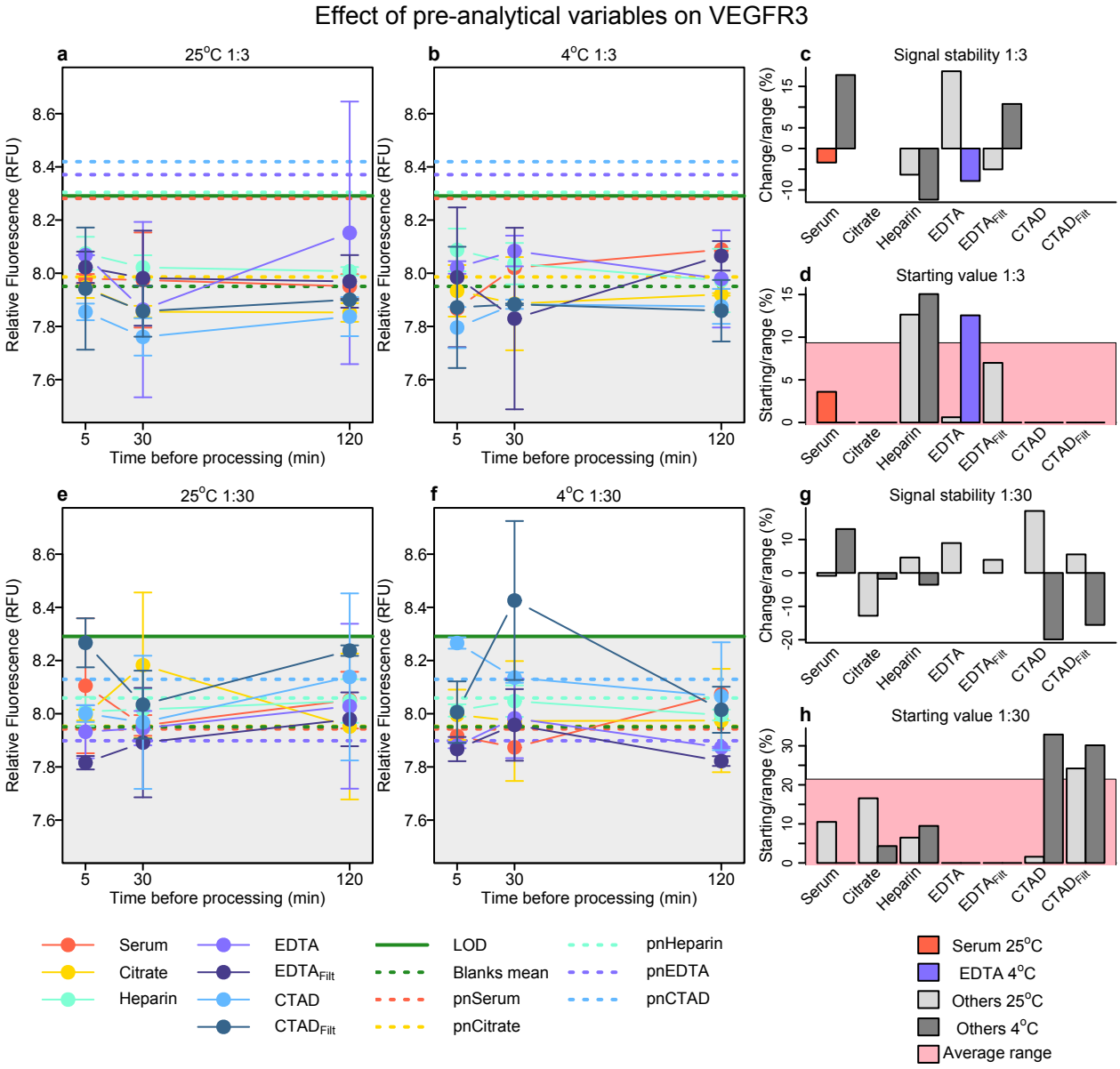

FIGURE I.S198: **Effect of pre-processing storage temperature on VEGFR3 stability and concentration.** Initial measured value and stability of VEGFR3 when stored at 25 °C (**a, e**) and 4 °C (**b, f**) before processing when collected in different tube types. The measured values are shown at low dilution of 1:3 (**a-b**) and high dilution of 1:30 (**e-f**). Stability before processing is expressed as an increase or decrease compared to the measurement range and is shown for low (**c**) and high (**g**) dilutions. Initial value is expressed as a portion of the measurement range when the linear regression is extrapolated to zero minutes and is shown for low (**d**) and high (**h**) dilutions. The pink box in graphs **d** and **h** indicate the region that is included by the *mean* ± *SD* of all the initial values and gives an indication of outliers when values lie outside this region. Red and purple bars in **c-d, g-h** are indicated at the measured dilution as the two choices for the TBI analysis.

TABLE I.S1: **Pre-analytical variables linear regression parameters in serum samples, low dilution.**

		Data	Blanks	Serum low dilution, 4 °C						Serum low dilution, 25 °C					
	Protein name	range (RFU)	mean (RFU)	Intercept (RFU)	Slope (RFU/min)	R^2	Span (RFU)	Increase (%)	Starting (%)	Intercept (RFU)	Slope (RFU/h)	R^2	Span (RFU)	Increase (%)	Starting (%)
1	AFP	3.35	1.56	2.3835	-0.0029	0.8143	0.3775	-11.57	28.26	2.2674	-0.0002	0.0076	0.1079	-0.6	24.28
2	AHSG	4.1	6.77	-	-	-	-	-	-	-	-	-	-	-	-
3	ALDH1L1	1.05	3.32	-	-	-	-	-	-	-	-	-	-	-	-
4	Amphiregulin	2.28	4.01	4.3693	-0.0001	0.0614	0.0588	-0.79	18.52	-	-	-	-	-	-
5	Ang1	3.33	0.96	3.6505	-0.0018	0.9364	0.2028	-7.5	96.03	3.5222	0	0.0001	0.0743	0.1	91.45
6	Ang2	0.88	5.07	-	-	-	-	-	-	-	-	-	-	-	-
8	BDNF	2.62	1.93	-	-	-	-	-	-	-	-	-	-	-	-
9	BMP2	0.78	3.25	-	-	-	-	-	-	-	-	-	-	-	-
10	BRAF	0.94	5.21	-	-	-	-	-	-	-	-	-	-	-	-
11	c-Kit	3.19	5.95	7.515	-0.0014	0.3984	0.2621	-5.62	55.32	7.4914	0.0001	0.002	0.0978	0.5	54.49
12	CA15-3	2.87	-1.56	-0.0607	-0.0042	0.4188	0.7847	-20.58	63.24	-0.4079	0.001	0.0139	0.2186	4.95	48.58
13	Cathepsin B	0.79	4.9	-	-	-	-	-	-	-	-	-	-	-	-
14	CCL5	3.76	7.11	-	-	-	-	-	-	-	-	-	-	-	-
15	CD14	4.06	-4.55	-2.3557	-0.0039	0.9899	0.4283	-15.24	75.57	-2.5458	0.0013	0.1903	0.1944	5.05	69.03
16	CEA	1.37	5.65	5.8755	0.0019	0.9953	0.2183	23.61	24.46	5.9443	0.0003	0.2719	0.0422	3.8	32.06
17	CRP	0.89	-1.03	-	-	-	-	-	-	-	-	-	-	-	-
18	CXCL12	1.43	6.56	-	-	-	-	-	-	-	-	-	-	-	-
19	E-cadherin	2.44	5.61	6.7196	0	0.0072	0.0243	-0.1	53.82	6.6865	-0.0007	0.2961	0.1055	-4.13	52.21
20	E-selectin	2.11	1.25	2.0869	-0.0019	0.4653	0.3346	-15.46	59.25	2.0423	-0.0001	0.0023	0.0365	-0.43	56.09
21	EGF	3.86	5.84	6.9242	-0.0015	0.6108	0.2388	-5.2	31.7	7.1407	0.0112	0.7985	1.3852	37.52	38.03
22	EGF-R	3.67	-2.28	0.5829	-0.0008	0.9992	0.0888	-2.75	89.41	0.5915	-0.0019	0.511	0.2411	-6.79	89.68
23	Endoglin	1.85	0.65	1.5757	-0.0003	0.0647	0.1413	-3	72.62	1.4427	-0.0006	0.1463	0.0844	-5.1	62.18
24	EpCAM	1.87	6.17	-	-	-	-	-	-	-	-	-	-	-	-
25	FAS	2.74	4.38	5.626	-0.0025	0.4291	0.4598	-12.04	52	5.3194	0.0011	0.0192	0.1558	5.2	39.2
26	FAS-L	1.18	-0.73	-0.2971	-0.0019	0.7529	0.2529	-27.65	55.79	-	-	-	-	-	-
28	FGFb	1.24	5.22	5.519	0.0003	0.8536	0.0414	4.13	31.68	5.5046	-0.0005	0.031	0.0831	-6.13	30.14
29	Flt-3	1.49	6.2	-	-	-	-	-	-	-	-	-	-	-	-
30	G-CSF	2.39	0.8	-	-	-	-	-	-	-	-	-	-	-	-
31	GFAP	2.62	0.12	0.9287	-0.0007	0.1641	0.1803	-3.42	36.28	0.906	0.0008	0.109	0.1154	4.07	35.26
32	GM-CSF	1.87	5.53	-	-	-	-	-	-	-	-	-	-	-	-
33	GRO-α	2.43	-8.01	-	-	-	-	-	-	-	-	-	-	-	-
34	HAI-1	1.98	5.42	5.786	-0.0001	0.0589	0.0615	-0.91	21.14	-	-	-	-	-	-
35	HE4	0.81	4.23	-	-	-	-	-	-	-	-	-	-	-	-
36	HER2	1.45	5.92	-	-	-	-	-	-	-	-	-	-	-	-
37	HER3	1.17	5.47	-	-	-	-	-	-	-	-	-	-	-	-
38	HGF	3.7	3.99	5.1171	-0.002	0.3011	0.4312	-6.74	32.55	4.8988	0.0002	0.0013	0.0228	0.7	26.23
39	HGF-R	3.75	1.35	4.2561	-0.0019	0.5035	0.3156	-6.7	91.36	4.0773	-0.0001	0.0004	0.2123	-0.32	85.74
40	HMGB1	1.11	1.01	-	-	-	-	-	-	-	-	-	-	-	-
41	HP	2.94	0.72	1.0752	-0.0008	0.1004	0.2504	-3.18	13.11	1.2533	-0.0025	0.3945	0.4425	-10.42	19.64
42	ICAM-1	4.35	-6.8	-4.6819	-0.0042	0.6563	0.6273	-13.28	57.98	-4.1027	-0.0005	0.0017	0.0942	-1.49	73.81
43	IFN-γ	1.63	1.13	-	-	-	-	-	-	-	-	-	-	-	-
44	IGFBP-1	3.52	4.77	7.298	0.001	0.7961	0.1271	3.44	77.96	7.3222	0.0012	0.2391	0.164	4.17	78.7
45	IGFBP-3	3.28	5.26	7.8946	-0.0001	0.0416	0.0398	-0.26	88.75	7.8733	0.0004	0.0967	0.0541	1.48	88.04
46	IGFBP-7	3.65	5.86	8.3873	0.0001	0.0179	0.0984	0.39	79.11	8.3654	0.0004	0.0355	0.071	1.31	78.42
47	IL-10	3	7.75	8.3964	-0.0011	0.3741	0.2176	-5.43	27.15	-	-	-	-	-	-
48	IL-12	2.4	-6.24	-	-	-	-	-	-	-	-	-	-	-	-
49	IL-15	2.34	6.06	-	-	-	-	-	-	-	-	-	-	-	-

Table I.S1 continued from previous page

	Protein name	Data range (RFU)	Blanks mean (RFU)	Serum low dilution, 4 °C						Serum low dilution, 25 °C					
				Intercept (RFU)	Slope (RFU/min)	R^2	Span (RFU)	Increase (%)	Starting (%)	Intercept (RFU)	Slope (RFU/h)	R^2	Span (RFU)	Increase (%)	Starting (%)
50	IL-18	2.91	-4.12	-2.6464	-0.0006	0.9535	0.0771	-3.31	67.73	-2.8398	-0.0003	0.0066	0.2885	-1.64	58.85
51	IL-1β	3.12	4.31	5.1507	-0.0022	0.5327	0.3592	-8.74	29.3	4.7763	-0.0007	0.0045	0.0741	-2.75	16.18
52	IL-1ra	2.24	-0.15	0.1469	-0.0015	0.556	0.2404	-9.1	16.12	-	-	-	-	-	-
53	IL-2	2.27	5.78	-	-	-	-	-	-	-	-	-	-	-	-
54	IL-3	2.37	-2.51	-	-	-	-	-	-	-	-	-	-	-	-
55	IL-4	1.26	3.71	-	-	-	-	-	-	-	-	-	-	-	-
56	IL-5	1.48	5.49	-	-	-	-	-	-	-	-	-	-	-	-
58	IL-7	2.47	-0.02	-	-	-	-	-	-	-	-	-	-	-	-
59	IL-8	2.22	0.05	-	-	-	-	-	-	-	-	-	-	-	-
60	IP-10	3.05	6.62	7.2345	-0.0021	0.3337	0.4312	-9.54	24.09	-	-	-	-	-	-
61	KLK14	2.82	-0.67	-	-	-	-	-	-	-	-	-	-	-	-
62	KLK8	0.79	5.1	-	-	-	-	-	-	-	-	-	-	-	-
63	Leptin	0.82	5.21	-	-	-	-	-	-	-	-	-	-	-	-
64	M-CSF	2.29	1.71	-	-	-	-	-	-	-	-	-	-	-	-
65	MCP1	1.1	5.53	-	-	-	-	-	-	-	-	-	-	-	-
66	MCP2	3.57	4.43	-	-	-	-	-	-	-	-	-	-	-	-
67	MCP3	2.73	6.63	-	-	-	-	-	-	-	-	-	-	-	-
68	MCP4	2.8	8.09	-	-	-	-	-	-	-	-	-	-	-	-
69	MIG	2.61	-1.78	-	-	-	-	-	-	-	-	-	-	-	-
70	MIP-1α	2.09	1.61	2.2223	-0.0008	0.9446	0.0878	-5.2	34.51	2.0626	-0.0002	0.001	0.1141	-0.98	25.5
71	MIP-1β	1.14	6.24	-	-	-	-	-	-	-	-	-	-	-	-
72	MMP-1	1.86	2.78	3.6453	-0.0011	0.9859	0.1193	-8.23	57.14	3.3842	-0.0008	0.0146	0.2004	-6.48	39.83
73	MMP-3	3.57	0.52	2.779	-0.0007	0.1579	0.203	-3.03	80.85	2.7711	-0.0009	0.1744	0.1681	-3.82	80.57
74	MMP-9	4.52	5.28	7.5918	-0.0015	0.7548	0.2041	-4.05	54.16	7.8071	0.0009	0.0285	0.1342	2.3	59.21
75	NCAM-1	2.76	4.08	6.4486	-0.0004	0.0395	0.1999	-1.66	95.69	6.2756	-0.0006	0.0305	0.0761	-2.89	88.71
76	NT-3	2.37	3.96	-	-	-	-	-	-	-	-	-	-	-	-
77	OPN	3.69	5.59	7.1917	-0.0002	0.1908	0.0629	-0.81	46.21	7.3446	0.0025	0.4927	0.3701	8.15	50.62
78	PAI-1	1.8	2.55	3.0239	0.0002	0.2735	0.0385	1.36	32.09	2.8877	0.0004	0.055	0.1219	3.47	22.95
79	PDGF-BB	3.59	5.72	7.3285	-0.0021	0.6691	0.2989	-7.27	48.01	7.5459	-0.0044	0.734	0.5273	-15.23	54.52
80	PRL	0.83	1.43	-	-	-	-	-	-	-	-	-	-	-	-
81	PSA	2.89	0.44	-	-	-	-	-	-	-	-	-	-	-	-
82	RBP4	0.82	5.18	-	-	-	-	-	-	-	-	-	-	-	-
83	S100B	1.21	2	-	-	-	-	-	-	-	-	-	-	-	-
85	SPARC	2.28	4.96	5.6762	-0.0016	0.9967	0.1763	-9.02	35.81	5.7215	-0.0002	0.0361	0.0269	-1.07	38.08
86	TF	1.72	1.93	-	-	-	-	-	-	-	-	-	-	-	-
87	TGF-α	2.36	4.12	-	-	-	-	-	-	-	-	-	-	-	-
88	TGF-β RII	2.45	4.3	-	-	-	-	-	-	-	-	-	-	-	-
89	TGF-β1	2.84	3.55	5.6033	-0.0021	0.8594	0.2688	-9.37	80.88	5.5639	-0.0027	0.4026	0.4081	-12.21	79.33
90	TGF-β2	1.64	5.81	-	-	-	-	-	-	-	-	-	-	-	-
91	THBS-1	3.71	0.26	3.1019	0	0.0011	0.1487	0.15	88.95	3.1206	0.0003	0.0516	0.0979	1.2	89.54
92	Tie-2	1.35	1.56	-	-	-	-	-	-	-	-	-	-	-	-
93	TIMP-1	2.51	5.71	6.3948	0.0007	0.8564	0.0975	4.07	32.39	6.6306	-0.0002	0.0044	0.0199	-0.86	43.54
94	TNF-α	2.12	2.04	-	-	-	-	-	-	-	-	-	-	-	-
95	TNF-RI	2.44	2.98	4.5803	-0.0021	0.9883	0.2383	-11.91	77.17	4.2862	0.0005	0.0149	0.0577	2.9	63
96	TNF-RII	3.3	-2.13	0.1623	-0.0033	0.5812	0.5243	-13.87	83.69	-0.1531	0.0013	0.083	0.2375	5.36	72.18
97	uPA	2.28	2.53	4.0459	-0.0001	0.0246	0.1013	-0.85	79.46	3.884	-0.001	0.13	0.1892	-6.04	70.96
98	uPA-R	2.38	6.54	-	-	-	-	-	-	-	-	-	-	-	-
99	VCAM-1	4.35	0.2	3.4472	-0.0016	0.2282	0.3919	-5	86.14	3.3154	0.0001	0.0003	0.1699	0.24	82.65
100	VEGF-A	4.09	4.94	7.654	-0.002	0.982	0.2176	-6.06	72.26	7.3625	0.0002	0.001	0.1282	0.57	64.51

Table I.S1 continued from previous page

	Protein name	Data range (RFU)	Blanks mean (RFU)	Serum low dilution, 4 °C						Serum low dilution, 25 °C					
				Intercept (RFU)	Slope (RFU/min)	R^2	Span (RFU)	Increase (%)	Starting (%)	Intercept (RFU)	Slope (RFU/h)	R^2	Span (RFU)	Increase (%)	Starting (%)
101	VEGF-D	0.98	2.95	-	-	-	-	-	-	-	-	-	-	-	-
102	VEGFR2	2.98	1.46	2.5814	0.0006	0.2905	0.1312	3.59	58.03	2.5279	0.0008	0.3023	0.0959	4.47	55.27
103	VEGFR3	1.24	7.95	-	-	-	-	-	-	-	-	-	-	-	-

TABLE I.S2: **Pre-analytical variables linear regression parameters in serum samples, high dilution.**

	Protein name	Data range (RFU)	Blanks mean (RFU)	Serum high dilution, 4 °C						Serum high dilution, 25 °C					
				Intercept (RFU)	Slope (RFU/min)	R^2	Span (RFU)	Increase (%)	Starting (%)	Intercept (RFU)	Slope (RFU/h)	R^2	Span (RFU)	Increase (%)	Starting (%)
1	AFP	3.35	1.56	-	-	-	-	-	-	-	-	-	-	-	-
2	AHSG	4.1	6.77	-	-	-	-	-	-	-	-	-	-	-	-
3	ALDH1L1	1.05	3.32	-	-	-	-	-	-	-	-	-	-	-	-
4	Amphiregulin	2.28	4.01	-	-	-	-	-	-	-	-	-	-	-	-
5	Ang1	3.33	0.96	3.0088	-0.0012	0.7858	0.1682	-5.13	73.1	3.1505	-0.0014	0.0658	0.3315	-5.79	78.17
6	Ang2	0.88	5.07	-	-	-	-	-	-	-	-	-	-	-	-
8	BDNF	2.62	1.93	-	-	-	-	-	-	-	-	-	-	-	-
9	BMP2	0.78	3.25	-	-	-	-	-	-	-	-	-	-	-	-
10	BRAF	0.94	5.21	-	-	-	-	-	-	-	-	-	-	-	-
11	c-Kit	3.19	5.95	6.7052	0.0019	0.4728	0.3384	7.83	26.75	6.955	-0.0021	0.151	0.4085	-8.43	35.56
12	CA15-3	2.87	-1.56	-	-	-	-	-	-	-	-	-	-	-	-
13	Cathepsin B	0.79	4.9	-	-	-	-	-	-	-	-	-	-	-	-
14	CCL5	3.76	7.11	-	-	-	-	-	-	-	-	-	-	-	-
15	CD14	4.06	-4.55	-2.5668	-0.0011	0.5421	0.1821	-4.39	68.31	-2.4902	-0.001	0.093	0.1318	-4.09	70.95
16	CEA	1.37	5.65	-	-	-	-	-	-	-	-	-	-	-	-
17	CRP	0.89	-1.03	-	-	-	-	-	-	-	-	-	-	-	-
18	CXCL12	1.43	6.56	-	-	-	-	-	-	6.8619	0.0016	0.0872	0.1914	18.06	30.53
19	E-cadherin	2.44	5.61	6.0876	-0.0009	0.9779	0.0974	-4.98	23.08	6.0359	0.0009	0.0832	0.1769	5.05	20.57
20	E-selectin	2.11	1.25	-	-	-	-	-	-	-	-	-	-	-	-
21	EGF	3.86	5.84	-	-	-	-	-	-	6.3587	0.0073	0.7764	0.7826	24.52	15.17
22	EGF-R	3.67	-2.28	-0.5398	0.0012	0.7991	0.1515	4.17	54.3	-0.196	-0.0005	0.0057	0.5859	-1.95	65.05
23	Endoglin	1.85	0.65	-	-	-	-	-	-	-	-	-	-	-	-
24	EpCAM	1.87	6.17	-	-	-	-	-	-	-	-	-	-	-	-
25	FAS	2.74	4.38	-	-	-	-	-	-	-	-	-	-	-	-
26	FAS-L	1.18	-0.73	-	-	-	-	-	-	-	-	-	-	-	-
28	FGFb	1.24	5.22	5.4294	0.0004	1	0.0434	4.64	22.09	-	-	-	-	-	-
29	Flt-3	1.49	6.2	-	-	-	-	-	-	-	-	-	-	-	-
30	G-CSF	2.39	0.8	-	-	-	-	-	-	-	-	-	-	-	-
31	GFAP	2.62	0.12	-	-	-	-	-	-	-	-	-	-	-	-
32	GM-CSF	1.87	5.53	-	-	-	-	-	-	-	-	-	-	-	-
33	GRO-α	2.43	-8.01	-	-	-	-	-	-	-	-	-	-	-	-
34	HAI-1	1.98	5.42	-	-	-	-	-	-	-	-	-	-	-	-
35	HE4	0.81	4.23	-	-	-	-	-	-	-	-	-	-	-	-
36	HER2	1.45	5.92	-	-	-	-	-	-	-	-	-	-	-	-
37	HER3	1.17	5.47	-	-	-	-	-	-	5.8689	-0.0022	0.1903	0.3445	-30.01	47.07
38	HGF	3.7	3.99	-	-	-	-	-	-	-	-	-	-	-	-
39	HGF-R	3.75	1.35	3.2787	0.0005	0.9976	0.0613	1.96	60.63	3.4888	-0.0014	0.3563	0.1725	-5.12	67.24

Table I.S2 continued from previous page

		Data	Blanks	Serum high dilution, 4 °C						Serum high dilution, 25 °C					
	Protein name	range (RFU)	mean (RFU)	Intercept (RFU)	Slope (RFU/min)	R^2	Span (RFU)	Increase (%)	Starting (%)	Intercept (RFU)	Slope (RFU/h)	R^2	Span (RFU)	Increase (%)	Starting (%)
40	HMGB1	1.11	1.01	-	-	-	-	-	-	-	-	-	-	-	-
41	HP	2.94	0.72	-	-	-	-	-	-	-	-	-	-	-	-
42	ICAM-1	4.35	-6.8	-5.2738	-0.0013	0.9953	0.1459	-4.08	41.8	-5.0996	-0.004	0.1727	0.4825	-12.66	46.56
43	IFN-γ	1.63	1.13	-	-	-	-	-	-	-	-	-	-	-	-
44	IGFBP-1	3.52	4.77	7.3085	0.0005	0.3172	0.1051	1.78	78.28	7.4107	-0.0008	0.085	0.1205	-2.98	81.43
45	IGFBP-3	3.28	5.26	7.2676	0.0004	0.9128	0.0474	1.45	67.67	7.233	-0.001	0.4585	0.1205	-3.8	66.5
46	IGFBP-7	3.65	5.86	8.0116	-0.0012	0.9588	0.1483	-4.35	67.34	7.9812	-0.0025	0.3703	0.3191	-8.92	66.39
47	IL-10	3	7.75	-	-	-	-	-	-	-	-	-	-	-	-
48	IL-12	2.4	-6.24	-	-	-	-	-	-	-	-	-	-	-	-
49	IL-15	2.34	6.06	-	-	-	-	-	-	-	-	-	-	-	-
50	IL-18	2.91	-4.12	-	-	-	-	-	-	-	-	-	-	-	-
51	IL-1β	3.12	4.31	-	-	-	-	-	-	-	-	-	-	-	-
52	IL-1ra	2.24	-0.15	-	-	-	-	-	-	-	-	-	-	-	-
53	IL-2	2.27	5.78	-	-	-	-	-	-	-	-	-	-	-	-
54	IL-3	2.37	-2.51	-	-	-	-	-	-	-	-	-	-	-	-
55	IL-4	1.26	3.71	-	-	-	-	-	-	-	-	-	-	-	-
56	IL-5	1.48	5.49	-	-	-	-	-	-	-	-	-	-	-	-
58	IL-7	2.47	-0.02	-	-	-	-	-	-	-	-	-	-	-	-
59	IL-8	2.22	0.05	-	-	-	-	-	-	-	-	-	-	-	-
60	IP-10	3.05	6.62	-	-	-	-	-	-	7.0401	0.0015	0.0662	0.2015	6.9	16.45
61	KLK14	2.82	-0.67	0.658	-0.0087	0.2732	1.9379	-42.58	56.4	0.2243	0.0014	0.0043	0.1674	7	38.01
62	KLK8	0.79	5.1	-	-	-	-	-	-	-	-	-	-	-	-
63	Leptin	0.82	5.21	-	-	-	-	-	-	-	-	-	-	-	-
64	M-CSF	2.29	1.71	-	-	-	-	-	-	-	-	-	-	-	-
65	MCP1	1.1	5.53	-	-	-	-	-	-	-	-	-	-	-	-
66	MCP2	3.57	4.43	-	-	-	-	-	-	-	-	-	-	-	-
67	MCP3	2.73	6.63	-	-	-	-	-	-	-	-	-	-	-	-
68	MCP4	2.8	8.09	-	-	-	-	-	-	-	-	-	-	-	-
69	MIG	2.61	-1.78	-	-	-	-	-	-	-	-	-	-	-	-
70	MIP-1α	2.09	1.61	-	-	-	-	-	-	-	-	-	-	-	-
71	MIP-1β	1.14	6.24	-	-	-	-	-	-	-	-	-	-	-	-
72	MMP-1	1.86	2.78	-	-	-	-	-	-	-	-	-	-	-	-
73	MMP-3	3.57	0.52	2.0024	0.0002	0.4448	0.0371	0.97	52.99	2.0862	-0.0011	0.0608	0.2531	-4.43	56
74	MMP-9	4.52	5.28	8.1617	0.0007	0.1696	0.1967	1.97	67.54	8.5831	-0.0014	0.0292	0.4204	-3.87	77.43
75	NCAM-1	2.76	4.08	5.6642	0.0005	0.6696	0.0667	2.19	64.06	5.6463	-0.0016	0.4842	0.2115	-7.58	63.33
76	NT-3	2.37	3.96	-	-	-	-	-	-	4.4277	0.0036	0.0569	0.4923	22.84	26
77	OPN	3.69	5.59	6.2906	-0.0004	0.9541	0.0536	-1.44	20.21	6.4269	0.0009	0.1652	0.1164	2.86	24.14
78	PAI-1	1.8	2.55	-	-	-	-	-	-	-	-	-	-	-	-
79	PDGF-BB	3.59	5.72	6.5349	-0.0033	0.2517	0.7626	-11.44	24.28	6.4564	0.0028	0.054	0.3288	9.66	21.93
80	PRL	0.83	1.43	-	-	-	-	-	-	-	-	-	-	-	-
81	PSA	2.89	0.44	-	-	-	-	-	-	-	-	-	-	-	-
82	RBP4	0.82	5.18	-	-	-	-	-	-	-	-	-	-	-	-
83	S100B	1.21	2	-	-	-	-	-	-	-	-	-	-	-	-
85	SPARC	2.28	4.96	-	-	-	-	-	-	-	-	-	-	-	-
86	TF	1.72	1.93	-	-	-	-	-	-	-	-	-	-	-	-
87	TGF-α	2.36	4.12	-	-	-	-	-	-	-	-	-	-	-	-
88	TGF-β RII	2.45	4.3	-	-	-	-	-	-	-	-	-	-	-	-
89	TGF-β1	2.84	3.55	4.2236	-0.0021	0.7088	0.3044	-9.74	26.44	-	-	-	-	-	-
90	TGF-β2	1.64	5.81	-	-	-	-	-	-	-	-	-	-	-	-

Table I.S2 continued from previous page

	Protein name	Data range (RFU)	Blanks mean (RFU)	Serum high dilution, 4 °C						Serum high dilution, 25 °C					
				Intercept (RFU)	Slope (RFU/min)	R^2	Span (RFU)	Increase (%)	Starting (%)	Intercept (RFU)	Slope (RFU/h)	R^2	Span (RFU)	Increase (%)	Starting (%)
91	THBS-1	3.71	0.26	3.1725	-0.0002	0.0611	0.107	-0.88	91.16	3.1503	0.0012	0.267	0.1426	4.41	90.46
92	Tie-2	1.35	1.56	-	-	-	-	-	-	-	-	-	-	-	-
93	TIMP-1	2.51	5.71	-	-	-	-	-	-	-	-	-	-	-	-
94	TNF-α	2.12	2.04	-	-	-	-	-	-	-	-	-	-	-	-
95	TNF-RI	2.44	2.98	3.4995	-0.0014	0.9855	0.1496	-7.51	25.08	-	-	-	-	-	-
96	TNF-RII	3.3	-2.13	-1.0579	0	0.0001	0.3754	-0.13	39.18	-1.1884	-0.0008	0.1348	0.0906	-3.44	34.42
97	uPA	2.28	2.53	-	-	-	-	-	-	2.8877	0.0012	0.1087	0.1366	7.26	18.67
98	uPA-R	2.38	6.54	-	-	-	-	-	-	-	-	-	-	-	-
99	VCAM-1	4.35	0.2	3.0816	0.001	0.2389	0.2271	2.95	76.45	3.0723	-0.001	0.0554	0.2298	-3.08	76.21
100	VEGF-A	4.09	4.94	6.1844	-0.001	0.8701	0.13	-3.07	33.18	5.8675	0.0003	0.0017	0.2972	0.84	24.75
101	VEGF-D	0.98	2.95	-	-	-	-	-	-	-	-	-	-	-	-
102	VEGFR2	2.98	1.46	-	-	-	-	-	-	-	-	-	-	-	-
103	VEGFR3	1.24	7.95	-	-	-	-	-	-	-	-	-	-	-	-

TABLE I.S3: **Pre-analytical variables linear regression parameters in citrate samples, low dilution.**

	Protein name	Data range (RFU)	Blanks mean (RFU)	Citrate low dilution, 4 °C						Citrate low dilution, 25 °C					
				Intercept (RFU)	Slope (RFU/min)	R^2	Span (RFU)	Increase (%)	Starting (%)	Intercept (RFU)	Slope (RFU/h)	R^2	Span (RFU)	Increase (%)	Starting (%)
1	AFP	3.35	1.56	2.4148	-0.0015	0.129	0.2056	-5.74	29.34	2.6749	-0.0034	0.6362	0.4047	-13.47	38.25
2	AHSG	4.1	6.77	-	-	-	-	-	-	-	-	-	-	-	-
3	ALDH1L1	1.05	3.32	-	-	-	-	-	-	-	-	-	-	-	-
4	Amphiregulin	2.28	4.01	-	-	-	-	-	-	-	-	-	-	-	-
5	Ang1	3.33	0.96	1.689	0.0028	0.1234	0.4383	11.56	25.95	1.7783	0.0012	0.1014	0.2842	4.88	29.14
6	Ang2	0.88	5.07	-	-	-	-	-	-	-	-	-	-	-	-
8	BDNF	2.62	1.93	-	-	-	-	-	-	-	-	-	-	-	-
9	BMP2	0.78	3.25	-	-	-	-	-	-	-	-	-	-	-	-
10	BRAF	0.94	5.21	-	-	-	-	-	-	-	-	-	-	-	-
11	c-Kit	3.19	5.95	7.2994	0.0005	0.0538	0.2129	2.2	47.71	7.3902	-0.0016	0.7276	0.1778	-6.63	50.92
12	CA15-3	2.87	-1.56	-0.2761	0.001	0.3505	0.1107	4.74	54.14	-0.1375	-0.0013	0.6604	0.1716	-6.25	60
13	Cathepsin B	0.79	4.9	-	-	-	-	-	-	-	-	-	-	-	-
14	CCL5	3.76	7.11	-	-	-	-	-	-	-	-	-	-	-	-
15	CD14	4.06	-4.55	-2.1955	0.0032	0.2429	0.4483	12.67	81.08	-2.0763	0.0021	0.2216	0.2682	8.11	85.19
16	CEA	1.37	5.65	5.9778	-0.0011	0.1685	0.1329	-13.88	35.77	-	-	-	-	-	-
17	CRP	0.89	-1.03	-	-	-	-	-	-	-	-	-	-	-	-
18	CXCL12	1.43	6.56	-	-	-	-	-	-	-	-	-	-	-	-
19	E-cadherin	2.44	5.61	7.3019	-0.0003	0.0222	0.1766	-1.57	82.14	7.2635	-0.0007	0.0296	0.1385	-4.02	80.27
20	E-selectin	2.11	1.25	-	-	-	-	-	-	2.0518	-0.0017	0.6254	0.1914	-13.93	56.76
21	EGF	3.86	5.84	-	-	-	-	-	-	-	-	-	-	-	-
22	EGF-R	3.67	-2.28	0.436	-0.0013	0.1066	0.3948	-4.83	84.81	0.3204	-0.0014	0.8722	0.1704	-5.18	81.2
23	Endoglin	1.85	0.65	1.3967	0	0.0002	0.0214	0.21	58.57	1.5201	-0.002	0.8774	0.239	-17.9	68.26
24	EpCAM	1.87	6.17	-	-	-	-	-	-	-	-	-	-	-	-
25	FAS	2.74	4.38	5.1441	0.0014	0.0783	0.3053	6.73	31.89	5.2332	-0.0016	0.1847	0.1917	-7.64	35.61
26	FAS-L	1.18	-0.73	-0.3644	0.0009	0.1542	0.1321	13.88	47.07	-0.2104	-0.0004	0.0534	0.1201	-6.54	67.02
28	FGFb	1.24	5.22	5.4817	-0.0008	0.1963	0.1094	-9.62	27.68	5.5005	-0.0022	0.7097	0.2722	-26.77	29.69
29	Flt-3	1.49	6.2	-	-	-	-	-	-	-	-	-	-	-	-

Table I.S3 continued from previous page

		Data	Blanks	Citrate low dilution, 4 °C						Citrate low dilution, 25 °C					
	Protein name	range (RFU)	mean (RFU)	Intercept (RFU)	Slope (RFU/min)	R^2	Span (RFU)	Increase (%)	Starting (%)	Intercept (RFU)	Slope (RFU/h)	R^2	Span (RFU)	Increase (%)	Starting (%)
30	G-CSF	2.39	0.8	-	-	-	-	-	-	-	-	-	-	-	-
31	GFAP	2.62	0.12	0.9537	-0.0007	0.0333	0.3795	-3.62	37.4	1.2319	-0.0054	0.9043	0.6019	-27.71	49.91
32	GM-CSF	1.87	5.53	-	-	-	-	-	-	-	-	-	-	-	-
33	GRO-α	2.43	-8.01	-	-	-	-	-	-	-	-	-	-	-	-
34	HAI-1	1.98	5.42	5.7218	-0.0006	0.0649	0.0683	-4.07	17.42	5.7516	-0.0019	0.4625	0.2143	-12.5	19.14
35	HE4	0.81	4.23	-	-	-	-	-	-	-	-	-	-	-	-
36	HER2	1.45	5.92	-	-	-	-	-	-	-	-	-	-	-	-
37	HER3	1.17	5.47	-	-	-	-	-	-	-	-	-	-	-	-
38	HGF	3.7	3.99	4.3992	-0.0006	0.0114	0.1375	-1.85	11.76	4.4611	-0.002	0.1165	0.217	-6.56	13.55
39	HGF-R	3.75	1.35	3.9342	0.0002	0.0013	0.0609	0.67	81.24	4.2291	-0.0035	0.4201	0.38	-12.78	90.51
40	HMGB1	1.11	1.01	1.4043	0.0002	0.0356	0.0294	2.52	46.01	1.4464	-0.0009	0.3729	0.1291	-12.3	50.91
41	HP	2.94	0.72	1.2188	-0.0002	0.0039	0.2953	-0.79	18.38	1.3665	-0.0032	0.9681	0.3539	-13.48	23.79
42	ICAM-1	4.35	-6.8	-4.1081	0.001	0.0061	0.1494	3.05	73.66	-4.0918	-0.0008	0.0041	0.1549	-2.63	74.11
43	IFN-γ	1.63	1.13	-	-	-	-	-	-	-	-	-	-	-	-
44	IGFBP-1	3.52	4.77	7.6284	-0.0009	0.1807	0.1388	-3.33	88.13	7.5433	0.0002	0.0014	0.2484	0.53	85.51
45	IGFBP-3	3.28	5.26	7.9213	-0.0012	0.2195	0.1767	-4.8	89.65	7.8576	-0.0001	0.0011	0.0109	-0.24	87.51
46	IGFBP-7	3.65	5.86	8.4668	-0.0006	0.0502	0.1088	-2.02	81.6	8.3655	0.0011	0.1454	0.2226	3.86	78.43
47	IL-10	3	7.75	-	-	-	-	-	-	-	-	-	-	-	-
48	IL-12	2.4	-6.24	-	-	-	-	-	-	-	-	-	-	-	-
49	IL-15	2.34	6.06	-	-	-	-	-	-	-	-	-	-	-	-
50	IL-18	2.91	-4.12	-2.8894	0.002	0.1184	0.2295	10.55	56.57	-2.8561	0.0013	0.1139	0.202	6.63	58.1
51	IL-1β	3.12	4.31	4.7688	0.0002	0.0006	0.0285	0.75	15.92	4.8965	-0.0015	0.041	0.1697	-5.89	20.39
52	IL-1ra	2.24	-0.15	0.2205	0.0001	0.0014	0.0619	0.78	20.05	0.3201	-0.0014	0.2833	0.1537	-8.61	25.37
53	IL-2	2.27	5.78	-	-	-	-	-	-	-	-	-	-	-	-
54	IL-3	2.37	-2.51	-2.2316	0.0012	0.056	0.1823	8.55	17.08	-2.0562	-0.0021	0.5724	0.2395	-15.11	28
55	IL-4	1.26	3.71	-	-	-	-	-	-	-	-	-	-	-	-
56	IL-5	1.48	5.49	-	-	-	-	-	-	-	-	-	-	-	-
58	IL-7	2.47	-0.02	-	-	-	-	-	-	0.4739	-0.0024	0.2635	0.2787	-13.43	23.98
59	IL-8	2.22	0.05	-	-	-	-	-	-	-	-	-	-	-	-
60	IP-10	3.05	6.62	7.2584	-0.0004	0.0102	0.3654	-1.94	25.03	7.2951	-0.002	0.1308	0.2586	-8.99	26.47
61	KLK14	2.82	-0.67	-	-	-	-	-	-	-	-	-	-	-	-
62	KLK8	0.79	5.1	-	-	-	-	-	-	-	-	-	-	-	-
63	Leptin	0.82	5.21	-	-	-	-	-	-	-	-	-	-	-	-
64	M-CSF	2.29	1.71	-	-	-	-	-	-	-	-	-	-	-	-
65	MCP1	1.1	5.53	-	-	-	-	-	-	-	-	-	-	-	-
66	MCP2	3.57	4.43	-	-	-	-	-	-	-	-	-	-	-	-
67	MCP3	2.73	6.63	-	-	-	-	-	-	-	-	-	-	-	-
68	MCP4	2.8	8.09	-	-	-	-	-	-	-	-	-	-	-	-
69	MIG	2.61	-1.78	-	-	-	-	-	-	-	-	-	-	-	-
70	MIP-1α	2.09	1.61	2.0054	-0.0023	0.2377	0.3151	-15.05	22.27	-	-	-	-	-	-
71	MIP-1β	1.14	6.24	-	-	-	-	-	-	-	-	-	-	-	-
72	MMP-1	1.86	2.78	-	-	-	-	-	-	-	-	-	-	-	-
73	MMP-3	3.57	0.52	2.7125	-0.0011	0.1437	0.2635	-4.67	78.46	2.7116	-0.0012	0.2113	0.2261	-5.05	78.43
74	MMP-9	4.52	5.28	7.5632	-0.0014	0.0609	0.2616	-3.72	53.49	7.6307	-0.0024	0.2641	0.4306	-6.51	55.07
75	NCAM-1	2.76	4.08	5.9683	-0.003	0.4723	0.3995	-13.91	76.32	5.8735	-0.0032	0.3629	0.3471	-14.75	72.49
76	NT-3	2.37	3.96	-	-	-	-	-	-	-	-	-	-	-	-
77	OPN	3.69	5.59	7.8084	-0.0005	0.0577	0.0772	-1.72	64	7.8369	-0.0014	0.4975	0.1578	-4.5	64.82
78	PAI-1	1.8	2.55	-	-	-	-	-	-	-	-	-	-	-	-
79	PDGF-BB	3.59	5.72	6.0651	0.0014	0.1646	0.165	4.73	10.23	-	-	-	-	-	-

Table I.S3 continued from previous page

	Protein name	Data range (RFU)	Blanks mean (RFU)	Citrate low dilution, 4 °C						Citrate low dilution, 25 °C					
				Intercept (RFU)	Slope (RFU/min)	R^2	Span (RFU)	Increase (%)	Starting (%)	Intercept (RFU)	Slope (RFU/h)	R^2	Span (RFU)	Increase (%)	Starting (%)
80	PRL	0.83	1.43	1.7639	-0.0002	0.023	0.1277	-4.21	56.37	1.7922	-0.0005	0.3532	0.0816	-10.39	61.08
81	PSA	2.89	0.44	-	-	-	-	-	-	-	-	-	-	-	-
82	RBP4	0.82	5.18	-	-	-	-	-	-	-	-	-	-	-	-
83	S100B	1.21	2	2.3184	0.0002	0.0673	0.029	2.53	36.92	2.3823	-0.0013	0.3843	0.1769	-18	44.37
85	SPARC	2.28	4.96	-	-	-	-	-	-	-	-	-	-	-	-
86	TF	1.72	1.93	-	-	-	-	-	-	-	-	-	-	-	-
87	TGF-α	2.36	4.12	-	-	-	-	-	-	-	-	-	-	-	-
88	TGF-β RII	2.45	4.3	-	-	-	-	-	-	-	-	-	-	-	-
89	TGF-β1	2.84	3.55	-	-	-	-	-	-	-	-	-	-	-	-
90	TGF-β2	1.64	5.81	-	-	-	-	-	-	-	-	-	-	-	-
91	THBS-1	3.71	0.26	2.8359	0.0018	0.1337	0.2815	6.63	80.64	3.0728	-0.0006	0.0389	0.2431	-2.18	88.04
92	Tie-2	1.35	1.56	1.909	-0.0009	0.0972	0.1686	-9.66	33.06	2.0111	-0.0027	0.469	0.3444	-29.35	42.86
93	TIMP-1	2.51	5.71	-	-	-	-	-	-	-	-	-	-	-	-
94	TNF-α	2.12	2.04	-	-	-	-	-	-	-	-	-	-	-	-
95	TNF-RI	2.44	2.98	4.2581	0.0004	0.0053	0.0542	2.06	61.64	4.2289	-0.0003	0.006	0.0582	-1.77	60.24
96	TNF-RII	3.3	-2.13	0.2521	0.0001	0.0008	0.1191	0.31	86.96	0.2631	0.0008	0.1597	0.0979	3.35	87.36
97	uPA	2.28	2.53	3.8478	-0.0003	0.0243	0.1748	-1.8	69.07	3.7015	0.0006	0.0762	0.1421	3.77	61.39
98	uPA-R	2.38	6.54	-	-	-	-	-	-	-	-	-	-	-	-
99	VCAM-1	4.35	0.2	3.5284	-0.0005	0.0423	0.1972	-1.55	88.29	3.5859	-0.0025	0.8439	0.2929	-7.68	89.81
100	VEGF-A	4.09	4.94	5.6847	-0.0019	0.146	0.3219	-5.69	19.89	5.4819	-0.0009	0.2679	0.1234	-2.85	14.5
101	VEGF-D	0.98	2.95	-	-	-	-	-	-	-	-	-	-	-	-
102	VEGFR2	2.98	1.46	2.6403	0.0015	0.12	0.1672	9.1	61.07	2.7196	-0.0007	0.0383	0.1099	-4.22	65.15
103	VEGFR3	1.24	7.95	-	-	-	-	-	-	-	-	-	-	-	-

TABLE I.S4: **Pre-analytical variables linear regression parameters in citrate samples, high dilution.**

	Protein name	Data range (RFU)	Blanks mean (RFU)	Citrate high dilution, 4 °C						Citrate high dilution, 25 °C					
				Intercept (RFU)	Slope (RFU/min)	R^2	Span (RFU)	Increase (%)	Starting (%)	Intercept (RFU)	Slope (RFU/h)	R^2	Span (RFU)	Increase (%)	Starting (%)
1	AFP	3.35	1.56	-	-	-	-	-	-	-	-	-	-	-	-
2	AHSG	4.1	6.77	-	-	-	-	-	-	-	-	-	-	-	-
3	ALDH1L1	1.05	3.32	-	-	-	-	-	-	-	-	-	-	-	-
4	Amphiregulin	2.28	4.01	-	-	-	-	-	-	-	-	-	-	-	-
5	Ang1	3.33	0.96	-	-	-	-	-	-	-	-	-	-	-	-
6	Ang2	0.88	5.07	-	-	-	-	-	-	-	-	-	-	-	-
8	BDNF	2.62	1.93	-	-	-	-	-	-	-	-	-	-	-	-
9	BMP2	0.78	3.25	-	-	-	-	-	-	-	-	-	-	-	-
10	BRAF	0.94	5.21	-	-	-	-	-	-	-	-	-	-	-	-
11	c-Kit	3.19	5.95	6.7684	-0.0013	0.4115	0.194	-5.37	28.98	6.7482	-0.0012	0.1059	0.1369	-4.8	28.27
12	CA15-3	2.87	-1.56	-0.9345	-0.0017	0.1394	0.336	-8.47	26.33	-0.9458	0.0002	0.016	0.0567	0.82	25.85
13	Cathepsin B	0.79	4.9	-	-	-	-	-	-	-	-	-	-	-	-
14	CCL5	3.76	7.11	-	-	-	-	-	-	-	-	-	-	-	-
15	CD14	4.06	-4.55	-2.6174	0.0001	0.0002	0.3479	0.22	66.57	-2.7247	-0.0004	0.0037	0.2529	-1.56	62.88
16	CEA	1.37	5.65	-	-	-	-	-	-	-	-	-	-	-	-
17	CRP	0.89	-1.03	-	-	-	-	-	-	-	-	-	-	-	-
18	CXCL12	1.43	6.56	-	-	-	-	-	-	-	-	-	-	-	-

Table I.S4 continued from previous page

		Data	Blanks	Citrate high dilution, 4 °C						Citrate high dilution, 25 °C					
	Protein name	range (RFU)	mean (RFU)	Intercept (RFU)	Slope (RFU/min)	R^2	Span (RFU)	Increase (%)	Starting (%)	Intercept (RFU)	Slope (RFU/h)	R^2	Span (RFU)	Increase (%)	Starting (%)
19	E-cadherin	2.44	5.61	5.9506	0.0015	0.422	0.1762	8.53	16.42	6.1447	-0.001	0.0776	0.1707	-5.34	25.86
20	E-selectin	2.11	1.25	-	-	-	-	-	-	-	-	-	-	-	-
21	EGF	3.86	5.84	-	-	-	-	-	-	-	-	-	-	-	-
22	EGF-R	3.67	-2.28	-0.4273	0.0007	0.0199	0.2689	2.47	57.82	-0.4832	-0.0024	0.0923	0.3771	-8.5	56.07
23	Endoglin	1.85	0.65	-	-	-	-	-	-	-	-	-	-	-	-
24	EpCAM	1.87	6.17	-	-	-	-	-	-	-	-	-	-	-	-
25	FAS	2.74	4.38	-	-	-	-	-	-	-	-	-	-	-	-
26	FAS-L	1.18	-0.73	-	-	-	-	-	-	-	-	-	-	-	-
28	FGFb	1.24	5.22	-	-	-	-	-	-	-	-	-	-	-	-
29	Flt-3	1.49	6.2	-	-	-	-	-	-	-	-	-	-	-	-
30	G-CSF	2.39	0.8	-	-	-	-	-	-	-	-	-	-	-	-
31	GFAP	2.62	0.12	-	-	-	-	-	-	-	-	-	-	-	-
32	GM-CSF	1.87	5.53	-	-	-	-	-	-	-	-	-	-	-	-
33	GRO-α	2.43	-8.01	-	-	-	-	-	-	-	-	-	-	-	-
34	HAI-1	1.98	5.42	-	-	-	-	-	-	-	-	-	-	-	-
35	HE4	0.81	4.23	-	-	-	-	-	-	-	-	-	-	-	-
36	HER2	1.45	5.92	-	-	-	-	-	-	-	-	-	-	-	-
37	HER3	1.17	5.47	-	-	-	-	-	-	-	-	-	-	-	-
38	HGF	3.7	3.99	-	-	-	-	-	-	-	-	-	-	-	-
39	HGF-R	3.75	1.35	2.9387	-0.0011	0.0294	0.3782	-3.82	49.94	3.2636	-0.0056	0.5834	0.607	-20.19	60.15
40	HMGB1	1.11	1.01	-	-	-	-	-	-	-	-	-	-	-	-
41	HP	2.94	0.72	-	-	-	-	-	-	-	-	-	-	-	-
42	ICAM-1	4.35	-6.8	-5.2758	0.0008	0.0411	0.1945	2.49	41.75	-4.7307	-0.0076	0.3132	1.0869	-23.84	56.65
43	IFN-γ	1.63	1.13	-	-	-	-	-	-	-	-	-	-	-	-
44	IGFBP-1	3.52	4.77	7.3007	0.0005	0.2297	0.075	1.88	78.04	7.3399	-0.0001	0.0138	0.0837	-0.48	79.25
45	IGFBP-3	3.28	5.26	7.4062	-0.0002	0.0529	0.0927	-0.7	72.33	7.3837	-0.0006	0.1609	0.1044	-2.44	71.57
46	IGFBP-7	3.65	5.86	7.6393	0.0012	0.4227	0.1731	4.45	55.67	7.8212	-0.0018	0.2119	0.3307	-6.63	61.37
47	IL-10	3	7.75	-	-	-	-	-	-	-	-	-	-	-	-
48	IL-12	2.4	-6.24	-	-	-	-	-	-	-	-	-	-	-	-
49	IL-15	2.34	6.06	-	-	-	-	-	-	-	-	-	-	-	-
50	IL-18	2.91	-4.12	-	-	-	-	-	-	-	-	-	-	-	-
51	IL-1β	3.12	4.31	-	-	-	-	-	-	-	-	-	-	-	-
52	IL-1ra	2.24	-0.15	-	-	-	-	-	-	-	-	-	-	-	-
53	IL-2	2.27	5.78	-	-	-	-	-	-	-	-	-	-	-	-
54	IL-3	2.37	-2.51	-	-	-	-	-	-	-	-	-	-	-	-
55	IL-4	1.26	3.71	-	-	-	-	-	-	-	-	-	-	-	-
56	IL-5	1.48	5.49	-	-	-	-	-	-	-	-	-	-	-	-
58	IL-7	2.47	-0.02	-	-	-	-	-	-	-	-	-	-	-	-
59	IL-8	2.22	0.05	-	-	-	-	-	-	-	-	-	-	-	-
60	IP-10	3.05	6.62	-	-	-	-	-	-	-	-	-	-	-	-
61	KLK14	2.82	-0.67	-	-	-	-	-	-	-	-	-	-	-	-
62	KLK8	0.79	5.1	-	-	-	-	-	-	-	-	-	-	-	-
63	Leptin	0.82	5.21	-	-	-	-	-	-	-	-	-	-	-	-
64	M-CSF	2.29	1.71	-	-	-	-	-	-	-	-	-	-	-	-
65	MCP1	1.1	5.53	-	-	-	-	-	-	-	-	-	-	-	-
66	MCP2	3.57	4.43	-	-	-	-	-	-	-	-	-	-	-	-
67	MCP3	2.73	6.63	-	-	-	-	-	-	-	-	-	-	-	-
68	MCP4	2.8	8.09	-	-	-	-	-	-	-	-	-	-	-	-
69	MIG	2.61	-1.78	-	-	-	-	-	-	-	-	-	-	-	-

Table I.S4 continued from previous page

	Protein name	Data range (RFU)	Blanks mean (RFU)	Citrate high dilution, 4 °C						Citrate high dilution, 25 °C					
				Intercept (RFU)	Slope (RFU/min)	R^2	Span (RFU)	Increase (%)	Starting (%)	Intercept (RFU)	Slope (RFU/h)	R^2	Span (RFU)	Increase (%)	Starting (%)
70	MIP-1α	2.09	1.61	-	-	-	-	-	-	-	-	-	-	-	-
71	MIP-1β	1.14	6.24	-	-	-	-	-	-	-	-	-	-	-	-
72	MMP-1	1.86	2.78	-	-	-	-	-	-	-	-	-	-	-	-
73	MMP-3	3.57	0.52	1.8705	0.0009	0.0856	0.1003	3.65	48.26	2.1801	-0.0024	0.1417	0.2817	-9.7	59.37
74	MMP-9	4.52	5.28	7.4702	0.0002	0.0064	0.1529	0.46	51.31	7.5077	0.0008	0.012	0.6249	2.17	52.19
75	NCAM-1	2.76	4.08	5.3485	-0.0001	0.0022	0.193	-0.6	51.32	5.3376	-0.0009	0.1808	0.14	-4.08	50.88
76	NT-3	2.37	3.96	-	-	-	-	-	-	-	-	-	-	-	-
77	OPN	3.69	5.59	6.7034	0.0011	0.315	0.1207	3.57	32.12	6.9821	-0.0018	0.0713	0.4255	-5.96	40.16
78	PAI-1	1.8	2.55	-	-	-	-	-	-	-	-	-	-	-	-
79	PDGF-BB	3.59	5.72	-	-	-	-	-	-	-	-	-	-	-	-
80	PRL	0.83	1.43	-	-	-	-	-	-	-	-	-	-	-	-
81	PSA	2.89	0.44	-	-	-	-	-	-	-	-	-	-	-	-
82	RBP4	0.82	5.18	-	-	-	-	-	-	-	-	-	-	-	-
83	S100B	1.21	2	-	-	-	-	-	-	-	-	-	-	-	-
85	SPARC	2.28	4.96	-	-	-	-	-	-	-	-	-	-	-	-
86	TF	1.72	1.93	-	-	-	-	-	-	-	-	-	-	-	-
87	TGF-α	2.36	4.12	-	-	-	-	-	-	-	-	-	-	-	-
88	TGF-β RII	2.45	4.3	-	-	-	-	-	-	-	-	-	-	-	-
89	TGF-β1	2.84	3.55	-	-	-	-	-	-	-	-	-	-	-	-
90	TGF-β2	1.64	5.81	-	-	-	-	-	-	-	-	-	-	-	-
91	THBS-1	3.71	0.26	2.8905	0.0017	0.1337	0.4693	6.09	82.34	3.1071	-0.0047	0.2431	0.5516	-16.71	89.11
92	Tie-2	1.35	1.56	-	-	-	-	-	-	-	-	-	-	-	-
93	TIMP-1	2.51	5.71	-	-	-	-	-	-	-	-	-	-	-	-
94	TNF-α	2.12	2.04	-	-	-	-	-	-	-	-	-	-	-	-
95	TNF-RI	2.44	2.98	-	-	-	-	-	-	-	-	-	-	-	-
96	TNF-RII	3.3	-2.13	-1.4702	0.0001	0.001	0.1261	0.43	24.14	-1.3426	-0.0024	0.3393	0.3107	-9.87	28.8
97	uPA	2.28	2.53	-	-	-	-	-	-	-	-	-	-	-	-
98	uPA-R	2.38	6.54	-	-	-	-	-	-	-	-	-	-	-	-
99	VCAM-1	4.35	0.2	3.0141	-0.0014	0.3716	0.1847	-4.11	74.67	2.8188	0.0004	0.0767	0.1358	1.17	69.49
100	VEGF-A	4.09	4.94	-	-	-	-	-	-	-	-	-	-	-	-
101	VEGF-D	0.98	2.95	-	-	-	-	-	-	-	-	-	-	-	-
102	VEGFR2	2.98	1.46	-	-	-	-	-	-	-	-	-	-	-	-
103	VEGFR3	1.24	7.95	-	-	-	-	-	-	-	-	-	-	-	-

TABLE I.S5: **Pre-analytical variables linear regression parameters in heparin samples, low dilution.**

	Protein name	Data range (RFU)	Blanks mean (RFU)	Heparin low dilution, 4 °C						Heparin low dilution, 25 °C					
				Intercept (RFU)	Slope (RFU/min)	R^2	Span (RFU)	Increase (%)	Starting (%)	Intercept (RFU)	Slope (RFU/h)	R^2	Span (RFU)	Increase (%)	Starting (%)
1	AFP	3.35	1.56	2.5148	-0.0017	0.494	0.2002	-6.8	32.76	2.2572	0.0006	0.1095	0.0762	2.27	32.76
2	AHSG	4.1	6.77	-	-	-	-	-	-	-	-	-	-	-	-
3	ALDH1L1	1.05	3.32	-	-	-	-	-	-	-	-	-	-	-	-
4	Amphiregulin	2.28	4.01	-	-	-	-	-	-	-	-	-	-	-	-
5	Ang1	3.33	0.96	1.8561	0.0037	0.2258	0.6964	15.38	31.92	1.4729	0.0065	0.6734	0.7386	26.65	31.92
6	Ang2	0.88	5.07	-	-	-	-	-	-	-	-	-	-	-	-
8	BDNF	2.62	1.93	-	-	-	-	-	-	-	-	-	-	-	-

Table I.S5 continued from previous page

		Data	Blanks	Heparin low dilution, 4 °C						Heparin low dilution, 25 °C					
	Protein name	range (RFU)	mean (RFU)	Intercept (RFU)	Slope (RFU/min)	R^2	Span (RFU)	Increase (%)	Starting (%)	Intercept (RFU)	Slope (RFU/h)	R^2	Span (RFU)	Increase (%)	Starting (%)
9	BMP2	0.78	3.25	-	-	-	-	-	-	-	-	-	-	-	-
10	BRAF	0.94	5.21	-	-	-	-	-	-	-	-	-	-	-	-
11	c-Kit	3.19	5.95	7.6788	-0.0006	0.2119	0.088	-2.33	61.1	7.5826	0.0012	0.3327	0.2047	4.73	61.1
12	CA15-3	2.87	-1.56	0.0407	-0.0012	0.0975	0.1879	-6.01	67.53	-0.0226	-0.0013	0.0826	0.4866	-6.39	67.53
13	Cathepsin B	0.79	4.9	-	-	-	-	-	-	-	-	-	-	-	-
14	CCL5	3.76	7.11	-	-	-	-	-	-	-	-	-	-	-	-
15	CD14	4.06	-4.55	-2.4221	-0.001	0.131	0.108	-3.89	73.29	-2.3712	-0.0006	0.0833	0.2233	-2.42	73.29
16	CEA	1.37	5.65	6.0147	-0.0008	0.1732	0.1123	-10.37	39.85	5.9629	0	0.0002	0.0758	0.31	39.85
17	CRP	0.89	-1.03	-	-	-	-	-	-	-	-	-	-	-	-
18	CXCL12	1.43	6.56	-	-	-	-	-	-	-	-	-	-	-	-
19	E-cadherin	2.44	5.61	6.7742	0.0001	0.0067	0.0159	0.32	56.48	6.8758	-0.0006	0.1511	0.0736	-3.56	56.48
20	E-selectin	2.11	1.25	2.2397	-0.0019	0.3784	0.2086	-15.47	70.1	2.0845	0.0002	0.0023	0.2599	1.23	70.1
21	EGF	3.86	5.84	-	-	-	-	-	-	-	-	-	-	-	-
22	EGF-R	3.67	-2.28	0.3913	-0.0008	0.5381	0.093	-2.83	83.42	0.4087	0.0006	0.1398	0.0921	2.26	83.42
23	Endoglin	1.85	0.65	1.6231	-0.0003	0.0493	0.0954	-2.66	76.33	1.6051	-0.0009	0.3022	0.1012	-8.52	76.33
24	EpCAM	1.87	6.17	-	-	-	-	-	-	-	-	-	-	-	-
25	FAS	2.74	4.38	5.4003	-0.0017	0.1433	0.1875	-8.27	42.58	5.2938	0.0011	0.0463	0.2662	5.31	42.58
26	FAS-L	1.18	-0.73	-	-	-	-	-	-	-	-	-	-	-	-
28	FGFb	1.24	5.22	5.5483	-0.0008	0.1229	0.1188	-10.19	34.81	5.4535	0.0007	0.2103	0.1094	8.98	34.81
29	Flt-3	1.49	6.2	-	-	-	-	-	-	-	-	-	-	-	-
30	G-CSF	2.39	0.8	-	-	-	-	-	-	-	-	-	-	-	-
31	GFAP	2.62	0.12	0.8596	0.0005	0.0499	0.1776	2.35	33.18	0.819	0.0012	0.2168	0.149	6.34	33.18
32	GM-CSF	1.87	5.53	-	-	-	-	-	-	-	-	-	-	-	-
33	GRO-α	2.43	-8.01	-	-	-	-	-	-	-	-	-	-	-	-
34	HAI-1	1.98	5.42	5.7494	-0.0008	0.0841	0.1052	-5.04	19.02	-	-	-	-	-	-
35	HE4	0.81	4.23	-	-	-	-	-	-	-	-	-	-	-	-
36	HER2	1.45	5.92	-	-	-	-	-	-	-	-	-	-	-	-
37	HER3	1.17	5.47	-	-	-	-	-	-	-	-	-	-	-	-
38	HGF	3.7	3.99	4.4673	-0.0013	0.0327	0.2787	-4.18	13.73	4.2388	0.0047	0.1923	0.5154	15.58	13.73
39	HGF-R	3.75	1.35	4.1306	-0.0009	0.0623	0.1676	-3.07	87.42	4.1208	-0.0007	0.055	0.3328	-2.39	87.42
40	HMGB1	1.11	1.01	-	-	-	-	-	-	-	-	-	-	-	-
41	HP	2.94	0.72	1.2522	-0.0006	0.0391	0.0965	-2.5	19.6	1.1287	-0.0004	0.0195	0.1038	-1.72	19.6
42	ICAM-1	4.35	-6.8	-3.9579	-0.0012	0.0071	0.1777	-3.71	77.77	-3.934	-0.0019	0.0205	0.2454	-6.12	77.77
43	IFN-γ	1.63	1.13	-	-	-	-	-	-	-	-	-	-	-	-
44	IGFBP-1	3.52	4.77	7.4403	-0.0001	0.0003	0.404	-0.34	82.34	7.4504	0.0004	0.0125	0.2329	1.34	82.34
45	IGFBP-3	3.28	5.26	8.0946	-0.0009	0.2128	0.1266	-3.56	95.47	8.0368	-0.0001	0.0033	0.1472	-0.5	95.47
46	IGFBP-7	3.65	5.86	8.5255	-0.0011	0.2596	0.1267	-4.13	83.44	8.4412	0.0001	0.0042	0.1006	0.41	83.44
47	IL-10	3	7.75	8.2014	-0.0013	0.0337	0.1804	-6.13	18.91	8.0762	0.0015	0.0651	0.1665	7.24	18.91
48	IL-12	2.4	-6.24	-	-	-	-	-	-	-	-	-	-	-	-
49	IL-15	2.34	6.06	-	-	-	-	-	-	-	-	-	-	-	-
50	IL-18	2.91	-4.12	-2.773	-0.0002	0.0039	0.0385	-1.1	61.92	-2.7668	0.0004	0.0455	0.0668	2.19	61.92
51	IL-1β	3.12	4.31	4.7486	-0.0007	0.0086	0.0823	-2.79	15.21	4.6648	0.001	0.0153	0.1076	3.89	15.21
52	IL-1ra	2.24	-0.15	-	-	-	-	-	-	-	-	-	-	-	-
53	IL-2	2.27	5.78	-	-	-	-	-	-	-	-	-	-	-	-
54	IL-3	2.37	-2.51	-	-	-	-	-	-	-	-	-	-	-	-
55	IL-4	1.26	3.71	-	-	-	-	-	-	-	-	-	-	-	-
56	IL-5	1.48	5.49	5.9873	-0.0017	0.3046	0.2148	-18.51	47.87	-	-	-	-	-	-
58	IL-7	2.47	-0.02	-	-	-	-	-	-	-	-	-	-	-	-
59	IL-8	2.22	0.05	-	-	-	-	-	-	-	-	-	-	-	-

Table I.S5 continued from previous page

		Data	Blanks	Heparin low dilution, 4 °C						Heparin low dilution, 25 °C					
	Protein name	range (RFU)	mean (RFU)	Intercept (RFU)	Slope (RFU/min)	R^2	Span (RFU)	Increase (%)	Starting (%)	Intercept (RFU)	Slope (RFU/h)	R^2	Span (RFU)	Increase (%)	Starting (%)
60	IP-10	3.05	6.62	7.6259	-0.0028	0.3126	0.3864	-12.78	39.46	7.4898	-0.0007	0.0191	0.4971	-3.34	39.46
61	KLK14	2.82	-0.67	-	-	-	-	-	-	-	-	-	-	-	-
62	KLK8	0.79	5.1	-	-	-	-	-	-	-	-	-	-	-	-
63	Leptin	0.82	5.21	-	-	-	-	-	-	-	-	-	-	-	-
64	M-CSF	2.29	1.71	-	-	-	-	-	-	-	-	-	-	-	-
65	MCP1	1.1	5.53	-	-	-	-	-	-	-	-	-	-	-	-
66	MCP2	3.57	4.43	-	-	-	-	-	-	-	-	-	-	-	-
67	MCP3	2.73	6.63	-	-	-	-	-	-	-	-	-	-	-	-
68	MCP4	2.8	8.09	-	-	-	-	-	-	-	-	-	-	-	-
69	MIG	2.61	-1.78	-	-	-	-	-	-	-	-	-	-	-	-
70	MIP-1α	2.09	1.61	2.1028	-0.0015	0.0449	0.2692	-9.51	27.77	1.9749	0.0009	0.0206	0.1445	6.11	27.77
71	MIP-1β	1.14	6.24	-	-	-	-	-	-	-	-	-	-	-	-
72	MMP-1	1.86	2.78	-	-	-	-	-	-	-	-	-	-	-	-
73	MMP-3	3.57	0.52	2.6899	0.0004	0.3229	0.0648	1.7	77.66	2.7767	0	0	0.1229	0.03	77.66
74	MMP-9	4.52	5.28	7.4962	-0.0008	0.0121	0.5731	-2.11	51.92	7.1355	0.003	0.2501	0.3513	8.04	51.92
75	NCAM-1	2.76	4.08	6.3314	-0.0006	0.0233	0.074	-2.64	90.96	6.2839	-0.0002	0.0037	0.0776	-0.85	90.96
76	NT-3	2.37	3.96	-	-	-	-	-	-	-	-	-	-	-	-
77	OPN	3.69	5.59	8.0225	-0.0016	0.2185	0.2044	-5.36	70.18	7.936	-0.0003	0.0092	0.2472	-1.04	70.18
78	PAI-1	1.8	2.55	2.9216	0	0.0006	0.1006	-0.32	25.23	2.9442	0.0009	0.251	0.1216	6.94	25.23
79	PDGF-BB	3.59	5.72	-	-	-	-	-	-	-	-	-	-	-	-
80	PRL	0.83	1.43	-	-	-	-	-	-	-	-	-	-	-	-
81	PSA	2.89	0.44	-	-	-	-	-	-	-	-	-	-	-	-
82	RBP4	0.82	5.18	-	-	-	-	-	-	-	-	-	-	-	-
83	S100B	1.21	2	-	-	-	-	-	-	-	-	-	-	-	-
85	SPARC	2.28	4.96	5.568	0.0026	0.3459	0.3451	15	30.38	5.8891	0	0	0.0137	-0.05	30.38
86	TF	1.72	1.93	-	-	-	-	-	-	-	-	-	-	-	-
87	TGF-α	2.36	4.12	-	-	-	-	-	-	-	-	-	-	-	-
88	TGF-β RII	2.45	4.3	-	-	-	-	-	-	-	-	-	-	-	-
89	TGF-β1	2.84	3.55	3.978	0.0045	0.4118	0.5987	20.31	16.74	3.8871	0.004	0.8876	0.5006	18.31	16.74
90	TGF-β2	1.64	5.81	-	-	-	-	-	-	-	-	-	-	-	-
91	THBS-1	3.71	0.26	2.8952	-0.0004	0.3739	0.041	-1.36	82.49	2.8739	0.0002	0.0198	0.1466	0.84	82.49
92	Tie-2	1.35	1.56	-	-	-	-	-	-	-	-	-	-	-	-
93	TIMP-1	2.51	5.71	6.5297	-0.0003	0.0158	0.1067	-1.4	38.77	6.5282	0.0009	0.0748	0.1233	5.06	38.77
94	TNF-α	2.12	2.04	-	-	-	-	-	-	-	-	-	-	-	-
95	TNF-RI	2.44	2.98	4.4199	-0.0013	0.1841	0.1533	-6.93	69.44	4.397	-0.0009	0.0612	0.1596	-4.78	69.44
96	TNF-RII	3.3	-2.13	0.0581	-0.0017	0.236	0.2438	-7.17	79.89	0.0177	0.0003	0.0064	0.3405	1.19	79.89
97	uPA	2.28	2.53	3.8027	-0.0012	0.1766	0.1615	-7.39	66.7	3.769	-0.0016	0.2998	0.1869	-9.42	66.7
98	uPA-R	2.38	6.54	-	-	-	-	-	-	-	-	-	-	-	-
99	VCAM-1	4.35	0.2	3.479	-0.0003	0.0074	0.1968	-0.95	86.98	3.6376	-0.0026	0.6771	0.3256	-8.03	86.98
100	VEGF-A	4.09	4.94	5.9526	0	0	0.3989	0.09	27.02	5.6688	0.0024	0.434	0.2948	7.24	27.02
101	VEGF-D	0.98	2.95	-	-	-	-	-	-	-	-	-	-	-	-
102	VEGFR2	2.98	1.46	2.473	-0.0002	0.0035	0.1262	-0.98	52.44	-	-	-	-	-	-
103	VEGFR3	1.24	7.95	-	-	-	-	-	-	-	-	-	-	-	-

TABLE I.S6: **Pre-analytical variables linear regression parameters in heparin samples, high dilution.**

		Data	Blanks	Heparin high dilution, 4 °C						Heparin high dilution, 25 °C					
	Protein name	range (RFU)	mean (RFU)	Intercept (RFU)	Slope (RFU/min)	R^2	Span (RFU)	Increase (%)	Starting (%)	Intercept (RFU)	Slope (RFU/h)	R^2	Span (RFU)	Increase (%)	Starting (%)
1	AFP	3.35	1.56	-	-	-	-	-	-	-	-	-	-	-	-
2	AHSG	4.1	6.77	-	-	-	-	-	-	-	-	-	-	-	-
3	ALDH1L1	1.05	3.32	-	-	-	-	-	-	-	-	-	-	-	-
4	Amphiregulin	2.28	4.01	-	-	-	-	-	-	-	-	-	-	-	-
5	Ang1	3.33	0.96	1.1629	0.0041	0.4713	0.5964	16.84	7.15	1.0339	0.0043	0.6485	0.4844	17.59	2.55
6	Ang2	0.88	5.07	-	-	-	-	-	-	-	-	-	-	-	-
8	BDNF	2.62	1.93	-	-	-	-	-	-	-	-	-	-	-	-
9	BMP2	0.78	3.25	-	-	-	-	-	-	-	-	-	-	-	-
10	BRAF	0.94	5.21	-	-	-	-	-	-	-	-	-	-	-	-
11	c-Kit	3.19	5.95	6.8711	0.0005	0.0211	0.156	1.88	32.6	6.8201	0.0017	0.3155	0.2197	6.91	30.8
12	CA15-3	2.87	-1.56	-1.0225	0.0007	0.0592	0.154	3.54	22.62	-1.0284	0.0022	0.3371	0.2694	10.68	22.37
13	Cathepsin B	0.79	4.9	-	-	-	-	-	-	-	-	-	-	-	-
14	CCL5	3.76	7.11	-	-	-	-	-	-	-	-	-	-	-	-
15	CD14	4.06	-4.55	-2.7724	0.0029	0.71	0.3723	11.44	61.24	-2.5163	-0.0008	0.3213	0.1205	-3.19	70.05
16	CEA	1.37	5.65	-	-	-	-	-	-	-	-	-	-	-	-
17	CRP	0.89	-1.03	-	-	-	-	-	-	-	-	-	-	-	-
18	CXCL12	1.43	6.56	-	-	-	-	-	-	-	-	-	-	-	-
19	E-cadherin	2.44	5.61	5.9362	0.0012	0.3825	0.1455	6.67	15.71	-	-	-	-	-	-
20	E-selectin	2.11	1.25	-	-	-	-	-	-	-	-	-	-	-	-
21	EGF	3.86	5.84	-	-	-	-	-	-	-	-	-	-	-	-
22	EGF-R	3.67	-2.28	-0.452	0.0007	0.0586	0.2286	2.5	57.05	-0.5129	0.0012	0.1086	0.1561	4.27	55.14
23	Endoglin	1.85	0.65	-	-	-	-	-	-	-	-	-	-	-	-
24	EpCAM	1.87	6.17	-	-	-	-	-	-	-	-	-	-	-	-
25	FAS	2.74	4.38	-	-	-	-	-	-	-	-	-	-	-	-
26	FAS-L	1.18	-0.73	-	-	-	-	-	-	-	-	-	-	-	-
28	FGFb	1.24	5.22	-	-	-	-	-	-	-	-	-	-	-	-
29	Flt-3	1.49	6.2	-	-	-	-	-	-	-	-	-	-	-	-
30	G-CSF	2.39	0.8	-	-	-	-	-	-	-	-	-	-	-	-
31	GFAP	2.62	0.12	-	-	-	-	-	-	-	-	-	-	-	-
32	GM-CSF	1.87	5.53	-	-	-	-	-	-	-	-	-	-	-	-
33	GRO-α	2.43	-8.01	-	-	-	-	-	-	-	-	-	-	-	-
34	HAI-1	1.98	5.42	-	-	-	-	-	-	-	-	-	-	-	-
35	HE4	0.81	4.23	-	-	-	-	-	-	-	-	-	-	-	-
36	HER2	1.45	5.92	-	-	-	-	-	-	-	-	-	-	-	-
37	HER3	1.17	5.47	5.8338	0.0001	0.0029	0.0238	1.59	42.94	5.7939	0.0012	0.3183	0.1357	16.44	38.26
38	HGF	3.7	3.99	-	-	-	-	-	-	-	-	-	-	-	-
39	HGF-R	3.75	1.35	3.2212	-0.0004	0.0181	0.1738	-1.55	58.82	3.1601	0.0003	0.0098	0.0345	1.05	56.9
40	HMGB1	1.11	1.01	-	-	-	-	-	-	-	-	-	-	-	-
41	HP	2.94	0.72	-	-	-	-	-	-	-	-	-	-	-	-
42	ICAM-1	4.35	-6.8	-5.1646	-0.0003	0.0022	0.2168	-0.98	44.79	-5.3037	0.0009	0.0101	0.1042	2.79	40.98
43	IFN-γ	1.63	1.13	-	-	-	-	-	-	-	-	-	-	-	-
44	IGFBP-1	3.52	4.77	7.2003	-0.0012	0.2802	0.1663	-4.25	74.95	7.1438	0.0001	0.0019	0.0154	0.47	73.21
45	IGFBP-3	3.28	5.26	7.4524	0	0.0004	0.0014	-0.05	73.88	7.4388	0	0.0001	0.0223	-0.03	73.42
46	IGFBP-7	3.65	5.86	7.8793	0.0003	0.0212	0.2084	1.26	63.19	7.8673	0.0006	0.0814	0.116	2.31	62.82
47	IL-10	3	7.75	-	-	-	-	-	-	-	-	-	-	-	-
48	IL-12	2.4	-6.24	-	-	-	-	-	-	-	-	-	-	-	-
49	IL-15	2.34	6.06	-	-	-	-	-	-	-	-	-	-	-	-

Table I.S6 continued from previous page

		Data	Blanks	Heparin high dilution, 4 °C						Heparin high dilution, 25 °C					
	Protein name	range (RFU)	mean (RFU)	Intercept (RFU)	Slope (RFU/min)	R^2	Span (RFU)	Increase (%)	Starting (%)	Intercept (RFU)	Slope (RFU/h)	R^2	Span (RFU)	Increase (%)	Starting (%)
50	IL-18	2.91	-4.12	-	-	-	-	-	-	-	-	-	-	-	-
51	IL-1β	3.12	4.31	-	-	-	-	-	-	-	-	-	-	-	-
52	IL-1ra	2.24	-0.15	-	-	-	-	-	-	-	-	-	-	-	-
53	IL-2	2.27	5.78	-	-	-	-	-	-	-	-	-	-	-	-
54	IL-3	2.37	-2.51	-	-	-	-	-	-	-	-	-	-	-	-
55	IL-4	1.26	3.71	-	-	-	-	-	-	-	-	-	-	-	-
56	IL-5	1.48	5.49	-	-	-	-	-	-	-	-	-	-	-	-
58	IL-7	2.47	-0.02	-	-	-	-	-	-	-	-	-	-	-	-
59	IL-8	2.22	0.05	-	-	-	-	-	-	-	-	-	-	-	-
60	IP-10	3.05	6.62	-	-	-	-	-	-	-	-	-	-	-	-
61	KLK14	2.82	-0.67	-	-	-	-	-	-	-	-	-	-	-	-
62	KLK8	0.79	5.1	-	-	-	-	-	-	-	-	-	-	-	-
63	Leptin	0.82	5.21	-	-	-	-	-	-	-	-	-	-	-	-
64	M-CSF	2.29	1.71	-	-	-	-	-	-	-	-	-	-	-	-
65	MCP1	1.1	5.53	-	-	-	-	-	-	-	-	-	-	-	-
66	MCP2	3.57	4.43	-	-	-	-	-	-	-	-	-	-	-	-
67	MCP3	2.73	6.63	-	-	-	-	-	-	-	-	-	-	-	-
68	MCP4	2.8	8.09	-	-	-	-	-	-	-	-	-	-	-	-
69	MIG	2.61	-1.78	-	-	-	-	-	-	-	-	-	-	-	-
70	MIP-1α	2.09	1.61	-	-	-	-	-	-	-	-	-	-	-	-
71	MIP-1β	1.14	6.24	-	-	-	-	-	-	-	-	-	-	-	-
72	MMP-1	1.86	2.78	-	-	-	-	-	-	-	-	-	-	-	-
73	MMP-3	3.57	0.52	1.7874	0.0033	0.8265	0.3648	13.63	45.28	1.8082	0.0021	0.245	0.2438	8.51	46.03
74	MMP-9	4.52	5.28	8.4183	-0.0022	0.1071	0.5246	-5.81	73.56	7.5909	0.0064	0.7677	0.7989	17.3	54.14
75	NCAM-1	2.76	4.08	5.5318	-0.0002	0.0173	0.1346	-1.15	58.71	5.4155	0.0006	0.0337	0.1137	2.77	54.02
76	NT-3	2.37	3.96	-	-	-	-	-	-	-	-	-	-	-	-
77	OPN	3.69	5.59	6.74	-0.0004	0.0122	0.2128	-1.34	33.18	6.677	0.0008	0.0275	0.0866	2.62	31.36
78	PAI-1	1.8	2.55	-	-	-	-	-	-	-	-	-	-	-	-
79	PDGF-BB	3.59	5.72	-	-	-	-	-	-	-	-	-	-	-	-
80	PRL	0.83	1.43	-	-	-	-	-	-	-	-	-	-	-	-
81	PSA	2.89	0.44	-	-	-	-	-	-	-	-	-	-	-	-
82	RBP4	0.82	5.18	-	-	-	-	-	-	-	-	-	-	-	-
83	S100B	1.21	2	-	-	-	-	-	-	-	-	-	-	-	-
85	SPARC	2.28	4.96	-	-	-	-	-	-	-	-	-	-	-	-
86	TF	1.72	1.93	-	-	-	-	-	-	-	-	-	-	-	-
87	TGF-α	2.36	4.12	-	-	-	-	-	-	-	-	-	-	-	-
88	TGF-β RII	2.45	4.3	-	-	-	-	-	-	-	-	-	-	-	-
89	TGF-β1	2.84	3.55	-	-	-	-	-	-	-	-	-	-	-	-
90	TGF-β2	1.64	5.81	-	-	-	-	-	-	-	-	-	-	-	-
91	THBS-1	3.71	0.26	2.6855	0.0023	0.2054	0.454	8.17	75.94	2.7172	0.0019	0.3293	0.2458	6.99	76.93
92	Tie-2	1.35	1.56	-	-	-	-	-	-	-	-	-	-	-	-
93	TIMP-1	2.51	5.71	-	-	-	-	-	-	-	-	-	-	-	-
94	TNF-α	2.12	2.04	-	-	-	-	-	-	-	-	-	-	-	-
95	TNF-RI	2.44	2.98	-	-	-	-	-	-	-	-	-	-	-	-
96	TNF-RII	3.3	-2.13	-1.3151	0.0009	0.1822	0.1925	3.96	29.8	-1.3408	0.0017	0.724	0.2148	7.23	28.86
97	uPA	2.28	2.53	-	-	-	-	-	-	-	-	-	-	-	-
98	uPA-R	2.38	6.54	-	-	-	-	-	-	-	-	-	-	-	-
99	VCAM-1	4.35	0.2	3.1752	-0.0011	0.6813	0.1305	-3.42	78.93	3.0168	0.0017	0.5463	0.1924	5.31	74.74
100	VEGF-A	4.09	4.94	-	-	-	-	-	-	-	-	-	-	-	-

Table I.S6 continued from previous page

	Protein name	Data range (RFU)	Blanks mean (RFU)	Heparin high dilution, 4 °C						Heparin high dilution, 25 °C					
				Intercept (RFU)	Slope (RFU/min)	R^2	Span (RFU)	Increase (%)	Starting (%)	Intercept (RFU)	Slope (RFU/h)	R^2	Span (RFU)	Increase (%)	Starting (%)
101	VEGF-D	0.98	2.95	-	-	-	-	-	-	-	-	-	-	-	-
102	VEGFR2	2.98	1.46	-	-	-	-	-	-	-	-	-	-	-	-
103	VEGFR3	1.24	7.95	-	-	-	-	-	-	-	-	-	-	-	-

TABLE I.S7: **Pre-analytical variables linear regression parameters in EDTA samples, low dilution.**

	Protein name	Data range (RFU)	Blanks mean (RFU)	EDTA low dilution, 4 °C						EDTA low dilution, 25 °C					
				Intercept (RFU)	Slope (RFU/min)	R^2	Span (RFU)	Increase (%)	Starting (%)	Intercept (RFU)	Slope (RFU/h)	R^2	Span (RFU)	Increase (%)	Starting (%)
1	AFP	3.35	1.56	2.5508	0.0005	0.0741	0.0735	2.11	34	2.5437	-0.0021	0.1668	0.3349	-8.28	33.75
2	AHSG	4.1	6.77	-	-	-	-	-	-	-	-	-	-	-	-
3	ALDH1L1	1.05	3.32	3.5447	0.0025	0.7389	0.284	34.99	26.9	-	-	-	-	-	-
4	Amphiregulin	2.28	4.01	4.2942	0.0009	0.065	0.1513	5.1	14.69	-	-	-	-	-	-
5	Ang1	3.33	0.96	1.4405	0.0011	0.0172	0.4956	4.6	17.08	1.1948	0.003	0.1028	0.3741	12.13	8.3
6	Ang2	0.88	5.07	-	-	-	-	-	-	-	-	-	-	-	-
8	BDNF	2.62	1.93	2.6082	0.003	0.0936	0.4642	18.89	37.23	2.5063	0.002	0.0749	0.4165	12.69	31.61
9	BMP2	0.78	3.25	-	-	-	-	-	-	-	-	-	-	-	-
10	BRAF	0.94	5.21	-	-	-	-	-	-	-	-	-	-	-	-
11	c-Kit	3.19	5.95	7.7847	0.0002	0.0184	0.0523	0.85	64.84	7.7165	0.0021	0.0959	0.4515	8.62	62.43
12	CA15-3	2.87	-1.56	0.0179	0.0015	0.0693	0.3691	7.47	66.56	0.0172	-0.0018	0.0392	0.256	-8.81	66.53
13	Cathepsin B	0.79	4.9	-	-	-	-	-	-	-	-	-	-	-	-
14	CCL5	3.76	7.11	-	-	-	-	-	-	-	-	-	-	-	-
15	CD14	4.06	-4.55	-2.6437	0.0037	0.3941	0.5058	14.68	65.67	-2.573	0.0019	0.2753	0.3257	7.56	68.1
16	CEA	1.37	5.65	6.1116	-0.0017	0.1109	0.365	-21.55	50.56	-	-	-	-	-	-
17	CRP	0.89	-1.03	-	-	-	-	-	-	-	-	-	-	-	-
18	CXCL12	1.43	6.56	-	-	-	-	-	-	-	-	-	-	-	-
19	E-cadherin	2.44	5.61	7.5563	-0.0025	0.4885	0.2831	-14.11	94.52	7.396	-0.003	0.5141	0.4332	-16.58	86.72
20	E-selectin	2.11	1.25	1.8999	0.0008	0.313	0.1312	6.42	45.98	-	-	-	-	-	-
21	EGF	3.86	5.84	-	-	-	-	-	-	6.2117	0.0034	0.0971	0.5739	11.46	10.87
22	EGF-R	3.67	-2.28	0.5618	-0.0022	0.4939	0.2821	-7.81	88.75	0.4489	0.0009	0.0322	0.2295	3.08	85.22
23	Endoglin	1.85	0.65	1.6246	0.0003	0.019	0.1113	2.43	76.45	1.6756	-0.001	0.0858	0.1143	-8.68	80.45
24	EpCAM	1.87	6.17	-	-	-	-	-	-	-	-	-	-	-	-
25	FAS	2.74	4.38	5.4173	0.0017	0.0508	0.2485	8.01	43.29	5.3562	-0.0007	0.004	0.2755	-3.5	40.74
26	FAS-L	1.18	-0.73	-0.4111	0.0019	0.28	0.266	28.04	41.02	-0.4209	0.001	0.0628	0.2555	14.29	39.74
28	FGFb	1.24	5.22	5.5371	0.0006	0.0897	0.1494	7.89	33.61	5.4483	0.0003	0.0083	0.0827	3.31	24.11
29	Flt-3	1.49	6.2	-	-	-	-	-	-	-	-	-	-	-	-
30	G-CSF	2.39	0.8	-	-	-	-	-	-	-	-	-	-	-	-
31	GFAP	2.62	0.12	0.9115	0.0024	0.6673	0.2742	12.31	35.51	0.9619	0.0012	0.1155	0.1328	6.26	37.77
32	GM-CSF	1.87	5.53	-	-	-	-	-	-	5.5979	0.0076	0.6273	0.8466	64.49	4.88
33	GRO-α	2.43	-8.01	-	-	-	-	-	-	-	-	-	-	-	-
34	HAI-1	1.98	5.42	5.7284	0.0004	0.0209	0.1473	2.55	17.81	5.6694	0.0009	0.0825	0.1751	6.18	14.39
35	HE4	0.81	4.23	4.5893	-0.0012	0.2182	0.1507	-24.43	64.28	-	-	-	-	-	-
36	HER2	1.45	5.92	-	-	-	-	-	-	-	-	-	-	-	-
37	HER3	1.17	5.47	-	-	-	-	-	-	-	-	-	-	-	-
38	HGF	3.7	3.99	4.6339	0.0012	0.0283	0.2447	3.84	18.56	4.5887	0.0001	0.0002	0.0396	0.33	17.25
39	HGF-R	3.75	1.35	4.26	-0.0009	0.1731	0.1614	-3.33	91.49	4.2509	0.0012	0.2054	0.3037	4.39	91.2

Table I.S7 continued from previous page

		Data	Blanks	EDTA low dilution, 4 °C						EDTA low dilution, 25 °C					
	Protein name	range (RFU)	mean (RFU)	Intercept (RFU)	Slope (RFU/min)	R^2	Span (RFU)	Increase (%)	Starting (%)	Intercept (RFU)	Slope (RFU/h)	R^2	Span (RFU)	Increase (%)	Starting (%)
40	HMGB1	1.11	1.01	1.2755	0.0005	0.0886	0.1323	6.93	31.02	1.2175	0.0014	0.2646	0.2103	18.85	24.26
41	HP	2.94	0.72	1.1776	0.001	0.3433	0.1149	4.09	16.87	1.4278	-0.0028	0.2591	0.4964	-11.66	26.04
42	ICAM-1	4.35	-6.8	-4.1261	0	0	0.3549	-0.08	73.17	-3.9765	-0.003	0.1828	0.4368	-9.55	77.26
43	IFN-γ	1.63	1.13	1.4939	0.0006	0.2218	0.0855	5.79	30.11	-	-	-	-	-	-
44	IGFBP-1	3.52	4.77	7.4957	0.0009	0.0941	0.2911	3.17	84.04	7.2248	0.0021	0.2504	0.3622	7.42	75.7
45	IGFBP-3	3.28	5.26	8.0875	-0.0009	0.3847	0.1411	-3.58	95.24	7.9228	0.0003	0.0097	0.1293	0.98	89.7
46	IGFBP-7	3.65	5.86	8.6754	-0.002	0.1777	0.3367	-7.32	88.14	8.5567	-0.0011	0.0285	0.5091	-3.88	84.42
47	IL-10	3	7.75	8.2625	-0.0011	0.017	0.2737	-5.32	21.5	8.009	0.0008	0.0095	0.1837	4.05	10.79
48	IL-12	2.4	-6.24	-	-	-	-	-	-	-	-	-	-	-	-
49	IL-15	2.34	6.06	-	-	-	-	-	-	-	-	-	-	-	-
50	IL-18	2.91	-4.12	-2.7943	0.0022	0.2697	0.2805	11.74	60.94	-2.8753	0.0027	0.5176	0.3823	14.17	57.22
51	IL-1β	3.12	4.31	4.7861	0.0019	0.0306	0.306	7.75	16.52	4.8402	0.0029	0.0567	0.32	11.57	18.42
52	IL-1ra	2.24	-0.15	0.042	0.0013	0.3952	0.1473	8.21	10.51	-0.0087	0.0026	0.8035	0.3145	15.7	7.81
53	IL-2	2.27	5.78	6.0121	0.0015	0.2037	0.1913	8.85	12.4	5.9407	0.0041	0.2943	0.4709	24.96	8.64
54	IL-3	2.37	-2.51	-	-	-	-	-	-	-	-	-	-	-	-
55	IL-4	1.26	3.71	-	-	-	-	-	-	3.9374	0.0029	0.2477	0.3472	33.42	22.5
56	IL-5	1.48	5.49	5.8302	0.0013	0.3016	0.1797	14.39	32.89	5.7028	0.0015	0.1315	0.2237	16.96	20.75
58	IL-7	2.47	-0.02	0.1998	0.0025	0.26	0.3265	14.05	10.63	-	-	-	-	-	-
59	IL-8	2.22	0.05	-	-	-	-	-	-	-	-	-	-	-	-
60	IP-10	3.05	6.62	7.7369	-0.0005	0.0045	0.2415	-2.23	43.82	7.8231	-0.0055	0.1768	0.7716	-24.66	47.21
61	KLK14	2.82	-0.67	0.2473	-0.0007	0.0101	0.3337	-3.56	38.99	0.2461	-0.004	0.1616	0.5361	-19.41	38.94
62	KLK8	0.79	5.1	5.3392	0.0003	0.0855	0.0399	5.99	41.73	-	-	-	-	-	-
63	Leptin	0.82	5.21	-	-	-	-	-	-	-	-	-	-	-	-
64	M-CSF	2.29	1.71	-	-	-	-	-	-	-	-	-	-	-	-
65	MCP1	1.1	5.53	-	-	-	-	-	-	5.5934	0.0037	0.8873	0.4031	58.32	8.55
66	MCP2	3.57	4.43	-	-	-	-	-	-	-	-	-	-	-	-
67	MCP3	2.73	6.63	-	-	-	-	-	-	-	-	-	-	-	-
68	MCP4	2.8	8.09	-	-	-	-	-	-	-	-	-	-	-	-
69	MIG	2.61	-1.78	-	-	-	-	-	-	-	-	-	-	-	-
70	MIP-1α	2.09	1.61	2.1723	-0.0005	0.0165	0.1476	-3.42	31.69	2.103	-0.0004	0.0045	0.1009	-2.69	27.77
71	MIP-1β	1.14	6.24	-	-	-	-	-	-	-	-	-	-	-	-
72	MMP-1	1.86	2.78	3.2271	0.0007	0.0121	0.1002	5.18	29.41	3.2641	0.0013	0.0428	0.1892	10.25	31.86
73	MMP-3	3.57	0.52	2.8371	-0.0004	0.0299	0.0508	-1.48	82.93	2.9899	-0.0001	0.0001	0.2818	-0.23	88.42
74	MMP-9	4.52	5.28	8.3333	-0.0008	0.0552	0.1249	-2.14	71.57	8.3708	0.0015	0.0504	0.2342	4.18	72.45
75	NCAM-1	2.76	4.08	6.0679	0.0008	0.055	0.1	3.53	80.34	6.0515	-0.002	0.0514	0.3	-9.09	79.67
76	NT-3	2.37	3.96	-	-	-	-	-	-	-	-	-	-	-	-
77	OPN	3.69	5.59	8.2854	-0.001	0.3694	0.1405	-3.36	77.77	8.2273	-0.0004	0.0084	0.3317	-1.32	76.09
78	PAI-1	1.8	2.55	3.1618	0.0005	0.042	0.0593	3.49	41.34	3.1359	0.0013	0.1812	0.1764	9.89	39.61
79	PDGF-BB	3.59	5.72	6.5443	0.0007	0.006	0.7173	2.28	24.56	6.2412	0.0011	0.055	0.1488	3.73	15.49
80	PRL	0.83	1.43	-	-	-	-	-	-	-	-	-	-	-	-
81	PSA	2.89	0.44	-	-	-	-	-	-	-	-	-	-	-	-
82	RBP4	0.82	5.18	-	-	-	-	-	-	-	-	-	-	-	-
83	S100B	1.21	2	-	-	-	-	-	-	-	-	-	-	-	-
85	SPARC	2.28	4.96	5.4836	0.0003	0.0069	0.2877	1.52	26.14	5.4405	0.0005	0.0273	0.1438	3.02	23.98
86	TF	1.72	1.93	-	-	-	-	-	-	-	-	-	-	-	-
87	TGF-α	2.36	4.12	-	-	-	-	-	-	4.3787	0.0036	0.1039	0.5218	21.65	13.46
88	TGF-β RII	2.45	4.3	-	-	-	-	-	-	-	-	-	-	-	-
89	TGF-β1	2.84	3.55	4.3898	0	0.0001	0.1972	-0.12	32.99	4.5031	-0.0034	0.5525	0.4112	-15.34	37.46
90	TGF-β2	1.64	5.81	-	-	-	-	-	-	-	-	-	-	-	-

Table I.S7 continued from previous page

	Protein name	Data range (RFU)	Blanks mean (RFU)	EDTA low dilution, 4 °C						EDTA low dilution, 25 °C					
				Intercept (RFU)	Slope (RFU/min)	R^2	Span (RFU)	Increase (%)	Starting (%)	Intercept (RFU)	Slope (RFU/h)	R^2	Span (RFU)	Increase (%)	Starting (%)
91	THBS-1	3.71	0.26	2.4678	0.0039	0.2796	0.6374	14.08	69.14	2.572	0.0033	0.4078	0.5022	11.87	72.39
92	Tie-2	1.35	1.56	1.9271	-0.0002	0.0008	0.453	-1.97	34.79	-	-	-	-	-	-
93	TIMP-1	2.51	5.71	6.7042	-0.002	0.5439	0.2287	-10.69	47.02	6.4279	0.0069	0.9079	0.7456	37.45	33.96
94	TNF-α	2.12	2.04	-	-	-	-	-	-	-	-	-	-	-	-
95	TNF-RI	2.44	2.98	4.2325	0.0015	0.1228	0.2114	8.05	60.41	4.2748	-0.0004	0.0203	0.0498	-2.33	62.45
96	TNF-RII	3.3	-2.13	-0.249	0.0031	0.253	0.5212	13.18	68.69	0.0228	-0.0011	0.0408	0.1373	-4.5	78.6
97	uPA	2.28	2.53	3.7964	-0.0011	0.2777	0.1519	-6.55	66.36	3.6954	-0.0005	0.0456	0.1399	-3.31	61.06
98	uPA-R	2.38	6.54	-	-	-	-	-	-	-	-	-	-	-	-
99	VCAM-1	4.35	0.2	3.4541	0.0021	0.2503	0.2932	6.25	86.32	3.511	-0.0013	0.059	0.1951	-4.08	87.83
100	VEGF-A	4.09	4.94	6.1572	-0.0021	0.0772	0.5823	-6.42	32.46	5.789	-0.002	0.0665	0.2988	-6.13	22.66
101	VEGF-D	0.98	2.95	-	-	-	-	-	-	-	-	-	-	-	-
102	VEGFR2	2.98	1.46	2.2225	0.002	0.1585	0.2942	11.79	39.53	-	-	-	-	-	-
103	VEGFR3	1.24	7.95	-	-	-	-	-	-	-	-	-	-	-	-

TABLE I.S8: **Pre-analytical variables linear regression parameters in EDTA samples, high dilution.**

	Protein name	Data range (RFU)	Blanks mean (RFU)	EDTA high dilution, 4 °C						EDTA high dilution, 25 °C					
				Intercept (RFU)	Slope (RFU/min)	R^2	Span (RFU)	Increase (%)	Starting (%)	Intercept (RFU)	Slope (RFU/h)	R^2	Span (RFU)	Increase (%)	Starting (%)
1	AFP	3.35	1.56	-	-	-	-	-	-	2.2395	-0.0031	0.799	0.3608	-12.03	23.33
2	AHSG	4.1	6.77	-	-	-	-	-	-	-	-	-	-	-	-
3	ALDH1L1	1.05	3.32	-	-	-	-	-	-	-	-	-	-	-	-
4	Amphiregulin	2.28	4.01	-	-	-	-	-	-	-	-	-	-	-	-
5	Ang1	3.33	0.96	-	-	-	-	-	-	-	-	-	-	-	-
6	Ang2	0.88	5.07	-	-	-	-	-	-	-	-	-	-	-	-
8	BDNF	2.62	1.93	-	-	-	-	-	-	-	-	-	-	-	-
9	BMP2	0.78	3.25	-	-	-	-	-	-	-	-	-	-	-	-
10	BRAF	0.94	5.21	-	-	-	-	-	-	-	-	-	-	-	-
11	c-Kit	3.19	5.95	6.8041	-0.0007	0.0203	0.1973	-2.95	30.24	6.7957	0.0012	0.0657	0.1568	5.02	29.94
12	CA15-3	2.87	-1.56	-0.6451	-0.0011	0.0867	0.1971	-5.32	38.56	-0.7129	0.0001	0.0004	0.0101	0.37	35.69
13	Cathepsin B	0.79	4.9	-	-	-	-	-	-	-	-	-	-	-	-
14	CCL5	3.76	7.11	-	-	-	-	-	-	-	-	-	-	-	-
15	CD14	4.06	-4.55	-2.3737	-0.0012	0.0311	0.1324	-4.59	74.95	-2.2911	-0.0021	0.7533	0.2588	-8.43	77.8
16	CEA	1.37	5.65	-	-	-	-	-	-	-	-	-	-	-	-
17	CRP	0.89	-1.03	-	-	-	-	-	-	-	-	-	-	-	-
18	CXCL12	1.43	6.56	-	-	-	-	-	-	-	-	-	-	-	-
19	E-cadherin	2.44	5.61	6.1191	0.0001	0.0017	0.015	0.4	24.61	6.2739	-0.0018	0.8582	0.2061	-9.9	32.14
20	E-selectin	2.11	1.25	-	-	-	-	-	-	-	-	-	-	-	-
21	EGF	3.86	5.84	-	-	-	-	-	-	-	-	-	-	-	-
22	EGF-R	3.67	-2.28	-0.5952	0.0009	0.0532	0.122	3.39	52.57	-0.4838	0.0006	0.0093	0.17	2.03	56.05
23	Endoglin	1.85	0.65	-	-	-	-	-	-	-	-	-	-	-	-
24	EpCAM	1.87	6.17	-	-	-	-	-	-	-	-	-	-	-	-
25	FAS	2.74	4.38	-	-	-	-	-	-	-	-	-	-	-	-
26	FAS-L	1.18	-0.73	-	-	-	-	-	-	-	-	-	-	-	-
28	FGFb	1.24	5.22	-	-	-	-	-	-	-	-	-	-	-	-
29	Flt-3	1.49	6.2	-	-	-	-	-	-	-	-	-	-	-	-

Table I.S8 continued from previous page

		Data	Blanks	EDTA high dilution, 4 °C						EDTA high dilution, 25 °C					
	Protein name	range (RFU)	mean (RFU)	Intercept (RFU)	Slope (RFU/min)	R^2	Span (RFU)	Increase (%)	Starting (%)	Intercept (RFU)	Slope (RFU/h)	R^2	Span (RFU)	Increase (%)	Starting (%)
30	G-CSF	2.39	0.8	-	-	-	-	-	-	-	-	-	-	-	-
31	GFAP	2.62	0.12	-	-	-	-	-	-	-	-	-	-	-	-
32	GM-CSF	1.87	5.53	-	-	-	-	-	-	-	-	-	-	-	-
33	GRO-α	2.43	-8.01	-	-	-	-	-	-	-	-	-	-	-	-
34	HAI-1	1.98	5.42	-	-	-	-	-	-	-	-	-	-	-	-
35	HE4	0.81	4.23	-	-	-	-	-	-	-	-	-	-	-	-
36	HER2	1.45	5.92	-	-	-	-	-	-	-	-	-	-	-	-
37	HER3	1.17	5.47	-	-	-	-	-	-	-	-	-	-	-	-
38	HGF	3.7	3.99	-	-	-	-	-	-	-	-	-	-	-	-
39	HGF-R	3.75	1.35	3.1145	0.0007	0.0747	0.1286	2.57	55.46	3.3104	-0.0014	0.0448	0.3179	-4.94	61.63
40	HMGB1	1.11	1.01	-	-	-	-	-	-	-	-	-	-	-	-
41	HP	2.94	0.72	-	-	-	-	-	-	0.9708	-0.0006	0.3306	0.0913	-2.63	9.29
42	ICAM-1	4.35	-6.8	-5.3833	-0.0017	0.0943	0.4188	-5.35	38.81	-5.1729	0.0001	0.0001	0.1944	0.24	44.56
43	IFN-γ	1.63	1.13	-	-	-	-	-	-	-	-	-	-	-	-
44	IGFBP-1	3.52	4.77	7.0636	0.0015	0.0144	0.9346	5.43	70.74	7.2774	0.0023	0.3985	0.3289	8.28	77.32
45	IGFBP-3	3.28	5.26	7.3413	-0.0008	0.0719	0.1327	-3.28	70.15	7.1769	0.0011	0.4027	0.1268	4.32	64.62
46	IGFBP-7	3.65	5.86	7.9352	-0.0007	0.0275	0.2653	-2.36	64.94	7.97	0.0001	0.0009	0.3156	0.53	66.03
47	IL-10	3	7.75	-	-	-	-	-	-	-	-	-	-	-	-
48	IL-12	2.4	-6.24	-	-	-	-	-	-	-	-	-	-	-	-
49	IL-15	2.34	6.06	-	-	-	-	-	-	-	-	-	-	-	-
50	IL-18	2.91	-4.12	-	-	-	-	-	-	-3.3936	-0.0026	0.7626	0.3064	-13.85	33.4
51	IL-1β	3.12	4.31	-	-	-	-	-	-	-	-	-	-	-	-
52	IL-1ra	2.24	-0.15	-	-	-	-	-	-	-	-	-	-	-	-
53	IL-2	2.27	5.78	-	-	-	-	-	-	-	-	-	-	-	-
54	IL-3	2.37	-2.51	-	-	-	-	-	-	-	-	-	-	-	-
55	IL-4	1.26	3.71	-	-	-	-	-	-	-	-	-	-	-	-
56	IL-5	1.48	5.49	-	-	-	-	-	-	-	-	-	-	-	-
58	IL-7	2.47	-0.02	-	-	-	-	-	-	-	-	-	-	-	-
59	IL-8	2.22	0.05	-	-	-	-	-	-	-	-	-	-	-	-
60	IP-10	3.05	6.62	-	-	-	-	-	-	-	-	-	-	-	-
61	KLK14	2.82	-0.67	-	-	-	-	-	-	0.4457	-0.0071	0.1403	0.7656	-34.81	47.4
62	KLK8	0.79	5.1	-	-	-	-	-	-	-	-	-	-	-	-
63	Leptin	0.82	5.21	-	-	-	-	-	-	-	-	-	-	-	-
64	M-CSF	2.29	1.71	-	-	-	-	-	-	-	-	-	-	-	-
65	MCP1	1.1	5.53	-	-	-	-	-	-	-	-	-	-	-	-
66	MCP2	3.57	4.43	-	-	-	-	-	-	-	-	-	-	-	-
67	MCP3	2.73	6.63	-	-	-	-	-	-	-	-	-	-	-	-
68	MCP4	2.8	8.09	-	-	-	-	-	-	-	-	-	-	-	-
69	MIG	2.61	-1.78	-	-	-	-	-	-	-	-	-	-	-	-
70	MIP-1α	2.09	1.61	-	-	-	-	-	-	-	-	-	-	-	-
71	MIP-1β	1.14	6.24	-	-	-	-	-	-	-	-	-	-	-	-
72	MMP-1	1.86	2.78	-	-	-	-	-	-	-	-	-	-	-	-
73	MMP-3	3.57	0.52	2.0505	0.0005	0.0546	0.107	2.16	54.72	2.0365	0.0021	0.3165	0.2307	8.82	54.22
74	MMP-9	4.52	5.28	8.5138	-0.003	0.1552	0.6721	-8.07	75.81	8.2163	0.0018	0.1275	0.2587	4.73	68.82
75	NCAM-1	2.76	4.08	5.0345	0.0004	0.0056	0.2797	1.69	38.66	5.1184	-0.0007	0.013	0.2329	-3.09	42.04
76	NT-3	2.37	3.96	-	-	-	-	-	-	4.5699	-0.0051	0.2181	0.6504	-32.47	33.9
77	OPN	3.69	5.59	7.0005	-0.0012	0.0468	0.1773	-3.99	40.69	6.7237	0.0022	0.12	0.2386	7.18	32.71
78	PAI-1	1.8	2.55	-	-	-	-	-	-	-	-	-	-	-	-
79	PDGF-BB	3.59	5.72	-	-	-	-	-	-	6.4011	-0.004	0.2251	0.4797	-13.86	20.28

Table I.S8 continued from previous page

	Protein name	Data range (RFU)	Blanks mean (RFU)	EDTA high dilution, 4 °C						EDTA high dilution, 25 °C					
				Intercept (RFU)	Slope (RFU/min)	R^2	Span (RFU)	Increase (%)	Starting (%)	Intercept (RFU)	Slope (RFU/h)	R^2	Span (RFU)	Increase (%)	Starting (%)
80	PRL	0.83	1.43	-	-	-	-	-	-	-	-	-	-	-	-
81	PSA	2.89	0.44	-	-	-	-	-	-	-	-	-	-	-	-
82	RBP4	0.82	5.18	-	-	-	-	-	-	-	-	-	-	-	-
83	S100B	1.21	2	-	-	-	-	-	-	-	-	-	-	-	-
85	SPARC	2.28	4.96	-	-	-	-	-	-	-	-	-	-	-	-
86	TF	1.72	1.93	-	-	-	-	-	-	-	-	-	-	-	-
87	TGF-α	2.36	4.12	-	-	-	-	-	-	-	-	-	-	-	-
88	TGF-β RII	2.45	4.3	-	-	-	-	-	-	-	-	-	-	-	-
89	TGF-β1	2.84	3.55	-	-	-	-	-	-	-	-	-	-	-	-
90	TGF-β2	1.64	5.81	-	-	-	-	-	-	-	-	-	-	-	-
91	THBS-1	3.71	0.26	2.9019	0.0015	0.0452	0.2995	5.38	82.7	2.8919	-0.0003	0.0019	0.3174	-1.23	82.39
92	Tie-2	1.35	1.56	-	-	-	-	-	-	-	-	-	-	-	-
93	TIMP-1	2.51	5.71	-	-	-	-	-	-	-	-	-	-	-	-
94	TNF-α	2.12	2.04	-	-	-	-	-	-	-	-	-	-	-	-
95	TNF-RI	2.44	2.98	-	-	-	-	-	-	3.5543	-0.0025	0.9394	0.267	-13.64	27.72
96	TNF-RII	3.3	-2.13	-1.0808	0.0003	0.005	0.0878	1.4	38.34	-0.9914	-0.0002	0.0024	0.1219	-0.93	41.61
97	uPA	2.28	2.53	-	-	-	-	-	-	-	-	-	-	-	-
98	uPA-R	2.38	6.54	-	-	-	-	-	-	-	-	-	-	-	-
99	VCAM-1	4.35	0.2	3.106	0.0004	0.036	0.0435	1.17	77.1	3.2668	-0.0005	0.0179	0.0605	-1.52	81.36
100	VEGF-A	4.09	4.94	-	-	-	-	-	-	-	-	-	-	-	-
101	VEGF-D	0.98	2.95	-	-	-	-	-	-	-	-	-	-	-	-
102	VEGFR2	2.98	1.46	-	-	-	-	-	-	-	-	-	-	-	-
103	VEGFR3	1.24	7.95	-	-	-	-	-	-	-	-	-	-	-	-

TABLE I.S9: **Pre-analytical variables linear regression parameters in $EDTA_{Filt}$ samples, low dilution.**

	Protein name	Data range (RFU)	Blanks mean (RFU)	$EDTA_{Filt}$ low dilution, 4 °C						$EDTA_{Filt}$ low dilution, 25 °C					
				Intercept (RFU)	Slope (RFU/min)	R^2	Span (RFU)	Increase (%)	Starting (%)	Intercept (RFU)	Slope (RFU/h)	R^2	Span (RFU)	Increase (%)	Starting (%)
1	AFP	3.35	1.56	2.4393	-0.0006	0.0095	0.373	-2.37	30.17	2.398	0.0007	0.0209	0.3875	2.72	28.76
2	AHSG	4.1	6.77	-	-	-	-	-	-	-	-	-	-	-	-
3	ALDH1L1	1.05	3.32	-	-	-	-	-	-	-	-	-	-	-	-
4	Amphiregulin	2.28	4.01	-	-	-	-	-	-	4.3728	-0.0003	0.0084	0.0959	-1.91	18.7
5	Ang1	3.33	0.96	1.1895	0.0055	0.2489	0.6806	22.74	8.11	1.3982	0.0017	0.0344	0.2596	6.92	15.56
6	Ang2	0.88	5.07	-	-	-	-	-	-	-	-	-	-	-	-
8	BDNF	2.62	1.93	2.8883	-0.0049	0.2255	0.6309	-31.14	52.67	2.814	0	0	0.0228	0.22	48.58
9	BMP2	0.78	3.25	-	-	-	-	-	-	-	-	-	-	-	-
10	BRAF	0.94	5.21	-	-	-	-	-	-	-	-	-	-	-	-
11	c-Kit	3.19	5.95	7.5911	0.0015	0.1324	0.2059	6.21	58.01	7.7745	0	0.0001	0.0407	-0.11	64.48
12	CA15-3	2.87	-1.56	-0.0786	-0.0011	0.0101	0.1469	-5.22	62.49	-0.0423	-0.0027	0.1658	0.3151	-13	64.02
13	Cathepsin B	0.79	4.9	-	-	-	-	-	-	-	-	-	-	-	-
14	CCL5	3.76	7.11	-	-	-	-	-	-	-	-	-	-	-	-
15	CD14	4.06	-4.55	-2.2598	-0.0032	0.2677	0.3724	-12.57	78.87	-2.2255	0.0003	0.0048	0.0947	1.13	80.05
16	CEA	1.37	5.65	-	-	-	-	-	-	5.9192	0.0011	0.3458	0.1433	13.49	29.29
17	CRP	0.89	-1.03	-	-	-	-	-	-	-	-	-	-	-	-
18	CXCL12	1.43	6.56	-	-	-	-	-	-	-	-	-	-	-	-

Table I.S9 continued from previous page

		Data	Blanks	EDTA$_{Filt}$ low dilution, 4 °C						EDTA$_{Filt}$ low dilution, 25 °C					
	Protein name	range (RFU)	mean (RFU)	Intercept (RFU)	Slope (RFU/min)	R^2	Span (RFU)	Increase (%)	Starting (%)	Intercept (RFU)	Slope (RFU/h)	R^2	Span (RFU)	Increase (%)	Starting (%)
19	E-cadherin	2.44	5.61	7.1286	0.002	0.1399	0.2514	11.22	73.72	7.0296	0.0028	0.2461	0.406	15.61	68.9
20	E-selectin	2.11	1.25	-	-	-	-	-	-	1.9556	-0.0001	0.0023	0.0753	-0.43	49.93
21	EGF	3.86	5.84	-	-	-	-	-	-	-	-	-	-	-	-
22	EGF-R	3.67	-2.28	0.3609	0.0012	0.2497	0.1264	4.21	82.47	0.3689	0.0006	0.0798	0.0805	2.18	82.72
23	Endoglin	1.85	0.65	1.5731	-0.0013	0.1134	0.1562	-11.64	72.41	1.4725	0.0006	0.0572	0.1225	5.32	64.52
24	EpCAM	1.87	6.17	-	-	-	-	-	-	-	-	-	-	-	-
25	FAS	2.74	4.38	5.2878	-0.0006	0.0024	0.0964	-2.99	37.89	5.4938	-0.0015	0.0267	0.175	-7.06	46.48
26	FAS-L	1.18	-0.73	-0.1206	-0.0028	0.6931	0.3163	-41.42	78.67	-0.2153	-0.0011	0.0755	0.1325	-16.44	66.39
28	FGFb	1.24	5.22	5.455	0.0007	0.0258	0.1622	8.63	24.82	5.4979	0.0011	0.1214	0.1284	13.06	29.42
29	Flt-3	1.49	6.2	-	-	-	-	-	-	-	-	-	-	-	-
30	G-CSF	2.39	0.8	-	-	-	-	-	-	-	-	-	-	-	-
31	GFAP	2.62	0.12	1.0288	-0.0006	0.018	0.0812	-2.86	40.78	0.9572	0.0015	0.2672	0.2444	7.97	37.56
32	GM-CSF	1.87	5.53	-	-	-	-	-	-	-	-	-	-	-	-
33	GRO-α	2.43	-8.01	-	-	-	-	-	-	-	-	-	-	-	-
34	HAI-1	1.98	5.42	5.6529	0.0006	0.0154	0.1339	3.74	13.44	5.7769	-0.0002	0.0081	0.0185	-1.08	20.61
35	HE4	0.81	4.23	4.5468	-0.0001	0.001	0.0801	-2.21	56.72	4.4495	0.001	0.4732	0.1313	19.87	39.41
36	HER2	1.45	5.92	-	-	-	-	-	-	-	-	-	-	-	-
37	HER3	1.17	5.47	-	-	-	-	-	-	5.9113	-0.0018	0.1476	0.257	-24.08	52.05
38	HGF	3.7	3.99	4.7095	-0.0008	0.0082	0.1685	-2.71	20.75	4.6785	-0.0002	0.0012	0.1733	-0.8	19.85
39	HGF-R	3.75	1.35	4.385	-0.0027	0.647	0.3238	-9.61	95.42	4.3682	-0.0004	0.025	0.1969	-1.45	94.89
40	HMGB1	1.11	1.01	1.3725	-0.0004	0.0632	0.0815	-5.98	42.31	1.2641	0.0009	0.4943	0.1143	12.45	29.69
41	HP	2.94	0.72	1.2176	0.0005	0.0292	0.077	2.09	18.33	1.4006	-0.0012	0.0739	0.3712	-5.08	25.04
42	ICAM-1	4.35	-6.8	-4.0419	0.0021	0.0399	0.431	6.52	75.47	-4.0451	-0.0001	0	0.0677	-0.2	75.38
43	IFN-γ	1.63	1.13	1.5772	-0.0016	0.307	0.2198	-15.39	36.92	-	-	-	-	-	-
44	IGFBP-1	3.52	4.77	7.2819	0.0011	0.0523	0.2832	3.97	77.46	7.4903	0.0013	0.3902	0.1643	4.68	83.88
45	IGFBP-3	3.28	5.26	7.8495	0.0017	0.2779	0.2798	6.39	87.23	7.9941	0.0005	0.1043	0.0676	1.76	92.1
46	IGFBP-7	3.65	5.86	8.2834	0.0038	0.4118	0.4222	13.53	75.86	8.4943	0.0004	0.02	0.1915	1.41	82.47
47	IL-10	3	7.75	8.1162	-0.0009	0.0064	0.3404	-4.32	15.32	8.0813	0.0011	0.0177	0.123	5.54	13.84
48	IL-12	2.4	-6.24	-	-	-	-	-	-	-	-	-	-	-	-
49	IL-15	2.34	6.06	-	-	-	-	-	-	-	-	-	-	-	-
50	IL-18	2.91	-4.12	-2.5073	-0.003	0.5818	0.3849	-15.68	74.12	-2.8189	0.002	0.1579	0.5222	10.33	59.81
51	IL-1β	3.12	4.31	4.9782	-0.0014	0.0162	0.2207	-5.72	23.25	4.9347	-0.0008	0.0107	0.2198	-3.37	21.73
52	IL-1ra	2.24	-0.15	0.208	-0.0011	0.5118	0.1457	-6.84	19.38	0.1724	0.0002	0.0095	0.1526	0.94	17.48
53	IL-2	2.27	5.78	-	-	-	-	-	-	-	-	-	-	-	-
54	IL-3	2.37	-2.51	-	-	-	-	-	-	-	-	-	-	-	-
55	IL-4	1.26	3.71	-	-	-	-	-	-	-	-	-	-	-	-
56	IL-5	1.48	5.49	-	-	-	-	-	-	5.9953	-0.0003	0.0099	0.0426	-2.89	48.63
58	IL-7	2.47	-0.02	0.4585	-0.0021	0.1894	0.3121	-11.82	23.23	-	-	-	-	-	-
59	IL-8	2.22	0.05	-	-	-	-	-	-	-	-	-	-	-	-
60	IP-10	3.05	6.62	7.4092	-0.0016	0.0143	0.2142	-7.13	30.95	7.5952	-0.0027	0.1388	0.383	-12	38.26
61	KLK14	2.82	-0.67	-	-	-	-	-	-	-	-	-	-	-	-
62	KLK8	0.79	5.1	5.2646	0.0016	0.3856	0.2361	32.73	28.69	5.3472	0.0009	0.0955	0.2978	18.22	43.13
63	Leptin	0.82	5.21	-	-	-	-	-	-	-	-	-	-	-	-
64	M-CSF	2.29	1.71	-	-	-	-	-	-	-	-	-	-	-	-
65	MCP1	1.1	5.53	-	-	-	-	-	-	-	-	-	-	-	-
66	MCP2	3.57	4.43	-	-	-	-	-	-	-	-	-	-	-	-
67	MCP3	2.73	6.63	-	-	-	-	-	-	-	-	-	-	-	-
68	MCP4	2.8	8.09	-	-	-	-	-	-	-	-	-	-	-	-
69	MIG	2.61	-1.78	-	-	-	-	-	-	-	-	-	-	-	-

Table I.S9 continued from previous page

		Data	Blanks	EDTA$_{Filt}$ low dilution, 4 °C						EDTA$_{Filt}$ low dilution, 25 °C					
	Protein name	range (RFU)	mean (RFU)	Intercept (RFU)	Slope (RFU/min)	R^2	Span (RFU)	Increase (%)	Starting (%)	Intercept (RFU)	Slope (RFU/h)	R^2	Span (RFU)	Increase (%)	Starting (%)
70	MIP-1α	2.09	1.61	2.0909	0.002	0.0692	0.3776	12.94	27.09	2.0401	0.0009	0.0196	0.0943	5.55	24.23
71	MIP-1β	1.14	6.24	6.1882	0.0048	0.9046	0.5496	73.03	0	-	-	-	-	-	-
72	MMP-1	1.86	2.78	3.2475	0.0008	0.0158	0.0943	6.27	30.76	-	-	-	-	-	-
73	MMP-3	3.57	0.52	2.692	0.0028	0.5204	0.3052	11.55	77.73	2.8437	0.0007	0.0273	0.1342	2.8	83.17
74	MMP-9	4.52	5.28	8.3227	0.0007	0.0639	0.1535	1.77	71.32	8.3375	-0.0006	0.0475	0.1619	-1.58	71.67
75	NCAM-1	2.76	4.08	5.8564	0.0022	0.0911	0.2551	10.15	71.8	6.0378	0.0003	0.0045	0.056	1.38	79.12
76	NT-3	2.37	3.96	-	-	-	-	-	-	-	-	-	-	-	-
77	OPN	3.69	5.59	8.1747	0.0007	0.0686	0.1002	2.37	74.57	8.1904	0.0001	0.0014	0.0833	0.23	75.03
78	PAI-1	1.8	2.55	3.1606	0.001	0.2264	0.1688	7.86	41.26	3.202	0.0009	0.1041	0.1748	6.69	44.04
79	PDGF-BB	3.59	5.72	6.096	0.0071	0.3887	0.8161	24.43	11.15	6.2356	0.0028	0.2051	0.3159	9.79	15.32
80	PRL	0.83	1.43	-	-	-	-	-	-	-	-	-	-	-	-
81	PSA	2.89	0.44	-	-	-	-	-	-	-	-	-	-	-	-
82	RBP4	0.82	5.18	-	-	-	-	-	-	-	-	-	-	-	-
83	S100B	1.21	2	-	-	-	-	-	-	-	-	-	-	-	-
85	SPARC	2.28	4.96	5.3659	0.0016	0.1319	0.2109	9.25	20.23	-	-	-	-	-	-
86	TF	1.72	1.93	-	-	-	-	-	-	-	-	-	-	-	-
87	TGF-α	2.36	4.12	-	-	-	-	-	-	-	-	-	-	-	-
88	TGF-β RII	2.45	4.3	-	-	-	-	-	-	-	-	-	-	-	-
89	TGF-β1	2.84	3.55	4.1673	0.0053	0.4544	0.6481	23.94	24.21	4.0813	0.0027	0.176	0.3625	12.35	20.82
90	TGF-β2	1.64	5.81	-	-	-	-	-	-	-	-	-	-	-	-
91	THBS-1	3.71	0.26	2.6798	0.0005	0.0084	0.4567	1.74	75.76	2.6784	0.0027	0.7781	0.3264	9.66	75.72
92	Tie-2	1.35	1.56	-	-	-	-	-	-	1.7707	0.0008	0.3255	0.1033	8.92	19.77
93	TIMP-1	2.51	5.71	6.5271	-0.0001	0.0031	0.0182	-0.68	38.65	6.5479	0.0009	0.0605	0.1792	4.69	39.63
94	TNF-α	2.12	2.04	-	-	-	-	-	-	-	-	-	-	-	-
95	TNF-RI	2.44	2.98	4.2709	-0.0003	0.004	0.0375	-1.6	62.26	4.2188	0.0012	0.1155	0.1331	6.52	59.75
96	TNF-RII	3.3	-2.13	-0.0677	-0.0028	0.2199	0.3168	-11.75	75.3	0.0066	-0.0025	0.3607	0.3252	-10.61	78.01
97	uPA	2.28	2.53	3.6641	0.0022	0.4001	0.3263	13.53	59.42	3.6493	0.0001	0.0011	0.1513	0.37	58.64
98	uPA-R	2.38	6.54	-	-	-	-	-	-	6.8584	0.0017	0.1989	0.3325	9.8	15.74
99	VCAM-1	4.35	0.2	3.4777	-0.0027	0.1765	0.333	-8.09	86.95	3.5564	-0.0022	0.3316	0.3498	-6.58	89.04
100	VEGF-A	4.09	4.94	5.6237	0.0058	0.3514	0.6604	17.84	18.27	5.7829	0.0013	0.0376	0.1743	3.85	22.5
101	VEGF-D	0.98	2.95	-	-	-	-	-	-	-	-	-	-	-	-
102	VEGFR2	2.98	1.46	2.4559	-0.001	0.0471	0.2286	-6	51.56	2.4575	0.0006	0.0576	0.1488	3.55	51.64
103	VEGFR3	1.24	7.95	-	-	-	-	-	-	-	-	-	-	-	-

TABLE I.S10: **Pre-analytical variables linear regression parameters in EDTA$_{Filt}$ samples, high dilution.**

		Data	Blanks	EDTA$_{Filt}$ high dilution, 4 °C						EDTA$_{Filt}$ high dilution, 25 °C					
	Protein name	range (RFU)	mean (RFU)	Intercept (RFU)	Slope (RFU/min)	R^2	Span (RFU)	Increase (%)	Starting (%)	Intercept (RFU)	Slope (RFU/h)	R^2	Span (RFU)	Increase (%)	Starting (%)
1	AFP	3.35	1.56	2.2334	-0.0018	0.1362	0.2854	-7.21	23.12	-	-	-	-	-	-
2	AHSG	4.1	6.77	-	-	-	-	-	-	-	-	-	-	-	-
3	ALDH1L1	1.05	3.32	-	-	-	-	-	-	-	-	-	-	-	-
4	Amphiregulin	2.28	4.01	-	-	-	-	-	-	-	-	-	-	-	-
5	Ang1	3.33	0.96	-	-	-	-	-	-	-	-	-	-	-	-
6	Ang2	0.88	5.07	-	-	-	-	-	-	-	-	-	-	-	-
8	BDNF	2.62	1.93	-	-	-	-	-	-	-	-	-	-	-	-

Table I.S10 continued from previous page

		Data	Blanks	$EDTA_{Filt}$ high dilution, 4 °C						$EDTA_{Filt}$ high dilution, 25 °C					
	Protein name	range (RFU)	mean (RFU)	Intercept (RFU)	Slope (RFU/min)	R^2	Span (RFU)	Increase (%)	Starting (%)	Intercept (RFU)	Slope (RFU/h)	R^2	Span (RFU)	Increase (%)	Starting (%)
9	BMP2	0.78	3.25	-	-	-	-	-	-	-	-	-	-	-	-
10	BRAF	0.94	5.21	-	-	-	-	-	-	-	-	-	-	-	-
11	c-Kit	3.19	5.95	6.6517	0.0006	0.0354	0.1729	2.63	24.86	6.6016	0.0038	0.2479	0.4898	15.36	23.1
12	CA15-3	2.87	-1.56	-0.7733	0.0008	0.1089	0.1719	3.92	33.14	-0.7877	0.0028	0.3201	0.3615	13.6	32.53
13	Cathepsin B	0.79	4.9	-	-	-	-	-	-	-	-	-	-	-	-
14	CCL5	3.76	7.11	-	-	-	-	-	-	-	-	-	-	-	-
15	CD14	4.06	-4.55	-2.22	-0.0011	0.0907	0.4328	-4.35	80.24	-2.256	-0.0001	0.0004	0.4958	-0.41	79
16	CEA	1.37	5.65	-	-	-	-	-	-	-	-	-	-	-	-
17	CRP	0.89	-1.03	-	-	-	-	-	-	-	-	-	-	-	-
18	CXCL12	1.43	6.56	-	-	-	-	-	-	-	-	-	-	-	-
19	E-cadherin	2.44	5.61	6.2233	-0.0006	0.2175	0.105	-3.17	29.68	6.0399	0.0014	0.5463	0.1765	7.99	20.76
20	E-selectin	2.11	1.25	-	-	-	-	-	-	-	-	-	-	-	-
21	EGF	3.86	5.84	-	-	-	-	-	-	-	-	-	-	-	-
22	EGF-R	3.67	-2.28	-0.557	0.0006	0.0103	0.2641	1.99	53.77	-0.5424	0.0033	0.5198	0.3749	11.99	54.22
23	Endoglin	1.85	0.65	-	-	-	-	-	-	-	-	-	-	-	-
24	EpCAM	1.87	6.17	-	-	-	-	-	-	-	-	-	-	-	-
25	FAS	2.74	4.38	-	-	-	-	-	-	-	-	-	-	-	-
26	FAS-L	1.18	-0.73	-	-	-	-	-	-	-	-	-	-	-	-
28	FGFb	1.24	5.22	-	-	-	-	-	-	-	-	-	-	-	-
29	Flt-3	1.49	6.2	-	-	-	-	-	-	-	-	-	-	-	-
30	G-CSF	2.39	0.8	-	-	-	-	-	-	-	-	-	-	-	-
31	GFAP	2.62	0.12	-	-	-	-	-	-	-	-	-	-	-	-
32	GM-CSF	1.87	5.53	-	-	-	-	-	-	-	-	-	-	-	-
33	GRO-α	2.43	-8.01	-	-	-	-	-	-	-	-	-	-	-	-
34	HAI-1	1.98	5.42	-	-	-	-	-	-	-	-	-	-	-	-
35	HE4	0.81	4.23	-	-	-	-	-	-	-	-	-	-	-	-
36	HER2	1.45	5.92	-	-	-	-	-	-	-	-	-	-	-	-
37	HER3	1.17	5.47	-	-	-	-	-	-	-	-	-	-	-	-
38	HGF	3.7	3.99	-	-	-	-	-	-	3.9827	0.0029	0.4243	0.3346	9.79	0
39	HGF-R	3.75	1.35	3.0742	0.0014	0.1492	0.16	5.05	54.2	3.2659	0.0001	0.0001	0.2089	0.26	60.23
40	HMGB1	1.11	1.01	-	-	-	-	-	-	-	-	-	-	-	-
41	HP	2.94	0.72	0.9566	-0.0003	0.1211	0.0729	-1.27	8.77	0.9594	0.0007	0.2517	0.0904	3.09	8.87
42	ICAM-1	4.35	-6.8	-5.3297	-0.0013	0.0659	0.1564	-4.15	40.28	-5.2901	0.0008	0.0174	0.3495	2.58	41.36
43	IFN-γ	1.63	1.13	-	-	-	-	-	-	-	-	-	-	-	-
44	IGFBP-1	3.52	4.77	7.4535	-0.0076	0.4645	0.8372	-26.93	82.74	7.3818	-0.0003	0.0039	0.2809	-0.9	80.54
45	IGFBP-3	3.28	5.26	7.1504	0.0005	0.0653	0.1727	1.94	63.73	7.2325	0.0006	0.0277	0.1305	2.25	66.49
46	IGFBP-7	3.65	5.86	7.885	-0.0009	0.0891	0.2113	-3.41	63.37	7.8031	0.0022	0.3716	0.263	7.83	60.8
47	IL-10	3	7.75	-	-	-	-	-	-	-	-	-	-	-	-
48	IL-12	2.4	-6.24	-	-	-	-	-	-	-	-	-	-	-	-
49	IL-15	2.34	6.06	-	-	-	-	-	-	-	-	-	-	-	-
50	IL-18	2.91	-4.12	-3.4172	0.0006	0.0525	0.1591	3.18	32.32	-	-	-	-	-	-
51	IL-1β	3.12	4.31	-	-	-	-	-	-	-	-	-	-	-	-
52	IL-1ra	2.24	-0.15	-	-	-	-	-	-	-	-	-	-	-	-
53	IL-2	2.27	5.78	-	-	-	-	-	-	-	-	-	-	-	-
54	IL-3	2.37	-2.51	-	-	-	-	-	-	-	-	-	-	-	-
55	IL-4	1.26	3.71	-	-	-	-	-	-	-	-	-	-	-	-
56	IL-5	1.48	5.49	-	-	-	-	-	-	-	-	-	-	-	-
58	IL-7	2.47	-0.02	-	-	-	-	-	-	-	-	-	-	-	-
59	IL-8	2.22	0.05	-	-	-	-	-	-	-	-	-	-	-	-

Table I.S10 continued from previous page

		Data	Blanks	$EDTA_{Filt}$ high dilution, 4 °C						$EDTA_{Filt}$ high dilution, 25 °C					
	Protein name	range (RFU)	mean (RFU)	Intercept (RFU)	Slope (RFU/min)	R^2	Span (RFU)	Increase (%)	Starting (%)	Intercept (RFU)	Slope (RFU/h)	R^2	Span (RFU)	Increase (%)	Starting (%)
60	IP-10	3.05	6.62	-	-	-	-	-	-	6.6343	0.005	0.6206	0.544	22.71	0.51
61	KLK14	2.82	-0.67	-	-	-	-	-	-	-0.7644	0.009	0.3245	1.082	42.05	0
62	KLK8	0.79	5.1	-	-	-	-	-	-	-	-	-	-	-	-
63	Leptin	0.82	5.21	-	-	-	-	-	-	-	-	-	-	-	-
64	M-CSF	2.29	1.71	-	-	-	-	-	-	-	-	-	-	-	-
65	MCP1	1.1	5.53	-	-	-	-	-	-	-	-	-	-	-	-
66	MCP2	3.57	4.43	-	-	-	-	-	-	-	-	-	-	-	-
67	MCP3	2.73	6.63	-	-	-	-	-	-	-	-	-	-	-	-
68	MCP4	2.8	8.09	-	-	-	-	-	-	-	-	-	-	-	-
69	MIG	2.61	-1.78	-	-	-	-	-	-	-	-	-	-	-	-
70	MIP-1α	2.09	1.61	-	-	-	-	-	-	-	-	-	-	-	-
71	MIP-1β	1.14	6.24	-	-	-	-	-	-	-	-	-	-	-	-
72	MMP-1	1.86	2.78	-	-	-	-	-	-	-	-	-	-	-	-
73	MMP-3	3.57	0.52	2.0746	-0.0007	0.1356	0.1762	-2.92	55.58	2.0419	0.0025	0.4308	0.278	10.14	54.41
74	MMP-9	4.52	5.28	8.2833	-0.0006	0.0435	0.1565	-1.75	70.4	8.2867	0.0006	0.0171	0.2564	1.57	70.47
75	NCAM-1	2.76	4.08	5.2121	-0.0012	0.0294	0.2118	-5.58	45.82	5.1737	-0.0025	0.1623	0.431	-11.66	44.27
76	NT-3	2.37	3.96	-	-	-	-	-	-	3.7349	0.0091	0.4924	1.0043	47.89	0
77	OPN	3.69	5.59	6.8118	0.0005	0.0133	0.2552	1.69	35.25	6.8893	-0.0007	0.0266	0.3472	-2.48	37.48
78	PAI-1	1.8	2.55	-	-	-	-	-	-	-	-	-	-	-	-
79	PDGF-BB	3.59	5.72	6.222	-0.0031	0.2082	0.4623	-10.56	14.92	5.7746	0.0059	0.4331	0.6806	20.32	1.54
80	PRL	0.83	1.43	-	-	-	-	-	-	-	-	-	-	-	-
81	PSA	2.89	0.44	-	-	-	-	-	-	-	-	-	-	-	-
82	RBP4	0.82	5.18	-	-	-	-	-	-	-	-	-	-	-	-
83	S100B	1.21	2	-	-	-	-	-	-	-	-	-	-	-	-
85	SPARC	2.28	4.96	-	-	-	-	-	-	-	-	-	-	-	-
86	TF	1.72	1.93	-	-	-	-	-	-	-	-	-	-	-	-
87	TGF-α	2.36	4.12	-	-	-	-	-	-	-	-	-	-	-	-
88	TGF-β RII	2.45	4.3	-	-	-	-	-	-	-	-	-	-	-	-
89	TGF-β1	2.84	3.55	-	-	-	-	-	-	-	-	-	-	-	-
90	TGF-β2	1.64	5.81	-	-	-	-	-	-	-	-	-	-	-	-
91	THBS-1	3.71	0.26	2.7245	0.0036	0.1132	0.4803	12.84	77.16	2.6937	0.0036	0.1006	0.5873	13.1	76.2
92	Tie-2	1.35	1.56	-	-	-	-	-	-	-	-	-	-	-	-
93	TIMP-1	2.51	5.71	-	-	-	-	-	-	-	-	-	-	-	-
94	TNF-α	2.12	2.04	-	-	-	-	-	-	-	-	-	-	-	-
95	TNF-RI	2.44	2.98	3.5252	-0.0011	0.3261	0.1604	-6.09	26.32	-	-	-	-	-	-
96	TNF-RII	3.3	-2.13	-1.1065	0.0007	0.0296	0.1526	3.09	37.41	-1.1399	0.0029	0.3746	0.4206	12.03	36.19
97	uPA	2.28	2.53	-	-	-	-	-	-	-	-	-	-	-	-
98	uPA-R	2.38	6.54	-	-	-	-	-	-	-	-	-	-	-	-
99	VCAM-1	4.35	0.2	3.0632	0.0006	0.0943	0.1746	1.97	75.97	3.0673	0.003	0.6767	0.3343	9.12	76.08
100	VEGF-A	4.09	4.94	-	-	-	-	-	-	-	-	-	-	-	-
101	VEGF-D	0.98	2.95	-	-	-	-	-	-	-	-	-	-	-	-
102	VEGFR2	2.98	1.46	-	-	-	-	-	-	-	-	-	-	-	-
103	VEGFR3	1.24	7.95	-	-	-	-	-	-	-	-	-	-	-	-

TABLE I.S11: **Pre-analytical variables linear regression parameters in CTAD samples, low dilution.**

		Data	Blanks	CTAD low dilution, 4 °C						CTAD low dilution, 25 °C					
	Protein name	range (RFU)	mean (RFU)	Intercept (RFU)	Slope (RFU/min)	R^2	Span (RFU)	Increase (%)	Starting (%)	Intercept (RFU)	Slope (RFU/h)	R^2	Span (RFU)	Increase (%)	Starting (%)
1	AFP	3.35	1.56	2.3411	0.0022	0.2175	0.4195	8.75	26.81	2.7653	-0.0008	0.0153	0.0939	-3.16	41.35
2	AHSG	4.1	6.77	-	-	-	-	-	-	-	-	-	-	-	-
3	ALDH1L1	1.05	3.32	-	-	-	-	-	-	-	-	-	-	-	-
4	Amphiregulin	2.28	4.01	-	-	-	-	-	-	-	-	-	-	-	-
5	Ang1	3.33	0.96	1.3731	0.0026	0.2999	0.3935	10.71	14.67	-	-	-	-	-	-
6	Ang2	0.88	5.07	-	-	-	-	-	-	-	-	-	-	-	-
8	BDNF	2.62	1.93	2.3725	0.0033	0.1313	0.4251	20.81	24.24	-	-	-	-	-	-
9	BMP2	0.78	3.25	-	-	-	-	-	-	-	-	-	-	-	-
10	BRAF	0.94	5.21	-	-	-	-	-	-	-	-	-	-	-	-
11	c-Kit	3.19	5.95	7.2179	0.0006	0.0707	0.0672	2.36	44.84	7.2091	-0.0003	0.0221	0.0394	-1.38	44.53
12	CA15-3	2.87	-1.56	-0.1074	-0.0022	0.2781	0.2531	-10.71	61.27	-0.1889	-0.0002	0.0033	0.0941	-0.81	57.83
13	Cathepsin B	0.79	4.9	-	-	-	-	-	-	-	-	-	-	-	-
14	CCL5	3.76	7.11	-	-	-	-	-	-	-	-	-	-	-	-
15	CD14	4.06	-4.55	-2.2465	0.0006	0.0325	0.2565	2.34	79.33	-2.4091	0.0012	0.053	0.2653	4.69	73.74
16	CEA	1.37	5.65	-	-	-	-	-	-	-	-	-	-	-	-
17	CRP	0.89	-1.03	-	-	-	-	-	-	-	-	-	-	-	-
18	CXCL12	1.43	6.56	-	-	-	-	-	-	-	-	-	-	-	-
19	E-cadherin	2.44	5.61	7.1093	0.0011	0.0347	0.1649	6.16	72.78	7.2871	-0.0005	0.0261	0.1007	-3.04	81.42
20	E-selectin	2.11	1.25	1.7953	0.0014	0.468	0.2456	11.83	38.55	1.829	0.0012	0.1299	0.1505	9.66	40.95
21	EGF	3.86	5.84	-	-	-	-	-	-	-	-	-	-	-	-
22	EGF-R	3.67	-2.28	0.1658	0	0.0002	0.0339	0.08	76.37	0.1262	-0.0006	0.0075	0.1954	-1.99	75.13
23	Endoglin	1.85	0.65	1.5665	0.0007	0.1652	0.0956	5.89	71.89	1.59	0.0007	0.5501	0.0871	6.04	73.73
24	EpCAM	1.87	6.17	-	-	-	-	-	-	-	-	-	-	-	-
25	FAS	2.74	4.38	5.0122	0.0015	0.0851	0.2182	7.24	26.38	4.8785	0.0013	0.292	0.143	6.22	20.8
26	FAS-L	1.18	-0.73	-	-	-	-	-	-	-	-	-	-	-	-
28	FGFb	1.24	5.22	5.3927	0.0011	0.1055	0.1763	13.41	18.16	5.3926	0.0008	0.2607	0.0913	9.4	18.15
29	Flt-3	1.49	6.2	-	-	-	-	-	-	-	-	-	-	-	-
30	G-CSF	2.39	0.8	-	-	-	-	-	-	-	-	-	-	-	-
31	GFAP	2.62	0.12	0.9815	0.0011	0.1406	0.1265	5.78	38.66	0.9408	0.0025	0.5467	0.3408	12.95	36.83
32	GM-CSF	1.87	5.53	-	-	-	-	-	-	-	-	-	-	-	-
33	GRO-α	2.43	-8.01	-	-	-	-	-	-	-	-	-	-	-	-
34	HAI-1	1.98	5.42	5.6052	0.0016	0.1807	0.1744	10.34	10.68	5.6314	0.0011	0.2365	0.1181	7.23	12.19
35	HE4	0.81	4.23	-	-	-	-	-	-	-	-	-	-	-	-
36	HER2	1.45	5.92	-	-	-	-	-	-	-	-	-	-	-	-
37	HER3	1.17	5.47	-	-	-	-	-	-	-	-	-	-	-	-
38	HGF	3.7	3.99	4.2064	0.002	0.1499	0.2215	6.78	6.17	4.2079	0.0032	0.5752	0.3814	10.78	6.22
39	HGF-R	3.75	1.35	4.1415	-0.0011	0.2305	0.1599	-3.93	87.76	3.962	0.0005	0.0554	0.077	1.84	82.12
40	HMGB1	1.11	1.01	1.3725	-0.0001	0.0176	0.0698	-1.7	42.31	1.3552	0	0.0004	0.0989	-0.5	40.29
41	HP	2.94	0.72	1.3967	-0.0017	0.2327	0.1884	-7.24	24.9	1.272	0.0004	0.0258	0.1893	1.79	20.33
42	ICAM-1	4.35	-6.8	-4.2613	0.0016	0.0159	0.183	5.14	69.47	-4.4418	0.0008	0.0023	0.1333	2.51	64.54
43	IFN-γ	1.63	1.13	1.3751	0.0024	0.2228	0.4436	22.99	20.4	-	-	-	-	-	-
44	IGFBP-1	3.52	4.77	7.0535	0.0017	0.0636	0.5404	5.92	70.43	7.0958	0.0028	0.2297	0.3229	9.8	71.73
45	IGFBP-3	3.28	5.26	7.7582	-0.0009	0.0909	0.1277	-3.33	84.17	7.6484	-0.0001	0.0067	0.078	-0.51	80.47
46	IGFBP-7	3.65	5.86	8.1714	-0.0004	0.0947	0.1151	-1.58	72.34	8.1154	-0.0005	0.0441	0.0638	-1.67	70.59
47	IL-10	3	7.75	-	-	-	-	-	-	-	-	-	-	-	-
48	IL-12	2.4	-6.24	-	-	-	-	-	-	-	-	-	-	-	-
49	IL-15	2.34	6.06	-	-	-	-	-	-	-	-	-	-	-	-

Table I.S11 continued from previous page

	Protein name	Data range (RFU)	Blanks mean (RFU)	CTAD low dilution, 4 °C						CTAD low dilution, 25 °C					
				Intercept (RFU)	Slope (RFU/min)	R^2	Span (RFU)	Increase (%)	Starting (%)	Intercept (RFU)	Slope (RFU/h)	R^2	Span (RFU)	Increase (%)	Starting (%)
50	IL-18	2.91	-4.12	-3.0164	0.0022	0.1224	0.3987	11.47	50.73	-3.0755	0.0025	0.8867	0.2763	13.08	48.02
51	IL-1β	3.12	4.31	4.5734	0.0011	0.0414	0.1466	4.37	9.07	4.5993	0.0014	0.0571	0.2001	5.8	9.98
52	IL-1ra	2.24	-0.15	0.1168	0.0012	0.2273	0.2221	7.56	14.51	0.0557	0.001	0.7502	0.1093	6.23	11.25
53	IL-2	2.27	5.78	-	-	-	-	-	-	-	-	-	-	-	-
54	IL-3	2.37	-2.51	-2.2027	0.0011	0.0913	0.2586	7.98	18.89	-	-	-	-	-	-
55	IL-4	1.26	3.71	-	-	-	-	-	-	-	-	-	-	-	-
56	IL-5	1.48	5.49	-	-	-	-	-	-	-	-	-	-	-	-
58	IL-7	2.47	-0.02	0.2627	0.0017	0.2635	0.2015	9.69	13.69	0.303	0.0012	0.3009	0.1363	6.6	15.65
59	IL-8	2.22	0.05	-	-	-	-	-	-	-	-	-	-	-	-
60	IP-10	3.05	6.62	7.2721	0.0011	0.0521	0.2571	4.85	25.56	-	-	-	-	-	-
61	KLK14	2.82	-0.67	-	-	-	-	-	-	-	-	-	-	-	-
62	KLK8	0.79	5.1	-	-	-	-	-	-	-	-	-	-	-	-
63	Leptin	0.82	5.21	-	-	-	-	-	-	-	-	-	-	-	-
64	M-CSF	2.29	1.71	-	-	-	-	-	-	-	-	-	-	-	-
65	MCP1	1.1	5.53	-	-	-	-	-	-	-	-	-	-	-	-
66	MCP2	3.57	4.43	-	-	-	-	-	-	-	-	-	-	-	-
67	MCP3	2.73	6.63	-	-	-	-	-	-	-	-	-	-	-	-
68	MCP4	2.8	8.09	-	-	-	-	-	-	-	-	-	-	-	-
69	MIG	2.61	-1.78	-	-	-	-	-	-	-	-	-	-	-	-
70	MIP-1α	2.09	1.61	1.8659	0.0011	0.0813	0.133	7.1	14.4	1.9707	0.0009	0.0296	0.1253	5.67	20.31
71	MIP-1β	1.14	6.24	-	-	-	-	-	-	-	-	-	-	-	-
72	MMP-1	1.86	2.78	-	-	-	-	-	-	-	-	-	-	-	-
73	MMP-3	3.57	0.52	2.6018	0.0002	0.0093	0.1027	0.84	74.49	2.631	-0.0006	0.1264	0.0932	-2.64	75.54
74	MMP-9	4.52	5.28	7.6352	0.0004	0.008	0.2751	1.19	55.18	8.024	0.0012	0.0151	0.5486	3.11	64.31
75	NCAM-1	2.76	4.08	5.9905	0.002	0.1078	0.223	9.46	77.22	6.0652	0.0013	0.0744	0.1457	5.86	80.23
76	NT-3	2.37	3.96	-	-	-	-	-	-	-	-	-	-	-	-
77	OPN	3.69	5.59	7.7123	0.0008	0.1686	0.1138	2.69	61.23	7.7044	0.0008	0.2088	0.1892	2.57	61
78	PAI-1	1.8	2.55	-	-	-	-	-	-	-	-	-	-	-	-
79	PDGF-BB	3.59	5.72	6.0222	0.0036	0.4528	0.5465	12.52	8.94	-	-	-	-	-	-
80	PRL	0.83	1.43	-	-	-	-	-	-	-	-	-	-	-	-
81	PSA	2.89	0.44	-	-	-	-	-	-	-	-	-	-	-	-
82	RBP4	0.82	5.18	-	-	-	-	-	-	-	-	-	-	-	-
83	S100B	1.21	2	-	-	-	-	-	-	-	-	-	-	-	-
85	SPARC	2.28	4.96	-	-	-	-	-	-	-	-	-	-	-	-
86	TF	1.72	1.93	-	-	-	-	-	-	-	-	-	-	-	-
87	TGF-α	2.36	4.12	-	-	-	-	-	-	-	-	-	-	-	-
88	TGF-β RII	2.45	4.3	-	-	-	-	-	-	-	-	-	-	-	-
89	TGF-β1	2.84	3.55	-	-	-	-	-	-	-	-	-	-	-	-
90	TGF-β2	1.64	5.81	-	-	-	-	-	-	-	-	-	-	-	-
91	THBS-1	3.71	0.26	2.9576	0.0011	0.2774	0.2057	4.12	84.44	3.0181	0.0009	0.2071	0.1624	3.31	86.33
92	Tie-2	1.35	1.56	1.9859	0.0009	0.1611	0.1342	9.73	40.44	2.0317	0.0003	0.0208	0.1663	3.71	44.85
93	TIMP-1	2.51	5.71	-	-	-	-	-	-	-	-	-	-	-	-
94	TNF-α	2.12	2.04	-	-	-	-	-	-	-	-	-	-	-	-
95	TNF-RI	2.44	2.98	4.184	0.0011	0.0398	0.124	5.83	58.07	4.165	0.0005	0.0216	0.1508	3	57.15
96	TNF-RII	3.3	-2.13	0.3334	-0.0009	0.2318	0.1081	-3.76	89.93	0.1902	-0.0012	0.1433	0.1786	-5.08	84.7
97	uPA	2.28	2.53	3.7369	0.0003	0.0105	0.1065	2.03	63.24	3.5746	0.0015	0.5611	0.1817	8.96	54.72
98	uPA-R	2.38	6.54	-	-	-	-	-	-	-	-	-	-	-	-
99	VCAM-1	4.35	0.2	3.561	-0.0015	0.2586	0.1788	-4.6	89.16	3.5664	-0.0004	0.0316	0.049	-1.29	89.3
100	VEGF-A	4.09	4.94	-	-	-	-	-	-	-	-	-	-	-	-

Table I.S11 continued from previous page

	Protein name	Data range (RFU)	Blanks mean (RFU)	CTAD low dilution, 4 °C						CTAD low dilution, 25 °C					
				Intercept (RFU)	Slope (RFU/min)	R^2	Span (RFU)	Increase (%)	Starting (%)	Intercept (RFU)	Slope (RFU/h)	R^2	Span (RFU)	Increase (%)	Starting (%)
101	VEGF-D	0.98	2.95	-	-	-	-	-	-	-	-	-	-	-	-
102	VEGFR2	2.98	1.46	2.5982	0.003	0.2738	0.3933	17.64	58.9	2.6269	0.0006	0.0254	0.0701	3.76	60.38
103	VEGFR3	1.24	7.95	-	-	-	-	-	-	-	-	-	-	-	-

TABLE I.S12: **Pre-analytical variables linear regression parameters in CTAD samples, high dilution.**

	Protein name	Data range (RFU)	Blanks mean (RFU)	CTAD high dilution, 4 °C						CTAD high dilution, 25 °C					
				Intercept (RFU)	Slope (RFU/min)	R^2	Span (RFU)	Increase (%)	Starting (%)	Intercept (RFU)	Slope (RFU/h)	R^2	Span (RFU)	Increase (%)	Starting (%)
1	AFP	3.35	1.56	2.0072	0.0015	0.1298	0.1631	5.89	15.37	-	-	-	-	-	-
2	AHSG	4.1	6.77	-	-	-	-	-	-	-	-	-	-	-	-
3	ALDH1L1	1.05	3.32	-	-	-	-	-	-	-	-	-	-	-	-
4	Amphiregulin	2.28	4.01	-	-	-	-	-	-	-	-	-	-	-	-
5	Ang1	3.33	0.96	-	-	-	-	-	-	-	-	-	-	-	-
6	Ang2	0.88	5.07	-	-	-	-	-	-	-	-	-	-	-	-
8	BDNF	2.62	1.93	-	-	-	-	-	-	-	-	-	-	-	-
9	BMP2	0.78	3.25	-	-	-	-	-	-	-	-	-	-	-	-
10	BRAF	0.94	5.21	-	-	-	-	-	-	-	-	-	-	-	-
11	c-Kit	3.19	5.95	6.6671	-0.0014	0.1663	0.3318	-5.7	25.41	6.6721	0.0001	0.001	0.0504	0.52	25.58
12	CA15-3	2.87	-1.56	-0.7905	-0.0029	0.7801	0.3255	-14.17	32.42	-1.0118	0.0016	0.2166	0.1773	7.73	23.07
13	Cathepsin B	0.79	4.9	-	-	-	-	-	-	-	-	-	-	-	-
14	CCL5	3.76	7.11	-	-	-	-	-	-	-	-	-	-	-	-
15	CD14	4.06	-4.55	-2.4623	0.0004	0.0083	0.0656	1.6	71.91	-2.1667	-0.0015	0.312	0.1813	-5.78	82.08
16	CEA	1.37	5.65	-	-	-	-	-	-	5.814	0.0012	0.6809	0.1281	14.84	17.66
17	CRP	0.89	-1.03	-	-	-	-	-	-	-	-	-	-	-	-
18	CXCL12	1.43	6.56	-	-	-	-	-	-	-	-	-	-	-	-
19	E-cadherin	2.44	5.61	6.1502	0.0004	0.0143	0.2017	2.12	26.12	6.0288	0.0014	0.6331	0.1505	7.55	20.22
20	E-selectin	2.11	1.25	-	-	-	-	-	-	-	-	-	-	-	-
21	EGF	3.86	5.84	-	-	-	-	-	-	-	-	-	-	-	-
22	EGF-R	3.67	-2.28	-0.5464	0.0011	0.4632	0.1383	4.04	54.1	-0.7583	0.0055	0.8869	0.606	19.86	47.47
23	Endoglin	1.85	0.65	-	-	-	-	-	-	-	-	-	-	-	-
24	EpCAM	1.87	6.17	-	-	-	-	-	-	-	-	-	-	-	-
25	FAS	2.74	4.38	-	-	-	-	-	-	-	-	-	-	-	-
26	FAS-L	1.18	-0.73	-	-	-	-	-	-	-	-	-	-	-	-
28	FGFb	1.24	5.22	-	-	-	-	-	-	5.3454	0.0016	0.6914	0.1918	19.69	13.09
29	Flt-3	1.49	6.2	-	-	-	-	-	-	-	-	-	-	-	-
30	G-CSF	2.39	0.8	-	-	-	-	-	-	-	-	-	-	-	-
31	GFAP	2.62	0.12	-	-	-	-	-	-	-	-	-	-	-	-
32	GM-CSF	1.87	5.53	-	-	-	-	-	-	-	-	-	-	-	-
33	GRO-α	2.43	-8.01	-	-	-	-	-	-	-	-	-	-	-	-
34	HAI-1	1.98	5.42	-	-	-	-	-	-	-	-	-	-	-	-
35	HE4	0.81	4.23	-	-	-	-	-	-	-	-	-	-	-	-
36	HER2	1.45	5.92	-	-	-	-	-	-	-	-	-	-	-	-
37	HER3	1.17	5.47	5.8351	-0.0009	0.1262	0.205	-11.63	43.1	-	-	-	-	-	-
38	HGF	3.7	3.99	-	-	-	-	-	-	-	-	-	-	-	-
39	HGF-R	3.75	1.35	2.94	-0.0026	0.3839	0.4584	-9.37	49.98	3.1827	0.0003	0.0051	0.1152	1.26	57.61

Table I.S12 continued from previous page

	Protein name	Data range (RFU)	Blanks mean (RFU)	CTAD high dilution, 4 °C						CTAD high dilution, 25 °C					
				Intercept (RFU)	Slope (RFU/min)	R^2	Span (RFU)	Increase (%)	Starting (%)	Intercept (RFU)	Slope (RFU/h)	R^2	Span (RFU)	Increase (%)	Starting (%)
40	HMGB1	1.11	1.01	-	-	-	-	-	-	-	-	-	-	-	-
41	HP	2.94	0.72	0.982	-0.0003	0.1127	0.0716	-1.47	9.7	0.8909	0.0012	0.2005	0.1352	4.93	6.36
42	ICAM-1	4.35	-6.8	-5.142	0.0046	0.1573	0.515	14.5	45.41	-5.339	0.0033	0.1855	0.4532	10.34	40.02
43	IFN-γ	1.63	1.13	-	-	-	-	-	-	-	-	-	-	-	-
44	IGFBP-1	3.52	4.77	7.6719	-0.0026	0.3932	0.3487	-9.32	89.47	7.1891	0.0037	0.3702	0.4622	13.03	74.6
45	IGFBP-3	3.28	5.26	7.3651	-0.0013	0.2918	0.1443	-4.95	70.95	7.2437	0.0004	0.073	0.1391	1.69	66.86
46	IGFBP-7	3.65	5.86	8.0909	0.001	0.1203	0.2479	3.69	69.82	7.6811	0.0032	0.8116	0.3956	11.47	56.98
47	IL-10	3	7.75	-	-	-	-	-	-	-	-	-	-	-	-
48	IL-12	2.4	-6.24	-	-	-	-	-	-	-	-	-	-	-	-
49	IL-15	2.34	6.06	-	-	-	-	-	-	-	-	-	-	-	-
50	IL-18	2.91	-4.12	-3.5675	0.0015	0.1746	0.1818	7.99	25.41	-3.2081	-0.0029	0.3921	0.3429	-15.21	41.92
51	IL-1β	3.12	4.31	-	-	-	-	-	-	-	-	-	-	-	-
52	IL-1ra	2.24	-0.15	-	-	-	-	-	-	-	-	-	-	-	-
53	IL-2	2.27	5.78	-	-	-	-	-	-	-	-	-	-	-	-
54	IL-3	2.37	-2.51	-	-	-	-	-	-	-	-	-	-	-	-
55	IL-4	1.26	3.71	-	-	-	-	-	-	-	-	-	-	-	-
56	IL-5	1.48	5.49	-	-	-	-	-	-	-	-	-	-	-	-
58	IL-7	2.47	-0.02	-	-	-	-	-	-	-	-	-	-	-	-
59	IL-8	2.22	0.05	-	-	-	-	-	-	-	-	-	-	-	-
60	IP-10	3.05	6.62	-	-	-	-	-	-	-	-	-	-	-	-
61	KLK14	2.82	-0.67	-	-	-	-	-	-	-	-	-	-	-	-
62	KLK8	0.79	5.1	5.4145	-0.0003	0.0228	0.1953	-6.43	54.89	5.3073	0.0021	0.5727	0.2317	42.09	36.15
63	Leptin	0.82	5.21	-	-	-	-	-	-	-	-	-	-	-	-
64	M-CSF	2.29	1.71	-	-	-	-	-	-	-	-	-	-	-	-
65	MCP1	1.1	5.53	6.0186	-0.0026	0.4386	0.3537	-40.6	67.21	-	-	-	-	-	-
66	MCP2	3.57	4.43	-	-	-	-	-	-	-	-	-	-	-	-
67	MCP3	2.73	6.63	-	-	-	-	-	-	-	-	-	-	-	-
68	MCP4	2.8	8.09	-	-	-	-	-	-	-	-	-	-	-	-
69	MIG	2.61	-1.78	-	-	-	-	-	-	-	-	-	-	-	-
70	MIP-1α	2.09	1.61	-	-	-	-	-	-	-	-	-	-	-	-
71	MIP-1β	1.14	6.24	-	-	-	-	-	-	-	-	-	-	-	-
72	MMP-1	1.86	2.78	-	-	-	-	-	-	-	-	-	-	-	-
73	MMP-3	3.57	0.52	1.9516	0.0003	0.0055	0.1118	1.11	51.17	1.8708	0.0019	0.4026	0.2505	7.87	48.27
74	MMP-9	4.52	5.28	7.9438	0.0011	0.2805	0.2239	3	62.42	7.8611	0.0053	0.1602	0.7525	14.19	60.48
75	NCAM-1	2.76	4.08	4.763	-0.0005	0.0553	0.073	-2.3	27.71	4.5686	0.0013	0.1709	0.1653	6.04	19.87
76	NT-3	2.37	3.96	-	-	-	-	-	-	-	-	-	-	-	-
77	OPN	3.69	5.59	7.6926	-0.0038	0.2453	0.5197	-12.5	60.66	7.0877	0.0033	0.2218	0.4151	10.82	43.21
78	PAI-1	1.8	2.55	-	-	-	-	-	-	-	-	-	-	-	-
79	PDGF-BB	3.59	5.72	-	-	-	-	-	-	-	-	-	-	-	-
80	PRL	0.83	1.43	-	-	-	-	-	-	-	-	-	-	-	-
81	PSA	2.89	0.44	-	-	-	-	-	-	-	-	-	-	-	-
82	RBP4	0.82	5.18	-	-	-	-	-	-	-	-	-	-	-	-
83	S100B	1.21	2	-	-	-	-	-	-	-	-	-	-	-	-
85	SPARC	2.28	4.96	-	-	-	-	-	-	-	-	-	-	-	-
86	TF	1.72	1.93	-	-	-	-	-	-	-	-	-	-	-	-
87	TGF-α	2.36	4.12	-	-	-	-	-	-	-	-	-	-	-	-
88	TGF-β RII	2.45	4.3	-	-	-	-	-	-	-	-	-	-	-	-
89	TGF-β1	2.84	3.55	-	-	-	-	-	-	-	-	-	-	-	-
90	TGF-β2	1.64	5.81	-	-	-	-	-	-	-	-	-	-	-	-

Table I.S12 continued from previous page

	Protein name	Data range (RFU)	Blanks mean (RFU)	CTAD high dilution, 4 °C Intercept (RFU)	Slope (RFU/min)	R^2	Span (RFU)	Increase (%)	Starting (%)	CTAD high dilution, 25 °C Intercept (RFU)	Slope (RFU/h)	R^2	Span (RFU)	Increase (%)	Starting (%)
91	THBS-1	3.71	0.26	2.1187	0.0019	0.0783	0.7676	6.97	58.23	2.1926	-0.0034	0.1419	0.8693	-12.06	60.54
92	Tie-2	1.35	1.56	-	-	-	-	-	-	-	-	-	-	-	-
93	TIMP-1	2.51	5.71	6.5655	-0.0052	0.6547	0.643	-28.55	40.47	6.5025	-0.0006	0.0096	0.1947	-3.37	37.49
94	TNF-α	2.12	2.04	-	-	-	-	-	-	-	-	-	-	-	-
95	TNF-RI	2.44	2.98	-	-	-	-	-	-	-	-	-	-	-	-
96	TNF-RII	3.3	-2.13	-1.6848	0.0024	0.5294	0.3548	10.14	16.31	-1.4065	-0.0005	0.0101	0.1607	-2.13	26.46
97	uPA	2.28	2.53	-	-	-	-	-	-	-	-	-	-	-	-
98	uPA-R	2.38	6.54	-	-	-	-	-	-	-	-	-	-	-	-
99	VCAM-1	4.35	0.2	2.9436	-0.0011	0.1333	0.2878	-3.43	72.8	2.792	0.0011	0.0904	0.1812	3.4	68.78
100	VEGF-A	4.09	4.94	-	-	-	-	-	-	-	-	-	-	-	-
101	VEGF-D	0.98	2.95	-	-	-	-	-	-	-	-	-	-	-	-
102	VEGFR2	2.98	1.46	-	-	-	-	-	-	-	-	-	-	-	-
103	VEGFR3	1.24	7.95	-	-	-	-	-	-	-	-	-	-	-	-

TABLE I.S13: **Pre-analytical variables linear regression parameters in $CTAD_{Filt}$ samples, low dilution.**

	Protein name	Data range (RFU)	Blanks mean (RFU)	$CTAD_{Filt}$ low dilution, 4 °C Intercept (RFU)	Slope (RFU/min)	R^2	Span (RFU)	Increase (%)	Starting (%)	$CTAD_{Filt}$ low dilution, 25 °C Intercept (RFU)	Slope (RFU/h)	R^2	Span (RFU)	Increase (%)	Starting (%)
1	AFP	3.35	1.56	2.6358	0	0.0006	0.0773	0.2	36.91	2.6455	0	0	0.0715	-0.02	37.24
2	AHSG	4.1	6.77	-	-	-	-	-	-	-	-	-	-	-	-
3	ALDH1L1	1.05	3.32	-	-	-	-	-	-	-	-	-	-	-	-
4	Amphiregulin	2.28	4.01	-	-	-	-	-	-	-	-	-	-	-	-
5	Ang1	3.33	0.96	-	-	-	-	-	-	-	-	-	-	-	-
6	Ang2	0.88	5.07	-	-	-	-	-	-	-	-	-	-	-	-
8	BDNF	2.62	1.93	2.658	-0.0039	0.3617	0.464	-24.72	39.98	2.6536	0.0001	0.0001	0.0136	0.63	39.73
9	BMP2	0.78	3.25	-	-	-	-	-	-	-	-	-	-	-	-
10	BRAF	0.94	5.21	-	-	-	-	-	-	-	-	-	-	-	-
11	c-Kit	3.19	5.95	7.2071	-0.0002	0.0052	0.1288	-0.84	44.46	7.1334	0.001	0.1638	0.1248	4.15	41.86
12	CA15-3	2.87	-1.56	-0.1847	0.0008	0.0815	0.1	3.89	58	-0.2336	-0.0005	0.0185	0.0578	-2.57	55.94
13	Cathepsin B	0.79	4.9	-	-	-	-	-	-	-	-	-	-	-	-
14	CCL5	3.76	7.11	-	-	-	-	-	-	-	-	-	-	-	-
15	CD14	4.06	-4.55	-2.0156	-0.006	0.7287	0.7874	-23.87	87.27	-2.2022	0.001	0.0487	0.2238	3.94	80.86
16	CEA	1.37	5.65	5.8186	0.0014	0.1668	0.155	17.72	18.16	-	-	-	-	-	-
17	CRP	0.89	-1.03	-	-	-	-	-	-	-	-	-	-	-	-
18	CXCL12	1.43	6.56	-	-	-	-	-	-	-	-	-	-	-	-
19	E-cadherin	2.44	5.61	7.1764	-0.0002	0.0016	0.1432	-1.05	76.04	7.1726	-0.001	0.0349	0.1662	-5.65	75.85
20	E-selectin	2.11	1.25	2.0946	-0.0034	0.7607	0.3809	-27.93	59.8	1.8955	0.0006	0.074	0.0705	4.81	45.67
21	EGF	3.86	5.84	-	-	-	-	-	-	-	-	-	-	-	-
22	EGF-R	3.67	-2.28	0.2334	-0.0021	0.5733	0.3315	-7.48	78.48	0.0419	0.0005	0.0168	0.055	1.78	72.49
23	Endoglin	1.85	0.65	1.6588	-0.0008	0.5628	0.1017	-7.46	79.13	1.6386	-0.0013	0.3199	0.1869	-11.72	77.55
24	EpCAM	1.87	6.17	-	-	-	-	-	-	-	-	-	-	-	-
25	FAS	2.74	4.38	5.1949	-0.0012	0.0398	0.1254	-5.57	34.01	5.0679	0.0001	0.0018	0.0173	0.64	28.71
26	FAS-L	1.18	-0.73	-0.298	-0.0016	0.636	0.2353	-24.07	55.67	-0.3243	-0.0009	0.4126	0.1103	-12.8	52.27
28	FGFb	1.24	5.22	-	-	-	-	-	-	5.4767	0.0001	0.0013	0.0527	1.05	27.14
29	Flt-3	1.49	6.2	-	-	-	-	-	-	-	-	-	-	-	-

Table I.S13 continued from previous page

		Data	Blanks	$CTAD_{Filt}$ low dilution, 4 °C						$CTAD_{Filt}$ low dilution, 25 °C					
	Protein name	range (RFU)	mean (RFU)	Intercept (RFU)	Slope (RFU/min)	R^2	Span (RFU)	Increase (%)	Starting (%)	Intercept (RFU)	Slope (RFU/h)	R^2	Span (RFU)	Increase (%)	Starting (%)
30	G-CSF	2.39	0.8	-	-	-	-	-	-	-	-	-	-	-	-
31	GFAP	2.62	0.12	0.8807	0.0013	0.0615	0.2368	6.64	34.13	0.9904	0.0007	0.0668	0.1208	3.66	39.05
32	GM-CSF	1.87	5.53	-	-	-	-	-	-	-	-	-	-	-	-
33	GRO-α	2.43	-8.01	-	-	-	-	-	-	-	-	-	-	-	-
34	HAI-1	1.98	5.42	5.755	-0.0008	0.0868	0.0991	-5.07	19.34	-	-	-	-	-	-
35	HE4	0.81	4.23	-	-	-	-	-	-	-	-	-	-	-	-
36	HER2	1.45	5.92	-	-	-	-	-	-	-	-	-	-	-	-
37	HER3	1.17	5.47	-	-	-	-	-	-	-	-	-	-	-	-
38	HGF	3.7	3.99	4.4184	-0.0008	0.0162	0.1021	-2.54	12.31	4.3078	0	0	0.1352	0	9.11
39	HGF-R	3.75	1.35	4.1022	-0.0041	0.5355	0.4732	-14.81	86.52	4.1136	-0.001	0.0932	0.1636	-3.58	86.88
40	HMGB1	1.11	1.01	1.4063	-0.0015	0.835	0.1686	-19.84	46.24	1.3401	0.0004	0.1646	0.1044	5.83	38.54
41	HP	2.94	0.72	1.2416	0.0002	0.0023	0.0176	0.66	19.21	1.2847	-0.0001	0.0015	0.0271	-0.6	20.79
42	ICAM-1	4.35	-6.8	-3.999	-0.003	0.0402	0.3419	-9.39	76.64	-4.2478	0.002	0.0223	0.4296	6.3	69.84
43	IFN-γ	1.63	1.13	-	-	-	-	-	-	-	-	-	-	-	-
44	IGFBP-1	3.52	4.77	7.3213	-0.0015	0.077	0.3109	-5.39	78.68	7.1768	0.0016	0.0687	0.4196	5.51	74.22
45	IGFBP-3	3.28	5.26	7.6642	-0.0003	0.0265	0.0487	-1.34	81	7.5834	0.0009	0.2241	0.109	3.61	78.28
46	IGFBP-7	3.65	5.86	8.1632	-0.0005	0.1138	0.1071	-1.65	72.09	8.1393	-0.0003	0.0241	0.0958	-0.96	71.34
47	IL-10	3	7.75	-	-	-	-	-	-	-	-	-	-	-	-
48	IL-12	2.4	-6.24	-	-	-	-	-	-	-	-	-	-	-	-
49	IL-15	2.34	6.06	-	-	-	-	-	-	-	-	-	-	-	-
50	IL-18	2.91	-4.12	-2.7953	-0.0016	0.1887	0.1854	-8.38	60.89	-2.7994	-0.0004	0.0101	0.1175	-2.01	60.7
51	IL-1β	3.12	4.31	4.8343	-0.0009	0.013	0.1229	-3.81	18.21	4.6268	-0.0001	0.0007	0.1665	-0.58	10.94
52	IL-1ra	2.24	-0.15	0.1919	-0.0016	0.4985	0.2417	-9.91	18.52	0.1761	0	0.0001	0.1664	-0.17	17.68
53	IL-2	2.27	5.78	-	-	-	-	-	-	-	-	-	-	-	-
54	IL-3	2.37	-2.51	-	-	-	-	-	-	-	-	-	-	-	-
55	IL-4	1.26	3.71	-	-	-	-	-	-	-	-	-	-	-	-
56	IL-5	1.48	5.49	-	-	-	-	-	-	-	-	-	-	-	-
58	IL-7	2.47	-0.02	0.4842	-0.0015	0.2152	0.1702	-8.49	24.48	-	-	-	-	-	-
59	IL-8	2.22	0.05	-	-	-	-	-	-	-	-	-	-	-	-
60	IP-10	3.05	6.62	7.4242	-0.0011	0.0701	0.1265	-4.82	31.54	7.3136	0.0001	0.0007	0.0123	0.35	27.19
61	KLK14	2.82	-0.67	-	-	-	-	-	-	-	-	-	-	-	-
62	KLK8	0.79	5.1	-	-	-	-	-	-	-	-	-	-	-	-
63	Leptin	0.82	5.21	-	-	-	-	-	-	-	-	-	-	-	-
64	M-CSF	2.29	1.71	-	-	-	-	-	-	-	-	-	-	-	-
65	MCP1	1.1	5.53	-	-	-	-	-	-	-	-	-	-	-	-
66	MCP2	3.57	4.43	-	-	-	-	-	-	-	-	-	-	-	-
67	MCP3	2.73	6.63	-	-	-	-	-	-	-	-	-	-	-	-
68	MCP4	2.8	8.09	-	-	-	-	-	-	-	-	-	-	-	-
69	MIG	2.61	-1.78	-	-	-	-	-	-	-	-	-	-	-	-
70	MIP-1α	2.09	1.61	1.9156	0.0026	0.3871	0.2781	16.64	17.2	-	-	-	-	-	-
71	MIP-1β	1.14	6.24	-	-	-	-	-	-	-	-	-	-	-	-
72	MMP-1	1.86	2.78	-	-	-	-	-	-	-	-	-	-	-	-
73	MMP-3	3.57	0.52	2.6979	-0.0022	0.3209	0.3098	-9.01	77.94	2.5859	0.0007	0.2063	0.0988	2.87	73.92
74	MMP-9	4.52	5.28	7.5515	0.0036	0.2781	0.4621	9.6	53.21	7.7604	0.0034	0.0696	0.5469	9.29	58.12
75	NCAM-1	2.76	4.08	6.0384	0.0001	0.0009	0.0895	0.61	79.15	6.0097	0.0014	0.1249	0.2527	6.47	77.99
76	NT-3	2.37	3.96	-	-	-	-	-	-	-	-	-	-	-	-
77	OPN	3.69	5.59	7.715	0.0009	0.4502	0.1231	3	61.31	7.7309	0.0004	0.062	0.05	1.41	61.77
78	PAI-1	1.8	2.55	-	-	-	-	-	-	-	-	-	-	-	-
79	PDGF-BB	3.59	5.72	-	-	-	-	-	-	-	-	-	-	-	-

Table I.S13 continued from previous page

		Data	Blanks	$CTAD_{Filt}$ low dilution, 4 °C						$CTAD_{Filt}$ low dilution, 25 °C					
	Protein name	range (RFU)	mean (RFU)	Intercept (RFU)	Slope (RFU/min)	R^2	Span (RFU)	Increase (%)	Starting (%)	Intercept (RFU)	Slope (RFU/h)	R^2	Span (RFU)	Increase (%)	Starting (%)
80	PRL	0.83	1.43	1.7349	-0.002	0.903	0.2153	-38.48	51.53	1.6717	0.0004	0.6184	0.0401	6.73	41.02
81	PSA	2.89	0.44	-	-	-	-	-	-	-	-	-	-	-	-
82	RBP4	0.82	5.18	-	-	-	-	-	-	-	-	-	-	-	-
83	S100B	1.21	2	-	-	-	-	-	-	-	-	-	-	-	-
85	SPARC	2.28	4.96	-	-	-	-	-	-	-	-	-	-	-	-
86	TF	1.72	1.93	-	-	-	-	-	-	-	-	-	-	-	-
87	TGF-α	2.36	4.12	-	-	-	-	-	-	-	-	-	-	-	-
88	TGF-β RII	2.45	4.3	-	-	-	-	-	-	-	-	-	-	-	-
89	TGF-β1	2.84	3.55	-	-	-	-	-	-	-	-	-	-	-	-
90	TGF-β2	1.64	5.81	-	-	-	-	-	-	-	-	-	-	-	-
91	THBS-1	3.71	0.26	2.2548	0.0038	0.2093	0.5166	13.73	62.48	2.4693	0.0036	0.6578	0.4848	12.99	69.18
92	Tie-2	1.35	1.56	1.9706	0.0003	0.0386	0.0519	3.65	38.98	2.0579	0.0001	0.0038	0.0314	1.61	47.36
93	TIMP-1	2.51	5.71	-	-	-	-	-	-	-	-	-	-	-	-
94	TNF-α	2.12	2.04	-	-	-	-	-	-	-	-	-	-	-	-
95	TNF-RI	2.44	2.98	4.2855	-0.0011	0.1437	0.1558	-5.91	62.96	4.2909	-0.0006	0.0405	0.0813	-3.59	63.22
96	TNF-RII	3.3	-2.13	0.2819	-0.0045	0.6432	0.4884	-19.04	88.05	0.1308	0.001	0.1641	0.1155	4.33	82.54
97	uPA	2.28	2.53	3.679	0.0002	0.0141	0.0308	1.15	60.21	3.7322	-0.0004	0.0918	0.0904	-2.58	62.99
98	uPA-R	2.38	6.54	-	-	-	-	-	-	-	-	-	-	-	-
99	VCAM-1	4.35	0.2	3.6613	-0.0023	0.7372	0.2644	-7.15	91.81	3.46	0.0005	0.0117	0.121	1.48	86.48
100	VEGF-A	4.09	4.94	5.2649	0.003	0.1996	0.3862	9.3	8.72	-	-	-	-	-	-
101	VEGF-D	0.98	2.95	-	-	-	-	-	-	-	-	-	-	-	-
102	VEGFR2	2.98	1.46	2.847	-0.0032	0.4491	0.3567	-18.97	71.72	2.8249	0	0.0001	0.0285	-0.21	70.58
103	VEGFR3	1.24	7.95	-	-	-	-	-	-	-	-	-	-	-	-

TABLE I.S14: **Pre-analytical variables linear regression parameters in $CTAD_{Filt}$ samples, high dilution.**

		Data	Blanks	$CTAD_{Filt}$ high dilution, 4 °C						$CTAD_{Filt}$ high dilution, 25 °C					
	Protein name	range (RFU)	mean (RFU)	Intercept (RFU)	Slope (RFU/min)	R^2	Span (RFU)	Increase (%)	Starting (%)	Intercept (RFU)	Slope (RFU/h)	R^2	Span (RFU)	Increase (%)	Starting (%)
1	AFP	3.35	1.56	-	-	-	-	-	-	-	-	-	-	-	-
2	AHSG	4.1	6.77	-	-	-	-	-	-	-	-	-	-	-	-
3	ALDH1L1	1.05	3.32	-	-	-	-	-	-	-	-	-	-	-	-
4	Amphiregulin	2.28	4.01	-	-	-	-	-	-	-	-	-	-	-	-
5	Ang1	3.33	0.96	-	-	-	-	-	-	-	-	-	-	-	-
6	Ang2	0.88	5.07	-	-	-	-	-	-	-	-	-	-	-	-
8	BDNF	2.62	1.93	-	-	-	-	-	-	-	-	-	-	-	-
9	BMP2	0.78	3.25	-	-	-	-	-	-	-	-	-	-	-	-
10	BRAF	0.94	5.21	-	-	-	-	-	-	-	-	-	-	-	-
11	c-Kit	3.19	5.95	6.831	-0.0028	0.3268	0.3439	-11.54	31.19	6.6089	0.0022	0.2408	0.2454	9.08	23.35
12	CA15-3	2.87	-1.56	-0.8137	-0.0021	0.3271	0.4207	-10.29	31.44	-0.9934	0.0012	0.1761	0.3058	6.04	23.84
13	Cathepsin B	0.79	4.9	-	-	-	-	-	-	-	-	-	-	-	-
14	CCL5	3.76	7.11	-	-	-	-	-	-	-	-	-	-	-	-
15	CD14	4.06	-4.55	-2.3165	-0.002	0.1692	0.249	-7.75	76.92	-2.3748	-0.0008	0.148	0.1351	-3.18	74.92
16	CEA	1.37	5.65	-	-	-	-	-	-	-	-	-	-	-	-
17	CRP	0.89	-1.03	-	-	-	-	-	-	-	-	-	-	-	-
18	CXCL12	1.43	6.56	-	-	-	-	-	-	-	-	-	-	-	-

Table I.S14 continued from previous page

		Data	Blanks	$CTAD_{Filt}$ high dilution, 4 °C						$CTAD_{Filt}$ high dilution, 25 °C					
	Protein name	range (RFU)	mean (RFU)	Intercept (RFU)	Slope (RFU/min)	R^2	Span (RFU)	Increase (%)	Starting (%)	Intercept (RFU)	Slope (RFU/h)	R^2	Span (RFU)	Increase (%)	Starting (%)
19	E-cadherin	2.44	5.61	6.0489	0.0013	0.4007	0.1719	7.34	21.2	6.0712	0.0008	0.0708	0.0983	4.35	22.28
20	E-selectin	2.11	1.25	-	-	-	-	-	-	-	-	-	-	-	-
21	EGF	3.86	5.84	-	-	-	-	-	-	-	-	-	-	-	-
22	EGF-R	3.67	-2.28	-0.5354	0.0002	0.0032	0.0208	0.55	54.44	-0.3084	-0.0001	0.0008	0.3204	-0.32	61.54
23	Endoglin	1.85	0.65	-	-	-	-	-	-	-	-	-	-	-	-
24	EpCAM	1.87	6.17	-	-	-	-	-	-	-	-	-	-	-	-
25	FAS	2.74	4.38	-	-	-	-	-	-	-	-	-	-	-	-
26	FAS-L	1.18	-0.73	-	-	-	-	-	-	-	-	-	-	-	-
28	FGFb	1.24	5.22	-	-	-	-	-	-	5.4026	0.001	0.1281	0.1502	12.02	19.22
29	Flt-3	1.49	6.2	-	-	-	-	-	-	-	-	-	-	-	-
30	G-CSF	2.39	0.8	-	-	-	-	-	-	-	-	-	-	-	-
31	GFAP	2.62	0.12	-	-	-	-	-	-	-	-	-	-	-	-
32	GM-CSF	1.87	5.53	-	-	-	-	-	-	-	-	-	-	-	-
33	GRO-α	2.43	-8.01	-	-	-	-	-	-	-	-	-	-	-	-
34	HAI-1	1.98	5.42	5.7261	-0.001	0.2646	0.1721	-6.44	17.67	-	-	-	-	-	-
35	HE4	0.81	4.23	-	-	-	-	-	-	-	-	-	-	-	-
36	HER2	1.45	5.92	-	-	-	-	-	-	-	-	-	-	-	-
37	HER3	1.17	5.47	5.832	-0.001	0.1639	0.2436	-13.27	42.73	5.8506	-0.0001	0.0045	0.0132	-1.21	44.91
38	HGF	3.7	3.99	-	-	-	-	-	-	-	-	-	-	-	-
39	HGF-R	3.75	1.35	3.1995	-0.0043	0.4669	0.5345	-15.55	58.14	3.1082	0	0	0.0543	0.06	55.27
40	HMGB1	1.11	1.01	-	-	-	-	-	-	-	-	-	-	-	-
41	HP	2.94	0.72	-	-	-	-	-	-	1.005	-0.0008	0.1317	0.0883	-3.22	10.54
42	ICAM-1	4.35	-6.8	-5.3562	0.0012	0.0123	0.1991	3.79	39.55	-5.2024	0.0009	0.0096	0.2769	2.8	43.75
43	IFN-γ	1.63	1.13	-	-	-	-	-	-	-	-	-	-	-	-
44	IGFBP-1	3.52	4.77	7.6394	-0.0013	0.0614	0.4584	-4.74	88.47	7.7699	-0.0016	0.256	0.2033	-5.55	92.48
45	IGFBP-3	3.28	5.26	7.3061	0	0.0004	0.0952	0.14	68.96	7.3252	-0.0002	0.02	0.0235	-0.64	69.61
46	IGFBP-7	3.65	5.86	7.8381	0.0019	0.1292	0.2573	6.89	61.9	7.9271	0.0012	0.0987	0.1406	4.23	64.69
47	IL-10	3	7.75	-	-	-	-	-	-	-	-	-	-	-	-
48	IL-12	2.4	-6.24	-	-	-	-	-	-	-	-	-	-	-	-
49	IL-15	2.34	6.06	-	-	-	-	-	-	-	-	-	-	-	-
50	IL-18	2.91	-4.12	-	-	-	-	-	-	-	-	-	-	-	-
51	IL-1β	3.12	4.31	-	-	-	-	-	-	-	-	-	-	-	-
52	IL-1ra	2.24	-0.15	-	-	-	-	-	-	-	-	-	-	-	-
53	IL-2	2.27	5.78	-	-	-	-	-	-	-	-	-	-	-	-
54	IL-3	2.37	-2.51	-	-	-	-	-	-	-	-	-	-	-	-
55	IL-4	1.26	3.71	-	-	-	-	-	-	-	-	-	-	-	-
56	IL-5	1.48	5.49	-	-	-	-	-	-	-	-	-	-	-	-
58	IL-7	2.47	-0.02	-	-	-	-	-	-	-	-	-	-	-	-
59	IL-8	2.22	0.05	-	-	-	-	-	-	-	-	-	-	-	-
60	IP-10	3.05	6.62	-	-	-	-	-	-	-	-	-	-	-	-
61	KLK14	2.82	-0.67	-	-	-	-	-	-	-	-	-	-	-	-
62	KLK8	0.79	5.1	5.3047	0.0009	0.1138	0.2057	17.82	35.7	5.4545	-0.0006	0.0381	0.2216	-12.59	61.88
63	Leptin	0.82	5.21	-	-	-	-	-	-	-	-	-	-	-	-
64	M-CSF	2.29	1.71	-	-	-	-	-	-	-	-	-	-	-	-
65	MCP1	1.1	5.53	-	-	-	-	-	-	-	-	-	-	-	-
66	MCP2	3.57	4.43	-	-	-	-	-	-	-	-	-	-	-	-
67	MCP3	2.73	6.63	-	-	-	-	-	-	-	-	-	-	-	-
68	MCP4	2.8	8.09	-	-	-	-	-	-	-	-	-	-	-	-
69	MIG	2.61	-1.78	-	-	-	-	-	-	-	-	-	-	-	-

Table I.S14 continued from previous page

	Protein name	Data range (RFU)	Blanks mean (RFU)	$CTAD_{Filt}$ high dilution, 4 °C						$CTAD_{Filt}$ high dilution, 25 °C					
				Intercept (RFU)	Slope (RFU/min)	R^2	Span (RFU)	Increase (%)	Starting (%)	Intercept (RFU)	Slope (RFU/h)	R^2	Span (RFU)	Increase (%)	Starting (%)
70	MIP-1α	2.09	1.61	-	-	-	-	-	-	-	-	-	-	-	-
71	MIP-1β	1.14	6.24	-	-	-	-	-	-	-	-	-	-	-	-
72	MMP-1	1.86	2.78	-	-	-	-	-	-	-	-	-	-	-	-
73	MMP-3	3.57	0.52	1.8905	0	0.0001	0.1358	-0.15	48.98	2.0843	0.0001	0.0008	0.3423	0.58	55.93
74	MMP-9	4.52	5.28	7.7873	0.0019	0.2107	0.3389	5.23	58.75	8.0473	0.0039	0.2038	0.4499	10.54	64.85
75	NCAM-1	2.76	4.08	4.5753	-0.0003	0.0152	0.2395	-1.52	20.14	4.6978	0.0001	0.0057	0.017	0.6	25.08
76	NT-3	2.37	3.96	-	-	-	-	-	-	-	-	-	-	-	-
77	OPN	3.69	5.59	7.3625	-0.0004	0.0049	0.321	-1.31	51.14	7.6023	-0.0014	0.1146	0.1607	-4.62	58.06
78	PAI-1	1.8	2.55	-	-	-	-	-	-	-	-	-	-	-	-
79	PDGF-BB	3.59	5.72	-	-	-	-	-	-	-	-	-	-	-	-
80	PRL	0.83	1.43	-	-	-	-	-	-	-	-	-	-	-	-
81	PSA	2.89	0.44	-	-	-	-	-	-	-	-	-	-	-	-
82	RBP4	0.82	5.18	-	-	-	-	-	-	-	-	-	-	-	-
83	S100B	1.21	2	-	-	-	-	-	-	-	-	-	-	-	-
85	SPARC	2.28	4.96	-	-	-	-	-	-	-	-	-	-	-	-
86	TF	1.72	1.93	-	-	-	-	-	-	-	-	-	-	-	-
87	TGF-α	2.36	4.12	-	-	-	-	-	-	-	-	-	-	-	-
88	TGF-β RII	2.45	4.3	-	-	-	-	-	-	-	-	-	-	-	-
89	TGF-β1	2.84	3.55	-	-	-	-	-	-	-	-	-	-	-	-
90	TGF-β2	1.64	5.81	-	-	-	-	-	-	-	-	-	-	-	-
91	THBS-1	3.71	0.26	0.4295	0.0076	0.5577	0.886	27.13	5.45	0.6583	0.0036	0.3779	0.518	13.08	12.6
92	Tie-2	1.35	1.56	-	-	-	-	-	-	-	-	-	-	-	-
93	TIMP-1	2.51	5.71	-	-	-	-	-	-	6.0869	0.003	0.1936	0.4084	16.58	17.83
94	TNF-α	2.12	2.04	-	-	-	-	-	-	-	-	-	-	-	-
95	TNF-RI	2.44	2.98	-	-	-	-	-	-	-	-	-	-	-	-
96	TNF-RII	3.3	-2.13	-1.1351	-0.0041	0.5343	0.5999	-17.37	36.37	-1.562	0.0023	0.2967	0.2967	9.65	20.79
97	uPA	2.28	2.53	-	-	-	-	-	-	-	-	-	-	-	-
98	uPA-R	2.38	6.54	-	-	-	-	-	-	-	-	-	-	-	-
99	VCAM-1	4.35	0.2	3.0461	-0.0006	0.0244	0.2262	-1.84	75.51	2.9325	0.0019	0.3413	0.2283	5.64	72.5
100	VEGF-A	4.09	4.94	-	-	-	-	-	-	-	-	-	-	-	-
101	VEGF-D	0.98	2.95	-	-	-	-	-	-	-	-	-	-	-	-
102	VEGFR2	2.98	1.46	-	-	-	-	-	-	-	-	-	-	-	-
103	VEGFR3	1.24	7.95	-	-	-	-	-	-	-	-	-	-	-	-

APPENDIX J

Potential biomarkers in TBI patients: Protein profiles in TBI patients

This appendix is a supplementary material to chapter chapter 6 that describes the time course profile of individual proteins in all sTBI and mTBI patients. Red lines in **b, h** show a threshold for a profile that is considered to have a peak, rather than being constant. The light red boxes in **d, e, f, j** show the threshold of comparison to the measured value compared.

Protein profiles in TBI patients

Electronic Supplementary Material

Time course proteomic analysis of matched microdialysis, cerebrospinal fluid and blood samples from severe and blood samples from mild traumatic brain injury patients

Veronique Laforte, Judith Marcoux, Rajeet Singh Saluja and David Juncker

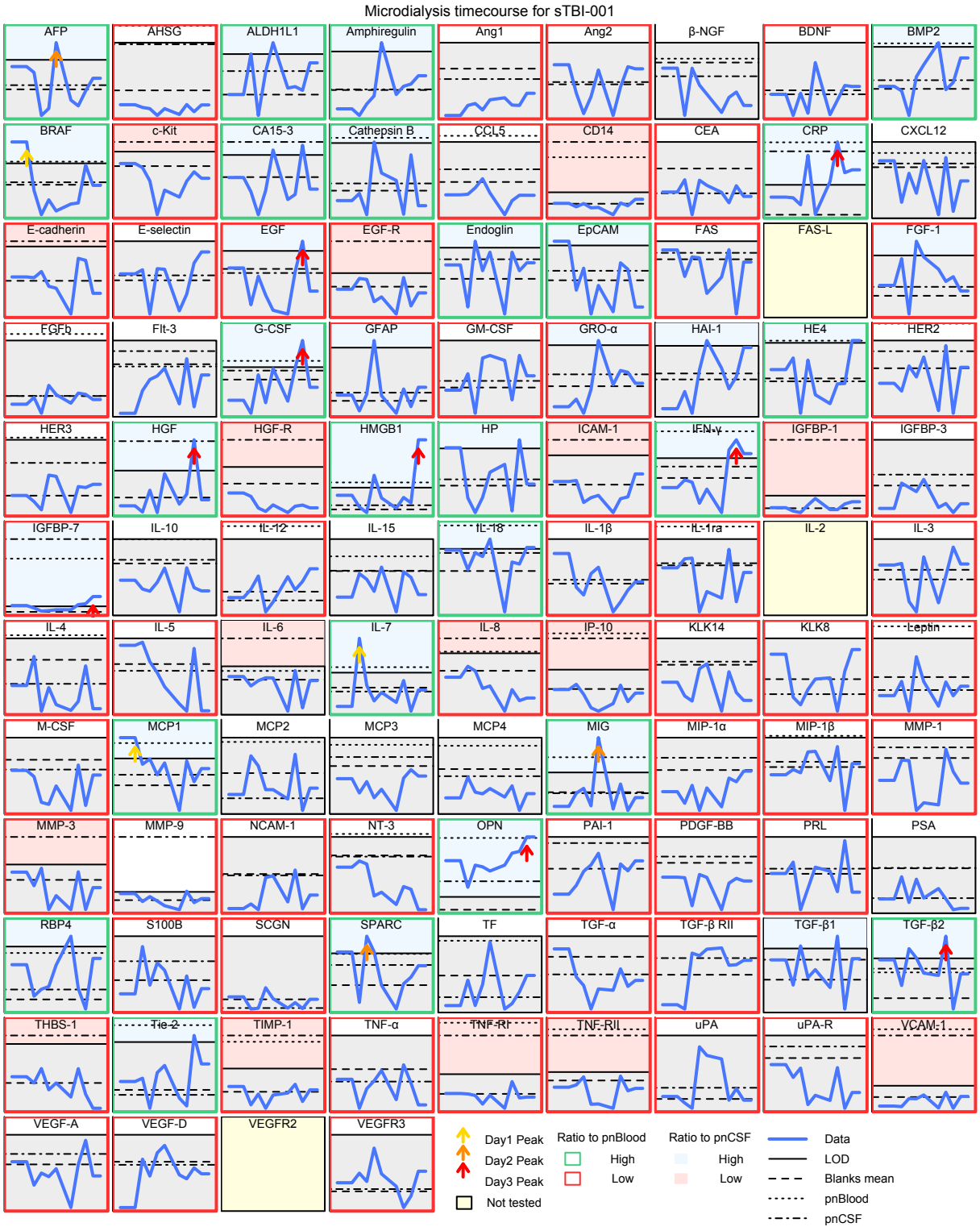

FIGURE J.S1: **Complete protein profiles in microdialysate for patient sTBI-001.** Protein profiles are extrapolated to account for missing values. Detected peaks are indicated by arrows, whose color indicates the day of the peak. Background and border colors indicate the mean of measurements is different from pnCSF and pnBlood, respectively. Time of sampling corresponds to 72 h started less than 24 h after injury.

FIGURE J.S2: **Complete protein profiles in CSF for patient sTBI-009.** Protein profiles are extrapolated to account for missing values. Detected peaks are indicated by arrows, whose color indicates the day of the peak. Background and border colors indicate the measurement is different from pnCSF and pnBlood, respectively. Time of sampling corresponds to 72 h started less than 24 h after injury.

FIGURE J.S3: **Complete protein profiles in blood for patient sTBI-009.** Protein profiles are extrapolated to account for missing values. Detected peaks are indicated by arrows, whose color indicates the day of the peak. Background and border colors indicate the measurement is different from pnCSF and pnBlood, respectively. Time of sampling corresponds to 72 h started less than 24 h after injury.

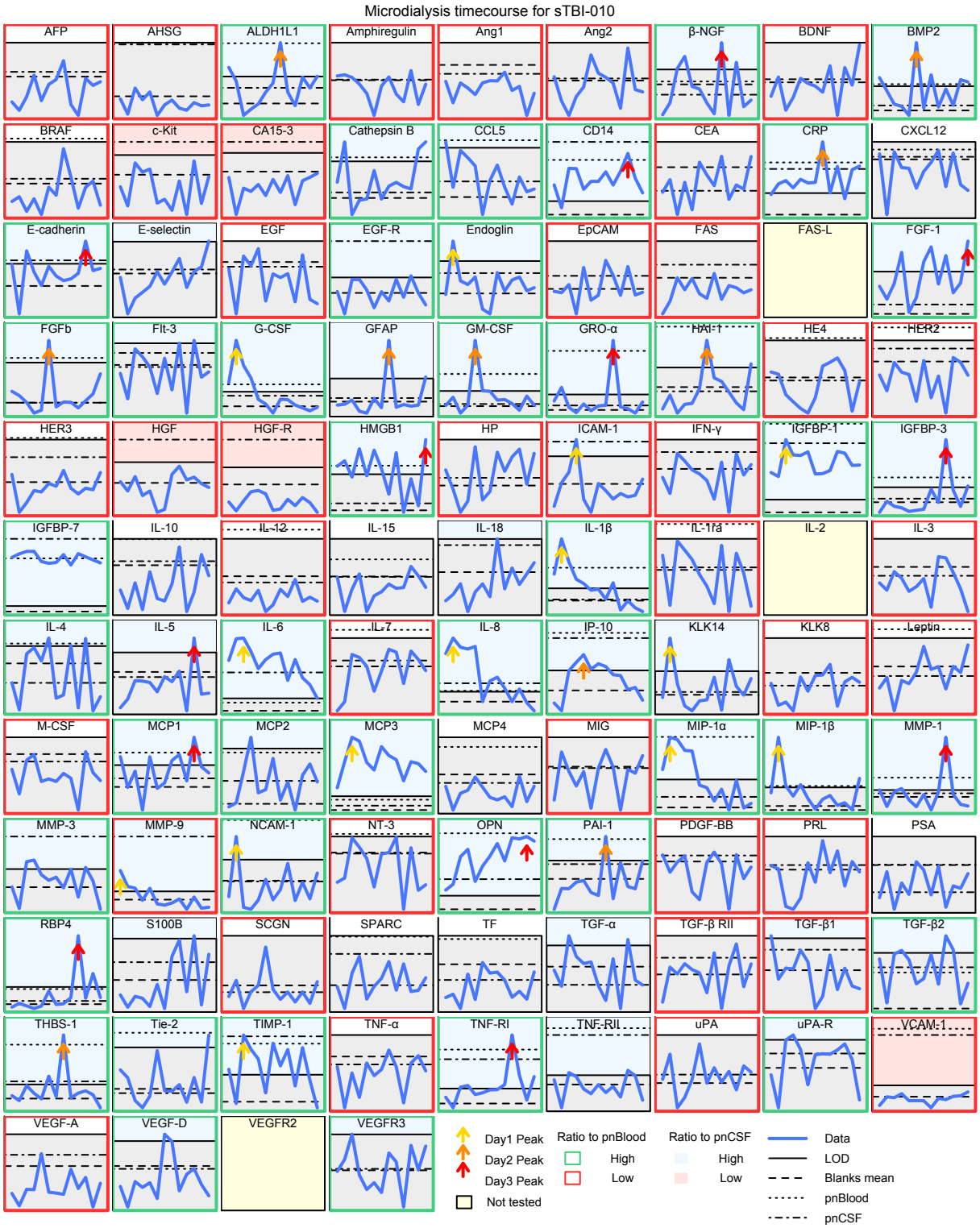

FIGURE J.S4: **Complete protein profiles in microdialysate for patient sTBI-010.** Protein profiles are extrapolated to account for missing values. Detected peaks are indicated by arrows, whose color indicates the day of the peak. Background and border colors indicate the mean of measurements is different from pnCSF and pnBlood, respectively. Time of sampling corresponds to 72 h started less than 24 h after injury.

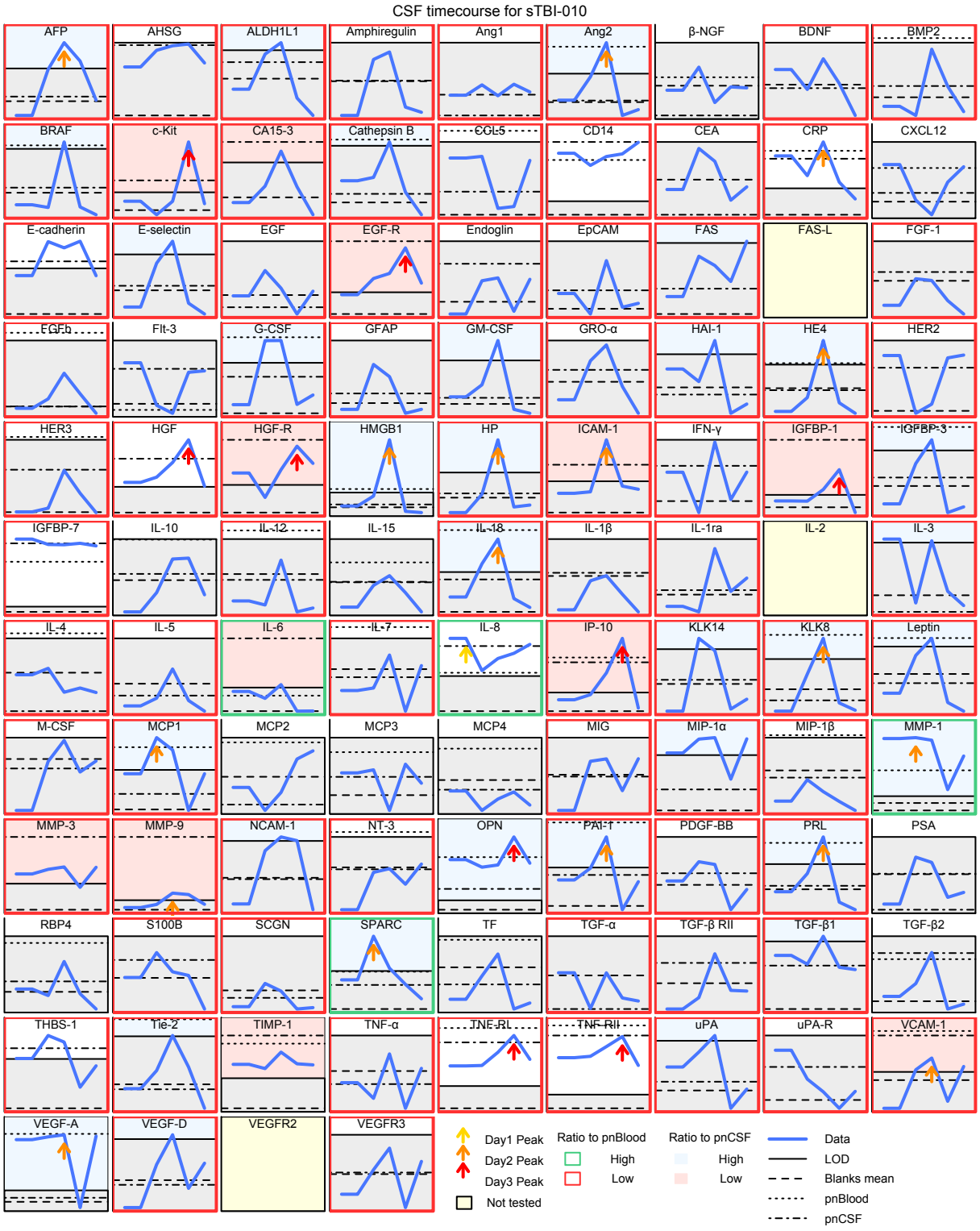

FIGURE J.S5: **Complete protein profiles in CSF for patient sTBI-010.** Protein profiles are extrapolated to account for missing values. Detected peaks are indicated by arrows, whose color indicates the day of the peak. Background and border colors indicate the mean of measurements is different from pnCSF and pnBlood, respectively. Time of sampling corresponds to 72 h started less than 24 h after injury.

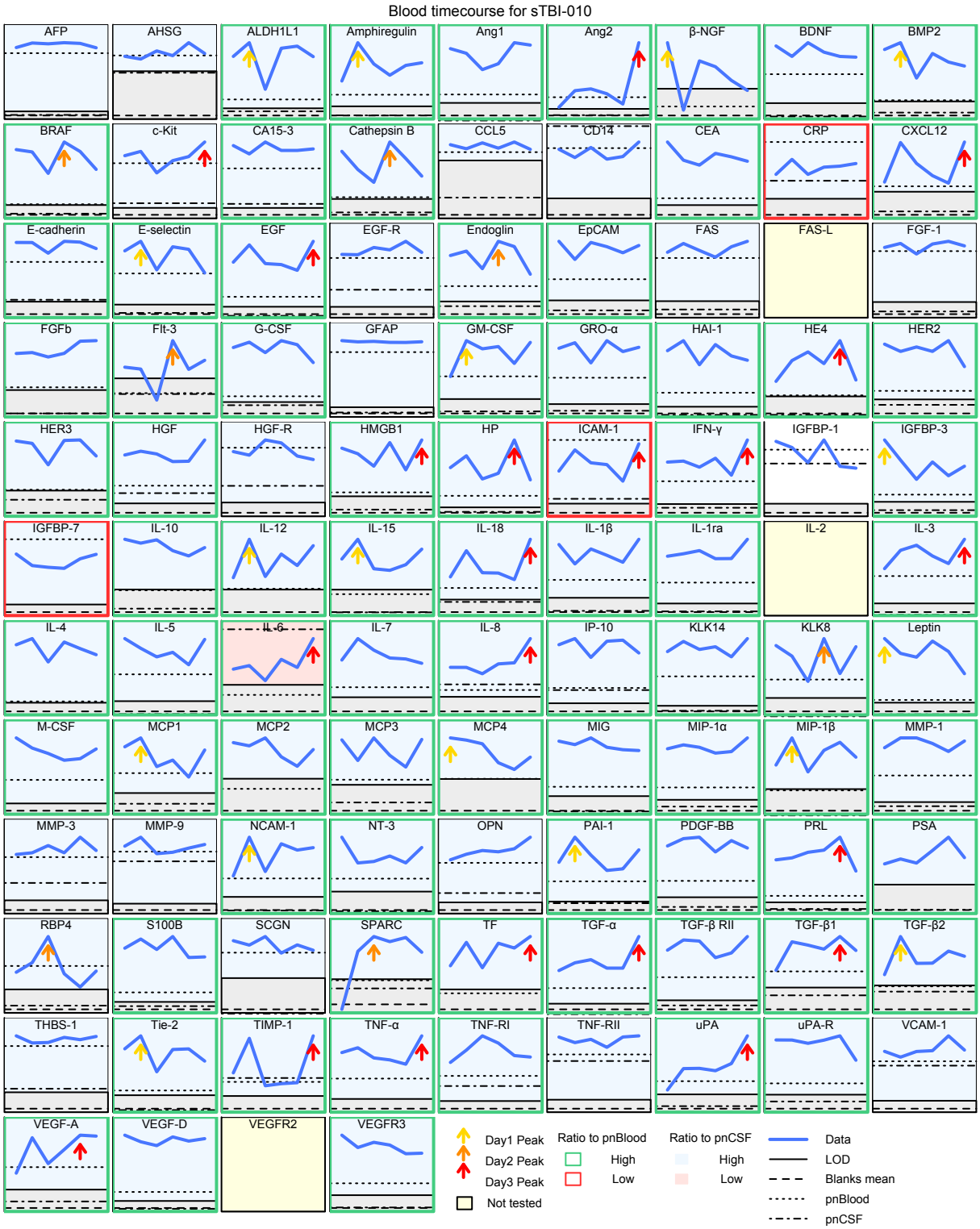

FIGURE J.S6: **Complete protein profiles in blood for patient sTBI-010.** Protein profiles are extrapolated to account for missing values. Detected peaks are indicated by arrows, whose color indicates the day of the peak. Background and border colors indicate the mean of measurements is different from pnCSF and pnBlood, respectively. Time of sampling corresponds to 72 h started less than 24 h after injury.

FIGURE J.S7: **Complete protein profiles in microdialysate for patient sTBI-011.** Protein profiles are extrapolated to account for missing values. Detected peaks are indicated by arrows, whose color indicates the day of the peak. Background and border colors indicate the mean of measurements is different from pnCSF and pnBlood, respectively. Time of sampling corresponds to 72 h started less than 24 h after injury.

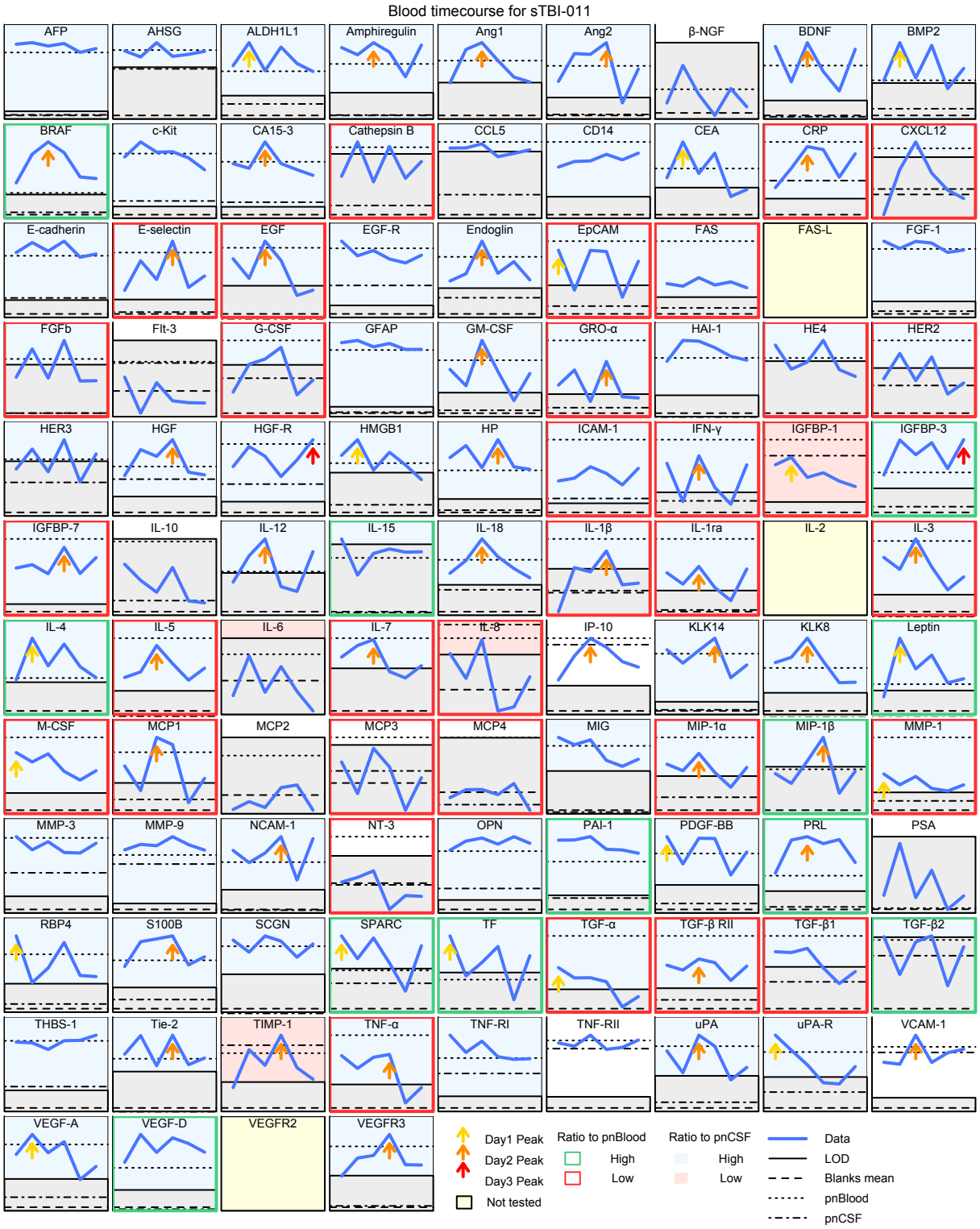

FIGURE J.S8: **Complete protein profiles in blood for patient sTBI-011.** Protein profiles are extrapolated to account for missing values. Detected peaks are indicated by arrows, whose color indicates the day of the peak. Background and border colors indicate the mean of measurements is different from pnCSF and pnBlood, respectively. Time of sampling corresponds to 72 h started less than 24 h after injury.

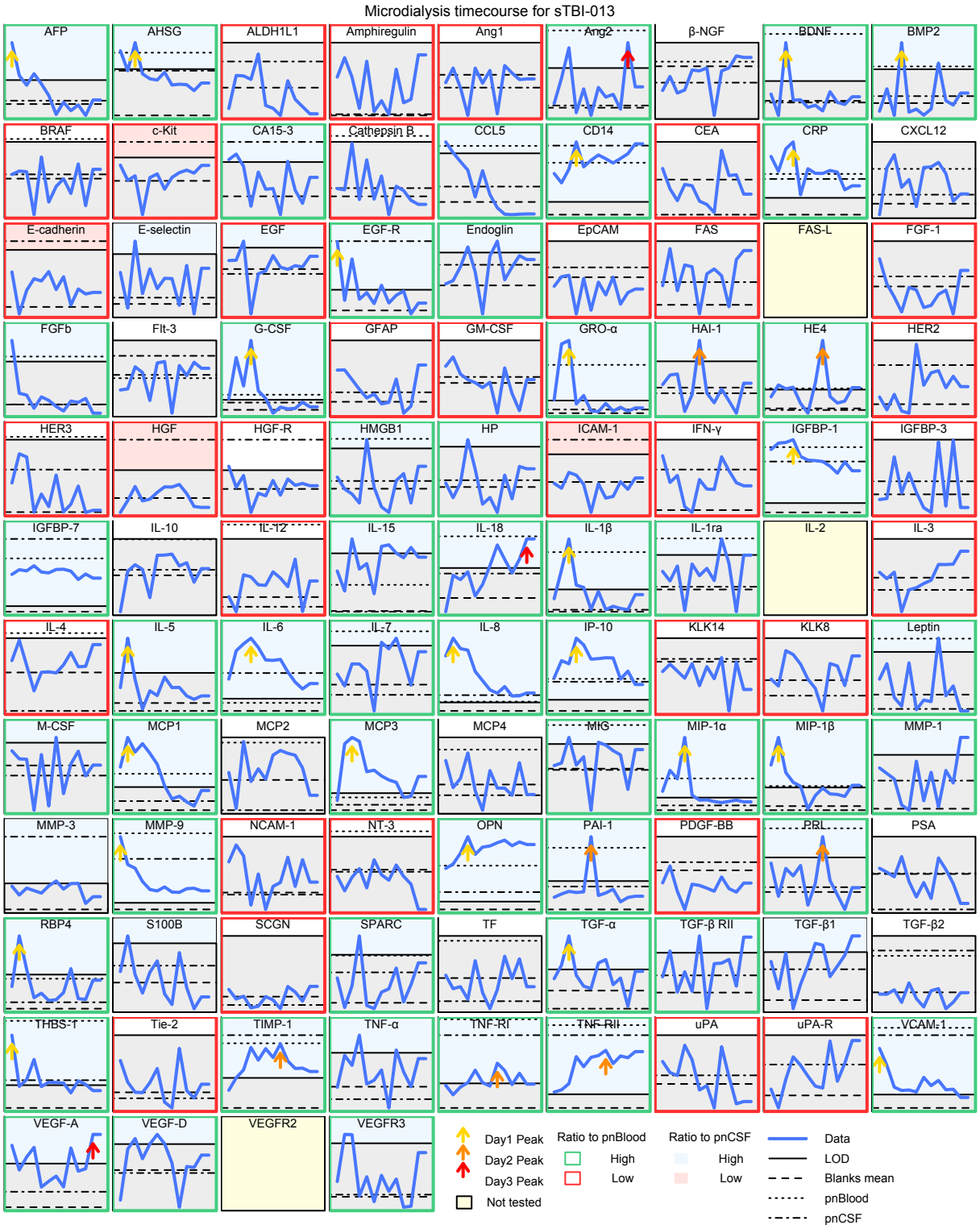

FIGURE J.S9: **Complete protein profiles in microdialysate for patient sTBI-013.** Protein profiles are extrapolated to account for missing values. Detected peaks are indicated by arrows, whose color indicates the day of the peak. Background and border colors indicate the mean of measurements is different from pnCSF and pnBlood, respectively. Time of sampling corresponds to 72 h started less than 24 h after injury.

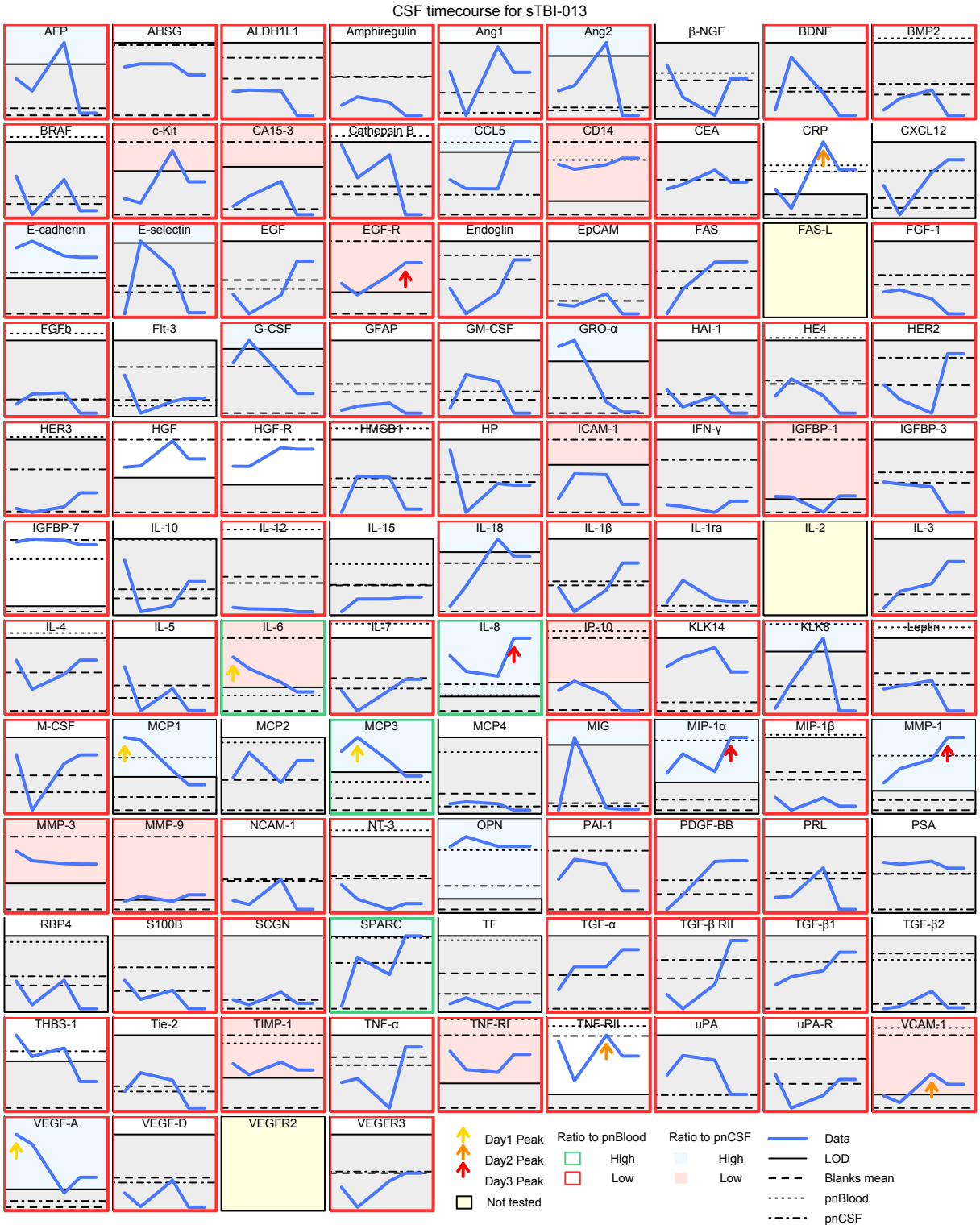

FIGURE J.S10: **Complete protein profiles in CSF for patient sTBI-013.** Protein profiles are extrapolated to account for missing values. Detected peaks are indicated by arrows, whose color indicates the day of the peak. Background and border colors indicate the mean of measurements is different from pnCSF and pnBlood, respectively. Time of sampling corresponds to 72 h started less than 24 h after injury.

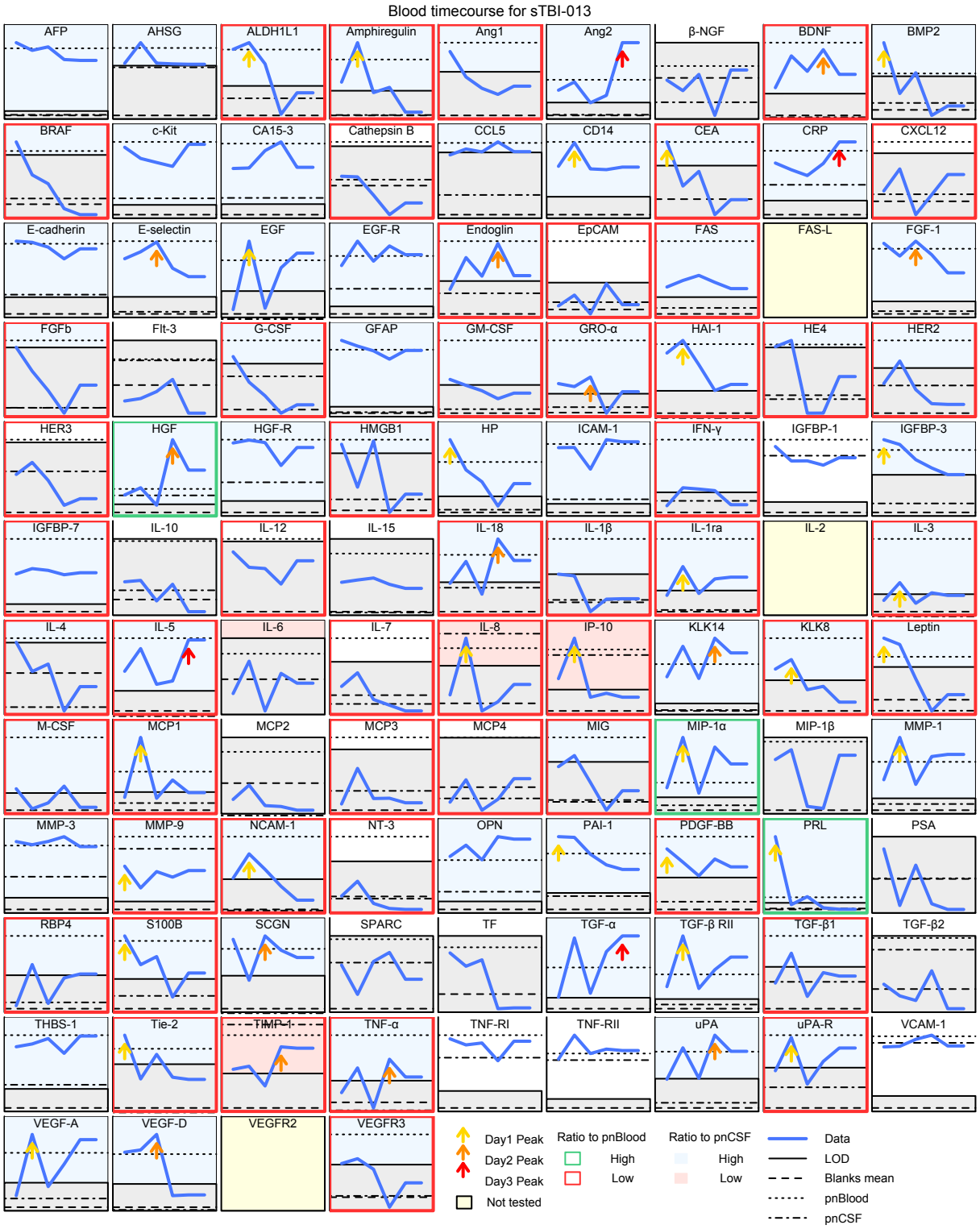

FIGURE J.S11: **Complete protein profiles in blood for patient sTBI-013.** Protein profiles are extrapolated to account for missing values. Detected peaks are indicated by arrows, whose color indicates the day of the peak. Background and border colors indicate the mean of measurements is different from pnCSF and pnBlood, respectively. Time of sampling corresponds to 72 h started less than 24 h after injury.

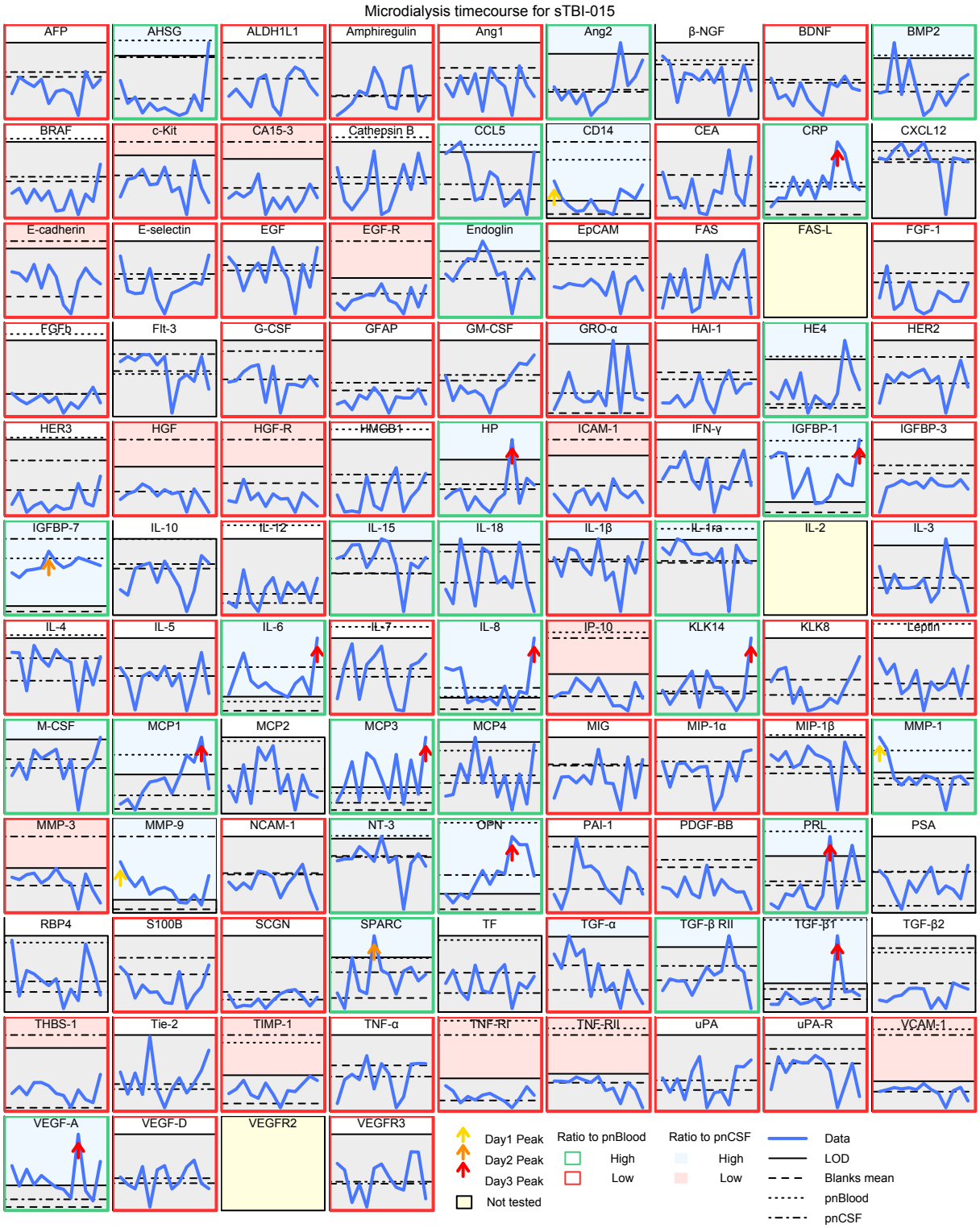

FIGURE J.S12: **Complete protein profiles in microdialysate for patient sTBI-015.** Protein profiles are extrapolated to account for missing values. Detected peaks are indicated by arrows, whose color indicates the day of the peak. Background and border colors indicate the mean of measurements is different from pnCSF and pnBlood, respectively. Time of sampling corresponds to 72 h started less than 24 h after injury.

FIGURE J.S13: **Complete protein profiles in CSF for patient sTBI-015.** Protein profiles are extrapolated to account for missing values. Detected peaks are indicated by arrows, whose color indicates the day of the peak. Background and border colors indicate the mean of measurements is different from pnCSF and pnBlood, respectively. Time of sampling corresponds to 72 h started less than 24 h after injury.

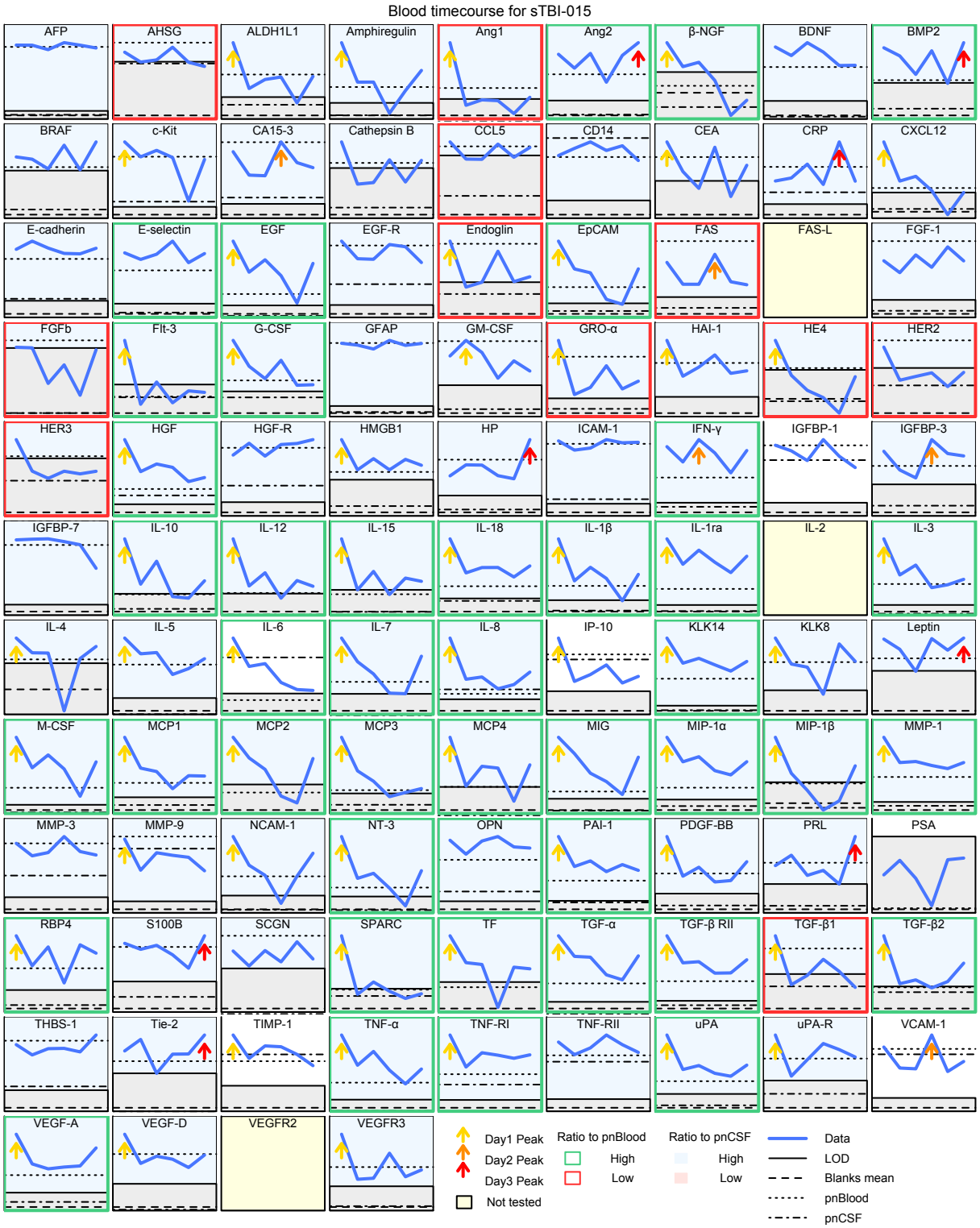

FIGURE J.S14: **Complete protein profiles in blood for patient sTBI-015.** Protein profiles are extrapolated to account for missing values. Detected peaks are indicated by arrows, whose color indicates the day of the peak. Background and border colors indicate the mean of measurements is different from pnCSF and pnBlood, respectively. Time of sampling corresponds to 72 h started less than 24 h after injury.

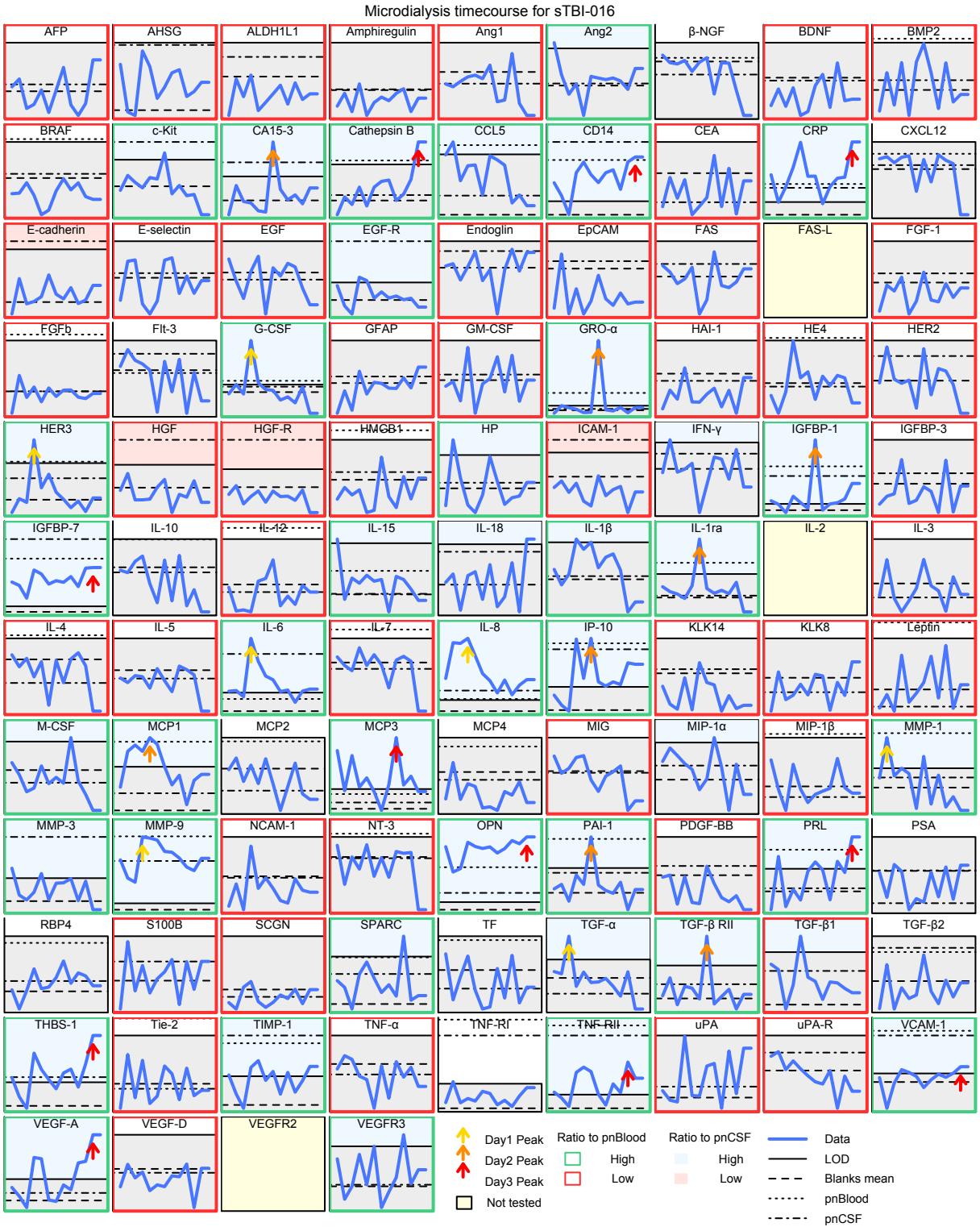

FIGURE J.S15: **Complete protein profiles in microdialysate for patient sTBI-016.** Protein profiles are extrapolated to account for missing values. Detected peaks are indicated by arrows, whose color indicates the day of the peak. Background and border colors indicate the mean of measurements is different from pnCSF and pnBlood, respectively. Time of sampling corresponds to 72 h started less than 24 h after injury.

FIGURE J.S16: **Complete protein profiles in CSF for patient sTBI-016.** Protein profiles are extrapolated to account for missing values. Detected peaks are indicated by arrows, whose color indicates the day of the peak. Background and border colors indicate the mean of measurements is different from pnCSF and pnBlood, respectively. Time of sampling corresponds to 72 h started less than 24 h after injury.

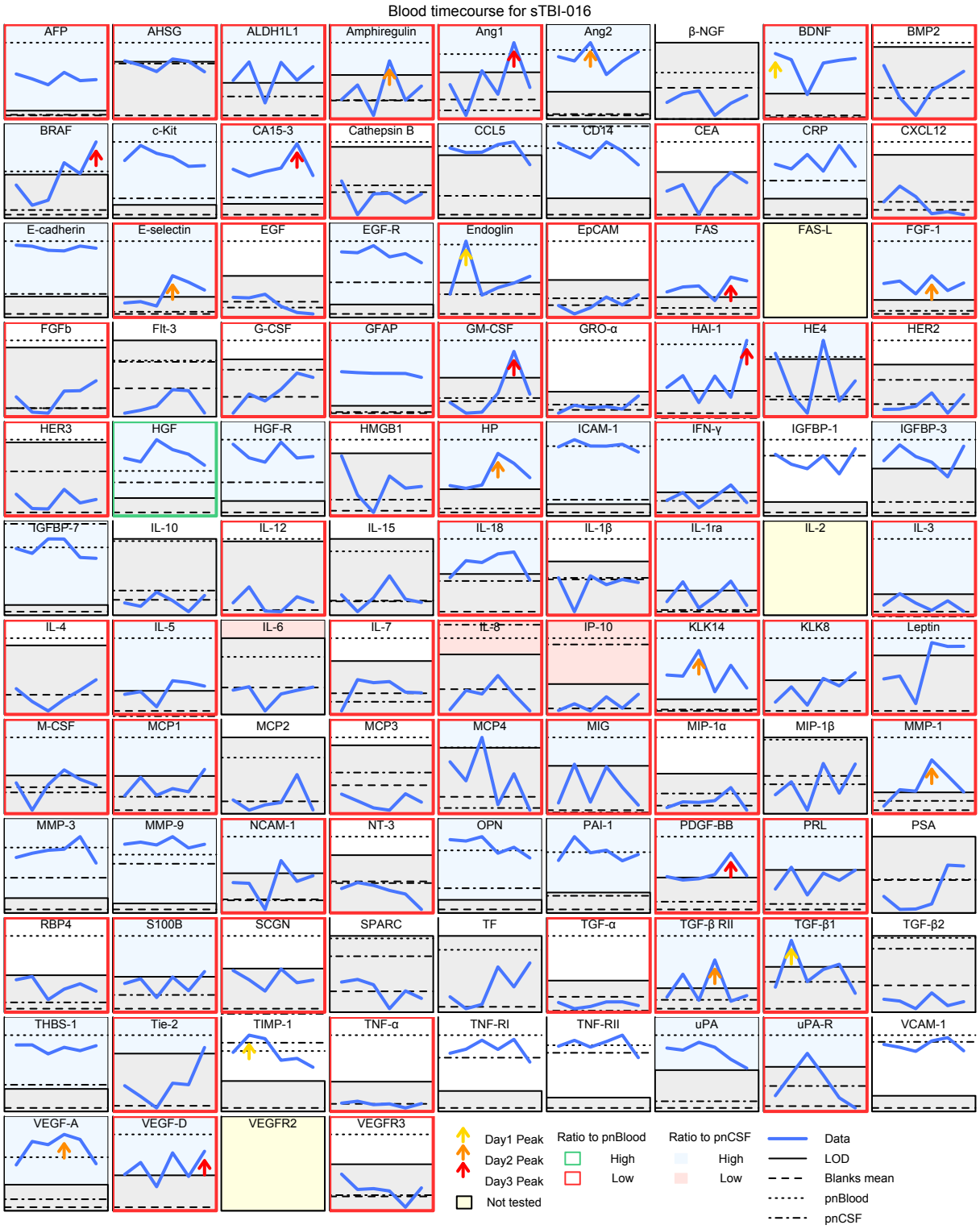

FIGURE J.S17: **Complete protein profiles in blood for patient sTBI-016.** Protein profiles are extrapolated to account for missing values. Detected peaks are indicated by arrows, whose color indicates the day of the peak. Background and border colors indicate the mean of measurements is different from pnCSF and pnBlood, respectively. Time of sampling corresponds to 72 h started less than 24 h after injury.

FIGURE J.S18: **Complete protein profiles in CSF for patient sTBI-017.** Protein profiles are extrapolated to account for missing values. Detected peaks are indicated by arrows, whose color indicates the day of the peak. Background and border colors indicate the mean of measurements is different from pnCSF and pnBlood, respectively. Time of sampling corresponds to 72 h started less than 24 h after injury.

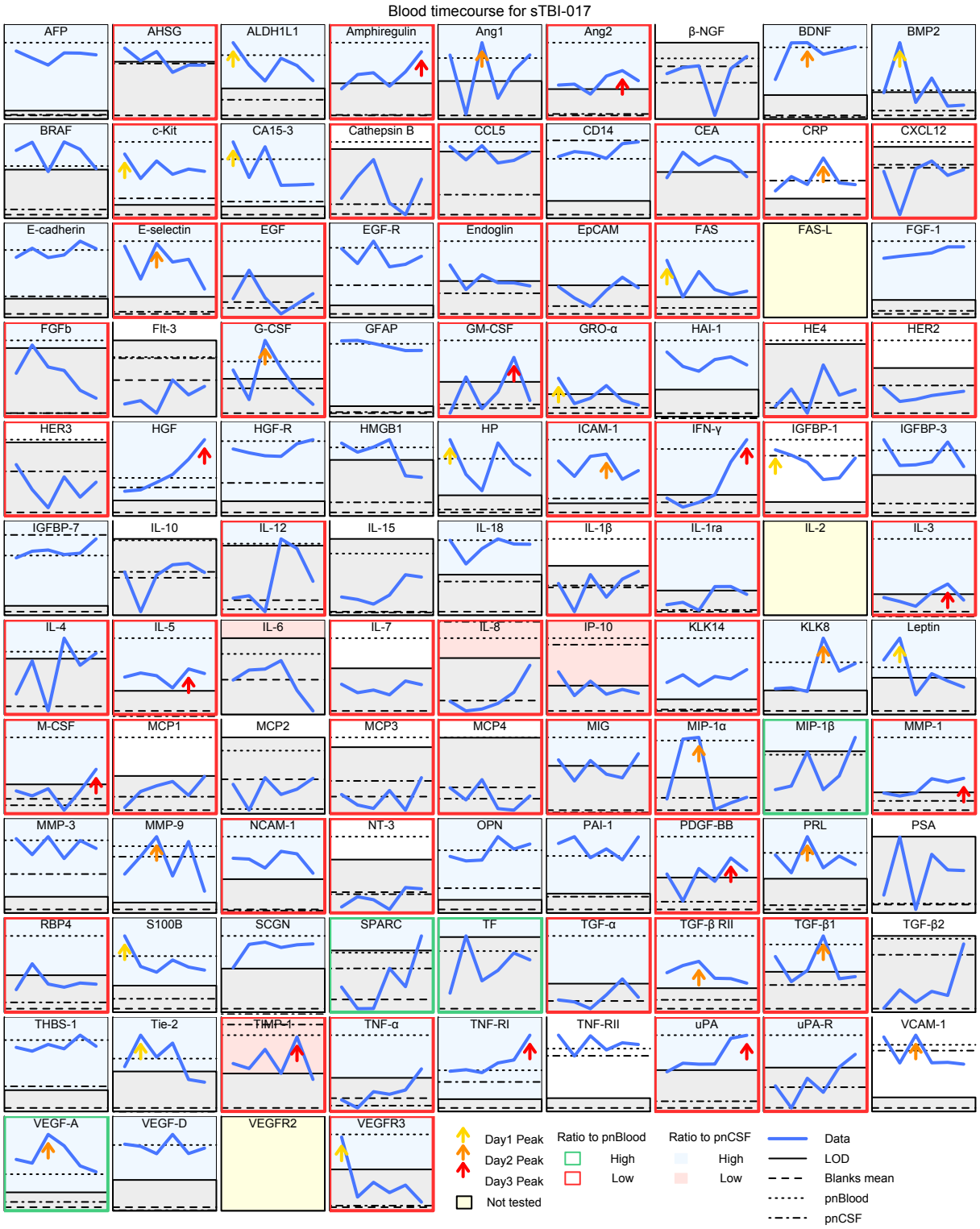

FIGURE J.S19: **Complete protein profiles in blood for patient sTBI-017.** Protein profiles are extrapolated to account for missing values. Detected peaks are indicated by arrows, whose color indicates the day of the peak. Background and border colors indicate the mean of measurements is different from pnCSF and pnBlood, respectively. Time of sampling corresponds to 72 h started less than 24 h after injury.

FIGURE J.S20: **Complete protein profiles in blood for patient mTBI-003.** Protein profiles are extrapolated to account for missing values. Detected peaks are indicated by arrows, whose color indicates the day of the peak. Border colors indicate the mean of measurements is different from pnBlood. Time of sampling corresponds to 72 h started less than 24 h after injury.

FIGURE J.S21: **Complete protein profiles in blood for patient mTBI-004.** Protein profiles are extrapolated to account for missing values. Detected peaks are indicated by arrows, whose color indicates the day of the peak. Border colors indicate the mean of measurements is different from pnBlood. Time of sampling corresponds to 72 h started less than 24 h after injury.

FIGURE J.S22: **Complete protein profiles in blood for patient mTBI-005.** Protein profiles are extrapolated to account for missing values. Detected peaks are indicated by arrows, whose color indicates the day of the peak. Border colors indicate the mean of measurements is different from pnBlood. Time of sampling corresponds to 72 h started less than 24 h after injury.

FIGURE J.S23: **Complete protein profiles in blood for patient mTBI-006.** Protein profiles are extrapolated to account for missing values. Detected peaks are indicated by arrows, whose color indicates the day of the peak. Border colors indicate the mean of measurements is different from pnBlood. Time of sampling corresponds to 72 h started less than 24 h after injury.

FIGURE J.S24: **Complete protein profiles in blood for patient mTBI-007.** Protein profiles are extrapolated to account for missing values. Detected peaks are indicated by arrows, whose color indicates the day of the peak. Border colors indicate the mean of measurements is different from pnBlood. Time of sampling corresponds to 72 h started less than 24 h after injury.

FIGURE J.S25: **Complete protein profiles in blood for patient mTBI-008.** Protein profiles are extrapolated to account for missing values. Detected peaks are indicated by arrows, whose color indicates the day of the peak. Border colors indicate the mean of measurements is different from pnBlood. Time of sampling corresponds to 72 h started less than 24 h after injury.

FIGURE J.S26: **Complete protein profiles in blood for patient mTBI-009.** Protein profiles are extrapolated to account for missing values. Detected peaks are indicated by arrows, whose color indicates the day of the peak. Border colors indicate the mean of measurements is different from pnBlood. Time of sampling corresponds to 72 h started less than 24 h after injury.

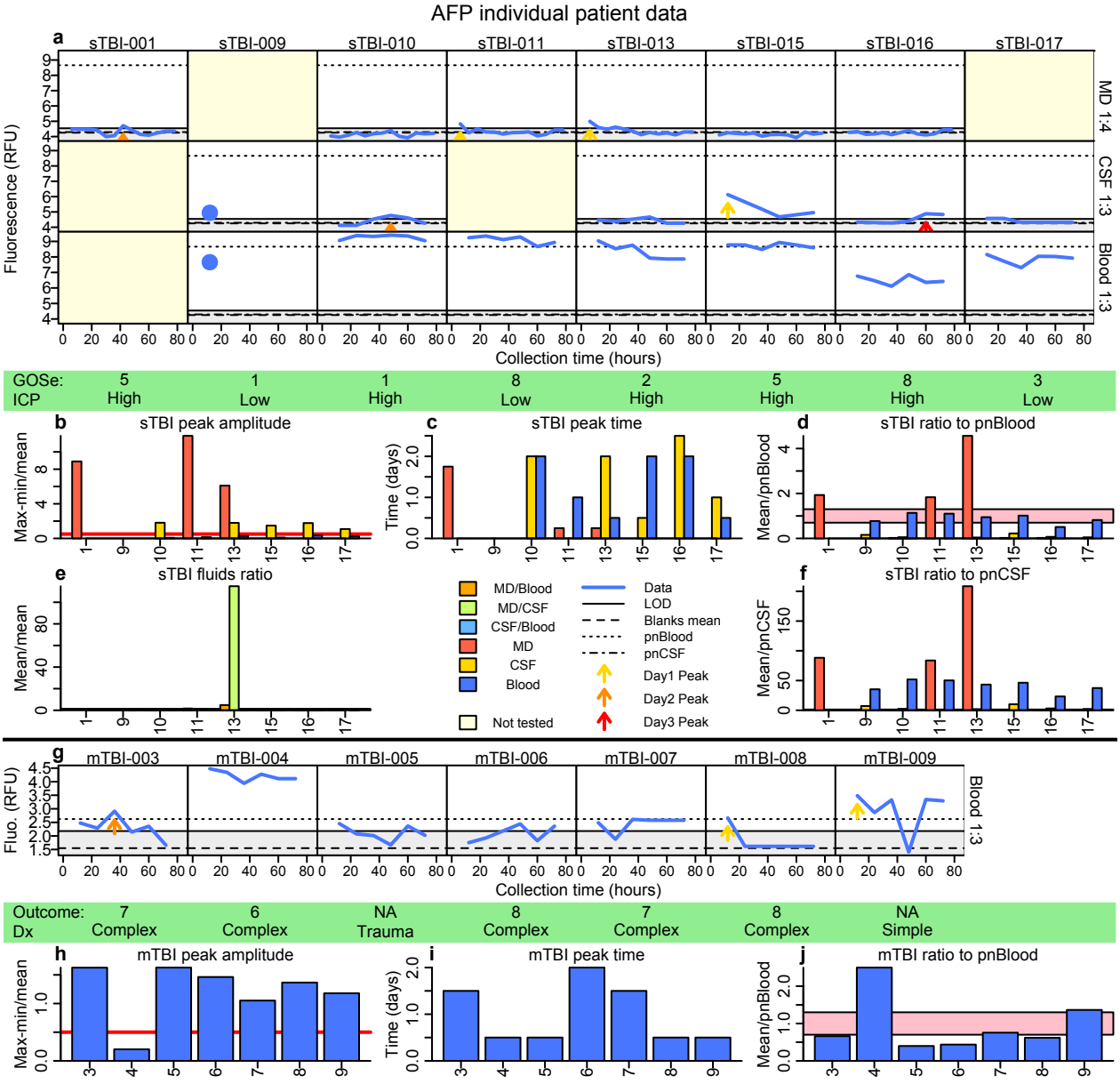

FIGURE J.S27: **Individual AFP protein profiles and peak and ratio analysis.** AFP concentration in microdialysate, CSF and blood samples of individual sTBI patients (**a**) and mTBI/trauma patients (**g**) was measured and peak amplitude and time, as well as ratio between mean time course values to value found in the pooled normal control (**b-f, h-j**) were calculated for each patient. Graphs **b-f** show calculations for individual sTBI patients, and graphs **h-j** show calculations for individual mTBI patients. Red lines in **b, h** show a threshold for a profile that is considered to have a peak, rather than being constant. The light red boxes in **d, e, f, j** show the threshold of comparison to the measured value compared.

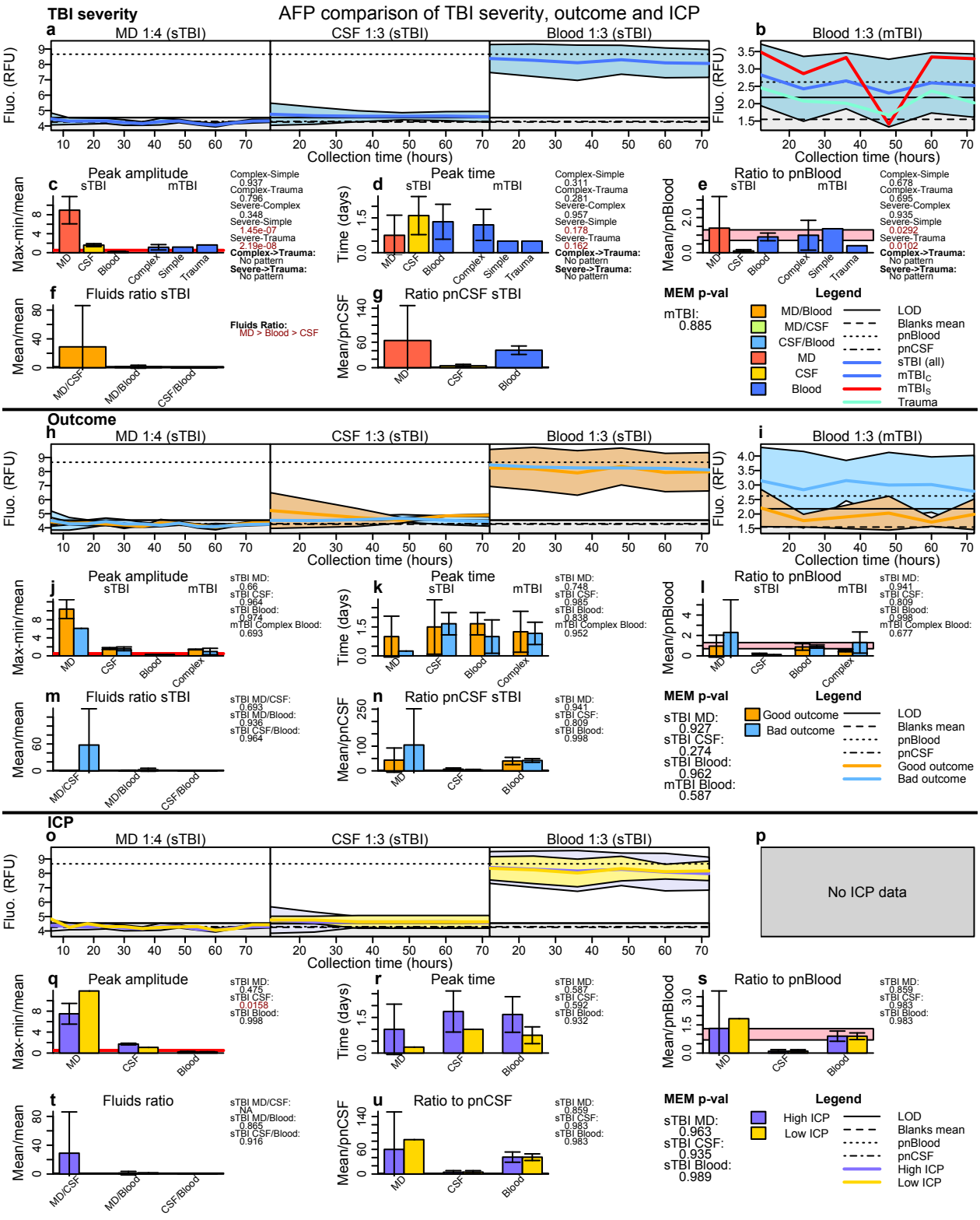

FIGURE J.S28: **Differential AFP protein profiles and peak and ratio analysis with respect to TBI severity, outcome and ICP.** Average AFP profiles are compared in terms of TBI severity (**a-g**), outcome (**h-n**) and ICP (**o-u**). Polygons in **a, b, h, i, o** indicate the mean value ±1 SD at each time point. Red lines in **c, j, q** show a threshold for a profile that is considered to have a peak, rather than being constant. The light red boxes in **e-g, l-n, s-u** show the threshold of comparison to the measured value compared. Benjamini–Hochberg adjusted p-values for comparisons are shown on the right of every graph.

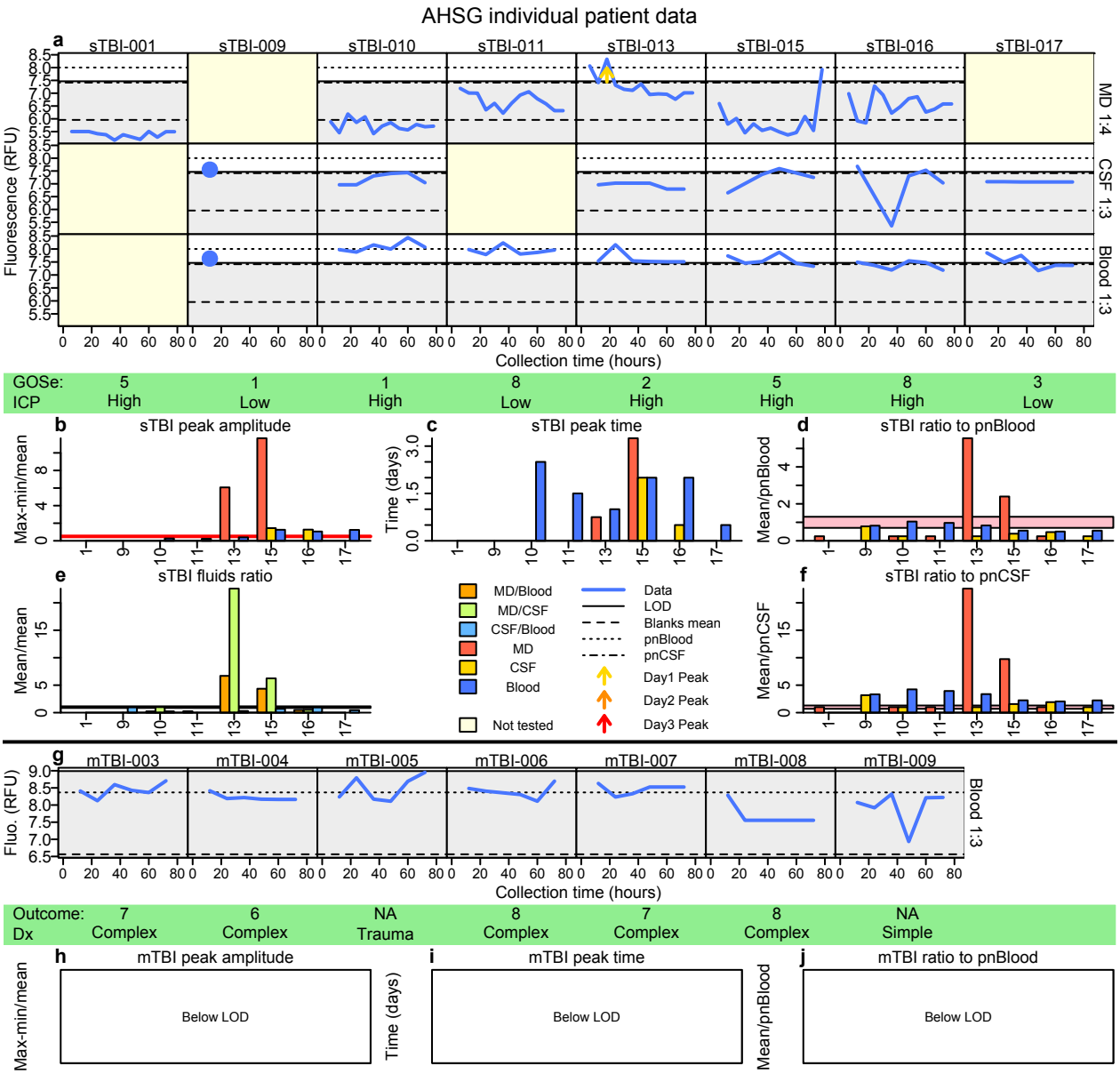

FIGURE J.S29: **Individual AHSG protein profiles and peak and ratio analysis.** AHSG concentration in microdialysate, CSF and blood samples of individual sTBI patients (**a**) and mTBI/trauma patients (**g**) was measured and peak amplitude and time, as well as ratio between mean time course values to value found in the pooled normal control (**b-f, h-j**) were calculated for each patient. Graphs **b-f** show calculations for individual sTBI patients, and graphs **h-j** show calculations for individual mTBI patients. Red lines in **b, h** show a threshold for a profile that is considered to have a peak, rather than being constant. The light red boxes in **d, e, f, j** show the threshold of comparison to the measured value compared. Graphs **b-f** show calculations for individual sTBI patients, and graphs **h-j** show calculations for individual mTBI patients. Red lines in **b, h** show a threshold for a profile that is considered to have a peak, rather than being constant. The light red boxes in **d, e, f, j** show the threshold of comparison to the measured value compared.

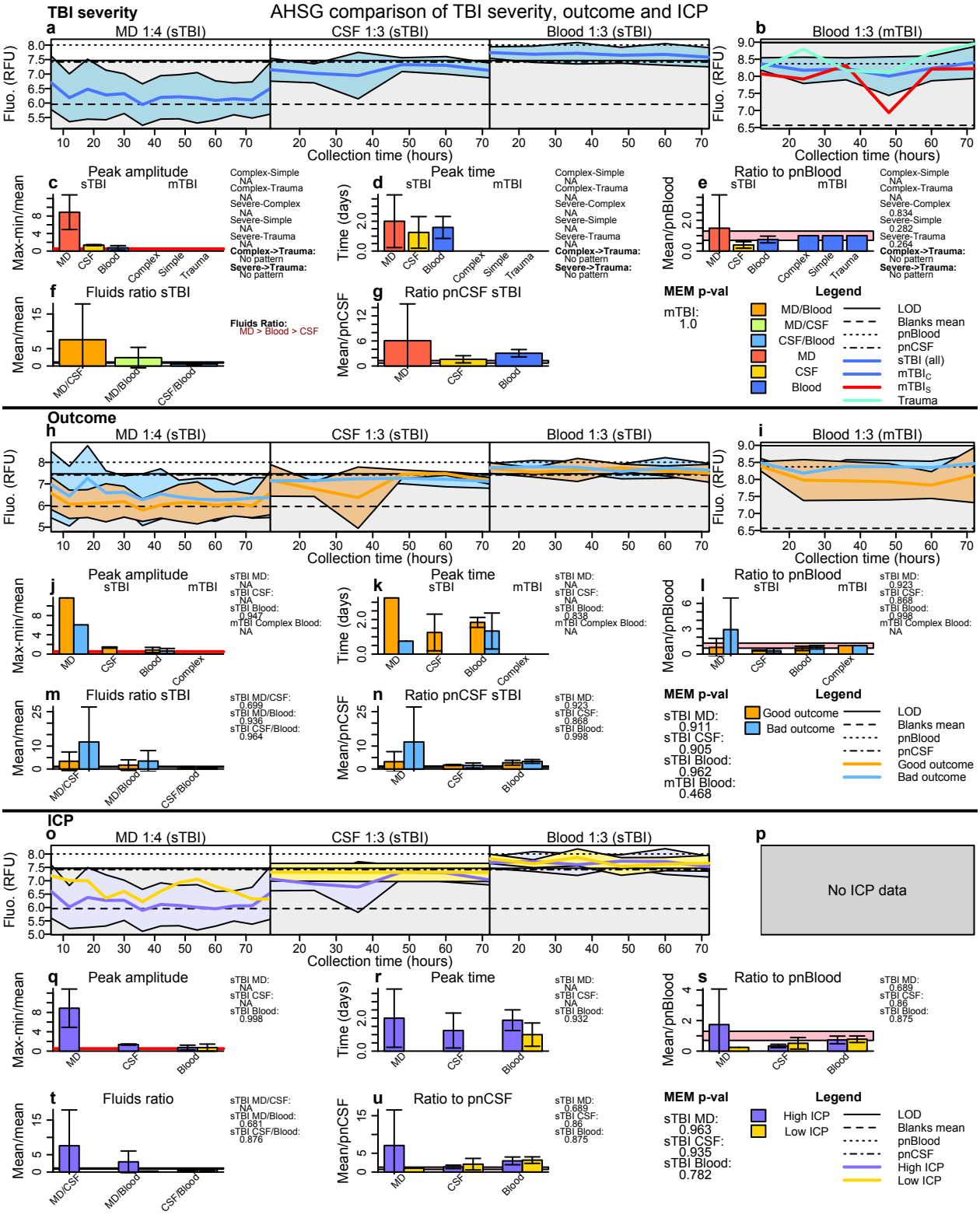

FIGURE J.S30: **Differential AHSG protein profiles and peak and ratio analysis with respect to TBI severity, outcome and ICP.** Average AHSG profiles are compared in terms of TBI severity (**a-g**), outcome (**h-n**) and ICP (**o-u**). Polygons in **a, b, h, i, o** indicate the mean value ±1 SD at each time point. Red lines in **c, j, q** show a threshold for a profile that is considered to have a peak, rather than being constant. The light red boxes in **e-g, l-n, s-u** show the threshold of comparison to the measured value compared. Benjamini–Hochberg adjusted p-values for comparisons are shown on the right of every graph.

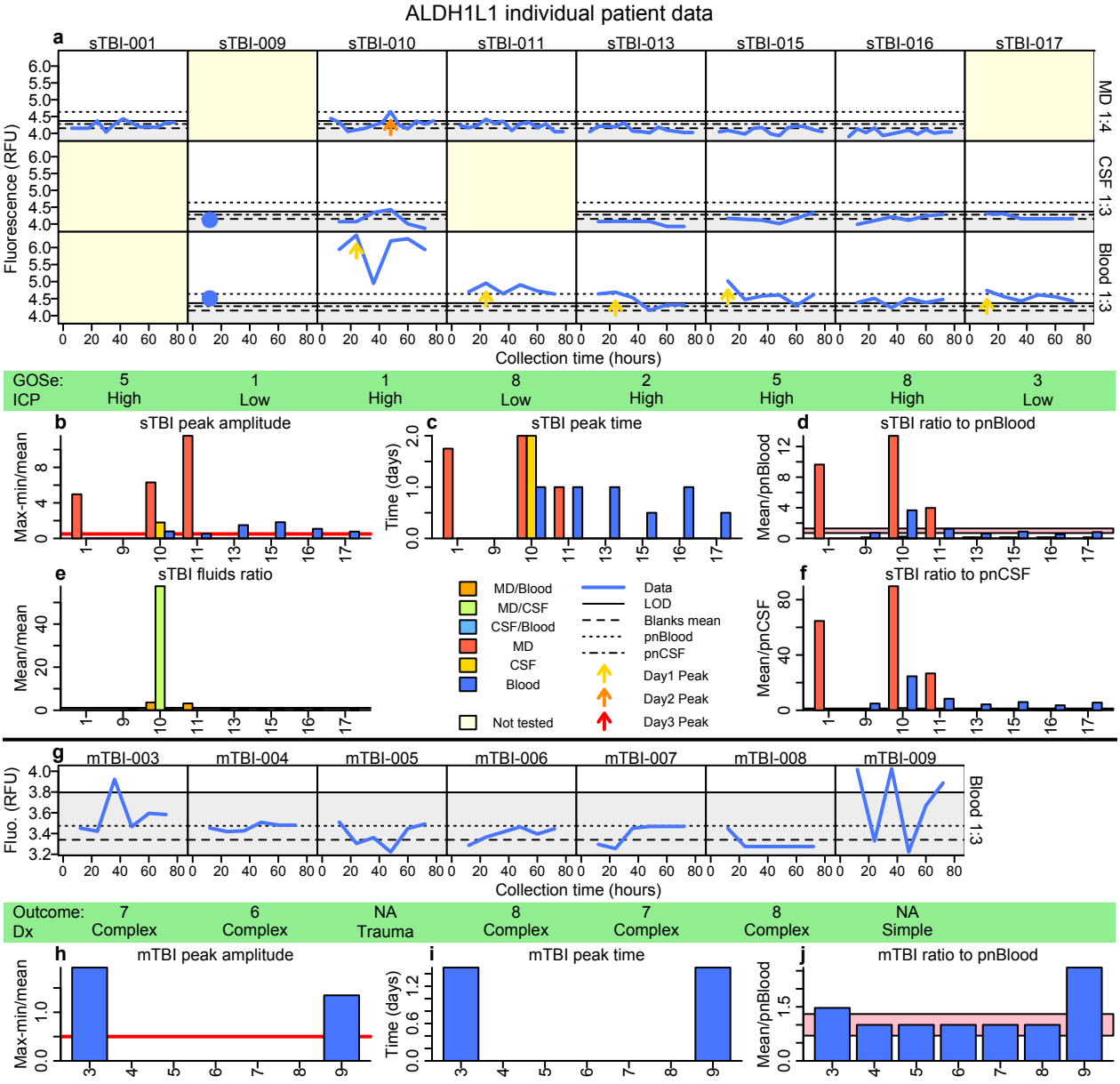

FIGURE J.S31: **Individual ALDH1L1 protein profiles and peak and ratio analysis.** ALDH1L1 concentration in microdialysate, CSF and blood samples of individual sTBI patients (**a**) and mTBI/trauma patients (**g**) was measured and peak amplitude and time, as well as ratio between mean time course values to value found in the pooled normal control (**b-f, h-j**) were calculated for each patient. Graphs **b-f** show calculations for individual sTBI patients, and graphs **h-j** show calculations for individual mTBI patients. Red lines in **b, h** show a threshold for a profile that is considered to have a peak, rather than being constant. The light red boxes in **d, e, f, j** show the threshold of comparison to the measured value compared.

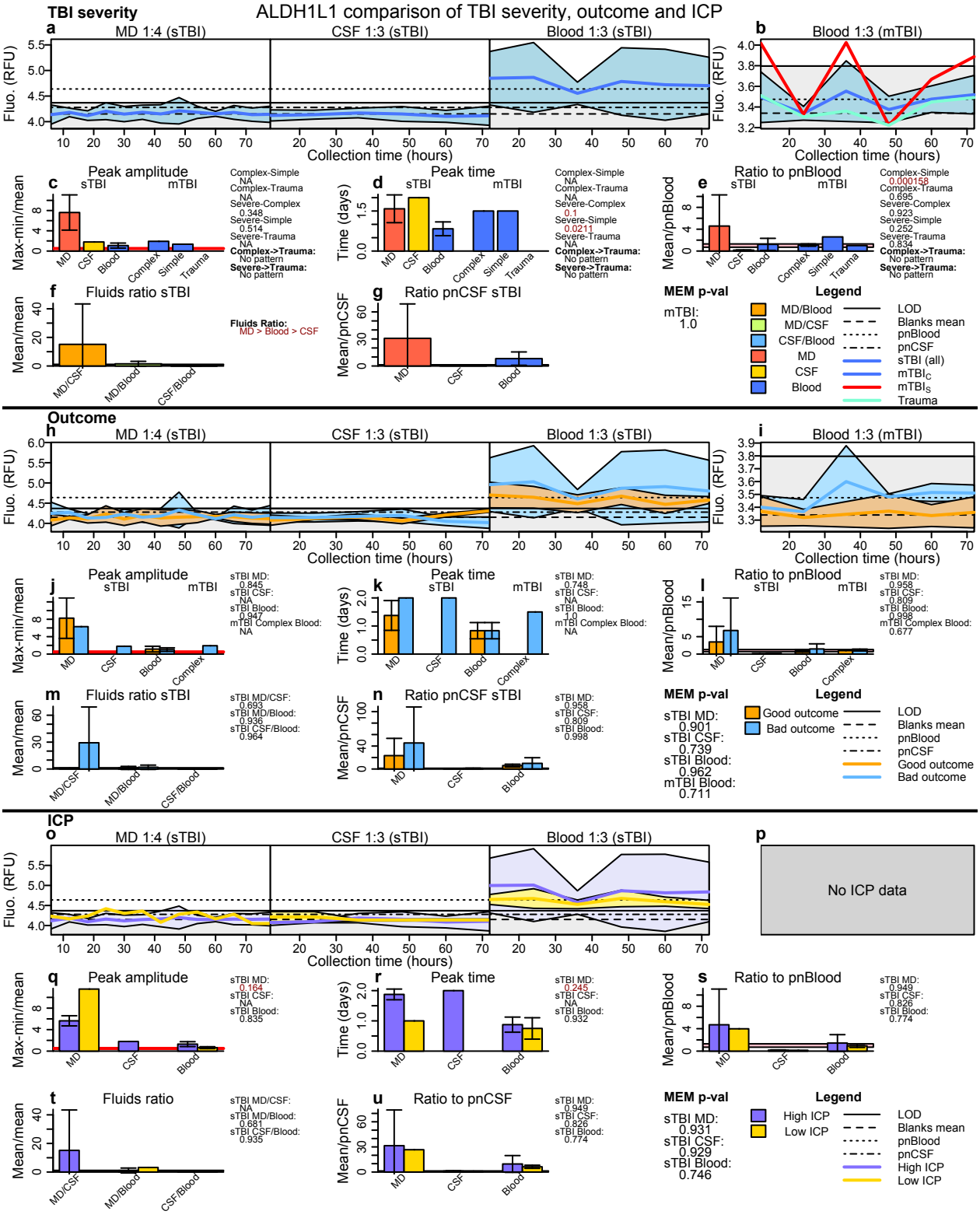

FIGURE J.S32: **Differential ALDH1L1 protein profiles and peak and ratio analysis with respect to TBI severity, outcome and ICP.** Average ALDH1L1 profiles are compared in terms of TBI severity (**a-g**), outcome (**h-n**) and ICP (**o-u**). Polygons in **a, b, h, i, o** indicate the mean value ±1 SD at each time point. Red lines in **c, j, q** show a threshold for a profile that is considered to have a peak, rather than being constant. The light red boxes in **e-g, l-n, s-u** show the threshold of comparison to the measured value compared. Benjamini–Hochberg adjusted p-values for comparisons are shown on the right of every graph.

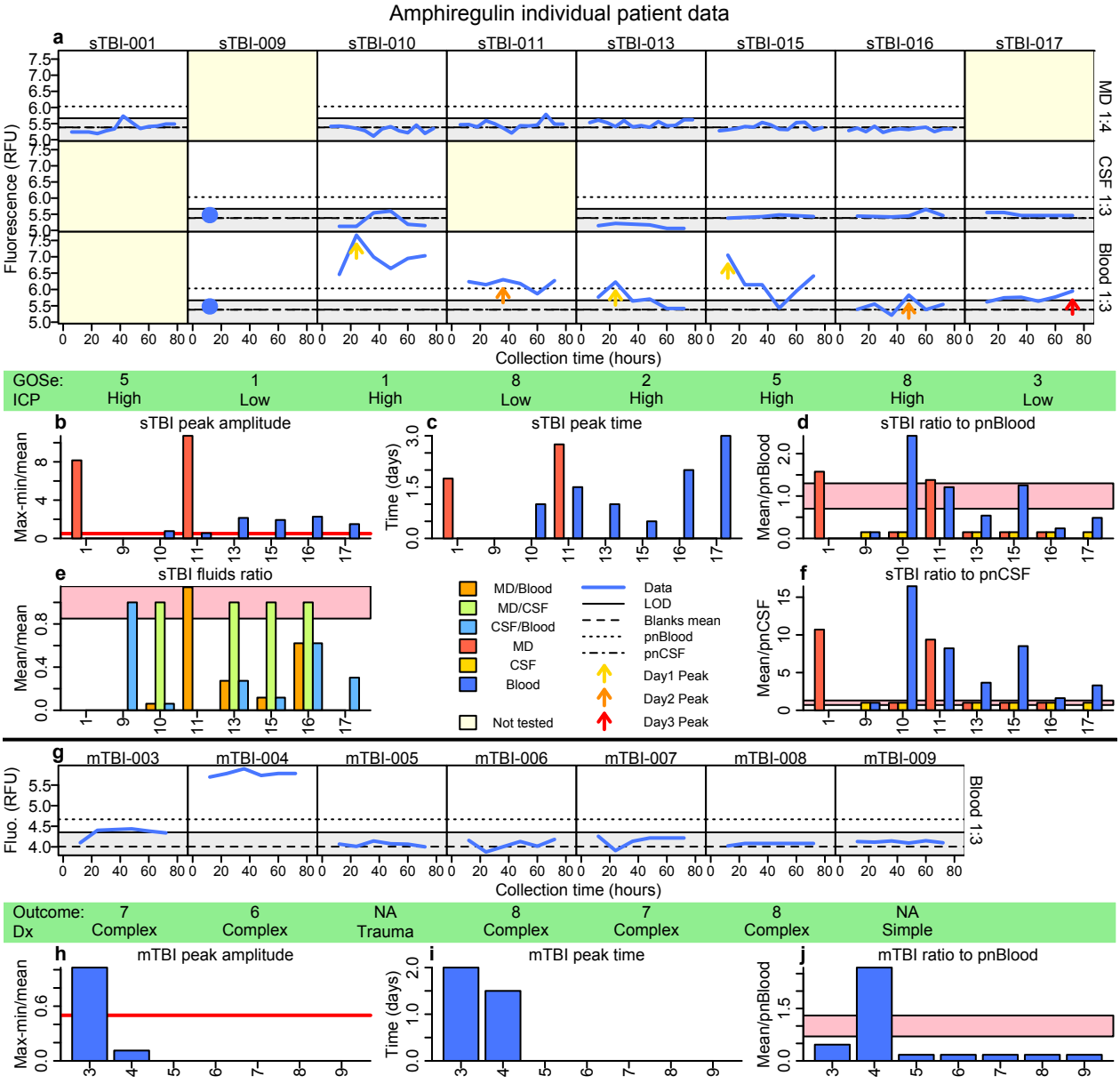

FIGURE J.S33: **Individual Amphiregulin protein profiles and peak and ratio analysis.** Amphiregulin concentration in microdialysate, CSF and blood samples of individual sTBI patients (**a**) and mTBI/trauma patients (**g**) was measured and peak amplitude and time, as well as ratio between mean time course values to value found in the pooled normal control (**b-f, h-j**) were calculated for each patient. Graphs **b-f** show calculations for individual sTBI patients, and graphs **h-j** show calculations for individual mTBI patients. Red lines in **b, h** show a threshold for a profile that is considered to have a peak, rather than being constant. The light red boxes in **d, e, f, j** show the threshold of comparison to the measured value compared.

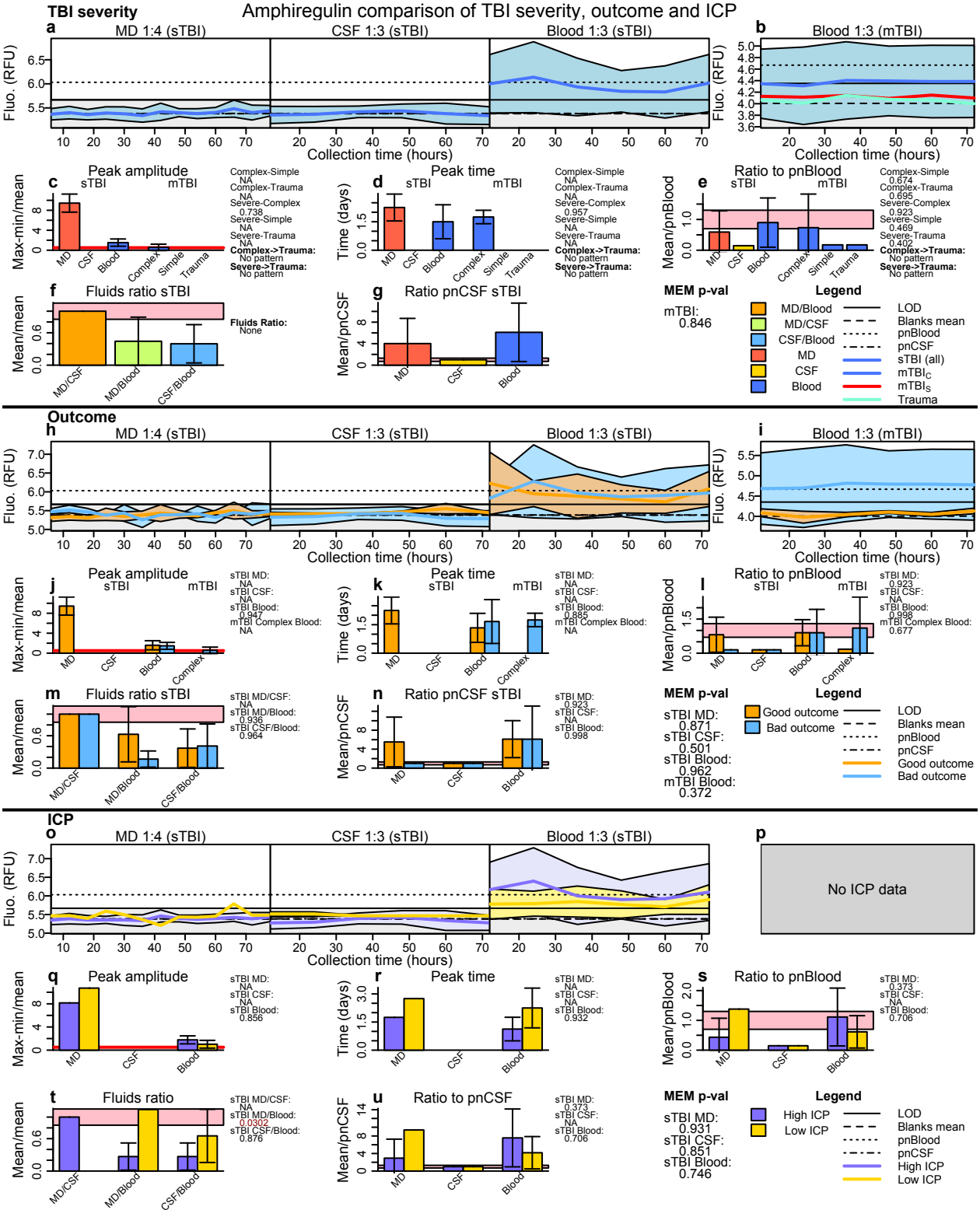

FIGURE J.S34: **Differential Amphiregulin protein profiles and peak and ratio analysis with respect to TBI severity, outcome and ICP.** Average Amphiregulin profiles are compared in terms of TBI severity (**a-g**), outcome (**h-n**) and ICP (**o-u**). Polygons in **a, b, h, i, o** indicate the mean value ±1 SD at each time point. Red lines in **c, j, q** show a threshold for a profile that is considered to have a peak, rather than being constant. The light red boxes in **e-g, l-n, s-u** show the threshold of comparison to the measured value compared. Benjamini–Hochberg adjusted p-values for comparisons are shown on the right of every graph.

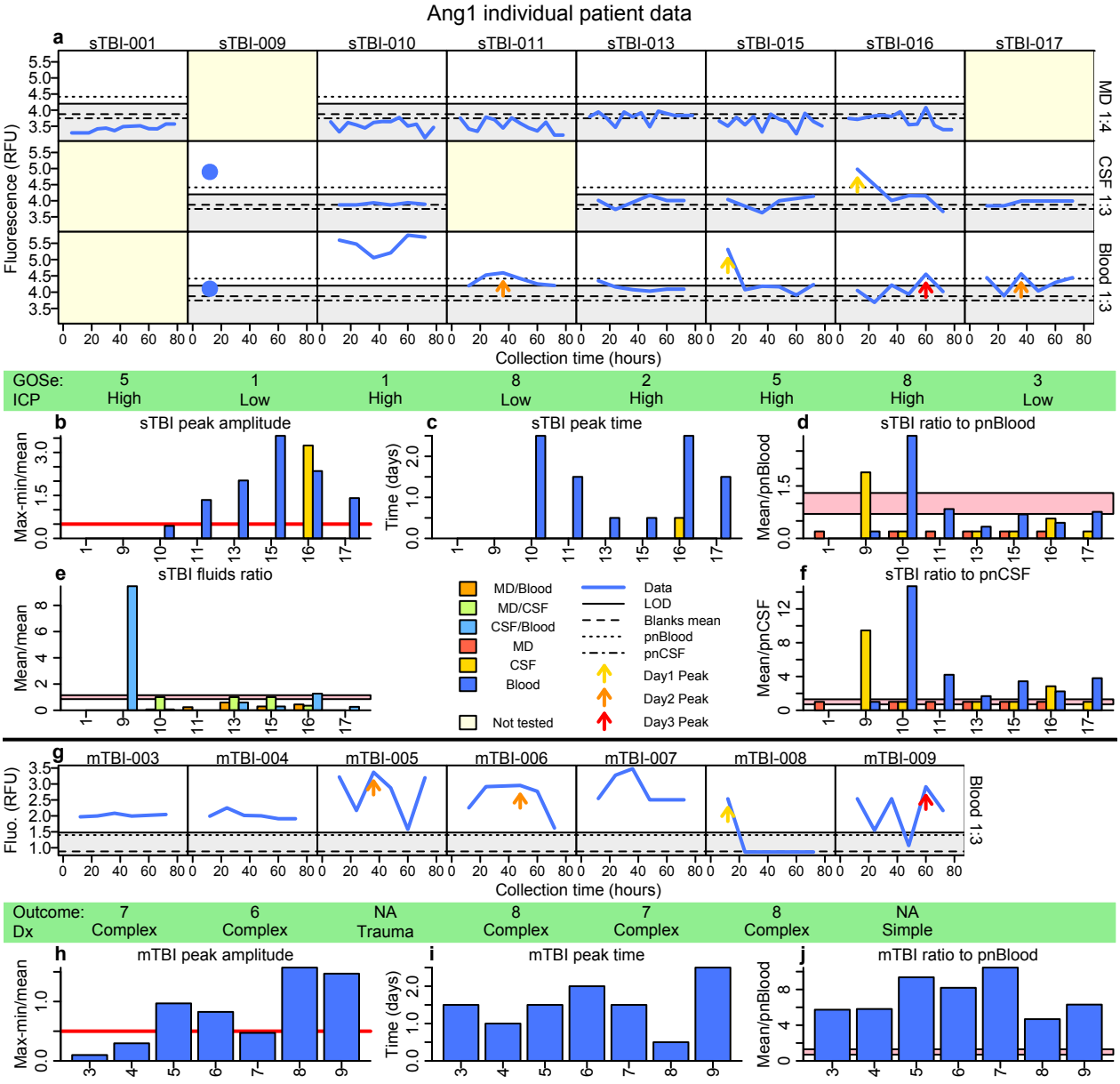

FIGURE J.S35: **Individual Ang1 protein profiles and peak and ratio analysis.** Ang1 concentration in microdialysate, CSF and blood samples of individual sTBI patients (**a**) and mTBI/trauma patients (**g**) was measured and peak amplitude and time, as well as ratio between mean time course values to value found in the pooled normal control (**b-f, h-j**) were calculated for each patient. Graphs **b-f** show calculations for individual sTBI patients, and graphs **h-j** show calculations for individual mTBI patients. Red lines in **b, h** show a threshold for a profile that is considered to have a peak, rather than being constant. The light red boxes in **d, e, f, j** show the threshold of comparison to the measured value compared.

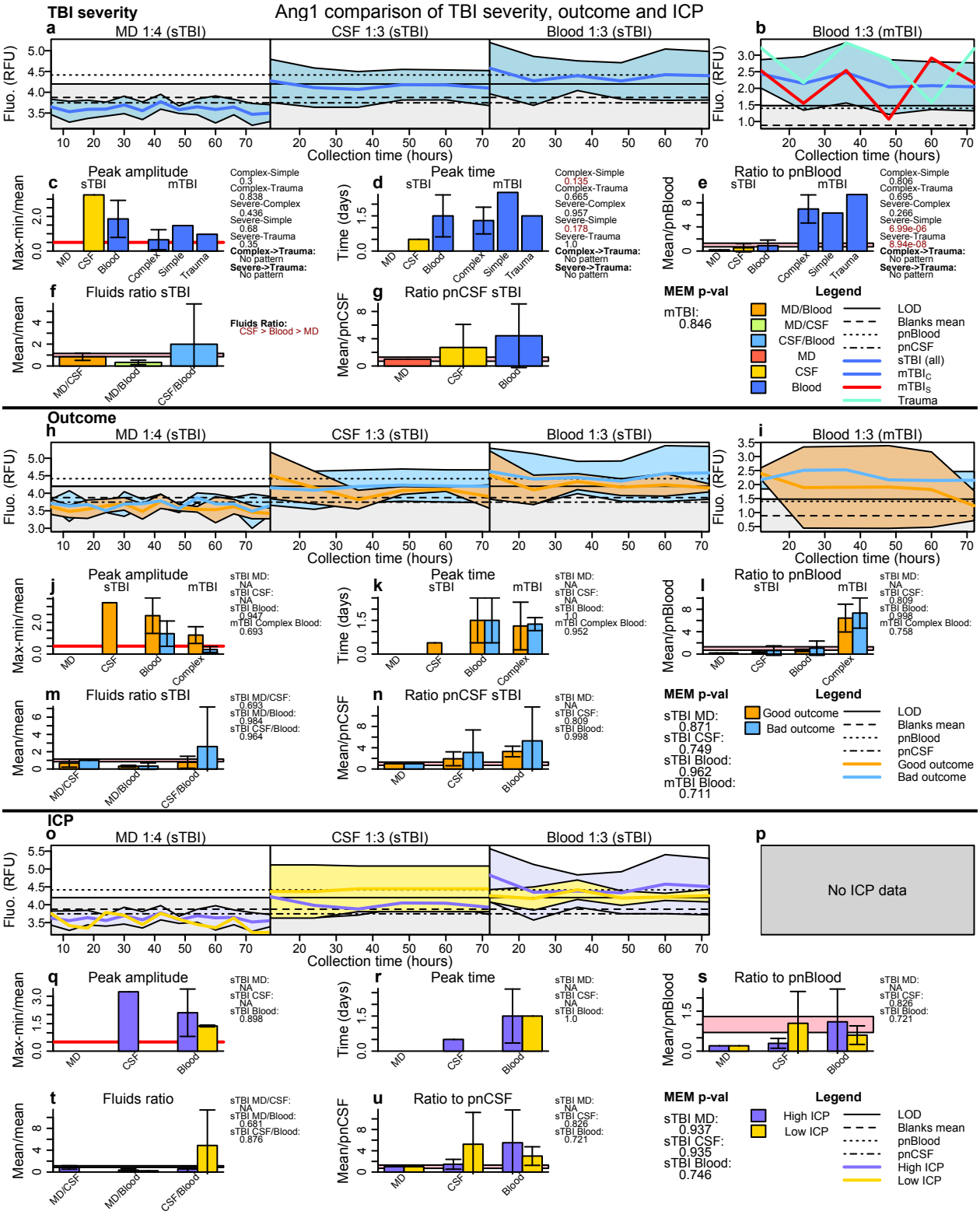

FIGURE J.S36: **Differential Ang1 protein profiles and peak and ratio analysis with respect to TBI severity, outcome and ICP.** Average Ang1 profiles are compared in terms of TBI severity (**a-g**), outcome (**h-n**) and ICP (**o-u**). Polygons in **a, b, h, i, o** indicate the mean value ±1 SD at each time point. Red lines in **c, j, q** show a threshold for a profile that is considered to have a peak, rather than being constant. The light red boxes in **e-g, l-n, s-u** show the threshold of comparison to the measured value compared. Benjamini–Hochberg adjusted p-values for comparisons are shown on the right of every graph.

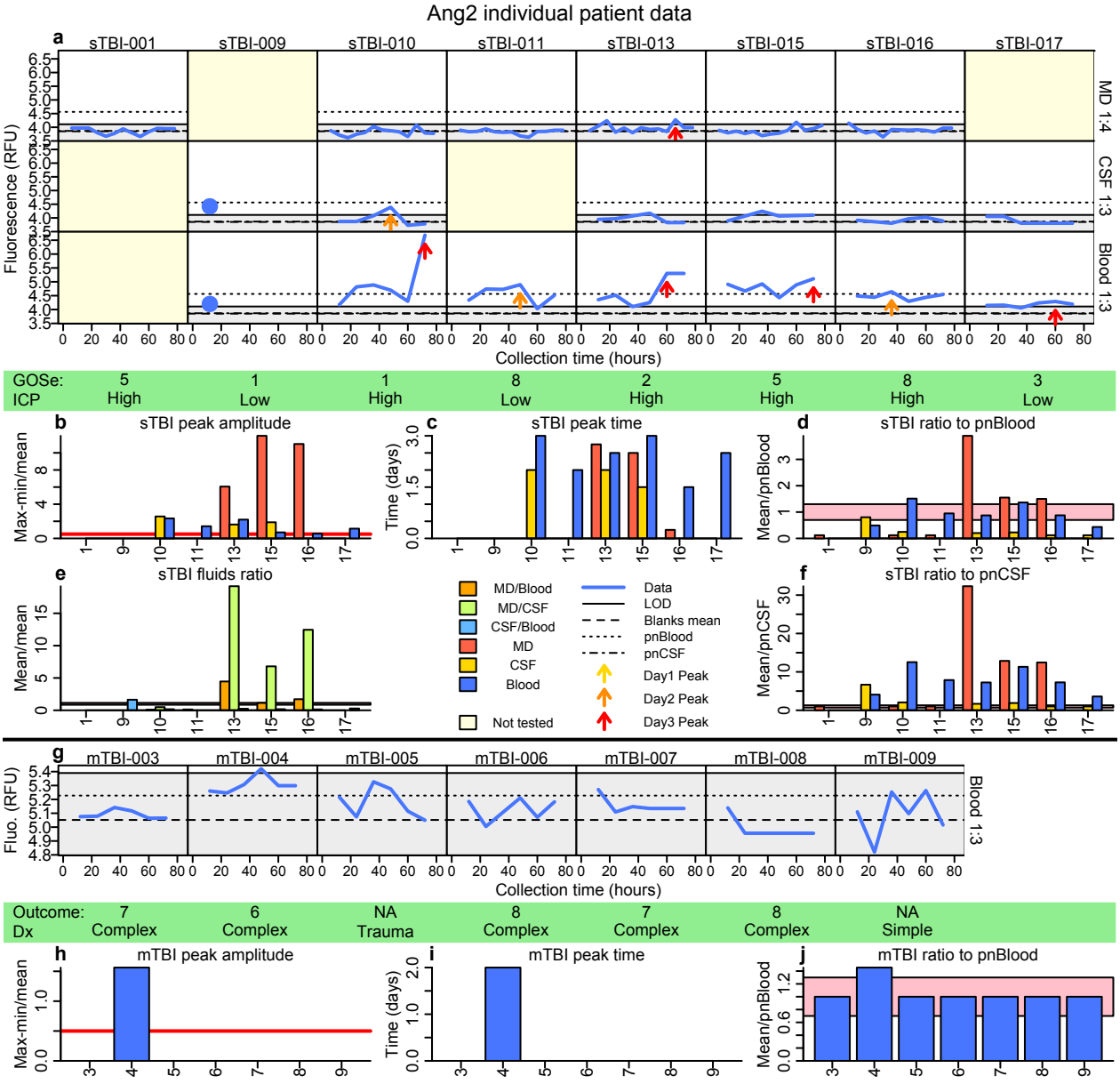

FIGURE J.S37: **Individual Ang2 protein profiles and peak and ratio analysis.** Ang2 concentration in microdialysate, CSF and blood samples of individual sTBI patients (**a**) and mTBI/trauma patients (**g**) was measured and peak amplitude and time, as well as ratio between mean time course values to value found in the pooled normal control (**b-f, h-j**) were calculated for each patient. Graphs **b-f** show calculations for individual sTBI patients, and graphs **h-j** show calculations for individual mTBI patients. Red lines in **b, h** show a threshold for a profile that is considered to have a peak, rather than being constant. The light red boxes in **d, e, f, j** show the threshold of comparison to the measured value compared.

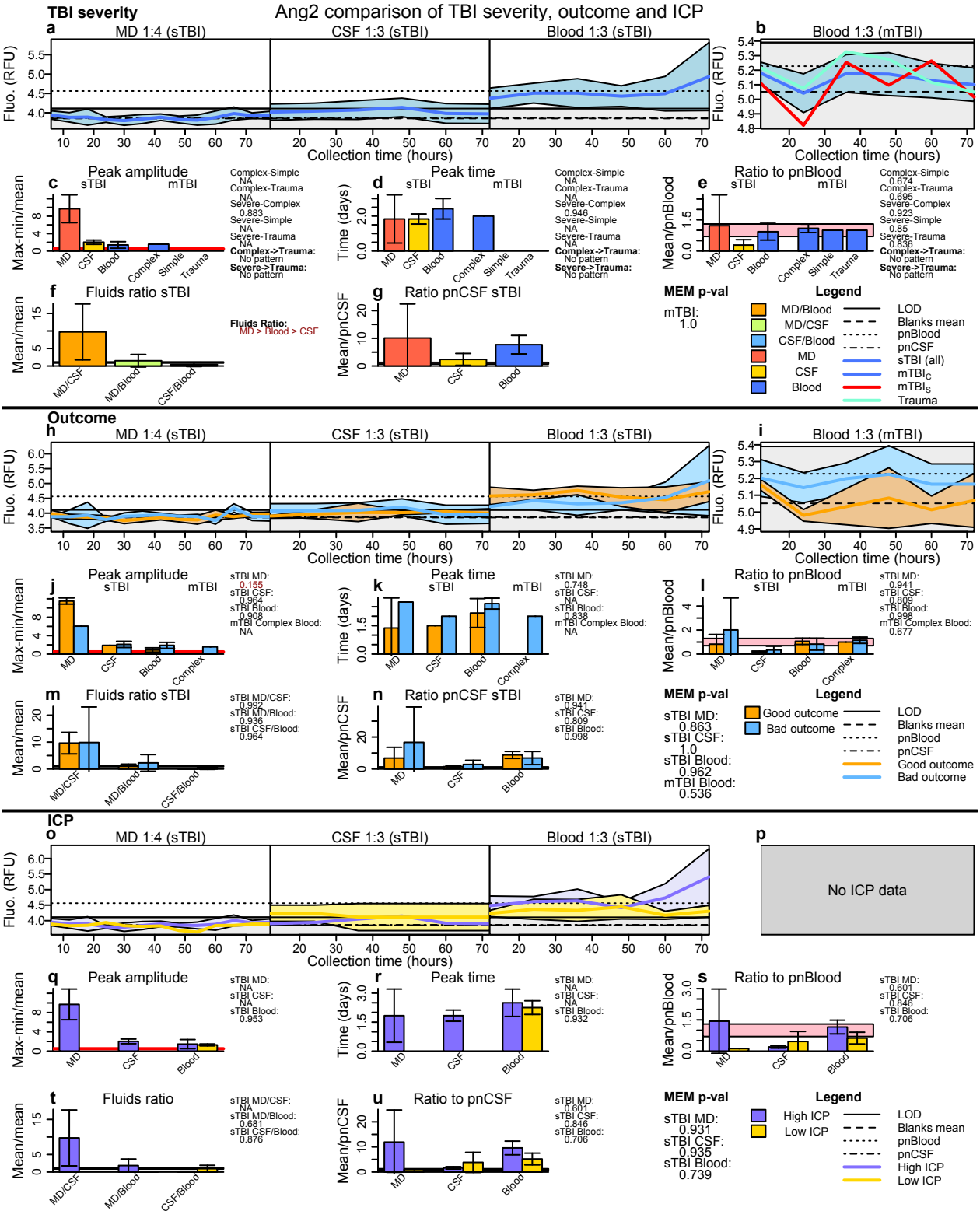

FIGURE J.S38: **Differential Ang2 protein profiles and peak and ratio analysis with respect to TBI severity, outcome and ICP.** Average Ang2 profiles are compared in terms of TBI severity (**a-g**), outcome (**h-n**) and ICP (**o-u**). Polygons in **a, b, h, i, o** indicate the mean value ±1 SD at each time point. Red lines in **c, j, q** show a threshold for a profile that is considered to have a peak, rather than being constant. The light red boxes in **e-g, l-n, s-u** show the threshold of comparison to the measured value compared. Benjamini–Hochberg adjusted p-values for comparisons are shown on the right of every graph.

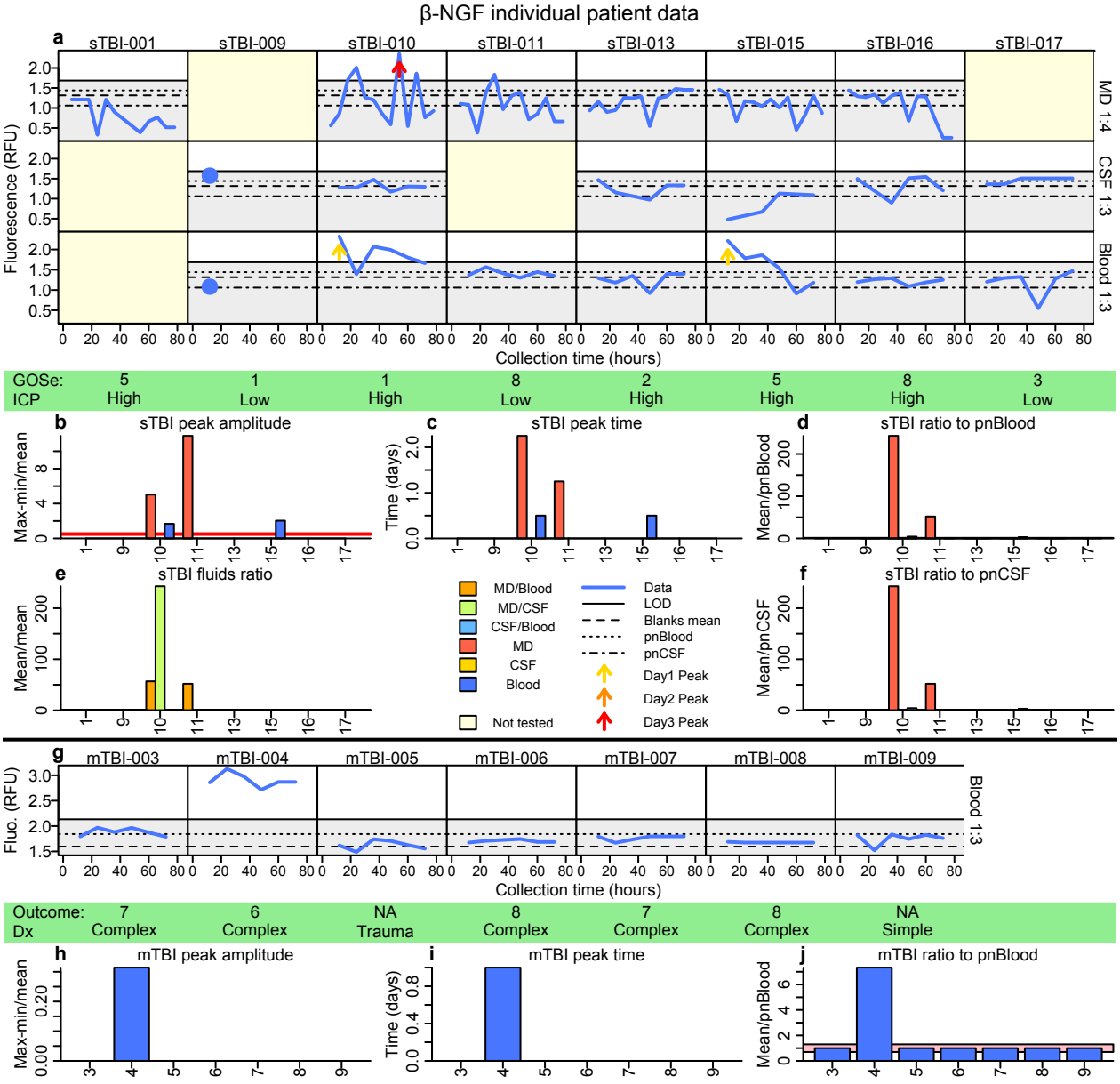

FIGURE J.S39: **Individual β-NGF protein profiles and peak and ratio analysis.** β-NGF concentration in microdialysate, CSF and blood samples of individual sTBI patients (**a**) and mTBI/trauma patients (**g**) was measured and peak amplitude and time, as well as ratio between mean time course values to value found in the pooled normal control (**b-f, h-j**) were calculated for each patient. Graphs **b-f** show calculations for individual sTBI patients, and graphs **h-j** show calculations for individual mTBI patients. Red lines in **b, h** show a threshold for a profile that is considered to have a peak, rather than being constant. The light red boxes in **d, e, f, j** show the threshold of comparison to the measured value compared.

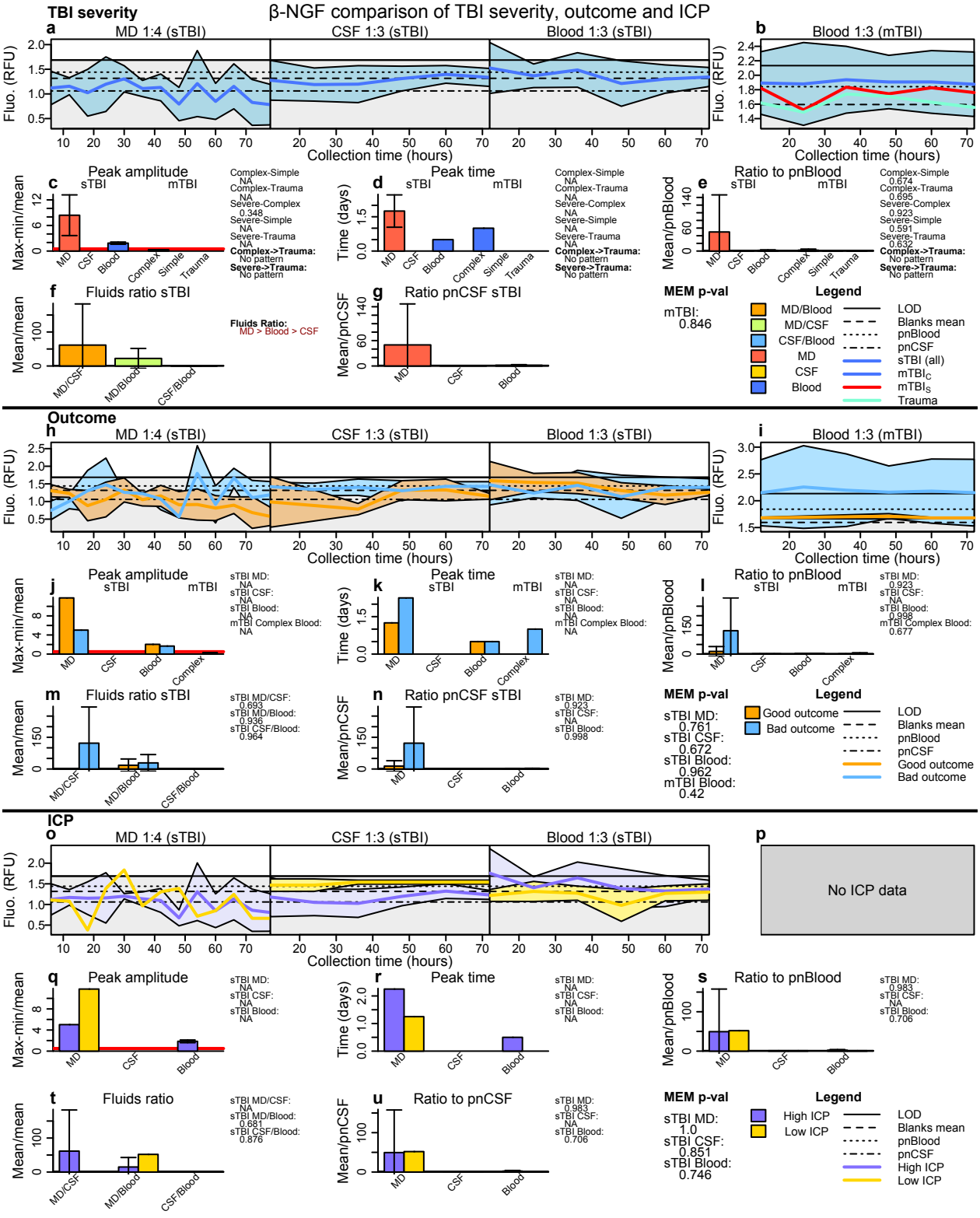

FIGURE J.S40: **Differential β-NGF protein profiles and peak and ratio analysis with respect to TBI severity, outcome and ICP.** Average β-NGF profiles are compared in terms of TBI severity (**a-g**), outcome (**h-n**) and ICP (**o-u**). Polygons in **a, b, h, i, o** indicate the mean value ± 1 SD at each time point. Red lines in **c, j, q** show a threshold for a profile that is considered to have a peak, rather than being constant. The light red boxes in **e-g, l-n, s-u** show the threshold of comparison to the measured value compared. Benjamini–Hochberg adjusted p-values for comparisons are shown on the right of every graph.

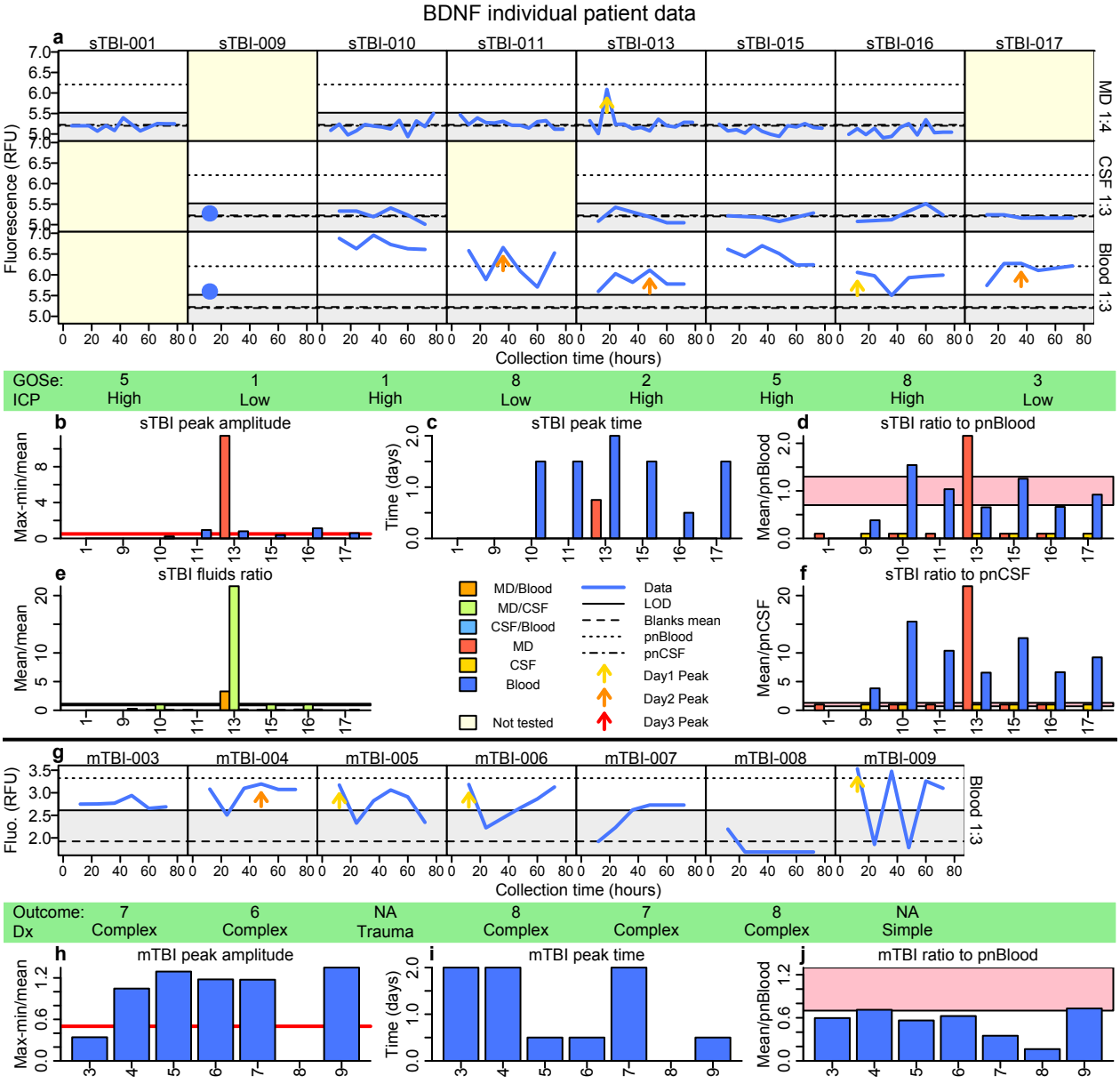

FIGURE J.S41: **Individual BDNF protein profiles and peak and ratio analysis.** BDNF concentration in microdialysate, CSF and blood samples of individual sTBI patients (**a**) and mTBI/trauma patients (**g**) was measured and peak amplitude and time, as well as ratio between mean time course values to value found in the pooled normal control (**b-f, h-j**) were calculated for each patient. Graphs **b-f** show calculations for individual sTBI patients, and graphs **h-j** show calculations for individual mTBI patients. Red lines in **b, h** show a threshold for a profile that is considered to have a peak, rather than being constant. The light red boxes in **d, e, f, j** show the threshold of comparison to the measured value compared.

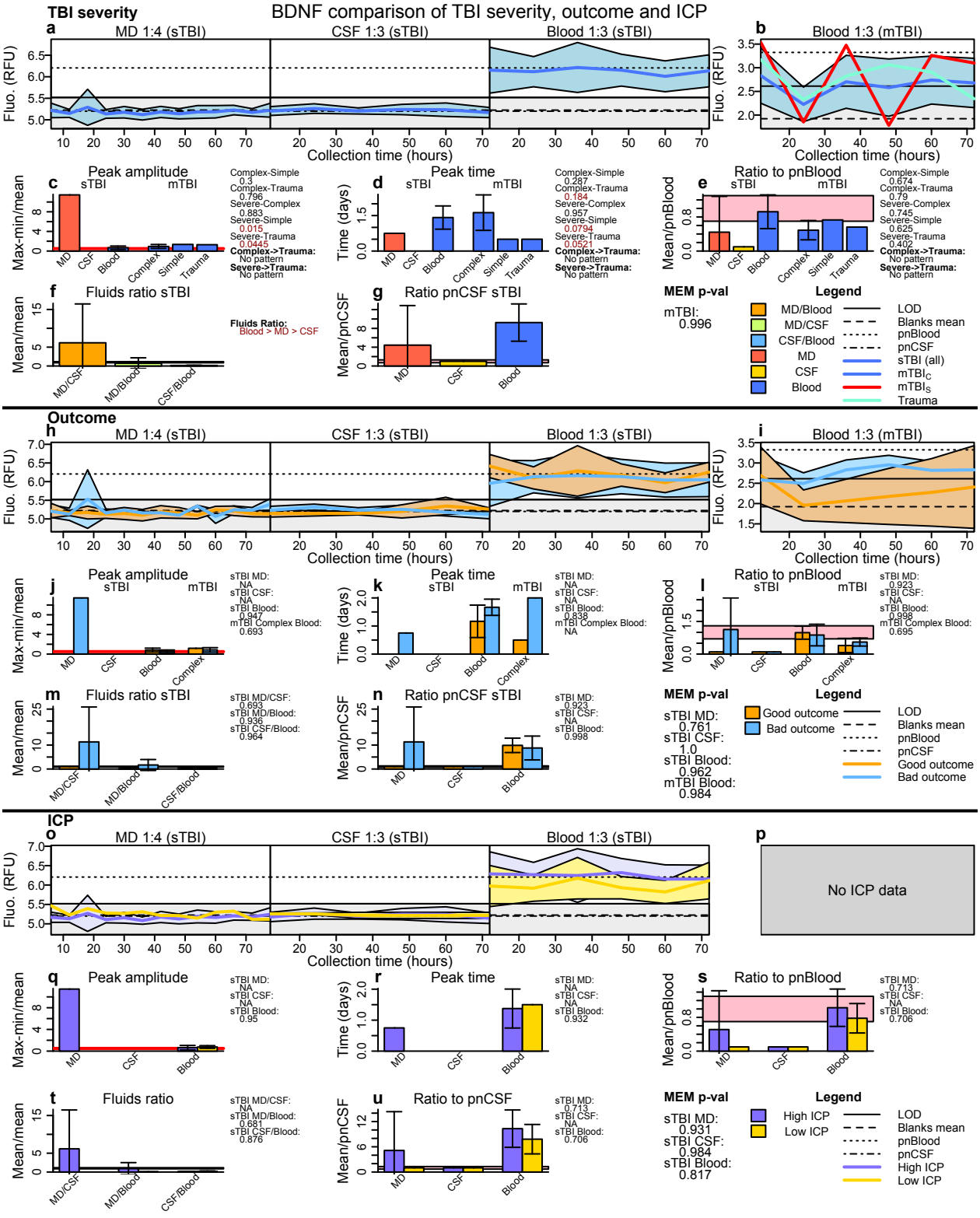

FIGURE J.S42: **Differential BDNF protein profiles and peak and ratio analysis with respect to TBI severity, outcome and ICP.** Average BDNF profiles are compared in terms of TBI severity (**a-g**), outcome (**h-n**) and ICP (**o-u**). Polygons in **a, b, h, i, o** indicate the mean value ±1 SD at each time point. Red lines in **c, j, q** show a threshold for a profile that is considered to have a peak, rather than being constant. The light red boxes in **e-g, l-n, s-u** show the threshold of comparison to the measured value compared. Benjamini–Hochberg adjusted p-values for comparisons are shown on the right of every graph.

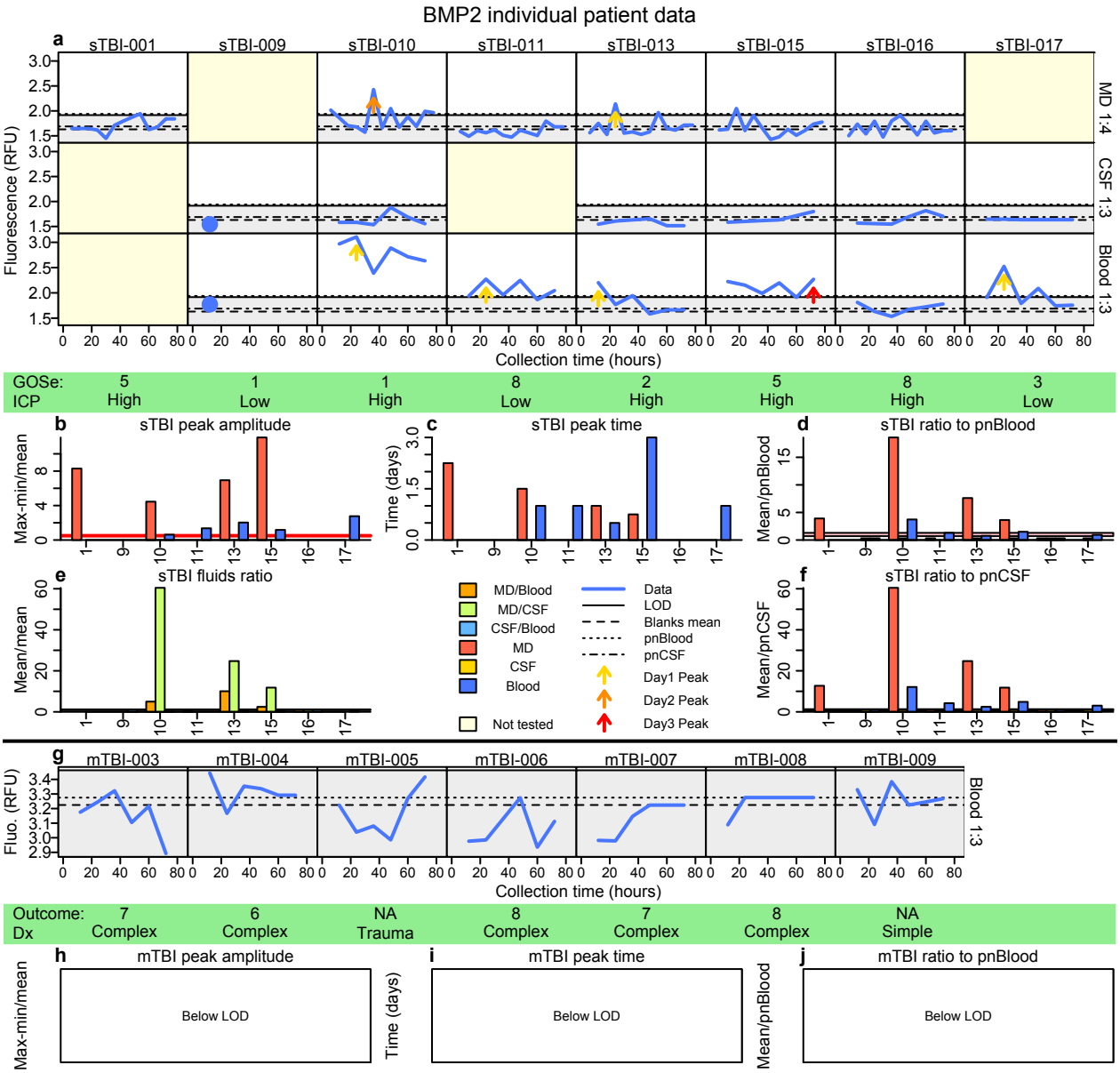

FIGURE J.S43: **Individual BMP2 protein profiles and peak and ratio analysis.** BMP2 concentration in microdialysate, CSF and blood samples of individual sTBI patients (**a**) and mTBI/trauma patients (**g**) was measured and peak amplitude and time, as well as ratio between mean time course values to value found in the pooled normal control (**b-f, h-j**) were calculated for each patient. Graphs **b-f** show calculations for individual sTBI patients, and graphs **h-j** show calculations for individual mTBI patients. Red lines in **b, h** show a threshold for a profile that is considered to have a peak, rather than being constant. The light red boxes in **d, e, f, j** show the threshold of comparison to the measured value compared.

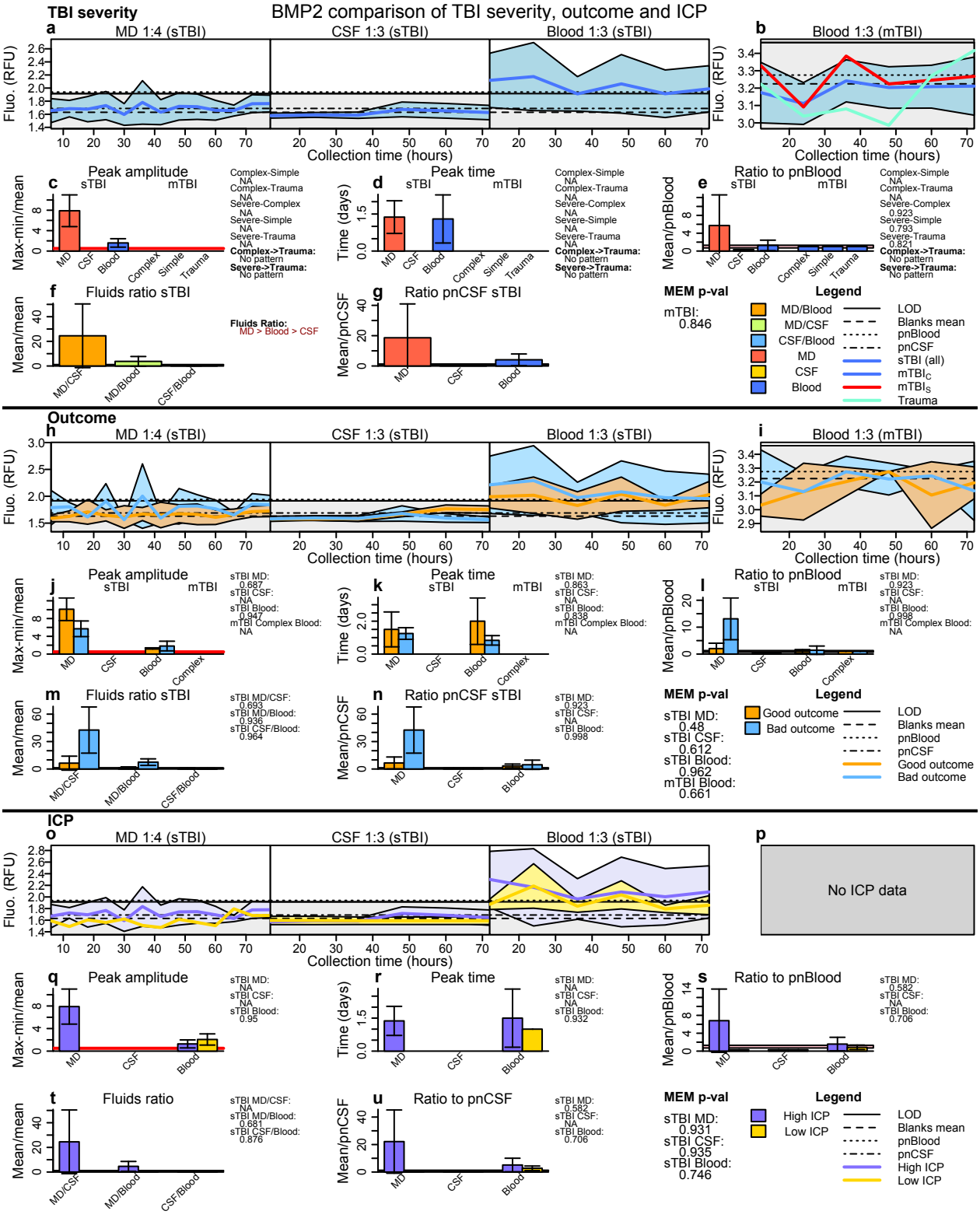

FIGURE J.S44: **Differential BMP2 protein profiles and peak and ratio analysis with respect to TBI severity, outcome and ICP.** Average BMP2 profiles are compared in terms of TBI severity (**a-g**), outcome (**h-n**) and ICP (**o-u**). Polygons in **a, b, h, i, o** indicate the mean value ±1 SD at each time point. Red lines in **c, j, q** show a threshold for a profile that is considered to have a peak, rather than being constant. The light red boxes in **e-g, l-n, s-u** show the threshold of comparison to the measured value compared. Benjamini–Hochberg adjusted p-values for comparisons are shown on the right of every graph.

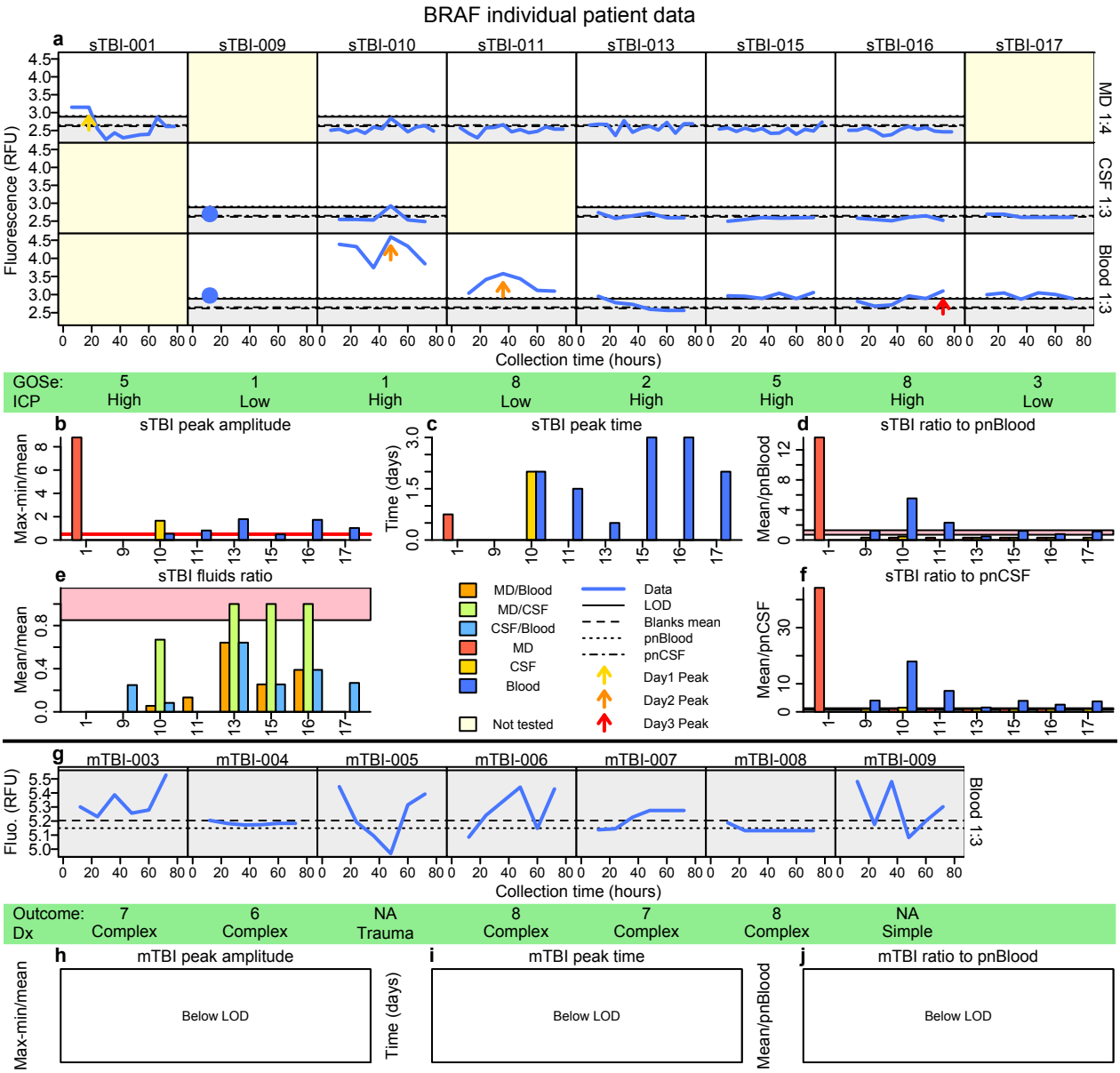

FIGURE J.S45: **Individual BRAF protein profiles and peak and ratio analysis.** BRAF concentration in microdialysate, CSF and blood samples of individual sTBI patients (**a**) and mTBI/trauma patients (**g**) was measured and peak amplitude and time, as well as ratio between mean time course values to value found in the pooled normal control (**b-f, h-j**) were calculated for each patient. Graphs **b-f** show calculations for individual sTBI patients, and graphs **h-j** show calculations for individual mTBI patients. Red lines in **b, h** show a threshold for a profile that is considered to have a peak, rather than being constant. The light red boxes in **d, e, f, j** show the threshold of comparison to the measured value compared.

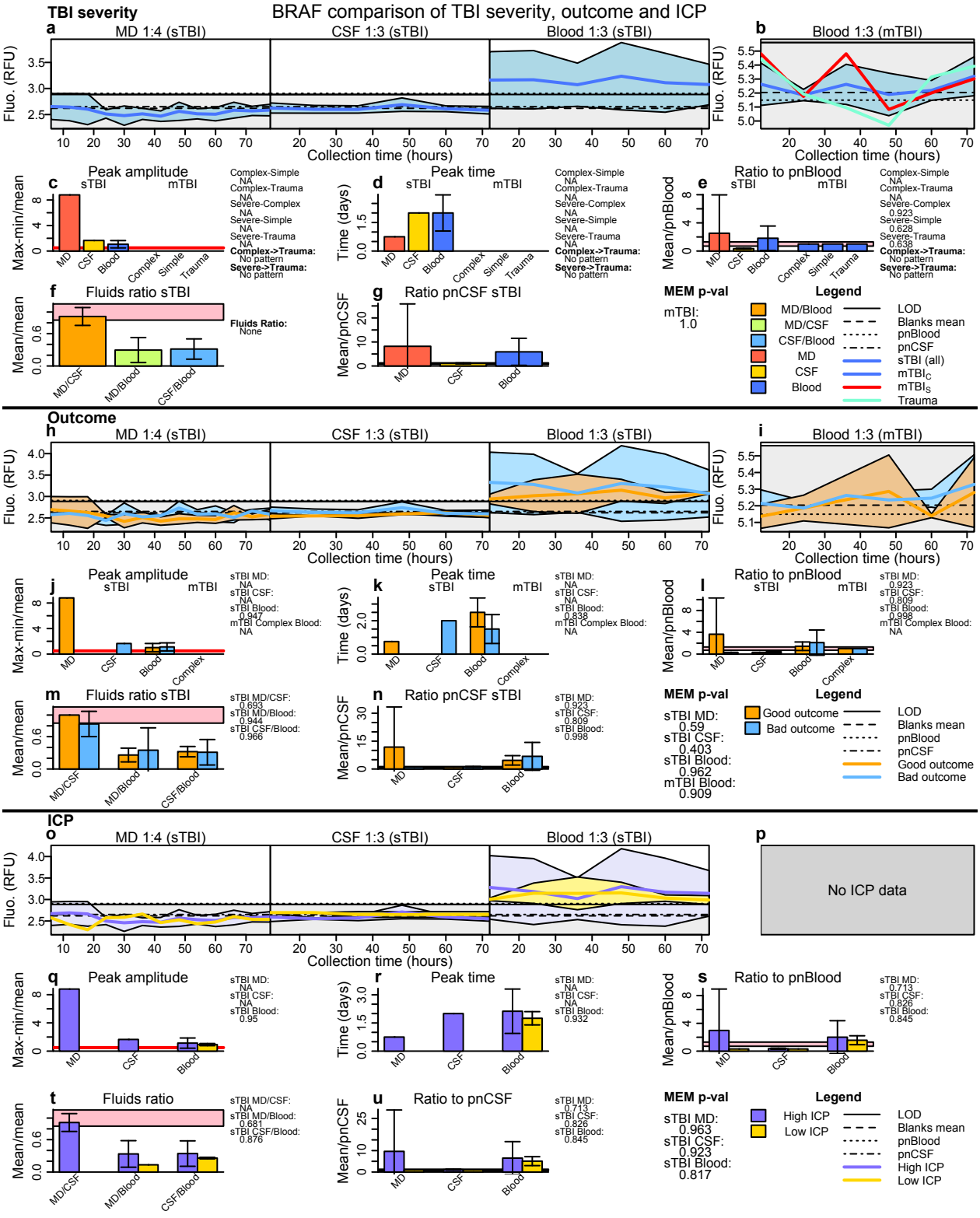

FIGURE J.S46: **Differential BRAF protein profiles and peak and ratio analysis with respect to TBI severity, outcome and ICP.** Average BRAF profiles are compared in terms of TBI severity (**a-g**), outcome (**h-n**) and ICP (**o-u**). Polygons in **a, b, h, i, o** indicate the mean value ±1 SD at each time point. Red lines in **c, j, q** show a threshold for a profile that is considered to have a peak, rather than being constant. The light red boxes in **e-g, l-n, s-u** show the threshold of comparison to the measured value compared. Benjamini–Hochberg adjusted p-values for comparisons are shown on the right of every graph.

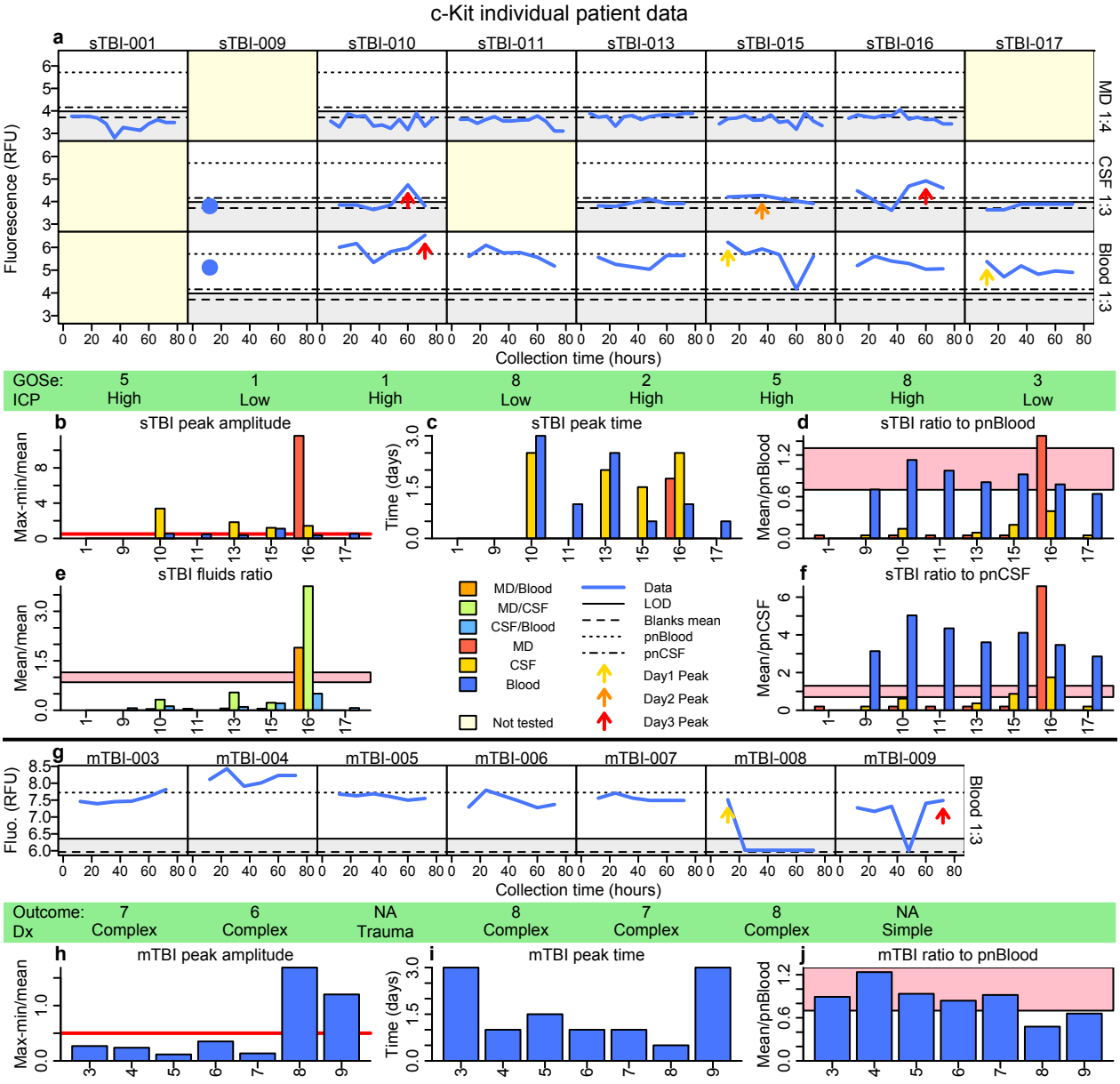

FIGURE J.S47: **Individual c-Kit protein profiles and peak and ratio analysis.** c-Kit concentration in microdialysate, CSF and blood samples of individual sTBI patients (**a**) and mTBI/trauma patients (**g**) was measured and peak amplitude and time, as well as ratio between mean time course values to value found in the pooled normal control (**b-f, h-j**) were calculated for each patient. Graphs **b-f** show calculations for individual sTBI patients, and graphs **h-j** show calculations for individual mTBI patients. Red lines in **b, h** show a threshold for a profile that is considered to have a peak, rather than being constant. The light red boxes in **d, e, f, j** show the threshold of comparison to the measured value compared.

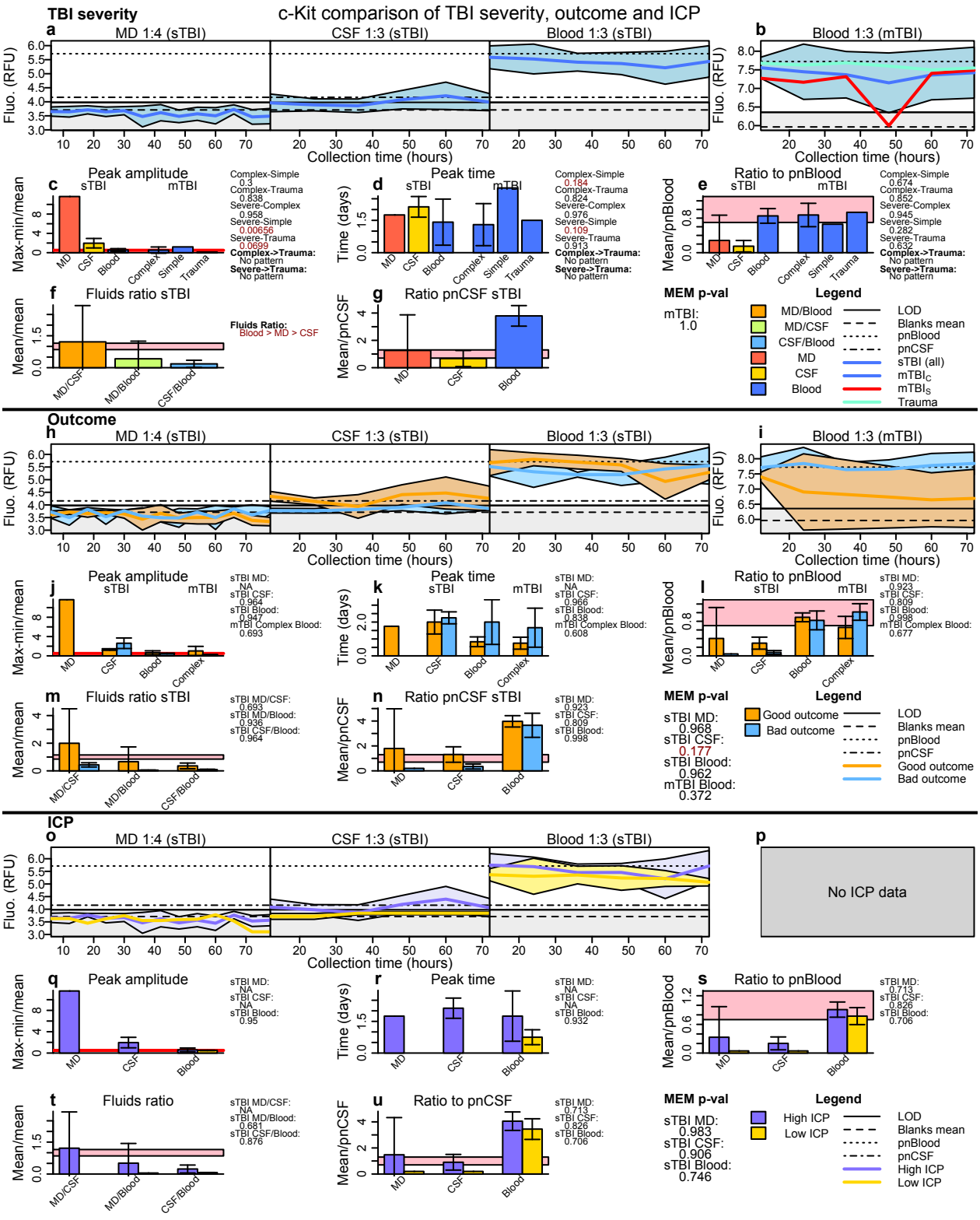

FIGURE J.S48: **Differential c-Kit protein profiles and peak and ratio analysis with respect to TBI severity, outcome and ICP.** Average c-Kit profiles are compared in terms of TBI severity (**a-g**), outcome (**h-n**) and ICP (**o-u**). Polygons in **a, b, h, i, o** indicate the mean value ±1 SD at each time point. Red lines in **c, j, q** show a threshold for a profile that is considered to have a peak, rather than being constant. The light red boxes in **e-g, l-n, s-u** show the threshold of comparison to the measured value compared. Benjamini–Hochberg adjusted p-values for comparisons are shown on the right of every graph.

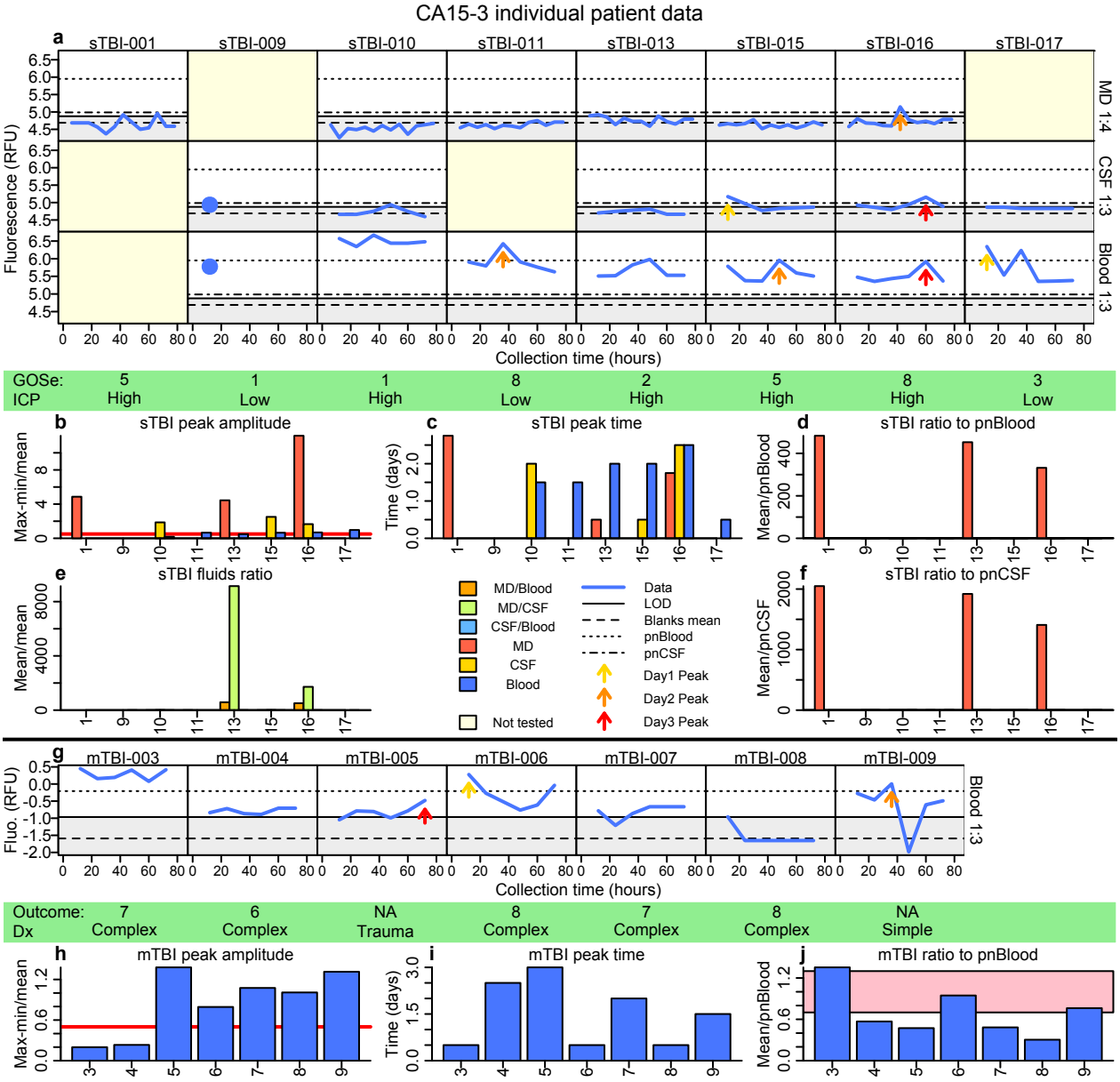

FIGURE J.S49: **Individual CA15-3 protein profiles and peak and ratio analysis.** CA15-3 concentration in microdialysate, CSF and blood samples of individual sTBI patients (**a**) and mTBI/trauma patients (**g**) was measured and peak amplitude and time, as well as ratio between mean time course values to value found in the pooled normal control (**b-f, h-j**) were calculated for each patient. Graphs **b-f** show calculations for individual sTBI patients, and graphs **h-j** show calculations for individual mTBI patients. Red lines in **b, h** show a threshold for a profile that is considered to have a peak, rather than being constant. The light red boxes in **d, e, f, j** show the threshold of comparison to the measured value compared.

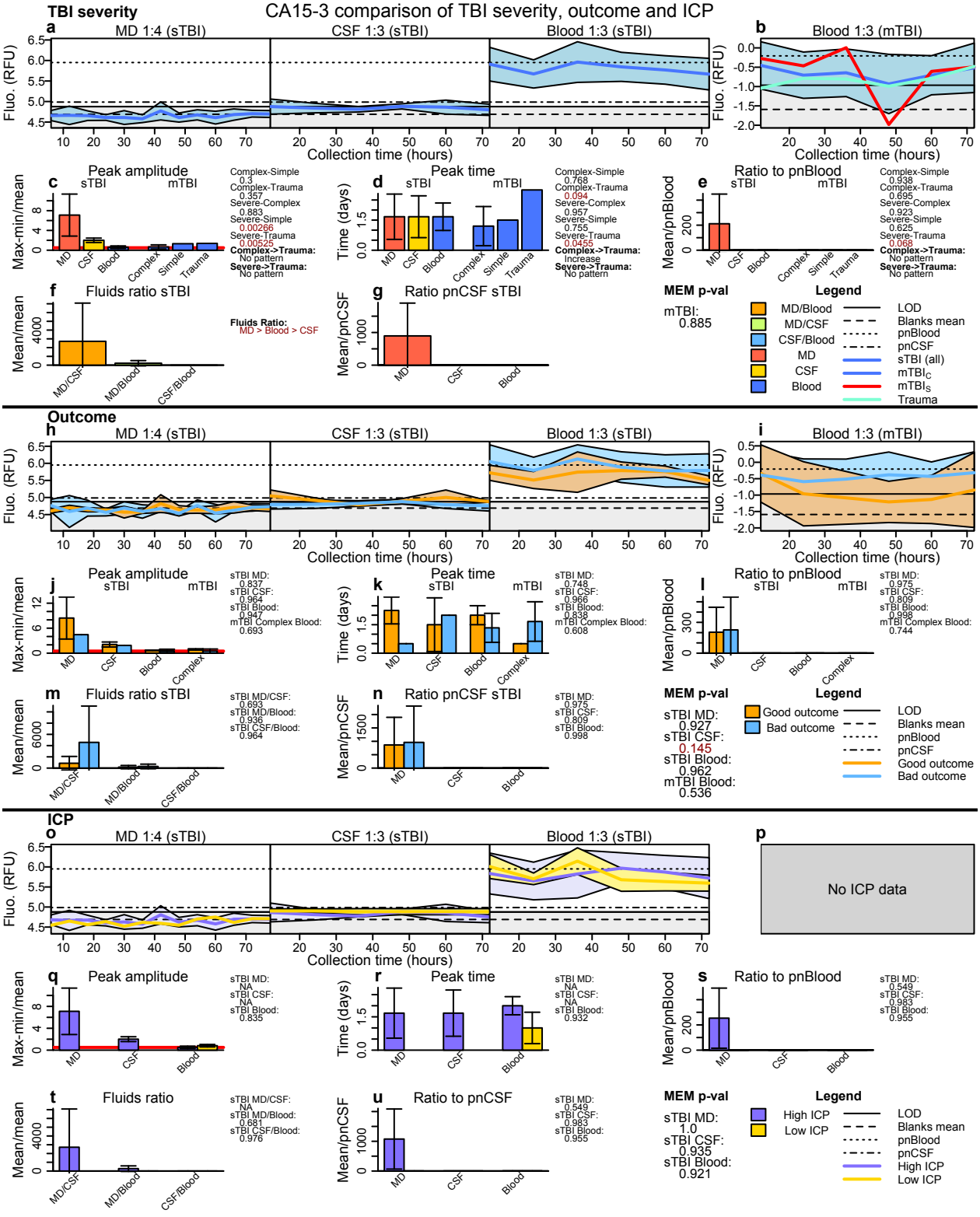

FIGURE J.S50: **Differential CA15-3 protein profiles and peak and ratio analysis with respect to TBI severity, outcome and ICP.** Average CA15-3 profiles are compared in terms of TBI severity (**a-g**), outcome (**h-n**) and ICP (**o-u**). Polygons in **a, b, h, i, o** indicate the mean value ±1 SD at each time point. Red lines in **c, j, q** show a threshold for a profile that is considered to have a peak, rather than being constant. The light red boxes in **e-g, l-n, s-u** show the threshold of comparison to the measured value compared. Benjamini–Hochberg adjusted p-values for comparisons are shown on the right of every graph.

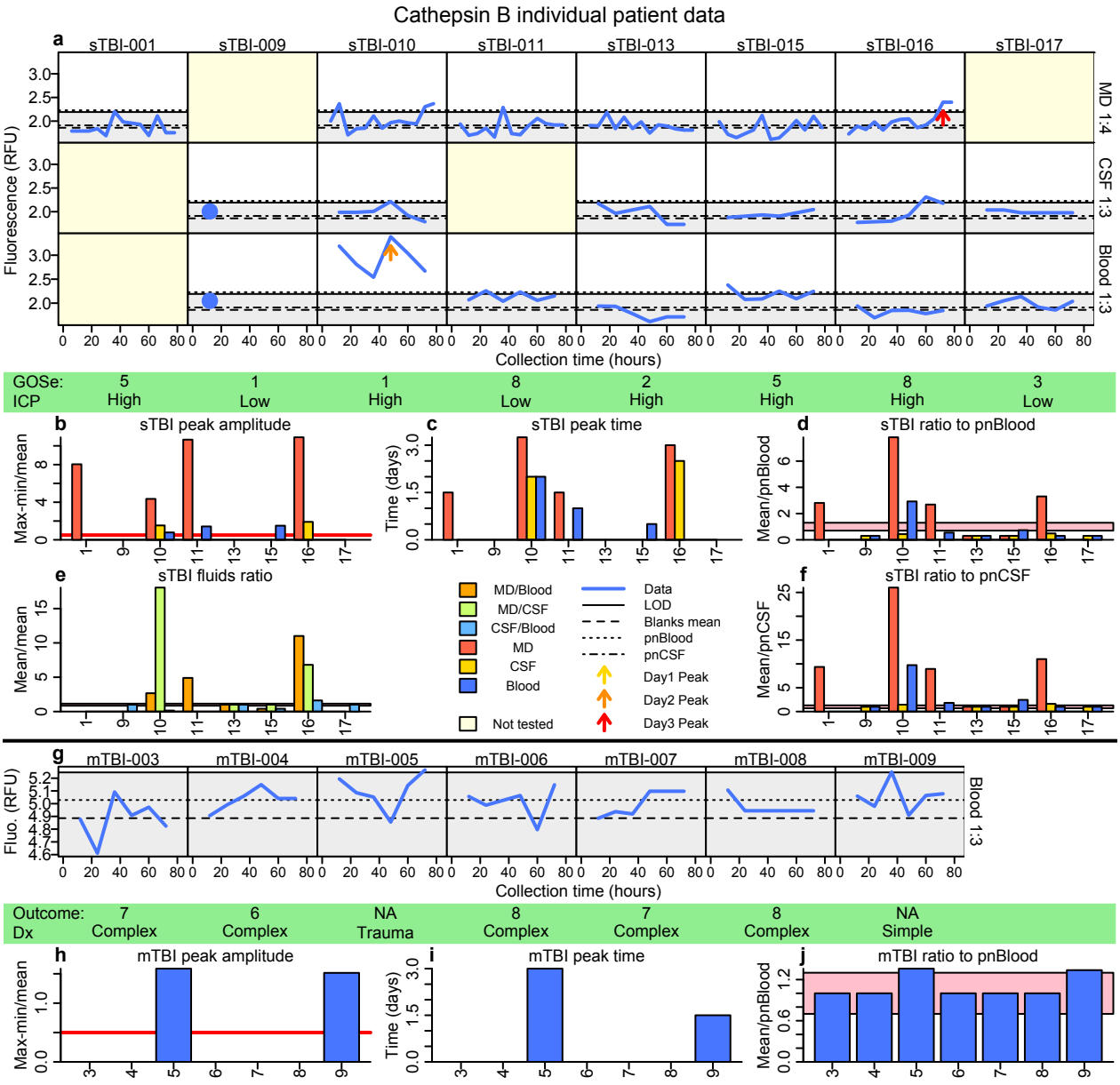

FIGURE J.S51: **Individual Cathepsin B protein profiles and peak and ratio analysis.** Cathepsin B concentration in microdialysate, CSF and blood samples of individual sTBI patients (**a**) and mTBI/trauma patients (**g**) was measured and peak amplitude and time, as well as ratio between mean time course values to value found in the pooled normal control (**b-f, h-j**) were calculated for each patient. Graphs **b-f** show calculations for individual sTBI patients, and graphs **h-j** show calculations for individual mTBI patients. Red lines in **b, h** show a threshold for a profile that is considered to have a peak, rather than being constant. The light red boxes in **d, e, f, j** show the threshold of comparison to the measured value compared.

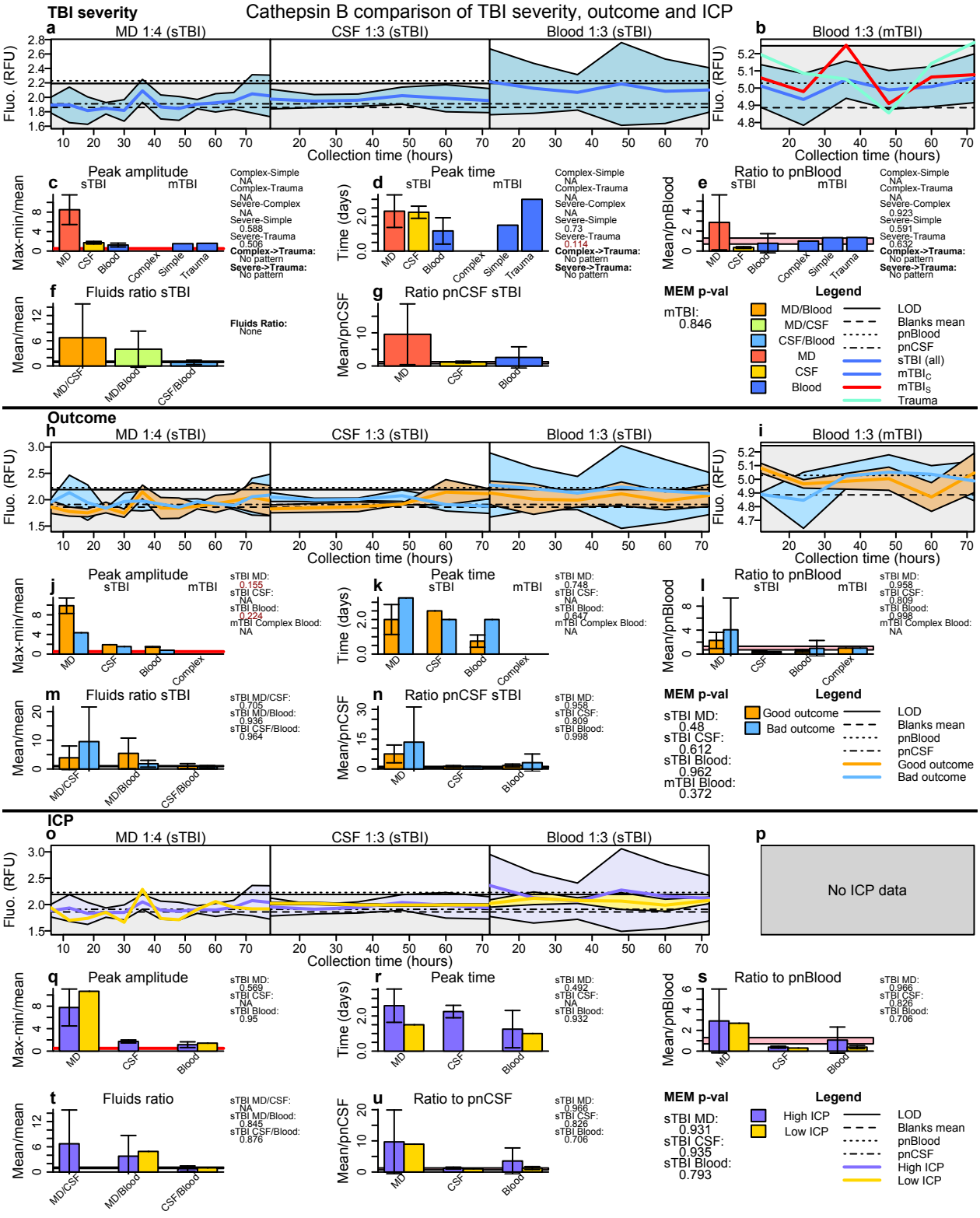

FIGURE J.S52: **Differential Cathepsin B protein profiles and peak and ratio analysis with respect to TBI severity, outcome and ICP.** Average Cathepsin B profiles are compared in terms of TBI severity (**a-g**), outcome (**h-n**) and ICP (**o-u**). Polygons in **a, b, h, i, o** indicate the mean value ±1 SD at each time point. Red lines in **c, j, q** show a threshold for a profile that is considered to have a peak, rather than being constant. The light red boxes in **e-g, l-n, s-u** show the threshold of comparison to the measured value compared. Benjamini–Hochberg adjusted p-values for comparisons are shown on the right of every graph.

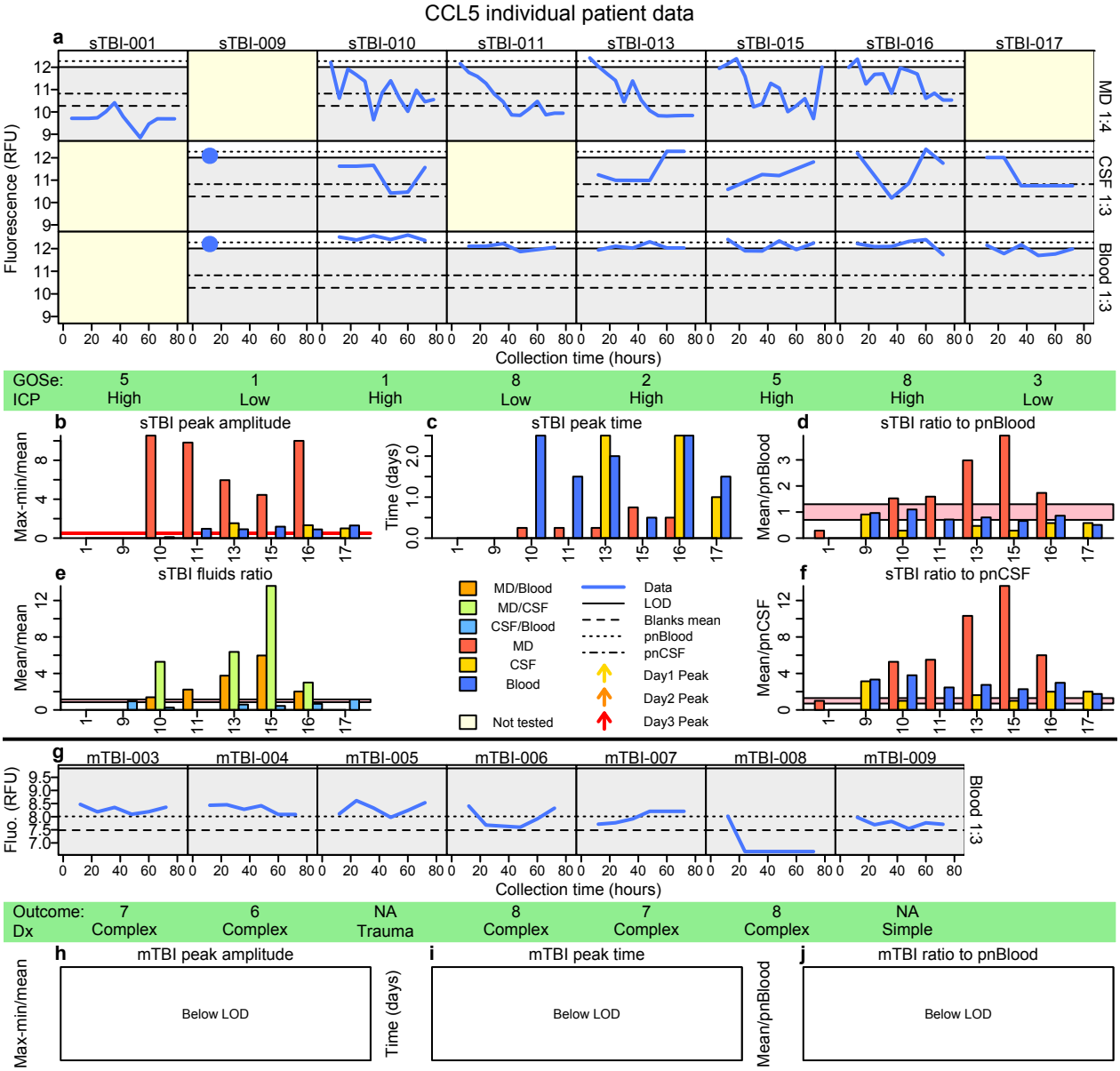

FIGURE J.S53: **Individual CCL5 protein profiles and peak and ratio analysis.** CCL5 concentration in microdialysate, CSF and blood samples of individual sTBI patients (**a**) and mTBI/trauma patients (**g**) was measured and peak amplitude and time, as well as ratio between mean time course values to value found in the pooled normal control (**b-f, h-j**) were calculated for each patient. Graphs **b-f** show calculations for individual sTBI patients, and graphs **h-j** show calculations for individual mTBI patients. Red lines in **b, h** show a threshold for a profile that is considered to have a peak, rather than being constant. The light red boxes in **d, e, f, j** show the threshold of comparison to the measured value compared.

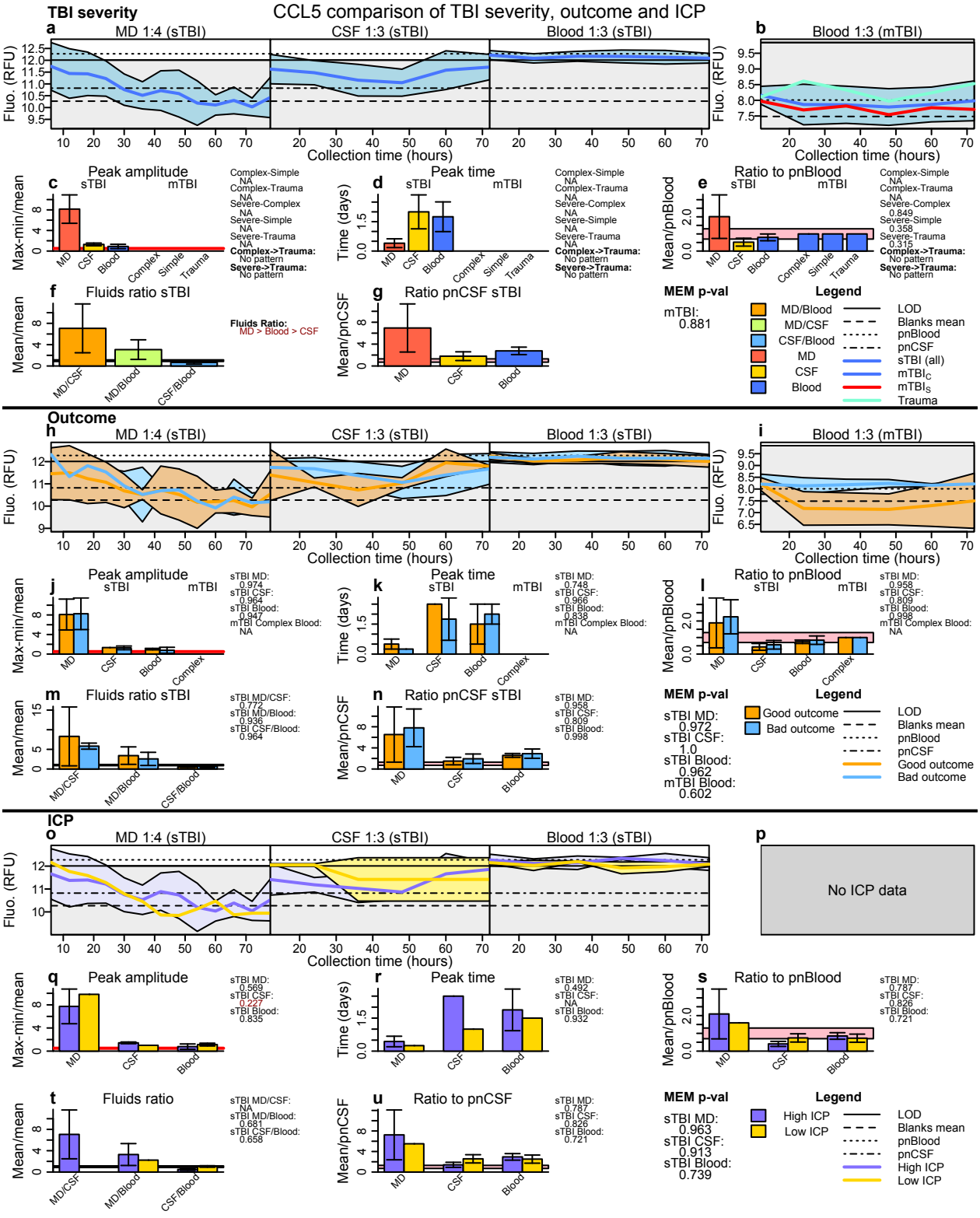

FIGURE J.S54: **Differential CCL5 protein profiles and peak and ratio analysis with respect to TBI severity, outcome and ICP.** Average CCL5 profiles are compared in terms of TBI severity (**a-g**), outcome (**h-n**) and ICP (**o-u**). Polygons in **a, b, h, i, o** indicate the mean value ±1 SD at each time point. Red lines in **c, j, q** show a threshold for a profile that is considered to have a peak, rather than being constant. The light red boxes in **e-g, l-n, s-u** show the threshold of comparison to the measured value compared. Benjamini–Hochberg adjusted p-values for comparisons are shown on the right of every graph.

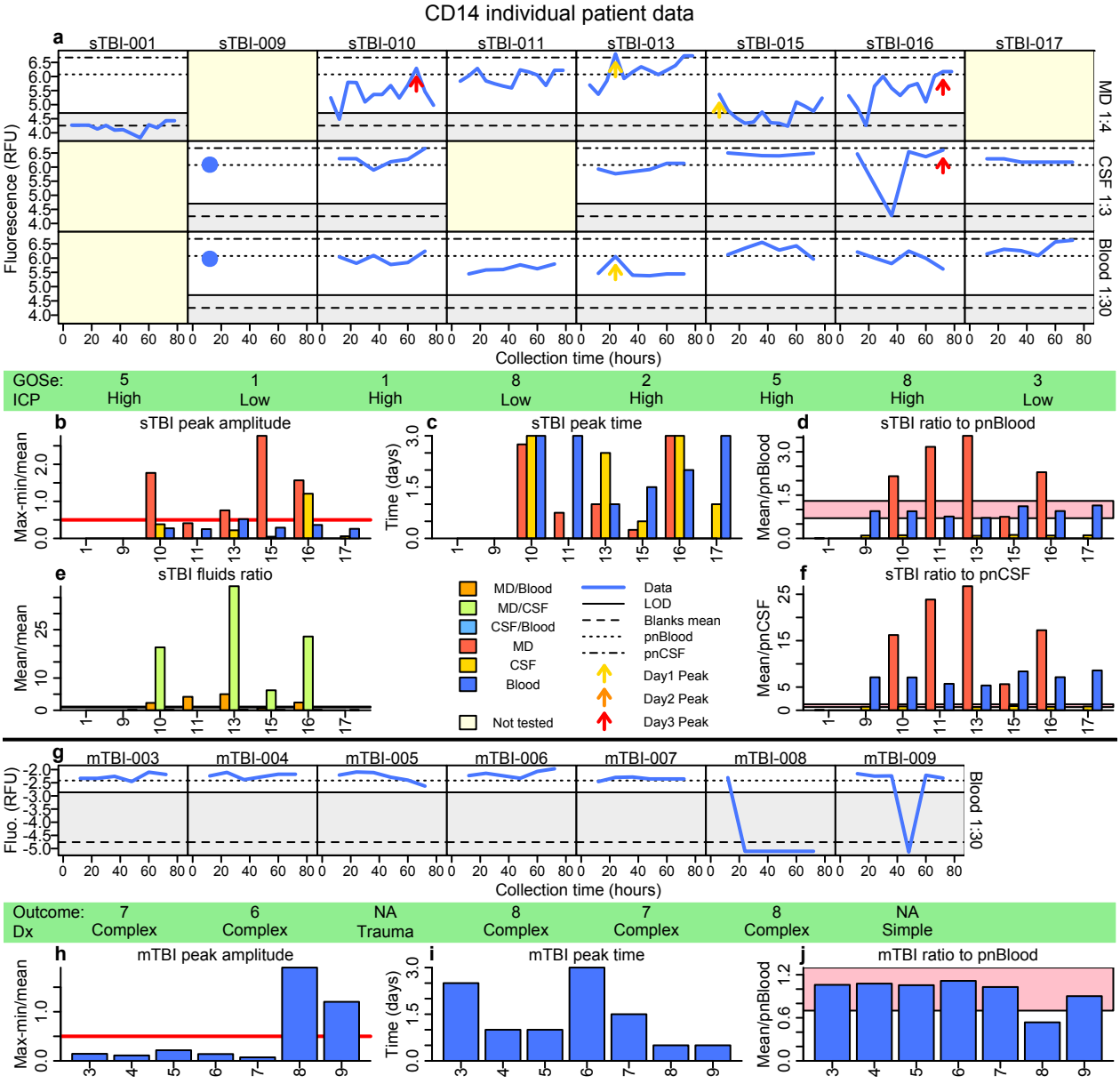

FIGURE J.S55: **Individual CD14 protein profiles and peak and ratio analysis.** CD14 concentration in microdialysate, CSF and blood samples of individual sTBI patients (**a**) and mTBI/trauma patients (**g**) was measured and peak amplitude and time, as well as ratio between mean time course values to value found in the pooled normal control (**b-f, h-j**) were calculated for each patient. Graphs **b-f** show calculations for individual sTBI patients, and graphs **h-j** show calculations for individual mTBI patients. Red lines in **b, h** show a threshold for a profile that is considered to have a peak, rather than being constant. The light red boxes in **d, e, f, j** show the threshold of comparison to the measured value compared.

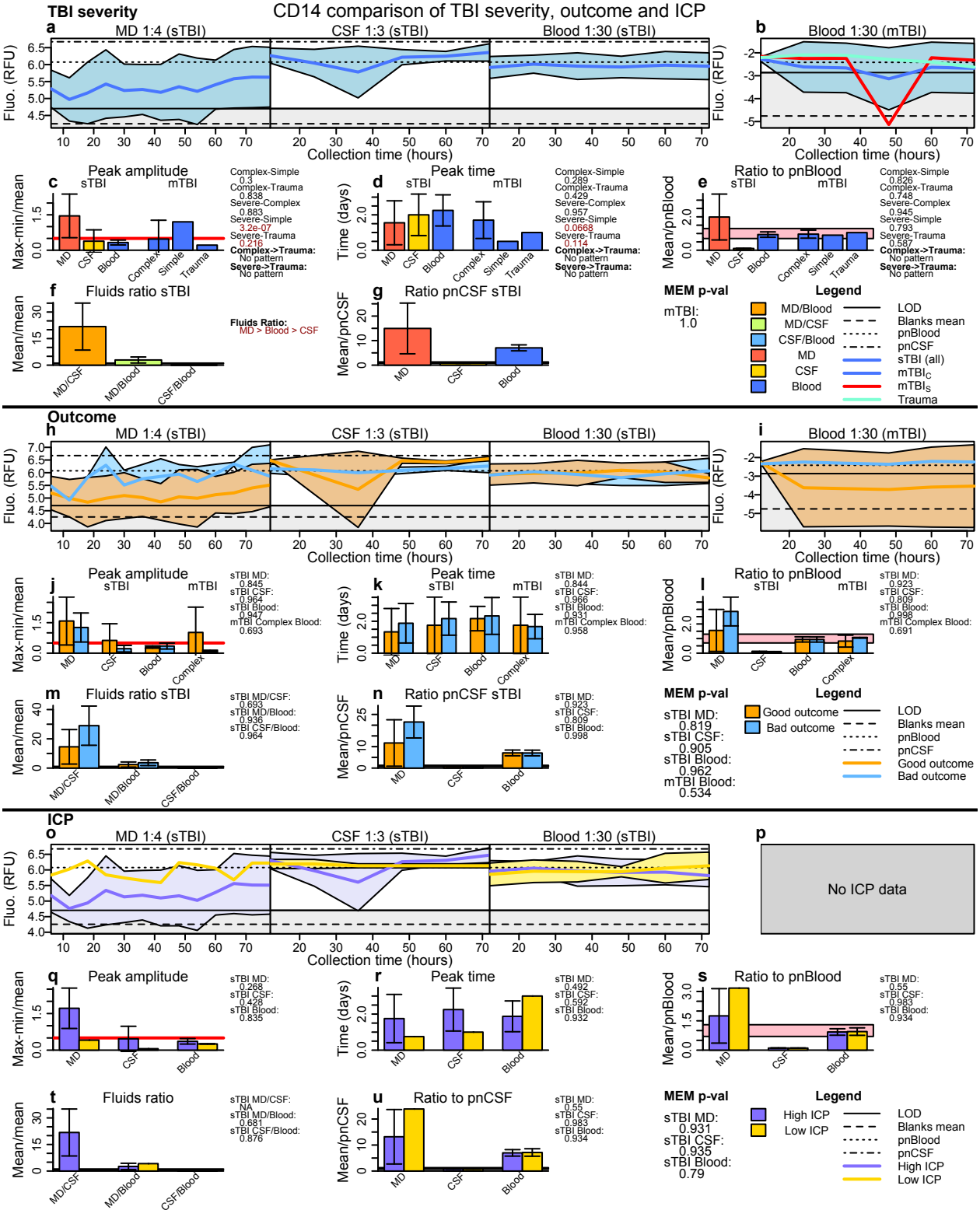

FIGURE J.S56: **Differential CD14 protein profiles and peak and ratio analysis with respect to TBI severity, outcome and ICP.** Average CD14 profiles are compared in terms of TBI severity (**a-g**), outcome (**h-n**) and ICP (**o-u**). Polygons in **a, b, h, i, o** indicate the mean value ±1 SD at each time point. Red lines in **c, j, q** show a threshold for a profile that is considered to have a peak, rather than being constant. The light red boxes in **e-g, l-n, s-u** show the threshold of comparison to the measured value compared. Benjamini–Hochberg adjusted p-values for comparisons are shown on the right of every graph.

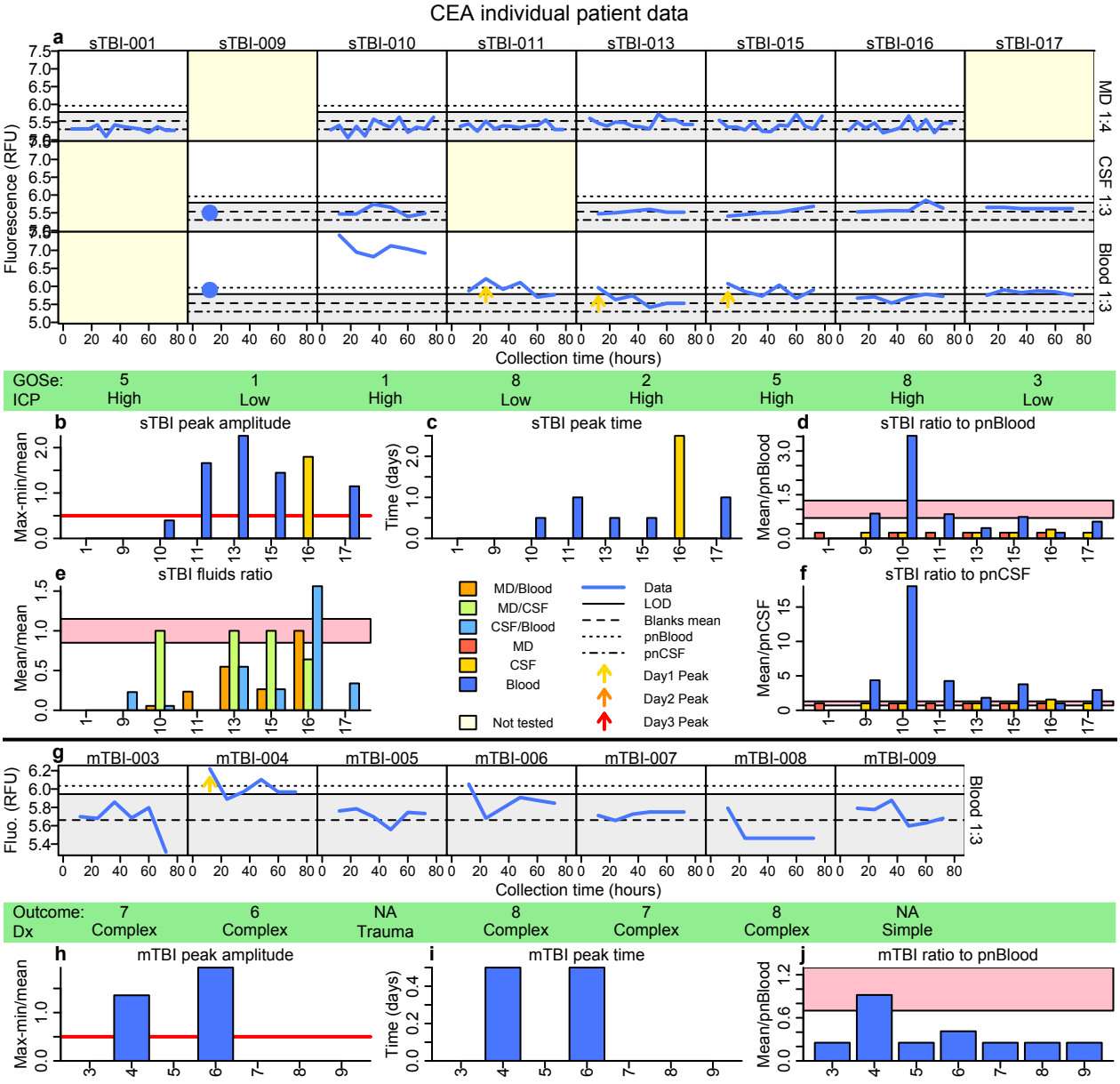

FIGURE J.S57: **Individual CEA protein profiles and peak and ratio analysis.** CEA concentration in microdialysate, CSF and blood samples of individual sTBI patients (**a**) and mTBI/trauma patients (**g**) was measured and peak amplitude and time, as well as ratio between mean time course values to value found in the pooled normal control (**b-f, h-j**) were calculated for each patient. Graphs **b-f** show calculations for individual sTBI patients, and graphs **h-j** show calculations for individual mTBI patients. Red lines in **b, h** show a threshold for a profile that is considered to have a peak, rather than being constant. The light red boxes in **d, e, f, j** show the threshold of comparison to the measured value compared.

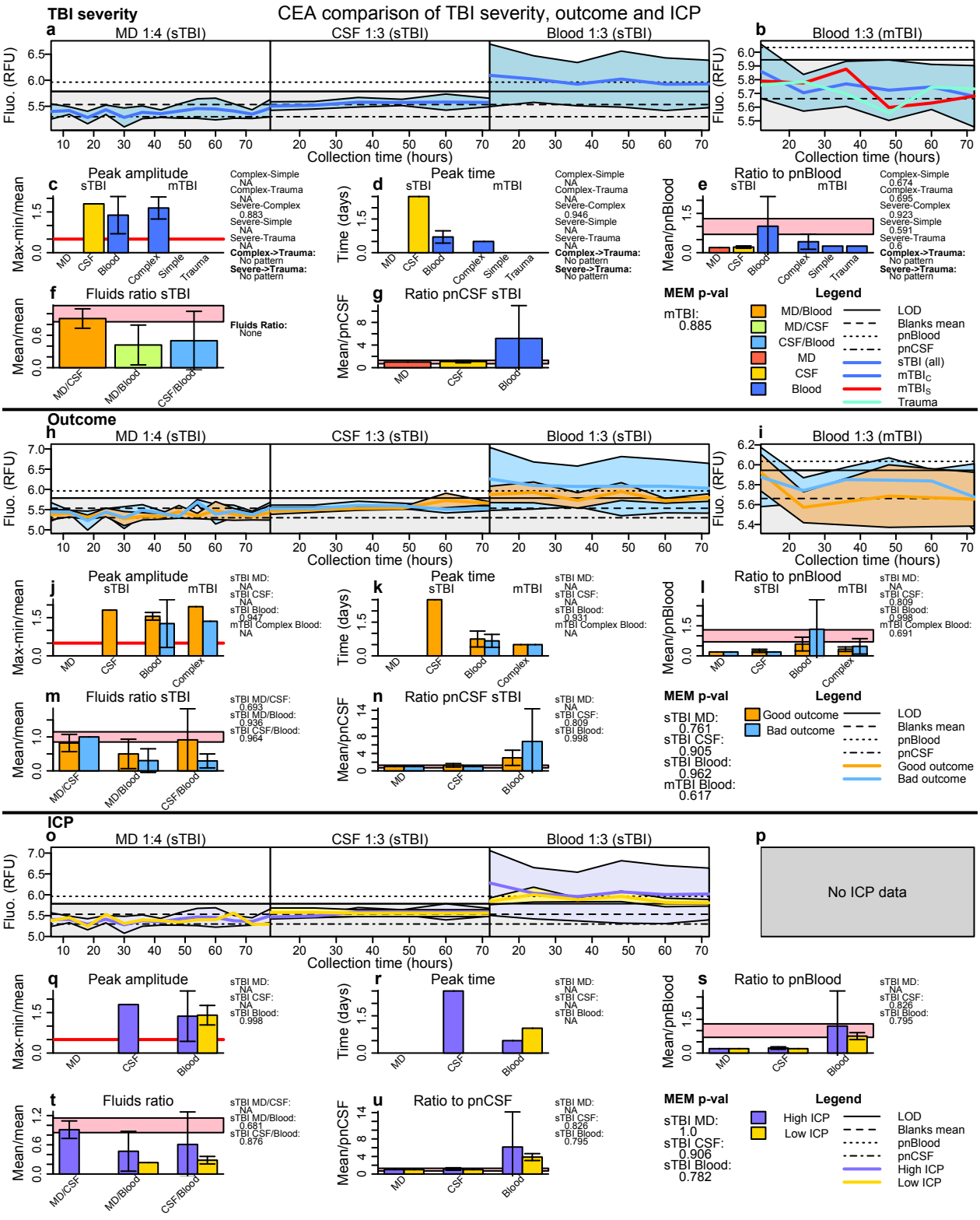

FIGURE J.S58: **Differential CEA protein profiles and peak and ratio analysis with respect to TBI severity, outcome and ICP.** Average CEA profiles are compared in terms of TBI severity (**a-g**), outcome (**h-n**) and ICP (**o-u**). Polygons in **a, b, h, i, o** indicate the mean value ±1 SD at each time point. Red lines in **c, j, q** show a threshold for a profile that is considered to have a peak, rather than being constant. The light red boxes in **e-g, l-n, s-u** show the threshold of comparison to the measured value compared. Benjamini–Hochberg adjusted p-values for comparisons are shown on the right of every graph.

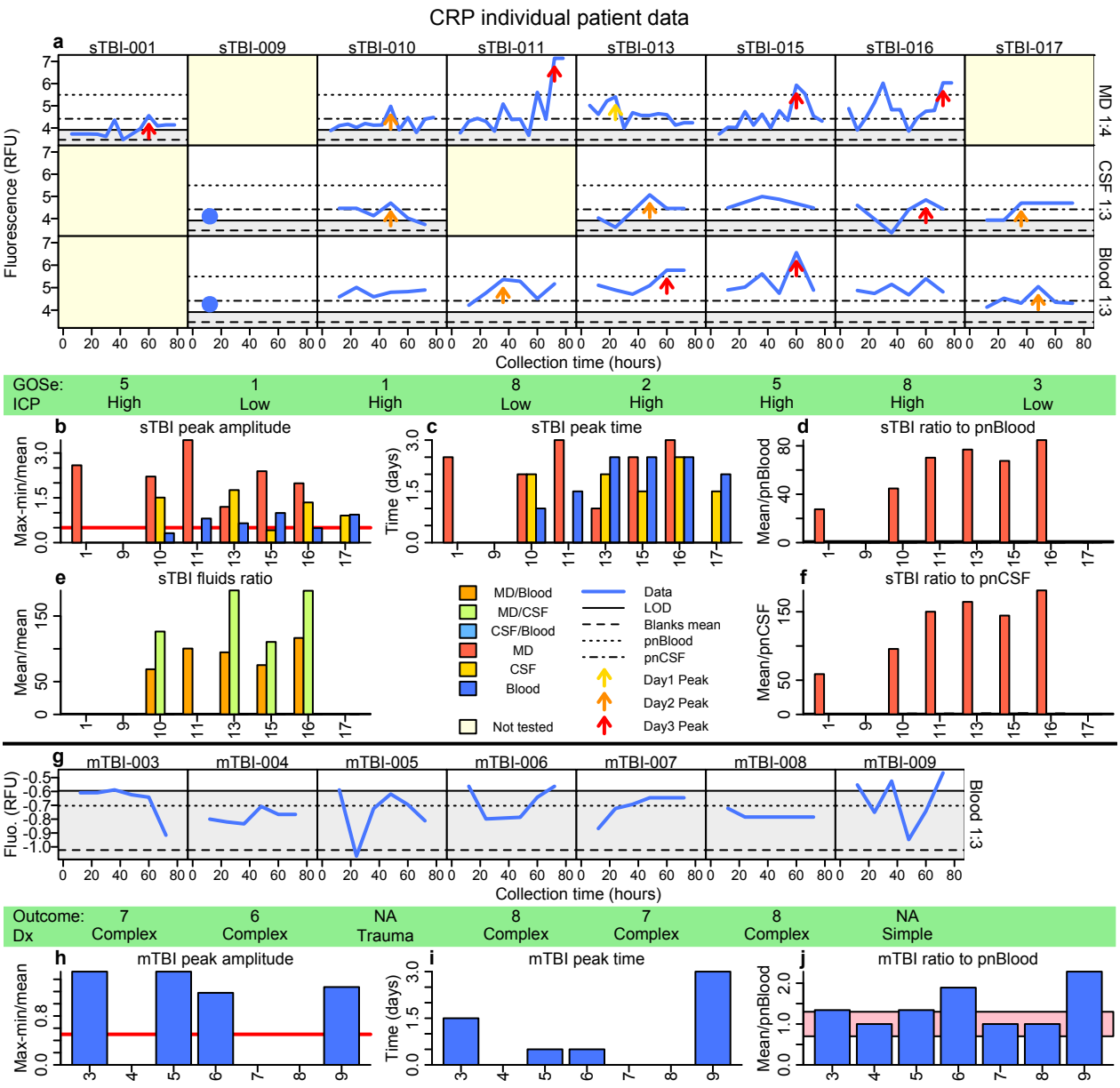

FIGURE J.S59: **Individual CRP protein profiles and peak and ratio analysis.** CRP concentration in microdialysate, CSF and blood samples of individual sTBI patients (**a**) and mTBI/trauma patients (**g**) was measured and peak amplitude and time, as well as ratio between mean time course values to value found in the pooled normal control (**b-f, h-j**) were calculated for each patient. Graphs **b-f** show calculations for individual sTBI patients, and graphs **h-j** show calculations for individual mTBI patients. Red lines in **b, h** show a threshold for a profile that is considered to have a peak, rather than being constant. The light red boxes in **d, e, f, j** show the threshold of comparison to the measured value compared.

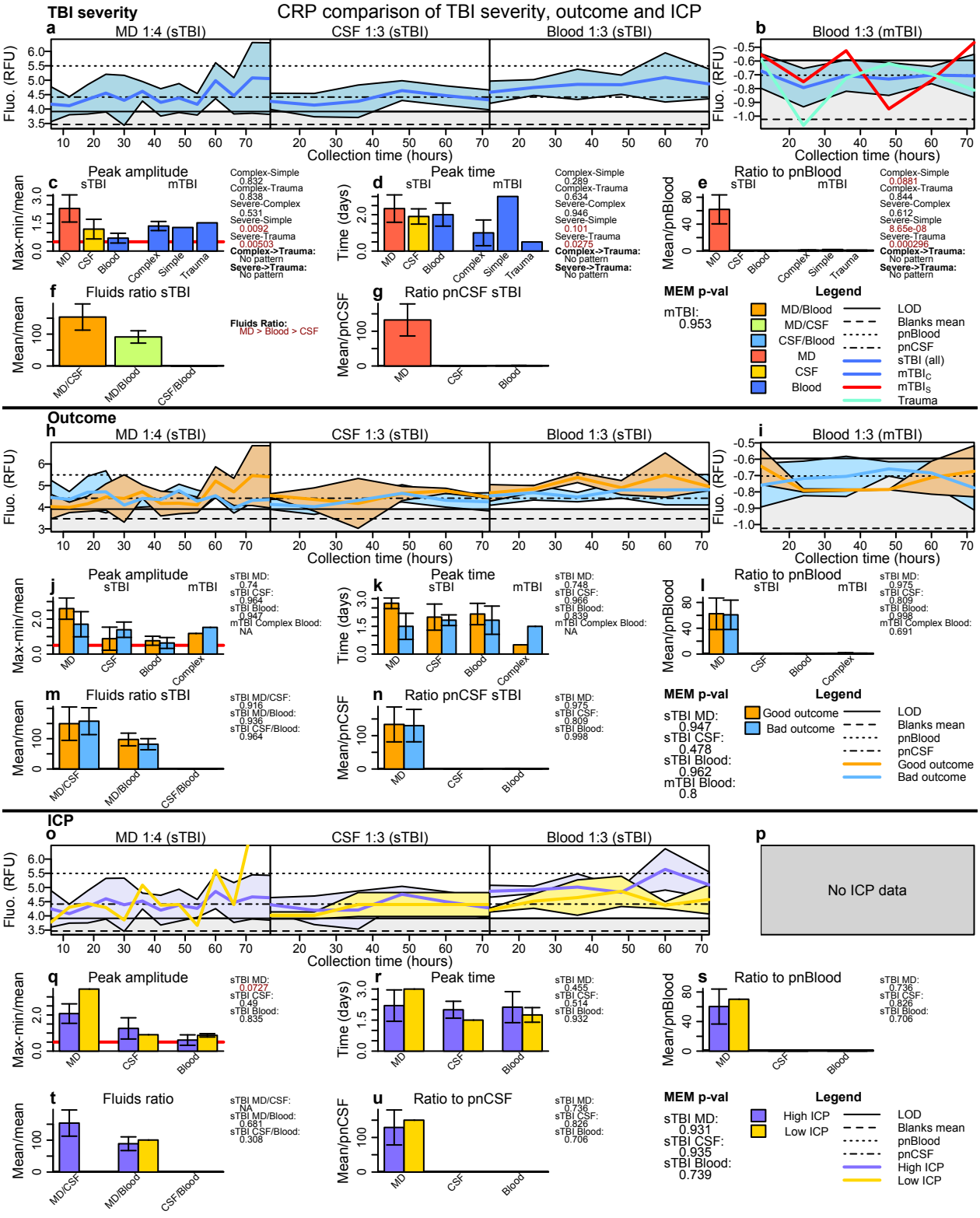

FIGURE J.S60: **Differential CRP protein profiles and peak and ratio analysis with respect to TBI severity, outcome and ICP.** Average CRP profiles are compared in terms of TBI severity (**a-g**), outcome (**h-n**) and ICP (**o-u**). Polygons in **a, b, h, i, o** indicate the mean value ±1 SD at each time point. Red lines in **c, j, q** show a threshold for a profile that is considered to have a peak, rather than being constant. The light red boxes in **e-g, l-n, s-u** show the threshold of comparison to the measured value compared. Benjamini–Hochberg adjusted p-values for comparisons are shown on the right of every graph.

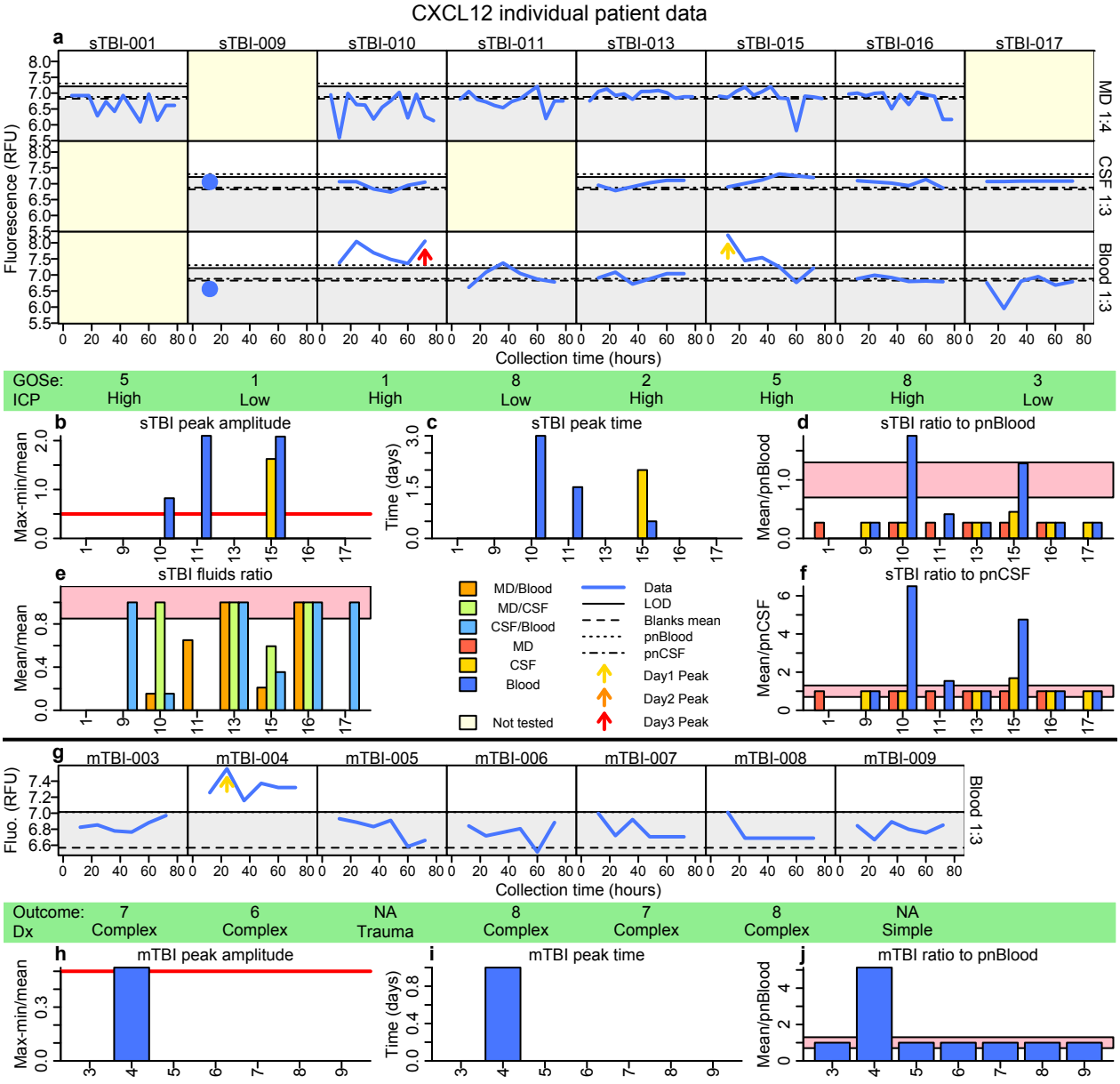

FIGURE J.S61: **Individual CXCL12 protein profiles and peak and ratio analysis.** CXCL12 concentration in microdialysate, CSF and blood samples of individual sTBI patients (**a**) and mTBI/trauma patients (**g**) was measured and peak amplitude and time, as well as ratio between mean time course values to value found in the pooled normal control (**b-f, h-j**) were calculated for each patient. Graphs **b-f** show calculations for individual sTBI patients, and graphs **h-j** show calculations for individual mTBI patients. Red lines in **b, h** show a threshold for a profile that is considered to have a peak, rather than being constant. The light red boxes in **d, e, f, j** show the threshold of comparison to the measured value compared.

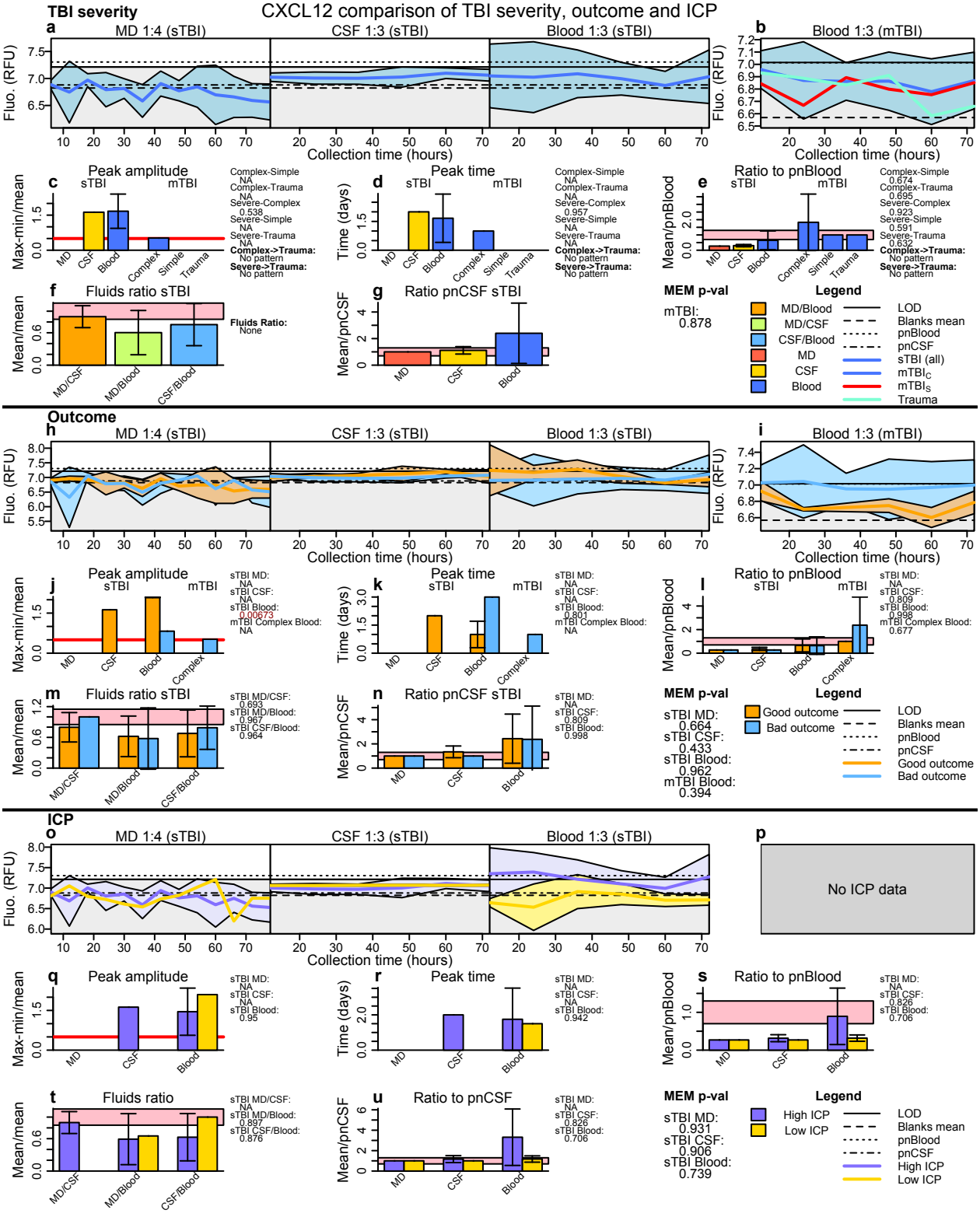

FIGURE J.S62: **Differential CXCL12 protein profiles and peak and ratio analysis with respect to TBI severity, outcome and ICP.** Average CXCL12 profiles are compared in terms of TBI severity (**a-g**), outcome (**h-n**) and ICP (**o-u**). Polygons in **a, b, h, i, o** indicate the mean value ±1 SD at each time point. Red lines in **c, j, q** show a threshold for a profile that is considered to have a peak, rather than being constant. The light red boxes in **e-g, l-n, s-u** show the threshold of comparison to the measured value compared. Benjamini–Hochberg adjusted p-values for comparisons are shown on the right of every graph.

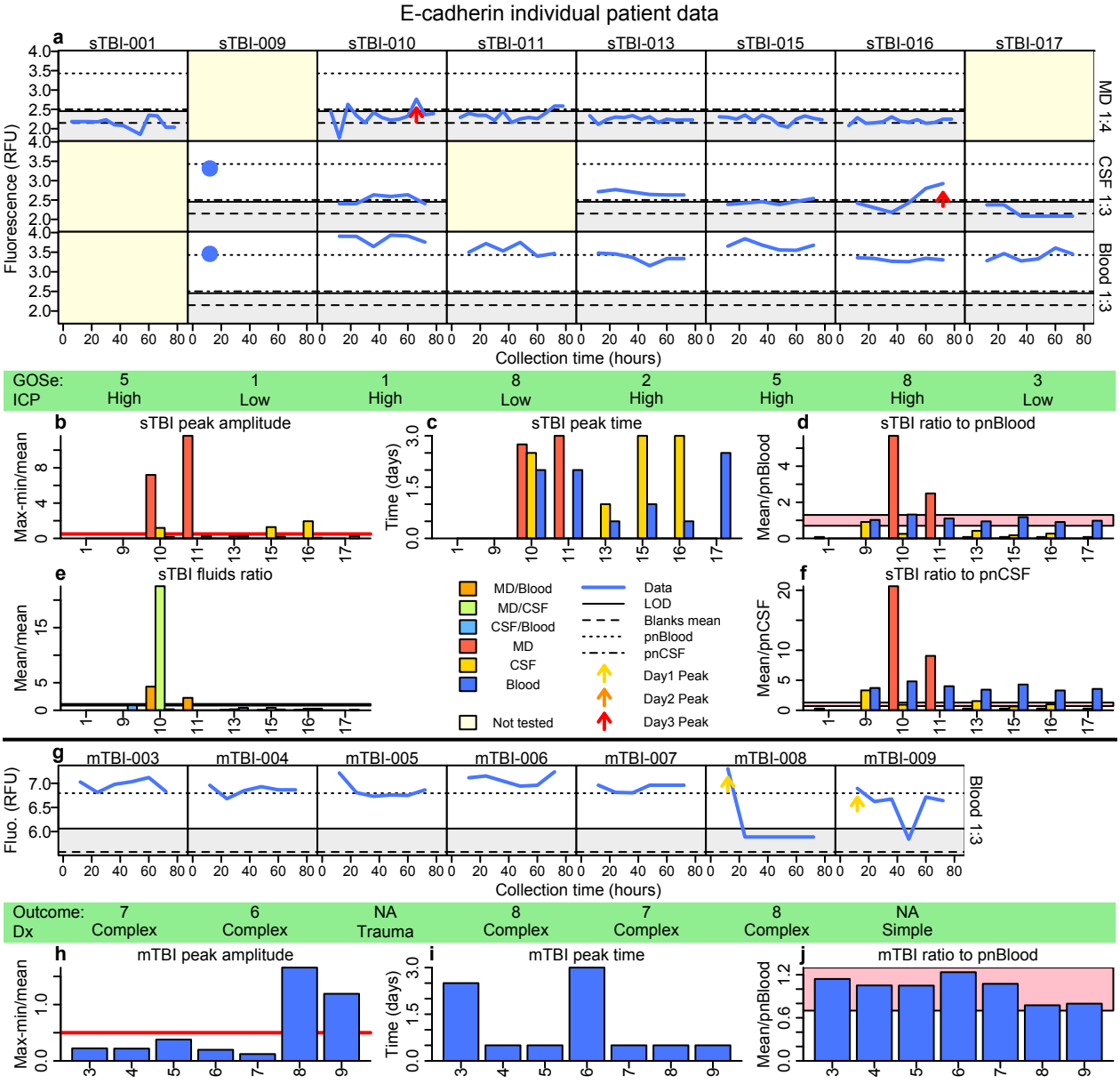

FIGURE J.S63: **Individual E-cadherin protein profiles and peak and ratio analysis.** E-cadherin concentration in microdialysate, CSF and blood samples of individual sTBI patients (**a**) and mTBI/trauma patients (**g**) was measured and peak amplitude and time, as well as ratio between mean time course values to value found in the pooled normal control (**b-f, h-j**) were calculated for each patient. Graphs **b-f** show calculations for individual sTBI patients, and graphs **h-j** show calculations for individual mTBI patients. Red lines in **b, h** show a threshold for a profile that is considered to have a peak, rather than being constant. The light red boxes in **d, e, f, j** show the threshold of comparison to the measured value compared.

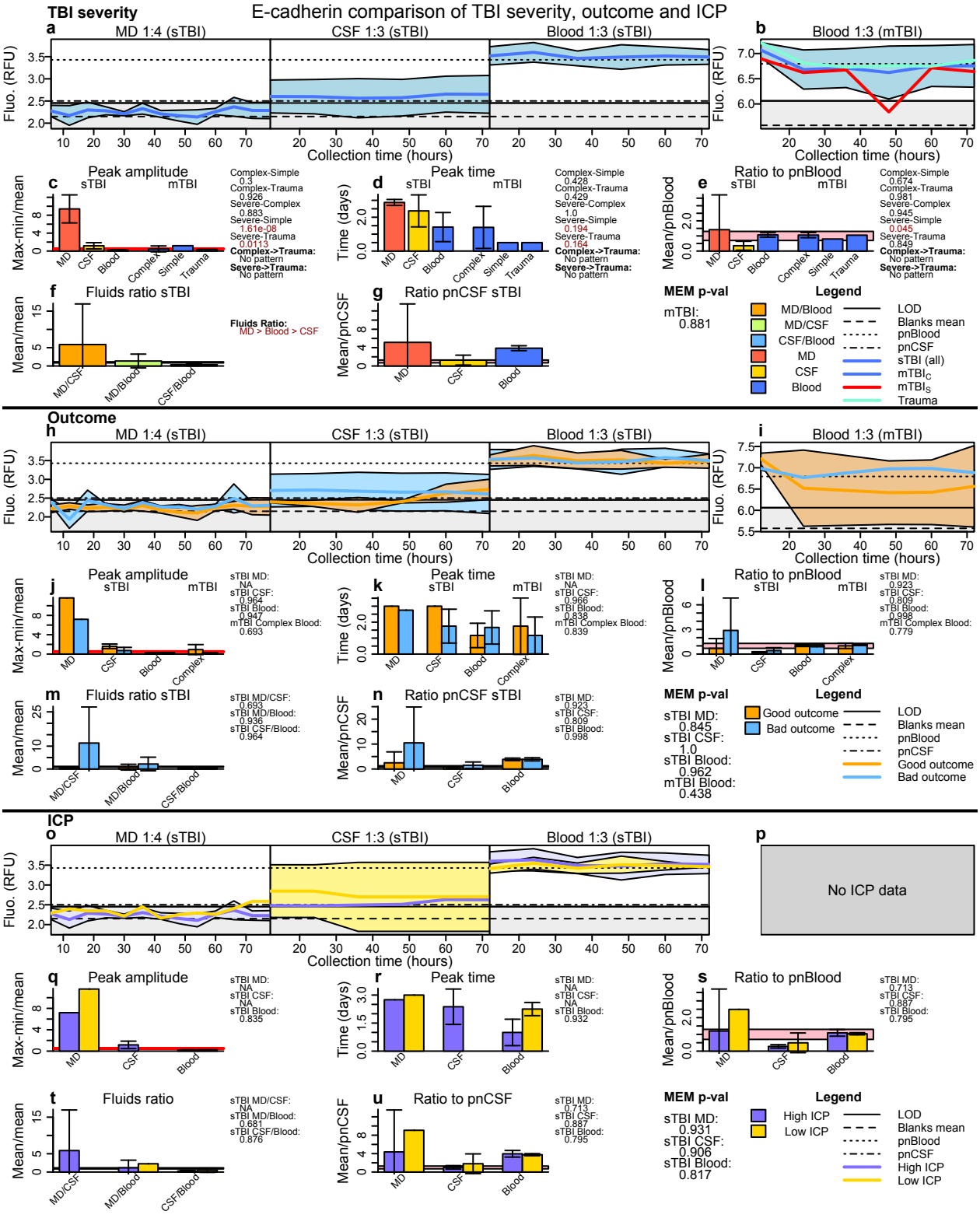

FIGURE J.S64: **Differential E-cadherin protein profiles and peak and ratio analysis with respect to TBI severity, outcome and ICP.** Average E-cadherin profiles are compared in terms of TBI severity (**a-g**), outcome (**h-n**) and ICP (**o-u**). Polygons in **a, b, h, i, o** indicate the mean value ±1 SD at each time point. Red lines in **c, j, q** show a threshold for a profile that is considered to have a peak, rather than being constant. The light red boxes in **e-g, l-n, s-u** show the threshold of comparison to the measured value compared. Benjamini–Hochberg adjusted p-values for comparisons are shown on the right of every graph.

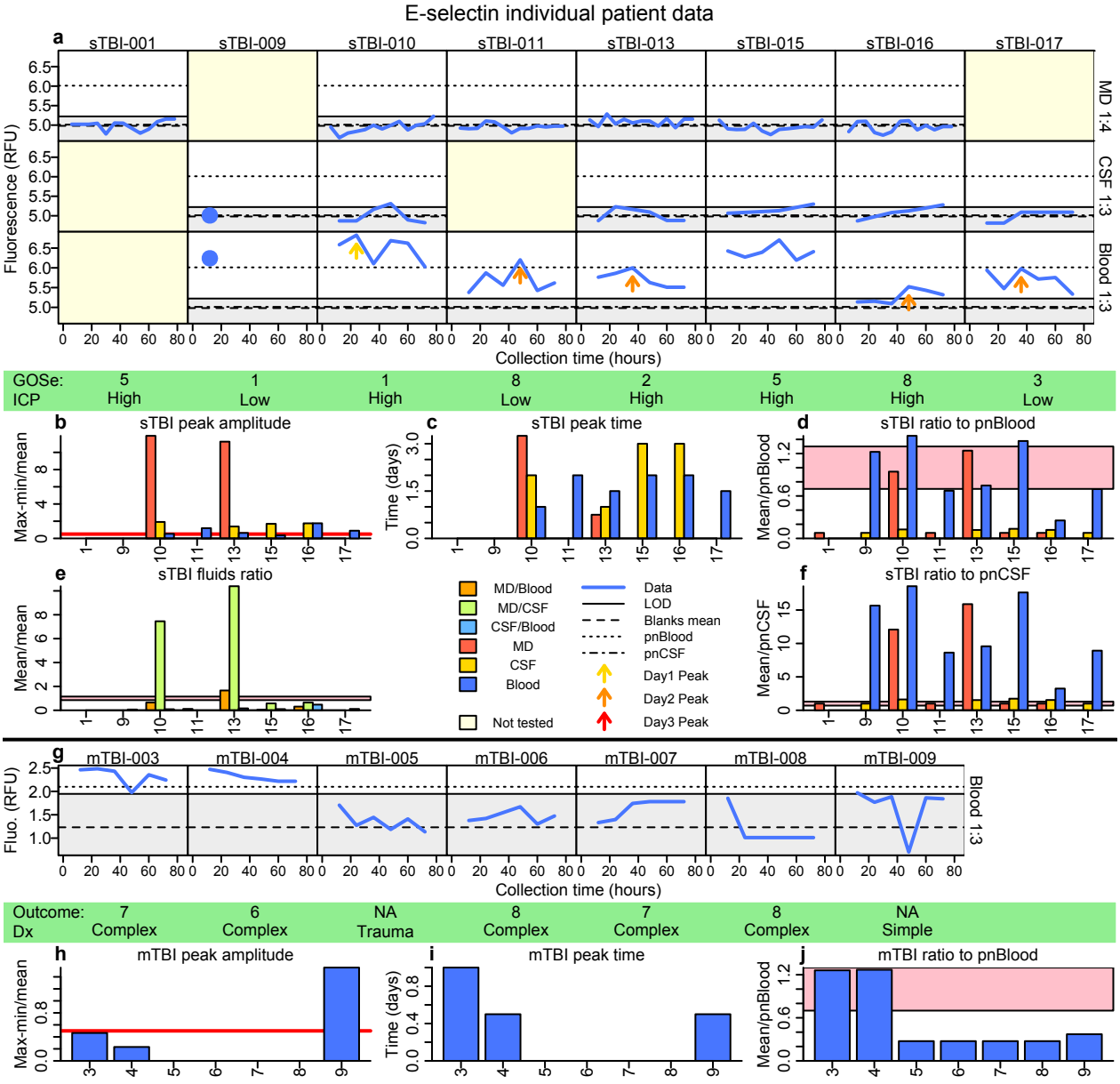

FIGURE J.S65: **Individual E-selectin protein profiles and peak and ratio analysis.** E-selectin concentration in microdialysate, CSF and blood samples of individual sTBI patients (**a**) and mTBI/trauma patients (**g**) was measured and peak amplitude and time, as well as ratio between mean time course values to value found in the pooled normal control (**b-f, h-j**) were calculated for each patient. Graphs **b-f** show calculations for individual sTBI patients, and graphs **h-j** show calculations for individual mTBI patients. Red lines in **b, h** show a threshold for a profile that is considered to have a peak, rather than being constant. The light red boxes in **d, e, f, j** show the threshold of comparison to the measured value compared.

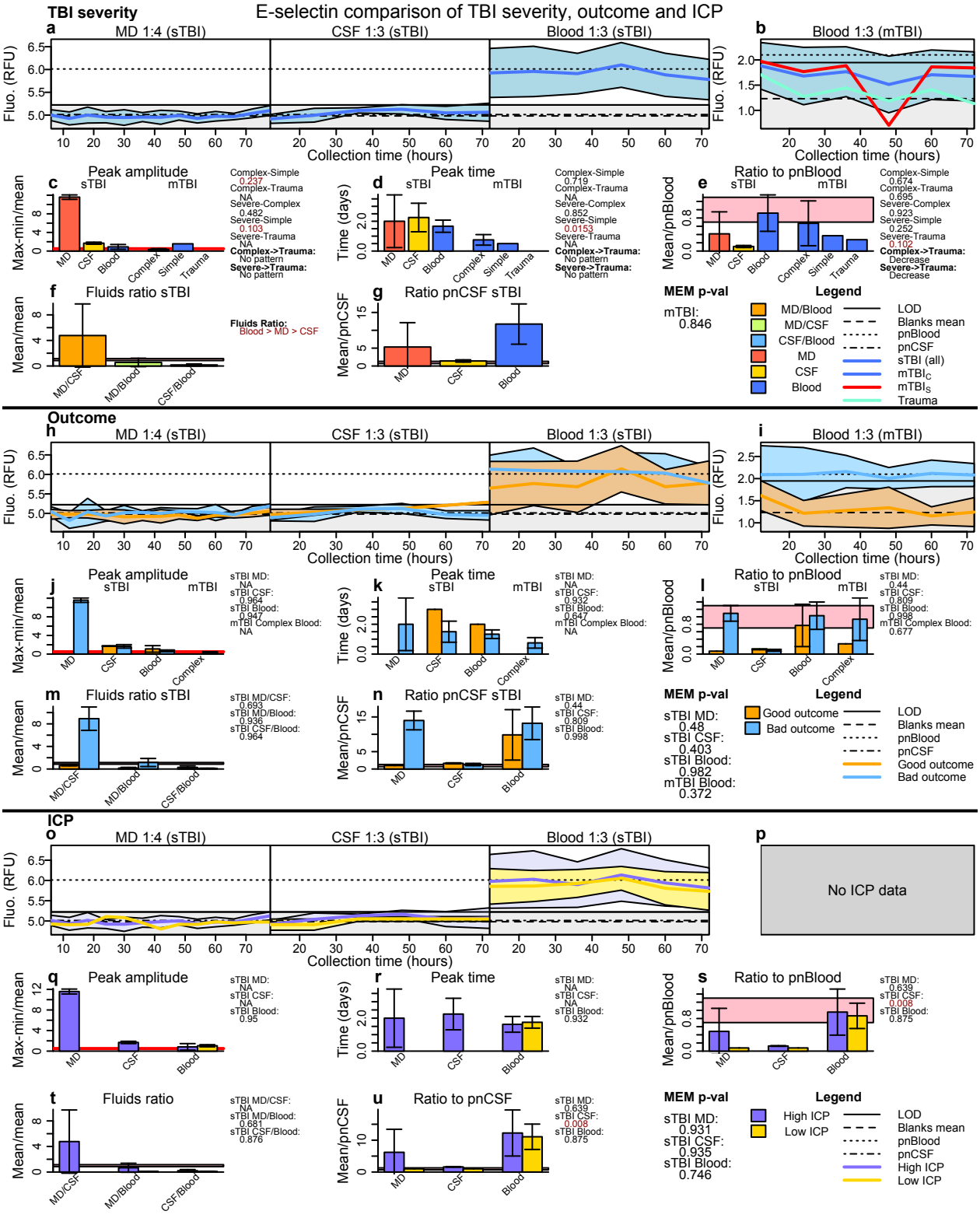

FIGURE J.S66: **Differential E-selectin protein profiles and peak and ratio analysis with respect to TBI severity, outcome and ICP.** Average E-selectin profiles are compared in terms of TBI severity (**a-g**), outcome (**h-n**) and ICP (**o-u**). Polygons in **a, b, h, i, o** indicate the mean value ±1 SD at each time point. Red lines in **c, j, q** show a threshold for a profile that is considered to have a peak, rather than being constant. The light red boxes in **e-g, l-n, s-u** show the threshold of comparison to the measured value compared. Benjamini–Hochberg adjusted p-values for comparisons are shown on the right of every graph.

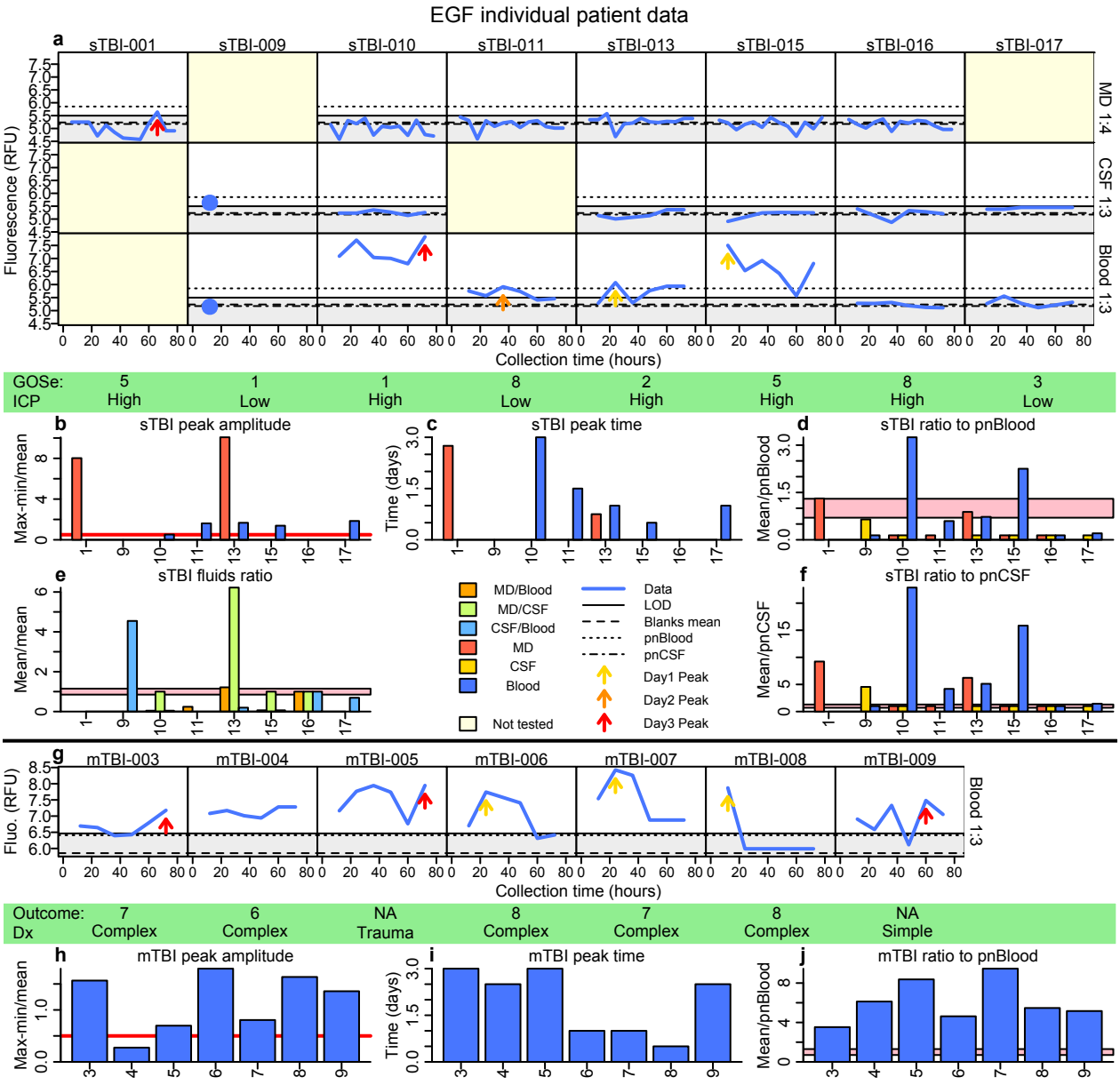

FIGURE J.S67: **Individual EGF protein profiles and peak and ratio analysis.** EGF concentration in microdialysate, CSF and blood samples of individual sTBI patients (**a**) and mTBI/trauma patients (**g**) was measured and peak amplitude and time, as well as ratio between mean time course values to value found in the pooled normal control (**b-f, h-j**) were calculated for each patient. Graphs **b-f** show calculations for individual sTBI patients, and graphs **h-j** show calculations for individual mTBI patients. Red lines in **b, h** show a threshold for a profile that is considered to have a peak, rather than being constant. The light red boxes in **d, e, f, j** show the threshold of comparison to the measured value compared.

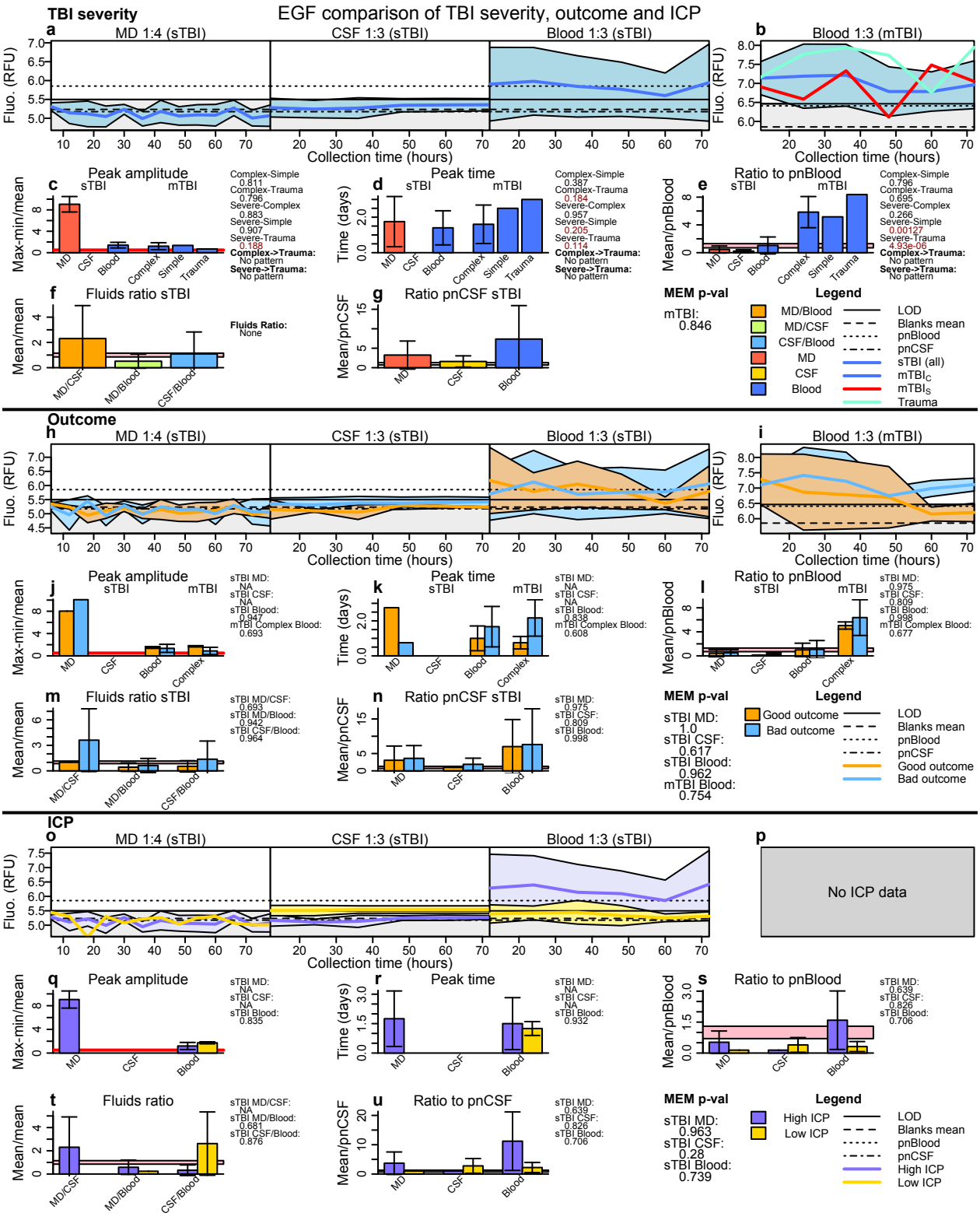

FIGURE J.S68: **Differential EGF protein profiles and peak and ratio analysis with respect to TBI severity, outcome and ICP.** Average EGF profiles are compared in terms of TBI severity (**a-g**), outcome (**h-n**) and ICP (**o-u**). Polygons in **a, b, h, i, o** indicate the mean value ±1 SD at each time point. Red lines in **c, j, q** show a threshold for a profile that is considered to have a peak, rather than being constant. The light red boxes in **e-g, l-n, s-u** show the threshold of comparison to the measured value compared. Benjamini–Hochberg adjusted p-values for comparisons are shown on the right of every graph.

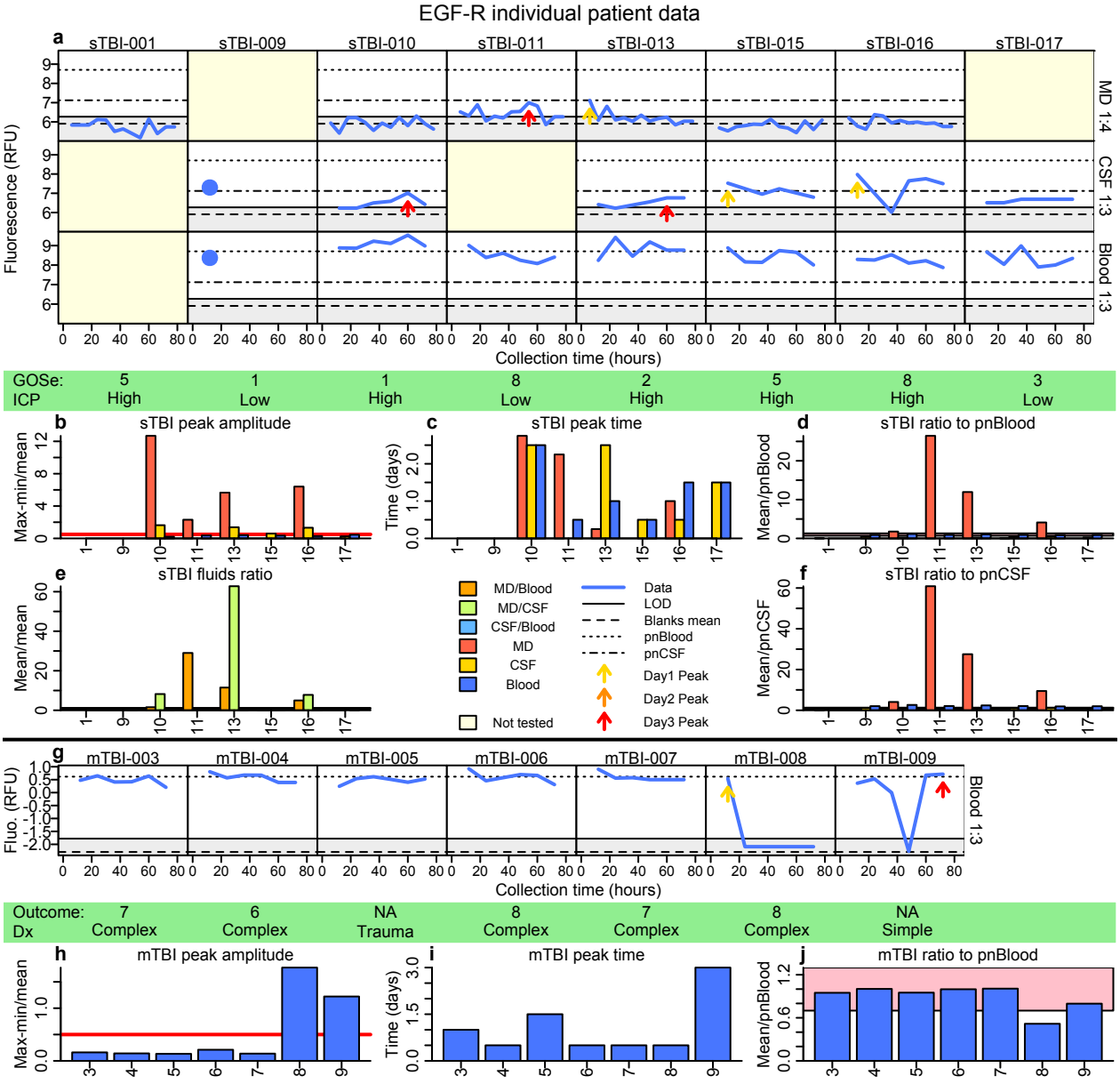

FIGURE J.S69: **Individual EGF-R protein profiles and peak and ratio analysis.** EGF-R concentration in microdialysate, CSF and blood samples of individual sTBI patients (**a**) and mTBI/trauma patients (**g**) was measured and peak amplitude and time, as well as ratio between mean time course values to value found in the pooled normal control (**b-f, h-j**) were calculated for each patient. Graphs **b-f** show calculations for individual sTBI patients, and graphs **h-j** show calculations for individual mTBI patients. Red lines in **b, h** show a threshold for a profile that is considered to have a peak, rather than being constant. The light red boxes in **d, e, f, j** show the threshold of comparison to the measured value compared.

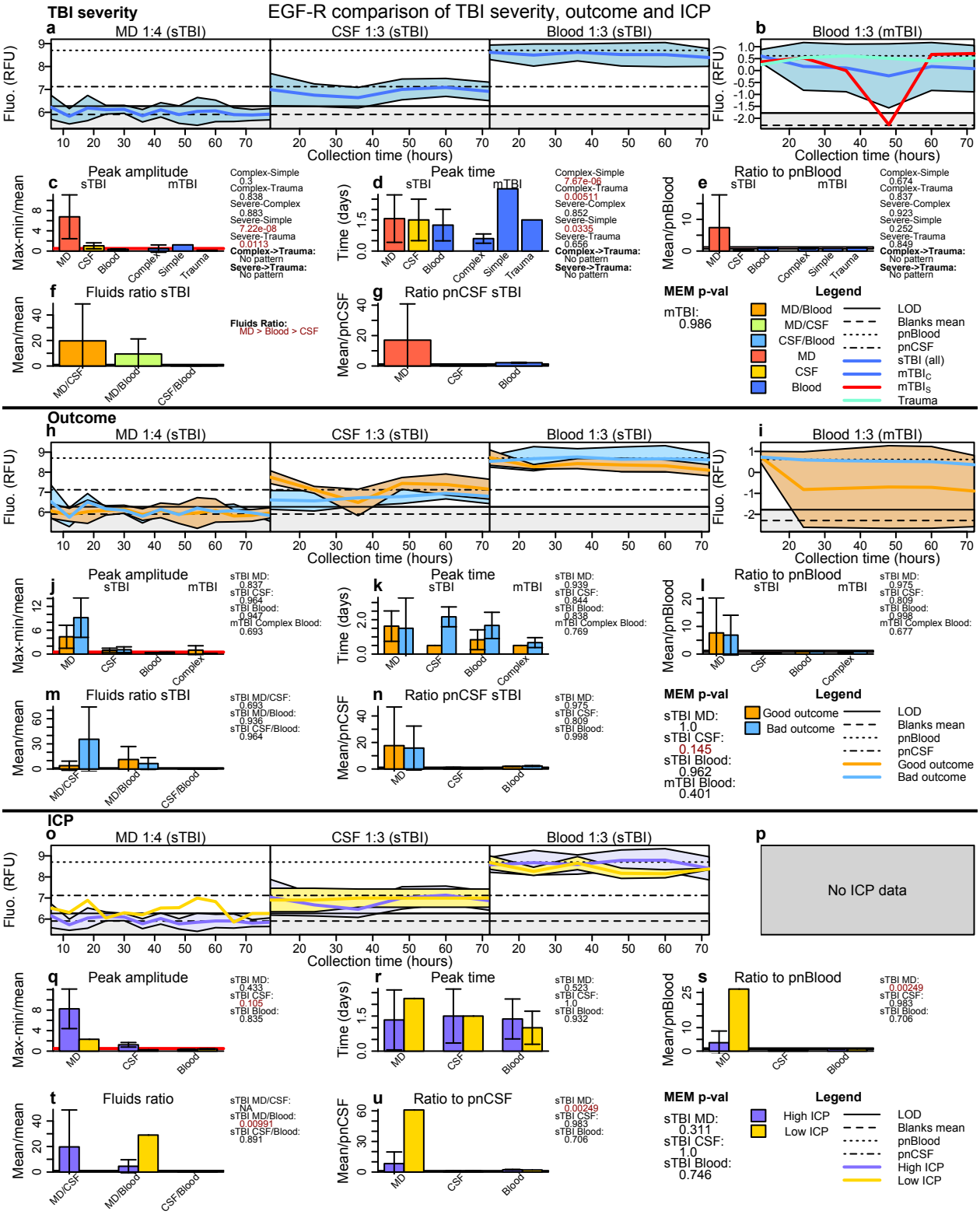

FIGURE J.S70: **Differential EGF-R protein profiles and peak and ratio analysis with respect to TBI severity, outcome and ICP.** Average EGF-R profiles are compared in terms of TBI severity (**a-g**), outcome (**h-n**) and ICP (**o-u**). Polygons in **a, b, h, i, o** indicate the mean value ±1 SD at each time point. Red lines in **c, j, q** show a threshold for a profile that is considered to have a peak, rather than being constant. The light red boxes in **e-g, l-n, s-u** show the threshold of comparison to the measured value compared. Benjamini–Hochberg adjusted p-values for comparisons are shown on the right of every graph.

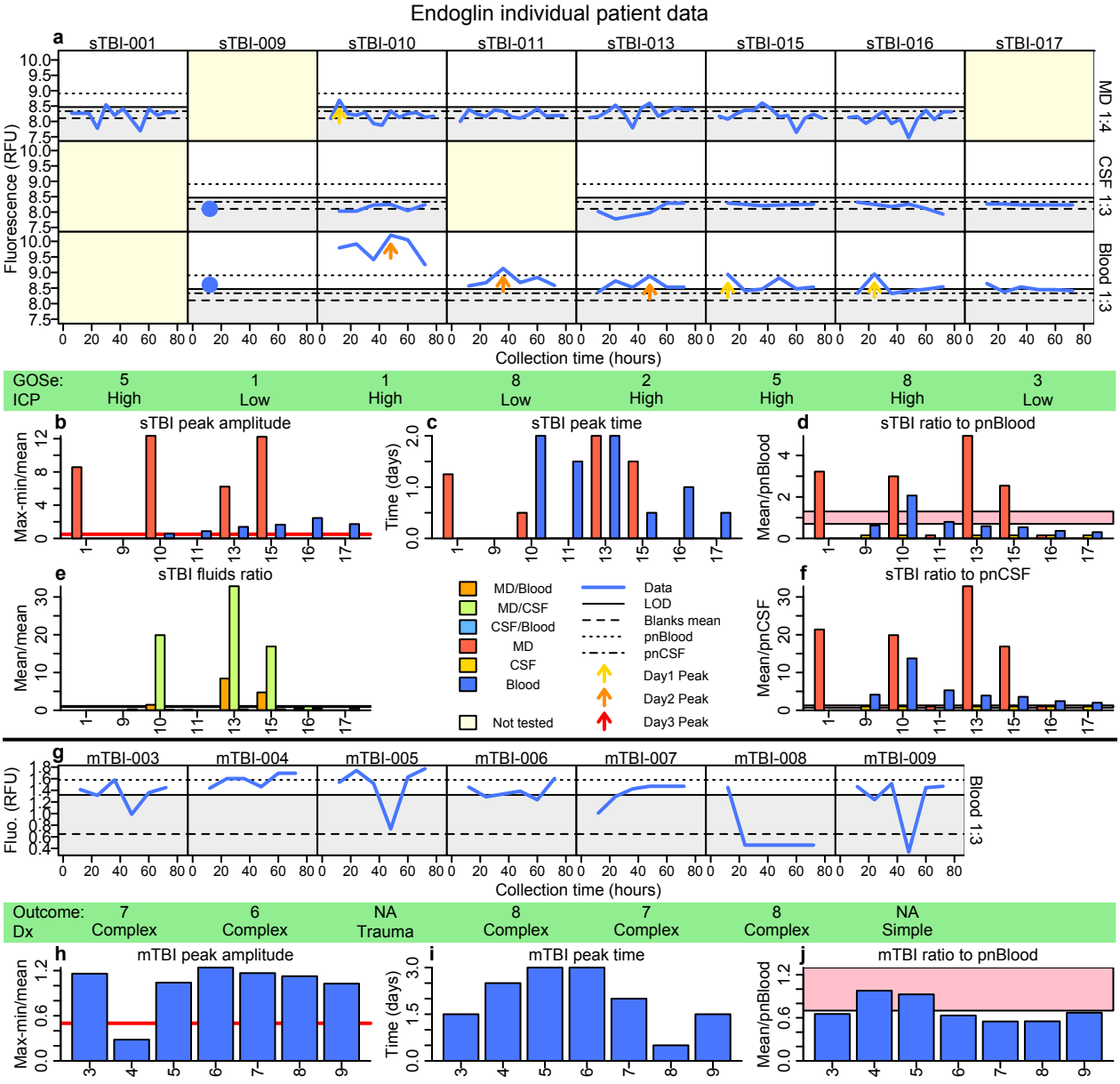

FIGURE J.S71: **Individual Endoglin protein profiles and peak and ratio analysis.** Endoglin concentration in microdialysate, CSF and blood samples of individual sTBI patients (**a**) and mTBI/trauma patients (**g**) was measured and peak amplitude and time, as well as ratio between mean time course values to value found in the pooled normal control (**b-f, h-j**) were calculated for each patient. Graphs **b-f** show calculations for individual sTBI patients, and graphs **h-j** show calculations for individual mTBI patients. Red lines in **b, h** show a threshold for a profile that is considered to have a peak, rather than being constant. The light red boxes in **d, e, f, j** show the threshold of comparison to the measured value compared.

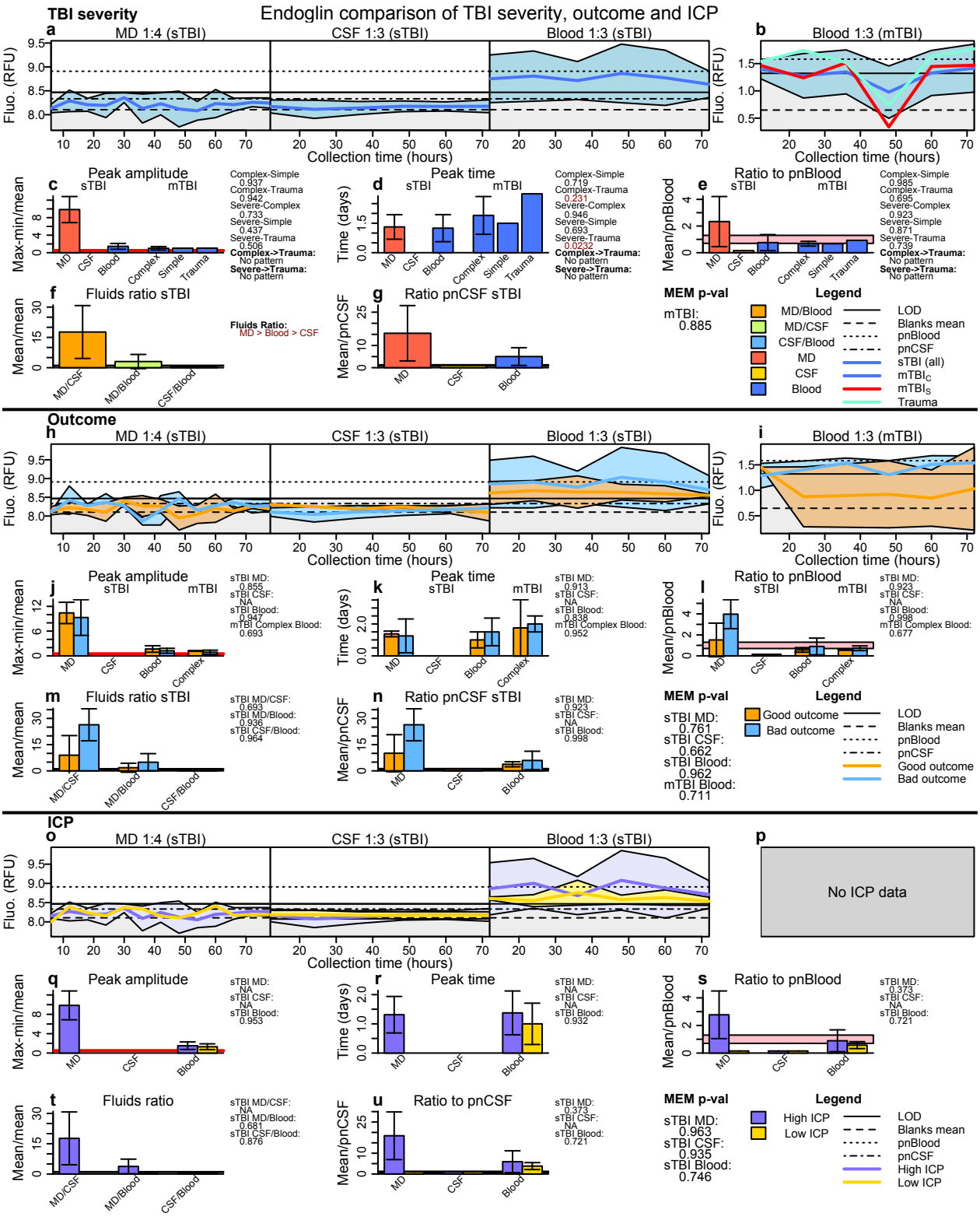

FIGURE J.S72: **Differential Endoglin protein profiles and peak and ratio analysis with respect to TBI severity, outcome and ICP.** Average Endoglin profiles are compared in terms of TBI severity (**a-g**), outcome (**h-n**) and ICP (**o-u**). Polygons in **a, b, h, i, o** indicate the mean value ±1 SD at each time point. Red lines in **c, j, q** show a threshold for a profile that is considered to have a peak, rather than being constant. The light red boxes in **e-g, l-n, s-u** show the threshold of comparison to the measured value compared. Benjamini–Hochberg adjusted p-values for comparisons are shown on the right of every graph.

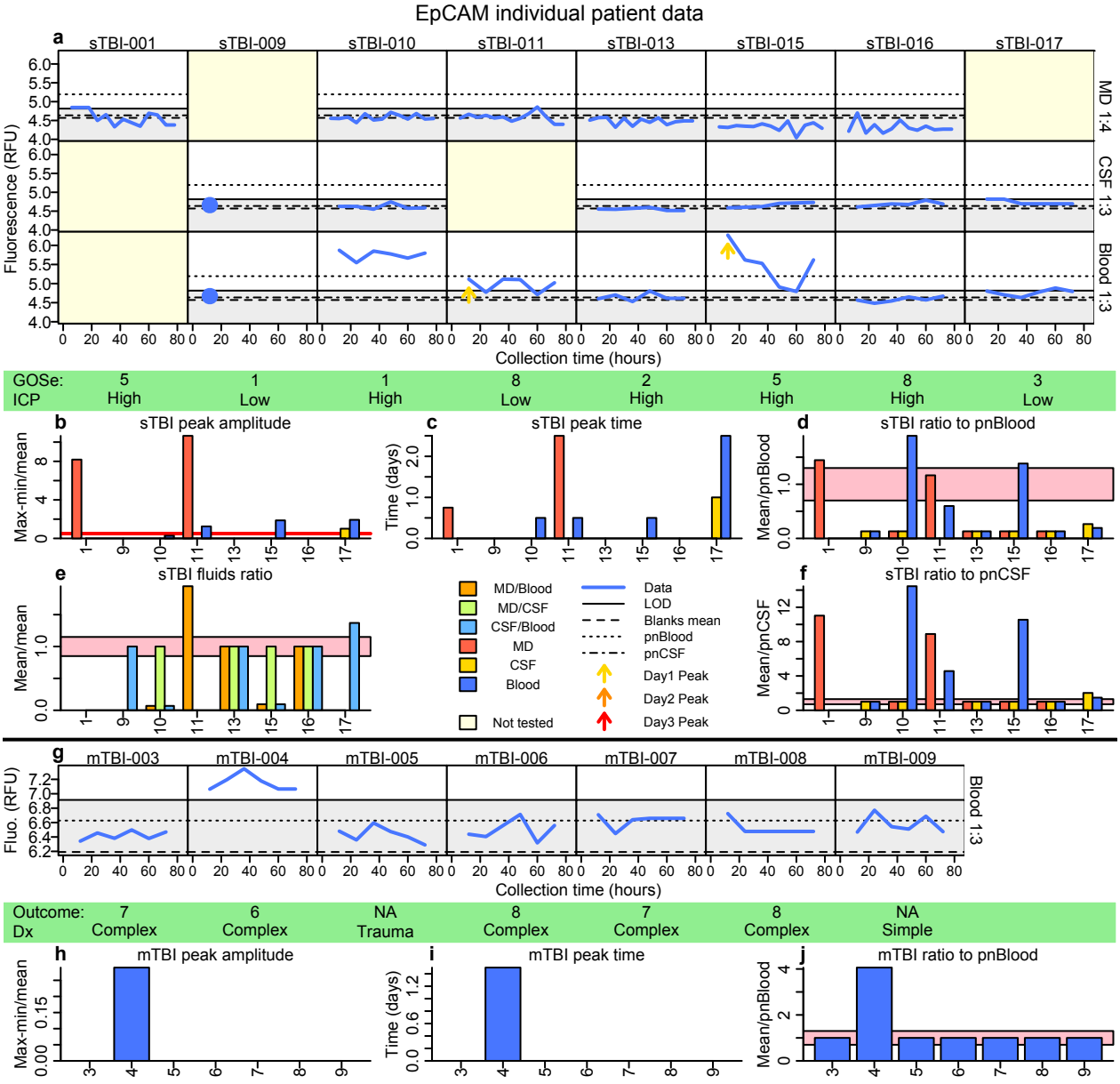

FIGURE J.S73: **Individual EpCAM protein profiles and peak and ratio analysis.** EpCAM concentration in microdialysate, CSF and blood samples of individual sTBI patients (**a**) and mTBI/trauma patients (**g**) was measured and peak amplitude and time, as well as ratio between mean time course values to value found in the pooled normal control (**b-f, h-j**) were calculated for each patient. Graphs **b-f** show calculations for individual sTBI patients, and graphs **h-j** show calculations for individual mTBI patients. Red lines in **b, h** show a threshold for a profile that is considered to have a peak, rather than being constant. The light red boxes in **d, e, f, j** show the threshold of comparison to the measured value compared.

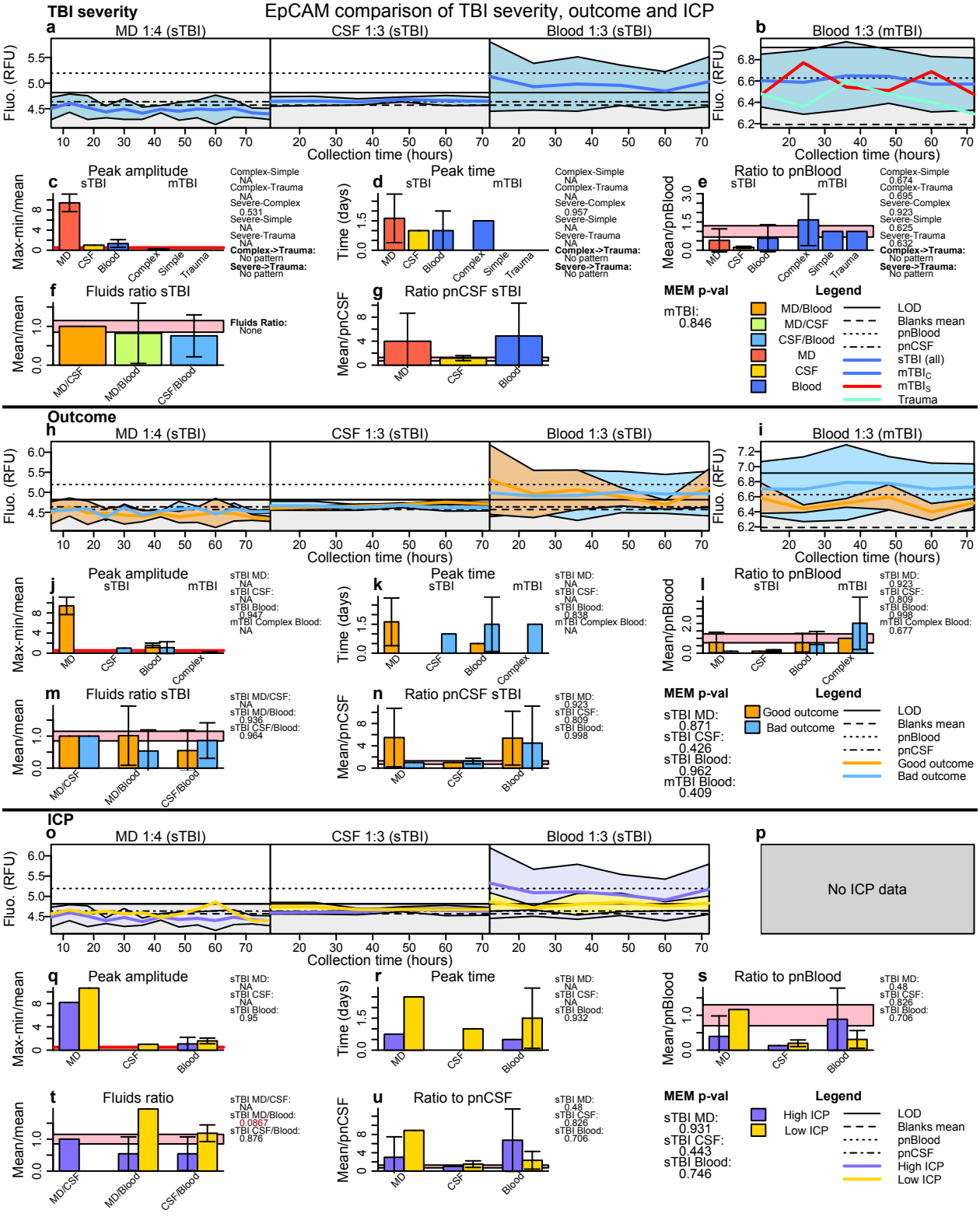

FIGURE J.S74: **Differential EpCAM protein profiles and peak and ratio analysis with respect to TBI severity, outcome and ICP.** Average EpCAM profiles are compared in terms of TBI severity (**a-g**), outcome (**h-n**) and ICP (**o-u**). Polygons in **a, b, h, i, o** indicate the mean value ±1 SD at each time point. Red lines in **c, j, q** show a threshold for a profile that is considered to have a peak, rather than being constant. The light red boxes in **e-g, l-n, s-u** show the threshold of comparison to the measured value compared. Benjamini–Hochberg adjusted p-values for comparisons are shown on the right of every graph.

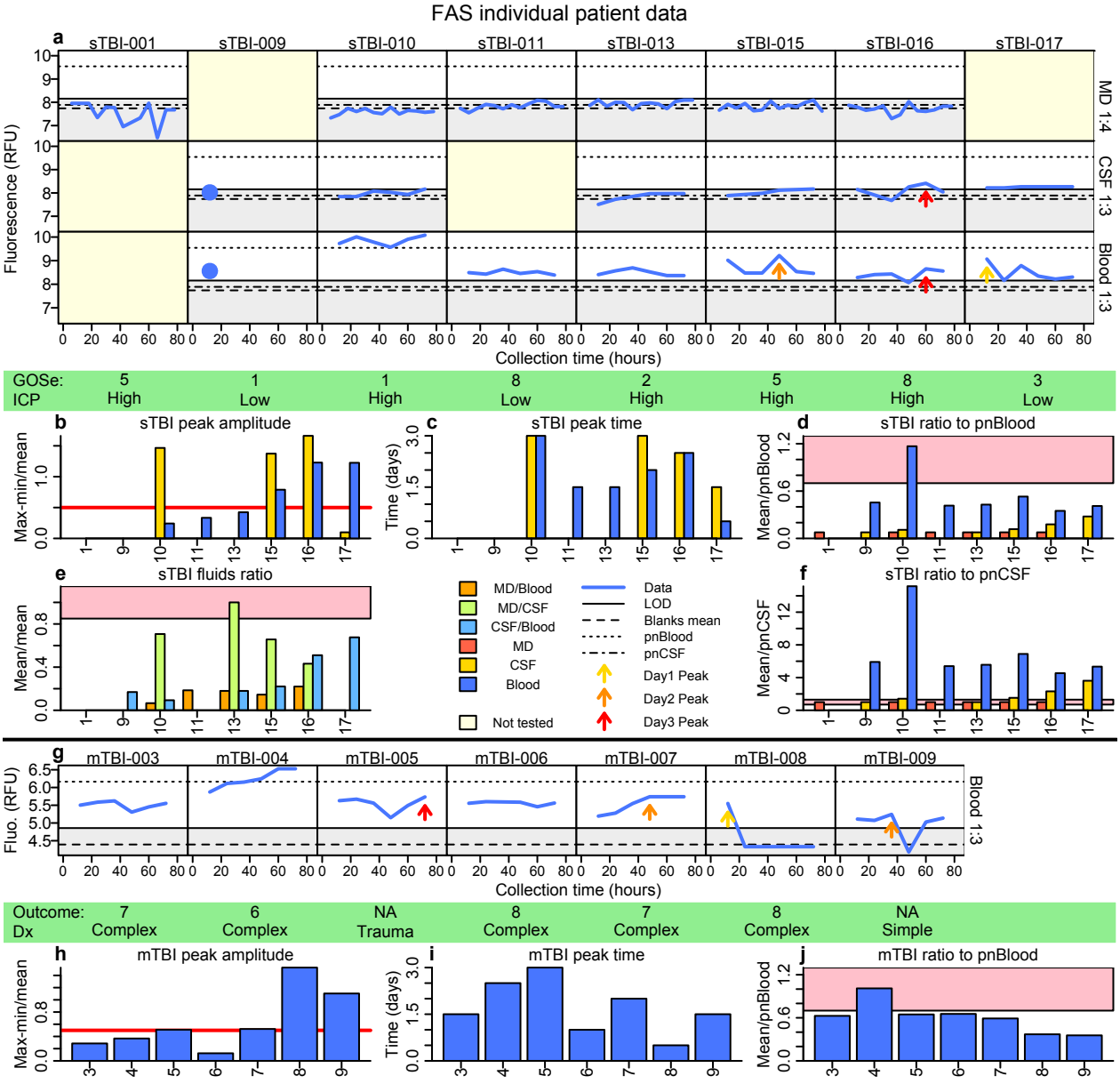

FIGURE J.S75: **Individual FAS protein profiles and peak and ratio analysis.** FAS concentration in microdialysate, CSF and blood samples of individual sTBI patients (**a**) and mTBI/trauma patients (**g**) was measured and peak amplitude and time, as well as ratio between mean time course values to value found in the pooled normal control (**b-f, h-j**) were calculated for each patient. Graphs **b-f** show calculations for individual sTBI patients, and graphs **h-j** show calculations for individual mTBI patients. Red lines in **b, h** show a threshold for a profile that is considered to have a peak, rather than being constant. The light red boxes in **d, e, f, j** show the threshold of comparison to the measured value compared.

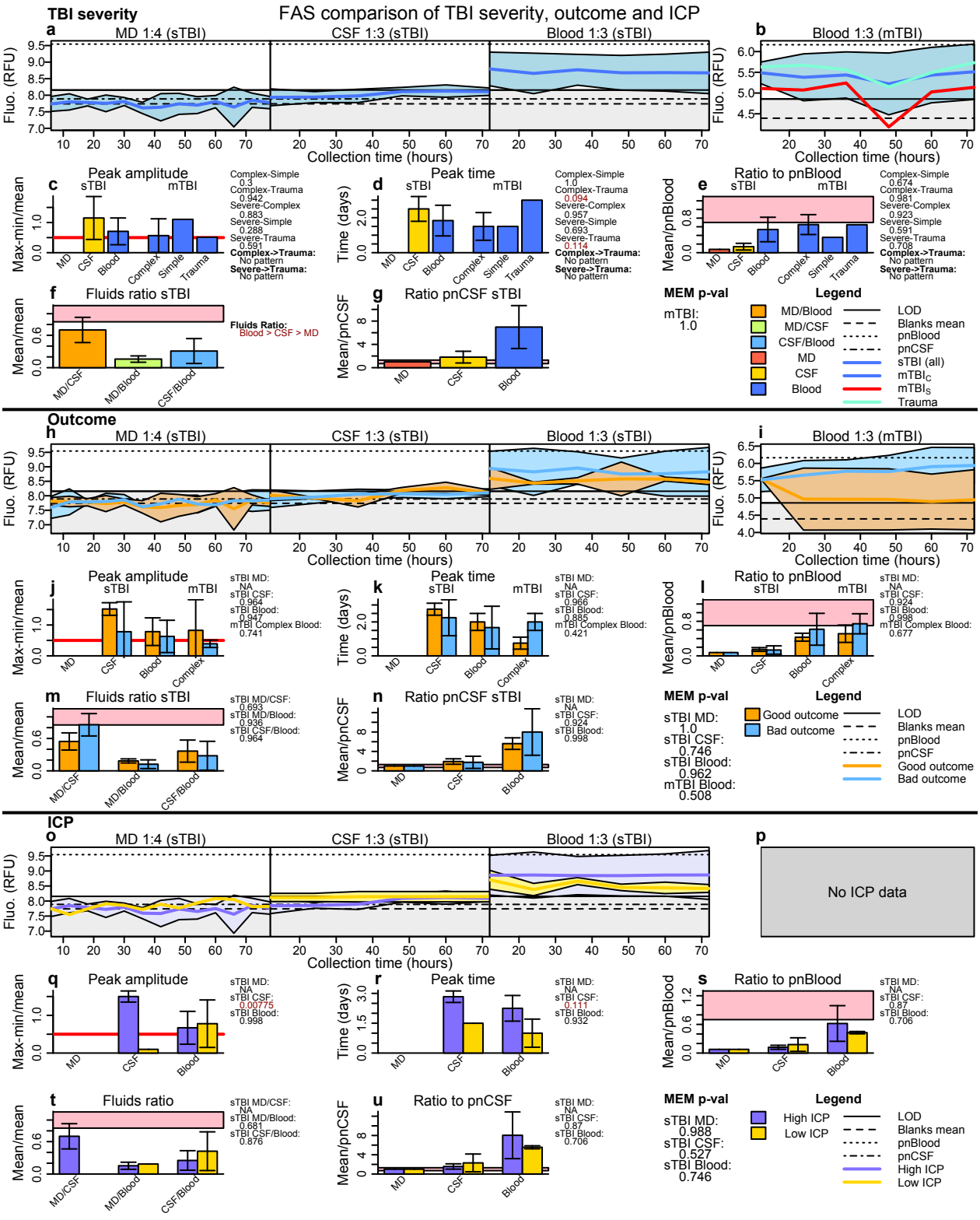

FIGURE J.S76: **Differential FAS protein profiles and peak and ratio analysis with respect to TBI severity, outcome and ICP.** Average FAS profiles are compared in terms of TBI severity (**a-g**), outcome (**h-n**) and ICP (**o-u**). Polygons in **a, b, h, i, o** indicate the mean value ±1 SD at each time point. Red lines in **c, j, q** show a threshold for a profile that is considered to have a peak, rather than being constant. The light red boxes in **e-g, l-n, s-u** show the threshold of comparison to the measured value compared. Benjamini–Hochberg adjusted p-values for comparisons are shown on the right of every graph.

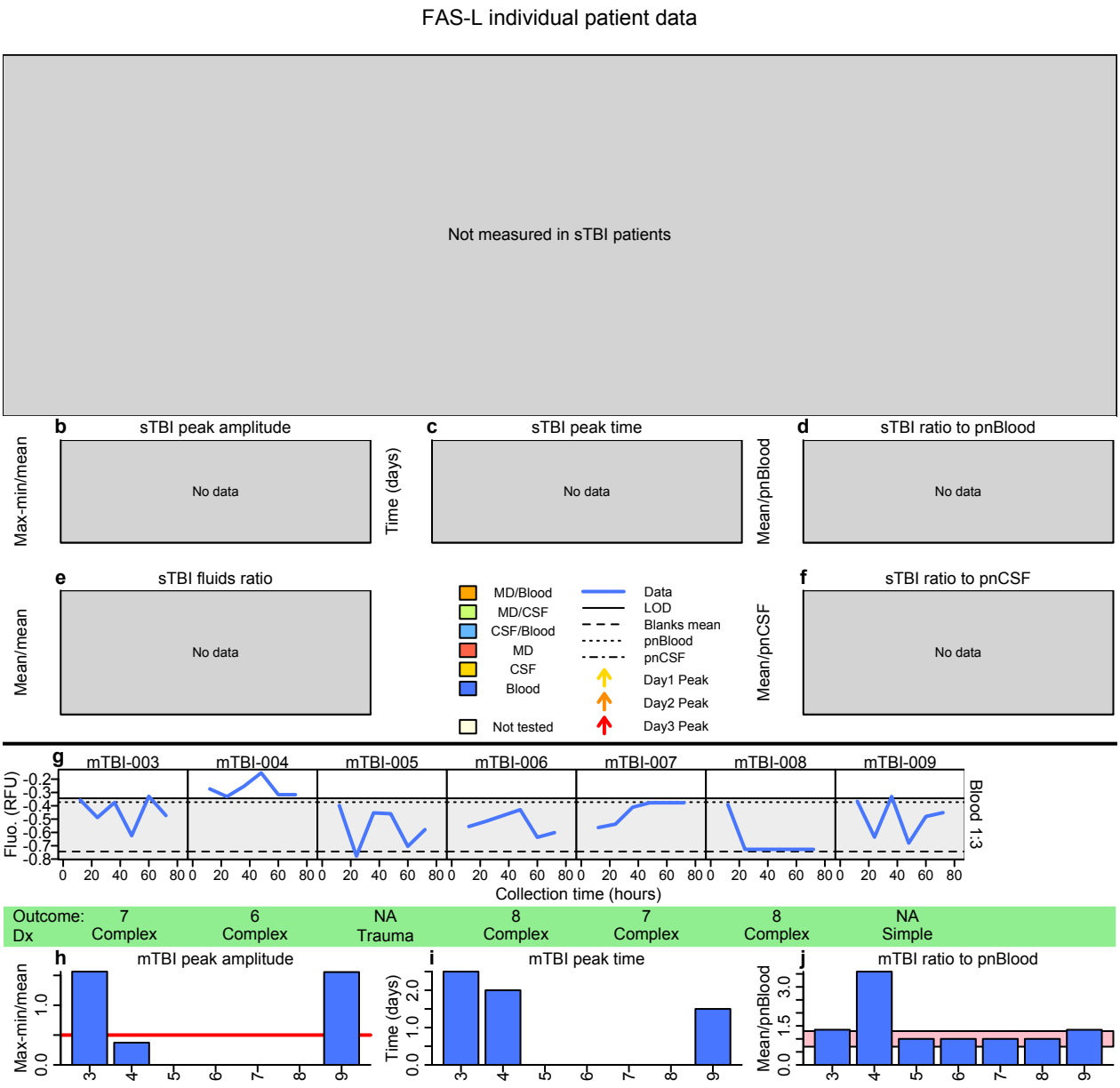

FIGURE J.S77: **Individual FAS-L protein profiles and peak and ratio analysis.** FAS-L concentration in microdialysate, CSF and blood samples of individual sTBI patients (**a**) and mTBI/trauma patients (**g**) was measured and peak amplitude and time, as well as ratio between mean time course values to value found in the pooled normal control (**b-f, h-j**) were calculated for each patient. Graphs **b-f** show calculations for individual sTBI patients, and graphs **h-j** show calculations for individual mTBI patients. Red lines in **b, h** show a threshold for a profile that is considered to have a peak, rather than being constant. The light red boxes in **d, e, f, j** show the threshold of comparison to the measured value compared.

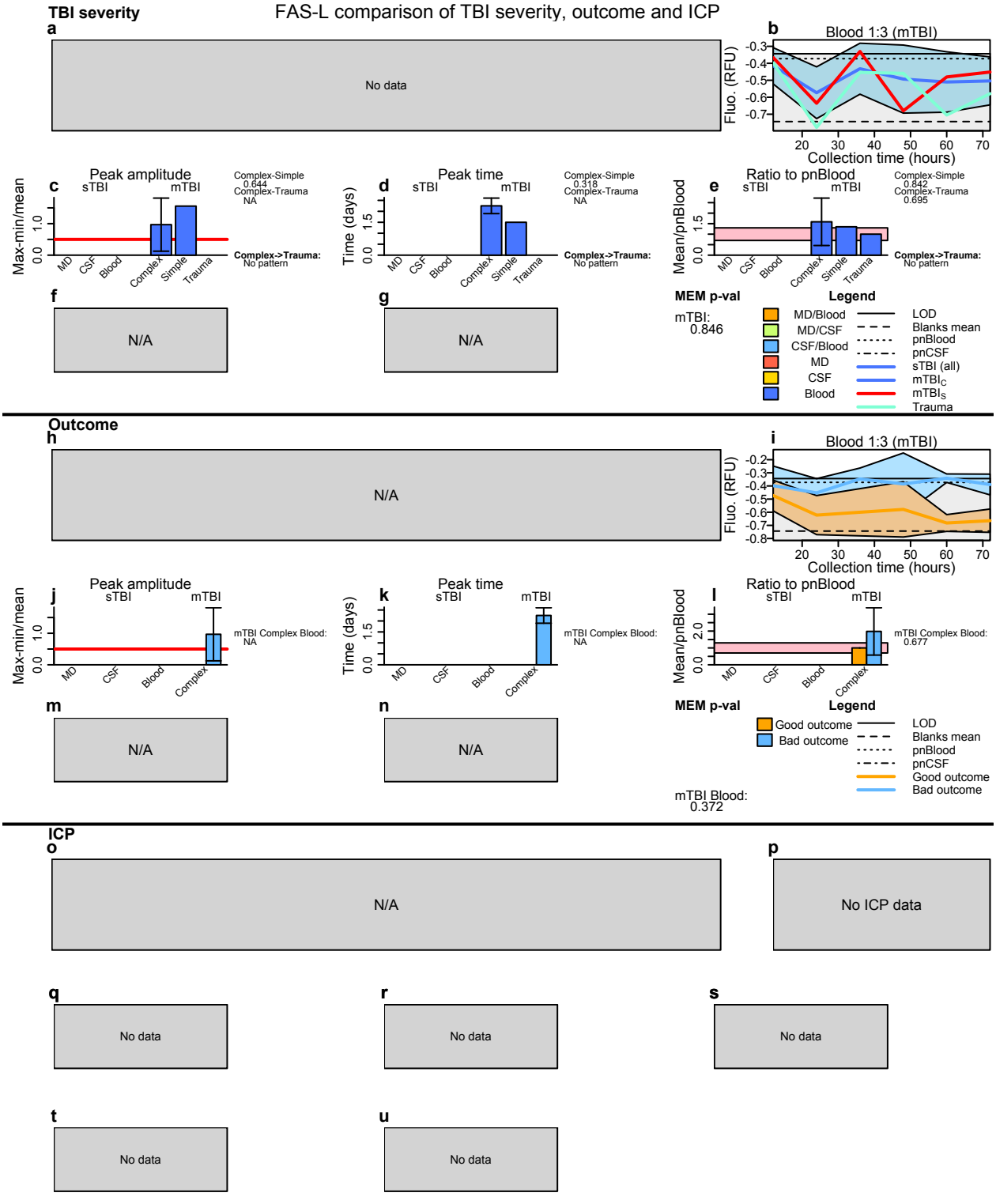

FIGURE J.S78: **Differential FAS-L protein profiles and peak and ratio analysis with respect to TBI severity, outcome and ICP.** Average FAS-L profiles are compared in terms of TBI severity (**a-g**), outcome (**h-n**) and ICP (**o-u**). Polygons in **a, b, h, i, o** indicate the mean value ±1 SD at each time point. Red lines in **c, j, q** show a threshold for a profile that is considered to have a peak, rather than being constant. The light red boxes in **e-g, l-n, s-u** show the threshold of comparison to the measured value compared. Benjamini–Hochberg adjusted p-values for comparisons are shown on the right of every graph.

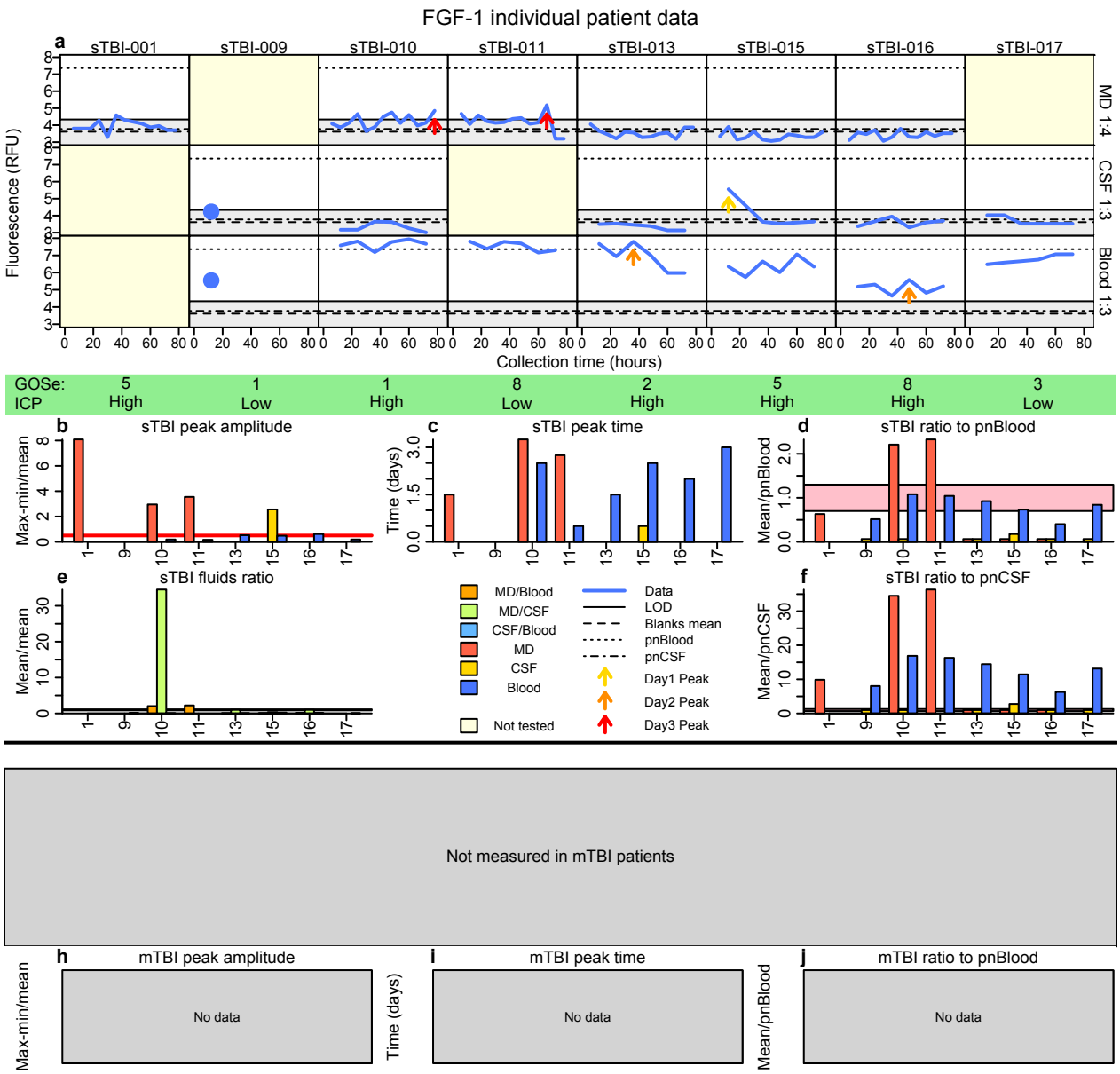

FIGURE J.S79: **Individual FGF-1 protein profiles and peak and ratio analysis.** FGF-1 concentration in microdialysate, CSF and blood samples of individual sTBI patients (**a**) and mTBI/trauma patients (**g**) was measured and peak amplitude and time, as well as ratio between mean time course values to value found in the pooled normal control (**b-f, h-j**) were calculated for each patient. Graphs **b-f** show calculations for individual sTBI patients, and graphs **h-j** show calculations for individual mTBI patients. Red lines in **b, h** show a threshold for a profile that is considered to have a peak, rather than being constant. The light red boxes in **d, e, f, j** show the threshold of comparison to the measured value compared.

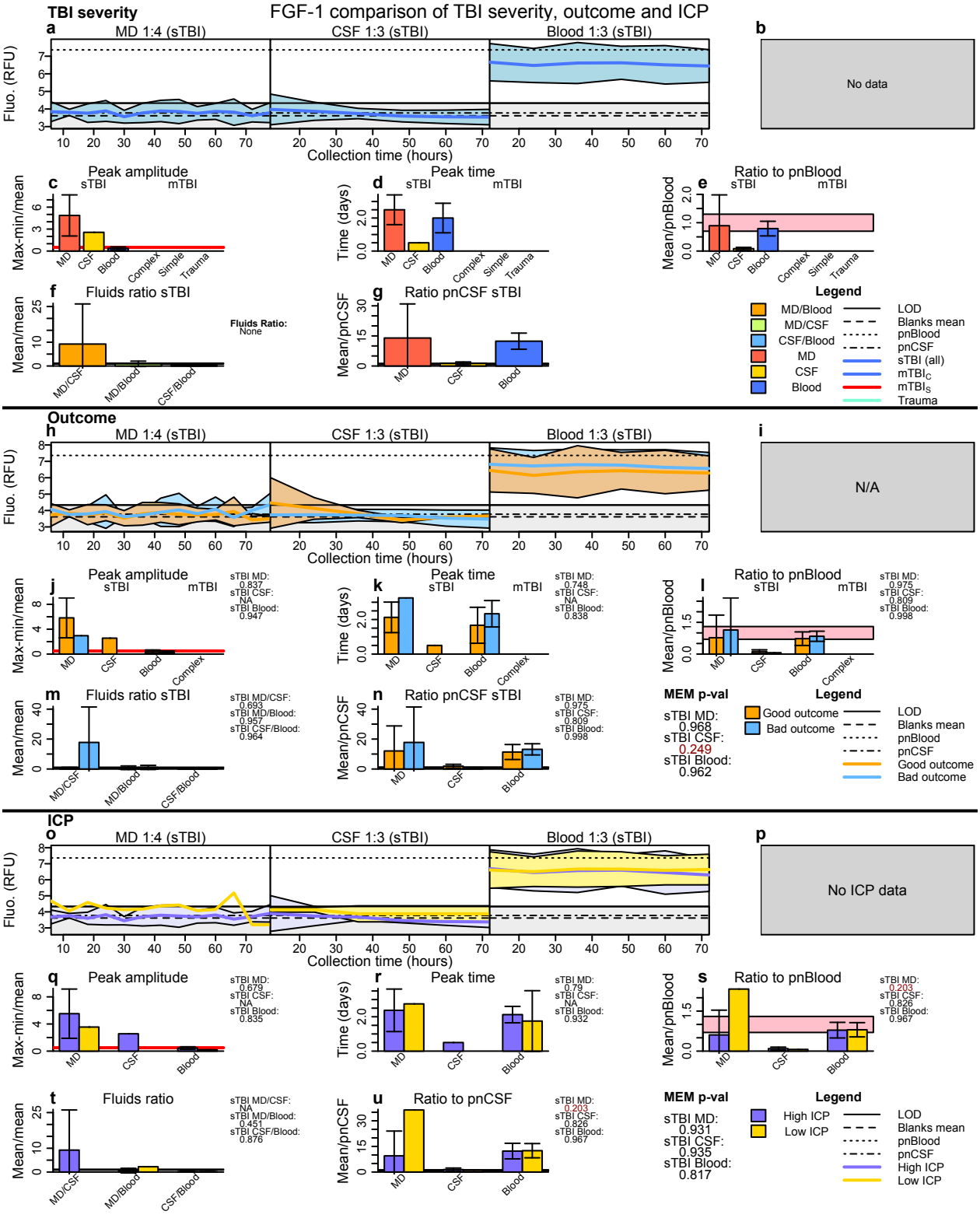

FIGURE J.S80: **Differential FGF-1 protein profiles and peak and ratio analysis with respect to TBI severity, outcome and ICP.** Average FGF-1 profiles are compared in terms of TBI severity (**a-g**), outcome (**h-n**) and ICP (**o-u**). Polygons in **a, b, h, i, o** indicate the mean value ±1 SD at each time point. Red lines in **c, j, q** show a threshold for a profile that is considered to have a peak, rather than being constant. The light red boxes in **e-g, l-n, s-u** show the threshold of comparison to the measured value compared. Benjamini–Hochberg adjusted p-values for comparisons are shown on the right of every graph.

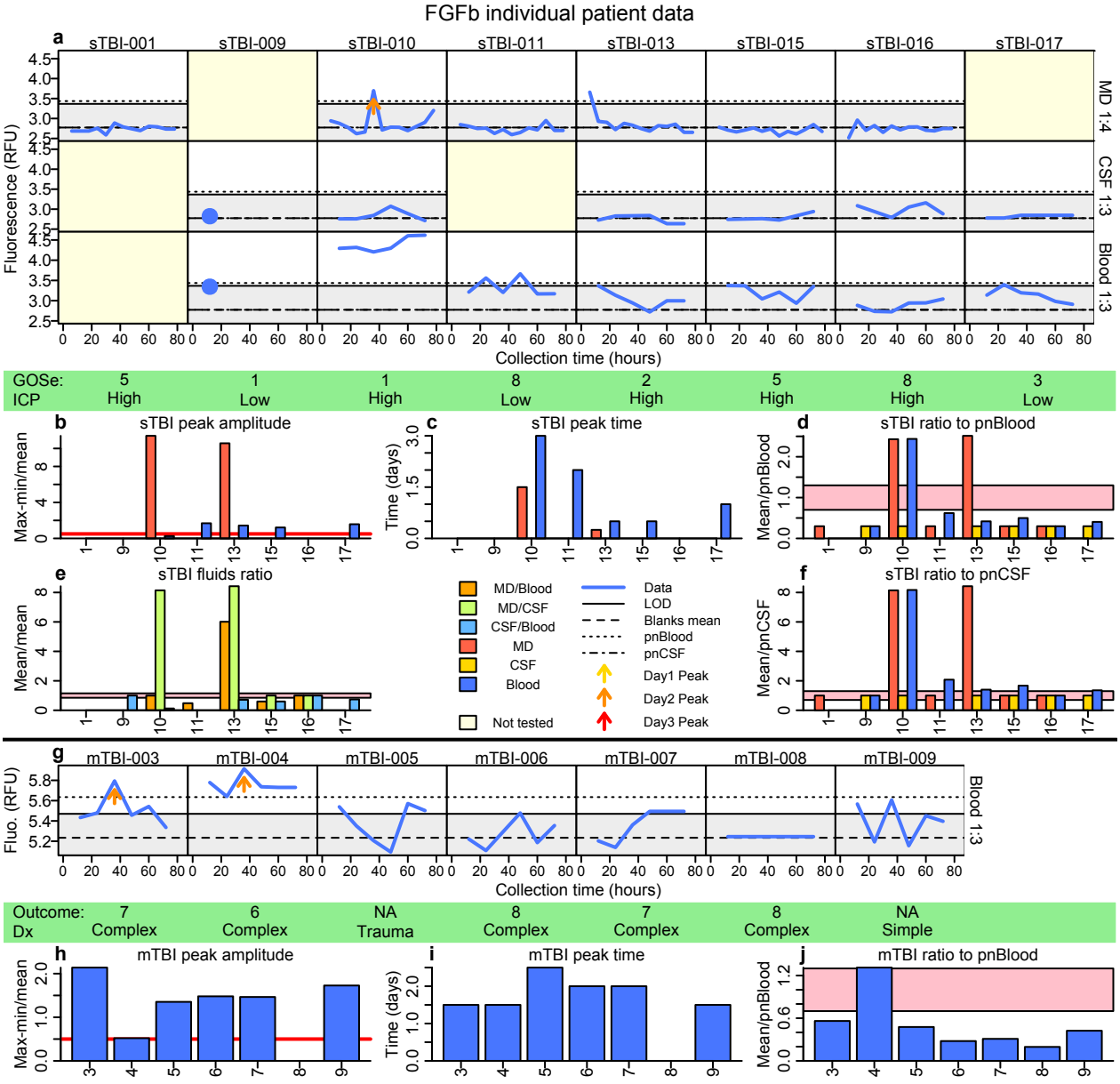

FIGURE J.S81: **Individual FGFb protein profiles and peak and ratio analysis.** FGFb concentration in microdialysate, CSF and blood samples of individual sTBI patients (**a**) and mTBI/trauma patients (**g**) was measured and peak amplitude and time, as well as ratio between mean time course values to value found in the pooled normal control (**b-f, h-j**) were calculated for each patient. Graphs **b-f** show calculations for individual sTBI patients, and graphs **h-j** show calculations for individual mTBI patients. Red lines in **b, h** show a threshold for a profile that is considered to have a peak, rather than being constant. The light red boxes in **d, e, f, j** show the threshold of comparison to the measured value compared.

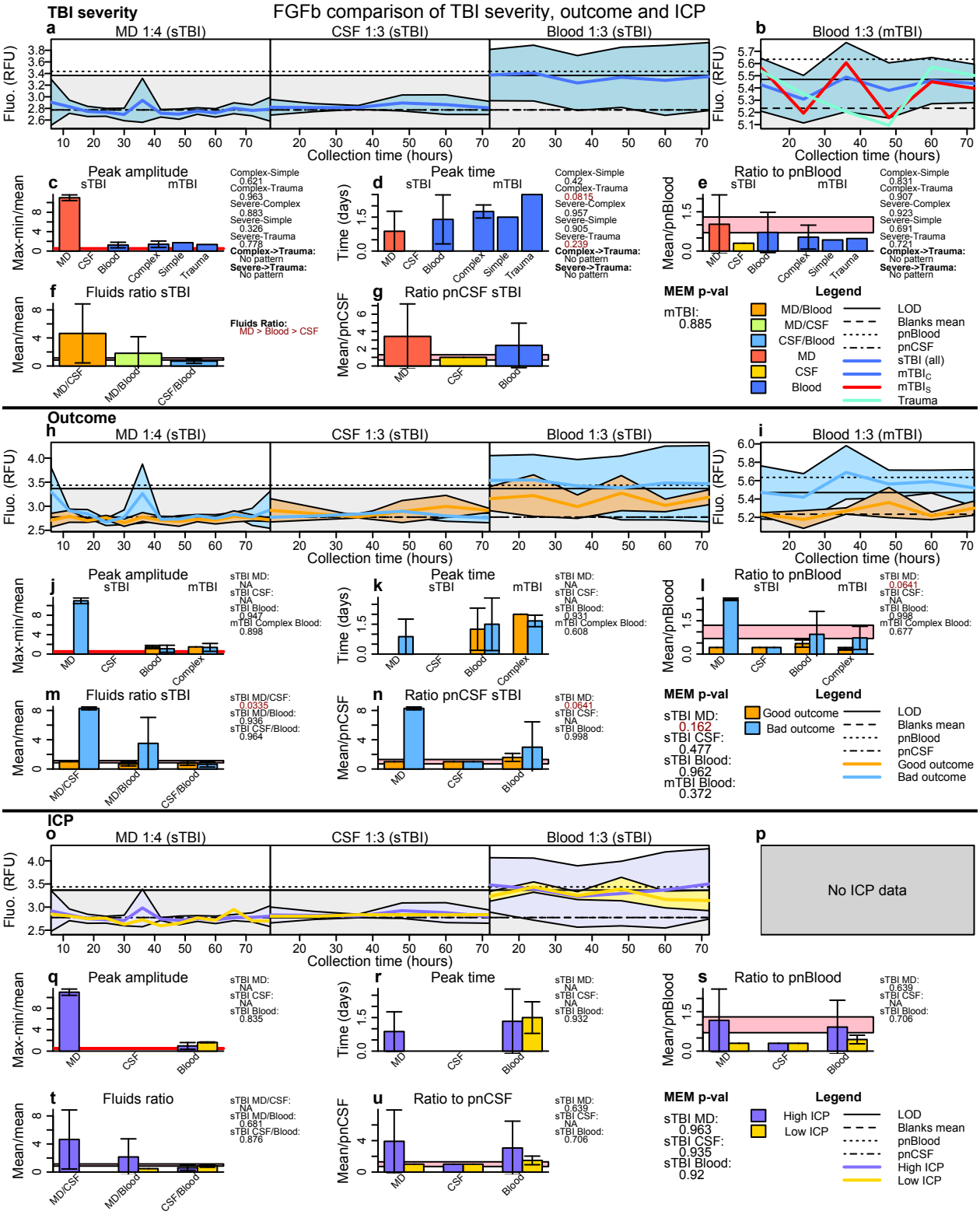

FIGURE J.S82: **Differential FGFb protein profiles and peak and ratio analysis with respect to TBI severity, outcome and ICP.** Average FGFb profiles are compared in terms of TBI severity (**a-g**), outcome (**h-n**) and ICP (**o-u**). Polygons in **a, b, h, i, o** indicate the mean value ±1 SD at each time point. Red lines in **c, j, q** show a threshold for a profile that is considered to have a peak, rather than being constant. The light red boxes in **e-g, l-n, s-u** show the threshold of comparison to the measured value compared. Benjamini–Hochberg adjusted p-values for comparisons are shown on the right of every graph.

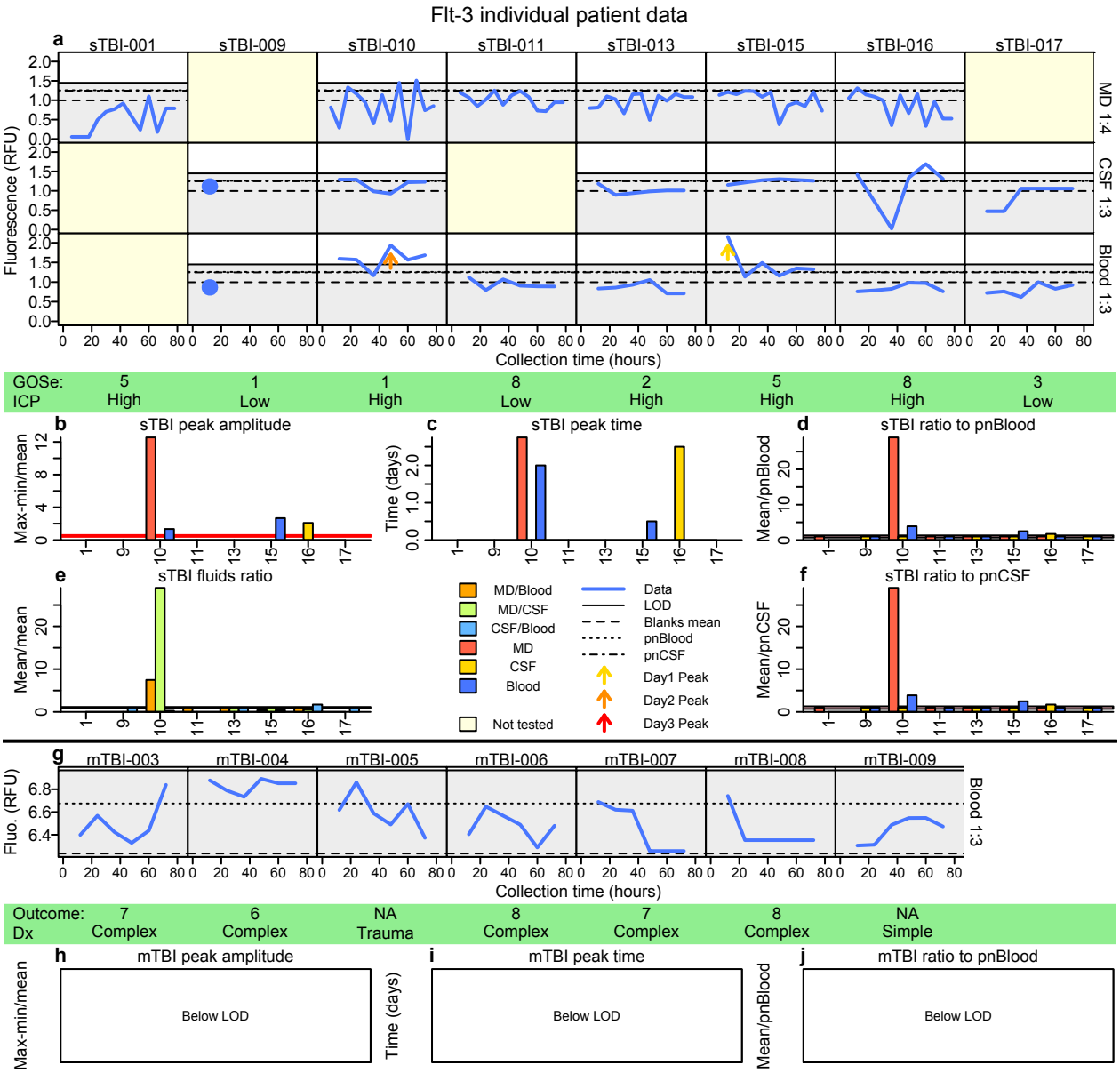

FIGURE J.S83: **Individual Flt-3 protein profiles and peak and ratio analysis.** Flt-3 concentration in microdialysate, CSF and blood samples of individual sTBI patients (**a**) and mTBI/trauma patients (**g**) was measured and peak amplitude and time, as well as ratio between mean time course values to value found in the pooled normal control (**b-f, h-j**) were calculated for each patient. Graphs **b-f** show calculations for individual sTBI patients, and graphs **h-j** show calculations for individual mTBI patients. Red lines in **b, h** show a threshold for a profile that is considered to have a peak, rather than being constant. The light red boxes in **d, e, f, j** show the threshold of comparison to the measured value compared.

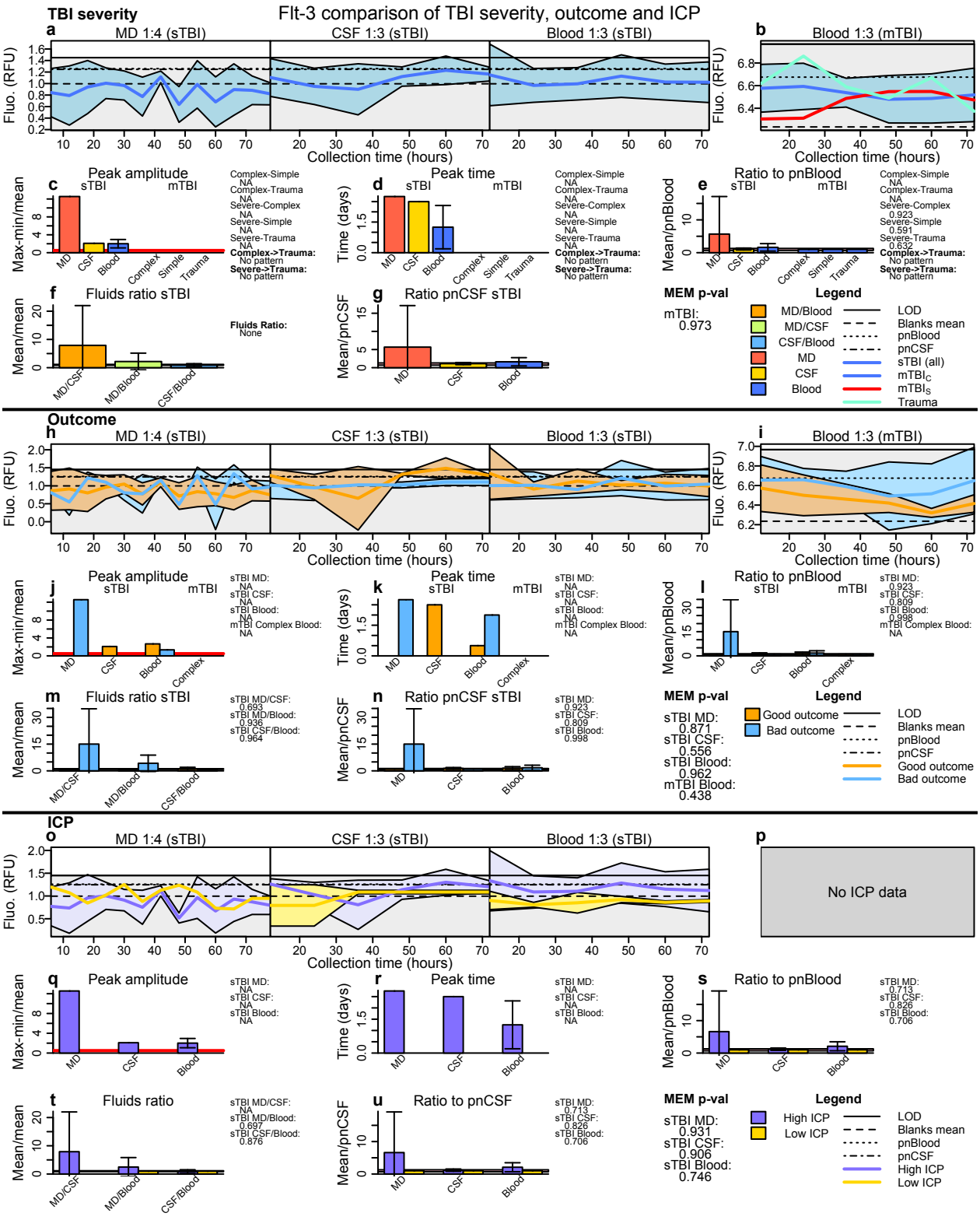

FIGURE J.S84: **Differential Flt-3 protein profiles and peak and ratio analysis with respect to TBI severity, outcome and ICP.** Average Flt-3 profiles are compared in terms of TBI severity (**a-g**), outcome (**h-n**) and ICP (**o-u**). Polygons in **a, b, h, i, o** indicate the mean value ±1 SD at each time point. Red lines in **c, j, q** show a threshold for a profile that is considered to have a peak, rather than being constant. The light red boxes in **e-g, l-n, s-u** show the threshold of comparison to the measured value compared. Benjamini–Hochberg adjusted p-values for comparisons are shown on the right of every graph.

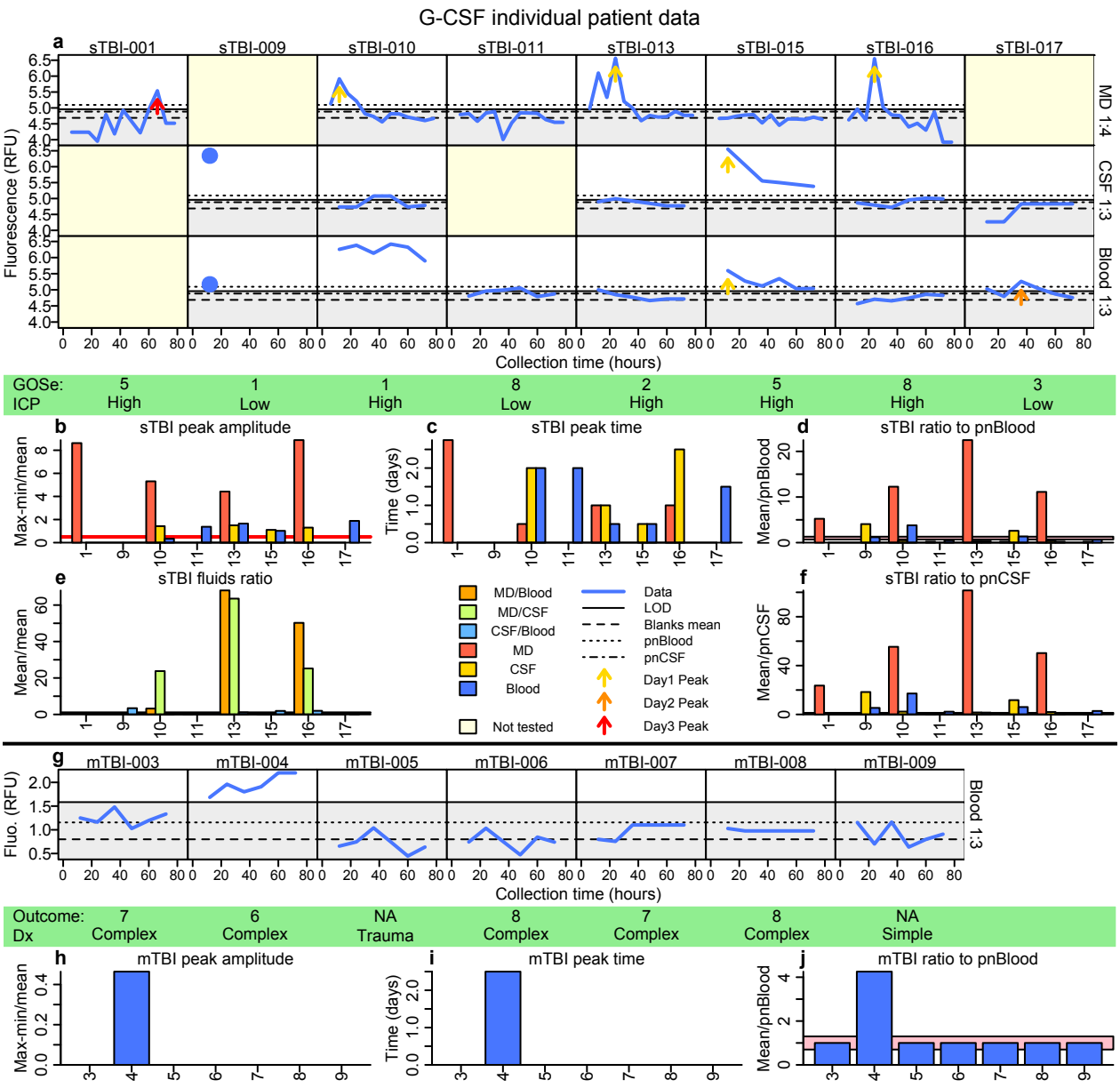

FIGURE J.S85: **Individual G-CSF protein profiles and peak and ratio analysis.** G-CSF concentration in microdialysate, CSF and blood samples of individual sTBI patients (**a**) and mTBI/trauma patients (**g**) was measured and peak amplitude and time, as well as ratio between mean time course values to value found in the pooled normal control (**b-f, h-j**) were calculated for each patient. Graphs **b-f** show calculations for individual sTBI patients, and graphs **h-j** show calculations for individual mTBI patients. Red lines in **b, h** show a threshold for a profile that is considered to have a peak, rather than being constant. The light red boxes in **d, e, f, j** show the threshold of comparison to the measured value compared.

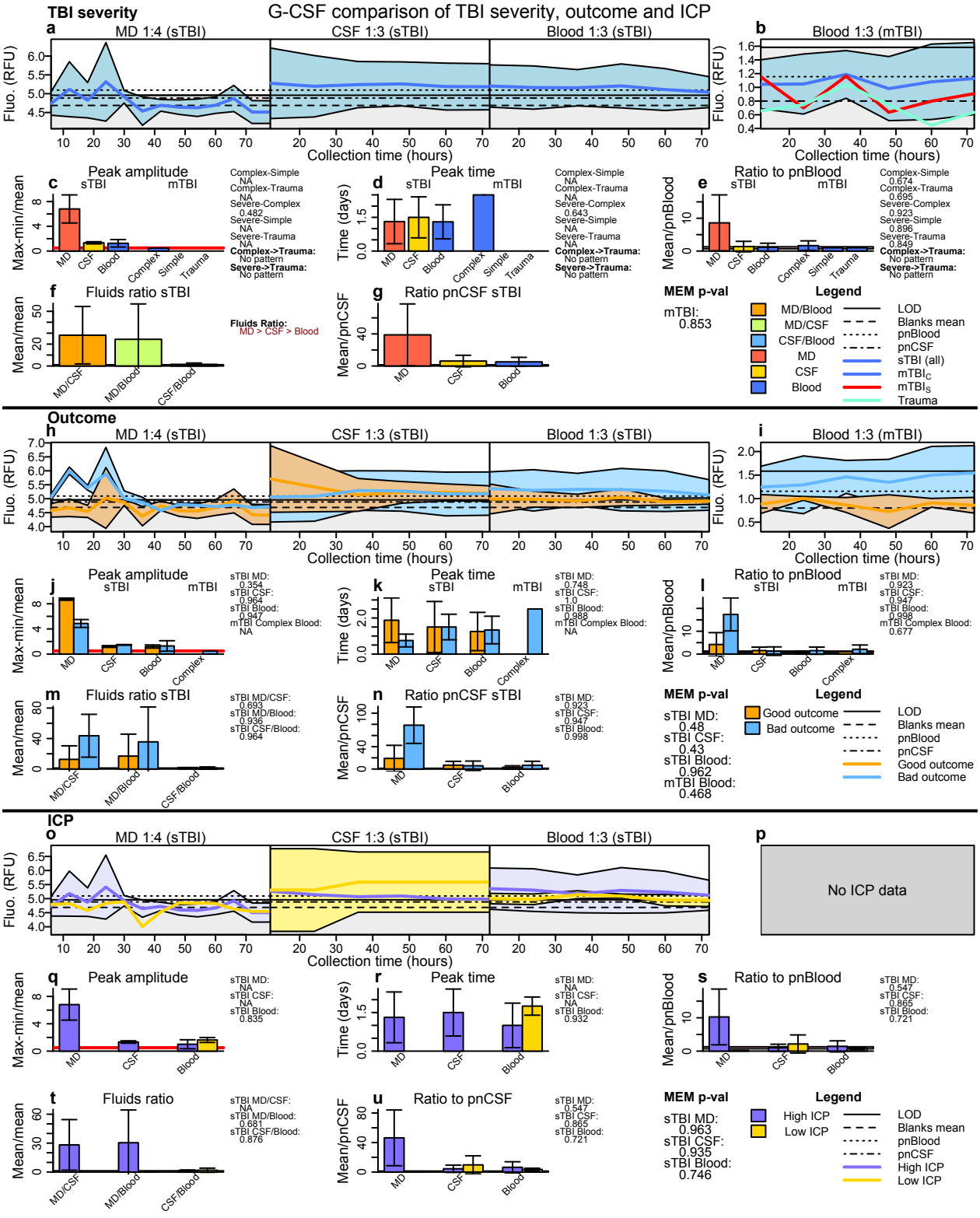

FIGURE J.S86: **Differential G-CSF protein profiles and peak and ratio analysis with respect to TBI severity, outcome and ICP.** Average G-CSF profiles are compared in terms of TBI severity (**a-g**), outcome (**h-n**) and ICP (**o-u**). Polygons in **a, b, h, i, o** indicate the mean value ±1 SD at each time point. Red lines in **c, j, q** show a threshold for a profile that is considered to have a peak, rather than being constant. The light red boxes in **e-g, l-n, s-u** show the threshold of comparison to the measured value compared. Benjamini–Hochberg adjusted p-values for comparisons are shown on the right of every graph.

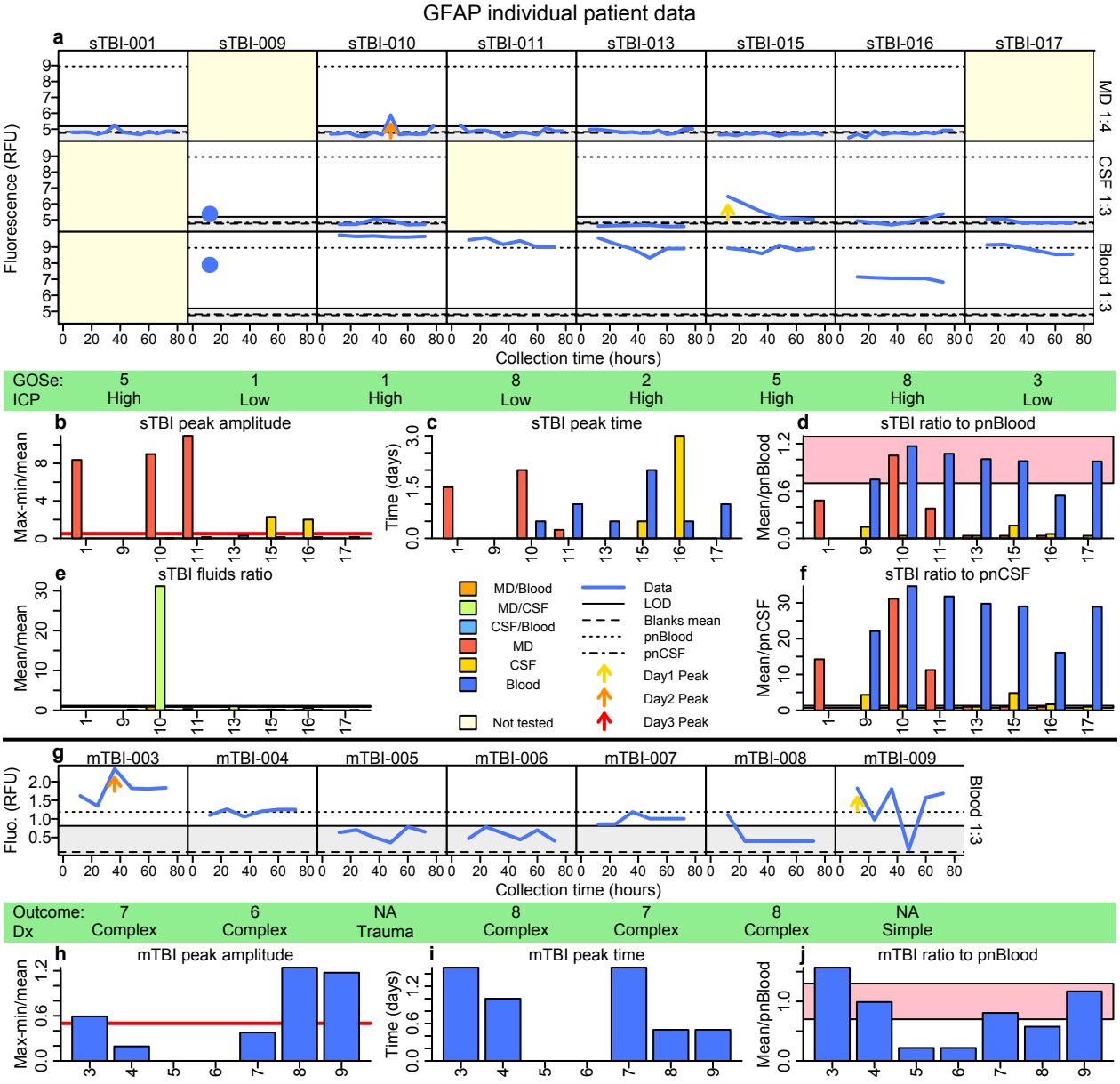

FIGURE J.S87: **Individual GFAP protein profiles and peak and ratio analysis.** GFAP concentration in microdialysate, CSF and blood samples of individual sTBI patients (**a**) and mTBI/trauma patients (**g**) was measured and peak amplitude and time, as well as ratio between mean time course values to value found in the pooled normal control (**b-f, h-j**) were calculated for each patient. Graphs **b-f** show calculations for individual sTBI patients, and graphs **h-j** show calculations for individual mTBI patients. Red lines in **b, h** show a threshold for a profile that is considered to have a peak, rather than being constant. The light red boxes in **d, e, f, j** show the threshold of comparison to the measured value compared.

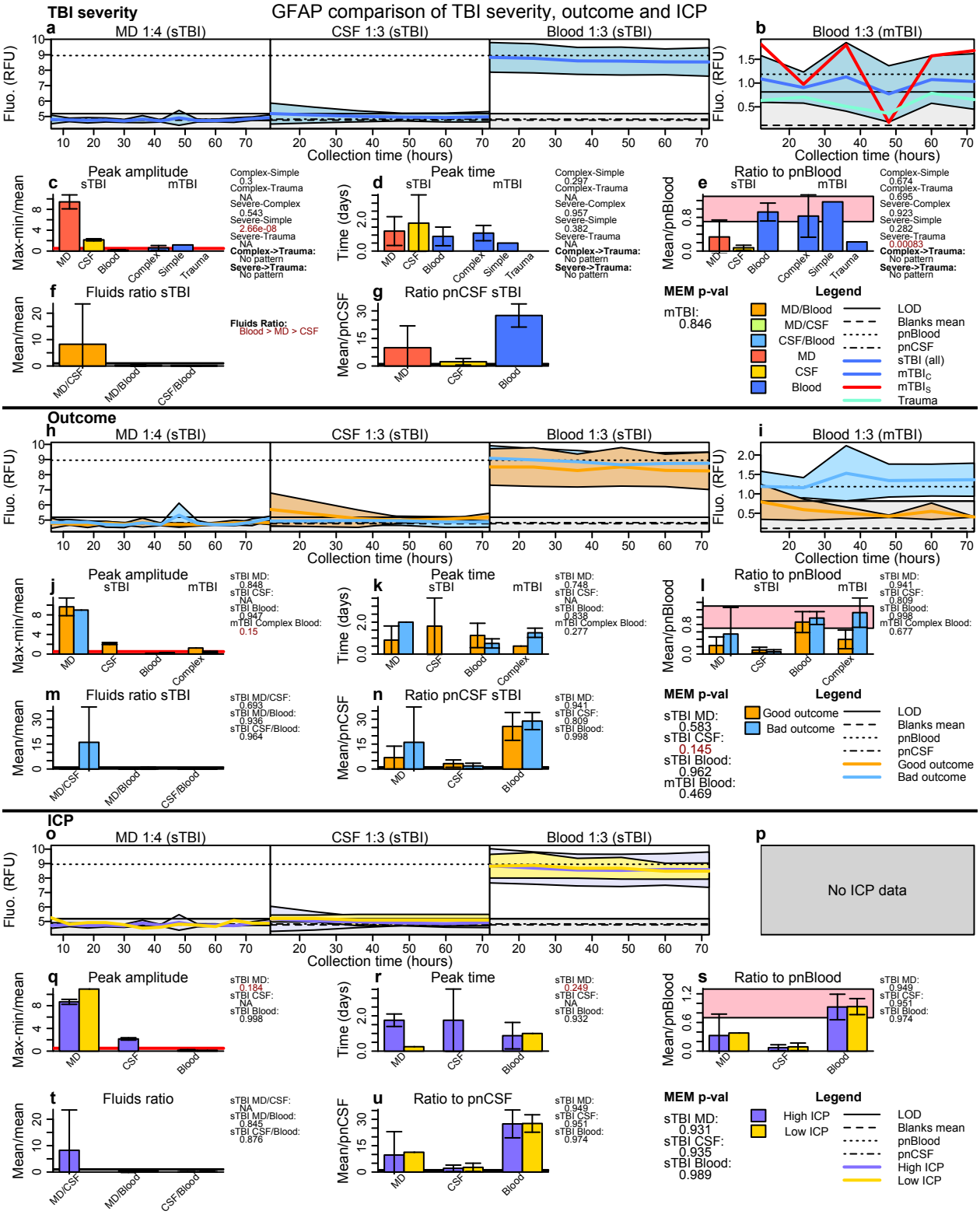

FIGURE J.S88: **Differential GFAP protein profiles and peak and ratio analysis with respect to TBI severity, outcome and ICP.** Average GFAP profiles are compared in terms of TBI severity (**a-g**), outcome (**h-n**) and ICP (**o-u**). Polygons in **a, b, h, i, o** indicate the mean value ±1 SD at each time point. Red lines in **c, j, q** show a threshold for a profile that is considered to have a peak, rather than being constant. The light red boxes in **e-g, l-n, s-u** show the threshold of comparison to the measured value compared. Benjamini–Hochberg adjusted p-values for comparisons are shown on the right of every graph.

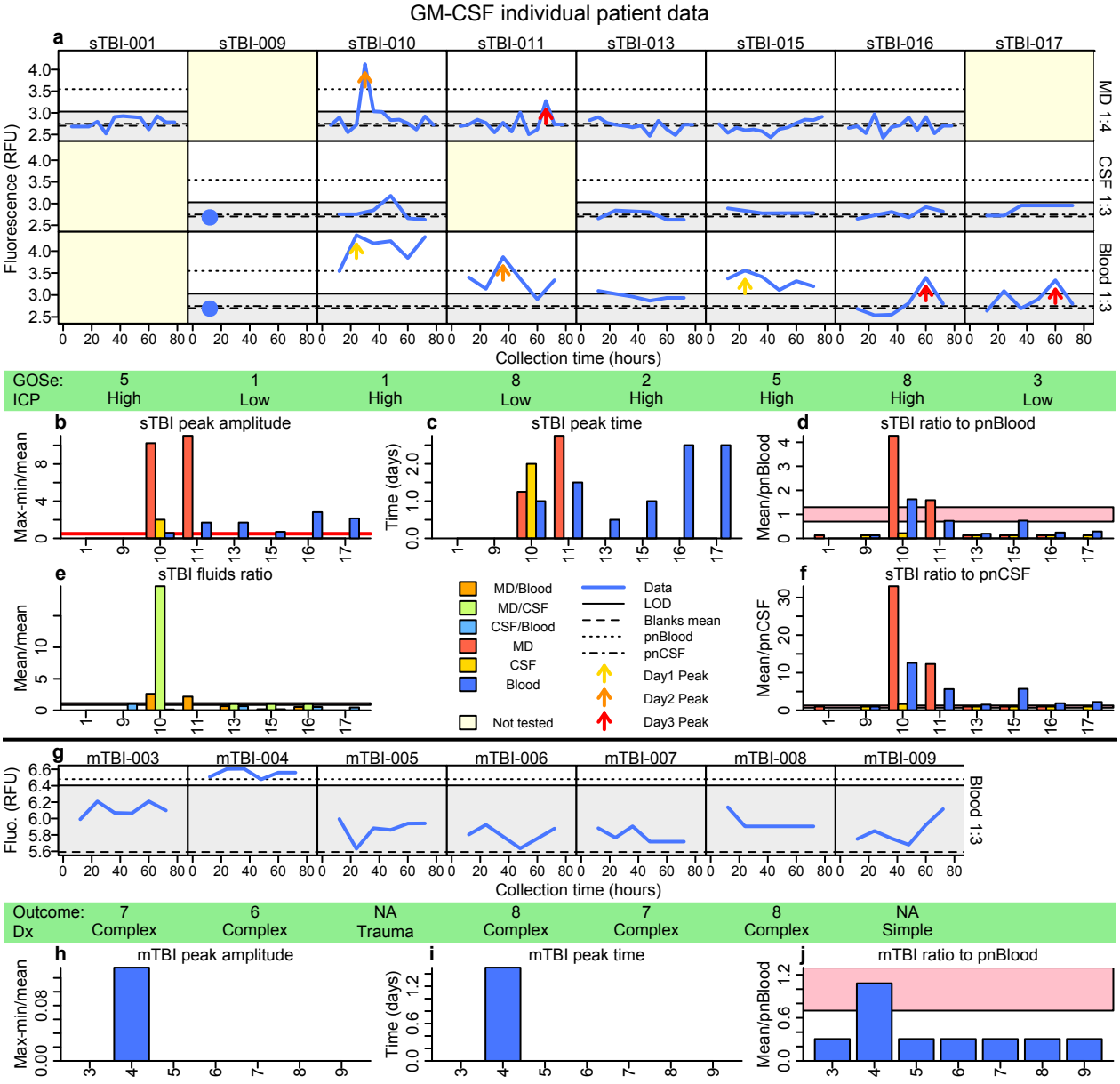

FIGURE J.S89: **Individual GM-CSF protein profiles and peak and ratio analysis.** GM-CSF concentration in microdialysate, CSF and blood samples of individual sTBI patients (**a**) and mTBI/trauma patients (**g**) was measured and peak amplitude and time, as well as ratio between mean time course values to value found in the pooled normal control (**b-f, h-j**) were calculated for each patient. Graphs **b-f** show calculations for individual sTBI patients, and graphs **h-j** show calculations for individual mTBI patients. Red lines in **b, h** show a threshold for a profile that is considered to have a peak, rather than being constant. The light red boxes in **d, e, f, j** show the threshold of comparison to the measured value compared.

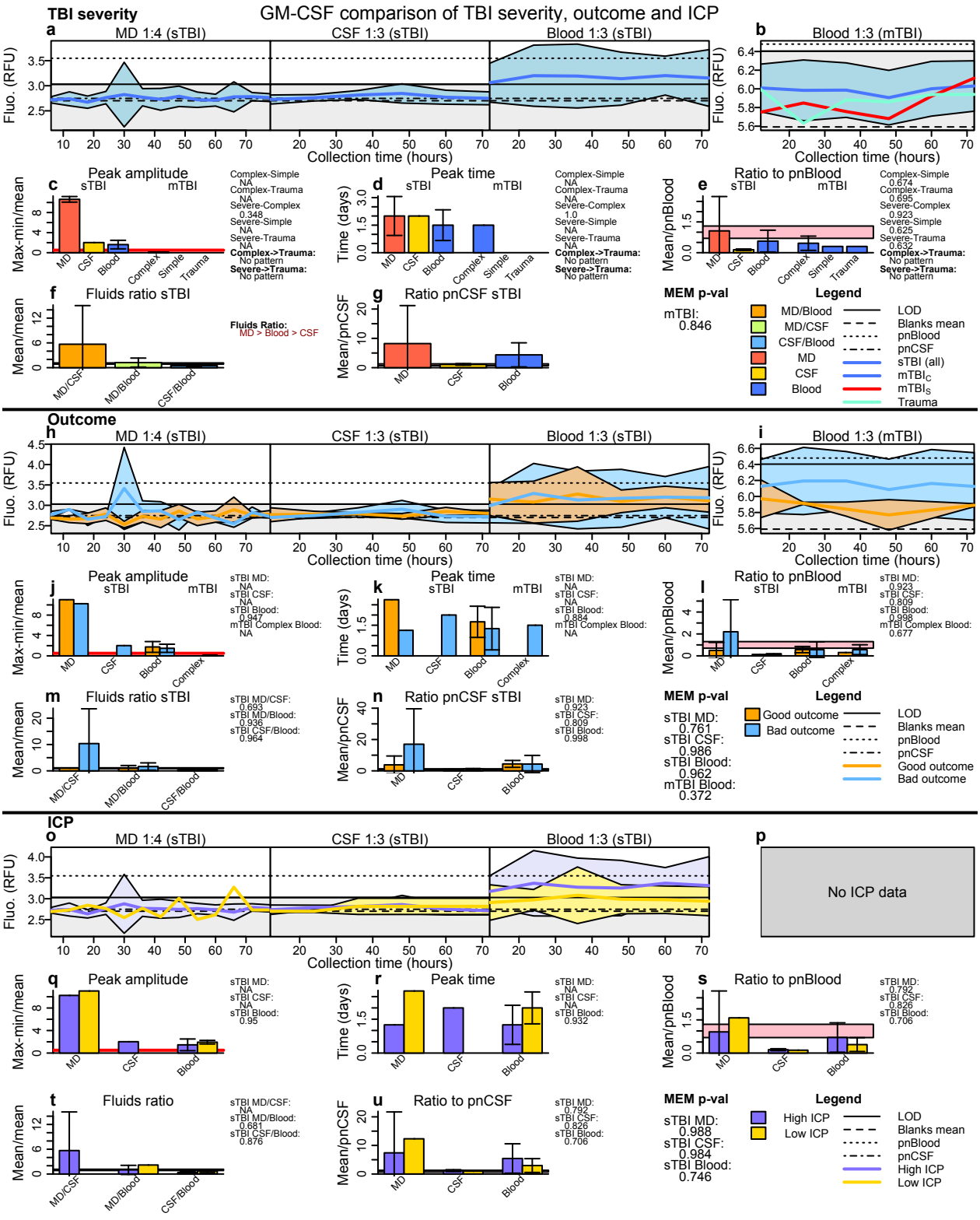

FIGURE J.S90: **Differential GM-CSF protein profiles and peak and ratio analysis with respect to TBI severity, outcome and ICP.** Average GM-CSF profiles are compared in terms of TBI severity (**a-g**), outcome (**h-n**) and ICP (**o-u**). Polygons in **a, b, h, i, o** indicate the mean value ±1 SD at each time point. Red lines in **c, j, q** show a threshold for a profile that is considered to have a peak, rather than being constant. The light red boxes in **e-g, l-n, s-u** show the threshold of comparison to the measured value compared. Benjamini–Hochberg adjusted p-values for comparisons are shown on the right of every graph.

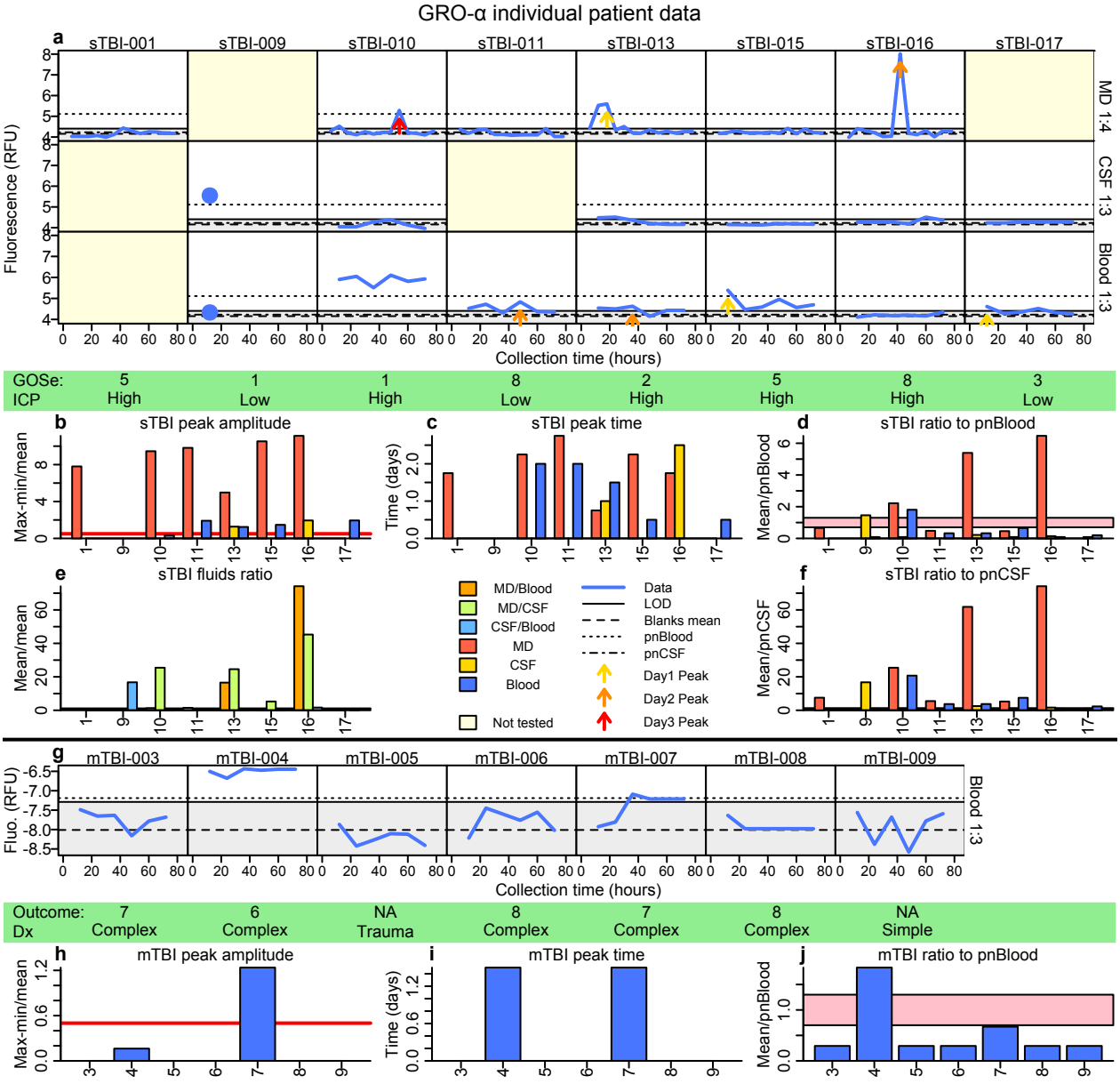

FIGURE J.S91: **Individual GRO-α protein profiles and peak and ratio analysis.** GRO-α concentration in microdialysate, CSF and blood samples of individual sTBI patients (**a**) and mTBI/trauma patients (**g**) was measured and peak amplitude and time, as well as ratio between mean time course values to value found in the pooled normal control (**b-f, h-j**) were calculated for each patient. Graphs **b-f** show calculations for individual sTBI patients, and graphs **h-j** show calculations for individual mTBI patients. Red lines in **b, h** show a threshold for a profile that is considered to have a peak, rather than being constant. The light red boxes in **d, e, f, j** show the threshold of comparison to the measured value compared.

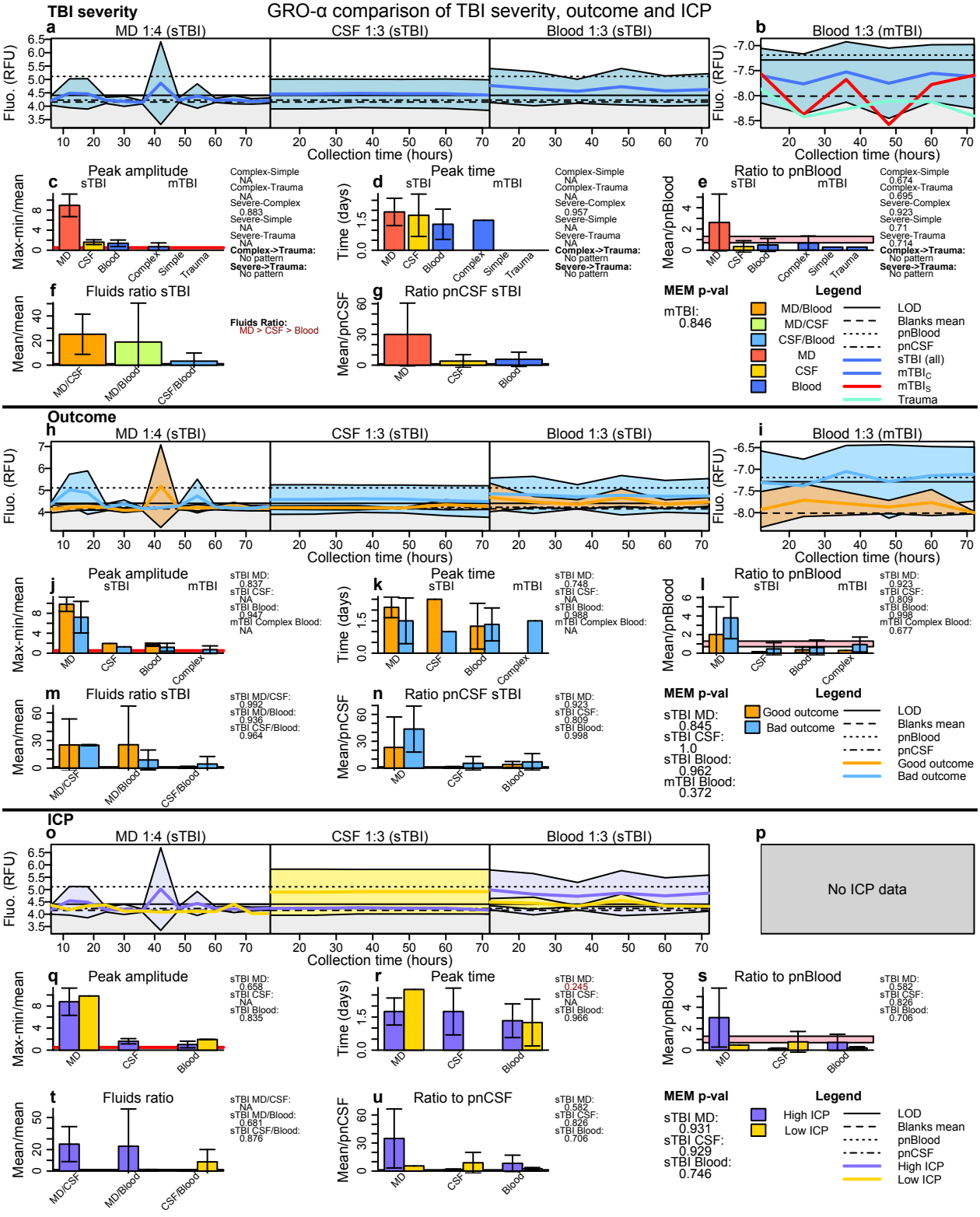

FIGURE J.S92: **Differential GRO-α protein profiles and peak and ratio analysis with respect to TBI severity, outcome and ICP.** Average GRO-α profiles are compared in terms of TBI severity (**a-g**), outcome (**h-n**) and ICP (**o-u**). Polygons in **a, b, h, i, o** indicate the mean value ± 1 SD at each time point. Red lines in **c, j, q** show a threshold for a profile that is considered to have a peak, rather than being constant. The light red boxes in **e-g, l-n, s-u** show the threshold of comparison to the measured value compared. Benjamini–Hochberg adjusted p-values for comparisons are shown on the right of every graph.

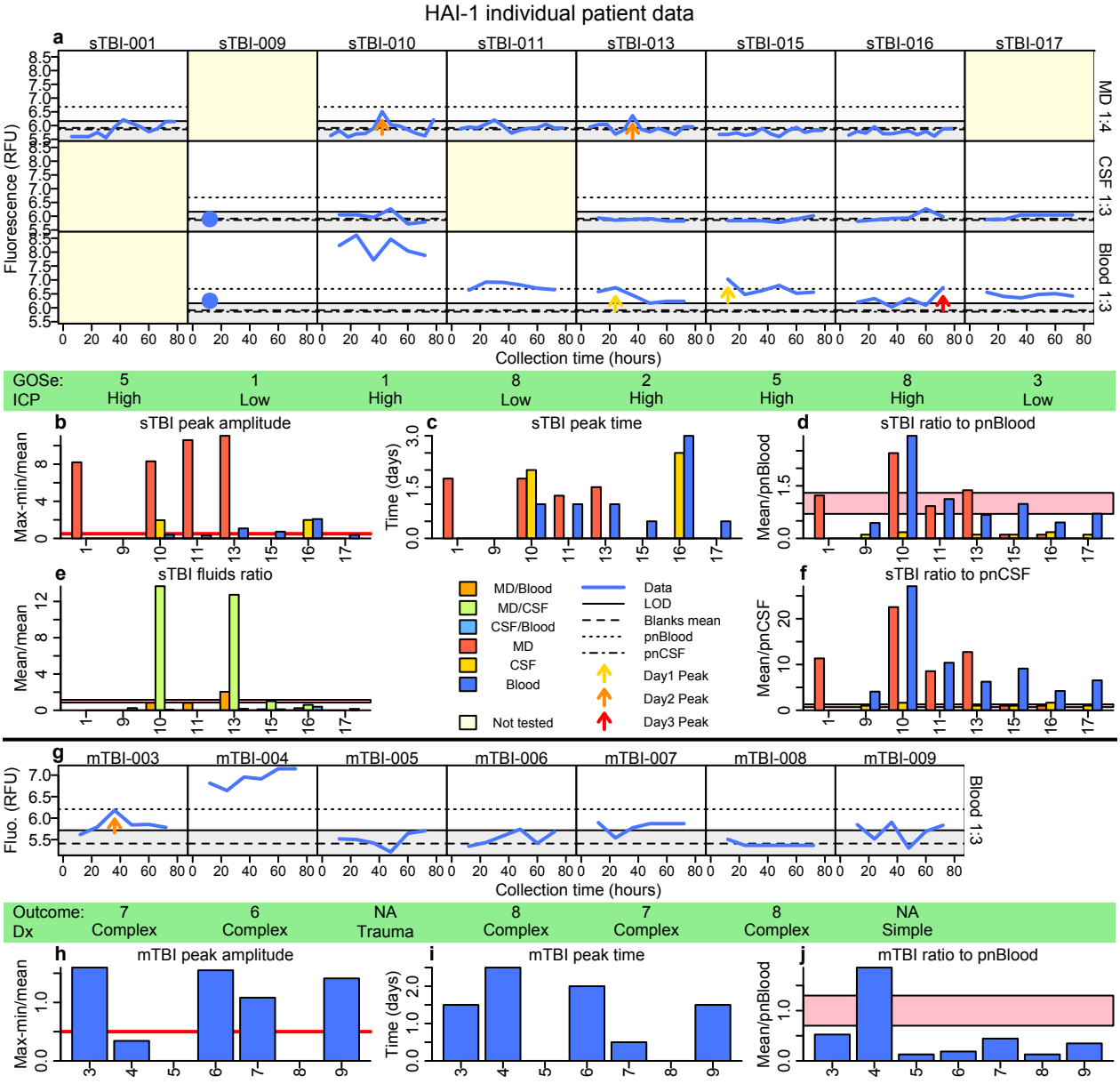

FIGURE J.S93: **Individual HAI-1 protein profiles and peak and ratio analysis.** HAI-1 concentration in microdialysate, CSF and blood samples of individual sTBI patients (**a**) and mTBI/trauma patients (**g**) was measured and peak amplitude and time, as well as ratio between mean time course values to value found in the pooled normal control (**b-f, h-j**) were calculated for each patient. Graphs **b-f** show calculations for individual sTBI patients, and graphs **h-j** show calculations for individual mTBI patients. Red lines in **b, h** show a threshold for a profile that is considered to have a peak, rather than being constant. The light red boxes in **d, e, f, j** show the threshold of comparison to the measured value compared.

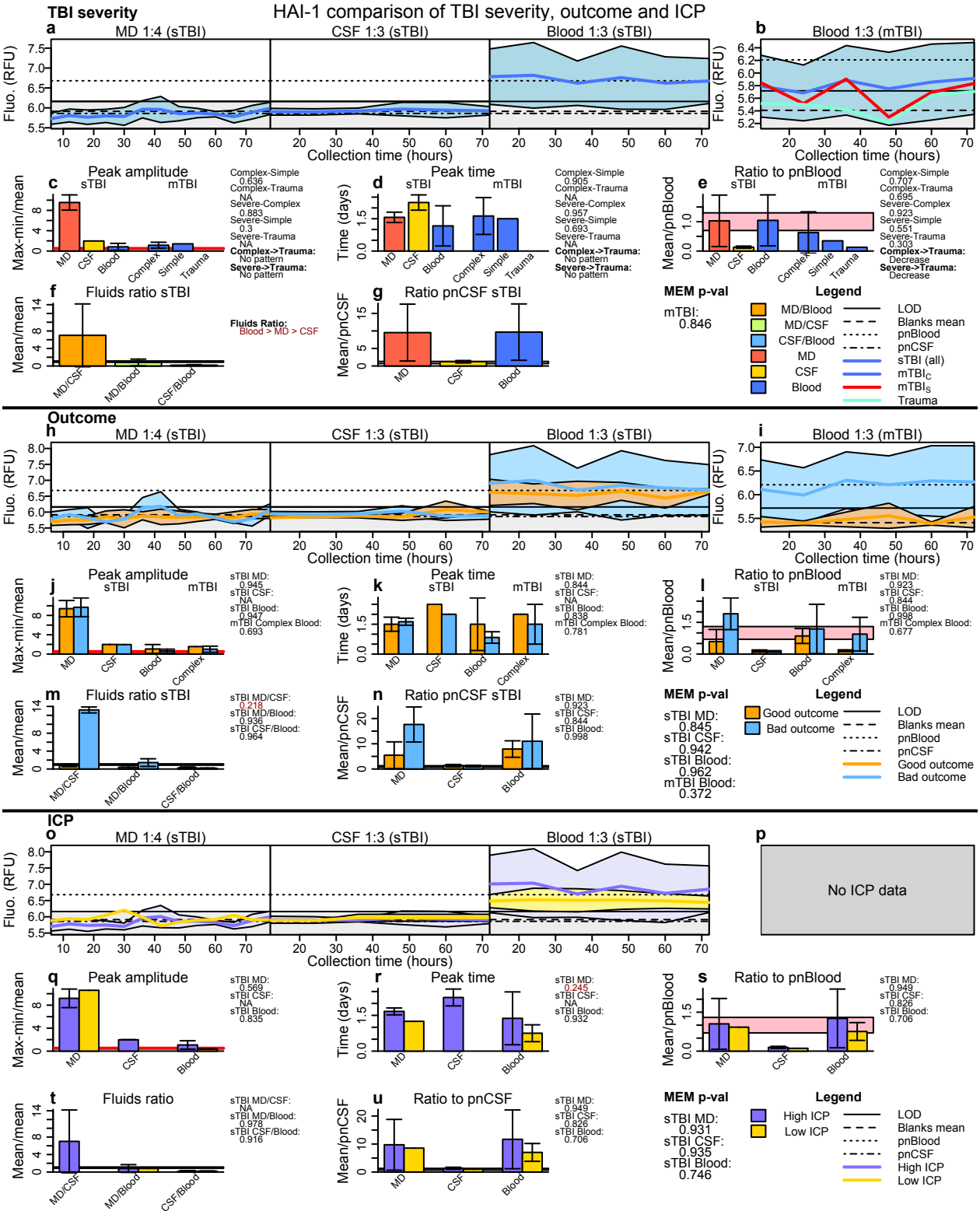

FIGURE J.S94: **Differential HAI-1 protein profiles and peak and ratio analysis with respect to TBI severity, outcome and ICP.** Average HAI-1 profiles are compared in terms of TBI severity (**a-g**), outcome (**h-n**) and ICP (**o-u**). Polygons in **a, b, h, i, o** indicate the mean value ±1 SD at each time point. Red lines in **c, j, q** show a threshold for a profile that is considered to have a peak, rather than being constant. The light red boxes in **e-g, l-n, s-u** show the threshold of comparison to the measured value compared. Benjamini–Hochberg adjusted p-values for comparisons are shown on the right of every graph.

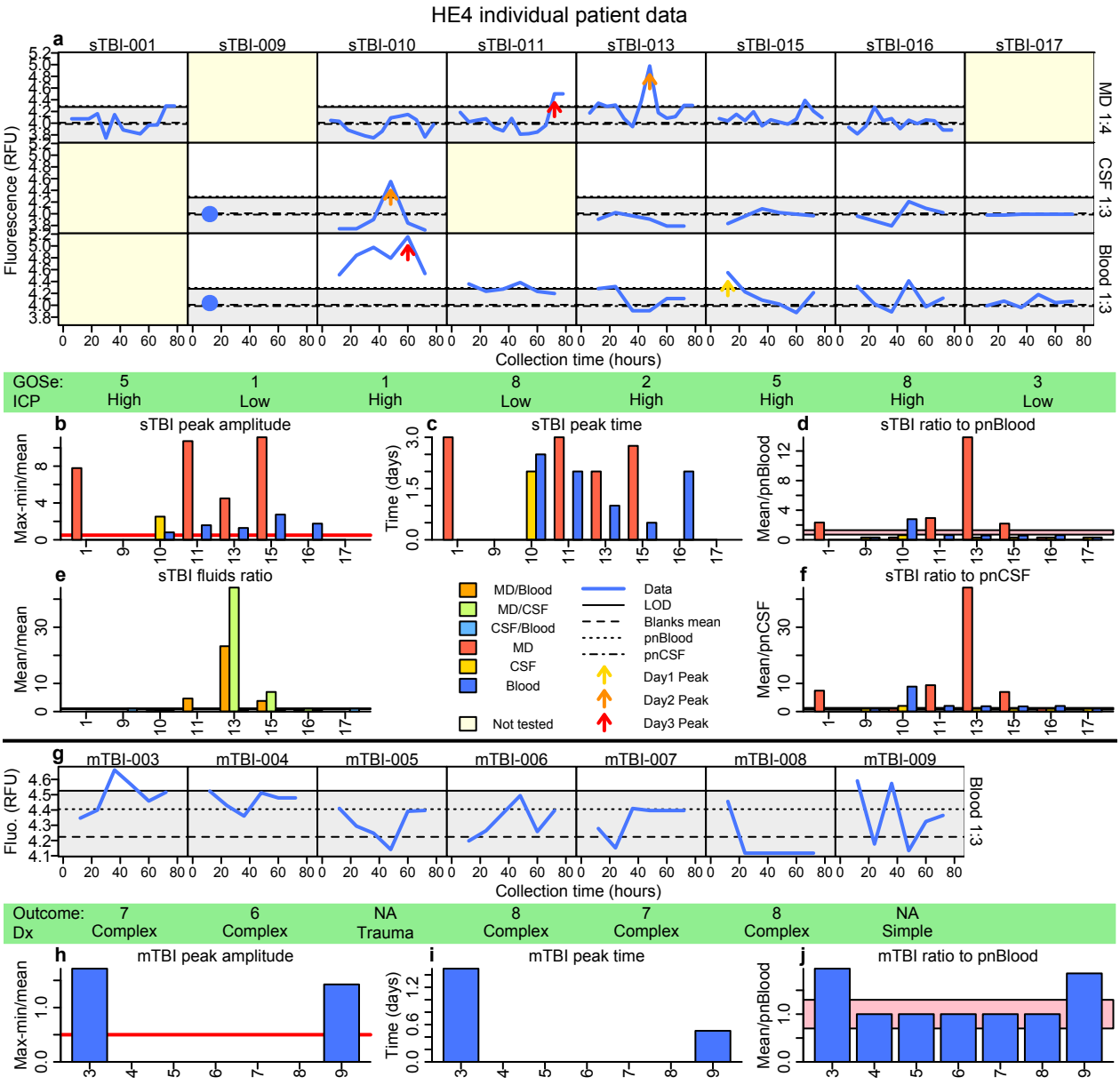

FIGURE J.S95: **Individual HE4 protein profiles and peak and ratio analysis.** HE4 concentration in microdialysate, CSF and blood samples of individual sTBI patients (**a**) and mTBI/trauma patients (**g**) was measured and peak amplitude and time, as well as ratio between mean time course values to value found in the pooled normal control (**b-f, h-j**) were calculated for each patient. Graphs **b-f** show calculations for individual sTBI patients, and graphs **h-j** show calculations for individual mTBI patients. Red lines in **b, h** show a threshold for a profile that is considered to have a peak, rather than being constant. The light red boxes in **d, e, f, j** show the threshold of comparison to the measured value compared.

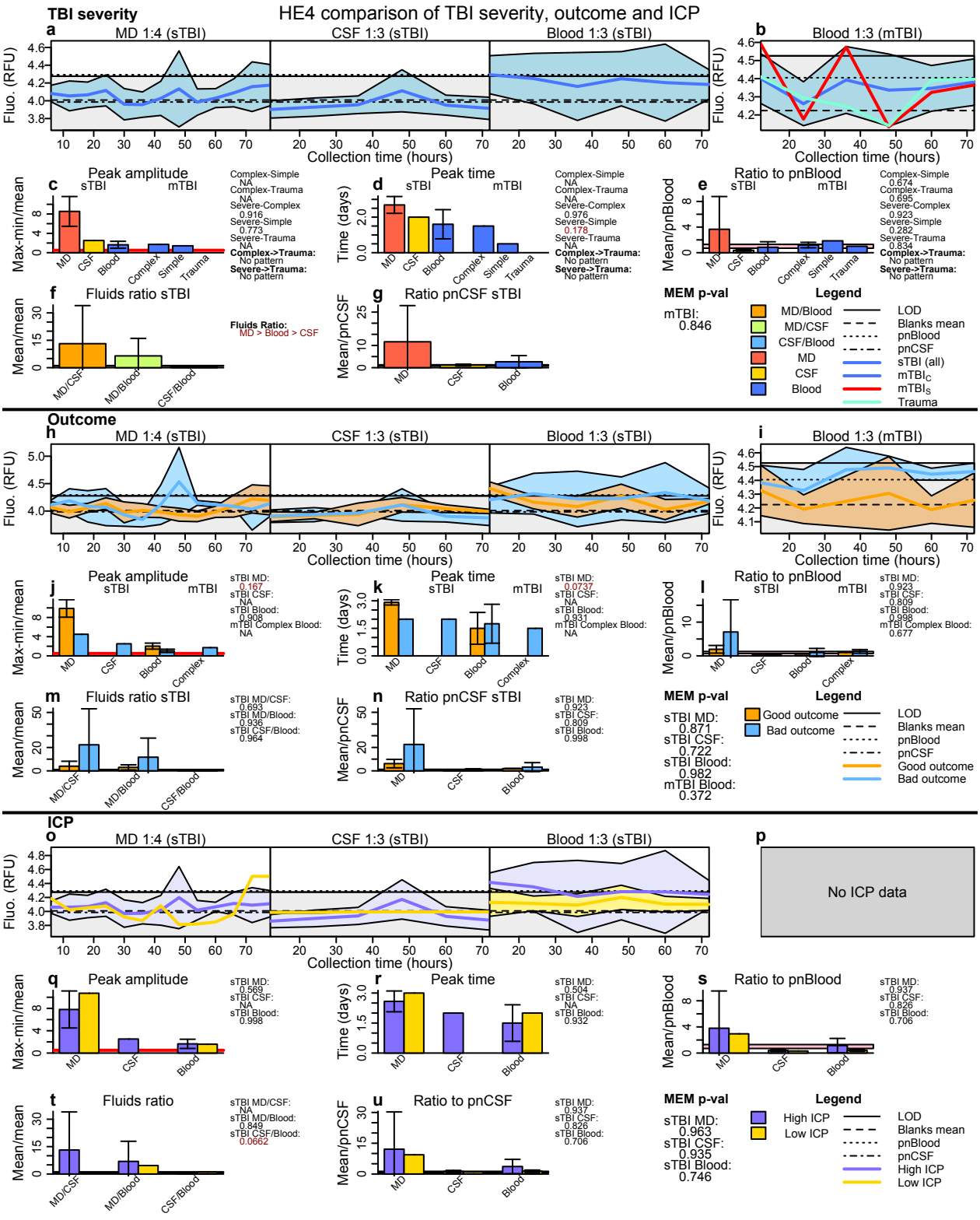

FIGURE J.S96: **Differential HE4 protein profiles and peak and ratio analysis with respect to TBI severity, outcome and ICP.** Average HE4 profiles are compared in terms of TBI severity (**a-g**), outcome (**h-n**) and ICP (**o-u**). Polygons in **a, b, h, i, o** indicate the mean value ±1 SD at each time point. Red lines in **c, j, q** show a threshold for a profile that is considered to have a peak, rather than being constant. The light red boxes in **e-g, l-n, s-u** show the threshold of comparison to the measured value compared. Benjamini–Hochberg adjusted p-values for comparisons are shown on the right of every graph.

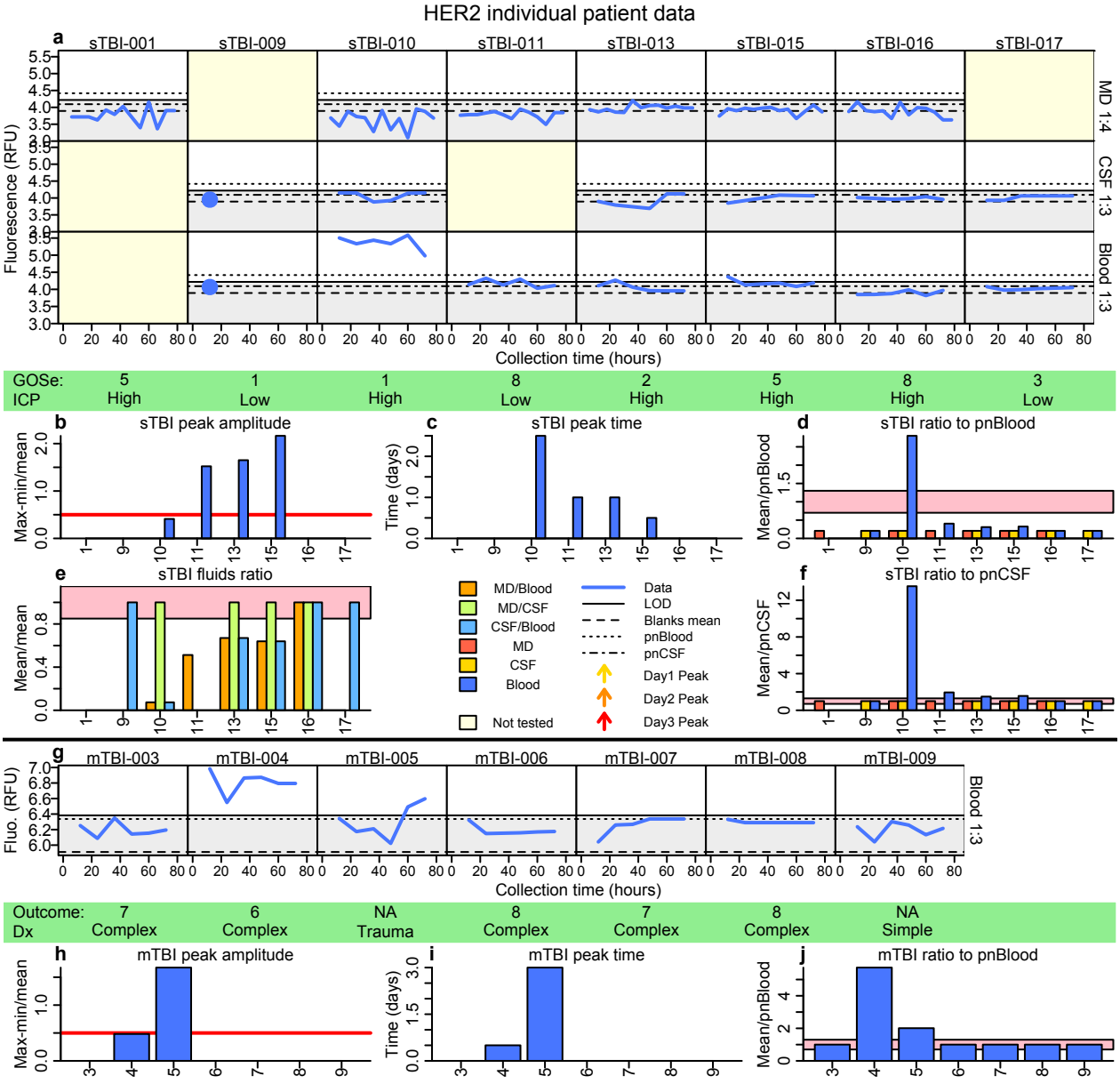

FIGURE J.S97: **Individual HER2 protein profiles and peak and ratio analysis.** HER2 concentration in microdialysate, CSF and blood samples of individual sTBI patients (**a**) and mTBI/trauma patients (**g**) was measured and peak amplitude and time, as well as ratio between mean time course values to value found in the pooled normal control (**b-f, h-j**) were calculated for each patient. Graphs **b-f** show calculations for individual sTBI patients, and graphs **h-j** show calculations for individual mTBI patients. Red lines in **b, h** show a threshold for a profile that is considered to have a peak, rather than being constant. The light red boxes in **d, e, f, j** show the threshold of comparison to the measured value compared.

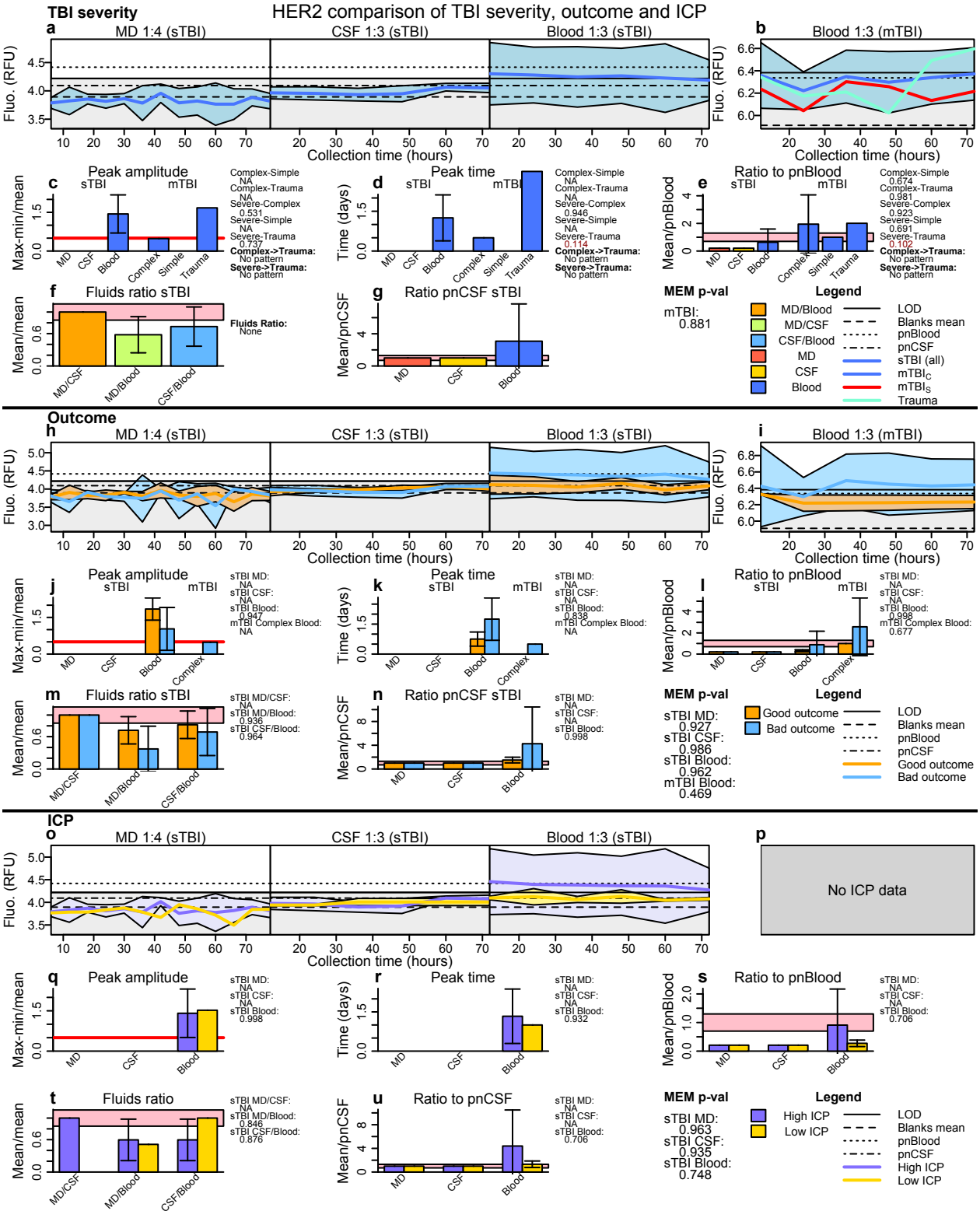

FIGURE J.S98: **Differential HER2 protein profiles and peak and ratio analysis with respect to TBI severity, outcome and ICP.** Average HER2 profiles are compared in terms of TBI severity (**a-g**), outcome (**h-n**) and ICP (**o-u**). Polygons in **a, b, h, i, o** indicate the mean value ±1 SD at each time point. Red lines in **c, j, q** show a threshold for a profile that is considered to have a peak, rather than being constant. The light red boxes in **e-g, l-n, s-u** show the threshold of comparison to the measured value compared. Benjamini–Hochberg adjusted p-values for comparisons are shown on the right of every graph.

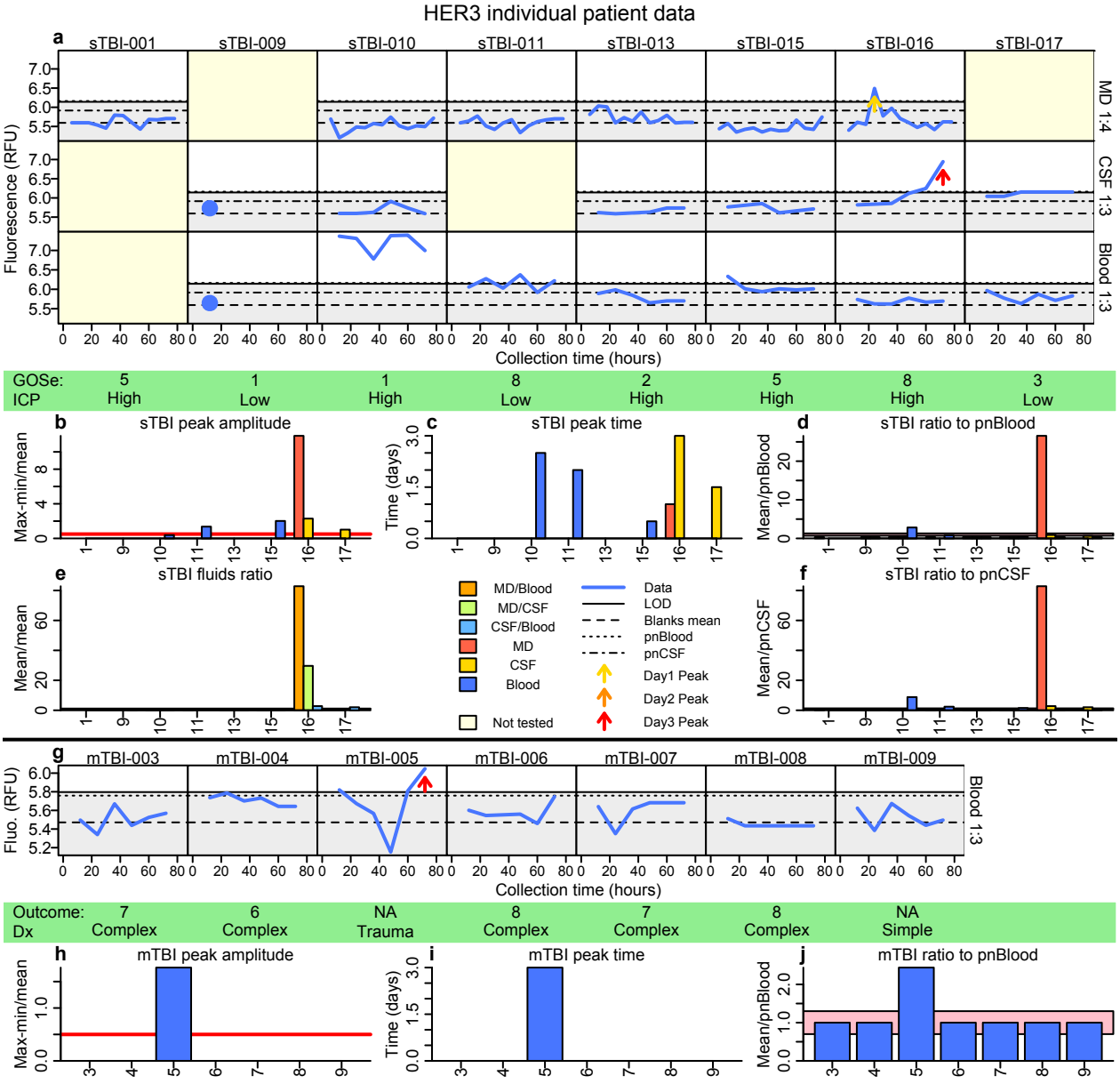

FIGURE J.S99: **Individual HER3 protein profiles and peak and ratio analysis.** HER3 concentration in microdialysate, CSF and blood samples of individual sTBI patients (**a**) and mTBI/trauma patients (**g**) was measured and peak amplitude and time, as well as ratio between mean time course values to value found in the pooled normal control (**b-f, h-j**) were calculated for each patient. Graphs **b-f** show calculations for individual sTBI patients, and graphs **h-j** show calculations for individual mTBI patients. Red lines in **b, h** show a threshold for a profile that is considered to have a peak, rather than being constant. The light red boxes in **d, e, f, j** show the threshold of comparison to the measured value compared.

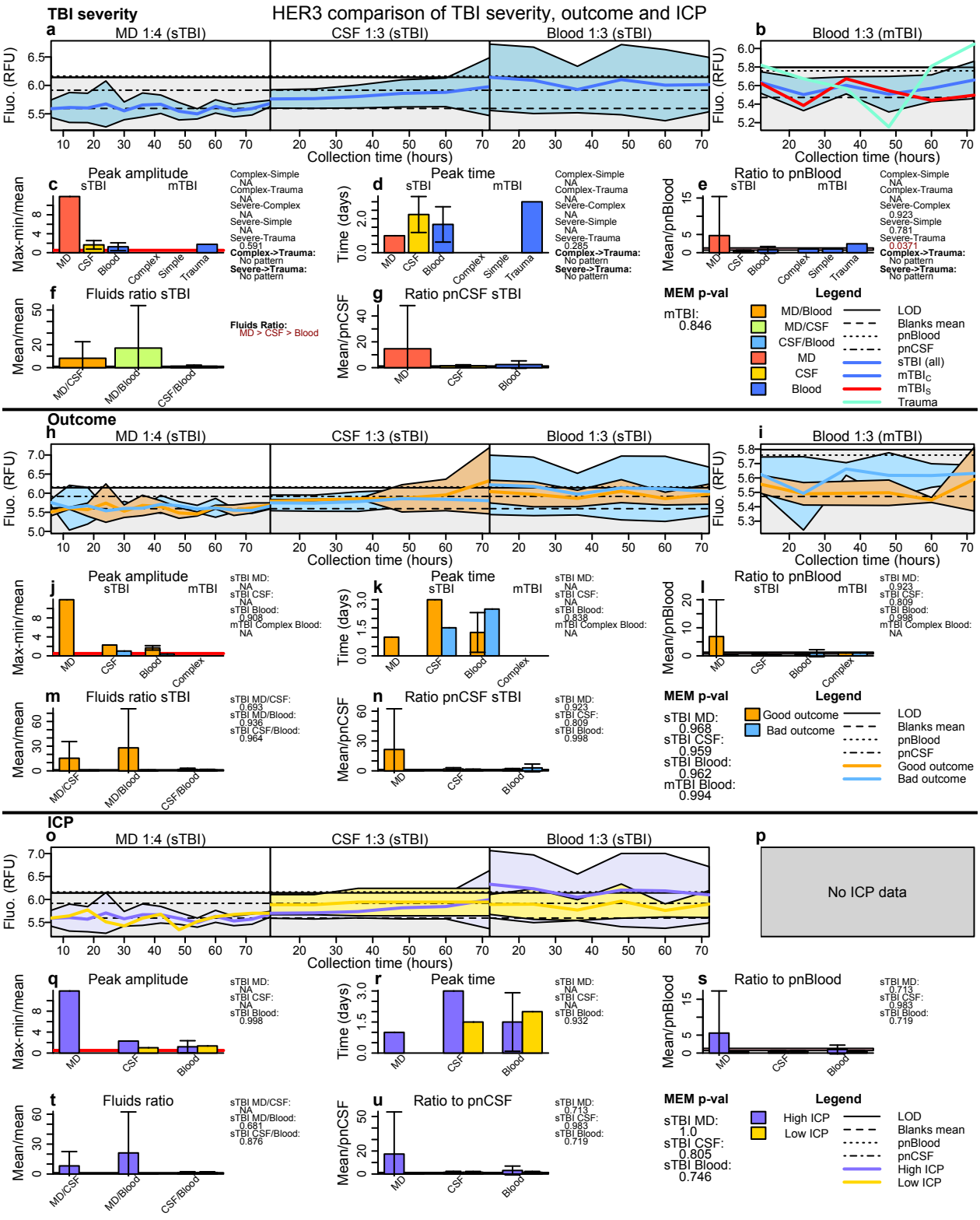

FIGURE J.S100: **Differential HER3 protein profiles and peak and ratio analysis with respect to TBI severity, outcome and ICP.** Average HER3 profiles are compared in terms of TBI severity (**a-g**), outcome (**h-n**) and ICP (**o-u**). Polygons in **a, b, h, i, o** indicate the mean value ±1 SD at each time point. Red lines in **c, j, q** show a threshold for a profile that is considered to have a peak, rather than being constant. The light red boxes in **e-g, l-n, s-u** show the threshold of comparison to the measured value compared. Benjamini–Hochberg adjusted p-values for comparisons are shown on the right of every graph.

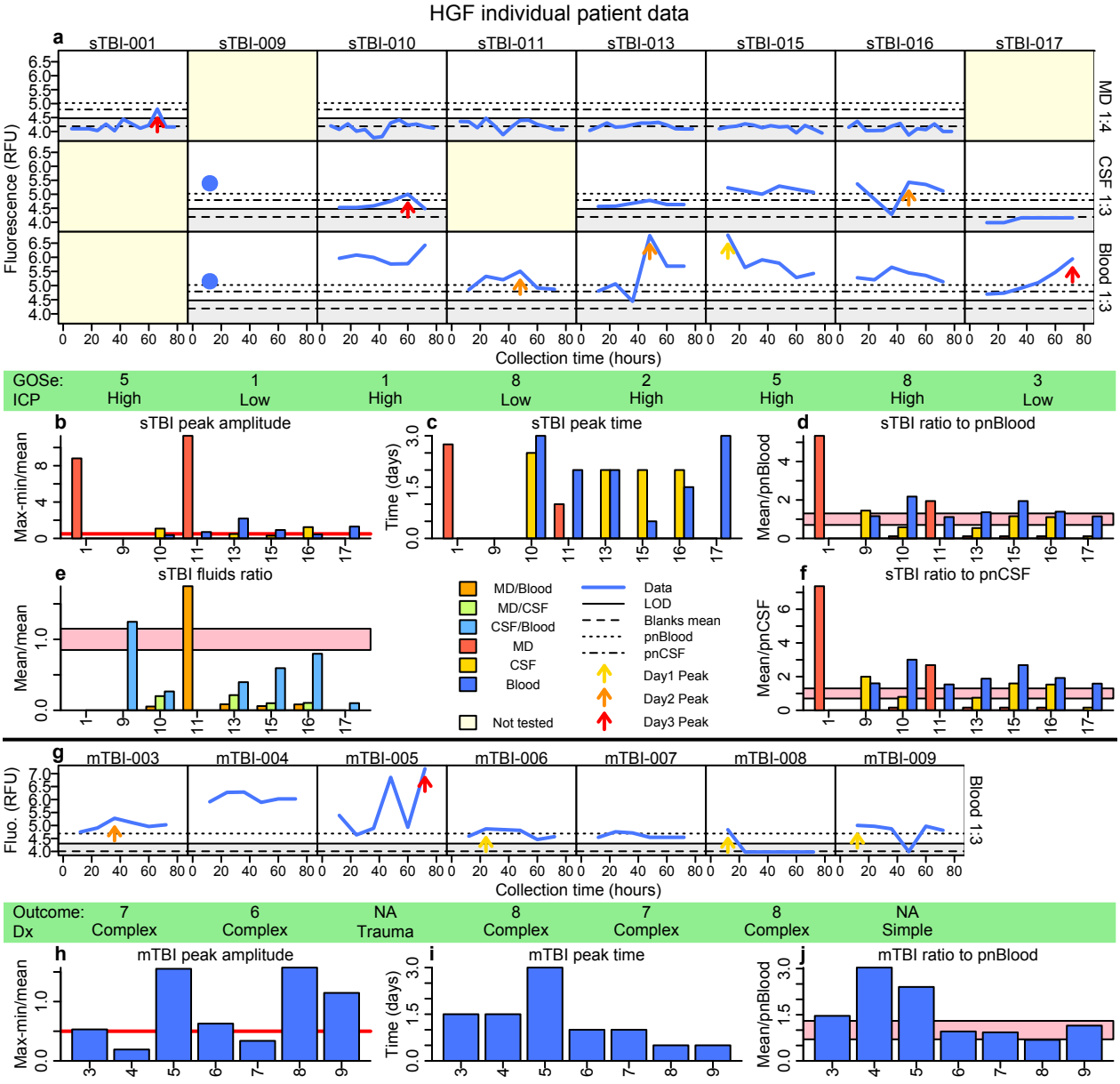

FIGURE J.S101: **Individual HGF protein profiles and peak and ratio analysis.** HGF concentration in microdialysate, CSF and blood samples of individual sTBI patients (**a**) and mTBI/trauma patients (**g**) was measured and peak amplitude and time, as well as ratio between mean time course values to value found in the pooled normal control (**b-f, h-j**) were calculated for each patient. Graphs **b-f** show calculations for individual sTBI patients, and graphs **h-j** show calculations for individual mTBI patients. Red lines in **b, h** show a threshold for a profile that is considered to have a peak, rather than being constant. The light red boxes in **d, e, f, j** show the threshold of comparison to the measured value compared.

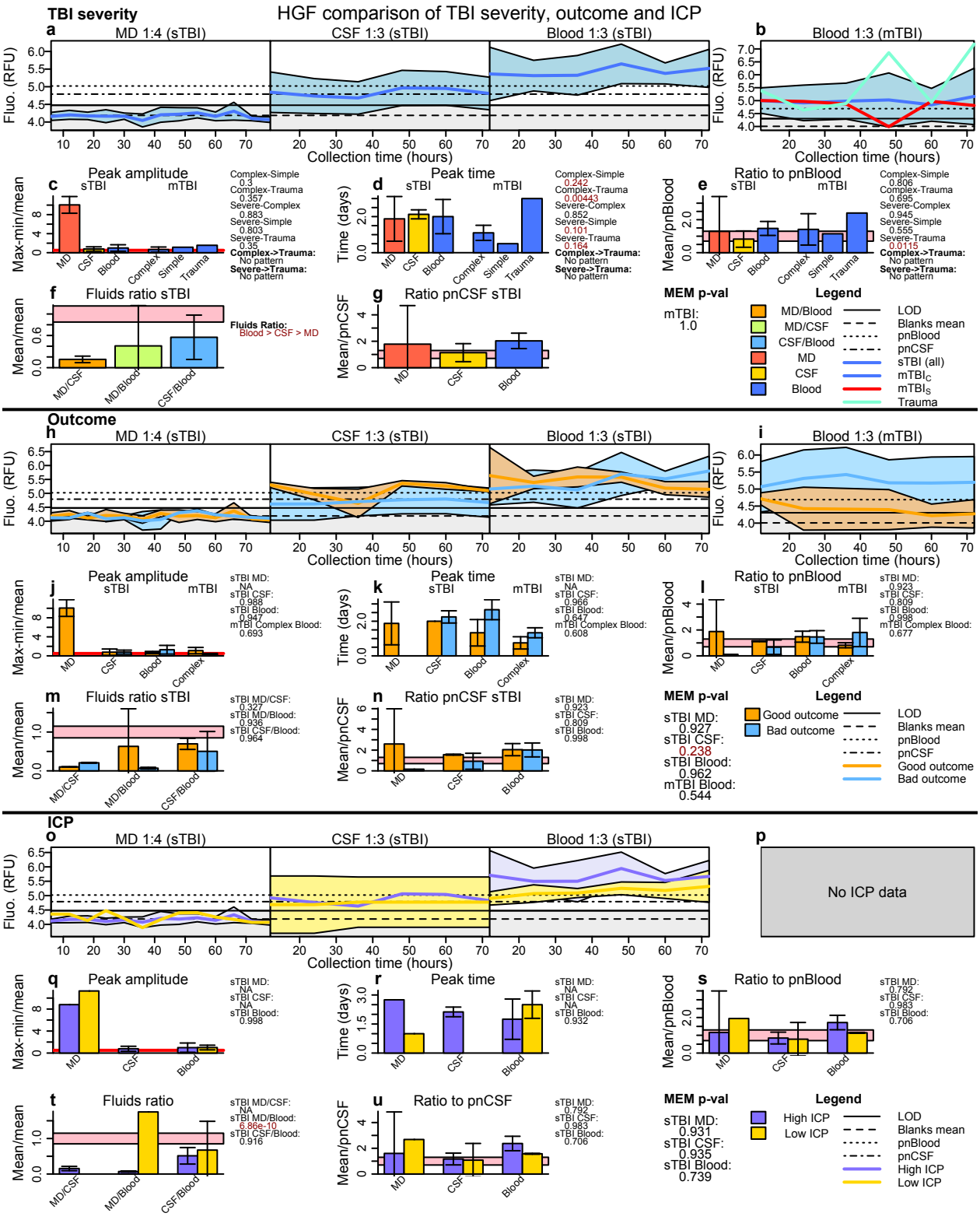

FIGURE J.S102: **Differential HGF protein profiles and peak and ratio analysis with respect to TBI severity, outcome and ICP.** Average HGF profiles are compared in terms of TBI severity (**a-g**), outcome (**h-n**) and ICP (**o-u**). Polygons in **a, b, h, i, o** indicate the mean value ±1 SD at each time point. Red lines in **c, j, q** show a threshold for a profile that is considered to have a peak, rather than being constant. The light red boxes in **e-g, l-n, s-u** show the threshold of comparison to the measured value compared. Benjamini–Hochberg adjusted p-values for comparisons are shown on the right of every graph.

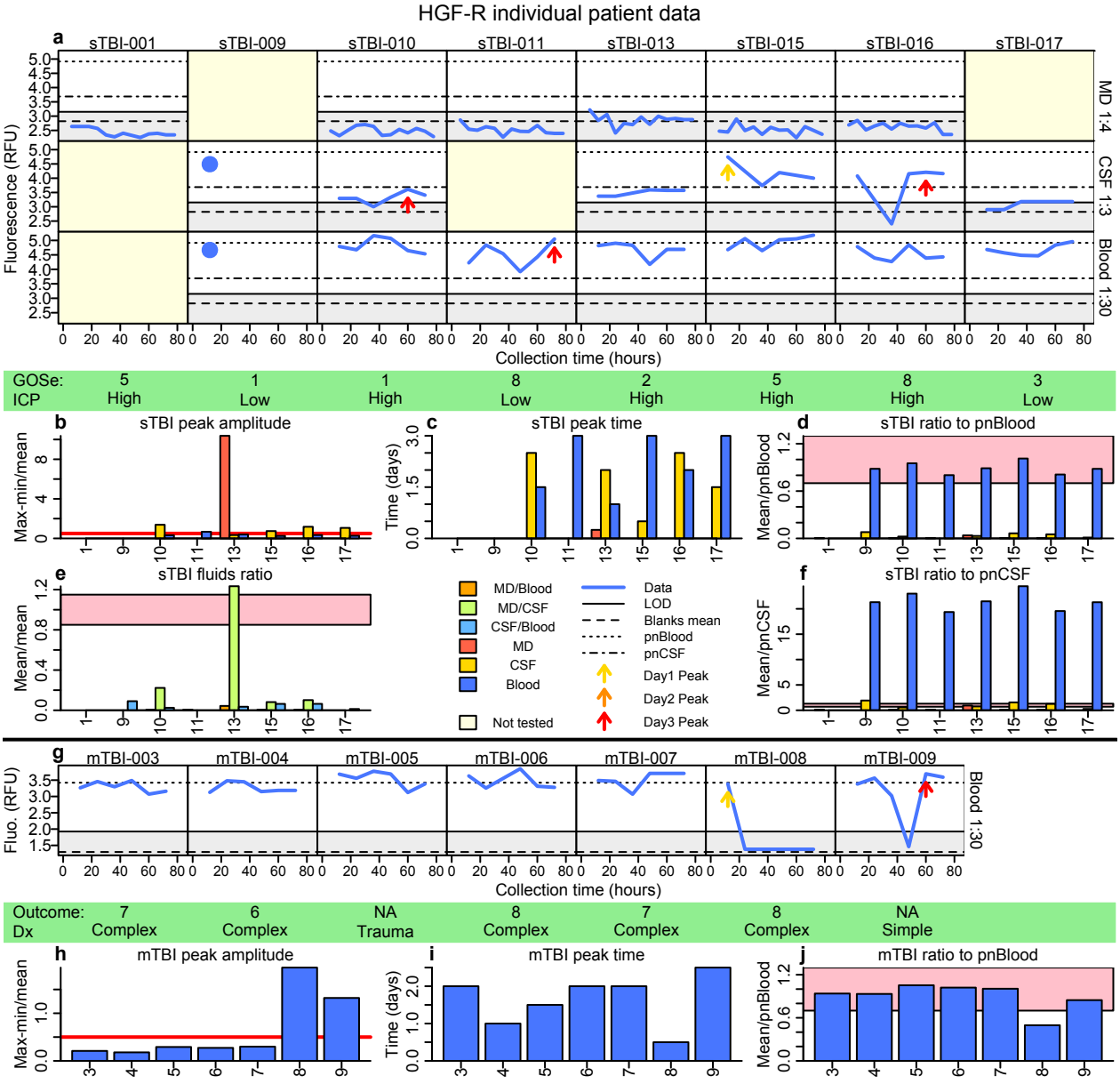

FIGURE J.S103: **Individual HGF-R protein profiles and peak and ratio analysis.** HGF-R concentration in microdialysate, CSF and blood samples of individual sTBI patients (**a**) and mTBI/trauma patients (**g**) was measured and peak amplitude and time, as well as ratio between mean time course values to value found in the pooled normal control (**b-f, h-j**) were calculated for each patient. Graphs **b-f** show calculations for individual sTBI patients, and graphs **h-j** show calculations for individual mTBI patients. Red lines in **b, h** show a threshold for a profile that is considered to have a peak, rather than being constant. The light red boxes in **d, e, f, j** show the threshold of comparison to the measured value compared.

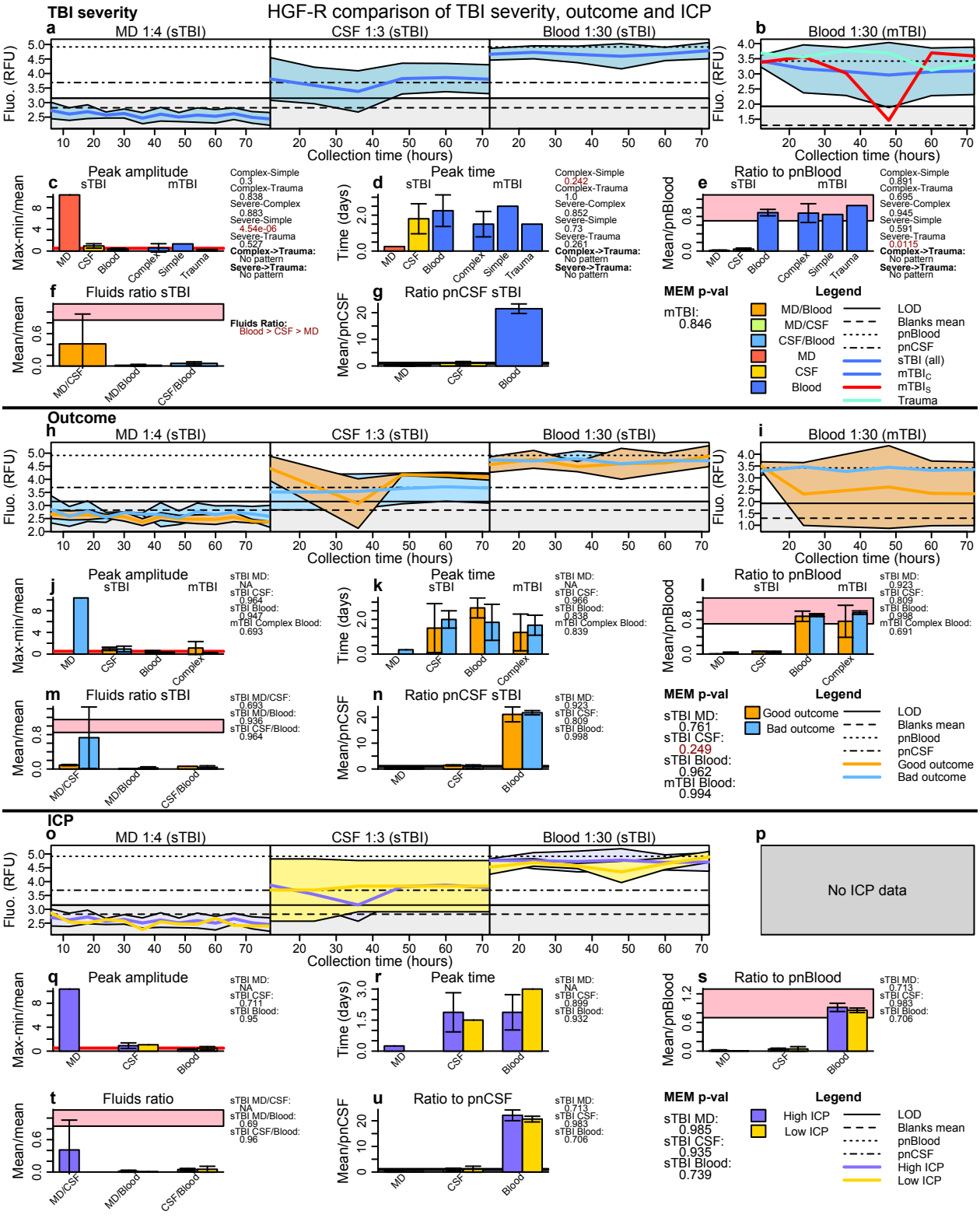

FIGURE J.S104: **Differential HGF-R protein profiles and peak and ratio analysis with respect to TBI severity, outcome and ICP.** Average HGF-R profiles are compared in terms of TBI severity (**a-g**), outcome (**h-n**) and ICP (**o-u**). Polygons in **a, b, h, i, o** indicate the mean value ±1 SD at each time point. Red lines in **c, j, q** show a threshold for a profile that is considered to have a peak, rather than being constant. The light red boxes in **e-g, l-n, s-u** show the threshold of comparison to the measured value compared. Benjamini–Hochberg adjusted p-values for comparisons are shown on the right of every graph.

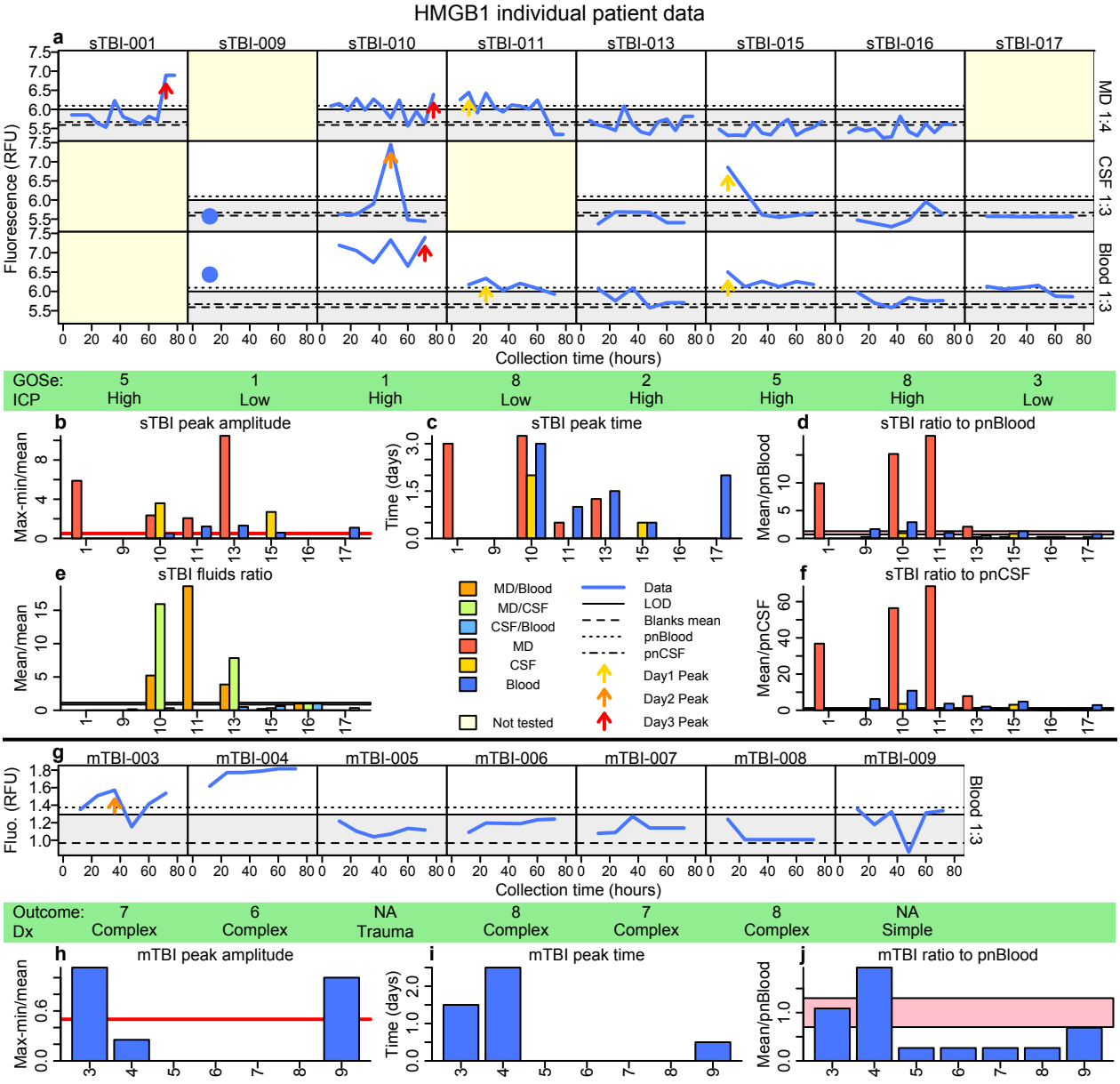

FIGURE J.S105: **Individual HMGB1 protein profiles and peak and ratio analysis.** HMGB1 concentration in microdialysate, CSF and blood samples of individual sTBI patients (**a**) and mTBI/trauma patients (**g**) was measured and peak amplitude and time, as well as ratio between mean time course values to value found in the pooled normal control (**b-f, h-j**) were calculated for each patient. Graphs **b-f** show calculations for individual sTBI patients, and graphs **h-j** show calculations for individual mTBI patients. Red lines in **b, h** show a threshold for a profile that is considered to have a peak, rather than being constant. The light red boxes in **d, e, f, j** show the threshold of comparison to the measured value compared.

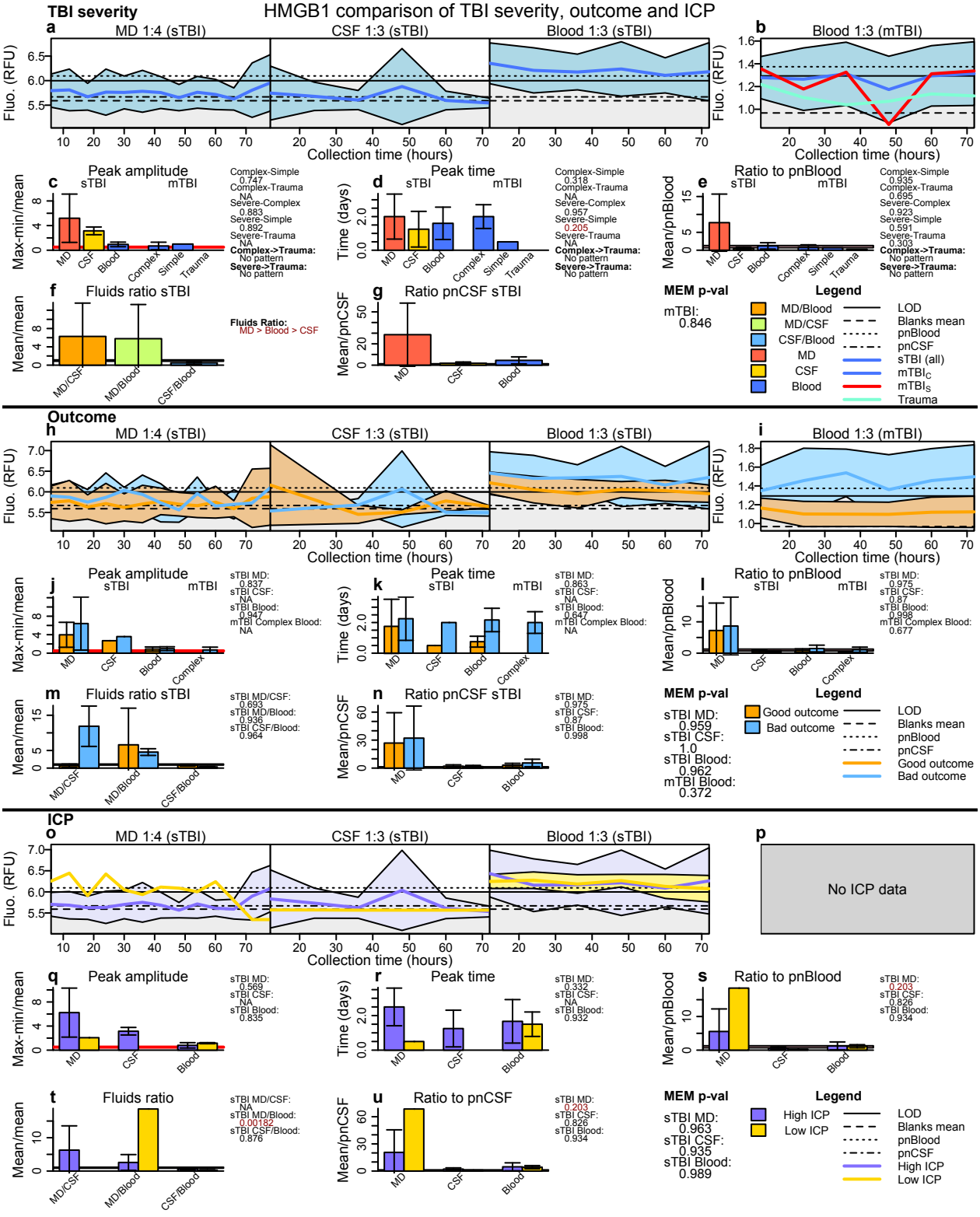

FIGURE J.S106: **Differential HMGB1 protein profiles and peak and ratio analysis with respect to TBI severity, outcome and ICP.** Average HMGB1 profiles are compared in terms of TBI severity (**a-g**), outcome (**h-n**) and ICP (**o-u**). Polygons in **a, b, h, i, o** indicate the mean value ±1 SD at each time point. Red lines in **c, j, q** show a threshold for a profile that is considered to have a peak, rather than being constant. The light red boxes in **e-g, l-n, s-u** show the threshold of comparison to the measured value compared. Benjamini–Hochberg adjusted p-values for comparisons are shown on the right of every graph.

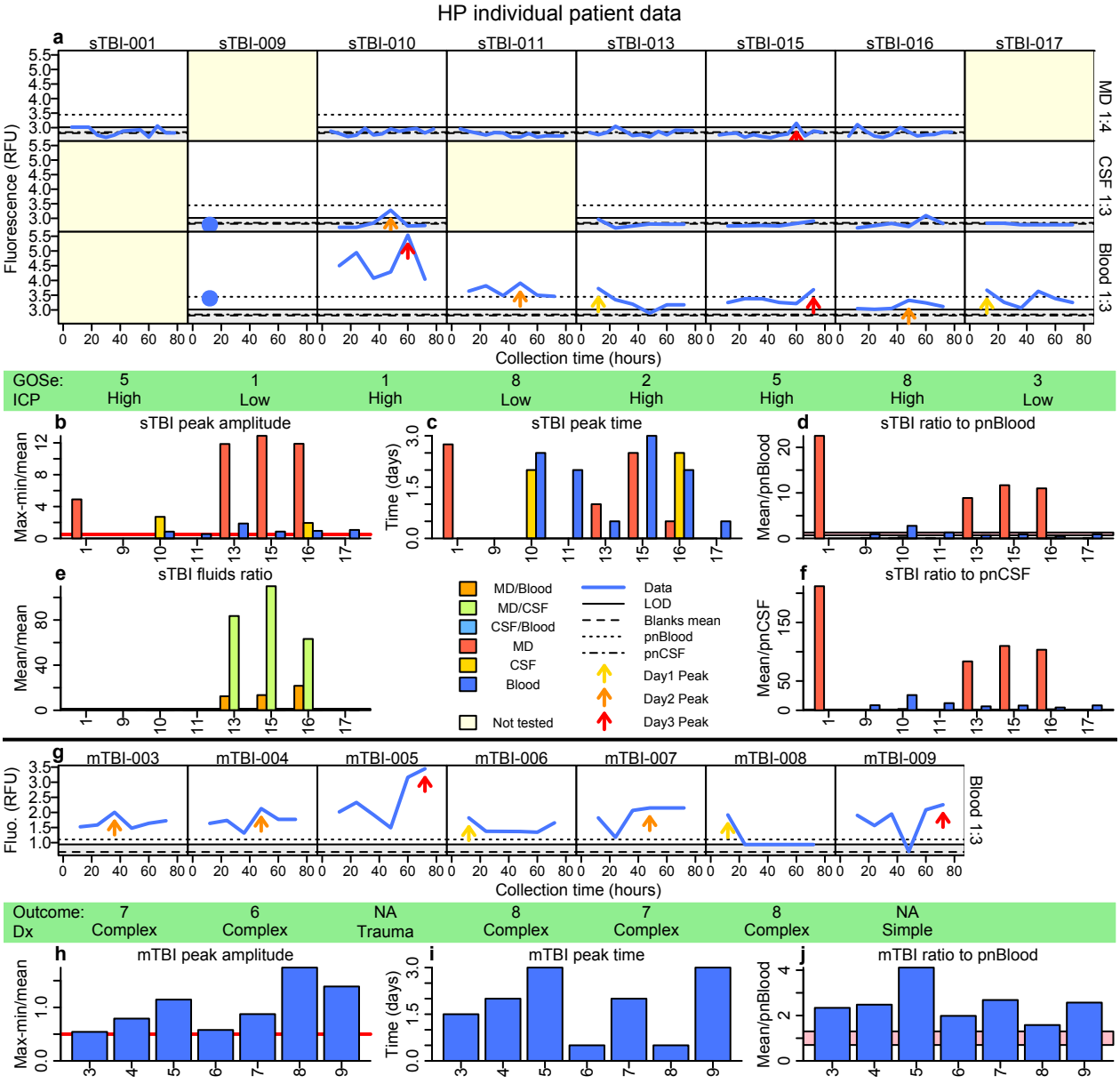

FIGURE J.S107: **Individual HP protein profiles and peak and ratio analysis.** HP concentration in microdialysate, CSF and blood samples of individual sTBI patients (**a**) and mTBI/trauma patients (**g**) was measured and peak amplitude and time, as well as ratio between mean time course values to value found in the pooled normal control (**b-f, h-j**) were calculated for each patient. Graphs **b-f** show calculations for individual sTBI patients, and graphs **h-j** show calculations for individual mTBI patients. Red lines in **b, h** show a threshold for a profile that is considered to have a peak, rather than being constant. The light red boxes in **d, e, f, j** show the threshold of comparison to the measured value compared.

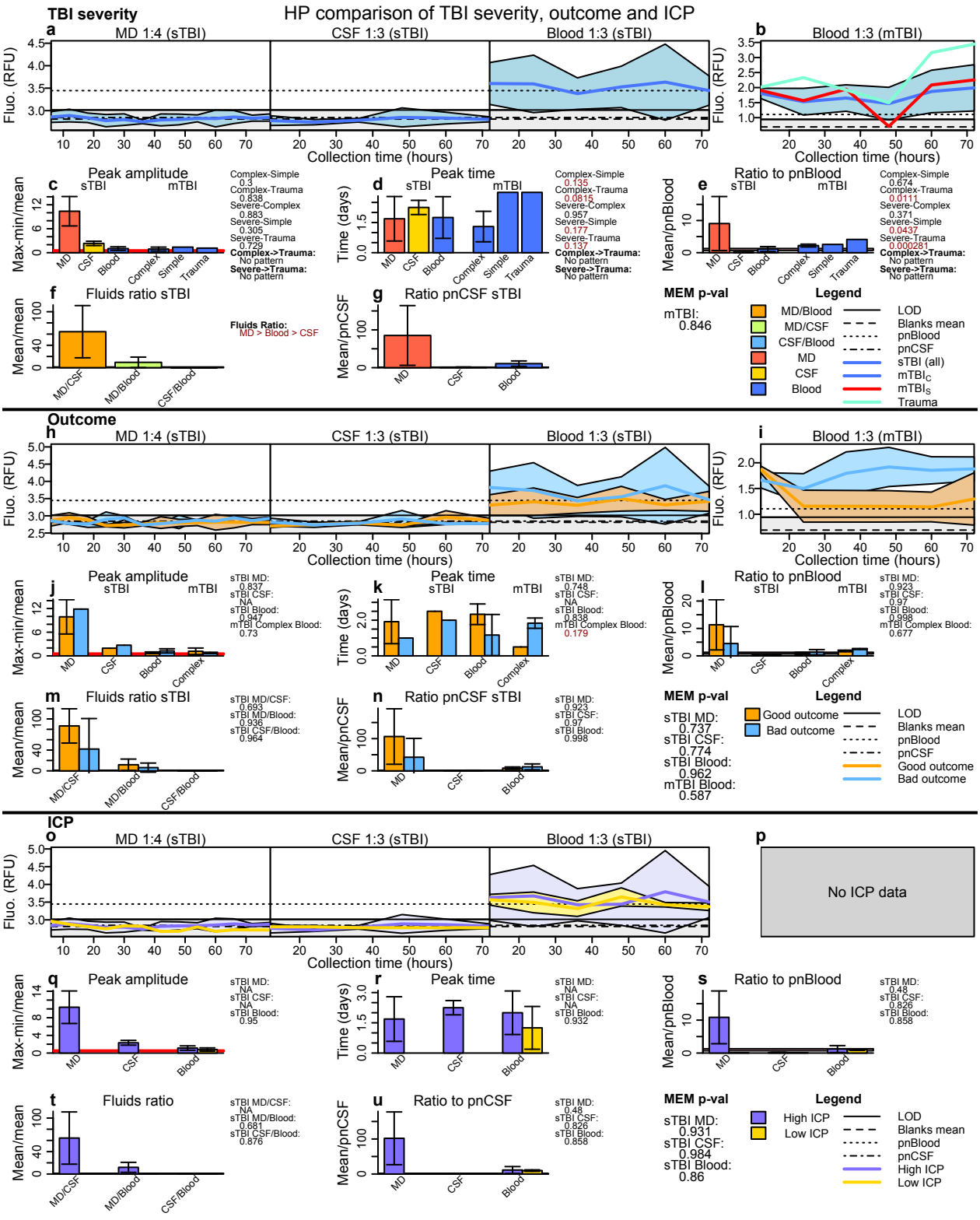

FIGURE J.S108: **Differential HP protein profiles and peak and ratio analysis with respect to TBI severity, outcome and ICP.** Average HP profiles are compared in terms of TBI severity (**a-g**), outcome (**h-n**) and ICP (**o-u**). Polygons in **a, b, h, i, o** indicate the mean value ±1 SD at each time point. Red lines in **c, j, q** show a threshold for a profile that is considered to have a peak, rather than being constant. The light red boxes in **e-g, l-n, s-u** show the threshold of comparison to the measured value compared. Benjamini–Hochberg adjusted p-values for comparisons are shown on the right of every graph.

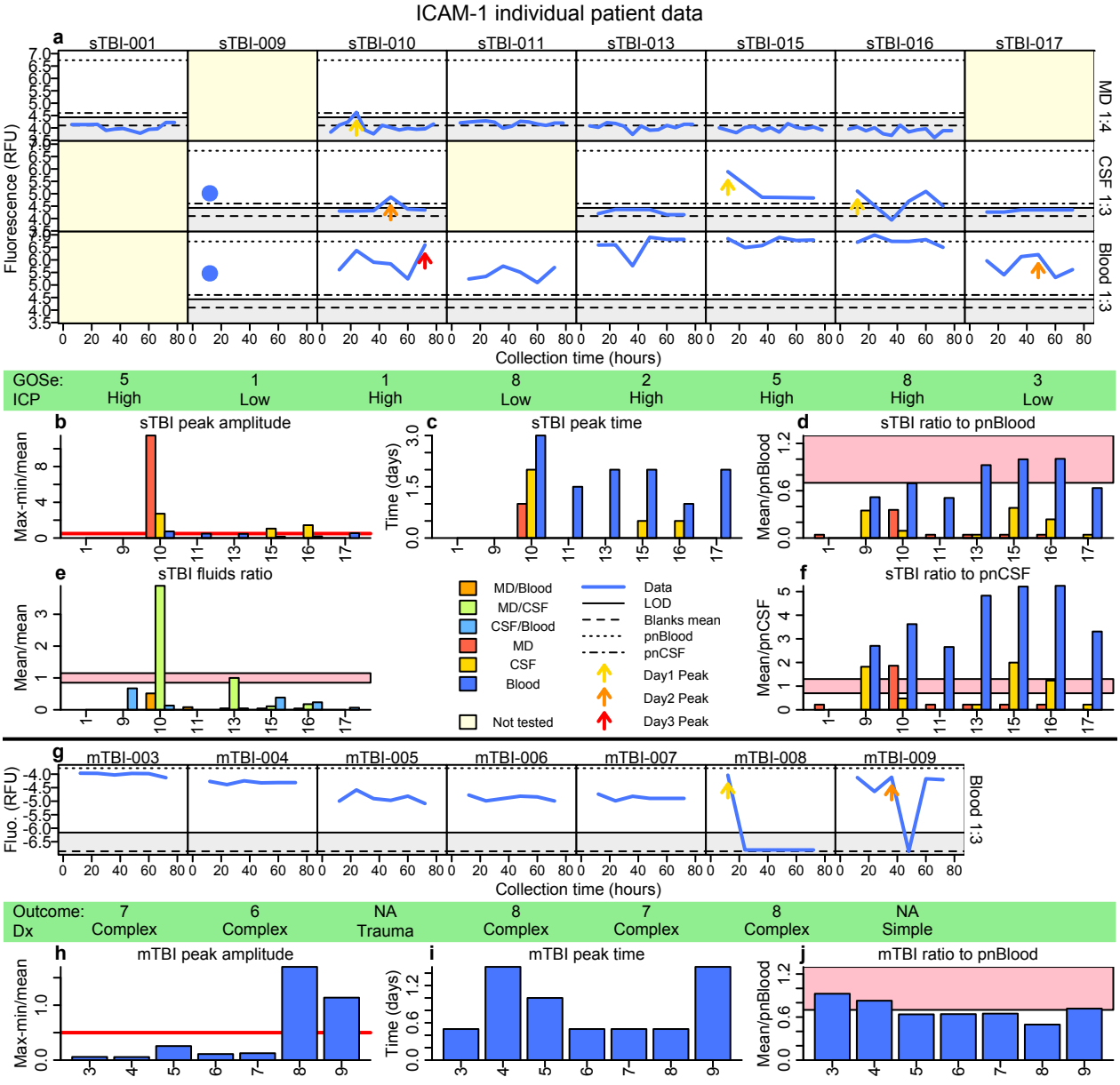

FIGURE J.S109: **Individual ICAM-1 protein profiles and peak and ratio analysis.** ICAM-1 concentration in microdialysate, CSF and blood samples of individual sTBI patients (**a**) and mTBI/trauma patients (**g**) was measured and peak amplitude and time, as well as ratio between mean time course values to value found in the pooled normal control (**b-f, h-j**) were calculated for each patient. Graphs **b-f** show calculations for individual sTBI patients, and graphs **h-j** show calculations for individual mTBI patients. Red lines in **b, h** show a threshold for a profile that is considered to have a peak, rather than being constant. The light red boxes in **d, e, f, j** show the threshold of comparison to the measured value compared.

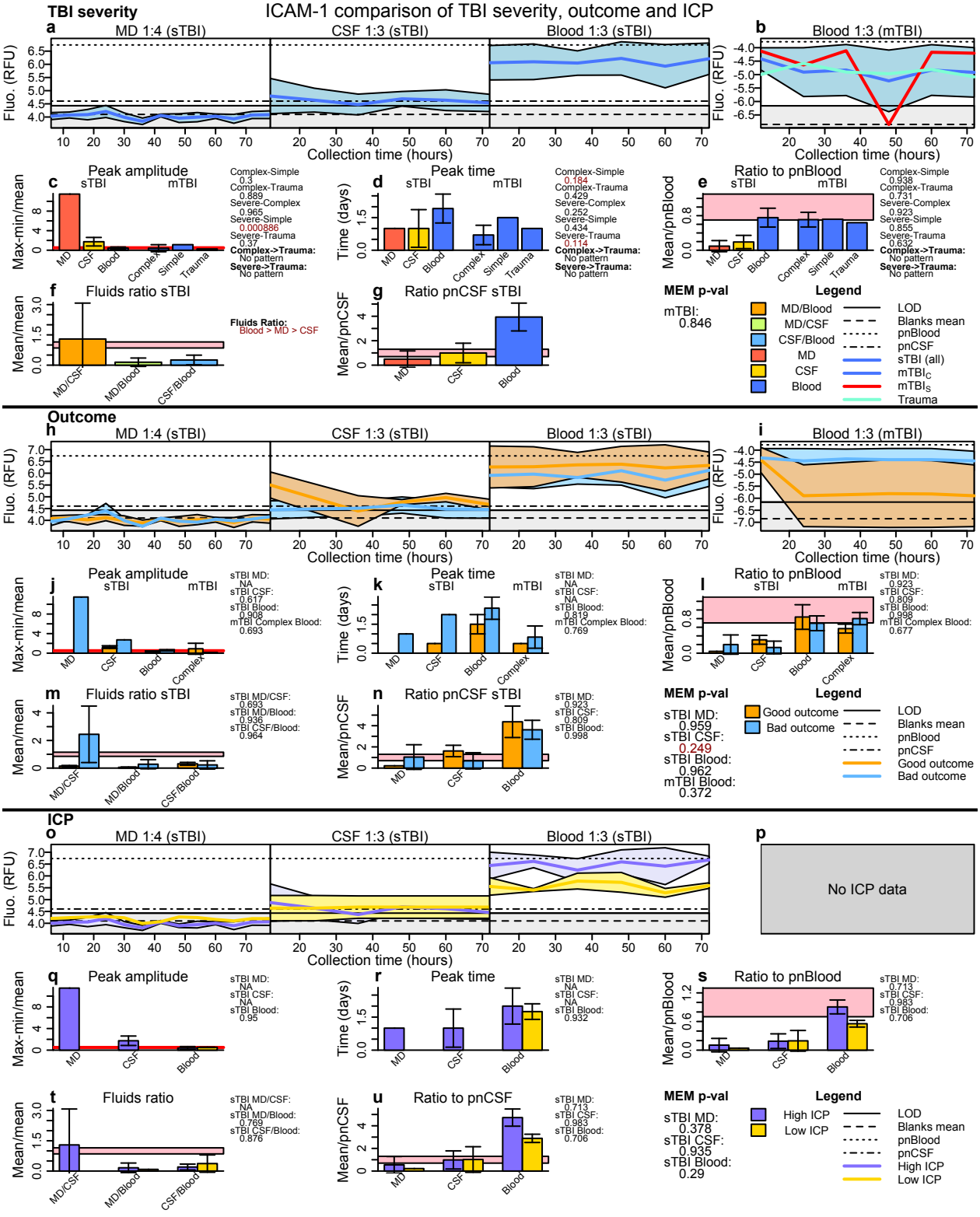

FIGURE J.S110: **Differential ICAM-1 protein profiles and peak and ratio analysis with respect to TBI severity, outcome and ICP.** Average ICAM-1 profiles are compared in terms of TBI severity (**a-g**), outcome (**h-n**) and ICP (**o-u**). Polygons in **a, b, h, i, o** indicate the mean value ±1 SD at each time point. Red lines in **c, j, q** show a threshold for a profile that is considered to have a peak, rather than being constant. The light red boxes in **e-g, l-n, s-u** show the threshold of comparison to the measured value compared. Benjamini–Hochberg adjusted p-values for comparisons are shown on the right of every graph.

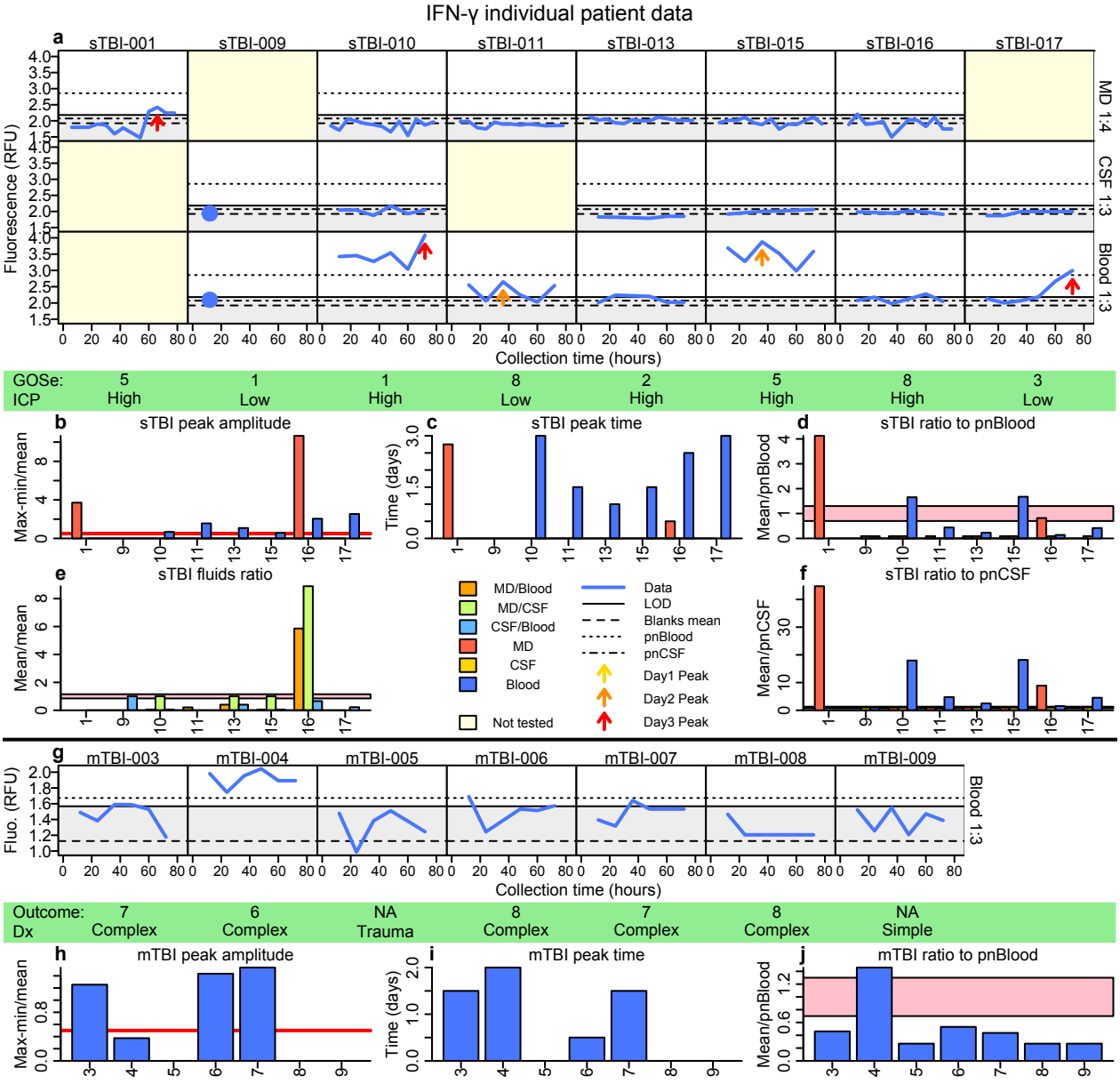

FIGURE J.S111: **Individual IFN-γ protein profiles and peak and ratio analysis.** IFN-γ concentration in microdialysate, CSF and blood samples of individual sTBI patients (**a**) and mTBI/trauma patients (**g**) was measured and peak amplitude and time, as well as ratio between mean time course values to value found in the pooled normal control (**b-f, h-j**) were calculated for each patient. Graphs **b-f** show calculations for individual sTBI patients, and graphs **h-j** show calculations for individual mTBI patients. Red lines in **b, h** show a threshold for a profile that is considered to have a peak, rather than being constant. The light red boxes in **d, e, f, j** show the threshold of comparison to the measured value compared.

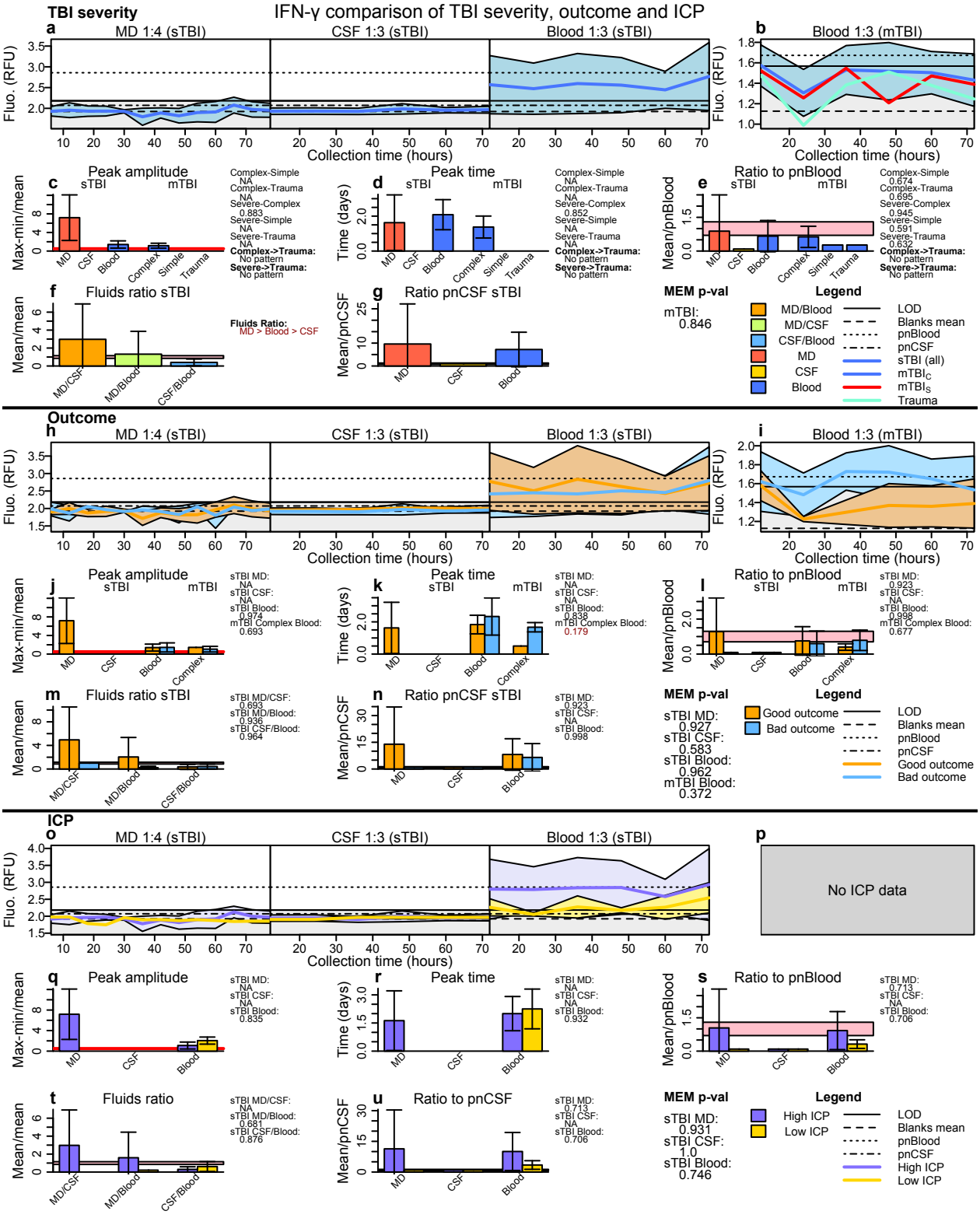

FIGURE J.S112: **Differential IFN-γ protein profiles and peak and ratio analysis with respect to TBI severity, outcome and ICP.** Average IFN-γ profiles are compared in terms of TBI severity (**a-g**), outcome (**h-n**) and ICP (**o-u**). Polygons in **a, b, h, i, o** indicate the mean value ± 1 SD at each time point. Red lines in **c, j, q** show a threshold for a profile that is considered to have a peak, rather than being constant. The light red boxes in **e-g, l-n, s-u** show the threshold of comparison to the measured value compared. Benjamini–Hochberg adjusted p-values for comparisons are shown on the right of every graph.

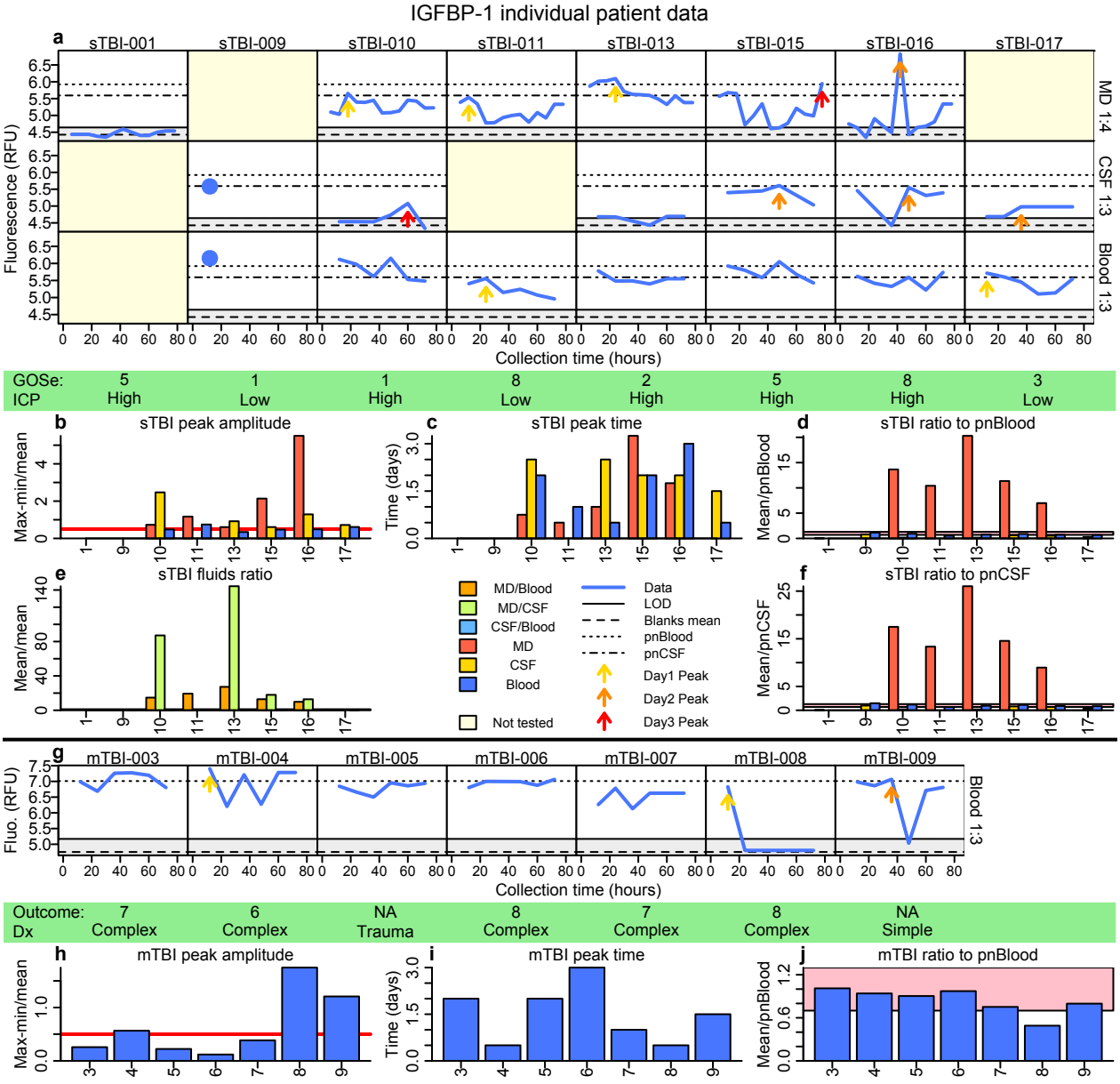

FIGURE J.S113: **Individual IGFBP-1 protein profiles and peak and ratio analysis.** IGFBP-1 concentration in microdialysate, CSF and blood samples of individual sTBI patients (**a**) and mTBI/trauma patients (**g**) was measured and peak amplitude and time, as well as ratio between mean time course values to value found in the pooled normal control (**b-f, h-j**) were calculated for each patient. Graphs **b-f** show calculations for individual sTBI patients, and graphs **h-j** show calculations for individual mTBI patients. Red lines in **b, h** show a threshold for a profile that is considered to have a peak, rather than being constant. The light red boxes in **d, e, f, j** show the threshold of comparison to the measured value compared.

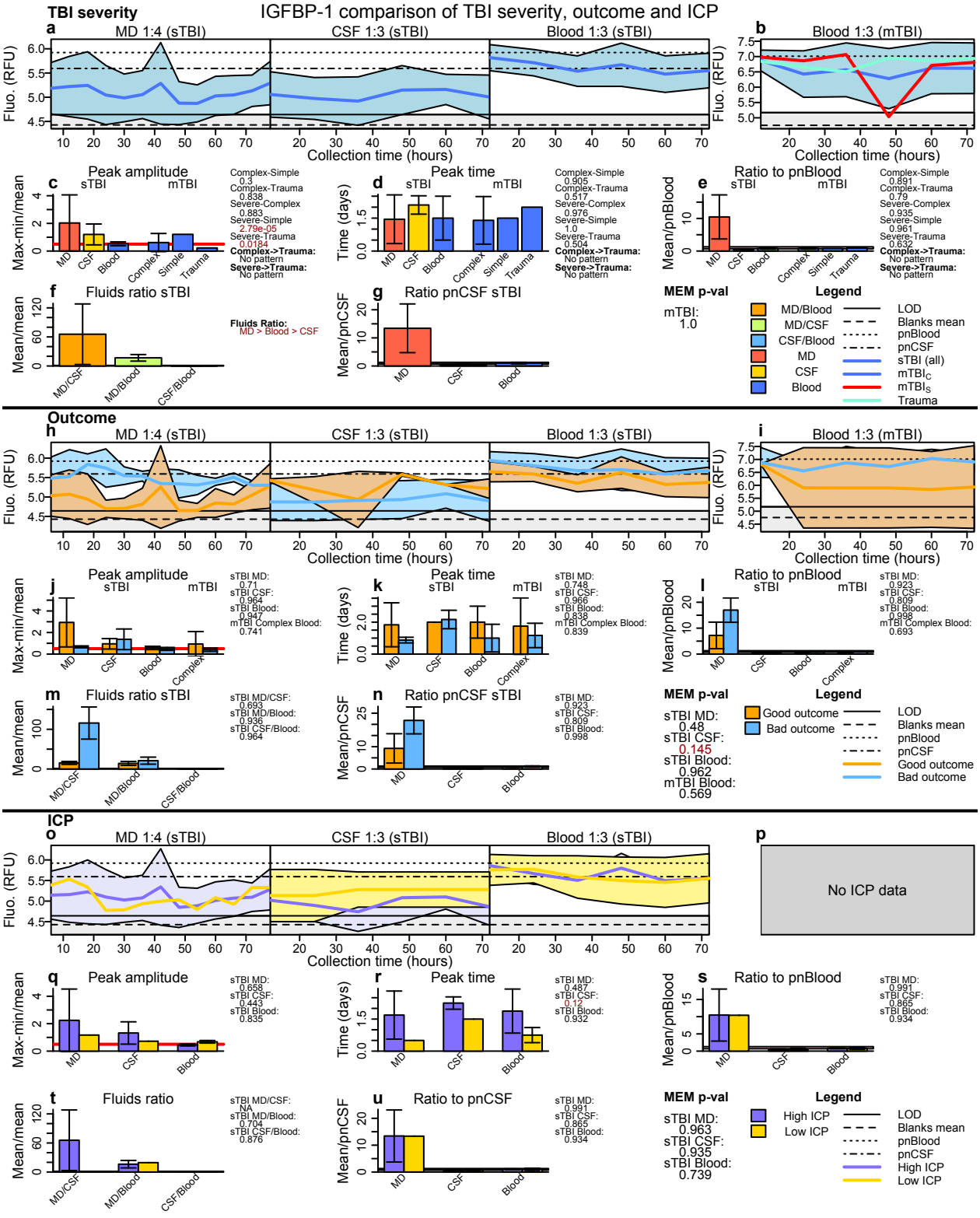

FIGURE J.S114: **Differential IGFBP-1 protein profiles and peak and ratio analysis with respect to TBI severity, outcome and ICP.** Average IGFBP-1 profiles are compared in terms of TBI severity (**a-g**), outcome (**h-n**) and ICP (**o-u**). Polygons in **a, b, h, i, o** indicate the mean value ±1 SD at each time point. Red lines in **c, j, q** show a threshold for a profile that is considered to have a peak, rather than being constant. The light red boxes in **e-g, l-n, s-u** show the threshold of comparison to the measured value compared. Benjamini–Hochberg adjusted p-values for comparisons are shown on the right of every graph.

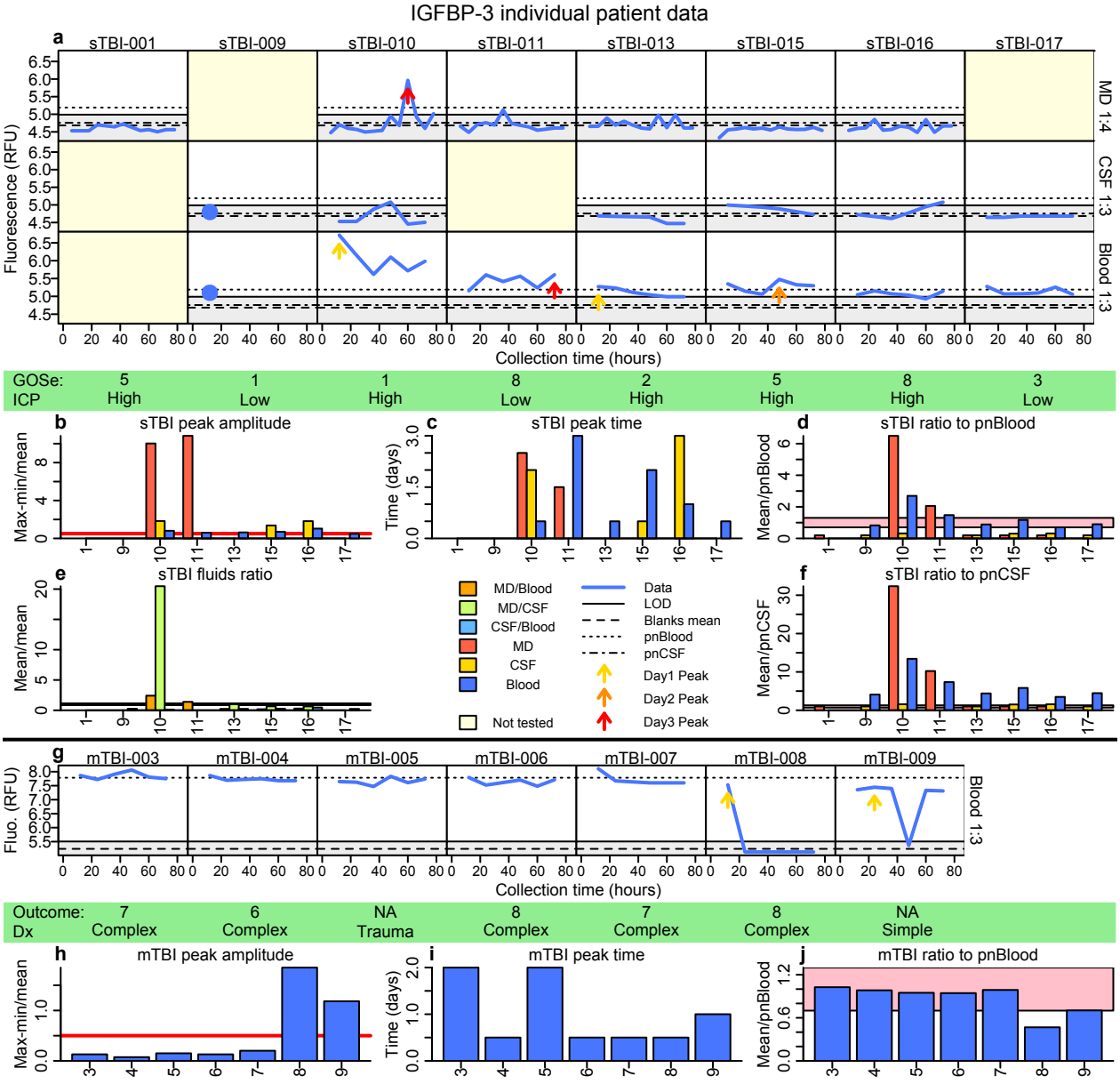

FIGURE J.S115: **Individual IGFBP-3 protein profiles and peak and ratio analysis.** IGFBP-3 concentration in microdialysate, CSF and blood samples of individual sTBI patients (**a**) and mTBI/trauma patients (**g**) was measured and peak amplitude and time, as well as ratio between mean time course values to value found in the pooled normal control (**b-f, h-j**) were calculated for each patient. Graphs **b-f** show calculations for individual sTBI patients, and graphs **h-j** show calculations for individual mTBI patients. Red lines in **b, h** show a threshold for a profile that is considered to have a peak, rather than being constant. The light red boxes in **d, e, f, j** show the threshold of comparison to the measured value compared.

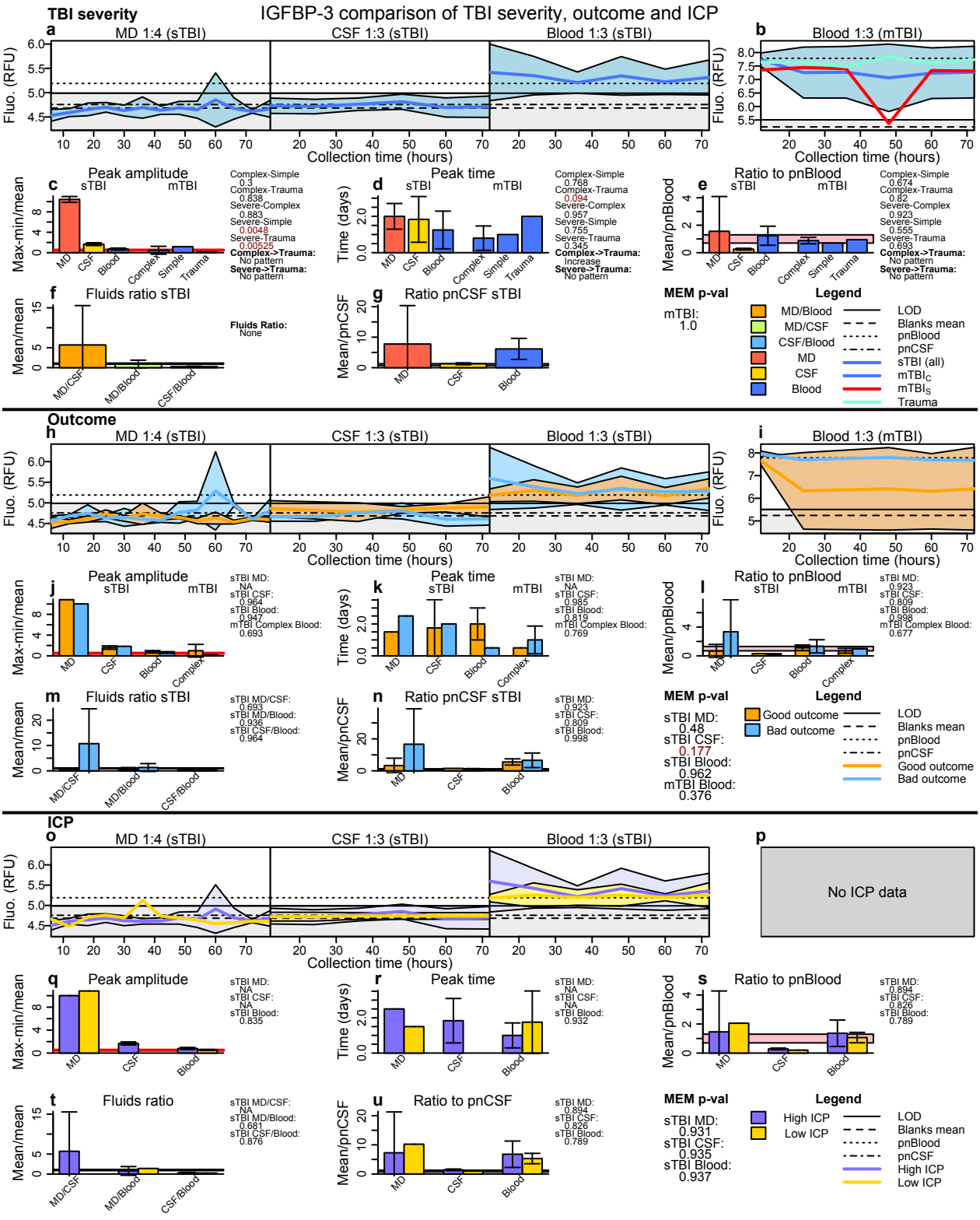

FIGURE J.S116: **Differential IGFBP-3 protein profiles and peak and ratio analysis with respect to TBI severity, outcome and ICP.** Average IGFBP-3 profiles are compared in terms of TBI severity (**a-g**), outcome (**h-n**) and ICP (**o-u**). Polygons in **a, b, h, i, o** indicate the mean value ±1 SD at each time point. Red lines in **c, j, q** show a threshold for a profile that is considered to have a peak, rather than being constant. The light red boxes in **e-g, l-n, s-u** show the threshold of comparison to the measured value compared. Benjamini–Hochberg adjusted p-values for comparisons are shown on the right of every graph.

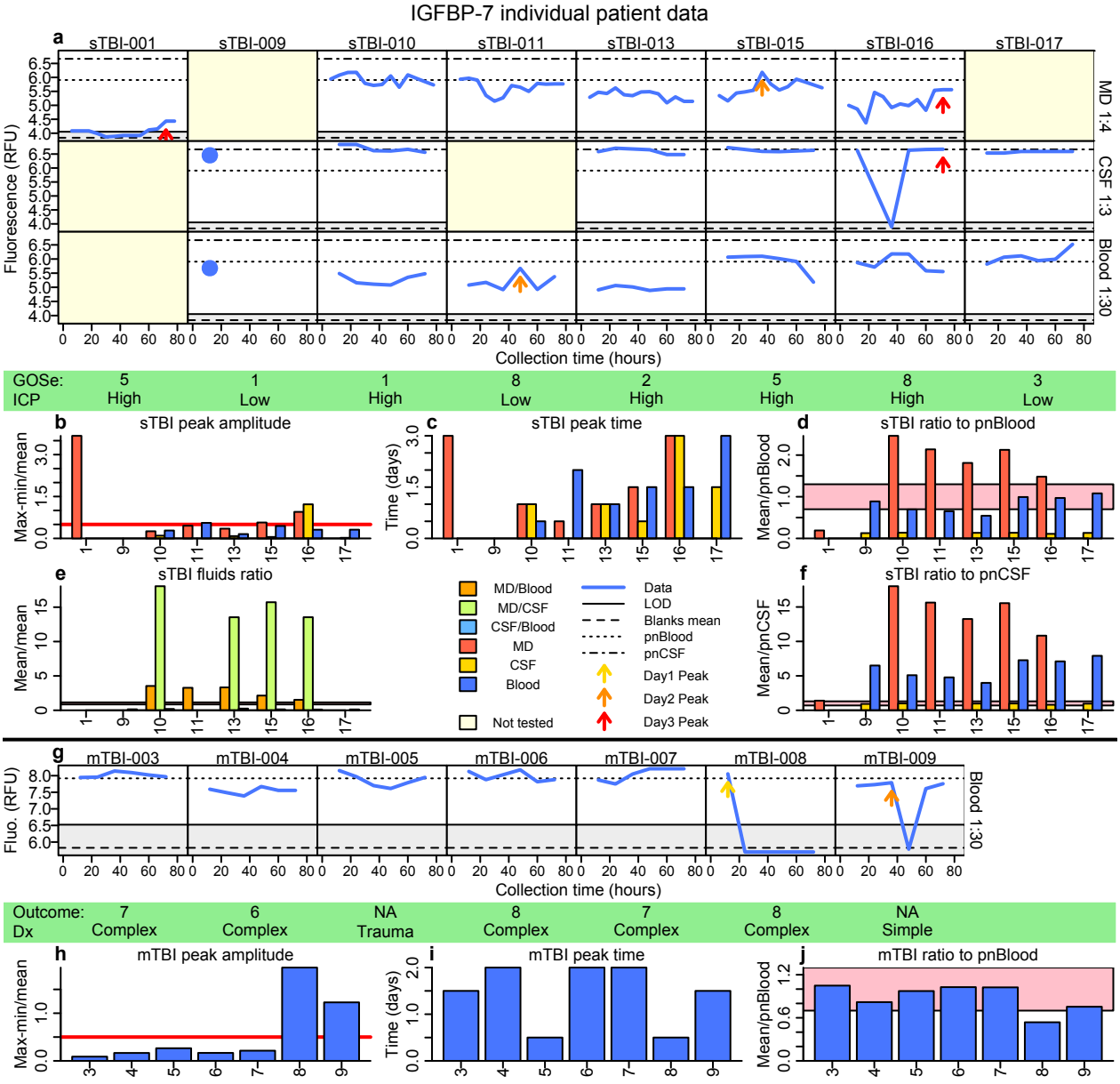

FIGURE J.S117: **Individual IGFBP-7 protein profiles and peak and ratio analysis.** IGFBP-7 concentration in microdialysate, CSF and blood samples of individual sTBI patients (**a**) and mTBI/trauma patients (**g**) was measured and peak amplitude and time, as well as ratio between mean time course values to value found in the pooled normal control (**b-f, h-j**) were calculated for each patient. Graphs **b-f** show calculations for individual sTBI patients, and graphs **h-j** show calculations for individual mTBI patients. Red lines in **b, h** show a threshold for a profile that is considered to have a peak, rather than being constant. The light red boxes in **d, e, f, j** show the threshold of comparison to the measured value compared.

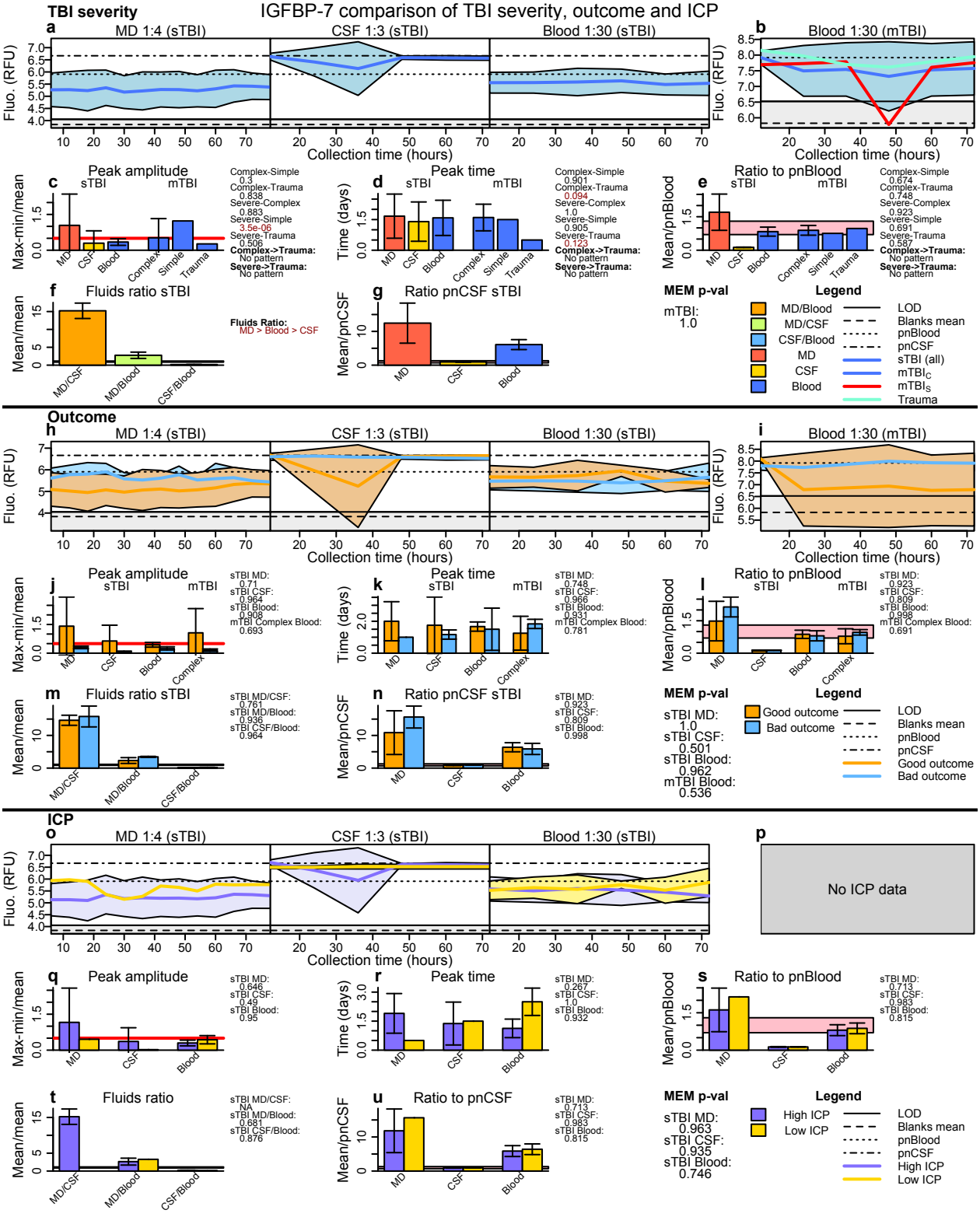

FIGURE J.S118: **Differential IGFBP-7 protein profiles and peak and ratio analysis with respect to TBI severity, outcome and ICP.** Average IGFBP-7 profiles are compared in terms of TBI severity (**a-g**), outcome (**h-n**) and ICP (**o-u**). Polygons in **a, b, h, i, o** indicate the mean value ±1 SD at each time point. Red lines in **c, j, q** show a threshold for a profile that is considered to have a peak, rather than being constant. The light red boxes in **e-g, l-n, s-u** show the threshold of comparison to the measured value compared. Benjamini–Hochberg adjusted p-values for comparisons are shown on the right of every graph.

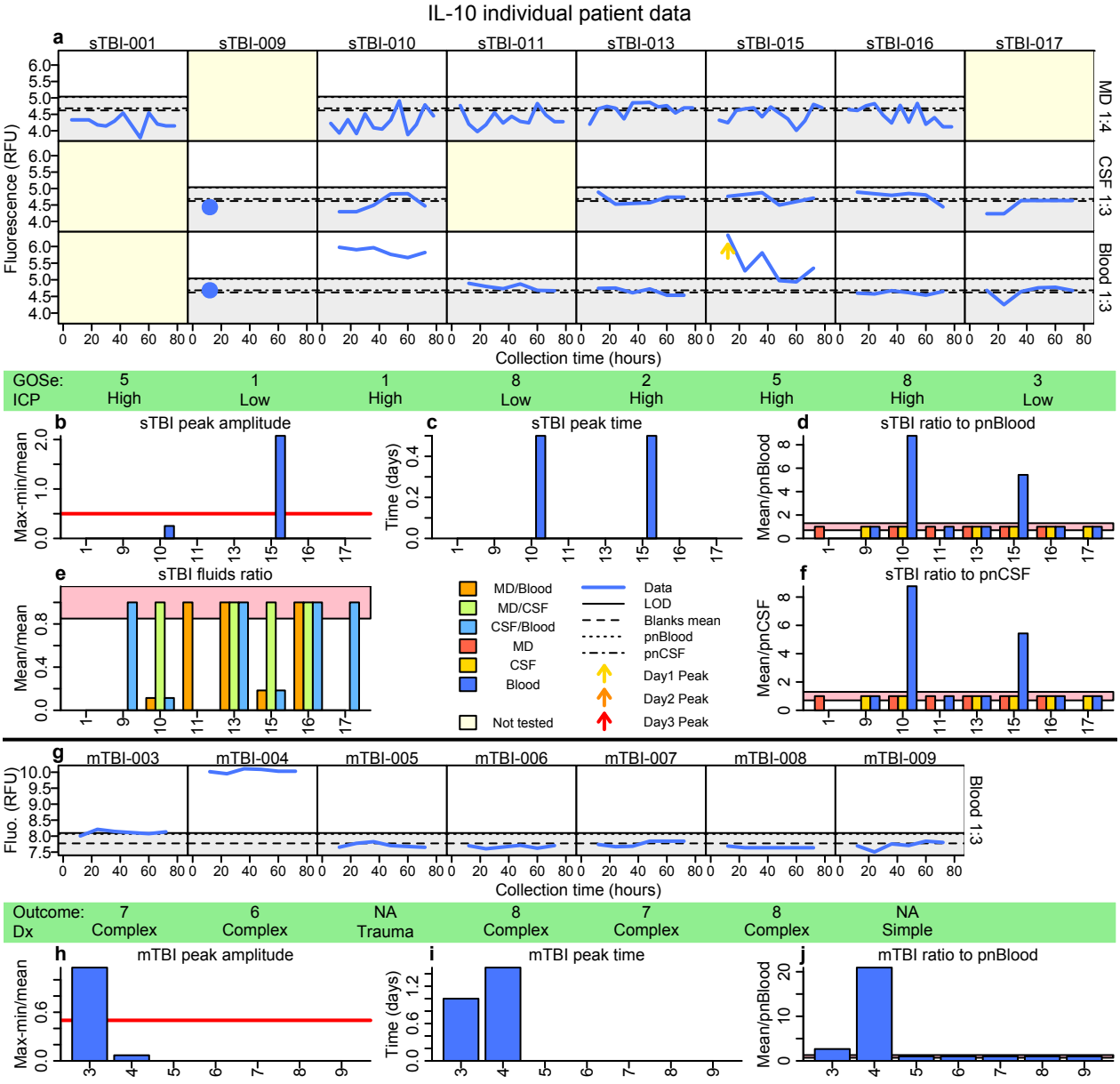

FIGURE J.S119: **Individual IL-10 protein profiles and peak and ratio analysis.** IL-10 concentration in microdialysate, CSF and blood samples of individual sTBI patients (**a**) and mTBI/trauma patients (**g**) was measured and peak amplitude and time, as well as ratio between mean time course values to value found in the pooled normal control (**b-f, h-j**) were calculated for each patient. Graphs **b-f** show calculations for individual sTBI patients, and graphs **h-j** show calculations for individual mTBI patients. Red lines in **b, h** show a threshold for a profile that is considered to have a peak, rather than being constant. The light red boxes in **d, e, f, j** show the threshold of comparison to the measured value compared.

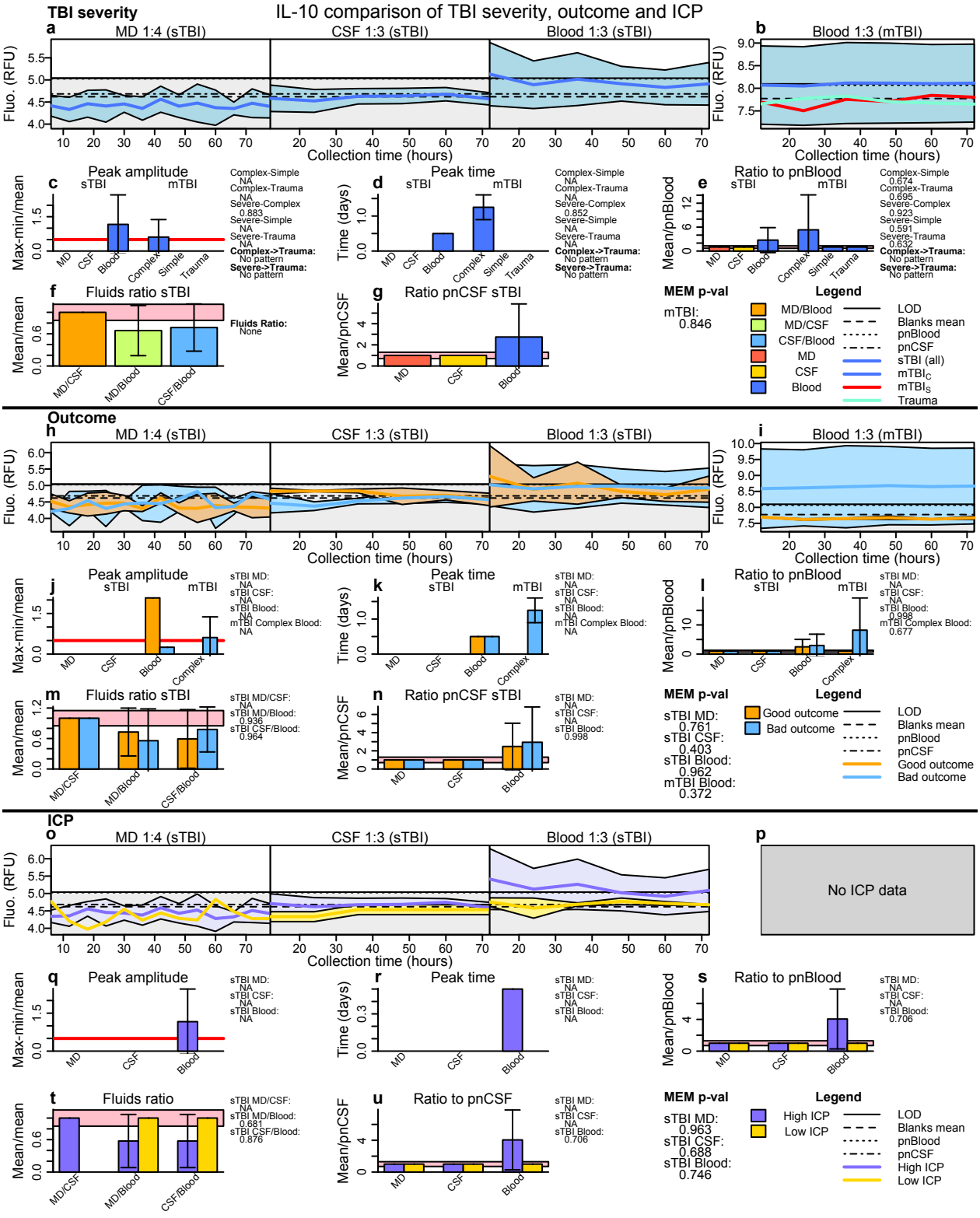

FIGURE J.S120: **Differential IL-10 protein profiles and peak and ratio analysis with respect to TBI severity, outcome and ICP.** Average IL-10 profiles are compared in terms of TBI severity (**a-g**), outcome (**h-n**) and ICP (**o-u**). Polygons in **a, b, h, i, o** indicate the mean value ±1 SD at each time point. Red lines in **c, j, q** show a threshold for a profile that is considered to have a peak, rather than being constant. The light red boxes in **e-g, l-n, s-u** show the threshold of comparison to the measured value compared. Benjamini–Hochberg adjusted p-values for comparisons are shown on the right of every graph.

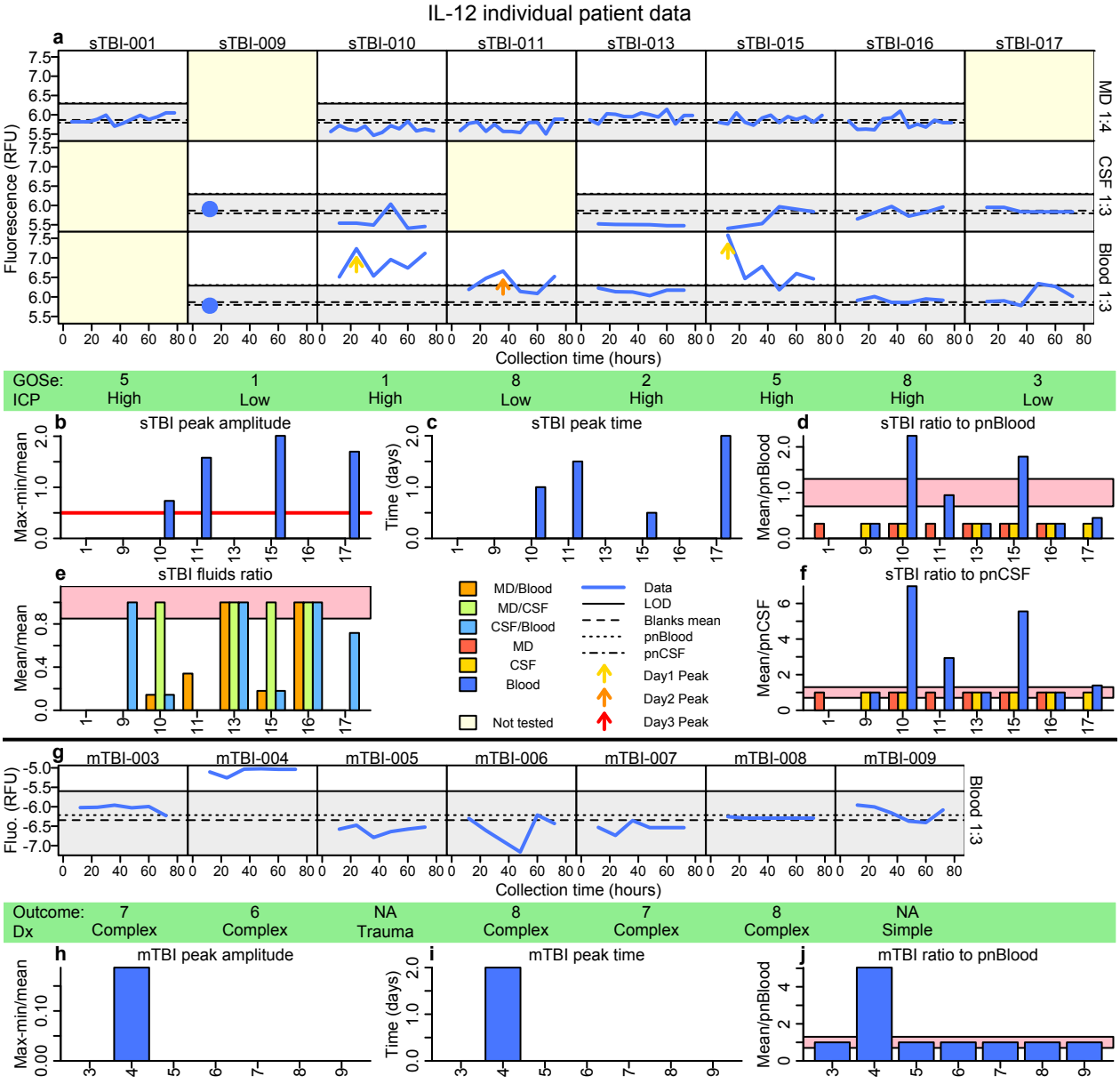

FIGURE J.S121: **Individual IL-12 protein profiles and peak and ratio analysis.** IL-12 concentration in microdialysate, CSF and blood samples of individual sTBI patients (**a**) and mTBI/trauma patients (**g**) was measured and peak amplitude and time, as well as ratio between mean time course values to value found in the pooled normal control (**b-f, h-j**) were calculated for each patient. Graphs **b-f** show calculations for individual sTBI patients, and graphs **h-j** show calculations for individual mTBI patients. Red lines in **b, h** show a threshold for a profile that is considered to have a peak, rather than being constant. The light red boxes in **d, e, f, j** show the threshold of comparison to the measured value compared.

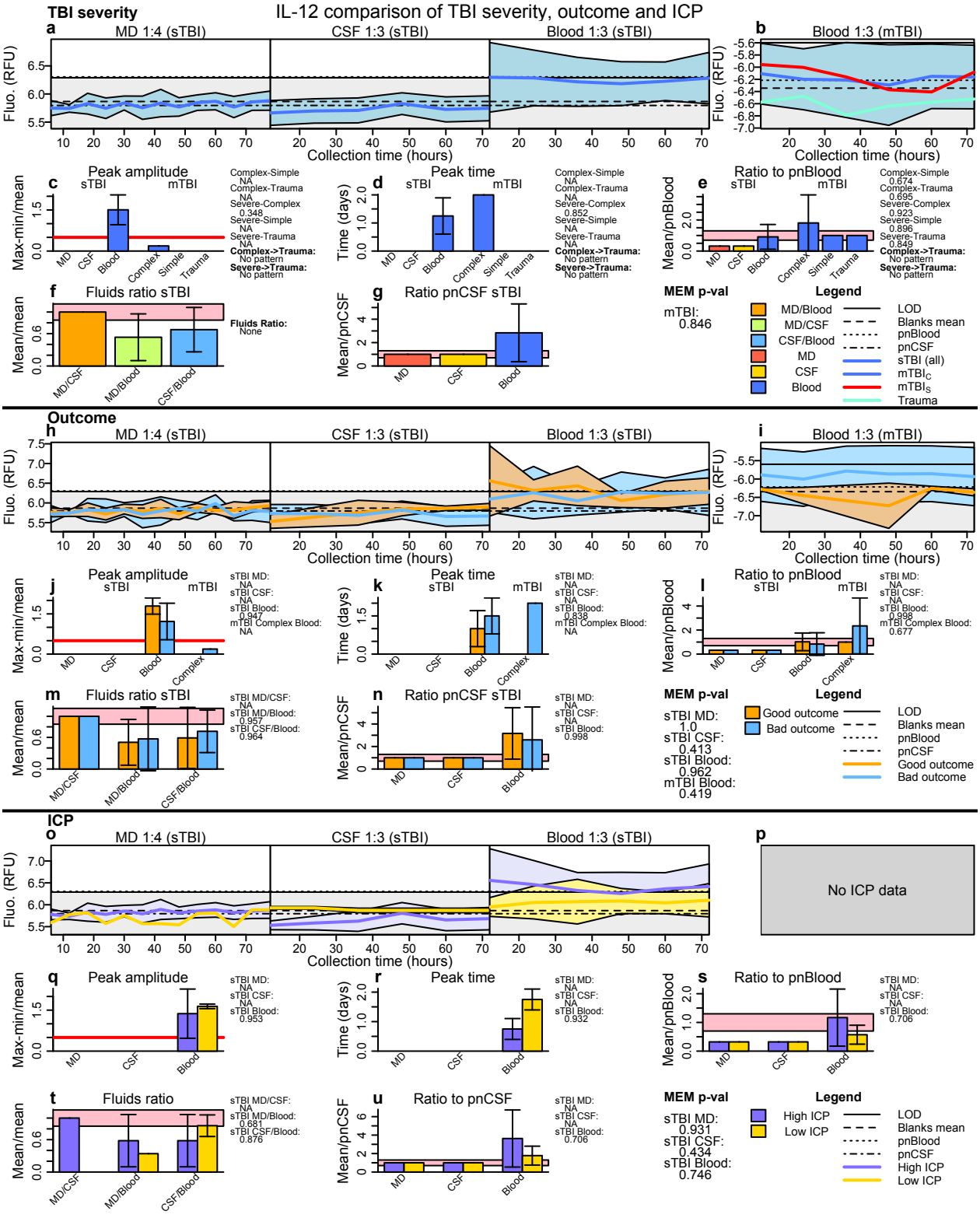

FIGURE J.S122: **Differential IL-12 protein profiles and peak and ratio analysis with respect to TBI severity, outcome and ICP.** Average IL-12 profiles are compared in terms of TBI severity (**a-g**), outcome (**h-n**) and ICP (**o-u**). Polygons in **a, b, h, i, o** indicate the mean value ±1 SD at each time point. Red lines in **c, j, q** show a threshold for a profile that is considered to have a peak, rather than being constant. The light red boxes in **e-g, l-n, s-u** show the threshold of comparison to the measured value compared. Benjamini–Hochberg adjusted p-values for comparisons are shown on the right of every graph.

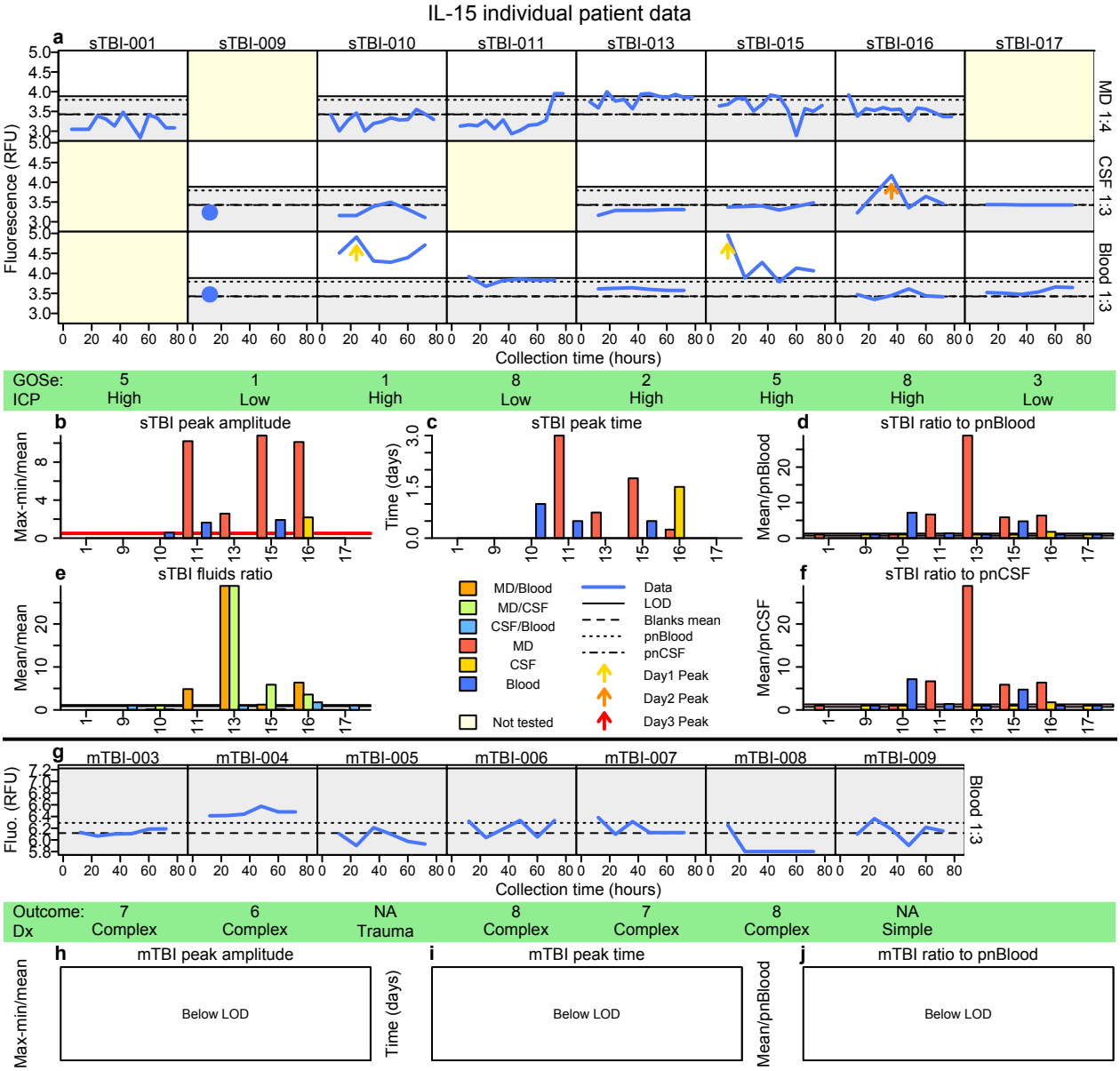

FIGURE J.S123: **Individual IL-15 protein profiles and peak and ratio analysis.** IL-15 concentration in microdialysate, CSF and blood samples of individual sTBI patients (**a**) and mTBI/trauma patients (**g**) was measured and peak amplitude and time, as well as ratio between mean time course values to value found in the pooled normal control (**b-f, h-j**) were calculated for each patient. Graphs **b-f** show calculations for individual sTBI patients, and graphs **h-j** show calculations for individual mTBI patients. Red lines in **b, h** show a threshold for a profile that is considered to have a peak, rather than being constant. The light red boxes in **d, e, f, j** show the threshold of comparison to the measured value compared.

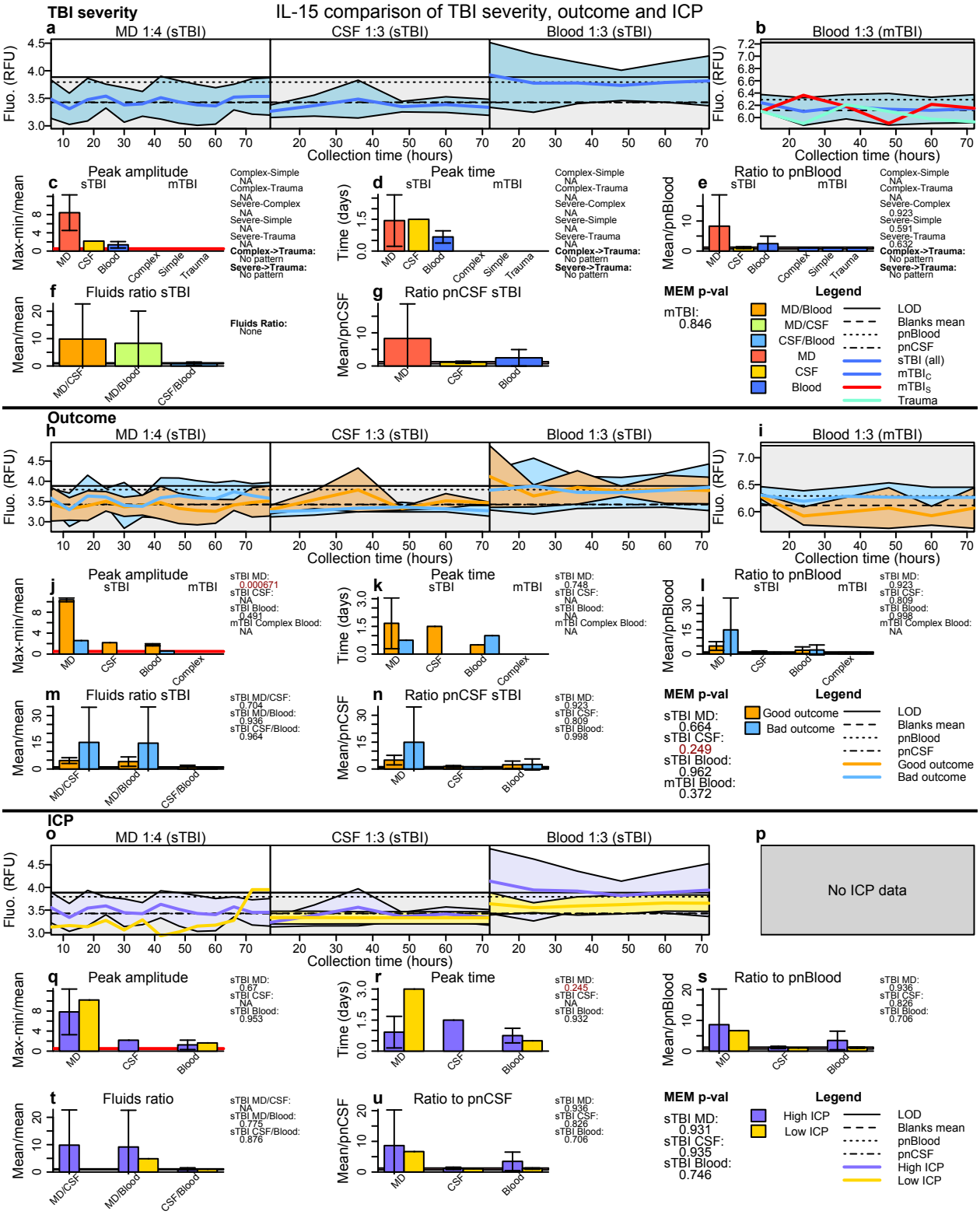

FIGURE J.S124: **Differential IL-15 protein profiles and peak and ratio analysis with respect to TBI severity, outcome and ICP.** Average IL-15 profiles are compared in terms of TBI severity (**a-g**), outcome (**h-n**) and ICP (**o-u**). Polygons in **a, b, h, i, o** indicate the mean value ±1 SD at each time point. Red lines in **c, j, q** show a threshold for a profile that is considered to have a peak, rather than being constant. The light red boxes in **e-g, l-n, s-u** show the threshold of comparison to the measured value compared. Benjamini–Hochberg adjusted p-values for comparisons are shown on the right of every graph.

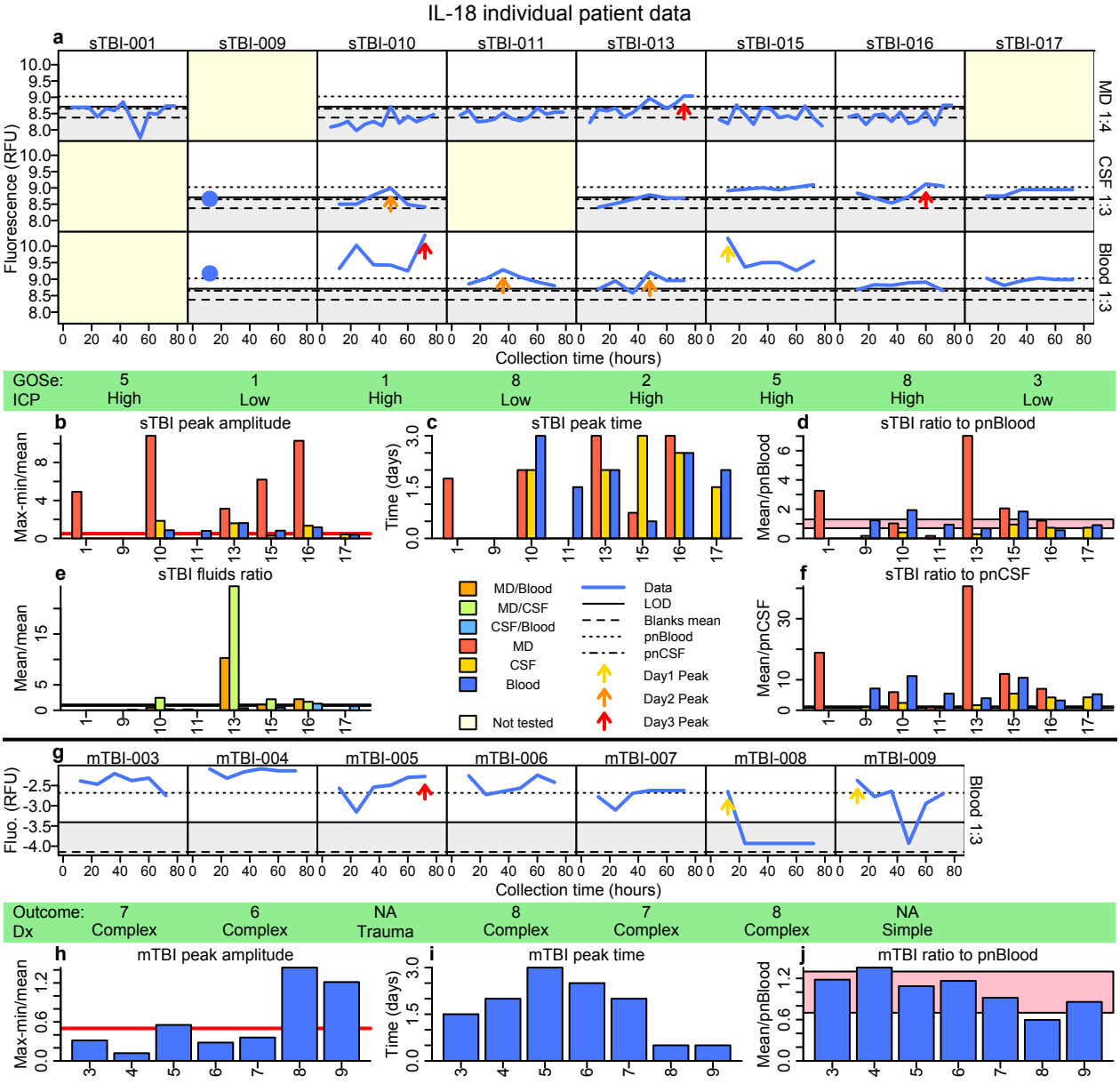

FIGURE J.S125: **Individual IL-18 protein profiles and peak and ratio analysis.** IL-18 concentration in microdialysate, CSF and blood samples of individual sTBI patients (**a**) and mTBI/trauma patients (**g**) was measured and peak amplitude and time, as well as ratio between mean time course values to value found in the pooled normal control (**b-f, h-j**) were calculated for each patient. Graphs **b-f** show calculations for individual sTBI patients, and graphs **h-j** show calculations for individual mTBI patients. Red lines in **b, h** show a threshold for a profile that is considered to have a peak, rather than being constant. The light red boxes in **d, e, f, j** show the threshold of comparison to the measured value compared.

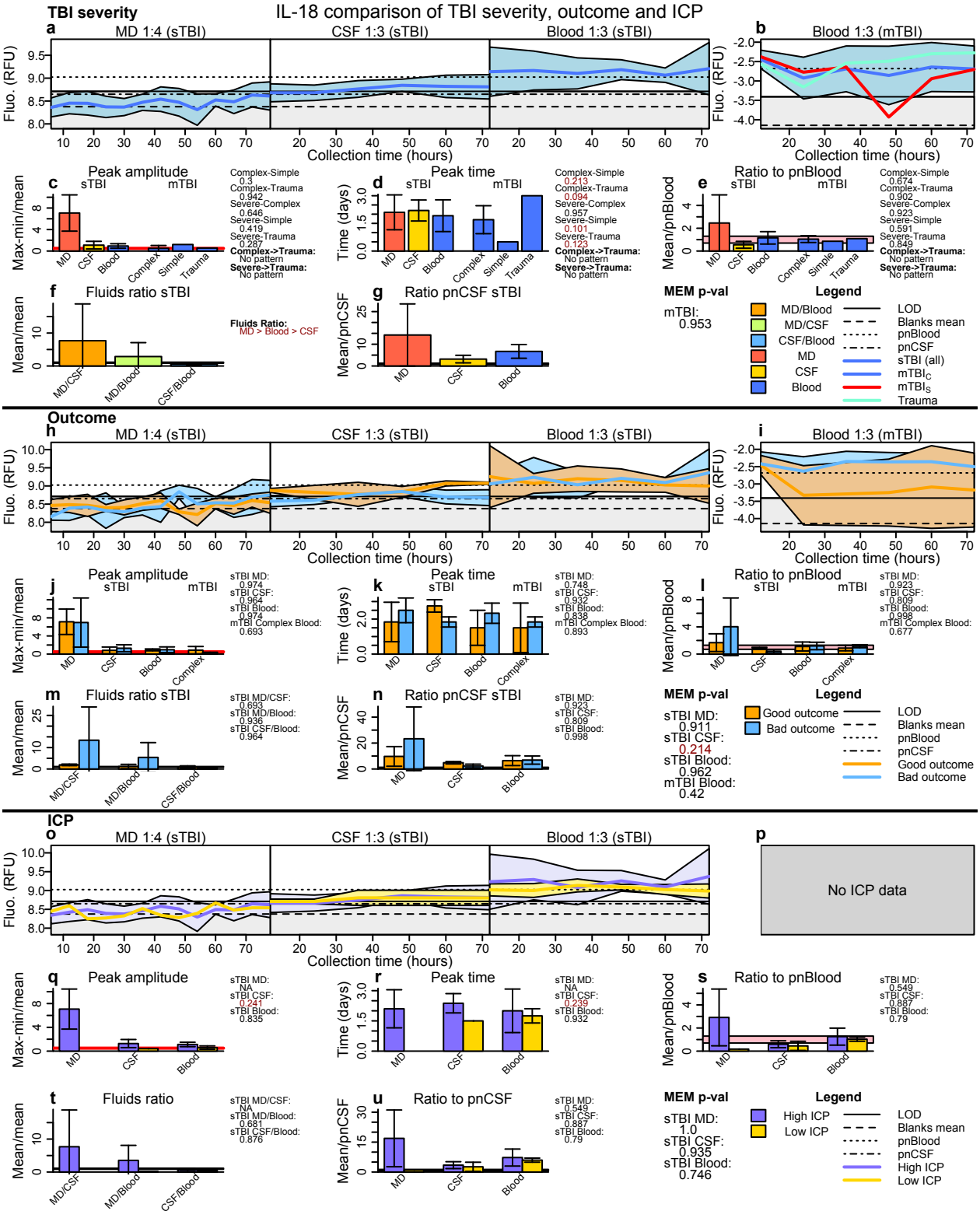

FIGURE J.S126: **Differential IL-18 protein profiles and peak and ratio analysis with respect to TBI severity, outcome and ICP.** Average IL-18 profiles are compared in terms of TBI severity (**a-g**), outcome (**h-n**) and ICP (**o-u**). Polygons in **a, b, h, i, o** indicate the mean value ±1 SD at each time point. Red lines in **c, j, q** show a threshold for a profile that is considered to have a peak, rather than being constant. The light red boxes in **e-g, l-n, s-u** show the threshold of comparison to the measured value compared. Benjamini–Hochberg adjusted p-values for comparisons are shown on the right of every graph.

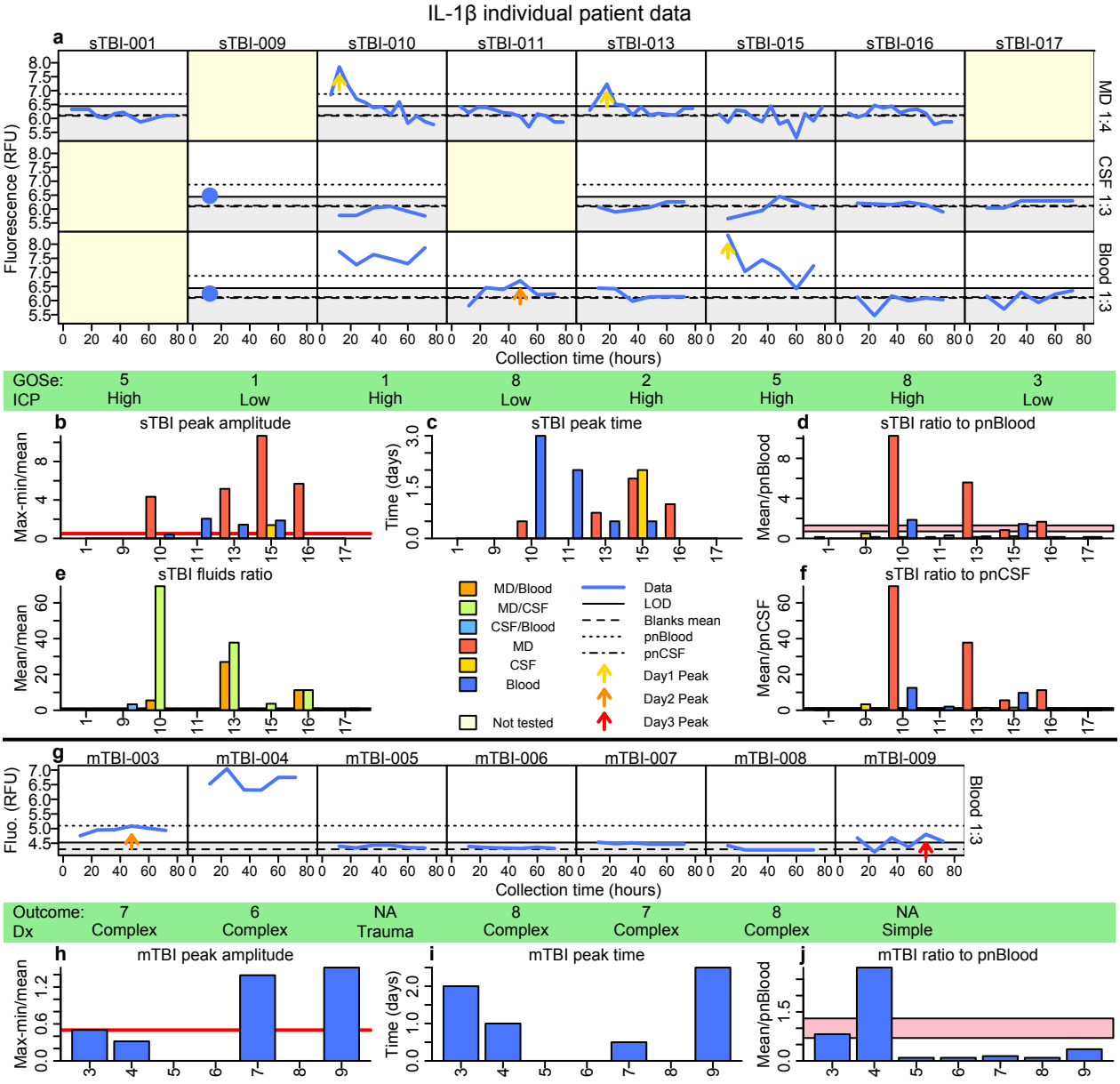

FIGURE J.S127: **Individual IL-1β protein profiles and peak and ratio analysis.** IL-1β concentration in microdialysate, CSF and blood samples of individual sTBI patients (**a**) and mTBI/trauma patients (**g**) was measured and peak amplitude and time, as well as ratio between mean time course values to value found in the pooled normal control (**b-f, h-j**) were calculated for each patient. Graphs **b-f** show calculations for individual sTBI patients, and graphs **h-j** show calculations for individual mTBI patients. Red lines in **b, h** show a threshold for a profile that is considered to have a peak, rather than being constant. The light red boxes in **d, e, f, j** show the threshold of comparison to the measured value compared.

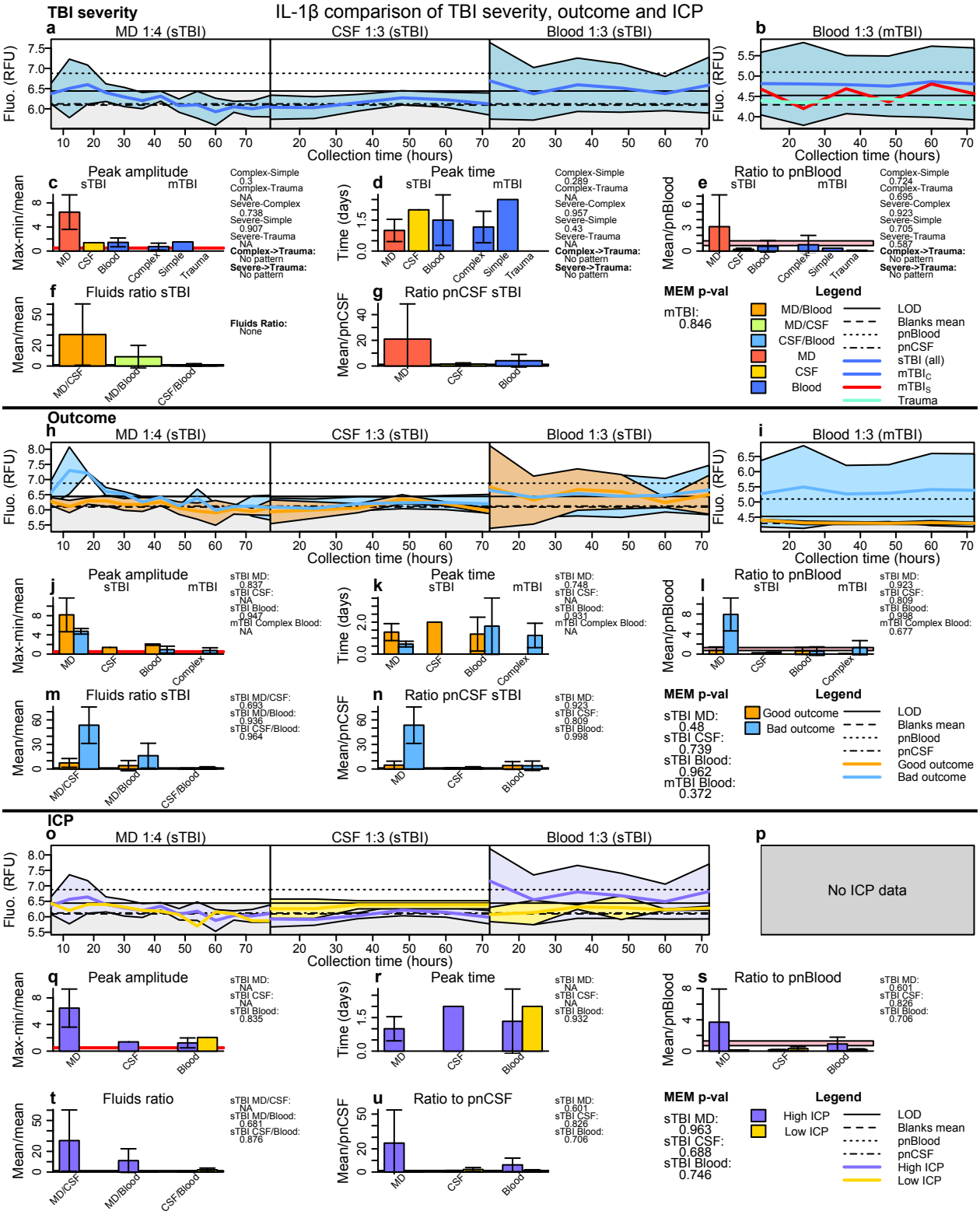

FIGURE J.S128: **Differential IL-1β protein profiles and peak and ratio analysis with respect to TBI severity, outcome and ICP.** Average IL-1β profiles are compared in terms of TBI severity (**a-g**), outcome (**h-n**) and ICP (**o-u**). Polygons in **a, b, h, i, o** indicate the mean value ± 1 SD at each time point. Red lines in **c, j, q** show a threshold for a profile that is considered to have a peak, rather than being constant. The light red boxes in **e-g, l-n, s-u** show the threshold of comparison to the measured value compared. Benjamini–Hochberg adjusted p-values for comparisons are shown on the right of every graph.

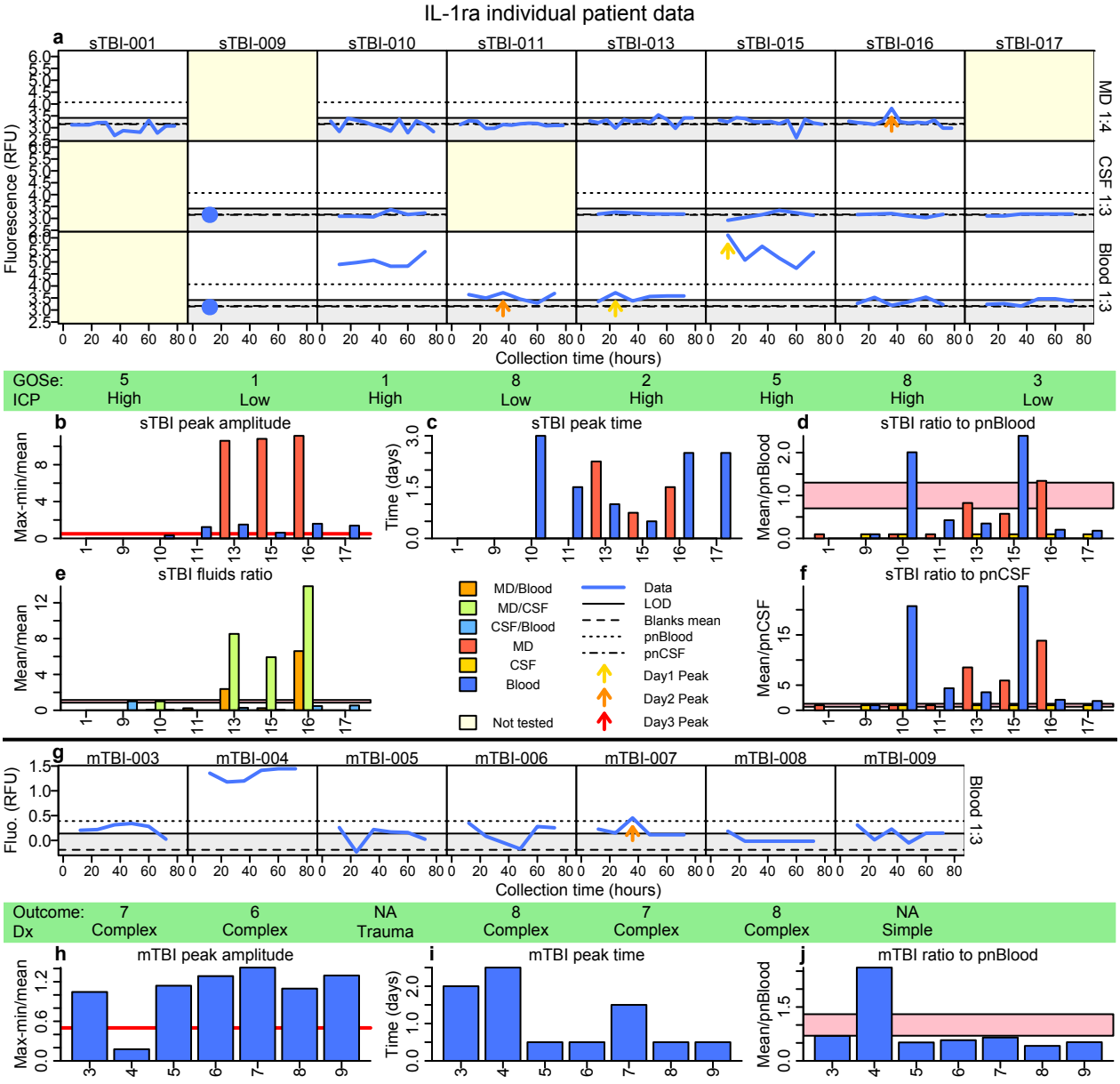

FIGURE J.S129: **Individual IL-1ra protein profiles and peak and ratio analysis.** IL-1ra concentration in microdialysate, CSF and blood samples of individual sTBI patients (**a**) and mTBI/trauma patients (**g**) was measured and peak amplitude and time, as well as ratio between mean time course values to value found in the pooled normal control (**b-f, h-j**) were calculated for each patient. Graphs **b-f** show calculations for individual sTBI patients, and graphs **h-j** show calculations for individual mTBI patients. Red lines in **b, h** show a threshold for a profile that is considered to have a peak, rather than being constant. The light red boxes in **d, e, f, j** show the threshold of comparison to the measured value compared.

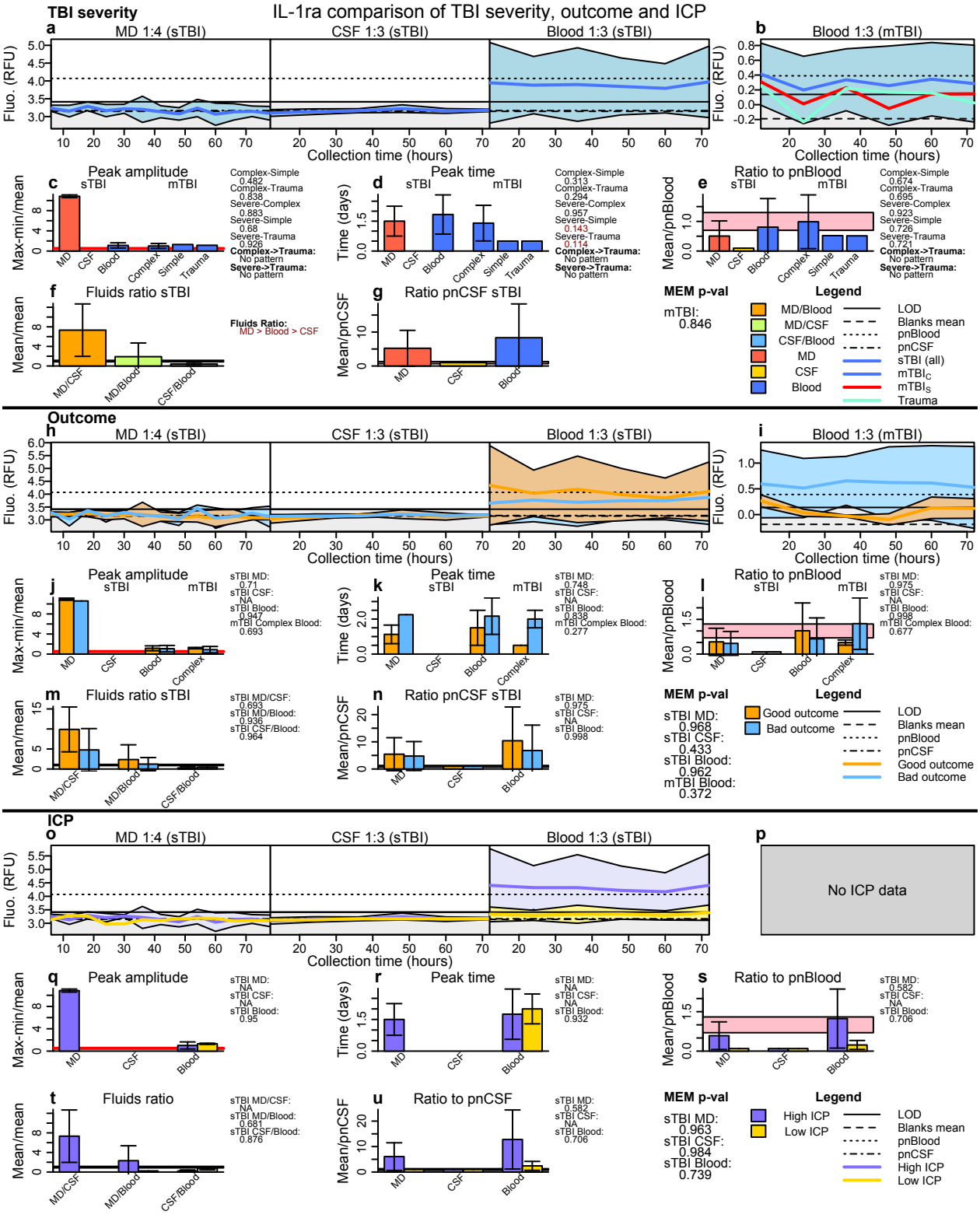

FIGURE J.S130: **Differential IL-1ra protein profiles and peak and ratio analysis with respect to TBI severity, outcome and ICP.** Average IL-1ra profiles are compared in terms of TBI severity (**a-g**), outcome (**h-n**) and ICP (**o-u**). Polygons in **a, b, h, i, o** indicate the mean value ±1 SD at each time point. Red lines in **c, j, q** show a threshold for a profile that is considered to have a peak, rather than being constant. The light red boxes in **e-g, l-n, s-u** show the threshold of comparison to the measured value compared. Benjamini–Hochberg adjusted p-values for comparisons are shown on the right of every graph.

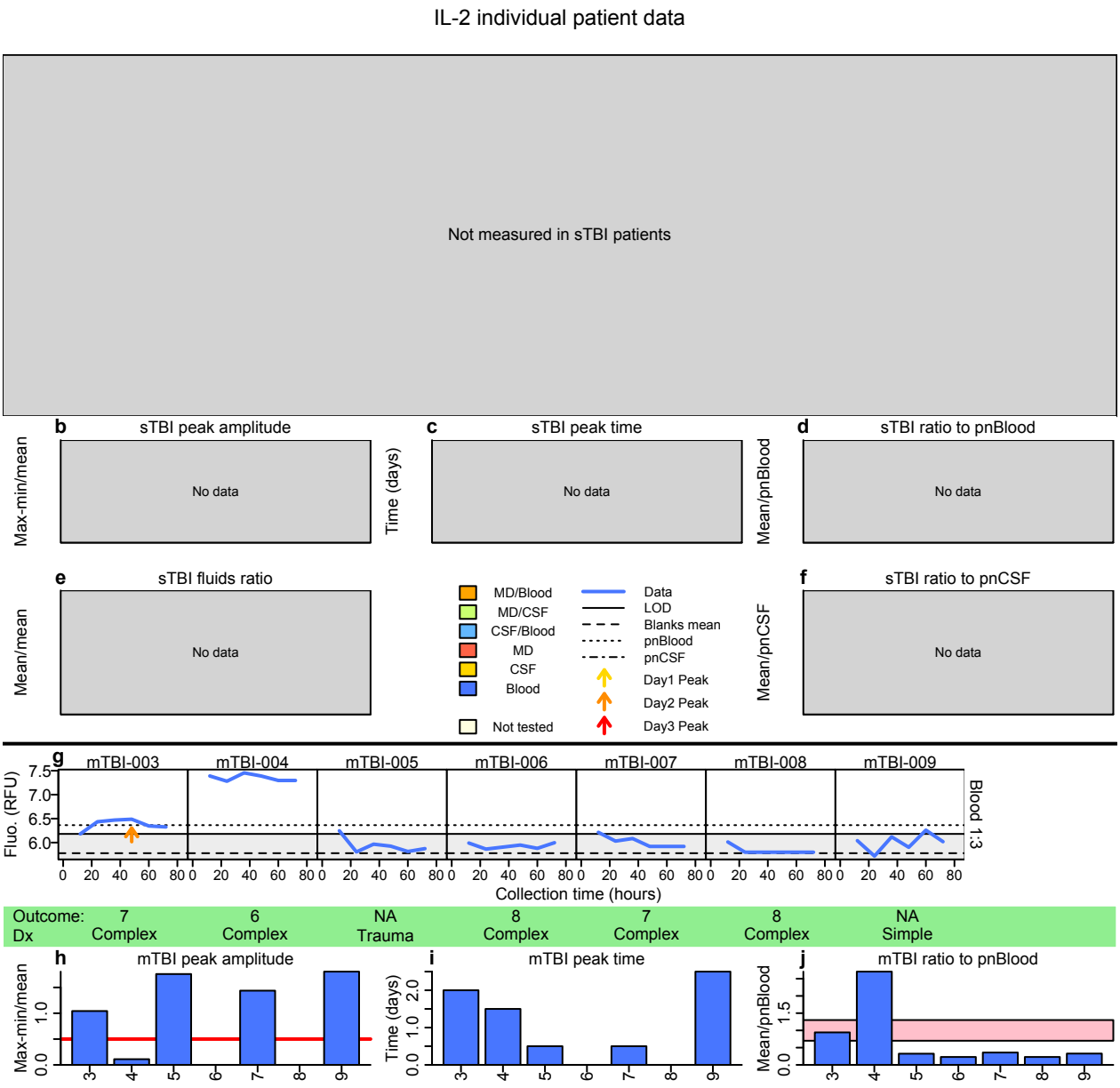

FIGURE J.S131: **Individual IL-2 protein profiles and peak and ratio analysis.** IL-2 concentration in microdialysate, CSF and blood samples of individual sTBI patients (**a**) and mTBI/trauma patients (**g**) was measured and peak amplitude and time, as well as ratio between mean time course values to value found in the pooled normal control (**b-f, h-j**) were calculated for each patient. Graphs **b-f** show calculations for individual sTBI patients, and graphs **h-j** show calculations for individual mTBI patients. Red lines in **b, h** show a threshold for a profile that is considered to have a peak, rather than being constant. The light red boxes in **d, e, f, j** show the threshold of comparison to the measured value compared.

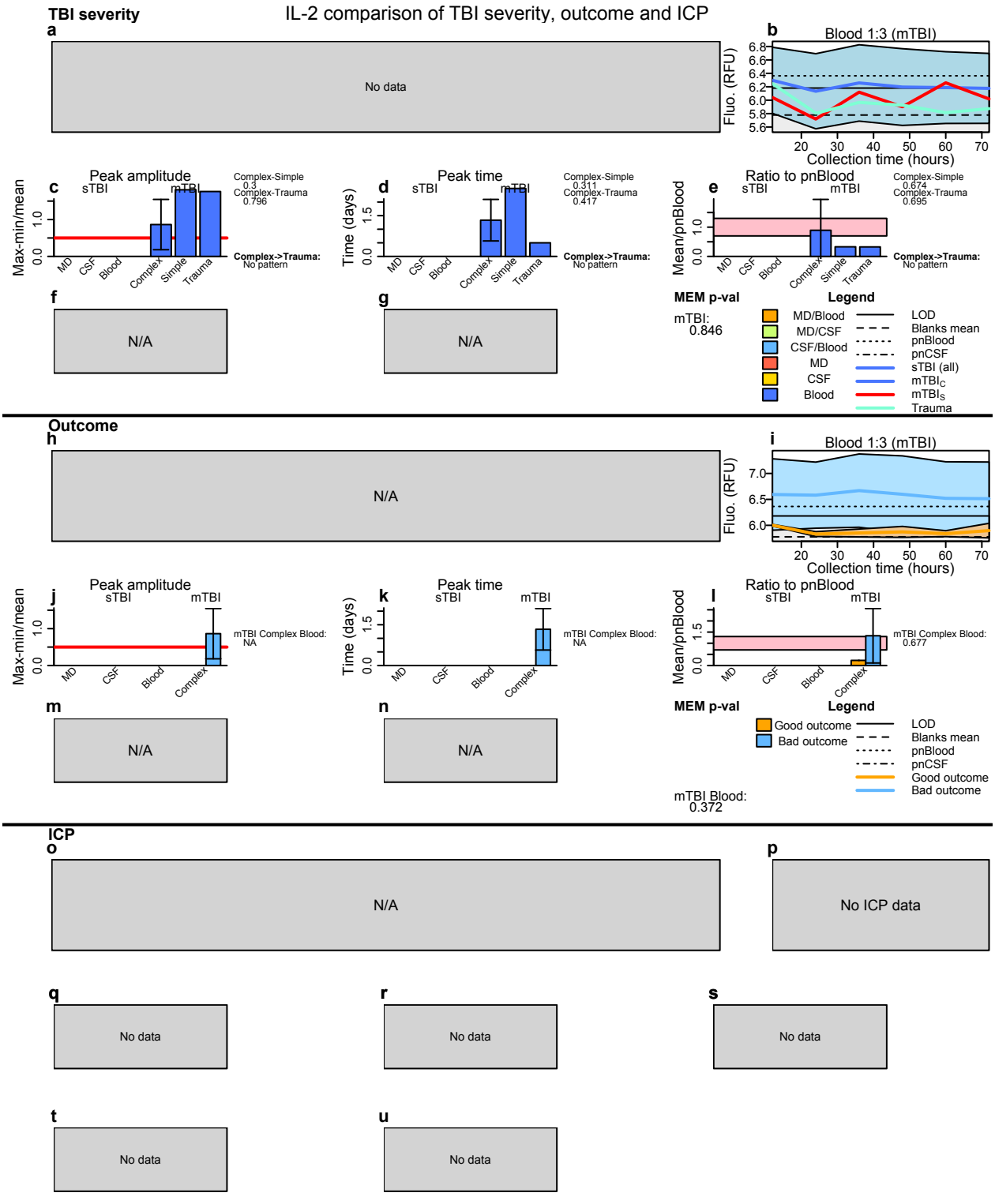

FIGURE J.S132: **Differential IL-2 protein profiles and peak and ratio analysis with respect to TBI severity, outcome and ICP.** Average IL-2 profiles are compared in terms of TBI severity (**a-g**), outcome (**h-n**) and ICP (**o-u**). Polygons in **a, b, h, i, o** indicate the mean value ±1 SD at each time point. Red lines in **c, j, q** show a threshold for a profile that is considered to have a peak, rather than being constant. The light red boxes in **e-g, l-n, s-u** show the threshold of comparison to the measured value compared. Benjamini–Hochberg adjusted p-values for comparisons are shown on the right of every graph.

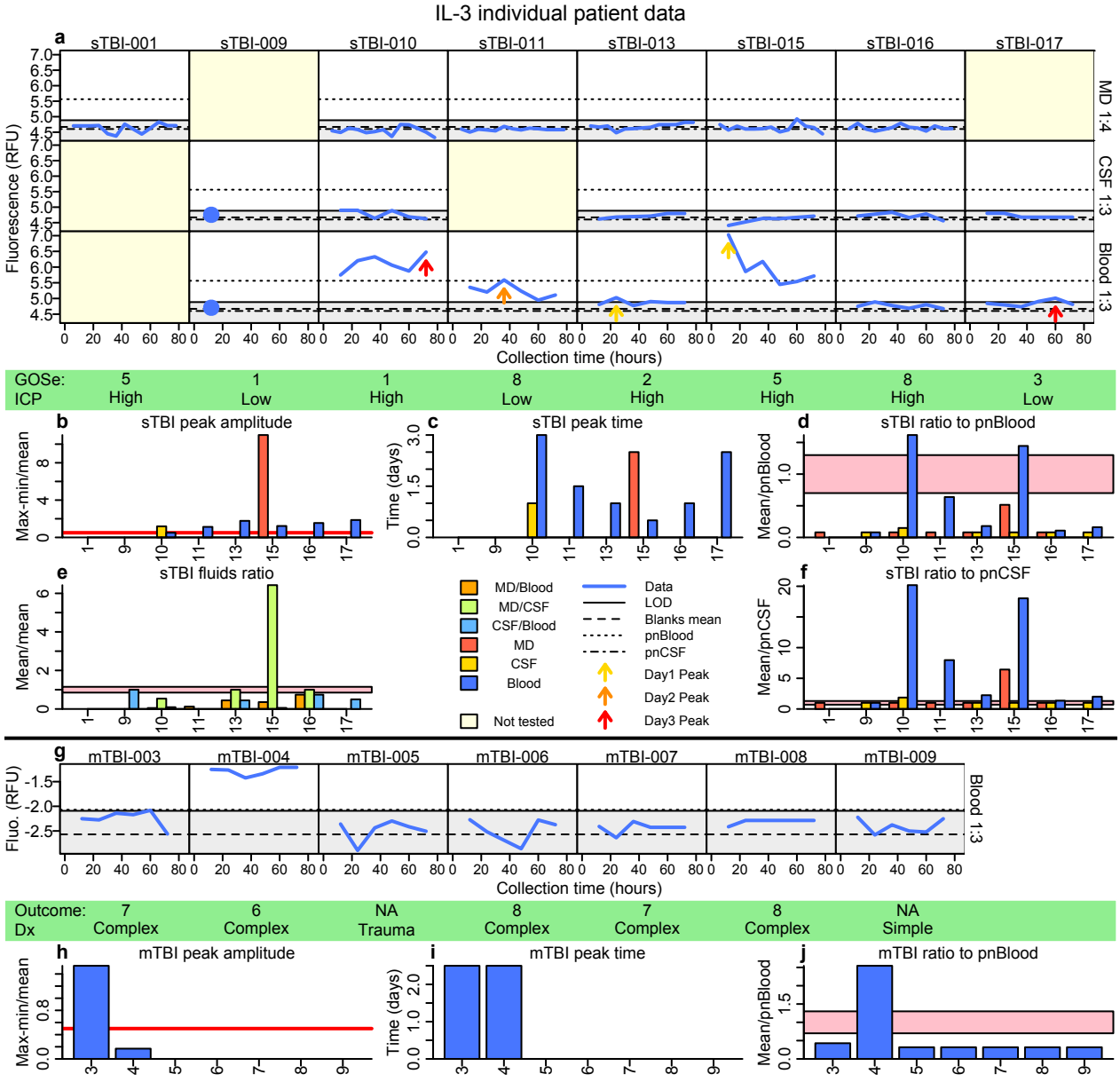

FIGURE J.S133: **Individual IL-3 protein profiles and peak and ratio analysis.** IL-3 concentration in microdialysate, CSF and blood samples of individual sTBI patients (**a**) and mTBI/trauma patients (**g**) was measured and peak amplitude and time, as well as ratio between mean time course values to value found in the pooled normal control (**b-f, h-j**) were calculated for each patient. Graphs **b-f** show calculations for individual sTBI patients, and graphs **h-j** show calculations for individual mTBI patients. Red lines in **b, h** show a threshold for a profile that is considered to have a peak, rather than being constant. The light red boxes in **d, e, f, j** show the threshold of comparison to the measured value compared.

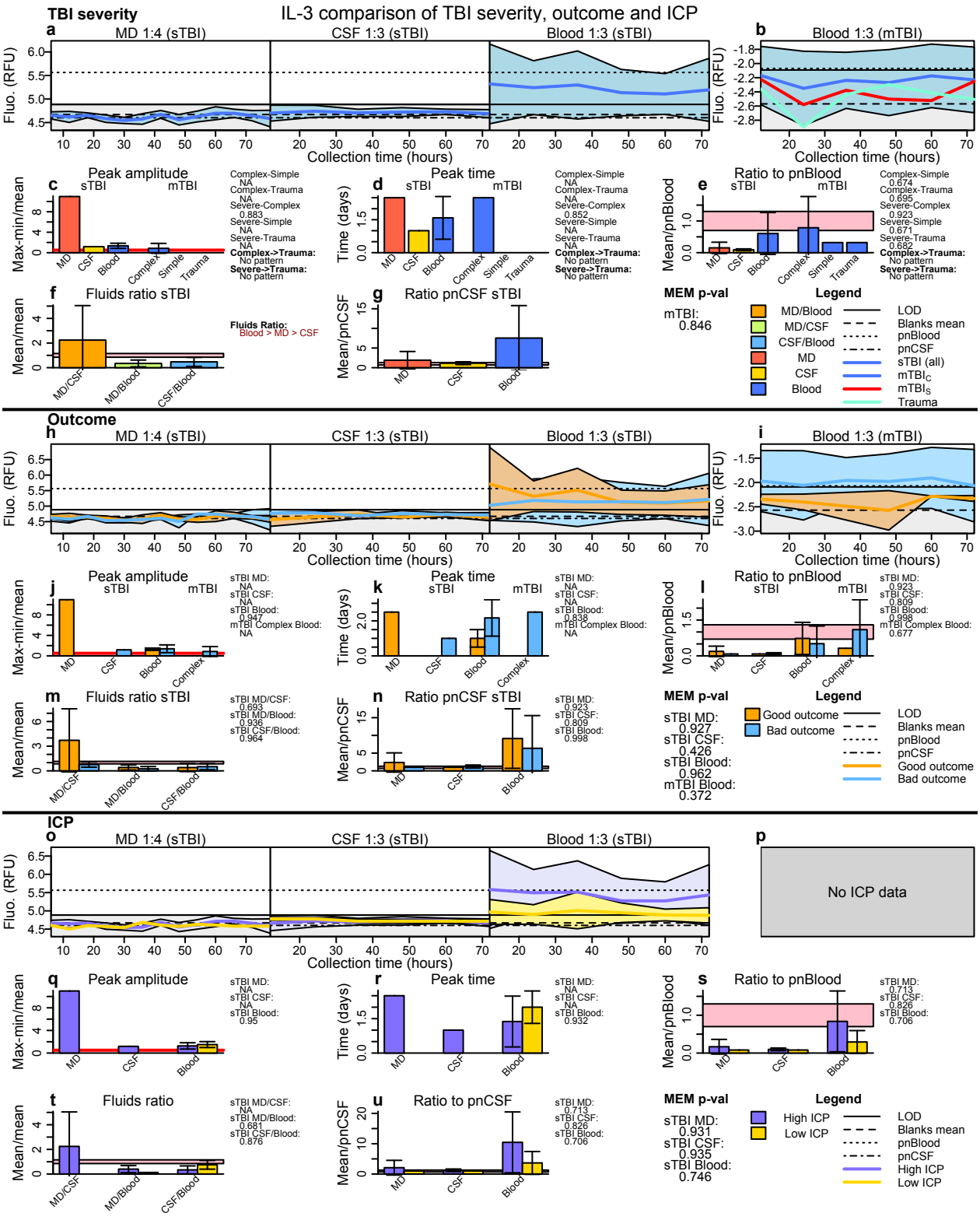

FIGURE J.S134: **Differential IL-3 protein profiles and peak and ratio analysis with respect to TBI severity, outcome and ICP.** Average IL-3 profiles are compared in terms of TBI severity (**a-g**), outcome (**h-n**) and ICP (**o-u**). Polygons in **a, b, h, i, o** indicate the mean value ±1 SD at each time point. Red lines in **c, j, q** show a threshold for a profile that is considered to have a peak, rather than being constant. The light red boxes in **e-g, l-n, s-u** show the threshold of comparison to the measured value compared. Benjamini–Hochberg adjusted p-values for comparisons are shown on the right of every graph.

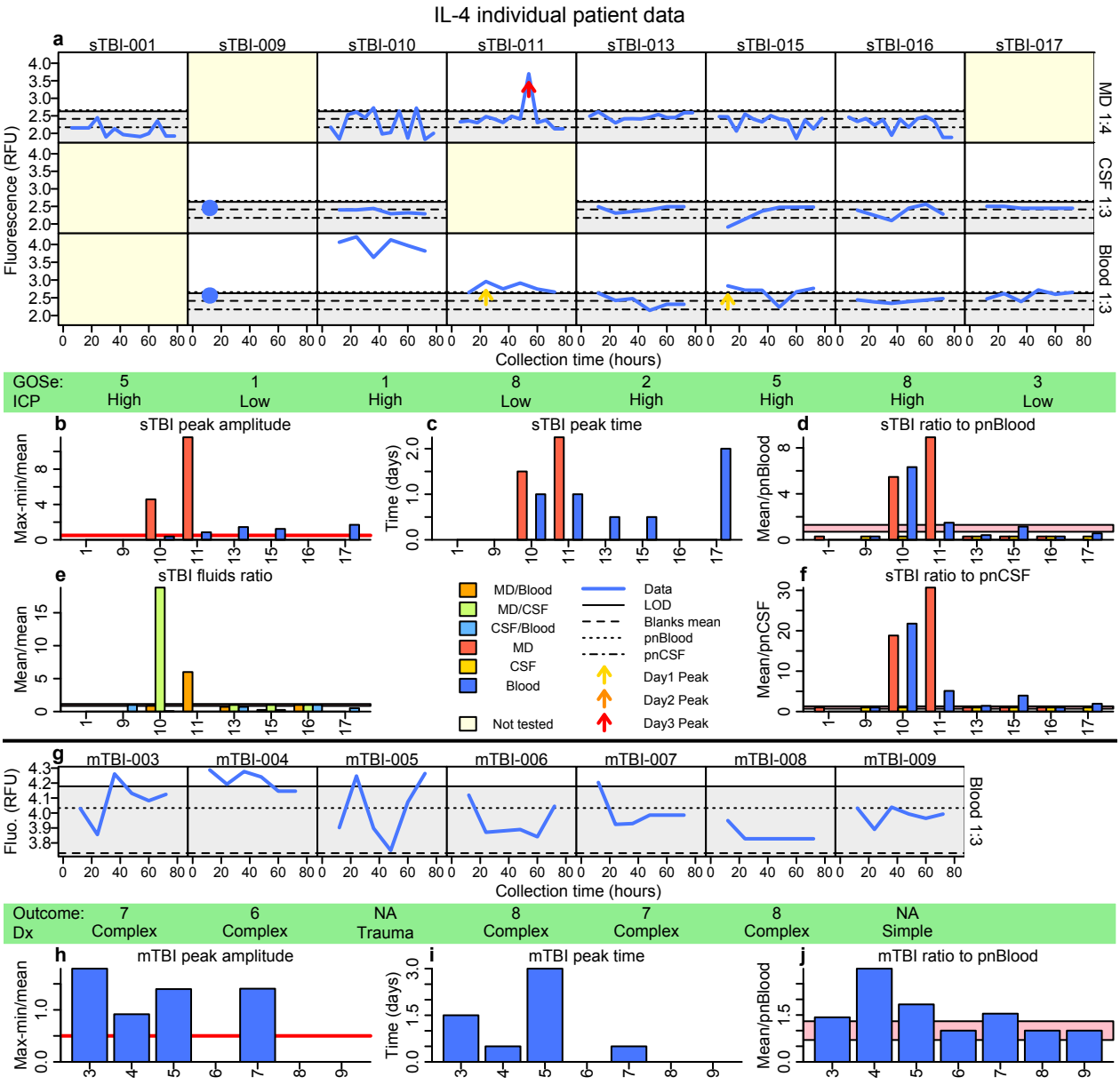

FIGURE J.S135: **Individual IL-4 protein profiles and peak and ratio analysis.** IL-4 concentration in microdialysate, CSF and blood samples of individual sTBI patients (**a**) and mTBI/trauma patients (**g**) was measured and peak amplitude and time, as well as ratio between mean time course values to value found in the pooled normal control (**b-f, h-j**) were calculated for each patient. Graphs **b-f** show calculations for individual sTBI patients, and graphs **h-j** show calculations for individual mTBI patients. Red lines in **b, h** show a threshold for a profile that is considered to have a peak, rather than being constant. The light red boxes in **d, e, f, j** show the threshold of comparison to the measured value compared.

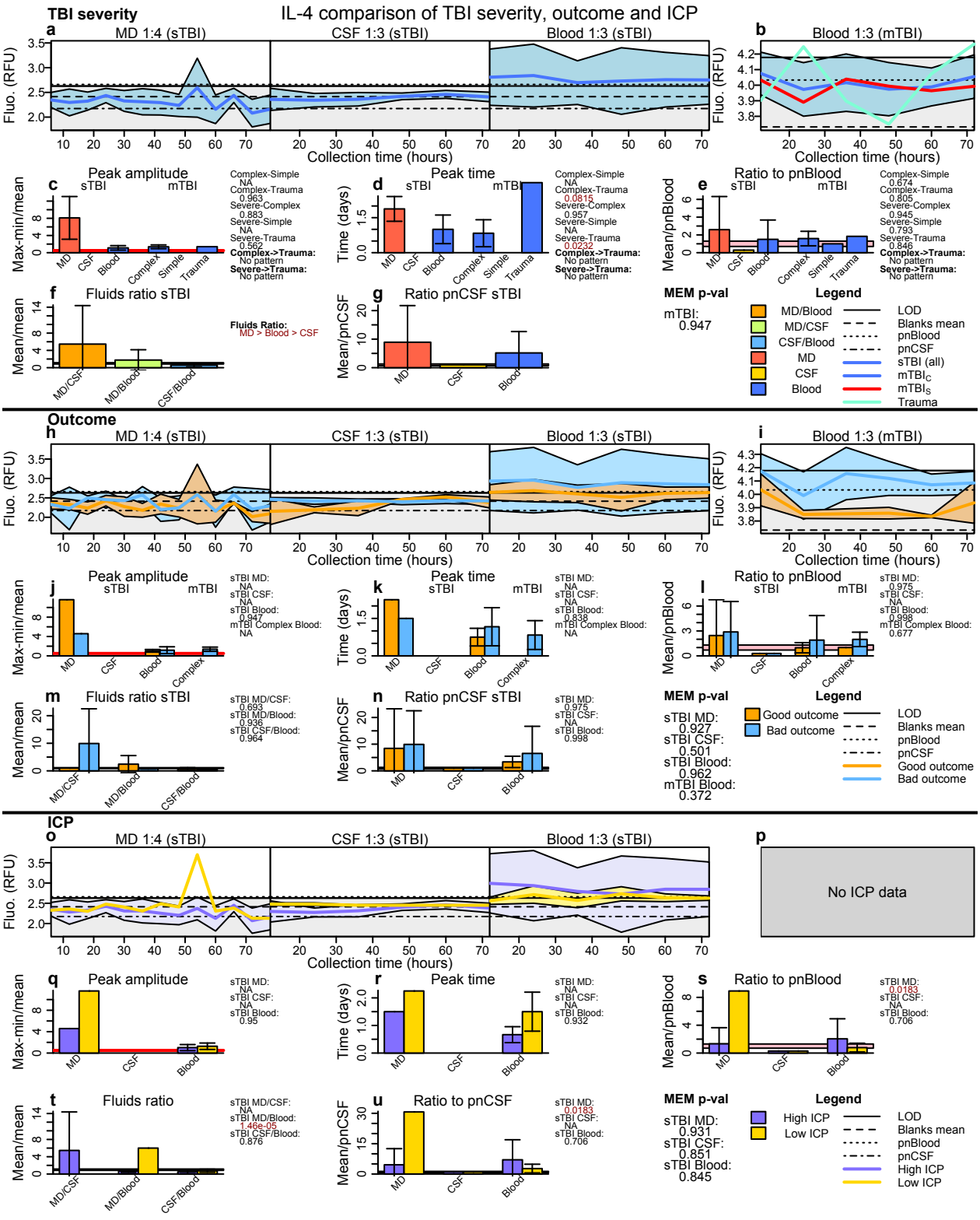

FIGURE J.S136: **Differential IL-4 protein profiles and peak and ratio analysis with respect to TBI severity, outcome and ICP.** Average IL-4 profiles are compared in terms of TBI severity (**a-g**), outcome (**h-n**) and ICP (**o-u**). Polygons in **a, b, h, i, o** indicate the mean value ±1 SD at each time point. Red lines in **c, j, q** show a threshold for a profile that is considered to have a peak, rather than being constant. The light red boxes in **e-g, l-n, s-u** show the threshold of comparison to the measured value compared. Benjamini–Hochberg adjusted p-values for comparisons are shown on the right of every graph.

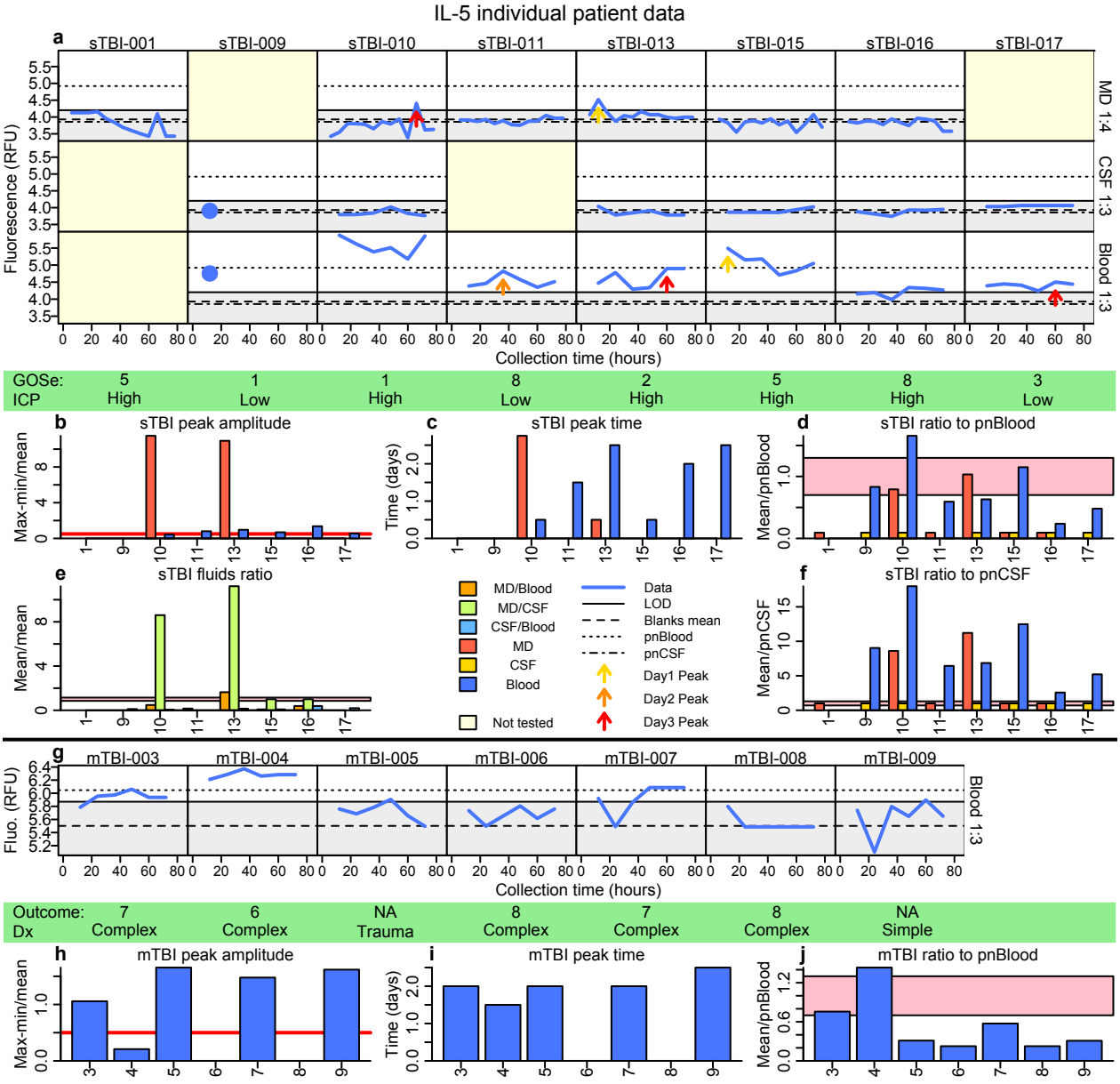

FIGURE J.S137: **Individual IL-5 protein profiles and peak and ratio analysis.** IL-5 concentration in microdialysate, CSF and blood samples of individual sTBI patients (**a**) and mTBI/trauma patients (**g**) was measured and peak amplitude and time, as well as ratio between mean time course values to value found in the pooled normal control (**b-f, h-j**) were calculated for each patient. Graphs **b-f** show calculations for individual sTBI patients, and graphs **h-j** show calculations for individual mTBI patients. Red lines in **b, h** show a threshold for a profile that is considered to have a peak, rather than being constant. The light red boxes in **d, e, f, j** show the threshold of comparison to the measured value compared.

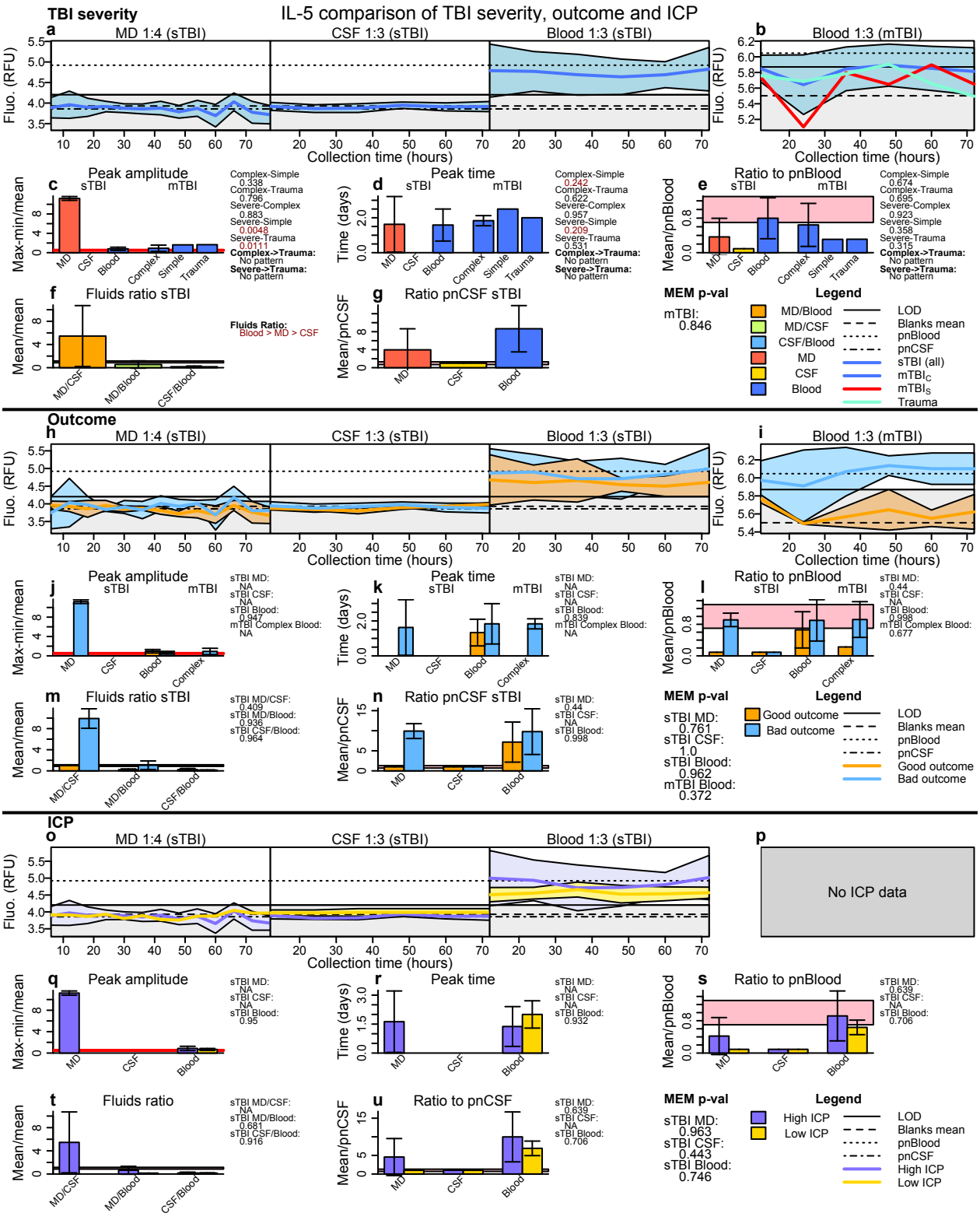

FIGURE J.S138: **Differential IL-5 protein profiles and peak and ratio analysis with respect to TBI severity, outcome and ICP.** Average IL-5 profiles are compared in terms of TBI severity (**a-g**), outcome (**h-n**) and ICP (**o-u**). Polygons in **a, b, h, i, o** indicate the mean value ±1 SD at each time point. Red lines in **c, j, q** show a threshold for a profile that is considered to have a peak, rather than being constant. The light red boxes in **e-g, l-n, s-u** show the threshold of comparison to the measured value compared. Benjamini–Hochberg adjusted p-values for comparisons are shown on the right of every graph.

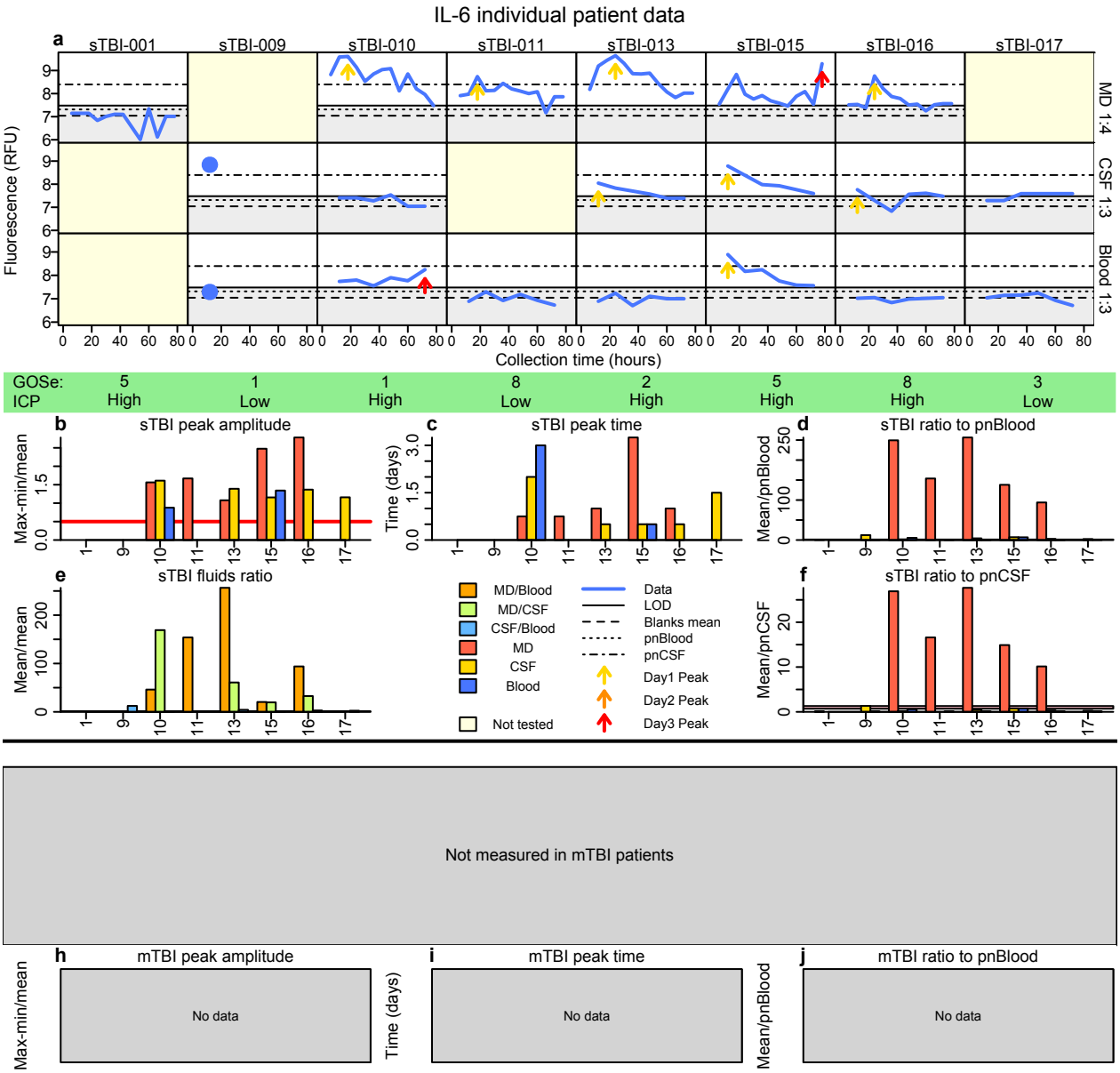

FIGURE J.S139: **Individual IL-6 protein profiles and peak and ratio analysis.** IL-6 concentration in microdialysate, CSF and blood samples of individual sTBI patients (**a**) and mTBI/trauma patients (**g**) was measured and peak amplitude and time, as well as ratio between mean time course values to value found in the pooled normal control (**b-f, h-j**) were calculated for each patient. Graphs **b-f** show calculations for individual sTBI patients, and graphs **h-j** show calculations for individual mTBI patients. Red lines in **b, h** show a threshold for a profile that is considered to have a peak, rather than being constant. The light red boxes in **d, e, f, j** show the threshold of comparison to the measured value compared.

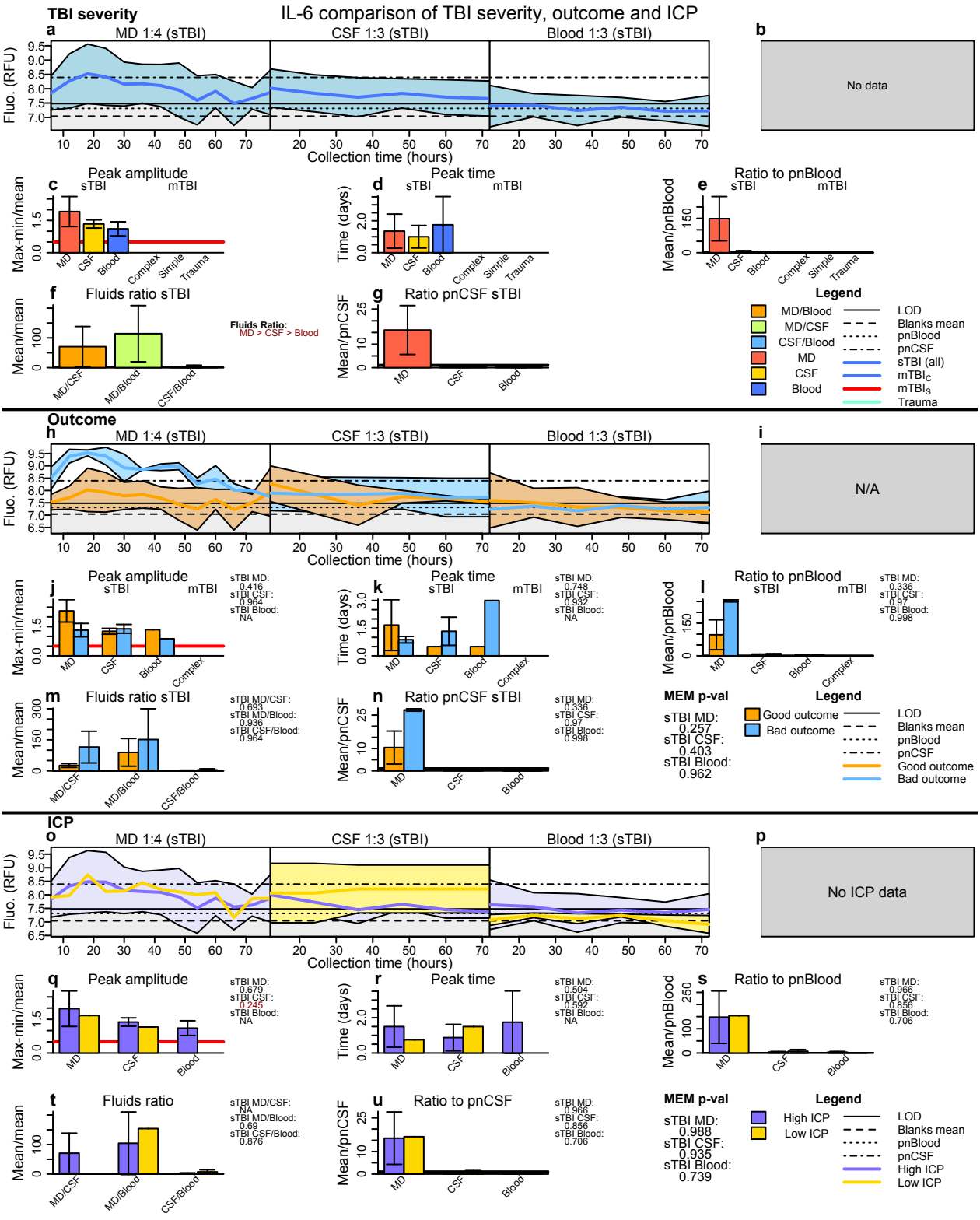

FIGURE J.S140: **Differential IL-6 protein profiles and peak and ratio analysis with respect to TBI severity, outcome and ICP.** Average IL-6 profiles are compared in terms of TBI severity (**a-g**), outcome (**h-n**) and ICP (**o-u**). Polygons in **a, b, h, i, o** indicate the mean value ±1 SD at each time point. Red lines in **c, j, q** show a threshold for a profile that is considered to have a peak, rather than being constant. The light red boxes in **e-g, l-n, s-u** show the threshold of comparison to the measured value compared. Benjamini–Hochberg adjusted p-values for comparisons are shown on the right of every graph.

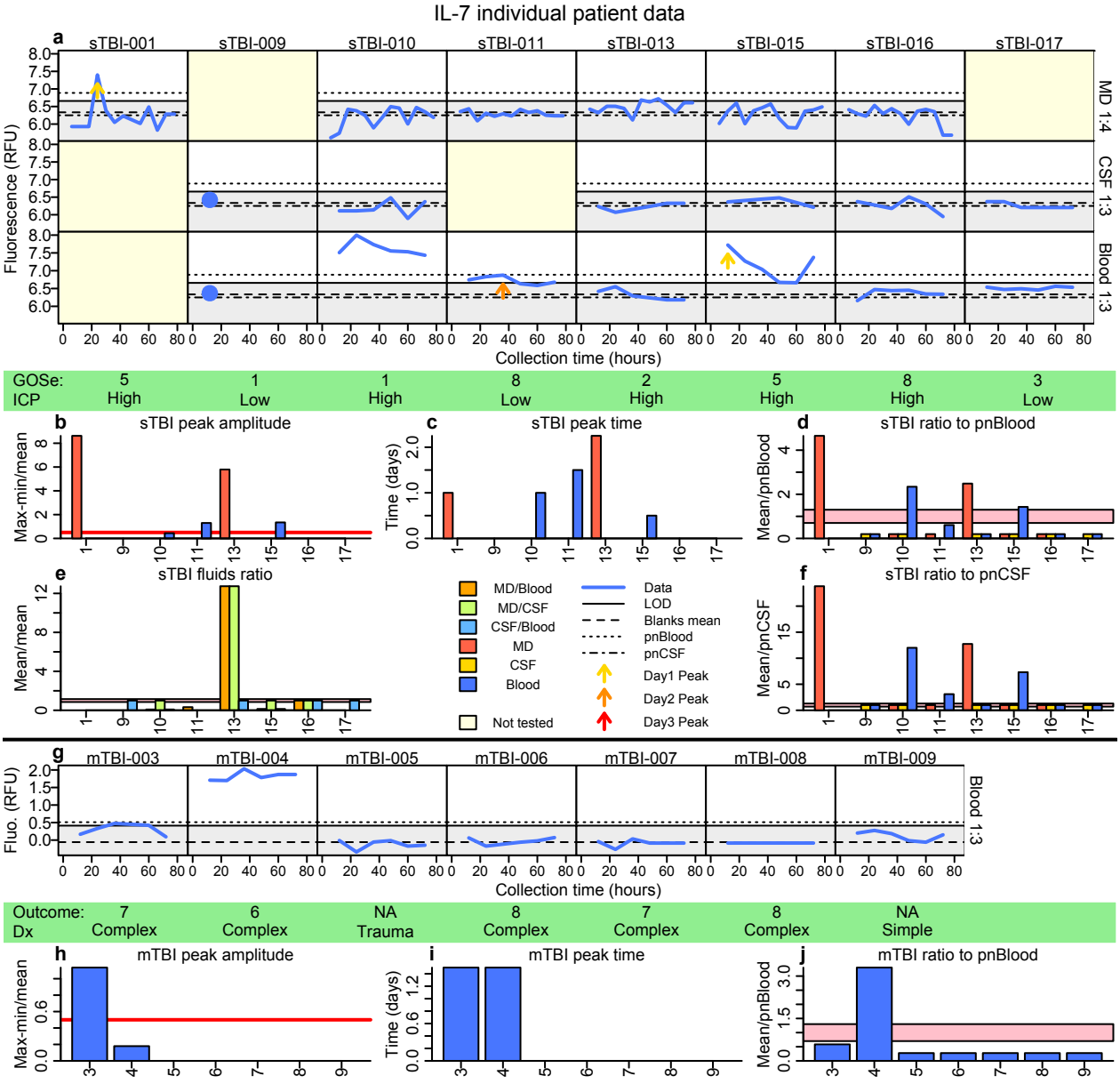

FIGURE J.S141: **Individual IL-7 protein profiles and peak and ratio analysis.** IL-7 concentration in microdialysate, CSF and blood samples of individual sTBI patients (**a**) and mTBI/trauma patients (**g**) was measured and peak amplitude and time, as well as ratio between mean time course values to value found in the pooled normal control (**b-f, h-j**) were calculated for each patient. Graphs **b-f** show calculations for individual sTBI patients, and graphs **h-j** show calculations for individual mTBI patients. Red lines in **b, h** show a threshold for a profile that is considered to have a peak, rather than being constant. The light red boxes in **d, e, f, j** show the threshold of comparison to the measured value compared.

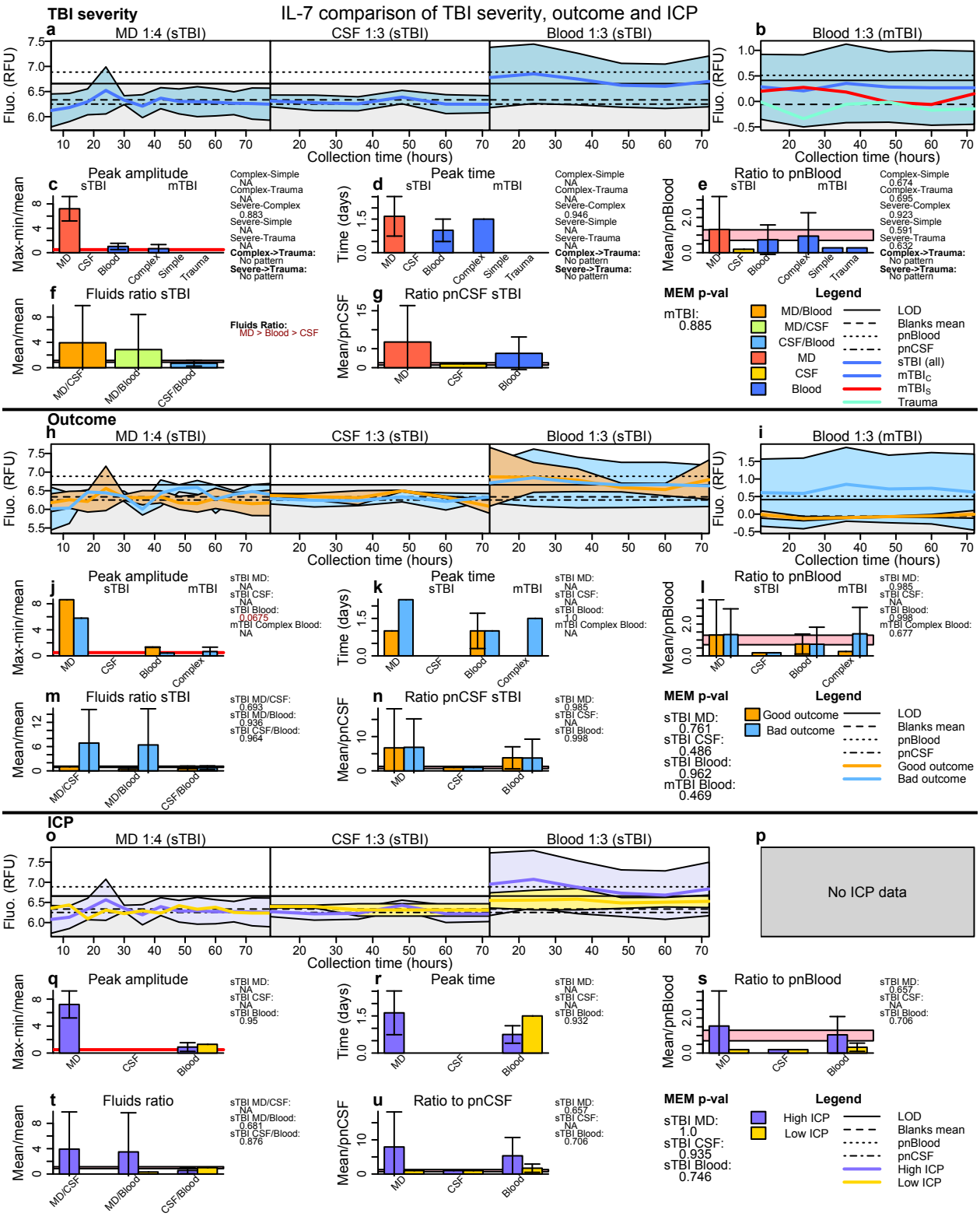

FIGURE J.S142: **Differential IL-7 protein profiles and peak and ratio analysis with respect to TBI severity, outcome and ICP.** Average IL-7 profiles are compared in terms of TBI severity (**a-g**), outcome (**h-n**) and ICP (**o-u**). Polygons in **a, b, h, i, o** indicate the mean value ±1 SD at each time point. Red lines in **c, j, q** show a threshold for a profile that is considered to have a peak, rather than being constant. The light red boxes in **e-g, l-n, s-u** show the threshold of comparison to the measured value compared. Benjamini–Hochberg adjusted p-values for comparisons are shown on the right of every graph.

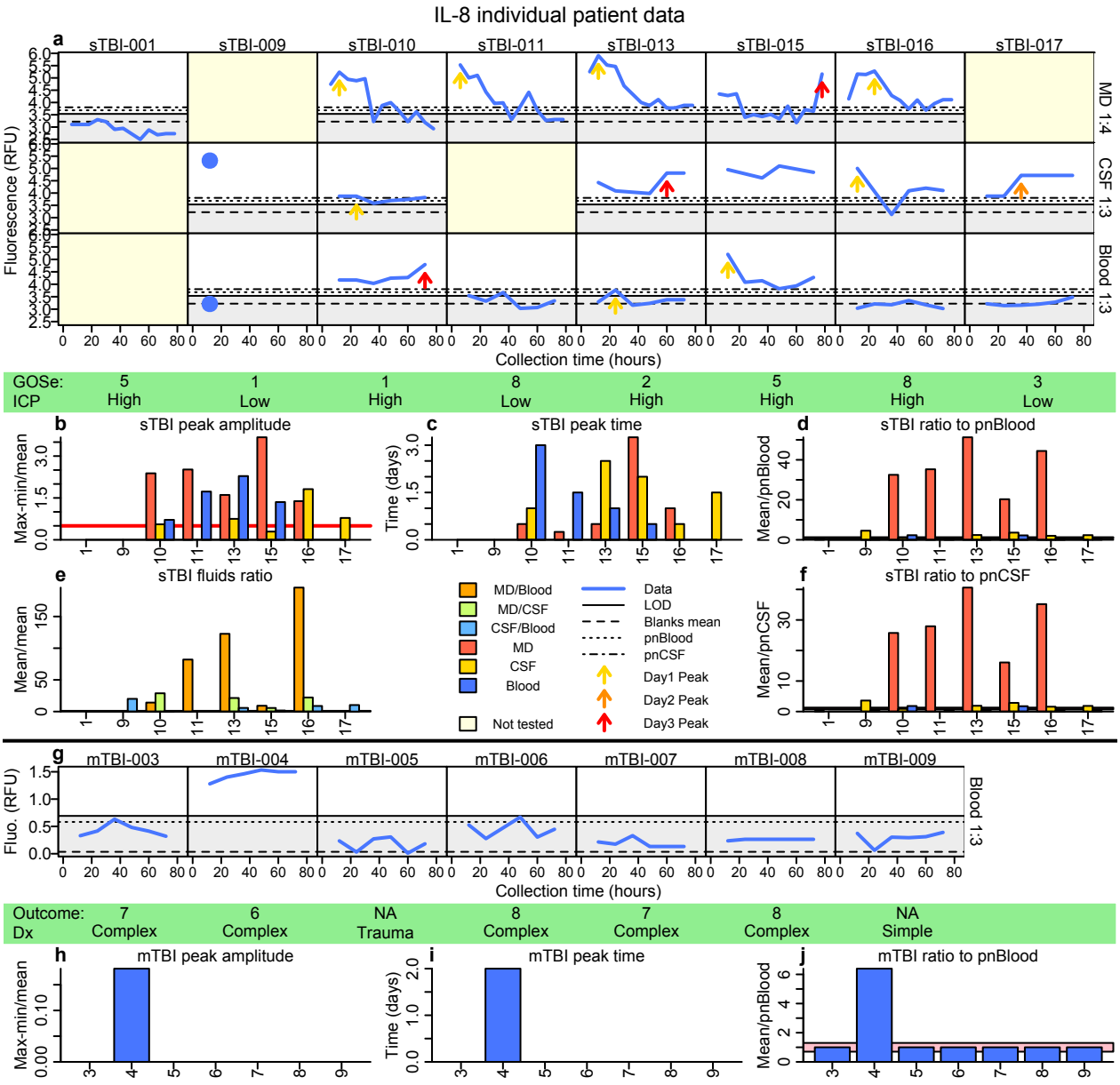

FIGURE J.S143: **Individual IL-8 protein profiles and peak and ratio analysis.** IL-8 concentration in microdialysate, CSF and blood samples of individual sTBI patients (**a**) and mTBI/trauma patients (**g**) was measured and peak amplitude and time, as well as ratio between mean time course values to value found in the pooled normal control (**b-f, h-j**) were calculated for each patient. Graphs **b-f** show calculations for individual sTBI patients, and graphs **h-j** show calculations for individual mTBI patients. Red lines in **b, h** show a threshold for a profile that is considered to have a peak, rather than being constant. The light red boxes in **d, e, f, j** show the threshold of comparison to the measured value compared.

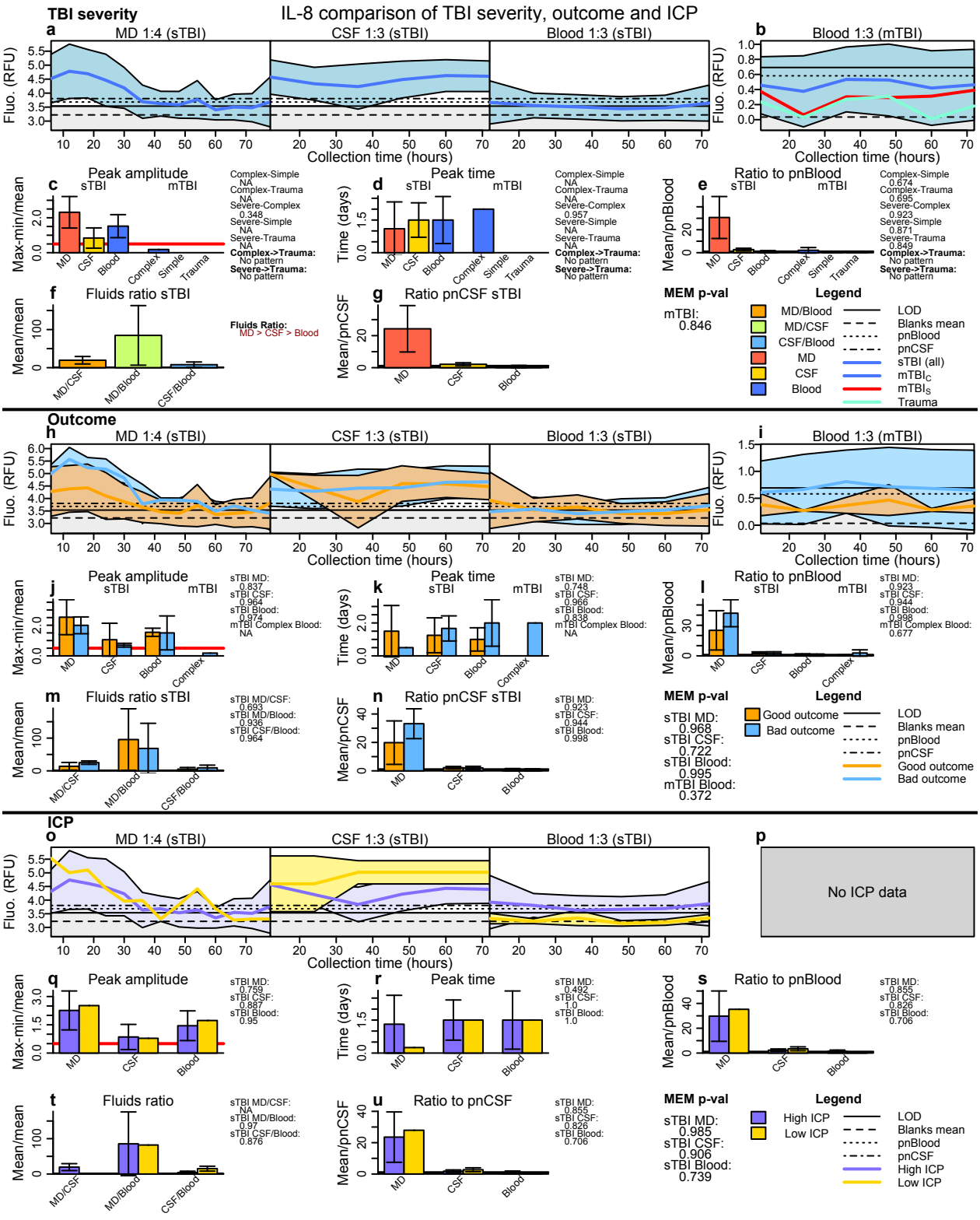

FIGURE J.S144: **Differential IL-8 protein profiles and peak and ratio analysis with respect to TBI severity, outcome and ICP.** Average IL-8 profiles are compared in terms of TBI severity (**a-g**), outcome (**h-n**) and ICP (**o-u**). Polygons in **a, b, h, i, o** indicate the mean value ±1 SD at each time point. Red lines in **c, j, q** show a threshold for a profile that is considered to have a peak, rather than being constant. The light red boxes in **e-g, l-n, s-u** show the threshold of comparison to the measured value compared. Benjamini–Hochberg adjusted p-values for comparisons are shown on the right of every graph.

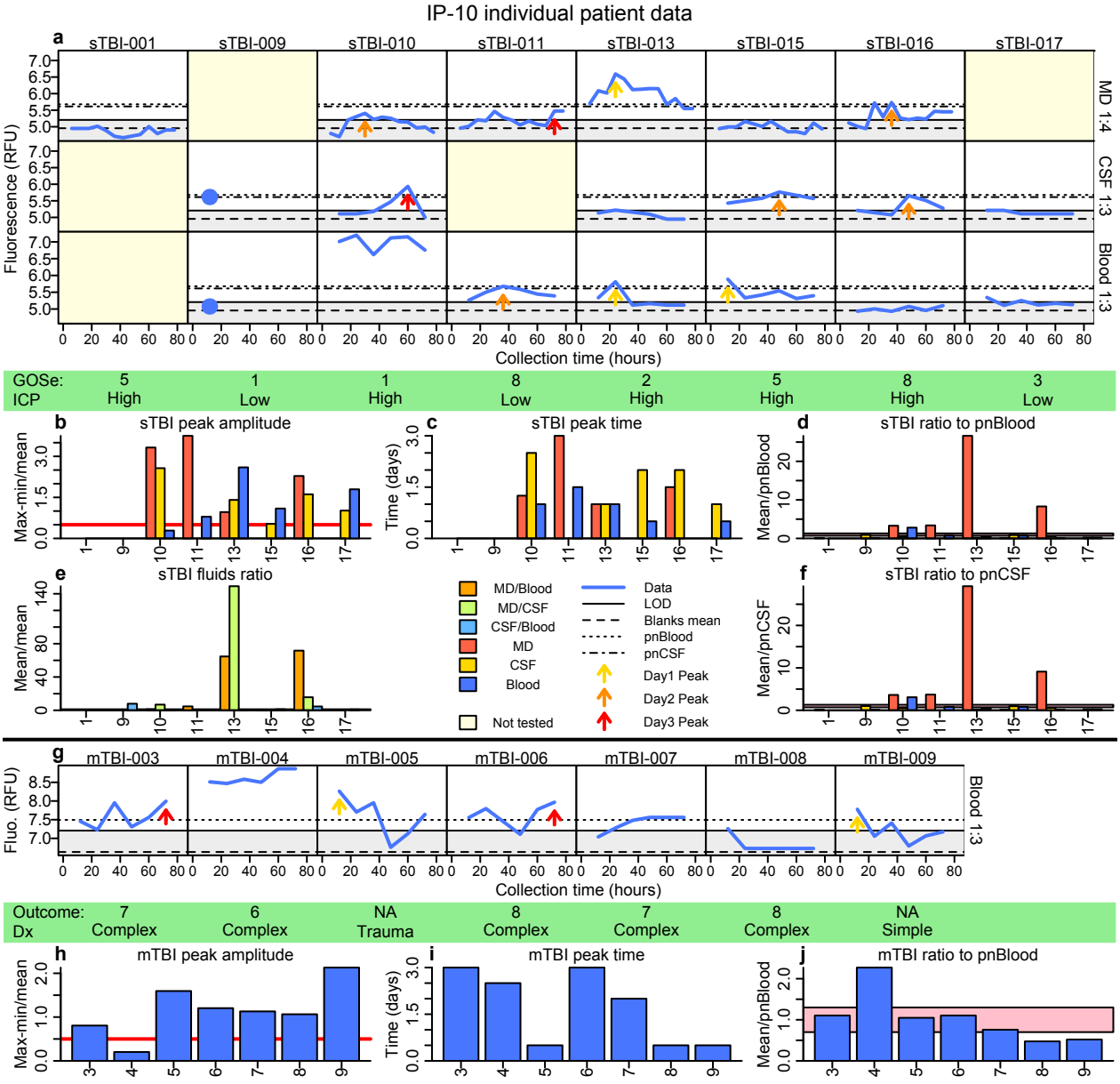

FIGURE J.S145: **Individual IP-10 protein profiles and peak and ratio analysis.** IP-10 concentration in microdialysate, CSF and blood samples of individual sTBI patients (**a**) and mTBI/trauma patients (**g**) was measured and peak amplitude and time, as well as ratio between mean time course values to value found in the pooled normal control (**b-f, h-j**) were calculated for each patient. Graphs **b-f** show calculations for individual sTBI patients, and graphs **h-j** show calculations for individual mTBI patients. Red lines in **b, h** show a threshold for a profile that is considered to have a peak, rather than being constant. The light red boxes in **d, e, f, j** show the threshold of comparison to the measured value compared.

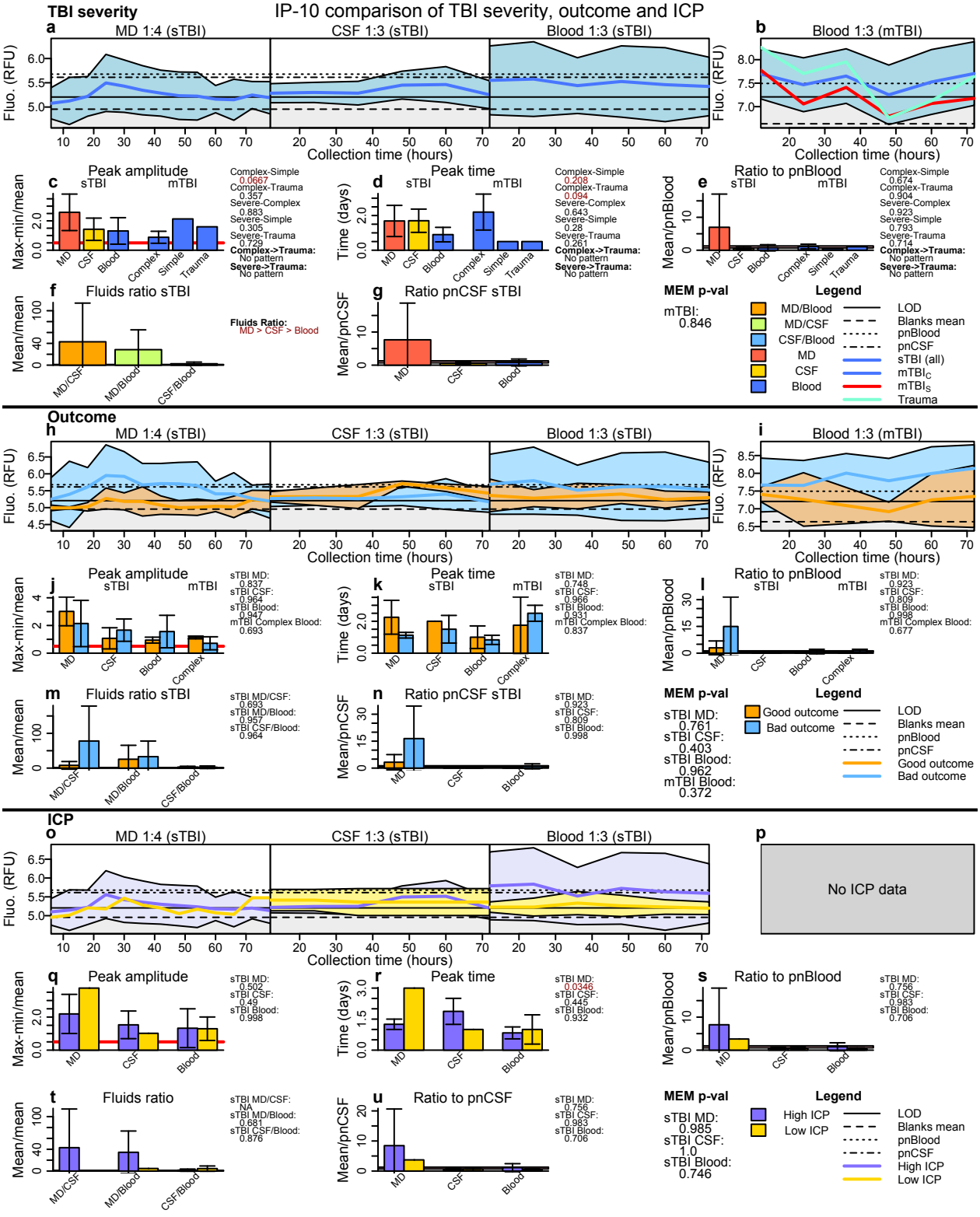

FIGURE J.S146: **Differential IP-10 protein profiles and peak and ratio analysis with respect to TBI severity, outcome and ICP.** Average IP-10 profiles are compared in terms of TBI severity (**a-g**), outcome (**h-n**) and ICP (**o-u**). Polygons in **a, b, h, i, o** indicate the mean value ±1 SD at each time point. Red lines in **c, j, q** show a threshold for a profile that is considered to have a peak, rather than being constant. The light red boxes in **e-g, l-n, s-u** show the threshold of comparison to the measured value compared. Benjamini–Hochberg adjusted p-values for comparisons are shown on the right of every graph.

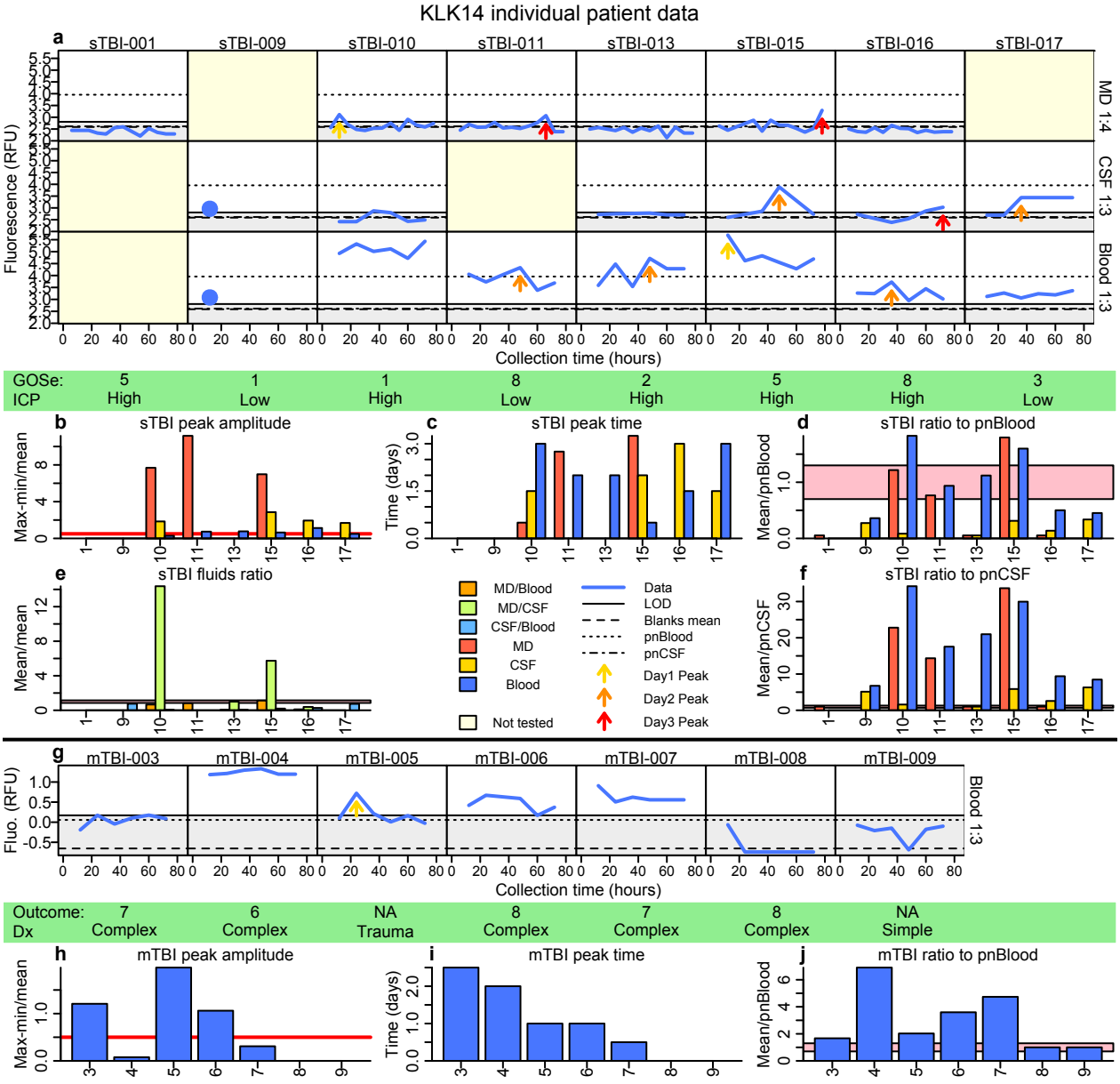

FIGURE J.S147: **Individual KLK14 protein profiles and peak and ratio analysis.** KLK14 concentration in microdialysate, CSF and blood samples of individual sTBI patients (**a**) and mTBI/trauma patients (**g**) was measured and peak amplitude and time, as well as ratio between mean time course values to value found in the pooled normal control (**b-f, h-j**) were calculated for each patient. Graphs **b-f** show calculations for individual sTBI patients, and graphs **h-j** show calculations for individual mTBI patients. Red lines in **b, h** show a threshold for a profile that is considered to have a peak, rather than being constant. The light red boxes in **d, e, f, j** show the threshold of comparison to the measured value compared.

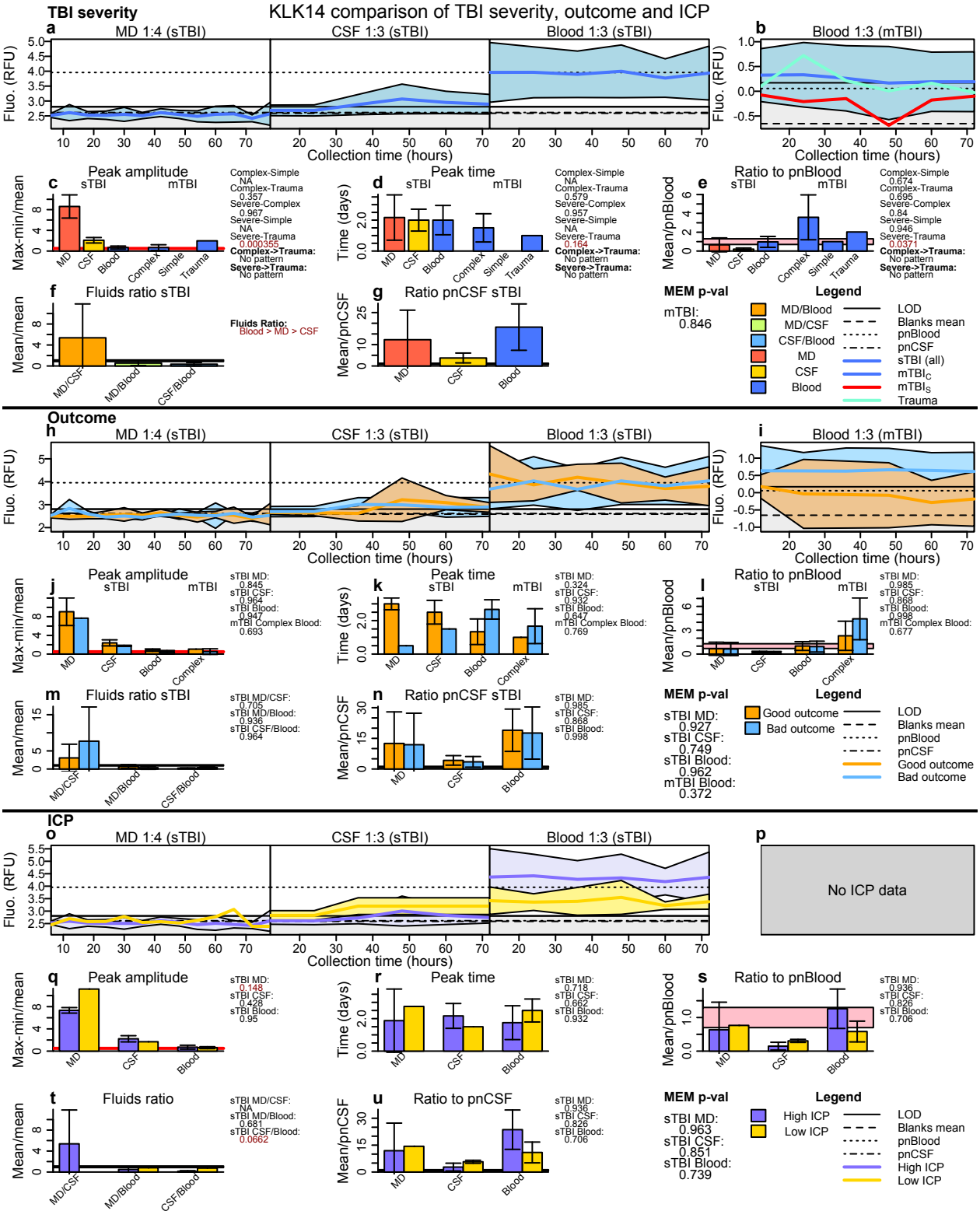

FIGURE J.S148: **Differential KLK14 protein profiles and peak and ratio analysis with respect to TBI severity, outcome and ICP.** Average KLK14 profiles are compared in terms of TBI severity (**a-g**), outcome (**h-n**) and ICP (**o-u**). Polygons in **a, b, h, i, o** indicate the mean value ±1 SD at each time point. Red lines in **c, j, q** show a threshold for a profile that is considered to have a peak, rather than being constant. The light red boxes in **e-g, l-n, s-u** show the threshold of comparison to the measured value compared. Benjamini–Hochberg adjusted p-values for comparisons are shown on the right of every graph.

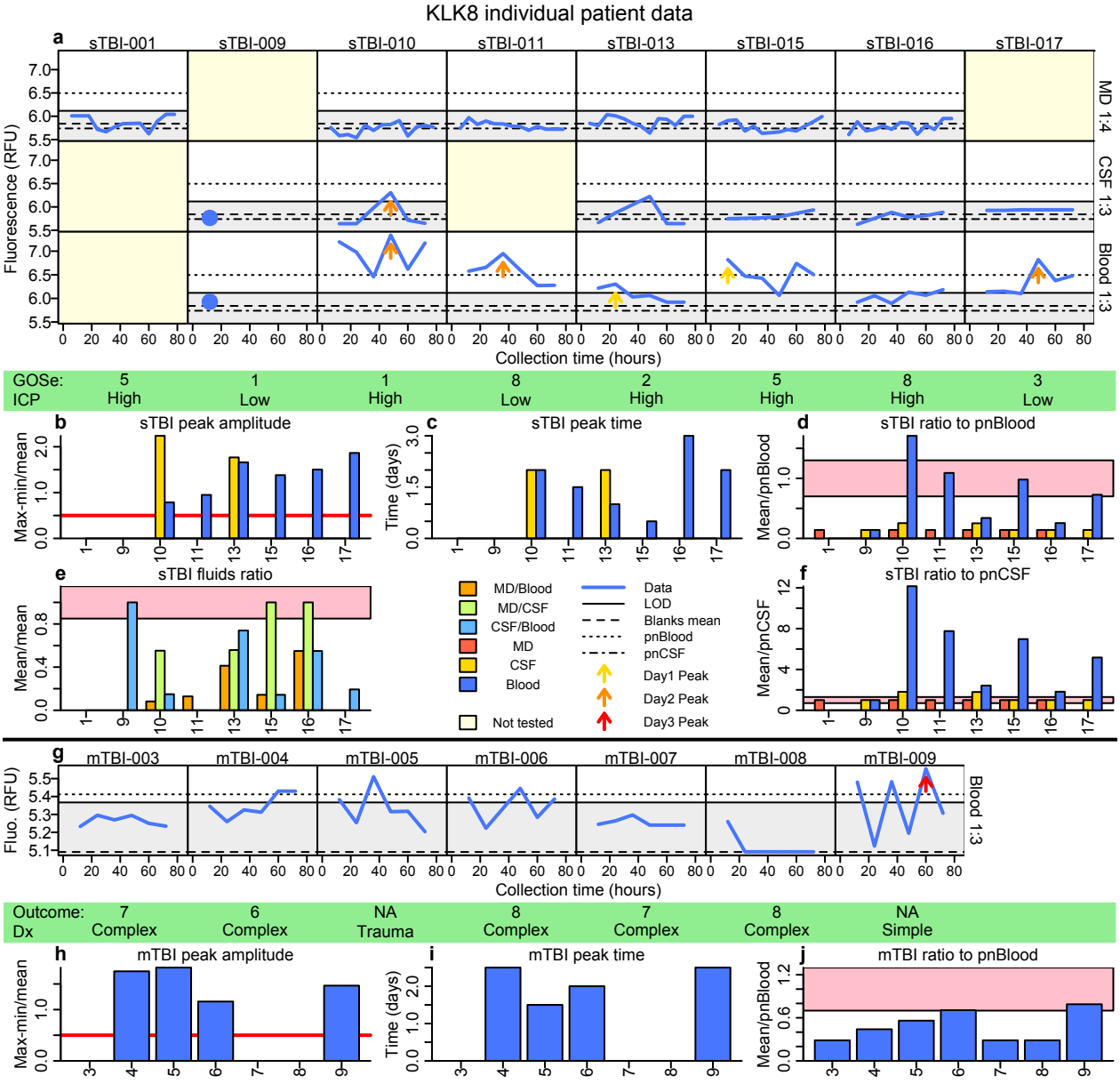

FIGURE J.S149: **Individual KLK8 protein profiles and peak and ratio analysis.** KLK8 concentration in microdialysate, CSF and blood samples of individual sTBI patients (**a**) and mTBI/trauma patients (**g**) was measured and peak amplitude and time, as well as ratio between mean time course values to value found in the pooled normal control (**b-f, h-j**) were calculated for each patient. Graphs **b-f** show calculations for individual sTBI patients, and graphs **h-j** show calculations for individual mTBI patients. Red lines in **b, h** show a threshold for a profile that is considered to have a peak, rather than being constant. The light red boxes in **d, e, f, j** show the threshold of comparison to the measured value compared.

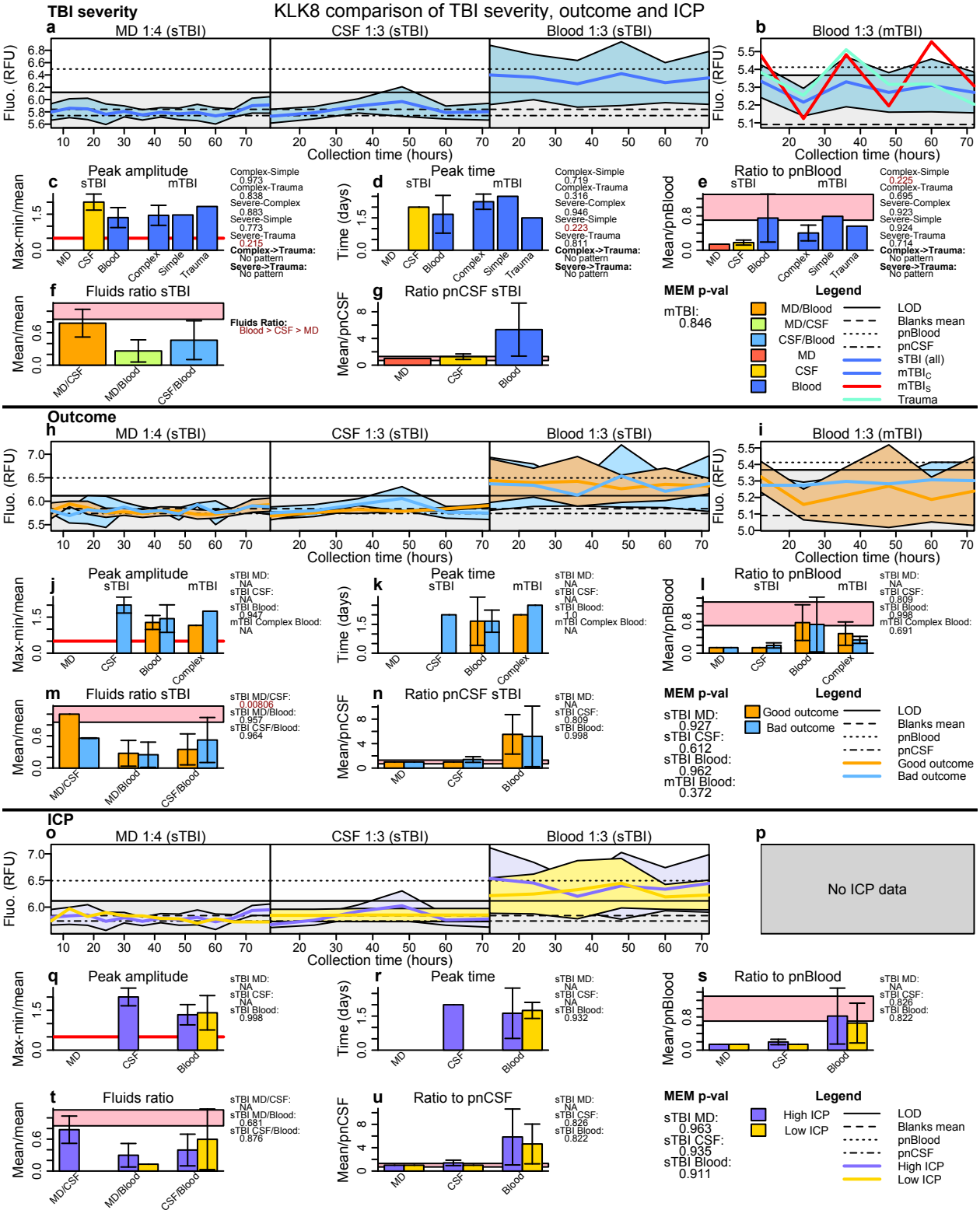

FIGURE J.S150: **Differential KLK8 protein profiles and peak and ratio analysis with respect to TBI severity, outcome and ICP.** Average KLK8 profiles are compared in terms of TBI severity (**a-g**), outcome (**h-n**) and ICP (**o-u**). Polygons in **a, b, h, i, o** indicate the mean value ±1 SD at each time point. Red lines in **c, j, q** show a threshold for a profile that is considered to have a peak, rather than being constant. The light red boxes in **e-g, l-n, s-u** show the threshold of comparison to the measured value compared. Benjamini–Hochberg adjusted p-values for comparisons are shown on the right of every graph.

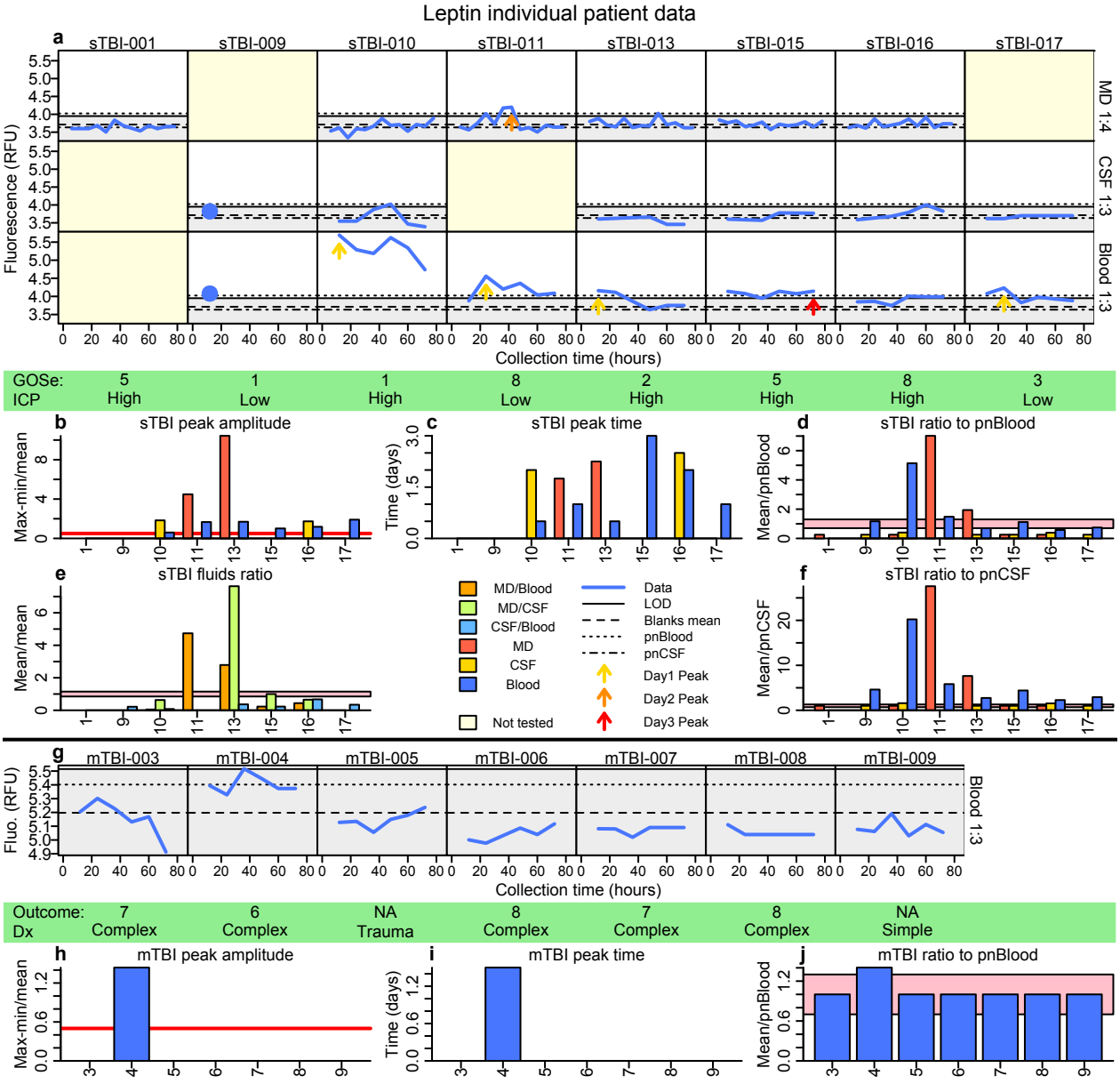

FIGURE J.S151: **Individual Leptin protein profiles and peak and ratio analysis.** Leptin concentration in microdialysate, CSF and blood samples of individual sTBI patients (**a**) and mTBI/trauma patients (**g**) was measured and peak amplitude and time, as well as ratio between mean time course values to value found in the pooled normal control (**b-f, h-j**) were calculated for each patient. Graphs **b-f** show calculations for individual sTBI patients, and graphs **h-j** show calculations for individual mTBI patients. Red lines in **b, h** show a threshold for a profile that is considered to have a peak, rather than being constant. The light red boxes in **d, e, f, j** show the threshold of comparison to the measured value compared.

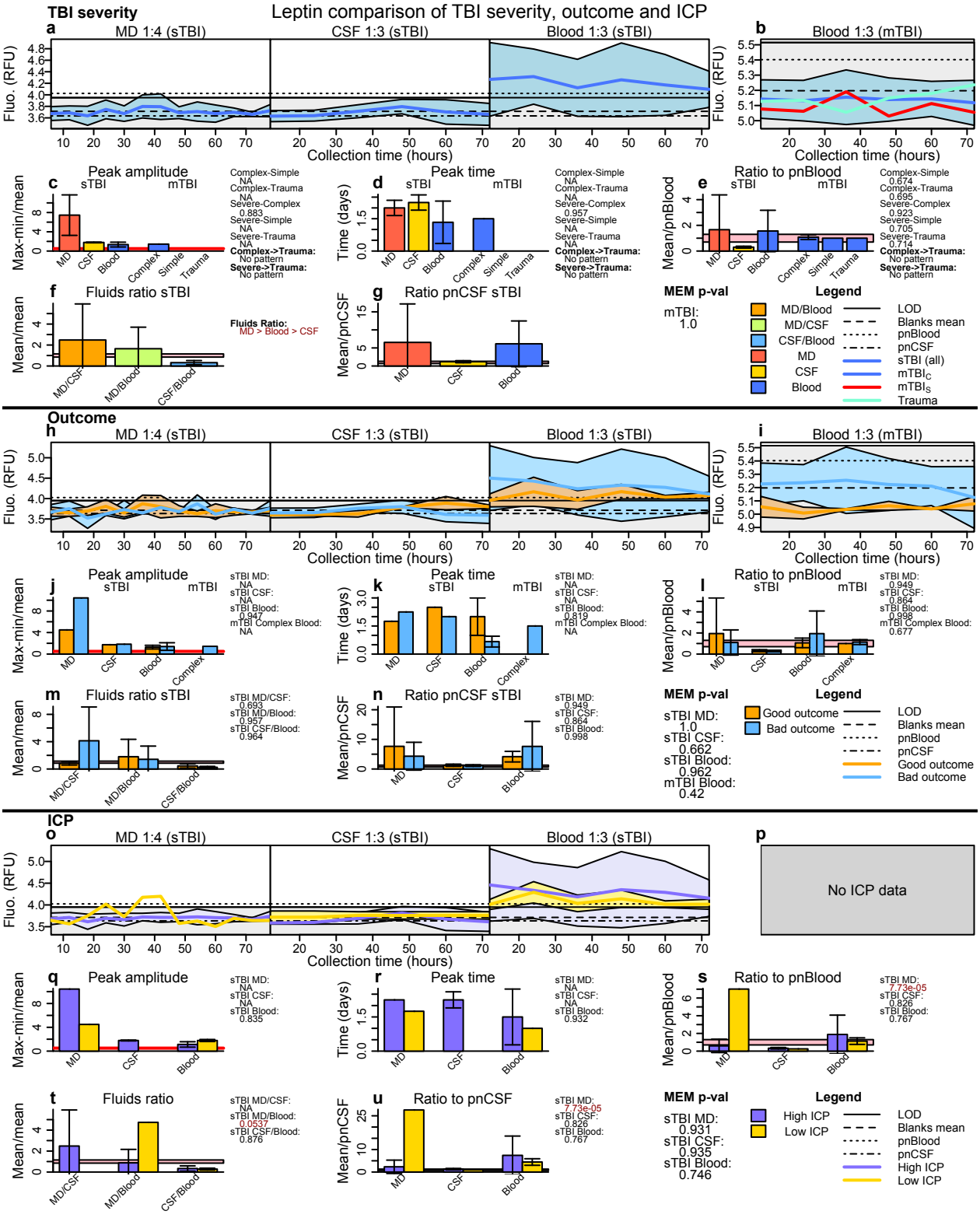

FIGURE J.S152: **Differential Leptin protein profiles and peak and ratio analysis with respect to TBI severity, outcome and ICP.** Average Leptin profiles are compared in terms of TBI severity (**a-g**), outcome (**h-n**) and ICP (**o-u**). Polygons in **a, b, h, i, o** indicate the mean value ±1 SD at each time point. Red lines in **c, j, q** show a threshold for a profile that is considered to have a peak, rather than being constant. The light red boxes in **e-g, l-n, s-u** show the threshold of comparison to the measured value compared. Benjamini–Hochberg adjusted p-values for comparisons are shown on the right of every graph.

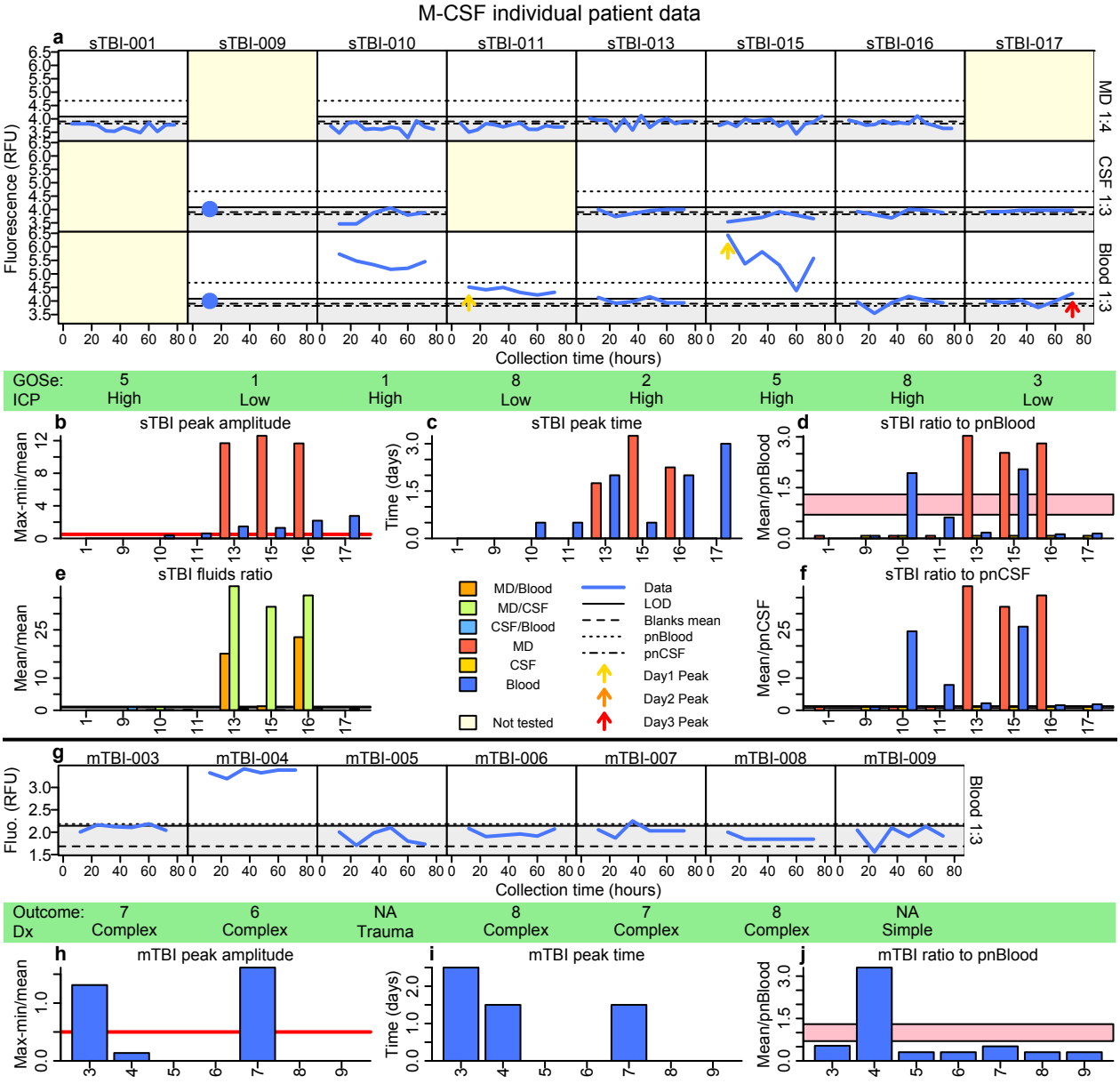

FIGURE J.S153: **Individual M-CSF protein profiles and peak and ratio analysis.** M-CSF concentration in microdialysate, CSF and blood samples of individual sTBI patients (**a**) and mTBI/trauma patients (**g**) was measured and peak amplitude and time, as well as ratio between mean time course values to value found in the pooled normal control (**b-f, h-j**) were calculated for each patient. Graphs **b-f** show calculations for individual sTBI patients, and graphs **h-j** show calculations for individual mTBI patients. Red lines in **b, h** show a threshold for a profile that is considered to have a peak, rather than being constant. The light red boxes in **d, e, f, j** show the threshold of comparison to the measured value compared.

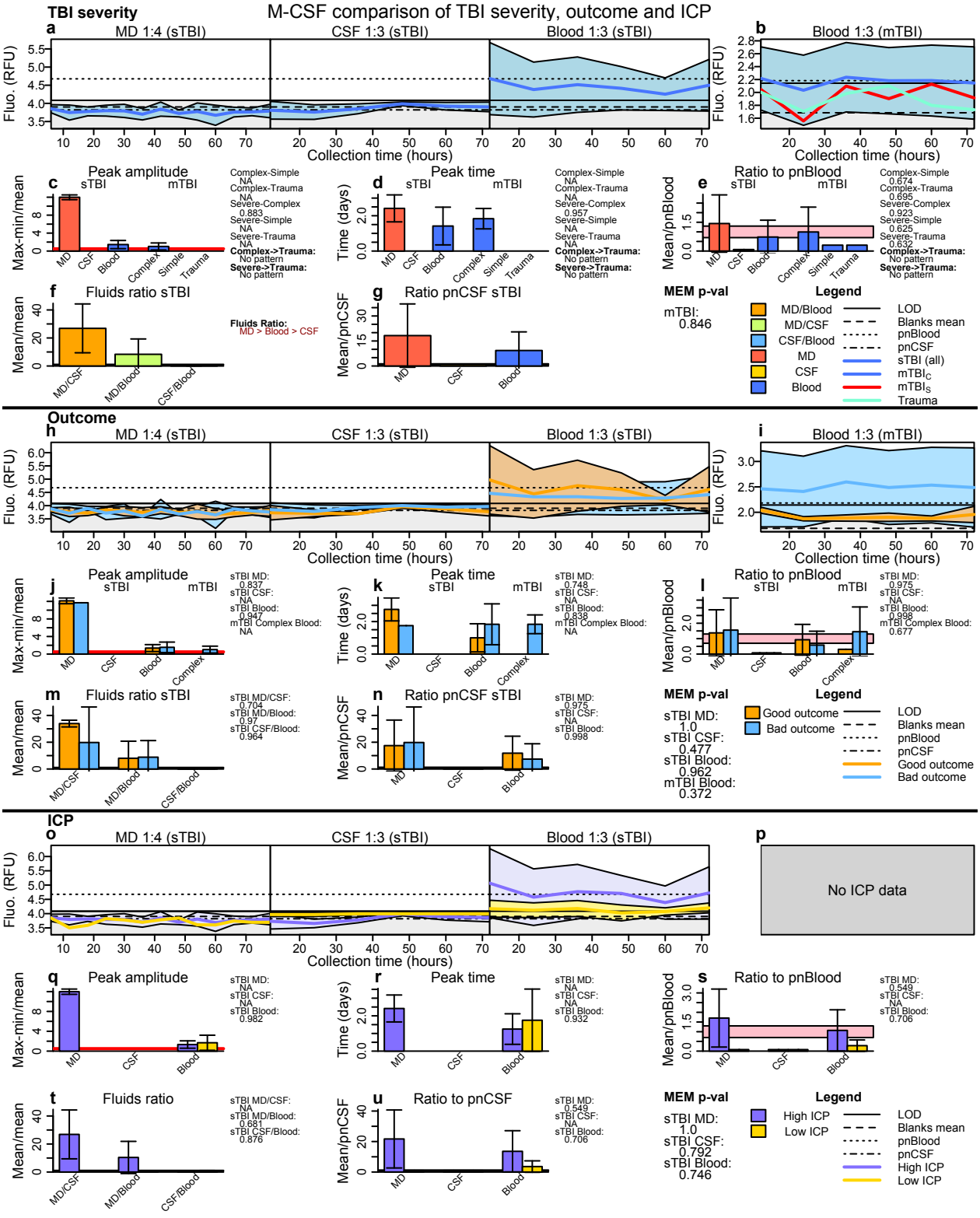

FIGURE J.S154: **Differential M-CSF protein profiles and peak and ratio analysis with respect to TBI severity, outcome and ICP.** Average M-CSF profiles are compared in terms of TBI severity (**a-g**), outcome (**h-n**) and ICP (**o-u**). Polygons in **a, b, h, i, o** indicate the mean value ±1 SD at each time point. Red lines in **c, j, q** show a threshold for a profile that is considered to have a peak, rather than being constant. The light red boxes in **e-g, l-n, s-u** show the threshold of comparison to the measured value compared. Benjamini–Hochberg adjusted p-values for comparisons are shown on the right of every graph.

FIGURE J.S155: **Individual MCP1 protein profiles and peak and ratio analysis.** MCP1 concentration in microdialysate, CSF and blood samples of individual sTBI patients (**a**) and mTBI/trauma patients (**g**) was measured and peak amplitude and time, as well as ratio between mean time course values to value found in the pooled normal control (**b-f, h-j**) were calculated for each patient. Graphs **b-f** show calculations for individual sTBI patients, and graphs **h-j** show calculations for individual mTBI patients. Red lines in **b, h** show a threshold for a profile that is considered to have a peak, rather than being constant. The light red boxes in **d, e, f, j** show the threshold of comparison to the measured value compared.

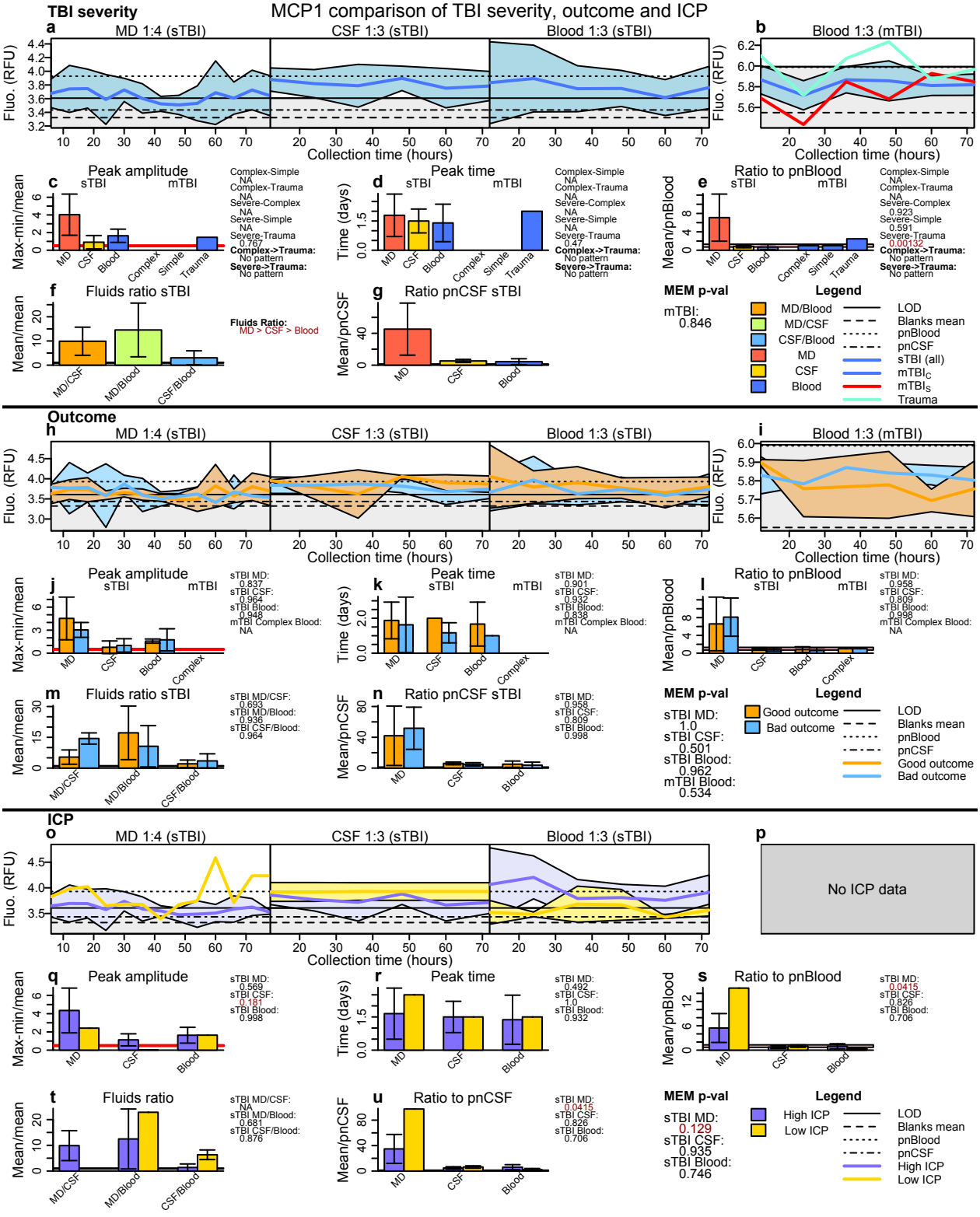

FIGURE J.S156: **Differential MCP1 protein profiles and peak and ratio analysis with respect to TBI severity, outcome and ICP.** Average MCP1 profiles are compared in terms of TBI severity (**a-g**), outcome (**h-n**) and ICP (**o-u**). Polygons in **a, b, h, i, o** indicate the mean value ±1 SD at each time point. Red lines in **c, j, q** show a threshold for a profile that is considered to have a peak, rather than being constant. The light red boxes in **e-g, l-n, s-u** show the threshold of comparison to the measured value compared. Benjamini–Hochberg adjusted p-values for comparisons are shown on the right of every graph.

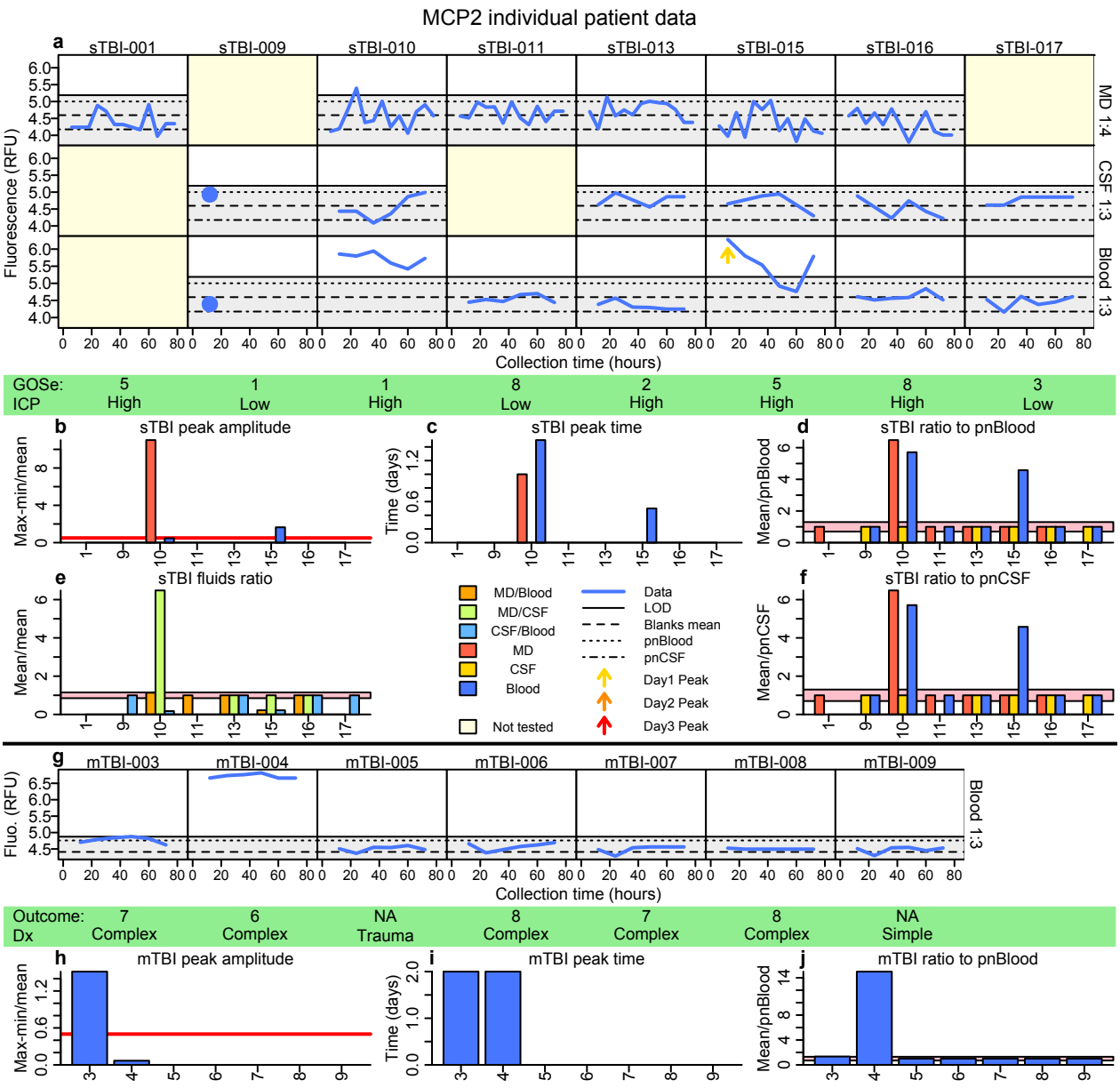

FIGURE J.S157: **Individual MCP2 protein profiles and peak and ratio analysis.** MCP2 concentration in microdialysate, CSF and blood samples of individual sTBI patients (**a**) and mTBI/trauma patients (**g**) was measured and peak amplitude and time, as well as ratio between mean time course values to value found in the pooled normal control (**b-f, h-j**) were calculated for each patient. Graphs **b-f** show calculations for individual sTBI patients, and graphs **h-j** show calculations for individual mTBI patients. Red lines in **b, h** show a threshold for a profile that is considered to have a peak, rather than being constant. The light red boxes in **d, e, f, j** show the threshold of comparison to the measured value compared.

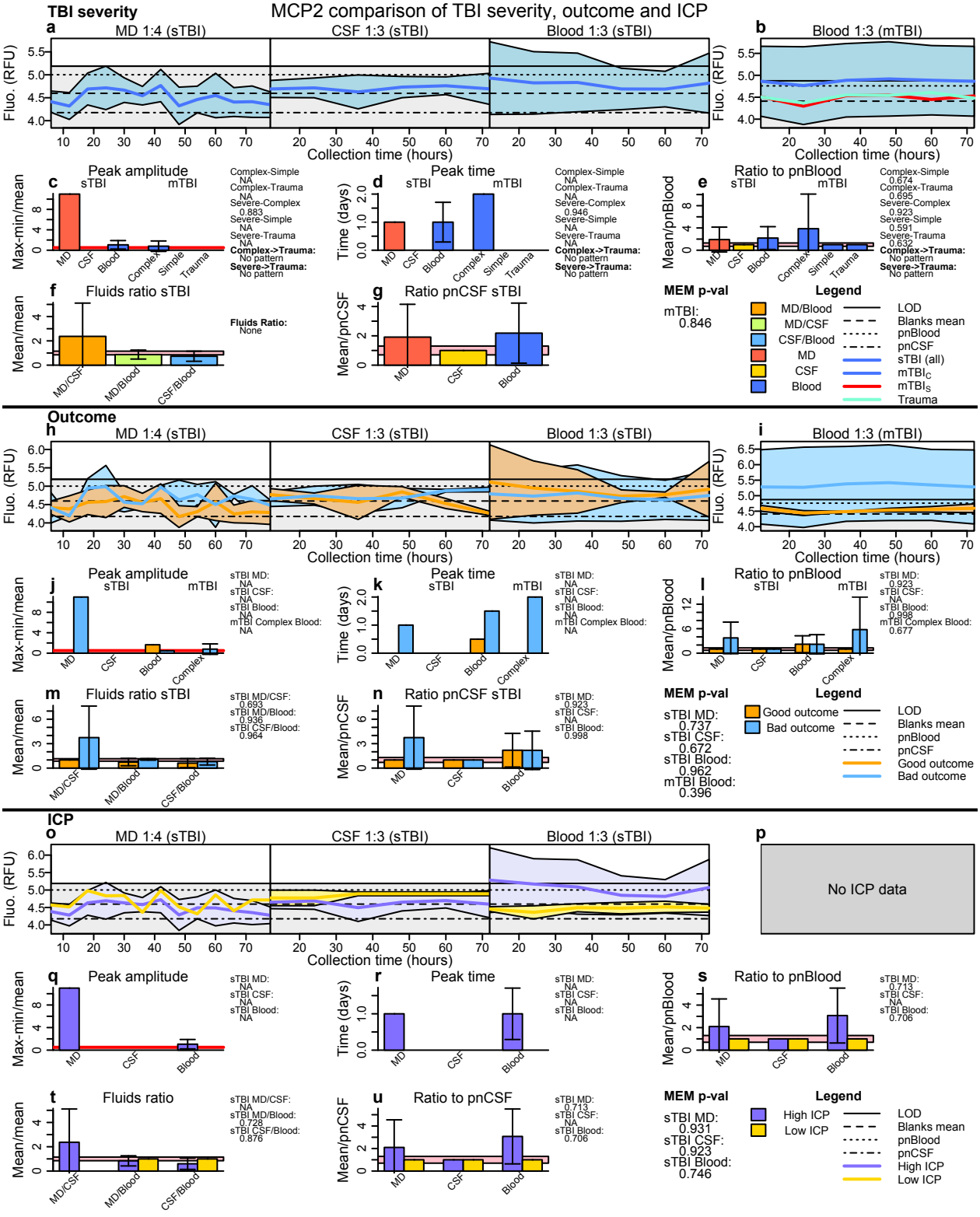

FIGURE J.S158: **Differential MCP2 protein profiles and peak and ratio analysis with respect to TBI severity, outcome and ICP.** Average MCP2 profiles are compared in terms of TBI severity (**a-g**), outcome (**h-n**) and ICP (**o-u**). Polygons in **a, b, h, i, o** indicate the mean value ±1 SD at each time point. Red lines in **c, j, q** show a threshold for a profile that is considered to have a peak, rather than being constant. The light red boxes in **e-g, l-n, s-u** show the threshold of comparison to the measured value compared. Benjamini–Hochberg adjusted p-values for comparisons are shown on the right of every graph.

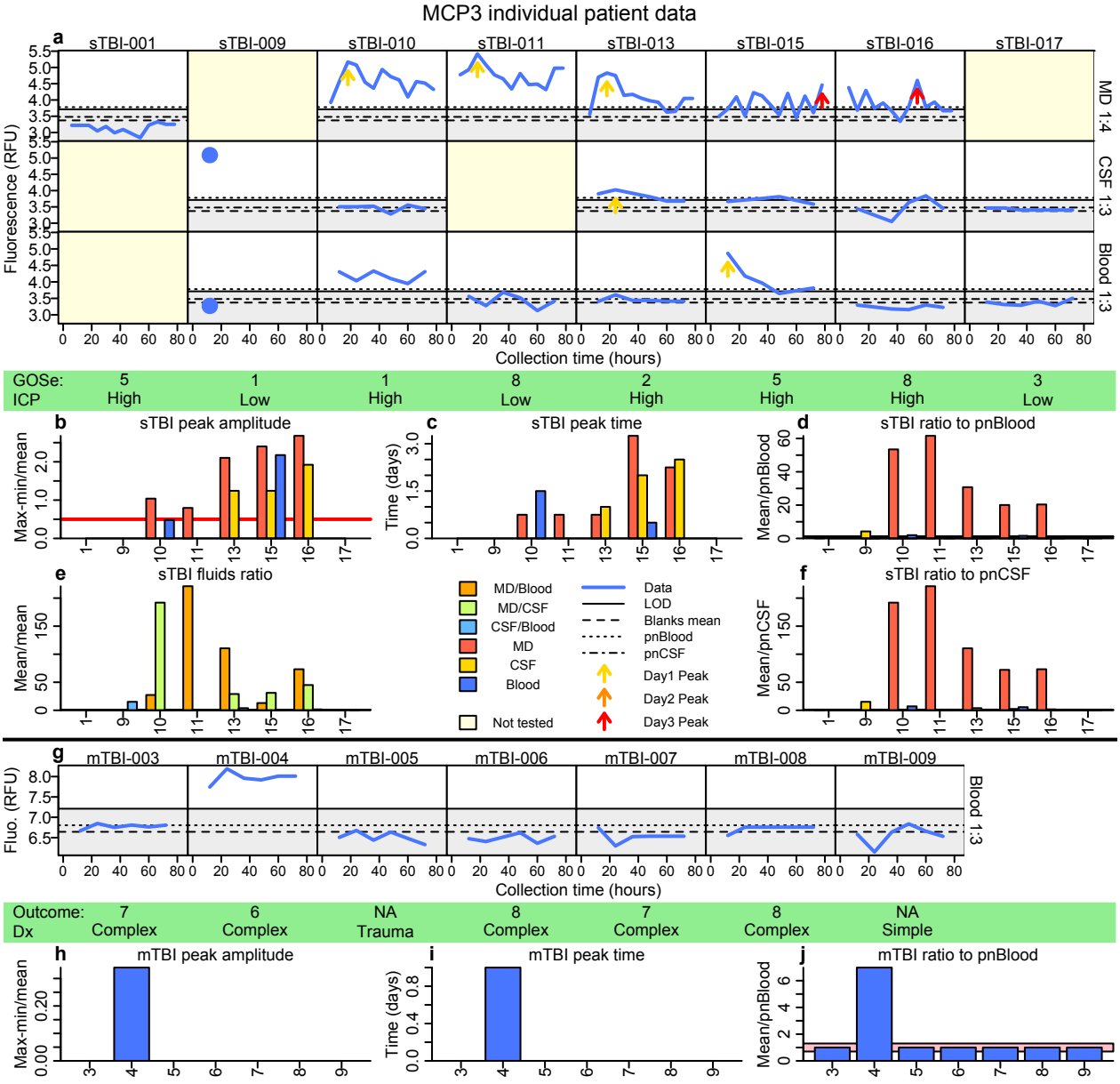

FIGURE J.S159: **Individual MCP3 protein profiles and peak and ratio analysis.** MCP3 concentration in microdialysate, CSF and blood samples of individual sTBI patients (**a**) and mTBI/trauma patients (**g**) was measured and peak amplitude and time, as well as ratio between mean time course values to value found in the pooled normal control (**b-f, h-j**) were calculated for each patient. Graphs **b-f** show calculations for individual sTBI patients, and graphs **h-j** show calculations for individual mTBI patients. Red lines in **b, h** show a threshold for a profile that is considered to have a peak, rather than being constant. The light red boxes in **d, e, f, j** show the threshold of comparison to the measured value compared.

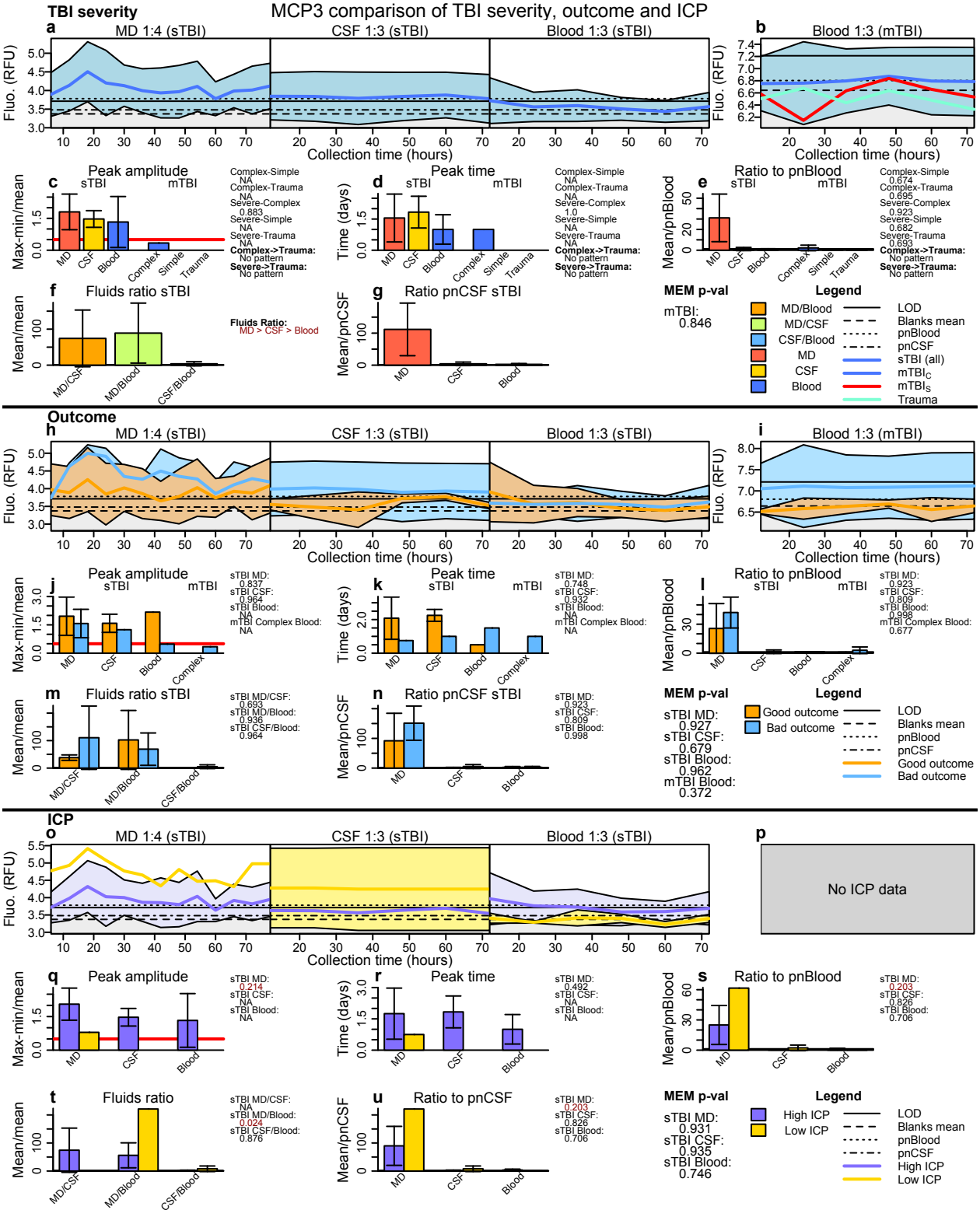

FIGURE J.S160: **Differential MCP3 protein profiles and peak and ratio analysis with respect to TBI severity, outcome and ICP.** Average MCP3 profiles are compared in terms of TBI severity (**a-g**), outcome (**h-n**) and ICP (**o-u**). Polygons in **a, b, h, i, o** indicate the mean value ±1 SD at each time point. Red lines in **c, j, q** show a threshold for a profile that is considered to have a peak, rather than being constant. The light red boxes in **e-g, l-n, s-u** show the threshold of comparison to the measured value compared. Benjamini–Hochberg adjusted p-values for comparisons are shown on the right of every graph.

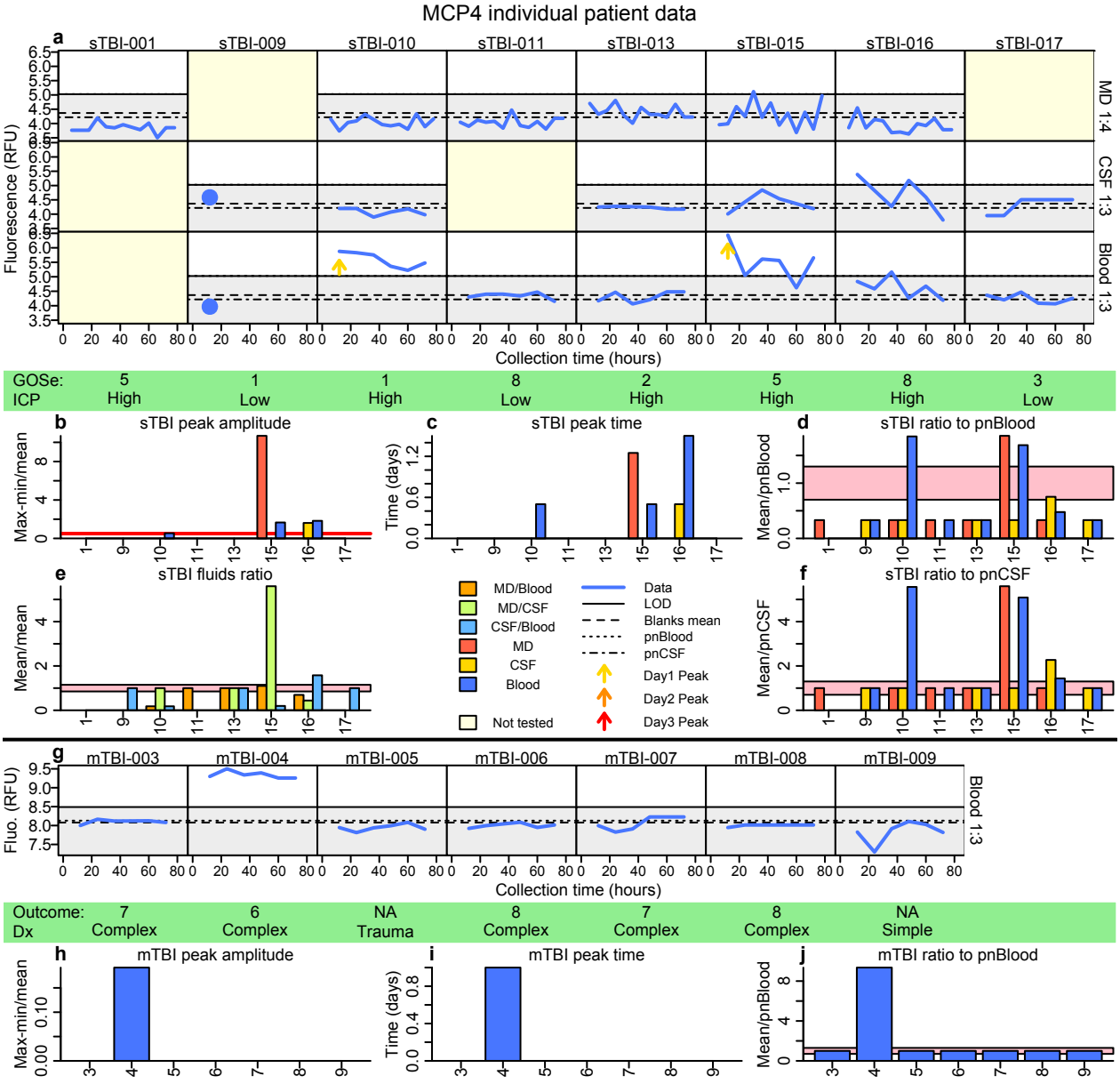

FIGURE J.S161: **Individual MCP4 protein profiles and peak and ratio analysis.** MCP4 concentration in microdialysate, CSF and blood samples of individual sTBI patients (**a**) and mTBI/trauma patients (**g**) was measured and peak amplitude and time, as well as ratio between mean time course values to value found in the pooled normal control (**b-f, h-j**) were calculated for each patient. Graphs **b-f** show calculations for individual sTBI patients, and graphs **h-j** show calculations for individual mTBI patients. Red lines in **b, h** show a threshold for a profile that is considered to have a peak, rather than being constant. The light red boxes in **d, e, f, j** show the threshold of comparison to the measured value compared.

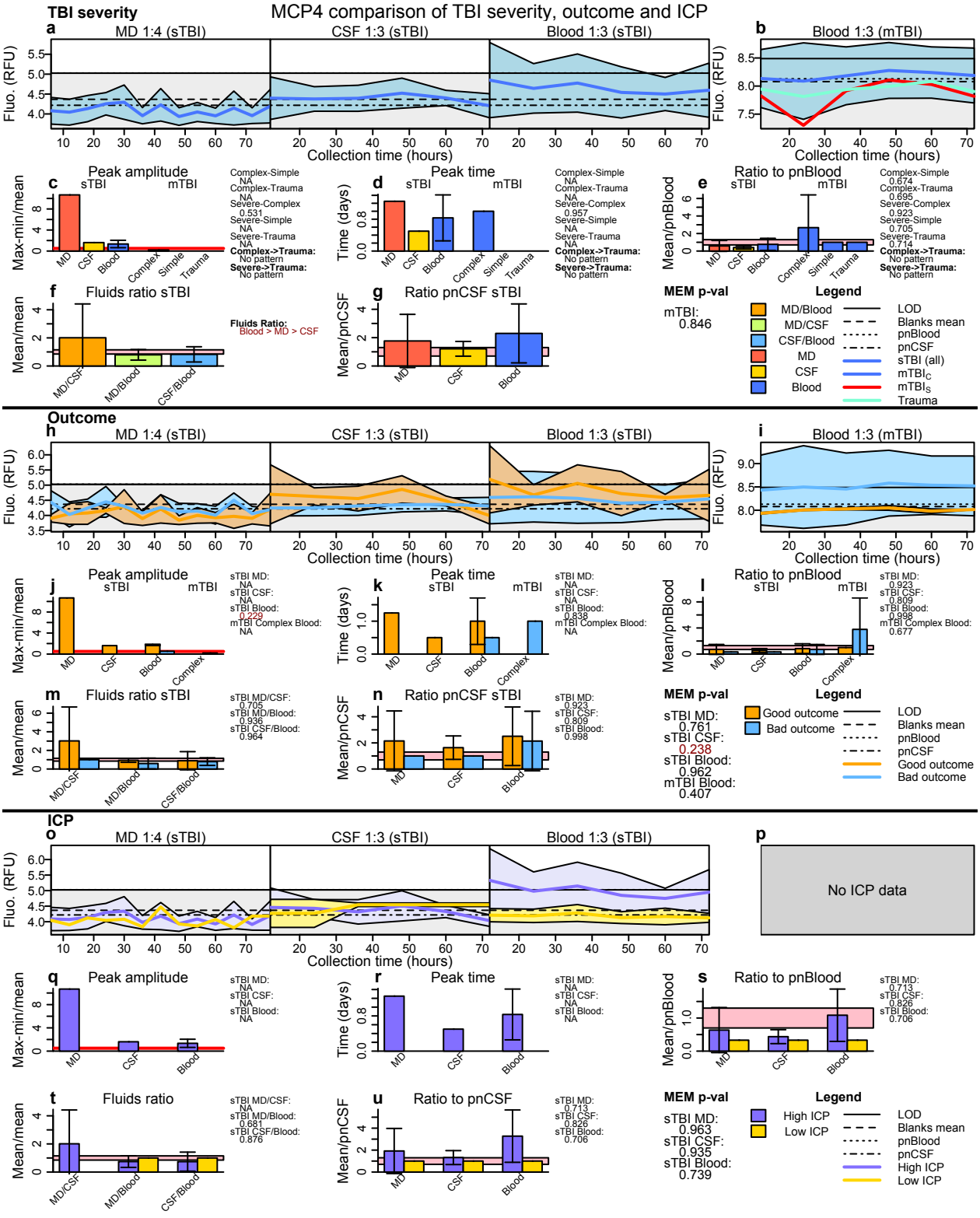

FIGURE J.S162: **Differential MCP4 protein profiles and peak and ratio analysis with respect to TBI severity, outcome and ICP.** Average MCP4 profiles are compared in terms of TBI severity (**a-g**), outcome (**h-n**) and ICP (**o-u**). Polygons in **a, b, h, i, o** indicate the mean value ±1 SD at each time point. Red lines in **c, j, q** show a threshold for a profile that is considered to have a peak, rather than being constant. The light red boxes in **e-g, l-n, s-u** show the threshold of comparison to the measured value compared. Benjamini–Hochberg adjusted p-values for comparisons are shown on the right of every graph.

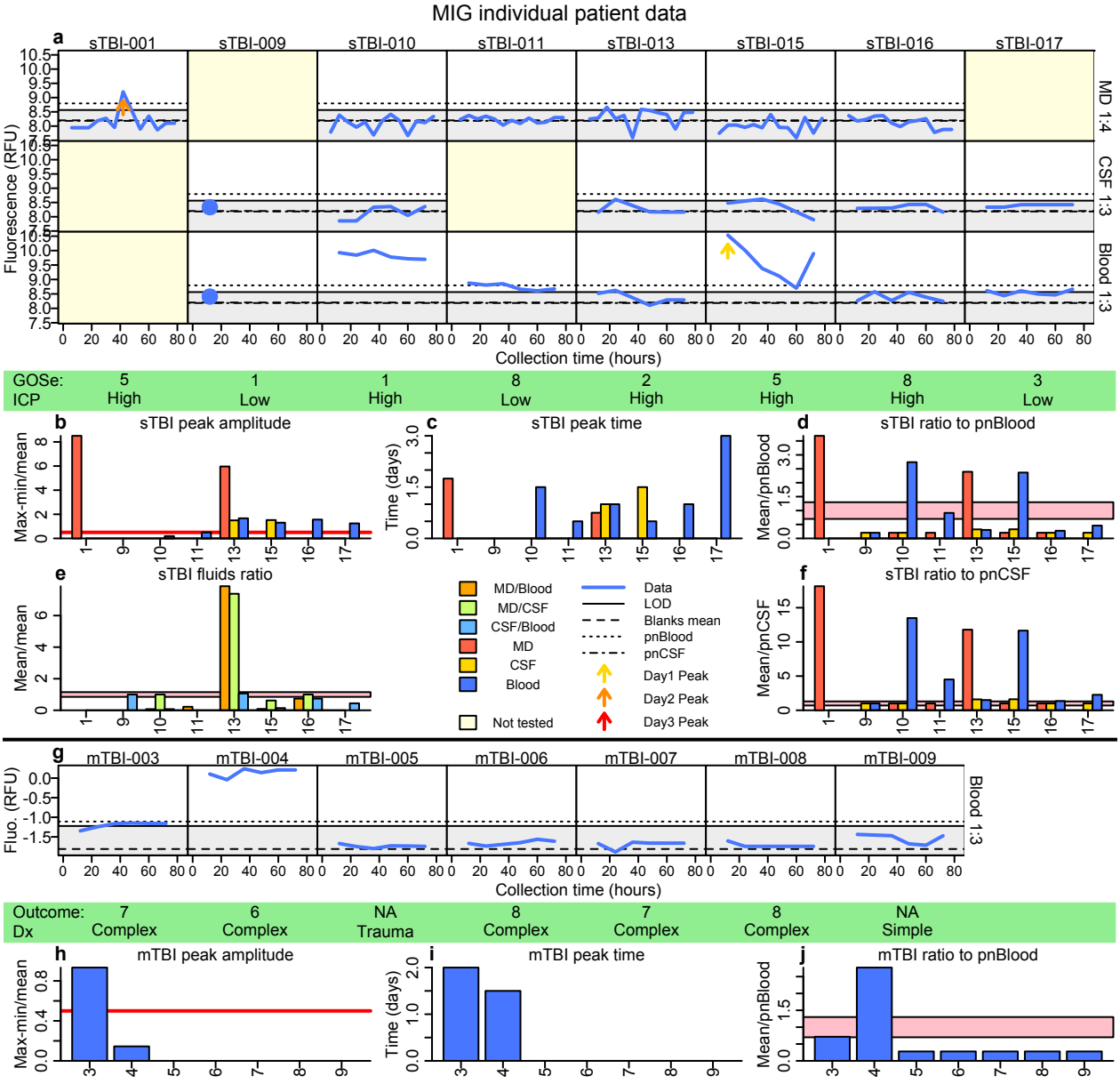

FIGURE J.S163: **Individual MIG protein profiles and peak and ratio analysis.** MIG concentration in microdialysate, CSF and blood samples of individual sTBI patients (**a**) and mTBI/trauma patients (**g**) was measured and peak amplitude and time, as well as ratio between mean time course values to value found in the pooled normal control (**b-f, h-j**) were calculated for each patient. Graphs **b-f** show calculations for individual sTBI patients, and graphs **h-j** show calculations for individual mTBI patients. Red lines in **b, h** show a threshold for a profile that is considered to have a peak, rather than being constant. The light red boxes in **d, e, f, j** show the threshold of comparison to the measured value compared.

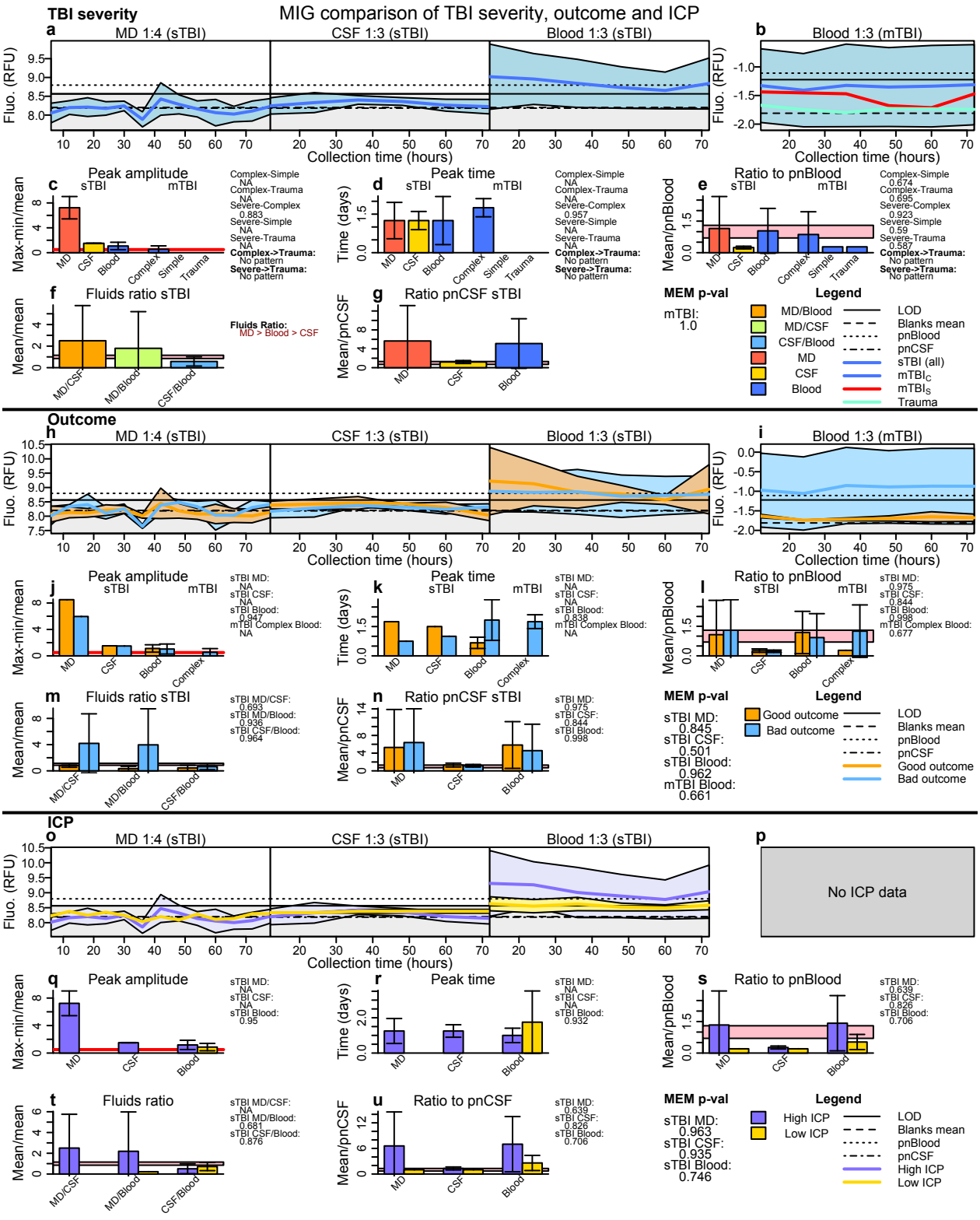

FIGURE J.S164: **Differential MIG protein profiles and peak and ratio analysis with respect to TBI severity, outcome and ICP.** Average MIG profiles are compared in terms of TBI severity (**a-g**), outcome (**h-n**) and ICP (**o-u**). Polygons in **a, b, h, i, o** indicate the mean value ±1 SD at each time point. Red lines in **c, j, q** show a threshold for a profile that is considered to have a peak, rather than being constant. The light red boxes in **e-g, l-n, s-u** show the threshold of comparison to the measured value compared. Benjamini–Hochberg adjusted p-values for comparisons are shown on the right of every graph.

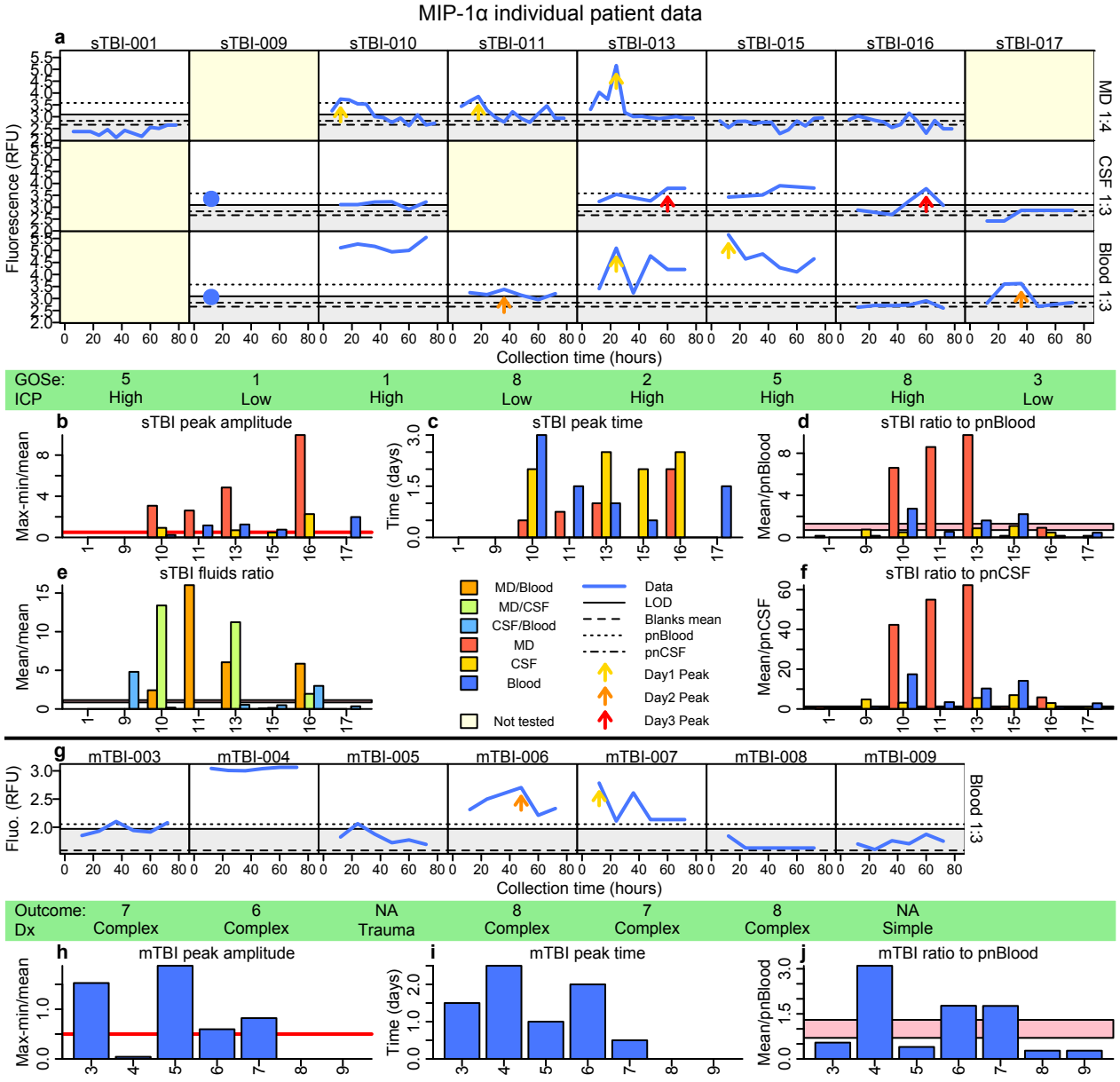

FIGURE J.S165: **Individual MIP-1α protein profiles and peak and ratio analysis.** MIP-1α concentration in microdialysate, CSF and blood samples of individual sTBI patients (**a**) and mTBI/trauma patients (**g**) was measured and peak amplitude and time, as well as ratio between mean time course values to value found in the pooled normal control (**b-f, h-j**) were calculated for each patient. Graphs **b-f** show calculations for individual sTBI patients, and graphs **h-j** show calculations for individual mTBI patients. Red lines in **b, h** show a threshold for a profile that is considered to have a peak, rather than being constant. The light red boxes in **d, e, f, j** show the threshold of comparison to the measured value compared.

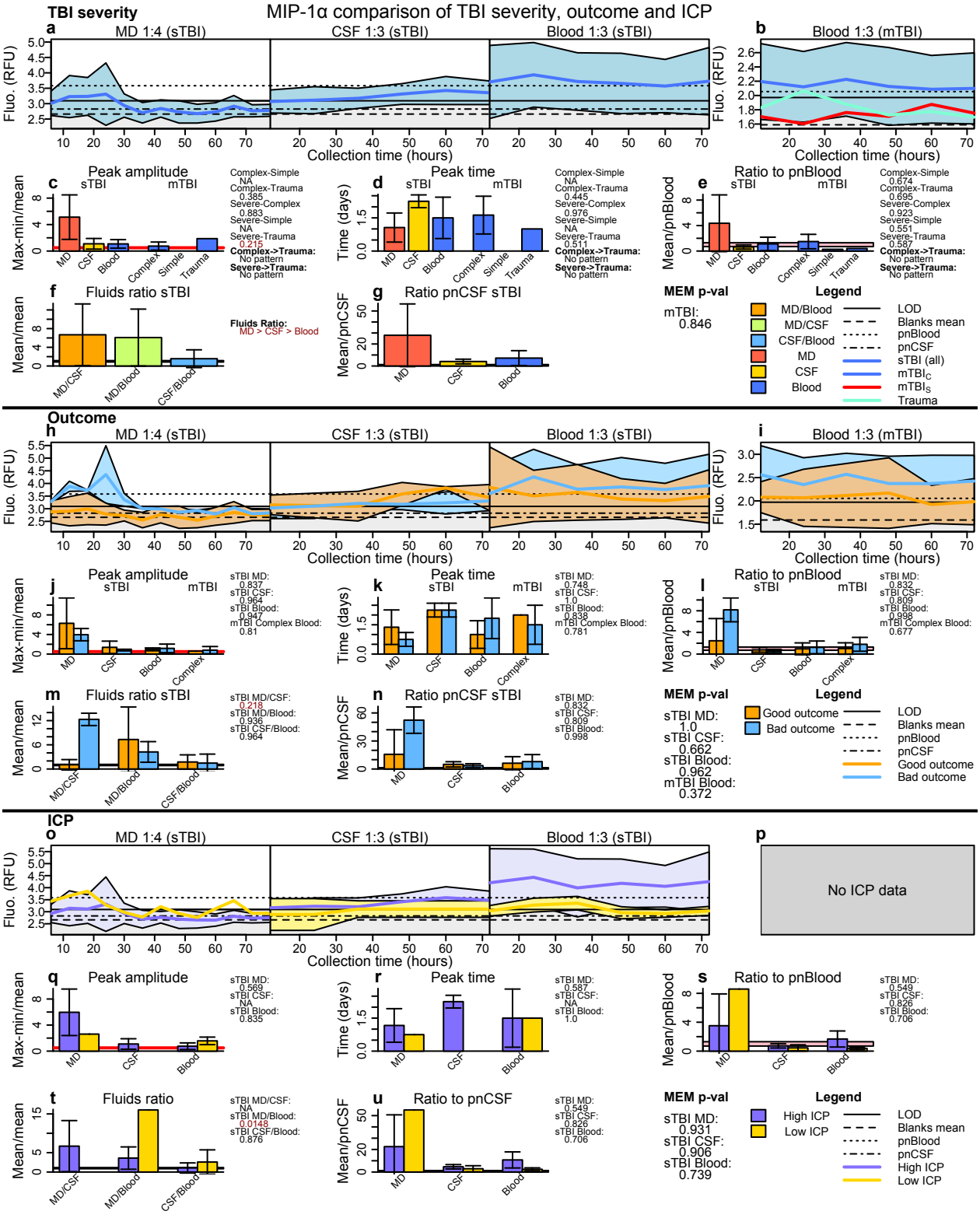

FIGURE J.S166: **Differential MIP-1α protein profiles and peak and ratio analysis with respect to TBI severity, outcome and ICP.** Average MIP-1α profiles are compared in terms of TBI severity (**a-g**), outcome (**h-n**) and ICP (**o-u**). Polygons in **a, b, h, i, o** indicate the mean value ± 1 SD at each time point. Red lines in **c, j, q** show a threshold for a profile that is considered to have a peak, rather than being constant. The light red boxes in **e-g, l-n, s-u** show the threshold of comparison to the measured value compared. Benjamini–Hochberg adjusted p-values for comparisons are shown on the right of every graph.

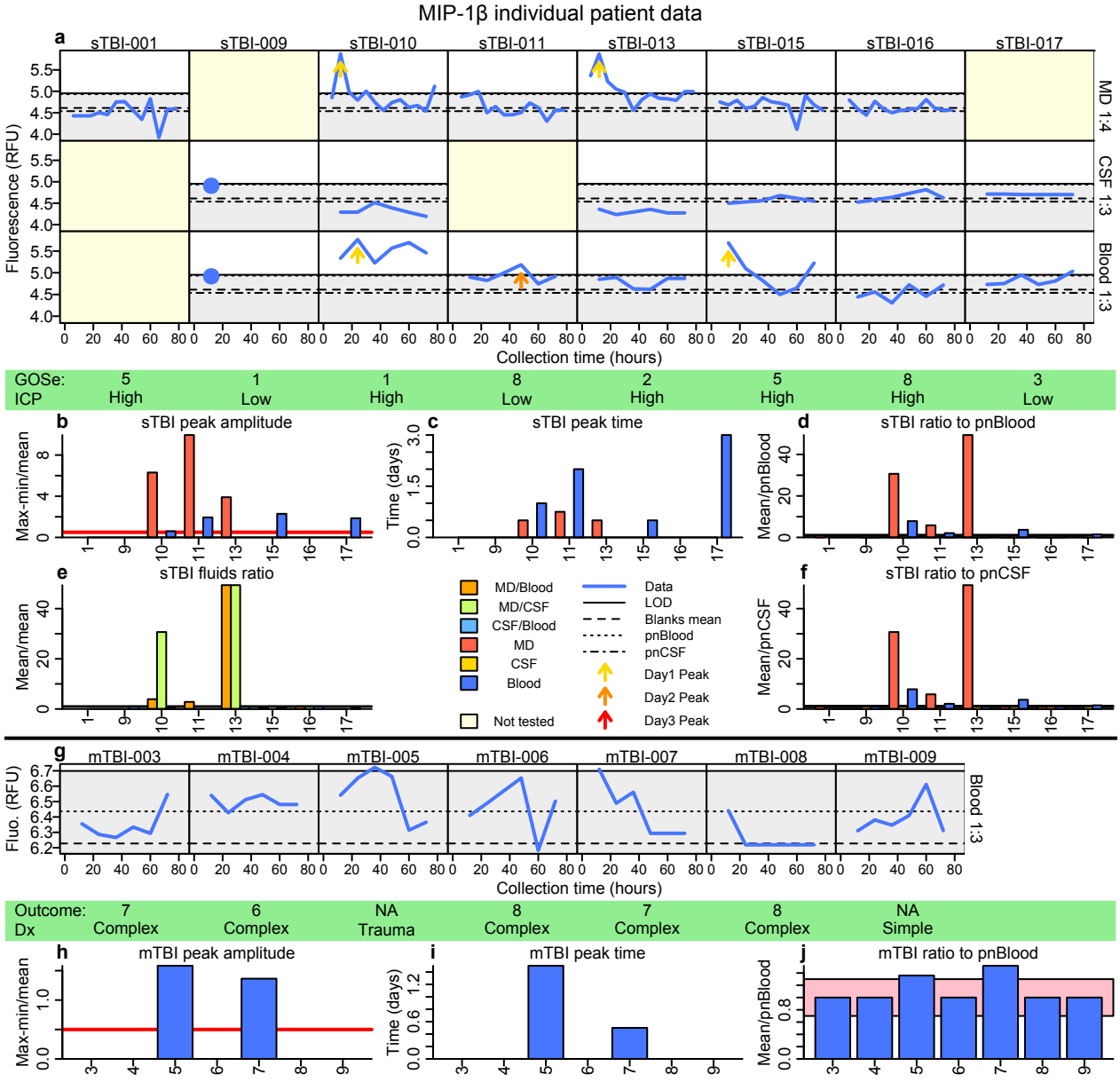

FIGURE J.S167: **Individual MIP-1β protein profiles and peak and ratio analysis.** MIP-1β concentration in microdialysate, CSF and blood samples of individual sTBI patients (**a**) and mTBI/trauma patients (**g**) was measured and peak amplitude and time, as well as ratio between mean time course values to value found in the pooled normal control (**b-f, h-j**) were calculated for each patient. Graphs **b-f** show calculations for individual sTBI patients, and graphs **h-j** show calculations for individual mTBI patients. Red lines in **b, h** show a threshold for a profile that is considered to have a peak, rather than being constant. The light red boxes in **d, e, f, j** show the threshold of comparison to the measured value compared.

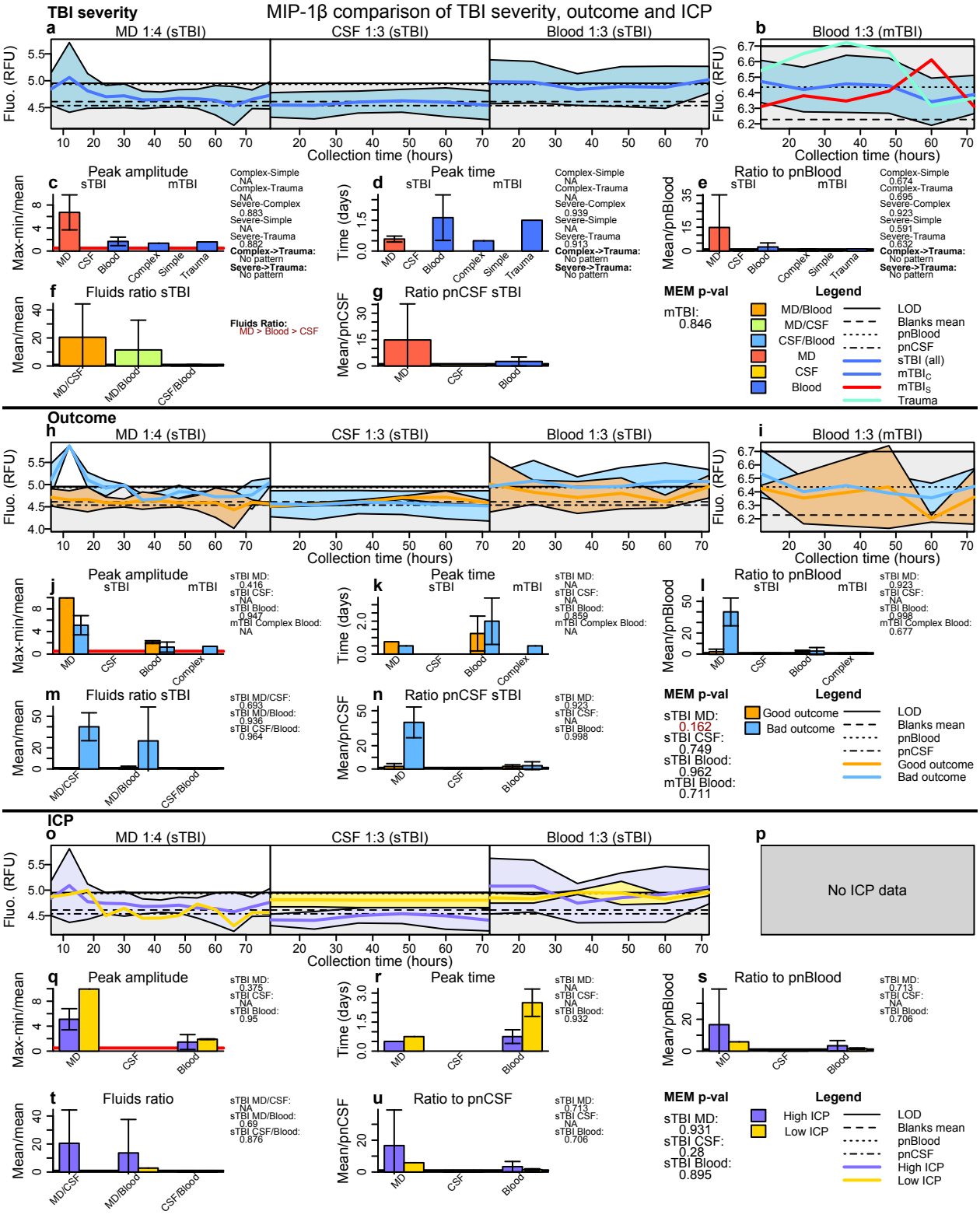

FIGURE J.S168: **Differential MIP-1β protein profiles and peak and ratio analysis with respect to TBI severity, outcome and ICP.** Average MIP-1β profiles are compared in terms of TBI severity (**a-g**), outcome (**h-n**) and ICP (**o-u**). Polygons in **a, b, h, i, o** indicate the mean value ± 1 SD at each time point. Red lines in **c, j, q** show a threshold for a profile that is considered to have a peak, rather than being constant. The light red boxes in **e-g, l-n, s-u** show the threshold of comparison to the measured value compared. Benjamini–Hochberg adjusted p-values for comparisons are shown on the right of every graph.

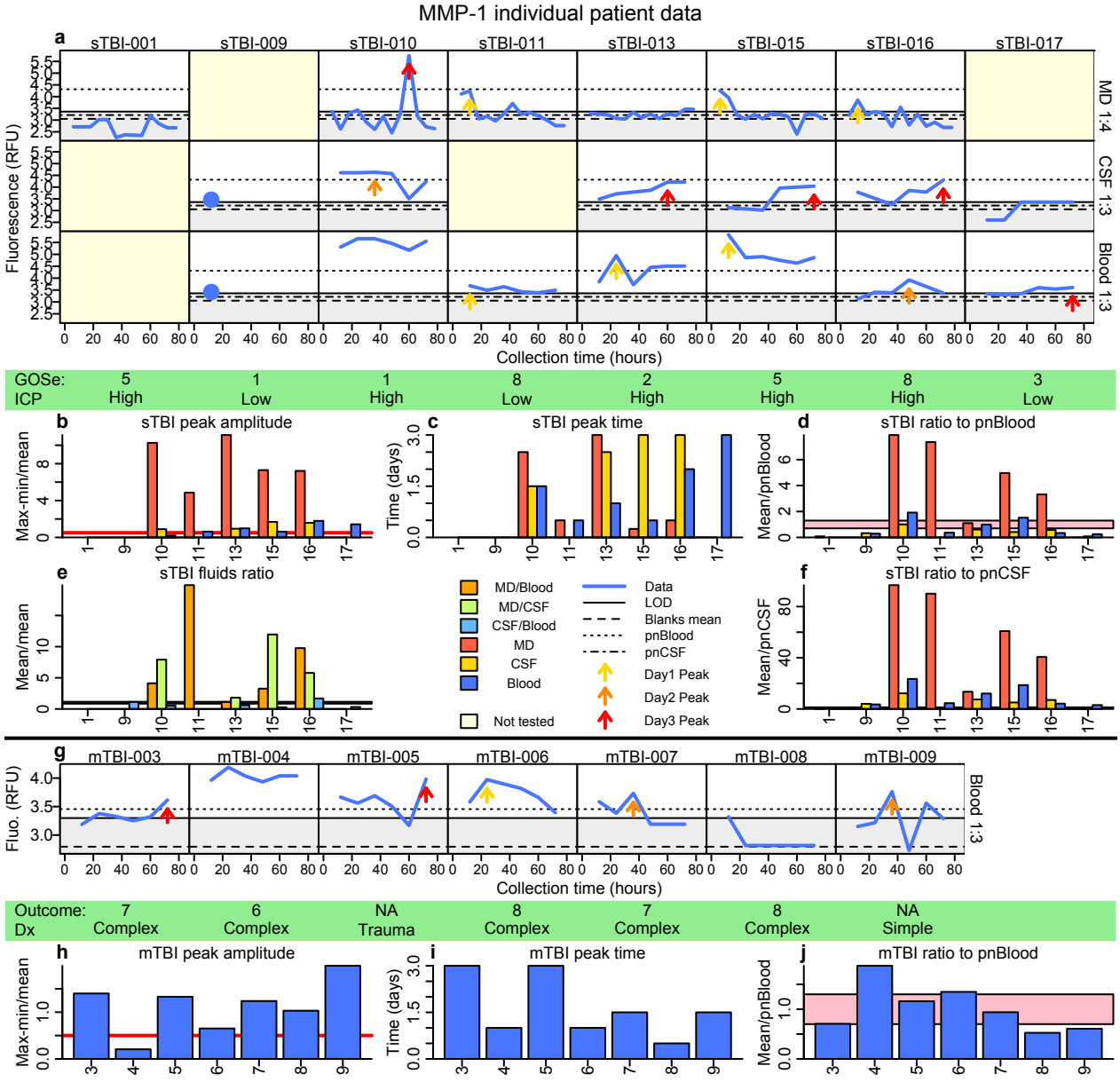

FIGURE J.S169: **Individual MMP-1 protein profiles and peak and ratio analysis.** MMP-1 concentration in microdialysate, CSF and blood samples of individual sTBI patients (**a**) and mTBI/trauma patients (**g**) was measured and peak amplitude and time, as well as ratio between mean time course values to value found in the pooled normal control (**b-f, h-j**) were calculated for each patient. Graphs **b-f** show calculations for individual sTBI patients, and graphs **h-j** show calculations for individual mTBI patients. Red lines in **b, h** show a threshold for a profile that is considered to have a peak, rather than being constant. The light red boxes in **d, e, f, j** show the threshold of comparison to the measured value compared.

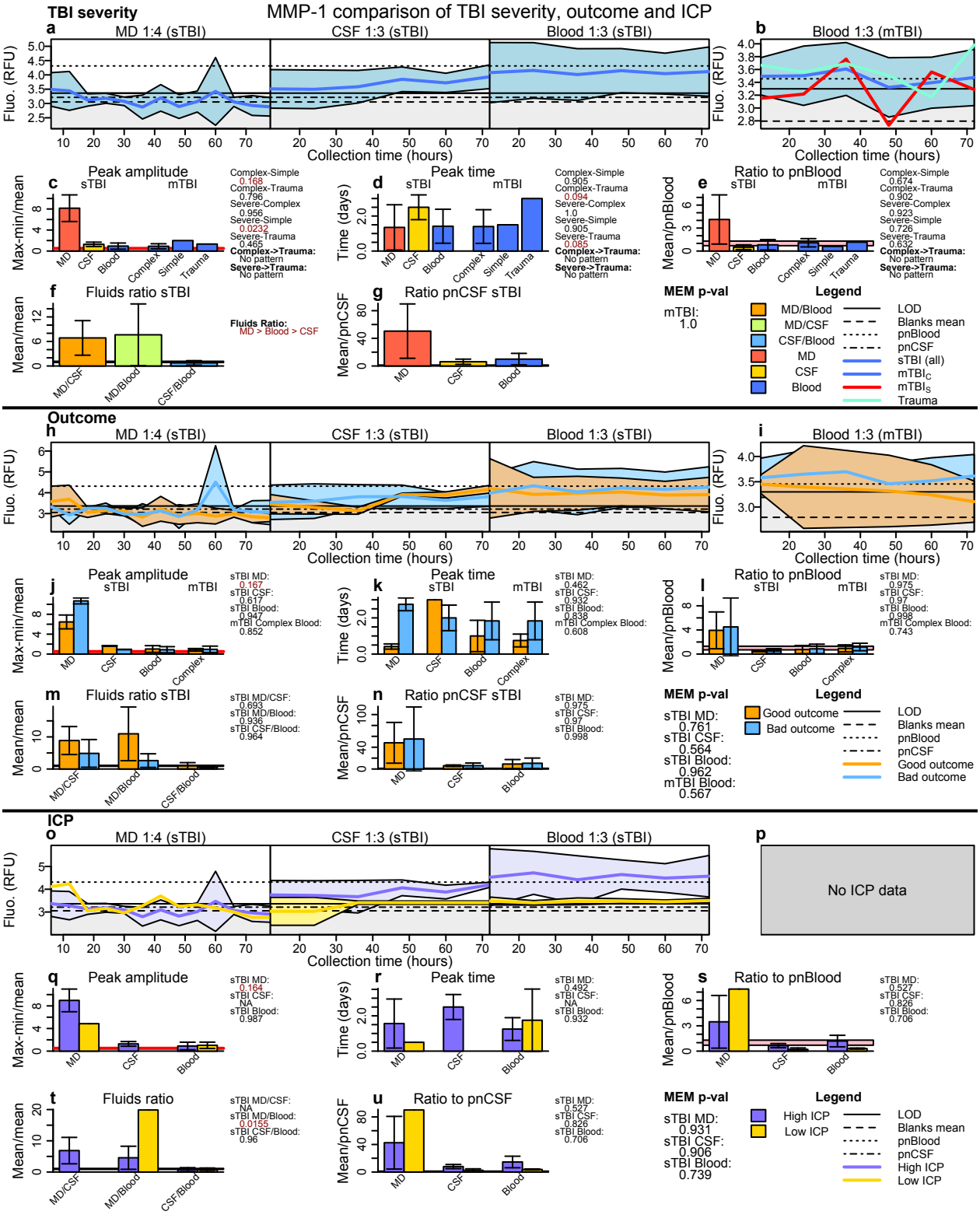

FIGURE J.S170: **Differential MMP-1 protein profiles and peak and ratio analysis with respect to TBI severity, outcome and ICP.** Average MMP-1 profiles are compared in terms of TBI severity (**a-g**), outcome (**h-n**) and ICP (**o-u**). Polygons in **a, b, h, i, o** indicate the mean value ±1 SD at each time point. Red lines in **c, j, q** show a threshold for a profile that is considered to have a peak, rather than being constant. The light red boxes in **e-g, l-n, s-u** show the threshold of comparison to the measured value compared. Benjamini–Hochberg adjusted p-values for comparisons are shown on the right of every graph.

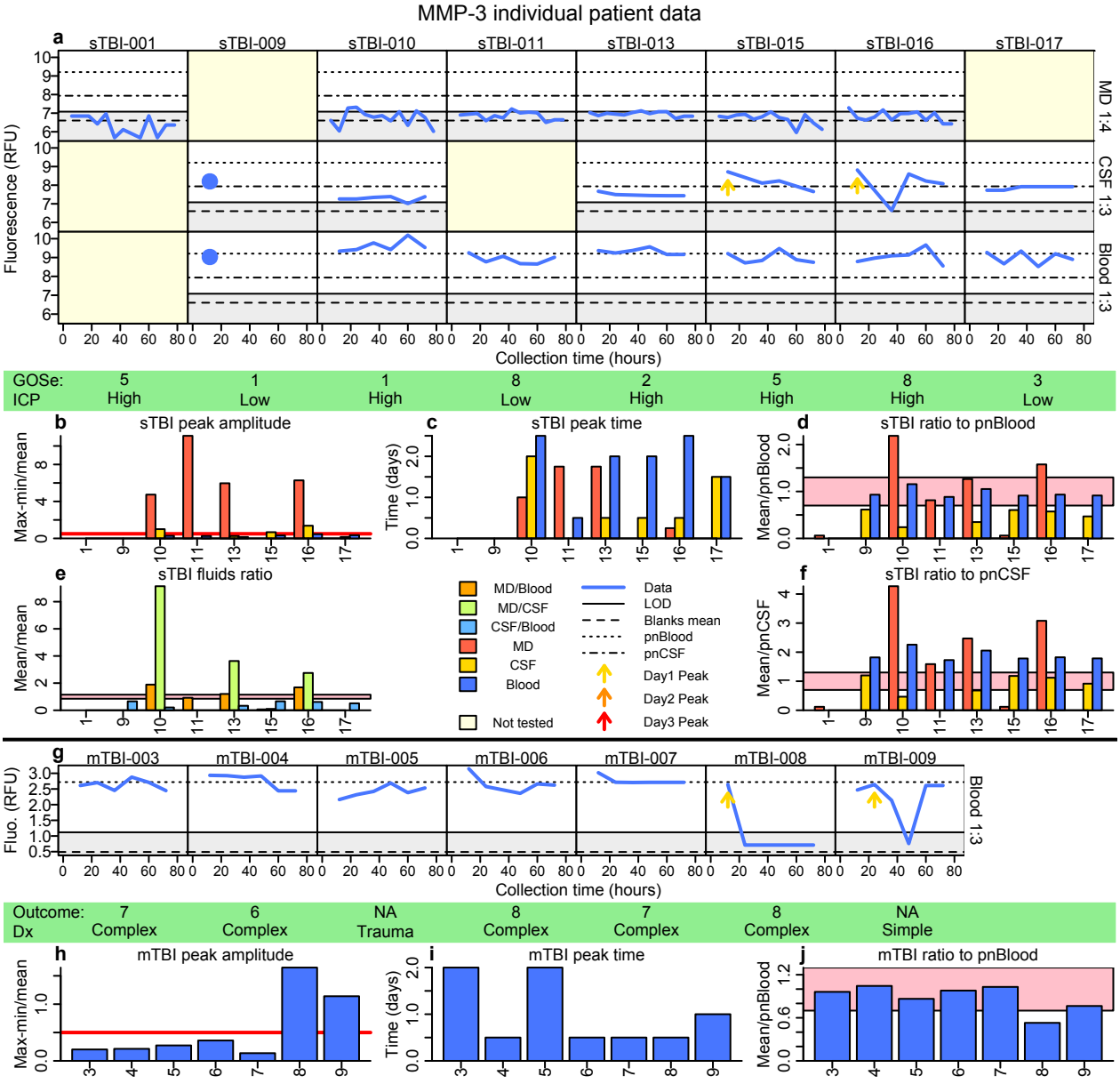

FIGURE J.S171: **Individual MMP-3 protein profiles and peak and ratio analysis.** MMP-3 concentration in microdialysate, CSF and blood samples of individual sTBI patients (**a**) and mTBI/trauma patients (**g**) was measured and peak amplitude and time, as well as ratio between mean time course values to value found in the pooled normal control (**b-f, h-j**) were calculated for each patient. Graphs **b-f** show calculations for individual sTBI patients, and graphs **h-j** show calculations for individual mTBI patients. Red lines in **b, h** show a threshold for a profile that is considered to have a peak, rather than being constant. The light red boxes in **d, e, f, j** show the threshold of comparison to the measured value compared.

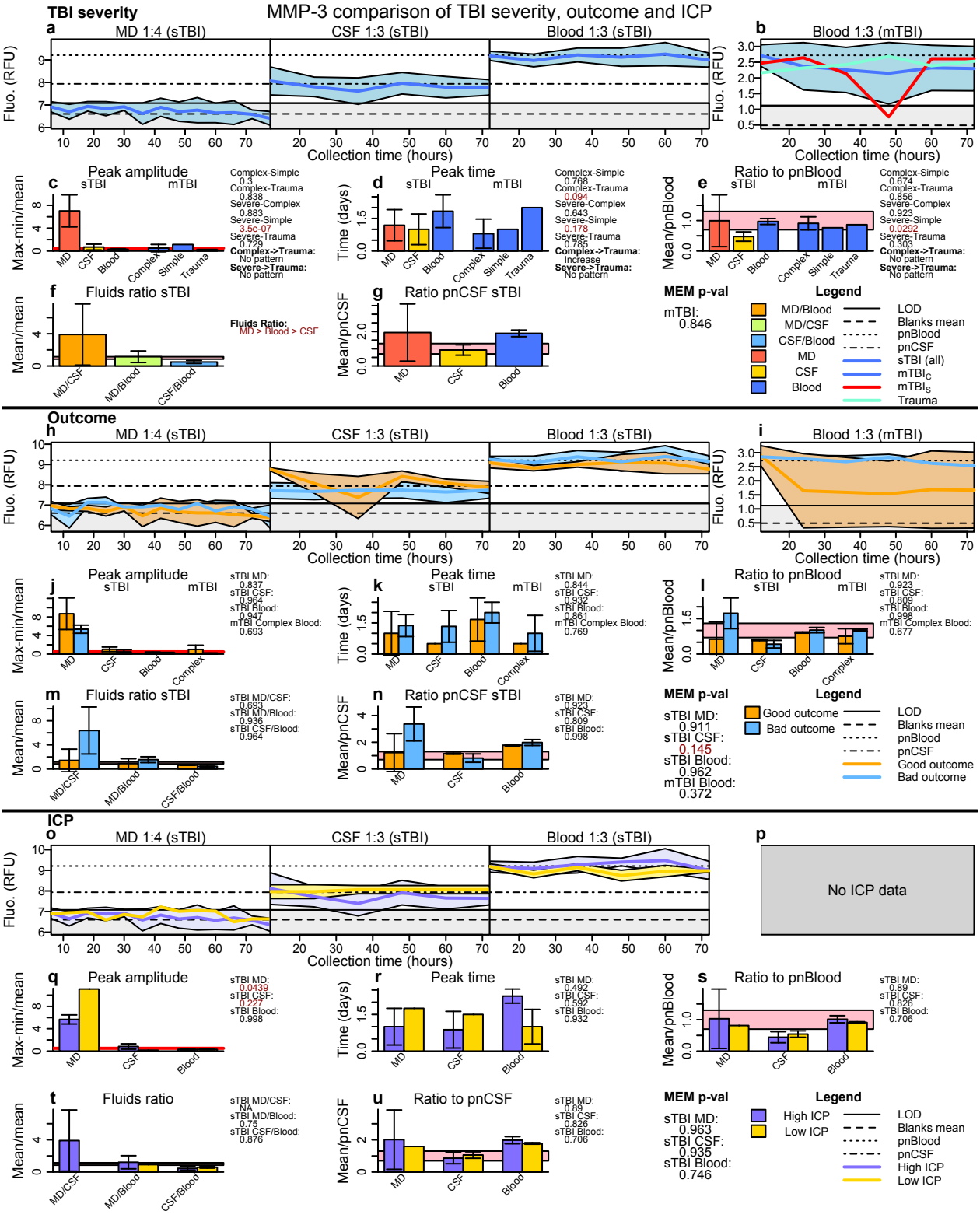

FIGURE J.S172: **Differential MMP-3 protein profiles and peak and ratio analysis with respect to TBI severity, outcome and ICP.** Average MMP-3 profiles are compared in terms of TBI severity (**a-g**), outcome (**h-n**) and ICP (**o-u**). Polygons in **a, b, h, i, o** indicate the mean value ±1 SD at each time point. Red lines in **c, j, q** show a threshold for a profile that is considered to have a peak, rather than being constant. The light red boxes in **e-g, l-n, s-u** show the threshold of comparison to the measured value compared. Benjamini–Hochberg adjusted p-values for comparisons are shown on the right of every graph.

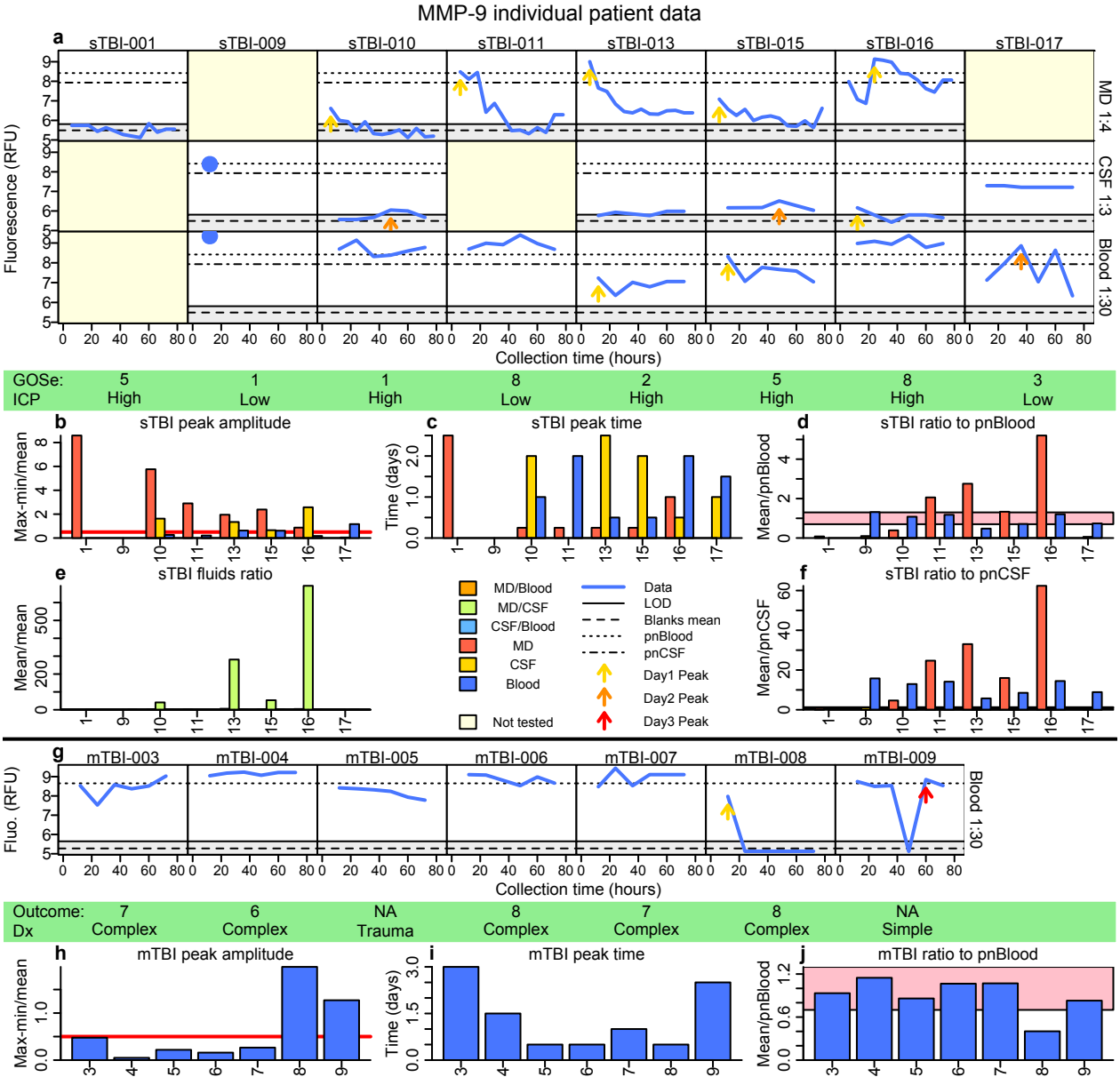

FIGURE J.S173: **Individual MMP-9 protein profiles and peak and ratio analysis.** MMP-9 concentration in microdialysate, CSF and blood samples of individual sTBI patients (**a**) and mTBI/trauma patients (**g**) was measured and peak amplitude and time, as well as ratio between mean time course values to value found in the pooled normal control (**b-f, h-j**) were calculated for each patient. Graphs **b-f** show calculations for individual sTBI patients, and graphs **h-j** show calculations for individual mTBI patients. Red lines in **b, h** show a threshold for a profile that is considered to have a peak, rather than being constant. The light red boxes in **d, e, f, j** show the threshold of comparison to the measured value compared.

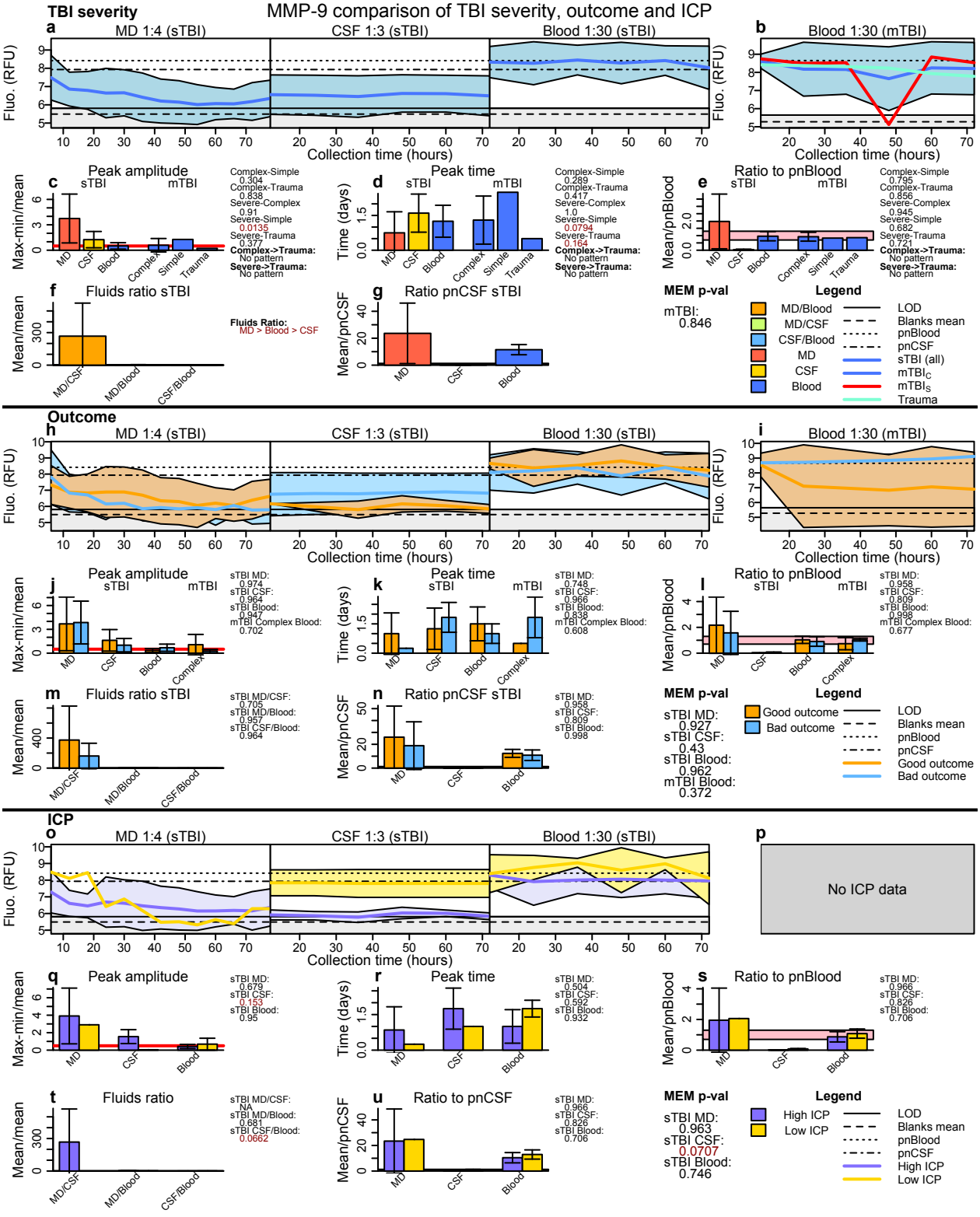

FIGURE J.S174: **Differential MMP-9 protein profiles and peak and ratio analysis with respect to TBI severity, outcome and ICP.** Average MMP-9 profiles are compared in terms of TBI severity (**a-g**), outcome (**h-n**) and ICP (**o-u**). Polygons in **a, b, h, i, o** indicate the mean value ±1 SD at each time point. Red lines in **c, j, q** show a threshold for a profile that is considered to have a peak, rather than being constant. The light red boxes in **e-g, l-n, s-u** show the threshold of comparison to the measured value compared. Benjamini–Hochberg adjusted p-values for comparisons are shown on the right of every graph.

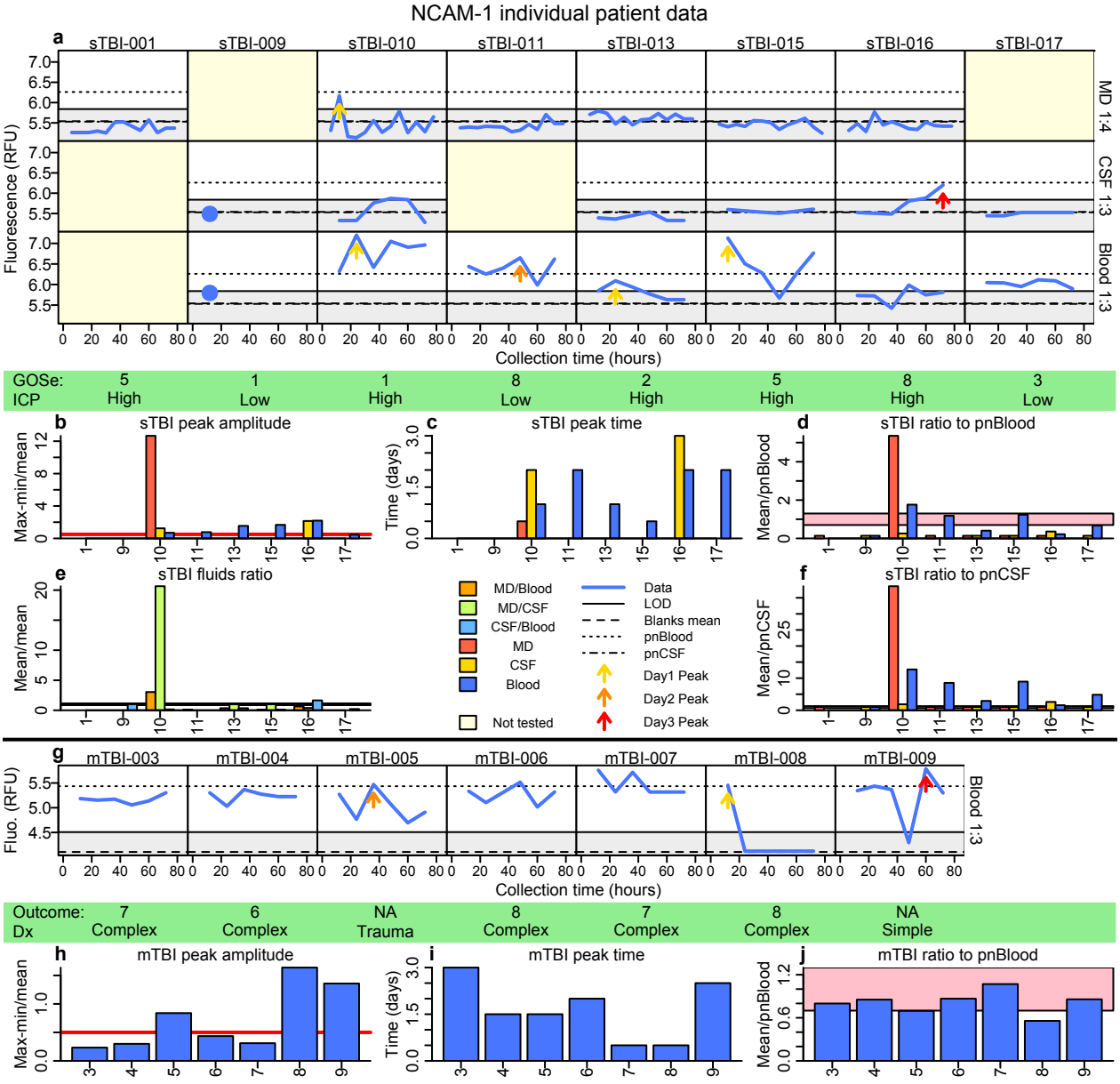

FIGURE J.S175: **Individual NCAM-1 protein profiles and peak and ratio analysis.** NCAM-1 concentration in microdialysate, CSF and blood samples of individual sTBI patients (**a**) and mTBI/trauma patients (**g**) was measured and peak amplitude and time, as well as ratio between mean time course values to value found in the pooled normal control (**b-f, h-j**) were calculated for each patient. Graphs **b-f** show calculations for individual sTBI patients, and graphs **h-j** show calculations for individual mTBI patients. Red lines in **b, h** show a threshold for a profile that is considered to have a peak, rather than being constant. The light red boxes in **d, e, f, j** show the threshold of comparison to the measured value compared.

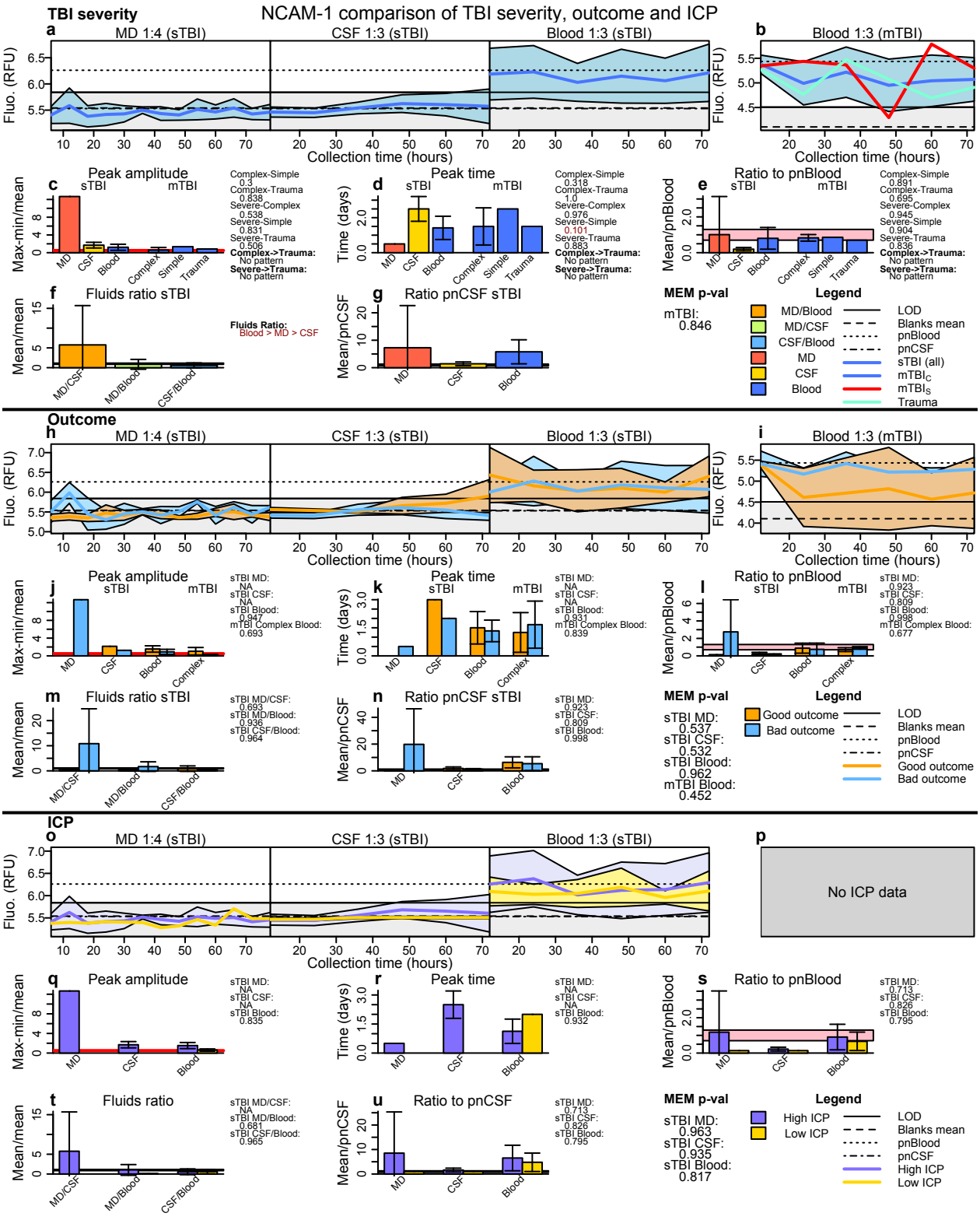

FIGURE J.S176: **Differential NCAM-1 protein profiles and peak and ratio analysis with respect to TBI severity, outcome and ICP.** Average NCAM-1 profiles are compared in terms of TBI severity (**a-g**), outcome (**h-n**) and ICP (**o-u**). Polygons in **a, b, h, i, o** indicate the mean value ±1 SD at each time point. Red lines in **c, j, q** show a threshold for a profile that is considered to have a peak, rather than being constant. The light red boxes in **e-g, l-n, s-u** show the threshold of comparison to the measured value compared. Benjamini–Hochberg adjusted p-values for comparisons are shown on the right of every graph.

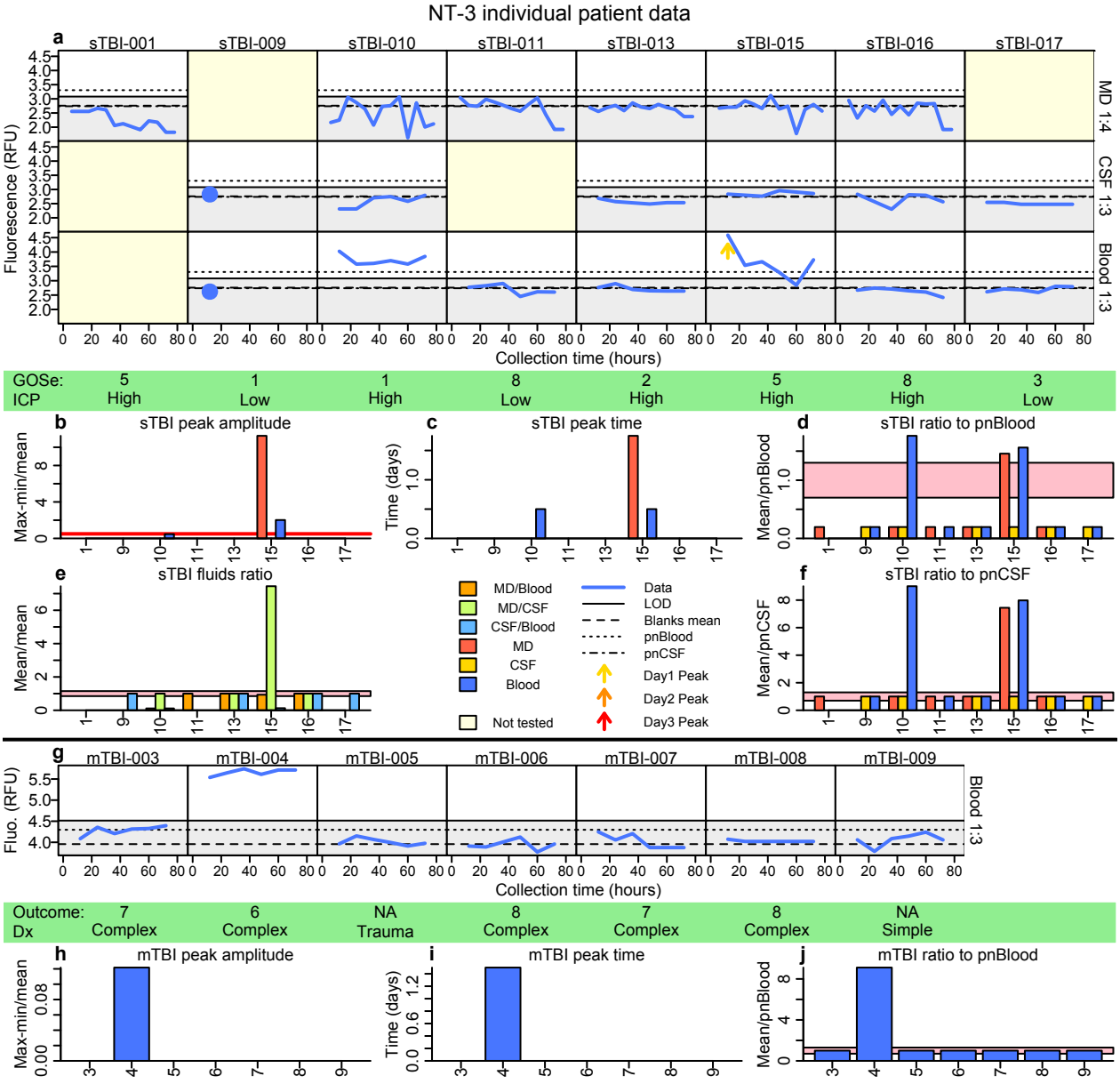

FIGURE J.S177: **Individual NT-3 protein profiles and peak and ratio analysis.** NT-3 concentration in microdialysate, CSF and blood samples of individual sTBI patients (**a**) and mTBI/trauma patients (**g**) was measured and peak amplitude and time, as well as ratio between mean time course values to value found in the pooled normal control (**b-f, h-j**) were calculated for each patient. Graphs **b-f** show calculations for individual sTBI patients, and graphs **h-j** show calculations for individual mTBI patients. Red lines in **b, h** show a threshold for a profile that is considered to have a peak, rather than being constant. The light red boxes in **d, e, f, j** show the threshold of comparison to the measured value compared.

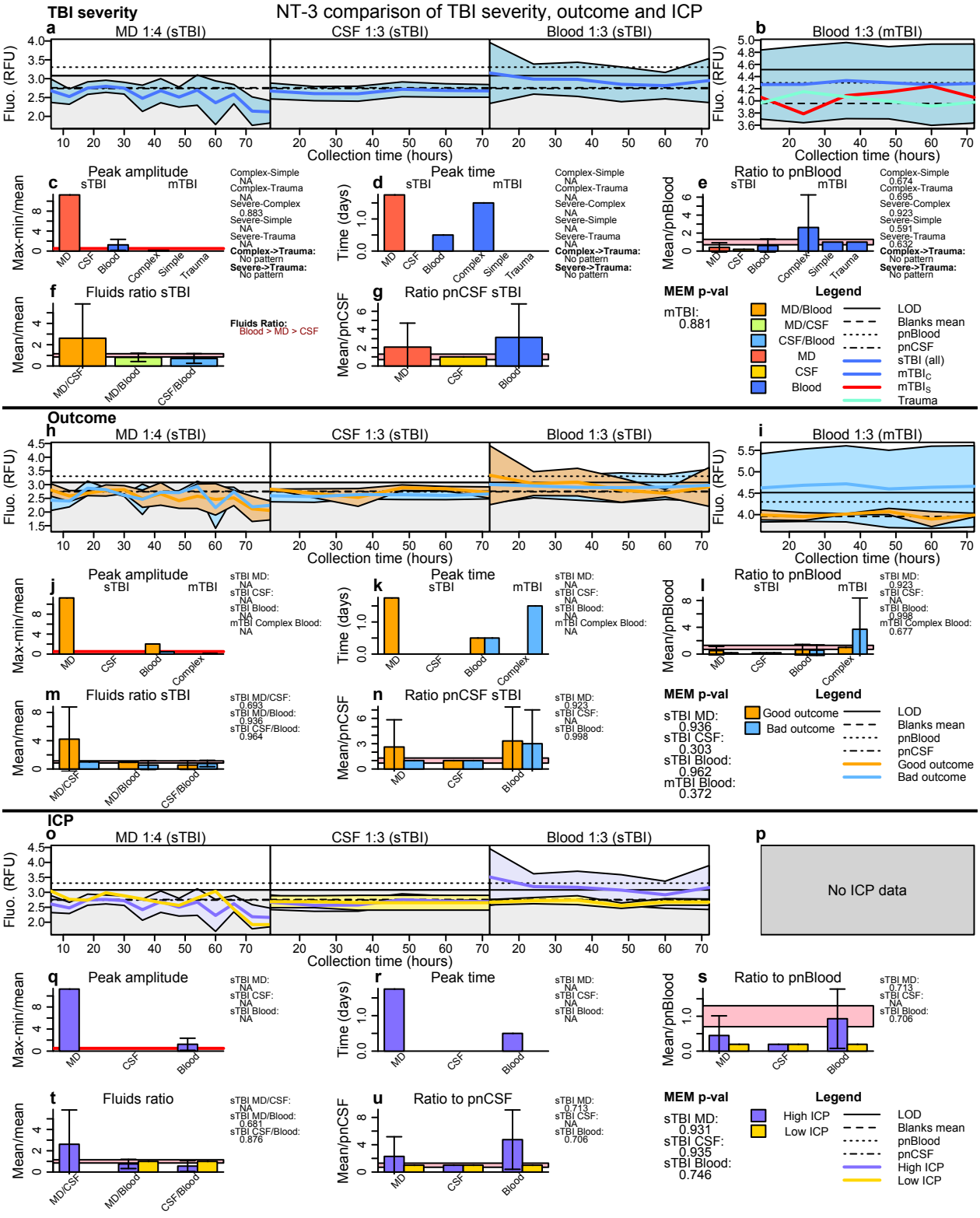

FIGURE J.S178: **Differential NT-3 protein profiles and peak and ratio analysis with respect to TBI severity, outcome and ICP.** Average NT-3 profiles are compared in terms of TBI severity (**a-g**), outcome (**h-n**) and ICP (**o-u**). Polygons in **a, b, h, i, o** indicate the mean value ±1 SD at each time point. Red lines in **c, j, q** show a threshold for a profile that is considered to have a peak, rather than being constant. The light red boxes in **e-g, l-n, s-u** show the threshold of comparison to the measured value compared. Benjamini–Hochberg adjusted p-values for comparisons are shown on the right of every graph.

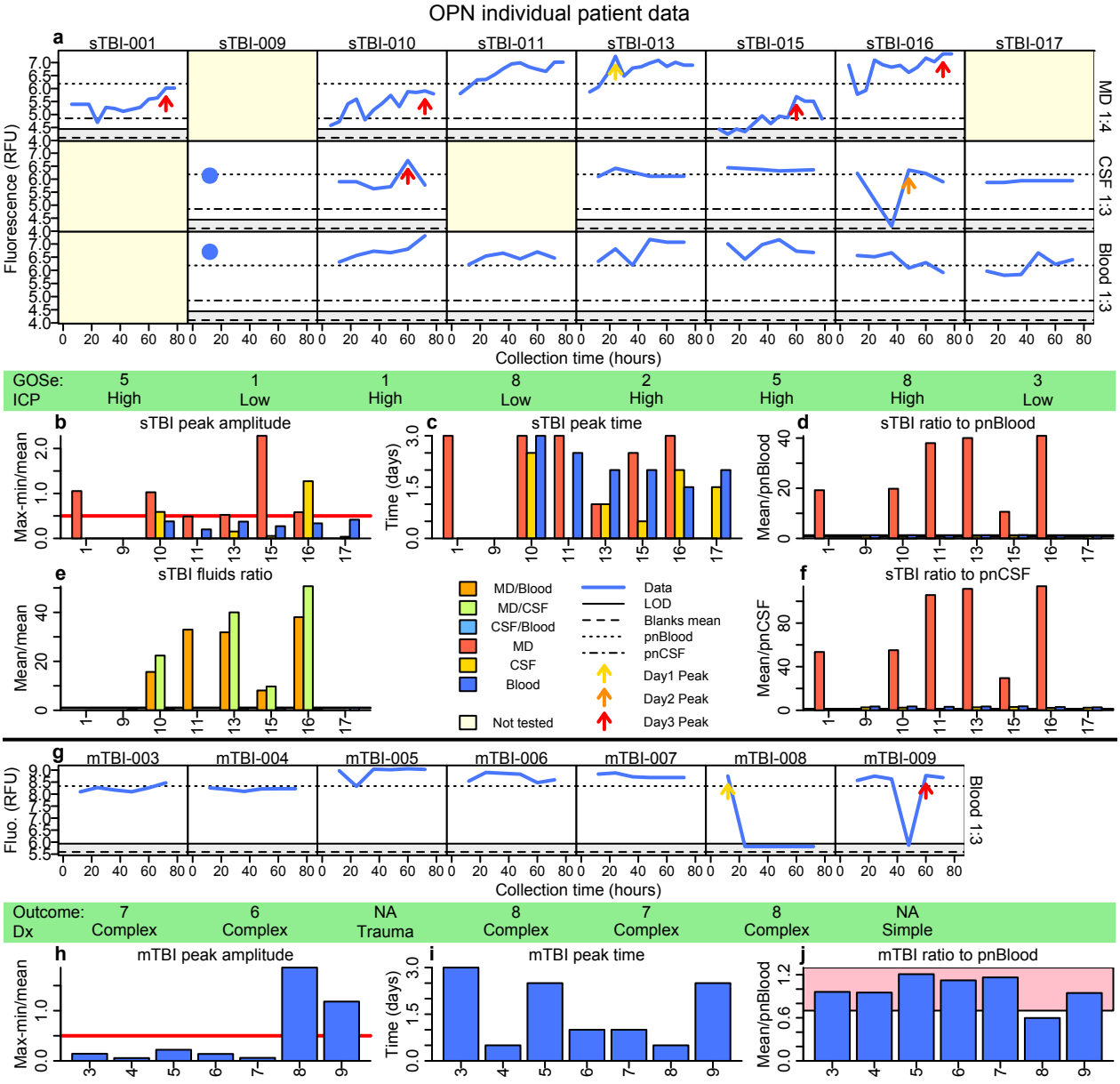

FIGURE J.S179: **Individual OPN protein profiles and peak and ratio analysis.** OPN concentration in microdialysate, CSF and blood samples of individual sTBI patients (**a**) and mTBI/trauma patients (**g**) was measured and peak amplitude and time, as well as ratio between mean time course values to value found in the pooled normal control (**b-f, h-j**) were calculated for each patient. Graphs **b-f** show calculations for individual sTBI patients, and graphs **h-j** show calculations for individual mTBI patients. Red lines in **b, h** show a threshold for a profile that is considered to have a peak, rather than being constant. The light red boxes in **d, e, f, j** show the threshold of comparison to the measured value compared.

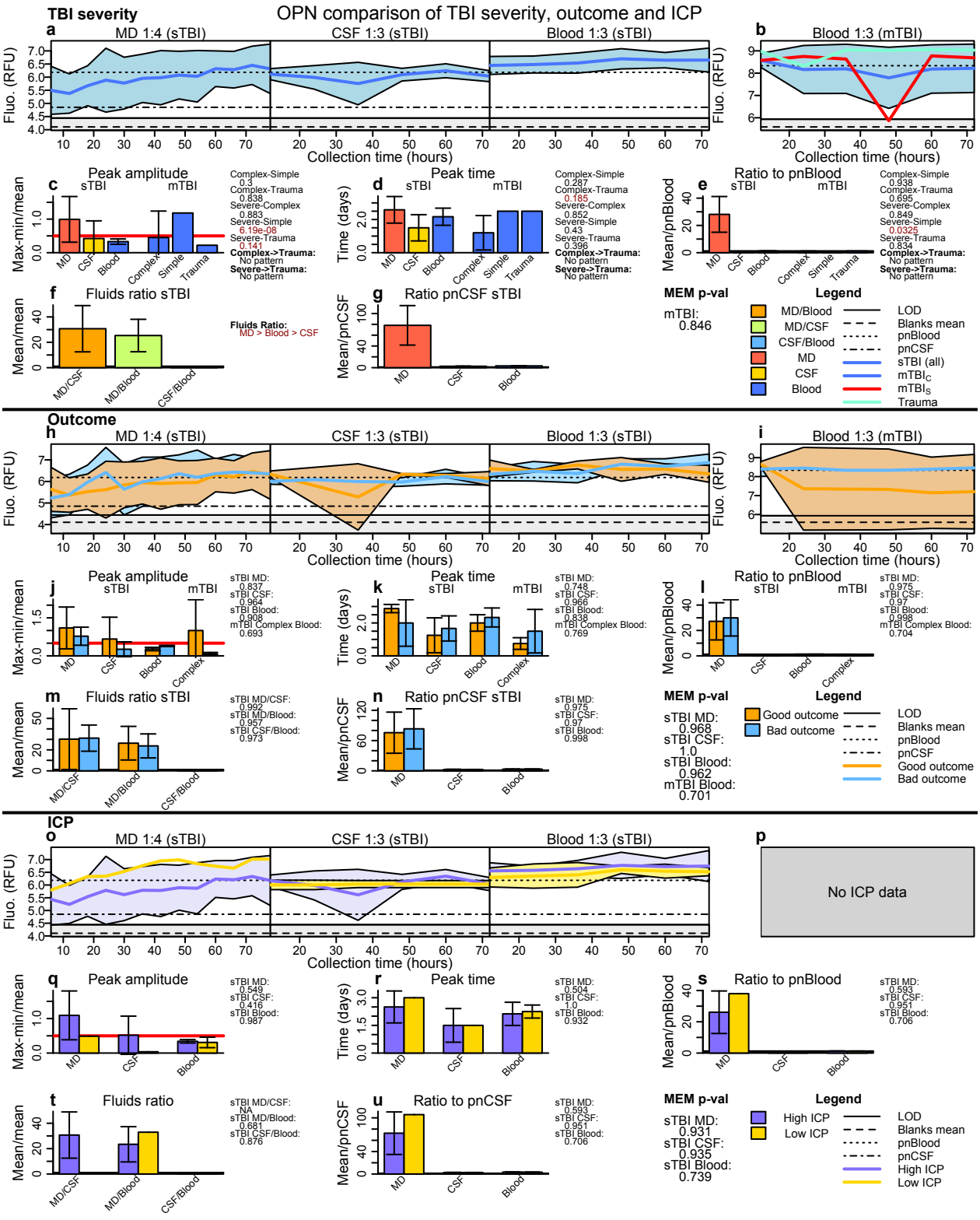

FIGURE J.S180: **Differential OPN protein profiles and peak and ratio analysis with respect to TBI severity, outcome and ICP.** Average OPN profiles are compared in terms of TBI severity (**a-g**), outcome (**h-n**) and ICP (**o-u**). Polygons in **a, b, h, i, o** indicate the mean value ±1 SD at each time point. Red lines in **c, j, q** show a threshold for a profile that is considered to have a peak, rather than being constant. The light red boxes in **e-g, l-n, s-u** show the threshold of comparison to the measured value compared. Benjamini–Hochberg adjusted p-values for comparisons are shown on the right of every graph.

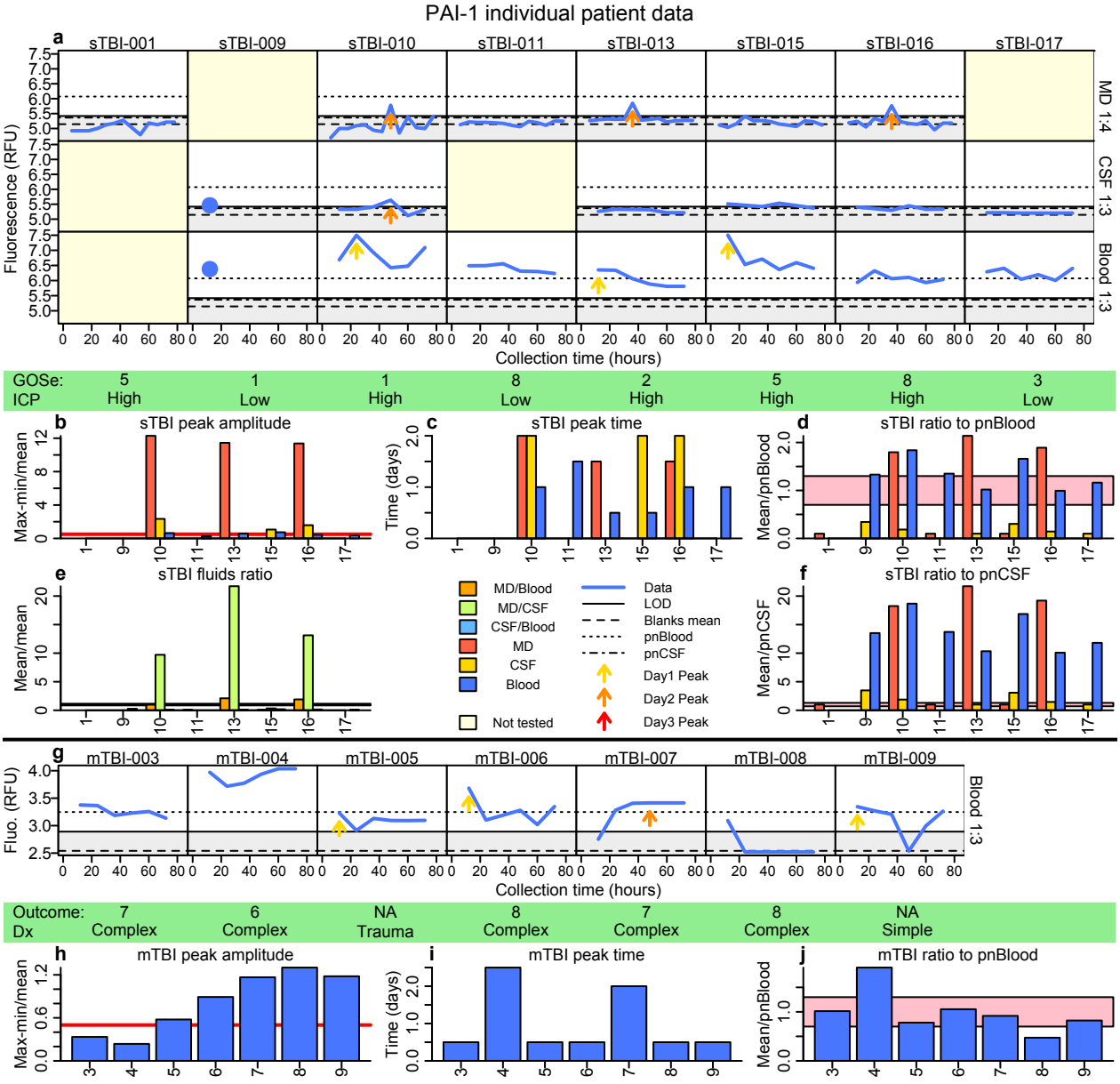

FIGURE J.S181: **Individual PAI-1 protein profiles and peak and ratio analysis.** PAI-1 concentration in microdialysate, CSF and blood samples of individual sTBI patients (**a**) and mTBI/trauma patients (**g**) was measured and peak amplitude and time, as well as ratio between mean time course values to value found in the pooled normal control (**b-f, h-j**) were calculated for each patient. Graphs **b-f** show calculations for individual sTBI patients, and graphs **h-j** show calculations for individual mTBI patients. Red lines in **b, h** show a threshold for a profile that is considered to have a peak, rather than being constant. The light red boxes in **d, e, f, j** show the threshold of comparison to the measured value compared.

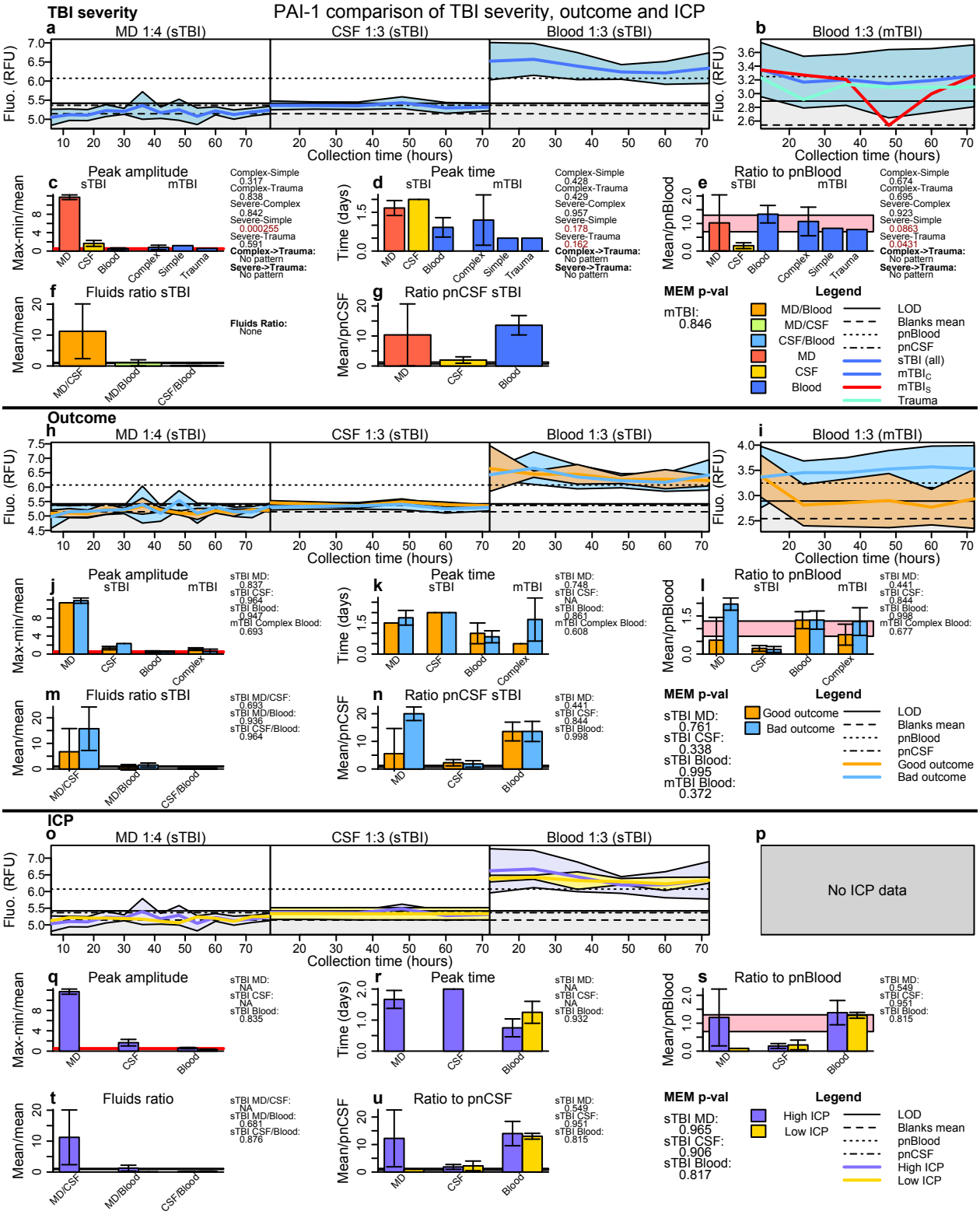

FIGURE J.S182: **Differential PAI-1 protein profiles and peak and ratio analysis with respect to TBI severity, outcome and ICP.** Average PAI-1 profiles are compared in terms of TBI severity (**a-g**), outcome (**h-n**) and ICP (**o-u**). Polygons in **a, b, h, i, o** indicate the mean value ±1 SD at each time point. Red lines in **c, j, q** show a threshold for a profile that is considered to have a peak, rather than being constant. The light red boxes in **e-g, l-n, s-u** show the threshold of comparison to the measured value compared. Benjamini–Hochberg adjusted p-values for comparisons are shown on the right of every graph.

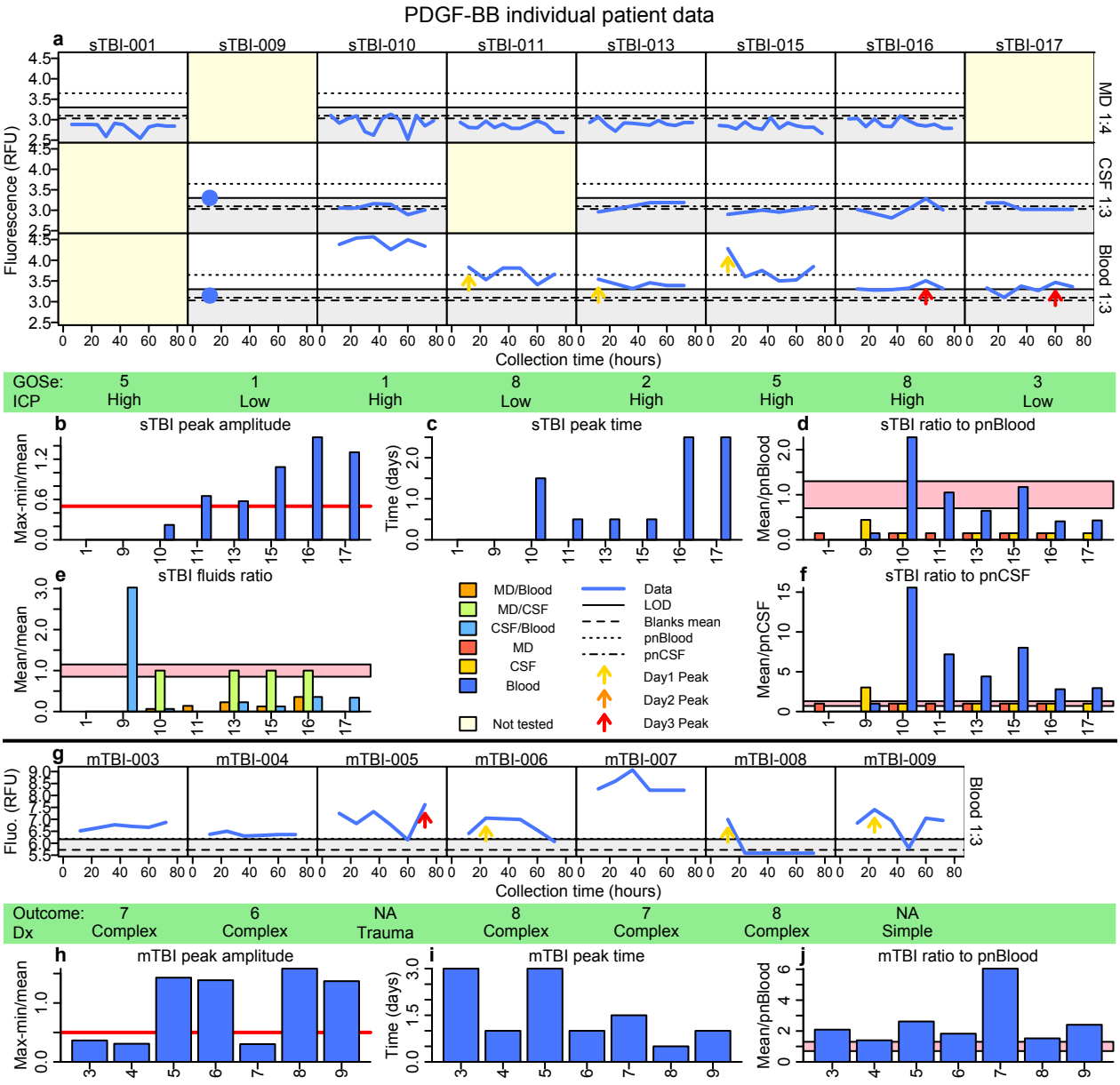

FIGURE J.S183: **Individual PDGF-BB protein profiles and peak and ratio analysis.** PDGF-BB concentration in microdialysate, CSF and blood samples of individual sTBI patients (**a**) and mTBI/trauma patients (**g**) was measured and peak amplitude and time, as well as ratio between mean time course values to value found in the pooled normal control (**b-f, h-j**) were calculated for each patient. Graphs **b-f** show calculations for individual sTBI patients, and graphs **h-j** show calculations for individual mTBI patients. Red lines in **b, h** show a threshold for a profile that is considered to have a peak, rather than being constant. The light red boxes in **d, e, f, j** show the threshold of comparison to the measured value compared.

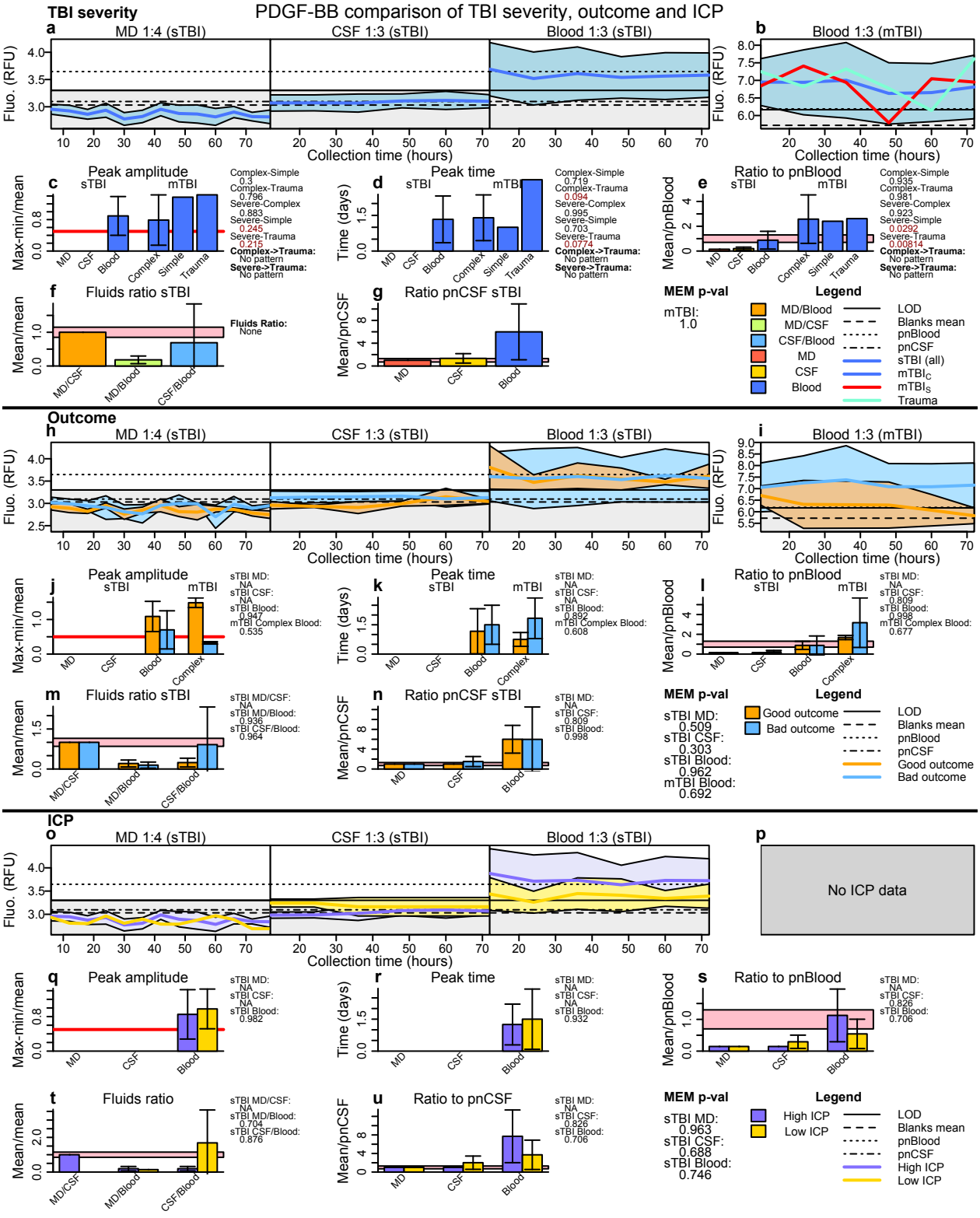

FIGURE J.S184: **Differential PDGF-BB protein profiles and peak and ratio analysis with respect to TBI severity, outcome and ICP.** Average PDGF-BB profiles are compared in terms of TBI severity (**a-g**), outcome (**h-n**) and ICP (**o-u**). Polygons in **a, b, h, i, o** indicate the mean value ±1 SD at each time point. Red lines in **c, j, q** show a threshold for a profile that is considered to have a peak, rather than being constant. The light red boxes in **e-g, l-n, s-u** show the threshold of comparison to the measured value compared. Benjamini–Hochberg adjusted p-values for comparisons are shown on the right of every graph.

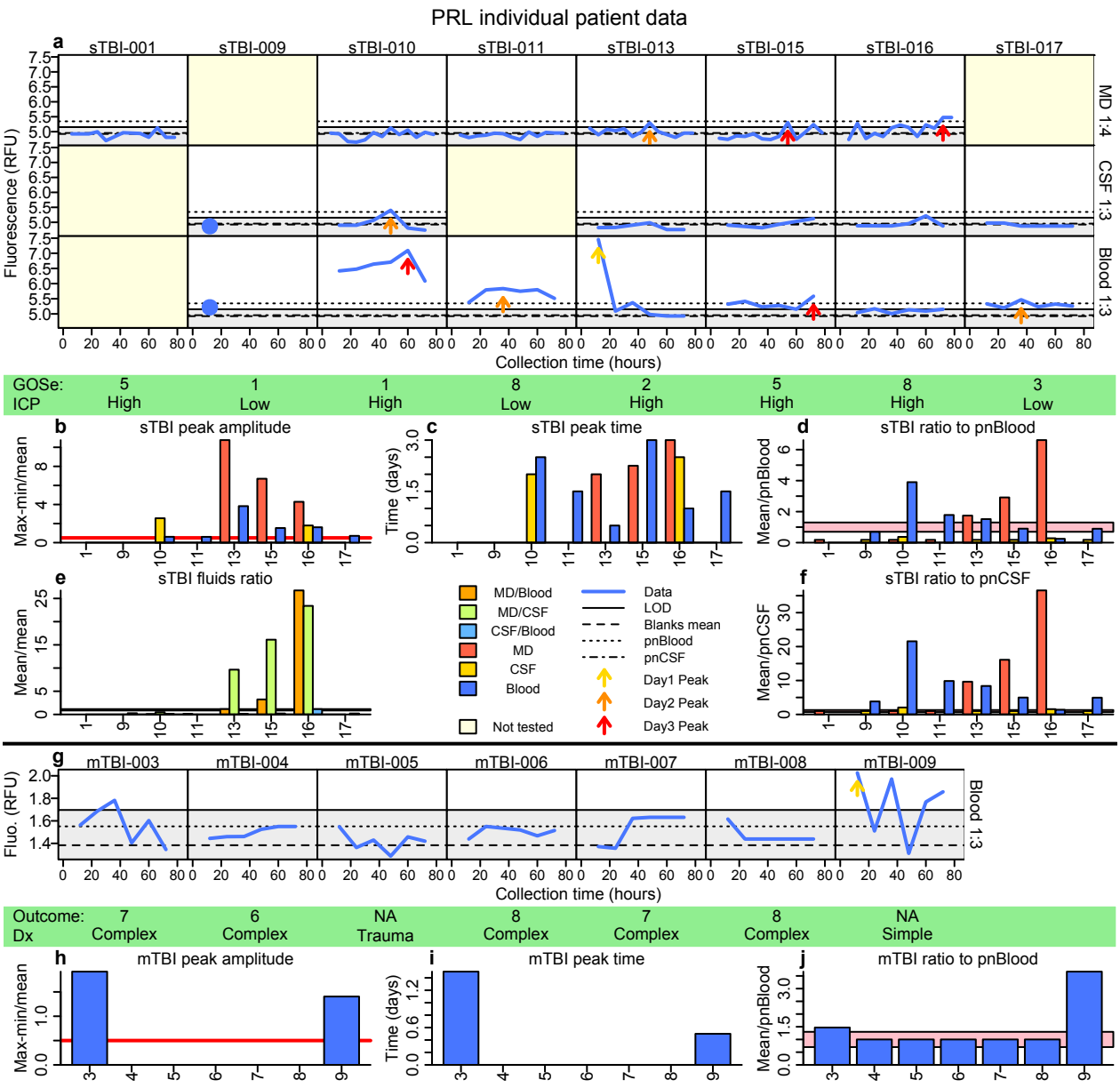

FIGURE J.S185: **Individual PRL protein profiles and peak and ratio analysis.** PRL concentration in microdialysate, CSF and blood samples of individual sTBI patients (**a**) and mTBI/trauma patients (**g**) was measured and peak amplitude and time, as well as ratio between mean time course values to value found in the pooled normal control (**b-f, h-j**) were calculated for each patient. Graphs **b-f** show calculations for individual sTBI patients, and graphs **h-j** show calculations for individual mTBI patients. Red lines in **b, h** show a threshold for a profile that is considered to have a peak, rather than being constant. The light red boxes in **d, e, f, j** show the threshold of comparison to the measured value compared.

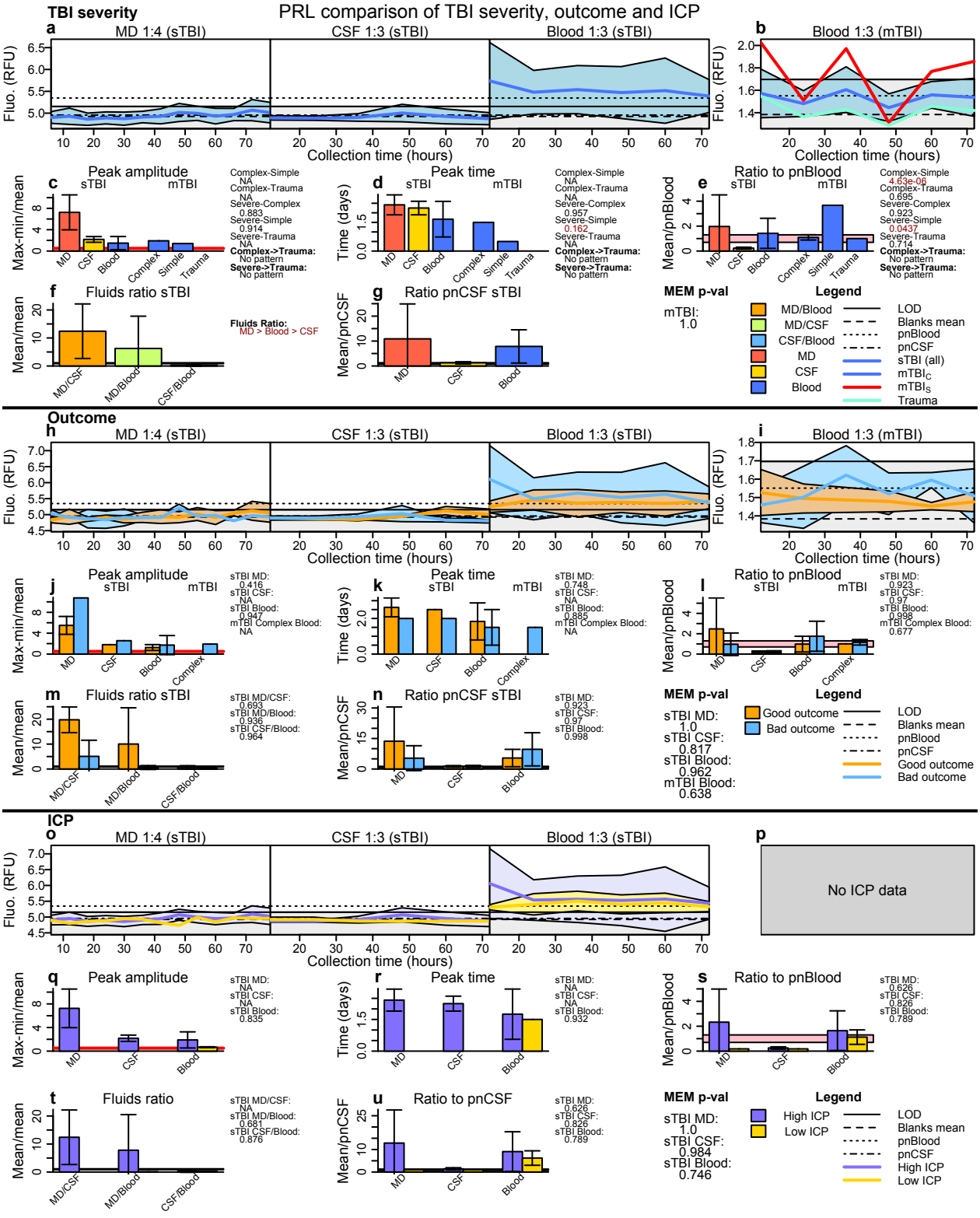

FIGURE J.S186: **Differential PRL protein profiles and peak and ratio analysis with respect to TBI severity, outcome and ICP.** Average PRL profiles are compared in terms of TBI severity (**a-g**), outcome (**h-n**) and ICP (**o-u**). Polygons in **a, b, h, i, o** indicate the mean value ±1 SD at each time point. Red lines in **c, j, q** show a threshold for a profile that is considered to have a peak, rather than being constant. The light red boxes in **e-g, l-n, s-u** show the threshold of comparison to the measured value compared. Benjamini–Hochberg adjusted p-values for comparisons are shown on the right of every graph.

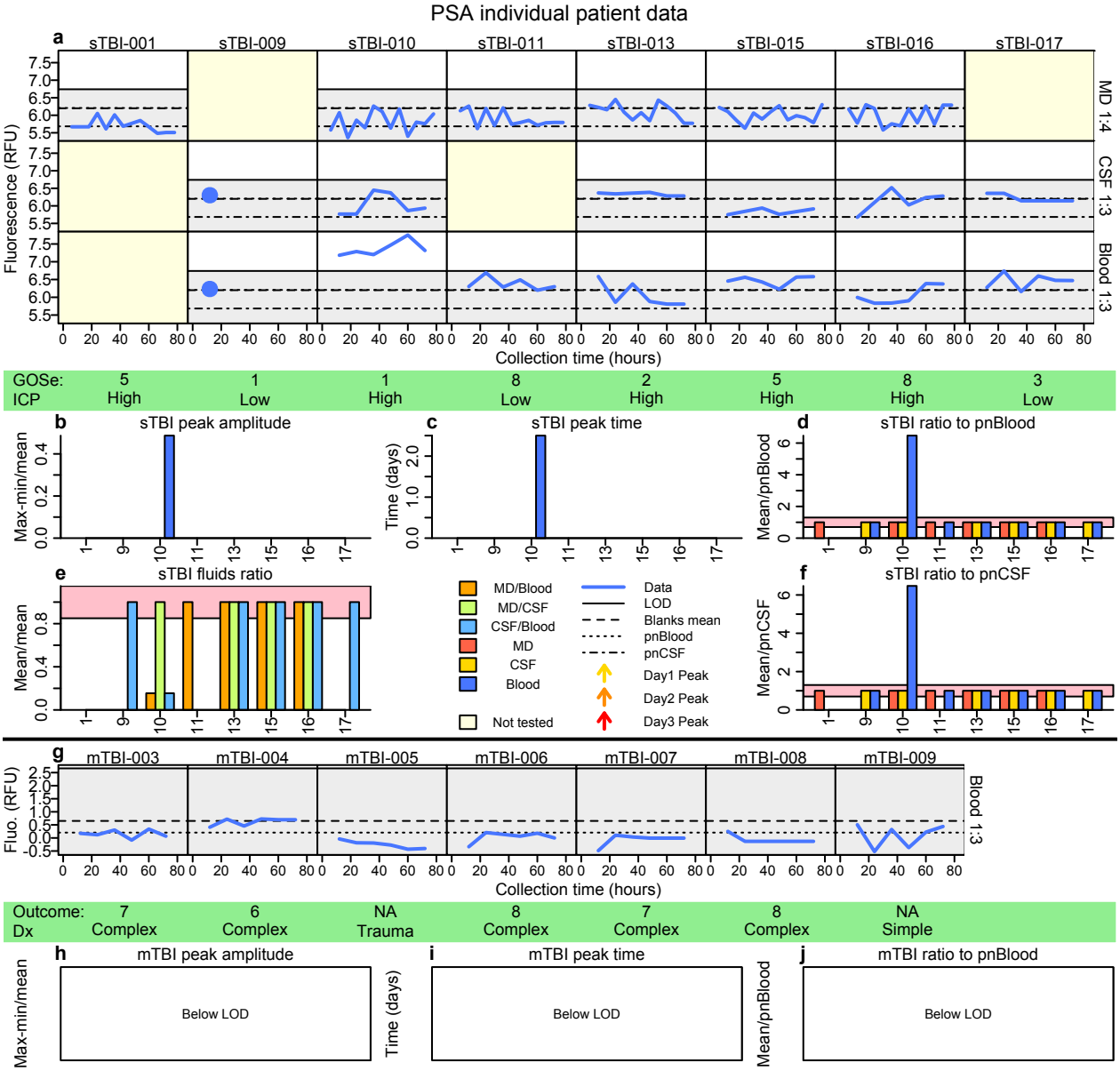

FIGURE J.S187: **Individual PSA protein profiles and peak and ratio analysis.** PSA concentration in microdialysate, CSF and blood samples of individual sTBI patients (**a**) and mTBI/trauma patients (**g**) was measured and peak amplitude and time, as well as ratio between mean time course values to value found in the pooled normal control (**b-f, h-j**) were calculated for each patient. Graphs **b-f** show calculations for individual sTBI patients, and graphs **h-j** show calculations for individual mTBI patients. Red lines in **b, h** show a threshold for a profile that is considered to have a peak, rather than being constant. The light red boxes in **d, e, f, j** show the threshold of comparison to the measured value compared.

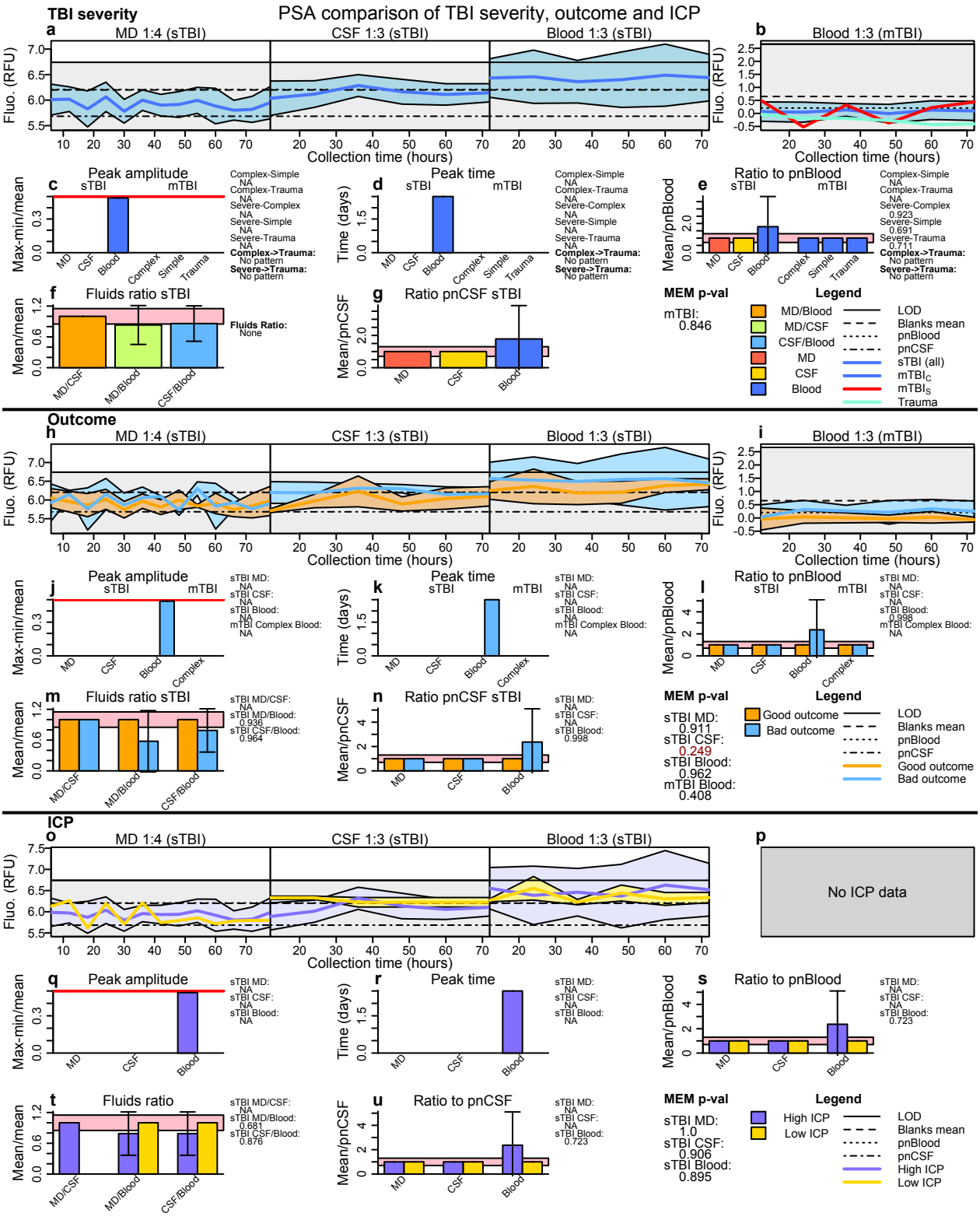

FIGURE J.S188: **Differential PSA protein profiles and peak and ratio analysis with respect to TBI severity, outcome and ICP.** Average PSA profiles are compared in terms of TBI severity (**a-g**), outcome (**h-n**) and ICP (**o-u**). Polygons in **a, b, h, i, o** indicate the mean value ±1 SD at each time point. Red lines in **c, j, q** show a threshold for a profile that is considered to have a peak, rather than being constant. The light red boxes in **e-g, l-n, s-u** show the threshold of comparison to the measured value compared. Benjamini–Hochberg adjusted p-values for comparisons are shown on the right of every graph.

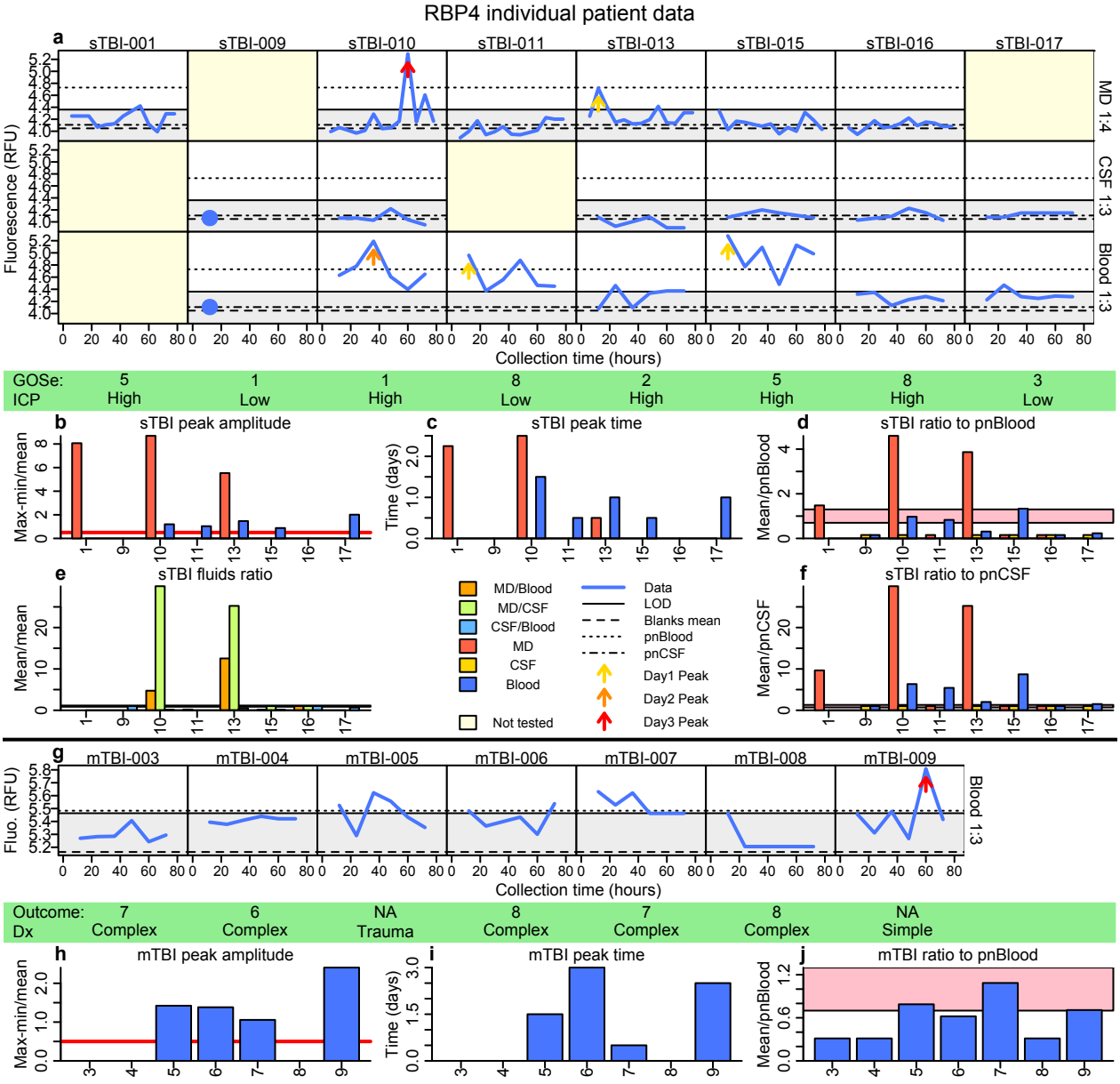

FIGURE J.S189: **Individual RBP4 protein profiles and peak and ratio analysis.** RBP4 concentration in microdialysate, CSF and blood samples of individual sTBI patients (**a**) and mTBI/trauma patients (**g**) was measured and peak amplitude and time, as well as ratio between mean time course values to value found in the pooled normal control (**b-f, h-j**) were calculated for each patient. Graphs **b-f** show calculations for individual sTBI patients, and graphs **h-j** show calculations for individual mTBI patients. Red lines in **b, h** show a threshold for a profile that is considered to have a peak, rather than being constant. The light red boxes in **d, e, f, j** show the threshold of comparison to the measured value compared.

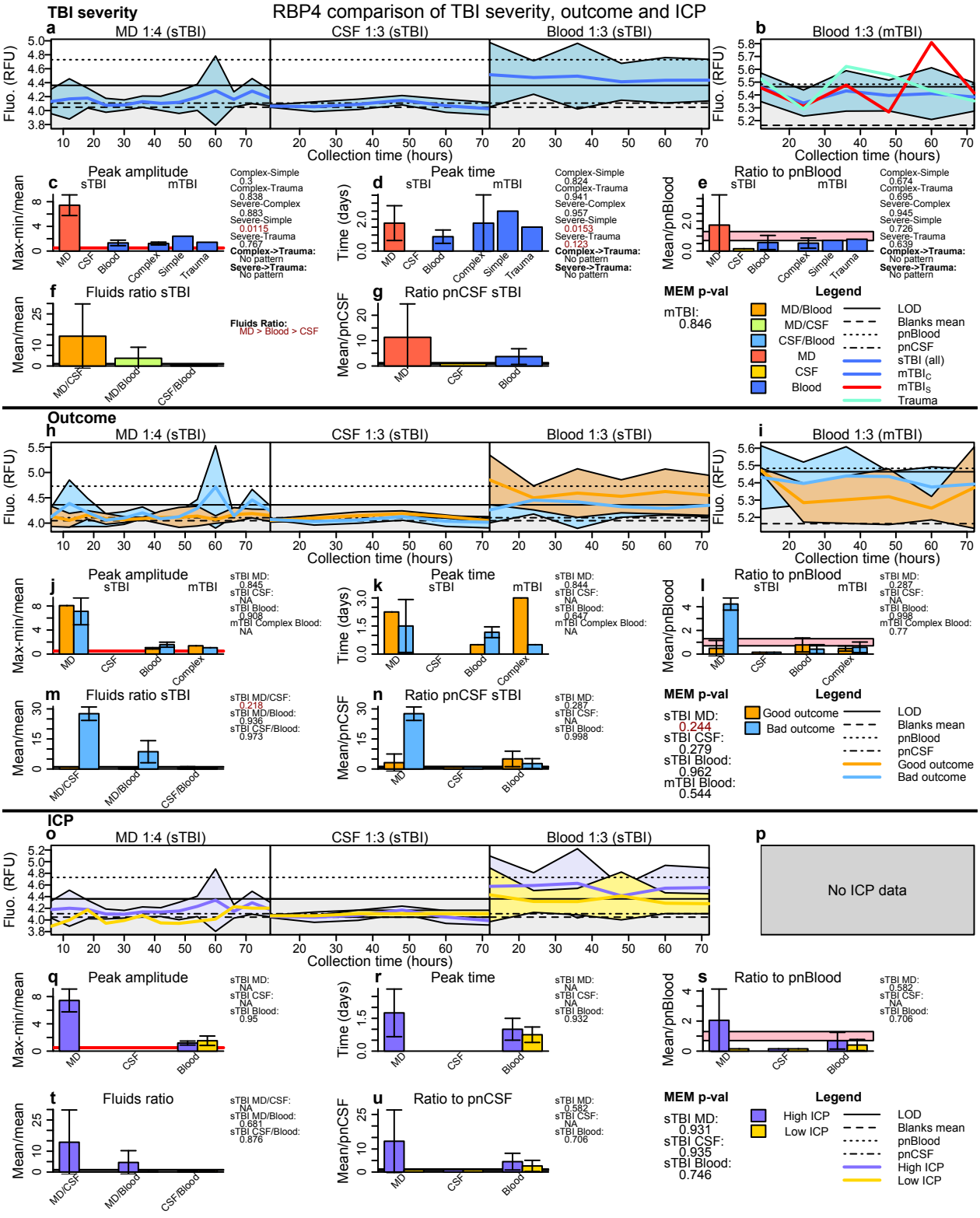

FIGURE J.S190: **Differential RBP4 protein profiles and peak and ratio analysis with respect to TBI severity, outcome and ICP.** Average RBP4 profiles are compared in terms of TBI severity (**a-g**), outcome (**h-n**) and ICP (**o-u**). Polygons in **a, b, h, i, o** indicate the mean value ±1 SD at each time point. Red lines in **c, j, q** show a threshold for a profile that is considered to have a peak, rather than being constant. The light red boxes in **e-g, l-n, s-u** show the threshold of comparison to the measured value compared. Benjamini–Hochberg adjusted p-values for comparisons are shown on the right of every graph.

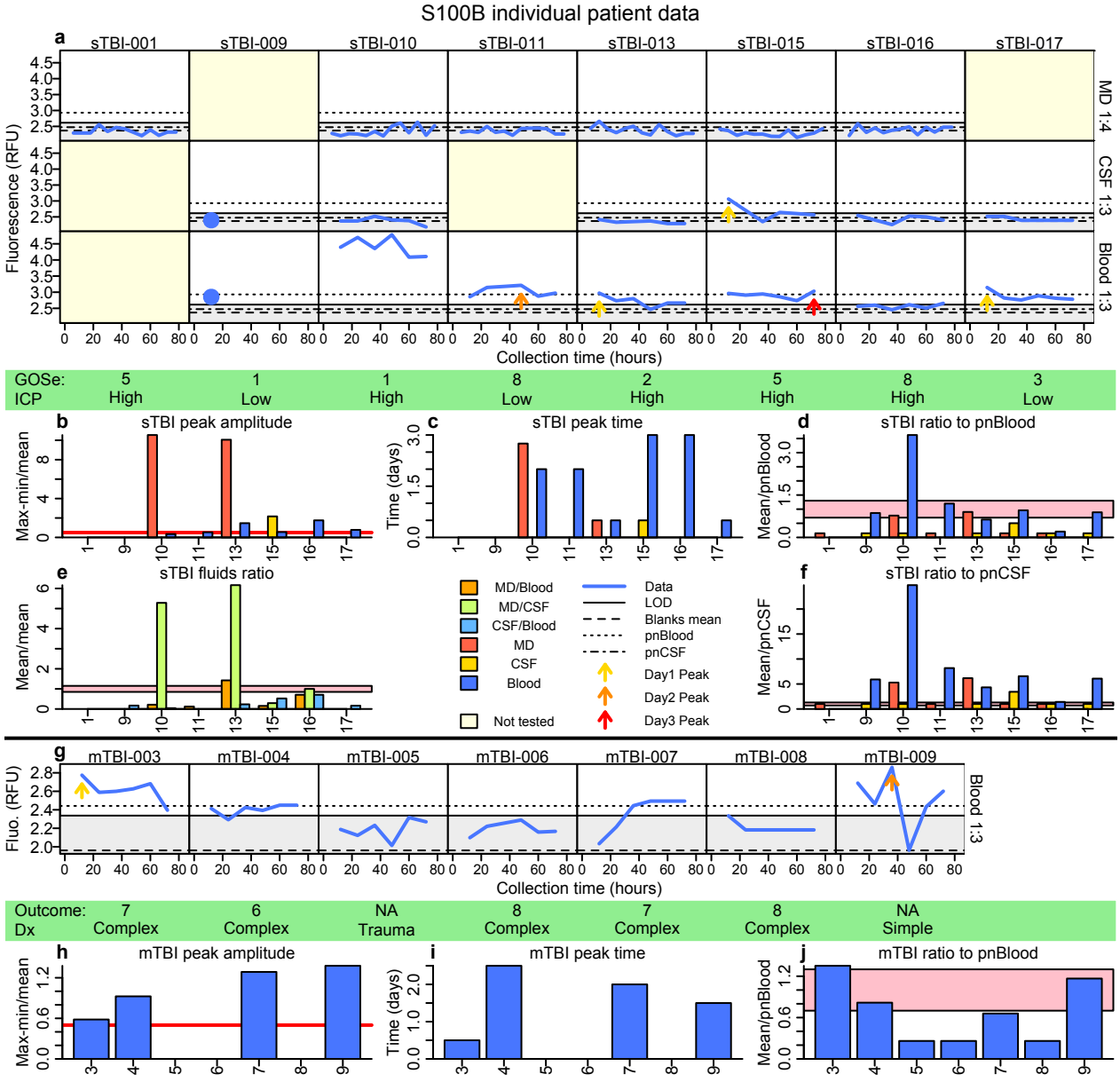

FIGURE J.S191: **Individual S100B protein profiles and peak and ratio analysis.** S100B concentration in microdialysate, CSF and blood samples of individual sTBI patients (**a**) and mTBI/trauma patients (**g**) was measured and peak amplitude and time, as well as ratio between mean time course values to value found in the pooled normal control (**b-f, h-j**) were calculated for each patient. Graphs **b-f** show calculations for individual sTBI patients, and graphs **h-j** show calculations for individual mTBI patients. Red lines in **b, h** show a threshold for a profile that is considered to have a peak, rather than being constant. The light red boxes in **d, e, f, j** show the threshold of comparison to the measured value compared.

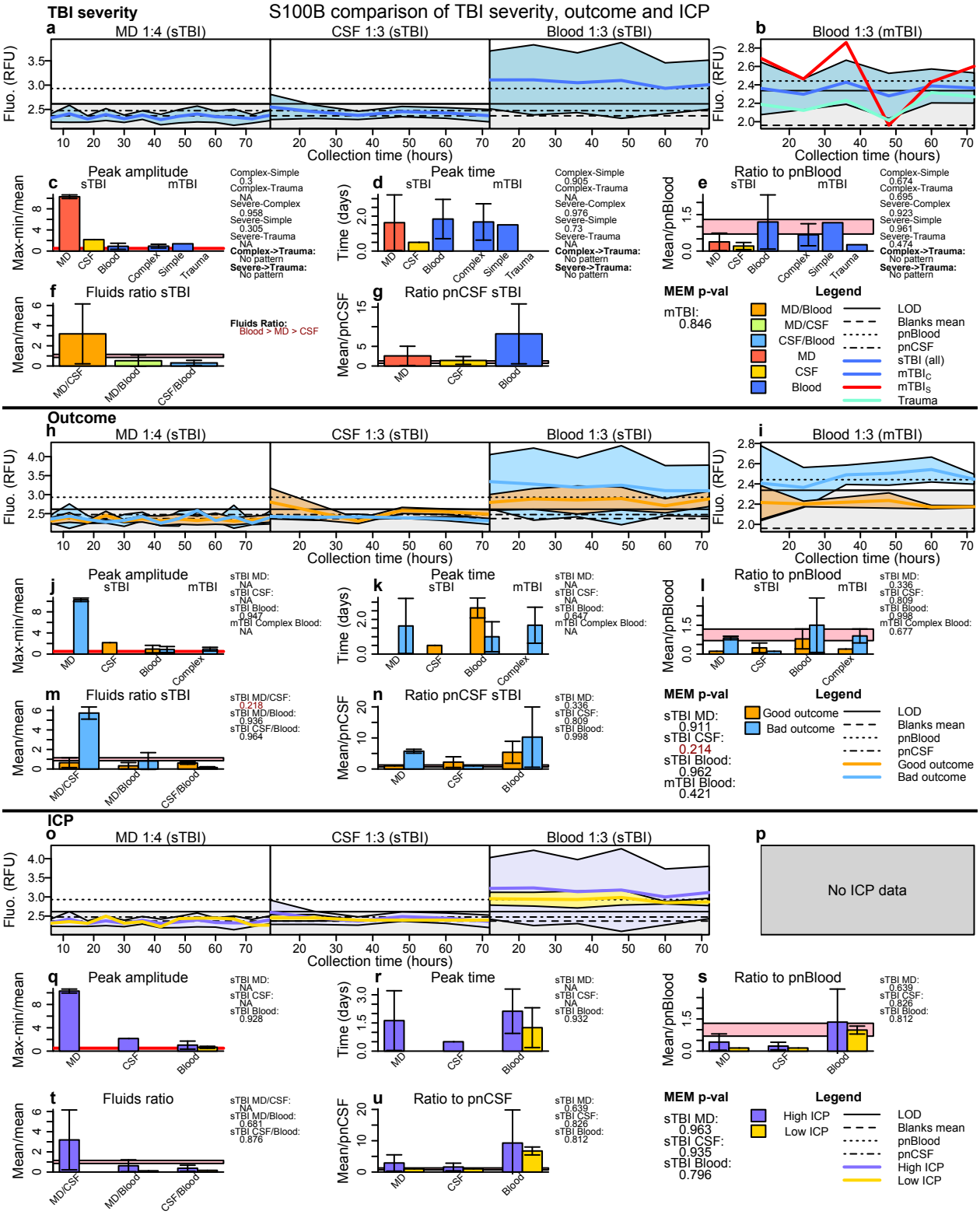

FIGURE J.S192: **Differential S100B protein profiles and peak and ratio analysis with respect to TBI severity, outcome and ICP.** Average S100B profiles are compared in terms of TBI severity (**a-g**), outcome (**h-n**) and ICP (**o-u**). Polygons in **a, b, h, i, o** indicate the mean value ±1 SD at each time point. Red lines in **c, j, q** show a threshold for a profile that is considered to have a peak, rather than being constant. The light red boxes in **e-g, l-n, s-u** show the threshold of comparison to the measured value compared. Benjamini–Hochberg adjusted p-values for comparisons are shown on the right of every graph.

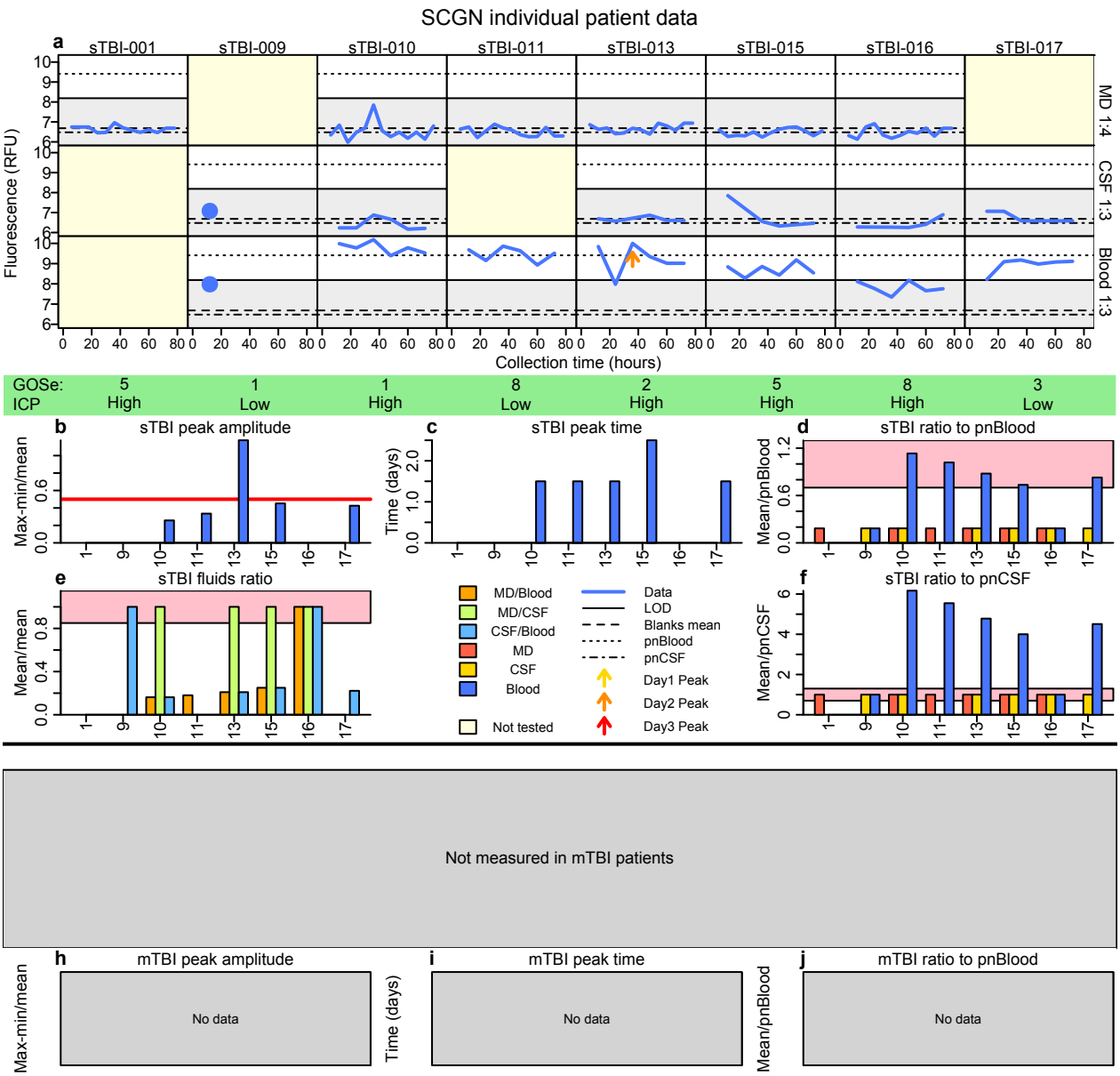

FIGURE J.S193: **Individual SCGN protein profiles and peak and ratio analysis.** SCGN concentration in microdialysate, CSF and blood samples of individual sTBI patients (**a**) and mTBI/trauma patients (**g**) was measured and peak amplitude and time, as well as ratio between mean time course values to value found in the pooled normal control (**b-f, h-j**) were calculated for each patient. Graphs **b-f** show calculations for individual sTBI patients, and graphs **h-j** show calculations for individual mTBI patients. Red lines in **b, h** show a threshold for a profile that is considered to have a peak, rather than being constant. The light red boxes in **d, e, f, j** show the threshold of comparison to the measured value compared.

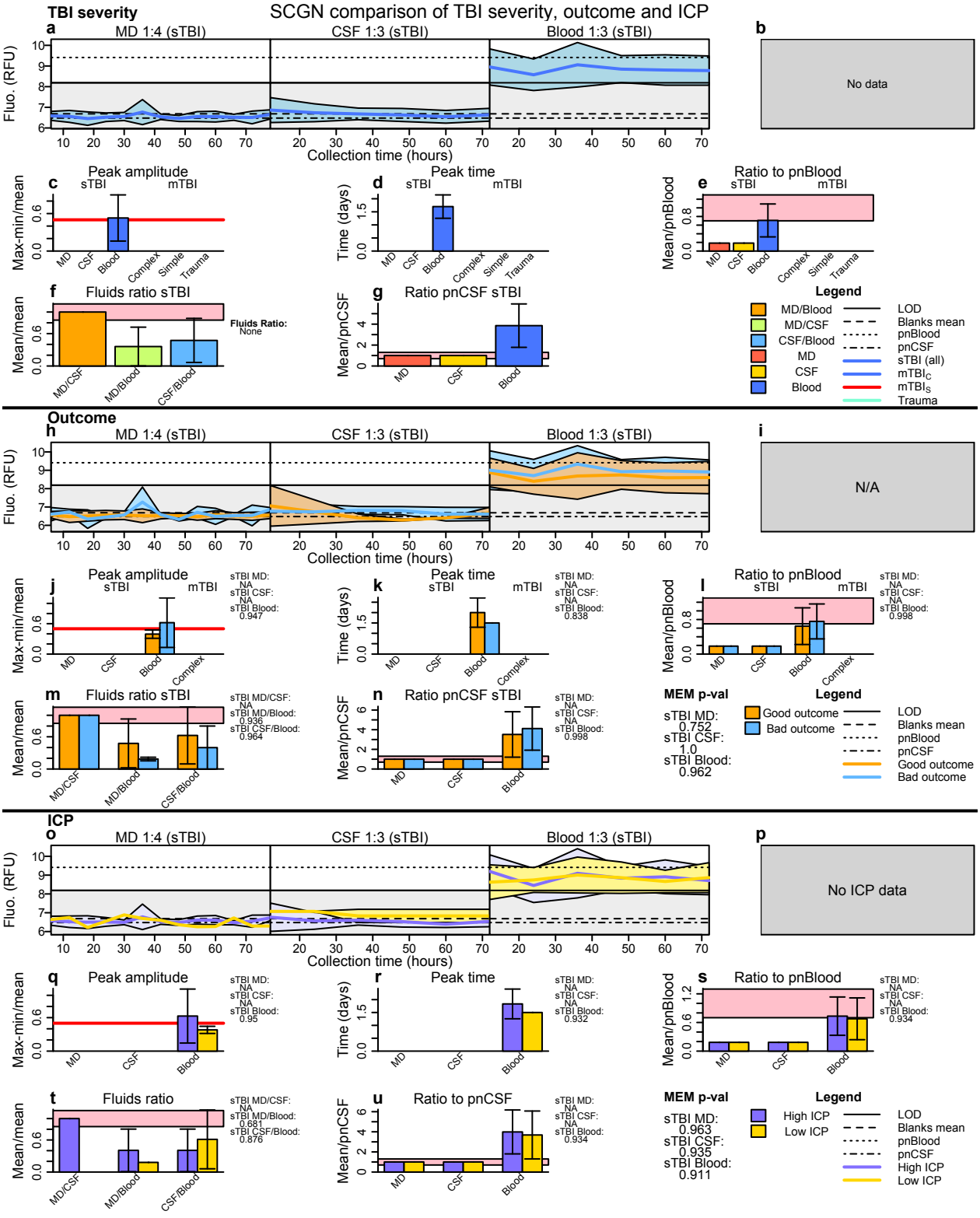

FIGURE J.S194: **Differential SCGN protein profiles and peak and ratio analysis with respect to TBI severity, outcome and ICP.** Average SCGN profiles are compared in terms of TBI severity (**a-g**), outcome (**h-n**) and ICP (**o-u**). Polygons in **a, b, h, i, o** indicate the mean value ±1 SD at each time point. Red lines in **c, j, q** show a threshold for a profile that is considered to have a peak, rather than being constant. The light red boxes in **e-g, l-n, s-u** show the threshold of comparison to the measured value compared. Benjamini–Hochberg adjusted p-values for comparisons are shown on the right of every graph.

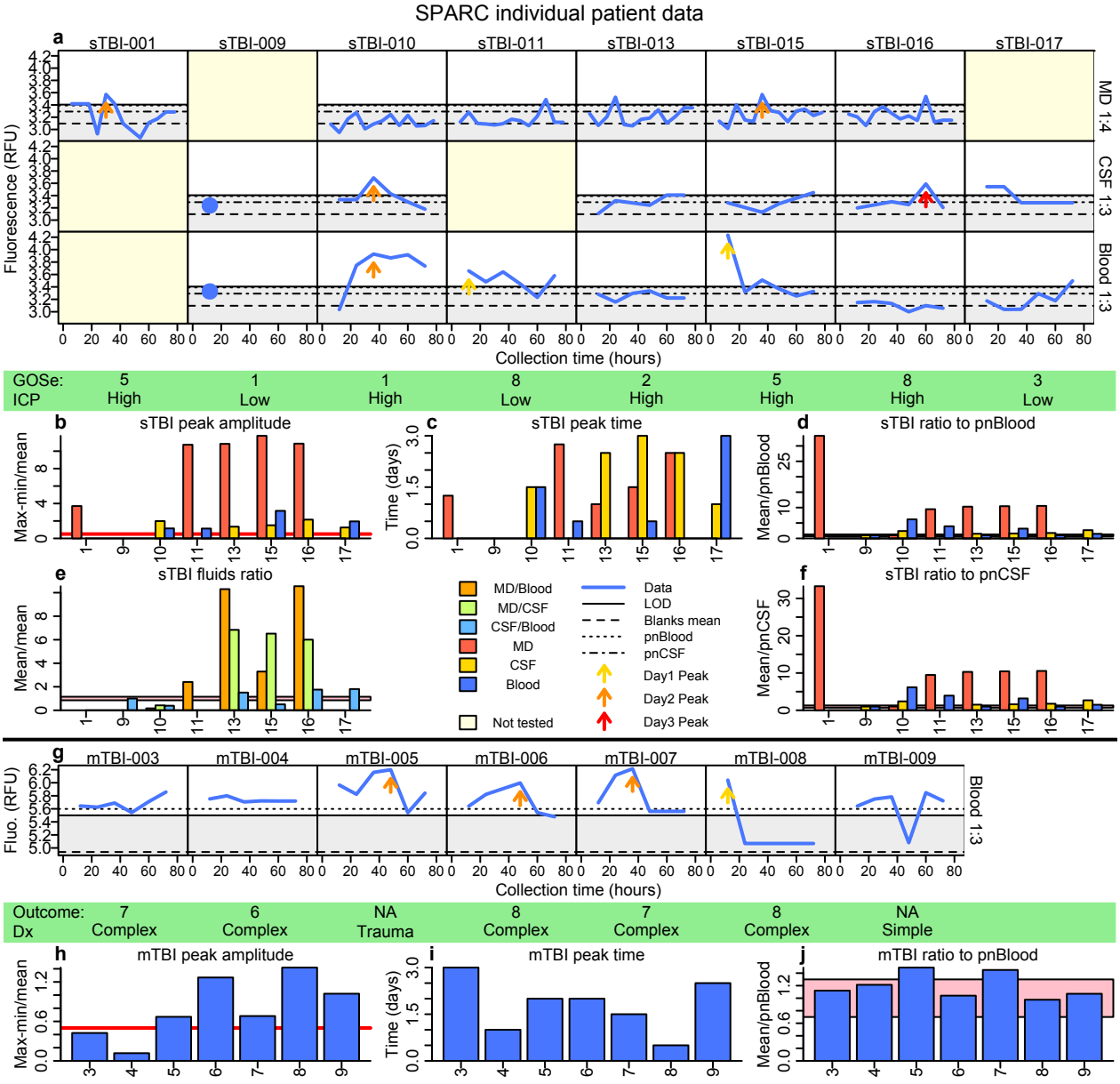

FIGURE J.S195: **Individual SPARC protein profiles and peak and ratio analysis.** SPARC concentration in microdialysate, CSF and blood samples of individual sTBI patients (**a**) and mTBI/trauma patients (**g**) was measured and peak amplitude and time, as well as ratio between mean time course values to value found in the pooled normal control (**b-f, h-j**) were calculated for each patient. Graphs **b-f** show calculations for individual sTBI patients, and graphs **h-j** show calculations for individual mTBI patients. Red lines in **b, h** show a threshold for a profile that is considered to have a peak, rather than being constant. The light red boxes in **d, e, f, j** show the threshold of comparison to the measured value compared.

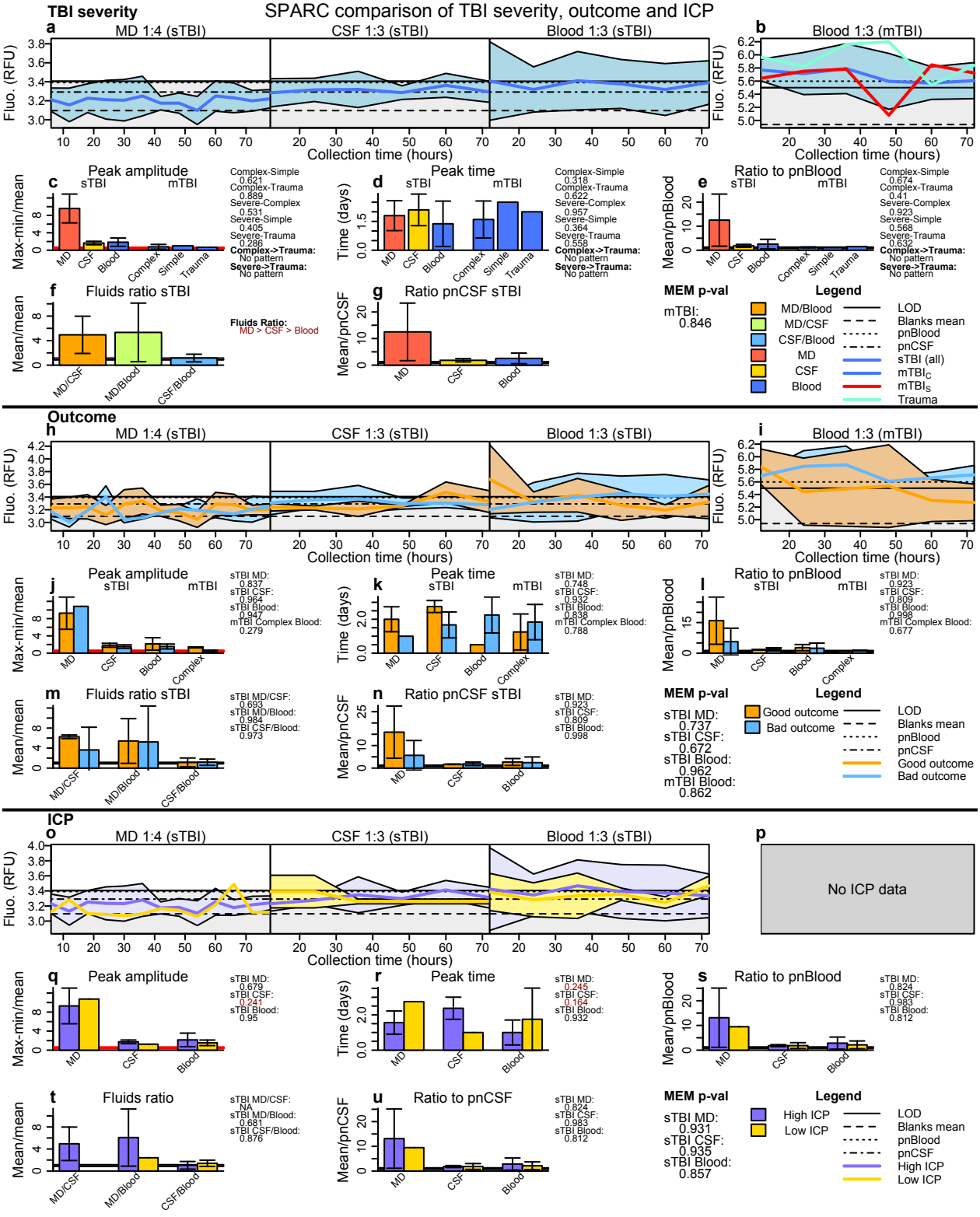

FIGURE J.S196: **Differential SPARC protein profiles and peak and ratio analysis with respect to TBI severity, outcome and ICP.** Average SPARC profiles are compared in terms of TBI severity (**a-g**), outcome (**h-n**) and ICP (**o-u**). Polygons in **a, b, h, i, o** indicate the mean value ±1 SD at each time point. Red lines in **c, j, q** show a threshold for a profile that is considered to have a peak, rather than being constant. The light red boxes in **e-g, l-n, s-u** show the threshold of comparison to the measured value compared. Benjamini–Hochberg adjusted p-values for comparisons are shown on the right of every graph.

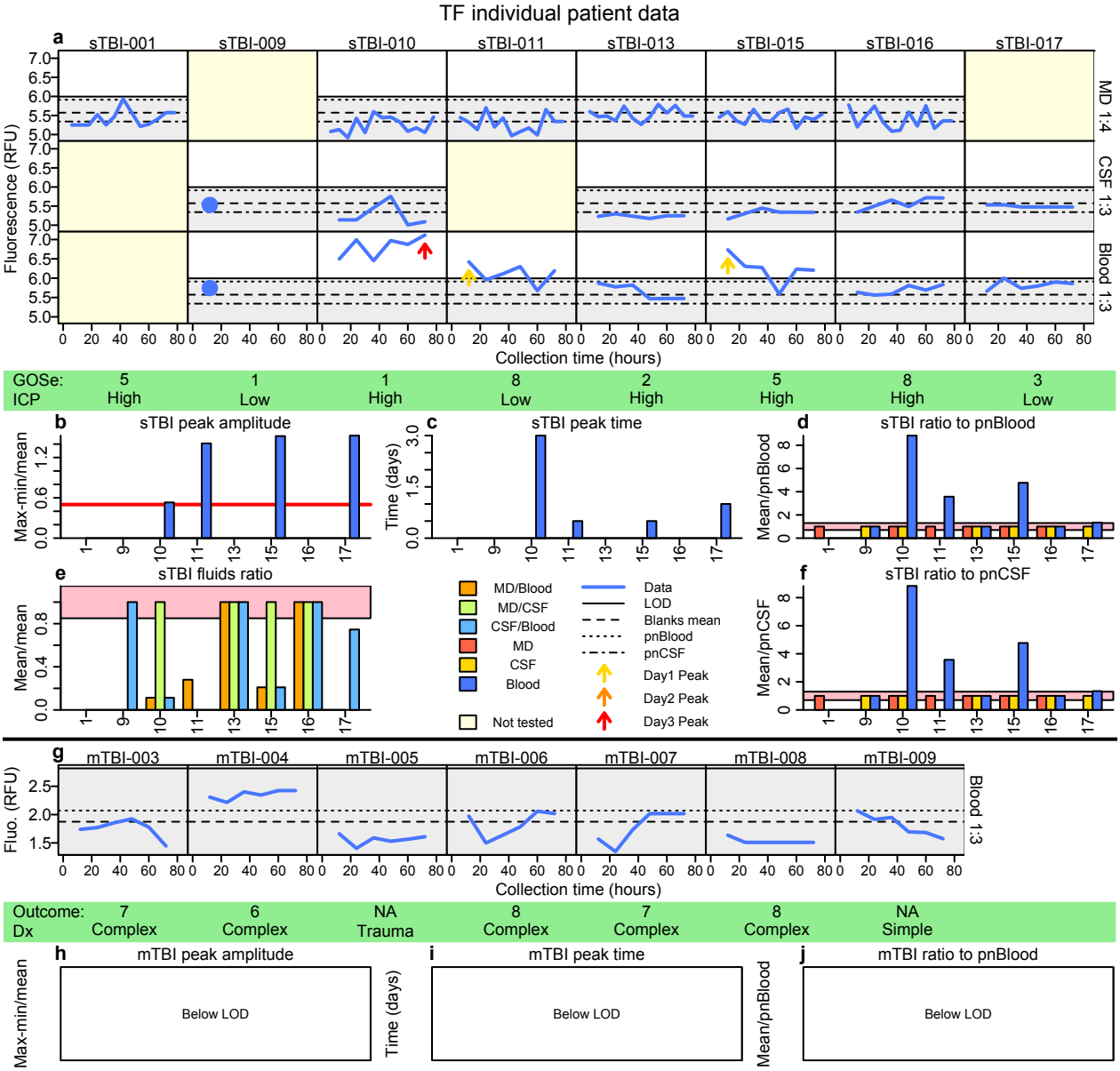

FIGURE J.S197: **Individual TF protein profiles and peak and ratio analysis.** TF concentration in microdialysate, CSF and blood samples of individual sTBI patients (**a**) and mTBI/trauma patients (**g**) was measured and peak amplitude and time, as well as ratio between mean time course values to value found in the pooled normal control (**b-f, h-j**) were calculated for each patient. Graphs **b-f** show calculations for individual sTBI patients, and graphs **h-j** show calculations for individual mTBI patients. Red lines in **b, h** show a threshold for a profile that is considered to have a peak, rather than being constant. The light red boxes in **d, e, f, j** show the threshold of comparison to the measured value compared.

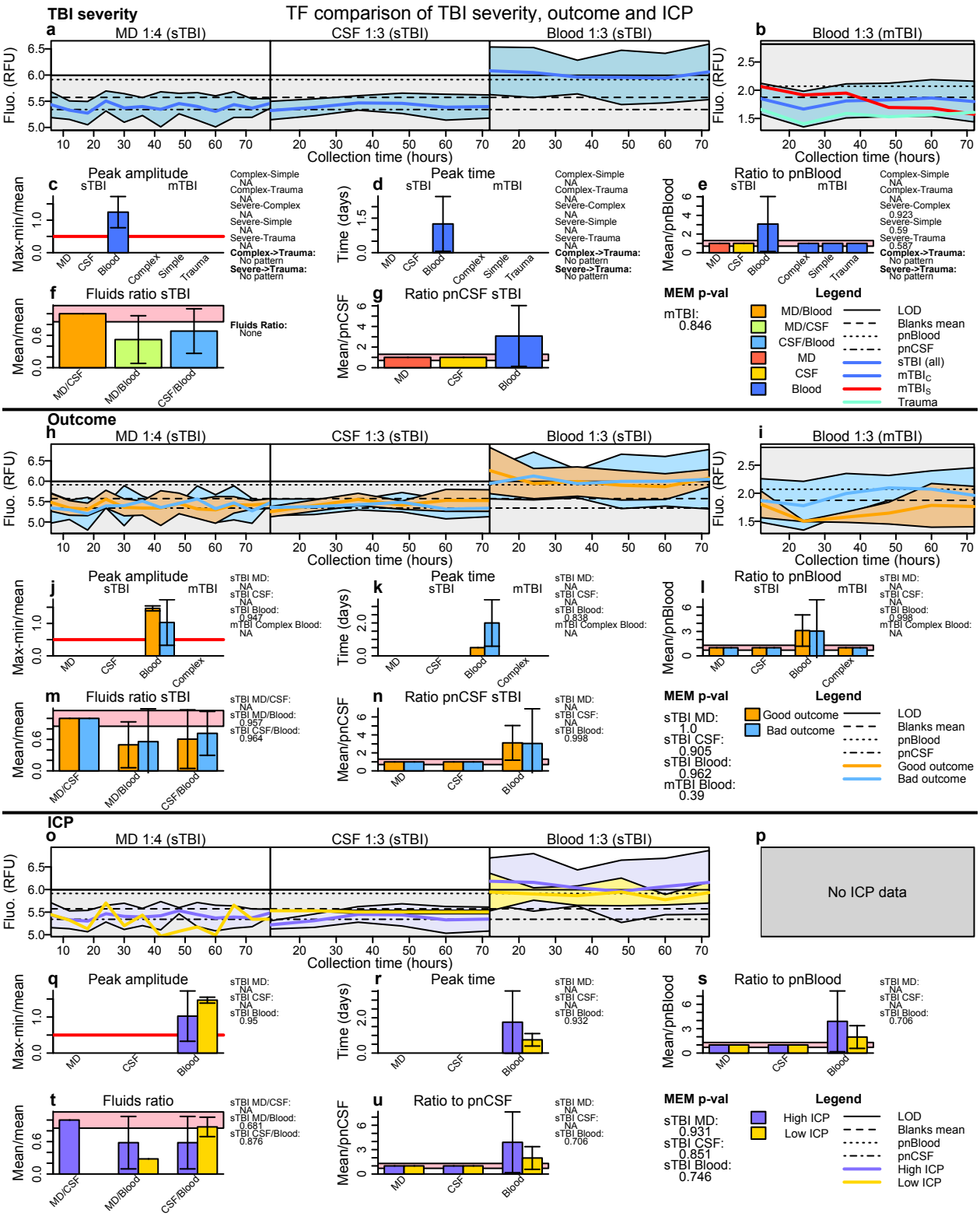

FIGURE J.S198: **Differential TF protein profiles and peak and ratio analysis with respect to TBI severity, outcome and ICP.** Average TF profiles are compared in terms of TBI severity (**a-g**), outcome (**h-n**) and ICP (**o-u**). Polygons in **a, b, h, i, o** indicate the mean value ±1 SD at each time point. Red lines in **c, j, q** show a threshold for a profile that is considered to have a peak, rather than being constant. The light red boxes in **e-g, l-n, s-u** show the threshold of comparison to the measured value compared. Benjamini–Hochberg adjusted p-values for comparisons are shown on the right of every graph.

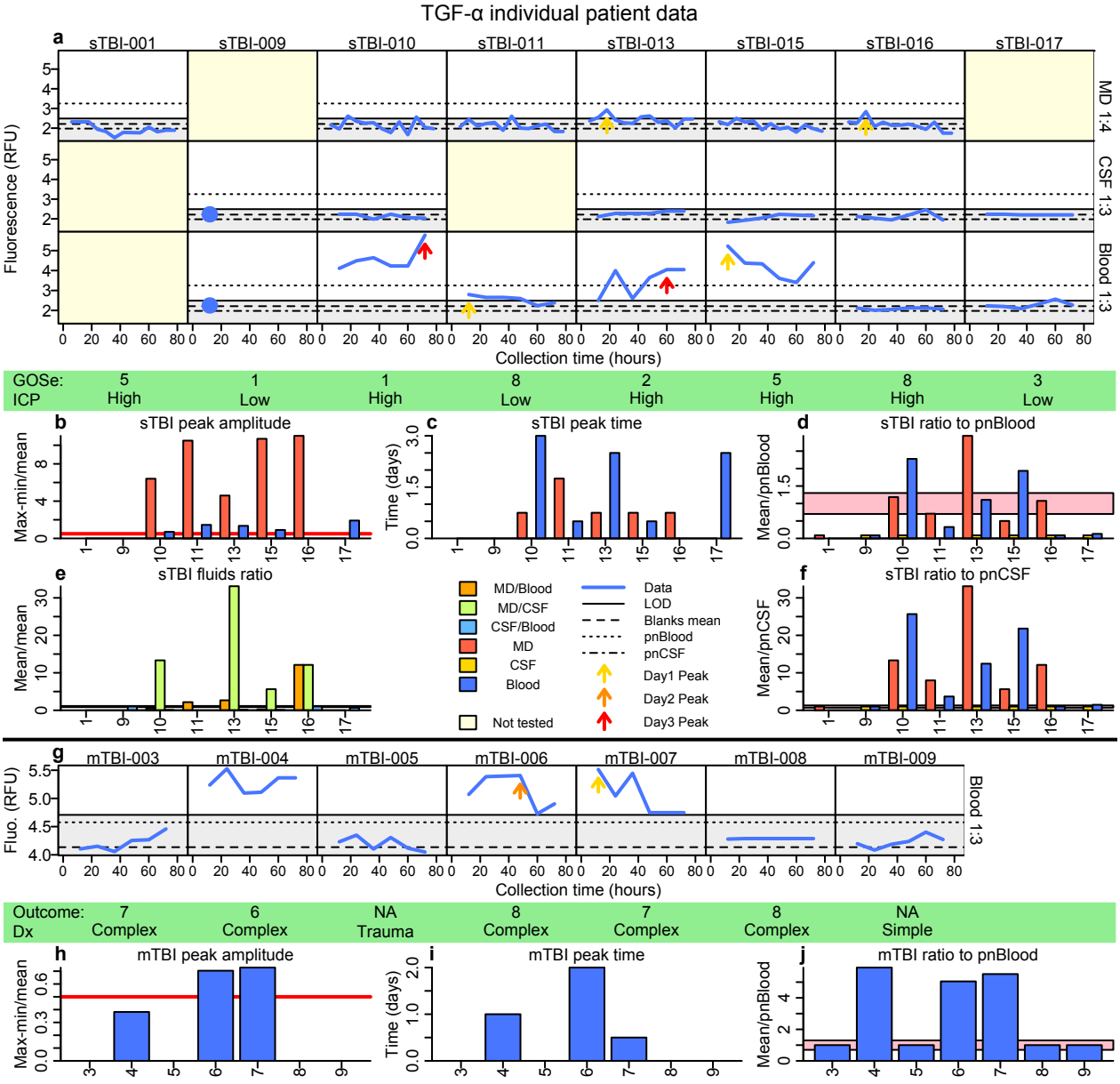

FIGURE J.S199: **Individual TGF-α protein profiles and peak and ratio analysis.** TGF-α concentration in microdialysate, CSF and blood samples of individual sTBI patients (**a**) and mTBI/trauma patients (**g**) was measured and peak amplitude and time, as well as ratio between mean time course values to value found in the pooled normal control (**b-f, h-j**) were calculated for each patient. Graphs **b-f** show calculations for individual sTBI patients, and graphs **h-j** show calculations for individual mTBI patients. Red lines in **b, h** show a threshold for a profile that is considered to have a peak, rather than being constant. The light red boxes in **d, e, f, j** show the threshold of comparison to the measured value compared.

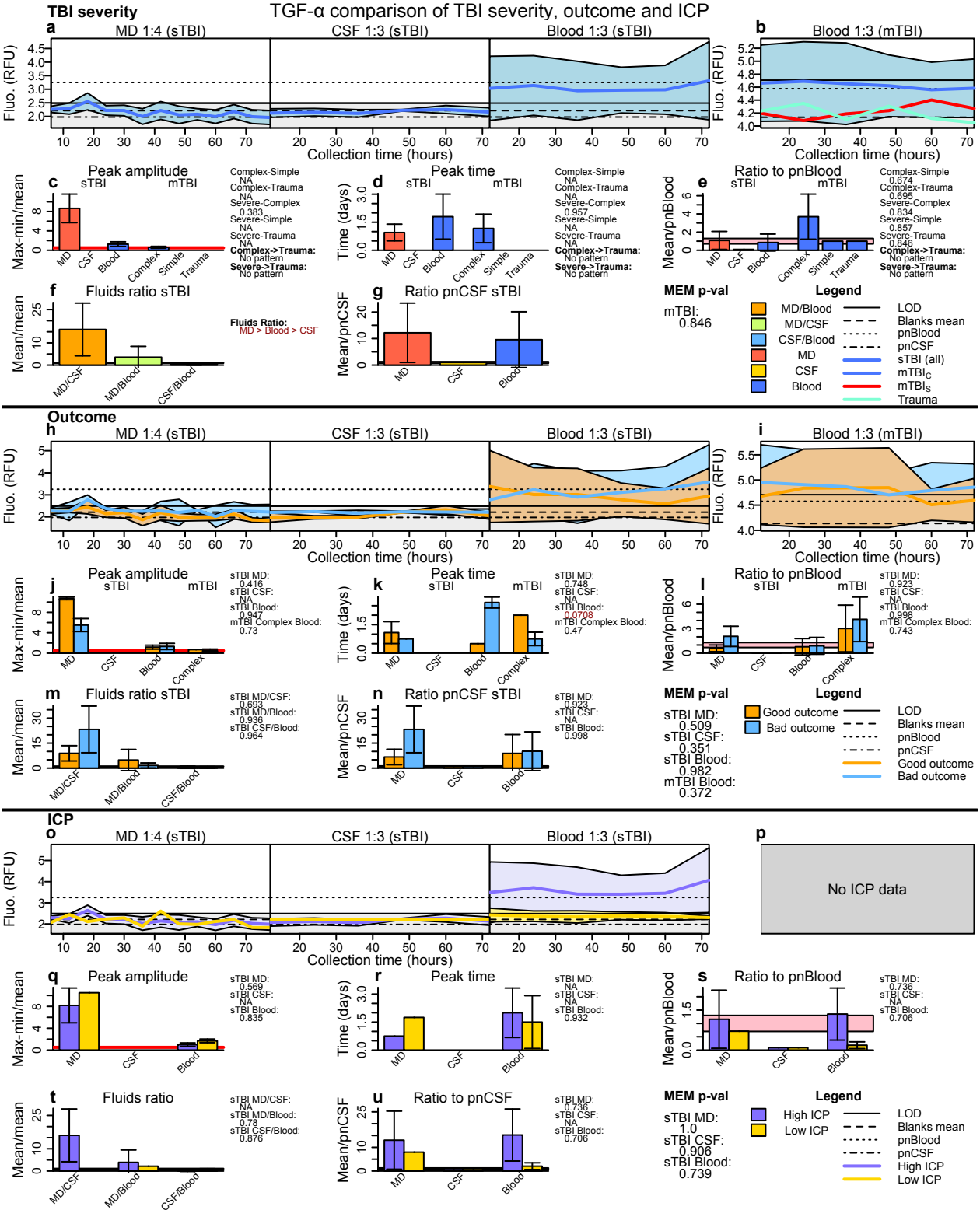

FIGURE J.S200: **Differential TGF-α protein profiles and peak and ratio analysis with respect to TBI severity, outcome and ICP.** Average TGF-α profiles are compared in terms of TBI severity (**a-g**), outcome (**h-n**) and ICP (**o-u**). Polygons in **a, b, h, i, o** indicate the mean value ± 1 SD at each time point. Red lines in **c, j, q** show a threshold for a profile that is considered to have a peak, rather than being constant. The light red boxes in **e-g, l-n, s-u** show the threshold of comparison to the measured value compared. Benjamini–Hochberg adjusted p-values for comparisons are shown on the right of every graph.

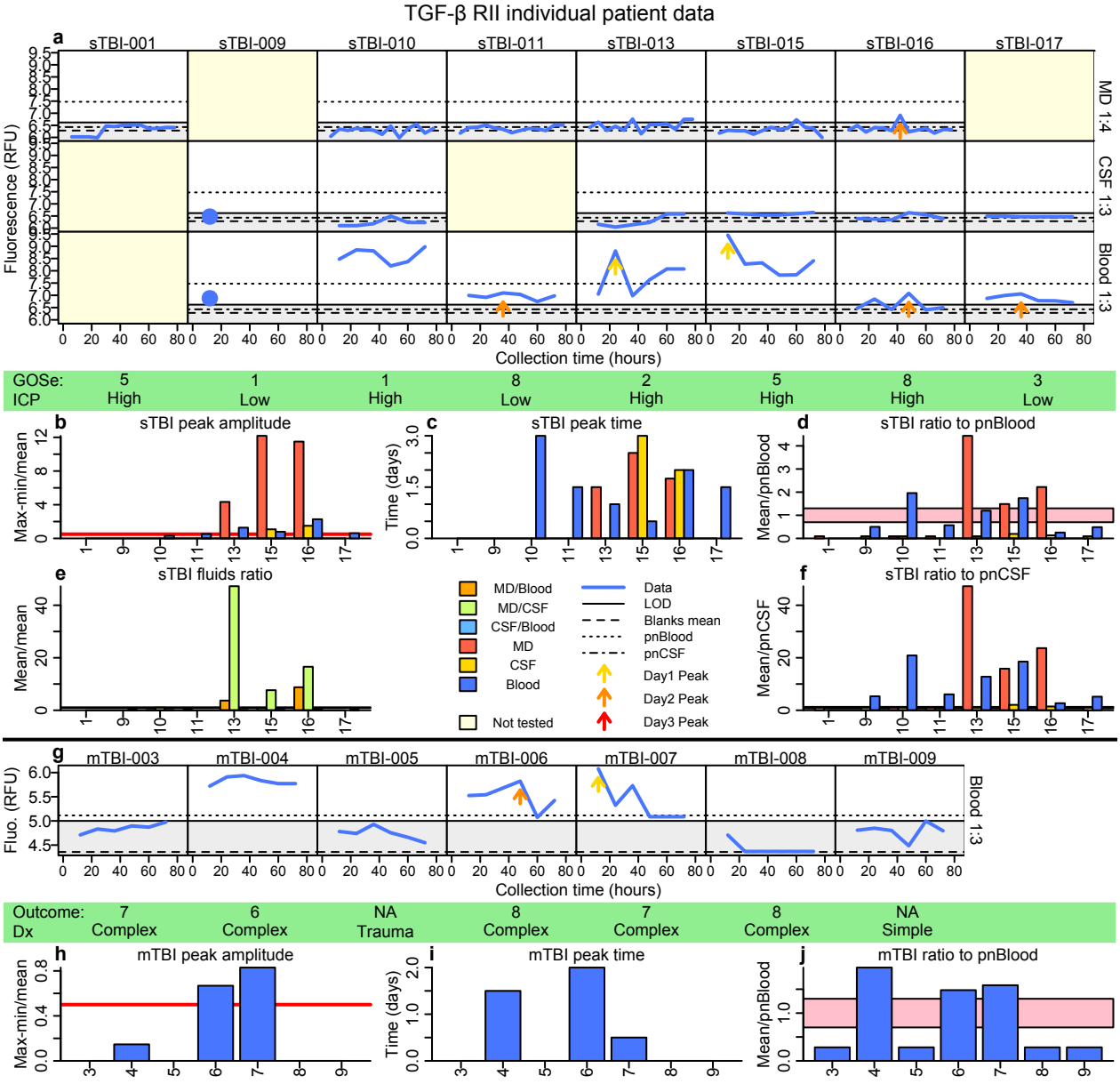

FIGURE J.S201: **Individual TGF-β RII protein profiles and peak and ratio analysis.** TGF-β RII concentration in microdialysate, CSF and blood samples of individual sTBI patients (**a**) and mTBI/trauma patients (**g**) was measured and peak amplitude and time, as well as ratio between mean time course values to value found in the pooled normal control (**b-f, h-j**) were calculated for each patient. Graphs **b-f** show calculations for individual sTBI patients, and graphs **h-j** show calculations for individual mTBI patients. Red lines in **b, h** show a threshold for a profile that is considered to have a peak, rather than being constant. The light red boxes in **d, e, f, j** show the threshold of comparison to the measured value compared.

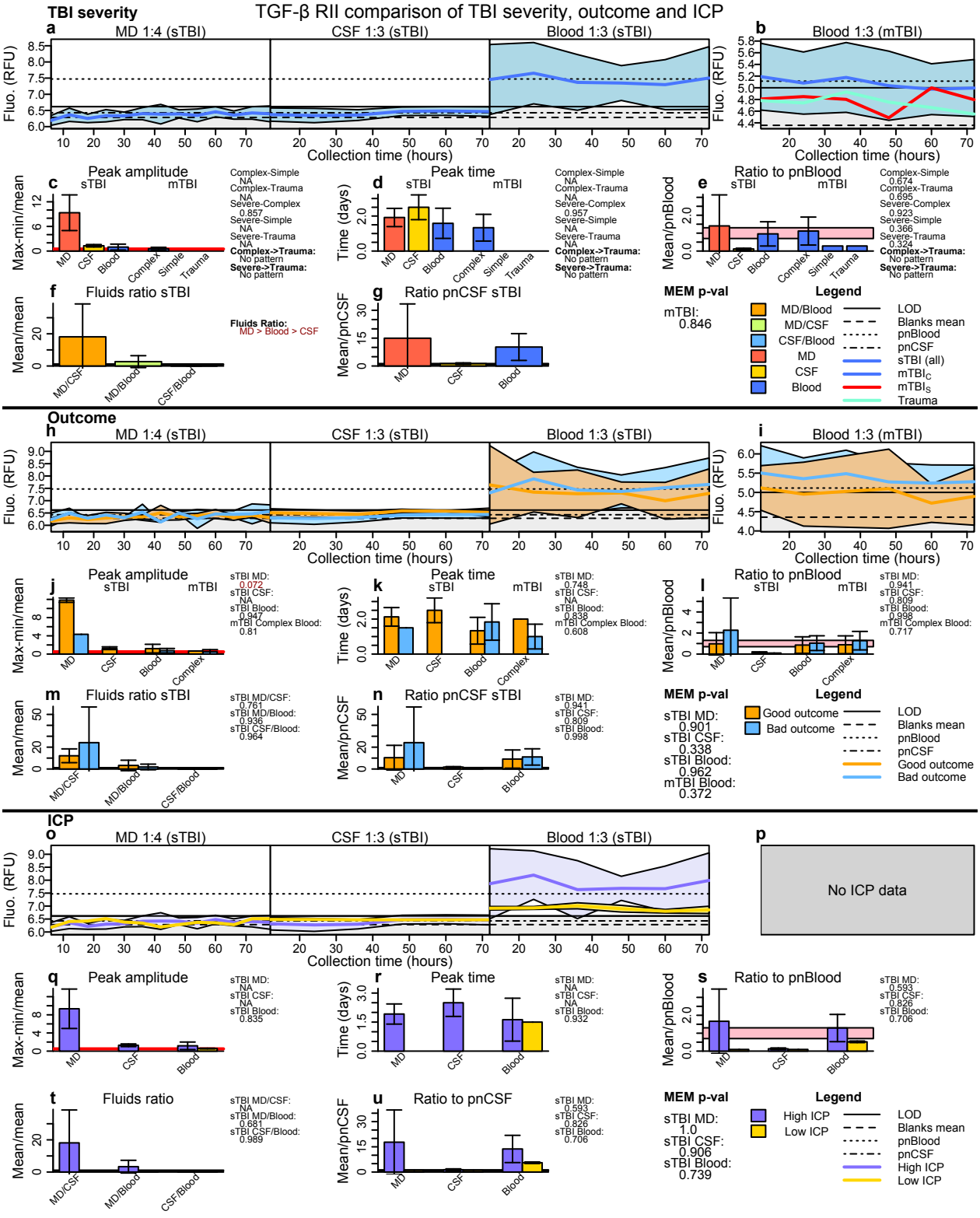

FIGURE J.S202: **Differential TGF-β RII protein profiles and peak and ratio analysis with respect to TBI severity, outcome and ICP.** Average TGF-β RII profiles are compared in terms of TBI severity (**a-g**), outcome (**h-n**) and ICP (**o-u**). Polygons in **a, b, h, i, o** indicate the mean value ± 1 SD at each time point. Red lines in **c, j, q** show a threshold for a profile that is considered to have a peak, rather than being constant. The light red boxes in **e-g, l-n, s-u** show the threshold of comparison to the measured value compared. Benjamini–Hochberg adjusted p-values for comparisons are shown on the right of every graph.

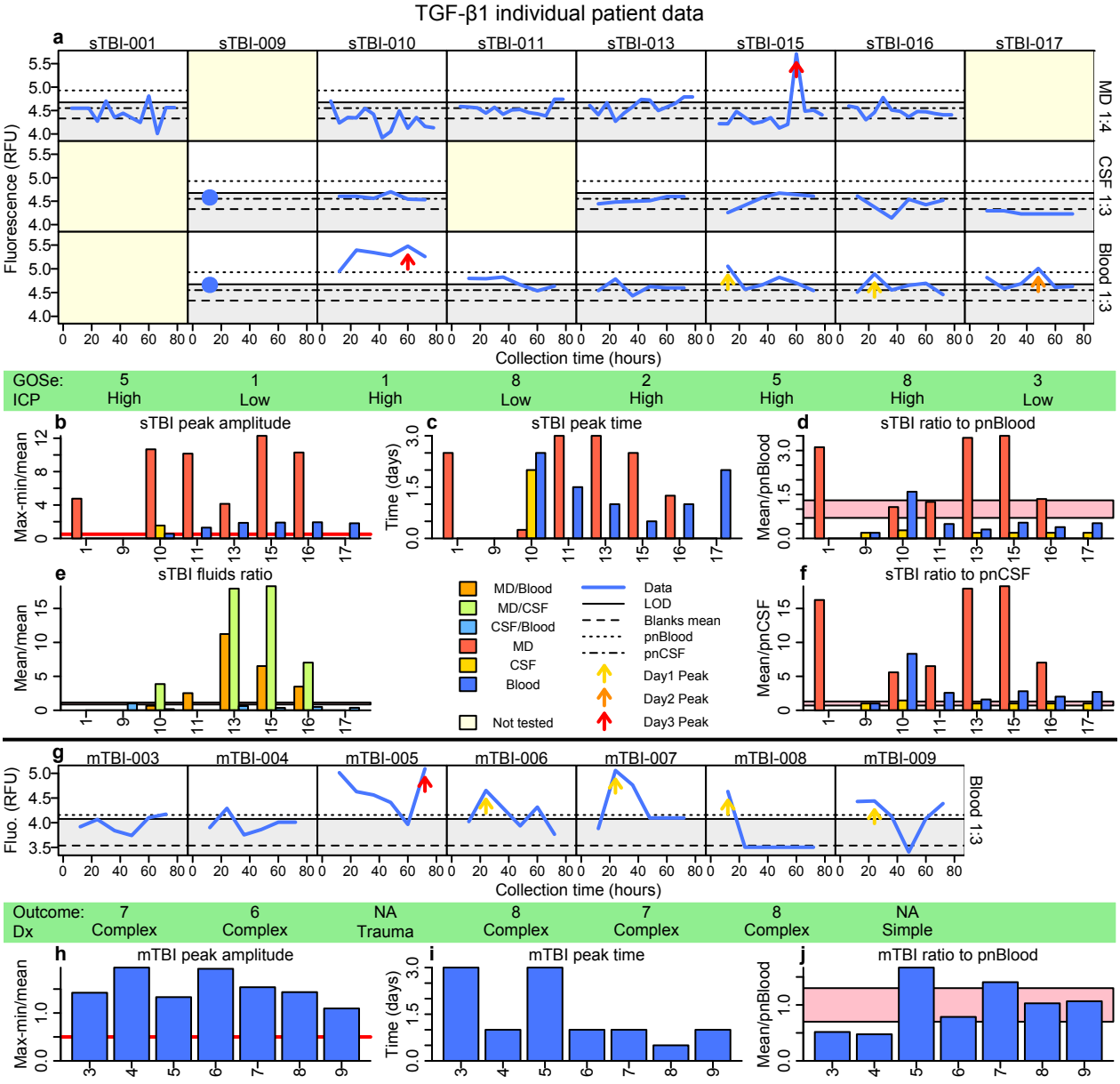

FIGURE J.S203: **Individual TGF-β1 protein profiles and peak and ratio analysis.** TGF-β1 concentration in microdialysate, CSF and blood samples of individual sTBI patients (**a**) and mTBI/trauma patients (**g**) was measured and peak amplitude and time, as well as ratio between mean time course values to value found in the pooled normal control (**b-f, h-j**) were calculated for each patient. Graphs **b-f** show calculations for individual sTBI patients, and graphs **h-j** show calculations for individual mTBI patients. Red lines in **b, h** show a threshold for a profile that is considered to have a peak, rather than being constant. The light red boxes in **d, e, f, j** show the threshold of comparison to the measured value compared.

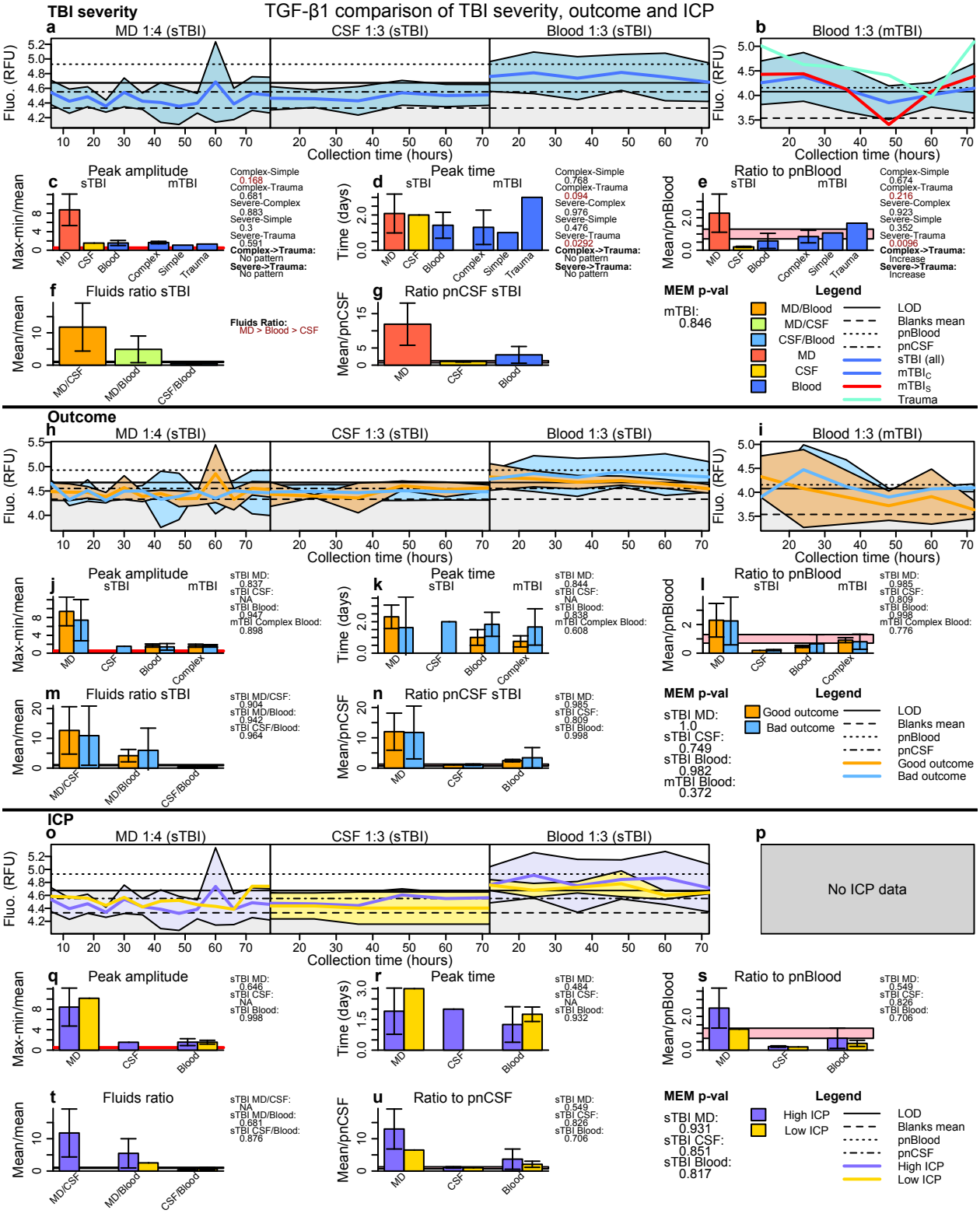

FIGURE J.S204: **Differential TGF-β1 protein profiles and peak and ratio analysis with respect to TBI severity, outcome and ICP.** Average TGF-β1 profiles are compared in terms of TBI severity (**a-g**), outcome (**h-n**) and ICP (**o-u**). Polygons in **a, b, h, i, o** indicate the mean value ± 1 SD at each time point. Red lines in **c, j, q** show a threshold for a profile that is considered to have a peak, rather than being constant. The light red boxes in **e-g, l-n, s-u** show the threshold of comparison to the measured value compared. Benjamini–Hochberg adjusted p-values for comparisons are shown on the right of every graph.

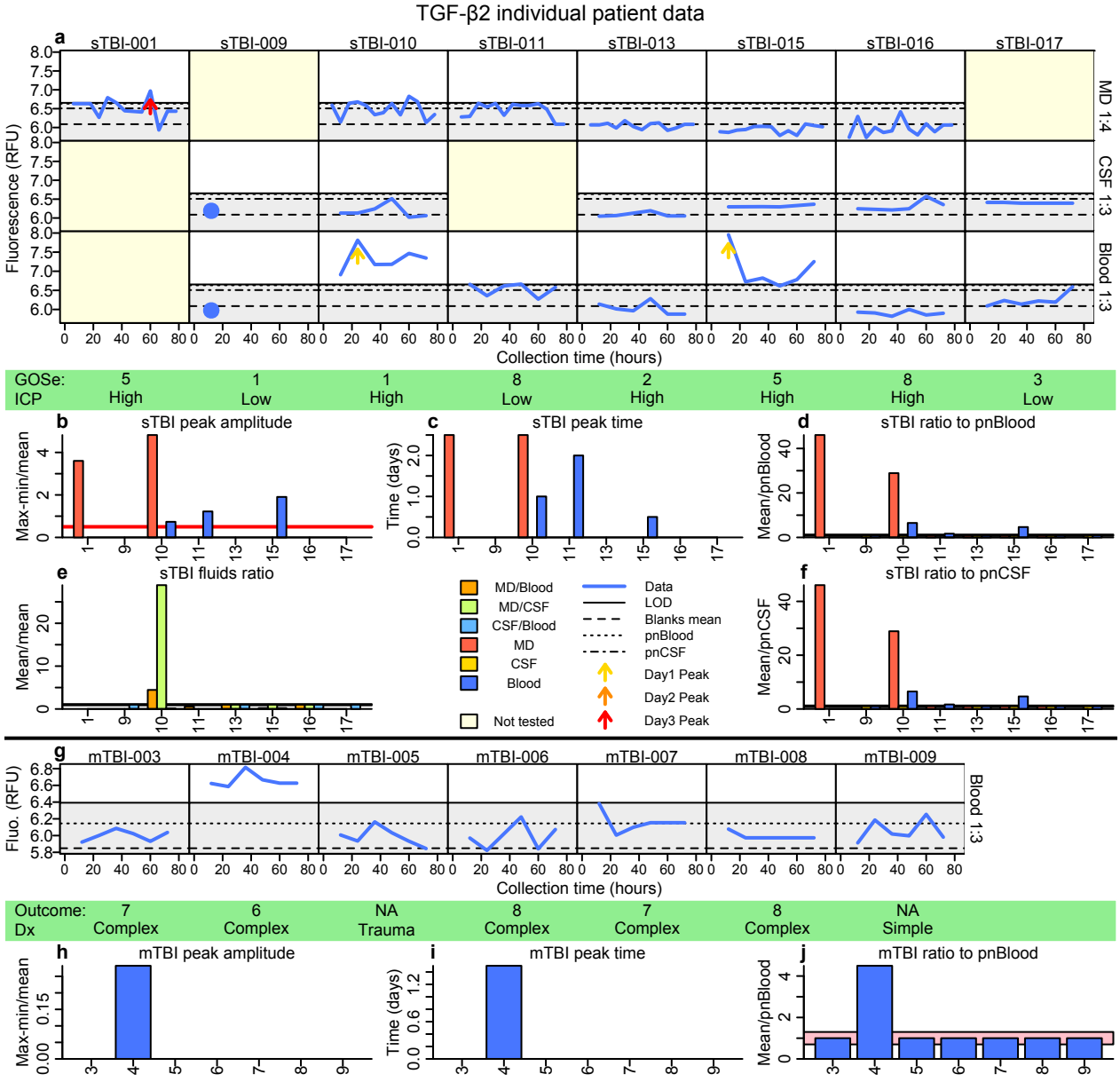

FIGURE J.S205: **Individual TGF-β2 protein profiles and peak and ratio analysis.** TGF-β2 concentration in microdialysate, CSF and blood samples of individual sTBI patients (**a**) and mTBI/trauma patients (**g**) was measured and peak amplitude and time, as well as ratio between mean time course values to value found in the pooled normal control (**b-f, h-j**) were calculated for each patient. Graphs **b-f** show calculations for individual sTBI patients, and graphs **h-j** show calculations for individual mTBI patients. Red lines in **b, h** show a threshold for a profile that is considered to have a peak, rather than being constant. The light red boxes in **d, e, f, j** show the threshold of comparison to the measured value compared.

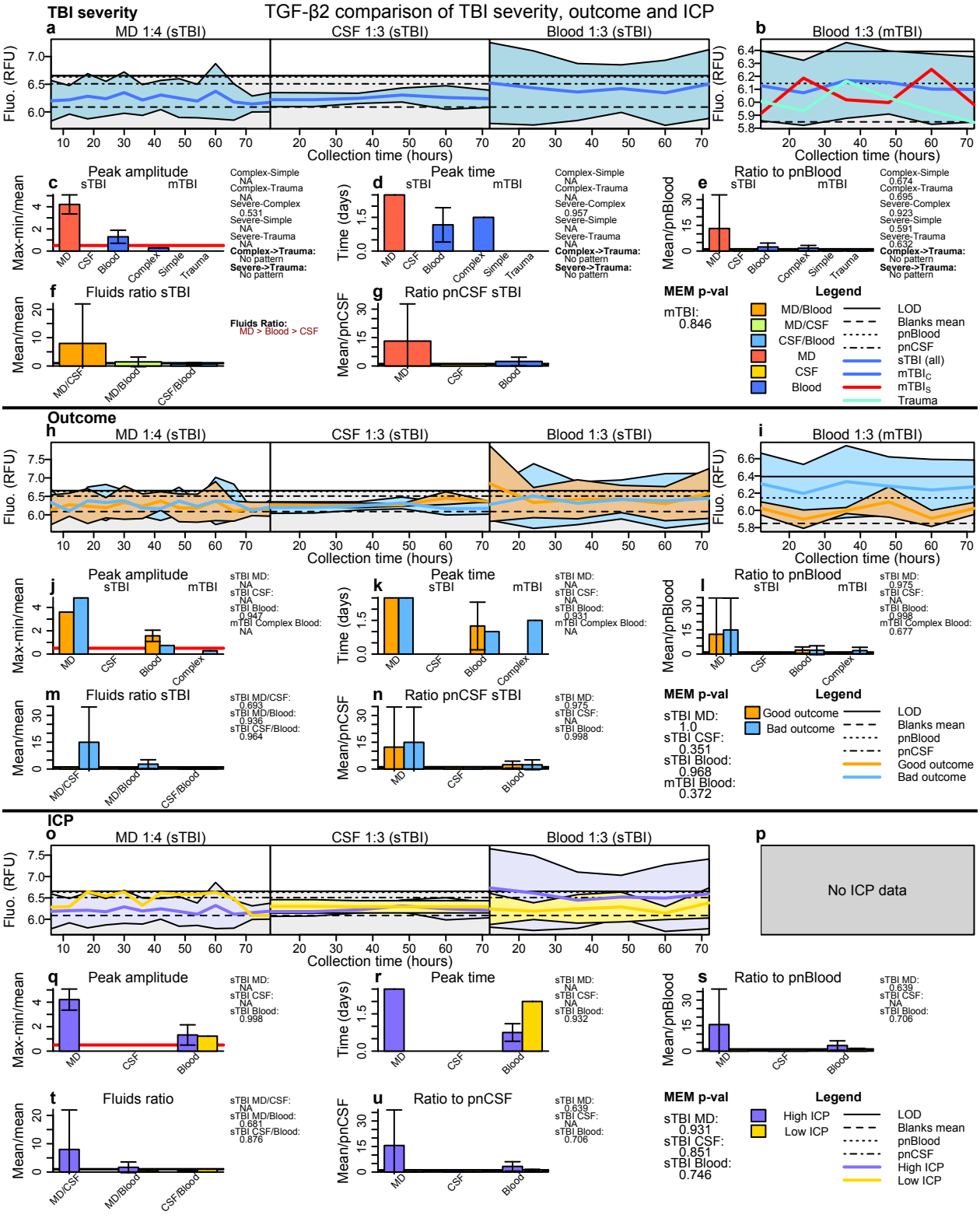

FIGURE J.S206: **Differential TGF-β2 protein profiles and peak and ratio analysis with respect to TBI severity, outcome and ICP.** Average TGF-β2 profiles are compared in terms of TBI severity (**a-g**), outcome (**h-n**) and ICP (**o-u**). Polygons in **a, b, h, i, o** indicate the mean value ± 1 SD at each time point. Red lines in **c, j, q** show a threshold for a profile that is considered to have a peak, rather than being constant. The light red boxes in **e-g, l-n, s-u** show the threshold of comparison to the measured value compared. Benjamini–Hochberg adjusted p-values for comparisons are shown on the right of every graph.

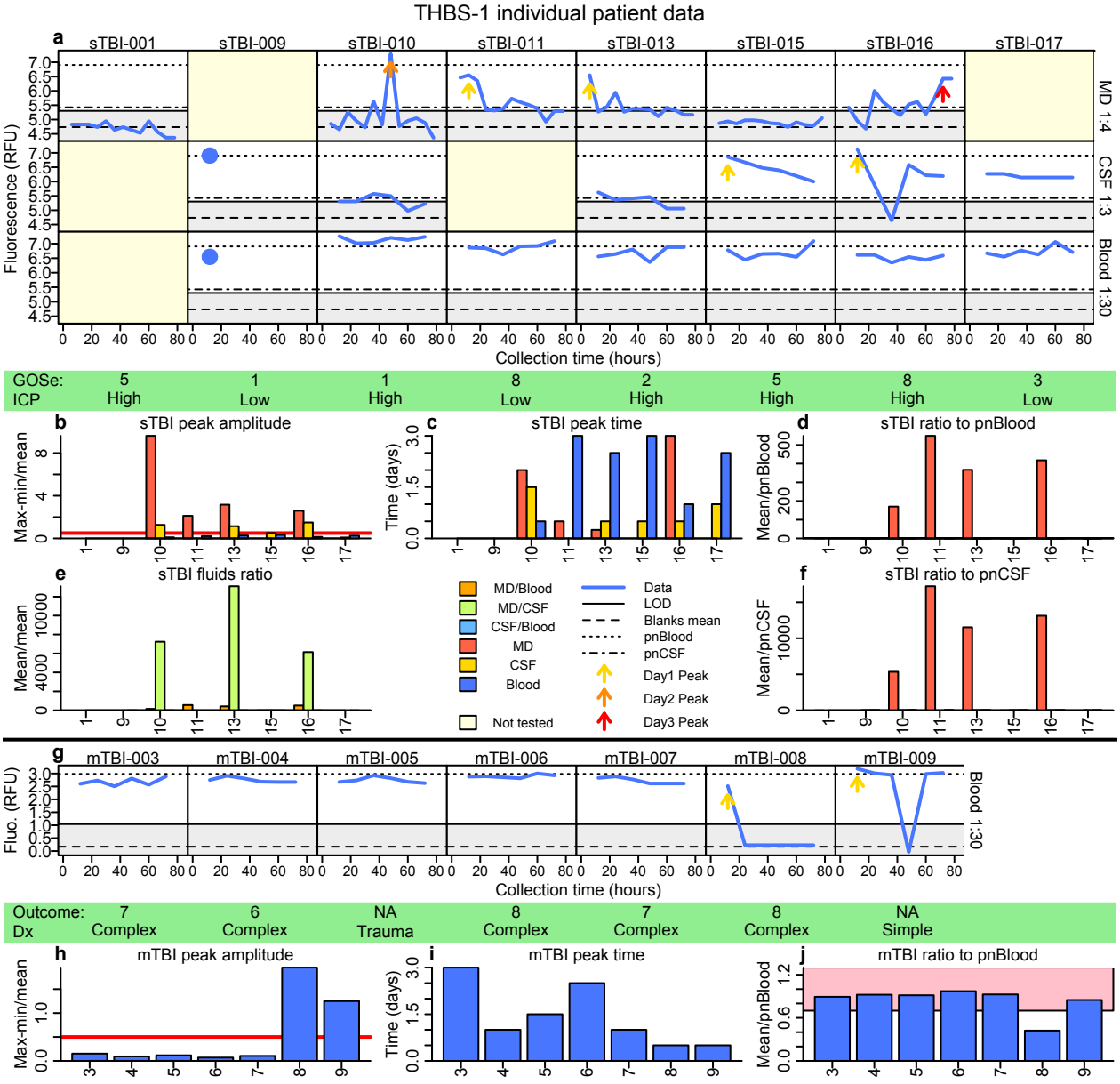

FIGURE J.S207: **Individual THBS-1 protein profiles and peak and ratio analysis.** THBS-1 concentration in microdialysate, CSF and blood samples of individual sTBI patients (**a**) and mTBI/trauma patients (**g**) was measured and peak amplitude and time, as well as ratio between mean time course values to value found in the pooled normal control (**b-f, h-j**) were calculated for each patient. Graphs **b-f** show calculations for individual sTBI patients, and graphs **h-j** show calculations for individual mTBI patients. Red lines in **b, h** show a threshold for a profile that is considered to have a peak, rather than being constant. The light red boxes in **d, e, f, j** show the threshold of comparison to the measured value compared.

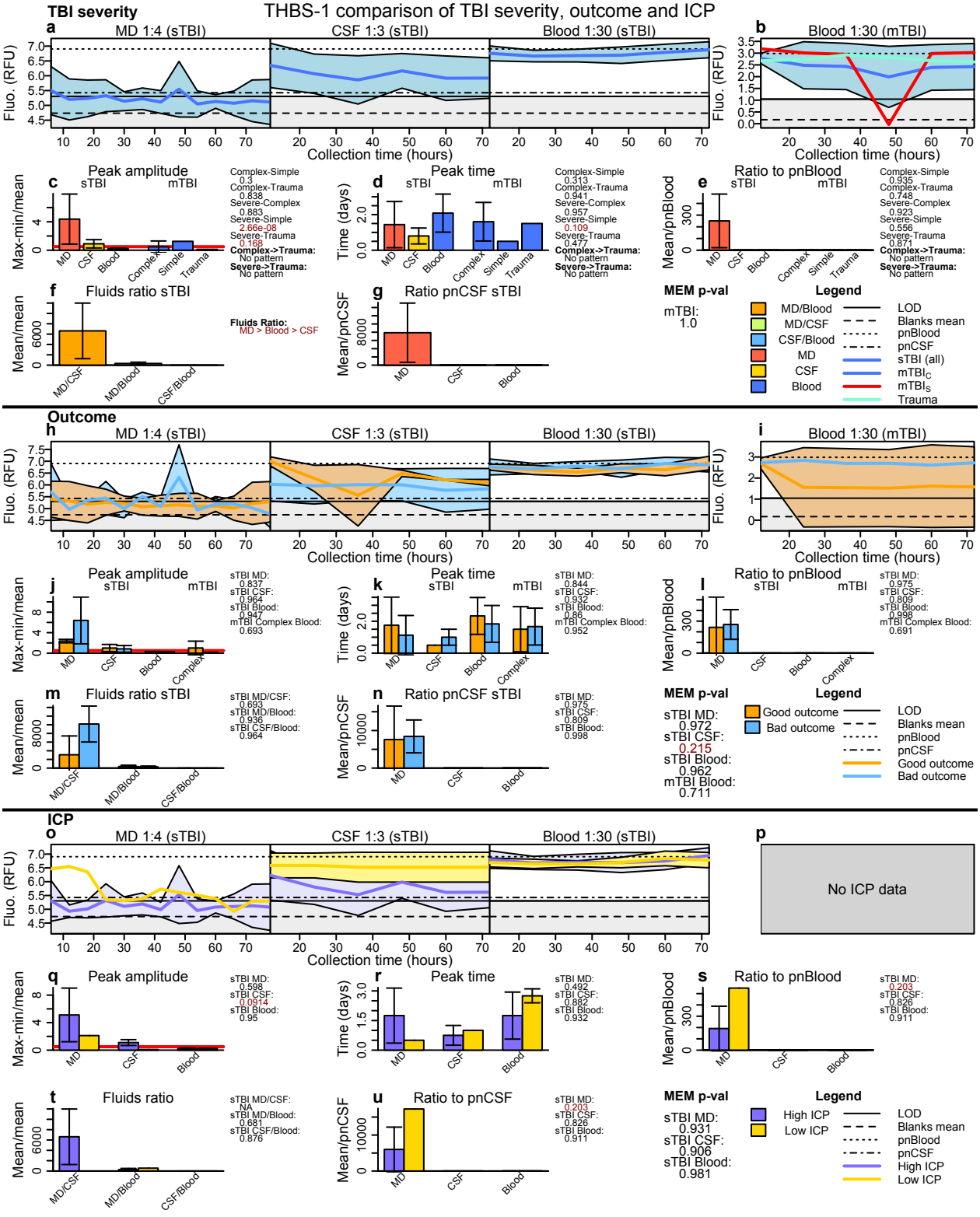

FIGURE J.S208: **Differential THBS-1 protein profiles and peak and ratio analysis with respect to TBI severity, outcome and ICP.** Average THBS-1 profiles are compared in terms of TBI severity (**a-g**), outcome (**h-n**) and ICP (**o-u**). Polygons in **a, b, h, i, o** indicate the mean value ±1 SD at each time point. Red lines in **c, j, q** show a threshold for a profile that is considered to have a peak, rather than being constant. The light red boxes in **e-g, l-n, s-u** show the threshold of comparison to the measured value compared. Benjamini–Hochberg adjusted p-values for comparisons are shown on the right of every graph.

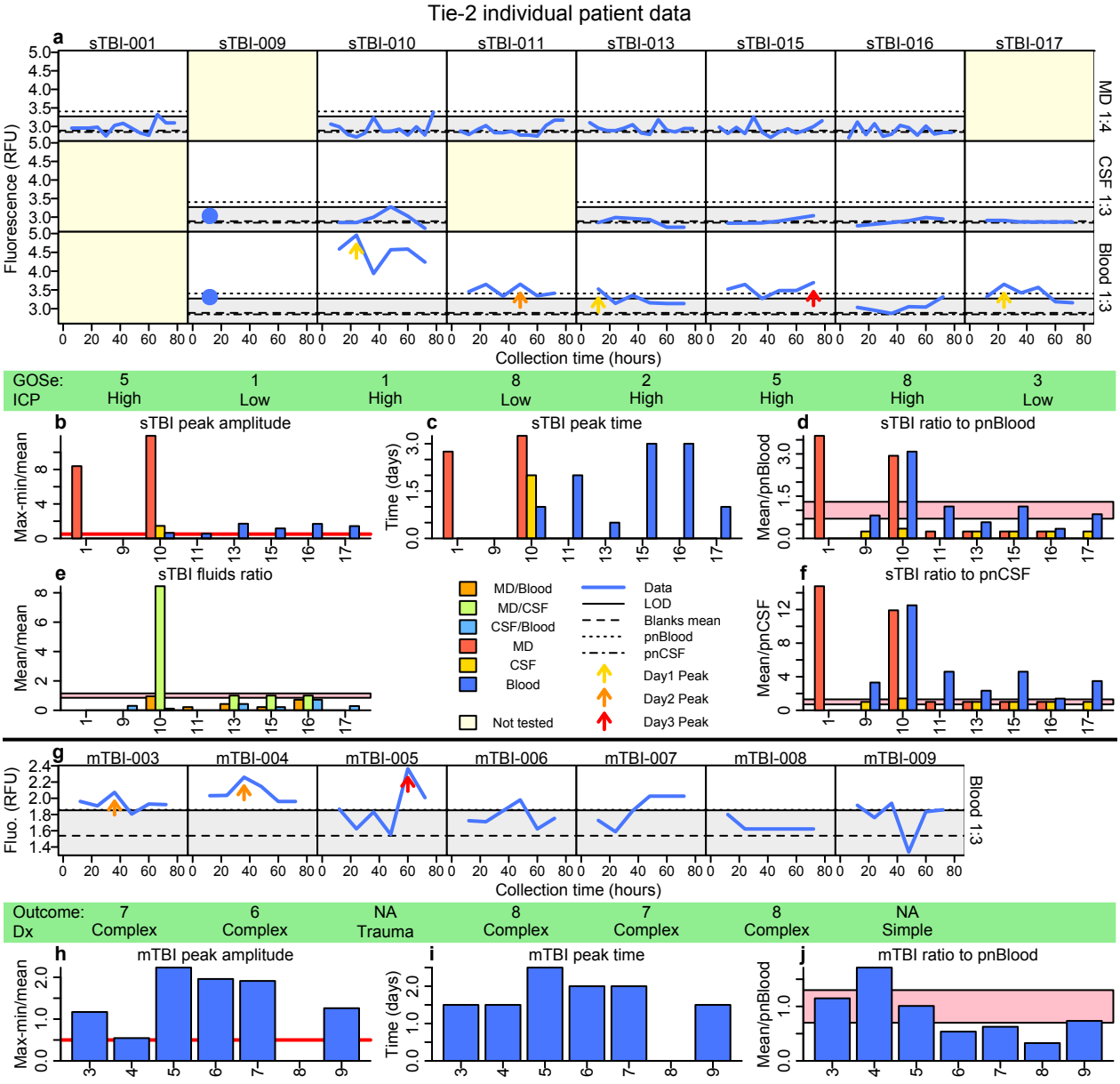

FIGURE J.S209: **Individual Tie-2 protein profiles and peak and ratio analysis.** Tie-2 concentration in microdialysate, CSF and blood samples of individual sTBI patients (**a**) and mTBI/trauma patients (**g**) was measured and peak amplitude and time, as well as ratio between mean time course values to value found in the pooled normal control (**b-f, h-j**) were calculated for each patient. Graphs **b-f** show calculations for individual sTBI patients, and graphs **h-j** show calculations for individual mTBI patients. Red lines in **b, h** show a threshold for a profile that is considered to have a peak, rather than being constant. The light red boxes in **d, e, f, j** show the threshold of comparison to the measured value compared.

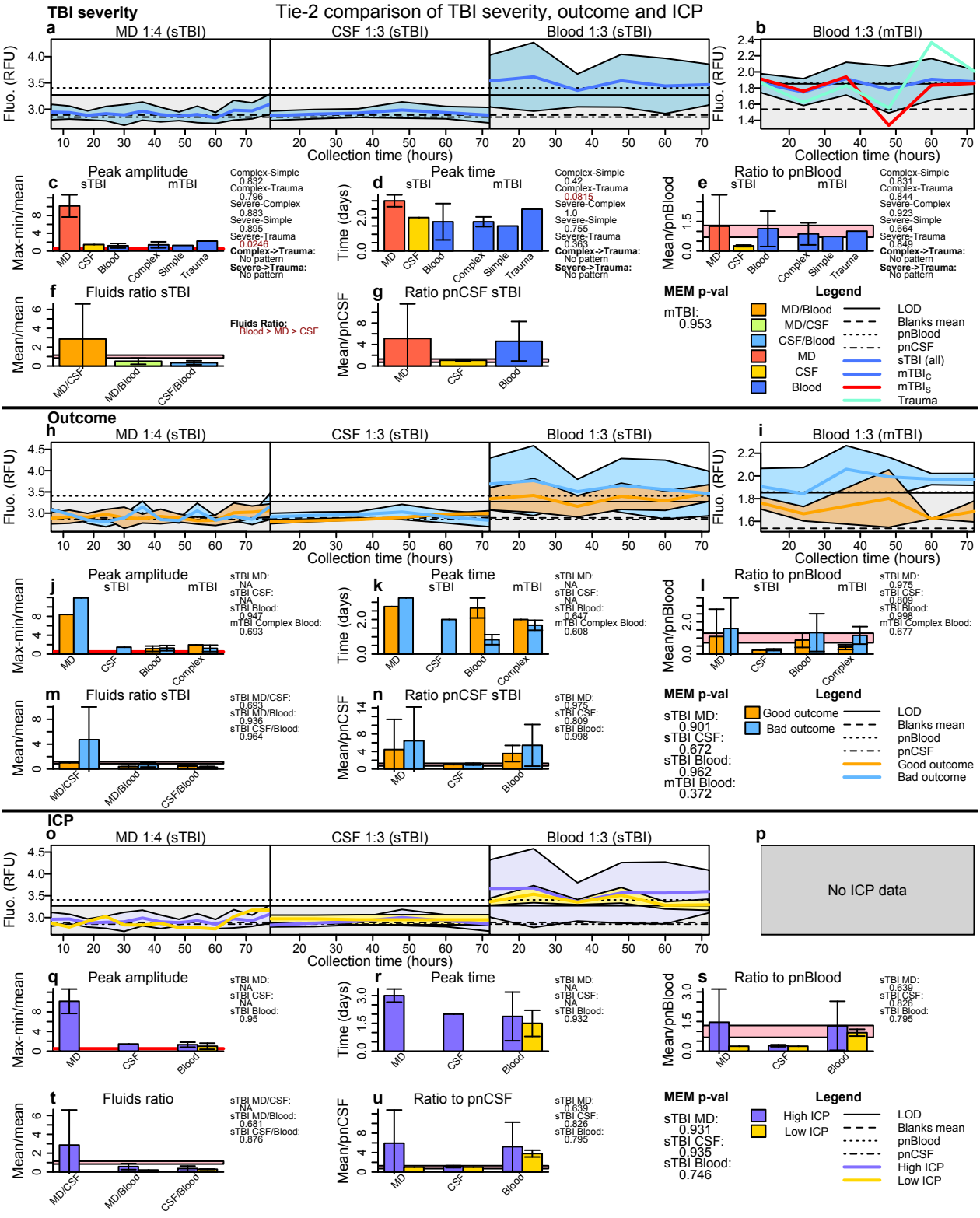

FIGURE J.S210: **Differential Tie-2 protein profiles and peak and ratio analysis with respect to TBI severity, outcome and ICP.** Average Tie-2 profiles are compared in terms of TBI severity (**a-g**), outcome (**h-n**) and ICP (**o-u**). Polygons in **a, b, h, i, o** indicate the mean value ±1 SD at each time point. Red lines in **c, j, q** show a threshold for a profile that is considered to have a peak, rather than being constant. The light red boxes in **e-g, l-n, s-u** show the threshold of comparison to the measured value compared. Benjamini–Hochberg adjusted p-values for comparisons are shown on the right of every graph.

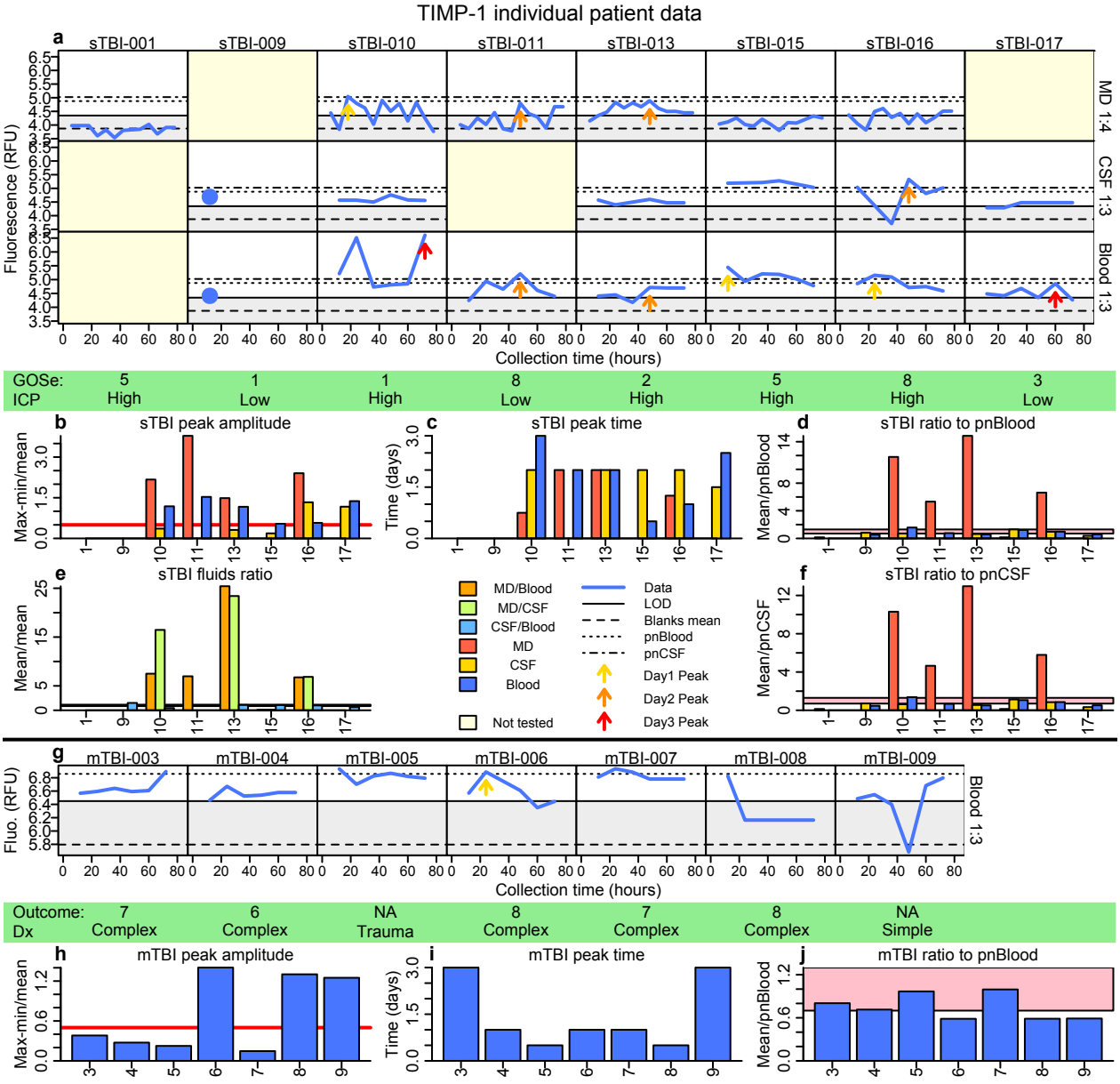

FIGURE J.S211: **Individual TIMP-1 protein profiles and peak and ratio analysis.** TIMP-1 concentration in microdialysate, CSF and blood samples of individual sTBI patients (**a**) and mTBI/trauma patients (**g**) was measured and peak amplitude and time, as well as ratio between mean time course values to value found in the pooled normal control (**b-f, h-j**) were calculated for each patient. Graphs **b-f** show calculations for individual sTBI patients, and graphs **h-j** show calculations for individual mTBI patients. Red lines in **b, h** show a threshold for a profile that is considered to have a peak, rather than being constant. The light red boxes in **d, e, f, j** show the threshold of comparison to the measured value compared.

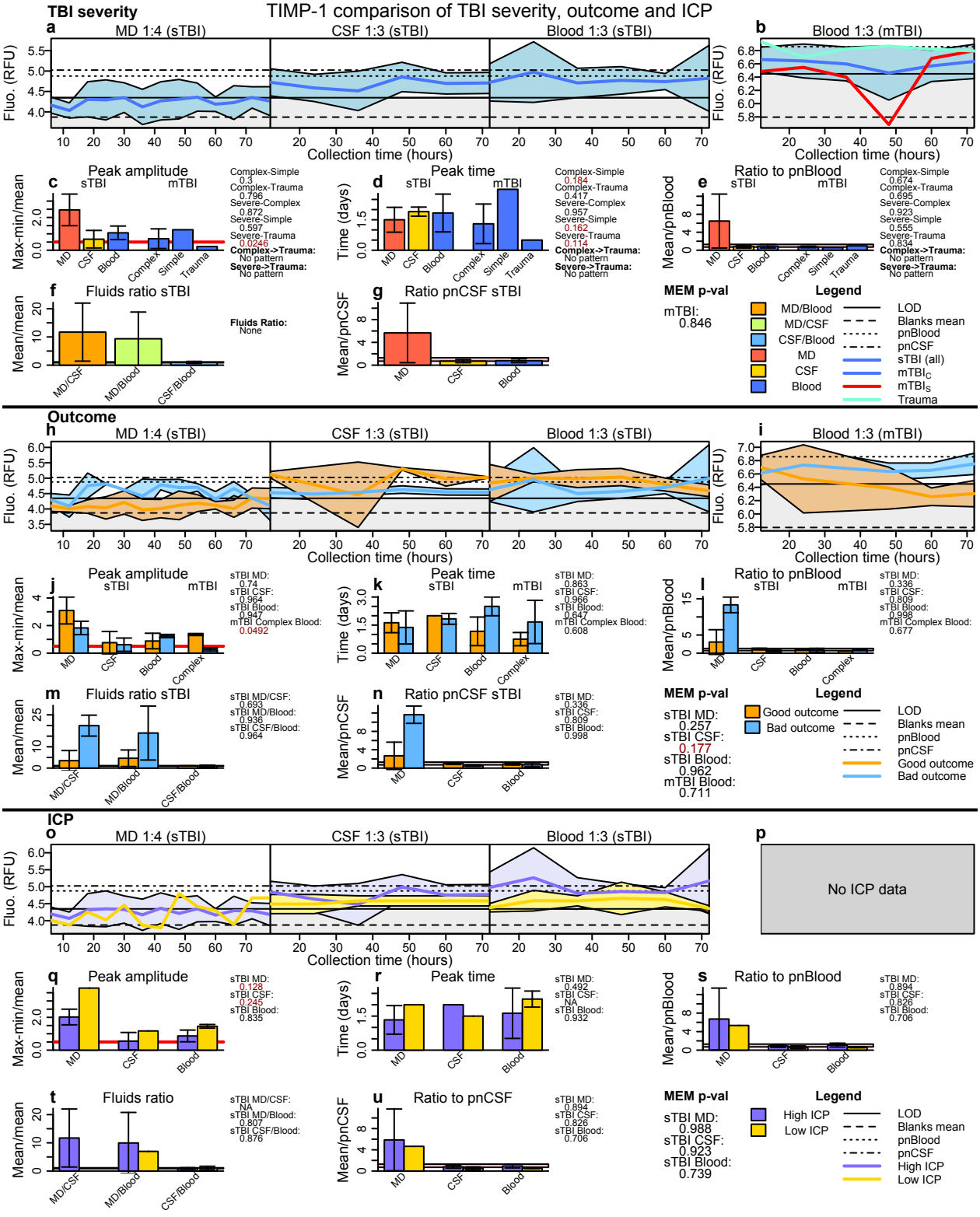

FIGURE J.S212: **Differential TIMP-1 protein profiles and peak and ratio analysis with respect to TBI severity, outcome and ICP.** Average TIMP-1 profiles are compared in terms of TBI severity (**a-g**), outcome (**h-n**) and ICP (**o-u**). Polygons in **a, b, h, i, o** indicate the mean value ±1 SD at each time point. Red lines in **c, j, q** show a threshold for a profile that is considered to have a peak, rather than being constant. The light red boxes in **e-g, l-n, s-u** show the threshold of comparison to the measured value compared. Benjamini–Hochberg adjusted p-values for comparisons are shown on the right of every graph.

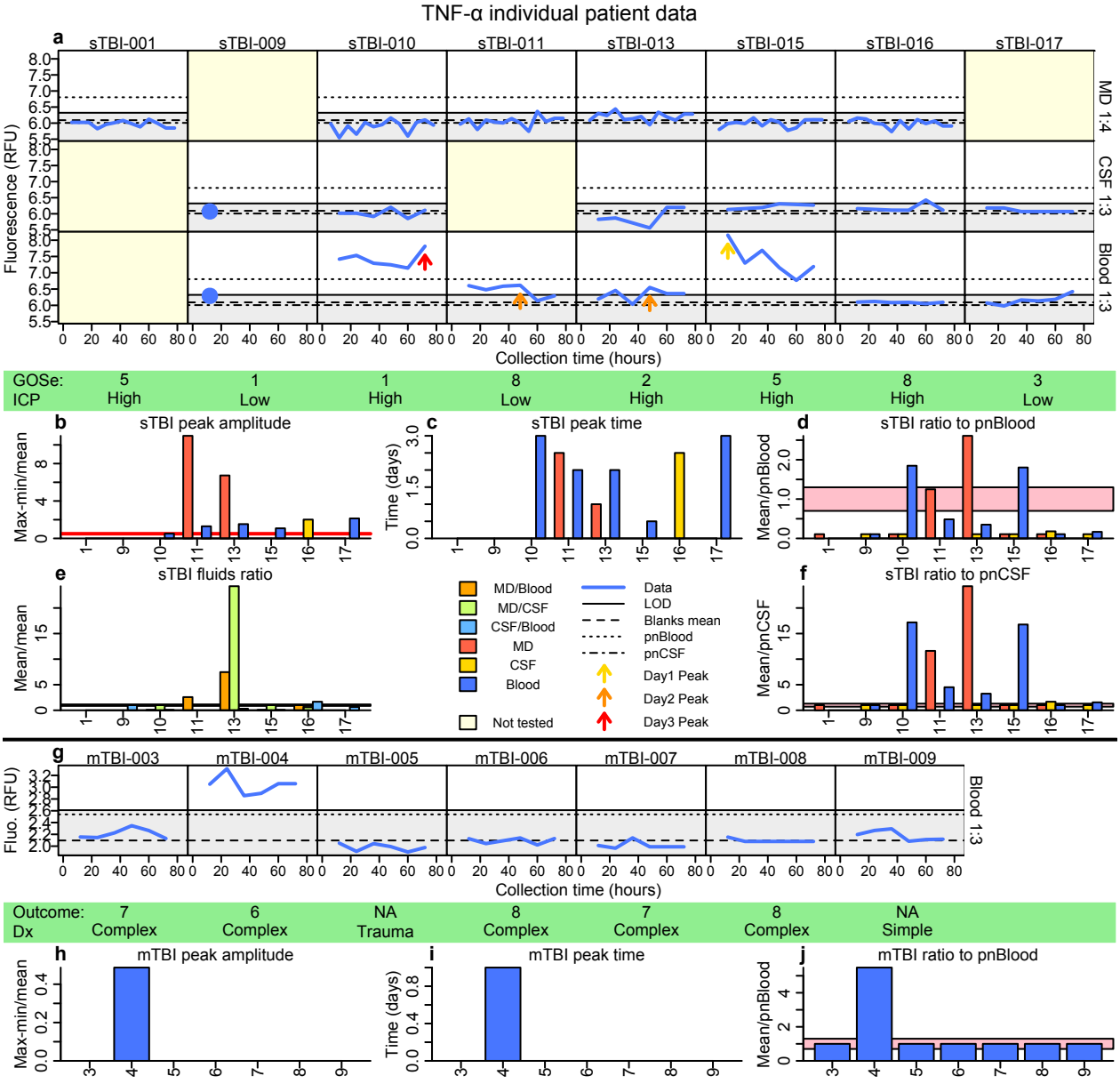

FIGURE J.S213: **Individual TNF-α protein profiles and peak and ratio analysis.** TNF-α concentration in microdialysate, CSF and blood samples of individual sTBI patients (**a**) and mTBI/trauma patients (**g**) was measured and peak amplitude and time, as well as ratio between mean time course values to value found in the pooled normal control (**b-f, h-j**) were calculated for each patient. Graphs **b-f** show calculations for individual sTBI patients, and graphs **h-j** show calculations for individual mTBI patients. Red lines in **b, h** show a threshold for a profile that is considered to have a peak, rather than being constant. The light red boxes in **d, e, f, j** show the threshold of comparison to the measured value compared.

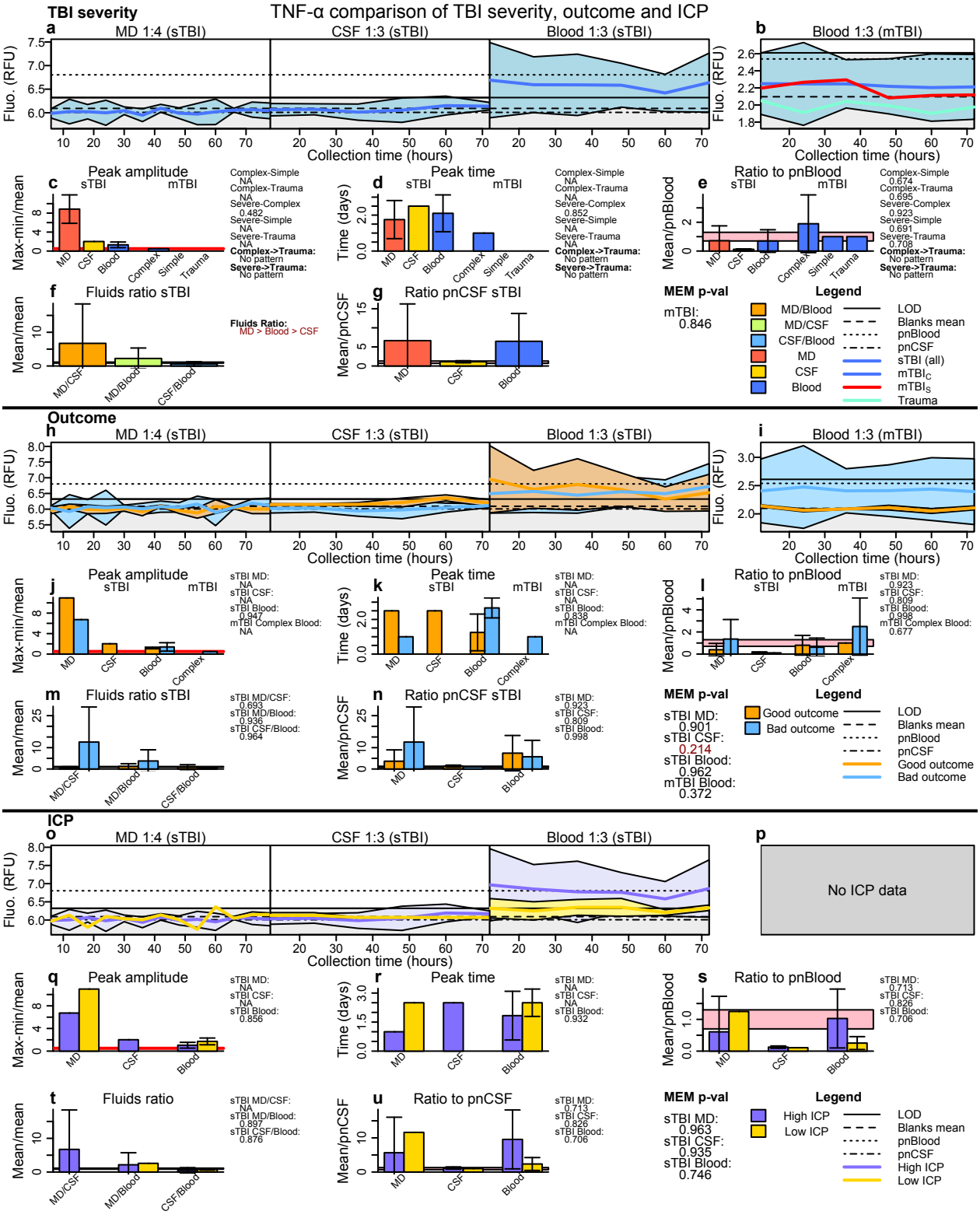

FIGURE J.S214: **Differential TNF-α protein profiles and peak and ratio analysis with respect to TBI severity, outcome and ICP.** Average TNF-α profiles are compared in terms of TBI severity (**a-g**), outcome (**h-n**) and ICP (**o-u**). Polygons in **a, b, h, i, o** indicate the mean value ± 1 SD at each time point. Red lines in **c, j, q** show a threshold for a profile that is considered to have a peak, rather than being constant. The light red boxes in **e-g, l-n, s-u** show the threshold of comparison to the measured value compared. Benjamini–Hochberg adjusted p-values for comparisons are shown on the right of every graph.

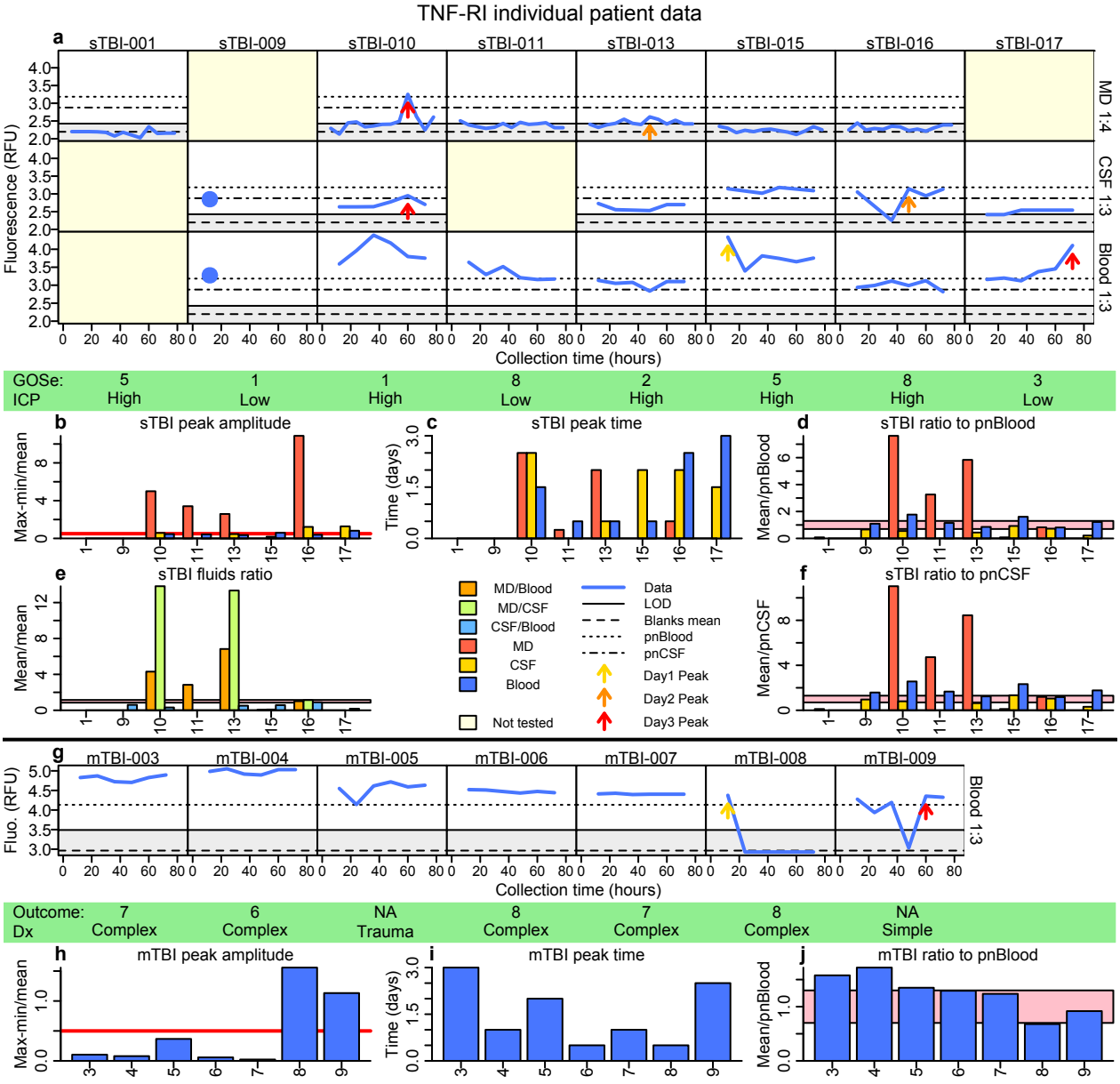

FIGURE J.S215: **Individual TNF-RI protein profiles and peak and ratio analysis.** TNF-RI concentration in microdialysate, CSF and blood samples of individual sTBI patients (**a**) and mTBI/trauma patients (**g**) was measured and peak amplitude and time, as well as ratio between mean time course values to value found in the pooled normal control (**b-f, h-j**) were calculated for each patient. Graphs **b-f** show calculations for individual sTBI patients, and graphs **h-j** show calculations for individual mTBI patients. Red lines in **b, h** show a threshold for a profile that is considered to have a peak, rather than being constant. The light red boxes in **d, e, f, j** show the threshold of comparison to the measured value compared.

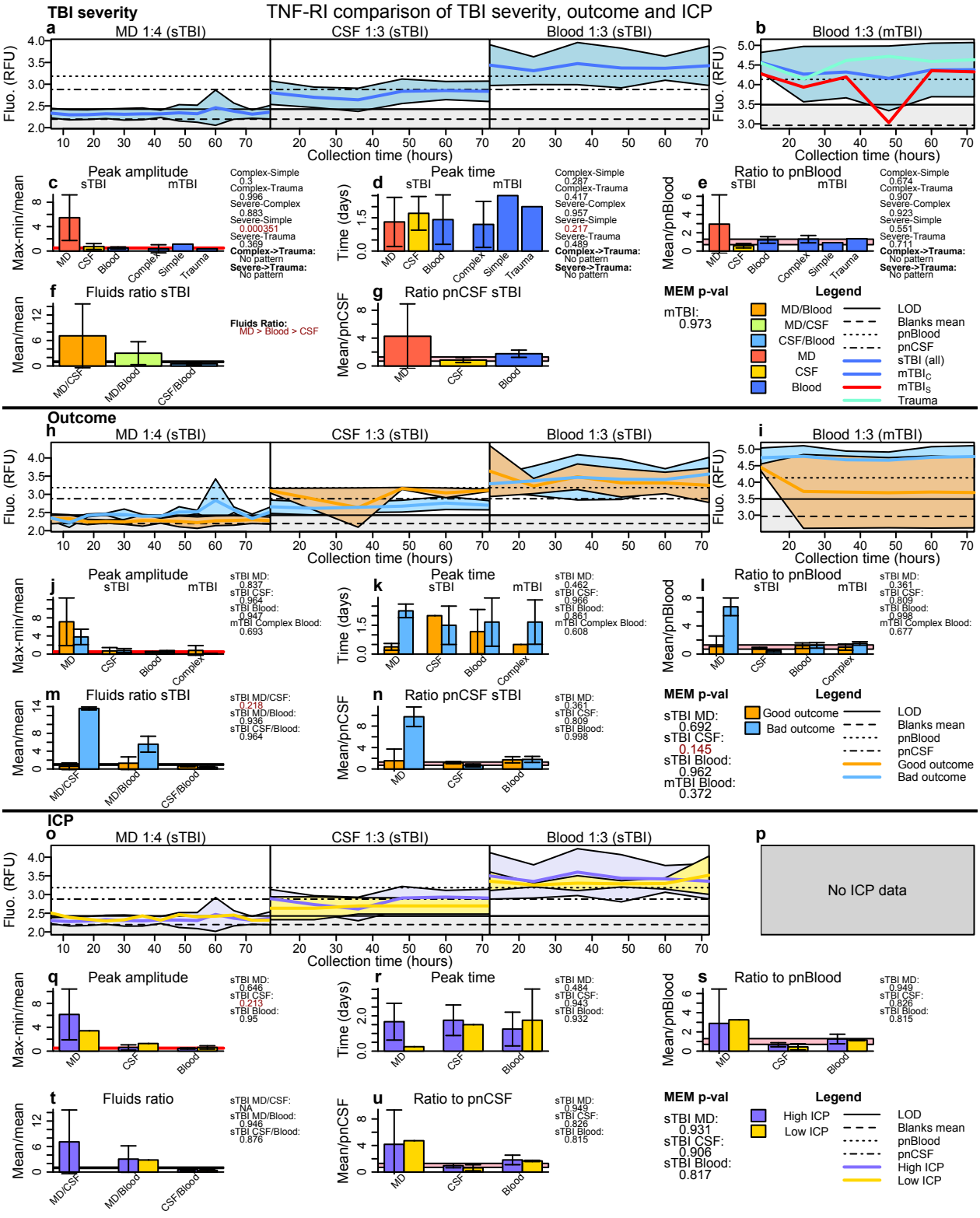

FIGURE J.S216: **Differential TNF-RI protein profiles and peak and ratio analysis with respect to TBI severity, outcome and ICP.** Average TNF-RI profiles are compared in terms of TBI severity (**a-g**), outcome (**h-n**) and ICP (**o-u**). Polygons in **a, b, h, i, o** indicate the mean value ±1 SD at each time point. Red lines in **c, j, q** show a threshold for a profile that is considered to have a peak, rather than being constant. The light red boxes in **e-g, l-n, s-u** show the threshold of comparison to the measured value compared. Benjamini–Hochberg adjusted p-values for comparisons are shown on the right of every graph.

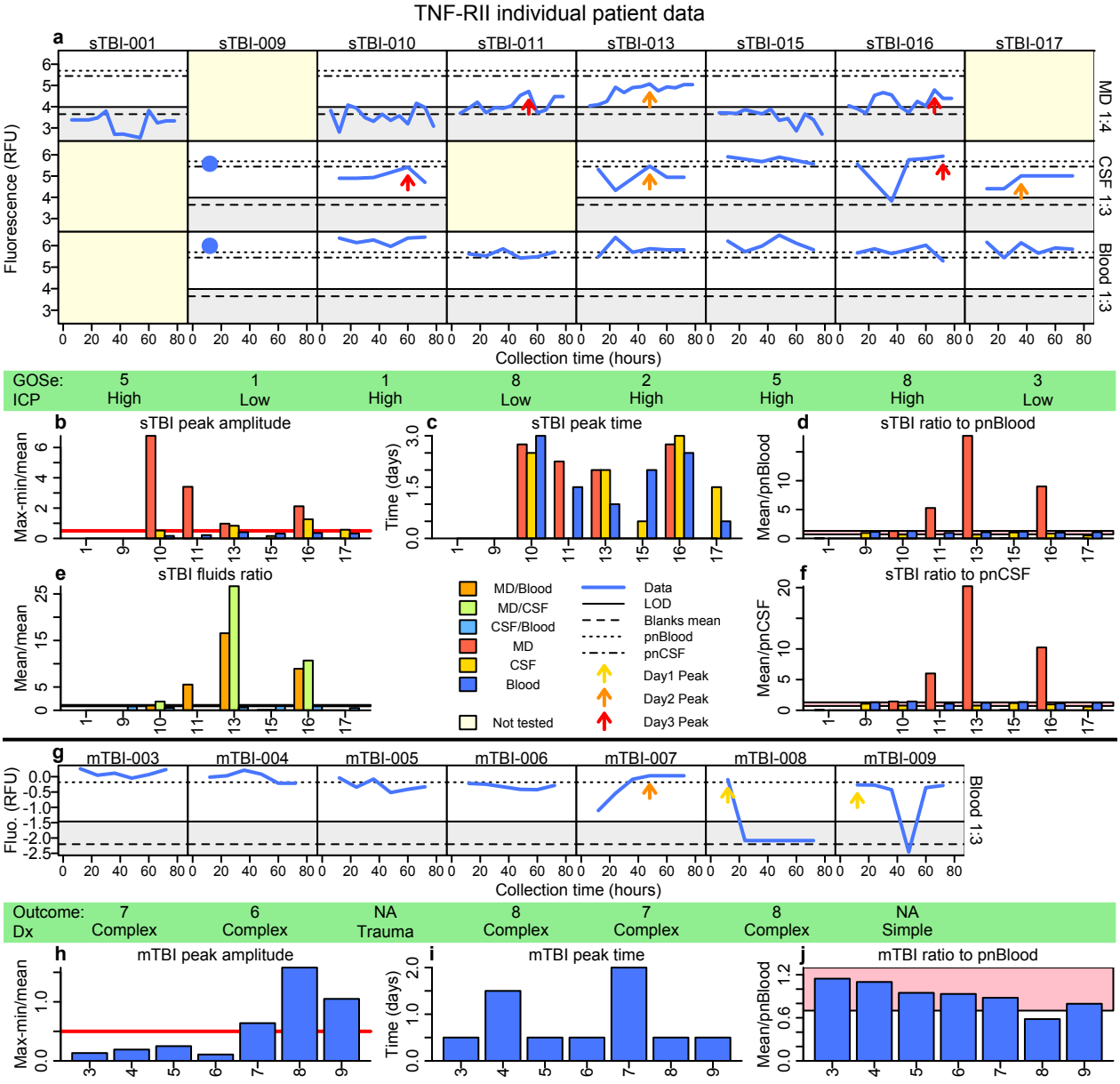

FIGURE J.S217: **Individual TNF-RII protein profiles and peak and ratio analysis.** TNF-RII concentration in microdialysate, CSF and blood samples of individual sTBI patients (**a**) and mTBI/trauma patients (**g**) was measured and peak amplitude and time, as well as ratio between mean time course values to value found in the pooled normal control (**b-f, h-j**) were calculated for each patient. Graphs **b-f** show calculations for individual sTBI patients, and graphs **h-j** show calculations for individual mTBI patients. Red lines in **b, h** show a threshold for a profile that is considered to have a peak, rather than being constant. The light red boxes in **d, e, f, j** show the threshold of comparison to the measured value compared.

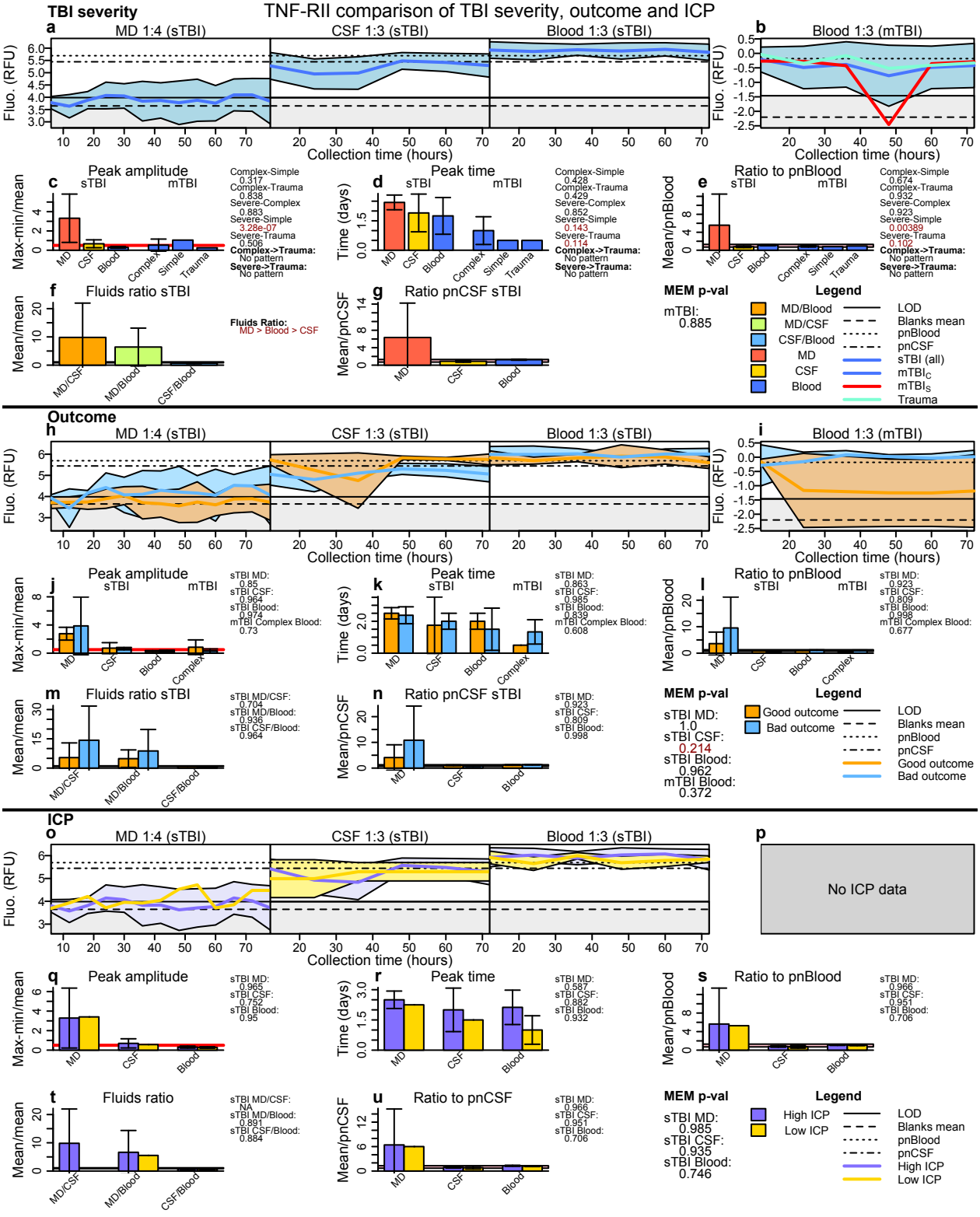

FIGURE J.S218: **Differential TNF-RII protein profiles and peak and ratio analysis with respect to TBI severity, outcome and ICP.** Average TNF-RII profiles are compared in terms of TBI severity (**a-g**), outcome (**h-n**) and ICP (**o-u**). Polygons in **a, b, h, i, o** indicate the mean value ±1 SD at each time point. Red lines in **c, j, q** show a threshold for a profile that is considered to have a peak, rather than being constant. The light red boxes in **e-g, l-n, s-u** show the threshold of comparison to the measured value compared. Benjamini–Hochberg adjusted p-values for comparisons are shown on the right of every graph.

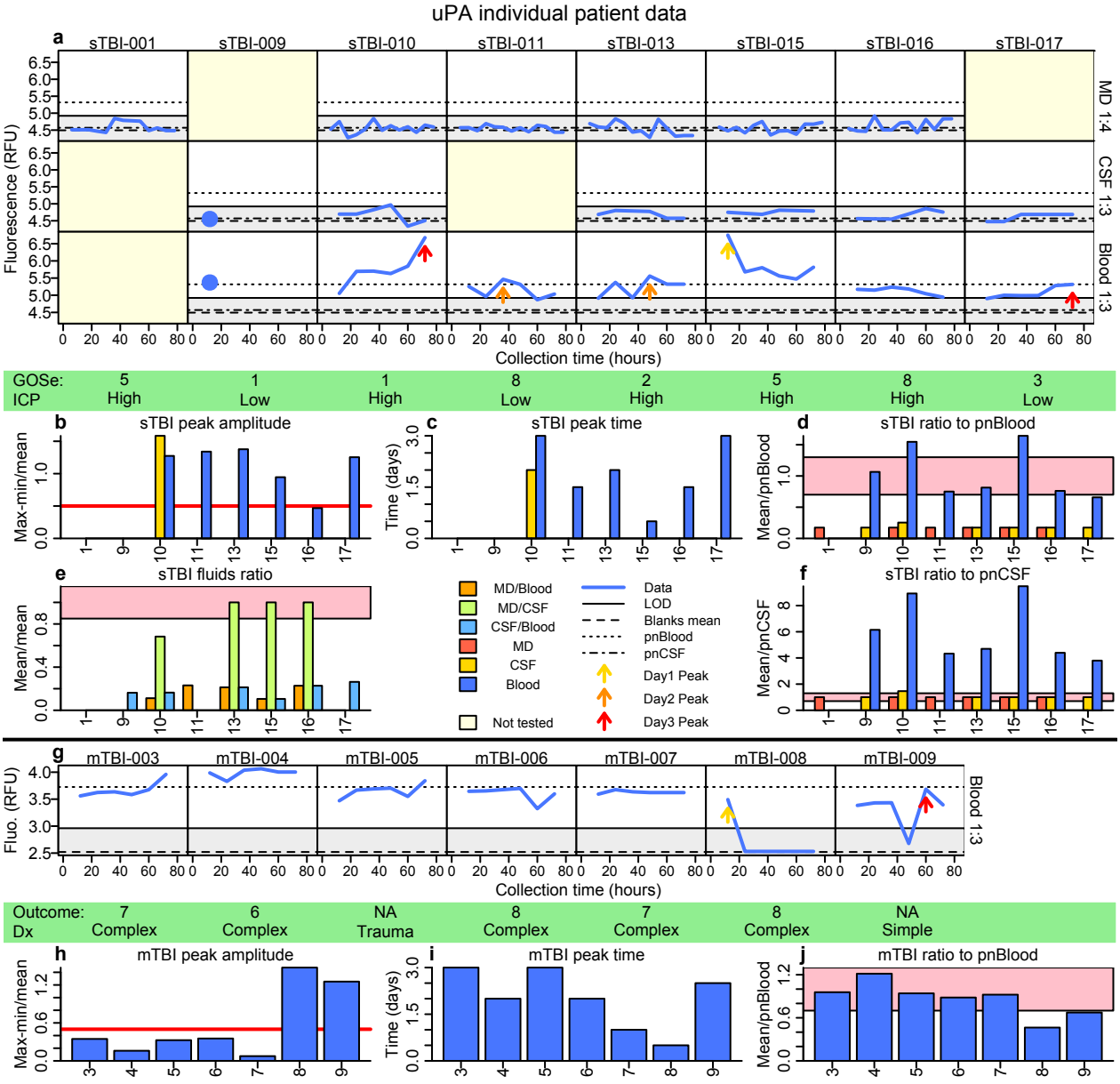

FIGURE J.S219: **Individual uPA protein profiles and peak and ratio analysis.** uPA concentration in microdialysate, CSF and blood samples of individual sTBI patients (**a**) and mTBI/trauma patients (**g**) was measured and peak amplitude and time, as well as ratio between mean time course values to value found in the pooled normal control (**b-f, h-j**) were calculated for each patient. Graphs **b-f** show calculations for individual sTBI patients, and graphs **h-j** show calculations for individual mTBI patients. Red lines in **b, h** show a threshold for a profile that is considered to have a peak, rather than being constant. The light red boxes in **d, e, f, j** show the threshold of comparison to the measured value compared.

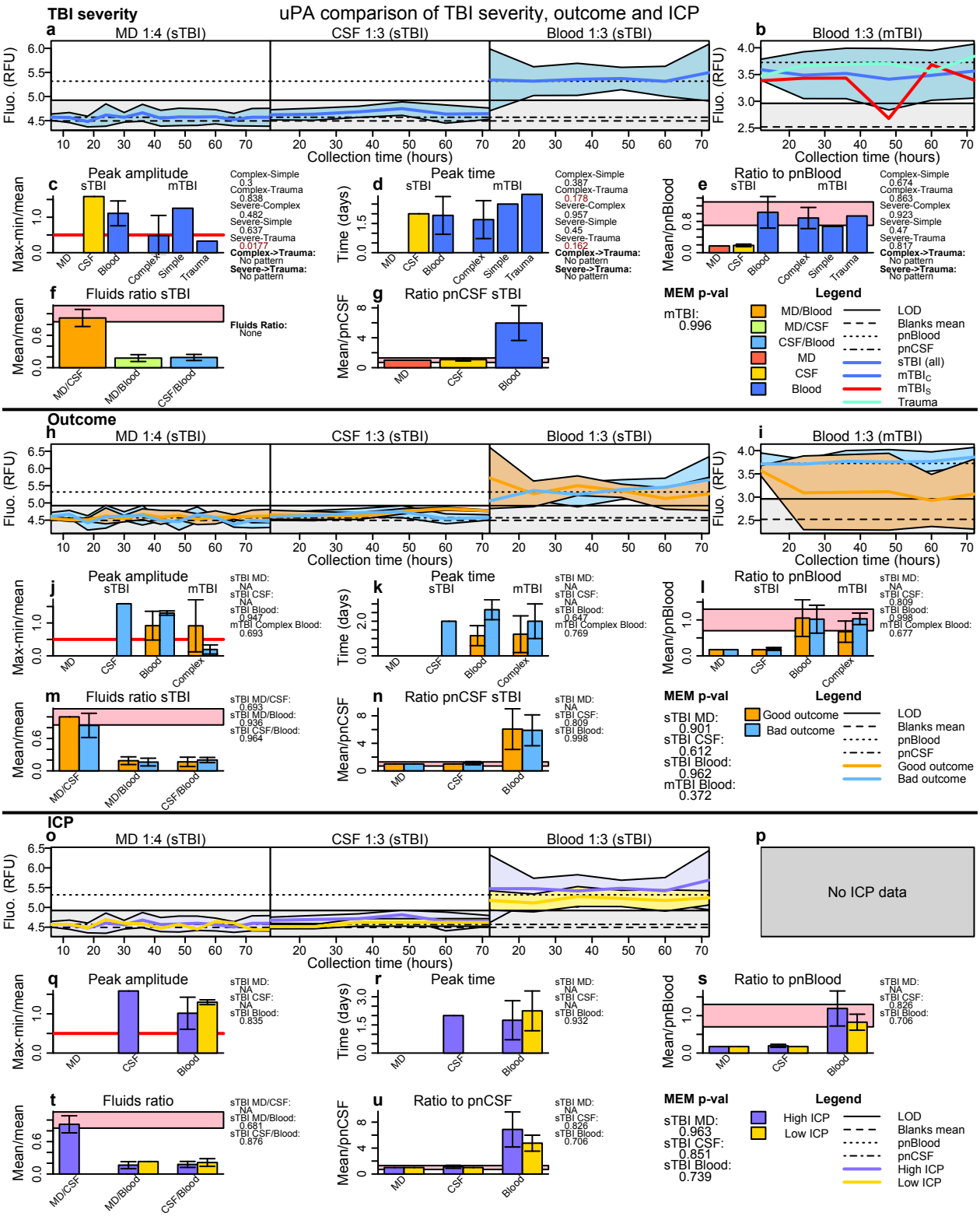

FIGURE J.S220: **Differential uPA protein profiles and peak and ratio analysis with respect to TBI severity, outcome and ICP.** Average uPA profiles are compared in terms of TBI severity (**a-g**), outcome (**h-n**) and ICP (**o-u**). Polygons in **a, b, h, i, o** indicate the mean value ±1 SD at each time point. Red lines in **c, j, q** show a threshold for a profile that is considered to have a peak, rather than being constant. The light red boxes in **e-g, l-n, s-u** show the threshold of comparison to the measured value compared. Benjamini–Hochberg adjusted p-values for comparisons are shown on the right of every graph.

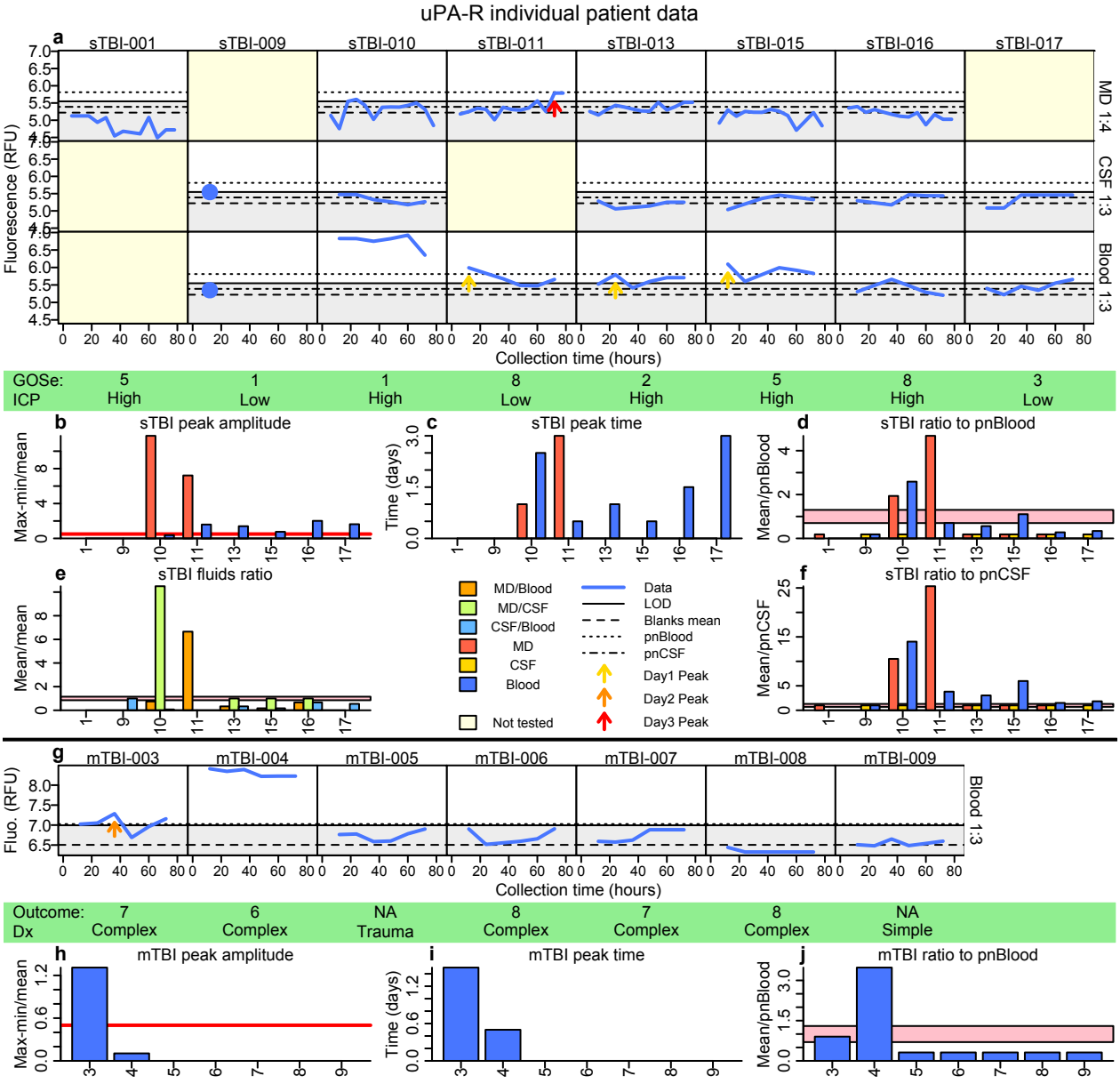

FIGURE J.S221: **Individual uPA-R protein profiles and peak and ratio analysis.** uPA-R concentration in microdialysate, CSF and blood samples of individual sTBI patients (**a**) and mTBI/trauma patients (**g**) was measured and peak amplitude and time, as well as ratio between mean time course values to value found in the pooled normal control (**b-f, h-j**) were calculated for each patient. Graphs **b-f** show calculations for individual sTBI patients, and graphs **h-j** show calculations for individual mTBI patients. Red lines in **b, h** show a threshold for a profile that is considered to have a peak, rather than being constant. The light red boxes in **d, e, f, j** show the threshold of comparison to the measured value compared.

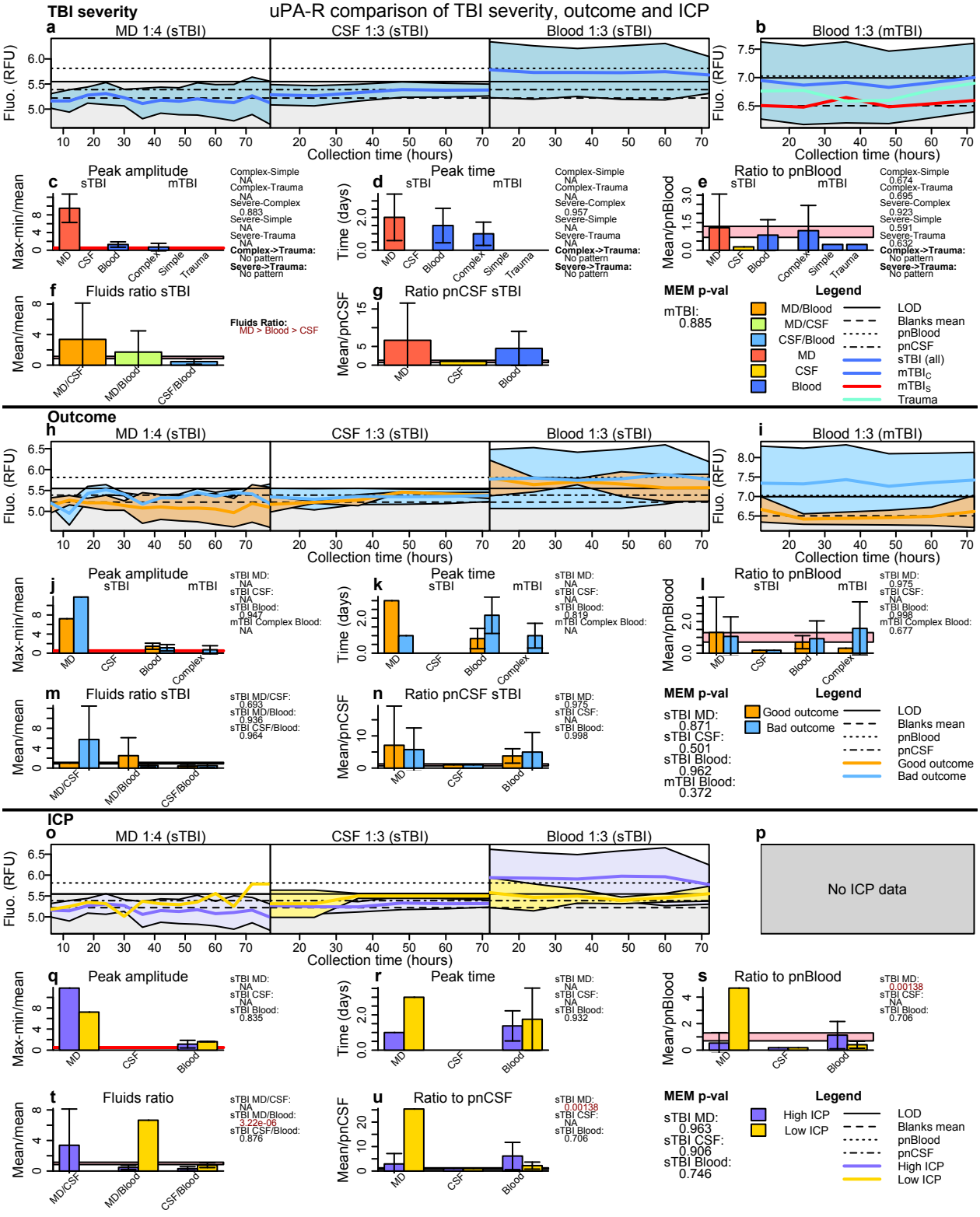

FIGURE J.S222: **Differential uPA-R protein profiles and peak and ratio analysis with respect to TBI severity, outcome and ICP.** Average uPA-R profiles are compared in terms of TBI severity (**a-g**), outcome (**h-n**) and ICP (**o-u**). Polygons in **a, b, h, i, o** indicate the mean value ±1 SD at each time point. Red lines in **c, j, q** show a threshold for a profile that is considered to have a peak, rather than being constant. The light red boxes in **e-g, l-n, s-u** show the threshold of comparison to the measured value compared. Benjamini–Hochberg adjusted p-values for comparisons are shown on the right of every graph.

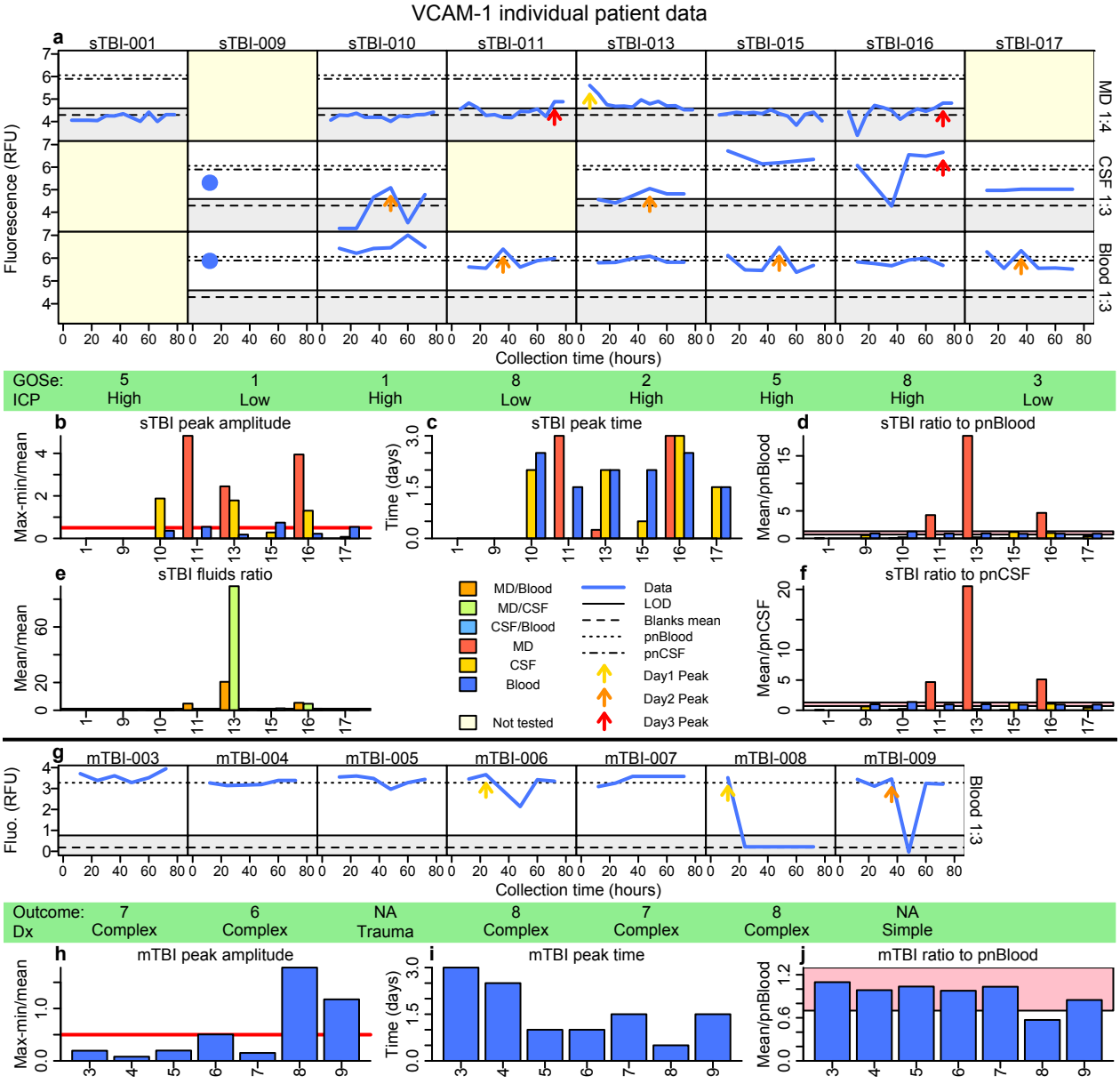

FIGURE J.S223: **Individual VCAM-1 protein profiles and peak and ratio analysis.** VCAM-1 concentration in microdialysate, CSF and blood samples of individual sTBI patients (**a**) and mTBI/trauma patients (**g**) was measured and peak amplitude and time, as well as ratio between mean time course values to value found in the pooled normal control (**b-f, h-j**) were calculated for each patient. Graphs **b-f** show calculations for individual sTBI patients, and graphs **h-j** show calculations for individual mTBI patients. Red lines in **b, h** show a threshold for a profile that is considered to have a peak, rather than being constant. The light red boxes in **d, e, f, j** show the threshold of comparison to the measured value compared.

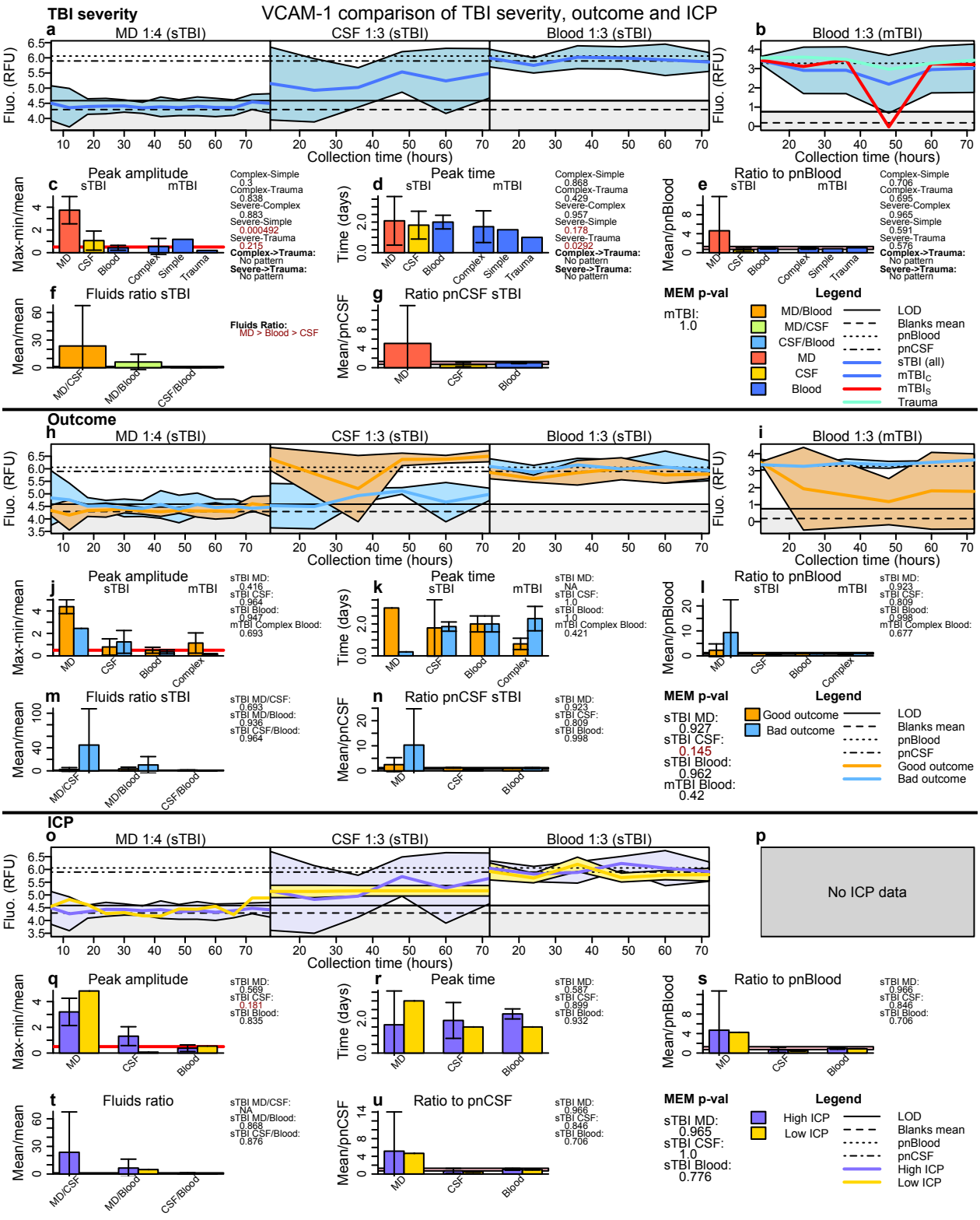

FIGURE J.S224: **Differential VCAM-1 protein profiles and peak and ratio analysis with respect to TBI severity, outcome and ICP.** Average VCAM-1 profiles are compared in terms of TBI severity (**a-g**), outcome (**h-n**) and ICP (**o-u**). Polygons in **a, b, h, i, o** indicate the mean value ±1 SD at each time point. Red lines in **c, j, q** show a threshold for a profile that is considered to have a peak, rather than being constant. The light red boxes in **e-g, l-n, s-u** show the threshold of comparison to the measured value compared. Benjamini–Hochberg adjusted p-values for comparisons are shown on the right of every graph.

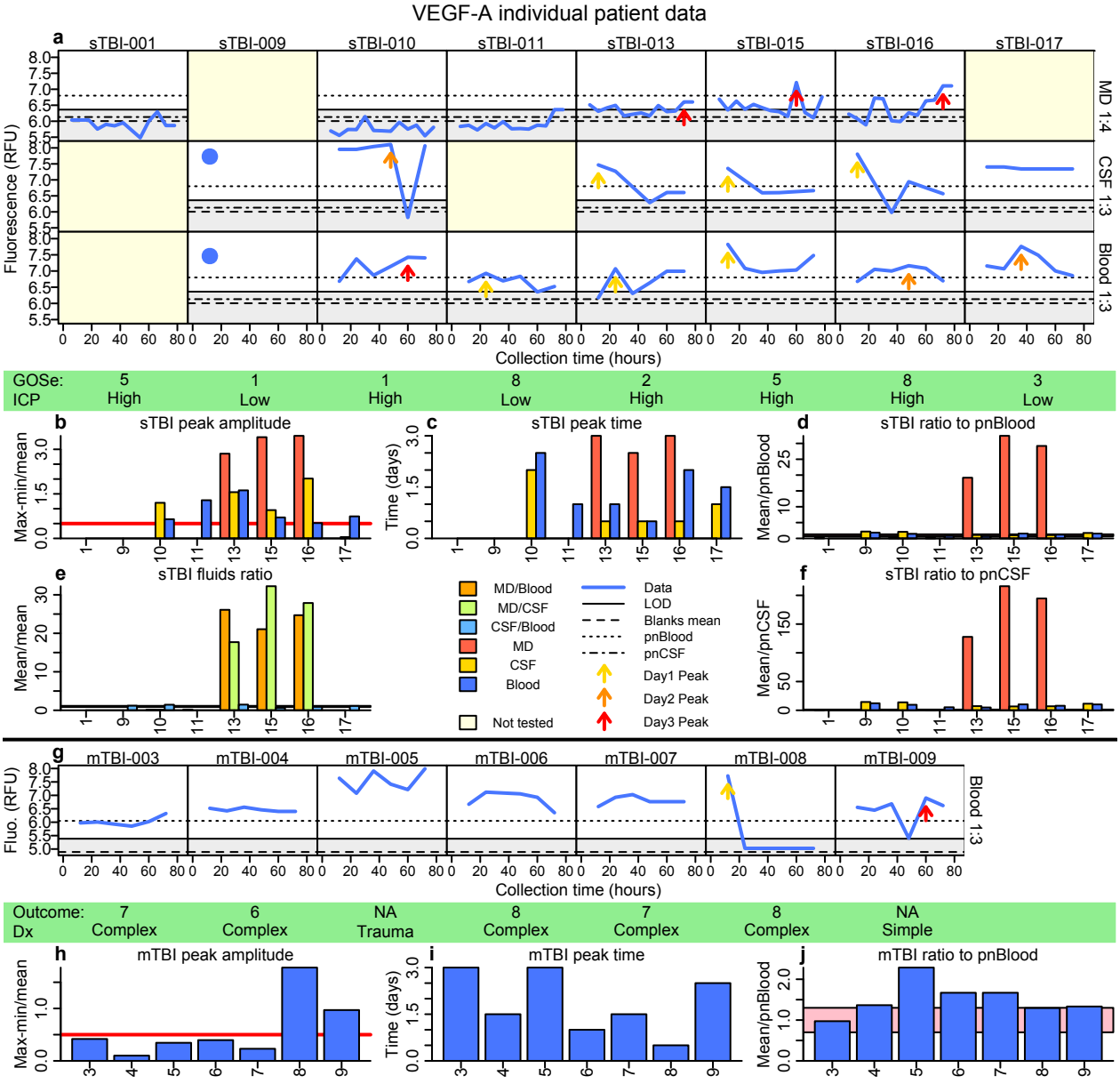

FIGURE J.S225: **Individual VEGF-A protein profiles and peak and ratio analysis.** VEGF-A concentration in microdialysate, CSF and blood samples of individual sTBI patients (**a**) and mTBI/trauma patients (**g**) was measured and peak amplitude and time, as well as ratio between mean time course values to value found in the pooled normal control (**b-f, h-j**) were calculated for each patient. Graphs **b-f** show calculations for individual sTBI patients, and graphs **h-j** show calculations for individual mTBI patients. Red lines in **b, h** show a threshold for a profile that is considered to have a peak, rather than being constant. The light red boxes in **d, e, f, j** show the threshold of comparison to the measured value compared.

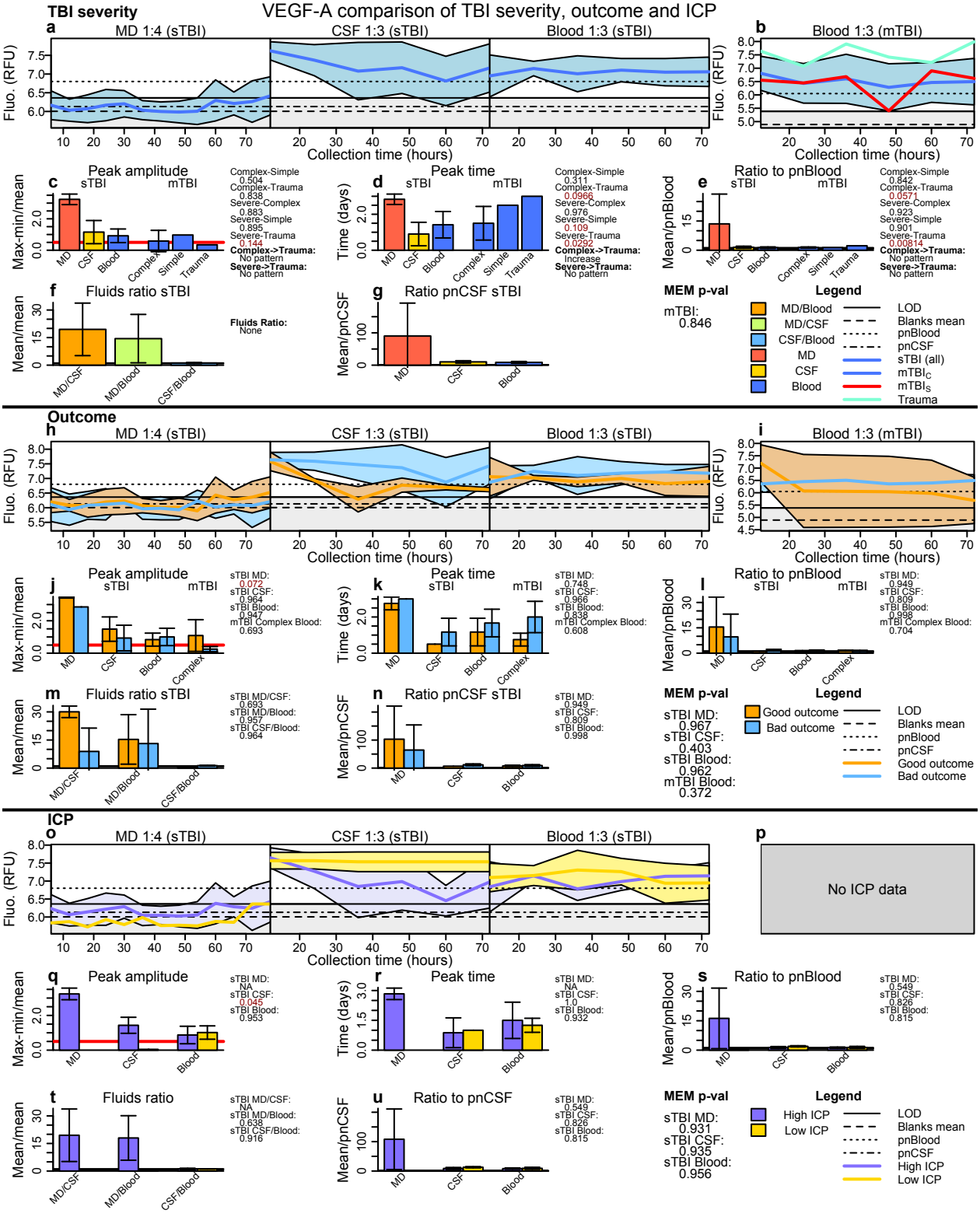

FIGURE J.S226: **Differential VEGF-A protein profiles and peak and ratio analysis with respect to TBI severity, outcome and ICP.** Average VEGF-A profiles are compared in terms of TBI severity (**a-g**), outcome (**h-n**) and ICP (**o-u**). Polygons in **a, b, h, i, o** indicate the mean value ±1 SD at each time point. Red lines in **c, j, q** show a threshold for a profile that is considered to have a peak, rather than being constant. The light red boxes in **e-g, l-n, s-u** show the threshold of comparison to the measured value compared. Benjamini–Hochberg adjusted p-values for comparisons are shown on the right of every graph.

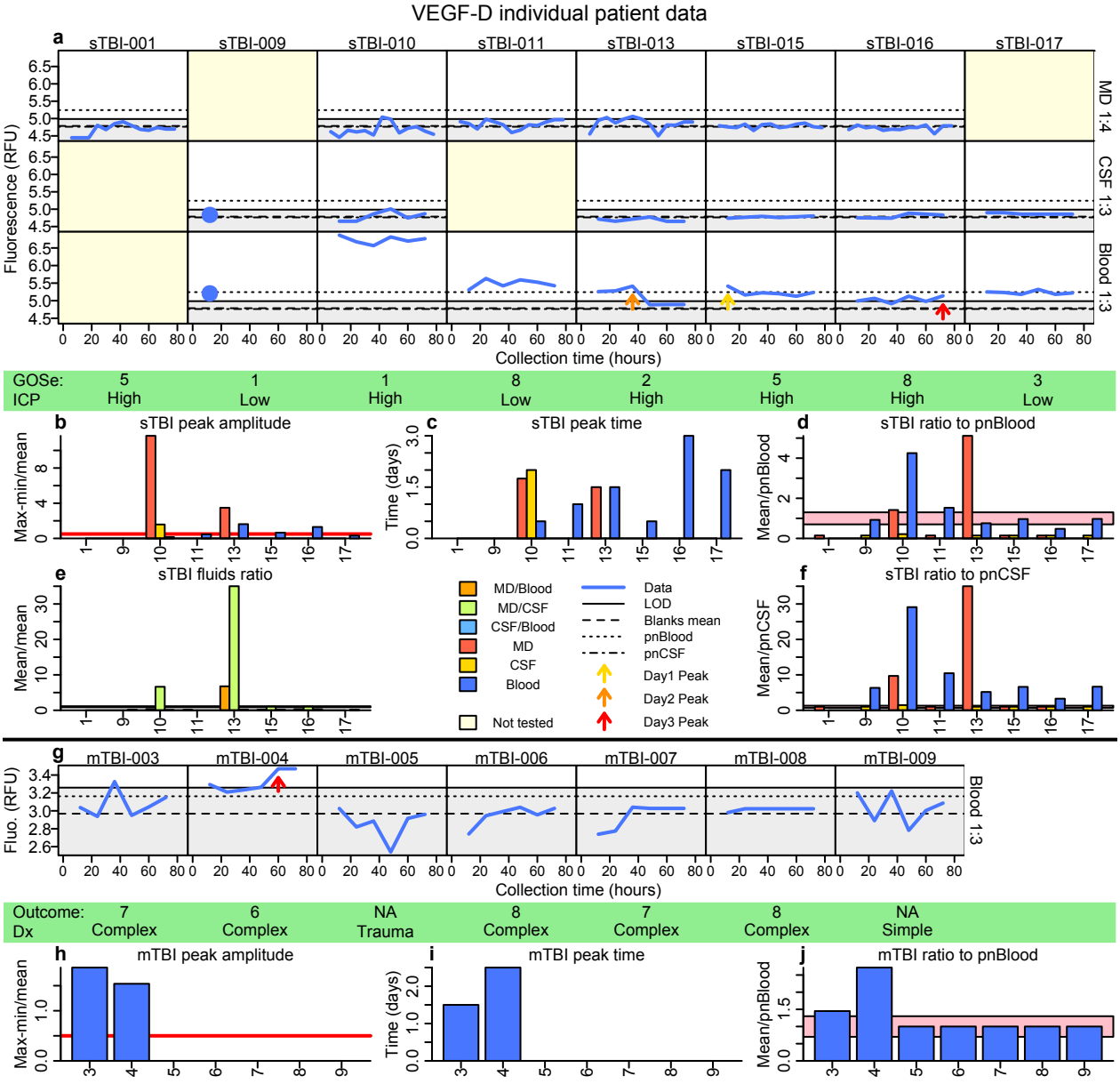

FIGURE J.S227: **Individual VEGF-D protein profiles and peak and ratio analysis.** VEGF-D concentration in microdialysate, CSF and blood samples of individual sTBI patients (**a**) and mTBI/trauma patients (**g**) was measured and peak amplitude and time, as well as ratio between mean time course values to value found in the pooled normal control (**b-f, h-j**) were calculated for each patient. Graphs **b-f** show calculations for individual sTBI patients, and graphs **h-j** show calculations for individual mTBI patients. Red lines in **b, h** show a threshold for a profile that is considered to have a peak, rather than being constant. The light red boxes in **d, e, f, j** show the threshold of comparison to the measured value compared.

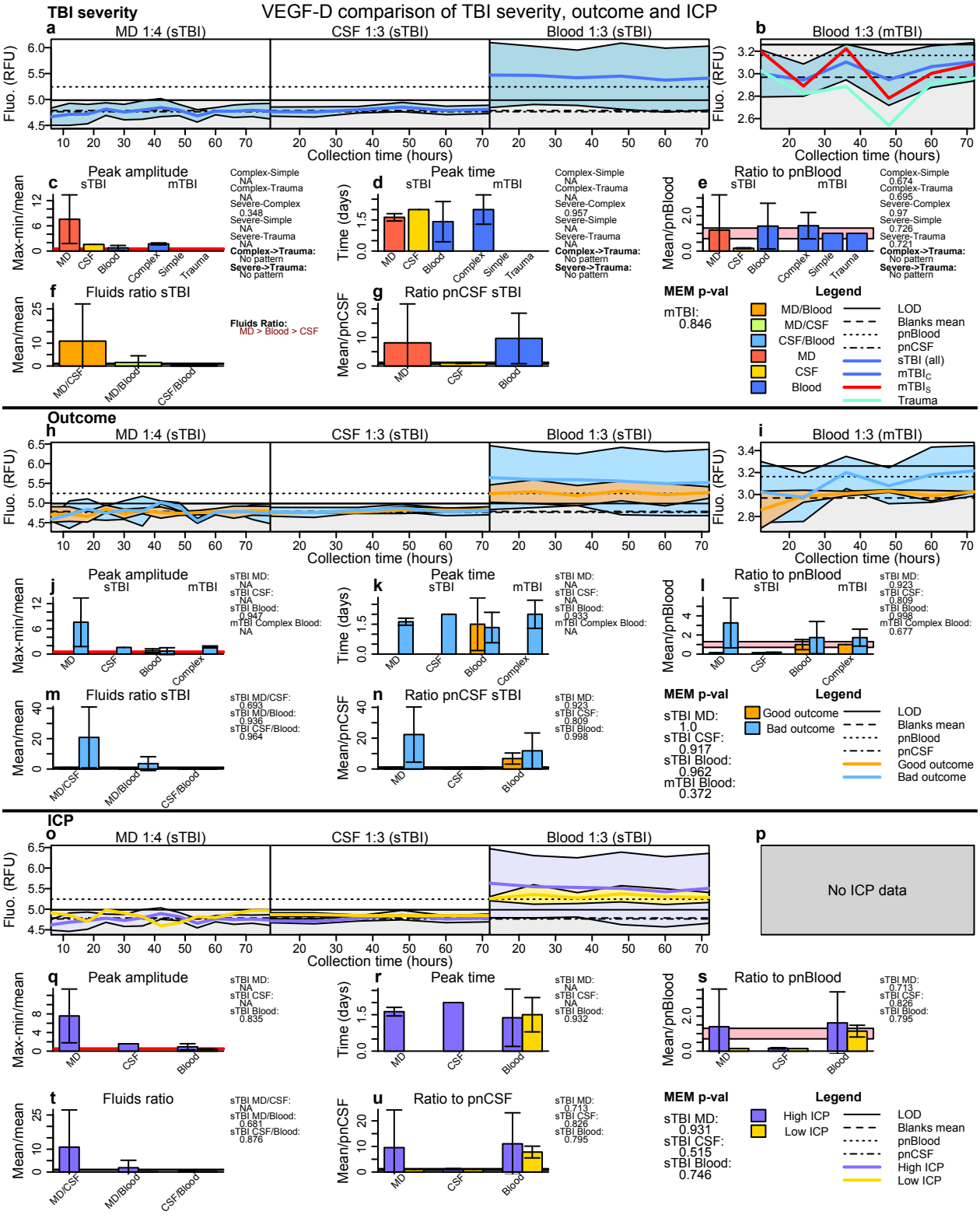

FIGURE J.S228: **Differential VEGF-D protein profiles and peak and ratio analysis with respect to TBI severity, outcome and ICP.** Average VEGF-D profiles are compared in terms of TBI severity (**a-g**), outcome (**h-n**) and ICP (**o-u**). Polygons in **a, b, h, i, o** indicate the mean value ±1 SD at each time point. Red lines in **c, j, q** show a threshold for a profile that is considered to have a peak, rather than being constant. The light red boxes in **e-g, l-n, s-u** show the threshold of comparison to the measured value compared. Benjamini–Hochberg adjusted p-values for comparisons are shown on the right of every graph.

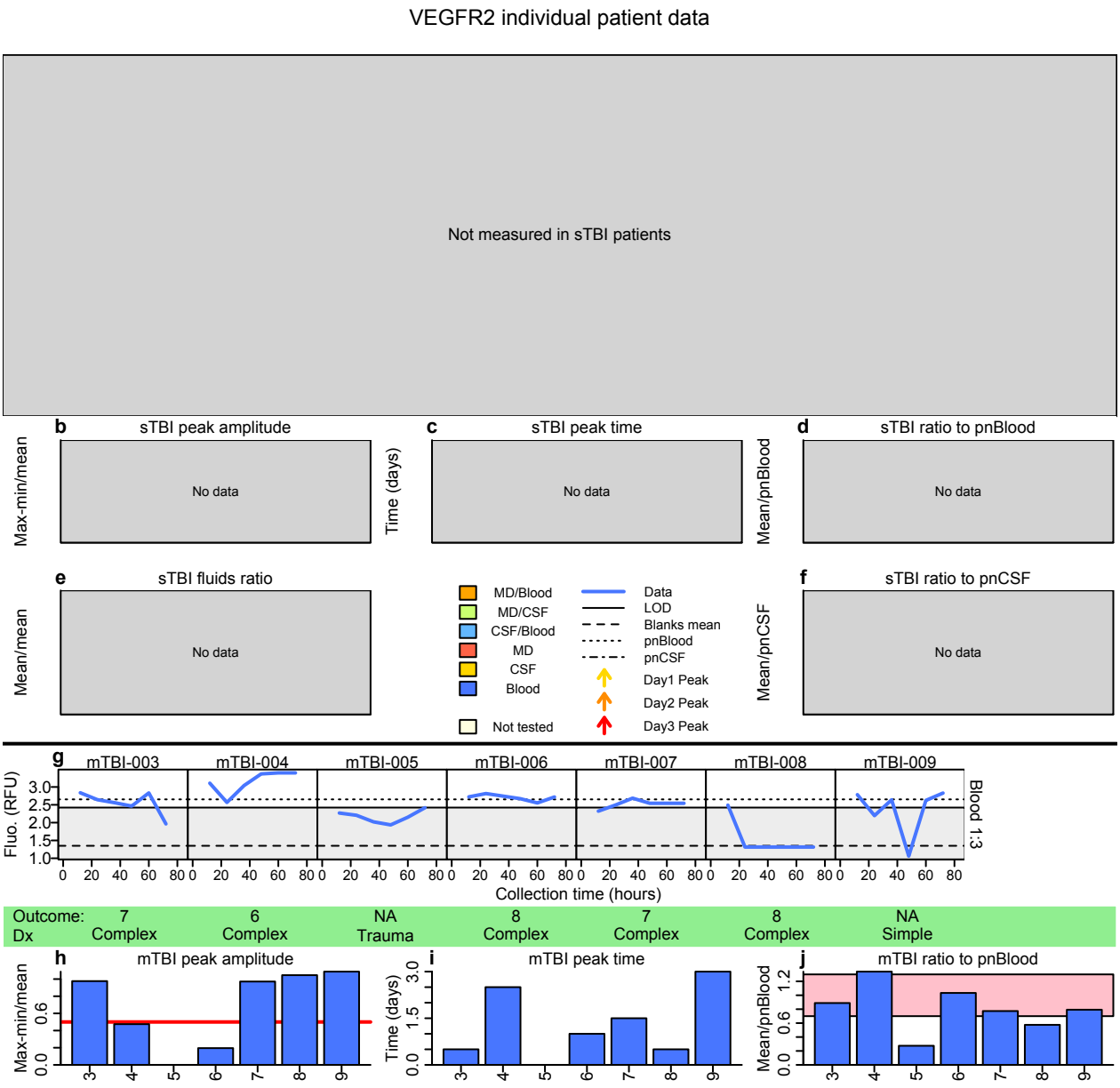

FIGURE J.S229: **Individual VEGFR2 protein profiles and peak and ratio analysis.** VEGFR2 concentration in microdialysate, CSF and blood samples of individual sTBI patients (**a**) and mTBI/trauma patients (**g**) was measured and peak amplitude and time, as well as ratio between mean time course values to value found in the pooled normal control (**b-f, h-j**) were calculated for each patient. Graphs **b-f** show calculations for individual sTBI patients, and graphs **h-j** show calculations for individual mTBI patients. Red lines in **b, h** show a threshold for a profile that is considered to have a peak, rather than being constant. The light red boxes in **d, e, f, j** show the threshold of comparison to the measured value compared.

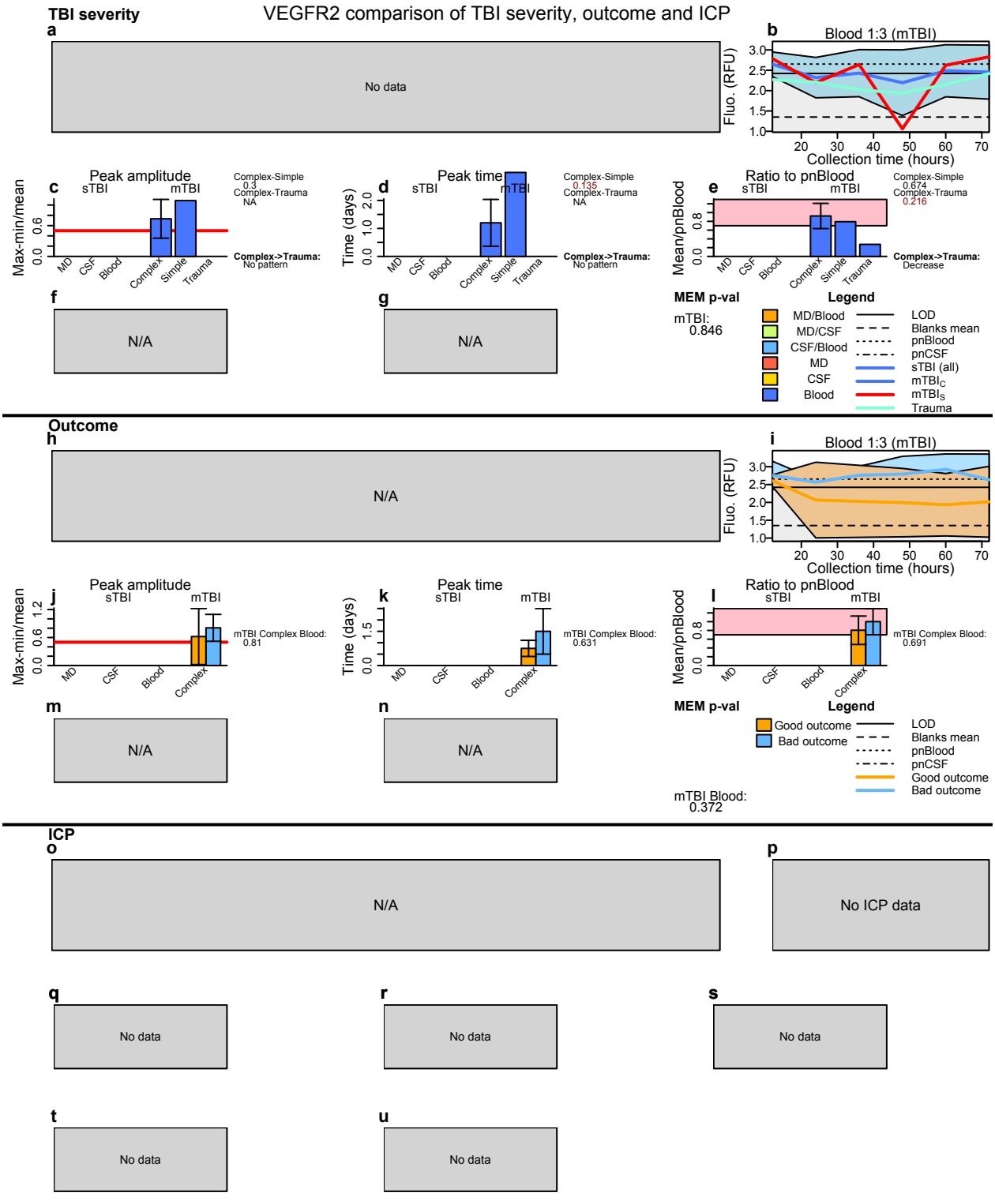

FIGURE J.S230: **Differential VEGFR2 protein profiles and peak and ratio analysis with respect to TBI severity, outcome and ICP.** Average VEGFR2 profiles are compared in terms of TBI severity (**a-g**), outcome (**h-n**) and ICP (**o-u**). Polygons in **a, b, h, i, o** indicate the mean value ±1 SD at each time point. Red lines in **c, j, q** show a threshold for a profile that is considered to have a peak, rather than being constant. The light red boxes in **e-g, l-n, s-u** show the threshold of comparison to the measured value compared. Benjamini–Hochberg adjusted p-values for comparisons are shown on the right of every graph.

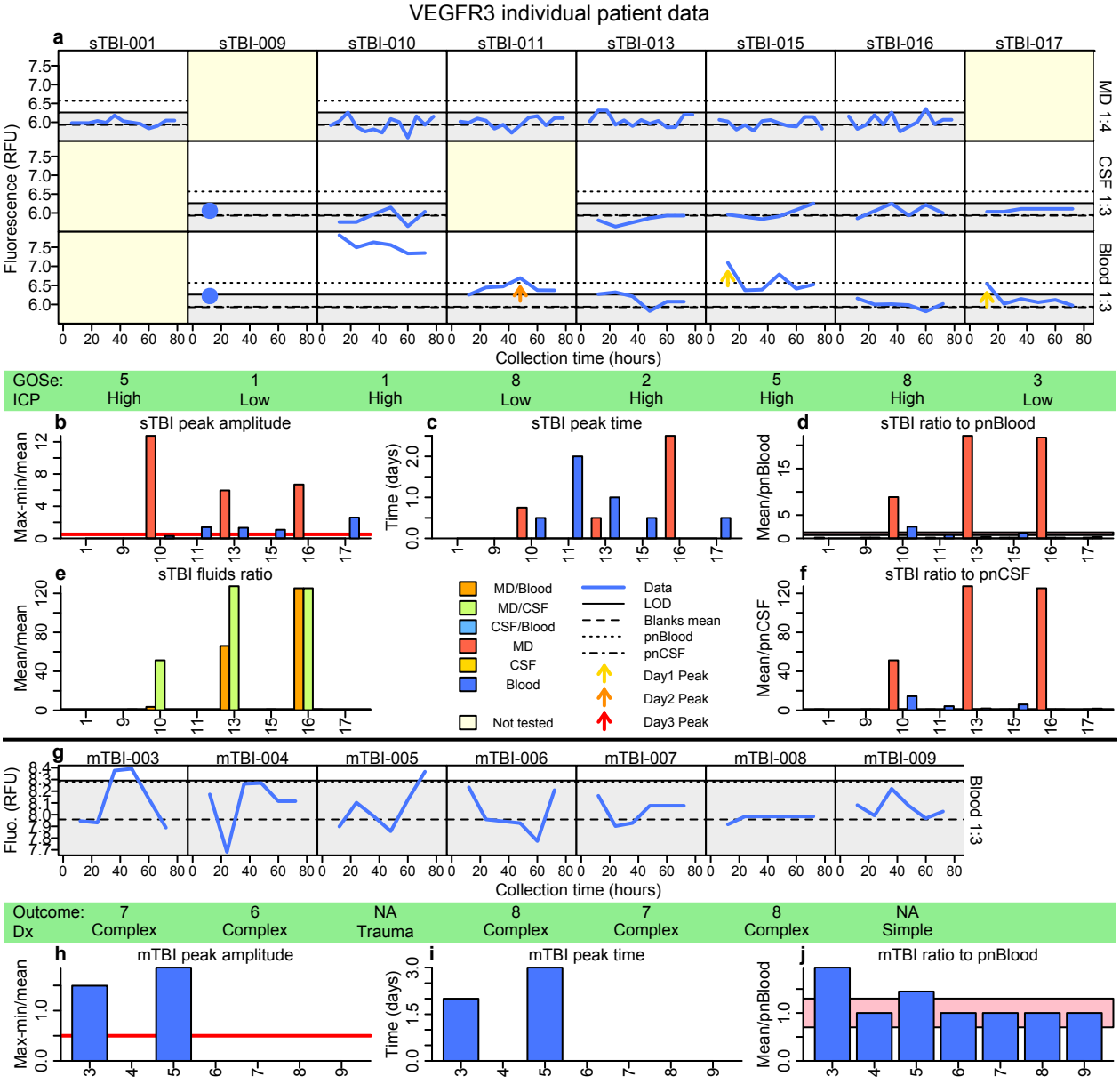

FIGURE J.S231: **Individual VEGFR3 protein profiles and peak and ratio analysis.** VEGFR3 concentration in microdialysate, CSF and blood samples of individual sTBI patients (**a**) and mTBI/trauma patients (**g**) was measured and peak amplitude and time, as well as ratio between mean time course values to value found in the pooled normal control (**b-f, h-j**) were calculated for each patient. Graphs **b-f** show calculations for individual sTBI patients, and graphs **h-j** show calculations for individual mTBI patients. Red lines in **b, h** show a threshold for a profile that is considered to have a peak, rather than being constant. The light red boxes in **d, e, f, j** show the threshold of comparison to the measured value compared.

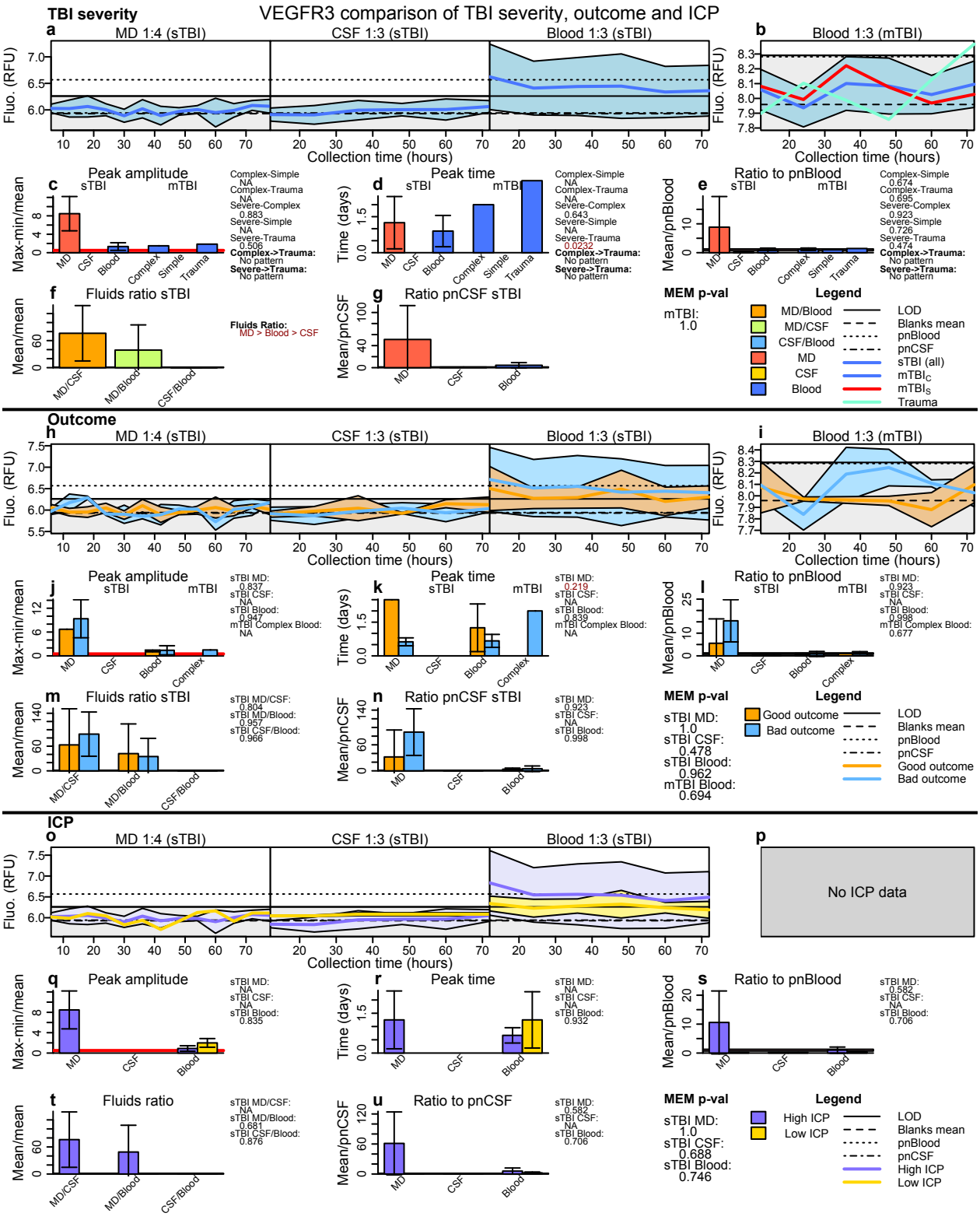

FIGURE J.S232: **Differential VEGFR3 protein profiles and peak and ratio analysis with respect to TBI severity, outcome and ICP.** Average VEGFR3 profiles are compared in terms of TBI severity (**a-g**), outcome (**h-n**) and ICP (**o-u**). Polygons in **a, b, h, i, o** indicate the mean value ±1 SD at each time point. Red lines in **c, j, q** show a threshold for a profile that is considered to have a peak, rather than being constant. The light red boxes in **e-g, l-n, s-u** show the threshold of comparison to the measured value compared. Benjamini–Hochberg adjusted p-values for comparisons are shown on the right of every graph.

Whole Bibliography

1. Nguyen, R., Fiest, K. M., McChesney, J., Kwon, C. S., Jette, N., Frolkis, A. D., Atta, C., Mah, S., Dhaliwal, H., Reid, A., Pringsheim, T., Dykeman, J. & Gallagher, C. The international incidence of traumatic brain injury: A systematic review and meta-analysis. *Canadian Journal of Neurological Sciences* **43,** 774–785 (2016).
2. Teasdale, G. & Jennett, B. Assessment of coma and impaired consciousness. *The Lancet* **2,** 81–84 (1974).
3. De Guise, E., Marcoux, J., Maleki, M., Leblanc, J., Dagher, J., Tinawi, S., Feyz, M. & Lamoureux, J. Trends in hospitalization associated with TBI in an urban level 1 trauma centre. *Canadian Journal of Neurological Sciences* **41,** 466–475 (2014).
4. Farhad, K., Khan, H. M. R., Ji, A. B., Yacoub, H. A., Qureshi, A. I. & Souayah, N. Trends in outcomes and hospitalization costs for traumatic brain injury in adult patients in the United States. *Journal of Neurotrauma* **30,** 84–90 (2013).
5. Lasry, O., Dendukuri, N., Marcoux, J. & Buckeridge, D. L. Accuracy of Administrative Health Data for Surveillance of Traumatic Brain Injury. *Epidemiology* **29,** 876–884 (2018).
6. Zumstein, M. A., Moser, M., Mottini, M., Ott, S. R., Sadowski-Cron, C., Radanov, B. P., Zimmermann, H. & Exadaktylos, A. Long-term outcome in patients with mild traumatic brain injury: A prospective observational study. *Journal of Trauma - Injury, Infection and Critical Care* **71,** 120–127 (2011).
7. Smith, J. A., Das, A., Ray, S. K. & Banik, N. L. Role of pro-inflammatory cytokines released from microglia in neurodegenerative diseases. *Brain Research Bulletin* **87,** 10–20 (2012).

8. Lannsjö, M, Backheden, M, Johansson, U, Geijerstam, J. L. & Borg, J. Does head CT scan pathology predict outcome after mild traumatic brain injury ? *European Journal of Neurology,* 124–129 (2012).

9. Carroll, L., Cassidy, J. D., Peloso, P., Borg, J., von Holst, H., Holm, L., Paniak, C. & Pépin, M. Prognosis for mild traumatic brain injury: results of the WHO collaborating centre task force on mild traumatic brain injury. *Journal of Rehabilitation Medicine* **36,** 84–105 (2004).

10. Ciurli, P, Formisano, R, Bivona, U, Cantagallo, A & Angelelli, P. Neuropsychiatric disorders in persons with severe traumatic brain injury: prevalence, phenomenology, and relationship with demographic, clinical, and functional features. *The Journal of Head Trauma Rehabilitation* **26,** 116–126 (2011).

11. Kang, J.-H. & Lin, H.-C. Increased risk of multiple sclerosis after traumatic brain injury: a nationwide population-based study. *Journal of Neurotrauma* **29,** 90–5 (2012).

12. Kontos, A. P., Kotwal, R. S., Elbin, R., Lutz, R. H., Forsten, R. D., Benson, P. J. & Guskiewicz, K. M. Residual Effects of Combat-Related Mild Traumatic Brain Injury. *Journal of Neurotrauma* **30,** 680–686 (2013).

13. Gardner, R. C., Byers, A. L., Barnes, D. E., Li, Y., Boscardin, J. & Yaffe, K. Mild TBI and risk of Parkinson disease. *Neurology* **90,** e1771–e1779 (2018).

14. Mendez, M. F. What is the Relationship of Traumatic Brain Injury to Dementia? *Journal of Alzheimer's Disease* **57,** 667–681 (2017).

15. DeKosky, S. T. & Asken, B. M. Injury cascades in TBI-related neurodegeneration. *Brain Injury* **31,** 1177–1182 (2017).

16. Ramlackhansingh, A. F., Brooks, D. J., Greenwood, R. J., Bose, S. K., Turkheimer, F. E., Kinnunen, K. M., Gentleman, S., Heckemann, R. a., Gunanayagam, K., Gelosa, G. & Sharp, D. J. Inflammation after trauma: microglial activation and traumatic brain injury. *Annals of Neurology* **70,** 374–83 (2011).

17. Pla-Roca, M., Leulmi, R. F., Tourekhanova, S., Bergeron, S., Laforte, V., Moreau, E., Gosline, S. J. C., Bertos, N., Hallett, M., Park, M. & Juncker, D. Antibody colocalization microarray: a scalable technology for multiplex protein analysis in complex samples. *Molecular & Cellular Proteomics* **11,** M111.011460 (2012).

18. Helmy, A., Carpenter, K. L. H., Menon, D. K., Pickard, J. D. & Hutchinson, P. J. A. The cytokine response to human traumatic brain injury : temporal profiles and evidence for cerebral parenchymal production. *Journal of Cerebral Blood Flow & Metabolism* **31,** 658–670 (2010).

19. Rosenbloom, A. J., Sipe, D. M. & Weedn, V. W. Microdialysis of proteins: Performance of the CMA/20 probe. *Journal of Neuroscience Methods* **148,** 147–153 (2005).

20. Rosenbloom, A. J., Ferris, R., Sipe, D. M., Riddler, S. A., Connolly, N. C., Abe, K. & Whiteside, T. L. In vitro and in vivo protein sampling by combined microdialysis and ultrafiltration. *Journal of Immunological Methods* **309,** 55–68 (2006).

21. Trickler, W. J. & Miller, D. W. Use of osmotic agents in microdialysis studies to improve the recovery of macromolecules. *Journal of Pharmaceutical Sciences* **92,** 1419–1427 (2003).

22. Quist, S. R., Kirbs, C., Kloft, C. & Gollnick, H. P. Cytokine and chemokine recovery is increased by colloid perfusates during dermal microdialysis. *Materials* **11,** 682 (2018).

23. Dahlin, A. P., Purins, K., Clausen, F., Chu, J., Sedigh, A., Lorant, T., Enblad, P., Lewe, A. & Hillered, L. Refined Microdialysis Method for Protein Biomarker Sampling in Acute Brain Injury in the Neurointensive Care Setting. *Analytical Chemistry* **86,** 8671–8679 (2014).

24. Giorgi-Coll, S., Blunt-Foley, H., Hutchinson, P. J. & Carpenter, K. L. H. Heparin-gold nanoparticles for enhanced microdialysis sampling. *Analytical and Bioanalytical Chemistry* **409,** 5031–5042 (2017).

25. Helmy, A, Carpenter, K. L., Skepper, J. N., Kirkpatrick, P. J., Pickard, J. D. & Hutchinson, P. J. Microdialysis of cytokines: methodological considerations, scanning electron microscopy, and determination of relative recovery. *Journal of Neurotrauma* **26,** 549–561 (2009).

26. Hillman, J., Åneman, O., Anderson, C., Sjögren, F., Säberg, C. & Mellergård, P. A microdialysis technique for routine measurement of macromolecules in the injured human brain. *Neurosurgery* **56,** 1264–1270 (2005).

27. Hutchinson, P. J., O'Connell, M. T., Rothwell, N. J., Hopkins, S. J., Nortje, J., Carpenter, K. L. H., Timofeev, I., Al-Rawi, P. G., Menon, D. K. & Pickard, J. D. Inflammation in human brain injury: intracerebral concentrations of IL-1alpha, IL-1beta, and their endogenous inhibitor IL-1ra. *Journal of Neurotrauma* **24,** 1545–57 (2007).

28. Rosdahl, H., Hamrin, K., Ungerstedt, U. & Henriksson, J. A microdialysis method for the in situ investigation of the action of large peptide molecules in human skeletal muscle: Detection of local metabolic effects of insulin. *International Journal of Biological Macromolecules* **28,** 69–73 (2000).

29. Molnar, C. & Gair, J. *Concepts of Biology - 1st Canadian Edition* (ed University, R.) (BC Open Textbook, 2019).

30. Shaw, N. A. The neurophysiology of concussion. *Progress in Neurobiology* **67,** 281–344 (2002).

31. Rehman, T., Ali, R., Tawil, I. & Yonas, H. Rapid progression of traumatic bifrontal contusions to transtentorial herniation: A case report. *Cases Journal* **1,** 1–4 (2014).

32. Riechers, R. G., Ramage, A., Brown, W., Kalehua, A., Rhee, P., Ecklund, J. M. & Ling, G. S. Physician Knowledge of the Glasgow Coma Scale. *Journal of Neurotrauma* **22,** 1327–1334 (2005).

33. Golan, J. D., Marcoux, J., Golan, E., Schapiro, R., Johnston, K. M., Maleki, M., Khetarpal, S. & Jacques, L. Traumatic brain injury in intoxicated patients. *Journal of Trauma - Injury, Infection and Critical Care* **63,** 365–369 (2007).

34. Baker, S. P., O'Neill, B., Haddon, W. & Long, W. B. The injury severity score: a method for describing patients with multiple injuries and evaluating emergency care. *The Journal of Trauma* **14,** 187–196 (1974).

35. Grote, S, Bocker, W, Mutschler, W, Bouillon, B & Lefering, R. Diagnostic value of the Glasgow Coma Scale for traumatic brain injury in 18,002 patients with severe multiple injuries. *Journal of Neurotrauma* **28,** 527–534 (2011).

36. Chen, J. W., Gombart, Z. J., Rogers, S, Gardiner, S. K., Cecil, S & Bullock, R. M. Pupillary reactivity as an early indicator of increased intracranial pressure: The introduction of the Neurological Pupil index. *Surgical Neurology international* **2,** 82 (2011).

37. Jacobs, B., Beems, T., Stulemeijer, M., van Vugt, A. B., van der Vliet, T. M., Borm, G. F. & Vos, P. E. Outcome Prediction in Mild Traumatic Brain Injury: Age and Clinical Variables Are Stronger Predictors than CT Abnormalities. *Journal of Neurotrauma* **27,** 655–668 (2010).

38. Kramer, A. H., Deis, N., Ruddell, S., Couillard, P., Zygun, D. A., Doig, C. J. & Gallagher, C. Decompressive Craniectomy in Patients with Traumatic Brain Injury: Are the Usual Indications Congruent with Those Evaluated in Clinical Trials? *Neurocritical Care* **25,** 10–19 (2016).

39. Hutchinson, P. J., Kolias, A. G., Tajsic, T., Adeleye, A., Aklilu, A. T., Apriawan, T., Bajamal, A. H., Barthélemy, E. J., Devi, B. I., Bhat, D., Bulters, D., Chesnut, R., Citerio, G., Cooper, D. J., Czosnyka, M., Edem, I., El-Ghandour, N. M., Figaji, A., Fountas, K. N., Gallagher, C., Hawryluk, G. W., Iaccarino, C., Joseph, M., Khan, T., Laeke, T., Levchenko, O., Liu, B., Liu, W., Maas, A., Manley, G. T., Manson, P., Mazzeo, A. T., Menon, D. K., Michael, D. B., Muehlschlegel, S., Okonkwo, D. O., Park, K. B., Rosenfeld, J. V., Rosseau, G., Rubiano, A. M., Shabani, H. K., Stocchetti, N., Timmons, S. D., Timofeev, I., Uff, C., Ullman, J. S., Valadka, A., Waran, V., Wells, A., Wilson, M. H. & Servadei, F. Consensus statement from

the International Consensus Meeting on the Role of Decompressive Craniectomy in the Management of Traumatic Brain Injury: Consensus statement. *Acta Neurochirurgica* **161,** 1261–1274 (2019).

40. Teasdale, G. & Jennett, B. Assessment and Prognosis of Coma After Head Injury. *Acta Neurochirurgica* **34,** 45–55 (1976).

41. Jennett, B., Snoek, J., Bond, M. R. & Brooks, N. Disability after severe head injury : observations on the use of the Glasgow Outcome Scale. *Journal of Neurology, Neurosurgery, and Psychiatry* **44,** 285–293 (1981).

42. Lu, J., Murray, G. D., Steyerberg, E. W., Butcher, I., McHugh, G. S., Lingsma, H., Mushkudiani, N., Choi, S., Maas, A. I. & Marmarou, A. Effects of Glasgow Outcome Scale misclassification on traumatic brain injury clinical trials. *Journal of Neurotrauma* **25,** 641–651 (2008).

43. De Guise, E., Leblanc, J., Dagher, J., Tinawi, S., Lamoureux, J., Marcoux, J., Maleki, M. & Feyz, M. Traumatic brain injury in the elderly: A level 1 trauma centre study. *Brain Injury* **29,** 558–564 (2015).

44. Julien, J., Alsideiri, G., Marcoux, J., Hasen, M., Correa, J. A., Feyz, M., Maleki, M. & de Guise, E. Antithrombotic agents intake prior to injury does not affect outcome after a traumatic brain injury in hospitalized elderly patients. *Journal of Clinical Neuroscience* **38,** 122–125 (2017).

45. Brown, A. W., Malec, J. F., McClelland, R. L., Diehl, N. N., Englander, J. & Cifu, D. X. Clinical Elements that Predict Outcome after Traumatic Brain Injury : A Prospective Multicenter Recursive Partitioning (Decision-Tree) Analysis. *Journal of Neurotrauma* **22,** 1040–1051 (2005).

46. Hou, D. J., Tong, K. A., Ashwal, S., Oyoyo, U., Joo, E., Shutter, L. & Obenaus, A. Diffusion-Weighted Magnetic Resonance Imaging Improves Outcome Prediction in Adult Traumatic Brain Injury. *Journal of Neurotrauma* **24,** 1558–1569 (2007).

47. Butcher, I., Maas, A. I., Lu, J., Marmarou, A., Murray, G. D., Mushkudiani, N. A., McHugh, G. S. & Steyerberg, E. W. Prognostic Value of Admission Blood Pressure in Traumatic Brain Injury: Results from The IMPACT Study. *Journal of Neurotrauma* **24,** 294–302 (2007).

48. Butcher, I, McHugh, G. S., Lu, J, Steyerberg, E. W., Hernandez, A. V., Mushkudiani, N, Maas, A. I., Marmarou, A & Murray, G. D. Prognostic value of cause of injury in traumatic brain injury: results from the IMPACT study. *Journal of Neurotrauma* **24,** 281–286 (2007).

49. Marmarou, A., Lu, J., Butcher, I., McHugh, G. S., Murray, G. D., Steyerberg, E. W., Mushkudiani, N. A., Choi, S. & Maas, A. I. Prognostic Value of The Glasgow Coma Scale And Pupil Reactivity in Traumatic Brain Injury Assessed Pre-Hospital And on Enrollment: An IMPACT Analysis. *Journal of Neurotrauma* **24,** 270–280 (2007).

50. Van Beek, J. G., Mushkudiani, N. A., Steyerberg, E. W., Butcher, I, McHugh, G. S., Lu, J, Marmarou, A, Murray, G. D. & Maas, A. I. Prognostic value of admission laboratory parameters in traumatic brain injury: results from the IMPACT study. *Journal of Neurotrauma* **24,** 315–328 (2007).

51. Hukkelhoven, C., Steyerberg, E., Habbema, J., Farace, E, Marmarou, A, Murray, G., Marshall, L. & Maas, A. Predicting Outcome after Traumatic Brain Injury: Admission Characteristics. *Journal of Neurotrauma* **22,** 1025–39 (2005).

52. Mondello, S., Jeromin, A., Buki, A., Bullock, R., Czeiter, E., Kovacs, N., Barzo, P., Schmid, K., Tortella, F., Wang, K. K. & Hayes, R. L. Glial Neuronal Ratio : A Novel Index for Differentiating Injury Type in Patients with Severe Traumatic Brain Injury. *Journal of Neurotrauma* **29,** 1096–1104 (2012).

53. Gan, Z. S., Stein, S. C., Swanson, R., Guan, S., Garcia, L., Mehta, D. & Smith, D. H. Blood biomarkers for traumatic brain injury: A quantitative assessment of diagnostic and prognostic accuracy. *Frontiers in Neurology* **10** (2019).

54. Papa, L., Robinson, G., Oli, M., Pineda, J., Demery, J., Brophy, G., Robicsek, S. A., Gabrielli, A., Robertson, C. S., Wang, K. K. & Hayes, R. L. Use of biomarkers for diagnosis and management of traumatic brain injury patients. *Expert Opinion on Medical Diagnostics* **2,** 937–945 (2008).

55. Papa, L., Akinyi, L., Liu, M. C., Pineda, J. a., Tepas, J. J., Oli, M. W., Zheng, W., Robinson, G., Robicsek, S. a., Gabrielli, A., Heaton, S. C., Hannay, H. J., Demery, J. a., Brophy, G. M., Layon, J., Robertson, C. S., Hayes, R. L. & Wang, K. K. W. Ubiquitin C-terminal hydrolase is a novel biomarker in humans for severe traumatic brain injury. *Critical Care Medicine* **38,** 138–44 (2010).

56. Papa, L., Lewis, L. M., Silvestri, S., Falk, J. L., Giordano, P., Brophy, G. M., Demery, J. A., Liu, M. C., Mo, J., Akinyi, L., Mondello, S., Schmid, K., Robertson, C. S., Tortella, F. C., Hayes, R. L. & Wang, K. K. Serum levels of ubiquitin C-terminal hydrolase distinguish mild traumatic brain injury from trauma controls and are elevated in mild and moderate traumatic brain injury patients with intracranial lesions and neurosurgical intervention. *Journal of Trauma and Acute Care Surgery* **72,** 1335–1344 (2012).

57. Herrmann, M., Curio, N., Jost, S., Wunderlich, M. T., Synowitz, H. & Wallesch, C. W. Protein S-100B and neuron specific enolase as early neurobiochemical markers of the severity of traumatic brain injury. *Restorative Neurology and Neuroscience* **14,** 109–114 (1999).

58. Thomas, D. G., Palfreyman, J. W. & Ratcliffe, J. G. Serum-Myelin-Basic-Protein Assay in Diagnosis and Prognosis of Patients With Head Injury. *The Lancet* **311,** 113–115 (1978).

59. Pelinka, L. E., Kroepfl, A., Schmidhammer, R., Krenn, M., Buchinger, W., Redl, H. & Raabe, A. Glial fibrillary acidic protein in serum after traumatic brain injury and multiple trauma. *Journal of Trauma - Injury, Infection and Critical Care* **57,** 1006–1012 (2004).

60. Berger, R. P., Pierce, M. C., Wisniewski, S. R., Adelson, P. D., Clark, R. S. B., Ruppel, R. A., Kochanek, P. M. & Background, A. Traumatic Brain Injury in Infants and Children. *Pediatrics* **109,** 2–7 (2002).

61. Chiaretti, A., Antonelli, A., Riccardi, R., Genovese, O., Pezzotti, P., Di Rocco, C., Tortorolo, L. & Piedimonte, G. Nerve growth factor expression correlates with severity and outcome of traumatic brain injury in children. *European Journal of Paediatric Neurology* **12,** 195–204 (2008).

62. Kleindienst, A. & Bullock, M. R. A critical analysis of the role of the neurotrophic protein S100B in acute brain injury. *Journal of Neurotrauma* **23,** 1185–1200 (2006).

63. Pike, B. R., Zhao, X., Newcomb, J. K., Posmantur, R. M., Wang, K. K. W. & Ca, R. L. H. Regional calpain and caspase-3 proteolysis of alpha-spectrin after traumatic brain injury. *Neuroreport* **9,** 2437–2442 (1998).

64. Ringger, N. C., O'Steen, B. E., Brabham, J. G., Silver, X, Pineda, J, Wang, K. K., Hayes, R. L. & Papa, L. A novel marker for traumatic brain injury: CSF alphaII-spectrin breakdown product levels. *Journal of Neurotrauma* **21,** 1443–1456 (2004).

65. Franz, G, Beer, R, Kampfl, A, Engelhardt, K, Schmutzhard, E, Ulmer, H & Deisenhammer, F. Amyloid beta 1-42 and tau in cerebrospinal fluid after severe traumatic brain injury. *Neurology* **60,** 1457–1461 (2003).

66. Shaw, G., Yang, C., Ellis, R., Anderson, K., Mickle, J. P., Scheff, S., Pike, B., Anderson, D. K. & Howland, D. R. Hyperphosphorylated neurofilament NF-H is a serum biomarker of axonal injury. *Biochemical and Biophysical Research Communications* **336,** 1268–1277 (2005).

67. Satchell, M. A., Lai, Y, Kochanek, P. M., Wisniewski, S. R., Fink, E. L., Siedberg, N. A., Berger, R. P., DeKosky, S. T., Adelson, P. D. & Clark, R. S. Cytochrome c, a biomarker of apoptosis, is increased in cerebrospinal fluid from infants with inflicted brain injury from child abuse. *Journal of Cerebral Blood Flow and Metabolism* **25,** 919–927 (2005).

68. Whalen, M. J., Carlos, T. M., Kochanek, P. M., Wisniewski, S. R., Bell, M. J., Carcillo, J. A., Clark, R. S., DeKosky, S. T. & Adelson, P. D. Soluble adhesion molecules in CSF are increased in children with severe head injury. *Journal of Neurotrauma* **15,** 777–787 (1998).

69. Pleines, U. E., Stover, J. F., Kossmann, T, Trentz, O & Morganti-Kossmann, M. C. Soluble ICAM-1 in CSF coincides with the extent of cerebral damage in patients with severe traumatic brain injury. *Journal of Neurotrauma* **15,** 399–409 (1998).

70. Beer, R, Franz, G, Srinivasan, A, Hayes, R. L., Pike, B. R., Newcomb, J. K., Zhao, X, Schmutzhard, E, Poewe, W & Kampfl, A. Temporal profile and cell subtype distribution of activated caspase-3 following experimental traumatic brain injury. *Journal of Neurochemistry* **75,** 1264–73 (2000).

71. Lenzlinger, P. M., Marx, A, Trentz, O, Kossmann, T & Morganti-Kossmann, M. C. Prolonged intrathecal release of soluble Fas following severe traumatic brain injury in humans. *Journal of Neuroimmunology* **122,** 167–174 (2002).

72. Vilalta, A, Sahuquillo, J, Rosell, A, Poca, M. A., Riveiro, M & Montaner, J. Moderate and severe traumatic brain injury induce early overexpression of systemic and brain gelatinases. *Intensive Care Medicine* **34,** 1384–1392 (2008).

73. Roberts, D. J., Jenne, C. N., Le, C., Kramer, A. H., Gallagher, C. N., Todd, S., Parney, I. F., Doig, C. J., Yong, V. W., Kubes, P. & Zygun, D. A. Association between the Cerebral Inflammatory and Matrix Metalloproteinase Responses after Severe Traumatic Brain Injury in Humans. *Journal of Neurotrauma* **30,** 1727–1736 (2013).

74. Roberts, D. J., Jenne, C. N., Léger, C., Kramer, A. H., Gallagher, C. N., Todd, S., Parney, I. F., Doig, C. J., Yong, V. W., Kubes, P. & Zygun, D. a. A prospective evaluation of the temporal matrix metalloproteinase response after severe traumatic brain injury in humans. *Journal of Neurotrauma* **30,** 1717–26 (2013).

75. Lu, K. T., Wang, Y. W., Yang, J. T., Yang, Y. L. & Chen, H. I. Effect of interleukin-1 on traumatic brain injury-induced damage to hippocampal neurons. *Journal of Neurotrauma* **22,** 885–895 (2005).

76. Michael, D. B., Byers, D. M. & Irwin, L. N. Gene expression following traumatic brain injury in humans: analysis by microarray. *Journal of Clinical Neuroscienceoscience* **12,** 284–290 (2005).

77. Buttram, S. D., Wisniewski, S. R., Jackson, E. K., Adelson, P. D., Feldman, K, Bayir, H, Berger, R. P., Clark, R. S. & Kochanek, P. M. Multiplex assessment of cytokine and chemokine levels in cerebrospinal fluid following severe pediatric traumatic brain injury: effects of moderate hypothermia. *Journal of Neurotrauma* **24,** 1707–1717 (2007).

78. Siman, R., Toraskar, N., Dang, A., McNeil, E., McGarvey, M., Plaum, J., Maloney, E. & Grady, M. S. A panel of neuron-enriched proteins as markers for traumatic brain injury in humans. *Journal of Neurotrauma* **26,** 1867–77 (2009).

79. Wilkinson, A. A., Simic, N., Frndova, H., Taylor, M. J., Choong, K., Fraser, D., Campbell, C., Dhanani, S., Kuehn, S., Beauchamp, M. H., Farrell, C., Anderson, V., Guerguerian, A. M., Dennis, M., Schachar, R. & Hutchison, J. S. Serum biomarkers help predict attention problems in critically ill children with traumatic brain injury. *Pediatric Critical Care Medicine* **17,** 638–648 (2016).

80. Di Battista, A. P., Rhind, S. G., Hutchison, M. G., Hassan, S., Shiu, M. Y., Inaba, K., Topolovec-Vranic, J., Neto, A. C., Rizoli, S. B. & Baker, A. J. Inflammatory cytokine and chemokine profiles are associated with patient outcome and the hyperadrenergic state following acute brain injury. *Journal of Neuroinflammation* **13,** 1–14 (2016).

81. Jastrow, K. M., Gonzalez, E. A., McGuire, M. F., Suliburk, J. W., Kozar, R. A., Iyengar, S., Motschall, D. A., McKinley, B. A., Moore, F. A. & Mercer, D. W. Early Cytokine Production Risk Stratifies Trauma Patients for Multiple Organ Failure. *Journal of the American College of Surgeons* **209,** 320–331 (2009).

82. Chiaretti, a, Barone, G, Riccardi, R, Antonelli, a, Pezzotti, P, Genovese, O, Tortorolo, L & Conti, G. Correlates With Severity and Outcome of Head Trauma in Children. *Neurology* (2009).

83. Mellergård, P., Sjögren, F. & Hillman, J. The Cerebral Extracellular Release of Glycerol, Glutamate, and FGF2 Is Increased in Older Patients following Severe Traumatic Brain Injury. *Journal of Neurotrauma* **29,** 112–118 (2011).

84. Dyhrfort, P., Shen, Q., Clausen, F., Thulin, M., Enblad, P., Kamali-Moghaddam, M., Lewén, A. & Hillered, L. Monitoring of Protein Biomarkers of Inflammation in Human Traumatic Brain Injury Using Microdialysis and Proximity Extension Assay Technology in Neurointensive Care. *Journal of Neurotrauma* **14,** 1–14 (2019).

85. Huie, J. R., Diaz-Arrastia, R., Yue, J. K., Sorani, M. D., Puccio, A. M., Okonkwo, D. O., Manley, G. T., Ferguson, A. R., Adeoye, O. M., Badjatia, N., Boase, K. D., Bodien-Guller, Y., Bullock, M. R., Chesnut, R. M., Corrigan, J. D., Crawford, K. L., Diaz-Arrastia, R., Dikmen, S. S., Duhaime, A.-C., Ellenbogen, R. G., Ezekiel, F., Feeser, V. R., Giacino, J. T., Goldman, D. P., Gonzales, L., Gopinath, S. P., Gullapalli, R. P., Hemphill, J. C., Hotz, G. A., Kramer, J. H., Levin, H., Lindsell, C. J., Machamer, J., Madden, C., Markowitz, A. J., Martin, A., Mathern, B. E., McAllister, T. W., McCrea, M. A., Merchant, R. E., Noel, F., Perl, D. P., Puccio, A. M., Rabinowitz, M., Robertson, C. S., Rosand, J., Sander, A. M., Satris, G., Schnyer, D. M., Seabury, S. A., Sergot, P., Sherer, M., Stein, D. M., Stein, M. B., Taylor, S. R., Temkin, N. R., Toga, A. W., Turtzo, L. C., Vespa, P. M., Wang, K. K., Zafonte, R. & Zhang, Z. Testing a Multivariate Proteomic Panel for Traumatic Brain Injury Biomarker Discovery: A TRACK-TBI Pilot Study. *Journal of Neurotrauma* **36,** 100–110 (2018).

86. Berger, R. P., Ta'asan, S., Rand, A., Lokshin, A. & Kochanek, P. Multiplex assessment of serum biomarker concentrations in well-appearing children with inflicted traumatic brain injury. *Pediatric Research* **65,** 97–102 (2009).

87. Robinson, S., Winer, J. L., Berkner, J., Chan, L. A. S., Denson, J. L., Maxwell, J. R., Yang, Y., Sillerud, L. O., Tasker, R. C., Meehan III, W. P., Mannix, R. & Jantzie, L. L. Imaging and serum biomarkers reflecting the functional efficacy of extended erythropoietin treatment in rats following infantile traumatic brain injury. *Journal of Neurosurgical Pediatry* **17,** 739–755 (2016).

88. Sankar, S. B., Pybus, A. F., Liew, A., Sanders, B., Shah, K. J., Wood, L. B. & Buckley, E. M. Low cerebral blood flow is a non-invasive biomarker of neuroinflammation after repetitive mild traumatic brain injury. *Neurobiology of Disease* **124,** 544–554 (2019).

89. Thelin, E. P., Just, D., Frostell, A., Häggmark-Månberg, A., Risling, M., Svensson, M., Nilsson, P. & Bellander, B. M. Protein profiling in serum after traumatic brain injury in rats reveals potential injury markers. *Behavioural Brain Research* **340,** 71–80 (2018).

90. Isoniemi, H, Tenovuo, O, Portin, R, Himanen, L & Kairisto, V. Outcome of traumatic brain injury after three decades–relationship to ApoE genotype. *Journal of Neurotrauma* **23,** 1600–1608 (2006).

91. McAllister, T. W., Tyler, A. L., Flashman, L. A., Rhodes, C. H., McDonald, B. C., Saykin, A. J., Tosteson, T. D., Tsongalis, G. J. & Moore, J. H. Polymorphisms in the Brain-Derived Neurotrophic Factor Gene Influence Memory and Processing Speed One Month after Brain Injury. *Journal of Neurotrauma* **29,** 1111–1118 (2011).

92. Dalla Libera, A. L., Regner, A., De Paoli, J., Centenaro, L., Martins, T. T. & Simon, D. IL-6 polymorphism associated with fatal outcome in patients with severe traumatic brain injury. *Brain Injury* **25,** 365–369 (2011).

93. Soustiel, J. F., Palzur, E., Nevo, O., Thaler, I. & Vlodavsky, E. Neuroprotective Anti-Apoptosis Effect of Estrogens in Traumatic Brain Injury. *Journal of Neurotrauma* **22,** 345–352 (2005).

94. Brotfain, E., E. Gruenbaum, S., Boyko, M., Kutz, R., Zlotnik, A. & Klein, M. Neuroprotection by Estrogen and Progesterone in Traumatic Brain Injury and Spinal Cord Injury. *Current Neuropharmacology* **14,** 641–653 (2016).

95. Bhomia, M., Balakathiresan, N. S., Wang, K. K., Papa, L. & Maheshwari, R. K. A Panel of Serum MiRNA Biomarkers for the Diagnosis of Severe to Mild Traumatic Brain Injury in Humans. *Scientific Reports* **6,** 1–12 (2016).

96. Parkin, G. M., Clarke, C., Takagi, M., Hearps, S., Babl, F. E., Davis, G. A., Anderson, V. & Ignjatovic, V. Plasma Tumor Necrosis Factor Alpha Is a Predictor of Persisting Symptoms Post-Concussion in Children. *Journal of Neurotrauma* **36,** 1768–1775 (2019).

97. Bromander, S., Anckarsäter, R., Kristiansson, M., Blennow, K., Zetterberg, H., Anckarsäter, H. & Wass, C. E. Changes in serum and cerebrospinal fluid cytokines in response to non-neurological surgery: an observational study. *Journal of Neuroinflammation* **9,** 242 (2012).

98. Papa, L., Ramia, M. M., Kelly, J. M., Burks, S. S., Pawlowicz, A. & Berger, R. P. Systematic Review of Clinical Research on Biomarkers for Pediatric Traumatic Brain Injury. *Journal of Neurotrauma* **30,** 324–338 (2013).

99. Oddo, M. & Hutchinson, P. J. Understanding and monitoring brain injury: the role of cerebral microdialysis. *Intensive Care Medicine* **44,** 1945–1948 (2018).

100. Blaus, B. Medical gallery of Blausen Medical. *WikiJournal of Medicine* **1** (2014).

101. Elson, J. A. *Red blood cell comparison* 2014.

102. Zetterström, T., Sharp, T., Marsden, C. A. & Ungerstedt, U. In Vivo Measurement of Dopamine and Its Metabolites by Intracerebral Dialysis: Changes After d-Amphetamine. *Journal of Neurochemistry* **41,** 1769–1773 (1983).

103. Meixensberger, J., Kunze, E., Barcsay, E., Vaeth, A. & Roosen, K. Clinical cerebral microdialysis: Brain metabolism and brain tissue oxygenation after acute brain injury. *Neurological Research* **23,** 801–806 (2001).

104. Vespa, P., Prins, M., Ronne-Engstrom, E., Caron, M., Shalmon, E., Hovda, D. A., Martin, N. A. & Becker, D. P. Increase in extracellular glutamate caused by reduced cerebral perfusion pressure and seizures after human traumatic brain injury: a microdialysis study. *Journal of Neurosurgery* **89,** 971–982 (1998).

105. Folkersma, H., Brevé, J. J. P., Tilders, F. J. H., Cherian, L., Robertson, C. S. & Vandertop, W. P. Cerebral microdialysis of interleukin (IL)-1ß and IL-6: extraction efficiency and production in the acute phase after severe traumatic brain injury in rats. *Acta Neurochirurgica* **150,** 1277–1284 (2008).

106. Afinowi, R, Tisdall, M, Keir, G, Smith, M, Kitchen, N & Petzold, A. Improving the recovery of S100B protein in cerebral microdialysis: implications for multimodal monitoring in neurocritical care. *Journal of Neuroscience Methods* **181,** 95–99 (2009).

107. Chen, J. W., Rogers, S. L., Gombart, Z. J., Adler, D. E. & Cecil, S. Implementation of cerebral microdialysis at a community-based hospital: A 5-year retrospective analysis. *Surgical Neurology international* **3,** 57 (2012).

108. Duo, J. & Stenken, J. A. Heparin-immobilized microspheres for the capture of cytokines. *Analytical and Bioanalytical Chemistry* **399,** 773–82 (2011).

109. Rossi, J. L., Ralay Ranaivo, H, Patel, F, Chrzaszcz, M, Venkatesan, C & Wainwright, M. S. Albumin causes increased myosin light chain kinase expression in astrocytes via p38 mitogen-activated protein kinase. *Journal of Neuroscience Research* **89,** 852–861 (2011).

110. Torres-Corzo, J. G., Tapia-Pérez, J. H., Sánchez-Aguilar, M., Della Vecchia, R. R., Chalita Williams, J. C. & Cerda-Gutiérrez, R. Comparison of cerebrospinal fluid obtained by ventricular endoscopy and by lumbar puncture in patients with hydrocephalus secondary to neurocysticercosis. *Surgical Neurology* **71,** 376–9 (2009).

111. Rosenling, T, Stoop, M. P., Smolinska, A, Muilwijk, B, Coulier, L, Shi, S, Dane, A, Christin, C, Suits, F, Horvatovich, P. L., Wijmenga, S. S., Buydens, L. M., Vreeken, R, Hankemeier, T, van Gool, A. J., Luider, T. M. & Bischoff, R. The Impact of Delayed Storage on the Measured Proteome and Metabolome of Human Cerebrospinal Fluid. *Clinical Chemistry* (2011).

112. Ranganathan, S, Polshyna, A, Nicholl, G, Lyons-Weiler, J & Bowser, R. Assessment of Protein Stability in Cerebrospinal Fluid Using Surface-Enhanced Laser Desorption/Ionization Time-of-Flight Mass Spectrometry Protein Profiling. *Clinical Proteomics* **2,** 91–101 (2006).

113. Banks, R. E., Stanley, A. J., Cairns, D. A., Barrett, J. H., Clarke, P, Thompson, D & Selby, P. J. Influences of blood sample processing on low-molecular-weight proteome identified by surface-enhanced laser desorption/ionization mass spectrometry. *Clinical Chemistry* **51,** 1637–1649 (2005).

114. Kälvegren, H., Jönsson, S. & Jonasson, L. Release of matrix metalloproteinases-1 and-2, but not-9, from activated platelets measured by enzyme-linked immunosorbent assay. *Platelets* **22,** 572–578 (2011).

115. O'Mullan, P., Craft, D., Yi, J. & Gelfand, C. A. Thrombin induces broad spectrum proteolysis in human serum samples. *Clinical Chemistry and Laboratory Medicine* **47,** 685–693 (2009).

116. Salazar, J.-F., Herbeth, B., Siest, G. & Leroy, P. Stability of blood homocysteine and other thiols: EDTA or acidic citrate? *Clinical Chemistry* **45,** 2016–2019 (1999).

117. Oddoze, C., Lombard, E. & Portugal, H. Stability study of 81 analytes in human whole blood, in serum and in plasma. *Clinical Biochemistry* **45,** 464–9 (2012).

118. Chan, B. Y. Y., Buckley, K. A., Durham, B. H., Gallagher, J. A. & Fraser, W. D. Effect of Anticoagulants and Storage Temperature on the Stability of Receptor Activator for Nuclear Factor-KB Ligand and Osteoprotegerin in Plasma and Serum. *Clinical Chemistry* **49,** 2083–2085 (2003).

119. Rai, A. J., Gelfand, C. A., Haywood, B. C., Warunek, D. J., Yi, J., Schuchard, M. D., Mehigh, R. J., Cockrill, S. L., Scott, G. B., Tammen, H., Schulz-Knappe, P., Speicher, D. W., Vitzthum, F., Haab, B. B., Siet, G. & Chan, D. W. HUPO Plasma Proteome Project specimen collection and handling: Towards the standardization of parameters for plasma proteome samples. *Proteomics* **5,** 3262–3277 (2005).

120. Hulmes, J. D., Bethea, D., Ho, K., Huang, S.-P., Ricci, D. L., Opiteck, G. J. & Hefta, S. A. An Investigation of Plasma Collection, Stabilization, and Storage Procedures for Proteomic Analysis of Clinical Samples. *Clinical Proteomics* **1,** 017–032 (2004).

121. Tammen, H, Schulte, I, Hess, R, Menzel, C, Kellmann, M, Mohring, T & Schulz-Knappe, P. Peptidomic analysis of human blood specimens: comparison between plasma specimens and serum by differential peptide display. *Proteomics* **5,** 3414–3422 (2005).

122. Jambunathan, K. & Galande, A. K. Sample collection in clinical proteomics - Proteolytic activity profile of serum and plasma. *Proteomics - Clinical Applications* **8,** 299–307 (2014).

123. Wilkins, M. R., Sanchez, J. C., Gooley, A. A., Appel, R. D., Humphery-Smith, I., Hochstrasser, D. F. & Williams, K. L. Progress with proteome projects: Why all proteins expressed by a genome should be identified and how to do it. *Biotechnology and Genetic Engineering Reviews* **13,** 19–50 (1996).

124. Garg, P., Morris, P., Fazlanie, A. L., Vijayan, S., Dancso, B., Dastidar, A. G., Plein, S., Mueller, C. & Haaf, P. Cardiac biomarkers of acute coronary syndrome: from history to high-sensitivity cardiac troponin. *Internal and Emergency Medicine* **12,** 147–155 (2017).

125. Whitcomb, D. C. What is personalized medicine and what should it replace? *Nature Reviews Gastroenterology and Hepatology* **9,** 418–424 (2012).

126. Haqqani, A. S., Hutchison, J. S., Ward, R & Stanimirovic, D. B. Biomarkers and diagnosis; protein biomarkers in serum of pediatric patients with severe traumatic brain injury identified by ICAT-LC-MS/MS. *Journal of Neurotrauma* **24,** 54–74 (2007).

127. Granger, J, Siddiqui, J, Copeland, S & Remick, D. Albumin depletion of human plasma also removes low abundance proteins including the cytokines. *Proteomics* **5,** 4713–4718 (2005).

128. Powers, T. W., Holst, S., Wuhrer, M., Mehta, A. S. & Drake, R. R. Two-dimensional N-glycan distribution mapping of hepatocellular carcinoma tissues by MALDI-imaging mass spectrometry. *Biomolecules* **5,** 2554–2572 (2015).

129. Thaitrong, N., Charlermroj, R., Himananto, O., Seepiban, C. & Karoonuthaisiri, N. Implementation of microfluidic sandwich ELISA for superior detection of plant pathogens. *PloS one* **8,** e83231 (2013).

130. Kuen, J. *Influence of 3D tumor cell/fibroblast co-culture on monocyte differentiation and tumor progression in pancreatic cancer* PhD thesis (Dec. 2017).

131. Shi, T., Fillmore, T. L., Sun, X., Zhao, R., Schepmoes, A. A., Hossain, M., Xie, F., Wu, S., Kim, J.-S., Jones, N., Moore, R. J., Pasa-Tolic, L., Kagan, J., Rodland, K. D., Liu, T., Tang, K., Camp, D. G., Smith, R. D. & Qian, W.-J. Antibody-free, targeted mass-spectrometric approach for quantification of proteins at low picogram per milliliter levels in human plasma/serum. *Proceedings of the National Academy of Sciences* **109,** 15395–15400 (2012).

132. Connor, D. E., Chaitanya, G. V., Chittiboina, P., McCarthy, P., Scott, L. K., Schrott, L., Minagar, A., Nanda, A. & Alexander, J. S. Variations in the cerebrospinal fluid proteome following traumatic brain injury and subarachnoid hemorrhage. *Pathophysiology* **24,** 169–183 (2017).

133. Crawford, F., Crynen, G., Reed, J., Mouzon, B., Bishop, A., Katz, B., Ferguson, S., Phillips, J., Ganapathi, V., Mathura, V., Roses, A. & Mullan, M. Identification of Plasma Biomarkers of TBI Outcome Using Proteomic Approaches in an APOE Mouse Model. *Journal of Neurotrauma* **29,** 246–260 (2012).

134. Hanrieder, J., Wetterhall, M., Enblad, P., Hillered, L. & Bergquist, J. Temporally resolved differential proteomic analysis of human ventricular CSF for monitoring traumatic brain injury biomarker candidates. *Journal of Neuroscience Methods* **177,** 469–478 (2009).

135. Kobeissy, F. H., Ottens, A. K., Zhang, Z, Liu, M. C., Denslow, N. D., Dave, J. R., Tortella, F. C., Hayes, R. L. & Wang, K. K. Novel differential neuroproteomics analysis of traumatic brain injury in rats. *Molecular & Cellular Proteomics* **5,** 1887–1898 (2006).

136. Lakshmanan, R, Angeles, L., Loo, J. A., Angeles, L., Drake, T, Angeles, L., Leblanc, J, Angeles, L., Ytterberg, A. J., Angeles, L., Mcarthur, D. L., Etchepare, M & Vespa, P. M. Metabolic Crisis After Traumatic Brain Injury is Associated with a Novel Microdialysis Proteome. *Neurocritical Care* **12,** 324–336 (2010).

137. Anada, R. P., Wong, K. T., Jayapalan, J. J., Hashim, O. H. & Ganesan, D. Panel of serum protein biomarkers to grade the severity of traumatic brain injury. *Electrophoresis* **39,** 2308–2315 (2018).

138. Engvall, E & Perlmann, P. Enzyme-linked immunosorbent assay (ELISA). Quantitative assay of immunoglobulin G. *Immunochemistry* **8,** 871–874 (1971).

139. De Koning, L., Liptak, C., Shkreta, A., Bradwin, G., Hu, F. B., Pradhan, A. D., Rifai, N. & Kellogg, M. D. A multiplex immunoassay gives different results than singleplex immunoassays which may bias epidemiologic associations. *Clinical Biochemistry* **45,** 848–851 (2012).

140. Phan, K., Sohn, K.-Y., Hill, S. a., Worster, A., You, J., Oremus, M., Devereaux, P. J., Jaffe, A. S. & Kavsak, P. a. Multiplex protein assay performance/evaluation and the requirement for precision and correlation to clinical assays. *Clinical Chemistry and Laboratory Medicine* **49,** 1915–8 (2011).

141. Li, H., Bergeron, S. & Juncker, D. Microarray-to-microarray transfer of reagents by snapping of two chips for cross-reactivity-free multiplex immunoassays. *Analytical Chemistry* **84,** 4776–4783 (2012).

142. Li, H., Munzar, J. D., Ng, A. & Juncker, D. A versatile snap chip for high-density sub-nanoliter chip-to-chip reagent transfer. *Scientific Reports* **5,** 11688 (2015).

143. Li, H., Bergeron, S., Larkin, H. & Juncker, D. Snap Chip for Cross-reactivity-free and Spotter-free Multiplexed Sandwich Immunoassays. *JoVE,* e56230 (2017).

144. Juncker, D., Bergeron, S., Laforte, V. & Li, H. Cross-reactivity in antibody microarrays and multiplexed sandwich assays: shedding light on the dark side of multiplexing. *Current Opinion in Chemical Biology* **18,** 29–37 (2014).

145. Assarsson, E., Lundberg, M., Holmquist, G., Björkesten, J., Thorsen, S. B., Ekman, D., Eriksson, A., Rennel Dickens, E., Ohlsson, S., Edfeldt, G., Andersson, A.-C., Lindstedt, P., Stenvang, J., Gullberg, M. & Fredriksson, S. Homogenous 96-Plex PEA Immunoassay Exhibiting High Sensitivity, Specificity, and Excellent Scalability. *PLoS ONE* **9,** e95192 (2014).

146. Bergeron, S., Laforte, V., Lo, P. S., Li, H. & Juncker, D. Evaluating mixtures of 14 hygroscopic additives to improve antibody microarray performance. *Analytical and Bioanalytical Chemistry* **407,** 8451–8462 (2015).

147. Barbulovic-Nad, I., Lucente, M., Sun, Y., Zhang, M., Wheeler, A. R. & Bussmann, M. Bio-microarray fabrication techniques–a review. *Critical Reviews in Biotechnology* **26,** 237–59 (2006).

148. Ellington, A. A., Kullo, I. J., Bailey, K. R. & Klee, G. G. Antibody-based protein multiplex platforms: technical and operational challenges. *Clinical Chemistry* **56,** 186–93 (2010).

149. Dufva, M. & Christensen, C. B. V. Optimization of oligonucleotide sets for DNA microarrays. *Methods in Molecular Biology* **381** (ed Rampal, J. B.) 93–103 (2007).

150. Kricka, L. J. & Master, S. R. Quality control and protein microarrays. *Clinical Chemistry* **55,** 1053–1055 (2009).

151. Deegan, R. D., Bakajin, O., Dupont, T. F., Huber, G., Nagel, S. R. & Witten, T. A. Capillary flow as the cause of ring stains from dried liquid drops. *Nature* **389,** 827–829 (1997).

152. Angulo, J. Polar Modelling and Segmentation of Genomic Microarray Spots Using Mathematical Morphology. *Image Analytical Stereology* **27,** 107–124 (2008).

153. Safavieh, R., Pla-Roca, M., Qasaimeh, M. A., Mirzaei, M. & Juncker, D. Straight SU-8 pins. *Journal of Micromechanics and Microengineering* **20,** 055001–055009 (2010).

154. Laforte, V., Olanrewaju, A. & Juncker, D. *Low-cost , high liquid volume silicon quill pins for robust and reproducible printing of antibody microarrays* in *MicroTAS: miniaturized systems for chemistry and life sciences* (Chemical and Biological Microsystems Society (CBMS), Freiburg, Germany, 2013), 485–487.

155. McQuain, M. K., Seale, K., Peek, J., Levy, S. & Haselton, F. R. Effects of relative humidity and buffer additives on the contact printing of microarrays by quill pins. *Analytical Biochemistry* **320,** 281–291 (2003).

156. Gutmann, O., Kuehlewein, R., Reinbold, S., Niekrawietz, R., Steinert, C. P., de Heij, B., Zengerle, R. & Daub, M. Fast and reliable protein microarray production by a new drop-in-drop technique. *Lab on a Chip* **5,** 675–81 (2005).

157. Hartmann, M., Sjödahl, J., Stjernström, M., Redeby, J., Joos, T. & Roeraade, J. Non-contact protein microarray fabrication using a procedure based on liquid bridge formation. *Analytical and Bioanalytical Chemistry* **393,** 591–598 (2009).

158. Liberski, A., Zhang, R. & Bradley, M. Inkjet fabrication of polymer microarrays and grids - Solving the evaporation problem. *Chemical Communications* **3,** 334–336 (2009).

159. Sun, Y., Zhou, X. & Yu, Y. A novel picoliter droplet array for parallel real-time polymerase chain reaction based on double-inkjet printing. *Lab on a Chip* **14,** 3603–3610 (2014).

160. Olle, E. W., Messamore, J, Deogracias, M. P., McClintock, S. D., Anderson, T. D. & Johnson, K. J. Comparison of antibody array substrates and the use of glycerol to normalize spot morphology. *Experimental and Molecular Pathology* **79,** 206–209 (2005).

161. González-González, M., Bartolome, R., Jara-Acevedo, R., Casado-Vela, J., Dasilva, N., Matarraz, S., García, J., Alcazar, J. A., Sayagues, J. M., Orfao, A. & Fuentes, M. Evaluation of homo- and hetero-functionally activated glass surfaces for optimized antibody arrays. *Analytical Biochemistry* **450,** 37–45 (2014).

162. Zuo, P., Zhang, Y., Liu, J. & Ye, B. C. Determination of β-adrenergic agonists by hapten microarray. *Talanta* **82,** 61–66 (2010).

163. Rodríguez-Seguí, S. A., Pons Ximénez, J. I., Sevilla, L., Ruiz, A., Colpo, P., Rossi, F., Martínez, E. & Samitier, J. Quantification of protein immobilization on substrates for cellular microarray applications. *Journal of Biomedical Materials Research - Part A* **98,** 245–256 (2011).

164. Liu, Y. S., Li, C. M., Yu, L. & Chen, P. Optimization of printing buffer for protein microarrays based on aldehyde-modified glass slides. *Frontiers in Bioscience* **12,** 3768–3773 (2007).

165. Ruwona, T. B., McBride, R., Chappel, R., Head, S. R., Ordoukhanian, P., Burton, D. R. & Law, M. Optimization of peptide arrays for studying antibodies to hepatitis C virus continuous epitopes. *Journal of Immunological Methods* **402,** 35–42 (2014).

166. Monroe, M. R., Reddington, A. P., Collins, A. D., LaBoda, C., Cretich, M., Chiari, M., Little, F. F. & Ünlü, M. S. Multiplexed method to calibrate and quantitate fluorescence signal for allergen-specific IgE. *Analytical Chemistry* **83,** 9485–9491 (2011).

167. Hegde, P., Qi, R., Abernathy, K., Gay, C., Dharap, S., Gaspard, R., Hughes, J. E., Snesrud, E., Lee, N. & Quackenbush, J. A concise guide to cDNA microarray analysis. *BioTechniques* **29,** 548–62 (2000).

168. Diehl, F., Grahlmann, S., Beier, M. & Hoheisel, J. D. Manufacturing DNA microarrays of high spot homogeneity and reduced background signal. *Nucleic Acids Research* **29,** E38 (2001).

169. Csonka, L. N., Ikeda, T. P., Fletcher, S. A. & Kustu, S. The accumulation of glutamate is necessary for optimal growth of *Salmonella typhimurium* in media of high osmolality but not induction of the proU operon. *Journal of Bacteriology* **176,** 6324–6333 (1994).

170. Preininger, C., Sauer, U., Dayteg, J. & Pichler, R. Optimizing processing parameters for signal enhancement of oligonucleotide and protein arrays on ARChip Epoxy. *Bioelectrochemistry* **67,** 155–162 (2005).

171. Lee, C.-S. & Kim, B.-G. Improvement of protein stability in protein microarrays. *Biotechnology Letters* **24,** 839–844 (2002).

172. Rickman, D. S., Herbert, C. J. & Aggerbeck, L. P. Optimizing spotting solutions for increased reproducibility of cDNA microarrays. *Nucleic Acids Research* **31,** e109 (2003).

173. Wu, P. & Grainger, D. W. Comparison of hydroxylated print additives on antibody microarray performance. *Journal of Proteome Research* **5,** 2956–2965 (2006).

174. *Glycerine : an overview* tech. rep. (The Soap and Detergent Association, New York, NY, 1990), 1–27.

175. Tamaru, S.-I., Yamaguchi, S. & Hamachi, I. Simple and Practical Semi-wet Protein/Peptide Array Utilizing a Micelle-mixed Agarose Hydrogel. *Chemistry Letters* **34,** 294–295 (2005).

176. Finch, C. A. *Polyvinyl alcohol, properties and applications* (John Wiley & Sons, Ltd, New York, NY, 1973).

177. Xu, B.-J., Jin, Q.-H. & Zhao, J.-L. A Novel Method of Producing Protein Microarray for Immunoassay. *Chinese Journal of Analytical Chemistry* **35,** 153–158 (2007).

178. *The Merck Index: An Encyclopedia of Chemicals, Drugs, and Biologicals* 15th ed. (ed O'Neil, M.) (Merck Sharp & Dohme Corp., Whitehouse Station, NJ, 2014).

179. Avseenko, N. V., Morozova, T. Y., Ataullakhanov, F. I. & Morozov, V. N. Immobilization of proteins in immunochemical microarrays fabricated by electrospray deposition. *Analytical Chemistry* **73,** 6047–52 (2001).

180. Moerman, R., Frank, J., Marijnissen, J. C. M., Schalkhammer, T. G. M. & van Dedem, G. W. K. Miniaturized electrospraying as a technique for the production of microarrays of reproducible micrometer-sized protein spots. *Analytical Chemistry* **73,** 2183–2189 (2001).

181. Moerman, R., van den Doel, L. R., Picioreanu, S., Frank, J., Marijnissen, J. P. A., van Dedem, G. W. K., Hjelt, K. H., Vellekoop, M. J., Sarro, P. M. & Young, I. T. *Microinjection of sigma-D-glucose standards and Amplex Red reagent on microarrays* in *Micro- and Nanofabricated Structures and Devices for Biomedical Environmental Applications II* (ed Ferrari, M.) **3606** (International Society for Optics and Photonics, San Jose, CA, USA, 1999), 119–128.

182. Haynes, W. N. *CRC Handbook of Chemistry and Physics* 95th ed. (CRC Press, 2014).

183. MacBeath, G. & Schreiber, S. L. Printing proteins as microarrays for high-throughput function determination. *Science* **289,** 1760–1763 (2000).

184. Ressine, A., Marko-Varga, G. & Laurell, T. Porous silicon protein microarray technology and ultra-/superhydrophobic states for improved bioanalytical readout. *Biotechnology Annual Review* **13,** 149–200 (2007).

185. Mueller, M., Loh, M. Q., Tee, D. H., Yang, Y. & Jungbauer, A. Liquid formulations for long-term storage of monoclonal IgGs. *Applied Biochemistry and Biotechnology* **169,** 1431–1448 (2013).

186. Zhou, G., Bergeron, S. & Juncker, D. High-performance low-cost antibody microarrays using enzyme-mediated silver amplification. *Journal of Proteome Research* **14,** 1872–1879 (2015).

187. Wingren, C., Ingvarsson, J., Dexlin, L., Szul, D. & Borrebaeck, C. A. K. Design of recombinant antibody microarrays for complex proteome analysis: choice of sample labeling-tag and solid support. *Proteomics* **7,** 3055–3065 (2007).

188. Guilleaume, B., Buness, A., Schmidt, C., Klimek, F., Moldenhauer, G., Huber, W., Arlt, D., Korf, U., Wiemann, S. & Poustka, A. Systematic comparison of surface coatings for protein microarrays. *Proteomics* **5,** 4705–4712 (2005).

189. Zhao, X., Pan, F., Cowsill, B., Lu, J. R., Garcia-Gancedo, L., Flewitt, A. J., Ashley, G. M. & Luo, J. Interfacial immobilization of monoclonal antibody and detection of human prostate-specific antigen. *Langmuir* **27,** 7654–7662 (2011).

190. Wolter, A., Niessner, R. & Seidel, M. Preparation and characterization of functional poly(ethylene glycol) surfaces for the use of antibody microarrays. *Analytical Chemistry* **79,** 4529–4537 (2007).

191. Delehanty, J. B. & Ligler, F. S. A Microarray Immunoassay for Simultaneous Detection of Proteins and Bacteria. *Analytical Chemistry* **74,** 5681–5687 (2002).

192. Luo, W., Pla-Roca, M. & Juncker, D. Taguchi design-based optimization of sandwich immunoassay microarrays for detecting breast cancer biomarkers. *Analytical Chemistry* **83,** 5767–5774 (2011).

193. Küster, S. K., Pabst, M., Zenobi, R. & Dittrich, P. S. Screening for protein phosphorylation using nanoscale reactions on microdroplet arrays. *Angewandte Chemie - International Edition* **54,** 1671–1675 (2015).

194. Chen, Z., Dodig-Crnković, T., Schwenk, J. M. & Tao, S. C. Current applications of antibody microarrays. *Clinical Proteomics* **15,** 1–15 (2018).

195. Sauer, U. Analytical protein microarrays: Advancements towards clinical applications. *Sensors (Switzerland)* **17,** 256 (2017).

196. Ko Ferrigno, P. Increasing experimental reproducibility, from antibodies to protein arrays. *Drug Discovery Today* **21,** 1197–1199 (2016).

197. Cretich, M., Damin, F. & Chiari, M. Protein microarray technology: How far off is routine diagnostics? *Analyst* **139,** 528–542 (2014).

198. Li, Z., Wen, F., Li, Z., Zheng, N., Jiang, J. & Xu, D. Simultaneous detection of α-Lactoalbumin, β-Lactoglobulin and Lactoferrin in milk by Visualized Microarray. *BMC Biotechnology* **17,** 72 (2017).

199. Gerdtsson, A., Dexlin-Mellby, L., Delfani, P., Berglund, E., Borrebaeck, C. & Wingren, C. Evaluation of Solid Supports for Slide- and Well-Based Recombinant Antibody Microarrays. *Microarrays* **5,** 16 (2016).

200. Ayling, K., Bowden, T., Tighe, P., Todd, I., Dilnot, E. M., Negm, O. H., Fairclough, L. & Vedhara, K. The application of protein microarray assays in psychoneuroimmunology. *Brain, Behavior, and Immunity* **59,** 62–66 (2017).

201. Van Hage, M., Schmid-Grendelmeier, P., Skevaki, C., Plebani, M., Canonica, W., Kleine-Tebbe, J., Nystrand, M., Jafari-Mamaghani, M. & Jakob, T. Performance evaluation of ImmunoCAP® ISAC 112: A multi-site study. *Clinical Chemistry and Laboratory Medicine* **55,** 571–577 (2017).

202. Brazma, A., Hingamp, P., Quackenbush, J., Sherlock, G., Spellman, P., Stoeckert, C., Aach, J., Ansorge, W., Ball, C. A., Causton, H. C., Gaasterland, T., Glenisson, P., Holstege, F. C., Kim, I. F., Markowitz, V., Matese, J. C., Parkinson, H., Robinson, A., Sarkans, U., Schulze-Kremer, S., Stewart, J., Taylor, R., Vilo, J. & Vingron, M. Minimum information about a microarray experiment (MIAME) - Toward standards for microarray data. *Nature Genetics* **29,** 365–371 (2001).

203. Martínez-Aranguren, R., Lizaso, M. T., Goikoetxea, M. J., García, B. E., Cabrera-Freitag, P., Trellez, O. & Sanz, M. L. Is the determination of specific IgE against components using ISAC 112 a reproducible technique? *PLoS ONE* **9,** 1–7 (2014).

204. Angenendt, P., Glökler, J., Murphy, D., Lehrach, H. & Cahill, D. J. Toward optimized antibody microarrays: a comparison of current microarray support materials. *Analytical Biochemistry* **309,** 253–260 (2002).

205. Harrison, A., Binder, H., Buhot, A., Burden, C. J., Carlon, E., Gibas, C., Gamble, L. J., Halperin, A., Hooyberghs, J., Kreil, D. P., Levicky, R., Noble, P. A., Ott, A., Pettitt, B. M., Tautz, D. & Pozhitkov, A. E. Physico-chemical foundations underpinning microarray and next-generation sequencing experiments. *Nucleic Acids Research* **41,** 2779–2796 (2013).

206. Löbke, C., Laible, M., Rappl, C., Ruschhaupt, M., Sahin, Ö., Arlt, D., Wiemann, S., Poustka, A., Sültmann, H. & Korf, U. Contact spotting of protein microarrays coupled with spike-in of normalizer protein permits time-resolved analysis of ERBB receptor signaling. *Proteomics* **8,** 1586–1594 (2008).

207. Ramani, S. R., Tom, I., Lewin-Koh, N., Wranik, B., Depalatis, L., Zhang, J., Eaton, D. & Gonzalez, L. C. A secreted protein microarray platform for extracellular protein interaction discovery. *Analytical Biochemistry* **420,** 127–138 (2012).

208. Olle, E. W., Sreekumar, A, Warner, R. L., McClintock, S. D., Chinnaiyan, A. M., Bleavins, M. R., Anderson, T. D. & Johnson, K. J. Development of an internally controlled antibody microarray. *Molecular & Cellular Proteomics* **4,** 1664–1672 (2005).

209. Zangar, R. C., Daly, D. S., White, A. M., Servoss, S. L., Tan, R. M. & Collett, J. R. ProMAT Calibrator : A Tool for Reducing Experimental Bias in Antibody Microarrays research articles. *Journal of Proteome Research* **8,** 3937–3943 (2009).

210. Jin, H. & Zangar, R. C. Antibody microarrays for high-throughput, multianalyte analysis. *Cancer Biomarkers* **6,** 281–290 (2009).

211. Ingvarsson, J., Larsson, A., Sjo, A. G., Truedsson, L., Jansson, B., Borrebaeck, C. A. K. & Wingren, C. Design of Recombinant Antibody Microarrays for Serum Protein Profiling : Targeting of Complement Proteins research articles. *Journal of Proteome Research* **6,** 3527–3536 (2007).

212. Hamelinck, D., Zhou, H., Li, L., Verweij, C., Dillon, D., Feng, Z., Costa, J. & Haab, B. B. Optimized Normalization for Antibody Microarrays and Application to Serum-Protein Profiling. *Molecular & Cellular Proteomics* **4,** 773–784 (2005).

213. Neuman de Vegvar, H. E., Amara, R. R., Steinman, L., Utz, P. J., Robinson, H. L. & Robinson, W. H. Microarray profiling of antibody responses against simian-human immunodeficiency virus: postchallenge convergence of reactivities independent of host histocompatibility type and vaccine regimen. *Journal of Virology* **77,** 11125–38 (2003).

214. Lv, L. L., Liu, B. C., Zhang, C. X., Tang, Z. M., Zhang, L. & Lu, Z. H. Construction of an antibody microarray based on agarose-coated slides. *Electrophoresis* **28,** 406–413 (2007).

215. Perlee, L., Christiansen, J, Dondero, R, Grimwade, B, Lejnine, S, Mullenix, M, Shao, W, Sorette, M, Tchernev, V., Patel, D. & Kingsmore, S. Development and standardization of multiplexed antibody microarrays for use in quantitative proteomics. *Proteome Science* **2,** 9 (2004).

216. List, M., Block, I., Pedersen, M. L., Christiansen, H., Schmidt, S., Thomassen, M., Tan, Q., Baumbach, J. & Mollenhauer, J. Microarray R-based analysis of complex lysate experiments with MIRACLE. *Bioinformatics* **30,** 631–638 (2014).

217. Rimini, R., Schwenk, J. M., Sundberg, M., Sjöberg, R., Klevebring, D., Gry, M., Uhlén, M. & Nilsson, P. Validation of serum protein profiles by a dual antibody array approach. *Journal of Proteomics* **73,** 252–66 (2009).

218. Sboner, A., Karpikov, A., Chen, G., Smith, M., Dawn, M., Freeman-cook, L., Schweitzer, B. & Gerstein, M. B. Robust-Linear-Model Normalization To Reduce Technical Variability in Functional Protein Microarrays. *Journal of Proteome Research* **8,** 5451–5464 (2009).

219. Laforte, V., Lo, P.-S., Li, H. & Juncker, D. Antibody Colocalization Microarray for Cross-Reactivity-Free Multiplexed Protein Analysis. *Methods in Molecular Biology* **1619** (eds Greening, D. W. & Simpson, R. J.) 239–261 (2017).

220. R Core Team. *R: A Language and Environment for Statistical Computing* R Foundation for Statistical Computing (Vienna, Austria, 2018).

221. Dag, O., Dolgun, A. & Konar, N. onewaytests: An R Package for One-Way Tests in Independent Groups Designs. *The R Journal* **10,** 175–199 (2018).

222. Komsta, L. *outliers: Tests for outliers* R package version 0.14 (2011).

223. Ritz, C., Baty, F., Streibig, J. C. & Gerhard, D. Dose-Response Analysis Using R. *PLOS ONE* **10** (12 2015).

224. Komsta, L. *mblm: Median-Based Linear Models* R package version 0.12 (2013).

225. Elzhov, T. V., Mullen, K. M., Spiess, A.-N. & Bolker, B. *minpack.lm: R Interface to the Levenberg-Marquardt Nonlinear Least-Squares Algorithm Found in MINPACK, Plus Support for Bounds* R package version 1.2-1 (2016).

226. Ritchie, M. E., Phipson, B., Wu, D., Hu, Y., Law, C. W., Shi, W. & Smyth, G. K. limma powers differential expression analyses for RNA-sequencing and microarray studies. *Nucleic Acids Research* **43,** e47 (2015).

227. Venables, W. N. & Ripley, B. D. *Modern Applied Statistics with S* Fourth. ISBN 0-387-95457-0 (Springer, New York, 2002).

228. Murphy, T. & Dendukuri, N. *R tutorial on fitting response curves for point-of-care diagnostic tests* http://weightinginbayesianmodels.github.io/poctcalibration/AMfunctions.html.

229. Saviranta, P., Okon, R., Brinker, A., Warashina, M., Eppinger, J. & Geierstanger, B. H. Evaluating sandwich immunoassays in microarray format in terms of the ambient analyte regime. *Clinical Chemistry* **50,** 1907–1920 (2004).

230. Yang, Y. H., Dudoit, S, Luu, P, Lin, D. M., Peng, V, Ngai, J & Speed, T. P. Normalization for cDNA microarray data: a robust composite method addressing single and multiple slide systematic variation. *Nucleic Acids Research* **30,** e15 (2002).

231. Babyak, M. What You See May Not Be What You Get: A Brief, Nontechnical Introduction to Overfitting in Regression-Type Models. *Psychosomatic Medicine,* 4–5 (2004).

232. Prüller, F., Wagner, J., Raggam, R. B., Hoenigl, M., Kessler, H. H., Truschnig-Wilders, M. & Krause, R. Automation of serum (1→3)-beta-D-glucan testing allows reliable and rapid discrimination of patients with and without candidemia. *Medical Mycology* **52,** 453–459 (2014).

233. Morschett, H., Wiechert, W. & Oldiges, M. Automation of a Nile red staining assay enables high throughput quantification of microalgal lipid production. *Microbial Cell Factories* **15,** 1–11 (2016).

234. Fu, Q., Kowalski, M. P., Mastali, M., Parker, S. J., Sobhani, K., Van Den Broek, I., Hunter, C. L. & Van Eyk, J. E. Highly Reproducible Automated Proteomics Sample Preparation Workflow for Quantitative Mass Spectrometry. *Journal of Proteome Research* **17,** 420–428 (2018).

235. Wang, S., Zhao, P. & Cao, B. Development and optimization of an antibody array method for potential cancer biomarker detection. *Journal of Biomedical Research* **25,** 63–70 (2011).

236. Wang, S., Oldenhof, H., Dai, X., Haverich, A., Hilfiker, A., Harder, M. & Wolkers, W. F. Protein stability in stored decellularized heart valve scaffolds and diffusion kinetics of protective molecules. *Biochimica et Biophysica Acta* **1844,** 430–438 (2014).

237. Vagenende, V., Yap, M. G. & Trout, B. L. Mechanisms of protein stabilization and prevention of protein aggregation by glycerol. *Biochemistry* **48,** 11084–11096 (2009).

238. Simpson, R. J. Stabilization of proteins for storage. *Cold Spring Harbor Protocols* **5** (2010).

239. Chen, X., Bhandari, B. & Zhou, P. Insight into the effect of glycerol on stability of globular proteins in high protein model system. *Food Chemistry* **278,** 780–785 (2019).

240. Pazhang, M., Mehrnejad, F., Pazhang, Y., Falahati, H. & Chaparzadeh, N. Effect of sorbitol and glycerol on the stability of trypsin and difference between their stabilization effects in the various solvents. *Biotechnology and Applied Biochemistry* **63,** 206–213 (2016).

241. Anfossi, L., Di Nardo, F., Profiti, M., Nogarol, C., Cavalera, S., Baggiani, C., Giovannoli, C., Spano, G., Ferroglio, E., Mignone, W. & Rosati, S. A versatile and sensitive lateral flow immunoassay for the rapid diagnosis of visceral leishmaniasis. *Analytical and Bioanalytical Chemistry* **410,** 4123–4134 (2018).

242. Bobosha, K., Tjon Kon Fat, E. M., van den Eeden, S. J. F., Bekele, Y., van der Ploeg-van Schip, J. J., de Dood, C. J., Dijkman, K., Franken, K. L. M. C., Wilson, L., Aseffa, A., Spencer, J. S., Ottenhoff, T. H. M., Corstjens, P. L. A. M. & Geluk, A. Field-Evaluation of a New Lateral Flow Assay for Detection of Cellular and Humoral Immunity against *Mycobacterium leprae*. *PLoS Neglected Tropical Diseases* **8** (2014).

243. Wang, Z., Zhi, D., Zhao, Y., Zhang, H., Wang, X., Ru, Y. & Li, H. Lateral flow test strip based on colloidal selenium immunoassay for rapid detection of melamine in milk, milk powder, and animal feed. *International Journal of Nanomedicine* **9,** 1699–1707 (2014).

244. Gussenhoven, G. C., Goris, M. G. A., Terpstra, W. J., Hartskeerl, R. A., Mol, B. E. N. W., W, C. O. R. & Smits, H. L. LEPTO Dipstick, a Dipstick Assay for Detection of Leptospira-Specific Immunoglobulin M Antibodies in Human Sera. *Microbiology* **35,** 92–97 (1997).

245. Ramachandran, S., Fu, E., Lutz, B. & Yager, P. Long-term dry storage of an enzyme-based reagent system for ELISA in point-of-care devices. *Analyst* **139,** 1456–1462 (2014).

246. Yu, C. Y., Ang, G. Y., Chua, A. L., Tan, E. H., Lee, S. Y., Falero-Diaz, G., Otero, O., Rodríguez, I., Reyes, F., Acosta, A., Sarmiento, M. E., Ghosh, S., Ramamurthy, T., Yean Yean, C., Lalitha, P. & Ravichandran, M. Dry-reagent gold nanoparticle-based lateral flow biosensor for the simultaneous detection of *Vibrio cholerae* serogroups O1 and O139. *Journal of Microbiological Methods* **86,** 277–282 (2011).

247. Nutt, S. L., Hodgkin, P. D., Tarlinton, D. M. & Corcoran, L. M. The generation of antibody-secreting plasma cells. *Nature Reviews Immunology* **15,** 160–171 (2015).

248. Berlier, J. E., Rothe, A., Buller, G., Bradford, J., Gray, D. R., Filanoski, B. J., Telford, W. G., Yue, S., Liu, J., Cheung, C. Y., Chang, W., Hirsch, J. D., Beechem, J. M., Haugland, R. P. & Haugland, R. P. Quantitative Comparison of Long-wavelength Alexa Fluor Dyes to Cy Dyes: Fluorescence of the Dyes and Their Bioconjugates. *Journal of Histochemistry and Cytochemistry* **51,** 1699–1712 (2003).

249. Tseng, G. C., Oh, M.-K., Rohlin, L., Liao, J. C. & Wong, W. H. Issues in cDNA microarray analysis: quality filtering, channel normalization, models of variations and assessment of gene effects. *Nucleic Acids Research* **29,** 2549–2557 (2001).

250. Sittampalam, G. S., Coussens, N. P., Nelson, H., Arkin, M., Auld, D., Austin, C., Bejcek, B., Glicksman, M., Inglese, J., Iversen, P. W., McGee, J., McManus, O., Minor, L., Napper, A., Peltier, J. M., Riss, T., Trask, O. J. & Weidner, J. *Assay Guidance Manual* tech. rep. (Eli Lilly & Company and the National Center for Advancing Translational Sciences, Bethesda, MD, 2016).

251. Paul, J., Sahaf, B., Perloff, S., Schoenrock, K., Wu, F., Nakasone, H., Coller, J. & Miklos, D. High-throughput allogeneic antibody detection using protein microarrays. *Journal of Immunological Methods* **432,** 57–64 (2016).

252. Schulz, M. K., Wang, L. P., Tange, M. & Bjerre, P. Cerebral microdialysis monitoring: determination of normal and ischemic cerebral metabolisms in patients with aneurysmal subarachnoid hemorrhage. *Journal of Neurosurgery* **93,** 808–814 (2000).

253. Hillman, J, Aneman, O, Persson, M, Andersson, C, Dabrosin, C & Mellergard, P. Variations in the response of interleukins in neurosurgical intensive care patients monitored using intracerebral microdialysis. *Journal of Neurosurgery* **106,** 820–825 (2007).

254. Mertes, P. M., Beck, B., Jaboin, Y., Stricker, A., Carteaux, J. P., Pinelli, G., El Abassi, K., Villemot, J. P., Burlet, C. & Boulangé, M. Microdialysis in the estimation of interstitial myocardial neuropeptide Y release. *Regulatory Peptides* **49,** 81–90 (1993).

255. Varrier, M. & Ostermann, M. Fluid composition and clinical effects. *Critical Care Clinics* **31,** 823–837 (2015).

256. Rosdahl, H., Ungerstedt, U. & Henriksson, J. Microdialysis in human skeletal muscle and adipose tissue at low flow rates is possible if dextran-70 is added to prevent loss of perfusion fluid. *Acta Physiologica Scandinavica* **159,** 261–262 (1997).

257. Hillman, J., Milos, P., Yu, Z. Q., Sjögren, F., Anderson, C. & Mellergård, P. Intracerebral microdialysis in neurosurgical intensive care patients utilising catheters with different molecular cut-off (20 and 100 kD). *Acta Neurochirurgica (Wien)* **148,** 319–324 (2006).

258. Dahlin, A. P., Wetterhall, M, Caldwell, K. D., Larsson, A, Bergquist, J, Hillered, L & Hjort, K. Methodological aspects on microdialysis protein sampling and quantification in biological fluids: an in vitro study on human ventricular CSF. *Analytical Chemistry* **82,** 4376–4385 (2010).

259. Chu, J., Koudriavtsev, V., Hjort, K. & Dahlin, A. P. Fluorescence imaging of macromolecule transport in high molecular weight cut-off microdialysis. *Analytical and Bioanalytical Chemistry* **406,** 7601–7609 (2014).

260. Clausen, F., Marklund, N. & Hillered, L. Acute inflammatory biomarker responses to diffuse traumatic brain injury in the rat monitored by a novel microdialysis technique. *Journal of Neurotrauma* **36,** 201–211 (2019).

261. Keeler, G. D., Durdik, J. M. & Stenken, J. A. Comparison of microdialysis sampling perfusion fluid components on the foreign body reaction in rat subcutaneous tissue. *European Journal of Pharmaceutical Sciences* **57,** 60–67 (2014).

262. Masuko, T., Minami, A., Iwasaki, N., Majima, T., Nishimura, S.-I. & Lee, Y. C. Carbohydrate analysis by a phenol-sulfuric acid method in microplate format. *Analytical Biochemistry* **339,** 69–72 (2005).

263. Kendrick, K. M. Use of Microdialysis in Neuroendocrinology. *Methods in Enzymology* **168,** 182–205 (1989).

264. Allen, M., Bjerke, M., Edlund, H., Nelander, S. & Westermark, B. Origin of the U87MG glioma cell line: Good news and bad news. *Science Translational Medicine* **8,** 354re3 (2016).

265. *Product Note 107 Microdialysis Pump* 8001243h. CMA Microdialysis (Feb. 2016).

266. Bellander, B. M., Cantais, E., Enblad, P., Hutchinson, P., Nordström, C. H., Robertson, C., Sahuquillo, J., Smith, M., Stocchetti, N., Ungerstedt, U., Unterberg, A. & Olsen, N. V. Consensus meeting on microdialysis in neurointensive care. *Intensive Care Medicine* **30,** 2166–2169 (2004).

267. Hutchinson, P. J., O'Connell, M. T., Nortje, J., Smith, P., Al-Rawi, P. G., Gupta, A. K., Menon, D. K. & Pickard, J. D. Cerebral microdialysis methodology — evaluation of 20 kDa and 100 kDa catheters. *Physiological Measurement* **26,** 423–428 (2005).

268. Kjellström, S., Appels, N., Ohlrogge, M., Laurell, T. & Marko-Varga, G. Microdialysis - a membrane based sampling technique for quantitative determination of proteins. *Chromatographia* **50,** 539–546 (1999).

269. Schutte, R. J., Oshodi, S. A. & Reichert, W. M. In vitro characterization of microdialysis sampling of macromolecules. *Analytical Chemistry* **76,** 6058–6063 (2004).

270. Tarassishin, L. & Lee, S. C. Interferon regulatory factor 3 alters glioma inflammatory and invasive properties. *Journal of Neuro-Oncology* **113,** 185–194 (2013).

271. Tarassishin, L., Lim, J., Weatherly, D. B., Angeletti, R. H. & Lee, S. C. Interleukin-1-induced changes in the glioblastoma secretome suggest its role in tumor progression. *Journal of Proteomics* **99,** 152–168 (2014).

272. Lönsmann Poulsen, H. Interstitial fluid concentrations of albumin and immunoglobulin G in normal men. *Scandinavian Journal of Clinical and Laboratory Investigation* **34,** 119–122 (1974).

273. Shiratori, T., Sato, A., Fukuzawa, M., Kondo, N. & Tanno, S. Severe Dextran-Induced Anaphylactic Shock during Induction of Hypertension-Hypervolemia-Hemodilution Therapy following Subarachnoid Hemorrhage. *Case Reports in Critical Care* **2015,** 1–5 (2015).

274. Hyder, A. A., Wunderlich, C. A., Puvanachandra, P., Gururaj, G. & Kobusingye, O. C. The impact of traumatic brain injuries: a global perspective. *NeuroRehabilitation* **22,** 341–353 (2007).

275. Gardner, R. C. & Yaffe, K. Epidemiology of mild traumatic brain injury and neurodegenerative disease. *Molecular and Cellular Neuroscience* **66,** 75–80 (2015).

276. Eierud, C., Craddock, R. C., Fletcher, S., Aulakh, M., King-Casas, B., Kuehl, D. & Laconte, S. M. Neuroimaging after mild traumatic brain injury: Review and meta-analysis. *NeuroImage: Clinical* **4,** 283–294 (2014).

277. Marmarou, A. Pathophysiology of traumatic brain edema: current concepts. *Acta Neurochirurgica. Supplement* **86,** 7–10 (2003).

278. Ichkova, A. & Badaut, J. New biomarker stars for traumatic brain injury. *Journal of Cerebral Blood Flow and Metabolism* **37,** 3276–3277 (2017).

279. Rodríguez-Rodríguez, A. & Egea-Guerrero, J. J. The utility of biomarkers in traumatic brain injury clinical management. *Critical Care* **20,** 5–6 (2016).

280. Goldstein, L. E. & McKee, A. C. Shining (laser) light on traumatic brain injury blood biomarkers. *JAMA Neurology* **74,** 1045 (2017).

281. Mondello, S., Schmid, K., Berger, R. P., Kobeissy, F., Italiano, D., Jeromin, A., Hayes, R. L., Tortella, F. C. & Buki, A. The Challenge of Mild Traumatic Brain Injury : Role of Biochemical Markers in Diagnosis of Brain Damage. *Medicinal Research Reviews* **34,** 503–531 (2014).

282. Tomar, G. S., Singh, G. P., Lahkar, D., Sengar, K., Nigam, R., Mohan, M. & Anindya, R. New biomarkers in brain trauma. *Clinica Chimica Acta* **487,** 325–329 (2018).

283. Rubenstein, R., Chang, B., Yue, J. K., Chiu, A., Winkler, E. A., Puccio, A. M., Diaz-Arrastia, R., Yuh, E. L., Mukherjee, P., Valadka, A. B., Gordon, W. A., Okonkwo, D. O., Davies, P., Agarwal, S., Lin, F., Sarkis, G., Yadikar, H., Yang, Z., Manley, G. T., Wang, K. K., Cooper, S. R., Dams-O'Connor, K., Borrasso, A. J., Inoue, T., Maas, A. I., Menon, D. K., Schnyer, D. M. & Vassar, M. J. Comparing plasma phospho tau, total tau, and phospho tau–total tau ratio as acute and chronic traumatic brain injury biomarkers. *JAMA Neurology* **74,** 1063–1072 (2017).

284. Orešič, M., Posti, J. P., Kamstrup-Nielsen, M. H., Takala, R. S., Lingsma, H. F., Mattila, I., Jäntti, S., Katila, A. J., Carpenter, K. L., Ala-Seppälä, H., Kyllönen, A., Maanpää, H. R., Tallus, J., Coles, J. P., Heino, I., Frantzén, J., Hutchinson, P. J., Menon, D. K., Tenovuo, O. & Hyötyläinen, T. Human Serum Metabolites Associate With Severity and Patient Outcomes in Traumatic Brain Injury. *EBioMedicine* **12,** 118–126 (2016).

285. Halford, J., Shen, S., Itamura, K., Levine, J., Chong, A. C., Czerwieniec, G., Glenn, T. C., Hovda, D. A., Vespa, P., Bullock, R., Dietrich, W. D., Mondello, S., Loo, J. A. & Wanner, I. B. New astroglial injury-defined biomarkers for neurotrauma assessment. *Journal of Cerebral Blood Flow and Metabolism* **37,** 3278–3299 (2017).

286. Diaz-arrastia, R., Wang, K. K. W., Papa, L., Sorani, M. D., Yue, J. K., Puccio, A. M., Mcmahon, P. J., Inoue, T., Yuh, E. L., Lingsma, H. F., Maas, A. I. R., Valadka, A. B., Okonkwo, D. O., Manley, G. T., Track-TBI Investigators, Casey, S. S., Cheong, M., Cooper, S. R., Connor, K. D.-o., Gordon, W. A., Hricik, A. J., Menon, D. K., Mukherjee, P., Schnyer, D. M., Sinha, T. K. & Vassar, M. J. Acute Biomarkers of Traumatic Brain Injury : Relationship

between Plasma Levels of Ubiquitin C-terminal Hydrolase-L1 and Glial Fibrillary Acidic Protein. *Journal of Neurotrauma* **31,** 19–25 (2014).

287. Poste, G. Bring on the biomarkers. *Nature* **469,** 156–157 (2011).

288. Ghoshal, S., Bondada, V., Saatman, K. E., Guttmann, R. P. & Geddes, W. J. Phage Display for Identification of Serum Biomarkers of Traumatic Brain Injury. *Journal of Neuroscience Methods* **272,** 33–37 (2016).

289. Bogoslovsky, T., Wilson, D., Chen, Y., Hanlon, D., Gill, J., Jeromin, A., Song, L., Moore, C., Gong, Y., Kenney, K. & Diaz-Arrastia, R. Increases of Plasma Levels of Glial Fibrillary Acidic Protein, Tau, and Amyloid β up to 90 Days after Traumatic Brain Injury. *Journal of Neurotrauma* **34,** 66–73 (2017).

290. Mellergård, P., Åneman, O., Sjögren, F., Säberg, C. & Hillman, J. Differences in cerebral extracellular response of interleukin-1β, interleukin-6, and interleukin-10 after subarachnoid hemorrhage or severe head trauma in humans. *Neurosurgery* **68,** 12–9; discussion 19 (2011).

291. Mellergård, P., Åneman, O., Sjögren, F., Pettersson, P. & Hillman, J. Changes in extracellular concentrations of some cytokines, chemokines, and neurotrophic factors after insertion of intracerebral microdialysis catheters in neurosurgical patients. *Neurosurgery* **62,** 151–158 (2008).

292. Kulbe, J. R. & Geddes, J. W. Current status of fluid biomarkers in mild traumatic brain injury. *Experimental Neurology* **275,** 334–352 (2016).

293. Aisiku, I. P., Yamal, J. M., Doshi, P., Benoit, J. S., Gopinath, S., Goodman, J. C. & Robertson, C. S. Plasma cytokines IL-6, IL-8, and IL-10 are associated with the development of acute respiratory distress syndrome in patients with severe traumatic brain injury. *Critical Care* **20,** 1–10 (2016).

294. Bukovics, P., Czeiter, E., Amrein, K., Kovacs, N., Pal, J., Tamas, A., Bagoly, T., Helyes, Z., Buki, A. & Reglodi, D. Changes of PACAP level in cerebrospinal fluid and plasma of patients with severe traumatic brain injury. *Peptides* **60,** 18–22 (2014).

295. De Vos, A., Bjerke, M., Brouns, R., De Roeck, N., Jacobs, D., Van den Abbeele, L., Guldolf, K., Zetterberg, H., Blennow, K., Engelborghs, S. & Vanmechelen, E. Neurogranin and tau in cerebrospinal fluid and plasma of patients with acute ischemic stroke. *BMC Neurology* **17,** 1–8 (2017).

296. Feng, G., Feng, J., Zhang, S., Tong, Y., Zhang, Q., Yang, X. & Zhang, H. Altered levels of α-melanocyte stimulating hormone in cerebrospinal fluid and plasma of patients with traumatic brain injury. *Brain Research* **1696,** 22–30 (2018).

297. Gopcevic, A., Mazul-Sunko, B., Marout, J., Sekulic, A., Antoljak, N., Siranovic, M., Ivanec, Z., Margaritoni, M., Bekavac-Beslin, M. & Zarkovic, N. Plasma Interleukin-8 as a Potential Predictor of Mortality in Adult Patients with Severe Traumatic Brain Injury. *The Tohoku Journal of Experimental Medicine* **211,** 387–393 (2007).

298. Grossetete, M., Phelps, J., Arko, L., Yonas, H. & Rosenberg, G. A. Elevation of MMP-3 and MMP-9 in CSF and Blood in Patients with Severe Traumatic Brain Injury. *Neurosurgery* **65,** 702–708 (2009).

299. Maier, B., Lehnert, M., Laurer, H. L. & Marzi, I. Biphasic elevation in cerebrospinal fluid and plasma concentrations of endothelin 1 after traumatic brain injury in human patients. *Shock* **27,** 610–614 (2007).

300. Mondello, S., Buki, A., Barzo, P., Randall, J., Provuncher, G., Hanlon, D., Wilson, D., Kobeissy, F. & Jeromin, A. CSF and Plasma Amyloid-β Temporal Profiles and Relationships with Neurological Status and Mortality after Severe Traumatic Brain Injury. *Scientific Reports* **3,** 2–7 (2014).

301. Morel, N, Morel, O, Petit, L, Hugel, B, Cochard, J. F., Freyssinet, J. M., Sztark, F & Dabadie, P. Generation of procoagulant microparticles in cerebrospinal fluid and peripheral blood after traumatic brain injury. *The Journal of Trauma* **64,** 698–704 (2008).

302. Saw, M. M., Chamberlain, J., Barr, M., Morgan, M. P., Burnett, J. R. & Ho, K. M. Differential disruption of blood-brain barrier in severe traumatic brain injury. *Neurocritical Care* **20,** 209–216 (2014).

303. Seifman, M. A., Adamides, A. A., Nguyen, P. N., Vallance, S. A., Cooper, D. J., Kossmann, T, Rosenfeld, J. V. & Morganti-Kossmann, M. C. Endogenous melatonin increases in cerebrospinal fluid of patients after severe traumatic brain injury and correlates with oxidative stress and metabolic disarray. *Journal of Cerebral Blood Flow and Metabolism* **28,** 684–696 (2008).

304. Singhal, A., Baker, A., Hare, G., Reinders, F., Schlichter, L. & Moulton, R. Association between Cerebrospinal Fluid Interleukin-6 Concentrations and Outcome after Severe Human Traumatic Brain Injury. *Journal of Neurotrauma* **19,** 929–937 (2002).

305. Zheng, K., Li, C., Shan, X., Liu, H., Fan, W., Wang, Z. & Zheng, P. Matrix metalloproteinases and their tissue inhibitors in serum and cerebrospinal fluid of patients with moderate and severe traumatic brain injury. *Neurology India* **61,** 606–609 (2013).

306. Sarrafzadeh, A., Schlenk, F., Gericke, C. & Vajkoczy, P. Relevance of cerebral interleukin-6 after aneurysmal subarachnoid hemorrhage. *Neurocritical Care* **13,** 339–346 (2010).

307. Clausen, F., Marklund, N., Lewén, A., Enblad, P., Basu, S. & Hillered, L. Interstitial F 2 - Isoprostane 8-Iso-PGF 2α As a Biomarker of Oxidative Stress after Severe Human Traumatic Brain Injury. *Journal of Neurotrauma* **29,** 766–775 (2011).

308. Chang, H. Y., Morrow, K., Bonacquisti, E., Zhang, W. Y. & Shah, D. K. Antibody pharmacokinetics in rat brain determined using microdialysis. *mAbs* **10,** 843–853 (2018).

309. Basso, D., Padoan, A., Laufer, T., Aneloni, V., Moz, S., Schroers, H., Pelloso, M., Saiz, A., Krapp, M., Fogar, P., Cornoldi, P., Zambon, C. F., Rossi, E., La Malfa, M., Marotti, A., Brefort, T., Weis, T. M., Katus, H. A. & Plebani, M. Relevance of pre-analytical blood management on the emerging cardiovascular protein biomarkers TWEAK and HMGB1 and on miRNA serum and plasma profiling. *Clinical Biochemistry* **50,** 186–193 (2017).

310. Pérez de Ciriza, C., Lawrie, A. & Varo, N. Influence of pre-analytical and analytical factors on osteoprotegerin measurements. *Clinical Biochemistry* **47,** 1279–1285 (2014).

311. Lanteri, P., Lombardi, G., Colombini, A., Grasso, D. & Banfi, G. Stability of osteopontin in plasma and serum. *Clinical Chemistry and Laboratory Medicineedicine* **50,** 1979–84 (2012).

312. Lev-Ran, A., Hwang, D. L. & Snyder, D. S. Human serum and plasma have different sources of epidermal growth factor. *American Journal of Physiology* **259,** R545–R548 (1990).

313. Benoy, I., Salgado, R., Colpaert, C., Weytjens, R., Vermeulen, P. B. & Dirix, L. Y. Serum interleukin 6, plasma VEGF, serum VEGF, and VEGF platelet load in breast cancer patients. *Clinical Breast Cancer* **2,** 311–315 (2002).

314. Friebe, A. & Volk, H. D. Stability of tumor necrosis factor alpha, interleukin 6, and interleukin 8 in blood samples of patients with systemic immune activation. *Archives of Pathology and Laboratory Medicine* **132,** 1802–1806 (2008).

315. Amadio, P., Sandrini, L., Ieraci, A., Tremoli, E. & Barbieri, S. S. Effect of clotting duration and temperature on BDNF measurement in human serum. *International Journal of Molecular Sciences* **18** (2017).

316. Tsuchimine, S., Sugawara, N., Ishioka, M. & Yasui-Furukori, N. Preanalysis storage conditions influence the measurement of brain-derived neurotrophic factor levels in peripheral blood. *Neuropsychobiology* **69,** 83–88 (2014).

317. Kaisar, M., Van Dullemen, L. F., Thézénas, M. L., Zeeshan Akhtar, M., Huang, H., Rendel, S., Charles, P. D., Fischer, R., Ploeg, R. J. & Kessler, B. M. Plasma degradome affected by variable storage of human blood. *Clinical Proteomics* **13,** 1–11 (2016).

318. Brain Trauma Foundation, American Association of Neurological Surgeons, Congress of Neurological Surgeons, Joint Section on Neurotrauma and Critical Care, AANS/CNS, Bratton, S. L., Chestnut, R. M., Ghajar, J., Hammond, F. F. M., Harris, O. A., Hartl, R., Manley, G. T., Nemecek, A., Newell, D. W., Rosenthal, G., Schouten, J., Shutter, L., Timmons, S. D., Ullman, J. S., Videtta, W., Wildberger, J. E. & Wright, D. W. Guidelines for the management of severe traumatic brain injury. VI. Indications for intracranial pressure monitoring. *Journal of Neurotrauma* **24,** S37–S44 (2007).

319. Marcoux, J, McArthur, D. A., Miller, C, Glenn, T. C., Villablanca, P, Martin, N. A., Hovda, D. A., Alger, J. R. & Vespa, P. M. Persistent metabolic crisis as measured by elevated cerebral microdialysis lactate-pyruvate ratio predicts chronic frontal lobe brain atrophy after traumatic brain injury. *Critical Care Medicine* **36,** 2871–2877 (2008).

320. Menon, D. K., Schwab, K., Wright, D. W. & Maas, A. I. Position statement: Definition of traumatic brain injury. *Archives of Physical Medicine and Rehabilitation* **91,** 1637–1640 (2010).

321. Wilson, J. T. L., Pettigrew, L. E. L. & Teasdale, G. M. Structured Interviews for the Glasgow Outcome Scale and the Extended Glasgow Outcome Scale: Guidelines for Their Use. *Journal of Neurotrauma* **15,** 573–585 (1998).

322. Bates, D., Mächler, M., Bolker, B. & Walker, S. Fitting Linear Mixed-Effects Models Using lme4. *Journal of Statistical Software* **67,** 1–48 (2015).

323. Ritchie, M. E., Phipson, B., Wu, D., Hu, Y., Law, C. W., Shi, W. & Smyth, G. K. limma powers differential expression analyses for RNA-sequencing and microarray studies. *Nucleic Acids Research* **43,** e47 (2015).

324. Hill, L. J., Di Pietro, V., Hazeldine, J., Davies, D., Tomman, E., Logan, A. & Belli, A. Cystatin D (CST5): An ultra-early inflammatory biomarker of traumatic brain injury. *Scientific Reports* **7,** 1–10 (2017).

325. Gómez, P. A., Castaño-Leon, A. M., De-la Cruz, J., Lora, D. & Lagares, A. Trends in epidemiological and clinical characteristics in severe traumatic brain injury: Analysis of the past 25 years of a single centre data base. *Neurocirugia* **25,** 199–210 (2014).

326. Feigin, V. L., Theadom, A., Barker-Collo, S., Starkey, N. J., McPherson, K., Kahan, M., Dowell, A., Brown, P., Parag, V., Kydd, R., Jones, K., Jones, A. & Ameratunga, S. Incidence of traumatic brain injury in New Zealand: A population-based study. *The Lancet Neurology* **12,** 53–64 (2013).

327. De Guise, E., LeBlanc, J., Dagher, J., Tinawi, S., Lamoureux, J., Marcoux, J., Maleki, M. & Feyz, M. Outcome in Women with Traumatic Brain Injury Admitted to a Level 1 Trauma Center. *International Scholarly Research Notices* **2014,** 1–9 (2014).

328. Gallagher, C. N., Carpenter, K. L., Grice, P., Howe, D. J., Mason, A., Timofeev, I., Menon, D. K., Kirkpatrick, P. J., Pickard, J. D., Sutherland, G. R. & Hutchinson, P. J. The human brain utilizes lactate via the tricarboxylic acid cycle: A 13C-labelled microdialysis and high-resolution nuclear magnetic resonance study. *Brain* **132,** 2839–2849 (2009).

329. Jalloh, I., Helmy, A., Howe, D. J., Shannon, R. J., Grice, P., Mason, A., Gallagher, C. N., Murphy, M. P., Pickard, J. D., Menon, D. K., Carpenter, T. A., Hutchinson, P. J. & Carpenter, K. L. A Comparison of Oxidative Lactate Metabolism in Traumatically Injured Brain and Control Brain. *Journal of Neurotrauma* **35,** 2025–2035 (2018).

330. Lama, S., Auer, R. N., Tyson, R., Gallagher, C. N., Tomanek, B. & Sutherland, G. R. Lactate storm marks cerebral metabolism following brain trauma. *Journal of Biological Chemistry* **289,** 20200–20208 (2014).

331. Tisdall, M. M. & Smith, M. Cerebral microdialysis: Research technique or clinical tool? *British Journal of Anaesthesia* **97,** 18–25 (2006).

332. Ståhl, N., Mellergård, P., Hallström, A., Ungerstedt, U. & Nordström, C. H. Intracerebral microdialysis and bedside biochemical analysis in patients with fatal traumatic brain lesions. *Acta Anaesthesiologica Scandinavica* **45,** 977–985 (2001).

333. Jones, E. V., Bernardinelli, Y., Zarruk, J. G., Chierzi, S. & Murai, K. K. SPARC and GluA1-Containing AMPA Receptors Promote Neuronal Health Following CNS Injury. *Frontiers in Cellular Neuroscience* **12,** 1–13 (2018).

334. Dandy, W. E. Internal Hydrocephalus. An Experimental, Clinical and Pathological Study. *Annals of Surgery* **70,** 129–142 (1919).

335. Kimelberg, H. K. Water homeostasis in the brain: Basic concepts. *Neuroscience* **129,** 851–860 (2004).

336. Orešković, D. & Klarica, M. The formation of cerebrospinal fluid: Nearly a hundred years of interpretations and misinterpretations. *Brain Research Reviews* **64,** 241–262 (2010).

337. Redzic, Z. Molecular biology of the blood-brain and the blood-cerebrospinal fluid barriers: Similarities and differences. *Fluids and Barriers of the CNS* **8,** 3 (2011).

338. Abbott, N. J., Pizzo, M. E., Preston, J. E., Janigro, D. & Thorne, R. G. The role of brain barriers in fluid movement in the CNS: is there a 'glymphatic' system? *Acta Neuropathologica* **135,** 387–407 (2018).

339. Legros, C., Chesneau, D., Boutin, J. A., Barc, C. & Malpaux, B. Melatonin from cerebrospinal fluid but not from blood reaches sheep cerebral tissues under physiological conditions. *Journal of Neuroendocrinology* **26,** 151–163 (2014).

340. Dietrich, M. O., Tort, A. B., Schaf, D. V., Farina, M., Gonçalves, C. A., Souza, D. O. & Portela, L. V. Increase in Serum S100B Protein Level After a Swimming Race. *Canadian Journal of Applied Physiology* **28,** 710–716 (2003).

341. Middeldorp, J. & Hol, E. M. GFAP in health and disease. *Progress in Neurobiology* **93,** 421–443 (2011).

342. Zhou, S., Yin, D. P., Wang, Y., Tian, Y., Wang, Z. G. & Zhang, J. N. Dynamic changes in growth factor levels over a 7-day period predict the functional outcomes of traumatic brain injury. *Neural Regeneration Research* **13,** 2134–2140 (2018).

343. Babcock, L., Zhang, N., Leach, J. & Wade, S. L. Are UCH-L1 and GFAP promising biomarkers for children with mild traumatic brain injury? *Brain Injury* **30,** 1231–1238 (2016).

344. Lewis, L. M., Schloemann, D. T., Papa, L., Fucetola, R. P., Bazarian, J., Lindburg, M. & Welch, R. D. Utility of Serum Biomarkers in the Diagnosis and Stratification of Mild Traumatic Brain Injury. *Academic Emergency Medicine* **24,** 710–720 (2017).

345. Papa, L., Brophy, G. M., Welch, R. D., Lewis, L. M., Braga, C. F., Tan, C. N., Ameli, N. J., Lopez, M. A., Haeussler, C. A., Mendez Giordano, D. I., Silvestri, S., Giordano, P., Weber, K. D., Hill-Pryor, C. & Hack, D. C. Time course and diagnostic accuracy of glial and neuronal blood biomarkers GFAP and UCH-L1 in a large cohort of trauma patients with and without mild traumatic brain injury. *JAMA Neurology* **73,** 551–560 (2016).

346. Plog, B. A., Dashnaw, M. L., Hitomi, E., Peng, W., Liao, Y., Lou, N., Deane, R. & Nedergaard, M. Biomarkers of Traumatic Injury Are Transported from Brain to Blood via the Glymphatic System. *The Journal of Neuroscience* **35,** 518–526 (2015).

347. Raheja, A., Sinha, S., Samson, N., Bhoi, S., Subramanian, A., Sharma, P. & Sharma, B. S. Serum biomarkers as predictors of long-term outcome in severe traumatic brain injury: analysis from a randomized placebo-controlled Phase II clinical trial. *Journal of Neurosurgery* **125,** 631–641 (2016).

348. Ercole, A., Thelin, E. P., Holst, A., Bellander, B. M. & Nelson, D. W. Kinetic modelling of serum S100b after traumatic brain injury. *BMC Neurology* **16,** 1–8 (2016).

349. Dixon, K. J. Pathophysiology of Traumatic Brain Injury. *Physical Medicine and Rehabilitation Clinics of North America* **28,** 215–225 (2017).

350. Ho, L., Zhao, W., Dams-O'Connor, K., Tang, C. Y., Gordon, W., Peskind, E. R., Yemul, S., Haroutunian, V. & Pasinetti, G. M. Elevated plasma MCP-1 concentration following traumatic brain injury as a potential "predisposition" factor associated with an increased risk for subsequent development of Alzheimer's Disease. *Journal of Alzheimer's Disease* **31,** 301–313 (2012).

351. Wang, Y., Sun, W. F., Liu, X. G., Deng, J., Yan, B. E., Jiang, W. Y. & Lin, X. B. Comparative study of serum BMP-2 and heterotopic ossification in traumatic brain injury and fractures patients. *China Journal of Orthopedics and Traumatology* **24,** 399–403 (2011).

352. Stein, D. M., Lindell, A, Murdock, K. R., Kufera, J. A., Menaker, J, Keledjian, K, Bochicchio, G. V., Aarabi, B & Scalea, T. M. Relationship of serum and cerebrospinal fluid biomarkers with intracranial hypertension and cerebral hypoperfusion after severe traumatic brain injury. *The Journal of Trauma* **70,** 1096–1103 (2011).

353. Stein, D. M., Lindel, A. L., Murdock, K. R., Kufera, J. A., Menaker, J. & Scalea, T. M. Use of serum biomarkers to predict secondary insults following severe traumatic brain injury. *Shock* **37,** 563–568 (2012).

354. Hergenroeder, G. W., Ward III, N. H., Clifton, G. L., Moore, A. N., Dash, P. K., McCoy Jr, J. P. & Samsel, L. Serum IL-6: A candidate biomarker for intracranial pressure elevation following isolated traumatic brain injury. *Journal of Neuroinflammation* **7,** 1–13 (2010).

355. Shiozaki, T., Hayakata, T., Tasaki, O., Hosotubo, H., Fuijita, K., Mouri, T., Tajima, G., Kajino, K., Nakae, H., Tanaka, H., Shimazu, T. & Sugimoto, H. Cerebrospinal fluid concentrations of anti-inflammatory mediators in early-phase severe traumatic brain injury. *Shock* **23,** 406–410 (2005).

356. Goyal, A., Failla, M. D., Niyonkuru, C., Amin, K., Fabio, A., Berger, R. P. & Wagner, A. K. S100b as a Prognostic Biomarker in Outcome Prediction for Patients with Severe Traumatic Brain Injury. *Journal of Neurotrauma* **30,** 946–957 (2013).

357. Heidari, K., Asadollahi, S., Jamshidian, M., Abrishamchi, S. N. & Nouroozi, M. Prediction of neuropsychological outcome after mild traumatic brain injury using clinical parameters, serum S100B protein and findings on computed tomography. *Brain Injury* **29,** 33–40 (2015).

358. Mondello, S., Kobeissy, F., Vestri, A., Hayes, R. L., Kochanek, P. M. & Berger, R. P. Serum Concentrations of Ubiquitin C-Terminal Hydrolase-L1 and Glial Fibrillary Acidic Protein after Pediatric Traumatic Brain Injury. *Scientific Reports* **6,** 1–8 (2016).

359. Rosenberg-Hasson, Y., Hansmann, L., Liedtke, M., Herschmann, I. & Maecker, H. T. Effects of serum and plasma matrices on multiplex immunoassays. *Immunologic Research* **58,** 224–233 (2014).

360. *https://www.olink.com/* 2019.

361. Schwickart, M., Vainshtein, I., Lee, R., Schneider, A. & Liang, M. Interference in immunoassays to support therapeutic antibody development in preclinical and clinical studies. *Bioanalysis* **6,** 1939–1951 (2014).

362. Abcam. *Technical tips for ELISA and multiplex immunoassay development* 2019.

363. R&D Systems. *ELISA Development Guide*

364. Glick, S. D., Dong, N., Jr., R. W. K. & Carlson, J. N. Estimating Extracellular Concentrations of Dopamine and 3,4-Dihydroxyphenylacetic Acid in Nucleus Accumbens and Striatum Using Microdialysis: Relationships Between In Vitro and In Vivo Recoveries. *Journal of Neurochemistry* **62,** 2017–2021 (1994).

365. Giorgi-Coll, S., Thelin, E. P., Lindblad, C., Tajsic, T., Carpenter, K., Hutchinson, P. J. & Helmy, A. Dextran 500 improves recovery of inflammatory markers: an in vitro microdialysis study. *Journal of Neurotrauma,* Epub ahead of print (2019).

366. Clancy, K. F., Dery, S., Laforte, V., Shetty, P., Juncker, D. & Nicolau, D. V. Protein microarray spots are modulated by patterning method, surface chemistry and processing conditions. *Biosensors and Bioelectronics* **130,** 397–407 (2019).

367. Rivas, L., Reuterswärd, P., Rasti, R., Herrmann, B., Mårtensson, A., Alfvén, T., Gantelius, J. & Andersson-Svahn, H. A vertical flow paper-microarray assay with isothermal DNA amplification for detection of Neisseria meningitidis. *Talanta* **183,** 192–200 (2018).

368. Frampton, J. P., White, J. B., Simon, A. B., Tsuei, M., Paczesny, S. & Takayama, S. Aqueous two-phase system patterning of detection antibody solutions for cross-reaction-free multiplex ELISA. *Scientific Reports* **4,** 4878 (2014).

369. Fredriksson, S., Dixon, W., Ji, H., Koong, A. C., Mindrinos, M. & Davis, R. W. Multiplexed protein detection by proximity ligation for cancer biomarker validation. *Nature Methods* **4,** 327–329 (2007).

370. Fredriksson, S., Gullberg, M., Jarvius, J., Olsson, C., Pietras, K., Gústafsdóttir, S. M., Östman, A. & Landegren, U. Protein detection using proximity-dependent DNA ligation assays. *Nature Biotechnology* **20,** 473–477 (2002).

371. Aldo, P., Marusov, G., Svancara, D., David, J. & Mor, G. Simple plex™: A novel multi-analyte, automated microfluidic immunoassay platform for the detection of human and mouse cytokines and chemokines. *American Journal of Reproductive Immunology* **75,** 678–693 (2016).

372. Blank, K., Lankenau, A., Mai, T., Schiffmann, S., Gilbert, I., Hirler, S., Albrecht, C., Benoit, M., Gaub, H. E. & Clausen-Schaumann, H. Double-chip protein arrays: force-based multiplex sandwich immunoassays with increased specificity. *Analytical and Bioanalytical Chemistry* **379,** 974–981 (2004).

373. Christendat, D., Yee, A., Dharamsi, A., Kluger, Y., Savchenko, A., Cort, J. R., Booth, V., Mackereth, C. D., Saridakis, V., Ekiel, I., Kozlov, G., Maxwell, K. L., Wu, N., McIntosh, L. P., Gehring, K., Kennedy, M. A., Davidson, A. R., Pai, E. F., Gerstein, M., Edwards, A. M. & Arrowsmith, C. H. Structural proteomics of an archaeon. *Nature Structural Biology* **7,** 903–909 (2000).

374. Kusnezow, W., Jacob, A., Walijew, A., Diehl, F. & Hoheisel, J. D. Antibody microarrays: An evaluation of production parameters. *Proteomics* **3,** 254–264 (2003).

375. Berlier, J. E., Rothe, A., Buller, G., Bradford, J., Gray, D. R., Filanoski, B. J., Telford, W. G., Yue, S., Liu, J., Cheung, C.-Y., Chang, W., Hirsch, J. D., Beechem, J. M., Haugland, R. P. & Haugland, R. P. Quantitative comparison of long-wavelength Alexa Fluor dyes to Cy dyes: fluorescence of the dyes and their bioconjugates. *The Journal of Histochemistry & Cytochemistry* **51,** 1699–1712 (2003).

376. Byerly, S., Sundin, K., Raja, R., Stanchfield, J., Bejjani, B. A. & Shaffer, L. G. Effects of ozone exposure during microarray posthybridization washes and scanning. *Journal of Molecular Diagnostics* **11,** 590–597 (2009).

377. Cox, W. G., Beaudet, M. P., Agnew, J. Y. & Ruth, J. L. Possible sources of dye-related signal correlation bias in two-color DNA microarray assays. *Analytical Biochemistry* **331,** 243–254 (2004).

378. Anderson, G. P. & Nerurkar, N. L. Improved fluoroimmunoassays using the dye Alexa Fluor 647 with the RAPTOR, a fiber optic biosensor. *Journal of Immunological Methods* **271,** 17–24 (2002).

379. Becker, W. Fluorescence lifetime imaging - techniques and applications. *Journal of Microscopy* **247,** 119–136 (2012).

380. Wilson, J. J., Burgess, R., Mao, Y. Q., Luo, S., Tang, H., Jones, V. S., Weisheng, B., Huang, R. Y., Chen, X. & Huang, R. P. Antibody Arrays in Biomarker Discovery. *Advances in Clinical Chemistry* **69,** 255–324 (2015).

381. Li, H., Bergeron, S., Annis, M. G., Siegel, P. M. & Juncker, D. Serial Analysis of 38 Proteins during the Progression of Human Breast Tumor in Mice Using an Antibody Colocalization Microarray. *Molecular & Cellular Proteomics* **14,** 1024–1037 (2015).

382. Wingren, C. & Borrebaeck, C. A. Antibody-based microarrays. *Methods in Molecular Biology* **509,** 57–84 (2009).

383. Gonzalez, R. M., Seurynck-Servoss, S. L., Crowley, S. A., Brown, M., Omenn, G. S., Hayes, D. F. & Zangar, R. C. Development and validation of sandwich ELISA microarrays with minimal assay interference. *Journal of Proteome Research* **7,** 2406–2414 (2008).

384. Rodbard, D., Feldman, Y., Jaffe, M. & Miles, L. Studies on the nature of the 'high-dose hook effect'. *Immunochemistry* **15,** 77–82 (1978).